frontiers | Research Topics

Prognosis prediction and risk stratification in head and neck cancer

Edited by
Heming Lu, Yong Yin, Qin Lin, Shiyu Song, Min Yao and Hui Wang

Published in
Frontiers in Oncology

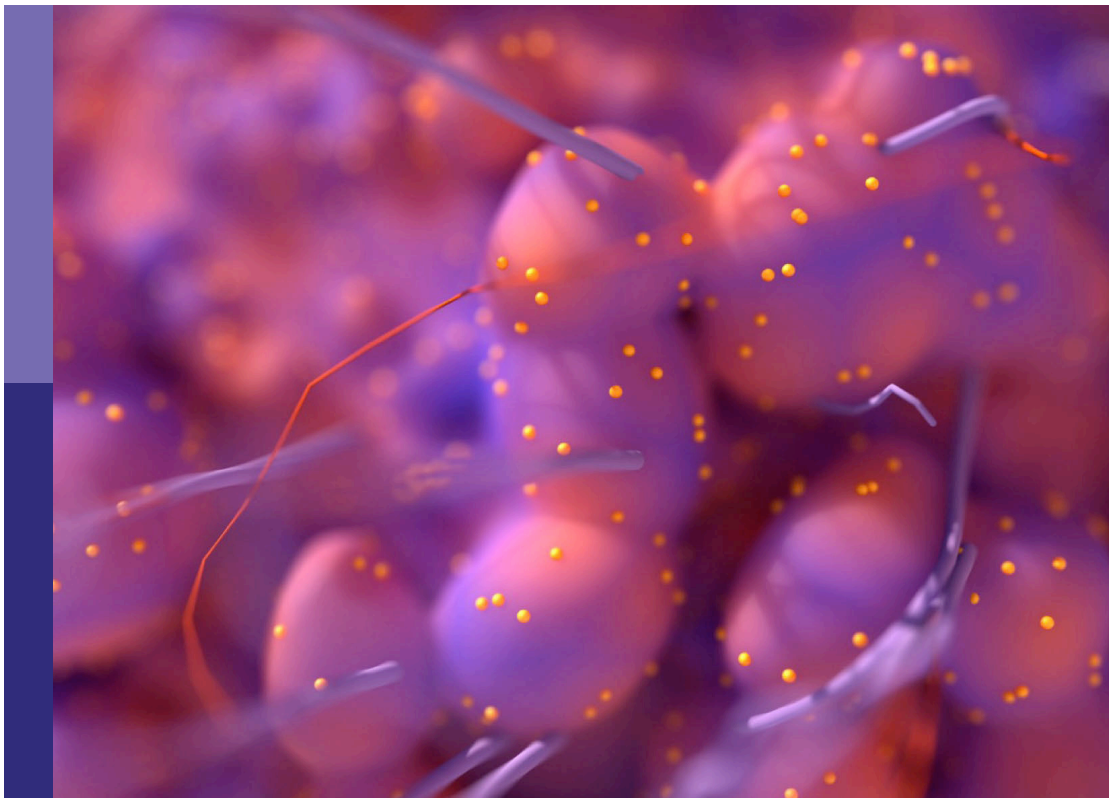

ISSN 1664-8714
ISBN 978-2-83251-320-0
DOI 10.3389/978-2-83251-320-0

About Frontiers

Frontiers is more than just an open access publisher of scholarly articles: it is a pioneering approach to the world of academia, radically improving the way scholarly research is managed. The grand vision of Frontiers is a world where all people have an equal opportunity to seek, share and generate knowledge. Frontiers provides immediate and permanent online open access to all its publications, but this alone is not enough to realize our grand goals.

Frontiers journal series

The Frontiers journal series is a multi-tier and interdisciplinary set of open-access, online journals, promising a paradigm shift from the current review, selection and dissemination processes in academic publishing. All Frontiers journals are driven by researchers for researchers; therefore, they constitute a service to the scholarly community. At the same time, the *Frontiers journal series* operates on a revolutionary invention, the tiered publishing system, initially addressing specific communities of scholars, and gradually climbing up to broader public understanding, thus serving the interests of the lay society, too.

Dedication to quality

Each Frontiers article is a landmark of the highest quality, thanks to genuinely collaborative interactions between authors and review editors, who include some of the world's best academicians. Research must be certified by peers before entering a stream of knowledge that may eventually reach the public - and shape society; therefore, Frontiers only applies the most rigorous and unbiased reviews. Frontiers revolutionizes research publishing by freely delivering the most outstanding research, evaluated with no bias from both the academic and social point of view. By applying the most advanced information technologies, Frontiers is catapulting scholarly publishing into a new generation.

What are Frontiers Research Topics?

Frontiers Research Topics are very popular trademarks of the *Frontiers journals series*: they are collections of at least ten articles, all centered on a particular subject. With their unique mix of varied contributions from Original Research to Review Articles, Frontiers Research Topics unify the most influential researchers, the latest key findings and historical advances in a hot research area.

Find out more on how to host your own Frontiers Research Topic or contribute to one as an author by contacting the Frontiers editorial office: frontiersin.org/about/contact

Prognosis prediction and risk stratification in head and neck cancer

Topic editors

Heming Lu — People's Hospital of Guangxi Zhuang Autonomous Region, China
Yong Yin — Department of Radiation Oncology, Shandong Cancer Hospital, China
Qin Lin — First Affiliated Hospital of Xiamen University, China
Shiyu Song — Virginia Commonwealth University Health System, United States
Min Yao — University Hospitals Cleveland Medical Center, United States
Hui Wang — Key Laboratory of Translational Radiation Oncology, Hunan Cancer Hospital, China

Citation

Lu, H., Yin, Y., Lin, Q., Song, S., Yao, M., Wang, H., eds. (2023). *Prognosis prediction and risk stratification in head and neck cancer*. Lausanne: Frontiers Media SA.
doi: 10.3389/978-2-83251-320-0

Table of contents

10 Editorial: Prognosis prediction and risk stratification in head and neck cancer
Tengxiang Li, Jie Lu, Yong Yin and Qingtao Qiu

17 Development and Validation of a Prognostic Nomogram for Hypopharyngeal Carcinoma
Shu Tian, Qin Li, Ruichen Li, Xinyu Chen, Zhonghua Tao, Hongli Gong, Xiaoshen Wang and Xichun Hu

27 Digital Pathology Scoring of Immunohistochemical Staining Reliably Identifies Prognostic Markers and Anatomical Associations in a Large Cohort of Oral Cancers
Julius Moratin, Andreas Mock, Sonja Obradovic, Karl Metzger, Christa Flechtenmacher, Karim Zaoui, Stefan Fröhling, Dirk Jäger, Jürgen Krauss, Jürgen Hoffmann, Kolja Freier, Dominik Horn, Jochen Hess and Christian Freudlsperger

38 The Prognostic Value of the DNA Repair Gene Signature in Head and Neck Squamous Cell Carcinoma
Ruijie Ming, Enhao Wang, Jiahui Wei, Jinxiong Shen, Shimin Zong and Hongjun Xiao

55 Prognostic Role of EGFR/p-EGFR in Patients With Nasopharyngeal Carcinoma: A Meta-Analysis
Xishan Chen, Renba Liang, Lin Lai, Kaihua Chen and Xiaodong Zhu

66 Are People With Blood Group O More Susceptible to Nasopharyngeal Carcinoma and Have Worse Survival Rates? A Systematic Review and Meta-Analysis
Shao-wu Jing, Qing Xu, Xin-yuan Zhang, Zhong-hao Jing, Zhi-jun Zhao, Ruo-hui Zhang, Feng-peng Wu and Jun Wang

74 Multivariate NTCP Model of Hypothyroidism After Intensity-Modulated Radiotherapy for Nasopharyngeal Carcinoma
Guanzhu Shen, Yinglin Peng, Jian Li, Haijun Wu, Guangshun Zhang, Chong Zhao and Xiaowu Deng

83 Prognostic Relevance of 18F-FDG-PET/CT-Guided Target Volume Delineation in Loco-Regionally Advanced Nasopharyngeal Carcinomas: A Comparative Study
Ouying Yan, Hui Wang, Yaqian Han, Shengnan Fu, Yanzhu Chen and Feng Liu

92 A Competing Risk Nomogram for Predicting Cancer-Specific Death of Patients With Maxillary Sinus Carcinoma
Mingbin Hu, Xiancai Li, Weiguo Gu, Jinhong Mei, Dewu Liu and Shaoqing Chen

103 Incidence and Prognostic Significance of PD-L1 Expression in High-Grade Salivary Gland Carcinoma
Qigen Fang, Yao Wu, Wei Du, Xu Zhang and Defeng Chen

110 Corrigendum: Incidence and Prognostic Significance of PD-L1 Expression in High-Grade Salivary Gland Carcinoma
Qigen Fang, Yao Wu, Wei Du, Xu Zhang and Defeng Chen

111 Prognostic Factors for Overall Survival in Nasopharyngeal Cancer and Implication for TNM Staging by UICC: A Systematic Review of the Literature
Chi Leung Chiang, Qiaojuan Guo, Wai Tong Ng, Shaojun Lin, Tiffany Sze Wai Ma, Zhiyuan Xu, Youping Xiao, Jishi Li, Tianzhu Lu, Horace Cheuk Wai Choi, Wenqi Chen, Eric Sze Chun Chau, Peter Ho Yin Luk, Shao Hui Huang, Brian O'Sullivan, Jianji Pan and Anne Wing Mui Lee

130 The Ratio of Preoperative Serum Biomarkers Predicts Prognosis in Patients With Oral Squamous Cell Carcinoma
Meng Ding, Yuxian Song, Junyan Jing, Mei Tian, Liang Ding, Qiang Li, Chongchong Zhou, Heng Dong, Yanhong Ni and Yongbin Mou

140 Residual Volume of Lymph Nodes During Chemoradiotherapy Based Nomogram to Predict Survival of Nasopharyngeal Carcinoma Patient Receiving Induction Chemotherapy
Yan Li, Jian Zang, Jingyi Liu, Shanquan Luo, Jianhua Wang, Bingxin Hou, Lina Zhao and Mei Shi

150 Radiomic Features Associated With HPV Status on Pretreatment Computed Tomography in Oropharyngeal Squamous Cell Carcinoma Inform Clinical Prognosis
Bolin Song, Kailin Yang, Jonathan Garneau, Cheng Lu, Lin Li, Jonathan Lee, Sarah Stock, Nathaniel M. Braman, Can Fahrettin Koyuncu, Paula Toro, Pingfu Fu, Shlomo A. Koyfman, James S. Lewis Jr and Anant Madabhushi

164 $CD68^+$ Macrophage Infiltration Associates With Poor Outcome of HPV Negative Oral Squamous Carcinoma Patients Receiving Radiation: Poly(I:C) Enhances Radiosensitivity of CAL-27 Cells but Promotes Macrophage Recruitment Through HMGB1
Dan Ai, Yu Dou, Zhaodi Nan, Ketao Wang, Huayang Wang, Lin Zhang, Zuoqing Dong, Jintang Sun, Chao Ma, Wanye Tan, Wenjuan Gao, Jia Liu, Lei Zhao, Shaohua Liu, Bingfeng Song, Qianqian Shao and Xun Qu

179 Prognostic Value of Plasma Epstein-Barr Virus DNA Levels Pre- and Post-Neoadjuvant Chemotherapy in Patients With Nasopharyngeal Carcinoma
Lisheng Zhu, Tao Ouyang, Ying Xiong, Li Ba, Qiuting Li, Mengjun Qiu, Zhenwei Zou and Gang Peng

193 Comparison of TPF and TP Induction Chemotherapy for Locally Advanced Nasopharyngeal Carcinoma Based on TNM Stage and Pretreatment Systemic Immune-Inflammation Index
Ying Xiong, Liangliang Shi, Lisheng Zhu and Gang Peng

202 Diagnostic and Prognostic Value of MicroRNAs in Metastasis and Recurrence of Head and Neck Squamous Cell Carcinoma: A Systematic Review and Meta-Analysis
Ke Qiu, Yao Song, Yufang Rao, Qiurui Liu, Danni Cheng, Wendu Pang, Jianjun Ren and Yu Zhao

212 A Tumor-Infiltration CD8+ T Cell-Based Gene Signature for Facilitating the Prognosis and Estimation of Immunization Responses in HPV+ Head and Neck Squamous Cell Cancer
Yingning Wu, Lingzhang Meng, Kai Cai, Jingjie Zhao, Siyuan He, Jiajia Shen, Qiuju Wei, Zechen Wang, Suren Sooranna, Hengguo Li and Jian Song

224 Survival-Weighted Health Profiles in Patients Treated for Advanced Oral Cavity Squamous Cell Carcinoma
Yao-Te Tsai, Wen-Cheng Chen, Cheng-Ming Hsu, Ming-Shao Tsai, Geng-He Chang, Yi-Chan Lee, Ethan I. Huang, Chiung-Cheng Fang and Chia-Hsuan Lai

234 Development and Validation of an Autophagy-Related LncRNA Prognostic Signature in Head and Neck Squamous Cell Carcinoma
Lin Shen, Na Li, Qin Zhou, Zhanzhan Li and Liangfang Shen

247 Subphrenic Lymph Node Metastasis Predicts Poorer Prognosis for Nasopharyngeal Carcinoma Patients With Metachronous Metastasis
Xue-Fang Zhang, Yan Zhang, Xu-Wei Liang, Jia-Luo Chen, Sheng-Fang Zhi, Wen-Jing Yin, Meng-Yao Wang, En-Lai Dong and Dong-Ping Chen

256 Transcriptomic Correlates of Immunologic Activation in Head and Neck and Cervical Cancer
Cristina Saiz-Ladera, Mariona Baliu-Piqué, Francisco J. Cimas, Aránzazu Manzano, Vanesa García-Barberán, Santiago Cabezas Camarero, Gonzalo Fernández Hinojal, Atanasio Pandiella, Balázs Győrffy, David Stewart, Juan J. Cruz-Hernández, Pedro Pérez-Segura and Alberto Ocana

272 Outcomes of Recurrent Nasopharyngeal Carcinoma Patients Treated With Salvage Surgery: A Meta-Analysis
Yekai Feng, Zhimei Dai, Ruicheng Yan, Feng Li, Xiaosheng Zhong, Haoxin Ye, Caiqing Chen, Shaochong Fan, Cheng Qing, Yong Pan and Haiying Sun

281 Comprehensive Analysis of Prognostic Alternative Splicing Signature Reveals Recurrence Predictor for Papillary Thyroid Cancer
Mian Liu, Rooh Afza Khushbu, Pei Chen, Hui-Yu Hu, Neng Tang, Deng-jie Ou-yang, Bo Wei, Ya-xin Zhao, Peng Huang and Shi Chang

295 Nomogram Predicting Cancer-Specific Death in Parotid Carcinoma: a Competing Risk Analysis
Xiancai Li, Mingbin Hu, Weiguo Gu, Dewu Liu, Jinhong Mei and Shaoqing Chen

307 Efficacy and Toxicity of Three Induction Chemotherapy Regimens in Locoregionally Advanced Nasopharyngeal Carcinoma: Outcomes of 10-Year Follow-Up
Hao Peng, Binbin Chen, Shuiqing He, Li Tian and Ying Huang

315 MicroRNA-483-5p Predicts Poor Prognosis and Promotes Cancer Metastasis by Targeting *EGR3* in Nasopharyngeal Carcinoma
Xi-Zhao Li, Yi-Jun Tu, Ting Zhou, Jiang-Bo Zhang, Ruo-Wen Xiao, Da-Wei Yang, Pei-Fen Zhang, Peng-Tao You and Xiao-Hui Zheng

324 Spatial Distribution of Immune Cells in Head and Neck Squamous Cell Carcinomas
Christian Idel, Julika Ribbat-Idel, Luise Klapper, Rosemarie Krupar, Karl-Ludwig Bruchhage, Eva Dreyer, Dirk Rades, Christina Polasky, Anne Offermann, Jutta Kirfel, Sven Perner and Barbara Wollenberg

335 Multidimensional Mutational Profiling of the Indian HNSCC Sub-Population Provides IRAK1, a Novel Driver Gene and Potential Druggable Target
Sagar Sanjiv Desai, Raksha Rao K, Anika Jain, Pushpinder Singh Bawa, Priyatam Dutta, Gaurav Atre, Anand Subhash, Vishal U. S. Rao, Suvratha J, Subhashini Srinivasan and Bibha Choudhary

352 Dose Prediction Using a Three-Dimensional Convolutional Neural Network for Nasopharyngeal Carcinoma With Tomotherapy
Yaoying Liu, Zhaocai Chen, Jinyuan Wang, Xiaoshen Wang, Baolin Qu, Lin Ma, Wei Zhao, Gaolong Zhang and Shouping Xu

361 The Integration of the Pre-Treatment Neutrophil-to-Lymphocyte Ratio in the Eighth Edition of the AJCC Staging System for Nasopharynx Cancer
Zhong-Guo Liang, Fan Zhang, Ye Li, Ling Li, Song Qu, Fang Su, Bin-Bin Yu, Ying Guan, Lu Han, Kai-Guo Li and Xiao-Dong Zhu

372 Identification of Prognostic Biomarkers Originating From the Tumor Stroma of Betel Quid-Associated Oral Cancer Tissues
Yi-Hong Liu, Yu-Lian Chen, Ting-Yu Lai, Ying-Chieh Ko, Yu-Fu Chou, Peir-Rong Chen, Jenn-Ren Hsiao, Jang-Yang Chang, Shine-Gwo Shiah, Jeng-Woei Lee, Jia-Ling Yang and Su-Fang Lin

386 Identification of Hypoxia-Related Molecular Classification and Associated Gene Signature in Oral Squamous Cell Carcinoma
Chen Li, Xin Chen, Xiaolin Ren, Jia-lin Chen, Hao Chen, Jing-jia Yu, Qiu-chi Ran, Shuang Kang, Xi-meng Chen and Zhen-jin Zhao

399 A Novel Lipid Prognostic Signature of ADCY2, LIPE, and OLR1 in Head and Neck Squamous Cell Carcinoma
Xiaolei Gao, Na Zhao, Liying Dong, Xuan Zheng, Yixin Zhang, Chong Ding, Shuyan Zhao, Zeyun Ma and Yixiang Wang

416 A New Dynamic Response to Therapy Assessment in Postoperative Patients With Low-Risk Differentiated Thyroid Cancer Treated Without Radioactive Iodine
Ping Dong, Li Wang, Liu Xiao, Liu Yang, Rui Huang and Lin Li

423 Worst Pattern of Perineural Invasion Redefines the Spatial Localization of Nerves in Oral Squamous Cell Carcinoma
Yong Fu, Xinwen Zhang, Zhuang Ding, Nisha Zhu, Yuxian Song, Xiaoxin Zhang, Yue Jing, Yijun Yu, Xiaofeng Huang, Lei Zhang, Qingang Hu, Yanhong Ni and Liang Ding

432 Comprehensive Analysis of m^{6}A Regulators Characterized by the Immune Cell Infiltration in Head and Neck Squamous Cell Carcinoma to Aid Immunotherapy and Chemotherapy
Zhiqiang Yang, Xiaoping Ming, Shuo Huang, Minlan Yang, Xuhong Zhou and Jiayu Fang

447 Predictive Value of a Combined Model Based on Pre-Treatment and Mid-Treatment MRI-Radiomics for Disease Progression or Death in Locally Advanced Nasopharyngeal Carcinoma
Le Kang, Yulin Niu, Rui Huang, Stefan (YUJIE) Lin, Qianlong Tang, Ailin Chen, Yixin Fan, Jinyi Lang, Gang Yin and Peng Zhang

459 Prognostic Value of an Immune-Related Gene Signature in Oral Squamous Cell Carcinoma
Chao Zhu, Liqun Gu, Mianfeng Yao, Jiang Li and Changyun Fang

472 Prediction Model of Distant Metastasis in Oral Cavity Squamous Cell Carcinoma With or Without Regional Lymphatic Metastasis
Hsueh-Ju Lu, Yu-Wei Chiu, Wen-San Lan, Chih-Yu Peng, Hsien-Chun Tseng, Chung-Han Hsin, Chun-Yi Chuang, Chun-Chia Chen, Wei-Shiou Huang and Shun-Fa Yang

483 Radiomics for Diagnosis and Radiotherapy of Nasopharyngeal Carcinoma
Yu-mei Zhang, Guan-zhong Gong, Qing-tao Qiu, Yun-wei Han, He-ming Lu and Yong Yin

491 An Immune Feature-Based, Three-Gene Scoring System for Prognostic Prediction of Head-and-Neck Squamous Cell Carcinoma
Yamin Zhang, Xiayan Luo, Jing Yu, Kejia Qian and Huiyong Zhu

505 Establishing a Predictive Nomogram for Cervical Lymph Node Metastasis in Patients With Papillary Thyroid Carcinoma
Qiao Hu, Wang-Jian Zhang, Li Liang, Ling-Ling Li, Wu Yin, Quan-Li Su and Fei-Fei Lin

515 A Robust Metabolic Enzyme-Based Prognostic Signature for Head and Neck Squamous Cell Carcinoma
Zizhao Mai, Huan Chen, Mingshu Huang, Xinyuan Zhao and Li Cui

527 Treatment Stratification in First-Line Recurrent or Metastatic Head and Neck Cancer, on Behalf of the EORTC Young Investigator Head and Neck Cancer Group
Konrad Klinghammer, Luigi Lorini, Daan Nevens, Christian Simon, Jean-Pascal Machiels and Paolo Bossi

533 Multi-Organ Omics-Based Prediction for Adaptive Radiation Therapy Eligibility in Nasopharyngeal Carcinoma Patients Undergoing Concurrent Chemoradiotherapy
Sai-Kit Lam, Yuanpeng Zhang, Jiang Zhang, Bing Li, Jia-Chen Sun, Carol Yee-Tung Liu, Pak-Hei Chou, Xinzhi Teng, Zong-Rui Ma, Rui-Yan Ni, Ta Zhou, Tao Peng, Hao-Nan Xiao, Tian Li, Ge Ren, Andy Lai-Yin Cheung, Francis Kar-Ho Lee, Celia Wai-Yi Yip, Kwok-Hung Au, Victor Ho-Fun Lee, Amy Tien-Yee Chang, Lawrence Wing-Chi Chan and Jing Cai

545 The Role of the EZH2 and H3K27me3 Expression as a Predictor of Clinical Outcomes in Salivary Duct Carcinoma Patients: A Large-Series Study With Emphasis on the Relevance to the Combined Androgen Blockade and HER2-Targeted Therapy
Natsuki Saigusa, Hideaki Hirai, Yuichiro Tada, Daisuke Kawakita, Masato Nakaguro, Kiyoaki Tsukahara, Satoshi Kano, Hiroyuki Ozawa, Takahito Kondo, Kenji Okami, Takafumi Togashi, Yukiko Sato, Makoto Urano, Manami Kajiwara, Tomotaka Shimura, Chihiro Fushimi, Akira Shimizu, Isaku Okamoto, Takuro Okada, Takayoshi Suzuki, Yorihisa Imanishi, Yoshihiro Watanabe, Akihiro Sakai, Koji Ebisumoto, Yuichiro Sato, Yoshitaka Honma, Keisuke Yamazaki, Yushi Ueki, Toyoyuki Hanazawa, Yuki Saito, Hideaki Takahashi, Mizuo Ando, Shinji Kohsaka, Takashi Matsuki and Toshitaka Nagao

561 A Comprehensive Risk Assessment and Stratification Model of Papillary Thyroid Carcinoma Based on the Autophagy-Related LncRNAs
Yongrun Mu, Fuling Song, Kai Yuan, Zili Zhang, Yan Lu, Rongzhan Fu and Dongsheng Zhou

574 Prognostic Impact of Pattern of Mandibular Involvement in Gingivo-Buccal Complex Squamous Cell Carcinomas: Marrow and Mandibular Canal Staging System
Abhishek Mahajan, Navnath Dhone, Richa Vaish, Ankita Singhania, Akshat Malik, Kumar Prabhash, Ankita Ahuja, Nilesh Sable, Pankaj Chaturvedi, Vanita Noronha, Sarbani Gosh Laskar, Ujjwal Agarwal, Shreya Shukla, Gouri Pantvaidya, Prathamesh Pai, Atanu Bhattacharjee, Vijay Patil, Asawari Patil, Munita Bal, Swapnil Rane, Shivakumar Thiagarajan and Anil D' Cruz

585 Integrative Pan-Cancer Analysis of KIF15 Reveals Its Diagnosis and Prognosis Value in Nasopharyngeal Carcinoma
Jinglin Mi, Shanshan Ma, Wei Chen, Min Kang, Meng Xu, Chang Liu, Bo Li, Fang Wu, Fengju Liu, Yong Zhang, Rensheng Wang and Li Jiang

602 Neoadjuvant Chemoradiotherapy for Oral Cavity Cancer: Predictive Factors for Response and Interim Analysis of the Prospective INVERT-Trial
Jens von der Grün, Ria Winkelmann, Iris Burck, Daniel Martin, Franz Rödel, Peter Johannes Wild, Katrin Bankov, Andreas Weigert, Ivan-Maximiliano Kur, Christian Brandts, Natalie Filmann, Christian Issing, Philipp Thönissen, Anna Maria Tanneberger, Claus Rödel, Shahram Ghanaati and Panagiotis Balermpas

615 The Prognostic Signature of Head and Neck Squamous Cell Carcinoma Constructed by Immune-Related RNA-Binding Proteins
Ruijie Ming, Xiangrui Li, Enhao Wang, Jiahui Wei, Bo Liu, Peng Zhou, Wenting Yu, Shimin Zong and Hongjun Xiao

633 Prognostic Factors for the Therapeutic Performance of Cisplatin in Head and Neck Malignancies
Frederic Jungbauer, Lena Huber, Sonja Ludwig, Nicole Rotter, Beatrice Walter, Lena Zaubitzer and Anne Lammert

645 Asporin Interacts With HER2 to Promote Thyroid Cancer Metastasis *via* the MAPK/EMT Signaling Pathway
Shaohua Zhan, Tianxiao Wang, Jingying Li, Hanyang Zhu, Wei Ge and Jinming Li

658 Does Reorganization of Clinicopathological Information Improve Prognostic Stratification and Prediction of Chemoradiosensitivity in Sinonasal Carcinomas? A Retrospective Study on 145 Patients
Marco Ferrari, Davide Mattavelli, Alberto Schreiber, Tommaso Gualtieri, Vittorio Rampinelli, Michele Tomasoni, Stefano Taboni, Laura Ardighieri, Simonetta Battocchio, Anna Bozzola, Marco Ravanelli, Roberto Maroldi, Cesare Piazza, Paolo Bossi, Alberto Deganello and Piero Nicolai

676 NTF2 Upregulation in HNSCC: a Predictive Marker and Potential Therapeutic Target Associated With Immune Infiltration
Guangxu Xuan, Xin Zhang, Min Zhang, Minghang Yu, Yujie Zhou, Xiaosong He, Xiaopeng Hu, Xi Wang and Liangfa Liu

688 Malignant Myoepithelioma of the Head and Neck: Demographics, Clinicopathological Characteristics, Treatment, and Prognosis
Jia-Qi Wang, Rong-Xin Deng, Hui Liu, Yuan Luo, Meng-Meng Lu and Zhi-Cheng Yang

frontiers | Frontiers in Oncology

TYPE Editorial
PUBLISHED 30 December 2022
DOI 10.3389/fonc.2022.1037001

OPEN ACCESS

EDITED AND REVIEWED BY
Jan Baptist Vermorken,
University of Antwerp, Belgium

*CORRESPONDENCE
Yong Yin
yinyongsd@126.com
Qingtao Qiu
qiuqingt@126.com

SPECIALTY SECTION
This article was submitted to Head and Neck Cancer, a section of the journal Frontiers in Oncology

RECEIVED 05 September 2022
ACCEPTED 20 December 2022
PUBLISHED 30 December 2022

CITATION
Li T, Lu J, Yin Y and Qiu Q (2022) Editorial: Prognosis prediction and risk stratification in head and neck cancer. *Front. Oncol.* 12:1037001. doi: 10.3389/fonc.2022.1037001

Editorial: Prognosis prediction and risk stratification in head and neck cancer

Tengxiang Li[1,2], Jie Lu[1], Yong Yin[1]* and Qingtao Qiu[1]*

[1]Department of Radiation Oncology Physics, Shandong Cancer Hospital and Institute, Shandong First Medical University and Shandong Academy of Medical Sciences, Jinan, China, [2]School of Nuclear Science and Technology, University of South China, Hengyang, China

KEYWORDS

head and neck cancer, prognosis, molecular biomarker, imaging biomarker, machine learning

Editorial on the Research Topic:
Prognosis prediction and risk stratification in head and neck cancer

Head and neck cancer is the seventh most common cancer worldwide, accounting for 3% of all cancers. For patients with early-stage disease, either surgery alone or definitive radiation therapy alone results in an excellent treatment outcome. However, the majority of newly diagnosed patients present with local-regionally advanced disease and require multimodality treatment. The treatment outcomes of these patients are far from satisfactory. It is widely recognized that treatment outcome is determined by a complex interaction of multiple factors, including biological, clinical, treatment, and environmental factors. However, current treatment decisions primarily rely on the clinical stage, which does not always reflect the variable clinical course and long-term outcomes. Recent advances in radiomics, genomics, proteomics, microbiome, AI technique and machine learning, and other potential imaging, biological, and clinical factors, alone or in combination, may provide new insights into the prognosis prediction and treatment response in head and neck cancer. Risk stratification based on these prognostic and predictive biomarkers will help design future clinical trials and personalized treatment strategies in head and neck cancer.

This paper aims to present the latest advances in basic, translational, and clinical research findings on predictions of treatment outcome and response and risk stratification in head and neck cancer, including nasopharyngeal carcinoma, and how these affect future clinical trials and treatment decisions in head and neck cancer.

1 Head and neck squamous cell carcinoma

By analyzing gene expression patterns in The Cancer Genome Atlas (TCGA) head and neck squamous cell carcinoma (HNSCC) dataset and GSE37991 dataset, Mai et al. examined possible prognostic indicators in head and neck carcinoma. The common differentially expressed metabolic enzymes were used to identify six expressed metabolic

enzymes (DEMEs). When investigated on a modest scale, this metabolic enzyme-based risk signature proved to be more accurate at predicting the prognosis of HNSCC than tumor, node, and distant metastasis (TNM) stage since it was simplified to six genes. While taking into account the loss of specific clinicopathological information, clinical data collection techniques and management procedures must be strictly adhered to for the application of this gene signature in real-world situations.

Deoxyribonucleic acid (DNA) repair capacity and the tolerance of DNA to radiation damage varies in cancers and healthy tissues, and they are linked to clinical manifestations, including cancer resistance and side effects. Ming's et al. developed a 13-diagnostic-related groups (13-DRG) signature for the prognosis of HNSCC, which could reliably and independently predict the patient's clinical outcome. The researchers also revealed the immune landscape, tumor mutation burden, and sensitivity to chemotherapy drugs in various risk groups, all of which may be used to inform clinical treatment choices.

The prospective evaluation of patient characteristics and the identification of novel potential prognostic biomarkers for cutting-edge treatment options is a crucial topic for stratifying personalized treatment for recurrent/metastatic HNSCC (RM HNSCC). The implementation of a relatively detailed assessment technique will make it easier to identify individuals who will likely benefit from immunotherapy, salvage surgery or (re)irradiation. In the first line of treatment for RM HNSCC, a variety of variables affect treatment decisions as indicated in a questionnaire by Klinghammer et al., including performance status, programmed cell death ligand 1 (PD-L1) expression, time from last systemic treatment above or below 6 months, and disease burden.

To evaluate the prognostic performance of HNSCC, including overall survival and immune profile performance, Gao et al. created a lipid-related prognostic signature. Their study suggests that predictors created for aberrant lipid metabolism have the potential to be used in the therapeutic assessment of HNSCC.

Individualized precision medicine and the assessment of cancer prognosis have become attractive study areas. To objectively quantify and identify trustworthy and clinically useful biomarkers, Moratin et al.'s research performed immunohistochemical staining and digital pathology algorithms. Overall and progression-free survival estimates were made with a substantial degree of accuracy using a combined score combining the epidermal growth factor receptor (EGFR) expression, neck node status, and immune cell characteristics.

For immune checkpoint inhibitors (ICI) therapy response, different immune cell distribution patterns within tumors may be essential. HNSCC patients have a relatively moderate response rate to therapy due to the absence of prognostic indicators. According to Idel et al.'s analysis of the spatial distribution differences between each immune cell type, programmed death-1 (PD-1) and PD-L1 expression levels in certain tumor types may be important for predicting treatment response.

Exome sequencing was undertaken by Desai et al., and this analysis revealed that several tumor suppressor genes had mutations. If those genes were driver genes and had the potential to be druggable, they might be the subject of an actionable mutation.

A significant prognostic factor for HNSCC is the incidence of neck lymph node metastasis (LNM). As a result, understanding the molecular mechanisms involved in HNSCC LNM has important clinical ramifications for risk assessment. Zhang et al. used Gene Ontology enrichment analysis to create a risk score for identifying lymphocytes that infiltrate tumors. When used to predict the survival of patients with HNSCC, the prediction model demonstrated discrimination capacity and agreement.

In a meta-analysis of the literature on the role of microRibonucleic acid (RNA)s in the clinical manifestations of HNSCC treatment, Qiu et al. discovered that microRNAs are highly accurate at identifying recurrent, metastatic, and lymph node metastatic HNSCC. This finding suggests risk grading and individualized treatment of patients in the clinic for abnormal microRNA manifestations.

In bioinformatics research, the investigation of diverse microlevel prognostic indicators is a prominent topic. Shen et al. developed a long noncoding long non-coding (Lnc)RNA prognostic signature for HNSCC, which had a higher impact on risk assessment but requires more research to demonstrate its potential practical value.

A common regulator of messenger (m)RNA expression called N6-Methyladenosine has drawn growing research interest. Although the importance of m6A in several biological processes, including the development and spread of malignancies, has been well established, studies of its potential on the tumor immune microenvironment (TIME) are few and far between. According to Yang et al.'s findings, m6A regulators and the TIME have a strong relationship. This has implications for research into immunotherapy and chemotherapy regimens for HNSCC.

Patients with HNSCC still receive treatment based on their disease stage and tumor site rather than tumor biology. Numerous biomolecular markers have been proposed to identify primary and secondary cancers in the early stages of the disease, including proteins, DNA, RNA, and microRNAs. Immune checkpoint inhibitors have become a novel therapeutic option for HNSCC, which is an immunosuppressive disease. It would be beneficial to look at how immune cells and their regulators function in the tumor microenvironment of HNSCC. Because RNA-binding proteins (RBPs) are essential for the post-transcriptional control of genes, it is important to investigate

how RBPs relate to HNSCC. An immune-related RBP predictive signature was developed by Ming et al.'s.

The majority of patients often receive a diagnosis of advanced HNSCC because of the asymptomatic nature of the early disease stages and the dearth of reliable screening techniques. Effective biomarkers must be found quickly in order to help doctors anticipate clinical outcomes with accuracy and provide references for specialized medical treatments to fight HNSCC. Nuclear transporter factor 2 (NTF2) was found as a potential diagnostic and prognostic biomarker for HNSCC *via* extensive analysis of its function by Xuan et al., which included RNA sequencing data and the associated clinical information.

Cisplatin is used as main or adjuvant (radio)chemotherapy for squamous cell carcinoma of the head and neck. There are two basic dosage regimens currently used, and the highest cumulative total dose of cisplatin is desired for the best results. The 3-weekly regimen had a larger cumulative total dose, according to Jungbauer et al.'s retrospective research. It can be concluded that the 3-weekly regimen is superior to the weekly regimen because this appears to favorably correlate with patient outcome. Functional organ systems, particularly those of the kidneys and bone marrow, are linked to a higher cumulative total dosage and can be thought of as predictive factors.

Primary surgery is followed with risk-adapted adjuvant radiotherapy (RT)/chemoradiotherapy (CRT) or definitive CRT for tumors that are functionally inoperable as the standard of care for locally advanced oral cavity cancer (LA-OCC). Patients with locally advanced HNSCC experience local recurrences and distant metastases after receiving combined modality therapy, and local control rates for the LA-OCC subgroup are still lower than those for LA-HNSCC, with the majority of locoregional failures occurring in the area of preceding RT. A prospective, single-arm experiment was initiated by Grün et al. to examine the feasibility and early efficacy of neoadjuvant chemoradiotherapy (nCRT) followed by surgery in LA-OCC, with a special emphasis on potential prognostic biomarkers.

The identification of cancers that will respond to treatment is required since targeting the immune system has proven to be a successful therapeutic approach for the management of different tumor types. Saiz-Ladera et al. discovered a collection of gene combinations connected to a greater presence of immune effector cells that are associated with better outcomes in HNSCC. This novel signature also recognizes a subset of cervical squamous cell carcinoma (CSCC), but not esophageal or lung squamous cell carcinoma (SCC). These findings can serve as a guide for choosing the focus of future studies.

It is important to determine whether human papillomavirus (HPV) immunotherapy effectiveness has a potential relationship with the tumor immune microenvironment since HPV+ or HPV- HNSCC patients have distinct prognostic outcomes.Wu et al.'s study used a single-cell RNA sequencing dataset and evaluated CD8+ T-cell based genes including ACAP1 (adenosine diphosphate ribosylation factor GTPase-activating proteins with Coiled-coil, Ankryin repeat and PH domains 1), ankyrin repeat domain 28 (ANKRD28), chromosome 12 open reading frame 75 (C12orf75), and mannose-6-phosphate receptor (M6PR) that could predict prognosis and immunization-correlated treatment responses.

2 Nasopharyngeal carcinoma

Nasopharyngeal carcinoma (NPC), which makes up a sizable fraction of head and neck tumors, has a considerable regional incidence. In a literature meta-analysis carried out by Chiang et al. for the eighth edition of TNM staging, clinical indicators were screened to suggest prognosis, such as upstaging paranasal sinus to T4. The conclusions obtained from this meta-analysis were all common clinical indicators, which are convenient and simple to use.

The commonly used clinical TNM staging may need to be taken into account for factors like varied EGFR expression for different outcomes over the same period since it does not specifically predict each patient's prognosis in nasopharyngeal carcinoma. High EGFR expression was found to be strongly related with poor overall survival (OS) and disease-free survival (DFS) in Chen et al.'s meta-analysis. It should be emphasized in practice that there was no significant link between various EGFR expression and progression-free survival (PFS), distant metastasis-free survival (DMFS), OS, etc., in the subgroup analysis.

Nasopharyngeal carcinoma is usually diagnosed beyond stage I because of the insidious location of the primary region. Induction chemotherapy combined with concurrent radiotherapy is commonly used in the clinical treatment of patients with locally advanced nasopharyngeal carcinoma. In Xiong et al.'s study, a comparison of the effectiveness of several chemotherapy regimens demonstrated that TPF (taxanes, cisplatin, and 5-fluorouracil) and TP (taxanes and cisplatin) led to different outcomes due to differences in toxicities in patients with NPC at N2-3 stages.

New options and approaches for investigating the diagnosis, therapy, and prognosis of NPC have been presented by the combination of radiomics and multimodal imaging. To diagnose and treat NPC, radiomics and machine learning have been combined. However, model selection is where machine learning in radiomics is most commonly used. Radiomics, a technology for extracting information from depth images, can help with NPC diagnosis and treatment, but it also presents a number of difficulties, including the need for large datasets for the development of tumor models, data sharing between various medical institutions, and different imaging protocols, as summarized by Zhang et al. To integrate radiomics models into clinical practice, significant progress is still needed. For

radiomics to promote individualized and intelligent treatment, more forward-looking research and applications are needed.

In a different meta-analysis on nasopharyngeal carcinoma, author Jing et al. analyzed the clinical manifestation of patients with various blood types and discovered that the incidence of nasopharyngeal carcinoma was lower in the Chinese population with blood group O. Worse 5-year OS, locoregional relapse-free survival (LRRFS) or DMFS rates were discovered in patients with blood group O. The study did not, however, analyze the distribution of blood types across various geographies or look into whether a person's blood type may be related to their onset of a certain disease.

The main factors influencing the occurrence of hypothyroidism in nasopharyngeal carcinoma patients following radiotherapy, specifically after intensity-modulated radiotherapy (IMRT), are the thyroid gland's volume and dosage. According to Shen et al.'s normal tissue complication probability (NTCP) model, which was built using multivariate construction, the best strategy to safeguard thyroid function was to reduce the average dose in the thyroid as much as possible.

Radiation therapy, along with other treatments including chemotherapy, is generally used to treat NPC. To improve the effectiveness of radiation therapy and limit the toxicity to normal tissue, the tumor target area of NPC ought to be precisely defined. According to Yan et al.'s study, the 50% standard uptake value (SUV)max threshold regimen for gross tumor volume (GTV) delineation with dose-painting appeared to be superior to the visual criterion or SUV2.5 threshold when it related to defining tumor volume in locoregionally progressed NPC with no increased toxicity.

Emerging radiomics has made it possible to reveal hidden biological characteristics and the genetic relationship between tumor and organ structures. There is growing evidence in the literature that radiomics may accurately predict treatment response based on volume shrinking in a variety of cancer types. To determine if patients with NPC were eligible for adaptive radiotherapy (ART), Lam et al. looked at the function of several multiorgan omics-based prediction models. Given the rising demand for ART in this particularly sensitive population of cancer patients during the period of IMRT, this study may offer the community helpful insights toward creating ART screening tools in the future.

According to the guidelines for the treatment of NPC, except for T1N0M0, which is treated with radiation alone, T2N0M0 and T1/2N1M0, and other stages are usually treated with a combination of radiotherapy and chemotherapy. Li et al. established residual volume of lymph nodes during chemoradiotherapy, which is useful in estimating 4-year OS, PFS and DMFS in NPC patients.

Peng et al. evaluated the therapeutic effects of CRT preceded by induction chemotherapy, which could consist of docetaxel plus cisplatin (TP), TP plus 5-fluorouracil (TPF) or cisplatin plus 5-fluorouracil (PF). These long-term follow-up studies are essential, and the results on OS and toxicity can be utilized when selecting chemotherapy regimens for patients with locally advanced NPC.

In addition to being extremely accurate in identifying soft tissues, magnetic resonance imaging (MRI) can distinguish between tumor invasion of bone structures and other symptoms in locally progressed NPC. Kang et al.'s study developed radiomics-based models of MRI images, which used pre- and in-treatment pictures with greater continuity and had superior local recurrence free survival (LRFS), DMFS, and OS predictions. These models were better at predicting disease progression or death. This concept may potentially be used in the diagnosis of various illnesses and as a tool for evaluating treatment effectiveness and prognosis, among other uses for MRI.

According to Liang et al.'s study, the eighth edition of the American Joint Committee on Cancer (AJCC) staging system for NPC in an endemic area integrating into the pretreatment neutrophil-to-lymphocyte ratio (NLR) may improve the ability to separate and discriminate between N classifications, but not within T classifications. Furthermore, the addition of adjuvant chemotherapy to concurrent chemoradiotherapy may be beneficial for individuals in the recursive partitioning analysis (RPA) 4 group. This statistical work aids in guiding the selection of a clinical treatment regimen.

The ability of epstein-barr virus (EBV) DNA levels in plasma before and after various treatments to predict the prognosis of NPC was examined in Zhu et al.'s study. It was discovered that pre-neoadjuvant chemotherapy (pre-NACT) and post-NACT EBV DNA levels can predict survival outcomes like PFS and OS in patients with NPC. The inability to forecast radiation efficiency using EBV DNA continues to be a significant drawback in its use.

Effective therapeutic target sites and corresponding treatment may improve survival of NPC patients. Li et al. explored the mechanism of action in NPC species based on the enrichment of MiR-483-5p microRNA in plasma, biopsy tissue, and tumor cells of patients with NPC in prior studies. This targeting site exists in tumor cells and has a high potential value in targeted immunotherapy.

Fewer studies have been conducted on distal lymph node metastasis in individuals with recurrence, compared to more studies on cervical lymph node metastasis in NPC. Subphrenic lymph node metastasis predicts a worse prognosis, according to Zhang et al.'s study, which was a two-center, small-sample study. The results of the study have strong implications for early recurrence detection and accurate prognosis assessment after expanding the geographical area, centers, and samples.

KIF15, a member of kinesin-12 family, has been shown to have an impact on the occurrence and progression of some types of human cancer and is essential for numerous biological processes. However, there have not been many thorough analyses on the function of KIF15 in human malignancies, and it is still unknown how KIF15 affects NPC diagnosis and prognosis. KIF15 was discovered to be highly expressed in NPC tissues, and this was

associated with a bad prognosis for NPC. KIF15 might be used as a therapeutic target in the management of NPC. Mi et al. examined KIF15's diagnostic and prognostic potential in NPC through a pancancer investigation.

3 Oral squamous cell carcinoma

Although many therapeutic approaches for oral squamous cell carcinoma (OSCC) have demonstrated encouraging results in the treatment of OSCC in recent years, the 5-year survival rate is still low. Ding et al. discovered preoperative the neutrophil-to-lymphocyte ratio (NLR), lymphocyte-to-monocyte ratio (LMR), neutrophil-to-white blood cell ratio (NWR), and lymphocyte-to-white blood cell ratio (LWR) in the peripheral blood as prognostic predictors of OSCC using studies like Kaplan–Meier curves, which are helpful in predicting OSCC progression.

OSCC patients with HPV-negative status typically have poor clinical outcomes and worse treatment outcomes. In patients with HPV negative OSCC who were receiving radiotherapy, Ai et al. discovered that CD68+ macrophage infiltration was related to poor overall survival. Radiation therapy, Poly(I:C), and drugs that target HMGB1 may improve OSCC's prognosis and responsiveness.

Perineural invasion (PNI), a crucial aspect of tumor invasion from a histological standpoint, aids in the spread of the tumor, however the prognostic significance of PNI is still up for debate. Traditional PNI was subclassified by Fu et al. to worst pattern of PNI (WPNI), and WPNI 3 was able to predict patients' prognoses on its own. Trichotomy provided more careful and exact pathology evidence for tumor-nerve interactions in OSCC patients.

Radiotherapy, chemotherapy, and other treatments are ineffective against hypoxic tumors. The recognition of various hypoxia patterns and the creation of a hypoxia-related risk score may improve our understanding of the tumor microenvironment of OSCC, according to Li et al.'s study. Determining the hypoxic state of tumors in various patients is a prerequisite for targeted and precise patient treatment.

In individuals with OSCC, the prognosis and immunotherapy response rates are dismal. The fundamental processes for how the tumor microenvironment affects the prognosis and development of tumors are still unknown. According to Zhu et al.'s research, the immune-related gene signature can predict overall survival and help OSCC patients receive individualized care. It can also identify patients who might benefit from immunotherapy as well as treatments that concentrate on metabolic pathways, DNA damage or repair, and spliceosomes.

Of all malignancies of the oral cavity, squamous cell carcinoma is the most prevalent. The prognosis is influenced by many variables, including T stage on size and depth of invasion, and degradation of the mandibular bone. In patients with gingivo-buccal complex squamous cell carcinoma (GBC-SCC), Mahajan et al. studied the pattern of mandibular involvement and its impact on oncologic outcomes. He proposed a staging system based on the pattern of bone involvement (MMC: Marrow and mandibular canal staging system), only marrow with or without mandibular canal involvement is linked to worse survival outcomes.

4 Papillary thyroid carcinoma

The incidence of papillary thyroid carcinoma (PTC), one of the most frequent malignant carcinomas of the endocrine system, is rising globally. Although there are now diagnostic and therapeutic options for thyroid cancer, the prognosis is still unknown. Cancer invasion, malignancy, metastasis, and medication resistance are all impacted by autophagy. Long noncoding RNAs (lncRNAs) have been implicated in the development of several forms of cancer, according to recent study. However, it is still unclear how the autophagy process and lncRNAs are linked, as well as the relevance of autophagy-related lncRNA for risk assessment, medication sensitivity prediction, and prognosis prediction in PTC patients. Based on the expression patterns of lncRNAs associated with autophagy, Mu et al. developed a unique risk classification system for PTC that may be utilized for prognosis prediction, drug sensitivity prediction, and risk assessment.

PTC is regarded as a benign, slow-growing tumor with a favorable prognosis and minimal malignancy; nonetheless, some individuals still have early cervical lymph node metastasis (CLNM), which increases the chance of local recurrence. The typical symptom of CLNM in PTC is a lateral cervical lymph node metastasis from the central lymph node. Although some PTCs may not develop central lymph node metastasis, they may develop direct lateral lymph node metastasis (LLNM). The most crucial factor for deciding the surgical technique prior to surgery is CLNM, which is the biggest risk factor for local recurrence and the prognosis of PTC patients. Hu et al. developed a nomogram that demonstrated an excellent prediction of CLNM in patients with PTC and was simple to employ.

PTC, which makes up a large portion of the histological subtypes of thyroid cancer, has a fast-rising morbidity and mortality rate due to lymph node metastases or distant metastases. We must develop a deeper understanding of the etiology of PTC patients with distant or lymph node metastases. Asporin was used by Zhan et al. to identify PTC patients with or without lymph node metastases using a TMT-based quantitative proteomics technique. Asporin's high expression in PTC tumorous tissues is a risk factor for a poor prognosis.

Alternative splicing (AS) events from Liu et al.'s study, through a limited analysis, could be regarded as trustworthy prognostic biomarkers for PTC. AS is crucial for the diversity of proteins and is closely linked to tumorigenicity, and these modifications are crucial for biological processes.

5 Oral cavity squamous cell carcinoma

Patients with distant metastases (DM) from oral cavity squamous cell carcinoma (OCSCC) have poor prognoses, and there are few reliable models for DM prediction. Although the DM growth mechanisms of the lymphatic and blood vessel systems may be different, DM development can happen directly through either of these systems. To build models for predicting DM in three years, Lu et al. used grouping factors and individually tailored micro parameters, such as age, surgical margin, early locoregional recurrence, lymphocyte-to-monocyte ratio, and presence of lymphovascular invasion.

The Cancer Genome Atlas' oral cavity malignancies have a unique clinicopathological characteristic called partial epithelial-mesenchymal transition (p-EMT). The tumor stroma must provide extra assistance to the p-EMT cells, which are at the invasion front, in order for them to move in concert. This assistance includes track clearance, extracellular matrix remodeling, and immune evasion. By combining disease-matched xenograft tissue and single-cell RNA-seq findings, Liu et al. found that transforming growth factor beta induced (TGFBI) and hyaluronidase genes 1 (HYAL1) could act as reliable predictive biomarkers for the prevention of oral cancer.

6 Parotid carcinoma

Multiple factors have been linked to the prognosis of patients with parotid carcinoma (PC). A competing risk nomogram developed in Li et al.'s single-center, long-term research can be utilized to estimate cancer-specific mortality in PC patients. For use as a guide for evaluation in the clinic, this nomogram must be verified across a number of locations.

Accurate computerized dose prediction can considerably increase the effectiveness and safety of clinical planning. In contrast to typical automatic plans, which concentrate on conventional accelerators, the Liu et al.'s study looked at tomotherapy plans using a patient-specific gap between organs at risk (OARs) and planning target volumes (PTVs) in the model-building process to improve a method for creating automatic tomotherapy planning.

7 Oropharyngeal squamous cell carcinoma

By examining imaging characteristics, radiomics is utilized to determine whether oropharyngeal squamous cell carcinoma (OPSCC) is caused by HPV+ or HPV- and to determine the prognosis. Song et al.'s, which used radiomics for the risk assessment of patients with OPSCC to enable individualized therapy and enhance outcomes, provided evidence for the role of radiomics in this regard.

8 Hypopharyngeal squamous cell carcinoma

The prognosis of patients with hypopharyngeal squamous-cell carcinoma (HSCC), a head and neck cancer, varies greatly. According to research by Tian et al., various demographic traits, clinicopathological variables, and treatment modalities are highly connected with the survival results of HSCC patients. The data are simple to gather, demonstrating the simplicity of using this nomogram in clinical practice to support the clinical evaluation of the risk level of HSCC patients and the creation of tailored treatment plans.

9 Differentiated thyroid cancer

For individuals with low-risk differentiated thyroid carcinoma, total thyroidectomy (TT) or lobectomy without radioactive iodine (RAI) is increasingly the standard of care (DTC). It is important to pay attention to the techniques used to evaluate the effectiveness of the therapies and the suggestions that might be made, especially in light of the numerous side effects. According to Dong et al.'s study, there is no regular advice for RAI following surgery in low-risk DTC patients due to patterns of suppressed serum thyroglobulin (Tg) and anti-thyroglobulin antibody (TgAb) levels and neck ultrasonography results.

10 Salivary gland carcinoma

PD-L1 expression and prognostic significance in high-grade salivary gland carcinoma (SGC) is one of the predictors of immunotherapy efficacy. According to Fang et al.'s research, PD-L1 expression in tumor cells of high-grade SGCs rather than in immune cells was a marker of a poor prognosis and was strongly correlated with tumor stage. This finding may indicate that treatment should focus on patients with this type of protein expression.

11 Maxillary sinus carcinoma

Maxillary sinus carcinoma (MSC) makes up a small percentage of head and neck cancers; studies based on just one medical facility have small sample numbers. MSC has a concealed anatomical site and a complicated neighboring connection that results in a vague prognosis. In people with

MSC, Hu et al.'s competing risk nomogram was successful in calculating the risk of cancer-specific death (CSD).

12 Salivary duct carcinoma

Salivary duct carcinoma (SDC) is a rare, extremely aggressive tumor that can develop both spontaneously and as part of pleomorphic adenoma. A majority of SDCs express the androgen receptor (AR), and approximately 40% are human epidermal growth factor receptor 2 (HER2)-positive. Treatments targeting AR and HER2 have recently been developed as a potential optional therapy in recurrent/metastatic or unresectable locally advanced SDCs based on these biomarker findings. For patients with SDC who tested positive for AR, AR-targeted treatment showed comparable effectiveness and less toxicity than traditional chemotherapy. Additionally, HER2-targeted therapy outperformed conventional or AR-targeted therapy in terms of effectiveness, with a greater response rate in HER2-positive SDC patients. However, choosing the best course of action is still challenging since SDCs frequently express both HER2 and AR. High expression of enhancer of zeste homolog 2 (EZH2) and histone H3 lysine 27 trimethylation (H3K27me3) in SDC was shown to be a potential indicator of the ineffectiveness of AR-targeted treatment, according to Saigusa et al.'s research.

13 Sinonasal carcinomas

Sinonasal carcinomas (SNCs) are difficult to categorize. As a result, prognosis and response prediction to nonsurgical treatment are frequently incorrect. The lack of prognostic and predictive tools is an unmet need, and the clinicopathological characteristics of the disease are the first logical source of information to be examined. In comparison to the current World Health Organization (WHO) categorization, Ferrari et al.'s analysis of cytomorphological, histomorphological, and locoregional extension offered a more accurate prediction. SNC chemo-radiosensitivity prediction, however, was not achieved.

14 Malignant myoepithelioma of the head and neck

The features and survival rates of malignant myoepithelioma of the head and neck (HNMM), a rare tumor, are not well defined. It will be important to investigate the epidemiology of HNMM and determine the criteria that will affect the prognosis of the condition. According to Wang et al., patients with HNMM frequently have a good prognosis, and factors including distant metastasis, pathological grade, and the use of surgery all help them survive. To assist doctors in the clinical care of this uncommon disease, the undifferentiated pathological grade and M1 in the M category were independent prognostic markers to predict OS and disease-specific survival (DSS) for HNMM patients.

We look forward to more researchers contributing more ideas, validations, reviews, etc., on head and neck cancer for prognosis and risk assessment, including but not limited to imaging biomarkers, molecular biomarkers including DNA, EBV-DNA, and HPV-DNA, microbiome, artificial intelligence technique and machine learning, and other potential biological or clinical factors, in combination with *in vitro*/*in vivo* validation. Additionally, we look forward to the prediction of treatment outcome and response and the latest development and validation of predictive models for head and neck cancer. Furthermore, we look forward to the outcomes of clinical trials based on prediction models established from above research and updated information about or preliminary results of ongoing clinical trials.

Author contributions

TL, JL, QQ and YY designed the study and wrote the manuscript. TL and QQ participated in the study designing and data collection. QQ and YY participated in offered guidance. All authors contributed to the article and approved the submitted version.

Funding

This study was supported by Natural Science Foundation of China (Grant Nos. 82001902, 82072094, and 12275162), Natural Science Foundation of Shandong Province (Grant Nos. ZR2019LZL017, ZR2020QH198, and ZR2020MH227), the Taishan Scholars Project of Shandong Province (Grant No. ts201712098).

Conflict of interest

The authors declare that the research was conducted in the absence of any commercial or financial relationships that could be construed as a potential conflict of interest.

Publisher's note

frontiers in Oncology

ORIGINAL RESEARCH
published: 21 June 2021
doi: 10.3389/fonc.2021.696952

Development and Validation of a Prognostic Nomogram for Hypopharyngeal Carcinoma

Shu Tian[1,2,3†], *Qin Li*[2,4†], *Ruichen Li*[3†], *Xinyu Chen*[1,2], *Zhonghua Tao*[1,2], *Hongli Gong*[5], *Xiaoshen Wang*[3*] and *Xichun Hu*[1,2*]

[1] Department of Medical Oncology, Fudan University Shanghai Cancer Center, Shanghai, China, [2] Department of Oncology, Shanghai Medical College, Fudan University, Shanghai, China, [3] Department of Radiation Oncology, Eye Ear Nose and Throat Hospital, Fudan University, Shanghai, China, [4] Fudan University Shanghai Cancer Center, Key Laboratory of Medical Epigenetics and Metabolism, Institutes of Biomedical Sciences, Fudan University, Shanghai, China, [5] Shanghai Key Clinical Disciplines of Otorhinolaryngology, Department of Otolaryngology, Eye Ear Nose and Throat Hospital, Fudan University, Shanghai, China

OPEN ACCESS

Edited by:
Heming Lu,
People's Hospital of Guangxi Zhuang Autonomous Region, China

Reviewed by:
Feng Mei,
Sichuan Cancer Hospital, China
Jingao Li,
Jiangxi Provincial Cancer Hospital, China

***Correspondence:**
Xichun Hu
huxichun2017@163.com
Xiaoshen Wang
ruijin702@163.com

[†]These authors have contributed equally to this work

Specialty section:
This article was submitted to Head and Neck Cancer, a section of the journal Frontiers in Oncology

Received: 18 April 2021
Accepted: 07 June 2021
Published: 21 June 2021

Citation:
Tian S, Li Q, Li R, Chen X, Tao Z, Gong H, Wang X and Hu X (2021) Development and Validation of a Prognostic Nomogram for Hypopharyngeal Carcinoma. Front. Oncol. 11:696952. doi: 10.3389/fonc.2021.696952

Hypopharyngeal squamous-cell carcinoma (HSCC) is a relatively rare head and neck cancer, with great variation in patient outcomes. This study aimed to develop a prognostic nomogram for patients with HSCC. From the Surveillance, Epidemiology, and End Results (SEER) database, we retrieved the clinical data of 2198 patients diagnosed with HSCC between 2010 and 2016. The patients were randomly assigned at a 4:1 ratio to the training set or the validation set. An external validation was performed by a set of 233 patients with locally advanced HSCC treated at our center. A Cox proportional hazards regression model was used to assess the relationship between each variable and overall survival (OS). Cox multivariate regression analysis was performed, and the results were used to develop a prognostic nomogram. The calibration curve and concordance index (C-index) were used to evaluate the accuracy of the prognostic nomogram. With a median overall follow-up time of 41 months (interquartile range: 20 to 61), the median OS for the entire cohort of SEER database was 24 months. The 3-year and 5-year OS rates were 41.3% and 32.5%, respectively. The Cox multivariate regression analysis of the training set showed that age, marital status, race, T stage, N stage, M stage, TNM stage, local treatment, and chemotherapy were correlated with OS. The nomogram showed a superior C-index over TNM stage (training set: 0.718 *vs* 0.627; validation set: 0.708 *vs* 0.598; external validation set: 0.709 *vs* 0.597), and the calibration curve showed a high level of concordance between the predicted OS and the actual OS. The nomogram provides a relatively accurate and applicable prediction of the survival outcome of patients with HSCC.

Keywords: hypopharyngeal carcinoma, nomogram, radiotherapy, surgery, prognosis, survival analysis

INTRODUCTION

Hypopharyngeal carcinoma is relatively rare and accounts for only approximately 3% of all head and neck tumors (1, 2). Approximately 95% of hypopharyngeal tumors are squamous-cell carcinoma (2). Hypopharyngeal squamous-cell carcinoma (HSCC) is often occult with atypical early symptoms due to its anatomical features, and approximately 80% of patients are already in stage III-IV at diagnosis (2, 3). A population cohort study of 2939 patients with hypopharyngeal carcinoma showed that 10.5% of patients were in tumor-node-metastasis (TNM) stage I, 12.1% were in stage II, 23.0% were in stage III, and 52.6% were in stage IV at diagnosis, with great variation in patient outcomes (3). The 5-year overall cancer-specific survival (CSS) rate is 33.4%, while the rate is 63.1% for stage I, 57.5% for stage II, 41.8% for stage III, and 22% for stage IV (3). However, the widely used American Joint Committee on Cancer (AJCC) TNM staging system remains has some limitations to assess prognosis in clinical practice. The outcomes of HSCC are also related to many clinical parameters, such as age (> 70 is an adverse prognostic factor) and primary site (piriform sinus tumor is associated with more favorable outcomes, followed by postcricoid region and then posterior pharyngeal wall) (4, 5). Treatment modalities probably affect patient survival, but the conclusions differ across studies (6–8). However, there is a lack of prognostic scoring systems that take those above clinical factors into account.

Nomogram is a visual statistical tool and can improve predictive accuracy for survival outcomes of tumor patients in clinical practice (9, 10). Several studies have shown that nomograms are superior to the TNM staging system in predicting prognoses (11, 12). By combining multiple clinical and pathological factors, nomograms can be used to assess the survival outcome of individual patient. However, few studies have yet been developed a prognostic nomogram for HSCC. The Surveillance, Epidemiology, and End Results (SEER) database is an authoritative source of cancer prevalence and survival in the United States, as it covers approximately 28% of the US population (6). Therefore, the SEER database can provide many cases for the development of predictive models for tumors, especially rare tumors. In this study, we retrieved the clinical data *via* the updated SEER database, including demographics, clinicopathological parameters, and treatment modalities, and established a nomogram to predict prognostic outcomes of patients with HSCC. We also performed internal and external validation.

PATIENTS AND METHODS

Patient Selection

We retrieved patient data from the updated SEER database (https://seer.cancer.gov), which included information on radiotherapy and chemotherapy (Incidence -SEER 18 Regs Custom Data with additional treatment fields, Nov 2018 Sub, 1975-2016 varying). We used SEER* Stat software (released: August 08, 2019, version 8.3.6; http://seer.cancer.gov/seerstat) to download the data. The screening criteria were as follows: 1) primary site: hypopharynx, which was coded as C12.9, C13.0, C13.1, C13.2, C13.8, or C13.9 according to the International Classification of Diseases for Oncology, Third Edition (ICD-O-3); 2) pathologically confirmed squamous-cell carcinoma, coded as 8050-8089 according to ICD-O-3; 3) complete follow-up data, including survival and cause of death; 4) a first primary tumor, confirmed in 2010 or later; and 5) detailed information on variables, including age, sex, marital status, race, insurance, and TNM stage at diagnosis, as well as treatment mode of the primary tumor, such as surgery, radiotherapy, and chemotherapy. In addition, for external validation, we selected patients with locally advanced HSCC who were treated in the Department of Radiation Oncology, Eye and ENT Hospital, Fudan University, between April 2014 and December 2017. In this study, HSCC patients from the SEER database and treated at our center were both staged according to the seventh edition of the AJCC TNM Cancer Staging Manual.

The HSCC cancer-specific survival and noncancer-specific survival were extracted from the SEER variables of cause-specific death classification and other cause-of-death classification. Information on surgery and radiotherapy was extracted from the following fields: radiation sequence with surgery, reason for no cancer-directed surgery, and radiation recode. Information on primary-site surgery was extracted from the field "RX Summ-Surg Prim Site". Primary-site surgery was coded as 20-52 according to the 2018 SEER program coding and staging manual.

Statistical Analysis

SPSS v22.0 (IBM, Armonk, NY, USA) and R for Windows v3.5.1 (https://www.r-project.org) were used for the statistical analysis. Categorical variables were analyzed using a chi-squared test. The Kaplan-Meier method and log-rank test were used for the survival analysis. A Cox proportional hazards regression model was used for the univariate and multivariate analyses to identify prognostic factors, and independent prognostic factors identified by the Cox multivariate analysis were used to develop the prognostic nomogram. The concordance index (C-index) and the Brier score were used to evaluate the performance of the prognostic nomogram, while the calibration curve was used for internal validation of the nomogram. We compared the predictive performance of the prognostic nomogram with that of TNM staging. We also performed a competing risk analysis because noncancer-specific death competed with cancer-specific death. All tests were two-sided, and $P < 0.05$ was considered statistically significant.

RESULTS

Patient Characteristics

We identified a total of 15,256 patients who were pathologically confirmed to have HSCC between 1975 and 2016 in the SEER database. Of these patients, 2001 patients were excluded due to a lack of complete follow-up data, 3145 patients were excluded

because HSCC was not their only tumor, 7613 patients were excluded because they were diagnosed before 2010 (no TNM staging information per the seventh edition of the AJCC Cancer Staging Manual), 292 patients were excluded due to unknown TNM stage, three patients were excluded because they were stage T0, and four patients were excluded due to unknown surgical details. Finally, 2198 patients were included in this study and were randomly assigned at a 4:1 ratio to the training set (n = 1758) or the validation set (n = 440). **Figure 1** illustrates the screening process. **Table 1** shows the demographics and clinical characteristics of the patients, 78.7% of whom were diagnosed with locally advanced HSCC (stages III-IVB). Moreover, 4.1% of the patients received surgery alone, 80.7% received radiotherapy alone, and 14.1% received both surgery and radiotherapy. The external validation set included 233 patients with locally advanced HSCC who were treated at our center, and **Table S1** shows their demographics and clinical characteristics.

For the 2198 patients, the median follow-up time was 41 months (interquartile range: 20 to 61). The 3-year and 5-year OS rates were 41.3% (95% CI, 38.9% to 43.7%) and 32.5% (95% CI, 30.0% to 35.0%), respectively; the 3-year and 5-year CSS rates were 50.2% (95% CI, 47.7% to 52.7%) and 44.0% (95% CI, 41.3% to 46.7%), respectively. The median OS of all patients was 24 months, and the median survival was 24 months in the training set and 29 months in the validation set. For the external validation set, the median follow-up time was 27.9 months (interquartile range: 19.3 to 38.3), and the 3-year OS rate was 64.6% (95% CI, 56.6% to 72.6%).

Construction of the Nomogram

For the training set, the Cox univariate regression analysis showed that the following parameters were significantly related to OS: age, marital status, race, insurance status, primary site, T stage, N stage, M stage, TNM stage, local treatment, and chemotherapy (**Table 2**). **Figure 2** shows the OS curves, which were based on the Kaplan-Meier method and log-rank test and accounted for the following parameters: age, marital status, race, insurance, primary site, pathological differentiation, T stage, N stage, M stage, TNM stage, local treatment, and chemotherapy. A competing risk analysis showed that age, marital status, race, T stage, N stage, M stage, local treatment, and chemotherapy were still correlated with HSCC-specific death (all $P < 0.05$, **Figure S1**). A subgroup analysis was also performed for T stage in patients with local resectable HSCC to analyze the relationship between local treatment and OS (**Figure 3**). In T3 patients, no significant difference was observed in OS among patients who received surgery alone, those who received radiotherapy alone, and those who received both surgery and radiotherapy ($P = 0.304$). In T4a patients, however, a significant between-group difference was observed in OS ($P < 0.001$), which was longest in patients who received both surgery and radiotherapy, followed by patients who received radiotherapy alone, and then patients who received surgery alone. Moreover, T3 and T4a patients who received systemic chemotherapy had a significantly longer OS than those who did not receive chemotherapy ($P < 0.001$). We further analyzed the overall survival of metastasis-free HSCC patients with different treatment modalities for each TNM stages, as shown in **Figure S2**. It was found that for locally advanced HSCC, the curative effect of single treatment modality was relatively poor, while that of combined therapy was relatively better (**Figures S2B–D**, $P < 0.001$).

A Cox multivariate regression analysis showed that age, marital status, race, T stage, N stage, M stage, local treatment,

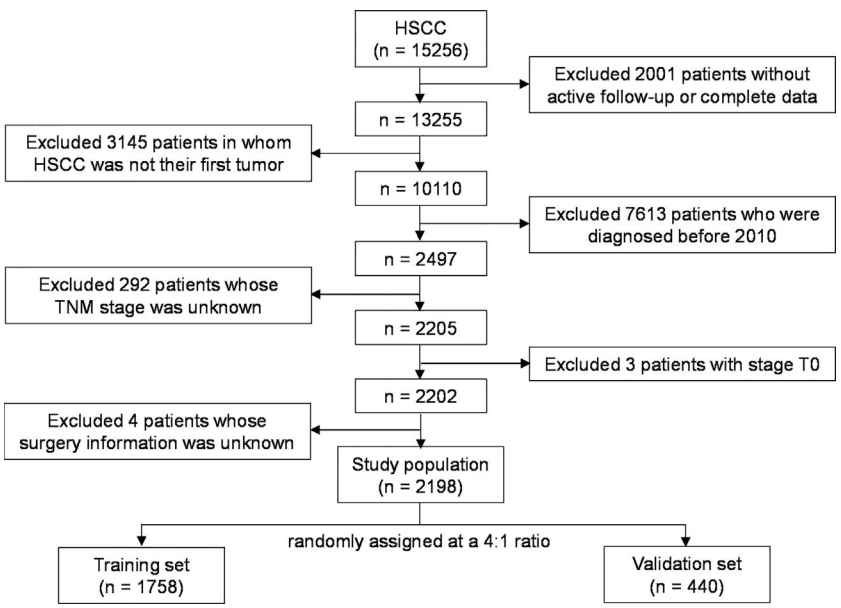

FIGURE 1 | Screening process.

TABLE 1 | Demographics and clinical characteristics of the HSCC training and validation sets from the SEER database.

Characteristic	All patients	Training set	Validation set
	(n = 2198) No. (%)	(n = 1758) No. (%)	(n = 440) No. (%)
Age			
≤50 years	206 (9.4)	171 (9.7)	35 (8)
51-60 years	719 (32.7)	562 (32)	157 (35.7)
61-70 years	749 (34.1)	607 (34.5)	142 (32.3)
>70 years	524 (23.8)	418 (23.8)	106 (24.1)
Sex			
Male	1825 (83)	1466 (83.4)	359 (81.6)
Female	373 (17)	292 (16.6)	81 (18.4)
Marital status			
Married	942 (42.9)	749 (42.6)	193 (43.9)
Others	1256 (57.1)	1009 (57.4)	247 (56.1)
Race			
White	1640 (74.6)	1325 (75.4)	315 (71.6)
Black	391 (17.8)	302 (17.2)	89 (20.2)
Others	167 (7.6)	131 (7.5)	36 (8.2)
Insurance			
No/unknown	150 (6.8)	128 (7.3)	22 (5)
Yes	2048 (93.2)	1630 (92.7)	418 (95)
Primary site			
Pyriform sinus	1272 (57.9)	1002 (57)	270 (61.4)
Postcricoid region	58 (2.6)	40 (2.3)	18 (4.1)
Posterior pharyngeal wall	151 (6.9)	127 (7.2)	24 (5.5)
NOS	717 (32.6)	589 (33.5)	128 (29.1)
Grade			
Well differentiated	82 (3.7)	61 (3.5)	21 (4.8)
Moderately differentiated	906 (41.2)	722 (41.1)	184 (41.8)
Poorly differentiated	728 (33.1)	587 (33.4)	141 (32)
Undifferentiated	19 (0.9)	10 (0.6)	9 (2)
Unknown	463 (21.1)	378 (21.5)	85 (19.3)
T stage			
T1	217 (9.9)	173 (9.8)	44 (10)
T2	778 (35.4)	626 (35.6)	152 (34.5)
T3	552 (25.1)	438 (24.9)	114 (25.9)
T4a	443 (20.2)	350 (19.9)	93 (21.1)
T4b	208 (9.5)	171 (9.7)	37 (8.4)
N stage			
N0	546 (24.8)	428 (24.3)	118 (26.8)
N1	401 (18.2)	333 (18.9)	68 (15.5)
N2	1124 (51.1)	894 (50.9)	230 (52.3)
N3	127 (5.8)	103 (5.9)	24 (5.5)
M stage			
M0	2016 (91.7)	1615 (91.9)	401 (91.1)
M1	182 (8.3)	143 (8.1)	39 (8.9)
TNM stage			
I	81 (3.7)	56 (3.2)	25 (5.7)
II	204 (9.3)	160 (9.1)	44 (10)
III	396 (18)	321 (18.3)	75 (17)
IVA	1075 (48.9)	865 (49.2)	210 (47.7)
IVB	260 (11.8)	213 (12.1)	47 (10.7)
IVC	182 (8.3)	143 (8.1)	39 (8.9)
Surgery and radiotherapy			
Surgery	91 (4.1)	64 (3.6)	27 (6.1)
Radiotherapy	1777 (80.8)	1440 (81.9)	337 (76.6)
Surgery +radiotherapy	309 (14.1)	237 (13.5)	72 (16.4)
Both not given	21 (1)	17 (1)	4 (0.9)
Chemotherapy			
No/unknown	654 (29.8)	514 (29.2)	140 (31.8)
Yes	1544 (70.2)	1244 (70.8)	300 (68.2)

HSCC, hypopharyngeal squamous cell carcinoma; NOS, not otherwise specified; TNM, tumor-node-metastasis.

and chemotherapy were independent prognostic factors for OS (**Table 2**). TNM stage was excluded from the multivariate analysis because it was not an independent variable, but rather, it is a combination of T, N, and M stages. The eight significant independent prognostic factors (age, marital status, race, T stage, N stage, M stage, local treatment, chemotherapy; $P < 0.05$) identified by the Cox multivariate regression analysis were used to develop a prognostic nomogram (**Figure 4**). The score of each prognostic factor was as follows (in descending order): age > 70: 52; marital status - other: 24; race - black: 26; T4b: 100; N3: 80; M1: 83; surgery and radiotherapy (no): 83; and chemotherapy (no): 59. The total score was used to predict each patient's 1-year, 3-year, and 5-year survival probabilities. For example, for a 65-year-old married Chinese patient diagnosed with HSCC T3N2bM0 who received radical chemoradiotherapy, the prognostic nomogram scored the age as 12, the marital status as 0, race as 0, T3 as 77, N2 as 40, M0 as 0, radiotherapy as 44, and chemotherapy as 0, which resulted in a total score of 173. Therefore, the model predicted that the 1-year, 3-year, and 5-year survival probabilities were 76%, 48%, and 37%, respectively.

Validation of the Nomogram

The nomogram was validated with both internal and external validation. For the internal validation, the calibration curve showed that the nomogram was accurate in its predictions (**Figure 5**). The X-axis represents the survival probability predicted by the nomogram, and the Y-axis represents the actual survival probability. The dotted line (45° diagonal line) indicates complete concordance between the actual probability and the predicted probability. The similarity between the solid line and the dotted line indicates a high level of accuracy in nomogram prediction. Next, the C-index and the Brier score were used to evaluate the performance of the prognostic nomogram, which was compared with that of the TNM staging system (**Table S2**). For the external validation, the patients in the validation set were rated with the nomogram, and then the total scores were incorporated into the Cox regression model to calculate the C-index. The C-index of the nomogram was greater than 0.7, which was higher than that of the TNM staging system (training set: 0.718 *vs* 0.627; validation set: 0.708 *vs* 0.598; external validation set: 0.709 *vs* 0.597). The nomogram also performed better than the TNM staging system as assessed by the Brier score (lower values indicate better model performance, **Table S2**). **Figure S3** shows that in the training set, the validation set, and the external validation set, the area under the curve (AUC) values for the 1-year, 3-year, and 5-year OS curves were higher for the nomogram than for the TNM staging system, which suggests that the nomogram is superior to the TNM staging system in predicting clinical outcomes.

Next, we divided the patients in the training and validation sets into the following three groups based on the 3-year survival probability predicted by the nomogram: the low-risk group (3-year survival probability ≥ 50%, score ≤ 170), the moderate-risk group (30% ≤ 3-year survival probability < 50%, 170 < score ≤ 213), and the high-risk group (3-year survival probability < 30%, score > 213). The Kaplan-Meier curve illustrates the good

TABLE 2 | Univariate and multivariate analyses of overall survival in the training set.

Variable	Univariate analysis		Multivariate analysis	
	HR (95% CI)	*P* value[a]	HR (95% CI)	*P* value
Age				
≤50 years	Reference			
51-60 years	1.176 (0.921-1.503)	0.193	1.138 (0.887-1.459)	0.308
61-70 years	1.168 (0.915-1.49)	0.212	1.248 (0.972-1.603)	0.083
>70 years	1.671 (1.305-2.138)	**<0.001**	1.947 (1.503-2.523)	**<0.001**
Sex				
Male	Reference			
Female	0.879 (0.737-1.048)	0.152	NA	
Marital status				
Married	Reference			
Others	1.487 (1.304-1.696)	**<0.001**	1.344 (1.173-1.541)	**<0.001**
Race				
White	Reference			
Black	1.677 (1.433-1.962)	**<0.001**	1.333 (1.13-1.573)	**0.001**
Others	0.991 (0.768-1.277)	0.942	0.968 (0.748-1.252)	0.803
Insurance				
No/unknown	Reference			
Yes	0.676 (0.542-0.841)	**<0.001**	0.814 (0.648-1.021)	0.075
Primary site				
Pyriform sinus	Reference			
Postcricoid region	1.187 (0.795-1.774)	0.402	1.214 (0.809-1.82)	0.349
Posterior pharyngeal wall	1.161 (0.903-1.492)	0.245	1.243 (0.963-1.604)	0.095
NOS	1.225 (1.068-1.404)	**0.004**	1.155 (1.006-1.326)	**0.042**
Grade				
Well differentiated	Reference		NA	
Moderately differentiated	1.18 (0.824-1.691)	0.366		
Poorly differentiated	1.049 (0.729-1.509)	0.797		
Undifferentiated	0.259 (0.062-1.082)	0.064		
Unknown	1.022 (0.703-1.487)	0.908		
T stage				
T1	Reference			
T2	1.602 (1.206-2.129)	**0.001**	1.66 (1.244-2.215)	**0.001**
T3	2.407 (1.808-3.204)	**<0.001**	2.575 (1.919-3.454)	**<0.001**
T4a	2.678 (1.999-3.588)	**<0.001**	2.958 (2.194-3.989)	**<0.001**
T4b	3.725 (2.721-5.101)	**<0.001**	3.403 (2.461-4.706)	**<0.001**
N stage				
N0	Reference			
N1	1.232 (1.007-1.508)	**0.043**	1.389 (1.128-1.709)	**0.002**
N2	1.43 (1.213-1.685)	**<0.001**	1.679 (1.408-2.002)	**<0.001**
N3	2.282 (1.737-3)	**<0.001**	2.795 (2.084-3.749)	**<0.001**
M stage				
M0	Reference			
M1	3.455 (2.85-4.188)	**<0.001**	2.686 (2.191-3.293)	**<0.001**
TNM stage				
I	Reference		NA	
II	2.117 (1.166-3.843)	**0.014**		
III	2.469 (1.4-4.354)	**0.002**		
IVA	3.31 (1.907-5.744)	**<0.001**		
IVB	5.2 (2.946-9.178)	**<0.001**		
IVC	10.754 (6.06-19.085)	**<0.001**		
Surgery and radiotherapy				
Surgery	Reference			
Radiotherapy	1.125 (0.786-1.61)	0.520	1.242 (0.857-1.801)	0.252
Surgery+ radiotherapy	0.715 (0.479-1.068)	0.101	0.724 (0.48-1.092)	0.123
Both not given	3.056 (1.649-5.665)	**<0.001**	2.088 (1.117-3.901)	**0.021**
Chemotherapy				
No/unknown	Reference			
Yes	0.6 (0.524-0.686)	**<0.001**	0.484 (0.416-0.564)	**<0.001**

HSCC, hypopharyngeal squamous cell carcinoma; NOS, not otherwise specified; TNM, tumor-node-metastasis; HR, hazard ratio; CI, confidence interval.
[a]*P values < 0.05 are indicated in bold.*

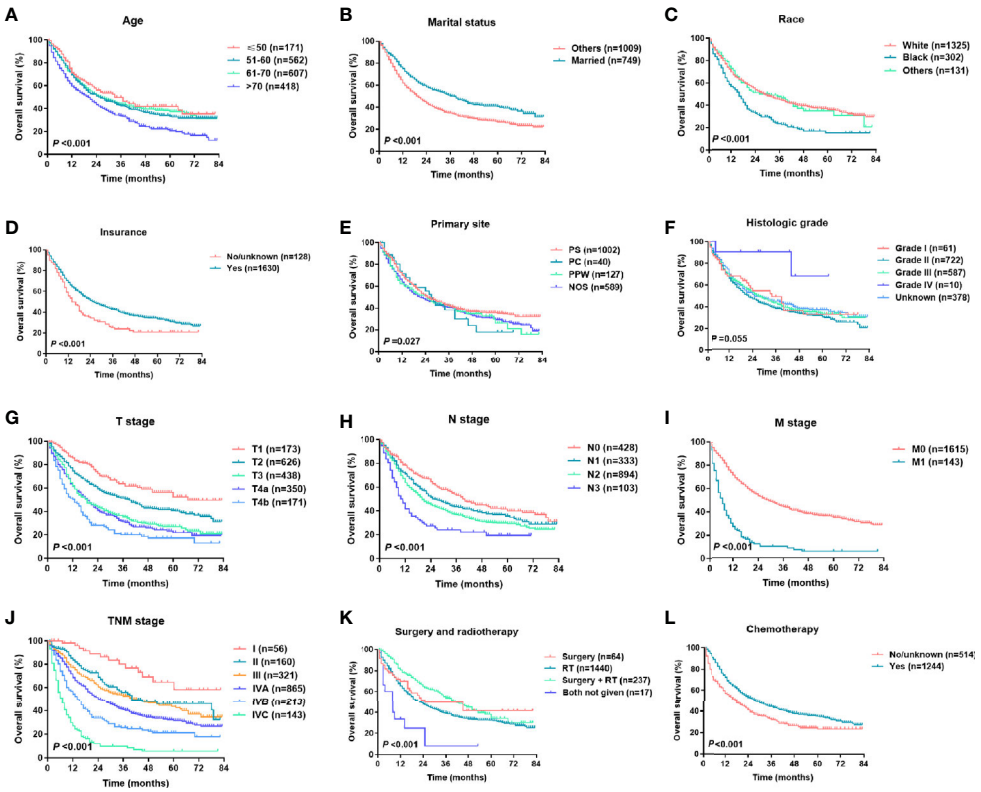

FIGURE 2 | Kaplan-Meier survival curves of HSCC patients in different subgroups: **(A)** age, **(B)** marital status, **(C)** race, **(D)** insurance status, **(E)** primary site, **(F)** histological grade, **(G)** T stage, **(H)** N stage, **(I)** M stage, **(J)** TNM stage, **(K)** surgery and radiotherapy, **(L)** chemotherapy.

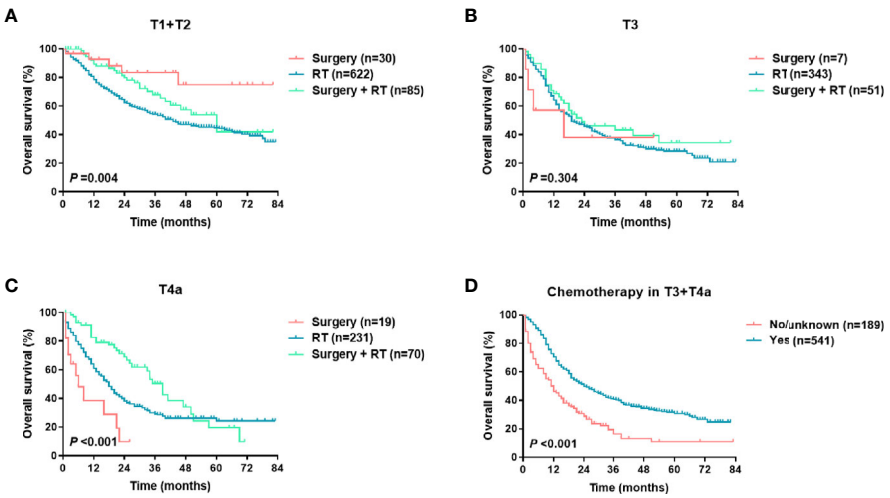

FIGURE 3 | OS of metastasis-free HSCC patients in different treatment groups (per T stage): **(A)** local treatment for T1 and T2 disease; **(B)** local treatment for T3 disease; **(C)** local treatment for T4a disease; **(D)** chemotherapy in T3 and T4a patients.

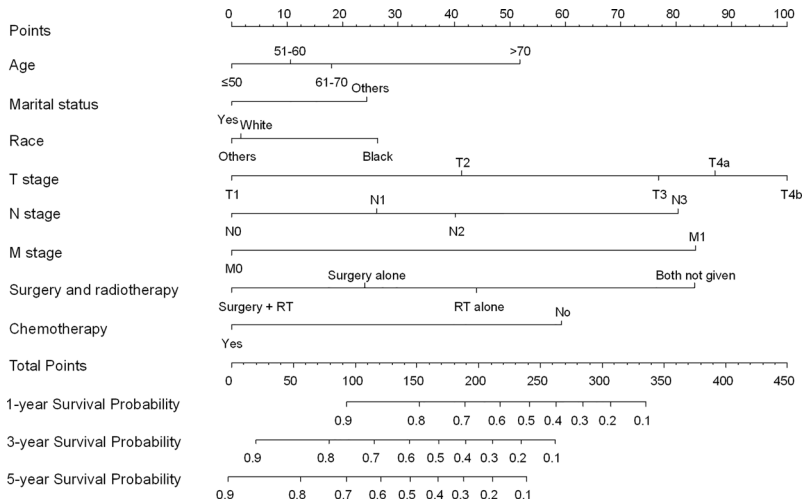

FIGURE 4 | Nomogram for predicting the survival probability of HSCC patients.

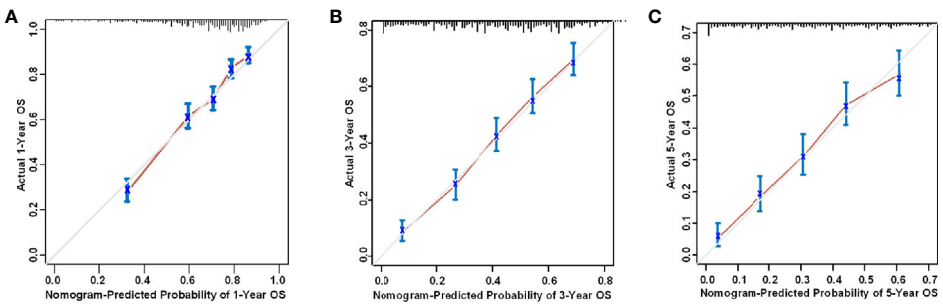

FIGURE 5 | Internal calibration curve of the nomogram for the prediction of the **(A)** 1-year, **(B)** 3-year, and **(C)** 5-year survival probability of HSCC patients.

prognostic discrimination of the nomogram ($P < 0.001$, **Figures 6A, B**). The patients in the external validation group were divided into the following two groups based on the 3-year survival probability predicted by the nomogram: the low-risk group (3-year survival probability ≥ 50%) and the high-risk group (3-year survival probability < 50%). The survival curves confirmed a significant between-group difference ($P < 0.001$, **Figure 6C**).

DISCUSSION

Previous SEER-based studies have analyzed the tumor characteristics, treatment, and survival of patients with HSCC (6–8). However, other than the TNM staging system, a unified prediction model for HSCC is lacking due to the low prevalence of this disease. This is the first SEER-based study to develop a nomogram prediction model of HSCC survival. Heng Y et al. recently developed a prognostic nomogram for Chinese patients with HSCC after tumor resection, which served as a stratification indication for postoperative adjuvant treatment (13). However, the optimal initial treatment modality for locally advanced HSCC has not been fully defined and was identified as an important prognostic factor (6–8). Thus, in this SEER-based study, we analyzed the effect of local treatment (surgery and/or radiotherapy) and chemotherapy on OS. We also analyzed the prognostic factors of HSCC, developed an intuitive nomogram to effectively predict OS, and confirmed the validity of the prediction model using both internal and external validation. The nomogram may be used to evaluate the survival probability of each HSCC patient and provide a reference for the clinical assessment of patient outcomes and treatment strategies.

According to the revised TNM staging system presented in 2002 in the sixth edition of the AJCC Cancer Staging Manual, stage T4 can be further classified as T4a (moderately advanced local disease) or T4b (very advanced local disease). As a result, stage IV is further classified as stage IVA (moderately advanced local/regional disease), stage IVB (very advanced local/regional disease), and stage IVC (distant metastatic disease) (14). According to the 2010 seventh edition of the AJCC Cancer

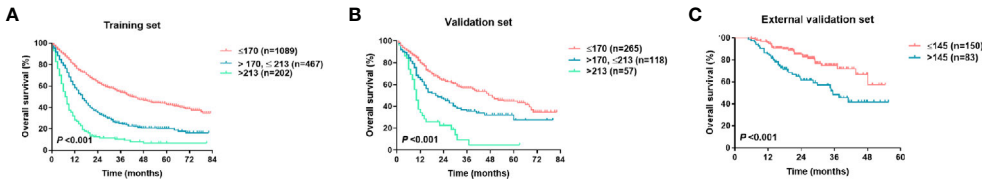

FIGURE 6 | Kaplan-Meier survival curves of the training set **(A)**, the validation set **(B)**, and the external validation **(C)** per nomogram score.

Staging Manual, HSCC-related esophageal involvement was revised from stage T4 (as described in the sixth edition) to stage T3 (15). In this study, we selected patients who were diagnosed in 2010 or later and who were staged according to the seventh edition of the AJCC Cancer Staging Manual. A survival analysis showed that the revised TNM stage was a good prognostic factor for HSCC (**Figures 2G–J**). However, we found limitations in the TNM stage. For example, the survival curve of stage T3 patients overlapped with that of stage T4a patients (**Figure 2G**), and no difference was observed in the OS prediction between stages II and III (**Figure 2J**), which suggests that the TNM staging prognostic system requires further improvement.

As in previous reports, this study showed that age was an important prognostic factor, and an age > 70 was associated with a more adverse prognosis (**Figure 2A**) (4, 5). In this SEER cohort, 23.8% of the patients were older than 70 at the time of HSCC diagnosis. The multivariate analysis showed that the hazard ratio was 1.947 (95% CI, 1.503-2.523, P < 0.001) in patients older than 70 relative to those aged 50 or below, in part because older patients tended to have more comorbidities and a shorter life expectancy and tended to receive more conservative treatment. The male: female ratio was approximately 5:1, which is similar to that reported in previous studies (4), but the univariate analysis revealed no difference in prognosis between the sexes. As shown in previous reports, this study reported that race, marital status, and insurance status were related to the OS of HSCC patients (**Figures 2B–D**), which to some extent reflected the effects of economic condition, social status, and emotional support on disease prognosis (16, 17). In this study, the univariate analysis showed that the primary site was a prognostic factor. "Primary site - not otherwise specified (NOS)" was associated with the worst prognosis, and no significant difference was observed in the prognosis of patients with tumors in other primary sites such as the piriform sinus, postcricoid region, and posterior pharyngeal wall (**Figure 2E**). In HSCC, it is often difficult to discern the primary site due to the large tumor size, which may explain the designation of "Primary site - NOS". We also analyzed pathological differentiation and found that most cases were moderately differentiated and that pathological differentiation was unrelated to HSCC prognosis.

For HSCC, radiotherapy and surgery are important local treatments that are usually administered alone or in combination based on disease stage and pathological risk factors (such as positive margins and extracapsular involvement of lymph nodes) (2, 18–20). In the early stages of the disease, both treatments are viable options; in locally advanced-stage disease, surgery plus radiotherapy helps improve the local control rate and the prognosis. In this study, radiotherapy and surgery were analyzed as a composite variable. Our SEER data showed that in America, radiotherapy alone is the most common treatment modality for HSCC (80.8%), followed by surgery plus radiotherapy (14.1%). Consistent with previous studies (6–8), this study showed that local treatment patterns were independent prognostic factors for survival (**Table 2** and **Figure 2K**). A population-based cohort study that involved 6647 HSCC patients showed that the best 5-year OS rate (48.5%) was achieved with a combination of surgery and radiation therapy. The 5-year OS rate of patients treated with surgery was significantly higher than that of those treated with radiotherapy alone in cases of local (63.3% *vs* 52.4%) or regionally advanced disease (41.3% *vs* 31.9%) (6). We then performed a subgroup analysis of T stage to determine the effect of local treatment on the survival of patients with HSCC without distant metastasis (**Figures 3A–C**). Among the HSCC patients with stages T1 and T2 disease, most received radiotherapy, although surgery alone was also effective (P = 0.004). Surgery plus radiotherapy was the best option for patients with stage T4a disease (P < 0.001), but this combination had no significant advantage in patients with stage T3 disease (P = 0.304). A population-based study in the Netherlands also indicated that overall survival of stage T3 patients was equal after total laryngectomy and (chemo)radiotherapy, but a survival benefit was achieved after primary surgery ± radiotherapy for T4 patients (18). In general, systemic chemotherapy improves HSCC prognosis (2, 7, 19). Our data demonstrated that chemotherapy significantly reduced mortality (HR 0.489, 95% CI 0.416-0.564, P < 0.001) (**Table 1** and **Figure 2L**), and this effect was even more pronounced in patients with locally advanced HSCC with stages T3 and T4 disease (**Figure 3D**).

In this study, eight prognostic factors were incorporated into our Cox multivariate analysis to develop a nomogram, including demographics (age, marital status, race, insurance status), clinicopathological parameters (primary site, T stage, N stage, M stage), and treatment (local treatment and chemotherapy). The selection of these parameters was reasonable, feasible, and practical. Further validation showed a high level of accuracy in the prediction ability of the nomogram, which was superior to that of the TNM staging system (**Figure S2**). Nevertheless, this study has some limitations. First, this is a SEER-based population cohort study. Patients with missing data were excluded from the study, which may have led to bias. Second, in the SEER database, chemotherapy was categorized as "No/Unknown" or "Yes", with

no details on modality, such as induction chemotherapy, concurrent chemotherapy, and adjuvant chemotherapy, and no details on the type or dose of chemotherapy drug, which may have led to information bias and may have affected the HR of the variables. Third, the SEER database does not include some of the known pathological prognostic factors for HSCC, such as positive margins or extracapsular involvement of lymph nodes. As a result, we were unable to incorporate these factors into the prediction model. Fourth, the SEER database provided OS and CSS data but not progression-free survival or local relapse-free survival data, which would have affected the survival prediction of the nomogram. Finally, the SEER database is based on the US population. Therefore, the nomogram may only serve as a reference for prognostic prediction in the Chinese HSCC population. In the future, large multicenter studies should be performed in Chinese patients to develop a prediction model for the Chinese population.

CONCLUSION

This SEER-based study shows that some demographic characteristics, clinicopathological parameters, and treatment strategies are significantly correlated with the survival outcomes of HSCC patients. We developed and validated a nomogram for HSCC that had superior discrimination and accuracy. The variables are easy to collect, which demonstrates the ease of use of this nomogram in clinical practice to aid in the clinical evaluation of the risk level of HSCC patients and the development of individualized treatment strategies.

DATA AVAILABILITY STATEMENT

Publicly available datasets were analyzed in this study. This data can be found here: SEER database (https://seer.cancer.gov): Incidence -SEER 18 Regs Custom Data with additional treatment fields, Nov 2018 Sub, 1975-2016 varying.

ETHICS STATEMENT

The studies involving human participants were reviewed and approved by The Institutional Review Board of the Eye Ear Nose and Throat Hospital, Fudan University. The patients/participants provided their written informed consent to participate in this study.

AUTHOR CONTRIBUTIONS

ST, XH, RL, and ZT conceived and designed the research. ST, QL, RL, and XC performed statistical analysis and analyzed the results. ST and HG followed the patients and collected clinical data. ST and XW wrote and revised the paper. All authors contributed to the article and approved the submitted version.

FUNDING

This work was funded by National Science and Technology Major Project (2020ZX09201-013) and Science and Technology Commission of Shanghai Municipality (19411961300).

ACKNOWLEDGMENTS

We would like to thank American Journal Experts for editing the language.

SUPPLEMENTARY MATERIAL

The Supplementary Material for this article can be found online at: https://www.frontiersin.org/articles/10.3389/fonc.2021.696952/full#supplementary-material

REFERENCES

1. Cooper JS, Porter K, Mallin K, Hoffman HT, Weber RS, Ang KK, et al. National Cancer Database Report on Cancer of the Head and Neck: 10-Year Update. *Head Neck* (2009) 31(6):748–58. doi: 10.1002/hed.21022
2. Pracy P, Loughran S, Good J, Parmar S, Goranova R. Hypopharyngeal Cancer: United Kingdom National Multidisciplinary Guidelines. *J Laryngol Otol* (2016) 130(S2):S104–S10. doi: 10.1017/S0022215116000529
3. Hoffman HT, Karnell LH, Shah JP, Ariyan S, Brown GS, Fee WE, et al. Hypopharyngeal Cancer Patient Care Evaluation. *Laryngoscope* (1997) 107 (8):1005–17. doi: 10.1097/00005537-199708000-00001
4. Spector JG, Sessions DG, Emami B, Simpson J, Haughey B, Fredrickson JM. Squamous Cell Carcinomas of the Aryepiglottic Fold: Therapeutic Results and Long-Term Follow-Up. *Laryngoscope* (1995) 105(7 Pt 1):734–46. doi: 10.1288/00005537-199507000-00012
5. Spector JG, Sessions DG, Emami B, Simpson J, Haughey B, Harvey J, et al. Squamous Cell Carcinoma of the Pyriform Sinus: A Nonrandomized Comparison of Therapeutic Modalities and Long-Term Results. *Laryngoscope* (1995) 105(4 Pt 1):397–406. doi: 10.1288/00005537-199504000-00012
6. Newman JR, Connolly TM, Illing EA, Kilgore ML, Locher JL, Carroll WR. Survival Trends in Hypopharyngeal Cancer: A Population-Based Review. *Laryngoscope* (2015) 125(3):624–9. doi: 10.1002/lary.24915
7. Kuo P, Sosa JA, Burtness BA, Husain ZA, Mehra S, Roman SA, et al. Treatment Trends and Survival Effects of Chemotherapy for Hypopharyngeal Cancer: Analysis of the National Cancer Data Base. *Cancer* (2016) 122(12):1853–60. doi: 10.1002/cncr.29962
8. Hochfelder CG, McGinn AP, Mehta V, Castellucci E, Kabarriti R, Ow TJ. Treatment Sequence and Survival in Locoregionally Advanced Hypopharyngeal Cancer: A Surveillance, Epidemiology, and End Results-Based Study. *Laryngoscope* (2020) 130(11):2611–21. doi: 10.1002/lary.28452
9. Iasonos A, Schrag D, Raj GV, Panageas KS. How to Build and Interpret a Nomogram for Cancer Prognosis. *J Clin Oncol* (2008) 26(8):1364–70. doi: 10.1200/JCO.2007.12.9791
10. Balachandran VP, Gonen M, Smith JJ, DeMatteo RP. Nomograms in Oncology: More Than Meets the Eye. *Lancet Oncol* (2015) 16(4):e173–80. doi: 10.1016/S1470-2045(14)71116-7
11. Zhou Z, Mo S, Dai W, Xiang W, Han L, Li Q, et al. Prognostic Nomograms for Predicting Cause-Specific Survival and Overall Survival of Stage I-III Colon

Cancer Patients: A Large Population-Based Study. *Cancer Cell Int* (2019) 19:355. doi: 10.1186/s12935-019-1079-4
12. Wang CY, Yang J, Zi H, Zheng ZL, Li BH, Wang Y, et al. Nomogram for Predicting the Survival of Gastric Adenocarcinoma Patients Who Receive Surgery and Chemotherapy. *BMC Cancer* (2020) 20(1):10. doi: 10.1186/s12885-019-6495-2
13. Heng Y, Zhu X, Zhou L, Zhang M, Li J, Tao L. A Prognostic Nomogram for Predicting the Long-Term Survival Outcome of Hypopharyngeal Squamous Cell Carcinoma Patients After Tumour Resection to Assist the Decision-Making of Postoperative Adjuvant Treatment. *Eur J Surg Oncol* (2020) 46 (2):245–51. doi: 10.1016/j.ejso.2019.09.005
14. Greene FL, Page DL, Fleming ID, Fritz AG, Balch CM, Haller DG, et al. *Cancer Staging Handbook. 6th ed*. New York: Springer (2002).
15. Edge SB, Byrd DR, Compton CC, Fritz AG, Greene FL, Trotti A, et al. *Cancer Staging Manual. 7th ed*. New York: Springer (2010).
16. Shi RL, Qu N, Lu ZW, Liao T, Gao Y, Ji QH. The Impact of Marital Status at Diagnosis on Cancer Survival in Patients With Differentiated Thyroid Cancer. *Cancer Med* (2016) 5(8):2145–54. doi: 10.1002/cam4.778
17. Zhan C, Yang X, Song X, Yan L. Radiotherapy vs Surgery for T1-2N0M0 Laryngeal Squamous Cell Carcinoma: A Population-Based and Propensity Score Matching Study. *Cancer Med* (2018) 7(7):2837–47. doi: 10.1002/cam4.1525
18. Petersen JF, Timmermans AJ, van Dijk BAC, Overbeek LIH, Smit LA, Hilgers FJM, et al. Trends in Treatment, Incidence and Survival of Hypopharynx Cancer: A 20-Year Population-Based Study in the Netherlands. *Eur Arch Otorhinolaryngol* (2018) 275(1):181–9. doi: 10.1007/s00405-017-4766-6
19. de Bree R. The Current Indications for Non-Surgical Treatment of Hypopharyngeal Cancer. *Adv Otorhinolaryngol* (2019) 83:76–89. doi: 10.1159/000492314
20. Eckel HE, Bradley PJ. Treatment Options for Hypopharyngeal Cancer. *Adv Otorhinolaryngol* (2019) 83:47–53. doi: 10.1159/000492308

Conflict of Interest: The authors declare that the research was conducted in the absence of any commercial or financial relationships that could be construed as a potential conflict of interest.

frontiers in Oncology

ORIGINAL RESEARCH
published: 29 July 2021
doi: 10.3389/fonc.2021.712944

Digital Pathology Scoring of Immunohistochemical Staining Reliably Identifies Prognostic Markers and Anatomical Associations in a Large Cohort of Oral Cancers

Julius Moratin[1], Andreas Mock[2,3], Sonja Obradovic[1], Karl Metzger[1], Christa Flechtenmacher[4], Karim Zaoui[5], Stefan Fröhling[3], Dirk Jäger[2], Jürgen Krauss[2], Jürgen Hoffmann[1], Kolja Freier[6], Dominik Horn[6], Jochen Hess[5] and Christian Freudlsperger[1]*

[1] Department of Oral and Cranio-Maxillofacial Surgery, University of Heidelberg, Heidelberg, Germany, [2] Department of Medical Oncology, National Center for Tumor Diseases (NCT) Heidelberg, Heidelberg University Hospital, Heidelberg, Germany, [3] Department of Translational Medical Oncology, National Center for Tumor Diseases (NCT) Heidelberg, German Cancer Research Center (DKFZ), Heidelberg, Germany, [4] Institute of Pathology, University of Heidelberg, Heidelberg, Germany, [5] Department of Otorhinolaryngology, University of Heidelberg, Heidelberg, Germany, [6] Department of Oral and Maxillofacial Surgery, Saarland University, Homburg, Germany

OPEN ACCESS

Edited by:
Heming Lu, People's Hospital of Guangxi Zhuang Autonomous Region, China

Reviewed by:
Philip Sloan, Newcastle upon Tyne Hospitals NHS Foundation Trust, United Kingdom
Carter Van Waes, National Institutes of Health Clinical Center (NIH), United States

***Correspondence:**
Julius Moratin
Julius.moratin@med.uni-heidelberg.de

Specialty section:
This article was submitted to Head and Neck Cancer, a section of the journal Frontiers in Oncology

Received: *21 May 2021*
Accepted: *09 July 2021*
Published: *29 July 2021*

Citation:
Moratin J, Mock A, Obradovic S, Metzger K, Flechtenmacher C, Zaoui K, Fröhling S, Jäger D, Krauss J, Hoffmann J, Freier K, Horn D, Hess J and Freudlsperger C (2021) Digital Pathology Scoring of Immunohistochemical Staining Reliably Identifies Prognostic Markers and Anatomical Associations in a Large Cohort of Oral Cancers. Front. Oncol. 11:712944. doi: 10.3389/fonc.2021.712944

Utilizing digital pathology algorithms for the objective quantification of immunohistochemical staining, this study aimed to identify robust prognostic biomarkers for oral cancer. Tissue microarrays with specimens of a large cohort of oral squamous cell carcinoma (n=222) were immunohistochemically stained to determine the expression of PD-L1, EGFR, and COX-2 and the amount of infiltrating NK cells and CD8-positive T cells. Immunoreactivity scores were assessed using both a classical manual scoring procedure and a digital semi-automatic approach using QuPath. Digital scoring was successful in quantifying the expression levels of different prognostic biomarkers (CD8: $p<0.001$; NK cells: $p=0.002$, PD-L1: $p=0.026$) and high levels of concordance with manual scoring results were observed. A combined score integrating EGFR expression, neck node status and immune cell signatures with a significant impact on overall and progression-free survival was identified ($p<0.001$). These data may contribute to the ongoing research on the identification of reliable and clinically relevant biomarkers for the individualization of primary and adjuvant treatment in oral cancer.

Keywords: immune cells, automated, quantification, biomarker, head and neck squamous cell carcinoma, oral squamous cell carcinoma

INTRODUCTION

In 2018, head and neck cancer was the seventh most common group of malignant tumors worldwide with approximately 900.000 new cases per year and squamous cell carcinomas arising from the oral mucosa (OSCC) form a major part of this entity (1–3). Metastases and locoregional disease recurrence are the main predicting factors for adverse clinical outcome and OSCC is responsible for about 1.5% of all cancer related deaths in the United States (4, 5). 5-year survival rates have remained at 40-60% over the last decades despite interdisciplinary multi-modal treatment (6–10).

Although, the introduction of immune checkpoint inhibition has brought new therapeutic options for patients with recurrent and/or metastatic head and neck squamous cell carcinoma (HNSCC), accurate biomarkers allowing for distinct risk-stratification and individualization of therapy and follow-up for patients with primary oral cancer are still limited (11, 12). Such markers might help to identify patients at risk of tumor progression, who may benefit from a more intensive interdisciplinary multi-modality therapy. While a plethora of publications reported on potential biomarkers, up to date, only few have been translated into clinical application due to a lack of prognostic relevance and clinical practicality.

A well-established method to identify and evaluate potential biomarkers is immunohistochemical staining of tumor sections to assess the expression pattern of potential candidate proteins. The use of tissue microarrays (TMAs) is a common and efficient technique to investigate expression levels of multiple markers in a large number of different tissue samples (13). The conventional way of manual inspection and counting of stained cells to assess the quantity and quality of potential biomarkers, such as different proteins or tumor-associated immune cells, is strongly observer-dependent and potentially error-prone. The introduction of automated digital image analysis has brought a new technique that may help to standardize and objectify pathological analysis including the assessment of biomarkers (14–16).

Lately, the shift towards a focus on the tumor immune microenvironment (TIME) led to the introduction of new potential biomarkers like immune-checkpoint-proteins (e. g. PD-L1) and tumor-associated immune cells in a variety of tumor entities including HNSCC. In the context of the newly introduced immunotherapy, especially PD-L1 and tumor infiltrating lymphocytes (TILs) are promising candidates with the potential to quantify both relevant aspects, the tumor immunogenicity and patients' immunological capacity (17–22). Additionally, EGFR and COX-2 have recently been identified as key regulators related to immune phenotypes in head and neck cancer with potential impact on the response to treatment immune checkpoint inhibition (ICI) (23).

Therefore, the purpose of this study was to apply digital pathology algorithms to investigate the expression levels of different potential biomarkers, including EGFR, COX-2 and PD-L1 and the infiltration of cytotoxic TILs like natural killer (NK) cells (defined by NK activation receptor CD335) and CD8+ T cells in tissue specimens of a cohort of 222 OSCCs. Protein expression and immune cell infiltration patterns were then analyzed regarding anatomic distribution and prognostic significance for overall and progression-free survival.

MATERIALS AND METHODS

Patients and Samples

The investigated cohort consisted of 222 patients with primary OSCCs. All patients received surgical treatment at the Department of Oral and Cranio-Maxillofacial Surgery of the University Hospital Heidelberg between the years 2010 and 2016. In case of residual disease, lymph node metastases or histopathological risk factors additional adjuvant radiotherapy or radio-chemotherapy was applied. Written informed consent was obtained from all patients and the study was approved by the ethics committee of the medical faculty of the University of Heidelberg (Ethic vote: S-360/2011). Follow-up data was assessed retrospectively *via* SAP patient management research software (SAP, Walldorf, Germany).

Tissue Microarray and Histological Slices

All TMAs and histological slices were prepared by the tissue bank of the National Center for Tumor Diseases (NCT) Heidelberg, Germany according to an established protocol as reported earlier (13). Hematoxylin-eosin-stained slides of the prepared tissue samples were examined by an expert pathologist for tumor content. Tumors were then marked to enable the selection of appropriate tissue samples. Via the tissue chip microarray (Beecher Instruments, Sun Prairie, Wisconsin, USA), tissue cores were extracted from the paraffin blocks. After transfer of the tissue cores into a recipient block, paraffin-embedding was used to create TMA blocks and slices were produced with a thickness of 2-3 µm for the staining procedure (Histo Bond, Marienfeld, Germany).

Immunohistochemistry

TMAs were stained using anti-PD-L1 (Cell Signaling Technology, Danvers, Massachusetts, USA), anti-Nkp46/CD335 (Thermo Fisher Scientific, Waltham, Massachusetts, USA), anti-Human CD8, (Clone C8/144B Dako, Agilent Technologies, Santa Clara, USA), anti-EGFR (D38B1, Cell Signaling Technology, Danvers, Massachusetts, USA), and anti-COX2 (SP21, Invitrogen/Thermo Fisher Scientific, Waltham, Massachusetts, USA) monoclonal antibodies, and the DAB Substrate Kit (Vector Laboratories, California, USA) following the manufacturer's instructions. Afterwards, TMAs were scanned using the Nanozoomer HT Scan System (Hamamatsu Photonics, Japan).

Manual and Digital Pathology-Based Scoring

The manual scoring procedure was performed with digital scans of the TMAs exclusively using the NDP.view2 software (Hamamatsu Photonics, Hamamatsu, Japan). The immunoreactivity score (IRS) was determined by three independent observers, who assessed the relative amounts of stained cells and the staining intensity. The observers were

blinded for the clinical data of the patients included in the study during the scoring procedures. For assessment of tumor cells, an ordinal scale was used based on the number of stained cells and staining intensity (amount of stained cells: 1 = no stained cells, 0%; 2 = < 33%; 3 = 33%-66%; 4 = >66%; staining intensity: 1 = no staining; 2 = low; 3 = medium; 4 = high). Median values of the three observes were used as final score. The two scores were then multiplied to create the final IRS with a range from 1 to 16. For immune cells, an ordinal scale was used based on the number of stained cells (amount of stained cells: 1 = no stained cells, 0%; 2 = < 33%; 3 = 33%-66%; 4 = >66%).

QuPath version v0.2.2 was used for semi-automatic digital quantification of immunohistochemical staining (24). In the first step, the TMA dearrayer function was used to infer the TMA grid. This step was followed by manually excluding invalid samples as well as staining artefacts from further analysis. Next, staining vectors were automatically determined for every TMA slide individually to ensure meaningful quantification between slides. Lastly, the positive cell detection function was used to quantify the number of positive cells for every sample. For every marker, the optimal score compartment was assessed by visual control (nucleus mean for CD8 cells, cytoplasm mean for CD335, EGFR and PD-L1 and cell mean for COX2). **Figure 1A** illustrates the procedure of semi-automatic digital scoring.

Anatogram of Immunostains

The illustration of the oral cavity was created using the vector-based graphic design software Vectornator X (Linearity GmbH, Karlsruhe). The exact tumor localization in relation to the graphic was determined for each patient using Microsoft Excel (Microsoft, Redmond, Washington). The tumor localization was

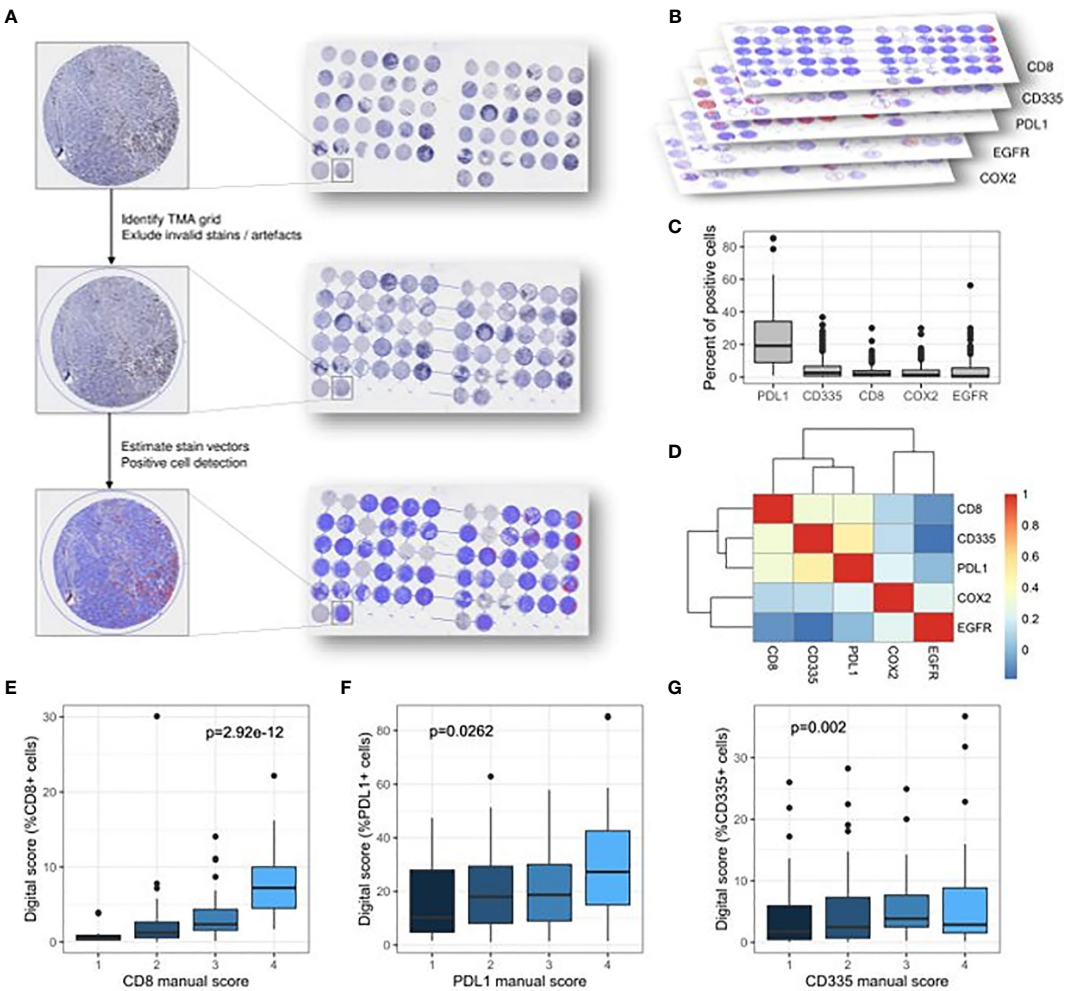

FIGURE 1 | Graphical abstract of the digital scoring procedure principles and the associations between score values obtained by different scoring techniques. **(A)** Identification and evaluation of tissue spots. Detection and quantification of stains. **(B)** Different biomarkers included in the analysis (CD8 cells, CD335/NK cells, PD-L1, EGFR, COX-2). **(C)** Percentage of positive cells for each stain across the samples. **(D)** Heatmap depicting the Spearman's correlation coefficient between different biomarkers. **(E–G)** Concordance between the classical manual scoring and the digital scoring technique for CD8 cells, CD335/NK cells and PD-L1.

projected onto the graphic and the various levels of expression (continuous scale) were mapped for each potential biomarker in R (version 4.0.2; www.r-project.org) to illustrate different levels of expression according to the tumor localization in the oral cavity.

Statistical Analysis

Statistical analyses were performed using Microsoft Excel (Microsoft, Redmond, Washington), SPSS 25 (SPSS for Windows, SPSS, Chicago, IL) and R (version 4.0.2; www.r-project.org).

Demographic, clinical and pathological features of the investigated cohort were analyzed using descriptive statistics. Median values of groups were analyzed using the Kruskal–Wallis one-way analysis of variance. The Wilcoxon rank-sum test was used for pairwise comparison of median values between groups. Correlation of expression levels of different biomarkers were evaluated using Spearman's correlation coefficient and concordance of values obtained by different scoring procedures was evaluated using linear regression modelling.

The optimal cut-off values to define high- and low-expressing groups in the digital scoring for all investigated biomarkers including the CD8/CD335 ratio were defined in a data-driven approach by finding meaningful local maxima in the distribution of p-values for all cut-offs in the inter-quartile range of expression values (see **Figure 3**).

Survival analysis was performed using the Kaplan-Meier method from date of diagnosis until death, disease recurrence or end of data collection and log-rank testing served to determine differences between the groups. Univariate and multivariate Cox regression models were applied to evaluate the impact of immune cell infiltration and protein expression on overall survival and progression-free survival together with relevant covariates.

A p-value of less than 0.05 was considered statistically significant.

RESULTS

Patient Cohort

Overall, tissue samples of 222 patients were included in the analysis. 137 patients (61.7%) were male and 85 (38.3%) were female. The age ranged from 27 to 88 years with a mean age of 64.3 ± 11.1 years. All patients suffered from primary squamous cell carcinoma of the oral cavity and received surgical treatment in the Department of Oral and Cranio-Maxillofacial Surgery of the University of Heidelberg between 2010 and 2016.

112 patients (50.5%) initially presented with early-stage disease (Stage I/II) and 110 (49.5%) with advanced disease (Stage III/IV). Adjuvant radiotherapy or radio-chemotherapy was applied for patients with advanced tumors (Stage III/IV), incomplete tumor resection (R+) or the presence of histopathological risk factors, such as perineural (PN+), lymphatic (L+) or vascular (V+) tumor infiltration. 89 patients (40.1%) received adjuvant treatment including radiotherapy (54 patients) and radio-chemotherapy (35 patients). 47 patients (21.2%) died during follow-up and 47 patients (21.2%) experienced disease recurrence. **Table 1** provides an overview of demographic and clinical features of the patient cohort.

Digital Pathology Scoring of Immunostaining and Comparison With Manual Scoring

The digital scoring of immunostaining was performed for CD8, CD335, PD-L1, EGFR and COX2 (**Figures 1B, C**). The immunostaining for CD8, CD335 and PD-L1 were also evaluated by manual scoring enabling a comparative analysis between both techniques. No significant correlation could be observed between all markers (**Figure 1D**). The highest concordance was achieved for CD8-positive T cells ($p<0.001$, **Figure 1E**), followed by Nkp46/CD335-positive NK cells ($p=0.002$, **Figure 1G**) and PD-L1 ($p=0.0262$, **Figure 1F**). Scoring of COX-2 and EGFR was performed using only the semi-automatic validation method, a comparison with the manual scoring method therefore was not possible.

Spatial Mapping of Expression Patterns

The distribution of tumors and the protein expression (digital scoring) for investigated biomarkers in dependence of the affected anatomic subunit of the oral cavity are shown in **Figure 2**. A subset of tumors which were localized in the border region between the oral cavity and oropharynx (n=16; soft palate and base of the tongue) were subsumed under the category "oropharynx". Overall, there was a dominance of tumors located in the lower section of the oral cavity with a higher frequency at the tongue, the floor of the mouth and the mandible (n=186, 83.8%; see **Table 1** and **Figure 2**).

The median expression values of the investigated biomarkers did not differ significantly between the anatomical subsites, except for PD-L1. Here, median expression values were significantly lower ($p<0.05$) for tumors located in the oropharynx as compared to the other subsites except for the maxilla (**Supplementary Figure 1** and **Supplementary Table 1**).

Survival Analysis

Assessing the clinical characteristics of the cohort revealed that the nodal status was the only parameter that was associated with OS (p=1.81E-05) or PFS (p=1.31E-05; **Figure 4**). To identify reliable expression biomarkers that could be applied by pathologist, expression values were not modelled as a continuous parameter in the survival time analysis but cut-offs were established. To this end, the distribution of p-values of the univariate cox proportional hazard model enabled to determine the robustness of cut-offs (**Figure 3**).

In the univariate survival analysis with overall survival (OS) as the endpoint, the CD8/CD335 ratio and PD-L1 but not CD8 showed a prognostic impact across a larger range of cut-offs. Both a higher CD8/CD335 ratio (ratio >2), i.e. a T cell dominance and a higher PD-L1 expression was associated with a shorter OS (-log10 hazard ratio < 0). Modelling progression free survival (PFS) as the endpoint identified the CD8/CD335 ratio and EGFR as significant biomarkers. Both markers were associated with a shorter PFS (**Figure 4**).

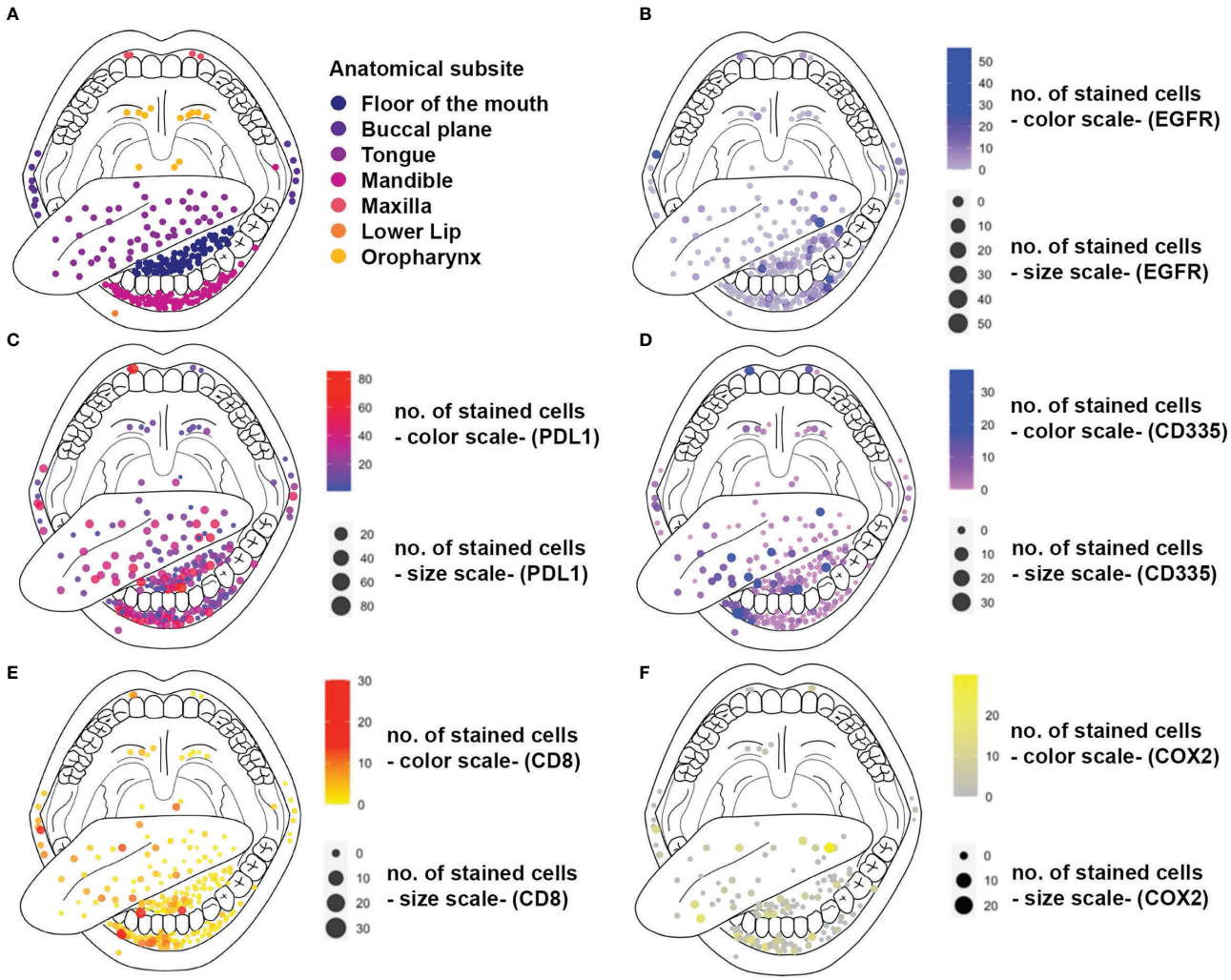

FIGURE 2 | Anatograms of immunostains for different biomarkers. Diameter and color of dots represent the number of stained cells for each biomarker. The localizations of dots meet the anatomic subsites affected by the tumor. **(A)** Localization of tumor tumors within the oral cavity and the oropharynx **(B)** EGFR expression **(C)** PD-L1 expression **(D)** CD335/NK cell Infiltration **(E)** CD8 cell infiltration **(F)** COX2 Expression

In the multivariate analysis of overall survival, the CD8/CD335 ratio and nodal status (N), but not PD-L1 were confirmed as independent prognostic markers (**Table 2**). The survival differences after stratification for pathological N status and CD8/CD335 ratio are illustrated in **Supplementary Figure 2B**. The best survival rates were observed for patients with N0 status and low CD8/CD335 ratio, while N+ with high CD8/CD335 ratio was associated with worse survival ($p<0.001$).

Similar results were observed for progression-free survival (PFS). Here, nodal status (N), the CD8/CD335 ratio and EGFR status were confirmed as independent prognostic markers (**Table 2**). **Supplementary Figure 2B** illustrates the survival rates after stratification for EGFR status, N status and CD8/CD335 ratio. Best survival rates were seen in patients with negative EGFR status and low CD8/CD335 ratio, irrespective of neck node status, while worst survival was observed for patients with positive EGFR status, presence of neck node metastases (N+) and high CD8/CD335 ratio ($p<0.001$).

DISCUSSION

The identification of reliable biomarkers is of critical importance for cancer research and to further individualize tumor therapy. While there have been advances in the definition of markers to prognosticate the therapeutic response to palliative medical therapy using immune checkpoint inhibition (ICI) by the evaluation of the tumor mutational burden (TMB) or the expression levels of PD-L1, there still is a lack on relevant

TABLE 1 | Demographic, clinical and pathological data of the investigated cohort of 222 oral and oropharyngeal cancers.

Parameter	Number of cases (%)
Gender	
Female	85 (38.3)
Male	137 (61.7)
Age	
<65 years	111 (50)
>65 years	111 (50)
T Stage	
T1	82 (36.9)
T2	72 (32.4)
T3	8 (3.6)
T4	60 (27.1)
N Stage	
0	147 (66.2)
1	27 (12.2)
2a	1 (0.5)
2b	28 (12.5)
2c	18 (8.1)
3	1 (0.5)
M Stage	
0	222 (100)
1	0
UICC	
1	69 (31.1)
2	44 (19.8)
3	23 (10.4)
4	86 (38.7)
Differentiation Grade	
1	17 (7.7)
2	153 (68.9)
3	46 (20.7)
Missing	6 (2.7)
R	
0	210 (94.6)
1	10 (4.5)
Missing	2 (0.9)
Location	
Floor of the mouth	64 (28.8)
Tongue	52 (23.4)
Mandible	70 (31.5)
Maxilla	5 (2.3)
Oropharynx	16 (7.2)
Buccal Plane	14 (6.3)
Lower lip	1 (0.5)
Recurrence	
yes	47 (21.2)
no	175 (78.8)

markers for the primary disease (25–27). A plethora of publications exists on the correlation of different markers with clinical parameters, such as tumor size, neck node status or survival, including proteins or genetic material (28, 29). However, none has been established so far in clinical practice to serve as an accurate prognostic or predictive marker for primary therapy. The major goal in the primary disease stage is to stratify patients' risks for tumor recurrence and, consequently, to allocate them to an adjusted primary and adjuvant treatment or more rigorous follow-up surveillance. Moreover, the introduction of new anti-cancer therapies is based on the identification of appropriate targets. The classical way of biomarker research is manual scoring of immunohistochemical staining to evaluate the expression levels of different proteins or to analyze quantity and distribution of tumor-associated immune cells. This technique is time-consuming and potentially hard to reproduce. This often results in numerous publications with contradictory conclusions due to differing methods of data generation, analysis and interpretation.

Hence, one of the goals of this study was to utilize digital pathology algorithms as a new standard procedure for the quantification of expression levels of potential biomarkers in oral cancer. The obtained IRS were then correlated with data obtained by manual scoring, associations with affected anatomic subsites, and prognostic significance to evaluate their conclusiveness.

Several biomarkers were chosen for this analysis including EGFR, COX-2, PD-L1, CD8-positive T cells and Nkp46/CD335-positive NK cells. The immune system has been identified as a key factor in the development of cancer and subsequently merged into the focus of cancer research. In the field of head and neck cancer, the introduction of immune checkpoint inhibition has further raised the importance of understanding the tumor-associated immune microenvironment and its potential influence on therapeutic success (11, 12, 30, 31). As response to immune checkpoint inhibition is restricted to a fraction of patients, surrogate markers for therapeutic success are needed. Here, several promising candidates have been proposed, including PD-L1 and tumor infiltration lymphocytes (TILs). PD-L1 has emerged as an independent prognostic marker in head and neck cancer patients and the application of immune-checkpoint-inhibition partly is based on PD-L1 expression levels (12, 32, 33). Several studies already reported on the high prognostic significance of TILs in various malignancies and their role as a marker for anti-tumor immune response (34–37). EGFR is an established prognostic marker, a key target in anti-cancer therapy and lately has been linked to different immune phenotypes and response to ICI treatment together with COX-2 (23, 38–40).

The primary aim of this study was to evaluate a digital pathology algorithm using the Qupath software approach to assess potential biomarkers in oral cancer. While different aspects of this method have been thoroughly described for a variety of diagnostic tasks including analysis of histological tumor samples, its utility for head and neck cancers remains to be confirmed in larger cohorts. Shaban et al. introduced a digital score for TIL abundance in OSCC investigating a cohort of 60 patients and described it as strong prognosticator for disease free survival. Moreover, they reported on the significantly higher impact of the digital TIL score in comparison to the manual score (14). de Ruiter et al. evaluated various T-cell markers in a cohort of 80 HPV-negative HNSCCs undergoing primary chemo-radiotherapy without finding relevant differences in overall and progression-free survival depending on T-cell infiltration (16). In another study, the authors used a digital pathology approach to determine PD-L1 expression and its prognostic significance in breast cancer. The authors concluded that the technique of digital pathology was effective in stratifying biomarker scores

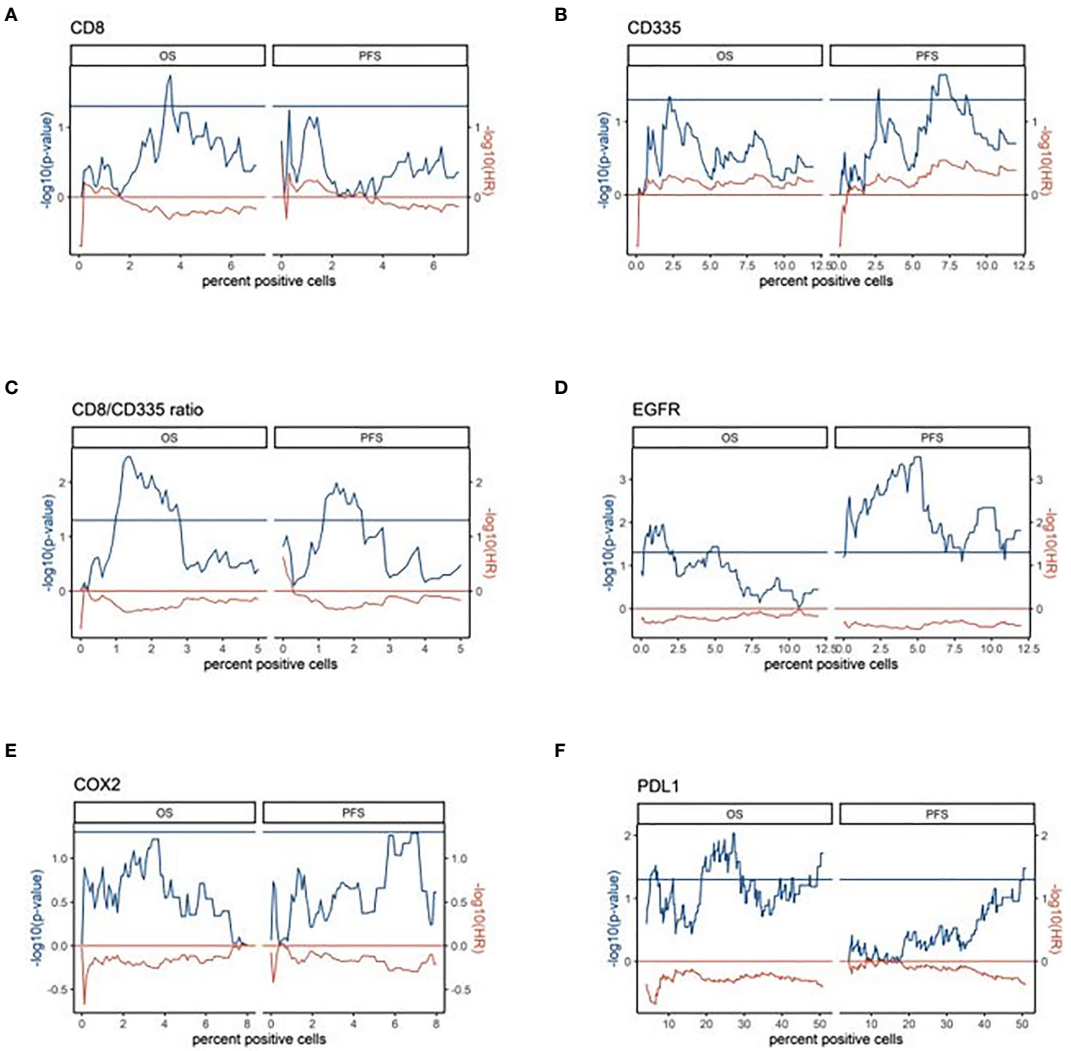

FIGURE 3 | Data-driven expression cut-offs of the digital scores for survival time analysis **(A–F)**. The p-values (cox proportional hazard model, -log10) and hazard ratios (-log10) of the univariate survival analysis are plotted over the percent of positive cells in the digital scoring. The left half of the respective plots show the results for OS and the right half for PFS. Horizontal lines illustrate the p-value cutoff ($p < 0.05$) and the direction of association (HR=1). Here, a negative –log10 HR corresponds to a shorter OS or PFS, respectively.

(41). In our study, the evaluation of expression levels of different proteins and the infiltrations patterns by manual scoring or semi-automatic scoring produced significantly correlated data sets. While the concordance was highest for CD8 cells, the correlations for NK cell and PD-L1 scores were weaker, possibly due to the greater variation of staining intensity and localization, especially for PD-L1.

All investigated biomarkers were analyzed regarding expression differences for distinct anatomical subsites by vector-designed anatograms depicting localization and staining intensity for each tumor and marker (**Figure 2**). Besides a dominance of tumors in the lower section of the oral cavity, there was a significant tendency towards lower median PD-L1 expression in tumors located in the oropharynx (base of the tongue and soft palate). All sixteen tumors that were subsumed under the term "oropharynx" were borderline tumors which affected the oral cavity and the oropharynx (e.g. maxilla-soft palate; tongue – base of the tongue). Those tumors were labeled as "oropharyngeal cancer" to sharpen the anatomical classifications for the analysis of spatial expression heterogeneity.

In the univariate survival analysis, several markers showed a prognostic impact on overall and progression-free survival, including PD-L1, EGFR, CD8 and NK cells. Furthermore, in the multivariate analysis, EGFR could be confirmed as independent prognostic marker for progression-free survival and the CD8/CD335 ratio for both, overall and progression-free survival. As reported before, this observation is in accordance with several other publications and confirms the validity of our data. Furthermore, this concordance strengthens

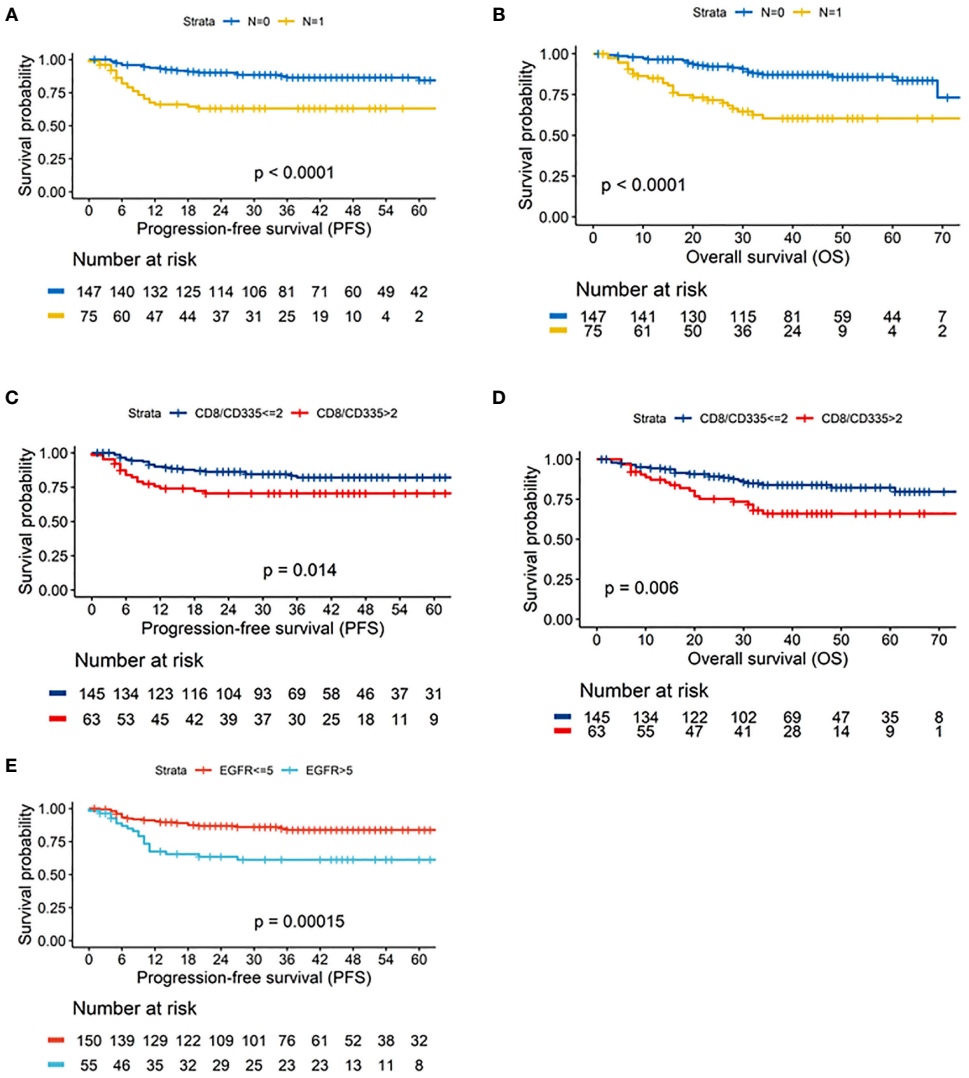

FIGURE 4 | Kaplan-Meier curves depicting the results of the univariate survival analysis for: Neck node status (N0/N1) – **(A)**. Progression-free survival (PFS) – **(B)**. overall survival (OS) CD8/CD335 ratio (CD8/CD335 ≤2/>2) – **(C)**. Progression-free survival (PFS) – **(D)**. overall survival (OS) EGFR status (EGFR ≤5/>5 – **(E)**. Progression-free survival (PFS).

TABLE 2 | Multivariate analysis of overall and progression-free survival.

Characteristics	Expression Cut-off	Overall survival		Progression-free survival	
		HR (95% CI)	p-value	HR (95% CI)	p-value
N status	**NA**	1.26 (0.65-1.87)	<0.001	1.44 (0.81-2.07)	<0.001
CD8/CD335 ratio	**2**	0.69 (0.09-1.29)	0.02	0.74 (0.13-1.35)	0.02
EGFR	**5**	–	–	1.16 (0.54-1.78)	0.002

The CD8/CD335 ratio and the EGFR expression were dichotomized according to the presented expression cut-offs. HR, hazard ratio.
NA, N Status does not have a cutoff.
Bold values mean for EGFR no significant impact on overall survival could be shown.

the technique of digital pathology as valid method of analysis for future studies. Several authors used different immune-scores including CD8-positive T cells to identify patients at risk for adverse outcome or those who had a higher chance to profit from a more intense multi-modal treatment including radio-chemotherapy (42–45). NK cells play a vital role in anti-tumor immunity and, in contrast to T cells, are independent of MHC related activation or prior immunization and their prognostic

impact on survival has been demonstrated for a variety of tumors (46–50). Their activity is mainly guided by inhibitory and activating signals *via* chemokines and blocking of inhibitory pathways has been shown to result in improved anti-tumor response (51, 52). While most of the mentioned publications on TILs in HNSCC reported on mixed cohorts of patients with primary and recurrent tumors of different subsites who mostly received different treatment modalities, our analysis focused on a large cohort of 222 patients with OSCC and primary surgical therapy. Here, we could confirm the prognostic significance of tumor-infiltrating lymphocytes (TILs) by evaluating NK cell and CD8 cell infiltration separately and in a CD8/CD335 ratio. In a multivariate analysis, the CD8/CD335 ratio was confirmed as independent prognostic factor for OS and PFS (p=0.02). The prognostic relevance of PD-L1 for oral cancer has been discussed in a plethora of studies and is supported by the data reported in this study (33).

The presented study has several limitations including the utilization of TMAs for the analyses considering the intratumor heterogeneity of several potential biomarkers such as PD-L1 (53). Further studies are warranted to evaluate the reported results using whole tissue slides and to validate the findings in a prospective setting. The translation of potential biomarkers into clinical practice is highly dependent of several factors, including prognostic value, reliability, and cost effectiveness. While singular biomarkers are prone to exhibit limitations regarding their clinical applicability, the definition of a set of several markers may synergize the strengths and compensate the weaknesses of single markers. The presented study contributed to this task by evaluating potential biomarker candidates using and validating a novel scoring approach with digital pathology on a large cohort of patients with oral cancer.

CONCLUSIONS

The assessment of immunohistochemical staining *via* digital pathology techniques was shown to be a feasible and efficient option for objective pathological analysis. The expression levels of different proteins and concentrations of tumor-infiltrating lymphocytes were successfully evaluated. Thereby, a set of clinical and histological markers with high prognostic relevance was identified. These findings provide a valuable contribution to the establishment of digital pathology as standard procedure for the identification and validation of existing and future biomarkers with clinical relevance to further enhance risk-stratification and individualization of tumor therapy in patients suffering from oral cancer.

DATA AVAILABILITY STATEMENT

The original contributions presented in the study are included in the article/**Supplementary Material**. Further inquiries can be directed to the corresponding author.

ETHICS STATEMENT

The studies involving human participants were reviewed and approved by Ethics Committee of the University of Heidelberg. Written informed consent for participation was not required for this study in accordance with the national legislation and the institutional requirements.

AUTHOR CONTRIBUTIONS

Conceptualization, JM, AM, JHe and CFr. Methodology, JM, AM, JHe, JK, CFr, SO. Formal analysis, JM, AM, SO, CFl, KZ, DJ, SF, JHe. Resources, JHo, JHe, JK, SF, DJ. Data curation, JM, AM, SO, DH, KF and KZ. Writing – original draft preparation, JM, AM, SO, DH, JHe and CFr. Writing – review and editing, CFl, CFr, DJ, SF, JHe, JHo, JK, KF, KZ and KM. visualization, JM, AM, SO and KM. All authors contributed to the article and approved the submitted version.

FUNDING

JM and AM are funded by the Physician-Scientist Program of the University of Heidelberg, Faculty of Medicine, JM is funded by the "Stiftung Tumorforschung Kopf-Hals".

ACKNOWLEDGMENTS

The TMA samples were provided by the tissue bank of the National Center for Tumor Diseases (NCT, Heidelberg, Germany) in accordance with the regulations of the tissue bank and the approval of the ethics committee of Heidelberg University. AM is a fellow of the DKTK (German Cancer Consortium) and the Cancer Core Europe TRYTRAC program.

SUPPLEMENTARY MATERIAL

The Supplementary Material for this article can be found online at: https://www.frontiersin.org/articles/10.3389/fonc.2021.712944/full#supplementary-material

REFERENCES

1. Ferlay J, Shin HR, Bray F, Forman D, Mathers C, Parkin DM. Estimates of Worldwide Burden of Cancer in 2008: GLOBOCAN 2008. *Int J Cancer* (2010) 127(12):2893–917. doi: 10.1002/ijc.25516
2. Bray F, Ferlay J, Soerjomataram I, Siegel RL, Torre LA, Jemal A. Global Cancer Statistics 2018: GLOBOCAN Estimates of Incidence and Mortality Worldwide for 36 Cancers in 185 Countries. *CA: A Cancer J Clin* (2018) 68 (6):394–424. doi: 10.3322/caac.21492
3. Shield KD, Ferlay J, Jemal A, Sankaranarayanan R, Chaturvedi AK, Bray F, et al. The Global Incidence of Lip, Oral Cavity, and Pharyngeal Cancers by Subsite in 2012. *CA: A Cancer J Clin* (2017) 67(1):51–64. doi: 10.3322/caac.21384
4. Siegel RL, Miller KD, Jemal A. Cancer Statistics, 2018. *CA: A Cancer J Clin* (2018) 68(1):7–30. doi: 10.3322/caac.21442

5. Krishna A, Singh RK, Singh S, Verma P, Pal US, Tiwari S. Demographic Risk Factors, Affected Anatomical Sites and Clinicopathological Profile for Oral Squamous Cell Carcinoma in a North Indian Population. *Asian Pac J Cancer Prev* (2014) 15(16):6755–60. doi: 10.7314/APJCP.2014.15.16.6755
6. D'Cruz AK, Vaish R, Kapre N, Dandekar M, Gupta S, Hawaldar R, et al. Elective Versus Therapeutic Neck Dissection in Node-Negative Oral Cancer. *N Engl J Med* (2015) 373(6):521–9. doi: 10.1056/NEJMoa1506007
7. Kligerman J, Lima RA, Soares JR, Prado L, Dias FL, Freitas EQ, et al. Supraomohyoid Neck Dissection in the Treatment of T1/T2 Squamous Cell Carcinoma of Oral Cavity. *Am J Surg* (1994) 168(5):391–4. doi: 10.1016/S0002-9610(05)80082-0
8. Akhtar S, Ikram M, Ghaffar S. Neck Involvement in Early Carcinoma of Tongue. Is Elective Neck Dissection Warranted? *J Pak Med Assoc* (2007) 57 (6):305–7.
9. Pignon JP, le Maitre A, Maillard E, Bourhis JGroup M-NC. Meta-Analysis of Chemotherapy in Head and Neck Cancer (MACH-NC): An Update on 93 Randomised Trials and 17,346 Patients. *Radiother Oncol* (2009) 92(1):4–14. doi: 10.1016/j.radonc.2009.04.014
10. Forastiere A, Koch W, Trotti A, Sidransky D. Head and Neck Cancer. *N Engl J Med* (2001) 345(26):1890–900. doi: 10.1056/NEJMra001375
11. Ferris RL, Blumenschein GJr., Fayette J, Guigay J, Colevas AD, Licitra L, et al. Nivolumab for Recurrent Squamous-Cell Carcinoma of the Head and Neck. *N Engl J Med* (2016) 375(19):1856–67. doi: 10.1056/NEJMoa1602252
12. Burtness B, Harrington KJ, Greil R, Soulieres D, Tahara M, de Castro GJr., et al. Pembrolizumab Alone or With Chemotherapy Versus Cetuximab With Chemotherapy for Recurrent or Metastatic Squamous Cell Carcinoma of the Head and Neck (KEYNOTE-048): A Randomised, Open-Label, Phase 3 Study. *Lancet* (2019) 394(10212):1915–28. doi: 10.1016/S0140-6736(19)32591-7
13. Freier K, Joos S, Flechtenmacher C, Devens F, Benner A, Bosch FX, et al. Tissue Microarray Analysis Reveals Site-Specific Prevalence of Oncogene Amplifications in Head and Neck Squamous Cell Carcinoma. *Cancer Res* (2003) 63(6):1179–82.
14. Shaban M, Khurram SA, Fraz MM, Alsubaie N, Masood I, Mushtaq S, et al. A Novel Digital Score for Abundance of Tumour Infiltrating Lymphocytes Predicts Disease Free Survival in Oral Squamous Cell Carcinoma. *Sci Rep* (2019) 9(1):13341. doi: 10.1038/s41598-019-49710-z
15. Almangush A, Leivo I, Makitie AA. Overall Assessment of Tumor-Infiltrating Lymphocytes in Head and Neck Squamous Cell Carcinoma: Time to Take Notice. *Acta Otolaryngol* (2020) 140(3):246–8. doi: 10.1080/00016489.2020.1720284
16. de Ruiter EJ, de Roest RH, Brakenhoff RH, Leemans CR, de Bree R, Terhaard CHJ, et al. Digital Pathology-Aided Assessment of Tumor-Infiltrating T Lymphocytes in Advanced Stage, HPV-Negative Head and Neck Tumors. *Cancer Immunol Immunother* (2020) 69(4):581–91. doi: 10.1007/s00262-020-02481-3
17. James FR, Jiminez-Linan M, Alsop J, Mack M, Song H, Brenton JD, et al. Association Between Tumour Infiltrating Lymphocytes, Histotype and Clinical Outcome in Epithelial Ovarian Cancer. *BMC Cancer* (2017) 17 (1):657. doi: 10.1186/s12885-017-3585-x
18. Jakubowska K, Kisielewski W, Kanczuga-Koda L, Koda M, Famulski W. Stromal and Intraepithelial Tumor-Infiltrating Lymphocytes in Colorectal Carcinoma. *Oncol Lett* (2017) 14(6):6421–32. doi: 10.3892/ol.2017.7013
19. Rakaee M, Kilvaer TK, Dalen SM, Richardsen E, Paulsen EE, Hald SM, et al. Evaluation of Tumor-Infiltrating Lymphocytes Using Routine H&E Slides Predicts Patient Survival in Resected non-Small Cell Lung Cancer. *Hum Pathol* (2018) 79:188–98. doi: 10.1016/j.humpath.2018.05.017
20. Heikkinen I, Bello IO, Wahab A, Hagstrom J, Haglund C, Coletta RD, et al. Assessment of Tumor-Infiltrating Lymphocytes Predicts the Behavior of Early-Stage Oral Tongue Cancer. *Am J Surg Pathol* (2019) 43(10):1392–6. doi: 10.1097/PAS.0000000000001323
21. Ward MJ, Thirdborough SM, Mellows T, Riley C, Harris S, Suchak K, et al. Tumour-Infiltrating Lymphocytes Predict for Outcome in HPV-Positive Oropharyngeal Cancer. *Br J Cancer* (2014) 110(2):489–500. doi: 10.1038/bjc.2013.639
22. Xu Q, Wang C, Yuan X, Feng Z, Han Z. Prognostic Value of Tumor-Infiltrating Lymphocytes for Patients With Head and Neck Squamous Cell Carcinoma. *Transl Oncol* (2017) 10(1):10–6. doi: 10.1016/j.tranon.2016.10.005
23. Feng B, Shen Y, Pastor Hostench X, Bieg M, Plath M, Ishaque N, et al. Integrative Analysis of Multi-Omics Data Identified EGFR and PTGS2 as Key Nodes in a Gene Regulatory Network Related to Immune Phenotypes in Head and Neck Cancer. *Clin Cancer Res* (2020) 26(14):3616–28. doi: 10.1158/1078-0432.CCR-19-3997
24. Bankhead P, Loughrey MB, Fernandez JA, Dombrowski Y, McArt DG, Dunne PD, et al. QuPath: Open Source Software for Digital Pathology Image Analysis. *Sci Rep* (2017) 7(1):16878. doi: 10.1038/s41598-017-17204-5
25. Osipov A, Lim SJ, Popovic A, Azad NS, Laheru DA, Zheng L, et al. Tumor Mutational Burden, Toxicity, and Response of Immune Checkpoint Inhibitors Targeting PD(L)1, CTLA-4, and Combination: A Meta-Regression Analysis. *Clin Cancer Res* (2020) 26(18):4842–51. doi: 10.1158/1078-0432.CCR-20-0458
26. Samstein RM, Lee CH, Shoushtari AN, Hellmann MD, Shen R, Janjigian YY, et al. Tumor Mutational Load Predicts Survival After Immunotherapy Across Multiple Cancer Types. *Nat Genet* (2019) 51(2):202–6. doi: 10.1038/s41588-018-0312-8
27. Cohen EEW, Soulieres D, Le Tourneau C, Dinis J, Licitra L, Ahn MJ, et al. Pembrolizumab Versus Methotrexate, Docetaxel, or Cetuximab for Recurrent or Metastatic Head-and-Neck Squamous Cell Carcinoma (KEYNOTE-040): A Randomised, Open-Label, Phase 3 Study. *Lancet* (2019) 393(10167):156–67. doi: 10.1016/S0140-6736(18)31999-8
28. Wang J, Lv N, Lu X, Yuan R, Chen Z, Yu J. Diagnostic and Therapeutic Role of microRNAs in Oral Cancer (Review). *Oncol Rep* (2021) 45(1):58–64. doi: 10.3892/or.2020.7854
29. Rajguru JP, Mouneshkumar CD, Radhakrishnan IC, Negi BS, Maya D, Hajibabaei S, et al. Tumor Markers in Oral Cancer: A Review. *J Family Med Prim Care* (2020) 9(2):492–6. doi: 10.4103/jfmpc.jfmpc_1036_19
30. Seiwert TY, Burtness B, Mehra R, Weiss J, Berger R, Eder JP, et al. Safety and Clinical Activity of Pembrolizumab for Treatment of Recurrent or Metastatic Squamous Cell Carcinoma of the Head and Neck (KEYNOTE-012): An Open-Label, Multicentre, Phase 1b Trial. *Lancet Oncol* (2016) 17(7):956–65. doi: 10.1016/S1470-2045(16)30066-3
31. Harrington KJ, Ferris RL, Blumenschein GJr., Colevas AD, Fayette J, Licitra L, et al. Nivolumab Versus Standard, Single-Agent Therapy of Investigator's Choice in Recurrent or Metastatic Squamous Cell Carcinoma of the Head and Neck (CheckMate 141): Health-Related Quality-of-Life Results From a Randomised, Phase 3 Trial. *Lancet Oncol* (2017) 18(8):1104–15. doi: 10.1016/S1470-2045(17)30421-7
32. Moratin J, Metzger K, Safaltin A, Herpel E, Hoffmann J, Freier K, et al. Upregulation of PD-L1 and PD-L2 in Neck Node Metastases of Head and Neck Squamous Cell Carcinoma. *Head Neck* (2019) 41(8):2484–91. doi: 10.1002/hed.25713
33. Lenouvel D, Gonzalez-Moles MA, Ruiz-Avila I, Gonzalez-Ruiz L, Gonzalez-Ruiz I, Ramos-Garcia P. Prognostic and Clinicopathological Significance of PD-L1 Overexpression in Oral Squamous Cell Carcinoma: A Systematic Review and Comprehensive Meta-Analysis. *Oral Oncol* (2020) 106:104722. doi: 10.1016/j.oraloncology.2020.104722
34. Fridman WH, Pages F, Sautes-Fridman C, Galon J. The Immune Contexture in Human Tumours: Impact on Clinical Outcome. *Nat Rev Cancer* (2012) 12 (4):298–306. doi: 10.1038/nrc3245
35. Fridman WH, Zitvogel L, Sautes-Fridman C, Kroemer G. The Immune Contexture in Cancer Prognosis and Treatment. *Nat Rev Clin Oncol* (2017) 14(12):717–34. doi: 10.1038/nrclinonc.2017.101
36. Galon J, Mlecnik B, Bindea G, Angell HK, Berger A, Lagorce C, et al. Towards the Introduction of the 'Immunoscore' in the Classification of Malignant Tumours. *J Pathol* (2014) 232(2):199–209. doi: 10.1002/path.4287
37. Angell H, Galon J. From the Immune Contexture to the Immunoscore: The Role of Prognostic and Predictive Immune Markers in Cancer. *Curr Opin Immunol* (2013) 25(2):261–7. doi: 10.1016/j.coi.2013.03.004
38. Keren S, Shoude Z, Lu Z, Beibei Y. Role of EGFR as a Prognostic Factor for Survival in Head and Neck Cancer: A Meta-Analysis. *Tumour Biol* (2014) 35 (3):2285–95. doi: 10.1007/s13277-013-1303-0
39. Vermorken JB, Mesia R, Rivera F, Remenar E, Kawecki A, Rottey S, et al. Platinum-Based Chemotherapy Plus Cetuximab in Head and Neck Cancer. *N Engl J Med* (2008) 359(11):1116–27. doi: 10.1056/NEJMoa0802656

40. Hashemi Goradel N, Najafi M, Salehi E, Farhood B, Mortezaee K. Cyclooxygenase-2 in Cancer: A Review. *J Cell Physiol* (2019) 234(5):5683–99. doi: 10.1002/jcp.27411
41. Humphries MP, Hynes S, Bingham V, Cougot D, James J, Patel-Socha F, et al. Automated Tumour Recognition and Digital Pathology Scoring Unravels New Role for PD-L1 in Predicting Good Outcome in ER-/HER2+ Breast Cancer. *J Oncol* (2018) 2018:2937012. doi: 10.1155/2018/2937012
42. Zhang XM, Song LJ, Shen J, Yue H, Han YQ, Yang CL, et al. Prognostic and Predictive Values of Immune Infiltrate in Patients With Head and Neck Squamous Cell Carcinoma. *Hum Pathol* (2018) 82:104–12. doi: 10.1016/j.humpath.2018.07.012
43. Balermpas P, Rodel F, Weiss C, Rodel C, Fokas E. Tumor-Infiltrating Lymphocytes Favor the Response to Chemoradiotherapy of Head and Neck Cancer. *Oncoimmunology* (2014) 3(1):e27403. doi: 10.4161/onci.27403
44. Balermpas P, Michel Y, Wagenblast J, Seitz O, Weiss C, Rodel F, et al. Tumour-Infiltrating Lymphocytes Predict Response to Definitive Chemoradiotherapy in Head and Neck Cancer. *Br J Cancer* (2014) 110 (2):501–9. doi: 10.1038/bjc.2013.640
45. Gooden MJ, de Bock GH, Leffers N, Daemen T, Nijman HW. The Prognostic Influence of Tumour-Infiltrating Lymphocytes in Cancer: A Systematic Review With Meta-Analysis. *Br J Cancer* (2011) 105(1):93–103. doi: 10.1038/bjc.2011.189
46. Caligiuri MA. Human Natural Killer Cells. *Blood* (2008) 112(3):461–9. doi: 10.1182/blood-2007-09-077438
47. Vivier E, Raulet DH, Moretta A, Caligiuri MA, Zitvogel L, Lanier LL, et al. Innate or Adaptive Immunity? The Example of Natural Killer Cells. *Science* (2011) 331(6013):44–9. doi: 10.1126/science.1198687
48. Muntasell A, Rojo F, Servitja S, Rubio-Perez C, Cabo M, Tamborero D, et al. NK Cell Infiltrates and HLA Class I Expression in Primary HER2(+) Breast Cancer Predict and Uncouple Pathological Response and Disease-Free Survival. *Clin Cancer Res* (2019) 25(5):1535–45. doi: 10.1158/1078-0432.CCR-18-2365
49. Zhou XH, Zhang XY, Liang JH, Zhu HY, Wang L, Xia Y, et al. Low Absolute NK Cell Counts in Peripheral Blood are Associated With Inferior Survival in Patients With Mantle Cell Lymphoma. *Cancer Biomark* (2019) 24(4):439–47. doi: 10.3233/CBM-182193
50. Pellegatta S, Eoli M, Cuccarini V, Anghileri E, Pollo B, Pessina S, et al. Survival Gain in Glioblastoma Patients Treated With Dendritic Cell Immunotherapy is Associated With Increased NK But Not CD8(+) T Cell Activation in the Presence of Adjuvant Temozolomide. *Oncoimmunology* (2018) 7(4): e1412901. doi: 10.1080/2162402X.2017.1412901
51. Childs RW, Carlsten M. Therapeutic Approaches to Enhance Natural Killer Cell Cytotoxicity Against Cancer: The Force Awakens. *Nat Rev Drug Discovery* (2015) 14(7):487–98. doi: 10.1038/nrd4506
52. Hofmann MH, Mani R, Engelhardt H, Impagnatiello MA, Carotta S, Kerenyi M, et al. Selective and Potent CDK8/19 Inhibitors Enhance NK-Cell Activity and Promote Tumor Surveillance. *Mol Cancer Ther* (2020) 19(4):1018–30. doi: 10.1158/1535-7163.MCT-19-0789
53. Rasmussen JH, Lelkaitis G, Hakansson K, Vogelius IR, Johannesen HH, Fischer BM, et al. Intratumor Heterogeneity of PD-L1 Expression in Head and Neck Squamous Cell Carcinoma. *Br J Cancer* (2019) 120(10):1003–6. doi: 10.1038/s41416-019-0449-y

Conflict of Interest: The authors declare that the research was conducted in the absence of any commercial or financial relationships that could be construed as a potential conflict of interest.

frontiers in Oncology

ORIGINAL RESEARCH
published: 30 July 2021
doi: 10.3389/fonc.2021.710694

The Prognostic Value of the DNA Repair Gene Signature in Head and Neck Squamous Cell Carcinoma

Ruijie Ming[†], *Enhao Wang*[†], *Jiahui Wei*, *Jinxiong Shen*[*], *Shimin Zong*[*] *and Hongjun Xiao*[*]

Department of Otorhinolaryngology, Union Hospital, Tongji Medical College, Huazhong University of Science and Technology, Wuhan, China

Purpose: To construct a prognostic signature composed of DNA repair genes to effectively predict the prognosis of patients with head and neck squamous cell carcinoma (HNSCC).

Methods: After downloading the transcriptome and clinical data of HNSCC from the Cancer Genome Atlas (TCGA), 499 patients with HNSCC were equally divided into training and testing sets. In the training set, 13 DNA repair genes were screened using univariate proportional hazard (Cox) regression analysis and least absolute shrinkage and selection operator (LASSO) Cox regression analysis to construct a risk model, which was validated in the testing set.

Results: In the training and testing sets, there were significant differences in the clinical outcomes of patients in the high- and low-risk groups showed by Kaplan-Meier survival curves ($P < 0.001$). Univariate and multivariate Cox regression analyses showed that the risk score had independent prognostic predictive ability ($P < 0.001$). At the same time, the immune cell infiltration, immune score, immune-related gene expression, and tumor mutation burden (TMB) of patients with HNSCC were also different between the high- and low-risk groups ($P < 0.05$). Finally, we screened several chemotherapeutics for HNSCC, which showed significant differences in drug sensitivity between the high- and low-risk groups ($P < 0.05$).

Conclusion: This study constructed a 13-DNA-repair-gene signature for the prognosis of HNSCC, which could accurately and independently predict the clinical outcome of the patient. We then revealed the immune landscape, TMB, and sensitivity to chemotherapy drugs in different risk groups, which might be used to guide clinical treatment decisions.

Keywords: head and neck squamous cell carcinoma, DNA repair gene, prognostic signature, immune microenvironment, tumor mutation burden, drug sensitivity

OPEN ACCESS

Edited by:
Heming Lu,
People's Hospital of Guangxi Zhuang Autonomous Region, China

Reviewed by:
Gunnar Wichmann,
University Hospital Leipzig, Germany
Lei Gao,
Second Hospital of Hebei Medical University, China

***Correspondence:**
Jinxiong Shen
sjxiong@sohu.com
Shimin Zong
2018XH0090@hust.edu.cn
Hongjun Xiao
xhjent_whxh@hust.edu.cn

[†]*These authors share first authorship*

Specialty section:
This article was submitted to Head and Neck Cancer, a section of the journal Frontiers in Oncology

Received: *17 May 2021*
Accepted: *12 July 2021*
Published: *30 July 2021*

Citation:
Ming R, Wang E, Wei J, Shen J, Zong S and Xiao H (2021) The Prognostic Value of the DNA Repair Gene Signature in Head and Neck Squamous Cell Carcinoma. Front. Oncol. 11:710694. doi: 10.3389/fonc.2021.710694

INTRODUCTION

Head and neck squamous cell carcinoma (HNSCC) is a type of tumor that originates from the squamous epithelium of the head and neck areas, including the mucous membranes of the lips, tongue, pharynx, larynx, and others (1). HNSCC is currently one of the most common malignant tumors worldwide, with morbidity and mortality accounting for 3.6 and 3.4% of all malignant

tumors in 2020, respectively (2). HNSCC is highly malignant, and there are no specific prognostic-related biomarkers for clinical application. Therefore, prognostic-related biomarkers with clinical applicability are urgently required.

DNA damage and repair play important roles throughout the life of a cell (3). DNA damage affects the expression of a variety of genes, including proto-oncogenes and cancer suppressor genes. Changes in the activity of proto-oncogenes and cancer suppressor genes are crucial in tumorigenesis (4). Several DNA repair genes have been confirmed to play an important role in the development and prognosis of HNSCC (5–7). Hence, constructing a risk model composed of DNA repair genes may be useful for predicting the prognosis of patients with HNSCC.

In this study, we aimed to establish a prognostic prediction model for HNSCC based on DNA repair genes. We first equally divided all patients with HNSCC into training and testing sets. In the training set, we screened prognostic-related DNA repair genes using univariate proportional hazard (Cox) regression analysis and least absolute shrinkage and selection operator (LASSO) regression analysis to construct a risk model (8). All patients with HNSCC were classified into high- and low-risk groups according to the median value of the training set risk score. Subsequently, we verified the prognostic relevance and prognostic predictive ability of the risk model in the training and testing sets. We also analyzed the tumor-infiltrating immune cells, immune-related gene expression, tumor mutation burden, and drug sensitivity of patients with HNSCC in the high- and low-risk groups. The results showed that the risk model composed of DNA repair genes could effectively distinguish patients with different clinical outcomes and has independent predictive prognostic ability.

METHODS

Data Download

The transcriptome profiling (RNA-seq) data harmonized to fragments per kilobase million (FPKM), clinical information, and tumor mutations in patients with HNSCC were downloaded from the Cancer Genome Atlas (TCGA) database (https://portal.gdc.cancer.gov/) in March 2021 (9). The pathologic stages were reconfirmed according to the seventh edition of the American Joint Committee on Cancer staging system (10). The gene transfer format (GTF) files were downloaded from Ensembl (http://asia.ensembl.org) for annotation (11). Immune-related genes were downloaded from the Tracking Tumor Immunophenotype (http://biocc.hrbmu.edu.cn/TIP/index.jsp) (12). The gene list, containing 569 DNA repair genes, was downloaded from Gene Set Enrichment Analysis (GSEA), "GO_DNA REPAIR" gene set (http://www.gsea-msigdb.org/gsea/msigdb/cards/GOBP_DNA_REPAIR.html) (13, 14). After annotation by the GTF files, 545 DNA repair genes were eventually used for subsequent analyses. GSE41613 (15), GSE27020 (16), GSE117973 (17), and GSE65858 (18) datasets with transcriptome and clinical data of patients with HNSCC were downloaded from Gene Expression Omnibus (https://www.ncbi.nlm.nih.gov/geo/) for external validation.

Construction of Risk Model

To construct the risk model, we first combined the transcriptome data and clinical information of patients with HNSCC to obtain 499 samples with complete clinical information and transcriptome information, and then randomly divided them into a training set and a testing set on average. Subsequently, LASSO regression analysis was performed to further screen out 13 more representative DNA repair genes for use in constructing the risk model, and the correlation coefficients (*Coef*) and expression (*EXP*) of these 13 genes were obtained using the "glmnet" package in R (19). Finally, the risk score of each patient was calculated by the following formula: Risk Score = $\Sigma_{i=1}^{n}$ *Expi* × *Coefi*, where *n* refers to the number of selected DNA repair genes, *Expi* indicates the expression levels of gene *i* in each HNSCC sample, and *Coefi* is the correlation coefficient of gene *i*. Finally, we classified all HNSCC samples into high- and low-risk groups based on the median value of the risk score of the training set.

Validation of the Risk Model

We verified the risk model separately in the training and testing sets. To this end, we first performed principal component analysis (PCA) in the training and testing sets to evaluate the discrimination of the risk model for patients in the high- and low-risk groups. We then utilized heat maps to show the expression patterns of the DNA repair genes in the risk model in the training and testing sets. The Kaplan-Meier survival curve was used to distinguish the difference in the clinical outcome of patients in the high- and low-risk groups, and the significant difference *P*-value was calculated by the log-rank test. The area under the curve (AUC) of the receiver operating characteristic (ROC) curve was used to evaluate the prognostic diagnostic accuracy of the risk score and clinical characteristics. Univariate and multivariate Cox regression analyses of risk score and clinical characteristics were used to evaluate the independent correlation between the risk score and prognosis of patients with HNSCC. We also performed the above verification in all patients with HNSCC. Then we divided all samples into multiple clinical subgroups based on clinical characteristics, and the Kaplan-Meier survival curve was performed in each subgroup to demonstrate the good prognostic ability of the risk score.

Evaluation of the Tumor Immune Microenvironment and Immune-Related Gene Expression

Before analyzing the immune-infiltration situation using the CIBERSORT algorithm, which contains 22 types of immune cells, we first standardized the gene expression data through the "CIBERSORT" package in R (20). The Wilcoxon test was used to compare the different infiltrations of the 22 immune cells in the high- and low-risk groups. The Pearson test was used to analyze the correlation between risk genes and tumor-infiltrating immune cells through Statistical Product and Service Solutions 25.0 (SPSS 25.0) (21). The ESTIMATE (Estimation of STromal

and Immune cells in MAlignant Tumors using Expression data) algorithm was used to evaluate the immune score, stromal cell content, and ESTIMATE score of each sample (22). We analyzed the expression of negative regulatory immune genes in the high- and low-risk groups using the Wilcoxon test. Finally, as the research on the role of immune checkpoint genes in various tumors is increasing, we analyzed the correlation between these genes and risk scores using the Spearman test and analyzed their differences in expression in the high- and low-risk patients using the Wilcoxon test.

Assessment of Tumor Mutation Burden

We displayed the 30 genes with the highest mutation rate in all HNSCC samples and calculated the tumor mutation burden (TMB) of all samples through the "maftools" package in R (23). We then divided the HNSCC samples into high- and low-TMB groups according to the best cut-off value of the TMB of each sample. The Kaplan-Meier survival curve showed the clinical outcome of the two groups of patients with HNSCC. By combining the TMB groups and the risk groups, we further evaluated the impact of the risk score and tumor mutation burden on the clinical outcome of patients with HNSCC and displayed them with survival curves.

Online Website Verification

We verified the influence of the expression of the 13 DNA repair genes on the Oncolnc website (http://www.oncolnc.org).

Analysis of Drug Sensitivity

To evaluate the model in the clinical treatment of HNSCC, we calculated the half-inhibitory concentration (IC50) of chemotherapeutic drugs for HNSCC. The difference in the IC50 between the high- and low-risk groups was compared by Wilcoxon signed-rank test using the "pRRophetic" package in R (24).

Statistical Analysis

The significance level of the *P*-value was set to <0.05. All statistical analyses were performed using R 4.0.4 (https://www.r-project.org/).

RESULTS

Development and Validation of the Prognostic Model

The flowchart of this research is shown in **Figure 1**. After merging the transcriptome data and the clinical data of patients with HNSCC downloaded from TCGA, we obtained 499 samples with complete information. We then divided all HNSCC samples into a training set (n = 251) and a testing set (n = 248). The basic clinical information of the two groups of patients is shown in **Table 1**. Subsequently, we screened out 82 prognostic-related genes among 545 DNA repair genes through univariate Cox regression analysis (**Table S1**, $P < 0.05$), of which 21 were risk genes (hazard ratio > 1). Subsequently, we screened out a further 13 representative DNA repair genes through LASSO Cox regression analysis, which were used to construct the risk model. The risk score was calculated based on the sum of the product of the expression (*Exp*) of all genes in the model and its correlation coefficient (*Coef*). The formula of the risk score was as follow: Risk Score = MORF4L2 * (0.0037) + COPS2 * (0.0063) + USP10 * (0.0255) + WAS * (–0.0123) + UVSSA * (–0.1324) + PRRX1 * (–0.0148) + ZBTB1 * (–0.0632) + DCLRE1C * (–0.0502) + MSH5 * (–0.3824) + DOT1L * (–0.1573) + ZBTB7A * (–0.00610) + POLR2C * (0.0085) + MORF4L1 * (0.0047). A negative correlation coefficient indicated that the gene was a protective factor in patients with HNSCC. In contrary, the gene with a positive correlation coefficient was a risk factor.

After calculating the risk scores of all patients with HNSCC, we divided the training set and testing set samples into high- and low-risk groups according to the median value of the training set risk score, as shown in **Figures 2A, G**. We found that in both the training and testing sets, the proportion of patients with HNSCC who died in the high-risk group was higher than that in the low-risk group (**Figures 2B, C, H, I**). The high- and low-risk groups were well distinguished (**Figures 2D, J**). Moreover, the DNA repair genes in the risk model showed the same expression pattern in the training and testing sets (**Figures 2E, K**). The Kaplan-Meier survival curve showed that the clinical outcomes of patients in the low-risk group were better than those in the high-risk group (**Figure 2L**), both in the training set (P = 8.439e–09; **Figure 2F**) and the testing set (P = 1.161e-04; **Figure 2L**).

To verify the ability and independence of our model to predict the prognosis of patients with HNSCC, we conducted ROC curves and univariate and multivariate Cox regression analyses in the training and testing sets, respectively. The sensitivity and specificity of the risk score were assessed using the ROC curve. In the training set, the area under the curve (AUC) of the 1-, 3-, and 5-year ROC curves of the risk score were all >0.7 (**Figure 3A**). The risk score had the largest AUCs of the 3-year ROC curve, compared to the clinical traits of patients with HNSCC (**Figure 3B**). In the testing set, the AUCs of the 1-, 3-, and 5-year ROC curves were all >0.65 (**Figure 3E**), and the risk score also had the largest AUCs of the 3-year ROC curve (**Figure 3F**). The hazard ratio (HR) value of the risk score was the largest in the univariate and multivariate Cox regression analyses of the risk score and multiple clinical features, which showed that the risk score was an independent prognostic factor (**Figures 3C, D**). The independence of the risk score for predicting the prognosis of HNSCC was confirmed in the test set (**Figures 3G, H**). **Table S2** shows the univariate and multivariate Cox regression analyses of the training and testing sets. Overall, the risk score was an independent prognostic factor for HNSCC. We were unable to find an external validation dataset with transcripts of all risk genes. However, we still verified the predictive ability of other genes except MSH5 in patients with HNSCC in GSE41613. We found that despite the lack of MSH, patients with HNSCC in the low-risk group showed better clinical outcomes than those in the high-risk group in our model ($P < 0.05$), and the expression pattern of the remaining genes was consistent with the training

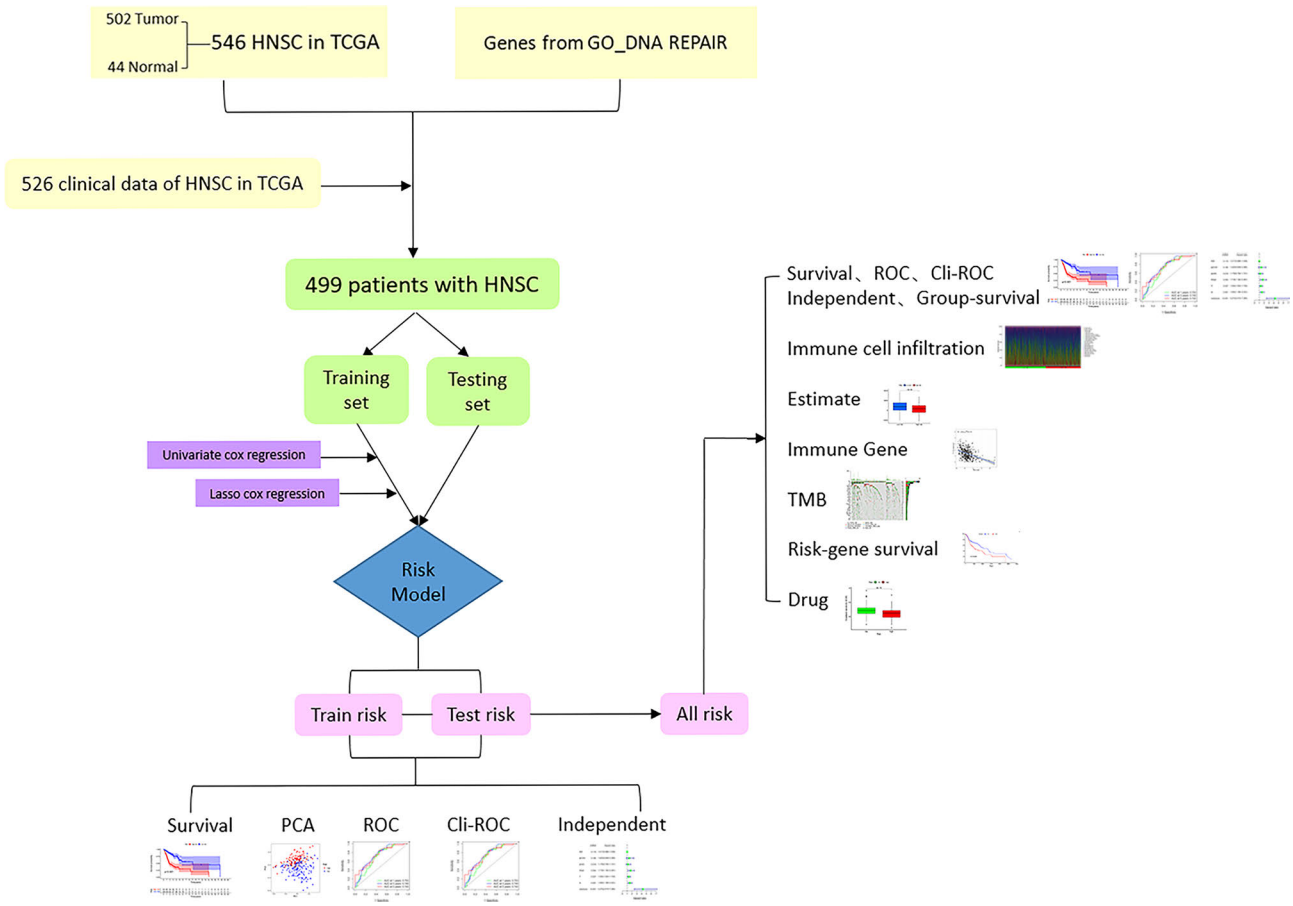

FIGURE 1 | Flowchart of this study.

TABLE 1 | Basic clinical information of training set and testing set.

Characteristics	Training set (n = 251)	Testing set (n = 248)
Age		
<=65	162	155
>65	89	93
Gender		
Female	70	63
Male	181	185
Stage		
Stage I-III	83	86
Stage IV	130	127
Unknown	36	35
Tumor		
T 1-2	85	87
T 3-4	136	134
Unknown	30	27
Lymph node		
N 0	84	83
N 1-3	122	118
Unknown	45	47

and testing sets (**Figure S1**). And we still verified in GSE117973 without transcript of UVSSA, GSE27020 without transcripts of MSH5 and UVSSA, and GSE65858 without transcripts of UVSSA and ZBTB1. The differences of prognosis of patients with HNSCC in the high- and low-risk groups were not significant ($P > 0.05$, **Figure S2**). For these external validation, we did a sensitivity analysis by using only 12 risk genes to recalculate the risk score. And we found that deleting every risk gene had little effect on the Kaplan-Meier survival curves (**Figures S3, S4**).

To further verify the accuracy of the model, we divided all samples into clinical subgroups based on different clinical traits, and we analyzed differences in the clinical outcomes of high- and low-risk samples in each clinical subgroup. Before clinical subgroup validation, we conducted a risk model validation for all samples. The Kaplan-Meier survival curve of all patients showed that the clinical outcomes of patients in the low-risk group were significantly better than those in the high-risk group ($P = 1.884e-11$; **Figure 4A**). The sensitivity and specificity of the risk scores of all HNSCC samples were assessed using the ROC curve. The AUCs of the ROC curves of risk score for 1-, 3-, and 5-year were all >0.65 (**Figure 4B**). The risk score had the largest AUCs of the ROC curves for 3-year compared to the clinical traits of patients with HNSCC (**Figure 4C**). PCA showed that patients in the high- and low-risk groups showed

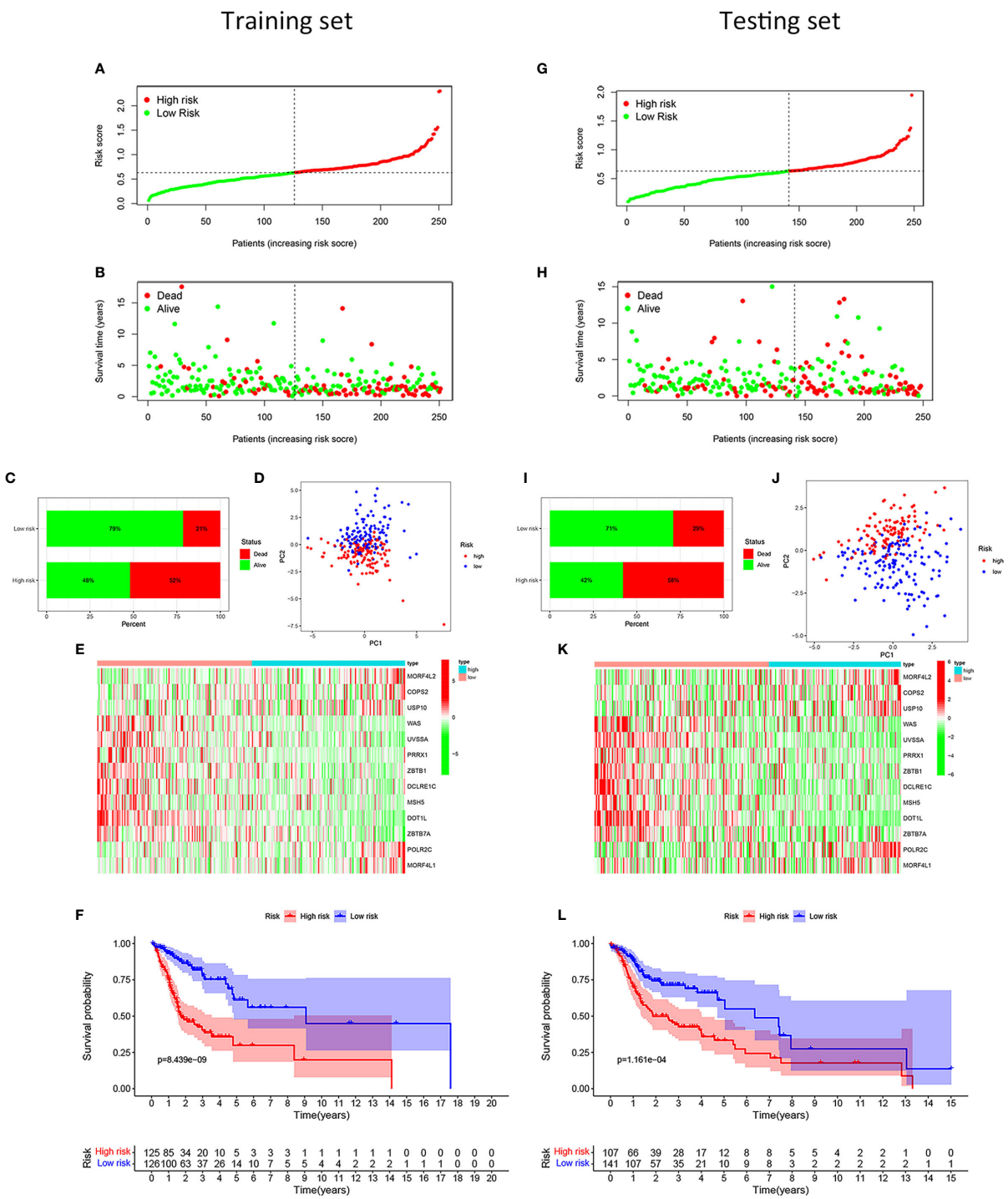

FIGURE 2 | Development and validation of the risk model for patients with HNSCC. Distribution of the HNSCC samples with different risk scores in the training set **(A)**. According to the median value, the HNSCC samples were divided into high- (red dot) and low-risk (green dot) groups. The distribution of survival status of HNSCC samples **(B)**. The red dot indicated dead status, and the green dot indicated alive status. Percentage of patients with HNSCC in alive or dead status **(C)**. The red bar meant dead status, and the green bar meant alive status. PCA of HNSCC samples **(D)**. The red dots indicated HNSCC samples in the high-risk group, while the blue dot meant low risk. Heat map depicting the expression patterns in the 13 DRGs between high- and low-risk groups **(E)**. Kaplan-Meier survival curve demonstrating the clinical outcome differences between high- and low-risk groups **(F)**. In the testing set, the distribution of the risk scores among all HNSCC samples **(G)**. The distribution of survival status of HNSCC samples **(H)**. Percentage of patients in survival status and death status **(I)**. PCA of HNSCC samples **(J)**. Heat map depicting the expression differences in the 13 DRGs between high- and low-risk groups **(K)**. Kaplan-Meier survival curve showing the clinical outcome differences between the two groups **(L)**.

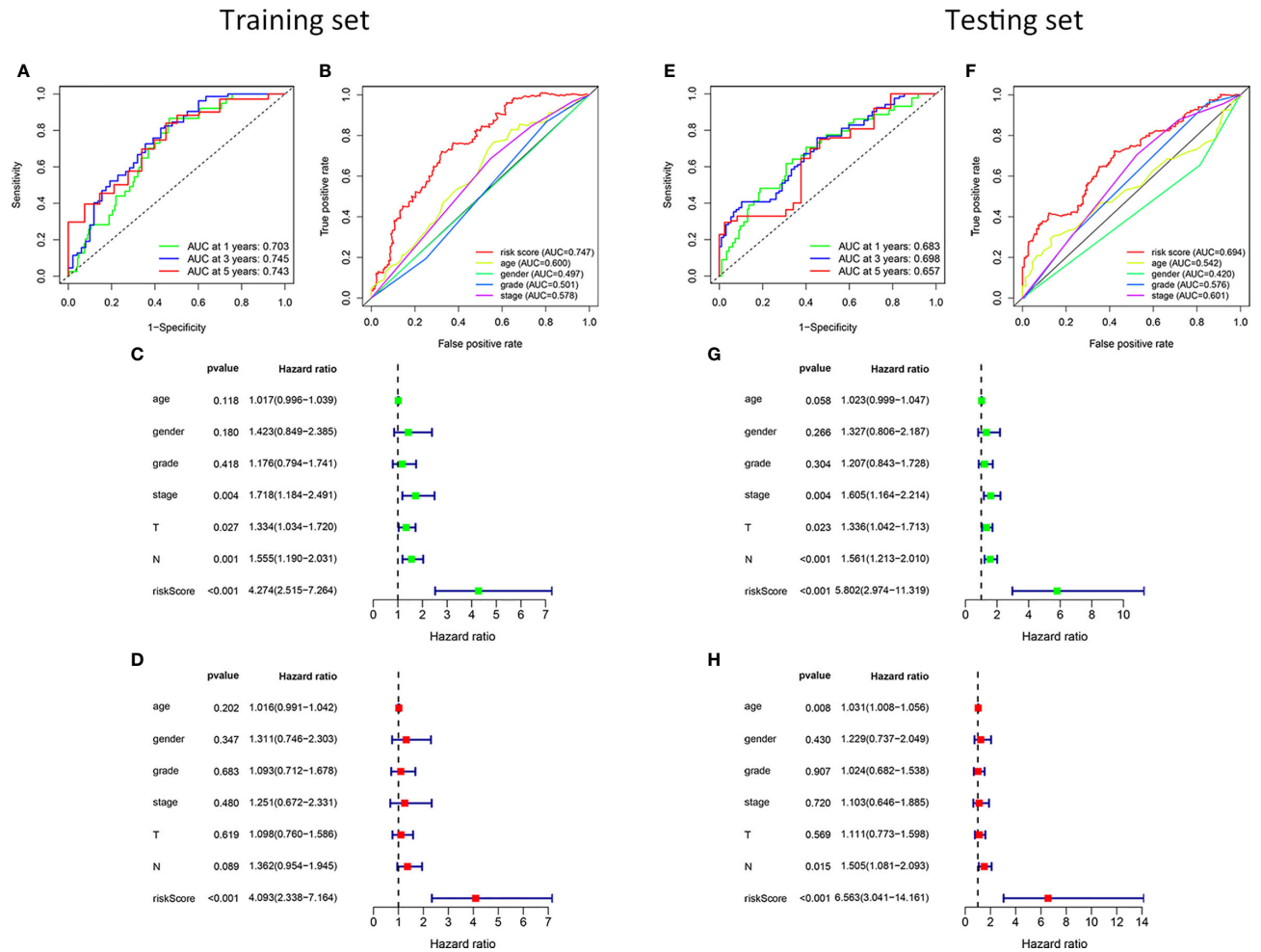

FIGURE 3 | Validation of the risk model. In the training set, the 1-, 3-, and 5-year ROC curves **(A)**. The ROC curves of clinicopathological characteristics and risk score for 3-year OS **(B)**. In the testing set, the ROC curves for 1-, 3-, and 5-year OS **(E)**. The ROC curves of clinicopathological characteristics and risk score for 3-year OS **(F)**. Univariate and multivariate Cox regression survival analysis was used to validate whether age, gender, grade, stage, T, N, and risk score could independently predict the clinical outcome of patients with HNSCC in the training **(C, D)** and testing sets **(G, H)**.

good discrimination (**Figure 4D**). The HR value of the risk score was the highest in the univariate and multivariate regression analyses of risk score and clinical characteristics (**Figures 4E, F**). Details of the univariate and multivariate Cox regression analyses of the training and testing sets are shown in **Table S3**. We divided all HNSCC samples into different clinical subgroups according to age, gender, stage, tumor (T), and lymph node (N) of patients with HNSCC. The clinical outcomes of patients in the low-risk group were significantly better than those in the high-risk group in all clinical subgroups, including those aged ≤65 years ($P < 0.001$, **Figure 4G**) and >65 years ($P < 0.001$, **Figure 4H**), male ($P < 0.001$, **Figure 4I**) and female ($P = 0.003$, **Figure 4J**), stage I-III (P = 0.007, **Figure 4K**), stage IV (P < 0.001, **Figure 4L**), T1-2 ($P < 0.001$, **Figure 4M**) and T3-4 ($P < 0.001$, **Figure 4N**), and N0 ($P = 0.011$, **Figure 4O**), and N1-3 ($P < 0.001$, **Figure 4P**).

Evaluation of the Immune Microenvironment and Expression of Immunoregulatory Genes

To reveal the differences in the immune microenvironment of high- and low-risk groups, including immune cell infiltration and expression of immunoregulatory and immune checkpoint genes, we first used the bioinformatics algorithm CIBERSORT to estimate 22 types of tumor-infiltrating immune cells in HNSCC. First, we found that among these 22 cell types, acquired immune-related immune cells infiltrated to a greater extent in HNSCC samples (**Figure 5A**). There were more naïve B cells ($P = 5.3e-05$, **Figure 5B**), resting mast cells ($P = 1.8e-06$, **Figure 5C**), T cells CD8 ($P = 0.0093$, **Figure 5D**), regulatory T cells (Tregs, $P = 6.7e-08$, **Figure 5E**), and follicular helper T cells ($P = 1.3e-05$, **Figure 5F**) in the low-risk group. In contrary, activated mast cells ($P = 0.00053$, **Figure 5G**), M0 macrophages ($P = 0.00026$,

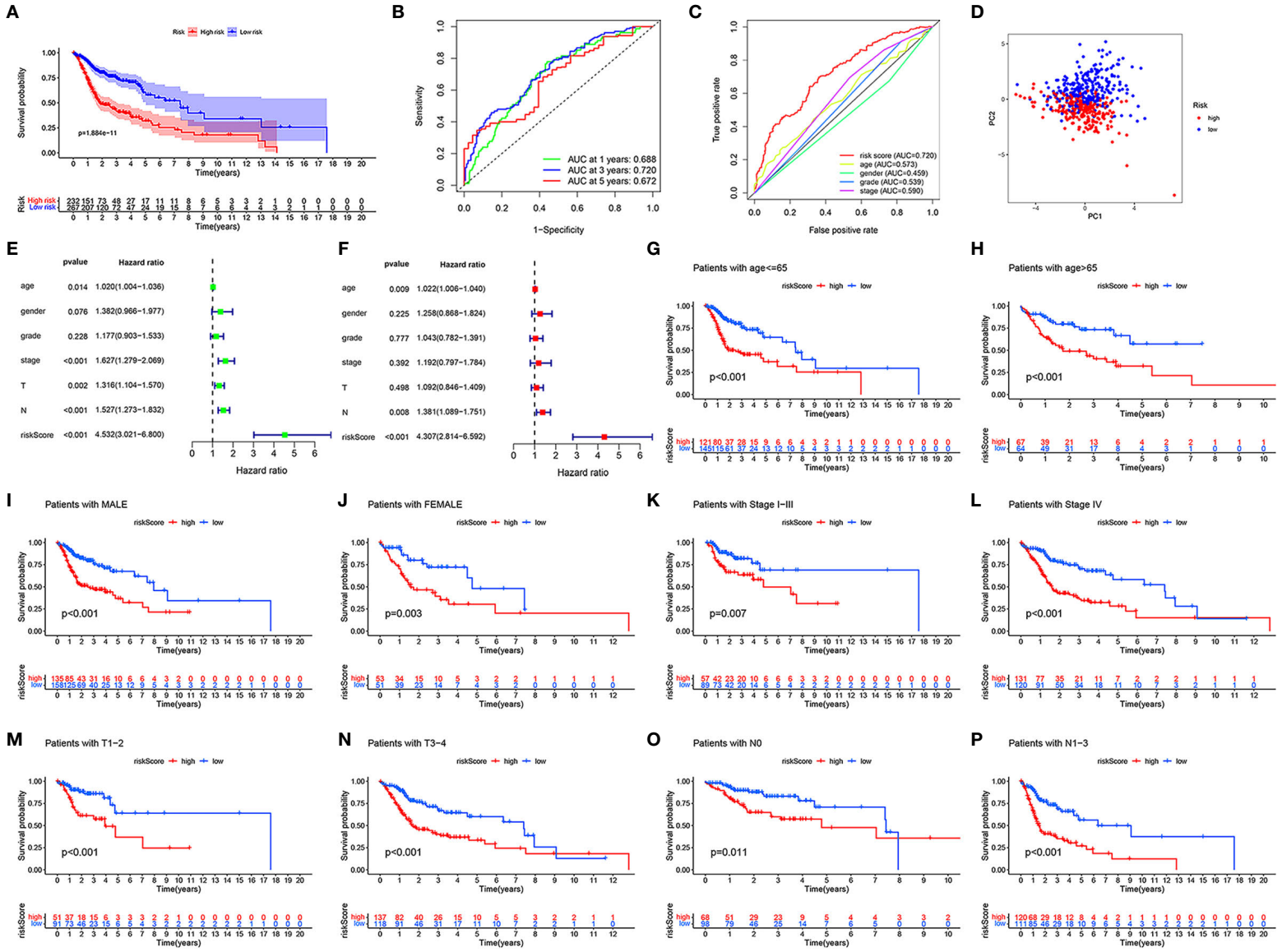

FIGURE 4 | Validation in different clinical traits subgroups. In all HNSCC samples, the Kaplan-Meier survival curve demonstrating the clinical outcome differences between the high- and low-risk groups **(A)**. The ROC curves for 1-, 3-, and 5-year OS **(B)**, ROC curves of clinicopathological characteristics and risk score **(C)** for 3-year OS. PCA of all HNSCC samples **(D)**. Univariate and multivariate Cox regression survival analysis validated whether age, gender, grade, stage, T, N, and risk score could independently predict the clinical outcomes of patients with HNSCC **(E, F)**. Kaplan-Meier curves showing the differences in prognosis between the high- and low- risk groups in different clinical subgroups, including ≤65 **(G)**, >65 **(H)**, male **(I)**, female **(J)**, stage I-III **(K)**, stage IV **(L)**, T1-2 **(M)**, T3-4 **(N)**, N0 **(O)**, and N1-3 **(P)**.

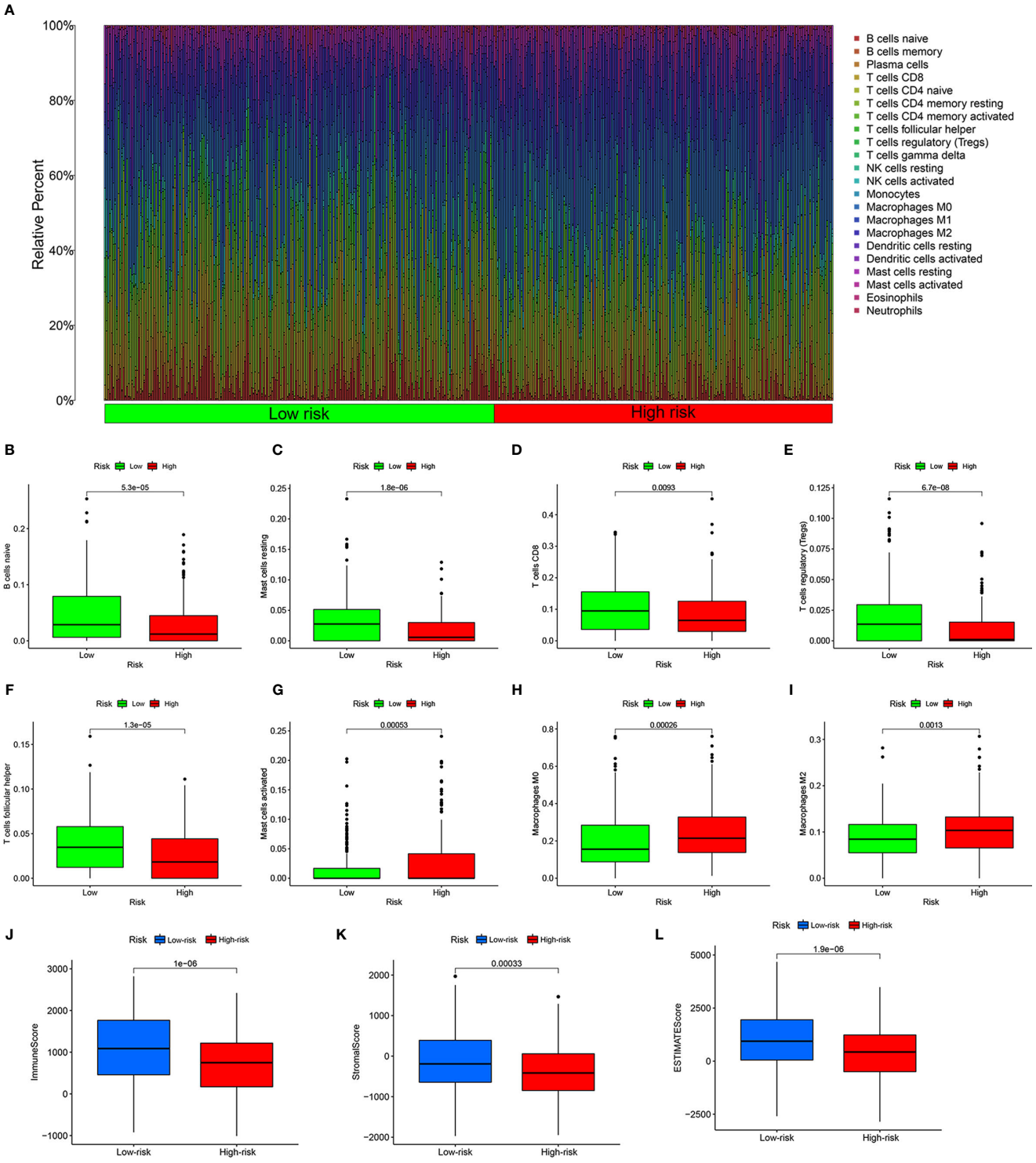

FIGURE 5 | Estimation of the immune microenvironment. **(A)** Relative percentage of 22 types of tumor-infiltrating immune cells from the CIRBERSORT. Greater infiltration of B cells naïve **(B)**, resting mast cells **(C)**, CD8 T cells **(D)**, regulatory T cells **(E)**, and follicular helper T cells **(F)** in the low-risk group, and more infiltrating activated mast cells **(G)**, M0 macrophages **(H)**, and M2 macrophages **(I)** in the high-risk group. Higher immune score **(J)**, stromal score **(K)**, and ESTIMATE score **(L)** calculated by ESTIMATE in the low-risk group.

Figure 5H), and M2 macrophages (P = 0.0013, **Figure 5I**) showed greater infiltration in the high-risk group. The HNSCC samples in the low-risk group had higher immune scores (P = 1e-06, **Figure 5J**), stromal scores (P = 0.00033, **Figure 5K**), and ESTIMATE scores (P = 1.9e-06, **Figure 5L**) evaluated by ESTIMATE than the high-risk group. In other words, the tumor purity of HNSCC was lower in the low-risk group. Naïve B cells were positively correlated with eight risk genes that had negative correlation coefficients and negatively correlated with MORF4L2, which had a positive correlation coefficient (P < 0.05). CD8+ T cells were positively correlated with five risk genes that had negative correlation coefficients and negatively correlated with eight risk genes that had negative correlation coefficients (P < 0.05). Tregs and follicular helper T cells were positively correlated with all risk genes that had negative correlation coefficients and negatively correlated with all risk genes that had positive correlation coefficients (P < 0.05). Monocytes and Macrophages M2 were negatively related to most risk genes (P < 0.05). Macrophages M0 were negatively correlated with some risk genes that had negative correlation coefficients and positively correlated with some risk genes that had positive correlation coefficients (P < 0.05). Details are shown in **Table S4**.

Next, we analyzed the relevant immune regulatory genes to further reveal the differences in the immune microenvironment of HNSCC in the high- and low-risk groups. Almost all negative immune regulatory genes in **Figure 6A** were highly expressed in the low-risk group, similar to CD4+ T cell and CD8+ T cell regulatory genes (**Figure 6B**). In addition, in recent years, immune checkpoint inhibitors have become increasingly common in the treatment of various tumors, including HNSCC. Therefore we investigated whether the risk model was related to immune checkpoint inhibitor-related biomarkers by Spearman correlation analysis, and we discovered that high risk scores were negatively correlated with the expression of CTLA4 (R = −0.34, P = 4.7e-15, **Figure 6C**), LAG3 (R = −0.28, P = 3e-10, **Figure 6D**), PD1 (R = −0.37, P < 2.2e-16, **Figure 6E**), PD-L1 (R = −0.16, P = 0.00051, **Figure 6F**), and TIM3 (R = −0.26, P = 7.4e-09, **Figure 6G**). A further Wilcoxon rank test also confirmed the expression pattern of CTLA4 (P = 4.8e-09, **Figure 6H**), LAG3 (P = 1.6e-06, **Figure 6I**), PD1 (P = 1.5e-11, **Figure 6J**), PD-L1 (P = 0.025, **Figure 6K**), and TIM3 (P = 6.2e-06, **Figure 6L**).

Assessment of Tumor Mutation Burden

To determine the tumor mutation burden (TMB), we first downloaded all the mutation data of HNSCC from TCGA and showed the top 30 mutation rate genes (**Figure 7A**). Subsequently, we identified the genes with the top 20 mutation rates in the high- and low-risk groups (**Figures 7B, C**). The tumor mutation rate of high-risk group samples was slightly higher than that of patients in the low-risk group, and the gene with the highest mutation rate in the high- and low-risk groups samples was TP53. According to the best cut-off point of TMB, all patients with HNSCC were divided into high- and low-TMB groups. The Kaplan-Meier survival curve showed that the clinical outcomes of patients with low TMB were significantly better than those of patients with high TMB (P = 0.003, **Figure 7D**). To further evaluate the influence of TMB and risk score on the prognosis of patients with HNSCC, we combined the TMB group with the risk group and analyzed the clinical outcomes of different groups using the Kaplan-Meier survival curve. The results showed that patients with low risk and low TMB had the best clinical outcome, followed by patients with low risk and high tumor mutation load, and that patients with high risk and high tumor mutation load had the worst clinical outcome (P < 0.001, **Figure 7E**). Considering the high mutation rate of TP53, we analyzed the correlation between TP53 and the risk score and its expression in the high- and low-risk groups. As a result, we found that TP53 was negatively correlated with the risk score (R = −0.31, P = 3.9e-12, **Figure 7F**) and was highly expressed in the low-risk group (P = 2.5e-05, **Figure 7G**).

Validation of the Website Oncolnc

We searched on the Oncolnc (http://www.oncolnc.org/) to verify the impact of high- and low-risk DRGs in the model on the prognosis of HNSCC and found that high-risk DRGs were correlated with poor prognosis and low-risk DRGs were associated with favorable patient prognosis. There were significant p-values for COPS2 (P = 0.000031, **Figure 8A**), DCLRE1C (P = 0.0051, **Figure 8B**), DOT1L (P = 0.0261, **Figure 8C**), UVSSA (P = 0.00589, **Figure 8D**), MORF4L2 (P = 0.00254, **Figure 8E**), POLR2C (P = 0.000262, **Figure 8F**), WAS (P = 0.0146, **Figure 8G**), ZBTB1 (P = 0.0153, **Figure 8H**), and USP10 (P = 0.0376, **Figure 8I**), whereas MORF4L1 (P = 0.088, **Figure 8J**), PRRX1 (P = 0.144, **Figure 8K**), ZBTB7A (P = 0.205, **Figure 8L**), and MSH5 (P = 0.391, **Figure 8M**) were not significant. The risk genes with negative correlation coefficients were also protective factors in the Oncolnc database.

Analysis of Drug Sensitivity

To evaluate the possible clinical application of the risk model, we analyzed the sensitivity difference of chemotherapy drugs for HNSCC in the current stage of clinical trials between the high- and low-risk groups, with the drug sensitivity expressed by IC50. We showed that patients in the high-risk group were more sensitive to erlotinib (P = 8.3e-16, **Figure 9A**), gefitinib (P = 0.00056, **Figure 9B**), paclitaxel (P = 2.9e-05, **Figure 9C**), docetaxel (P = 2e-10, **Figure 9D**), and sorafenib (P = 2.7e-05, **Figure 9E**), whereas patients in low-risk group were more sensitive to methotrexate (P = 6e-07, **Figure 9F**), vinorelbine (P = 8.3e-05, **Figure 9G**), and rapamycin (P = 0.00015, **Figure 9H**), which indicated that the model could be used as a potential predictor of chemotherapy sensitivity.

DISCUSSION

An increasing number of studies have shown that DNA damage and repair play important roles in malignant tumors, including HNSCC (25). DNA repair has been proven to be widely involved in the development, prognosis, and metastasis of HNSCC (26). Further studies on the expression profile of DNA repair genes in

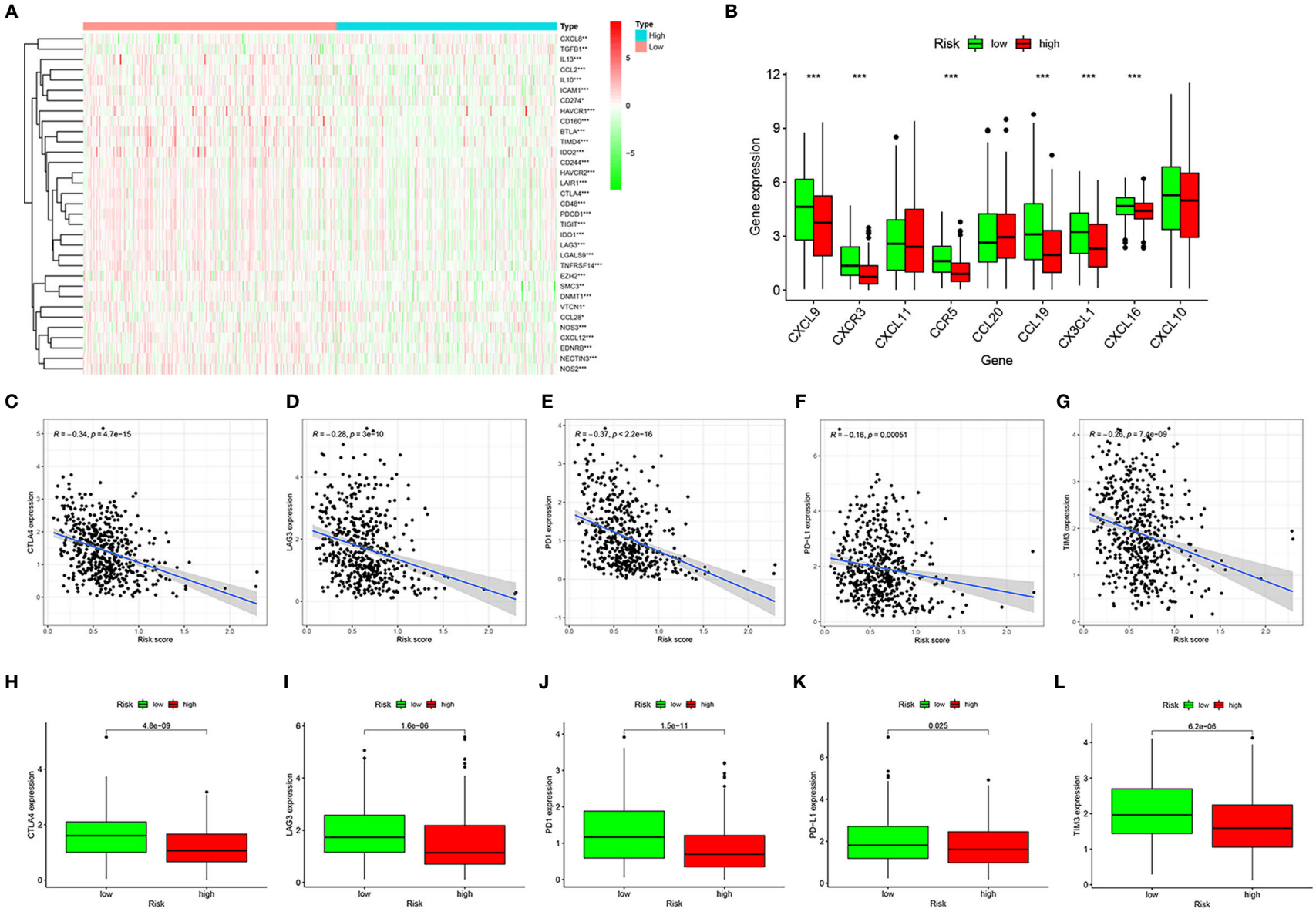

FIGURE 6 | Estimation of immune regulatory gene expression. Heatmap of negative immune regulatory gene expression **(A)**. Differential expression of CD4+ T cell and CD8+ T cell regulatory genes in the high- and low-risk groups **(B)**. Correlation between gene expression and risk scores of CTLA4 **(C)**, LAG3 **(D)**, PD1 **(E)**, PD-L1 **(F)**, and TIM3 **(G)**. Differential expression of CTLA4 **(H)**, LAG3 **(I)**, PD1 **(J)**, PD-L1 **(K)**, and TIM3 **(L)** genes in high- and low-risk groups. $^{*}P < 0.05$, $^{**}P < 0.01$, $^{***}P < 0.001$.

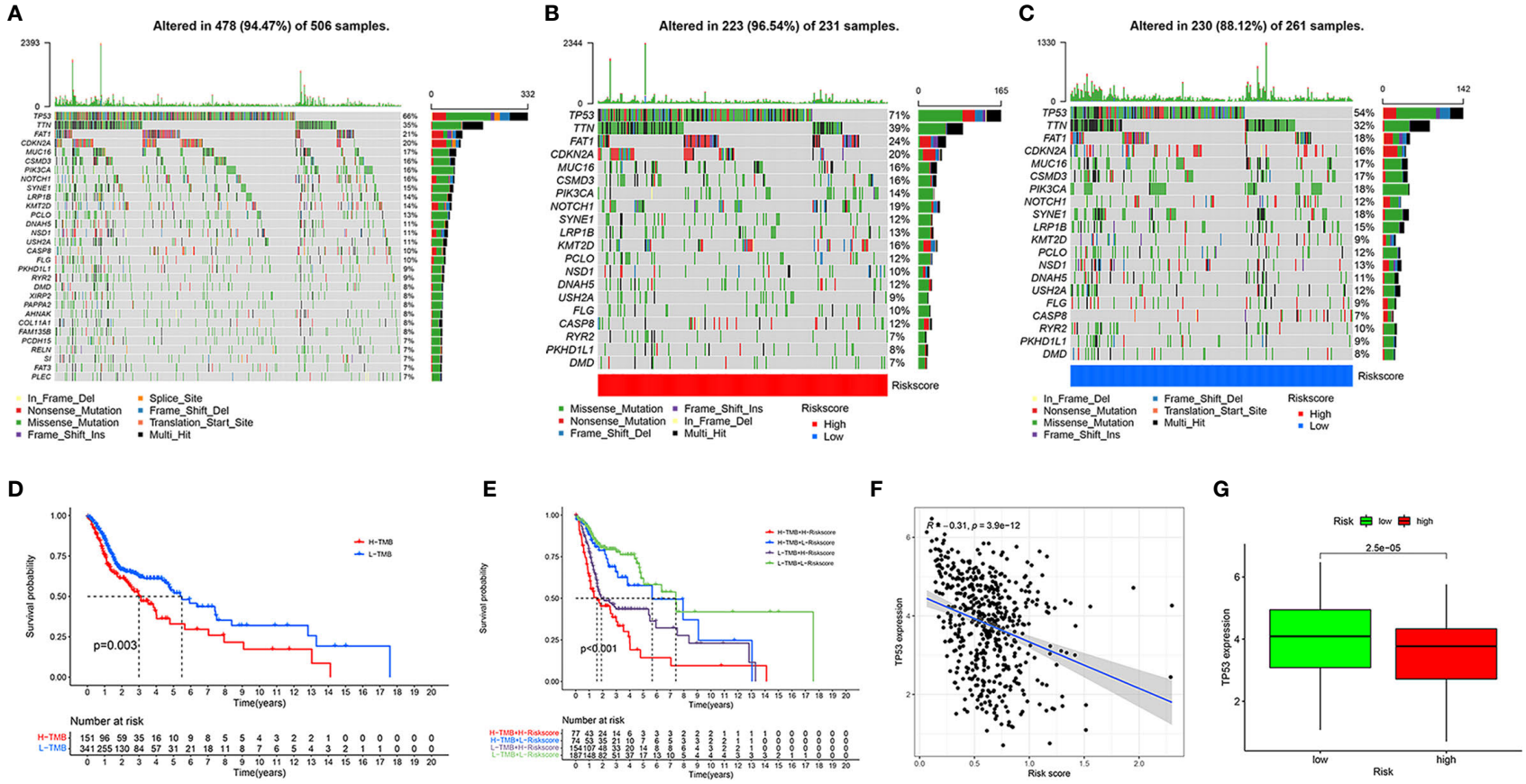

FIGURE 7 | Assessment of tumor mutation burden of HNSCC. Top 30 mutant genes of all HNSCC samples **(A)**. Top 20 mutant genes of high- **(B)** and low-risk **(C)** groups. Kaplan-Meier survival curve showing the OS differences between the high- and low-TMB groups **(D)**. Kaplan-Meier survival curve showing the OS differences in the four combinations of TMB and risk **(E)**. Correlation of TP53 expression and risk score **(F)**. Different expression of TP53 in high- and low-risk groups **(G)**.

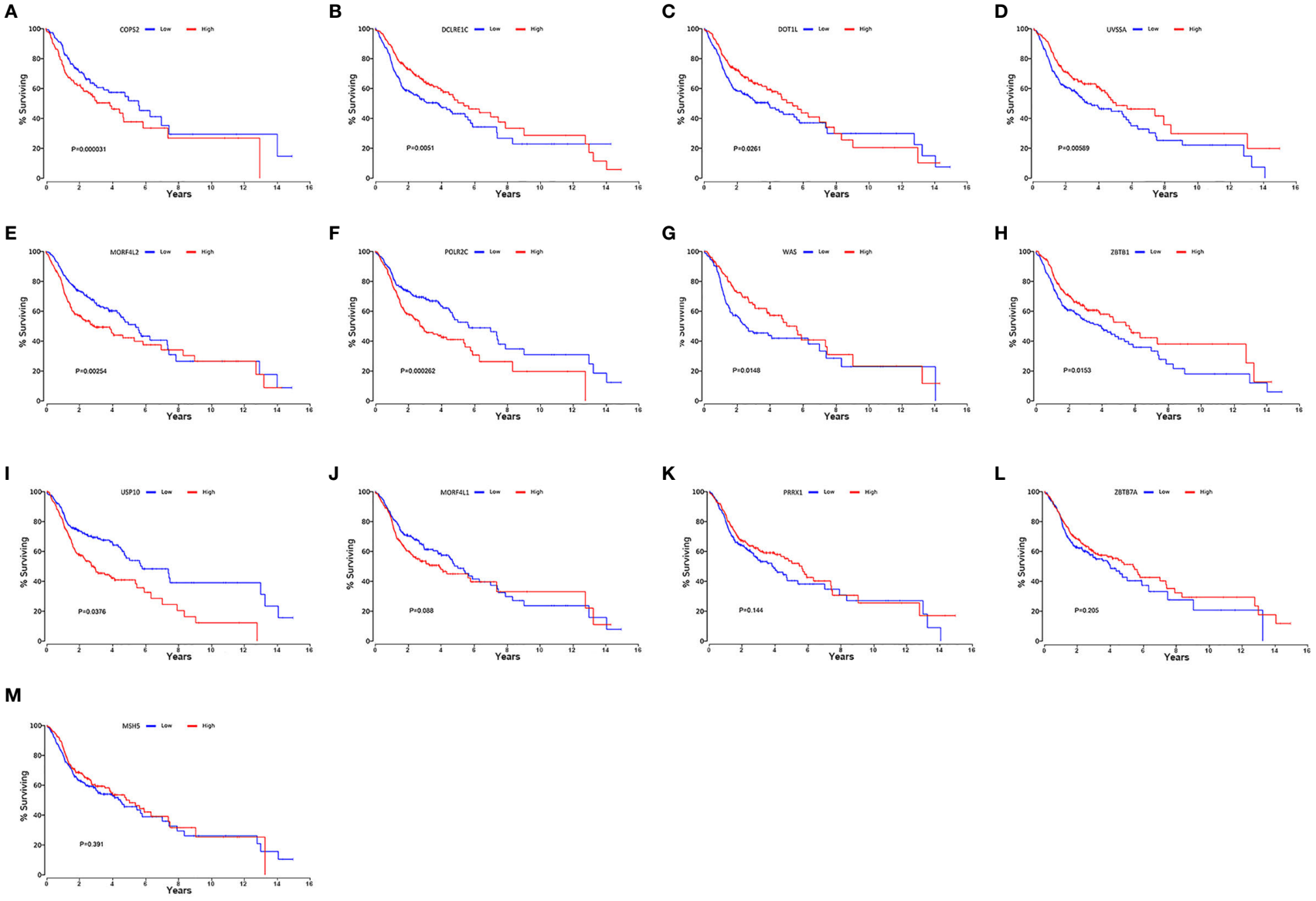

FIGURE 8 | Verification of online website Oncolnc. Kaplan-Meier survival curve from Oncolnc (http://www.oncolnc.org/) of COPS2 **(A)**, DCLRE1C **(B)**, DOT1L **(C)**, UVSSA **(D)**, MORF4L2 **(E)**, POLR2C **(F)**, WAS **(G)**, ZBTB1 **(H)** and USP10 **(I)**, MORF4L1 **(J)**, PRRX1 **(K)**, ZBTB7A **(L)**, and MSH5 **(M)** for HNSCC.

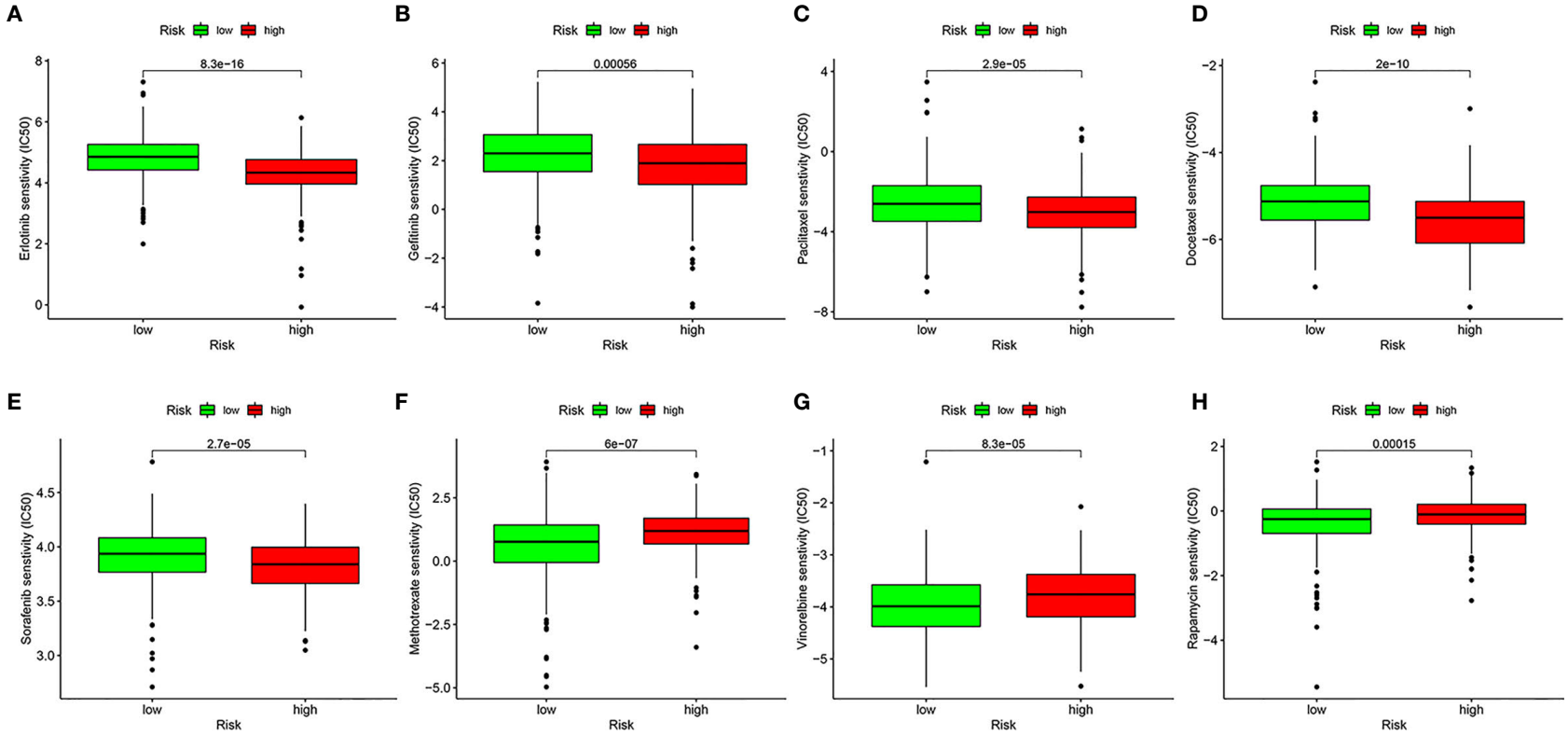

FIGURE 9 | Analysis of drug sensitivity. Difference in inhibitory centration (IC50) of Erlotinib **(A)**, Gefitinib **(B)**, Paclitaxel **(C)**, Docetaxel **(D)**, Sorafenib **(E)**, Methotrexate **(F)**, Vinorelbine **(G)**, and Rapamycin **(H)** for treatment of HNSCC in the high- and low-risk groups.

HNSCC specimens may provide new ideas to improve the clinical prognosis of patients.

A total of 545 DNA repair genes were obtained from the "GO_DNA REPAIR" gene set of the GSEA database for subsequent analysis. Through univariate and LASSO Cox regression analyses in the training set, we constructed a risk model that included 13 DNA repair genes. Patients in high-risk group had worse clinical outcomes than low-risk patients. The AUC of the ROC at 1-, 3-, and 5-year confirmed the good prediction performance of the risk score. In addition, prediction accuracy and independence were verified using univariate and multivariate Cox regression analyses. We also performed clinical subgroup validation in the internal dataset and further validated the model in the online database Oncolnc, which reflected good accuracy and repeatability of the risk model.

We illustrated the immune landscape of patients with HNSCC using CIBERSORT and ESTIMATE, including tumor-infiltrating immune cells, immune score, immune regulatory genes, and immune checkpoint genes, all of which are considered important in HNSCC (27). Comprehensive analysis revealed that the risk score was more negatively related to tumor-infiltrating cells such as naïve B cells, resting mast cells, CD8+ T cells, Tregs, and follicular helper T cells, and positively related to activated mast cells and macrophages. According to **Table S4**, the correlation between risk score and tumor-infiltrating immune cells was contributed by the influence of all risk genes on tumor-infiltrating immune cells. Tumor-infiltrating immune cells both correlated with eight gene transcripts that have a negative correlation coefficient and five gene transcripts having a positive correlation coefficient. In addition, patients in the low-risk group had higher immune scores, stromal scores, and ESTIMATE scores, which indicated that their tumor purity was lower.

In this study, some of the DRGs in the risk model have already been identified as having an important role in the immune system while others have not been well studied in the immune system at present. Decreasing the activity of DOT1L (DOT1 like histone lysine methyltransferase) through silencing or an inhibitor preferentially suppressed the production of interleukin 6 (IL-6) and interferon β (IFN-β) but not of tumor necrosis factor α (TNF-α) in macrophages triggered by Toll-like receptor (TLR) ligands or virus infection. DOT1L-mediated selective histone 3 lysine 79 (H3K79me2/3) modifications at the IL-6 and IFN-β1 promoters are required for the full activation of innate immune responses (28). DO1L plays an important role in regulating the differentiation and complete function of CD4+, CD8+T cells and B cells in the process of acquired immunity, while DO1L knockdown or mutation invalidates acquired immunity (29–32). ZBTB1 (zinc finger and BTB domain containing 1) prevents DNA damage in replicating immune progenitors, allowing the generation of B cells, T cells, and myeloid cells (33). In alveolar macrophages, antigen presentation was ZBTB7A (zinc finger and BTB domain containing 7A)-dependent where alveolar macrophages deficient in ZBTB7A failed to induce antibody production and T cell responses (34).

CD8+ T cell infiltration indicates better prognosis of patients with HNSCC (35). Because of the negative correlation between the risk score and tumor-infiltrating cells, we investigated the differential expression of negative immune regulatory genes, CD4+ T cell and CD8+ T cell regulatory genes in different groups. The results showed that almost all of these genes were highly expressed in the low-risk group, potentially due to increased infiltration of immune cells in the low-risk group samples. Subsequently, the correlation between the risk score and the expression of five immune checkpoint genes, CTLA4, LAG3, PD1, PD-L1, and TIM3, indicated that the expression of immune checkpoint genes was negatively correlated with the risk score and was highly expressed in the low-risk group, suggesting that immune checkpoint inhibitors may be beneficial to patients with HNSCC with low risk scores.

In recent years, there has been an increasing number of studies on the TMB of various tumors, including HNSCC, not only in the context of its use as a biomarker, but also in the treatment of immune checkpoint inhibitors (36). In our study, TMB was positively correlated with risk score and poorer clinical outcomes. Because TP53 showed the highest mutation rate, we compared its expression in different groups and found that it was negatively correlated with the risk score and highly expressed in the low-risk group. Our model suggested that patients with HNSCC with high risk scores were more sensitive to biological inhibitors such as erlotinib, gefitinib, and sorafenib, instead of chemotherapeutics like methotrexate. These analyses of drug sensitivity were based on "pRRophetic" package in R (20). Although the authenticity of the difference in drug sensitivity of these drugs among patients with HNSCC in different risk groups needs to be verified by further clinical trials, this model based on DNA repair genes provides the possibility for guiding clinical drug use. We speculated that the effect of immunotherapy on HNSCC would be better than that of traditional chemotherapy.

In this study, some of the DRGs in the process of modeling that have already been identified play an important role in the malignant phenotypes of various cancer types. DOT1L is involved in tumorigenesis and tumor metabolism or metastasis of ovarian cancer (37, 38), prostate cancer (39, 40), leukemia (41, 42), neuroblastoma (43), colorectal cancer (44), and breast cancer (45). PRRX1 (paired related homeobox 1), a homeodomain transcriptional factor, has been demonstrated to be important in pancreatic cancer, especially in the regulation of epithelial-to-mesenchymal transition (EMT) in pancreatic cancer (46–49). Moreover, UPS10 (ubiquitin-specific peptidase 10), a deubiquitinase, promotes proliferation of hepatocellular carcinoma by deubiquitinating and stabilizing YAP/TAZ, and suppresses lung tumorigenesis by deubiquitinating and stabilizing KLF4 (50, 51). ZBTB7A (zinc finger and BTB domain containing 7A) acts as a tumor suppressor through transcriptional repression in several carcinomas (52–54). Moreover, its mutation or downregulation promotes cancer progression (55, 56). Furthermore, its homologous gene, ZBTB1, participates in regulating the treatment effectiveness and resistance to chemotherapy (57, 58). At present, other DRGs in the model have not been studied in depth in tumors.

In general, the prognosis model constructed based on the DNA repair gene transcripts and clinical information of patients

with HNSCC in TCGA can well predict the prognosis of patients with HNSCC in the high- and low-risk groups. And this model systematically elaborated the molecular characteristics and immune microenvironment of HNSCC. The internal verification established based on the TCGA database also proved the stability of the model and provided reference value for prediction of the clinical outcomes of patients with HNSCC. In addition, the significant differences of multiple immune checkpoint genes between the high- and low-risk groups point out possible directions for the immunotherapy of patients with HNSCC.

However, we recognized that there were limitations to this study. On the one hand, the HNSCC samples involved in this study were not sufficient, and the DNA repair gene transcripts and clinical information of multiple GEO databases were incomplete, which hindered our external verification. On the other hand, the immaturity of the biobank of our institution was not enough to verify. Nevertheless, we still successfully completed external verification with the remaining genes in GSE41613 without MSH5 transcript, which further confirmed the availability and stability of the prognostic model. However, there were no significant differences in the Kaplan-Meier survival curves validated in the GSE117973 (without UVSSA), GSE27020 (without UVSSA and MSH5), and GSE65858 (without ZBTB1 and UVSSA). We assumed that the lack of a relatively important gene would reduce the predictive ability of the model, which might be the reason for the failure of the verification in GSE27020, GSE117973, and GSE65858.

CONCLUSION

In conclusion, this study constructed a 13-DRG signature for the prognosis of HNSCC, which could accurately and independently predict the clinical outcome of the patient. We then revealed the immune landscape, TMB, and sensitivity to chemotherapy drugs in different risk groups, which might be used to guide clinical treatment decisions.

DATA AVAILABILITY STATEMENT

Publicly available datasets were analyzed in this study. This data can be found here: https://portal.gdc.cancer.gov/

http://asia.ensembl.org

http://biocc.hrbmu.edu.cn/TIP/index.jsp http://www.gsea-msigdb.org/gsea/msigdb/cards/GOBP_DNA_REPAIR.html

http://www.oncolnc.org/

https://www.r-project.org/

https://www.ncbi.nlm.nih.gov/geo/.

AUTHOR CONTRIBUTIONS

RM and EW designed the study, performed the experiments and plotted the data. RM and JW validated the data. RM and EW drafted the manuscript. HX, SZ, and JS reviewed and edited the manuscript. HX and SZ supervised the project. HX and SZ funded the experiments for the study. All authors contributed to the article and approved the submitted version.

FUNDING

This study was supported by grants from the National Natural Science Foundation of China (Grant numbers 81771002, 82071057).

ACKNOWLEDGMENTS

The authors gratefully acknowledge the data generated by all public datasets utilized in this research. The authors are very thankful to all researchers for developing R package tools. The authors are very grateful to these authors for their selfless dedication to TCGA database and standardizing these data work from TCGA. The authors cherish these precious public database resources very much. We thank Editage (https://editage.com/frontiers/) for improving the English text of a draft of this manuscript.

SUPPLEMENTARY MATERIAL

The Supplementary Material for this article can be found online at: https://www.frontiersin.org/articles/10.3389/fonc.2021.710694/full#supplementary-material

REFERENCES

1. Puram SV, Rocco JW. Molecular Aspects of Head and Neck Cancer Therapy. *Hematol Oncol Clin North Am* (2015) 29(6):971–92. doi: 10.1016/j.hoc.2015.07.003
2. Bray F, Ferlay J, Soerjomataram I, Siegel RL, Torre LA, Jemal A. Global Cancer Statistics 2018: GLOBOCAN Estimates of Incidence and Mortality Worldwide for 36 Cancers in 185 Countries. *CA: A Cancer J Clin* (2018) 68 (6):394–424. doi: 10.3322/caac.21492
3. Lans H, Hoeijmakers JHJ, Vermeulen W, Marteijn JA. The DNA Damage Response to Transcription Stress. *Nat Rev Mol Cell Biol* (2019) 20(12):766–84. doi: 10.1038/s41580-019-0169-4
4. Stover EH, Konstantinopoulos PA, Matulonis UA, Swisher EM. Biomarkers of Response and Resistance to DNA Repair Targeted Therapies. *Clin Cancer Res* (2016) 22(23):5651–60. doi: 10.1158/1078-0432.Ccr-16-0247
5. Borchiellini D, Etienne-Grimaldi MC, Bensadoun RJ, Benezery K, Dassonville O, Poissonnet G, et al. Candidate Apoptotic and DNA Repair Gene Approach Confirms Involvement of ERCC1, ERCC5, TP53 and MDM2 in Radiation-Induced Toxicity in Head and Neck Cancer. *Oral Oncol* (2017) 67:70–6. doi: 10.1016/j.oraloncology.2017.02.003
6. Fan CY, Liu KL, Huang HY, Barnes EL, Swalsky PA, Bakker A, et al. Frequent Allelic Imbalance and Loss of Protein Expression of the DNA Repair Gene Hogg1 in Head and Neck Squamous Cell Carcinoma. *Lab Invest* (2001) 81 (10):1429–38. doi: 10.1038/labinvest.3780356

7. Lima LM, de Souza LR, da Silva TF, Pereira CS, Guimarães AL, de Paula AM, et al. DNA Repair Gene Excision Repair Cross Complementing-Group 1 (ERCC1) in Head and Neck Squamous Cell Carcinoma: Analysis of Methylation and Polymorphism (G19007A), Protein Expression and Association With Epidemiological and Clinicopathological Factors. *Histopathology* (2012) 60(3):489–96. doi: 10.1111/j.1365-2559.2011.04062.x
8. Tibshirani R. The Lasso Method for Variable Selection in the Cox Model. *Stat Med* (1997) 16(4):385–95. doi: 10.1002/(sici)1097-0258(19970228)16:4<385::aid-sim380>3.0.co;2-3
9. Mounir M, Lucchetta M, Silva TC, Olsen C, Bontempi G, Chen X, et al. New Functionalities in the TCGAbiolinks Package for the Study and Integration of Cancer Data From GDC and GTEx. *PLoS Comput Biol* (2019) 15(3): e1006701. doi: 10.1371/journal.pcbi.1006701
10. Edge SB, Compton CC. The American Joint Committee on Cancer: The 7th Edition of the AJCC Cancer Staging Manual and the Future of TNM. *Ann Surg Oncol* (2010) 17(6):1471–4. doi: 10.1245/s10434-010-0985-4
11. Howe KL, Achuthan P, Allen J, Allen J, Alvarez-Jarreta J, Amode MR, et al. Ensembl 2021. *Nucleic Acids Res* (2021) 49(D1):D884–d891. doi: 10.1093/nar/gkaa942
12. Xu L, Deng C, Pang B, Zhang X, Liu W, Liao G, et al. TIP: A Web Server for Resolving Tumor Immunophenotype Profiling. *Cancer Res* (2018) 78 (23):6575–80. doi: 10.1158/0008-5472.Can-18-0689
13. Blake JA, Dolan M, Drabkin H, Hill DP, Li N, Sitnikov D, et al. Gene Ontology Annotations and Resources. *Nucleic Acids Res* (2013) 49(Database issue): D530–5. doi: 10.1093/nar/gks1050
14. Reimand J, Isserlin R, Voisin V, Kucera M, Tannus-Lopes C, Rostamianfar A, et al. Pathway Enrichment Analysis and Visualization of Omics Data Using G: Profiler, GSEA, Cytoscape and EnrichmentMap. *Nat Protoc* (2019) 14(2):482–517. doi: 10.1038/s41596-018-0103-9
15. Lohavanichbutr P, Méndez E, Holsinger FC, Rue TC, Zhang Y, Houck J, et al. A 13-Gene Signature Prognostic of HPV-Negative OSCC: Discovery and External Validation. *Clin Cancer Res* (2013) 19(5):1197–203. doi: 10.1158/1078-0432.Ccr-12-2647
16. Fountzilas E, Kotoula V, Angouridakis N, Karasmanis I, Wirtz RM, Eleftheraki AG, et al. Identification and Validation of a Multigene Predictor of Recurrence in Primary Laryngeal Cancer. *PLoS One* (2013) 8(8):e70429. doi: 10.1371/journal.pone.0070429
17. Mock A, Plath M, Moratin J, Tapken MJ, Jäger D, Krauss J, et al. EGFR and PI3K Pathway Activities Might Guide Drug Repurposing in HPV-Negative Head and Neck Cancers. *Front Oncol* (2021) 11:678966. doi: 10.3389/fonc.2021.678966
18. Wichmann G, Rosolowski M, Krohn K, Kreuz M, Boehm A, Reiche A, et al. The Role of HPV RNA Transcription, Immune Response-Related Gene Expression and Disruptive TP53 Mutations in Diagnostic and Prognostic Profiling of Head and Neck Cancer. *Int J Cancer* (2015) 137(12):2846–57. doi: 10.1002/ijc.29649
19. Friedman J, Hastie T, Tibshirani R. Regularization Paths for Generalized Linear Models via Coordinate Descent. *J Stat Softw* (2010) 33(1):1–22. doi: 10.18637/jss.v033.i01
20. Newman AM, Liu CL, Green MR, Gentles AJ, Feng W, Xu Y, et al. Robust Enumeration of Cell Subsets From Tissue Expression Profiles. *Nat Methods* (2015) 12(5):453–7. doi: 10.1038/nmeth.3337
21. Weaver B, Wuensch KL. SPSS and SAS Programs for Comparing Pearson Correlations and OLS Regression Coefficients. *Behav Res Methods* (2013) 45 (3):880–95. doi: 10.3758/s13428-012-0289-7
22. Yoshihara K, Shahmoradgoli M, Martínez E, Vegesna R, Kim H, Torres-Garcia W, et al. Inferring Tumour Purity and Stromal and Immune Cell Admixture From Expression Data. *Nat Commun* (2013) 4:2612. doi: 10.1038/ncomms3612
23. Mayakonda A, Lin DC, Assenov Y, Plass C, Koeffler HP. Maftools: Efficient and Comprehensive Analysis of Somatic Variants in Cancer. *Genome Res* (2018) 28(11):1747–56. doi: 10.1101/gr.239244.118
24. Geeleher P, Cox N, Huang RS. Prrophetic: An R Package for Prediction of Clinical Chemotherapeutic Response From Tumor Gene Expression Levels. *PLoS One* (2014) 9(9):e107468. doi: 10.1371/journal.pone.0107468
25. Nickoloff JA, Jones D, Lee SH, Williamson EA, Hromas R. Drugging the Cancers Addicted to DNA Repair. *J Natl Cancer Inst* (2017) 109(11):djx059. doi: 10.1093/jnci/djx059
26. Moutafi M, Economopoulou P, Rimm D, Psyrri A. PARP Inhibitors in Head and Neck Cancer: Molecular Mechanisms, Preclinical and Clinical Data. *Oral Oncol* (2021) 117:105292. doi: 10.1016/j.oraloncology.2021.105292
27. Cillo AR, Kürten CHL, Tabib T, Qi Z, Onkar S, Wang T, et al. Immune Landscape of Viral- and Carcinogen-Driven Head and Neck Cancer. *Immunity* (2020) 52(1):183–99.e9. doi: 10.1016/j.immuni.2019.11.014
28. Chen X, Liu X, Zhang Y, Huai W, Zhou Q, Xu S, et al. Methyltransferase Dot1l Preferentially Promotes Innate IL-6 and IFN-β Production by Mediating H3K79me2/3 Methylation in Macrophages. *Cell Mol Immunol* (2020) 17 (1):76–84. doi: 10.1038/s41423-018-0170-4
29. Scheer S, Runting J, Bramhall M, Russ B, Zaini A, Ellemor J, et al. The Methyltransferase DOT1L Controls Activation and Lineage Integrity in CD4(+) T Cells During Infection and Inflammation. *Cell Rep* (2020) 33 (11):108505. doi: 10.1016/j.celrep.2020.108505
30. Kwesi-Maliepaard EM, Aslam MA, Alemdehy MF, van den Brand T, McLean C, Vlaming H, et al. The Histone Methyltransferase DOT1L Prevents Antigen-Independent Differentiation and Safeguards Epigenetic Identity of CD8(+) T Cells. *Proc Natl Acad Sci USA* (2020) 117(34):20706–16. doi: 10.1073/pnas.1920372117
31. Kealy L, Di Pietro A, Hailes L, Scheer S, Dalit L, Groom JR, et al. The Histone Methyltransferase DOT1L Is Essential for Humoral Immune Responses. *Cell Rep* (2020) 33(11):108504. doi: 10.1016/j.celrep.2020.108504
32. Aslam MA, Alemdehy MF, Kwesi-Maliepaard EM, Muhaimin FI, Caganova M, Pardieck IN, et al. Histone Methyltransferase DOT1L Controls State-Specific Identity During B Cell Differentiation. *EMBO Rep* (2021) 22(2): e51184. doi: 10.15252/embr.202051184
33. Cao X, Lu Y, Zhang X, Kovalovsky D. Zbtb1 Safeguards Genome Integrity and Prevents P53-Mediated Apoptosis in Proliferating Lymphoid Progenitors. *J Immunol* (2016) 197(4):1199–211. doi: 10.4049/jimmunol.1600013
34. Nayak DK, Zhou F, Xu M, Huang J, Tsuji M, Yu J, et al. Zbtb7a Induction in Alveolar Macrophages Is Implicated in Anti-HLA-Mediated Lung Allograft Rejection. *Sci Transl Med* (2017) 9(398):eaal1243. doi: 10.1126/scitranslmed.aal1243
35. Mandal R, Şenbabaoğlu Y, Desrichard A, Havel JJ, Dalin MG, Riaz N, et al. The Head and Neck Cancer Immune Landscape and its Immunotherapeutic Implications. *JCI Insight* (2016) 1(17):e89829. doi: 10.1172/jci.insight.89829
36. Chan TA, Yarchoan M, Jaffee E, Swanton C, Quezada SA, Stenzinger A, et al. Development of Tumor Mutation Burden as an Immunotherapy Biomarker: Utility for the Oncology Clinic. *Ann Oncol* (2019) 30(1):44–56. doi: 10.1093/annonc/mdy495
37. Zhang X, Liu D, Li M, Cao C, Wan D, Xi B, et al. Prognostic and Therapeutic Value of Disruptor of Telomeric Silencing-1-Like (DOT1L) Expression in Patients With Ovarian Cancer. *J Hematol Oncol* (2017) 10(1):29. doi: 10.1186/s13045-017-0400-8
38. Salvati A, Gigantino V, Nassa G, Giurato G, Alexandrova E, Rizzo F, et al. The Histone Methyltransferase DOT1L Is a Functional Component of Estrogen Receptor Alpha Signaling in Ovarian Cancer Cells. *Cancers (Basel)* (2019) 11(11):1720. doi: 10.3390/cancers11111720
39. Vatapalli R, Sagar V, Rodriguez Y, Zhao JC, Unno K, Pamarthy S, et al. Histone Methyltransferase DOT1L Coordinates AR and MYC Stability in Prostate Cancer. *Nat Commun* (2020) 11(1):4153. doi: 10.1038/s41467-020-18013-7
40. Thomas T. DOT1L in Prostate Cancer. *Nat Rev Urol* (2020) 17(10):544. doi: 10.1038/s41585-020-0374-0
41. Daigle SR, Olhava EJ, Therkelsen CA, Majer CR, Sneeringer CJ, Song J, et al. Selective Killing of Mixed Lineage Leukemia Cells by a Potent Small-Molecule DOT1L Inhibitor. *Cancer Cell* (2011) 20(1):53–65. doi: 10.1016/j.ccr.2011.06.009
42. Okada Y, Feng Q, Lin Y, Jiang Q, Li Y, Coffield VM, et al. Hdot1l Links Histone Methylation to Leukemogenesis. *Cell* (2005) 121(2):167–78. doi: 10.1016/j.cell.2005.02.020
43. Wong M, Tee AEL, Milazzo G, Bell JL, Poulos RC, Atmadibrata B, et al. The Histone Methyltransferase DOT1L Promotes Neuroblastoma by Regulating Gene Transcription. *Cancer Res* (2017) 77(9):2522–33. doi: 10.1158/0008-5472.Can-16-1663
44. Yang L, Lei Q, Li L, Yang J, Dong Z, Cui H. Silencing or Inhibition of H3K79 Methyltransferase DOT1L Induces Cell Cycle Arrest by Epigenetically Modulating C-Myc Expression in Colorectal Cancer. *Clin Epigenet* (2019) 11(1):199. doi: 10.1186/s13148-019-0778-y

45. Byun WS, Kim WK, Han HJ, Chung HJ, Jang K, Kim HS, et al. Targeting Histone Methyltransferase DOT1L by a Novel Psammaplin A Analog Inhibits Growth and Metastasis of Triple-Negative Breast Cancer. *Mol Ther Oncolytics* (2019) 15:140–52. doi: 10.1016/j.omto.2019.09.005
46. Takano S, Reichert M, Bakir B, Das KK, Nishida T, Miyazaki M, et al. Prrx1 Isoform Switching Regulates Pancreatic Cancer Invasion and Metastatic Colonization. *Genes Dev* (2016) 30(2):233–47. doi: 10.1101/gad.263327.115
47. Reichert M, Takano S, von Burstin J, Kim SB, Lee JS, Ihida-Stansbury K, et al. The Prrx1 Homeodomain Transcription Factor Plays a Central Role in Pancreatic Regeneration and Carcinogenesis. *Genes Dev* (2013) 27(3):288–300. doi: 10.1101/gad.204453.112
48. Marchand B, Pitarresi JR, Reichert M, Suzuki K, Laczkó D, Rustgi AK. PRRX1 Isoforms Cooperate With FOXM1 to Regulate the DNA Damage Response in Pancreatic Cancer Cells. *Oncogene* (2019) 38(22):4325–39. doi: 10.1038/s41388-019-0725-6
49. Feldmann K, Maurer C, Peschke K, Teller S, Schuck K, Steiger K, et al. Mesenchymal Plasticity Regulated by Prrx1 Drives Aggressive Pancreatic Cancer Biology. *Gastroenterology* (2021) 160(1):346–61.e24. doi: 10.1053/j.gastro.2020.09.010
50. Wang X, Xia S, Li H, Wang X, Li C, Chao Y, et al. The Deubiquitinase USP10 Regulates KLF4 Stability and Suppresses Lung Tumorigenesis. *Cell Death Differ* (2020) 27(6):1747–64. doi: 10.1038/s41418-019-0458-7
51. Zhu H, Yan F, Yuan T, Qian M, Zhou T, Dai X, et al. USP10 Promotes Proliferation of Hepatocellular Carcinoma by Deubiquitinating and Stabilizing YAP/TAZ. *Cancer Res* (2020) 80(11):2204–16. doi: 10.1158/0008-5472.Can-19-2388
52. Shi DB, Wang YW, Xing AY, Gao JW, Zhang H, Guo XY, et al. C/Ebpα-Induced miR-100 Expression Suppresses Tumor Metastasis and Growth by Targeting ZBTB7A in Gastric Cancer. *Cancer Lett* (2015) 369(2):376–85. doi: 10.1016/j.canlet.2015.08.029
53. Liu XS, Haines JE, Mehanna EK, Genet MD, Ben-Sahra I, Asara JM, et al. ZBTB7A Acts as a Tumor Suppressor Through the Transcriptional Repression of Glycolysis. *Genes Dev* (2014) 28(17):1917–28. doi: 10.1101/gad.245910.114
54. Han D, Chen S, Han W, Gao S, Owiredu JN, Li M, et al. ZBTB7A Mediates the Transcriptional Repression Activity of the Androgen Receptor in Prostate Cancer. *Cancer Res* (2019) 79(20):5260–71. doi: 10.1158/0008-5472.Can-19-0815
55. Liu XS, Liu Z, Gerarduzzi C, Choi DE, Ganapathy S, Pandolfi PP, et al. Somatic Human ZBTB7A Zinc Finger Mutations Promote Cancer Progression. *Oncogene* (2016) 35(23):3071–8. doi: 10.1038/onc.2015.371
56. Alam H, Li N, Dhar SS, Wu SJ, Lv J, Chen K, et al. Hp1γ Promotes Lung Adenocarcinoma by Downregulating the Transcription-Repressive Regulators NCOR2 and ZBTB7A. *Cancer Res* (2018) 78(14):3834–48. doi: 10.1158/0008-5472.Can-17-3571
57. Zhang P, Yang Y, Qian K, Li L, Zhang C, Fu X, et al. A Novel Tumor Suppressor ZBTB1 Regulates Tamoxifen Resistance and Aerobic Glycolysis Through Suppressing HER2 Expression in Breast Cancer. *J Biol Chem* (2020) 295(41):14140–52. doi: 10.1074/jbc.RA119.010759
58. Williams RT, Guarecuco R, Gates LA, Barrows D, Passarelli MC, Carey B, et al. ZBTB1 Regulates Asparagine Synthesis and Leukemia Cell Response to L-Asparaginase. *Cell Metab* (2020) 31(4):852–61.e6. doi: 10.1016/j.cmet.2020.03.008

Conflict of Interest: The authors declare that the research was conducted in the absence of any commercial or financial relationships that could be construed as a potential conflict of interest.

Publisher's Note: All claims expressed in this article are solely those of the authors and do not necessarily represent those of their affiliated organizations, or those of the publisher, the editors and the reviewers. Any product that may be evaluated in this article, or claim that may be made by its manufacturer, is not guaranteed or endorsed by the publisher.

frontiers in Oncology

SYSTEMATIC REVIEW
published: 19 August 2021
doi: 10.3389/fonc.2021.697369

Prognostic Role of EGFR/p-EGFR in Patients With Nasopharyngeal Carcinoma: A Meta-Analysis

Xishan Chen[1†], Renba Liang[2†], Lin Lai[2†], Kaihua Chen[3] and Xiaodong Zhu[2,3]*

[1] Department of Oncology, The Fourth Affiliated Hospital of Guangxi Medical University, Liuzhou, China, [2] Department of Oncology, Wuming Hospital of Guangxi Medical University, Nanning, China, [3] Department of Radiation Oncology, Guangxi Medical University Cancer Hospital, Nanning, China

Background: The prognostic value of epidermal growth factor receptor (EGFR)/phosphorylated EGFR (p-EGFR) expression in nasopharyngeal carcinoma remains controversial. A meta-analysis was performed to investigate prognostic significance of EGFR/p-EGFR expression in patients with nasopharyngeal carcinoma.

Methods: Literatures published before November 2020 were systematically searched in relevant databases, including PubMed, Web of Science, Embase, China National Knowledge Infrastructure (CNKI), and Wan fang databases. STATA 13 statistical software was used to analyze the pooled hazard ratio (HR) and 95% confidence interval (CI). Heterogeneity of the studies was examined by I^2. Sensitivity and subgroup analysis were performed to explore sources of heterogeneity. The potential publication bias was assessed using both Egger's and Begg's tests.

Results: A total of 20 literatures with 1545 patients were included for the meta-analysis. The meta-analysis results suggested that high expression of EGFR was significantly associated with poor overall survival (OS) (HR = 1.70, 95% CI: 1.24–3.15, P = 0.001) and disease-free survival (DFS) (HR = 2.58, 95% CI: 1.87–3.56, P = 0.000). However, it was not significantly associated with progression-free survival (PFS) (HR = 1.85, 95% CI: 0.90–3.82, P = 0.09) and distant metastasis-free survival (DMFS) (HR = 1.39, 95% CI: 0.73–2.67, P = 0.319). The subgroup analysis indicated that patients with EGFR high expression in studies of higher TNM stage (III–IV) ratio had significantly poor OS (HR = 2.27, 95% CI: 1.09–4.73, P = 0.03), but heterogeneity existed in studies (I^2 = 95.1%, P = 0.000). Sensitivity analyses revealed that EGFR expression did not significantly affect OS by an individual study solely, indicating there was inherent heterogeneity in OS cohorts. There was no significant heterogeneity among eight studies in the DFS cohorts (I^2 = 0%, P = 0.606). There was significant heterogeneity between EGFR expression and DMFS (I^2 = 82.8%, P = 0.000). Sub-group analysis in differentiated carcinoma demonstrated a smaller heterogeneity (I^2 = 33.2%). In addition, p-EGFR high expression had no significant correlation with OS (HR = 1.00, 95% CI: 0.88–1.14, P = 0.982) and DMFS (HR = 1.21, 95% CI: 0.96–1.52, P = 0.112). The heterogeneity

OPEN ACCESS

Edited by:
Heming Lu,
People's Hospital of Guangxi Zhuang Autonomous Region, China

Reviewed by:
Vito Carlo Alberto Caponio, University of Foggia, Italy
Li Rongqing, The First Affiliated Hospital of Kunming Medical University, China

****Correspondence:***
Xiaodong Zhu
zhuxdonggxmu@126.com

[†]These authors have contributed equally to this work

Specialty section:
This article was submitted to Head and Neck Cancer, a section of the journal Frontiers in Oncology

Received: *19 April 2021*
Accepted: *29 July 2021*
Published: *19 August 2021*

Citation:
Chen X, Liang R, Lai L, Chen K and Zhu X (2021) Prognostic Role of EGFR/p-EGFR in Patients With Nasopharyngeal Carcinoma: A Meta-Analysis. Front. Oncol. 11:697369. doi: 10.3389/fonc.2021.697369

among p-EGFR and OS studies was small (I^2 = 21%, P = 0.26). There was no significant heterogeneity in the DMFS cohorts (I^2 = 0%, P = 0.497).

Conclusion: EGFR high-expression was significantly associated with poor OS and DFS, which may serve as a prognostic predictor for nasopharyngeal cancer.

Systematic Review Registration: [https://www.crd.york.ac.uk/PROSPERO], identifier [number CRD42021258457].

Keywords: EGFR, nasopharyngeal carcinoma, meta-analysis, prognosis, p-EGFR

INTRODUCTION

Nasopharyngeal carcinoma (NPC) is a malignancy that arises from the epithelium of nasopharynx, having obvious regional characteristics and high incidence in China and southeast Asia (1). According to national cancer registry data in China, the incidence and mortality of NPC in Guangxi province rank first (2). Currently, the clinical TNM staging system is the principal prognostic indicator for NPC (3). However, clinical outcomes are different among patients with the same TNM stage (4). It seems that TNM stage alone is insufficient to predict individual clinical outcome. Several studies have shown that varied biological behavior and different prognosis was presented in the NPC patients with the same classification (5–7). Therefore, a reliable prognostic biomarker is necessary to improve individualized patient treatment and predict outcomes.

EGFR, belonging to the receptor tyrosine kinase family, plays an important role in regulation of proliferation and survival of tumor cells (8, 9). After ligand binding, EGFR is activated and forms homodimers or heterodimers, resulting in the phosphorylation and activation of multiple downstream signaling pathways, such as cellular differentiation, proliferation, and carcinogenesis (10, 11). Studies have demonstrated that EGFR is frequently overexpressed in NPC (12, 13). However, the relationship between EGFR expression and prognosis remains controversial. Several researches reported that high expression of EGFR was associated with poor prognosis (14–16), while other studies found no association between EGFR and prognostic value in NPC patients (17–19). Differences in study population's characteristics and cutoff values may explain the discrepancies among different studies.

Phosphorylated-EGFR (p-EGFR) may be more predictive of patient outcome. Recent studies demonstrated that p-EGFR high-expression was associated with poorer prognosis in patients with sarcoma (20) and non-small cell lung cancer (21). In addition, some studies found that p-EGFR high-expression was closely related to nasopharyngeal cancer development (22, 23). Hence, we performed this updated meta-analysis to evaluate prognostic significance of EGFR/p-EGFR expression in patients with NPC.

MATERIALS AND METHODS

Search Strategy

This meta-analysis was reported according to the Preferred Reporting Items for Systematic Reviews and Meta-Analyses (PRISMA) Statement and was registered at International Prospective Register of Systematic Reviews (number CRD42021258457). PubMed, Embase, Web of Science, CNKI, and Wan Fang Data were searched to identify relevant studies which were published before November 2020. The following words in English were used for retrieval of relevant studies: (((((((EGFR) OR EGFR transcription factor) OR (epidermal growth factor receptor)) OR EGFR protein) OR pEGFR) OR phospho-EGFR) OR (phosphorylated signal epidermal growth factor receptor)) OR phosphorylated EGFR transcription factor) OR protein EGFR OR (erbB1)) OR (HER1) AND (((NPC) OR (nasopharyngeal carcinoma)) OR (nasopharyngeal neoplasm)) OR (nasopharyngeal cancer). In addition, the following words in Chinese were searched for relevant studies: nasopharyngeal cancer, EGFR, and phospho-EGFR.

Inclusion Criteria

The following inclusion criteria were used in this study. (1) The tissue samples were from clinically diagnosed nasopharyngeal cancer patients. (2) Immunohistochemical (IHC) assay was performed to examine EGFR/p-EGFR expression. (3) HR and 95% CI was used to evaluate the association between EGFR/p-EGFR overexpression and survival time, or Kaplan-Meier (K-M) curves were used to estimate survival time. (4) When the results were reported in multiple publications, the most complete and recently reported data was extracted.

Exclusion Criteria

The exclusion criteria were as follows: (1) recurrent or metastatic NPC tissue samples, (2) unable to obtain HR and 95% CI date or K-M curves or insufficient data, (3) the results collected from NPC cell lines or animal experiments, and (4) literatures published as letters, reviews, conference abstracts, case reports, or expert consensus.

Data Collection

All articles were independently screened by the two investigators, and those studies not meeting the inclusion criteria were excluded. Any discrepancy was discussed and resolved by seeking opinions from a third party. The content of data extraction includes the following: (1) general information: first author, publication year, country, or region; (2) basic characteristics of studies: types of researches, number of patients, study size, patients' mean age, follow-up time, detection method, ICH cutoff value, histological differentiation, TNM stage (I–II *vs.* III–IV), etc.; (3) primary data: HR and 95% CI of survival outcomes, including overall survival (OS) and/or disease-free survival (DFS)/progression-free survival (PFS)/distant metastasis-free survival (DMFS). The HRs and its

95% CI were extracted from the text indirectly or calculated from the K-M survival curve using Engauge Digitizer (version 12.2.1).

Quality Assessment

Quality assessment was performed by two investigators separately according to the method of Hayden et al. (24) and the Reporting Recommendations for Tumor Marker Prognostic Studies (REMARK) (25), as previously reported by Almangush et al. (26). A score ≥10 was considered to indicate high quality articles.

STATISTICAL ANALYSIS

HRs with 95% CI were used to evaluate the correlation of EGFR/p-EGFR high expression with the survival time of NPC patients. Meta-analysis was performed using Stata software (version 13.0). Heterogeneity among studies was assessed with the Cochran Q test and I^2 test. The fixed effects model was used if there was no heterogeneity among studies (P ≥0.1, I^2 < 50% in heterogeneity test). Otherwise, it was considered to have significant heterogeneity (P<0.1, I^2 ≥ 50% in heterogeneity test), the random effect model was used, and the source of heterogeneity was explored using subgroup analysis or sensitivity analysis. The potential publication bias was evaluated using both Egger's and Begg's tests, and P > 0.05 was considered to have no publication bias.

RESULTS

Literature Search Results, Characteristics and Quality Assessment of Included Studies

A total of 1286 studies were identified, among which 680 articles were published in English and 606 in Chinese. After initial screening, 1211 studies were excluded, and 75 trials were retrieved for detailed assessment. After full-text screening, 20 studies with 1545 patients were eligible and included for our systematic review (12, 14–19, 22, 23, 27–35), of which three studies were published in Chinese and the others in English. These eligible studies were published from 2002 to 2019, and 19 of which were on EGFR and 3 on p-EGFR. The literature search flow is shown in **Figure 1**. The basic characteristics and quality assessment of the included studies are shown in **Tables 1** and **2**.

Meta-Analysis Between EGFR/p-EGFR Expression and Prognosis

EGFR/p-EGFR Expression and OS

We observed a high degree of heterogeneity among the 17 studies reporting EGFR and OS (I^2 = 92%, P = 0. 006). Despite this, the pooled HR indicated a significantly shorter OS in patients with higher expression of EGFR (HR = 1.70, 95% CI: 1.24–2.35, P = 0.001) (**Figure 2A**). For all three studies about p-EGFR and OS, the pooled HR was 1.00 (95% CI: 0.88–1.14, P = 0.982),

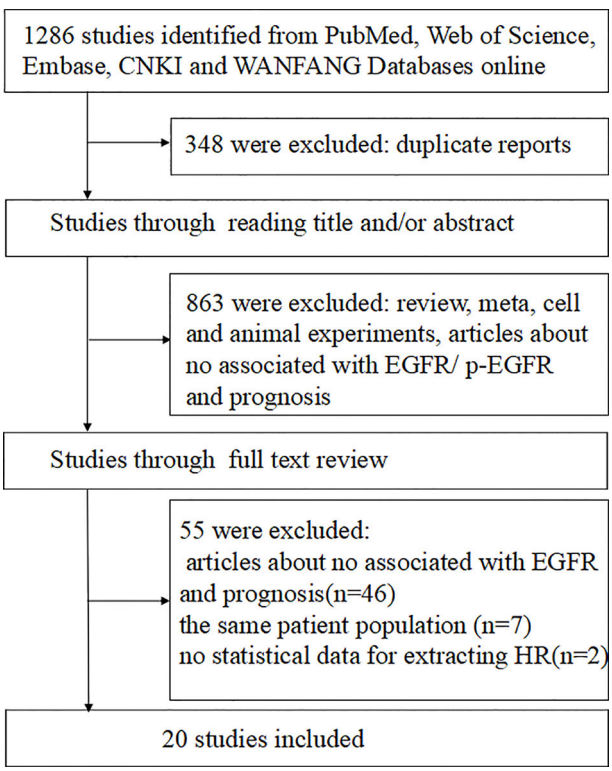

FIGURE 1 | Flow chart of studies selection procedure.

TABLE 1 | Characteristics of included studies.

Author	Year	Type	Country	Study type	N	Age	Follo-up	Detection method	Histological differentiation (C *vs.* UC)	Clinical stage (I–II *vs.* III– IV)	Clinical outcome	EGFR effect	Treatment	Quality score
Fujii et al. (17)	2002	EGFR	Japan	RE	53	49	90.9m	IHC	45,8	24,29	DFS	NS	NACT+RT	9
Ma et al. (22)	2003	EGFR	China (Hong Kong)	PR	78	48	46m	IHC	0,78	29,49	OS DFS	S S	CCRT/RT	10
Chua et al. (27)	2004	EGFR	China (Hong Kong)	RE	54	NA	52m	IHC	0,54	23,31	DFS DMFS	S S	NACT+ RT	10
Leong et al. (28)	2004	EGFR	Singapore	PR	75	46	28.6m	IHC	0,75	26,49	OS DFS	NS NS	NA	8
Wang et al. (29)	2006	EGFR	China	RE	55	NA	NA	IHC	NA	7,48	OS	S	RT	7
Fang et al. (18)	2007	EGFR	China (Taiwan)	RE	30	17	NA	IHC	13,17	11,19	OS DFS	NS NS	CCRT/RT+-AC	8
Yuan et al. (23)	2008	EGFR	China	RE	110	47	65m	IHC	110,0	27,83	OS DMFS	NS NS	CCRT/RT+-NAC	7
	2008	p-EGFR	China	RE	110	47	65m	IHC	110,0	27,83	OS DMFS	NS S	CCRT/RT+-NAC	7
Yuan et al. (36)	2008	EGFR	China	RE	75	45	NA	IHC	75,0	24,51	OS	S	NA	8
Taheri-Kadkhoda et al. (14)	2009	EGFR	Sweden	RE	45	56	96m	IHC	NA	12,33	OS DFS DMFS	S S	NACT+-AC+ERBT	10
Huang et al. (12)	2010	EGFR	China (Taiwan)	RE	170	46	68m	IHC	76,94	71,99	OS DMFS	NS NS	CCRT/RT	10
	2010	p-EGFR	China (Taiwan)	RE	170	46	68m	IHC	76,94	71,99	OS DMFS	NS NS	CCRT/RT	10
Qi (33)	2010	EGFR	China	RE	55	45	60m	IHC	55,0	13,42	OS	NS	NACT+-CCRT/CCRT/ RT	8
Kim et al. (30)	2010	EGFR	Korea	RE	38	48	30m	IHC	7,31	6,32	OS PFS	NS NS	NA	10
Kim et al. (19)	2010	EGFR	Korea	RE	69	50	54m	IHC	9,60	17,52	OS	NS	CCRT/ICRT/RT	10
Cao et al. (15)	2011	EGFR	China	RE	127	45	60m	IHC	NA	0,127	OS DFS	S S	IC+CCRT	8
Pan et al. (16)	2013	EGFR	China	RE	111	46	NA	IHC	NA	41,70	OS DFS DMFS	S S	CCRT/RT	9
Zhang et al. (37)	2014	EGFR	China	RE	96	49	NA	IHC	NA	45,51	OS	S	CCRT/ICRT+-AC	9
Wu (34)	2015	p-EGFR	China	RE	107	50	31m	IHC	0,107	12,95	OS PFS	NS NS	ICRT/CCRT	9
Kang et al. (31)	2016	EGFR	Korea	RE	46	60	52m	IHC	NA	20,26	OS	NS	CCRT/RT	10
Mao et al. (32)	2019	EGFR	China	RE	31	44	NA	IHC	NA	3,28	OS	S	CCRT/ICRT+-AC, CTX	9
Wang et al. (35)	2019	EGFR	China	RE	120	55	43m	IHC	16,104	40,80	OS PFS	S S	CCRT/ICRT+-AC	8

RE, retrospective; PR, prospective; N, number of patients; NA, not available; S, significant (identifying EGFR/p-EGFR high-expression as a poor prognostic factor); NS, not significant; IRS, immunoreactive score; IC, induction chemotherapy; NACT, ICRT, induction chemotherapy followed by radiation Therapy; neoadjuvant chemotherapy; CCRT, concurrent chemoradiotherapy; AC, adjuvant chemotherapy; RT, radiotherapy; ERBT, external beam radiotherapy; CTX, cetuximab.

TABLE 2 | Included studies were evaluated according to the REMARK guidelines.

Author (year)	Samples	Clinical data	Immunohistochemistry	Prognostication	Statistics	Classical Prognostic Factors
Fujii et al. (17)	A	A	A	I	I	A
Ma et al. (22)	A	A	A	A	I	A
Chua et al. (27)	A	A	A	I	A	I
Leong et al. (28)	A	A	A	A	I	I
Wang et al. (29)	I	A	A	I	I	I
Fang et al. (18)	A	A	A	A	A	A
Yuan et al. (23)	I	A	A	I	A	A
Yuan et al. (23)	I	A	A	I	I	I
Taheri-Kadkhoda et al. (14)	A	A	A	I	I	A
Huang et al. (12)	A	A	A	A	A	A
Qi (33)	I	A	A	A	A	I
Kim YJ et al. (30)	I	A	A	A	I	I
Kim TJ et al. (19)	I	A	A	A	A	A
Cao XJ et al. (15)	A	A	A	A	A	A
Pan et al. (16)	I	A	A	A	A	A
Zhang et al. (37)	A	A	A	I	I	I
Wu (34)	I	A	A	I	I	I
Kang et al. (31)	I	A	A	I	A	A
Mao et al. (32)	A	A	A	A	A	A
Wang et al. (35)	I	A	A	A	A	A

A, Adequate; I, Inadequate.

indicating that p-EGFR high-expression had no significant correlation with OS in patients with NPC (**Figure 2B**). In addition, there was no obvious heterogeneity between these studies (I^2 = 38.4%, P = 0.197).

EGFR/p-EGFR Expression and DFS/PFS/DMFS

Eight studies exploring the association between EGFR and DFS showed that EGFR high-expression was predictor of poorer DFS (HR = 2.58, 95% CI: 1.87–3.56, P = 0.000; I^2 = 0%, P = 0.606) (**Figure 3A**), which was similar to the results of EGFR and OS. In two studies reporting EGFR and PFS, the pooled HR was 1.85 (95% CI: 0.90–3.82, P = 0.09), suggesting that patients with EGFR high-expression had a poor prognosis and there was an acceptable heterogeneity among studies (I^2 = 45.4%, P = 0.176). In the five studies about DMFS, no significant association was found between DMFS and high-expression of EGFR with a pooled HR of 1.39 (95% CI:0.73–2.67, P = 0.319) (**Figure 3B**), but heterogeneity was significant among the studies (I^2 = 82.8%, P = 0.000) (**Figure 3C**). On the other hand, in two studies reporting p-EGFR and DMFS, the pooled HR was 1.21 (95% CI: 0.96–1.52, P = 0.112) without heterogeneity (I^2 = 0%, P = 0.497) (**Figure 3D**), revealing that high-expression of p-EGFR was not related to DMFS of patients with NPC.

Subgroup and Sensitivity Analysis

As shown in **Table 3**, subgroup analyses showed that patients with EGFR high-expression in studies of higher TNM stage (III–IV) ratio divided using a median percentage of TNM stage I–II samples in entire samples had significantly poor OS (HR = 2.27, 95% CI: 1.09–4.73, P = 0.03). However, the heterogeneity still existed in those studies (I^2 = 95.1%, P = 0.000). In addition, the prognostic value of EGFR was not significantly associated with the country, sample size, IHC cutoff value, and histological differentiation. Moreover, sensitivity analyses revealed that EGFR expression did not significantly affect OS by an individual study solely, indicating there was inherent heterogeneity in OS cohorts (**Figure 4A**). A subgroup analysis was performed for studies among EGFR and DMFS, finding that the heterogeneity obviously decreased in differentiated carcinoma subgroup (I^2 = 33.2%) (**Figure 4B**).

Publication Bias

Publication bias was evaluated using Begg's test and Egger's test. No significant publication bias was found among studies about EGFR and OS, DFS, and DMFS (all P-values were >0.05) (**Figure 5**).

DISCUSSION

EGFR high-expression and activation of downstream signaling pathways can promote cellular differentiation and contribute to aggressive tumor behaviors, such as increasing metastatic and migratory potential, chemotherapy and radiotherapy resistance, and stemness (38, 39). p-EGFR is an active form of EGFR and is crucial for EGFR signaling (40). It has been reported that p-EGFR was associated with poor prognosis of non-small cell lung cancer patients (21). Besides, patients with high expression of p-EGFR had shorter DMFS compared with those with low p-EGFR expression. However, the prognostic value of EGFR/p-EGFR expression in NPC remains controversial. Thus, the evaluation of relationship between EGFR/p-EGFR expression and prognosis may provide a more suitable strategy for individualized treatment of NPC.

Our meta-analysis showed EGFR could predict the outcome of patients with NPC. The pooled HRs for both OS and DFS indicate an important prognostic role for EGFR in NPC. Furthermore, the results of this meta-analysis are in accordance with the findings of previous meta-analysis (41, 42). However, the association between p-EGFR expression and the prognosis of NPC has not yet been

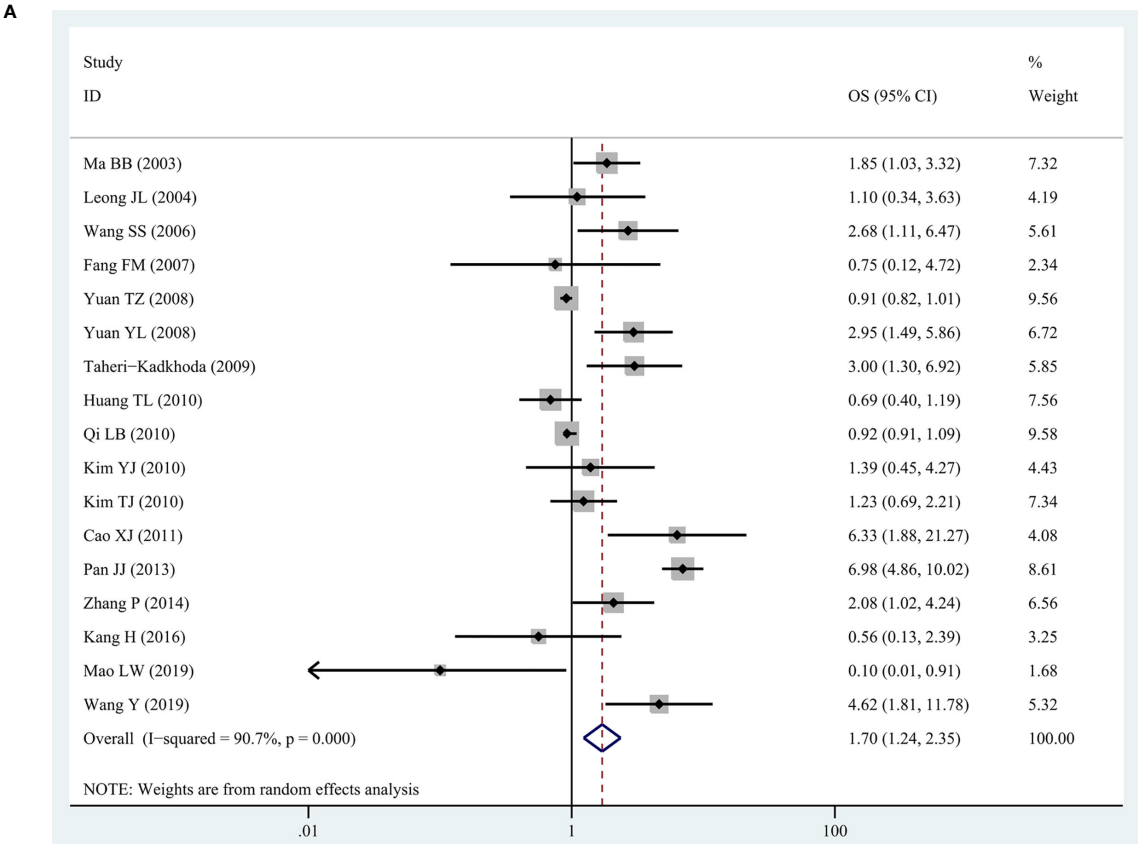

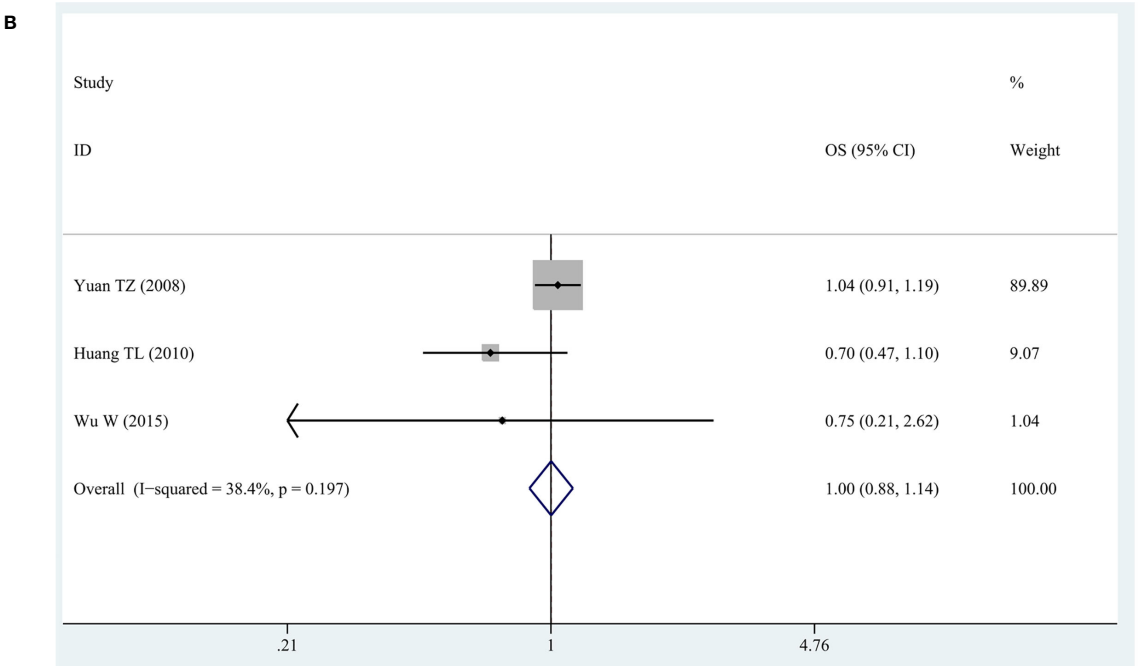

FIGURE 2 | The forest map for relationship between EGFR/p-EGFR and OS in NPC. **(A)** EGFR and OS. **(B)** p-EGFR and OS.

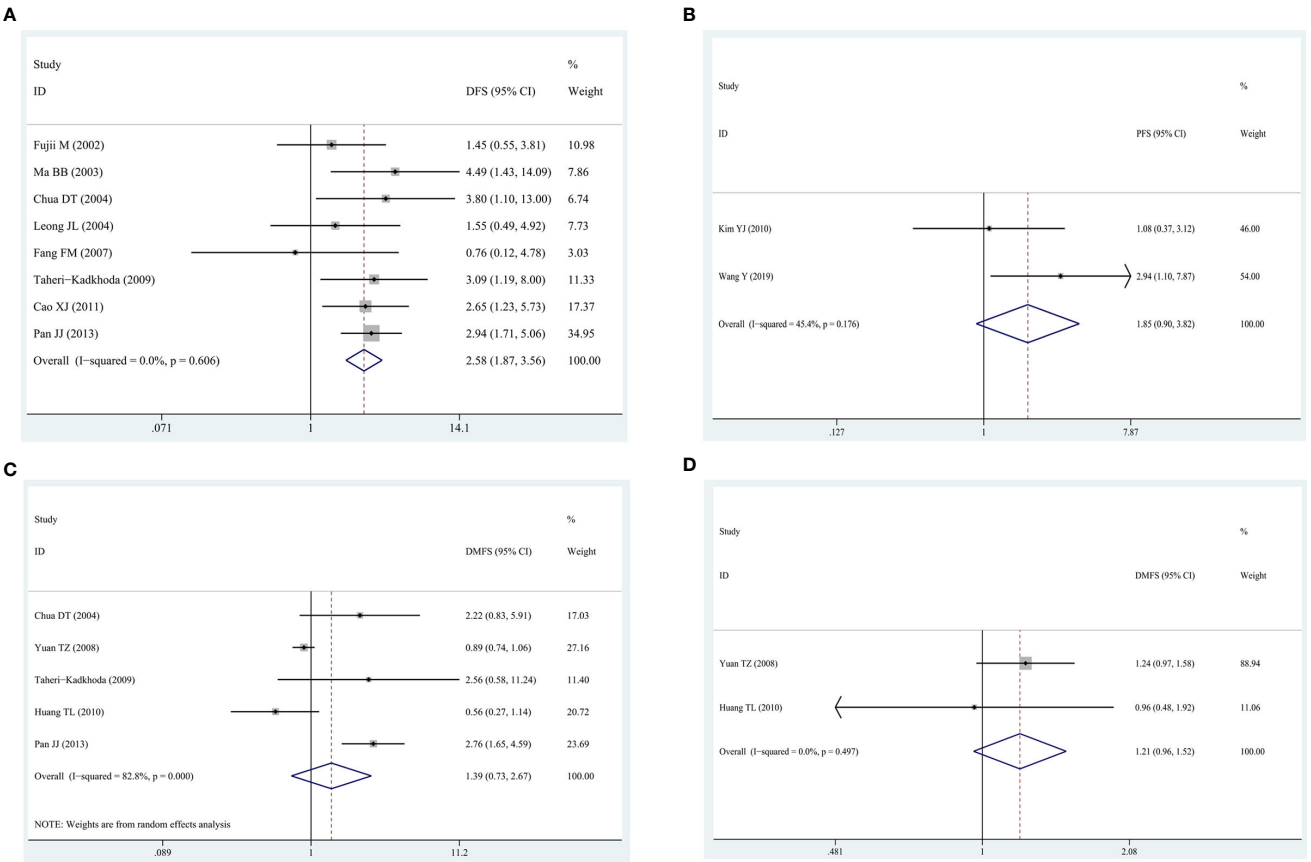

FIGURE 3 | The forest map for relationship between EGFR/p-EGFR and DFS/PFS/DMFS in NPC. **(A)** EGFR and DFS. **(B)** EGFR and PFS. **(C)** EGFR and DFMS. **(D)** p-EGFR and DMFS.

assessed in the previous meta-analysis. In our meta-analysis, high-expression of p-EGFR was not significantly associated with OS (HR = 1.00, 95% CI: 0.88–1.14) and DMFS (HR = 1.21, 95% CI: 0.96–1.52). Additionally, heterogeneity testing displayed significant heterogeneity when analyzing OS and DMFS. Subgroup analyses revealed that patients with EGFR high expression in studies of higher TNM stage (III–IV) ratio had significantly poor OS, but heterogeneity existed in studies (I^2 = 95.1%, P = 0.000). EGFR high-expression was not significantly associated with the country, sample size, IHC cutoff value, and histological differentiation. Sensitivity analyses also revealed that EGFR expression did not significantly affect OS by an individual study solely, indicating there was inherent heterogeneity in OS cohorts. In subgroup analysis with EGFR and DMFS, heterogeneity was reduced to I^2 = 33.2% when we combined studies of differentiated carcinoma, indicating that the difference in tumor histology may be another source of heterogeneity and undifferentiated carcinoma was more likely to metastasize. In this study, no publication bias was observed according to both Begg's test and Egger's test in studies reporting OS, DFS, and DMFS, which proved the stability of our study.

TABLE 3 | Subgroup analysis of relationship between EGFR and OS.

Marker	Survival outcome	N	Model	HR (95% CI)	P	Heterogeneity (I^2, P)
EGFR	OS for Asian	16	R	1.65 (1.19–2.29)	0.003	91.0%, P = 0.000
EGFR	OS for higher rate in differentiated tumor	3	R	1.00 (0.81–1.23)	0.993	82%, P = 0.004
EGFR	OS for higher rate in undifferentiated tumor	7	R	1.38 (0.85–2.23)	0.189	57.4%, P = 0.029
EGFR	OS for cutoff 10%	7	R	1.53 (1.00–2.35)	0.052	95.1%, P = 0.000
EGFR	OS for cutoff 25%	5	R	2.04 (0.92–4.55)	0.081	78.4%, P = 0.001
EGFR	OS for higher TNM stage (I, II *vs*. III, IV)	8	R	2.27 (1.09–4.73)	0.03	95.1%, P = 0.000
EGFR	OS for lower TNM stage (I, II *vs*. III, IV)	9	R	1.29 (0.81–2.06)	0.289	65.4%, P = 0.003
EGFR	OS for number of samples (N > 100)	5	R	2.52 (0.84–7.54)	0.098	97%, P = 0.000
EGFR	OS for number of samples (N ≤ 100)	12	R	1.47 (1.00–2.16)	0.051	71.3%, P = 0.000

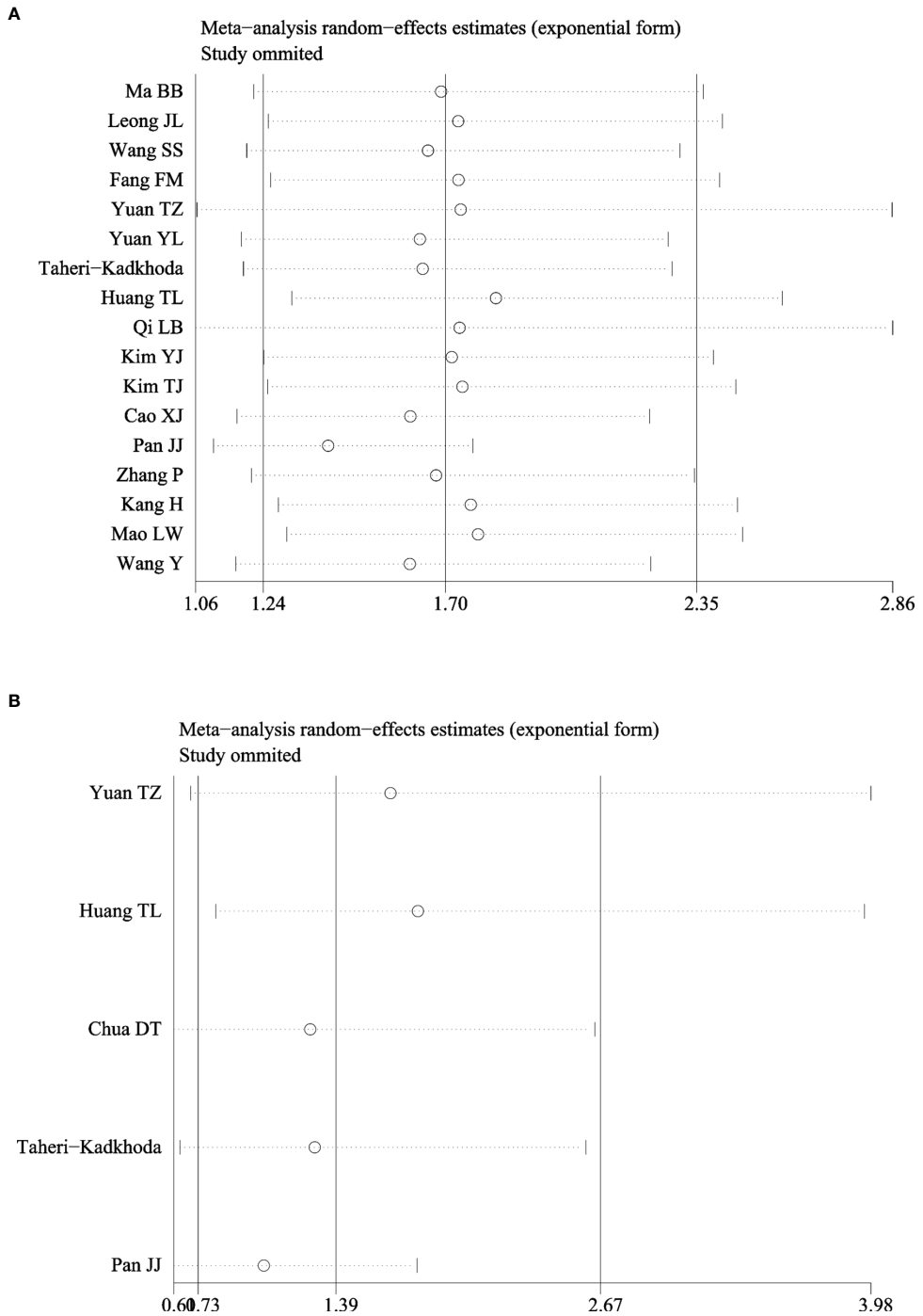

FIGURE 4 | Sensitivity analysis of hazard ratios of EGFR for OS and DMFS. **(A)** EGFR and OS. **(B)** EGFR and DMFS.

Some of the included studies had deficiencies in some parameters according to the REMARKS guidelines, such as a potential ambiguity in the distinction between OS and disease specific survival in some of the included studies. There is no doubt that our study has serval limitations. Firstly, the studies included mainly focused on the patients in China, with insufficient data to examine the differences in trends by ethnic groups. Secondly, differences in quality of all included studies may affect the reliability of the results. Thirdly, the reliability and stability of the IHC results is related to the detection levels of research institutions and researchers themselves. Finally, we calculated the HR estimates from the K-M survival curves

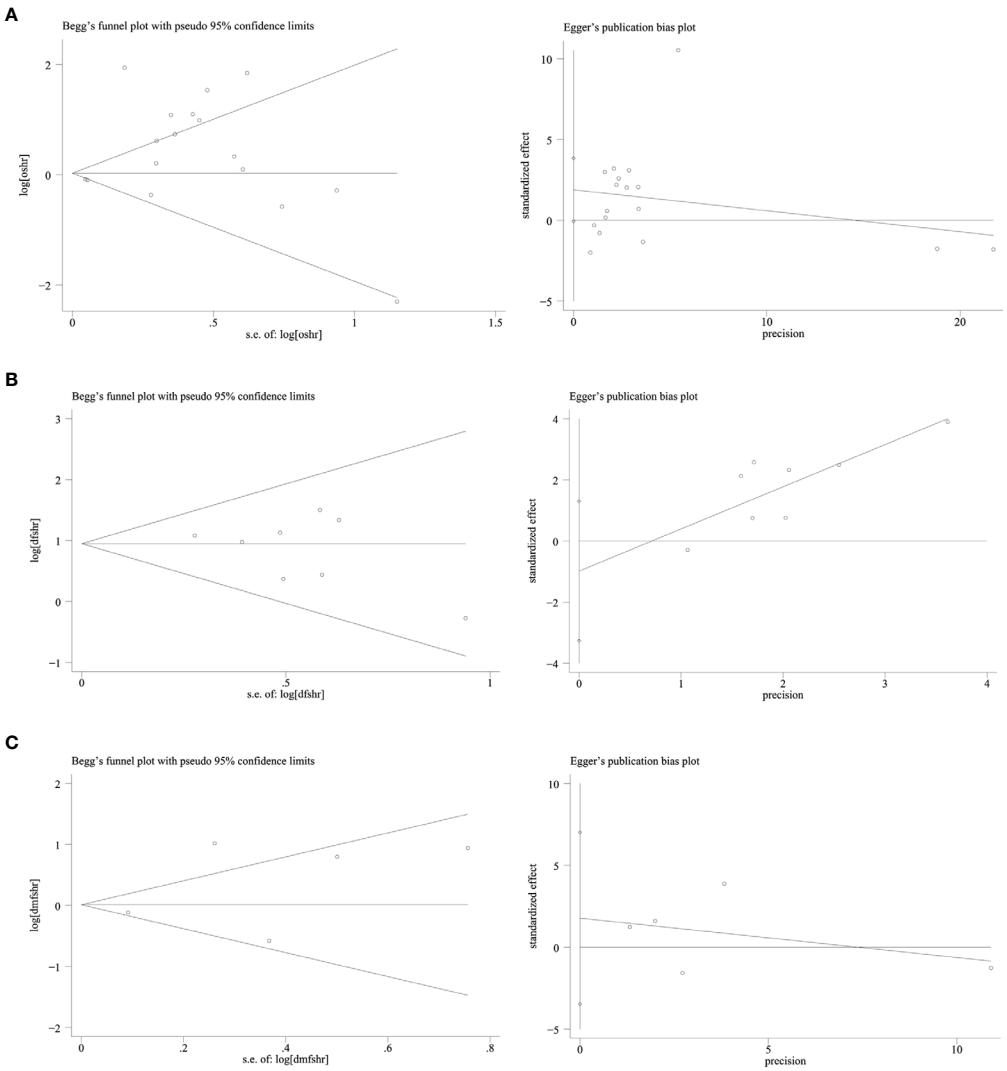

FIGURE 5 | Publication bias funnel plot of EGFR and OS, DFS, DMFS: Begg's test and Egger's test. **(A)** EGFR and OS. **(B)** EGFR and DFS. **(C)** EGFR and DMFS.

when some of the HRs with 95% CI were not directly extracted from the studies, which may be different from actual value.

In conclusion, EGFR high-expression is associated with shorter OS and DFS, suggesting that it may serve as a potential prognostic factor for patients with NPC. However, p-EGFR expression may not be used as a predictor of survival prognosis in patients with NPC, which needs to be confirmed in additional prospective, multicenter studies in the future.

DATA AVAILABILITY STATEMENT

The original contributions presented in the study are included in the article/supplementary material. Further inquiries can be directed to the corresponding author.

AUTHOR CONTRIBUTIONS

All authors listed have made a substantial, direct, and intellectual contribution to the work and approved it for publication.

FUNDING

This work was supported by National Natural Science Foundation of China (81760544), the Key Research and Development Program Project of Guangxi Zhuang Autonomous Region (Grant No. GuikeAB18221007), the Independent Project of Key Laboratory of Early Prevention & Treatment for Regional High-Incidence-Tumor (Grant No. GKE2019-17), Guangxi Science and Nature Foundation Project (2017GXNSFBA198005), the Scientific

Research & Technical Development Project of Wuming District, Nanning city (No. 20200214), Liuzhou City Science and technology research projects (2019AF10601), Liuzhou City Science and technology research projects (2018BJ10303), and Department of Health of Guangxi Zhuang Autonomous Region Self-Raised Funds Project (Z20200269 and 20200856). The Basic Ability Enhancement Program for Young and Middle-aged Teachers in Higher Education Institutions of Guangxi (No.2021KY0283, No. 2021KY0091) and Science Foundation for Distinguished Young Scholars of Guangxi University of Chinese Medicine (No. 2020JQ001).

REFERENCES

1. Chen YP, Chan ATC, Le QT, Blanchard P, Sun Y, Ma J. Nasopharyngeal Carcinoma. *Lancet* (2019) 394(10192):64–80. doi: 10.1016/s0140-6736(19)30956-0
2. Wei KR, Zheng RS, Zhang SW, Liang ZH, Li ZM, Chen WQ. Nasopharyngeal Carcinoma Incidence and Mortality in China, 2013. *Chin J Cancer* (2017) 36(1):90. doi: 10.1186/s40880-017-0257-9
3. Sun R, Qiu HZ, Mai HQ, Zhang Q, Hong MH, Li YX, et al. Prognostic Value and Differences of the Sixth and Seventh Editions of the UICC/AJCC Staging Systems in Nasopharyngeal Carcinoma. *J Cancer Res Clin Oncol* (2013) 139(2):307–14. doi: 10.1007/s00432-012-1333-9
4. Chua MLK, Wee JTS, Hui EP, Chan ATC. Nasopharyngeal Carcinoma. *Lancet* (2016) 387(10022):1012–24. doi: 10.1016/s0140-6736(15)00055-0
5. Han L, Lin SJ, Pan JJ, Chen CB, Zhang Y, Zhang XC, et al. Prognostic Factors of 305 Nasopharyngeal Carcinoma Patients Treated With Intensity-Modulated Radiotherapy. *Chin J Cancer* (2010) 29(2):145–50. doi: 10.5732/cjc.009.10332
6. Chen FM, Zhang YX, Li XF, Gao JF, Ma H, Wang XL, et al. The Prognostic Value of Deficient Mismatch Repair in Stage II-IVa Nasopharyngeal Carcinoma in the Era of IMRT. *Sci Rep* (2020) 10(1):9690. doi: 10.1038/s41598-020-66678-3
7. Huang CL, Guo R, Li JY, Xu C, Mao YP, Tian L, et al. Nasopharyngeal Carcinoma Treated With Intensity-Modulated Radiotherapy: Clinical Outcomes and Patterns of Failure Among Subsets of 8th AJCC Stage IVa. *Eur Radiol* (2020) 30(2):816–22. doi: 10.1007/s00330-019-06500-5
8. Paci A, Ciarimboli G, Ferdeghini M. Growth Factors and Oncogenes in Development and Carcinogenesis. Role of the Epidermal Growth Factor System. *Minerva Med* (1994) 85(9):467–90.
9. Hardbower DM, Coburn LA, Asim M, Singh K, Sierra JC, Barry DP, et al. EGFR-Mediated Macrophage Activation Promotes Colitis-Associated Tumorigenesis. *Oncogene* (2017) 36(27):3807–19. doi: 10.1038/onc.2017.23
10. Ch'ng S, Low I, Ng D, Brasch H, Sullivan M, Davis P, et al. Epidermal Growth Factor Receptor: A Novel Biomarker for Aggressive Head and Neck Cutaneous Squamous Cell Carcinoma. *Hum Pathol* (2008) 39(3):344–9. doi: 10.1016/j.humpath.2007.07.004
11. Zhang L, Chen QY, Liu H, Tang LQ, Mai HQ. Emerging Treatment Options for Nasopharyngeal Carcinoma. *Drug Design Dev Ther* (2013) 7:37–52. doi: 10.2147/dddt
12. Huang TL, Li CF, Huang HY, Fang FM. Correlations Between Expression of Epidermal Growth Factor Receptor (EGFR), Phosphorylated EGFR, Cyclooxygenase-2 and Clinicopathological Variables and Treatment Outcomes in Nasopharyngeal Carcinomas. *Chang Gung Med J* (2010) 33(6):619–27.
13. Yang Y, Xuan J, Yang Z, Han A, Xing L, Yue J, et al. The Expression of Epidermal Growth Factor Receptor and Ki67 in Primary and Relapse Nasopharyngeal Cancer: A Micro-Evidence for Anti-EGFR Targeted Maintenance Therapy. *Med Oncol* (2012) 29(3):1448–55. doi: 10.1007/s12032-011-0028-4
14. Taheri-Kadkhoda Z, Magnusson B, Svensson M, Mercke C, Björk-Eriksson T. Expression Modes and Clinical Manifestations of Latent Membrane Protein 1, Ki-67, Cyclin-B1, and Epidermal Growth Factor Receptor in Nonendemic Nasopharyngeal Carcinoma. *Head Neck* (2009) 31(4):482–92. doi: 10.1002/hed.21002
15. Cao XJ, Hao JF, Yang XH, Xie P, Liu LP, Yao CP, et al. Prognostic Value of Expression of EGFR and Nm23 for Locoregionally Advanced Nasopharyngeal Carcinoma. *Med Oncol* (2012) 29(1):263–71. doi: 10.1007/s12032-010-9782-y
16. Pan J, Tang T, Xu L, Lu JJ, Lin S, Qiu S, et al. Prognostic Significance of Expression of Cyclooxygenase-2, Vascular Endothelial Growth Factor, and Epidermal Growth Factor Receptor in Nasopharyngeal Carcinoma. *Head Neck* (2013) 35(9):1238–47. doi: 10.1002/hed.23116
17. Fujii M, Yamashita T, Ishiguro R, Tashiro M, Kameyama K. Significance of Epidermal Growth Factor Receptor and Tumor Associated Tissue Eosinophilia in the Prognosis of Patients With Nasopharyngeal Carcinoma. *Auris Nasus Larynx* (2002) 29(2):175–81. doi: 10.1016/s0385-8146(01)00135-3
18. Fang FM, Li CF, Chien CY, Rau KM, Huang HY. Immunohistochemical Expression of Epidermal Growth Factor Receptor and Cyclooxygenase-2 in Pediatric Nasopharyngeal Carcinomas: No Significant Correlations With Clinicopathological Variables and Treatment Outcomes. *Int J Pediatr Otorhinolaryngol* (2007) 71(3):447–55. doi: 10.1016/j.ijporl.2006.11.019
19. Kim TJ, Lee YS, Kang JH, Kim YS, Kang CS. Prognostic Significance of Expression of VEGF and Cox-2 in Nasopharyngeal Carcinoma and Its Association With Expression of C-Erbb2 and EGFR. *J Surg Oncol* (2011) 103(1):46–52. doi: 10.1002/jso.21767
20. Yang JL, Gupta RD, Goldstein D, Crowe PJ. Significance of Phosphorylated Epidermal Growth Factor Receptor and Its Signal Transducers in Human Soft Tissue Sarcoma. *Int J Mol Sci* (2017) 18(6):1159. doi: 10.3390/ijms18061159
21. Sonnweber B, Dlaska M, Skvortsov S, Dirnhofer S, Schmid T, Hilbe W. High Predictive Value of Epidermal Growth Factor Receptor Phosphorylation But Not of EGFRvIII Mutation in Resected Stage I Non-Small Cell Lung Cancer (NSCLC). *J Clin Pathol* (2006) 59(3):255–9. doi: 10.1136/jcp.2005.027615
22. Ma BB, Poon TC, To KF, Zee B, Mo FK, Chan CM, et al. Prognostic Significance of Tumor Angiogenesis, Ki 67, P53 Oncoprotein, Epidermal Growth Factor Receptor and HER2 Receptor Protein Expression in Undifferentiated Nasopharyngeal Carcinoma–A Prospective Study. *Head Neck* (2003) 25(10):864–72. doi: 10.1002/hed.10307
23. Yuan TZ, Li XX, Cao Y, Qian CN, Zeng MS, Guo X. Correlation of Epidermal Growth Factor Receptor Activation to Metastasis-Free Survival of Nasopharyngeal Carcinoma Patients. *Ai zheng* (2008) 27(5):449–54.
24. Hayden JA, Côté P, Bombardier C. Evaluation of the Quality of Prognosis Studies in Systematic Reviews. *Ann Internal Med* (2006) 144(6):427–37. doi: 10.7326/0003-4819-144-6-200603210-00010
25. Altman DG, McShane LM, Sauerbrei W, Taube SE. Reporting Recommendations for Tumor Marker Prognostic Studies (REMARK): Explanation and Elaboration. *PloS Med* (2012) 9(5):e1001216. doi: 10.1371/journal.pmed.1001216
26. Almangush A, Heikkinen I, Mäkitie AA, Coletta RD, Läärä E, Leivo I, et al. Prognostic Biomarkers for Oral Tongue Squamous Cell Carcinoma: A Systematic Review and Meta-Analysis. *Br J Cancer* (2017) 117(6):856–66. doi: 10.1038/bjc.2017.244
27. Chua DT, Nicholls JM, Sham JS, Au GK. Prognostic Value of Epidermal Growth Factor Receptor Expression in Patients With Advanced Stage Nasopharyngeal Carcinoma Treated With Induction Chemotherapy and Radiotherapy. *Int J Radiat Oncol Biol Phys* (2004) 59(1):11–20. doi: 10.1016/j.ijrobp.2003.10.038
28. Leong JL, Loh KS, Putti TC, Goh BC, Tan LK. Epidermal Growth Factor Receptor in Undifferentiated Carcinoma of the Nasopharynx. *Laryngoscope* (2004) 114(1):153–7. doi: 10.1097/00005537-200401000-00029
29. Wang SS, Guan ZZ, Xiang YQ, Wang B, Lin TY, Jiang WQ, et al. Significance of EGFR and P-ERK Expression in Nasopharyngeal Carcinoma. *Zhonghua Zhong Liu Za Zhi* (2006) 28(1):28–31.
30. Kim YJ, Go H, Wu HG, Jeon YK, Park SW, Lee SH. Immunohistochemical Study Identifying Prognostic Biomolecular Markers in Nasopharyngeal Carcinoma Treated by Radiotherapy. *Head Neck* (2011) 33(10):1458–66. doi: 10.1002/hed.21611
31. Kang H, Kwon M, Park JJ, Kim JP, Woo SH, Ahn SK, et al. Clinical Implications of Human Papilloma Virus and Other Biologic Markers in Nasopharyngeal Cancer. *Oral Oncol* (2016) 55:e7–10. doi: 10.1016/j.oraloncology.2016.02.002
32. Mao L, Tan J, Wang F, Luo Y, Liu W, Zeng F, et al. Retrospective Study Comparing Anti-EGFR Monoclonal Antibody Plus Cisplatin-Based

Chemoradiotherapy *Versus* Chemoradiotherapy Alone for Stage II-IVb Nasopharyngeal Carcinoma and Prognostic Value of EGFR and VEGF Expression. *Clin Otolaryngol: Off J ENT-UK Off J Netherlands Soc Oto-Rhino-Laryngol Cervico-Facial Surg* (2019) 44(4):572–80. doi: 10.1111/coa.13340

33. Qi LB. Expression and Clinical Significance of EGFR Receptor in Nasopharyngeal Carcinoma. *Chin J Primary Med Pharm* (2010) 17 (20):2755–7.
34. Wu W. Study on the Relationship Between the Phosphorylated Epidermal Grow the Factor Receptor and the Prognosis of Patients With Nasopharyngeal Carcinoma. *Med Innovation China* (2015) 12(30):50–3. doi: 10.3969/j.issn.1674-4985.2015.30.017
35. Wang Y, Wu B, Sun HL, Hu W, Xiong HC, Li CD, et al. Expression of EGFR and HLA-F in Nasopharyngeal Carcinoma and Their Prognostic Value. *Zhejiang Med J* (2019) 41(17):1826–30. doi: 10.12056/j.issn.1006-2785.2019.41.17.2018-2721
36. Yuan Y, Zhou X, Song J, Qiu X, Li J, Ye L, et al. Expression and Clinical Significance of Epidermal Growth Factor Receptor and Type 1 Insulin-Like Growth Factor Receptor in Nasopharyngeal Carcinoma. *Ann Otol Rhinol Laryngol* (2008) 117(3):192–200. doi: 10.1177/000348940811700306
37. Zhang P, Wu SK, Wang Y, Fan ZX, Li CR, Feng M, et al. p53, MDM2, eIF4E and EGFR Expression in Nasopharyngeal Carcinoma and Their Correlation With Clinicopathological Characteristics and Prognosis: A Retrospective Study. *Oncol Lett* (2015) 9(1):113–8. doi: 10.3892/ol.2014.2631
38. Blume-Jensen P, Hunter T. Oncogenic Kinase Signalling. *Nature* (2001) 411 (6835):355–65. doi: 10.1038/35077225
39. Hynes NE, Lane HA. ERBB Receptors and Cancer: The Complexity of Targeted Inhibitors. *Nat Rev Cancer* (2005) 5(5):341–54. doi: 10.1038/nrc1609
40. Yamano S, Gi M, Tago Y, Doi K, Okada S, Hirayama Y, et al. Role of Deltanp63(Pos)CD44v(pos) Cells in the Development of N-Nitroso-Tris-Chloroethylurea-Induced Peripheral-Type Mouse Lung Squamous Cell Carcinomas. *Cancer Sci* (2016) 107(2):123–32. doi: 10.1111/cas.12855
41. Sun W, Long G, Wang J, Mei Q, Liu D, Hu G. Prognostic Role of Epidermal Growth Factor Receptor in Nasopharyngeal Carcinoma: A Meta-Analysis. *Head Neck* (2014) 36(10):1508–16. doi: 10.1002/hed.23481
42. Ma X, Huang J, Wu X, Li X, Zhang J, Xue L, et al. Epidermal Growth Factor Receptor Could Play a Prognostic Role to Predict the Outcome of Nasopharyngeal Carcinoma: A Meta-Analysis. *Cancer Biomark: Section A Dis Markers* (2014) 14(4):267–77. doi: 10.3233/cbm-140401

Conflict of Interest: The authors declare that the research was conducted in the absence of any commercial or financial relationships that could be construed as a potential conflict of interest.

Publisher's Note: All claims expressed in this article are solely those of the authors and do not necessarily represent those of their affiliated organizations, or those of the publisher, the editors and the reviewers. Any product that may be evaluated in this article, or claim that may be made by its manufacturer, is not guaranteed or endorsed by the publisher.

frontiers in Oncology

SYSTEMATIC REVIEW
published: 20 August 2021
doi: 10.3389/fonc.2021.698113

Are People With Blood Group O More Susceptible to Nasopharyngeal Carcinoma and Have Worse Survival Rates? A Systematic Review and Meta-Analysis

*Shao-wu Jing[1], Qing Xu[2], Xin-yuan Zhang[1], Zhong-hao Jing[1], Zhi-jun Zhao[3], Ruo-hui Zhang[1], Feng-peng Wu[1] and Jun Wang[1]**

[1] Department of Radiation Oncology, Fouth Hospital of Hebei Medical University, Shijiazhuang, China, [2] Department of Ultrasound, Fouth Hospital of Hebei Medical University, Shijiazhuang, China, [3] Otorhinolaryngology Head and Neck Surgery, Fouth Hospital of Hebei Medical University, Shijiazhuang, China

OPEN ACCESS

Edited by:
Yong Yin,
Shandong Cancer Hospital, China

Reviewed by:
Jinghao Duan,
Shandong University, China
Marcos Santos,
University of Brasilia, Brazil

***Correspondence:**
Jun Wang
wangjunzr@163.com

Specialty section:
This article was submitted to Head and Neck Cancer, a section of the journal Frontiers in Oncology

Received: *20 April 2021*
Accepted: *02 August 2021*
Published: *20 August 2021*

Citation:
Jing S-w, Xu Q, Zhang X-y, Jing Z-h, Zhao Z-j, Zhang R, Wu F-p and Wang J (2021) Are People With Blood Group O More Susceptible to Nasopharyngeal Carcinoma and Have Worse Survival Rates? A Systematic Review and Meta-Analysis. Front. Oncol. 11:698113. doi: 10.3389/fonc.2021.698113

Objective: Nasopharyngeal carcinoma (NPC) is a common malignant tumour in Southeast Asia, especially in southern China. ABO blood groups have been proven to play an important role in many cancers. However, it is still controversial whether the ABO blood group has a definite relationship to susceptibility to NPC and the prognosis of NPC patients. This meta-analysis was performed to elucidate the correlation between ABO blood group and NPC to provide more data for clinical practice.

Methods: A systematic search was performed of the Chinese National Knowledge Infrastructure (CNKI), Wanfang, Web of Science, EMBASE, and PubMed databases up to December 31, 2020. Stata 11.0 statistical software was used for this meta-analysis.

Results: According to the inclusion and exclusion criteria, a total of 6 studies including 6938 patients with NPC were selected. Blood group O was relevant to Chinese NPC patients, and patients with blood group O had a significantly lower incidence of NPC, while blood group A had no correlation with susceptibility to NPC. There was no difference in the 3-year overall survival (OS), locoregional relapse-free survival (LRRFS) or distant metastasis-free survival (DMFS) rates between patients with blood group O and those with non-O blood groups; worse 5-year OS, LRRFS and DMFS rates were found in patients with blood group O, whereas blood group A was not related to prognosis.

Conclusion: Blood group O in Chinese patients with NPC seems to be a protective factor for morbidity. However, once patients with blood group O are diagnosed with NPC, this blood group often indicates unfavourable OS, LRRFS and DMFS rates. It is recommended that more attention should be paid to the influence of blood group factor on patients in the treatment of NPC.

Keywords: nasopharyngeal carcinoma, ABO blood group, susceptibility, prognosis, meta analysis

INTRODUCTION

Nasopharyngeal carcinoma (NPC) is a common malignant head and neck neoplasm in Southeast Asia, especially in southern China (1). Some studies have demonstrated that several factors increase the risk for NPC, such as Epstein–Barr virus infection, smoking, alcohol consumption, and family history of cancer (2–6). Moreover, ethnicity, environmental factors, and host genetic susceptibility are all recognized to be risk factors for the pathogenesis of NPC, contributing to the variation in individual susceptibility to cancer.

BO blood group antigens, the most immunogenic of all blood group antigens, are of clinical importance in transfusion medicine. Aside from erythrocytes, a wide variety of human tissues and most epithelial and endothelial cells express ABO blood group antigens (7). Alterations in ABO antigen expression can change the interactions between individual cells or between cells and the extracellular matrix. This change is believed to play an important role in tumorigenesis and cancer progression (8). Many studies have reported that patients with different blood groups possess different biological characteristics; for example, pancreatic cancer patients with blood group O have higher risk and more advanced disease than those with a non-O blood group (9), blood group O is associated with decreased frequency in pancreatic ductal adenocarcinoma (10), poor recurrence-free survival and overall survival (OS) rates are observed in cervical cancer patients with a non-O blood group (11), higher recurrence and progression is observed in bladder cancer patients with blood group O (12), and a decreased OS rate is found in renal carcinoma patients with a non-O blood group (13). However, whether such an association exists between ABO blood group and the incidence of NPC remains controversial (14–17). Some studies have shown that patients with blood group A have an increased risk for NPC (15, 16) and that blood group O reduces susceptibility (15), while others have shown no correlation between ABO blood group and NPC (14, 17).

With the combination of precision radiotherapy and potent chemotherapy strategies, the OS rates of NPC have been considerably improved (18, 19). However, local recurrence and distant metastasis still occur after treatment in approximately 5%-15% and 15%-30% of patients, respectively (20). Although a relationship between the ABO blood group and the prognosis of NPC has been reported (21–25), the conclusions are still inconsistent. Additionally, no evidence-based results have been reported to date. Given the above, we performed this meta-analysis to elucidate the correlation between ABO blood group and NPC, including incidence and prognosis, to provide more data for clinical practice.

METHODS

Literature Search Strategy

We performed a literature search of the Chinese National Knowledge Infrastructure (CNKI), Wanfang, Web of Science, EMBASE, and PubMed databases for all original articles relevant to the relationship between ABO blood groups and NPC up to December 31, 2020. Keywords utilized in the search included "nasopharyngeal carcinoma", "nasopharyngeal cancer", or "nasopharyngeal neoplasm", and "ABO blood group", with language restricted to Chinese and English. After identification, articles were manually filtered by review of the abstracts and/or full texts.

Inclusion and Exclusion Criteria

The eligible criteria for study inclusion were the following: (1) domestic literature published in the national core journals collected at Peking University Library, and foreign literature published in full-text English; (2) studies conducted in humans with NPC with the diagnosis confirmed by pathology; (3) information of serologically determined blood groups collected before treatment; (4) advanced radiation techniques other than two-dimensional radiotherapy were utilized; (5) detailed original material, including reliable data, clear results, appropriate application of statistical methods, and available odds ratio (OR), hazard ratio (HR), and 95% confidence intervals (CI) or the data required to calculate these.

Quality Assessment

An evaluation guide for case-control studies was used for each independent study to assess whether there was bias the extent of its influence (26), including the following aspects: (1) whether the baseline characteristics such as gender, age, and TNM stage were clear; (2) whether TNM staging standard was provided; (3) whether there was a significant difference in gender, TNM stage, pathological type etc. between NPC patients and cancer-free controls; (4) whether it was a multi-centre study; and (5) whether the existence of bias in research was discussed. Each of the above 5 items represented 1 point; a study with a score of 3 or more was considered to be of high quality. According to the unified quality standards, two investigators independently extracted relevant data from the included studies and summarized it. Any disagreements that appeared were resolved by consulting an adjudicating senior author.

Statistical Analysis

This systematic review was conducted basically following the "Preferred Reporting Items for Systematic Reviews and Meta-Analyses" (PRISMA) guidelines (27) and the Cochrane Handbook (28). Stata 11.0 statistical software provided by the Cochrane collaboration was used for this meta-analysis. To determine the effect size, the OR and its 95% CI were calculated. We estimated the prognostic significance of ABO blood groups in NPC by directly using the HR and its 95% CI reported in the original articles when available; otherwise, the Kaplan–Meier curve was used to obtain the HR and its 95% CI using the method provided by Tierney et al. (29) A Q test was applied to identify heterogeneity. When there was heterogeneity (p value $\nleq 0.05$), a random effects model was used; otherwise, a fixed effects model was employed. The Z test was used to determine whether there was a significant difference in the pooled OR and HR. Publication bias was assessed by determining whether the funnel chart was symmetric. Egger's linear regression was used for the publication bias test.

RESULTS

Retrieval Results and Quality Evaluation

Seventeen studies were found initially; out of these, 3 domestic studies were excluded because they were not published in core journals of the Peking University Library. Out of the remaining articles, 4 were repeat publications, 2 were not case-control studies, and 2 lacked complete data. Ultimately, a total of 6 studies (14–17, 22, 23) including 6938 patients with NPC were selected for this meta-analysis (**Figure 1**). The baseline characteristics of the analyzed cohort were shown in **Tables 1**, **2**. The scores of the studies were greater than or equal to 3, which meant they were of high quality. The proportion of blood group O in NPC patients was 24.83%-41.95%, and the proportion of blood group A was 25.09%-52.35%. In each study, the proportion of patients with blood group A plus blood group O exceeded 65%.

Blood Group O Status

Blood group O was analyzed in NPC patients and cancer-free controls in a total of 4 studies (14–17). A random effects model was used owing to statistical heterogeneity between the two groups (p = 0.040). The results showed that the distribution of blood group O was irrelevant between NPC patients and cancer-free controls (OR: 1.190; 95% CI: 0.629-1.079; p = 0.159, **Figure 2A**). Of these 4 studies, 3 were Chinese, and 1 was Turkish. A sensitivity analysis was conducted by removing the Turkish study data (15), and the pooled OR and its 95% CI were 1.130 and 1.018-1.254, respectively, (p = 0.022<0.05, **Figure 2B**), which indicated that if the analysis was limited to Chinese patients, blood group O was associated with a lower incidence of NPC.

Blood Group A Status

Blood group A in NPC patients was analyzed using the same 4 studies. There was no significant difference between NPC patients and cancer-free controls (OR: 0.824; 95% CI: 0.982-1.441; p = 0.076), as shown in **Figure 3A**. A sensitivity analysis was also performed by deleting the study of Turkoz FP et al. (15). The pooled OR was 0.933, and the 95% CI was 0.832-1.047 (p = 0.241>0.05, **Figure 3B**), which indicated that blood group A had no correlation with NPC.

The 3- and 5-Year OS Rates

Two studies (22, 23) compared the 3- and 5-year OS rates of patients with blood group O and those with a non-O blood group (A, B, and AB). It was revealed that there was no significant

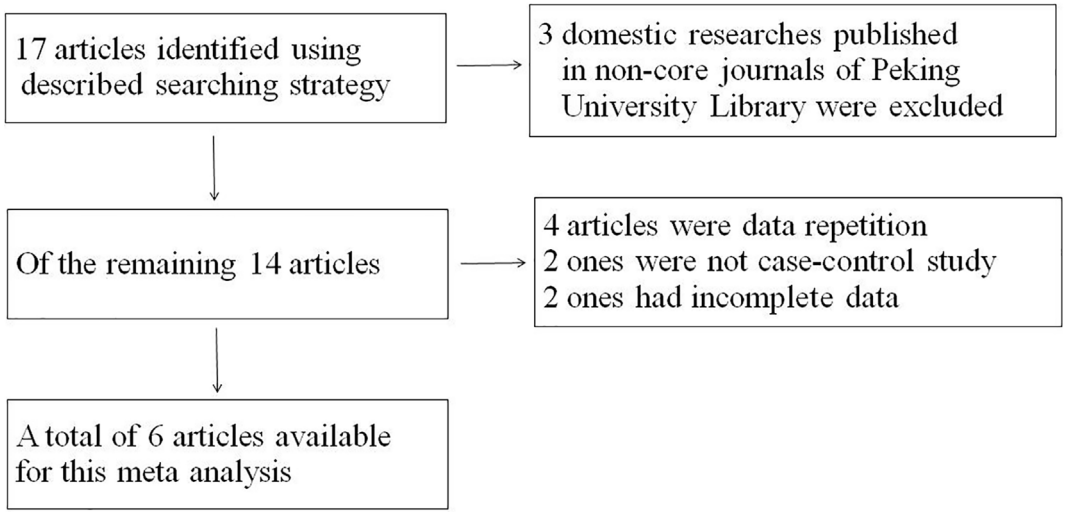

FIGURE 1 | Flow chart for article search and selection process.

TABLE 1 | Basic characteristic of the included studies.

Author	Year	Country	Race	Blood group status (%)		Quality assessment				
				O	A	1	2	3	4	5
Seow LJ et al. (14)	1964	China	Mongolia	92 (39.65)	63 (27.15)	1	1	1	0	0
Turkoz FP et al. (15)	2011	Turkey	Europa	37 (24.83)	78 (52.35)	1	1	1	1	0
Sheng LM et al. (16)	2013	China	Mongolia	575 (37.39)	471 (30.62)	1	1	1	0	0
Lin K et al. (17)	2018	China	Mongolia	472 (41.55)	285 (25.09)	1	1	1	0	1
Peng H et al. (22)	2016	China	Mongolia	586 (41.95)	372 (26.63)	1	1	1	0	0
Wang GN et al. (23)	2019	China	Mongolia	977 (40.06)	641 (26.28)	1	1	1	0	0

TABLE 2 | Disease-related outcomes of the eligible studies.

Author	Group	OS (%)		LRRFS (%)		DMFS (%)		Treatment Plan
		3-year	5-year	3-year	5-year	3-year	5-year	
Peng H et al. (22)	O	90.4	67.8	83.1	56.8	86.5	58.8	Prescribed doses were 66-72Gy at 2.12-2.43Gy/fraction to PTV of the GTV-nx, 64-70Gy to the PTV of the GTV-nd, 60-63Gy to the PTV of high-risk CTV, and 54-56Gy to the PTV of low-risk CTV. Neoadjuvant or adjuvant chemotherapy consisted of cisplatin with 5-fluorouracil or cisplatin with docetaxel administered every three weeks for two or three cycles. Concurrent chemotherapy consisted of cisplatin given weekly or on weeks 1, 4 and 7 of radiotherapy.
	non-O	89.3	71.1	84.8	65.6	84.5	65.9	
	A	87.1	68.8	82.8	66.9	83.8	67.5	
	non-A	90.7	69.3	85.2	65.8	85.8	67.0	
Wang GN et al. (23)	O	79.4	63.8	77.8	61.5	76.5	61.8	GTV was defined as GTV-nx and GTV-nd and was prescribed 66-70Gy in 30-32 fractions. CTV1 was defined as GTVnx plus a margin of 5-10 mm and was prescribed 60Gy in 30-32 fractions. CTV2 was defined by adding a margin of 5-10 mm to CTV1 and included the retropharyngeal lymph nodal regions, clivus, skull base, pterygoid fossae, parapharyngeal space, inferior sphenoid sinus, and posterior edge of the nasal cavity and maxillary sinuses, and was prescripted 54Gy in 30-32 fractions. Chemotherapy regimen was mainly based on platinum.
	non-O	81.1	67.4	78.8	65.5	78.4	65.8	
	A	81.1	67.7	78.9	65.5	78.9	65.8	
	non-A	80.1	65.4	78.2	63.3	77.2	63.6	

OS, overall survival; LRRFS, locoregional relapse-free survival; DMFS, distant metastasis-free survival.

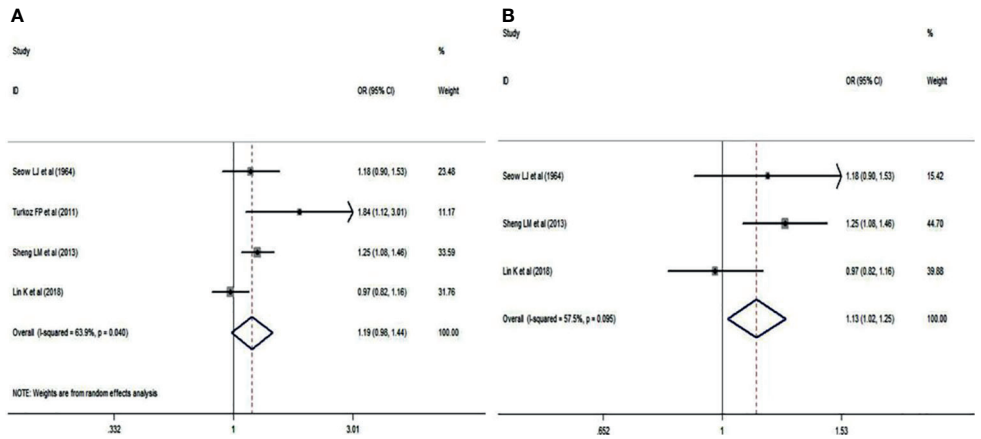

FIGURE 2 | Forest plots of blood group O status. **(A)** Distribution of blood group O in the whole involved patients with NPC; **(B)** Distribution of blood group O in Chinese patients with NPC.

difference in the 3-year OS rate between blood groups (HR: 0.966; 95% CI: 0.785-1.188; p = 0.742), as shown in **Figure 4A**, whereas the difference in the 5-year OS rate neared significance (HR: 0.860; 95% CI: 0.739-1.001; p = 0.051) (**Figure 4B**), indicating that NPC patients with blood group O had a worse trend in 5-year OS rates than those with a non-O blood group.

The 3- and 5-Year LRRFS Rates

These two studies also compared the 3- and 5-year LRRFS rates of patients with blood group O and those with a non-O blood group. It was revealed that there was no significant difference in the 3-year LRRFS rate (HR: 0.945; 95% CI: 0.802-1.112; p = 0.496), as shown in **Figure 5A**, but there was a significant difference in the 5-year LRRFS rate (HR: 0.838; 95% CI: 0.720-0.975; p = 0.022<0.05) (**Figure 5B**), which indicated that NPC patients with blood group O had a worse 5-year LRRFS rate than those with a non-O blood group.

The 3- and 5-year DMFS Rates

The same two studies also provided 3- and 5-year DMFS rate data for patients with blood group O and those with a non-O blood group. Although the 3-year DMFS rate was not significantly different (HR: 1.002; 95% CI: 0.770-1.305; p = 0.986), as shown in **Figure 6A**, the 5-year DMFS rate was significantly different (HR: 0.849; 95% CI: 0.730-0.988; p = 0.034<0.05) (**Figure 6B**), which indicated that compared with the non-O group, NPC patients with blood group O also had a worse 5-year DMFS rate.

Relationship Between Blood Group A and Prognosis of NPC

The 3- and 5-year OS, LRRFS, and DMFS rates of patients with blood group A and those with a non-A blood group (O, B, and AB) could also be analyzed from these two studies (22, 23). The results showed that blood group A had no correlation with the prognosis of NPC (all P values>0.05), regardless of whether the 3- or 5-year OS, LRRFS, or DMFS rate was analyzed (**Table 3**).

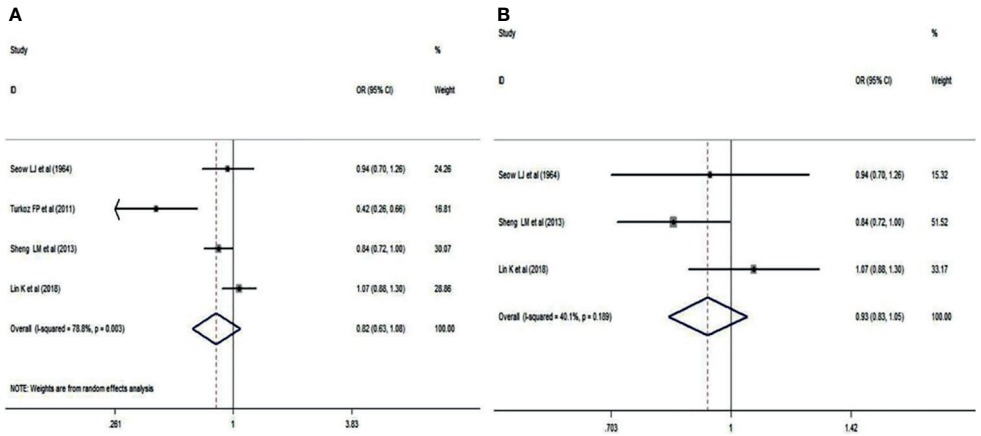

FIGURE 3 | Forest plots of blood group A status. **(A)** Distribution of blood group A in the whole involved patients with NPC; **(B)** Distribution of blood group A in Chinese patients with NPC.

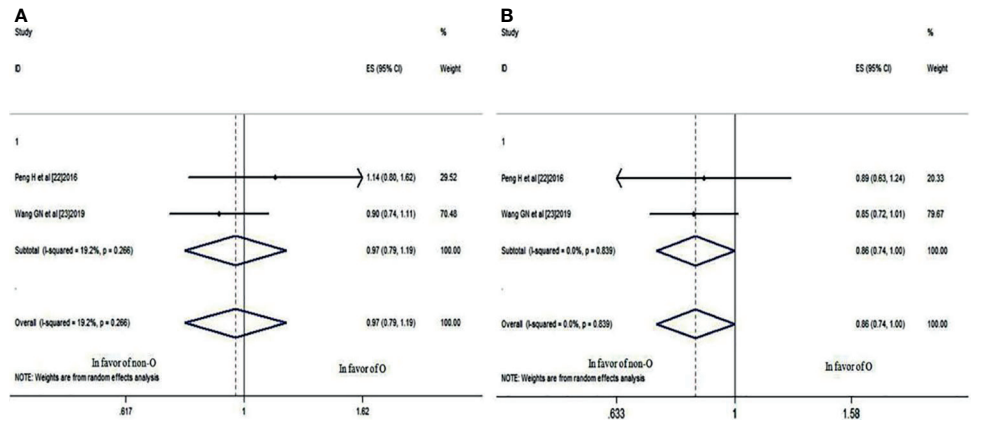

FIGURE 4 | Forest plots of OS in patients with NPC. **(A)** 3-year OS between blood group O and non-O; **(B)** 5-year OS between blood group O and non-O.

Publication Bias Analysis

Egger's test was performed to assess publication bias. **Table 4** showed that there was no indication of publication bias for blood group O or blood group A (both P values >0.05). Because there were only two studies on prognosis, publication bias tests and sensitivity analyses could not be performed.

DISCUSSION

The antigens of the ABO blood group system were discovered as the first human genetic markers in 1900 (30). The ABO gene encodes a glycosyl transferase that synthesizes A and B agglutinogens to form ABO blood groups (31). Many studies have reported that the ABO blood group is correlated with susceptibility to many malignancies. For instance, a definite correlation has been established between the ABO blood group and pancreatic cancer. Patients with a non-O blood group have an increased risk for pancreatic cancer (32).

The correlation between the ABO blood group and NPC is ambiguous. The initial research by Seow et al. (14) demonstrated that there was no association between ABO blood groups and NPC, but in 2011, Turkoz FP et al. (15) indicated that ABO blood groups were related to NPC susceptibility. Blood group A was reported to increase risk, but blood group O showed a protective effect. To date, two more relevant studies have been published. Sheng LM et al. (16) showed that compared with subjects with blood group O, a relatively higher risk was observed among patients with blood group A, while Lin K et al. (17) found no significant difference in ABO blood group between the NPC group and the control group. To date, there is no published meta-analysis providing evidence-based data to show the relevant results of ABO blood group and NPC susceptibility studies. According to the inclusion and exclusion criteria, 6 studies of high quality were included in this meta-analysis; 4 of

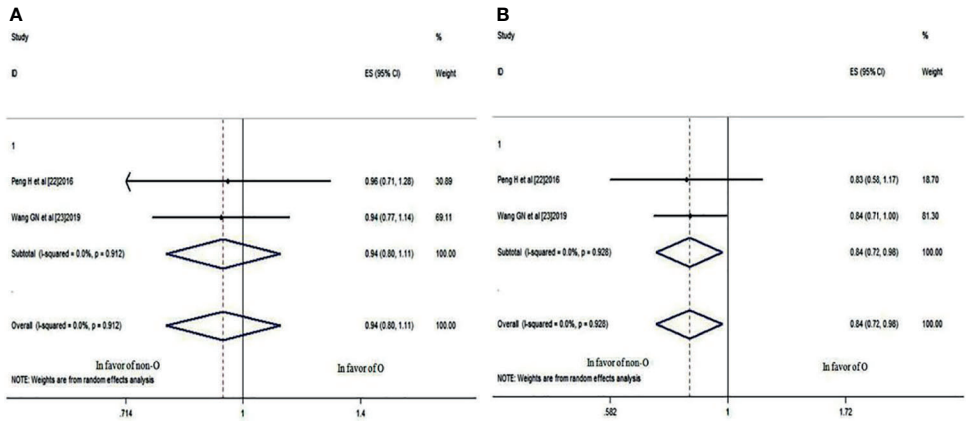

FIGURE 5 | Forest plots of LRRFS in patients with NPC. **(A)** 3-year LRRFS between blood group O and non-O; **(B)** 5-year LRRFS between blood group O and non-O.

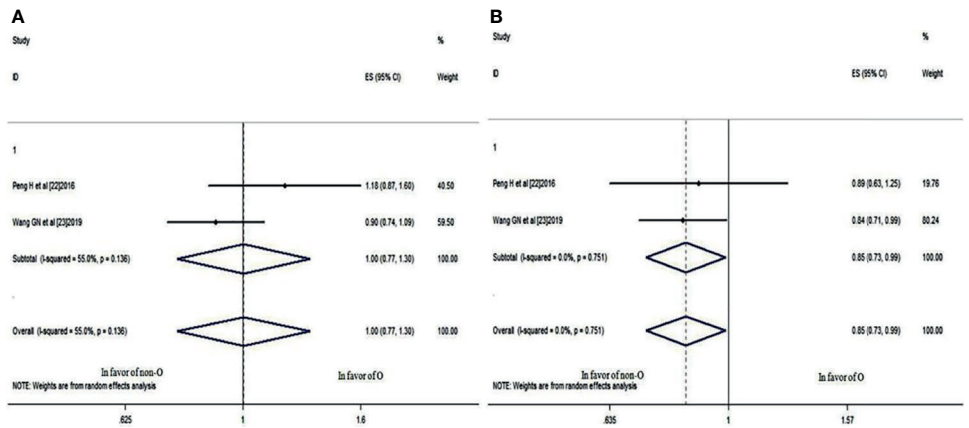

FIGURE 6 | Forest plots of DMFS in patients with NPC. **(A)** 3-year DMFS between blood group O and non-O; **(B)** 5-year DMFS between blood group O and non-O.

TABLE 3 | Relationship between blood group A and prognosis of NPC.

Statistic index	HR	95% CI		P-value
3-year OS	1.445	0.345	6.050	0.615
5-year OS	1.105	0.932	1.310	0.252
3-year LRRFS	0.965	0.787	1.183	0.730
5-year LRRFS	1.101	0.929	1.303	0.267
3-year DMFS	1.003	0.788	1.276	0.984
5-year DMFS	1.087	0.918	1.288	0.331

TABLE 4 | Publication bias of the included studies.

Statistic index	t	95% CI		P-value
Blood group O status	0.90	-8.035	12.280	0.463
Blood group A status	-1.18	-16.464	9.394	0.360

the studies concerned the relationship between ABO blood group with NPC incidence, and 2 studies focused on the relationship between ABO blood group and NPC patient prognosis. Our results showed that there was no significant overall difference in the incidence of blood group O between NPC patients and cancer-free controls, but a sensitivity analysis demonstrated that if the analysis was restricted to Chinese individuals, group O was associated with significantly lower susceptibility to NPC, whereas no differences in blood group A were observed between the two groups, indicating that blood group O seems to be a protective factor in the Chinese population.

Due to anatomic constraints and a high degree of radiosensitivity, radiotherapy is the main treatment for non-metastatic NPC. The prognosis of early-stage NPC is satisfactory; however, for patients with locally advanced NPC, the prognosis

is still poor despite the combination of concurrent and neoadjuvant chemotherapy (33). Immune therapies targeting the PD-1/PD-L1 axis have shown significant anti-tumour effects against some types of tumours, including melanoma and non-small cell lung cancer (34); however Huang ZL et al. (35) indicated that higher/positive expression of PD-L1/PD-1 may not serve as a suitable prognostic biomarker for NPC. Additional novel prognostic factors are needed to identify patients at high risk to help devise individual treatment strategies. Given the controversial results regarding the ABO blood group as a prognostic factor for NPC, we conducted this systematic review to assess the role of different blood groups in NPC and patient survival. The data from two studies (22, 23) were pooled for this meta-analysis. Although there was no difference in the 3-year OS, LRRFS or DMFS rate, a trend towards worse 5-year OS rates and significantly worse 5-year LRRFS and DMFS rates were found in NPC patients with blood group O (HR: 0.860, 95% CI: 0.739-1.001, $p = 0.051$; HR: 0.838, 95% CI: 0.720-0.975, $p = 0.022$; HR: 0.849, 95% CI: 0.730-0.988, $p = 0.034$, respectively), while there was no significant difference between patients with blood group A and a non-A blood group, regardless of whether the 3- and 5-year OS, LRRFS or DMFS rate was analyzed. However, Ouyang PY et al. (25) reported lower OS and DMFS rates associated with blood type A when the analysis was restricted to male patients; unfortunately, we could not conduct further subgroup analysis because of insufficient data available from the included studies.

The mechanism of how ABO blood groups influence NPC progression is still unclear. Neoplastic transformation is characterized by a dramatic aberration in cellular cohesive interaction. Adhesion molecules have been shown to facilitate tumour cell mobility, adhesion, and the host inflammatory response to cancer (36). Paré G et al. (37) found that the concentration of soluble intercellular adhesion molecule-1 is higher in women with blood group O and is related to worse survival in NPC (38). Edgren G et al. (39) showed that individuals with blood group O may have an increased inflammatory response. Maeda K et al. (40) indicated that inflammation plays an important role in the radiosensitivity of tumours. Persistent and severe inflammation is usually associated with radioresistance, which may increase the risk of tumour recurrence. These findings may explain why NPC patients with blood group O have worse OS, LRRFS and DMFS rates.

This meta-analysis has potential shortcomings. (1) due to the extremely unbalanced global distribution, the overwhelming majority of the subjects in the included studies were Chinese; thus, bias may be present; (2) the detection method for the ABO blood group was not provided in all six studies, therefore possible differences in methods may have affected the results; (3) because of limited data extracted from the included studies, further stratified analysis was impossible to perform; and (4) the included studies were all openly published, and were in Chinese and English only. Unpublished literature and language bias may also have affected the results.

In conclusion, blood group O in the Chinese population seems to be a protective factor against NPC. However, when patients with blood group O are diagnosed with NPC, this blood group often indicates unfavourable OS, LRRFS and DMFS rates. It is recommended that more attention should be paid to the influence of blood group factor on patients in the treatment of NPC.

DATA AVAILABILITY STATEMENT

The original contributions presented in the study are included in the article/supplementary materials. Further inquiries can be directed to the corresponding author.

AUTHOR CONTRIBUTIONS

S-wJ, QX, and JW conceived and designed the study. X-yZ and Z-hJ collected data. Z-jZ, R-hZ, and F-pW performed the analysis. S-wJ wrote the draft of this manuscript. JW edited the manuscript. All authors contributed to the article and approved the submitted version.

FUNDING

This work was supported by the Key Research Projects of Medical Science in Hebei Province (ZL20140174).

REFERENCES

1. Shield KD, Ferlay J, Jemal A, Sankaranarayanan R, Chaturvedi AK, Bray F, et al. The Global Incidence of Lip, Oral Cavity, and Pharyngeal Cancers by Subsite in 2012. *CA Cancer J Clin* (2017) 67:51–64. doi: 10.3322/caac.21384
2. Shen GP, Pan QH, Hong MH, Qin HD, Xu YF, Chen LZ, et al. Human Genetic Variants of Homologous Recombination Repair Genes First Found to be Associated With Epstein-Barr Virus Antibody Titers in Healthy Cantonese. *Int J Cancer* (2011) 129:1459–66. doi: 10.1002/ijc.25759
3. Wang JH, Shi M, Hsia YS, Luo SQ, Zhao LN, Xu M, et al. Failure Patterns and Survival in Patients With Nasopharyngeal Carcinoma Treated With Intensity Modulated Radiation in Northwest China: A Pilot Study. *Radiat Oncol* (2012) 7:2. doi: 10.1186/1748-717X-7-2
4. Chen C, Shen LJ, Li BF, Gao J, Xia YF. Smoking is a Poor Prognostic Factor for Male Nasopharyngeal Carcinoma Treated With Radiotherapy. *Radiother Oncol* (2014) 110:409–15. doi: 10.1016/j.radonc.2013.08.003
5. Chen YP, Zhao BC, Chen C, Lei XX, Shen LJ, Chen G, et al. Alcohol Drinking as an Unfavorable Prognostic Factor for Male Patients With Nasopharyngeal Carcinoma. *Sci Rep* (2016) 6:19290. doi: 10.1038/srep19290
6. Nor Hashim NA, Ramzi NH, Velapasamy S, Alex L, Chahil JK, Lye SH, et al. Identification of Genetic and Non-Genetic Risk Factors for Nasopharyngeal Carcinoma in a Southeast Asian Population. *Asian Pac J Cancer Prev* (2012) 13:6005–10. doi: 10.7314/apjcp.2012.13.12.6005
7. Schuessler MH, Pintado S, Welt S, Real FX, Melamed MR, Lloyd KO, et al. Blood-Group and Blood-Group-Related Antigens in Normal Pancreas and Pancreas Cancer: Enhanced Expression of Precursor Type 1, Tn and Sialyl-Tn in Pancreas Cancer. *Int J Cancer* (1991) 47:180–7. doi: 10.1002/ijc.2910470204

8. Zhou J, Yang LC, He ZY, Li FY, Wu SG, Sun JY, et al. Prognostic Impact of ABO Blood Group on the Survival in Patients With Ovarian Cancer. *J Cancer* (2015) 6:970–5. doi: 10.7150/jca.12471
9. Ben QW, Wang KX, Yuan YZ, Li ZS. Pancreatic Cancer Incidence and Outcome in Relation to ABO Blood Groups Among Han Chinese Patients: A Case-Control Study. *Int J Cancer* (2011) 128:1179–86. doi: 10.1002/ijc.25426
10. Hofmann BT, Stehr A, Dohrmann T, Güngör C, Herich L, Hiller J, et al. ABO Blood Group Igm Isoagglutinins Interact With Tumor-Associated O-Glycan Structures in Pancreatic Cancer. *Clin Cancer Res* (2014) 20:6117–26. doi: 10.1158/1078-0432.CCR-14-0716
11. Hanprasertpong J, Jiamset I, Atjimakul T. Prognostic Value of ABO Blood Group in Patients With Early Stage Cervical Cancer Treated With Radical Hysterectomy With Pelvic Node Dissection. *Tumour Biol* (2016) 37:7421–30. doi: 10.1007/s13277-015-4626-1
12. Ohno Y. Words of Wisdom. Re: Impact of ABO Blood Type on Outcomes in Patients With Primary Nonmuscle Invasive Bladder Cancer. *Eur Urol* (2014) 66:391. doi: 10.1016/j.eururo.2014.05.023
13. Kaffenberger SD, Morgan TM, Stratton KL, Boachie AM, Barocas DA, Chang SS, et al. ABO Blood Group is a Predictor of Survival in Patients Undergoing Surgery for Renal Cell Carcinoma. *BJU Int* (2012) 110:E641–6. doi: 10.1111/j.1464-410X.2012.11366.x
14. Seow LJ, Kwa SB, Teoh CK. A Preliminary Survey of ABO Blood Group Frequency in Nasopharyngeal Carcinoma in Chinese Patients. *Singapore Med J* (1964) 4:93–5.
15. Turkoz FP, Celenkoglu G, Dogu GG, Kalender ME, Coskun U, Alkis N, et al. Risk Factors of Nasopharyngeal Carcinoma in Turkey-an Epidemiological Survey of the Anatolian Society of Medical Oncology. *Asian Pac J Cancer Prev* (2011) 12:3017–21.
16. Sheng LM, Sun XJ, Zhang LZ, Su D. ABO Blood Group and Nasopharyngeal Carcinoma Risk in a Population of Southeast China. *Int J Cancer* (2013) 133:893–7. doi: 10.1002/ijc.28087
17. Lin K, Qiu F, Chen SL, He X, Peng SG, Chen H. Lack of Association Between the Distribution of ABO Blood Groups and Nasopharyngeal Carcinoma in a Population of Southern China. *J Cancer Res Ther* (2018) 14:785–8. doi: 10.4103/jcrt.JCRT_567_17
18. Lee AW, Ng WT, Chan LL, Hung WM, Chan CC, Sze HC, et al. Evolution of Treatment for Nasopharyngeal Cancer-Success and Setback in the Intensity-Modulated Radiotherapy Era. *Radiother Oncol* (2014) 110:377–84. doi: 10.1016/j.radonc.2014.02.003
19. Zhang B, Mo Z, Du W, Wang Y, Liu L, Wei Y. Intensity-Modulated Radiation Therapy Versus 2D-RT or 3D-CRT for the Treatment of Nasopharyngeal Carcinoma: A Systematic Review and Meta-Analysis. *Oral Oncol* (2015) 51:1041–6. doi: 10.1016/j.oraloncology.2015.08.005
20. Lee AW, Ma BB, Ng WT, Chan AT. Management of Nasopharyngeal Carcinoma: Current Practice and Future Perspective. *J Clin Oncol* (2015) 33:3356–64. doi: 10.1200/JCO.2015.60.9347
21. Zhang YX, Kang SY, Chen G, Fang WF, Wu X, You HJ, et al. ABO Blood Group, Epstein-Barr Virus Infection and Prognosis of Patients With non-Metastatic Nasopharyngeal Carcinoma. *Asian Pac J Cancer Prev* (2014) 15:7459–65. doi: 10.7314/apjcp.2014.15.17.7459
22. Peng H, Chen L, Li WF, Zhang Y, Liu LZ, Tian L, et al. Prognostic Correlations Between ABO Blood Group and Pre-Treatment Plasma Epstein-Barr Virus DNA in Patients With Nasopharyngeal Carcinoma Receiving Intensity-Modulated Radiotherapy. *PloS One* (2016) 11:e0166194. doi: 10.1371/journal.pone.0166194
23. Wang GN, Zhou S, Chen C, Chang H, Tao YL, Liu S, et al. O Blood Type Is Associated With Unfavorable Distant Metastasis-Free Survival in Female Patients With Nasopharyngeal Carcinoma: A Retrospective Study of 2439 Patients From Epidemic Area. *J Cancer* (2019) 10:1297–306. doi: 10.7150/jca.28372
24. Li G, Zheng RH, Qiu B, Huang LJ, Xia YF. Correlation Between ABO Blood Group and Prognosis of Nasopharyngeal Carcinoma. *J Pract Med* (2019) 35:2061–4. doi: 10.3969/j.issn.1006-5725.2019.13.007
25. Ouyang PY, Su Z, Mao YP, Xie FY. Prognostic Value of ABO Blood Group in Southern Chinese Patients With Established Nasopharyngeal Carcinoma. *Br J Cancer* (2013) 109:2462–6. doi: 10.1038/bjc.2013.559
26. Lichtenstein MJ, Mulrow CD, Elwood PC. Guidelines for Reading Case-Control Studies. *J Chronic Dis* (1987) 40:893–903. doi: 10.1016/0021-9681(87)90190-1
27. Liberati A, Altman DG, Tetzlaff J, Mulrow C, Gøtzsche PC, Ioannidis JP, et al. The PRISMA Statement for Reporting Systematic Reviews and Meta-Analyses of Studies That Evaluate Health Care Interventions: Explanation and Elaboration. *J Clin Epidemiol* (2009) 62:e1–34. doi: 10.1371/journal.pmed.1000100
28. Higgins JPT, Green S. *Cochrane Handbook for Systematic Reviews of Interventions Version 5.1.0. The Cochrane Collaboration*. (2011), Available: http://www.cochrane-handbook.org/. (Accessed 24 January 2011).
29. Tierney JF, Stewart LA, Ghersi D, Burdett S, Sydes MR. Practical Methods for Incorporating Summary Time-to-Event Data Into Meta-Analysis. *Trials* (2007) 8:16. doi: 10.1186/1745-6215-8-16
30. Aymard JP. Karl Landsteiner (1868-1943) and the Discovery of Blood Groups. *Transfus Clin Biol* (2012) 19:244–8. doi: 10.1016/j.tracli.2012.08.127
31. Yamamoto F, Clausen H, White T, Marken J, Hakomori S. Molecular Genetic Basis of the Histo-Blood Group ABO System. *Nature* (1990) 345:229–33. doi: 10.1038/345229a0
32. Wolpin BM, Kraft P, Gross M, Helzlsouer K, Bueno-de-Mesquita HB, Steplowski E, et al. Pancreatic Cancer Risk and ABO Blood Group Alleles: Results From the Pancreatic Cancer Cohort Consortium. *Cancer Res* (2010) 70:1015–23. doi: 10.1158/0008-5472.CAN-09-2993
33. Yi JL, Gao L, Huang XD, Li SY, Luo JW, Cai WM, et al. Nasopharyngeal Carcinoma Treated by Radical Radiotherapy Alone: Ten-Year Experience of a Single Institution. *Int J Radiat Oncol Biol Phys* (2006) 65:161–8. doi: 10.1016/j.ijrobp.2005.12.003
34. Chen LP, Han X. Anti-PD-1/PD-L1 Therapy of Human Cancer: Past, Present, and Future. *J Clin Invest* (2015) 125:3384–91. doi: 10.1172/JCI80011
35. Huang ZL, Liu S, Wang GN, Zheng SH, Ding SR, Tao YL, et al. The Prognostic Significance of PD−L1 and PD−1 Expression in Patients With Nasopharyngeal Carcinoma: A Systematic Review and Meta−Analysis. *Cancer Cell Int* (2019) 19:141. doi: 10.1186/s12935-019-0863-5
36. Benekli M, Güllü IH, Tekuzman G, Savaş MC, Hayran M, Hasçelik G, et al. Circulating Intercellular Adhesion Molecule-1 and E-Selectin Levels in Gastric Cancer. *Br J Cancer* (1998) 78:267–71. doi: 10.1038/bjc.1998.476
37. Paré G, Chasman DI, Kellogg M, Zee RY, Rifai N, Badola S, et al. Novel Association of ABO Histo-Blood Group Antigen With Soluble ICAM-1: Results of a Genome-Wide Association Study of 6,578 Women. *PloS Genet* (2008) 4:e1000118. doi: 10.1371/journal.pgen.1000118
38. Yu YQ, Dong WD, Zhou XR, Li SH. The Significance of Serum Soluble Intercellular Adhesion Molecule 1 and Transforming Growth Factor Alpha in Patients With Nasopharyngeal Carcinoma. *Arch Otolaryngol Head Neck Surg* (2004) 130:1205–8. doi: 10.1001/archotol.130.10.1205
39. Edgren G, Hjalgrim H, Rostgaard K, Norda R, Wikman A, Melbye M, et al. Risk of Gastric Cancer and Peptic Ulcers in Relation to ABO Blood Type: A Cohort Study. *Am J Epidemiol* (2010) 172:1280–5. doi: 10.1093/aje/kwq299
40. Maeda K, Shibutani M, Otani H, Nagahara H, Ikeya T, Iseki Y, et al. Inflammation Based Factors and Prognosis in Patients With Colorectal Cancer. *World J Gastrointest Oncol* (2015) 7:111–7. doi: 10.4251/wjgo.v7.i8.111

Conflict of Interest: The authors declare that the research was conducted in the absence of any commercial or financial relationships that could be construed as a potential conflict of interest.

frontiers in Oncology

ORIGINAL RESEARCH
published: 23 August 2021
doi: 10.3389/fonc.2021.714536

Multivariate NTCP Model of Hypothyroidism After Intensity-Modulated Radiotherapy for Nasopharyngeal Carcinoma

Guanzhu Shen[1,2†], Yinglin Peng[1,3†], Jian Li[4], Haijun Wu[5], Guangshun Zhang[1], Chong Zhao[1] and Xiaowu Deng[1*]*

[1] Department of Radiation Oncology, State Key Laboratory of Oncology in South China, Collaborative Innovation Center for Cancer Medicine, Sun Yat-sen University Cancer Center, Guangzhou, China, [2] Department of Radiation Oncology, The Third Affiliated Hospital of Sun Yat-sen University, Guangzhou, China, [3] School of Biomedical Engineering, Sun Yat-sen University, Guangzhou, China, [4] Department of Radiation Oncology, Central Hospital of Guangdong Nongken, Zhanjiang, China, [5] Department of Radiation Oncology, Cancer Center, First People's Hospital of Foshan, Affiliated Foshan Hospital of Sun Yat-sen University, Foshan, China

OPEN ACCESS

Edited by:
Yong Yin,
Shandong Cancer Hospital, China

Reviewed by:
Zhenjiang Li,
Shandong Cancer Hospital, China
Ye Tian,
Second Affiliated Hospital of Soochow University, China

***Correspondence:**
Xiaowu Deng
dengxw@sysucc.org.cn
Chong Zhao
zhaochong@sysucc.org.cn

[†]These authors have contributed equally to this work

Specialty section:
This article was submitted to Head and Neck Cancer, a section of the journal Frontiers in Oncology

Received: *25 May 2021*
Accepted: *06 August 2021*
Published: *23 August 2021*

Citation:
Shen G, Peng Y, Li J, Wu H, Zhang G, Zhao C and Deng X (2021) Multivariate NTCP Model of Hypothyroidism After Intensity-Modulated Radiotherapy for Nasopharyngeal Carcinoma. Front. Oncol. 11:714536. doi: 10.3389/fonc.2021.714536

Objective: To evaluate the incidence of hypothyroidism in patients with nasopharyngeal carcinoma after intensity-modulated radiotherapy (IMRT), analyze its correlation with multiple influencing factors such as thyroid exposure dose, thyroid volume, and gender, and construct a multivariate-based normal tissue complication probability (NTCP) model for the occurrence of hypothyroidism after IMRT.

Materials and Methods: The thyroid hormone levels of patients at different points in time before and after radiotherapy were tested, and statistics on the incidence of hypothyroidism after treatment were obtained. The dose-volume data of patients' thyroids were converted into EQD2 equivalent dose values. The correlation between hypothyroidism after radiotherapy and thyroid exposure dose, thyroid volume, gender, and other factors was analyzed, and an NTCP model was constructed.

Results: A total of 69 patients with nasopharyngeal carcinoma were enrolled in this study. Twelve months after radiotherapy, a total of 24 patients (34.8%) developed hypothyroidism. Univariate analysis and multivariate analysis revealed that the average thyroid dose and thyroid volume are the most important factors affecting hypothyroidism after radiotherapy. The NTCP model constructed based on the average dose and thyroid volume has a good degree of fit.

Conclusion: The volume and average dose of the thyroid gland are the key factors affecting the occurrence of hypothyroidism in patients with nasopharyngeal carcinoma after radiotherapy. The NTCP model constructed based on multivariate construction suggests that reducing the average dose of the thyroid to the greatest extent is an effective way to protect thyroid functions.

Keywords: nasopharyngeal carcinoma, intensity-modulated radiotherapy, hypothyroidism, EQD2, NTCP mode

INTRODUCTION

Radiotherapy-induced hypothyroidism (RHT) is one of the common late-stage toxic reactions in patients who have received cervical radiotherapy, and its incidence is as high as 20%–40% (1–3), which is higher than the incidence in the normal population. The occurrence of hypothyroidism after radiotherapy in most studies was concentrated within 5 years after radiotherapy, and it generally reached a peak approximately 1 to 3 years after radiotherapy (4–6).

Intensity-modulated radiation therapy (IMRT) is the main treatment for nasopharyngeal carcinoma. Notably, 70% to 80% of patients with nasopharyngeal carcinoma had cervical lymph node metastasis at the first diagnosis (7, 8), and prophylactic irradiation of the neck lymph node drainage area is inevitable. The thyroid is located in the prophylactic irradiation area of the neck and is exposed to higher doses of radiation. However, there are currently few reports on the incidence of hypothyroidism in nasopharyngeal cancer patients after IMRT. Huang et al. retrospectively analyzed the data of 98 nasopharyngeal cancer patients who received IMRT. The lower neck prophylactic irradiation area was given a prescribed dose of 54 Gy. The median follow-up period was 17 months, and the results showed that the average thyroid dose was 49.72 Gy, and the incidence of hypothyroidism was 33.7% (9). Hypothyroidism due to radiotherapy generally has an insidious onset and lacks typical symptoms and signs; therefore, it is often ignored by clinicians and patients.

Gender (10–12), age (5, 13, 14), and thyroid volume (10, 15) are factors that affect hypothyroidism after radiotherapy, but thyroid exposure dose is the most important factor (11, 16). The incidence of hypothyroidism increases with the exposure dose, and its specific threshold is still inconclusive. Kim et al. reported the follow-up results of 114 patients with head and neck tumors after radical radiotherapy. V45 = 50% is the threshold for hypothyroidism (17), and subsequent meta-analysis results additionally support this conclusion (18). However, some studies believe that V30 or V50 is the dose threshold for hypothyroidism (19–21).

The equivalent dose in 2 Gy fractions (EQD2) is the dose required to achieve the same biological effect as conventional fractionated radiotherapy with fractions of 2 Gy. IMRT can deliver different fractionated doses of radiation to target areas and organs at risk in the irradiation field. In the treatment of nasopharyngeal carcinoma using the simultaneous measurement technique, the fractionated dose of the primary tumor target area often exceeds the conventional fractions of 2 Gy/time, and the fractionated dose of organs at risk is often lower than that of conventional fractionation. However, the dose tolerance value of each organ at risk is calculated based on the biological effects of fractionated irradiation with 2 Gy fractions of conventional radiotherapy. It is impossible to accurately assess the biological effects and probability of possible damage depending on the physical dose for organs-at-risk obtained using an IMRT treatment planning system (TPS) alone. The thyroid is a late-reacting tissue and is greatly affected by fractionated doses. Therefore, in the case of IMRT, the threshold value of the dose-volume factor based on the physical dose cannot be a reference for the limited conditions of the plan design. Additionally, it is impossible to select a reasonable IMRT dose limit level directly based on the relationship between the thyroid injury probability and the dose-volume under conventional fractionated irradiation.

This study aims to assess the incidence of hypothyroidism after radiotherapy in patients with nasopharyngeal carcinoma, analyze the correlation between hypothyroidism after radiotherapy and possible influencing factors, and construct a normal tissue complication probability (NTCP) model for the occurrence of hypothyroidism after IMRT, based on the equivalent dose in 2 Gy fractions (EQD2). In addition, this model is used to guide the search for more reasonable conditions for thyroid dose optimization in IMRT.

MATERIALS AND METHODS

Case Screening

All patients were pathologically diagnosed with nasopharyngeal carcinoma and received nasopharyngeal + cervical IMRT at Sun Yat-sen University Cancer Center. No distant metastasis was observed in the first diagnosis. Further, there was no history of hyperthyroidism, thyroiditis, and other thyroid-related diseases before treatment and no history of thyroid surgery, as well as no medical or surgical history corresponding to pituitary-related diseases. Moreover, the thyroid functions [including thyroid stimulating hormone (TSH)] were normal before treatment, and regular follow-up and thyroid function tests were performed as required after the treatment.

Before treatment, and three months and twelve months after treatment, venous blood was drawn from the patients *via* the electrochemiluminescence method for thyroid function tests. The test items include free triiodothyronine 3 (fT3), free triiodothyronine 4 (fT4), TSH, and thyroid peroxidase antibody. The clinical diagnosis of hypothyroidism depends on the related symptoms and signs of hypothyroidism, the extent to which the serum TSH is higher than the normal upper limit, and the extent to which fT3 and fT4 are lower than the normal lower limit. If the patient has no clinical manifestations, but the TSH in the blood circulation is higher than the normal upper limit with or without fT3 and fT4 level abnormalities, the patient can be diagnosed with subclinical hypothyroidism.

Intensity-Modulated Radiotherapy and Dose Conversion

The target area delineation method and prescription dose administration of IMRT are described in our previously published literature (22). The treatment planning system (TPS) used Eclipse 11.0. The thyroid delineation entailed a layer-by-layer delineation of the thyroid structure based on enhanced CT scan images. The delineation range included the entire left and right lobes and isthmus of the thyroid, but no restriction was set for the thyroid dose.

The patients' IMRT regimen was exported from the TPS to an EQD2 calculation and evaluation software in DICOM RT format. The calculation software automatically calculated the pixel-by-pixel conversion of EQD2 according to the set thyroid

α/β value and the mature linear quadratic model calculation formula of radiobiology, and reconstructed the relevant EQD2 dose-volume parameters.

The EQD2 calculation formula is as follows: $EQD2 = D\frac{d+\alpha/\beta}{2+\alpha/\beta}$ where D is the total dose and d is the fractionated dose. We consulted reports in authoritative literature (23) and set the α/β value of the thyroid gland to be 3 Gy. The overlap between the thyroid and PTV2 was calculated according to the thyroid α/β value.

Data collection included the maximum thyroid dose Dmax, minimum dose Dmin, average dose Dmean, fractionated dose, V10 (percentage of thyroid volume where the exposure dose exceeded 10 Gy), V20, V30, V40, V45, V50, V60, V70, and thyroid volume after conversion to EQD2.

Data Analysis

SPSS 16.0 statistical analysis software was used for the analysis. Patients were divided into a hypothyroidism group and normal thyroid function group according to whether hypothyroidism occurred 12 months after treatment. If Dmean, age, and thyroid volume between the two groups conformed to the condition of normal homogeneity of variance, an independent sample T test was performed; otherwise, the rank sum test of independent samples was used, and the chi-square test was used for the comparison of categorical data such as gender, staging, and other factors. The thyroid hormone levels at different points in time (if they conformed to the normal homogeneity of variance) were analyzed by repeated measures analysis of variance and pairwise tests, and $p < 0.05$ was considered to indicate statistical significance.

According to whether hypothyroidism occurred 12 months after treatment, factors that may affect thyroid function, including gender, age, T stage, N stage, clinical stage, thyroid volume, Dmax, Dmin, Dmean, fractionated dose and V10 to V70, were analyzed by logistic regression analysis, one by one, to select independent influencing factors with statistical significance. Spearman correlation analysis was used to analyze the correlation between various factors, and representative factors were selected to perform logistic regression multi-factor analysis, by the forward method, to select the factors affecting the occurrence of thyroid function after radiotherapy and derive the logistic regression equation through fitting.

NTCP Model Construction

The NTCP model equation determined the mixture model for calculation (24, 25); the formula is as follows.

$$\mathrm{NTCP} = (1 + e^{-s})^{-1}$$

where *S* is the logistic regression equation derived through the fitting with factors selected by multi-factor analysis.

RESULTS

General Data of Patients

From August 2012 to January 2014, a total of 69 patients met the enrollment requirements and entered the study. Among them, 53 were males and 16 were females, with a median age of 43 years (11–64 years). The general data of all patients are shown in **(Table 1)**.

Changes in Thyroid Hormone Levels After Radiotherapy Compared to Those Before Radiotherapy

There was no significant difference in serum fT3 levels between different points in time. Twelve months after radiotherapy, the level of fT4 was significantly lower than that before radiotherapy ($p < 0.001$). The TSH level showed a continuous upward trend from before to after radiotherapy (pairwise comparison showed each $p < 0.001$). Twelve months after radiotherapy, the level of A-Thyroid peroxidase (A-TPO) was significantly higher than that before radiotherapy ($p = 0.011$) **(Figure 1)**.

Thyroid Dose and Volume

After converting the thyroid physical dose into EQD2, the median value of Dmin of the whole group was 21.34 ± 10.71 Gy (0.80 to 35.69 Gy); the median value of Dmax was 63.89 ± 4.39 Gy (51.42 to 74.89 Gy); the median value of Dmean was 41.79 ± 11.02 Gy (10.31 to 51.46 Gy); and the median value of fractionated dose was 1.37 ± 0.35 Gy (0.34 to 1.83 Gy).

The median thyroid volume was 16.60 ± 6.38 cc (8.19 – 42.00 cc). Through the K–S test (Kolmogorov–Smirnov test), it was known that the thyroid volume distribution approximately conformed to a normal distribution (Kolmogorov–Smirnov $Z = 0.968$, $p = 0.306$), as shown in **(Figure 2)**.

Hypothyroidism After Radiotherapy

The thyroid hormone levels of all patients before radiotherapy were within the normal range. Three months after radiotherapy,

TABLE 1 | Patient and treatment characteristics.

	No.	Percentage
Gender		
Male	53	76.8
Female	16	23.2
Age	43 (11–64) years old	
T stage*		
T1	5	7.3
T2	17	24.6
T3	35	50.7
T4	12	17.4
N stage*		
N0	11	15.9
N1	29	42.0
N2	27	39.1
N3	2	2.9
Clinical stage*		
I	2	2.9
II	17	24.6
III	38	55.1
IV	12	17.4
Treatment method		
Radiotherapy alone	11	15.9
Radiotherapy+chemotherapy	58	84.1

**According to the AJCC 7th Edition staging system.*

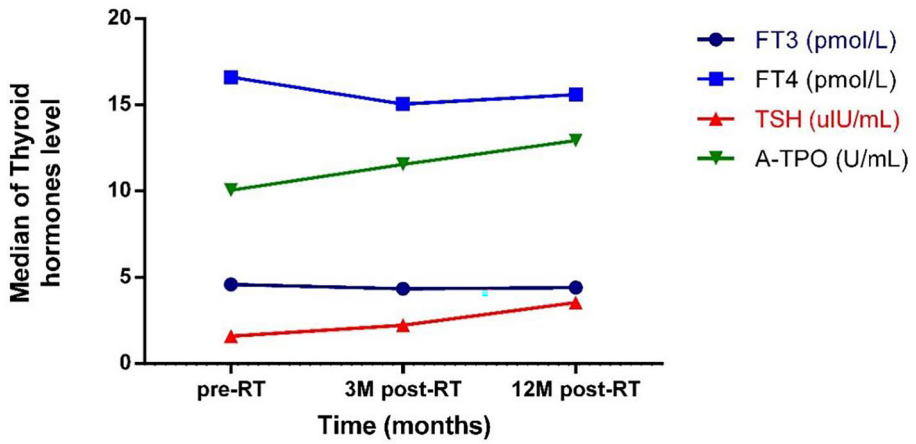

FIGURE 1 | The trend of the change of thyroid hormones level with time. pre-RT, previous radiotherapy; 3M post-RT, 3 months post radiotherapy; 12M post-RT, 12 months post radiotherapy; FT3, Free triiodothyronine 3; FT4, Free triiodothyronine 4; TSH, Thyroid stimulating hormone; A-TPO, A-Thyroid peroxidase.

6 patients developed hypothyroidism, the prevalence rate was 8.7%, of which 5 cases had subclinical hypothyroidism, including 3 males and 2 females. Additionally, there was a case of clinical hypothyroidism in a 45-year-old male patient. Twelve months after radiotherapy, there were 24 cases of abnormal thyroid function, including 2 cases of clinical hypothyroidism and 22 cases of subclinical hypothyroidism. The total incidence of hypothyroidism was 34.8%, of which 16 patients were male and 8 patients were female and both patients with clinical hypothyroidism were male. The patients were categorized into the hypothyroidism group (24 cases) and normal thyroid function group (45 cases) according to whether hypothyroidism occurred twelve months after radiotherapy, and the differences between the two groups were statistically analyzed. There was a significant difference in age between the two groups (median age: 39 years in the hypothyroid group *vs.* 45 years in the normal

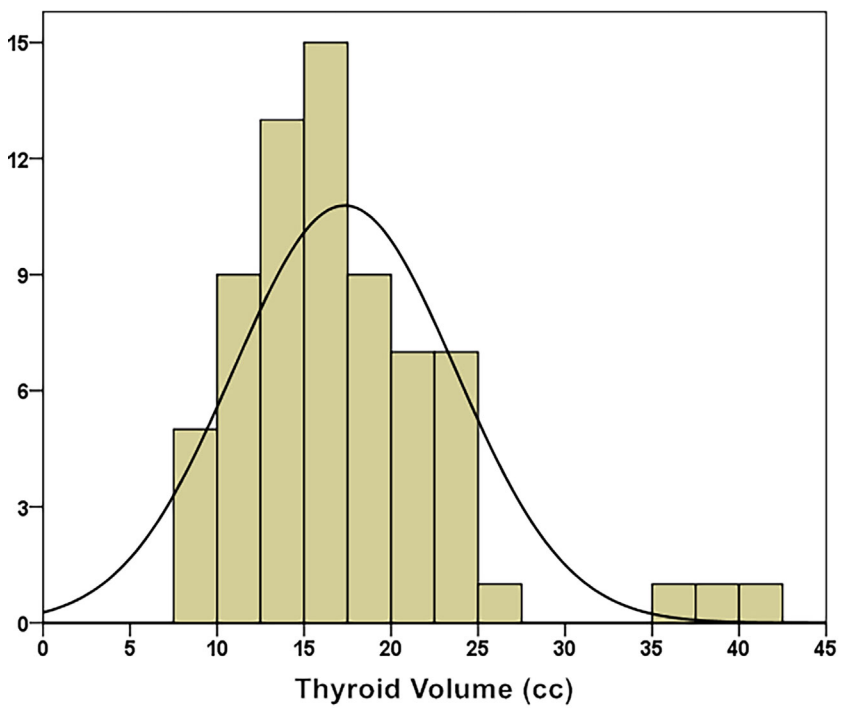

FIGURE 2 | Thyroid volume distribution of 69 patients.

group, p = 0.005). There was no statistical difference in gender, T, N staging, and clinical staging.

The median value of Dmin in the two groups was 24.86 ± 7.92 Gy in the hypothyroidism group *vs.* 16.00 ± 10.65 Gy in the normal group (p = 0.001). The median values of Dmax were: 64.29 ± 4.61 Gy in the hypothyroidism group *vs.* 63.62 ± 4.31 Gy in the normal group (p = 0.681). The median value of Dmean was 46.54 ± 7.37 Gy in the hypothyroidism group *vs.* 38.44 ± 11.45 Gy in the normal group, (p = 0.001). The median thyroid volumes of the two groups were: 13.46 ± 3.86 cc (8.19 to 20.50 cc) in the hypothyroidism group *vs.* 17.10 ± 6.80 cc (8.80 to 42.00 cc) in the normal group (p = 0.001); the thyroid volume in the hypothyroidism group was significantly smaller than that of the normal thyroid function group.

Logistic Univariate Analysis and Multivariate Analysis

Logistic univariate regression analysis revealed that age, Dmin, Dmean, V20 to V50, and thyroid volume were all related factors that affected the occurrence of hypothyroidism. Because there might be certain correlations between the above-mentioned related factors, Spearman correlation analysis was used to analyze the related factors that affected the occurrence of hypothyroidism, and Spearman coefficient > 0.8 was used as the criterion to select representative factors. The results showed that Dmean had a strong correlation with Dmin, V20 to V50 (Spearman correlation coefficients were all > 0.8), while age and thyroid volume had a relatively weak correlation with other factors.

The three independent factors of age, Dmean, and thyroid volume were analyzed by logistic multivariate regression analysis. The results showed that Dmean (p = 0.016) and thyroid volume (p = 0.011) were independent prognostic factors **(Table 2)**.

The logistic equation obtained after fitting is

$$S = -1.385 + (0.093 \times \text{Dmean}) + (-0.188 \times \text{thyroid volume})$$

Normal Tissue Complication Probability Model

According to the calculation method of the mixture model, the following NTCP calculation formula is obtained:

NTCP = $(1 + e^{S})^{-1}$, where S = -1.385 + (0.093 × Dmean) + (-0.188 × thyroid volume), the unit of Dmean is Gy, and the unit of thyroid volume is cc. This equation has passed the goodness of fit test (Hosmer–Lemeshow: p = 0.698) and has a good degree of fit, indicating that the probability of hypothyroidism is positively correlated with the average thyroid dose, and it increases with an increase in the average thyroid dose (OR value = 1.098/Gy, 95% confidence interval of the OR value: 1.018 to 1.184). Contrastingly, the probability of hypothyroidism is negatively correlated with thyroid volume: as the thyroid volume decreases, the probability of hypothyroidism increases (OR value = 0.829/cc, 95% confidence interval of OR value: 0.717 to 0.958).

In this study, the thyroid volume of 69 patients was mostly concentrated from 10 cc to 25 cc; thus, the thyroid volume was divided into four levels: 10 cc, 15 cc, 20 cc, and 25 cc, and the corresponding NTCP curves were drawn, as shown in **(Figure 3)**. There were two variables in the NTCP model, and the distribution of thyroid volume conformed to the normal distribution. Taking the median thyroid volume of 16.60 cc, the TD5/1 and TD10/1 of RHT were calculated as 16.67Gy and 24.77Gy, respectively.

DISCUSSION

Hypothyroidism is one of the common complications of head and neck tumors and nasopharyngeal cancer among patients

TABLE 2 | Univariate analysis and multivariate analysis of radiation induced hypothyroidism.

Parameters	Univariate		Multivariate	
	Hazard ratio (95% CI)	P-value	Hazard ratio (95% CI)	P-value
Gender	2.312 (0.738-7.245)	0.15		
Age	0.934 (0.887-0.984)	0.01	0.957 (0.906-1.011)	0.12
T-classification	1.920 (0.973-3.789)	0.06		
N-classification	1.579 (0.830-3.107)	0.186		
Clinical stage	1.702 (0.820-3.531)	0.153		
Chemotherapy	6.571 (0.787-54.851)	0.082		
Fractionated dose	1.358 (0.869-2.123)	0.179		
Dmin	1.001 (1.000-1.002)	0.002		
Dmax	1.000 (0.999-1.001)	0.676		
Dmean	1.001 (1.000-1.002)	0.004	1.001 (1.000-1.002)	0.016
V10	1.046 (0.999-1.095)	0.053		
V20	1.046 (1.006-1.088)	0.023		
V30	1.038 (1.012-1.066)	0.004		
V40	1.046 (1.020-1.073)	0.001		
V45	1.046 (1.018-1.075)	0.001		
V50	1.052 (1.017-1.089)	0.004		
V60	1.056 (0.979-1.139)	0.156		
V70	0.580 (0.026-12.933)	0.731		
Volume	0.808 (0.703-0.928)	0.003	0.838 (0.721-0.975)	0.011

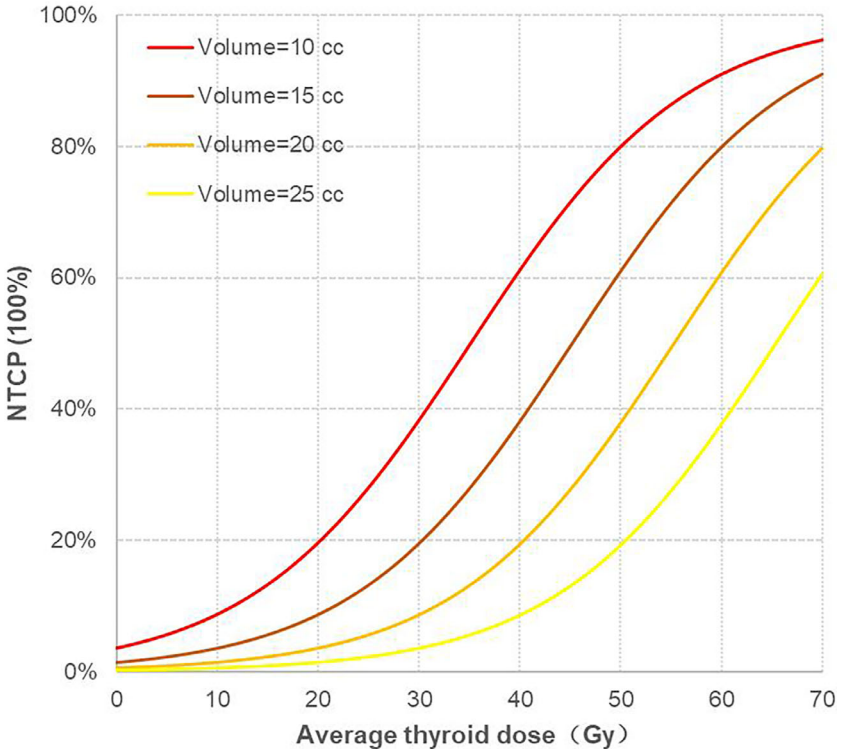

FIGURE 3 | Corresponding NTCP curves of four different thyroid volume levels. NTCP, normal tissue complication probability.

after receiving cervical radiotherapy. Previous studies mostly involved patients who received radiotherapy for head and neck tumors. However, patients with head and neck tumors often underwent surgery before radiotherapy. The results of a meta-analysis show that patients who underwent hemithyroidectomy or surgery in the neck that did not involve the thyroid gland had a higher incidence of hypothyroidism (18). Radiotherapy is the main treatment for nasopharyngeal cancer, in contrast with the case of head and neck tumors. Previously, there were few reports of hypothyroidism in patients with nasopharyngeal carcinoma after radiotherapy. Wu et al. reported the occurrence of hypothyroidism in 408 patients with nasopharyngeal carcinoma who received conventional radiotherapy or three-dimensional radiotherapy; the incidence of hypothyroidism after 5 years of treatment was 24.7% (2). After the treatment of nasopharyngeal carcinoma entered the era of IMRT, the incidence of hypothyroidism has increased. Studies have shown that among nasopharyngeal carcinoma patients who received IMRT, 33.7% of patients had hypothyroidism at a median period of 17 months after radiotherapy (9); Zhai et al. reported that after patients with nasopharyngeal carcinoma received IMRT, the incidence of hypothyroidism after 2 and 3 years was 29.6% and 43.9%, respectively (26). In this study, 34.8% of patients who used IMRT had hypothyroidism 12 months after radiotherapy, which was close to the results of previous studies. The main reason for the significant increase in the incidence of hypothyroidism may be as follows: In IMRT, the radiation dose in the prophylactic cervical irradiation area, especially the metastatic cervical lymph nodes, is significantly higher than that of conventional radiotherapy to obtain a better area control rate, and the exposure dose of the thyroid, which is close to the prophylactic cervical irradiation area, is correspondingly increased; secondly, when conventional radiotherapy is used for prophylactic irradiation of the neck, a 3 cm wide lead shield is usually set in the front tangent field of the neck to protect the spinal cord. Therefore, the thyroid can be partially blocked by the lead shield, thereby avoiding exposure to higher doses of radiation.

In this study, it can be observed from the trend of hormone levels that the thyroid fT3 level decreased slightly after radiotherapy; the serum fT4 level decreased significantly, while the serum TSH level and A-TPO level continued to increase after treatment. This trend is consistent with the previous research results of Lin et al. (27). Studies have confirmed that thyroid autoantibodies are one of the important factors in the occurrence of hypothyroidism after radiotherapy (14, 28, 29). The study by Lin et al. found that the serum A-TPO level of nasopharyngeal carcinoma patients who had hypothyroidism after radiotherapy was significantly higher than that of patients with normal thyroid function, and the serum A-TPO level of patients was negatively correlated with fT4 levels (27). A study observed significant increases in thyroid inflammation-related indicators such as thyroid vascular pulsatility index and resistance index after radiotherapy under Doppler ultrasound, and it is believed that thyroid inflammation due to radiation damage is an important link in the occurrence of hypothyroidism after radiotherapy (30). Moreover, inflammation of the thyroid can

stimulate the production of A-TPO, which may further aggravate the damage to the thyroid.

Since the nasopharynx is adjacent to the sphenoid bone and the pituitary fossa, the pituitary is often exposed to higher doses due to its proximity to the target area. Central hypothyroidism due to insufficient secretion of the trophic hormone by the pituitary gland is characterized by serum TSH levels that are lower than normal, with or without abnormal serum fT3 and fT4 levels. A recent report retrospectively analyzed 135 cases of hypothyroidism in nasopharyngeal carcinoma patients after IMRT treatment. The median follow-up period was 34.1 months. Notably, 28.9% (39/135) of the patients had primary hypothyroidism and no central hypothyroidism occurred (26), which is similar to the results reported by McDowell et al. (31). Additionally, there are many studies showing that the pituitary dose does not affect the occurrence of central hypothyroidism after radiotherapy, and the thyroid radiation dose is an influencing factor for the occurrence of primary hypothyroidism after radiotherapy (32, 33). In this study, only 2 patients in the entire group showed a continuous small drop in serum TSH levels three months and twelve months after radiotherapy compared with the levels before radiotherapy, but no patients had serum TSH levels lower than normal after radiotherapy, proving that no patients experienced the decompensation of pituitary functions.

In this study, the NTCP model of hypothyroidism constructed based on EQD2 showed that thyroid volume and average dose are two independent factors that affect the occurrence of hypothyroidism after radiotherapy, which is consistent with the results of multiple previous studies (15, 20, 24). However, some researchers tend to believe that a specific dose-volume value, such as VS60, V40, or V50, is a risk factor for hypothyroidism (5, 19, 34). The results of this study show that Dmean is one of the most important factors influencing the occurrence of hypothyroidism after radiotherapy, and its impact is greater than that of any of the indicators among V20 to V50, which additionally means that the occurrence of hypothyroidism is not affected only by the percentage of the volume of the thyroid that receives high doses of radiation. Because even if the percentage of thyroid volume exposed to high doses is very small, the overall thyroid exposure dose Dmean can still be high and increase the risk of hypothyroidism. This is in line with the relevant previous hypothesis about the mechanism of hypothyroidism after radiotherapy: that is, in addition to the damage to thyroid acinar cells, radiation can cause damage to the endothelial cells of thyroid nutrient vessels, leading to atherosclerosis, narrowing of the lumen, and insufficient blood supply to the thyroid gland (29, 30, 35, 36). In addition, thyroid inflammation due to radiotherapy leads to increased levels of thyroid autoantibodies, and autoimmune reactions between thyroid autoantibodies such as A-TPO and the thyroid may additionally play a damaging role in the occurrence of hypothyroidism (27, 37). Although the percentage of thyroid volume exposed to high doses is very small, local ischemia and the autoantibody immune response of thyroid can still affect the secretory function of the entire thyroid. Therefore, when evaluating IMRT plans for patients with nasopharyngeal carcinoma, simply using a certain dose-volume threshold such as V20 to V50 for the thyroid dose assessment may underestimate the risk of hypothyroidism, and it may be more reasonable to use Dmean for the assessment.

Thyroid volume is another key factor that affects the occurrence of hypothyroidism after radiotherapy. Studies have shown that for every 1 cc increase in the thyroid volume before treatment, the incidence of hypothyroidism can be reduced by 7% (6). Additionally, our study observed that there is a negative correlation between the thyroid volume and the occurrence of hypothyroidism, that is, the larger the thyroid volume before treatment, the lower the risk of hypothyroidism after radiotherapy. Thyroid volume is a protective factor for hypothyroidism after radiotherapy. which is consistent with the results of multiple previous studies (1, 6, 24).

The cases number met the enrollment criteria and entered this study were relatively small at the time, it was not able to create an adequate validation data set for external verification of the NTCP model. In addition, the time of follow-up was not long enough to assess the incidence of hypothyroidism at 3 or 5 years after radiotherapy. Muthy et al. (38) reported the hypothyroidism after radiotherapy in 122 patients with advanced head and neck tumors in a median follow-up time of 41 months, the peak of hypothyroidism occurred about 1 year after receiving radiotherapy (median time of subclinical hypothyroidism was 11.5 months, and median time of clinical hypothyroidism was 14.5 months). For the median thyroid volume of 16.60 cc, our study shown that the TD5/1 and TD10/1 of radiation induced hypothyroidism were 16.67Gy and 24.77Gy, respectively. Further study to expand and verify the model is undergoing and will be reported when enough cases are collected.

Overall, this study constructed an EQD2-based NTCP model of hypothyroidism after IMRT for nasopharyngeal carcinoma, which can provide an accurate basis for a more optimized thyroid dose restriction strategy. Accurately delineating the scope of the thyroid gland and regarding it as an organ at risk for dose restriction according to the NTCP model is the basis for reducing the occurrence of hypothyroidism. For a certain thyroid volume, the average thyroid dose should be reduced to the greatest extent. When selecting IMRT techniques, a multi-leave-collimator with a higher resolution should be used to maximize the dose conformity of the target area and increase the dose gradient between the radiotherapy target zone and the thyroid, which is a feasible dose optimization scheme.

DATA AVAILABILITY STATEMENT

The datasets presented in this study can be found in online repositories. The names of the repository/repositories and accession number(s) can be found below: https://www.researchdata.org.cn (RDD number: RDDA2021001995).

ETHICS STATEMENT

Our study was reviewed and approved by the IRB committee of Sun Yat-sen University Cancer Center, with

the approval number of B2021-234. As this study is only a retrospective analysis, informed consent exemption was approved.

AUTHOR CONTRIBUTIONS

XD and CZ contributed conception and design of the study. GS, YP, JL, HW, and GZ organized the database. YP, JL, HW, and GZ performed the statistical analysis. GS wrote the first draft of the manuscript. GS and YP wrote sections of the manuscript. All authors contributed to the article and approved the submitted version.

FUNDING

This work was jointly supported by National Natural Science Foundation of China (12005316), and Cancer Precision Radiotherapy Spark Program of China International Medical Foundation (2019-N-11-20).

SUPPLEMENTARY MATERIAL

The Supplementary Material for this article can be found online at: https://www.frontiersin.org/articles/10.3389/fonc.2021.714536/full#supplementary-material

REFERENCES

1. Ronjom MF, Brink C, Bentzen SM, Hegedus L, Overgaard J, Johansen J. Hypothyroidism After Primary Radiotherapy for Head and Neck Squamous Cell Carcinoma: Normal Tissue Complication Probability Modeling With Latent Time Correction. *Radiother Oncol* (2013) 109:317–22. doi: 10.1016/j.radonc.2013.06.029
2. Wu YH, Wang HM, Chen HW, Lin CY, Chen YC, Fan KH, et al. Hypothyroidism After Radiotherapy for Nasopharyngeal Cancer Patients. *Int J Radiat Oncol Biol Phys* (2010) 76:1133–9. doi: 10.1016/j.ijrobp.2009.03.011
3. Peng L, Mao YP, Huang CL, Guo R, Tang LL. A New Model for Predicting Hypothyroidism After Intensity-Modulated Radiotherapy for Nasopharyngeal Carcinoma. *Front Oncol* (2020) 10:551255. doi: 10.3389/fonc.2020.551255
4. Lin Z, Yang Z, He B, Wang D, Gao X, Shing-Yau T, et al. Pattern of Radiation-Induced Thyroid Gland Changes in Nasopharyngeal Carcinoma Patients in 48 Months After Radiotherapy. *PloS One* (2018) 13:e200310. doi: 10.1371/journal.pone.0200310
5. Sommat K, Ong WS, Hussain A, Soong YL, Fong KW. Thyroid V40 Predicts Primary Hypothyroidism After Intensity Modulated Radiation Therapy for Nasopharyngeal Carcinoma. *Int J Radiat Oncol Biol Phys* (2017) 98:574–80. doi: 10.1016/j.ijrobp.2017.03.007
6. Diaz R, Jaboin JJ, Morales-Paliza M, Koehler E, Phillips JG, Stinson S, et al. Hypothyroidism as a Consequence of Intensity-Modulated Radiotherapy With Concurrent Taxane-Based Chemotherapy for Locally Advanced Head-and-Neck Cancer. *Int J Radiat Oncol Biol Phys* (2010) 77:468–76. doi: 10.1016/j.ijrobp.2009.05.018
7. Guo R, Wu H, Wang J, Lian CL, He ZY, Zhang WW, et al. Lymph Node Status and Outcomes for Nasopharyngeal Carcinoma According to Histological Subtypes: A SEER Population-Based Retrospective Analysis. *Adv Ther* (2019) 36(11):3123–33. doi: 10.1007/s12325-019-01100-7
8. Shen G, Xiao W, Han F, Fan W, Lin PX, Lu L, et al. Advantage of PET/CT in Target Delineation of MRI-Negative Cervical Lymph Nodes In Intensity-Modulated Radiation Therapy Planning for Nasopharyngeal Carcinoma. *J Cancer* (2017) 8:4117–23. doi: 10.7150/jca.21582
9. Huang S, Wang X, Hu C, Ying H. Hypothalamic-Pituitary-Thyroid Dysfunction Induced by Intensity-Modulated Radiotherapy (IMRT) for Adult Patients With Nasopharyngeal Carcinoma. *Med Oncol* (2013) 30:710. doi: 10.1007/s12032-013-0710-9
10. Luo R, Wu VWC, He B, Gao X, Xu Z, Wang D, et al. Development of a Normal Tissue Complication Probability (NTCP) Model for Radiation-Induced Hypothyroidism in Nasopharyngeal Carcinoma Patients. *BMC Cancer* (2018) 18:575. doi: 10.1186/s12885-018-4348-z
11. Xu Y, Shao Z, Tang T, Liu G, Yao Y, Wang J, et al. A Dosimetric Study on Radiation-Induced Hypothyroidism Following Intensity-Modulated Radiotherapy in Patients With Nasopharyngeal Carcinoma. *Oncol Lett* (2018) 16:6126–32. doi: 10.3892/ol.2018.9332
12. Siala W, Mnejja W, Abid M, Ghorbel A, Frikha M, Daoud J. Thyroid Toxicity After Radiotherapy of Nasopharyngeal Carcinoma. *Ann Endocrinol (Paris)* (2011) 72:19–23. doi: 10.1016/j.ando.2010.06.005
13. Ulger S, Ulger Z, Yildiz F, Ozyar E. Incidence of Hypothyroidism After Radiotherapy for Nasopharyngeal Carcinoma. *Med Oncol* (2007) 24:91–4. doi: 10.1007/BF02685908
14. Hancock SL, McDougall IR, Constine LS. Thyroid Abnormalities After Therapeutic External Radiation. *Int J Radiat Oncol Biol Phys* (1995) 31:1165–70. doi: 10.1016/0360-3016(95)00019-U
15. Ronjom MF, Brink C, Bentzen SM, Hegedüs L, Overgaard J, Petersen JBB, et al. External Validation of a Normal Tissue Complication Probability Model for Radiation-Induced Hypothyroidism in an Independent Cohort. *Acta Oncol* (2015) 54:1301–9. doi: 10.3109/0284186X.2015.1064160
16. Haciislamoglu E, Canyilmaz E, Gedik S, Aynaci O, Serdar L, Yoney A. Effect of Dose Constraint on the Thyroid Gland During Locoregional Intensity-Modulated Radiotherapy in Breast Cancer Patients. *J Appl Clin Med Phys* (2019) 20:135–41. doi: 10.1002/acm2.12668
17. Kim MY, Yu T, Wu HG. Dose-Volumetric Parameters for Predicting Hypothyroidism After Radiotherapy for Head and Neck Cancer. *JPN J Clin Oncol* (2014) 44:331–7. doi: 10.1093/jjco/hyt235
18. Vogelius IR, Bentzen SM, Maraldo MV, Petersen PM, Specht L. Risk Factors for Radiation-Induced Hypothyroidism: A Literature-Based Meta-Analysis. *CANCER-AM Cancer Soc* (2011) 117:5250–60. doi: 10.1002/cncr.26186
19. Sachdev S, Refaat T, Bacchus ID, Sathiaseelan V, Mittal BB. Thyroid V50 Highly Predictive of Hypothyroidism in Head-and-Neck Cancer Patients Treated With Intensity-Modulated Radiotherapy (IMRT). *Am J Clin Oncol* (2017) 40:413–7. doi: 10.1097/COC.0000000000000165
20. Akgun Z, Atasoy BM, Ozen Z, Yavuz D, Gulluoglu B, Sengoz M, et al. V30 as a Predictor for Radiation-Induced Hypothyroidism: A Dosimetric Analysis in Patients Who Received Radiotherapy to the Neck. *Radiat Oncol* (2014) 9:104. doi: 10.1186/1748-717X-9-104
21. Zhou L, Chen J, Shen W, Chen ZL, Huang S, Tao CJ, et al. Thyroid V50 is a Risk Factor for Hypothyroidism in Patients With Nasopharyngeal Carcinoma Treated With Intensity-Modulated Radiation Therapy: A Retrospective Study. *Radiat Oncol* (2020) 15:68. doi: 10.1186/s13014-020-01490-x
22. Peng YL, Chen L, Shen GZ, Li YN, Yao JJ, Xiao WW, et al. Interobserver Variations in the Delineation of Target Volumes and Organs at Risk and Their Impact on Dose Distribution in Intensity-Modulated Radiation Therapy for Nasopharyngeal Carcinoma. *Oral Oncol* (2018) 82:1–7. doi: 10.1016/j.oraloncology.2018.04.025
23. Bakhshandeh M, Hashemi B, Mahdavi SR, Nikoofar A, Vasheghani M, Kazemnejad A. Normal Tissue Complication Probability Modeling of Radiation-Induced Hypothyroidism After Head-and-Neck Radiation Therapy. *Int J Radiat Oncol Biol Phys* (2013) 85:514–21. doi: 10.1016/j.ijrobp.2012.03.034
24. Boomsma MJ, Bijl HP, Christianen ME, Beetz I, Langendijk JA. A Prospective Cohort Study on Radiation-Induced Hypothyroidism: Development of an NTCP Model. *Int J Radiat Oncol Biol Phys* (2012) 84:e351–6. doi: 10.1016/j.ijrobp.2012.05.020

25. Bentzen SM, Thames HD, Travis EL, Ang KK, Emmanuelet VDS, Dewit L, et al. Direct Estimation of Latent Time for Radiation Injury in Late-Responding Normal Tissues: Gut, Lung, and Spinal Cord. *Int J Radiat Biol* (1989) 55:27–43. doi: 10.1080/09553008914550041
26. Zhai RP, Kong FF, Du CR, Hu CS, Ying HM. Radiation-Induced Hypothyroidism After IMRT for Nasopharyngeal Carcinoma: Clinical and Dosimetric Predictors in a Prospective Cohort Study. *Oral Oncol* (2017) 68:44–9. doi: 10.1016/j.oraloncology.2017.03.005
27. Lin Z, Chen L, Fang Y, Cai A, Zhang T, Wu VWC. Longitudinal Study on the Correlations of Thyroid Antibody and Thyroid Hormone Levels After Radiotherapy in Patients With Nasopharyngeal Carcinoma With Radiation-Induced Hypothyroidism. *Head Neck* (2014) 36:171–5. doi: 10.1002/hed.23285
28. Cutuli B, Quentin P, Rodier JF, Barakat P, Grob JC. Severe Hypothyroidism After Chemotherapy and Locoregional Irradiation for Breast Cancer. *Radiother Oncol* (2000) 57:103–5. doi: 10.1016/S0167-8140(00)00183-3
29. Cannon CR. Hypothyroidism in Head and Neck Cancer Patients: Experimental and Clinical Observations. *Laryngoscope* (1994) 104:1–21. doi: 10.1288/00005537-199411001-00001
30. Bakhshandeh M, Hashemi B, Mahdavi SR, Nikoofar A, Edraki HR, Kazemnejad A. Evaluation of Thyroid Disorders During Head-and-Neck Radiotherapy by Using Functional Analysis and Ultrasonography. *Int J Radiat Oncol Biol Phys* (2012) 83:198–203. doi: 10.1016/j.ijrobp.2011.05.064
31. Mcdowell LJ, Rock K, Wei X, Chan B, Ringash J. Long-Term Late Toxicity, Quality of Life, and Emotional Distress in Patients With Nasopharyngeal Carcinoma Treated With Intensity Modulated Radiation Therapy. *Int J Radiat Oncol Biol Phys* (2018) 102:340–52. doi: 10.1016/j.ijrobp.2018.05.060
32. Lin Z, Wang X, Xie W, Yang Z, Che K, Wu VW. Evaluation of Clinical Hypothyroidism Risk Due to Irradiation of Thyroid and Pituitary Glands in Radiotherapy of Nasopharyngeal Cancer Patients. *J Med Imaging Radiat Oncol* (2013) 57:713–8. doi: 10.1111/1754-9485.12074
33. Bhandare N, Kennedy L, Malyapa RS, Morris CG, Mendenhall WM. Primary and Central Hypothyroidism After Radiotherapy for Head-and-Neck Tumors. *Int J Radiat Oncol Biol Phys* (2007) 68:1131–9. doi: 10.1016/j.ijrobp.2007.01.029
34. Lertbutsayanukul C, Kitpanit S, Prayongrat A, Kannarunimit D, Netsawang B, Chakkabat C. Validation of Previously Reported Predictors for Radiation-Induced Hypothyroidism in Nasopharyngeal Cancer Patients Treated With Intensity-Modulated Radiation Therapy, a Post Hoc Analysis From a Phase III Randomized Trial. *J Radiat Res* (2018) 59:446–55. doi: 10.1093/jrr/rry036
35. Zhang SY, Park KW, Oh S, Cho HJ, Lee MM. NF-kappaB Decoy Potentiates the Effects of Radiation on Vascular Smooth Muscle Cells by Enhancing Apoptosis. *Exp Mol Med* (2005) 37:18–26. doi: 10.1038/emm.2005.3
36. Feehs RS, McGuirt WF, Bond MG, Strickland HL, Craven TE, Hiltbrand JB. Irradiation. A Significant Risk Factor for Carotid Atherosclerosis. *Arch Otolaryngol Head Neck Surg* (1991) 117:1135–7. doi: 10.1001/archotol.1991.01870220083014
37. Lo GA, Remco DB, Kuik DJ, Lips PTAM, Mary B, Blomberg BME, Agrawal JP. The Prevalence of Hypothyroidism After Treatment for Laryngeal and Hypopharyngeal Carcinomas: Are Autoantibodies of Influence? *Acta Otolaryngol* (2007) 127:312–7. doi: 10.1080/00016480600818096
38. Murthy V, Narang K, Ghosh-Laskar S, Gupta T, Budrukkar A, et al. Hypothyroidism After 3-Dimensional Conformal Radiotherapy and Intensity-Modulated Radiotherapy for Head and Neck Cancers: Prospective Data From 2 Randomized Controlled Trials. *Head Neck* (2014) 36:1573–80. doi: 10.1002/hed.23482

Conflict of Interest: The authors declare that the research was conducted in the absence of any commercial or financial relationships that could be construed as a potential conflict of interest.

Publisher's Note: All claims expressed in this article are solely those of the authors and do not necessarily represent those of their affiliated organizations, or those of the publisher, the editors and the reviewers. Any product that may be evaluated in this article, or claim that may be made by its manufacturer, is not guaranteed or endorsed by the publisher.

frontiers in Oncology

ORIGINAL RESEARCH
published: 23 August 2021
doi: 10.3389/fonc.2021.709622

Prognostic Relevance of 18F-FDG-PET/CT-Guided Target Volume Delineation in Loco-Regionally Advanced Nasopharyngeal Carcinomas: A Comparative Study

*Ouying Yan[1,2], Hui Wang[1], Yaqian Han[1], Shengnan Fu[1,2], Yanzhu Chen[1,2] and Feng Liu[1]**

[1] Department of Radiation Oncology, Hunan Cancer Hospital and The Affiliated Cancer Hospital of Xiangya School of Medicine, Central South University, Changsha, China, [2] The Affiliated Cancer Hospital of Xiangya School of Medicine, Central South University, Changsha, China

OPEN ACCESS

Edited by:
Moran Amit,
University of Texas MD Anderson Cancer Center, United States

Reviewed by:
Shorook Na'Ara,
University of California, San Francisco, United States
Wenbing Lv,
Southern Medical University, China

***Correspondence:**
Feng Liu
liufeng820111@163.com

Specialty section:
This article was submitted to Head and Neck Cancer, a section of the journal Frontiers in Oncology

Received: *14 May 2021*
Accepted: *04 August 2021*
Published: *23 August 2021*

Citation:
Yan OY, Wang H, Han YQ, Fu SN, Chen YZ and Liu F (2021) Prognostic Relevance of 18F-FDG-PET/CT-Guided Target Volume Delineation in Loco-Regionally Advanced Nasopharyngeal Carcinomas: A Comparative Study. Front. Oncol. 11:709622. doi: 10.3389/fonc.2021.709622

Introduction: An optimal approach to define tumor volume in locoregionally advanced nasopharyngeal carcinoma (NPC) using 18F-fluorodeoxyglucose positron emission tomography/computed tomography (FDG-PET/CT) remains unclear. This retrospective study aimed at comparing the outcomes and toxicities of different FDG-PET/CT-guided techniques for primary tumor volume delineation in locoregionally advanced NPC.

Methods: From August 2015 to February 2018, 292 patients with stage III-IVB NPC received FDG-PET/CT-guided IMRT. Three PET/CT-based techniques were used to determine the gross tumor volume (GTV) as follows: visual criteria (group A; n = 98), a standard uptake value (SUV) threshold of 2.5 (group B; n = 95), and a threshold of 50% maximal intensity (group C, n = 99) combined with a dose-painting technique.

Results: In groups A, B, and C, the 5-year LRFS rates were 89.4%, 90.0%, and 97.8%, respectively (p = 0.043). The 5-year DMFS rates were 75.1%, 76.0%, and 87.7%, respectively (p = 0.043). The 5-year DFS rates were 70.9%, 70.3%, and 82.2%, respectively (p = 0.048). The 5-year OS rates were 73.5%, 73.9%, and 84.9%, respectively (p = 0.038). Group C showed significantly higher 5-year LRFS, LRRFS, DMFS, DFS, and OS than those in groups A and B ($p < 0.05$). No statistically significant differences were observed between the three study groups in the cumulative incidences of grade 3-4 acute and late toxicities. Multivariate analyses showed that the PET/CT-guided technique for target volume delineation was an independent prognostic factor for 5-year LRFS, DFS, DMFS, and OS (p = 0.039, p = 0.030, p = 0.035 and p = 0.028, respectively), and was marginally significant in predicting LRRFS (p = 0.080).

Conclusions: The 50% SUVmax threshold regimen for GTV delineation with dose-painting appeared to be superior to the visual criteria or SUV2.5 threshold in locoregionally advanced NPC, and there was no increased toxicity.

Keywords: FDG-PET/CT, prognosis, nasopharyngeal carcinoma, chemoradiotherapy, intensity-modulated radiation therapy

INTRODUCTION

Nasopharyngeal carcinoma (NPC) is a radiosensitive neoplasm. Radiotherapy (RT) is the primary treatment strategy for NPC, and concurrent chemoradiotherapy is extensively used for locally advanced NPC (1, 2). However, the treatment response is unsatisfactory, with rates of local recurrence varying from 16.8% to 23% (3, 4). Since the mortality rate associated with NPC is directly related to the rates of local recurrence, it is important to develop methods for the improvement of treatment outcomes in patients with locoregionally advanced disease. Boosting the radiotherapy dose can provide better local control. However, dose escalation for NPC may increase treatment-related comorbidities due to the high-dose irradiation of normal tissues (5). Thus, determining the appropriate tumor volume to prescribe high radiation dose treatment remains a major challenge.

18F-fluorodeoxyglucose positron emission tomography/computed tomography (FDG-PET-CT) is a powerful molecular imaging tool based on the activity of cancer cell metabolism. Delineation of biological characteristics prior to the therapy facilitates individual adaptation and optimization of treatment schedules and ensures improved prognosis and decreased treatment toxicity (6). Previous studies have indicate that 18F-FDG PET can be used for target volume delineation in radiotherapy for head and neck squamous cell carcinomas (including NPC) (3, 6–13). Several approaches have been proposed for outlining FDG-avid tumors, including auto-contouring at SUV threshold ≥ 2.5, ≥ 40% to 50% of maximal SUV (SUVmax) and visual delineation (14). In our previous study, we compared FDG-PET/CT guided dose escalation IMRT with CT-based IMRT in locoregionally advanced NPC. Relative to CT-based IMRT, FDG-PET/CT-guided dose-painting IMRT (DP-IMRT) is a powerful technique with survival benefit which does not increase the incidence of toxicities (3).

To the best of our knowledge, the methods and thresholds based on SUV have not been clearly defined till date. Additionally, clinical trials directly comparing the long-term results of IMRT based on different PET/CT-derived GTV delineation in NPC patients are not available. The primary aim of this study was to retrospectively analyze the comparative efficacy and toxicity of PET/CT-guided IMRT using three PET/CT-derived methods for primary tumor volume delineation in locoregionally advanced NPC patients, and to determine if there was a difference between PET/CT-guided dose-painting and PET/CT-based IMRT in locally advanced NPC prognosis.

METHODS

Patient Selection

Between August 2015 and February 2018, 292 patients with locoregionally advanced NPC from the Hunan Cancer Hospital (The Affiliated Cancer Hospital of Xiangya School of Medicine, Central South University) were selected for the present study. Eligible patients between the ages of 18-70 years with non-distant metastatic, histologically confirmed WHO types II-III, stage III, and IVB nasopharyngeal carcinoma. Patients were required to provide written informed consent prior to undergoing chemoradiotherapy. Patients with a history of previous radiotherapy, in-complete radiotherapy, secondary malignancy, evidence of distant metastasis, pregnancy, or lactating females were excluded from the study. We were able to identify the information of participants during and after data collection. This retrospective study was approved by the Ethics Committee of our hospital.

Radiotherapy

All patients received both pre-treatment contrast-enhanced CT of the head and neck and 18F-FDG-PET/CT of the whole body. The scope of the CT simulation scan from the head to the manubriosternal joint was at 2.5-mm increments. The FDG-PET/CT scans were performed within 3 days of CT scans of the same location and in same the postural position. At 1-hour post-injection of 190-240 MBq of FDG, FDG-PET scans were conducted. Data acquisition was within 3 minutes per bed position (3, 9). The images were then converted from FDG-PET to SUV, and PET/CT and CT images were used for image fusion. Three FDG-PET/CT-based methods for gross tumor volume (GTV) delineation were compared: visual criteria (group A), a standard uptake value (SUV) threshold of 2.5, (SUV2.5) (group B), and a threshold of 50% of the maximum standardized uptake value (50% SUVmax) (group C), combined with dose-painting technique. The target volumes were based on FDG-PET/CT by a group of experienced radiation oncologists, with the assistance of experienced nuclear medicine physicians. In group A, the criteria for defining the GTV of the nasopharynx (GTVnx) in FDG-PET/CT were based on visual observation (volume) (10, 12, 13). In group B, the primary tumor area with SUV2.5 threshold was defined as GTVnx (volume 2.5) (8, 11, 14). In group C, the visual criteria were used for GTVnx delineation. Using a dose-painting technique for simultaneous integrated boost (SIB), a sub-volume GTVnx-PET (volume 50%) in the GTVnx was defined as the 50% threshold of the maximum standardized uptake value (3, 9, 11, 14, 15).

In all the groups, IMRT was performed using linear accelerators (16–18). The GTVnx was enlarged by 5 mm (containing the whole nasopharyngeal mucosa and submembrane) (17), and defined as PGTVnx. The dose for T1-2 patients was DT 70.4 Gy/32 Fx, and for T3-4 patients was DT 72.6 Gy/33 Fx, with 2.2 Gy per fraction. The irradiation doses of lymph node GTV (GTVnd) was 69.96-72.6 Gy/32-33 Fx, with 2.12-2.2 Gy per fraction; for high-risk subclinical lesions (planned target volume, PTV1), it was 60.06-64 Gy/32-33 Fx, with 1.82-2.0 Gy per fraction, and for low-risk subclinical diseases (PTV2) it was 50.96-56.0 Gy/26-28 Fx, at the rate of 1.82-2.0 Gy per fraction. Radiotherapy was performed daily from Monday to Friday and lasted for 32 to 33 days. The Pinnacle3 inverse planning system was used to design and optimize the regimens. Group C was subjected to PET/CT-guided DP-IMRT. The dose administered to the GTVnx-PET was increased to DT 75.2 Gy/32 Fx gradually in T1-2 patients, and DT 77.55 Gy/33 Fx in T3-4 patients, at 2.35 Gy per fraction. Other dose target volumes were prescribed in a manner similar to those in groups

A and B. The doses of critical structures were within the tolerance limits of the Radiation Therapy Oncology Group (RTOG) 0615 (16) and RTOG 0225 protocols (18).

Chemotherapy

Induction chemotherapy was administered every 3 weeks, which consisted of intravenous 3 cycles of docetaxel (60 mg/m2) and cisplatin (60 mg/m2) on day 1, followed by uninterrupted intravenous fluorouracil administration (600 mg/m2) per day from day 1 to day 5, for three cycles before concurrent chemoradiotherapy. The prescription of concurrent chemotherapy was 80-100 mg/m2 cisplatin alone every three weeks, at the same time as IMRT.

Follow-Up

The follow-up period was calculated from day one of the therapy through the last date of follow-up (April 16, 2021) or until death. We classified chemotherapy-related toxicities based on the Common Terminology Criteria for Adverse Events (version 4.0) and evaluated the toxicities of radiotherapy based on the RTOG scoring criteria for acute and late radiation incidences. The tumor complete response (CR) was assessed by physical examination of the head and neck, fiberoptic nasopharyngoscopy, and MRI at 3 months after radiotherapy completion. Classification of tumor response was based on WHO response standard (16, 19).

Statistical Analysis

All analyses were performed using SPSS (version 20.0; IBM Corporation, Armonk, NY, USA). The overall survival (OS) was defined as the time from diagnosis to the last available follow-up; disease-free survival (DFS), survival without any local, regional, or distant failure; distant metastasis-free survival (DMFS), as survival without distant metastasis; local recurrence-free survival (LRFS), as survival without local relapse; regional recurrence-free survival (RRFS), survival without local relapse in cervical or regional lymph nodes, and locoregional recurrence-free survival (LRRFS), as survival without local relapse in the lymph nodes of the nasopharynx or cervical.

The classification variables were analyzed using χ^2 test. Kaplan-Meier survival curves and log-rank tests were used to calculate time-to-event endpoints between the three groups. Multivariable analyses were performed to assess the significance of independent prognosis using the Cox proportional hazards model. The potential prognostic factors included age, sex, tumor stage, node stage, pre-treatment Epstein-Barr virus deoxyribonucleic acid (EBV DNA) concentration (20), and PET/CT-guided GTV (50% SUVmax threshold *vs.* visual criteria or SUV2.5 threshold). Statistical significance was set at $p<0.05$.

RESULTS

Patient Characteristics

The number of patients in groups A, B, and C were 98, 95, and 99, respectively. The median age was 47 years (range: 18-70 years). The median follow-up time for all patients was 60.5 months (range: 13-68 months) and 62 months for the surviving patients (range: 39-68 months). The median SUVmax value for nasopharyngeal masses was 10.6 (range: 4.2-25.3) for all patients. The patient baseline features are listed in **Table 1**. Clinical features and baseline demographics were balanced between the three groups.

Impact of PET/CT-Derived GTV Delineation on Primary Tumor Volume

The median primary tumor volumes of the GTVnx for group A (visual volume), group B (volume 2.5), and group C were 41.9 mL (range: 6.2-184.6 mL), 36.5 mL (range: 4.6-162.2 mL), and 39.4 mL (range: 5.8-176.8 mL), respectively. The median volume of the GTVnx-PET (volume 50%) in group C was 13.2 mL (range: 1.4-32.6 mL). The volume 50% in group C was significantly lower than the visual volume in group A ($p < 0.001$), volume 2.5 in group B ($p < 0.001$), and GTVnx in group C ($p < 0.001$). No significant differences were found in GTVnx for the three groups (group A *vs.* group B, $p = 0.056$; group A *vs.* group C, $p = 0.141$; group B *vs.* group C, $p = 0.704$).

Response

The complete response (CR) rate in group C was 100% (99/99) as compared to 92.9% (91/98) in group A ($p = 0.007$) and 94.7% (90/95) in group B ($p = 0.021$). The CR rate did not differ significantly between groups A and B ($p = 0.607$). Two patients in group A and one in group B showed residual nasopharyngeal tumors. Six patients in group A and four in group B showed residual neck lymph nodes. Three patients had residual nasopharyngeal neoplasms received salvage chemotherapy. Six months after the completion of radiotherapy, no patient with residual nasopharyngeal tumors was observed and only 2 patients in group A and 1 patient in group B were diagnosed with residual neck lymph nodes, and were successfully treated with salvage neck dissection.

Adverse Events

All patients in the cohorts completed the established RT regimen. All patients received concurrent chemotherapy. 71 patients (24.3%) underwent induction chemotherapy. 29 (9.9%) patients received adjuvant chemotherapy after completion of radiotherapy (**Table 1**). Chemotherapy was discontinued due to severe liver dysfunction, neutropenia, and refusal of treatment. Mucositis and hematologic toxicity were the most frequently recorded grade 3-4 acute adverse events. Three patients experienced grade 3-4 late toxicities, including skin fibrosis and xerostomia (dry mouth) (**Table 2**). No treatment-related deaths occurred during treatment. Tumor responses and toxicities were similar among the three groups (**Table 2**).

Treatment Failure

24 patients (24.5%) in group A, 22 patients (23.2%) in group B, and 12 patients (12.5%) in group C had tumor recurrence. The median time to recurrence was 25.5 (8–38) months for local recurrence, 26 (8–42) months for regional recurrence and was 29

TABLE 1 | Clinical demographics of patients with loco-regionally advanced NPC.

Characteristics	Visual criteria group	SUV 2.5 group	50% SUV max group	P value*
	No. of patients (%)	No. of patients (%)	No. of patients (%)	
Total	98	95	99	
Age, y				
Median	47	47	46	
Range	18-66	19-69	22-70	
Sex				
Male	71 (72.4)	68 (71.6)	67 (67.7)	0.736
Female	27 (27.6)	27 (28.4)	32 (32.3)	
Pathology				
WHO type 2	30 (30.6)	30 (31.6)	29 (29.3)	0.941
WHO type 3	68 (69.4)	65 (68.4)	70 (70.7)	
T stage				
T1	11 (11.2)	10 (10.5)	9 (9.1)	0.989
T2	25 (25.5)	24 (25.3)	27 (27.3)	
T3	28 (28.6)	25 (26.3)	30 (30.3)	
T4	34 (34.7)	36 (37.9)	33 (33.3)	
N stage				
N0	3 (3.1)	3 (3.2)	3 (3.0)	0.974
N1	6 (6.1)	7 (7.4)	10 (10.1)	
N2	68 (69.4)	63 (66.3)	65 (65.7)	
N3	21 (21.4)	22 (23.2)	21 (21.2)	
AJCC stage group				
III	52 (53.0)	47 (49.5)	48 (48.5)	0.971
IVA	27 (27.6)	28 (29.5)	31 (31.3)	
IVB	19 (19.4)	20 (21.1)	20 (20.2)	
Concurrent chemotherapy				
Yes	98 (100.0)	95 (100.0)	99 (100.0)	.
No	0 (0.0)	0 (0.0)	0 (0.0)	
Induction chemotherapy				
Yes	23 (23.5)	26 (27.4)	22 (22.2)	0.686
No	75 (76.5)	69 (72.6)	77 (77.8)	
Adjuvant chemotherapy				
Yes	11 (11.2)	10 (10.5)	8 (8.1)	0.741
No	87 (88.8)	85 (89.5)	91 (91.9)	

**P values were calculated using chi-square test.*

TABLE 2 | Grade 3-4 toxicity.

Adverse events	Visual criteria group	SUV 2.5 group	50% SUV max group	P value*
	No. of patients (%)	No. of patients (%)	No. of patients (%)	
Acute adverse events				
Anemia	2 (2.0)	1 (1.1)	1 (1.0)	0.788
Neutropenia	8 (8.2)	10 (10.5)	8 (8.1)	0.796
Leukopenia	18 (18.4)	15 (15.8)	15 (15.2)	0.813
Thrombocytopenia	2 (2.0)	0	1 (1.0)	0.372
Liver dysfunction	1 (1.0)	0	0	0.370
Nephrotoxicity	0	0	0	.
Nausea	17 (17.3)	16 (16.8)	14 (14.1)	0.805
Vomiting	11 (11.2)	13 (13.7)	10 (10.1)	0.730
Mucositis	34 (34.7)	28 (29.5)	31 (31.3)	0.731
Dermatitis	12 (12.2)	12 (12.6)	9 (9.1)	0.692
Dysphagia or odynophagia	4 (4.1)	3 (3.2)	3 (3.0)	0.907
Dry mouth	5 (5.1)	5 (5.3)	3 (3.0)	0.700
Ototoxicity	1 (1.0)	0	0	0.370
Late adverse events				
Skin fibrosis	1 (1.0)	1 (1.0)	0	0.600
Dry mouth	1 (1.0)	0	0	0.370
Ototoxicity	0	0	0	.
Trismus	0	0	0	.
Nasopharyngeal ulceration	0	0	0	.

**P values were calculated using chi-square test.*

(8–42) months for loco-regional recurrence. 52 patients experienced metastases to distant organs, of whom 46 had bone metastases, 18 had liver metastases, and 30 had lung metastases. 32 patients had more than one metastatic site. In conformity with standard practice, salvage treatments were conducted for the patients with relapse, involving re-irradiation, chemotherapy, and surgery.

Survival

64 patients (26 in group A, 25 in group B, and 13 in group C) died, which included 48 deaths due to distant metastases, 9 due to loco-regional recurrence, and 7 due to other medical conditions. In groups A, B, and C, the 5-year LRFS rates were 89.4%, 90.0%, and 97.8%, respectively ($p = 0.043$). The 5-year RRFS rates were 87.3%, 87.0%, and 93.4%, respectively ($p = 0.170$). The 5-year LRRFS rates were 84.3%, 84.9%, and 93.4%, respectively ($p = 0.054$). The 5-year DMFS rates were 75.1%, 76.0%, and 87.7%, respectively ($p = 0.043$). The 5-year DFS rates were 70.9%, 70.3%, and 82.2%, respectively ($p = 0.048$), and the 5-year OS rates were 73.5%, 73.9%, and 84.9%, respectively ($p = 0.038$). No statistically significant differences in LRFS, RRFS, LRRFS, DMFS, DFS, and OS were observed between groups A and B (**Figure 1**). Group C showed significantly higher 5-year LRFS, LRRFS, DMFS, DFS, and OS ($p < 0.05$, **Figure 1**) as compared with group A or group B.

Prognostic Factors

In the univariate analysis, the PET/CT-guided GTV (50% SUVmax threshold *vs.* visual criteria or SUV2.5 threshold) was an important prognostic factor for 5-year LRFS, LRRFS, DMFS, DFS, and OS ($p = 0.013$, $p = 0.016$, $p= 0.012$, $p= 0.014$, and $p = 0.011$, respectively). EBV DNA was identified as an important prognostic factor for 5-year LRFS, RRFS, LRRFS, DMFS, DFS, and OS ($p < 0.001$, $p = 0.017$, $p = 0.003$, $p < 0.001$, $p < 0.001$, and $p < 0.001$, respectively). There was a significant correlation between sex and DMFS ($p = 0.035$). However, age, T-category, and N-category were not significant factors for LRFS, RRFS, LRRFS, DMFS, DFS, or OS. Multivariate analyses revealed that PET/CT-guided GTV was an independent prognostic indicator of 5-year LRFS, DFS, DMFS, and OS ($p = 0.039$, $p = 0.030$, $p = 0.035$ and $p = 0.028$, respectively), and was marginally significant for LRRFS ($p = 0.080$). EBV DNA was a favorable independent prognostic indicator of 5-year LRFS, LRRFS, DFS, DMFS, and OS ($p = 0.010$, $p = 0.043$, $p < 0.001$, $p< 0.001$, and $p < 0.001$,

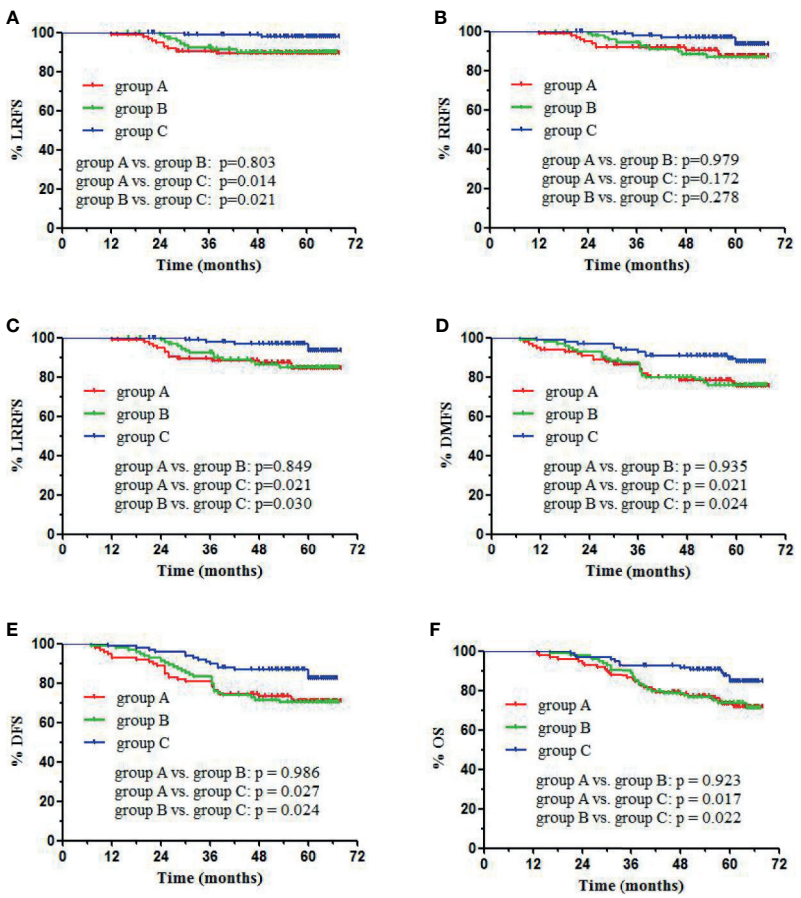

FIGURE 1 | Kaplan-Meier survival curves of different groups: visual criteria, SUV2.5, and 50% SUVmax group. **(A)** LRFS, **(B)** RRFS, **(C)** LRRFS, **(D)** DMFS, **(E)** DFS, **(F)** OS.

respectively). The outcomes from the multivariate Cox regression analyses are listed in **Table 3**.

DISCUSSION

Chemoradiotherapy is the primary treatment for locoregionally advanced NPCs. Its clinical outcomes have greatly improved with IMRT (21–23). However, residual tumor and local recurrence are challenging because of the highly invasive and metastatic nature of the disease (3, 4, 23). During IMRT planning, the precise definition of tumor volume is crucial for predicting patient prognosis. Usually, the GTV in NPC is evaluated using CT imaging. However, previous studies have found that 18F-FDG-PET/CT can greatly enhance the value of TNM staging, treatment assessment, and prognosis of NPC (24–28), and has been increasingly used to plan RT (29). Moreover, 18F-FDG-PET integrated with IMRT is more likely to facilitate target volume delineation and dose escalation (30), thereby being more favorable for the main clinical outcomes.

TABLE 3 | Multivariable analysis of prognostic factors in loco-regionally advanced NPC.

Endpoint	HR (95% CI)	P value*
Local recurrence-free survival		
Sex	0.631 (0.254-1.570)	0.322
Age	1.350 (0.565-3.225)	0.500
T stage	1.001 (0.401-2.501)	0.998
N stage	0.000 (0.000-0.000)	0.977
EBV DNA level	0.070 (0.009-0.526)	0.010
PET-guided GTV	4.655 (1.081-20.047)	0.039
Loco-regional recurrence-free survival		
Sex	0.657 (0.293-1.472)	0.308
Age	1.094 (0.503-2.379)	0.820
T stage	0.819 (0.350-1.920)	0.646
N stage	0.369 (0.049-2.802)	0.335
EBV DNA level	0.381 (0.150-0.968)	0.043
PET-guided GTV	2.392 (0.900-6.359)	0.080
Disease-free survival		
Sex	1.175 (0.672-2.063)	0.572
Age	1.410 (0.885-2.249)	0.149
T stage	1.216 (0.737-2.008)	0.445
N stage	1.047 (0.441-2.488)	0.917
EBV DNA level	0.251 (0.136-0.464)	<0.001
PET-guided GTV	1.863 (1.063-3.264)	0.030
Distant metastasis-free survival		
Sex	1.935 (0.912-4.107)	0.086
Age	1.566 (0.920-2.666)	0.099
T stage	1.139 (0.638-2.033)	0.086
N stage	1.131 (0.437-2.930)	0.099
EBV DNA level	0.230 (0.111-0.478)	<0.001
PET-guided GTV	2.047 (1.051-3.986)	0.035
Overall survival		
Sex	1.190 (0.656-2.156)	0.567
Age	1.258 (0.767-2.064)	0.363
T stage	1.225 (0.721-2.079)	0.453
N stage	0.751 (0.266-2.119)	0.588
EBV DNA level	0.217 (0.109-0.432)	<0.001
PET-guided GTV	1.988 (1.077-3.668)	0.028

**P values were calculated using an adjusted Cox proportional-hazards model.*

SUV is the primary quantitative indicator for tumor detection using 18F-FDG-PET (9). Several methods for tumor delineation using FDG-PET have been studied. A simple and most commonly used strategy is based on the visual interpretation of FDG-PET images by practiced radiation oncologists or nuclear medicine physicians (10, 12, 13). However, visual delineation of neoplasms is highly operator-dependent and leads to significant inter-observer differences (14). Other techniques of threshold determination have also been used to define target volumes, such as the percentage of maximum peak SUV (50% SUVmax), a fixed SUV threshold of 2.5, or a threshold that is adaptive to the signal-to-background ratio (SBR), although their prognostic value remains controversial (8–11, 14, 15). The lack of a unified standardization technique poses a major challenge in using FDG-PET in delineating tumor volume. Currently, there is no formally recognized method for defining the optimal tumor volume using FDG-PET/CT. Therefore, our research team conducted the current study to ascertain the optimal SUV-based methods to define the primary tumor volume in locoregionally advanced NPC and to compare the difference between PET/CT-guided dose escalation and PET/CT-based (without dose escalation) IMRT for locally advanced NPC prognosis.

Previous studies have combined FDG-PET (or PET/CT) with RT planning and compared the major neoplasm volume using PET and CT (and/or MRI) in patients with NPC (8, 10, 14, 15, 31, 32). Most results showed significant variations between the different modalities. Hung et al. (14) compared different PET-based thresholds (for e.g., SUV2.5, 40% Max, and 50% Max) for primary tumor delineation in 32 NPC patients, and reported that the SUV2.5 method generated the largest volume and the 50% Max method resulted in the smallest tumor volume. In our study, no significant difference was observed between the visual volume and volume 2.5 groups. The primary neoplasm volumes evaluated using the visual and SUV2.5 methods were significantly larger than those derived from the 50% SUVmax method, which is consistent with the findings of Hung et al. (14).

Yu et al. (11) reported that since the volume based SUV50% max isocontour was significantly smaller than the volume derived from the SUV2.5 threshold, the areas of 50% SUVmax may not be sufficient for GTVnx. Therefore, we used similar visual criteria to define GTVnx in the 50% SUVmax group and used dose-painting technique to dose boost for the threshold of 50% SUVmax (GTVnx-PET), which based on our previous study and ongoing clinical trials (9, 15). However, larger target volumes may result in higher doses of irradiation to normal tissues and, thus, increase treatment-related complications. Therefore, our study did not escalate the dose to the PET target volume based on the SUV2.5 threshold and visual delineation.

All patients in our study received concurrent chemoradiotherapy. The CR rate after chemoradiotherapy for locoregionally advanced NPC has been reported to range from 82.8% to 99% (1, 20, 33). We previously reported that FDG-PET/CT-guided DP-IMRT significantly advanced CR rates (99.0%) compared with those by the CT-based IMRT (92.9%) (3). In the present study, the CR rate was significantly higher in group C (100%) than in group A (92.9%)

and group B (94.7%). Our results suggest that the risk of local residual tumor was reduced by DP-IMRT using dose escalation to the 50% SUVmax sub-volume.

Very few studies have used PET/CT-guided IMRT to study the nasopharyngeal carcinoma. Wang et al. (8) included 67 patients with locally advanced NPC and analyzed the results of conventional RT, CT-based IMRT, and PET/CT-guided IMRT. The PET/CT-guided IMRT group, which used the SUV2.5 method for delineating GTV, when statistically compared with the traditional RT group, showed a better 3-year local progression-free survival rate (LPFS: 100% *vs*. 95.8%, P<0.05) and DFS (95.2% *vs*. 79.2%, P<0.05). However, the difference in the survival rate between the PET/CT-guided IMRT and CT-based IMRT groups was not statistically significant. We have previously demonstrated that FDG-PET/CT-guided DP-IMRT increased 3-year OS, DFS, DMFS, LFFS, and LRFFS in comparison to the CT-based IMRT (3). Based on these results, we compared the efficacy of PET/CT-guided IMRT using three PET/CT-derived methods for primary tumor volume delineation in patients with locoregionally advanced NPC in the present study. The results showed that the 5-year LRFS, DMFS, DFS, and OS were higher in the 50%SUVmax group than in the visual and SUV2.5 groups. In the current study, dose escalation of the SUV 50%max isocontour improved the treatment efficacy while decreasing collateral damage in comparison to that of the visual criteria and threshold of SUV2.5. Distant metastasis is the primary cause of treatment failure following chemoradiotherapy. Our results suggest that the risk of distant metastasis was highly reduced with an increase in local control rates and, hence, enhanced the DFS and OS. We had a relatively large sample size; thus, the results of our analysis have some instructive significance.

Wang et al. (8) reported that for PET/CT-guided IMRT, the most common acute toxicities included acute mucositis and late toxicities included xerostomia, subcutaneous fibrosis, and ototoxicity. The patients treated with PET/CT-guided or CT-based IMRT showed similar acute and late toxicities. In our study, a single (1.0%) patient with extensive tumor migration to the unilateral parotid gland and metastatic lymph node invasion to the contralateral parotid gland had grade 3 xerostomia in the visual criteria group. To ensure that the dose delivered to the PTV could sufficiently control the tumor, the mean dose of the bilateral parotid gland was increased to 34 Gy in this patient. Bakst et al. (5) evaluated the results of 25 NPC patients (stage II-IVB) who received DP-IMRT combined with chemotherapy. The prescription dose in their trial was 70.2 Gy in 2.34-Gy fractions to the GTV. One patient developed hearing loss of grade 3, and 12% of the patients experienced temporal lobe necrosis. In our study, no patient developed severe ototoxicity or brain toxicity. Compared to the study by Bakst et al., the lower incidence of brain toxicity in our study was likely attributed to a lower fractionated dose in the visual and SUV2.5 groups, and the 50% SUVmax group showed overall smaller dose-escalation volumes. Our PET/CT-based-IMRT regimen did not increase acute and late toxicities in comparison to the CT-based IMRT in NPC patients reported by Lin et al. (17) and Lee et al. (16). Our previous studies found no statistically significant differences in acute and late-presenting toxicities between CT-based IMRT and PET/CT-guided DP-IMRT (3). Likewise, in this study, we did not observe significant differences in acute or late toxicities among the three groups, and no grade 5 acute toxicities were found, which is consistent with prior studies.

Several studies have reported varying levels of prognosis in NPC treated with IMRT combined with chemotherapy (1, 3, 17, 20, 22, 33, 34). However, to date, no prior research has investigated the prognostic value of different techniques in the PET/CT-guided GTV delineation of NPC. Our data showed that PET/CT-guided IMRT (50% SUVmax threshold with dose escalation *vs*. visual criteria or SUV2.5 threshold) was a significant and independent prognostic factor for LRFS, DFS, DMFS, and OS. Thus, the 50% SUVmax method for dose escalation by DP-IMRT is a reasonable recommendation for improving the survival of patients with locoregionally advanced NPC. The therapeutic benefit of a 50%SUVmax threshold regimen for DP-IMRT encourages further exploration in other prospective studies. The present study had several limitations. Our study was limited by its retrospective nature. Although concurrent chemoradiotherapy was the major treatment regimen, induction chemotherapy was administered to 24.3% of patients, which may have influenced the treatment homogeneity. In addition, further follow-up is required to assess the long-term survival of patients with NPC, and more comprehensive PET/CT-guided GTV delineation methods also needed to explore in our future prospective clinical trials to ascertain the most favorable treatment.

CONCLUSION

Overall, our results indicated that PET/CT-guided dose escalation IMRT combined with chemotherapy is effective for patients with locoregionally advanced NPC. The 50% SUVmax threshold regimen for DP-IMRT significantly improved survival without any increase in toxicity compared with the visual criteria or SUV2.5 threshold. Further, prospective trials are required to fully investigate the PET/CT-based methods of contouring the tumor to determine an optimal regimen for survival.

DATA AVAILABILITY STATEMENT

The original contributions presented in the study are included in the article/supplementary material. Further inquiries can be directed to the corresponding author.

ETHICS STATEMENT

The studies involving human participants were reviewed and approved by Ethics Committee of Hunan Cancer Hospital. Written informed consent for participation was not required for this study in accordance with the national legislation and the institutional requirements.

AUTHOR CONTRIBUTIONS

Conceived and designed the experiments: FL and HW. Performed the experiments: FL, OY, and YH. Analyzed the data: FL, SF, YC, and OY. Contributed reagents/materials/analysis tools: FL, OY, SF, and YC. Wrote the paper: FL, OY, and YH. All authors contributed to the article and approved the submitted version.

FUNDING

This study was supported by grants from Beijing Hope Run Special Fund of Cancer Foundation of China (No. LC2016W05 and LC2016W06), Changsha Science and Technology Bureau (No. kq2004133), and Health Commission of Hunan Province (C2017044). The funders had no role in study design, data collection, and analysis, decision to publish, or preparation of the manuscript.

ACKNOWLEDGMENTS

We would like to thank Editage (www.editage.cn) for English language editing.

REFERENCES

1. Ribassin-Majed L, Marguet S, Lee AWM, Ng WT, Ma J, Chan ATC, et al. What Is the Best Treatment of Locally Advanced Nasopharyngeal Carcinoma? An Individual Patient Data Network Meta-Analysis. *J Clin Oncol* (2017) 35(5):498–505. doi: 10.1200/jco.2016.67.4119
2. Zhang Y, Chen L, Hu GQ, Zhang N, Zhu XD, Yang KY, et al. Gemcitabine and Cisplatin Induction Chemotherapy in Nasopharyngeal Carcinoma. *N Engl J Med* (2019) 381(12):1124–35. doi: 10.1056/NEJMoa1905287
3. Liu F, Xi XP, Wang H, Han YQ, Xiao F, Hu Y, et al. PET/CT-Guided Dose-Painting *Versus* CT-Based Intensity Modulated Radiation Therapy in Locoregional Advanced Nasopharyngeal Carcinoma. *Radiat Oncol (Lond Engl)* (2017) 12(1):15. doi: 10.1186/s13014-016-0739-y
4. Qiu S, Lin S, Tham IW, Pan J, Lu J, Lu JJ. Intensity-Modulated Radiation Therapy in the Salvage of Locally Recurrent Nasopharyngeal Carcinoma. *Int J Radiat Oncol Biology Phys* (2012) 83(2):676–83. doi: 10.1016/j.ijrobp.2011.07.006
5. Bakst RL, Lee N, Pfister DG, Zelefsky MJ, Hunt MA, Kraus DH, et al. Hypofractionated Dose-Painting Intensity Modulated Radiation Therapy With Chemotherapy for Nasopharyngeal Carcinoma: A Prospective Trial. *Int J Radiat Oncol Biology Phys* (2011) 80(1):148–53. doi: 10.1016/j.ijrobp.2010.01.026
6. Hoeben BA, Bussink J, Troost EG, Oyen WJ, Kaanders JH. Molecular PET Imaging for Biology-Guided Adaptive Radiotherapy of Head and Neck Cancer. *Acta Oncol (Stockholm Sweden)* (2013) 52(7):1257–71. doi: 10.3109/0284186x.2013.812799
7. Perez-Romasanta LA, Bellon-Guardia M, Torres-Donaire J, Lozano-Martin E, Sanz-Martin M, Velasco-Jimenez J. Tumor Volume Delineation in Head and Neck Cancer With 18-Fluor-Fluorodeoxiglucose Positron Emission Tomography: Adaptive Thresholding Method Applied to Primary Tumors and Metastatic Lymph Nodes. *Clin Trans Oncol: Off Publ Fed Spanish Oncol Societies Natl Cancer Inst Mexico* (2013) 15(4):283–93. doi: 10.1007/s12094-012-0914-z
8. Wang J, Zheng J, Tang T, Zhu F, Yao Y, Xu J, et al. A Randomized Pilot Trial Comparing Position Emission Tomography (PET)-Guided Dose Escalation Radiotherapy to Conventional Radiotherapy in Chemoradiotherapy Treatment of Locally Advanced Nasopharyngeal Carcinoma. *PLoS One* (2015) 10(4):e0124018. doi: 10.1371/journal.pone.0124018
9. Houweling AC, Wolf AL, Vogel WV, Hamming-Vrieze O, van Vliet-Vroegindeweij C, van de Kamer JB, et al. FDG-PET and Diffusion-Weighted MRI in Head-and-Neck Cancer Patients: Implications for Dose Painting. *Radiother Oncol* (2013) 106(2):250–4. doi: 10.1016/j.radonc.2013.01.003
10. Delouya G, Igidbashian L, Houle A, Bélair M, Boucher L, Cohade C, et al. ^{18}F-FDG-PET Imaging in Radiotherapy Tumor Volume Delineation in Treatment of Head and Neck Cancer. *Radiother Oncol* (2011) 101(3):362–8. doi: 10.1016/j.radonc.2011.07.025
11. Yu H, Caldwell C, Mah K, Poon I, Balogh J, MacKenzie R, et al. Automated Radiation Targeting in Head-and-Neck Cancer Using Region-Based Texture Analysis of PET and CT Images. *Int J Radiat Oncol Biology Phys* (2009) 75(2):618–25. doi: 10.1016/j.ijrobp.2009.04.043
12. Breen SL, Publicover J, De Silva S, Pond G, Brock K, O'Sullivan B, et al. Intraobserver and Interobserver Variability in GTV Delineation on FDG-PET-CT Images of Head and Neck Cancers. *Int J Radiat Oncol Biology Phys* (2007) 68(3):763–70. doi: 10.1016/j.ijrobp.2006.12.039
13. Zheng XK, Chen LH, Wang QS, Wu HB, Wang HM, Chen YQ, et al. Influence of FDG-PET on Computed Tomography-Based Radiotherapy Planning for Locally Recurrent Nasopharyngeal Carcinoma. *Int J Radiat Oncol Biology Phys* (2007) 69(5):1381–8. doi: 10.1016/j.ijrobp.2007.05.033
14. Hung GU, Wu IS, Lee HS, You WC, Chen HC, Chen MK. Primary Tumor Volume Measured by FDG PET and CT in Nasopharyngeal Carcinoma. *Clin Nucl Med* (2011) 36(6):447–51. doi: 10.1097/RLU.0b013e31821738b8
15. Guido A, Fuccio L, Rombi B, Castellucci P, Cecconi A, Bunkheila F, et al. Combined 18F-FDG-PET/CT Imaging in Radiotherapy Target Delineation for Head-and-Neck Cancer. *Int J Radiat Oncol Biology Phys* (2009) 73(3):759–63. doi: 10.1016/j.ijrobp.2008.04.059
16. Lee NY, Zhang Q, Pfister DG, Kim J, Garden AS, Mechalakos J, et al. Addition of Bevacizumab to Standard Chemoradiation for Locoregionally Advanced Nasopharyngeal Carcinoma (RTOG 0615): A Phase 2 Multi-Institutional Trial. *Lancet Oncol* (2012) 13(2):172–80. doi: 10.1016/s1470-2045(11)70303-5
17. Lin S, Pan J, Han L, Guo Q, Hu C, Zong J, et al. Update Report of Nasopharyngeal Carcinoma Treated With Reduced-Volume Intensity-Modulated Radiation Therapy and Hypothesis of the Optimal Margin. *Radiother Oncol* (2014) 110(3):385–9. doi: 10.1016/j.radonc.2014.01.011
18. Lee N, Harris J, Garden AS, Straube W, Glisson B, Xia P, et al. Intensity-Modulated Radiation Therapy With or Without Chemotherapy for Nasopharyngeal Carcinoma: Radiation Therapy Oncology Group Phase II Trial 0225. *J Clin Oncol* (2009) 27(22):3684–90. doi: 10.1200/jco.2008.19.9109
19. Chen QY, Wen YF, Guo L, Liu H, Huang PY, Mo HY, et al. Concurrent Chemoradiotherapy *vs* Radiotherapy Alone in Stage II Nasopharyngeal Carcinoma: Phase III Randomized Trial. *J Natl Cancer Inst* (2011) 103(23):1761–70. doi: 10.1093/jnci/djr432
20. Liu LT, Tang LQ, Chen QY, Zhang L, Guo SS, Guo L, et al. The Prognostic Value of Plasma Epstein-Barr Viral DNA and Tumor Response to Neoadjuvant Chemotherapy in Advanced-Stage Nasopharyngeal Carcinoma. *Int J Radiat Oncol Biology Phys* (2015) 93(4):862–9. doi: 10.1016/j.ijrobp.2015.08.003
21. Guo Q, Lu T, Hui Huang S, O'Sullivan B, Zong J, Xiao Y, et al. Depicting Distant Metastatic Risk by Refined Subgroups Derived From the 8th Edition Nasopharyngeal Carcinoma TNM. *Oral Oncol* (2019) 91:113–20. doi: 10.1016/j.oraloncology.2019.02.021
22. He Y, Wang Y, Shen L, Zhao Y, Cao P, Lei M, et al. Prognostic Value of the Distance Between the Primary Tumor and Brainstem in the Patients With Locally Advanced Nasopharyngeal Carcinoma. *BMC Cancer* (2016) 16:114. doi: 10.1186/s12885-016-2148-x
23. Sun XS, Liu SL, Luo MJ, Li XY, Chen QY, Guo SS, et al. The Association Between the Development of Radiation Therapy, Image Technology, and Chemotherapy, and the Survival of Patients With Nasopharyngeal Carcinoma: A Cohort Study From 1990 to 2012. *Int J Radiat Oncol Biol Phys* (2019) 105(3):581–90. doi: 10.1016/j.ijrobp.2019.06.2549
24. Ren YY, Li YC, Wu HB, Wang QS, Han YJ, Zhou WL, et al. Whole-Body (18)F-FDG PET/CT for M Staging in the Patient With Newly Diagnosed Nasopharyngeal Carcinoma: Who Needs? *Eur J Radiol* (2017) 89:200–7. doi: 10.1016/j.ejrad.2017.02.002

25. Lin P, Min M, Lee M, Holloway L, Forstner D, Bray V, et al. Prognostic Utility of (18)F-FDG PET-CT Performed Prior to and During Primary Radiotherapy for Nasopharyngeal Carcinoma: Index Node Is a Useful Prognostic Imaging Biomarker Site. *Radiother Oncol: J Eur Soc Ther Radiol Oncol* (2016) 120 (1):87–91. doi: 10.1016/j.radonc.2016.05.021
26. Ma G, Gu B, Hu J, Kong L, Zhang J, Li Z, et al. Pretreatment (18)F-FDG Uptake Heterogeneity can Predict Treatment Outcome of Carbon Ion Radiotherapy in Patients With Locally Recurrent Nasopharyngeal Carcinoma. *Ann Nucl Med* (2021) 35(7):834–42. doi: 10.1007/s12149-021-01621-8
27. Chan SC, Yeh CH, Chang JT, Chang KP, Wang JH, Ng SH. Combing MRI Perfusion and (18)F-FDG PET/CT Metabolic Biomarkers Helps Predict Survival in Advanced Nasopharyngeal Carcinoma: A Prospective Multimodal Imaging Study. *Cancers* (2021) 13(7):1550. doi: 10.3390/cancers13071550
28. Xiao BB, Lin DF, Sun XS, Zhang X, Guo SS, Liu LT, et al. Nomogram for the Prediction of Primary Distant Metastasis of Nasopharyngeal Carcinoma to Guide Individualized Application of FDG PET/Ct. *Eur J Nucl Med Mol Imaging* (2021) 48(8):2586–98. doi: 10.1007/s00259-020-05128-8
29. Peng L, Hong X, Yuan Q, Lu L, Wang Q, Chen W. Prediction of Local Recurrence and Distant Metastasis Using Radiomics Analysis of Pretreatment Nasopharyngeal [18F]FDG PET/CT Images. *Ann Nucl Med* (2021) 35(4):458–68. doi: 10.1007/s12149-021-01585-9
30. Berwouts D, Olteanu LA, Duprez F, Vercauteren T, De Gersem W, De Neve W, et al. Three-Phase Adaptive Dose-Painting-by-Numbers for Head-and-Neck Cancer: Initial Results of the Phase I Clinical Trial. *Radiother Oncol* (2013) 107(3):310–6. doi: 10.1016/j.radonc.2013.04.002
31. Geets X, Lee JA, Castadot P, Bol A, Grégoire V. Potential Place of FDG-PET for the GTV Delineation in Head and Neck and Lung Cancers. *Cancer Radiother* (2009) 13(6-7):594–9. doi: 10.1016/j.canrad.2009.06.025
32. Deantonio L, Beldì D, Gambaro G, Loi G, Brambilla M, Inglese E, et al. FDG-PET/CT Imaging for Staging and Radiotherapy Treatment Planning of Head and Neck Carcinoma. *Radiat Oncol (Lond Engl)* (2008) 3:29. doi: 10.1186/1748-717x-3-29
33. Au KH, Ngan RKC, Ng AWY, Poon DMC, Ng WT, Yuen KT, et al. Treatment Outcomes of Nasopharyngeal Carcinoma in Modern Era After Intensity Modulated Radiotherapy (IMRT) in Hong Kong: A Report of 3328 Patients (HKNPCSG 1301 Study). *Oral Oncol* (2018) 77:16–21. doi: 10.1016/j.oraloncology.2017.12.004
34. Zhang Y, Li WF, Liu X, Chen L, Sun R, Sun Y, et al. Nomogram to Predict the Benefit of Additional Induction Chemotherapy to Concurrent Chemoradiotherapy in Locoregionally Advanced Nasopharyngeal Carcinoma: Analysis of a Multicenter, Phase III Randomized Trial. *Radiother Oncol* (2018) 129(1):18–22. doi: 10.1016/j.radonc.2017.12.002

Conflict of Interest: The authors declare that the research was conducted in the absence of any commercial or financial relationships that could be construed as a potential conflict of interest.

Publisher's Note: All claims expressed in this article are solely those of the authors and do not necessarily represent those of their affiliated organizations, or those of the publisher, the editors and the reviewers. Any product that may be evaluated in this article, or claim that may be made by its manufacturer, is not guaranteed or endorsed by the publisher.

frontiers in Oncology

ORIGINAL RESEARCH
published: 24 August 2021
doi: 10.3389/fonc.2021.698955

A Competing Risk Nomogram for Predicting Cancer-Specific Death of Patients With Maxillary Sinus Carcinoma

Mingbin Hu[1†], Xiancai Li[2†], Weiguo Gu[1], Jinhong Mei[3], Dewu Liu[2*] and Shaoqing Chen[1*]*

[1] Department of Oncology, The First Affiliated Hospital of Nanchang University, Nanchang, China, [2] Department of Burns, The First Affiliated Hospital of Nanchang University, Nanchang, China, [3] Department of Pathology, The First Affiliated Hospital of Nanchang University, Nanchang, China

OPEN ACCESS

Edited by:
Heming Lu,
People's Hospital of Guangxi Zhuang Autonomous Region, China

Reviewed by:
Qishuai Guo,
Chongqing University, China
Ali-Farid Safi,
Klinik Professor Sailer, Switzerland
Takumi Kumai,
Asahikawa Medical University, Japan

***Correspondence:**
Shaoqing Chen
1075017867@qq.com
Dewu Liu
dewuliu2@126.com
Jinhong Mei
mjhdoctor@126.com

[†]These authors have contributed equally to this work and share first authorship

Specialty section:
This article was submitted to Head and Neck Cancer, a section of the journal Frontiers in Oncology

Received: *22 April 2021*
Accepted: *30 July 2021*
Published: *24 August 2021*

Citation:
Hu M, Li X, Gu W, Mei J, Liu D and Chen S (2021) A Competing Risk Nomogram for Predicting Cancer-Specific Death of Patients With Maxillary Sinus Carcinoma. Front. Oncol. 11:698955. doi: 10.3389/fonc.2021.698955

Objectives: Herein, we purposed to establish and verify a competing risk nomogram for estimating the risk of cancer-specific death (CSD) in Maxillary Sinus Carcinoma (MSC) patients.

Methods: The data of individuals with MSC used in this study was abstracted from the (SEER) Surveillance, Epidemiology, and End Results data resource as well as from the First Affiliated Hospital of Nanchang University (China). The risk predictors linked to CSD were identified using the CIF (cumulative incidence function) along with the Fine-Gray proportional hazards model on the basis of univariate analysis coupled with multivariate analysis implemented in the R-software. After that, a nomogram was created and verified to estimate the three- and five-year CSD probability.

Results: Overall, 478 individuals with MSC were enrolled from the SEER data resource, with a 3- and 5-year cumulative incidence of CSD after diagnosis of 42.1% and 44.3%, respectively. The Fine-Gray analysis illustrated that age, histological type, N stage, grade, surgery, and T stage were independent predictors linked to CSD in the SEER-training data set (n = 343). These variables were incorporated in the prediction nomogram. The nomogram was well calibrated and it demonstrated a remarkable estimation accuracy in the internal validation data set (n = 135) abstracted from the SEER data resource and the external validation data set (n = 200). The nomograms were well-calibrated and had a good discriminative ability with concordance indexes (c-indexes) of 0.810, 0.761, and 0.755 for the 3- and 5-year prognosis prediction of MSC-specific mortality in the training cohort, internal validation, and external validation cohort, respectively.

Conclusions: The competing risk nomogram constructed herein proved to be an optimal assistant tool for estimating CSD in individuals with MSC.

Keywords: maxillary sinus carcinoma, nomogram, cancer-specific death, SEER, competing risk

INTRODUCTION

Maxillary sinus carcinoma (MSC) accounts for 1%–4% of all head and neck cancers (1). Early diagnosis of maxillary sinus is difficult because of its hidden anatomical site and complex adjacent relationship. In most patients it has already invaded the bone wall and surrounding tissues when they are diagnosed, meaning they have a poorly defined prognosis (2). Numerous reports have documented the prognosis of general oral cancer (3) and Nasopharyngeal carcinoma (4), but few have addressed MSC. Numerous reports have documented the survival of individuals with MSC. Nonetheless, most reports are based on single medical institutions, with small sample sizes (5). Therefore, it is critical to strengthen research on MSC prognosis.

Surveillance, Epidemiology, and End Results (SEER), a population-based data resource, has data for about 28% of the US population. Hence, particularly for rare tumors, there are a number of relevant cases in the SEER data resource that can be used for establishing competitive risk prediction models (6). The information of MSC cases herein was abstracted from the SEER data resource, which guarantees the sufficiency, as well as authenticity of the data. Generally, patients with cancer are often predisposed to more than two risks, however only one event finally occurs (7). The risks other than the one of interest are referred to as competing risks. Competing risks are censored in a traditional survival analysis, but can be improved *via* a competing risk analysis.

A nomogram is a visualization of a linear prognostic model that is employed to quickly predict survival probabilities (8). Each value of these characteristics reflects a score on the nomogram graph, with the overall score mapping the survival likelihood. Some researches only focus on the traditional Kaplan-Meier method along with Cox proportional hazard model, while some studies are centered on population-based assessments (9, 10). Nevertheless, a remarkable amount of research has explored the overall survival along with cancer cause-distinct survival analysis, neglecting the involvement of competing causes of death in non-metastatic MSC prognosis. The competing risks of death influence the long-time survival prognosis to a remarkable extent; therefore, they should be taken into account when predicting the survival outcomes.

Herein, we aimed to develop a competing risk nomogram on the basis of the data abstracted from the SEER data resource for estimating cancer-specific death (CSD) in individuals with MSC. This could help clinicians in making decisions regarding individualized MSC treatment, as well as making accurate estimations of disease outcomes.

MATERIAL AND METHODS

Surveillance, Epidemiology, and End Results Database Patients

This was a retrospective analysis that analyzed the data of individuals with MSC between 2000 and 2017. The data of the individuals with MSC used in this study were abstracted from the publicly accessible SEER data resource.

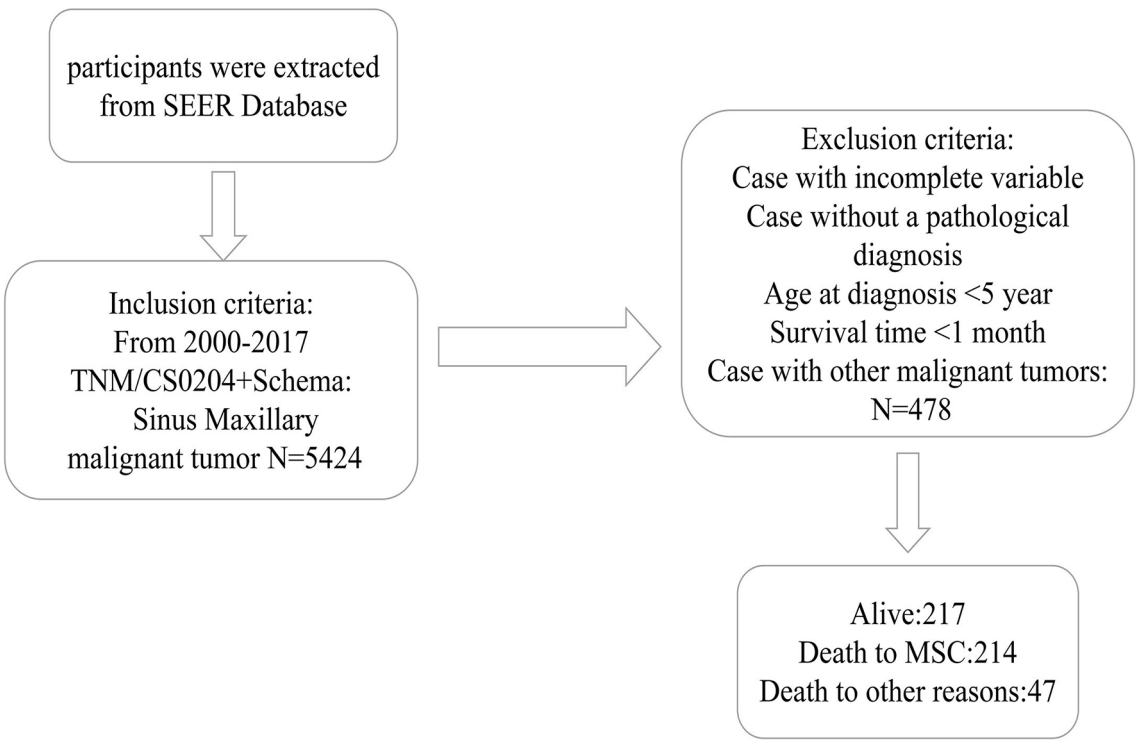

FIGURE 1 | The Flow diagram of patient selection. SEER, Surveillance, Epidemiology, and End Results; MSC, Maxillary Sinus Carcinoma.

SEER 18 Regs custom data (with additional treatment fields) uploaded in November 2019 (1975–2017 varying) were selected. All individuals diagnosed with MSC (site recode NM7/CS v0204+ Schema of "Sinus Maxillary" and behavior recode ICD-O-3 of "malignant") were enrolled. Participants who were less than 5 years old at diagnosis, with a survival period of less than or equal to one month lacking a pathological diagnosis or lacking complete data were excluded from the study.

Our Medical Center Patients

Overall, we enrolled 200 individuals with MSC from the First Affiliated Hospital of Nanchang University (China) from 2006 to 2017. All patients were confirmed by pathology, and had no history of other cancers. The approval of this study was granted by the Ethics Committee of First Affiliated Hospital of Nanchang University (No. 2020140).

Variable Selection

The variables consisting of Age, Race, Sex, AJCC (American Joint Committee on Cancer) stage, T stage, N stage, M stage, Surgery, Grade, Radiation, histological type, follow-up time as well as survival outcomes were abstracted from the SEER data resource. The X-tile software (https://x-tile.software.informer.com/) was employed to explore the optimal cut-point values. The age at the time of diagnosis of the patients was categorized into two groups, i.e., <65 and ≥65 years. The AJCC staging approach, seventh edition was utilized herein. The ICD-O-3 codes was employed to stratify the MSC histological type into two classes, i.e., SCC (squamous cell carcinoma) and none SCC (consisting of adenomas and adenocarcinomas, cystic, adnexal and skin appendage neoplasms, mucinous, serous neoplasms, and mucoepidermoid neoplasms, etc.) on the basis of the WHO classification approach. Tumor-specific survival was the primary

TABLE 1 | Basic characteristics of Maxillary Sinus Carcinoma patients in the training, internal validation, and external validation cohorts.

Characteristics	SEER database		Our medical center	p-value
	Training cohort (n = 343) n (%)	Internal validation cohort (n = 135) n (%)	External validation cohort (n = 200) n (%)	
Age(years)				<0.001
<65	219 (63.8)	100 (74.1)	166 (83.0)	
≥65	124 (36.2)	35 (25.9)	34 (17.0)	
Race				0.247
White	246 (71.7)	99 (73.3)		
Black	56 (16.3)	20 (14.8)		
Others	41 (12.0)	16 (11.9)	200 (100)	
Sex				0.966
Male	234 (68.2)	93 (68.9)	78 (39.0)	
Female	109 (31.8)	42 (31.1)	122 (61.0)	
AJCC stage				<0.001
I	21 (6.1)	15 (11.1)	14 (7.0)	
II	81 (23.6)	14 (10.4)	49 (24.5)	
III	121 (35.3)	50 (37.0)	101 (50.5)	
IV	120 (35.0)	56 (41.5)	36 (18.0)	
T stage				<0.001
T1	29 (8.5)	8 (6.0)	16 (8.0)	
T2	34 (9.9)	17 (12.5)	69 (34.5)	
T3	81 (23.6)	25 (18.5)	83 (41.5)	
T4	199 (58.0)	85 (63.0)	32 (16.0)	
N stage				<0.001
N0	265 (77.3)	107 (79.3)	114 (57.0)	
N1	30 (9.2)	7 (5.2)	71 (35.5)	
N2	48 (13.5)	21 (15.5)	15 (7.5)	
M stage				0.7098
M0	324 (94.5)	130 (96.3)	190 (95.0)	
M1	19 (5.5)	5(3.7)	10 (5.0)	
Surgery				<0.001
No	101 (29.4)	31 (23.0)	11 (5.5)	
Yes	242 (70.6)	104 (77.0)	189 (94.5)	
Grade				<0.001
Well	36 (11.1)	28(20.7)	60 (30.0)	
Moderate	160 (46.6)	42 (31.1)	26 (13.0)	
Poorly/Undifferentiated	147 (42.3)	65 (48.2)	114 (57.0)	
Radiation				<0.001
No	138 (40.2)	49 (36.3)	48 (24.0)	
Yes	205 (60.8)	86 (64.7)	152 (76.0)	
Histologic type				<0.001
SCC	190 (55.5)	74 (54.8)	135 (67.5)	
None SCC	153 (45.5)	61 (45.2)	65 (32.5)	

AJCC, American Joint Committee on Cancer; SCC, squamous cell carcinoma.

endpoint in this study, which was computed as the time from MSC diagnosis to the death of the participant resulting from MSC or a censored event. Deaths resulting from accidents or diseases apart from MSC were regarded as competitive risks.

Statistical Analyses

All analyses were implemented in the R-software (V.4.0.4; packages: foreign, cmprsk, mstate, rms, crrstep, pec, survivial, and riskRegression). P-value was two-sided, $p < 0.05$ defining statistical significance. First, we determined the CIF (cumulative incidence function) for 3- to 5-year time points. Additional subgroup analyses were carried out between various subgroups, and respective CIF curves were constructed for these variables. Remarkable differences in the CIF values among subgroups were explored with the Gray's test. Secondly, we randomly split the enrolled SEER data resource participants into a training data set and a validation data set at a ratio of 7:3. The external validation data set consisted of subjects with MSC enrolled from our hospital. The training data set was utilized to construct the nomogram that was employed to estimate CSD. The two validation data sets were used in verifying the accuracy of the constructed nomogram. Univariate along with multivariate analyses were utilized to determine the independent risk factors of CSD in the training data set. The Fine-Gray proportional hazards model was employed to construct the competing risk nomogram.

The nomogram efficiency was first assessed in the training data set and then in the validation data sets regarding the C-index, AUC, as well as calibration curve. The C-index was employed to quantify the estimation potential of the model. It ranged between 0.5 and 1.0, which reflected a random chance from revealing no discrimination to revealing perfect

TABLE 2 | Cumulative incidence of cancer-specific death in Maxillary Sinus Carcinoma.

Characteristics	Total number of pateints (n)	Cumulative incidence		P-value
		3-year	5-year	
Age(years)				<0.001
<65	319	43.3%	54%	
≥65	159	56%	56.2%	
Race				0.611
White	345	46.7%	49%	
Black	76	53.5%	53.5%	
Others	57	42.9%	47.9%	
Sex				0.742
Male	327	48.4%	67.7%	
Female	151	45.8%	47,0%	
AJCC stage				<0.001
I	36	18.9%	18.9%	
II	95	49.7%	53%	
III	171	57%	77%	
IV	176	64%	70%	
T stage				<0.001
T1	37	15.6%	16.8%	
T2	51	33.2%	35.3%	
T3	106	55.6%	58.3%	
T4	284	57.7%	61.2%	
N stage				<0.001
N0	372	19.3%	21.6%	
N1	37	47.3%	49.4%	
N2	69	60.3%	60.9%	
M stage				<0.001
M0	454	32.5%	34.6%	
M1	24	82.6%	87.0%	
Surgery				<0.001
No	132	63.1%	64.2%	
Yes	346	41.6%	44.2%	
Grade				<0.001
Well	64	28%	29.7%	
Moderate	202	47.2%	51%	
Poorly/Undifferentiated	212	51.2%	52.5%	
Radiation				<0.001
No	187	63.9%	63.9%	
Yes	291	38.6%	41.6%	
Histology type				<0.001
SCC	264	35.5%	38.9%	
None SCC	214	26.0%	27.5%	

AJCC, American Joint Committee on Cancer; SCC, squamous cell carcinoma.

discrimination (11). The AUC exhibits the overall prognostic value across all thresholds (12), with an optimum estimation value yielding an AUC of 1.0. DCA (decision curve analysis) was employed to establish the clinical net benefit of diverse prognostic thresholds for a prospective clinical effect (13), and evaluated the nomogram performance in comparison with the AJCC staging system visually.

RESULTS

Baseline Characteristics

As indicated in **Figure 1**, initially, the data of 5,424 individuals with MSC was abstracted from the SEER data resource. Following the thorough screening, 478 individuals with MSC were enrolled in the final analysis. The median age of the patients was 64 (15–85) years at diagnosis (males = 66.7%). Most of the patients were of the white race (n = 345, 72.2%). Of the 478 MSC cases, 264 (55.2%) were SCC, including 202 (42.3%) cases of moderate differentiation. Stage IV was the most prevalent tumor stage (n = 176, 36.8%), followed by stage III (n = 171, 35.8%), II (n = 95, 19.9%), and I (n = 36, 7.5%). A remarkable number of the patients were classified as T4 (59.4%), followed by T3 (22.2%), T2 (10.7%), and T1 (7.7%). More than 50% of the cases were without lymph node (LN) metastasis (N0, 77.8%), and most cases had no distant metastasis (M0, 95.0%). A remarkable number of the patients were treated with surgery (n = 346, 72.4%). According to the observation of clinical characteristics in the three cohorts, there were differences in age, AJCC stage, T stage, N stage, surgery, radiation, and histologic type ($P < 0.05$). **Table 1** provides a detailed summary of the demographic along with the clinical features of the enrolled participants.

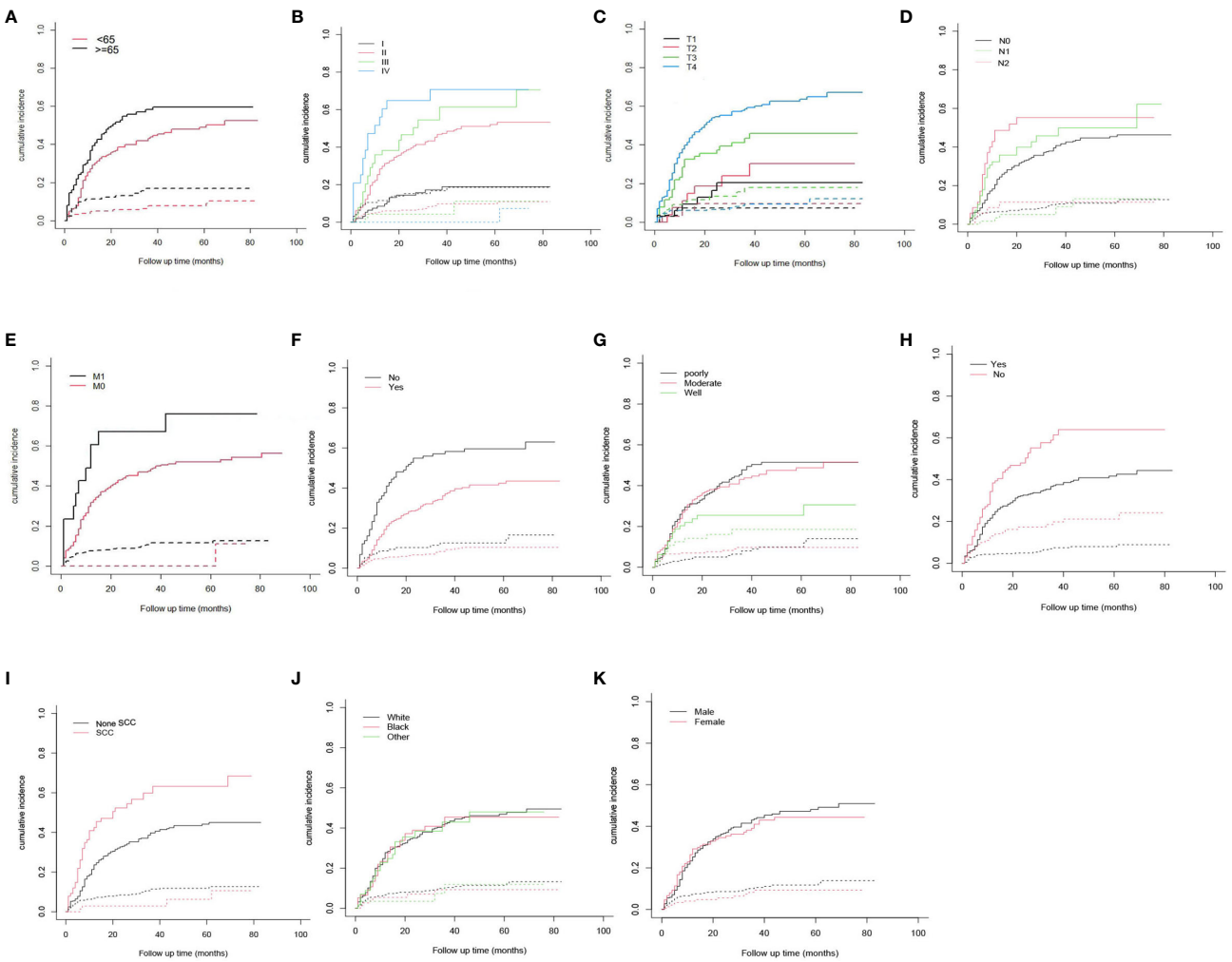

FIGURE 2 | Cumulative incidence estimates of cancer-specific death in Maxillary Sinus Carcinoma. **(A)** Age; **(B)** AJCC stage; **(C)** T stage; **(D)** N stage; **(E)** M stage; **(F)** Surgery; **(G)** Grade; **(H)** radiation; **(I)** Histologic type; **(J)** Race; **(K)** Sex. Solid line represents cause-specific death, dotted line represents other causes of death. AJCC, American Joint Committee on Cancer; SCC, squamous cell carcinoma.

Cumulative Incidence Function Survival Analysis

Table 2 illustrates the results of our competing risk model. The median follow-up period was 26 (1–83) months. Overall, there were 261 deaths (54.6%) by the end of follow-up, with 214 (82.0%) being CSDs and 47 (18.0%) caused by other events. The 3-year cumulative incidence of CSD was 42.1%, while that of the 5-year was 44.3%. The result of the CIF subgroup analysis illustrated that a high CSD primarily occurred in patients aged ≥65 years (**Figure 2A**); who had an advanced AJCC stage (**Figure 2B**), T stage (**Figure 2C**), N stage (**Figure 2D**), and M1 stage (**Figure 2E**); who were not treated with surgery (**Figure 2F**) nor radiation (**Figure 2H**); who had a poorly/undifferentiated grade (**Figure 2G**); and SCC (**Figure 2I**). Nonetheless, no remarkable difference in CSD was observed in race, as well as sex subgroup analyses (**Figures 2J, K**).

Nomogram Construction

As illustrated in **Table 2**, the individuals with MSC abstracted from the SEER database were randomized into a training data set (n = 343) and a validation data set (n = 135) at a ratio of 7:3. The multivariate analysis of the Fine-Gray proportional sub-distribution hazards model on the basis of the Akaike information criterion (AIC) indicated that age, histological type, stage, grade, N stage, M stage, and surgery were independent predictors affecting CSD in MSC patients of the training group ($P < 0.05$). After the optimization of the model on the basis of Bayesian information criterion (BIC), six variables were finally included in the prediction model (**Table 3**). A competing risk nomogram was constructed to estimate the 3- and 5-year likelihoods of CSD on the basis of these predictors (**Figure 3**). An individual patient chance of death from MSC at diverse time points could be easily calculated through this prediction model *via* adding the scores of each incorporated variable.

TABLE 3 | Results of univariate and multivariate analyses by Fine-Gray proportional sub-distribution hazards model in the training cohort.

Characteristics	Univariate analysis		Multivariate analysis (AIC)		Multivariate analysis (BIC)	
	HR(95% CI)	P-value	HR(95% CI)	P-value	HR(95% CI)	P-value
Age(years)						
<65	Ref		Ref		Ref	
≥65	1.610 (1.300–1.980)	<0.001	1.444(1.140–1.830)	0.002	1.438 (1.136–1.821)	0.003
Race						
White	Ref					
Black	1.070 (0.746–1.550)	0.700				
Others	0.080 (0.588–1.090)	0.160				
Sex						
Male	Ref					
Female	1.110 (0.89–1.370)	0.340				
AJCC stage						
I	Ref					
II	1.670 (1.140–2.450)	0.009				
III	3.130 (2.150–4.540)	<0.001				
IV	6.580 (4.810–9.010)	<0.001				
T stage						
T1	Ref		Ref		Ref	
T2	2.020 (1.520–2.690)	<0.001	1.284 (0.951–1.734)	0.100	1.296 (0.960–1.751)	0.090
T3	4.010 (2.810–5.740)	<0.001	2.244 (1.545–3.258)	<0.001	2.215 (1.514–3.240)	<0.001
T4	4.710 (3.480–6.380)	<0.001	1.808 (1.253–2.610)	<0.001	1.937 (1.353–2.775)	<0.001
N stage						
N0	Ref		Ref		Ref	
N1	2.690 (2.020–3.580)	<0.001	1.848 (1.353–2.525)	<0.001	1.939 (1.426–2.638)	<0.001
N2	4.640 (3.650–5.890)	<0.001	2.981 (2.235–3.978)	<0.001	3.217 (2.437–4.247)	<0.001
M stage						
M0	Ref		Ref			
M1	5.460 (3.640–8.180)	<0.001	2.028 (1.087–3.783)	0.026		
Surgery						
No	Ref		Ref		Ref	
Yes	0.254 (0.200–0.322)	<0.001	0.462 (0.342–0.623)	<0.001	0.451 (0.336–0.606)	<0.001
Radiation						
No	Ref					
Yes	1.54 (1.00–2.325)	<0.001				
Grade						
Well	Ref		Ref			
Moderately	1.510 (1.160–1.960)	<0.001	1.058 (0.803–1.394)	0.847	1.023 (0.723–1.425)	0.423
Poorly/Undifferentiated	2.440 (1.790–3.330)	<0.001	1.495 (1.050–2.129)	0.026	1.235 (1.058–1.919)	<0.001
Histologic type						
SCC	Ref		Ref		Ref	
None SCC	0.169 (0.096–0.296)	<0.001	0.312 (0.176–0.552)	<0.001	0.314 (0.152–0.616)	<0.001

AJCC, American Joint Committee on Cancer; SCC, squamous cell carcinoma.

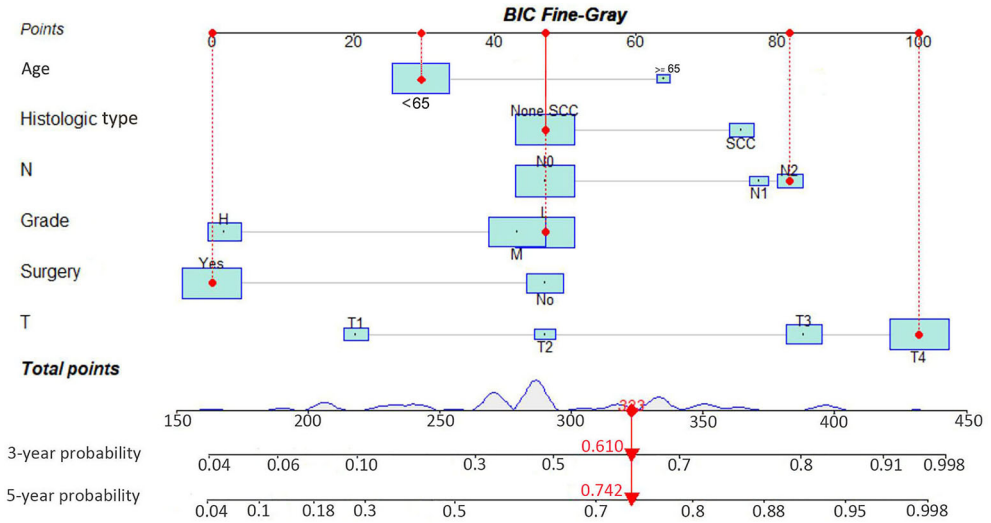

FIGURE 3 | Interactive nomogram for predicting the 3- and 5-year probabilities of cancer-specific death in Maxillary Sinus Carcinoma. BIC, Bayesian information criterion; SCC, squamous cell carcinoma.

Nomogram Verification

The C-index of the competing risk nomogram model for estimating the probability of CSD was 0.810 in the training cohort, 0.761 in the internal validation data set, and 0.755 in the external validation cohort. The AUC of our nomogram model for estimating the 3- and 5-year likelihoods of CSD was 0.792 and 0.812 in the training data set, 0.783 and 0.764 in the internal validation data set, and 0.756 and 0.783 in the external validation data set. The calibration graphs exhibited an excellent agreement between the actual and the nomogram-estimated likelihoods in the training (**Figures 4A, B**) and validation data sets (**Figures 4C–F**). Altogether, these data demonstrated the excellent estimation potential along with the remarkable confidence of the constructed nomogram.

Decision Curve Analysis

DCA was conducted in the three study data sets. In all three cohorts, the nomogram illustrated a higher net benefit along with a wider range of threshold likelihood relative to the AJCC staging approach, which depicts that the nomogram showed a high clinical utility value (**Figures 5A–F**).

DISCUSSION

Maxillary sinus carcinoma is one of the most frequent malignant tumors in the department of otolaryngology. The incidence of MSC is second only to nasopharyngeal carcinoma and laryngeal carcinoma in China, accounting for 2%–3% of head and neck tumors. Previous studies on sinonasal malignancies using the data abstracted from the SEER data resource have focused on incidence, as well as survival patterns (14, 15). For the first time, herein, we constructed prognostic models for the prognosis of individuals with MSC in a competitive event model and established more accurate predictors. The large data samples abstracted from the SEER data resource reduced the error of this study. In contrast with the traditional survival analysis, the competitive event model ensures that the chosen influencing factors have the most direct association with the prognosis of cancer. Although the AJCC staging system is a widely used system at present, it is unable to make a more personalized evaluation on the patient prognosis. For instance, the AJCC TNM staging approach for cutaneous melanoma was suggested to be used in vulva melanoma (16); however, treatment choices, for instance, chemotherapy, surgery, or radiotherapy, were not incorporated in this staging tool. Instead, a nomogram can make a more comprehensive and personalized evaluation because it integrates multiple factors.

Of the 11 parameters discovered herein, nine (age, M stage, radiation, AJCC stage, grade, T stage, surgery, N stage, as well as histological type) were demonstrated to be independent predictors of CSD in individuals with MSC through univariate along with multivariate competing risk analysis. In the univariate analysis, sex and race were not included, implying that they have no impact on CSD in individuals with MSC. The multivariate competing risk analysis data demonstrated that AJCC stage is not an independent predictor, which is linked to its comprehensive assessment of the T, N, and M stages. Following BIC optimization, six parameters (age, histological type, N stage, grade, surgery, and T stage) were included in the model.

It is critical to note that age was found to be an independent factor, which is consistent with Shen et al., who established a nomogram to study the prognosis of MSC. Le et al. explored the staging of MSCs and illustrated that the age of patients, favoring the young, is a remarkable independent predictor after correcting for other confounders, which may be a result of older patients having more comorbidities, as well as higher perioperative risks

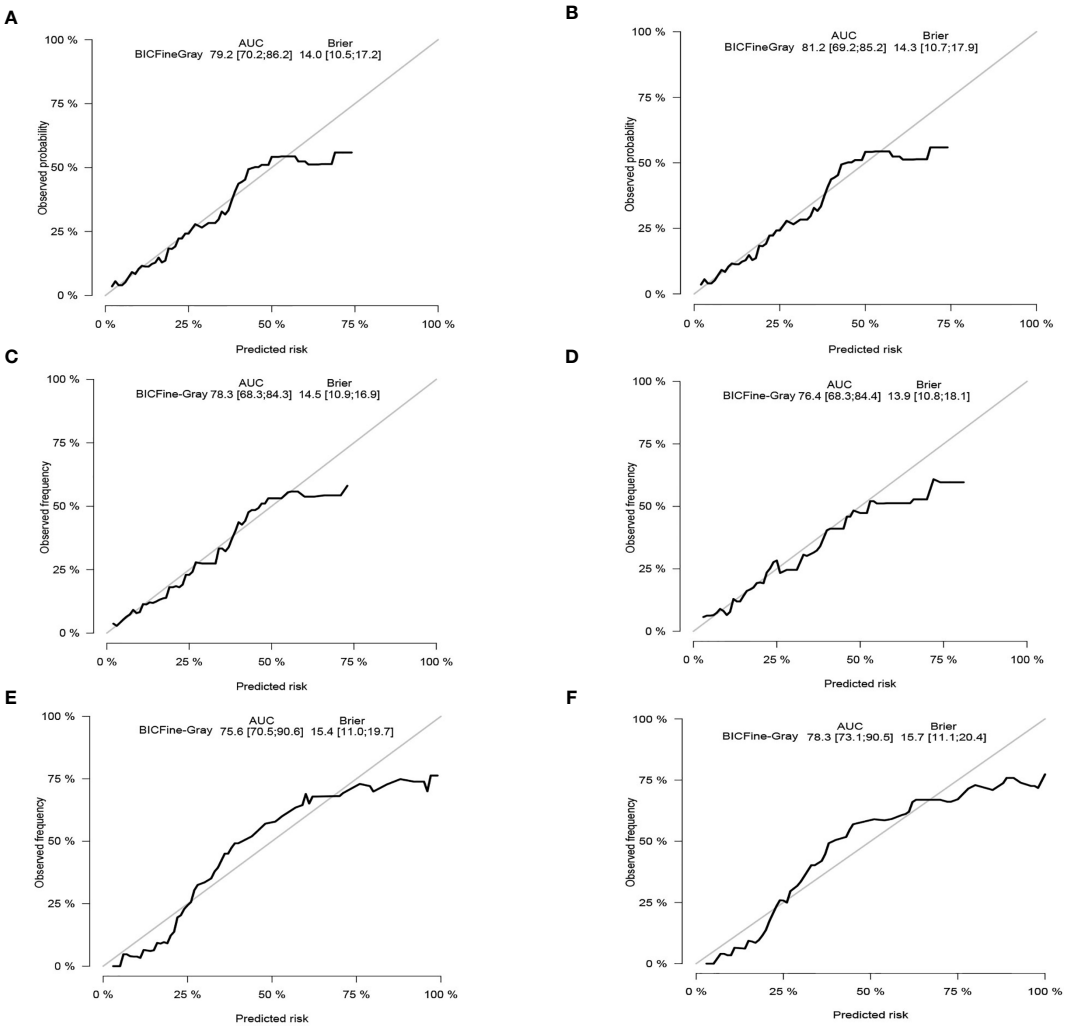

FIGURE 4 | Calibration curves. In the training cohort, the 3-and 5-year probabilities of cancer-specific death **(A, B)**. In the internal validation cohort, the 3- and 5-year probabilities of cancer-specific death **(C, D)**. In the external validation cohort, the 3- and 5-year probabilities of cancer-specific death **(E, F)**. BIC, Bayesian information criterion; AUC, area under the curve.

(15, 17, 18). The result about race in our study is similar with Shen et al., who reported that there was no significant difference in the prognosis among different races (15). There is also no direct evidence of survival differences between races. The research of Wang et al. illustrated that sex had no influence on cancer-specificity survival of Maxillary sinus SCC patients, which is consistent with our research (5). The data illustrated that higher pathological stage (grade) along with M stage and radiation were independent predictors for individuals with MSC, which is congruent with the data of previous studies (19). Nonetheless, the three factors above were removed in the process of using MSC to optimize the model to avoid overfitting.

Most clinicians prefer surgical therapy for MSC at all stages, although on the basis of the NCCN guidelines, surgery is remarkably recommended as the preferred approach for a resectable Maxillary sinus squamous cell carcinoma (MSSCC) (T1–T4a) (20). Our data illustrated that treatment with surgery remarkably reduced the CSD risks in individuals with MSC, which is congruent with the clinical experience of most doctors. However, whether a clinically negative neck in patients with MSC should be treated with an elective neck dissection or irradiated prophylactically is controversial in Europe and the United States (21, 22). In the study of Shen et al., surgery improved survival on the basis of the log-rank test. Nevertheless, in the Cox model, they demonstrated that this protective influence applies only to individuals with negative lymph nodes (15).

MSSCC is the most frequent pathological type in MSC, responsible for about 30%–50% of malignant paranasal sinus tumors (23, 24). Studies have avoided making a comparative analysis between SCC and other kinds of oral cancer. Herein, SCC was responsible for 55.2% of all MSC cases, and we established that the risk of CSD in individuals with SCC was remarkably higher in contrast with that in other kinds of MSC,

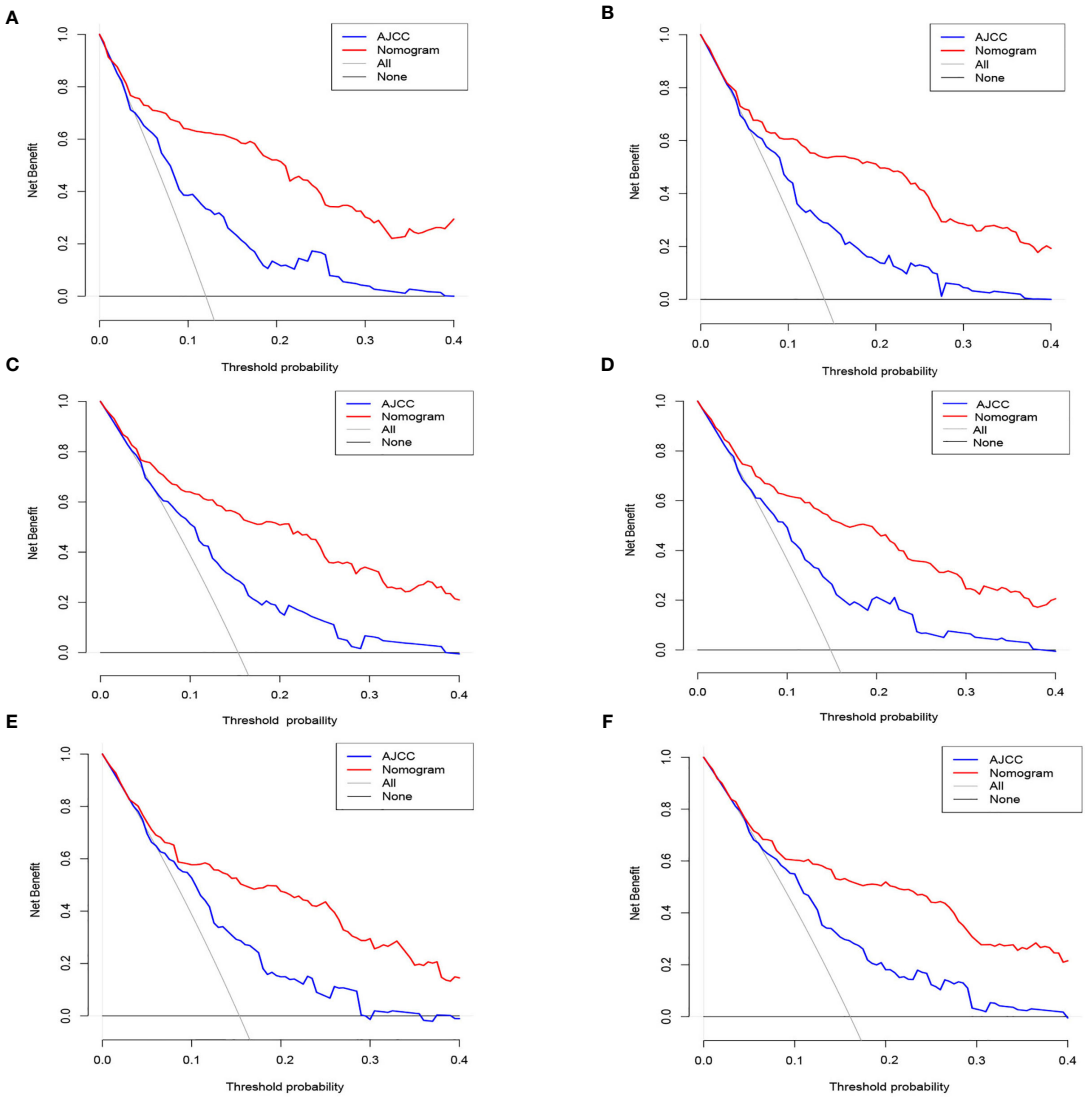

FIGURE 5 | The nomogram of the Decision curve analysis and the nomogram of the AJCC staging system in the prediction of the cancer-specific death of patients at the 3- and 5-year point in the training **(A, B)**, internal validation **(C, D)** and external validation **(E, F)** cohorts.

including adenoid cystic carcinoma, adenocarcinomas, mucoepidermoid neoplasms, and neuroendocrine carcinoma. This is congruent with the findings of Unsal et al., and van der Laan et al. in lung cancer (19, 25). This could be attributed to the high invasive, as well as metastatic ability of squamous cell carcinoma.

Previous reports on sinonasal malignancies that used the SEER program data have focused on incidence along with survival patterns (24, 26), while we centered on constructing estimation models herein. The treatment of MSC and the assessment of the prognosis presently depend on the AJCC staging approach. Our predictive model is appropriate for all individuals with MSC and could be broadly utilized at all levels of medical centers. The comprehensiveness of this nomogram could compensate the inefficiencies of the AJCC staging tool, and allow a precise assessment of the prognosis of individuals with MSC. In addition, a user-friendly graphic interface of the prediction model could enhance communication between clinicians and patients. Besides, we employed a validation data set for external verification, and the results were remarkably linked to the actual survival probabilities.

It is undeniable that this study has some limitations. Firstly, the SEER data resource lacks some critical variables linked to prognosis, such as chemotherapy, perineural infiltration, and smoking and sinusitis history. In addition, we used the sixth or seventh edition of the AJCC staging approach herein, which lacks two critical variables (depth of infiltration and extranodal extension) relative to the eighth edition. Third, the SEER data resource additionally does not collect data on tumor volume, which is regarded as a remarkable prognostic variable for

sinonasal malignancies. Although this study included data on radiotherapy, the SEER data resource lacks detailed information on the clinical treatment. Finally, although the SEER data resource provided a large sample size for this study, there are still some errors when it is applied in a global context. Larger-sample multi-center prospective research is required to further improve our prediction model and verify its clinical utility value.

CONCLUSION

We have established a competing risk analysis nomogram for individuals with MSC using the data abstracted from the SEER data resource. Our well-calibrated nomogram could be employed to make clinical decisions with regard to the prognosis and individualized treatment of individuals with MSC.

DATA AVAILABILITY STATEMENT

The data of MSC patients searched in SEER database are freely available. The data collected from our hospital generated and analyzed during the current study are available from the corresponding author on reasonable request.

ETHICS STATEMENT

Written informed consent was obtained from the individual(s) for the publication of any potentially identifiable images or data included in this article.

AUTHOR CONTRIBUTIONS

WG and MH were involved in the collecting of data and follow-up of the patients. XL and MH were responsible for the conception and design of the study, assisted with the statistical analysis, and wrote and revised the manuscript. SC, DL, and JM contributed their help on the data analysis, revised the English language and grammar, and corrected parts of the discussion. All authors contributed to the article and approved the submitted version.

FUNDING

This work was supported by the National Natural Science Foundation of China (NO.81560410) and Postgraduate Innovation Special Foundation of Jiangxi Province (YC2020-B043).

REFERENCES

1. Cancer JS for H, Committee CR. *Japan Society for Head and Neck Cancer, Cancer Registry Committee. Report of Head and Neck Cancer Registry of Japan Clinical Statistics of Registered Patients*. (2016). Available at: http://www.jshnc.umin.ne.jp/pdf/2016syourei_houkok.pdf (Accessed August 14, 2020).
2. Ferrari M, Ioppi A, Schreiber A, Gualtieri T, Mattavelli D, Rampinelli V, et al. Malignant Tumors of the Maxillary Sinus: Prognostic Impact of Neurovascular Invasion in a Series of 138 Patients. *Oral Oncol* (2020) 106:104672. doi: 10.1016/j.oraloncology.2020.104672
3. Cheraghlou S, Schettino A, Zogg CK, Judson BL. Changing Prognosis of Oral Cancer: An Analysis of Survival and Treatment Between 1973 and 2014. *Laryngoscope* (2018) 128(12):2762–9. doi: 10.1002/lary.27315
4. Wu CF, Lv JW, Lin L, Mao YP, Deng B, Zheng WH, et al. Development and Validation of a Web-Based Calculator to Predict Individualized Conditional Risk of Site-Specific Recurrence in Nasopharyngeal Carcinoma: Analysis of 10,058 Endemic Cases. *Cancer Commun (Lond)* (2021) 41(1):37–50. doi: 10.1002/cac2.12113
5. Wang Y, Yang R, Zhao M, Guo W, Zhang L, Zhang W, et al. Retrospective Analysis of 98 Cases of Maxillary Sinus Squamous Cell Carcinoma and Therapeutic Exploration. *World J Surg Oncol* (2020) 18(1):90. doi: 10.1186/s12957-020-01862-3
6. Doll KM, Rademaker A, Sosa JA. Practical Guide to Surgical Data Sets: Surveillance, Epidemiology, and End Results (SEER) Database. *JAMA Surg* (2018) 153(6):588–9. doi: 10.1001/jamasurg.2018.0501
7. Dignam JJ, Zhang Q, Kocherginsky M. The Use and Interpretation of Competing Risks Regression Models. *Clin Cancer Res an Off J Am Assoc Cancer Res* (2012) 18:2301–8. doi: 10.1158/1078-0432.CCR-11-2097
8. Li J, Zheng Q, Zhao X, Zhao J, An T, Wu M, et al. Nomogram Model for Predicting Cause-Specific Mortality in Patients With Stage I Small-Cell Lung Cancer: A Competing Risk Analysis. *BMC Cancer* (2020) 20(1):793. doi: 10.1186/s12885-020-07271-9
9. Yang Y, Chen ZJ, Yan S. The Incidence, Risk Factors and Predictive Nomograms for Early Death Among Patients With Stage IV Gastric Cancer: A Population-Based Study. *J Gastrointest Oncol* (2020) 11(5):964–82. doi: 10.21037/jgo-20-217
10. Dibas M, Ghozy S, Morsy S, Salah Abbas A, Alkahtani S, Bin-Jumah M, et al. Novel Nomograms Predicting Overall and Cancer-Specific Survival of Malignant Ependymoma Patients: A Population-Based Study. *J Neurosurg Sci* (2020). doi: 10.23736/S0390-5616.20.05033-X
11. Wang Y, Wu J, He H, Ma H, Hu L, Wen J, et al. Nomogram Predicting Cancer-Specific Mortality in Early-Onset Rectal Cancer: A Competing Risk Analysis. *Int J Colorectal Dis* (2020) 35(5):795–804. doi: 10.1007/s00384-020-03527-9
12. Mo S, Dai W, Xiang W, Li Q, Wang R, Cai G. Predictive Factors of Synchronous Colorectal Peritoneal Metastases: Development of a Nomogram and Study of Its Utilities Using Decision Curve Analysis. *Int J Surg* (2018) 54(Pt A):149–55. doi: 10.1016/j.ijsu.2018.04.051
13. Vickers AJ, Cronin AM, Elkin EB, Gonen M. Extensions to Decision Curve Analysis, A Novel Method for Evaluating Diagnostic Tests, Prediction Models and Molecular Markers. *BMC Med Inform Decis Mak* (2008) 8:53. doi: 10.1186/1472-6947-8-53
14. Quan H, Yan L, Zhang H, Zou L, Yuan W, Wang S. Development and Validation of a Nomogram for Prognosis of Sinonasal Squamous Cell Carcinoma. *Int Forum Allergy Rhinol* (2019) 9(9):1030–40. doi: 10.1002/alr.22354
15. Shen W, Sakamoto N, Yang L. Prognostic Models and Nomograms for Predicting Survival of Patients With Maxillary Sinus Carcinomas. *Int Forum Allergy Rhinol* (2017) 7(7):741–8. doi: 10.1002/alr.21950
16. Leitao MM Jr, Cheng X, Hamilton AL, Siddiqui NA, Jurgenliemk-Schulz I, Mahner S, et al. Gynecologic Cancer InterGroup (GCIG) Consensus Review for Vulvovaginal Melanomas. *Int J Gynecol Cancer* (2014) 24:S117–22. doi: 10.1097/IGC.0000000000000198
17. Le QT, Fu KK, Kaplan M, Terris DJ, Fee WE, Goffinet DR. Treatment of Maxillary Sinus Carcinoma: A Comparison of the 1997 and 1977 American Joint Committee on Cancer Staging Systems. *Cancer* (1999) 86:1700–11. doi: 10.1002/(SICI)1097-0142(19991101)86:9<1700::AID-CNCR11>3.0.CO;2-4
18. Nishio N, Fujimoto Y, Hiramatsu M, Maruo T, Tsuzuki H, Mukoyama N, et al. Maxillary Sinus Carcinoma Outcomes Over 60 Years: Experience at a Single Institution. *Nagoya J Med Sci* (2018) 80(1):91–8. doi: 10.18999/nagjms.80.1.91
19. van der Laan TP, Iepsma R, Witjes MJ, van der Laan BF, Plaat BE, Halmos GB. Meta-Analysis of 701 Published Cases of Sinonasal Neuroendocrine Carcinoma: The Importance of Differentiation Grade in Determining Treatment Strategy. *Oral Oncol* (2016) 63:1–9. doi: 10.1016/j.oraloncology.2016.10.002

20. Pfister DG, Spencer S, Adelstein D, Adkins D, Anzai Y, Brizel DM, et al. Head and Neck Cancers, Version 2.2020, NCCN Clinical Practice Guidelines in Oncology. *J Natl Compr Canc Netw* (2020) 18(7):873–98. doi: 10.6004/jnccn.2020.0031
21. Takes RP, Ferlito A, Silver CE, Rinaldo A, Medina JE, Robbins KT, et al. The Controversy in the Management of the N0 Neck for Squamous Cell Carcinoma of the Maxillary Sinus. *Eur Arch Otorhinolaryngol* (2013) 116:887–93. doi: 10.1007/s00405-013-2591-0
22. Rinaldo A, Ferlito A, Shaha AR, Wei WI. Is Elective Neck Treatment Indicated in Patients With Squamous Cell Carcinoma of the Maxillary Sinus? *Acta Otolaryngol* (2002) 122:443–7. doi: 10.1080/00016480260000175
23. Byrd JK, Clair JM, El-Sayed I. AHNS Series: Do You Know Your Guidelines? Principles for Treatment of Cancer of the Paranasal Sinuses: A Review of the National Comprehensive Cancer Network Guidelines. *Head Neck* (2018) 40 (9):1889–96. doi: 10.1002/hed.25143
24. Turner JH, Reh DD. Incidence and Survival in Patients With Sinonasal Cancer: A Historical Analysis of Population-Based Data. *Head Neck* (2012) 34(6):877–85. doi: 10.1002/hed.21830
25. Unsal AA, Chung SY, Zhou AH, Baredes S, Eloy JA. Sinonasal Adenoid Cystic Carcinoma: A Population-Based Analysis of 694 Cases. *Int Forum Allergy Rhinol* (2017) 7(3):312–20. doi: 10.1002/alr.21875
26. Dubal PM, Bhojwani A, Patel TD, Zuckerman O, Baredes S, Liu JK, et al. Squamous Cell Carcinoma of the Maxillary Sinus: A Population-Based Analysis. *Laryngoscope* (2016) 126(2):399–404. doi: 10.1002/lary.25601

Conflict of Interest: The authors declare that the research was conducted in the absence of any commercial or financial relationships that could be construed as a potential conflict of interest.

Publisher's Note: All claims expressed in this article are solely those of the authors and do not necessarily represent those of their affiliated organizations, or those of the publisher, the editors and the reviewers. Any product that may be evaluated in this article, or claim that may be made by its manufacturer, is not guaranteed or endorsed by the publisher.

frontiers in Oncology

ORIGINAL RESEARCH
published: 26 August 2021
doi: 10.3389/fonc.2021.701181

Incidence and Prognostic Significance of PD-L1 Expression in High-Grade Salivary Gland Carcinoma

Qigen Fang, Yao Wu, Wei Du, Xu Zhang and Defeng Chen*

Department of Head Neck and Thyroid, Affiliated Cancer Hospital of Zhengzhou University, Henan Cancer Hospital, Zhengzhou, China

Objective: PD-L1 is one of the predictors of immunotherapy efficacy. Our goal was to analyze its expression and prognostic significance in high-grade salivary gland carcinoma (SGC).

Methods: PD-L1 expression was evaluated using paraffin-embedded specimens from patients with surgically treated high-grade SGC, and it was scored by the tumor proportion score (TPS), combined positive score (CPS), and immune cell (IC) score. Associations between clinicopathological variables, disease-free survival (DFS), overall survival (OS) and PD-L1 expression were assessed.

Results: TPS≥1% occurred in 47 patients with an incidence of 43.1%, and it was significantly related to an advanced tumor stage. In patients with TPS<1%, TPS ranging from 1% to 20%, and TPS≥20%, the 5-year DFS rates were 36%, 26%, and 13%, respectively, and the difference was significant. In patients with TPS<1%, TPS ranging from 1% to 20%, and TPS≥20%, the 5-year OS rates were 49%, 24%, and 13%, respectively, and the difference was significant. CPS≥1 occurred in 87 patients with an incidence of 79.8%. IC scores of 0, 1, 2, and 3 were noted in 24 (22.0%), 37 (33.9%), 31 (28.4%), and 17 (15.6%) patients, respectively. Both CPS and IC scores had no impact on DFS or OS.

Conclusions: The expression of PD-L1 in tumor cells of high-grade SGCs was not uncommon, and it was significantly associated with tumor stage. PD-L1 expression in tumor cells rather than in immune cells indicated a poor prognosis.

Keywords: salivary gland carcinoma, PD-L1, immunotherapy, high-grade salivary gland carcinoma, survival

OPEN ACCESS

Edited by:
Hui Wang,
Hunan Cancer Hospital, China

Reviewed by:
Naomi Kiyota,
Kobe University Hospital, Japan
Shahram Ghanaati,
Goethe University Frankfurt, Germany

****Correspondence:***
Qigen Fang
qigenfang@126.com

Specialty section:
This article was submitted to Head and Neck Cancer, a section of the journal Frontiers in Oncology

Received: *27 April 2021*
Accepted: *10 August 2021*
Published: *26 August 2021*

Citation:
Fang Q, Wu Y, Du W, Zhang X and Chen D (2021) Incidence and Prognostic Significance of PD-L1 Expression in High-Grade Salivary Gland Carcinoma. Front. Oncol. 11:701181. doi: 10.3389/fonc.2021.701181

INTRODUCTION

Salivary gland carcinoma (SGC) is a relatively uncommon malignancy and accounts for less than 10% of all head and neck cancers (1). Based on the 2017 WHO classification, SGCs consist of 24 different histologic types (2). Due to their different biological behaviors and prognoses, SGCs are divided into three grades: low, intermediate, and high (3). Usually, high-grade SGC is the least frequent but has the worst prognosis. Even when treated with systemic therapies, many patients can still develop a recurrence (4, 5). More effective treatments are required to improve their prognosis.

Immune checkpoint inhibitors, such as programmed death 1 (PD-1) inhibitors, have been confirmed to be effective in controlling many malignant tumors (6). Expression of programmed death ligand-1 (PD-L1) is recognized as an important predictor of immunotherapy efficacy. A number of pioneers have analyzed PD-L1 expression in SGCs (7–9), but conflicting data have been reported, some researchers have described that about 20% of the patients show PD-L1 expression in SGC cells, and it is associated with poor disease free survival and overall survival (7, 8), but some have noted there is little relationship between PD-L1 expression and the disease specific survival (9). The scientific value of these studies is limited by no uniform standards of cutoff values, tissue specimens, antibodies, and scoring criteria for evaluating PD-L1 expression, there is still a lot of unknown knowledge regarding expression pattern and prognostic significance of PD-L1 especially in high grade SGCs, which is rarely analyzed, as far as we know, there are only four reports available for learning (10–13), according to the literature, the incidence of PD-L1 expression ranged from 26% to 53%, Xu et al. (10) and Sato et al. (11) would agree that high PD-L1 expression in salivary duct carcinoma was strongly associated with unfavorable prognosis, but Hamza et al. (12) and Schvartsman et al. (13) might not support this statement but presented PD-L1 expression had no effect on the survival. Therefore, in the current study, we aimed to evaluate the expression pattern and survival significance of PD-L1 in high-grade SGCs to explore the potential benefit of immunotherapy in this specific group.

PATIENTS AND METHODS

Ethics

Our hospital institutional research committee approved this study, and all participants signed an informed consent agreement. All procedures performed were in conducted in accordance with the ethical standards of the institutional and/or national research committee and the 1964 Helsinki Declaration and its later amendments or comparable ethical standards.

Patient Selection

From January 2010 to January 2021, the medical records of patients with surgically treated SGCs were retrospectively reviewed, and the enrolled patients met the following criteria: the disease was primary and classified as high grade based on the 2017 WHO classification (2); there was no history of other cancers; and there was enough paraffin-embedded tissue available for the PD-L1 expression test. Patients without sufficient demographic, pathologic, or follow-up data were excluded from the analysis. Information regarding age, sex, TNM stage (8^{th} AJCC system), pathologic reports, treatment, and follow-up was extracted and analyzed.

PD-L1 Expression Test

PD-L1 expression was tested by immunohistochemistry staining using 4μm thick sections of formalin-fixed, paraffin-embedded specimens and a monoclonal antibody targeting PD-L1 (SP263). The antibody was intended for diagnostic use *in vitro* and was employed according to the instructions of the manufacturer's protocol. The sections were rehydrated through graded ethanol at room temperature followed by deparaffinized in xylene. They were incubated with primary antibody for 30 minutes firstly, and then with biotinylated secondary antibodies. Immunoreactions were visualized using a 3-amino-9-ethylcarbazole as a substrate (Ventana OptiView DAB IHC detection KIT, Ref: 760-700, Mannheim, Germany). Human non-neoplastic tonsillar tissue was used as a positive control for the antibody.

TPS referred to the percentage of viable tumor cells showing partial or complete membrane PD-L1 staining at any intensity; CPS referred to the number of PD-L1 stained cells (tumor cells, lymphocytes, macrophages) divided by the total number of viable tumor cells multiplied by 100; and IC referred to the percentage of tumor area covered by PD-L1+ immune cells (4-tiered score: 0: <1%, 1: 1-5%, 2: 5-10%, 3: >10%). All PD-L1 expression evaluation was performed with high power microscope (×200).

Treatment Principle

In our cancer center, a definite diagnosis of SGC is usually made based on postoperative pathology. If a high-grade SGC was confirmed, adjuvant radiotherapy and/or chemotherapy were always administered. Neck dissection was performed if there was a cN+ neck. After discharge from the hospital, the patients were routinely followed every 3 months for the first two years and then every 6 to 12 months for the next 3 years. If disease recurrence was suspected, active interference was immediately performed.

Statistical Analysis

Associations between clinicopathological variables and PD-L1 expression were evaluated by the chi-square test. The Kaplan-Meier method was used to analyze disease-free survival (DFS) and overall survival (OS). The DFS was calculated from the date of surgery to the date of recurrence or the last follow-up visit, and OS was calculated from the date of surgery to the date of death or last follow-up visit. Factors that were significant in univariate analysis were then analyzed in a Cox proportional hazards regression model to study the independent effects on survival. All statistical analyses were performed by SPSS 20.0, and $p<0.05$ was considered to be significant.

RESULTS

Baseline Information of the Patients

A total of 109 patients were included for analysis; there were 60 (55.0%) men and 49 (45.0%) women, and the mean age was 45.6 ± 10.4 years. Primary sites were distributed in the parotid gland in 55 (50.5%) patients, submandibular gland in 27 (24.8%) patients, sublingual gland in 15 (13.8%) patients, and minor gland in 12 (11.0%) patients.

Tumor stages were classified as T1 in 17 (15.6%) patients, T2 in 45 (41.3%) patients, T3 in 35 (32.1%) patients, and T4 in 12 (11.0%) patients. Neck lymph node stages were classified as N0

in 68 (62.4%) patients and N+ in 41 (37.6%) patients. The most common histologic type was high-grade mucoepidermoid carcinoma (MEC), followed by salivary duct carcinoma (SDC), which occurred in 47 (43.1%) and 33 (30.3%) patients, respectively. Adenocarcinoma, not otherwise specified, developed in 15 (13.8%) patients. Squamous cell carcinoma occurred in 8 (7.3%) patients. The least common histologic types were small cell carcinoma, large cell carcinoma, and spindle cell carcinoma, which all developed in 2 (1.8%) patients each. Perineural invasion (PNI) and lymphovascular invasion (LVI) were noted in 37 (33.9%) and 33 (30.3%) patients, respectively. A positive margin occurred in 9 (8.3%) patients.

All patients underwent surgical treatments, 60 (55.0%) patients also underwent neck dissection, and pathologic lymph node metastasis occurred in 45 (75.0%, 45/60) patients. All patients received adjuvant radiotherapy, and 24 (22.0%) patients also underwent adjuvant chemotherapy (**Table 1**).

TABLE 1 | Demographic and pathologic information of the patients.

Variables	Number (%)
Age	
≥45	48 (44.0%)
<45	61 (56.0%)
Gender	
Male	60 (55.0%)
Female	49 (45.0%)
Primary site	
Parotid gland	55 (50.5%)
Submandibular gland	27 (24.8%)
Sublingual gland	15 (13.8%)
Minor gland	12 (11.0%)
Histologic type	
High grade mucoepidermoid carcinoma	47 (43.1%)
Salivary duct carcinoma	33 (30.3%)
Adenocarcinoma not otherwise specified	15 (13.8%)
Squamous cell carcinoma	8 (7.3%)
Small cell carcinoma	2 (1.8%)
Large cell carcinoma	2 (1.8%)
Spindle cell carcinoma	2 (1.8%)
Perineural invasion	37 (33.9%)
Lymphovascular invasion	33 (30.3%)
Tumor stage	
T1-T2	62 (56.9%)
T3-T4	47 (43.1%)
Neck lymph node stage	
N0	68 (62.4%)
N+	41 (37.6%)
Positive margin	9 (8.3%)
Radiotherapy	109 (100%)
Chemotherapy	24 (22.0%)

PD-L1 Expression

TPS≥1% occurred in 47 patients with an incidence of 43.1%; in these 47 patients, 32 cases had a TPS<20%, and 15 cases had a TPS≥20%. CPS≥1 occurred in 87 patients with an incidence of 79.8%; of these 87 patients, 47 had a CPS<20, and 40 had a CPS≥20. IC scores of 0, 1, 2, and 3 were noted in 24 (22.0%), 37 (33.9%), 31 (28.4%), and 17 (15.6%) patients, respectively.

Predictors of PD-L1 Expression

As **Table 2** describes, in patients with T1-T2 tumors, 42 cases had TPS<1%, 17 cases had a TPS ranging from 1% to 20%, and

TABLE 2 | Association between clinicopathological variables and PD-L1 expression.

Variable	Tumor proportion score			p	Combined positive score			p	Immune cell score		p
	<1%	1-20%	≥20%		<1	1-20	≥20		0/1	2/3	
Age											
≥45	27	16	5		10	23	15		29	19	
<45	35	16	10	0.558	12	24	25	0.557	32	29	0.406
Gender											
Male	33	18	9		13	27	20		35	25	
Female	29	14	6	0.882	9	20	20	0.717	26	23	0.581
Primary site											
Parotid gland	32	16	7		10	26	19		27	28	
Submandibular gland	16	7	4		7	10	10		16	11	
Sublingual gland	8	5	2		3	6	6		9	6	
Minor gland	6	4	2	0.997	2	5	5	0.973	9	3	0.386
Histologic type											
High grade mucoepidermoid carcinoma	28	12	7		9	20	18		26	21	
Salivary duct carcinoma	19	9	5		8	15	10		20	13	
Adenocarcinoma not otherwise specified	7	6	2		3	7	5		8	7	
Others	8	5	1	0.932	2	5	7	0.931	7	7	0.910
Perineural invasion	22	10	7	0.588	8	17	12	0.803	20	17	0.232
Lymphovascular invasion	19	8	6	0.588	6	17	10	0.498	19	14	0.823
Tumor stage											
T1-T2	42	17	3		14	27	21		37	25	
T3-T4	20	15	12	0.003	8	20	19	0.695	24	23	0.370
Neck lymph node stage											
N0	43	16	9		13	30	25		39	29	
N+	19	16	6	0.182	9	17	15	0.931	22	19	0.707

3 cases had a TPS≥20%; in patients with T3-T4 tumors, 20 cases had TPS<1%, 15 cases had a TPS ranging from 1% to 20%, and 12 cases had a TPS≥20%, and the difference was significant (p=0.003). No apparent associations between any other variables and TPS were noted (all p>0.05). Furthermore, there were no significant relationships between any of the clinicopathological variables and the CPS or IC score (all p>0.05).

Survival Analysis

After a follow-up with a mean time of 3.8 (range: 0.6-9.6) years, disease recurrence occurred in 71 patients, and 62 patients died. The overall 5-year DFS and OS rates were 30.0% and 36%, respectively.

In patients with TPS<1%, the 5-year DFS rate was 36%; in patients with TPS ranging from 1% to 20%, the 5-year DFS rate was 26%; and in patients with TPS≥20%, the 5-year DFS rate was 13%, and the difference was significant (p<0.001, **Figure 1**). In patients with TPS<1%, the 5-year OS rate was 49%; in patients with TPS ranging from 1% to 20%, the 5-year OS rate was 24%; and in patients with TPS≥20%, the 5-year OS rate was 13%, and the difference was significant (p<0.001, **Figure 2**). Further, the Cox model confirmed the independence of TPS's correlation with DFS and OS (**Tables 3** and **4**).

In patients with CPS<1, the 5-year DFS rate was 44%; in patients with CPS ranging from 1 to 20, the 5-year DFS rate was 24%; and in patients with CPS≥20, the 5-year DFS rate was 30%, and the difference was not significant (p=0.635, **Figure 3**). In patients with CPS<1, the 5-year OS rate was 44%; in patients with CPS ranging from 1 to 20, the 5-year OS rate was 21%; and in patients with CPS≥20, the 5-year OS rate was 53%, and the difference was not significant (p=0.540, **Figure 4**).

In patients with an IC score of 0/1, the 5-year DFS rate was 28%; in patients with an IC score of 2/3, the 5-year DFS rate was 34%, and the difference was not significant (p=0.600, **Figure 5**). In patients with an IC score of 0/1, the 5-year OS rate was 32%; in patients with an IC score of 2/3, the 5-year OS rate was 41%, and the difference was not significant (p=0.422, **Figure 6**).

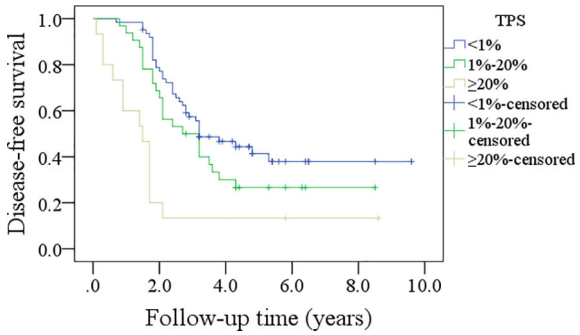

FIGURE 1 | Comparison of disease-free survival in patients with different tumor proportion scores (TPSs), combined positive score (CPS), and immune cell (IC) score.

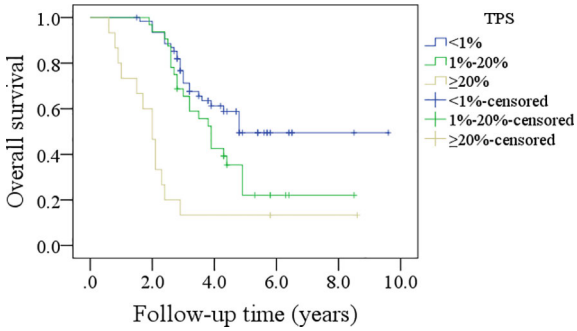

FIGURE 2 | Comparison of overall survival in patients with different tumor proportion scores (TPSs).

TABLE 3 | Survival effect of PD-L1 expression on disease free survival in high grade salivary gland carcinoma.

Variable	Univariate	Cox model	
	p	p	HR [95%CI]
Age (≥45 *vs* <45)	0.354		
Gender (Male *vs* female)	0.267		
Primary site (Parotid *vs* others)	0.004	0.002	1.896 [1.046-4.332]
Histologic type (Mucoepidermoid carcinoma *vs* others)	0.154		
Perineural invasion	<0.001	<0.001	2.006 [1.356-5.337]
Lymphovascular invasion	<0.001	<0.001	1.675 [1.114-3.008]
Tumor stage (T3+T4 *vs* T1+T2)	<0.001	<0.001	4.675 [2.337-9.988]
Neck lymph node stage (N+ *vs* N0)	<0.001	<0.001	3.285 [2.217-7.447]
Tumor proportion score			
<1%			
1% to 20%		0.015	1.994 [1.175-2.887]
≥20%	<0.001	<0.001	3.063 [2.000-6.326]
Combined positive score			
<1			
1 to 20			
≥20	0.635		
Immune cell score (2/3 *vs* 0/1)	0.600		

DISCUSSION

The most significant finding in the current study was that PD-L1 expression was not uncommon in high-grade SGC cells. TPS was associated with tumor stage and prognosis, and a greater TPS indicated worse survival. Both CPS and IC scores had no relationship with clinicopathological variables or prognosis. Our study provided valuable evidence that TPS could represent a better target for immune checkpoint inhibition than the CPS and IC scores.

The PD-L1/PD-1 axis mediates immune tolerance and promotes tumor growth and progression *via* the inhibition of anti-tumor immunity. Blocking the interaction between PD-L1 and PD-1 was clinically shown to be beneficial in maintaining the anti-tumor functions of the adaptive immune system (14). It was important to explore the PD-L1 expression level in solid malignancies, but it is not frequently analyzed in SGCs. Mukaigawa et al. (7) might be the first to investigate this

TABLE 4 | Survival effect of PD-L1 expression on overall survival in high grade salivary gland carcinoma.

Variable	Univariate p	Cox model p	Cox model HR [95%CI]
Age (≥45 *vs* <45)	0.632		
Gender (Male *vs* female)	0.227		
Primary site (Parotid *vs* others)	<0.001	0.002	2.976 [1.365-4.338]
Histologic type (Mucoepidermoid carcinoma *vs* others)	0.641		
Perineural invasion	<0.001	<0.001	2.156 [1.227-4.307]
Lymphovascular invasion	<0.001	<0.001	1.998 [1.032-3.098]
Tumor stage (T3+T4 *vs* T1+T2)	<0.001	<0.001	3.876 [1.578-7.447]
Neck lymph node stage (N+ *vs* N0)	<0.001	<0.001	3.002 [1.674-6.885]
Tumor proportion score			
<1%			
1% to 20%		0.021	2.075 [1.275-4.886]
≥20%	<0.001	<0.001	3.328 [1.998-6.356]
Combined positive score			
<1			
1 to 20			
≥20	0.540		
Immune cell score (2/3 *vs* 0/1)	0.422		

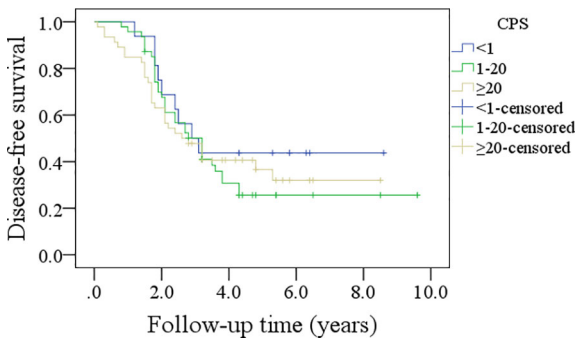

FIGURE 3 | Comparison of disease-free survival in patients with different combined positive scores (CPSs).

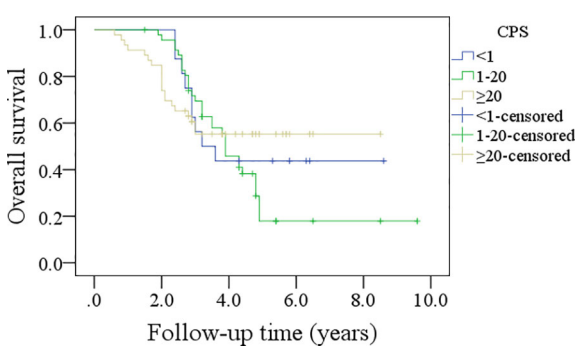

FIGURE 4 | Comparison of overall survival in patients with different combined positive scores (CPSs).

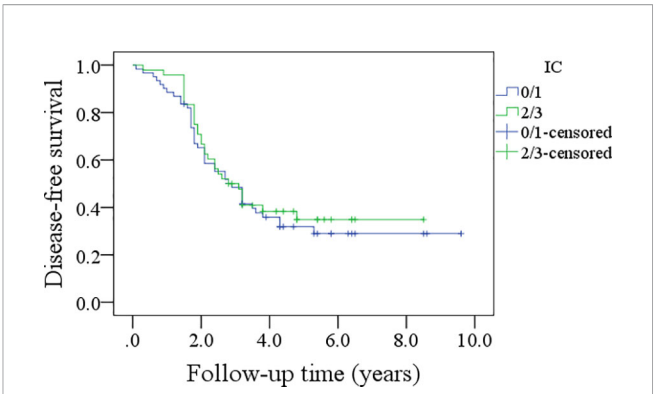

FIGURE 5 | Comparison of disease-free survival in patients with different immune cell (IC) scores.

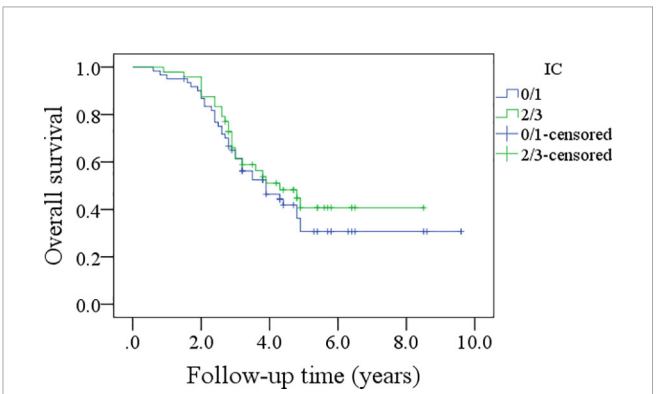

FIGURE 6 | Comparison of overall survival in patients with different immune cell (IC) scores.

issue and found that 22.8% of 219 surgically resected SGC specimens had PD-L1 expression. Moreover, the expression of PD-L1 in cancer cells was significantly related to age, sex, tumor location, pathologic tumor and nodal stages, histologic type, and pathologic grade. However, in this study, the authors defined PD-L1 expression positivity as a case showing complete membranous expression of PD-L1 in more than 1% of the carcinoma cells, which was apparently different from other studies. Vital et al. (8) considered positivity for PD-L1 if there was any unequivocal membranous staining of at least 1% of the tumor cells; in their 167 SGC patients, 17% showed PD-L1 positivity, and PD-L1 expression in tumor cells was associated with a higher tumor grade. A similar definition of PD-L1 expression positivity was used by Higashino et al. (9); the authors reported a rate of 28.3%, and it was more common in tumors with a higher stage, a higher grade, and node-positive cases. However, none of these three studies focused on high-grade SGCs, which usually have a worse prognosis than low- and intermediate-grade SGCs and deserve more attention (4, 15).

Very few researchers have examined the significance of PD-L1 expression in high-grade SGCs. Hamza et al. (12) evaluated

salivary duct carcinoma specimens from 113 patients and found that 26% of the samples had positive PD-L1 expression (TPS≥1%), but the authors did not analyze the association between PD-L1 expression and clinicopathological variables. Another paper enrolling 17 salivary duct carcinoma patients reported that there was a positive PD-L1 expression rate as high as 53% (13), but in our research, we noted that the rate was 42.4%. This inconsistency might be attributed to several possibilities. First, the antibodies used in immunohistochemistry were different, and a previous study confirmed that the positive rate of PD-L1 expression was significantly affected by the antibody clones (16). Second, the specimens used for PD-L1 detection were different. We used full-face sections, but some used tissue microarray sections. When comparing these two methods, cases with high expression of PD-L1 did not have good concordance (17).

In addition, the term high-grade SGC has been used not only for salivary duct carcinoma but also to refer to some other types of cancer. This was the first study to focus on this small, specific group. We noted that the overall rate of TPS≥1% patients was 43.1%, which was associated with the tumor stage but not the histologic type. This finding was interesting and suggested that the high-grade SGC microenvironment exhibited similar immunogenicity independent of histologic type but was affected by tumor stage. Similarly, Kesar et al. (18) previously noted in their 84 patients that the two most common malignant tumor types presenting with PD-L1 expression were adenocarcinoma not otherwise specified and squamous cell carcinoma.

There are no official standards for reporting PD-L1 expression detection, and three scoring criteria are available: TPS, CPS and the IC score. In the current study, 79.8% and 44.0% of the patients had CPS≥1 and IC scores of 2 or 3, respectively. These incidences were consistent with the reports by Xu et al. (10), Witte et al. (19), and Szewczyk et al. (20). However, there was a discrepancy in the association between PD-L1 expression and clinicopathological variables. Witte et al. (18) noted that both TPS and the IC score were not related to node-positive disease, but a higher CPS means a higher frequency of lymph node metastasis. Possible explanations were differences between the studied cases and the different antibodies used.

The survival effect of PD-L1 expression in SGC is another important issue for analysis. Mukaigawa et al. (7) found that in 219 SGC patients, the 5-year DFS rates of patients showing tumor cell PD-L1 positivity and PD-L1 negativity were 20.2% and 54.6%, respectively, and the difference was significant. The 5-year OS rates of patients with tumor cell PD-L1 positivity and PD-L1 negativity were 40.8% and 80.9%, respectively, and the difference was also significant. In a paper by Xu et al. (10), the authors described that PD-L1 immunopositivity in at least 25% of tumor cells was associated with decreased disease-specific survival. Similar results were also confirmed by Sato et al. (11, 21), Nakano et al. (22), and our results. This suggested a negative survival effect of high TPS. It was the strongest point of current study, we firstly employed the three established predictive scoring criteria on this small and specific group of high grade SGC, and uncovered that TPS rather than CPS or IC score showed better promising target for immuno-oncologic treatment.

However, there were also totally different viewpoints. Higashino et al. (9) showed that in their 127 patients, disease-specific survival was 86.9% for those with PD-L1-negative tumors and 82.2% for patients with PD-L1-positive tumors, and there was no significant difference. In their subgroup analysis of high grade cancers, it was 52.7% in 23 patients with PD-L1-negative tumors and 62.5% in 21 patients with PD-L1-positive tumors, again showing no significant difference, and it remained the same in low- and intermediate grade cases. Even when expression by 10% of tumor cells was used as the threshold for defining PD-L1 positivity, no significant difference in disease-specific survival was observed. Hamza et al. (12) included 113 patients, and the authors reported that the OS rates at 3, 5 and 10 years were 52.6%, 37.9% and 25.6%, respectively. There was no significant difference in survival between patients with PD-L1-immunoreactive tumors and those without. Similar findings were also reported by Schvartsman et al. (13) and Witte et al. (19). Vital et al. (8) reported that PD-L1 expression in tumor cells did not have any correlation with DFS and OS in 167 patients with SGC, but PD-L1 positivity in tumor-infiltrating immune cells predicted a worse DFS and OS in salivary duct carcinoma. Xu et al. (10) noted PD-L1 immunopositivity determined with a cutoff of CPS≥1 was associated with improved disease-specific survival and DFS in salivary duct carcinoma. The presence of PD-1-positive immune cells was associated with improved survival regardless of the expression level. However, in our study, we failed to note a positive relationship between prognosis and CPS/IC score. The differences might be explained by that the authors investigated only PD-L1 positive tumor cells and did not check the PD-1 positive immune cells, and more importantly, even if there were many PD-L1 positive tumor cells, sometimes there were few PD-1 positive immune cells around the tumor cells. Usually, PD-1 positive immune cells induced PD-L1 positive tumor cells as a result of immune response. However, sometimes tumor cells expressed PD-L1 with innate immune response.

Limitations in the current study must be acknowledged. First, our sample size was relatively small. Second, this was a retrospective study, and it had inherent bias. Third, we used paraffin-embedded specimens and not fresh tissue to assess PD-L1 expression, which might affect the accuracy of PD-L1 expression evaluation. Fourth, PD-L1 expression level showed heterogeneity among different PD-L1 antibodies used and different pathologists, and also it showed intra-tumoral heterogeneity, more studies were needed to clarify the PD-L1 expression level in high-grade SGCs.

In summary, the expression of PD-L1 in tumor cells of high-grade SGCs was not uncommon, TPS was associated with tumor stage and prognosis, and a greater TPS indicated worse survival. Both CPS and IC scores had no relationship with clinicopathological variables or prognosis. Patients with high TPS might benefit from immunotherapy.

DATA AVAILABILITY STATEMENT

The original contributions presented in the study are included in the article/**Supplementary Material**. Further inquiries can be directed to the corresponding author.

ETHICS STATEMENT

The studies involving human participants were reviewed and approved by Henan cancer hospital institutional research committee approved this study, and all participants signed an informed consent agreement. The patients/participants provided their written informed consent to participate in this study.

AUTHOR CONTRIBUTIONS

All authors contributed to the article and approved the submitted version.

SUPPLEMENTARY MATERIAL

The Supplementary Material for this article can be found online at: https://www.frontiersin.org/articles/10.3389/fonc.2021.701181/full#supplementary-material

REFERENCES

1. Gatta G, Guzzo M, Locati LD, McGurk M, Prott FJ. Major and Minor Salivary Gland Tumours. *Crit Rev Oncol Hematol* (2020) 152:102959. doi: 10.1016/j.critrevonc.2020.102959
2. El-Nagger AKCJ, Grandis JR, Takata T, Slootweg PJ. *WHO Classification of Head and Neck Tumours*. Lyon, France: International Agency for Research on Cancer (IARC (2017).
3. Dahan LS, Giorgi R, Vergez S, Le Taillandier de Gabory L, Costes-Martineau V, Herman P, et al. REFCOR Members. Mucoepidermoid Carcinoma of Salivary Glands: A French Network of Rare Head and Neck Tumors (REFCOR) Prospective Study of 292 Cases. *Eur J Surg Oncol* (2020) 47:1376–83. doi: 10.1016/j.ejso.2020.11.123
4. Fang Q, Wu J, Liu F. Oncologic Outcome and Potential Prognostic Factors in Primary Squamous Cell Carcinoma of the Parotid Gland. *BMC Cancer* (2019) 19:752. doi: 10.1186/s12885-019-5969-6
5. Shi S, Fang Q, Liu F, Zhong M, Sun C. Prognostic Factors and Survival Rates for Parotid Duct Carcinoma Patients. *J Craniomaxillofac Surg* (2014) 42:1929–31. doi: 10.1016/j.jcms.2014.08.001
6. Lei Y, Li X, Huang Q, Zheng X, Liu M. Progress and Challenges of Predictive Biomarkers for Immune Checkpoint Blockade. *Front Oncol* (2021) 11:617335. doi: 10.3389/fonc.2021.617335
7. Mukaigawa T, Hayashi R, Hashimoto K, Ugumori T, Hato N, Fujii S. Programmed Death Ligand-1 Expression Is Associated With Poor Disease Free Survival in Salivary Gland Carcinomas. *J Surg Oncol* (2016) 114:36–43. doi: 10.1002/jso.24266
8. Vital D, Ikenberg K, Moch H, Rössle M, Huber GF. The Expression of PD-L1 in Salivary Gland Carcinomas. *Sci Rep* (2019) 9:12724. doi: 10.1038/s41598-019-49215-9
9. Higashino M, Kawata R, Nishikawa S, Terada T, Haginomori SI, Kurisu Y, et al. Programmed Death Ligand-1 Expression Is Associated With Stage and Histological Grade of Parotid Carcinoma. *Acta Otolaryngol* (2020) 140:175–80. doi: 10.1080/00016489.2019.1683604
10. Xu B, Jungbluth AA, Frosina D, Alzumaili B, Aleynick N, Slodkowska E, et al. The Immune Microenvironment and Expression of PD-L1, PD-1, PRAME and MHC I in Salivary Duct Carcinoma. *Histopathology* (2019) 75:672–82. doi: 10.1111/his.13944
11. Sato F, Akiba J, Kawahara A, Naito Y, Ono T, Takase Y, et al. The Expression of Programed Death Ligand-1 Could be Related With Unfavorable Prognosis in Salivary Duct Carcinoma. *J Oral Pathol Med* (2018) 47:683–90. doi: 10.1111/jop.12722
12. Hamza A, Roberts D, Su S, Weber RS, Bell D, Ferrarotto R. PD-L1 Expression by Immunohistochemistry in Salivary Duct Carcinoma. *Ann Diagn Pathol* (2019) 40:49–52. doi: 10.1016/j.anndiagpath.2019.04.001
13. Schvartsman G, Bell D, Rubin ML, Tetzlaff M, Hanna E, Lee JJ, et al. The Tumor Immune Contexture of Salivary Duct Carcinoma. *Head Neck* (2021) 43:1213–9. doi: 10.1002/hed.26587
14. Yajuk O, Baron M, Toker S, Zelter T, Fainsod-Levi T, Granot Z. The PD-L1/PD-1 Axis Blocks Neutrophil Cytotoxicity in Cancer. *Cells* (2021) 10:1510. doi: 10.3390/cells10061510
15. Fang Q, Wu J, Du W, Zhang X. Predictors of Distant Metastasis in Parotid Acinic Cell Carcinoma. *BMC Cancer* (2019) 19:475. doi: 10.1186/s12885-019-5711-4
16. Parra ER, Villalobos P, Mino B, Rodriguez-Canales J. Comparison of Different Antibody Clones for Immunohistochemistry Detection of Programmed Cell Death Ligand 1 (PD-L1) on Non-Small Cell Lung Carcinoma. *Appl Immunohistochem Mol Morphol* (2018) 26:83–93. doi: 10.1097/PAI.0000000000000531
17. Gniadek TJ, Li QK, Tully E, Chatterjee S, Nimmagadda S, Gabrielson E. Heterogeneous Expression of PD-L1 in Pulmonary Squamous Cell Carcinoma and Adenocarcinoma: Implications for Assessment by Small Biopsy. *Mod Pathol* (2017) 30:530–8. doi: 10.1038/modpathol.2016.213
18. Kesar N, Winkelmann R, Oppermann J, Ghanaati S, Martin D, Neumayer T, et al. Prognostic Impact of CD8-Positive Tumour-Infiltrating Lymphocytes and PD-L1 Expression in Salivary Gland Cancer. *Oral Oncol* (2020) 111:104931. doi: 10.1016/j.oraloncology.2020.104931
19. Witte HM, Gebauer N, Lappöhn D, Umathum VG, Riecke A, Arndt A, et al. Prognostic Impact of PD-L1 Expression in Malignant Salivary Gland Tumors as Assessed by Established Scoring Criteria: Tumor Proportion Score (TPS), Combined Positivity Score (CPS), and Immune Cell (IC) Infiltrate. *Cancers (Basel)* (2020) 12:873. doi: 10.3390/cancers12040873
20. Szewczyk M, Marszałek A, Sygut J, Golusiński P, Golusiński W. Prognostic Markers in Salivary Gland Cancer and Their Impact on Survival. *Head Neck* (2019) 41:3338–47. doi: 10.1002/hed.25857
21. Sato F, Ono T, Kawahara A, Matsuo K, Kondo R, Sato K, et al. Prognostic Value of Tumor Proportion Score in Salivary Gland Carcinoma. *Laryngoscope* (2021) 131:E1481–8. doi: 10.1002/lary.29120
22. Nakano T, Takizawa K, Uezato A, Taguchi K, Toh S, Masuda M. Prognostic Value of Programed Death Ligand-1 and Ligand-2 Co-Expression in Salivary Gland Carcinomas. *Oral Oncol* (2019) 90:30–7. doi: 10.1016/j.oraloncology.2019.01.015

Conflict of Interest: The authors declare that the research was conducted in the absence of any commercial or financial relationships that could be construed as a potential conflict of interest.

Publisher's Note: All claims expressed in this article are solely those of the authors and do not necessarily represent those of their affiliated organizations, or those of the publisher, the editors and the reviewers. Any product that may be evaluated in this article, or claim that may be made by its manufacturer, is not guaranteed or endorsed by the publisher.

frontiers in Oncology

CORRECTION
published: 30 December 2021
doi: 10.3389/fonc.2021.836903

Corrigendum: Incidence and Prognostic Significance of PD-L1 Expression in High-Grade Salivary Gland Carcinoma

Qigen Fang, Yao Wu, Wei Du, Xu Zhang and Defeng Chen*

Department of Head Neck and Thyroid, Affiliated Cancer Hospital of Zhengzhou University, Henan Cancer Hospital, Zhengzhou, China

Keywords: salivary gland carcinoma, PD-L1, immunotherapy, high-grade salivary gland carcinoma, survival

OPEN ACCESS

Approved by:
Frontiers Editorial Office, Frontiers Media SA, Switzerland

****Correspondence:***
Qigen Fang
qigenfang@126.com

Specialty section:
This article was submitted to Head and Neck Cancer, a section of the journal Frontiers in Oncology

Received: *16 December 2021*
Accepted: *16 December 2021*
Published: *30 December 2021*

Citation:
Fang Q, Wu Y, Du W, Zhang X and Chen D (2021) Corrigendum: Incidence and Prognostic Significance of PD-L1 Expression in High-Grade Salivary Gland Carcinoma. Front. Oncol. 11:836903. doi: 10.3389/fonc.2021.836903

A Corrigendum on:

Incidence and Prognostic Significance of PD-L1 Expression in High-Grade Salivary Gland Carcinoma

By Fang Q, Wu Y, Du W, Zhang X, Chen D. (2021) Front Oncol. 11:701181. doi: 10.3389/fonc.2021.701181

In the published article, there was an error in affiliation order. Instead of "Department of Head Neck and Thyroid, Henan Cancer Hospital, Affiliated Cancer Hospital of Zhengzhou University, Zhengzhou, China", it should be "Department of Head Neck and Thyroid, Affiliated Cancer Hospital of Zhengzhou University, Henan Cancer Hospital, Zhengzhou, China".

The authors apologize for this error and state that this does not change the scientific conclusions of the article in any way. The original article has been updated.

frontiers in Oncology

SYSTEMATIC REVIEW
published: 02 September 2021
doi: 10.3389/fonc.2021.703995

Prognostic Factors for Overall Survival in Nasopharyngeal Cancer and Implication for TNM Staging by UICC: A Systematic Review of the Literature

Chi Leung Chiang[1,2], Qiaojuan Guo[3], Wai Tong Ng[1,2], Shaojun Lin[3], Tiffany Sze Wai Ma[2], Zhiyuan Xu[1], Youping Xiao[3], Jishi Li[1], Tianzhu Lu[3], Horace Cheuk Wai Choi[2], Wenqi Chen[1], Eric Sze Chun Chau[2], Peter Ho Yin Luk[2], Shao Hui Huang[4], Brian O'Sullivan[4], Jianji Pan[3] and Anne Wing Mui Lee[1,2]**

[1] Clinical Oncology Center, The University of Hong Kong-Shenzhen Hospital, Shenzhen, China, [2] Department of Clinical Oncology, Li Ka Shing Faculty of Medicine, The University of Hong Kong, Hong Kong, Hong Kong, [3] Department of Radiation Oncology, Fujian Cancer Hospital & Fujian Medical University Cancer Hospital, Fuzhou, China, [4] Department of Radiation Oncology, University of Toronto, Princess Margaret Cancer Centre, Toronto, ON, Canada

This study aims to identify prognostic factors in nasopharyngeal carcinoma (NPC) to improve the current 8th edition TNM classification. A systematic review of the literature reported between 2013 and 2019 in PubMed, Embase, and Scopus was conducted. Studies were included if (1) original clinical studies, (2) ≥50 NPC patients, and (3) analyses on the association between prognostic factors and overall survival. The data elements of eligible studies were abstracted and analyzed. A level of evidence was synthesized for each suggested change to the TNM staging and prognostic factors. Of 5,595 studies screened, 108 studies (44 studies on anatomical criteria and 64 on non-anatomical factors) were selected. Proposed changes/factors with strong evidence included the upstaging paranasal sinus to T4, defining parotid lymph node as N3, upstaging N-category based on presence of lymph node necrosis, as well as the incorporation of non-TNM factors including EBV-DNA level, primary gross tumor volume (GTV), nodal GTV, neutrophil-lymphocyte ratio, lactate dehydrogenase, C-reactive protein/albumin ratio, platelet count, SUVmax of the primary tumor, and total lesion glycolysis. This systematic review provides a useful summary of suggestions and prognostic factors that potentially improve the current staging system. Further validation studies are warranted to confirm their significance.

Keywords: nasopharyngeal carcinoma, prognostic factors, AJCC/UICC staging system, TMN classification, systematic review, anatomical criteria

OPEN ACCESS

Edited by:
Yong Yin,
Shandong Cancer Hospital, China

Reviewed by:
Maria Grazia Ghi,
Veneto Institute of Oncology (IRCCS), Italy
Qiqi Xie,
Affiliated Hospital of Qinghai University, China

****Correspondence:***
Chi-Leung Chiang
chiangcl@hku.hk
Anne Wing Mui Lee
awmlee@hku.hk

Specialty section:
This article was submitted to Head and Neck Cancer, a section of the journal Frontiers in Oncology

Received: *01 May 2021*
Accepted: *29 July 2021*
Published: *02 September 2021*

Citation:
Chiang CL, Guo Q, Ng WT, Lin S, Ma TSW, Xu Z, Xiao Y, Li J, Lu T, Choi HCW, Chen W, Chau ESC, Luk PHY, Huang SH, O'Sullivan B, Pan J and Lee AWM (2021) Prognostic Factors for Overall Survival in Nasopharyngeal Cancer and Implication for TNM Staging by UICC: A Systematic Review of the Literature. Front. Oncol. 11:703995. doi: 10.3389/fonc.2021.703995

INTRODUCTION

Nasopharyngeal carcinoma (NPC) is an important global health burden with approximately 130,000 new cases diagnosed and more than 70,000 deaths in 2018 (1). It is a unique disease with distinctive natural behavior, epidemiology, and histopathology that differs from other head and neck cancers. Estimation of prognosis is a fundamental step in patient management. Among the various prognostic factors, the tumor–node–metastasis (TNM) staging, which has been jointly adopted by the American Joint Committee on Cancer (AJCC) and the Union for International Cancer Control (UICC), remains the most robust factor for global application. The TNM 5th Edition issued in 1997, which introduced a customized staging system for NPC by merging the strengths of the AJCC/UICC 4th edition and Ho's system, is a historic milestone with worldwide acceptance. Subsequent revisions refined the staging system based on diagnostic and therapeutic advances (2, 3); the current 8th Edition, released in 2017, is another milestone with the unification of the TNM and the Chinese staging systems (4).

In addition to the refinement of TNM parameters, there is a growing interest in the incorporation of non-anatomical prognostic factors that reflect biological tumor behavior. These factors are potentially useful for providing biomarkers on personalized risk stratification, especially with regard to metastatic risk, for tailoring the treatment intensity. There is increasing evidence that incorporation of these factors/biomarkers with TNM staging system could further improve risk stratification (5, 6).

To provide the best available evidence for the upcoming TNM 9th Edition and associated prognostic grouping, a comprehensive systematic review was carried out to identify potentially important suggestions on anatomic and non-anatomic prognostic factors. These suggestions will then be confirmed by a multicenter validation study before the final recommendation to UICC and AJCC for consideration. The current paper is our summary of suggested prognostic factors that warrant further validation.

MATERIALS AND METHODS

Study Protocol

This review adhered to the Preferred Reporting Items for Systematic Reviews and Meta-Analysis (PRISMA) guideline (7). A systematic search of PubMed, Scopus, and Embase for relevant literature published from January 1, 2013, to September 13, 2019, was performed. This timeframe was selected because the construction of TNM 8th Edition was based on literature reviews up to December 31, 2012. Both English and Chinese literatures were accepted, although unpublished studies were not included in the search. The search terms (**Supplementary Table 1**) were as follows: ("staging" or "TNM" or "prognostic") and ("nasopharyngeal carcinoma" or "nasopharyngeal cancer" or "nasopharyngeal neoplasm").

Inclusion Process and Criteria

From the literature identified in the initial search, the following studies were excluded after screening their titles and citations: duplicated studies, conference abstracts, reviews, letters, editorials, case reports, book chapters, and basic science studies. The remaining studies were further assessed to determine eligibility, which included original clinical studies, either prospective or retrospective, with a sample size of at least 50 NPC patients, treated with intensity modulated radiotherapy (IMRT) or equivalent, and showing a significant association between prognostic factors and overall survival (OS). Novel prognostic markers with limited potential for global applicability (e.g., radiomics, micro-RNA, circulating tumor cells, and genetic signatures) were excluded from this review. In cases of multiple studies from one institution, the study with the largest number of patients and the most recently published study was prioritized.

Two independent teams (University of Hong Kong–Shenzhen Hospital and Fujian Cancer Hospital) performed the first review to exclude the ineligible studies. Three independent reviewers (AL, W-TN, and C-LC) further assessed papers that generated disagreements based on the inclusion/exclusion before a final decision was made on the list of studies to be selected for inclusion in this review.

Data Extraction and Analyses

The primary data from the articles were extracted. The primary endpoint for the assessment of prognostic value in this review was OS; the secondary endpoints of distant-metastasis-free survival (DMFS) and local-relapse-free survival (LRFS) were included if they were reported by the original study.

We used the QUality In Prognosis Studies (QUIPS) tool to assess the risk of bias within individual studies (8). The QUIPS tool was originally designed to assess bias in studies of prognostic factors. The tool originally comprised six domains—Study Participation, Prognostic Factor Measurement, Outcome Measurement, Statistical Analysis and Reporting, Study Confounding, and Study Attrition—each of which is guided by three to seven prompting items. Based on the risk of bias, the overall quality of each study was determined as high (score 5–6), moderate (score 3–4), or low (score 0–2); low-quality studies were excluded from this review.

The criteria adopted in this systematic review were designed to synthesize the level of evidence (9), which was defined as "strong," if there were consistent recommendations (≥75%) in multiple high-quality cohorts; "moderate," if recommendations were consistent in ≥67% of multiple high-quality cohorts; "limited," if the recommendation was based on a single cohort; and "inconclusive," if there were inconsistent recommendations.

RESULTS

Study Selection

An initial search of the three databases identified 5,595 studies that fit the search terms. Following the exclusion of ineligible articles (based on the predefined study eligibility criteria), two independent teams were constituted to identify new suggestions for improving the current TNM 8th Edition. Among the 2,200 studies evaluated, 34 original studies were selected for inclusion

by both teams, whereas 198 studies were selected by only one team. The studies with a discrepancy in agreement were further reviewed by three independent reviewers, and 74 were accepted for inclusion. Thus, a total of 108 original studies were included in this in-depth systematic review.

Study Characteristics

The characteristics of the 108 studies are presented in **Supplementary Tables 2–6**. Only six studies are prospective analyses, while the rest (n = 102) were retrospective. The majority of studies (n = 101) included only patients without distant metastasis. Forty-four studies focused on anatomical criteria: 22 studies on primary tumor (T-classification) (6, 10–30), 20 on nodal disease (N-classification) (14, 22, 23, 31–47), 5 studies on metastatic disease (M-classification) (48–52), and 3 studies included more than one category. In the 64 studies that evaluated non-anatomical factors, 22 studies focused on plasma Epstein-Barr virus (EBV) deoxyribonucleic acid (DNA) level (53–71), 12 studies on tumor volume (63, 65, 72–81), 18 studies on inflammatory/hematological factors (54, 82–98), and 15 studies on the parameters of fluorodeoxyglucose (FDG) positron emission tomography (PET) (99–113). Three studies had more than one non-anatomical category.

Risks of Bias

The assessment on study quality using the QUIPS tool showed that 62 (57.4%) of the included articles were classified as high quality and 46 (42.6%) as moderate quality. **Supplementary Figure 1** presents an algorithm of the study selection process, and **Supplementary Tables 2–6** list the QUIPS scores of the included studies. Suggestions from well-conducted studies with large sample sizes or with evidence supported by multiple studies were identified for inclusion in this review.

Proposed Changes and Prognostic Factors

Summary of the level of evidence on the recommendations and studied prognostic factors is summarized in **Table 1**. Among the 44 reports on TNM parameters (**Table 2**), 13 proposed changes to current TNM-8 were identified: six on T-category, eight on N-category, and one on M-category. The recommendations that were considered to have a strong level of evidence included the involvement of the paranasal sinus (PNS) as T4 disease (16, 18–20), parotid lymph node (PLN) as N3 disease (34, 35), and the upstaging of N-classification in the presence of lymph node necrosis (LNN) (39, 40, 42).

Among the 64 studies on non-TNM factors, 18 proposed parameters were identified. Prognostic factors with consistent support from multiple studies included EBV-DNA level (**Table 3**), primary gross tumor volume (GTV) (63, 72–74, 76, 78–81), nodal GTV (**Table 4**) (74, 75, 77, 81), neutrophil-lymphocyte ratio (NLR) (**Table 5**) (83, 85, 91, 92, 97), C-reactive protein (CRP)/albumin ratio (83, 89, 98), anemia (84, 87, 96), platelet count (82, 86), lactate dehydrogenase (LDH) (88, 95), and SUV_{max} of the primary tumor (99–101, 103, 108, 111, 113) and total lesion glycolysis (TLG) (**Table 6**) (104, 111).

DISCUSSION

To our understanding, this systematic review that evaluated the prognostic factors for NPC patients in 108 articles published from 2013 to 2019 is the most comprehensive review on this topic. The TNM 8th Edition, based entirely on the anatomical tumor extent, is the most widely used prognostic tool for NPC and remains the most robust factor for guiding treatment decisions, evaluating treatment results, and comparing outcomes between institutions worldwide. However, continuous improvement is necessary in view of the advances in investigations and treatments. Furthermore, refinement of prognostic tools by the incorporation of novel proposals based on functional imaging, plasma biomarkers, and molecular tumor characteristics is desirable in the current era of personalized oncology. For tumors with disease sites such as the prostate, breast, and skin (i.e., melanoma), non-anatomical factors have been successfully incorporated while still maintaining essential anatomical information. For NPC, considerable progress on both anatomical and non-anatomical prognostic factors have been made since the publication of the TNM 8th Edition. This systematic review reviewed the latest evidence to facilitate the formulation of a comprehensive proposal for designing the upcoming TNM 9th Edition.

T-Classification

A major change in the TNM 8th Edition was the replacement of the ambiguous terms IF/masseter space involvement with a clear specification of extensive soft tissue infiltration beyond the lateral surface of LP as T4, and the downstaging of MP/LP/PM to T2. This change was supported by two studies (10, 13, 14). However, five studies showed that MP and/or LP involvement was associated with a worse prognosis than T2 and should be upstaged; suggestions included categorizing MP as T3 and LP as T4 disease (n = 1) (16), MP as T2 and LP as T4 (n = 3) (13, 15, 30), and both MP and LP as T3 disease (n = 1) (10). Thus, further validation of the prognostic significance of MP/LP is recommended.

Three studies, comprising a total of 1,348 patients, showed that PNS involvement should be upstaged from current T3 to T4 disease given its poorer outcomes (5-year OS rate of 53.7–83.7%) (16, 19, 20). Of note, Zhang et al. reported worse prognoses among patients with ethmoid sinus or maxillary sinus involvement as T4 disease, but better prognosis in those with sphenoid sinus invasion alone as T3 disease (18); further studies on the relapse risks of various PNS are warranted.

The widespread use of magnetic resonance imaging (MRI) has improved the accuracy of detection of the extent of involvement of the skull base and of intracranial extension. With better disease characterization, Li et al. proposed the subdivision of skull base involvement into T3-slight (pterygoid process and/or base of the

TABLE 1 | Proposed prognostic factors and the level of evidence for recommendations.

	Strong*	Moderate*	Inconclusive*	Limited*
T-classification	PNS involvement (T4)		MP (upstaged to T3/4)	Skull base (T3 slight *vs.* T3 severe)
			LP (upstaged to T3/4)	Intra-cranial extension (T4a *vs.* T4b)
			Merging of T-classification (Merging of T1/T2, T1/T2/T3, or T2/3)	
N-classification	PLN (N3)	ENE (upstaging of N-classification or N3)	RLN	PLV LN
	LNN (upstaging of N-classification)			Cervical LN level
				Number of LN regions
				Merging of N classification (N2/N3)
M-classification			Subclassification of M-stage (based on number of lesions, number of organ involvement, liver involvement)	
EBV-DNA level	Pretreatment EBV-DNA level (Range: 1,500–25,000 copies/ml)			
Tumor volume	Primary GTV volume (Range: 20–50 ml)			
	Nodal GTV volume (Range: 7.2–35.7 ml)			
Inflammatory or hematological markers	NLR (Range: 2.28–3.0)			Hs-CRP
	CRP/albumin ratio (Range: 0.03–0.141)			PNI and AGR
	Anemia (Range: 11–13 g/dl)			D-dimer
	Platelet count (Range: 266–300 × 10^9/L)			TIL
	LDH (Range: 220–229 U/L)			PDW
FDG-PET parameters	SUV_{max} of the primary tumor (Range: 8–18.8)		SUV_{max} of nodal disease	MTV
	TLG (Range: 322.7–382.2)		SUV_{max} of metastatic disease	

PNS, paranasal sinus; IF, infratemporal fossa; PM, prevertebral muscle; MP, medial pterygoid; LP, lateral pterygoid; PLN, parotid lymph node; LNN, lymph node necrosis; ENE, extra-nodal extension; PLV LN, posterior to level V lymph node; LN, lymph node; RLN, retropharyngeal lymph node; EBV-DNA, Epstein-Barr virus deoxyribonucleic acid; GTV, gross tumor volume; NLR, neutrophil-lymphocyte ratio; CRP, C-reactive protein; PDW, platelet distribution width; LDH, lactate dehydrogenase; Hs-CRP, high-sensitivity CRP; PNI, prognostic nutrition index; AGR, albumin/globulin ratio; TIL, tumor-infiltrating lymphocytes; SUV_{max}, maximum standardized uptake ratio; TLG, total lesion glycolysis; MTV, metabolic tumor volume.
**Level of evidence: "strong," if there were consistent recommendations (≥75%) in multiple high-quality cohorts; "moderate," if recommendations were consistent in ≥67% of multiple high-quality cohorts; "limited," if the recommendation was based on a single cohort; and "inconclusive," if there were inconsistent recommendations.*

pterygoid bone only) and T3-severe (others) (24); similarly, Cao et al. suggested the subdivision of T4 into T4a (without intracranial extension) and T4b (with intracranial extension) based on the presence of intracranial extension (29). Further studies are needed to validate these findings.

With the technological advances in both diagnostics and treatment, the differences in survival and local control in the T-category has diminished. Eight of the included studies proposed the simplification of the T-category (6, 21–27); these included three studies that suggested the merging of T1 and T2 disease (21, 23, 24), one suggested combining of T1, T2, and T3 disease (22), and one proposed a merging of T2 and T3 (27). Other studies proposed simplification of the definition of T-classification, refinement of T2–T4 disease, and reclassification as T1 and T2 only (6, 25, 26).

Level of Evidence:

Strong: PNS involvement (T4 disease)

Moderate: Nil

Inconclusive: MP (upstaged to T3/4), LP (upstaged to T3/4), and merging of T-classification (T1–T2, T1, T2, and T3, or T2–T3)

Limited: Skull base (T3 slight *vs.* T3 severe) and intracranial extension (T4a *vs.* T4b).

N-Classification

Despite the rarity of PLN metastasis (0.4–2.8%), consistent findings were noted on its adverse prognostic outcome, which was similar to those with N3 disease, as demonstrated in two studies that included a total of 11,742 patients. Both reports recommended PLN involvement as the criteria for N3 classification (34, 35). Also, suspicion of PLN metastasis, especially in patients with advanced nodal diseases, should be raised on pretreatment imaging, and biopsy is indicated in the suspected case.

Furthermore, in five studies, there was consensus that LNN was an adverse prognostic factor (hazard ratio [HR]: 1.75–5.79) (38–42). In the largest study by Lan et al., patients with LNN had worse OS and DMFS (OS, 78.8 *vs.* 91.8%; DMFS, 78.4 *vs.* 91.6%,

TABLE 2 | Characteristics of studies of T-, N-, and M-classification prognostic factors and survival (n=44).

(I) T-classification (n=22)

Study (Author/ Year of publication)	Study design (P/R)	Sample size	TNM/UICC staging	Prognostic factor	HR (high vs. low)	95% CI	*P* value	Survival probabilities	*P* value	Proposed changes	Quality score
(A) Medial pterygoid (MP), lateral pterygoid (LP), prevertebral muscle (PM), infratemporal fossa (IF), and others											
Luo (2014) (10)	R	742	7th Edition Stage III–IVB	MP or LP (Yes vs. No)	1.658	1.058–2.596	NA	5-year OS: 82.5% vs.70.9%	0.001	MP/LP should be staged as T3	5
Sze (2014) (11)	R	1104 (all) 434 (T3)	7th Edition Stage I–IVB	MP ± LP	1.16	0.76–1.76	0.49	–	–	MP ± LP should be classified as T2	5
Zhang (2014) (30)	R	808	7th Edition Stage I–IVB	Masticator space involvement	1.309	1.061–1.615	0.012	–	–	Medial involvement to be classified as T2; lateral involvement to be classified as T4	4
Xiao Y, Pan J, Chen Y (2015) (12)	R	816	7th Edition Stage I–IVB	MP	1.572	1.191–2.074	0.007	5-year OS: w/MP: 69.6%	–	MP similar to T2 prognosis	4
Zhang (2015)(13)	R	1504	7th Edition Stage I–IVB	MP	0.623	0.445–0.873	0.006	–	–	T2: Mild invasion (involvement of medial pterygoid muscle of masticator space or pre-styloid, carotid, prevertebral, or retropharyngeal spaces) T4: extensive invasion (involvement of lateral pterygoid muscle and beyond the masticator space or parotid space).	3
				LP	1.572	1.143–2.163	0.005	–	–		
				Posterior carotid space	1.085	0.787–1.497	0.618	–	–		
				Parapharyngeal extension	1.169	0.756–1.809	0.482	–	–		
Pan (2016) (14)	R	1609	7th Edition Stage I–IVB	MP/LP/PM	1.008	1.004–1.013	<0.001	–	–	MP/LP/PM as T2	6
Zhou (2017) (16)	R	358	7th Edition Stage III–IVb	MP, LP, PNS, skull base, cavernous sinus, CN	–	–	–	5-year OS: Without MP vs. with MP: 86.9% vs. 83.1% without LP vs with LP: 67% vs. 81.6%	<0.001	T3: MP and skull base T4: LP, PNS, MS beyond LP, cavernous sinus, and CN	5
Kang M, Zhou P, Liao X (2017) (15)	R	608	8th Edition Stage I–IVB	MP/LP	3.410	2.016–5.766	<0.001	5-year OS: 75.6% vs. 86.7%	0.043	LP should be graded as T4 MP: T2	4
(B) Skull base involvement											
Li (2019) (17)	R	1225	8th Edition Stage I–IVB	Skull base (T3 slight: pterygoid process and/or base of pterygoid bone vs. T3 severe)	1.117	0.557–2.241	0.775	5-year OS: 93.0% vs. 83.5%	0.014	Patients with **T3 slight** (base of pterygoid bone and pterygoid process) should be T2; **T3 severe** remains as T3	6
(C) Paranasal sinus (PNS) involvement											
Zhang (2016) (18)	R	1811	7th Edition Stage I–IVB	PNS	2.614	1.455–4.695	0.001	–	–	T3: Sphenoid sinus T4: Ethmoid and maxillary sinuses	5

(Continued)

TABLE 2 | Continued

Study (Author/ Year of publication)	Study design (P/R)	Sample size	TNM/UICC staging	Prognostic factor	HR (high vs. low)	95% CI	*P* value	Survival probabilities	*P* value	Proposed changes	Quality score
(I) T-classification (n=22)											
Zhou (2017) (16)	R	358	7th Edition Stage III–IVb	MP, LP, PNS, skull base, cavernous sinus, CN	–	–	–	5-year OS: 66.3% vs. 84.1%	<0.001	T3: MP and skull base T4: LP, PNS, MS beyond LP, cavernous sinus, and CN	5
Wang Y, Zhao J, Zhao Y (2018) (19)	R	295	8th Edition T3–4, M0	PNS	1.919	1.128–3.264	0.016	5-year OS: 53.7% vs. 80.4%	0.001	PNS to be moved to T4	3
Cao (2019) (20)	R	695	8th Edition Stage I–IVb	PNS	–	–	–	5-year OS: 83.7% vs. 92.2%	0.011	PNS to be reclassified to T4	5
(D) Intracranial extension or cranial nerve involvement											
Zong (2014) (28)	R	375	7th Edition Stage III–IVB	Cranial nerve involvement	–	–	–	5-year OS: with MRI-detected CN 71.9% vs. without MRI-detected CN 77.7%	0.134	MRI-detected CN should not be reclassified as T4 to avoid excessive treatment	4
Cao (2017) (29)	R	335	7th Edition T4	Intracranial invasion	0.572	0.389–0.839	0.004	1- / 3- / 5-year: T4a: 95.9% / 83.1% / 71.5% vs. T4b: 91.2% / 69.7% / 51.6%	–	To subclassify T4: (a) without intracranial invasion, (b) with intracranial invasion	5
(E) Simplification of T-classification											
Zong (2015) (21)	R	1241	7th Edition Stage I–IVB	T1 vs. T2 vs. T3	1.792	1.295–2.48	<0.001	5-year OS: 88.1%		Merge T1–T2	4
Kang (2016) (22)	R	492	7th Edition Stage I–IVB	T1 vs. T2 vs. T3 vs. T4	1.657	1.101–2.495	0.016	5-year OS: 100% vs 98.2% vs 97.9% vs 88.2%	0.001	Merge T1–T3 to T1, T4 as T2	4
Liang (2016) (23)	R	752	7th Edition Stage I–IVB	T1 vs. T2 vs. T3 vs. T4	–	–	–	–	–	Merge T1–T2 to T1, T3 as T2, T4 as T3	4
Kang M, Zhou P, Wei T (2017) (26)	P	492	7th Edition Stage I–IVB	T1 vs. T2 vs. T3 vs. T4	–	–	–	–	–	T1 (nasopharynx, nasal cavity, parapharyngeal space, oropharynx, skull base, and MP); T2 (LP, paranasal sinus, infratemporal fossa, orbit, cranial nerves, cavernous sinus, and intracalvarium)	5
Li (2018) (24)	R	382	7th Edition Stage I–IVB	T1 vs. T2 vs. T3 vs. T4	2.366	1.685–3.322	<0.001	5-year OS: 92.4% vs. 92.0% vs. 87.3% vs. 76.5%	0.001	Merge T1–T2	6
Yang (2018) (25)	R	1317	7th/8th Edition Stage I–IVB	T1 vs. T2 vs. T3 vs. T4	–	–	–	–	–	Refinement of T2–T4 needed as no difference in LRFS in T2–T4; and OS difference in T2 and T3	6
Pan (2019) (6)	R	325	8th Edition Stage I–IVB	T1-T4	–	–	–	–	–	Simplification of the definition of T1, T2, T3, and T4	4

(Continued)

TABLE 2 | Continued

(I) T-classification (n=22)

Study (Author/ Year of publication)	Study design (P/R)	Sample size	TNM/UICC staging	Prognostic factor	HR (high vs. low)	95% CI	*P* value	Survival probabilities	*P* value	Proposed changes	Quality score
Tang (2019) (27)	R	2191 (training set); 414 (validation set)	8th Edition Stage I–IVB	Merging T2 and T3 (proT1, proT2, and proT3)	proT2: 1.379 proT3: 2.644	pro T2: 0.896–2.121 proT3: 1.667–4.193	–	5-year OS: 93.8% vs. 87.5% vs. 76.0%	<0.001	Merging of T2 and T3 to proposed T2 (proT2)	6

(II) N-classification (n=19)

Study (Author/ Year of publication)	Study design (P/R)	Sample size	TNM/UICC staging	Prognostic factor	HR (high vs. low)	95% CI	*P* value	Survival probabilities	*P* value	Proposed changes	Quality score
(A) Retropharyngeal LN (RPLN)											
Shi (2014) (31)	R	142	7th Edition N1 disease	CLN+RLN	–	–	–	5-year OS: 85.3% vs. 95.1%	0.119	Better prognosis: CLN or RLN-only > CLN + RLN	5
Tang (2014) (32)	R	749	7th Edition Stage I–IVB	RLN	–	–	–	83.9%	–	Better prognosis: RLN-only > Other N1 disease; No difference in unilateral vs. bilateral RLN	5
Huang L, Zhang Y, Liu Y (2019) (33)	R	1225	8th Edition Stage I–IVB	RLN Bilateral vs. non-bilateral	1.628	1.178–2.250	0.003	5-year OS: Bilateral: 76.58% vs. Non-bilateral: 88.97%	<0.001	Upgrading bilateral RLN metastasis from N1 to N2	6
(B) Parotid LN (PLN)											
Xu (2017) (34)	R	1616	7th Edition Stage I–IVB	PLN	–	–	–	–	0.001	PLN similar prognosis of N3	6
Zhang (2019) (35)	R	10126	8th Edition Stage I–IVB	PLN	–	–	–	–	–	PLN similar prognosis as that of N3	5
(C) Extra-nodal extension (ENE)											
Ai (2019) (36)	R	546	8th Edition Stage I–IVB	ENE	G1: 0.637 G2: 1.989	0.396–1.023 1.145–3.457	0.062 0.015	5-year OS: 52.4%	–	Grade 2 ENE (muscle/skin/salivary gland) classified as N3	5
Lu (2019) (37)	R	1616	8th Edition Stage II	ENE	–	–	–	7-year OS: 81.9% vs 89.9%	0.05	ENE associated with poorer prognosis	5
(D) Lymph node necrosis (LNN)											
Guo (2015) (38)	R	1197	7th Edition Stage I–IVB	Nodal level (RLN) Extracapsular spread Necrosis Laterality Maximal axial diameter	1.295 - - 1.663 1.326	1.047–1.602 - - 1.200–2.304 0.995–1.767	0.017 - - 0.002 0.054	- -	- NS (0.629) NS (0.130) - -	ENE and LNN is not prognostic	6

(Continued)

TABLE 2 | Continued

Study (Author/ Year of publication)	Study design (P/R)	Sample size	TNM/UICC staging	Prognostic factor	HR (high vs. low)	95% CI	*P* value	Survival probabilities	*P* value	Proposed changes	Quality score
(I) T-classification (n=22)											
Lan (2015) (39)	R	1800	7th Edition Stage I–IVB	LNN	2.03	1.50–2.75	<0.001	5-year OS: LNN 78.8% vs. non-LNN 91.8%	<0.01	N1 with LNN = N2 no LNN N2 with LNN = N3	4
Luo Y, Ren J, Zhou P (2016) (40)	R	189	7th Edition Stage III–IVB	LNN	1.754	1.061–2.899	0.028	5-year OS: 75.8% vs. 59.5%	0.033	N1 with LNN = N2 no LNN N2 with LNN = N3	5
Lu L, Wei X, Li YH (2017) (41)	R	252	7th Edition Stage II–IVB	LNN	2.1	1.57–2.64	<0.01	5-year OS: LNN 74.6% vs. non-LNN 89.7%	<0.01	No suggestion	4
Ting (2017) (44)	R	257	7th Edition Stage I–IVB	Cystic lymph node metastasis (CLNM)	5.785	–	<0.001	N/A	–	CLNM can categorize N2 patients into two prognostic groups	5
Feng (2019) (42)	R	616	8th Edition Stage I–IVB	LNN	2.154	1.282–3.620	0.029	5-year OS: LNN 82.9% vs. non-LNN 93.0%	<0.001	N1 with LNN = N2 no LNN N2 with LNN = N3	6
(E) Simplification of N-classification											
Kang (2016) (22)	R	492	7th Edition Stage I–IVB	N3a+ N3b vs. N2	New N3 vs. N2: 2.507	1.508–4.169	<0.001	–	–	Merge N3a and N3b into N3	6
Pan (2016) (14)	R	1609	7th Edition Stage I–IVB	Caudal border of cricoid cartilage to differentiate N2 vs. N3, merging of N3a and N3b	New N3: 4.24	2.57–7.00	<0.001	5-year OS: 7th edition N2/N3a/ N3b: 75% vs. 75% vs. 69% Proposed 8th edition: N2/N3: 75% vs 70%	<0.001 <0.001	Merge N3a and N3b into N3	5
Liang (2016) (23)	R	752	7th Edition Stage I–IVB	N1 vs. N2 vs. N3	–	–	–	–	–	Merge N1 and N2	4
(F) Others											
Jiang (2017) (43)	R	406	7th Edition N1–3M0	Posterior to level V (PLV) LN	3.431	1.088–10.822	0.035	3-year OS: 51.5% vs. 88.4%	–	PLV LN should be defined as a new lymph node segment	3
Kang (2018) (45)	P	492	7th Edition Stage I–IVB	Cervical LN level	Level VIIa: 1.080 Level III: 1.520 Level IVa: 2.124 Level Va: 0.462 Level	0.475–2.452 0.934–2.474 1.041–4.335 0.063–3.381 2.057–13.667 2.483–44.318	–	5-year OS: Level II: 82.7% Level III: 75.2% Level IVa: 67.0% Level Va: 92.3% Level Vb: 37.0% Level IVb, Vc: 33.3% Level VIIa:78.9%	<0.001	N1 [RLN or/and unilateral upper cervical (I, II, III, Va, VIIb, VIII, IX, and X regions) LNs], N2 [bilateral upper cervical LN] and N3 (LN in IVa and Vb regions and their lower regions)	6

(Continued)

TABLE 2 | Continued

(I) T-classification (n=22)

Study (Author/ Year of publication)	Study design (P/R)	Sample size	TNM/UICC staging	Prognostic factor	HR (high vs. low)	95% CI	*P* value	Survival probabilities	*P* value	Proposed changes	Quality score
					Vb: 5.302 Level IVb, Vc: 10.491						
Zhou (2018) (46)	R	354	8th Edition Stage I–IVB	Number of lymph node regions (LNR)	2–6: 4.59 ≥7: 9.78	1.36–15.49 2.88–33.25	0.039 0.002	5-year OS: 0–1: 97.1% 2–6: 84.9% ≥7: 74.2%	–	New N classification based on LNR: 0–1, 2–6, ≥7	6

(III) M-classification (n=5)

Study (Author/ Year of publication)	Study design (P/R)	Sample size	Prognostic factor	HR (95% CI)	P value	OS probabilities	Survival probabilities	P value	Proposed changes	Quality score
Shen LJ, Wang SY, Xie GF (2015) (49)	R	505	M1a: single lesion to isolated organ (except for the liver) M1b: single lesion to the liver, or multiple lesions in other organs M1c: multiple lesions in the liver	M1b vs. M1a: 1.69 (1.16–2.48) M1c vs. M1a: 2.64 (1.75–3.98)	0.007 <0.001	3-year OS	M1a: 62.1% M1b: 36.1% M1c: 17.9%	0.001	Recategorization of M stage: M1a: single lesion to isolated organ (except for the liver) M1b: single lesion to the liver, or multiple lesions in other organs M1c: multiple lesions in the liver	4
Shen (2016) (48)	R	1172	M1a, a single lesion in a single organ or location M1b, multiple lesions in a single organ or location; and M1c, metastases in multiple locations	M1b vs. M1a: 2.28 (1.71–3.05) M1c vs. M1a: 3.65 (2.75–4.85)	–	–	–	–	Subdivision of the M1 stage: M1a, a single lesion in a single organ or location M1b, multiple lesions in a single organ or location; and M1c, metastases in multiple locations	5

(Continued)

TABLE 2 | Continued

(I) T-classification (n=22)

Study (Author/ Year of publication)	Study design (P/R)	Sample size	TNM/UICC staging	Prognostic factor	HR (high vs. low)	95% CI	*P* value	Survival probabilities	*P* value	Proposed changes	Quality score
Jiang (2016) (50)	R	347	To use ten-signature classifier * as a classifier for M1a and M1b.	3.45 (2.59–4.60)	<0.001	2-year OS	71.4% vs 18.8%	0.001	To use ten-signature classifier * as a classifier for M1a and M1b.	5	
Tian (2016) (51)	R	263	M1a: 5 single-organ metastases or 1–5 lesions M1b: 5 multiorgan metastases or >6 lesions	N/A	N/A	5-year OS	M1a: 38.7% vs. M1b: 7.0%	<0.001	M1a: oligo metastasis without liver involvement M1b, multiple metastases without liver involvement M1c, liver involvement irrespective of metastatic lesions.	5	
Zou (2017) (52)	R	462 (training set) 272, 243 (internal and external validation set)	M1a: oligometastasis without liver involvement M1b, multiple metastases without liver involvement M1c, liver involvement irrespective of metastatic lesions	M1b vs. M1a: 1.63 (1.17–2.26) M1c vs. M1a: 2.96 (2.14–4.10)	0.004 <0.001	3-year OS	M1a: 54.5–72.8%, M1b: 34.3–41.6%, M1c: 2.6–23.6%	<0.001	M1a: 5 single-organ metastases or 1–5 lesions M1b: 5 multiorgan metastases or >6 lesions	4	

***** *Ten-signature classifier: oligometastases, extra-regional LN metastases, N-stage, EB-VCA IgA, neutrophil count, platelet count, hemoglobin, glutamic-pyruvic transaminase, glutamyl transpeptidase, and monocyte count*
Study design: prospective (P)/retrospective (R); HR, hazard ratio; CI, confidence interval; OS, overall survival.

both $p < 0.001$); the authors proposed that patients with LNN should be upstaged in their respective N-category (39).

In addition to the proposals identified in the current literature search, extra-nodal extension (ENE) was recently advocated as a new criterion for N3-classification in the TNM 8th Edition for other head and neck cancers, but not for NPC. Specifically, Ai et al. proposed the categorization, as N3 disease, of ENE with infiltration into the adjacent muscle/skin/salivary gland (36). Lu et al. showed that ENE was a poor prognostic factor for NPC and proposed to categorize ENE as G0: lymph nodes without ENE; G1: tumor infiltration beyond the individual nodal capsule(s) into the surrounding fat plane; G2: coalescent nodal mass with unequivocal evidence of ENE; G3: tumor infiltration beyond the nodal capsule into adjacent structures (37). Only G2/G3 ENE, but not G1, was independently prognostic of death; the authors hence proposed a refined N-classification: New-N1: N1/N2 without G2-/G3-ENE; New-N2: N1 with G2-ENE; New-N3: N2 with G2-ENE, N1/N2 with G3-rENE, or N3. On the contrary, Guo et al. suggested that ENE was not a poor prognostic factor; but the definition of ENE was not mentioned in their study (38).

The current TNM 8th Edition categorizes retropharyngeal lymph node involvement (≤6 cm) as N1 disease, regardless of its unilateral or bilateral involvement. Tang et al. supported the current classification (32), but Study by Huang et al. on 1,225 patients (33) suggested upstaging bilateral retropharyngeal lymph node involvement as N2 disease, as they have worse 5-year OS (89.4 *vs.* 82.6%) and DMFS (91.5 *vs.* 82.9%).

Furthermore, four studies proposed the simplification of the N-classification and supported the current N3 disease with merging of the previous N3a and N3b (14, 23, 45, 47). Other studies on PLV LN, cervical LN level, and the number of LN regions had limited evidence (22, 43, 44, 46).

Level of Evidence:

Strong: PLN (N3 disease), LNN (Upstaging of N-classification)

Moderate: ENE (Upstaging of N-classification or N3)

Inconclusive: RLN involvement

Limited: PLV LN, cervical LN level, number of LN regions, merging of N2 and N3

M-Classification

Several suggestions have been made on the subcategorization of *de novo* oligo-metastatic disease based on the number of metastatic lesions and the site(s) of involvement (48–52). However, given the diversity of definition and management of patients with oligo-metastasis, no conclusive recommendation could be made. Most studies have shown that the number of metastatic lesions and the number of organ involvements were independent poor prognostic factors. Furthermore, both Shen et al. and Zou et al. reported that single (or oligo-) metastatic lesions without liver involvement had better prognoses compared with lesions with liver involvement (49, 52). In a multicenter study of 977 patients that was reported by Zou et al., liver metastases represented a worse prognostic factor regardless of the number of metastatic lesions with a 3-year OS rate of 34.3–72.8% *vs.* 22.6–23.6% (52).

Level of Evidence:

Inconclusive: Subclassification of M-category

Plasma EBV-DNA Level

The measurement of EBV-DNA concentration is widely used in diagnosis, prognostication, treatment monitoring, and the surveillance of recurrence. In concordance with previous meta-analyses (115–117), we found that the pretreatment plasma EBV-DNA level was a prognostic factor; the risk of mortality, local failure, and metastases was 1.3- to 8.4-fold, 1.1- to 3.1-fold, and 1.4- to 8.1-fold higher, respectively, for patients with high EBV-DNA levels compared to patients with low EBV-DNA levels (53–71, 114).

Several studies have highlighted the important role of EBV-DNA to refine the prognosis of patients with similar TNM stage groups. In a study of 385 patients with Stage II (TNM 7th edition) disease, the 3-year PFS, LRFS, and DMFS rates for the detectable and undetectable EBV-DNA groups were 89.1 *vs.* 96.4%, 94.3 *vs.* 98.2%, and 94.2 *vs.* 98.6%, respectively ($p = 0.005$, 0.039, and 0.017, respectively) (63). For locally advanced disease, Zhang et al. revealed that patients with stage II–III (TNM 7th Edition) and a high EBV-DNA level had worse survival than those with stage IVa–b and a low EBV-DNA level (5-year OS: 82.7 *vs.* 92.9%, PFS: 70.7 *vs.* 89%) (57). Similarly, Jin et al. showed that the prognosis of patients with stage IVa–b (TNM 7th Edition) and low EBV-DNA level was similar to that of patients with Stage III disease and high EBV-DNA level (61).

Furthermore, two studies demonstrated that recursive partitioning analysis (RPA), which integrated stage groups and the plasma EBV-DNA level, had better survival predictive ability compared to the TNM 8th Edition (67, 71). Guo et al. proposed the following RPA classes: Stage RI (T1N0), RIIA (T2–T3N0 or T1–T3N1, EBV-DNA ≤2,000 copies/ml), Stage RIIB (T2–T3N0 or T1–T3N1, EBV-DNA >2,000 copies/ml; T1–T3N2, EBV-DNA ≤2,000 copies/ml), Stage RIII (T1–T3N2, EBV-DNA >2,000 copies/ml; T4N0–N2), and Stage RIVA (any T and N3) (67). The 5-year PFS rate was 100, 87.9, 76.7, 68.7, and 50.4% for the proposed stages RI, RIIA, RIIB, RIII, and RIV, respectively ($p < 0.001$). In a similar study by Lee VH et al., RPA derived four new stages: RPA-I (T1–T4, N0–N2, and EBV-DNA <500 copies/ml), RPA-II (T1–T4, N0–N2, and EBV-DNA ≥500 copies/ml), RPA-III (T1–T2 and N3), and RPA-IVA (T3–T4 and N3) (71).

The EBV-DNA concentration could provide biological information of tumors beyond the anatomical factors and thereby improve the prognostic performance of the staging system. Nonetheless, the heterogeneity of cutoff values has hindered the wide application of EBV-DNA in NPC staging. The EBV-DNA cutoff values varied markedly among our included studies (1,500–25,000 copies/ml), with 4,000 copies/ml being the most frequently used cutoff value (54, 57, 59, 66). Plasma EBV-DNA is a laboratory-developed test with heterogeneity based on different DNA extraction, purification, and stabilization methods; different instruments used; different primers and probes that target a different part of the EBV genome; and different quantification controls (118). An earlier study showed that different PCR assays using primer/probe sets for latent membrane protein-2 (LMP-2) and BamHI-W might yield slightly different plasma EBV-DNA concentrations from that in the same sample (119). Also, the low

TABLE 3 | Association of overall survival with the pretreatment EBV DNA level (n=16).

Study (Author/Year of publication)	Study design(P/R) [a]	Sample size	Cutoff value [b]	HR (high vs. low)	95% CI	*P* value	Survival probabilities	*P* value	Quality score
Chen M, Yin L, Wu J (2015) (53)	P	165	Positive vs negative	–	–	–	2-year OS: Negative EBV 100% vs. positive EBV 94%	1.000	5
Tang (2015) (54)	P/R	6337	4000	8.44	(6.15–11.57)	<0.001	–	–	4
Yang (2015) (55)	R	1168	3760	1.41	(1.06–1.88)	0.017	–	–	4
Zhao (2015) (56)	R	637	1500	1.83	(0.79–4.24)	0.161	–	–	4
Chen (2016) (57)	R	404	4000	3.75	(1.701–8.284)	<0.001	3-year OS: 85% vs. 98%	<0.001	4
Lv (2016) (59)	R	1501	4000	1.97	(1.42 – 2.75)	<0.001	5-year OS: 81% vs. 91%	<0.001	6
Peng H, Chen L, Zhang Y (2016) (117)	R	1106	Positive vs negative	1.83	(1.08–3.11)	0.026	4-year OS: 86% vs. 94%	<0.001	3
Peng H, Guo R, Chen L (2016) (60)	R	584	2010	4.581	(1.58–13.26)	0.005	3-year OS: 92.3% vs. 98.9%	<0.001	3
Zhang (2016) (57)	R	1467	4000	3.44	(2.32–5.09)	<0.001	5-year OS: 83% vs. 95%	<0.001	6
Jin YN, Yao JJ, Zhang F (2017) (61)	R	1036	1500	1.65	(1.10–2.47)	N/A	5-year OS: 79% vs. 87%	0.002	6
Du (2019) (66)	R	607	4000	2.16	(1.25–3.71)	0.005	5-year OS: 85% vs. 97%	<0.001	4
Guo (2019) (67)	R	979	N/A	1.29	(1.13–1.48)	0.001	–	–	4
Huang CL, Sun ZQ, Guo R (2019) (68)	R	949	7000	1.86	(0.77–4.53)	0.171	3-year OS: 95% vs. 89%	0.138	5
Sun XS, Chen WH, Liu SL (2019) (70)	R	2742	1460	3.58	(2.50–5.13)	<0.001	–	–	4
Sun XS, Liang YJ, Liu SL (2019) (69)	R	226	25000	1.91	(1.23–2.96)	0.004	–	–	3
Sun XS, Liu LT, Liu SL (2019) (69)	R	502	Detectable vs undetectable	–	–	–	3-year OS: 34% vs. 69%	<0.001	4

(deleted)[a]Study design: prospective (P)/retrospective (R). [b] Cutoff values: pretreatment EBV DNA level (copies/mL).
HR, hazard ratio; CI, confidence interval; OS, overall survival.
N/A, Not available.

sensitivity of EBV-DNA assays in patients with low-volume NPC is another concern (120). Thus, further international efforts are encouraged to harmonize the assay and validate it in large prospective cohorts to ensure that plasma EBV-DNA can unleash its full potential and be incorporated into the staging system.

Level of Evidence:

Strong: Pretreatment EBV-DNA level

Tumor Volume

There were 12 studies with 8,403 patients in the current systematic review that evaluated the significance of tumor volumes (GTV-P and/or GTV-N). Seven papers focused on the primary tumor volume (GTV-P; n = 7) (63, 72, 73, 76, 78–80), two on the nodal tumor volume (GTV-N; n = 2) (75, 77), and two on the total tumor volume including primary and node (GTV-P and GTV-N; n = 2) (74, 81). One study did not include a cutoff for GTV-N and GTV-P (65).

The findings suggested that large GTV-P was an independent predictor of OS (HR 1.56–3.23) (63, 72–74, 76, 78–80), DMFS (HR 1.01–3.23) (63, 65, 77–81), and LRFS (HR 1.01–2.79) (63, 73, 76, 78–81). Similarly, large GTV-N was an adverse prognostic factor for OS (HR 1.56–3.41) (75, 77) and DMFS (HR 2.72–6.33) (75, 81). However, the proposed cutoff values varied widely among the studies included in this review (**Table 4**): GTV-P ranged from 20 to 50 ml (median 33 ml), and GTV-N ranged from 7.2 to 35.7 ml (median 15 ml).

The current T- and N-classifications of the staging system are primarily based on the extent of tumor invasion and the maximum diameter of the LN, respectively. Tumor volume might correlate better with the number of clonogenic tumor cells, leading to a more accurate prediction of the chance of cure (121). Volumetric stratification has been demonstrated to improve the prognostic ability of the TNM staging system. Jeong et al. divided stage II–IV (TNM 8th Edition) into the volume subgroup and found that the 5-year OS was significantly better in participants with GTV-P ≤33 ml compared to those with GTV-P >33 ml (87.3 *vs.* 66.7%) (80); Chen et al. showed that among 385 TNM-8th Edition classified Stage II patients, those with a total GTV <30 cm^3 was associated with a better prognosis than those with a total GTV ≥30 cm^3 (63).

Despite the growing body of evidence, tumor volume is yet to be used for cancer staging in routine clinical practice for several reasons. Firstly, there are significant intra- and inter-observer variations in volume delineation. Secondly, the malignant tumor often grows into irregular shapes, and accurate measurement of tumor volume is hard to achieve with conventional imaging. Furthermore, the cutoff value of the tumor volume is difficult to define due to the differences in assessment software, measurement timing, and methods of statistical analysis (122, 123). Future efforts are needed to overcome these challenges before tumor volume can be used as a widely applied prognostic marker.

Level of Evidence:

Strong: Primary GTV volume and nodal GTV volume

Blood Inflammatory/Hematological Markers

In the 18 studies that were included, nine inflammatory/hematological markers were evaluated: the most frequently

TABLE 4 | Association of overall survival with tumor volume (n=11).

Study (Author/Year of publication)	Study design (P/R)[a]	Sample size	Primary (P) or nodal (N) cutoff volume (cm^3)	HR(high vs. low)	95% CI	*P* value	Survival probabilities [b]	*P* value	Quality score
Tian (2015) (72)	R	229	38 (P)	–	–	–	5-year OS: 15.2% vs. 48.7%	<0.01	4
He (2016) (73)	R	358	46.4 (P)	2.46	1.48–4.10	0.001	3-year OS: 75.5% vs. 90.5%	<0.001	5
Lu (2016) (74)	P	180	20 (P)	–	–	–	5-year OS: 70.6% vs. 95.1%	0.001	4
Qin (2016) (76)	P	249	33 (P)	1.01 (per cm^3)	1.003–1.018	0.04	5-year OS: 70.5% vs. 86.1%	0.006	3
Luo Y, Gao Y, Yang G (2016) (75)	R	110	14.1 (N)	1.875	1.001–3.512	0.050	5-year OS: 53.0% vs. 75.6%	0.028	4
Chen (2017) (77)	R	1230	7.2/35.7 (N)	1.72 (7.2–35.7 vs. ≤7.2) / 3.41(>35.7 vs. ≤7.2)	1.09–2.69 1.93–6.04	0.019 <0.001	5-year OS: ≤7.2: 90.2% vs. 7.2–35.7: 88.2% vs. >35.7: 62.3%	<0.001	6
Liang (2017) (79)	R	455	28 (P)	3.231	1.776–5.878	<0.001	4-year OS: 75.4% vs. 95.1%	<0.001	4
Liu T, Lv J, Qin Y (2017) (81)	P	143	43.5 (P) 15.0 (N)	7.81 3.55	1.79–33.3 1.33–9.43	0.006 0.011	5-year OS: 68% vs. 97% 5-year OS: 74% vs. 91%	<0.001 <0.001	5
Zhang (2017) (78)	R	393	23 (P)	2.05	1.11–3.80	0.022	–	–	3
Chen (2018) (63)	P	385	30 (P)	–	–	–	3-year PFS: 89% vs. 96%	0.008	4
Jeong (2018) (80)	R	133	33 (P)	2.93	1.16–7.42	0.013	5-year OS: 67% vs. 87%	0.021	5

[a]*Study design: prospective (P)/retrospective (R).* [b]*Survival outcomes: OS, overall survival; PFS, progression-free survival. HR, hazard ratio; CI, confidence interval*

proposed marker (n = 5) is NLR (83, 85, 91, 92, 97), followed by anemia (n = 3) (84, 87, 96), LDH (n = 2) (88, 95), platelet count (n = 2) (82, 86), and the CRP/albumin ratio (n = 3) (83, 89, 98). Other proposals with limited supporting evidence included high-sensitivity CRP (hs-CRP; n = 1) (54), platelet distribution width (PDW) (86), prognostic nutrition index (PNI) and albumin/globulin ratio (AGR) (n = 1) (93), D-dimer (n = 1) (94), and tumor-infiltrating lymphocytes (TIL; n = 1) (90).

The results of 2,225 NPC patients in five studies showed that elevated pretreatment NLR was consistently associated with worse OS (HR 1.19–2.38), DMFS (HR 1.45), and LRFS (HR 1.35) (**Supplementary Table 5**) (83, 85, 91, 92, 97). Evidence suggested that proinflammatory tumor microenvironments are closely related to cancer development and progression. Lymphocytes are immune cells that exhibit an antitumor function, while neutrophils are inflammatory cells that influence the cytotoxic activity of the immune system. Therefore, an increased NLR, with an elevated neutrophil count and/or reduced lymphocyte count, is a biomarker that reflects an imbalance in pro- and antitumor activities in the host's immune system. Various cutoff

TABLE 5 | Association of overall survival with neutrophil-lymphocyte ratio (NLR) (n=4).

Study (Author/Year of publication)	Study design (P/R)[a]	Sample size	Prognostic factors	Cut off point	HR(high vs. low)	95% CI	*P* value	Survival probabilities	*P* value	Quality score
Lu AY, Li HF, Zheng YM (2019) (85)	R	140	NLR	≥2.28	2.383	1.041–5.457	0.040	5-year OS: ≥2.28: 70.3% <2.28: 87.8%	0.010	4
Ye (2018) (91)	R	427	NLR	≥2.32	1.699	1.005–2.873	0.048	5-year OS: ≥2.32: 81.8% <2.32: 90.0%	0.015	4
Akcay (2019) (92)	R	62	NLR	≥3	1.19	1.04–2.35	0.002	NA	NA	5
Yao (2019) (97)	R	1550	NLR	>2.50	1.72	1.31–2.24	<0.001	5-year OS: >2.50: 82.5% ≤2.50: 90.3%	<0.0001	6

[a]*Study design: prospective (P)/retrospective (R).*
HR, hazard ratio; CI, confidence interval; OS, overall survival.
N/A, Not available.

TABLE 6 | Association of overall survival with PET parameters (n=10).

Study(Author/Year of publication)	Study design(P/R)[a]	Sample size	Nature of PET parameters	Cutoff value	HR (high vs. low)	95% CI	*P* value	Survival probabilities (overall survival)	*P* value	Quality score
Yoon (2014) (99)	R	53	SUV_{max}-T MTV-$T_{2.5}$ MTV-$T_{3.0}$	≥8.9 ≥31.45 cm^3 ≥23.01 cm^3	1.08 5.03 5.03	0.25–7.71 1.04–24.24 1.04–24.24	0.74 0.029 0.029	–	–	3
Zaghloul (2014) (100)	R	70	SUV_{max}-T	≥8.0	–	–	0.034 (U)	–	–	3
Hsieh (2015) (101)	R	174	SUV_{max}-T	≥8.35	3.91	1.45–10.53	0.007	5-year OS: 69.2% vs. 93.4%	0.001	4
Shen T, Tang LQ, Luo DH (2015) (102)	R	194 (107: LR; 87: DM)	SUV_{max}-T or SUV_{max}-M	≥8.65 (LR) ≥13.55 (DM)	4.882 2.415	1.06–22.59 0.96–6.10	0.042 0.062	–	–	4
Xiao W, Xu A, Han F (2015) (103)	R	179	SUV_{max}-T	≥10.22	–	–	–	5-year OS: 66.6% vs. 87.6%	<0.001	5
Yoon (2016) (104)	R	97	TLG	322.7	0.29	0.11–0.79	0.02	5-year OS: 54.0% vs. 85.7%	0.003	6
Lee (2017) (108)	R	53	SUV_{max}-T SUV_{max}-N	≥13.2 ≥13.4	- 7.799	- 1.51–40.40	- 0.014	- 3-year OS: 33.1% vs. 55.5%	- 0.003	5
Liu F, Xi XP, Wang H (2017) (109)	R	213	PET-CT-guided dose-painting IMRT vs CT-based IMRT	–	0.425	0.18–1.009	0.052	3-year OS: 82.6% vs. 91.8%	0.049	5
Alessi (2019) (111)	R	160	SUV_{max}-T SUV_{mean}-T TLG	18.8 9.5 382.2	1.07 1.07 1.003	- - -	0.01 0.01 0.01	–	–	3
Sun XS, Liang YJ, Liu SL (2019) (113)	R	253	SUV_{max}-T, SUV_{max}-N SUV_{max}-M	17.0 12.7 6.9	- 1.40 1.72	- 0.95–2.06 1.13–2.78	- 0.087 0.012	3-year OS: SUV_{max}-T: >17 vs. ≤17: 47.7% vs. 57.3% 3-year OS: SUV_{max}-N: >12.7 vs. ≤12.7: 46.5% vs. 65.1% 3-year OS: SUV_{max}-M: >6.9 vs. ≤6.9: 49.2% vs. 65.4%	SUV_{max}-T: 0.48 SUV_{max}-N: 0.005 SUV_{max}-M: 0.005	5

[a]*Study design: prospective (P)/retrospective (R).*

HR, hazard ratio; CI, confidence interval; SUV_{max}, maximum standardized uptake value; SUV_{mean}, mean standardized uptake value; MTV, metabolic tumor volume; TLG, total lesion glycolysis; T, primary tumor; N, lymph node; M, metastasis; LR, local recurrence.

values of NLR have been suggested (range 2.28–3.00, median 2.32), and the analysis suggested that NLR was a reliable prognostic marker regardless of the cutoff value (124).

Other hematological markers such as hemoglobin, platelet count, LDH, and CRP have the advantages of easy accessibility, inexpensive measurement, and high reproducibility and therefore possess a promising potential for integration into the international prognostic system. In particular, the significance of LDH and CRP have long been recognized (125–127), and these parameters had been incorporated in various recently published prognostic nomograms of NPC (128–130). Accordingly, further validations of these findings are encouraged.

Level of Evidence:

Strong: NLR, CRP/albumin ratio, anemia, PDW and platelet count, and LDH

Limited: Hs-CRP, PNI and AGR, D-dimer, and TIL

FDG-PET Parameters

Among the 15 studies on FDG-PET included in the current review, most evaluated the maximum SUV (SUV_{max}), either alone (n = 11) (100–103, 105–108, 110, 112, 113); some also proposed other metabolic parameters, such as metabolic tumor volume (MTV; n = 1) (99) or TLG (n = 2) (104, 111) (**Supplementary Table 6**). A single study further evaluated the difference in prognosis between PET-CT-guided dose-painting intensity-modulated radiation therapy (IMRT) and CT-based IMRT (109).

Four studies consistently showed that the high SUV_{max} of the primary tumor was associated with poor OS (HR 1.07–4.88) (99, 101, 102, 111); however, conflicting results were shown with regard to the high SUV_{max} of nodal and metastatic disease (102, 113). High TLG was associated with inferior OS in two studies, and MTV was a poor prognostic factor in one study

(**Supplementary Table 6**) (99, 104, 111). Therefore, we recommend further validation of the role of the high SUV_{max} of the primary tumor and high TLG.

The metabolic information of FDG-PET could predict tumor aggressiveness and be correlated with patient survival (131). The majority of FDG-PET studies evaluated the prognostic role of the SUV_{max} of the tumor mass; however, the SUV_{max} was limited by representing only the maximum uptake within the volume of interest (VOI) instead of within the entire mass. Emerging metabolic parameters such as TLG and MTV have been proposed to overcome these limitations: MTV is measured by contouring margins defined by thresholds, whereas TLG is calculated by multiplying the MTV by the mean SUV. Additional studies are encouraged to define the prognostic role of the abovementioned factor. However, the diverse range of cutoff values of these PET parameters used in different studies are attributable to several reasons. First, variables such as tumor delineation and definition of VOI may affect the MTV and TLG values; second, the cutoff values are established by the statistical parameters of each institution without cross-validation. Based on the evidence in the current literature, we cannot recommend a concrete cutoff value for further validation as the wide range of values has limited its reproducibility and global applicability.

Level of Evidence:

Strong: High SUV_{max} of the primary tumor and TLG

Limited: MTV

Inconclusive: High SUV_{max} of nodal disease and SUV_{max} of metastatic disease

Limitations

The limitations of this research merit discussion. Firstly, despite the exclusion of poor-quality studies, most of the included studies had a retrospective observational design, which is prone to biases. Secondly, the majority of the included studies that evaluated the non-anatomical markers used dichotomous variables to determine the prognostic value. The cutoff value of parameters varied among different studies, as it was calculated statistically in each study to achieve the most significant prognostic effect; therefore, the generalizability of the findings is uncertain. Thirdly, due to the heterogeneity of study designs, study populations, measurement techniques, and cutoff values, we were unable to perform a meta-analysis to estimate a pooled value reliably. Also, some of the studies of plasma EBV-DNA in early years were not included in the present analysis; however, our conclusion remains consistent with the previous findings (115–117). Lastly, some of the novel markers, such as radiomics, micro-RNA, circulating tumor cells, and genetic signatures, were not included in this review due to their limited global applicability at present.

Summary Remarks

This systematic review has identified a comprehensive list of prognostic factors and suggestions that could contribute toward more accurate risk stratification for designing personalized treatment for NPC. Further studies for the validation of these factors are needed to confirm reproducibility and define the optimal cutoff criterion, to formulate the recommendations for designing the upcoming 9th Edition of the TNM staging system.

DATA AVAILABILITY STATEMENT

The original contributions presented in the study are included in the article/**Supplementary Material**. Further inquiries can be directed to the corresponding author.

AUTHOR CONTRIBUTIONS

WN, JP, and AL: conception and design. CC, QG, TM, ZX, HC, and JL: collection and assembly of data. CC, WN, HC, JP, and AL: data analysis and interpretation. CC, WN, and AL: manuscript writing. All authors contributed to the article and approved the submitted version.

SUPPLEMENTARY MATERIAL

The Supplementary Material for this article can be found online at: https://www.frontiersin.org/articles/10.3389/fonc.2021.703995/full#supplementary-material

REFERENCES

1. Ferlay J, Ervik M, Lam F, Colombet M, Mery L, Pineros M, et al. *Global Cancer Observatory: Cancer Today* (2018). International Agency for Research on Cancer. Available at: https://gco.iarc.fr/today (Accessed 25 February, 2020).
2. *AJCC Cancer Staging Manual. sixth edition*. PL Greene, DL Page, ID Fleming, AG Fritz, CM Balch, DG Haller, et al. New York: Springer (2002).
3. *AJCC Cancer Staging Handbook. Seventh edition*. S Edge, DR Byrd, CC Compton, FL Greene, A Trotti. New York: Springer-Verlag (2010).
4. Chinese Committee for Staging of Nasopharyngeal Carcinoma. Report on Revision of the Chinese 1992 Staging System for Nasopharyngeal Carcinoma. *J Radiat Oncol* (2013) 2:233–40. doi: 10.1007/s13566-013-0088-5
5. Guo R, Mao YP, Tang LL, Chen L, Sun Y, Ma J. The Evolution of Nasopharyngeal Carcinoma Staging. *Br J Radiol* (2019) 92(1102):20190244. doi: 10.1259/bjr.20190244
6. Pan XX, Tong LH, Chen YF, Li FL, Tang WB, Liu YJ, et al. A Simplified T Classification Based on the 8th Edition of the UICC/AJCC Staging System for Nasopharyngeal Carcinoma. *Cancer Manag Res* (2019) 11:3163–9. doi: 10.2147/CMAR.S185860
7. Moher D, Liberati A, Tetzlaff J, Altman DG, Group P. Preferred Reporting Items for Systematic Reviews and Meta-Analyses: The PRISMA Statement. *BMJ* (2009) 339:b2535. doi: 10.1136/bmj.b2535
8. Hayden JA, van der Windt DA, Cartwright JL, Cote P, Bombardier C. Assessing Bias in Studies of Prognostic Factors. *Ann Intern Med* (2013) 158 (4):280–6. doi: 10.7326/0003-4819-158-4-201302190-00009
9. Bosma SE, Ayu O, Fiocco M, Gelderblom H, Dijkstra PDS. Prognostic Factors for Survival in Ewing Sarcoma: A Systematic Review. *Surg Oncol* (2018) 27(4):603–10. doi: 10.1016/j.suronc.2018.07.016
10. Luo DH, Yang J, Qiu HZ, Shen T, Chen QY, Huang PY, et al. A New T Classification Based on Masticator Space Involvement in Nasopharyngeal Carcinoma: A Study of 742 Cases With Magnetic Resonance Imaging. *BMC Cancer* (2014) 14:653. doi: 10.1186/1471-2407-14-653
11. Sze H, Chan LL, Ng WT, Hung AW, Lee MC, Chang AT, et al. Should All Nasopharyngeal Carcinoma With Masticator Space Involvement be Staged

as T4? *Oral Oncol* (2014) 50(12):1188–95. doi: 10.1016/j.oraloncology.2014.09.001
12. Xiao Y, Pan J, Chen Y, Lin S, Zong J, Chen Y, et al. The Prognosis of Nasopharyngeal Carcinoma Involving Masticatory Muscles: A Retrospective Analysis for Revising T Subclassifications. *Med (Baltimore)* (2015) 94(4): e420. doi: 10.1097/MD.0000000000000420
13. Zhang GY, Huang Y, Hu XF, Chen XP, Xu T, Liu LZ, et al. Prognostic Value of Classifying Parapharyngeal Extension in Nasopharyngeal Carcinoma Based on Magnetic Resonance Imaging. *BioMed Res Int* (2015) 2015:749515. doi: 10.1155/2015/749515
14. Pan JJ, Ng WT, Zong JF, Chan LL, O'Sullivan B, Lin SJ, et al. Proposal for the 8th Edition of the AJCC/UICC Staging System for Nasopharyngeal Cancer in the Era of Intensity-Modulated Radiotherapy. *Cancer* (2016) 122(4):546–58. doi: 10.1002/cncr.29795
15. Kang M, Zhou P, Liao X, Xu M, Wang R. Prognostic Value of Masticatory Muscle Involvement in Nasopharyngeal Carcinoma Patients Treated With Intensity-Modulated Radiation Therapy. *Oral Oncol* (2017) 75:100–5. doi: 10.1016/j.oraloncology.2017.11.002
16. Zhou Q, He Y, Zhao Y, Wang Y, Kuang W, Shen L. A Study of 358 Cases of Locally Advanced Nasopharyngeal Carcinoma Receiving Intensity-Modulated Radiation Therapy: Improving the Seventh Edition of the American Joint Committee on Cancer T-Staging System. *BioMed Res Int* (2017) 2017:1419676. doi: 10.1155/2017/1419676
17. Li HJ, Hu YY, Huang L, Zhou J, Li JJ, Xie CB, et al. Subclassification of Skull-Base Invasion for Nasopharyngeal Carcinoma Using Cluster, Network and Survival Analyses: A Double-Center Retrospective Investigation. *Radiother Oncol* (2019) 134:37–43. doi: 10.1016/j.radonc.2019.01.021
18. Zhang Y, Peng H, Guo R, Li WF, Chen L, Liu X, et al. Should All Nasopharyngeal Carcinoma With Paranasal Sinus Invasion be Staged as T3 in the Intensity-Modulated Radiotherapy Era? A Study of 1811 Cases. *J Cancer* (2016) 7(10):1353–9. doi: 10.7150/jca.15141
19. Wang Y, Zhao J, Zhao Y, Yang Z, Lei M, Li Z, et al. Impact of Paranasal Sinus Invasion on Advanced Nasopharyngeal Carcinoma Treated With Intensity-Modulated Radiation Therapy: The Validity of Advanced T Stage of AJCC/UICC Eighth Edition Staging System. *Cancer Med* (2018) 7(7):2826–36. doi: 10.1002/cam4.1506
20. Cao C, Jiang F, Jin Q, Jin T, Huang S, Hu Q, et al. Paranasal Sinus Invasion in Nasopharyngeal Carcinoma After Intensity-Modulated Radiotherapy. *Cancer Res Treat* (2019) 51(1):73–9. doi: 10.4143/crt.2017.607
21. Zong J, Lin S, Lin J, Tang L, Chen B, Zhang M, et al. Impact of Intensity-Modulated Radiotherapy on Nasopharyngeal Carcinoma: Validation of the 7th Edition AJCC Staging System. *Oral Oncol* (2015) 51(3):254–9. doi: 10.1016/j.oraloncology.2014.10.012
22. Kang M, Long J, Li G, Yan H, Feng G, Liu M, et al. A New Staging System for Nasopharyngeal Carcinoma Based on Intensity-Modulated Radiation Therapy: Results of a Prospective Multicentric Clinical Study. *Oncotarget* (2016) 7(12):15252–61. doi: 10.18632/oncotarget.7553
23. Liang ZG, Chen XQ, Niu ZJ, Chen KH, Li L, Qu S, et al. Recommendations for Updating T and N Staging Systems for Nasopharyngeal Carcinoma in the Era of Intensity-Modulated Radiotherapy. *PloS One* (2016) 11(12):e0168470. doi: 10.1371/journal.pone.0168470
24. Li Y, Ou X, Hu C. Validation and Suggestion of Eighth T Classifications of the UICC/AJCC Staging System for Nasopharyngeal Carcinoma Patients: A Retrospective Analysis. *Jpn J Clin Oncol* (2018) 48(10):927–33. doi: 10.1093/jjco/hyy109
25. Yang XL, Wang Y, Liang SB, He SS, Chen DM, Chen HY, et al. Comparison of the Seventh and Eighth Editions of the UICC/AJCC Staging System for Nasopharyngeal Carcinoma: Analysis of 1317 Patients Treated With Intensity-Modulated Radiotherapy at Two Centers. *BMC Cancer* (2018) 18 (1):606. doi: 10.1186/s12885-018-4419-1
26. Kang M, Zhou P, Wei T, Zhao T, Long J, Li G, et al. A New T Staging System for Nasopharyngeal Carcinoma Based on Intensity-Modulated Radiation Therapy: Results From a Prospective Multicentric Clinical Study. *Am J Cancer Res* (2017) 7(2):346–56. doi: 10.1016/j.ijrobp.2016.06.1489
27. Tang LL, Liang SB, Huang CL, Zhang F, Xu C, Mao YP, et al. The Development and External Validation of Simplified T Category Classification for Nasopharyngeal Carcinoma to Improve the Prognostic Value in the Intensity-Modulated Radiotherapy Era. *Cancer Med* (2019) 8 (5):2213–22. doi: 10.1002/cam4.2131
28. Zong J, Lin S, Chen Y, Wang B, Xiao Y, Lin J, et al. Does MRI-Detected Cranial Nerve Involvement Affect the Prognosis of Locally Advanced Nasopharyngeal Carcinoma Treated With Intensity Modulated Radiotherapy? *PloS One* (2014) 9 (6):e100571. doi: 10.1371/journal.pone.0100571
29. Cao C, Luo J, Gao L, Yi J, Huang X, Li S, et al. Magnetic Resonance Imaging-Detected Intracranial Extension in the T4 Classification Nasopharyngeal Carcinoma With Intensity-Modulated Radiotherapy. *Cancer Res Treat* (2017) 49(2):518–25. doi: 10.4143/crt.2016.299
30. Zhang GY, Huang Y, Cai XY, Chen XP, Xu T, Wu J, et al. Prognostic Value of Grading Masticator Space Involvement in Nasopharyngeal Carcinoma According to MR Imaging Findings. *Radiology* (2014) 273(1):136–43. doi: 10.1148/radiol.14132745
31. Shi Q, Shen C, Kong L, Wang X, Ding J, Gao Y, et al. Involvement of Both Cervical Lymph Nodes and Retropharyngeal Lymph Nodes has Prognostic Value for N1 Patients With Nasopharyngeal Carcinoma. *Radiat Oncol* (2014) 9:7. doi: 10.1186/1748-717X-9-7
32. Tang LL, Guo R, Zhou G, Sun Y, Liu LZ, Lin AH, et al. Prognostic Value and Staging Classification of Retropharyngeal Lymph Node Metastasis in Nasopharyngeal Carcinoma Patients Treated With Intensity-Modulated Radiotherapy. *PloS One* (2014) 9(10):e108375. doi: 10.1371/journal.pone.0108375
33. Huang L, Zhang Y, Liu Y, Li H, Wang S, Liang S, et al. Prognostic Value of Retropharyngeal Lymph Node Metastasis Laterality in Nasopharyngeal Carcinoma and a Proposed Modification to the UICC/AJCC N Staging System. *Radiother Oncol* (2019) 140:90–7. doi: 10.1016/j.radonc.2019.04.024
34. Xu Y, Chen X, Zhang M, Xiao Y, Zong J, Guo Q, et al. Prognostic Effect of Parotid Area Lymph Node Metastases After Preliminary Diagnosis of Nasopharyngeal Carcinoma: A Propensity Score Matching Study. *Cancer Med* (2017) 6(10):2213–21. doi: 10.1002/cam4.1154
35. Zhang Y, Zhang ZC, Li WF, Liu X, Liu Q, Ma J. Prognosis and Staging of Parotid Lymph Node Metastasis in Nasopharyngeal Carcinoma: An Analysis in 10,126 Patients. *Oral Oncol* (2019) 95:150–6. doi: 10.1016/j.oraloncology.2019.06.013
36. Ai QY, King AD, Poon DMC, Mo FKF, Hui EP, Tong M, et al. Extranodal Extension is a Criterion for Poor Outcome in Patients With Metastatic Nodes From Cancer of the Nasopharynx. *Oral Oncol* (2019) 88:124–30. doi: 10.1016/j.oraloncology.2018.11.007
37. Lu T, Hu Y, Xiao Y, Guo Q, Huang SH, O'Sullivan B, et al. Prognostic Value of Radiologic Extranodal Extension and its Potential Role in Future N Classification for Nasopharyngeal Carcinoma. *Oral Oncol* (2019) 99:104438. doi: 10.1016/j.oraloncology.2019.09.030
38. Guo Q, Pan J, Zong J, Zheng W, Zhang C, Tang L, et al. Suggestions for Lymph Node Classification of UICC/AJCC Staging System: A Retrospective Study Based on 1197 Nasopharyngeal Carcinoma Patients Treated With Intensity-Modulated Radiation Therapy. *Med (Baltimore)* (2015) 94(20): e808. doi: 10.1097/MD.0000000000000808
39. Lan M, Huang Y, Chen CY, Han F, Wu SX, Tian L, et al. Prognostic Value of Cervical Nodal Necrosis in Nasopharyngeal Carcinoma: Analysis of 1800 Patients With Positive Cervical Nodal Metastasis at MR Imaging. *Radiology* (2015) 276(2):619. doi: 10.1148/radiol.15154020
40. Luo Y, Ren J, Zhou P, Gao Y, Yang G, Lang J. Cervical Nodal Necrosis is an Independent Survival Predictor in Nasopharyngeal Carcinoma: An Observational Cohort Study. *Onco Targets Ther* (2016) 9:6775–83. doi: 10.2147/OTT.S110558
41. Lu L, Wei X, Li YH, Li WB. Sentinel Node Necrosis is a Negative Prognostic Factor in Patients With Nasopharyngeal Carcinoma: A Magnetic Resonance Imaging Study of 252 Patients. *Curr Oncol* (2017) 24(3):e220–5. doi: 10.3747/co.24.3168
42. Feng Y, Cao C, Hu Q, Chen X. Prognostic Value and Staging Classification of Lymph Nodal Necrosis in Nasopharyngeal Carcinoma After Intensity-Modulated Radiotherapy. *Cancer Res Treat* (2019) 51(3):1222–30. doi: 10.4143/crt.2018.595
43. Jiang C, Zhang T, Gao H, Zhang L. Prognosis of Cervical and Posterior to Level V Lymph Node Metastasis in 406 Cases of Nasopharyngeal Carcinoma. *Chin J Clin Onco* (2017) 44:1019–23.

44. Ting Y, Chee J, Charn TC, Loh KS, Choong CC, Ting E, et al. Prognostic Significance of Cystic Lymph Nodal Metastasis in Nasopharyngeal Carcinoma. *Head Neck* (2017) 39(9):1832–9. doi: 10.1002/hed.24844
45. Kang M, Zhou P, Wei T, Zhao T, Long J, Li G, et al. A Novel N Staging System for NPC Based on IMRT and RTOG Guidelines for Lymph Node Levels: Results of a Prospective Multicentric Clinical Study. *Oncol Lett* (2018) 16(1):308–16. doi: 10.3892/ol.2018.8676
46. Zhou X, Ou X, Yang Y, Xu T, Shen C, Ding J, et al. Quantitative Metastatic Lymph Node Regions on Magnetic Resonance Imaging are Superior to AJCC N Classification for the Prognosis of Nasopharyngeal Ccarcinoma. *J Oncol* (2018) 2018:9172585. doi: 10.1155/2018/9172585
47. Yue D, Xu YF, Zhang F, Lin L, Mao YP, Li WF, et al. Is Replacement of the Supraclavicular Fossa With the Lower Level Classification Based on Magnetic Resonance Imaging Beneficial in Nasopharyngeal Carcinoma? *Radiother Oncol* (2014) 113(1):108–14. doi: 10.1016/j.radonc.2014.08.036
48. Shen L, Li W, Wang S, Xie G, Zeng Q, Chen C, et al. Image-Based Multilevel Subdivision of M1 Category in TNM Staging System for Metastatic Nasopharyngeal Carcinoma. *Radiology* (2016) 280(3):805–14. doi: 10.1148/radiol.2016151344
49. Shen LJ, Wang SY, Xie GF, Zeng Q, Chen C, Dong AN, et al. Subdivision of M Category for Nasopharyngeal Carcinoma With Synchronous Metastasis: Time to Expand the M Categorization System. *Chin J Cancer* (2015) 34 (10):450–8. doi: 10.1186/s40880-015-0031-9
50. Jiang R, You R, Pei XQ, Zou X, Zhang MX, Wang TM, et al. Development of a Ten-Signature Classifier Using a Support Vector Machine Integrated Approach to Subdivide the M1 Stage Into M1a and M1b Stages of Nasopharyngeal Carcinoma With Synchronous Metastases to Better Predict Patients' Survival. *Oncotarget* (2016) 7(3):3645–57. doi: 10.18632/oncotarget.6436
51. Tian YH, Zou WH, Xiao WW, Zeng L, Yuan X, Bai L, et al. Oligometastases in AJCC Stage IVc Nasopharyngeal Carcinoma: A Subset With Better Overall Survival. *Head Neck* (2016) 38(8):1152–7. doi: 10.1002/hed.24345
52. Zou X, You R, Liu H, He YX, Xie GF, Xie ZH, et al. Establishment and Validation of M1 Stage Subdivisions for De Novo Metastatic Nasopharyngeal Carcinoma to Better Predict Prognosis and Guide Treatment. *Eur J Cancer* (2017) 77:117–26. doi: 10.1016/j.ejca.2017.02.029
53. Chen M, Yin L, Wu J, Gu JJ, Jiang XS, Wang DJ, et al. Impact of Plasma Epstein-Barr Virus-DNA and Tumor Volume on Prognosis of Locally Advanced Nasopharyngeal Carcinoma. *BioMed Res Int* (2015) 2015:617949. doi: 10.1155/2015/617949
54. Tang LQ, Li CF, Chen QY, Zhang L, Lai XP, He Y, et al. High-Sensitivity C-Reactive Protein Complements Plasma Epstein-Barr Virus Deoxyribonucleic Acid Prognostication in Nasopharyngeal Carcinoma: A Large-Scale Retrospective and Prospective Cohort Study. *Int J Radiat Oncol Biol Phys* (2015) 91(2):325–36. doi: 10.1016/j.ijrobp.2014.10.005
55. Yang L, Hong S, Wang Y, Chen H, Liang S, Peng P, et al. Development and External Validation of Nomograms for Predicting Survival in Nasopharyngeal Carcinoma Patients After Definitive Radiotherapy. *Sci Rep* (2015) 5:15638. doi: 10.1038/srep15638
56. Zhao FP, Liu X, Chen XM, Lu J, Yu BL, Tian WD, et al. Levels of Plasma Epstein-Barr Virus DNA Prior and Subsequent to Treatment Predicts the Prognosis of Nasopharyngeal Carcinoma. *Oncol Lett* (2015) 10(5):2888–94. doi: 10.3892/ol.2015.3628
57. Chen WH, Tang LQ, Guo SS, Chen QY, Zhang L, Liu LT, et al. Prognostic Value of Plasma Epstein-Barr Virus DNA for Local and Regionally Advanced Nasopharyngeal Carcinoma Treated With Cisplatin- Based Concurrent Chemoradiotherapy in Intensity-Modulated Radiotherapy Era. *Med (Baltimore)* (2016) 95(5):e2642. doi: 10.1097/MD.0000000000002642
58. Du XJ, Tang LL, Mao YP, Guo R, Sun Y, Lin AH, et al. Circulating EBV DNA, Globulin and Nodal Size Predict Distant Metastasis After Intensity-Modulated Radiotherapy in Stage II Nasopharyngeal Carcinoma. *J Cancer* (2016) 7(6):664–70. doi: 10.7150/jca.14183
59. Lv JW, Chen YP, Zhou GQ, Tang LL, Mao YP, Li WF, et al. Cigarette Smoking Complements the Prognostic Value of Baseline Plasma Epstein-Barr Virus Deoxyribonucleic Acid in Patients With Nasopharyngeal Carcinoma Undergoing Intensity-Modulated Radiation Therapy: A Large-Scale Retrospective Cohort Study. *Oncotarget* (2016) 7(13):16806–17. doi: 10.18632/oncotarget.7609
60. Peng H, Guo R, Chen L, Zhang Y, Li WF, Mao YP, et al. Prognostic Impact of Plasma Epstein-Barr Virus DNA in Patients With Nasopharyngeal Carcinoma Treated Using Intensity-Modulated Radiation Therapy. *Sci Rep* (2016) 6:22000. doi: 10.1038/srep22000
61. Jin YN, Yao JJ, Zhang F, Wang SY, Zhang WJ, Zhou GQ, et al. Is Pretreatment Epstein-Barr Virus DNA Still Associated With 6-Year Survival Outcomes in Locoregionally Advanced Nasopharyngeal Carcinoma? *J Cancer* (2017) 8(6):976–82. doi: 10.7150/jca.18124
62. Yao JJ, Zhou GQ, Wang YQ, Wang SY, Zhang WJ, Jin YN, et al. Prognostic Values of the Integrated Model Incorporating the Volume of Metastatic Regional Cervical Lymph Node and Pretreatment Serum Epstein-Barr Virus DNA Copy Number in Predicting Distant Metastasis in Patients With N1 Nasopharyngeal Carcinoma. *Chin J Cancer* (2017) 36(1):98. doi: 10.1186/s40880-017-0264-x
63. Chen QY, Guo SY, Tang LQ, Lu TY, Chen BL, Zhong QY, et al. Combination of Tumor Volume and Epstein-Barr Virus DNA Improved Prognostic Stratification of Stage II Nasopharyngeal Carcinoma in the Intensity Modulated Radiotherapy Era: A Large-Scale Cohort Study. *Cancer Res Treat* (2018) 50(3):861–71. doi: 10.4143/crt.2017.237
64. He SS, Wang Y, Bao Y, Cai XY, Yang XL, Chen DM, et al. Dynamic Changes in Plasma Epstein-Barr Virus DNA Load During Treatment Have Prognostic Value in Nasopharyngeal Carcinoma: A Retrospective Study. *Cancer Med* (2018) 7(4):1110–7. doi: 10.1002/cam4.1381
65. Peng L, Yang Y, Guo R, Mao YP, Xu C, Chen YP, et al. Relationship Between Pretreatment Concentration of Plasma Epstein-Barr Virus DNA and Tumor Burden in Nasopharyngeal Carcinoma: An Updated Interpretation. *Cancer Med* (2018) 7(12):5988–98. doi: 10.1002/cam4.1858
66. Du YY, Luo DH, Sun XS, Tang LQ, Mai HQ, Chen QY, et al. Combining Pretreatment Plasma Epstein-Barr Virus DNA Level and Cervical Node Necrosis Improves Prognostic Stratification in Patients With Nasopharyngeal Carcinoma: A Cohort Study. *Cancer Med* (2019) 8 (16):6841–52. doi: 10.1002/cam4.2481
67. Guo R, Tang LL, Mao YP, Du XJ, Chen L, Zhang ZC, et al. Proposed Modifications and Incorporation of Plasma Epstein-Barr Virus DNA Improve the TNM Staging System for Epstein-Barr Virus-Related Nasopharyngeal Carcinoma. *Cancer* (2019) 125(1):79–89. doi: 10.1002/cncr.31741
68. Huang CL, Sun ZQ, Guo R, Liu X, Mao YP, Peng H, et al. Plasma Epstein-Barr Virus DNA Load After Induction Chemotherapy Predicts Outcome in Locoregionally Advanced Nasopharyngeal Carcinoma. *Int J Radiat Oncol Biol Phys* (2019) 104(2):355–61. doi: 10.1016/j.ijrobp.2019.01.007
69. Sun XS, Liu LT, Liu SL, Guo SS, Wen YF, Xie HJ, et al. Identifying Optimal Candidates for Local Treatment of the Primary Tumor Among Patients With De Novo Metastatic Nasopharyngeal Carcinoma: A Retrospective Cohort Study Based on Epstein-Barr Virus DNA Level and Tumor Response to Palliative Chemotherapy. *BMC Cancer* (2019) 19(1):92. doi: 10.1186/s12885-019-5281-5
70. Sun XS, Chen WH, Liu SL, Liang YJ, Chen QY, Guo SS, et al. Individualized Concurrent Chemotherapy by Pretreatment Plasma Epstein-Barr Viral DNA in II-III Stage Nasopharyngeal Carcinoma: A Propensity Score Matching Analysis Using a Large Cohort. *Cancer Med* (2019) 8(9):4214–25. doi: 10.1002/cam4.2343
71. Lee VH, Kwong DL, Leung TW, Choi CW, O'Sullivan B, Lam KO, et al. The Addition of Pretreatment Plasma Epstein-Barr Virus DNA Into the Eighth Edition of Nasopharyngeal Cancer TNM Stage Classification. *Int J Cancer* (2019) 144(7):1713–22. doi: 10.1002/ijc.31856
72. Tian YM, Xiao WW, Bai L, Liu XW, Zhao C, Lu TX, et al. Impact of Primary Tumor Volume and Location on the Prognosis of Patients With Locally Recurrent Nasopharyngeal Carcinoma. *Chin J Cancer* (2015) 34(6):247–53. doi: 10.1186/s40880-015-0019-5
73. He YX, Wang Y, Cao PF, Shen L, Zhao YJ, Zhang ZJ, et al. Prognostic Value and Predictive Threshold of Tumor Volume for Patients With Locally Advanced Nasopharyngeal Carcinoma Receiving Intensity-Modulated Radiotherapy. *Chin J Cancer* (2016) 35(1):96. doi: 10.1186/s40880-016-0159-2
74. Lu L, Li J, Zhao C, Xue W, Han F, Tao T, et al. Prognostic Efficacy of Combining Tumor Volume With Epstein-Barr Virus DNA in Patients Treated

With Intensity-Modulated Radiotherapy for Nasopharyngeal Carcinoma. *Oral Oncol* (2016) 60:18–24. doi: 10.1016/j.oraloncology.2016.06.013
75. Luo Y, Gao Y, Yang G, Lang J. Clinical Outcome and Prognostic Factors of Intensity-Modulated Radiotherapy for T4 Stage Nasopharyngeal Carcinoma. *BioMed Res Int* (2016) 2016:4398498. doi: 10.1155/2016/4398498
76. Qin L, Wu F, Lu H, Wei B, Li G, Wang R. Tumor Volume Predicts Survival Rate of Advanced Nasopharyngeal Carcinoma Treated With Concurrent Chemoradiotherapy. *Otolaryngol Head Neck Surg* (2016) 155(4):598–605. doi: 10.1177/0194599816644408
77. Chen FP, Zhou GQ, Qi ZY, Lin L, Hu J, Wang XJ, et al. Prognostic Value of Cervical Nodal Tumor Volume in Nasopharyngeal Carcinoma: Analysis of 1230 Patients With Positive Cervical Nodal Metastasis. *PloS One* (2017) 12 (5):e0176995. doi: 10.1371/journal.pone.0176995
78. Zang J, Li C, Zhao LN, Wang JH, Xu M, Luo SQ, et al. Prognostic Model of Death and Distant Metastasis for Nasopharyngeal Carcinoma Patients Receiving 3DCRT/IMRT in Nonendemic Area of China. *Med (Baltimore)* (2016) 95(21):e3794. doi: 10.1097/MD.0000000000003794
79. Liang SB, Teng JJ, Hu XF, Yang XL, Luo M, Fang XN, et al. Prognostic Value of Total Tumor Volume in Patients With Nasopharyngeal Carcinoma Treated With Intensity-Modulated Radiotherapy. *BMC Cancer* (2017) 17 (1):506. doi: 10.1186/s12885-017-3480-5
80. Jeong Y, Lee SW. Tumor Volume/Metabolic Information can Improve the Prognostication of Anatomy Based Staging System for Nasopharyngeal Cancer? Evaluation of the 8th Edition of the AJCC/UICC Staging System for Nasopharyngeal Cancer. *Radiat Oncol J* (2018) 36(4):295–303. doi: 10.3857/roj.2018.00430
81. Liu T, Lv J, Qin Y. Standardized Tumor Volume: An Independent Prognostic Factor in Advanced Nasopharyngeal Carcinoma. *Oncotarget* (2017) 8(41):70299–309. doi: 10.18632/oncotarget.20313
82. Chen YP, Zhao BC, Chen C, Shen LJ, Gao J, Mai ZY, et al. Pretreatment Platelet Count Improves the Prognostic Performance of the TNM Staging System and Aids in Planning Therapeutic Regimens for Nasopharyngeal Carcinoma: A Single-Institutional Study of 2,626 Patients. *Chin J Cancer* (2015) 34(3):137–46. doi: 10.1186/s40880-015-0006-x
83. Li JP, Chen SL, Liu XM, He X, Xing S, Liu YJ, et al. A Novel Inflammation-Based Stage (I Stage) Predicts Overall Survival of Patients With Nasopharyngeal Carcinoma. *Int J Mol Sci* (2016) 17(11):1900. doi: 10.3390/ijms17111900
84. Li X, Chang H, Tao Y, Wang X, Gao J, Zhang W, et al. Revalidation of a Prognostic Score Model Based on Complete Blood Count for Nasopharyngeal Carcinoma Through a Prospective Study. *Chin J Cancer Res* (2016) 28(5):467–77. doi: 10.21147/j.issn.1000-9604.2016.05.01
85. Lu AY, Li HF, Zheng YM, Tang MZ, Li J, Wu HH, et al. Prognostic Significance of Neutrophil to Lymphocyte Ratio, Lymphocyte to Monocyte Ratio, and Platelet to Lymphocyte Ratio in Patients With Nasopharyngeal Carcinoma. *BioMed Res Int* (2017) 2017:3047802. doi: 10.1155/2017/3047802
86. Xie X, Zeng X, Cao S, Hu X, Shi Q, Li D, et al. Elevated Pretreatment Platelet Distribution Width and Platelet Count Predict Poor Prognosis in Nasopharyngeal Carcinoma. *Oncotarget* (2017) 8(62):106089–97. doi: 10.18632/oncotarget.22528
87. Zhang LL, Zhou GQ, Li YY, Tang LL, Mao YP, Lin AH, et al. Combined Prognostic Value of Pretreatment Anemia and Cervical Node Necrosis in Patients With Nasopharyngeal Carcinoma Receiving Intensity-Modulated Radiotherapy: A Large-Scale Retrospective Study. *Cancer Med* (2017) 6 (12):2822–31. doi: 10.1002/cam4.1233
88. Zhou JY, Chen T, Li W, Ye K, ZB W. Effect of Pretreatment Serum LDH and ALP Levels on the Prognosis of Patients With Nasopharyngeal Carcinoma. *Lin Chung Er Bi Yan Hou Tou Jing Wai Ke Za Zhi* (2017) 31:1069–73. doi: 10.13201/j.issn.1001-1781.2017.14.004
89. Wang Y, Yang L, Xia L, Chen Y. High C-Reactive Protein/Albumin Ratio Predicts Unfavorable Distant Metastasis-Free Survival in Nasopharyngeal Carcinoma: A Propensity Score-Matched Analysis. *Cancer Manag Res* (2018) 10:371–81. doi: 10.2147/CMAR.S155604
90. Wang YQ, Chen YP, Zhang Y, Jiang W, Liu N, Yun JP, et al. Prognostic Significance of Tumor-Infiltrating Lymphocytes in Nondisseminated Nasopharyngeal Carcinoma: A Large-Scale Cohort Study. *Int J Cancer* (2018) 142(12):2558–66. doi: 10.1002/ijc.31279
91. Ye L, Oei RW, Kong F, Xu T, Shen C, Wang X, et al. Prognostic Values of Hematological Biomarkers in Nasopharyngeal Carcinoma Patients Treated With Intensity-Modulated Radiotherapy. *Eur Arch Otorhinolaryngol* (2018) 275(5):1309–17. doi: 10.1007/s00405-018-4956-x
92. Akcay M, Etiz D, Ozen A, Saylisoy S. Neutrophil/lymphocyte Ratio and Prognosis in Patients With non-Metastatic Nasopharyngeal Cancer: A Single-Center Experience. *Turk Oncol Derg* (2019) 34(2):92–9. doi: 10.5505/tjo.2019.1845
93. Gundog M, Basaran H. Pretreatment Low Prognostic Nutritional Index and Low Albumin-Globulin Ratio are Predictive for Overall Survival in Nasopharyngeal Cancer. *Eur Arch Oto-Rhino-L* (2019) 276(11):3221–30. doi: 10.1007/s00405-019-05595-2
94. He SS, Wang Y, Wang CT, Zhu MY, Yang XL, Chen DM, et al. A Combined Marker Based on Plasma D-Dimer and Serum Albumin Levels in Patients With Nasopharyngeal Carcinoma is Associated With Poor Survival Outcomes in a Retrospective Cohort Study. *J Cancer* (2019) 10(16):3691–7. doi: 10.7150/jca.32387
95. Long GX, Tang WH, Fu XG, Liu DB, Zhang LL, Hu GY, et al. Pre-Treatment Serum Lactate Dehydrogenase Predicts Distant Metastasis and Poor Survival in Nasopharyngeal Carcinoma. *J Cancer* (2019) 10(16):3657–64. doi: 10.7150/jca.32716
96. Topkan E, Ekici NY, Ozdemir Y, Besen AA, Yildirim BA, Mertsoylu H, et al. Baseline Hemoglobin <11.0 G/dL has Stronger Prognostic Value Than Anemia Status in Nasopharynx Cancers Treated With Chemoradiotherapy. *Int J Biol Marker* (2019) 34:139–47. doi: 10.1177/1724600818821688
97. Yao JJ, Zhu FT, Dong J, Liang ZB, Yang LW, Chen SY, et al. Prognostic Value of Neutrophil-to-Lymphocyte Ratio in Advanced Nasopharyngeal Carcinoma: A Large Institution-Based Cohort Study From an Endemic Area. *BMC Cancer* (2019) 19:37. doi: 10.1186/s12885-018-5236-2
98. Tao CJ, Chen YY, Jiang F, Feng XL, Jin QF, Jin T, et al. The C-Reactive Protein/Albumin Ratio is an Independent Prognostic Factor for Overall Survival in Patients With Nasopharyngeal Carcinoma Receiving Intensity-Modulated Radiotherapy. *J Cancer* (2016) 7(14):2005–11. doi: 10.7150/jca.16210
99. Yoon YH, Lee SH, Hong SL, Kim SJ, Roh HJ, Cho KS. Prognostic Value of Metabolic Tumor Volume as Measured by Fluorine-18-Fluorodeoxyglucose Positron Emission Tomography/Computed Tomography in Nasopharyngeal Carcinoma. *Int Forum Allergy Rhinol* (2014) 4(10):845–50. doi: 10.1002/alr.21363
100. Zaghloul HA, Khedr GA, Rostom Y, Refaat T. The Predictive Value of Pretreatment (18)-F-FDG-PET-CT in Locally Advanced Nasopharyngeal Cancer Patients Treated Definitively With Induction Chemotherapy Followed by Concurrent Chemo-Radiotherapy. *J Nucl Med Radiat Ther* (2014) 5(1):166. doi: 10.4172/2155-9619.1000166
101. Hsieh TC, Hsieh CY, Yang TY, Chen TT, Lin CY, Lin CC, et al. [18F]-Fluorodeoxyglucose Positron Emission Tomography Standardized Uptake Value as a Predictor of Adjuvant Chemotherapy Benefits in Patients With Nasopharyngeal Carcinoma. *Oncologist* (2015) 20(5):539–45. doi: 10.1634/theoncologist.2014-0291
102. Shen T, Tang LQ, Luo DH, Chen QY, Li PJ, Mai DM, et al. Different Prognostic Values of Plasma Epstein-Barr Virus DNA and Maximal Standardized Uptake Value of 18F-FDG PET/CT for Nasopharyngeal Carcinoma Patients With Recurrence. *PloS One* (2015) 10(4):e0122756. doi: 10.1371/journal.pone.0122756
103. Xiao W, Xu A, Han F, Lin X, Lu L, Shen G, et al. Positron Emission Tomography-Computed Tomography Before Treatment is Highly Prognostic of Distant Metastasis in Nasopharyngeal Carcinoma Patients After Intensity-Modulated Radiotherapy Treatment: A Prospective Study With Long-Term Follow-Up. *Oral Oncol* (2015) 51(4):363–9. doi: 10.1016/j.oraloncology.2015.01.009
104. Yoon HI, Kim KH, Lee J, Roh YH, Yun M, Cho BC, et al. The Clinical Usefulness of (18)F-Fluorodeoxyglucose Positron Emission Tomography (PET) to Predict Oncologic Outcomes and PET-Based Radiotherapeutic Considerations in Locally Advanced Nasopharyngeal Carcinoma. *Cancer Res Treat* (2016) 48(3):928–41. doi: 10.4143/crt.2015.275
105. Zhang Y, Li WF, Mao YP, Zhou GQ, Peng H, Sun Y, et al. Establishment of an Integrated Model Incorporating Standardised Uptake Value and N-Classification for Predicting Metastasis in Nasopharyngeal Carcinoma. *Oncotarget* (2016) 7(12):13612–20. doi: 10.18632/oncotarget.7253
106. Jeong Y, Baek S, Park JW, Joo JH, Kim JS, Lee SW. Lymph Node Standardized Uptake Values at Pre-Treatment (18)F-Fluorodeoxyglucose

Positron Emission Tomography as a Valuable Prognostic Factor for Distant Metastasis in Nasopharyngeal Carcinoma. *Br J Radiol* (2017) 90 (1071):20160239. doi: 10.1259/bjr.20160239
107. Jin YN, Yao JJ, Wang SY, Zhang WJ, Zhou GQ, Zhang F, et al. Prognostic Value of Primary Gross Tumor Volume and Standardized Uptake Value of (18)F-FDG in PET/CT for Distant Metastasis in Locoregionally Advanced Nasopharyngeal Carcinoma. *Tumour Biol* (2017) 39(7):1010428317717843. doi: 10.1177/1010428317717843
108. Lee SJ, Kay CS, Kim YS, Son SH, Kim M, Lee SW, et al. Prognostic Value of Nodal SUVmax of 18F-FDG PET/CT in Nasopharyngeal Carcinoma Treated With Intensity-Modulated Radiotherapy. *Radiat Oncol J* (2017) 35(4):306–16. doi: 10.3857/roj.2017.00115
109. Liu F, Xi XP, Wang H, Han YQ, Xiao F, Hu Y, et al. PET/CT-Guided Dose-Painting Versus CT-Based Intensity Modulated Radiation Therapy in Locoregional Advanced Nasopharyngeal Carcinoma. *Radiat Oncol* (2017) 12(1):15. doi: 10.1186/s13014-016-0739-y
110. Zhong L, Li C, Ren Y, Wu D. Prognostic Value of (18)F-Fluorodeoxyglucose PET Parameters and Inflammation in Patients With Nasopharyngeal Carcinoma. *Oncol Lett* (2017) 14(4):5004–12. doi: 10.3892/ol.2017.6816
111. Alessi A, Lorenzoni A, Cavallo A, Padovano B, Iacovelli NA, Bossi P, et al. Role of Pretreatment 18F-FDG PET/CT Parameters in Predicting Outcome of non-Endemic EBV DNA-Related Nasopharyngeal Cancer (NPC) Patients Treated With IMRT and Chemotherapy. *Radiol Med* (2019) 124(5):414–21. doi: 10.1007/s11547-018-0980-6
112. Fei Z, Chen C, Huang Y, Qiu X, Li Y, Li L, et al. Metabolic Tumor Volume and Conformal Radiotherapy Based on Prognostic PET/CT for Treatment of Nasopharyngeal Carcinoma. *Med (Baltimore)* (2019) 98(28):e16327. doi: 10.1097/MD.0000000000016327
113. Sun XS, Liang YJ, Liu SL, Chen QY, Guo SS, Wen YF, et al. Maximal Standard Uptake Values of (18)F-Fluoro-2-Deoxy-D-Glucose Positron Emission Tomography Compared With Epstein-Barr Virus DNA as Prognostic Indicators in De Novo Metastatic Nasopharyngeal Carcinoma Patients. *BMC Cancer* (2019) 19(1):908. doi: 10.1186/s12885-019-6106-2
114. Peng H, Chen L, Zhang Y, Guo R, Li WF, Mao YP, et al. Survival Analysis of Patients With Advanced-Stage Nasopharyngeal Carcinoma According to the Epstein-Barr Virus Status. *Oncotarget* (2016) 7(17):24208–16. doi: 10.18632/oncotarget.8144
115. Zhang J, Shu C, Song YL, Li QF, Huang JW, Ma XL. Epstein-Barr Virus DNA Level as a Novel Prognostic Factor in Nasopharyngeal Carcinoma: A Meta-Analysis. *Medicine* (2016) 95(40):e5130. doi: 10.1097/MD.0000000000005130
116. Zhang WN, Chen YP, Chen L, Guo R, Zhou GQ, Tang LL, et al. The Clinical Utility of Plasma Epstein-Barr Virus DNA Assays in Nasopharyngeal Carcinoma: The Dawn of a New Era? A Systematic Review and Meta-Analysis of 7836 Cases. *Medicine* (2015) 94(20):e845. doi: 10.1097/MD.0000000000000845
117. Qu H, Huang Y, Zhao S, Zhou Y, Lv W. Prognostic Value of Epstein-Barr Virus DNA Level for Nasopharyngeal Carcinoma: A Meta-Analysis of 8128 Cases. *Eur Arch Otorhinolaryngol* (2020) 277(1):9–18. doi: 10.1007/s00405-019-05699-9
118. Kim KY, Le Q-T, Yom SS, Pinsky BA, Bratman SV, Ng RHW. Current State of PCR-Based Epstein- Barr Virus DNA Testing for Nasopharyngeal Cancer. *J Natl Cancer Inst* (2017) 109(4). doi: 10.1093/jnci/djx007
119. Le QT, Zhang Q, Cao H, Cheng AJ, Pinsky BA, Hong RL, et al. An International Collaboration to Harmonize the Quantitative Plasma Epstein-Barr Virus DNA Assay for Future Biomarker-Guided Trials in Nasopharyngeal Carcinoma. *Clin Cancer Res* (2013) 19(8):2208–15. doi: 10.1158/1078-0432.CCR-12-3702
120. Nicholls JM, Lee VH, Chan SK, Tsang KC, Choi CW, Kwong DL, et al. Negative Plasma Epstein-Barr Virus DNA Nasopharyngeal Carcinoma in an Endemic Region and Its Influence on Liquid Biopsy Screening Programmes. *Br J Cancer* (2019) 121(8):690–8. doi: 10.1038/s41416-019-0575-6
121. Wu Z, Zeng RF, Su Y, Gu MF, Huang SM. Prognostic Significance of Tumor Volume in Patients With Nasopharyngeal Carcinoma Undergoing Intensity-Modulated Radiation Therapy. *Head Neck* (2013) 35(5):689–94. doi: 10.1002/hed.23010
122. Arens AI, Troost EG, Hoeben BA, Grootjans W, Lee JA, Gregoire V, et al. Semiautomatic Methods for Segmentation of the Proliferative Tumour Volume on Sequential FLT PET/CT Images in Head and Neck Carcinomas and Their Relation to Clinical Outcome. *Eur J Nucl Med Mol Imaging* (2014) 41(5):915–24. doi: 10.1007/s00259-013-2651-0
123. Bhatia KS, King AD, Yu KH, Vlantis AC, Tse GM, Mo FK, et al. Does Primary Tumour Volumetry Performed Early in the Course of Definitive Concomitant Chemoradiotherapy for Head and Neck Squamous Cell Carcinoma Improve Prediction of Primary Site Outcome? *Br J Radiol* (2010) 83(995):964–70. doi: 10.1259/bjr/27631720
124. Yin J, Qin Y, Luo YK, Feng M, Lang JY. Prognostic Value of Neutrophil-to-Lymphocyte Ratio for Nasopharyngeal Carcinoma: A Meta-Analysis. *Med (Baltimore)* (2017) 96(29):e7577. doi: 10.1097/MD.0000000000007577
125. Zhou GQ, Tang LL, Mao YP, Chen L, Li WF, Sun Y, et al. Baseline Serum Lactate Dehydrogenase Levels for Patients Treated With Intensity-Modulated Radiotherapy for Nasopharyngeal Carcinoma: A Predictor of Poor Prognosis and Subsequent Liver Metastasis. *Int J Radiat Oncol Biol Phys* (2012) 82(3):e359–65.
126. Wan XB, Wei L, Li H, Dong M, Lin Q, Ma XK, et al. High Pretreatment Serum Lactate Dehydrogenase Level Correlates With Disease Relapse and Predicts an Inferior Outcome in Locally Advanced Nasopharyngeal Carcinoma. *Eur J Cancer* (2013) 49(10):2356–64. doi: 10.1016/j.ejca.2013.03.008
127. Turen S, Ozyar E, Altundag K, Gullu I, Atahan IL. Serum Lactate Dehydrogenase Level is a Prognostic Factor in Patients With Locoregionally Advanced Nasopharyngeal Carcinoma Treated With Chemoradiotherapy. *Cancer Invest* (2007) 25(5):315–21. doi: 10.1080/07357900701209103
128. Tang XR, Li YQ, Liang SB, Jiang W, Liu F, Ge WX, et al. Development and Validation of a Gene Expression-Based Signature to Predict Distant Metastasis in Locoregionally Advanced Nasopharyngeal Carcinoma: A Retrospective, Multicentre, Cohort Study. *Lancet Oncol* (2018) 19(3):382–93. doi: 10.1016/S1470-2045(18)30080-9
129. Tang LQ, Li CF, Li J, Chen WH, Chen QY, Yuan LX, et al. Establishment and Validation of Prognostic Nomograms for Endemic Nasopharyngeal Carcinoma. *J Natl Cancer Inst* (2016) 108(1):djv291. doi: 10.1093/jnci/djv291
130. Xia WX, Zhang HB, Shi JL, Lu X, Wang L, Ye YF, et al. A Prognostic Model Predicts the Risk of Distant Metastasis and Death for Patients With Nasopharyngeal Carcinoma Based on Pre-Treatment Serum C-Reactive Protein and N-Classification. *Eur J Cancer* (2013) 49(9):2152–60. doi: 10.1016/j.ejca.2013.03.003
131. Chen WS, Li JJ, Hong L, Xing ZB, Wang F, Li CQ. Comparison of MRI, CT and 18F-FDG PET/CT in the Diagnosis of Local and Metastatic of Nasopharyngeal Carcinomas: An Updated Meta Analysis of Clinical Studies. *Am J Transl Res* (2016) 8(11):4532–47. doi: 10.1016/j.oraloncology.2015.10.010

Conflict of Interest: CC: Consulting or Advisory Role: AstraZeneca, Eiasi; Research funding: AstraZeneca, Merck Kgga.

The remaining authors declare that the research was conducted in the absence of any commercial or financial relationships that could be construed as a potential conflict of interest.

Publisher's Note: All claims expressed in this article are solely those of the authors and do not necessarily represent those of their affiliated organizations, or those of the publisher, the editors and the reviewers. Any product that may be evaluated in this article, or claim that may be made by its manufacturer, is not guaranteed or endorsed by the publisher.

frontiers in Oncology

ORIGINAL RESEARCH
published: 06 September 2021
doi: 10.3389/fonc.2021.719513

The Ratio of Preoperative Serum Biomarkers Predicts Prognosis in Patients With Oral Squamous Cell Carcinoma

Meng Ding[1†], Yuxian Song[2†], Junyan Jing[3], Mei Tian[1], Liang Ding[2], Qiang Li[3], Chongchong Zhou[1], Heng Dong[3], Yanhong Ni[2*] and Yongbin Mou[3*]*

[1] Nanjing Stomatological Hospital, Medical School of Nanjing University, Nanjing, China, [2] Central Laboratory, Nanjing Stomatological Hospital, Medical School of Nanjing University, Nanjing, China, [3] Department of Oral Implantology, Nanjing Stomatological Hospital, Medical School of Nanjing University, Nanjing, China

OPEN ACCESS

Edited by:
Qin Lin,
First Affiliated Hospital of Xiamen University, China

Reviewed by:
Wan Maria Nabillah Ghani,
University of Malaya, Malaysia
Jian Zhou,
Fudan University, China

***Correspondence:**
Yongbin Mou
yongbinmou@163.com
Yanhong Ni
niyanhong12@163.com
Heng Dong
dongheng90@smail.nju.edu.cn

[†]These authors have contributed equally to this work

Specialty section:
This article was submitted to Head and Neck Cancer, a section of the journal Frontiers in Oncology

Received: *02 June 2021*
Accepted: *17 August 2021*
Published: *06 September 2021*

Citation:
Ding M, Song Y, Jing J, Tian M, Ding L, Li Q, Zhou C, Dong H, Ni Y and Mou Y (2021) The Ratio of Preoperative Serum Biomarkers Predicts Prognosis in Patients With Oral Squamous Cell Carcinoma. Front. Oncol. 11:719513. doi: 10.3389/fonc.2021.719513

Background: Dynamic changes in circulating immune-inflammatory cells have been regarded as simple and convenient prognostic biomarkers in various cancers. However, studies on the prognostic values of their ratios in oral squamous cell carcinoma (OSCC) remain limited.

Materials and Methods: A total of 493 OSCC patients were included in the present study. Here, we investigated the prognostic values of the neutrophil-to-lymphocyte ratio (NLR), lymphocyte-to-monocyte ratio (LMR), neutrophil-to-white blood cell ratio (NWR), and lymphocyte-to-white blood cell ratio (LWR) in OSCC. The correlations of the NLR, LMR, NWR, and LWR with clinicopathological characteristics were statistically analyzed using the Chi-square test, Kaplan-Meier curves, and univariate and multivariate Cox regression models.

Result: Kaplan-Meier analyses revealed that OSCC patients with a high LMR and low NWR had prolonged overall survival (OS, $P<0.001$) and disease-free survival (DFS, $P<0.001$ and $P=0.003$, respectively), but there were no significant differences in metastasis-free survival (MFS, $P=0.053$ and $P=0.052$, respectively). In contrary, a high NLR and low LWR were associated with poor OS ($P<0.001$ and $P=0.0016$, respectively), DFS ($P=0.0014$ and 0.0012, respectively) and MFS ($P=0.021$ and 0.008, respectively). Additionally, Cox multivariate analyses showed that the LMR was an independent prognostic factor for both OS ($P=0.007$) and DFS ($P=0.017$), while the LWR was an independent prognostic factor for MFS ($P=0.009$).

Conclusion: Preoperative NLR, LMR, NWR, and LWR in the peripheral blood are significant prognostic factors for OSCC and might be helpful in predicting OSCC progression.

Keywords: oral squamous cell carcinoma, neutrophil-to-lymphocyte ratio, lymphocyte-to-monocyte ratio, neutrophil-to-white blood cell ratio, lymphocyte-to-white blood cell ratio, overall survival, disease-free survival, metastasis-free survival

INTRODUCTION

Oral squamous cell carcinoma (OSCC) refers to a malignant tumor that originates from the mouth and is dominated by squamous cells (1). Cancer cells can occur in the gingiva, hard palate, tongue, buccal mucosa, lip and other organs, and the number of confirmed OSCC cases is predicted to rise to 856,000 cases by 2035 worldwide (2). Although many therapeutic strategies for OSCC have shown promising effects in the treatment of OSCC in recent decades, the 5-year survival rate remains at approximately 65% (3). In addition, the survival rates of patients are affected by the stage of cancer progression. For localized OSCC, the 5-year survival rate is 84% but decreases to 65% in regional cases and to 39% if distant metastasis is present (4). In other words, a high survival rate relies largely on early detection, which is the key to improving the quality of life of OSCC patients. To avoid distant metastasis of OSCC due to a missed diagnosis, local and precise approaches are urgently needed to prevent, screen, and intervene in OSCC.

The traditional tumor staging system is based on the primary tumor classification (T), quantification of nodal metastasis (N), and presence of distant metastasis (M) (5). However, patients with the same TNM stages often show significantly different prognoses, which indicates that the TNM staging system remains far from optimal in predicting OSCC outcomes, especially the clinical TNM (cTNM) (6, 7), which largely relies on the radiological evaluation. It is well known that the radiological examination can be influenced by the limitations of imaging techniques or technicians, which may result in inaccurate classification (8). Thus, some studies considered introducing a prognostic evaluation using serum biomarkers (such as neutrophils, lymphocytes, and monocytes) to optimally stratify patients, select treatment strategies and predict prognosis in the clinic (9, 10). The main strength of the novel method is that the information can be obtained from routine blood tests before surgery, without any extra effort, making it a simple, economical, and real-time prediction tool.

Numerous studies have indicated that changes in circulating immune-inflammatory cells, such as monocytes, lymphocytes, neutrophils, and platelets, in the peripheral blood could be novel prognostic biomarkers in soft tissue sarcomas or oropharyngeal cancer (10, 11). However, whether assessing the circulating immune-inflammatory in peripheral blood is suitable for OSCC is still unclear. Tsai et al. studied 202 OSCC patients and found that the pretreatment circulating monocyte count increased with advanced clinical stage (12). In a retrospective study of 309 patients with OSCC, a high platelet count, high neutrophil count and low lymphocyte count were found to be associated with reduced overall survival (OS) and disease-free survival (DFS) (13). Some studies have also indicated that an increased pretreatment neutrophil-to-lymphocyte ratio (NLR) is associated with poor outcomes in hepatocellular carcinoma, colorectal cancer, endometrial cancer, and gastric cancer (14–17). However, few studies have reported the prognostic values of the ratios of immune-inflammatory cells, such as the NLR, lymphocyte-to-monocyte ratio (LMR), neutrophil-to-white blood cell ratio (NWR), and lymphocyte-to-white blood cell ratio (LWR), especially in patients with OSCC. Moreover, previous studies have focused on the relationship between serum biomarkers and OS or DFS, but the predictive capacity of these biomarkers for metastasis has not yet been reported.

Therefore, the current study aimed to evaluate the association of the NLR, LMR, NWR, and LWR with clinicopathological characteristics, as well as their prognostic value for OS, DFS, and MFS in OSCC patients.

Abbreviations: OSCC, oral squamous cell carcinoma; NLR, neutrophil-to-lymphocyte ratio; LMR, lymphocyte-to-monocyte ratio; NWR, neutrophil-to-white blood cell ratio; LWR, lymphocyte-to-white blood cell ratio; OS, overall survival; DFS, disease-free survival; MFS, metastasis-free survival; T, tumor; N, nodal metastasis; M, distant metastasis; CBCT, cone beam computed tomography; AJCC, American Joint Committee on Cancer; WBCs, white blood cells; HR, hazard ratio; CI, confidence interval.

MATERIALS AND METHODS

Inclusion and Exclusion Criteria of Participants

The clinical data used in the present study were obtained from a database that collected demographic data, clinical characteristics, treatments, and follow-ups of all patients with OSCC who were primary diagnosed and surgically treated at Nanjing Stomatological Hospital from 2012 to 2015.

The inclusion criteria for the study were as follows: (1) primary OSCC without any previous treatment; (2) tumor resected completely by surgical ablation and neck lymph node dissection (if necessary); and (3) availability of complete follow-up data, including survival, metastasis, and cause of death. Patients who met the following conditions were excluded: (1) patients with incomplete clinical and laboratory data; (2) patients who received chemotherapy or radiotherapy prior to surgery; (3) patients who were diagnosed with nonsquamous carcinoma, such as adenoid cystic carcinoma and mucoepidermoid carcinoma; and (4) patients with blood and lymphatic system disorders.

Data Collection

Patients underwent standard workups according to the OSCC clinical pathway. Before the operation, a record of a clear medical history, a complete physical examination, results of laboratory and hematological investigations, results of cone beam computed tomography (CBCT) or head and neck computed tomography, and chest radiographs were obtained. Tumors were excised with adequate margins under intraoperative frozen-section control, and pathological TNM classification was performed according to the American Joint Committee on Cancer (AJCC) Staging Manual (7th Edition).

For each patient, the following information was obtained: age, sex, T stage, N stage, M stage, relapse, lesion site, smoking status, and survival status. The lymphocyte count, monocyte count, neutrophil count, and white blood cell count were retrieved from preoperative blood tests; the NLR, LMR, NWR, and LWR were further derived from these values. All patients were regularly followed up bimonthly until August 31, 2018. Recurrence was

defined as the presence of tumors with similar histological characteristics after treatment. Metastasis was defined as tumor recurrence within distant organs.

Ethics

This study was approved by the Ethics Committee of Nanjing Stomatological Hospital, Medical School of Nanjing University (2015NL-018KS), and written informed consent was obtained from the patients or their families.

Statistical Analysis

The endpoints of this study included OS (time between diagnosis and death from any cause), DFS (time between end of primary treatment to recurrence/second primary/last follow-up), and MFS (time between diagnosis and the occurrence of distant metastasis).

The associations between the NLR, LMR, NWR, LWR, and clinicopathological parameters were evaluated by the Chi-square test. The continuous variables NLR, LMR, NWR, and LWR were analyzed as dichotomous variables according to the optimal cutoff value. The associations of the NLR, LMR, NWR, and LWR with the state of metastasis were judged by Student's t test. Patients' clinical endpoints were calculated using Kaplan-Meier curves and compared by the log-rank test. Backward stepwise multivariate Cox proportion analysis was performed to determine the influence of age, sex, TNM stage, nodal status, metastasis, smoking, NLR, LMR, NWR, and LWR on OS, DFS, and MFS. The results from the Cox analysis are reported as relative risks with the corresponding 95% confidence intervals (CIs). Statistical analyses were performed with SPSS software (version 19, SPSS Inc., Chicago, IL, USA). $P < 0.05$ was considered statistically significant.

TABLE 1 | Clinico-pathological characteristics of patients with OSCC.

Characteristics	*N* = 493	Percentage (%)
Age (years)		
<60	208	42.2
≥60	285	57.8
Gender		
Male	261	52.9
Female	232	47.1
Smoking		
Yes	132	27
No	361	73
Tumor size		
T1	164	33.3
T2	246	49.9
T3	34	6.9
T4	49	9.9
Lymph node status		
N0	352	71.4
N1	88	17.8
N2	53	10.8
N3	0	0
Relapse		
Yes	30	6.1
No	463	93.9
Metastasis		
Yes	44	8.9
No	449	91.1
Site of the lesions		
Tongue	218	44.2
Buccal mucosa	121	24.6
Gingiva	88	17.8
Floor of the mouth	34	6.9
Palate	20	4.1
Lip	12	2.4
Survival status		
Alive	416	84.4
Dead	77	15.6

RESULTS

Patient Characteristics

A total of 493 patients fulfilled the inclusion criteria of this study, and all their clinicopathological characteristics are presented in **Table 1**. Briefly, there were a total of 261 males and 232 females; among whom 208 patients were <60 years old, 285 patients were ≥ 60 years old, and 132 patients had a smoking habit, and 361 patients did not. According to tumor stage, a total of 164 (33.3%) cases were T1 (tumor diameter ≤ 2 cm), 246 (49.9%) were T2 (2 cm < tumor diameter ≤ 4 cm), 34 (6.9%) were T3 (tumor diameter > 4 cm), and 49 (9.9%) were T4 (the tumor spread to the surrounding structure). Among the 493 patients, 30 had local relapse, and 44 had distant metastasis. Until the last follow-up, 416 (84.4%) patients remained alive, whereas 77 (15.6%) patients died due to disease recurrence, metastasis, or other reasons. All data are shown in the **Table 1**.

Associations of Serum Biomarkers With Clinicopathological Characteristics of Patients With OSCC

In the present study, patients were stratified using optimum cutoff values for the NLR (2.9), LMR (3.4), NWR (0.67), and LWR (0.23), which were determined according to the highest χ^2 value defined by Kaplan-Meier survival analysis and log-rank tests. The associations of the above hematological parameters with the clinicopathological characteristics of patients with OSCC are shown in **Table 2**. Older age was associated more with a high NLR (P=0.01) and low LWR (P=0.005). Males were more strongly associated with a high NLR (P=0.01), high NWR (P=0.031), low LMR (P<0.001), and low LWR (P=0.003) than females. Both a high NLR and high NWR were demonstrated to be associated with the presence of metastasis (P=0.031 and P<0.001, respectively), while a low LWR was demonstrated to be associated with the presence of metastasis (P=0.012).

Associations of the NLR, LMR, NWR, and LWR With the State of Metastasis and Survival

Student's t test was used to compare the NLR, LMR, NWR and LWR with the state of metastasis. The results showed that a high NLR and NWR and a low LWR were associated with metastasis (P<0.05) (**Figure 1**). To evaluate the prognostic values of the NLR, LMR, NWR, and LWR on OS (**Figure 2**), DFS (**Figure 3**), and MFS (**Figure 4**), the Kaplan-Meier method was used. The analysis of the results revealed that patients with a high NLR (P<0.001) or NWR (P<0.001) had significantly worse OS, while

TABLE 2 | Associations of NLR, LMR, NWR, and LWR with clinicopathological characteristics.

Parameter	NLR			LMR			NWR			LWR		
	Low n (%)	High n (%)	*P*-Value	Low n (%)	High n (%)	*P*-Value	Low n (%)	High n (%)	*P*-Value	Low n (%)	High n (%)	*P*-Value
Age (years)												
< 60	168 (45.5)	40 (32.3)	**0.01**	45 (436.3)	163 (44.2)	0.124	165 (44.7)	43 (34.7)	0.05	39 (31.5)	169 (45.8)	**0.005**
≥ 60	201 (54.5)	84 (67.7)		79 (63.7)	206 (55.8)		204 (55.3)	81 (65.3)		85 (68.5)	200 (54.2)	
Gender												
Male	183 (49.6)	78 (62.9)	**0.01**	87 (70.2)	174 (47.2)	**<0.001**	185 (50.1)	76 (61.3)	**0.031**	80 (64.5)	181 (49.1)	**0.003**
Female	186 (50.4)	46 (37.1)		37 (29.8)	195 (52.8)		184 (49.9)	48 (38.7)		44 (35.5)	188 (50.9)	
Tumor size												
T1-T2	313 (84.8)	97 (78.2)	0.089	102 (82.3)	308 (83.5)	0.093	313 (84.8)	97 (78.2)	0.089	99 (79.8)	311 (84.3)	0.253
T3-T4	56 (15.2)	27 (21.8)		22 (17.7)	61 (16.5)		56 (15.2)	27 (21.8)		25 (20.2)	58 (15.7)	
Lymph node stage												
N0	268 (72.6)	83 (66.9)	0.226	82 (66.1)	269 (72.9)	0.605	264 (71.5)	87 (70.2)	0.769	81 (65.3)	270 (73.2)	0.095
N1-N3	101 (27.4)	41 (33.1)		42 (33.9)	100 (27.1)		105 (28.5)	37 (29.8)		43 (34.7)	99 (26.8)	
Relapse												
No	347 (94.0)	116 (93.5)	0.884	115 (92.7)	348 (94.3)	0.528	347 (94.0)	116 (93.5)	0.884	116 (93.5)	347 (94.0)	0.844
Yes	22 (6.0)	8 (6.5)		9 (7.3)	21 (5.7)		22 (6.0)	8 (6.5)		8 (6.5)	22 (6.0)	
Metastasis												
No	342 (92.7)	107 (86.3)	**0.031**	108 (87.1)	341 (92.4)	0.072	341 (88.1)	108 (75.0)	**<0.001**	106 (85.5)	343 (93.0)	**0.012**
Yes	27 (7.3)	17 (13.7)		16 (12.9)	28 (7.6)		28 (11.9)	16 (25.0)		18 (14.5)	26 (7.0)	

NLR, neutrophil-to-lymphocyte ratio; LMR, lymphocyte-to-monocyte ratio; NWR, neutrophil-to-white blood cell ratio; LWR, lymphocyte-to- white blood cell ratio.
Bold indicates statistical significance.

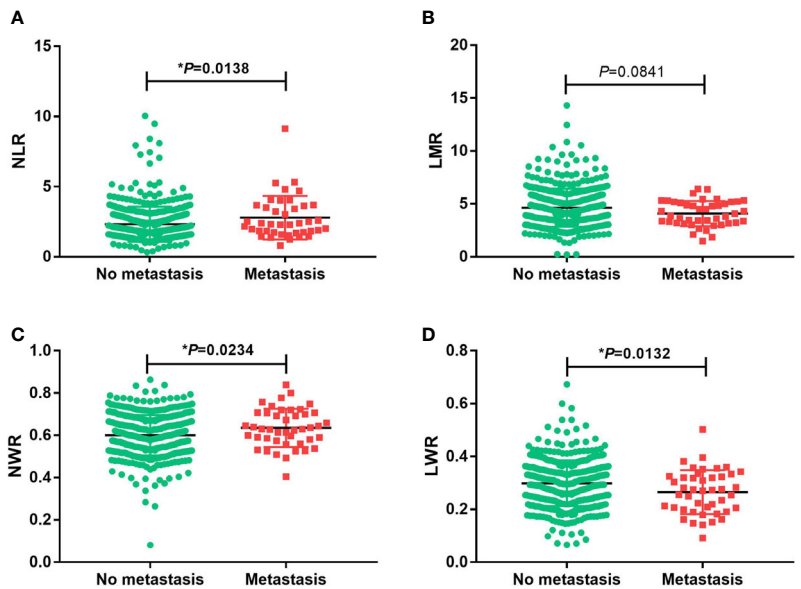

FIGURE 1 | Associations of the prognostic values with the state of metastasis in oral squamous cell carcinoma. **(A)** neutrophil-to-lymphocyte ratio (NLR), **(B)** lymphocyte-to-monocyte ratio (LMR), **(C)** neutrophil-to-white blood cell ratio (NWR) and **(D)** lymphocyte-to-white blood cell ratio (LWR). Asterisks (*) indicate statistical significance.

those with a high LMR (P<0.001) or LWR (P=0.0016) had better OS. Similar differences were also observed in DFS. **Figure 3** shows that patients with a high NLR (P=0.0014) or NWR (P=0.003) had significantly worse DFS, while those with a high LMR (P<0.001) or LWR (P=0.0012) had better DFS. However, with regard to MFS, only the NLR and LWR were significantly associated with MFS. Specifically, patients with a high NLR and low LWR had significantly poor MFS (P=0.021 and 0.008, respectively).

Univariate and Multivariate Analyses of Prognostic Factors

To further verify the prognostic values of the NLR, LMR, NWR, and LWR, univariate and multivariate analyses of OS, DFS and MFS were performed. As shown in **Table 3**, the univariate analysis demonstrated that nodal status (P<0.001), metastasis (P<0.001), the NLR (P=0.001), the LMR (P<0.001), the NWR (P=0.001), and the LWR (P=0.002) were significantly associated

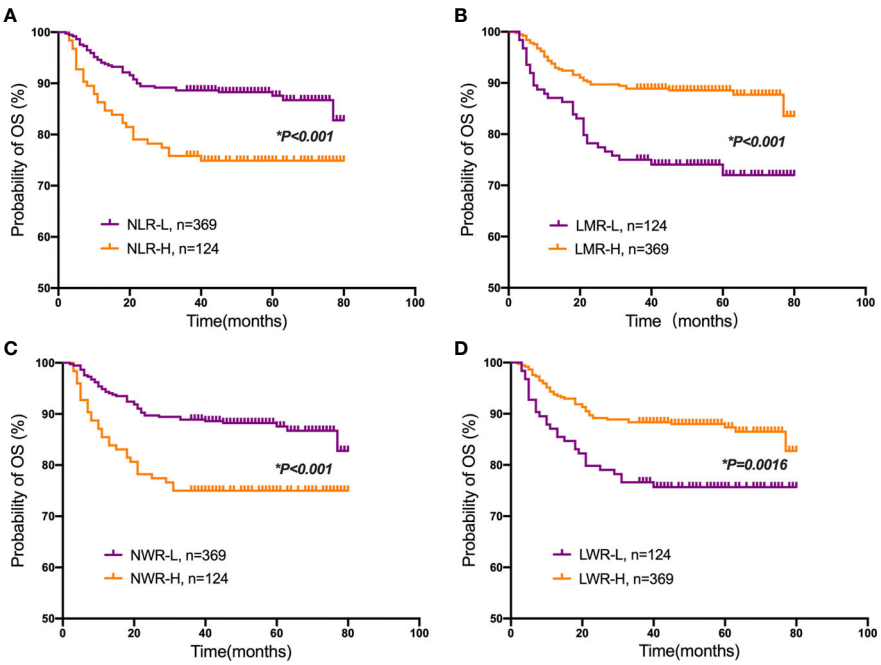

FIGURE 2 | Kaplan-Meier plots for the probability of overall survival (OS). OS rates of the patient subgroups stratified by the **(A)** neutrophil-to-lymphocyte ratio (NLR), **(B)** lymphocyte-to-monocyte ratio (LMR), **(C)** neutrophil-to-white blood cell ratio (NWR) and **(D)** lymphocyte-to-white blood cell ratio (LWR). Asterisks (*) indicate statistical significance.

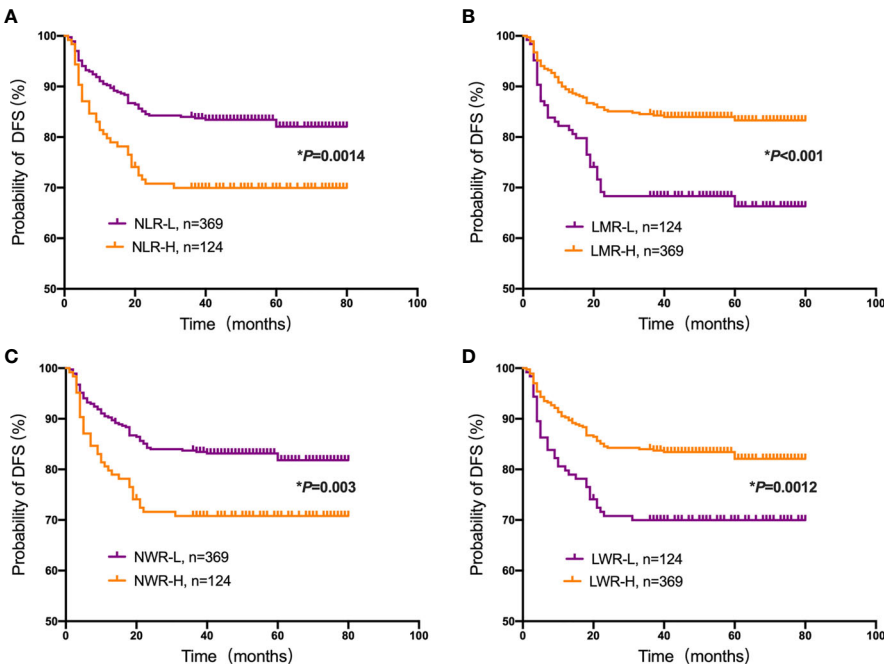

FIGURE 3 | Kaplan-Meier plots for the probability of disease-free survival (DFS). DFS rates of the patient subgroups stratified by the **(A)** neutrophil-to-lymphocyte ratio (NLR), **(B)** lymphocyte-to-monocyte ratio (LMR), **(C)** neutrophil-to-white blood cell ratio (NWR) and **(D)** lymphocyte-to-white blood cell ratio (LWR). Asterisks (*) indicate statistical significance.

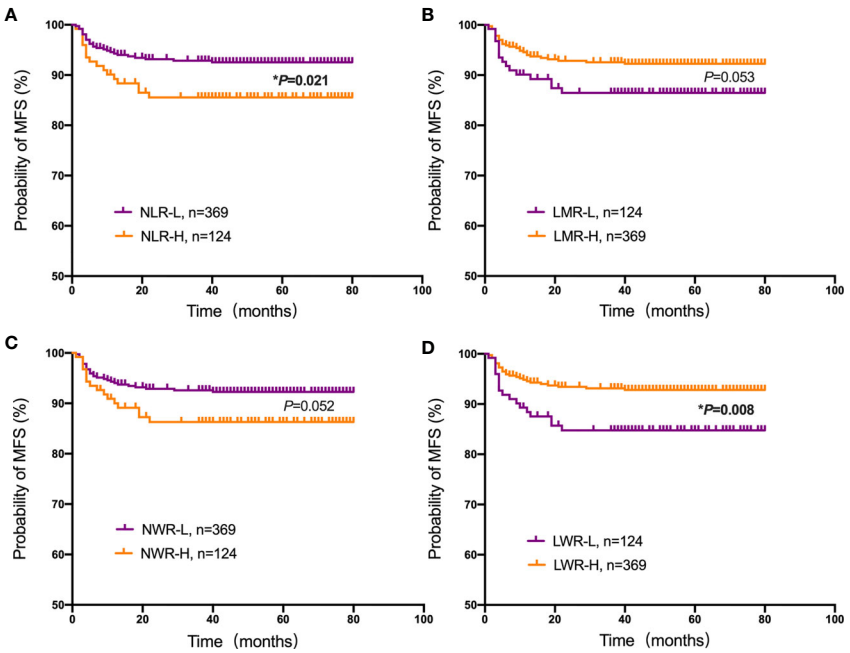

FIGURE 4 | Kaplan-Meier plots for the probability of metastasis-free survival (MFS). MFS rates of the patient subgroups stratified by the **(A)** neutrophil-to-lymphocyte ratio (NLR), **(B)** lymphocyte-to-monocyte ratio (LMR), **(C)** neutrophil-to-white blood cell ratio (NWR) and **(D)** lymphocyte-to-white blood cell ratio (LWR). Asterisks (*) indicate statistical significance.

TABLE 3 | Univariate and multivariate analysis for OS.

Parameter	Univariate analysis		Multivariate analysis	
	HR (95%CI)	*P*-Value	HR (95%CI)	*P*-Value
Age (years): ≥60 *vs.* <60	1.505 (0.938-2.414)	0.090		0.215
Gender: female *vs.* male	1.079 (0.690-1.686)	0.740		0.633
Tumor size: T3-T4 *vs.* T1-T2	1.304 (0.752-2.261)	0.345		0.520
Nodal status: N+ *vs.* N0	3.297 (2.106-5.161)	**<0.001**	2.912 (1.853- 4.575)	**<0.001**
Metastasis: Yes *vs.* No	9.371 (5.883-14.925)	**<0.001**	8.008 (4.988-12.857)	**<0.001**
Smoking: Yes *vs.* No	0.834 (0.492-1.414)	0.500		0.205
NLR: ≥2.9 *vs.* <2.9	2.173 (1.378-3.427)	**0.001**		0.437
LMR: <3.4 *vs.* ≥3.4	0.414 (0.263-0.650)	**<0.001**	0.532 (0.336-0.840)	**0.007**
NWR: ≥0.67 *vs.* <0.67	2.196 (1.392-3.463)	**0.001**		0.147
LWR: ≥0.23 *vs.*< 0.23	0.486 (0.308-0.769)	**0.002**		0.677

OS, overall survival; NLR, neutrophil-to-lymphocyte ratio; LMR, lymphocyte-to-monocyte ratio; NWR, neutrophil-to-white blood cell ratio; LWR, lymphocyte-to- white blood cell ratio; HR, hazard ratio; CI, confidence interval.

Bold indicates statistical significance.

Adjusted for age, gender, tumor size, nodal status, metastasis, smoking in logistic regression models.

with OS. Subsequently, these parameters were further analyzed with multivariate Cox regression analysis, and the results revealed that nodal status (hazard ratio [HR]=2.912, 95% CI=1.853-4.575, p<0.001), metastasis (HR=8.008, 95% CI=4.988-12.857, *P*<0.001), and the LMR (HR=0.532, 95% CI=0.336-0.840, *P*=0.007) were significantly associated with OS, indicating that nodal status, metastasis, and the LMR are independent prognostic factors for OS.

For DFS, the univariate analysis showed that nodal status (*P*<0.001), metastasis (*P*<0.001), the NLR (*P*=0.002), the LMR (*P*<0.001), the NWR (*P*=0.004), and the LWR (*P*=0.002) were significantly associated with prognosis (**Table 4**). However, only nodal status (HR=1.960, 95% CI=1.316-2.919, *P*=0.001), metastasis (HR=21.561, 95% CI=13.878-33.496, *P*<0.001) and the LMR (HR=0.609, 95% CI=0.406-0.915, *P*=0.017) remained significant, indicating that nodal status, metastasis and the LMR are independent prognostic factors for DFS in OSCC patients.

The univariate analysis shown in **Table 5** revealed that nodal status (*P*=0.04), the NLR (*P*=0.024) and the LWR (*P*=0.009) were significantly associated with MFS. However, in the multivariate analyses using the Cox proportional hazards model for MFS, only the LWR (HR=0.451, 95% CI=0.247-0.823, *P*=0.009) was identified as a significant prognostic factor.

TABLE 4 | Univariate and multivariate analysis for DFS.

Parameter	Univariate analysis		Multivariate analysis	
	HR (95%CI)	*P*-Value	HR (95%CI)	*P*-Value
Age (years): ≥60 *vs.* <60	1.178 (0.788-1.761)	0.424		0.831
Gender: female *vs.* male	1.073 (0.725-1.588)	0.724		0.505
Tumor size: T3-T4 *vs.* T1-T2	1.077 (0.647-1.794)	0.776		0.673
Nodal status: N+ *vs.* N0	2.410 (1.626-3.573)	**<0.001**	1.960 (1.316-2.919)	**0.001**
Metastasis: Yes *vs.* No	24.460 (15.864-37.715)	**<0.001**	21.561 (13.878-33.496)	**<0.001**
Smoking: Yes *vs.* No	0.968 (0.619-1.514)	0.887		0.336
NLR: ≥2.9 *vs.* <2.9	1.914 (1.275-2.872)	**0.002**		0.932
LMR: <3.4 *vs.* ≥3.4	0.460 (0.308-0.686)	**<0.001**	0.609 (0.406-0.915)	**0.017**
NWR: ≥0.67 *vs.* <0.67	1.831 (1.217-2.755)	**0.004**		0.940
LWR: ≥0.23 *vs.* < 0.23	0.520 (0.346-0.780)	**0.002**		0.670

DFS, disease free survival; NLR, neutrophil-to-lymphocyte ratio; LMR, lymphocyte-to-monocyte ratio; NWR, neutrophil-to-white blood cell ratio; LWR, lymphocyte-to- white blood cell ratio; HR, hazard ratio; CI, confidence interval.

Bold indicates statistical significance.

Adjusted for age, gender, tumor size, nodal status, metastasis, smoking in logistic regression models.

TABLE 5 | Univariate and multivariate analysis for MFS.

Parameter	Univariate analysis		Multivariate analysis	
	HR (95%CI)	*P*-Value	HR (95%CI)	*P*-Value
Age (years): ≥60 *vs.* <60	1.804 (0.944-3.447)	0.074		0.131
Gender: female *vs.* male	1.125 (0.623-2.032)	0.695		0.455
Tumor size: T3-T4 *vs.* T1-T2	0.782 (0.331-1.850)	0.576		0.501
Nodal status: N+ *vs.* N0	1.877 (1.029-3.425)	**0.040**		0.058
Smoking: Yes *vs.* No	0.902 (0.456-1.784)	0.766		0.723
NLR: ≥2.9 *vs.* <2.9	2.008 (1.094-3.685)	**0.024**		0.429
LMR:<3.4 *vs.* ≥3.4	0.551 (0.298-1.019)	0.058		0.641
NWR: ≥0.67 *vs.* <0.67	1.817 (0.983-3.359)	0.057		0.708
LWR: ≥0.23 *vs.*< 0.23	0.451 (0.247-0.823)	**0.009**	0.451 (0.247-0.823)	**0.009**

MFS, metastasis free survival; NLR, neutrophil-to-lymphocyte ratio; LMR, lymphocyte-to-monocyte ratio; NWR, neutrophil-to-white blood cell ratio; LWR, lymphocyte-to- white blood cell ratio; HR, hazard ratio; CI, confidence interval.

Bold indicates statistical significance.

Adjusted for age, gender, tumor size, nodal status, metastasis, smoking in logistic regression models.

DISCUSSION

OSCC is a highly malignant tumor type (18), and the development of effective methods to diagnose and treat OSCC represents an urgent task (19). Inflammation is a basic and important pathologic response of the body triggered by damage that can occur alone or accompany tumors (20). Carcinogenesis not only recruits WBCs to and around neoplasms but also causes tissue damage through physical and chemical mechanisms, leading to wide, nonspecific inflammatory responses and systemic inflammatory responses (21). Thus, changes the counts and component proportions of white blood cells (WBCs) are changed. In the present study, the clinicopathological characteristics, follow-up data, and various peripheral blood component ratios of 493 patients with OSCC were analyzed to verify the correlations between cancer-associated systemic inflammation and OSCC outcomes. We found that a high NLR and low LWR were associated with older age. We also found that males were more strongly associated with a high NLR, high NWR, low LMR, and low LWR than females, consistent with previous studies (22). In addition, a high NLR, high NWR and low LWR were found to be associated with the presence of metastasis. However, relationships between serum biomarkers and other clinicopathological characteristics, including tumor stage, lymph node stage and relapse, were not found. This suggests that the predictive effect of the NLR, NWR, LMR and LWR may be independent of the TNM staging system. We can use these serum biomarkers to complement the diagnosis of OSCC, to evaluate prognosis and to assess treatment.

Regarding cancer-associated inflammatory responses, a previous study demonstrated a moderate correlation between monocytes and neutrophils, as they both have a negative impact on the prognosis of patients with oropharyngeal cancer, whereas lymphocytes have the opposite effect (23). The NLR, which reflects the balance between a protumor inflammatory status and an antitumor immune status, is the most widely used parameter for prognostic prediction. Most studies have reported that an increased NLR is related to worse disease control and poor survival (24–26). Similarly, in the current study, we also observed that patients with a high NLR were associated with a significant downward trend of survival probability according to the 80-month Kaplan-Meier curves for OS, DFS and MFS. Unfortunately, the multivariate analysis demonstrated that the NLR is not an

independent prognostic factor for OS, DFS or MFS. The LWR is another predictive biomarker related to the prognosis of various cancers, including gastric cancer and non-small-cell lung cancer (27, 28). However, we did not find any literature reporting an association between the LWR and OSCC. According to the results of the univariate and multivariate analyses in our study, the LWR is an independent prognostic factor for MFS. This might be the first report to state a cutoff value for the LWR in predicting metastasis and demonstrated that a low LWR is a poor prognostic factor in patients with OSCC. The prognostic value of the LMR has been investigated by many schoolers while studying various cancers, including breast, lung, esophageal, gastric, colorectal, pancreatic, bladder, and cervical cancers (29). Lin et al. studied 256 patients with newly diagnosed metastatic nasopharyngeal carcinoma who received chemotherapy and found that a high LMR was associated with a good prognosis (30). The data of our study demonstrate that the LMR is the only serum biomarker independently related to both OS and DFS (according to the multivariate analysis).

Based on upon evidence, we speculate that the NLR, NWR, and LWR might affect the survival rate in an indirect way (*i.e.*, by relating to poor clinicopathological manifestations or promoting the migration of cancer cells), while the LMR directly reflects patient survival duration after treatment. Although the underlying mechanisms of the relationship between the LMR and prognosis are not well understood, the LMR is thought to reflect the balance between the prognosis-improving effect of lymphocytes and the adverse effect of monocytes.

According to previous studies, the prognosis of OSCC is highly heterogeneous, with an overall 5-year survival rate of approximately 64%, and the median survival duration for patients with locoregionally recurrent or metastatic OSCC is 8~10 months (31, 32). Oral malignancies progress through four stages; in the early stage (stages I and II), the 5-year survival rate is approximately 80%. However, it is reduced to approximately 50% in patients with locoregional metastasis (stages III, IVA, and IVB) and approximately 25% if distant metastasis is present (stage IVC) (33, 34). Therefore, it is of great significance to understand the relationship between metastasis and inflammatory cells in predicting the prognosis of OSCC. In general, metastasis comprises the sequential occurrence of uncontrolled cancer cell proliferation, invasion into the blood or lymph circulation, and crosstalk with various components of the new microenvironment, including parenchymal, stromal and inflammatory cells. However, the precise mechanism of the process has not yet been clarified, and the factors affecting its occurrence are mostly uncertain. Based on the above results, lymph node metastasis is closely correlated with poor survival, and it was also proven in our study that metastasis is an independent predictor for poor survival. In addition, we found that a high NLR and NWR and a low LWR were associated with metastasis, whereas the LWR was an independent prognostic factor for predicting MFS. If these results can be verified by further evidence, patients who have a high risk of metastasis will receive direct benefits.

We enrolled 493 patients in the present study, with the longest follow-up exceeding 80 months. The main strength of the current study was that a large number of patients treated at a single institution were included, with a relatively long follow-up duration, and data were collected by using uniform database templates to ensure consistency, which improved the quality of the evidence. However, some inherent limitations were inevitable because of its retrospective nature. For example, patients who had blood or lymphatic system disorders were excluded because of a strict eligibility criterion, which may have caused patient selection bias. In addition, the therapy strategies were not uniform but varied based on the patient's condition, and the effect of different treatment-related factors on prognosis was not evaluated. Therefore, a prospective study designed to confirm the prognostic value of the pretreatment NLR, LMR, NWR, and LWR is needed. Despite the limitations of this study, pretreatment serum biomarkers can be quick, simple, easily obtainable, and cost-effective tools to predict the outcome of OSCC.

CONCLUSION

The results of this study showed that OSCC patients with a high LMR and low NWR had prolonged OS and DFS, while a high NLR and low LWR were associated with poor OS, DFS and MFS. Moreover, once the prognostic significance of these novel markers is defined and verified by researchers, they can be widely applied in the clinic and help doctors identify patients at high risk for disease recurrence and tumor progression.

DATA AVAILABILITY STATEMENT

The original contributions presented in the study are included in the article/supplementary material. Further inquiries can be directed to the corresponding authors.

ETHICS STATEMENT

The studies involving human participants were reviewed and approved by Ethics Committee of Nanjing Stomatological Hospital, Medical School of Nanjing University. The patients/participants provided their written informed consent to participate in this study.

AUTHOR CONTRIBUTIONS

The authors contributed in the following manner: Study conception and design: YM and YN. Acquisition of data: YS, JJ, and MT. Statistical analysis: MD, YS, and CZ. Manuscript preparation: MD. English editing: QL. Critical manuscript revision: LD and HD. MD and YS contributed equally to this work. All authors contributed to the article and approved the submitted version.

FUNDING

The authors are grateful for grants from the National Natural Science Foundation of China (Nos. 81371680, 81571800, and 81772880), the Development of Science and Technology of

Nanjing (No. 201803036), Jiangsu Provincial Medical Talent (No. ZDRCC2016016), the Nanjing Medical Science and Technique Development Foundation (QRX17083, ZKX18035), YKK18124, YKK20151, and YKK19094).

REFERENCES

1. Li Q, Dong H, Yang G, Song Y, Mou Y, Ni Y. Mouse Tumor-Bearing Models as Preclinical Study Platforms for Oral Squamous Cell Carcinoma. *Front Oncol* (2020) 10:212. doi: 10.3389/fonc.2020.00212
2. Du M, Nair R, Jamieson L, Liu Z, Bi P. Incidence Trends of Lip, Oral Cavity, and Pharyngeal Cancers: Global Burden of Disease 1990-2017. *J Dent Res* (2020) 99:143–51. doi: 10.1177/0022034519894963
3. Ferrari E, Pezzi ME, Cassi D, Pertinhez TA, Spisni A, Meleti M. Salivary Cytokines as Biomarkers for Oral Squamous Cell Carcinoma: A Systematic Review. *Int J Mol Sci* (2021) 22:6795. doi: 10.3390/ijms22136795
4. Siegel RL, Miller KD, Jemal A. Cancer Statistics, 2020. *CA Cancer J Clin* (2020) 70:7–30. doi: 10.3322/caac.21590
5. Patel SG, Shah JP. TNM Staging of Cancers of the Head and Neck: Striving for Uniformity Among Diversity. *CA Cancer J Clin* (2005) 55:242–58; quiz 261-2, 264. doi: 10.3322/canjclin.55.4.242
6. Zhou J, Li H, Cheng B, Cao R, Zou F, Yang D, et al. Derivation and Validation of a Prognostic Scoring Model Based on Clinical and Pathological Features for Risk Stratification in Oral Squamous Cell Carcinoma Patients: A Retrospective Multicenter Study. *Front Oncol* (2021) 11:652553. doi: 10.3389/fonc.2021.652553
7. Pollaers K, Hinton-Bayre A, Friedland PL, Farah CS. AJCC 8th Edition Oral Cavity Squamous Cell Carcinoma Staging - Is it an Improvement on the AJCC 7th Edition? *Oral Oncol* (2018) 82:23–8. doi: 10.1016/j.oraloncology.2018.04.018
8. Almangush A, Bello IO, Heikkinen I, Hagstrom J, Haglund C, Kowalski LP, et al. Improving Risk Stratification of Early Oral Tongue Cancer With TNM-Immune (TNM-I) Staging System. *Cancers (Basel)* (2021) 13:3235. doi: 10.3390/cancers13133235
9. Mascitti M, Togni L, Rubini C, Troiano G, Lo Muzio L, Santarelli A. Tumour-Associated Tissue Eosinophilia (TATE) in Oral Squamous Cell Carcinoma: A Comprehensive Review. *Histol Histopathol* (2021) 36:113–22. doi: 10.14670/HH-18-250
10. Takahashi H, Sakakura K, Tada H, Kaira K, Oyama T, Chikamatsu K. Prognostic Significance and Population Dynamics of Peripheral Monocytes in Patients With Oropharyngeal Squamous Cell Carcinoma. *Head Neck* (2019) 41:1880–8. doi: 10.1002/hed.25625
11. Kagedal A, Rydberg Millrud C, Hayry V, Kumlien Georen S, Lidegran M, Munck-Wikland E, et al. Oropharyngeal Squamous Cell Carcinoma Induces an Innate Systemic Inflammation, Affected by the Size of the Tumour and the Lymph Node Spread. *Clin Otolaryngol* (2018) 43:1117–21. doi: 10.1111/coa.13122
12. Tsai YD, Wang CP, Chen CY, Lin LW, Hwang TZ, Lu LF, et al. Pretreatment Circulating Monocyte Count Associated With Poor Prognosis in Patients With Oral Cavity Cancer. *Head Neck* (2014) 36:947–53. doi: 10.1002/hed.23400
13. Diao P, Wu Y, Ge H, Li J, Zhang W, Huang R, et al. Preoperative Circulating Platelet, Neutrophil, and Lymphocyte Counts Predict Survival in Oral Cancer. *Oral Dis* (2019) 25:1057–66. doi: 10.1111/odi.13049
14. Ren L, Chen D, Xu W, Xu T, Wei R, Suo L, et al. Predictive Potential of Nomogram Based on GMWG for Patients With Hepatocellular Carcinoma After Radical Resection. *BMC Cancer* (2021) 21:817. doi: 10.1186/s12885-021-08565-2
15. Kuramochi H, Yamada T, Yoshida Y, Matsuda A, Kamiyama H, Kosugi C, et al. The Pre-Treatment Lymphocyte-To-Monocyte Ratio Predicts Efficacy in Metastatic Colorectal Cancer Treated With TAS-102 and Bevacizumab. *Anticancer Res* (2021) 41:3131–7. doi: 10.21873/anticanres.15098
16. Aoyama T, Takano M, Miyamoto M, Yoshikawa T, Kato K, Sakamoto T, et al. Pretreatment Neutrophil-To-Lymphocyte Ratio Was a Predictor of Lymph Node Metastasis in Endometrial Cancer Patients. *Oncology* (2019) 96:259–67. doi: 10.1159/000497184
17. Zhu Z, Gao J, Liu Z, Li C, Xue Y. Preoperative Platelet-To-Lymphocyte Ratio (PLR) for Predicting the Survival of Stage I-III Gastric Cancer Patients With a MGC Component. *BioMed Res Int* (2021) 2021:9678363. doi: 10.1155/2021/9678363
18. Dong H, Su H, Chen L, Liu K, Hu HM, Yang W, et al. Immunocompetence and Mechanism of the DRibble-DCs Vaccine for Oral Squamous Cell Carcinoma. *Cancer Manag Res* (2018) 10:493–501. doi: 10.2147/CMAR.S155914
19. Yang D, Chen F, He S, Shen H, Hu Y, Feng N, et al. One-Pot Growth of Triangular SnS Nanopyramids for Photoacoustic Imaging and Photothermal Ablation of Tumors. *New J Chem* (2019) 43:13256–62. doi: 10.1039/C9NJ03045J
20. Chen L, Kong X, Yan C, Fang Y, Wang J. The Research Progress on the Prognostic Value of the Common Hematological Parameters in Peripheral Venous Blood in Breast Cancer. *Onco Targets Ther* (2020) 13:1397–412. doi: 10.2147/OTT.S227171
21. Li L, Yu R, Cai T, Chen Z, Lan M, Zou T, et al. Effects of Immune Cells and Cytokines on Inflammation and Immunosuppression in the Tumor Microenvironment. *Int Immunopharmacol* (2020) 88:106939. doi: 10.1016/j.intimp.2020.106939
22. Grimm M, Rieth J, Hoefert S, Krimmel M, Rieth S, Teriete P, et al. Standardized Pretreatment Inflammatory Laboratory Markers and Calculated Ratios in Patients With Oral Squamous Cell Carcinoma. *Eur Arch Otorhinolaryngol* (2016) 273:3371–84. doi: 10.1007/s00405-016-3950-4
23. Huang SH, Waldron JN, Milosevic M, Shen X, Ringash J, Su J, et al. Prognostic Value of Pretreatment Circulating Neutrophils, Monocytes, and Lymphocytes in Oropharyngeal Cancer Stratified by Human Papillomavirus Status. *Cancer* (2015) 121:545–55. doi: 10.1002/cncr.29100
24. Schwartz PB, Poultsides G, Roggin K, Howard JH, Fields RC, Clarke CN, et al. PLR and NLR Are Poor Predictors of Survival Outcomes in Sarcomas: A New Perspective From the USSC. *J Surg Res* (2020) 251:228–38. doi: 10.1016/j.jss.2020.01.008
25. Duan J, Pan L, Yang M. Preoperative Elevated Neutrophil-to-Lymphocyte Ratio (NLR) and Derived NLR are Associated With Poor Prognosis in Patients With Breast Cancer: A Meta-Analysis. *Med (Baltimore)* (2018) 97:e13340. doi: 10.1097/MD.0000000000013340
26. Nam KW, Kim TJ, Lee JS, Kwon HM, Lee YS, Ko SB, et al. High Neutrophil-To-Lymphocyte Ratio Predicts Stroke-Associated Pneumonia. *Stroke* (2018) 49:1886–92. doi: 10.1161/STROKEAHA.118.021228
27. Feng F, Sun L, Zheng G, Liu S, Liu Z, Xu G, et al. Low Lymphocyte-to-White Blood Cell Ratio and High Monocyte-to-White Blood Cell Ratio Predict Poor Prognosis in Gastric Cancer. *Oncotarget* (2017) 8:5281–91. doi: 10.18632/oncotarget.14136
28. Yuan C, Li N, Mao X, Liu Z, Ou W, Wang SY. Elevated Pretreatment Neutrophil/White Blood Cell Ratio and Monocyte/Lymphocyte Ratio Predict Poor Survival in Patients With Curatively Resected Non-Small Cell Lung Cancer: Results From a Large Cohort. *Thorac Cancer* (2017) 8:350–8. doi: 10.1111/1759-7714.12454
29. Pan YC, Jia ZF, Cao DH, Wu YH, Jiang J, Wen SM, et al. Preoperative Lymphocyte-to-Monocyte Ratio (LMR) Could Independently Predict Overall Survival of Resectable Gastric Cancer Patients. *Med (Baltimore)* (2018) 97:e13896. doi: 10.1097/MD.0000000000013896
30. Lin GN, Peng JW, Liu DY, Xiao JJ, Chen YQ, Chen XQ. Increased Lymphocyte to Monocyte Ratio Is Associated With Better Prognosis in Patients With Newly Diagnosed Metastatic Nasopharyngeal Carcinoma Receiving Chemotherapy. *Tumour Biol* (2014) 35:10849–54. doi: 10.1007/s13277-014-2362-6
31. Beltramini GA, Belloni LM, Fusco N, Sacconi A, Muti P, Baj A, et al. Comparing Prognostic Utility Between the 8th Edition of TNM Staging System and the Lymph Node Ratio for Oral Squamous Cell Carcinoma. *Head Neck* (2021). doi: 10.1002/hed.26769
32. Bai XX, Zhang J, Wei L. Analysis of Primary Oral and Oropharyngeal Squamous Cell Carcinoma in Inhabitants of Beijing, China-A 10-Year

Continuous Single-Center Study. *BMC Oral Health* (2020) 20:208. doi: 10.1186/s12903-020-01192-6
33. Gold KA, Lee HY, Kim ES. Targeted Therapies in Squamous Cell Carcinoma of the Head and Neck. *Cancer* (2009) 115:922–35. doi: 10.1002/cncr.24123
34. Mahieu R, den Toom IJ, Boeve K, Lobeek D, Bloemena E, Donswijk ML, et al. Contralateral Regional Recurrence in Lateralized or Paramedian Early-Stage Oral Cancer Undergoing Sentinel Lymph Node Biopsy-Comparison to a Historic Elective Neck Dissection Cohort. *Front Oncol* (2021) 11:644306. doi: 10.3389/fonc.2021.644306

Conflict of Interest: The authors declare that the research was conducted in the absence of any commercial or financial relationships that could be construed as a potential conflict of interest.

Publisher's Note: All claims expressed in this article are solely those of the authors and do not necessarily represent those of their affiliated organizations, or those of the publisher, the editors and the reviewers. Any product that may be evaluated in this article, or claim that may be made by its manufacturer, is not guaranteed or endorsed by the publisher.

frontiers in Oncology

ORIGINAL RESEARCH
published: 06 September 2021
doi: 10.3389/fonc.2021.739103

Residual Volume of Lymph Nodes During Chemoradiotherapy Based Nomogram to Predict Survival of Nasopharyngeal Carcinoma Patient Receiving Induction Chemotherapy

Yan Li†, Jian Zang†, Jingyi Liu, Shanquan Luo, Jianhua Wang, Bingxin Hou, Lina Zhao and Mei Shi**

Department of Radiation Oncology, Xijing Hospital, Fourth Military Medical University, Xi'an, China

OPEN ACCESS

Edited by:
Heming Lu,
People's Hospital of Guangxi Zhuang Autonomous Region, China

Reviewed by:
Ling Guo,
Sun Yat-sen University Cancer Center (SYSUCC), China
Gayani Pitiyage,
University of London, United Kingdom

***Correspondence:**
Mei Shi
mshi82@hotmail.com
Lina Zhao
zhaolinazln@outlook.com

†These authors have contributed equally to this work

Specialty section:
This article was submitted to Head and Neck Cancer, a section of the journal Frontiers in Oncology

Received: *10 July 2021*
Accepted: *16 August 2021*
Published: *06 September 2021*

Citation:
Li Y, Zang J, Liu J, Luo S, Wang J, Hou B, Zhao L and Shi M (2021) Residual Volume of Lymph Nodes During Chemoradiotherapy Based Nomogram to Predict Survival of Nasopharyngeal Carcinoma Patient Receiving Induction Chemotherapy. Front. Oncol. 11:739103. doi: 10.3389/fonc.2021.739103

Purpose: To accurately stratify nasopharyngeal carcinoma (NPC) patients who were benefit from induction chemotherapy (IC) followed by chemoradiotherapy (CCRT), we established residual volume of lymph nodes during chemoradiotherapy based nomogram to predict survival for NPC patients.

Methods: Cox regression analysis were used to evaluate predictive effects of tumor volume parameters. Multivariate Cox regression analysis was used to identify the prognostic factors, and nomogram models were developed to predict survival of NPC patients receiving IC followed by CCRT.

Results: Compared with other tumor volumetric parameters, midRT GTVnd was the best predictive factor for OS (HR: 1.043, 95%CI: 1.031-1.055), PFS (HR: 1.040, 95%CI: 1.030- 1.051), and DMFS (HR: 1.046, 95%CI: 1.034 – 1.059) according to the HR of Cox regression analysis. Based on multivariate analysis, three nomograms included midRT GTVnd were constructed to predict 4-year survival. The C-index of nomograms for each survival endpoints were as follow (training cohort *vs*. validation cohort): 0.746 *vs*. 0.731 for OS; 0.747 *vs*. 0.735 for PFS; 0.768 *vs*. 0.729 for DMFS, respectively. AUC showed a good discriminative ability. Calibration curves demonstrated a consistence between actual results and predictions. Decision curve analysis (DCA) showed that the nomograms had better clinical predictive effects than current TNM staging system.

Conclusion: We identified the best volumetric indicator associated with prognosis was the residual volume of lymph nodes at the fourth week of chemoradiotherapy for patients receiving IC followed by CCRT. We developed and validated three nomograms to predict specific probability of 4-year OS, PFS and DMFS for NPC patient receiving IC followed by CCRT.

Keywords: nasopharyngeal carcinoma, tumor volume, induction chemotherapy, adaptive chemoradiotherapy, nomogram

INTRODUCTION

More than 70% of newly diagnosed NPC are classified as locoregionally advanced disease (1). Based on results of several clinical randomized control studies, induction chemotherapy (IC) followed by concurrent chemoradiotherapy (CCRT) has been recommended as a preferred regimen for locoregionally advanced NPC (LA-NPC) by guideline of National Comprehensive Cancer Network (NCCN) and Chinese Society of Clinical Oncology (CSCO) (2, 3). Unfortunately, approximate 20-30% patients could not benefit from IC-CCRT regime, and the toxicities were increased compared with CCRT (4, 5). Therefore, it's important to identify the patients who could benefit from IC followed by CCRT (4–8).

Emerging evidences show that pretreatment tumor volume is a prognostic factor for disease progression and survival of NPC (9–11). Recent study reported that post IC primary gross tumor and lymph node volume also had prognostic value for overall survival (OS) of LA-NPC (12). The changing rate of primary tumor volume before and after IC has also been demonstrated to predict the survival outcome of NPC (13). However, in clinical practice, tumor with poor response to IC could still respond to chemoradiotherapy and residual tumor with good response to IC could resist to chemoradiotherapy. Because adaptive radiotherapy (ART) can compensate for the dosimetric impacts induced by anatomic and geometric variations in patients, it has been widely used to treat head neck cancer (14, 15). Meanwhile, it also provides opportunity to dynamically evaluate the changing of tumor volume during radiotherapy (16). Several studies found changing of primary tumor volume during CCRT or radiotherapy could impact on patient survival in many cancers (17, 18). With regard to NPC, changing rate of total volume during radiotherapy included primary site and lymph nodes was also reported as a better prognostic factor for NPC patients receiving adaptive CCRT (19). Therefore, the tumor volume change related to IC alone was not adequate for outcomes prediction of NPC patients receiving IC followed by CCRT.

To our knowledge, no study has thus far investigated the detailed volumetric parameters and volume change rate before and after IC as well as during radiotherapy. Therefore, the purpose of the present research was to investigate the predictive volumetric parameters in the whole process of IC followed by CCRT treatment, and further to establish the nomogram to stratify LA-NPC patients who could benefit from IC followed by CCRT.

MATERIALS AND METHODS

Patients

We consecutively reviewed 262 LA-NPC patients at the XiJing Hospital between July 2010 and September 2017. All patients had complete history and physical examinations, blood work and direct fiberoptic nasopharyngoscopy, imaged by computed tomography (CT) and magnetic resonance imaging (MRI) of head and neck, and chest images, abdominal sonography, and whole-body bone scan. Patients were re-staged according to the 8th edition of American Joint Committee for Cancer Staging (AJCC) system. Two radiologists reviewed all the imaging records and disagreements were resolved by consensus. The eligibility criteria in the study included: (1) age≥18 years and Karnofsky performance score ≥70; (2) histologically confirmed newly diagnostic nasopharyngeal squamous cell carcinoma; (3) stages III–IV without distant metastasis; (4) receiving IC+CCRT as initial treatment modality; (5) treated with intensity-modulated radiotherapy (IMRT); (5) re-scanning and re-planning were conducted during chemoradiotherapy. The exclusion criteria included: (1) non-squamous cell carcinoma of nasopharynx; (2) not complete the prescribed course of radiotherapy, (3) without adaptive re-planning during radiotherapy course. Ultimately, a total of 253 patients were included for analysis. The protocol was approved by the appropriate ethical review boards of XiJing hospital, and the study was conducted in accordance with the principles of the Declaration of Helsinki.

Radiation Therapy and Chemotherapy

The treatment planning approaches were described by our previous studies (20–22). In general, patients were immobilized in the supine position with head, neck, and shoulder thermoplastic mask, and CT simulation according to standard procedures. The target of nasopharynx tumor was delineated manually according to MRI before and after chemotherapy and during radiotherapy. For tumor involved cavity, such as nasal cavity, nasopharynx cavity or oropharynx cavity, the delineation would be changed if primary tumor shrunk in these sites after chemotherapy and during radiotherapy. However, the delineation of primary tumor volume was not changed after chemotherapy and during radiotherapy for tumor involved submucosal sites, skull base, cervical vertebra and intracranial extension. The target of lymph node was delineated according to the imaging before and after chemotherapy and during radiotherapy. If changing of lymph node was observed after chemotherapy and during radiotherapy, the target would be modified according to imaging. The prescribed radiation doses were defined as follows: a total of 72.6 Gy in 33 fractions at 2.2 Gy per fraction to the primary tumor of nasopharynx, 66–72.6 Gy to metastatic lymph nodes, 55–60 Gy to high-risk clinical target, and 50 Gy to low-risk clinical target. All patients were treated with 1 fraction daily for 5 days per week. The doses received by each organ at risk (OAR) should be no more than its tolerance (23).

The induction chemotherapy included TP regimen (docetaxel 75mg/m^2, cisplatin 75mg/m^2), GP regimen (gemcitabine 1000mg/m^2, cisplatin 75mg/m^2) and TPF regimen (docetaxel 75mg/m^2, cisplatin 75 mg/m^2, 5-FU 750 mg/m^2 days1 to 5) every 3 weeks for 2–3 cycles. Radiotherapy began at 3 weeks after the last cycle of induction chemotherapy. Concurrent chemotherapy was only consisted of cisplatin (100mg/m^2) every three weeks.

Tumor Volume Measurement

Three simulation CT scans were performed for every patient: before induction chemotherapy, before radiotherapy and the fourth week of radiotherapy. The primary tumor and the metastatic lymph nodes were delineated on simulation CT images according to the MRI and CT fused images. The

volume was automatically measured by Eclipse 10.0 treatment planning system (Varian, CA, USA). The definitions of tumor volume were listed as follows: pre-induction chemotherapy gross primary tumor (preIC GTVnx) and lymph node (preIC GTVnd)、post-induction chemotherapy gross primary tumor (postIC GTVnx) and lymph node (postIC GTVnd), gross primary tumor at fourth week of radiotherapy (midRT GTVnx) and lymph node (midRT GTVnd).

Evaluation and Statistical Analysis

The follow-up time was calculated from the end of treatment to the last follow-up or death. Patients were regularly evaluated every 3 months during the first two years, every 6 months in the third–fifth years, and then once every year thereafter. The endpoints in this study included overall survival (OS), progression-free survival (PFS) and distant metastasis-free survival (DMFS). OS was defined as the time from end of treatment to death; PFS was measured from the end of treatment to the date of disease progression or death from any causes; DMFS, was defined as the time from end of treatment to first detection of distant metastasis.

The clinical features in different groups were evaluated by the Pearson Chi-square or Fisher's test. The hazard ratio (HR) of COX proportional regression is used to re-evaluate the prediction of volumetric parameters. Multivariate Cox proportional hazard regression analysis was conducted to explore significant factors associated with OS, PFS and DMFS, and the proportional-hazards assumption was tested with Schoenfeld residuals. Variable risk was expressed as a hazard ratio (HR) with a corresponding 95% confidence interval (95% CI).

Based on the results of multivariable Cox regression analysis, nomogram models were formulated to predict 4-year OS、PFS and DMFS. The performance of the models was evaluated by ROC analysis and calibration curve using 1000 bootstrap resamples based on the training cohort and validation cohort validity. The value of Concordance index (C-index) and the area under the ROC curve (AUC) were used to evaluate the discriminative ability of nomogram, which ranged from 0.5 to 1.0, with 0.5 indicating a random chance while closer to 1.0 indicating a better ability to correctly discriminate the outcome. Decision curve analysis (DCA) was performed in present study as a method for determining the clinical application value of the prediction models by quantifying the net benefit to the patient under different threshold probabilities, and was applied to compare the predictive validity of the nomogram and 8th edition TNM stage in the training cohort and validation cohort (12, 24). Statistical analyses were performed using IBM SPSS Statistics (Version 25.0) and R program (version 3.6.3). The statistical tests were two-sided, and a p-value of < 0.05 was considered statistically significant difference.

RESULTS

Patient Characteristics and Survival

The baseline characteristics of 253 LA-NPC patients were listed in **Supplementary Table 1**. There were more men than women (ratio, 2.46:1). The median patient age was 47 years (range:18-70 years). 44.3% (112 of 253) of patients had history of smoking and 29.2% (74 of 253) had history of drinking. Most patients (74.3%) had WHO nonkeratinizing undifferentiated subtype, and the remaining 25.7% of the patients had WHO nonkeratinizing differentiated subtype. Most patients (60.9%) had clinical stage IV disease. EBV DNA copies were detected only in 54 patients (17.8%) using quantitative PCR assay. In total, 73.1% of patients received TP regimen as induction chemotherapy, 22.9% received GP regimen and only 4% received TPF regimen.

At a median follow-up time of 52 months (rang:4-120 months), 66 patients (26.1%) had died, 26 patients (10.3%) experienced locoregional recurrence, 54 patients (21.3%) developed distant metastasis during the follow-up period. The estimated 4-year OS, PFS and DMFS rates were 76.9%, 68.5% and 78.1%, respectively.

Comparison of Predictive Performance of Tumor Volumetric Parameters

The detailed tumor volumetric parameters were shown in **Supplementary Table 2**. As continuous variables, we quantitatively analyzed and compared the prediction performance of different tumor volumetric parameters for OS, PFS and DMFS. Compared with other parameters, midRT GTVnd was the best predictive factor for OS (HR: 1.043, 95%CI: 1.031-1.055), PFS (HR: 1.040, 95%CI: 1.030- 1.051), and DMFS (HR: 1.046, 95%CI: 1.034 – 1.059) (**Table 1**). For the convenience of subsequent analysis, midRT GTVnd as continuous variables were divided into four groups as follow according to interquartile ranges (IQR): ≤7.85 cm^3, 7.85-14.70 cm^3, 14.70-27.50cm^3 and > 27.50cm^3.

Nomogram Development

For constructing the nomogram model to predict prognosis of NPC patients received IC followed by CCRT, a total of 253 patients were randomly divided into two independent cohorts according to a 7:3 ratio: training cohort (n = 177) and validation cohort (n =76) (**Table 2**). Univariate and multivariate analysis were conducted to identify prognostic factors associated with survival in the training cohort. The

TABLE 1 | Univariate Cox analysis of volumetric parameters in different endpoints.

Parameter	HR (95%CI)		
	OS	PFS	DMFS
preIC GTVnx	1.007 (1.002-1.012)	1.008 (1.003-1.013)	1.005 (0.999-1.011)
postIC GTVnx	1.012 (1.005-1.018)	1.013 (1.007-1.018)	1.008 (1.001-1.015)
midRT GTVnx	1.013 (1.006-1.019)	1.014 (1.008-1.019)	1.009 (1.002-1.016)
preIC GTVnd	1.007 (1.002-1.012)	1.008 (1.003-1.012)	1.009 (1.004-1.014)
postIC GTVnd	1.025 (1.018-1.033)	1.025 (1.019-1.032)	1.028 (1.020-1.036)
midRT GTVnd	1.043 (1.031-1.055)	1.040 (1.030-1.051)	1.046 (1.034-1.059)

HR, hazard ratio; CI, confidence interval; OS, overall survival; PFS, progression-free survival; DMFS, distant metastasis-free survival; preIC GTVnx and preIC GTVnd, pre-induction chemotherapy gross primary tumor and lymph node; postIC GTVnx and postIC GTVnd, post-induction chemotherapy gross primary tumor and lymph node; midRT GTVnx and midRT GTVnd, gross primary tumor at fourth week of radiotherapy and lymph node.

covariates included sex, age, smoking history, drinking history, histological WHO types, T stage, N stage, clinical stage, midRT GTVnd. Based on the multivariate analysis, histological type (P=0.02), T stage (P=0.015), N stage (P=0.027) and midRT GTVnd (P < 0.001) were correlated with OS. For PFS and DMFS, histological type, T stage and midRT GTVnd were detected as independently prognostic factors (P < 0.05) (**Supplementary Tables 3–5**). Based on predictive factors identified from the multivariate analysis in training cohort, we developed three nomograms to predict 4-year OS, PFS and DMFS, respectively (**Figure 1**).

TABLE 2 | Characteristics of Patients in the Primary and Validation Cohorts.

Characteristic	Training cohort (n=177)	Validation cohort (n=76)	P value
Sex			0.559
Male	124 (70.1%)	56 (73.7%)	
Female	53 (29.9%)	20 (26.3%)	
Age (years)			
Median age (range)	46.85 (18-70)	47.66 (18-66)	0.555
≤45	72 (40.7%)	30 (39.5%)	0.858
>45	105 (59.3%)	46 (60.5%)	
Smoking			0.922
Yes	78 (44.1%)	34 (44.7%)	
No	99 (55.9%)	42 (55.3%)	
Drinking			0.816
Yes	51 (28.8%)	23 (30.3%)	
No	126 (71.2%)	53 (69.7%)	
Histological type			0.644
non-keratinizing undifferentiation	133 (75.1%)	55 (72.4%)	
non-keratinizing differentiation	44 (24.9%)	21 (27.6%)	
T stage			0.443
T1	12 (6.8%)	3 (3.9%)	
T2	73 (41.2%)	34 (44.7%)	
T3	36 (20.3%)	8 (10.5%)	
T4	56 (31.6%)	31 (40.8%)	
N stage			0.372
N0	1 (0.6%)	0 (0%)	
N1	12 (6.8%)	5 (6.6%)	
N2	100 (56.5%)	49 (64.5%)	
N3	64 (36.2%)	22 (28.9%)	
Disease stage			0.441
III	72 (40.7%)	27 (35.5%)	
IV	105 (59.3%)	49 (64.5%)	
EBV DNA copies			0.820
undetected	147 (83.1%)	64 (84.2%)	
detected	30 (16.9%)	12 (15.8%)	
IC regimens			0.425
TP	127 (71.8%)	58 (76.3%)	
GP	42 (23.7%)	16 (21.1%)	
TPF	8 (4.5%)	2 (2.6%)	
IC cycles			0.442
1 Cycle	1 (0.6%)	2 (2.6%)	
2 Cycles	99 (55.9%)	36 (47.4%)	
3 Cycles	77 (43.5%)	38 (50.0%)	
mid-RT GTVnd			0.201
Median volume (cc) (range)	14.7 (0-99.75)	12.5 (0.1-83.7)	

IC, induction chemotherapy; midRT GTVnd, gross primary tumor at fourth week of radiotherapy.

Nomogram Validation and Evaluation

Each nomogram was validated internally and externally. The C-index of nomogram to predict OS was 0.746 (95%CI: 0.676-0.816) in training cohort and 0.731 (95%CI: 0.628-0.834) in validation cohort. The AUC showed a good discriminative ability in both cohorts (training cohort, AUC: 0.774, 95%CI 0.712-0.863; validation cohort, AUC: 0.768,95%CI 0.648-0.888). For PFS, The C-index of nomogram was 0.747 (95%CI: 0.684-0.809) in training cohort and 0.735 (95%CI: 0.634-0.836) in validation cohort. And AUC showed a good discriminative ability in both cohorts (training cohort, AUC: 0.771, 95%CI: 0.701-0.860; validation cohort, AUC: 0.772, 95%CI: 0.676-0.893). The C-index of nomogram to predict DMFS was 0.768 (95 CI: 0.699-0.837) in training cohort and 0.729 (95%CI: 0.605-0.852) in validation cohort. The AUC also showed a good discriminative ability in both cohorts (training cohort, AUC: 0.776, 95%CI: 0.707-0.869; validation cohort, AUC: 0.758, 95%CI: 0.643-0.927) (**Figure 2**). Moreover, the calibration plot of each nomogram demonstrated a good consistency between the actual clinical results and the predicted outcomes (**Figure 3**). Then we compared the midRT GTVnd based nomogram against the 8th TNM schema. The DCA showed that the midRT GTVnd based nomogram model was the better reliable clinical tools for predict disease relapse and death (**Figure 4**).

DISCUSSION

Tumor volume is closely associated with prognosis of NPC has been widely reported (9, 10). Although several studies found pretreatment tumor volume and changing rate of tumor volume before and after IC had prognostic value for NPC, it was not be enough to accurately stratify patients who are benefit from IC followed by CCRT. In this study, we firstly compared the predictive performance of different tumor volumetric parameters in different treatment phase in patients receiving IC followed by CCRT. We found the residual volume of lymph nodes at the fourth week of chemoradiotherapy (midRT GTVnd) had the best predictive effects for OS, PFS and DMFS according to HR of Cox regression analysis, indicating midRT GTVnd was the optimal choice as prognostic factor among all kinds of tumor volumetric parameters in the whole process of IC followed by CCRT. The time point of ART may be a potential factor to impact the predictive effect of midRT GTVnd because tumor volume would be changed along with different ART time point. Although it is still confused to identify the optimal time point of ART, several prospective studies reported change of dose distribution varied markedly at the third or fourth week of radiotherapy in patients with NPC (25, 26). According to these studies, ART is routinely conducted at the fourth week of radiotherapy in our center. Whether other time points of ART could result in different prognostic effects of midRT GTVnd still need to be further investigated for NPC patients.

It has been a consensus that lymph nodes metastasis is associated with poor prognosis of NPC patients. Some specific features of lymph node have also been reported as poor

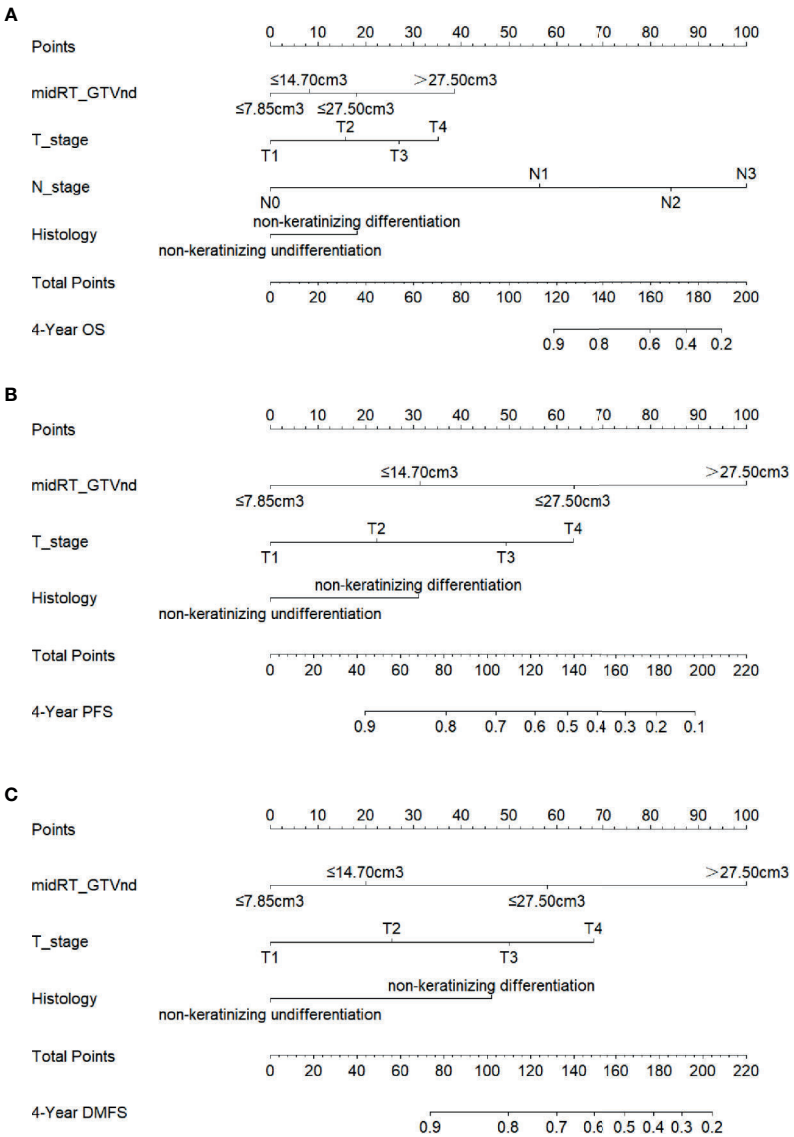

FIGURE 1 | Nomogram to predictive survival. **(A)**, Nomogram for the probability of 4-year OS was developed based on four factors including midRT GTVnd, T stage, N stage and histological type; **(B)**, Nomogram for the probability of 4-year PFS was developed based on three factors including midRT GTVnd, T stage and histological type; **(C)**, Nomogram for the probability of 4-year DMFS was developed based on three factors including midRT GTVnd, T stage, and histological type. The probability could be obtained as function of total points calculated as the sum of points for each specific variable. Points was assigned for each factor by drawing a line upward from the corresponding values to the 'point' line. The total sum of points added by each factor was plotted on the "total points" line. A line was drawn down to read the corresponding predictions of probability.

prognostic factors for NPC, such as extracapsular invasion, necrosis, coalescence and bulky disease (>6 cm) which are closely related to the treatment sensitivity (27). In this study, we reported midRT GTVnd was a new feature which could reflect treatment sensitivity because it was defined as the residual volume of lymph nodes after IC plus at least half course of chemoradiotherapy. Analyzing from the potential mechanism, residual volume of lymph nodes might contain large number of treatment resistant cells. It has been confirmed that these cells always contribute to tumor recurrence and metastasis, and further to negatively impact patient survival (28, 29).

On multivariate analysis, we identified histological types, T stage, N stage and midRT GTVnd were independently prognostic factors for OS. In this study, 25.7% of patients had nonkeratinizing differentiated subtype which was associated with poor survival. This result was consistent with our previous studies (20, 30). All patients enrolled in this study were from the Northwest China where were considered as a typical non-

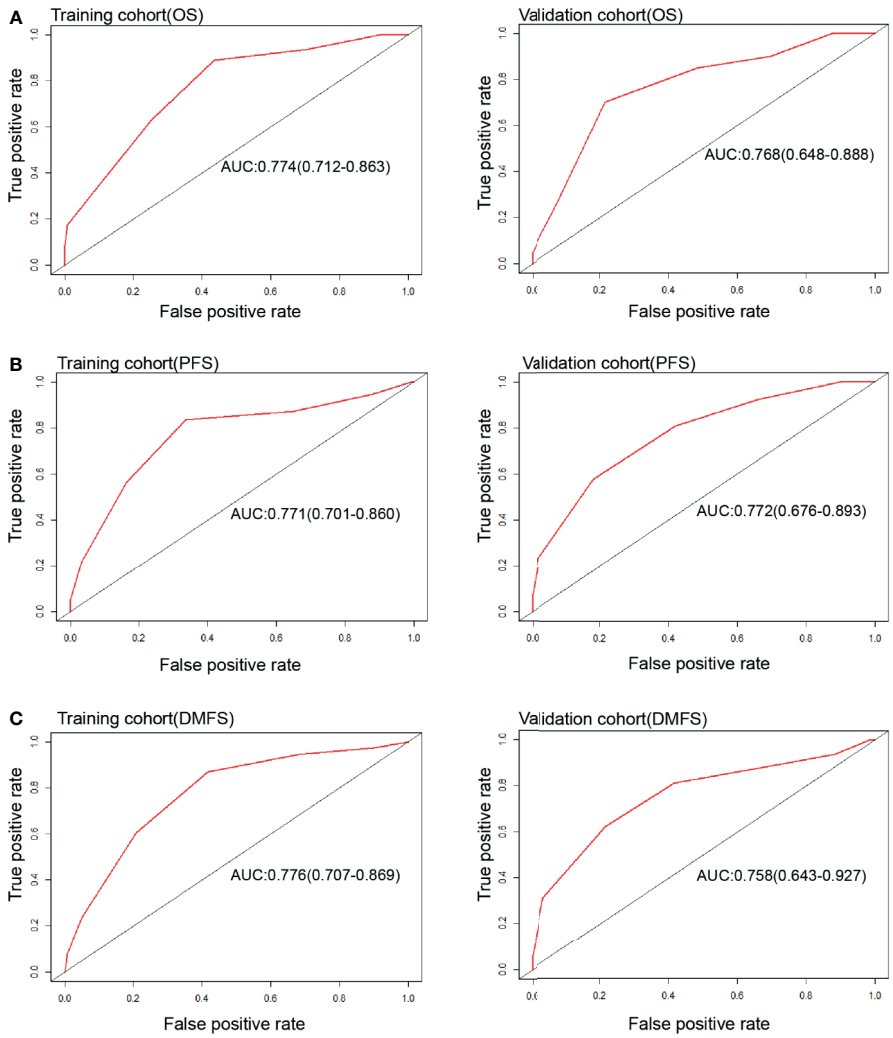

FIGURE 2 | ROC curves of Nomograms to predict 4-year OS **(A)**, PFS **(B)** and DMFS **(C)** in both training and validation cohort.

endemic area for NPC. Although the prognostic value of histological type for NPC remains controversial in endemic area, given the potentially distinctive pathogenesis, geographical and ethnic origin in Northwest China, the nonkeratinizing differentiated subtype may be an efficient prognostic indicator. We failed to detect a positive correlation between N stage and distant metastatic disease on multivariate analysis. The reason may be explained by unclassified N stage was used to analyze. After patients were divided into two groups: N0-N2 and N3, patients with stage N3 had significantly higher rate of distant metastatic disease than those with stage N0 to N2 using log-rank test (data was not shown).

In view of the prognostic value of midRT GTVnd for OS, PFS and DMFS, we developed and validated three midRT GTVnd based nomograms to predict probability of 4-year survival for LA-NPC patients treated with IC followed by CCRT. The identification and calibration of the nomograms confirmed these prognostic models had wide range of applicability. Compared with the 8th edition of TNM staging system, DCA curves showed the nomogram models had better prediction accuracy for death and disease relapse in patients with LA-NPC receiving IC followed by CCRT. Unlike other risk scores could provide a probability of prognosis before treatment, our models focused on the treatment sensitivity and prognosis at end of the IC followed by CCRT. This would help clinicians to design appropriate strategies of follow-up and adjuvant treatment for each patient.

Although phase 3 trials confirm that adjuvant chemotherapy consist of cisplatin and fluorouracil following chemoradiotherapy fails to yield further benefits in LA-NPC (31, 32), several retrospective studies imply metronomic adjuvant uracil plus tegafur may reduce distant metastasis and improve survival in high-risk patients (33, 34). Plasma Epstein-Barr virus (EBV) DNA of post radiotherapy is often used to guide adjuvant

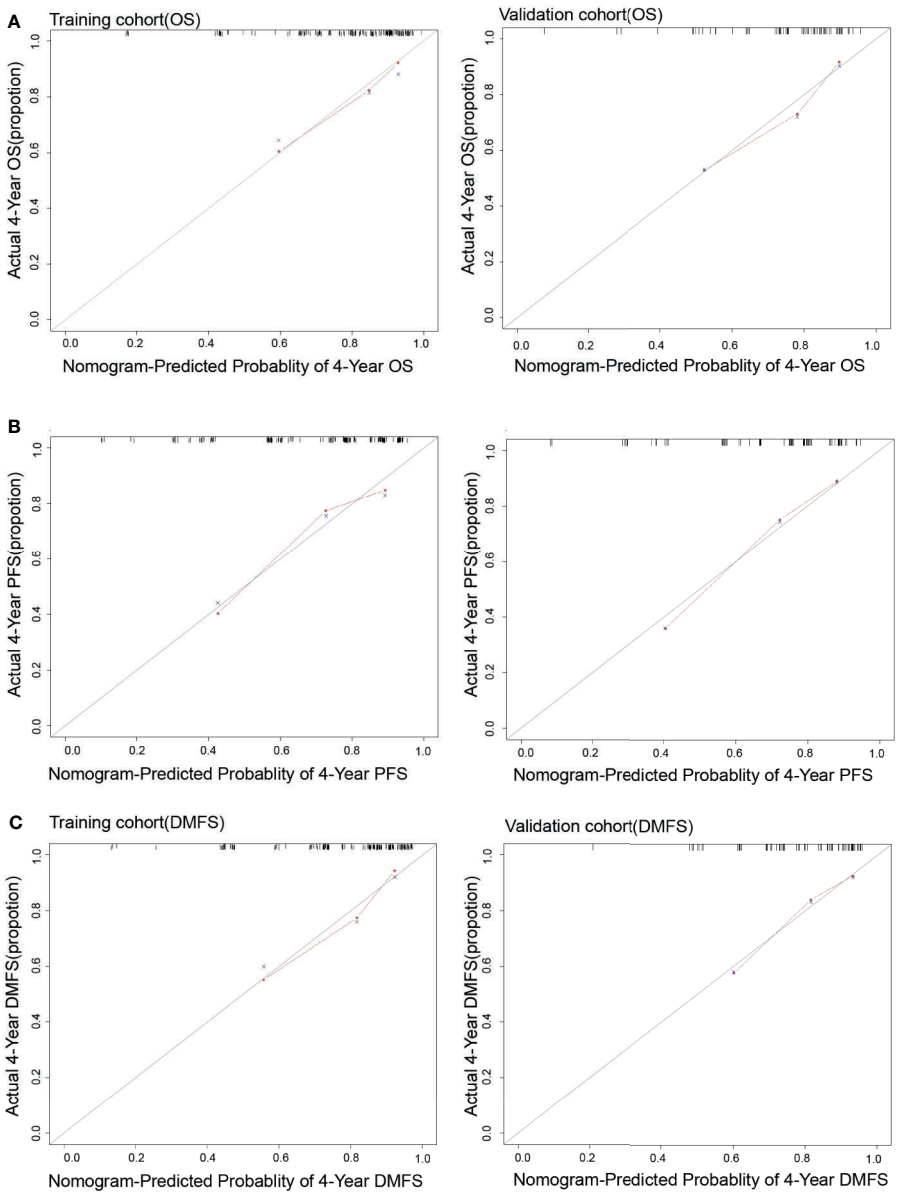

FIGURE 3 | The calibration curves of Nomograms to predict 4-year OS **(A)**, PFS **(B)** and DMFS **(C)** in both training and validation cohort.

therapy (35). However, different segments of the same viral DNA or different viral genes might result in vary sensitivities in quantitative PCR assay (34). In our center, although plasma EBV DNA is detected routinely using quantitative PCR assay for each patient before treatment and in the whole follow-up period, EBV DNA copies can be detected only in a few plasma samples of patients. Under this situation, these nomogram models established by this study may provide information to stratify high-risk patients without known its plasma EBV DNA status to receive adjuvant chemotherapy. These clinically high-risk features-guided approaches are feasible during daily practice in all hospitals.

The current study may have a few weak points. First, because of its retrospective nature, selection bias might have been unavoidable. Thus, the results need validation of further large sample prospective studies. Second, our data based on a single non-endemic center from the Northwest China, and thus, external validation with other centers in endemic region is needed. Finally, there is a possibility of inter- and/or intra-physician variation in GTV measurements. Despite these limitations, the discriminatory performance of the volumetric parameters in the whole process of IC-CCRT treatment could be utilized as an indicator for tailoring therapy on an individual patient basis.

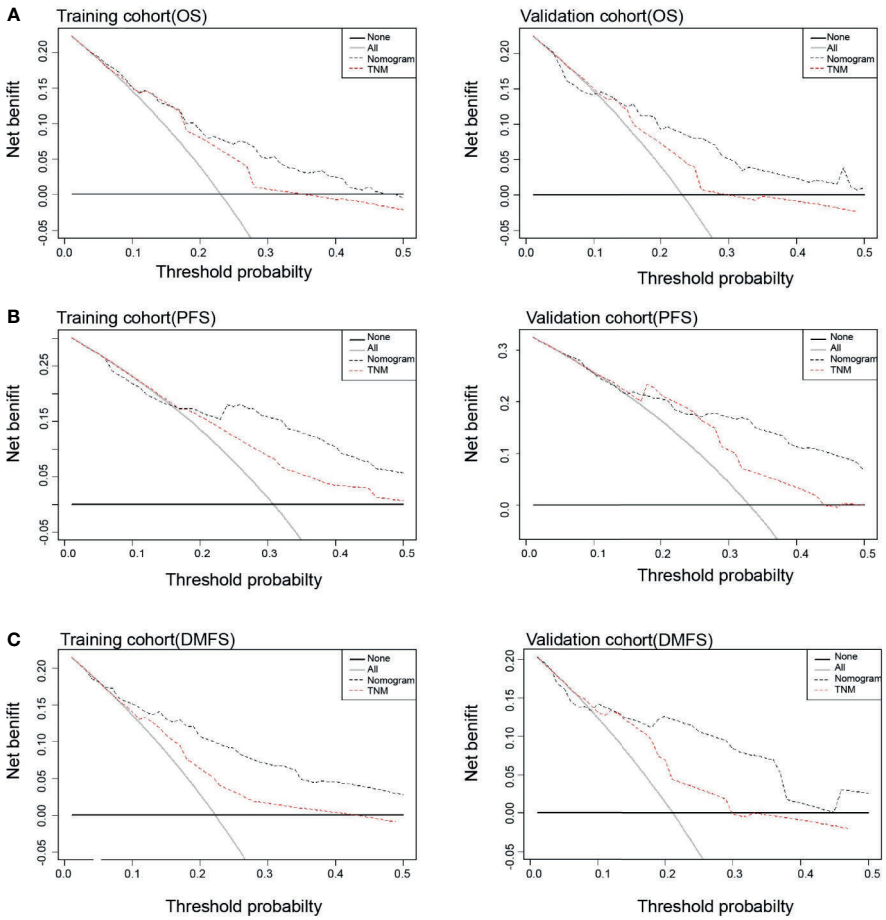

FIGURE 4 | Decision curve analysis of prognostic effects between Nomograms and TNM stage for OS **(A)**, PFS **(B)** and DMFS **(C)** in both training and validation cohort.

In this study, we identified the best volumetric factor indicator associated with prognosis was the residual volume of lymph nodes at the fourth week of chemoradiotherapy for NPC patients receiving IC followed by CCRT. Based on the volumetric factor and clinical risk factors, we developed and validated three different nomograms to predict specific probability of 4-year OS, PFS and DMFS for LA-NPC patient, respectively.

DATA AVAILABILITY STATEMENT

The raw data supporting the conclusions of this article will be made available by the authors, without undue reservation.

ETHICS STATEMENT

The studies involving human participants were reviewed and approved by Medical Ethics Committee of the First Affiliated Hospital of the Fourth Military Medical University. Written informed consent for participation was not required for this study in accordance with the national legislation and the institutional requirements.

AUTHOR CONTRIBUTIONS

Study concepts: MS. Study design: YL, JZ, and LZ. Data acquisition: JZ, JL, SL, JW, and BH. Quality control of data and algorithms: YL and MS. Data analysis and interpretation: JZ, JL, YL, LZ, and MS. Statistical analysis: JZ and YL. Manuscript preparation: YL. Manuscript editing: JZ and JL. Manuscript review: MS. All authors contributed to the article and approved the submitted version.

SUPPLEMENTARY MATERIAL

The Supplementary Material for this article can be found online at: https://www.frontiersin.org/articles/10.3389/fonc.2021.739103/full#supplementary-material

REFERENCES

1. Mao YP, Xie FY, Liu LZ, Sun Y, Li L, Tang LL, et al. Re-Evaluation of 6th Edition of AJCC Staging System for Nasopharyngeal Carcinoma and Proposed Improvement Based on Magnetic Resonance Imaging. *Int J Radiat Oncol Biol Phys* (2009) 73:1326–34. doi: 10.1016/j.ijrobp.2008.07.062
2. Sun Y, Li WF, Chen NY, Zhang N, Hu GQ, Xie FY, et al. Induction Chemotherapy Plus Concurrent Chemoradiotherapy *Versus* Concurrent Chemoradiotherapy Alone in Locoregionally Advanced Nasopharyngeal Carcinoma: A Phase 3, Multicentre, Randomised Controlled Trial. *Lancet Oncol* (2016) 17:1509–20. doi: 10.1016/s1470-2045(16)30410-7
3. Zhang Y, Chen L, Hu GQ, Zhang N, Zhu XD, Yang KY, et al. Gemcitabine and Cisplatin Induction Chemotherapy in Nasopharyngeal Carcinoma. *N Engl J Med* (2019) 381:1124–35. doi: 10.1056/NEJMoa1905287
4. Liu LT, Liang YJ, Guo SS, Mo HY, Guo L, Wen YF, et al. Induction Chemotherapy Followed by Radiotherapy *Versus* Concurrent Chemoradiotherapy in the Treatment of Different Risk Locoregionally Advanced Nasopharyngeal Carcinoma. *Ther Adv Med Oncol* (2020) 12:1758835920928214. doi: 10.1177/1758835920928214
5. Zhang LL, Huang MY, Fei X, Wang KX, Song D, Wang T, et al. Risk Stratification for Nasopharyngeal Carcinoma: A Real-World Study Based on Locoregional Extension Patterns and Epstein-Barr Virus DNA Load. *Ther Adv Med Oncol* (2020) 12:1758835920932052. doi: 10.1177/1758835920932052
6. Lei Y, Li YQ, Jiang W, Hong XH, Ge WX, Zhang Y, et al. A Gene-Expression Predictor for Efficacy of Induction Chemotherapy in Locoregionally Advanced Nasopharyngeal Carcinoma. *J Natl Cancer Inst* (2021) 113:471–80. doi: 10.1093/jnci/djaa100
7. Qiang M, Li C, Sun Y, Sun Y, Ke L, Xie C, et al. A Prognostic Predictive System Based on Deep Learning for Locoregionally Advanced Nasopharyngeal Carcinoma. *J Natl Cancer Inst* (2021) 113:606–15. doi: 10.1093/jnci/djaa149
8. Liang Y, Li J, Li Q, Tang L, Chen L, Mao Y, et al. Plasma Protein-Based Signature Predicts Distant Metastasis and Induction Chemotherapy Benefit in Nasopharyngeal Carcinoma. *Theranostics* (2020) 10:9767–78. doi: 10.7150/thno.47882
9. Guo R, Sun Y, Yu XL, Yin WJ, Li WF, Chen YY, et al. Is Primary Tumor Volume Still a Prognostic Factor in Intensity Modulated Radiation Therapy for Nasopharyngeal Carcinoma? *Radiother Oncol* (2012) 104:294–9. doi: 10.1016/j.radonc.2012.09.001
10. Chen MK, Chen TH, Liu JP, Chang CC, Chie WC. Better Prediction of Prognosis for Patients With Nasopharyngeal Carcinoma Using Primary Tumor Volume. *Cancer* (2004) 100:2160–6. doi: 10.1002/cncr.20210
11. Xue F, Ou D, Ou X, Zhou X, Hu C, He X. Prognostic Efficacy of Extensive Invasion of Primary Tumor Volume for T3-4 Nasopharyngeal Carcinoma Receiving Intensity-Modulated Radiotherapy. *Oral Oncol* (2020) 100:104478. doi: 10.1016/j.oraloncology.2019.104478
12. Chen FP, Wen DW, Li F, Lin L, Kou J, Zheng WH, et al. The Role of Post-Neoadjuvant Chemotherapy Tumor Volume for Prognostication and Treatment Guidance in Loco-Regionally Advanced Nasopharyngeal Carcinoma. *Cancers (Basel)* (2019) 11:1632. doi: 10.3390/cancers11111632
13. Yang H, Liu Y, Zhang R, Ye Y, Chen Q, Qin Q, et al. Prognostic Value of the Tumor Volume Reduction Rate After Neoadjuvant Chemotherapy in Patients With Locoregional Advanced Nasopharyngeal Carcinoma. *Oral Oncol* (2020) 110:104897. doi: 10.1016/j.oraloncology.2020.104897
14. Yu TT, Lam SK, To LH, Tse KY, Cheng NY, Fan YN, et al. Pretreatment Prediction of Adaptive Radiation Therapy Eligibility Using MRI-Based Radiomics for Advanced Nasopharyngeal Carcinoma Patients. *Front Oncol* (2019) 9:1050. doi: 10.3389/fonc.2019.01050
15. Gensheimer MF, Le QT. Adaptive Radiotherapy for Head and Neck Cancer: Are We Ready to Put it Into Routine Clinical Practice? *Oral Oncol* (2018) 86:19–24. doi: 10.1016/j.oraloncology.2018.08.010
16. Tan W, Ye J, Xu R, Li X, He W, Wang X, et al. The Tumor Shape Changes of Nasopharyngeal Cancer During Chemoradiotherapy: The Estimated Margin to Cover the Geometrical Variation. *Quant Imaging Med Surg* (2016) 6:115–24. doi: 10.21037/qims.2016.03.07
17. Huang R, Guo H, Chen J, Zhai T, Chen J, Lin K, et al. Intratreatment Tumor Volume Change During Definitive Chemoradiotherapy is Predictive for Treatment Outcome of Patients With Esophageal Carcinoma. *Cancer Manag Res* (2020) 12:7331–9. doi: 10.2147/cmar.S246500
18. Watanabe Y, Nakamura S, Ichikawa Y, Ii N, Kawamura T, Kondo E, et al. Early Alteration in Apparent Diffusion Coefficient and Tumor Volume in Cervical Cancer Treated With Chemoradiotherapy or Radiotherapy: Incremental Prognostic Value Over Pretreatment Assessments. *Radiother Oncol* (2021) 155:3–9. doi: 10.1016/j.radonc.2020.09.059
19. Lee H, Ahn YC, Oh D, Nam H, Noh JM, Park SY. Tumor Volume Reduction Rate During Adaptive Radiation Therapy as a Prognosticator for Nasopharyngeal Cancer. *Cancer Res Treat* (2016) 48:537–45. doi: 10.4143/crt.2015.081
20. Zang J, Li C, Zhao LN, Wang JH, Xu M, Luo SQ, et al. Prognostic Model of Death and Distant Metastasis for Nasopharyngeal Carcinoma Patients Receiving 3DCRT/IMRT in Nonendemic Area of China. *Med (Baltimore)* (2016) 95:e3794. doi: 10.1097/md.0000000000003794
21. Zhao LN, Zhou B, Shi M, Wang JH, Xiao F, Xu M, et al. Clinical Outcome for Nasopharyngeal Carcinoma With Predominantly WHO II Histology Treated With Intensity-Modulated Radiation Therapy in Non-Endemic Region of China. *Oral Oncol* (2012) 48:864–9. doi: 10.1016/j.oraloncology.2012.03.001
22. Wang J, Shi M, Hsia Y, Luo S, Zhao L, Xu M, et al. Failure Patterns and Survival in Patients With Nasopharyngeal Carcinoma Treated With Intensity Modulated Radiation in Northwest China: A Pilot Study. *Radiat Oncol* (2012) 7:2. doi: 10.1186/1748-717x-7-2
23. Lee N, Harris J, Garden AS, Straube W, Glisson B, Xia P, et al. Intensity-Modulated Radiation Therapy With or Without Chemotherapy for Nasopharyngeal Carcinoma: Radiation Therapy Oncology Group Phase II Trial 0225. *J Clin Oncol* (2009) 27:3684–90. doi: 10.1200/jco.2008.19.9109
24. Vickers AJ, Elkin EB. Decision Curve Analysis: A Novel Method for Evaluating Prediction Models. *Med Decis Making* (2006) 26:565–74. doi: 10.1177/0272989x06295361
25. Nishi T, Nishimura Y, Shibata T, Tamura M, Nishigaito N, Okumura M. Volume and Dosimetric Changes and Initial Clinical Experience of a Two-Step Adaptive Intensity Modulated Radiation Therapy (IMRT) Scheme for Head and Neck Cancer. *Radiother Oncol* (2013) 106:85–9. doi: 10.1016/j.radonc.2012.11.005
26. Yang H, Hu W, Wang W, Chen P, Ding W, Luo W. Replanning During Intensity Modulated Radiation Therapy Improved Quality of Life in Patients With Nasopharyngeal Carcinoma. *Int J Radiat Oncol Biol Phys* (2013) 85:e47–54. doi: 10.1016/j.ijrobp.2012.09.033
27. Lu T, Hu Y, Xiao Y, Guo Q, Huang SH, O'Sullivan B, et al. Prognostic Value of Radiologic Extranodal Extension and its Potential Role in Future N Classification for Nasopharyngeal Carcinoma. *Oral Oncol* (2019) 99:104438. doi: 10.1016/j.oraloncology.2019.09.030
28. Yu X, Liu Y, Yin L, Peng Y, Peng Y, Gao Y, et al. Radiation-Promoted CDC6 Protein Stability Contributes to Radioresistance by Regulating Senescence and Epithelial to Mesenchymal Transition. *Oncogene* (2019) 38:549–63. doi: 10.1038/s41388-018-0460-4
29. Yeung DCM, Yeung Z, Wong EWY, Vlantis AC, Chan JYK. Neck Lymph Node Status on Survival of Regionally Recurrent or Persistent Nasopharyngeal Carcinoma. *Sci Rep* (2020) 10:5622. doi: 10.1038/s41598-020-62625-4
30. Zang J, Li C, Xu M, Xu W, Kang X, Wang J, et al. Induction Chemotherapy Followed by Concurrent Chemoradiotherapy is Benefit for Advanced Stage Nasopharyngeal Carcinoma With Different Nonkeratinizing Carcinoma Subtypes. *Sci Rep* (2018) 8:13318. doi: 10.1038/s41598-018-31050-z
31. Chan ATC, Hui EP, Ngan RKC, Tung SY, Cheng ACK, Ng WT, et al. Analysis of Plasma Epstein-Barr Virus DNA in Nasopharyngeal Cancer After Chemoradiation to Identify High-Risk Patients for Adjuvant Chemotherapy: A Randomized Controlled Trial. *J Clin Oncol* (2018) 11:3192–100. doi: 10.1200/jco.2018.77.7847
32. Chen L, Hu CS, Chen XZ, Hu GQ, Cheng ZB, Sun Y, et al. Concurrent Chemoradiotherapy Plus Adjuvant Chemotherapy *Versus* Concurrent Chemoradiotherapy Alone in Patients With Locoregionally Advanced Nasopharyngeal Carcinoma: A Phase 3 Multicentre Randomised Controlled Trial. *Lancet Oncol* (2012) 13:163–71. doi: 10.1016/s1470-2045(11)70320-5
33. Twu CW, Wang WY, Chen CC, Liang KL, Jiang RS, Wu CT, et al. Metronomic Adjuvant Chemotherapy Improves Treatment Outcome in Nasopharyngeal Carcinoma Patients With Postradiation Persistently Detectable Plasma Epstein-Barr Virus Deoxyribonucleic Acid. *Int J Radiat Oncol Biol Phys* (2014) 89:21–9. doi: 10.1016/j.ijrobp.2014.01.052

34. Liu YC, Wang WY, Twu CW, Jiang RS, Liang KL, Wu CT, et al. Prognostic Impact of Adjuvant Chemotherapy in High-Risk Nasopharyngeal Carcinoma Patients. *Oral Oncol* (2017) 64:15–21. doi: 10.1016/j.oraloncology.2016.11.008
35. Zhang L, Huang Y, Hong S, Yang Y, Yu G, Jia J, et al. Gemcitabine Plus Cisplatin *Versus* Fluorouracil Plus Cisplatin in Recurrent or Metastatic Nasopharyngeal Carcinoma: A Multicentre, Randomised, Open-Label, Phase 3 Trial. *Lancet* (2016) 388:1883–92. doi: 10.1016/s0140-6736(16)31388-5

Conflict of Interest: The authors declare that the research was conducted in the absence of any commercial or financial relationships that could be construed as a potential conflict of interest.

frontiers in Oncology

ORIGINAL RESEARCH
published: 07 September 2021
doi: 10.3389/fonc.2021.744250

Radiomic Features Associated With HPV Status on Pretreatment Computed Tomography in Oropharyngeal Squamous Cell Carcinoma Inform Clinical Prognosis

*Bolin Song[1], Kailin Yang[2], Jonathan Garneau[3], Cheng Lu[1], Lin Li[1], Jonathan Lee[4], Sarah Stock[4], Nathaniel M. Braman[1], Can Fahrettin Koyuncu[1], Paula Toro[1], Pingfu Fu[5], Shlomo A. Koyfman[2], James S. Lewis Jr[6] and Anant Madabhushi[1,7]**

[1] Center for Computational Imaging and Personalized Diagnostics, Case Western Reserve University, Cleveland, OH, United States, [2] Department of Radiation Oncology, Taussig Cancer Center, Cleveland Clinic, Cleveland, OH, United States, [3] Department of Otolaryngology and Head and Neck Surgery, University of Virginia, Charlottesville, VA, United States, [4] Imaging Institute, Cleveland Clinic, Cleveland, OH, United States, [5] Department of Population and Quantitative Health Sciences, Case Western Reserve University, Cleveland, OH, United States, [6] Department of Pathology, Microbiology, and Immunology, Vanderbilt University Medical Center, Nashville, TN, United States, [7] Louis Stokes Cleveland Veterans Administration Medical Center, Cleveland, OH, United States

OPEN ACCESS

Edited by:
Min Yao,
University Hospitals Cleveland Medical Center, United States

Reviewed by:
Amit Gupta,
Royal Marsden NHS Foundation Trust, United Kingdom
Gayani Pitiyage,
St George's, University of London, United Kingdom

***Correspondence:**
Anant Madabhushi
axm788@case.edu

Specialty section:
This article was submitted to Head and Neck Cancer, a section of the journal Frontiers in Oncology

Received: 20 July 2021
Accepted: 16 August 2021
Published: 07 September 2021

Citation:
Song B, Yang K, Garneau J, Lu C, Li L, Lee J, Stock S, Braman NM, Koyuncu CF, Toro P, Fu P, Koyfman SA, Lewis JS Jr and Madabhushi A (2021) Radiomic Features Associated With HPV Status on Pretreatment Computed Tomography in Oropharyngeal Squamous Cell Carcinoma Inform Clinical Prognosis. Front. Oncol. 11:744250. doi: 10.3389/fonc.2021.744250

Purpose: There is a lack of biomarkers for accurately prognosticating outcome in both human papillomavirus-related (HPV+) and tobacco- and alcohol-related (HPV–) oropharyngeal squamous cell carcinoma (OPSCC). The aims of this study were to i) develop and evaluate radiomic features within (intratumoral) and around tumor (peritumoral) on CT scans to predict HPV status; ii) investigate the prognostic value of the radiomic features for both HPV– and HPV+ patients, including within individual AJCC eighth edition-defined stage groups; and iii) develop and evaluate a clinicopathologic imaging nomogram involving radiomic, clinical, and pathologic factors for disease-free survival (DFS) prediction for HPV+ patients.

Experimental Design: This retrospective study included 582 OPSCC patients, of which 462 were obtained from The Cancer Imaging Archive (TCIA) with available tumor segmentation and 120 were from Cleveland Clinic Foundation (CCF, denoted as S_{CCF}) with HPV+ OPSCC. We subdivided the TCIA cohort into training (S_T, 180 patients) and validation (S_V, 282 patients) based on an approximately 3:5 ratio for HPV status prediction. The top 15 radiomic features that were associated with HPV status were selected by the minimum redundancy–maximum relevance (MRMR) using S_T and evaluated on S_V. Using 3 of these 15 top HPV status-associated features, we created radiomic risk scores for both HPV+ (RRS_{HPV+}) and HPV– patients (RRS_{HPV-}) through a Cox regression model to predict DFS. RRS_{HPV+} was further externally validated on S_{CCF}. Nomograms for the HPV+ population (M_{p+RRS}) were constructed. Both RRS_{HPV+} and M_{p+RRS} were used to prognosticate DFS for the AJCC eighth edition-defined stage I, stage II, and stage III patients separately.

Results: RRS_{HPV+} was prognostic for DFS for i) the whole HPV+ population [hazard ratio (HR) = 1.97, 95% confidence interval (CI): 1.35–2.88, $p < 0.001$], ii) the AJCC eighth stage I population (HR = 1.99, 95% CI: 1.04–3.83, $p = 0.039$), and iii) the AJCC eighth stage II population (HR = 3.61, 95% CI: 1.71–7.62, $p < 0.001$). HPV+ nomogram M_{p+RRS} (C-index, 0.59; 95% CI: 0.54–0.65) was also prognostic of DFS (HR = 1.86, 95% CI: 1.27–2.71, $p = 0.001$).

Conclusion: CT-based radiomic signatures are associated with both HPV status and DFS in OPSCC patients. With additional validation, the radiomic signature and its corresponding nomogram could potentially be used for identifying HPV+ OPSCC patients who might be candidates for therapy deintensification.

Keywords: oropharyngeal squamous cell carcinoma, human papillomavirus, radiomics, prognosis prediction, nomograms

INTRODUCTION

The rise in the incidence of human papillomavirus (HPV)-related cancers has caused a significant epidemiological shift (1) in oropharyngeal squamous cell carcinoma (OPSCC). It is estimated that HPV causes more than 70% of OPSCC cases in the United States (2). HPV+ OPSCC differs from its HPV− counterpart in response to treatment and disease aggressiveness (3). In order to account for this, the most recent American Joint Committee on Cancer (AJCC) eighth edition tumor staging system was modified to incorporate HPV status, with different staging systems for HPV (p16) positive and negative tumors (4). HPV+ patients tend to respond better to definitive radiotherapy or combined chemoradiotherapy protocols and are less likely than HPV− patients to develop disease recurrence and metastases. Thus, it has become critical to develop biomarkers within the HPV+ and HPV− populations for risk stratification.

Treatment of OPSCC patients is on the cusp of a paradigm shift; current clinical trials are geared toward reducing treatment toxicity for HPV+ patients without compromising survival outcomes since low-risk patients typically could benefit from a lower dose of radiotherapy or less invasive surgical operations (treatment deintensification) (5). However, it is challenging to tailor the most optimal treatment strategy for each patient. Although high T (T3/T4) and N (N3) stages as well as tobacco use are clinically accepted risk factors for HPV+ OPSCC patients, these categorical predictors neglect the oncogenic differences between individual patients (6). A recent phase II randomized controlled trial NRG HN002 reported that patients who are grouped as candidates for treatment de-escalation using a combination of clinicopathologic factors did not meet the goal of 2-year disease-free survival (DFS) in the radiotherapy only arm (7). This exhibits a clear unmet clinical need for the development of objective biomarkers to identify patients who could truly benefit from treatment de-escalation.

On the other hand, the unmet need for HPV− patients is to precisely identify patients at high risk of developing local or regional failure after treatment, patients who might be candidates for targeted treatment escalation (8). While the eighth edition of the AJCC staging modifications that separate HPV+ and HPV− patients is a major advance (9), it still may not be sufficient for accurate risk stratification as it de-emphasizes the importance of nodal metastasis by diagnosing most of the new p16+ OPSCC patients into stages I and II (10).

Radiomics is the process of computational extraction of large numbers of quantitative imaging features, such as texture features, from routine radiologic scans (e.g., MRI and CT) for characterization of the disease (11). These features are able to detect subtle changes in imaging intensity patterns within a local region which in turn may help better describe the cancer phenotype as well as the tumor microenvironment. While radiomic features in the immediate vicinity outside the tumor have shown significant value in differentiating disease subtypes for lung (12) and breast (13) cancers, we are not aware of any work that has attempted to collectively evaluate the role of textural patterns from both within (intratumoral) and outside the tumor (peritumoral) to predict HPV status or to identify their association with disease-specific survival in OPSCC.

In this study, we sought to explore the prognostic value of both intratumoral and peritumoral HPV status-associated radiomic features on CT scans and compared and combined them with clinical and pathologic factors on over 500 OPSCC patients. The prognostic radiomic biomarker for HPV+ OPSCC was validated both internally (237 patients) and externally (120 patients) on two different cohorts. We also evaluated the utility of the radiomic signature to prognosticate DFS within each individual AJCC eighth edition-defined stage group. Finally, this study also involved creation and validation of a clinicopathologic nomogram for estimating DFS for HPV+ OPSCC patients. **Figure 1** shows the overall methodology comprising radiomic feature extraction and selection, prognostic signatures, and radiomic nomogram construction and validation.

MATERIALS AND METHODS

Patients

Two OPSCC cohorts were included in this study: The Cancer Imaging Archive (TCIA, $n = 462$) OPC-Radiomics cohort (10)

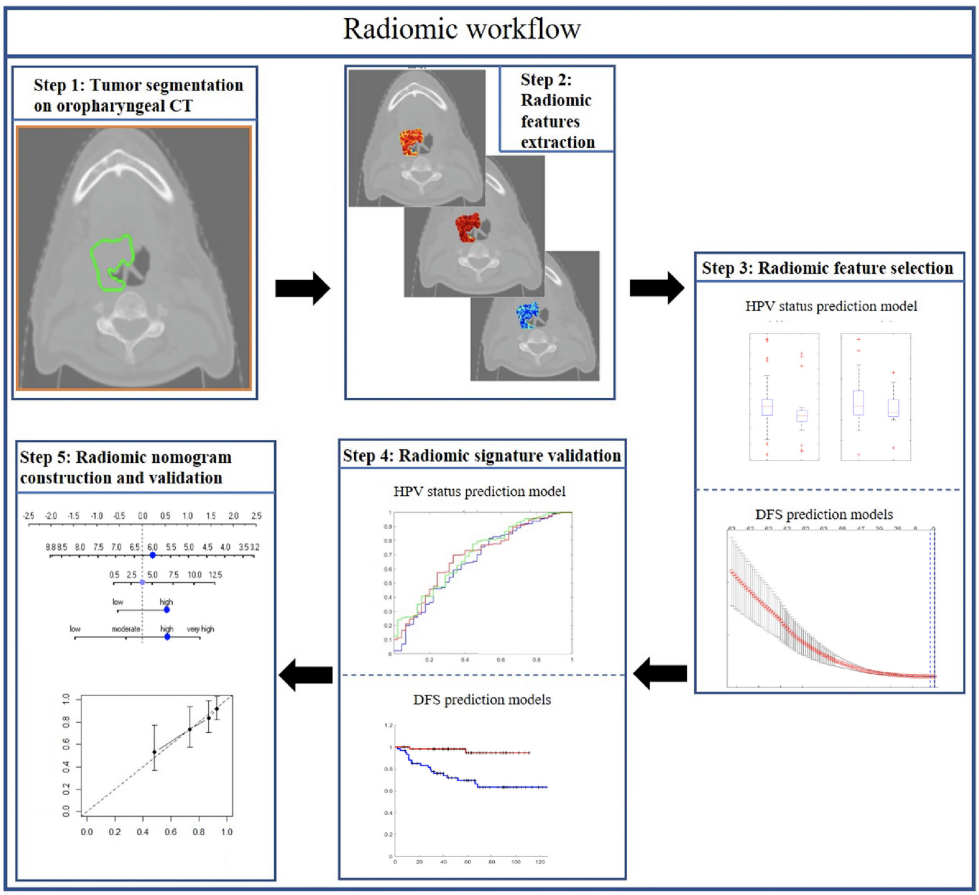

FIGURE 1 | Diagram of the overall radiomic workflow.

and the Cleveland Clinic Foundation (CCF) cohort (n = 120). All patients had undergone pretreatment radiotherapy planning CT. TCIA is an open archive of deidentified cancer-specific medical images and associated clinical metadata accessible for public download (14). Clinicopathologic and outcome information for patients in the CCF cohort were collected after obtaining approval from the Institutional Review Board of Cleveland Clinic. Demographic data are shown in **Table 1**. For the TCIA cohort, a total of 473 patients with OPSCC treated with curative intent at the Princess Margaret Cancer Center between 2005 and 2010 were reviewed. Histopathologic confirmation was used for the diagnosis of OPSCC and p16 immunohistochemistry was used to assess HPV status. Patients were triaged using inclusion criteria that involved the availability of i) radiotherapy planning CT scans with matched clinical information (HPV status by p16 immunohistochemistry, survival information) and ii) binary mask for gross tumor volume (GTV). Fourteen patients with the following criteria were excluded: i) CT images containing artifact (n = 6); ii) number of voxels within tumor is less than 200, which was deemed to be insufficient for feature extraction (n = 5); and iii) tumor mask contains normal brain tissue (n = 3). Following the patient exclusion criteria, 462 patients from the TCIA cohort and 120 patients from the CCF cohort were included for subsequent radiomic analysis. The flowchart for patient enrollment is illustrated in **Supplementary Figure S1**.

CT Imaging

The CT images for the TCIA cohort were acquired (10) from one of the following CT scanners: General Electric Discovery ST, General Electric Lightspeed Plus, or Toshiba Medical Systems Aquillion ONE. CT scans were acquired in helical mode with a slice thickness of 2.5 mm (General Electric) or 2 mm (Toshiba), at 120 kVp and 300 mAs tube current. Image resolution was 1 mm for all the scans. The CT images for the CCF cohort were acquired from either The General Electric Medical System or The Siemens Medical System. CT scans were acquired in helical mode with a slice thickness of 3 mm, at 120 kVp and 235 mAs tube current. Image resolution is between 0.4 and 0.5 mm for most of the patients, with an image matrix of 512 × 512.

Intratumoral and Peritumoral Compartment Definitions

The binary intratumoral masks which outlined the primary GTV were obtained using the Radiation Therapy Structures

TABLE 1 | Clinicopathologic data for HPV+ and HPV– patients included in this study.

Clinical parameter	Patient demographics						
	HPV+ patients				HPV– patients		
	TCIA training (S_T, n = 100)	TCIA validation (S_V, n = 237)	CCF validation (S_{CCF}, n = 120)	p-value	TCIA training (S_T, n = 80)	TCIA validation (S_V, n = 45)	p-value
Age	60.4 ± 9.07	58.3 ± 9.43	59.45 ± 9.52	0.11	65.54 ± 10.39	64.87 ± 9.63	0.63
Gender							
Male	82 (82%)	197 (83.1%)	108 (90%)	0.16	58 (72.5%)	31 (68.9%)	0.82
Female	18 (18%)	40 (16.9%)	12 (10%)		22 (27.5%)	14 (31.1%)	
Smoking history							
Non-smoker	41 (41%)	83 (35%)	47 (35%)		5 (6.3%)	7 (15.6%)	0.18
Ex-smoker	39 (39%)	95 (40.1%)	51 (40.1%)	0.59	30 (37.5%)	18 (40%)	
Current	20 (20%)	59 (24.9%)	22 (24.9%)		45 (56.2%)	20 (44.4%)	
Drinking history							
Non-/light drinker	82 (82%)	191 (80.6%)	102 (85%)	0.39	39 (48.8%)	22 (48.9%)	0.70
Ex-drinker	6 (6%)	12 (5.1%)	9 (7.5%)		9 (11.2%)	9 (20%)	
Heavy drinker	12 (12%)	34 (14.3%)	9 (7.5%)		32 (40%)	14 (31.1%)	
T stage							
T1	23 (23%)	45 (19%)	27 (22.5%)	0.35	7 (8.7%)	3 (6.7%)	0.91
T2	36 (36%)	81 (34.2%)	46 (38.3%)		23 (28.8%)	15 (33.3%)	
T3	30 (30%)	65 (27.4%)	24 (20%)		30 (37.5%)	15 (33.3%)	
T4	11 (11%)	46 (19.4%)	23 (19.2%)		20 (25%)	12 (26.7%)	
N stage							
N0	13 (13%)	26 (11%)	12 (10%)	0.93	23 (28.7%)	14 (31.1%)	0.99
N1	53 (53%)	132 (55.7%)	73 (60.8%)		32 (40%)	18 (40%)	
N2	27 (27%)		29 (24.2%)		19 (23.8%)	10 (22.2%)	
N3	7 (7%)	57 (24.1%)22 (9.2%)	6 (5%)		6 (7.5%)	3 (6.7%)	
Overall stage (AJCC eighth edition)							
I	42 (42%)	98 (41.4%)	62 (51.7%)	0.07	22 (27.5%)	13 (28.9%)	0.97
II	41 (41%)	76 (32%)	30 (25%)		32 (40%)	17 (37.8%)	
III	17 (17%)	63 (26.6%)	27 (22.5%)		26 (32.5%)	15 (33.3%)	
IV	0 (0%)	0 (0%)	1 (0.8%)		0 (0%)	0 (0%)	

(RTSTRUCT) for the TCIA cohort (10). Primary tumors on the CCF cohort were manually segmented by two board-certified head and neck radiologists JL (with 5 years of clinical expertise) and SS (with 6 years of clinical expertise) across all of the two-dimensional CT sections using a hand-annotation tool in axial view. Morphologic dilation operations were then performed for all patients on intratumoral masks to define the annular ring region outside the tumor up to a radial distance of 15 mm based on previous studies in lung (15) and breast cancer (13), where peritumoral margins >15 mm were not associated with disease recurrence. The intratumoral masks were then subtracted from the dilated masks to obtain the peritumoral regions, which were then subdivided into three peritumoral rings of 5-mm-radius increments. Implementation details on peritumoral masks are provided in **Appendix E1**, section 1.

Radiomic Feature Extraction

A total of 664 intratumoral and 1,485 peritumoral (495 × 3 peritumoral rings) radiomic features were extracted for all patients on all the compartments on a per-pixel basis. The feature sets for each study utilized included 16 gray-level intensity features (quantifying statistics of the raw intensity within a specific window size of 3 × 3, 5 × 5, 7 × 7, and 9 × 9), 40 intensity gradient-based features (quantifying intensity gradient variability), 52 gray-level co-occurrence matrix (GLCM) Haralick features (capturing disorder patterns of the adjacent pixel intensities within local pixel neighborhoods) (16), 20 Laws energy (capturing combinations of five irregular texture enhancement patterns: levels, spots, edges, waves and ripples in an image) (17), 28 Gabor wavelet-based features (capturing structural detail at seven orientations of 22.5°, 45°, 67.5°, 90°, 112.5°, 135°, 157.5°, and 4 scales of 2, 4, 8, and 12 pixels) (18), and 52 CoLlAGe features (capturing textural heterogeneity by applying GLCM metrics to local anisotropic gradient orientations) (19). All of these texture features were extracted in both intratumoral and peritumoral compartments (0–5, 5–10, and 10–15 mm) on all slices containing the tumor. Statistics of mean, median, standard deviation, skewness, and kurtosis were calculated from the feature responses of all pixels within the region of interest. A list of the extracted features is summarized in **Supplementary Table S1**, with their detailed descriptions provided in **Appendix E1**, section 2. All feature values were transformed into new scores with a mean of 0 and a SD of 1 (z-score transformation). Both intratumoral and peritumoral feature extraction pipelines are now publicly available at https://github.com/ccipd.

Statistical Analysis

Within the TCIA cohort, 462 patients were randomly allocated to S_T (180 patients: 100 HPV+ and 80 HPV–) and S_V (282 patients: 237 HPV+ and 45 HPV–) in an approximately 3:5 ratio. For both HPV+ and HPV– patients, the ratio of non-censored

patients in S_T and S_V was kept balanced. The clinical end points of interest for this study were HPV status and DFS. DFS was defined as the time interval from the radiotherapy end date to the date of either last follow-up (censored) or local, regional, distant failure and death (event), whichever happened first. The difference of continuous variables (i.e., age) between cohorts (i.e., S_T, S_V, and S_{CCF}) was determined using the analysis of variance (ANOVA) and the association between categorical factors was estimated using the chi-square test.

Since there were no HPV− patients in the CCF cohort, we used only the TCIA cohort for HPV status prediction. A machine learning classifier was first constructed using a combination of intratumoral and peritumoral features for the prediction of HPV status using S_T. To remove redundant features, all possible pairs of features in S_T were tested for correlation by calculating the Spearman correlation coefficient (SCC). For any pair of features with SCC greater than 0.80, the feature with the higher Wilcoxon rank sum *p*-value was removed. A linear discriminant analysis (LDA) machine-learning classifier was subsequently trained in conjunction with the minimum redundancy–maximum relevance (MRMR) (20) feature selection approach using a 100-run, 3-fold cross-validation setting. The top 15 most frequently selected radiomic features (F_t) that best discriminated between HPV+ vs. HPV− across all iterations were identified from S_T. An unadjusted *p*-value <0.05 (using two-sided Wilcoxon rank sum tests) was employed to indicate statistical significance. These features were then evaluated *via* the LDA classifier in terms of HPV status prediction on S_V using the area under the receiver operating characteristic curve (AUC) metric.

We also developed dedicated radiomic risk score classifiers for patients within the individual HPV+ (RRS_{HPV+}) and HPV− (RRS_{HPV-}) categories. The least absolute shrinkage and selection operator (LASSO) method was applied to F_t using the cases in S_T for both HPV+ and HPV− patients. After identifying the top ranked features, the corresponding LASSO coefficients were used for constructing risk classifiers for the HPV+ (RRS_{HPV+}) and HPV− (RRS_{HPV-}), respectively. Both RRS_{HPV+} and RRS_{HPV-} were calculated for each patient *via* a linear combination of selected features that were weighted by corresponding coefficients:

$$RRS_{HPV+/-} = \Sigma_{i=1}^{n} \beta_i * x_i$$

where *n* (ranging from 0 to 15) is the number of features selected by LASSO for HPV+ or HPV− patients, x_i refers to the HPV status-associated feature value, and β_i is the corresponding weighted coefficient. The potential association of RRS_{HPV+} and RRS_{HPV-} with DFS was first assessed in S_T and then evaluated in S_V. The prognostic ability of RRS_{HPV+} was further externally validated in S_{CCF}. Patients were classified into high or low risk based on the median value of the RRS_{HPV+} or RRS_{HPV-} in S_T, which was then applied to S_V and S_{CCF}. Kaplan–Meier survival curves were used to visualize the survival rate for the high- and low-risk groups. At any given point on the survival curve, the probability that a patient in either the high-risk or low-risk group remains alive is presented (21). The log-rank test and hazard ratio were used to compare the survival differences between the two groups. The same Kaplan–Meier survival analyses were further performed for each cancer stage group defined by the AJCC eighth edition on the dataset combining S_V and S_{CCF}. The final values for *n* were determined when the hazard ratio for high risk over low risk reached the highest in S_V for HPV+ patients (**Supplementary Figure S4**). The value of the tuning parameter in the LASSO-Cox model (λ) was averaged out by 10 cross-validation to minimize the error within S_T. Constructions of RRS_{HPV+} and RRS_{HPV-} were performed using in-house software implemented in the MATLAB R2019b platform (MathWorks).

Univariate Cox proportional hazards analysis on the effect of RRS_{HPV+}, RRS_{HPV-}, and the individual clinicopathologic variables (gender, smoking status, drinking status, T stage, N stage, and AJCC eighth edition of overall stage) on DFS was evaluated. Variables significant in univariate analysis were included for multivariable Cox proportional hazards analysis to investigate the relationships between the various covariates (including the RRS_{HPV+}, RRS_{HPV-}, and the clinicopathologic variables).

To further investigate the independent prognostic value of the RRS_{HPV+} with existing clinical factors (gender, smoking, and drinking status) and pathological staging factors (T stage, N stage, and the AJCC stage eighth edition), we constructed nomogram models for HPV+ patients comprising i) only the clinical factors (M_c) of gender, smoking, and drinking history; ii) only the pathologic staging factors (M_p) of AJCC eighth edition overall stage and N stage; and iii) both the pathologic T stage and the RRS_{HPV+} (M_{p+RRS}) using S_T and validated them in S_V and S_{CCF}. The prognostic ability of M_{p+RRS} was compared against M_c and M_p for HPV+ populations in terms of the concordance index (C-index). The nomograms were validated using 1,000 bootstrap resampling to calculate C-index with confidence intervals. Calibration curve analysis was performed to compare the nomogram-predicted DFS with the actual DFS. Decision curve analysis was adopted to calculate the net benefit for M_{p+RRS} in comparison with M_c and M_p, for verification of the clinical usefulness of the nomogram (22). Nomogram construction, calibration plot, and decision curve were implemented using the "rms" and "SvyNom" packages under R statistical software (version 4.0.3; R Foundation for Statistical Computing, Vienna, Austria).

RESULTS

Clinicopathologic Characteristics

The clinical and pathologic characteristics of patients in the TCIA training set (S_T), TCIA internal validation set (S_V), and CCF external validation set (S_{CCF}) are summarized in **Table 1**. No significant differences were found in most features among S_T, S_V, and S_{CCF}. All patients included in this study underwent radiotherapy. Eighty-seven of the 180 patients in S_T (48.3%) and 145 of the 282 patients in S_V (51.4%) were also treated with chemotherapy. The median DFS for HPV+ patients was 6.19 years in S_T and 6.24 years in S_V. The median DFS for HPV− patients was 1.27 years in S_T and 1.55 years in S_V. Thirty-three

percent (33/100, 6 local) and 33% (79/237) of HPV+ patients were not censored in S_T and S_V, respectively, while 77.5% (62/80) and 68.9% (31/45) of HPV− patients were not censored in S_T and S_V, respectively. There were 62 (18.4%) recurrences (15 local, 8 regional, and 39 distant) for HPV+ patients and 64 (51.2%) recurrences (30 local, 11 regional, and 23 distant) for HPV− patients.

Experiment 1: Prediction of HPV Status

Within S_T, 454 uncorrelated intratumoral and peritumoral features were obtained after feature pruning. From these uncorrelated features, the top 15 were identified for predicting HPV status by MRMR feature selection, of which 11 were peritumoral features and 4 were intratumoral features (**Table 2**).

Changes in classification performance on account of differently selected features in S_T are provided in **Supplementary Figure S2**. Standard deviation of CoLlAGe sum of variance from the 0–5-mm rings (**Figure 2C**) was identified as the most discriminating peritumoral feature ($p < 0.001$), while the median of Haralick correlation-info1 (**Figure 2B**) was identified as the most discriminating feature ($p < 0.001$) within the tumor. Both features were differentially expressed on CT scans between HPV+ and HPV− patients, and representative examples are illustrated *via* colormaps of the feature representations overlaid on the tumor areas or the annular ring regions around the tumor (**Figure 2A**). Noticeably, three of the four selected Haralick features were measures of correlation applied with different statistics on both intratumoral and peritumoral regions, suggesting that there might be significant pixel correlation-related pattern differences between the HPV+ and HPV− patients. We also observed consistently higher Laws feature values for HPV− patients compared with HPV+ across S_T and S_V. These features quantify intensity smoothness, abrupt edge changes, and ripple patterns on CT scans. Interestingly, all the selected Laws and Gabor features were from regions outside the tumor. Further details on the selected features are provided in **Supplementary Figure S3**.

The areas under the curve (AUCs) for using intratumoral and peritumoral alone on S_T are 0.82 (95% CI: 0.76, 0.88) and 0.87 (95% CI: 0.81, 0.92), respectively. The corresponding AUCs on S_V are 0.58 (95% CI: 0.49, 0.67) and 0.67 (95% CI: 0.58, 0.76). When combining the intratumoral and peritumoral features, ROC analysis on S_T yielded an accuracy of 0.79 and AUC of 0.84 (95% CI: 0.78, 0.90), with a sensitivity of 0.89 and specificity of 0.68 when using a threshold of 0.4. For S_V, we obtained an accuracy of 0.74 and an AUC of 0.70 (95% CI: 0.62, 0.79), with a sensitivity of 0.78 and specificity of 0.53 when the same threshold from S_T was applied. **Figure 2D** illustrates that using combined peritumoral and intratumoral features improved AUC compared with only using the intratumoral features and using only the peritumoral features for predicting HPV status.

Experiment 2: Prognosticate DFS for Both HPV− and HPV+ Patients, Including Within Individual AJCC Eighth Edition-Defined Stage Groups

A three-feature radiomic signature was identified as having the best prediction of DFS for both HPV+ and HPV− patients (**Supplementary Figure S4**). The radiomic risk scores for HPV+ patients (RRS_{HPV+}) and HPV− patients (RRS_{HPV-}) across S_T, S_V, and S_{CCF} are illustrated in **Supplementary Figure S5**. Details of the features selected are provided in **Table 2**, with their coefficients in the Cox model provided in **Supplementary Figure S6**. RRS_{HPV+} was constructed using two peritumoral and one intratumoral features, while RRS_{HPV-} was constructed using three peritumoral features. The median RRS_{HPV+} value (−0.0809) in S_T was used as the cutoff threshold for defining high- and low-risk groups, resulting in statistically significant

TABLE 2 | Top 15 features for HPV status prediction and notation of involvement in HPV status-specific prognostic prediction in experiment 2.

Feature names (parameters)	ROI	Rank sum *p*-value (unadjusted)	Contribute to DFS prediction for HPV +?	Contribute to DFS prediction for HPV −?
CoLlAGe (Std of sum-variance)	Peritumoral 0–5 mm	3.0×10^{-7}	✗	✗
Haralick (mean of Info1)	Peritumoral 0–5 mm	1.3×10^{-8}	✗	✗
Gabor (median, $\lambda = 3$, $\theta = 0.1$ rad)	Peritumoral 5–10 mm	8.5×10^{-6}	✓	✓
CoLlAGe (skewness of sum-average)	Peritumoral 5–10 mm	0.0046	✗	✓
CoLlAGe (kurtosis of diff-average)	Peritumoral 0–5 mm	1.78×10^{-4}	✗	✗
Haralick (Std of Info1)	Peritumoral 5–10 mm	4.7×10^{-4}	✗	✗
Gabor (skewness, $\lambda = 5$, $\theta = 0.0$ rad)	Peritumoral 10–15 mm	0.001	✗	✗
Laws (median of E5L5)	Peritumoral 10–15 mm	0.0335	✗	✗
Laws (skewness L5R5)	Peritumoral 0–5 mm	6.5×10^{-4}	✗	✗
Gabor (kurtosis, $\lambda = 3$, $\theta = 0.6$ rad)	Peritumoral 0–5 mm	4.8×10^{-6}	✗	✓
CoLlAGe (Std of sum-average)	Peritumoral 0–5 mm	5.3×10^{-5}	✓	✗
Haralick (median of info1)	Intratumoral	1.8×10^{-5}	✗	✗
CoLlAGe (skewness of diff-variance)	Intratumoral	4.4×10^{-4}	✗	✗
Gray (median of mean intensity)	Intratumoral	0.001	✓	✗
Haralick (skewness of diff-variance)	Intratumoral	0.005	✗	✗

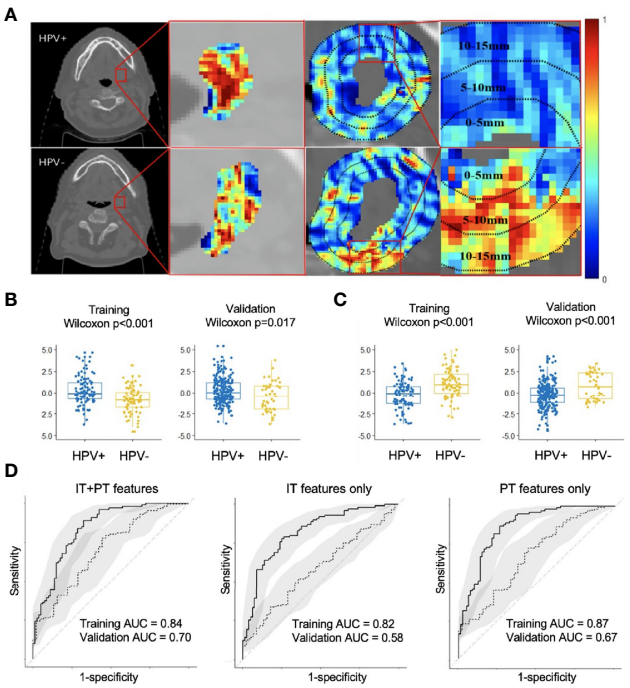

FIGURE 2 | Feature map for the best intratumoral and peritumoral features expressing differently on the example HPV+ and HPV– CT slices overlaid with either tumor or annular ring areas around the tumor **(A)**. Boxplots showing distribution differences for the best intratumoral **(B)** and peritumoral feature **(C)** between HPV+ and HPV– patients in both training (S_T) and validation (S_V). Receiver operating characteristic (ROC) analysis of radiomic features for predicting HPV status on training (S_T, n = 180) and validation (S_V, n = 282) cohorts with confidence intervals **(D)**. Using combined intratumoral and peritumoral features yielded the best result in S_V. IT, intratumoral; PT, peritumoral.

DFS prediction by KM analysis in S_T (log-rank test, p = 0.026, HR = 2.18), S_V (log-rank test, p = 0.003, HR = 1.94), S_{CCF} (log-rank test, p = 0.033, HR = 2.32), and S_V+S_{CCF} (log-rank test, p < 0.001, HR = 1.97) as illustrated in **Figures 3A–D**, respectively. The median RRS_{HPV-} value (0.0076) in S_T also resulted in a statistically significant prediction of DFS by Kaplan–Meier analysis in both the S_T (log-rank test, p < 0.001, HR = 2.49) and S_V (log-rank test, p = 0.023, HR = 2.41), as illustrated in **Figures 3E, F**, respectively.

The prognostic ability of the radiomic risk score (RRS_{HPV+}) was further evaluated for the patients within the AJCC eighth edition-defined different stage groups in S_V+S_{CCF}. The HRs of predicting DFS using RRS_{HPV+} for stage I (**Figure 4A**), stage II (**Figure 4B**), and stage III (**Figure 4C**) HPV+ patients were 1.99 (95% CI: 1.04–3.83, p = 0.039), 3.61 (1.71–7.62, p < 0.001), and 1.4 (0.746–2.63, p = 0.294), respectively.

Results of the univariable analysis are shown in **Table 3**. T3 stage, a moderate or heavy drinking history, and a higher RRS_{HPV+} were significantly associated with worse DFS for the HPV+ population in S_T. N2 stage and a higher RRS_{HPV-} were significantly associated with worse DFS for the HPV– population in S_T. In multivariable analysis, RRS_{HPV+} (DFS hazard ratio, 30.12, 95% CI: 5.67–159.96, p < 0.001) and T3 stage (DFS hazard ratio, 2.94, 95% CI: 1.02–8.45, p = 0.04) remained independent prognostic factors for HPV+ patients in the Cox proportional hazards model (**Table 4**). For HPV– patients, RRS_{HPV-} (DFS hazard ratio, 3.37, 95% CI: 1.93–5.88, p < 0.001), N1 stage (DFS hazard ratio, 2.08, 95% CI: 1.06–4.07, p = 0.03), and N2 stage (DFS hazard ratio, 2.55, 95% CI: 1.21–5.36, p = 0.01) were the independent prognostic factors in the multivariable Cox proportional hazards model.

Experiment 3: Using Radiomic Nomogram M_{p+RRS} to Prognosticate DFS Among HPV+ OPSCC

Variables significant in both univariable and multivariable analyses (pathologic T stage and RRS_{HPV+}) were used to develop the radiomic nomogram M_{p+RRS} (**Figure 5A**) for HPV+ patients. The calibration curve of M_{p+RRS} for estimating DFS showed good agreement between the predicted and the observed survival probability in both S_T (**Figure 5B**) and the combined validation set S_V+S_{CCF} (**Figure 5C**). The C-index of M_{p+RRS} for estimating DFS in S_T was 0.72 (95% CI: 0.62–0.81), while the C-index for the pathologic staging nomogram M_p was 0.62 (95% CI: 0.51–0.72), and that for the nomogram M_c using gender, smoking, and drinking history was 0.59 (95% CI: 0.49–0.69). When evaluated on S_V+S_{CCF}, M_{p+RRS} yielded a C-index of 0.59 (95% CI: 0.54–0.65) for DFS prediction, while for M_p and M_c, the C-indices were 0.59 (95% CI: 0.53–0.64) and 0.56 (95% CI: 0.51–0.61), respectively. The Kaplan–Meier survival curves for M_{p+RRS} in S_T and in S_V+S_{CCF} are shown in **Figures 3G, H**. In addition, M_{p+RRS} was significantly associated with DFS, independent of M_c and M_p in the multivariable analysis when evaluated on S_T+S_V+S_{CCF} (**Table 5**). In the decision curve analysis, M_{p+RRS} yielded a better net benefit compared with M_c or M_p individually when the threshold probability <0.35 (**Figure 5D**).

When evaluating the prognostic ability of M_{p+RRS} for HPV+ patients in S_V+S_{CCF} within each AJCC eighth edition-defined stage group, univariable Cox proportional hazard regression yielded HRs of 1.25 (95% CI: 0.66–2.36, p = 0.493) for stage I, 2.07 (0.915–4.68, p = 0.081) for stage II, and 2.32 (1.22–4.41, p = 0.01) for stage III patients. The corresponding KM curves are shown in **Figures 4D–F**.

DISCUSSION

HPV+ OPSCC has better clinical prognosis and treatment response than the alcohol- and tobacco-related HPV– OPSCC (23). Because of this, treatment deintensification to reduce therapy-related morbidity in "low-risk" HPV+ OPSCC patients is being considered. However, a recent phase II randomized controlled trial by Yom et al. reported that patients in whom therapy was deintensified based on traditional TNM staging information did not meet the goal of 2-year DFS >85% (7). This was likely due to the lack of biomarkers for identifying patients who would most benefit from therapy deintensification. Although the AJCC eighth edition staging system represents a

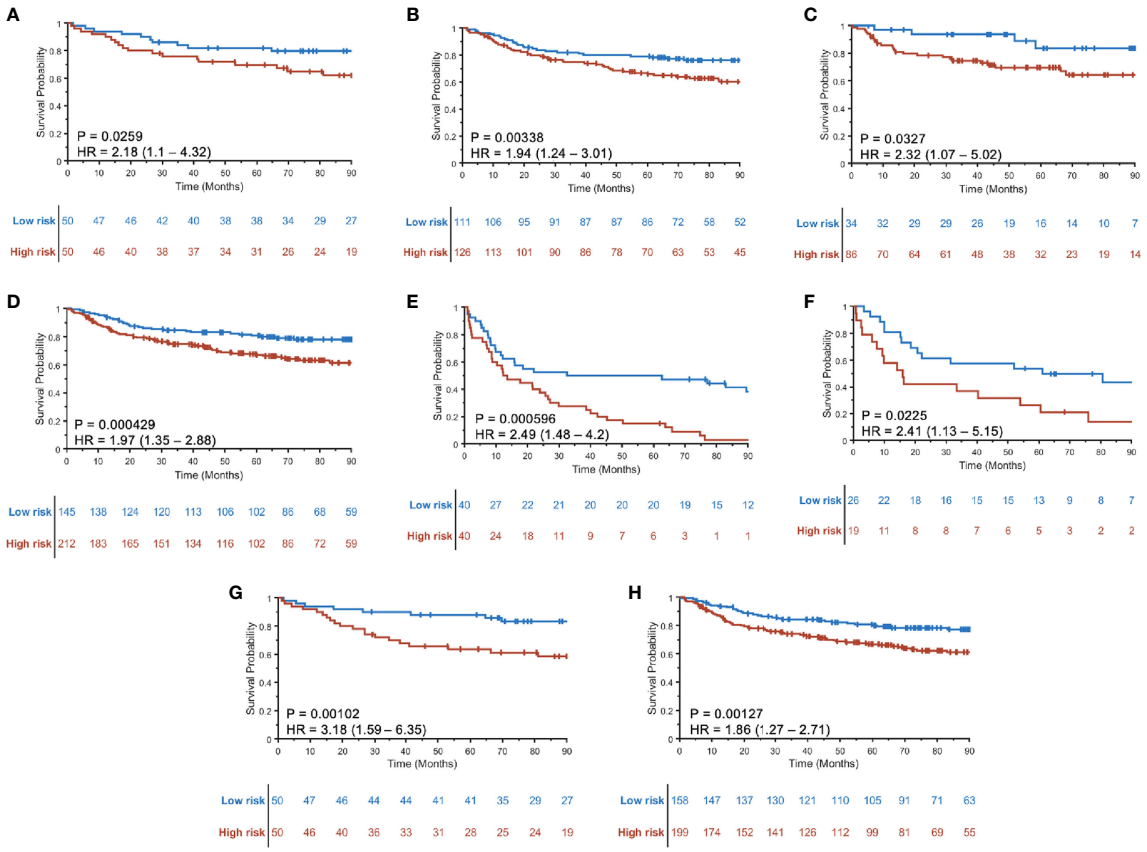

FIGURE 3 | Kaplan–Meier curves for disease-free survival (DFS) using RRS_{HPV+} in training S_T **(A)**, internal validation S_V **(B)**, external validation S_{CCF} **(C)**, and the combined validation set S_V+S_{CCF} **(D)**. Kaplan–Meier curves for DFS prediction using RRS_{HPV-} in S_T **(E)** and S_V **(F)**. DFS prediction for HPV+ patients in the S_T **(G)** and S_V+S_{CCF} set **(H)** using radiomic nomogram (M_{p+RRS}), which contains pathologic tumor stage and the RRS_{HPV+}.

major improvement over the seventh edition, better and more reliable methods for pretreatment prognostication are needed for therapeutic decision-making. The radiomic biomarkers presented in this study aimed to identify those truly low-risk HPV+ patients within both the whole and AJCC eighth edition stage 1 population groups, for whom treatment deintensification should be considered.

In this work, we investigated the ability of both intratumoral and peritumoral radiomic biomarkers on CT scans to predict HPV status for a large cohort of 462 OPSCC patients. Additionally, we addressed the OPSCC prognosis prediction problem independently within the HPV+ and HPV– populations. The radiomic signature which was prognostic for the whole HPV+ population was also prognostic within the AJCC eighth edition stage I and stage II patients. Finally, the radiomic features were combined with pathologic staging factors to form a radiomic nomogram for individualized prognosis estimation for HPV+ OPSCC patients.

Currently, measuring p16 protein expression *via* immunohistochemistry is the recommended test for determining HPV status. However, distinct populations of patients exist in whom the tumors overexpress p16 but are in fact negative for HPV-DNA or mRNA expression and vice versa (24). Consequently, using p16 testing alone to determine HPV status results in some misclassified patients. Additional biomarkers are needed to complement the p16 testing. In the first experiment, we demonstrated that radiomic features from within the tumor and annular rings of 0–15 mm outside the tumor on CT imaging could reasonably predict HPV status of OPSCC, with an overall accuracy of 76%. A recent study by Leijenaar et al. designed a statistical framework for HPV status prediction, and they found that HPV+ tumors are more homogeneous in CT densities (25). This finding is in alignment with the result of this study. Specifically, HPV+ tumors possess a more homogeneous morphologic appearance in terms of CT texture patterns compared with HPV– tumors, which in turn is characterized by the Haralick correlation of information measured within the tumor (**Figure 2A**, second column). A higher value of the Haralick correlation indicates less pixel intensity disorders and decreased morphologic appearance heterogeneity for HPV+ tumors compared with HPV– tumors. Similar to the findings we report, Bagher-Ebadian et al. reported that HPV+ tumors have consistently lower energy components for seven frequency bands quantified by the DOST features (26). Although the discriminating textural features we identified are

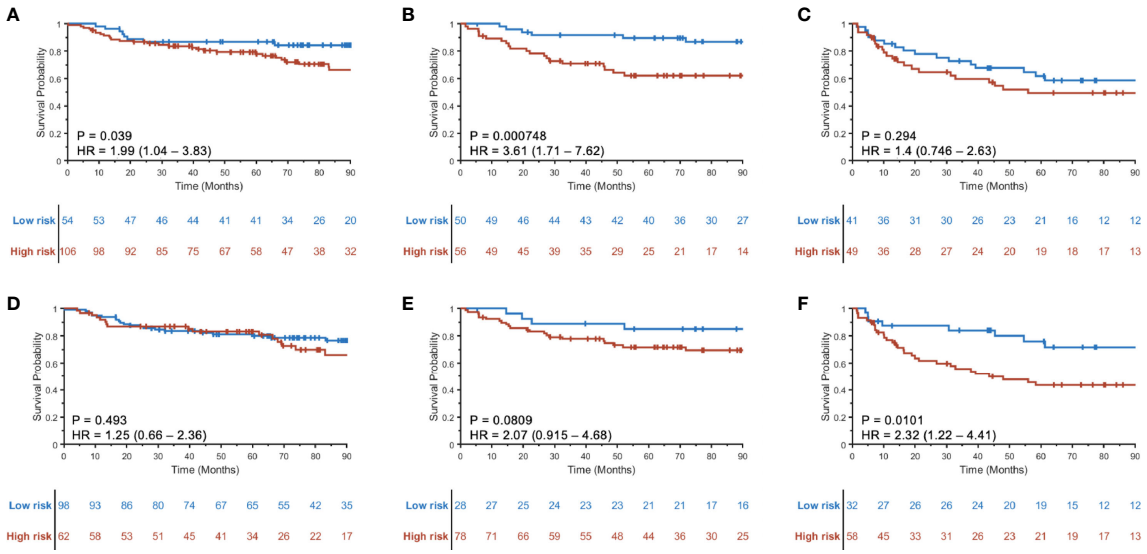

FIGURE 4 | Kaplan–Meier curves for prognostication using RRSHPV+ within the AJCC eighth edition-defined overall stage I **(A)**, II **(B)**, and III **(C)** HPV+ OPSCC patients. Similarly, Kaplan–Meier curves using the radiomic nomogram M_{p+RRS} for prognostication within overall stage I **(D)**, II **(E)**, and III **(F)** HPV+ OPSCC patients.

different from previous studies, the interpretations of the features are similar. However, we also found higher gray-level intensity values of HPV+ tumors compared with HPV– tumors on CT, which appears to be at odds to the findings of the study by Leijenaar et al. (25). In addition, our study represents the first study for integrating CT radiomic both within and around the tumor for OPSCC HPV status prediction. We demonstrate the superior discriminability of peritumoral CT radiomic features, which appears to suggest discriminable differences of the microenvironment in the regions immediately outside the tumor. HPV– patients are best characterized by a combination of local intensity disorder and microscale heterogeneity in gradient orientation, particularly outside the tumor. Specifically, a higher peritumoral variation of the gradient orientation defined by the CoLlAGe sum of variance was observed in HPV– compared with HPV+ tumors. Reduced expression of Haralick information

TABLE 3 | Univariable Cox proportional hazard model analysis in the training set (S_T) for HPV+ and HPV– patients.

Variables	HPV+ patients		HPV– patients	
	HR (95% CI)	*p*-value	HR (95% CI)	*p*-value
Gender (female *vs.* male)	1.32 (0.78–1.84)	0.41	1.12 (0.63–1.86)	0.97
Smoking history (current smoker *vs.* non-/ex-smoker)	1.36 (0.54–3.39)	0.39	1.04 (0.63–1.73)	0.87
Drinking history (moderate/heavy drinker *vs.* non-/ex-/light drinker)	1.66 (1.05–2.42)	**0.02**	1.21 (0.72–2.05)	0.47
T stage				
T1	Ref		Ref	
T2	1.26 (0.42–3.78)	0.82	0.88 (0.32–2.39)	0.80
T3	2.9 (1.03–8.15)	**0.03**	1.11 (0.42–2.91)	0.83
T4	2.9 (0.84–10.13)	0.09	1.17 (0.42–3.22)	0.76
N stage				
N0	Ref		Ref	
N1	0.71 (0.26–1.96)	0.51	2.12 (0.89–4.13)	0.14
N2	0.82 (0.27–2.46)	0.72	2.61 (1.25–5.41)	**0.01**
N3	1.47 (0.35–6.20)	0.59	2.40 (0.85–6.75)	0.10
Overall stage (AJCC eighth edition)				
I	Ref		Ref	
II	1.81 (0.82–3.99)	0.14	1.02 (0.55–1.90)	0.94
III	2.19 (0.85–5.68)	0.11	1.27 (0.66–2.42)	0.47
RRS_{HPV+} ($RRS_{HPV–}$)	29.45 (7.2–120)	**<0.0001**	6.28 (2.06–19.16)	**0.0007**

Bold values refer to significant p values < 0.05.

TABLE 4 | Multivariable Cox proportional hazard model analysis in the training set (S_T) for HPV+ and HPV– patients.

HPV+ patients			HPV– patients		
Variables	**HR (95% CI)**	***p*-value**	**Variables**	**HR (95% CI)**	***p*-value**
Drinking history (moderate/heavy drinker *vs.* non-/ex-/light drinker)	0.81 (0.36–1.82)	0.61	N stage		
			N0	Ref	
			N1	2.08 (1.06–4.07)	**0.03**
			N2	2.55 (1.21–5.36)	**0.01**
			N3	2.80 (0.98–7.97)	0.054
T stage			RRS_{HPV-}	3.37 (1.93–5.88)	**<0.0001**
T1	Ref				
T2	1.22 (0.38–3.92)	0.74			
T3	2.94 (1.02–8.45)	**0.04**			
T4	2.56 (0.70–9.35)	0.16			
RRS_{HPV+}	30.12 (5.67–159.96)	**<0.0001**			

Bold values refer to significant p values < 0.05.

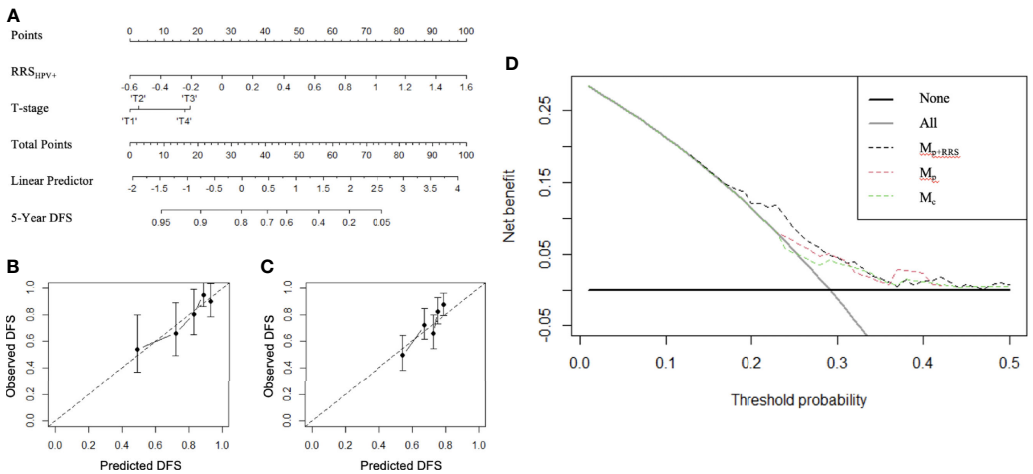

FIGURE 5 | The constructed radiomic nomogram M_{p+RRS} **(A)** integrating the pathologic tumor stage (T stage) with the RRS_{HPV+}. RRS_{HPV+} has more effect on DFS than the T stage, as indicated by a wider range of the total points. Calibration curves have good agreement between predicted and actual survival probability on S_T **(B)** and S_V +S_{CCF} **(C)**. Decision curve on S_T+S_V+S_{CCF}
(D) compared the clinical usefulness of radiomic nomogram M_{p+RRS} (black dash line) in DFS prediction against the pathologic staging nomogram M_p (red dash line) and the clinical nomogram M_c (green dash line).

TABLE 5 | Comparison between the radiomic nomogram M_{p+RRS}, the pathologic staging nomogram M_p, and the clinical factors nomogram M_c for DFS prediction in S_T+S_V+S_{CCF}.

M_{p+RRS}, M_c, and M_p (S_T+S_V+S_{CCF}, *N* = 457, 136 died or had recurrence)				
Model	**HR (95% CI)**	**C-index (95% CI)**	**Univariable *p*-value**	**Multivariable *p*-value**
M_{p+RRS}	1.6 (1.4–2)	0.62 (0.57–0.67)	<0.001***	<0.001***
M_p	2.2 (1.4–3.5)	0.59 (0.55–0.64)	<0.001***	0.057
M_c	2.1 (1.4–3)	0.57 (0.52–0.61)	<0.001***	0.072

****refers to extreme significant p values < 0.001.*

capturing low level of correlation between adjacent pixels was also an important component of the peritumoral radiomic signature for HPV– patients. Furthermore, HPV– peritumoral regions were characterized by abrupt changes in edges, ripples, and intensity smoothness, as detected by the elevated expression of Laws features. These findings are consistent with previous studies, which showed that HPV+ tumors have less stroma overall, have smoother borders to the nests and leading edges, and are more homogeneously cellular usually without keratin production (27–29).

In the second experiment, we evaluated the prognostic ability of the HPV status-associated radiomics features found in experiment

1, to separately stratify HPV+ and HPV− OPSCC patients into high- and low-risk groups based on DFS. We constructed dedicated radiomic risk scores (RRS_{HPV+}, RRS_{HPV-}), which yielded significant risk stratification based on DFS in the validation set for both HPV+ and HPV− populations. A previous study by Leijenaar et al. externally validated the prognostic value of intratumoral radiomic signatures in a larger cohort of 542 OPSCC (C-index = 0.628, $p < 0.001$) but did not consider the variation of the results by HPV status (30). Vallières et al. used radiomic features from pretreatment FDG-PET and CT images of 300 patients from four different cohorts to prognosticate outcomes in head and neck cancer (31). They obtained C-indices of 0.63, 0.88, and 0.60 for local, regional, and distant recurrence-free survival. Aerts et al. trained a prognostic radiomic model on 422 patients with lung cancer and validated on 231 patients with head and neck cancers (32), achieving a concordance index of 0.69 ($p < 0.001$) on the validation set. However, unlike our study, this study did not consider HPV status as an independent prognostic indicator for outcome prediction. The prognostic ability of the radiomic risk score (RRS_{HPV+}) was also evaluated within each of the AJCC eighth edition-defined stage groups. Although various treatment deintensification strategies have been proposed by multiple clinical trials based on clinicopathologic factors, there is a lack of reliable biomarkers for risk-stratifying OPSCC patients within individual stage groups. In the HN002 trial, patients meeting criteria of either T1-T2 N1-N2b M0 or T3 N0 N-2b M0 (AJCC seventh ed.) with a ≤10 pack-year smoking history are selected as candidates for therapy deintensification (7). Their results showed that patients randomly assigned to the non-chemotherapy arm did not meet the goal of 2-year DFS >85%. The authors also reported that for these patients using a low-than-standard-dose radiotherapy resulted in a higher rate of locoregional failure. This indicates that risk stratification based on grouping of clinicopathologic factors alone is not robust and there is a clear unmet clinical need for developing more granular and more objective biomarkers to identify patients who could truly benefit from treatment de-escalation. Clinically, stage I and stage II patients are the current target for treatment de-escalation. However, a subset of these patients still had poor survival outcome and would not benefit from treatment de-escalation (33). The CT radiomic risk score developed in this study represents a potential useful tool for guiding treatment intensities within the early-stage HPV+ OPSCC patients. By applying the threshold defined from the training set, the learned radiomic risk scores could further separate the stage I and stage II HPV+ patients into high- vs. low-risk groups based on disease-free survival. As such, the radiomic biomarker presented in this study could potentially help to distinguish patients within the current AJCC eighth edition definition of low risk as to which patients will benefit from treatment deintensification vs. those who will not. The findings of this study are consistent with a recently published study, where a histology-based imaging biomarker (MuNi) was found to be associated with survival for stage I and stage II patients (34). Noticeably, the prognostic radiomic features identified in this study are mainly from peritumoral compartments. One possible explanation for this is that the peritumoral radiomic features are associated with tumor-infiltrating HPV-specific immune responses prior to treatment, which have been more commonly found floating around the tumor without actual penetration or action into the tumor core and are strongly associated with prognosis (35, 36).

In the third experiment, we developed a radiomic nomogram M_{p+RRS} for HPV+ DFS prediction. Currently, the conventional TNM and AJCC staging systems are routinely used for risk stratification and prognosis estimation. They reflect tumor size (T), lymph node status (N), and cancer metastasis (M). However, these staging factors could not capture the intratumor heterogeneity, which has been shown to be a significant prognostic factor. The radiomic nomogram combined the pathologic staging information with the radiomic features extracted from the entire tumor on CT scans, enabling for robust pretreatment survival estimation. Combining the RRS_{HPV+} from experiment 2 with the pathologic T stage resulted in a nomogram that leads to a more individualized prognosis prediction. With refinement and improvement, this type of radiomic approach might guide more tailored treatment for patients with better survival outcome. Compared with risk stratification using only the conventional staging factors, the radiomic nomogram had an improved DFS estimation. A previous study by Fakhry et al. showed that a nomogram integrating clinicopathologic factors (i.e., HPV status, T and N stages) could reliably predict progression-free survival (37), which is in alignment with our results. Based on our results, T3 stage is significantly associated with worse DFS for HPV+ patients, while N1 and N2 stages are significantly associated with worse DFS for HPV− patients in both univariable and multivariable analyses. With regard to the radiomic nomogram for head and neck cancer, Zhang et al. built multiparametric MRI-based radiomic nomograms for predicting nasopharyngeal carcinoma prognosis and obtained C-index of 0.776 for PFS prediction (38). Yuan et al. proved that a nomogram consisting of MRI radiomic signatures and TNM stage could better predict head and neck cancer prognosis with a C-index of 0.72 on the validation set (39). The prognostic performance difference between our new CT-based nomogram and the MRI-based nomogram may be on the higher image resolution offered by multiparametric MRI, although CT tends to be used more routinely compared with MRI for head and neck cancer. We also noted that both patient cohorts from Zhang et al. (38) and Yuan et al. (39) comprised a majority of advanced stage head and neck cancer patients (100% and 70.6%), while our training and validation cohorts consist of only 17% and 26.6% of stage III and no stage IV OPSCC patients. This may also influence the performance of the model since intratumor heterogeneity could be more easily captured within those aggressive tumors.

Our study does have several limitations. First, the prognostic biomarker validation on a single cohort was done in a retrospective manner. Second, we predicted neither benefit of existing treatments for the two populations nor treatment response within the individual AJCC eighth edition-defined stage groups. These aims will be part of our future study involving large multisite and multimodality evaluation of radiomic signatures in predicting treatment response for the two populations. Third, we acknowledge the limitation of our

dataset from the TCIA in terms of HPV status based on p16 testing which may not accurately reflect the true transcriptionally active HPV status, at least for a small percentage of patients. Nonetheless, this study demonstrates that CT radiomic features could, in theory, complement the existing p16 testing method in distinguishing HPV status.

Despite the aforementioned limitations, this study is the first to show the role of combined intratumoral and peritumoral radiomic features in predicting HPV status of OPSCC patients. It is also the first study to incorporate both radiomic signatures and corresponding nomograms for prognosis prediction for HPV+ and HPV− patients. If confirmed in prospective clinical trials, this radiomic nomogram pipeline could enrich the existing AJCC eighth staging systems for risk-stratifying OPSCC patients. One can imagine a strategy where numerous sources of data go into predictive models for patient care. Especially attractive here is that all patients received pretreatment cross-sectional CT scans so the data are already garnered in digitized form, easily available for radiomics-based nomograms for prognosis prediction.

DATA AVAILABILITY STATEMENT

The raw data supporting the conclusions of this article will be made available by the authors, without undue reservation.

ETHICS STATEMENT

The studies involving human participants were reviewed and approved by Cleveland Clinic. The patients/participants provided their written informed consent to participate in this study.

AUTHOR CONTRIBUTIONS

BS: conceptualization, data curation, formal analysis, methodology, investigation, writing—original draft, and writing—review and editing. KY: conceptualization, investigation, and writing—review and editing. JG: writing—review and editing. CL: writing—review and editing. LL: formal analysis and investigation. NB: writing—review and editing. CK: writing—review and editing. PT: resources and investigation. PF: conceptualization, investigation, and writing—review and editing. SK: resources, investigation, and writing—review and editing. JSL: resources, investigation, and writing—review and editing. AM: conceptualization, methodology, investigation, supervision, funding acquisition, project administration, and writing—review and editing. All authors contributed to the article and approved the submitted version.

FUNDING

Research reported in this publication was supported by the National Cancer Institute under award numbers 1U24CA199374-01, R01 CA24999201A1, R01CA202752-01A1, R01CA208236-01A1, R01CA216579-01A1, R01CA220581-01A1, 1U01CA239055-01, 1U01CA248226-01, and 1U54CA254566-01; National Heart, Lung and Blood Institute 1R01HL15127701A1; National Institute for Biomedical Imaging and Bioengineering 1R43EB028736-01; National Center for Research Resources under award number 1 C06 RR12463-01; VA Merit Review Award IBX004121A from the United States Department of Veterans Affairs Biomedical Laboratory Research and Development Service; the Office of the Assistant Secretary of Defense for Health Affairs, through the Breast Cancer Research Program (W81XWH-19-1-0668), the Prostate Cancer Research Program (W81XWH-15-1-0558, W81XWH-20-1-0851), the Lung Cancer Research Program (W81XWH-18-1-0440, W81XWH-20-1-0595), and the Peer Reviewed Cancer Research Program (W81XWH-18-1-0404); the Kidney Precision Medicine Project (KPMP) Glue Grant; the Ohio Third Frontier Technology Validation Fund; the Clinical and Translational Science Collaborative of Cleveland (UL1TR0002548) from the National Center for Advancing Translational Sciences (NCATS) component of the National Institutes of Health and NIH roadmap for Medical Research; and the Wallace H. Coulter Foundation Program in the Department of Biomedical Engineering at Case Western Reserve University. KY was supported by the Computational Genomic Epidemiology of Cancer (CoGEC) Program at Case Comprehensive Cancer Center (T32CA094186).

ACKNOWLEDGMENTS

The authors would like to thank Dr. Christina Buzzy and Katherine Gullett for manuscript revisions.

SUPPLEMENTARY MATERIAL

The Supplementary Material for this article can be found online at: https://www.frontiersin.org/articles/10.3389/fonc.2021.744250/full#supplementary-material

REFERENCES

1. Stein AP, Saha S, Kraninger JL, Swick AD, Yu M, Lambert PF, et al. Prevalence of Human Papillomavirus in Oropharyngeal Cancer: A Systematic Review. *Cancer J* (2015) 21:138–46. doi: 10.1097/PPO.0000000000000115
2. Ang KK, Harris J, Wheeler R, Weber R, Rosenthal DI, Nguyen-Tân PF, et al. Human Papillomavirus and Survival of Patients With Oropharyngeal Cancer. *N Engl J Med* (2010) 363:24–35. doi: 10.1056/NEJMoa0912217
3. Fakhry C, Westra WH, Li S, Cmelak A, Ridge JA, Pinto H, et al. Improved Survival of Patients With Human Papillomavirus-Positive Head and Neck Squamous Cell Carcinoma in a Prospective Clinical Trial. *J Natl Cancer Inst* (2008) 100:261–9. doi: 10.1093/jnci/djn011
4. Machczyński P, Majchrzak E, Niewinski P, Marchlewska J, Golusiński W. A Review of the 8th Edition of the AJCC Staging System for Oropharyngeal Cancer According to HPV Status. *Eur Arch Otorhinolaryngol* (2020) 277:2407–12. doi: 10.1007/s00405-020-05979-9

5. Howard J, Dwivedi RC, Masterson L, Kothari P, Quon H, Holsinger FC. De-Intensified Adjuvant (Chemo)Radiotherapy Versus Standard Adjuvant Chemoradiotherapy Post Transoral Minimally Invasive Surgery for Resectable HPV-Positive Oropharyngeal Carcinoma. *Cochrane Database Syst Rev* (2018) 12:CD012939. doi: 10.1002/14651858.CD012939.pub2
6. Amin MB, Greene FL, Edge SB, Compton CC, Gershenwald JE, Brookland RK, et al. The Eighth Edition AJCC Cancer Staging Manual: Continuing to Build a Bridge From a Population-Based to a More "Personalized" Approach to Cancer Staging. *CA Cancer J Clin* (2017) 67:93–9. doi: 10.3322/caac.21388
7. Yom SS, Torres-Saavedra P, Caudell JJ, Waldron JN, Gillison ML, Xia P, et al. Reduced-Dose Radiation Therapy for HPV-Associated Oropharyngeal Carcinoma (NRG Oncology HN002). *J Clin Oncol* (2021) 39:956–65. doi: 10.1200/JCO.20.03128
8. Würdemann N, Wagner S, Sharma SJ, Prigge E-S, Reuschenbach M, Gattenlöhner S, et al. Prognostic Impact of AJCC/UICC 8th Edition New Staging Rules in Oropharyngeal Squamous Cell Carcinoma. *Front Oncol* (2017) 7:129. doi: 10.3389/fonc.2017.00129
9. Becker C, Hofauer BG, Mansour N, Ketterer MC, Schulz T, Knopf A. The 8th Edition of the TNM Staging System-A Curse or a Bfor Oropharyngeal Carcinoma? *HNO* (2021) 69(2):89–94. doi: 10.1007/s00106-020-00875-4
10. Kwan JYY, Su J, Huang SH, Ghoraie LS, Xu W, Chan B, et al. *Radiomic Biomarkers to Refine Risk Models for Distant Metastasis in HPV-related Oropharyngeal Carcinoma*. *Int J Radiat Oncol Biol Phys* (2018) 102 (4):1107–16. doi: 10.1016/j.ijrobp.2018.01.057
11. Wong AJ, Kanwar A, Mohamed AS, Fuller CD. Radiomics in Head and Neck Cancer: From Exploration to Application. *Transl Cancer Res* (2016) 5:371–82. doi: 10.21037/tcr.2016.07.18
12. Beig N, Khorrami M, Alilou M, Prasanna P, Braman N, Orooji M, et al. Perinodular and Intranodular Radiomic Features on Lung CT Images Distinguish Adenocarcinomas From Granulomas. *Radiology* (2019) 290:783–92. doi: 10.1148/radiol.2018180910
13. Braman N, Prasanna P, Whitney J, Singh S, Beig N, Etesami M, et al. Association of Peritumoral Radiomics With Tumor Biology and Pathologic Response to Preoperative Targeted Therapy for HER2 (ERBB2)-Positive Breast Cancer. *JAMA Netw Open* (2019) 2(4):e192561. doi: 10.1001/jamanetworkopen.2019.2561
14. Clark K, Vendt B, Smith K, Freymann J, Kirby J, Koppel P, et al. The Cancer Imaging Archive (TCIA): Maintaining and Operating a Public Information Repository. *J Digit Imaging* (2013) 26:1045–57. doi: 10.1007s10278-013-9622-7
15. Mohiuddin K, Haneuse S, Sofer T, Gill R, Jaklitsch MT, Colson YL, et al. Relationship Between Margin Distance and Local Recurrence Among Patients Undergoing Wedge Resection for Small (≤2 cm) Non-Small Cell Lung Cancer. *J Thorac Cardiovasc Surg* (2014) 147:1169–75; discussion 1175-1177. doi: 10.1016/j.jtcvs.2013.11.056
16. Haralick RM, Shanmugam K, Dinstein I. Textural Features for Image Classification In: *IEEE Transactions on Systems, Man, and Cybernetics*, vol. SMC-3, no. 6. (1973) pp. 610–21 doi: 10.1109/TSMC.1973.4309314
17. Gillett WD. Image Classification Using Laws' Texture Energy Measures. All Computer Science and Engineering Research. (1987). Report Number: WUCS-87-25.
18. Fogel I, Sagi D. Gabor Filters as Texture Discriminator. *Biol Cybern* (1989) 61:103–13. doi: 10.1007/BF00204594
19. Prasanna P, Tiwari P, Madabhushi A. Co-Occurrence of Local Anisotropic Gradient Orientations (CoLlAGe): A New Radiomics Descriptor. *Sci Rep* (2016) 6:37241. doi: 10.1038/srep37241
20. Shirzad MB, Keyvanpour MR. A Feature Selection Method Based on Minimum Redundancy Maximum Relevance for Learning to Rank. *AI Robotics (IRANOPEN)* (2015) 2015:1–5. doi: 10.1109/RIOS.2015.7270735
21. Beig N, Bera K, Prasanna P, Antunes J, Correa R, Singh S, et al. Radiogenomic-Based Survival Risk Stratification of Tumor Habitat on Gd-T1w MRI Is Associated With Biological Processes in Glioblastoma. *Clin Cancer Res* (2020) 26:1866–76. doi: 10.1158/1078-0432.CCR-19-2556
22. Vickers AJ, van Calster B, Steyerberg EW. A Simple, Step-by-Step Guide to Interpreting Decision Curve Analysis. *Diagn Progn Res* (2019) 3:18. doi: 10.1186/s41512-019-0064-7
23. Taberna M, Mena M, Pavón MA, Alemany L, Gillison ML, Mesía R. Human Papillomavirus-Related Oropharyngeal Cancer. *Ann Oncol* (2017) 28:2386–98. doi: 10.1093/annonc/mdx304
24. Singhi AD, Westra WH. Comparison of Human Papillomavirus *in Situ* Hybridization and P16 Immunohistochemistry in the Detection of Human Papillomavirus-Associated Head and Neck Cancer Based on a Prospective Clinical Experience. *Cancer* (2010) 116:2166–73. doi: 10.1002/cncr.25033
25. Leijenaar RT, Bogowicz M, Jochems A, Hoebers FJ, Wesseling FW, Huang SH, et al. Development and Validation of a Radiomic Signature to Predict HPV (P16) Status From Standard CT Imaging: A Multicenter Study. *Br J Radiol* (2018) 91:20170498. doi: 10.1259/bjr.20170498
26. Bagher-Ebadian H, Lu M, Siddiqui F, Ghanem AI, Wen N, Wu Q, et al. Application of Radiomics for the Prediction of HPV Status for Patients With Head and Neck Cancers. *Med Phys* (2020) 47:563–75. doi: 10.1002/mp.13977
27. Chernock RD. Morphologic Features of Conventional Squamous Cell Carcinoma of the Oropharynx: "Keratinizing" and "Nonkeratinizing" Histologic Types as the Basis for a Consistent Classification System. *Head Neck Pathol* (2012) 6 Suppl 1:S41–47. doi: 10.1007/s12105-012-0373-4
28. Westra WH. The Morphologic Profile of HPV-Related Head and Neck Squamous Carcinoma: Implications for Diagnosis, Prognosis, and Clinical Management. *Head Neck Pathol* (2012) 6 Suppl 1:S48–54. doi: 10.1007/s12105-012-0371-6
29. Chernock RD, El-Mofty SK, Thorstad WL, Parvin CA, Lewis JS. HPV-Related Nonkeratinizing Squamous Cell Carcinoma of the Oropharynx: Utility of Microscopic Features in Predicting Patient Outcome. *Head Neck Pathol* (2009) 3:186–94. doi: 10.1007/s12105-009-0126-1
30. Leijenaar RTH, Carvalho S, Hoebers FJP, Aerts HJWL, van Elmpt WJC, Huang SH, et al. External Validation of a Prognostic CT-Based Radiomic Signature in Oropharyngeal Squamous Cell Carcinoma. *Acta Oncol* (2015) 54:1423–9. doi: 10.3109/0284186X.2015.1061214
31. Vallières M, Kay-Rivest E, Perrin LJ, Liem X, Furstoss C, Aerts HJWL, et al. Radiomics Strategies for Risk Assessment of Tumour Failure in Head-and-Neck Cancer. *Sci Rep* (2017) 7:10117. doi: 10.1038/s41598-017-10371-5
32. Aerts HJWL, Velazquez ER, Leijenaar RTH, Parmar C, Grossmann P, Carvalho S, et al. Decoding Tumour Phenotype by Noninvasive Imaging Using a Quantitative Radiomics Approach. *Nat Commun* (2014) 5:4006. doi: 10.1038/ncomms5006
33. Oguejiofor K, Hall J, Slater C, Betts G, Hall G, Slevin N, et al. Stromal Infiltration of CD8 T Cells is Associated With Improved Clinical Outcome in HPV-Positive Oropharyngeal Squamous Carcinoma. *Br J Cancer* (2015) 113:886–93. doi: 10.1038/bjc.2015.277
34. Koyuncu CF, Lu C, Bera K, Zhang Z, Xu J, Toro P, et al. Computerized Tumor Multinucleation Index (MuNI) is Prognostic in P16+ Oropharyngeal Carcinoma. *J Clin Invest* (2021) 131(8):e145488. doi: 10.1172/JCI145488
35. Sinha P, Lewis JS, Kallogjeri D, Nussenbaum B, Haughey BH. Soft Tissue Metastasis in P16-Positive Oropharynx Carcinoma: Prevalence and Association With Distant Metastasis. *Oral Oncol* (2015) 51:778–86. doi: 10.1016/j.oraloncology.2015.05.004
36. Hanoteau A, Newton JM, Krupar R, Huang C, Liu H-C, Gaspero A, et al. Tumor Microenvironment Modulation Enhances Immunologic Benefit of Chemoradiotherapy. *J Immunother Cancer* (2019) 7:10. doi: 10.1186/s40425-018-0485-9
37. Fakhry C, Zhang Q, Nguyen-Tân PF, Rosenthal DI, Weber RS, Lambert L, et al. Development and Validation of Nomograms Predictive of Overall and Progression-Free Survival in Patients With Oropharyngeal Cancer. *J Clin Oncol* (2017) 35:4057–65. doi: 10.1200/JCO.2016.72.0748
38. Zhang B, Tian J, Dong D, Gu D, Dong Y, Zhang L, et al. Radiomics Features of Multiparametric MRI as Novel Prognostic Factors in Advanced Nasopharyngeal Carcinoma. *Clin Cancer Res* (2017) 23:4259–69. doi: 10.1158/1078-0432.CCR-16-2910
39. Yuan Y, Ren J, Shi Y, Tao X. MRI-Based Radiomic Signature as Predictive Marker for Patients With Head and Neck Squamous Cell Carcinoma. *Eur J Radiol* (2019) 117:193–8. doi: 10.1016/j.ejrad.2019.06.019

Author Disclaimer: The content is solely the responsibility of the authors and does not necessarily represent the official views of the National Institutes of Health, the U.S. Department of Veterans Affairs, the Department of Defense, or the United States Government.

Conflict of Interest: AM is an equity holder in Elucid Bioimaging and in Inspirata Inc. In addition, he has served as a scientific advisory board member for Inspirata Inc., AstraZeneca, Bristol Myers Squibb, and Merck. Currently, he serves on the advisory board of Aiforia Inc. He also has sponsored research agreements with Philips, AstraZeneca, Boehringer Ingelheim, and Bristol Myers Squibb. His technology has been licensed to Elucid Bioimaging. He is also involved in a NIH U24 grant with PathCore Inc. and three different R01 grants with Inspirata Inc. SK is a consultant for Merck and Regeneron, receives research support from Merck and Bristol Myers Squibb, and reports honoraria from UpToDate.

The remaining authors declare that the research was conducted in the absence of any commercial or financial relationships that could be construed as a potential conflict of interest.

Publisher's Note: All claims expressed in this article are solely those of the authors and do not necessarily represent those of their affiliated organizations, or those of the publisher, the editors and the reviewers. Any product that may be evaluated in this article, or claim that may be made by its manufacturer, is not guaranteed or endorsed by the publisher.

frontiers in Oncology

ORIGINAL RESEARCH
published: 09 September 2021
doi: 10.3389/fonc.2021.740622

CD68$^+$ Macrophage Infiltration Associates With Poor Outcome of HPV Negative Oral Squamous Carcinoma Patients Receiving Radiation: Poly(I:C) Enhances Radiosensitivity of CAL-27 Cells but Promotes Macrophage Recruitment Through HMGB1

Dan Ai[1,2], Yu Dou[3], Zhaodi Nan[1,2], Ketao Wang[4], Huayang Wang[5], Lin Zhang[5], Zuoqing Dong[4], Jintang Sun[2], Chao Ma[2], Wanye Tan[4], Wenjuan Gao[2], Jia Liu[2], Lei Zhao[2], Shaohua Liu[4], Bingfeng Song[2], Qianqian Shao[2] and Xun Qu[2]**

[1] Laboratory of Basic Medical Sciences, Qilu Hospital, Cheeloo College of Medicine, Shandong University, Jinan, China, [2] Laboratory of Basic Medical Sciences, Qilu Hospital of Shandong University, Jinan, China, [3] School and Hospital of Stomatology, Cheelo College of Medicine, Shandong University, Jinan, China, [4] Department of Oral and Maxillofacial Surgery, Qilu Hospital of Shandong University & Institute of Stomatology, Shandong University, Jinan, China, [5] Department of Clinical Laboratory Medicine, Qilu Hospital of Shandong University, Jinan, China

OPEN ACCESS

Edited by:
Yong Yin,
Shandong Cancer Hospital, China

Reviewed by:
Dawei Chen,
Shandong Cancer Hospital, China
Jian-Guo Zhou,
University of Erlangen Nuremberg, Germany

***Correspondence:**
Xun Qu
quxun@sdu.edu.cn
Yu Dou
yu.dou@sdu.edu.cn

Specialty section:
This article was submitted to Head and Neck Cancer, a section of the journal Frontiers in Oncology

Received: 13 July 2021
Accepted: 12 August 2021
Published: 09 September 2021

Citation:
Ai D, Dou Y, Nan Z, Wang K, Wang H, Zhang L, Dong Z, Sun J, Ma C, Tan W, Gao W, Liu J, Zhao L, Liu S, Song B, Shao Q and Qu X (2021) CD68$^+$ Macrophage Infiltration Associates With Poor Outcome of HPV Negative Oral Squamous Carcinoma Patients Receiving Radiation: Poly(I:C) Enhances Radiosensitivity of CAL-27 Cells but Promotes Macrophage Recruitment Through HMGB1. Front. Oncol. 11:740622. doi: 10.3389/fonc.2021.740622

Patients with human papillomavirus (HPV) negative oral squamous cell carcinoma (OSCC) generally have poor clinical outcomes and worse responses to radiotherapy. It is urgent to explore the underlining mechanisms of the distinct prognoses between HPV negative and HPV positive OSCC and to develop effective therapy strategy to increase the survival rate of HPV negative OSCC patients. We conducted a retrospective cohort of 99 resected OSCC patients to evaluate the prognosis of HPV negative and HPV positive OSCC patients receiving radiation or not. We further addressed the association of CD68$^+$ macrophage infiltration with HPV status and the effects on survival of OSCC patients. We also used the TCGA-OSCC cohort for further verification. Based on the cohort study, we applied a synthetic dsRNA polymer, polyriboinosinic-polyribocytidylic acid (poly(I:C)), on CAL-27 (HPV negative OSCC cells). We co-cultured its condition medium with THP-1 derived macrophage and examined the cytokines and macrophage migration. We found that high CD68$^+$ macrophage infiltration associated with poor overall survival in HPV negative OSCC patients receiving radiation. *In vitro*, poly(I:C) could induce apoptosis and enhance the radiosensitivity, but increase macrophage recruitment. Targeting HMGB1 could inhibit IL-6 induction and macrophage recruitment. Our findings indicated that CD68$^+$ macrophage might play an important role in the outcomes of HPV negative OSCC patients receiving radiation. Our findings also suggested that radiation combined poly(I:C)

might be a potential therapy strategy to increase the radiation response and prognosis of HPV negative OSCC. Notably, HMGB1 should be targeted to inhibit macrophage recruitment and enhance overall therapy effects.

Keywords: oral squamous cell carcinoma, human papillomavirus, radiosensitivity, poly(I:C), HMGB1

INTRODUCTION

Oral cancer, the most common head and neck cancer (HNC), accounts for more than 300,000 new cases of and 170,000 deaths occur worldwide per year (1). Oral squamous cell carcinoma (OSCC) comprises approximately 90% of these cases with a 5-year survival rate of 40–60% (2). Patients with human papillomavirus (HPV) negative OSCC generally have a poor prognosis and worse response to radiotherapy or chemoradiotherapy (3–5). HPV negative and positive OSCC exhibit distinct clinic-pathological features and heterogeneous microenvironments; however, the factors responsible for the distinct responses and prognoses remained obscure (6). Therefore, it is urgent to explore the underlining mechanisms of the distinct prognoses between HPV negative and positive OSCC, so as to optimize therapy strategy of HPV negative OSCC patients and increase overall survival rate.

Radiotherapy affects the tumor microenvironment, which in turn affects radiation-induced anticancer efficacy (7). Recent studies showed that enriched inflammatory lymphocyte infiltration in tumor microenvironment associated with HPV positive HNC and favorable prognosis (8–11). Macrophages are crucial drivers of tumor-promoting inflammation (12, 13). Macrophage polarization has also been reported to increase radiosensitivity in HPV positive HNC (14). So far, however, it is not clear whether macrophage infiltration associates with response to radiotherapy and survival of HPV negative and HPV positive OSCC. On the other hand, Hanoteau et al. reported that immune modulation of tumor microenvironment enhanced response to chemoradiotherapy of HNC (15). Sato-Kaneko et al. found that adjuvant toll like receptor (TLR) agonists could enhance tumor suppression and metastasis prevention of checkpoint inhibitors in HNC (16). Therefore, we hypothesized that TLR agonists might modulate tumor microenvironment and enhance the radiosensitivity of HPV negative OSCC, the majority population of OSCC.

We conducted a retrospective cohort of 99 resected OSCC patients and validated the findings using TCGA-OSCC cohort. We evaluated the association of $CD68^+$ macrophage infiltration with HPV status and overall and disease-free survival of OSCC patients receiving or not receiving post operation radiation. Based on the findings of the cohort study, *in vitro*, we applied a synthetic dsRNA polymer, polyriboinosinic-polyribocytidylic acid [poly(I:C)], as a TLR agonist on CAL-27 (HPV negative OSCC cells). We assessed the apoptosis and proliferation of CAL-27 in response to poly(I:C) or combined with radiation. We co-cultured its condition medium with THP-1 derived macrophage and examined the induced cytokine profile and macrophage migration. We also addressed the role of a radiation injury associated molecule, High Mobility Group Box 1 (HMGB1), in above effects on macrophage.

MATERIALS AND METHODS

Patient and Study Design

The specimens were obtained from 99 primary OSCC patients admitted in Qilu Hospital of Shandong University between 2006 and 2015. All patients received surgical resections without preoperative chemotherapy or radiotherapy. The ethical approval of this study was obtained from the Ethics Committee of Qilu Hospital of Shandong University. The patients were subject to radiotherapy according to TNM stage, tumor differentiation, and the patients' intentions. The patients were followed up until May 2019 (median: 60 months). The baseline clinic-pathological characteristics were shown in **Supplementary Table S1**.

The Cancer Genome Atlas (TCGA)-HNSCC cohort was used for validation. The clinical characteristics of TCGA-HNSCC cohort were obtained from the Genomic Data Commons (GDC, https://portal.gdc.cancer.gov/). Gene expression data of TCGA-HNSCC RNA-sequencing (RNA-seq) dataset was obtained from UCSC Xena (https://xena.ucsc.edu/). HPV status was determined based on Cao et al. (17). Patients with HPV-supporting reads > 100 were defined as HPV positive. Updated follow-up information was used based on Liu et al. (18). Patients without HPV status or follow-up information were excluded. Patients with histories of malignancies and/or adjuvant therapies were also excluded. At last, a total of 278 OSCC patients were used for validation. The baseline clinic-pathological characteristics were shown in **Supplementary Table S2**. CIBERSORT, a deconvolution algorithm, was used to analyze the infiltration of macrophages in the tumor microenvironment (19) (https://cibersort.stanford.edu/index.php). Twenty-two human immune cell types were inferred. The landscape of immune infiltration is shown in **Figure 1A**. Another deconvolution tool, Estimating the Proportions of Immune and Cancer cells (EPIC), was also used to estimate the proportions of macrophages (20) (http://epic.gfellerlab.org). Seven human cell types were inferred by ERIC, and the landscape is shown in **Figure 1B**.

Immunohistochemistry of p16 and CD68

P16 and CD68 were used to determine HPV status (4, 21) and macrophage infiltration (12, 22), respectively. Formalin-fixed paraffin-embedded tumor specimens were cut into 5-μm sections and processed for immunohistochemistry. Briefly, after incubation with a mouse anti-P16INK4a monoclonal antibody (1:50, 550834, BD Pharmingen, USA) or a mouse anti-CD68 (PG-M1) monoclonal antibody (ZM-0464, ZSGB-bio, China) at 4°C overnight, the sections were processed using biotin-streptavidin horseradish peroxidase detection system (SP-9000, SPlink Detection Kit, ZSGB-bio, Beijing, China). The slides

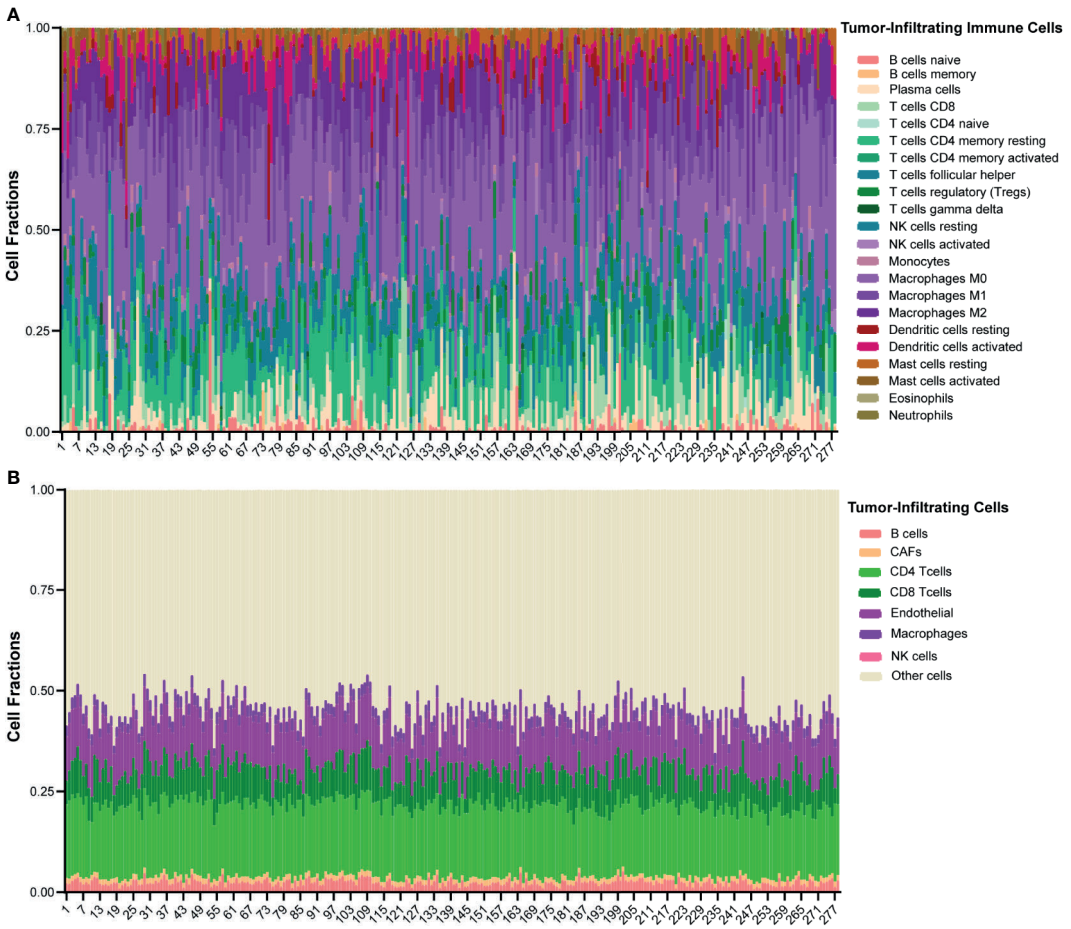

FIGURE 1 | The landscape of immune infiltration of 278 OSCC patients in TCGA cohort. **(A)** Heatmap of 22 types of tumor-infiltrating immune cells deconvolved using CIBERSORT in OSCC. **(B)** Heatmap of 7 types of tumor-infiltrating cells deconvolved using EPIC in OSCC.

were viewed under the Olympus IX81 microscope (Olympus, Japan), and the images were produced using DP Controller (Olympus, Japan).

P16 expression was evaluated based on staining intensity (0: no staining, 1: weak, 2: moderate, or 3: strong) and the proportion of stained tumor cells (0: 0–5%, 1: 6–25%, 2: 26–50%, 3: 51–75%, or 4: greater than 75%). P16 status was considered positive if staining intensity was strong (score 3) and the proportion of stained tumor cells was greater than 25% (score 2–4), or the staining intensity was moderate (score 2) and the proportion of stained tumor cells was greater than 75% (score 4). For CD68 evaluation, we counted the numbers of positively stained cells in five random fields (400×) in tumor nest of each specimen. The average number of $CD68^+$ cells infiltrated in tumor nest per field was calculated. The level of $CD68^+$ macrophages was determined according to its median value (12.67 per filed). All cases with number ≤ 12.67 per field were considered low, the number > 12.67 considered high. The evaluations of p16 and CD68 were performed by two pathologists and confirmed by another experienced pathologist.

Cell Culture and Treatment

CAL-27 (HPV-negative human oral squamous cell line) and THP-1 (human monocytic cell line) were obtained from American Type Culture Collection (ATCC). All cells were cultured in phenol red-free Roswell Park Memorial Institute (RPMI) 1640 medium (HyClone, USA) supplemented with 10% charcoal stripped fetal bovine serum (HyClone, USA) at 37°C, 5% CO2.

CAL-27 were treated with 10 μg/ml poly(I:C) (TOCRIS, R&D, USA) or PBS for specific period of time (2 or 24 h). The cells were exposed with a serial of doses of radiation (0, 2, 6, or 8 Gy). Conditioned cells and conditioned medium (CM) were collected after culture for 24 h. Radiation was carried out using Varian 23EX 554 accelerator radiation platform in Department of Radiotherapy of Qilu Hospital of Shandong University. The required doses, 2, 6, and 8 Gy, were calculated according to 6MV X-ray PDD table of Varian 23EX 554 accelerator. The vertical irradiation field was 20 cm × 20 cm.

To generate THP-1-derived macrophages, THP-1 cells (1×10^6 cells/well) were treated with 100 ng/ml phorbol myristate

acetate (R&D, USA) for 6 h. For cytokine induction, the medium of THP-1-derived macrophages was replaced with 50% CAL-27 CM (or no CM control), which was the supernatants of CAL-27 treated with/without poly(I:C) for 24 h and/or 8 Gy radiation. The cells were continued to culture for 42 h before changing fresh medium and were further incubated for 24 h. IL-6 NAb neutralizing antibody or its isotype antibody (NAb/IsoAb, 10 μg/ml, R&D, USA), or HMGB1 NAb/IsoAb (1 μg/ml, Sigma, USA) was applied for the specific treatment groups as indicated.

Cell Proliferation Assay

Cell proliferation was measured by CCK-8 assay (Bioss, China). CAL-27 cells were seeded in 96-well plates at a density of 2×10^3 cells/200 μl. At the end of poly(I:C) and radiation treatments, the medium was replaced and CCK-8 solution (10 μg) was added to each well. At last, the optical density was measured at 450 nm with a microplate microscope after incubated in darkness for 2 h.

Apoptosis Assay

Apoptosis was measured using Annexin V-FITC/PI apoptosis detection kit (BestBio, China). CAL-27 cells described above were collected and washed with cold PBS. The cells were then resuspended in 500 μl binding buffer containing 5 μl Annexin V-FITC and 5 μl propidium iodide and incubated for 15 min before analyzed for flow cytometry (NovoCyte, ACEA Biosciences, USA).

Enzyme-Linked Immunosorbent Assay

The concentration of High Mobility Group Box 1 (HMGB1) in CAL-27 CM was determined by Human HMGB1 ELISA kit (Elabscience, China) according to the manufacturer's instructions.

Cytokine Assay

The supernatants of THP-1-derived macrophages after incubation with CAL-27 CM were collected and stored at -80°C after removal of the cell debris. Bio-Plex ProTM Human Th17 Cytokine Assay (Bio-rad, USA) was used to detect the levels of cytokines in above supernatants according to the manufacturer's instructions.

Migration Assay

The 24-well Transwell culture inserts (8 μm, BD Biosciences, USA) were used for cell migration assay according to the manufacturer's instructions. THP-1-derived macrophages (1×10^5) were resuspended in 100 μl of serum-free RPMI-1640 medium and seeded into the upper compartment of each well. RPMI-1640 medium (600 μl) with 10% FBS and 50% CAL-27 CM was added into the lower chamber of the plate. RPMI-1640 medium with 10% FBS but without CAL-27 CM was used as control. IL-6 NAb/IsoAb (10 μg/ml, R&D, USA) or HMGB1 NAb/IsoAb (1 μg/ml) was added into CAL-27 CM as indicated. After incubation at 37°C in 5% CO2 for 24 h, the migrated cells were fixed using 10% formalin and stained with eosin. Cell numbers of five random fields were counted, and images were taken.

Statistical Analysis

Data were presented as mean ± standard deviation (SD) unless indicated. Student's t test, Mann-Whitney U test, or ANOVA was used to determine the statistical significances as indicated. Chi-square test or Fisher's exact test was used to determine the differences of clinicopathological characteristics between different groups. Kaplan-Meier analysis was used, and the log-rank test was used to discriminate the differences. Univariate and multivariate cox regressions were used to assess the association with overall or disease-free survival. Factors associated with cancer-specific survival with a P value lower than 0.1 and those shown to associate with cancer outcomes were further tested in multivariate cox regression. A two-tailed P value less than 0.05 was considered as statistical significance. For statistical analyses of cohort studies, IBM SPSS software version 25.0 (SPSS Inc., USA) was used. For statistical analyses of *in vitro* experiments, Graphpad Prism 8 software (La Jolla, USA) was used. All statistical graphs were generated using Graphpad Prism 8 software.

RESULTS

Poor Overall Survival of HPV Negative OSCC Patients Receiving Radiation

To analyze HPV status in OSCC, tumor specimens from 99 OSCC patients in our cohort were stained for p16 (**Figure 2A**), a marker of HPV. To investigate the association of HPV status with the outcomes of OSCC patients, we analyzed the survivals between HPV negative and HPV positive OSCC patients and between those received or not received radiation in our cohort. We observed a poor overall survival (OS) and a poor disease-free survival (DFS) in HPV negative patients with OSCC, however, the differences were not significant (P = 0.056 and P = 0.085, respectively, **Figures 2B, C**). Accordingly, there was no significant association between HPV status and OS or DFS in patients with OSCC in univariate or multivariate cox regression (hazard ratio: 0.439, 95% confidence interval: 0.183–1.053, P = 0.065 for OS, hazard ratio: 0.536, 95% confidence interval: 0.259–1.110, P = 0.093 for DFS, **Supplementary Tables S3, S4**). Furthermore, radiation treated OSCC patients with HPV negative status showed worse OS and DFS compared to those with HPV positive status; however, the differences were not significant either (P = 0.063 and P = 0.075, respectively, **Figures 2D, E**).

We further validated the findings in TCGA-OSCC cohort. OSCC patients (278) were selected from TCGA-HNSCC cohort as described in Materials and Method section. Trends of poor OS and DFS in HPV negative patients with OSCC were observed, however, the differences were not significant (P = 0.169 and P = 0.288, respectively, **Supplementary Figure S1A, B**). Accordingly, there was no association between HPV status and OS or DFS in patients with OSCC in univariate or multivariate cox regression (hazard ratio: 0.674, 95% confidence interval: 0.328–1.387, P = 0.284 for OS, hazard ratio: 0.623, 95% confidence interval: 0.327–1.188, P = 0.151 for DFS, **Supplementary Tables S5, S6**) in TCGA-OSCC cohort. In addition, radiation treated OSCC patients with HPV negative status showed a trend of worse OS compared to those with HPV positive status, but without statistical significance (P = 0.085, **Supplementary Figure S1C**).

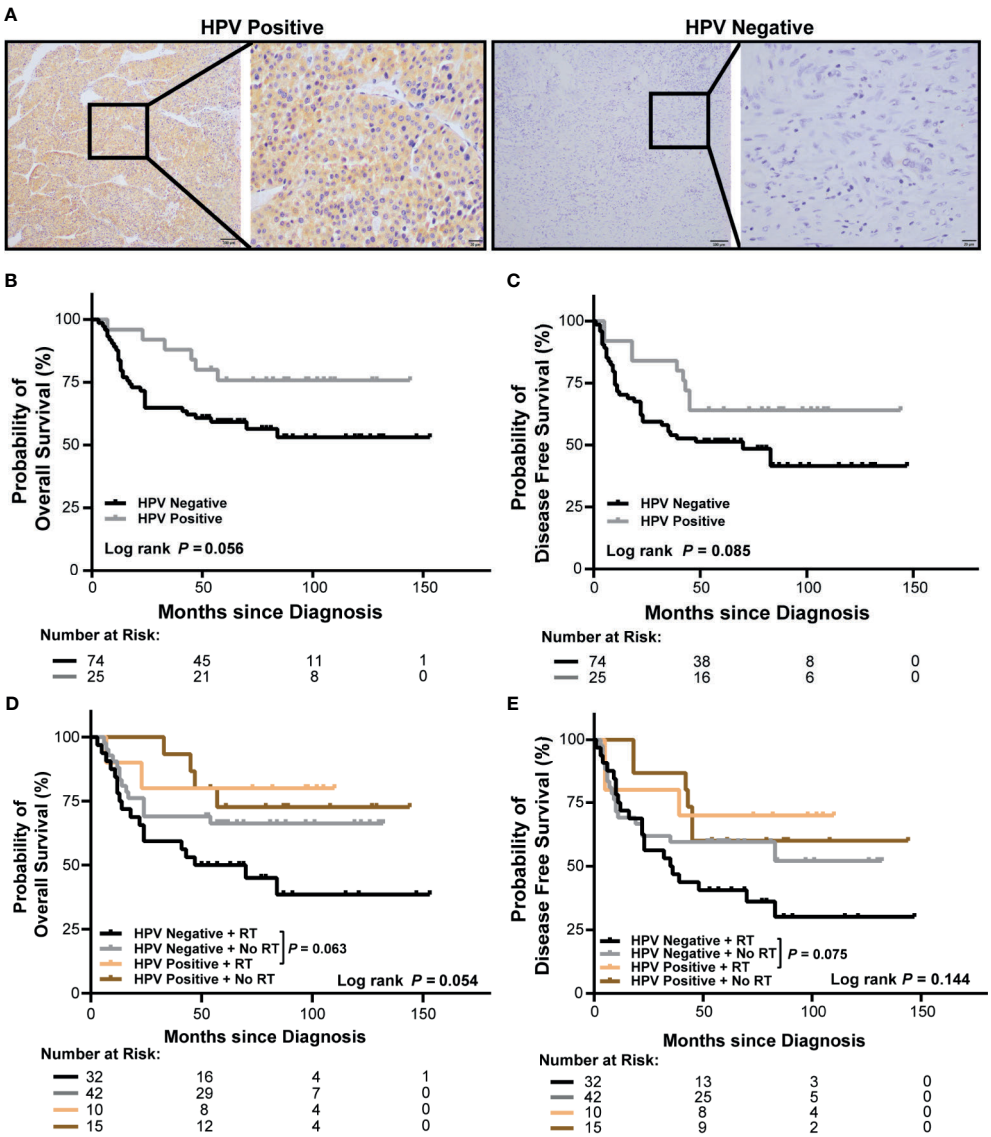

FIGURE 2 | Association of HPV status and radiation with survival of OSCC patients in our cohort. **(A)** Representative immunohistochemical images of p16 positive and negative OSCC (left: 100×, right: 400×). **(B, C)** Kaplan-Meier curves show overall survival **(B)** and disease-free survival **(C)** of HPV negative and HPV positive OSCC patients. **(D, E)** Kaplan-Meier curves show overall survival **(D)** and disease-free survival **(E)** of HPV negative and HPV positive OSCC patients receiving radiation or no radiation. Log-rank test and/or pair wised comparison was used for significance. RT, radiation.

The correlations between HPV status and clinic-pathological characteristics were also analyzed. No significant correlation was found in our cohort (**Supplementary Table S1**). More HPV negative patients were found in late stage OSCC patients in TCGA cohort (**Supplementary Table S2**).

Intratumor CD68$^+$ Macrophage Infiltration Is Not Correlated HPV Status or Outcomes of OSCC Patients

To analyze macrophage infiltration in OSCC, tumor specimens from 99 OSCC patients in our cohort were stained for CD68, a marker of human macrophages. As shown in **Figure 3A**, CD68$^+$ cells present throughout the tumor core. Intratumor infiltration of CD68$^+$ macrophages were evenly distributed in patients with HPV negative and HPV positive OSCC (**Figure 3B**). There was no association of CD68$^+$ macrophage infiltration with overall or disease-free survival using log-rank test (**Figures 3C, D**) or univariate or multivariate cox regression (**Supplementary Tables S3, S4**). The association was not different either considering HPV status (**Figures 3E, F**).

We validated the findings in TCGA-OSCC cohort. Accordingly, macrophage infiltration deconvolved using CIBERSOFT was not correlated with HPV status (**Supplementary Figure S2A**). There was no association of

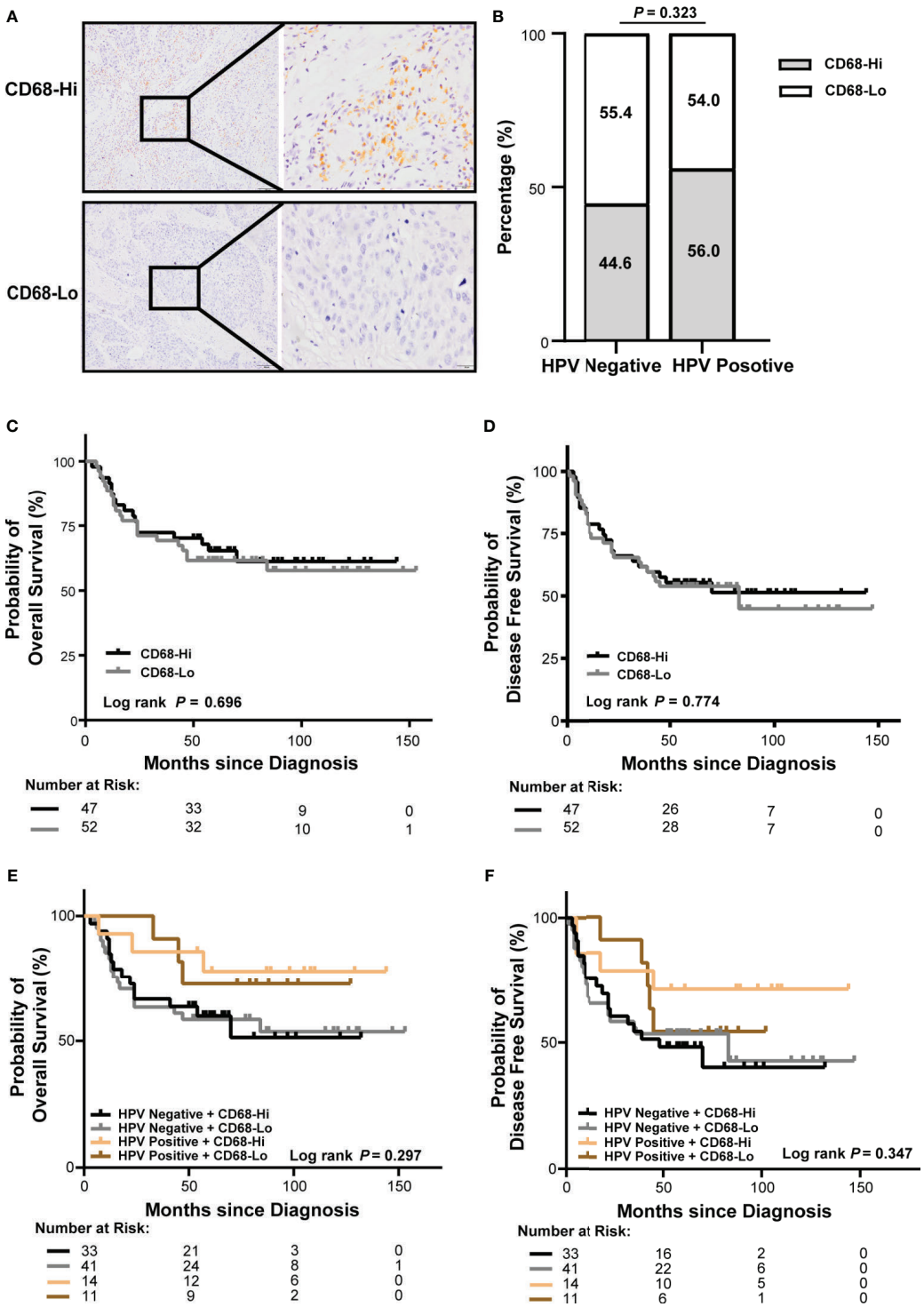

FIGURE 3 | Association of CD68$^+$ macrophage infiltration and HPV status with survival of OSCC patients in our cohort. **(A)** Representative immunohistochemical images of high or low level of CD68$^+$ macrophages in OSCC (left: 100×, right: 400×). **(B)** Proportion of high or low level of CD68$^+$ macrophages in patients with HPV negative and HPV positive OSCC. **(C, D)** Kaplan-Meier curves exhibit overall survival **(C)** and disease-free survival **(D)** in high or low level of CD68$^+$ macrophage infiltrated OSCC patients. **(E, F)** Kaplan-Meier curves exhibit overall survival **(E)** and disease-free survival **(F)** in high or low level of CD68$^+$ macrophage infiltrated OSCC patients with HPV negative and HPV positive status. Log-rank test and/or pair wised comparison was used for significance. CD68-Hi, CD68-High; CD68-Lo, CD68-Low; RT, radiation.

macrophage infiltration with overall or disease-free survival (**Supplementary Figures S2B, C** and **Supplementary Tables S5, S6**). The association was not different either considering HPV status (**Supplementary Figures S2D, E**). Similar results were also observed in macrophage infiltration deconvolved using EPIC (**Supplementary Figure S3**).

Notably, we found that $CD68^+$ macrophage infiltration was significantly correlated with differentiation in patients with HPV negative OSCC ($P = 0.014$), but not in those with HPV positive OSCC ($P = 0.072$, **Table 1**) in our cohort. In TCGA-OSCC cohort, we found that macrophage infiltration deconvolved using CIBERSOFT was correlated with the histological grade ($P = 0.012$, **Table 2**), especially in patients with HPV negative OSCC ($P = 0.011$, **Table 3**). In addition, we found that macrophage infiltration deconvolved using EPIC was also correlated with the histological grade in patients with HPV negative OSCC ($P = 0.022$, **Table 4**).

Intratumor $CD68^+$ Macrophage Infiltration Associates With Poor Survival of HPV Negative OSCC Patients Receiving Radiation

We next evaluated the role of $CD68^+$ macrophage infiltration in the outcomes of radiation treated OSCC patients in HPV negative and HPV positive subgroups in our cohort. We observed a poor OS and a poor DFS in high $CD68^+$ macrophage infiltrated OSCC patients received radiation in all OSCC patients ($P = 0.009$ and $P = 0.021$, respectively, **Figure 4A, B**). In univariate cox regression model, high $CD68^+$ macrophage infiltration was associated with poor OS and DFS of OSCC patients received radiation (hazard ratio: 3.492, 95% confidence interval: 1.287–9.476, $P = 0.014$ for OS, hazard ratio: 2.610, 95% confidence interval: 1.112–6.123, $P = 0.027$ for DFS, **Figure 4C, D** and **Supplementary Tables S7, S8**). Notably, similar results only appeared in the HPV negative OSCC subgroup ($P = 0.011$ and $P = 0.016$, respectively, **Figures 5A, B**). Accordingly, radiation was associated with poor OS and DFS of high $CD68^+$ macrophage infiltrated OSCC patients in HPV negative subgroup in univariate cox regression model (hazard ratio: 3.746, 95% confidence interval: 1.248–11.244, $P = 0.019$ for OS, hazard ratio: 3.012, 95% confidence interval: 1.161–7.814, $P = 0.023$ for DFS, **Figures 5C, D** and **Supplementary Tables S9, S10**). However, the associations remained not statistically significant after adjusting for age, gender, tumor size, lymph node metastasis, and differentiation in multivariate cox regression model (**Supplementary Tables S9, S10**). In addition, there were no associations in HPV positive OSCC subgroup (**Supplementary Figure S4** and **Supplementary Tables S11** and **S12**) in our cohort. We also validated these findings in TCGA-OSCC cohort. However, no association of macrophage

TABLE 1 | Correlation of intratumor $CD68^+$ macrophage infiltration with clinic-pathological characteristics of HPV positive and negative OSCC patients in our cohort.

Clinic-pathological characteristics	Total 25 *N* (%)	HPV positive patients		P^a value	Total 74 *N* (%)	HPV negative patients		P^b value
		CD68-high 14 (56.0%) *N* (%)	CD68-low 11 (44.0%) *N* (%)			CD68-high 33 (44.6%) *N* (%)	CD68-low 41 (55.4%) *N* (%)	
Age				0.697				0.065
≤59 years	15 (60.0)	9 (64.3)	6 (54.5)		36 (48.6)	20 (60.6)	16 (39.0)	
>59 years	10 (40.0)	5 (35.7)	5 (46.5)		38 (51.4)	13 (39.4)	25 (61.0)	
Gender				0.241				0.080
Male	15 (60.0)	10 (71.4)	5 (46.5)		41 (55.4)	22 (66.7)	19 (46.3)	
Female	10 (40.0)	4 (28.6)	6 (54.5)		33 (44.6)	11 (33.3)	22 (53.7)	
Smoking status				1.000				0.609
Smoking	12 (48.0)	7 (50.0)	5 (46.5)		29 (39.2)	14 (42.4)	15 (36.6)	
Non-smoking	13 (52.0)	7 (50.0)	6 (54.5)		45 (60.8)	19 (57.6)	26 (63.4)	
Drinking status				0.414				0.239
Drinking	10 (40.0)	7 (50.0)	3 (27.3)		26 (35.1)	14 (42.4)	12 (29.3)	
Non-drinking	15 (60.0)	7 (50.0)	8 (72.7)		48 (64.9)	19 (57.6)	29 (70.7)	
Tumor size				1.000				0.694
≤2 cm	14 (56.0)	8 (57.1)	6 (54.5)		34 (45.9)	16 (48.5)	18 (43.9)	
>2 cm	11 (44.0)	6 (42.9)	5 (46.5)		40 (54.1)	17 (51.5)	23 (56.1)	
Lymph node				1.000				0.093
Positive	8 (32.0)	5 (35.7)	3 (27.3)		28 (37.8)	9 (27.3)	19 (46.3)	
Negative	17 (68.0)	9 (64.3)	8 (72.7)		46 (62.2)	24 (72.7)	22 (53.7)	
TNM stage				1.000				0.419
Stage I–II	14 (56.0)	8 (57.1)	6 (54.5)		41 (55.4)	20 (60.6)	21 (51.2)	
Stage III–IV	11 (44.0)	6 (42.9)	5 (46.5)		33 (44.6)	13 (39.4)	20 (48.8)	
Differentiation				0.072				0.014
High	17 (68.0)	12 (86.0)	5 (46.5)		48 (64.9)	16 (48.5)	32 (78.0)	
Moderate	6 (24.0)	1 (7.0)	5 (46.5)		16 (21.6)	12 (36.4)	4 (9.8)	
Poor	2 (8.0)	1 (7.0)	1 (7.0)		10 (13.5)	5 (15.1)	5 (12.2)	
Radiotherapy				1.000				0.549
Yes	10 (40.0)	6 (42.9)	4 (36.4)		32 (43.2)	13 (39.4)	19 (46.3)	
No	15 (60.0)	8 (57.1)	7 (63.6)		42 (56.8)	20 (60.6)	22 (53.7)	

a: Fisher's exact test. b: $\chi 2$ test.

TABLE 2 | Correlation of macrophage infiltration deconvolved using CIBERSOFT and EPIC with clinic-pathological characteristics of OSCC patients in TCGA cohort.

Clinic-pathological characteristics	All patients 278 (100%) *N (%)*	CIBERSORT		*P*[b] value	EPIC		*P*[b] value
		Macrophages-high 139 (50.0%) *N (%)*	Macrophages-low 139 (50.0%) *N (%)*		Macrophages-high 139 (50.0%) *N (%)*	Macrophages-low 139 (50.0%) *N (%)*	
Age				0.093			0.093
≤ 61 years	142 (51.1)	64 (46.0)	78 (56.1)		64 (46.0)	78 (56.1)	
>61 years	136 (48.9)	75 (54.0)	61 (43.9)		75 (54.0)	61 (43.9)	
Gender				0.305			0.073
Male	188 (67.6)	90 (64.7)	98 (70.5)		87 (62.6)	101 (72.7)	
Female	90 (32.4)	49 (35.3)	41 (29.5)		52 (37.4)	38 (27.3)	
Lymph node				0.102			0.421
Positive	143 (51.4)	69 (49.7)	74 (53.3)	0.936*	71 (51.1)	72 (51.8)	0.763*
Negative	111 (39.9)	53 (38.1)	58 (41.7)		53 (38.1)	58 (41.7)	
NA	24 (8.7)	17 (12.2)	7 (5.0)		15 (10.8)	9 (6.5)	
TNM stage				0.403[a]			0.494[a]
Stage I–II	73 (26.3)	41 (29.5)	32 (23.0)	0.204*	35 (25.2)	38 (27.3)	0.602*
Stage III–IV	198 (71.2)	94 (67.6)	104 (74.8)		102 (73.4)	96 (69.1)	
NA	7 (2.5)	4 (2.9)	3 (2.2)		2 (1.4)	5 (3.6)	
Histological grade				0.013[a]	0.013		0.057[a]
G1-G2	218 (78.4)	100 (72.0)	118 (84.9)	0.012*	102 (73.4)	116 (83.5)	0.052*
G3-G4	59 (21.2)	38 (27.3)	21 (15.1)		36 (25.9)	23 (16.5)	
NA	1 (0.4)	1 (0.7)	0 (0.0)		1 (0.7)	0 (0.0)	
Radiotherapy				1.000			0.054
Yes	154 (55.4)	77 (55.4)	77 (55.4)		85 (61.2)	69 (49.6)	
No	124 (44.6)	62 (44.6)	62 (44.6)		54 (38.8)	70 (50.4)	

*a: Fisher's exact test. b: χ2 test except for those marked with a. *Pairwise comparison without NA group.*

TABLE 3 | Correlation of macrophage infiltration deconvolved using CIBERSOFT with clinic-pathological characteristics of HPV positive and negative OSCC patients in TCGA cohort.

Clinic-pathological characteristics	Total 33 (100%) *N (%)*	HPV positive patients		*P*[b] value	Total 2 (100%) *N (%)* Total	HPV negative patients		*P*[b] value
		Macrophages-high 17 (51.5%) *N (%)*	Macrophages-low 16 (48.5%) *N (%)*			Macrophages- high 122 (49.8%) *N (%)*	Macrophages- low 123 (50.2%) *N (%)*	
Age				0.080				0.308
≤ 61 years	19 (57.6)	7 (41.2)	12 (75.0)		123 (50.2)	57 (46.7)	66 (53.7)	
>61 years	14 (42.4)	10 (58.8)	4 (25.0)		122 (49.8)	65 (53.3)	58 (46.3)	
Gender				1.000				0.261
Male	27 (81.8)	14 (82.4)	13 (81.3)		161 (65.7)	76 (62.3)	85 (69.1)	
Female	6 (18.2)	3 (17.6)	3 (18.7)		84 (34.3)	46 (37.7)	38 (30.9)	
Lymph node				0.857				0.052
Positive	18 (54.5)	10 (58.8)	8 (50.0)	1.000*	125 (51.0)	59 (48.4)	66 (53.7)	0.974*
Negative	14 (42.4)	7 (41.2)	7 (43.8)		97 (39.6)	46 (37.7)	51 (41.4)	
NA	1 (3.1)	0 (0.0)	1 (6.2)		23 (9.4)	17 (13.9)	6 (4.9)	
TNM stage				1.000				0.505[a]
Stage I–II	11 (33.3)	6 (35.3)	5 (31.3)	1.000*	62 (25.3)	35 (28.7)	27 (22.0)	0.224*
Stage III–IV	17 (21.2)	8 (47.1)	9 (56.2)		181 (73.9)	86 (70.5)	95 (77.2)	
NA	5 (45.5)	3 (17.6)	2 (12.5)		2 (0.8)	1 (0.8)	1 (0.8)	
Histological grade				1.000				0.011[a]
G1–G2	28 (84.8)	14 (82.4)	14 (87.5)	1.000*	190 (77.6)	86 (70.5)	104 (84.6)	0.011*
G3–G4	5 (15.2)	3 (17.6)	2 (12.5)		54 (22.0)	35 (28.7)	19 (15.4)	
NA	0 (0.0)	0 (0.0)	0 (0.0)		1 (0.4)	1 (0.8)	0 (0.0)	
Radiotherapy				0.296				0.658
Yes	20 (60.6)	12 (70.6)	8 (50.0)		134 (54.7)	65 (53.3)	69 (56.1)	
No	13 (39.4)	5 (29.4)	8 (50.0)		111 (45.3)	57 (46.7)	54 (43.9)	

*a: Fisher's exact test. b: χ2 test except for those marked with a. *Pairwise comparison without NA group.*

TABLE 4 | Correlation of macrophage infiltration deconvolved using EPIC with clinic-pathological characteristics of HPV positive and negative OSCC patients in TCGA cohort.

Clinic-pathological characteristics	Total 33 (100%) *N (%)*	HPV positive patients		P^b value	Total 245 (100%) *N (%)*	HPV negative patients		P^b value
		Macrophages-high 18 (54.5%) *N (%)*	Macrophages-low 15 (45.5%) *N (%)*			Macrophages- high 121 (49.4%) *N (%)*	Macrophages- low 124 (50.6%) *N (%)*	
Age				1.000				0.085
≤ 61 years	19 (57.6)	10 (55.6)	9 (60.0)		123 (50.2)	54 (44.6)	69 (55.6)	
>61 years	14 (42.4)	8 (44.4)	6 (40.0)		122 (49.8)	67 (55.4)	55 (44.4)	
Gender				1.000				0.043
Male	27 (81.8)	15 (83.3)	12 (80.0)		161 (65.7)	72 (62.3)	89 (69.1)	
Female	6 (18.2)	3 (16.7)	3 (20.0)		84 (34.3)	49 (37.7)	35 (30.9)	
Lymph node				0.482				0.230
Positive	18 (54.5)	9 (50.0)	9 (60.0)	0.490*	125 (51.0)	62 (51.2)	63 (50.8)	0.531*
Negative	14 (42.4)	9 (50.0)	5 (33.3)		97 (39.6)	44 (36.4)	53 (42.7)	
NA	1 (3.1)	0 (0.0)	1 (6.7)		23 (9.4)	15 (12.4)	8 (6.5)	
TNM stage				0.132				0.942[a]
Stage I–II	11 (33.3)	5 (27.8)	6 (40.0)	0.248*	62 (25.3)	30 (24.8)	32 (25.8)	0.856*
Stage III–IV	17 (21.2)	12 (66.7)	5 (33.3)		181 (73.9)	90 (74.4)	91 (73.4)	
NA	5 (45.5)	1 (5.6)	4 (26.7)		2 (0.8)	1 (0.8)	1 (0.8)	
Histological grade				1.000				0.025[a]
G1–G2	28 (84.8)	13 (86.7)	15 (83.3)		190 (77.6)	86 (71.1)	104 (83.9)	0.022*
G3–G4	5 (15.2)	2 (13.3)	3 (16.7)		54 (22.0)	34 (28.1)	20 (16.1)	
NA	0 (0.0)	0 (0.0)	0 (0.0)		1 (0.4)	1 (0.8)	0 (0.0)	
Radiotherapy				0.039				0.216
Yes	20 (60.6)	14 (70.6)	6 (50.0)		134 (54.7)	71 (58.7)	63 (50.8)	
No	13 (39.4)	4 (29.4)	9 (50.0)		111 (45.3)	50 (41.3)	61 (49.2)	

*a: Fisher's exact test. b: $\chi 2$ test except for those marked with a. *Pairwise comparison without NA group.*

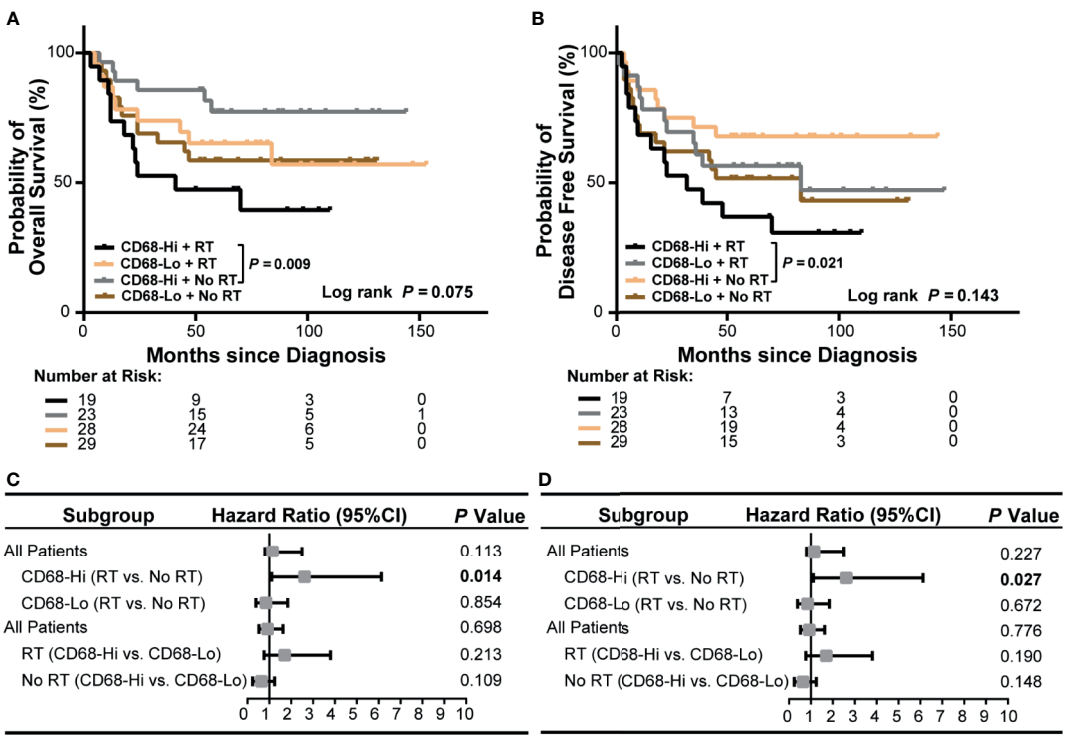

FIGURE 4 | Association of $CD68^+$ macrophage infilatration and radiation with survival of all OSCC patients in our cohort. **(A, B)** Kaplan-Meier curves show overall survival **(A)** and disease-free survival **(B)** in high or low level of $CD68^+$ macrophage infiltrated OSCC patients receiving radiation or no radiation. Log-rank test and/or pair wised comparison was used for significance. **(C, D)** Forest plots illustrate hazard ratios of subgroup univariate cox regression of overall survival **(C)** and disease-free survival **(D)**. CD68-Hi, CD68-High; CD68-Lo, CD68-Low; RT, radiation.

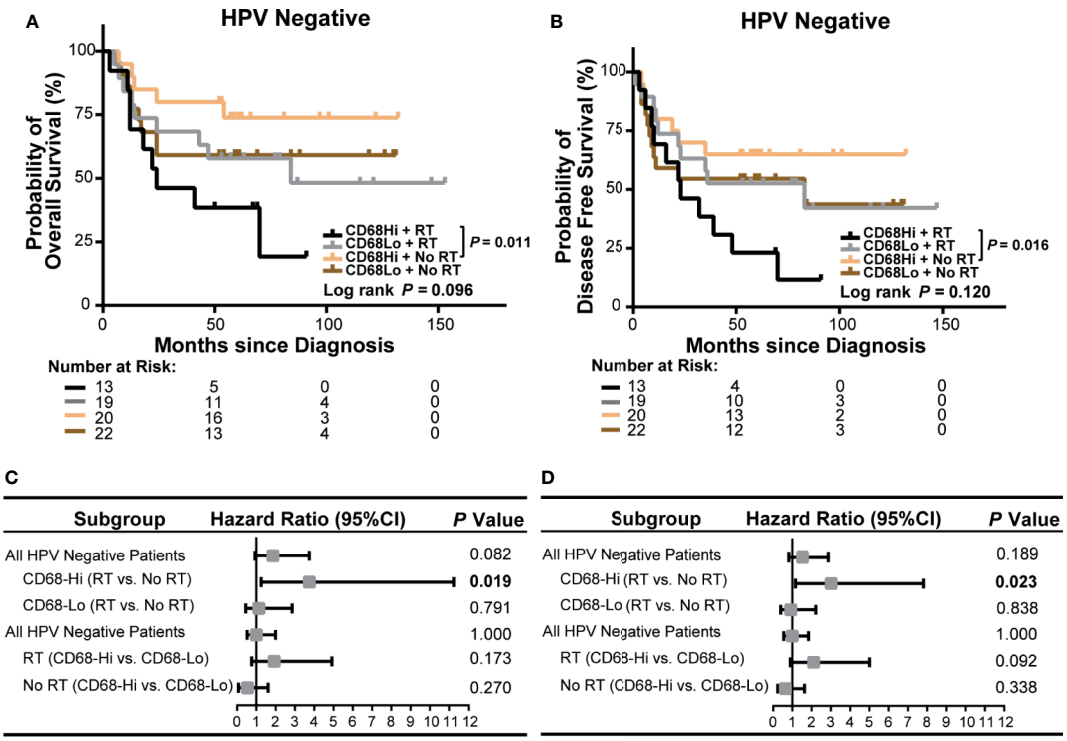

FIGURE 5 | Association of CD68$^+$ macrophage infilatration and radiation with survival of HPV negative OSCC patients in our cohort. **(A, B)** Kaplan-Meier curves exhibit overall survival **(A)** and disease-free survival **(B)** in high or low level of CD68$^+$ macrophage infiltrated HPV negative OSCC patients receiving radiation or no radiation. Log-rank test and/or pair wised comparison was used for significance. **(C, D)** Forest plots illustrate hazard ratios of subgroup univariate cox regression of overall survival **(C)** and disease-free survival **(D)**. CD68-Hi, CD68-High; CD68-Lo, CD68-Low; RT, radiation.

infiltration deconvolved using CIBERSOFT or EPIC and prognosis was observed in all OSCC patients (**Supplementary Figures S5, S6** and **Supplementary Tables S13–S16**), HPV negative OSCC subgroup (**Supplementary Figures S7, S8** and **Supplementary Tables S17–S20**), or HPV positive OSCC subgroup (data not shown). These results suggested that CD68$^+$ macrophage might play an important role in the distinct prognoses of HPV negative and positive OSCC patients receiving radiation or not.

Poly(I:C) Induces Apoptosis of CAL-27 and Enhances Its Radiosensitivity

In the above cohort studies, we observed trends of poor OS and DFS of radiation treated OSCC patients in HPV negative subgroup. To explore whether virus affects the radiosensitivity of HPV negative OSCC cells, *in vitro*, we applied a viral dsRNA mimic, poly(I:C), on CAL-27 cells. We performed apoptosis assay of flow cytometry of CAL-27 treated with poly(I:C) combined with radiation (**Figure 6A–D**). We demonstrated that the apoptotic rates of CAL-27 were significantly increased by increasing of radiation dose. On the other hand, poly(I:C) further increased the apoptosis rates of CAL-27 treated with radiation. Similarly, the proliferation of CAL-27 was also significantly decreased by increasing radiation dose (**Figure 6E**). Poly(I:C) had a further inhibitory effect on the proliferation of CAL-27 treated with radiation. Together, these results suggested that poly(I:C) not only induced apoptosis of CAL-27, but also enhanced the radiosensitivity of CAL-27.

Poly(I:C) Alters Cytokine Induction and Recruitment of Macrophage Cocultured With Radiation Stimulated CAL-27

In the above cohort studies, we found that radiation was associated with poor OS and DFS of high CD68$^+$ macrophage infiltrated OSCC patients in HPV negative subgroup. To explore the effect of poly(I:C) and/or radiation treated CAL-27 on cytokine secretion of macrophage, we treated THP-1-derived macrophages with CAL-27 conditioned medium (CM) and evaluated the levels of cytokines using Th17 Cytokine Assay (**Figure 7A**). M1-type cytokines, IL-1β, IL-6, IL-17 and TNF-α of THP-1-derived macrophages were induced in response to radiation stimulated CAL-27 CM. Moreover, the inductions of IL-1β and IL-6 were also significantly increased in response to poly(I:C) combined radiation stimulated CAL-27 CM. The inductions of IL-17 and TNF-α were significantly decreased in response to poly(I:C) combined radiation stimulated CAL-27 CM. On the other hand, radiation-stimulated CAL-27 CM significantly inhibited the secretion of IL-7 in THP-1-derived macrophage, and the addition of poly(I:C) further inhibited the secretion of IL-7. Furthermore, poly(I:C) treated CAL-27 CM

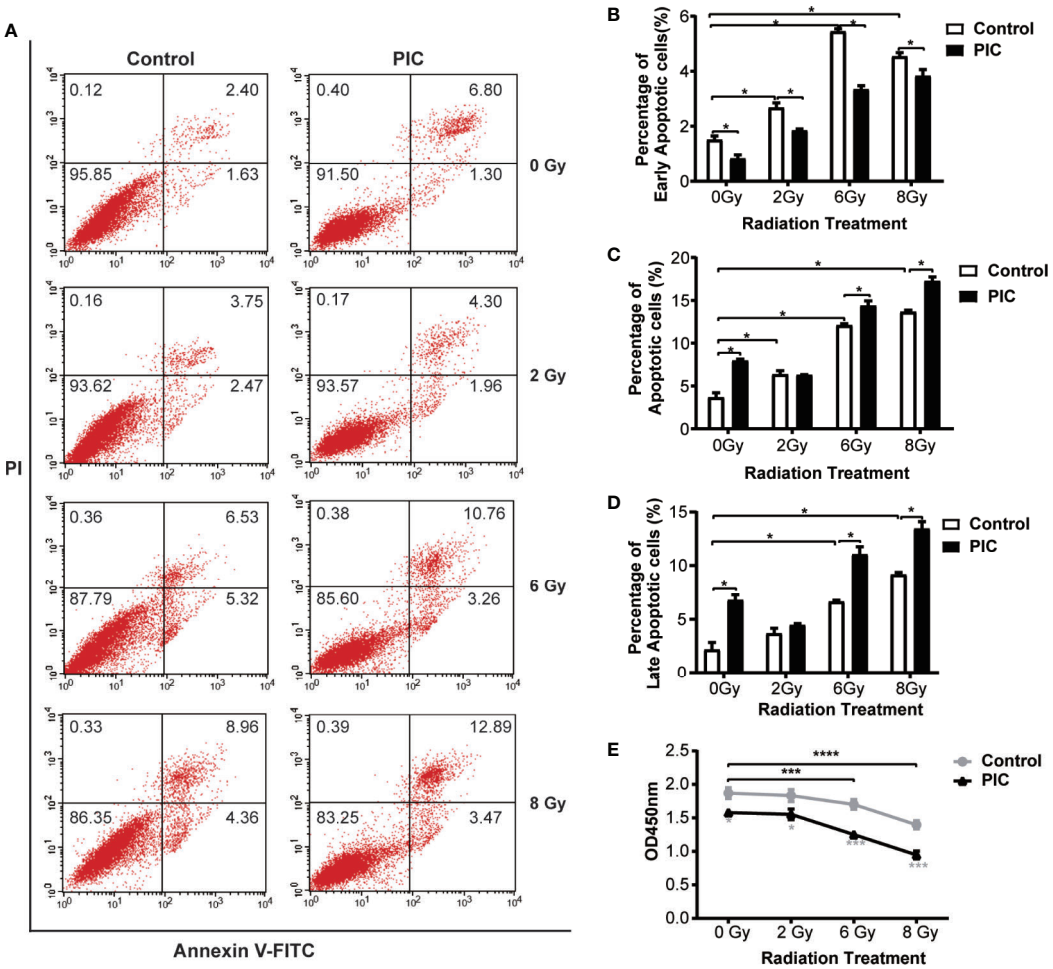

FIGURE 6 | Poly(I:C) enhances radiation-induced apoptosis and inhibits proliferation of CAL-27. CAL-27 cells were treated with poly(I:C) or PBS for 24 h followed by radiation. **(A)** Representative plots illustrate apoptosis of CAL-27 according to annexin V and/or propidium iodide (PI) staining. **(B)** Bar plots indicate the quantifications of early apoptotic cells ((annexin V+/PI-) of the bottom right quadrant. **(C)** Bar plots indicate the quantifications of late apoptotic cells (annexin V+/PI+) of the top right quadrant. **(D)** Bar plots indicate the quantifications of total apoptotic cells (annexin V+) of the top right and bottom right quadrants. **(E)** The proliferation curve shows the proliferation of CAL-27 detected by CCK-8 assay. Student's t-test was used for significance determination of flowcytometry (mean ± SD, n = 3). ANOVA was used for significance determination of CCK-8 assay (mean ± SD, n = 5). * indicates $P < 0.05$, *** indicates $P < 0.001$ and **** indicates $P < 0.0001$. PIC, poly (I:C).

inhibited IL-12p70 secretion of THP-1-derived macrophages regardless of radiation treatment. These results addressed the importance of M1-type cytokine, IL-6, which was induced most significantly in response to both radiation and poly(I:C) stimulated CAL-27 CM.

Based on the evidences of HMGB1 in macrophage function and radiation damage, we further explored the induction of HMGB1 in poly(I:C) and/or radiation treated CAL-27 CM (**Figure 7B**) and its role in IL-6 induction (**Figure 7C**). HMGB1 induction of CAL-27 CM was significantly promoted in response to radiation in a dose dependent manner. On the other hand, poly(I:C) significantly promoted HMGB1 induction of CAL-27 in a time dependent manner regardless of radiation. Notably, poly(I:C) treatment for 24h combined 8Gy radiation showed the most significant induction of HMGB1. Furthermore, neutralizing HMGB1 significantly inhibited IL-6 induction of THP-1-derived macrophage in response to CAL-27 CM treated with poly(I:C) for 24h and 8Gy radiation.

To investigate the role of IL-6 in macrophage recruitment, we established an *in vitro* macrophage migration model using transwell chambers. We co-cultured THP-1-derived macrophages with CAL-27 CM treated with poly(I:C) and radiation. We found that poly(I:C) or radiation treated CAL-27 CM promoted the recruitment of THP-1-derived macrophages. The recruitment was significantly enhanced by combining poly(I:C) and radiation. However, the recruitment was depleted by neutralizing IL-6 (**Figures 7D, E**). These suggested the key role of IL-6 in macrophage recruitment by CAL-27 CM. Furthermore, neutralizing HMGB1 also significantly inhibited the recruitment of THP-1-derived macrophages by in response to CAL-27 CM (**Figures 7F, G**). These results suggested

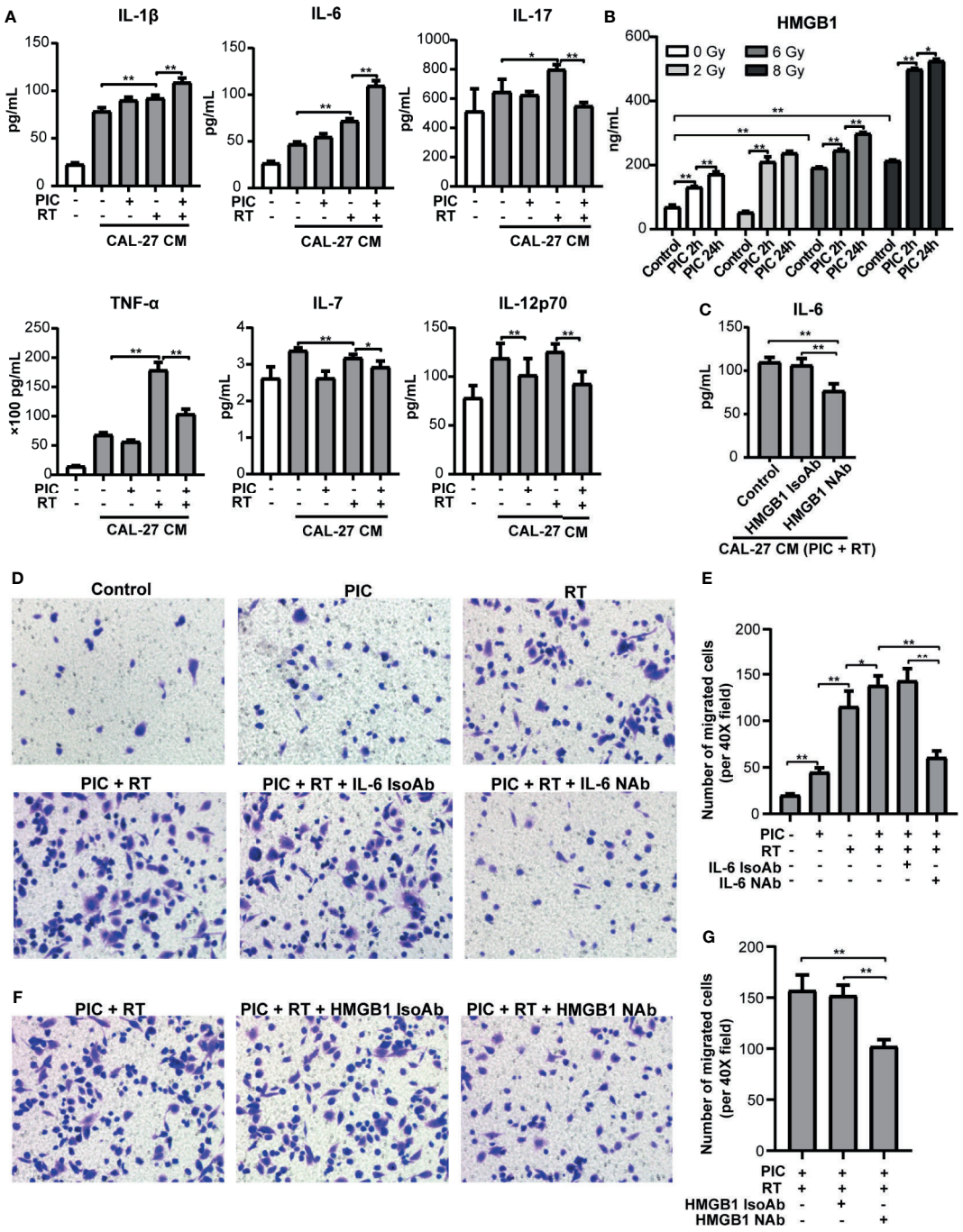

FIGURE 7 | Poly(I:C) and radiation-stimulated CAL-27 alters cytokine secretion of macrophages and promotes macrophage recruitment through IL-6 and HMGB1. CAL-27 cells were treated with poly(I:C) or PBS for 24 h followed by 8 Gy or 0 Gy radiation. THP-1-derived macrophages were treated with above CAL-27 CM (or no CM control) and continued to culture for 42 h before incubation for 24 h with fresh medium. **(A)** The concentrations of IL-1β, IL-6, IL-17, TNF-α, IL-7, and IL-12p70 in the supernatants were detected by cytokine assay. ANOVA was used (mean ± SD, n = 5). **(B)** Bar plot shows HMGB1 concentrations in CAL-27 CM detected by ELISA. Mann-Whitney U-test was used (mean ± SD, n = 3). **(C)** Bar plot shows the concentration of IL-6 in the supernatants of THP-1-derived macrophages treated with CAL-27 CM (poly (I:C) 24 h combined 8 Gy radiation) or pretreated with HMGB1 neutralizing antibody or isotype antibody. **(D, E)** Representative images (×200) and quantifications of the migrated THP-1-derived macrophages treated with CAL-27 CM and IL-6 neutrolizing antibody (or isotype). **(F, G)** Representative images (×200) and quantifications of the migrated THP-1-derived macrophages treated with CAL-27 CM and HMGB1 neutrolizing antibody (or isotype). ANOVA was used (mean ± SD, n = 5). * indicates $P < 0.05$ and ** indicates $P < 0.01$. PIC, poly (I:C); CM, condition medium; RT, radiation. NAb, neutralizing antibody; IsoAb, isotype antibody.

that poly(I:C) and radiation stimulated CAL-27 CM promoted macrophage recruitment could be inhibited by targeting HMGB1.

DISCUSSION

The need to explore the underlining mechanisms of the distinct prognoses of HPV negative and positive OSCC is urgent for precise medicine. Lymphocyte infiltration of tumor microenvironment and its modulation have been shown associated with HPV positive HNC patients and their favorable prognosis and better therapy response (8–11, 15, 16). Nonetheless, the role of macrophage has been overlooked. We observed a poor OS and a poor DFS in high $CD68^+$ macrophage infiltrated OSCC patients receiving radiation in HPV negative subgroup in our cohort. Based on the cohort results, we further conducted *in vitro* experiments, we found that poly(I:C) could not only induce apoptosis, but also enhanced the radiosensitivity of CAL-27. Furthermore, neutralizing IL-6 or HMGB1 could inhibit macrophage recruitment. A schematic diagram was made to depict the above mechanisms (**Figure 8**).

To explore the association of macrophage infiltration with HPV status and survival of OSCC patients, we conducted a retrospective cohort. In our study, we found that $CD68^+$ macrophage infiltration was not associated with OS or DFS of OSCC patients. The association of $CD68^+$ macrophages with survival of OSCC patients is controversial. Some studies showed that high $CD68^+$ macrophage associated with poor survival of OSCC (23–27) or with favorable survival of OSCC (28). Consistent with our results, there are also studies demonstrated no association of $CD68^+$ macrophage infiltration with prognosis of OSCC patients (29, 30). However, we observed a poor OS and a poor DFS in radiation treated OSCC patients with high $CD68^+$ macrophage infiltration, especially in HPV negative subgroup, but not in HPV positive subgroup. However, the lack of association between macrophage infiltration and radiation response in HPV positive OSCC patients might also result from the limited number of HPV positive subgroup. These findings indicated that $CD68^+$ macrophage might associate with poor radiation response and prognosis of HPV negative OSCC patients, and that $CD68^+$ macrophage infiltration might need to be reduced before radiation therapy for HPV negative OSCC patients.

Since HPV negative OSCC patients receiving radiation obtained worse survival than HPV positive OSCC patients, we applied radiation and/or poly(I:C) to CAL-27 cells in an attempt to examine whether viral mimic could affect radiosensitivity of HPV negative OSCC. We found that poly(I:C) could induce apoptosis of CAL-27. This is consistent with previous studies of pancreatic cancer (31, 32), glioblastoma (33), and neuroblastoma (34). We also found that poly(I:C) could enhance the radiosensitivity of CAL-27. This is consistent with Mikulandra's finding using poly(I:C) and cisplatin in HNSCC-derived cells (35) and Sato's finding in lung adenocarcinoma (36). Together, these suggested that radiation combined with poly(I:C) could be potentially used for OSCC suppression.

On the other hand, we found that M1-type cytokines were induced in THP-1 derived macrophages in response to radiation and poly(I:C) stimulated CAL-27 CM. IL-6, the most significantly induced cytokine, played a key role in macrophage recruitment by CAL-27 CM. We also demonstrated that the process was dependent of HMGB1. It has been shown as a key damage-related molecular pattern to induce inflammation in response to radiation (37–39). However, HMGB1 has also been shown to promote hepatocellular carcinoma (40) and associate with

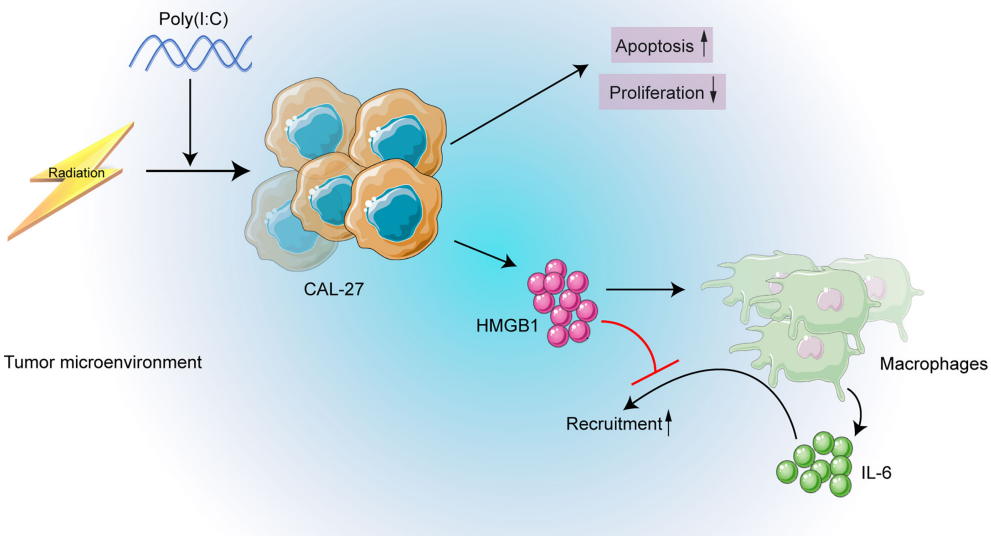

FIGURE 8 | The schematic diagram depicting the strategy of targeting HMGB1 may enhance radiosensitivity of CAL-27 cells by inhibiting macrophage recruitment induced by poly(I:C).

radiation resistance of bladder cancer cells (41). Accordingly, in our study, neutralizing HMGB1 could inhibit IL-6 induction and macrophage recruitment. Taken together, our findings suggested that although poly(I:C) could enhance radiosensitivity of OSCC, neutralizing HMGB1 should also be used to inhibit macrophage recruitment promoted by poly(I:C) and radiation CAL-27 CM.

In summary, we demonstrated that $CD68^+$ macrophage infiltration might associate with poor prognosis of HPV negative OSCC patients receiving radiation using our cohort. We found that treating CAL-27 with a viral mimic, poly(I:C), could induce apoptosis and enhance the radiosensitivity. Furthermore, HMGB1 should be targeted to inhibit macrophage recruitment and may enhance the overall therapy effects. Our findings may supply a potential therapy strategy to increase the radiation response and prognosis of HPV negative OSCC and provide new insights in understanding the molecular mechanisms.

DATA AVAILABILITY STATEMENT

The original contributions presented in the study are included in the article/**Supplementary Material**. Further inquiries can be directed to the corresponding authors.

ETHICS STATEMENT

The studies involving human participants were reviewed and approved by The Ethics Committee of Qilu Hospital of Shandong University. Written informed consent for participation was not required for this study in accordance with the national legislation and the institutional requirements.

AUTHOR CONTRIBUTIONS

XQ and YD conceived and designed the project. KW, ZD, WT, and SL performed the surgeries and collected the clinical characteristics data. ZN, HW, LZhang and LZhao completed the follow-ups. DA, JS, and CM performed the immunohistochemistry and histological analyses. YD, DA, and ZN performed the survival analysis of the cohort. DA, HW, WG, JL, BS, and QS performed in vitro experiments and analyzed the data. YD and DA wrote the manuscript. All authors contributed to the article and approved the submitted version.

FUNDING

This work was supported by the grants of XQ (81772879) and YD (81902770) from National Natural Science Foundation of China.

SUPPLEMENTARY MATERIAL

The Supplementary Material for this article can be found online at: https://www.frontiersin.org/articles/10.3389/fonc.2021.740622/full#supplementary-material

REFERENCES

1. Bray F, Ferlay J, Soerjomataram I, Siegel RL, Torre LA, Jemal A. Global Cancer Statistics 2018: GLOBOCAN Estimates of Incidence and Mortality Worldwide for 36 Cancers in 185 Countries. *CA Cancer J Clin* (2018) 68 (6):394–424. doi: 10.3322/caac.21492
2. Cohen EE, LaMonte SJ, Erb NL, Beckman KL, Sadeghi N, Hutcheson KA, et al. American Cancer Society Head and Neck Cancer Survivorship Care Guideline. *CA: Cancer J Clin* (2016) 66(3):203–39. doi: 10.3322/caac.21343
3. Bryant AK, Sojourner EJ, Vitzthum LK, Zakeri K, Shen H, Nguyen C, et al. Prognostic Role of P16 in Nonoropharyngeal Head and Neck Cancer. *J Natl Cancer Inst* (2018) 110(12):1393–9. doi: 10.1093/jnci/djy072
4. Chung CH, Zhang Q, Kong CS, Harris J, Fertig EJ, Harari PM, et al. P16 Protein Expression and Human Papillomavirus Status as Prognostic Biomarkers of Nonoropharyngeal Head and Neck Squamous Cell Carcinoma. *J Clin Oncol* (2014) 32(35):3930–8. doi: 10.1200/JCO.2013.54.5228
5. Budach V, Tinhofer I. Novel Prognostic Clinical Factors and Biomarkers for Outcome Prediction in Head and Neck Cancer: A Systematic Review. *Lancet Oncol* (2019) 20(6):e313–e26. doi: 10.1016/s1470-2045(19)30177-9
6. Chi AC, Day TA, Neville BW. Oral Cavity and Oropharyngeal Squamous Cell Carcinoma–an Update. *CA Cancer J Clin* (2015) 65(5):401–21. doi: 10.3322/caac.21293
7. Jarosz-Biej M, Smolarczyk R, Cichoń T, Kułach N. Tumor Microenvironment as A "Game Changer" in Cancer Radiotherapy. *Int J Mol Sci* (2019) 20 (13):3212. doi: 10.3390/ijms20133212
8. Chen YP, Wang YQ, Lv JW, Li YQ, Chua MLK, Le QT, et al. Identification and Validation of Novel Microenvironment-Based Immune Molecular Subgroups of Head and Neck Squamous Cell Carcinoma: Implications for Immunotherapy. *Ann Oncol* (2019) 30(1):68–75. doi: 10.1093/annonc/mdy470
9. Cillo AR, Kurten CHL, Tabib T, Qi Z, Onkar S, Wang T, et al. Immune Landscape of Viral- and Carcinogen-Driven Head and Neck Cancer. *Immunity* (2020) 52(1):183–99 e9. doi: 10.1016/j.immuni.2019.11.014
10. Wieland A, Patel MR, Cardenas MA, Eberhardt CS, Hudson WH, Obeng RC, et al. Defining HPV-Specific B Cell Responses in Patients With Head and Neck Cancer. *Nature* (2020). doi: 10.1038/s41586-020-2931-3
11. Balermpas P, Rodel F, Rodel C, Krause M, Linge A, Lohaus F, et al. CD8+ Tumour-Infiltrating Lymphocytes in Relation to HPV Status and Clinical Outcome in Patients With Head and Neck Cancer After Postoperative Chemoradiotherapy: A Multicentre Study of the German Cancer Consortium Radiation Oncology Group (DKTK-ROG). *Int J Cancer* (2016) 138(1):171–81. doi: 10.1002/ijc.29683
12. Mantovani A, Marchesi F, Malesci A, Laghi L, Allavena P. Tumour-Associated Macrophages as Treatment Targets in Oncology. *Nat Rev Clin Oncol* (2017) 14(7):399–416. doi: 10.1038/nrclinonc.2016.217
13. Dijkgraaf EM, Heusinkveld M, Tummers B, Vogelpoel LT, Goedemans R, Jha V, et al. Chemotherapy Alters Monocyte Differentiation to Favor Generation of Cancer-Supporting M2 Macrophages in the Tumor Microenvironment. *Cancer Res* (2013) 73(8):2480–92. doi: 10.1158/0008-5472.Can-12-3542
14. Chen X, Fu E, Lou H, Mao X, Yan B, Tong F, et al. IL-6 Induced M1 Type Macrophage Polarization Increases Radiosensitivity in HPV Positive Head and Neck Cancer. *Cancer Lett* (2019) 456:69–79. doi: 10.1016/j.canlet.2019.04.032
15. Hanoteau A, Newton JM, Krupar R, Huang C, Liu HC, Gaspero A, et al. Tumor Microenvironment Modulation Enhances Immunologic Benefit of Chemoradiotherapy. *J Immunother Cancer* (2019) 7(1):10. doi: 10.1186/s40425-018-0485-9

16. Sato-Kaneko F, Yao S, Ahmadi A, Zhang SS, Hosoya T, Kaneda MM, et al. Combination Immunotherapy With TLR Agonists and Checkpoint Inhibitors Suppresses Head and Neck Cancer. *JCI Insight* (2017) 2(18):e93397. doi: 10.1172/jci.insight.93397
17. Cao S, Wendl MC, Wyczalkowski MA, Wylie K, Ye K, Jayasinghe R, et al. Divergent Viral Presentation Among Human Tumors and Adjacent Normal Tissues. *Sci Rep* (2016) 6:28294. doi: 10.1038/srep28294
18. Liu J, Lichtenberg T, Hoadley KA, Poisson LM, Lazar AJ, Cherniack AD, et al. An Integrated TCGA Pan-Cancer Clinical Data Resource to Drive High-Quality Survival Outcome Analytics. *Cell* (2018) 173(2):400–16 e11. doi: 10.1016/j.cell.2018.02.052
19. Newman AM, Liu CL, Green MR, Gentles AJ, Feng W, Xu Y, et al. Robust Enumeration of Cell Subsets From Tissue Expression Profiles. *Nat Methods* (2015) 12(5):453–7. doi: 10.1038/nmeth.3337
20. Racle J, de Jonge K, Baumgaertner P, Speiser DE, Gfeller D. Simultaneous Enumeration of Cancer and Immune Cell Types From Bulk Tumor Gene Expression Data. *Elife* (2017) 6:e26476. doi: 10.7554/eLife.26476
21. Schlecht NF, Brandwein-Gensler M, Nuovo GJ, Li M, Dunne A, Kawachi N, et al. A Comparison of Clinically Utilized Human Papillomavirus Detection Methods in Head and Neck Cancer. *Mod. Pathol* (2011) 24(10):1295–305. doi: 10.1038/modpathol.2011.91
22. Taylor PR, Martinez-Pomares L, Stacey M, Lin HH, Brown GD, Gordon S. Macrophage Receptors and Immune Recognition. *Annu Rev Immunol* (2005) 23:901–44. doi: 10.1146/annurev.immunol.23.021704.115816
23. Wolf GT, Chepeha DB, Bellile E, Nguyen A, Thomas D, McHugh J. Tumor Infiltrating Lymphocytes (TIL) and Prognosis in Oral Cavity Squamous Carcinoma: A Preliminary Study. *Oral Oncol* (2015) 51(1):90–5. doi: 10.1016/j.oraloncology.2014.09.006
24. Balermpas P, Rodel F, Liberz R, Oppermann J, Wagenblast J, Ghanaati S, et al. Head and Neck Cancer Relapse After Chemoradiotherapy Correlates With CD163+ Macrophages in Primary Tumour and CD11b+ Myeloid Cells in Recurrences. *Br J Cancer* (2014) 111(8):1509–18. doi: 10.1038/bjc.2014.446
25. Costa NL, Valadares MC, Souza PP, Mendonça EF, Oliveira JC, Silva TA, et al. Tumor-Associated Macrophages and the Profile of Inflammatory Cytokines in Oral Squamous Cell Carcinoma. *Oral Oncol* (2013) 49(3):216–23. doi: 10.1016/j.oraloncology.2012.09.012
26. Lu CF, Huang CS, Tjiu JW, Chiang CP. Infiltrating Macrophage Count: A Significant Predictor for the Progression and Prognosis of Oral Squamous Cell Carcinomas in Taiwan. *Head Neck* (2010) 32(1):18–25. doi: 10.1002/hed.21138
27. Liu SY, Chang LC, Pan LF, Hung YJ, Lee CH, Shieh YS. Clinicopathologic Significance of Tumor Cell-Lined Vessel and Microenvironment in Oral Squamous Cell Carcinoma. *Oral Oncol* (2008) 44(3):277–85. doi: 10.1016/j.oraloncology.2007.02.007
28. Wirsing AM, Ervik IK, Seppola M, Uhlin-Hansen L, Steigen SE, Hadler-Olsen E. Presence of High-Endothelial Venules Correlates With a Favorable Immune Microenvironment in Oral Squamous Cell Carcinoma. *Modern Pathol.: An Off J United States Can Acad Pathol. Inc* (2018) 31(6):910–22. doi: 10.1038/s41379-018-0019-5
29. Fang J, Li X, Ma D, Liu X, Chen Y, Wang Y, et al. Prognostic Significance of Tumor Infiltrating Immune Cells in Oral Squamous Cell Carcinoma. *BMC Cancer* (2017) 17(1):375. doi: 10.1186/s12885-017-3317-2
30. Kwon M, Yeo SC, Lee JS, Park JJ. Not CD68 But Stabilin-1 Expression is Associated With the Risk of Recurrence in Patients With Oral Cavity Squamous Cell Carcinoma. *Head Neck* (2019) 41(7):2058–64. doi: 10.1002/hed.25654
31. Bhoopathi P, Quinn BA, Gui Q, Shen XN, Grossman SR, Das SK, et al. Pancreatic Cancer-Specific Cell Death Induced *In Vivo* by Cytoplasmic-Delivered Polyinosine-Polycytidylic Acid. *Cancer Res* (2014) 74(21):6224–35. doi: 10.1158/0008-5472.can-14-0819
32. Duewell P, Beller E, Kirchleitner SV, Adunka T, Bourhis H, Siveke J, et al. Targeted Activation of Melanoma Differentiation-Associated Protein 5 (MDA5) for Immunotherapy of Pancreatic Carcinoma. *Oncoimmunology* (2015) 4(10):e1029698. doi: 10.1080/2162402x.2015.1029698
33. Glas M, Coch C, Trageser D, Dassler J, Simon M, Koch P, et al. Targeting the Cytosolic Innate Immune Receptors RIG-I and MDA5 Effectively Counteracts Cancer Cell Heterogeneity in Glioblastoma. *Stem Cells (Dayton Ohio)* (2013) 31(6):1064–74. doi: 10.1002/stem.1350
34. Hsu WM, Huang CC, Lee HY, Wu PY, Wu MT, Chuang HC, et al. MDA5 Complements TLR3 in Suppression of Neuroblastoma. *Oncotarget* (2015) 6 (28):24935–46. doi: 10.18632/oncotarget.4511
35. Mikulandra M, Kobescak A, Verillaud B, Busson P, Matijevic Glavan T. Radio-Sensitization of Head and Neck Cancer Cells by a Combination of Poly (I:C) and Cisplatin Through Downregulation of Survivin and C-IAP2. *Cell Oncol (Dordrecht)* (2019) 42(1):29–40. doi: 10.1007/s13402-018-0403-7
36. Sato Y, Yoshino H, Kashiwakura I, Tsuruga E. DAP3 Is Involved in Modulation of Cellular Radiation Response by RIG-I-Like Receptor Agonist in Human Lung Adenocarcinoma Cells. *Int J Mol Sci* (2021) 22(1):420. doi: 10.3390/ijms22010420
37. Candéias SM, Testard I. The Many Interactions Between the Innate Immune System and the Response to Radiation. *Cancer Lett* (2015) 368(2):173–8. doi: 10.1016/j.canlet.2015.02.007
38. Anuranjani BM. Concerted Action of Nrf2-ARE Pathway, MRN Complex, HMGB1 and Inflammatory Cytokines - Implication in Modification of Radiation Damage. *Redox Biol* (2014) 2:832–46. doi: 10.1016/j.redox.2014.02.008
39. Yanai H, Ban T, Wang Z, Choi MK, Kawamura T, Negishi H, et al. HMGB Proteins Function as Universal Sentinels for Nucleic-Acid-Mediated Innate Immune Responses. *Nature* (2009) 462(7269):99–103. doi: 10.1038/nature08512
40. Jiang J, Wang GZ, Wang Y, Huang HZ, Li WT, Qu XD. Hypoxia-Induced HMGB1 Expression of HCC Promotes Tumor Invasiveness and Metastasis *via* Regulating Macrophage-Derived IL-6. *Exp Cell Res* (2018) 367(1):81–8. doi: 10.1016/j.yexcr.2018.03.025
41. Shrivastava S, Mansure JJ, Almajed W, Cury F, Ferbeyre G, Popovic M, et al. The Role of HMGB1 in Radioresistance of Bladder Cancer. *Mol Cancer Ther* (2016) 15(3):471–9. doi: 10.1158/1535-7163.Mct-15-0581

Conflict of Interest: The authors declare that the research was conducted in the absence of any commercial or financial relationships that could be construed as a potential conflict of interest.

The handling editor and the reviewer DC declared a shared affiliation, though no other collaboration, with the authors at the time of the review.

Publisher's Note: All claims expressed in this article are solely those of the authors and do not necessarily represent those of their affiliated organizations, or those of the publisher, the editors and the reviewers. Any product that may be evaluated in this article, or claim that may be made by its manufacturer, is not guaranteed or endorsed by the publisher.

frontiers in Oncology

ORIGINAL RESEARCH
published: 16 September 2021
doi: 10.3389/fonc.2021.714433

Prognostic Value of Plasma Epstein-Barr Virus DNA Levels Pre- and Post-Neoadjuvant Chemotherapy in Patients With Nasopharyngeal Carcinoma

Lisheng Zhu[1†], Tao Ouyang[2†], Ying Xiong[1], Li Ba[1], Qiuting Li[3], Mengjun Qiu[3], Zhenwei Zou[1] and Gang Peng[1*]*

[1] Cancer Center, Union Hospital, Tongji Medical College, Huazhong University of Science and Technology, Wuhan, China, [2] Department of Radiology, Union Hospital, Tongji Medical College, Huazhong University of Science and Technology, Wuhan, China, [3] Division of Gastroenterology, Liyuan Hospital, Tongji Medical College, Huazhong University of Science and Technology, Wuhan, China

Background: In this study, we evaluated the prognostic value of the plasma levels of Epstein-Barr virus (EBV) DNA in patients with nasopharyngeal carcinoma (NPC) at different treatment stages.

Methods: We retrospectively analyzed the Data of 206 patients with NPC. Pre-neoadjuvant chemotherapy (pre-NACT), post-NACT, post-radiotherapy, and post-treatment plasma EBV DNA levels were used to establish prognostic nomograms. The concordance index (C-index) and calibration curves were used to compare the prognostic accuracy of the nomograms. The results were confirmed in a validation cohort consisting of patients who were tested for EBV DNA levels at all four stages of treatment. The Kaplan-Meier method was used to calculate the progression-free survival (PFS) and overall survival (OS). Survival differences were calculated using the log-rank test.

Results: EBV DNA-positive patients had worse 3-year PFS and 5-year OS than EBV DNA-negative patients; this was true for pre-NACT (PFS: 82.7% *vs*. 57.3%, $P < 0.001$; OS: 90.9% *vs*. 68.7%, $P = 0.08$) and post-NACT (PFS: 85.0% *vs*. 50.6%, $P < 0.001$; OS: 91.7% *vs*. 65.7%; $P = 0.001$) EBV DNA levels but not for post-radiotherapy (PFS: 72.2% *vs*. 60.9%, $P = 0.192$; OS: 73.1% *vs*. 77.2%, $P = 0.472$) or post-treatment (PFS: 77.3% *vs*. 59.2%, $P = 0.063$; OS: 77.5% *vs*. 79.7%, $P = 0.644$) levels. Nomograms combining pre-NACT and post-NACT EBV DNA levels had a superior prognostic ability than those of post-radiotherapy and post-treatment EBV DNA levels.

OPEN ACCESS

Edited by:
Shiyu Song,
Virginia Commonwealth University Health System, United States

Reviewed by:
Christopher McLaughlin,
University of Virginia Cancer Center, United States
Alexander Slade,
Stony Brook Medicine, United States

***Correspondence:**
Gang Peng
penggang1977@aliyun.com
Zhenwei Zou
zouzhenwei@hust.edu.cn

[†]These authors have contributed equally to this work

Specialty section:
This article was submitted to Head and Neck Cancer, a section of the journal Frontiers in Oncology

Received: *25 May 2021*
Accepted: *09 August 2021*
Published: *16 September 2021*

Citation:
Zhu L, Ouyang T, Xiong Y, Ba L, Li Q, Qiu M, Zou Z and Peng G (2021) Prognostic Value of Plasma Epstein-Barr Virus DNA Levels Pre- and Post-Neoadjuvant Chemotherapy in Patients With Nasopharyngeal Carcinoma. Front. Oncol. 11:714433. doi: 10.3389/fonc.2021.714433

Conclusion: Pre-NACT EBV DNA levels combined with post-NACT EBV DNA levels can more reliably predict survival outcomes in patients with NPC.

Keywords: nasopharyngeal carcinoma, Epstein-Barr virus DNA, neoadjuvant chemotherapy, prognostic factor, nomogram

INTRODUCTION

Nasopharyngeal carcinoma (NPC) is relatively common in Southeast Asian countries due to the high prevalence of Epstein-Barr virus (EBV) infections (1). The recent advances in intensity-modulated radiotherapy (IMRT) and concurrent chemoradiotherapy (CCRT) have greatly improved the prognosis and survival outcomes of patients with NPC (2). However, some patients with NPC develop local recurrence or metastasis within 2 years of treatment (3). Patients with NPC receive different neoadjuvant chemotherapy (NACT) and adjuvant chemotherapy (ACT) regimens depending on their TNM stage. A phase III clinical trial showed that ACT with cisplatin and fluorouracil did not significantly improve the failure-free survival in patients with a locally advanced NPC (4). However, NACT with gemcitabine and cisplatin increased the 3-year recurrence-free survival from 76.5% to 85.3% in patients with a locally advanced NPC (5). In another study, three cycles of NACT improved the disease-free survival in patients with advanced NPC, although no significant changes were observed in the overall survival (OS) (6). Furthermore, the combination of NACT and ACT had no effect on the distant metastasis-free survival and OS in patients with advanced, high-risk NPC, despite a moderate improvement in the prognosis of low-risk patients (7, 8). Hence, the clinical benefit of NACT and ACT in patients with NPC merits further investigation.

EBV infection is associated with an increased risk of NPC (9–12). The relationship between the EBV DNA levels and the prognosis of patients at different stages of treatment has also been reported (13–16). Pre-treatment and post-treatment EBV DNA levels are considered as an indicator of tumor load and tumor malignancy. Notably, pre-treatment EBV DNA levels in the plasma of patients with NPC were significantly correlated with distant metastasis (6), relapse (17), and long-term OS (18, 19). Additionally, post-radiotherapy EBV DNA levels in the plasma of patients with NPC predicted locoregional failure, distant metastasis, and death (20). Post-treatment plasma EBV DNA levels also predicted distant metastasis (21) and tumor recurrence (22); thus, additional treatment in patients with high post-treatment EBV DNA levels may prevent relapse (14). Many NPC prognostic models are based on the EBV characteristics and serological indicators (19, 23, 24). The predictive ability of the nomograms of the circulating EBV DNA levels is higher than that of nomograms of the TNM stage (25). These findings suggest that plasma EBV DNA levels are useful in risk stratification and prognosis prediction in patients with NPC (23, 26). Furthermore, evaluating the plasma EBV DNA levels may improve the prediction of the PFS and OS (27, 28).

Nevertheless, the relevance of the dynamic changes in EBV DNA levels in NPC prognosis remains unclear. In this study, we evaluated the prognostic value of plasma EBV DNA levels at different treatment stages and the relationship between plasma EBV levels and NACT outcomes. We also developed a nomogram by combining pre-NACT and post-NACT EBV levels with other traditional risk factors.

METHODS

Patients

>We retrospectively reviewed the data of 696 patients diagnosed with NPC who underwent radiotherapy with NACT at Wuhan Union Hospital Cancer Center between July 2012 and October 2018; 490 patients were excluded because of the lack of information on the plasma EBV DNA levels. Among the 206 NPC patients, the plasma EBV DNA levels were evaluated before NACT (hereafter referred to as pre-NACT) in 178 patients, after NACT and before radiotherapy (hereafter referred to as post-NACT) in 161 patients, post-radiotherapy in 118 patients, and post-treatment in 133 patients. There was an intersection between the different groups of patients. The validation cohort consisted of 76 patients with known EBV DNA levels at all four treatment stages. The eligibility criteria were as follows: (1) pathological diagnosis of primary NPC; (2) no history of cancer treatment; (3) at least one plasma EBV DNA level evaluation (pre-NACT, post-NACT, post-radiotherapy, or post-treatment); (4) treatment with IMRT; (5) NACT treatment; (6) availability of baseline clinical data, including routine blood indicators and liver and kidney function. The experimental design is shown in **Figure 1**.

Diagnosis and Treatment

Baseline demographic and clinicopathological characteristics, including gender, age, and smoking status, were collected for all patients. Blood samples were collected before treatment to assess the levels of white blood cells, hemoglobin (HGB), platelets (PLT), lactate dehydrogenase (LDH), and EBV DNA. The clinical tumor stage was determined according to the AJCC TNM staging guidelines, seventh edition. All patients received IMRT and NACT, with or without adjuvant chemotherapy (ACT). NACT regimens were as follows: 1) 75 mg/m^2 of docetaxel and 75 mg/m^2 of cisplatin on day 1, and 750 mg/m^2 of fluorouracil for 5 days; 2) 1,000 mg/m^2 of gemcitabine on day 1 and day 8, 80 mg/m^{2}of cisplatin on day 1; 3) 75 mg/m^2 of docetaxel and 75 mg/m^2 of cisplatin on day 1. Each regimen was given in three-week cycles for a total of three cycles. Details on NACT regimens can be found in **Tables 1** and **S2**.

Plasma Epstein-Barr Virus DNA Evaluation

Plasma EBV DNA levels were assessed by quantitative PCR (qPCR) as previously described (23). Samples with EBV DNA

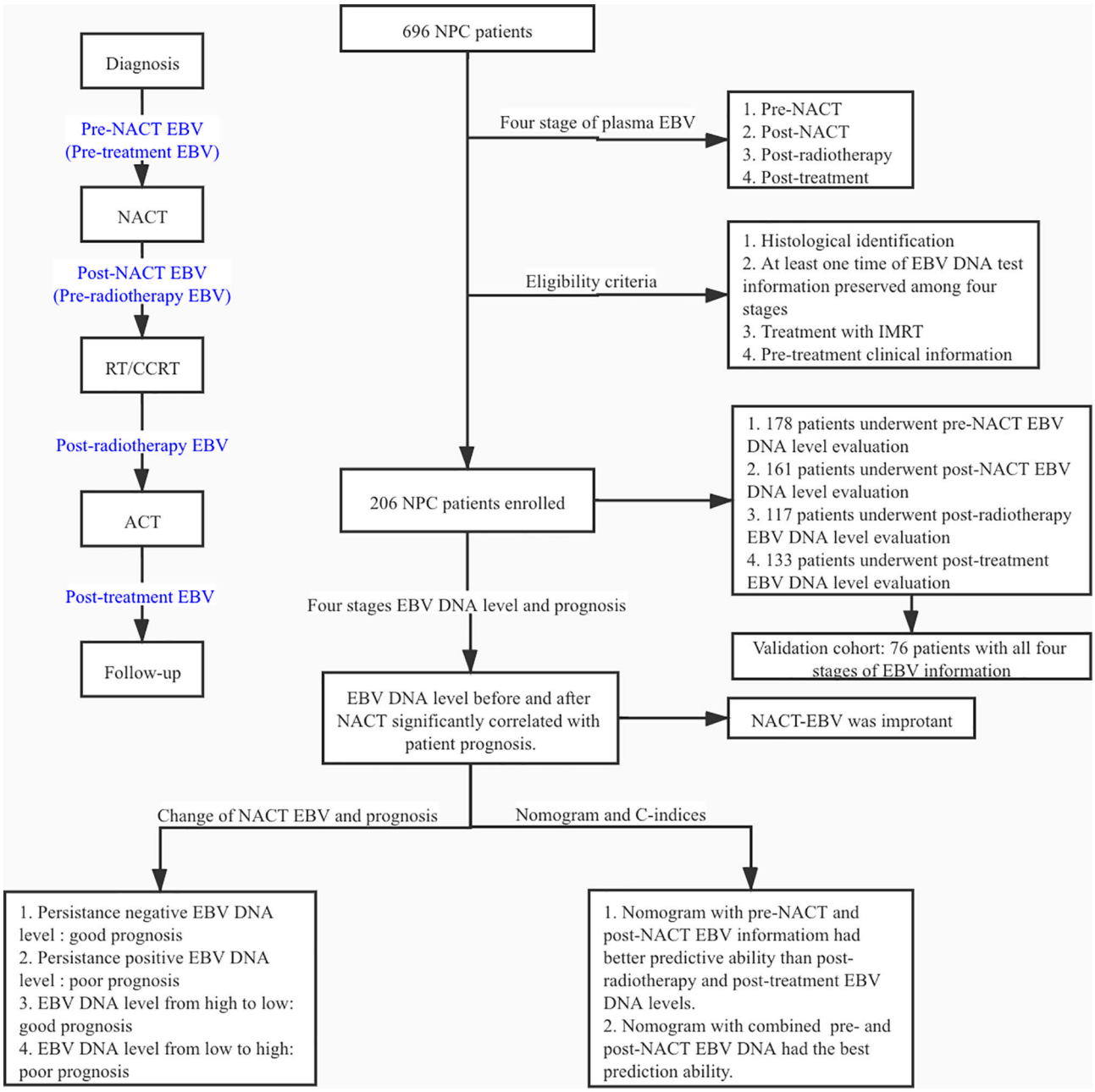

FIGURE 1 | Flow chart of this study.

levels higher than 400 copies/mL were considered EBV-positive. As not all patients had been evaluated for the EBV DNA levels at all four stages, we separately assessed patients with available data on pre-NACT, post-NACT, post-radiotherapy, and post-therapy plasma EBV DNA levels.

Patient Follow-Up

Patients were followed up every three months in the first three years after treatment and every six months thereafter. The primary endpoint of the study was PFS, defined as the time from diagnosis to disease progression or any-cause death. The secondary endpoint was OS, defined as the time from diagnosis to any-cause death. Patients were censored at the last follow-up date (January 2020).

Statistical Analysis

Statistical analyses were conducted using R version 3.6.3 (http://www.R-project.org). The Kaplan-Meier method was used to calculate the PFS and OS; survival differences were compared using the log-rank test. Patient characteristics were compared

TABLE 1 | Patient demographic and clinical characteristics.

Characteristic	Patients No. (%)
Age, y	
≤45	91 (44.2)
>45	115 (55.8)
Gender	
Female	49 (23.8)
Male	157 (76.2)
Clinical stage	
I/II	29 (14.1)
III	87 (42.2)
IVa	74 (35.9)
IVb	16 (7.8)
Tumor stage	
T1	3 (1.5)
T2	70 (34.0)
T3	78 (37.9)
T4	55 (26.7)
Node stage	
N0	9 (4.4)
N1	57 (27.7)
N2	102 (49.5)
N3	38 (18.4)
M stage	
M0	190 (92.2)
M1	16 (7.8)
Treatment	
NACT+RT ± ACT	140 (68.0)
NACT+CCRT ± ACT	66 (32.0)
NACT	
DCF	112 (54.4)
DP	59 (28.6)
GP	35 (17.0)
LDH, g/L	
<245	187 (93.2)
≥245	19 (6.8)
WBC, 10^9/L	
<4	21 (10.2)
4–10	173 (84.0)
≥10	12 (5.8)
HGB, g/L	
<120	33 (16.0)
120–150	133 (64.6)
≥150	40 (19.4)
PLT, 10^9/L	
<100	3 (1.5)
100–300	174 (84.5)
≥300	29 (14.1)
Smoking	
No	111 (53.9)
Yes	95 (46.1)
Alcohol	
No	138 (67.0)
Yes	68 (33.0)
EBV levels	
Negative	–
Positive	–
Clinical Outcome	
No progress	152 (73.8)
Local recurrence	32 (15.5)
Distant metastasis	22 (10.7)
Death	31 (15.0)

NACT, neoadjuvant chemotherapy; RT, radiotherapy; CCRT, concurrent chemoradiotherapy; ACT, adjuvant chemotherapy; DCF, docetaxel plus cisplatin and fluorouracil; DP, docetaxel plus cisplatin; GP, gemcitabine plus cisplatin; LDH, lactate dehydrogenase; WBC, white blood cells; HGB, hemoglobin; PLT, platelets; Positive EBV level was defined as serum EBV DNA load higher than 400 copies/mL; otherwise, was negative. N = 206.

using the χ^2 or Fisher's exact test. Significant factors in univariate analysis were used in the multivariable Cox regression analysis. A prognostic nomogram was established, and the concordance index (C-index) and calibration curve were used to determine the accuracy and discriminative ability of the nomogram. Two-sided *P*-values < 0.05 were considered statistically significant.

RESULTS

Patient Characteristics

In this retrospective study, we analyzed the data of 206 patients with NPC. There were no differences in the baseline characteristics between the included and excluded patients (**Table S1**). Plasma EBV DNA levels were determined pre-NACT in 178 patients, post-NACT in 161 patients, post-radiotherapy in 118 patients, and post-treatment in 133 patients. The patient demographics and clinical characteristics are presented in **Table 1**. The median follow-up time was 36.4 months (range, 3.8–91.6 months). A total of 54 (26.1%) patients had recurrent disease and distant metastasis, and 31 (15.0%) patients died. All patients received NACT before radiotherapy or CCRT.

Plasma Epstein-Barr DNA Levels Before and After Neoadjuvant Chemotherapy Are Significantly Associated With Patient Prognosis

The 3-year PFS rate of EBV DNA-negative patients before NACT was significantly higher than that of EBV DNA-positive patients (82.7% *vs*. 57.3%, $P < 0.001$; **Figure 2**). The risk of disease progression in patients positive for EBV DNA after NACT was 4.105 times (95% CI, 1.975–8.533) higher than that of patients negative for EBV DNA after NACT. Additionally, the 3-year PFS and 5-year OS rates were significantly lower in patients positive for EBV DNA after NACT than in EBV DNA-negative patients (3-year PFS: 50.6% *vs*. 85.0%, $P < 0.001$; 5-year OS: 91.7% *vs*. 65.7%; $P = 0.001$). There were no significant differences in the 3-year PFS and 5-year OS between patients stratified by post-radiotherapy EBV DNA levels (3-year PFS: 72.2% *vs*. 60.9%, $P = 0.192$; 5-year OS: 73.1% *vs*. 77.2%, $P = 0.472$). The prognosis of patients with high post-treatment EBV DNA levels tended to be worse than that of patients with low EBV DNA levels (3-year PFS: 59.2% *vs*. 77.3%, $P = 0.063$; 5-year OS: 77.5% *vs*. 79.7%, $P = 0.644$).

Because pre-NACT and post-NACT EBV DNA levels were strongly associated with PFS, we further investigated the relationship between NACT-associated EBV DNA levels and patient prognosis. Interestingly, the prognosis of patients with an EBV DNA-negative status all along was significantly better than that of patients who were EBV DNA-positive either before or after NACT and who were EBV DNA-positive both before and after NACT (3-year PFS: 88.8% *vs*. 71.5% *vs*. 40.1%, $P < 0.001$; 5-year OS: 94.3% *vs*. 84.7% *vs*. 56.4%, $P < 0.001$; **Figures 3A, B**).

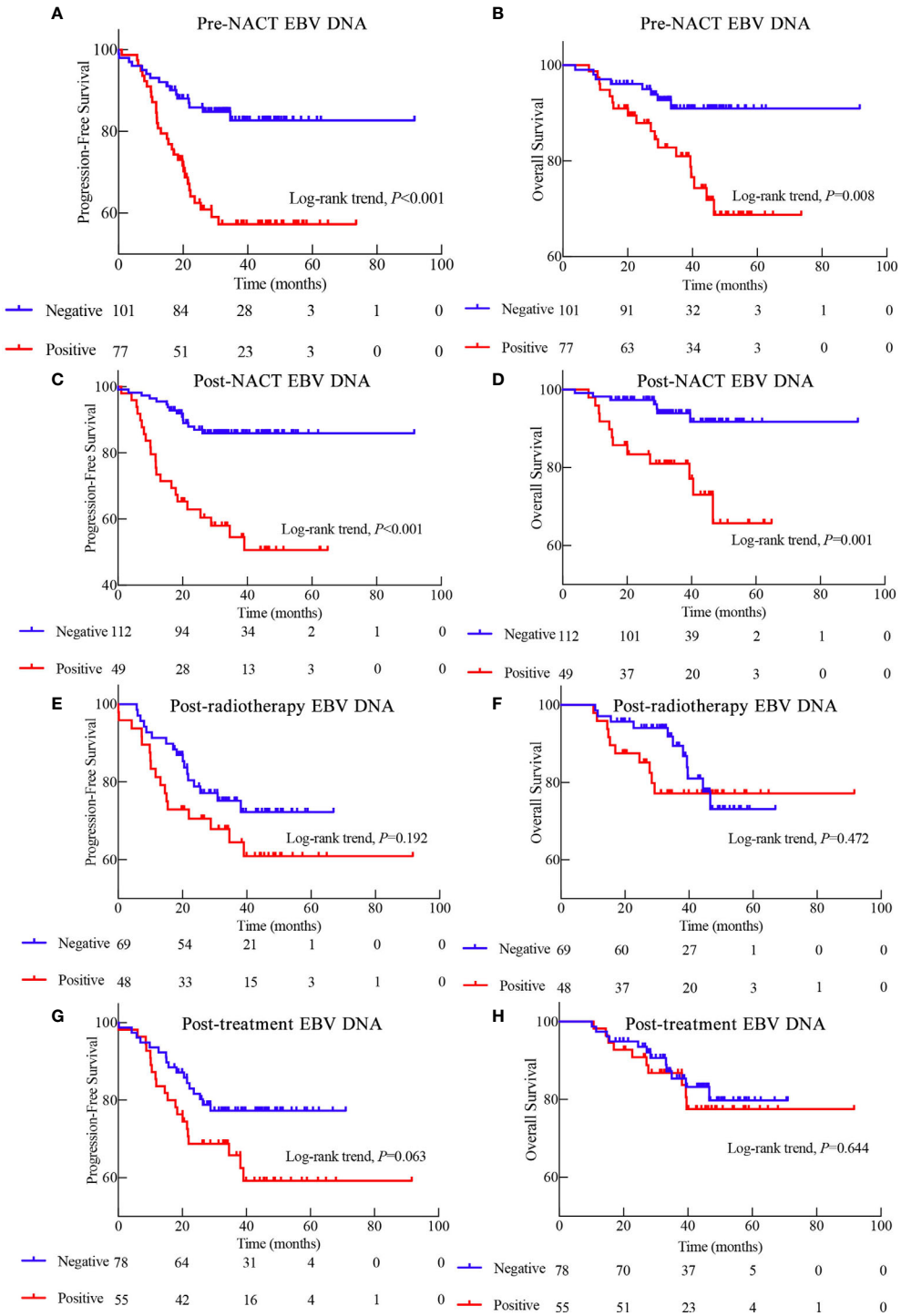

FIGURE 2 | Kaplan-Meier survival curves showing the progression-free survival (PFS) and overall survival (OS) of patients with EBV tested during different stages of treatment. **(A)** PFS based on pre- neoadjuvant chemotherapy (NACT) EBV DNA levels. **(B)** OS based on pre-NACT EBV DNA levels. **(C)** PFS based on post-NACT EBV DNA levels. **(D)** OS based on post-NACT EBV DNA levels. **(E)** PFS based on post-radiotherapy EBV DNA levels. **(F)** OS based on post-radiotherapy EBV DNA levels. **(G)** PFS based on post-treatment EBV DNA levels. **(H)** OS based on post-treatment EBV DNA levels.

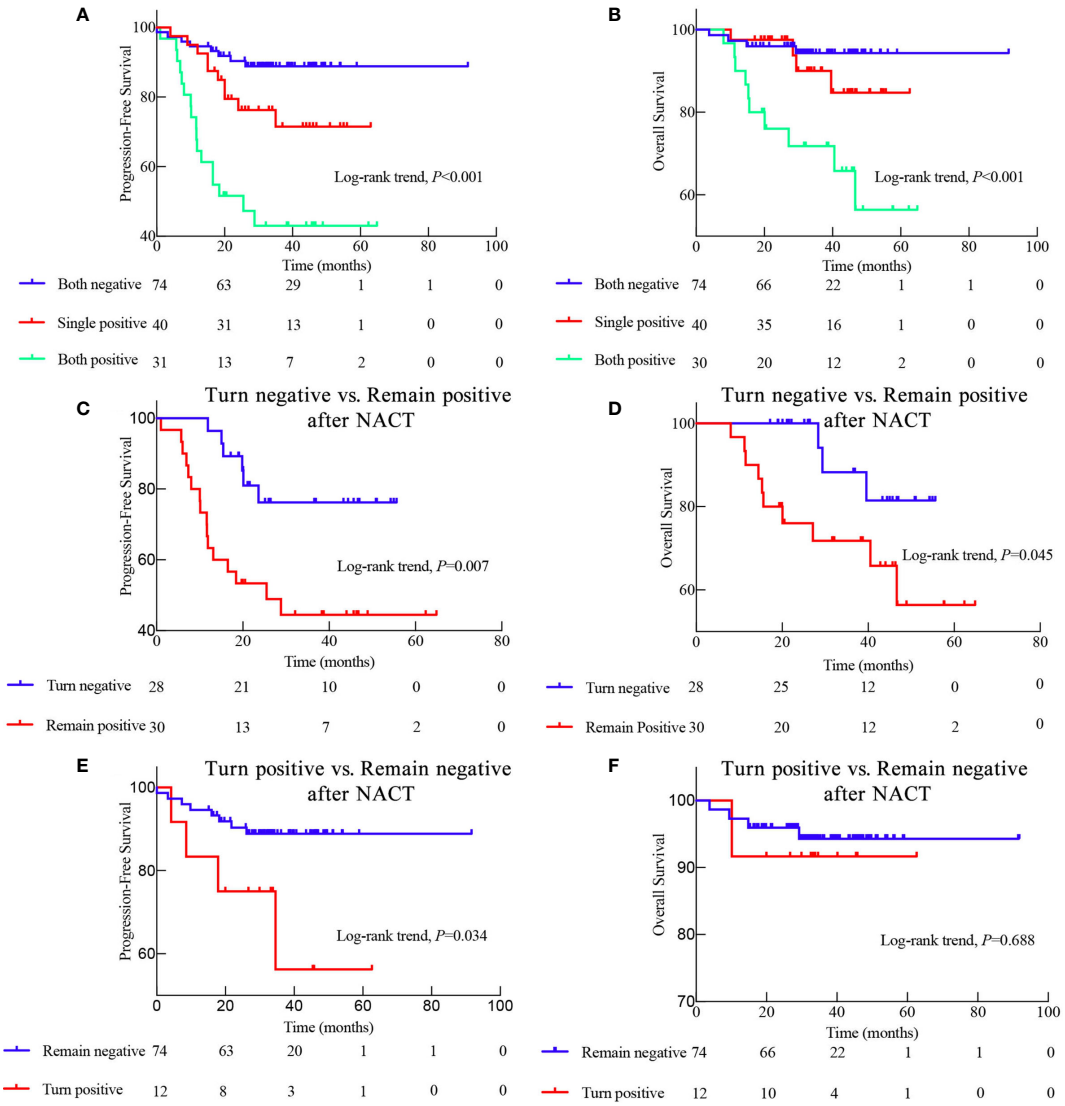

FIGURE 3 | Kaplan-Meier survival curves displaying the progression-free survival (PFS) and overall survival (OS) of patients with different EBV status during neoadjuvant chemotherapy (NACT). **(A)** PFS and **(B)** OS of patients with different EBV status throughout NACT as follows: Both negative means EBV DNA-negative before and after NACT; Single positive means EBV DNA-positive either before or after NACT; Both positive means EBV DNA-positive both before and after NACT; **(C)** Comparison of the PFS and **(D)** OS between patients whose EBV DNA status switched from positive to negative after NACT and those who remained EBV DNA-positive after NACT; **(E)** Comparison of the PFS and **(F)** OS between patients with EBV DNA status changing from negative to positive and those who remained EBV DNA-negative after NACT.

Switch From Epstein-Barr Virus DNA-Positive Level to Negative Epstein-Barr Virus DNA Level After Neoadjuvant Chemotherapy Is Associated With a Favorable Prognosis

We also evaluated the prognostic significance in the conversion from EBV DNA-positive to EBV DNA-negative after NACT. The prognosis of patients who exhibited a conversion from EBV DNA-positive to EBV DNA-negative after NACT was significantly better than that of patients who remained EBV DNA-positive (3-year PFS: 76.2% *vs.* 44.4%, $P = 0.007$; 5-year OS: 81.4% *vs.* 56.4%, $P = 0.045$; **Figures 3C, D**). Consistently, the 3-year PFS was significantly worse in patients who displayed conversion from EBV DNA-negative to EBV DNA-positive after NACT than in those who remained EBV DNA-negative (3-year-PFS: 56.3% *vs.* 88.8%, $P = 0.034$; **Figures 3E, F**). However, the prognostic ability of the conversion from EBV DNA-negative to EBV DNA-positive, and vice versa, after RT and ACT, was less profound (**Figure S1**). These findings suggest that the changes in the EBV DNA levels during NACT may be a

better predictor of prognosis than the changes in the EBV DNA levels during RT or ACT.

We also evaluated whether the plasma EBV DNA levels were affected by the different NACT regimens. We observed no significant differences in the plasma EBV DNA levels based on the NACT regimen (**Table 1**). Similarly, there was also no significant difference in the NACT regimens between patients with different EBV levels (**Table S2**). Moreover, the OS and PFS were similar between patients receiving different NACT regimens (**Figure S2**).

Prognostic Factors in Nasopharyngeal Cancer

Univariate analysis indicated that the TNM stage, LDH levels, HGB levels, pre-NACT EBV DNA levels, and post-NACT EBV DNA levels were associated with the PFS in patients with NPC (**Table 2**). Multivariable analysis using these factors revealed that the TNM stage, LDH levels, HGB levels, pre-NACT EBV DNA levels, and post-NACT EBV DNA levels were independent risk factors predicting treatment failure (**Table 3**).

Prognostic Value of the Nomograms of Pre- NACT and Post-NACT Epstein-Barr Virus DNA Levels

Next, we established nomograms to predict the PFS in patients with NPC (**Figures 4A, B**; **Figures S3A, B**). Calibration graphs were generated to confirm the accuracy of the prediction model (**Figures 5A, B, D, E**). In these graphs, the x-axes indicated the 3-year or 5-year PFS, and the y-axes indicated the actual survival. The prediction power of the nomograms of pre-NACT and post-NACT EBV DNA levels was higher than that of the nomograms with post-radiotherapy and post-treatment EBV DNA levels, with C-indices of 0.758, 0.780, 0.739, and 0.737, respectively (**Table 4**). The C-indexes of nomogram A and nomogram B were significantly higher than those of EBV DNA levels alone and the TNM staging system, with values of 0.626 (95% CI, 0.555–0.697) and 0.745 (95% CI, 0.697–0.819) in the pre-NACT group and 0.666 (95% CI, 0.588–0.744) and 0.724 (95% CI, 0.655–0.815) in the post-NACT group. We also found that the C-indexes of the nomograms of EBV DNA levels before and after NACT were higher than those of the nomograms of EBV DNA levels after radiotherapy and after treatment. These findings suggest that the plasma EBV DNA levels pre-NACT and post-NACT are promising prognostic factors in patients with NPC.

To confirm the prognostic accuracy of the nomogram, we evaluated its prognostic performance in a validation cohort of 76 patients with available data on the EBV load for all four treatment stages. In this validation cohort, the C-indexes of nomograms A and B were higher than those of nomograms C and D (A: 0.796, 95% CI, 0.704–0.888; B: 0.794, 95% CI, 0.698–0.890; C: 0.743, 95% CI, 0.631–0.855; D: 0.759, 95% CI, 0.663–0.855; **Table 4**; **Figures 5C, F** and **Figures S4C, F**). The prognostic power of pre-NACT and post-NACT EBV DNA levels was higher than that of post-radiotherapy and post-treatment EBV DNA levels.

The Combination of Pre-NACT and Post-NACT Epstein-Barr Virus DNA Levels Improves the Prognostic Accuracy

We also investigated whether the combination of pre- and post-NACT EBV DNA levels can improve the accuracy of the prognostic model. EBV DNA levels were classified as double-positive, single-positive, or double-negative. This classification method based on EBV DNA levels significantly improved the prognostic accuracy of the nomogram for PFS, providing C-indices of 0.791 (95% CI, 0.728–0.854: **Figure 6A**) in the primary cohort and 0.819 (95% CI, 0.735–0.903) in the validation cohort (**Table 5**). C-indices of EBV alone were also improved, which were 0.710 (95% CI, 0.622–0.798) in the primary cohort and 0.738 (95% CI, 0.624–0.852) in the validation cohort. The calibration curves confirmed the high prognostic power of the combination of pre-NACT and post-NACT EBV DNA levels (**Figures 6B–D**).

DISCUSSION

To the best of our knowledge, this is the first study combining pre-NACT and post-NACT plasma EBV DNA levels to predict patient prognosis. We found significant variations in the EBV DNA levels depending on the treatment stage. We also found that pre-NACT and post-NACT plasma EBV levels were a robust prognostic biomarker independent of the NACT regimen. Patients who were negative for EBV DNA before and after NACT had a better prognosis than EBV DNA-positive patients. Notably, EBV-positive to EBV-negative conversion after NACT was strongly associated with a favorable prognosis. The C-indices of the nomogram combining pre-NACT and post-NACT plasma EBV DNA levels were higher than those of other nomograms in the primary and validation cohorts.

Plasma EBV DNA levels are an accurate and reliable predictor of NPC progression. Changes in the plasma EBV DNA levels can provide insights into the relationship between EBV infection and NPC. Tang and Hong reported that pre-treatment EBV DNA levels were an important prognostic marker (6, 23). Similarly, Leung et al. demonstrated that plasma EBV DNA levels during radiotherapy predicted clinical outcomes (29). By monitoring the plasma EBV DNA levels at different stages of chemotherapy and radiotherapy, Rui et al. found that EBV DNA levels before, after, and during NACT predicted the risk of metastasis in patients with NPC (16). Consistently, we found that pre-NACT and post-NACT EBV DNA levels strongly predicted survival in patients with NPC. The 3-year PFS of patients with EBV DNA level decline during NACT was 31.8% higher than that of patients who remained EBV-positive after NACT. Detectable EBV DNA levels after first-line therapy were associated with local

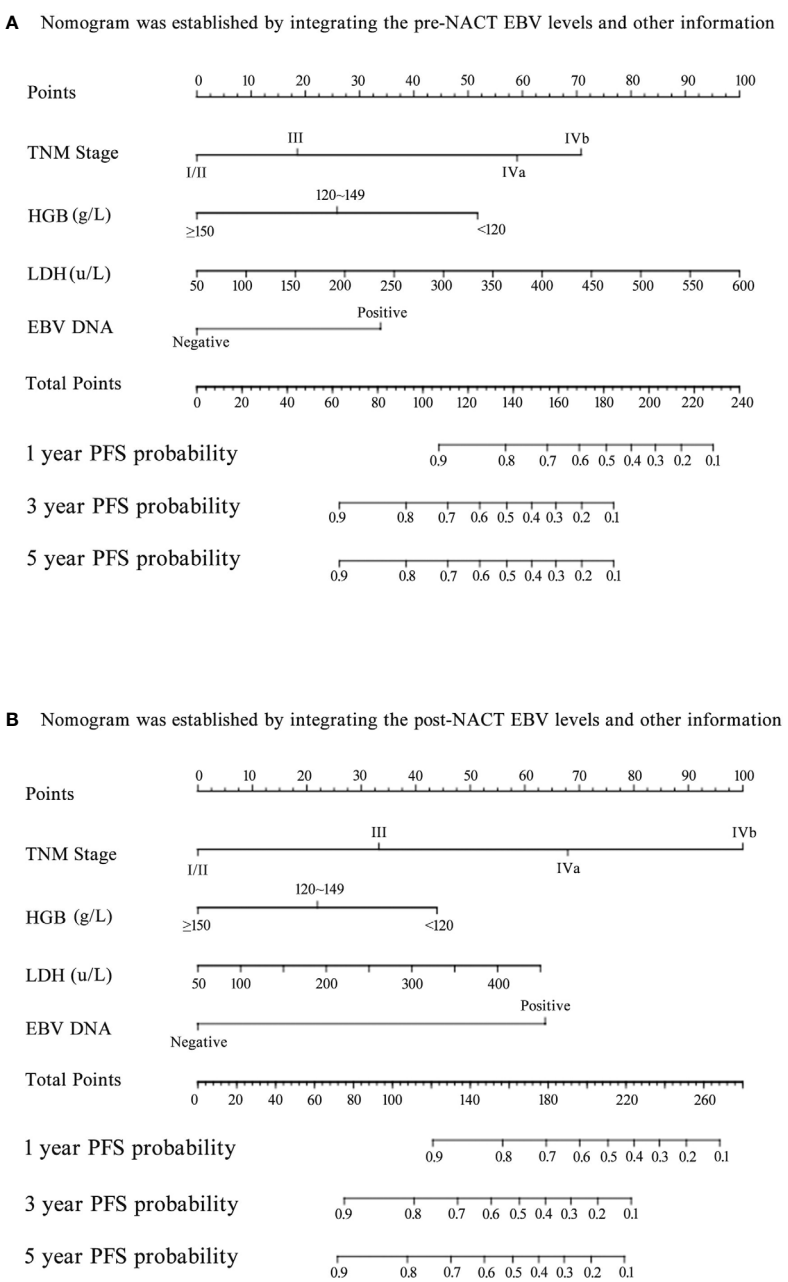

FIGURE 4 | Nomogram for predicting the 1-year, 3-year, and 5-year progression-free survival (PFS) of patients. **(A)** The nomogram was established by integrating the TNM stage, HGB, LDH, and pre-neoadjuvant chemotherapy (NACT) EBV levels; **(B)** The nomogram was established by integrating the TNM stage, HGB, LDH, and post-NACT EBV levels.

recurrence, distant metastasis, and disease progression, consistent with the findings of Lv et al. (25) These findings suggest that active EBV infection is associated with aggressive tumor phenotypes in NPC. EBV DNA decrease after NACT level might indicate early tumors response. As previously reported, NACT response is associated with a favorable prognosis in patients with NPC and can be used to risk-stratify patients (30, 31). Early tumor response is associated with size reduction in primary tumor lesions detected by imaging methods; however, biomarkers of early tumor response are lacking (32, 33). Our findings suggest that changes in EBV DNA levels during NACT may be a reliable biomarker of early response in patients with NACT. Consistently, Chen et al. used changes in EBV DNA levels and (18)F-FDG PET-derived parameters to evaluate the early response in patients with NPC (34).

TABLE 2 | Univariate analysis for the progression-free survival of the primary cohort (N = 206).

Variable	Patients	
	HR	*P*
Gender		
Female	Reference	
Male	1.409 (0.709–2.800)	0.328
Age, y		
≤45	Reference	
>45	1.005 (0.983–1.028)	0.639
TNM stage		
I/II	Reference	
III	2.220 (0.501–9.841)	0.294
IVa	7.289 (1.743–30.481)	**0.007****
IVb	10.361 (2.198–48.834)	**0.003****
WBC, 10^9/L		
<4	Reference	
4–10	0.939 (0.400–2.206)	0.886
≥10	1.302 (0.367–4.614)	0.683
Neutrophil, 10^9/L		
<2	Reference	
2–7	0.969 (0.432–2.176)	0.939
≥7	0.643 (0.245–1.690)	0.370
Lymphocyte		
<1	Reference	
1–2	0.803 (0.318–2.026)	0.643
≥2	1.127 (0.326–3.893)	0.850
PLT, 10^9/L		
<100	Reference	
100–300	~	0.996
≥300	~	0.996
LDH, U/L	1.006 (1.003–1.009)	**<0.001*****
HGB, g/L		
~119/120–149/150~	0.533 (0.337–0.841)	**0.007****
Smoking		
No	Reference	
Yes	1.008 (0.990–1.026)	0.413
Alcohol		
No	Reference	
Yes	1.097 (0.628–1.918)	0.744
EBV DNA		
Pre-NACT		
Negative	Reference	
Positive	3.065 (1.646–5.705)	**<0.001*****
Post- NACT		
Negative	Reference	
Positive	3.941 (2.029–7.654)	**<0.001*****
Post-radiotherapy		
Negative	Reference	
Positive	1.608 (0.812–3.184)	0.173
Post-treatment		
Negative	Reference	
Positive	1.869 (0.971–3.598)	0.061

*NACT, neoadjuvant chemotherapy. **P < 0.01; ***P < 0.001; bold means statistically significant.*

TABLE 3 | Multivariate analysis for the progression-free survival of the primary cohort (N = 206).

Variable	Patients	
	HR	*P*
TNM stage		
I/II	Reference	
III	1.951 (0.439–8.670)	0.379
IVa	5.929 (1.409–24.946)	**0.015***
IVb	7.519 (1.575–35.905)	**0.011***
LDH, U/L	1.005 (1.002–1.008)	**<0.001*****
HGB, g/L		
~119/120–149/150~	0.546 (0.340–0.878)	**0.012***
EBV DNA		
Pre-NACT		
Negative	Reference	
Positive	2.461 (1.303–4.645)	**0.005****
Post- NACT		
Negative	Reference	
Positive	3.783 (1.893–7.561)	**<0.001*****
Post-radiotherapy		
Negative	Reference	
Positive	1.265 (0.617–2.592)	0.521
Post-treatment		
Negative	Reference	
Positive	1.834 (0.927–3.626)	0.081

*NACT, neoadjuvant chemotherapy. *P < 0.05; **P < 0.01; ***P < 0.001; bold means statistically significant.*

Tang et al. found that the C-index of a nomogram with EBV DNA levels was significantly higher than that of a nomogram without an EBV load (23). Nomograms of EBV DNA levels can also predict tumor recurrence and survival in patients with NPC (35, 36). In another study, EBV DNA levels predicted metastasis within six months after treatment (37). Therefore, EBV DNA levels could be used to risk-stratify patients and guide clinical decision making (35). However, all previous studies used pre-treatment EBV DNA levels to predict the prognosis. However, our findings suggest that monitoring the changes in EBV DNA levels during treatment may be a better predictor of prognosis in patients with NPC. We found that the C-indices of the prediction model based on the EBV DNA levels both before and after NACT were higher than those of the traditional nomograms of EBV DNA levels only before or after treatment. Thus, the clinical implementation of combined pre-NACT and post-NACT EBV DNA testing may improve the prognostic accuracy in patients with NPC. Given the strong relationship between pre-NACT and post-NACT EBV DNA levels and treatment outcomes, we believe that dynamic plasma EBV DNA may serve as a valuable marker to help predict prognosis, as well as guide NPC screening and treatment (9, 38–40). According to our findings, NACT may be continued until EBV DNA levels have reached <400 copies/mL. In patients who persistently have high plasma levels of EBV DNA, aggressive treatments (e.g., EBV-targeted cytotoxic T lymphocytes) may be needed (41, 42).

The current study had a few limitations. Importantly, not all the patients had complete EBV test results for all treatment stages. Plasma EBV DNA levels at all four treatment stages were known for only 76 patients, and the small cohort size may have led to a sampling bias. Additionally, we did not take into account different ACT strategies. However, differences in ACT regimens may lead to different clinical outcomes. Additionally, the primary endpoint of the study, PFS, is unreliable in retrospective studies due to the expected inconsistency in determining the events other than death. Another limitation is that post-NACT, post-radiotherapy, and post-treatment EBV DNA levels were assessed between the last date of the former treatment and the first date of later therapy.

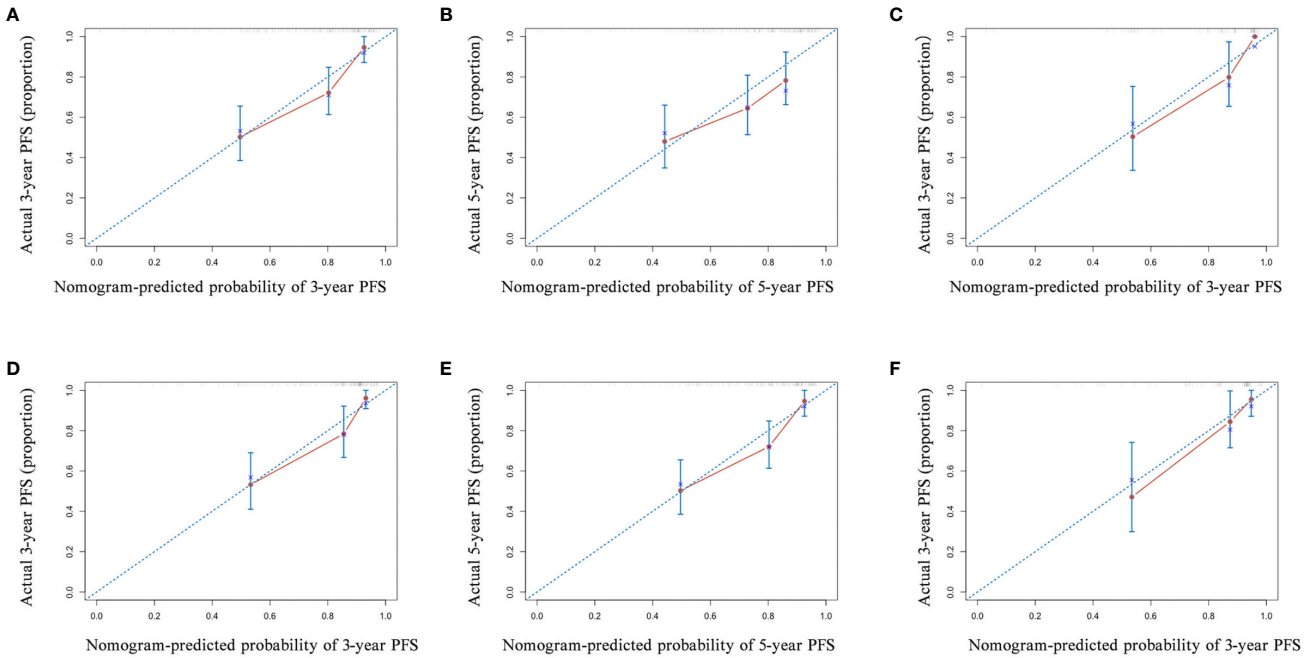

FIGURE 5 | The calibration curve of the nomogram for predicting the progression-free survival (PFS) with pre-neoadjuvant chemotherapy (NACT) or post-NACT EBV DNA levels. **(A)** 3-year and **(B)** 5-year in nomogram with pre-NACT EBV DNA levels in the primary cohort and **(C)** 3-year in the validation cohort; **(D)** 3-year and **(E)** 5-year in nomogram with post-NACT EBV DNA levels in the primary cohort and **(F)** 3-year in the validation cohort. Actual PFS is plotted on the y-axis; nomogram-predicted probability of PFS is plotted on the x-axis.

TABLE 4 | The C-indices of nomograms, TNM stage + HGB + LDH, and EBV DNA for the prediction of the progression-free survival (PFS) in the primary cohort and validation cohort .

Factor	Primary cohort		Validation cohort	
	C-index (CI)	*P*	C-index (CI)	*P*
Pre-NACT				
Nomogram A	0.758 (0.697–0.819)	**<0.001*** **	0.796 (0.704–0.888)	**<0.001*** **
Stage+HGB+LDH	0.745 (0.676–0.814)	**<0.001*** **	0.736 (0.624–0.848)	**0.02***
EBV	0.626 (0.555–0.697)	**<0.001*** **	0.677 (0.565–0.789)	**0.005****
Post-NACT				
Nomogram B	0.780 (0.713–0.847)	**<0.001*** **	0.794 (0.698–0.890)	**<0.001*** **
Stage+HGB+LDH	0.724 (0.644–0.804)	**<0.001*** **	0.736 (0.624–0.848)	**<0.02***
EBV	0.666 (0.588–0.744)	**<0.001*** **	0.685 (0.573–0.797)	**<0.001*** **
Post-radiotherapy				
Nomogram C	0.739 (0.657–0.821)	**<0.001*** **	0.743 (0.631–0.855)	**0.03***
Stage+HGB+LDH	0.735 (0.655–0.815)	**<0.001*** **	0.736 (0.624–0.848)	**0.02***
EBV	0.570 (0.484–0.656)	0.1	0.569 (0.447–0.691)	0.2
Post-treatment				
Nomogram D	0.737 (0.661–0.813)	**<0.001*** **	0.759 (0.663–0.855)	**0.03***
Stage+HGB+LDH	0.703 (0.621–0.785)	**<0.001*** **	0.736 (0.624–0.848)	**0.02***
EBV	0.579 (0.499–0.659)	**0.04***	0.543 (0.423–0.663)	0.4

*Nomogram A, including four high risk factors (Stage, HGB, LDH, and pre-NACT EBV levels); Nomogram B, including four high risk factors (Stage, HGB, LDH, and post-NACT EBV levels); Nomogram C, including four high risk factors (Stage, HGB, LDH, and post-radiotherapy EBV levels); Nomogram D, including four high risk factors (Stage, HGB, LDH, and post-treatment EBV levels); NACT, neoadjuvant chemotherapy; C-index, concordance index; CI, confidence interval. *P < 0.05; **P < 0.01; ***P < 0.001; bold means statistically significant.*

CONCLUSION

We evaluated the relationship between the plasma EBV DNA levels and treatment outcomes in patients with NPC. Our findings suggest that the combination of pre-NACT and post-NACT plasma EBV DNA levels accurately predicts survival in patients with NPC. We also provided evidence that tracking plasma EBV DNA may benefit patients undergoing NACT for

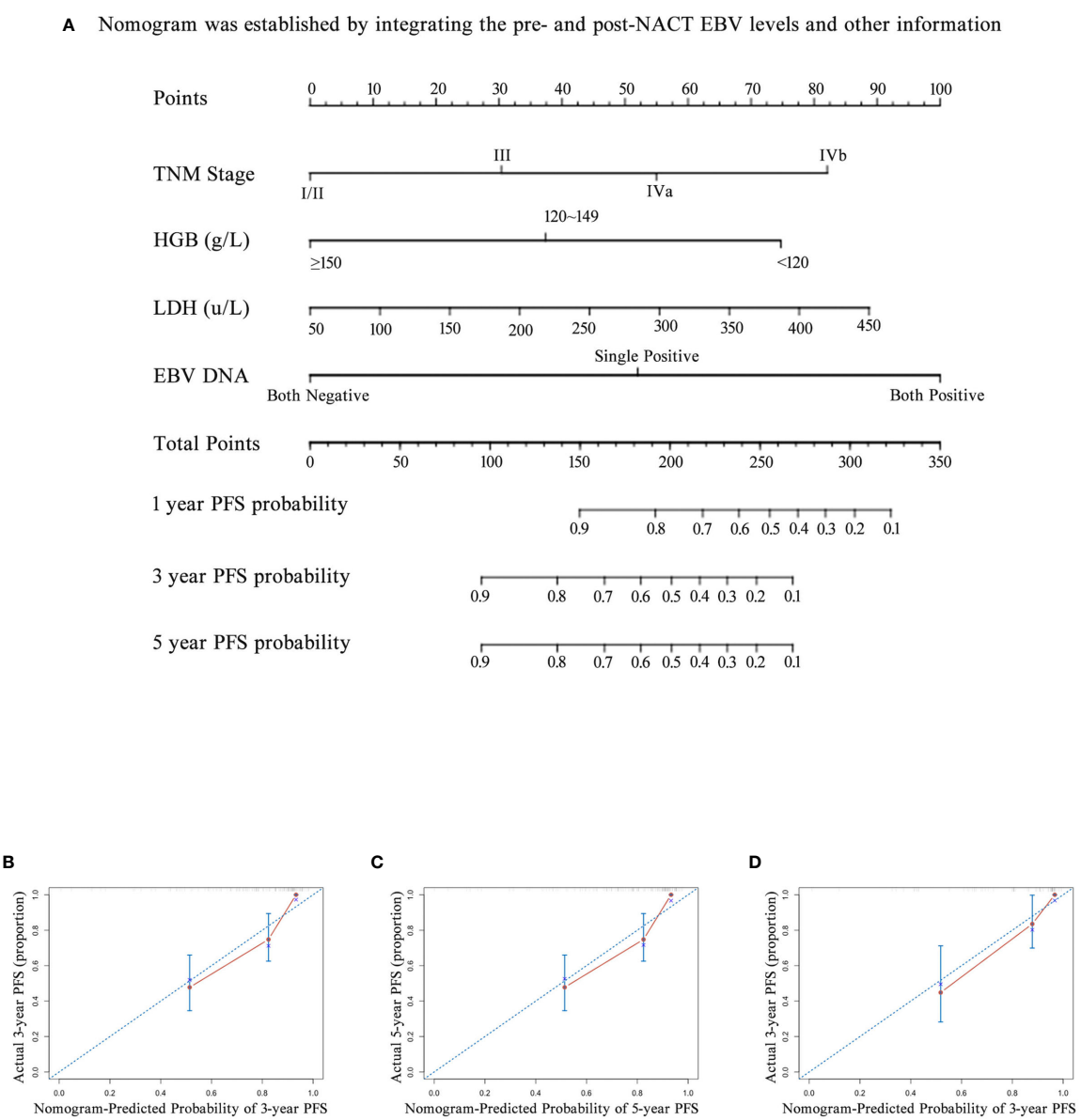

FIGURE 6 | The nomogram and its calibration curve established by using pre- and post- neoadjuvant chemotherapy (NACT) EBV levels. **(A)** Nomogram; The calibration curves for predicting patient PFS at **(B)** 3-year and **(C)** 5-year in the primary cohort and **(D)** 3-year in the validation cohort. Actual PFS is plotted on the y-axis; nomogram-predicted probability of PFS is plotted on the x-axis. PFS, progression-free survival.

TABLE 5 | The C-indices of nomograms, TNM stage + HGB + LDH, and combined pre- and post-NACT EBV DNA for the prediction of the progression-free survival (PFS) in the primary cohort and validation cohort.

Factor	Primary cohort		Validation cohort	
	C-index (CI)	*P*	C-index (CI)	*P*
nomogram	0.791 (0.728–0.854)	**<0.001*** **	0.819 (0.735–0.903)	**<0.001*** **
Stage+HGB+LDH	0.732 (0.650–0.814)	**<0.001*** **	0.736 (0.624–0.848)	**<0.001*** **
EBV	0.710 (0.622–0.798)	**<0.001*** **	0.738 (0.624–0.852)	**<0.001*** **

*Nomogram A, including four high risk factors (Stage, HGB, LDH, and combined pre- and post-NACT EBV levels); C-index, concordance index; CI, confidence interval. N (Primary cohort) = 206; N (Validation cohort) = 76. ***P < 0.001; bold means statistically significant.*

NPC. Future multicenter, randomized, controlled trials are required to confirm the prognostic value of EBV DNA levels in patients with NPC.

DATA AVAILABILITY STATEMENT

The original contributions presented in the study are included in the article/**Supplementary Materials**, further inquiries can be directed to the corresponding authors.

ETHICS STATEMENT

The studies involving human participants were reviewed and approved by Regional Ethics Committee of Tongji Medical College, Huazhong University of Science and Technology. The patients/participants provided their written informed consent to participate in this study.

AUTHOR CONTRIBUTIONS

Conceptualization: ZZ and GP. Methodology: GP and LZ. Software: TO. Validation: YX, LB, and MQ. Formal analysis: LZ and QL. Investigation: LZ and TO. Data curation: QL. Writing—original draft preparation: LZ and TO. Writing—review and editing: GP and ZZ. Visualization: YX and LB. Supervision: QL, LB, and MQ. Funding acquisition: ZZ and GP. All authors contributed to the article and approved the submitted version.

FUNDING

This work was supported by National Natural Science Foundation of China (Grant No. 81874232 and 82071067).

SUPPLEMENTARY MATERIAL

The Supplementary Material for this article can be found online at: https://www.frontiersin.org/articles/10.3389/fonc.2021.714433/full#supplementary-material

Supplementary Figure 1 | Kaplan-Meier survival curves displaying progression-free survival (PFS) and overall survival (OS) of patients with different EBV status in different treatment stages. **(A)** Comparison of PFS and **(B)** OS between patients with EBV-DNA status changing from positive to negative and remaining positive after radiotherapy; **(C)** Comparison of PFS and **(D)** OS between patients with EBV-DNA status turning from negative to positive and remaining negative after radiotherapy; **(E)** Comparison of PFS and **(F)** OS between patients with EBV-DNA status switching from positive to negative and remaining positive after adjuvant chemotherapy (ACT); **(G)** Comparison of PFS and **(H)** OS between patients with EBV-DNA status turning from negative to positive and remaining negative after ACT.

Supplementary Figure 2 | The relationship between neoadjuvant chemotherapy (NACT) regimens and prognosis in different subgroups. **(A)** PFS and **(B)** OS in group of pre-NACT; **(C)** PFS and **(D)** OS in group of post-NACT; **(E)** PFS and **(F)** OS in group of post-radiotherapy; **(G)** PFS and **(H)** OS in group of post-treatment. PFS, Progression-free survival (PFS); OS, Overall survival; DCF, docetaxel plus cisplatin and fluorouracil; GP, gemcitabine plus cisplatin; DP, docetaxel plus cisplatin.

Supplementary Figure 3 | Nomogram for predicting patients' 1-year, 3-year and 5-year progression-free survival (PFS). **(A)** The nomogram was established by integrating the TNM stage, HGB, LDH and post- radiotherapy EBV levels; **(B)** The nomogram was established by integrating the TNM stage, HGB, LDH and post-treatment EBV levels.

Supplementary Figure 4 | The calibration curve of nomogram for predicting progression-free survival (PFS) by using post-radiotherapy EBV DNA levels or post-treatment EBV DNA levels. **(A)** 3-year and **(B)** 5-year in nomogram with post-radiotherapy EBV DNA levels in the primary cohort and **(C)** 3-year in the validation cohort; **(D)** 3-year and **(E)** 5-year in nomogram with post-treatment EBV DNA levels in the primary cohort and **(F)** 3-year in the validation cohort. Actual PFS is plotted on the y-axis; nomogram- predicted probability of PFS is plotted on the x-axis.

Supplementary Table 1 | Patient demographic and clinical characteristics of inclusion patients, exclusion patients and validation patients.

Supplementary Table 2 | NACT regimens of four subgroups in NPC patients with different EBV DNA levels. NACT, neoadjuvant chemotherapy; DCF, docetaxel plus cisplatin and fluorouracil; GP, gemcitabine plus cisplatin; DP, docetaxel plus cisplatin.

REFERENCES

1. Torre LA, Bray F, Siegel RL, Ferlay J, Lortet-Tieulent J, Jemal A. Global Cancer Statistics, 2012. *CA: Cancer J Clin* (2015) 65(2):87–108. doi: 10.3322/caac.21262
2. Al-Sarraf M, LeBlanc M, Giri PG, Fu KK, Cooper J, Vuong T, et al. Chemoradiotherapy Versus Radiotherapy in Patients With Advanced Nasopharyngeal Cancer: Phase III Randomized Intergroup Study 0099. *J Clin Oncol: Off J Am Soc Clin Oncol* (1998) 16(4):1310–7. doi: 10.1200/jco.1998.16.4.1310
3. Chen L, Zhang Y, Lai SZ, Li WF, Hu WH, Sun R, et al. 10-Year Results of Therapeutic Ratio by Intensity-Modulated Radiotherapy Versus Two-Dimensional Radiotherapy in Patients With Nasopharyngeal Carcinoma. *Oncol* (2019) 24(1):e38–45. doi: 10.1634/theoncologist.2017-0577
4. Chen L, Hu CS, Chen XZ, Hu GQ, Cheng ZB, Sun Y, et al. Concurrent Chemoradiotherapy Plus Adjuvant Chemotherapy Versus Concurrent Chemoradiotherapy Alone in Patients With Locoregionally Advanced Nasopharyngeal Carcinoma: A Phase 3 Multicentre Randomised Controlled Trial. *Lancet Oncol* (2012) 13(2):163–71. doi: 10.1016/s1470-2045(11)70320-5
5. Zhang Y, Chen L, Hu GQ, Zhang N, Zhu XD, Yang KY, et al. Gemcitabine and Cisplatin Induction Chemotherapy in Nasopharyngeal Carcinoma. *New Engl J Med* (2019) 381(12):1124–35. doi: 10.1056/NEJMoa1905287
6. Hong RL, Hsiao CF, Ting LL, Ko JY, Wang CW, Chang JTC, et al. Final Results of a Randomized Phase III Trial of Induction Chemotherapy Followed by Concurrent Chemoradiotherapy Versus Concurrent Chemoradiotherapy Alone in Patients With Stage IVA and IVB Nasopharyngeal Carcinoma-Taiwan Cooperative Oncology Group (TCOG) 1303 Study. *Ann Oncol: Off J Eur Soc Med Oncol* (2018) 29(9):1972–9. doi: 10.1093/annonc/mdy249
7. Liu LT, Chen QY, Tang LQ, Guo SS, Guo L, Mo HY, et al. Neoadjuvant or Adjuvant Chemotherapy Plus Concurrent CRT Versus Concurrent CRT Alone in the Treatment of Nasopharyngeal Carcinoma: A Study Based on EBV DNA. *J Natl Compr Cancer Netw: JNCCN* (2019) 17(6):703–10. doi: 10.6004/jnccn.2018.7270
8. Yao JJ, Zhou GQ, Zhang F, Zhang WJ, Lin L, Tang LL, et al. Neoadjuvant and Concurrent Chemotherapy Have Varied Impacts on the Prognosis of Patients With the Ascending and Descending Types of Nasopharyngeal Carcinoma Treated With Intensity-Modulated Radiotherapy. *PloS One* (2016) 11(10):e0161878. doi: 10.1371/journal.pone.0161878

9. Ji MF, Sheng W, Cheng WM, Ng MH, Wu BH, Yu X, et al. Incidence and Mortality of Nasopharyngeal Carcinoma: Interim Analysis of a Cluster Randomized Controlled Screening Trial (PRO-NPC-001) in Southern China. *Ann Oncol: Off J Eur Soc Med Oncol* (2019) 30(10):1630–7. doi: 10.1093/annonc/mdz231
10. Hu B, Sun M, Wang Z, Zheng Y, Cai W, Shi HH, et al. Prognostic Value of Programmed Cell Death-Ligand 1 Expression in Tumor-Infiltrating Lymphocytes and Viral Load in Peripheral Blood Mononuclear Cells for Epstein-Barr Virus-Positive Nasopharyngeal Carcinoma. *Clin Chem* (2020) 66 (9):1219–27. doi: 10.1093/clinchem/hvaa170
11. Xie L, Shi F, Li Y, Li W, Yu X, Zhao L, et al. Drp1-Dependent Remodeling of Mitochondrial Morphology Triggered by EBV-LMP1 Increases Cisplatin Resistance. *Signal Transduction Targeted Ther* (2020) 5(1):56. doi: 10.1038/s41392-020-0151-9
12. Yoshizaki T, Kondo S, Wakisaka N, Murono S, Endo K, Sugimoto H, et al. Pathogenic Role of Epstein-Barr Virus Latent Membrane Protein-1 in the Development of Nasopharyngeal Carcinoma. *Cancer Lett* (2013) 337(1):1–7. doi: 10.1016/j.canlet.2013.05.018
13. Zhang Y, Tang LL, Li YQ, Liu X, Liu Q, Ma J. Spontaneous Remission of Residual Post-Therapy Plasma Epstein-Barr Virus DNA and its Prognostic Implication in Nasopharyngeal Carcinoma: A Large-Scale, Big-Data Intelligence Platform-Based Analysis. *Int J Cancer* (2019) 144(9):2313–9. doi: 10.1002/ijc.32021
14. Liang SB, Zhang N, Chen DM, Yang XL, Chen BH, Zhao H, et al. Prognostic Value of Gross Tumor Regression and Plasma Epstein Barr Virus DNA Levels at the End of Intensity-Modulated Radiation Therapy in Patients With Nasopharyngeal Carcinoma. *Radiother Oncol: J Eur Soc Ther Radiol Oncol* (2019) 132:223–9. doi: 10.1016/j.radonc.2018.10.010
15. Huang CL, Sun ZQ, Guo R, Liu X, Mao YP, Peng H, et al. Plasma Epstein-Barr Virus DNA Load After Induction Chemotherapy Predicts Outcome in Locoregionally Advanced Nasopharyngeal Carcinoma. *Int J Radiat Oncol Biol Phys* (2019) 104(2):355–61. doi: 10.1016/j.ijrobp.2019.01.007
16. You R, Liu YP, Lin M, Huang PY, Tang LQ, Zhang YN, et al. Relationship of Circulating Tumor Cells and Epstein-Barr Virus DNA to Progression-Free Survival and Overall Survival in Metastatic Nasopharyngeal Carcinoma Patients. *Int J Cancer* (2019) 145(10):2873–83. doi: 10.1002/ijc.32380
17. Twu CW, Wang WY, Liang WM, Jan JS, Jiang RS, Chao J, et al. Comparison of the Prognostic Impact of Serum Anti-EBV Antibody and Plasma EBV DNA Assays in Nasopharyngeal Carcinoma. *Int J Radiat Oncol Biol Phys* (2007) 67(1):130–7. doi: 10.1016/j.ijrobp.2006.07.012
18. Jin YN, Yao JJ, Zhang F, Wang SY, Zhang WJ, Zhou GQ, et al. Is Pretreatment Epstein-Barr Virus DNA Still Associated With 6-Year Survival Outcomes in Locoregionally Advanced Nasopharyngeal Carcinoma? *J Cancer* (2017) 8 (6):976–82. doi: 10.7150/jca.18124
19. Li JY, Huang CL, Luo WJ, Zhang Y, Tang LL, Peng H, et al. An Integrated Model of the Gross Tumor Volume of Cervical Lymph Nodes and Pretreatment Plasma Epstein-Barr Virus DNA Predicts Survival of Nasopharyngeal Carcinoma in the Intensity-Modulated Radiotherapy Era: A Big-Data Intelligence Platform-Based Analysis. *Ther Adv Med Oncol* (2019) 11:1758835919877729. doi: 10.1177/1758835919877729
20. Chan ATC, Hui EP, Ngan RKC, Tung SY, Cheng ACK, Ng WT, et al. Analysis of Plasma Epstein-Barr Virus DNA in Nasopharyngeal Cancer After Chemoradiation to Identify High-Risk Patients for Adjuvant Chemotherapy: A Randomized Controlled Trial. *J Clin Oncol: Off J Am Soc Clin Oncol* (2018) 36(31):3091–9. doi: 10.1200/jco.2018.77.7847
21. Li WF, Zhang Y, Huang XB, Du XJ, Tang LL, Chen L, et al. Prognostic Value of Plasma Epstein-Barr Virus DNA Level During Posttreatment Follow-Up in the Patients With Nasopharyngeal Carcinoma Having Undergone Intensity-Modulated Radiotherapy. *Chin J Cancer* (2017) 36(1):87. doi: 10.1186/s40880-017-0256-x
22. Wong ECY, Hung JLC, Ng WT. Potential Pitfalls in Incorporating Plasma Epstein-Barr Virus DNA in the Management of Nasopharyngeal Carcinoma. *Head Neck* (2020) 42(3):446–55. doi: 10.1002/hed.26018
23. Tang LQ, Li CF, Li J, Chen WH, Chen QY, Yuan LX, et al. Establishment and Validation of Prognostic Nomograms for Endemic Nasopharyngeal Carcinoma. *J Natl Cancer Institute* (2016) 108(1). doi: 10.1093/jnci/djv291
24. Li J, Chen S, Peng S, Liu Y, Xing S, He X, et al. Prognostic Nomogram for Patients With Nasopharyngeal Carcinoma Incorporating Hematological Biomarkers and Clinical Characteristics. *Int J Biol Sci* (2018) 14(5):549–56. doi: 10.7150/ijbs.24374
25. Lv J, Chen Y, Zhou G, Qi Z, Tan KRL, Wang H, et al. Liquid Biopsy Tracking During Sequential Chemo-Radiotherapy Identifies Distinct Prognostic Phenotypes in Nasopharyngeal Carcinoma. *Nat Commun* (2019) 10 (1):3941. doi: 10.1038/s41467-019-11853-y
26. Zhang LL, Huang MY, Fei X, Wang KX, Song D, Wang T, et al. Risk Stratification for Nasopharyngeal Carcinoma: A Real-World Study Based on Locoregional Extension Patterns and Epstein-Barr Virus DNA Load. *Ther Adv Med Oncol* (2020) 12:1758835920932052. doi: 10.1177/1758835920932052
27. Lee VH, Kwong DL, Leung TW, Choi CW, O'Sullivan B, Lam KO, et al. The Addition of Pretreatment Plasma Epstein-Barr Virus DNA Into the Eighth Edition of Nasopharyngeal Cancer TNM Stage Classification. *Int J Cancer* (2019) 144(7):1713–22. doi: 10.1002/ijc.31856
28. Guo R, Tang LL, Mao YP, Du XJ, Chen L, Zhang ZC, et al. Proposed Modifications and Incorporation of Plasma Epstein-Barr Virus DNA Improve the TNM Staging System for Epstein-Barr Virus-Related Nasopharyngeal Carcinoma. *Cancer* (2019) 125(1):79–89. doi: 10.1002/cncr.31741
29. Leung SF, Chan KC, Ma BB, Hui EP, Mo F, Chow KC, et al. Plasma Epstein-Barr Viral DNA Load at Midpoint of Radiotherapy Course Predicts Outcome in Advanced-Stage Nasopharyngeal Carcinoma. *Ann Oncol: Off J Eur Soc Med Oncol* (2014) 25(6):1204–8. doi: 10.1093/annonc/mdu117
30. Peng H, Chen L, Li WF, Guo R, Mao YP, Zhang Y, et al. Tumor Response to Neoadjuvant Chemotherapy Predicts Long-Term Survival Outcomes in Patients With Locoregionally Advanced Nasopharyngeal Carcinoma: A Secondary Analysis of a Randomized Phase 3 Clinical Trial. *Cancer* (2017) 123(9):1643–52. doi: 10.1002/cncr.30520
31. Peng H, Chen L, Zhang Y, Li WF, Mao YP, Liu X, et al. The Tumour Response to Induction Chemotherapy has Prognostic Value for Long-Term Survival Outcomes After Intensity-Modulated Radiation Therapy in Nasopharyngeal Carcinoma. *Sci Rep* (2016) 6:24835. doi: 10.1038/srep24835
32. Qiang M, Li C, Sun Y, Ke L, Xie C, Zhang T, et al. A Prognostic Predictive System Based on Deep Learning for Locoregionally Advanced Nasopharyngeal Carcinoma. *J Natl Cancer Institute* (2020) 113(5):606–15. doi: 10.1093/jnci/djaa149
33. Yongfeng P, Chuner J, Lei W, Fengqin Y, Zhimin Y, Zhenfu F, et al. The Usefulness of Pretreatment MR-Based Radiomics on Early Response of Neoadjuvant Chemotherapy in Patients With Locally Advanced Nasopharyngeal Carcinoma. *Oncol Res* (2021) 28(6):605–13. doi: 10.3727/096504020x16022401878096
34. Liu LT, Tang LQ, Chen QY, Zhang L, Guo SS, Guo L, et al. The Prognostic Value of Plasma Epstein-Barr Viral DNA and Tumor Response to Neoadjuvant Chemotherapy in Advanced-Stage Nasopharyngeal Carcinoma. *Int J Radiat Oncol Biol Phys* (2015) 93(4):862–9. doi: 10.1016/j.ijrobp.2015.08.003
35. Chen FP, Lin L, Qi ZY, Zhou GQ, Guo R, Hu J, et al. Pretreatment Nomograms for Local and Regional Recurrence After Radical Radiation Therapy for Primary Nasopharyngeal Carcinoma. *J Cancer* (2017) 8 (13):2595–603. doi: 10.7150/jca.20255
36. He Y, Yang D, Zhou T, Xue W, Zhang J, Li F, et al. Epstein-Barr Virus DNA Loads in the Peripheral Blood Cells Predict the Survival of Locoregionally-Advanced Nasopharyngeal Carcinoma Patients. *Cancer Biol Med* (2021) 18 (3):888–9. doi: 10.20892/j.issn.2095-3941.2020.0464
37. Lu ZJ, Liu LT, Sun XS, Guo SS, Yang Q, Liu S, et al. Establishment and Validation of a Prognostic Nomogram to Predict Early Metastasis in Nasopharyngeal Carcinoma Patients Within Six Months After Radiotherapy and to Guide Intensive Treatment. *Radiother Oncol: J Eur Soc Ther Radiol Oncol* (2021) 162:202–11. doi: 10.1016/j.radonc.2021.03.035
38. Tay JK, Siow CH, Goh HL, Lim CM, Hsu PP, Chan SH, et al. A Comparison of EBV Serology and Serum Cell-Free DNA as Screening Tools for Nasopharyngeal Cancer: Results of the Singapore NPC Screening Cohort. *Int J Cancer* (2020) 146(10):2923–31. doi: 10.1002/ijc.32774
39. Ji MF, Huang QH, Yu X, Liu Z, Li X, Zhang LF, et al. Evaluation of Plasma Epstein-Barr Virus DNA Load to Distinguish Nasopharyngeal Carcinoma Patients From Healthy High-Risk Populations in Southern China. *Cancer* (2014) 120(9):1353–60. doi: 10.1002/cncr.28564
40. Tan R, Phua SKA, Soong YL, Oon LLE, Chan KS, Lucky SS, et al. Clinical Utility of Epstein-Barr Virus DNA and Other Liquid Biopsy Markers in

Nasopharyngeal Carcinoma. *Cancer Commun (London England)* (2020) 40 (11):564–85. doi: 10.1002/cac2.12100
41. Comoli P, Pedrazzoli P, Maccario R, Basso S, Carminati O, Labirio M, et al. Cell Therapy of Stage IV Nasopharyngeal Carcinoma With Autologous Epstein-Barr Virus-Targeted Cytotoxic T Lymphocytes. *J Clin Oncol: Off J Am Soc Clin Oncol* (2005) 23(35):8942–9. doi: 10.1200/jco.2005.02.6195
42. Straathof KC, Bollard CM, Popat U, Huls MH, Lopez T, Morriss MC, et al. Treatment of Nasopharyngeal Carcinoma With Epstein-Barr Virus–Specific T Lymphocytes. *Blood* (2005) 105(5):1898–904. doi: 10.1182/blood-2004-07-2975

Conflict of Interest: The authors declare that the research was conducted in the absence of any commercial or financial relationships that could be construed as a potential conflict of interest.

Publisher's Note: All claims expressed in this article are solely those of the authors and do not necessarily represent those of their affiliated organizations, or those of the publisher, the editors and the reviewers. Any product that may be evaluated in this article, or claim that may be made by its manufacturer, is not guaranteed or endorsed by the publisher.

frontiers in Oncology

ORIGINAL RESEARCH
published: 20 September 2021
doi: 10.3389/fonc.2021.731543

Comparison of TPF and TP Induction Chemotherapy for Locally Advanced Nasopharyngeal Carcinoma Based on TNM Stage and Pretreatment Systemic Immune-Inflammation Index

Ying Xiong†, *Liangliang Shi*†, *Lisheng Zhu* and *Gang Peng**

Cancer Center, Union Hospital, Tongji Medical College, Huazhong University of Science and Technology, Wuhan, China

OPEN ACCESS

Edited by:
Heming Lu,
People's Hospital of Guangxi Zhuang Autonomous Region, China

Reviewed by:
Man Hu,
Shandong University, China
Xiaozhong Chen,
University of Chinese Academy of Sciences, China

***Correspondence:**
Gang Peng
penggangunion@163.com

†*These authors have contributed equally to this work*

Specialty section:
This article was submitted to Head and Neck Cancer, a section of the journal Frontiers in Oncology

Received: *27 June 2021*
Accepted: *31 August 2021*
Published: *20 September 2021*

Citation:
Xiong Y, Shi L, Zhu L and Peng G (2021) Comparison of TPF and TP Induction Chemotherapy for Locally Advanced Nasopharyngeal Carcinoma Based on TNM Stage and Pretreatment Systemic Immune-Inflammation Index. Front. Oncol. 11:731543. doi: 10.3389/fonc.2021.731543

Purpose: To evaluate the efficacy and toxicity of the two IC (induction chemotherapy) regimens, TPF (taxanes, cisplatin, and 5-fluorouracil) and TP (taxanes and cisplatin) combined with concurrent chemoradiotherapy (CCRT) in locally advanced nasopharyngeal carcinoma (LA-NPC) patients.

Methods: Ultimately, we enrolled 213 patients at stage III-IVA in this retrospective study. The prognosis of TPF and TP was compared by Kaplan-Meier and Cox proportional hazard regression. The toxicities were evaluated according to CTCAE v4.0 and RTOG criteria.

Results: TPF was found to have a higher 5-year DMFS in stage IVA and N2-3 patients. The optimal value of pretreatment SII was 432.48. A further subgroup analysis revealed that patients in stage IVA combined with SII ≥432.48 showed superior OS (*P*=0.038) and DMFS (*P*=0.028) from TPF. Also, SII was proved to be a prognostic element for PFS (HR 2.801, P=0.018) and DMFS (HR 3.735, P=0.032) in multivariate analysis, and IC regimen (HR 2.182, P=0.049) for predicting DMFS. The rate of grade 3–4 leukopenia (*P*=0.038), neutropenia (*P*=0.021), radiation oral mucositis (*P*=0.048), diarrhea (*P*=0.036), and ear damage (*P*=0.046) were more common in TPF group.

Conclusion: Our study revealed that TPF regimen showed a higher 5-year DMFS for stage IVA and N2-3 patients, while for stage III and N0-1, TP might be ample. In high-risk LA-NPC patients (stage IVA combined with pretreatment SII ≥432.48), TPF had a higher 5-year OS and DMFS, with more grade 3–4 toxicities, but most of them were endurable.

Keywords: locally advanced nasopharyngeal carcinoma, induction chemotherapy, systemic immune-inflammation index, prognosis, toxicity

INTRODUCTION

Nasopharyngeal carcinoma (NPC) is a malignant head and neck tumor that occurs at the top and lateral wall of the nasopharyngeal cavity, with a relatively higher incidence in China and Southeast Asia and 129,000 new cases diagnosed worldwide (1). Early symptoms are hidden, and 75% patients have been diagnosed with NPC at stage III or IVA. Due to its special anatomy and sensitivity to radiation, concurrent chemoradiotherapy (CCRT) is regarded as the main treatment in locally advanced NPC (LA-NPC). As intensity-modulated radiotherapy (IMRT) improving, local control rates of LA-NPC were improved; however, distant metastasis still remains a major failure pattern.

Accumulating studies confirms that induction chemotherapy (IC) could help to control subclinical micrometastasis (2). A phase III trial (3) showed that IC followed by CCRT could improve overall survival (OS), distant metastasis-free survival (DMFS), and disease-free survival (DFS) in LA-NPC when compared with CCRT. A recent study (4) showed that IC plus CCRT could increase OS (P<0.001), PFS (P<0.001), DMFS (P<0.001), and LRFS (P<0.001) in LA-NPC. Similarly, the survival benefits brought by IC followed by CCRT have been confirmed in many other studies (5). As a result, based on the National Comprehensive Cancer Network (NCCN) guideline, IC followed by CCRT is suggested in the category 1A recommendations for LA-NPC (6).

As we know, the first-line IC regimens including Docetaxel, cisplatin, and 5-fluorouracil (TPF), Docetaxel and cisplatin (TP), cisplatin and 5-fluorouracil (PF), Gemcitabine and cisplatin (GP) have brought some survival advantages in studies (7). At present, TPF is the main regimen, but accompanied by its long treatment time and adverse reactions caused by 5-FU, such as myelosuppression and diarrhea. Therefore, it is crucial whether the TP regimen can reduce the related toxicities while ensuring the survival benefit. A previous research performed by Wang et al. (8) in LA-NPC showed that, TPF (docetaxel 60 mg/m^2, cisplatin 25 mg/m^2, days 1–3, 5-FU 500 mg/m^2, days 1–3) had similar efficacy compared to TP, and the grade 3–4 toxicity in TP group is lower, which provided an idea for TP regimen as an alternative to TPF. However, the standard dose of 5-FU was lowered as considering the tolerance of patients, so we could not completely rule out the potential effect of dose. At present, there is still no consensus about the efficacy and safety of the two regimens. Therefore, this paper was conducted to compare the survival efficacy and treatment-related toxicity of TPF and TP regimen in LA-NPC patients, in order to explore the feasibility of alternative TP regimen.

In addition, the TNM staging system is still considered as the reference standard for evaluating the survival in patients, but the prognosis of patients who received similar treatment in the same period is different, as the internal tumor heterogeneity is not taken into account by TNM staging. Nowadays, accumulating evidence have shown that inflammation contributes to the development, growth, and metastasis of cancer cells (9). And systemic immune-inflammation index (SII), a new hematological index, has been identified as a prognostic biomarker in NPC (10). It is worth pointing out that patients with NPC in our analysis were divided into different subgroups according to the pretreatment SII levels, which was not reported in previous studies.

MATERIALS AND METHODS

Patients

A total of 213 patients diagnosed with LA-NPC at Union Hospital Cancer Center from January 2013 and December 2017 were enrolled. The inclusion criteria were as follows: (1) pathologically verified NPC at the first diagnosis; (2) Karnofsky performance status (KPS) ≥70; (3) age between 16 and 70 years; (4) a complete examination, including nasopharyngeal speculum, lung CT, enhanced MRI of the nasopharynx and neck, abdominal ultrasound, and a whole-body bone scan (or whole-body PET-CT), and finally re-staged as III-IVA according to the 8th edition of the AJCC staging system; and (5) complete data of hematological parameters, including neutrophil, lymphocyte, and platelet counts within 7 days before treatment. The exclusion criteria were as follows: (1) a history of second primary malignant tumor; (2) a history of anticancer therapy; (3) an unfinished IC followed by CCRT; (4) a poor function of heart, lung, liver, and renal; and (5) complicated with acute infection or autoimmune diseases. Written consent was obtained from enrolled patients, and the study was approved by Cancer Center of Union Hospital of Tongji Medical College of Huazhong University of Science and Technology.

Methods

IMRT was conducted with 6MV X-ray linear accelerator. And principles of target delineation are as follows: Gross tumor volume of the nasopharynx (GTVnx): 66–76 Gy/33F; Gross tumor volume of the positive neck lymph nodes (GTVnd): 66–70 Gy/33F; Clinical target volume 1 (CTV1): 60–66 Gy/33F; Clinical target volume 2 (CTV2): 54–60 Gy/33F. The fractionated dose was 1.8 to 2.2 Gy at one fraction per day and 5 days per week. PTV (Planning target volume) was expanded by adding 3 mm to the GTV and CTV, respectively. The IC regimens were as follows: (1) TPF regimen: docetaxel (75 mg/m^2/day, day 1), cisplatin (75 mg/m^2/day, day 1), and 5-fluorouracil (750 mg/m^2/day, days 1–5); and (2) TP regimen: docetaxel (75 mg/m^2/day, day 1) and cisplatin (75 mg/m^2/day, day 1). IC were conducted every 21 days for three cycles. Besides, the cumulative dose of cisplatin during the concurrent chemotherapy was 200 mg/m^2.

Data Collection and Clinical Endpoints

The clinical data of all patients before treatment were collected were sex, age, smoking and drinking history, EBV-DNA status, T stage, N stage, clinical stage, and IC regimen. Hematological data before treatment were peripheral blood neutrophils, lymphocytes, and platelet count. SII is defined as total platelet count (10^9/L) × neutrophil count (10^9/L)/total lymphocyte count (10^9/L). The follow-up data: the time of beginning of follow-up, death, disease progression, and the deadline of follow-up.

The endpoints were as follows: OS, defined as the time from pathological diagnosis to death of any cause or the last follow-up; Progression-free survival (PFS), the time from pathological

diagnosis to tumor progression or death for any cause; Locoregional relapse-free survival (LRFS), the time from pathological diagnosis to local recurrence; DMFS, the time from the pathological diagnosis to the distant metastasis.

Treatment-related side effects between the groups were evaluated according to CTCAE V4.0 (Common Terminology Criteria for Adverse Events V4.0) (11) and RTOG (Radiation Therapy Oncology Group) criteria (12).

Follow-Up

The frequency of follow-up after treatment was every 3 months in the first 2 years, every 6 months in the 3 to 5 years, and then annually after 5 years. The follow-up included complete medical records. All patients were followed up by each clinical examination in the hospital or telephone calls.

Statistical Analyses

SPSS 25.0 and GraphPad Prism 8.0 software were used to analyze the data. The optimal cutoff value of SII was decided according to the receiver operating characteristic (ROC) curve. The measurement data were tested by independent sample t-test or Mann-Whitney U test, and the classified variables were tested by chi-square test. Survival curves were analyzed by Kaplan-Meier method and univariate analysis by Log-rank. Cox proportional hazard regression model was adopted in multivariate analysis. *P* value less than 0.05 was considered as statistically significant.

RESULTS

Baseline Characteristics and Follow-Up

Ultimately, 213 patients diagnosed at stage III-IVA were enrolled, with 128 and 85 patients in the TPF and TP group, respectively, whose baseline characteristics are shown in **Table 1**. Among them, 155 (72.77%) were males and 58 (27.23%) were females, with a median age of 45 years. One hundred one (47.42%) and 87 (40.85%) patients had a history of smoking and drinking, respectively. In the cohort, 121 (56.81%) patients were diagnosed with positive EBV DNA status. Based on the TNM staging system, 115 (53.99%) and 98 (46.01%) patients were re-staged in stage III and IVA, respectively. According to the ROC curve, the optimal cutoff value of pretreatment SII was 432.48 (*P*=0.011, Sensitivity: 95.0%, Specificity: 34.7%, AUC=0.673) (**Figure 1**), with 67 (31.46%) cases in low SII group (SII < 432.48) and 146 (68.64%) cases in a higher SII group, respectively.

As shown in the table, there was no significant difference in the two regimen groups ($P > 0.05$). In whole, the follow-up time ranged from 26 to 83 months. Finally, 20 (9.39%) patients died, and 54 (25.35%) patients suffered from tumor progression, of which 28 (51.85%) and 26 (48.15%) patients had local progression and distant metastasis, respectively. The 5-year OS, PFS, LRFS, and DMFS rates in TPF and TP groups were 89.0 *vs* 82.4%, 76.8 *vs* 68.4%, 85.9 *vs* 86.9% and 90.2 *vs* 81.3%, respectively.

Survival Analysis Based on TNM Staging System

Survival curves based on the different IC regimens were analyzed using the Kaplan-Meier method. As was shown in **Figure 2**, the

TABLE 1 | Baseline characteristics of patients in the TPF and TP groups.

Variables	TPF (n = 128) (%)	TP (n = 85) (%)	*P*
Age (years)			0.166
<45	38 (29.69)	33 (38.82)	
≥45	90 (70.31)	52 (61.18)	
Sex			0.127
Female	30 (23.44)	28 (32.94)	
Male	98 (76.56)	57 (67.06)	
Smoke			
No	60 (46.88)	52 (61.18)	0.051
Yes	68 (53.12)	33 (38.82)	
Drink			0.290
No	72 (56.25)	54 (63.53)	
Yes	56 (43.75)	31 (36.47)	
EBV DNA status			0.628
Negative	57 (44.53)	35 (41.18)	
Positive	71 (55.47)	50 (58.82)	
Tumor classification			0.406
T1	1 (0.78)	0 (0.00)	
T2	18 (14.06)	18 (21.17)	
T3	56 (43.75)	38 (44.71)	
T4	53 (41.41)	29 (34.12)	
Nodal classification			0.213
N0	2 (1.56)	3 (3.53)	
N1	30 (23.44)	15 (17.65)	
N2	78 (60.94)	47 (55.29)	
N3	18 (14.06)	20 (23.53)	
Clinical stage			0.756
III	60 (46.88)	38 (44.71)	
IVA	68 (53.12)	47 (55.29)	
Pretreatment SII level			0.824
<432.48	41 (32.03)	26 (30.59)	
≥432.48	87 (67.97)	59 (69.41)	

TPF, docetaxel, cisplatin, and 5-fluorouracil; TP, docetaxel and cisplatin; EBV DNA, Epstein-Barr virus DNA; SII, systemic immune-inflammation index.

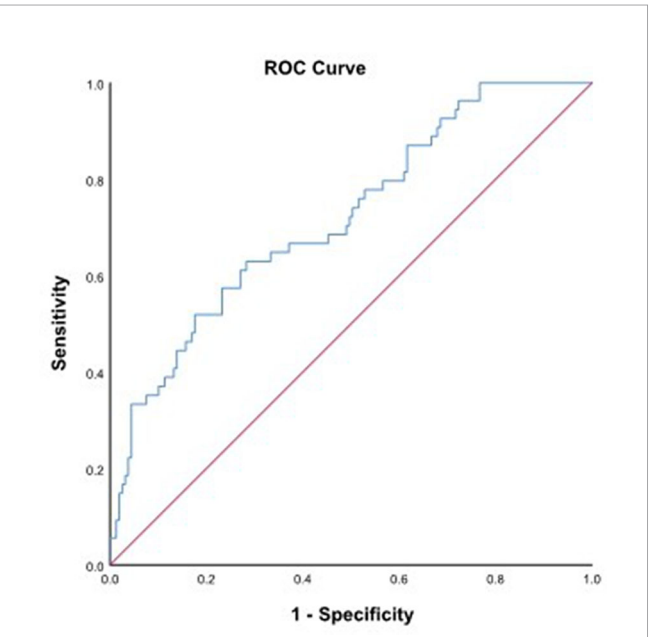

FIGURE 1 | ROC curve for pretreatment SII = 432.48 based on OS (*P*=0.011, Sensitivity: 95.0%, Specificity: 34.7%, AUC=0.673). ROC, receiver operating characteristic; SII, systemic immune-inflammation index; OS, overall survival.

patients in TPF group showed superior 5-year DMFS (90.2 *vs* 81.3%, $P = 0.043$, **Figure 2D**). However, no evident difference was found in OS, PFS, and LRFS between the two groups ($P > 0.050$).

Patients in different TNM stages showed different tumor load and treatment failure rate. Therefore, survival differences among patients in different clinical and N stage subgroups were conducted separately, with 98 in stage III and 115 in stage IVA. Since only five stage N0 patients were included, in order to minimize the deviation of statistical analysis, we divided N stage into N0-1 and N2-3 subgroups, including 50 and 163 cases, respectively. As shown in **Figure 3**, no significant survival difference was found in stage IVA patients between the two groups, and the TPF group had superior PFS ($P = 0.042$, **Figure 3B**) and DMFS ($P = 0.033$, **Figure 3D**). Similarly, we found that stage N2-3 patients in TPF also showed a significant trend in a higher DMFS ($P = 0.057$, **Supplementary Figure 3**). However, in patients with stage III and N0-1, no survival difference was found ($P > 0.050$, **Supplementary Figure 3**).

Survival Analysis in Stage IVA Patients Combined With Pretreatment SII

Moreover, SII is a promising factor in predicting prognosis of NPC patients. Therefore, based on the different pretreatment SII levels, we separated patients at stage IVA into low- and high-risk groups. Interestingly, our results revealed that in the high-risk group (SII ≥432.48), TPF showed significantly better OS ($P = 0.038$, **Figure 4A**) and DMFS ($P = 0.028$, **Figure 4D**) than TP, while not applicable for PFS (P = 0.099, **Figure 4B**) and LRFS (P = 0.667, **Figure 4C**). Further analysis was conducted and revealed that no significant survival difference was found in the low-risk group (SII <432.48); however, there were only 16 and 10 cases in TPF and TP groups, respectively, which required larger samples to confirm.

Univariate and Multivariate Analyses

In our univariate analysis, EBV DNA status, TNM stage, and pretreatment SII were corroborated as potential factors affecting all survival outcomes (**Table 2**). Patients with N0-1 stage were found to have a higher DMFS rate than that of N2-3 (88.3 *vs* 84.6%, $P = 0.038$). And in different IC regimens, the TPF regimen showed greater 5-year DMFS rate (90.2 *vs* 81.3%, $P = 0.043$). Considering the confounding factors, only statistically significant variables in univariate analysis were further researched in multivariate cox regression analysis. As shown in **Table 3**, EBV DNA status and clinical stage were related factors affecting all survival outcomes ($P < 0.050$). Also, pretreatment SII was considered as a related prognostic element for PFS (HR 2.801, 95% CI 1.195–6.565, $P = 0.018$) and DMFS (HR 3.735, 95% CI 1.121–12.441, $P = 0.032$). At the same time, IC regimen (HR 2.182, 95% CI 1.002–4.751, $P = 0.049$) and N stage (HR 4.076, 95% CI 0.962–7.267, $P = 0.046$) can also be used as effective indicators for predicting DMFS in LA-NPC patients.

Toxicities

As shown in **Table 4**, no significant difference was found in grade 1–2 toxicities between the TPF and TP groups ($P > 0.050$).

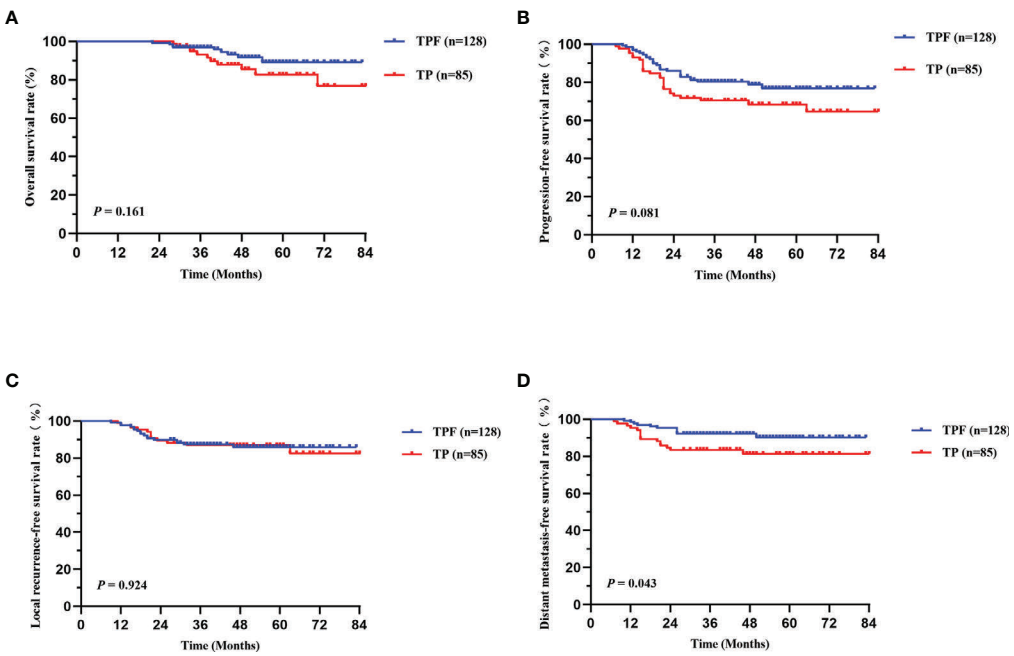

FIGURE 2 | Kaplan-Meier survival curves of OS **(A)**, PFS **(B)**, LRFS **(C)**, and DMFS **(D)** between TPF and TP groups in locally advanced patients. TPF, docetaxel, cisplatin, and 5-fluorouracil; TP, docetaxel and cisplatin; OS, overall survival; PFS, progression-free survival; LRFS, locoregional relapse-free survival; DMFS, distant metastasis-free survival.

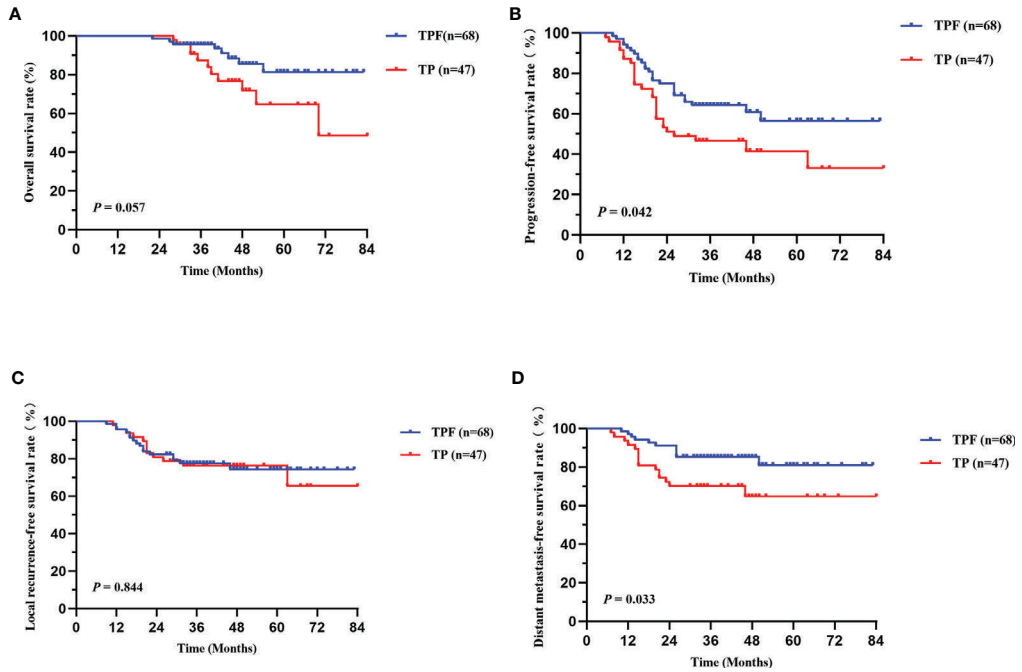

FIGURE 3 | Kaplan-Meier survival curves of OS **(A)**, PFS **(B)**, LRFS **(C)**, and DMFS **(D)** between TPF and TP groups in patients with stage IVA. TPF, docetaxel, cisplatin, and 5-fluorouracil; TP, docetaxel and cisplatin; OS, overall survival; PFS, progression-free survival; LRFS, locoregional relapse-free survival; DMFS, distant metastasis-free survival.

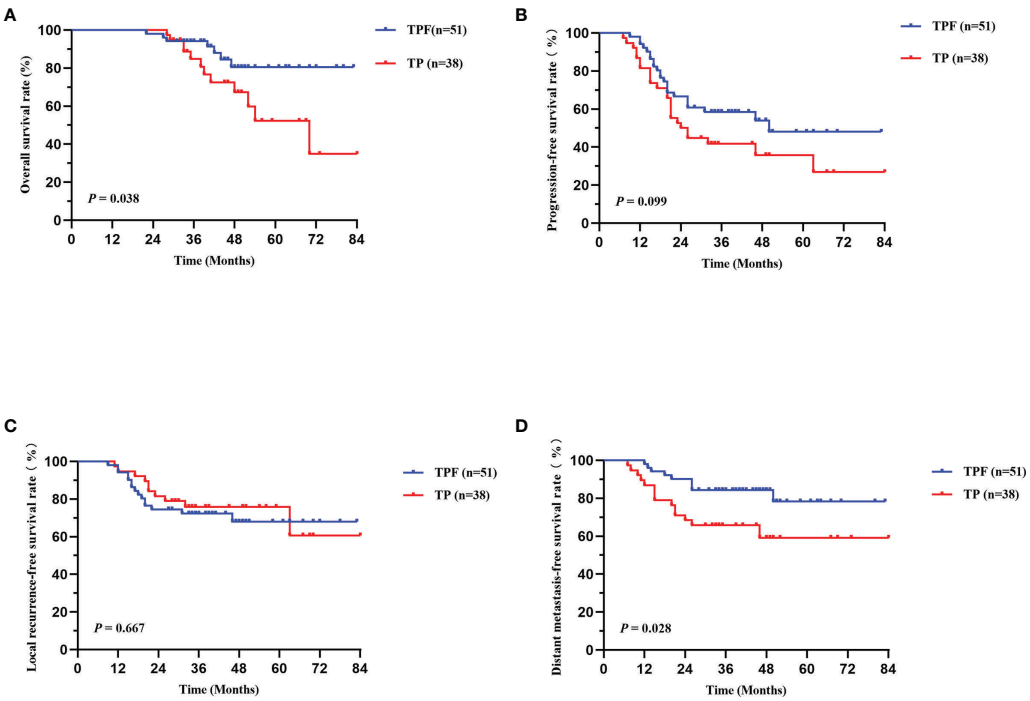

FIGURE 4 | Kaplan-Meier survival curves of OS **(A)**, PFS **(B)**, LRFS **(C)**, and DMFS **(D)** between TPF and TP groups in stage IVA patients with high SII (SII≥432.48). TPF, docetaxel, cisplatin, and 5-fluorouracil; TP, docetaxel and cisplatin; OS, overall survival; PFS, progression-free survival; LRFS, locoregional relapse-free survival; DMFS, distant metastasis-free survival.

TABLE 2 | Univariate analysis of prognostic factors for LA-NPC patients.

Variables	5-year OS (%)	*P*	5-year PFS (%)	*P*	5-year LRFS (%)	*P*	5-year DMFS (%)	*P*
Age (years)		0.494		0.636		0.537		0.298
<45	88.0		72.0		88.7		83.2	
≥45	86.1		74.1		85.1		88.4	
Sex		0.800		0.688		0.392		0.624
Female	84.9		70.8		81.0		89.7	
Male	87.6		74.4		88.3		85.4	
Smoke		0.533		0.655		0.781		0.500
No	88.4		74.5		85.6		88.0	
Yes	85.0		72.3		87.1		85.1	
Drink		0.798		0.599		0.700		0.164
No	86.2		74.7		85.6		89.1	
Yes	87.1		71.4		87.2		83.0	
EBV DNA status		0.004		0.000		0.001		0.000
Negative	96.0		93.3		95.5		97.8	
Positive	80.8		59.0		79.4		78.5	
Tumor classification		0.393		0.259		0.333		0.535
T1-2	90.3		81.0		90.5		90.5	
T3-4	85.7		71.2		85.1		85.4	
Nodal classification		0.289		0.479		0.307		0.038
N0-1	91.6		68.1		78.8		88.3	
N2-3	85.7		73.3		88.0		84.6	
Clinical stage		0.000		0.001		0.001		0.000
III	99.0		99.0		99.0		99.0	
IVA	75.0		50.2		75.1		74.3	
Pretreatment SII level		0.002		0.000		0.008		0.021
<432.48	100		91.0		95.5		95.5	
≥432.48	80.9		65.5		82.1		82.5	
IC regimen		0.154		0.080		0.924		0.043
TPF	89.0		76.8		85.9		90.2	
TP	82.4		68.4		86.9		81.3	

EBV DNA, Epstein-Barr virus DNA; SII, systemic immune-inflammation index; IC, induction chemotherapy; TPF, docetaxel, cisplatin, and 5-fluorouracil; TP, docetaxel and cisplatin; OS, overall survival; PFS, progression-free survival; LRFS, locoregional relapse-free survival; DMFS, distant metastasis-free survival.

Compared with TP regimen, we found that the rate of grade 3–4 leukopenia (40.62 *vs* 36.47%, $P = 0.038$), neutropenia (27.34 *vs* 14.12%, $P = 0.021$), radiation oral mucositis (28.91 *vs* 14.12%, $P = 0.048$), diarrhea (27.34 *vs* 10.59%, $P = 0.036$), and ear damage (14.06 *vs* 10.59%, $P = 0.046$) was higher in the TPF group. All the patients with toxicities were improved after treatment, and no interruption of treatment occurred.

DISCUSSION

Due to the special anatomical structure and its sensitivity to radiation, radiotherapy is the main treatment for NPC. And as the IMRT advanced, the local control rate has been improved, while local recurrence and distant metastasis are still the main failure (13). Increasing evidences suggested that IC can promote the eradication of micrometastasis, alleviate clinical symptoms caused in short term, and improve radiosensitivity (14). Furthermore, IC has been confirmed to be effective with LA-NPC in several phase III trials (15) and is widely applied. Hence, IC followed by CCRT is suggested to improve survival benefit in LA-NPC. However, it is quite important to find effective IC regimens with fewer side effects. Currently, studies on IC regimens commonly used in LA-NPC include TPF, TP, PF, and GP (16). Zhao et al. (17) found that compared with PF regimen, both GP and TP regimens could significantly improve DFS and OS, and no severe toxicities occurred. And Peng et al. (18) revealed that for NPC patients receiving a cumulative cisplatin dose (CCD) <200 mg/m^2, TPF showed better survival than TP and PF, while no significant difference was found in patients receiving a CCD ≥200 mg/m^2.

At present, TPF is the main regimen for LA-NPC, but accompanied by its long treatment time and adverse toxicities caused by 5-FU, such as myelosuppression and diarrhea. In a previous study on locally advanced head and neck squamous cell carcinoma (19), it was found that the total effective rate of TP regimen was 65.4%. The 3-year PFS rate and OS rate were similar as TPF. What is known to us all, different tumors of the head and neck were included in that study, and the response rate of TP regimen was taken as the main endpoint. Wang et al. (8) further found that TPF (docetaxel 60 mg/m2, cisplatin 25 mg/m2, days 1–3, 5-FU 500 mg/m2, days 1–3) showed similar efficacy compared to TP. No significant difference in 3-year survival outcomes was found ($P > 0.050$) between the two IC regimens. And multivariate analysis in this study also reached the same conclusion; however, the grade 3–4 toxicity in TP group is lower and tolerable. On accounting of the toxicities of 5-FU, patients were given lower dosage, so the potential effect of insufficient dose cannot be completely ruled out. At present, there is still no consensus about the efficacy and safety of the two regimens.

TABLE 3 | Multivariate cox regression analysis of prognostic factors for LA-NPC patients.

Variables	HR (95% CI)	*P*
OS		
EBV DNA status (positive *vs* negative)	6.456 (1.496–7.871)	0.012
Nodal classification (N2-3 *vs* N0-1)	2.167 (0.500–9.391)	0.301
Clinical stage (IVA *vs* III)	9.355 (2.588–14.731)	0.004
Pretreatment SII level (≥432.48 *vs* <432.48)	3.977 (0.709–7.314)	0.073
IC regimen (TP *vs* TPF)	1.880 (0.778–4.545)	0.161
PFS		
EBV DNA status (positive *vs* negative)	5.254 (2.242–12.314)	0.001
Nodal classification (N2-3 *vs* N0-1)	0.887 (0.637–1.236)	0.480
Clinical stage (IVA *vs* III)	4.956 (5.898–12.845)	0.001
Pretreatment SII level (≥432.48 *vs* <432.48)	2.801 (1.195–6.565)	0.018
IC regimen (TP *vs* TPF)	1.604 (0.941–2.736)	0.083
LRFS		
EBV DNA status (positive *vs* negative)	3.358 (1.162–9.700)	0.025
Nodal classification (N2-3 *vs* N0-1)	0.665 (0.303–1.463)	0.311
Clinical stage (IVA *vs* III)	1.479 (2.477–7.839)	0.004
Pretreatment SII level (≥432.48 *vs* <432.48)	0.665 (0.303–1.463)	0.086
IC regimen (TP *vs* TPF)	1.036 (0.495–2.172)	0.924
DMFS		
EBV DNA status (positive *vs* negative)	9.871 (2.332–4.774)	0.002
Nodal classification (N2-3 *vs* N0-1)	4.076 (0.962–7.267)	0.046
Clinical stage (IVA *vs* III)	5.201 (2.769–5.011)	0.010
Pretreatment SII level (≥432.48 *vs* <432.48)	3.735 (1.121–12.441)	0.032
IC regimen (TP *vs* TPF)	2.182 (1.002–4.751)	0.049

EBV DNA, Epstein-Barr virus DNA; SII, systemic immune-inflammation index; IC, induction chemotherapy; TPF, docetaxel, cisplatin, and 5-fluorouracil; TP, docetaxel and cisplatin; OS, overall survival; PFS, progression-free survival; LRFS, locoregional relapse-free survival; DMFS, distant metastasis-free survival; HR, hazard ratio; CI, confidence interval.

Therefore, this paper was conducted to compare the efficacy and toxicity of TPF and TP regimen in LA-NPC, in order to explore the feasibility of alternative TP regimen.

Finally, 213 LA-NPC patients were enrolled in our study. It was found that compared to TP, the TPF regimen showed similar short-term efficacy (total effective rate was 79.7 *vs* 78.8%), and no significance in 5-year OS, PFS, and LRFS ($P > 0.050$), which were consistent with Peng (18) and Wang et al. (8). Variously, in our study, TPF was found to have a higher 5-year DMFS rate (90.2 *vs* 81.3% 750 mg/m^2, $P = 0.043$), which may be due to the therapeutic benefits of 5-FU. Compared with the study of Wang et al. (8) (5-FU 500 mg/m^2, days 1–3), the dose in our hospital reached 750 mg/m^2 (days 1–5) in TPF regimen. Similarly, in the NPC-9901 and NPC-9902 study (20), the dose of 5-FU during CCRT was confirmed to improve DFFS, with an explanation that 5-FU could reduce the risk of disease, and this may also be applicable to the IC phase. Nowadays, the TNM staging system is still considered as a critical factor related to prognosis, and we further analyzed survival differences between patients in stage III and IVA, respectively. Interestingly, the same results were found in stage IVA patients. In previous studies, patients with advanced N category (N2–3) were more prone to distant metastasis (21); in our N category subgroups, fortunately, we observed that the TPF group had a trend in higher 5-year DMFS ($P = 0.057$), which was not applicable in N0-1. One possible statement is that TPF can reduce distant metastases from patients with high metastatic burdens (N2–3). Similarly, Guo et al. (22) found that N3 is an independent prognostic factor for LA-NPC, with poorer survival. These findings are similar to the results of our study, that is, compared with TP regimen, TPF regimen can show better survival in LA-NPC, especially in N2-3 patients. For N0-1 patients, the choice of TP regimen with fewer treatment-related toxicities may be enough.

In recent years, more and more evidences supported systemic inflammation contributed to the biological behavior of tumor cells, such as growth, infiltration, and metastasis (23). SII is associated with poor prognosis of NPC as a new biomarker (10), which is defined as an integration of peripheral platelet, neutrophil, and lymphocyte count. It is a comprehensive and objective tool that integrates three indicators together, and it is simpler and cheaper. Oei et al. (24) revealed that pretreatment SII level was an effective predictor for OS, PFS, and DMFS ($P < 0.05$). In our study, it was also confirmed that pretreatment SII was a significant prognostic factor of PFS (HR 2.801, $P = 0.018$) and DMFS (HR 3.735, $P = 0.032$), which was similar as the previous results. Nevertheless, the optimal threshold of SII level before treatment is not consistent in various studies, which may be related to the baseline characteristics in enrolled patients and reference standards for different instruments, and further

TABLE 4 | Treatment-related toxicities between the TPF and TP groups.

Variables	TPF (n = 128)			TP (n = 85)			*P*	
	Grade 0 (%)	Grade 1-2 (%)	Grade 3-4 (%)	Grade 0 (%)	Grade 1-2 (%)	Grade 3-4 (%)	Grade 1-2	Grade 3-4
Leukopenia	20 (15.63)	56 (43.75)	52 (40.62)	24 (28.24)	30 (35.29)	31 (36.47)	0.380	0.038
Neutropenia	28 (21.88)	65 (50.78)	35 (27.34)	33 (38.82)	40 (47.06)	12 (14.12)	0.465	0.021
Anemia	46 (35.94)	78 (60.94)	4 (3.12)	36 (42.35)	47 (55.29)	2 (2.36)	0.583	0.154
Thrombocytopenia	44 (34.38)	82 (64.06)	2 (1.56)	28 (32.94)	56 (65.88)	1 (1.18)	0.435	0.083
Abnormal liver function	46 (35.94)	81 (63.28)	1 (0.78)	26 (30.59)	58 (68.23)	1 (1.18)	0.363	0.215
Abnormal renal function	48 (37.50)	79 (61.72)	1 (0.78)	32 (37.65)	53 (62.35)	0 (0.00)	0.672	0.276
Vomiting	23 (17.97)	90 (70.31)	15 (11.72)	12 (14.12)	59 (69.41)	14 (16.47)	0.574	0.426
Oral mucositis	26 (20.31)	65 (50.78)	37 (28.91)	23 (27.06)	50 (58.82)	12 (14.12)	0.375	0.048
Diarrhea	18 (14.06)	75 (58.60)	35 (27.34)	17 (20.00)	59 (69.41)	9 (10.59)	0.584	0.036
Osteonecrosis	126 (98.44)	2 (1.56)	0 (0.00)	84 (98.82)	1 (1.18)	0 (0.00)	0.746	0.548
Ear (deafness/otitis)	89 (69.53)	21 (16.41)	18 (14.06)	65 (76.47)	11 (12.94)	9 (10.59)	0.147	0.046
Radiation-induced malignancy	0 (0.00)	0 (0.00)	0 (0.00)	0 (0.00)	0 (0.00)	0 (0.00)	–	–

TPF, docetaxel, cisplatin, and 5-fluorouracil; TP, docetaxel and cisplatin.

prospective research to determine the appropriate cutoff value will be more accurate.

The mechanism of SII affecting prognosis may be related to its components. In inflammatory cells, neutrophils are a part of the tumor microenvironment and are closely related to cancer progression, which can promote the development and metastasis of cancer cells by secreting inflammatory mediators, like TNF and IL-6 (25). Similarly, for lymphocytes, tumor growth can be regulated by secreting cytokines, like IFN-γ and TNF-α. And then, platelets are able to increase the number of tumor cells in circulation and further induce epithelial mesenchymal transformation, thus promoting the extravasation of tumor cells to the metastatic site (26). In addition, some evidence suggests that both neutrophils and platelets can further enhance tumor angiogenesis by secreting vascular endothelial cell factors, like fibroblast growth factor and angiopoietin. Hence, a higher SII, defined as a combination of high neutrophil count, high platelet count, and low lymphocyte count, can promote unlimited proliferation and distant metastasis of tumor cells and contribute to a poor prognosis. As far as we know, the prognostic value of IC regimens based on pretreatment SII and TNM stage in LA-NPC was not reported before. According to ROC curve, the patients in stage IVA with SII≥432.48 was defined high-risk group. Interestingly, our results revealed that in the high-risk group, compared with TP, the TPF regimen showed a superior OS (P = 0.038) and DMFS (P = 0.028); unfortunately, due to a limited sample size in the low SII group, a consistent conclusion has not been reached. Hence, TPF could be considered as the more effective regimen, particularly in high-risk (IVA combined with SII≥432.48) patients. Furthermore, multivariate analysis showed that IC regimen (HR 2.182, P = 0.049) and N stage (HR 4.076, P = 0.046) could also be used as effective indicators for predicting DMFS in LA-NPC patients.

About the treatment-related side effects, obviously, combinations of three drugs produce more grade 3–4 toxicities. In our study, we found that compared with TP, the rate of grade 3–4 leukopenia (P = 0.038), neutropenia (P = 0.021), radiation oral mucositis (P = 0.048), diarrhea (P = 0.036), and ear damage (P = 0.046) were more common in the TPF group, which was consistent as previously reported (8, 27). This difference could be attributed to the anti-tumor therapy of 5-FU, since myelosuppression and diarrhea are the common toxicities.

Whereas, there are also some limitations in this study. First of all, this study is a retrospective analysis in a single center and with a small sample size, which is inevitably accompanied by the deviation of data selection. Second, we only studied SII levels before treatment; a dynamic analysis would be more meaningful. Therefore, further multicenter, large-sample, prospective randomized controlled trials are needed to comprehensively compare the effects of different IC regimens on the efficacy and prognosis in LA-NPC patients.

CONCLUSION

In summary, our study revealed that TPF regimen showed a higher 5-year DMFS for LA-NPC patients with stage IVA and N2-3, while TP may be enough for stage III and N0-1. In stage IVA combined with pretreatment SII ≥ 432.48 patients, TPF had higher 5-year OS and DMFS, although grade 3–4 toxicities were more common, but most of them can be tolerable.

DATA AVAILABILITY STATEMENT

The raw data supporting the conclusions of this article will be made available by the authors, without undue reservation. Requests to access these datasets should be directed to xiongying0604@163.com.

ETHICS STATEMENT

The studies involving human participants were reviewed and approved by Union Hospital of Tongji Medical College of Huazhong University of Science and Technology. The patients/participants provided their written informed consent to participate in this study.

AUTHOR CONTRIBUTIONS

XY: topic selection, data collection, and article writing. LZ: image editing. LS: suggestions and amendments to experimental methods and data. GP: article guidance and revision. All authors contributed to the article and approved the submitted version.

FUNDING

This work was supported by National Natural Science Foundation of China (Grant No. 82071067).

SUPPLEMENTARY MATERIAL

The Supplementary Material for this article can be found online at: https://www.frontiersin.org/articles/10.3389/fonc.2021.731543/full#supplementary-material

REFERENCES

1. Bray F, Ferlay J, Soerjomataram I, Siegel RL, Torre LA, Jemal A. Global Cancer Statistics 2018: GLOBOCAN Estimates of Incidence and Mortality Worldwide for 36 Cancers in 185 Countries. *CA: Cancer J Clin* (2018) 68 (6):394–424. doi: 10.3322/caac.21492
2. Liu T, Sun Q, Chen J, Li B, Qin W, Wang F, et al. Neoadjuvant Chemotherapy With Fluorouracil Plus Nedaplatin or Cisplatin for Locally Advanced Nasopharyngeal Carcinoma: A Retrospective Study. *J Cancer* (2018) 9 (20):3676–82. doi: 10.7150/jca.27198
3. Yang Q, Cao S-M, Guo L, Hua Y-J, Huang P-Y, Zhang X-L, et al. Induction Chemotherapy Followed by Concurrent Chemoradiotherapy Versus Concurrent Chemoradiotherapy Alone in Locoregionally Advanced Nasopharyngeal Carcinoma: Long-Term Results of a Phase III Multicentre Randomised Controlled Trial. *Eur J Cancer* (2019) 119:87–96. doi: 10.1016/j.ejca.2019.07.007

4. Wang Q, Xu G, Xia Y, Zuo J, Zeng G, Xue Z, et al. Comparison of Induction Chemotherapy Plus Concurrent Chemoradiotherapy and Induction Chemotherapy Plus Radiotherapy in Locally Advanced Nasopharyngeal Carcinoma. *Oral Oncol* (2020) 111:104925. doi: 10.1016/j.oraloncology.2020.104925
5. Li W-F, Chen N-Y, Zhang N, Hu G-Q, Xie F-Y, Sun Y, et al. Concurrent Chemoradiotherapy With/Without Induction Chemotherapy in Locoregionally Advanced Nasopharyngeal Carcinoma: Long-Term Results of Phase 3 Randomized Controlled Trial. *Int J Cancer* (2019) 145(1):295–305. doi: 10.1002/ijc.32099
6. Pfister DG, Spencer S, Adelstein D, Adkins D, Anzai Y, Brizel DM, et al. Head and Neck Cancers, Version 2.2020, NCCN Clinical Practice Guidelines in Oncology. *J Natl Compr Canc Netw* (2020) 18(7):873–98. doi: 10.6004/jnccn.2020.0031
7. Wang F, Chuner J, Lei W, Fengqin Y, Zhimin Y, Quanquan S, et al. Optimal Induction Chemotherapeutic Regimen Followed by Concurrent Chemotherapy Plus Intensity-Modulated Radiotherapy as First-Line Therapy for Locoregionally Advanced Nasopharyngeal Carcinoma. *Med (Baltimore)* (2020) 99(39):e22283. doi: 10.1097/MD.0000000000022283
8. Fangzheng W, Chuner J, Lei W, Fengqin Y, Zhimin Y, Quanquan S, et al. Addition of 5-Fluorouracil to First-Line Induction Chemotherapy With Docetaxel and Cisplatin Before Concurrent Chemoradiotherapy Does Not Improve Survival in Locoregionally Advanced Nasopharyngeal Carcinoma. *Oncotarget* (2017) 8(53):91150–61. doi: 10.18632/oncotarget.20017
9. Kinoshita T, Goto T. Links Between Inflammation and Postoperative Cancer Recurrence. *J Clin Med* (2021) 10(2):228. doi: 10.3390/jcm10020228
10. Jiang W, Chen Y, Huang J, Xi D, Chen J, Shao Y, et al. Systemic Immune-Inflammation Index Predicts the Clinical Outcome in Patients With Nasopharyngeal Carcinoma: A Propensity Score-Matched Analysis. *Oncotarget* (2017) 8(39):66075–86. doi: 10.18632/oncotarget.19796
11. Liu Y-J, Zhu G-P, Guan X-Y. Comparison of the NCI-CTCAE Version 4.0 and Version 3.0 in Assessing Chemoradiation-Induced Oral Mucositis for Locally Advanced Nasopharyngeal Carcinoma. *Oral Oncol* (2012) 48(6):554–9. doi: 10.1016/j.oraloncology.2012.01.004
12. Cox JD, Stetz J, Pajak TF. Toxicity Criteria of the Radiation Therapy Oncology Group (RTOG) and the European Organization for Research and Treatment of Cancer (EORTC). *Int J Radiat Oncol Biol Phys* (1995) 31(5):1341–6. doi: 10.1016/0360-3016(95)00060-C
13. Sun X, Su S, Chen C, Han F, Zhao C, Xiao W, et al. Long-Term Outcomes of Intensity-Modulated Radiotherapy for 868 Patients With Nasopharyngeal Carcinoma: An Analysis of Survival and Treatment Toxicities. *Radiother Oncol* (2014) 110(3):398–403. doi: 10.1016/j.radonc.2013.10.020
14. Cao S-M, Yang Q, Guo L, Mai H-Q, Mo H-Y, Cao K-J, et al. Neoadjuvant Chemotherapy Followed by Concurrent Chemoradiotherapy Versus Concurrent Chemoradiotherapy Alone in Locoregionally Advanced Nasopharyngeal Carcinoma: A Phase III Multicentre Randomised Controlled Trial. *Eur J Cancer* (2017) 75:14–23. doi: 10.1016/j.ejca.2016.12.039
15. Peng H, Chen L, Zhang J, Li W-F, Mao Y-P, Zhang Y, et al. Induction Chemotherapy Improved Long-Term Outcomes of Patients With Locoregionally Advanced Nasopharyngeal Carcinoma: A Propensity Matched Analysis of 5-Year Survival Outcomes in the Era of Intensity-Modulated Radiotherapy. *J Cancer* (2017) 8(3):371–7. doi: 10.7150/jca.16732
16. Hui EP, Ma BB, Leung SF, King AD, Mo F, Kam MK, et al. Randomized Phase II Trial of Concurrent Cisplatin-Radiotherapy With or Without Neoadjuvant Docetaxel and Cisplatin in Advanced Nasopharyngeal Carcinoma. *J Clin Oncol: Off J Am Soc Clin Oncol* (2009) 27(2):242–9. doi: 10.1200/JCO.2008.18.1545
17. Zhao L, Xu M, Jiang W, Pan H, Zang J, Luo S, et al. Induction Chemotherapy for the Treatment of non-Endemic Locally Advanced Nasopharyngeal Carcinoma. *Oncotarget* (2017) 8(4):6763–74. doi: 10.18632/oncotarget.14279
18. Peng H, Tang L-L, Chen B-B, Chen L, Li W-F, Mao Y-P, et al. Optimizing the Induction Chemotherapy Regimen for Patients With Locoregionally Advanced Nasopharyngeal Carcinoma: A Big-Data Intelligence Platform-Based Analysis. *Oral Oncol* (2018) 79:40–6. doi: 10.1016/j.oraloncology.2018.02.011
19. Noronha V, Goswami C, Patil S, Joshi A, Patil VM, Murthy V, et al. Response to Docetaxel and Cisplatin Induction Chemotherapy of Locally Advanced Head and Neck Squamous Cell Carcinoma: A Multicenter, non-Comparative, Open-Label Interventional Pilot Study. *J Laryngol Otol* (2016) 130(9):833–42. doi: 10.1017/S0022215116008513
20. Lee AWM, Tung SY, Ngan RKC, Chappell R, Chua DTT, Lu TX, et al. Factors Contributing to the Efficacy of Concurrent-Adjuvant Chemotherapy for Locoregionally Advanced Nasopharyngeal Carcinoma: Combined Analyses of NPC-9901 and NPC-9902 Trials. *Eur J Cancer* (2011) 47(5):656–66. doi: 10.1016/j.ejca.2010.10.026
21. Zhang Y, Chen M, Chen C, Kong L, Lu JJ, Xu B. The Efficacy and Toxicities of Intensive Induction Chemotherapy Followed by Concurrent Chemoradiotherapy in Nasopharyngeal Carcinoma Patients With N Disease. *Sci Rep* (2017) 7(1):3668. doi: 10.1038/s41598-017-03963-8
22. Guo Q, Pan J, Zong J, Zheng W, Zhang C, Tang L, et al. Suggestions for Lymph Node Classification of UICC/AJCC Staging System: A Retrospective Study Based on 1197 Nasopharyngeal Carcinoma Patients Treated With Intensity-Modulated Radiation Therapy. *Med (Baltimore)* (2015) 94(20): e808. doi: 10.1097/MD.0000000000000808
23. Fernandes JV, Cobucci RNO, Jatobá CAN, Fernandes T, de Azevedo JWV, de Araújo JMG. The Role of the Mediators of Inflammation in Cancer Development. *Pathol Oncol Res* (2015) 21(3):527–34. doi: 10.1007/s12253-015-9913-z
24. Oei RW, Ye L, Kong F, Du C, Zhai R, Xu T, et al. Prognostic Value of Inflammation-Based Prognostic Index in Patients With Nasopharyngeal Carcinoma: A Propensity Score Matching Study. *Cancer Manag Res* (2018) 10:2785–97. doi: 10.2147/CMAR.S171239
25. Tecchio C, Scapini P, Pizzolo G, Cassatella MA. On the Cytokines Produced by Human Neutrophils in Tumors. *Semin Cancer Biol* (2013) 23(3):159–70. doi: 10.1016/j.semcancer.2013.02.004
26. Mego M, Gao H, Cohen EN, Anfossi S, Giordano A, Tin S, et al. Circulating Tumor Cells (CTCs) are Associated With Abnormalities in Peripheral Blood Dendritic Cells in Patients With Inflammatory Breast Cancer. *Oncotarget* (2017) 8(22):35656–68. doi: 10.18632/oncotarget.10290
27. Bae WK, Hwang JE, Shim HJ, Cho SH, Lee JK, Lim S-C, et al. Phase II Study of Docetaxel, Cisplatin, and 5-FU Induction Chemotherapy Followed by Chemoradiotherapy in Locoregionally Advanced Nasopharyngeal Cancer. *Cancer Chemother Pharmacol* (2010) 65(3):589–95. doi: 10.1007/s00280-009-1152-0

Conflict of Interest: The authors declare that the research was conducted in the absence of any commercial or financial relationships that could be construed as a potential conflict of interest.

frontiers in Oncology

SYSTEMATIC REVIEW
published: 27 September 2021
doi: 10.3389/fonc.2021.711171

Diagnostic and Prognostic Value of MicroRNAs in Metastasis and Recurrence of Head and Neck Squamous Cell Carcinoma: A Systematic Review and Meta-Analysis

Ke Qiu[1†], Yao Song[1†], Yufang Rao[1†], Qiurui Liu[1], Danni Cheng[1], Wendu Pang[1], Jianjun Ren[1,2,3] and Yu Zhao[1*]*

[1] Department of Oto-Rhino-Laryngology, West China Hospital, Sichuan University, Chengdu, China, [2] West China Biomedical Big Data Center, West China Hospital/West China School of Medicine, Sichuan University, Chengdu, China, [3] Medical Big Data Center, Sichuan University, Chengdu, China

OPEN ACCESS

Edited by:
Hui Wang,
Hunan Cancer Hospital, China

Reviewed by:
Shahram Ghanaati,
Goethe University Frankfurt, Germany
Vito Carlo Alberto Caponio,
University of Foggia, Italy

***Correspondence:**
Yu Zhao
yutzhao@VIP.163.com
Jianjun Ren
juneent2016@163.com

[†]These authors have contributed equally to this work

Specialty section:
This article was submitted to Head and Neck Cancer, a section of the journal Frontiers in Oncology

Received: 18 May 2021
Accepted: 01 September 2021
Published: 27 September 2021

Citation:
Qiu K, Song Y, Rao Y, Liu Q, Cheng D, Pang W, Ren J and Zhao Y (2021) Diagnostic and Prognostic Value of MicroRNAs in Metastasis and Recurrence of Head and Neck Squamous Cell Carcinoma: A Systematic Review and Meta-Analysis. Front. Oncol. 11:711171. doi: 10.3389/fonc.2021.711171

MicroRNAs have been proven to make remarkable differences in the clinical behaviors of head and neck squamous cell carcinoma (HNSCC). This study aims to systematically analyze whether differential expression levels of microRNAs are related to recurrence or metastasis in patients with HNSCC. A comprehensive search of the PubMed, EMBASE, and CENTRAL was conducted up to July 24th, 2021. Data were collected and combined from studies reporting recurrence-free survival (RFS) of HNSCC patients with high microRNA expression compared to those with low expression. Besides, studies providing necessary data for evaluating the diagnostic value of microRNAs for detecting recurrence and metastasis based on their expression levels were also included and combined. The pooled hazard ratio (HR) value for the outcomes of RFS in 1,093 HNSCC samples from 10 studies was 2.51 (95%CI: 2.13–2.96). A sensitivity of 0.79 (95% CI: 0.72–0.85) and specificity of 0.77 (95%CI: 0.68–0.83) were observed in three studies, of which 93 patients with recurrence and 82 nonrecurrence controls were included, and the area under the curve (AUC) was 0.85 (95% CI: 0.81–0.88). Additionally, high diagnostic accuracy of microRNAs in detecting lymph node metastasis (LNM) was also reported. In conclusion, two panels of microRNAs showed the potential to predict recurrence or diagnose recurrence in HNSCC patients, respectively, which could facilitate prognosis prediction and diagnosis of clinical behaviors in HNSCC patients.

Systematic Review Registration: PROSPERO (https://www.crd.york.ac.uk/prospero), identifier CRD42020161117.

Keywords: microRNA, head and neck squamous cell carcinoma (HNSCC), recurrence-free survival (RFS), metastasis, diagnostic accuracy, meta-analysis

INTRODUCTION

Head and neck squamous cell carcinomas (HNSCCs), visualized as the most common form of human solid tumors in the head and neck region, account for a large proportion of cancer mortality worldwide (1, 2). A multiple process that accumulates genetic mutations sequentially is believed to play a critical role in the formation of HNSCCs. And these highly heterogeneous tumors are derived from stratified epithelial cells of various anatomical subsites, mainly including the oral cavity, tongue, nasal cavity, larynx, and pharynx (3, 4). However, recent studies had illustrated similarities in genomic, genetic, and epigenetic alterations between HNSCCs from different subsites, which suggested the existence of certain common mechanisms underlying the initiation and progression of HNSCCs (3, 5, 6). It is estimated that approximately 1/3 of HNSCC patients develop recurrence or metastasis after receiving standard therapies, and the majority of them ended with poor prognosis (7, 8). Currently, tumor-node-metastasis (TNM) staging based on imaging modalities and biopsy represents the leading way to predict HNSCCs' biological behaviors, especially for metastasis and recurrence; however, accuracy varied among HNSCCs with different origins (9, 10). Therefore, reliable and detectable biomarkers may contribute to the diagnosis and prediction of metastasis and recurrence of SCCs.

MicroRNAs, a special class of noncoding RNAs (19–23 nucleotides in length), are capable of binding to their target mRNAs and regulating gene expression at the post-transcriptional level (11). In the past decade, microRNAs had been proven to make remarkable differences in HNSCC carcinogenesis and cancer progression, making them potential biomarkers to predict biological behaviors of HNSCCs (12–18). This meta-analysis aimed at evaluating the diagnostic and prognostic values of microRNAs in the recurrence and metastasis of human SCCs.

METHODS AND MATERIALS

Protocol and Eligibility Criteria

This study was conducted in accordance with the PRISMA (Preferred Reporting Items for Systematic Reviews and Meta-Analysis) guidelines (19) and was already registered on prospero (registration number: CRD42020161117).

The inclusion criteria were as follows: 1) studies written in English; 2) the diagnosis of HNSCC was confirmed by histopathology; 3) studies demonstrating the expression levels of microRNA by quantitative polymerase chain reaction (qPCR), *in situ* hybridization (ISH), fluorescent *in situ* hybridization (FISH), or RNA sequencing; 4) studies reporting HR with 95% confidence interval (CI) or Kaplan–Meier curves related to the correlation of microRNA expression with RFS; and 5) studies providing necessary data for evaluating the diagnostic value of microRNAs in predicting recurrence and metastasis.

The exclusion criteria were as follows: 1) studies related to nonhuman samples; 2) studies providing combined outcomes of more than one microRNA or insufficient data; 3) duplicate studies; 4) studies in the form of reviews, letters, editorials, meeting abstracts, or case reports; and 5) studies reporting SCC not originated from the head and neck region.

More specifically, for the meta-analysis evaluating the predictive values of microRNAs, we aimed to address the question of whether HNSCC patients with a higher expression level of microRNAs had different risk of cancer recurrence compared to HNSCC patients with a lower expression level of microRNAs. And for the meta-analysis evaluating the diagnostic values of microRNAs, we aimed to address the question of whether the expression level of microRNAs in human biospecimen could be used as indicators for distinguishing the HNSCC patients with recurrence/metastasis or not.

Information Sources and Search Strategies

A comprehensive search of the PubMed, EMBASE, and CENTRAL was conducted from the beginning of each database to July 24th, 2021. Meanwhile, additional records from other sources, e.g., the references of included studies and original studies mentioned in reviews, were also screened.

A Boolean combination of Mesh terms and free text words were used as search strategies, mainly including "Carcinoma, Squamous Cell"[Mesh], "MicroRNA", "MiRNAs", "MicroRNAs"[Mesh], "Metastasis", "Metastases", "Recurrences", "Relapse", and "Recurrence"[Mesh]. Detailed search strategies were presented in **Supplementary Material**.

Study Selection, Data Collection Process, and Data Items

The initial screening of titles and abstracts were conducted independently by two authors, and full texts would be reviewed if the titles and abstracts were ambiguous. Any discrepancy was solved by consensus, and a third author would participate if necessary. Finally, studies fulfilling all inclusion criteria were included in the systematic review.

Data extraction for studies investigating the RFS and diagnostic value was also independently performed and cross-checked by two authors. The agreement between authors KQ and YS was determined by Cohen's kappa score. And the extracted items were as follows: year of publication, first author, country, microRNAs studied, type of microRNA dysregulation, sample sizes, duration of follow-up, tumor sites, metastasis sites, detection assay, sample types, and cutoffs for the expression of microRNAs.

Risk of Bias Assessment, Summary Measures, and Statistical Analyses

The risk of bias within each included prognostic study was evaluated by the Newcastle-Ottawa Scale (NOS) (http://www.ohri.ca/programs/clinical_epidemiology/oxford.asp), and the risk of bias within each included diagnostic study was evaluated by the tool provided by Quality Assessment of Diagnostic Accuracy Studies—2 (QUADAS-2) (20), while the risk of bias across studies was evaluated by the Cochran Q test

and Higgins index (I^2). Heterogeneity was considered significant if $P < 0.05$ in Q test, and subgroup analyses were applied to find the potential sources of heterogeneity. Besides, overall effects were analyzed by a fixed-effect model if $I^2 < 50\%$; otherwise, a random-effects model would be applied.

For studies investigating RFS, ln[HR] and standard error (SE) were synthesized (21). The publication bias was tested by Begg's test. For studies investigating diagnostic values, we calculated the pooled sensitivity and specificity. The summary receiver operator characteristic (SROC) curve and the area under the SROC curve (AUC) were constructed and calculated to explore the diagnostic accuracy of microRNAs in metastasis/recurrence. Additionally, the publication bias was tested by Deek's funnel plot asymmetry test.

The STATA 12.0 (Stata Corp, College Station, TX, USA) and Review Manager (Version5.4, The Cochrane Collaboration, 2020) software was used for all meta-analysis, and $P < 0.05$ was considered significant.

RESULTS

Study Selection

A total of 3,349 records were retrieved through the initial comprehensive search. A total of 1,860 articles remained after excluding duplicates and were screened according to titles and abstracts. Subsequently, 398 studies remained and underwent full-text screening. A total of 14 studies that fully met the inclusion criteria were included for further analysis, among which 10 studies (22–31) were included for meta-analysis of HR for RFS, 3 studies (32–34) were included for meta-analysis of diagnostic accuracy for recurrence, and another 1 study (14) was included for systematic review of diagnostic accuracy for metastasis. Detailed selection process and reasons of exclusion were presented in **Figure 1**.

Study Characteristics

For the 10 included studies investigating RFS, a cumulative number of 1,093 SCC samples were analyzed. Tumor subsites were confined to head and neck regions, including the oral cavity, larynx, hypopharynx, and oropharynx. The duration of follow-up ranged from 28 months to more than 120 months, and all outcomes were evaluated by multivariate Cox regression models. Detailed characteristics of each study are presented in **Table 1**.

For the three included studies investigating diagnostic accuracy for recurrence, a total of 93 recurrence patients and 82 nonrecurrence controls were analyzed. Tumor subsites were confined to head and neck regions, including larynx and oral cavity. And the recurrence sites were not reported in most of the studies. Detailed characteristics of each study are presented in **Table 2**.

Similarly, for the included study investigating diagnostic accuracy for metastasis, a total of 25 metastasis patients and 23 nonmetastasis controls were analyzed. Tumor subsites were confined to head and neck regions. And the metastasis sites were reported to be the lymph node. Detailed characteristics of each study are presented in **Table 2**.

Synthesis of RFS and Subgroup Analysis

The pooled HR value for the outcomes of RFS in all HNSCC patients was 2.51 (95%CI: 2.13–2.96) (**Figure 2**). Poorer RFS correlated with upregulation of 14 microRNAs (miR-205-5p, miR-429, miR-21-3p, miR-331-3p, miR-200a-3p, miR-19a-3p, miR-21-5p, miR-151a-3p, miR-17-3p, miR-18b-5p, miR-324-5p, miR-96-5p, miR-141-3p, and miR-130a) and with downregulation of 7 microRNAs (miR-29c, miR-200b, miR-375, miR-422a, miR-15b-5p, miR-204, and miR-200c).

We further conducted a subgroup analysis based on anatomical subsites, and the results showed that pooled HR values for the outcomes of RFS were 2.02 (95%CI: 1.10–3.71) in oropharyngeal squamous cell carcinoma (OPSCC) patients and 2.12 (95%CI: 1.64–2.73) in oral squamous cell carcinoma (OSCC) patients (**Figure 3**). And in OPSCC patients, poorer RFS correlated with downregulation of miR-422a and miR-375. While in OSCC patients, poorer RFS correlated with upregulation of five microRNAs (miR-21-3p, miR-130b-3p, miR-96-5p, miR-141-3p, and miR-130a) and with downregulation of three microRNAs (miR-375, miR-204, and miR-200c) (**Figure 3A**). Meanwhile, we also conducted a subgroup analysis for individual microRNAs with more than two outcomes. And the expression levels of miR-21-3p, miR-96-5p, and miR-375 showed strong association with RFS, especially miR-21-3p, with a pooled HR value of 3.59 (95%CI: 1.91-6.76) (**Figure 3B**).

Taken together, our results showed that a panel of 21 microRNAs (miR-205-5p, miR-429, miR-21-3p, miR-331-3p, miR-200a-3p, miR-19a-3p, miR-21-5p, miR-151a-3p, miR-17-3p, miR-18b-5p, miR-324-5p, miR-96-5p, miR-141-3p, miR-130a, miR-29c, miR-200b, miR-375, miR-422a, miR-15b-5p, miR-204, and miR-200c) might have the potential to predict the prognosis of patients with HNSCCs, of which 2 microRNAs were associated with the prognosis of OPSCC patients, and 8 microRNAs were associated with the prognosis of OSCC patients.

Study Quality and Risk of Bias in Prognostic Studies

NOS scores of each prognostic study are listed in **Table S1**, of which eight studies (80%) were of "good" quality and deemed to have low risk of bias, while the other two studies (20%) were of "poor" quality and deemed to have high risk of bias mainly due to the lack of adjustment for important confounding variables. A Cohen's kappa score of 0.76 revealed great agreement beyond chance between the two authors. Besides, no statistically significant heterogeneity ($P > 0.1$) and publication bias (Begg's test: $P = 0.333$, **Figure S1**) was observed in the pooled analysis of RFS.

Pooled Diagnostic Accuracy of microRNAs for HNSCC Recurrence

The evaluation for the sensitivity and specificity of a panel of four microRNAs in diagnosing the recurrence of SCCs is illustrated in **Figure 4A** (miR-34c-5p, miR-186-5p, miR-3651,

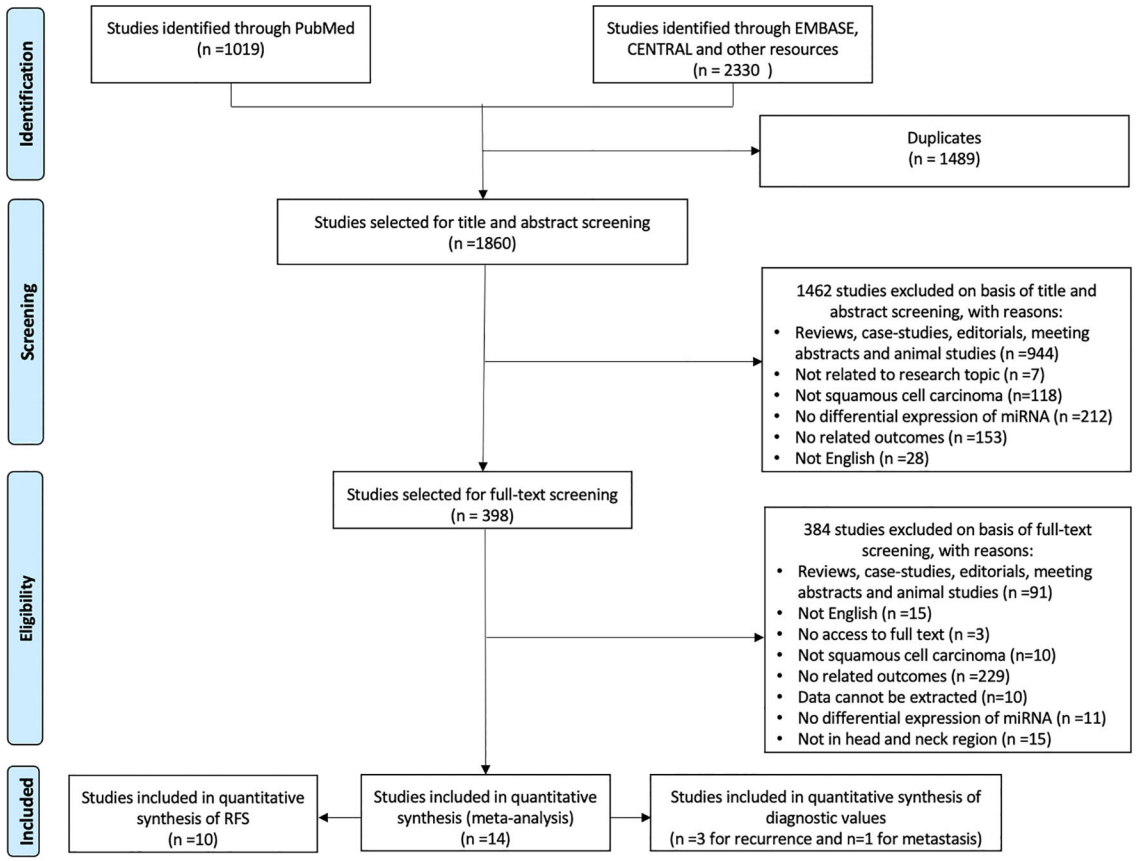

FIGURE 1 | Flow diagram summarizing the selection process of the systematic review.

and miR-494-5p). A sensitivity of 0.79 (95% CI: 0.72–0.85) and a specificity of 0.77 (95% CI: 0.68–0.83) were observed in patients with recurrence and nonrecurrence controls. The AUC was 0.85 (95% CI: 0.81–0.88), and the corresponding SROC curve is presented in **Figure 4B**.

Study Quality and Risk of Bias in Diagnostic Studies

As is shown in **Figure S2**, nearly all included diagnostic studies showed low risk of bias in patient selection, reference standard, and flow and timing; however, all of these three studies showed high risk of bias in index test mainly due to their retrospective nature, in which the index test results cannot be interpreted without knowledge of the results of the reference standard. Besides, the diagnostic thresholds in these studies were not confined and also not prespecified, which might cause some concerns on applicability. Meanwhile, no significant heterogeneity ($P > 0.1$) and publication bias ($P = 0.53$, **Figure S3**) was observed.

Overview of Diagnostic Accuracy of microRNAs for LNM in HNSCC

Only one study reporting the diagnostic accuracy of four independent microRNAs for LNM in HNSCC met our eligibility criteria. However, given the high risk of bias for pooled analysis of four tests derived from the same study, meta-analysis was not conducted. de Carvalho et al. reported the diagnostic accuracy of miRNA-200a (sensitivity 0.76; specificity:0.88; AUC: 0.92), miRNA-200c (sensitivity: 0.88; specificity: 1.00; AUC: 0.94), miRNA-203 (sensitivity: 1.00; specificity: 1.00; AUC: 1.00), and miRNA-205 (sensitivity: 1.00; specificity: 1.00; AUC: 1.00) in distinguishing 25 HNSCC patients with LNM from 23 HNSCC patients without LNM (14). All of these four microRNAs showed high diagnostic accuracy for detecting LNM in HNSCC patients; however, their performance was evaluated in the same cohort of which the sample size is not large enough. Thus, whether microRNAs have the potential for detecting LNM in HNSCC still needs to be validated by more studies with larger sample sizes.

DISCUSSION

In this review, we systematically analyzed 1,093 HNSCC samples from 10 studies (22–31) and identified a panel of 21 microRNAs related to poor RFS in HNSCC patients for the first time. Besides, we investigated the diagnostic accuracy of microRNAs for

TABLE 1 | Detailed characteristics and NOS scores of included studies investigating RFS.

Author and Year	Country	MicroRNA	Tumor sites and sample size	Assay	Type of samples	Dysregulation	Cutoff value	Follow-up time	Survival analysis
Ganci et al. (24)	Italy	miR-205-5p miR-429 miR-21-3p miR-331-3p miR-200a-3p miR-19a-3p miR-21-5p miR-151a-3p miR-17-3p miR-18b-5p miR-324-5p miR-96-5p	Oral cavity (n=73), larynx (n=29), hypopharynx (n=9) and oropharynx (n=10)	qPCR	Fresh frozen (tumor tissue)	Upregulation	According to special signal code	73M	Multivariate
Ganci et al. (25)	Italy	miR-429 miR-21-5p miR-96-5p miR-21-3p	Head and neck (n=106)	qPCR	FFPE (peritumor tissue)	Upregulation	According to special signal code	31M on average	Multivariate
Hudcova et al. (28)	Czech	miR-29c miR-200b miR-375	Head and neck (n=42)	qPCR	Fresh frozen (tumor tissue)	Downregulation	Not reported	30M	Multivariate
Bonnin et al. (23)	France	miR-422a	Oropharynx (n=75)	qPCR	Fresh frozen (tumor tissue)	Downregulation	Not reported	Unclear (more than 120M)	Multivariate
Ganci et al. (26)	Italy	miR-141-3p	Oral cavity (n=69)	qPCR	Fresh frozen (tumor tissue)	Upregulation	According to special signal code	50M	Multivariate
Harris et al. (27)	America	miR-375	Oral cavity (n=43)	qPCR	Fresh frozen (tumor tissue)	Downregulation	25-percentile	Unclear (more than 60M)	Multivariate
Harris et al. (27)	America	miR-375	Oropharynx (n=37)	qPCR	Fresh frozen (tumor tissue)	Downregulation	25-percentile	Unclear (more than 60M)	Multivariate
Harris et al. (27)	America	miR-375	Larynx (n=43)	qPCR	Fresh frozen (tumor tissue)	Downregulation	25-percentile	Unclear (more than 60M)	Multivariate
Ahmad et al. (22)	Czech	miR-15b-5p	Oral cavity (n=6), Hypopharynx (n=6), Larynx (n=8), Oropharynx (n=23)	qPCR	FFPE (tumor tissue)	Downregulation	Not reported	Unclear (more than 60M)	Multivariate
He et al. (29)	China	miR-130a	Oral cavity (n=92)	qPCR	Fresh frozen (plasma)	Upregulation	Median relative expression level	36M	Multivariate
Rajthala et al. (30)	Norway	miRNA-204	Oral cavity (n=158)	qPCR	FFPE (tumor tissue)	Downregulation	Not reported	8.6Y on average	Multivariate
Song et al. (31)	China	miR–200c	Oral cavity (n=204)	qPCR	Fresh frozen (tumor tissue)	Downregulation	Median relative expression level	36M	Multivariate

TABLE 2 | Detailed characteristics of included studies investigating diagnostic values of microRNAs for recurrence and LNM.

Author and Year	Country	MicroRNA	Tumor sites and sample size	Assay	Type of samples	Number of samples		Metastasis/Recurrence sites
						M (+) OR R (+)	M (-) OR R (-)	
de Carvalho et al. (14)	Brazil	miR-200a miR-200c miR-203 miR-205	Head and neck (n=48)	qPCR	FFPE (lymph node)	25	23	Lymph node (metastasis)
Re et al. (32)	Italy	miR-34c-5p	Larynx (n=90)	qPCR	FFPE (tumor tissue)	49	41	Not reported (recurrence)
Re et al. (33)	Italy	miR-34c-5p	Larynx (n=43)	qPCR	FFPE (tumor tissue)	23	20	Not reported (recurrence)
Ries et al. (34)	Austria	miR-186-5p miR-3651 miR-494-5p	Oral cavity (n=42)	qPCR	Fresh frozen (whole blood)	21	21	Not reported (recurrence)

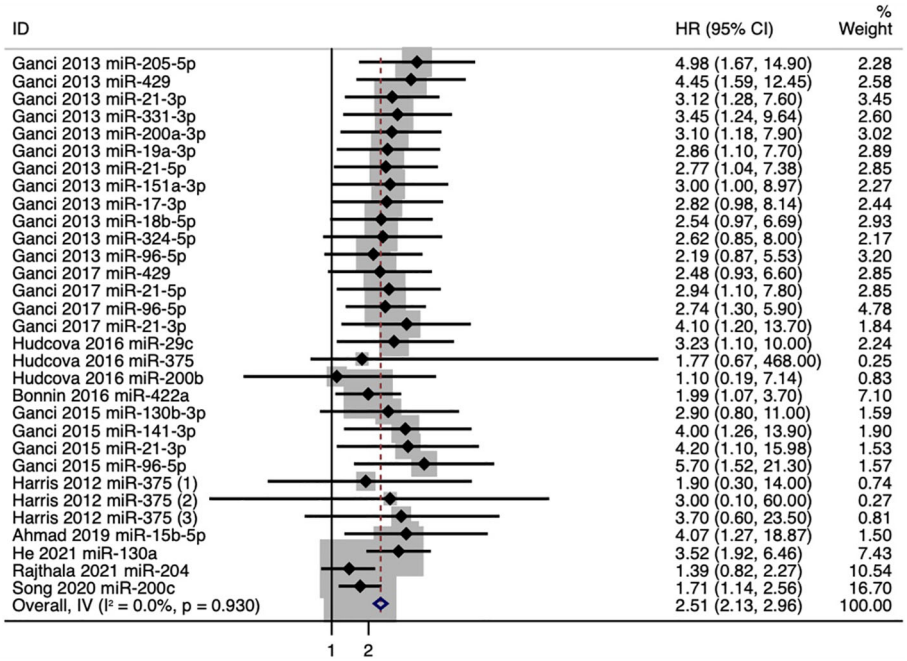

FIGURE 2 | Forest plot for the association between microRNA expression and recurrence-free survival (RFS).

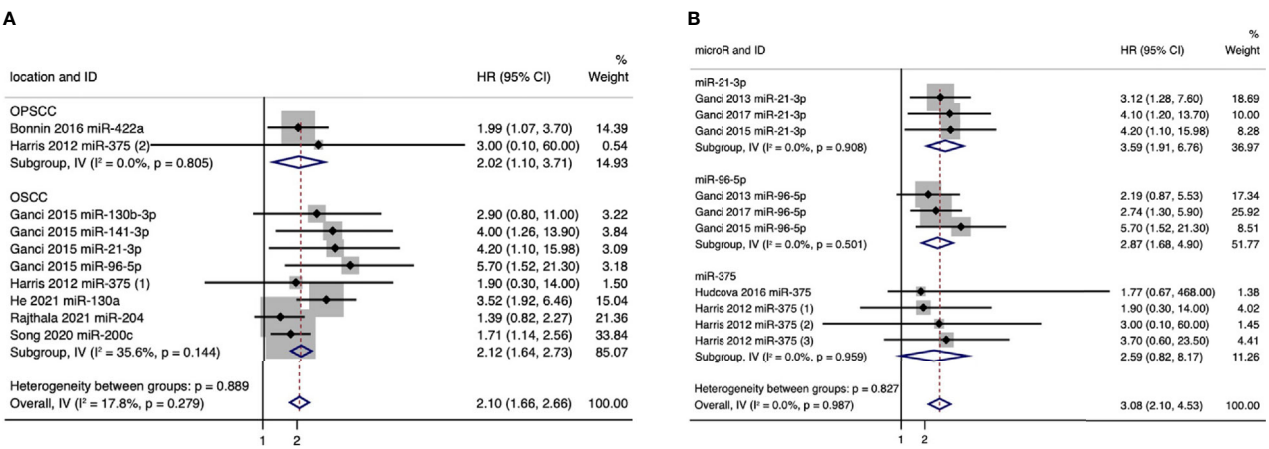

FIGURE 3 | **(A)** Forest plot for subgroup analysis of the association between microRNA expression and recurrence-free survival (RFS) based on anatomical subsites. **(B)** Forest plot for subgroup analysis of the association between microRNA expression and recurrence-free survival (RFS) based on microRNAs (only individual microRNAs with more than two outcomes were presented).

recurrence (by analyzing 93 recurrence patients and 82 nonrecurrence controls from 3 studies) (32–34) and LNM (by presenting an overview of 25 metastasis patients and 23 nonmetastasis controls from another study) (14). We observed relatively high diagnostic accuracy of microRNAs in diagnosing recurrence and LNM for HNSCCs, which have the potential to assist imaging modalities and histopathology biopsy in the diagnosis and prognosis for HNSCC patients.

In the current study, we specifically took recurrence and metastasis as the outcomes. Our results showed that a panel of 21 microRNAs might be suitable biomarkers for predicting the recurrence of HNSCCs (pooled HR:2.51, 95%CI: 2.13–2.96, $I^2 = 0$), among which poor RFS correlated with upregulation of 14 microRNAs (miR-205-5p, miR-429, miR-21-3p, miR-331-3p, miR-200a-3p, miR-19a-3p, miR-21-5p, miR-151a-3p, miR-17-3p, miR-18b-5p, miR-324-5p, miR-96-5p, miR-141-3p, and

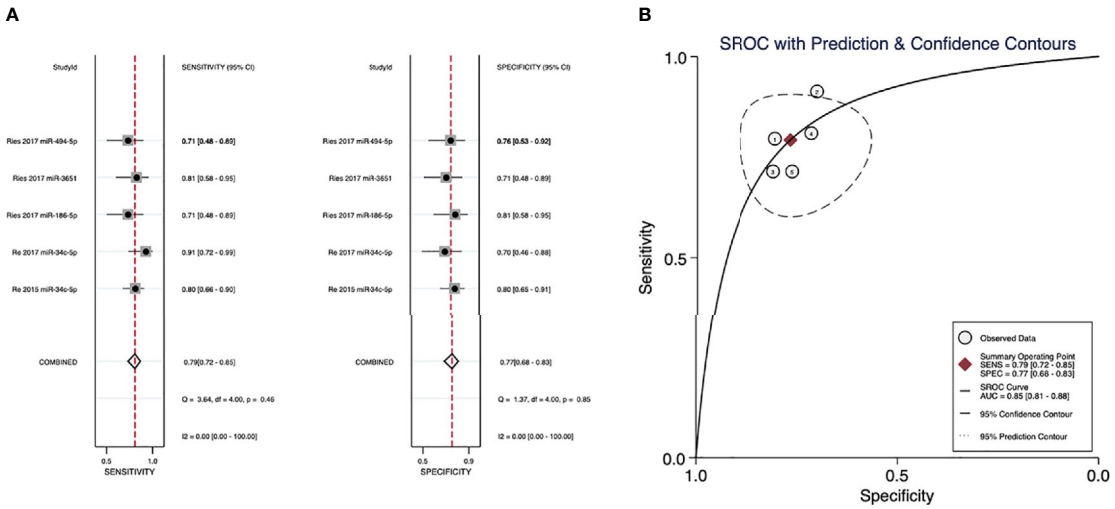

FIGURE 4 | **(A)** Sensitivity and specificity of microRNAs in diagnosing recurrence. **(B)** The summary receiver operating characteristic (SROC) curves of the diagnostic performance of microRNAs for recurrence.

miR-130a) or with downregulation of 7 microRNAs (miR-29c, miR-200b, miR-375, miR-422a, miR-15b-5p, miR-204, and miR-200c). Besides, subgroup analyses revealed similar trends in OSCC and OPSCC patients as well as identified miR-21-3p, miR-96-5p, and miR-375, which showed strong association with RFS. Our quality assessments showed that 80% of the included studies investigating RFS were of good quality, and the meta-analysis was of low risk of bias, which reinforced the reliability of our results. Meanwhile, the diagnostic accuracy of microRNAs in HNSCC recurrence was decent (sensitivity: 0.79, 95% CI: 0.72–0.85; specificity: 0.77, 95%CI: 0.68–0.83; AUC: 0.85, 95% CI: 0.81–0.88), together with a low rate of heterogeneity and low risk of publication bias. Additionally, the diagnostic accuracy of microRNAs in LNM of HNSCC reported by de Carvalho et al. was relatively high but needs further validation.

We further summarized these analyzed microRNAs and explored their well-known biological functions related to tumor malignant behaviors in **Table S2**. As expected, the downregulation of microRNAs, which had been previously reported to be related to tumor suppressing functions, including inhibiting tumor cell proliferation, migration, and invasion (18, 35–61), was associated with poorer RFS in our study. Similarly, the upregulation of microRNAs, which had been previously reported to function as enhancers of tumor malignant behaviors (62–83), were associated with poorer RFS. Besides, the modulation of epithelial to mesenchymal transition (EMT), an essential early step of tumor metastasis, was identified as the most commonly reported mechanism, through which those microRNAs regulate malignant behaviors of other types of tumor. Meanwhile, surprisingly, we found five members of the microRNA-200 family (miR-200a, miR-200b, miR-200c, miR-429, and miR-141), which are known for their regulatory function on EMT, and their combination might act as a strong prognosis predictor (**Figure S3**) (39, 84–88). Thus, we hypothesized that the modulation of EMT and subsequent cell migration and invasion might also act as the key pathophysiological mechanisms of the interplay between microRNAs and HNSCC, which still needs to be further confirmed by mechanistical studies.

There were some limitations in this study. First, given the fact that most of the included studies performed their analyses in HNSCC samples with mixed subsites, which cannot be strictly separated, therefore subgroup analysis could only be available in OSCC and OPSCC patients. And consequently, whether our conclusions can be generalized to SCC derived from other subsites remained to be verified by further studies with larger sample sizes and a wider spectrum of HNSCC subsites. Second, it is also a pity that most of these included studies have not performed subgroup analyses based on HPV status; thus, we were not able to properly investigate the influence of the HPV status. However, most of these included studies have adjusted the HPV status in their multivariate analysis, which might reduce its influence to some extent. Third, the outcomes of four independent microRNAs for LNM in HNSCC were retrieved from the same study. Thus, pooled analysis was not conducted due to the potential high risk of bias. And the reported high diagnostic accuracy still needs to be further validated. Additionally, our results should be explained cautiously since our panels have significance when these microRNAs are taken as a whole, not individually.

DATA AVAILABILITY STATEMENT

The datasets generated for this study are available on request to the corresponding authors.

AUTHOR CONTRIBUTIONS

JR and YZ contributed to the study conception and design. Material preparation was performed by QL and WP, data collection was performed by YR, and analysis was performed by KQ, YS, YR, and DC. The first draft of the manuscript was written by KQ and YS, and all authors commented on previous versions of the manuscript. All authors contributed to the article and approved the submitted version.

FUNDING

This work was supported by West China Hospital, Sichuan University (YZ, grant # 2019HXFH003, grant # ZYJC21027); Chengdu Science and Technology Bureau (JR, grant # 20GJHZ0193); Sichuan University (YZ, grant # 20ZDYF3010, RJJ, grant # 2019HXBH079, #2020SCU12049); The Science and Technology Department of Sichuan Province (YZ, grant # 2020YFH0090, RJJ, grant#2020YFS0111); The Health Department of Sichuan Province (JR, grant # 20PJ030); China Postdoctoral Science Foundation (JR, grant # 2020M673250); The Foundation of National Clinical Research Center for Geriatrics (SH, grant # Z20201013); and National Natural Youth Science Foundation of China (JR, grant # 82002868).

SUPPLEMENTARY MATERIAL

The Supplementary Material for this article can be found online at: https://www.frontiersin.org/articles/10.3389/fonc.2021.711171/full#supplementary-material

REFERENCES

1. Torre LA, Bray F, Siegel RL, Ferlay J, Lortet-Tieulent J, Jemal A. Global Cancer Statistic. *CA Cancer J Clin* (2015) 65(2):87–108. doi: 10.3322/caac.21262
2. Torre LA, Siegel RL, Ward EM, Jemal A. Global Cancer Incidence and Mortality Rates and Trends–An Update. *Cancer Epidemiol Biomarkers Prev Publ Am Assoc Cancer Research cosponsored by Am Soc Prev Oncol* (2016) 25 (1):16–27. doi: 10.1158/1055-9965.EPI-15-0578
3. Sanchez-Danes A, Blanpain C. Deciphering the Cells of Origin of Squamous Cell Carcinomas. *Nat Rev Cancer* (2018) 18(9):549–61. doi: 10.1038/s41568-018-0024-5
4. Alsahafi E, Begg K, Amelio I, Raulf N, Lucarelli P, Sauter T, et al. Clinical Update on Head and Neck Cancer: Molecular Biology and Ongoing Challenges. *Cell Death Dis* (2019) 10(8):540. doi: 10.1038/s41419-019-1769-9
5. Dotto GP, Rustgi AK. Squamous Cell Cancers: A Unified Perspective on Biology and Genetics. *Cancer Cell* (2016) 29(5):622–37. doi: 10.1016/j.ccell.2016.04.004
6. Mathelier A, Shi W, Wasserman WW. Identification of Altered Cis-Regulatory Elements in Human Disease. *Trends Genet* (2015) 31(2):67–76. doi: 10.1016/j.tig.2014.12.003
7. Argiris A, Karamouzis MV, Raben D, Ferris RL. Head and Neck Cancer. *Lancet* (2008) 371(9625):1695–709. doi: 10.1016/S0140-6736(08)60728-X
8. Svider PF, Blasco MA, Raza SN, Shkoukani M, Sukari A, Yoo GH, et al. Head and Neck Cancer. *Otolaryngol Head Neck Surg* (2017) 156(1):10–3. doi: 10.1177/0194599816674672
9. Huang SH, O'Sullivan B. Overview of the 8th Edition TNM Classification for Head and Neck Cancer. *Curr Treat Options Oncol* (2017) 18(7):40. doi: 10.1007/s11864-017-0484-y
10. Denaro N, Russi EG, Merlano MC. Pros and Cons of the New Edition of TNM Classification of Head and Neck Squamous Cell Carcinoma. *Oncology* (2018) 95(4):202–10. doi: 10.1159/000490415
11. Jonas S, Izaurralde E. Towards a Molecular Understanding of microRNA-Mediated Gene Silencing. *Nat Rev Genet* (2015) 16(7):421–33. doi: 10.1038/nrg3965
12. Benaich N, Woodhouse S, Goldie SJ, Mishra A, Quist SR, Watt FM. Rewiring of an Epithelial Differentiation Factor, miR-203, to Inhibit Human Squamous Cell Carcinoma Metastasis. *Cell Rep* (2014) 9(1):104–17. doi: 10.1016/j.celrep.2014.08.062
13. Chang WM, Lin YF, Su CY, Peng HY, Chang YC, Lai TC, et al. Dysregulation of RUNX2/Activin-A Axis Upon miR-376c Downregulation Promotes Lymph Node Metastasis in Head and Neck Squamous Cell Carcinoma. *Cancer Res* (2016) 76(24):7140–50. doi: 10.1158/0008-5472.CAN-16-1188
14. de Carvalho AC, Scapulatempo-Neto C, Maia DC, Evangelista AF, Morini MA, Carvalho AL, et al. Accuracy of microRNAs as Markers for the Detection of Neck Lymph Node Metastases in Patients With Head and Neck Squamous Cell Carcinoma. *BMC Med* (2015) 13:108. doi: 10.1186/s12916-015-0350-3
15. Hiyoshi Y, Kamohara H, Karashima R, Sato N, Imamura Y, Nagai Y, et al. MicroRNA-21 Regulates the Proliferation and Invasion in Esophageal Squamous Cell Carcinoma. *Clin Cancer Res an Off J Am Assoc Cancer Res* (2009) 15(6):1915–22. doi: 10.1158/1078-0432.CCR-08-2545
16. Huang WC, Chan SH, Jang TH, Chang JW, Ko YC, Yen TC, et al. miRNA-491-5p and GIT1 Serve as Modulators and Biomarkers for Oral Squamous Cell Carcinoma Invasion and Metastasis. *Cancer Res* (2014) 74(3):751–64. doi: 10.1158/0008-5472.CAN-13-1297
17. Huang WC, Jang TH, Tung SL, Yen TC, Chan SH, Wang LH. A Novel miR-365-3p/EHF/keratin 16 Axis Promotes Oral Squamous Cell Carcinoma Metastasis, Cancer Stemness and Drug Resistance *via* Enhancing Beta5-Integrin/C-Met Signaling Pathway. *J Exp Clin Cancer Res CR* (2019) 38 (1):89. doi: 10.1186/s13046-019-1091-5
18. Kong KL, Kwong DL, Chan TH, Law SY, Chen L, Li Y, et al. MicroRNA-375 Inhibits Tumour Growth and Metastasis in Oesophageal Squamous Cell Carcinoma Through Repressing Insulin-Like Growth Factor 1 Receptor. *Gut* (2012) 61(1):33–42. doi: 10.1136/gutjnl-2011-300178
19. Liberati A, Altman DG, Tetzlaff J, Mulrow C, Gøtzsche PC, Ioannidis JPA, et al. The PRISMA Statement for Reporting Systematic Reviews and Meta-Analyses of Studies That Evaluate Health Care Interventions: Explanation and Elaboration. *J Clin Epidemiol* (2009) 62(10):e1–e34. doi: 10.1016/j.jclinepi.2009.06.006
20. Whiting PF, Rutjes AW, Westwood ME, Mallett S, Deeks JJ, Reitsma JB, et al. QUADAS-2: A Revised Tool for the Quality Assessment of Diagnostic Accuracy Studies. *Ann Intern Med* (2011) 155(8):529–36. doi: 10.7326/0003-4819-155-8-201110180-00009
21. Tierney JF, Stewart LA, Ghersi D, Burdett S, Sydes MR. Practical Methods for Incorporating Summary Time-to-Event Data Into Meta-Analysis. *Trials* (2007) 8:16–. doi: 10.1186/1745-6215-8-16
22. Ahmad P, Sana J, Slavik M, Gurin D, Radova L, Gablo NA, et al. MicroRNA-15b-5p Predicts Locoregional Relapse in Head and Neck Carcinoma Patients Treated With Intensity-Modulated Radiotherapy. *Cancer Genomics Proteomics* (2019) 16(2):139–46. doi: 10.21873/cgp.20119
23. Bonnin N, Armandy E, Carras J, Ferrandon S, Battiston-Montagne P, Aubry M, et al. MiR-422a Promotes Loco-Regional Recurrence by Targeting NT5E/CD73 in Head and Neck Squamous Cell Carcinoma. *Oncotarget* (2016) 7 (28):44023–38. doi: 10.18632/oncotarget.9829
24. Ganci F, Sacconi A, Bossel Ben-Moshe N, Manciocco V, Sperduti I, Strigari L, et al. Expression of TP53 Mutation-Associated microRNAs Predicts Clinical Outcome in Head and Neck Squamous Cell Carcinoma Patients. *Ann Oncol Off J Eur Soc Med Oncol* (2013) 24(12):3082–8. doi: 10.1093/annonc/mdt380
25. Ganci F, Sacconi A, Manciocco V, Covello R, Benevolo M, Rollo F, et al. Altered Peritumoral microRNA Expression Predicts Head and Neck Cancer Patients With a High Risk of Recurrence. *Modern Pathol an Off J United States Can Acad Pathol Inc* (2017) 30(10):1387–401. doi: 10.1038/modpathol.2017.62

26. Ganci F, Sacconi A, Manciocco V, Sperduti I, Battaglia P, Covello R, et al. MicroRNA Expression as Predictor of Local Recurrence Risk in Oral Squamous Cell Carcinoma. *Head Neck* (2016) 38 Suppl 1:E189–97. doi: 10.1002/hed.23969
27. Harris T, Jimenez L, Kawachi N, Fan J-B, Chen J, Belbin T, et al. Low-Level Expression of miR-375 Correlates With Poor Outcome and Metastasis While Altering the Invasive Properties of Head and Neck Squamous Cell Carcinomas. *Am J Pathol* (2012) 180(3):917–28. doi: 10.1016/j.ajpath.2011.12.004
28. Hudcova K, Raudenska M, Gumulec J, Binkova H, Horakova Z, Kostrica R, et al. Expression Profiles of miR-29c, miR-200b and miR-375 in Tumour and Tumour-Adjacent Tissues of Head and Neck Cancers. *Tumour Biol J Int Soc Oncodevelopmental Biol Med* (2016) 37(9):12627–33. doi: 10.1007/s13277-016-5147-2
29. He T, Guo X, Li X, Liao C, Wang X, He K. Plasma-Derived Exosomal microRNA-130a Serves as a Noninvasive Biomarker for Diagnosis and Prognosis of Oral Squamous Cell Carcinoma. *J Oncol* (2021) 2021:5547911. doi: 10.1155/2021/5547911
30. Rajthala S, Dongre H, Parajuli H, Min A, Nginamau ES, Kvalheim A, et al. Combined *In Situ* Hybridization and Immunohistochemistry on Archival Tissues Reveals Stromal microRNA-204 as Prognostic Biomarker for Oral Squamous Cell Carcinoma. *Cancers (Basel)* (2021) 13(6):1370. doi: 10.3390/cancers13061307
31. Song J, Zhang N, Cao L, Xiao D, Ye X, Luo E, et al. Down-Regulation of miR-200c Associates With Poor Prognosis of Oral Squamous Cell Carcinoma. *Int J Clin Oncol* (2020) 25(6):1072–8. doi: 10.1007/s10147-020-01649-2
32. Re M, Ceka A, Rubini C, Ferrante L, Zizzi A, Gioacchini FM, et al. MicroRNA-34c-5p is Related to Recurrence in Laryngeal Squamous Cell Carcinoma. *Laryngoscope* (2015) 125(9):E306–12. doi: 10.1002/lary.25475
33. Re M, Magliulo G, Gioacchini FM, Bajraktari A, Bertini A, Ceka A, et al. Expression Levels and Clinical Significance of miR-21-5p, miR-Let-7a, and miR-34c-5p in Laryngeal Squamous Cell Carcinoma. *BioMed Res Int* (2017) 2017:3921258. doi: 10.1155/2017/3921258
34. Ries J, Baran C, Wehrhan F, Weber M, Neukam FW, Krautheim-Zenk A, et al. Prognostic Significance of Altered miRNA Expression in Whole Blood of OSCC Patients. *Oncol Rep* (2017) 37(6):3467–74. doi: 10.3892/or.2017.5639
35. Liu N, Tang LL, Sun Y, Cui RX, Wang HY, Huang BJ, et al. MiR-29c Suppresses Invasion and Metastasis by Targeting TIAM1 in Nasopharyngeal Carcinoma. *Cancer Lett* (2013) 329(2):181–8. doi: 10.1016/j.canlet.2012.10.032
36. Wang H, Zhu Y, Zhao M, Wu C, Zhang P, Tang L, et al. miRNA-29c Suppresses Lung Cancer Cell Adhesion to Extracellular Matrix and Metastasis by Targeting Integrin β1 and Matrix Metalloproteinase2 (MMP2). *PloS One* (2013) 8(8):e70192. doi: 10.1371/journal.pone.0070192
37. Wang L, Yu T, Li W, Li M, Zuo Q, Zou Q, et al. The miR-29c-KIAA1199 Axis Regulates Gastric Cancer Migration by Binding With WBP11 and PTP4A3. *Oncogene* (2019) 38(17):3134–50. doi: 10.1038/s41388-018-0642-0
38. Zhang JX, Mai SJ, Huang XX, Wang FW, Liao YJ, Lin MC, et al. MiR-29c Mediates Epithelial-to-Mesenchymal Transition in Human Colorectal Carcinoma Metastasis *via* PTP4A and GNA13 Regulation of β-Catenin Signaling. *Ann Oncol* (2014) 25(11):2196–204. doi: 10.1093/annonc/mdu439
39. Cheng YX, Zhang QF, Hong L, Pan F, Huang JL, Li BS, et al. MicroRNA-200b Suppresses Cell Invasion and Metastasis by Inhibiting the Epithelial-Mesenchymal Transition in Cervical Carcinoma. *Mol Med Rep* (2016) 13(4):3155–60. doi: 10.3892/mmr.2016.4911
40. Humphries B, Wang Z, Li Y, Jhan JR, Jiang Y, Yang C. ARHGAP18 Downregulation by miR-200b Suppresses Metastasis of Triple-Negative Breast Cancer by Enhancing Activation of RhoA. *Cancer Res* (2017) 77(15):4051–64. doi: 10.1158/0008-5472.CAN-16-3141
41. Li J, Yuan J, Yuan X, Zhao J, Zhang Z, Weng L, et al. MicroRNA-200b Inhibits the Growth and Metastasis of Glioma Cells *via* Targeting ZEB2. *Int J Oncol* (2016) 48(2):541–50. doi: 10.3892/ijo.2015.3267
42. Li Y, Guan B, Liu J, Zhang Z, He S, Zhan Y, et al. MicroRNA-200b is Downregulated and Suppresses Metastasis by Targeting LAMA4 in Renal Cell Carcinoma. *EBioMedicine* (2019) 44:439–51. doi: 10.1016/j.ebiom.2019.05.041
43. Williams LV, Veliceasa D, Vinokour E, Volpert OV. miR-200b Inhibits Prostate Cancer EMT, Growth and Metastasis. *PloS One* (2013) 8(12):e83991. doi: 10.1371/journal.pone.0083991
44. Cao ZH, Cheng JL, Zhang Y, Bo CX, Li YL. MicroRNA−375 Inhibits Oral Squamous Cell Carcinoma Cell Migration and Invasion by Targeting Platelet −Derived Growth Factor−a. *Mol Med Rep* (2017) 15(2):922–8. doi: 10.3892/mmr.2016.6057
45. Cui F, Wang S, Lao I, Zhou C, Kong H, Bayaxi N, et al. miR-375 Inhibits the Invasion and Metastasis of Colorectal Cancer *via* Targeting SP1 and Regulating EMT-Associated Genes. *Oncol Rep* (2016) 36(1):487–93. doi: 10.3892/or.2016.4834
46. Jimenez L, Sharma VP, Condeelis J, Harris T, Ow TJ, Prystowsky MB, et al. MicroRNA-375 Suppresses Extracellular Matrix Degradation and Invadopodial Activity in Head and Neck Squamous Cell Carcinoma. *Arch Pathol Lab Med* (2015) 139(11):1349–61. doi: 10.5858/arpa.2014-0471-OA
47. Wang F, Li Y, Zhou J, Xu J, Peng C, Ye F, et al. miR-375 is Down-Regulated in Squamous Cervical Cancer and Inhibits Cell Migration and Invasion *via* Targeting Transcription Factor SP1. *Am J Pathol* (2011) 179(5):2580–8. doi: 10.1016/j.ajpath.2011.07.037
48. Yang S, Yang R, Lin R, Si L. MicroRNA-375 Inhibits the Growth, Drug Sensitivity and Metastasis of Human Ovarian Cancer Cells by Targeting PAX2. *J buon* (2019) 24(6):2341–6.
49. Yi J, Jin L, Chen J, Feng B, He Z, Chen L, et al. MiR-375 Suppresses Invasion and Metastasis by Direct Targeting of SHOX2 in Esophageal Squamous Cell Carcinoma. *Acta Biochim Biophys Sin (Shanghai)* (2017) 49(2):159–69. doi: 10.1093/abbs/gmw131
50. Liu M, Xiusheng H, Xiao X, Wang Y. Overexpression of miR-422a Inhibits Cell Proliferation and Invasion, and Enhances Chemosensitivity in Osteosarcoma Cells. *Oncol Rep* (2016) 36(6):3371–8. doi: 10.3892/or.2016.5182
51. Sun J, Chen Z, Xiong J, Wang Q, Tang F, Zhang X, et al. MicroRNA−422a Functions as a Tumor Suppressor in Glioma by Regulating the Wnt/β−Catenin Signaling Pathway *via* RPN2. *Oncol Rep* (2020) 44(5):2108–20. doi: 10.3892/or.2020.7741
52. Wang H, Tang C, Na M, Ma W, Jiang Z, Gu Y, et al. miR-422a Inhibits Glioma Proliferation and Invasion by Targeting IGF1 and IGF1R. *Oncol Res* (2017) 25(2):187–94. doi: 10.3727/096504016X14732772150389
53. Zhang J, Yang Y, Yang T, Yuan S, Wang R, Pan Z, et al. Double-Negative Feedback Loop Between microRNA-422a and Forkhead Box (FOX)G1/Q1/E1 Regulates Hepatocellular Carcinoma Tumor Growth and Metastasis. *Hepatology* (2015) 61(2):561–73. doi: 10.1002/hep.27491
54. Chava S, Reynolds CP, Pathania AS, Gorantla S, Poluektova LY, Coulter DW, et al. miR-15a-5p, miR-15b-5p, and miR-16-5p Inhibit Tumor Progression by Directly Targeting MYCN in Neuroblastoma. *Mol Oncol* (2020) 14(1):180–96. doi: 10.1002/1878-0261.12588
55. Chung TK, Lau TS, Cheung TH, Yim SF, Lo KW, Siu NS, et al. Dysregulation of microRNA-204 Mediates Migration and Invasion of Endometrial Cancer by Regulating FOXC1. *Int J Cancer* (2012) 130(5):1036–45. doi: 10.1002/ijc.26060
56. Fan X, Fang X, Liu G, Xiong Q, Li Z, Zhou W. MicroRNA-204 Inhibits the Proliferation and Metastasis of Breast Cancer Cells by Targeting PI3K/AKT Pathway. *J buon* (2019) 24(3):1054–9.
57. Hu WB, Wang L, Huang XR, Li F. MicroRNA-204 Targets SOX4 to Inhibit Metastasis of Lung Adenocarcinoma. *Eur Rev Med Pharmacol Sci* (2019) 23(4):1553–62. doi: 10.26355/eurrev_201902_17114
58. Shi L, Zhang B, Sun X, Lu S, Liu Z, Liu Y, et al. MiR-204 Inhibits Human NSCLC Metastasis Through Suppression of NUAK1. *Br J Cancer* (2014) 111(12):2316–27. doi: 10.1038/bjc.2014.580
59. Yang S, Chen B, Zhang B, Li C, Qiu Y, Yang H, et al. Mir−204−5p Promotes Apoptosis and Inhibits Migration of Gastric Cancer Cells by Targeting HER−2. *Mol Med Rep* (2020) 22(4):2645–54. doi: 10.3892/mmr.2020.11367
60. Yu Y, Wang Y, Xiao X, Cheng W, Hu L, Yao W, et al. MiR-204 Inhibits Hepatocellular Cancer Drug Resistance and Metastasis Through Targeting NUAK1. *Biochem Cell Biol* (2019) 97(5):563–70. doi: 10.1139/bcb-2018-0354
61. Zhang B, Cui H, Sun Y, Wang X, Jia Q, Li J, et al. Up-Regulation of miR-204 Inhibits Proliferation, Invasion and Apoptosis of Gallbladder Cancer Cells by Targeting Notch2. *Aging (Albany NY)* (2021) 13(2):2941–58. doi: 10.18632/aging.202444
62. Cao W, Zhao Y, Wang L, Huang X. Circ0001429 Regulates Progression of Bladder Cancer Through Binding miR-205-5p and Promoting VEGFA Expression. *Cancer biomark* (2019) 25(1):101–13. doi: 10.3233/CBM-182380

63. De Cola A, Lamolinara A, Lanuti P, Rossi C, Iezzi M, Marchisio M, et al. MiR-205-5p Inhibition by Locked Nucleic Acids Impairs Metastatic Potential of Breast Cancer Cells. *Cell Death Dis* (2018) 9(8):821. doi: 10.1038/s41419-018-0854-9
64. Lang Y, Xu S, Ma J, Wu J, Jin S, Cao S, et al. MicroRNA-429 Induces Tumorigenesis of Human Non-Small Cell Lung Cancer Cells and Targets Multiple Tumor Suppressor Genes. *Biochem Biophys Res Commun* (2014) 450 (1):154–9. doi: 10.1016/j.bbrc.2014.05.084
65. Doberstein K, Bretz NP, Schirmer U, Fiegl H, Blaheta R, Breunig C, et al. miR-21-3p is a Positive Regulator of L1CAM in Several Human Carcinomas. *Cancer Lett* (2014) 354(2):455–66. doi: 10.1016/j.canlet.2014.08.020
66. Tseng HH, Tseng YK, You JJ, Kang BH, Wang TH, Yang CM, et al. Next-Generation Sequencing for microRNA Profiling: MicroRNA-21-3p Promotes Oral Cancer Metastasis. *Anticancer Res* (2017) 37(3):1059–66. doi: 10.21873/anticanres.11417
67. Chang RM, Yang H, Fang F, Xu JF, Yang LY. MicroRNA-331-3p Promotes Proliferation and Metastasis of Hepatocellular Carcinoma by Targeting PH Domain and Leucine-Rich Repeat Protein Phosphatase. *Hepatology* (2014) 60 (4):1251–63. doi: 10.1002/hep.27221
68. Chen HH, Zong J, Wang SJ. LncRNA GAPLINC Promotes the Growth and Metastasis of Glioblastoma by Sponging miR-331-3p. *Eur Rev Med Pharmacol Sci* (2019) 23(1):262–70. doi: 10.26355/eurrev_201901_16772
69. Sarkar A, Rahaman A, Biswas I, Mukherjee G, Chatterjee S, Bhattacharjee S, et al. Tgfβ Mediated LINC00273 Upregulation Sponges Mir200a-3p and Promotes Invasion and Metastasis by Activating ZEB1. *J Cell Physiol* (2020) 235(10):7159–72. doi: 10.1002/jcp.29614
70. Feng S, Zhu X, Fan B, Xie D, Li T, Zhang X. Mir−19a−3p Targets PMEPA1 and Induces Prostate Cancer Cell Proliferation, Migration and Invasion. *Mol Med Rep* (2016) 13(5):4030–8. doi: 10.3892/mmr.2016.5033
71. Jiang XM, Yu XN, Liu TT, Zhu HR, Shi X, Bilegsaikhan E, et al. microRNA-19a-3p Promotes Tumor Metastasis and Chemoresistance Through the PTEN/Akt Pathway in Hepatocellular Carcinoma. *BioMed Pharmacother* (2018) 105:1147–54. doi: 10.1016/j.biopha.2018.06.097
72. Li Q, Li B, Li Q, Wei S, He Z, Huang X, et al. Exosomal miR-21-5p Derived From Gastric Cancer Promotes Peritoneal Metastasis *via* Mesothelial-to-Mesenchymal Transition. *Cell Death Dis* (2018) 9(9):854. doi: 10.1038/s41419-018-0928-8
73. Zhang R, Xia T. Long Non-Coding RNA XIST Regulates PDCD4 Expression by Interacting With miR-21-5p and Inhibits Osteosarcoma Cell Growth and Metastasis. *Int J Oncol* (2017) 51(5):1460–70. doi: 10.3892/ijo.2017.4127
74. Zhu Y, Bo H, Chen Z, Li J, He D, Xiao M, et al. LINC00968 can Inhibit the Progression of Lung Adenocarcinoma Through the miR-21-5p/SMAD7 Signal Axis. *Aging (Albany NY)* (2020) 12(21):21904–22. doi: 10.18632/aging.104011
75. Liu H, Cheng Y, Xu Y, Xu H, Lin Z, Fan J, et al. The Inhibition of Tumor Protein P53 by microRNA-151a-3p Induced Cell Proliferation, Migration and Invasion in Nasopharyngeal Carcinoma. *Biosci Rep* (2019) 39(10): BSR20191357. doi: 10.1042/BSR20191357
76. Lu D, Tang L, Zhuang Y, Zhao P. miR-17-3P Regulates the Proliferation and Survival of Colon Cancer Cells by Targeting Par4. *Mol Med Rep* (2018) 17 (1):618–23. doi: 10.3892/mmr.2017.7863
77. Yang X, Du WW, Li H, Liu F, Khorshidi A, Rutnam ZJ, et al. Both Mature miR-17-5p and Passenger Strand miR-17-3p Target TIMP3 and Induce Prostate Tumor Growth and Invasion. *Nucleic Acids Res* (2013) 41 (21):9688–704. doi: 10.1093/nar/gkt680
78. Wang YY, Yan L, Yang S, Xu HN, Chen TT, Dong ZY, et al. Long Noncoding RNA AC073284.4 Suppresses Epithelial-Mesenchymal Transition by Sponging miR-18b-5p in Paclitaxel-Resistant Breast Cancer Cells. *J Cell Physiol* (2019) 234(12):23202–15. doi: 10.1002/jcp.28887
79. Yang Y, Xia S, Zhang L, Wang W, Chen L, Zhan W. MiR-324-5p/PTPRD/CEBPD Axis Promotes Papillary Thyroid Carcinoma Progression via Microenvironment Alteration. *Cancer Biol Ther* (2020) 21(6):522–32. doi: 10.1080/15384047.2020.1736465
80. Liu ZM, Wu ZY, Li WH, Wang LQ, Wan JN, Zhong Y. MiR-96-5p Promotes the Proliferation, Invasion and Metastasis of Papillary Thyroid Carcinoma Through Down-Regulating CCDC67. *Eur Rev Med Pharmacol Sci* (2019) 23 (8):3421–30. doi: 10.26355/eurrev_201904_17706
81. Wei S, Zheng Y, Jiang Y, Li X, Geng J, Shen Y, et al. The circRNA circPTPRA Suppresses Epithelial-Mesenchymal Transitioning and Metastasis of NSCLC Cells by Sponging miR-96-5p. *EBioMedicine* (2019) 44:182–93. doi: 10.1016/j.ebiom.2019.05.032
82. Zhang H, Chen R, Shao J. MicroRNA-96-5p Facilitates the Viability, Migration, and Invasion and Suppresses the Apoptosis of Cervical Cancer Cells Bynegatively Modulating Sfrp4. *Technol Cancer Res Treat* (2020) 19:1533033820934132. doi: 10.1177/1533033820934132
83. Chen J, Yan D, Wu W, Zhu J, Ye W, Shu Q. MicroRNA-130a Promotes the Metastasis and Epithelial-Mesenchymal Transition of Osteosarcoma by Targeting PTEN. *Oncol Rep* (2016) 35(6):3285–92. doi: 10.3892/or.2016.4719
84. Gregory PA, Bert AG, Paterson EL, Barry SC, Tsykin A, Farshid G, et al. The miR-200 Family and miR-205 Regulate Epithelial to Mesenchymal Transition by Targeting ZEB1 and SIP1. *Nat Cell Biol* (2008) 10(5):593–601. doi: 10.1038/ncb1722
85. Chen H, Li Z, Zhang L, Zhang L, Zhang Y, Wang Y, et al. MicroRNA-200c Inhibits the Metastasis of Triple-Negative Breast Cancer by Targeting ZEB2, an Epithelial-Mesenchymal Transition Regulator. *Ann Clin Lab Sci* (2020) 50 (4):519–27.
86. Tan T, Xu XH, Lu XH, Wang XW. MiRNA-200a-3p Suppresses the Proliferation, Migration and Invasion of Non-Small Cell Lung Cancer Through Targeting IRS2. *Eur Rev Med Pharmacol Sci* (2020) 24(2):712–20. doi: 10.26355/eurrev_202001_20050
87. Chen J, Wang L, Matyunina LV, Hill CG, McDonald JF. Overexpression of miR-429 Induces Mesenchymal-to-Epithelial Transition (MET) in Metastatic Ovarian Cancer Cells. *Gynecol Oncol* (2011) 121(1):200–5. doi: 10.1016/j.ygyno.2010.12.339
88. Hou X, Yang L, Jiang X, Liu Z, Li X, Xie S, et al. Role of microRNA-141-3p in the Progression and Metastasis of Hepatocellular Carcinoma Cell. *Int J Biol Macromol* (2019) 128:331–9. doi: 10.1016/j.ijbiomac.2019.01.144

Conflict of Interest: The authors declare that the research was conducted in the absence of any commercial or financial relationships that could be construed as a potential conflict of interest.

frontiers in Oncology

ORIGINAL RESEARCH
published: 28 September 2021
doi: 10.3389/fonc.2021.749398

A Tumor-Infiltration CD8+ T Cell-Based Gene Signature for Facilitating the Prognosis and Estimation of Immunization Responses in HPV+ Head and Neck Squamous Cell Cancer

Yingning Wu[1,2,3†], Lingzhang Meng[2†], Kai Cai[4†], Jingjie Zhao[5†], Siyuan He[2], Jiajia Shen[2], Qiuju Wei[2,6], Zechen Wang[2], Suren Sooranna[7], Hengguo Li[1] and Jian Song[2,8*]*

[1] Medical Imaging Center, The First Affiliated Hospital of Jinan University, Guangzhou, China, [2] Center for Systemic Inflammation Research (CSIR), School of Preclinical Medicine, Youjiang Medical University for Nationalities, Baise, China, [3] Department of Radiation, The Affiliated Hospital of Youjiang Medical University for Nationalities, Baise, China, [4] Radiation Therapy Center, The First Affiliated Hospital of Guangxi University of Chinese Medicine, Nanning, China, [5] Life Science and Clinical Research Center, The Affiliated Hospital of Youjiang Medical University for Nationalities, Baise, China, [6] School of Pharmacy, Youjiang Medical University for Nationalities, Baise, China, [7] Department of Metabolism, Digestion and Reproduction, Imperial College London, Chelsea & Westminster Hospital, London, United Kingdom, [8] Department of Radiation Oncology, Renji Hospital, School of Medicine, Shanghai Jiao Tong University, Shanghai, China

Background: CD8+ T cells, which play a vital role in response to adaptive immunity, are closely related to the immunization responses to kill tumor cells. Understanding the effects exerted by tumor-infiltrated CD8+ T cells in HPV+ and HPV- head and neck squamous cell carcinoma (HNSCC) patients is critical for predicting their prognosis as well as their responses towards immunization-related therapy.

Materials and Methods: HNSCC single cell transcriptome was used to screen for differentially expressed genes (DEGs) based on CD8+ T cells. A gene signature associated with CD8+ T cells was built and verified with the cancer genome atlas dataset with a view to predicting the prognosis of HNSCC patients. Risk scores were calculated for HNSCC cases and categorized into either high- or low-risk cohorts. The prognosis-correlated data of the risk scores were analyzed by using Kaplan-Meier survival curves and multi-variate Cox regression plots. In addition, the possibility of using the genetic profiles to predict responses toward immunization-related therapy was explored.

Results: From the DEGs screened from the sequencing of single-cell RNA, a gene signature of 4 genes (ACAP1, ANKRD28, C12orf75, and M6PR) were identified. It was

OPEN ACCESS

Edited by:
Hui Wang,
Hunan Cancer Hospital, China

Reviewed by:
Xu Wang,
Affiliated Hospital of Jiangsu University, China
Shu-Heng Jiang,
Shanghai Cancer Institute, China

***Correspondence:**
Jian Song
sjjhm@hotmail.com
Hengguo Li
lhgjnu@263.net

†These authors have contributed equally to this work

Specialty section:
This article was submitted to Head and Neck Cancer, a section of the journal Frontiers in Oncology

Received: *29 July 2021*
Accepted: *09 September 2021*
Published: *28 September 2021*

Citation:
Wu Y, Meng L, Cai K, Zhao J, He S, Shen J, Wei Q, Wang Z, Sooranna S, Li H and Song J (2021) A Tumor-Infiltration CD8+ T Cell-Based Gene Signature for Facilitating the Prognosis and Estimation of Immunization Responses in HPV+ Head and Neck Squamous Cell Cancer. Front. Oncol. 11:749398. doi: 10.3389/fonc.2021.749398

seen that these genes could predict overall survival in HPV+ HNSCC patients. In addition, high- and low-risk HPV+ HNSCC patients showed marked differences in their CD8+ T-cell infiltration due to immunization when clinical characteristics were taken into consideration. This correlated with their immunization therapy responses.

Conclusions: Our work provides insights into explaining the restricted responses of current immunization checkpoint inhibiting substances in HPV+ HNSCC patients. A novel genetic signature to predict the prognosis and immunization-correlated therapeutic responses is presented. This will provide potential new therapeutic opportunities for HPV+ HNSCC patients.

Keywords: CD8+ T cells, HPV, immunization-correlated genes, immunization-correlated therapy, differentially expressed genes, predicted prognosis, head and neck squamous cell carcinoma

INTRODUCTION

Head and neck squamous cell carcinoma (HNSCC) refers to cancer of the oral cavity, oropharynx and larynx, and is the sixth commonest carcinoma globally (1). More than 550,000 new patients are reported each year, accounting for approximately 4% of carcinomas worldwide (2). Because most cases present with locally advanced disease, HNSCC is correlated with poor prognosis and results in high mortality (3). Conventional treatments exhibit limited effectiveness, and new therapeutic strategies capable of broadening the existing treatment options for HNSCC are urgently required (4). Recent clinical trials have demonstrated that programmed death ligand 1 (PD-L1) or programmed death 1 (PD-1) blockade exhibit clinically meaningful anti-tumor activity together with an acceptable safety profile when used in the treatment of HNSCC patients (5, 6). However, despite this progress, only about 20-30% of HNSCC cases survived after anti-PD-1/PD-L1 therapies, and the response towards PD-1/PD-L1 blockade is still far from satisfactory. Therefore, there is an urgent need to further understand the immunization state of the cell during this disease and identify features correlated to the response ability of existing immunization therapies, thereby paving the way to the development of new single and multi-drug immunization therapies.

HNSCC, is a type of carcinoma that can arise due to genetic alteration caused by either exposure to carcinogens (such as alcohol and/or tobacco) or *via* malignant conversion due to HPV infection (7, 8). There is an alarming growth of HPV + HNSCC in western countries, with up to half of all HNSCC patients residing in the US, as the presence of HPV infections is considered to increase the risk of the disease (9). However, HPV-correlated HNSCC is suggested to exhibit distinctive biological and clinically-associated characteristics, with the presence of HPV conferring a survival advantage when compared to its absence (10). Distinct tumor-infiltration immunization populations were identified in HNSCC patients, with a greater proportion of dysfunctional CD8+ T cells seen in HPV- HNSCC (11). A higher rate of response towards PD-1/PD-L1 was also identified in HPV+ patients compared to those who were HPV-. Thus, the presence of HPV may well be a factor that can be used to classify HNSCC. However, the underlying mechanisms and potential associations between the HPV state and the tumor immunization environment still needs to be characterized.

In the present study, we attempted to elucidate the correlation between the HPV state and immunization environment-related factors by using a multicenter database. A single-cell RNA sequencing dataset was used to assess the various subpopulations of immune cells and particular genes that may differ in HPV+ and HPV- HNSCC patients. Using a combination of RNA-seq data from a large number of HNSCC cases and their corresponding clinical information, a gene signature for tumor-infiltrated CD8+ T cells was established using multiple machine learning algorithms. This risk-associated gene signature was verified using the gene expression profiles and clinically associated information from an independent cancer genome atlas (TCGA) provisional dataset. The genetic signature obtained may provide future targets for increasing our knowledge of the mechanisms that govern HPV+ and HPV- HNSCC. This study may also increase immunization checkpoint blockade therapy efficacy with respect to treatment of this disease.

MATERIALS AND METHODS

CD8+ T Cell Estimation in HNSCC Patients

The TIMER2.0 database (http://timer.comp-genomics.org/) was utilized to explore the relationship between tumor infiltration of CD8+ T cells and the prognosis of HNSCC in patients (12). We analyzed the immunization infiltration CD8+ T cells in different carcinoma types by multiple immunization deconvolution approaches, by using Cox regression correlation and Kaplan-Meier survival curves. These data obtained were used to correlate the prognosis data of the relevant immunization infiltration data in a range of carcinoma categories.

Research of CD8+ T Cell-Correlated Immunization-Correlated Genes in HNSCC

Single cell transcriptomes include 130,721 cells from HPV- HNSCC and HPV+ HNSCC (10). Both cohorts consist of PBMC and tumor infiltrated leukocytes (TIL). In the current analysis we have only included 60,676 cells from the TIL.

Single-Cell RNA-Seq Data Analysis

Specific to the integrated investigation of single-cell data, these were normalized with the SCTransform approach and then analyzed by conducting a mutual principal unit investigation (PCA) (https://satijalab.org/seurat/v3.1/integration.html) (13). The PCA analysis was also conducted on the integrated datasets with the cluster analysis being performed with uniform manifold approximation and projection (UMAP). Cluster analysis of single-cells was performed using Seurat's graph-based clustering approach [R software package Seurat (version 2.3.4)] with the FindClusters feature resolution set to 0.1. Subsequently, the clusters were visualized by using the UMAP (version 0.2.6.0) graph. For quality control, unique molecular identifier counts of less than 500 and double multiples were removed. Furthermore, cells with > 5% mitochondrial genes and > 50% ribosomal genes were filtered out.

Collection and Processing of the HNSCC RNAseq Dataset

The RNA sequencing dataset for HNSCC and the corresponding clinically related data originated from the TCGA database (https://portal.gdc.carcinoma.gov/), which consists of 279 samples. The validation cohort dataset is TCGA provisional database, consisting of 249 samples. The raw gene expression dataset was processed. Probe IDs received the annotation toward the gene from the corresponding platform annotation profile of the GDC website and the raw matrix data received the quantile normalization and log2 conversion. Samples with missing data were excluded.

Building a CD8+ T Cell-Correlated Gene Signature

Single-cell data was classified into specific cell types and divided according to their respective tissue sources. The corresponding transcriptome investigation data were compared in order to screen for DEGs. To increase the efficiency of the study the candidate DEGs were taken as min.pct > 0.25 and | Log2 (FC) | > 0.5.

The association between HNSCC tumor-infiltration CD8+ T cell-correlated DEGs and overall survival time in TCGA HNSCC cases was studied. Univariate Cox regression analysis was carried out for identifying the genes associated with survival (p value < 0.05). Subsequently, the significance of candidate genes was selected using variable importance in a randomized survival forest (RSF) algorithm. A risk score model with the selected DEGs was built using multivariate Cox regression approaches. In addition, the Kaplan-Meier test was employed for a number of gene features and p-values (log) were determined. Receiver operating characteristic (ROC) analysis was carried out for 3- and 5-year overall survival rates and area under the curves (AUCs) were determined for assessing the specificity and sensitivity of the gene signature. In addition, for testing the robustness of the results, the HNSCC tumor-infiltration CD8+ T cell-correlated gene signature was further verified with the TCGA HNSCC dataset.

The Effects of Age, Gender, Alcohol and Smoking on HNSCC Patients

To assess the correlation of risk score distribution and clinically related characteristics, HNSCC patients were grouped according to age and gender as well as their status regarding alcohol consumption and smoking. In addition, risk scores were calculated in order to assess the patients' prognosis for HNSCC in the presence and absence of HPV by using multivariate Cox regression correlations.

Statistical Analysis

Statistics investigations were carried out with R software (version 3.6.0). Kaplan-Meier tests and ROC analysis were performed with the "survivor" and "survROC" software packages (14). Optimal cutoff data points were calculated using the "survminer" package (15). Single-variate and multi-variate Cox regression correlations were used to assess the prognosis-correlated factors of interest. Hazard ratios (HR) and 95% confidence intervals (95% CI) were presented for all the prognosis-correlated factors. In statistical tests, $P<0.05$ was considered statistically significant.

RESULTS

A Comparison of CD8+ T Cells in HPV– and HPV+ HNSCC Patients

From the TIMER2.0 website, a number of immunization deconvolution approaches including "XCELL (16)", "MCPCOUNTER (17)", "QUANTISEQ (18)", "CIBERSORT-ABS" and "CIBERSORT (19)" were employed for estimating immunization infiltration of CD8+ T cells in HPV– and HPV+ HNSCC patients. With the single-variate Cox proportional risk model, the found that the tumor-infiltrated CD8+ T cells were protective for cases with HPV+ HNSCC, but this was not seen in HPV– HNSCC patients (**Figure 1A**). According to the Kaplan-Meier curves obtained, the survival period of the high tumor-infiltration CD8+ T-cell cohort was significantly longer than that of the low CD8+ T tumor infiltration seen in HNSCC patients who also had HPV, irrespective of the deconvolution approach used (**Figure 1B**).

Single-Cell RNA-Seq-Based DEGs Identification

The RNA-seq based on single cells consisted of 130,721 immunization cells from the tumor infiltrated leukocyte (TIL) samples obtained from HNSCC patients. Using the UMAP algorithm, this mixture of 11 cell types including CD8 T, CD4 T, dendritic, CD8+ T, mast, natural killer (NK) and plasma cells as well as mon/macrophages were unambiguously clustered and annotated (**Figure 2A**). Single-cell clustering was also based on the presence and absence of HPV (**Figure 2B**). According to the pie chart, the number of CD8+ T cells was an important unit of the HNSCC TILs (**Figure 2C**). The bar graphs also indicated that CD8+ T cells accounted for the greatest proportion of infiltration of all the immunization cells into the HPV– and HPV+ tumors in HNSCC patients (**Figure 2D**). The gene expression of LAG3 showed that exhausting T cells account for majority of the CD8 T cells (**Figure 2E**).

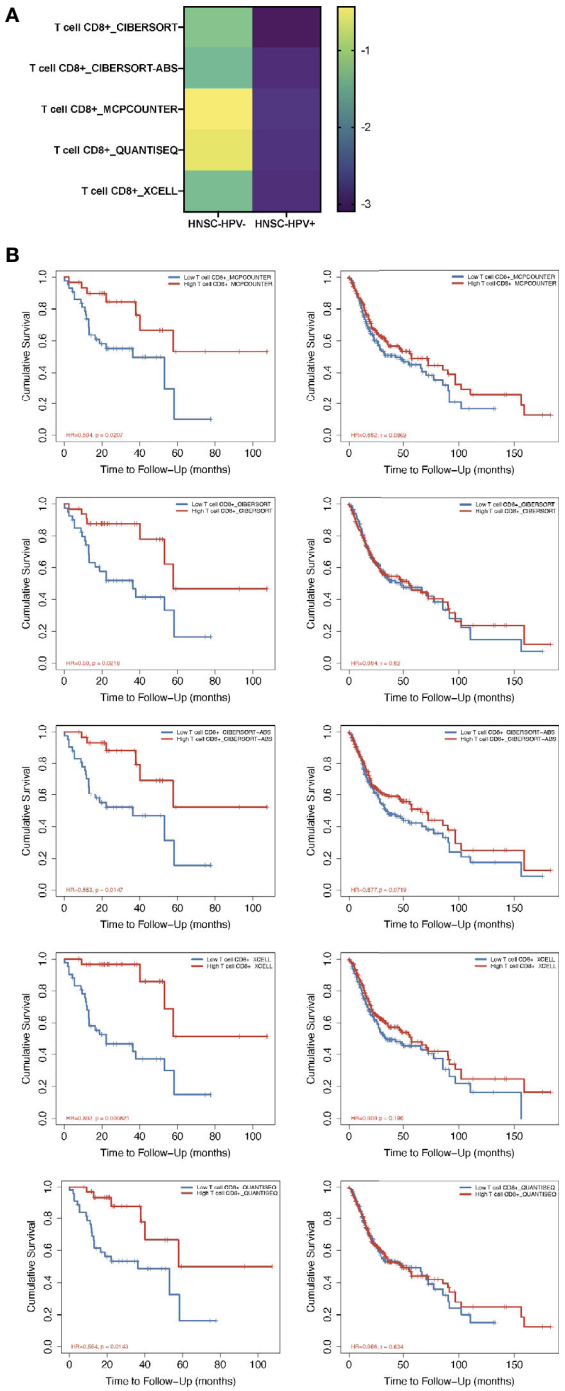

FIGURE 1 | Prognosis-correlated data of CD8+ T cells from patients with HPV– and HPV+ HNSCC. **(A)** A heat map of data from the multiple-variate Cox proportional risk model in terms of CD8+ T cells from patients with HPV– *versus* HPV+ HNSCC. The z-scores represent the risk scores. **(B)** Kaplan-Meier survival analysis showing the levels of CD8+ T cells from patients with HPV– (right column) and HPV+ (left column) HNSCC by using MCPcounter, CIBERSORT, CIBERSORT-ABS, XCELL and QUANTISEQ approaches.

Building a CD8+ T Cell-Correlated Gene Signature

Subsequently, the HPV+ HNSCC tumor-infiltration CD8+ T cell-correlated DEGs were screened based on the selection criteria in the approaches used (**Figure 3A**). To screen for the crucial survival-related factors, the DEGs from the CD8+ T cells of HPV+ HNSCC were analyzed using single-variate Cox regression for the TCGA dataset, and a total of 21 DEGs were

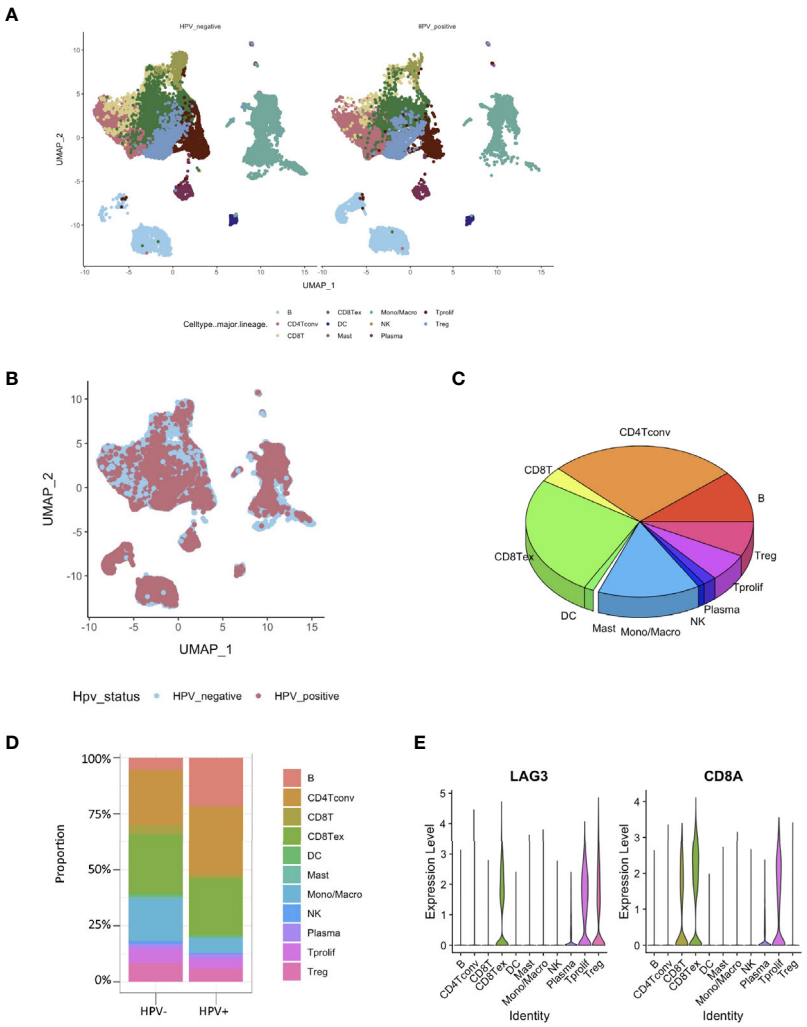

FIGURE 2 | Identification of HPV– and HPV+ HNSCC tumor-infiltration of CD8+ T cell-correlated genes. **(A)** View of single cell samples from HPV– and HPV+ TIL. The annotated UMAP plot identifying 11 distinctive cell types. **(B)** The annotated UMAP plot of HPV– and HPV+ HNSCC TIL. **(C)** A pie chart of the seven cell types that make up the TIL of HNSCC. **(D)** Bar graphs of the cell proportions in the TIL of HPV– and HPV+ HNSCC. **(E)** Violin plots illustrating the expression of CD8A and exhausting T cell marker LAG3 in different TIL cell types.

identified to be significantly correlated to survival in these patients ($p < 0.05$) (**Figure 3B**). Based on the random forest algorithm, the top 5 significant genes, ACAP1, ANKRD28, C12orf75, M6PR and RGCC, were screened (**Figure 3C**).

Further, we studied the expression of the significant genes in different immune cell subsets and found the association of ACAP1, ANKRD28, C12orf75 and M6PR, but not RGCC, with CD8+ T cells (**Figure 4A**). Also, we checked the TCGA data using CIBERSORT deconvolution and TIMER2 website, which demonstrated a substantial fraction of CD8+ T cells and the 4 signature genes in HPV+ compared to HPV- HNSCC (**Figures 4B, C**). RGCC was detectable, and therefore excluded from the signature genes.

The risk scoring system was then built using these 4 genes with multi-variate Cox analysis using the TCGA dataset. In accordance with the formula, a risk score was calculated for the respective cases. The HPV+HNSCC cases in the TCGA dataset were then divided into high-risk and low-risk cohorts with the optimal cutoff data for the risk scores. Kaplan-Meier curves showed that the high-risk group survived for longer periods in comparison with those patients in the low-risk cohort (**Figure 5A**). In comparison, there was no clear distinction in the high-risk cohort of HPV- HNSCC case survival (**Figure 5B**). This was further validated in the TCGA provisional dataset for HPV+ HNSCC (**Figure 5C**). To estimate the predictive power of genetic characteristics, ROC curve analysis of the HPV+ HNSCC cases were plotted and this showed an AUC of 1 and 0.739 for 3 year-survival (**Figure 5D**), while ROC survival curves for the HPV- HNSCC patients were less significant (**Figure 5E**). This was verified by

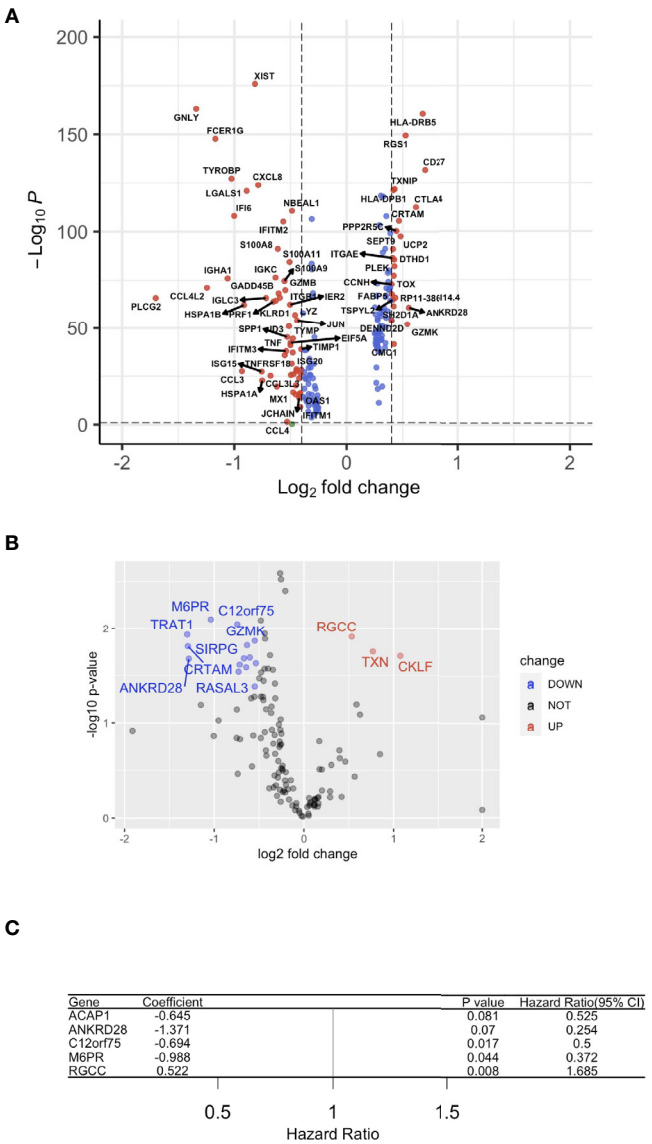

FIGURE 3 | A gene signature using infiltrated CD8+ T cells. **(A)** A volcano plot of the differentially expressed genes (DEGs) between HPV+ and HPV– HNSCC tumor-infiltrated CD8+ T cells. **(B)** A volcano plot showing the DEGs obtained from Cox regression analysis of survival-related HPV+ HNSCC-infiltrated CD8+ T cells. **(C)** Forest plot lines of the top 4 genes screened by using random survival forest analysis of HNSCC patients.

using the TCGA provisional dataset which showed an AUC curve of 0.839 for 3 year-survival (**Figure 5F**).

Correlation of Risk Score Distribution and Clinical Characteristics of HNSCC Patients

HPV+ HNSCC cases in the TCGA dataset were categorized according to high or low risk score cohorts with the best cutoff data obtained. Box plots showed that age, sex and alcohol consumption were not correlated with the risk score (**Figure 6A**). However, smoking (**Figure 6B**) did show a correlation with the risk score. Furthermore, risk scores of HPV- HNSCC cases were also evaluated according to their gene signatures as established with the scRNA and TCGA datasets (**Figures 6C, D**). No correlation of the risk scores were found when the cases were divided according to their age and sex as well as alcohol consumption and smoking status. This revealed a specificity of the current gene signature for the assessment of smoking in HPV+ HNSCC patients.

In order to compare the prognosis-correlated factors to those general factors, risk scores for genetic characteristics and clinically-related variables were analyzed by multi-variate Cox regression (**Figures 6E, F**). The forest plots did not show any significance that the current risks examined, thus revealing the significance of the current gene signature and risk scoring system used in this study.

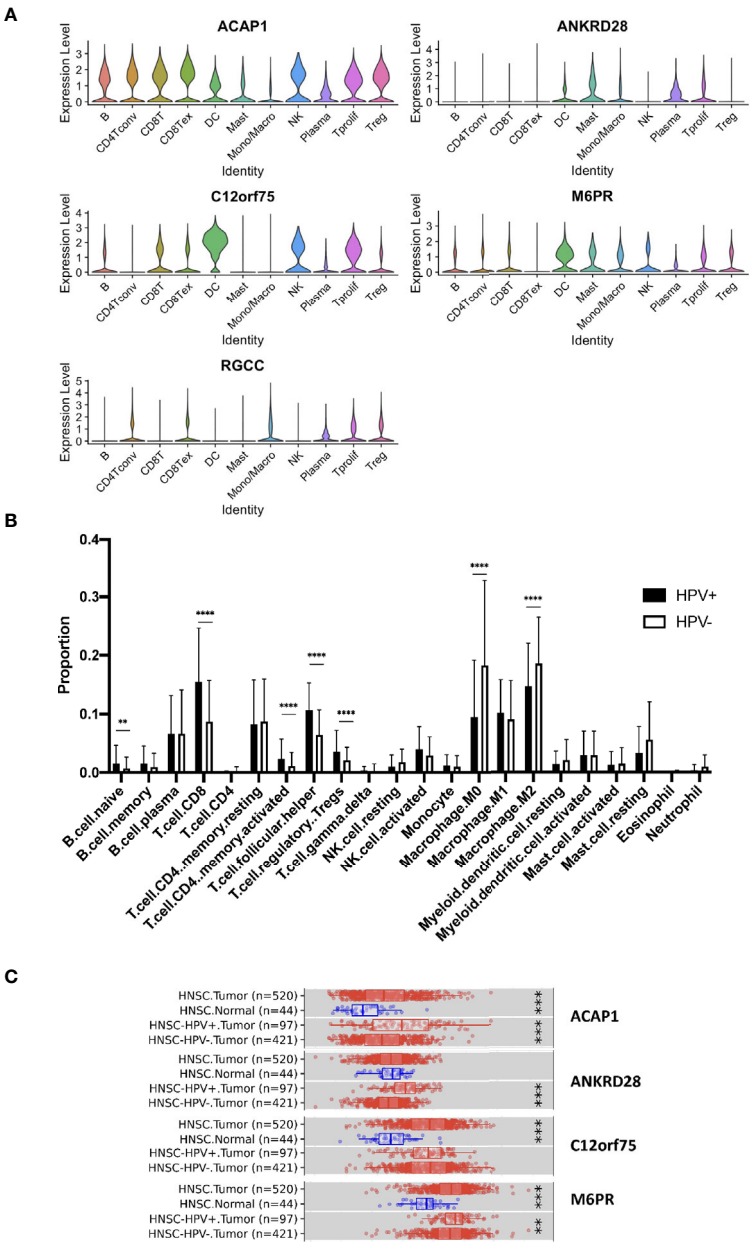

FIGURE 4 | Expression of the signature genes. **(A)** Violin plots illustrating the expression of the survival related signature genes in different TIL cell types of scRNA data. **(B)** Bulk seq data were deconvoluted using CIBERSORT method. Bar graph illustrating the proportion of infiltrated immune cells of HPV+ and HPV– HNSCC. **(C)** Expression of signature genes were analyzed using TIMER2 website. Box charts showed the expression of the signature genes of the TCGA data. "**" refers $p < 0.01$, "***" refers $p < 0.001$ and "****" refers $p < 0.0001$.

Profiling the Gene Expression of the HPV+ HNSCC Risk Groups

With the signature genes, we separated the HPV+ HNSCC into high and low risk groups. We investigated the DEGs between high and low risk groups of HPV+ HNSCC TCGA samples (**Figure 7A**). The gene ontology (GO) and KEGG pathways studies showed that the risk DEGs are enriched in the T cell activation and differentiation (**Figures 7B, C**), indicating the involvement of the signature genes in the T cells function. We further investigated the correlation of the signature genes with the immune checkpoint genes and found a decent correlation with CTLA4, LAG3 and PDCD1, but not with the DAMP signal gene S100A8 (**Figures 8A–D**). Especially, a strong correlation was detected between ACAP1 and the checkpoint related genes (**Figure 8E**).

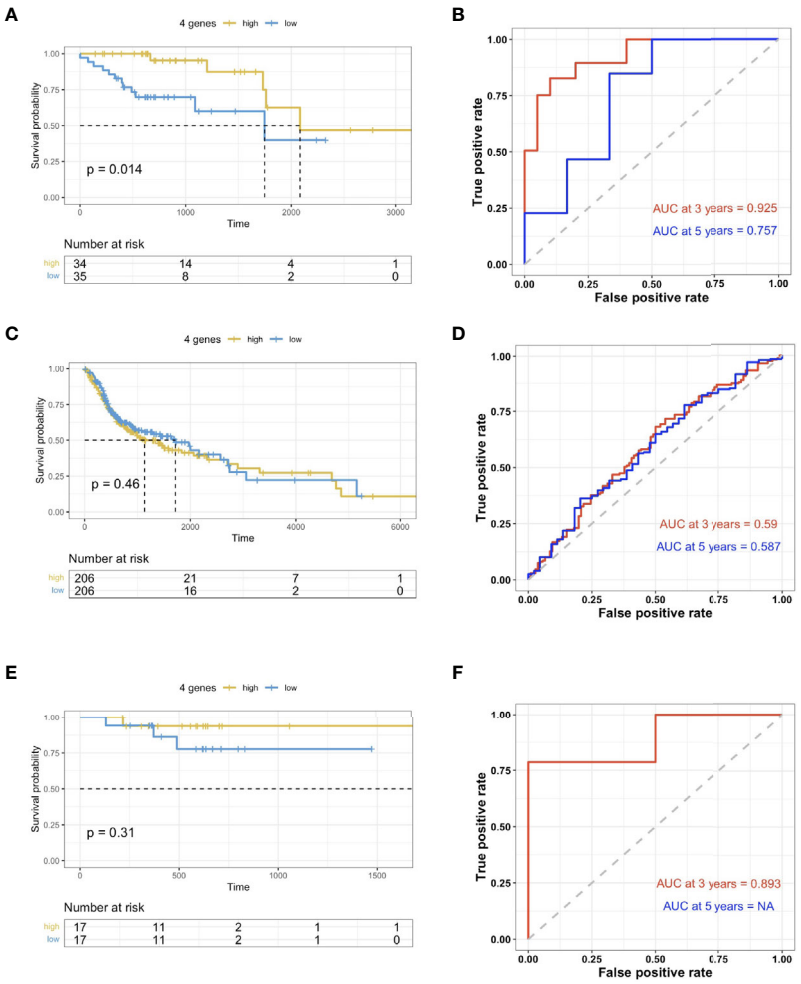

FIGURE 5 | Validation of prognosis gene labels for HNSCC cases. **(A)** Kaplan-Meier (KM) analysis of the risk group that were defined with CD8+ T cell-correlated gene tags in the TCGA dataset for HPV+ HNSCC. **(B)** KM analysis of the risk group that were defined with CD8+ T cell-correlated gene tags in the TCGA dataset for HPV- HNSCC. **(C)** KM analysis of the risk group that were defined with CD8+ T cell-correlated gene tags in the TCGA provisional dataset for HPV+ HNSCC. **(D)** Three- and five-year ROC survival curves from the TCGA dataset for HPV+ HNSCC. **(E)** Three- and five-year ROC survival curves from the HPV- HNSCC TCGA dataset. **(F)** Three- and five-year ROC survival curves from the TCGA provisional dataset for HPV+ HNSCC.

DISCUSSION

Using a single-variate Cox proportional risk model, we identified that the tumor-infiltration of CD8+ T cells were protective for cases with HPV+ HNSCC, but not for HPV- HNSCC cases. Further, the tumor immunization environment was explored using single-cell sequencing and screened for CD8+ T cell-specific gene feature differences between HPV+ and HPV- HNSCC patients. In addition, we built a prognosis-correlated genetic signature that divided the overall survival of HPV+ HNSCC into two risk groups with the high-risk cases showing poorer prognoses. A prognosis-correlated gene signature consisting of 4 genes with low risk. Then the association between CD8+ T cell genetic traits and clinically related parameters were determined using TCGA dataset and verified in TCGA provisional dataset, to demonstrate the accuracy of genetic traits for prognosis-correlated prediction.

According to the single-cell data, there were significant differences between the immune profiles of HPV- *versus* HPV+ HNSCC patients, which is of significance when designing their immunotherapy regimens. Although the proportion infiltrating CD8 cells were similar in the two HNSCC types, the CD8 gene cell expression profiles were not identical, so more tailored therapies will be required in order to improve the survival rates of patients. The distinct immune profiles in the microenvironment of HPV+ and HPV- HNSCC patients may result from the presence of viral antigens throughout the carcinogenesis process, resulting in the early innate immune responses and the enhancement of the T cells adaptive immune response (20, 21). Further comparisons of the gene

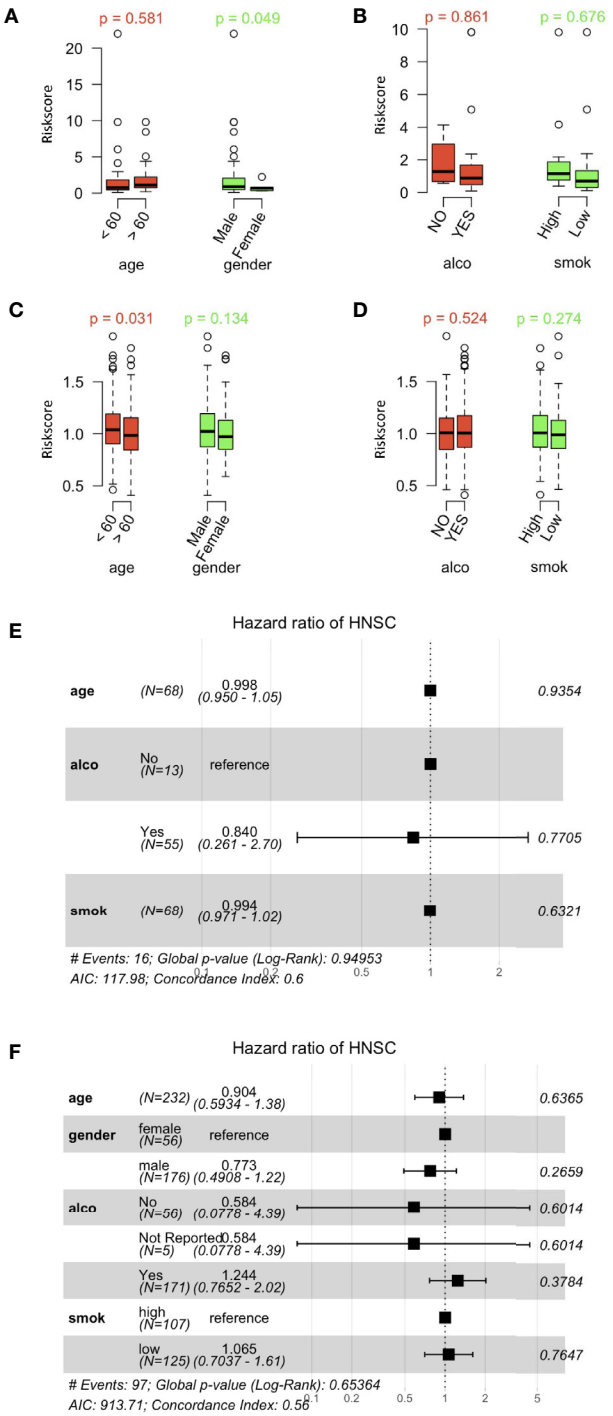

FIGURE 6 | Correlation between risk scores and clinically related characteristics of HNSCC patients. **(A)** Distribution of risk scores obtained when patients' data obtained from the HPV+ HNSCC TCGA dataset were separated by age and sex. **(B)** Risk score distributions for alcohol and smoking in the HPV+ HNSCC TCGA dataset. **(C)** Distribution of risk scores obtained when patients' data obtained from the HPV- HNSCC TCGA dataset were separated by age and sex. **(D)** Risk score distributions for alcohol and smoking in the HPV- HNSCC TCGA dataset. **(E)** Multi-variate Cox regression forest plots of the risk scores and clinically related characteristics in the HPV+ HNSCC TCGA dataset. **(F)** Multi-variate Cox regression forest plots of risk scores and clinically related characteristics in the HPV- HNSCC TCGA dataset. Alco and Smok refer to alcohol consumer and smoker.

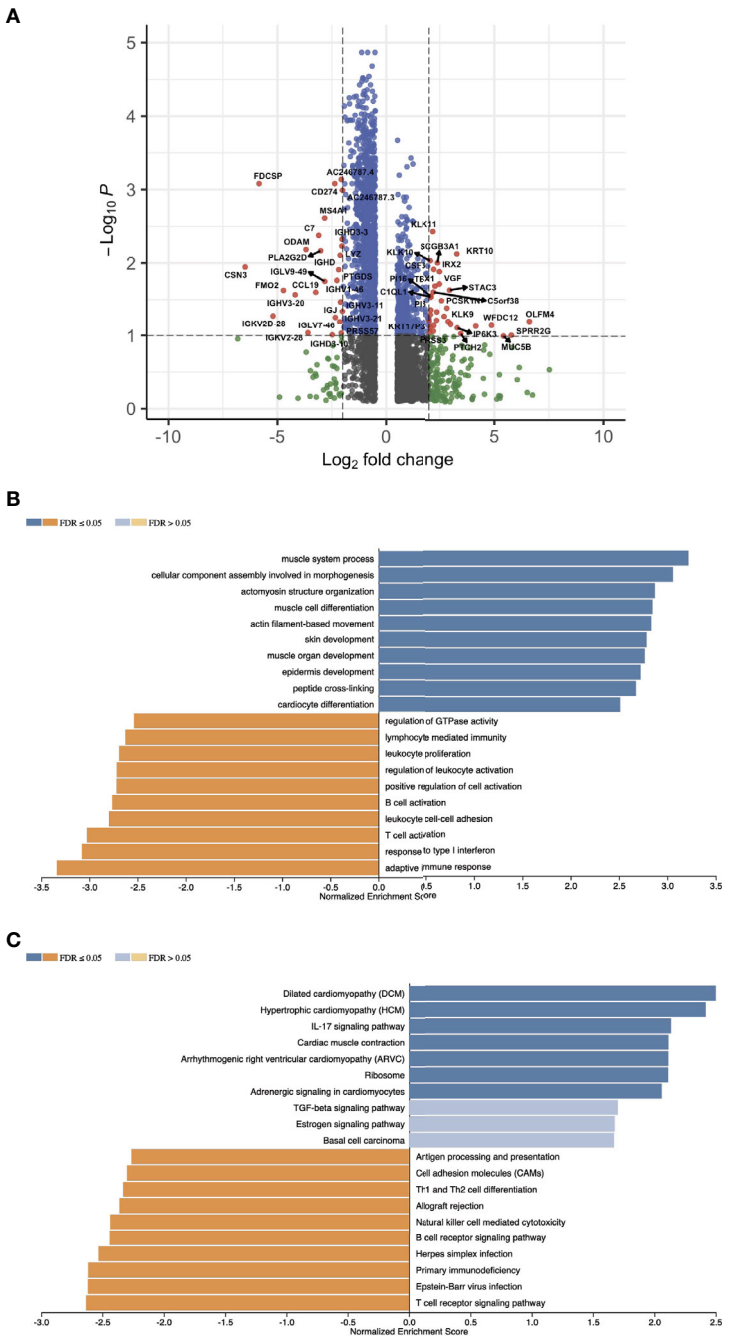

FIGURE 7 | Profiling the gene expression of the HPV+ HNSCC risk groups. **(A)** A volcano plot of the DEGs between high and low risk groups of HPV+ HNSCC TCGA samples. **(B)** Bar graphs showing the enriched gene ontology (GO) Biological Process of the risk DEGs and **(C)** the enriched KEGG pathways.

transcriptomes of cells with and without the presence of viral antigens throughout the carcinogenesis process is needed to enable the true cause of immune profile differences seen in the presence and absence of HPV in HNSCC patients.

In line with our current results, a recent study noted that between nearly 10% of the infiltrating T cells present in HNSCC were such CD8-positive T cells that target HPV and express PD-1 (22). One of these cells has stem cell characteristics and can expand in large numbers to treat head and neck cancer if cancer immunotherapy is used. Current conventional treatments for head and neck cancer include radiotherapy and chemotherapy, but they may affect the number of immune cells in the body. Therefore, better results may be achieved if immunotherapy is used first and then combined with conventional modalities.

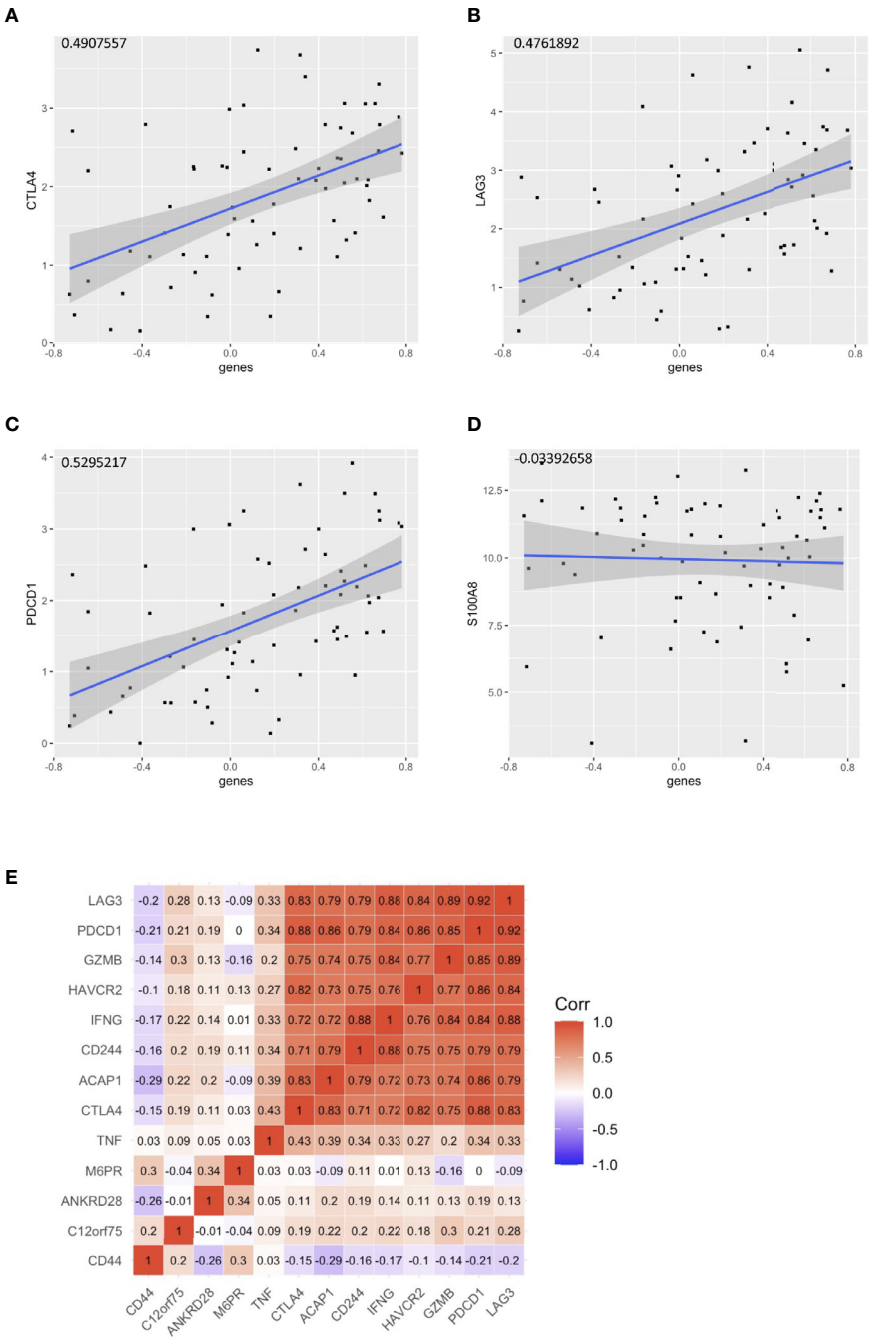

FIGURE 8 | Correlation of the signature genes with the checkpoint related genes. Correlation of the signature genes with **(A)** CTLA4 **(B)**LAG3 and **(C)** PDCD1. **(D)** S100A8 was used as control. **(E)** A corr plot showing the signature genes with the checkpoint related genes.

The shortcoming of our current study is the small size of the test group, which, although showing a good trend, somehow lacks statistical significance. Further studies are needed to examine not only HPV+ samples but also specific epitopes of HPV infection.

DATA AVAILABILITY STATEMENT

The original contributions presented in the study are included in the article/**Supplementary Material**. Further inquiries can be directed to the corresponding authors.

ETHICS STATEMENT

The studies involving human participants were reviewed and approved by Youjiang Medical University for Nationalities. The patients/participants provided their written informed consent to participate in this study.

AUTHOR CONTRIBUTIONS

JS and HL designed this study. YW, LM, KC, and JZ analyzed the scRNA-seq data. HL, SH, and JS analyzed the bulk sequencing data. QW, ZW, and SS contributed to scRNA-seq data and helped organize this manuscript. All authors contributed to the article and approved the submitted version.

FUNDING

This research work was funded by the National Natural Science Foundation of China (#31970745).

SUPPLEMENTARY MATERIAL

The Supplementary Material for this article can be found online at: https://www.frontiersin.org/articles/10.3389/fonc.2021.749398/full#supplementary-material

REFERENCES

1. Argiris A, Karamouzis MV, Raben D, Ferris RL. Head and Neck Cancer. *Lancet* (2008) 371:1695–709. doi: 10.1016/S0140-6736(08)60728-X
2. Geng X, Zhang Y, Zeng Z, Zhu Z, Wang H, Yu W, et al. Molecular Characteristics, Prognostic Value, and Immune Characteristics of M(6)A Regulators Identified in Head and Neck Squamous Cell Carcinoma. *Front Oncol* (2021) 11:629718. doi: 10.3389/fonc.2021.629718
3. Timar J, Csuka O, Remenar E, Repassy G, Kasler M. Progression of Head and Neck Squamous Cell Cancer. *Cancer Metastasis Rev* (2005) 24:107–27. doi: 10.1007/s10555-005-5051-5
4. Topalian SL, Hodi FS, Brahmer JR, Gettinger SN, Smith DC, McDermott DF, et al. Safety, Activity, and Immune Correlates of Anti-PD-1 Antibody in Cancer. *N Engl J Med* (2012) 366:2443–54. doi: 10.1056/NEJMoa1200690
5. Burtness B, Harrington KJ, Greil R, Soulieres D, Tahara M, de Castro GJr., et al. Pembrolizumab Alone or With Chemotherapy *Versus* Cetuximab With Chemotherapy for Recurrent or Metastatic Squamous Cell Carcinoma of the Head and Neck (KEYNOTE-048): A Randomised, Open-Label, Phase 3 Study. *Lancet* (2019) 394:1915–28. doi: 10.1016/S0140-6736(19)32591-7
6. Ferris RL, Licitra L, Fayette J, Even C, Blumenschein G Jr, Harrington KJ, et al. Nivolumab in Patients With Recurrent or Metastatic Squamous Cell Carcinoma of the Head and Neck: Efficacy and Safety in CheckMate 141 by Prior Cetuximab Use. *Clin Cancer Res* (2019) 25:5221–30. doi: 10.1158/1078-0432.CCR-18-3944
7. Ang KK, Harris J, Wheeler R, Weber R, Rosenthal DI, Nguyen-Tan PF, et al. Human Papillomavirus and Survival of Patients With Oropharyngeal Cancer. *N Engl J Med* (2010) 363:24–35. doi: 10.1056/NEJMoa0912217
8. Carvalho AL, Nishimoto IN, Califano JA, Kowalski LP. Trends in Incidence and Prognosis for Head and Neck Cancer in the United States: A Site-Specific Analysis of the SEER Database. *Int J Cancer* (2005) 114:806–16. doi: 10.1002/ijc.20740
9. LeHew CW, Weatherspoon DJ, Peterson CE, Goben A, Reitmajer K, Sroussi H, et al. The Health System and Policy Implications of Changing Epidemiology for Oral Cavity and Oropharyngeal Cancers in the United States From 1995 to 2016. *Epidemiol Rev* (2017) 39:132–47. doi: 10.1093/epirev/mxw001
10. Cillo AR, Kurten CHL, Tabib T, Qi Z, Onkar S, Wang T, et al. Immune Landscape of Viral- and Carcinogen-Driven Head and Neck Cancer. *Immunity* (2020) 52:183–99.e9. doi: 10.1016/j.immuni.2019.11.014
11. Kansy BA, Concha-Benavente F, Srivastava RM, Jie HB, Shayan G, Lei Y, et al. PD-1 Status in CD8(+) T Cells Associates With Survival and Anti-PD-1 Therapeutic Outcomes in Head and Neck Cancer. *Cancer Res* (2017) 77:6353–64. doi: 10.1158/0008-5472.CAN-16-3167
12. Li T, Fu J, Zeng Z, Cohen D, Li J, Chen Q, et al. TIMER2.0 for Analysis of Tumor-Infiltrating Immune Cells. *Nucleic Acids Res* (2020) 48:W509–14. doi: 10.1093/nar/gkaa407
13. Stuart T, Butler A, Hoffman P, Hafemeister C, Papalexi E, Mauck WM3rd, et al. Comprehensive Integration of Single-Cell Data. *Cell* (2019) 177:1888–1902 e21. doi: 10.1016/j.cell.2019.05.031
14. Therneau TM, Li H. Computing the Cox Model for Case Cohort Designs. *Lifetime Data Anal* (1999) 5:99–112. doi: 10.1023/A:1009691327335
15. Zeng L, Fan X, Wang X, Deng H, Zhang K, Zhang X, et al. Bioinformatics Analysis Based on Multiple Databases Identifies Hub Genes Associated With Hepatocellular Carcinoma. *Curr Genomics* (2019) 20:349–61. doi: 10.2174/1389202920666191011092410
16. Aran D, Hu Z, Butte AJ. Xcell: Digitally Portraying the Tissue Cellular Heterogeneity Landscape. *Genome Biol* (2017) 18:220. doi: 10.1186/s13059-017-1349-1
17. Becht E, Giraldo NA, Lacroix L, Buttard B, Elarouci N, Petitprez F, et al. Estimating the Population Abundance of Tissue-Infiltrating Immune and Stromal Cell Populations Using Gene Expression. *Genome Biol* (2016) 17:218. doi: 10.1186/s13059-016-1070-5
18. Finotello F, Mayer C, Plattner C, Laschober G, Rieder D, Hackl H, et al. Molecular and Pharmacological Modulators of the Tumor Immune Contexture Revealed by Deconvolution of RNA-Seq Data. *Genome Med* (2019) 11:34. doi: 10.1186/s13073-019-0638-6
19. Newman AM, Liu CL, Green MR, Gentles AJ, Feng W, Xu Y, et al. Robust Enumeration of Cell Subsets From Tissue Expression Profiles. *Nat Methods* (2015) 12:453–7. doi: 10.1038/nmeth.3337
20. Menezes FDS, Fernandes GA, Antunes JLF, Villa LL, Toporcov TN. Global Incidence Trends in Head and Neck Cancer for HPV-Related and -Unrelated Subsites: A Systematic Review of Population-Based Studies. *Oral Oncol* (2021) 115:105177. doi: 10.1016/j.oraloncology.2020.105177
21. Kobayashi K, Hisamatsu K, Suzui N, Hara A, Tomita H, Miyazaki T. A Review of HPV-Related Head and Neck Cancer. *J Clin Med* (2018) 7(9):241. doi: 10.3390/jcm7090241
22. Eberhardt CS, Kissick HT, Patel MR, Cardenas MA, Prokhnevska N, Obeng RC, et al. Functional HPV-Specific PD-1(+) Stem-Like CD8 T Cells in Head and Neck Cancer. *Nature* (2021) 597(7875):279–84. doi: 10.1038/s41586-021-03862-z

Conflict of Interest: The authors declare that the research was conducted in the absence of any commercial or financial relationships that could be construed as a potential conflict of interest.

Publisher's Note: All claims expressed in this article are solely those of the authors and do not necessarily represent those of their affiliated organizations, or those of the publisher, the editors and the reviewers. Any product that may be evaluated in this article, or claim that may be made by its manufacturer, is not guaranteed or endorsed by the publisher.

frontiers in Oncology

ORIGINAL RESEARCH
published: 29 September 2021
doi: 10.3389/fonc.2021.754412

Survival-Weighted Health Profiles in Patients Treated for Advanced Oral Cavity Squamous Cell Carcinoma

*Yao-Te Tsai[1], Wen-Cheng Chen[2], Cheng-Ming Hsu[1], Ming-Shao Tsai[1], Geng-He Chang[1], Yi-Chan Lee[3], Ethan I. Huang[1], Chiung-Cheng Fang[2] and Chia-Hsuan Lai[2]**

[1] Department of Otorhinolaryngology-Head and Neck Surgery, Chang Gung Memorial Hospital, Chiayi, Taiwan, [2] Department of Radiation Oncology, Chang Gung Memorial Hospital, Chiayi, Taiwan, [3] Department of Otorhinolaryngology-Head and Neck Surgery, Chang Gung Memorial Hospital, Keelung, Taiwan

Objectives: For patients with oral cavity squamous cell carcinoma (OSCC), particularly for those with advanced disease, quality of life (QoL) is a key outcome measure. Therefore, we estimated survival-weighted psychometric scores (SWPS), life expectancy (LE), and quality-adjusted LE (QALE) in patients with advanced OSCC.

Methods and Materials: For estimation of survival function, we enrolled 2313 patients with advanced OSCC diagnosed between January 1, 2007, and December 31, 2013. The patients were followed until death or December 31, 2014. To acquire the QoL data, data from 194 patients were collected by employing the Taiwan Chinese versions of the Quality of Life Questionnaire Core 30 and Quality of Life Questionnaire Head and Neck 35 developed by the European Organisation for Research and Treatment of Cancer and the EQ-5D-3L between October 1, 2013, and December 31, 2017. The LE of the patients with OSCC were estimated through linear extrapolation of a logit-transformed curve. SWPS and QALE were determined by integrating the LE and corresponding QoL outcomes.

Results: For the patients with advanced OSCC, the estimated LE and QALE were 8.7 years and 7.7 quality-adjusted life years (QALYs), respectively. The loss of LE and QALE was 19.0 years and 20.0 QALYs, respectively. The estimated lifetime impairments of swallowing, speech, cognitive functioning, physical functioning, social functioning, and emotional functioning were 8.3, 6.5, 6.5, 6.1, 5.7, and 5.4 years, respectively. The estimated lifetime problems regarding mouth opening, teeth, social eating, and social contact were 6.6, 6.1, 7.5, and 6.1 years, respectively. The duration of feeding tube dependency was estimated to be 1.6 years.

Conclusions: Patients with advanced OSCC had an estimated LE of 8.7 years and QALE of 7.7 QALYs. SWPS provided useful information regarding how advanced OSCC affects the subjective assessment of QoL. Our study results may serve as a reference for the allocation of cancer treatment resources.

Keywords: oral cavity squamous cell carcinoma, quality of life, survival-weighted psychometric scores, life expectancy, quality-adjusted life expectancy

OPEN ACCESS

Edited by:
Heming Lu,
People's Hospital of Guangxi Zhuang Autonomous Region, China

Reviewed by:
Imran Petkar,
Guy's and St Thomas' NHS Foundation Trust, United Kingdom
Jared Shenson,
University of Texas MD Anderson Cancer Center, United States

***Correspondence:**
Chia-Hsuan Lai
chiahsuan7092@gmail.com

Specialty section:
This article was submitted to Head and Neck Cancer, a section of the journal Frontiers in Oncology

Received: *06 August 2021*
Accepted: *15 September 2021*
Published: *29 September 2021*

Citation:
Tsai Y-T, Chen W-C, Hsu C-M, Tsai M-S, Chang G-H, Lee Y-C, Huang EI, Fang C-C and Lai C-H (2021) Survival-Weighted Health Profiles in Patients Treated for Advanced Oral Cavity Squamous Cell Carcinoma. Front. Oncol. 11:754412. doi: 10.3389/fonc.2021.754412

INTRODUCTION

Oral squamous cell carcinoma (OSCC) is the sixth most common cancer in the world, and its incidence has been increasing, with an annual incidence approaching 500,000 (1, 2). In Taiwan, because of the high prevalence of betel nut chewing and cigarette smoking (3), OSCC is the fourth most common cancer among men. Approximately 60% of patients with OSCC present with locoregionally advanced disease (stage III or IV) at diagnosis (1), and the 5-year survival rate is only 10%–40% (2). Both OSCC and its treatments can significantly impair patients' quality of life (QoL) and functional status. Conventionally, the outcome assessments for OSCC consider both physician and patient perspectives, with physicians objectively reporting survival, local control, and complication rates and patients subjectively reporting physical, emotional, social, and psychological outcomes (3). Patient reported outcomes are increasingly studied (4), and OSCC patients have reported varying degrees of physical problems [e.g., eating and speaking changes (5)], mental stress [e.g., fatigue, anxiety, and depression (6, 7)], and altered interpersonal relationships [e.g. social isolation, work impairment, and disrupted social relationships (5, 8)]. Among head and neck cancer (HNC) patients, OSCC patients experience the worst QoL and function (9). Patients with advanced OSCC frequently experience moderate to severe QoL and functional impairments attributable to their extensive tumor invasion or multidisciplinary treatments, such as ablative surgery and radiation therapy (9, 10). Surgery plus adjuvant radiotherapy can result in more severe and prolonged QoL disturbance compared with radiotherapy alone (11), and psychosocial and functional impairment may persist for a long time (5, 8). Hence, periodic review of QoL and the use of questionnaires may facilitate communication between patients and physicians and thereby optimize cancer treatments and nutritional interventions, potentially improving survival in patients with OSCC (12).

The quality-adjusted life-expectancy (QALE) that considers both survival and QoL is widely applied for cancer patient care and clinical research (13, 14). Studies have compared and quantified QALE in patients with HNC by estimating life expectancy (LE) and quality-adjusted LE (QALE) (14, 15). However, these studies enrolled highly heterogeneous samples and did not consider survival-weighted psychometric scores (SWPS). In the present study, we investigated the feasibility of estimating QALE and SWPS by combining mean QoL scores at various intervals with survival function in patients with advanced OSCC.

MATERIALS AND METHODS

Patients

Figure 1 presents the study flowchart. Patients diagnosed as having OSCC between January 1, 2007, and December 31, 2013, were retrospectively analyzed for survival estimation. Eligibility criteria were the following: (1) aged 18 to 75 years; (2) had newly diagnosed locally advanced OSCC (stage III or IV); (3) underwent curative treatments; and (4) had an Eastern Cooperative Oncology Group performance status of 0 to 2. We excluded patients who (1) underwent palliative treatment; (2) had a history of any cancer; (3) whose OSCC had already metastasized at diagnosis; or (4) had another cancer in addition to OSCC. Finally, a cohort of 2313 patients with advanced OSCC diagnosed during the study period was enrolled from our cancer registry database. Patients with OSCC who underwent treatments and follow-up at our hospital from October 1, 2013, to December 31, 2017, were prospectively enrolled for QoL questionnaire completion. Informed consent was obtained from all participants, and the institutional review board of our hospital approved the study protocol (No. 102-2668B). This study was performed in compliance with the tenets of the Declaration of Helsinki.

Treatment Protocol

Each patient underwent a routine workup consisting of comprehensive history taking, physical examination, flexible fiberoptic laryngoscopy, plain chest radiography, abdominal sonography, and pretreatment computed tomography or magnetic resonance imaging of the head and neck. In addition, the computed tomography of chest will be arranged if there is any abnormal finding on the plain chest radiography, and the positron emission tomography/computed tomography scan will be performed in patients with stage IV disease or if there is any finding suspicious for metastasis in the aforementioned studies. All patients underwent either primary ablative surgery with adjuvant therapy or radiotherapy (RT)/chemoradiotherapy (CRT) with curative intent. The cancer staging manual of the American Joint Committee on Cancer (2010) was used for OSCC staging. The types of adjuvant therapy were determined by the tumor board conference according to institutional guidelines. The detailed adjuvant treatment guidelines in our institute and their comparison with the National Comprehensive Cancer Network guidelines have been reported by Lin et al. (16). In brief, patients diagnosed as having a pathologic T4 disease and single metastatic neck lymphadenopathy are provided adjuvant RT, whereas those diagnosed as having extranodal extension, multiple metastatic lymphadenopathies, or positive surgical margins are administered adjuvant CRT. If indicated, the intensity-modulated RT (2 Gy/d, 5 d/week) was used to treat patients, and the radiation dose was 60–66 Gy in an adjuvant setting and 70–72 in a definitive setting. Platinum-based agents were used if chemotherapy was indicated. All patients were regularly followed up, at which time questionnaires were completed. Follow-up visits occurred during years 1–3 every three months and in years 4+ every six months. At every follow-up visit, all patients were reviewed by speech-language pathologists and dietician and underwent complete physical examination including the fiberoptic laryngoscopy. Moreover, during the follow-up period, we executed head and neck magnetic resonance imaging or computed tomography at 6-month intervals during the first 2 years and annually thereafter.

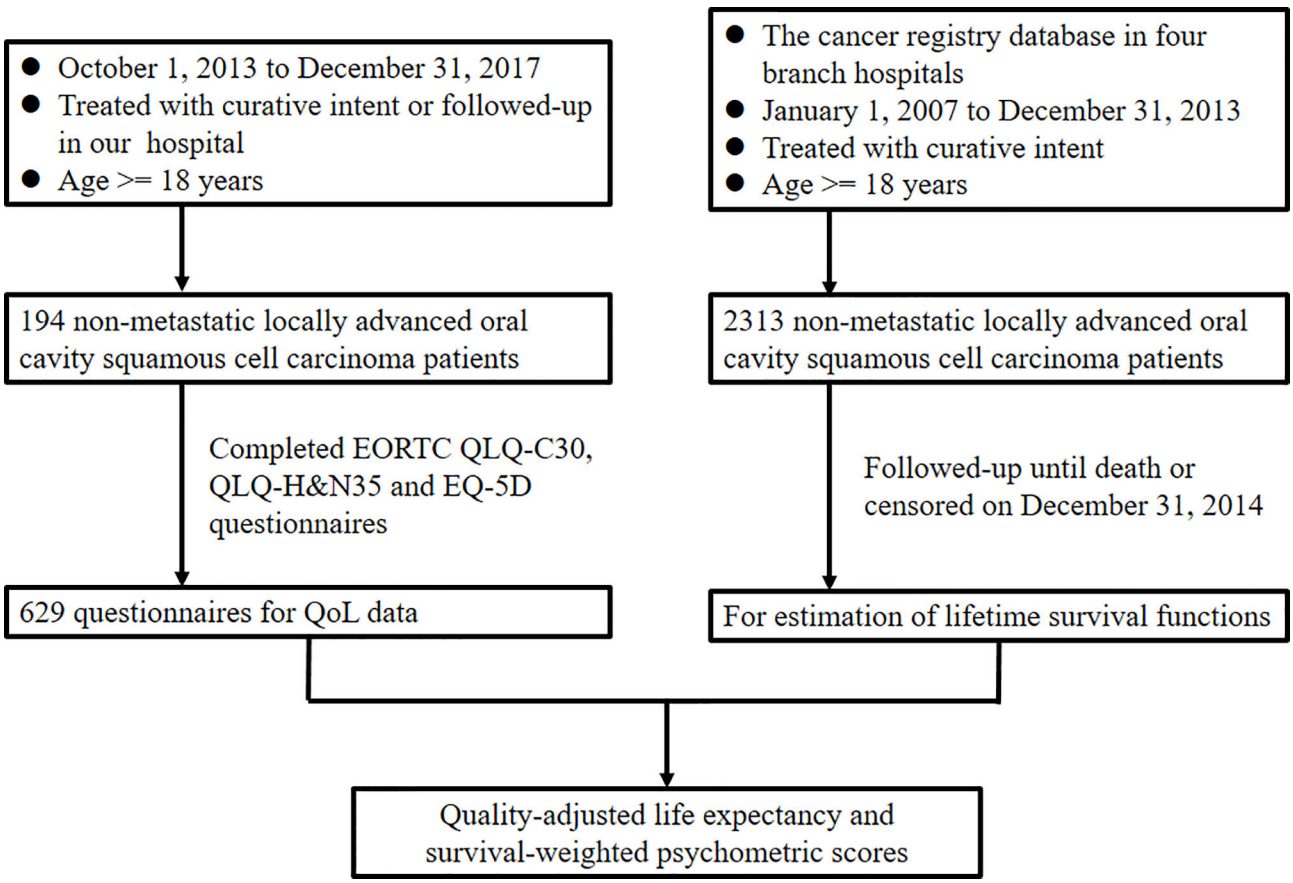

FIGURE 1 | Study design flowchart. EORTC, European Organisation for Research and Treatment of Cancer; H&N, head and neck; QLQ, quality of life questionnaire; QoL, quality of life.

QoL Instruments

The Taiwan Chineseversions of the European Organisation for Research and Treatment of Cancer (EORTC) Quality of Life Questionnaire Core 30 (EORTC QLQ-C30) and EORTC Quality of Life Questionnaire Head and Neck 35 (EORTC QLQ-H&N35) were used to assess QoL (17–19); these instruments, in translation and after cross-cultural adaptation to a Mandarin-speaking population, have been validated (20, 21). Per the EORTC scoring manual, for both instruments, scores were linearly transformed; all scales (multiple or single item) were scored 0–100 (22). A higher functioning score and QoL scale score indicated high functioning or QoL. By contrast, high scores on the symptom scales indicated more severe symptoms.

The EQ-5D-3L; Taiwanese version) was employed to assess general health and analyze cost utility (23). The EQ-5D-3L has five domains (pain/discomfort, mobility, anxiety/depression, self-care, and activities of daily living) and three levels of classification (no, some, and extreme problems). The health information derived from the five domains was transformed into health-related utility values by the time trade-off method (24). The utility value indicated the degree of general health status on a scale from 0 to 1, with 0 representing death and 1 representing perfect health.

Statistical Analysis

Numbers with percentages were used for categorical variables, and means with standard deviations were used to indicate continuous variables. The survival duration of the 2313 patients from the cancer registration database was defined as the duration from the date of curative treatment to death or censoring on December 31, 2014. We then plotted the Kaplan–Meier curves for overall survival estimation. On the basis of the life table of the general population in Taiwan, the Monte Carlo method was applied to determine the survival function of the reference population (matched for age and sex) (25). Linear extrapolation of a logit-transformed curve of the survival ratio between patients with OSCC and the reference population was performed to obtain the LE of the patients with OSCC (25–27). Kernel smoothing of the QoL data from 194 patients was applied to estimate average QoL function (27). The functional disabilities or symptoms were plotted against time at the beginning of curative treatment. From then until the attainment of every QoL follow-up data point, the survival outcomes were combined with the psychometric scores or utility values to calculate the SWPS or QALE (3). In brief, the utility values or psychometric scores at different time points were multiplied with the

corresponding lifetime survival probabilities over the course of cancer to obtain the quality-adjusted survival curve, of which the area under the curve would be the QALE or SWPS (28). The LE implies the expected total duration of living under a certain degree of unhealthy status after the treatments; the QALE can be interpreted as the expected total duration of living under a perfect healthy condition after the treatments. Each SWPS in a psychometric item can be interpreted as the expected total duration of living under a condition with a problem in that item after the treatments. The utility value was assumed to be 1 for the reference population during the study period. Hwang et al. proposed a minimum sample size of 50 for generating the mean QoL function curve (27). Considering the 7-year follow-up data and extrapolation to 50 years of survival, we estimated the LE, QALE, and SWPS of patients with OSCC. SPSS Statistics for Windows, version 17.0 (SPSS Inc., Chicago, IL, USA) was used for statistical analysis, and $p < .05$ was considered to indicate statistical significance. Survival extrapolation was performed using iSQoL [http://sites.stat.sinica.edu.tw/isqol/; validated in (13, 29, 30)].

RESULTS

Patient Characteristics

Table 1 presents the patients' baseline characteristics. The survival data of 2313 patients with OSCC were used for lifetime survival estimates. Another 194 patients were selected for QoL questionnaire completion. Among the enrolled patients, the most common stage of OSCC was stage IVA (n = 1413, 61.1%), followed by stage III (n = 602, 26.0%) and stage IVB (n = 298, 12.9%). Two thousand one hundred five (91%) patients received ablative surgery as their primary treatment modality; 1088 (47%) patients underwent postoperative adjuvant CRT, and 448 (19.4%) patients received adjuvant RT. Given the presence of the unresectable T4b disease, significant underlying comorbidities [e.g. end-stage liver disease (31) and severely reduced ejection fraction (32)], and the patient's willingness, approximately 10% of patients underwent definitive RT/CRT as their primary treatment (33, 34). **Table 2** presents the results of the 629 valid responses to the EORTC QLQ-C30 and QLQ-H&N35 completed by 194 patients with OSCC, which were stratified by time periods: post-treatment <1 year, 1–3 years, and >3 years.

Survival Outcome, LE, and QALE

Among the 2313 patients with OSCC, the 5-year overall survival rate was 54.2% (median follow-up: 31.4 months; range: 0.7–97.1 months). The LE and QALE for the reference cohort in Taiwan is 27.7 years and 27.7 quality-adjusted life years (QALYs). In our cohort of patients with OSCC, the estimated LE and QALE was 8.7 years (95% confidence interval [CI]: 6.3–14.8 years) and 7.7 QALYs (95% CI: 5.5–13.1 QALYs), respectively (**Figure 2**); thus, the estimated loss was 19.0 years and 20.0 QALYs, respectively (**Figures 3A, B**, respectively).

Symptoms and Impaired Function

The median period between curative treatments and questionnaire completion was 1.7 months (range: 1–158.2 months). We estimated that patients with OSCC experienced pain and consumed painkillers for 4.9 and 2.0 years, respectively (**Figure 4**). Regarding functional disabilities, the durations of impairments in cognitive, physical, social, emotional, and role functioning were estimated to be 6.5 (95% CI: 4.8-11.6), 6.1 (95% CI: 4.6-11.5), 5.7 (95% CI: 4.4-10.0), 5.4 (95% CI: 4.1-10.0), and 2.8 (95% CI: 2.0-4.9) years, respectively (**Figure 5**). The durations of impairments in swallowing, speech, taste, and smell were estimated to be 8.3 (95% CI: 6.4-15.0), 6.5 (95% CI: 4.9-11.7), 3.6 (95% CI: 2.7-6.6), and 3.0 (95% CI: 2.2-4.1) years, respectively (**Figure 6**). The patients experienced problems involving mouth opening, teeth, social eating, and social contact for an estimated 6.6 (95% CI: 5.0-11.4), 6.1 (95% CI: 4.5-11.0), 7.5 (95% CI: 5.7-13.3), and 6.1 (95% CI: 4.3-11.1) years, respectively (**Figure 6**). The estimated duration of tube feeding dependence was 1.6 (95% CI: 1.1-2.8) years. In addition, the dynamic changes of the utility values and functional impairments (**Figure 7**) as well as different problems (**Figure 8**) were also demonstrated.

Extrapolation Validity

The model-extrapolated 8-year overall survival outcomes (using the initial 7-year follow-up data of 2313 patients) was compared with the survival outcomes measured using the Kaplan–Meier method. As shown in **Figure 9**, the observed survival data were highly consistent with the estimated survival curve. The mean ± standard deviation of estimated survival among the patients with OSCC was 58.9 ± 1.0 months, indicating a relative bias of only 0.3% from the observed survival (59.1 ± 0.8 months) at the end of the 8-year follow-up period.

TABLE 1 | Baseline patient characteristics.

Variables	OSCC patients (n = 2313)	Patients completed QoL questionnaires (n = 194)
Age at diagnosis (years, mean ± SD)	51.9 ± 10.9	52.4 ± 9.8
Gender		
Male	2147 (92.8%)	192 (99.0%)
Female	166 (7.2%)	2 (1.0%)
Overall stage		
III	602 (26.0%)	56 (28.9%)
IVA	1413 (61.1%)	113 (58.2%)
IVB	298 (12.9%)	25 (12.9%)
T classification		
T1	124 (5.4%)	16 (8.2%)
T2	496 (21.4%)	46 (23.7%)
T3	428 (18.5%)	23 (11.9%)
T4A	988 (42.7%)	84 (43.3%)
T4B	277 (12.0%)	25 (12.9%)
N classification		
N0	870 (37.6%)	105 (54.1%)
N1	514 (22.2%)	28 (14.5%)
N2	918 (39.7%)	60 (30.9%)
N3	11 (0.5%)	1 (0.5%)
Curative treatment		
Surgery	2105 (91.0%)	174 (89.7%)
Adjuvant CRT	1088 (47.0%)	123 (63.4%)
Adjuvant RT	448 (19.4%)	51 (26.3%)
Curative RT/CRT	208 (9.0%)	20 (10.3%)

CRT, chemoradiotherapy; QoL, quality of life; OSCC, oral cavity squamous cell carcinoma; RT, radiotherapy; SD, standard deviation.

TABLE 2 | The mean scores of the EORTC QOL scales in different periods of time.

	T1 scores (± SD)	T2 scores (± SD)	T3 scores (± SD)
EORTC QLQ-30			
Global quality of life	51 (± 22)	58 (± 20)	60 (± 22)
Physical functioning	73 (± 24)	80 (± 21)	87 (± 15)
Emotional functioning	72 (± 26)	78 (± 23)	79 (± 24)
Cognitive functioning	78 (± 24)	75 (± 20)	77 (± 19)
Social functioning	59 (± 35)	65 (± 29)	72 (± 32)
Role functioning	75 (± 34)	80 (± 31)	88 (± 23)
Fatigue	41 (± 27)	27 (± 26)	25 (± 23)
Nausea/vomiting	10 (± 19)	03 (± 13)	04 (± 11)
Pain	35 (± 31)	18 (± 22)	14 (± 20)
Dyspnea	15 (± 23)	15 (± 22)	15 (± 23)
Insomnia	35 (± 36)	24 (± 30)	26 (± 30)
Appetite loss	28 (± 32)	13 (± 22)	11 (± 19)
Constipation	17 (± 22)	17 (± 27)	12 (± 19)
Diarrhea	13 (± 23)	7 (± 15)	10 (± 17)
Financial problems	46 (± 39)	44 (± 35)	36 (± 36)
EORTC QLQ-H&N35			
Pain	29 (± 26)	18 (± 24)	12 (± 14)
Swallowing	45 (± 28)	38 (± 25)	44 (± 26)
Senses (taste/smell)	30 (± 29)	32 (± 33)	17 (± 27)
Speech	34 (± 29)	29 (± 28)	35 (± 30)
Social eating	48 (± 30)	42 (± 31)	47 (± 34)
Social contact	26 (± 27)	22 (± 25)	27 (± 28)
Sexuality	33 (± 34)	29 (± 32)	24 (± 28)
Teeth	33 (± 37)	42 (± 41)	44 (± 34)
Opening mouth	49 (± 35)	47 (± 36)	54 (± 40)
Dry mouth	48 (± 37)	53 (± 35)	48 (± 34)
Sticky saliva	50 (± 35)	34 (± 33)	33 (± 35)
Coughing	33 (± 30)	31 (± 23)	26 (± 25)
Feeling ill	45 (± 35)	26 (± 26)	21 (± 25)

T1, within the first year after treatment beginning; T2, post-treatment 1–3 years; T3, post-treatment 3 years and thereafter.
EORTC, European Organization for Research and Treatment of Cancer; QLQ, quality of life; H&N, head and neck; SD, standard deviation.

DISCUSSION

Patients with locally advanced OSCC tend to have more symptoms, more severe functional disabilities, and greater reductions in QoL due to aggressive tumor extension and metastatic lymphadenopathy necessitating extensive surgical interventions or RT/CRT (4). Multidisciplinary management and advancements in treatment have facilitated the control of advanced OSCC (35); therefore, understanding the lifetime health burden of these patients is critical (36). To the best of our knowledge, this is the first study to describe QALE and lifetime symptoms or functional impairments in patients with locally advanced OSCC undergoing curative treatments. The estimated durations of problems concerning the teeth, mouth opening, social contact, and social eating all exceeded 6 years, consistent with results from a previous study (37). This may be explained by the significant lasting changes in oral structures, facial appearance, and social adaptation after curative treatment. We also observed that all the QoL domains excepting role function impairment (2.8 years), namely social, emotional, cognitive, and physical functioning, were adversely affected for over 5 years. This finding may be ascribable to the relatively young age of the patients at diagnosis, as well as to their active social participation and sufficient family support. The LE and QALE of the average patient with OSCC in Taiwan are approximately 12.2 years and 11.3 QALYs, respectively (15). Our estimates of LE and QALE, which were lower, are reasonable because we enrolled only patients with locally advanced disease. By integrating the QoL data from the QLQ-C30, QLQ-H&N35, and EQ-5D-3L questionnaires with the survival function, we generated a multidimensional health profile from the patient perspective, enabling an intuitive understanding of the changes of QoL in patients with advanced

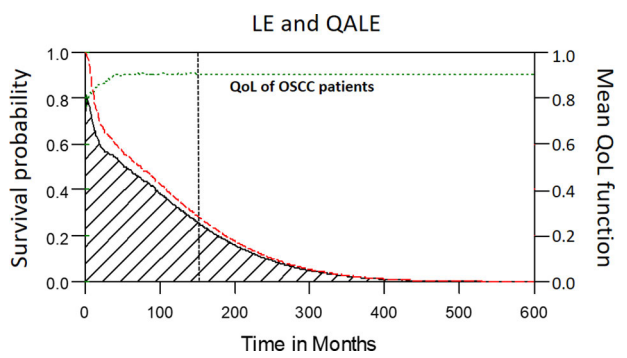

FIGURE 2 | The mean QoL (utility) function (green dashed line) was multiplied with the corresponding lifetime survival probabilities (red dashed line) to obtain the quality-adjusted survival curve (black solid line). The area under the red dashed line is the LE. The area under the black solid line is the QALE. The vertical black dotted line stands for the starting month of extrapolation.

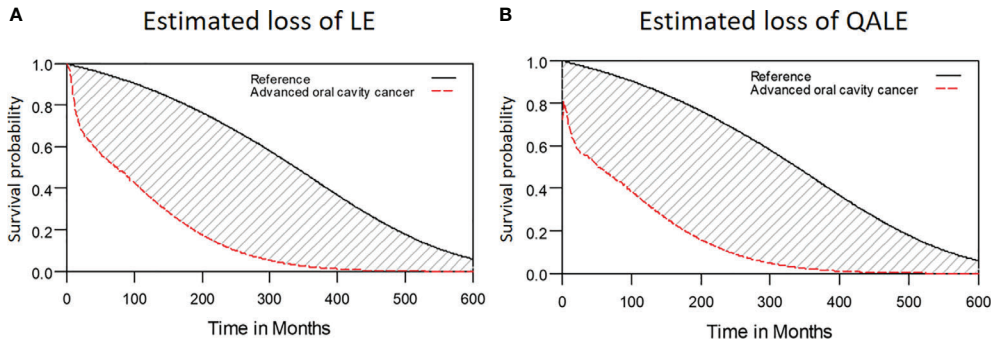

FIGURE 3 | Estimated loss of LE and QALE for advanced OSCC patients. **(A)** Estimated loss of LE; **(B)** Estimated loss of QALE.

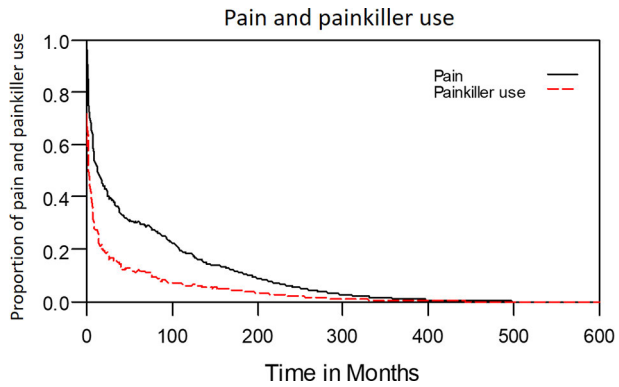

FIGURE 4 | Dynamic changes in pain and painkiller use in patients with locally advanced OSCC.

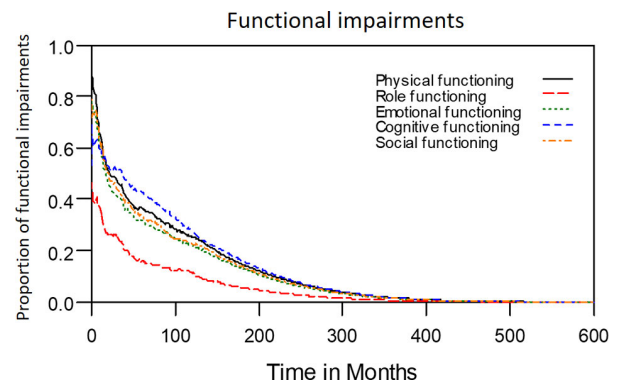

FIGURE 5 | Functional impairments in patients with advanced OSCC. The estimated persistence of functional impairments is represented by the area under the quality-adjusted survival curve. Duration of functional impairments (years): Role—2.8; Physical—6.1; Emotional—5.4; Cognitive—6.5; Social—5.7.

OSCC. Of note, OSCC and its treatments negatively impact patient QoL, particularly in those treated with ablative surgery (11). Extensive surgery considerably changes the facial appearance of patients with HNC, causing problems in social eating, swallowing, and speech and leading to social isolation and depression (38, 39). Given that 90% of our patients were treated with primary ablative surgery, their prolonged functional disabilities may be partially explained by the impacts of this extensive procedure. This highlights the necessity of developing psychosocial rehabilitation strategies for patients with advanced OSCC (40).

Our study results may extend the literature concerning QoL function in patients with locally advanced OSCC in several regards. First, because disease severity and treatment courses may influence various facets of QoL, a comprehensive assessment of psychometric scores for each QoL facet may yield a more holistic view. For instance, acute cancer- or treatment-related symptoms, such as pain and nausea or vomiting, may resolve gradually during follow-up. By contrast, patients with OSCC may experience prolonged physical distress and social functioning impairment that may or may not recover even after long-term disease remission is achieved (41). Multidimensional assessment may reflect the changes in QoL after the diagnosis of OSCC and may thus increase the feasibility of using QoL as an endpoint of treatment efficacy (42). Because the substantial change of the patient's QoL usually happened within the first 2 months after curative treatments due to the surgical morbidity, treatment related toxicity and its recovery, and most symptom burden tended to be stable after 1 year (43). Hence, we collected the QoL data more frequently in the first 2 months after treatments for better estimation of QALE or SWPS. In addition, the QoL after the last data collection time point is assumed to be the same thereafter. Accordingly, even >50% of QoL data points came from within the first 2 months after treatments, it may cause little impact on the lifelong extrapolation. Second, patients' subjective judgments of QoL may change over time (44). Hence, we used the extrapolation method, which entails a simulation approach, for estimating the lifetime survival function. By integrating the extrapolated survival outcomes and the psychometric data, we acquired the

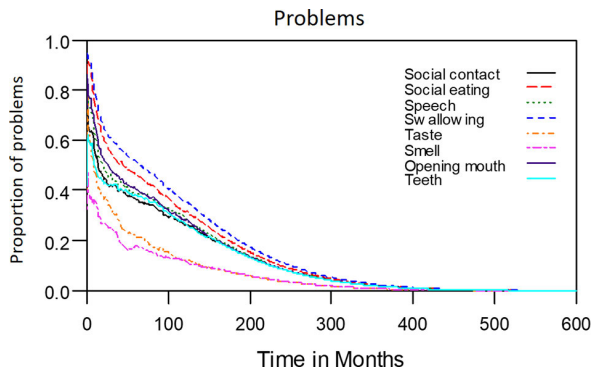

FIGURE 6 | Problems in patients with advanced OSCC. The estimated persistence of impairments or problems are represented by the area under the quality-adjusted survival curve. Duration of functional impairments or problems (years): Taste—3.6; Smell—3.0; Speech—6.5; Swallow—8.3. Problem—years endured: Open mouth—6.6; Dentition—6.1; Social eating—7.5; Social contact—6.1.

SWPS for lifetime QoL assessments in patients with advanced OSCC. Changes in QoL scores over time correspond to the cancer treatment courses and disease severity in patients with cancer, and the QoL profile is particularly informative regarding emotional distress, physical performance, and social function (45); these findings accord with ours. Overall, SWPS may constitute a comprehensive approach for determining the lifetime QoL function of patients with advanced OSCC.

The health costs and economic burden of OSCC are comparable with or higher than those of other cancers (46). Despite their poorer survival outcomes, the patients with advanced OSCC used more resources (corresponding to higher expenditures) than did those with early-stage OSCC. This is attributable to the need of this patient group for multidisciplinary treatment, supportive care, and palliative care following repeated relapse (47). The results of this study demonstrated that compared with the reference population, patients with locally advanced OSCC had substantial losses of LE (19.0 years) and QALE (20.0 QALYs). Given that the QALY metric is commonly used to assess value in health care decision-

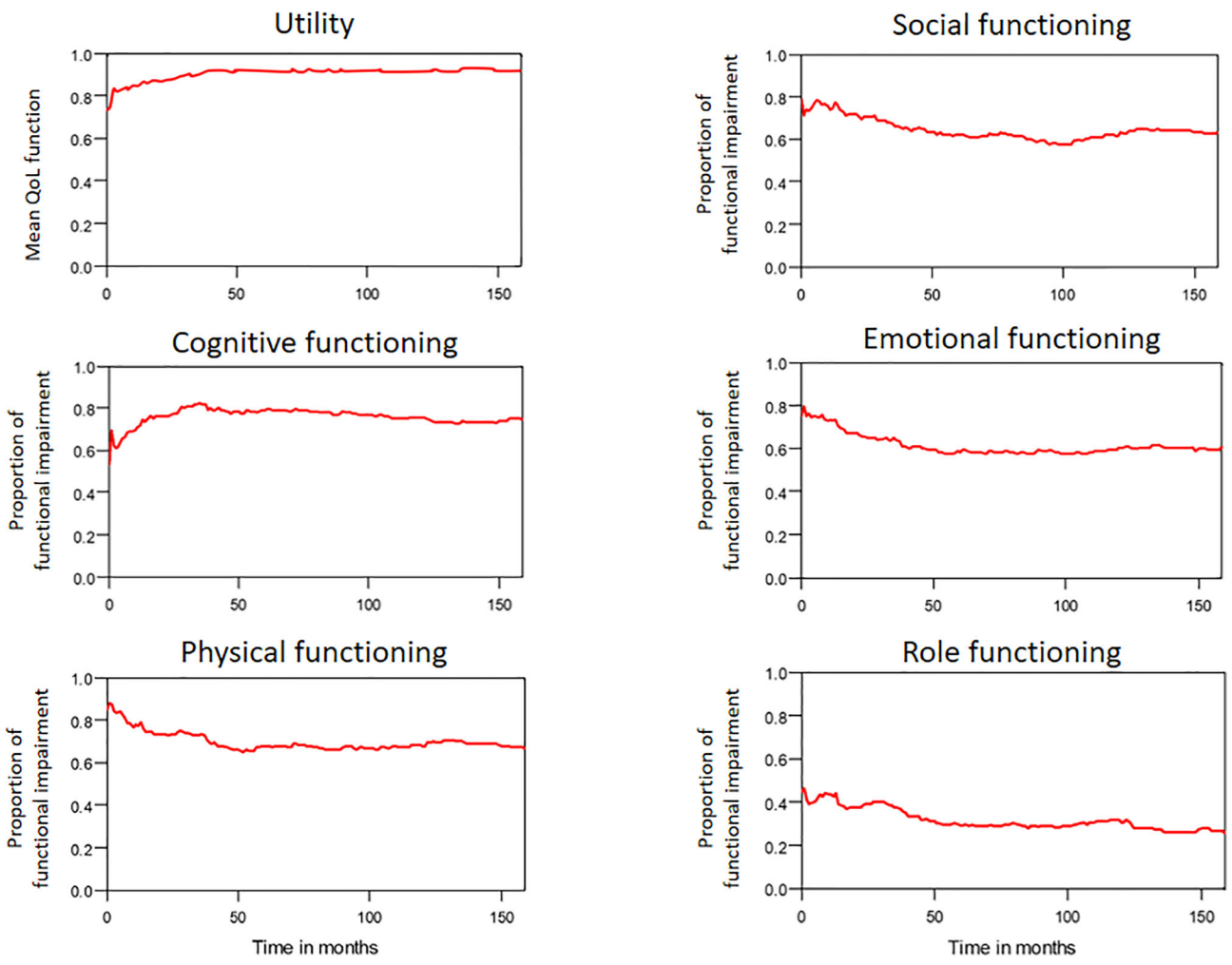

FIGURE 7 | The trends of mean QoL (utility) function and functional impairments in patients with OSCC.

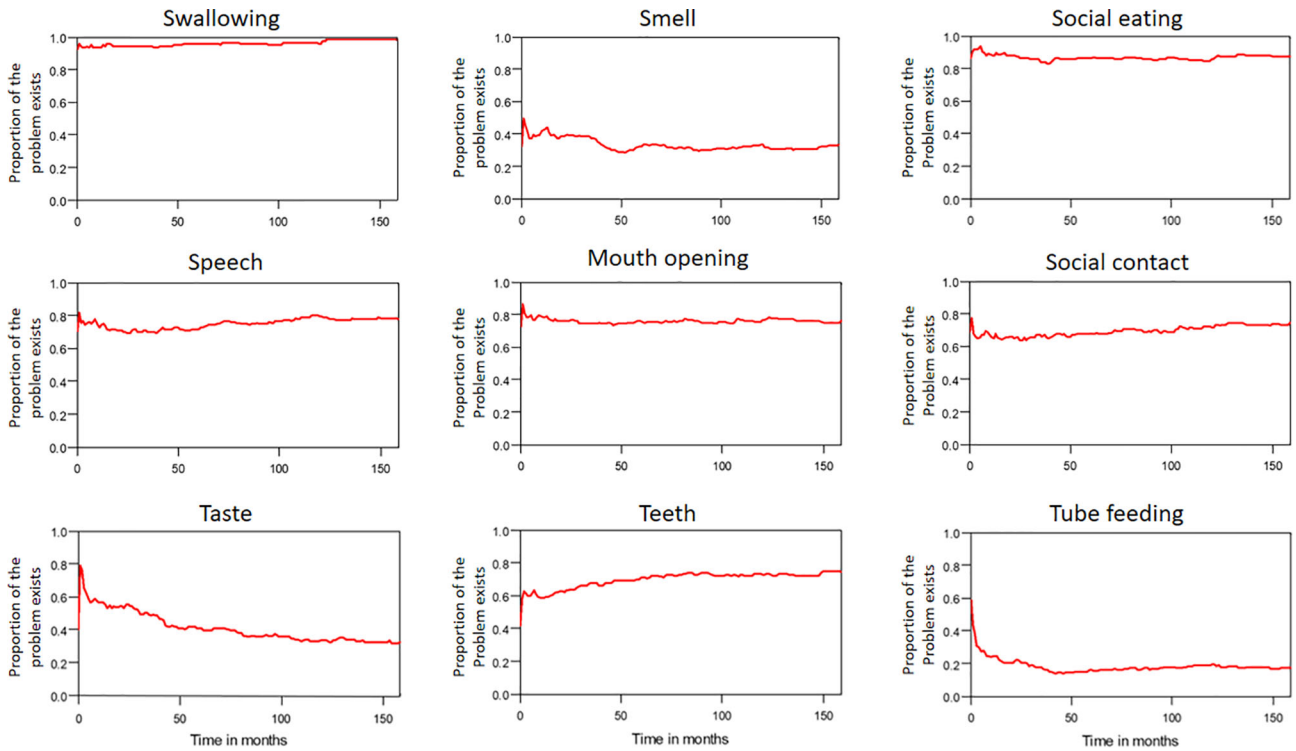

FIGURE 8 | The trends of different problems in patients with OSCC.

making (48), our data could yield useful information about resource allocation in advanced OSCC care.

This study has several limitations. First, the QALE and SWPS may have been overestimated for the following reasons. During extrapolation, the assumption of a constant level of QoL near the end of follow-up may have been distorted because real QoL usually declines with age (49). Moreover, patients who survived longer might have had a better QoL and completed more questionnaires (50). Further studies involving the administration of long-term QoL questionnaires and longer follow-up periods are warranted to confirm our findings. Second, the reference population utility was assumed to be 1 for the survival duration. Therefore, the loss of QALE among patients with OSCC may have been overestimated. Notably, Chung et al. indicated that women had an older mean age at diagnosis, less LE reduction, and a longer estimated QALE than men (15). However, our cohort had only two women with OSCC who completed the QoL questionnaires. Given that the computed tomography of chest was not routinely performed during staging workup in this study, small lung metastasis may have been underestimated and could negatively impact the patient's prognosis and QoL (51). This potential confounding factor may need to be considered in the results interpretation. Another potential confounding factor is that the improvement of the surgeon's technique and experience may lead to the better survival and QoL outcomes in patients who were treated in the later period of this study. Although our results involve intuitive assessment and appear reasonable, their interpretation should be made with these limitations in mind.

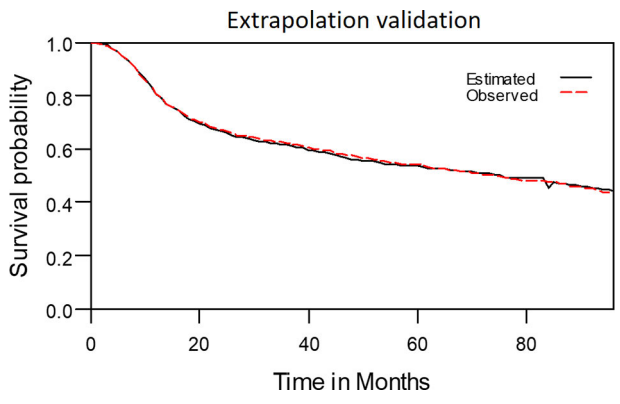

FIGURE 9 | The observed 8-year survival curve and the estimated 8-year survival curve matched properly.

In conclusion, patients with advanced OSCC had an estimated LE and QALE of 8.7 years and 7.7 QALYs, respectively, and estimated LE and QALE losses of 19.0 years and 20.0 QALYs, respectively. The data on SWPS indicated that patients experienced multiple ongoing problems and functional disabilities over a long period of time following curative treatments. Future studies should evaluate whether information obtained from data on QALE and SWPS can be used to allocate health care resources and assess the

impacts of surgery with different neoadjuvant or adjuvant protocols in patients with OSCC.

DATA AVAILABILITY STATEMENT

The raw data supporting the conclusions of this article will be made available by the authors, without undue reservation.

ETHICS STATEMENT

The studies involving human participants were reviewed and approved by Institutional review board of Chang Gung Memorial Hospital (No. 102-2668B). The patients/participants provided their written informed consent to participate in this study.

AUTHOR CONTRIBUTIONS

C-HL and W-CC were involved in the conception and design. M-ST, C-MH, and G-HC were involved in the analysis and data interpretation. Y-TT and CHL drafted the manuscript. Y-CL, C-CF, and EH revised the manuscript critically for intellectual content. All authors contributed to the article and approved the submitted version.

FUNDING

This study was supported by the Chang Gung Memorial Hospital (grant numbers: CORPG6D0251-3).The funding source had no role in the design of this study and had no role during its execution, analyses, interpretation of the data, or decision to submit results.

REFERENCES

1. Vokes EE, Weichselbaum RR, Lippman SM, Hong WK. Head and Neck Cancer. *N Engl J Med* (1993) 328(3):184–94. doi: 10.1056/NEJM199301213280306
2. Onizawa K, Nishihara K, Yamagata K, Yusa H, Yanagawa T, Yoshida H. Factors Associated With Diagnostic Delay of Oral Squamous Cell Carcinoma. *Oral Oncol* (2003) 39(8):781–8. doi: 10.1016/s1368-8375(03)00075-7
3. Lai CH, Chen WC, Fang CC, Chen MF. Survival-Weighted Health Profiles in Nasopharyngeal Cancer Patients. *Front Oncol* (2021) 11:635667. doi: 10.3389/fonc.2021.635667
4. Abbas S, Tariq MUU, Raheem A, Saeed J, Hashmi SS, Karim M, et al. Assessment of Factors Affecting Quality of Life in Oral Squamous Cell Carcinoma Patients Using University of Washington Quality of Life Questionnaire. *Cureus* (2019) 11(1):e3904. doi: 10.7759/cureus.3904
5. List MA, Ritter-Sterr CA, Baker TM, Colangelo LA, Matz G, Pauloski BR, et al. Longitudinal Assessment of Quality of Life in Laryngeal Cancer Patients. *Head Neck* (1996) 18(1):1–10. doi: 10.1002/(SICI)1097-0347(199601/02)18:1<1::AID-HED1>3.0.CO;2-7
6. Neilson KA, Pollard AC, Boonzaier AM, Corry J, Castle DJ, Mead KR, et al. Psychological Distress (Depression and Anxiety) in People With Head and Neck Cancers. *Med J Aust* (2010) 193(S5):S48–51. doi: 10.5694/j.1326-5377.2010.tb03928.x
7. Sawada NO, de Paula JM, Sonobe HM, Zago MM, Guerrero GP, Nicolussi AC. Depression, Fatigue, and Health-Related Quality of Life in Head and Neck Cancer Patients: A Prospective Pilot Study. *Support Care Cancer* (2012) 20(11):2705–11. doi: 10.1007/s00520-012-1390-2
8. Penedo FJ, Traeger L, Benedict C, Thomas G, Dahn JR, Krause MH, et al. Perceived Social Support as a Predictor of Disease-Specific Quality of Life in Head-and-Neck Cancer Patients. *J Support Oncol* (2012) 10(3):119–23. doi: 10.1016/j.suponc.2011.09.002
9. Borggreven PA, Verdonck-de Leeuw IM, Muller MJ, Heiligers ML, de Bree R, Aaronson NK, et al. Quality of Life and Functional Status in Patients With Cancer of the Oral Cavity and Oropharynx: Pretreatment Values of a Prospective Study. *Eur Arch Otorhinolaryngol* (2007) 264(6):651–7. doi: 10.1007/s00405-007-0249-5
10. Rathmell AJ, Ash DV, Howes M, Nicholls J. Assessing Quality of Life in Patients Treated for Advanced Head and Neck Cancer. *Clin Oncol (R Coll Radiol)* (1991) 3(1):10–6. doi: 10.1016/s0936-6555(05)81034-9
11. McDonough EM, Varvares MA, Dunphy FR, Dunleavy T, Dunphy CH, Boyd JH. Changes in Quality-of-Life Scores in a Population of Patients Treated for Squamous Cell Carcinoma of the Head and Neck. *Head Neck* (1996) 18(6):487–93. doi: 10.1002/(SICI)1097-0347(199611/12)18:6<487::AID-HED1>3.0.CO;2-Z
12. de Oliveira Faria S, Howell D, Vamondes Kulcsar MA, Eluf-Neto J. Nutritional Outcomes in Head and Neck Cancer Patients: Is Intensive Nutritional Care Worth It? *Cancer Treat Res Commun* (2020) 25:100233. doi: 10.1016/j.ctarc.2020.100233
13. Hsu C, Wang JD, Hwang JS, Tien HF, Chang SM, Cheng AL, et al. Survival-Weighted Health Profile for Long-Term Survivors of Acute Myelogenous Leukemia. *Qual Life Res* (2003) 12(5):503–17. doi: 10.1023/a:1025043113819
14. Lai CH, Chen MF, Fang FM, Chen WC. Estimation of Life Expectancy and Quality-Adjusted Life Expectancy in Non-Metastatic Nasopharyngeal Cancer Patients Treated by Intensity-Modulated Radiotherapy With or Without Chemotherapy. *Oral Oncol* (2014) 50(7):646–50. doi: 10.1016/j.oraloncology.2014.03.011
15. Chung CH, Hu TH, Wang JD, Hwang JS. Estimation of Quality-Adjusted Life Expectancy of Patients With Oral Cancer: Integration of Lifetime Survival With Repeated Quality-of-Life Measurements. *Value Health Reg Issues* (2020) 21:59–65. doi: 10.1016/j.vhri.2019.07.005
16. Lin CY, Fan KH, Lee LY, Hsueh C, Yang LY, Ng SH, et al. Precision Adjuvant Therapy Based on Detailed Pathologic Risk Factors for Resected Oral Cavity Squamous Cell Carcinoma: Long-Term Outcome Comparison of Cgmh and Nccn Guidelines. *Int J Radiat Oncol Biol Phys* (2020) 106(5):916–25. doi: 10.1016/j.ijrobp.2019.08.058
17. Aaronson NK, Ahmedzai S, Bergman B, Bullinger M, Cull A, Duez NJ, et al. The European Organization for Research and Treatment of Cancer Qlq-C30: A Quality-of-Life Instrument for Use in International Clinical Trials in Oncology. *J Natl Cancer Inst* (1993) 85(5):365–76. doi: 10.1093/jnci/85.5.365
18. Bjordal K, Hammerlid E, Ahlner-Elmqvist M, de Graeff A, Boysen M, Evensen JF, et al. Quality of Life in Head and Neck Cancer Patients: Validation of the European Organization for Research and Treatment of Cancer Quality of Life Questionnaire-H&N35. *J Clin Oncol* (1999) 17(3):1008–19. doi: 10.1200/JCO.1999.17.3.1008
19. Bjordal K, Kaasa S. Psychometric Validation of the Eortc Core Quality of Life Questionnaire, 30-Item Version and a Diagnosis-Specific Module for Head and Neck Cancer Patients. *Acta Oncol* (1992) 31(3):311–21. doi: 10.3109/02841869209108178
20. Chie WC, Hong RL, Lai CC, Ting LL, Hsu MM. Quality of Life in Patients of Nasopharyngeal Carcinoma: Validation of the Taiwan Chinese Version of the Eortc Qlq-C30 and the Eortc Qlq-H&N35. *Qual Life Res* (2003) 12(1):93–8. doi: 10.1023/a:1022070220328
21. Yang Z, Meng Q, Luo J, Lu Q, Li X, Li G, et al. Development and Validation of the Simplified Chinese Version of Eortc Qlq-H&N35 for Patients With Head and Neck Cancer. *Support Care Cancer* (2012) 20(7):1555–64. doi: 10.1007/s00520-011-1247-0
22. King MT. The Interpretation of Scores From the Eortc Quality of Life Questionnaire Qlq-C30. *Qual Life Res* (1996) 5(6):555–67. doi: 10.1007/BF00439229
23. Chang TJ, Tarn YH, Hsieh CL, Liou WS, Shaw JW, Chiou XG. Taiwanese Version of the Eq-5d: Validation in a Representative Sample of the Taiwanese

Population. *J Formos Med Assoc* (2007) 106(12):1023–31. doi: 10.1016/S0929-6646(08)60078-9
24. Lee HY, Hung MC, Hu FC, Chang YY, Hsieh CL, Wang JD. Estimating Quality Weights for Eq-5d (Euroqol-5 Dimensions) Health States With the Time Trade-Off Method in Taiwan. *J Formos Med Assoc* (2013) 112(11):699–706. doi: 10.1016/j.jfma.2012.12.015
25. Hwang JS, Wang JD. Monte Carlo Estimation of Extrapolation of Quality-Adjusted Survival for Follow-Up Studies. *Stat Med* (1999) 18(13):1627–40. doi: 10.1002/(sici)1097-0258(19990715)18:13<1627::aid-sim159>3.0.co;2-d
26. Hwang JS, Tsauo JY, Wang JD. Estimation of Expected Quality Adjusted Survival by Cross-Sectional Survey. *Stat Med* (1996) 15(1):93–102. doi: 10.1002/(SICI)1097-0258(19960115)15:1<93::AID-SIM155>3.0.CO;2-2
27. Hwang JS, Wang JD. Integrating Health Profile With Survival for Quality of Life Assessment. *Qual Life Res* (2004) 13(1):1–10; discussion 11-4. doi: 10.1023/B:QURE.0000015299.45623.38
28. Lai WW, Chung CH, Lin CN, Yang SC, Hwang JS, Wang JD. Qalys and Medical Costs Saved From Prevention of a Cancer: Analysis of Nation-Wide Real-World Data of Taiwan With Lifetime Horizon. *J Formos Med Assoc* (2021). doi: 10.1016/j.jfma.2021.04.023
29. Chu PC, Wang JD, Hwang JS, Chang YY. Estimation of Life Expectancy and the Expected Years of Life Lost in Patients With Major Cancers: Extrapolation of Survival Curves Under High-Censored Rates. *Value Health* (2008) 11 (7):1102–9. doi: 10.1111/j.1524-4733.2008.00350.x
30. Lee HY, Hwang JS, Jeng JS, Wang JD. Quality-Adjusted Life Expectancy (Qale) and Loss of Qale for Patients With Ischemic Stroke and Intracerebral Hemorrhage: A 13-Year Follow-Up. *Stroke* (2010) 41(4):739–44. doi: 10.1161/STROKEAHA.109.573543
31. Kao HK, Guo LF, Cheng MH, Chen IH, Liao CT, Fang KH, et al. Predicting Postoperative Morbidity and Mortality by Model for Endstage Liver Disease Score for Patients With Head and Neck Cancer and Liver Cirrhosis. *Head Neck* (2011) 33(4):529–34. doi: 10.1002/hed.21486
32. Healy KO, Waksmonski CA, Altman RK, Stetson PD, Reyentovich A, Maurer MS. Perioperative Outcome and Long-Term Mortality for Heart Failure Patients Undergoing Intermediate- and High-Risk Noncardiac Surgery: Impact of Left Ventricular Ejection Fraction. *Congest Heart Fail* (2010) 16 (2):45–9. doi: 10.1111/j.1751-7133.2009.00130.x
33. Foster CC, Melotek JM, Brisson RJ, Seiwert TY, Cohen EEW, Stenson KM, et al. Definitive Chemoradiation for Locally-Advanced Oral Cavity Cancer: A 20-Year Experience. *Oral Oncol* (2018) 80:16–22. doi: 10.1016/j.oraloncology.2018.03.008
34. Stenson KM, Kunnavakkam R, Cohen EE, Portugal LD, Blair E, Haraf DJ, et al. Chemoradiation for Patients With Advanced Oral Cavity Cancer. *Laryngoscope* (2010) 120(1):93–9. doi: 10.1002/lary.20716
35. Liao CT, Kang CJ, Lee LY, Hsueh C, Lin CY, Fan KH, et al. Association Between Multidisciplinary Team Care Approach and Survival Rates in Patients With Oral Cavity Squamous Cell Carcinoma. *Head Neck* (2016) 38 Suppl 1:E1544–53. doi: 10.1002/hed.24276
36. Wu TY, Chung CH, Lin CN, Hwang JS, Wang JD. Lifetime Risks, Loss of Life Expectancy, and Health Care Expenditures for 19 Types of Cancer in Taiwan. *Clin Epidemiol* (2018) 10:581–91. doi: 10.2147/CLEP.S155601
37. Nemeth D, Zaleczna L, Huremovic A, Engelmann J, Poeschl PW, Strasz M, et al. Importance of Chewing, Saliva, and Swallowing Function in Patients With Advanced Oral Cancer Undergoing Preoperative Chemoradiotherapy: A Prospective Study of Quality of Life. *Int J Oral Maxillofac Surg* (2017) 46 (10):1229–36. doi: 10.1016/j.ijom.2017.05.005
38. Bjordal K, Freng A, Thorvik J, Kaasa S. Patient Self-Reported and Clinician-Rated Quality of Life in Head and Neck Cancer Patients: A Cross-Sectional Study. *Eur J Cancer B Oral Oncol* (1995) 31B(4):235–41. doi: 10.1016/0964-1955(95)00010-f
39. Langius A, Bjorvell H and Lind MG. Functional Status and Coping in Patients With Oral and Pharyngeal Cancer Before and After Surgery. *Head Neck* (1994) 16(6):559–68. doi: 10.1002/hed.2880160611
40. Rapoport Y, Kreitler S, Chaitchik S, Algor R, Weissler K. Psychosocial Problems in Head-and-Neck Cancer Patients and Their Change With Time Since Diagnosis. *Ann Oncol* (1993) 4(1):69–73. doi: 10.1093/oxfordjournals.annonc.a058365
41. Howren MB, Christensen AJ, Karnell LH, Funk GF. Psychological Factors Associated With Head and Neck Cancer Treatment and Survivorship: Evidence and Opportunities for Behavioral Medicine. *J Consult Clin Psychol* (2013) 81(2):299–317. doi: 10.1037/a0029940
42. Pourel N, Peiffert D, Lartigau E, Desandes E, Luporsi E, Conroy T. Quality of Life in Long-Term Survivors of Oropharynx Carcinoma. *Int J Radiat Oncol Biol Phys* (2002) 54(3):742–51. doi: 10.1016/s0360-3016(02)02959-0
43. de Graeff A, de Leeuw JR, Ros WJ, Hordijk GJ, Blijham GH, Winnubst JA. Long-Term Quality of Life of Patients With Head and Neck Cancer. *Laryngoscope* (2000) 110(1):98–106. doi: 10.1097/00005537-200001000-00018
44. Brazier JE, Dixon S, Ratcliffe J. The Role of Patient Preferences in Cost-Effectiveness Analysis: A Conflict of Values? *Pharmacoeconomics* (2009) 27 (9):705–12. doi: 10.2165/11314840-000000000-00000
45. Velikova G, Wright P, Smith AB, Stark D, Perren T, Brown J, et al. Self-Reported Quality of Life of Individual Cancer Patients: Concordance of Results With Disease Course and Medical Records. *J Clin Oncol* (2001) 19 (7):2064–73. doi: 10.1200/JCO.2001.19.7.2064
46. Lang K, Menzin J, Earle CC, Jacobson J, Hsu MA. The Economic Cost of Squamous Cell Cancer of the Head and Neck: Findings From Linked Seer-Medicare Data. *Arch Otolaryngol Head Neck Surg* (2004) 130(11):1269–75. doi: 10.1001/archotol.130.11.1269
47. Schernberg A, Sagaon-Teyssier L, Schwarzinger MGroup ES. Clinical and Economic Burden of Head and Neck Cancer: A Nationwide Retrospective Cohort Study From France. *Clinicoecon Outcomes Res* (2019) 11:441–51. doi: 10.2147/CEOR.S198312
48. Garau M, Shah KK, Mason AR, Wang Q, Towse A, Drummond MF. Using Qalys in Cancer: A Review of the Methodological Limitations. *Pharmacoeconomics* (2011) 29(8):673–85. doi: 10.2165/11588250-000000000-00000
49. Orpana HM, Ross N, Feeny D, McFarland B, Bernier J, Kaplan M. The Natural History of Health-Related Quality of Life: A 10-Year Cohort Study. *Health Rep* (2009) 20(1):29–35.
50. Fryback DG, Dunham NC, Palta M, Hanmer J, Buechner J, Cherepanov D, et al. Us Norms for Six Generic Health-Related Quality-of-Life Indexes From the National Health Measurement Study. *Med Care* (2007) 45(12):1162–70. doi: 10.1097/MLR.0b013e31814848f1
51. Langendijk JA, de Jong MA, Leemans CR, de Bree R, Smeele LE, Doornaert P, et al. Postoperative Radiotherapy in Squamous Cell Carcinoma of the Oral Cavity: The Importance of the Overall Treatment Time. *Int J Radiat Oncol Biol Phys* (2003) 57(3):693–700. doi: 10.1016/s0360-3016(03)00624-2

Conflict of Interest: The authors declare that the research was conducted in the absence of any commercial or financial relationships that could be construed as a potential conflict of interest.

Publisher's Note: All claims expressed in this article are solely those of the authors and do not necessarily represent those of their affiliated organizations, or those of the publisher, the editors and the reviewers. Any product that may be evaluated in this article, or claim that may be made by its manufacturer, is not guaranteed or endorsed by the publisher.

frontiers in Oncology

ORIGINAL RESEARCH
published: 01 October 2021
doi: 10.3389/fonc.2021.743611

Development and Validation of an Autophagy-Related LncRNA Prognostic Signature in Head and Neck Squamous Cell Carcinoma

Lin Shen, Na Li, Qin Zhou, Zhanzhan Li and Liangfang Shen*

Department of Oncology, Xiangya Hospital, Central South University, Changsha, China

Head and neck squamous cell carcinoma (HNSCC) is one of the greatest public challenges because of delayed diagnosis and poor prognosis. In this study, we established an autophagy-associated long non-coding (Lnc)RNA prognostic signature to assess the prognosis of HNSCC patients. The LncRNA expression profiles and clinical information of 499 HNSCC samples were available in The Cancer Genome Atlas. Autophagic LncRNAs were analyzed using Pearson correlation. A co-expression network showed the interactions between autophagic genes and LncRNAs. An autophagic LncRNAs prognostic signature, consisting of MYOSLID, AL139287.1, AC068580.1, AL022328.2, AC104083.1, AL160006.1, AC116914.2, LINC00958, and AL450992.2, was developed through uni- and multivariate Cox regressions. High- and low-risk groups were classified based on the median risk scores. The high-risk group had significantly worse overall survival according to Kaplan–Meier curve analysis. Multivariate Cox regression demonstrated that risk scores were a significant independent prognostic factor (hazard ratio = 1.739, 95% confidence interval: 1.460–2.072), with an area under the curve of 0.735. Principal component analysis distinguished two categories based on the nine-LncRNA prognostic signature. In conclusion, this novel autophagic LncRNA signature is an independent prognostic factor and may suggest novel therapeutic targets for HNSCC.

Keywords: autophagy, head and neck squamous carcinoma, long non-coding RNA, overall survival, prognostic signature

OPEN ACCESS

Edited by:
Heming Lu,
People's Hospital of Guangxi Zhuang Autonomous Region, China

Reviewed by:
Lingzhang Meng,
Youjiang Medical University for Nationalities, China
Min Kang,
Guangxi Medical University, China

****Correspondence:***
Zhanzhan Li
lizhanzhan@csu.edu.cn

Specialty section:
This article was submitted to Head and Neck Cancer, a section of the journal Frontiers in Oncology

Received: *19 July 2021*
Accepted: *08 September 2021*
Published: *01 October 2021*

Citation:
Shen L, Li N, Zhou Q, Li Z and Shen L (2021) Development and Validation of an Autophagy-Related LncRNA Prognostic Signature in Head and Neck Squamous Cell Carcinoma. Front. Oncol. 11:743611. doi: 10.3389/fonc.2021.743611

INTRODUCTION

Head and neck squamous cell carcinomas (HNSCCs) are common tumors that rank eighth worldwide in terms of incidence and mortality. HNSCCs are epithelial carcinomas derived from the oral cavity, nasal cavity, larynx, hypopharynx, and pharynx (1). They have a heterogeneous etiology based on multistage progression, genetic alterations, and environmental factors (2).

Excessive smoking, alcohol consumption, and human papillomavirus infections are known risk factors for HNSCC development (3, 4). The initial symptoms, such as nasal congestion, oral ulcers, sore throat, and hoarseness, mimic common illnesses and often lead to late diagnoses. Although the diagnostic and treatment modalities for HNSCCs are rapidly improving, the 5-year survival rate has not increased significantly in the past few years, and the prognosis remains poor (5).

Long non-coding RNAs (LncRNAs) are non-protein-coding transcribed RNAs with more than 200 base pairs (6). LncRNAs were previously regarded as "dark matter" and "transcriptional noise" without biofunctions, but recent studies have demonstrated that many LncRNAs are involved in important bioactivities, such as chromatin modification, transcriptional activation and interference, and cell differentiation and proliferation (7–9). LncRNAs are mostly found in the nucleus, particularly in the chromatin fraction, which underlines their regulatory role in gene transcription. Moreover, genome-wide tumor association studies have revealed that thousands of LncRNAs are associated with tumorigenesis and metastasis (10, 11). LncRNAs are considered novel biomarkers for guiding treatment due to recent advances in our understanding the molecular mechanisms underlying cancer-related LncRNAs (12, 13).

Autophagy is a physiological process that membrane-encloses damaged or degenerated proteins and organelles, and delivers them to lysosomes for degradation (14). Autophagic dysregulation is related to various diseases, including neurodegenerative, inflammatory, cardiovascular, and neoplastic disorders (15–18). Predictive functions of autophagy in various cancers are gradually being explored. An autophagy-related gene signature was recently reported to be closely related with HNSCC outcomes (19, 20). Another autophagic LncRNA signature was found to accurately predict the prognoses of bladder urothelial carcinomas (21). Although autophagic genes and LncRNAs can reportedly serve as HNSCC biomarkers, their prognostic value remains unclear. Our study aimed to clarify the prognostic functions of autophagy-associated LncRNAs in HNSCC.

METHODS

Data Acquisition

Messenger RNA (mRNA) sequences and clinical data of HNSCC patients and controls (peritumor tissues) were acquired from The Cancer Genome Atlas (TCGA; https://cancergenome.nih.gov/). The inclusion criteria were HNSCC patients; complete LncRNA expression data and clinical information; and follow-up duration longer than 30 days. Complete clinical information, including age, sex, tumor grade, American Joint Committee on Cancer (AJCC) stage, TNM stage, and survival data, were downloaded for analysis. Autophagic genes were acquired from the Human Autophagy Database (http://autophagy.lu/index.html). Simple nucleotide variations of HNSCC were also downloaded from TCGA.

As our data were publicly available, no specific ethical approval or informed consent was required.

Identification of Autophagic LncRNAs

LncRNA expression profiles of HNSCC patients were obtained from TCGA. All data were standardized using the limma package for R software (v.3.6.3; R Foundation for Statistical Computing, Vienna, Austria) before further analysis. Pearson correlation analyses were performed on LncRNAs and autophagic genes in HNSCC patients using R software (v.3.6.3). A correlation coefficient (R) > 0.3 and p-value < 0.001 were considered significant for autophagic LncRNAs. A co-expression network between autophagic LncRNAs and genes was also built using Cytoscape (v.3.8.2).

Establishment of Prognostic Signature

Uni- and multivariate Cox regression analyses were performed to establish potential prognostic signatures. First, the association between autophagic LncRNAs and survival rates was assessed by univariate Cox regression. $p < 0.01$ was regarded significant for prognosis-related LncRNAs in HNSCC patients. Multivariate Cox regression analysis was then performed for the selected prognostic LncRNAs. A risk-score-based prognostic signature was computed as follows: risk score = $\mathrm{lncRNA1}_{\beta\times\mathrm{Expression}}$ + $\mathrm{lncRNA2}_{\beta\times\mathrm{Expression}}$ + $\mathrm{lncRNA(N)}_{\beta\times\mathrm{Expression}}$ (22).

Prognosis Prediction

According to the formula above, HNSCC patients were classified into high- and low-risk groups based on median risk scores. A Kaplan–Meier curve was plotted to compare survival between groups using the two-sided log-rank test. Uni- and multivariate Cox regressions were performed to evaluate the effect of clinical variables on survival in HNSCC patients and to determine if the risk scores were independent prognostic factors. Predictive accuracy was determined by calculating the area under the receiver operating characteristic (ROC) curve (AUC). We also investigated the association of the expression level of each autophagic LncRNA with overall survival (OS) in HNSCC patients using Kaplan–Meier curves. To clarify the impact of single autophagy-related LncRNAs on HNSCC prognosis, we assessed their associations with the various clinical characteristics using Student's t-test or one-way analysis of variance (ANOVA).

Functional Analysis

Principal component analysis (PCA) was performed to determine similarities and differences between the autophagic-LncRNA and whole expression profiles of HNSCC patients. Functional enrichment was assessed using gene set enrichment analysis (GSEA; v.4.0.3; http://www.broadinstitute.org/gsea/index.jsp). We verified whether or not differentially expressed genes between high- and low-risk groups were enriched in autophagy-related processes.

Prognostic Signature Validation

We detected the expression of nine autophagic LncRNAs in 190 HNSCC patients, which were used for prognostic signature

validation. The validation data were provided by the Ethics Committee of Xiangya Hospital, Central South University. All HNSCC cases were pathologically confirmed; the clinical characteristics are shown in **Table S1**.

The expression levels of target LncRNAs were measured using real-time polymerase chain reaction (RT-PCR). Total RNA was extracted from the tissue specimens using the GeneJET RNA purification kit (Thermo Fisher Scientific, Waltham, MA, USA) according to manufacturer's instructions. Complementary DNAs (cDNAs) were synthesized using SuperScript III Reverse Transcriptase (Invitrogen; Thermo Fisher Scientific). LncRNA expression was assessed by RT-PCR ([model]; Bio-Rad Laboratories Inc., Hercules, CA, USA). Expression levels were quantified using the $2^{-\Delta\Delta Ct}$ method.

Statistical Analysis

All statistical analyses were performed using R software (v.4.0.5). Survival probabilities were compared between groups using Kaplan–Meier curve analysis. The diagnostic accuracy of the signature was evaluated by ROC curve analysis. Nomographs were plotted to estimate the 1-, 3-, and 5-year OS rates of individuals according to different risk scores and clinical parameters. Pearson and Spearman correlation analyses were performed. Simple nucleotide variations were analyzed using the maftools R package. $p < 0.05$ was considered significant.

RESULTS

Identification of Prognostic Autophagy-Related LncRNAs

We identified 14,142 LncRNAs by RNA-sequence analysis of HNSCC patients from TCGA. We also obtained 257 autophagy-related genes from a public database (**Table S2**). In total, 910 autophagy-related LncRNAs met the criteria ($R > 0.3$ and $p < 0.001$). Cox regression analyses were then performed to determine the autophagy-related LncRNAs with potential prognostic value for HNSCC (**Table S3**). Of the 910 LncRNAs, 18 were linked with the OS of HNSCC patients. Multivariate Cox regression showed that 9 of those 18 LncRNAs (MYOSLID, AL139287.1, AC068580.1, AL022328.2, AC104083.1, AL160006.1, AC116914.2, LINC00958, and AL450992.2) were involved in the prognostic signature (**Figures 1A**, **S1A–I** and **Table S4**).

Establishment of the Nine-LncRNA Prognostic Signature

The risk score of the HNSCC patients was calculated as follows: risk score = $(0.0236 \times Exp_{MYOSLID}) + (-0.0890 \times Exp_{AL139287.1}) + (-0.3069 \times Exp_{AC068580.1}) + (0.2869 \times Exp_{AL022328.2}) + (-0.0802 \times Exp_{AC104083.1}) + (-0.2112 \times Exp_{AL160006.1}) + (-0.4007 \times Exp_{AC116914.2}) + (0.0140 \times Exp_{LINC00958}) + (-0.0425 \times Exp_{AL450992.2})$. The prognostic value of this nine-LncRNA risk signature for HNSCC patients was evaluated. Based on the median risk scores, 249 and 205 HNSCC patients were classified as high and low risk, respectively. Kaplan–Meier curve analysis revealed significant differences in OS between the groups; OS was worse in the high-risk group (**Figure 1B**). We ranked the HNSCC patients according to their risk scores based on the nine-LncRNA prognostic signature (**Figure 1C**). The scatter diagram demonstrated that the survival rates of the HNSCC patients were correlated with the risk scores; the mortality rate increased with an increased risk score (**Figure 1D**). The AUC value of the nine lncRNAs was 0.735. The AUC values for age, sex, tumor grade, AJCC stage, T stage, N stage, and M stage were 0.602, 0.451, 0.593, 0.657, 0.594, 0.620, and 0.566, respectively (**Figure 1E**). These results confirmed that the nine-LncRNA prognostic signature could predict the survival outcomes of HNSCC patients.

The LncRNA Signature Was Independently Associated With Prognosis

Multivariate Cox regression based on risk scores and clinical characteristics was performed to determine whether the nine-LncRNA prognostic signature was an independent prognostic factor. Univariate Cox regression demonstrated that the risk score was significantly correlated with OS (**Figure 1F**). Multivariate Cox regression also showed a significant association between the risk score and OS in HNSCC patients (**Figure 1G**).

Clinical Significance of the Prognostic Signature

A nomogram was plotted to evaluate 1-, 3-, and 5-year survival based on the risk score of the prognostic signature and clinical data. The nomogram demonstrated that the risk score was the most significant contributor to the 3- and 5-year OS of HNSCC patients (**Figure 2**). We then investigated the associations of high- and low-risk status with clinical parameters using the Chi-square test. No significant differences in clinical parameters were observed between groups ($p > 0.05$; **Figure 3A**). We also analyzed risk scores according to clinical parameters and found significant differences in relation to survival status and T stage. Patients with poor survival status and advanced T stage had higher risk scores ($p < 0.05$; **Figures 3B, C**). To verify the utility of the prognosis signature, we also performed subgroup analyses based on age (≤ 60 vs. > 60 years; **Figures 4A, B**), sex (**Figures 4C, D**), grade (T1–2 vs. T3–4; **Figures 4E, F**), AJCC stage (stage I–II vs. stage III–IV; **Figures 4G, H**), T stage (T1–2 vs. T3–4; **Figures 4I, J**), and M stage (M0 vs. M1; **Figures 4K, L**). We found that the prognostic signature was related to OS in all strata of the population. The high-risk group had worse OS than the low-risk group.

In addition, we investigated LncRNA expression levels according to the various clinical characteristics. The expression levels of AC116914.2 and AL022328.2 were higher in males compared to females (**Figure S2A**). The expression levels of AL022328.2 and AL450992.2 were higher for higher grades, but the expression of MYOSLID had no correlation with grade (**Figure S2B**). No significant differences were found in expression levels by AJCC stage (**Figure S2C**). The expression levels of AC068580.1, LINC00958, and MYOSLID increased from T1 to T3, but were decreased for T4 (**Figure S2D**).

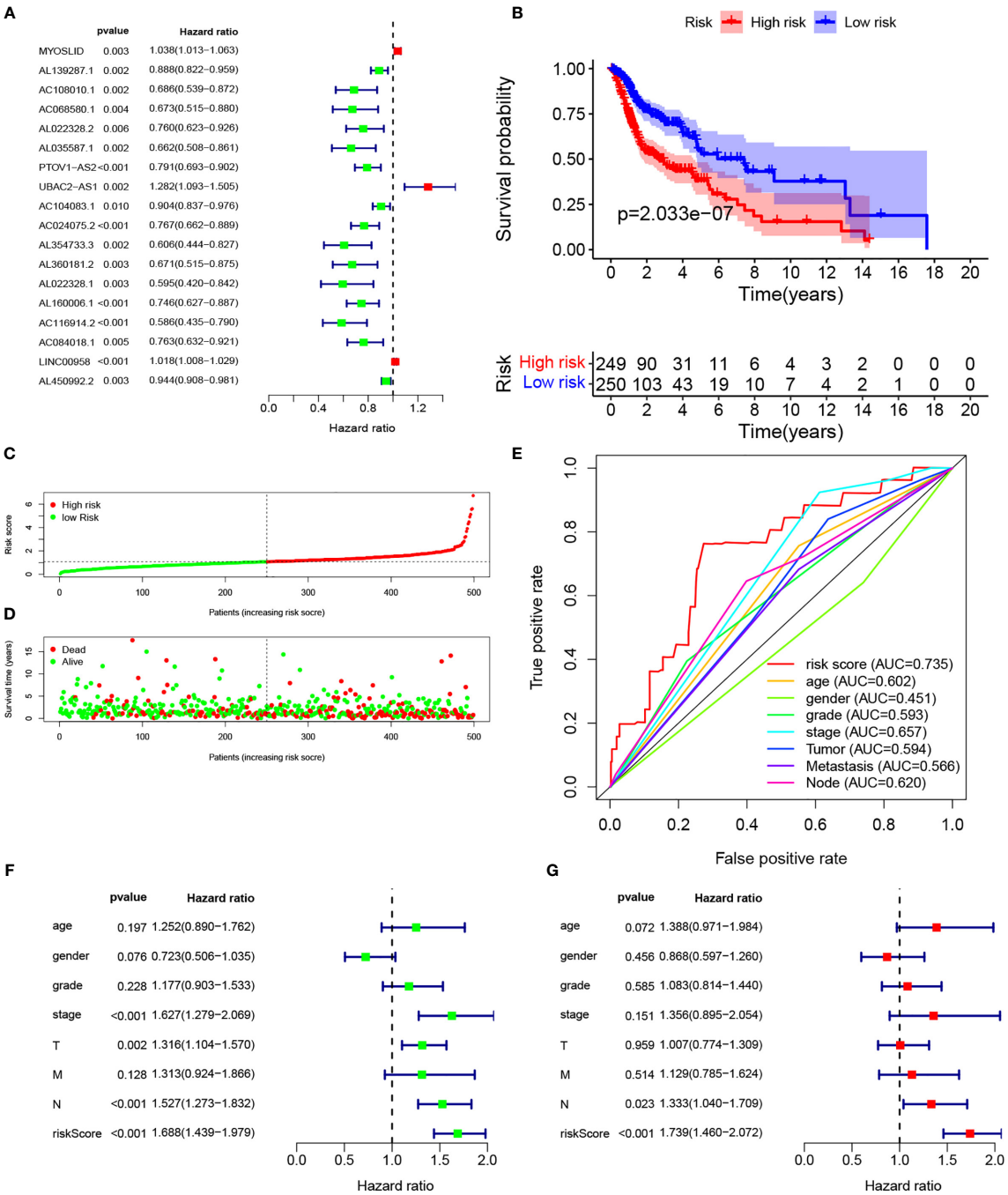

FIGURE 1 | Establishment of autophagy-related lncRNA signature for HNSCC patients. **(A)** Forest plot of univariate Cox regression for autophagic lncRNAs correlated with HNSCC prognosis. **(B)** Kaplan–Meier curves of overall survival for high- and low-risk groups. **(C)** Risk scores of the high- and low-risk groups. **(D)** Scatterplot of risk scores and survival time/survival outcomes. **(E)** ROC curves of prognostic signature and other clinical parameters. **(F, G)** Forest plots of univariate and multivariate Cox regressions, respectively, for association between risk score and overall survival.

The results regarding the N stage were similar to those for the AJCC stages (**Figure S2E**). In terms of the M stage, AL022328.2 and AL139287.1 expression levels were higher, but AC116914.2 expression was lower, in the M1 stage (**Figure S2F**).

Gene Mutations

We analyzed the gene mutation profiles of 492 HNSCC patients based on the risk scores. The high- and low-risk groups consisted of 245 (49.1%) and 247 (49.5%) samples, respectively, while 7

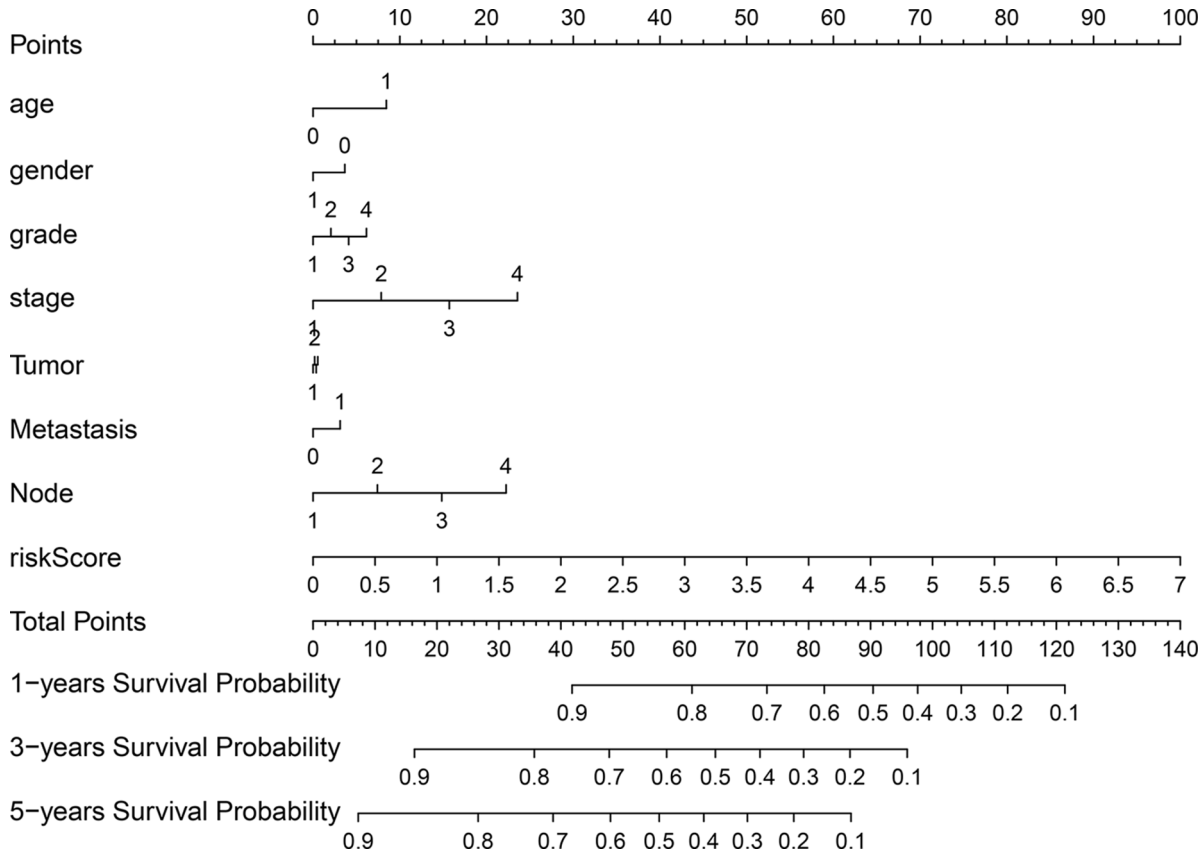

FIGURE 2 | Nomograph of 1-, 3-, and 5-year overall survival probabilities predicted based on autophagy-related LncRNA signature.

(1.4%) samples were excluded because of a lack of mutation data. Waterfall plots were used to evaluate the genes of the patients in the two groups (**Figures 5A, B**). The top 10 mutated genes in the high-risk group were TP53, TTN, FAT1, CDKN2A, NOTCH1, PIK3CA, CASP8, LRP1B, MUC16, and CSMD3. Although some mutated genes overlapped between groups, several genes were more frequent in the high-risk group, including TP53 (p = 0.004), HRAS (p = 0.001), and CASP8 (p = 0.001). Missense mutations accounted for most of the mutations in both groups (**Figures 5C, D**). The single-nucleotide variant was the most common type (**Figures 5E, F**), and C-to-T transversions were the most common single-nucleotide variant (**Figures 5G, H**). The gene cloud plots showed the top mutated genes in the two groups (**Figures 5I, J**).

Co-Expression Network of Autophagy-Related LncRNAs and mRNAs

Studies have suggested that mutual regulation between LncRNAs and mRNAs is critical for tumor progression. We established a co-expression network using Cytoscape. There were 48 mRNAs associated with nine target LncRNAs ($R > 0.3$, $p < 0.001$; **Figure 6A**). Associations among co-expressed mRNAs and LncRNAs in the prognostic signature and risk types were visualized using a Sankey diagram (**Figure 6B**). AL022328.2 was the major component of overall risk, while MYOSLID and LINC00958 accounted for small proportions (**Figure 7B**). The corresponding mRNAs were ATF4, ATG16L2, ATG4B, ATG4D, CAPN10, CDKN1B, HDAC6, IKBKB, ITGA3, MAP2K7, PELP1, RAB24, TSC1, TSC2, ULK3, and WDR45. Among these mRNAs, CAPN10, which is involved in degradation of the extracellular matrix and nitric oxide synthase signaling, was most strongly correlated with AL022328.2. We performed Kyoto Encyclopedia of Genes and Genomes (KEGG) enrichment analysis to identify the co-expressed mRNAs most associated with autophagic LncRNAs, and determined that the top five enriched signaling pathways were involved in autophagy, human papillomavirus infection, PI3K–Akt pathway, human cytomegalovirus infection, and apoptosis (**Figure 6C**).

Functional Analysis

PCA was performed to determine differences in gene distribution between the high- and low-risk groups. No significant differences were found in the whole gene expression profiles of the two groups (**Table S5**), but significant differences were observed within the autophagic-LncRNA set (**Figures 7A, B**). GSEA was used to investigate the functional enrichment of genes. We analyzed 178

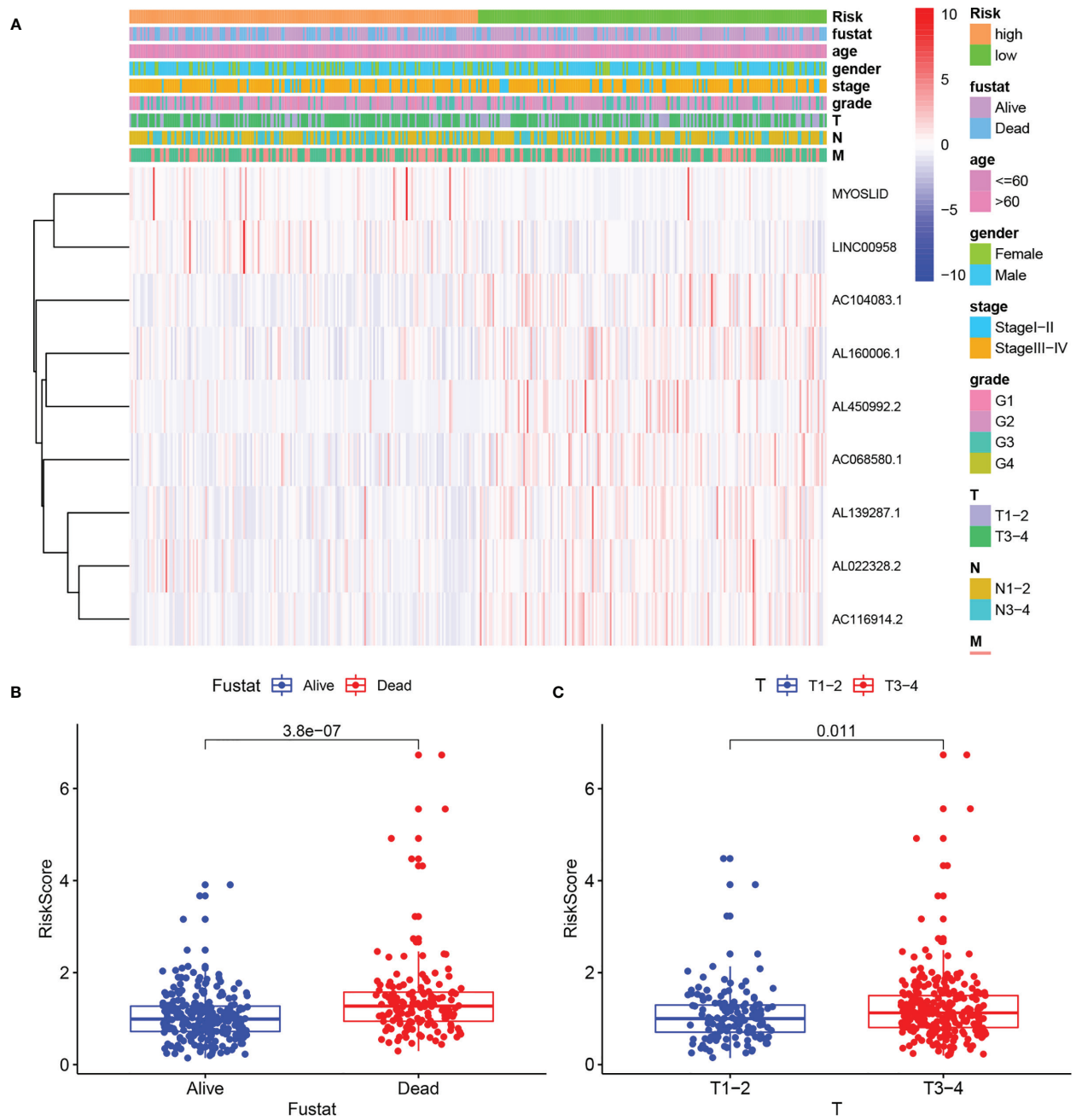

FIGURE 3 | Correlation of risk score with clinical parameters. **(A)** Heatmaps of clinical parameters and autophagy-related LncRNAs between high- and low-risk groups. **(B)** Boxplot of risk score difference between alive and dead groups. **(C)** Boxplot of risk score difference between T stage1–2 and T stage 3–4.

gene sets and found that 14 and 164 were upregulated in the high-risk (**Table S6**) and low-risk (**Table S7**) groups, respectively. KEGG pathway analysis revealed that the proteasome pathways and ribosomes were significantly enriched in the high-risk group (**Figures 7C, D**). ATP-binding cassette transporters (**Figure 7E**), acute myeloid leukemia (**Figure 7F**), B-cell receptor pathway (**Figure 7G**), FC epsilon RI pathway (**Figure 7H**), inositol phosphate metabolism (**Figure 7I**), non-small cell lung cancer (**Figure 7J**), and the phosphatidylinositol system (**Figure 7K**) were highly enriched in the low-risk group.

LncRNA Expression Levels

The expression levels of nine LncRNAs were compared between 502 tumor tissue and 44 normal tissue specimens from TCGA (**Figure S3A**). The results showed that MYOSLID, LINC00958, and AL022328.2 were expressed more, while AL450992.2 and

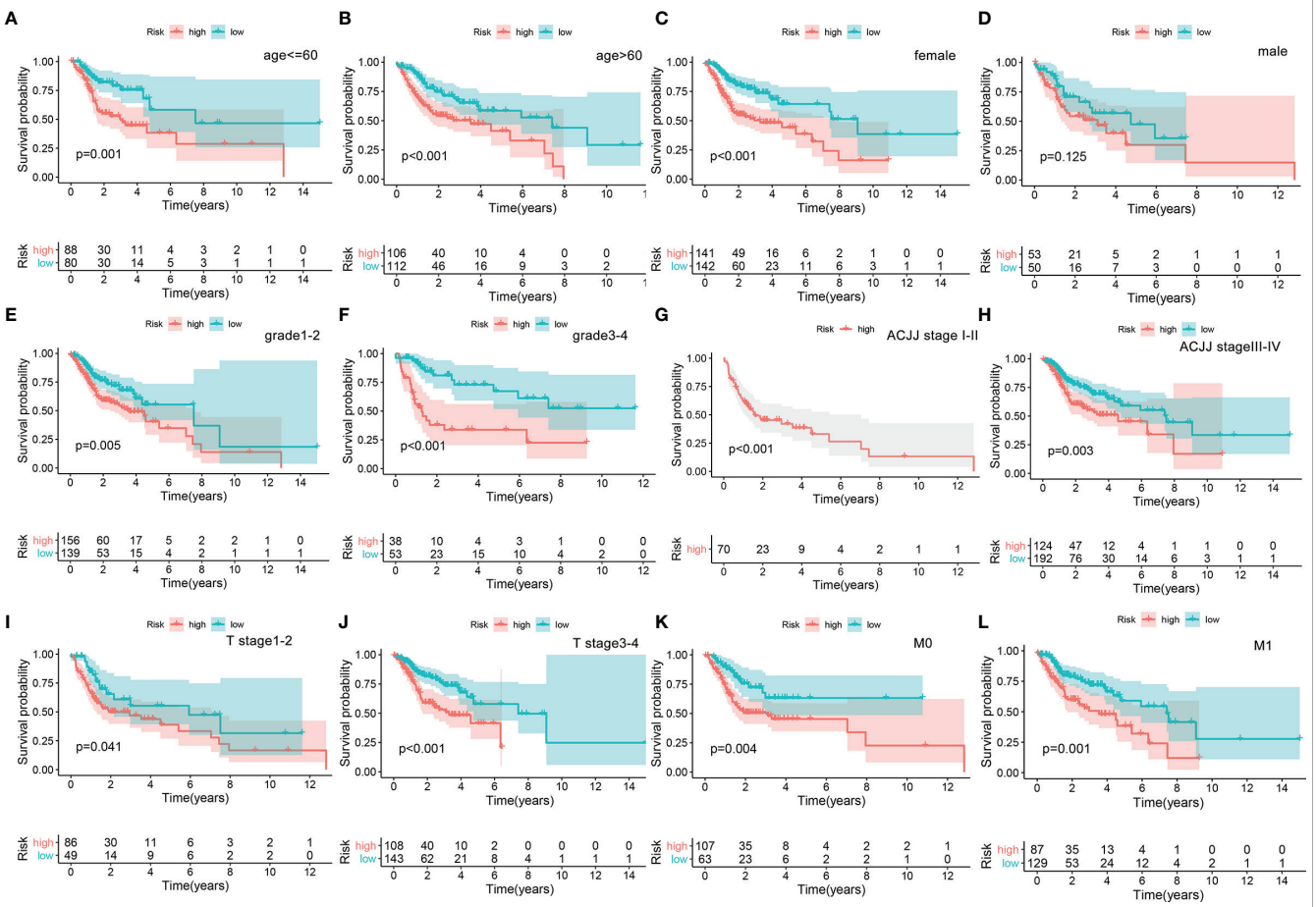

FIGURE 4 | Overall survival difference between high- and low-risk groups for HNSCC patients stratified by clinical parameters, including age [age ≤60, ag e>60, **(A, B)**], gender [female, male, **(C, D)**], grade [G1–2, G3–4, **(E, F)**], AJCC stage [Stage I–II, Stage III–IV, **(G, H)**], T stage [Stage 1–2, Stage 3–4, **(I, J)**], and M stage [M0, M1, **(K, L)**].

AC068580.1 were expressed less, in tumor compared to normal tissues (**Figure S3B**). These results were consistent with our analysis. However, AL104083.1 and AC116914.2 were significant risk factors in multivariate analysis. AL139287.1 and AL160006.1 showed no significant differences between tumor and normal tissues. The expression levels of the nine lncRNAs are presented in **Figure 8E**.

Validation of Prognostic Signature

For HNSCC data validation, we analyzed 190 HNSCC patients, separated into high- and low-risk groups based on the risk score. The results indicated that the high-risk group had worse OS than the low-risk group ($p < 0.05$; **Figure 8A**). The AUC value of the validated data was 0.742 (**Figure 8B**). Univariate Cox regression demonstrated that risk scores (hazard ratio [HR] = 2.035, 95% confidence interval [CI]: 1.541–2.688, $p < 0.001$, **Figure 8C**) and M stage (HR = 1.950, 95% CI: 1.110–3.425, $p = 0.020$) were related to poor OS. Multivariate Cox regression demonstrated that risk scores (HR = 2.082, 95% CI: 1.563–2.773, $p < 0.001$, **Figure 8D**) and M stage (HR = 2.039, 95% CI: 1.140–3.648, $p = 0.016$) were independently correlated with OS.

DISCUSSION

Head and neck cancers are among the most common malignancies worldwide, and about 90% of these are squamous cell carcinomas (23). Surgery combined with chemoradiotherapy provides favorable outcomes in early-stage HNSCC (24, 25). However, early-stage HNSCC patients usually have no obvious symptoms. Most patients are diagnosed at moderate or advanced stages, and about 17% of patients miss the window for surgery. Advanced HNSCCs have a poor prognosis and high recurrence rates (26). Therefore, there is an urgent need to identify potential prognostic biomarkers. Many reports have suggested that biomarkers identified through database mining may predict HNSCC prognosis (27–29). Autophagy can remove harmful substances from the body and keep the internal environment stable (30). However, autophagy can also promote tumor growth

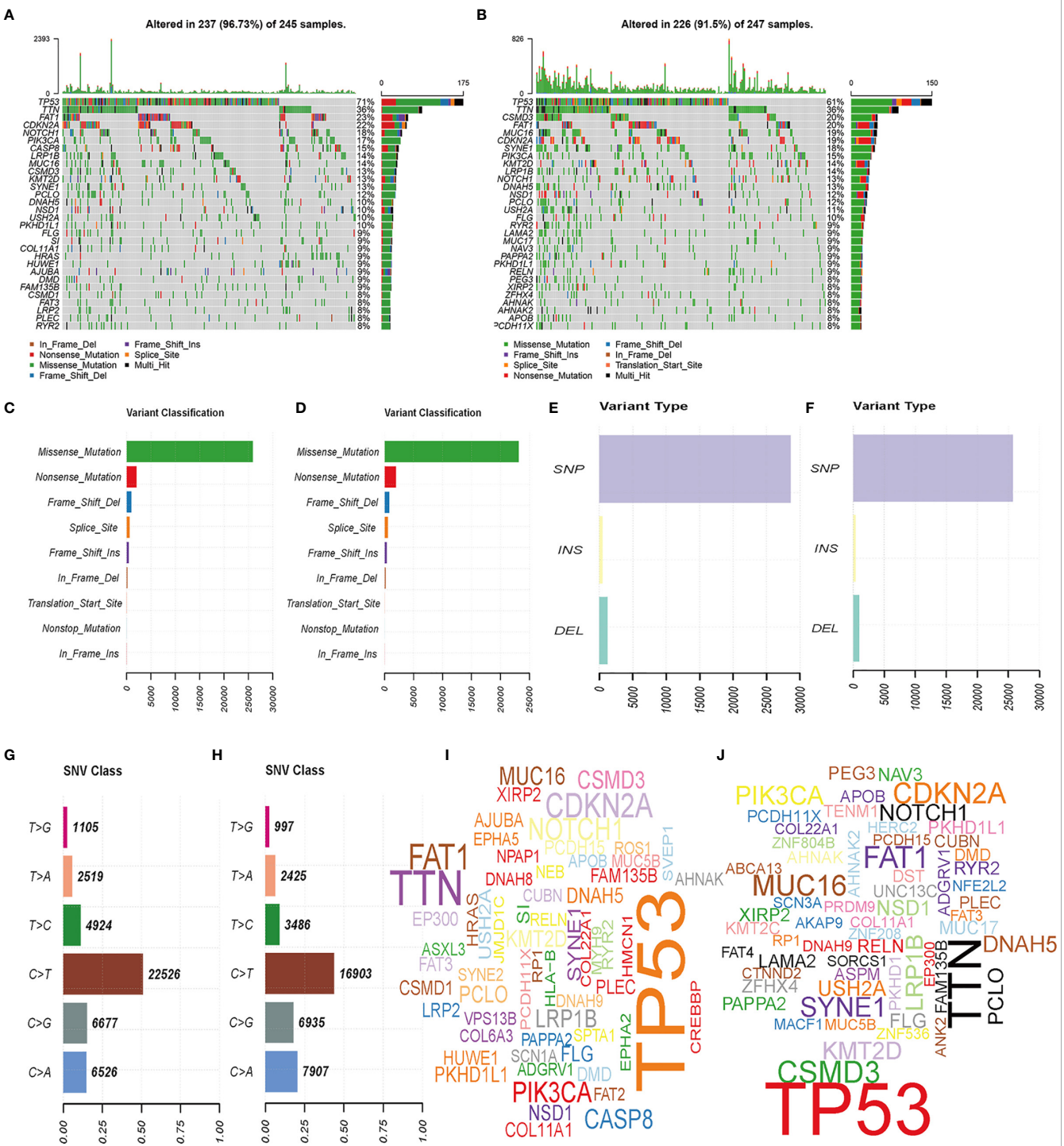

FIGURE 5 | Landscape of mutation profiles between high- and low-risk HNSCC patients. **(A, B)** Waterfall plots of mutation information in each sample. **(C, D)** Variant classification. **(E, F)** Distribution of genetic alterations. **(G, H)** SNV classes. **(I, J)** Gene clouds of mutation frequencies in HNSCC patients.

by providing energy. LncRNAs have been widely investigated as autophagy-related regulators of tumorigenesis (31).

Autophagy is closely related with oncogenesis and is important in the treatment and prognosis of various cancers (32). In the oncogenesis stage of HNSCC, smoking can induce autophagy and lead to oxidative stress (33). Moreover, knockdown of essential autophagy genes and biochemical inhibition of autophagy can remarkably enhance HPV

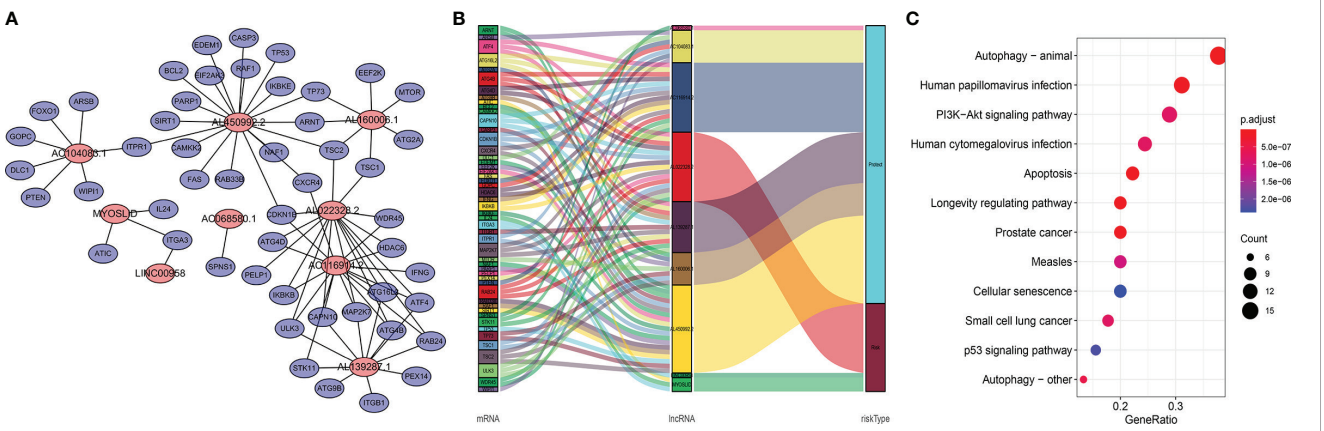

FIGURE 6 | Functional annotations of autophagic LncRNAs prognostic signature as per co-expressed mRNA. **(A)** Co-expressed regulatory network of LncRNAs-mRNA based on the signature. **(B)** Sankey diagram of co-occurrences of LncRNAs, mRNAs, and factors. **(C)** KEGG enrichment analysis of co-expressed mRNAs related with the LncRNA signature.

infectivity (34). During treatment, autophagy is known to be correlated with chemo- and radioresistance due to autophagy-mediated cell death or survival (35). Autophagy is also significantly related to HNSCC prognosis; for example, an autophagic gene signature is reportedly a strong predictor of HNSCC prognosis (27). LncRNAs are increasingly being considered as novel biomarkers and prognostic markers of cancers. Autophagy-related LncRNA signatures can also predict the prognosis of colon adenocarcinoma and breast cancer (36, 37). However, there are no reports on the predictive potential of autophagic LncRNA signatures for HNSCC. Therefore, this study was performed to evaluate the role of autophagic LncRNAs in HNSCC.

We identified a prognostic signature based on nine LncRNAs, namely, MYOSLID, AL139287.1, AC068580.1, AL022328.2, AC104083.1, AL160006.1, AC116914.2, LINC00958, and AL450992.2, to predict OS in HNSCC patients. Among them, AL139287.1, AC068580.1, AC104083.1, AL160006.1, AC116914.2, and AL450992.2 were protection-related, while MYOSLID, AL022328.2, and LINC00958 were risk-related, based on the Sankey diagram. MYOSLID reportedly promotes invasion and metastasis by regulating the partial epithelial–mesenchymal transition in HNSCCs (38). LINC00958 plays a role in multiple cancers by upregulating the microRNA-625/NUAK pathway and contributes to nasopharyngeal carcinomas (39). LINC00958 regulates the miR-627-5p/YBX2 axis to facilitate cell proliferation and migration in oral squamous cell carcinoma (40). In this study, a co-expression network between these nine LncRNAs and the autophagic genes with which they interact was used to determine the mechanisms potentially underlying the autophagy-related LncRNA signature and HNSCC prognosis. The risk score increased as the expression levels of the three risk-related LncRNAs increased and those of the six protection-related LncRNAs decreased. Kaplan–Meier curve analysis revealed that the high-risk group had significantly poorer OS. The AUC value was 0.735, which indicates the reliability and stability of the prognostic signature. In addition, analysis of single autophagy-related LncRNAs showed that higher expression levels of two risk-related LncRNAs were associated with a poor prognosis, while higher levels of the remaining LncRNAs were related to a better prognosis. Multivariate Cox regression demonstrated that the autophagic LncRNA signature is an independent prognostic factor ($p < 0.001$). PCA of whole gene expression profile data revealed no significant differences between groups, but significant differences were seen when analyzing the autophagy-related LncRNA set. GSEA demonstrated that the 14 autophagy-related gene sets, which mainly participate in proteasome and ribosome pathways, were more common in the high-risk group. Proteasomes constitute a degradation system for oxidatively damaged proteins and are involved in cancer development because the ubiquitin–proteasomal system is a key regulator of various molecular pathways (41). Ribosomes are required to convert the information contained in mRNAs into functional proteins; therefore, promoting ribosome and protein synthesis to maintain tumor cell growth and division is essential (42). More importantly, both of these pathways may be involved in autophagy (43, 44). Autophagy-related genes enriched in these pathways may shed light on the mechanisms underlying the poor prognosis of the high-risk group. Autophagy is associated with immune filtration in tumor patients (45). Considering the important role of immune functions, future studies should investigate immune changes in HNSCC patients.

There were several limitations to this study. First, HNSCC encompasses several types of cancers, each of which require separate, detailed analyses. The present risk model was based on a public database, so validation with larger samples is required. Finally, additional experiments are required to elucidate the molecular mechanisms and potential treatment targets.

Our analyses highlight the prognostic value of the nine-LncRNA signature for HNSCC patients, which could guide clinical decisions and treatment plans, and thus improve prognosis.

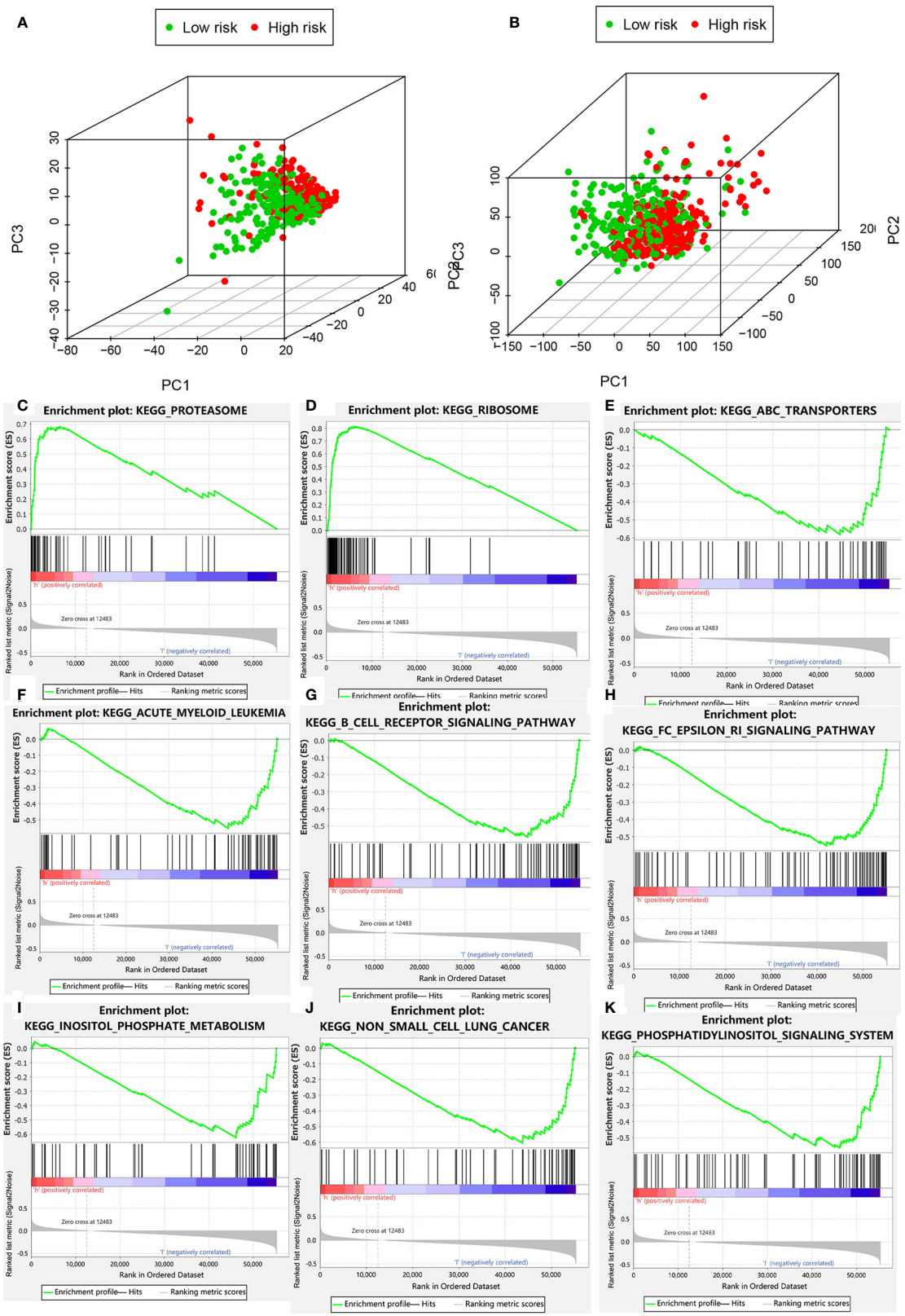

FIGURE 7 | Clustering analysis based on risk score. **(A)** PCA of two categories. **(B)** PCA for genome-wide expression profiles between high- and low-risk groups. **(C–K)** Enrichment plot for KEGG pathways analysis.

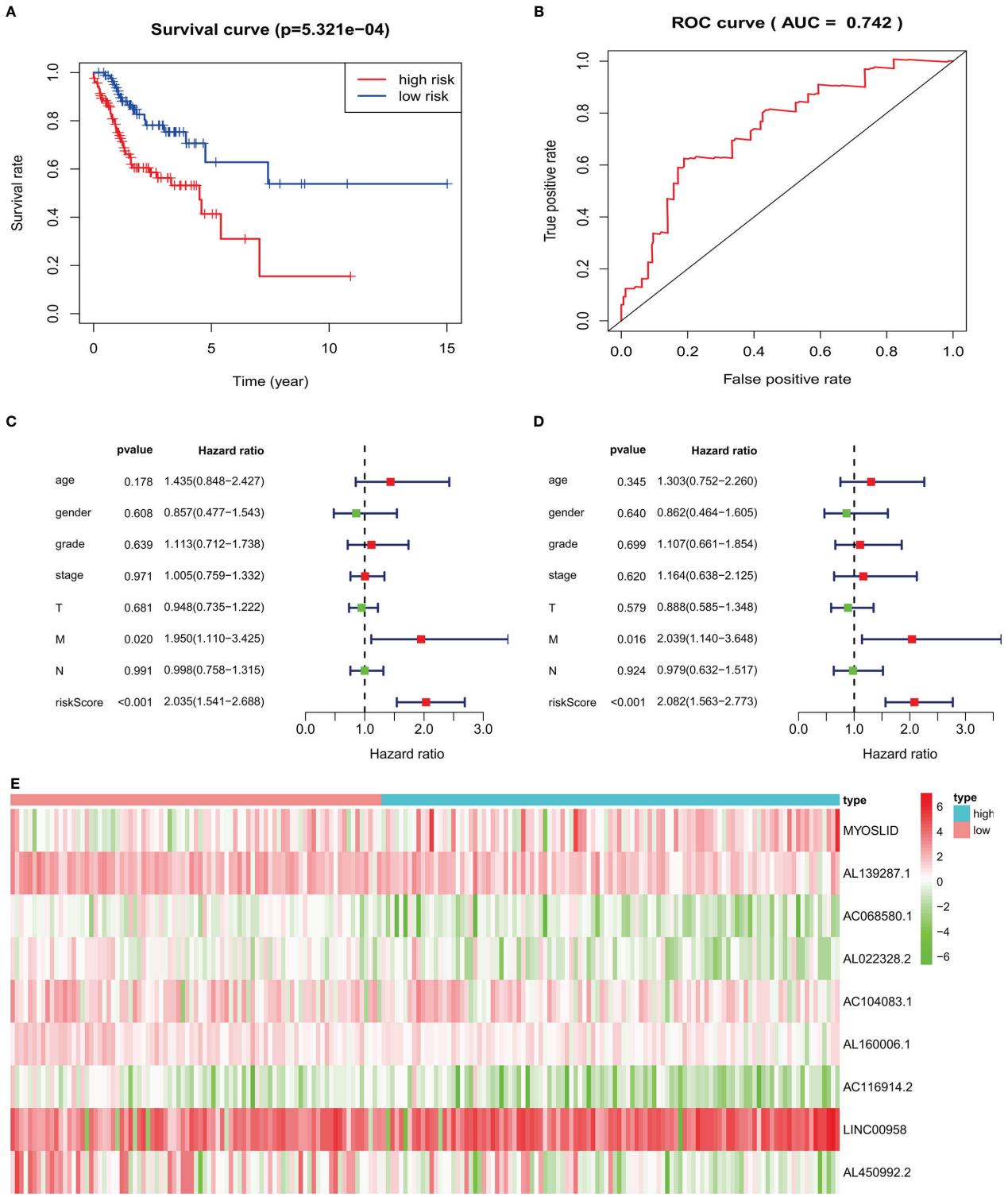

FIGURE 8 | Validation of prognostic signature in an independent HNSCC population: **(A)** high-risk HNSCC patients have poorer overall survival. **(B)** ROC curves of prognostic signature in validated HNSCC patients. **(C, D)** Forest plots of univariate and multivariate Cox regression, respectively, about association between risk score and overall survival in validated HNSCC patients. **(E)** Heatmap of nine target LncRNAs in high-risk and low-risk groups.

DATA AVAILABILITY STATEMENT

The datasets presented in this study can be found in online repositories. The names of the repository/repositories and accession number(s) can be found in the article/**Supplementary Material**.

ETHICS STATEMENT

The studies involving human participants were reviewed and approved by the Ethics Committee of Xiangya Hospital, Central South University (201404355). The patients/participants provided their written informed consent to participate in this study.

AUTHOR CONTRIBUTIONS

ZL designed this study and directed the research group in all aspects, including planning, execution, and analysis of the study. LinS drafted the manuscript. NL and QZ collected the data. ZL provided the statistical software, performed the data analysis, and arranged the figures and tables. ZL and LiaS revised the manuscript. All authors contributed to the article and approved the submitted version.

FUNDING

This study was supported by the National Natural Science Foundation of China (No. 82003239), the Hunan Province Natural Science Foundation (Youth Foundation Project) (No. 2019JJ50945), and the Science Foundation of Xiangya Hospital for Young Scholar (No. 2018Q012).

SUPPLEMENTARY MATERIAL

The Supplementary Material for this article can be found online at: https://www.frontiersin.org/articles/10.3389/fonc.2021.743611/full#supplementary-material

Supplementary Figure 1 | Kaplan-Meier curves of associations between signature lncRNAs and prognosis in HNSCC patients. **(A)** MYOSLID; **(B)** LINC00958; **(C)** AL450992.2; **(D)** AL160006.1; **(E)** AL139287.1; **(F)** AL022328.2; **(G)** AC116914.2; **(H)** AC104083.1; **(I)** AC068580.1.

Supplementary Figure 2 | Relation between autophagic signature lncRNAs and clinical parameters. **(A)** gender (female vs. male); **(B)** grade (G1, G2, G3, G4); **(C)** AJCC Stage (Stage I, II, III, IV); **(D)** T stage (T1, T2, T3, T4); **(E)** Stage N (N0, N1, N2, N3); **(F)** Stage M [M0, M1, MX (unknown)].

Supplementary Figure 3 | Expression levels of signature lncRNAs between normal tissues (n=44) and tumor tissues (n=502). **(A)** heatmap and **(B)** boxplot.

Supplementary File S1 | Original data.

REFERENCES

1. Marur S, Forastiere AA. Head and Neck Squamous Cell Carcinoma: Update on Epidemiology, Diagnosis, and Treatment. *Mayo Clin Proc* (2016) 91:386–96. doi: 10.1016/j.mayocp.2015.12.017
2. Johnson DE, Burtness B, Leemans CR, Lui V, Bauman JE, Grandis JR. Head and Neck Squamous Cell Carcinoma. *Nat Rev Dis Primers* (2020) 6:92. doi: 10.1038/s41572-020-00224-3
3. Stein AP, Saha S, Kraninger JL, Swick AD, Yu M, Lambert PF, et al. Prevalence of Human Papillomavirus in Oropharyngeal Cancer: A Systematic Review. *Cancer J* (2015) 21:138–46. doi: 10.1097/PPO.0000000000000115
4. Isayeva T, Li Y, Maswahu D, Brandwein-Gensler M. Human Papillomavirus in Non-Oropharyngeal Head and Neck Cancers: A Systematic Literature Review. *Head Neck Pathol* (2012) 6 Suppl 1:S104–20. doi: 10.1007/s12105-012-0368-1
5. Gnanasekaran T, Low H, Gupta R, Gao K, Clark J. Prognosis of Metastatic Head and Neck Squamous Cell Carcinoma Over the Last 30 Years. *Anz J Surg* (2018) 88:1158–62. doi: 10.1111/ans.14833
6. Mattick JS. The State of Long Non-Coding RNA Biology. *Noncoding RNA* (2018) 4:17. doi: 10.3390/ncrna4030017
7. Maenner S, Muller M, Becker PB. Roles of Long, Non-Coding RNA in Chromosome-Wide Transcription Regulation: Lessons From Two Dosage Compensation Systems. *Biochimie* (2012) 94:1490–8. doi: 10.1016/j.biochi.2011.12.026
8. Dykes IM, Emanueli C. Transcriptional and Post-Transcriptional Gene Regulation by Long Non-Coding RNA. *Genomics Proteomics Bioinf* (2017) 15:177–86. doi: 10.1016/j.gpb.2016.12.005
9. Wei B, Wei W, Zhao B, Guo X, Liu S. Long Non-Coding RNA HOTAIR Inhibits miR-17-5p to Regulate Osteogenic Differentiation and Proliferation in Non-Traumatic Osteonecrosis of Femoral Head. *PloS One* (2017) 12: e169097. doi: 10.1371/journal.pone.0169097
10. Liao WJ, Mao YL. Regulatory Effects of Long Non-Coding RNA on Tumorigenesis. *Zhongguo Yi Xue Ke Xue Yuan Xue Bao* (2015) 37:358–63. doi: 10.3881/j.issn.1000-503X.2015.03.023
11. Chen B, Li Y, He Y, Xue C, Xu F. The Emerging Roles of Long Non-Coding RNA in Gallbladder Cancer Tumorigenesis. *Cancer Biomark* (2018) 22:359–66. doi: 10.3233/CBM-170979
12. Zhou M, Zhao H, Xu W, Bao S, Cheng L, Sun J. Discovery and Validation of Immune-Associated Long Non-Coding RNA Biomarkers Associated With Clinically Molecular Subtype and Prognosis in Diffuse Large B Cell Lymphoma. *Mol Cancer* (2017) 16:16. doi: 10.1186/s12943-017-0580-4
13. Yang S, Xu J, Zeng X. A Six-Long Non-Coding RNA Signature Predicts Prognosis in Melanoma Patients. *Int J Oncol* (2018) 52:1178–88. doi: 10.3892/ijo.2018.4268
14. Hurley JH, Young LN. Mechanisms of Autophagy Initiation. *Annu Rev Biochem* (2017) 86:225–44. doi: 10.1146/annurev-biochem-061516-044820
15. Kesidou E, Lagoudaki R, Touloumi O, Poulatsidou KN, Simeonidou C. Autophagy and Neurodegenerative Disorders. *Neural Regener Res* (2013) 8:2275–83. doi: 10.3969/j.issn.1673-5374.2013.24.007
16. Kimura T, Isaka Y, Yoshimori T. Autophagy and Kidney Inflammation. *Autophagy* (2017) 13:997–1003. doi: 10.1080/15548627.2017.1309485
17. Bravo-San PJ, Kroemer G, Galluzzi L. Autophagy and Mitophagy in Cardiovascular Disease. *Circ Res* (2017) 120:1812–24. doi: 10.1161/CIRCRESAHA.117.311082
18. Kimmelman AC, White E. Autophagy and Tumor Metabolism. *Cell Metab* (2017) 25:1037–43. doi: 10.1016/j.cmet.2017.04.004
19. Ren Z, Zhang L, Ding W, Luo Y, Shi Z, Shrestha B, et al. Development and Validation of a Novel Survival Model for Head and Neck Squamous Cell Carcinoma Based on Autophagy-Related Genes. *Genomics* (2020) 113:1166–75. doi: 10.1016/j.ygeno.2020.11.017
20. Feng H, Zhong L, Yang X, Wan Q, Pei X, Wang J. Development and Validation of Prognostic Index Based on Autophagy-Related Genes in Patient With Head and Neck Squamous Cell Carcinoma. *Cell Death Discovery* (2020) 6:59. doi: 10.1038/s41420-020-00294-y
21. Sun Z, Jing C, Xiao C, Li T. An Autophagy-Related Long Non-Coding RNA Prognostic Signature Accurately Predicts Survival Outcomes in Bladder Urothelial Carcinoma Patients. *Aging (Albany NY)* (2020) 12:15624–37. doi: 10.18632/aging.103718

22. Zhang K, Xiao M, Jin X, Jiang H. NR5A2 Is One of 12 Transcription Factors Predicting Prognosis in HNSCC and Regulates Cancer Cell Proliferation in a P53-Dependent Manner. *Front Oncol* (2021) 11:691318. doi: 10.3389/fonc.2021.691318
23. Siegel RL, Miller KD, Jemal A. Cancer Statistics, 2019. *CA Cancer J Clin* (2019) 69:7–34. doi: 10.3322/caac.21551
24. Charous SJ. Early Stage Head and Neck Cancer-Surgery. *Cancer Treat Res* (2003) 114:85–113. doi: 10.1007/0-306-48060-3_4
25. Donato V, Iacari V, Zurlo A, Nappa M, Martelli M, Banelli E, et al. Radiation Therapy and Chemotherapy in the Treatment of Head and Neck Extranodal Non-Hodgkin's Lymphoma in Early Stage With a High Grade of Malignancy. *Anticancer Res* (1998) 18:547–54.
26. Lorch JH, Goloubeva O, Haddad RI, Cullen K, Sarlis N, Tishler R, et al. Induction Chemotherapy With Cisplatin and Fluorouracil Alone or in Combination With Docetaxel in Locally Advanced Squamous-Cell Cancer of the Head and Neck: Long-Term Results of the TAX 324 Randomised Phase 3 Trial. *Lancet Oncol* (2011) 12:153–9. doi: 10.1016/S1470-2045(10)70279-5
27. Azad AK, Bairati I, Samson E, Cheng D, Mirshams M, Qiu X, et al. Validation of Genetic Sequence Variants as Prognostic Factors in Early-Stage Head and Neck Squamous Cell Cancer Survival. *Clin Cancer Res* (2012) 18:196–206. doi: 10.1158/1078-0432.CCR-11-1759
28. Misawa K, Mochizuki D, Imai A, Endo S, Mima M, Misawa Y, et al. Prognostic Value of Aberrant Promoter Hypermethylation of Tumor-Related Genes in Early-Stage Head and Neck Cancer. *Oncotarget* (2016) 7:26087–98. doi: 10.18632/oncotarget.8317
29. Zhang X, Yang H, Lee JJ, Kim E, Lippman SM, Khuri FR, et al. MicroRNA-Related Genetic Variations as Predictors for Risk of Second Primary Tumor and/or Recurrence in Patients With Early-Stage Head and Neck Cancer. *Carcinogenesis* (2010) 31:2118–23. doi: 10.1093/carcin/bgq177
30. Schaaf MB, Houbaert D, Mece O, Agostinis P. Autophagy in Endothelial Cells and Tumor Angiogenesis. *Cell Death Differ* (2019) 26:665–79. doi: 10.1038/s41418-019-0287-8
31. Zhou J, Li Y, Liu X, Long Y, Chen J. LncRNA-Regulated Autophagy and Its Potential Role in Drug-Induced Liver Injury. *Ann Hepatol* (2018) 17:355–63. doi: 10.5604/01.3001.0011.7381
32. Keulers TG, Schaaf MB, Rouschop KM. Autophagy-Dependent Secretion: Contribution to Tumor Progression. *Front Oncol* (2016) 6:251. doi: 10.3389/fonc.2016.00251
33. Ding S, Hou X, Wang G, Qiu H, Liu Y, Zhou Y, et al. Autophagy Flux Contributes to Regulation of Components of Eclipta Prostrata L. @ on Cigarette Smoking-Induced Injury of Bronchial Epithelial Cells. *Front Pharmacol* (2018) 9:107. doi: 10.3389/fphar.2018.00107
34. Cui X, Wang X, Zhou X, Jia J, Chen H, Zhao W. miR-106a Regulates Cell Proliferation and Autophagy by Targeting LKB1 in HPV-16-Associated Cervical Cancer. *Mol Cancer Res* (2020) 18:1129–41. doi: 10.1158/1541-7786.MCR-19-1114
35. Das CK, Mandal M, Kogel D. Pro-Survival Autophagy and Cancer Cell Resistance to Therapy. *Cancer Metastasis Rev* (2018) 37:749–66. doi: 10.1007/s10555-018-9727-z
36. Zhou W, Zhang S, Li HB, Cai Z, Tang S, Chen LX, et al. Development of Prognostic Indicator Based on Autophagy-Related lncRNA Analysis in Colon Adenocarcinoma. *BioMed Res Int* (2020) 2020:9807918. doi: 10.1155/2020/9807918
37. Li X, Jin F, Li Y. A Novel Autophagy-Related lncRNA Prognostic Risk Model for Breast Cancer. *J Cell Mol Med* (2020) 25:4–14. doi: 10.1111/jcmm.15980
38. Xiong HG, Li H, Xiao Y, Yang QC, Yang LL, Chen L, et al. Long Noncoding RNA MYOSLID Promotes Invasion and Metastasis by Modulating the Partial Epithelial-Mesenchymal Transition Program in Head and Neck Squamous Cell Carcinoma. *J Exp Clin Cancer Res* (2019) 38:278. doi: 10.1186/s13046-019-1254-4
39. Chen M, Xu Z, Zhang Y, Zhang X. LINC00958 Promotes The Malignancy Of Nasopharyngeal Carcinoma by Sponging microRNA-625 and Thus Upregulating Nuak1. *Onco Targets Ther* (2019) 12:9277–90. doi: 10.2147/OTT.S216342
40. Chen F, Liu M, Yu Y, Sun Y, Li J, Hu W, et al. LINC00958 Regulated miR-627-5p/YBX2 Axis to Facilitate Cell Proliferation and Migration in Oral Squamous Cell Carcinoma. *Cancer Biol Ther* (2019) 20:1270–80. doi: 10.1080/15384047.2019.1617571
41. Manasanch EE, Orlowski RZ. Proteasome Inhibitors in Cancer Therapy. *Nat Rev Clin Oncol* (2017) 14:417–33. doi: 10.1038/nrclinonc.2016.206
42. Kim HJ, Maiti P, Barrientos A. Mitochondrial Ribosomes in Cancer. *Semin Cancer Biol* (2017) 47:67–81. doi: 10.1016/j.semcancer.2017.04.004
43. Bassham DC, MacIntosh GC. Degradation of Cytosolic Ribosomes by Autophagy-Related Pathways. *Plant Sci* (2017) 262:169–74. doi: 10.1016/j.plantsci.2017.05.008
44. Wang Y, Le WD. Autophagy and Ubiquitin-Proteasome System. *Adv Exp Med Biol* (2019) 1206:527–50. doi: 10.1007/978-981-15-0602-4_25
45. Cui B, Lin H, Yu J, Yu J, Hu Z. Autophagy and the Immune Response. *Adv Exp Med Biol* (2019) 1206:595–634. doi: 10.1007/978-981-15-0602-4_27

Conflict of Interest: The authors declare that the research was conducted in the absence of any commercial or financial relationships that could be construed as a potential conflict of interest.

Publisher's Note: All claims expressed in this article are solely those of the authors and do not necessarily represent those of their affiliated organizations, or those of the publisher, the editors and the reviewers. Any product that may be evaluated in this article, or claim that may be made by its manufacturer, is not guaranteed or endorsed by the publisher.

frontiers in Oncology

ORIGINAL RESEARCH
published: 01 October 2021
doi: 10.3389/fonc.2021.726179

Subphrenic Lymph Node Metastasis Predicts Poorer Prognosis for Nasopharyngeal Carcinoma Patients With Metachronous Metastasis

Xue-Fang Zhang[1†], Yan Zhang[1†], Xu-Wei Liang[1], Jia-Luo Chen[1], Sheng-Fang Zhi[2], Wen-Jing Yin[3], Meng-Yao Wang[3], En-Lai Dong[3] and Dong-Ping Chen[3]*

[1] Radiotherapy Department, Affiliated Dongguan Hospital, Southern Medical University, Dongguan, China, [2] Nuclear Medicine Department, Affiliated Dongguan Hospital, Southern Medical University, Dongguan, China, [3] Department of Radiation Oncology, Affiliated Cancer Hospital and Institute of Guangzhou Medical University, Guangzhou, China

OPEN ACCESS

Edited by:
Heming Lu,
People's Hospital of Guangxi Zhuang Autonomous Region, China

Reviewed by:
Fei Han,
Sun Yat-sen University Cancer Center (SYSUCC), China
Weiren Luo,
The Second Affiliated hospital of Southern University of Science and Technology, China

***Correspondence:**
Dong-Ping Chen
chen_dpgz@163.com

[†]These authors share first authorship

Specialty section:
This article was submitted to Head and Neck Cancer, a section of the journal Frontiers in Oncology

Received: *16 June 2021*
Accepted: *25 August 2021*
Published: *01 October 2021*

Citation:
Zhang X-F, Zhang Y, Liang X-W, Chen J-L, Zhi S-F, Yin W-J, Wang M-Y, Dong E-L and Chen D-P (2021) Subphrenic Lymph Node Metastasis Predicts Poorer Prognosis for Nasopharyngeal Carcinoma Patients With Metachronous Metastasis. Front. Oncol. 11:726179. doi: 10.3389/fonc.2021.726179

Aim: We retrospectively analyzed the distribution of distant lymph node metastasis and its impact on prognosis in patients with metastatic NPC after treatment.

Methods: From 2010 to 2016, 219 NPC patients out of 1,601 (182 from the Affiliated Cancer Hospital and Institute of Guangzhou Medical University, and 37 from the Affiliated Dongguan Hospital, Southern Medical University) developed distant metastasis after primary radiation therapy. Metastatic lesions were divided into groups according to location: bones above the diaphragm (supraphrenic bone, SUP-B); bones below the diaphragm (subphrenic bone, SUB-B); distant lymph nodes above the diaphragm (supraphrenic distant lymph nodes, SUP-DLN); distant lymph nodes below the diaphragm (subphrenic distant lymph nodes, SUB-DLN), liver, lung, and other lesions beyond bone/lung/distant lymph node above the diaphragm (supraphrenic other lesions, SUP-OL); other lesions beyond bone/liver/distant lymph node below the diaphragm (subphrenic other lesions, SUB-OL); the subtotal above the diaphragm (supraphrenic total lesions, SUP-TL); and the subtotal below the diaphragm (subphrenic total lesions, SUB-TL). Kaplan–Meier methods were used to estimate the probability of patients' overall survival (OS). Univariate and multivariate analyses were applied using the Cox proportional hazard model to explore prediction factors of OS.

Results: The most frequent metastatic locations were bone (45.2%), lung (40.6%), liver (32.0%), and distant lymph nodes (20.1%). The total number of distant lymph node metastasis was 44, of which 22 (10.0%) were above the diaphragm, 18 (8.2%) were below the diaphragm, and 4 (1.8%) were both above and below the diaphragm. Age (HR: 1.02, 95% CI: 1.00, 1.03, p = 0.012), N stage (HR: 1.26, 95% CI: 1.04, 1.54, p = 0.019), number of metastatic locations (HR: 1.39, 95% CI: 1.12, 1.73, p = 0.003), bone (HR: 1.65, 95% CI: 1.20, 2.25, p = 0.002), SUB-B (HR: 1.51, 95% CI: 1.07, 2.12, p = 0.019), SUB-DLN (HR: 1.72, 95% CI: 1.03, 2.86, p = 0.038), and SUB-O L(HR: 4.46, 95% CI: 1.39, 14.3, p = 0.012) were associated with OS. Multivariate analyses revealed that a higher N stage (HR: 1.23, 95% CI: 1.00, 1.50, p = 0.048), SUB-DLN (HR: 1.72, 95% CI: 1.02, 2.90,

p = 0.043), and SUB-OL (HR: 3.72, 95% CI: 1.14, 12.16, p = 0.029) were associated with worse OS.

Conclusion: Subphrenic lymph node metastasis predicts poorer prognosis for NPC patients with metachronous metastasis; however, this needs validation by large prospective studies.

Keywords: nasopharyngeal carcinoma (NCP), metachronous metastasis, subphrenic lymph node metastasis, distant lymph node metastasis, prognosis

INTRODUCTION

Nasopharyngeal carcinoma (NPC) is one of the most common malignant tumors in South China with 18%–50% of treatment failure due to distant metastasis (1). As there are many lymphatic capillaries in the mucosa of the nasopharynx, NPC is prone to lymph node metastasis, with cervical lymph node involvement as high as 85%–90% in newly diagnosed NPC patients (2–4). Tumor cells use the lymphatic duct and lymph nodes for metastasis and the colonization of peripheral organs (5).

Brown et al. confirmed that cancer cells not only pass through the sentinel lymph nodes and then enter the lymphatic duct to metastasize to distant organs but also directly enter the bloodstream through blood vessels in the lymph nodes (6). Ethel R. Pereira et al. found that isolated cancer cells in the lymph nodes were located within 5 mm of blood vessels and that mice with complete lymph nodes had more circulating tumor cells and lung metastasis than those that underwent lymph node resection (7), proving that lymph node metastasis is diffused from lymph nodes invading the blood vessels rather than by exporting lymph vessels. This poses an important question: does the location of distant lymph node NPC metastasis impact prognosis, and if so, how?

In this paper, we retrospectively analyzed the distribution of distant lymph node metastasis and its impact on prognosis in patients with metastatic NPC after treatment. We hope that the study of tumor characteristics according to the location and route of metastasis will help to determine the biological explanation of tumor behavior, explain the related survival results, and guide disease monitoring and treatment selection.

MATERIALS AND METHODS

Patients

In this retrospective study, 1,601 NPC patients from 2010 to 2016 were initially treated at the Affiliated Cancer Hospital and Institute of Guangzhou Medical University (1,214) and the Affiliated Dongguan Hospital, Southern Medical University (387). Two hundred nineteen patients (182 from the Affiliated Cancer Hospital and Institute of Guangzhou Medical University and 37 from the Affiliated Dongguan Hospital, Southern Medical University) developed distant metastasis after primary radiation therapy (RT).

This study's inclusion criteria were i) histologically confirmed NPC and ii) radiographically detectable metastatic disease after initial radiation therapy (more than 3 months) on the basis of subsequent follow-up. The exclusion criteria were i) other malignancies and ii) HIV, tuberculosis, or other chronic inflammatory diseases (e.g., inflammatory bowel disease).

All clinical data were collected when metastasis was diagnosed, including magnetic resonance imaging of the head and neck regions, radiographs or computed tomography (CT) of the chest, ultrasonography or CT scans of the abdomen, and whole-body bone scans. Positron emission tomography with 2-deoxy-2-[fluorine-18]fluoro-D-glucose integrated with computed tomography(18F FDG PET/CT) were performed to confirm the metastasis of 44 patients (7 from the Affiliated Cancer Hospital and Institute of Guangzhou Medical University and 37 from the Affiliated Dongguan Hospital, Southern Medical University).

All 219 patients were treated with intensity-modulated radiation therapy (IMRT) during the initial treatment. Among them, 14 (6.4%) did not receive chemotherapy, and the other 205 (93.6%) received chemotherapy. One hundred seventy-one (78.1%) were treated with concurrent chemotherapy, including 19 (8.68%) with concurrent chemotherapy, 73 (33.3%) with neoadjuvant chemotherapy plus concurrent chemotherapy, 12 (5.5%) with concurrent chemotherapy plus adjuvant chemotherapy, and 67 (30.6%) with neoadjuvant chemotherapy plus concurrent chemotherapy plus adjuvant chemotherapy; 34 (15.5%) received non-concurrent chemotherapy, among which 26 (11.87%) received neoadjuvant chemotherapy, 1 (0.5%) received adjuvant chemotherapy, and 7 (3.2%) received neoadjuvant chemotherapy plus adjuvant chemotherapy.

After distant metastasis, cisplatin-based combination chemotherapy was recommended for most patients (209, 95.4%). Other agents were 5-fluorouracil, paclitaxel (albumin paclitaxel or paclitaxel liposomal), docetaxel, gemcitabine, cyclophosphamide, vincristine, bleomycin, capecitabine, and S-1. Supportive management with no anticancer treatment was provided for four patients (4,1.8%). Surgical resection, radiation therapy, radiofrequency ablation, and trans-arterial chemoembolization were prescribed if the doctors thought it was valuable to do so.

This study was approved by the ethics committee of the Affiliated Cancer Hospital and Institute of Guangzhou Medical University with the approval number: ZN2021-05.

Distribution of Metastatic Lesions and Other Variables

The criteria for distant lymph node (DLN) metastasis were i) CT/MRI showing a minimum lymph node diameter of ≥10 mm; ii) central necrosis or annular reinforcement; iii) extracapsular

invasion of the lymph nodes (irregular enhancement of the lymph node margin; iv) some or all of the surrounding fat spaces not visible; v) lymph nodes fused with each other; and vi) 18F FDG PET/CT: SUV of the lymph nodes higher than the abdominal aorta, and/or CT images with the above features (8).

Metastatic lesions were divided into groups according to location: bones above the diaphragm (supraphrenic bone, SUP-B); bones below the diaphragm (subphrenic bone, SUB-B); distant lymph nodes above the diaphragm (supraphrenic distant lymph nodes, SUP-DLN); distant lymph nodes below the diaphragm (subphrenic distant lymph nodes, SUB-DLN), liver, lung, other lesions above the diaphragm (supraphrenic other lesions beyond bone/lung/distant lymph node, SUP-OL); other lesions below the diaphragm (subphrenic other lesions beyond bone/liver/distant lymph node, SUB-OL); the subtotal above the diaphragm (supraphrenic total lesions, SUP-TL); and the subtotal below the diaphragm (subphrenic total lesions, SUB-TL).

SUP-TL included SUP-B, SUP-DLN, lung, and SUP-OL. SUB-TL included SUB-B, SUB-DLN, liver, and SUB-OL. SUP-B is defined as lesions of the C-spine, T-spine, ribs, sternum, scapula, humerus, and clavicle. SUB-B is defined as lesions of the L-spine, sacrum, pelvic bone, and femur. SUP-DLN is defined as mediastinal LN, axillary LN, and hilar LN (excluding neck LN). SUB-DLN is defined as retroperitoneal LN, pelvic LN, hepatic hilar LN, and inguinal LN. SUP-OL is defined as other metastases above the diaphragm and beyond the bone/lung/distant lymph node such as the pleura and thyroid. SUB-OL is defined as other metastases below the diaphragm and beyond the bone/liver/distant lymph node such as the spleen and adrenal glands.

The primary disease, NPC, was T and N staged according to the American Joint Committee on Cancer (AJCC) Cancer Staging Manual (8th Edition) (9). The variables assessed in this study included sex, age, body mass index before primary therapy (BMI1), body mass index during metastasis (BMI2), the T/N/TNM staging of the primary disease NPC, disease-free interval (DFI), local recurrence, overall survival (OS), and the total organs of the metastatic lesions (organs-n).

Follow-Up and Endpoints

Patients were routinely followed up every two cycles during systemic chemotherapy and every 2 to 3 months during no anticancer treatment until death. OS was defined as the interval between the date of distant metastasis to the date of death of any cause. DFI was defined as the interval from the date of initial diagnosis of NPC to the date of distant metastasis. Data from patients alive at the end of study (December 31, 2020) were censored. We verified survival status on August 31, 2020, by direct telecommunication with the patient or family members and by checking the clinic attendance records.

Statistical Analysis

Continuous variables were described using mean and standard deviation (SD) for normally distributed data and median and interquartile [IQR] for non-normally distributed data. The Student t-test or Mann–Whitney U test were used for continuous variables between groups. Frequency and percentage were used to describe the categorical data, and the chi-square test to test the difference.

The Kaplan–Meier method was used to estimate the probability of patients' OS. Survival curves were drawn to compare the difference between/among covariate groups, and the log-rank test was applied accordingly. Univariate and multivariate analyses were applied using the Cox proportional hazard model to explore prediction factors of OS. Variables with a $p<0.1$ in the univariate model were kept for multivariate analyses. A stepwise variable selection procedure (with iterations between the "forward" and "backward" steps) was applied to obtain the best candidate for the final Cox proportional hazards model. The chosen significance level for entry (SLE) and for stay (SLS) was 0.25. A p value <0.05 was considered statistically significant. All statistical analyses were performed using R (software version 6.3, https://www.r-project.org/).

RESULTS

Patient Characteristics

The patient characteristics of metachronous metastatic NPC (n = 219) are described in **Table 1**. The mean age at diagnosis of metastatic NPC was 50.2 years (SD, 11.4). One hundred and six (48.4%) were more than 50 years old. One hundred seventy-four (79.5%) were male, and 45 (20.5%) were female. Before the first radiotherapy treatment, 32 (14.6%), 29 (13.2%), 122 (55.7%), and 36 (16.4%) were T1, T2, T3, and T4 stages, respectively. Eleven (5.0%), 91 (41.6%), 76 (34.7%), and 41 (18.7%) were N0, N1, N2, and N3 stages, respectively.

The median OS of metachronous metastatic NPC was 13.2 months (IQR, 7.3, 25.3), and the median DFI was 20.1 months (IQR, 10.0, 33.6). The most frequent metastatic locations were bone (99/219, 45.2%), lung (89/219, 40.6%), liver (70/219, 32.0%), and distant lymph nodes (44/219, 20.1%). There were 142 (64.8%), 52 (23.7%), 24 (11.0%), and 1 (0.5%) patients with one, two, three, and four metastatic locations, respectively.

Distribution of Distant Lymph Node Metastasis

The distribution of distant lymph node metastasis is described in **Table 2**. The total number of distant lymph node metastasis was 44/219 (20.1%), of which 22/219 (10.0%) were above the diaphragm, 18/219 (8.2%) were below the diaphragm, and 4/219 (1.8%) were both above and below the diaphragm. The median number of distant lymph node metastasis in 44 patients was 3 (range, 1–7), 10 (22.7%) had one DLN metastasis, 24 (54.5%) had two to four DLN metastases, and 10 (22.7%) had five or more than five DLN metastases.

Distant lymph node metastases above the diaphragm were located in the mediastinal LN (18/219, 8.2%), axillary LN (8/219, 3.7%), hilar LN (3/219, 1.4%), and the internal mammary lymph nodes (2/219, 0.9%). For distant lymph node metastasis below

TABLE 1 | Patient characteristics.

	Level	Overall	DLN (-)	DLN (+)	p
No (%)		219 (100%)	175 (79.9%)	44 (20.1%)	
Sex no. (%)	Male	174 (79.5)	142 (81.1)	32 (72.7)	0.305
	Female	45 (20.5)	33 (18.9)	12 (27.3)	
Age no. (%)	≤50	106 (48.4)	79 (45.1)	27 (61.4)	0.079
	>50	113 (51.6)	96 (54.9)	17 (38.6)	
BMI1 [median (IQR)]		21.4 [19.9, 23.5]	21.5 [20.1, 23.5]	20.6 [18.9, 23.5]	0.074
BMI2 [median (IQR)]		20.3 [18.7, 21.9]	20.3 [18.8, 21.9]	19.4 [18.2, 21.8]	0.150
T no. (%)	1	32 (14.6)	25 (14.3)	7 (15.9)	0.256
	2	29 (13.2)	20 (11.4)	9 (20.5)	
	3	122 (55.7)	98 (56.0)	24 (54.5)	
	4	36 (16.4)	32 (18.3)	4 (9.1)	
N no. (%)	0	11 (5.0)	11 (6.3)	0 (0.0)	0.311
	1	91 (41.6)	74 (42.3)	17 (38.6)	
	2	76 (34.7)	58 (33.1)	18 (40.9)	
	3	41 (18.7)	32 (18.3)	9 (20.5)	
TNM no. (%)	I	1 (0.5)	1 (0.6)	0 (0.0)	0.355
	II	29 (13.2)	20 (11.4)	9 (20.5)	
	III	119 (54.3)	95 (54.3)	24 (54.5)	
	IVa	70 (32.0)	59 (33.7)	11 (25.0)	
Recurrence no. (%)	No	175 (79.9)	137 (78.3)	38 (86.4)	0.325
	Yes	44 (20.1)	38 (21.7)	6 (13.6)	
DFI [median (IQR)]		20.1 [10.0, 33.6]	18.0 [9.3, 31.4]	28.3 [17.0, 42.8]	0.003
OS no. (%)	No	58 (26.5)	45 (25.7)	13 (29.5)	0.746
	Yes	161 (73.5)	130 (74.3)	31 (70.5)	
OS time [median (IQR)]		13.2 [7.3, 25.3]	13.7 [7.1, 26.1]	11.0 [7.7, 20.5]	0.464
Organ N [mean (SD)]		1.5 (0.7)	1.3 (0.6)	2.2 (0.8)	<0.001
Bone no. (%)	No	120 (54.8)	91 (52.0)	29 (65.9)	0.137
	Yes	99 (45.2)	84 (48.0)	15 (34.1)	
Liver no. (%)	No	149 (68.0)	121 (69.1)	28 (63.6)	0.604
	Yes	70 (32.0)	54 (30.9)	16 (36.4)	
Lung no. (%)	No	130 (59.4)	100 (57.1)	30 (68.2)	0.246
	Yes	89 (40.6)	75 (42.9)	14 (31.8)	
Other lesion no. (%)	No	199 (90.9)	162 (92.6)	37 (84.1)	0.138
	Yes	20 (9.1)	13 (7.4)	7 (15.9)	
SUP-OL no. (%)	No	202 (92.2)	165 (94.3)	37 (84.1)	0.051
	Yes	17 (7.8)	10 (5.7)	7 (15.9)	
SUB-OL no. (%)	No	216 (98.6)	173 (98.9)	43 (97.7)	0.492
	Yes	3 (1.4)	2 (1.1)	1 (2.3)	
SUP-B no. (%)	No	149 (68.0)	119 (68.0)	30 (68.2)	1.000
	Yes	70 (32.0)	56 (32.0)	14 (31.8)	
SUB-B no. (%)	No	165 (75.3)	132 (75.4)	33 (75.0)	1.000
	Yes	54 (24.7)	43 (24.6)	11 (25.0)	
SUP-TL no. (%)	No	65 (29.7)	55 (31.4)	10 (22.7)	0.356
	Yes	154 (70.3)	120 (68.6)	34 (77.3)	
SUB-TL no. (%)	No	106 (48.4)	87 (49.7)	19 (43.2)	0.501
	Yes	113 (51.6)	88 (50.3)	25 (56.8)	

DLN, distant lymph nodes; no., number; BMI1, body mass index before primary therapy; BMI2, body mass index during metastasis; T, T staging of the primary disease of NPC; N, N staging of the primary disease of NPC; TNM, TNM staging of the primary disease of NPC; DFI, disease-free interval; OS, overall survival; SUP-OL, supraphrenic other lesions; SUB-OL, subphrenic other lesions; SUP-B, supraphrenic bone; SUB-B, subphrenic bone; SUP-TL, supraphrenic total lesions; SUB-TL, subphrenic total lesions.

the diaphragm, there were 20/219 (10.0%) in the retroperitoneal LN, 1/219 (0.4%) in the pelvic LN, 1/219 (0.4%) in the hepatic hilar LN, and 2/219 (0.9%) in the inguinal LN.

Distant Lymph Node Metastasis Below the Diaphragm Indicates Poorer Prognosis

Survival analysis showed that patients with distant lymph node metastasis below the diaphragm had poorer OS than those without distant lymph node metastasis below the diaphragm (p = 0.036) (**Figure 1**). As shown in **Table 3**, in the univariate analysis, age (HR: 1.02, 95% CI: 1.00, 1.03, p = 0.012), a higher N stage of the primary disease NPC (HR: 1.26, 95% CI: 1.04, 1.54, p = 0.019), more metastatic locations (HR: 1.39, 95% CI: 1.12, 1.73, p = 0.003), bone (HR: 1.65, 95% CI: 1.20, 2.25, p = 0.002), SUB-B (HR: 1.51, 95% CI: 1.07, 2.12, p = 0.019), SUB-DLN (HR: 1.72, 95% CI: 1.03, 2.86, p = 0.038), and SUB-OL (HR: 4.46, 95% CI: 1.39, 14.3, p = 0.012) were associated with worse OS.

Subsequent multivariate analyses revealed that a higher N stage (HR: 1.23, 95% CI: 1.00, 1.50, p = 0.048), SUB-DLN (HR: 1.72, 95% CI: 1.02, 2.90, p = 0.043), and SUB-OL (HR: 3.72, 95% CI: 1.14, 12.16, p = 0.029) were associated with worse OS. Kaplan–Meier survival analysis of patients with and without

TABLE 2 | The distribution of distant lymph node metastasis.

Site	No. (%)
SUP-DLN	22 (10.0%)
SUB-DLN	18 (8.2%)
SUP-LN and SUB-LN	4 (1.8%)
Mediastinal LN	18 (8.2%)
Axillary LN	8 (3.7%)
Hilar LN	3 (1.4%)
Internal mammary lymph nodes	2 (0.9%)
Retroperitoneal LN	20 (9.1%)
Pelvic LN	1 (0.4%)
Hepatic hilar LN	1 (0.4%)
Inguinal LN	2 (0.8%)

No., number; SUP-DLN, supraphrenic distant lymph node; SUB-DLN, subphrenic distant lymph node.

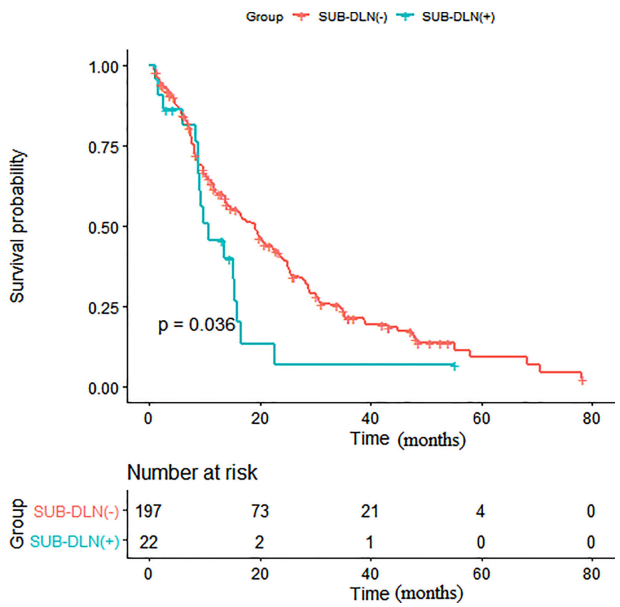

FIGURE 1 | Kaplan-Meier survival analysis of patients with and without SUB-DLN. (SUB-DLN, subphrenic distant lymph node).

SUB-DLN is shown in **Figure 1**. Kaplan–Meier survival analysis of patients with and without SUP-B/SUB-B/SUB-TL is shown in **Figures 2–4**.

DISCUSSION

Lymph nodes are the central transport center of circulating immune cells, with the lymphatic drainage system of the body a coherent whole separated by particular anatomical boundaries (10–12). Patients with extra-regional lymph node metastasis are considered to have better prognosis than those with solid organ metastasis among some metastatic malignancies. The research by Hong Pan showed that patients with distant lymph node metastasis (DLNM) had similar breast cancer–specific survival (BCSS) and OS as those with ipsilateral supraclavicular lymph node metastasis (ISLM), whereas those with distant metastasis (not DLNM) had significantly poorer BCSS and OS (12). Similarly, Francesca Magnoni found that although contralateral axillary lymph node metastasis after treatment belongs to distant metastasis (distant lymph node metastasis), its OS is significantly better than the distant metastasis of other organs (13). Yuki Mukai also found that cervical cancer without metastasis of other organs but with distant lymph node metastasis (supraclavicular/mesentery/mediastinum lymph node) had a good local control rate. The 2-year overall, cancer-specific, and progression-free survival as well as the local control of primary tumor rates were 51.3%, 51.3%, 46.9%, and 67.9%, respectively (14).

The lymphatic drainage routes of the body's organs are local lymph nodes, retroperitoneal lymph nodes, the thoracic duct, and the left supraclavicular lymph node (15, 16). The left supraclavicular lymph nodes, often called the Virchow lymph node, is near the junction of the thoracic duct and the left subclavian vein, from which most of the body's lymph flows into systemic circulation. For breast, cervical, prostate, and even gastrointestinal cancer, lymph diffusion may be along the abovementioned lymphatic drainage routes. Therefore, distant lymph node metastasis of non-solid organs is more contained and has a better prognosis than solid organ metastasis for these malignant tumors.

The diaphragm is an important anatomical structure. It is a natural barrier of the lymphatic system, and it divides the lymphatic system into two regions according to space. Multiple lymph node involvement on one side of the diaphragm has better prognosis than involvement on both sides in regard to Hodgkin's disease (17). Subphrenic LN (retroperitoneal lymph nodes) are regional lymph nodes in cervical cancer and prostate cancer, which have better prognosis than those with metastasis (18–20).

The nasopharynx is prone to lymph node metastasis because of its well-developed network of lymphatics (21). Yali Xu included 2,994 patients (M1, 299/10.0%) with primary nasopharyngeal carcinoma diagnosed in the SEER database from 2006 to 2015. Compared with the N0/N1 group, the HR of the 5-year overall survival (OS) in the N2 group was 1.311 (95% CI: 1.135–1.514, $p < 0.001$), and the HR of OS in the N3 group was 1.625 (95% CI: 1.357–1.945, $p < 0.01$). In addition, the HR of cancer-specific survival (CSS) was 1.351 (95% CI: 1.156–1.580, $p < 0.001$) in the N2 group and 1.630 (95% CI: 1.342–1.979, $p < 0.01$) in the N3 group (22).The article gave the tips that the more regional lymph node metastasis in nasopharyngeal carcinoma is, the worse of the prognosis is.

Metachronous metastatic nasopharyngeal carcinoma with different locations has different prognosis. Lujun Shen found that the number of metastatic foci (multiple and single), the number of metastatic sites (multiple and single), liver involvement, and bone involvement were independent prognostic factors of OS, but that distant lymph node metastasis was not associated with overall survival (23). Zixun Zeng and others also analyzed the prognostic factors of 860 patients with metachronous NPC metastasis and found that age, the International Union for Cancer Control (UICC), N stage, Karnofsky Performance Status (KPS), serum lactate

TABLE 3 | Univariate analysis and multivariate analyses of clinicopathologic characteristics.

Characteristic	Univariate analysis			Multivariate analyses		
	HR	95% CI	p-value	HR	95% CI	p-value
Sex	0.88	0.59, 1.30	0.521			
Age	1.02	1.00, 1.03	0.012			
BMI1	0.99	0.94, 1.04	0.629			
BMI2	0.98	0.92, 1.04	0.451			
T	0.96	0.80, 1.15	0.612			
N	1.26	1.04, 1.54	0.019	1.23	1.00,1.50	0.048
TNM	1.22	0.95, 1.56	0.110			
Recurrence	1.02	0.68, 1.53	0.928			
DFI	1.00	0.99,1.01	0.855			
Organ_n	1.39	1.12, 1.73	0.003			
Bone	1.65	1.20,2.25	0.002			
SUP-B	1.27	0.92, 1.75	0.146			
SUB-B	1.51	1.07, 2.12	0.019	1.36	0.96,1.93	0.083
Liver	1.20	0.86, 1.67	0.281			
Lung	0.92	0.67, 1.27	0.624			
SUP-OL	1.03	0.57, 1.85	0.933			
SUB-OL	4.46	1.39, 14.3	0.012	3.72	1.14, 12.16	0.029
DLN	1.09	0.73,1.61	0.674			
DLN_n▲	1.08	0.89,1.30	0.459			
SUP-DLN	0.89	0.54, 1.46	0.643			
SUB-DLN	1.72	1.03, 2.86	0.038	1.72	1.02, 2.90	0.043
SUP-TL	1.04	0.73, 1.48	0.828			
SUB-TL	1.30	0.95, 1.77	0.104			

▲ *DLN_n:1/2-4/≥5.*

HR, hazard ratio; CI, confidence interval; BMI1, body mass index before primary therapy; BMI2, body mass index during metastasis; T, T staging of the primary disease of NPC; N, N staging of the primary disease of NPC; TNM, TNM staging of the primary disease of NPC; DFI, disease-free interval; Organ_n, number of metastatic locations; SUP-B, supraphrenic bone; SUB-B, subphrenic bone; SUP-OL, supraphrenic other lesions; SUB-OL, subphrenic other lesions; DLN, distant lymph node; DLN_n, number of distant lymph node; SUP-DLN, supraphrenic distant lymph node; SUB-DLN, subphrenic distant lymph node; SUP-TL, supraphrenic total lesions; SUB-TL, subphrenic total lesions.

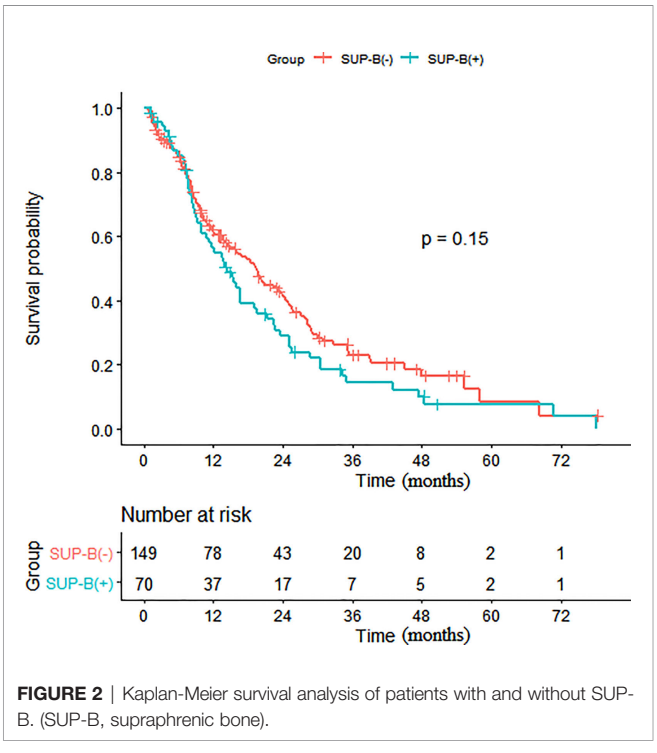

FIGURE 2 | Kaplan-Meier survival analysis of patients with and without SUP-B. (SUP-B, supraphrenic bone).

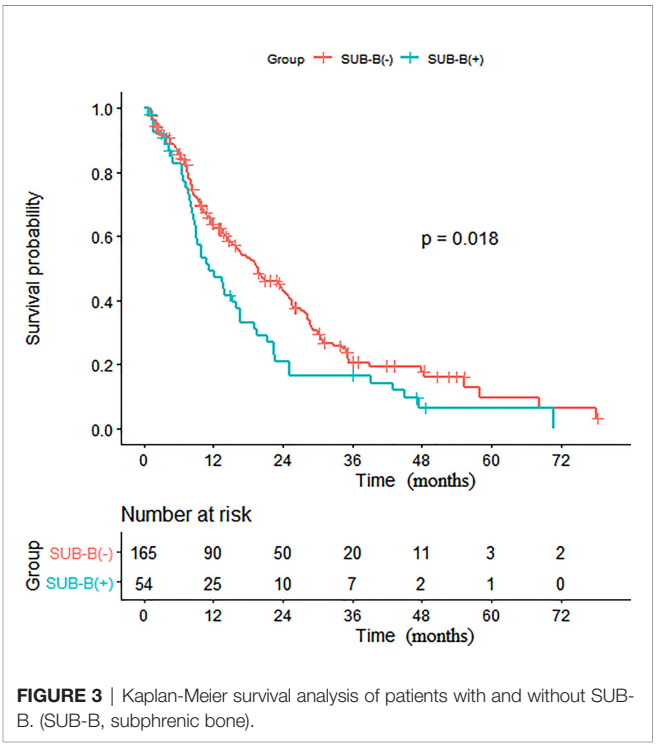

FIGURE 3 | Kaplan-Meier survival analysis of patients with and without SUB-B. (SUB-B, subphrenic bone).

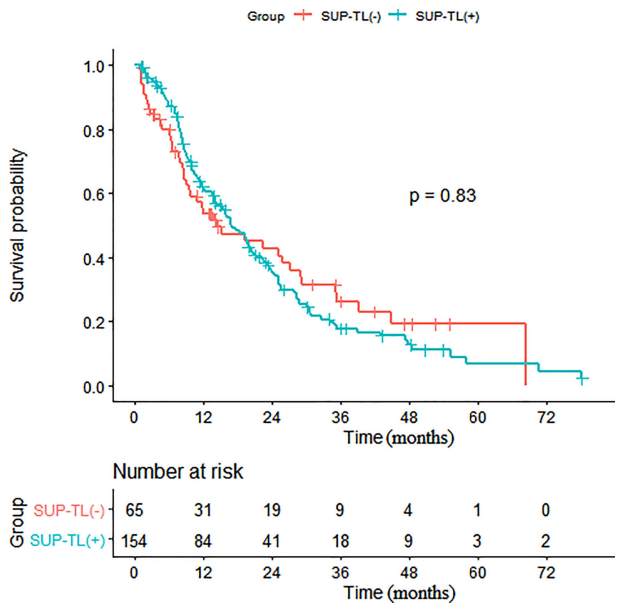

FIGURE 4 | Kaplan-Meier survival analysis of patients with and without SUP-TL. (SUP-TL, supraphrenic total lesions).

dehydrogenase (SLDH), the number of metastases, liver involvement, and bone involvement were prognostic factors affecting the OS of patients with NPC metastasis (24).Jihyun Chang found that distant lung metastasis is a good prognostic factor for metastatic NPC after treatment (25), while most other studies found that heterochronous metastatic NPC with liver metastasis had a poor OS (23, 24, 26, 27).

Distant lymph node NPC metastasis is a common metastasis site besides the liver, bone, lung, and brain (28). In this study, we firstly defined distant lymph nodes as supra- and sub-distant lymph nodes based on the diaphragm and explored the influence of supra- and sub-diaphragmatic distant lymph node metastasis on the prognosis of NPC with metachronous metastasis. Our results showed that subphrenic lymph node metastasis is associated with poorer prognosis. This finding is contrary to the conclusion of the prognosis of distant lymph node metastasis of thoracic, abdominal, and pelvic malignant tumors. It may be that for NPC, distant lymph node metastasis comes from the lymph reflux after the metastasis of peripheral organs. We found that distant lymph nodes were associated with multiple metastasis locations: the mean number of metastatic locations in the group without distant lymph node metastasis was 1.3 (SD, 0.6), and 2.2 (SD, 0.8) in the group with distant lymph node metastasis ($p < 0.001$). Although metastases of the liver, lung, and supraseptal lymph nodes were not found to predict prognosis in this study, the metastases of subseptal lymph nodes and other organs were found to predict poorer prognosis. However, due to the small sample size of this study, we were unable to detect the impact of liver and lung metastases on prognosis. We speculate that the diaphragm may block the further spread of tumor cells through the lymphatic duct in NPC, which migrates to the surrounding lymph nodes from peripheral organ metastasis (lung, liver, and bone). Once subphrenic lymph node metastasis occurs, it has a worse prognosis than surrounding organ metastasis (liver, subphrenic bone). Yet, supraphrenic lymph nodes do not have a predictive effect for metachronous metastasis NPC due to the better prognosis of the lungs.

While considering from the perspective of molecular mechanism, we may see the other side of SUB-DLN metastases. Lymphatic circulation plays an important role in the occurrence and development of cancer. The dissemination of tumor cells to other organs is usually mediated by lymphatic vessels as catheters, which is often referred to as tumor-associated lymphangiogenesis. When the tumor microenvironment stimulates tumor cells, tumor stromal cells, and tumor-infiltrating cells to induce a series of lymphangiogenic factors, gene lymphangiogenesis related to tumor will occur (29). It was found that miR-129-5p inhibited lymphangiogenesis and lymph node metastasis of nasopharyngeal carcinoma by blocking the zinc finger ZIC2 mediated hedgehog signaling pathway. ZIC2 was highly expressed in nasopharyngeal carcinoma compared with normal tissues. The exogenous expression of miR-129-5p resulted in decreased expression of ZIC2 and other hedgehog signaling components (30). Chuanghua Luo demonstrated that the pigment epithelium-derived factor (PEDF) is lowly expressed in human NPC tissues with poor prognosis and is negatively correlated with lymphatic vessel density (LVD). It was found that PEDF inhibits lymphangiogenesis and lymphatic metastasis of NPC *in vivo* experiments. PEDF also reduced the expression and secretion of vascular endothelial growth factor C (VEGF-C) through the nuclear factor-κB (NF-κB) signaling pathway in NPC cells. Their research showed that PEDF plays a vital role in lymphatic metastasis by targeting both lymphatic endothelial cells and NPC cells (31). The mechanism of nasopharyngeal lymphangiogenesis and lymphatic metastasis needs further exploration, which can explain the influence of different lymph node metastases in NPC on prognosis and also provide a candidate drug for the treatment of NPC metastasis.

This study has several limitations. One, the follow-up treatment of some patients with metastatic NPC was not uniform, and the influence of treatment factors on prognosis was not included in this study. Two, because the EBV DNA level was not available in most of the cases, we cannot analyze its impact on prognosis. Three, only a small number of patients (44/219, 20.1%) were diagnosed with metastases by whole-body 18F FDG PET-CT, and the vast majority of patients were diagnosed *via* chest and abdominal CT; therefore, the incidence of lymph node metastasis may be underestimated. Four, due to the small sample size, the above factors may lead to bias. Further prospective studies are needed to verify the above conclusions.

CONCLUSION

Subseptal lymph node metastasis predicts poorer prognosis for NPC patients with metachronous metastasis; however, this needs validation by large prospective studies. This is the first study to divide distant lymph node metastasis into upper and lower parts with the diaphragm as an anatomical boundary. This research provides another perspective and future direction to further

explore the relationship between lymph node dissemination and NPC and help us find the treatment for NPC metastasis.

DATA AVAILABILITY STATEMENT

The raw data supporting the conclusions of this article will be made available by the authors, without undue reservation.

AUTHOR CONTRIBUTIONS

D-PC and X-FZ designed the study. YZ, X-WL, J-LC, S-FZ, W-JY, M-YW, and E-LD acquired the data. YZ and X-FZ analyzed the data. X-FZ drafted the manuscript. D-PC critically revised the manuscript's intellectual content. All authors contributed to the article and approved the submitted version.

ACKNOWLEDGMENTS

All of the authors would like to thank the patients and the staff at the Affiliated Dongguan Hospital, Southern Medical University, and the Affiliated Cancer Hospital and Institute of Guangzhou Medical University. We thank Mrs. Jingrong Shi from Guangzhou Tianpeng Computer Technology Co., Ltd., for her contributions and assistance in terms of data analysis.

REFERENCES

1. Lee AW, Poon YF, Foo W, Law SC, Cheung FK, Chan DK, et al. Retrospective Analysis of 5037 Patients With Nasopharyngeal Carcinoma Treated During 1976-1985: Overall Survival and Patterns of Failure. *Int J Radiat Oncol Biol Phys* (1992) 23:261–70. doi: 10.1016/0360-3016(92)90740-9
2. Lee AW, Foo W, Law SC, Poon YF, Sze WM, SK O, et al. Nasopharyngeal Carcinoma: Presenting Symptoms and Duration Before Diagnosis. *Hong Kong Med J* (1997) 3:355–61.
3. Geara FB, Sanguineti G, Tucker SL, Garden AS, Ang KK, Morrison WH, et al. Carcinoma of the Nasopharynx Treated by Radiotherapy Alone: Determinants of Distant Metastasis and Survival. *Radiother Oncol* (1997) 43:53–61. doi: 10.1016/S0167-8140(97)01914-2
4. Perez CA, Devineni VR, Marcial-Vega V, Marks JE, Simpson JR.Kucik N. Carcinoma of the Nasopharynx: Factors Affecting Prognosis. *Int J Radiat Oncol Biol Phys* (1992) 23:271–80. doi: 10.1016/0360-3016(92)90741-Y
5. Hellman S. Karnofsky Memorial Lecture. Natural History of Small Breast Cancers. *J Clin Oncol* (1994) 12:2229–34. doi: 10.1200/JCO.1994.12.10.2229
6. Brown M, Assen FP, Leithner A, Abe J, Schachner H, Asfour G, et al. Lymph Node Blood Vessels Provide Exit Routes for Metastatic Tumor Cell Dissemination in Mice. *Science* (2018) 359:1408–11. doi: 10.1126/science.aal3662
7. Pereira ER, Kedrin D, Seano G, Gautier O, Meijer EFJ, Jones D, et al. Lymph Node Metastases can Invade Local Blood Vessels, Exit the Node, and Colonize Distant Organs in Mice. *Science* (2018) 359:1403–7. doi: 10.1126/science.aal3622
8. van den Brekel MW. Lymph Node Metastases: CT and MRI. *Eur J Radiol* (2000) 33:230–38. doi: 10.1016/S0720-048X(99)00145-X
9. Tang LL, Chen YP, Mao YP, Wang ZX, Guo R, Chen L, et al. Validation of the 8th Edition of the UICC/AJCC Staging System for Nasopharyngeal Carcinoma From Endemic Areas in the Intensity-Modulated Radiotherapy Era. *J Natl Compr Canc Netw* (2017) 15:913–19. doi: 10.6004/jnccn.2017.0121
10. Brito RA, Valero V, Buzdar AU, Booser DJ, Ames F, Strom E, et al. Long-Term Results of Combined-Modality Therapy for Locally Advanced Breast Cancer With Ipsilateral Supraclavicular Metastases: The University of Texas M.D. Anderson Cancer Center Experience. *J Clin Oncol* (2001) 19:628–33. doi: 10.1200/JCO.2001.19.3.628
11. Chen SC, Chang HK, Lin YC, Leung WM, Tsai CS, Cheung YC, et al. Prognosis of Breast Cancer After Supraclavicular Lymph Node Metastasis: Not a Distant Metastasis. *Ann Surg Oncol* (2006) 13:1457–65. doi: 10.1245/s10434-006-9012-1
12. Pan H, Wang H, Qian M, Mao X, Shi G, Ma G, et al. Comparison of Survival Outcomes Among Patients With Breast Cancer With Distant vs Ipsilateral Supraclavicular Lymph Node Metastases. *JAMA Netw Open* (2021) 4:e211809. doi: 10.1001/jamanetworkopen.2021.1809/
13. Magnoni F, Colleoni M, Mattar D, Corso G, Bagnardi V, Frassoni S, et al. Contralateral Axillary Lymph Node Metastases From Breast Carcinoma: Is it Time to Review TNM Cancer Staging. *Ann Surg Oncol* (2020) 27:4488–99. doi: 10.1245/s10434-020-08605-4
14. Mukai Y, Yokota NR, Sugiura M, Mizushima T, Taniuchi R, Imai Y, et al. Outcome of Radiation Therapy for Stage IVB Uterine Cervical Cancer With Distant Lymph Nodes Metastases; Sequential Irradiation for Distant Lymph Nodes Metastases. *In Vivo* (2021) 35:1169–76. doi: 10.21873/invivo.12365
15. Siosaki MD, Souza AT. Images in Clinical Medicine. Virchow's Node. *N Engl J Med* (2013) 368:e7. doi: 10.1056/NEJMicm1204740
16. Baumgart DC, Fischer A. Virchow's Node. *Lancet* (2007) 370:1568. doi: 10.1016/S0140-6736(07)61661-4
17. Lister TA, Crowther D, Sutcliffe SB, Glatstein E, Canellos GP, Young RC, et al. Report of a Committee Convened to Discuss the Evaluation and Staging of Patients With Hodgkins Disease: Cotswolds Meeting. *J Clin Oncol* (1989) 7:1630–36. doi: 10.1200/JCO.1989.7.11.1630
18. Brierley JD, Mary KG, Wittekind C. *TNM Classification of Malignant Tumors. 8th edn*. Chichester, West Sussex, UK Wiley Blackwell: UICC International Union Against Cancer (2017).
19. Olthof EP, Mom CH, van der Velden J. More Attention is Needed for the Corrigendum to the Revised FIGO Staging for Carcinoma of the Cervix Uteri. *Int J Gynecol Cancer* (2020) 30:1850. doi: 10.1136/ijgc-2020-001959
20. Bhatla N, Berek JS, Cuello Fredes M, Denny LA, Grenman S, Karunaratne K, et al. Revised FIGO Staging for Carcinoma of the Cervix Uteri. *Int J Gynaecol Obstet* (2019) 145:129–35. doi: 10.1002/ijgo.12749
21. Sham JS, Choy D, Wei WI. Nasopharyngeal Carcinoma: Orderly Neck Node Spread. *Int J Radiat Oncol Biol Phys* (1990) 19:929–33. doi: 10.1016/0360-3016(90)90014-B
22. Xu Y, Huang T, Fan L, Jin W, Chen X, Chen J. Patterns and Prognostic Value of Lymph Node Metastasis on Distant Metastasis and Survival in Nasopharyngeal Carcinoma: A Surveillance, Epidemiology, and End Results Study, 2006-2015. *J Oncol* (2019) 2019:4094395. doi: 10.1155/2019/4094395
23. Shen L, Li W, Wang S, Xie G, Zeng Q, Chen C, et al. Image-Based Multilevel Subdivision of M1 Category in TNM Staging System for Metastatic Nasopharyngeal Carcinoma. *Radiology* (2016) 280:805–14. doi: 10.1148/radiol.2016151344
24. Zeng Z, Shen L, Wang Y, Shi F, Chen C, Wu M, et al. A Nomogram for Predicting Survival of Nasopharyngeal Carcinoma Patients With Metachronous Metastasis. *Med (Baltimore)* (2016) 95:e4026. doi: 10.1097/MD.0000000000004026
25. Chang JH, Ahn YC, Park H, Oh D, Noh JM, Sun JM, et al. Fate of Patients With Nasopharyngeal Cancer Who Developed Distant Metastasis as First Failure After Definitive Radiation Therapy. *Head Neck* (2016) 38 Suppl 1: E293–9. doi: 10.1002/hed.23988
26. Jiang R, Cai XY, Yang ZH, Yan Y, Zou X, Guo L, et al. Elevated Peripheral Blood Lymphocyte-to-Monocyte Ratio Predicts a Favorable Prognosis in the Patients With Metastatic Nasopharyngeal Carcinoma. *Chin J Cancer* (2015) 34:237–46. doi: 10.1186/s40880-015-0025-7
27. Shen LJ, Wang SY, Xie GF, Zeng Q, Chen C, Dong AN, et al. Subdivision of M Category for Nasopharyngeal Carcinoma With Synchronous Metastasis: Time

to Expand the M Categorization System. *Chin J Cancer* (2015) 34:450–58. doi: 10.1186/s40880-015-0031-9
28. Zheng WH, He XJ, Chen FP, Lin L, Huang XD, Zhou HQ, et al. Establishing M1 Stage Subdivisions by Incorporating Radiological Features and Epstein-Barr Virus DNA for Metastatic Nasopharyngeal Carcinoma. *Ann Transl Med* (2020) 8:83. doi: 10.21037/atm.2020.01.13
29. Md Yusof K, Rosli R, Abdullah MA, Avery-Kiejda K. The Roles of Non-Coding RNAs in Tumor-Associated Lymphangiogenesis. *Cancers (Basel)* (2020) 12:1–27. doi: 10.3390/cancers12113290
30. Yu D, Han GH, Zhao X, Liu X, Xue K, Wang D, et al. MicroRNA-129-5p Suppresses Nasopharyngeal Carcinoma Lymphangiogenesis and Lymph Node Metastasis by Targeting ZIC2. *Cell Oncol (Dordr)* (2020) 43:249–61. doi: 10.1007/s13402-019-00485-5
31. Luo C, Yin H, Gao T, Ma C, Liu J, Zhang T, et al. PEDF Inhibits Lymphatic Metastasis of Nasopharyngeal Carcinoma as a New Lymphangiogenesis Inhibitor. *Cell Death Dis* (2021) 12:295. doi: 10.1038/s41419-021-03583-1

Conflict of Interest: The authors declare that the research was conducted in the absence of any commercial or financial relationships that could be construed as a potential conflict of interest.

Publisher's Note: All claims expressed in this article are solely those of the authors and do not necessarily represent those of their affiliated organizations, or those of the publisher, the editors and the reviewers. Any product that may be evaluated in this article, or claim that may be made by its manufacturer, is not guaranteed or endorsed by the publisher.

frontiers in Oncology

ORIGINAL RESEARCH
published: 06 October 2021
doi: 10.3389/fonc.2021.714550

Transcriptomic Correlates of Immunologic Activation in Head and Neck and Cervical Cancer

Cristina Saiz-Ladera[1†], Mariona Baliu-Piqué[1†], Francisco J. Cimas[2], Aránzazu Manzano[1], Vanesa García-Barberán[1], Santiago Cabezas Camarero[1], Gonzalo Fernández Hinojal[1], Atanasio Pandiella[3], Balázs Győrffy[4,5,6], David Stewart[7], Juan J. Cruz-Hernández[3], Pedro Pérez-Segura[1] and Alberto Ocana[1,2]*

[1] Experimental Therapeutics Unit, Medical Oncology Department, Hospital Clínico Universitario San Carlos (HCSC), Instituto de Investigación Sanitaria (IdISSC), Madrid, Spain, [2] Translational Oncology Laboratory, Centro Regional de Investigaciones Biomedicas, Castilla-La Mancha University (CRIB-UCLM), Albacete, Spain, [3] Instituto de Biología Molecular y Celular del Cáncer and Centro de Investigación Biomédica en Red de Cáncer (CIBERONC), Centro Superior de Investigaciones Científicas (CSIC), Salamanca, Spain, [4] Department of Bioinformatics, Faculty of Medicine, Semmelweis University, Budapest, Hungary, [5] 2nd Department of Pediatrics, Faculty of Medicine, Semmelweis University, Budapest, Hungary, [6] Institute of Enzymology, Research Centre of Nature Sciences, Budapest, Hungary, [7] Ottawa University Hospital, University of Ottawa, Ottawa, ON, Canada

Targeting the immune system has emerged as an effective therapeutic strategy for the treatment of various tumor types, including Head and Neck Squamous Cell Carcinoma (HNSCC) and Non-small-Cell Lung Cancer (NSCLC), and checkpoint inhibitors have shown to improve patient survival in these tumor types. Unfortunately, not all cancers respond to these agents, making it necessary to identify responsive tumors. Several biomarkers of response have been described and clinically tested. As of yet what seems to be clear is that a pre-activation state of the immune system is necessary for these agents to be efficient. In this study, using established transcriptomic signatures, we identified a group of gene combination associated with favorable outcome in HNSCC linked to a higher presence of immune effector cells. *CD2*, *CD3D*, *CD3E*, and *CXCR6* combined gene expression is associated with improved outcome of HNSCC patients and an increase of infiltrating immune effector cells. This new signature also identifies a subset of cervical squamous cell carcinoma (CSCC) patients with favorable prognosis, who show an increased presence of immune effector cells in the tumor, which outcome shows similarities with the HP-positive HNSCC cohort of patients. In addition, *CD2*, *CD3D*, *CD3E*, and *CXCR6* signature is able to predict the best favorable prognosis in terms of overall survival of CSSC patients. Of note, these findings were not reproduced in other squamous cell carcinomas like esophageal SCC or lung SCC. Prospective confirmatory studies should be employed to validate these findings.

Keywords: head and neck squamous cell carcinoma (HNSCC), human papillomavirus, transcriptome signature, immune gene signatures, cervical squamous cell carcinoma (CSCC)

OPEN ACCESS

Edited by:
Hui Wang,
Hunan Cancer Hospital, China

Reviewed by:
Maud Kamal,
Institut Curie, France
Sheng Yang,
Nanjing Medical University, China

****Correspondence:***
Alberto Ocana
alberto.ocana@salud.madrid.org

†These authors have contributed equally to this work and share first authorship

Specialty section:
This article was submitted to Head and Neck Cancer, a section of the journal Frontiers in Oncology

Received: *25 May 2021*
Accepted: *13 September 2021*
Published: *06 October 2021*

Citation:
Saiz-Ladera C, Baliu-Piqué M, Cimas FJ, Manzano A, García-Barberán V, Camarero SC, Hinojal GF, Pandiella A, Győrffy B, Stewart D, Cruz-Hernández JJ, Pérez-Segura P and Ocana A (2021) Transcriptomic Correlates of Immunologic Activation in Head and Neck and Cervical Cancer. Front. Oncol. 11:714550. doi: 10.3389/fonc.2021.714550

INTRODUCTION

Squamous Cell Carcinoma (SCC) includes a wide range of tumors originated from diverse anatomical locations that share common molecular and genetic features (1). SCCs arise from squamous and non-squamous epithelial tissues, and they are classified according to their location as head and neck, esophagus, lung, and cervix, among others (2). SCCs are in many occasions incurable diseases particularly in their advanced stages (1). This is the case for Head and Neck Squamous Cell Carcinoma (HNSCC) and Cervical Squamous Cell Carcinoma (CSCC), since the therapeutic options for both tumors, when diagnosed in the metastatic setting, are limited and outcome is severely compromised (3, 4). In both tumors, human papilloma virus (HPV) infection plays a central oncogenic role in a substantial proportion of cases and associates with aggressiveness and clinical outcome particularly in HNSCC (5). The classical treatment for HNSCC includes chemotherapies based on platinum agents and taxanes combined with anti-EGFR antibodies, which has demonstrated to improve survival (3). Recently, immunomodulators, particularly immune checkpoint inhibitors like pembrolizumab or nivolumab, have shown to improve relapse-free survival (RFS) and overall survival (OS) (5–8). Although this has dramatically changed the expected survival of HNSCC patients, the metastatic setting, nevertheless, remained an incurable condition (9). In a similar manner, immunotherapy has shown efficacy in CSCC patients with recurrent or metastatic cancers with disease progression or after chemotherapy when tumors express PD-L1 (Combined Positive Score, CPS ≥1) (10). In other tumor types like non-small-cell lung (NSCLC) or bladder cancer, checkpoint inhibitors have also demonstrated to provide clinical efficacy (6–8, 11). However, blocking of immune inhibitory signals with antibodies against PD1 or PD-L1 does not always result in clinical response (12, 13). Activation of the immune system, including the presence of effector T cells in the tumor, is a main requisite for these therapies to be effective (14). In addition, expression of PD1 or PD-L1 or the presence of Tumor Infiltrating Lymphocytes (TIL) is associated with favorable survival, independently of the therapy administered, confirming the relevant role of the immune system in the antitumoral action (15, 16).

Identification of genomic correlations of immune activation is an approach that could permit the selection of tumors susceptible to respond to immunotherapies. In this context, the mutational burden or altered mismatch repair mechanisms have been described as predictors of response to immunotherapies in several types of tumors (17–19). Likewise, some molecular alterations have been described as linked to the lack of activity of immunotherapeutic agents including JAK2 or B2M mutations (20). Regardless, recognition of immune pre-activated tumors, usually associated with favorable prognosis, is a requisite for most immune therapies to be efficient.

In this article we explored gene sets that predict favorable prognosis in HNSCC, with the aim to identify pre-activated immune tumors. We identified a transcriptomic signature associated with favorable outcome and linked with the infiltration of effector immune cells in this tumor. Similar findings were observed in Cervical SCC (CSCC), confirming its relevance.

MATERIAL AND METHODS

Immune Gene Signatures

Previously described immune signatures, i.e., expanded immune gene signature (CD3D, IL2RG, CXCL10, IDO1, NKG7, CIITA, HLA-E, HLA-DRA, CD3E, CXCR6, STAT1, CCL5, LAG3, GZMK, TAGAP, CD2, STAT1, CXCL13, GZMB), IFN gamma signature (IDO1, CXCL10, CXCL9, HLA-DRA, IRF9, IFNG, STAT1), cytotoxic T lymphocyte (CTL) signature (CD8A, CD8B, GZMA, GZMB, and PRF1), and HLA genes (HLA-A, HLA-B) were used to study the prognostic capacity of the genes composing each signature (21–23).

Clinical Outcome Analysis of Individual Genes and Signatures

The KM Plotter Online Tool (http://www.kmplot.com) (24, 25) was used to explore the relationship between the expression of described gene signatures (expanded immune gene signature, IFN gamma signature, CTL signature, and HLA genes) and the newly identified signature (*CD2*, *CD3D*, *CD3E*, and *CXCR6*) with patient clinical outcomes. We evaluated the prognostic values of mRNA expression of previously described gene signatures, for overall survival (OS) in a cohort of HNSCC patients (n=527) in all stages from the Cancer Genome Atlas (TCGA) database.

Briefly, publicly available RNA-seq HTSeq count files obtained from Illumina HiSeq 2000 RNA Sequencing Version 2 platform were analyzed for quantification of mRNA expression. Negative binomial distribution method was used through DESeq package to normalize the raw count data, and Bioconductor AnnotationDbi package (http://bioconductor.org/packages/AnnotationDbi/) was employed to annotate Ensembl transcript IDs with gene symbols (n = 25,228). After that, second scaling normalization was performed to calculate the mean expression of all genes in each patient sample to 1,000 to reduce batch effects.

In order to determine the correlation between gene expression and OS, Cox proportional hazards regression analysis was performed by using the Survival R package v2.38 (http://CRAN.R-project.org/package=survival/). Log-rank P values, hazard ratios (HR), and 95% confidence intervals (CI) were calculated. In terms of statistical analysis, false discovery rate (FDR) was computed to correct for multiple hypothesis testing, and the result was only accepted as significant in the case of FDR < 10%. Each possible cutoff was evaluated between the highest and lowest quartile of expression, and the best performing threshold with the lowest p value was used in the final analysis when drawing the Kaplan–Meier plot. In addition, multivariate survival analysis was performed for the gene expression and clinical features to assess independence from known epidemiological and clinical variables, including race, sex, age, tumor stage, and tumor grade when available. Finally, only genes associated with good outcome (HR<0.65, p<0.05, and FDR≤ 5%) were selected after screening through KM Plotter.

According to the results, the gene expression of the individual genes and the newly identified signature (*CD2*, *CD3D*, *CD3E*, and *CXCR6*) were assessed for OS in the different cohorts including HNSCC (n= 527), Esophageal SCC (n=81), Lung SCC (n=501), and

Cervical SCC (n=254). In case we identified an association with multiple genes, the mean expression of the selected genes was used. Patients were divided according to the best cutoff values of the gene expression [lowest p-value (*p*)] into high *vs* low expression.

For graphical representation, a heatmap plot was performed using *GraphPad Prism 8.0* tool. Survival HR parameter was represented as labels overlaid on the graph. The scale color meaning was represented as follows: blue, favorable outcome; red, detrimental outcome. Detailed information about the patients and clinical variables that were included in this study are resumed in **Table 1**.

Analysis of Tumor Mutational Burden and HPV

Clinicopathological characteristics of patients, including stage, grade, sex, race, including tumor mutational burden (TMB), were available and allowed to restrict the analysis in the cited KM Plotter Online Tool (http://www.kmplot.com).

The TMB was determined from whole-exome sequencing data from TCGA datasets used as the number of genes with a mutation. A gene was assigned "mutated" in case it had, at least, one mutation. Then, the median number of mutations across all samples within each tumor type was determined and was used as a cutoff: samples that had more "mutated" genes were determined as "high TMB," and samples that had fewer "mutated" genes were assigned to the "low TMB" cohort.

In terms of HPV status detection, the Cancer Genomic Atlas (TCGA) dataset used the HPV16 DNA genotyping and mRNA expression to detect HPV oncoprotein transcripts.

Association Between Tumor Immune Infiltrates and Gene Expression

The correlation between gene expression and the presence of tumor immune infiltrates ($CD8^+$T cells, NK cells, macrophages, and dendritic cells) in HNSCC and CSCC was analyzed using the Tumor Immune Estimation Resource (TIMER 2.0) platform (http://cistrome.org/TIMER/) (26, 27), a dataset that contains 10,897 samples from diverse cancer types available in the TCGA database. To analyze the relationship between tumor gene expression and immune infiltration, the available "Gene Module" from TIMER 2.0 was used. TIMER 2.0 uses an R package that integrates six computational algorithms to associate the tumor immune infiltrate populations with genomic and transcriptomic changes in the tumors (based on microarrays or RNAsequencing data), providing an estimation of immune infiltration levels for TCGA database or user-provided tumor profiles. To make the estimations of the immune cell populations, the cited algorithms are based on gene signature-based approaches utilizing a list of cell-type-specific gene

TABLE 1 | Patients' clinical characteristics.

Clinical data available	HNSCC		Lung SCC		CSCC	
Total n	527		504		254	
Median age	61 years		NA		47 years	
Gender (male)	73%		74%		0%	
Smoking history	76%		96%		NA	
Alcohol history	68%		NA		NA	
Median follow-up	21.4 months		22.2 months		22.4 months	
Stage	***n***	***%***	***n***	***%***	***n***	***%***
Stage 1	27	5.90%	246	48.90%	126	51.10%
Stage 2	74	16.30%	165	32.80%	62	25.10%
Stage 3	82	18.10%	85	16.90%	43	17.40%
Stage 4	270	59.60%	7	1.40%	16	6.50%
Grade	***n***	***%***	***n***	***%***	***n***	***%***
Grade 1	63	12.50%	NA	NA	12	5.30%
Grade 2	311	61.50%	NA	NA	110	48.70%
Grade 3	125	24.70%	NA	NA	103	45.60%
Grade 4	7	1.38%	NA	NA	1	0.40%
Stage	***n***	***%***	***n***	***%***	***n***	***%***
T1	NA	NA	114	22.62%	111	56.35%
T2	NA	NA	295	58.53%	58	29.44%
T3	NA	NA	71	14.09%	19	9.64%
T4	NA	NA	24	4.76%	9	4.57%
Lymph Node	***n***	***%***	***n***	***%***	***n***	***%***
N0	NA	NA	320	64.26%	105	67.31%
N1	NA	NA	133	26.71%	51	32.69%
N2	NA	NA	40	8.03%	0	0%
N3	NA	NA	5	1.00%	0	0%
Metastasis	***n***	***%***	***n***	***%***	***n***	***%***
M0	NA	NA	414	98.34%	102	93.58%
M1	NA	NA	7	1.66%	7	6.42%

Epidemiological data including age (median years), gender, smoking and alcohol history (in corresponding percentages, %), and median follow-up (in months) of included patients per each SCC type in this study are displayed in the table. In addition, the corresponding total number (n) and the percentage (%) of included patients of each SCC type are showed by stage (1 to 4), grade (1 to 4), and TNM staging system (T1 to T4, N0 to N3, and M0 to M1).
NA, Not Available.

sets and using the expression values of these signature gene sets in tissue samples. Specific tissue types, distinct cancer-cell intrinsic gene expression, and different immune cell types are considered to establish Spearman's correlations between the expression of the input gene and the abundance of the immune cell type as well as its subtypes across cancer types under study. These algorithms were applied to the expression profiles of the Cancer Genome Atlas (TCGA) tumors, allowing to explore various associations between immune infiltrates and genetic features in the TCGA cohorts. The association between the immune infiltrates and the clinical features, such as HPV infection condition, was possible sorting patient cohorts in case of HNSCC. The results are displayed as a functional heatmap, and by clicking on each box of the heatmap, subsequently it generates a scatter plot showing the association of the gene expression with the infiltrated immune cell type. "Purity adjusted" option was selected (the correlation of the given gene expression with tumor purity as proportion of cancer cells in a sample), and the most immune cell types are negatively correlated with tumor purity (data not shown). Partial Spearman's correlation was used to perform this association analysis, and statistical significance was expressed (p<0.05). Correlation value was displayed by "Rho" parameter. Positive correlation is associated with Rho>0 values, and negative correlation is associated with Rho<0 values.

RESULTS

Evaluation of Immune Activated Signatures and Clinical Outcome in HNSCC

With the main goal to identify immunologic correlates associated with prognosis in HNSCC, we took advantage of previous published immune transcriptomic signatures (21–23). We first explored the association of the genes included in each signature with favorable prognosis, and latter their correlation with immune populations as described in *Materials and Methods* (**Figure 1A**). The correlation analysis between each immune signature and the 32 individual genes with OS is displayed as a heatmap in **Figure 1B** and **Table 2**.

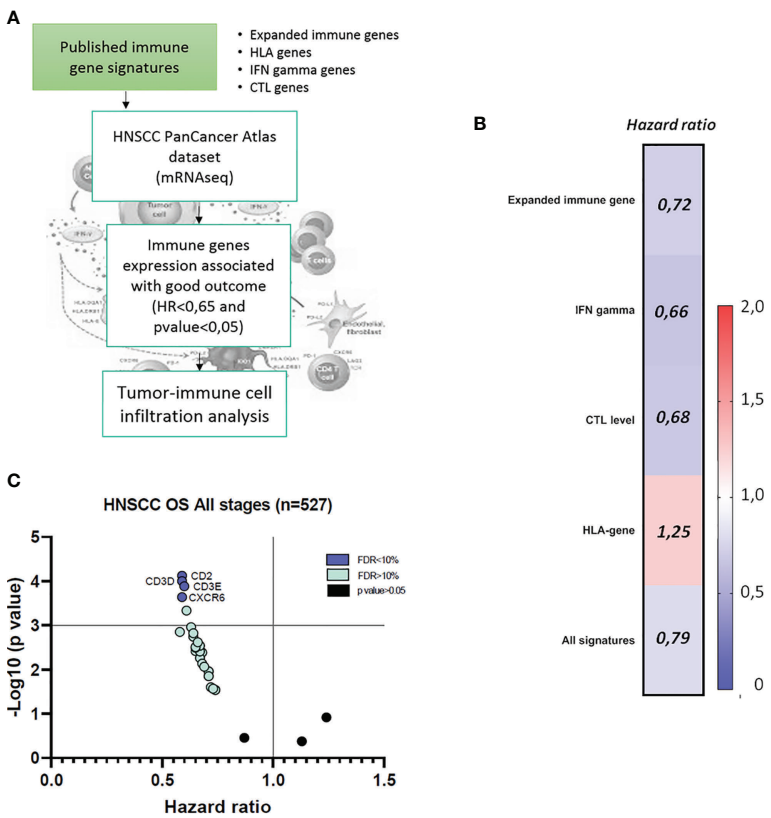

FIGURE 1 | Evaluation of the impact of immune gene signatures (*Expanded* immune genes, *IFN gamma genes*, *CTL level*, and *HLA genes*) on clinical outcome in Head and Neck Squamous Cell Carcinoma (HNSCC) patients. **(A)** Flow chart of the analysis of the four published immune gene signatures and the transcriptomic expression effect in HNSCC patients' clinical outcome and the correlation with tumor immune cell infiltrate composition. **(B)** Hazard ratio (HR) heat map for risk of death of each published immune gene signatures (*Expanded immune genes*, *IFN gamma genes*, *CTL levels*, and *HLA genes)* and combined, in association with overall survival (OS) in HNSCC patients at all stages (n = 527), using data from TCGA database as described in *Materials and Methods*. HR < 1 discriminates a risk reduction. Blue color represents favorable prognosis, and red color represents detrimental prognosis, with 95% confidence interval (CI) and p value < 0.05. **(C)** Graph representation of immune genes with the most favorable outcome in HNSCC (HR < 1, p value < 0.05 and FDR < 10%), in blue spots. Green spots represent immune genes with good prognosis and FDR > 10% and p < 0.05. Black spots represent immune genes without statistical significance (p value > 0.05).

Favorable survival was observed for the expanded immune genes signature (HR=0.72; 95% confidence intervals CI=0.55–0.94; log rank p=0.016), the IFN gamma signature (HR=0.66; 95% CI=0.50–0.87; log rank p=0.0028), and the CTL level signature (HR=0.68; 95% CI=0.52–0.89; log rank p=0.0053) (**Figure 1B**). Only the HLA signature predicted unfavorable survival (HR=1.25; 95% CI=0.92–1.70; log rank p=0.150) (**Figure 1B**). For the whole population of tumors (all stages, n=527), most individual genes were associated with favorable outcome (**Table 2**). The different gene signatures did not predict for better OS in comparison with some individual transcripts, particularly with CD2 (HR=0.59; 95% CI=0.45–0.77; log rank p= 7.5e−05), CD3D (HR=0.59; 95% CI=0.45–0.77; log rank p=0.0001), CD3E (HR=0.60; 95% CI=0.46–0.78; log rank p=0.00013), and CXCR6 (HR=0.59; 95% CI=0.45–0.78; log rank p=0.00023) (**Table 2**). In addition, these individual genes presented a smaller FDR (FDR<10%) compared with the other analyzed genes and signatures (**Figure 1C**).

Considering these results, we decided to analyze the gene set combination of *CD2*, *CD3D*, *CD3E*, and *CXRC6*.

The expression of PDL1 or PD1 is associated with favorable clinical outcome and improved response to immunotherapy including HNSCC tumors (5–8). We identified a positive correlation between the new immune gene signature (*CD2*, *CD3D*, *CD3E*, *CXCR6*) and *CD274* (*PD-L1*) expression in HNSCC patients (Spearman rank correlation coefficient = 0.56; $P=2.4E^{-43}$), which could support the outcome prediction in this group.

The Combined Gene Signature *CD2*, *CD3D*, *CD3E*, and *CXCR6* Predicted Favorable Prognosis in Different HNSCC Clinical Stages

Next, we tested whether a new signature composed by *CD2*, *CD3D*, *CD3E*, and *CXRC6* could improve the potential prediction capacity in HNSCC patients. The combined immune signature demonstrated a higher prediction in the stage II and III patient subgroups, even with a small number of patients: for stage II (n=69), HR=0.39; 95% CI=0.15–0.99; log rank p=0.041; and stage III subgroup: (n=78), HR=0.31; 95% CI=0.15–0.66; log rank p=0.0012). For all stages the combined signature also predicted favorable survival: (n=527), HR=0.58; 95% CI=0.44–0.76; log rank $p=8e^{-05}$). Results in stage IV were also significant but with less

TABLE 2 | Clinical outcome of individual immune genes from the four immune gene signatures in terms of overall survival (OS) of HNSCC patients.

Signature	OS N = 527 (All stages)				
	Gene symbol	**HR**	**CI**	**pValue**	**FDR**
Expanded immune genes	CXCL13	0,58	0,41–0,81	0,0014	50%
	CD2	**0,59**	**0,45–0,77**	**0,000075**	**5%**
	CD3D	**0,59**	**0,45–0,77**	**0,0001**	**5%**
	CXCR6	**0,59**	**0,45–0,78**	**0,00023**	**2%**
	CD3E	**0,60**	**0,46–0,78**	**0,00013**	**5%**
	GZMK	0,61	0,46–0,81	0,00046	20%
	GZMB	0,63	0,48–0,83	0,0011	20%
	IL2RG	0,64	0,48–0,85	0,0018	10%
	TAGAP	0,65	0,49–0,87	0,0032	50%
	LAG3	0,67	0,51–0,89	0,0055	50%
	NKG7	0,67	0,52–0,88	0,0039	50%
	CIITA	0,67	0,51–0,87	0,0029	50%
	CCL5	0,68	0,52–0,9	0,0073	>50%
	IDO1	0,71	0,54–0,92	0,011	>50%
	CXCL10	0,71	0,54–0,93	0,014	>50%
	HLA-DRA	0,73	0,55–0,97	0,027	>50%
	STAT1	0,74	0,56–0,97	0,029	>50%
	HLA-E	0,87	0,65–1,16	0,35	100%
IFN gamma genes	CXCL9	0,65	0,49–0,87	0,0038	>50%
	IFNG	0,68	0,52–0,88	0,0041	>50%
	IDO1	0,71	0,54–0,92	0,011	>50%
	CXCL10	0,71	0,54–0,93	0,014	>50%
	IRF9	0,72	0,53–0,96	0,025	>50%
	HLA-DRA	0,73	0,55–0,97	0,027	>50%
	STAT1	0,74	0,56–0,97	0,029	>50%
CTL level	GZMB	0,63	0,48–0,83	0,0011	20%
	GZMA	0,64	0,49–0,85	0,0015	50%
	PRF1	0,65	0,48–0,86	0,0031	>50%
	CD8A	0,66	0,5–0,86	0,0024	50%
	CD8B	0,69	0,52–0,91	0,0086	>50%
HLA genes	HLA-B	1,13	0,84–1,5	0,42	100%
	HLA-A	1,24	0,95–1,61	0,12	100%

Table shows the list of individual genes belonging to the four previous published immune gene signatures. HR < 1 discriminates a risk reduction. The 95% confidence interval (CI) and p value are displayed. p value < 0.05 and FDR (False Discovery Rate) to correct for multiple hypothesis testing are displayed.
The bold values represent those genes that stand out with the best clinical outcome (HR < 0.65, FDR < 10%, p < 0.05).

magnitude of benefit compared with the other subgroups: (n=259), HR=0.62; 95% CI=0.43–0.89; log rank p=0.0089) (**Figure 2**).

CD2, *CD3D*, *CD3E*, and *CXCR6* Expression Is Associated With Infiltration of Memory CD8+ T, Activated NK, Dendritic Cells, and M1 Macrophages in HPV-Positive HNSCC

We next explored the association of the expression at an individual transcriptomic level of *CD2*, *CD3D*, *CD3E*, and *CXRC6* with the presence of tumor-infiltrating immune cell populations. All genes had a negative correlation with tumor purity, demonstrating the high presence of immune populations.

In HPV-positive HNSCC tumors (n=98), we observed the strongest positive correlation with central memory $CD8^+$ T cell subpopulation (*CD2:* Rho=0.904, *CD3D:* Rho=0.933, *CD3E:* Rho=0.938 and *CXCR6:* Rho=0.886) and also a positive correlation with effector memory $CD8^+$ T cells (*CD2:* Rho=0.612, *CD3D:* Rho=0.693, *CD3E:* Rho=0.623 and *CXCR6:* Rho=0.606) (**Figure 3**). In the case of NK cells, the stronger association was found for activated NK cells (*CD2:* Rho=0.573,

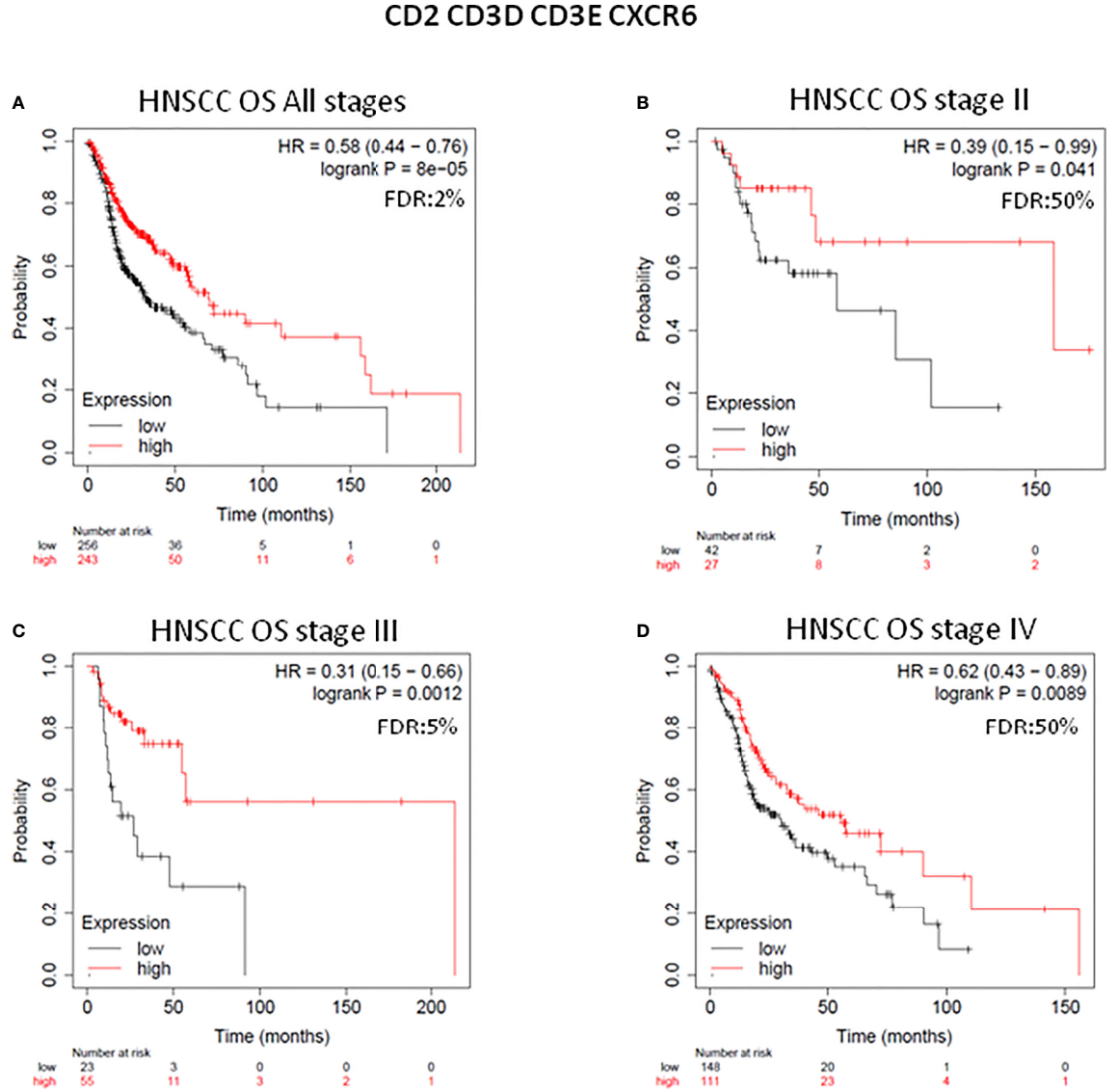

FIGURE 2 | Clinical outcome analysis of *CD2*, *CD3D*, *CD3E*, *CXCR6* immune gene-set combination in each stage of HNSCC patients. Survival plots of the combination of four immune genes with the most favorable prognosis (HR < 0.65, *p* value < 0.05, and FDR < 10%) at all stages of HNSC patients (n = 527) **(A)**, at stage II (n = 69) **(B)**, at stage III (n = 78) **(C)**, and at stage IV (n = 259) **(D)** are displayed. Patients whose tumors harbor high gene expression levels predicted better survival (red line), and those with low gene expression levels predicted worse survival (black line). Number of patients at risk at every time (months), with high (in red) and low gene expression (in black) are displayed. HR for risk of death and OS are displayed. HR < 0.65 discriminates a risk reduction. FDR is also displayed. The gene combination is displayed at the top of the figure.

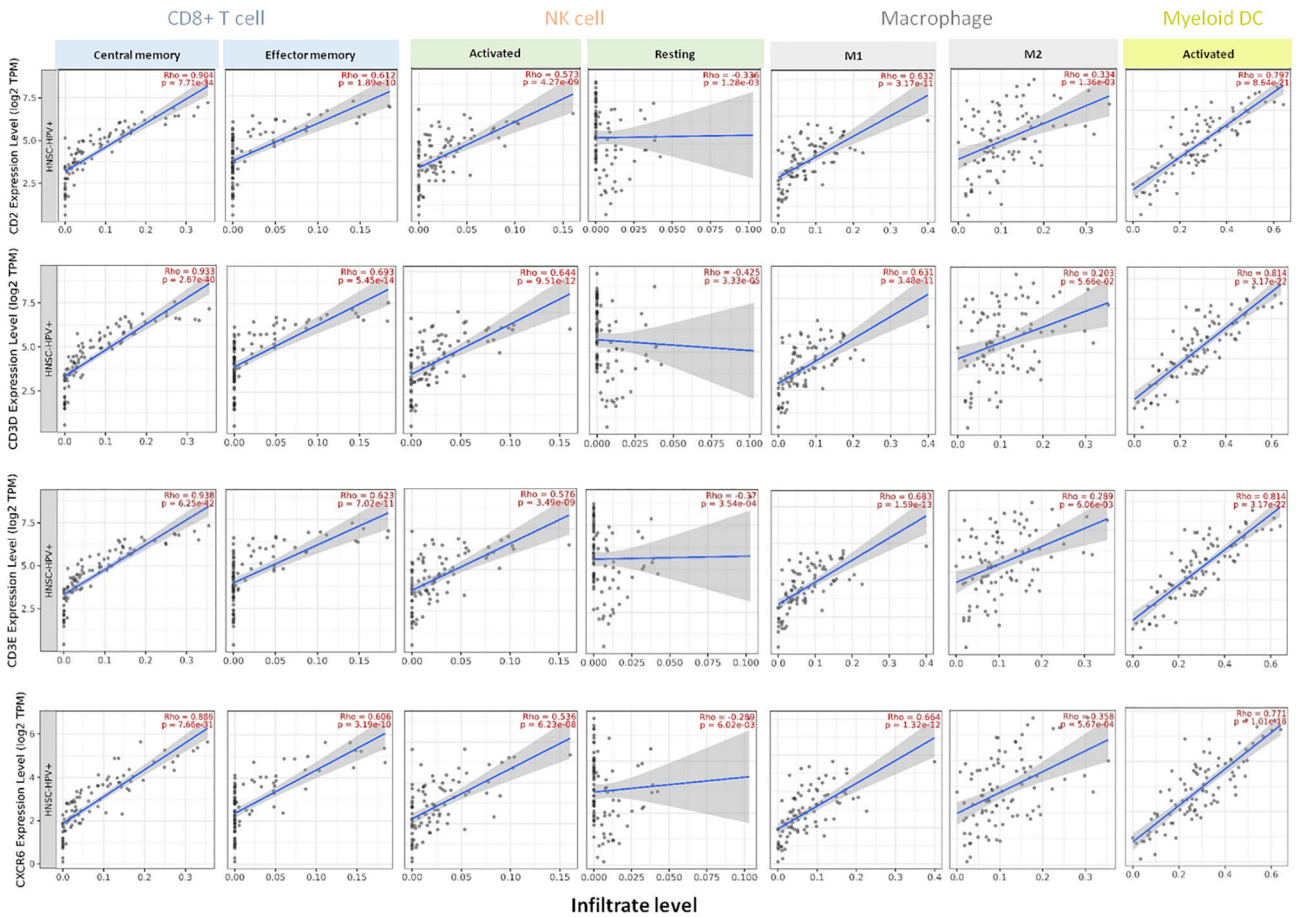

FIGURE 3 | Association of the expression of *CD2*, *CD3D*, *CD3E*, *CXCR6* with specific tumor-infiltrating immune cell populations in HPV-positive HNSCC patients. Expression of each gene and association with the presence of CD8+ T cells (central memory and effector memory subsets), NK cells (activated and resting), macrophages (M1 and M2 types), and activated myeloid dendritic cells in HPV-positive HNSCC (n = 98). Each panel presents the relationship between infiltrates estimation value with the purity-adjusted spearman's correlation parameter Rho and gene expression join p value < 0.001. Rho value > 0 represents a positive correlation, and Rho < 0 represents a negative correlation. Association with immune cell populations was provided by *TIMER 2.0* software and was correlated with transcriptome expression level of each immune gene, as described in *Material and Methods*.

CD3D: Rho=0.644, *CD3E:* Rho=0.576 and *CXCR6:* Rho=0.536), compared with a negative association with resting NK cells (*CD2:* Rho=−0.336, *CD3D:* Rho=−0.425, *CD3E:* Rho=−0.370 and *CXCR6:* Rho=−0.289). Regarding the macrophage population, HPV-positive tumors showed a positive correlation with both subtypes (M1 and M2): M1 (*CD2:* Rho=0.632, *CD3D:* Rho=0.631, *CD3E:* Rho=0.683, and *CXCR6:* Rho=0.664), and less significant for the M2 subtype (*CD2:* Rho=0.334, *CD3D:* Rho=0.203, *CD3E:* Rho=0.289, and *CXCR6:* Rho=0.358) (**Figure 3**). For the activated dendritic cell population, a strong correlation was observed (*CD2:* Rho=*0.797*, *CD3D:* Rho=0.814, *CD3E:* Rho=0.814, and *CXCR6:* Rho=0.771) (**Figure 3**).

In case of HPV-negative HNSCC tumors (n=422), we found a positive correlation between the gene expression level of *CD2*, *CD3D*, *CD3E*, and *CXRC6*, and $CD8^+$ T cells subpopulations, finding the higher correlation with CD8+ central memory cells (*CD2:* Rho=0.817, *CD3D:* Rho=0.800, *CD3E:* Rho=0.826, and *CXCR6:* Rho=0.797). A less significant association was observed for the CD8+ effector memory cells (*CD2:* Rho=0.570, *CD3D:* Rho=0.592, *CD3E:* Rho=0.550, and *CXCR6:* Rho=0.570) (**Figure 4**). In addition, we found a positive association between the gene expression level of *CD2*, *CD3D*, *CD3E*, and *CXRC6* and the activated fraction of NK cells present in the tumor (*CD2:* Rho=0.442, *CD3D:* Rho=0.460, *CD3E:* Rho=0.423, and *CXCR6:* Rho=0.401). A negative association with resting NK cells (*CD2:* Rho=−0.059, *CD3D:* Rho=−0.111, *CD3E:* Rho=−0.039, and *CXCR6:* Rho=0.02) was observed. Similar findings were observed for M1 macrophage infiltrates (*CD2:* Rho=0.760, *CD3D:* Rho=0.706, *CD3E:* Rho=0.747, and *CXCR6:* Rho=0.744) and M2 macrophages (*CD2:* Rho=0.753, *CD3D:* Rho=0.667, *CD3E:* Rho=0.748, and *CXCR6:* Rho=0.715), being the association with M2 macrophages higher than those observed for HPV-positive HNSCC tumors. Finally, we analyzed the activation state of the myeloid dendritic cell subpopulation, observing a high correlation with activated dendritic cells (*CD2:* Rho=0.829, *CD3D:* Rho=0.796, *CD3E:* Rho=0.796, and *CXCR6:* Rho=0.760) (**Figure 4**).

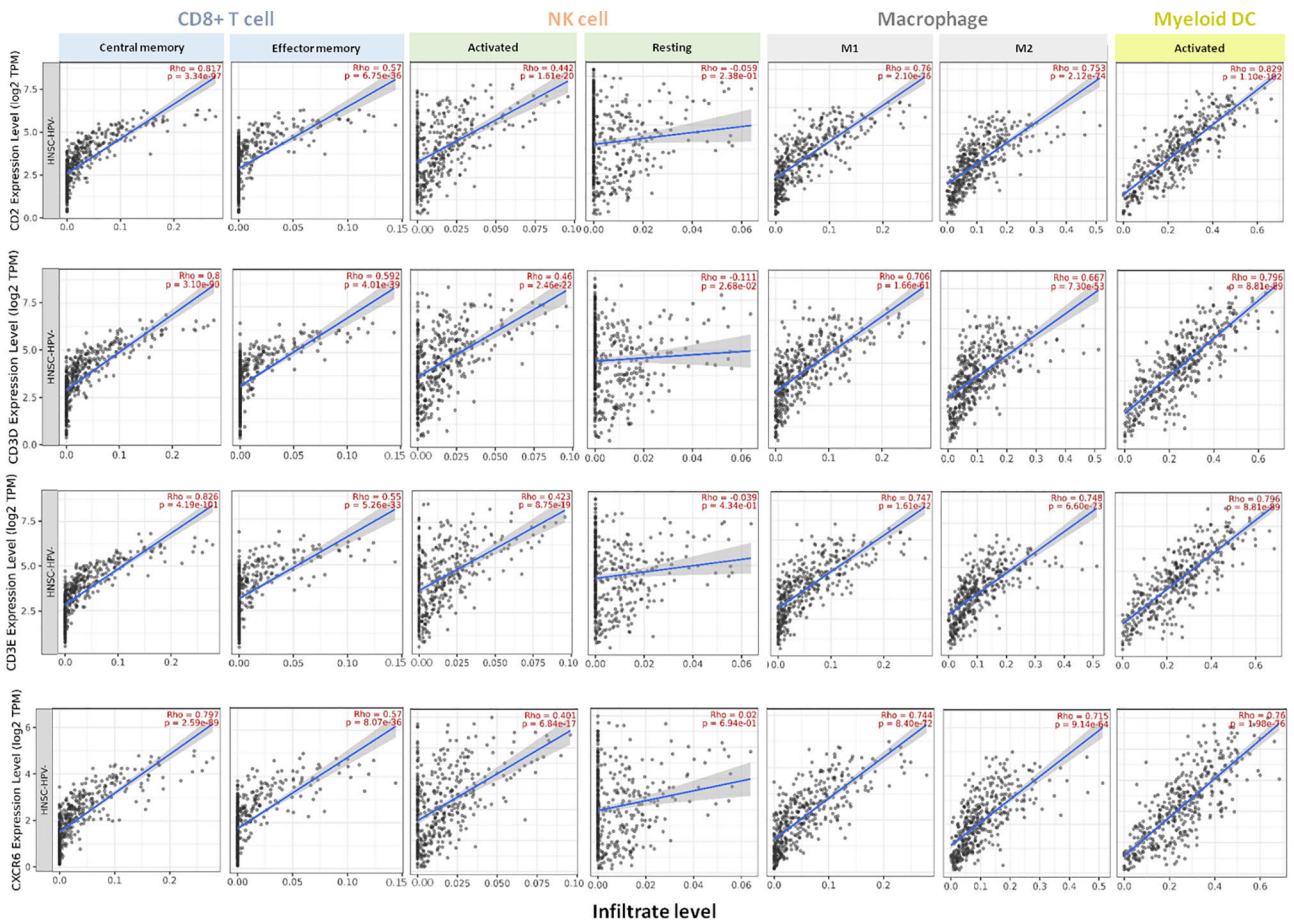

FIGURE 4 | Association of the expression of *CD2*, *CD3D*, *CD3E*, *CXCR6* with specific tumor-infiltrating immune cell populations in HPV-negative HNSCC patients. Expression of each gene and association with the presence of CD8+ T cells (central memory and effector memory subsets), NK cells (activated and resting), macrophages (M1 and M2 types), and activated myeloid dendritic cells in HPV-negative HNSCC (n = 422). Each panel presents the relationship between infiltrates estimation value with the purity-adjusted spearman's correlation parameter Rho and gene expression join p value < 0.001. Rho value > 0 represents a positive correlation, and Rho < 0 represents a negative correlation. Association with immune cell populations was provided by *TIMER 2.0* software and was correlated with transcriptome expression level of each immune gene.

Evaluation of Immune Activated Genes in Other Squamous Cell Tumors

SCCs arise in a different locations and share molecular and genetic alterations (1). In this context, we decided to explore if the expression of four previous published immune gene signatures (Expanded immune genes, IFN gamma genes, CTL genes, and HLA) and the new identified *CD2*, *CD3D*, *CD3E*, and *CXCR6* gene combination were able to classify patients with different outcome in lung, esophageal, and cervical SCC. Unexpectedly, no significant effect of four previous published immune gene signatures was observed in lung SCC (data not shown), neither in the case of the evaluated 32 individual genes (**Table 3**) or in case of the new *CD2*, *CD3D*, *CD3E*, and *CXCR6* signature: (n=504), HR=0.85, 95% CI=0.64–1.13; log rank p=0.27 (**Supplementary Figure 1**). However, a detrimental outcome was observed for both, the 32 individual genes (**Table 4**), and the new signature in esophageal SCC (n=81; HR=2.92; 95% CI=1.19–7.18; log rank p=0.015) (**Supplementary Figure 1**).

In CSCC we found that the expression of the analyzed immune signatures (Expanded immune genes, IFN gamma genes, CTL genes, and HLA genes) were associated with favorable OS in all stages (HR=0.6; 95% CI=0.35–1.04; log rank p=0.068) (**Figure 5A** and **Table 5**), showing similar results with that in the of case of HNSCC. Most individual genes were associated with favorable outcome at all stages (n: 254; **Table 5**), and the previously selected genes showed the most favorable prediction capacity: CD2 (HR=0.41; 95% CI=0.26–0.66; log rank p= 0,0001), CD3D (HR=0.39; 95% CI=0.24–0.64; log rank p= $8{,}5e^{-05}$), CD3E (HR=0.42; 95% CI=0.26–0.67; log rank p=0.0002), and *CXCR6* (HR=0.44; 95% CI=0.27–0.70; log rank p=0.0004). Of note, in the CSCC cohort, we identified that expression of LAG3 was associated with very favorable outcome (HR=0.3; 95% CI=0.15–0.61; log rank p= 0,0004). We next

TABLE 3 | Clinical outcome of individual immune genes from the four immune gene signatures in terms of overall survival (OS) of LSCC patients.

Signature	OS N = 504 (All stages)				
	Gene symbol	HR	CI	pValue	FDR
Expanded immune genes	CXCL13	0,79	0,6–1,05	0,1	100%
	CD2	0,80	0,63–1,09	0,19	100%
	CD3D	0,83	0,6–1,1	0,2	100%
	CXCR6	0,84	0,62–1,14	0,27	100%
	CD3E	0,88	0,66–1,17	0,38	100%
	GZMK	0,79	0,61–1,04	0,092	100%
	GZMB	0,82	0,61–1,11	0,2	100%
	IL2RG	1,14	0,86–1,53	0,36	100%
	TAGAP	1,21	0,92–1,59	0,16	100%
	LAG3	0,71	0,52–0,96	0,024	>50%
	NKG7	0,87	0,65–1,17	0,35	100%
	CIITA	0,87	0.66–1,14	0,31	100%
	CCL5	0.79	0,6–1,04	0,093	100%
	IDO1	0.83	0.63–1,11	0,21	100%
	CXCL10	0,82	0,61–1,1	0.19	100%
	HLA-DRA	1,11	0,82–1,52	0,49	100%
	STAT1	1,24	0,95–1,63	0,11	100%
	HLA-E	1,39	1,04–1,86	0,024	>50%
IFN gamma genes	CXCL9	0,73	0,55–0,58	0,034	>50%
	IFNG	0,71	0,54–0,93	0,013	>50%
	IDO1	0.83	0.63–1,11	0,21	100%
	CXCL10	0,82	0,61–1,1	0.19	100%
	IRF9	1,25	0,95–1,64	0,11	100%
	HLA-DRA	1,11	0,82–1,52	0,49	100%
	STAT1	1,24	0,95–1,63	0,11	100%
CTL level	GZMB	0,82	0,61–1,11	0,2	100%
	GZMA	0,84	0,63–1,12	0,23	100%
	PRF1	1,19	0,9–1,56	0,22	100%
	CD8A	0,83	0,62–1,1	0,19	100%
	CD8B	0,81	0,6–1,08	0,15	100%
HLA genes	HLA-B	1,26	0,96–1,65	0,095	100%
	HLA-A	1,15	0,85–1,57	0,37	100%

Table shows the list of individual genes belonging to the four previous published immune gene signatures. HR < 1 discriminates a risk reduction. The 95% confidence interval (CI) and p value are displayed. p value < 0.05 and FDR (False Discovery Rate) to correct for multiple hypothesis testing are displayed.

TABLE 4 | Clinical outcome of individual immune genes from the four immune gene signatures in terms of overall survival (OS) of ESCC patients.

Signature	OS N= 81 (All stages)				
	Gene symbol	HR	CI	pValue	FDR
Expanded immune genes	CXCL13	1,68	0,57–4,92	0,34	100%
	CD2	2,5	1,08–5,74	0,027	>50%
	CD3D	2,56	1,06–6,18	0,03	>50%
	CXCR6	2,37	1,05–5,34	0,032	>50%
	CD3E	2,71	1,11–6,62	0,023	>50%
	GZMK	2,05	0,82–5,13	0,12	100%
	GZMB	2,34	1,03–5,33	0,038	>50%
	IL2RG	2,27	0,9–5,74	0,076	100%
	TAGAP	2,71	1,11–6,63	0,023	>50%
	LAG3	1.92	0,83–4,45	0,12	100%
	NKG7	2,41	0,99–5,87	0.046	>50%
	CIITA	1,46	0,62–3,44	0,38	100%
	CCL5	2,16	0,85–5,47	0,097	100%
	IDO1	2,1	0,91–4,85	0,076	100%
	CXCL10	2,18	0,8–5,89	0,12	100%
	HLA-DRA	2,12	0,87–5,2	0,093	100%
	STAT1	2,63	1,03–6,71	0,036	>50%
	HLA-E	3,53	1,46–8,51	0,0029	10%
IFN gamma genes	CXCL9	2,28	0,94–5,53	0,062	100%
	IFNG	2,78	1,04–7,43	0,034	>50%
	IDO1	2,1	0,91–4,85	0,076	100%
	CXCL10	2,18	0,8–5,89	0,12	100%
	IRF9	2,53	1,02–6,29	0,038	>50%
	HLA-DRA	2,12	0,87–5,2	0,093	100%
	STAT1	2,63	1,03–6,71	0,036	>50%
CTL level	GZMB	2,34	1,03–5,33	0,038	>50%
	GZMA	2,81	1,18–6,67	0,015	50%
	PRF1	2,75	1,14–6,64	0,02	>50%
	CD8A	1,72	0,77–3,84	0,18	100%
	CD8B	2,89	0,98–8,51	0,045	>50%
HLA genes	HLA-B	3,67	1,42–9,45	0,0041	20%
	HLA-A	2,52	1,1–5,75	0,024	>50%

Table shows the list of individual genes belonging to the four previous published immune gene signatures. HR < 1 discriminates a risk reduction. The 95% confidence interval (CI) and p value are displayed. p value < 0.05 and FDR (False Discovery Rate) to correct for multiple hypothesis testing are displayed.

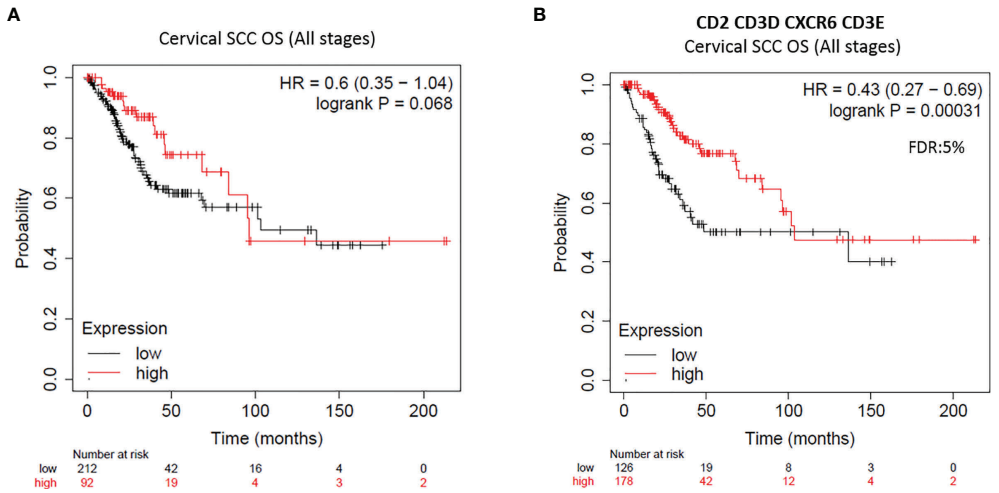

FIGURE 5 | Expression of *CD2*, *CD3D*, *CD3E*, *CXCR6* immune gene combination shows better clinical outcome of CSSC patients. Clinical outcome of survival plots in CSCC at all stages (n = 254) with transcriptomic expression of all four previous published immune signatures **(A)** and with the new immune gene-set combination *CD2*, *CD3D*, *CD3E*, *CXCR6* (HR < 0.65 and FDR = 5%) **(B)**. HR for risk of death and OS are displayed. HR < 0.65 discriminates a risk reduction. FDR is also displayed.

evaluated the combined effect of the identified immune gene signature (combining *CD2*, *CD3D*, *CD3E*, and *CXCR6*), demonstrating a favorable prognosis (HR=0.43; 95% CI=0.27–0.69; log rank p=0.00031) with a low FDR (<5%) (**Figure 5B**).

The assessment of the new immune gene signature (*CD2*, *CD3D*, *CD3E*, and *CXCRC6*) in the CSCC cohort per tumor stage was not possible because sample size was too low for a meaningful analysis when we filtered data by stage.

Expression of *CD2*, *CD3D*, *CD3E*, and *CXCR6* Is Linked to a High Expression of Memory CD8+ T Cells, Activated NK Cells, and M1 Macrophages in CSCC

Since *CD2*, *CD3D*, *CD3E*, and *CXCR6* predict very favorable prognosis in CSCC, we evaluated the association of this new signature at transcriptomic level with the presence of tumor-infiltrating immune cell populations in CSCC. All genes showed a negative correlation with tumor purity. As in the case of HNSCC patients, we found a positive correlation between the gene expression of *CD2*, *CD3D*, *CD3E*, and *CXCR6* and $CD8^+$ T cells (central and effector memory subpopulations), and the strongest correlation was observed for the central memory $CD8^+$ T cells (*CD2:* Rho=0.881, *CD3D:* Rho=0.883, *CD3E:* Rho=0.896, and *CXCR6:* Rho=0.850) (**Figure 6**). A positive association was also observed for the CD8+ effector memory subpopulation (*CD2:* Rho=0.665, *CD3D:* Rho=0.700, *CD3E:* Rho=0.631, and *CXCR6:* Rho=0.636) (**Figure 6**).

In case of the NK cell population, the strongest correlation was found with the activated fraction (*CD2:* Rho=0.637, *CD3D:* Rho=0.613, *CD3E:* Rho=0.713, and *CXCR6:* Rho=0.649). In the macrophage population, the highest association was identified for the M1 group (*CD2:* Rho=0.719, *CD3D:* Rho=0.651, *CD3E:* Rho=0.706, and *CXCR6:* Rho=0.664) compared with the M2 macrophage population (*CD2:* Rho=0.503, *CD3D:* Rho=0.408, *CD3E:* Rho=0.510, and *CXCR6:* Rho=0.469). For activated dendritic cells, the results were as follow: *CD2:* Rho=0.739, *CD3D:* Rho=0.743, *CD3E:* Rho=0.705, and *CXCR6:* Rho=0.620) (**Figure 6**).

Clinical Outcome in HNSCC and CSSC With Expression of *CD2, CD3D, CD3E, CXCR6* and High Mutation Burden

As the mutational burden has been associated with response to immune-modulatory drugs (18, 19), we explored if the expression of the identified immune signature *CD2*, *CD3D*, *CD3E*, *CXCR6* was able to predict a better outcome in HNSCC and in CSCC with high mutational burden. In HNSCC with high mutational burden, the presence of the immune signature was able to predict favorable OS (n=251; HR=0.53; 95% CI=0.37–0.76; log rank p=0.00051; FDR=5%) (**Figure 7A**). Similarly, in CSCC tumors with high mutational burden, the presence of the immune signature predicted strongly favorable survival (n=143; HR=0.19; 95% CI=0.09–0.39; log rank p=4.5e-07, FDR=1%) (**Figure 7B**). This result suggests that outcome prediction of the aforementioned immune signature is much more effective in HSCC and CSCC tumors with high mutational burden.

DISCUSSION

In the present article we describe immune genomic signatures associated with favorable outcome in HNSCC and CSCC. Identification of genomic immune correlates that predict outcome as an indirect measure of immune activation is a key task in oncology.

SCCs comprise a large family of tumors from epithelial tissues that arise from different locations but that share some common biological characteristics like genomic instability, dysfunction of

TABLE 5 | Clinical outcome of individual immune genes from the four immune gene signatures in terms of overall survival (OS) of CSCC patients.

Signature	OS N = 254 (All stages)				
	Gene symbol	HR	CI	pValue	FDR
Expanded immune genes	CXCL13	0,55	0,35–0,88	0,012	>50%
	CD2	**0,41**	**0,26–0,66**	**0,0001**	**2%**
	CD3D	**0,39**	**0,24–0,64**	**8,5e-05**	**1%**
	CXCR6	**0,44**	**0,27–0,70**	**0,0004**	**5%**
	CD3E	**0,42**	**0,26–0,67**	**0.0002**	**2%**
	GZMK	0,47	0,27–0,81	0,0059	>50%
	GZMB	0,41	0,22–0,78	0,005	>50%
	IL2RG	0,62	0,39–1,00	0,046	>50%
	TAGAP	0,64	0,39–1,06	0.079	100%
	LAG3	0,3	0,15–0,61	0,0004	5%
	NKG7	0,45	0,24–0,84	0,01	>50%
	CIITA	0,54	0,33–0,89	0,014	>50%
	CCL5	0,47	0,29–0,76	0,0015	20%
	IDO1	0,5	0,28–0,89	0,017	>50%
	CXCL10	0,63	0,39–1,01	0,053	100%
	HLA-DRA	0,48	0,3–0,79	0,0033	50%
	STAT1	0,65	0,4–1,03	0,065	100%
	HLA-E	0,68	0,41–1,12	0,13	100%
IFN gamma genes	CXCL9	0,42	0,22–0,8	0,0069	>50%
	IFNG	0,36	0,19–0,71	0,002	20%
	IDO1	0,5	0,28–0,89	0,017	>50%
	CXCL10	0,63	0,39–1,01	0,053	100%
	IRF9	0,63	0,39–1,00	0,049	>50%
	HLA-DRA	0,48	0,3–0,79	0,0033	50%
	STAT1	0,65	0,4–1,03	0,065	100%
CTL level	GZMB	0,41	0,22–0,78	0,005	>50%
	GZMA	0,48	0,25–0,92	0,023	>50%
	PRF1	0,56	0,34–0,94	0,026	>50%
	CD8A	0,45	0,28–0,72	0,0006	10%
	CD8B	0,49	0,3–0,78	0,002	20%
HLA genes	HLA-B	0,7	0,42–1,15	0,15	100%
	HLA-A	0,66	0,41–1,07	0,091	100%

Table shows the list of individual genes belonging to the four previous published immune gene signatures. HR < 1 discriminates a risk reduction. The 95% confidence interval (CI) and p value are displayed. p value < 0.05 and FDR (False Discovery Rate) to correct for multiple hypothesis testing are displayed.
The bold values represent those genes that stand out with the best clinical outcome (HR < 0.65, FDR < 10%, p < 0.05).

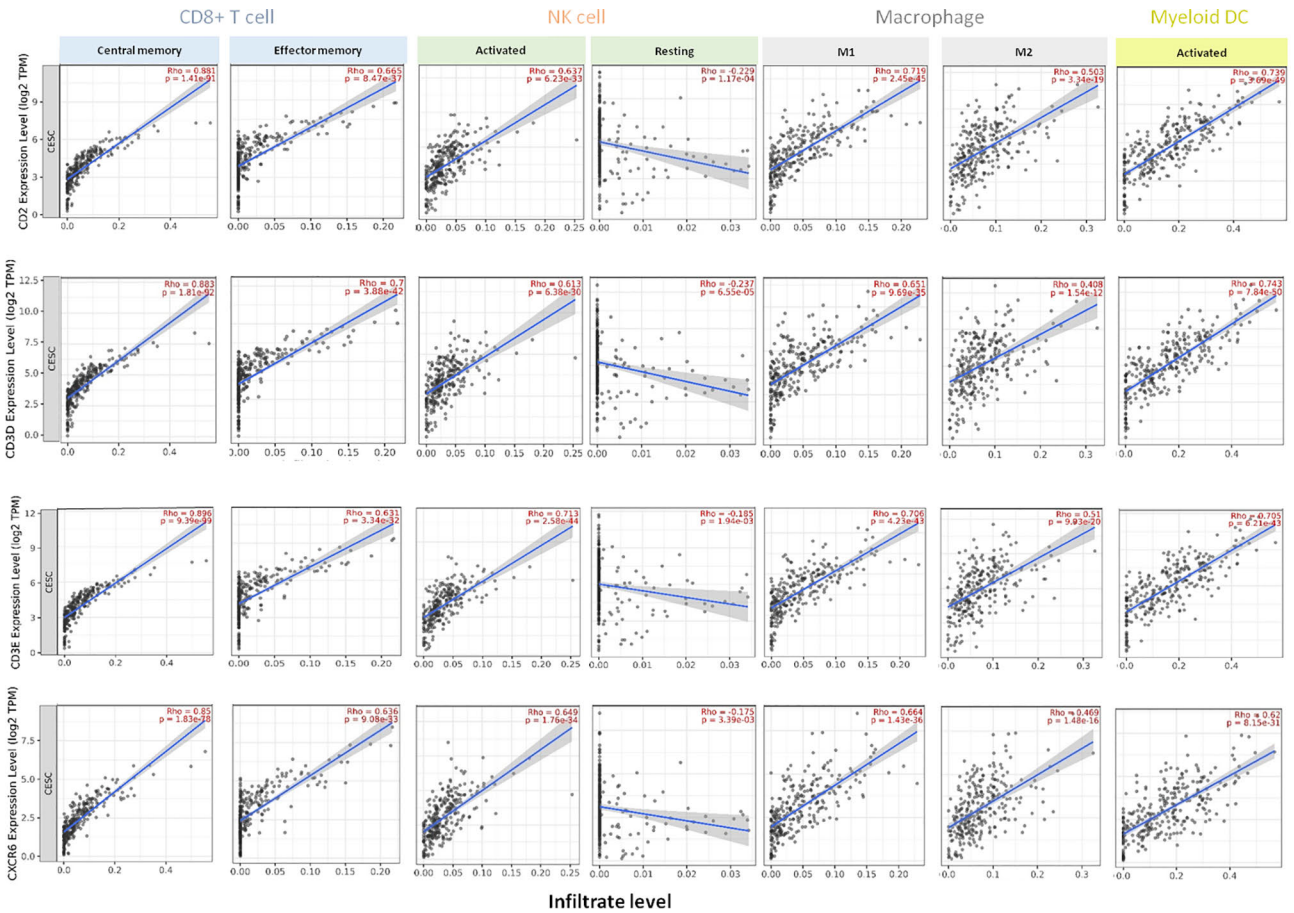

FIGURE 6 | Association of *CD2*, *CD3D*, *CD3E*, *CXCR6* transcriptomic expression with specific tumor-infiltrating immune cell populations in CSCC patients. Expression of each gene in association with the presence of CD8+ T cells (central memory and effector memory subsets), NK cells (activated or resting), macrophages (M1 and M2 types), and activated myeloid dendritic infiltrates in CSSC patients (n = 254). Each panel presents the relationship between infiltrates estimation value with the purity-adjusted spearman's correlation parameter Rho and gene expression, join p value < 0.001. Rho value > 0 represents a positive correlation, and Rho < 0 represents a negative correlation. Association with immune cell populations was provided by *TIMER 2.0* software and was correlated with transcriptome expression level of each immune gene.

DNA repair mechanisms, or relative sensibility to therapeutic agents that induce DNA damage or affect DNA repair mechanisms (1). In addition, some of them have shown to be more sensitive to immunologic agents probably due to the retained viral antigens produced by the presence of HPV infection (4, 5).

Using previously described transcriptomic signatures associated with immune activation, we aimed to identify genes that were linked with favorable outcome in HNSCC patients. We found a correlation with outcome of most of the signatures except for the HLA one. The fact that some genes correlated better than the whole signature let us explore a combination of transcripts that could increase the prediction capacity, and this was the case for a signature that included only four genes: *CD2*, *CD3D*, *CD3E*, and *CXCR6*. Of note, these findings were reproduced in CSCC and with minor significance in esophagus tumors. The association between gene expression profile and clinical outcome in patients selecting by HPV condition was not available with KM Plotter Online Tool in the case of the HNSCC cohort of patients.

A remarkable finding is the fact that the identified results were not reproduced in other squamous cell lung cancers. These results, although surprising, confirm the heterogeneity of tumors at a location and histology level (28, 29). Probably, the results have been conditioned by the presence of HPV in these two indications: HNSCC and CSCC (most CSCC tumors are HPV positive), a situation that is not observed in other squamous cell tumors like esophagus or lung. These tumors lack the presence of HPV infection, so they do not exhibit the viral neoantigens or molecules likely recognized by the identified immune cell populations in HNSCC and CSCC.

The immune gene signature comprised several genes. CD3D and CD3E are part of the TCR-CD3 complex present on T-lymphocyte cell surface (30, 31). CD3 chains contain immunoreceptor tyrosine-based activation motifs (ITAMs) in their cytoplasmic domain, and after T-cell receptor engagement,

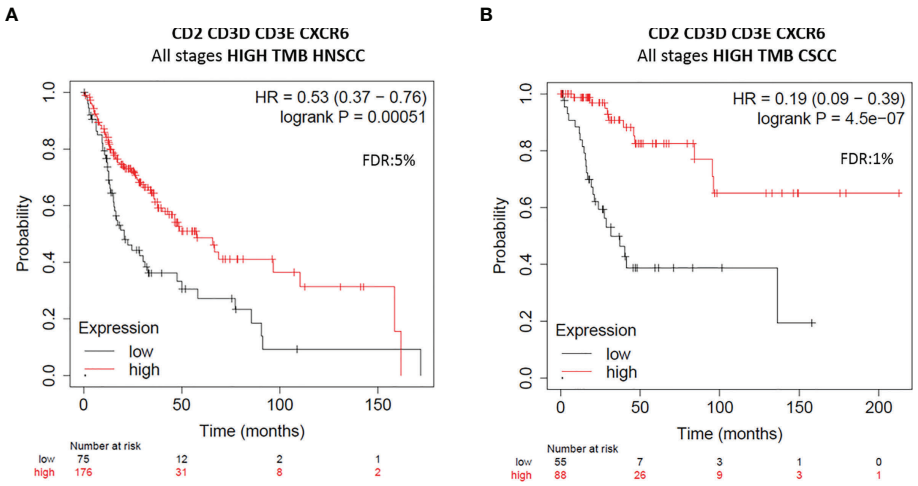

FIGURE 7 | Clinical outcome analysis of *CD2*, *CD3D*, *CD3E*, *CXCR6* immune gene signature expression in HNSCC and CSCC tumors with high mutational burden. Clinical outcomes of survival plots of new immune gene signature with improved favorable prognosis at all stages of HNSCC tumors (n = 251) **(A)** and CSCC tumors (n = 143) **(B)** with high mutational burden (TMB) are displayed. Red line represents survival of patients whose tumors harbor high gene expression levels, and those with low gene expression levels show in black line. Number of patients at risk at every time (months), with high (in red) and low gene expression (in black), is displayed. HR for risk of death and OS are displayed. HR < 0.65 discriminates a risk reduction. FDR is also displayed. The gene combination is displayed at the top of each figure.

they transmit the activation signaling by phosphorylation of SRC (30). In this context, the presence of these two genes is an indirect measure of the existence of activated T cells. It is not surprising to see that their presence has also been described as linked with prognosis (32). CD2 is a cell adhesion protein expressed on the T cell and NK cell surface and has been used as a specific marker for these two populations (33). Finally, CXCR6 has been described as a chemokine associated with the activation of IFN gamma effector cells, therefore can constitute an adequate marker to select active T cells (34).

The presence of the selected genes correlated with low tumor purity in HNSCC and CSCC. Moreover, we observed a very clear and strong association with the presence of populations of cells involved in adaptive immune cell response including activated T cells and dendritic cells. In addition, we observed an increase in M1 macrophages and in activated NK cells, demonstrating that the innate immunity was also present and therefore can have a role in the antitumoral action. This finding is relevant as a single signature of four genes can identify an immunologic state that is linked with a favorable prognosis compromising an adaptive and innate activated immune response. Unfortunately, no evaluation of immune populations in esophageal SCC was performed, since data are not publicly available.

When exploring differences between HNSCC HPV-positive and HPV-negative tumors, we did not observe major discrepancies beyond the fact that HPV-positive tumors had a stronger presence of the described immune cells (35). In fact, almost all CSCC tumors are HPV positive. As mentioned before, tumors in which a viral infection is a key oncogenic event can have a wider presence of neoantigens and therefore an increase presence of immune activated cells, what suggests that could be more sensitive to agents that modulate the immune system. In fact, we observed that the expression of the new immune signature correlated with the same composition of tumoral immune cell infiltrates in HNSCC and CSCC (see and compare **Figure 3** and **Figure 6**), maybe since both types of tumors shared the same pattern of neoantigens.

A relevant finding of our study is the discrimination in outcome between those tumors with a high tumor mutational burden (TMB). In this context, not all tumors with TMB respond to immune modulators, which suggests that the identification of biomarkers within this population will also be of help.

We acknowledge that our study has limitations. This is an *in silico* analysis using datasets from different sources. However, all the datasets included in this study are publicly available and have been incorporated in several studies that support their consideration as representative of the general population. Of note, the compilation and integration of molecular biology and clinical data into the available datasets is sometimes scarce. For instance, we could not explore if in terms of expression our new signature had different prediction in the HNSCC cohort per HPV status. This was not the case in CSCC where all patients are HPV positive.

In conclusion, we describe a set of genes that are able to identify immune activated tumors involving adaptive and innate immune response, associated with favorable prognosis in HNSCC and CSCC. Prospective studies should be performed to confirm these results.

DATA AVAILABILITY STATEMENT

Publicly available datasets were analyzed in this study. This data can be found here: https://kmplot.com/analysis/, http://cistrome.org/TIMER/download.html.

AUTHOR CONTRIBUTIONS

AO, CS-L, MB-P, and AM have contributed to conception and design of the study. AO has performed the main design of the work. CS-L and MB-P have carried out the acquisition, analysis, or interpretation of data for the work. All authors contributed to the article and approved the submitted version.

FUNDING

This work has been supported by Instituto de Salud Carlos III (PI16/01121 and PI19/00808), ACEPAIN; Diputación de Albacete, CIBERONC and CRIS Cancer Foundation (to AO). Ministry of Economy and Competitiveness of Spain (BFU2015-71371-R), the Instituto de Salud Carlos III through the Spanish Cancer Centers Network Program (RD12/0036/0003) and CIBERONC, the scientific foundation of the AECC and the CRIS Foundation (to AP). The work carried out in our laboratories receive support from the European Community through the regional development funding program (FEDER).

SUPPLEMENTARY MATERIAL

The Supplementary Material for this article can be found online at: https://www.frontiersin.org/articles/10.3389/fonc.2021.714550/full#supplementary-material

Supplementary Figure 1 | Clinical outcome analysis of *CD2*, *CD3D*, *CD3E*, *CXCR6* immune gene signature expression in lung SCC and esophageal SCC tumors. Clinical outcomes of survival plots of new immune gene signature with no prediction at all stages of lung SCC tumors (n = 501) **(A)** and poor prognosis at all stages in esophageal SCC tumors (n = 81) **(B)** are displayed. Red line represents survival of patients whose tumors harbor high gene expression levels, and black line represents those with low gene expression levels. Number of patients at risk at every time (months) is displayed. HR for risk of death and overall survival (OS) are displayed. HR < 0.65 discriminates a risk reduction. FDR is also displayed. The gene combination is displayed at the top of each figure.

REFERENCES

1. Chow LQM. Head and Neck Cancer. *N Engl J Med* (2020) 382(1):60–72. doi: 10.1056/NEJMra1715715
2. Sánchez-Danés A, Blanpain C. Deciphering the Cells of Origin of Squamous Cell Carcinomas. *Nat Rev Cancer* (2018) 18(9):549–61. doi: 10.1038/s41568-018-0024-5
3. Cramer JD, Burtness B, Le QT, Ferris RL. The Changing Therapeutic Landscape of Head and Neck Cancer. *Nat Rev Clin Oncol* (2019) 16 (11):669–83. doi: 10.1038/s41571-019-0227-z
4. Wendel Naumann R, Leath CA3rd. Advances in Immunotherapy for Cervical Cancer. *Curr Opin Oncol* (2020) 32(5):481–7. doi: 10.1097/CCO.0000000000000663
5. Cohen EEW, Soulières D, Le Tourneau C, Dinis J, Licitra L, Ahn M-J, et al. Pembrolizumab Versus Methotrexate, Docetaxel, or Cetuximab for Recurrent or Metastatic Head-and-Neck Squamous Cell Carcinoma (KEYNOTE-040): A Randomised, Open-Label, Phase 3 Study. *Lancet (London England)* (2019) 393(10167):156–67. doi: 10.1016/S0140-6736(18)31999-8
6. Chow LQM, Haddad R, Gupta S, Mahipal A, Mehra R, Tahara M, et al. Antitumor Activity of Pembrolizumab in Biomarker-Unselected Patients With Recurrent and/or Metastatic Head and Neck Squamous Cell Carcinoma: Results From the Phase Ib KEYNOTE-012 Expansion Cohort. *J Clin Oncol Off J Am Soc Clin Oncol* (2016) 34(32):3838–45. doi: 10.1200/JCO.2016.68.1478
7. Ferris RL, Blumenschein GJ, Fayette J, Guigay J, Colevas AD, Licitra L, et al. Nivolumab for Recurrent Squamous-Cell Carcinoma of the Head and Neck. *N Engl J Med* (2016) 375(19):1856–67. doi: 10.1056/NEJMoa1602252
8. Seiwert TY, Burtness B, Mehra R, Weiss J, Berger R, Eder JP, et al. Safety and Clinical Activity of Pembrolizumab for Treatment of Recurrent or Metastatic Squamous Cell Carcinoma of the Head and Neck (KEYNOTE-012): An Open-Label, Multicentre, Phase 1b Trial. *Lancet Oncol* (2016) 17(7):956–65. doi: 10.1016/S1470-2045(16)30066-3
9. Miyauchi S, Kim SS, Pang J, Gold KA, Gutkind JS, Califano JA, et al. Immune Modulation of Head and Neck Squamous Cell Carcinoma and the Tumor Microenvironment by Conventional Therapeutics. *Clin Cancer Res an Off J Am Assoc Cancer Res* (2019) 25(14):4211–23. doi: 10.1158/1078-0432.CCR-18-0871
10. Chung HC, Ros W, Delord J-P, Perets R, Italiano A, Shapira-Frommer R, et al. Efficacy and Safety of Pembrolizumab in Previously Treated Advanced Cervical Cancer: Results From the Phase II KEYNOTE-158 Study. *J Clin Oncol Off J Am Soc Clin Oncol* (2019) 37(17):1470–8. doi: 10.1200/JCO.18.01265
11. Mirza AH, Thomas G, Ottensmeier CH, King EV. Importance of the Immune System in Head and Neck Cancer. *Head Neck* (2019) 41(8):2789–800. doi: 10.1002/hed.25716
12. Mahoney KM, Rennert PD, Freeman GJ. Combination Cancer Immunotherapy and New Immunomodulatory Targets. *Nat Rev Drug Discov* (2015) 14(8):561–84. doi: 10.1038/nrd4591
13. Ribas A, Wolchok JD. Cancer Immunotherapy Using Checkpoint Blockade. *Science* (2018) 359(6382):1350–5. doi: 10.1126/science.aar4060
14. Topalian SL, Taube JM, Anders RA, Pardoll DM. Mechanism-Driven Biomarkers to Guide Immune Checkpoint Blockade in Cancer Therapy. *Nat Rev Cancer* (2016) 16(5):275–87. doi: 10.1038/nrc.2016.36
15. Adams S, Gray RJ, Demaria S, Goldstein L, Perez EA, Shulman LN, et al. Prognostic Value of Tumor-Infiltrating Lymphocytes in Triple-Negative Breast Cancers From Two Phase III Randomized Adjuvant Breast Cancer Trials: ECOG 2197 and ECOG 1199. *J Clin Oncol Off J Am Soc Clin Oncol* (2014) 32(27):2959–66. doi: 10.1200/JCO.2013.55.0491
16. Loi S, Michiels S, Salgado R, Sirtaine N, Jose V, Fumagalli D, et al. Tumor Infiltrating Lymphocytes are Prognostic in Triple Negative Breast Cancer and Predictive for Trastuzumab Benefit in Early Breast Cancer: Results From the FinHER Trial. *Ann Oncol Off J Eur Soc Med Oncol* (2014) 25(8):1544–50. doi: 10.1093/annonc/mdu112
17. Goodman AM, Kato S, Bazhenova L, Patel SP, Frampton GM, Miller V, et al. Tumor Mutational Burden as an Independent Predictor of Response to Immunotherapy in Diverse Cancers. *Mol Cancer Ther* (2017) 16(11):2598–608. doi: 10.1158/1535-7163.MCT-17-0386
18. Le DT, Durham JN, Smith KN, Wang H, Bartlett BR, Aulakh LK, et al. Mismatch Repair Deficiency Predicts Response of Solid Tumors to PD-1 Blockade. *Science* (2017) 357(6349):409–13. doi: 10.1126/science.aan6733
19. Mandal R, Samstein RM, Lee K-W, Havel JJ, Wang H, Krishna C, et al. Genetic Diversity of Tumors With Mismatch Repair Deficiency Influences Anti-PD-1 Immunotherapy Response. *Science* (2019) 364(6439):485–91. doi: 10.1126/science.aau0447
20. Havel JJ, Chowell D, Chan TA. The Evolving Landscape of Biomarkers for Checkpoint Inhibitor Immunotherapy. *Nat Rev Cancer* (2019) 19(3):133–50. doi: 10.1038/s41568-019-0116-x
21. Rooney MS, Shukla SA, Wu CJ, Getz G, Hacohen N. Molecular and Genetic Properties of Tumors Associated With Local Immune Cytolytic Activity. *Cell* (2015) 160(1–2):48–61. doi: 10.1016/j.cell.2014.12.033
22. Ayers M, Lunceford J, Nebozhyn M, Murphy E, Loboda A, Kaufman DR, et al. IFN-γ-Related mRNA Profile Predicts Clinical Response to PD-1 Blockade. *J Clin Invest* (2017) 127(8):2930–40. doi: 10.1172/JCI91190
23. Jiang P, Gu S, Pan D, Fu J, Sahu A, Hu X, et al. Signatures of T Cell Dysfunction and Exclusion Predict Cancer Immunotherapy Response. *Nat Med* (2018) 24(10):1550–8. doi: 10.1038/s41591-018-0136-1
24. Győrffy B, Lanczky A, Eklund AC, Denkert C, Budczies J, Li Q, et al. An Online Survival Analysis Tool to Rapidly Assess the Effect of 22,277 Genes on

Breast Cancer Prognosis Using Microarray Data of 1,809 Patients. *Breast Cancer Res Treat* (2010) 123(3):725–31. doi: 10.1007/s10549-009-0674-9
25. Nagy Á, Lánczky A, Menyhárt O, Győrffy B. Validation of miRNA Prognostic Power in Hepatocellular Carcinoma Using Expression Data of Independent Datasets. *Sci Rep* (2018) 8(1):9227. doi: 10.1038/s41598-018-27521-y
26. Li B, Severson E, Pignon J-C, Zhao H, Li T, Novak J, et al. Comprehensive Analyses of Tumor Immunity: Implications for Cancer Immunotherapy. *Genome Biol* (2016) 17(1):174. doi: 10.1186/s13059-016-1028-7
27. Li T, Fan J, Wang B, Traugh N, Chen Q, Liu JS, et al. TIMER: A Web Server for Comprehensive Analysis of Tumor-Infiltrating Immune Cells. *Cancer Res* (2017) 77(21):e108–10. doi: 10.1158/0008-5472.CAN-17-0307
28. Lu J, Wang W, Xu M, Li Y, Chen C, Wang X. A Global View of Regulatory Networks in Lung Cancer: An Approach to Understand Homogeneity and Heterogeneity. *Semin Cancer Biol* (2017) 42:31–8. doi: 10.1016/j.semcancer.2016.11.004
29. Lin L, Lin D-C. Biological Significance of Tumor Heterogeneity in Esophageal Squamous Cell Carcinoma. *Cancers (Basel)* (2019) 11(8):1156. doi: 10.3390/cancers11081156
30. Delgado P, Fernández E, Dave V, Kappes D, Alarcón B. CD3delta Couples T-Cell Receptor Signalling to ERK Activation and Thymocyte Positive Selection. *Nature* (2000) 406(6794):426–30. doi: 10.1038/35019102
31. Pan Q, Gollapudi AS, Dave VP. Biochemical Evidence for the Presence of a Single CD3delta and CD3gamma Chain in the Surface T Cell Receptor/CD3 Complex. *J Biol Chem* (2004) 279(49):51068–74. doi: 10.1074/jbc.M406145200
32. Zuo Z, Xiong J, Zeng C, Jiang Y, Xiong K, Tao H, et al. Exploration of a Robust and Prognostic Immune Related Gene Signature for Cervical Squamous Cell Carcinoma. *Front Mol Biosci* (2021) 8:625470. doi: 10.3389/fmolb.2021.625470
33. Sanchez-Madrid F, Krensky AM, Ware CF, Robbins E, Strominger JL, Burakoff SJ, et al. Three Distinct Antigens Associated With Human T-Lymphocyte-Mediated Cytolysis: LFA-1, LFA-2, and LFA-3. *Proc Natl Acad Sci USA* (1982) 79(23):7489–93. doi: 10.1073/pnas.79.23.7489
34. Calabresi PA, Yun SH, Allie R, Whartenby KA. Chemokine Receptor Expression on MBP-Reactive T Cells: CXCR6 Is a Marker of IFNgamma-Producing Effector Cells. *J Neuroimmunol* (2002) 127(1–2):96–105. doi: 10.1016/S0165-5728(02)00106-6
35. Wang J, Sun H, Zeng Q, Guo X-J, Wang H, Liu H-H, et al. HPV-Positive Status Associated With Inflamed Immune Microenvironment and Improved Response to Anti-PD-1 Therapy in Head and Neck Squamous Cell Carcinoma. *Sci Rep* (2019) 9(1):13404. doi: 10.1038/s41598-019-49771-0

Conflict of Interest: The authors declare that the research was conducted in the absence of any commercial or financial relationships that could be construed as a potential conflict of interest.

Publisher's Note: All claims expressed in this article are solely those of the authors and do not necessarily represent those of their affiliated organizations, or those of the publisher, the editors and the reviewers. Any product that may be evaluated in this article, or claim that may be made by its manufacturer, is not guaranteed or endorsed by the publisher.

frontiers in Oncology

SYSTEMATIC REVIEW
published: 08 October 2021
doi: 10.3389/fonc.2021.720418

Outcomes of Recurrent Nasopharyngeal Carcinoma Patients Treated With Salvage Surgery: A Meta-Analysis

Yekai Feng[1], Zhimei Dai[1], Ruicheng Yan[1], Feng Li[2], Xiaosheng Zhong[1], Haoxin Ye[1], Caiqing Chen[1], Shaochong Fan[1], Cheng Qing[3], Yong Pan[1] and Haiying Sun[3]**

[1] Department of Otolaryngology–Head and Neck Surgery, The Forth Affiliated Hospital of Guangzhou Medical University, Guangzhou, China, [2] Department of Otolaryngology–Head and Neck Surgery, Affiliated Hospital of Guangdong Medical University, Zhanjiang, China, [3] Department of Otorhinolaryngology, Union Hospital, Tongji Medical College, Huazhong University of Science and Technology, Wuhan, China

OPEN ACCESS

Edited by:
Heming Lu,
People's Hospital of Guangxi Zhuang Autonomous Region, China

Reviewed by:
Xicai Sun,
Fudan University, China
Ivan Tham,
Gleneagles Hospital, Singapore

***Correspondence:**
Yong Pan
ppyy221@163.com
Haiying Sun
sunhaiying120@163.com

Specialty section:
This article was submitted to Head and Neck Cancer, a section of the journal Frontiers in Oncology

Received: *04 June 2021*
Accepted: *09 September 2021*
Published: *08 October 2021*

Citation:
Feng Y, Dai Z, Yan R, Li F, Zhong X, Ye H, Chen C, Fan S, Qing C, Pan Y and Sun H (2021) Outcomes of Recurrent Nasopharyngeal Carcinoma Patients Treated With Salvage Surgery: A Meta-Analysis. Front. Oncol. 11:720418. doi: 10.3389/fonc.2021.720418

Objective: To assess the efficacy of treatment outcomes of salvage surgery for recurrent nasopharyngeal carcinoma (rNPC).

Methods: We conducted a detailed search of the literatures in biomedical databases published from January 1990 to December 2020. The main research features and results of interest were retrieved from the articles that met the selection criteria for meta-analysis.

Results: A total of 21 articles with 778 patients were included, 17 of which met the meta-analysis inclusion criteria. The pooled 2-year overall survival (OS), 5-year OS, and 2-year disease-free survival (DFS) were 71%, 50% and 61%, respectively. Subgroup analysis was conducted with postoperative adjuvant therapy. The pooled 2-year OS, 5-year OS and 2-year DFS of the postoperative adjuvant therapy group compared with the surgery alone group were 69% vs 72%, 44% vs 56%, and 77% vs 54%, respectively. Univariate and multivariate analyses were performed on 178 patients with detailed individual postoperative survival data in 10 articles. On multivariate analysis, recurrent T (RT) stage and adjuvant therapy were independent predictors of outcomes.

Conclusions: This meta-analysis indicated that recurrent NPC patients can obtain survival benefits from salvage surgery. Accurately assessing the RT stage of the tumor and choosing the appropriate surgical method are important to the success of the surgery. Although the prognostic factors influencing outcome have been studied, conclusive data on the survival benefits are still lacking. Random controlled trials (RCTs) to compare surgery alone and postoperative adjuvant therapy are needed in patients with positive margin status after salvage surgery.

Keywords: outcome, adjuvant therapy, surgery, recurrent nasopharyngeal carcinoma, meta-analysis

INTRODUCTION

Nasopharyngeal carcinoma (NPC), which originates from nasopharyngeal epithelial cells, is a coon malignant tumor that occurs in the head and neck (1). The primary treatment strategy for NPC is radiotherapy with or without chemotherapy (2). However, approximately 7% to 15% of patients have persistent or recurrent disease after radical radiotherapy, and 10% to 40% of patients experience recurrence within 1 to 2 years after initial treatment (2, 3).

At present, there is still no standardized management strategy for recurrent NPC (rNPC). Surgery is often the first choice for recurrent locoregional NPC. Intensity-modulated radiotherapy (IMRT) can be chosen as a salvage treatment for unresectable disease. Targeted therapy and chemotherapy can be considered for patients who cannot undergo or refuse to receive reirradiation. Palliative chemotherapy is the main choice for patients with distant metastasis (4, 5). Radiotherapy resistance is the main reason of NPC relapse within 1 year and fatal complications caused by irradiation makes the situation more worse (6). It is reasonable that further radiotherapy (RT) or chemotherapy (CHT) might lead to undesirable survival outcomes. The development of salvage surgery provides an alternative treatment.

In this study, we carried out a meta-analysis of the long-term results of patients who underwent surgery with or without adjuvant therapy for recurrent NPC. The combined OS and DFS rates outcomes were reported. At the same time, subgroup analysis of postoperative adjuvant therapy was performed. We also performed univariate and multivariate analyses to identify prognostic factors in a series of patients with detailed postoperative survival data.

MATERIALS AND METHODS

Search Strategy

A systematic search of the PubMed, Embase, Cochrane Library, and Web of Science databases and 2 major Chinese databases, CNKI and Wanfang, were conducted in December 2020. The search strategy was predefined. The following free terms and medical subject headings were included: "nasopharyngeal," "nasopharyngeal diseases," "nasopharyngeal neoplasms," "nasopharyngeal carcinoma," "recurrence," "surgery," and "survival." We limited the scope of our research to studies that only targeted humans and published in Chinese and English. The publication time was restricted from 1990 to 2020.

Inclusion and Exclusion Criteria

Studies that met all of the following inclusion criteria were selected: (1) Study population: patients with histologically proven, locally recurrent, nonmetastatic NPC receiving a primary and radical radiotherapy; (2) Treatment modality: salvage surgery for rNPC patients with or without adjuvant therapy; (3) Outcomes: the results of OS rate and DFS rate in patients who treated postoperative adjuvant therapy and surgery alone; (4) Study design: randomized controlled trials, retrospective and prospective cohort, and case series were included. Case reports, repeatedly published data, studies without adequate data and studies without full text were excluded.

Data Collection and Extraction

Data were extracted by two independent reviewers (Y.F. and Z.D.). The following data were collected from the full text of articles: The characteristics of author, publication language, number of patients, main clinical features of patients, treatment approaches, postoperative adjuvant therapy and survival rate; The Kaplan-Meier survival curve was used in the way introduced by Parmerl et al. (7) to obtain the required survival data when the survival data were not obtained directly from the articles; Data from studies with detailed individual postoperative adjuvant treatment data were extracted separately.

Assessment of Study Quality

Each study's quality was assessed by the Methodological Index For Non-randomized Studies (MINORS) (8). There are total of 12 evaluation indicators, each of which is divided into 0 to 2 points. Scoring method: 0 point means not reported; 1 point means reported but insufficient information; 2 point means reported and provided sufficient information. The first 8 items are designed for no-control studies. The last 4 and the first 8 items are designed for studies with the control group. Articles with a score of 0-8 are low-quality, 9-16 are classified as medium quality, and 17-24 are classified as high-quality. Two reviewers scored independently. If the scoring results are inconsistent, it will be determined through discussion or consultation with a third independent senior oncologist, and finally an agreement is reached.

Statistical Analysis

In this study, we conducted the meta-analysis using software STATA version 15.0 (StataCorp LLC, College Station, TX). The random effects model (9) was adopted when heterogeneity was detected ($I^2 > 50\%$). Sensitivity analysis, Meta-regression and subgroup analyses were used to explore the source of the heterogeneity among the studies. The univariate and multivariate analysis of 178 patients with detailed survival data was performed by the IBM SPSS Statistics Version 21. OS and DFS were calculated by the Kaplan-Meier method and compared by the log-rank test. A 2-tailed $p < 0.05$ indicated statistical difference. Factors that achieved significance on univariate were included in the Cox proportional rate hazard model for multivariate analysis to identify independent significant prognostic factors.

RESULTS

A total of 4976 related publications were retrieved. 4881 articles were excluded because they were duplicates, systematic reviews, animal experiments, case reports, or unrelated to the current

analysis. In addition, 95 studies were evaluated later. After reading the full texts, 74 articles were excluded. The main reasons for exclusion are listed in **Figure 1**. Finally, 21 articles were screened out, 17 of which were included in the meta-analysis since they had a sample size of greater than 10 (10–26). Ten articles provided detailed survival data (21–30). The average MINORS score of the included articles was approximately 10 points. There was a medium quality of methodological heterogeneity in this research.

The main clinical characteristics are shown in **Table 1**. The pooled 2-year OS, 5-year OS, and 2-year DFS that experienced surgery with or without adjuvant therapy for rNPC were 71% (95% CI, 62%-80%, I^2 = 83.2%, p < 0.05, **Figure 2A**), 50% (95% CI, 34%-66%, I^2 = 94%, p < 0.05, **Figure 2B**), and 61% (95% CI, 46%-75%, I^2 = 77.5%, p < 0.05, **Figure 2C**), respectively. There was high heterogeneity indicated by the I^2 value being > 50%; thus, the potential causes of heterogeneity and bias were further investigated.

Meta-regression analysis showed that rT stage (Tau^2 = 0.02315; p = *0.209*), postoperative adjuvant therapy (Tau^2 = 0.0266; p = *0.718*), margin status (Tau^2 = 0.02377; p = *0.14*), and surgical approach (Tau^2 = 0.027; p = *0.514*) may not associated with heterogeneity. We further conducted a subgroup analysis of postoperative adjuvant therapy. In this subgroup analysis, we

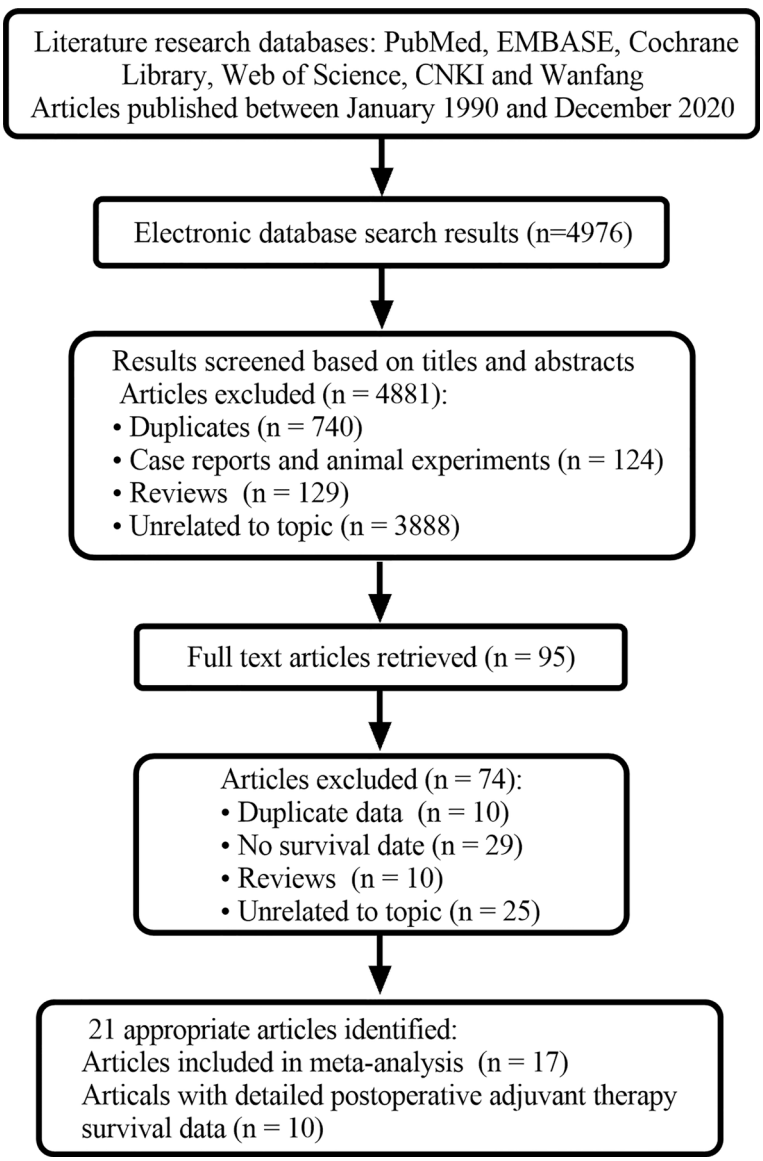

FIGURE 1 | PRISMA flow diagram.

TABLE 1 | Main characteristics of the articles included in the meta-analysis.

Author	Published language	Year	M/F (n)	n (rT classification)	Approach		Margins		Adjuvant therapy	Reported outcome of interest			MINORS
					Endoscopic	Open	Positive	Negative or Close		2-year OS (%)	2-year DFS (%)	5-year OS (%)	
Mao et al. (11)	Chinese	2018	21/10	31rT1	31	0	1	30	0	96.6	67.5	96.6	9
Tao et al. (16)	Chinese	2011	23/14	37(-)	8	29	12	0	12			33	10
							0	25	19				
Bian et al. (15)	English	2011	50/21	71(27rT1, 29rT2, 14rT3, 11rT4)	0	71	27	44	0	62.1		42.1	10
Wong et al. (12)	English	2016	9/6	15(2rT3, 13rT4)	15	0	6	9	0	66.7	40		10
Tsang et al. (21)	English	2014	7/5	12(8rT1, 4rT3)	-		0	11	0	81.8	66.7		9
							1	0	1				
Ko et al. (22)	English	2009	21/7	28(12rT1, 16rT2a)	28	0	0	25	0	51.9	37.1		10
							3	0	3				
King et al. (20)	English	2000	28/3	31(20rT1, 9rT2, 2rT3)	0	31		23	23	93.6	89	57.6	11
								7	0	29	29	-	
Shu et al. (26)	English	2000	24/4	28(16rT1, 9rT2, 2rT3, 1rT4)	0	28	0	21	0	49.2		34.5	11
							7	0	7	57.1		42.9	
Chang et al. (24)	English	2004	30/8	38(16rT1, 4rT2, 11rT3, 7rT4)	0	38	0	30	0	86.7		78.8	8
							8	0	8	42.9			
Hsu et al. (19)	English	2001	47/13	60(10rT1, 18rT2, 22rT3, 10rT4)	0	60	32	0	29	58		35	10
							0	28	0	56		25	
Ng et al. (14)	English	2015	14/6	20(18rT1, 2rT2)	0	20	0	20	0	95.3	73.6	66.7	11
Vlantis et al. (18)	English	2007	61/18	79(39rT1, 28rT2, 10rT3, 2rT4)	0	79	0	36	22				10
							0	13 close	13	77		46	
							30	0	25				
Li et al. (10)	English	2020	132/57	189(55rT1, 42rT2, 64rT3, 28rT4)	189	0	32	1	33			51	11
							0	156	0			41.7	
Chen et al. (17)	English	2009	-	37(17rT1, 18rT2, 2rT3)	37	0	1	36	0	84.2			9
Choi and Lee (23)	English	2005	7/4	11(4rT1, 4rT2, 2rT3, 1rT4)	0	11	2	9	0	72.7			9
Hall et al. (25)	English	2003	12/6	18(1rTx, 6rT1, 7rT2, 1rT3, 3rT4)	0	18		-	18	67		33.5	10
Weng et al. (13)	English	2017	26/10	36(8rT1, 9rT2, 8rT3, 11rT4)	36	0	3	33	36	66	64		11

–, not available; DFS, disease-free survival; OS, overall survival; F, female; M, male; MINORS, Methodological Index for Non-Randomized Studies.

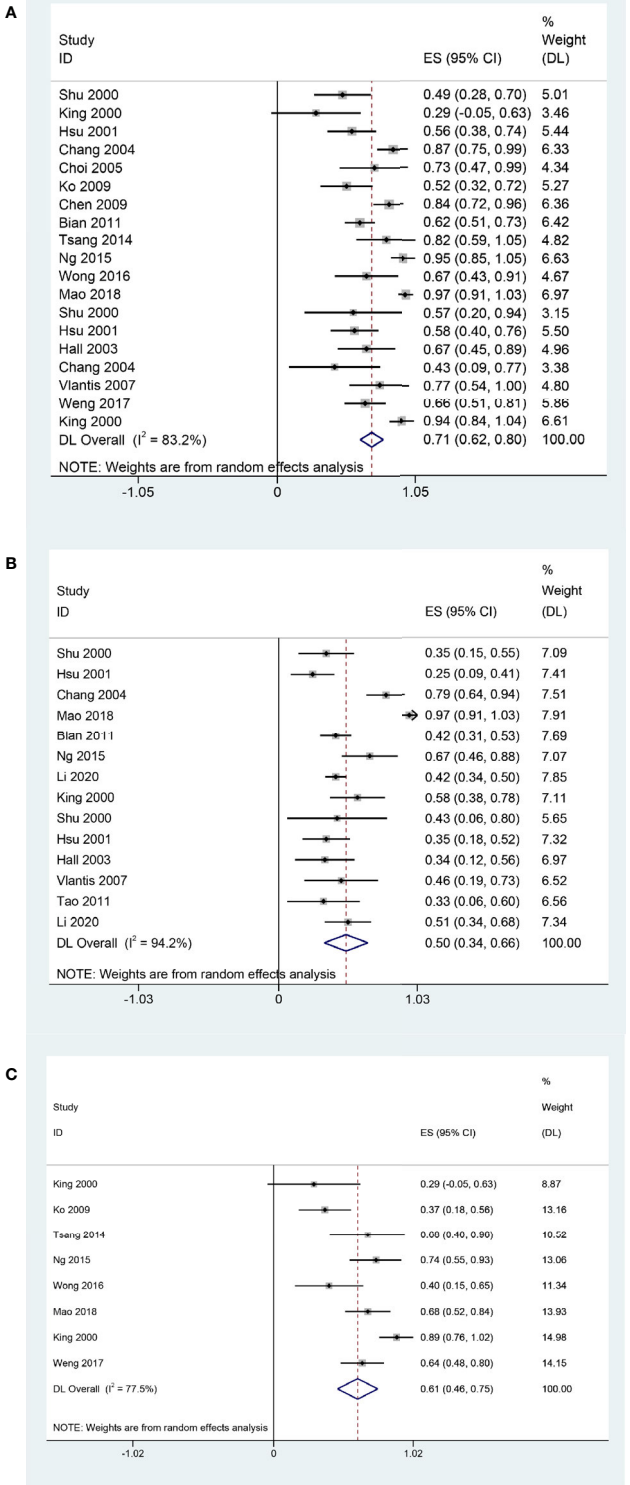

FIGURE 2 | Forest plot of meta-analysis Pooled 2-year OS **(A)**; Pooled 5-year OS **(B)**; Pooled 2-year DFS **(C)**.

performed exploratory sensitivity analysis to find potential causes of heterogeneity. Sensitivity analysis of the pooled 2-year OS revealed that the postoperative adjuvant treatment outcomes of King et al. (20) might have had an influence on clinical heterogeneity.

In the subgroup analysis, patients underwent surgery alone had a better 2-year OS rate (72%, 95% CI, 61%-83%, $I^2 = 86.3\%$, $p < 0.05$, **Figure 3A**) than those underwent surgery and adjuvant therapy (64%, 95% CI, 55%-73%, $I^2 = 0.00\%$, $p = 0.641$, **Figure 3A**). The 5-year OS was 44% (95% CI, 35%-52%, $I^2 = 0.00\%$, $p = 0.543$, **Figure 3B**) in the postoperative adjuvant therapy group and 56% (95% CI, 31%-80%, $I^2 = 96.9\%$, $p < 0.05$, **Figure 3B**) in the surgery alone group. The 2-year DFS of the postoperative adjuvant therapy group was 77% (95% CI, 52%-1.01%, $I^2 = 77.5\%$, $p < 0.05$, **Figure 3C**), which was higher than that of the surgery alone group (54%, 95% CI, 39%-70%, $I^2 = 64.5\%$, $p < 0.05$, **Figure 3C**).

We conducted univariate and multivariate analysis on 178 patients with detailed survival data related to postoperative adjuvant treatment. There were 131 males and 47 females. Their follow-up time was 1-117 months, and the average follow-up time was 26 months. Sixty-six patients underwent RT after surgery, 12 underwent surgery and CHT, and 125 patients underwent surgery alone. The detailed data of each patients are suarized in **Supplemental Table S1**.

There was no significant difference in the distribution of gender, margin status, and recurrent T stage between the open surgery group and the endoscopic surgery group. However, we found there was significant association between surgical approach and adjuvant therapy ($p = 0.010$). In the open surgery group, 62 (65.3%) patients underwent surgery alone, and 33 (34.7%) patients received adjuvant RT after surgery. In the endoscopic surgery group, 63 (75.9%) received surgery alone, 3 (3.6%) received adjuvant RT, 12 (14.4%) received adjuvant CHT, and 5 (6.1%) received postoperative concurrent chemoradiotherapy (CCRT). We further compared the patients who treated with surgery alone, the 5-year OS was 77.0% in the open surgery group and 82.5% in the endoscopic surgery group ($p > 0.05$), the 2-year DFS was 85.0% in the open surgery group and 72.5% in the surgery alone group ($p > 0.05$). In the open surgery group, the 5-year OS was 35.2% in the postoperative RT group and 77.0% in the surgery alone group ($p < 0.05$). The 2-year DFS was 37.3% in the postoperative RT group and 85.0% in the surgery alone group ($p < 0.05$). In the endoscopic surgery group, 12 patients received adjuvant CHT. Compared with the 2-year OS (82.5%) in the surgery alone group, the 2-year OS was 67.3% in the adjuvant CHT group ($p < 0.05$).

The prognostic factors for recurrent NPC are shown in the **Table 2**. Margin status (**Figure 4B**), recurrent T stage (**Figures 4C, D**), adjuvant therapy (**Figures 4E, F**) affected the survival outcomes of patients. The variables considered significant in the univariate were included in the Cox multivariate analyses. Two variables (recurrent T stage and adjuvant therapy) were independent risk factors for the DFS of recurrent NPC in the Cox multivariate analyses (**Table 3**).

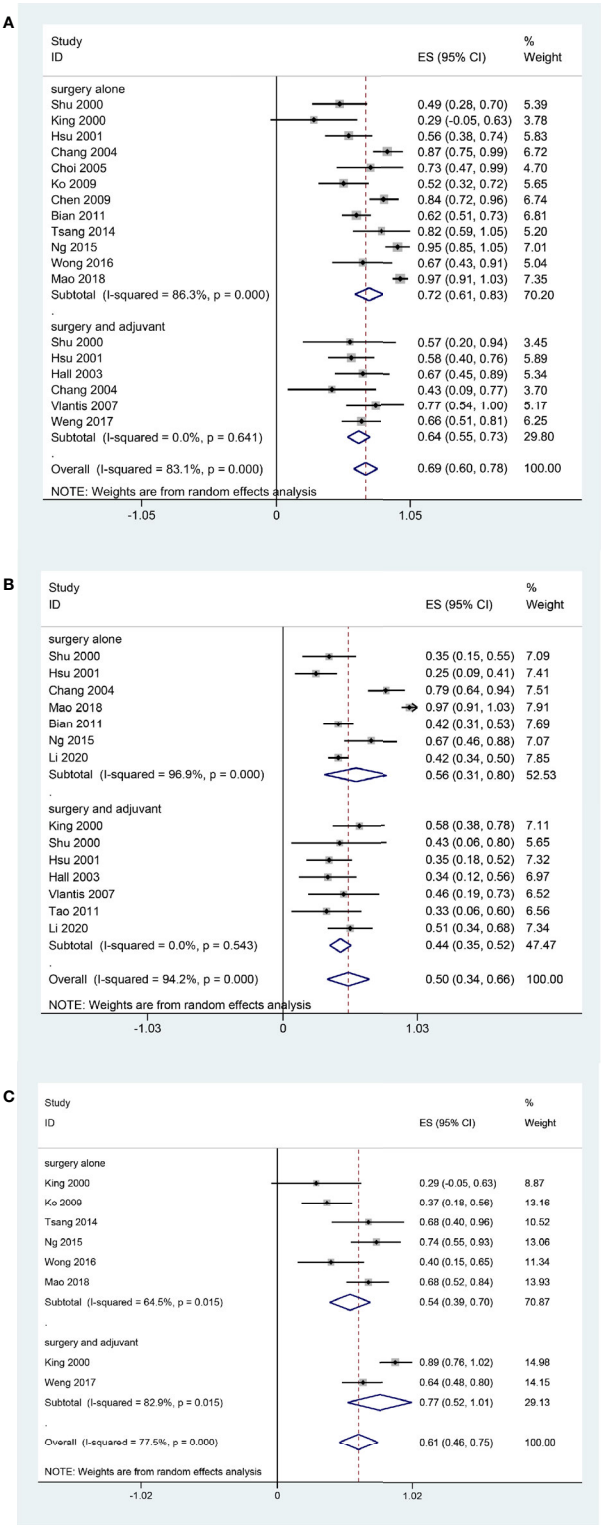

FIGURE 3 | Forest plot of subgroup meta-analysis Pooled 2-year OS **(A)**; Pooled 5-year OS **(B)**; Pooled 2-year DFS **(C)**. Subgroups were stratified according to the postoperative adjuvant therapy status of the patients in each study.

TABLE 2 | Clinical Characteristics and univariate analysis of prognostic factors.

Variables	No. of patients(%)	P Value	
		DFS	OS
Sex		0.640	0.940
Male	131 (73.6)		
Female	47 (27.7)		
Surgical Approach		0.795	0.097
open	95 (53.4)		
endoscopic	83 (44.6)		
Margin Status		0.034	0.333
negative or close	121 (82.9)		
positive	25 (17.1)		
Recurrent T Stage (4 levels: T1, T2, T3, T4)		0.000	0.000
T1	84 (47.5)		
T2	50 (28.2)		
T3	30 (16.9)		
T4	13 (7.3)		
Adjuvant Therapy		0.000	0.002
(3 levels: not given, RT, CHT)			
No	125 (72.3)		
RT	36 (20,8)		
CHT	12 (6.9)		

OS, overall survival; DFS, dieases free survival; RT, radiotherapy; CHT, chemotherapy.

DISCUSSION

Reirradiation, with or without chemotherapy, is a treatment strategy for rNPC. However, it is related with normal tissue injury that results in a rise of mortality and treatment-related morbidity and influences the quality of patients' life (31, 32). Salvage surgery can achieve a better survival rate with lower treatment-related complications than IMRT or two-dimensional conventional radiotherapy (17, 29, 33). In this study, we aim to assess the efficacy of treatment outcomes in salvage surgery for recurrent nasopharyngeal carcinoma.

In our study, the results of meta-analysis showed that the pooled 2-year OS, 5-year OS and 2-year DFS rates were 71%, 50% and 61%, respectively, indicating that the majority of these patients can obtain survival benefits from surgery, which is comparable to the survival rate of 189 patients reported by Wang et al. (10). In this subgroup analysis, the 2-year OS rate and 5-year OS rate in the surgery alone group were superior to those in the postoperative adjuvant therapy group. The 2-year DFS rate in the postoperative adjuvant therapy group was 77%, which was higher than that the surgery alone group (54%). We further retrieved individual patient data with detailed survival results to compare the survival rate of 178 patients who underwent surgery, and found that recurrent T stage and adjuvant therapy were independent risk factors for the DFS of recurrent NPC in the Cox multivariate analyses.

Studies on the effects of adjuvant therapy on the prognosis of patients have been reported. According to following up 79 patients who were treated with surgery, Vlantis et al. (18) found that the adjuvant radiotherapy may not associate with an additional benefit. That is because the clear margin group, of whom only 61% received postoperative radiotherapy, showed a better survival rate than the positive margin group, of whom 83% received postoperative radiotherapy. You et al. (33) published a

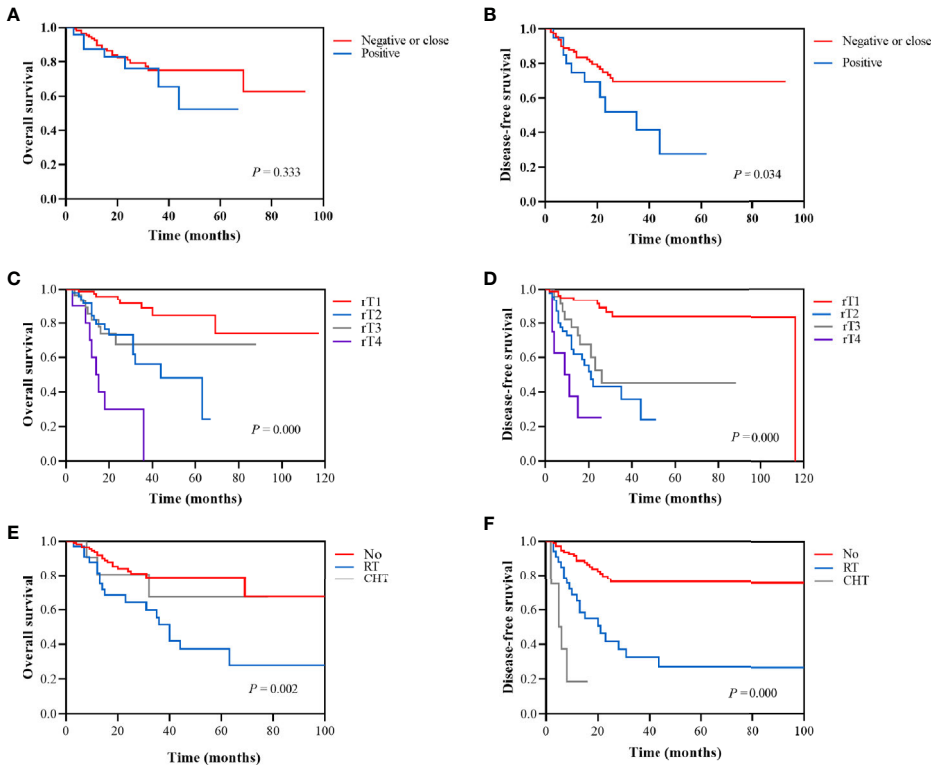

FIGURE 4 | Kaplan-Meier survival analysis according to margin status (negative or close vs positive): **(A)** 2-year OS was 81.0% vs 76.2%. **(B)** 2-year DFS was 73.3% vs 52.0%. Kaplan-Meier survival analysis according to recurrent T stage (rT1, rT2, rT3, and rT4): **(C)** 2-year OS was 93.7%, 73.1%, 67.6%, and 30.0%, respectively. **(D)** 2-year DFS was 93.3%, 43.1%, 52.5%, and 25.0%, respectively. Kaplan-Meier survival analysis according to adjuvant therapy (No, RT, and CHT): **(E)** 2-year OS was 82.6%, 64.1%, and 80.8%, respectively. **(F)** 1-year DFS was 88.7%, 65.3%, and 16.7%, respectively.

TABLE 3 | Cox multivariate regression analysis of disease free survival at 2 years.

Variables	P Value	HR	95% CI	
			Lower	Upper
Margin Status	0.082	4.169	0.834	20.82437
Recurrent T Stage				
T1	0.000			
T2	0.000	8.832	3.384	23.052
T3	0.003	5.382	1.755	16.508
T4	0.000	12.814	3.099	52.989
Adjuvant Therapy				
No	0.000			
RT	0.033	6.098	1.157	32.138
CHT	0.000	35.744	9.917	128.832

CI, confifence intervals; HR, hazard ratio compared to the first mentioned variable; RT, radiotherapy; CHT, chemoterapy.

case-matched study comparing salvage endoscopic nasopharyngectomy with IMRT for selected local recurrent T1-T3 NPC patients. Their results suggested that the improvement in the OS rate in patients who treated with salvage endoscopic nasopharyngectomy compared with salvage IMRT may be associated with a reduction in the risk of reirradiation injury, rather than the elimination of radiation-resistant disease or a reduction in the risk of local recurrence and distant metastasis. However, A meta-analysis published in 2014 showed that postoperative adjuvant therapy is an effective treatment, with 5-year OS rates of 67% vs 39% in the postoperative adjuvant therapy group compared the surgery alone group (34). King et al. (20) previously described those 31 patients routinely received postoperative radiotherapy and found that nasopharyngectomy supplemented by postoperative radiotherapy achieved significant survival and tumor control in selected recurrent NPC. In our study, there was no significant difference in OS between the clear margin group, of whom only 1.7% received postoperative RT and 6.7% received postoperative CHT, and the positive margin group, of whom 76.2% received postoperative RT and 9.5% received postoperative CHT. Patients with positive margins are recoended to receive RT after surgery. In addition, considering that only two studies were included in the postoperative adjuvant therapy group in the DFS subgroup analysis, there is insufficient data to demonstrate an improved DFS benefit for patients who underwent adjuvant therapy after surgery. Due to the limited number of cases, it is difficult to conduct control studies with large samples, and there is still a lack of convincing evidence-based medicine. We cannot ignore the deviation of highly selected patients.

In the past, advanced tumor invading the internal carotid artery (ICA) and skull base is considered unresectable. With the refinement of imaging, cooperation with ophthalmologist and neurosurgeons, and the development of endoscopic surgery and equipment, more selected advanced tumor including invasion of the ICA can be radically removed (10). However, most surgeons mainly focus on early rNPC, ignoring the research of advanced rNPC. Endoscopic nasopharyngectomy reported by Mao et al. (11) described a 5-year OS rate is 96.6% in 31 early rNPC patients. Liu et al. (35) showed that the 2-year OS rates in rT1, rT2, rT3, rT4 were 82.2%, 47.4%, 70.5%, and 36.8%, respectively. Ng et al. analyzed 20 patients (18 with rT1, 2 with rT2) treated with open surgery, and the results of 2-year OS was 95% (14). Bian et al. (15) showed that the 2-year OS rates for recurrent T1, T2, T3, and T4 disease after open surgery were 79.8%, 66.7%, 42.5%, and 10.6%, respectively. Hao reported the 5-year OS rates in stage I, stage II, stage III, and stage IV disease after open surgery were 64.8%, 38.1%, 25.9%, and 46.9%, respectively (36). In our study, rT3 group is superior to rT2 group, because most patients with rT3 are highly selective patients, and the lesions are confined to paranasal sinus. rT2 tumor confined to the parapharyngeal tissues is adjacent to ICA, so extended resection will be more challenging for surgeons. Therefore, the salvage surgery achieved better survival results in rT1-T2 patients and partial selected rT3 patients, and the efficacy of salvage surgeries on rT4 was significantly different in each study.

Although the prognostic factors influencing outcome have been studied, conclusive data on the survival benefits are still lacking. RCTs to compare surgery alone and surgery with adjuvant therapy are needed in patients with positive margin status. As a result of the importance of margin status, the goal of nasopharyngectomy is to obtain a microscopically negative margin (37). For patients with positive surgical margin status, further resection should be performed as soon as possible if the operation is feasible. In recent years, there is increasing evidence that histologically normal margins may have underlying genetic mutations that lead to negative margin results (38, 39). This has motived researchers to search for novel molecular markers to accurately predict local tumor recurrence after surgery (40).

Our study has several limitations. First, patients undergoing surgery alone are highly selected, with a greater chance of negative margins and better survival outcomes, which may increase the bias. The use of an open approach in patients with extensive invasion of the skull base or intracranial area also increase the potential bias. Second, based on the current research, it is not possible to recoend the optimal total dose, fractionated dose and fractionated method of exposure, which may lead to different results in different centers and thus lead to bias. Third, some raw survival data could not be obtained directly from the studies, and data obtained through statistical methods may not be accurate.

CONCLUSION

The meta-analysis indicated that recurrent NPC patients can obtain survival benefits from salvage surgery. Accurately assessing the rT stage of the tumor and choosing the appropriate surgical method is of great significance to the success of the surgery. Although the prognostic factors influencing outcome have been studied, conclusive data on the survival benefits are still lacking, and RCTs to compare surgery alone and postoperative adjuvant therapy are necessary in patients with positive margin status after salvage surgery.

DATA AVAILABILITY STATEMENT

The original contributions presented in the study are included in the article/**Supplementary Material**. Further inquiries can be directed to the corresponding authors.

AUTHOR CONTRIBUTIONS

YF participated in the retrieval and analysis of the article and drafted the manuscript. YF and ZD participated in the screening and data statistics of the article. RY, XZ, HY, CQ, CC, and SF reviewed and edited the manuscript. YP and HS participated in article screening and management, and reviewed, and edited the manuscript. All authors contributed to the article and approved the submitted version.

FUNDING

This work was supported by National Nature Science Foundation of China #81600801 (HS).

SUPPLEMENTARY MATERIAL

The Supplementary Material for this article can be found online at: https://www.frontiersin.org/articles/10.3389/fonc.2021.720418/full#supplementary-material

REFERENCES

1. Tang LL, Chen WQ, Xue WQHY, Zheng RS, Zeng YX, Jia WH. Global Trends in Incidence and Mortality of Nasopharyngeal Carcinoma - ScienceDirect. *Cancer Lett* (2016) 374:22–30. doi: 10.1016/j.canlet.2016.01.040
2. Chee J, Ting Y, Ong YK, Chao SS, Loh KS, Lim CM. Relapse Status as a Prognostic Factor in Patients Receiving Salvage Surgery for Recurrent or Residual Nasopharyngeal Cancer After Definitive Treatment. *Head Neck* (2016) 38:1393–400. doi: 10.1002/hed.24451
3. Lee AW, Ma BB, Ng WT, Chan AT. Management of Nasopharyngeal Carcinoma: Current Practice and Future Perspective. *J Clin Oncol Off J Am Soc Clin Oncol* (2015) 33(29):3356–64. doi: 10.1200/JCO.2015.60.9347
4. Yu Pei C, Chan ATC, Quynh Thu L, Pierre B, Ying S, Jun M. Nasopharyngeal Carcinoma. *Lancet* (2019) 394:64–80. doi: 10.1016/S0140-6736(19)30956-0
5. Lin SJ, Chen XZ, Li JG, Hu CS. Expert Consensus on the Treatment of Recurrent Nasopharyngeal Carcinoma. *Chin J Radiat Oncol* (2018) 27:16–22. doi: 10.3760/cma.j.issn.1004-4221.2018.01.004
6. Hu J, Bao C, Gao J, Guan X, Hu W, Yang J, et al. Salvage Treatment Using Carbon Ion Radiation in Patients With Locoregionally Recurrent

Nasopharyngeal Carcinoma: Initial Results. *Cancer Am Cancer Soc* (2018) 124:2427–37. doi: 10.1002/cncr.31318
7. Parmar MK, Torri V, Stewart L. Extracting Suary Statistics to Perform Meta-Analyses of the Published Literature for Survival Endpoints. *Stat Med* (1998) 17:2815–34. doi: 10.1002/(SICI)1097-0258(19981230)17:24<2815::AID-SIM110>3.0.CO;2-8
8. Slim K, Nini E, Forestier D, Kwiatkowski F, Panis Y, Chipponi J. Methodological Index for Non-Randomized Studies (Minors): Development and Validation of a New Instrument. *Anz J Surg* (2003) 73:712–6. doi: 10.1046/j.1445-2197.2003.02748.x
9. DerSimonian R, Laird N. Meta-Analysis in Clinical Trials Revisited. *Contemp Clin Trials* (2015) 45:139–45. doi: 10.1016/j.cct.2015.09.002
10. Li W, Lu H, Wang H, Zhang H, Sun X, Hu L, et al. Salvage Endoscopic Nasopharyngectomy in Recurrent Nasopharyngeal Carcinoma: Prognostic Factors and Treatment Outcomes. *Am J Rhinol Allergy* (2020) 35(4):458–66. doi: 10.1177/1945892420964054
11. Mao X, Xiang Y, Jiang L, Nie X, Zheng C. Endoscopic Nasopharyngectomy for Recurrent Nasopharyngeal Carcinoma: A Review of 31 Patients and Analysis of the Prognostic Factors. *J Chin Physician* (2018) 20:1159–63. doi: 10.3760/cma.j.issn.1008-1372.2018.08.011
12. Wong EHC, Liew YT, Abu Bakar MZ, Lim EYL, Prepageran N. A Preliminary Report on the Role of Endoscopic Endonasal Nasopharyngectomy in Recurrent Rt3 and Rt4 Nasopharyngeal Carcinoma. *Eur Arch Oto Rhino L* (2017) 274:275–81. doi: 10.1007/s00405-016-4248-2
13. Weng J, Wei J, Si J, Qin Y, Li M, Liu F, et al. Clinical Outcomes of Residual or Recurrent Nasopharyngeal Carcinoma Treated With Endoscopic Nasopharyngectomy Plus Chemoradiotherapy or With Chemoradiotherapy Alone: A Retrospective Study. *PeerJ* (2017) 5:e3912. doi: 10.7717/peerj.3912
14. Ng LS, Lim CM, Loh KS. Long-Term Outcomes of Nasopharyngectomy Using Partial Maxillectomy Approach. *Laryngoscope* (2016) 126:1103–7. doi: 10.1002/lary.25777
15. Bian X, Chen H, Liao L. A Retrospective Study of Salvage Surgery for Recurrent Nasopharyngeal Carcinoma. *Int J Clin Oncol* (2012) 17:212–7. doi: 10.1007/s10147-011-0276-5
16. Tao Z, Si Y, Lan S, Zhang Z, Deng Z, Huang B, et al. Choice of Surgical Approaches for Salvage Surgery of Primary Lesion Recurrence and Residual Cases of Nasopharyngeal Carcinoma. *Chin J Otorhinolaryngol Head Neck Surg* (2011) 108–13. doi: 10.1631/jzus.B1000197
17. Chen M, Wen W, Guo X, Yang A, Qian C, Hua Y, et al. Endoscopic Nasopharyngectomy for Locally Recurrent Nasopharyngeal Carcinoma. *Laryngoscope* (2009) 119:516–22. doi: 10.1002/lary.20133
18. Vlantis AC, Tsang RKYu BK, Kam MK., Tong MC, Lo PS, et al. Nasopharyngectomy and Surgical Margin Status. *Arch Otolaryngol Head Neck Surg* (2007). doi: 10.1001/archotol.133.12.1296
19. Hsu, Hong RL, Ting LL, Ko JY, Sheen TS, Lou PJ. Factors Affecting the Overall Survival After Salvage Surgery in Patients With Recurrent Nasopharyngeal Carcinoma at the Primary Site: Experience With 60 Cases. *Arch Otolaryngol Head Neck Surg* (2001) 127:798–802. doi: 10-1001/pubs.Arch Otolaryngol. Head Neck Surg.-ISSN-0886-4470-127-7-ooa00198
20. King WWK, Ku PKM, Mok CO, Teo PML. Nasopharyngectomy in the Treatment of Recurrent Nasopharyngeal Carcinoma: A Twelve-Year Experience. *Head Neck* (2000) 22:215–22. doi: 10.1002/(SICI)1097-0347(200005)22:3<215::AID-HED2>3.0.CO;2-B
21. Tsang RK, To VS, Ho AC, Ho WK, Chan JY, Wei WI. Early Results of Robotic Assisted Nasopharyngectomy for Recurrent Nasopharyngeal Carcinoma. *Head Neck* (2015) 37:788–93. doi: 10.1002/hed.23672
22. Ko JY, Wang CP, Ting LL, Yang TL, Tan CT. Endoscopic Nasopharyngectomy With Potassium-Titanyl-Phosphate (KTP) Laser for Early Locally Recurrent Nasopharyngeal Carcinoma. *Head Neck* (2009) 31:1309–15. doi: 10.1002/hed.21091
23. Choi JY, Lee WS. Curative Surgery for Recurrent Nasopharyngeal Carcinoma *via* the Infratemporal Fossa Approach. *Arch Otolaryngology–Head Neck Surg* (2005) 131:213. doi: 10.1001/archotol.131.3.213
24. Chang KP, Hao SP, Tsang NM, Ueng SH. Salvage Surgery for Locally Recurrent Nasopharyngeal Carcinoma—A 10-Year Experience. *Otolaryngol - Head Neck Surg* (2004) 131:497–502. doi: 10.1016/j.otohns.2004.02.049
25. Hall CEJ, Harris R, A'Hern R, Archer DJ, Rhys-Evans P, Henk JM, et al. Le Fort I Osteotomy and Low-Dose Rate Ir192 Brachytherapy for Treatment of Recurrent Nasopharyngeal Tumours. *Radiother Oncol* (2003) 66:41. doi: 10.1016/S0167-8140(02)00309-2
26. Shu CH, Cheng H, Lirng JF, Chang FC, Chao Y, Chi KH, et al. Salvage Surgery for Recurrent Nasopharyngeal Carcinoma. *Laryngoscope* (2000) 110:1483–8. doi: 10.1097/00005537-200009000-00014
27. Hsu NI, Shen PH, Chao SS, Ong YK, Li CS. En Bloc Resection Concept for Endoscopic Endonasal Nasopharyngectomy: Surgical Anatomy and Outcome. *Chin Med J (Engl)* (2014) 127:2934–9. doi: 10.3760/cma.j.issn.0366-6999.20133189
28. Emanuelli E, Albu S, Cazzador D, Pedruzzi B, Babighian G, Martini A. Endoscopic Surgery for Recurrent Undifferentiated Nasopharyngeal Carcinoma. *J Craniofac Surg* (2014) 25:1003–8. doi: 10.1097/SCS.0000000000000698
29. Ho AS, Kaplan MJ, Fee WE, Yao M, Sunwoo JB, Hwang PH. Targeted Endoscopic Salvage Nasopharyngectomy for Recurrent Nasopharyngeal Carcinoma. *Int Forum Allergy RH* (2012) 2:166–73. doi: 10.1002/alr.20111
30. Castelnuovo P, Dallan I, Bignami M, Battaglia P, Nicolai P. Nasopharyngeal Endoscopic Resection in the Management of Selected Malignancies: Ten-Year Experience. *Rhinology* (2010) 48:84–9. doi: 10.4193/Rhin09.079
31. Tian YM, Zhao C, Guo Y, Huang Y, Huang SM, Deng XW, et al. Effect of Total Dose and Fraction Size on Survival of Patients With Locally Recurrent Nasopharyngeal Carcinoma Treated With Intensity-Modulated Radiotherapy: A Phase 2, Single-Center, Randomized Controlled Trial. *Cancer AM Cancer Soc* (2014) 120:3502–9. doi: 10.1002/cncr.28934
32. Kong L, Wang L, Shen C, Hu C, Wang L, Lu JJ. Salvage Intensity-Modulated Radiation Therapy (IMRT) for Locally Recurrent Nasopharyngeal Cancer After Definitive IMRT: A Novel Scenario of the Modern Era. *Sci Rep* (2016) 6:32883. doi: 10.1038/srep32883
33. You R, Zou X, Hua YJ, Han F, Li L, Zhao C, et al. Salvage Endoscopic Nasopharyngectomy is Superior to Intensity-Modulated Radiation Therapy for Local Recurrence of Selected T1-T3 Nasopharyngeal Carcinoma - A Case-Matched Comparison. *Radiother Oncol* (2015) 115:399–406. doi: 10.1016/j.radonc.2015.04.024
34. Na'Ara S, Amit M, Billan S, Cohen JT, Gil Z. Outcome of Patients Undergoing Salvage Surgery for Recurrent Nasopharyngeal Carcinoma: A Meta-Analysis. *Ann Surg Oncol* (2014) 21:3056–62. doi: 10.1245/s10434-014-3683-9
35. Liu J, Yu H, Sun X, Wang D, Gu Y, Liu Q, et al. Salvage Endoscopic Nasopharyngectomy for Local Recurrent or Residual Nasopharyngeal Carcinoma: A 10-Year Experience. *Int J Clin Oncol* (2017) 22(5):834–42. doi: 10.1007/s10147-017-1143-9
36. Hao SP, Tsang NM, Chang KP, Hsu YS, Chen CK, Fang KH. Nasopharyngectomy for Recurrent Nasopharyngeal Carcinoma: A Review of 53 Patients and Prognostic Factors. *Acta Otolaryngol* (2008) 128:473–81. doi: 10.1080/00016480701813806
37. Chan JY, To VS, Chow VL, Wong ST, Wei WI. Multivariate Analysis of Prognostic Factors for Salvage Nasopharyngectomy *via* the Maxillary Swing Approach. *Head Neck* (2014) 36:1013–7. doi: 10.1002/hed.23403
38. Bilde A, von Buchwald C, Dabelsteen E, Therkildsen MH, Dabelsteen S. Molecular Markers in the Surgical Margin of Oral Carcinomas. *J Oral Pathol Med* (2009) 38:72–8. doi: 10.1111/j.1600-0714.2008.00715.x
39. Nathan CO, Amirghahri N, Rice C, Abreo FW, Shi R, Stucker FJ. Molecular Analysis of Surgical Margins in Head and Neck Squamous Cell Carcinoma Patients. *Laryngoscope* (2002) 112:2129–40. doi: 10.1097/00005537-200212000-00003
40. Chan JY, Wei WI. Impact of Resection Margin Status on Outcome After Salvage Nasopharyngectomy for Recurrent Nasopharyngeal Carcinoma. *Head Neck* (2016) 38 Suppl 1:E594–9. doi: 10.1002/hed.24046

Conflict of Interest: The authors declare that the research was conducted in the absence of any commercial or financial relationships that could be construed as a potential conflict of interest.

Publisher's Note: All claims expressed in this article are solely those of the authors and do not necessarily represent those of their affiliated organizations, or those of the publisher, the editors and the reviewers. Any product that may be evaluated in this article, or claim that may be made by its manufacturer, is not guaranteed or endorsed by the publisher.

frontiers in Oncology

ORIGINAL RESEARCH
published: 13 October 2021
doi: 10.3389/fonc.2021.705929

Comprehensive Analysis of Prognostic Alternative Splicing Signature Reveals Recurrence Predictor for Papillary Thyroid Cancer

Mian Liu[1], Rooh Afza Khushbu[1], Pei Chen[1], Hui-Yu Hu[1], Neng Tang[1], Deng-jie Ou-yang[1], Bo Wei[1], Ya-xin Zhao[1], Peng Huang[1,2] and Shi Chang[1,2,3]**

[1] Department of General Surgery, Xiangya Hospital Central South University, Changsha, China, [2] Clinical Research Center for Thyroid Disease in Hunan Province, Changsha, China, [3] National Clinical Research Center for Geriatric Disorders, Xiangya Hospital, Changsha, China

OPEN ACCESS

Edited by:
Hui Wang,
Hunan Cancer Hospital, China

Reviewed by:
Maria Cossu Rocca,
European Institute of Oncology (IEO), Italy
Haixia Guan,
Guangdong Provincial People's Hospital, China
Haijun TU,
Hunan University, China

***Correspondence:**
Peng Huang
xiangyahp@csu.edu.cn
Shi Chang
changshi@csu.edu

Specialty section:
This article was submitted to Head and Neck Cancer, a section of the journal Frontiers in Oncology

Received: *06 May 2021*
Accepted: *27 September 2021*
Published: *13 October 2021*

Citation:
Liu M, Khushbu RA, Chen P, Hu H-Y, Tang N, Ou-yang D-j, Wei B, Zhao Y-x, Huang P and Chang S (2021) Comprehensive Analysis of Prognostic Alternative Splicing Signature Reveals Recurrence Predictor for Papillary Thyroid Cancer. Front. Oncol. 11:705929. doi: 10.3389/fonc.2021.705929

Background: Alternative splicing (AS) plays a key role in the diversity of proteins and is closely associated with tumorigenicity. The aim of this study was to systemically analyze RNA alternative splicing (AS) and identify its prognostic value for papillary thyroid cancer (PTC).

Methods: AS percent-splice-in (PSI) data of 430 patients with PTC were downloaded from the TCGA SpliceSeq database. We successfully identified recurrence-free survival (RFS)-associated AS events through univariate Cox regression, LASSO regression and multivariate regression and then constructed different types of prognostic prediction models. Gene function enrichment analysis revealed the relevant signaling pathways involved in RFS-related AS events. Simultaneously, a regulatory network diagram of AS and splicing factors (SFs) was established.

Results: We identified 1397 RFS-related AS events which could be used as the potential prognostic biomarkers for PTC. Based on these RFS-related AS events, we constructed a ten-AS event prognostic prediction signature that could distinguish high-and low-risk patients and was highly capable of predicting PTC patient prognosis. ROC curve analysis revealed the excellent predictive ability of the ten-AS events model, with an area under the curve (AUC) value of 0.889; the highest prediction intensity for one-year RFS was 0.923, indicating that the model could be used as a prognostic biomarker for PTC. In addition, the nomogram constructed by the risk score of the ten-AS model also showed high predictive efficiency for the prognosis of PTC patients. Finally, the constructed SF-AS network diagram revealed the regulatory role of SFs in PTC.

Conclusion: Through the limited analysis, AS events could be regarded as reliable prognostic biomarkers for PTC. The splicing correlation network also provided new insight into the potential molecular mechanisms of PTC.

Keywords: alterative splicing, papillary thyroid cancer, recurrence-free survival, prognosis, splicing factor

INTRODUCTION

Thyroid cancer is the most rapidly increasing malignancy worldwide in both men and women (1). Papillary thyroid cancer (PTC), the most common thyroid carcinoma type, comprise 80% of all cases (1). PTC has several subtypes, including classical papillary cancers, less aggressive variants, such as follicular, oxyphilic, and cribriform-morular variants, and more aggressive variants, such as diffuse-sclerosing, tall-cell, columnar-cell and solid variants (2). In general, PTC has an excellent prognosis, with a 5-year survival rate over 97%, and PTC tumors measuring less than 1 cm have a 10-year disease-specific survival rate over 99% (3). Although PTC is associated with low mortality, the incidence of disease recurrence or metastasis is 20-30%, and is even higher in patients with the more aggressive variants (4, 5). It is important to assess the PTC recurrence risk accurately for ensuring patients to receive the most appropriate treatment strategy. Over the past few decades, great efforts have been made in exploring prognostic biomarkers for PTC, in particular gene markers, such as mutations in the *BRAF, RAS, PIK3CA, P53, PTEN, P53* and *ALK* genes (6, 7). Although these studies showed promising results, they only focused on the factors driven by mutation and the level of transcription while ignoring the diversity of RNA isoform resulting from posttranscriptional modifications. Currently, there is no consensus on assessing the prognosis of PTC patients.

Alternative splicing (AS) is a significant molecular posttranscriptional modification mechanism that converts mRNA into different RNA transcripts which are then translated into different protein products, thus greatly increasing the diversity of protein species (8, 9). Recent studies have shown that more than 90% of human genes have AS modifications and these modifications play an important role in biological processes (10, 11). The dysregulation of AS is involved in a variety of physiological and pathological processes, including tumorigenesis. Since tumor cells tend to generate sub-isoform changes, which lead to the functional loss of tumor suppressor genes and the activation of oncogenic genes (12). These multiple AS events are conducive to tumor cell proliferation, invasion and metastasis, drug resistance and immune escape (13). For example, exon 13 skipping in CD46 and the exon 13-containing CD46 isoform play opposite roles in bladder cancer development, and exon 13 skipping remarkably accelerated DNA synthesis, cancer cell proliferation, migration and invasion (14). KLF6-SV1, an oncogenic alternatively-spliced isoform of KLF6 produced by alternative 5′ splice sites, is often highly expressed in various human malignancies including non-small cell lung cancer and hepatocellular carcinoma (15–17). *BRCA1/2* germline mutations are most commonly seen in breast and ovarian cancer patients who benefit from treatment with PARP inhibitors (PARPis) or platinum compounds, but BRCA1-Δ11q splice variants lacking the majority of exon 11 contribute to therapeutic resistance (18, 19). We found that prognostic models constructed from AS events data had good efficiency for evaluating the survival time of adrenocortical carcinoma, cervical cancer and prostate cancer patients (20–22).

In addition, some studies have shown that AS events could be intricately regulated by key splicing factors (SFs) (23). The abnormal expression of SFs cause subversive alteration in tumor-specific AS events, which affects the initiation and progression of carcinoma (24). In recent years, the development of genome-wide sequencing technology has provided new opportunities to explore and identify tumor-specific molecules and prognostic markers (25, 26). A comprehensive analysis of AS events and underlying SF-AS regulatory networks can provide new insight into the molecular mechanism of PTC and prognosis-related biomarkers for PTC patients. Preliminary studies in AS have provided evidence of prognosis value, while the function and mechanism of AS in PTC remains unknown.

In our study, we revealed a large number of RFS-related AS events in PTC through a systemic analysis of the AS events of all genes in the PTC cohort from the TCGA SpliceSeq dataset. We constructed a prognostic prediction model based on the identification of RFS-associated AS events, and presented the clinicopathological characteristics and a nomogram of AS prognostic predictors, which could predict the recurrence-free survival rate of PTC patients. Finally, development of an SF-AS relationship network diagram showed the potential regulatory mechanisms involved in PTC recurrence and patient prognosis.

MATERIALS AND METHODS

The flowchart of the study is shown in **Figure 1**.

Acquisition of AS Data

The percent splice-in (PSI) data of AS events in PTC were downloaded from the TCGA SpliceSeq (https://bioinformatics.mdanderson.org/TCGASpliceSeq/) database, which provides the overview of AS events across 33 types of tumors based on TCGA RNA-seq data. AS events for 7 types have been identified so far, namely Alternate Acceptor site (AA), Alternate Donor site (AD), Alternate Promoter (AP), Alternate Terminator (AT), Exon Skip (ES), Mutually Exclusive Exons (ME) and Retained Intron (RI) (27). The annotation of the AS event consists of the parent gene symbol, the unique ID number and the splicing type. PSI values are used to quantify AS events, and its range is from zero to one. In order to acquire a credible AS events data set, we set a strict screening condition that the proportion of samples contain PSI values over 75%. We filtered out the data with AS events missing rate over than 20%, then replaced the missing value with median values.

Analysis of RFS-Related AS Events, Function and Pathway Enrichment Analysis and Gene Interaction Network

The clinical information of the PTC cohort was obtained from the cBioPortal (http://www.cbioportal.org) database, including recurrence-free survival status and time. Patients were divided into high and low PSI subgroups based on the median value of PSI, and then univariate Cox regression analysis was used to explore

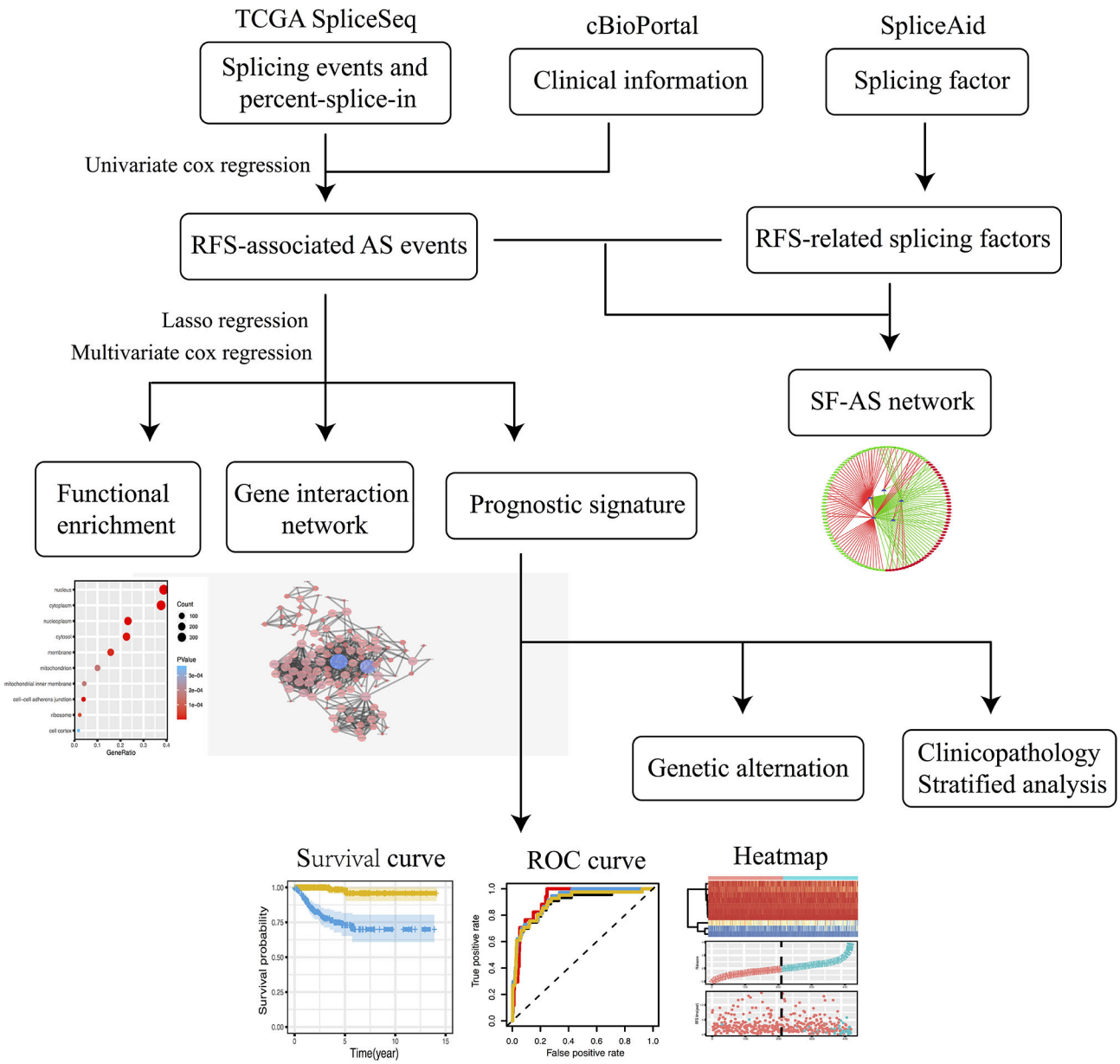

FIGURE 1 | The flowchart of the study.

RFS-associated seven types AS events respectively, p values less than 0.05 considered as statistically significant. UpSetR mapping was used to analyze the interaction between the RFS-related AS events for each splicing type and corresponding parent genes. Target genes network were constructed *via* the Search Tool for the Retrieval of Interacting Genes (STRING, https://string-db.org) and Cytoscape (version 3.7.1). Database for Annotation, Visualization and Integrated Discovery (DAVID) online functional annotation tool (https://david.ncifcrf.gov/tools.jsp) was used to complete genetic function and pathway enrichment analysis, and use RStudio drawing.

Construction of the AS Model for Predicting Recurrence of PTC Patients

First, LASSO regression analysis was performed on the RFS-associated AS events obtained of 7 types by univariate Cox regression analysis. In order to avoid overfitting of the model, multivariate Cox regression analysis was used to further screen the candidate AS events and identify independent prognostic predictors. We calculated the risk score for each patient based on each predictor and the calculation formula is as follows: Risk score = $PSI_{AS\ event1} \times coefficient_{\ AS\ event1} + PSI_{AS\ event2} \times coefficient_{\ AS\ event2} + \cdots + PSI_{AS\ eventn} \times coefficient_{\ AS\ eventn}$. According to the

median risk score, PTC patients were divided into high and low risk subgroups, and Kaplan-Meier analysis was used to evaluate the accuracy of each prognostic prediction signature. In addition, the receiver operating characteristic (ROC) curve by the survival ROC package was used to calculate the corresponding area under the curve (AUC) value. Furthermore, the cBioPortal online database was used to analyze mutations and expression changes in corresponding parental genes.

The Verification of Prognostic Value of AS Predictor

The modeling dataset was random divided into two validation datasets (50 percent vs 50 percent, n=215), Kaplan-Meier survival curve and ROC curve were used to evaluate the performance of the model. Besides, we also performed a pan-cancer survival analysis based on data from TCGA.

To further analyze the independent risk factor associated with recurrence of PTC, AS prognostic predictor signature along with all clinicopathological variable mentioned above were performed by univariate Cox regression analysis. The candidate variables were subjected to multivariate regression analysis to screen out independent prognostic predictors.

In addition, we analyzed the clinicopathological characteristics of the high- and low-risk subgroups. Judge and verify the prognostic performance of the final AS prediction model in the stratified survival analysis, such as age, sex, histologic subtype, tumor grade, lymph node grade, and pathological stage.

Analysis of RFS-Related SFs and Construction of SF-AS Relationship Network

Splicing factors (SFs) were obtained from SpliceAid 2 (www.introni.it/spliceaid.html) database. The normalized mRNA expression data of the SFs were obtained from UCSC Xena (https://xena.ucsc.edu) database. The Protein expression level of SFs was obtained from The Human Protein Atlas (https://www.proteinatlas.org/) database. Univariate Cox regression analysis was used to screen out RFS-related SFs. Spearman correlation analysis was used to detect the relationship between RFS-related AS events and SFs, P value less than 0.05 and the correlation coefficient greater than 0.4 as cutoff value. Finally, Cytoscape is used to construct a potential SF-AS relationship network diagram.

RESULTS

A Complete Overview of AS Events in the TCGA PTC Cohort

Through integrating all AS events of PTC patients from the TCGA SpliceSeq database, we discovered 37833 AS events involving 18231 genes, including 10219 ESs in 3904 genes, 9127 APs in 3653 genes, 8597 ATs in 3753 genes, 3683 AAs in 2592 genes, 3190 ADs in 2240 genes, 2787 RIs in 1865 genes, and 232 MEs in 224 genes (see **Supplementary Figure 1A**). The figures showed that one gene can produce multiple types of AS events in PTC patients. Among these 7 types of AS events, the most frequent splicing type was ES, while the least type was ME (see **Supplemental Figure 1A**).

Detection of RFS-Related AS Events and Analysis of Function and Pathway Enrichment

The survival and clinical information for PTC was obtained from the cBioPortal database (**Supplementary Table 1**). There was a total of 430 PTC patients with available recurrence-free survival time data and complete clinical information in our analysis. In PTC cohort, univariate Cox analysis of all AS events revealed that 1396 AS events were significantly related to the RFS ($P<0.05$, **Supplementary Tables 2**). In order to better visualize the intersection of different types of AS events and corresponding parent genes, an UpSet plot was constructed, as shown in **Supplementary Figure 1B**. Interestingly, we found that one gene can produce 3 different types of AS events in this study. The different types of prognoses associated AS events, except ME, in the top 20 genes are clearly exhibited in **Figure 2**. Next, we performed functional and pathway enrichment of 989 parent genes of RFS-associated AS events. The results showed that a total of 130 GO terms and 3 KEGG terms were significantly involved in prognosis ($p<0.05$), and **Figures 3A–D** showed the top 10 GO functional enrichment and KEGG pathways. To further explore the biological association between the corresponding paternal genes in PTC, we used STRING and Cytoscape to create a gene interaction network. **Figure 3E** shows a network diagram of the parental genes. The larger the node, the greater the degree of association with other genes, and the top 3 genes identified were UBA52, UBB and RPL31, they may be closely related to the occurrence and progression of PTC.

Establishment of AS Recurrence Prediction Model for PTC Patients

We performed LASSO regression analysis for the significant RFS-associated AS events in each AS type (**Supplementary Figure 2A–G**). In order to avoid model overfitting, the above results of each AS type were further analyzed by multivariate Cox regression analysis to screen out the most suitable predictor for AS recurrence models. Seven types of AS models (AA, AT, ME, RI, AD, AP and ES) were constructed, and the formula corresponding to each model was shown in **Table 1**. Based on the formula, we calculated the risk score of each patient and divided into high and low risk groups. The Kaplan-Meier survival analysis showed that the recurrence model of each AS type had good predictive power to distinguish between good and poor survival results (**Figures 4A–G**). To further evaluate and compare the efficiency of the model, ROC curves were used to calculate the AUC value predicting the 1-year, 3-year, 5-year and 10-year recurrence-free survival rate (**Figures 4a–g**). The AUC values of the seven types of models at different times did not exceed 0.04. The largest AUC value of the ROC for the 1-year, 5-year and 10-year RFS rate was obtained with the AA prognostic predictor (0.860, 0.824 and 0.827 respectively), and the largest AUC value for the 3-year survival rate was obtained with the AP model (0.825). Importantly, a ten-AS event predictor was

obtained by the overall analysis of prognostic-related AS events using LASSO regression and multivariate Cox regression analysis (**Supplementary Figure 2H**). The calculation used for the risk score is shown in **Tables 1** and **2**, the high-risk group showed a worse significant survival outcome than low-risk (**Figure 5A**). The 1-year, 3-year, 5-year and 10-year AUC values of the ROC curve for the combined model were calculated as 0.923, 0.916, 0.900 and 0.889 respectively. These values were higher than those obtained by the seven separate models individually, suggesting that the mixed AS model had the highest-level performance among all prognostic models (**Figure 5B**). The distribution of patient survival status and survival time, risk score for the prognostic predictors and the PSI of the ten AS events for final recurrence model, as illustrated in **Figure 5C**, the results showed that the shorter the patient's survival time and the more recurrent cases, the higher the risk score of the model was significantly higher ($P < 0.05$, **Figure 5C**).

In addition, parental genetic alteration of the ten-AS event model is shown in **Figure 6A**. The mutation of these ten genes rarely appeared in PTC patients from the TCGA dataset, but the mRNA expression level of most of the genes were altered; for example, *NUD16* expression was decreased in 71% of PTC samples compared to normal tissue (**Figure 6A**). We detected the relationship between the expression level of parental genes and the RFS rate of PTC patients. There was a statistically significant relationship between PTC patient's prognosis and the expression of *SPHK2, SLC22A17, NUDT16, FXN, ADIRF, MARK3* and *MTURN*. The representative survival curves showed that *NUDT16*, *MTURN* and *FXN* had the most changes, and high expression was a favorable prognostic factor (**Figures 6B–D**, **Supplementary Figure 3**). The changes in mRNA may be caused by AS events, but AS events are not limited to changes in mRNA levels as they are also involved in the specific functions of protein regions.

The Efficiency of AS Prognostic Predictor in Stratified Clinicopathologic Subgroups in PTC Patients

According to the ten-AS prognostic model, PTC patients were divided into two risk levels (high or low). The clinicopathologic characteristics of the two groups as shown in **Table 3**, PTC patients with high risk tended to be over the age of 55 and had tumors with a higher grade ($p<0.05$). Moreover, we analyzed the predictive performance of ten-AS prognostic model in stratified PTC patients (**Table 3**). The prognostic model identified high-risk patients with worse RFS rates in each subgroup except T1 and Stage II, which may result from the small number of endpoint events in these two subgroups (**Table 3**). In order to further explore the potential factors related to recurrence in PTC patients, the clinicopathologic variables along with the risk score of the ten-AS prognostic predictor were subjected to univariate Cox regression analysis. Age <55, female sex, histologic type-classical PTC, pathologic T1, pathologic N1 and pathologic stage I were set as references. The results showed that age, tall cell type, T3, T4, N1b, stage III, stage IV and risk score were significantly related to PTC recurrence (**Table 4**). Furthermore, the meaningful factors were analyzed by multivariate Cox regression analysis, and the results uncovered that the ten-AS prognostic model was the only independent recurrence prognostic factor (**Table 4**). The risk score of the ten-AS model, the independent predictive factor, was used to establish nomogram (**Supplementary Figure 4**). Our results suggested that the ten-AS prognostic predictor had a better efficiency in predicting PTC recurrence than clinicopathological characteristics, and predictive value in stratified subgroups well.

The Verification of Prognostic Value of the Ten-AS Signature

Internal validation in two datasets shown good performance of the ten-AS signature, PTC patients with high glycolysis scores exhibited worse prognosis (see **Supplementary Figure 5**). Besides, we also evaluated the prognostic values of the ten-AS prognostic model in various cancers. In our results, the ten-AS prognostic model also applied to prostate adenocarcinoma (PRAD) and lung adenocarcinoma (LUAD), PRAD or LUAD patients with high-risk scores exhibited worse prognosis (see **Supplementary Figure 6**).

Detection of RFS-Associated SFs and Construction of SF-AS Relationship Network

In order to explore the upstream regulatory factors of dysregulated AS, the expression of 71 SFs was extracted from level 3 RNA-seq data of TCGA PTC. The results for univariate Cox regression analysis exhibited that 5 SFs (KHSRP, NOVA2, PTBP2, SRSF3 and RBM9) were significantly correlated to the RFS rate of PTC patients (**Supplementary Table 3**). The recurrence-free survival time curve with high and low expression of these 5 SFs shown as **Figures 7A–E**, among them, KHSRP was oncogenic factor, while NOVA2, PTBP2, SRSF3 and RBM9 were tumor inhibitor. We further searched The Protein Atlas database to detect the protein level of the 5 SFs in PTC. The immunohistochemistry (IHC) results showed that KHSRP, SRSF3 and RBM9 were located in nucleus, and the expression of SRSF3 and RBM9 were significantly lower in cancer than normal thyroid, while there was no significantly different between KHSRP, NOVA2 and PTBP2 in carcinoma and normal tissues (**Figure 7F**). The mRNA expression level of PTBP2 in normal tissues was higher than PTC, and NOVA2 expression was significantly involved in tumor stage, high expression in I-II stages and low expression in III-IV stage for PTC (**Figures 7G, H**). In addition, we used Spearman's test to detect the relationship between the expression of these 5 SFs and PSI values of RFS-associated AS events. The relationship network diagram showed that RFS-related 5 SFs (blue rectangles) were significantly associated with 117 AS events, with P value less than 0.05 and Spearman coefficient greater than or 0.4 as the cutoff value ($p<0.05$, Spearman≥ 0.4, **Figure 8B**). Interestingly, we found that the expression of KHSRP was positively correlated (red lines) with most of adverse survival prognostic AS events (red dots) but negatively correlated (green lines) with most of favorable AS events (green dots), however, the tumor suppressor SFs were inversely related to AS events. For example, **Figure 8A** exhibited

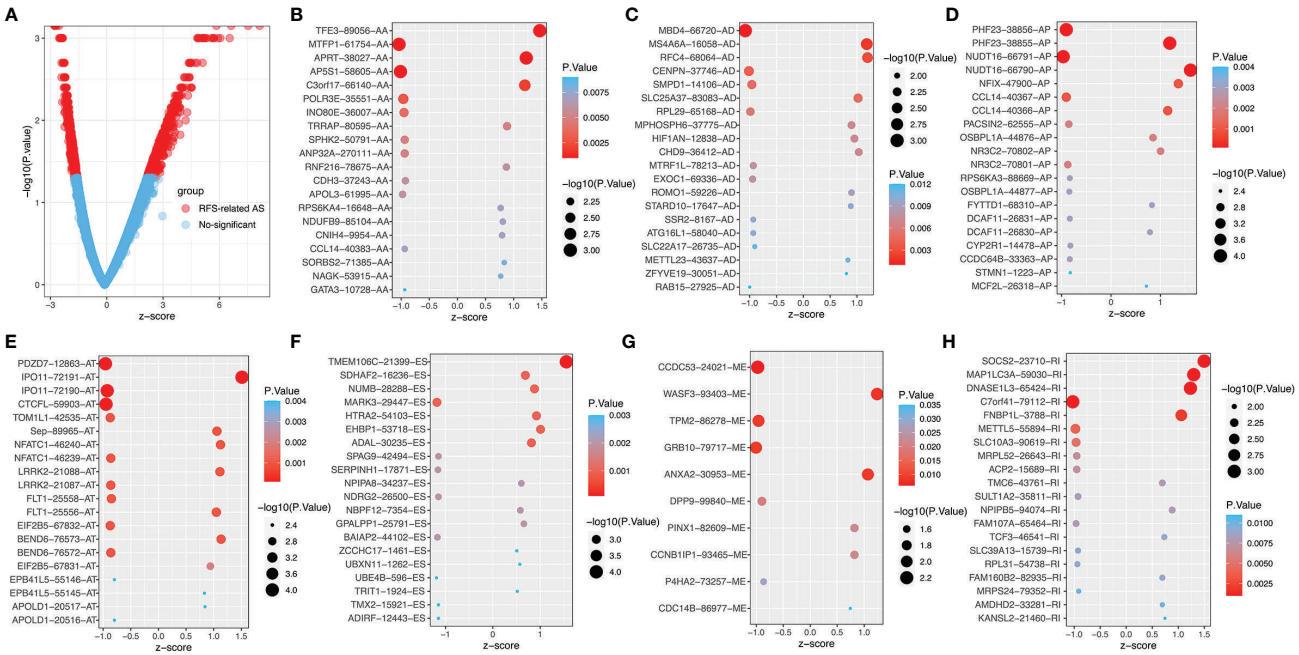

FIGURE 2 | The top 20 RFS-associated AS events. **(A)** Volcano map of AS event, red dots represent RFS- related AS. The top 20 AS events related to recurrence outcomes in different splice types in PTC, including **(B)** AA, alternate acceptor site. **(C)** AD, alternate donor site. **(D)** AP, alternate promoter. **(E)** AT, alternate terminator. **(F)** ES, exon skip. **(G)** ME, mutually exclusive exons. **(H)** RI, retained intron.

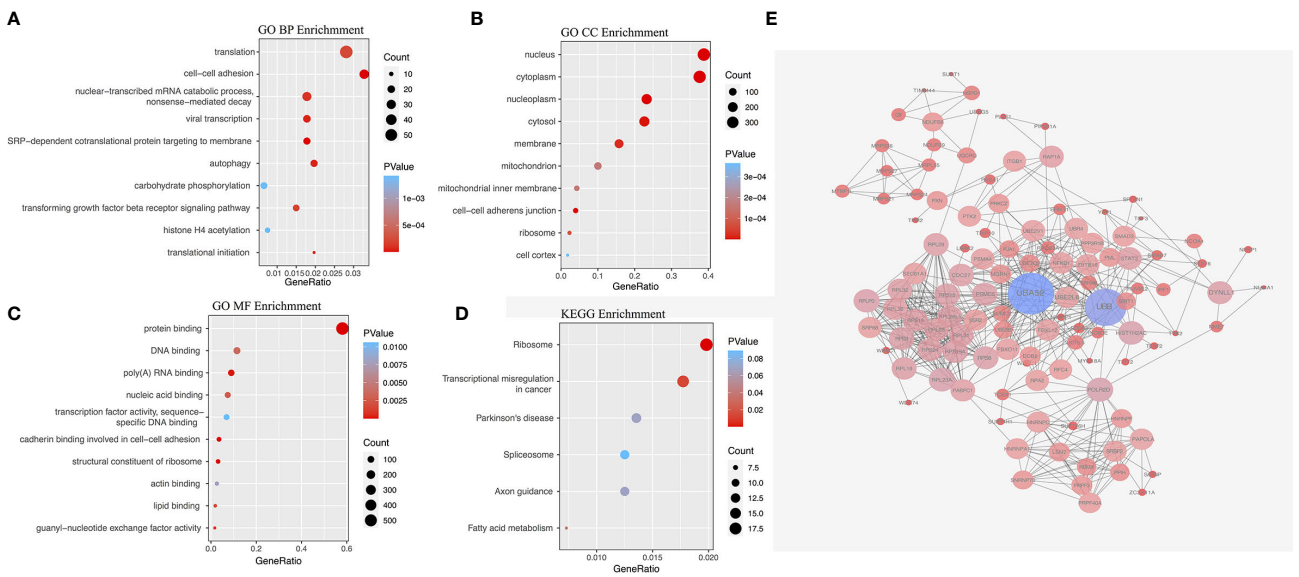

FIGURE 3 | The gene interaction network of RFS-associated AS events, functional and pathway analysis. **(A)** GO biological processes (BP) enrichment. **(B)** GO cellular component (CC) enrichment. **(C)** GO molecular function (MF) enrichment. **(D)** KEGG pathway enrichment analysis. **(E)** Parent genes interaction network.

the representative scatter plots of SFs and AS events correlation. Based on our preliminary exploration, we proposed the hypothesis that antineoplastic SFs play a key role in dysregulated AS, which may lead to tumor progression in PTC.

DISCUSSION

In this study, we first recognized diversified AS events with prognostic power using PSI of PTC AS data obtained from the

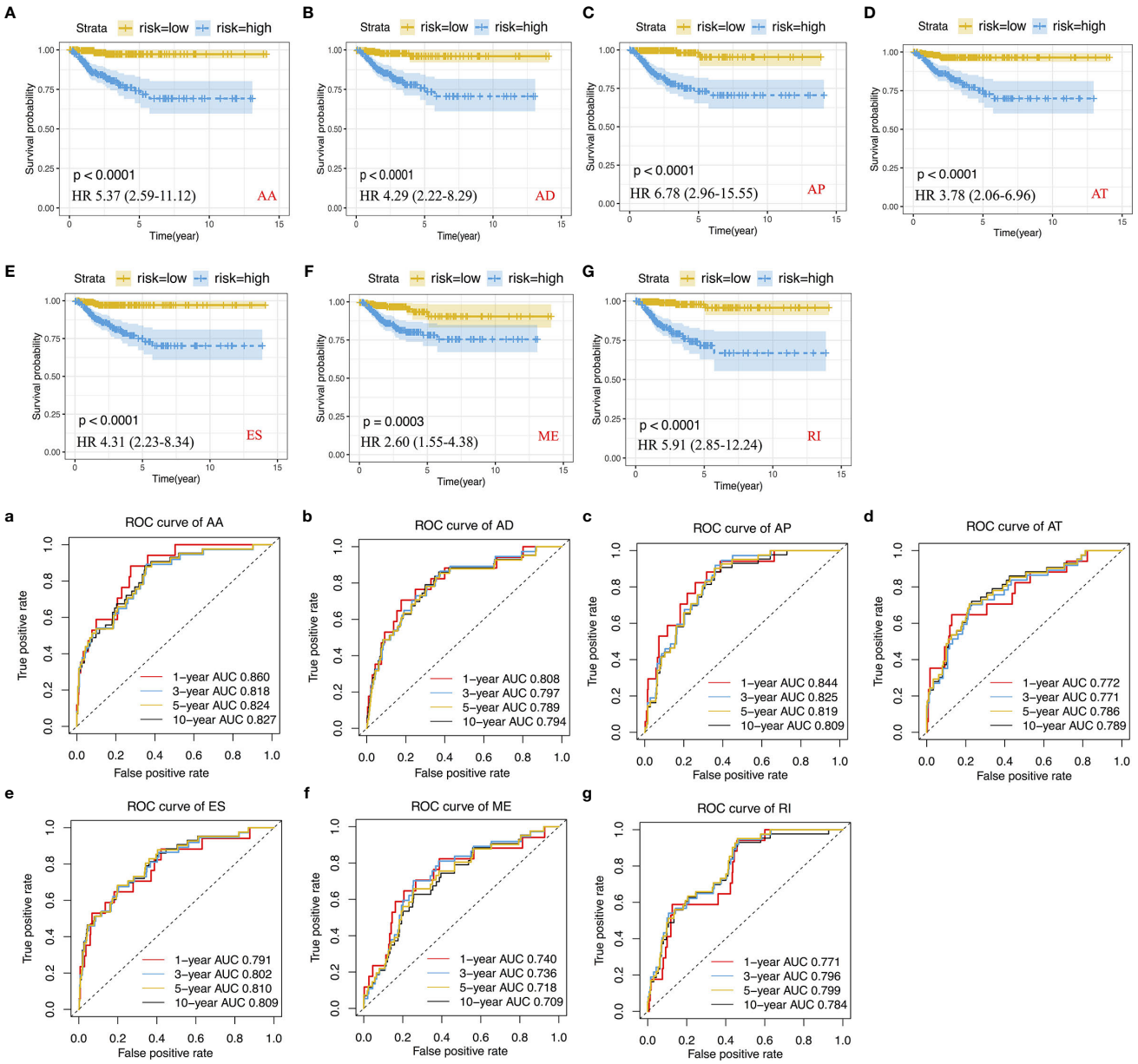

FIGURE 4 | Construction of Kaplan-Meier survival curve and ROC curve and calculation of AUC values for recurrence prognostic predictors. **(A–G)** Kaplan-Meier survival curve for AA, AD, AP, AT, ES, ME and RI prediction models. **(a–g)** ROC curve for AA, AD, AP, AT, ES, ME and RI prediction models.

TCGA. By using TCGA data, reported studies involved to PTC prognostic have shown that long noncoding RNA (lncRNAs), microRNA, and methylation data can work as prognostic factors. Chen et al., using binding motif data from Ensembl Biomart, predicted transcription factors (TFs) for affected genes to construct a TF/lncRNA/mRNA network, which predicted PTC prognosis with an AUC of 0.794 (28). Wang et al. established an N6-methyladenosine (m6A) RNA methylation-related risk signature of disease-free survival for a total PTC cohort with an AUC of 0.817. These models have also shown favorable prognostic predictions (29). We explored all events and established a ten-AS event signature to evaluate the RFS rate of PTC patients. The AUC values of the ROC curve for the 1-year, 3-year, 5-year and 10-year recurrence-free survival rate of PTC patients were 0.923, 0.916, 0.900 and 0.889 respectively, and we obtained more efficient prediction values from this model than with others. Importantly, the present ten-AS event signature has been confirmed with universality in predicting the prognosis of a wide range of tumors, including PRAD and LUAD patients.

AS is a key regulatory factor in the diversity of protein translation and gene phenotype, which is not only involved in normal physiological process but also plays an important role in

TABLE 1 | Formula of each prognostic signature for PTC.

Type	Formula
AA	DGKZ|15545|AA× (-2.68) + ZC3H14|28713|AA× (1.44) + LRRC28|32640|AA× (-1.20) + INO80E|36008|AA× (-4.92) + APRT|38027|AA× (5.86) + INO80C|45175|AA× (0.09) + SPHK2|50791|AA× (-4.97) + NR4A2|55620|AA× (1.23) + AP5S1|58605|AA× (-2.60) + CHCHD10|61315|AA × (-1.08) + MTFP1|61754|AA × (-1.17)
AD	STARD10|17647|AD× (0.45) + N4BP2L2|25597|AD × (-4.02) + SPINT1|30056|AD × (-0.48) + CHD9|36412|AD × (0.68) + IFI35|41177|AD× (-0.05) + SEC14L1|43713|AD × (-2.90) + MBD4|66720|AD × (-3.60)
AP	SLC22A17|26733|AP× (-2.64) + DCAF11|26830|AP × (0.22) + CCL14|40366|AP × (1.51) + NUDT16|66790|AP × (-22.52)
AT	FAM72A|9578|AT × (0.41) + ABCC4|26108|AT × (2.78) + SUPT16H|26571|AT × (5.75) + TOM1L1|42535|AT × (-4.95) + GDPD1|42768|AT × (7.27) + Mar|73177|AT × (-0.44) +COBL|79728|AT × (2.49) + FXN|86527|AT × (8.97) + KIF4A|89372|AT × (-0.06)
ES	PTER|10876|ES × (0.40) + ADIRF|12443|ES × (-24.30) + CS|22419|ES × (0.84) + C14orf159|28857|ES × (4.56) + NDUFB1|28987|ES × (3.98) + MARK3|29447|ES × (-1.31) + COX5A|31814|ES × (-3.68) + NPIPA8|34237|ES × (1.35)
ME	CCDC53|24021|ME × (-1.02) + WASF3|93403|ME × (-1.12)
RI	SOCS2|23710|RI× (0.35) + USHBP1|48248|RI × (0.89) + DNASE1L3|65424|RI × (0.07) + MTURN|79112|RI × (-3.98) + FAM160B2|82935|RI × (1.44)
All	SPHK2|50791|AA × (-2.33) + SEC14L1|43713|AD × (-0.42) + SLC22A17|26733|AP × (-0.21) + CCL14|40366|AP × (1.02) + NUDT16|66790|AP × (15.52) + FXN|86527|AT × (6.72) + ADIRF|12443|ES × (-23.02) + MARK3|29447|ES × (-0.69) + TNFSF13|38976|ES × (-0.29) + MTURN|79112|RI × (-3.57)

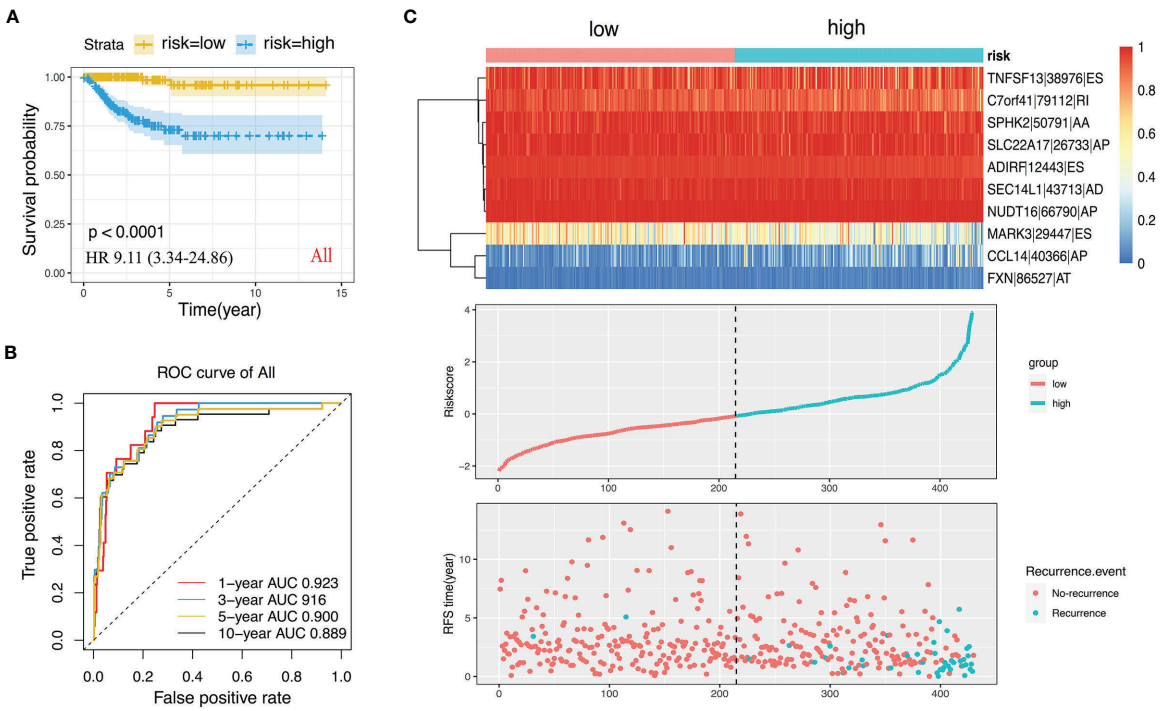

FIGURE 5 | The ten-AS events signature as the best prognostic predictive model in PTC cohort. **(A)** Kaplan-Meier curve of the ten-AS prognostic predictor. **(B)** ROC curve of the ten-AS prognostic predictor. **(C)** The upper part showed the heatmap of PSI score of AS events involved in the prognostic predictor. The middle part was risk score of each individual. The bottom was the recurrence status and RFS time of each PTC patients.

TABLE 2 | Prognostic predictors for PTC.

Gene	AS id	type	Exons	HR	Lower95	Upper95	P-value	Index
SPHK2	50791	AA	3.3:3.4	0.51	0.32	0.82	0.005	-2.33
SEC14L1	43713	AD	4.2	0.57	0.35	0.9	0.017	-0.42
SLC22A17	26733	AP	1	0.54	0.34	0.85	0.008	-0.21
CCL14	40366	AP	1	2.41	1.45	4	0.001	1.02
NUDT16	66790	AP	2	2.86	1.66	4.92	0.0001	15.52
FXN	86527	AT	7	1.57	1.01	2.44	0.047	6.72
ADIRF	12443	ES	2	0.48	0.3	0.79	0.01	-23.02
MARK3	29447	ES	17	0.45	0.27	0.72	0.001	-0.69
TNFSF13	38976	ES	2.2:3	0.52	0.32	0.82	0.005	-0.29
MTURN	79112	RI	4.2	0.46	0.28	0.73	0.001	-3.57

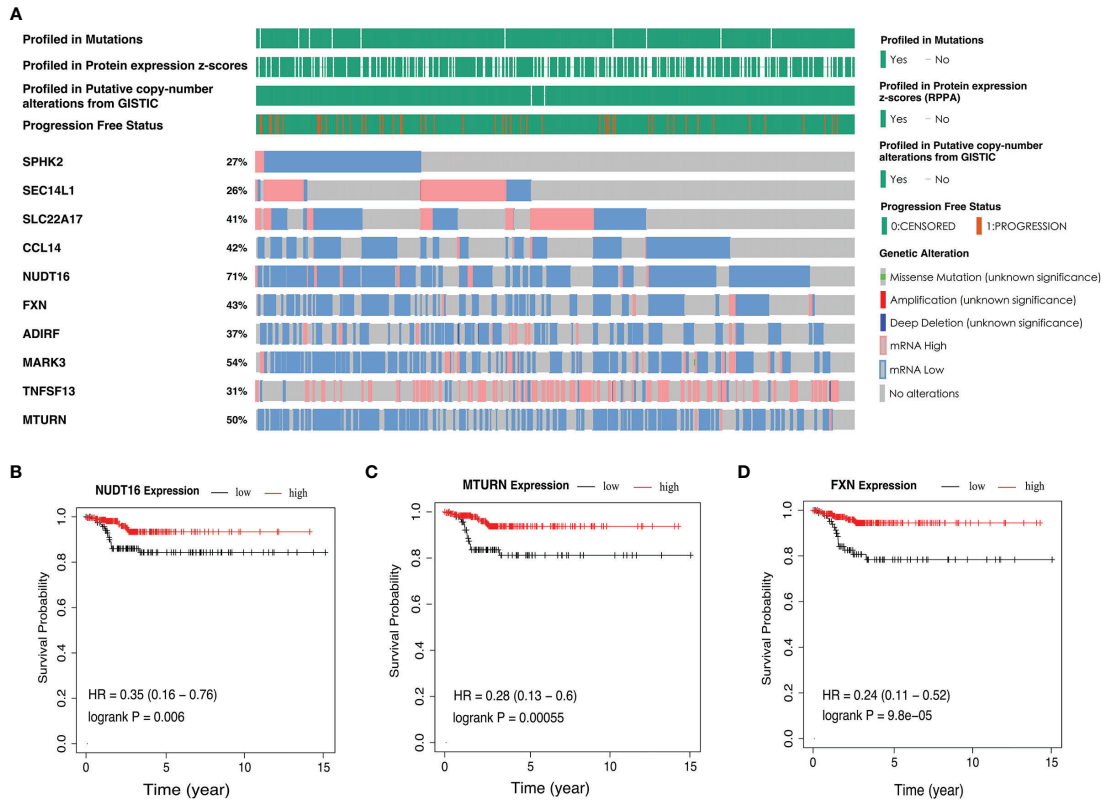

FIGURE 6 | The parent genetic alteration in PTC cases. **(A)** In the PTC cohort, waterfall plot of parent genes variation and expression from the ten-AS models. **(B–D)** Kaplan-Meier survival curves of NUDT16, MTURN and FXN gene expression.

the occurrence and development of human diseases, including PTC. For example, the alternatively spliced variant of thyroid stimulating hormoneβ (TSHβ), TSHβv (exon 2 deleted, exon 3 retained) has been associated with autoimmune thyroiditis in humans, which is also a high-risk factor for thyroid carcinoma (30). Circadian clock-independent AS events that play an important role in the homeostasis of the endocrine system, such as alternatively spliced *Clock* and *Bmal1*, are regulated by thyroid hormone receptor-associated protein 3 (THRAP3) and are closely associated with endocrine diseases including PTC (31, 32). Therefore, we could design different primers to evaluate the presence of AS events and types by PCR experiments and verified them by sanger sequence, which is relatively simple and effective.

In the ten-AS event prognostic prediction signature, some parental genes have been reported to play a key role in oncologic progression. Two spliced variants of *MARK3* (exon 16 included and exon 16 skipped) are differentially expressed by neural progenitors and neuronal cells and contribute to the important molecular regulation of cortical development (33). *TNFSF13*, a tumor necrosis factor, plays a significant role in tumor development and autoimmune diseases, and hypoxia promotes the retention of the intron of *TNFSF13* and suppresses the spliced isoform in MCF7 cells, which may contribute to a tumor suppressor effect (34, 35). *SEC14L1* with 3 alternatively spliced exons spanning exon 11 was specifically expressed in human peripheral blood leukocytes, and different protein isoforms may show differential expression in breast and ovarian cancer development (36). Nonetheless, few studies have reported the functional characteristic and of other parental genes in this prognostic signature. Moreover, we found that changes in the mRNA levels of the parental genes in most PTC samples were associated with patient prognosis. AS events can affect the level of transcription and proteome expression. Whether the change in mRNA levels is caused by the corresponding AS events needs to be verified with further experiments. However, there were no statistically significant associations between some genes and prognosis, and the loss or gain of regions resulting from AS events might produce meaningful biological behaviors. Therefore, the underlying molecular mechanisms of these AS events in the final model is unclear, and further functional experimental research is necessary.

In addition, we also explored the correlation between clinicopathological characteristics and the RFS rate of PTC patients, and the results of the univariate analysis demonstrated that age greater than 55 years, tall cell variant PTC, T3 and T4, lateral neck lymph node metastasis and pathological stage III and IV are indicative of poor prognosis. However, further multivariate analysis showed that the risk score of the ten-AS model was the only independent prognostic factor of PTC. In addition, we found that the subgroup of high-risk AS signatures was associated with

TABLE 3 | Clinicopathology feature of the final AS signature and prognostic analysis in stratified PTC cohorts.

	Low-risk (cases)	High-risk (cases)	P.value	Survival (P.value)
Age			**0.0054**	
<55	159	132		<0.0001
≥55	56	83		<0.0001
Gender			0.126	
Female	151	165		<0.0001
Man	64	50		<0.0001
Subtype			0.538	
Follicular	44	36		<0.0001
Classical	155	163		0.013
Tall Cell	19	16		0.0021
Pathologic T			**0.0087**	
T1	80	48		0.098
T2	62	76		0.0011
T3	64	82		<0.0001
T4	9	9		<0.0001
Pathologic N			0.613	
N0	112	109		<0.0001
N1	27	28		0.03
N1a	46	39		0.0056
N1b	30	39		0.0035
Stage			0.168	
Stage I	132	111		0.0001
Stage II	16	25		0.11
Stage III	46	51		0.0004
Stage IV	21	28		0.001

Variables with statistical significance were shown in bold.

TABLE 4 | Univariate and multivariate Cox regression analysis for clinicopathology variables.

	Univariate analysis			Multivariate analysis		
	HR	**(95% CI)**	**P-value**	**HR**	**(95% CI)**	**P-value**
Age						
<55		Ref			Ref	
≥55	1.75	1.14-2.67	**0.01**	0.68	0.33-1.4	0.296
Gender						
Female		Ref			/	
Man	1.42	0.75-2.68	0.285	/	/	/
Subtype						
Follicular		Ref			Ref	
Classical	1.4	0.54-3.59	0.49	1.22	0.39-3.82	0.731
Tall Cell	3.45	1.09-10.89	**0.035**	2.1	0.47-9.34	0.329
Pathologic T						
T1		Ref			Ref	
T2	2.7	0.87-8.39	0.085	1.26	0.37-4.28	0.71
T3	5.04	1.74-14.59	**0.003**	1.77	0.53-5.91	0.354
T4	6.28	1.56-25.18	**0.01**	1.31	0.22-7.7	0.762
Pathologic N						
N0		Ref			Ref	
N1	2.05	0.89-4.69	0.091	2.14	0.75-6.06	0.153
N1a	1.51	0.66-3.45	0.329	0.99	0.38-2.62	0.99
N1b	2.65	1.19-5.92	**0.017**	2.82	0.96-8.29	0.059
Stage						
Stage I		Ref			Ref	
Stage II	1.05	0.31-3.61	0.935	1.02	0.2-5.15	0.979
Stage III	2.53	1.25-5.12	**0.01**	2.03	0.68-6.11	0.207
Stage IV	3.52	1.55-7.98	**0.003**	0.99	0.29-3.35	0.986
Risk score	16.06	9.58-26.9	**<0.0001**	20	10.23-39.11	**<0.0001**

Variables with statistical significance were shown in bold.

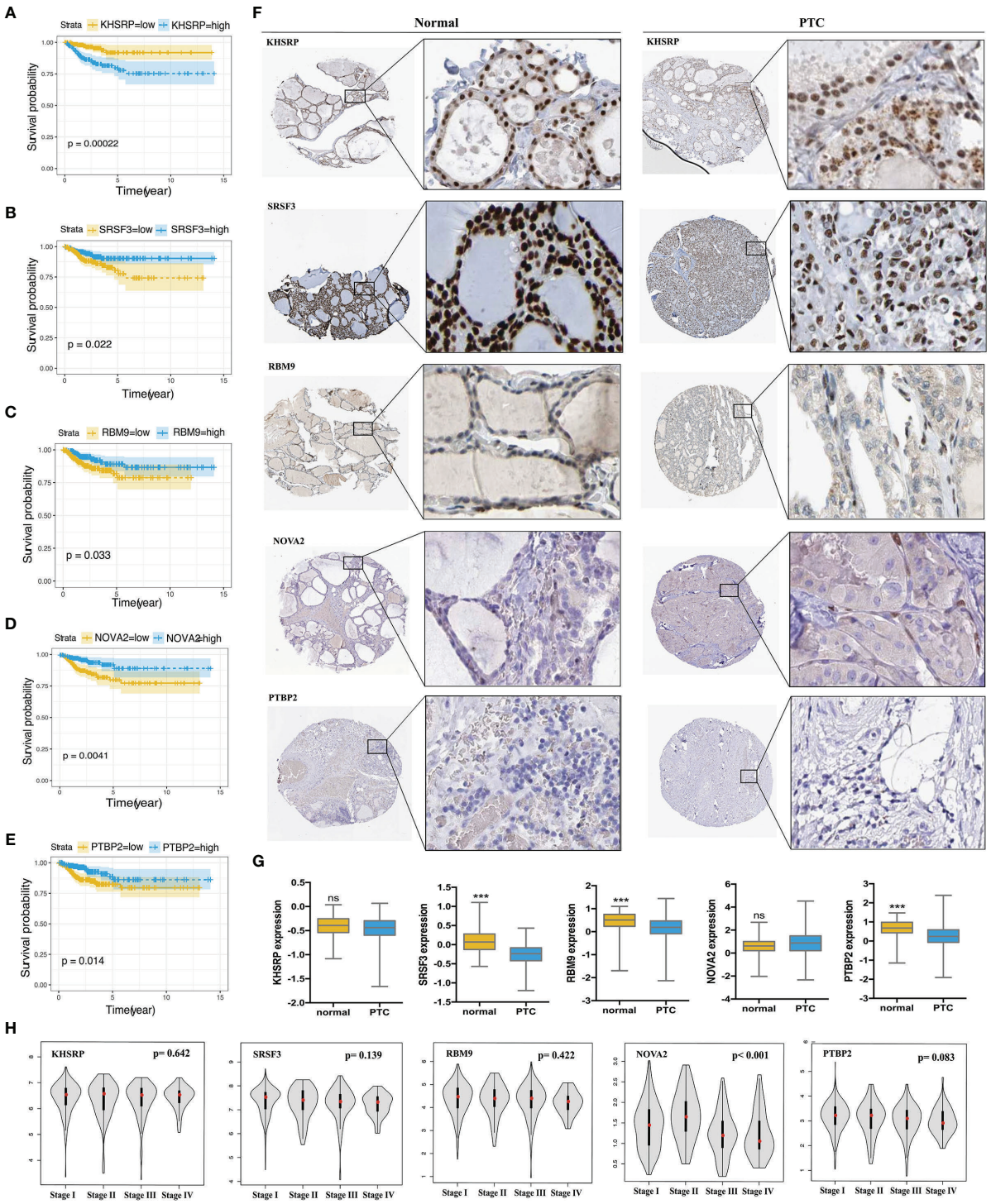

FIGURE 7 | Validation the prognostic correlation of the targeting SFs and the expression in PTC tissues. Kaplan-Meier curves of **(A)** KHSRP **(B)** SRSF3 **(C)** RBM9 **(D)** NOVA2 **(E)** PTBP2 for PTC. **(F)** Immunohistochemistry (IHC) staining shown the expression of KHSRP, SRSF3, RBM9, NOVA2 and PTBP2 in normal thyroid tissues and PTC, data obtained from the HUMAN PROTEIN ATLAS database (HPA, https://www.proteinatlas.org/). **(G)** Comparison of the expression level of KHSRP, SRSF3, RBM9, NOVA2 and PTBP2 in normal thyroid tissues and PTC, data obtained from the Cancer Genome Atlas (TCGA, https://portal.gdc.cancer.gov) Student's t-test, ***p < 0.001; ns mean no significance. **(H)** Comparison of the expression level of KHSRP, SRSF3, RBM9, NOVA2 and PTBP2 in different stage (I, II, III and IV stage) of PTC from GEPAI database (http://gepia.cancer-pku.cn/).

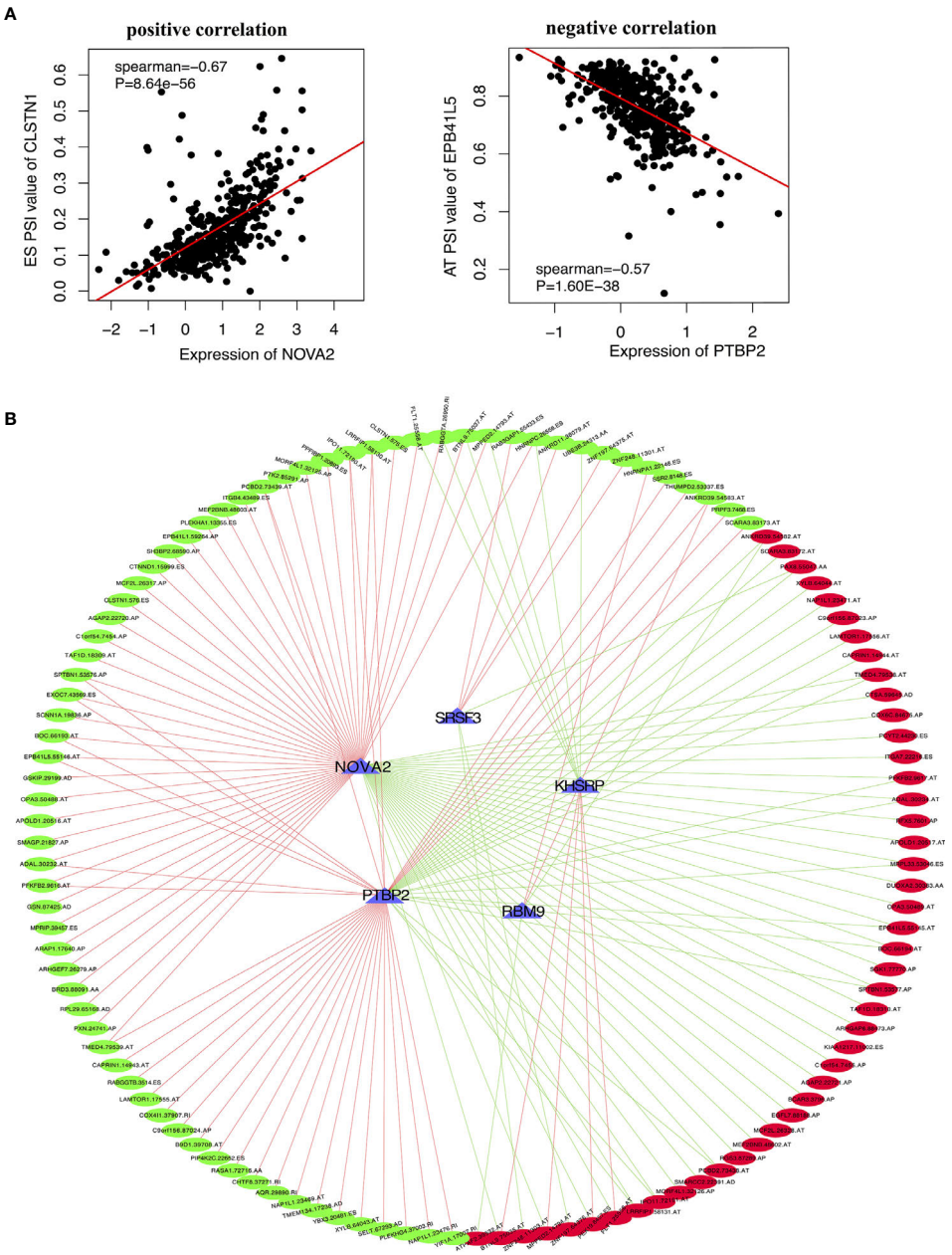

FIGURE 8 | The correlation between the targeting SFs with AS events in PTC. **(A)** Two representative scatter plots showed the relevance between the expression of SFs and AS events, (left) positive correlation between NOVA2 and CLSTN1.575.ES PSI value, (right) negative correlation between PTBP2 and EPB41L5.55145.AT PSI value. **(B)** Interaction network of SF-AS (P<0.05, Spearman>0.4). Blue triangles represent RFS-associated SFs. Red lines represent SFs positively correlated with AS events, and green lines represent SFs negatively correlated with AS events. Red dots represent adverse AS events, and green dots represent favorable AS events.

age and tumor stage, which also showed that tumor-specific AS events play a role in cancer progression and metastasis. Moreover, biological function enrichment and pathway analysis of RFS-related AS events showed that cell-cell adhesion and the transforming growth factor beta receptor signaling pathway promote PTC tumor cell growth, invasion and metastasis (37, 38). KEGG enrichment revealed ribosome and transcriptional mis-regulation in cancer that was associated with the tumorigenesis and prognosis of PTC (39). Therefore, we hypothesized that carcinoma-related outcomes due to changes in AS may involve these pathways.

SFs are the main regulators of AS events and influence splicing sites by recognizing and binding precursor mRNAs. In our study, we identified five SFs related to the prognosis of PTC patients.

KHSRP was reported to be oncogenic in non-small lung cancer, colorectal cancer and PTC (40–42). Overexpression of *KHSRP* activated IFN-αJAK-STAT1 signaling pathway and induced lung cancer cell invasion and metastasis (40). *KHSRP* might be a target mRNA regulated by the STAU1-mediated mRNA decay (SMD) pathway in PTC; however, the detailed mechanism is unclear (41). *NOVA2*, a key AS regulator of vascular morphogenesis, was overexpressed in lung carcinoma but its expression was negatively correlated with the prognosis of PTC patients in our analysis (43, 44). Finally, an obvious trend for SF-AS correlation network that the most of favorable prognostic AS events were positively correlated with the tumor suppressor SFs, while negatively correlated with oncogenic SFs expression, however, there was opposite relationship between adverse AS events and SFs. The role of 5 SFs in PTC and the regulation of alternative splice events remains to be verified by more experiments. This study provides a deeper understanding of the mechanism of SFs in the regulation and associated splicing patterns, which will help us to further explore the potential mechanism of AS events in the development and progression of PTC.

Although well performance of the present model has been watched, some limitations are inevitably existed in this study. First, this research lacks repeatability data that could be obtained from assessing the established prognostic predictors in other independent cohorts of PTC patients. Second, the prognostic significance of these potential therapeutic targets and diagnostic biomarkers for PTC still needs to be validated with further biological function experiments, mouse model and clinical trial. Nevertheless, our comprehensive analysis of recurrence-related SFs and AS events provides new knowledge and a new perspective for studying intrinsic molecular mechanisms and identifying potential therapeutic strategies for PTC.

CONCLUSION

We performed a systematic analysis of AS events in PTC and constructed prognostic signatures that can be used to predict the recurrence-free survival rate for PTC patients. The ten-AS event signature involves genes including *SPHK2*, *SEC14L1*, *SLC22A17*, *CCL14*, *NUDT16*, *FXN*, *ADIRF*, *MARK3*, *TNFSF13* and *MTURN*, which can affect the prognosis and biological progression of PTC. The identification of prognosis-related AS events and SF regulatory network increases the understanding of the underlying mechanisms of PTC development and provides a new avenue for developing treatment strategies.

DATA AVAILABILITY STATEMENT

The original contributions presented in the study are included in the article/**Supplementary Material**. Further inquiries can be directed to the corresponding authors.

AUTHOR CONTRIBUTIONS

Conceptualization, ML, PH, SC, and RK. Resources, RK, ML, PC, HYH, NT, D-jO and BW. Data Curation, ML, RK, PC, HH, D-jO, Y-xZ, and NT. Writing, ML, D-jO and PH. Supervision, D-jO, PH, SC, and RK. Funding Acquisition, PH and SC. All authors contributed to the article and approved the submitted version.

FUNDING

This work was supported by grants from the National Natural Science Foundation of China (81974423, 81902729), the Key Research and Development Programme of Hunan Province (2019SK2031), the Natural Science Foundation of Hunan Province of China (2020JJ5904) and China Postdoctoral Science Foundation (2020M672517).

SUPPLEMENTARY MATERIAL

The Supplementary Material for this article can be found online at: https://www.frontiersin.org/articles/10.3389/fonc.2021.705929/full#supplementary-material

REFERENCES

1. Siegel RL, Miller KD, Jemal A. Cancer Statistics, 2020. *CA Cancer J Clin* (2020) 70(1):7–30. doi: 10.3322/caac.21590
2. Schneider D, Chen H. New Developments in the Diagnosis and Treatment of Thyroid Cancer. *CA Cancer J Clin* (2013) 63(6):374–94. doi: 10.3322/caac.21195
3. Yu X, Wan Y, Sippel RS, Chen H. Should All Papillary Thyroid Microcarcinomas be Aggressively Treated? An Analysis of 18,445 Cases. *Ann Surg* (2011) 254 (4):653–60. doi: 10.1097/SLA.0b013e318230036d
4. Brown R, de Souza J, Cohen E. Thyroid Cancer: Burden of Illness and Management of Disease. *J Cancer* (2011) 2:193–9. doi: 10.7150/jca.2.193
5. Mazzaferri E, Jhiang S. Long-Term Impact of Initial Surgical and Medical Therapy on Papillary and Follicular Thyroid Cancer. *Am J Med* (1994) 97 (5):418–28. doi: 10.1016/0002-9343(94)90321-2
6. Cell J. Integrated Genomic Characterization of Papillary Thyroid Carcinoma. *Cell* (2014) 159(3):676–90. doi: 10.1016/j.cell.2014.09.050
7. Liu M, Chen P, Hu HY, Ou-Yang DJ, Khushbu RA, Tan HL, et al. Kinase Gene Fusions: Roles and Therapeutic Value in Progressive and Refractory Papillary Thyroid Cancer. *J Cancer Res Clin Oncol* (2021) 147(2):323–37. doi: 10.1007/s00432-020-03491-5
8. Keren H, Lev-Maor G, Ast G. Alternative Splicing and Evolution: Diversification, Exon Definition and Function. *Nat Rev Genet* (2010) 11 (5):345–55. doi: 10.1038/nrg2776
9. Tress M, Abascal F, Valencia A. Alternative Splicing May Not Be the Key to Proteome Complexity. *Trends Biochem Sci* (2017) 42(2):98–110. doi: 10.1016/j.tibs.2016.08.008
10. Matera A, Wang Z. A Day in the Life of the Spliceosome. *Nat Rev Mol Cell Biol* (2014) 15(2):108–21. doi: 10.1038/nrm3742
11. Kahles A, Lehmann K, Toussaint N, Hüser M, Stark S, Sachsenberg T, et al. Comprehensive Analysis of Alternative Splicing Across Tumors From 8,705 Patients. *Cancer Cell* (2018) 34(2):211–24.e6. doi: 10.1016/j.ccell.2018.07.001
12. Dvinge H, Guenthoer J, Porter P, Bradley R. RNA Components of the Spliceosome Regulate Tissue- and Cancer-Specific Alternative Splicing. *Genome Res* (2019) 29(10):1591–604. doi: 10.1101/gr.246678.118
13. Bonnal S, López-Oreja I, Valcárcel J. Roles and Mechanisms of Alternative Splicing in Cancer - Implications for Care. *Nat Rev Clin Oncol* (2020) 17 (8):457–74. doi: 10.1038/s41571-020-0350-x

14. Zeng J, Xu H, Huang C, Sun Y, Xiao H, Yu G, et al. CD46 Splice Variant Enhances Translation of Specific mRNAs Linked to an Aggressive Tumor Cell Phenotype in Bladder Cancer. *Mol Ther Nucleic Acids* (2021) 24:140–53. doi: 10.1016/j.omtn.2021.02.019
15. Zhang N, Yan Q, Lu L, Shao J, Sun Z. The KLF6 Splice Variant KLF6-SV1 Promotes Proliferation and Invasion of non-Small Cell Lung Cancer by Up-Regultating PI3K-AKT Signaling Pathway. *J Cancer* (2019) 10(22):5324–31. doi: 10.7150/jca.34212
16. Hu K, Zheng QK, Ma RJ, Ma C, Sun ZG, Zhang N. Kruppel-Like Factor 6 Splice Variant 1: An Oncogenic Transcription Factor Involved in the Progression of Multiple Malignant Tumors. *Front Cell Dev Biol* (2021) 9:661731. doi: 10.3389/fcell.2021.661731
17. Lopez-Canovas JL, Del Rio-Moreno M, Garcia-Fernandez H, Jimenez-Vacas JM, Moreno-Montilla MT, Sanchez-Frias ME, et al. Splicing Factor SF3B1 Is Overexpressed and Implicated in the Aggressiveness and Survival of Hepatocellular Carcinoma. *Cancer Lett* (2021) 496:72–83. doi: 10.1016/j.canlet.2020.10.010
18. Wang Y, Bernhardy AJ, Cruz C, Krais JJ, Nacson J, Nicolas E, et al. The BRCA1-Delta11q Alternative Splice Isoform Bypasses Germline Mutations and Promotes Therapeutic Resistance to PARP Inhibition and Cisplatin. *Cancer Res* (2016) 76(9):2778–90. doi: 10.1158/0008-5472.CAN-16-0186
19. Gelli E, Colombo M, Pinto AM, De Vecchi G, Foglia C, Amitrano S, et al. Usefulness and Limitations of Comprehensive Characterization of mRNA Splicing Profiles in the Definition of the Clinical Relevance of BRCA1/2 Variants of Uncertain Significance. *Cancers (Basel)* (2019) 11(3):295. doi: 10.3390/cancers11030295
20. Liang W, Sun F. Prognostic Alternative mRNA Splicing in Adrenocortical Carcinoma. *Front Endocrinol (Lausanne)* (2021) 12:538364. doi: 10.3389/fendo.2021.538364
21. Zhao J, Chang L, Gu X, Liu J, Sun B, Wei X. Systematic Profiling of Alternative Splicing Signature Reveals Prognostic Predictor for Prostate Cancer. *Cancer Sci* (2020) 111(8):3020–31. doi: 10.1111/cas.14525
22. Ouyang D, Yang P, Cai J, Sun S, Wang Z. Comprehensive Analysis of Prognostic Alternative Splicing Signature in Cervical Cancer. *Cancer Cell Int* (2020) 20:221. doi: 10.1186/s12935-020-01299-4
23. Tripathi V, Ellis J, Shen Z, Song D, Pan Q, Watt A, et al. The Nuclear-Retained Noncoding RNA MALAT1 Regulates Alternative Splicing by Modulating SR Splicing Factor Phosphorylation. *Mol Cell* (2010) 39(6):925–38. doi: 10.1016/j.molcel.2010.08.011
24. Ladomery M. Aberrant Alternative Splicing Is Another Hallmark of Cancer. *Int J Cell Biol* (2013) 2013:463786. doi: 10.1155/2013/463786
25. de Klerk E, t Hoen P. Alternative mRNA Transcription, Processing, and Translation: Insights From RNA Sequencing. *Trends Genet* (2015) 31(3):128–39. doi: 10.1016/j.tig.2015.01.001
26. Katz Y, Wang E, Airoldi E, Burge C. Analysis and Design of RNA Sequencing Experiments for Identifying Isoform Regulation. *Nat Methods* (2010) 7 (12):1009–15. doi: 10.1038/nmeth.1528
27. Ryan M, Wong W, Brown R, Akbani R, Su X, Broom B, et al. TCGASpliceSeq a Compendium of Alternative mRNA Splicing in Cancer. *Nucleic Acids Res* (2016) 44:D1018–22. doi: 10.1093/nar/gkv1288
28. Chen Y, Jiang B, Wang W, Su D, Xia F, Li X. Identifying the Transcriptional Regulatory Network Associated With Extrathyroidal Extension in Papillary Thyroid Carcinoma by Comprehensive Bioinformatics Analysis. *Front Genet* (2020) 11:453. doi: 10.3389/fgene.2020.00453
29. Wang X, Fu X, Zhang J, Xiong C, Zhang S, Lv Y. Identification and Validation of M(6)A RNA Methylation Regulators With Clinical Prognostic Value in Papillary Thyroid Cancer. *Cancer Cell Int* (2020) 20:203. doi: 10.1186/s12935-020-01283-y
30. Klein J. Novel Splicing of Immune System Thyroid Stimulating Hormone β-Subunit-Genetic Regulation and Biological Importance. *Front Endocrinol (Lausanne)* (2019) 10:44. doi: 10.3389/fendo.2019.00044
31. Zhang D, Jones R, James P, Kitahara C, Xiao Q. Associations Between Artificial Light at Night and Risk for Thyroid Cancer: A Large US Cohort Study. *Cancer* (2021) 127(9):1448–58. doi: 10.1002/cncr.33392
32. Marcheva B, Perelis M, Weidemann BJ, Taguchi A, Lin H, Omura C, et al. A Role for Alternative Splicing in Circadian Control of Exocytosis and Glucose Homeostasis. *Genes Dev* (2020) 34(15-16):1089–105. doi: 10.1101/gad.338178.120
33. Liu J, Geng A, Wu X, Lin R, Lu Q. Alternative RNA Splicing Associated With Mammalian Neuronal Differentiation. *Cerebral Cortex* (2018) 28(8):2810–6. doi: 10.1093/cercor/bhx160
34. Xiao Y, Motomura S, Podack E. APRIL (TNFSF13) Regulates Collagen-Induced Arthritis, IL-17 Production and Th2 Response. *Eur J Immunol* (2008) 38(12):3450–8. doi: 10.1002/eji.200838640
35. Han J, Li J, Ho JC, Chia GS, Kato H, Jha S, et al. Hypoxia Is a Key Driver of Alternative Splicing in Human Breast Cancer Cells. *Sci Rep* (2017) 7(1):4108. doi: 10.1038/s41598-017-04333-0
36. Kalikin LM, Bugeaud EM, Palmbos PL, Lyons RH Jr, Petty EM. Genomic Characterization of Human SEC14L1 Splice Variants Within a 17q25 Candidate Tumor Suppressor Gene Region and Identification of an Unrelated Embedded Expressed Sequence Tag. *Mamm Genome* (2001) 12 (12):925–9. doi: 10.1007/s00335-001-2073-3
37. Vasko V, Espinosa A, Scouten W, He H, Auer H, Liyanarachchi S, et al. Gene Expression and Functional Evidence of Epithelial-to-Mesenchymal Transition in Papillary Thyroid Carcinoma Invasion. *Proc Natl Acad Sci U S A* (2007) 104 (8):2803–8. doi: 10.1073/pnas.0610733104
38. He J, Jin Y, Zhou M, Li X, Chen W, Wang Y, et al. Solute Carrier Family 35 Member F2 Is Indispensable for Papillary Thyroid Carcinoma Progression Through Activation of Transforming Growth Factor-β Type I Receptor/Apoptosis Signal-Regulating Kinase 1/Mitogen-Activated Protein Kinase Signaling Axis. *Cancer Sci* (2018) 109(3):642–55. doi: 10.1111/cas.13478
39. Jeong S, Kim I, Kim H, Choi M, Lee J, Jo YJE, et al. Liver X Receptor β Related to Tumor Progression and Ribosome Gene Expression in Papillary Thyroid Cancer. *Endocrinol Metab (Seoul)* (2020) 35(3):656–68. doi: 10.3803/EnM.2020.667
40. Yan M, Sun L, Li J, Yu H, Lin H, Yu T, et al. RNA-Binding Protein KHSRP Promotes Tumor Growth and Metastasis in non-Small Cell Lung Cancer. *J Exp Clin Cancer Res* (2019) 38(1):478. doi: 10.1186/s13046-019-1479-2
41. Gou Q, Gao L, Nie X, Pu W, Zhu J, Wang Y, et al. Long Noncoding RNA AB074169 Inhibits Cell Proliferation via Modulation of KHSRP-Mediated CDKN1a Expression in Papillary Thyroid Carcinoma. *Cancer Res* (2018) 78 (15):4163–74. doi: 10.1158/0008-5472.CAN-17-3766
42. Caiazza F, Oficjalska K, Tosetto M, Phelan J, Noonan S, Martin P, et al. KH-Type Splicing Regulatory Protein Controls Colorectal Cancer Cell Growth and Modulates the Tumor Microenvironment. *Am J Pathol* (2019) 189(10):1916–32. doi: 10.1016/j.ajpath.2019.07.004
43. Angiolini F, Belloni E, Giordano M, Campioni M, Forneris F, Paronetto M, et al. A Novel L1CAM Isoform With Angiogenic Activity Generated by NOVA2-Mediated Alternative Splicing. *eLife* (2019) 8:e44305. doi: 10.7554/eLife.44305
44. Li C, Liu H, Niu Q, Gao JJC. Circ_0000376, a Novel circRNA, Promotes the Progression of Non-Small Cell Lung Cancer Through Regulating the miR-1182/NOVA2 Network. *Cancer Manag Res* (2020) 12:7635–47. doi: 10.2147/cmar.S258340

Conflict of Interest: The authors declare that the research was conducted in the absence of any commercial or financial relationships that could be construed as a potential conflict of interest.

The handling editor declared a shared affiliation with the authors at time of review.

frontiers in Oncology

ORIGINAL RESEARCH
published: 13 October 2021
doi: 10.3389/fonc.2021.698870

Nomogram Predicting Cancer-Specific Death in Parotid Carcinoma: a Competing Risk Analysis

Xiancai Li[1,2†], *Mingbin Hu*[1†], *Weiguo Gu*[1†], *Dewu Liu*[2*], *Jinhong Mei*[3*] *and Shaoqing Chen*[1*]

[1] Department of Oncology, The First Affiliated Hospital of Nanchang University, Nanchang, China, [2] Department of Burn, The First Affiliated Hospital of Nanchang University, Nanchang, China, [3] Department of Pathology, The First Affiliated Hospital of Nanchang University, Nanchang, China

OPEN ACCESS

Edited by:
Yong Yin,
Shandong Cancer Hospital, China

Reviewed by:
Peiguo Wang,
Tianjin Medical University Cancer Institute and Hospital, China
Jingao Li,
Jiangxi Provincial Cancer Hospital, China

***Correspondence:**
Shaoqing Chen
1075017867@qq.com
Jinhong Mei
mjhdoctor@126.com
Dewu Liu
dewuliu2@126.com

[†]These authors have contributed equally to this work

Specialty section:
This article was submitted to Head and Neck Cancer, a section of the journal Frontiers in Oncology

Received: 22 April 2021
Accepted: 17 September 2021
Published: 13 October 2021

Citation:
Li X, Hu M, Gu W, Liu D, Mei J and Chen S (2021) Nomogram Predicting Cancer-Specific Death in Parotid Carcinoma: a Competing Risk Analysis. Front. Oncol. 11:698870. doi: 10.3389/fonc.2021.698870

Purpose: Multiple factors have been shown to be tied to the prognosis of individuals with parotid cancer (PC); however, there are limited numbers of reliable as well as straightforward tools available for clinical estimation of individualized mortality. Here, a competing risk nomogram was established to assess the risk of cancer-specific deaths (CSD) in individuals with PC.

Methods: Data of PC patients analyzed in this work were retrieved from the Surveillance, Epidemiology, and End Results (SEER) data repository and the First Affiliated Hospital of Nanchang University (China). Univariate Lasso regression coupled with multivariate Cox assessments were adopted to explore the predictive factors influencing CSD. The cumulative incidence function (CIF) coupled with the Fine-Gray proportional hazards model was employed to determine the risk indicators tied to CSD as per the univariate, as well as multivariate analyses conducted in the R software. Finally, we created and validated a nomogram to forecast the 3- and 5-year CSD likelihood.

Results: Overall, 1,467 PC patients were identified from the SEER data repository, with the 3- and 5-year CSD CIF after diagnosis being 21.4% and 24.1%, respectively. The univariate along with the Lasso regression data revealed that nine independent risk factors were tied to CSD in the test dataset (n = 1,035) retrieved from the SEER data repository. Additionally, multivariate data of Fine-Gray proportional subdistribution hazards model illustrated that N stage, Age, T stage, Histologic, M stage, grade, surgery, and radiation were independent risk factors influencing CSD in an individual with PC in the test dataset ($p < 0.05$). Based on optimization performed using the Bayesian information criterion (BIC), six variables were incorporated in the prognostic nomogram. In the internal SEER data repository verification dataset (n = 432) and the external medical center verification dataset (n = 473), our nomogram was well calibrated and exhibited considerable estimation efficiency.

Conclusion: The competing risk nomogram presented here can be used for assessing cancer-specific mortality in PC patients.

Keywords: SEER, parotid cancer, cancer-specific death, competing risk, nomogram

INTRODUCTION

Parotid cancers are responsible for about 70% of malignant tumors in the salivary gland, characterized by pathological/histological differences (1, 2). The present crude incidence of primary cancers of the salivary is 0.9 per 100,000, of which approximately 80% of these cases arise in the parotid salivary gland (3). The prognosis of individuals with PC differs significantly, with some clinical features considerably influencing the disease-free survival (DSF) along with (OS) overall survival. Its mortality rate has remained the same over the past decade, with a 5-year OS of approximately 60% dependent on the histological type, as well as the anatomical site, and specifically the treatment option (4, 5). Presently, the AJCC staging criteria are the main approach to estimating prognosis in individuals with parotid cancer. Nonetheless, remarkable differences in the clinical outcomes among individuals with parotid cancer at the same stage receiving similar treatments have been reported (6). This demonstrates that the AJCC staging method is far from being a perfect system for making a prognosis, as well as treatment decisions. Such a method is only ideal for estimating distant metastasis (M stage), tumor size along with extension (T stage), and lymph node (LN) involvement without taking into account other factors, e.g., histological types, demographical factors, and treatments. Recently, numerous researches have documented the prognosis of common head and neck cancer, such as laryngeal carcinoma (7) and nasopharyngeal carcinoma (8), but few have addressed PC. The survival of individuals with PC has been investigated by other research groups; nonetheless, most investigations are from single institutions lacking the assessment of CSD risk factors. Hence, it is pivotal to conduct more research on PC prognosis.

Surveillance, Epidemiology, and End Results (SEER), a data repository based on populations, represents an estimated 28% of the US population. Therefore, the datasets retrieved from the SEER data repository provide adequate cases of creating prognostic models, particularly for rare cancers (9). The data of PC cases utilized in this research were retrieved from the SEER data repository, which can guarantee the authenticity and sufficiency of the data. Overall, cancer patients frequently experience more than two events, but only one event occurs (10). The events excluding that of interest are termed as competing risks. In traditional survival assessment, censoring of competing risks is done and can be enhanced through competing risk assessment.

A nomogram visualizes the linear prognosis of a disease (11). Each characteristic value on the nomogram plot signifies a score, with the total score mapping the survival estimate. In many studies, survival outcomes are determined using the Kaplan-Meier approach coupled with the Cox proportional hazard, although the population-based approaches are also applied (12, 13). Nonetheless, a significance of the studies analyzed the OS along with the cancer-specific survival assessment, while neglecting the role played by other competing causes of death in the prognosis of nonmetastatic PC. Prolonged survival is dependent on the competing risks of death to a remarkable degree. The competing risk should be considered when forecasting survival outcomes.

In this work, we aimed to construct a competing risk nomogram using data retrieved from the SEER data repository to assist in predicting death linked to PC. The nomogram will help clinicians in making patient-specific decisions in treating PC as well as precise predictions of disease outcomes.

MATERIAL AND METHODS

SEER Database Patients

We retrospectively analyzed data from the SEER data repository spanning from 1992 to 2017. The SEER data repository (https://seer.cancer.gov/) is publicly accessible.

A selection of SEER 13 Regs Custom Data (with additional treatment fields) uploaded in November 2019 (1992–2017 varying) was done. All subjects with primary PC diagnosis (site recode NM7/CS v0204+ Schema of "parotid gland" along with the ICD-O-3 behavior recode of "malignant") were enrolled in the analysis. Exclusion criteria consisted of PC individuals who were less than 5 years old, those with a survival time of ≤1 month, and patients lacking complete data or a pathological diagnosis.

Our Medical Center Patients

We collected data from 473 individuals with PC who were admitted to the First Affiliated Hospital of Nanchang University (China) spanning from 2006 to 2017. The subjects confirmed by pathology had no history of other malignant tumors. The Ethics Committee of the First Affiliated Hospital of Nanchang University approved this retrospective cohort study. The principles of the Helsinki Declaration were followed with regards to data confidentiality.

Variable Selection

Factors including age, T stage, AJCC stage, N stage, race, M stage, sex, histological type, surgery, radiation, grade, follow-up time, and survival outcomes were retrieved from the SEER data repository. We adopted the X-tile software to determine the optimal threshold values. The age of the subjects at diagnosis was classified into two classes, i.e., ≥70 and <70 years. The AJCC stage was employed as the staging approach. The ICD-O-3 codes were adopted to categorize the PC histological type into two classes, i.e., mucoepidermoid carcinoma (MEC) and none MEC (squamous cell carcinoma, myoepithelial carcinoma, polymorphous adenocarcinoma NOS, adenoid cystic carcinoma, and acinic cell carcinoma, among others) as per the WHO categorization approach. Cancer-distinct survival constituted the primary end-point and included the time beginning from cancer diagnosis to death emerging from PC or a censored risk. Deaths linked to accidents or diseases excluding PC constituted the competition risks.

Statistical Analyses

We conducted all the analysis using R (V.4.0.4: survivial, crrstep, cmprsk, pec, rms, riskRegression, mstate, and foreign packages) to perform the statistical analyses. Two-sided and $p < 0.05$

defined statistical significance. Firstly, we computed the CIF for 3 to 5 years. We further carried out subgroup analysis between diverse subgroups, and matching CIF curves were created for these variables. Gray's test was implemented to determine the drastic differences in values of CIF among subgroups. Secondly, patients from the SEER data repository were split at random into a test data set along with the verification data set, with a 7:3 ratio. Patients recruited from our hospital served as the external verification dataset. The test dataset was employed to create the prediction nomogram for estimating of CSD, whereas the verification datasets were employed to validate the efficiency of our nomogram. Univariate coupled with the Lasso Cox regression model assessments were implemented to explore the independent predictors of CSDs in the test dataset. All different variables were further identified by AIC and BIC models. The Fine-Gray proportional hazards model was adopted to develop the competing risk nomogram.

The performance of our nomogram was first explored in the test cohort and subsequently in the verification cohorts with respect to the C-index, AUC, and the calibration curve. The estimation capacity of our nomogram was quantified with the C-index and ranged from 0.5 to 1.0, representing a random probability from indicating no discrimination to indicating optimal discrimination (14). The AUC reflects the overall estimation value for all the thresholds (15), with a perfect prediction value exhibiting an AUC of 1.0. We adopted decision curve analysis (DCA) to determine the clinical net benefit of different probability thresholds for a possible clinical consequence (16) and explored the nomogram efficiency in contrast with the AJCC staging approach visually.

RESULTS

Baseline Features of Participants

As illustrated in **Figure 1**, we initially retrieved 2,304 patient cases from the SEER data repository. Strict screening was carried out, yielding 1,467 patient cases with PC who were recruited in the study. The subjects' median age was 50.7 years (5–85) at diagnosis with males accounting for 43.6%. Most participants were white (n = 1,142, 77.8%). Of the 1,467 PC cases, 621 (42.3%) were MEC, consisting of 599 (40.8%) incidences of moderate differentiation. Besides, stage I constituted the most frequent tumor stage (n = 454, 30.9%), followed by stages IV (n = 420, 28.6%), II (n = 334, 22.8%), and III (n = 259, 17.7%). Most PC subjects were classified as T1 (35.0%), followed by T2 (28.9%), T3 (19.9%), and T4 (16.2%). More than half of the PC subjects lacked lymph node (LN) metastases (N0, 72.1%), and most patients did not exhibit distant metastases (M0, 96.4%). A significant number of the PC individuals were treated using surgical therapy (n = 1,375, 93.7%) and 35.5% of the patients received radiotherapy. The detailed demographic, as well as clinical characteristics of the recruited participants, are given in **Table 1**.

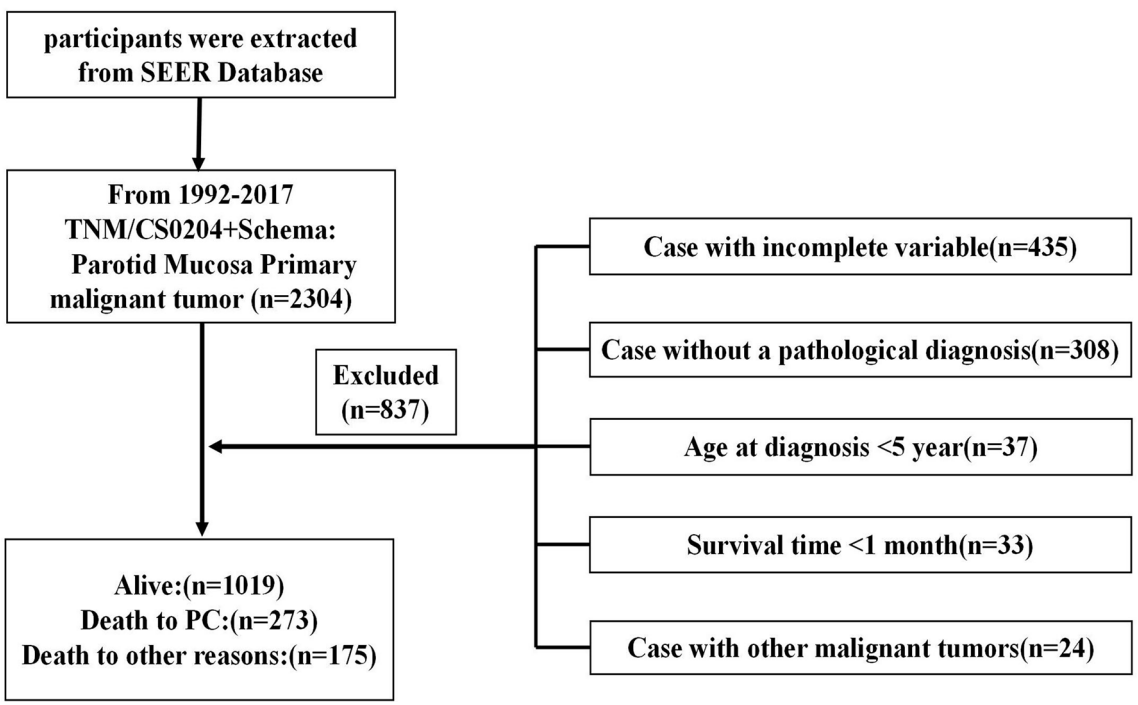

FIGURE 1 | Flow diagram illustrating recruitment of patients. SEER, Surveillance, Epidemiology, and End Results; PC, parotid cancer.

CIF Survival Analysis

The median follow-up time was 43 months (1–95) based on the results of the nomogram (**Table 2**). In total, 448 patients (30.5%) had died by the end of follow-up, among which 273 (60.9%) patients died from cancer and 175 (39.1%) patients died from other causes. The 3- and 5-year CSD CIF was 21.4% and 24.1%, respectively. The CIF subgroup assessment data exhibited that high CSD majorly occurred in individuals with PC aged ≥70 years (**Figure 2A**) with advanced AJCC stage (**Figure 2B**), advanced T stage (**Figure 2C**), advanced N stage (**Figure 2D**), along with M1 stage (**Figure 2E**), as well as the patients who did not undergo surgical treatment (**Figure 2F**), radiation treatment (**Figure 2H**), and with undifferentiated/poor grade (**Figure 2G**) and MEC (**Figure 2I**). Nevertheless, no considerable difference in CSD was reported and race and sex subgroup assessments (**Figures 2J, K**).

Nomogram Development

As illustrated in **Table 1**, the patients from the SEER data repository were stratified at random into a test group (n = 1,035) and a verification group (n = 432) at a ratio of 7:3. We implemented univariate and Lasso Cox assessments in the test dataset to determine independent predictors affecting CDS. A total of nine predictive factors (AJCC stage, surgery, age, T stage, M stage, grade, N stage, histologic, and radiation) were incorporated in the predictive model (**Figures 3A, B**). All variables were further identified by the multivariate assessment of Fine-Gray proportional subdistribution hazards model. As per the AIC assessment, age, T stage, surgery, N stage, histologic, M stage, grade, as well as radiation were independent predictors influencing cancer-distinct death in individuals with PC of the test cohort ($p < 0.05$). Following the optimization of the nomogram as per the BIC, we finally incorporated six variables

TABLE 1 | Basic characteristics of parotid cancer patients in the training, internal validation, and external validation cohorts.

Characteristics	SEER database		Our medical center
	Training cohort (n = 1,035) n (%)	Internal validation cohort (n = 432) n (%)	External validation cohort (n = 473) n (%)
Age (years)			
<70	689 (66.6)	291 (67.4)	416 (87.9)
≥70	346 (33.4)	141 (32.6)	57 (12.1)
Race			
White	795 (76.8)	347 (80.3)	
Black	93 (9.0)	37 (8.6)	
Others	147 (14.2)	48 (11.1)	473 (100.0)
Sex			
Male	446 (43.1)	193 (44.7)	261 (55.2)
Female	589 (56.9)	239 (55.3)	212 (44.8)
AJCC stage			
I	331 (32.0)	123 (28.5)	123 (26)
II	228 (22.0)	106 (24.5)	184 (38.9)
III	176 (17.0)	83 (19.2)	121 (25.6)
IV	300 (29.0)	120 (27.8)	45 (9.5)
T stage			
T1	365 (35.3)	149 (34.5)	119 (25.2)
T2	291 (28.1)	134 (31.0)	201 (42.5)
T3	206 (19.9)	86 (19.9)	126 (26.6)
T4	173 (16.7)	63 (14.6)	27 (5.7)
N stage			
N0	747 (72.2)	311 (72.0)	375 (79.3)
N1	110 (10.6)	49 (11.3)	61 (12.9)
N2	178 (17.2)	72 (16.7)	37 (7.8)
M stage			
M0	997 (96.3)	417 (96.5)	462 (97.7)
M1	38 (3.7)	15 (3.5)	11 (2.3)
Surgery			
No	64 (6.2)	28 (6.5)	14 (3.0)
Yes	971 (93.8)	404 (93.5)	459 (97.0)
Grade			
Well	241 (23.3)	94 (21.8)	207 (43.8)
Moderate	422 (40.8)	177 (41.0)	89 (18.8)
Poorly/undifferentiated	372 (35.9)	161 (37.3)	177 (37.4)
Radiation			
No	668 (64.5)	278 (64.4)	263 (55.6)
Yes	367 (35.5)	154 (35.6)	210 (44.4)
Histologic type			
MEC	445 (43)	176 (40.7)	185 (39.1)
No-MEC	590 (57)	256 (59.3)	288 (60.9)

TABLE 2 | Cumulative incidence of cancer-specific death in parotid cancer.

Characteristics	Total number of patients (*n* = 1,467)	Cumulative incidence		*p*-value
		3 years	5 years	
Age (years)				<0.001
<70	980	11.8%	14.3%	
≥70	487	27.9%	29.9%	
Race				0.556
White	130	8.9%	11.1%	
Black	195	17.1%	19.3%	
Others	1,142	13.9%	15.0%	
Sex				0.282
Male	639	10.3%	11.4%	
Female	828	12.4%	14.9%	
AJCC stage				<0.001
I	454	2.0%	2.8%	
II	334	6.1%	6.6%	
III	259	18.0%	21.9%	
IV	420	41.8%	46.4%	
T stage				<0.001
T1	514	2.6%	3.7%	
T2	425	12.7%	13.5%	
T3	292	26.8%	31.8%	
T4	236	44.7%	49.2%	
N stage				<0.001
N0	1,058	8.8%	10.5%	
N1	159	32.1%	33.3%	
N2	250	43.0%	49.0%	
M stage				<0.001
M0	1,414	15.2%	17.5%	
M1	53	74.0%	81.6%	
Surgery				<0.001
No	92	51.6%	55.9%	
Yes	1,375	14.9%	17.1%	
Grade				<0.001
Well	599	0.9%	0.9%	
Moderate	533	11.2%	13.2%	
Poorly/undifferentiated	335	34.3%	38.7%	
Radiation				<0.001
No	946	5.5%	7.1%	
Yes	521	38.2%	42.0%	
Histology type				<0.001
MEC	521	15.1%	17.0%	
No-MEC	846	19.1%	21.9%	

in the estimation model (**Table 3**). A competing event nomogram was created to assess the 3- and 5-year chances of CSD by using these variables (**Figure 4**). Each patient's likelihood of death caused by PC at various time points was computed *via* this model through the addition of the scores of each of the integrated variables.

Nomogram Verification

The C-indexes of the developed nomogram for prediction of the likelihood of CSD in the test data set were 0.862, and the internal verification datasets were 0.843 and 0.795 in the external verification. The AUC of the competing risk nomogram model for forecasting 3- and 5-year likelihoods of CSD was 0.851 and 0.861 in the test cohort, 0.834 and 0.843 in the internal verification cohort, and 0.761 and 0.751 in the external verification cohort. The calibration plots demonstrated optimal consistency of the actual likelihood with the nomogram-forecasted likelihoods in the test (**Figures 5A, D**), as well as verification datasets (**Figures 5B, C, E, F**). The above data illustrated the good estimation potential along with the high confidence of our nomogram.

Decision Curve Analysis

The DCA was carried out in the test, internal verification, and external verification datasets. The estimation model exhibited an elevated net benefit coupled with a wide range of cutoff likelihood in contrast with the AJCC categorization criteria, illustrating that our prognostic model exhibited a high clinical application value (**Figures 6A–F**).

DISCUSSION

Salivary gland tumors (SGT) are rare, representing less than 3% of all head and neck tumors (17). On the basis of literature, 22%–35% of SGT are malignant, with the percentage of malignant

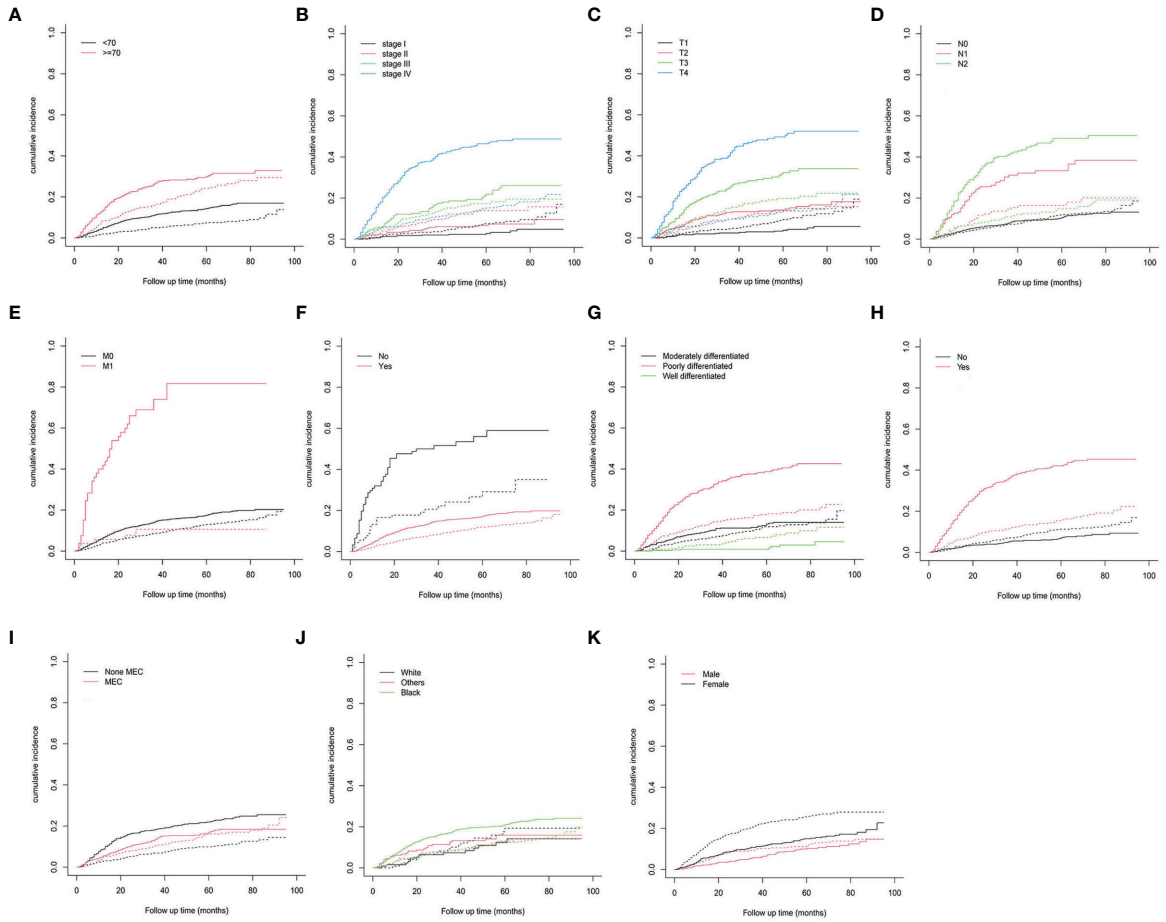

FIGURE 2 | Cumulative incidence predictions of CSD in parotid carcinoma. **(A)** Age; **(B)** AJCC stage; **(C)** T stage; **(D)** N stage; **(E)** M stage; **(F)** surgery; **(G)** grade; **(H)** radiation; **(I)** histologic type; **(J)** race; **(K)** sex. Solid line designates CSD; dotted line designates other causes of death. AJCC, American Joint Committee on Cancer; MEC, mucoepidermoid carcinoma.

SGT in the parotid being 15%–25% (1, 18). The pathological types of PC are very complex. Different types of tumors have different clinical and imaging manifestations, treatment, and prognosis. Herein, for the first time, a nomogram for the prognosis of persons with PC was created in a competitive risk nomogram and determined more precise indicators. The large-sized samples available in the SEER data repository reduce errors in this research. Relative to prevailing tools for assessing survival outcomes, the developed nomogram ensures that the chosen variables can be directly associated with a prognosis of cancer. Currently, the most widely used prognostic tool for all solid tumors, including salivary gland tumors, is the TNM staging system (19), but this staging system did not include treatment options such as surgery, chemotherapy, and radiotherapy. However, a nomogram can allow individualized examination of patient prognosis since it incorporates numerous variables.

Of the 11 variables determined in this study, these predictors have been proven in other studies (20, 21). Nine (age, AJCC stage, radiation, T stage, M stage, grade, surgery, N stage, and histological type) were established as indicators of CSD in persons with PC *via* univariate coupled with the Lasso Cox regression model competing risk assessment. Sex and race were excluded in the univariate assessment, illustrating that they do not influence CSD in persons with PC. Assessment of multiple variables using the competing nomogram showed that the AJCC stage was not an independent indicator of patient prognosis. Finally, six variables (age, T stage, M stage, surgery, radiation, and grade) were used to construct the nomogram.

Similar to a study by Sun et al., age was found to independently influence the prognosis of parotid gland mucoepidermoid carcinoma (20). Lyu et al. investigated staging of PC and documented that patient age, favoring 40–60-year-old patients, which is a considerable independent indicator after adjusting for other confounders, might be because older patients have more comorbidities coupled with elevated perioperative risks (22, 23). This finding was congruent with Sun et al. who documented that the prognosis was not remarkably different across races (20) and survival differences between races are not remarkable. Fang et al. documented that sex had no effect on cancer-distinct survival of PC patients,

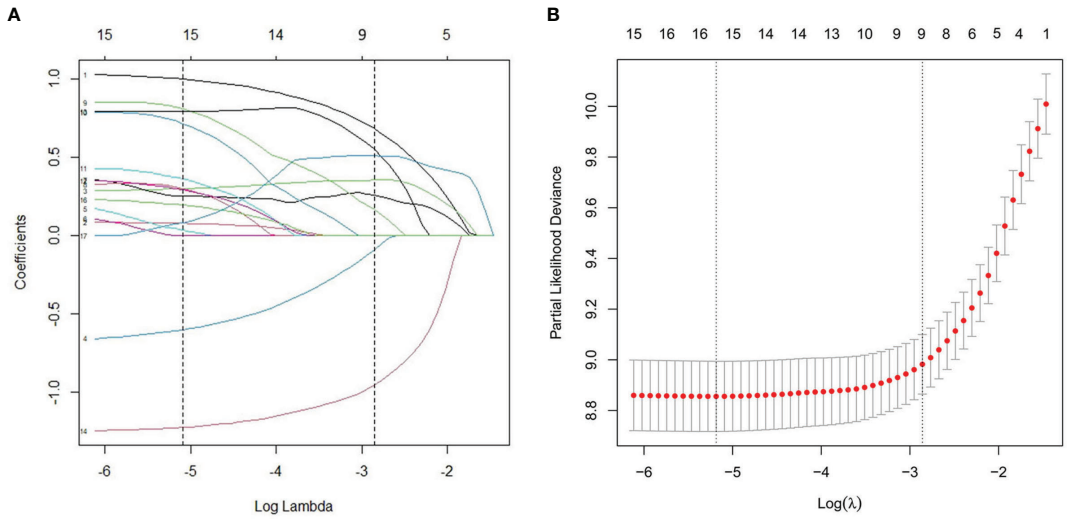

FIGURE 3 | L1-penalized (Lasso) regression model were adopted to determine further predictive variables in test dataset. **(A)** LASSO coefficient patterns of the features. **(B)** Ten-time cross-verification for tuning parameter selection in the Lasso model.

TABLE 3 | Results of univariate and multivariate analyses by Fine-Gray proportional subdistribution hazards model in the training cohort.

Characteristics	Univariate analysis		Multivariate analysis (AIC)		Multivariate analysis (BIC)	
	HR (95% CI)	*p*-value	HR (95% CI)	*p*-value	HR (95% CI)	*p*-value
Age (years)						
<70	Ref		Ref		Ref	
≥70	3.274 (2.461–11.718)	<0.001	2.543 (2.082–3.107)	0.001	1.997 (1.53–2.605)	0.003
Race						
Black	Ref					
White	0.991 (0.606–1.833)	0.376228				
Others	0.756 (0.408–1.503)	0.973185				
Sex						
Male	Ref					
Female	1.168 (0.87–2.387)	0.301423				
AJCC stage						
I	Ref					
II	0.595 (0.239–0.969)	0.009				
III	0.57 (0.232–0.974)	<0.001				
IV	0.575 (0.163–0.985)	<0.001				
T stage						
T1	Ref		Ref		Ref	
T2	2.861 (1.326–3.767)	0.008	2.098 (1.176–3.742)	0.012	2.072 (1.262–3.113)	0.090
T3	4.719 (2.298–9.959)	<0.001	3.134 (1.826–5.377)	<0.001	3.374 (1.392–5.919)	<0.001
T4	4.368 (1.945–6.993)	<0.001	3.223 (1.807–5.746)	<0.001	4.716 (2.994–7.885)	<0.001
N stage						
N0	Ref		Ref			
N1	1.352 (1.131–1.88)	<0.001	2.139 (1.3–3.522)	<0.001		
N2	1.865 (1.238–2.554)	0.007	2.36 (1.495–3.726)	<0.001		
M stage						
M0	Ref		Ref		Ref	
M1	2.696 (1.231–3.425)	0.01	2.51 (1.733–3.636)	0.001	2.678 (1.707–4.202)	<0.001
Surgery						
No	Ref		Ref		Ref	
Yes	0.17 (0.09–0.995)	<0.001	0.312 (0.235–0.414)	<0.001	0.338 (0.236–0.482)	<0.001
Radiation						
No	Ref		Ref		Ref	
Yes	2.116 (1.219–2.268)	<0.001	2.139 (1.3–3.522)	<0.001	1.817 (1.117–3.603)	<0.001

(Continued)

TABLE 3 | Continued

Characteristics	Univariate analysis		Multivariate analysis (AIC)		Multivariate analysis (BIC)	
	HR (95% CI)	*p*-value	HR (95% CI)	*p*-value	HR (95% CI)	*p*-value
Grade						
Well	Ref		Ref		Ref	
Moderately	1.267 (1.061–1.938)	<0.001	1.223 (1.101–3.742)	<0.001	1.684 (1.131–2.132)	<0.001
Poorly/undifferentiated	2.78 (1.847–6.338)	<0.001	2.529 (1.811–3.532)	0.001	1.964 (1.054–3.659)	0.03
Histologic type						
MEC	Ref		Ref			
None MEC	2.602 (1.64–5.155)	<0.001	2.477 (1.715–3.576)	<0.001		

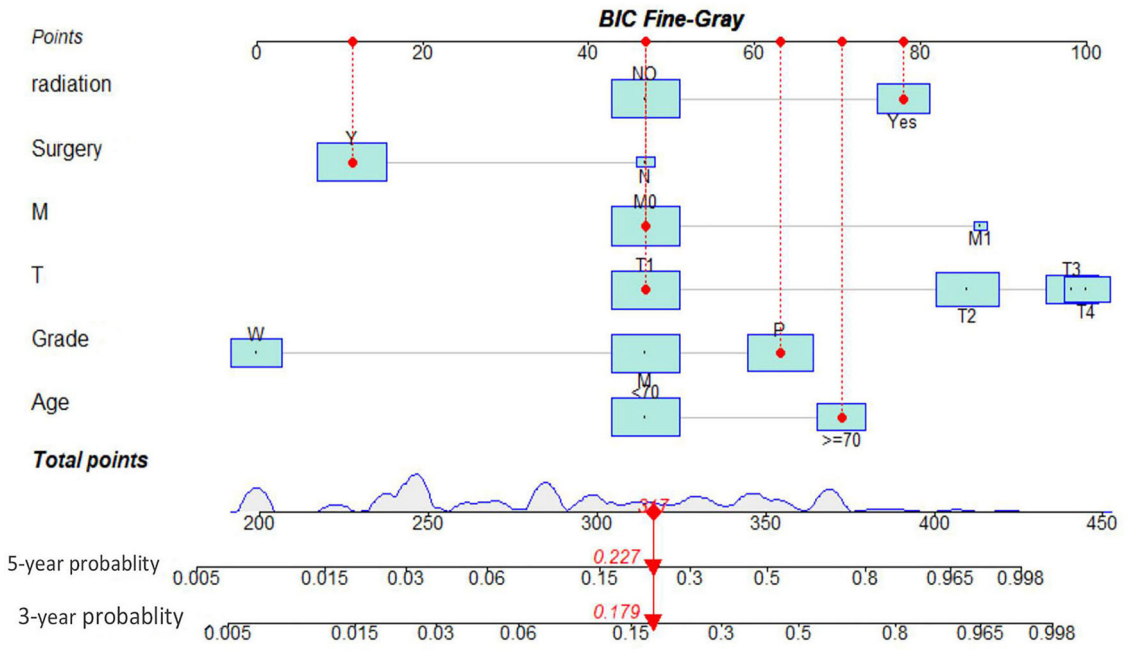

FIGURE 4 | Interactive nomogram for predicting 3- and 5-year likelihoods of CSD in parotid carcinoma. BIC, Bayesian information criterion; MEC, mucoepidermoid carcinoma.

which is congruent with our work (24). The findings also showed that histology type and N stage were independent indicators for PC patients, which is in agreement with previous findings in malignant salivary gland tumor research (25). To prevent overfitting, the aforementioned factors were omitted using PC to improve the performance of the model.

Surgical treatment is the most frequently used therapy for PC at all stages, although according to the guidelines published by the NCCN, surgery is highly recommended for resectable PC (T1–T4a) (26). The data herein demonstrated that surgical therapy could remarkably diminish the tumor-distinct risk of death in individuals with PC; this has been confirmed by most clinicians. However, neck dissection is a controversial subject in parotid malignant tumors. In the presence of a clinically palpable lymph node, there is a consensus on the application of elective neck dissection with a primary parotid surgery (27), some authors support elective neck dissection depending on the tumor histology, size, and grade (28, 29). However, in the study by Ali et al., they suggested that the neck is susceptible to be a target region for metastatic diseases; therefore, complete neck dissection between levels I to V is recommended (30). We established that radiation therapy could remarkably suppress deaths in PC patients, but whether radiotherapy can significantly improve the prognosis of patients is still controversial. In the study by Kaur et al., they believe that postoperative radiotherapy (PORT) has shown a survival benefit in patients with major salivary gland carcinoma (31). For patients with resected T1–2 tumors, the present protocols advocate radiation treatment after operation for individuals with adenoid cystic pathology, close (<1 mm) perineural, or lymphovascular infiltration, or positive

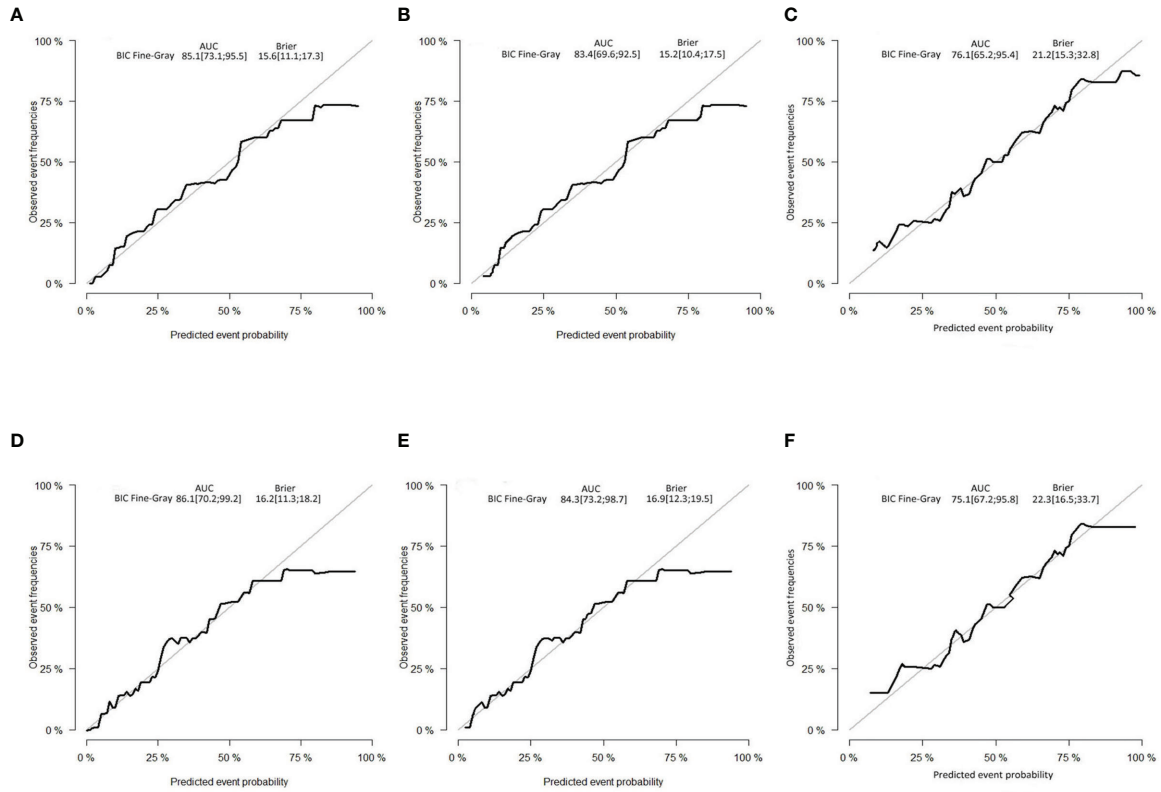

FIGURE 5 | Calibration curves. **(A)** Three-year and **(D)** 5-year likelihoods of CSD in the test dataset. **(B)** Three-year and **(E)** 5-year likelihoods of CSD in the internal verification dataset. **(C)** Three-year and **(F)** 5-year likelihoods of CSD in the external verification dataset. BIC, Bayesian information criterion; AUC, area under the curve.

margins, lymph node metastasis, as well as intermediate- or high-grade histology (26). In a parotid gland infiltrating ductal carcinoma (IDC) research, they found that PORT only enhanced survival of individuals with parotid gland IDC within T3–4, N1, and TNM III subgroups (32).

Mucoepidermoid carcinoma (MEC), the most prevalent type of PC, constitutes approximately 30–50% of malignant salivary glands (33, 34) However, there is no prognostic analysis of different pathological types of parotid carcinoma. Herein, MEC accounted for 42.3% of all PC cases, and we exhibited that the risk of CSD in persons with MEC was not remarkably higher relative to that in other types of PC such as adenoid cystic carcinoma and polymorphous adenocarcinoma, adenocarcinoma NOS, and myoepithelial carcinoma. This is consistent with the result of Filho OVO et in a retrospective analysis of 193 patients (25). Nevertheless, Baddour et al. and Kokemueller et al. revealed higher survival rates at 5, 10, and 15 years for MEC in relation to other types of PC (35, 36). We think that this should be related to the difference in diagnosis and treatment level between different regions.

Previous investigation on parotid carcinoma based on the SEER data repository focused on incidence, along with survival trends (37, 38), while we focused on creating a prognostic nomogram herein. The clinical therapy of PC and the evaluation of prognosis currently depends on the AJCC staging method. Our prognostic model is suitable for all persons with PC and could be extensively applied in all levels of medical centers. The comprehensive nature of the nomogram may cover the shortcomings of the AJCC staging method, and allow individualized treatment, as well as the precise examination of the prognosis of individuals with PC. Besides, the user-friendly graphic interface of the nomogram could promote the interaction of clinicians with patients. Additionally, a verification data set was utilized for external verification, and the data were drastically congruent with actual survival likelihoods.

However, this research had some shortcomings. In the first place, the SEER data repository lacks some pivotal factors tied to prognosis, including perineural invasion, smoking history, chronic parotitis history, comorbidities, and lack of genetic records of patients. Besides, we adopted the sixth or seventh edition of the AJCC staging method, which lacks two pivotal variables (depth of invasion, as well as an extranodal extension) in contrast with the eighth edition. Moreover, the SEER repository lacks data on tumor volume, which is considered a significant prognostic factor for Salivary gland tumors. Even though this work incorporated the data on chemotherapy and radiotherapy, but the SEER database lacks detailed data on cycles number and doses of chemotherapy, the radiotherapy approaches, and the follow-up treatment after relapse. These variables can also influence the prognosis. Lastly,

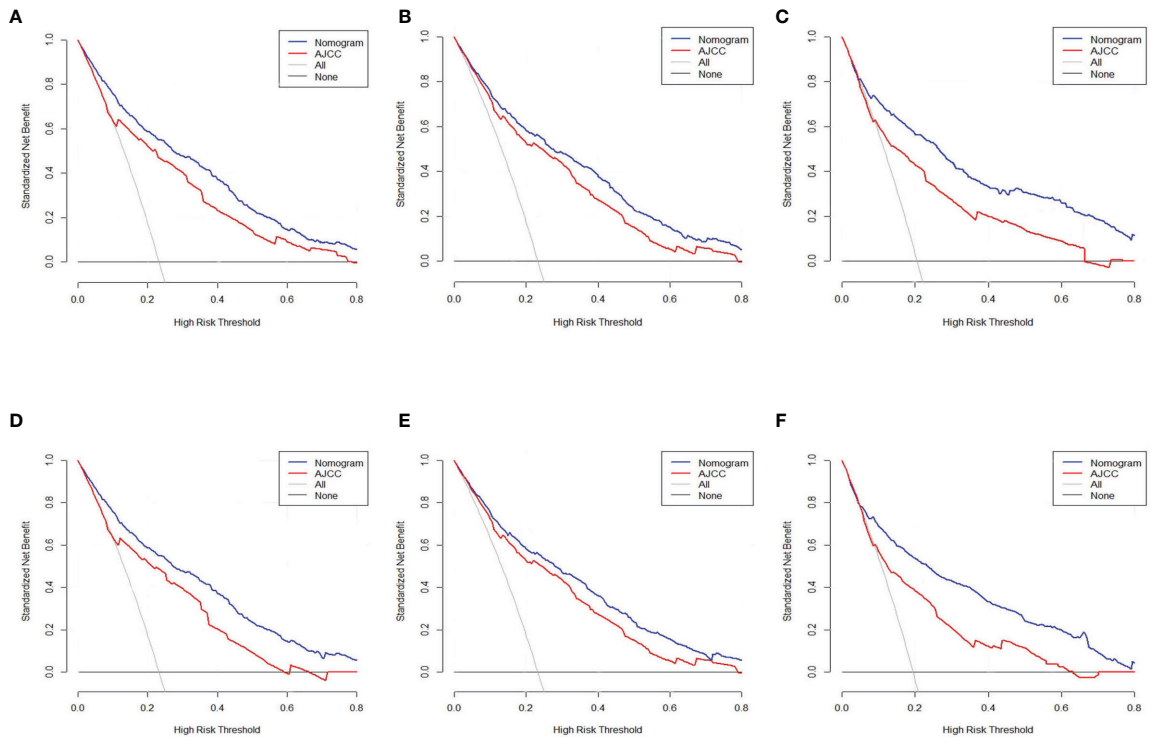

FIGURE 6 | Decision curve assessment of the nomogram along with the AJCC staging approach in the estimation of the CSD of individuals with PC at 3 and 5 years in the test cohort **(A, D)**, internal verification **(B, E)**, and external verification **(C, F)** cohorts.

even though the SEER data repository provided an extensive range of samples for this analysis, errors exist when this database is utilized in the global context. Besides, the data of the external verification are only from a single province in China. It has been reported that even in China, there are different epidemiological differences between the north and the south (1, 39). Therefore larger-sample multicenter study should be conducted to further improve our estimation model and validate its clinical application significance.

CONCLUSION

We have created a competing risk nomogram for PC patients using the data retrieved from the SEER data repository and carried out external verification to show the precision and reliability of our nomogram. This well-calibrated nomogram could be utilized in making clinical decisions regarding the prognosis as well as personalized treatment of PC patients.

DATA AVAILABILITY STATEMENT

The original contributions presented in the study are included in the article/supplementary material. Further inquiries can be directed to the corresponding authors.

ETHICS STATEMENT

Written informed consent was obtained from the individual(s) for the publication of any potentially identifiable images or data included in this article.

AUTHOR CONTRIBUTIONS

XL and MH were responsible for the conception and design of the study, assisted with the statistical analysis, and wrote and revised the manuscript. MH and WG were involved in the collecting of data and follow up of the patients. SC and JM contributed their help on the data analysis, revised the English language and grammar, and corrected parts of the discussion. DL has made the primary contribution in the later stage in the writing and modification of the paper and the review of the finalized article. All authors contributed to the article and approved the submitted version.

FUNDING

This study was supported by the National Natural Science Foundation of China (No. 81560410) and the Postgraduate Innovation Special Foundation of Jiangxi Province (YC2020-B043).

REFERENCES

1. Gao M, Hao Y, Huang MX, Ma DQ, Chen Y, Luo HY, et al. Salivary Gland Tumours in a Northern Chinese Population: A 50-Year Retrospective Study of 7190 Cases. *Int J Oral Maxillofac Surg* (2017) 46(3):343–9. doi: 10.1016/j.ijom.2016.09.021
2. da Silva LP, Serpa MS, Viveiros SK, Sena DAC, de Carvalho Pinho RF, de Abreu Guimarães LD, et al. Salivary Gland Tumors in a Brazilian Population: A 20-Year Retrospective and Multicentric Study of 2292 Cases. *J Craniomaxillofac Surg* (2018) 46(12):2227–33. doi: 10.1016/j.jcms.2018.09.028
3. de Ridder M, Balm AJ, Smeele LE, Wouters MW, van Dijk BA. An Epidemiological Evaluation of Salivary Gland Cancer in the Netherlands (1989–2010). *Cancer Epidemiol* (2015) 39(1):14–20. doi: 10.1016/j.canep.2014.10.007
4. McHugh CH, Roberts DB, El-Naggar AK, Hanna EY, Garden AS, Kies MS, et al. Prognostic Factors in Mucoepidermoid Carcinoma of the Salivary Glands. *Cancer* (2012) 118:3928–36. doi: 10.1002/cncr.26697
5. Chen AM, Lau VH, Farwell DG, Luu Q, Donald PJ. Mucoepidermoid Carcinoma of the Parotid Gland Treated by Surgery and Postoperative Radiation Therapy: Clinicopathologic Correlates of Outcome. *Laryngoscope* (2013) 123(12):3049–55. doi: 10.1002/lary.24238
6. Ali S, Palmer FL, Yu C, DiLorenzo M, Shah JP, Kattan MW, et al. A Predictive Nomogram for Recurrence of Carcinoma of the Major Salivary Glands. *JAMA Otolaryngol Head Neck Surg* (2013) 139(7):698–705. doi: 10.1001/jamaoto.2013.3347
7. Cui J, Wang L, Zhong W, Chen Z, Tan X, Yang H, et al. Development and Validation of Nomogram to Predict Risk of Survival in Patients With Laryngeal Squamous Cell Carcinoma. *Biosci Rep* (2020) 40(8): BSR20200228. doi: 10.1042/BSR20200228
8. Li J, Chen S, Peng S, Liu Y, Xing S, He X, et al. Prognostic Nomogram for Patients With Nasopharyngeal Carcinoma Incorporating Hematological Biomarkers and Clinical Characteristics. *Int J Biol Sci* (2018) 14(5):549–56. doi: 10.7150/ijbs.24374
9. Doll KM, Rademaker A, Sosa JA. Practical Guide to Surgical Data Sets: Surveillance, Epidemiology, and End Results (SEER) Database. *JAMA Surg* (2018) 153(6):588–9. doi: 10.1001/jamasurg.2018.0501
10. Dignam JJ, Zhang Q, Kocherginsky M. The Use and Interpretation of Competing Risks Regression Models. *Clin Cancer Res* (2012) 18(8):2301–8. doi: 10.1158/1078-0432.CCR-11-2097
11. Li J, Zheng Q, Zhao X, Zhao J, An T, Wu M, et al. Nomogram Model for Predicting Cause-Specific Mortality in Patients With Stage I Small-Cell Lung Cancer: A Competing Risk Analysis. *BMC Cancer* (2020) 20(1):793. doi: 10.1186/s12885-020-07271-9
12. Yang Y, Chen ZJ, Yan S. The Incidence, Risk Factors and Predictive Nomograms for Early Death Among Patients With Stage IV Gastric Cancer: A Population-Based Study. *J Gastrointest Oncol* (2020) 11(5):964–82. doi: 10.21037/jgo-20-217
13. Dibas M, Ghozy S, Morsy S, Salah Abbas A, Alkahtani S, Bin-Jumah M, et al. Novel Nomograms Predicting Overall and Cancer-Specific Survival of Malignant Ependymoma Patients: A Population-Based Study. *J Neurosurg Sci* (2020). doi: 10.23736/S0390-5616.20.05033-X
14. Li J, Li X, Gu J, Ma X, Xue F. A Competing-Risks Nomogram for Predicting Probability of Death From CRC in Chinese Han Patients With Stage I-III CRC. *Jpn J Clin Oncol* (2018) 48(12):1088–95. doi: 10.1093/jjco/hyy136
15. van Steenbeek CD, van Maaren MC, Siesling S, Witteveen A, Verbeek XAAM, Koffijberg H. Facilitating Validation of Prediction Models: A Comparison of Manual and Semi-Automated Validation Using Registry-Based Data of Breast Cancer Patients in the Netherlands. *BMC Med Res Methodol* (2019) 19(1):117. doi: 10.1186/s12874-019-0761-5
16. Fei Z, Qiu X, Li M, Chen C, Li Y, Huang Y. Prognosis Viewing for Nasopharyngeal Carcinoma Treated With Intensity-Modulated Radiation Therapy: Application of Nomogram and Decision Curve Analysis. *Jpn J Clin Oncol* (2020) 50(2):159–68. doi: 10.1093/jjco/hyz165
17. Ito FA, Ito K, Vargas PA, de Almeida OP, Lopes MA. Salivary Gland Tumors in a Brazilian Population: A Retrospective Study of 496 Cases. *Int J Oral Maxillofac Surg* (2005) 34(5):533–6. doi: 10.1016/j.ijom.2005.02.005
18. Israel Y, Rachmiel A, Ziv G, Nagler R. Benign and Malignant Salivary Gland Tumors - Clinical and Demographic Characteristics. *Anticancer Res* (2016) 36 (8):4151–4.
19. Webber C, Gospodarowicz M, Sobin LH, Wittekind C, Greene FL, Mason MD, et al. Improving the TNM Classification: Findings From a 10-Year Continuous Literature Review. *Int J Cancer* (2014) 135(2):371–8. doi: 10.1002/ijc.28683
20. Sun J, Sun Y, Yang F, Zhou Q, Liu W, Cheng Y. Nomogram to Predict the Prognosis of Parotid Gland Mucoepidermoid Carcinoma: A Population-Based Study of 1306 Cases. *Peer J* (2019) 7:e7237. doi: 10.7717/peerj.7237
21. Chakrabarti S, Nair D, Malik A, Qayyumi B, Nair S, Agrawal JP, et al. Prognostic Factors in Parotid Cancers: Clinicopathological and Treatment Factors Influencing Outcomes. *Indian J Cancer* (2018) 55(1):98–104. doi: 10.4103/ijc.IJC_503_17
22. Lyu HX, Wang ZR, Gao YQ, Yu M, Li BQ, Zhang ZB. Clinical Pathologic Analysis on 3 724 Cases of Salivary Gland Tumors. *Zhonghua Kou Qiang Yi Xue Za Zhi* (2019) 54(1):10–6. doi: 10.3760/cma.j.issn.1002-0098.2019.01.003
23. Nakano T, Yasumatsu R, Kogo R, Hashimoto K, Asai K, Ohga S, et al. Parotid Gland Carcinoma: 32 Years' Experience From a Single Institute. *J Laryngol Otol* (2019) 133(7):604–9. doi: 10.1017/S0022215119001130
24. Fang Q, Wu J, Liu F. Oncologic Outcome and Potential Prognostic Factors in Primary Squamous Cell Carcinoma of the Parotid Gland. *BMC Cancer* (2019) 19(1):752. doi: 10.1186/s12885-019-5969-6
25. Filho OVO, Rêgo TJRD, Mendes FHO, Dantas TS, Cunha MDPSS, Malta CEN, et al. Prognostic Factors and Overall Survival in a 15-Year Followup of Patients With Malignant Salivary Gland Tumors: A Retrospective Analysis of 193 Patients. *Braz J Otorhinolaryngol* (2020) S1808-8694(20):30116–6. doi: 10.1016/j.bjorl.2020.06.016
26. Pfister DG, Spencer S, Adelstein D, Adkins D, Anzai Y, Brizel DM, et al. Head and Neck Cancers, Version 2.2020, NCCN Clinical Practice Guidelines in Oncology. *J Natl Compr Canc Netw* (2020) 18(7):873–98. doi: 10.6004/jnccn.2020.0031
27. Hanna EYN, Suen JY. Malignant Tumors of the Salivary Glands. In: EN Myers, JY Suen, JN Myers, EYN Hanna, editors. *Cancer of the Head and Neck, 4th ed.* Philadelphia: Saunders (2003). p. 475–510. doi: 10.1007/0-387-21701-0_9
28. Armstrong JG, Harrison LB, Thaler HT, Friedlander-Klar H, Fass DE, Zelefsky MJ, et al. The Indications for Elective Treatment of the Neck in Cancer of the Major Salivary Glands. *Cancer* (1992) 69(3):615–9. doi: 10.1002/1097-0142(19920201)69:3<615::aid-cncr2820690303>3.0.co;2-9
29. Lloyd S, Yu JB, Ross DA, Wilson LD, Decker RH. A Prognostic Index for Predicting Lymph Node Metastasis in Minor Salivary Gland Cancer. *Int J Radiat Oncol Biol Phys* (2010) 76(1):169–75. doi: 10.1016/j.ijrobp.2009.01.021
30. Ali S, Palmer FL, DiLorenzo M, Shah JP, Patel SG, Ganly I. Treatment of the Neck in Carcinoma of the Parotid Gland. *Ann Surg Oncol* (2014) 21(9):3042–8. doi: 10.1245/s10434-014-3681-y
31. Kaur J, Goyal S, Muzumder S, Bhasker S, Mohanti BK, Rath GK. Outcome of Surgery and Post-Operative Radiotherapy for Major Salivary Gland Carcinoma: Ten Year Experience From a Single Institute. *Asian Pac J Cancer Prev* (2014) 15(19):8259–63. doi: 10.7314/apjcp.2014.15.19.8259
32. Lv T, Wang Y, Wang X. Subgroups of Parotid Gland Infiltrating Ductal Carcinoma Benefit From Postoperative Radiotherapy: A Population-Based Study. *Future Oncol* (2019) 15(8):885–95. doi: 10.2217/fon-2018-0495
33. Brandwein MS, Ivanov K, Wallace DI, Hille JJ, Wang B, Fahmy A, et al. Mucoepidermoid Carcinoma: A Clinicopathologic Study of 80 Patients With Special Reference to Histological Grading. *Am J Surg Pathol* (2001) 25(7):835–45. doi: 10.1097/00000478-200107000-00001
34. Lydiatt WM, Patel SG, O'Sullivan B, Brandwein MS, Ridge JA, Migliacci JC, et al. Head and Neck Cancers-Major Changes in the American Joint Committee on Cancer Eighth Edition Cancer Staging Manual. *CA Cancer J Clin* (2017) 67(2):122–37. doi: 10.3322/caac.21389
35. Baddour HMJr, Fedewa SA, Chen AY. Five- and 10-Year Cause-Specific Survival Rates in Carcinoma of the Minor Salivary Gland. *JAMA Otolaryngol Head Neck Surg* (2016) 142(1):67–73. doi: 10.1001/jamaoto.2015.2805
36. Kokemueller H, Swennen G, Brueggemann N, Brachvogel P, Eckardt A, Hausamen JE. Epithelial Malignancies of the Salivary Glands: Clinical Experience of a Single Institution-a Review. *Int J Oral Maxillofac Surg* (2004) 33(5):423–32. doi: 10.1016/j.ijom.2004.02.007
37. Chen MM, Roman SA, Sosa JA, Judson BL. Histologic Grade as Prognostic Indicator for Mucoepidermoid Carcinoma: A Population-

Level Analysis of 2400 Patients. *Head Neck* (2014) 36(2):158–63. doi: 10.1002/hed.23256
38. Rutt AL, Hawkshaw MJ, Lurie D, Sataloff RT. Salivary Gland Cancer in Patients Younger Than 30 Years. *Ear Nose Throat J* (2011) 90(4):174–84. doi: 10.1177/014556131109000409
39. Li LJ, Li Y, Wen YM, Liu H, Zhao HW. Clinical Analysis of Salivary Gland Tumor Cases in West China in Past 50 Years. *Oral Oncol* (2008) 44(2):187–92. doi: 10.1016/j.oraloncology.2007.01.016

Conflict of Interest: The authors declare that the research was conducted in the absence of any commercial or financial relationships that could be construed as a potential conflict of interest.

Publisher's Note: All claims expressed in this article are solely those of the authors and do not necessarily represent those of their affiliated organizations, or those of the publisher, the editors and the reviewers. Any product that may be evaluated in this article, or claim that may be made by its manufacturer, is not guaranteed or endorsed by the publisher.

frontiers in Oncology

ORIGINAL RESEARCH
published: 14 October 2021
doi: 10.3389/fonc.2021.765378

Efficacy and Toxicity of Three Induction Chemotherapy Regimens in Locoregionally Advanced Nasopharyngeal Carcinoma: Outcomes of 10-Year Follow-Up

Hao Peng[1†], Binbin Chen[2†], Shuiqing He[3], Li Tian[4] and Ying Huang[3*]*

[1] Center for Translational Medicine, Precision Medicine Institute, The First Affiliated Hospital, Sun Yat-sen University, Guangzhou, China, [2] Department of Clinical Nutrition, Sun Yat-sen University Cancer Center, State Key Laboratory of Oncology in South China, Collaborative Innovation Center of Cancer Medicine, Guangzhou, China, [3] Department of Radiation Oncology, Sun Yat-sen University Cancer Center, State Key Laboratory of Oncology in South China, Collaborative Innovation Center of Cancer Medicine, Guangzhou, China, [4] Imaging Diagnosis and Interventional Center, Sun Yat-sen University Cancer Center, State Key Laboratory of Oncology in South China, Collaborative Innovation Center of Cancer Medicine, Guangzhou, China

OPEN ACCESS

Edited by:
Hui Wang,
Hunan Cancer Hospital, China

Reviewed by:
Xia He,
Nanjing Medical University, China
Lirong Wu,
Nanjing Medical University, China

***Correspondence:**
Hao Peng
pengh67@mail.sysu.edu.cn
Ying Huang
huangying@sysucc.org.cn

[†]These authors have contributed equally to this work

Specialty section:
This article was submitted to Head and Neck Cancer, a section of the journal Frontiers in Oncology

Received: *27 August 2021*
Accepted: *22 September 2021*
Published: *14 October 2021*

Citation:
Peng H, Chen B, He S, Tian L and Huang Y (2021) Efficacy and Toxicity of Three Induction Chemotherapy Regimens in Locoregionally Advanced Nasopharyngeal Carcinoma: Outcomes of 10-Year Follow-Up. Front. Oncol. 11:765378. doi: 10.3389/fonc.2021.765378

Background/Objective: We aimed to compare the 10-year survival outcomes of induction docetaxel plus cisplatin and 5-fluorouracil (TPF), docetaxel plus cisplatin (TP), and cisplatin plus 5-fluorouracil (PF) regimens additional to concurrent chemoradiotherapy (CRT) in locoregionally advanced nasopharyngeal carcinoma (NPC).

Methods: Eligible patients with newly diagnosed stage III-IVA NPC were included. Propensity score matching (PSM) was used to balance prognostic covariates. Survival outcomes and toxicities between different groups were compared.

Results: A total of 855 patients between 2009 and 2012 were included, with 395 (46.2%), 258 (30.2%), and 202 (23.6%) receiving TPF plus CRT, TP plus CRT, and PF plus CRT regimens, respectively. After a median follow-up of 111.8 months, multivariate analysis both in the whole cohort and PSM selected 202 pairs showed that TPF plus CRT and TP plus CRT achieved significantly better 10-year overall survival (OS) than PF plus CRT. Sensitivity analysis after excluding patients with T3-4N0 disease demonstrated that TPF plus CRT still achieved significantly better OS than PF plus CRT (HR, 0.580; 95% CI, 0.395-0.852; $P = 0.005$), while the difference between TP plus CRT and PF plus CRT was marginally significant (HR, 0.712; 95% CI, 0.503-1.008; $P = 0.056$). With regard to toxicity profile, PF regimen achieved the lowest grade 3–5 toxicities (27.3%).

Conclusion: TPF plus CRT and TP plus CRT were better than PF plus CRT in improving the 10-year OS of patients with stage III-IVA NPC.

Keywords: nasopharyngeal carcinoma, induction chemotherapy, 10-year outcomes, radiotherapy, concurrent chemoradiotherapy (CCRT)

BACKGROUND

As an aggressive and relatively rare head and neck cancer, nasopharyngeal carcinoma (NPC) has an extremely unbalanced geographical distribution worldwide; it is endemic in Southern China and Southeast Asia but very rare in western countries (1, 2). Different from other head and neck cancers, nondisseminated NPC is cured by radiotherapy. A 10-year overall survival (OS) of 87.1–100% could be achieved in patients with stage I-II disease; however, the corresponding survival outcome of patients with stage III-IVA disease was only 75.5–55.6%, and distant metastasis has come as the main failure patter (3). Unfortunately, more than 80% of patients presented with advanced diseases at initial diagnosis (2, 4). Therefore, how to reduce distant metastasis and improve the therapeutic outcomes of patients with advanced disease have been widely studied.

Induction chemotherapy (IC), usually a combination of two or three cytotoxic drugs, is given before radiotherapy to eliminate clinically undetectable micrometastatic lesions, thereby reducing the rate of distant failure and improving survival. Indeed, several phase III clinical trials conducted in recent years have showed that IC additional to concurrent chemoradiotherapy (CRT) could improve both distant metastasis-free survival (DMFS) and OS (5–9). This evidence strengthened the role of IC in locoregionally advanced NPC, and IC plus CRT was therefore approved as the preferable treatment strategy worldwide for advanced NPC. Despite these advances, the most effective IC regimen, however, is still unknown since various regimens all achieved positive results (5–8, 10, 11). A previously retrospective study uncovered that a triple combination of docetaxel plus cisplatin and 5-fluorouracil (TPF) was better than docetaxel plus cisplatin (TP) and cisplatin plus 5-fluorouracil (PF) regimens in patients with stage III-IVA NPC (excluding T3N0) (12). However, the insufficient follow-up duration (median, 46.1 months) and inclusion of patients who did not receive concurrent chemotherapy made these results inconclusive.

Based on this premise, we conducted this study to compare the 10-year survival outcomes of patients with locoregionally advanced NPC receiving induction TPF, TP, or PF plus CRT in the era of intensity-modulated radiotherapy (IMRT).

RESULTS

Baseline Information of Included Patients

A total of 855 patients treated between April 2009 and December 2012 were included in our study, with 395 (46.2%) receiving TPF plus CRT, 258 (30.2%) receiving TP plus CRT, and 202 (23.6%) receiving PF plus CRT. Baseline information of these patients is shown in **Table 1**. The whole cohort had a median age of 44 years and a male-to-female ratio of 3.3. The PF plus CRT group had significantly lower percentages of T4 (29.4% *vs*. 39.3% *vs*. 35.2%, $P = 0.007$), N3 (14.7% *vs*. 20.7% *vs*. 23.3%, $P = 0.173$), and stage IVA (41.1% *vs*. 55.7% *vs*. 52.0%, $P = 0.001$) diseases compared with TPF plus CRT and TP plus CRT groups. More patients in the TPF plus CRT group received three or more cycles than in the TP plus CRT and PF plus CRT groups (69.6% *vs*. 22.3% *vs*. 26.7%, $P < 0.0001$). Notably, the TP plus CRT group had the lowest percentage of patients receiving a cumulative cisplatin dose (CCD) ≥ 200 mg/m^2 (8.9% *vs*. 23.0% *vs*. 21.7%, $P < 0.0001$). A total of 278 patients received weekly cisplatin/nedaplatin during radiotherapy, with 80 (20.3%), 136 (52.7%), and 62 (29.7%) in the TPF, TP, and PF groups, respectively.

Treatment Failure Pattern

Up to the last follow-up (August 20, 2021), the median follow-up duration was 111.8 months (range, 4.57–149.63 months) for the whole cohort and 120.9 months (range, 7.43–149.63 months) for those alive. Among the patients survived, 9.6% (56/586) of them were lost to follow-up, and only 5 (0.9%) of the remaining patients were followed for less than 9 years (range, 105.2–107.6 months). A total of 269 (31.6%) deaths were observed, with 124 (31.4%) in the TPF plus CRT group, 78 (38.6%) in the PF plus CRT group, and 67 (26.0%) in the TP plus CRT group. Moreover, 85 (21.5%), 45 (11.4%), and 40 (10.1%) patients in the TPF plus CRT group suffered distant, local, and regional recurrence, respectively. The corresponding numbers were 49 (24.3%), 23 (11.4%), and 20 (9.9%) in the PF plus CRT group, and 45 (17.4%), 20 (7.8%), and 8 (3.1%) in the TP plus CRT group. Intriguingly, 29 (3.4%) patients still survived after disease progression and salvage treatments, with 18 (4.6%) in the TPF plus CRT group, 4 (2.0%) in the PF plus CRT group, and 7 (2.7%) in the TP plus CRT group. Notably, 39 new events, which accounted for 13.1% of all events, occurred after 5 years, with 21 (5.3%) in the TPF plus CRT group, 11 (5.4%) in the PF plus CRT group, and 7 (2.7%) in the TP plus CRT group (**Supplementary Table S1**).

Survival Outcomes Comparison

The estimated 10-year OS, DFS, DMFS, and LFFS rates were 67.8%, 64.9%, 78.4%, and 83.8% for the whole cohort, respectively. With regard to the three groups, the estimated 10-year survival rates of TPF *vs*. TP *vs*. PF were 67.7% *vs*. 73.5% *vs*. 60.5% ($P_{\text{TPF vs. TP}} = 0.153$, $P_{\text{TPF vs. PF}} = 0.058$, $P_{\text{PF vs. TP}} = 0.003$) for OS, 63.6% *vs*. 71.1% *vs*. 59.2% ($P_{\text{TPF vs. TP}} = 0.055$, $P_{\text{TPF vs. PF}} = 0.262$, $P_{\text{PF vs. TP}} = 0.007$) for DFS, 77.7% *vs*. 82.3% *vs*. 74.5% ($P_{\text{TPF vs. TP}} = 0.209$, $P_{\text{TPF vs. PF}} = 0.39$, $P_{\text{PF vs. TP}} = 0.063$) for DMFS, and 81.2% *vs*. 89.5% *vs*. 81.8% ($P_{\text{TPF vs. TP}} = 0.006$, $P_{\text{TPF vs. PF}} = 0.968$, $P_{\text{PF vs. TP}} = 0.015$; **Supplementary Figure S1**) for LFFS. After adjusting for various factors by an adjusted Cox proportional hazards model, TPF plus CRT (OS: HR, 0.672; 95% CI, 0.491–0.920; $P = 0.013$; DFS: HR, 0.753; 95% CI, 0.544–0.994; $P = 0.045$) and TP plus CRT (OS: HR, 0.664; 95% CI, 0.478–0.922; $P = 0.015$; DFS: HR, 0.701; 95% CI, 0.510–0.963; $P = 0.029$) were associated with significantly better OS and DFS compared with PF plus CRT (**Table 2**).

We used PSM to balance independent prognostic factors identified above (tumor stage, alcohol intake, age, and gender) and further performed survival analysis in the selected 202 pairs (**Supplementary Table S2**). Correspondingly, the 10-year OS, DFS, DMFS, and LFFS rates for TPF *vs*. PF *vs*. TP were 68.9% *vs*. 70.3% *vs*. 60.5% ($P_{\text{TPF vs. TP}} = 0.83$, $P_{\text{TPF vs. PF}} = 0.068$, $P_{\text{PF vs. TP}} =$

TABLE 1 | Baseline information of 855 patients receiving different IC regimens.

Characteristics	TPF No. (%)	PF No. (%)	TP No. (%)	*P* value
Gender				0.589
Male	304 (77.0)	150 (74.3)	202 (78.3)	
Female	91 (23.0)	52 (25.7)	56 (21.7)	
Age (years)				0.461[b]
Median (range)	43 (16-72)	46 (12-72)	45 (18-76)	
≥ 50	114 (28.9)	71 (35.1)	77 (29.8)	
< 50	281 (71.1)	131 (64.9)	181 (70.2)	
Smoking				0.584
Yes	158 (40)	72 (35.6)	100 (38.8)	
No	237 (60)	130 (64.4)	158 (61.2)	
Alcohol intake				0.781
Yes	54 (13.7)	24 (11.9)	36 (14.0)	
No	341 (86.3)	178 (88.1)	222 (86.0)	
Family history of cancer				0.64
Yes	106 (26.8)	47 (23.3)	66 (25.6)	
No	289 (73.2)	155 (76.7)	192 (74.4)	
T category[a]				0.007
T1	21 (5.3)	13 (6.4)	4 (1.6)	
T2	30 (7.6)	18 (8.9)	20 (7.8)	
T3	189 (47.8)	100 (49.5)	158 (61.2)	
T4	155 (39.3)	71 (35.2)	76 (29.4)	
N category[a]				0.173
N0	18 (4.6)	11 (5.4)	19 (7.4)	
N1	198 (50.1)	91 (45.1)	139 (53.9)	
N2	97 (24.6)	53 (26.2)	62 (24.0)	
N3	82 (20.7)	47 (23.3)	38 (14.7)	
Overall stage[a]				0.001
III	175 (44.3)	97 (48.0)	152 (58.9)	
IVA	220 (55.7)	105 (52.0)	106 (41.1)	
IC cycle				<0.0001
2	120 (30.4)	157 (77.7)	189 (73.3)	
3	243 (61.5)	32 (15.9)	55 (21.3)	
4	32 (8.1)	13 (6.4)	14 (5.4)	
CCD (mg/m^2)				<0.0001[b]
Median (range)	160 (40-300)	160 (30-300)	160 (30-300)	
≥ 200	91 (23.0)	18 (8.9)	56 (21.7)	
< 200	304 (77.0)	184 (91.1)	202 (78.3)	

IC, induction chemotherapy; TPF, docetaxel plus cisplatin and 5-fluorouracil; PF, cisplatin plus 5-fluorouracil; TP, docetaxel plus cisplatin; CCD, cumulative cisplatin dose during radiotherapy.

[a]*According to the eighth edition of the AJCC/UICC manual.*

[b]*P values were calculated by one-way ANOVA.*

0.043), 64.8% *vs.* 67.6% *vs.* 59.2% ($P_{TPF\ vs.\ TP} = 0.585$, $P_{TPF\ vs.\ PF} = 0.219$, $P_{PF\ vs.\ TP} = 0.074$), 79.5% *vs.* 79.3% *vs.* 74.5% ($P_{TPF\ vs.\ TP} = 0.929$, $P_{TPF\ vs.\ PF} = 0.269$, $P_{PF\ vs.\ TP} = 0.310$), and 81.9% *vs.* 89.7% *vs.* 81.8% ($P_{TPF\ vs.\ TP} = 0.039$, $P_{TPF\ vs.\ PF} = 0.784$, $P_{PF\ vs.\ TP} = 0.021$; **Figure 1**). Results of multivariate analysis revealed that TPF plus CRT (HR, 0.617; 95% CI, 0.426–0.894; $P = 0.011$) and TP plus CRT (HR, 0.699; 95% CI, 0.498–0.982; $P = 0.039$) groups were associated with significantly improved OS but marginally significant DFS (TPF plus CRT: HR, 0.701; 95% CI, 0.491–1.002; $P = 0.051$; TP plus CRT: HR, 0.738; 95% CI, 0.532–1.025; $P = 0.07$) compared with PF plus CRT (**Supplementary Table S3**).

Sensitivity Analysis

We performed sensitivity analysis by excluding stage T3-4N0 disease, which was regarded as low risk of distant metastasis by previous trials (5, 7). In total, 32 patients were excluded, and 189 pairs were selected by PSM from the remaining patients (**Supplementary Table S4**). Consistent with the results above, TPF plus CRT and TP plus CRT still achieved higher 10-year OS (70.1% *vs.* 69.3% *vs.* 60.6%), DFS (65.7% *vs.* 66.4% *vs.* 60.2%) and DMFS (79.8% *vs.* 78.5% *vs.* 74.4%) rates than PF plus CRT (**Figure 2**). Multivariate analysis demonstrated a significant difference in OS between TPF plus CRT and PF plus CRT (HR, 0.580; 95% CI, 0.395–0.852; $P = 0.005$), while this difference between TP plus CRT and PF plus CRT was marginally significant (HR, 0.712; 95% CI, 0.503–1.008; $P = 0.056$; **Supplementary Table S5**).

Toxicity Comparison

Treatment adverse events of different IC regimens are shown in **Table 3**. As expected, the PF regimen achieved the lowest percentages of grade 3–5 toxicities (27.3%), and the TP regimen had the highest rate of grade 3–5 toxicities, which were mainly grade 3–5 neutropenia (97.1%) and febrile neutropenia (11.8%). This should be due to the application of

TABLE 2 | Results of multivariate analysis.

Endpoint	Factor	Hazard ratio (95% CI)	*P* value
OS	Alcohol intake (Yes *vs*. No)	1.421 (1.033-1.950)	0.031
	Age (≥ 50y *vs*. < 50y)	1.351 (1.054-1.730)	0.017
	N category (N2-3 *vs*. N0-1)	1.771 (1.363-2.301)	<0.0001
	Overall stage (IVA *vs*. III)	1.757 (1.354-2.282)	<0.0001
	Treatment (TPF plus CRT *vs*. PF plus CRT)	0.672 (0.491-0.920)	0.013
	Treatment (TP plus CRT *vs*. PF plus CRT)	0.664 (0.478-0.922)	0.015
DFS	Alcohol intake (Yes *vs*. No)	1.477 (1.093-1.998)	0.011
	T category (T3-4 *vs*. T1-2)	1.508 (1.043-2.180)	0.029
	N category (N2-3 *vs*. N0-1)	1.925 (1.501-2.467)	<0.0001
	Overall stage (IVA *vs*. III)	1.644 (1.286-2.101)	<0.0001
	Treatment (TPF plus CRT *vs*. PF plus CRT)	0.753 (0.544-0.994)	0.045
	Treatment (TP plus CRT *vs*. PF plus CRT)	0.701 (0.510-0.963)	0.029
DMFS	Gender (Female *vs*. male)	0.620 (0.416-0.923)	0.018
	N category (N2-3 *vs*. N0-1)	2.458 (1.179-3.364)	<0.0001
	Overall stage (IVA *vs*. III)	1.902 (1.387-2.610)	<0.0001
	Treatment (TPF plus CRT *vs*. PF plus CRT)	0.784 (0.531-1.158)	0.221
	Treatment (TP plus CRT *vs*. PF plus CRT)	0.774 (0.515-1.164)	0.219
LFFS	T category (T3-4 *vs*. T1-2)	2.069 (1.081-3.961)	0.028
	N category (N2-3 *vs*. N0-1)	1.627 (1.120-2.363)	0.011
	Treatment (TPF plus CRT *vs*. PF plus CRT)	1.002 (0.664-1.514)	0.991
	Treatment (TP plus CRT *vs*. PF plus CRT)	0.565 (0.336-0.949)	0.031

OS, overall survival; DFS, disease-free survival; DMFS, distant metastasis-free survival; LFFS, locoregional failure-free survival; CI, confidence interval; IC, induction chemotherapy; CRT, concurrent chemoradiotherapy; Pre-DNA, pre-treatment plasma EBV DNA.

P-values were calculated using an adjusted Cox proportional hazards model with backward elimination, and the following variables were included: gender (female vs. male), age (≥ 50 years vs. < 50 years), smoking (yes vs. no), drinking (yes vs. no), family history of cancer (yes vs. no), T category (T3-4 vs. T1-2), N category (N2-3 vs. N0-1), overall stage (IVA vs. III), cumulative cisplatin dose during radiotherapy (≥ 200 vs. < 200 mg/m^2), induction chemotherapy cycle (2 vs. 3-4), and treatment groups (TPF plus CRT vs. PF plus CRT, TP plus CRT vs. PF plus CRT).

a higher dose of docetaxel (75 mg/m^2). Otherwise, grade 3–5 nonhematologic toxicities were uncommon in the TP group. Compared with the PF regimen, the TPF regimen had higher grade 3–5 neutropenia (35.6% *vs*. 14.7%, $P < 0.001$), leukopenia (27.2% *vs*. 5%, $P < 0.001$), and mucositis (6.3% *vs*. 1.3%, $P = 0.004$). Undoubtedly, docetaxel additional to PF would result in greater toxicities.

DISCUSSION

Our current study reported the 10-year survival outcomes of patients with stage III-IVA NPC receiving different IC regimens plus CRT in the era of IMRT. We found that TPF plus CRT and TP plus CRT achieved significantly better OS than PF plus CRT both in the whole cohort and the selected pairs by PSM. Toxicity analysis showed that the PF regimen had the lowest percentages of grade 3–5 adverse events. To date, our study is the first one to report the 10-year therapeutic outcomes of locoregionally advanced NPC treated by IC plus CRT in the era of IMRT.

Our study only recruited patients receiving induction TPF, TP, and PF regimens because these three regimens have been used most frequently and for the longest time in our center. Their efficacy in locoregionally advanced NPC has also been verified by clinical trials (5, 6, 8–11). Although gemcitabine plus cisplatin (GP) is also effective and may have fewer adverse events (7), the insufficient follow-up duration of patients receiving this regimen precludes them from being enrolled into this study. As previous study showed that two cycles of IC could achieve comparable outcomes as three or more cycles (13), we therefore only recruited patients receiving at least two cycles to reduce the impact of the IC cycle. Consistent with previous findings (13), results of multivariate analysis in our study also did not identify the IC cycle (2 *vs*. 3-4) as an independent prognostic factor. Another interesting finding was that patients receiving the TP regimen achieved lower CCD dose than those receiving the TPF regimen. The mainly responsible reason may be that a higher dose of docetaxel (75 mg/m^2) may reduce patients' tolerance to concurrent cisplatin/nedaplatin.

Notably, 39 new events occurred 5 years after radiotherapy, accounting for 13.1% of all events. Therefore, intensive follow-up is still needed after 5 years. Among the 39 new events, distant metastasis only accounted for 30.7% and noncancer-related death accounted for 33.3%. These results indicated that distant metastasis was no longer the main cause of treatment failure after 5 years for patients receiving IC plus CRT, and we should pay attention to noncancer-related death, which may be due to treatment-related sequelae.

When analyzing all the 855 patients together, both the TPF plus CRT and TP plus CRT groups achieved significantly better OS and DFS than the PF plus CRT group. However, some comparisons in PSM or sensitivity analysis only showed marginally significant difference. The main reason contributing to this should be the decreased sample sizes, which reduced statistical power in PSM and sensitivity analysis. Generally, induction TPF and TP regimens should be more effective than the PF regimen, which was consistent with the findings of a meta-analysis that taxanes-based IC could decrease the risk of distant metastasis by above 10% for patients with stage IVA disease (14). Moreover, the effect of docetaxel additional to induction PF regimen has also been verified in head and neck

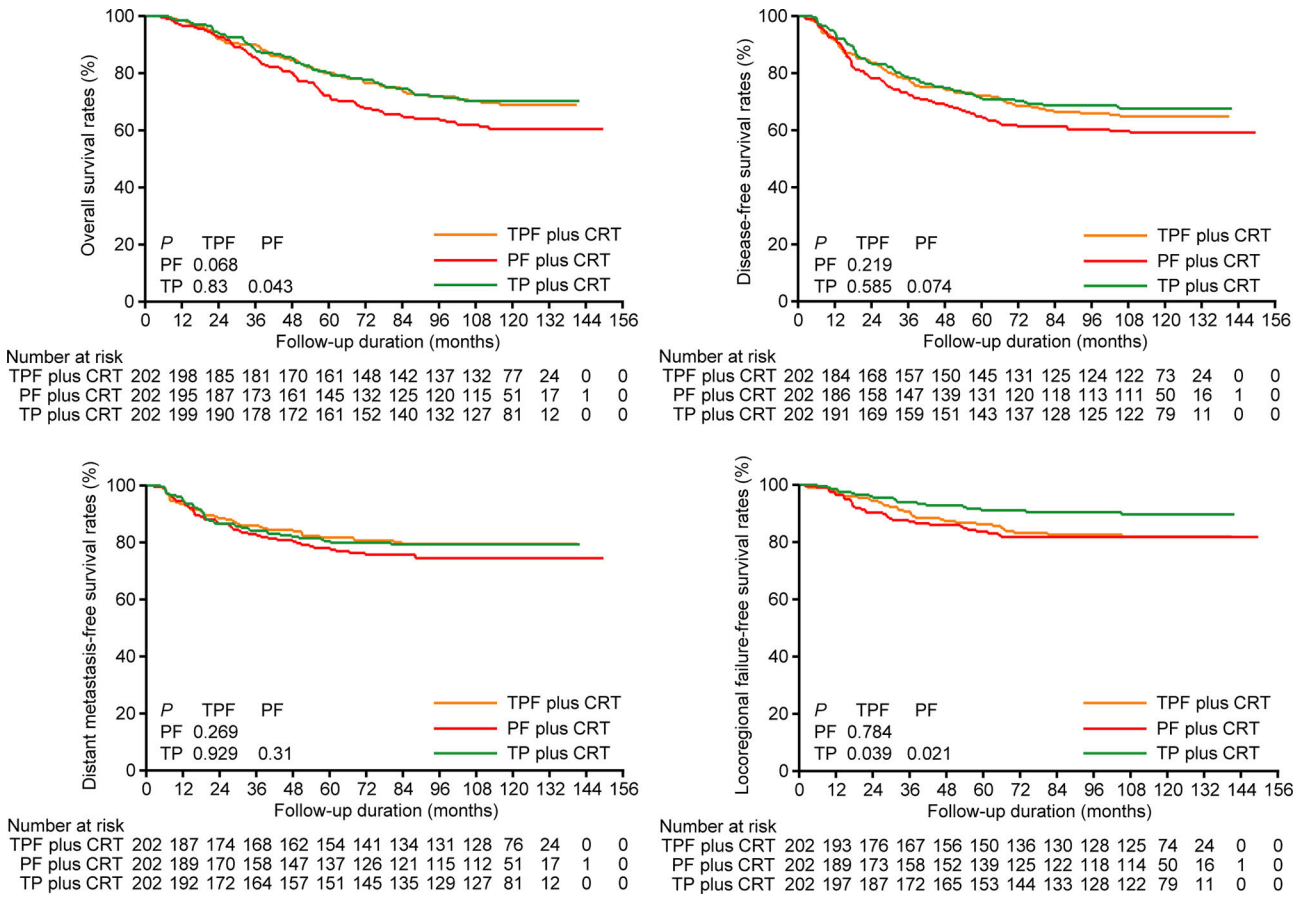

FIGURE 1 | Kaplan-Meier overall survival, disease-free survival, distant metastasis-free survival, and locoregional failure-free survival curves of patients receiving induction TPF, PF, and TP plus CRT in the 202 pairs selected by propensity score matching. TPF, docetaxel plus cisplatin and fluorouracil; PF, cisplatin plus fluorouracil; TP, docetaxel plus cisplatin.

cancers (15–18). Different from previous results that TPF was significantly better than TP with regard to DFS and OS endpoints (12), survival endpoints except LFFS did not significantly differ between the TPF plus CRT and TP plus CRT groups. There may be three reasons attributing to this discrepancy. First, the follow-up duration was much longer in our study. Second, patients with stage T3N0 were excluded in that study. Third, patients who did not receive concurrent chemotherapy were also included in that study.

Limitations of our study should also be addressed. First, many potential bias may exist in our retrospective study. We therefore set strict enrollment criteria and balanced various prognostic factors by PSM to reduce bias. Moreover, we performed sensitivity analysis to further validate our findings. Second, toxic data during IC are unavailable for most of the patients due to the retrospective nature of our study. We therefore extracted these data from previously published clinical trials. To minimize the impact of ethnic differences on adverse events, we only recruited the three clinical trials (5, 6, 10) conducted in the endemic area (mainly South China). Despite this, this result should be interpreted discreetly. Third, the relatively small sample size, especially in PSM and sensitivity analysis, precluded the production of significant differences for some endpoints, although the survival curves showed obvious differences.

MATERIALS AND METHODS

Patient Inclusion Criteria

We retrospectively reviewed the data of patients with newly diagnosed NPC who were treated at our center between 2009 and 2012. Patients would be enrolled for this study after meeting the following criteria: (1) newly diagnosed stage III-IVA disease; (2) receiving IC plus CRT; (3) IC regimens were TPF, TP, and PF and IC cycles ≥ 2; (4) concurrent chemotherapy regimen should be single-agent platinum; (5) treated by IMRT and received a total dose of at least 66 Gy; (6) no other malignancy. Notably, we included patients receiving TPF, TP, and PF regimens because they were most frequently used at that time. Moreover, the efficacy of these regimens has also been validated in

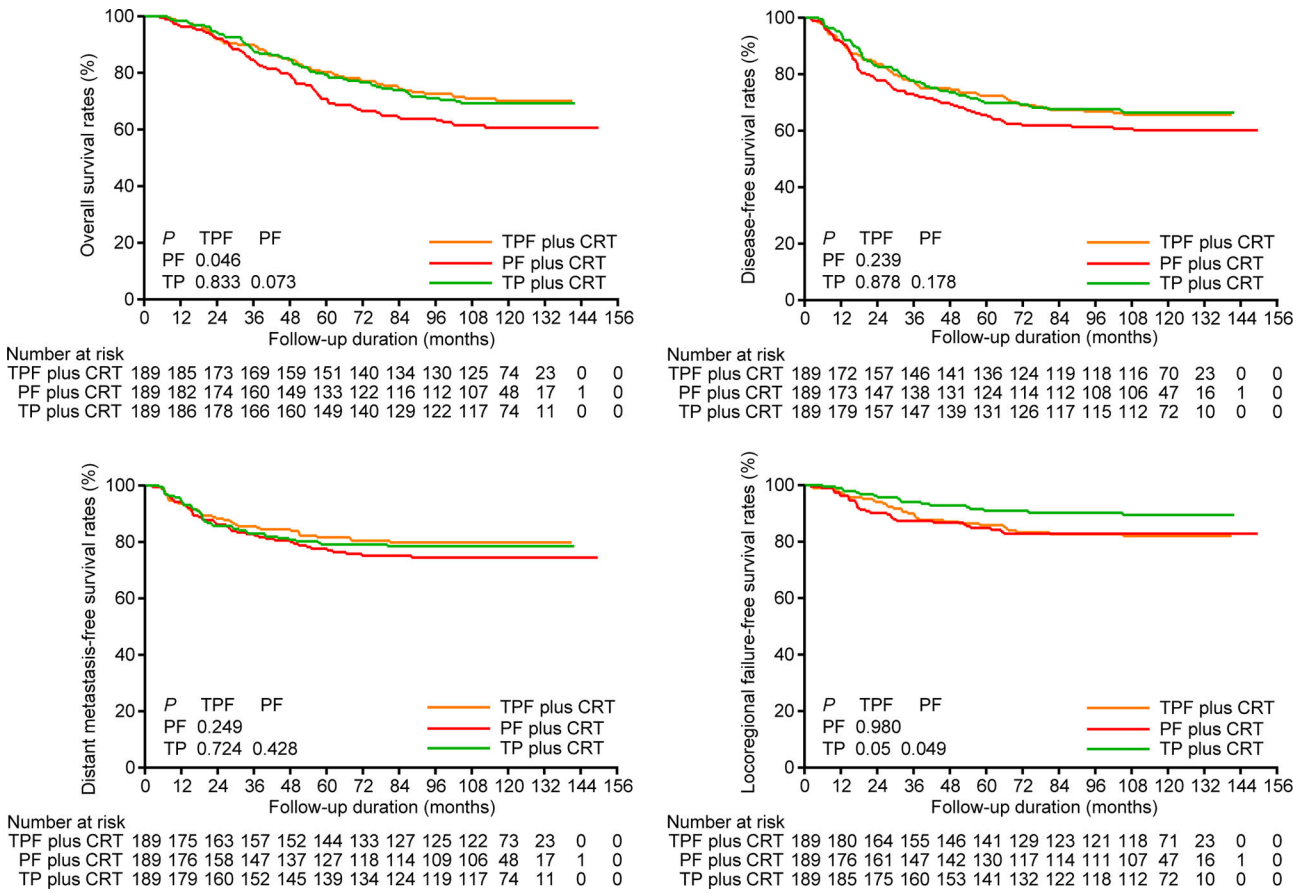

FIGURE 2 | Kaplan-Meier overall survival, disease-free survival, distant metastasis-free survival, and locoregional failure-free survival curves of patients receiving induction TPF, PF, and TP plus CRT in the 189 pairs of sensitivity analysis. TPF, docetaxel plus cisplatin and fluorouracil; PF, cisplatin plus fluorouracil; TP, docetaxel plus cisplatin.

TABLE 3 | Acute toxicity comparison during induction chemotherapy.

	TPF (n = 239)	TP (n = 34)	PF (n = 238)	*P* value
Overall Grade 3-5 (%)	43.1 (103/239)	/	27.3 (65/238)	< 0.001
Grade 3-5 Hematologic				
Neutropenia	35.6 (85/239)	97.1 (33/34)	14.7 (35/238)	< 0.001
Febrile Neutropenia	1.7 (4/239)	11.8 (4/34)	/	< 0.001
Neutropenia infection	0.8 (2/239)	/	/	/
Leukopenia	27.2 (65/239)	/	5 (12/238)	< 0.001
Anemia	0.4 (1/239)	/	0.4 (1/238)	NS
Thrombocytopenia	0	/	0	NS
Grade 3-5 Non-hematologic				
Diarrhea	7.9 (19/239)	/	/	/
Mucositis	6.3 (15/239)	/	1.3 (3/238)	0.004
Nausea/vomiting	7.5 (18/239)	8.8 (3/34)	4.2 (10/238)	NS
Hepatoxicity	2.5 (6/239)	/	0.8 (2/238)	NS
Allergic reaction	0.8 (2/239)	/	0.4 (1/238)	NS
Fatigue	/	5.9 (2/34)	/	/
Ototoxicity	0	/	0	NS
Nephrotoxicity	0	/	0	NS

TPF, docetaxel plus cisplatin with 5-fluorouracil; TP, docetaxel plus cisplatin; PF, 5-fluorouracil plus cisplatin; NS, not significant.

randomized clinical trials. The protocol of our study was approved by the Research Ethics Committee of our center, and all the analyses were carried out in accordance with the Declaration of Helsinki. Written informed consent was obtained from all patients.

Pretreatment Staging Workup

Potential patients with indicated symptoms in our hospital would receive routine staging workup including physical examination, enhanced magnetic resonance imaging (MRI) of head and neck, chest computed tomography (CT) or X-ray, abdominal CT or sonography, and whole body bone scan. ^{18}F-FDG positron emission tomography (PET)-CT would also be recommended to patients who presented with massive lymph node or bilateral cervical lymph node metastasis. Patients were restaged by one radiologist (LT) and one radiation oncologist (YH) separately, both with more than 10-year experience in the diagnosis and treatment of NPC at our center, based on the imaging data and the eighth edition of the International Union against Cancer/American Joint Committee on Cancer (UICC/AJCC) manual (19).

Induction and Concurrent Chemotherapy Treatment

IC was delivered every 3 weeks for two to four cycles, and the regimens consisted of docetaxel (75 mg/m^2, d1) plus cisplatin (75 mg/m^2, d1), cisplatin (80 mg/m^2 d1) plus 5-fluorouracil (1,000 mg/m^2 d1-d5, 120 h infusion), or docetaxel (60–75 mg/m^2, d1) plus cisplatin (60–75 mg/m^2, d1) and 5-fluorouracil (600–750 mg/m^2, d1-d5, 120-h infusion). Concurrent chemotherapy was delivered during radiotherapy and consisted of weekly cisplatin/nedaplatin (30–40 mg/m^2, d1) or tri-weekly cisplatin/nedaplatin (80–100 mg/m^2, d1).

Radiotherapy

All the patients received pre-radiotherapy evaluation to exclude any contraindication. IMRT was delivered using the simultaneous integrated boost (SIB) technique. The prescribed doses were 66–70 Gy at 2.0–2.27 Gy per fraction to the planning target volume (PTV) of nasopharynx lesion and metastatic neck lymph nodes, 56–60 Gy at 30–35 fractions to the PTV of clinically high-risk regions, and 50–56 Gy at 30–35 fractions to the PTV of clinically low-risk regions. Radiotherapy fractions were delivered once per day from Monday to Friday each week.

Toxicity of Induction Chemotherapy

Due to the retrospective nature of our study, IC-related adverse events were not recorded for most of the patients. Therefore, we extracted toxicity data from three previous clinical trials conducted in endemic areas (mainly in South China) (5, 6, 10) to perform indirect comparisons between TPF, TP, and PF regimens.

Follow-Up Strategy and Endpoints

Patients finishing the treatment would be followed according to the institutional follow-up strategies, which included enhanced MRI of head and neck, chest CT or X-ray, abdominal CT or sonography, and whole bone scan (optional) every 3 months during the first 2 years after radiotherapy, every 6 months during the third to fifth years, and annually thereafter. For patients who lived far away from our hospital, we recommended them to receive these imaging workups at local medical centers and they would be followed by telephone. Disease recurrence including local, regional, and distant metastasis (except bone) was diagnosed by pathology. Bone metastasis was mainly confirmed by imaging methods like MRI, CT, or PET-CT.

Endpoints evaluated at our study included OS (time from diagnosis to death), disease-free survival (DFS, time from diagnosis to disease progression including noncancer-related death), distant metastasis-free survival (DMFS, time from diagnosis to first distant failure), and locoregional failure-free survival (LFFS, time from diagnosis to first local or regional recurrence or both).

Statistical Methods

T-test or one-way ANOVA was applied to determine the difference between continuous variables, and chi-square test or Fisher's exact test was used for categorical variables. Propensity score matching (PSM) (20) was employed to balance covariates (T category, N category, overall stage, gender, age, alcohol intake) between the three groups. Estimated 10-year survival outcomes of OS, DFS, DMFS, and LFFS were obtained from Kaplan-Meier methods, and the differences were compared by log-rank test. Independent prognostic factors and their corresponding hazard ratios (HRs) and 95% confidence intervals (CIs) were identified by the multivariate Cox proportional hazard model. All statistical analyses were conducted using the Stata Statistical Package 12 (StataCorp LP, College Station, TX, USA), and a two-sided $P < 0.05$ indicated statistical significance.

CONCLUSION

Based on the 10-year follow-up, our current study reported and compared the efficacy of three IC regimens and uncovered that TPF plus CRT and TP plus CRT were better than PF plus CRT in improving the OS of patients with locoregionally advanced NPC. Further comparisons of TPF or TP with the GP regimen by future studies are needed to identify the optimal treatment strategy for NPC patients with locoregionally advanced disease.

DATA AVAILABILITY STATEMENT

The raw data supporting the conclusions of this article will be made available by the authors, without undue reservation.

ETHICS STATEMENT

The studies involving human participants were reviewed and approved by Sun Yat-sen University Cancer Center. Written

informed consent to participate in this study was provided by the participants' legal guardian/next of kin.

AUTHOR CONTRIBUTIONS

HP and YH contributed to study design. BC, SH, and LT collected the study data. HP, BC, and YH contributed to data analysis and interpretation. BC and SH contributed to manuscript writing. HP and YH reviewed the manuscript and contributed to quality control. All authors contributed to the article and approved the submitted version.

FUNDING

This work was funded by the National Natural Science Foundation of China (82002981).

SUPPLEMENTARY MATERIAL

The Supplementary Material for this article can be found online at: https://www.frontiersin.org/articles/10.3389/fonc.2021.765378/full#supplementary-material

REFERENCES

1. Bray F, Ferlay J, Soerjomataram I, Siegel RL, Torre LA, Jemal A. Global Cancer Statistics 2018: GLOBOCAN Estimates of Incidence and Mortality Worldwide for 36 Cancers in 185 Countries. *CA Cancer J Clin* (2018) 68:394–424. doi: 10.3322/caac.21492
2. Chen YP, Chan ATC, Le QT, Blanchard P, Sun Y, Ma J. Nasopharyngeal Carcinoma. *Lancet* (2019) 394:64–80. doi: 10.1016/S0140-6736(19)30956-0
3. Wu LR, Liu YT, Jiang N, Fan YX, Wen J, Huang SF, et al. Ten-Year Survival Outcomes for Patients With Nasopharyngeal Carcinoma Receiving Intensity-Modulated Radiotherapy: An Analysis of 614 Patients From a Single Center. *Oral Oncol* (2017) 69:26–32. doi: 10.1016/j.oraloncology.2017.03.015
4. Mao YP, Xie FY, Liu LZ, Sun Y, Li L, Tang LL, et al. Re-Evaluation of 6th Edition of AJCC Staging System for Nasopharyngeal Carcinoma and Proposed Improvement Based on Magnetic Resonance Imaging. *Int J Radiat Oncol Biol Phys* (2009) 73:1326–34. doi: 10.1016/j.ijrobp.2008.07.062
5. Sun Y, Li WF, Chen NY, Zhang N, Hu GQ, Xie FY, et al. Induction Chemotherapy Plus Concurrent Chemoradiotherapy Versus Concurrent Chemoradiotherapy Alone in Locoregionally Advanced Nasopharyngeal Carcinoma: A Phase 3, Multicentre, Randomised Controlled Trial. *Lancet Oncol* (2016) 17:1509–20. doi: 10.1016/S1470-2045(16)30410-7
6. Cao SM, Yang Q, Guo L, Mai HQ, Mo HY, Cao KJ, et al. Neoadjuvant Chemotherapy Followed by Concurrent Chemoradiotherapy Versus Concurrent Chemoradiotherapy Alone in Locoregionally Advanced Nasopharyngeal Carcinoma: A Phase III Multicentre Randomised Controlled Trial. *Eur J Cancer* (2017) 75:14–23. doi: 10.1016/j.ejca.2016.12.039
7. Zhang Y, Chen L, Hu GQ, Zhang N, Zhu XD, Yang KY, et al. Gemcitabine and Cisplatin Induction Chemotherapy in Nasopharyngeal Carcinoma. *N Engl J Med* (2019) 381:1124–35. doi: 10.1056/NEJMoa1905287
8. Frikha M, Auperin A, Tao Y, Elloumi F, Toumi N, Blanchard P, et al. A Randomized Trial of Induction Docetaxel-Cisplatin-5FU Followed by Concomitant Cisplatin-RT Versus Concomitant Cisplatin-RT in Nasopharyngeal Carcinoma (GORTEC 2006-02). *Ann Oncol* (2018) 29:731–6. doi: 10.1093/annonc/mdx770
9. Yang Q, Cao SM, Guo L, Hua YJ, Huang PY, Zhang XL, et al. Induction Chemotherapy Followed by Concurrent Chemoradiotherapy Versus Concurrent Chemoradiotherapy Alone in Locoregionally Advanced Nasopharyngeal Carcinoma: Long-Term Results of a Phase III Multicentre Randomised Controlled Trial. *Eur J Cancer* (2019) 119:87–96. doi: 10.1016/j.ejca.2019.07.007
10. Hui EP, Ma BB, Leung SF, King AD, Mo F, Kam MK, et al. Randomized Phase II Trial of Concurrent Cisplatin-Radiotherapy With or Without Neoadjuvant Docetaxel and Cisplatin in Advanced Nasopharyngeal Carcinoma. *J Clin Oncol* (2009) 27:242–9. doi: 10.1200/JCO.2008.18.1545
11. Li WF, Chen NY, Zhang N, Hu GQ, Xie FY, Sun Y, et al. Concurrent Chemoradiotherapy With/Without Induction Chemotherapy in Locoregionally Advanced Nasopharyngeal Carcinoma: Long-Term Results of Phase 3 Randomized Controlled Trial. *Int J Cancer* (2019) 145:295–305. doi: 10.1002/ijc.32099
12. Peng H, Tang LL, Chen BB, Chen L, Li WF, Mao YP, et al. Optimizing the Induction Chemotherapy Regimen for Patients With Locoregionally Advanced Nasopharyngeal Carcinoma: A Big-Data Intelligence Platform-Based Analysis. *Oral Oncol* (2018) 79:40–6. doi: 10.1016/j.oraloncology.2018.02.011
13. Peng H, Chen L, Li WF, Zhang Y, Liu LZ, Tian L, et al. Optimize the Cycle of Neoadjuvant Chemotherapy for Locoregionally Advanced Nasopharyngeal Carcinoma Treated With Intensity-Modulated Radiotherapy: A Propensity Score Matching Analysis. *Oral Oncol* (2016) 62:78–84. doi: 10.1016/j.oraloncology.2016.10.014
14. Zhang LN, Gao YH, Lan XW, Tang J, OuYang PY, Xie FY. Effect of Taxanes-Based Induction Chemotherapy in Locoregionally Advanced Nasopharyngeal Carcinoma: A Large Scale Propensity-Matched Study. *Oral Oncol* (2015) 51:950–6. doi: 10.1016/j.oraloncology.2015.07.004
15. Posner MR, Lefebvre JL. Docetaxel Induction Therapy in Locally Advanced Squamous Cell Carcinoma of the Head and Neck. *Br J Cancer* (2003) 88:11–7. doi: 10.1038/sj.bjc.6600685
16. Posner MR, Hershock DM, Blajman CR, Mickiewicz E, Winquist E, Gorbounova V, et al. Cisplatin and Fluorouracil Alone or With Docetaxel in Head and Neck Cancer. *N Engl J Med* (2007) 357:1705–15. doi: 10.1056/NEJMoa070956
17. Vermorken JB, Remenar E, van Herpen C, Gorlia T, Mesia R, Degardin M, et al. Cisplatin, Fluorouracil, and Docetaxel in Unresectable Head and Neck Cancer. *N Engl J Med* (2007) 357:1695–704. doi: 10.1056/NEJMoa071028
18. Pointreau Y, Garaud P, Chapet S, Sire C, Tuchais C, Tortochaux J, et al. Randomized Trial of Induction Chemotherapy With Cisplatin and 5-Fluorouracil With or Without Docetaxel for Larynx Preservation. *J Natl Cancer Inst* (2009) 101:498–506. doi: 10.1093/jnci/djp007
19. Pan JJ, Ng WT, Zong JF, Chan LL, O'Sullivan B, Lin SJ, et al. Proposal for the 8th Edition of the AJCC/UICC Staging System for Nasopharyngeal Cancer in the Era of Intensity-Modulated Radiotherapy. *Cancer* (2016) 122:546–58. doi: 10.1002/cncr.29795
20. Austin PC. The Relative Ability of Different Propensity Score Methods to Balance Measured Covariates Between Treated and Untreated Subjects in Observational Studies. *Med Decis Making* (2009) 29:661–77. doi: 10.1177/0272989X09341755

Conflict of Interest: The authors declare that the research was conducted in the absence of any commercial or financial relationships that could be construed as a potential conflict of interest.

Publisher's Note: All claims expressed in this article are solely those of the authors and do not necessarily represent those of their affiliated organizations, or those of the publisher, the editors and the reviewers. Any product that may be evaluated in this article, or claim that may be made by its manufacturer, is not guaranteed or endorsed by the publisher.

frontiers in Oncology

ORIGINAL RESEARCH
published: 15 October 2021
doi: 10.3389/fonc.2021.720835

MicroRNA-483-5p Predicts Poor Prognosis and Promotes Cancer Metastasis by Targeting *EGR3* in Nasopharyngeal Carcinoma

Xi-Zhao Li[1†], Yi-Jun Tu[2†], Ting Zhou[1], Jiang-Bo Zhang[1], Ruo-Wen Xiao[1], Da-Wei Yang[1], Pei-Fen Zhang[1], Peng-Tao You[2] and Xiao-Hui Zheng[1*]*

[1] State Key Laboratory of Oncology in South China, Collaborative Innovation Center for Cancer Medicine, Guangdong Key Laboratory of Nasopharyngeal Carcinoma Diagnosis and Therapy, Sun Yat-sen University Cancer Center, Guangzhou, China, [2] Hubei Key Laboratory of Resources and Chemistry of Chinese Medicine, College of Pharmacy, Hubei University of Chinese Medicine, Wuhan, China

Background: MicroRNAs, as small non-coding RNAs, play an important role in tumorigenesis. MiR-483-5p was found to have a significant increase as a diagnostic biomarker of nasopharyngeal carcinoma (NPC), not only in plasma from NPC patients but also in tumor cell lines and biopsy tissues in our previous study. However, its function and mechanism in NPC are still unclear.

Methods: Tissue microarray including 178 primary NPC and 35 adjacent non-cancerous nasopharyngeal mucosal tissues was used to further validate the overexpression of miR-483-5p. Wound healing and invasion assays were conducted to verify its biological function. RNA sequencing (RNA-seq) and dual-luciferase reporter assay was performed to explore its target, and it was verified in fresh biopsy tissues from 23 NPC patients and 9 patients with chronic nasopharyngitis.

Results: MiR-483-5p was highly expressed in NPC tissues than in adjacent non-cancerous tissues. It was found to have a significant correlation with poor overall survival (OS) [hazard ratio (HR) = 2.89, 95% confidence interval (CI) = 1.00–8.35, p = 0.041] and progression-free survival (PFS) (HR = 1.95, 95%CI = 1.06–3.60, p = 0.029) of NPC patients. Silencing of its expression inhibited the migratory and invasive capacities of NPC cells *in vitro*. *EGR3* (early growth response 3) was identified as a direct target, and inhibiting miR-483-5p expression markedly enhanced the expression of *EGR3* at both the mRNA and protein levels. Besides, a significant decrease of *EGR3* expression was found in fresh biopsy tissues from NPC patients, in contrast to miR-483-5p expression. Furthermore, directly decreasing the expression of *EGR3* could enhance the migration and invasion of NPC cells.

OPEN ACCESS

Edited by:
Yong Yin,
Shandong Cancer Hospital, China

Reviewed by:
Michael Kharouta,
University Hospitals Seidman Cancer Center, United States
Hongxing Liu,
First Affiliated Hospital of Guangzhou Medical University, China
Yong-Chao Qiao,
Guilin Medical University, China

***Correspondence:**
Peng-Tao You
tptyou@hbtcm.edu.cn
Xiao-Hui Zheng
zhengxh@sysucc.org.cn

[†]These authors have contributed equally to this work

Specialty section:
This article was submitted to Head and Neck Cancer, a section of the journal Frontiers in Oncology

Received: 05 June 2021
Accepted: 28 September 2021
Published: 15 October 2021

Citation:
Li X-Z, Tu Y-J, Zhou T, Zhang J-B, Xiao R-W, Yang D-W, Zhang P-F, You P-T and Zheng X-H (2021) MicroRNA-483-5p Predicts Poor Prognosis and Promotes Cancer Metastasis by Targeting EGR3 in Nasopharyngeal Carcinoma. Front. Oncol. 11:720835. doi: 10.3389/fonc.2021.720835

Conclusion: The newly identified miR-483-5p/*EGR3* pathway provides further insights into the development and metastasis of NPC and may provide a potential therapeutic target for NPC treatment in order to improve survival of NPC patients.

Keywords: nasopharyngeal carcinoma, *EGR3*, miR-483-5p, prognosis, metastasis

INTRODUCTION

Nasopharyngeal carcinoma (NPC) is a common head and neck malignancy. Globally, the highest incident of NPC is found in southern China and southeastern Asia, where the annual incidence is about 20–50 cases per 100,000 people (1, 2). Previous studies have demonstrated that genetic susceptibility, endemic environmental factors, and Epstein–Barr virus (EBV) infection constitute the three etiological contributors to NPC (3). Although the overall survival rate is approximately 90% in patients with early clinical stage after therapy, unfortunately, most patients are diagnosed with advanced stage at their first visit, and the survival rate decreases to less than 50% (4). Recurrence and metastasis, especially high metastasis, are the major reasons for treatment failure (5). Therefore, there is a great need to fully disclose the molecular mechanism underlying the recurrence and metastasis of NPC.

MicroRNAs (miRNAs) are non-coding RNA molecules, about 19–25 nucleotides in length, negatively regulating gene expression at the posttranscriptional level through base paring with the 3′ untranslated region (3′-UTR) of the messenger RNA (mRNA) transcripts (6). In tumor biology, many studies have proven the importance of miRNAs in promoting tumor growth, metastasis, angiogenesis, and immune evasion through controlling the expressions of their target genes (7, 8). Besides, miRNAs have been developed as important biomarkers in predicting tumor prognosis (9). They provide new therapeutic targets in supporting personalized tumor therapy.

In NPC, certain amounts of valuable miRNAs have been identified in previous studies (10, 11). Some miRNAs have low expressions in tumor tissues and act as tumor suppressor genes, while some other miRNAs are highly expressed and act as oncogenes. They play important roles in the pathogenesis of NPC by regulating specific target genes that are involved in various cellular processes and pathways. The potential utility of some miRNAs as prognostic biomarkers has also been discussed (12, 13). Because of the deep influence of EBV infection, some EBV-related miRNAs have also been found to play roles in NPC (14–16). Despite great achievements having been reached, discovering more functional miRNAs is still necessary to help fully understand the mechanism of occurrence and development of NPC.

In our previous study, miR-483-5p was found to be highly expressed in plasma from NPC patients, showing its potential application in the diagnosis of NPC. Furthermore, its high expression was also validated in tumor cell lines and frozen biopsy tissues, indicating its role in causing NPC (17). In this study, the mechanism of miR-483-5p in promoting NPC was focused on. Firstly, miR-483-5p was found to have potential application in the prediction of poor prognosis. Secondly, it exerted a function in the promotion of metastasis by enhancing tumor migration and invasion. Finally, *EGR3* (early growth response 3) was identified as a functional target gene and validated by the luciferase reporter assay. Consistent with the effect of a high expression of mir-483-5p, silencing of *EGR3* could enhance the migration and invasion of NPC cell lines. The newly identified miR-483-5p/*EGR3* pathway expands our understanding of the role of mir-483-5p and may provide prognostic indicators and a novel therapeutic target for the treatment of NPC.

MATERIALS AND METHODS

Cell Lines and Clinical Specimens

Human NPC cell lines (CNE-1 and 5-8F) were maintained in RPMI-1640 (Invitrogen, Carlsbad, CA, USA) supplemented with 10% fetal bovine serum (FBS) (Gibco, Grand Island, NY, USA). Formalin-fixed paraffin-embedded tissues of 178 primary NPC tissues and 35 adjacent non-cancerous nasopharyngeal mucosal tissues were included in the NPC tissue microarray. The detailed characteristics of the study population are presented in **Supplementary Table S1**. Besides, 32 fresh biopsy tissues from 23 NPC patients and nine patients with chronic nasopharyngitis were used for the detection of *EGR3*. The characteristics of these patients are presented in **Supplementary Table S2**. The biopsy tissues were collected at the time of diagnosis and were preserved using RNAlater (Invitrogen) in a −80°C cryogenic refrigerator before use. All samples were collected from Sun Yat-sen University Cancer Center (SYSUCC; Guangzhou, China) and reviewed by pathologists to confirm the diagnosis. The research protocols were approved by the Institutional Ethical Review Board of Sun Yat-sen University Cancer Center, and informed consent was obtained from each patient.

RNA Extraction, Reverse Transcription, and Quantitative RT-PCR

Total RNA from cell lines and fresh biopsy tissues was extracted with TRIzol (Invitrogen) according to the manufacturer's instructions. Complementary DNA (cDNA) was synthesized with the PrimeScript RT Reagent Kit (Takara, Tokyo, Japan). GAPDH was used as the internal control for the quantification of *EGR3*. Quantitative RT-PCR was carried out on the Roche LightCycler®480 96 Real-Time PCR platform, and gene expression was quantified using the $2^{-\Delta\Delta CT}$ method.

In Situ Hybridization

In situ hybridization (ISH) was conducted on the tissue microarray, which included 178 primary NPC tissues and 35

adjacent non-cancerous nasopharyngeal mucosal tissues. MiR-483-5p expression was detected by the digoxigenin (DIG)-labeled locked nucleic acid (LNA)-based probe (Qiagen, Hilden, Germany). Washing and scanning were carried out according to the manufacturer's protocols. The sections were scored independently by two pathologists, and the staining index was generated as the product of the staining intensity (0, no staining; 1, weak, light yellow; 2, moderate, yellow brown; 3, strong, brown) and the proportion of positive cells (1, 0%–25%; 2, 26%–50%; 3, 51%–75%; 4, 76%–100%).

Vectors and Transfection

The miRNA inhibitor, scrambled negative control (NC) oligonucleotides, and *EGR3* small interfering RNA (siRNA) were purchased from RiBoBio (Guangzhou, China). Transient transfection was performed using Lipofectamine 2000 (Invitrogen) in OPTI-MEM media according to the manufacturer's protocol.

Wound Healing and Invasion Assays

Cell migration was measured with a scratch wound healing assay. Transfected 5-8F cells were seeded into six-well plates, subjected to serum starvation for 24 h in serum-free media, then an artificial wound was created in the confluent cell monolayer using a 200-μl pipette tip. Images were taken at 0 and 24 h using an inverted microscope. For invasion assays, 5×10^4 cells were placed into a Matrigel-coated Transwell chamber (BD Biosciences, Wokingham, UK) with an 8-μm pore size. The non-invading cells in the bottom of the chamber were fixed with 100% methanol and stained with crystal violet. The experiments were performed in triplicate.

Luciferase Reporter Assay

The *EGR3* wild-type (Wt) and mutant (Mt) 3′-UTR sequences were synthesized and sub-cloned into the psiCHECK luciferase reporter plasmid (Promega, Madison, WI, USA). 5-8F was seeded into a 12-well plate at a density of 5×10^6 and each recombinant luciferase reporter plasmid and the miR-483-5p mimic were co-transfected using Lipofectamine 2000 reagent (Invitrogen) according to the manufacturer's instructions. The psiCHECK promoter vector was used as the control, and the pRL-SV40 Renilla luciferase vector (Promega) was used to normalize the activity of firefly luciferase. Twenty-four hours later, the luciferase activity in each well was detected using the Dual-Luciferase Reporter Assay System (Promega).

Western Blot

Total protein was extracted from cultured cells using RIPA buffer containing phenylmethanesulfonyl fluoride (PMSF) and quantified using a bicinchoninic acid (BCA) protein assay kit (Beyotime, Haimen, China). Protein lysates were subjected to SDS-PAGE and transferred onto polyvinylidene fluoride membranes (Millipore, Billerica, MA, USA), followed by incubation first with an *EGR3* antibody (Invitrogen) and then with a secondary antibody. β-actin antibody was used as the loading control, and the bands were detected by enhanced chemiluminescence.

Treatment and Follow-Up

All patients involved in the tissue array were treated following the routine practice of SYSUCC. Patients were followed up every 3 months during the first 2 years, semi-annually during years 3–5, and annually thereafter until death or loss to follow-up. Our primary endpoint was overall survival (OS; time from NPC diagnosis to death from any cause or censored at the date of last follow-up) and the secondary endpoint was progression-free survival (PFS; time from NPC diagnosis to the first local regional recurrence, or distant metastasis, or death from any cause, or censored at the date of last follow-up).

Statistical Analysis

Data are presented as the mean ± SD. Student's *t*-test was used for comparisons between groups. Univariate and multivariate logistic regressions were performed to assess the associations between the clinical characteristics and the ISH scores. For survival analyses, survival curves were depicted using the Kaplan–Meier method and compared using the log-rank test. Multivariate Cox regression analyses including age, gender, American Joint Committee on Cancer (AJCC) stage, and the ISH sores were performed. All statistical analysis was performed using R software, version 4.0.2 (http://www.r-project.org), and a two-sided p-value <0.05 was considered statistically significant.

RESULTS

Overexpression of miR-483-5p Was Associated With Poor Prognosis in NPC Patients

High expressions of miR-483-5p were found in the plasma, tumor cell lines, and frozen tumor tissues from NPC patients in our previous study. To further validate its high expression, the expression level of miR-483-5p was determined using ISH in paraffin-embedded tissue microarray, which contained 178 NPC tissues and 35 non-cancerous nasopharyngeal mucosal tissues. The results showed that the ISH scores of miR-483-5p were significantly higher in tumor tissues than those in non-tumor tissues ($p < 0.0001$) (**Figure 1A**). An optimal cutoff value (COV) (ISH score = 7) for high and low miR-483-5p expressions was determined (**Figure 1B**), and 59 of the 178 (33.2%) samples were classified as high-miR-483-5p-expressing tissues (ISH scores >7). Further survival analysis established that NPC patients with a high miR-483-5p expression had significantly poorer OS ($p = 0.041$) (**Figure 1C**) and PFS ($p = 0.029$) (**Figure 1D**). Furthermore, multivariate Cox regression analysis found that miR-483-5p expression was an independent prognostic factor for PFS (HR = 1.87, 95%CI = 1.01–3.45, $p = 0.046$) (**Supplementary Table S3**). However, no significant correlations were found between miR-483-5p and any other clinical features (**Supplementary Table S4**). These results suggest that the expression level of miR-483-5p is correlated with clinical outcomes and may be a promising prognostic biomarker in NPC patients.

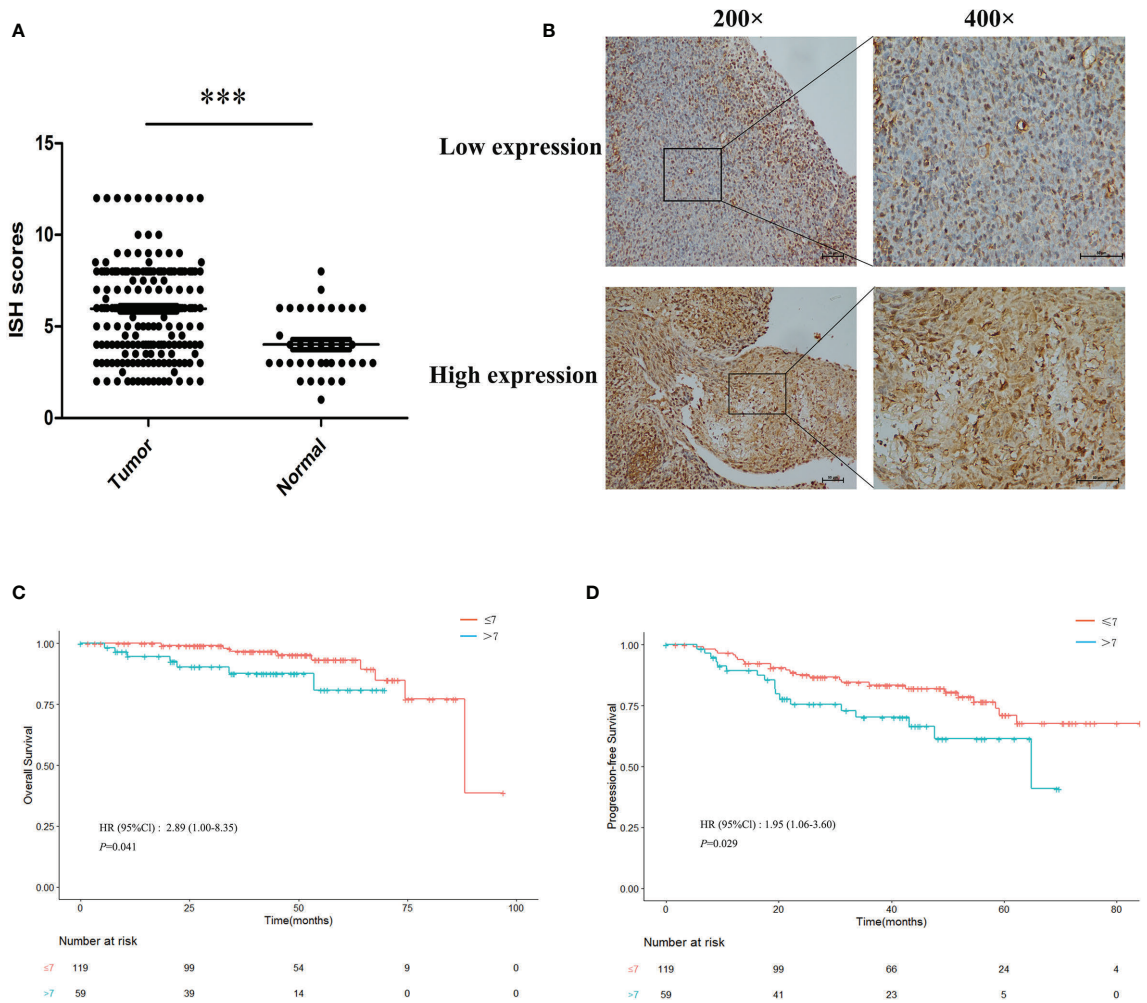

FIGURE 1 | Overexpression of miR-483-5p was associated with poor prognosis in nasopharyngeal carcinoma (NPC) patients. **(A)** *In situ* hybridization (ISH) scores in NPC tissues compared with non-tumor tissues. **(B)** ISH staining of miR-483-5p in representative NPC cases with low and high miR-483-5p expressions (magnification, ×200 and ×400). **(C, D)** Survival curves for patients with NPC according to the ISH scores. ***P < 0.001.

MiR-483-5p Promoted NPC Cell Migration and Invasion *In Vitro*

To determine whether ectopic expression of miR-483-5p could affect the migration and invasion abilities of NPC cells *in vitro*, wound healing and invasion assays were performed in the 5-8F and CNE-1 tumor cell lines. Because of its high expression, interfering with the miR-483-5p expression was adopted in this study. In the scratch wound healing assays, it was shown that 5-8F and CNE-1 cells transfected with the miR-483-5p inhibitor both migrated much more slowly than those transfected with the miR-Ctrl and NC (**Figure 2A**). The invasion assays showed that transfection of the miR-483-5p inhibitor significantly reduced the invasion abilities of 5-8F and CNE-1 cells (**Figure 2B**). These results suggest that the high expression of miR-483-5p promoted NPC cell migration and invasion. However, change of cell proliferation was not observed (data not shown).

EGR3 Was a Direct Target of miR-483-5p in 5-8F NPC Cell Line

To further explore the molecular mechanism by which miR-483-5p exerts its biological function, whole-transcriptome sequencing assays were performed in the Majorbio cloud platform (https://cloud.majorbio.com). There were 101 genes with significant differences (adjusted $p < 0.05$). According to the fold change, seven genes, namely, *CCL5*, *S100A8*, *FGF21*, *S100P*, *WNT6*, *CEBPE*, and *EGR3*, were selected as the candidate targets of miR-483-5p (**Supplementary Table S5**). Afterwards, *EGR3* was predicted as a potential target gene of miR-483-5p, performed using RNA22Sites (https://cm.jefferson.edu/rna22/Interactive/). To confirm whether *EGR3* was negatively regulated by miR-483-5p, luciferase reporter vectors were constructed containing the Wt or Mt miR-483-5p target sequences of the *EGR3* 3′-UTR (**Figure 3A**). Overexpression of

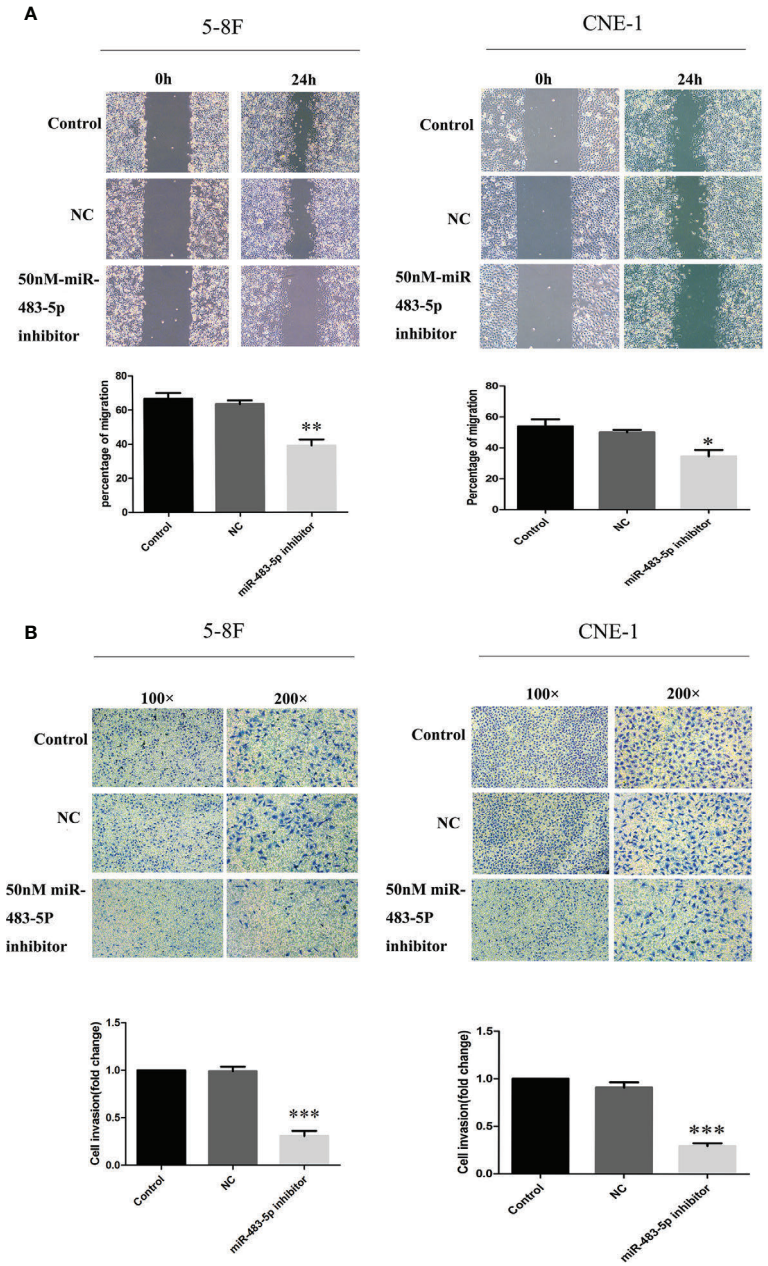

FIGURE 2 | MiR-483-5p promoted the migration and invasion of nasopharyngeal carcinoma (NPC) cells *in vitro*. **(A)** Cell migration ability measured by the scratch wound healing assay. **(B)** Cell invasion ability measured by Boyden chamber assays with Matrigel. $^{*}p < 0.05$, $^{**}p < 0.01$, $^{***}p < 0.001$.

miR-483-5p significantly inhibited the luciferase activity of the Wt *EGR3* 3′-UTR reporter gene, but not the Mt reporter gene (**Figure 3B**). In addition, it was further found that the inhibition of miR-483-5p expression increased the expression of *EGR3* at both the protein and mRNA levels (**Figures 3C, D**, respectively) in cell lines. These results demonstrate that *EGR3* is a direct target gene of miR-483-5p.

EGR3 Was Decreased in NPC Clinical Specimens and Its Decrease Could Enhance NPC Cell Migration and Invasion *In Vitro*

The mRNA expression level of *EGR3* was further measured in fresh biopsy tissues containing 23 NPC tissues and nine non-cancerous nasopharyngeal mucosal tissues by quantitative PCR (q-PCR).

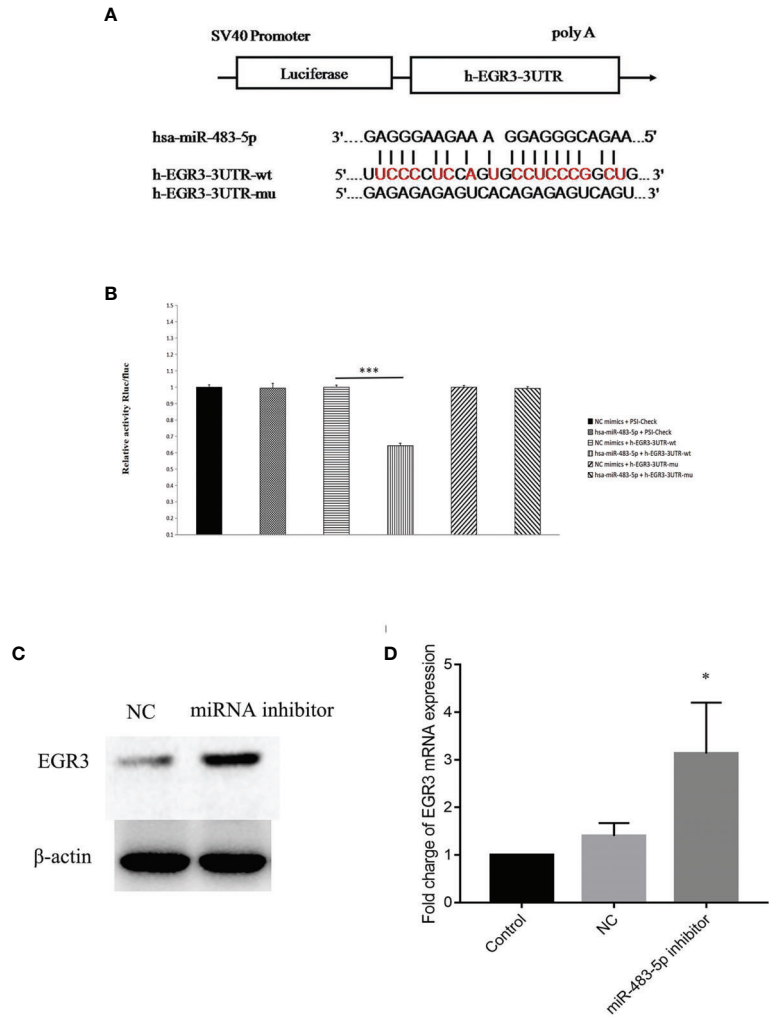

FIGURE 3 | *EGR3* was a direct target of miR-483-5p in nasopharyngeal carcinoma (NPC) cell lines. **(A)** Wild-type (Wt) or mutant (Mt) target sequences of the *EGR3* mRNA 3′-UTR. **(B)** The luciferase reporter assay was performed in 5-8F cells transfected with the psiCHECK luciferase reporter plasmid containing the Wt 3′-UTR of *EGR3*, Mt 3′-UTR of *EGR3*, a miR-483-5p mimic, and the negative control. **(C)** Western blot assay of the protein level of *EGR3* in 5-8F cells after transfection with the miR-483-5p inhibitor. **(D)** Relative quantification of the mRNA expression of *EGR3* by quantitative RT-PCR in 5-8F cells after transfection with the miR-483-5p inhibitor.*$p < 0.05$, ***$p < 0.001$.

As expected, the results showed that *EGR3* was significantly downregulated in tumor tissues compared with non-tumor tissues ($p = 0.0002$) (**Figure 4A**). As the inhibition of miR-483-5p has been shown to decrease the migration and invasion of NPC cells, we supposed that inhibiting the expression of *EGR3*, being a target gene of miR-483-5p, might play an opposite role in NPC. To test this hypothesis, endogenous *EGR3* in 5-8F cells was silenced by the EGR3-specific siRNA oligo (**Figure 4B**). In the wound healing assays, 5-8F cells transfected with siEGR3 migrated faster than those transfected with scrambled siRNA control and NC (**Figure 4C**). In the invasion assays, transfection with siEGR3 significantly increased the invasion ability of 5-8F cells (**Figure 4D**). Taken together, our study demonstrates that *EGR3* is a direct and functional mediator of miR-483-5p in NPC.

DISCUSSION

In a previous work, we found that miR-483-5p was overexpressed in the plasma, tumor cell lines, and frozen biopsy tissues from NPC patients. These results highly indicated its role in promoting NPC occurrence (17). However, there are few studies exploring its role in NPC. In this study, our results further showed that a high expression of miR-483-5p was correlated with inferior OS and PFS in NPC patients. It could promote the cell migration and invasion abilities of NPC *in vitro* by targeting *EGR3*. These findings provide new insights into the molecular functions of miR-483-5p, which could be used as a promising prognostic biomarker and a potential therapeutic target for NPC patients.

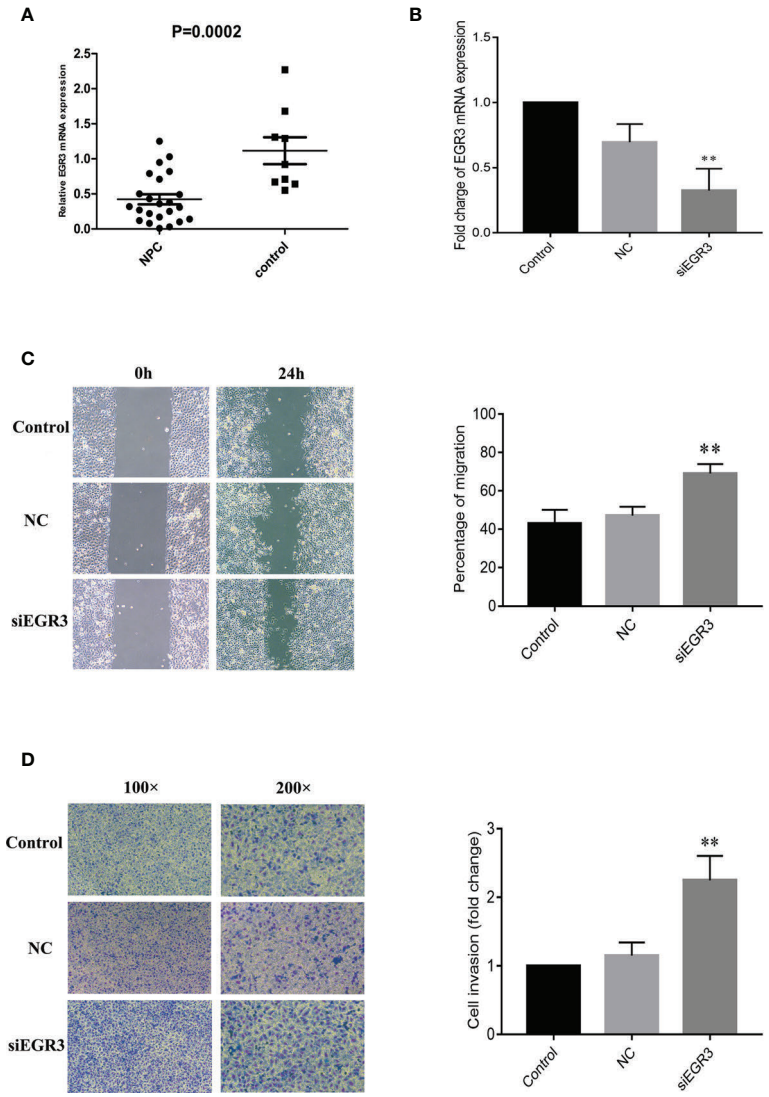

FIGURE 4 | *EGR3* was decreased in nasopharyngeal carcinoma (NPC) clinical specimens, and its decrease could enhance NPC cell migration and invasion *in vitro*. **(A)** Relative expression of *EGR3* mRNA by quantitative RT-PCR in NPC tissues compared with non-tumor tissues. **(B)** Relative expression of *EGR3* mRNA by quantitative RT-PCR in 5-8F cells after transfection with siRNA. **(C)** Cell migration ability measured by the scratch wound healing assay. **(D)** Cell invasion ability measured by Boyden chamber assays with Matrigel. $^{**}p < 0.01$.

Reliable molecular biomarkers are needed for accurate prognosis. In NPC, some molecular signatures have shown potential application in prognosis prediction. For example, Liu et al. reported that a molecular signature containing five miRNAs (miR-142-3p, miR-29c, miR-26a, miR-30e, and miR-93) was significantly associated with overall, disease-free, and distant metastasis-free survival (12). Another study reported a non-overlapping four-miRNA prognostic signature, namely, miR-34c, miR-140, miR-154, and miR-449b, associated with distant metastasis in NPC (18). Considering their association with tumor metastasis, these abnormally expressed miRNAs may play roles in promoting tumor migration and invasion. Therefore, further validation studies will be essential for driving the use of these miRNAs in clinical practice for NPC. On the one hand, a high expression of miR-483-5p was not only found in the plasma, tumor cell lines, and frozen biopsy tissues from NPC patients in our study but it was also validated in the plasma from NPC patients in another study (19). On the other hand, the prognostic ability of miR-483-5p was observed in other tumors, such as in esophageal cancer (20), adrenocortical cancer (21), and hepatocellular carcinoma (22). These results provide strong evidence for its further application in prognosis prediction. As expected, miR-483-5p was further found to be associated with OS and PFS in NPC in this study (**Figure 1**).

Consistent overexpression of miR-483-5p was found in multiple types of clinical samples, such as plasma, tumor cell clines, frozen biopsy tissues, and paraffin-embedded tissues from NPC patients. These strongly suggest the potential role of miR-483-5p in NPC. Therefore, further experiments were conducted, and miR-483-5p was found to play a role in regulating tumor cell migration and invasion,

but not proliferation (**Figure 2**). Two representative cell lines, a highly metastatic cell line (5-8F) and a low metastatic cell line (CNE1), were both tested. Inhibition of miR-483-5p significantly reduced the migration and invasion of NPC cell lines. Therefore, it was identified as an oncogene in NPC. However, a different function of miR-483-5p in different cancers has been shown. For example, it was found to promote cancer progression, migration, or invasion in esophageal cancer (20), gastric cancer (23), and prostate cancer (24). In contrast, it was reported to exert a function in inhibiting cell proliferation or metastasis in Wilms' tumor (25), renal cell carcinoma (26), and glioma (27). However, its effects on the promotion of metastasis in NPC have not been reported previously.

MiRNAs exert their function by interacting with their target genes *via* base pairing to the 3′-UTR of mRNA (7, 8). Several genes such as *KCNQ1* (20), *PRM5* (24), *MKNK1* (25), and *ERK1* (27) have been identified as the target genes of mir-483-5p in esophageal cancer, prostate cancer, Wilms' tumor, and glioma, respectively. Therefore, it seems that miR-483-5p carried out its function by regulating different target genes. Several candidate genes were identified by RNA sequencing (RNA-seq), and *EGR3* was finally validated as the direct target gene (**Figure 3**). *EGR3* is a zinc finger transcription factor and has been studied primarily in the context of neurodevelopment, autoimmunity, inflammation, and angiogenesis (28–32). Recently, several studies have shown that the expression of *EGR3* was frequently dysregulated in a variety of cancer types (33, 34). To the best of our knowledge, these observations provide the first evidence of miR-483-5p acting as a repressor of *EGR3*. The decreased expression of *EGR3* was also further validated in fresh biopsy tissues, and its decrease in tumor cell line was also found to promote the migration and invasion capacity (**Figure 4**). Besides, some other genes were found to be highly expressed, with high mir-483-5p expression, by RNA-seq. Therefore, these genes might be indirectly regulated by mir-483-5p through targeting other genes.

In conclusion, we provided the first evidence that miR-483-5p promoted the migration of NPC cell by targeting *EGR3* and may serve as a promising prognostic biomarker and therapeutic target for NPC patients. The causal link between miRNAs and tumor initiation and progression further underscores their potential utility as accurate and reliable biomarkers.

DATA AVAILABILITY STATEMENT

The original contributions presented in the study are included in the article/**Supplementary Material**. Further inquiries can be directed to the corresponding authors.

ETHICS STATEMENT

The studies involving human participants were reviewed and approved by the Institutional Ethical Review Board of Sun Yat-sen University Cancer Center. The patients/participants provided written informed consent to participate in this study. Written informed consent was obtained from the individual(s) for the publication of any potentially identifiable images or data included in this article.

AUTHOR CONTRIBUTIONS

P-TY and X-HZ conceived, designed the study, and wrote the final draft. X-ZL carried out the experiments and drafted the manuscript. Y-JT carried out the experiments. J-BZ, R-WX, and P-FZ assisted in the experiments. TZ and D-WY performed data collection and analysis. All authors contributed to the article and approved the submitted version.

FUNDING

This work was supported by the National Natural Science Foundation of China (grant no. 81802708), the Key Area Research and Development Program of Guangdong Province, China (grant no. 2019B110233004), the Science and Technology Planning Project of Guangdong Province, China (grant no. 2019B030316031), the Science and Technology Planning Project of Guangzhou City, China (grant nos. 201804020094 and 201904010467), the Fundamental Research Funds for the Central Universities (grant no. 19ykpy185), and the Sino-Sweden Joint Research Program (grant no. 81861138006). The funder had no role in the study design, participant recruitment, data collection, data analysis, data interpretation, or writing of the report.

SUPPLEMENTARY MATERIAL

The Supplementary Material for this article can be found online at: https://www.frontiersin.org/articles/10.3389/fonc.2021.720835/full#supplementary-material

REFERENCES

1. Torre LA, Bray F, Siegel RL, Ferlay J, Lortet-Tieulent J, Jemal A. Global Cancer Statistics, 2012. *CA Cancer J Clin* (2015) 65(2):87–108. doi: 10.3322/caac.21262
2. McDermott AL, Dutt SN, Watkinson JC. The Aetiology of Nasopharyngeal Carcinoma. *Clin Otolaryngol Allied Sci* (2001) 26(2):82–92. doi: 10.1046/j.1365-2273.2001.00449.x
3. Young LS, Rickinson AB. Epstein-Barr Virus: 40 Years on. *Nat Rev Cancer* (2004) 4(10):757–68. doi: 10.1038/nrc1452
4. Razak AR, Siu LL, Liu FF, Ito E, O'Sullivan B, Chan K. Nasopharyngeal Carcinoma: The Next Challenges. *Eur J Cancer (Oxford Engl 1990)* (2010) 46 (11):1967–78. doi: 10.1016/j.ejca.2010.04.004
5. Zhang Y, Chen L, Hu GQ, Zhang N, Zhu XD, Yang KY, et al. *Et Al*: Gemcitabine and Cisplatin Induction Chemotherapy in Nasopharyngeal Carcinoma. *N Engl J Med* (2019) 381(12):1124–35. doi: 10.1056/NEJMoa1905287
6. Lee R, Feinbaum R, Ambros V. A Short History of a Short RNA. *Cell* (2004) 116(2 Suppl):S89–92, 81 p following S96. doi: 10.1016/S0092-8674(04)00035-2

7. Kasinski AL, Slack FJ. Epigenetics and Genetics. MicroRNAs En Route to the Clinic: Progress in Validating and Targeting microRNAs for Cancer Therapy. *Nat Rev Cancer* (2011) 11(12):849–64. doi: 10.1038/nrc3166
8. Stahlhut C, Slack FJ. MicroRNAs and the Cancer Phenotype: Profiling, Signatures and Clinical Implications. *Genome Med* (2013) 5(12):111. doi: 10.1186/gm516
9. Condrat CE, Thompson DC, Barbu MG, Bugnar OL, Boboc A, Cretoiu D, et al. miRNAs as Biomarkers in Disease: Latest Findings Regarding Their Role in Diagnosis and Prognosis. *Cells* (2020) 9(2):276. doi: 10.3390/cells9020276
10. Spence T, Bruce J, Yip KW, Liu FF. MicroRNAs in Nasopharyngeal Carcinoma. *Chin Clin Oncol* (2016) 5(2):17. doi: 10.21037/cco.2016.03.09
11. Wang S, Claret FX, Wu W. MicroRNAs as Therapeutic Targets in Nasopharyngeal Carcinoma. *Front Oncol* (2019) 9:756. doi: 10.3389/fonc.2019.00756
12. Liu N, Chen NY, Cui RX, Li WF, Li Y, Wei RR, et al. Prognostic Value of a microRNA Signature in Nasopharyngeal Carcinoma: A microRNA Expression Analysis. *Lancet Oncol* (2012) 13(6):633–41. doi: 10.1016/S1470-2045(12)70102-X
13. Zhao L, Fong AHW, Liu N, Cho WCS. Molecular Subtyping of Nasopharyngeal Carcinoma (NPC) and a microRNA-Based Prognostic Model for Distant Metastasis. *J Biomed Sci* (2018) 25(1):16. doi: 10.1186/s12929-018-0417-5
14. Jiang C, Li L, Xiang YQ, Lung ML, Zeng T, Lu J, et al. Epstein-Barr Virus miRNA BART2-5p Promotes Metastasis of Nasopharyngeal Carcinoma by Suppressing Rnd3. *Cancer Res* (2020) 80(10):1957–69. doi: 10.1158/0008-5472.CAN-19-0334
15. Lin C, Zong J, Lin W, Wang M, Xu Y, Zhou R, et al. EBV-miR-BART8-3p Induces Epithelial-Mesenchymal Transition and Promotes Metastasis of Nasopharyngeal Carcinoma Cells Through Activating NF-κb and Erk1/2 Pathways. *J Exp Clin Cancer Res CR* (2018) 37(1):283. doi: 10.1186/s13046-018-0953-6
16. Gao W, Wong TS, Lv KX, Zhang MJ, Tsang RK, Chan JY. Detection of Epstein-Barr Virus (EBV)-Encoded microRNAs in Plasma of Patients With Nasopharyngeal Carcinoma. *Head Neck* (2019) 41(3):780–92. doi: 10.1002/hed.25544
17. Zheng XH, Cui C, Ruan HL, Xue WQ, Zhang SD, Hu YZ, et al. Plasma microRNA Profiling in Nasopharyngeal Carcinoma Patients Reveals miR-548q and miR-483-5p as Potential Biomarkers. *Chin J Cancer* (2014) 33 (7):330–8. doi: 10.5732/cjc.013.10246
18. Bruce JP, Hui AB, Shi W, Perez-Ordonez B, Weinreb I, Xu W, et al. Identification of a microRNA Signature Associated With Risk of Distant Metastasis in Nasopharyngeal Carcinoma. *Oncotarget* (2015) 6(6):4537–50. doi: 10.18632/oncotarget.3005
19. Wang HY, Yan LX, Shao Q, Fu S, Zhang ZC, Ye W, et al. Profiling Plasma microRNA in Nasopharyngeal Carcinoma With Deep Sequencing. *Clin Chem* (2014) 60(5):773–82. doi: 10.1373/clinchem.2013.214213
20. Chen Y, Wang H, Zhu S, Lan X. miR-483-5p Promotes Esophageal Cancer Progression by Targeting KCNQ1. *Biochem Biophys Res Commun* (2020) 531 (4):615–21. doi: 10.1016/j.bbrc.2020.07.037
21. Soon PS, Tacon LJ, Gill AJ, Bambach CP, Sywak MS, Campbell PR, et al. miR-195 and miR-483-5p Identified as Predictors of Poor Prognosis in Adrenocortical Cancer. *Clin Cancer Res an Off J Am Assoc Cancer Res* (2009) 15(24):7684–92. doi: 10.1158/1078-0432.CCR-09-1587
22. Tang S, Chen Y, Feng S, Yi T, Liu X, Li Q, et al. MiR-483-5p Promotes IGF-II Transcription and is Associated With Poor Prognosis of Hepatocellular Carcinoma. *Oncotarget* (2017) 8(59):99871–88. doi: 10.18632/oncotarget.21737
23. Wu K, Ma L, Zhu J. Mir−483−5p Promotes Growth, Invasion and Self −Renewal of Gastric Cancer Stem Cells by Wnt/β−Catenin Signaling. *Mol Med Rep* (2016) 14(4):3421–8. doi: 10.3892/mmr.2016.5603
24. Yang ZG, Ma XD, He ZH, Guo YX. miR-483-5p Promotes Prostate Cancer Cell Proliferation and Invasion by Targeting RBM5. *Int Braz J Urol Off J Braz Soc Urol* (2017) 43(6):1060–7. doi: 10.1590/s1677-5538.ibju.2016.0595
25. Liu K, He B, Xu J, Li Y, Guo C, Cai Q, et al. miR-483-5p Targets MKNK1 to Suppress Wilms' Tumor Cell Proliferation and Apoptosis *In Vitro* and *In Vivo*. *Med Sci monitor Int Med J Exp Clin Res* (2019) 25:1459–68. doi: 10.12659/MSM.913005
26. Wang XG, Zhu YW, Wang T, Chen B, Xing JC, Xiao W. MiR-483-5p Downregulation Contributed to Cell Proliferation, Metastasis, and Inflammation of Clear Cell Renal Cell Carcinoma. *Kaohsiung J Med Sci* (2020) 37(3):192–9. doi: 10.1002/kjm2.12320
27. Wang L, Shi M, Hou S, Ding B, Liu L, Ji X, et al. MiR-483-5p Suppresses the Proliferation of Glioma Cells *via* Directly Targeting ERK1. *FEBS Lett* (2012) 586(9):1312–7. doi: 10.1016/j.febslet.2012.03.035
28. Safford M, Collins S, Lutz MA, Allen A, Huang CT, Kowalski J, et al. Egr-2 and Egr-3 are Negative Regulators of T Cell Activation. *Nat Immunol* (2005) 6 (5):472–80. doi: 10.1038/ni1193
29. Nishimura Y, Takizawa R, Koike S, Kinoshita A, Satomura Y, Kawasaki S, et al. Association of Decreased Prefrontal Hemodynamic Response During a Verbal Fluency Task With EGR3 Gene Polymorphism in Patients With Schizophrenia and in Healthy Individuals. *NeuroImage* (2014) 85 Pt 1:527–34. doi: 10.1016/j.neuroimage.2013.08.021
30. Liu D, Evans I, Britton G, Zachary I. The Zinc-Finger Transcription Factor, Early Growth Response 3, Mediates VEGF-Induced Angiogenesis. *Oncogene* (2008) 27(21):2989–98. doi: 10.1038/sj.onc.1210959
31. Li S, Miao T, Sebastian M, Bhullar P, Ghaffari E, Liu M, et al. The Transcription Factors Egr2 and Egr3 are Essential for the Control of Inflammation and Antigen-Induced Proliferation of B and T Cells. *Immunity* (2012) 37(4):685–96. doi: 10.1016/j.immuni.2012.08.001
32. Baron VT, Pio R, Jia Z, Mercola D. Early Growth Response 3 Regulates Genes of Inflammation and Directly Activates IL6 and IL8 Expression in Prostate Cancer. *Br J Cancer* (2015) 112(4):755–64. doi: 10.1038/bjc.2014.622
33. Liao F, Ji MY, Shen L, Qiu S, Guo XF, Dong WG. Decreased EGR3 Expression is Related to Poor Prognosis in Patients With Gastric Cancer. *J Mol Histol* (2013) 44(4):463–8. doi: 10.1007/s10735-013-9493-8
34. Salotti J, Sakchaisri K, Tourtellotte WG, Johnson PF. An Arf-Egr-C/Ebpβ Pathway Linked to Ras-Induced Senescence and Cancer. *Mol Cell Biol* (2015) 35(5):866–83. doi: 10.1128/MCB.01489-14

Conflict of Interest: The authors declare that the research was conducted in the absence of any commercial or financial relationships that could be construed as a potential conflict of interest.

frontiers in Oncology

ORIGINAL RESEARCH
published: 28 October 2021
doi: 10.3389/fonc.2021.712788

Spatial Distribution of Immune Cells in Head and Neck Squamous Cell Carcinomas

Christian Idel[1†], Julika Ribbat-Idel[2†], Luise Klapper[2], Rosemarie Krupar[3], Karl-Ludwig Bruchhage[1], Eva Dreyer[2], Dirk Rades[4], Christina Polasky[1], Anne Offermann[2], Jutta Kirfel[2], Sven Perner[2,3†] and Barbara Wollenberg[5†]*

[1] Department of Otorhinolaryngology, University of Luebeck, Luebeck, Germany, [2] Institute of Pathology, University of Luebeck and University Hospital Schleswig-Holstein, Luebeck, Germany, [3] Pathology, Research Center Borstel, Leibniz Lung Center, Borstel, Germany, [4] Department of Radiation Oncology, University of Luebeck, Lübeck, Germany, [5] Department of Otorhinolaryngology, MRI Technical University Munich, Munich, Germany

OPEN ACCESS

Edited by:
Heming Lu,
People's Hospital of Guangxi Zhuang Autonomous Region, China

Reviewed by:
Maud Kamal,
Institut Curie, France
Arutha Kulasinghe,
The University of Queensland, Australia

***Correspondence:**
Christian Idel
Christian.Idel@uksh.de

†These authors have contributed equally to this work

Specialty section:
This article was submitted to Head and Neck Cancer, a section of the journal Frontiers in Oncology

Received: *21 May 2021*
Accepted: *08 October 2021*
Published: *28 October 2021*

Citation:
Idel C, Ribbat-Idel J, Klapper L, Krupar R, Bruchhage K-L, Dreyer E, Rades D, Polasky C, Offermann A, Kirfel J, Perner S and Wollenberg B (2021) Spatial Distribution of Immune Cells in Head and Neck Squamous Cell Carcinomas. Front. Oncol. 11:712788. doi: 10.3389/fonc.2021.712788

Background: Head and neck squamous cell carcinomas (HNSCCs) have a very moderate response rate to immune checkpoint inhibitor (ICI) treatment compared to other cancer types. Lacking predictive markers for treatment response, we analyzed the immune status of HNSCC and assessed the spatial distribution of immune cells.

Materials and Methods: *Via* assessing hematoxylin–eosin (H&E) stains, we divided HNSCCs by the immune cell distribution in hot, cold, and excluded tumors. For each group, each with 10 tumors, we performed serial immunohistochemical (IHC) staining of the immune cell markers, checkpoint molecules, and immune regulators.

Results: The spatial distributions were different for each immune cell type, allocating regulatory T cells (Tregs) and CD11b cells predominantly in the stroma. CD4 and CD8 cells were present either in the tumor stroma or between cancer cells. Interestingly, the expressions of PD-1 (programmed cell death 1 receptor) and PD-L1 (programmed death-ligand 1) were higher in hot tumors in comparison to cold and excluded tumors. The expression of pSMAD [indicating active transforming growth factor beta (TGF-β)] was higher in excluded tumors.

Conclusion: Different immune cell distribution patterns within tumors might be crucial for ICI treatment response since hot tumors have the highest expressions of PD-1 and PD-L1. TGF-β might be a key regulator for immune cell distribution and a promising therapeutic target that determines the formation of hot or excluded immune patterns.

Keywords: HNSCC, immune landscape, spatial distribution, TGF-β, PD-L1, PD-1, immune checkpoint

INTRODUCTION

Head and neck squamous cell carcinoma (HNSCC) is the sixth most common cancer worldwide (1–3). The most common therapeutic options are surgery and/or chemoradiotherapy. But these therapies are often linked to severe side effects that are hard to endure for patients. They suffer from functional impairment such as permanent voice changes or dysphagia. Surgery leads to scars and

visible deformations, and a lot of patients are adversely affected by chronic pain. It has been long known that chemoradiotherapy very often leads to xerostomia, fibrosis, and necrosis of the bone and soft tissue in the head and neck region (4). Also, changes in the therapy regimens of a combined irradiation and chemotherapy only had a moderate impact on the reduction of toxicity (5, 6). Despite great research efforts, overlooking studies in the time period from 1987 up until today, the prognosis is still rather poor. In p16-negative tumors, the 5-year survival is still only 40%–60% if all tumor stages are pooled. For stages III and IV, as classified by the Union for International Cancer Control (UICC), the 2-year survival is even less since 30%–50% of patients develop local or regional recurrence, and in patients with a recurrent or a metastatic disease, the median overall survival (OS) was 10–13 months prior to the introduction of immune therapies (7–11). Tumors may originate from different locations within the group of HNSCCs, i.e., the oral cavity, oropharynx, hypopharynx, and larynx. There is growing evidence that HNSCCs of these different sites of origin differ in tumor biology. The clearest difference is seen in oropharyngeal cancers, in which human papillomavirus (HPV) has a huge impact on the OS of patients. But HPV has so far not had any impact on OS in cancers of the oral cavity, the hypopharynx, and the larynx (12). Also, HNSCCs of the different sites of origin differ in the response toward irradiation. Primary tumors of the hypopharynx have the worst response toward radiotherapy (13).

The introduction of immune therapies for solid cancers by the use of the so-called immune checkpoint inhibitors (ICIs) increased the OS rates of many patients regardless of the cancer type. The most severe impact was observed in malignant melanoma therapy, extending to cancer types such as lung cancer, where ICI treatment is very promising as well (14–16). Therefore, high hopes were set for the treatment of patients with HNSCC. The results of several phase III clinical trials showed a significant improvement compared to the standard chemotherapeutic regimen, but with mostly only a moderate improvement of the OS at the primary analysis (17–19). The 2-year follow-up data again confirm the superiority of ICI to various chemotherapy protocols, especially in patients with a higher programmed death-ligand 1 (PD-L1) expression score, but miss to achieve a stable plateau in the survival curve (20).

The results of the clinical trials have already altered the therapeutic algorithms (9), but the OS rates remain lower than those in other epithelial cancers, even other squamous cell cancers (21).

The reason for this very different impact of ICIs in the treatments of various cancers is not understood so far. Research in this field is vastly expanding at the moment.

In the clinical setting, tremendous efforts are undertaken to enroll patients in clinical trials that combine two checkpoint targeting drugs, but especially from melanoma patients, we learned that this is associated with an increased risk of severe adverse events (22, 23). The second major step comprises the use of an ICI backbone and additional targeting of a second cancer-relevant pathway.

Clinical development is severely hampered by the lack of biomarkers. Most studies are being performed as all-comer studies, lacking the right assay to predefine the most suitable patients for the drugs tested. Currently, in clinical practice, tumor response is correlated with the lymphocytic infiltrate in the tumor and the expression of PD-L1.

The immune status of HNSCC might serve as an explanation for the low impact of ICI treatment in HNSCC. Saloura et al. analyzed the genomes of two HNSCC cohorts for cytokine expression and defined two patterns, namely, high and low $CD8^+$ T-cell-inflamed phenotype (24). Kulasinghe et al. gave a first impression of the distribution of immune cells within HNSCC using multiplex immunohistochemistry (IHC) to predict the response to ICI treatment. Due to the low number of samples, they have not identified a predictive marker so far (25).

Other authors divided tumors into different immune profiles, such as hot, cold, and excluded tumors, based on the infiltration of $CD8^+$ T cells (26, 27). To better understand the immune profile of HNSCC, we first analyzed the immune cell distribution in tumors of primary HNSCC patients who underwent surgery as a first-line treatment in whole tissue slides. But instead of a CD8 IHC, we used hematoxylin–eosin (H&E) staining to describe the following immune status of HNSCC phenotypes:

- cold (almost no immune cells visible),
- excluded (immune cells within the tumor, but only in the stroma), and
- hot (immune cells in the stroma and between cancer cells).

In each group of 10 HNSCC patients of the hot, excluded, or cold status, we examined serial immunohistological stains. This way, we were able to establish a pattern of various immune cells linked to the degree of lymphocytic infiltrates in HNSCC. There are several markers to find first signs of regulators forming the different types of immune status.

MATERIAL AND METHODS

The study was conducted in accordance with the Declaration of Helsinki, and the protocol was approved by the Ethics Committee of the University of Luebeck (project code AZ 16-277).

Patient Selection

We established an HNSCC cohort as previously described by obtaining archived tissue samples (28). The cohort contained hot, cold, and excluded tumor tissues. We randomly selected 10 patients from each group to perform the comparative analyses, as described below. All tumors were from therapy-naive patients (PT), and none of them received ICI treatment later since ICI treatment is not yet part of the standard treatment for primary HNSCC. More details on the tumor location, tumor node metastases (TNM) stage, and later therapy are shown in **Tables 1**, **2**.

Immunohistochemistry

Immune profiles (hot, cold, or excluded) were assigned after H&E evaluation by a board-certified pathologist. For 10 cases from each group, we performed IHC on 4-µm-thick sections of a formalin-fixed paraffin-embedded (FFPE) specimen after

TABLE 1 | Clinicopathological data of patients.

Clinicopathological parameters	*n*	Immune distribution		
		Hot	Excluded	Cold
Gender				
Male	24	9	6	9
Female	6	1	4	1
Age (years)				
≤63	18	6	7	5
>63	12	4	3	5
Karnofsky scale				
≤70	6	1	1	4
>70	16	7	7	2
n/a	8	2	2	4
Smoking				
Yes	26	7	10	9
No	3	3	0	0
n/a	1	–/–	–/–	1
Alcohol abuse				
Yes	14	4	6	4
No	15	6	4	5
n/a	1	–/–	–/–	1
Tumor site				
Larynx	6	1	2	3
Oral cavity	10	3	2	5
Hypopharynx	3	1	2	0
Oropharynx	11	5	4	2
T stage				
T1–T2	19	6	8	5
T3–T4	11	4	2	5
Lymph node metastasis				
N (0)	8	2	3	3
N (+)	22	8	7	7
Distant metastasis				
M (0)	24	9	7	8
M (+)	6	1	3	2
Pathological grade				
G1	0	0	0	0
G2	19	7	6	6
G3	11	3	4	4
UICC stage				
I–II	9	3	3	3
III–IV	21	7	7	7
p16				
Positive	9	4	3	2
Negative	21	6	7	8
Recurrence				
Yes	4	0	4	0
No	26	10	6	10

n/a, not applicable; UICC, Union for International Cancer Control.

deparaffinization. We employed the IView DAB Detection Kit on a Ventana BenchMark (Roche, Basel, Switzerland). Immunostaining was performed followed by microwave-based antigen retrieval as previously described (29).

The following antibodies were used:

- CD4 [rabbit monoclonal antibody, clone SP35, ready to use (RTU); Ventana Medical Systems Roche, Oro Valley, AZ, USA]
- CD8 (rabbit monoclonal antibody, clone SP57, RTU; Ventana Medical Systems Roche)
- CD11b (rabbit monoclonal antibody, clone ER1345y C-terminal ab52478, 1:200; Abcam, Cambridge, UK)
- FOXP3 (mouse monoclonal antibody, clone 236A/E7, 1:100; Invitrogen Thermo Fisher Scientific, Rockford, IL, USA)
- PD-1 (mouse monoclonal antibody, clone NAT105, RTU; Cell Marque Sigma-Aldrich, Rocklin, CA, USA)
- PD-L1 (rabbit monoclonal antibody, clone E1L3N, RTU; Cell Signaling, Danvers, MA, USA)

Evaluation and Scoring of Slides

For CD4, CD8, and CD11b, the percentage of immune cells and the location of positive cells (stromal *versus* diffuse) were determined. The share of FOXP3-positive cells among the CD4-positive cells was estimated. For pSMAD3, the percentage of positive tumor cells and the staining intensity were assessed and the immunoreactive score of Remmele and Stegner (IRS) was calculated. For PD-L1 evaluation, all three established scoring systems were employed, namely, the tumor positivity score (TPS), immune cell (IC) score, and the combined positivity score (CPS). For the TPS, all PD-L1-positive cancer cells were counted and put into relation to all viable cancer cells. Values are presented as percentages. For the IC score, PD-L1-positive immune cells were estimated by tumor area. For the CPS, all PD-L1-positive cells (cancer cells and immune cells) were counted and put into relation to the number of all viable cancer cells. This number was then multiplied by 100. This score has no unit. Programmed cell death 1 protein (PD-1) receptor was assessed using CPS in analogy to the CPS of PD-L1. CPS is so far the only marker for PD-L1 expression that is used for clinical decisions in HNSCC (9).

Statistical Analyses and Graphical Visualization

Statistical analysis was performed with an unpaired *t*-test for all data presented here. *P*-values <0.05 were considered to be statistically significant. This research has made use of the statistical analyses and visualization in R software (version 4.0.2; R Foundation, Vienna, Austria; http://www.R-project.org).

We used the following software to create artwork and to edit the photomicrographs: Inkspace (version 0.92.4; The Inkscape Project c/o Software Freedom Conservancy, Brooklyn, NY, USA; https://inkscape.org/) and GIMP (version 2.10.14; The GIMP Project c/o GNOME Foundation, Orinda, CA, USA; https://www.gimp.org).

Ethics

The study was conducted in accordance with the Declaration of Helsinki, and the protocol was approved by the Ethics Committee of the University of Luebeck (project code AZ 16-277).

RESULTS

Patient Criteria

As expected for HNSCC, the majority of patients were males and middle-aged. A majority were smokers and p16-negative. They mostly presented with clinically advanced stages and lymph node metastases, and most suffered from a recurrence. Primary tumors

TABLE 2 | Details of all patients.

T stage	N stage	M stage	Grade	UICC stage	p16	Pack years	Alcohol	Recurrence	Follow-up (months)	Death	OP	Chemotherapy	Radiotherapy
T3	N2	M0	2	IV	Negative	30	Yes	No	56	No	Yes	No	Yes
T2	N2	M0	2	II	Positive	20	No	No	48	No	Yes	Yes	Yes
T2	N0	M0	2	II	Negative	0	Yes	No	47	No	Yes	No	Yes
T2	N1	M0	3	III	Positive	0	No	No	47	No	Yes	No	Yes
T3	N2	M0	2	IV	Negative	40	Yes	No	11	Yes	Yes	No	Yes
T4	N3	M1	2	IV	Negative	45	No	No	44	No	Yes	Yes	Yes
T1	N3	M0	2	IV	Negative	35	Yes	No	6	Yes	Yes	Yes	Yes
T2	N1	M0	3	III	Positive	0	No	No	69	No	Yes	No	Yes
T2	N2	M0	3	II	Positive	20	No	No	62	No	Yes	Yes	Yes
T3	N0	M0	2	III	Negative	30	No	No	56	No	Yes	No	No
T2	N1	M1	3	II	Positive	40	No	No	84	No	Yes	No	Yes
T1	N2	M1	3	IV	Negative	40	Yes	Yes	29	No	Yes	Yes	Yes
T2	N0	M0	3	II	Negative	10	Yes	No	84	No	Yes	No	No
T2	N2	M1	3	IV	Negative	20	Yes	Yes	15	Yes	Yes	No	No
T4	N0	M0	2	IV	Negative	30	Yes	No	83	No	Yes	Yes	Yes
T1	N2	M0	2	IV	Negative	30	Yes	Yes	10	Yes	Yes	No	Yes
T3	N1	M0	2	III	Negative	50	No	Yes	83	No	Yes	Yes	Yes
T1	N2	M0	2	IV	Negative	50	Yes	No	57	No	Yes	No	Yes
T2	N1	M0	2	III	Positive	30	No	No	64	No	Yes	No	Yes
T2	N0	M0	2	II	Positive	140	No	No	57	No	Yes	No	No
T1	N0	M0	2	I	Negative	75	Yes	No	53	No	Yes	No	No
T1	N2	M0	2	IV	Positive	3	No	No	45	No	Yes	No	No
T3	N2	M0	2	IV	Negative	40	No	No	18	Yes	Yes	No	No
T4	N2	M1	2	IV	Negative	60	No	No	6	Yes	Yes	Yes	Yes
T4	N2	M0	2	IV	Negative	60	Yes	No	0	Yes	Yes	No	No
T2	N2	M0	2	IV	Negative	17	No	No	38	No	Yes	No	Yes
T1	N0	M0	3	I	Negative	30	Yes	No	39	No	Yes	No	No
T2	N0	M0	3	II	Negative	n/a	n/a	No	0	Yes	Yes	No	No
T4	N1	M0	3	IV	Positive	60	No	No	55	No	Yes	Yes	Yes
T4	N2	M1	3	IV	Negative	35	Yes	No	7	Yes	Yes	Yes	Yes

n/a, not applicable; UICC, Union for International Cancer Control.

were located in the oral cavity, oropharynx, larynx, and hypopharynx. Details are presented in **Tables 1**, **2**.

Different Immune Cell Influx But the Same Immune Cell Proportions in the Three Immune Phenotypes

By reading the H&E slides, we established three distinct categories of immune cell infiltrates in HNSCC. In "cold" tumors, there were only very few immune cells overall. The other categories contained more intratumoral immune cells than did the cold tumors, but differed in their distribution: hot tumors contained immune cells diffusely throughout the tumor bulk, whereas in excluded tumors the immune cells were restricted to the stromal areas. By estimating the expressions of CD8 (CD8 T cells), CD4 (CD4 T cells), FoxP3 (regulatory T cells, Tregs), and CD11b (myeloid-derived cells), it was found that there was no significant difference in the proportion of each in the three immune types (**Figure 1**). There was a trend of a higher proportion of CD11b-positive myeloid cells in the excluded tumors, but this difference was not statistically significant ($p > 0.05$).

Different Distribution Patterns in the Three Immune Phenotypes

As mentioned above, the immune types were defined by the morphology of the H&E stain, whereas the distribution of the immune cell subtypes within the tumor was analyzed by IHC of CD8 and CD4 T cells, FoxP3, and CD11b (**Figure 1**). In cold tumors, there were only very few detectable cells of each analyzed immune cell subtype. In one tumor, there were no immune cells at all. In the other nine tumors, CD11b cells were only detectable in the tumor stroma, with CD4 T cells in the majority of cases in the stroma as well (seven tumors only in the stroma and two tumors in the tumor cells and the stroma). FoxP3 cells represented only a small fraction of the CD4 T cells, and if detectable, they were located in the stroma. In the nine cases with few immune cells, CD8 T cells were found in the stroma and in between the cancer cells. In excluded tumors, all four immune cell types were mainly in the stroma of the tumors and not in between the cancer cells. In hot tumors, the CD4 T cells and FoxP3 cells were found in 4 out of 10 tumors in the stroma and in between the cancer cells; in 6 out of 10 cases, only within the stroma. CD11b cells were detectable in the stroma and in between the cancer cells in 7 out of 10 tumors and only within the stroma in 3 out of 10 cases. CD8 T cells were located in the stroma and in between the cancer cells in 10 out of 10 tumors (**Figure 2**).

Higher pSMAD Expression in Excluded Than in Hot HNSCC

pSMAD was measured using IHC in cancer cells and in immune cells as an indicator for an activated transforming growth factor

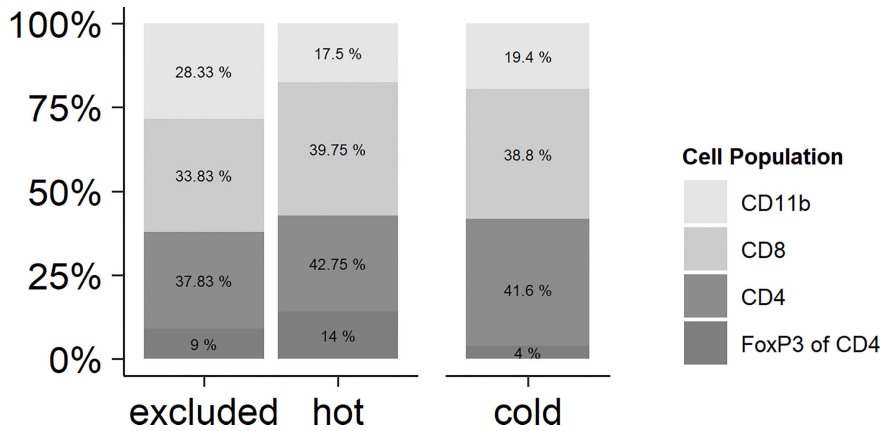

FIGURE 1 | Relationships of the immune cell types in hot, cold, and excluded tumors. While the total number of immune cells differed between hot and excluded tumors on the one hand and especially cold tumors on the other hand, the relationships of CD11b-positive myeloid cells, CD8-positive T lymphocytes, and CD4 T positive lymphocytes were very similar in all three tumor immune types. There was a trend of a higher proportion of CD11b-positive myeloid cells in excluded tumors, but this difference was not statistically significant ($p > 0.05$). In CD4-positive T lymphocytes, the percentage of FoxP3-positive regulatory T cells (Tregs) was related to all CD4-positive cells. There was no significant difference in the proportion of Tregs between hot, cold, and excluded tumors.

beta (TGF-β) pathway. There was a significantly higher pSMAD expression pattern observed in the cancer cells of the excluded tumors than that in cancer cells of hot tumors ($p = 0.0381$). The expression of pSMAD in the cancer cells of cold tumors was in between that of hot and excluded tumors. Comparing the expression of pSMAD in hot and cold tumors showed no significant difference ($p = 0.5032$), and neither did the comparison between cold and excluded tumors ($p = 0.1317$) (**Figures 3**, **4**).

Furthermore, the immune cells within the sections were identified and scored based on their staining by a board-certified pathologist. The expression of pSMAD in immune cells showed no significant difference between the excluded and hot tumors ($p = 0.2053$), while there were almost no immune cells in cold tumors.

Higher PD-1 Expression in Hot HNSCC

The expression of PD-1 was detected with IHC and the CPS was applied. The CPS of PD-1 was significantly higher in hot tumors in comparison with those in cold and excluded tumors (hot *vs.* excluded, $p = 0.0027$; hot *vs.* cold, $p = 0.0304$). The CPS of PD-1 in excluded tumors was not significantly different from that in cold tumors ($p = 0.5538$) (**Figures 5**, **6**).

Higher PD-L1 Expression in Hot HNSCC

The expression of PD-L1 was detected with IHC (**Figure 7**) and evaluated using the TPS, IC score, and CPS. The TPS of PD-L1 was significantly higher in hot tumors in comparison to those in cold and excluded tumors (hot *vs.* excluded, $p = 0.0422$; hot *vs.* cold, $p = 0.0127$). The TPS of PD-L1 in excluded tumors was not significantly different from that in cold tumors ($p = 0.2477$) (**Figure 8**). The IC score in hot tumors was not significantly higher than that in excluded tumors (hot *vs.* excluded, $p = 0.3078$; hot *vs.* cold, $p = 0.1196$). The CPS of PD-L1 was significantly higher in hot tumors in comparison with those in cold and excluded tumors (hot *vs.* excluded, $p = 0.0011$; hot *vs.* cold, $p = 0.0085$).

DISCUSSION

The prognosis for patients with advanced HNSCC is still very poor. Even the introduction of ICI therapy in HNSCC has not shown prognostic improvements so far (30). To better understand the differences of HNSCC in contrast to other cancer entities with a good ICI response, a lot of research was done that included RNA sequencing. Saloura et al. studied the cytokine expression patterns in HNSCC genome cohorts and proposed that the depletion of Tregs and M2 macrophages might improve the outcomes of HNSCC patients with an ICI treatment (24). It has been indicated that an IFN-γ-related profile can predict the response to treatment with the PD-1 inhibitor pembrolizumab in melanoma. This might hold true for HNSCC as well (31). In a very detailed analysis of the RNA sequencing profiles, Chen et al. described the so-called immune class of HNSCC, which contained tumors with enriched inflammatory response, enhanced cytolytic activity, and active IFN-γ signaling (32). However, RNA sequencing is still rather expensive and time-consuming. In comparison, IHC staining is more cost-effective and can be established easily without the need for expensive technical equipment. This is why, in the study presented here, we focused on IHC-based analysis to better understand the landscape of immune cells in HNSCC. In other IHC-based studies of HNSCC, the focus was on a more general description of the relation of the immune cell types rather than their spatial distribution (25, 33) or on a single location such as that of oral tongue cancers (34). The study of Meehan et al. included a mixture of PT and recurrent disease (RD) HNSCC of the tongue. As the response rate in recurrent tumors to ICI treatment is still low, some studies have

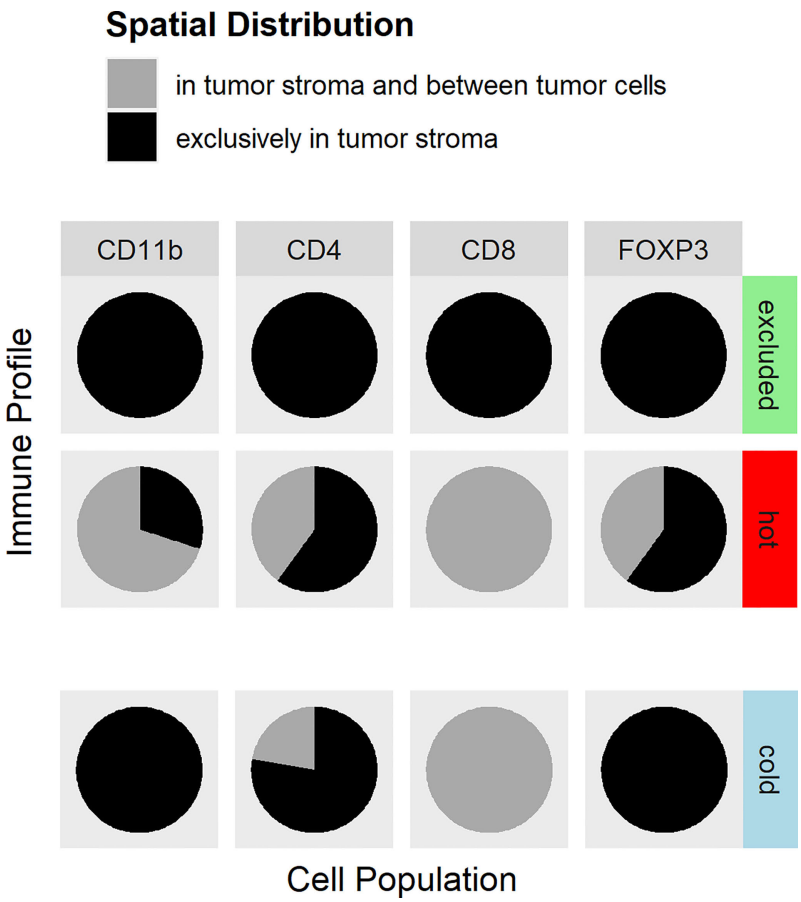

FIGURE 2 | Distribution of immune cell antigens in hot, cold, and excluded tumors. The distributions of CD4 lymphocytes, CD8 lymphocytes, CD11b-positive myeloid cells, and regulatory T cells (Tregs) within tumor tissues differed between hot, cold, and excluded tumors. In excluded tumors, all four cell types are found in the tumor stroma (*black*), but not in between cancer cells. In cold tumors, there were only very few immune cells at all (indicated by the *slight offset*). The few CD8 T cells were found in the stroma and in between cancer cells (*gray*), CD4 T cells were, in most cases, in the stroma (*black*) and only in a few cases in between cancer cells and in the stroma (*gray*), while Tregs and myeloid cells were only in the stroma (*black*) in cold tumors. In hot tumors, CD8 T lymphocytes were found in the tumor stroma and in between cancer cells (*gray*). CD4 T lymphocytes and Tregs were located exclusively in the tumor stroma in most hot tumors (*black*), and in fewer cases, CD4 T lymphocytes were between cancer cells and in the stroma (*gray*). CD11b cells were in the stroma and in between cancer cells (*gray*) in most hot tumors, but in some hot tumors, they were only found in the stroma (*black*).

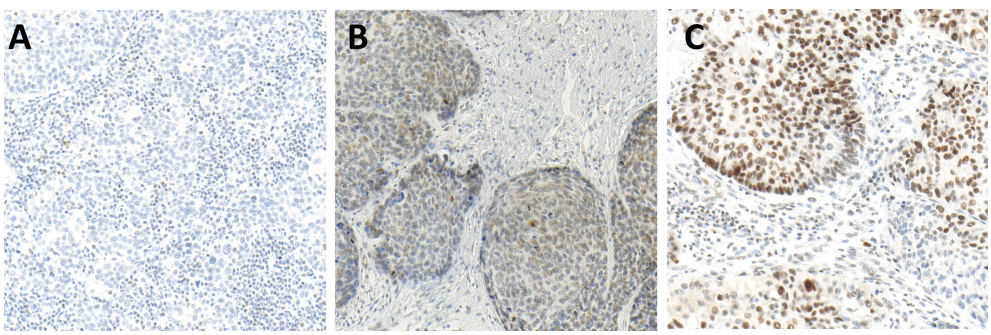

FIGURE 3 | Immunohistochemistry (IHC) of pSMAD expression in hot **(A)**, cold **(B)**, and excluded **(C)** head and neck squamous cell carcinomas (HNSCCs). Hot HNSCCs **(A)** showed very low pSMAD expression, while excluded HNSCCs **(C)** had very high pSMAD expression. In cold HNSCC **(B)**, the pSMAD expression was in between.

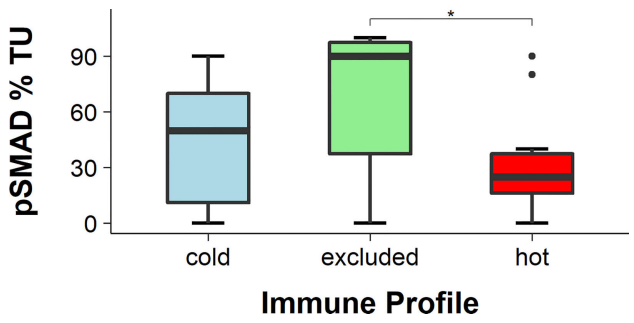

FIGURE 4 | Percentage of pSMAD-positive cancer cells. The expression of pSMAD was the highest in cancer cells of excluded tumors and the lowest in hot tumors, while in cold tumors it was in between. The difference in pSMAD expression between excluded and hot tumors was statistically significant ($p < 0.05$), while the expression difference in cold tumors was not statistically significant in either of the two other tumor immune types (both $p > 0.05$), * means p<0.05.

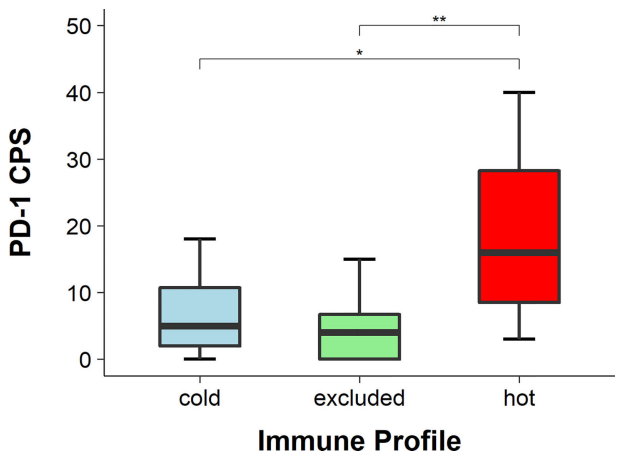

FIGURE 6 | PD-1 scores in hot, cold, and excluded head and neck squamous cell carcinomas (HNSCCs; combined positivity score, CPS). The CPS of PD-1 was the highest in hot tumors and the lowest in excluded tumors, while in cold tumors it was in between. The differences in the CPS of PD-1 between hot and excluded tumors and between hot and cold tumors were statistically significant (both $p < 0.05$), while the difference between cold and excluded tumors was not statistically significant ($p > 0.05$), * means p<0.05, ** means p<0.005.

tested the use of ICI in the treatment of primary HNSCC, such as KEYNOTE-689 [Study of Pembrolizumab Given Prior to Surgery and in Combination With Radiotherapy Given Post-Surgery for Advanced Head and Neck Squamous Cell Carcinoma (MK-3475-689), full text view, ClinicalTrials.gov] or ADRISK (Postoperative aRCH With Cisplatin Versus aRCH With Cisplatin and Pembrolizumab in Locally Advanced Head and Neck Squamous Cell Carcinoma, ClinicalTrials.gov). In the study presented here, we focused on treatment-naive primary HNSCC as well. The analyzed tumors were divided into three distribution patterns of immune cells. The first category, named cold tumors, had almost no immune cells in the tumor, either in the stroma or between the cancer cells. The second category, called excluded tumors, showed immune cells in the tumor, but they were limited to locations in the stroma surrounding the cancer cell areas without getting in between the cancer cells. The third type, so-called hot tumors, presented with immune cells both in the stroma and in between cancer cells.

Interestingly, mainly the CD8 T lymphocytes showed a distribution in between the cancer cells in the so-called hot tumors, while CD11b-positive myeloid cells and CD4 T lymphocytes were less frequently found in between cancer cells. By showing that in all H&E stains defining hot tumors the CD8 T lymphocytes were in the stroma and in between the cancer cells, we have provided proof that a simple H&E stain is enough for the definition of hot, cold, and excluded tumors and that CD8 IHC is not needed, as done in other studies (27). But to address the poor response to ICI in HNSCC, the expression levels of PD-1 and PD-L1 were analyzed as well. In routine diagnostics, the TPS and CPS for the expression of PD-L1 are common tools used to address the possible administration of pembrolizumab therapy in HNSCC patients (30). Also, the IC score was assessed since this score is examined for the decision about ICI treatment in lung cancer. The TPS and CPS for PD-L1 were significantly higher in hot tumors in comparison to those in excluded and cold tumors, but the IC score was not. Since the IC score only considers PD-L1 expression in

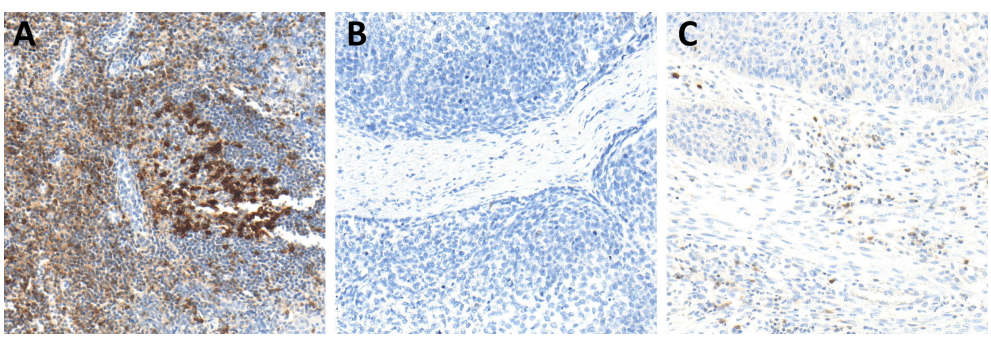

FIGURE 5 | Immunohistochemistry (IHC) of PD-1 expression in hot **(A)**, cold **(B)**, and excluded **(C)** head and neck squamous cell carcinomas (HNSCCs). In hot HNSCCs **(A)**, the expression of PD-1 was very high, while it was very low in cold **(B)** and excluded **(C)** HNSCCs.

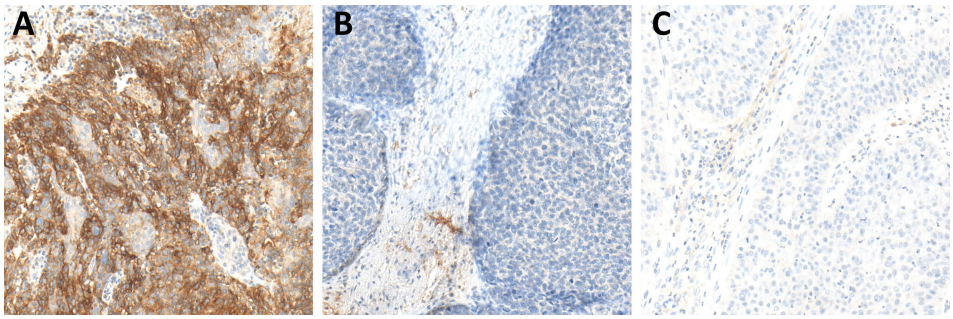

FIGURE 7 | Programmed death-ligand 1 (PD-L1) expression in hot **(A)**, cold **(B)**, and excluded **(C)** head and neck squamous cell carcinomas (HNSCCs). In hot HNSCCs **(A)**, the expression of PD-L1 was very high, while it was very low in cold **(B)** and excluded **(C)** HNSCCs.

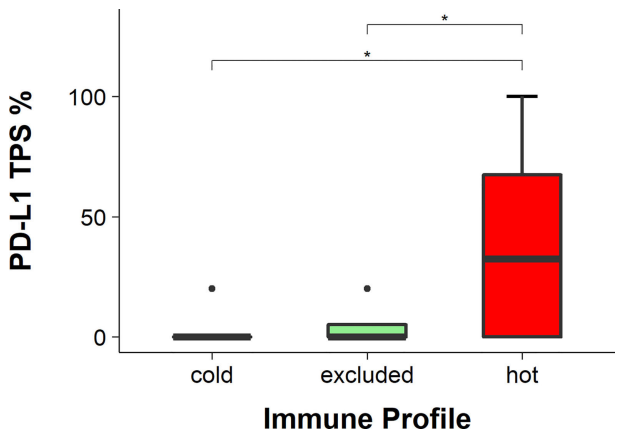

FIGURE 8 | Programmed death-ligand 1 (PD-L1) scores in hot, cold, and excluded head and neck squamous cell carcinomas (HNSCC; tumor positivity score, TPS). The TPS of PD-1 was the highest in hot tumors and the lowest in cold tumors, while in excluded tumors it was in between. The differences in the TPS of PD-1 between hot and excluded tumors and between hot and cold tumors were statistically significant (both $p < 0.05$), while the difference between cold and excluded tumors was not statistically significant ($p > 0.05$), * means p<0.05.

immune cells—the TPS includes PD-L1 expression in cancer cells and the CPS includes PD-L1 expression in cancer and immune cells—it underlines that the main PD-L1 expression in hot tumors is in cancer cells. In a previous study, we found worse prognosis for cold tumors in comparison to those in hot and excluded tumors in a cohort of 419 HNSCC patients. This was independent of other known risk classifications such as the T stage, UICC stage, p16 expression, grading, sex, and age. Interestingly, there was no difference between p16-positive and p16-negative cancers in relation to excluded, cold, and hot cases, with 52.8% excluded, 24.8% cold, and 22.4% hot HNSCC in the p16-negative group *versus* 53.5% excluded, 23,9% cold, and 22.5% hot HNSCC in the p16-positive group (28). In the present study, we wanted to provide initial insights into the distribution of the different immune cell types in hot, cold, and excluded HNSCC.

Nivolumab and pembrolizumab are so far the two approved ICI medications for recurrent HNSCC. Since these antibodies are directed against PD-1, the expression patterns of PD-1 were analyzed as well. For this, the CPS of PD-1 was employed as PD-1 is mainly expressed on T cells, but less so in cancer cells. The binding of PD-L1 by PD-1 on T cells led to a decreased activation of the mammalian target of rapamycin (mTOR) *via* the PI3K/AKT pathway. In some cancer entities such as melanoma, PD-1 activation in cancer cells led to mTOR activation, in turn leading to cancer progression; so far, it has not been described for cancer cells in HNSCC (35, 36). Interestingly, the CPS of PD-1 was significantly higher in hot tumors in comparison to those in excluded and cold tumors. The higher PD-1 and PD-L1 expressions might make hot tumors more prone to anti-PD-1 treatment, but this needs further investigation.

Interestingly, the cancer cells of excluded tumors had a significantly higher pSMAD expression, indicating a higher TGF-β expression. TGF-β has multiple roles in physiological settings such as cell proliferation and differentiation, wound healing, and immune system, but it is very important in several pathologies, for example, in skeletal diseases, fibrosis, and cancer. In epithelial cells, it has a bifunctional role. On the one hand, it can inhibit the epidermal growth factor (EGF)-mediated cell proliferation; on the other hand, it can work synergistically with EGF in epithelial cell proliferation. Several cancer types have higher TGF-β levels than those in healthy tissues, and in several cancers, a higher TGF-β expression level is associated with cancer progression and poorer survival (37). In HNSCC, TGF-β promotes cancer cell growth. A high TGF-β expression is associated with poor prognosis and epithelial–mesenchymal transition (EMT), which might lead to metastasis (38, 39). A high TGF-β expression level also makes HNSCC cells less sensitive to cisplatin treatment by reducing the cisplatin-induced apoptosis (40). HNSCCs with high TGF-β expressions also have worse outcomes when treated with anti-PD-1 (41). In several tumor types, it was shown that TGF-β impairs the function of cytotoxic CD8 T cells (42). In the data presented here, in the immune cells of excluded and hot tumors, there was no significant difference in pSMAD expression. This might indicate that TGF-β in cancer cell areas does not directly affect the influx of immune cells into the stroma, but it is assumed that the TGF-β

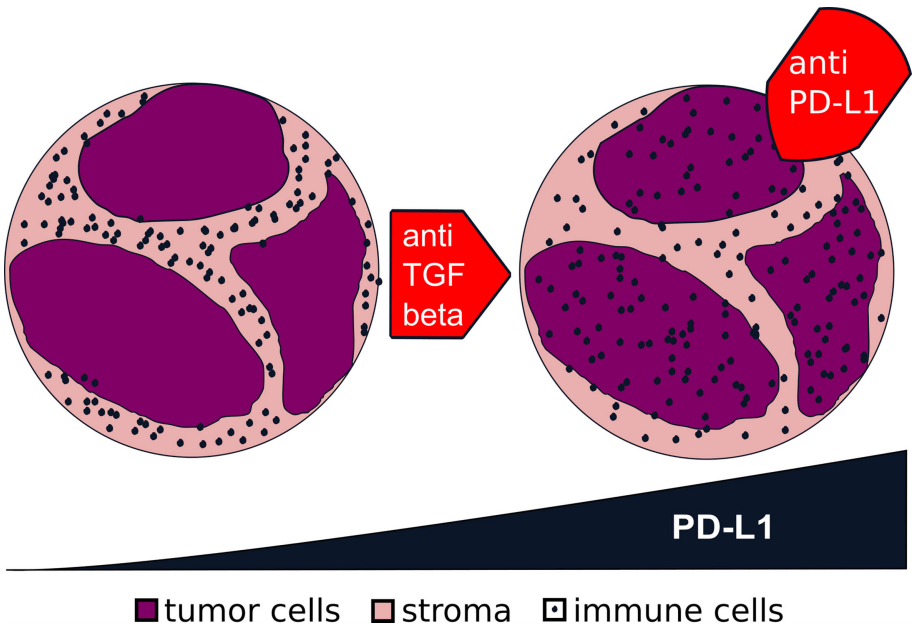

FIGURE 9 | Transformation from excluded to hot tumors *via* transforming growth factor beta (TGF-β). From the data presented in this study, we generated the hypothesis for future studies: that a blockage of TGF-β in an excluded tumor (*left*) might turn it into a hot tumor (*right*). The higher expression of programmed death-ligand 1 (PD-L1) in a hot tumor might make it more prone to a blockage of the interaction of PD-1/PD-L1.

expression in cancer cell areas might be a barrier for immune cell infiltration in between cancer cells. In a murine model of colorectal cancer metastasis, the inhibition of TGF-β led to a higher immune cell infiltration. In this model, a single anti-PD-L1 therapy did not affect metastasis. But the combination of an anti-PD-L1 ICI with an inhibitor of TGF-β eradicated most metastasis and prolonged recurrence-free survival (43). This might also be possible in HNSCC, that the inhibition of TGF-β leads to a transformation of excluded tumors toward hot tumors. Since hot tumors have significantly higher expressions of PD-1 and PD-L1 in comparison to excluded tumors, they might be more prone to ICI treatments.

We appreciate the limitations of our study as it provides plain descriptive data and a limited number of cases. More functional analysis is needed to determine the underlying mechanisms defining hot, cold, and excluded HNSCCs and the prognostic role of TGF-β. Identifying these might lead to a better understanding of cancer progression, treatment failure, and, therefore, the optimization of therapy. With the study presented here, we wanted to give first insights into the immune cell distribution in HNSCC and a possible explanation for a high TGF-β expression being associated with worse outcomes of anti-PD-1 treatment in HNSCC. With the limited number of patients, we cannot provide any prognostic value of the TGF-β expression. But as we described worse OS for cold tumors in our previous study (28) and as all of these tumors were not treated with ICIs, we do not expect a prognostic value of TGF-β expression for the established standard therapy regimens of HNSCC. However, we are keen to learn about TGF-β analyses in future cohorts receiving ICI treatments.

Since the introduction of ICI therapy has not had a large impact on the prognosis of HNSCCs in comparison to other solid tumor types, we still need a better understanding of the underlying mechanisms. The different distribution patterns of immune cells within tumors might be an explanation since only hot tumors do have high expressions of PD-1 and PD-L1. TGF-β might be a key regulator and will serve as a promising therapeutic target, which determines the formation of a hot or an excluded immune pattern (**Figure 9**).

DATA AVAILABILITY STATEMENT

The raw data supporting the conclusions of this article will be made available by the authors, without undue reservation.

ETHICS STATEMENT

The studies involving human participants were reviewed and approved by the Ethics Committee of the University of Luebeck (project code AZ 16-277). Written informed consent for participation was not required for this study, in accordance with the national legislation and the institutional requirements.

AUTHOR CONTRIBUTIONS

SP, BW, and CI designed the study concept and approach. SP, JR-I, and CI designed the experiments. JR-I, LK, and CI performed

the experiments. SP, JR-I, and ED prepared the tissues. JR-I and CI analyzed and interpreted the data, did the statistics, and wrote the manuscript. JR-I prepared the figures and created the artwork. AO provided technical advice and helped develop the methodology. JK and DR assisted with the discussion. SP, BW, RK, K-LB, and CP revised the manuscript. All authors contributed to the article and approved the submitted version.

FUNDING

The study was supported by a clinical scientist fellowship of the Medical Faculty of the University of Luebeck (J26-2018) to CI and Fellowships of the Mildred Scheel Doctoral Program of the German Cancer Aid awarded to LK (grant no. 70113940).

REFERENCES

1. Ferlay J, Colombet M, Soerjomataram I, Mathers C, Parkin DM, Pineros M, et al. Estimating the Global Cancer Incidence and Mortality in 2018: GLOBOCAN Sources and Methods. *Int J Cancer* (2019) 144:1941–53. doi: 10.1002/ijc.31937
2. Lin W, Chen M, Hong L, Zhao H, Chen Q. Crosstalk Between PD-1/PD-L1 Blockade and Its Combinatorial Therapies in Tumor Immune Microenvironment: A Focus on HNSCC. *Front Oncol* (2018) 8:532. doi: 10.3389/fonc.2018.00532
3. Shield KD, Ferlay J, Jemal A, Sankaranarayanan R, Chaturvedi AK, Bray F, et al. The Global Incidence of Lip, Oral Cavity, and Pharyngeal Cancers by Subsite in 2012. *CA Cancer J Clin* (2017) 67:51–64. doi: 10.3322/caac.21384
4. Larson DL, Lindberg RD, Lane E, Goepfert H. Major Complications of Radiotherapy in Cancer of the Oral Cavity and Oropharynx. A 10 Year Retrospective Study. *Am J Surg* (1983) 146:531–6. doi: 10.1016/0002-9610(83)90247-7
5. Jacinto JK, Co J, Mejia MB, Regala EE. The Evidence on Effectiveness of Weekly vs Triweekly Cisplatin Concurrent With Radiotherapy in Locally Advanced Head and Neck Squamous Cell Carcinoma (HNSCC): A Systematic Review and Meta-Analysis. *Br J Radiol* (2017) 90:20170442. doi: 10.1259/bjr.20170442
6. Mehanna H, Robinson M, Hartley A, Kong A, Foran B, Fulton-Lieuw T, et al. Radiotherapy Plus Cisplatin or Cetuximab in Low-Risk Human Papillomavirus-Positive Oropharyngeal Cancer (De-ESCALaTE HPV): An Open-Label Randomised Controlled Phase 3 Trial. *Lancet (London England)* (2019) 393:51–60. doi: 10.1016/s0140-6736(18)32752-1
7. Bernier J. A Multidisciplinary Approach to Squamous Cell Carcinomas of the Head and Neck: An Update. *Curr Opin Oncol* (2008) 20:249–55. doi: 10.1097/CCO.0b013e3282faa0b1
8. Chin D, Boyle GM, Porceddu S, Theile DR, Parsons PG, Coman WB. Head and Neck Cancer: Past, Present and Future. *Expert Rev Anticancer Ther* (2006) 6:1111–8. doi: 10.1586/14737140.6.7.1111
9. Cohen EEW, Bell RB, Bifulco CB, Burtness B, Gillison ML, Harrington KJ, et al. The Society for Immunotherapy of Cancer Consensus Statement on Immunotherapy for the Treatment of Squamous Cell Carcinoma of the Head and Neck (HNSCC). *J Immunother Cancer* (2019) 7:184. doi: 10.1186/s40425-019-0662-5
10. Ervin TJ, Clark JR, Weichselbaum RR, Fallon BG, Miller D, Fabian RL, et al. An Analysis of Induction and Adjuvant Chemotherapy in the Multidisciplinary Treatment of Squamous-Cell Carcinoma of the Head and Neck. *J Clin Oncol* (1987) 5:10–20. doi: 10.1200/jco.1987.5.1.10
11. Vokes EE, Weichselbaum RR, Lippman SM, Hong WK. Head and Neck Cancer. *N Engl J Med* (1993) 328:184–94. doi: 10.1056/nejm199301213280306
12. Chaudhary S, Ganguly K, Muniyan S, Pothuraju R, Sayed Z, Jones DT, et al. Immunometabolic Alterations by HPV Infection: New Dimensions to Head and Neck Cancer Disparity. *J Natl Cancer Inst* (2019) 111:233–44. doi: 10.1093/jnci/djy207
13. Petersen JF, Timmermans AJ, van Dijk BAC, Overbeek LIH, Smit LA, Hilgers FJM, et al. Trends in Treatment, Incidence and Survival of Hypopharynx Cancer: A 20-Year Population-Based Study in the Netherlands. *Eur Arch Otorhinolaryngol* (2018) 275:181–9. doi: 10.1007/s00405-017-4766-6
14. An Q, Liu Z. Comparative Efficacy and Safety of Combination Therapies for Advanced Melanoma: A Network Meta-Analysis. *BMC Cancer* (2019) 19:43. doi: 10.1186/s12885-018-5259-8
15. Ichiki Y, Taira A, Chikaishi Y, Matsumiya H, Mori M, Kanayama M, et al. Prognostic Factors of Advanced or Postoperative Recurrent Non-Small Cell Lung Cancer Targeted With Immune Check Point Inhibitors. *J Thorac Dis* (2019) 11:1117–23. doi: 10.21037/jtd.2019.04.41
16. McArthur GA, Ribas A. Targeting Oncogenic Drivers and the Immune System in Melanoma. *J Clin Oncol* (2013) 31:499–506. doi: 10.1200/jco.2012.45.5568MEEHAN
17. Cohen EEW, Soulieres D, Le Tourneau C, Dinis J, Licitra L, Ahn MJ, et al. Pembrolizumab Versus Methotrexate, Docetaxel, or Cetuximab for Recurrent or Metastatic Head-and-Neck Squamous Cell Carcinoma (KEYNOTE-040): A Randomised, Open-Label, Phase 3 Study. *Lancet (London England)* (2019) 393:156–67. doi: 10.1016/s0140-6736(18)31999-8
18. Cramer JD, Burtness B, Le QT, Ferris RL. The Changing Therapeutic Landscape of Head and Neck Cancer. *Nat Rev Clin Oncol* (2019) 16:669–83. doi: 10.1038/s41571-019-0227-z
19. Larkins E, Blumenthal GM, Yuan W, He K, Sridhara R, Subramaniam S, et al. FDA Approval Summary: Pembrolizumab for the Treatment of Recurrent or Metastatic Head and Neck Squamous Cell Carcinoma With Disease Progression on or After Platinum-Containing Chemotherapy. *Oncologist* (2017) 22:873–8. doi: 10.1634/theoncologist.2016-0496
20. Ferris RL, Blumenschein GJr., Fayette J, Guigay J, Colevas AD, Licitra L, et al. Nivolumab vs Investigator's Choice in Recurrent or Metastatic Squamous Cell Carcinoma of the Head and Neck: 2-Year Long-Term Survival Update of CheckMate 141 With Analyses by Tumor PD-L1 Expression. *Oral Oncol* (2018) 81:45–51. doi: 10.1016/j.oraloncology.2018.04.008
21. Hirsch L, Zitvogel L, Eggermont A, Marabelle A. PD-Loma: A Cancer Entity With a Shared Sensitivity to the PD-1/PD-L1 Pathway Blockade. *Br J Cancer* (2019) 120:3–5. doi: 10.1038/s41416-018-0294-4
22. Hao C, Tian J, Liu H, Li F, Niu H, Zhu B. Efficacy and Safety of Anti-PD-1 and Anti-PD-1 Combined With Anti-CTLA-4 Immunotherapy to Advanced Melanoma: A Systematic Review and Meta-Analysis of Randomized Controlled Trials. *Medicine* (2017) 96:e7325. doi: 10.1097/md.0000000000007325
23. Rotte A. Combination of CTLA-4 and PD-1 Blockers for Treatment of Cancer. *J Exp Clin Cancer Res* (2019) 38:255. doi: 10.1186/s13046-019-1259-z
24. Saloura V, Izumchenko E, Zuo Z, Bao R, Korzinkin M, Ozerov I, et al. Immune Profiles in Primary Squamous Cell Carcinoma of the Head and Neck. *Oral Oncol* (2019) 96:77–88. doi: 10.1016/j.oraloncology.2019.06.032
25. Kulasinghe A, Taheri T, O'Byrne K, Hughes BGM, Kenny L, Punyadeera C. Highly Multiplexed Digital Spatial Profiling of the Tumor Microenvironment of Head and Neck Squamous Cell Carcinoma Patients. *Front Oncol* (2021) 10:607349. doi: 10.3389/fonc.2020.607349
26. Chen DS, Mellman I. Elements of Cancer Immunity and the Cancer-Immune Set Point. *Nature* (2017) 541:321–30. doi: 10.1038/nature21349
27. Kather JN, Suarez-Carmona M, Charoentong P, Weis CA, Hirsch D, Bankhead P, et al. Topography of Cancer-Associated Immune Cells in Human Solid Tumors. *eLife* (2018) 7. doi: 10.7554/eLife.36967
28. Ribbat-Idel J, Perner S, Kuppler P, Klapper L, Krupar R, Watermann C, et al. Immunologic "Cold" Squamous Cell Carcinomas of the Head and Neck Are Associated With an Unfavorable Prognosis. *Front Med* (2021) 8. doi: 10.3389/fmed.2021.622330
29. Braun M, Goltz D, Shaikhibrahim Z, Vogel W, Bohm D, Scheble V, et al. ERG Protein Expression and Genomic Rearrangement Status in Primary and Metastatic Prostate Cancer–a Comparative Study of Two Monoclonal Antibodies. *Prostate Cancer Prostatic Dis* (2012) 15:165–9. doi: 10.1038/pcan.2011.67
30. Pai SI, Faivre S, Licitra L, Machiels JP, Vermorken JB, Bruzzi P, et al. Comparative Analysis of the Phase III Clinical Trials of Anti-PD1

Monotherapy in Head and Neck Squamous Cell Carcinoma Patients (CheckMate 141 and KEYNOTE 040). *J Immunother Cancer* (2019) 7:96. doi: 10.1186/s40425-019-0578-0
31. Ayers M, Lunceford J, Nebozhyn M, Murphy E, Loboda A, Kaufman DR, et al. IFN-Gamma-Related mRNA Profile Predicts Clinical Response to PD-1 Blockade. *J Clin Invest* (2017) 127:2930–40. doi: 10.1172/jci91190
32. Chen YP, Wang YQ, Lv JW, Li YQ, Chua MLK, Le QT, et al. Identification and Validation of Novel Microenvironment-Based Immune Molecular Subgroups of Head and Neck Squamous Cell Carcinoma: Implications for Immunotherapy. *Ann Oncol* (2019) 30:68–75. doi: 10.1093/annonc/mdy470
33. Succaria F, Kvistborg P, Stein JE, Engle EL, McMiller TL, Rooper LM, et al. Characterization of the Tumor Immune Microenvironment in Human Papillomavirus-Positive and -Negative Head and Neck Squamous Cell Carcinomas. *Cancer Immunol Immunother* (2021) 70:1227–37. doi: 10.1007/s00262-020-02747-w
34. Meehan K, Leslie C, Lucas M, Jacques A, Mirzai B, Lim J, et al. Characterization of the Immune Profile of Oral Tongue Squamous Cell Carcinomas With Advancing Disease. *Cancer Med* (2020) 9:4791–807. doi: 10.1002/cam4.3106
35. Kleffel S, Posch C, Barthel SR, Mueller H, Schlapbach C, Guenova E, et al. Melanoma Cell-Intrinsic PD-1 Receptor Functions Promote Tumor Growth. *Cell* (2015) 162:1242–56. doi: 10.1016/j.cell.2015.08.052
36. Riley JL. PD-1 Signaling in Primary T Cells. *Immunol Rev* (2009) 229:114–25. doi: 10.1111/j.1600-065X.2009.00767.x
37. Morikawa M, Derynck R, Miyazono K. TGF-Beta and the TGF-Beta Family: Context-Dependent Roles in Cell and Tissue Physiology. *Cold Spring Harb Perspect Biol* (2016) 8:1–26.. doi: 10.1101/cshperspect.a021873
38. Liu L, Ning SB, Fu S, Mao Y, Xiao M, Guo B. Effects of lncRNA ANRIL on Proliferation and Apoptosis of Oral Squamous Cell Carcinoma Cells by Regulating TGF-Beta/Smad Pathway. *Eur Rev Med Pharmacol Sci* (2019) 23:6194–201. doi: 10.26355/eurrev_201907_18435
39. Suzuki S, Toyoma S, Tsuji T, Kawasaki Y, Yamada T. CD147 Mediates Transforming Growth Factor-Beta1-Induced Epithelial-Mesenchymal Transition and Cell Invasion in Squamous Cell Carcinoma of the Tongue. *Exp Ther Med* (2019) 17:2855–60. doi: 10.3892/etm.2019.7230
40. Oshimori N, Oristian D, Fuchs E. TGF-Beta Promotes Heterogeneity and Drug Resistance in Squamous Cell Carcinoma. *Cell* (2015) 160:963–76. doi: 10.1016/j.cell.2015.01.043
41. Wu X, Gu Z, Chen Y, Chen B, Chen W, Weng L, et al. Application of PD-1 Blockade in Cancer Immunotherapy. *Comput Struct Biotechnol J* (2019) 17:661–74. doi: 10.1016/j.csbj.2019.03.006
42. Batlle E, Massague J. Transforming Growth Factor-Beta Signaling in Immunity and Cancer. *Immunity* (2019) 50:924–40. doi: 10.1016/j.immuni.2019.03.024
43. Tauriello DVF, Palomo-Ponce S, Stork D, Berenguer-Llergo A, Badia-Ramentol J, Iglesias M, et al. TGFbeta Drives Immune Evasion in Genetically Reconstituted Colon Cancer Metastasis. *Nature* (2018) 554:538–43. doi: 10.1038/nature25492

Conflict of Interest: The authors declare that the research was conducted in the absence of any commercial or financial relationships that could be construed as a potential conflict of interest.

Publisher's Note: All claims expressed in this article are solely those of the authors and do not necessarily represent those of their affiliated organizations, or those of the publisher, the editors and the reviewers. Any product that may be evaluated in this article, or claim that may be made by its manufacturer, is not guaranteed or endorsed by the publisher.

frontiers in Oncology

ORIGINAL RESEARCH
published: 02 November 2021
doi: 10.3389/fonc.2021.723162

Multidimensional Mutational Profiling of the Indian HNSCC Sub-Population Provides IRAK1, a Novel Driver Gene and Potential Druggable Target

Sagar Sanjiv Desai[1,2†], Raksha Rao K[1†], Anika Jain[3], Pushpinder Singh Bawa[1], Priyatam Dutta[1], Gaurav Atre[1], Anand Subhash[4], Vishal U. S. Rao[4], Suvratha J[1], Subhashini Srinivasan[1] and Bibha Choudhary[1]*

[1] Department of Biotechnology and Bioinformatics, Institute of Bioinformatics and Applied Biotechnology, Bangalore, India, [2] Graduate Student Registered Under Manipal Academy of Higher Education, Manipal, India, [3] Department of Biotechnology, School of Biosciences and Technology, Vellore Institute of Technology, Vellore Campus, Katpadi, Vellore, India, [4] Healthcare Global Enterprises Ltd, Cancer Centre, Bangalore, India

OPEN ACCESS

Edited by:
Yong Yin,
Shandong Cancer Hospital, China

Reviewed by:
Marcos Santos,
University of Brasilia, Brazil
Jharna Datta,
The Ohio State University,
United States

***Correspondence:**
Bibha Choudhary
vibha@ibab.ac.in

[†]These authors share first authorship

Specialty section:
This article was submitted to Head and Neck Cancer, a section of the journal Frontiers in Oncology

Received: 10 June 2021
Accepted: 28 September 2021
Published: 02 November 2021

Citation:
Desai SS, K RR, Jain A, Bawa PS, Dutta P, Atre G, Subhash A, Rao VUS, J S, Srinivasan S and Choudhary B (2021) Multidimensional Mutational Profiling of the Indian HNSCC Sub-Population Provides IRAK1, a Novel Driver Gene and Potential Druggable Target. Front. Oncol. 11:723162. doi: 10.3389/fonc.2021.723162

Head and neck squamous cell carcinomas (HNSCC) include heterogeneous group of tumors, classified according to their anatomical site. It is the sixth most prevalent cancer globally. Among South Asian countries, India accounts for 40% of HNC malignancies with significant morbidity and mortality. In the present study, we have performed exome sequencing and analysis of 51 Head and Neck squamous cell carcinoma samples. Besides known mutations in the oncogenes and tumour suppressors, we have identified novel gene signatures differentiating buccal, alveolar, and tongue cancers. Around 50% of the patients showed mutation in tumour suppressor genes TP53 and TP63. Apart from the known mutations, we report novel mutations in the genes AKT1, SPECC1, and LRP1B, which are linked with tumour progression and patient survival. A highly curated process was developed to identify survival signatures. 36 survival-related genes were identified based on the correlation of functional impact of variants identified using exome-seq with gene expression from transcriptome data (GEPIA database) and survival. An independent LASSO regression analysis was also performed. Survival signatures common to both the methods led to identification of 4 dead and 3 alive gene signatures, the accuracy of which was confirmed by performing a ROC analysis (AUC=0.79 and 0.91, respectively). Also, machine learning-based driver gene prediction tool resulted in the identification of IRAK1 as the driver (p-value = 9.7 e-08) and also as an actionable mutation. Modelling of the IRAK1 mutation showed a decrease in its binding to known IRAK1 inhibitors.

Keywords: HNSCC, IRAK1, survival, driver gene, LASSO, ROC, whole exome sequencing

INTRODUCTION

Head and Neck cancer (HNC) is a heterogeneous disease that encompasses tumors of majorly three regions, oral cavity, oropharynx, and larynx, and together they account for more than 660000 new cases and over 320000 deaths worldwide wide, while India has contributed to 36%, 20.9% and 18.8% of the total cases of each type respectively, in 2020 (https://gco.iarc.fr) (1). More than 90% of the HNCs are diagnosed as squamous cell carcinomas (HNSCC). The common risk factors worldwide are smoking tobacco, alcohol consumption, improper diet, whereas chewing areca nuts, chewing tobacco, smoking bidis, etc., are rampant in India (1, 2). Over the past 3-4 decades, various treatment regimens like surgery, adjuvant chemotherapy, radiation therapy, immunotherapy, etc. have been employed, yet only 50 % improvement in survival rates have been achieved for HNSCC (3–5).

Several studies have reported drivers of Head and Neck cancer oncogenesis. The drivers can be broadly classified into tumor suppressors and oncogenes. Alterations in oncogene families like *ras* family of genes, *myc* family and EGFR family have been implicated in oral and head and neck cancers. High frequency of mutations in *HRAS*, copy number alterations and aberrant expression levels in *KRAS, NRAS, MYC* and *EGFR* have been reported in relation with development of many squamous cell carcinomas. Driver Genes like *CCND1, MAPK* family and *PIK3CA* are involved in the progression of HNSCC (4, 6, 7). Early stages of head and neck cancers have been associated with inactivated *CDKN2A* and *TP53*, loss of function copy alterations is associated with aggressive cancers. HPV+ve HNSCC cancers are characterized by frequent mutations and chromosomal deletions in tumor suppressors like *PTEN*, E-cadherins and *RB1 (*4, 6, 8). One of the first steps of oncogenesis involves the evasion of immune system. In HNSCC, *IRAK1* overexpression is associated with tumor progression and low survival (9). *IRAK1* is a kinase, activated downstream of TLRs and is activated upon radiation therapy in HNSCC (10, 11)

Several models have been proposed as predictive biomarkers for the prognosis of HNSCC patients. A recent study reported a 6 gene signature for predicting survival in patients using random forest sampling and Cox regression analysis. Exome seq analysis has led to the identification of SNPs in the genes, which can be used as independent prognostic markers (12, 13). Oncogenic driver mutations in genes commonly associated with HNSCC, like *P53, PI3-AKT* pathway, *HRAS, CCND1* and others, have been associated with poor survival and have been identified as important factors for outcome predictions in HNSCC cohorts (4, 8). Accumulation of structural variants such as Copy number variation (CNV), Loss of Heterozygosity (LOH) in oncogenes, and tumor suppressors like *c-MYC, EGFR, CDKN2A*, respectively, have been associated with recurrence of squamous cell carcinomas, and poor prognosis and outcome predictions have been linked to rapid occurrence rates of SCNAs across tumor genomes (4, 14, 15). The genomic analyses of HNSCC from (110 patients) Indian population led to the identification of 5 new frequently mutated (10-22% of the patients) genes associated with OSCC-GB, namely, *USP9X, MLL4, ARID2, UNC13C* and *TRPM3* (16).

In this study, we have performed exome sequencing of 51 individuals from diverse anatomical sites and correlated the clinical phenotype to the genotype. We report distinct anatomical site-specific signatures and heterogeneity within each group. We have also identified novel driver mutations using Oncodrivclustl. We identified alive and dead signatures using two different approaches. The first approach was based on the correlation of functional impact of variants using exome-seq with gene expression using transcriptome data (GEPIA database) and the second was LASSO regression. The signatures were validated using a receiver operating characteristics (ROC) model. We have identified 2 missense mutations in IRAK1, one of which causes structural changes in the protein, possibly leading to change in its activity.

METHODOLOGY

Subjects for the Study

We obtained 51 FFPE (Formalin Fixed Paraffin Embedded) samples diagnosed with oral cancer at the Healthcare Global Enterprises Ltd, Bengaluru, Karnataka, India. The protocol was approved by the institutional review board of HCG and Institute of Bioinformatics and Applied Biotechnology. The clinical details of every patient are mentioned in **Table 1**. Informed consent was obtained from all the participants.

Exome Library Preparation

To prepare libraries for Whole Exome Sequencing, 100ng-1µg of genomic DNA was sheared with the Covaris S220 (Covaris, Woburn, MA, USA), followed by end-repair, 3' end Adenylation and ligation with paired-end adaptors. Post ligation, 15µl of the purified libraries were PCR amplified, all the above steps were performed using the Agilent SureSelect^{XT} kit and every step was followed by DNA purification on a magnetic stand using AMPure XP Reagent beads (Beckman Coulter Genomics, Danvers, MA, USA). Afterward, size (approx 225-275 bp) and quantity (>800ng) were verified employing the Agilent

TABLE 1 | A table summarizing clinical data of the samples in the study.

Characteristics		Number of Samples
Age (years)	<= 55	25
	> 55	21
Survival Status	Alive	23
	Dead	14
Gender	Female	15
	Male	31
Tumor Stage	T1	9
	T2	5
	T3	5
	T4	11
Habits	Smoking	18
	Alcohol	8
	Quit	3
	None	15

Tapestation 2200 system followed by hybridization and probe capture using Exome SureSelect Human All Exon V6+UTR probes (Agilent). Dynabeads MyOne Streptavidin T1 magnetic beads (Thermofisher). Finally, Captured Libraries were amplified with 12 cycles of PCR using indexing primers containing 8-bp indices, followed by an amplification using AMPure XP beads (Beckman Coulter). Final libraries were checked for quality (each fragment size approx. 300-400 bp) and quantity using Agilent Tapestation 2200 system.

Whole Exome Sequencing and Analysis

The libraries were multiplexed and pooled followed by a 100-bp paired-end sequencing with ~100X exome coverage depth per sample (Approx. 60-90 mb exome size) on the Illumina HiSeq 2500 platform. The exome sequencing raw data is available at https://www.ncbi.nlm.nih.gov/sra/PRJNA740146. Filtered high exome-sequencing reads generated on HiSeq 2500 were analyzed using FastQC for quality checking (https://www.bioinformatics.babraham.ac.uk/projects/fastqc/). Bowtie2 (17) aligner was used for alignment and mapping of reads against the hg38 version of the human genome, with default parameter settings. SAMtools (18) was used for conversion of SAM files to BAM files. PCR duplicates were removed using Picard tools (http://broadinstitute.github.io/picard/). Variant calling was performed using the best practices Mutect2 module of GATK (Genome Analysis Toolkit, Broad Institute) including local realignment around insertions/deletions and base-quality score recalibration (19). Duplicate removed alignment files were subjected to another format Variant calling using pileup utilities from BCFtools (18). Variants common to pileup approach and GATK process, and the ones being spanned by more than 3 reads were annotated using the SnpEff and SnpSift tools (20, 21). Only the variants not present in the 1000G database were considered for further analysis (22).

Obtaining Mutation Profiles

All the vcf files were primarily processed using shell scripts. Mutation frequency of genes known to be implicated in Head and Neck cancer was depicted using a waterfall plot from the R package GenVisR (23). The samples were grouped into categories based on age (0-40 yrs.; 40-50 yrs.; 50-60 yrs.; 60-70 yrs.; 70-80 yrs.), habits (alcohol; tobacco; all; none; quit), stage of tumor at the time of biopsy (early; advanced; recurrent) and site of tumor (alveolar; buccal mucosa; tongue). Total number of mutations, number of high impact mutations and number of protein coding mutations (high impact + missense variants), per sample, from each category were obtained. Mutation signatures were obtained using the SomaticSignatures package of R (24). CNV analysis was performed using CNVkit (25).

Driver Gene Analysis

To predict the driver genes, vcf files of all the samples were merged into a single file using the BCFtools toolkit which included all the mutations present in each and every sample. This merged vcf file was given as an input to OncodriveCLUSTL for driver gene analysis (24, 26). The resulting genes were filtered based on their p-value significance and frequency of mutation. Further we checked for the effect of mutations being harbored by these genes on patient survival and it was seen that none of the mutations showed a significant difference in survival. We also checked for an association between expression patterns of these genes and patient survival from the GEPIA database (24, 26, 27) and the genes showing a significant correlation were further shortlisted followed by generating a lolliplots of the mutations present in the shortlisted genes using G3Viz (28).

IRAK1 Structure Modeling and Validation

The IRAK1 protein (identified as one of the driver genes) structure and its two mutants S532L and F196S were modeled using the 712-residue sequence from UniProt (UniProt ID: P51617) on the Robetta web server (29). The structure obtained is further energy minimized on Swiss-PdbViewer using a GROMOS 43B1 force field to repair distorted geometries (30). The energy minimized protein structure of IRAK1 was further validated using the SAVES webserver (https://saves.mbi.ucla.edu/) which employs tools such as ERRAT (30, 31), PROVE (32), PROCHECK (32, 33), WHATCHECK (34) and VERIFY 3D (35). Site Directed Mutator (SDM) and I-Mutant 2.0 (36, 37). Webservers were used to predict the effect of mutation on the stability of the protein structure and the Gibbs free energy change(ddG). Autodock 4.0 was used to blind dock the ligand JH-X-119-01 (a selective inhibitor for IRAK1) (36–38) with the wild type IRAK1 structure as well as the S532L and F196S mutant structures to study the change in ligand binding upon mutation. The active site of *IRAK1* (Serine/Threonine Protein Kinase) corresponds to residues 336-348. The binding site of *IRAK1*(Protein Kinase, ATP Binding Site) corresponds to residues 218-239 as indicated by InterPro. LigPlot+ software (36–39) was used to visualize the ligand interactions. To understand the change in interaction between the residues in the protein structure upon mutation, Residue Interaction Analysis was performed. RING web server was used to generate a Residue Interaction Network (RIN) wherein the nodes represent the residues and the arcs represent the physico-chemical interactions (40). The network thus generated is visualized in Cytoscape to study the change in interactions of residue 196 and 532 upon mutation (41).

Survival Models

Mutation profiles and the associated clinical data of 178 Oral cancer patients from Indian Cohort were downloaded from the ICGC database. For survival analysis, ICGC and inhouse data were clubbed. To associate demographic and clinical parameters with survival time and to assess the effect of variants on it, construction of Kaplan-Meyer plots and hazard ratio (HR with 95% CI) calculations were performed by employing univariate and multivariate Cox analysis using the survminer (https://github.com/kassambara/survminer) and survival (42) packages of R. From the inhouse data, a total of 36 genes were shortlisted based on an initial scrutiny, 19 fitting the dead signature criteria and 17 fitting the alive signature criteria, 6 genes were shortlisted based on the significant association of their mutation profiles with alive and dead samples (Chi-square analysis performed in R) and an

association of expression patterns with survival analysis from GEPIA database (Gene Expression Profiling Interactive Analysis). Further functional annotations were performed using information databases such as UCSC and GeneCards.

Lasso Regression Model

LASSO stands for Least Absolute Shrinkage and Selection Operator. It is a linear form of regularization technique (to minimize the error because of overfitting of data while constructing a model). As the name suggests, it uses a "shrinkage/penalty term(lambda)" in its regression equation to be able to predict with accuracy and precision.

Mathematical equation:

$$\sum_{i=1}^{n}\left(y_i - \sum_j x_{ij} \quad \beta_j\right)^2 + \lambda\sum_{j=1}^{p}|\beta_j|$$

where, λ, the penalty factor (or the shrinkage parameter) and β are the coefficients related to p features (43). The significant genes were found by computing the coefficients of Lasso regression of the cox survival data. This was achieved by using the "sksurv" or "scikit-survival" module of python, present as a part of "scikit-learn".

The equation the module sksurv.linear_model. CoxnetSurvivalAnalysis uses is as follows:-

$$\arg\max_{\beta} \log PL(\beta) - \alpha\left(\sum_{j=1}^{p}|\beta_j| + \frac{1-r}{2}\sum_{j=1}^{p}\beta_j^2\right)$$

This equation represents the "elastic net regression". Here α is the same as γ which is mentioned in the Lasso regression introduction equation. By giving a l1_ratio value of 1.0 we are eliminating the Ridge regression term (second term) and only keeping the Lasso regression term. Steps followed for each dataset; 1. The dataset was processed by "CoxnetSurvivalAnalysis" with a subset of 100 random alpha values, a l1_ratio of 1.0(complete Lasso regression), alpha_min_ratio is set to auto depending on the no. of samples and no. of features. This gives us a subset of coefficients corresponding to that particular alpha value. To obtain the best alpha value by a 5-fold cross validation, we use the following modules and their utility classes a. Sklearn.pipeline.make_pipeline b. sklearn.preprocessing.StandardScaler c. sklearn.model_selection.KFold d. sklearn.model_selection.GridSearchCV. After the best alpha value for the dataset is obtained, we obtain the coefficients for all the features pertaining to that alpha value.

Statistical Analysis

Chi-square analysis was performed to determine the significance in difference between number of alive and dead patients per gene. Survival time was defined as days from the initial diagnosis to the death or the last follow-up. The hazard ratio and their 95% confidence intervals (95% CI) for the associations of clinical variables with survival time were calculated by univariate Cox proportional hazard analysis using the survival and survminer packages of R (42). The associations between SNPs and patient survival (for the additive 4 dead and 3 alive gene models) were analyzed by multivariate Cox regression models. The difference in survival time between different patients based on genotypes of the dead and alive signature genes, using an additive model, was assessed by Kaplan-Meier curves, the significance of the influence of the clinical parameters and the additive gene models on patient survival was determined using log-rank test. Receiver Operating characteristic (ROC) curve was constructed and the area under the curve (AUC) was used to assess the performance of the model. The results were considered significant if the p-value was less than 0.05.

RESULTS

Identification of Mutation Burden and Signatures Associated With the Age and Stage of HNC Tumor

Variant analysis was performed for 50 Head and Neck Squamous Cell Carcinoma (HNSCC) tumor samples using exome-seq. The depth covered per sample was approximately 100X with an average of 61 million reads (**Supplementary Table 1**). To identify if there was a chromosome bias for mutations, we analyzed the mutations from all the samples. The number and density of mutation was highest on ChrX (average 794 variants) followed by Chr1 (average 400 variants), while chr18 had the least number of variants (average 60 variants) (**Figure 1A**).

To check whether the number of mutations correlate with disease progression, habit and age of the individual, we catalogued the number of mutations per individual, habit and age. On comparison across different age groups, we observed the lowest number of total variants (approx. 3000/sample) in patients aged < 40 years, while the number was as high as 5000 variants/sample in patients belonging 70-80 years of age (**Figure 1B**). Patients consuming alcohol or tobacco had relatively a smaller number of variants (approx. 2500/sample) as compared to the patients consuming both (approx. 3000/sample) and the ones having quit these habits, surprisingly, showed the least number of mutations (**Figure 1C**). Recurrent tumor samples obtained from the buccal mucosa and alveolar sockets harbored the maximum number of variants (approx. 5000/sample) as compared to tumors of other sites in the oral cavity (**Figure 1D**). Interestingly, a stage-wise distribution showed that tumors at the earliest stage have the highest number of mutations, followed by a gentle decline in the number of variants in the case of advanced and recurrent stages (**Figure 1E**). We further investigated mutational signatures mutational burden/Mb in tumors from patients with different habits and mild distinctions were observed. C>T followed by T>C mutations were seen in high abundance across all the habits with the highest being in the quit category, while the patients with alcohol consumption showed a relatively higher C>A signature and the ones with tobacco consumption had higher levels of C>G mutation as compared to other habit categories (**Figure 1F**). Patients consuming both alcohol and Tobacco displayed the maximum tumor mutational burden (TMB) and yet again, the samples having quit these habits show the lowest TMB (**Figure 3A**).

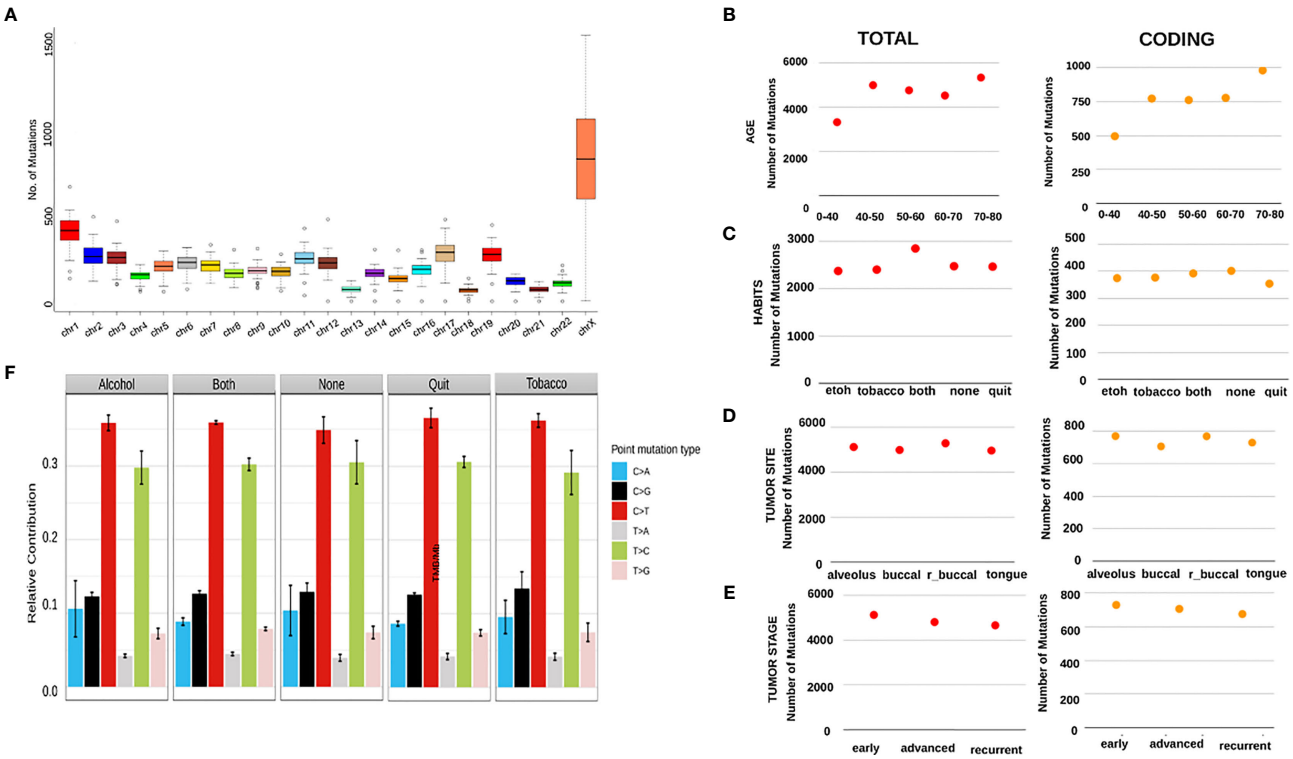

FIGURE 1 | **(A)** A boxplot showing an aggregate of number of mutations in every sample per Mb of across all the chromosomes. It can be seen that chrX shows the highest number of mutations with the highest number of variations between the samples, with the next highest being chr1. X-axis shows the chromosome numbers and Y-axis depicts the number of mutations per Mb. **(B–E)** The scatter plots here show varying patterns of average number of all mutations and average number of coding mutations per category. **(A)** shows the average numbers across age groups, **(C)** shows the average numbers across patient habits, **(D)** shows average numbers across tumor sites and **(E)** shows the numbers across stages of tumors. **(F)** This is a bar graph showing the relative contribution of 6 mutational signatures in patients categorized by habits.

Unique Signature in Cell Cycle, Apoptotic and Wnt Signaling Pathway Segregate Tumors of the Buccal Cavity From Tongue and Alveolus

A set of genes known to harbor somatic mutations and classified as driver genes in HNSCC were identified and a waterfall plot generated (**Figure 2**). As expected, *TP53*, a known tumor suppressor, and *TP63* had the highest frequency of mutation (greater than 60%) in the HNSC cohort. Transcription factors like *NOTCH1* (16%) and *KMT2B* (16%), *UNC13C* (14%), another tumor suppressor, *ERCC2* (14%) involved in nucleotide excision repair pathway, were recurrently mutated, whereas genes like *CDKN2A, MLH1, FGFR1, EGFR*, etc. had a less than 10% mutation frequency. Interestingly, *CCND1*, known to be associated with HNSCC due to copy number alterations, and *APEX1* which is known to be associated with a high risk of HNC showed negligible mutation frequency (**Figure 2**). Notably, among variations in the coding region, missense variants, stop gained variants, and structural interaction variants showed the highest frequency (**Figure 2**).

We categorized 19 patients based on anatomical sites, alveolar, buccal mucosa, and tongue and constructed waterfall plot. The genes uniquely mutated in each category were from a known list of proteins belonging to various categories namely, tumor suppressors, WNT signaling, Cell cycle, Apoptosis, EMT, Replication, etc. Tumor site data was available for only 19 of the patients. Tumour site data was available for only 19 of the patients. It was seen that *APC4*, a gene involved in Cell cycle progression, harboring a structural interaction variant showed the highest frequency being present in 18 out of 19 patients across all the tumor sites. 50-60% of the samples showed mutations in genes involved in Apoptosis, like CASP10, ATF4, PARP1, and TNFSF10, most of which were either missense or structural interaction variants, respectively. The alveolar tumours were characterized by mutations in cell cycle genes, PRKCG, RBL2, RFC2, WEE1, MCM2, CDKN2A, SMAD4, MCM3, and PRKDC proto-oncogenes like HRAS, NRAS, LMNB2. Mutational signatures in the patients with buccal mucosa category belong to the Apoptosis pathway (*MAPK10, CTSW, DAXX, ATM, HTRA2, BIRC3, CASP6*) and WNT signaling pathway (*WISP1, NOTUM, NFATC1, ROR2, CTNNB1, CACYBP*) and EMT pathway related genes, namely, *RNASEH2B, DAB2IP, MMP9* and *SNAI* were observed. Interestingly, the mutation in transcription factor *TFDP1* involved in the cell cycle was observed only in 2 samples both of them had recurrence. The least number of genes with

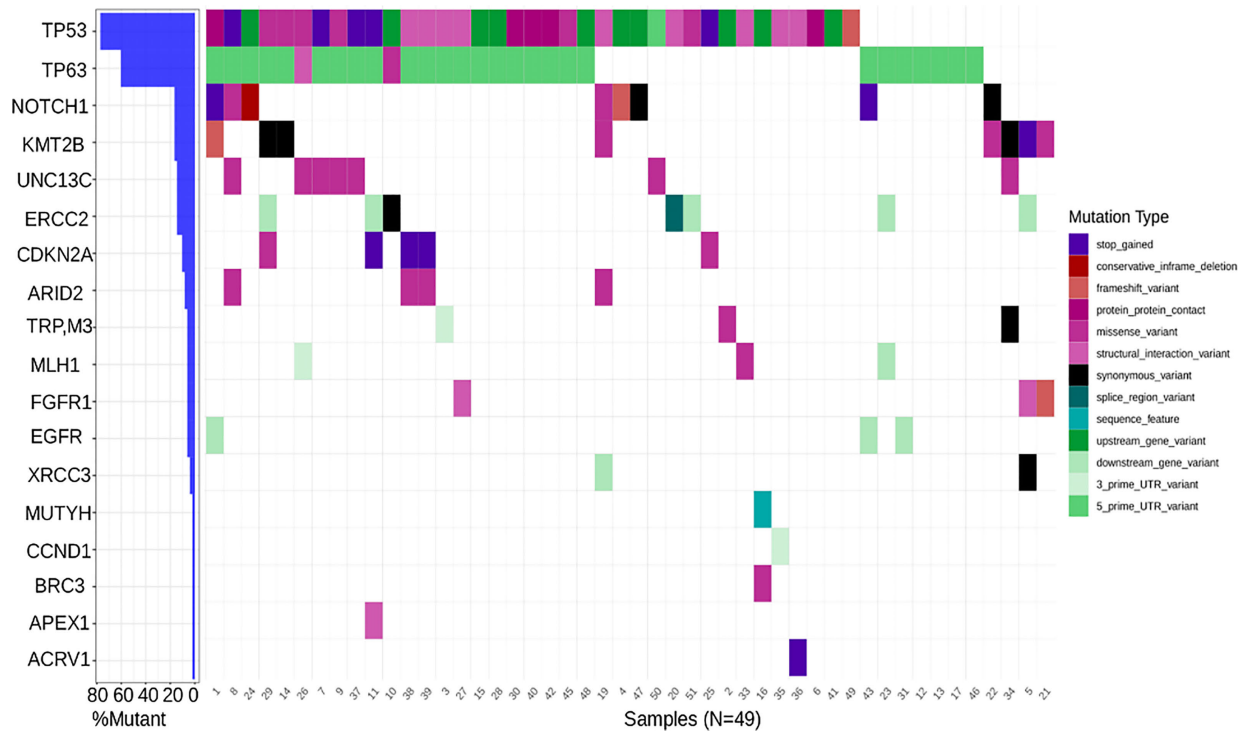

FIGURE 2 | Waterfall plot depicting mutation frequency of genes known to be implicated in HNSCC across patients with the highest frequency being that of TP53 and the lowest being that of ACRV1 along with a varying frequency across tumor suppressors, cell cycle genes, DNA damage and repair genes etc.

mutational signatures were obtained in tongue cancer. Tongue cancer was characterized by unique mutations in the cell cycle genes MCM4, RNASEH2A, HDAC1, CCNB1, WNT signalling pathway LRP5, NFATC4, and WNT11, and TP53 tumour suppressor gene (**Supplementary Figure S1**). We also observed patient specific mutation within each category depicting heterogeneity in each of the samples.

Combination of Radiotherapy, Chemotherapy, and Surgery Is Associated With Worse Patient Survival Compared to Surgery and Chemotherapy or Surgery and Radiotherapy

Differential survival within different clinical properties was illustrated using Kaplan-Meier plots. Within the habit's category, significantly ($p=0.0083 < 0.01$) low survival was observed for patients who consumed alcohol and tobacco, compared to patients having neither and the ones who have quit (**Figure 3B**). Among various forms of treatment, patients having undergone only Surgery and the ones with Surgery + Radiotherapy had a significantly higher probability of survival as compared to the patients having been administered with all three, Chemotherapy + Surgery + Radiotherapy ($p<0.0001$) (**Figure 3C**). For comparison, Oral cancer whole exome data of the Indian Cohort consisting of 178 samples, was downloaded from the ICGC database along with the clinical parameters of the patients. On clubbing the in-house and ICGC survival data, it was observed that patients that underwent surgery + radiation therapy showed significantly better survival ($p=0.00036$) as compared to the ones with only surgery and surgery + chemotherapy + radiation. In conclusion, the samples that were given surgery + chemotherapy + surgery showed the lowest probability of survival in both scenarios. As expected, the patients with no treatment administered exhibited the least survival probability (**Figure 3D**). The tumor stage of patients along with recurrence was also analyzed and it was seen that patient showing recurrence at any stage of the tumor displayed a significantly lower probability of survival ($p<0.0001$) with the recurrent T4 stage showing the lowest of survival as compared to the patients with stages without recurrence. A similar trend was seen in the inhouse data but the result was only mildly significant (p-value=0.07) (**Figure 3E**, **Supplementary Figure S2A**). A multivariate Cox proportional hazards analysis of the clinical parameters revealed that the tumor stage and treatment (Hazard Ratio 1.6 and 2.0 respectively) significantly (p-value < 0.001) influence the patients' risk of death (**Figure 3F**).

Identification of IRAK1 and UMODl1 as Driver Genes and Potential Therapeutic Targets

After getting a general idea of the mutation spectrum and survival trends associated with clinical parameters, we checked for oncogenic driver genes using OncodriveCLUSTL. Among the

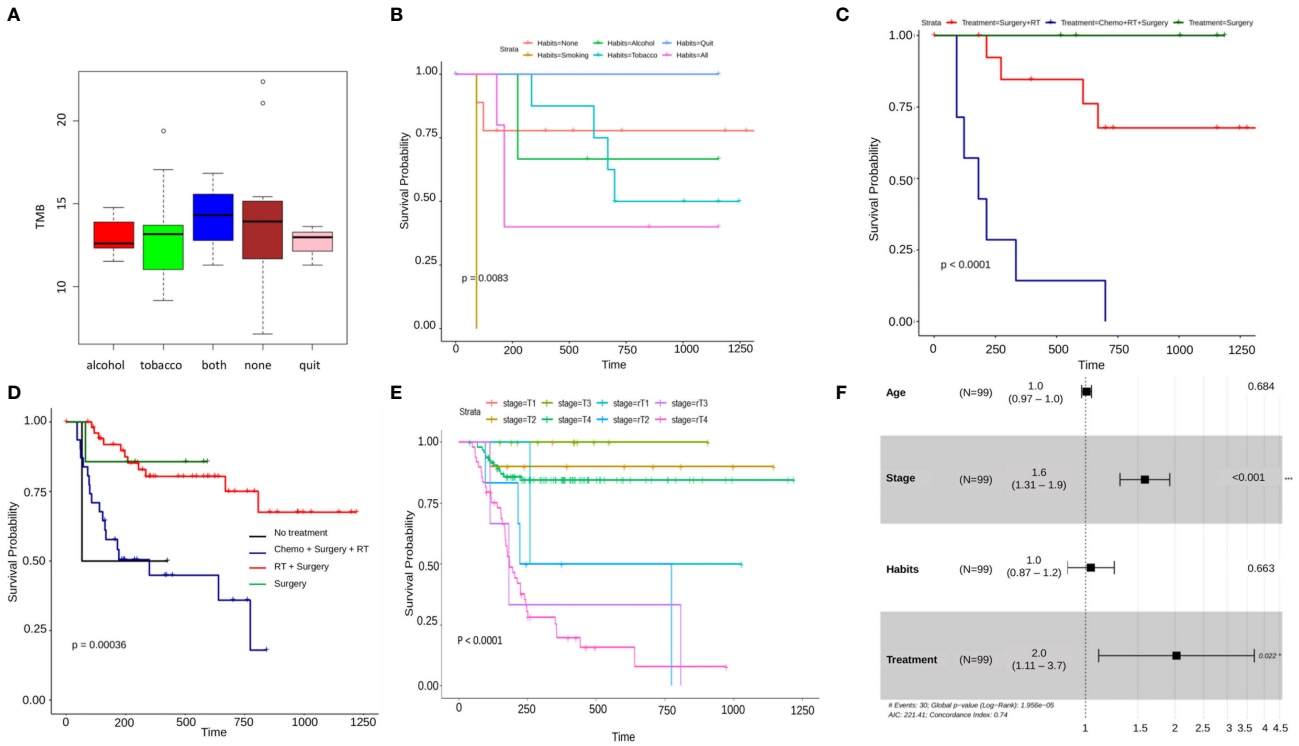

FIGURE 3 | **(A)** A boxplot of average tumor mutation burden of patients categorized by habits. Patients having both the habits of alcohol consumption and tobacco usage, show the highest amount of average tmb, lowest is seen to be in the patients with alcohol consumption and those who have quit either of the habits. Surprisingly, it is seen to be high in the patients having none of the habits. **(B–E)** Kaplam-Meier plots showing significant differential survival probabilities between different clinical categories. **(B)** This plot shows a significantly lower survival in patients with the habit of smoking as compared to any other category. **(C)** This Kaplan-Meier plot depicts a significantly lower survival probability in patients with a combined treatment regimen of chemotherapy, radiation therapy and Surgery as against any other individual or combined treatment type. This pattern gets reflected again in **(D)** where the data from ICGC Indian oral cancer cohort has been combined with in-house data and finally, **(E)** shows A differential survival plot of patients from ICGC and in-house data showing a significantly lower survival probability in patients with recurrent tumor stages as against their non-recurrent counterparts. **(F)** A cox-proportional hazard ratios forest plot, depicting the fact that there is a significant difference between various categories tumor stage and treatment regimens.

significant genes obtained, top two genes *THAP7* and *CDK3* (p-value=1.11e$^{-19,}$ had mutations present in almost all the samples) (**Figure 4A**). *THAP7* harbored a missense mutation which was present in 48 out of 51 samples whereas *CDK3* had a downstream gene variant being a part of *CDK3-TEN1* fusion present in 42 samples. Further, in order to screen the other genes from the output, we started by referring to the GEPIA database. From the significant list of genes, we checked for the ones displaying a significant difference in survival from the HNSCC transcriptome dataset in GEPIA and we obtained two driver genes that had a significantly high frequency of mutations across all the patients. The first was *IRAK1*, with two missense mutations, present in 21 and 19 patients respectively (**Figure 4D**), on either side of its kinase domain with a p-value for its mutation cluster being 9.70e^{-08} (**Figure 4F**) and significant differential survival from GEPIA (Hazards Ratio = 1.3, p-value = 0.038) (**Figure 4C**). The second was *UMODL1* with one missense mutation in its EGF-like calcium-binding (EGF_CA) domain, present in 29 patients (**Figure 4E**) as part of a significant mutation cluster with p-value = 1.11^{e-19} (**Figure 4F**) and yet again, a significant differential survival from GEPIA (Hazards Ratio = 0.74, p-value = 0.029) (**Figure 4B**).

Mutations in *IRAK1* Lead to Structural Changes Impacting Stability and Binding of an Inhibitor

We chose *IRAK1* for further analysis based on its function as a modulator of the innate immune system and its association with survival. It is known that cancer cells escape the immune system due to faulty signalling.

The *IRAK1* protein structure and its two mutants S532L and F196S were modeled using the 712-residue sequence from UniProt (UniProt ID: P51617) on the Robetta web server. The modeled structure was then energy minimized, validated and the effects of the two mutations on stability and Gibbs free energy were analyzed. The energy of the structure modeled was found to decrease drastically upon energy minimization, from -22736.7 to -33353.3 for wildtype, from -22663.424 to -33286.121 for S53L and from -23651.352 to -33606.613 for F196S, indicating better structures for all the three (**Table 2**). The overall quality factor of the three structures, as predicted by SAVES web server was above 94, with the Wild structure having a factor of 96.1207 and S532L and F196S structures having a quality factor of 95.265 and 94.1176 respectively. In the case of S532L, the stability of

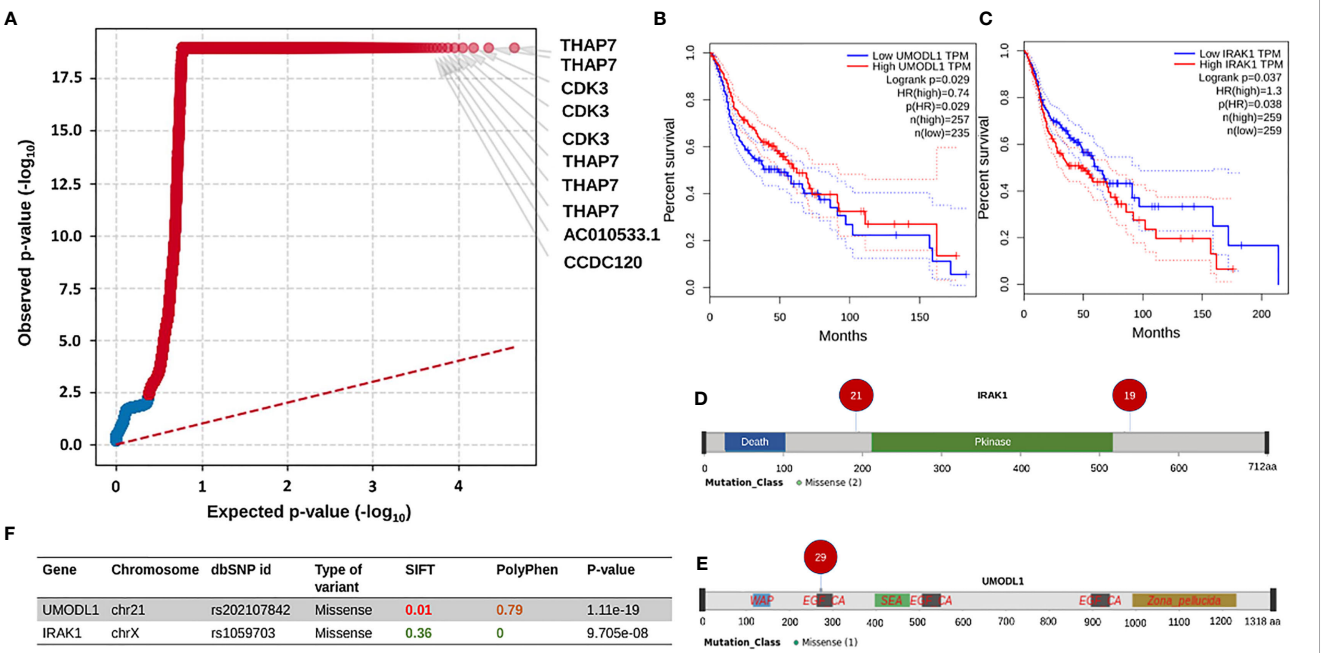

F

Gene	Chromosome	dbSNP id	Type of variant	SIFT	PolyPhen	P-value
UMODL1	chr21	rs202107842	Missense	0.01	0.79	1.11e-19
IRAK1	chrX	rs1059703	Missense	0.36	0	9.705e-08

FIGURE 4 | This entire panel of figures represents results from driver genes prediction and the subsequent analyses performed. **(A)** This is a quantile plot generated by oncodriveclutstl that depicts significant driver genes predicted as per frequency of mutations. This plot shows THAP7 and CDK3 as the most significant driver genes. **(B, C)** Show expression-based survival plots of two more driver genes, UMODL1 and IRAK1, respectively, from the HNSCC dataset in GEPIA2 database. Both have a significant difference in survival probability between high and low expression categories. **(F)** Table showing the details of the UMODL1 and IRAK1 mutations. It can be seen that the missense mutations in both of them have been previously reported, are deleterious and probably damaging based on the SIFT and PolyPhen values. The p-value in the last column is the significance measure from oncodriveclustl prediction. **(D, E)** Are lollipop plots depicting the amino acid position and the number of patients of the missense mutations in UMODL1 and IRAK1 linear protein structures respectively.

IRAK1 structure increased up to a ddG value of 1.53 and decreased to a value of -0.52 for the F196S mutant as shown by Site Directed Mutator (SDM). Similar results were obtained using I-Mutant 2.0 (**Table 3**). JH-X-119-01, an inhibitor of IRAK1 (36) was docked on to the wild type *IRAK1* structure as well as the S532L and F196S mutant structures to study the change in ligand binding upon mutation. The active site of *IRAK1* (Serine/Threonine Protein Kinase) corresponds to residues 336-348. The binding site of *IRAK1*(Protein Kinase, ATP Binding Site) corresponds to residues 218-239. JH-X-119-01 interacts with Tyr236, Val235, and Arg228 on the wild type structure with a binding energy of -6.66 (**Figure 5A**, **Table 4**) and residues Arg232 and Tyr236 on the F196S mutant structure, with a slightly reduced binding energy of -5.46 (**Supplementary Figure S3A**, **Table 4**). The ligand did not have any favorable interactions with active site or binding site residues in the S532L mutant structure (**Table 4**). Ser532 on the wild type structure interacts with residue Ala535 only (**Figure 5C**) but Leu532 on the mutant type structure interacts with three residues (Val528, Ser536 and Ala535) (**Figure 5D**). This increase in residue interaction could explain the increase in stability upon mutation. Phe196 on the wild type structure interacts with three residues (Pro13, His17 and Phe18) but Ser196 on the mutant structure interacts with only one residue (Tyr20). This loss of two interactions could explain the decrease in stability upon mutation (**Supplementary Figures S3B, C**).

TABLE 2 | Change in structure energy upon minimization.

Molecule Type	Structure Energy before minimization (in KJ/mol)	Structure Energy after minimization (in KJ/mol)
Wild	-22736.748	-33353.344
S532L	-22663.424	-33286.121
F196S	-23651.352	-33606.613

TABLE 3 | ddG values for S532L and F196S mutants on SDM and I-Mutant 2.0.

Mutation	S532L	F196S
SDM	1.53	-0.52
I-Mutant 2.0	1.02	-1.62

Multivariate Prediction of Prognostic Markers Based on Survival Trends

To identify survival associated markers, we used two approaches: we had the survival details of 37/51 samples, of which 23 were alive and 14 dead. To start with, we defined cut-off percentages for mutations to be considered as alive or dead signatures. We considered a particular variant as an alive signature only if the

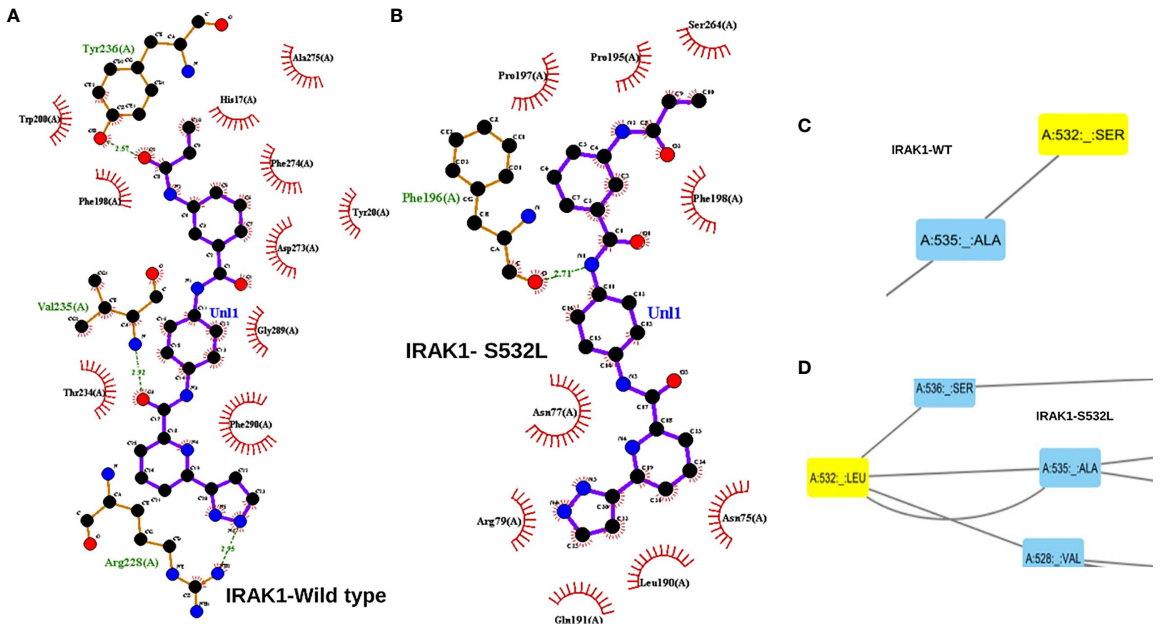

FIGURE 5 | **(A)** A ligplot interaction image showing the interaction of JH-X-119-01 an IRAK1 inhibitor interacting with 3 residues of the wild type IRAK1 molecule. **(B)** Ligplot interaction image showing the interaction of JH-X-119-01 with just one residue of the S532L mutant IRAK1 molecule. The interactions in a and b have been marked in red circles. **(C)** A cytoscape screen shot showing the interaction of just two residues within the IRAK1 wildtype molecule. **(D)** Cytoscape screen shot showing increased interaction of 4 residues within the S532L mutant IRAK1 molecule.

variant in a gene was present in at least 70% of the alive patients (~16/23) and present in utmost 40% (~6/14) or 50% (~7/14) of the dead patients. Similarly, for a variant to be considered a dead signature, we stated that it should be present in at least 60% of the dead patients (~10/14) and utmost 40% (~9/23) to 50% (~12/23) of the alive patients. Additionally, we also selected genes having mutations exclusively in alive or dead patients. By following these criteria, we shortlisted 17 genes for the alive signature and 19 genes for the dead signature (**Supplementary Table 1**). To screen these 36 genes further, we again referred to the HNSC differential survival dataset, based on the transcriptome, from the GEPIA database which resulted in 6 genes (**Supplementary Figure S4**). For alive signatures, we identified mutations in 3 genes, *BCAP31, TCEB2* and *NID1*. For dead signatures, we identified missense mutations in 3 genes, *AHRR, ZNF568* and *CEP112*. On performing a Chi-squared comparison test, there was a significant difference found between the alive and dead percentages of individuals for these 6 genes (**Figure 6A**). To check for differential survival concerning these 6 genes, Kaplan Meier plots were generated. Out of the 6 genes, *NID1* was the only gene that showed a significant differential survival between patients with mutations present in *NID1* and those with no mutation (p-value=0.014) (**Figure 6B**). The rest of the 5 genes, individually, did not show any significant differential survival with respect to presence or absence of mutations (**Supplementary Figures S5A–E**), though *BCAP31* showed borderline significance in its Kaplan-Meier plot (p-value=0.093) (**Supplementary Figure S5A**), and a significant difference in survival on clubbing it with *TP53* a known tumor suppressor (p=0.031) (**Supplementary Figure S5F**). Next, on clubbing the 3 genes alive and the 3 dead signature mutation data separately, we find a significant difference in survival (p-value=0.0048) for the dead signature as compared to the alive signature (p-value = 0.073) (**Supplementary Figures S5G**, **Figure 6C**). Additionally on performing a Multivariate Cox Proportional Hazards analysis of all the Clinical parameters clubbed with all the genes, it was observed that treatment group variables have a significant influence on patients' risk of death (HR=18.7, p-value=0.044) (**Supplementary Figure S5H**) and in cases where clinical properties were clubbed with the individual genes one by one, only *TCEB2* and Treatment group variables, showed a significant influence on patient's probability of survival (HR=0.013, p-value=0.021) and their risk of death (HR=17.003, p-value=0.002), respectively (**Supplementary Figure S5I**). Finally, we looked for the survival probabilities of

TABLE 4 | Docking energies and ligand-residue interactions.

Mutation Type	IRAK1 residues JH-X-119-01 interacts with	Binding Energy
Wild	Arg228 Val235 Tyr236	-6.66
F196S	Thr141 Arg232 Tyr236	-5.46
S532L	None of the docking conformations interacted with the active site or the binding site	

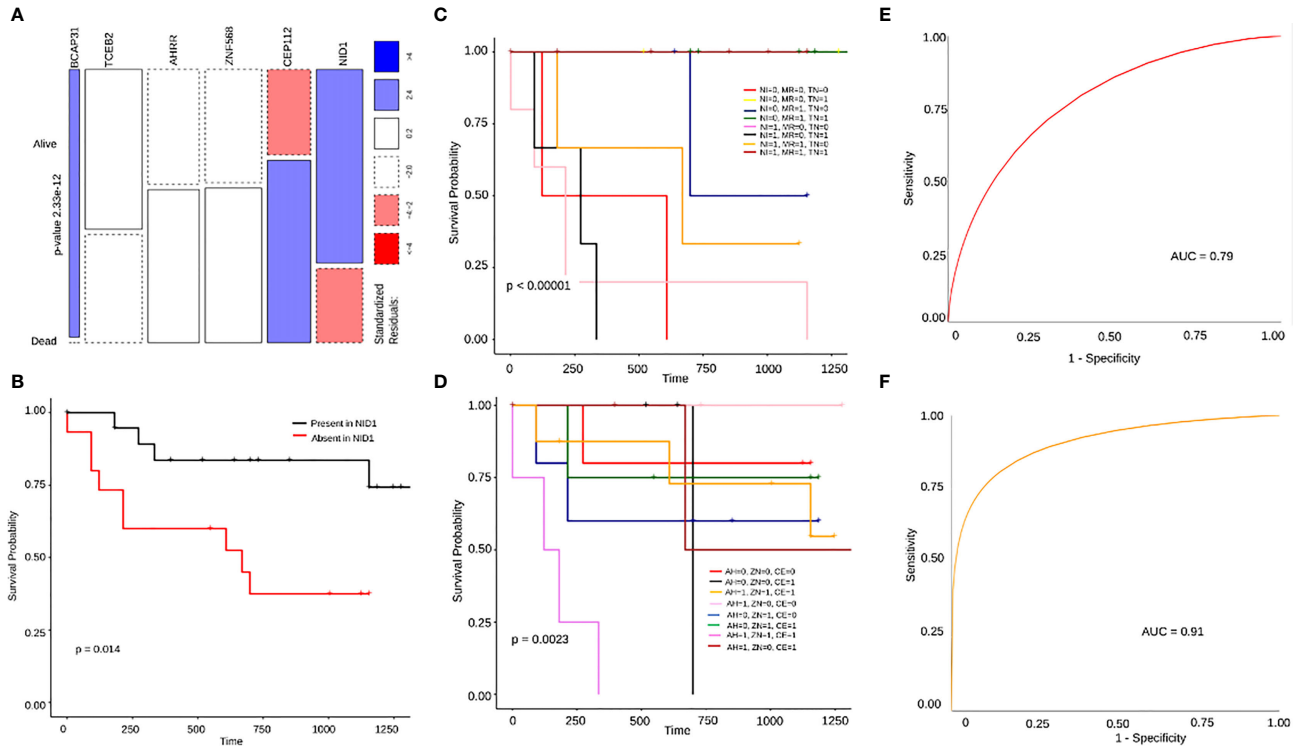

FIGURE 6 | **(A)** A mosaic plot for chi square test showing significant difference between the number of alive and dead patients harboring mutations in BCAP31, TCEB2, AHRR, ZNF568, CEP112 and NID1. **(B)** A Kaplan Meier plot showing significant difference in survival probability between patients with and without NID1 mutation. **(C, D)** Are differential survival plots for the 3 dead and 3 alive gene signatures respectively. In **(C)** AH stands for AHRR, ZN stands for ZNF568 and CE stands for CEP112 where the difference in survival probabilities is much more significant with p=0.0023. In **(D)** NI stands for NID1, MR stands for MRPL23, and TN stands for TNS2, and the difference in survival between presence of mutations in different combinations of genes is significant with p<0.0001. **(E)** This is an ROC curve representing the 3 gene dead signature model with a high accuracy of 79% (AUC=0.79). **(F)** An ROC curve representing the 3 gene alive signature model with an even higher accuracy of 91% (AUC=0.91).

these 6 genes in the HNSCC WEX data from the TCGA database and none of them showed a significant difference in survival. On analyzing the initial 36 genes again, independent of the GEPIA transcriptome data, we found significant differences in survival trends of 6 genes with an alive signature, *MRPL23, TNS2, SPECC1*, *TBP* and *PLXNA3*, and 2 genes, *MARCH10* and *COL4A6* as dead signature. The second approach was LASSO regression detailed below.

Lasso Regression Models for Prediction of Prognostic Markers

In order to additionally screen for prognostic genes, we used LASSO regression to perform reduction analysis on two sets of genes; 1) The set of 36 genes obtained by applying our own cut-off criteria for dead and alive signatures, 2) Genes with only missense mutations present in at least 4 patient samples. The datasets were analyzed using python's Scikit-learn module. The data was processed using 100 random penalty (alpha) values for 10000 iterations to obtain the best alpha value after 5-fold cross-validation. The best alpha values for both the datasets were 0.09 and.0817, respectively. On obtaining the best alpha value, we further obtained the coefficients for that particular alpha value which determine the significance of the associated genes. The genes with coefficients of 0 were eliminated. From the first dataset, we obtained *MRPL23* (-0.85), *COL4A6* (0.45), *TBP* (-0.45), *MARCH10* (0.38), *SPECC1* (-0.35), *TNS2* (-0.3) *CEP112* (0.28), and *NID1* (-0.3) as the genes with significant variants (**Figure 7A**). The same signatures were obtained from the second dataset: *MRPL23*, *TNS2*, *NID1*, and *MARCH10* (**Figure 7B**). Individual Kaplan-Meier plots of these genes showed significant differences in survival as well (**Supplementary Figures S6A–C**). Taking the genes common to the LASSO regression results using the two datasets and our initial independent scrutiny of significant survival genes, we observe that *MARCH10, MRPL23*, *NID1* and *TNS2* are statistically robust genes for a prognostic model prediction. All the above results were confirmed using the R package glmnet. To check if *MRPL23, TNS2 and NID1* would act as better alive gene signatures, we combined the survival data of all three and the difference in survival was significant (p-value < 0.0001) (**Figure 6D**). Adding *MARCH10* to the existing dead signature (*AHRR, ZNF568 and TCEB2*), resulted in a significant 4 gene signature (p-value = 0.012) (**Supplementary Figure S6D**). To check the accuracy of both the models, we performed and Receiver Operating Curve analysis (ROC) for both of them and the 3 gene alive model ROC curve resulted in an accuracy

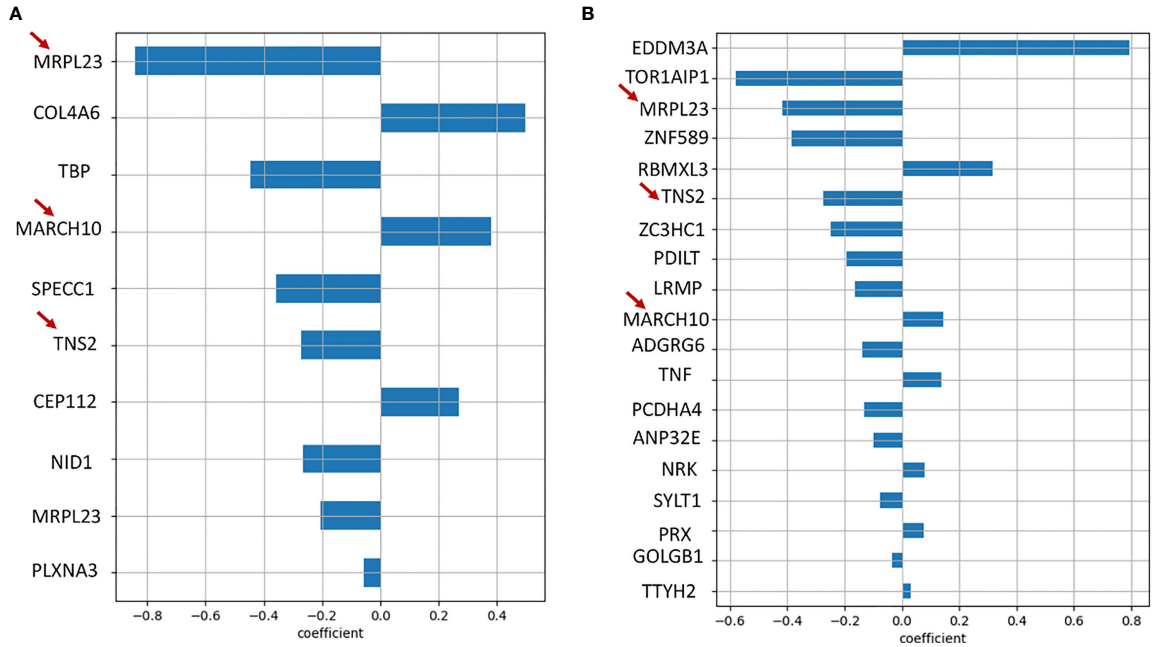

FIGURE 7 | **(A)** Bar graph showing genes obtained as significant prognostic markers from Lasso regression algorithm of the initial 36 alive/dead genes. **(B)** Bar graph showing genes obtained as significant prognostic markers from Lasso regression algorithm of all genes with missense mutations, run using 100 random alpha values and 10000 iterations. It is interesting to note that MRPL23, TNS2 and MARCH10, marked with red arrows, are common to both the results.

of 91% (AUC=0.91) and the 4 gene dead model (including *MARCH10*) had an accuracy of close to 80% (AUC=0.79). These results confirm the presence of two robust and accurate survival models; a 3 gene alive signature; *NID1, MRPL3* and *TNS2* and a 4 gene dead signature, *AHRR, ZNF568, CEP112* and *MARCH10* (**Figures 6E, F**). On comparing results from models of three sets of iterations, i.e., 10000, 1000, and 100 we observe a recurring occurrence of 2 genes *EDDM3A*, a secretory protein, and *TOR1AIP1*, nuclear laminar protein involved in the mTOR pathway (**Figure 7B**). Interestingly, both the genes also showed significant differences in survival when plotting Kaplan Meier graphs individually (**Supplementary Figure S6E, F**).

Identification of a Novel and Deleterious Variant in Cancer Gene Census in Indian HNSCC

To check for the presence of novel variants in our data, from the merged vcf file of all the samples containing all the mutations, we separated out the first 5 columns namely the chromosome, the position of the mutation, reference allele, alternate allele, and the quality score and uploaded it onto the Ensembl Variant Effect Predictor (VEP). From the output file of VEP we filtered out the variants having neither a dbSNP -rs ID nor any COSMIC ID associated with it and termed these 10767 variants as novel variants. Further, we extracted pathogenic variants based on the "deleterious" factor from Sift and "probably_damaging" factor from the PolyPhen databases and obtained a list of unique genes associated with 114 novel variants of which 35 were oncogenes and 11 were tumor suppressors (**Figure 8A, B**). On referring to the HNSCC whole exome data of these 114 genes from TCGA database we found that only 8 of them were a part of the Cancer Gene Census of which only 3 genes, *AKT1, LRP1B*, and *SPECC1* showed a significant difference in survival from the TCGA whole exome data associated with these genes (**Figure 8A**). Further, we looked into the association of the variants and the survival of the above-mentioned 3 genes in our data and found that *SPECC1* showed a significant difference in survival (p=0.035) (**Supplementary Figure 7A**). Surprisingly, the *SPECC1* variant that showed significant survival difference was an intron variant. We performed a network analysis of 114 genes associated with novel variants using the STRING and REACTOME database. Interestingly, the pathways with variants belonged to Collagen biosynthesis and degradation, mTOR signalling, and ECM signalling pathways (**Figure 8C, D**, **Supplementary Figure 7B**). The gene *AKT1*, a known oncogene, had the most significant number of interactions, interconnecting all the three major clusters observed.

Copy Number Analysis

CNVkit was used to perform CNV analysis of all the samples. Varying patterns of copy number gains and losses were seen in all the chromosomes across all the samples (**Figure 9A**). Based on initial results, 10 samples were excluded from further analysis as their patterns were collectively distinct from the rest 41. The remaining 41 samples chr3, chr7, chr8, chr17, chr19, and chrX (**Figure 9C**) showed distinct variations in copy number across

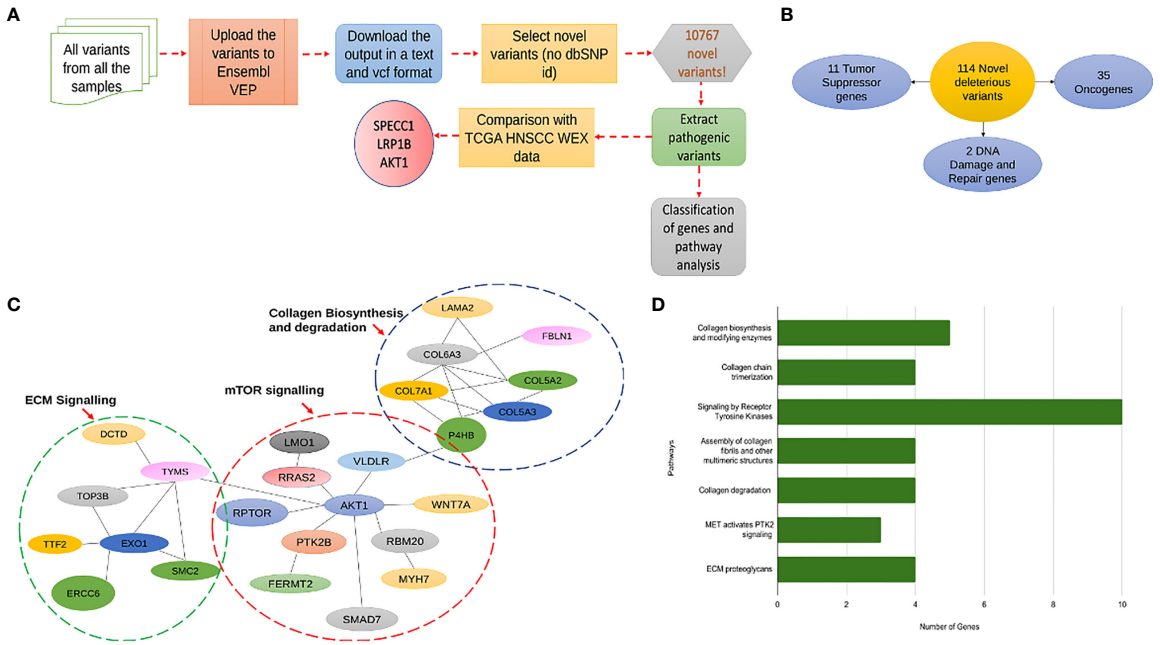

FIGURE 8 | **(A)** A flowchart explaining the pipeline followed for prediction of novel deleterious variants from in-house data. **(B)** This diagram shows the classification of 114 novel deleterious variants into 11 Tumor suppressor genes, 35 oncogenes and 2 DNA damage and Repair genes. **(C)** This figure shows the distribution of the 114 novel deleterious variants into 3 significant pathway interaction networks, namely Collagen Biosynthesis and Degradation, mTOR signaling and ECM Signaling. **(D)** A bar graph showing all the significantly mutated pathways by the number of genes mutated with the most significant pathway being receptor tyrosine kinase signaling.

their chromosome lengths. On continuing with chr3, which had the most striking number of variations, it was seen that within the chromosome, samples 21, 40, 41, 43, 50, 65, 71, and 72 displayed the most significant difference in copy number gain and loss between extreme ends of the chromosome (**Figures 9B, C**). Further, the last 70 Mb region of the chromosome in these 8 samples was analyzed and it was seen that *ZBTB38, ATP1B3, GK5, ZIC4, AGTR1, GYG1*, and *SERP1* genes showed a significant gain in Copy number (**Figure 9D**).

DISCUSSION

One of the main objectives of our study was to identify prognostic signatures linked to survival prediction in the Indian HNSCC cohort. In HNSCC, mutations in a known set of tumor suppressors and oncogenes, namely TP53, CCND1, NOTCH1, PIK3CA, MYC, CDKN2A, PTEN, and FBXW7, have been reported, but most of them are not associated with survival (4, 44). Several studies have reported a correlation of survival with specific signatures using either exome, or transcriptome, or small RNA signature (13, 45, 46). Several predictive models using machine learning algorithms such as random forest and lasso- cox regression have been developed to identify genes associated with treatment outcomes, survival, and prognosis of head and neck cancers (47, 48). There are no studies from India correlating survival with gene signatures. We have utilized LASSO-COX and developed a new method using integrated variant signature and gene expression to identify survival-associated genes. The variants identified from exome-see segregated the cancer of the buccal cavity from the tongue and alveolus. Previous studies from the Indian subpopulation on oral cancer and oesophageal cancer have identified mutations specific to the population (16, 49). We have identified novel mutations in AKT1, LRP1B, and SPECC1. Network analysis using all the novel variants identified Collagen biosynthesis and degradation, mTOR signalling, and ECM signalling pathways.

Preliminary variant analysis revealed that of the genes known to be mutated in HNSCC patients, *TP53 and TP63* were the ones with the highest frequency of mutation. Both these tumor suppressors are known to be mutated in HNSCC and loss of expression of the same has been linked to cancer progression while *TP63* is known to promote survival in HNSCC patients (4, 50, 51). Most of the other proto-oncogenes like *NOTCH1, FGFR1, EGFR, CCND1* or tumor suppressors like *CDKN2A, ARID2 and MLH1*, a mismatch repair gene, that are known to be frequently mutated in oral or head and neck squamous cell carcinomas in general were seen to have less than or equal to 20% mutation frequency. The frequency of these proteins being lower than usual, suggests heterogeneity especially in the Indian cohort.

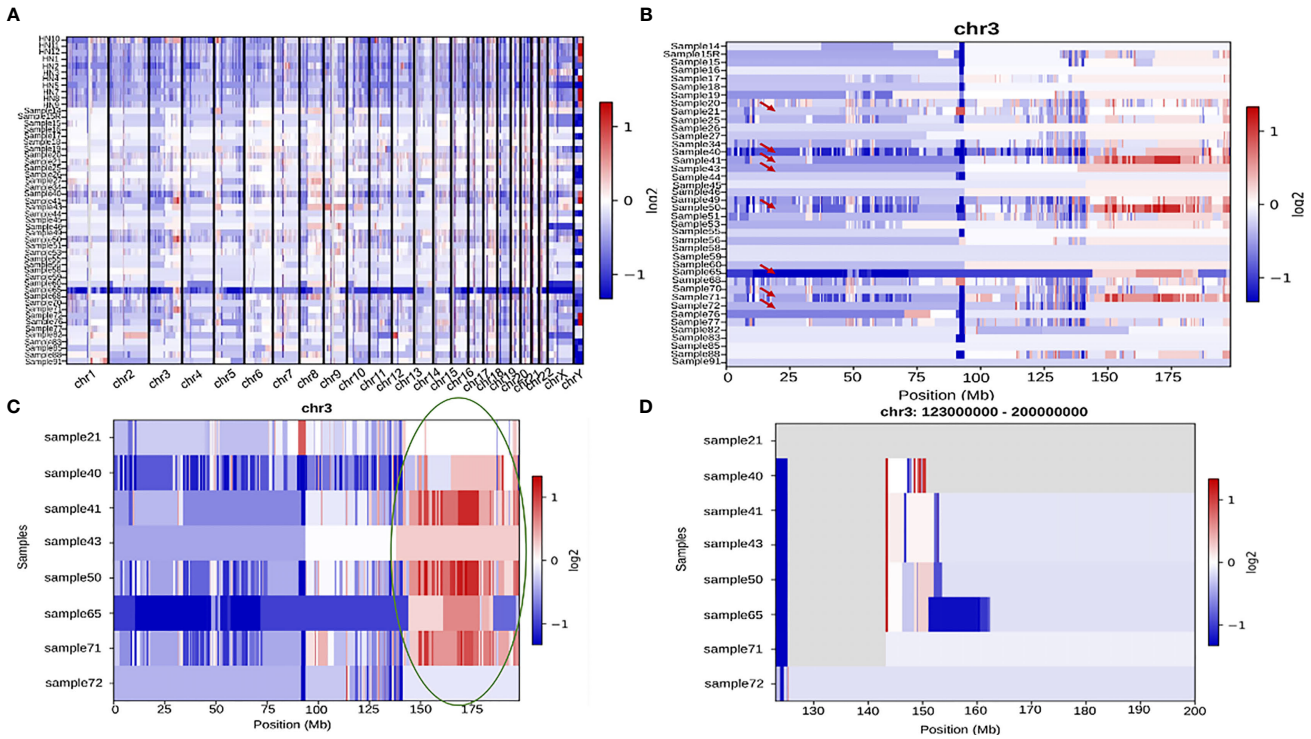

FIGURE 9 | **(A)** A comprehensive heatmap showing copy number variation in all the samples across all the chromosomes. **(B)** Heatmap showing copy number variation across the entire length of chr3 in all the samples. Samples 21, 40, 41, 43, 50, 65, 71, and 72 are indicated by a red arrow since they show the most significant amount of variation amongst all the 41 samples. **(C)** A heatmap representing the above-mentioned subset of samples with a high amount of variation towards the end of chromosome 3. The last ~70 Mb (150Mb-200Mb) have been highlighted with a green oval which have been zoomed into in **(D)**.

On performing a tumor site-based signature analysis we came across several interesting results. To start with, *APC*, Adenomatous Polyposis Coli, a tumor suppressor in the WNT pathways, previously seen to have very low mutation rates in HNSCC was seen to have a structural interaction variant in 18 out of the 19 patients categorized. This suggests that the mutation was an inactivating mutation, contributing to the progression of HNC (52). Next, *GPC4*, Glypican 4, a known regulator of WNT signaling, known to be downregulated in breast cancer and ovarian cancer, and upregulated in colorectal cancer was seen to be mutated in 50% of the patients (52–54). The other genes with approximately 50% mutation frequency *WNT16, PARP1 and ATF4*. *PARP1* is known to have high expression levels in oral cancer and hence a more than 30% mutation frequency in our data, suggests an activating mutation in all tumor sites (55). The role of WNT16, a part of the canonical WNT signaling pathway family of genes, in cancer progression remains unknown, although expression of WNT16 is downregulated in Basal cell carcinoma (56).

Alveolar signatures were associated with mutations in cell cycle regulators such as *PRKCG, WEE1 and RBL2*. *PRKCG and WEE1*, when upregulated, are known to be good prognostic markers in Glioblastoma, while high mRNA levels of RBL2 are known to be associated with HPV+ head and neck tumors (57). Oncogenes like *FGFR1, HRAS, NRAS*, and a tumor suppressor CDKN2A are known to have mutations in HNSCC (4). Tumor suppressor *SMAD4*, involved in the EMT pathway was seen to have a stop gained mutation. It has been reported earlier that a somatic LOH mutation was present in a high frequency of lymph node metastatic tumors in HNSCC (58). The Buccal cavity signatures revealed a mutation in the cell cycle associated gene TFDP1, specific to the recurrent buccal sample. *TFDP1* amplification has been associated with lung cancer in a previous study and has been stated as a potential oncogene. Its role in head and neck cancer is unknown (59). *CASP8* and *ATM* were the signatures present in buccal cavity. Mutation frequency of 34% has been observed in *CAPS8* gene which is also associated with reduced survival in hnscc patients (60). Mutations in *ATM*, which is a well characterized tumor suppressor has been associated with oral cancer, lung cancer and breast cancer (61–63). The presence of a missense variant in a buccal mucosa tumor patient indicates that the mutation might be an inactivating mutation. Apart from *TP53*, which has previously been identified as a driver gene in oral tongue squamous cell carcinoma (64), novel gene cluster specific to tongue cancer has been identified which needs validation in larger cohort..

We investigated several potential prognostic markers based on a correlation of mutations occurring in genes and their

corresponding survival outcomes. A comparison with the transcriptome data from the GEPIA database resulted in an initial set of 6 genes, 3 genes as a survival signature and 3 as dead. The most important finding out of the 6 survival signatures is the third alive signature gene *NID1*. Apart from showing a significant difference in survival from GEPIA, it was the only one that showed a significant difference in survival with in-house exome data. Nidogen 1 is a protein that interacts with several components of the extracellular matrix and its overexpression is known to correlate with drug resistance in ovarian cancer and increased metastasis in women affected with Breast Cancer (65, 66). Also, from GEPIA, high *NID1* levels correspond to low survival probability, while patients with *NID1* mutation show higher probability in our dataset, which suggests that the mutation is an inactivating mutation. Since the none of the other individual genes showed any significant difference in survival, we were encouraged to go back to our initial list of 36 genes and additionally screen through all the missense mutations in the data. A lasso regression model was built using python and R and the two datasets (36 genes and all missense mutations) were screened in order to obtain significant prognostic markers. From the algorithms and the initial curation results, we obtained 3 common alive signatures genes, MRPL23, TNS2 and NID1, and four dead signatures, MARCH10, AHRR, ZNF568 and CEP112. The individual association of survival probabilities of MRPL23, TNS2, MARCH10 and NID1 was significant.

Interestingly combined association of dead signatures showed a significant difference in survival. *AHRR*, an Aryl hydrocarbon receptor repressor, a known tumor suppressor has been associated with smokers in lung cancer patients in an epigenetic manner (67, 68). A mutation in the gene contributing to a dead signature suggests that its tumor suppressor potential was inactivated. The second dead signature gene was *CEP112*, a centrosomal protein involved in cell division, known to play a key role in the maintenance of genomic stability in association with *BRCA1 (*69) and *ZNF568*, with the most significant contribution to the dead gene signature with a particular mutation present in 12 dead and 10 alive patients, indicating *ZNF568* role in tumor suppression.

Two ROC models were built to assess the accuracy of the 3 gene additive alive and the 4 gene dead signatures and it was observed that the alive signature was more accurate with an AUC of 0.91 while the accuracy of the dead signature was 0.79. There have been cancer studies where prognostic ROC models have been greater than 0.65 but have rarely crossed 0.87, which suggests that an AUC of 0.91 represents a significant predictive model (70, 71). Combining two different methods and selecting genes based on functionality rather than just the top signatures gave better accuracy than alone any of the methods, suggesting the potential robustness of this alternative approach towards screening of prognostic markers.

From these different sets of results, it is noteworthy that the predictive survival signatures are quite different when one considers the only exome as compared to when it is considered in concert with transcriptome analysis. Since the focus was on missense mutations, the same analysis also revealed targets with clinical implications and survival. We are aware that the cohorts for transcriptome and exome are not the same, exome is from our in-house Indian cohort while transcriptome is from GEPIA, representing mostly Caucasian population, nevertheless, the expression pattern with some degree of difference, more or less would be similar.

None of the Survival signatures showed significant survival differences in the Caucasian HNSCC cohort, which suggests the presence of population specific prognostic markers. We also performed preliminary Copy number analysis and obtained a signature differentiating a set of samples from another. Correlations between the clinical data/survival parameters with the copy number results are being investigated.

From the driver gene analysis, we saw that the second mutation of *IRAK1*, S532L showed significant results. S532L *IRAK1* mutant depicted the greatest deviation from the wild type in Docking studies and Residue Interaction Studies. The inhibitor (JH-X-119-01) was unable to interact with any active/binding site residues on the S532L mutant while it formed hydrogen bonds with the ATP binding site residues of the wild type and F196S variant. S532L mutant residue had added interactions with two residues which could have played a role in blocking the binding of the ligand to the binding site of the S532L mutant structure. F196S mutant residue had a loss of two interactions but was able to provide the binding pocket for ligand binding similar to the wild type. Further residue interaction analysis with the range of active site and binding site residues may shed light on the deviation in inhibitor binding behavior of the S532L mutant from the Wild Type *IRAK1*. Hence S532L seems to have a greater effect on the structure and ligand binding and can be targeted for further studies.

The small sample size of patients in the study is a definite shortcoming, but the use of multiple statistically significant methods supporting the findings of our alternate screening method, also resulting in a druggable protein target, reflects on the potential robustness of our method but the signatures obtained in this study need to be validated with a large set of patient samples.

CONCLUSION

Exome sequencing and analysis of 51 HNSCC samples identified tumor site-specific biomarkers and a recurrence signature. The combined LASSO-COX and exome-transcriptome analysis of mutational profiles with clinical data resulted in 4 dead and 3 alive gene signatures linked to survival. The three genes alive signature identified can predict survival of HNSCC patients with 91% accuracy. We also identified novel mutations and a druggable driver gene target IRAK1. However, our results need validation with a larger sample size.

DATA AVAILABILITY STATEMENT

The datasets presented in this study can be found in online repositories. The names of the repository/repositories and accession number(s) can be found below: BioProject PRJNA740146.

ETHICS STATEMENT

The study has been approved by the Institutional Ethics Committee of IBAB and HCG (IBABIEC-03/PR02/010518). Informed consent was collected from all the patients participating in the study.

AUTHOR CONTRIBUTIONS

BC and SD conceived and coordinated the study. AS and VR, provided the samples. BC, SD, and RR collected the samples. PS and RR performed the exome library preparation of the FFPE samples. BC, SD, RR, PD, GA, AJ, and SJ designed and performed the experiments. BC, SD, PD, and GA interpreted the data and wrote the manuscript. All authors contributed to the article and approved the submitted version.

FUNDING

We thank the Department of Information Technology, Biotechnology and Science & Technology, Govt. of Karnataka, India, and Department of Science and Technology (SR/FST/LSI-536/2012), India for infrastructure grant and the Bio-IT grant. SD is supported by Department of Biotechnology (Ref. no BT/PR13458/COE/34/33/2015 and BT/PR13616/GET/119/9/2015), Govt. of India, India.

ACKNOWLEDGMENTS

We acknowledge Professor Narayan Rao Yathindra for his constant guidance and support throughout the study.

SUPPLEMENTARY MATERIAL

The Supplementary Material for this article can be found online at: https://www.frontiersin.org/articles/10.3389/fonc.2021.723162/full#supplementary-material

Supplementary Figure S1 | A waterfall plot showing site wise signatures mutations across patients with site of tumor originating from alveolus, buccal mucosa and tongue.

Supplementary Figure S2 | (A) A K-M plot showing difference in survival probabilities between different stages of tumor. **(B)** A K-M plot showing significant difference in survival probabilities between different types of chemotherapy regimens.

Supplementary Figure S3 | (A) A ligplot image showing the interaction of JH-X-119-01 with F196S mutant IRAK1 molecule, marked in red circles. **(B)** A cytoscape image showing internal IRAK1 wildtype interactions. **(C)** Cytoscape image showing a reduced number of interactions within the IRAK1 molecule.

Supplementary Figure S4 | A panel of KM plots from GEPIA showing significant differences in survival probabilities of BCAP31, AHRR, ZNF568, TCEB2, CEP112 and NID1 based on high and low expression categories.

Supplementary Figure S5 | (A–E) Showing K-M plots of BCAP31, AHRR, ZNF568, CEP112 and TCEB2 based on presence or absence of mutations. Note that the differences in survival probabilities are not significant. **(F)** A KM plot of BCAP31 and TP53 combined showing significant difference in survival based on presence or absence of mutations in both the genes. **(G)** An additive differential survival plot of the initial 3 alive gene signature, BCAP31, TCEB2 and NID1, showing a low significance value of 0.073. **(H)** A multivariate analysis forest plot showing significant influence of Treatment group of variables on patients' risk of death. **(I)** A multivariate forest plot showing significant influence of Treatment group of variables on patients' risk of death.

Supplementary Figure S6 | (A–C) K-M plots showing significant difference in survival probabilities between absence and presence of mutations in 3 genes, MRPL23, MARCH10 and TNS2. **(D)** And additive differential plot of the 4 gene dead signature, AHRR, ZNF568, CEP112 and MARCH10, showing significant difference in survival probabilities. **(E)** A K-M plot showing significant difference in survival between two categories of EDDM3A gene based on presence or absence of mutations. **(F)** A K-M plot showing significant difference in survival between two categories of TOR1AIP1 gene based on presence or absence of mutations.

Supplementary Figure S7 | (A) A K-M plot showing significant difference in survival between two categories of SPECC1 gene based on presence or absence of an intron variant. **(B)** An interaction network obtained from the STRING database, showing 3 significant pathways from the novel deleterious genes linked by AKT1.

REFERENCES

1. Argiris A, Eng C. Epidemiology, Staging, and Screening of Head and Neck Cancer. *Cancer Treat Res* (2003) 114:15–60. doi: 10.1007/0-306-48060-3_2
2. Sanderson RJ, Ironside JAD. Squamous Cell Carcinomas of the Head and Neck. *BMJ* (2002) 325:822–7. doi: 10.1136/bmj.325.7368.822
3. Laramore GE, Scott CB, al-Sarraf M, Haselow RE, Ervin TJ, Wheeler R, et al. Adjuvant Chemotherapy for Resectable Squamous Cell Carcinomas of the Head and Neck: Report on Intergroup Study 0034. *Int J Radiat Oncol Biol Phys* (1992) 23:705–13. doi: 10.1016/0360-3016(92)90642-U
4. Mountzios G, Rampias T, Psyrri A. The Mutational Spectrum of Squamous-Cell Carcinoma of the Head and Neck: Targetable Genetic Events and Clinical Impact. *Ann Oncol* (2014) 25:1889–900. doi: 10.1093/annonc/mdu143
5. Chow LQM. Head and Neck Cancer. *N Engl J Med* (2020) 382:60–72. doi: 10.1056/NEJMra1715715
6. Field JK. Oncogenes and Tumour-Suppressor Genes in Squamous Cell Carcinoma of the Head and Neck. *Eur J Cancer Part B: Oral Oncol* (1992) 28:67–76. doi: 10.1016/0964-1955(92)90016-t
7. Nagai MA. Genetic Alterations in Head and Neck Squamous Cell Carcinomas. *Braz J Med Biol Res* (1999) 32:897–904. doi: 10.1590/s0100-879x1999000700015
8. Hackermüller J, Reiche K, Otto C, Hösler N, Blumert C, Brocke-Heidrich K, et al. Cell Cycle, Oncogenic and Tumor Suppressor Pathways Regulate Numerous Long and Macro Non-Protein-Coding RNAs. *Genome Biol* (2014) 15:R48. doi: 10.1186/gb-2014-15-3-r48
9. Wee ZN, Yatim SMJM, Kohlbauer VK, Feng M, Goh JY, Bao Y, et al. IRAK1 is a Therapeutic Target That Drives Breast Cancer Metastasis and Resistance to Paclitaxel. *Nat Commun* (2015) 6:8746. doi: 10.1038/ncomms9746
10. Liu PH, Shah RB, Li Y, Arora A, Ung PM-U, Raman R, et al. An IRAK1-PIN1 Signalling Axis Drives Intrinsic Tumour Resistance to Radiation Therapy. *Nat Cell Biol* (2019) 21:203–13. doi: 10.1038/s41556-018-0260-7

11. Liu PH, Sidi S. Targeting the Innate Immune Kinase IRAK1 in Radioresistant Cancer: Double-Edged Sword or One-Two Punch? *Front Oncol* (2019) 9:1174. doi: 10.3389/fonc.2019.01174
12. Wang J, Chen X, Tian Y, Zhu G, Qin Y, Chen X, et al. Six-Gene Signature for Predicting Survival in Patients With Head and Neck Squamous Cell Carcinoma. *Aging* (2020) 12:767–83. doi: 10.18632/aging.102655
13. He Y, Ji P, Li Y, Wang R, Ma H, Yuan H. Genetic Variants Were Associated With the Prognosis of Head and Neck Squamous Carcinoma. *Front Oncol* (2020) 10:372. doi: 10.3389/fonc.2020.00372
14. Chen Y, Chen C. DNA Copy Number Variation and Loss of Heterozygosity in Relation to Recurrence of and Survival From Head and Neck Squamous Cell Carcinoma: A Review. *Head Neck* (2008) 30:1361–83. doi: 10.1002/hed.20861
15. Gross AM, Orosco RK, Shen JP, Egloff AM, Carter H, Hofree M, et al. Multi-Tiered Genomic Analysis of Head and Neck Cancer Ties TP53 Mutation to 3p Loss. *Nat Genet* (2014) 46:939–43. doi: 10.1038/ng.3051
16. India Project Team of the International Cancer Genome Consortium. Mutational Landscape of Gingivo-Buccal Oral Squamous Cell Carcinoma Reveals New Recurrently-Mutated Genes and Molecular Subgroups. *Nat Commun* (2013) 4:2873. doi: 10.1038/ncomms3873
17. Langmead B, Salzberg SL. Fast Gapped-Read Alignment With Bowtie 2. *Nat Methods* (2012) 9:357–9. doi: 10.1038/nmeth.1923
18. Li H, Handsaker B, Wysoker A, Fennell T, Ruan J, Homer N, et al. 1000 Genome Project Data Processing Subgroup. The Sequence Alignment/Map Format and SAMtools. *Bioinformatics* (2009) 25:2078–9. doi: 10.1093/bioinformatics/btp352
19. DePristo MA, Banks E, Poplin R, Garimella KV, Maguire JR, Hartl C, et al. A Framework for Variation Discovery and Genotyping Using Next-Generation DNA Sequencing Data. *Nat Genet* (2011) 43:491–8. doi: 10.1038/ng.806
20. Cingolani P, Platts A, Wang LL, Coon M, Nguyen T, Wang L, et al. A Program for Annotating and Predicting the Effects of Single Nucleotide Polymorphisms, SnpEff: SNPs in the Genome of Drosophila Melanogaster Strain W1118; Iso-2; Iso-3. *Fly* (2012) 6:80–92. doi: 10.4161/fly.19695
21. Cingolani P, Patel VM, Coon M, Nguyen T, Land SJ, Ruden DM, et al. Using Drosophila Melanogaster as a Model for Genotoxic Chemical Mutational Studies With a New Program, SnpSift. *Front Genet* (2012) 3:35. doi: 10.3389/fgene.2012.00035
22. 1000 Genomes Project Consortium, Auton A, Brooks LD, Durbin RM, Garrison EP, Kang HM, et al. A Global Reference for Human Genetic Variation. *Nature* (2015) 526:68–74. doi: 10.1038/nature15393
23. Skidmore ZL, Wagner AH, Lesurf R, Campbell KM, Kunisaki J, Griffith OL, et al. GenVisR: Genomic Visualizations in R. *Bioinformatics* (2016) 32:3012–4. doi: 10.1093/bioinformatics/btw325
24. Gehring JS, Fischer B, Lawrence M, Huber W. SomaticSignatures: Inferring Mutational Signatures From Single-Nucleotide Variants. *Bioconductor* (2015) 31(22):3673–3675. doi: 10.1093/bioinformatics/btv408
25. Talevich E, Shain AH, Botton T, Bastian BC. CNVkit: Genome-Wide Copy Number Detection and Visualization From Targeted DNA Sequencing. *PloS Comput Biol* (2016) 12:e1004873. doi: 10.1371/journal.pcbi.1004873
26. Arnedo-Pac C, Mularoni L, Muiños F, Gonzalez-Perez A, Lopez-Bigas N. OncodriveCLUSTL: A Sequence-Based Clustering Method to Identify Cancer Drivers. *Bioinformatics* (2019) 35:4788–90. doi: 10.1093/bioinformatics/btz501
27. Tang Z, Li C, Kang B, Gao G, Li C, Zhang Z. GEPIA: A Web Server for Cancer and Normal Gene Expression Profiling and Interactive Analyses. *Nucleic Acids Res* (2017) 45:W98–W102. doi: 10.1093/nar/gkx247
28. Guo X, Zhang B, Zeng W, Zhao S, Ge D. G3viz: An R Package to Interactively Visualize Genetic Mutation Data Using a Lollipop-Diagram. *Bioinformatics* (2019) 36:928–9. doi: 10.1093/bioinformatics/btz631
29. Kim DE, Chivian D, Baker D. Protein Structure Prediction and Analysis Using the Robetta Server. *Nucleic Acids Res* (2004) 32:W526–31. doi: 10.1093/nar/gkh468
30. Arnold K, Bordoli L, Kopp J, Schwede T. The SWISS-MODEL Workspace: A Web-Based Environment for Protein Structure Homology Modelling. *Bioinformatics* (2006) 22:195–201. doi: 10.1093/bioinformatics/bti770
31. Colovos C, Yeates TO. Verification of Protein Structures: Patterns of Nonbonded Atomic Interactions. *Protein Sci* (1993) 2:1511–9. doi: 10.1002/pro.5560020916
32. Pontius J, Richelle J, Wodak SJ. Deviations From Standard Atomic Volumes as a Quality Measure for Protein Crystal Structures. *J Mol Biol* (1996) 264:121–36. doi: 10.1006/jmbi.1996.0628
33. Laskowski RA, MacArthur MW, Moss DS, Thornton JM. PROCHECK: A Program to Check the Stereochemical Quality of Protein Structures. *J Appl Crystallogr* (1993) 26:283–91. doi: 10.1107/S0021889892009944
34. Hooft RW, Vriend G, Sander C, Abola EE. Errors in Protein Structures. *Nature* (1996) 381(6580):272. doi: 10.1038/381272a0
35. Bowie JU, Luthy R. Eisenberg D. A Method to Identify Protein Sequences That Fold Into a Known Three-Dimensional Structure. *Science* (1991) 253:164–70. doi: 10.1126/science.1853201
36. Worth CL, Preissner R, Blundell TL. SDM—A Server for Predicting Effects of Mutations on Protein Stability and Malfunction. *Nucleic Acids Res* 39 (suppl_2):W215–W222. doi: 10.1093/nar/gkr363
37. Capriotti E, Fariselli P, Casadio R. I-Mutant2.0: Predicting Stability Changes Upon Mutation From the Protein Sequence or Structure. *Nucleic Acids Res* (2005) 33:W306–10. doi: 10.1093/nar/gki375
38. Hatcher JM, Yang G, Wang L, Ficarro SB, Buhrlage S, Wu H, et al. Discovery of a Selective, Covalent IRAK1 Inhibitor With Antiproliferative Activity in MYD88 Mutated B-Cell Lymphoma. *ACS Med Chem Lett* (2020) 11:2238–43. doi: 10.1021/acsmedchemlett.0c00378
39. Laskowski RA, Swindells MB. LigPlot+: Multiple Ligand-Protein Interaction Diagrams for Drug Discovery. *J Chem Inf Model* (2011) 51:2778–86. doi: 10.1021/ci200227u
40. Piovesan D, Minervini G, Tosatto SCE. The RING 2.0 Web Server for High Quality Residue Interaction Networks. *Nucleic Acids Res* (2016) 44:W367–74. doi: 10.1093/nar/gkw315
41. Shannon P, Markiel A, Ozier O, Baliga NS, Wang JT, Ramage D, et al. Cytoscape: A Software Environment for Integrated Models of Biomolecular Interaction Networks. *Genome Res* (2003) 13:2498–504. doi: 10.1101/gr.1239303
42. Therneau TM, Grambsch PM. *Modeling Survival Data: Extending the Cox Model*. Springer-Verlag New York: Springer Science & Business Media (2013).
43. Tibshirani R. THE LASSO METHOD FOR VARIABLE SELECTION IN THE COX MODEL. *Stat Med* (1997) 16:385–95. doi: 10.1002/(sici)1097-0258(19970228)16:4<385::aid-sim380>3.0.co;2-3
44. Fernández-Mateos J, Pérez-García J, Seijas-Tamayo R, Mesía R, Rubió-Casadevall J, García-Girón C, et al. Oncogenic Driver Mutations Predict Outcome in a Cohort of Head and Neck Squamous Cell Carcinoma (HNSCC) Patients Within a Clinical Trial. *Sci Rep* (2020) 10. doi: 10.1038/s41598-020-72927-2
45. Rock LD, Minatel BC, Marshall EA, Guisier F, Sage AP, Barros-Filho MC, et al. Expanding the Transcriptome of Head and Neck Squamous Cell Carcinoma Through Novel MicroRNA Discovery. *Front Oncol* (2019) 9:1305. doi: 10.3389/fonc.2019.01305
46. Serafini MS, Lopez-Perez L, Fico G, Licitra L, De Cecco L, Resteghini C. Transcriptomics and Epigenomics in Head and Neck Cancer: Available Repositories and Molecular Signatures. *Cancers Head Neck* (2020) 5:1–10. doi: 10.1186/s41199-020-0047-y
47. Plath M, Gass J, Hlevnjak M, Li Q, Feng B, Hostench XP, et al. Unraveling Most Abundant Mutational Signatures in Head and Neck Cancer. *Int J Cancer* (2021) 148:115–27. doi: 10.1002/ijc.33297
48. Schomberg J. Identification of Targetable Pathways in Oral Cancer Patients *via* Random Forest and Chemical Informatics. *Cancer Inform* (2019) 18:1176935119889911. doi: 10.1177/1176935119889911
49. Mangalaparthi KK, Patel K, Khan AA, Manoharan M, Karunakaran C, Murugan S, et al. Mutational Landscape of Esophageal Squamous Cell Carcinoma in an Indian Cohort. *Front Oncol* (2020) 10:1457. doi: 10.3389/fonc.2020.01457
50. Lakshmanachetty S, Balaiya V, High WA, Koster MI. Loss of TP63 Promotes the Metastasis of Head and Neck Squamous Cell Carcinoma by Activating MAPK and STAT3 Signaling. *Mol Cancer Res* (2019) 17:1279–93. doi: 10.1158/1541-7786.MCR-18-1355
51. Rocco JW, Leong C-O, Kuperwasser N, DeYoung MP, Ellisen LW. P63 Mediates Survival in Squamous Cell Carcinoma by Suppression of P73-Dependent Apoptosis. *Cancer Cell* (2006) 9:45–56. doi: 10.1016/j.ccr.2005.12.013

52. Takei S, Ueno Y, Yoda J, Tamura S, Hotomi M, Fujihara K, et al. Roles of Beta-Catenin Overexpression and Adenomatous Polyposis Coli Mutation in Head and Neck Cancer. *Nihon Jibiinkoka Gakkai Kaiho* (2003) 106:692–9. doi: 10.3950/jibiinkoka.106.692
53. Li N, Spetz MR, Ho M. The Role of Glypicans in Cancer Progression and Therapy. *J Histochem Cytochem* (2020) 68:841–62. doi: 10.1369/0022155420933709
54. Munir J, Van Ngu T, Na Ayudthaya PD, Ryu S. Downregulation of Glypican-4 Facilitates Breast Cancer Progression by Inducing Cell Migration and Proliferation. *Biochem Biophys Res Commun* (2020) 526:91–7. doi: 10.1016/j.bbrc.2020.03.064
55. Kossatz S, Brand C, Gutiontov S, Liu JTC, Lee NY, Gönen M, et al. Detection and Delineation of Oral Cancer With a PARP1 Targeted Optical Imaging Agent. *Sci Rep* (2016) 6:21371. doi: 10.1038/srep21371
56. Carmo NG DO, Sakamoto LHT, Pogue R, DO Couto Mascarenhas C, Passos SK, Felipe MSS, et al. Altered Expression of PRKX, WNT3 and WNT16 in Human Nodular Basal Cell Carcinoma. *Anticancer Res* (2016) 36:4545–51. doi: 10.21873/anticanres.11002
57. Johnson ME, Cantalupo PG, Pipas JM. Identification of Head and Neck Cancer Subtypes Based on Human Papillomavirus Presence and E2F-Regulated Gene Expression. *mSphere* (2018) 3. doi: 10.1128/mSphere.00580-17
58. Lin L-H, Chang K-W, Cheng H-W, Liu C-J. Somatic Mutations in Head and Neck Carcinoma Are Associated With Tumor Progression. *Front Oncol* (2019) 9:1379. doi: 10.3389/fonc.2019.01379
59. Castillo SD, Angulo B, Suarez-Gauthier A, Melchor L, Medina PP, Sanchez-Verde L, et al. Gene Amplification of the Transcription Factor DP1 and CTNND1 in Human Lung Cancer. *J Pathol* (2010) 222:89–98. doi: 10.1002/path.2732
60. Singh R, Das S, Datta S, Mazumdar A, Biswas NK, Maitra A, et al. Study of Caspase 8 Mutation in Oral Cancer and Adjacent Precancer Tissues and Implication in Progression. *PloS One* (2020) 15:e0233058. doi: 10.1371/journal.pone.0233058
61. He Y, Chen Q, Li B. ATM in Oral Carcinogenesis: Association With Clinicopathological Features. *J Cancer Res Clin Oncol* (2008) 134:1013–20. doi: 10.1007/s00432-008-0365-7
62. Choi M, Kipps T, Kurzrock R. ATM Mutations in Cancer: Therapeutic Implications. *Mol Cancer Ther* (2016) 15:1781–91. doi: 10.1158/1535-7163.MCT-15-0945
63. Schneider J, Illig T, Rosenberger A, Bickeböller H, Wichmann H-E. Detection of ATM Gene Mutations in Young Lung Cancer Patients: A Population-Based Control Study. *Arch Med Res* (2008) 39:226–31. doi: 10.1016/j.arcmed.2007.08.004
64. Campbell BR, Chen Z, Faden DL, Agrawal N, Li RJ, Hanna GJ, et al. The Mutational Landscape of Early- and Typical-Onset Oral Tongue Squamous Cell Carcinoma. *Cancer* (2021) 127:544–53. doi: 10.1002/cncr.33309
65. Zhou Y, Zhu Y, Fan X, Zhang C, Wang Y, Zhang L, et al. NID1, a New Regulator of EMT Required for Metastasis and Chemoresistance of Ovarian Cancer Cells. *Oncotarget* (2017) 8:33110–21. doi: 10.18632/oncotarget.16145
66. Urooj T, Wasim B, Mushtaq S, Haider G, Shah SNN, Ghani R, et al. Increased NID1 Expression Among Breast Cancer Lung Metastatic Women; A Comparative Analysis Between Naive and Treated Cases. *Recent Pat Anticancer Drug Discov* (2020) 15:59–69. doi: 10.2174/1574892815666200302115438
67. Zudaire E, Cuesta N, Murty V, Woodson K, Adams L, Gonzalez N, et al. The Aryl Hydrocarbon Receptor Repressor Is a Putative Tumor Suppressor Gene in Multiple Human Cancers. *J Clin Invest* (2008) 118:640–50. doi: 10.1172/JCI30024
68. Grieshober L, Graw S, Barnett MJ, Thornquist MD, Goodman GE, Chen C, et al. AHRR Methylation in Heavy Smokers: Associations With Smoking, Lung Cancer Risk, and Lung Cancer Mortality. *BMC Cancer* (2020) 20:905. doi: 10.1186/s12885-020-07407-x
69. Panda S, Setia M, Kaur N, Shepal V, Arora V, Singh DK, et al. Noncoding RNA Ginir Functions as an Oncogene by Associating With Centrosomal Proteins. *PloS Biol* (2018) 16:e2004204. doi: 10.1371/journal.pbio.2004204
70. Liu Y, Yin S. A Novel Prognostic Index Based on the Analysis of Glycolysis-Related Genes in Head and Neck Squamous Cell Carcinomas. *J Oncol* (2020) 2020. doi: 10.1155/2020/7353874
71. Liu Z, Cao Y, Diao W, Cheng Y, Jia Z, Peng X. Radiomics-Based Prediction of Survival in Patients With Head and Neck Squamous Cell Carcinoma Based on Pre- and Post-Treatment F-PET/CT. *Aging* (2020) 12:14593–619. doi: 10.18632/aging.103508

Conflict of Interest: Authors AS and VR are employed by HealthCare Global Enterprises Ltd.

The remaining authors declare that the research was conducted in the absence of any commercial or financial relationships that could be construed as a potential conflict of interest.

Publisher's Note: All claims expressed in this article are solely those of the authors and do not necessarily represent those of their affiliated organizations, or those of the publisher, the editors and the reviewers. Any product that may be evaluated in this article, or claim that may be made by its manufacturer, is not guaranteed or endorsed by the publisher.

frontiers in Oncology

ORIGINAL RESEARCH
published: 11 November 2021
doi: 10.3389/fonc.2021.752007

Dose Prediction Using a Three-Dimensional Convolutional Neural Network for Nasopharyngeal Carcinoma With Tomotherapy

Yaoying Liu[1,2], Zhaocai Chen[3], Jinyuan Wang[1], Xiaoshen Wang[1], Baolin Qu[1], Lin Ma[1], Wei Zhao[2], Gaolong Zhang[2] and Shouping Xu[1]**

[1] Department of Radiation Oncology, the First Medical Center of the People's Liberation Army General Hospital, Beijing, China, [2] School of Physics, Beihang University, Beijing, China, [3] Manteia Technologies Co., Ltd, Xiamen, China

OPEN ACCESS

Edited by:
Heming Lu,
People's Hospital of Guangxi Zhuang Autonomous Region, China

Reviewed by:
Yinglin Peng,
Sun Yat-sen University Cancer Center (SYSUCC), China
Changsheng Ma,
Shandong University, China

***Correspondence:**
Shouping Xu
shouping_xu@yahoo.com
Gaolong Zhang
zgl@buaa.edu.cn

Specialty section:
This article was submitted to Head and Neck Cancer, a section of the journal Frontiers in Oncology

Received: *02 August 2021*
Accepted: *21 October 2021*
Published: *11 November 2021*

Citation:
Liu Y, Chen Z, Wang J, Wang X, Qu B, Ma L, Zhao W, Zhang G and Xu S (2021) Dose Prediction Using a Three-Dimensional Convolutional Neural Network for Nasopharyngeal Carcinoma With Tomotherapy. Front. Oncol. 11:752007. doi: 10.3389/fonc.2021.752007

Purpose: This study focused on predicting 3D dose distribution at high precision and generated the prediction methods for nasopharyngeal carcinoma patients (NPC) treated with Tomotherapy based on the patient-specific gap between organs at risk (OARs) and planning target volumes (PTVs).

Methods: A convolutional neural network (CNN) is trained using the CT and contour masks as the input and dose distributions as output. The CNN is based on the "3D Dense-U-Net", which combines the U-Net and the Dense-Net. To evaluate the model, we retrospectively used 124 NPC patients treated with Tomotherapy, in which 96 and 28 patients were randomly split and used for model training and test, respectively. We performed comparison studies using different training matrix shapes and dimensions for the CNN models, i.e., 128 ×128 ×48 (for Model I), 128 ×128 ×16 (for Model II), and 2D Dense U-Net (for Model III). The performance of these models was quantitatively evaluated using clinically relevant metrics and statistical analysis.

Results: We found a more considerable height of the training patch size yields a better model outcome. The study calculated the corresponding errors by comparing the predicted dose with the ground truth. The mean deviations from the mean and maximum doses of PTVs and OARs were 2.42 and 2.93%. Error for the maximum dose of right optic nerves in Model I was 4.87 ± 6.88%, compared with 7.9 ± 6.8% in Model II (p=0.08) and 13.85 ± 10.97% in Model III (p<0.01); the Model I performed the best. The gamma passing rates of PTV_{60} for 3%/3 mm criteria was 83.6 ± 5.2% in Model I, compared with 75.9 ± 5.5% in Model II (p<0.001) and 77.2 ± 7.3% in Model III (p<0.01); the Model I also gave the best outcome. The prediction error of D_{95} for PTV_{60} was 0.64 ± 0.68% in Model I, compared with 2.04 ± 1.38% in Model II (p<0.01) and 1.05 ± 0.96% in Model III (p=0.01); the Model I was also the best one.

Conclusions: It is significant to train the dose prediction model by exploiting deep-learning techniques with various clinical logic concepts. Increasing the height (Y direction) of training patch size can improve the dose prediction accuracy of tiny OARs and the

whole body. Our dose prediction network model provides a clinically acceptable result and a training strategy for a dose prediction model. It should be helpful to build automatic Tomotherapy planning.

Keywords: dose prediction, deep learning, Tomotherapy, nasopharyngeal carcinoma, radiotherapy plan

INTRODUCTION

Radiotherapy (RT) Plan optimization is a time-consuming process in routine clinical practice. It may cost several hours to constrain the dose distribution to meet the optimal clinical criteria. The plan quality, which the total voxel information can guide the RT plan optimization and ensure, depends on the medical dosimetrist or the medical physicist's clinical experience and skills. It can minimize the uncertainty of the planning outcome due to different planners handling the planning process (1–3).

Recently, artificial intelligence (AI) and deep learning (DL) methods have been extensively involved in radiotherapy workflow, such as dose prediction (4–7). The DL-based methods perform well in automatic feature extraction and mapping transformation (5, 8). The dose prediction model can make an end-to-end mapping transformation between patients' anatomical and dose distribution information with organs-at-risk (OARs) constraints (9–12). Compared with using the conventional treatment planning system (TPS), using the DL model to generate predicted dose distribution reduces planning time significantly (13–16).

Tomotherapy is a superior RT modality for treating advanced cancers, such as head and neck cancer. Compared to conventional RT treatment, Tomotherapy plan optimization is a time-consuming process. To make a plan with desirable quality, the planner needs to adjust the dose-volume histogram (DVH) limitation and plan criteria to update the plan weights iteratively. In this context, the total voxel information becomes a crucial consideration in dose prediction. It can guide Tomotherapy plan optimization, reducing the iteration times by lessening TPS optimization's adjustment steps and minimizing the planning outcome uncertainty caused by anthropogenic factors. Different planners may handle the planning process.

Due to the complex anatomy, it is highly challenging to make a plan that can precisely deliver the prescribed dose to the target for the head and neck cancer patients (17, 18). They carry great essential functions for humans, and they need to be protected from unnecessary doses to guarantee which could still function well after the treatment (safe during the treatment). It results in more difficulty in achieving the desirable dose for planning target volumes (PTVs).

This study aims to establish the underlying relationship between anatomical and dose distribution information for nasopharyngeal carcinoma (NPC) patients treated with Tomotherapy using deep-learning approaches. Since few studies have been performed to investigate dose prediction for NPC, this study should be potentially exciting and valuable as guidance or reference for future RT planning.

MATERIALS AND METHODS

Data Collection and Preparation

One hundred twenty-four NPC patients were treated with Tomotherapy, and our study collected their data. PTVs, the OARs, and the external contour (Body) were labeled as the contoured structures. We added a 3 mm margin around the gross tumor volume of the nasopharynx (GTVnx) and clinical target volume (CTV) to create the planning GTVnx (pGTVnx) and PTV, respectively. The PTVs include PTV_{60} (a prescription dose of 60 Gy) and PTV_{54} (54 Gy). The OARs included Brainstem, Spinal-cord, Eyes, Lens, Larynx-esophagus-trachea (L-E-T), Optic-nerves, Oral-cavity, Parotid-glands (PGs), Pituitary, Thyroid, Submaxillary-glands (SMGs). The study collected Digital Imaging and Communications in Medicine (DICOM) files for each case, including CT series, RT Plan, RT Structure, and RT Dose files. All cases corresponding DICOM files involved in our study have been done for particular quality assurance (QA) and delivered.

The collected cases have good consistency: have all PTV_{60} (with prescription dose of 60 Gy) and have the same types of OARs. We did the data preprocessing before the model training. It ensures the CNN network could load and correctly process the mapping transformation between the patient's anatomical and dose distribution information. We extracted the 3D CT matrix from CT DICOM files, and the voxel values were normalized for each case. The normalized CT matrix holds a zero mean value and one as the variance. The study converted the region of interest (ROI) information to a binary mask, which means the pixels inside the contouring area with a value of 1 and pixels outside the contouring area with 0. The spacing and matrix shapes of the ROI contouring mask were adjusted equal to the corresponding CT matrix. We obtained the dose array from RT Dose files, with dose values (from 0 to 74 Gy) directly recorded in the dose matrix. All data preprocessing had been done by Python codes. NumPy, pydicom, and other python packages were used to conserve the raw data to the "npy" format.

3D Neural Network

The 3D Dense-U-Net was built as the neural network architecture (**Figure 1**). "U-Net" is a famous well-behaved CNN network specializing in end-to-end matrix mapping (19). The U-Net architecture consists of down-sampling and up-sampling blocks concatenated across the bottleneck symmetrically, thus allowing the model to extract features for high, middle, and low level (20). The Dense-U-Net structure preserves the up-sampling and down-sampling portions and adds the densely connected layers within each hierarchical level to create the "Dense structure" (21). Every hierarchical

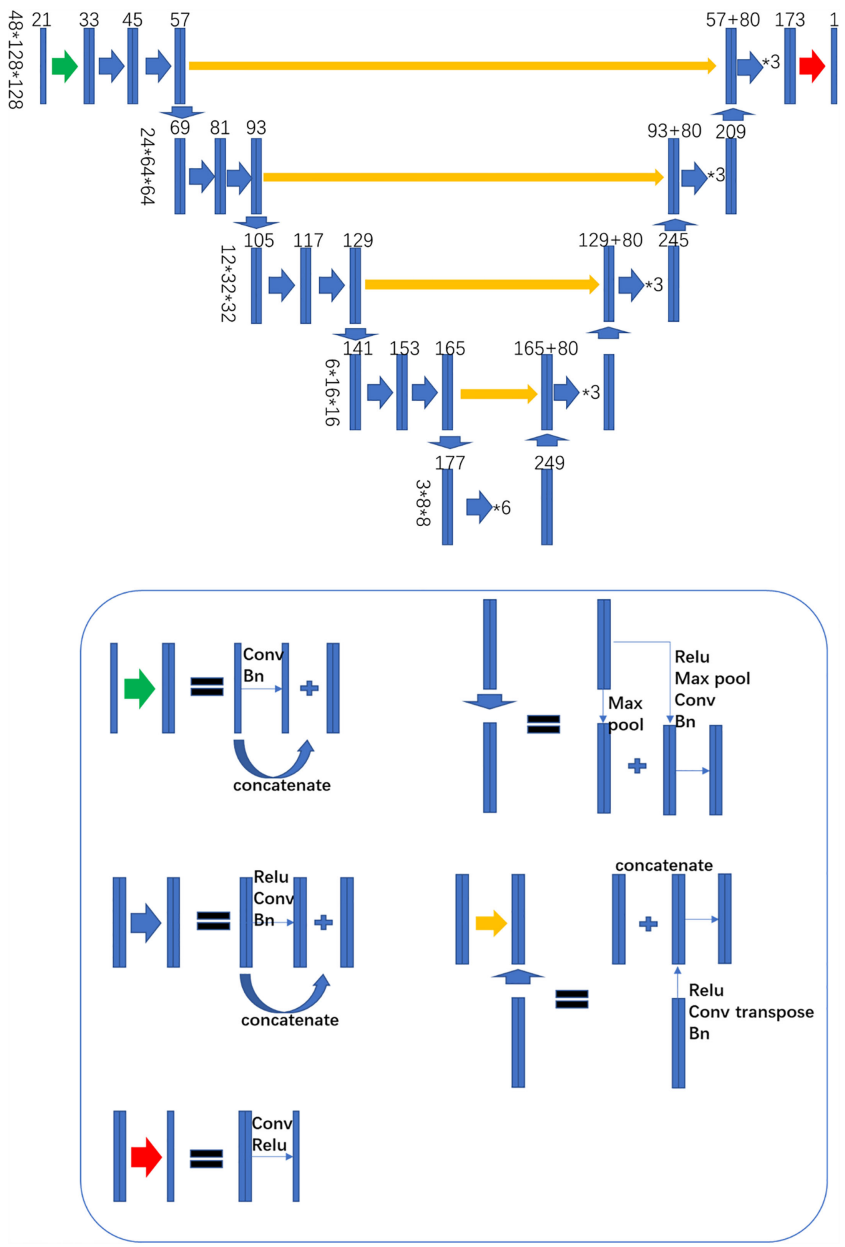

FIGURE 1 | 3D Dense-U-NET structure.

level of Dense-U-Net preserves all features from previous layers. It allows the features to be reused and propagated along with successive layers. The 3D Dense-U-Net is the 3D version of the Dense U-Net model. Compared to the 2D Dense U-Net, the 3D one can directly process the input 3D matrix's information and capture features along the Y direction.

Training and Testing

For the 124 nasopharyngeal carcinoma cases, we randomly chose 96 cases for training and 28 cases for testing. The model input matrix contained 21 channels. The first channel is for CT image information, and the 2–21 channels contain ROIs contour information, which includes pGTVnx, PTV_{60}, PTV_{54}, Body, Brainstem, Spinal-cord, Eye-L, Eye-R, Lens-L, Lens-R, L-E-T, Optic-nerve-L, Optic-nerve-R, Oral-cavity, Parotid-L, Parotid-R, Pituitary, Thyroid, SMG-L, and SMG-R. In this study, the ground truth is the dose distribution from the collected RT DOSE DICOM files. Due to the GPU memory limitation, we specified the patch-training strategy. The 128×128×48 shape matrix for training was randomly selected from the 3D dose matrix. The 3D Dense-U-Net model was built up by connection of Dense Block. Every Dense Block includes a Relu activation process, followed by convolution

(kernel size 3×3×3), batch normalization, and concatenation with the previous layer. We used zero paddings in each convolution, and each convolution layer had 12 channels. The 3D Dense-U-NET model went through four times down-sampled by max-pooling (kernel size 2×2×2) and symmetrically with four times up-sampled by deconvolution (kernel size 2×2×2, channel =80). The down-sampling process reduced the initial input matrix size from 128×128×48(128➔64➔32➔16➔8) to 8×8×3. It allows the network to be able to extract features both locally and globally; the up-sampling restored the matrix size from 8×8×3 to 128×128×48. The final hierarchical layer of convolution forms a single channel matrix and becomes the output matrix. We used the Adam optimizer (22) with the MAE loss function ($\frac{1}{n}\Sigma_{i=1}^{n}|f(x)-y|$) and settled the batch size as 4. The learning rate decayed from 10^{-4} to 10^{-6} during CNN network training. When the loss values and learning rate stabilized, the process stopped training. And an Nvidia RTX 3090 GPU accelerated the entire training and testing process in this study. The deep learning framework was TensorFlow and Keras.

This study used 28 untrained cases for the model testing. The CT images and ROI contours were used as the model input data, and dose distribution was the model output (**Figure 2**). The matrix height (Y direction) of the testing case patch was 64. We concatenated the full-body dose distribution after the model generated the predicted dose distribution for each testing case patch.

We trained two comparative models with different Y lengths (height) to verify whether the 3D model with a large-height training patch could extract more interrelation information from different OAR-PTV distances in the Y direction. From our statistics results, the distance between specific OARs to PTV varies a lot among different patients. For example, the optic nerves' distances to PTV ranged from 0 to 30 mm, which already equals 10 slices thickness of a CT scan with 3 mm thickness. Model I used the above model training method, and the shape of the training matrix was 128×128×48. Model II reduced the height of the training matrix to 128×128×16 shape. Training Model II aimed to verify whether the increase of height of the training matrix would be helpful to modulate the model to provide more accurate dose prediction for OARs. If the maximum distance from the optic nerve to PTV was 10 slices, and the height of the training matrix was just 16 slice distances, the training matrix may not be able to find enough spatial relationship from optic-organ to PTV. Increasing the height of

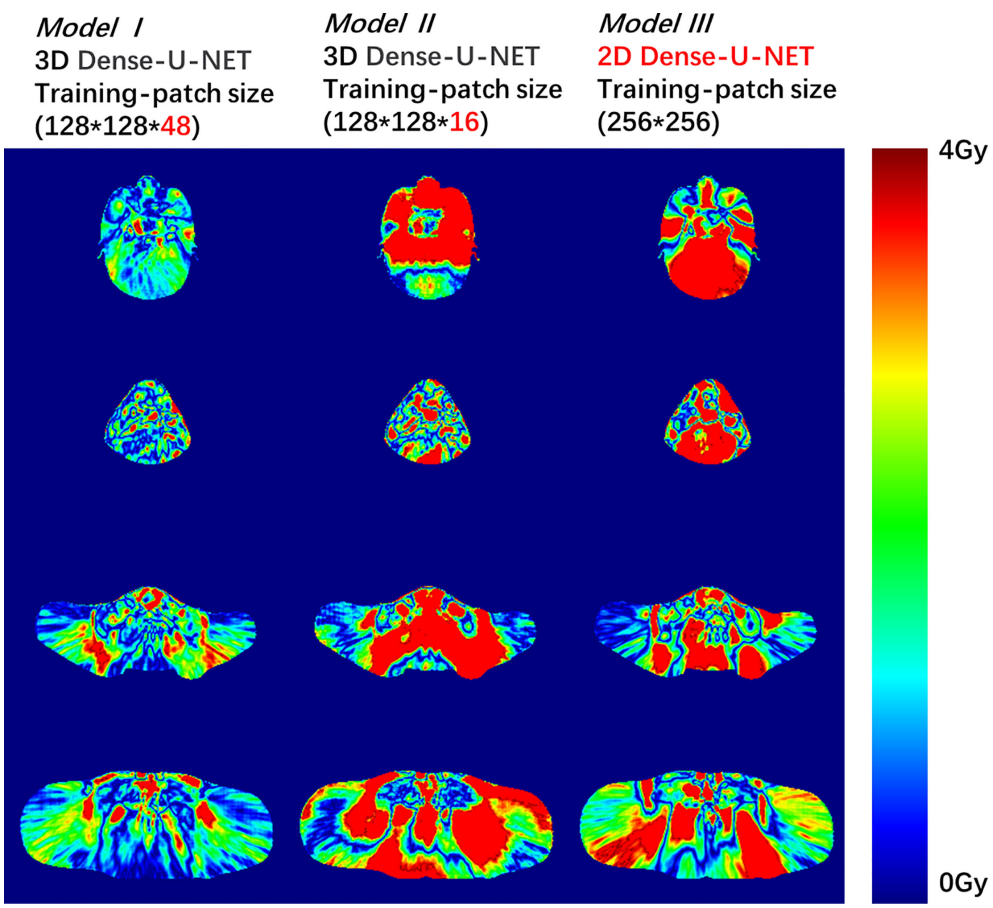

FIGURE 2 | Dose difference between the predicted dose distribution and the ground truth for Model I, II, or III. The deep red color shows the dose difference beyond 4 Gy.

the training matrix may allow the model to explore a more spatial relationship between the optic nerves and PTV, therefore, to generate more accurate OAR dose prediction. Model III used 2D Dense U-net. It is a simplified change from 3D Dense-U-net to a 2D version. Model III was designed to eliminate the "Y-direction distance" influence in the learning process. Model III can be seen as a comparison experiment to verify if the OAR-PTV distance in the Y direction would be a factor affecting the DL model output.

Quantitative Evaluation

Percentage of errors (δDi), p-value, and gamma passing rate were calculated to evaluate our three models' accuracy. The formula of the percentage of errors was:

$$\delta Di = \frac{\left|Di_{Ground-truth} - Di_{predicted}\right|}{prescription\ dose}$$

We calculated δDi of D_{98}, D_{95}, D_{50}, D_2 for PTV_{60}, and D_{mean}, D_{max} for all ROIs. All corresponding δDi for 28 test patients were counted and formed mean and standard deviation (Mean ± SD) for each ROI. The p-value of the two models' δDi was calculated using a T-test; when the p-value<0.05, the prediction results have no statistical correlation. The gamma passing rates with the 3%/3 mm criteria and 10% threshold for the three approaches were calculated by 3D Slicer 4.10.2 [National Institutes of Health (NIH), USA] software.

RESULTS

The mean deviations from the mean and maximum dose of PTVs and OARs were 2.42 and 2.93%, respectively. Error for the maximum dose of optic nerves-R in Model I was 4.87 ± 6.88%, compared with 7.9 ± 6.8% in Model II (p=0.08) and 13.85 ± 10.97% in Model III (p<0.01); Model I showed well. The gamma passing rate of PTV_{60} for 3%/3 mm criteria was 83.6 ± 5.2% in Model I, compared with 75.9 ± 5.5% in Model II (p<0.001) and 77.2 ± 7.3% in Model III (p<0.01); Model I also did the best job. The prediction error of D_{95} for PTV_{60} was 0.64 ± 0.68% in Model I, compared with 2.04 ± 1.38% in Model II (p<0.01) and 1.05 ± 0.96% in Model III (p=0.01); Model I still performed well. The details of prediction errors are presented in **Table 1** and **Table 2**.

To compare the three models' accuracy intuitively, we randomly selected a test patient. We showed the dose difference between the predicted dose and the ground truth in **Figure 2** and the DVH plots of ROIs in **Figure 3**. Figures of the dose differences and DVH plots showed that Model I has the best prediction among the three models and an advantage in predicting the optic organs' dose.

DISCUSSION

Precise automatic dose prediction can significantly improve clinical planning efficiency and safety (23). 3D dose prediction results can refer to current RT plan optimization in TPS (24, 25). Here, we built CNN-based dose prediction on the previous approved delivered plans. Since, in daily clinical practice, different medical physicists handled the planning process, which provided a source of uncertainty of the RT planning outcome. Using CNN-based dose prediction results guiding plan optimization can reduce the uncertainty of the planning outcomes and improve the plan optimization speed (26). A few fluence-prediction-based auto-planning researches have been

TABLE 1 | Mean and standard deviation (Mean ± SD) of maximum and mean values between the predicted dose and the ground truth received on PTVs and OARs relative to the prescription dose.

ROI	Error of D_{mean} (%)					Error of D_{max} (%)				
	Model I	Model II	Model III	p^{a*}	p^{b*}	Model I	Model II	Model III	p^{a*}	p^{b*}
Body	0.58 ± 0.49	1.70 ± 1.17	0.64 ± 0.56	<0.01	0.67	2.09 ± 1.19	1.91 ± 1.07	1.97 ± 1.18	0.55	0.69
Brainstem	3.36 ± 3.00	5.63 ± 4.03	4.54 ± 3.38	0.02	0.16	2.90 ± 2.49	4.85 ± 3.66	3.61 ± 3.23	0.02	0.35
Spinal-cord	3.18 ± 4.56	8.65 ± 3.83	3.49 ± 4.06	<0.01	0.78	2.83 ± 2.41	4.84 ± 2.61	3.26 ± 274	<0.01	0.52
Eye-L	1.35 ± 1.14	1.61 ± 1.78	2.87 ± 2.30	0.50	<0.01	4.40 ± 3.41	7.08 ± 5.60	7.09 ± 5.13	0.03	0.02
Eye-R	1.48 ± 1.59	2.59 ± 2.92	2.31 ± 2.29	0.07	0.11	3.64 ± 3.31	9.89 ± 7.12	4.36 ± 495	<0.01	0.51
Lens-L	0.39 ± 0.34	0.48 ± 0.39	0.80 ± 0.61	0.31	<0.01	0.80 ± 0.66	0.80 ± 0.55	1.23 ± 0.96	0.99	0.05
Lens-R	0.52 ± 0.42	0.44 ± 0.35	0.63 ± 0.60	0.47	0.39	0.75 ± 0.59	0.69 ± 0.43	0.83 ± 0.77	0.67	0.66
L-E-T	2.20 ± 2.05	9.23 ± 3.92	2.73 ± 2.50	<0.01	0.38	2.49 ± 1.59	3.85 ± 3.61	2.28 ± 2.07	0.06	0.67
Optic-nerve-L	5.10 ± 4.40	7.67 ± 5.02	11.47 ± 9.38	0.04	<0.01	5.84 ± 5.21	8.30 ± 5.11	13.15 ± 11.58	0.07	<0.01
Optic-nerve-R	4.71 ± 5.12	7.90 ± 5.77	11.06 ± 8.11	0.03	<0.01	4.87 ± 6.88	7.93 ± 6.80	13.85 ± 10.97	0.08	<0.01
Oral-cavity	2.40 ± 2.20	2.63 ± 2.47	2.43 ± 2.13	0.70	0.96	2.12 ± 1.94	2.32 ± 1.95	2.21 ± 2.22	0.69	0.87
Parotid-L	2.13 ± 1.57	3.70 ± 2.60	1.60 ± 1.43	0.01	0.17	3.41 ± 2.62	3.90 ± 2.93	2.83 ± 2.08	0.50	0.35
Parotid-R	2.84 ± 2.29	4.00 ± 2.65	2.47 ± 2.29	0.08	0.53	3.46 ± 2.58	3.34 ± 3.03	3.37 ± 2.48	0.87	0.89
pGTVnx	0.56 ± 0.33	0.98 ± 0.65	0.68 ± 0.42	<0.01	0.24	1.92 ± 1.15	1.91 ± 0.86	1.81 ± 1.07	0.97	0.69
Pituitary	4.01 ± 5.36	4.23 ± 4.96	10.06 ± 9.59	0.87	<0.01	3.87 ± 4.17	4.47 ± 3.81	7.19 ± 8.76	0.57	0.07
PTV1	0.80 ± 0.49	1.27 ± 0.69	0.73 ± 0.77	<0.01	0.71	2.09 ± 1.19	1.91 ± 1.07	1.97 ± 1.18	0.55	0.69
PTV2	0.54 ± 0.54	1.29 ± 0.96	0.45 ± 0.32	<0.01	0.46	2.82 ± 2.01	2.49 ± 2.03	4.28 ± 3.33	0.53	0.04
Thyroid	3.66 ± 3.26	7.53 ± 4.16	4.59 ± 3.54	<0.01	0.29	2.23 ± 1.61	3.76 ± 2.78	2.01 ± 1.83	0.01	0.61
Mandible-L	3.77 ± 5.11	6.32 ± 5.94	6.21 ± 5.97	0.08	0.09	3.20 ± 2.67	5.09 ± 3.71	3.76 ± 3.20	0.03	0.47
Mandible-R	2.43 ± 1.97	3.23 ± 3.23	3.19 ± 4.13	0.26	0.37	2.71 ± 2.06	2.96 ± 2.63	2.09 ± 209	0.69	0.25

*: p_a, p value between Model I and Model II; p_b, p value between Model I and Model III.

TABLE 2 | Means and standard deviations (Mean ± SD) of absolute differences for clinical DVH metrics between the predicted and ground truth doses.

	PTV_{60} error (%)				
	Model I	**Model II**	**Model III**	p_a*	p_b*
D_{98}	1.24 ± 1.52	3.20 ± 2.18	1.19 ± 1.44	<0.01	0.68
D_{95}	0.64 ± 0.68	2.04 ± 1.38	1.05 ± 0.96	<0.01	0.01
D_{50}	1.07 ± 1.04	1.14 ± 1.31	0.93 ± 1.18	0.13	<0.01
D_2	1.37 ± 0.80	1.52 ± 1.00	0.94 ± 0.89	0.65	<0.01

*: p_a, p value between Model I and Model II; p_b, p value between Model I and Model.

done in the past few years. They mentioned that dose distribution could be predicted utilizing a fluence map as well. Furthermore, this enlightens us to get the dose prediction based on an auto-planning system (27, 28). Dose prediction studies can be the basis for much RT-relevant research and technology development.

NPC cases with Tomotherapy have great value in deep-learning dose prediction research. As we know, NPC patients with Tomotherapy are relatively rare in clinical RT practice. And in the past, studies about dose prediction of NPC patients with Tomotherapy were also not too many. Our study for dose prediction found that using a 3D CNN network for training could provide a better outcome than using a 2D CNN network, and the dose prediction accuracy has reached the clinical standard (the mean deviations for the mean and maximum doses of PTVs and OARs were 2.42 and 2.93%, respectively). It can refer to future dose prediction of NPC patients with Tomotherapy, even though this method still needs more research to improve its accuracy.

Our dose prediction model performed well in OARs and PTV areas but didn't work well in the outside area of OARs and PTVs. Although the outcome accuracy in this study met the clinical requirements, the evaluating indicators included the deviations for the mean and maximum doses for ROIs, the gamma passing rates for PTV, and the DVH plots. But there are still some problems, such as the passing rate for Body was 70.2 ± 9.8%, which was relatively poor. That means further research should focus on how to predict accurate doses in no-contoured areas.

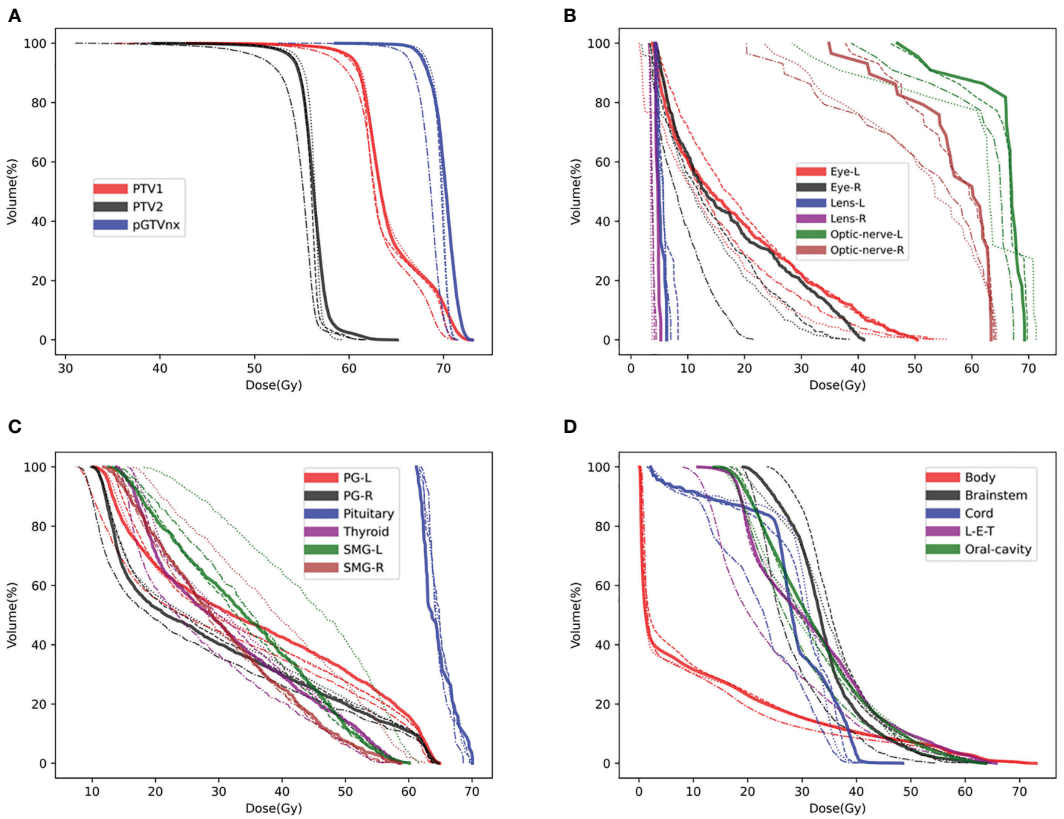

FIGURE 3 | DVH plots for a test patient, such as **(A)** DVH plot of PTVs, **(B)** DVH plot of optic organs, **(C, D)** DVH plots of the other OARs. DVH, Ground-truth (Solid line), Model I (Dashed line), Model II (Dashed and dotted line), Model III (Dotted line).

Future studies recommend inputting more features such as the help region and the outward expansion area or controlling training data's consistency, such as only using the designed plan from the same planner.

Besides building a dose prediction model, there is another critical factor that needs to be thought over (1). Training with the CNN network should follow the clinical logic concept (2). Training strategy should not directly duplicate from other studies, considering the dataset's features should be ahead of training.

In this study, the network structure is similar to some medical imaging segmentation networks. Previous studies showed that the U-net could perform very well in dose prediction and CT image segmentation tasks. But the training strategy should be suitable for the specific prediction tasks. For example, the 2D U-Net can perform pretty well in the task of CT image segmentation (19, 29, 30). Slice by slice segmentation prediction is similar to the clinical logic flow. As is well known, clinical staff always creates the contouring slice by slice, which affirms that each single CT slice should contain enough segmentation information. But as shown in the study, directly using the 2D network to predict dose distribution slice by slice cannot give us the wanted outcome, which may be due to the loss of Y-direction information as shown in the results, the OARs (such as Spinal-cord), which were close to PTV in the Y direction. It didn't show the different results using the 2D or 3D network to predict the dose distribution. But for OARs far from PTV in the Y direction, such as the optic organs, the dose-prediction results of the 2D network brought out lacks ability. The reason for the outcome difference could be that the algorithm logic is different from the clinical logic. When a medical physicist or dosimetrist makes a treatment plan, the staff should consider the relationship of the relative location between OAR and PTVs. We can quickly understand that it is difficult to avoid unnecessary doses for NPC patients if the optic organs are close to PTV. On the other hand, if the organs are far from PTV, they would be protected from radiation more efficiently. So, using the 3D network for training can allow the model to get the relative location between OARs and PTV. This action conforms to the clinical logic flow. Thus, a good outcome could meet.

Meanwhile, it is necessary to formulate the training strategy by considering the dataset's features. Some deep-learning-based dose prediction studies have been made for cervical carcinoma. The studies used a general 3D-model-patch-training strategy with 16 pixels height matrix to train (shape of n×n×16) or directly used a 2D network for data training (5, 31, 32). From some dose prediction studies proposed, 2D network training is good enough to provide excellent results of dose prediction. But in transplanting the patch-training strategy to this project, using (n×n×16) shape matrix to train or using the 2D network gives different results. We found that the results were not so good. Reviewing the patient's anatomic structure, we finally uncovered the dependency between the dose prediction results and the patient's anatomic information. Using an (n×n×16) shape training matrix/patch, we got an ideal dose prediction for the patients whose PTV was close to the eyes. But for the patients whose PTV was far from the eyes, it resulted in a wrong prediction. The statistics results showed that the optic nerve's dose delivered was negatively correlated with the distance from PTV to it. For all patients involved in the study, the maximum dose for optic nerves ranged from 9.7 to 71.4 Gy; the distance from the optic nerves to PTV ranged from 0 to 30 mm. The deep-learning model needs to know the spatial relationship between OARs and PTV. Since the predicted doses of optic nerves were highly related to its distance to PTV, using (n×n×16) shape matrix for training, it wouldn't get an accurate dose prediction for the cases with sizeable PTV-eye distance. We believe that the (n×n×16) shape training matrix fitted better to extract anatomic information in pelvic cancer because the pelvic tissues were generally compact to PTV. For NPC patients, the PTV-eye distance varies from 0 to several centimeters. If the training patch's height is small such as 16 pixels, it may be difficult for the deep-learning network to find the PTV-eye spatial relationship. PTVs have usually more than 70 slices thickness height for NPC patients. Suppose the training patch's matrix with a considerable height, such as height = 48 pixels, and the model could extract more features of the spatial relationship among the PTV-eye voxels.

Clinical and actual treatment logic concept includes a lot of information, which are greatly important. We could utilize them to optimize the deep-learning network performance relevant to the RT aspect. The training matrix should be considered the network's field of view from which the model could find the transformation relationship. Training with the 3D Dense-U-NET could predict each pixel's dose value by considering the full input matrix. Increasing the input matrix height (Y direction) would be a strategy realized the extraction combination features of model training and clinical logic concepts. Increasing the height of the input matrix (increases the local sense of field) can make the DL model find more spatial features and relationships correlated to PTV-OAR distance, which provides a more accurate outcome for dose prediction.

The deep-learning-based dose prediction method still has many problems that need to be solved. Firstly, previous research never focused on excavating the data's internal features and comparing the data differences. The anatomical information holds tremendous differences among different patients. Secondly, we can't directly use the previous researchers' method for deep learning, for different tumor types and treatment techniques have specific dose prediction methods. According to the tumor type and treatment mode, developing a specific dose prediction method can be a better way to improve dose prediction efficiency and accuracy. Our research was focused on adding the clinical logic concept with the deep-learning method together. Therefore, we developed a more reasonable deep-learning model training strategy.

A deep-learning-based study focuses on the relevant software and hardware, the clinical logic concepts, and the collected data characteristic. Combining computer technology, clinical logic flow, and data characteristics would be an ideal pathway to develop an excellent-performance dose prediction model.

CONCLUSIONS

In this study, we successfully developed an accurate dose prediction model using a 3D convolutional neural network. It proves well for NPC patients with Tomotherapy. It also tells that exploring the spatial features between OARs and PTV is necessary for dose prediction. We found that a 3D DL model with a larger Y-dimension training matrix increases the accuracy of dose prediction outcomes. With this extra consideration, our accuracy improvement method of dose prediction is good enough to be considered a milestone for the automatic planning process with Tomotherapy and other RT techniques. The predicted results could be used as a reference or guidance for systematic clinical RT planning.

DATA AVAILABILITY STATEMENT

The original contributions presented in the study are included in the article/supplementary material. Further inquiries can be directed to the corresponding authors.

ETHICS STATEMENT

This study was approved by the Ethics Committee of the Chinese PLA General Hospital (approved no. S2016-122-01). Written informed consent to participate in this study was provided by the participant's legal guardian.

AUTHOR CONTRIBUTIONS

YL: Experiment design and code implementation; article writing. ZC: Technical support. JW: Data collection. XW: Technical support. BQ: Data collection. LM: Data collection. WZ: Technical support, article modification. SX: Experiment design, article modification. GZ: Article modification. All authors contributed to the article and approved the submitted version.

FUNDING

This work was supported by the Medical Big Data AI R&D Project (2019MBD-043).

REFERENCES

1. Barragan-Montero AM, Nguyen D, Lu W, Lin MH, Norouzi-Kandalan R, Geets X, et al. Three-Dimensional Dose Prediction for Lung IMRT Patients With Deep Neural Networks: Robust Learning From Heterogeneous Beam Configurations. *Med Phys* (2019) 46(8):3679–91. doi: 10.1002/mp.13597
2. Chen X, Men K, Li Y, Yi J, Dai J. A Feasibility Study on an Automated Method to Generate Patient-Specific Dose Distributions for Radiotherapy Using Deep Learning. *Med Phys* (2019) 46(1):56–64. doi: 10.1002/mp.13262
3. Kajikawa T, Kadoya N, Ito K, Takayama Y, Chiba T, Tomori S, et al. A Convolutional Neural Network Approach for IMRT Dose Distribution Prediction in Prostate Cancer Patients. *J Radiat Res* (2019) 60(5):685–93. doi: 10.1093/jrr/rrz051
4. Nguyen D, Jia X, Sher D, Lin M-H, Iqbal Z, Liu H, et al. Three-Dimensional Radiotherapy Dose Prediction on Head and Neck Cancer Patients With a Hierarchically Densely Connected U-Net Deep Learning Architecture. *Phys Med Biol* (2019) 64(6):065020. doi: 10.1088/1361-6560/ab039b
5. Ma M, Kovalchuk N, Buyyounouski MK, Xing L, Yang Y. Incorporating Dosimetric Features Into the Prediction of 3D VMAT Dose Distributions Using Deep Convolutional Neural Network. *Phys Med Biol* (2019) 64 (12):125017. doi: 10.1088/1361-6560/ab2146
6. Boldrini L, Bibault J-E, Masciocchi C, Shen Y, Bittner M-I. Deep Learning: A Review for the Radiation Oncologist. *Front Oncol* (2019) 9:977. doi: 10.3389/fonc.2019.00977
7. Kandalan RN, Nguyen D, Rezaeian NH, Barragán-Montero AM, Breedveld S, Namuduri K, et al. Dose Prediction With Deep Learning for Prostate Cancer Radiation Therapy: Model Adaptation to Different Treatment Planning Practices. *Radiother Oncol* (2020) 153:228–35. doi: 10.1016/j.radonc.2020.10.027
8. LeCun Y, Bengio Y, Hinton G. Deep Learning. *Nature* (2015) 521(7553):436–44. doi: 10.1038/nature14539
9. Guerreiro F, Seravalli E, Janssens G, Maduro J, Knopf A, Langendijk J, et al. Deep Learning Prediction of Proton and Photon Dose Distributions for Paediatric Abdominal Tumours. *Radiother Oncol* (2021) 156:36–42. doi: 10.1016/j.radonc.2020.11.026
10. Gronberg MP, Gay SS, Netherton TJ, Rhee DJ, Court LE, Cardenas CE. Dose Prediction for Head and Neck Radiotherapy Using a Three-Dimensional Dense Dilated U-Net Architecture. *Med Phys* (2021) 48(9):5567–73. doi: 10.1002/mp.14827
11. Zimmermann L, Faustmann E, Ramsl C, Georg D, Heilemann G. Dose prediction for radiation therapy using feature-based losses and One Cycle Learning. *Med Phys* (2021) 48(9):5562–6. doi: 10.1002/mp.14774
12. Kearney V, Chan JW, Wang T, Perry A, Descovich M, Morin O, et al. DoseGAN: A Generative Adversarial Network for Synthetic Dose Prediction Using Attention-Gated Discrimination and Generation. *Sci Rep* (2020) 10 (1):1–8. doi: 10.1038/s41598-020-68062-7
13. Liang B, Tian Y, Chen X, Yan H, Yan L, Zhang T, et al. Prediction of Radiation Pneumonitis With Dose Distribution: A Convolutional Neural Network (CNN) Based Model. *Front Oncol* (2020) 9:1500. doi: 10.3389/fonc.2019.01500
14. Hu J, Song Y, Wang Q, Bai S, Yi Z. Incorporating Historical Sub-Optimal Deep Neural Networks for Dose Prediction in Radiotherapy. *Med Image Anal* (2021) 67:101886. doi: 10.1016/j.media.2020.101886
15. Bakx N, Bluemink H, Hagelaar E, van der Sangen M, Theuws J, Hurkmans C. Development and Evaluation of Radiotherapy Deep Learning Dose Prediction Models for Breast Cancer. *Phys Imaging Radiat Oncol* (2021) 17:65–70. doi: 10.1016/j.phro.2021.01.006
16. Barragán-Montero AM, Thomas M, Defraene G, Michiels S, Haustermans K, Lee JA, et al. Deep Learning Dose Prediction for IMRT of Esophageal Cancer: The Effect of Data Quality and Quantity on Model Performance. *Physica Med* (2021) 83:52–63. doi: 10.1016/j.ejmp.2021.02.026
17. Caudell JJ, Torres-Roca JF, Gillies RJ, Enderling H, Kim S, Rishi A, et al. The Future of Personalised Radiotherapy for Head and Neck Cancer. *Lancet Oncol* (2017) 18(5):e266–73. doi: 10.1016/S1470-2045(17)30252-8
18. Castelli J, Simon A, Lafond C, Perichon N, Rigaud B, Chajon E, et al. Adaptive Radiotherapy for Head and Neck Cancer. *Acta Oncol* (2018) 57(10):1284–92. doi: 10.1080/0284186X.2018.1505053
19. Jin J, Zhu H, Zhang J, Ai Y, Zhang J, Teng Y, et al. Multiple U-Net-Based Automatic Segmentations and Radiomics Feature Stability on Ultrasound Images for Patients With Ovarian Cancer. *Front Oncol* (2021) 10:614201. doi: 10.3389/fonc.2020.614201
20. Ronneberger O, Fischer P, Brox T. U-Net: Convolutional Networks for Biomedical Image Segmentation. In: *International Conference on Medical Image Computing and Computer-Assisted Intervention*. Munich, Germany: Springer (2015).
21. Huang G, Liu Z, van der Maaten L, Weinberger KQ. Densely Connected Convolutional Networks. In: *Proceedings of the IEEE Conference on Computer Vision and Pattern Recognition*. Honolulu, HI, United States (2017).

22. Kingma DP, Ba J. Adam: A Method for Stochastic Optimization. In: *International Conference on Learning Representations 2015 (ICLR 2015)*. San Diego, California, United States (2014).
23. Ma J, Nguyen D, Bai T, Folkerts M, Jia X, Lu W, et al. A Feasibility Study on Deep Learning–Based Individualized 3d Dose Distribution Prediction. *Med Phys* (2021) 48(8):4438–47. doi: 10.1002/mp.15025
24. Bai X, Wang B, Wang S, Wu Z, Gou C, Hou Q. Radiotherapy Dose Distribution Prediction for Breast Cancer Using Deformable Image Registration. *Biomed Eng Online* (2020) 19:1–20. doi: 10.1186/s12938-020-00783-2
25. Norouzi Kandalan R, Nguyen D, Hassan Rezaeian N, Barragan-Montero AM, Breedveld S, Namuduri K, et al. Dose Prediction With Deep Learning for Prostate Cancer Radiation Therapy: Model Adaptation to Different Treatment Planning Practices. *Radiother Oncol* (2020) 153:228–35. doi: 10.1016/j.radonc.2020.10.027
26. Sun Y, Yang Y, Qian J, Tian Y. Evaluation and Prediction of Pelvic Dose in Postoperative IMRT for Cervical Cancer. *Chin J Radiat Oncol* (2020) 6 (2020):136–40.
27. Zhong Y, Yu L, Zhao J, Fang Y, Yang Y, Wu Z, et al. Clinical Implementation of Automated Treatment Planning for Rectum Intensity-Modulated Radiotherapy Using Voxel-Based Dose Prediction and Post-Optimization Strategies. *Front Oncol* (2021) 11:697995. doi: 10.3389/fonc.2021.697995
28. Nilsson V, Gruselius H, Zhang T, De Kerf G, Claessens M. Probabilistic Dose Prediction Using Mixture Density Networks for Automated Radiation Therapy Treatment Planning. *Phys Med Biol* (2021) 66(5):055003. doi: 10.1088/1361-6560/abdd8a
29. He K, Liu X, Shahzad R, Reimer R, Thiele F, Niehoff J, et al. Advanced Deep Learning Approach to Automatically Segment Malignant Tumors and Ablation Zone in the Liver With Contrast-Enhanced CT. *Front Oncol* (2021) 11:669437. doi: 10.3389/fonc.2021.669437
30. Liu X, Li K-W, Yang R, Geng L-S. Review of Deep Learning Based Automatic Segmentation for Lung Cancer Radiotherapy. *Front Oncol* (2021) 11:717039. doi: 10.3389/fonc.2021.717039
31. Kajikawa T, Kadoya N, Ito K, Takayama Y, Chiba T, Tomori S, et al. Automated Prediction of Dosimetric Eligibility of Patients With Prostate Cancer Undergoing Intensity-Modulated Radiation Therapy Using a Convolutional Neural Network. *Radiol Phys Technol* (2018) 11(3):320–7. doi: 10.1007/s12194-018-0472-3
32. Ma M, Buyyounouski K, Vasudevan M,V, Xing L, Yang Y. Dose Distribution Prediction in Isodose Feature-Preserving Voxelization Domain Using Deep Convolutional Neural Network. *Med Phys* (2019) 46(7):2978–87. doi: 10.1002/mp.13618

Conflict of Interest: Manteia Technologies Co., Ltd employed author ZC.

The remaining authors declare that the research was conducted in the absence of any commercial or financial relationships that could be construed as a potential conflict of interest.

frontiers in Oncology

ORIGINAL RESEARCH
published: 11 November 2021
doi: 10.3389/fonc.2021.724467

The Integration of the Pre-Treatment Neutrophil-to-Lymphocyte Ratio in the Eighth Edition of the AJCC Staging System for Nasopharynx Cancer

Zhong-Guo Liang[1†], Fan Zhang[2†], Ye Li[1†], Ling Li[1], Song Qu[1], Fang Su[1], Bin-Bin Yu[1], Ying Guan[1], Lu Han[1], Kai-Guo Li[1] and Xiao-Dong Zhu[1]*

[1] Department of Radiation Oncology, Guangxi Medical University Cancer Hospital, Cancer Institute of Guangxi Zhuang Autonomous Region, Nanning, China, [2] Microbiome Research Centre, St George and Sutherland Clinical School, The University of New South Wales Sydney, St George Hospital, Kogarah, NSW, Australia

OPEN ACCESS

Edited by:
Yong Yin,
Shandong Cancer Hospital, China

Reviewed by:
Aline Lauda Freitas Chaves,
DOM Clinica de Oncologia, Brazil
Arnab Pal,
Post Graduate Institute of Medical Education and Research (PGIMER), India

***Correspondence:**
Xiao-Dong Zhu
zhuxdonggxmu@126.com

[†]These authors have contributed equally to this work

Specialty section:
This article was submitted to Head and Neck Cancer, a section of the journal Frontiers in Oncology

Received: *13 June 2021*
Accepted: *15 October 2021*
Published: *11 November 2021*

Citation:
Liang Z-G, Zhang F, Li Y, Li L, Qu S, Su F, Yu B-B, Guan Y, Han L, Li K-G and Zhu X-D (2021) The Integration of the Pre-Treatment Neutrophil-to-Lymphocyte Ratio in the Eighth Edition of the AJCC Staging System for Nasopharynx Cancer. Front. Oncol. 11:724467. doi: 10.3389/fonc.2021.724467

Objective: The present study aimed to evaluate the role of integrating the pretreatment neutrophil-to-lymphocyte ratio (NLR) into the eighth edition of the AJCC staging system for nasopharynx cancer in an endemic region.

Methods: Between May 2007 and December 2012, a total of 713 cases with NPC were retrospectively analyzed. The separation ability in terms of overall survival (OS), local failure-free survival (LFFS), distant metastasis-free survival (DMFS), and failure-free survival (FFS) was evaluated. The discriminatory ability was assessed using Harrell's concordance index (c-index). Recursive partitioning analysis (RPA) was conducted and incorporated with pretreatment NLR.

Results: When integrated with NLR, the separate and discriminatory abilities for N classifications were improved in terms of OS and DMFS, but not for T categories. By using Recursive partitioning analysis, five subgroups were generated. Compared with the overall stage, the integration of NLR could not enhance the separate and discriminatory abilities. However, patients in the RPA 4 group gained significant benefits in terms of OS (HR 0.390 (95%CI 0.212-0.716), P = 0.002) and FFS (HR 0.548 (95%CI 0.314-0.958), P = 0.032) from the additional adjuvant chemotherapy after concurrent chemoradiotherapy.

Conclusion: The integration of NLR into the 8th edition of the AJCC staging system could enhance the separation and discriminatory abilities for N classifications, but not for T categories. In addition, patients in the RPA 4 group could benefit from the addition of adjuvant chemotherapy to concurrent chemoradiotherapy.

Keywords: nasopharynx cancer (NPC), neutrophil-to-lymphocyte ratio (NLR), neoplasm staging, concurrent chemoradiotherapy (CCRT), adjuvant chemotherapy

INTRODUCTION

Nasopharynx carcinoma (NPC) is prevalent in South-Eastern China, Malaysia, Indonesia, Singapore, Eastern Asia, and Northern Africa, with a high incidence rate of 15-50/100,000 cases per year (1, 2). Radiotherapy in combination with chemotherapy is the main therapeutic regimen for NPC. With improvements in diagnostic imaging and radiotherapy technology and the broader application of systemic therapy, the prognosis of NPC has improved significantly (3–5).

The American Joint Committee on Cancer (AJCC) Tumor-Node-Metastasis (TNM) staging system has been widely applied to estimate curative effects and to help develop therapeutic strategies. We previously reported recommendations for updating the T and N staging systems for NPC by comparing the 2008 Chinese staging system and the 7th AJCC staging system (6). Recently, the 8th edition of the AJCC staging system for NPC was released and is based on large-sample clinical trials using magnetic resonance imaging (MRI) and intensity modulated radiation therapy (IMRT) technology (7).

Clinically, patients with the same TNM stage may have different prognoses, which indicates the heterogeneity among patients. Therefore, it is essential to integrate other prognostic factors into the TNM staging system. A set of studies have shown that when integrated with some biomarkers, the separation and discriminatory ability can be enhanced in several tumors, including prostate cancer (8), breast cancer (9), lymphoma (10), and seminoma (11). Pre-treatment neutrophil-lymphocyte ratio (NLR) have been proved as an useful biomarker to predict overall survival in several cancers, such as gastric cancer (12), breast cancer (13), and nasopharyngeal carcinoma (14, 15). Several studies have demonstrated that NPC patients with an elevated pre-treatment NLR had poorer survival (14, 15). The present study aimed to investigate the role of integration of the pre-treatment NLR with the eighth edition of the AJCC staging system for nasopharynx cancer in an endemic region. In addition, an accurate staging system could not only predict prognosis, but also guide clinicians in making treatment decisions. Currently, controversy exists regarding the role of adjuvant chemotherapy after concurrent chemoradiotherapy for NPC (16, 17). Therefore, we also aimed to explore whether the integration of NLR could help stratify who may benefit from the additional adjuvant chemotherapy.

METHODS AND MATERIALS

Patients

A total of 713 patients with NPC were retrospectively analyzed between May 2007 and December 2012. Patients who met the following criteria were included: (1) differentiated or undifferentiated nonkeratinizing NPC; (2) no distant metastases upon diagnosis; (3) pretreatment evaluations, including a complete patient history, physical and neurological examinations, nasopharynx and neck MRI scans, chest X-ray or computed tomography (CT) scans, abdominal ultrasonography scans, and whole-body bone scans; and (4) use of IMRT as the radiotherapy technology. Three patients had keratinizing carcinoma, and all the other patients were diagnosed with nonkeratinizing carcinoma. The median age was 45 years old. A total of 557 patients were male, and 175 were female. Stage classifications were identified according to the 8th edition of the AJCC staging system by two radiation oncologists. If discordance existed between the two radiologists, a third physician's opinion was obtained. The patient characteristics are shown in **Table 1**. Blood routine, including the items of neutrophil and lymphocyte counts, is conducted by automatic blood analyzer before treatment (China, Shenzhen, Mindray BC6900). Considering several studies had demonstrated that NPC patients with an elevated pre-treatment NLR had poorer survival, and the median of pre-treatment NLR of 713 patients was 2.07 (range, 0.63-12.03), so it was chosen as the cut-off. The Ethics Committee of Guangxi Medical University Cancer Hospital approved the study protocol, and informed consent forms were signed by participants. The data were anonymously analyzed, and all the participants' personal information is confidential. The research was performed in accordance with relevant guidelines and regulations.

TABLE 1 | Characteristics of patients with nasopharyngeal carcinoma.

Characteristics	Number of patients (%)
Sex	
male	544 (76.3%)
female	169 (23.7%)
Age, years†	45 (16-86)
KPS	
70-80	274 (38.4%)
90-100	439 (61.6%)
T classification*	
T1	69 (9.7%)
T2	215 (30.2%)
T3	286 (40.1%)
T4	143 (20.1%)
N classification*	
N0	62 (8.7%)
N1	252 (35.3%)
N2	294 (41.2%)
N3	105 (14.7%)
Clinical stage*	
I	16 (2.2%)
II	139 (19.5%)
III	329 (46.1%)
IV A	229 (32.1%)
Neutrophil, k/cc†	4.03 (0.74-14.32)
Lymphocyte, g/L†	1.93 (0.43-5.57)
NLR	
≤2.07	358 (50.2%)
>2.07	355 (49.8%)
Treatment regimens	
IMRT	79 (11.1%)
CCRT	184 (25.8%)
CCRT+AC	331 (46.4%)
IC+CCRT	51 (7.2%)
IC+CCRT+AC	53 (7.4%)
IC+IMRT	8 (1.1%)
IC+IMRT+AC	7 (1.0%)

**The 8th edition American Joint Committee on Cancer staging system; †The median and the range of values; NLR, Neutrophil-to-lymphocyte ratio; IMRT, Intensity modulated radiotherapy; CCRT, Concurrent chemoradiotherapy; IC, Induction chemotherapy; AC, Adjuvant chemotherapy.*

Treatment Strategies

A detailed description of IMRT has been previously published (18). The prescribed dose was 68-74 Gy applied to the primary tumor, 60-71 Gy applied to any involved cervical lymph nodes, 60-66 Gy applied to the high-risk regions, and 54-60 Gy applied to the low-risk regions in 30-32 fractions/6-7 weeks. Those with stage I disease underwent IMRT alone. For patients with stage II-IVb disease, IMRT was administered in combination with a platinum-based chemotherapy regimen.

Follow-Up and Statistical Analysis

Follow-up was conducted from the day of diagnosis to either the day of death or the day of the last follow-up. Patients were evaluated every 3 months during the first two years, every 6 months during the next three to five years, and annually thereafter until death.

Statistical analyses were performed with SPSS software (version 16.0, SPSS Inc., Chicago, IL). The endpoints, including overall survival (OS), distant metastasis-free survival (DMFS), local failure-free survival (LFFS), and failure-free survival (FFS) were calculated using the Kaplan-Meier method, and the differences were assessed with the log-rank test. Multivariate analyses with the Cox proportional hazards model were carried out. The discriminatory performance was evaluated *via* Harrell's concordance index (c-index) (19). The c-index was calculated using the package "rms" (20) in R version 3.5.1 (http://www.r-project.org/). To compare the c-indexes, bootstrap datasets with 1000 repetitions were performed. Recursive partitioning analysis (RPA) for OS was conducted with ordinal T- and N- categories and pre-treatment NLR to derive RPA stages objectively. The RPA algorithm is based on the optimized binary partition of T- or N- categories or NLR, which would result in subgroups with relatively homogeneous survival performance. All P-values were two-sided, and $P \leq 0.05$ was considered statistically significant.

RESULTS

With a median follow-up of 77 months (range, 2-134 months), a total of 171 (24%) patients died, 121 (17%) developed distant metastasis, and 65 (9.1%) developed local recurrence. Univariate analysis showed that patients with a pretreatment NLR > 2.07 had poor OS (HR 1.710 (95%CI 1.257-2.325), P = 0.001), DMFS (HR 1.476 (95%CI 1.029-2.118), P = 0.033), and FFS (HR 1.475 (95%CI 1.125-1.934), P = 0.005) than those with a NLR ≤ 2.07, while no significant difference was found in LFFS (HR 1.194 (95%CI 0.734-2.118), P = 0.475) (**Figure 1**). The univariate analysis also indicated that sex, age (continuous), and T and N classifications were significant prognostic factors for OS. The multivariate analysis revealed that age (continuous), pre-treatment NLR, and T and N classifications were significant factors for OS (details are shown in **Table 2**).

T Classification

The OS and LFFS curves for the T categories are shown in **Figure 2**. Based on the 8th edition staging system, there were significant differences in OS between the T subgroups, except in the comparison of the T1 and T2 classifications (details are shown in **Figure 2A**). However, there only existed a significant difference in LFFS between T4 and the other T categories ($P < 0.05$; **Figure 2B**). When integrated with NLR, a significant difference in OS was found between "T1-2 & NLR ≤ 2.07" and "T1-2 & NLR > 2.07", but no significant differences existed between "T1-2 & NLR > 2.07" and "T3-4 & NLR ≤ 2.07", "T3-4 & NLR ≤ 2.07" and "T3-4 & NLR > 2.07" (**Figure 2C**). Regarding LFFS, significant differences were only observed between "T1-2 & NLR ≤ 2.07" and "T3-4 & NLR ≤ 2.07", "T1-2 & NLR ≤ 2.07" and "T3-4 & NLR > 2.07" (**Figure 2D**). After integration of NLR, the C-index became smaller for both OS and LFFS (details are shown in **Table 3**), which meant that the discriminatory ability was not improved.

N Classification

The OS and DMFS curves for the N subsets are shown in **Figure 3**. Significant differences were found between the N subsets in terms of OS and DMFS for the 8th edition AJCC staging system, except for comparison of the N0 and N1 as well as N2 and N3 classifications (details are shown in **Figures 3A, B**). After integration of NLR, there were significant differences in OS between the updated subgroups except for the comparison of "N0-1 & NLR > 2.07" and "N2-3 & NLR ≤ 2.07" (**Figure 3C**). In terms of DMFS, there were still no significant differences between the "N0-1 & NLR ≤ 2.07" and "N0-1 & NLR > 2.07" subgroups and between the "N2-3 & NLR ≤ 2.07" and "N2-3 & NLR > 2.07" subgroups. Cox multivariate regression analysis showed that the N classifications were independent prognostic indicators of DMFS and OS in the two staging systems ($P < 0.001$). When integrated with NLR, significant improvements in the C-index of OS and DMFS were observed (details are shown in **Table 3**).

Recursive Partitioning Analysis

Recursive partitioning analysis classified NPC patients into eight categories with disparate outcomes for OS (**Figure 4**). Then 5-year overall survival rates in each group were calculated by using the Kaplan-Meier method, with 95.9%, 87.2%, 87.4%, 82.0%, 83.7%, 79.5%, 74.0%, and 67.8% in eight subgroups, respectively. Those with 5-year OS > 90% were classified as the best prognosis group (RPA1), and those with 5-year OS ≤70% were classified as the poor prognosis group (RPA5). Those with 5-year OS > 70%, and ≤80% were identified the intermediate prognosis group (RPA4). Those with 5-year OS > 80%, and ≤90% were identified as the good prognosis group. The good prognosis group consisted of four subgroups, and the 5-year rates of OS were 87.2%, 87.4%, 82.0%, and 83.7%, respectively. Then the good prognosis group was divided into two groups. The two subgroups with 5-year OS of 87.2% and 87.4% were merged into RPA2, and the other two subgroups with 5-year OS of 82.0%, and 83.7% were merged into RPA3 (**Figure 4**). Five-year OS was significantly different between RPA groupings (RPA1 to RPA5: 95.9%, 87.3%, 83.0%, 76.4%, and 67.8%, respectively). **Figure 5** shows the FFS and OS curves for the overall stage and RPA groups. According to the 8th AJCC staging system, significant differences were found between the clinical stages in terms of OS and FFS, except for comparison of stages I and II (details are

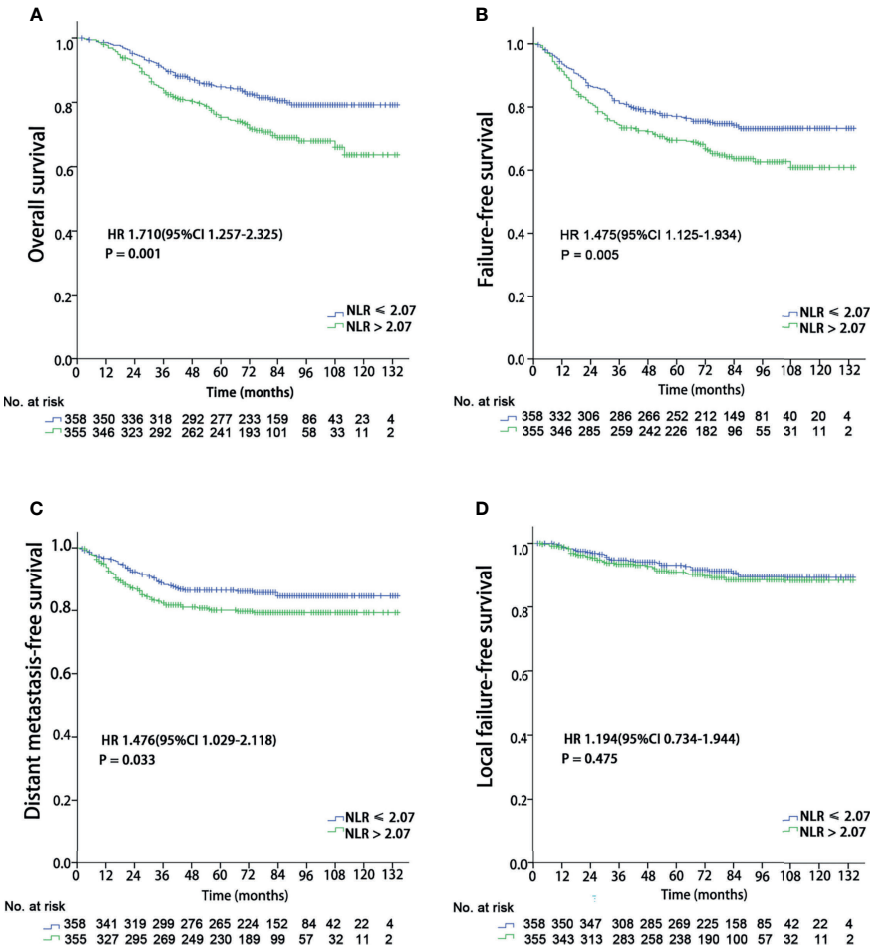

FIGURE 1 | Kaplan–Meier survival curves for 713 patients stratified by the cutoff of NLR. NLR, Neutrophil-to-lymphocyte ratio. **(A)** Overall survival; **(B)** Failure-free survival; **(C)** Distant metastasis failure-free survival; **(D)** Local failure-free survival.

TABLE 2 | Univariate and multivariate analyses for the overall survival using Cox regression model.

Endpoints	Univariate analysis	P	Multivariate analysis	P
	HR (95%CI)		HR (95%CI)	
Sex				
Female *vs* male	0.680 (0.461-1.004)	0.05	0.753 (0.508-1.115)	0.156
Age				
Continuous	1.042 (1.029-1.056)	<0.001	1.047 (1.033-1.062)	<0.001
Chemotherapy				
Yes *vs* No	0.976 (0.612-1.558)	0.919		
T classification				
T3-4 *vs* T1-2	2.490 (1.751-3.540)	<0.001	2.036 (1.422-2.915)	<0.001
N classification				
N2-3 *vs* N0-1	1.849 (1.342-2.547)	<0.001	1.941 (1.398-2.695)	<0.001
NLR				
>2.07 *vs* ≤2.07	1.710 (1.257-2.325)	0.001	1.593 (1.166-2.177)	0.003

HR, Hazard Ratio; NLR, Neutrophil-to-lymphocyte ratio.

shown in **Figures 5A, B**). When using the RPA stages, patients with RPA1 stage had better OS than those with RPA2 stage, but no significant differences were observed between patients with the RPA2 and RPA3 stages, between the RPA3 and RPA4 stages, and between the RPA4 and RPA5 stages (**Figure 5C**). Regarding FFS, significant differences were found between the subgroups, except for the comparisons of the RPA1 and RPA2, RPA2 and RPA3, and RPA3 and RPA4 groups (**Figure 5D**). The

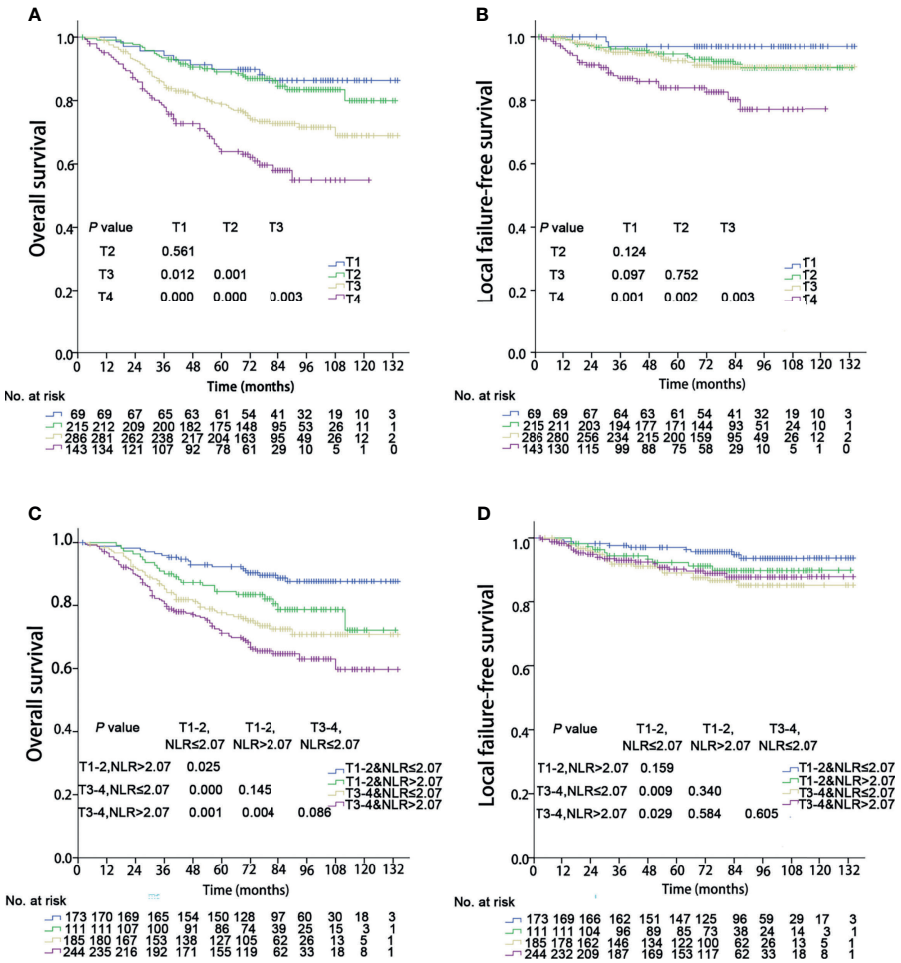

FIGURE 2 | Kaplan–Meier survival curves of 713 patients stratified by the T and T & NLR classifications. NLR, Neutrophil-to-lymphocyte ratio. **(A, C)** Overall survival; **(B, D)** Local failure-free survival.

c-indexes of OS and FFS were not improved when using RPA classifications (details are shown in **Table 4**).

We performed subgroup analyses to explore whether the integration of NLR could help identify who may benefit from the additional adjuvant chemotherapy by comparing concurrent chemoradiotherapy followed by adjuvant chemotherapy *versus* concurrent chemoradiotherapy alone. When using the 8th edition AJCC staging system, no significant benefits of adjuvant chemotherapy were found in any stage groups. For those 206 patients in RPA4, 77.2% (159/206) patients received concurrent chemoradiotherapy alone or concurrent chemoradiotherapy followed by adjuvant chemotherapy. We observed that patients in the RPA 4 group gained significant OS benefits (HR 0.390 (95%CI 0.212-0.716), P = 0.002) and FFS (HR 0.548 (95%CI 0.314-0.958), P = 0.032) from the additional adjuvant chemotherapy (**Figure 6**). However, no significant survival benefits were found for the additional adjuvant chemotherapy to concurrent chemoradiotherapy for other RPA groups. Meanwhile, the value of induction chemotherapy was also investigated. A total of 119 patients (16.7%) received induction chemotherapy, with 9 in RPA 1, 17 in RPA 2, 20 in RPA 3, 34 in RPA 4, and 39 in RPA 5, respectively. Then we compared the efficacy of the treatment regimens with or without induction chemotherapy in RPA 4 and 5 groups. It was found that no survival benefits were gained from induction chemotherapy in both RPA 4 and 5 groups.

DISCUSSION

In the present study, we explored the role of integrating pre-treatment NLR with the 8th edition AJCC staging system. We observed that the integration of NLR could enhance the separate and discriminatory abilities for the N category, but not for the T classification. In addition, it could help identify who may benefit from the additional adjuvant chemotherapy after concurrent chemoradiotherapy.

In a meta-analysis involving 7,031 patients, an increased NLR was related to a poor OS and PFS (PFS) (21), which was consistent with the present study. In another two retrospective

TABLE 3 | Univariate analysis for T and N classifications associated with overall survival, local failure-free survival, and distant metastasis free survival.

	HR (95%CI)	P	C-index		HR (95%CI)	P	C-index	P*
OS				OS				
T1	reference			T1-2&NLR ≤ 2.07	reference			<0.001
T2	1.231 (0.587-2.579)	0.583	0.632	T1-2&NLR>2.07	1.947 (1.054-3.598)	0.033	0.628	
T3	2.409 (1.205-4.815)	0.013	(0.590-0.674)	T3-4&NLR ≤ 2.07	2.803 (1.647-4.772)	<0.001	(0.585-0.671)	
T4	4.119 (2.031-8.353)	<0.001		T3-4&NLR>2.07	3.826 (2.320-6.308)	<0.001		
LFFS				LFFS	0.088			
T1	reference			T1-2&NLR ≤ 2.07	reference			<0.001
T2	2.956 (0.683-12.798)	0.147	0.626	T1-2&NLR>2.07	1.859 (0.755-4.577)	0.177	0.580	
T3	3.259 (0.768-13.832)	0.109	(0.558-0.694)	T3-4&NLR ≤ 2.07	2.666 (1.227-5.796)	0.013	(0.511-0.649)	
T4	7.680 (1.808-32.629)	0.006		T3-4&NLR>2.07	2.299 (1.067-4.953)	0.034		
OS				OS				
N0	reference			N0-1&NLR ≤ 2.07	reference			<0.001
N1	1.245 (0.628-2.468)	0.531	0.593	N0-1&NLR>2.07	2.104 (1.225-3.614)	0.007	0.610	
N2	2.002 (1.035-3.875)	0.039	(0.552-0.635)	N2-3&NLR ≤ 2.07	2.229 (1.329-3.737)	0.002	(0.567-0.653)	
N3	2.810 (1.395-5.663)	0.004		N2-3&NLR>2.07	3.268 (2.003-5.332)	<0.001		
DMFS				DMFS				
N0	reference			N0-1&NLR ≤ 2.07	reference			<0.001
N1	1.551 (0.538-4.472)	0.416	0.640	N0-1&NLR>2.07	1.238 (0.590-2.596)	0.573	0.644	
N2	3.683 (1.339-10.131)	0.012	(0.591-0.689)	N2-3&NLR ≤ 2.07	2.611 (1.411-4.830)	0.002	(0.593-0.694)	
N3	5.549 (1.962-15.697)	0.001		N2-3&NLR>2.07	3.770 (2.098-6.775)	<0.001		

P < 0.05 was considered statistically significant difference between the two c-indexes. HR, Hazard Ratio; NLR, Neutrophil-to-lymphocyte ratio; OS, Overall survival; LFFS, Local failure-free survival; DMFS, Distant metastasis-free survival.*

studies, Liao et al. and Ye et al. also observed that patients with a high NLR had significantly lower PFS and OS (15, 22). What is the potential mechanism by which NLR can affect tumor prognosis? As is well known, the tumor microenvironment (TME) plays a key role in tumorigenesis, proliferation, invasion, and metastasis. As inflammatory markers, neutrophils and lymphocytes are both important components of TME (23, 24). Neutrophils can activate tumor initiation by inducing the formation of reactive oxygen species (ROS), reactive nitrogen species (RNS) and proteases, as well as promoting tumor proliferation (23). In addition, neutrophils can also motivate metastasis formation *via* inhibiting natural killer function and facilitating the extravasation of tumor cells through the secretion of IL1β and matrix metalloproteinases (25). Several studies have reported the potential mechanism why neutrophil correlate with poor prognosis of cancer patients. Wang et al. found that patients with gastric cancer showed a significantly higher neutrophil infiltration in tumors, and the tumor-activated neutrophils fostered immune suppression and disease progression through granulocyte-macrophage colony-stimulating factor-PD-L1 (GM-CSF-PD-L1) pathway (26). In 2021, Kajioka et al. reported that neutrophil extracellular traps (NETs) induced the epithelial to mesenchymal transition in pancreatic cancer cells and thereby promoted their migration and invasion (27). Lymphocyte, including cytotoxic T cells, Th1 helper cells and B cells, can orchestrate tumor cell elimination (24). Therefore, an abundance of lymphocytes may result in poor prognoses. That is to say if patients have higher level of neutrophil and lower level of lymphocyte, their prognoses may be poor.

The peripheral NLR may become an easily measured, cost-effective and reproducible marker associated with clinical practice. However, there still exist some issues that need to be resolved. For example, the cutoff of NLR is not unique in different research institutes, ranging from 2.28 to 5.0 according to the published results (21). It is also unclear whether the level of NLR can be altered to improve prognosis by targeted treatment. Therefore, more studies need to be performed to assess the widespread use of this biomarker.

In the era of precision medicine, heterogeneities among patients require oncologists to integrate other prognostic factors into the TNM staging system. For example, prostatic specific antigen (PSA), as a powerful biomarker for prostate cancer, has been merged into the AJCC staging system to help divide patients into different risk groups (8). The expression levels of estrogen receptors (ER) and progesterone receptors (PR), as well as Her-2 for breast cancer, guide oncologists in predicting prognosis and developing the corresponding therapeutic strategies (9). Our study showed that the integration of NLR could help improve the separation and discriminatory abilities for the N category, but not for T classification. It is urgent to conduct multicenter studies to identify the role of integrating NLR with the TNM staging system for NPC.

Currently, the role of adjuvant chemotherapy (AC) after concurrent chemoradiotherapy (CCRT) for NPC is still unclear. A multicenter randomized controlled trial and a retrospective study with 2,263 patients both showed that the addition of adjuvant chemotherapy to CCRT could not provide significant survival benefits (16, 28). However, a multi-

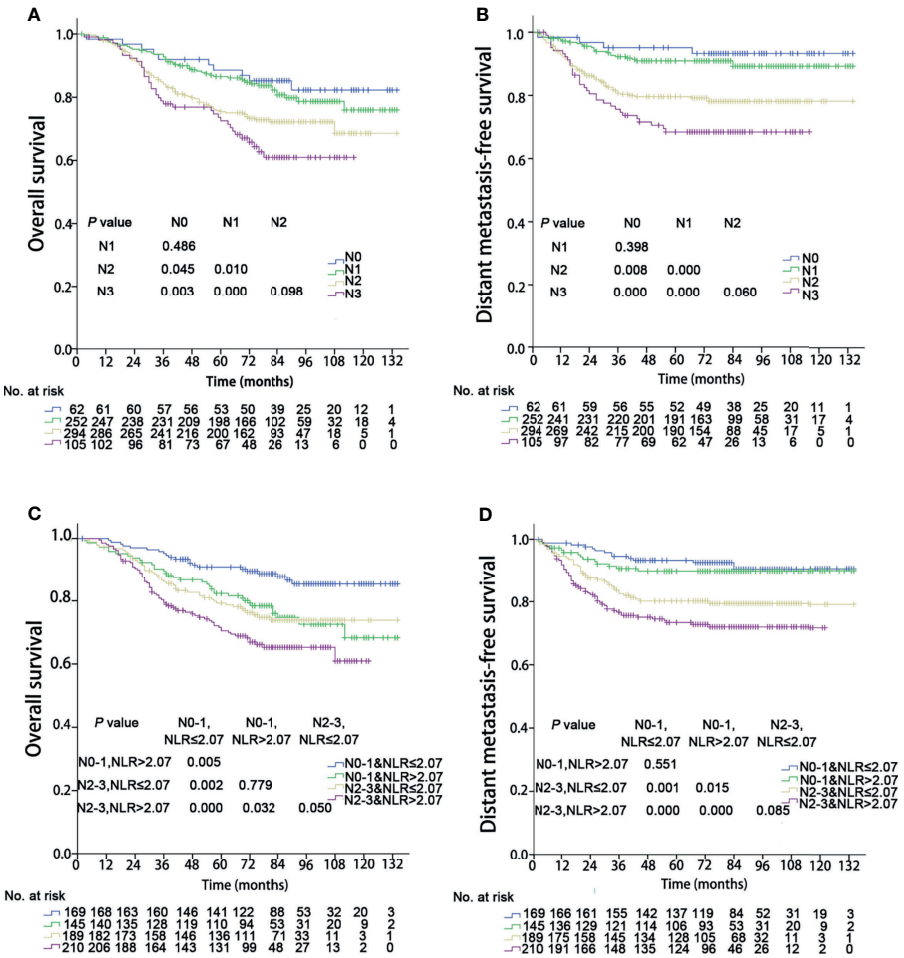

FIGURE 3 | Kaplan–Meier survival curves of 713 patients stratified by the N and N & NLR classifications. NLR, Neutrophil-to-lymphocyte ratio. **(A, C)** Overall survival; **(B, D)** Distant metastasis failure-free survival.

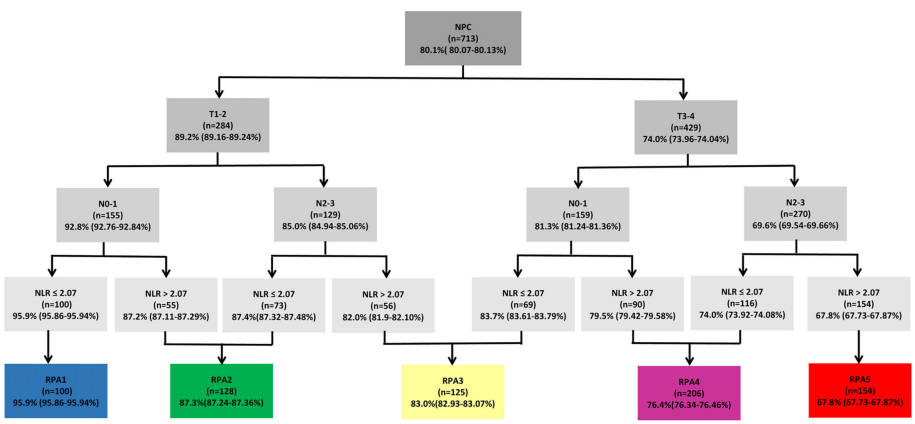

FIGURE 4 | Recursive partitioning analysis for the endpoint of 5-year overall survival of 713 patients, based on the optimized binary partition of T-, N- categories and NLR. RPA, Recursive partitioning analysis; NLR, Neutrophil-to-lymphocyte ratio.

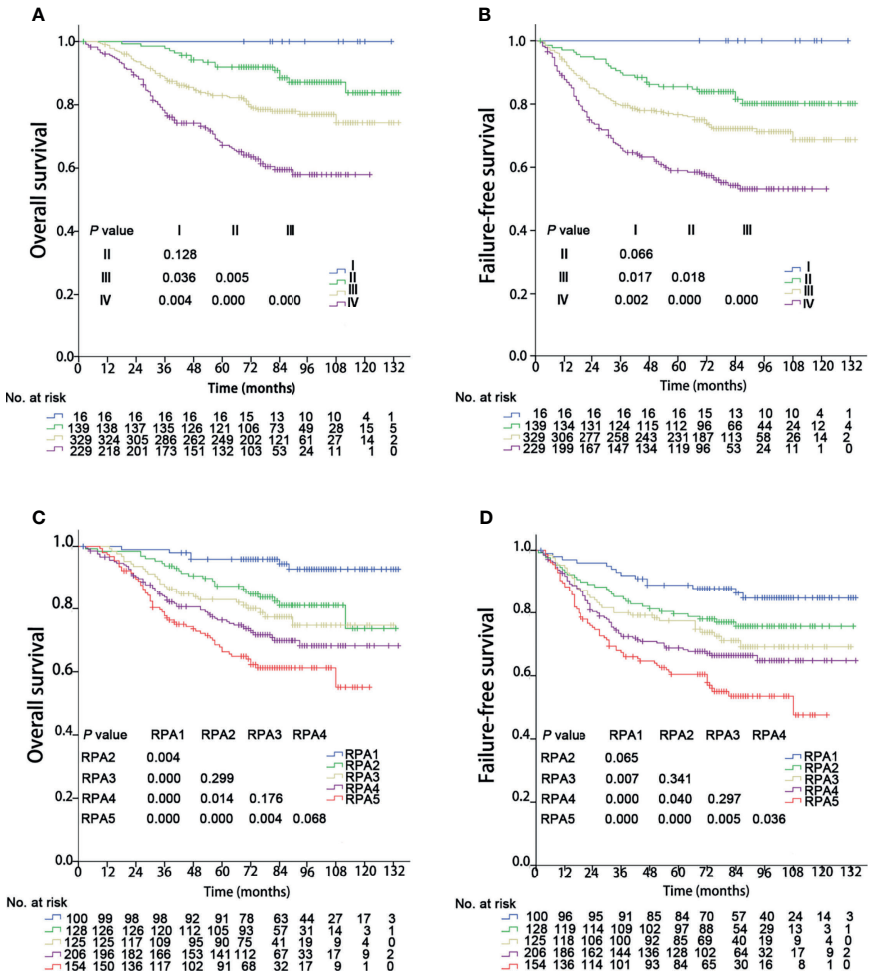

FIGURE 5 | Kaplan–Meier survival curves of 713 patients stratified by the overall stage and RPA groups. RPA, Recursive partitioning analysis. **(A, C)** Overall survival; **(B, D)** Failure-free survival.

TABLE 4 | Univariate analysis for the overall stage and RPA classes associated with overall survival, and failure-free survival.

	HR (95%CI)	P	C-index		HR (95%CI)	P	C-index	P*
OS				OS				
I-II	reference		0.646	RPA 1	reference		0.646	0.863
III	2.396 (1.391-4.128)	0.002	(0.605 - 0.687)	RPA 2	3.268 (1.330-8.032)	0.010	(0.603-0.690)	
IV	4.893 (2.862-8.367)	<0.001		RPA 3	4.337 (1.789-10.516)	0.001		
				RPA 4	5.939 (2.560-13.779)	<0.001		
				RPA 5	8.424 (3.626-19.571)	<0.001		
FFS				FFS				
I-II	reference		0.619	RPA 1	reference		0.611	<0.001
III	1.906 (1.223-2.970)	0.004	(0.583 - 0.656)	RPA 2	1.798 (0.953-3.391)	0.070	(0.572- 0.649)	
IV	3.509 (2.262-5.445)	<0.001		RPA 3	2.280 (1.226-4.240)	0.009		
				RPA 4	2.834 (1.594-5.040)	<0.001		
				RPA 5	4.066 (2.285-7.235)	<0.001		

RPA, Recursive partitioning analysis; P < 0.05 was considered statistically significant difference between the two c-indexes; HR, Hazard Ratio; NLR, Neutrophil-to-lymphocyte ratio; OS, Overall survival; FFS, Failure-free survival.*

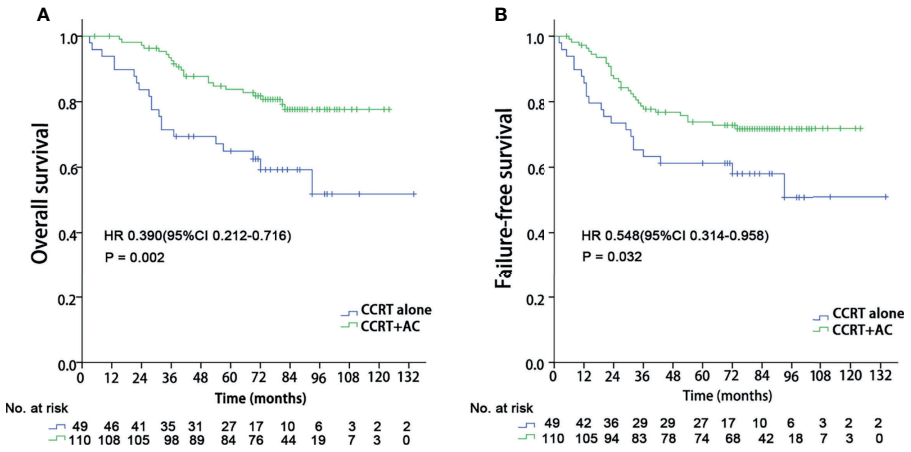

FIGURE 6 | Kaplan–Meier survival curves in the CCRT + AC and CCRT alone arms for patients in the RPA 4 group. CCRT, Concurrent chemoradiotherapy; AC, Adjuvant chemotherapy; RPA, Recursive partitioning analysis; **(A)** Overall survival; **(B)** Failure-free survival.

institutional retrospective study with 380 patients in the CCRT alone arm and 327 patients in the CCRT-AC arm revealed that AC can significantly improve survival (17). In the present study, we observed that patients in the group RPA 4 (T3-4N0-1&NLR>2.07, or T3-4N2-3&NLR ≤ 2.07) may gain a survival benefit from the addition of adjuvant chemotherapy to concurrent chemoradiotherapy. However, the samples in both arms were not large. It is essential to conduct prospective trials with large samples to verify the results.

There are some limitations of the present study. First, as a retrospective study, selection bias may have occurred because patients were included only if they met specific selection criteria. However, these findings can help us design and conduct prospective studies to investigate the truth. Second, the sample size was not large. Third, the patients were from a single hospital, which may result in selection bias. Finally, a set of studies has shown that the presence of Epstein-Barr viral DNA (EBV DNA) in plasma (29) has a significant influence on the prognosis of NPC patients. However, these relevant data are not available for all patients, and plasma EBV DNA assay by RT-PCR (reverse transcription-polymerase chain reaction) is not yet a routine investigation in many centres, especially in low income countries and cities. Additionally, most published studies are based on laboratory-derived test of the individual institute: the lowest detection limit varies widely among different institutions, resulting in variation in false-negative rates and recommended cutoff values (30). Therefore, considering that the updated stage system should have wide popularization and application prospects, we did not include this factor in the analysis.

In summary, the integration of NLR into the 8th edition of the AJCC staging system could significantly improve the separation and discriminatory abilities for N classification, but not for T category. Additionally, it could help stratify patients who may gain a survival benefit from the addition of adjuvant chemotherapy to concurrent chemoradiotherapy. More prospective trials with large samples are essential to verify these results.

DATA AVAILABILITY STATEMENT

The original contributions presented in the study are included in the article/supplementary material. Further inquiries can be directed to the corresponding author.

ETHICS STATEMENT

The studies involving human participants were reviewed and approved by The Ethics Committee of Guangxi Medical University Cancer Hospital. Written informed consent to participate in this study was provided by the participants' legal guardian/next of kin.

AUTHOR CONTRIBUTIONS

X-DZ contributed to conception and design of the study. Z-GL, FZ, K-GL, LH, and FS organized the database. Z-GL and FZ performed the statistical analysis. Z-GL, FZ, and YL wrote the first draft of the manuscript. LL, SQ, B-BY, and YG wrote sections of the manuscript. All authors contributed to manuscript revision, read, and approved the submitted version.

FUNDING

This work was sponsored by grants from the National Natural Science Foundation of China (No. 81760544), Key R&D

Program of Guangxi (AB18221007), Project of Guangxi Medical and Health Appropriate Technology Development and Extension Application (No. S2018001), Guangxi Natural Science Foundation (No. 2020GXNSFBA159002), the Health Commission of Guangxi Zhuang Autonomous Region (No.Z20200333). The funders had no role in study design, data collection and analysis, decision to publish, or preparation of the manuscript.

REFERENCES

1. Petersson F. Nasopharyngeal Carcinoma: A Review. *Semin Diagn Pathol* (2015) 32:54–73. doi: 10.1053/j.semdp.2015.02.021
2. Bray F, Ferlay J, Soerjomataram I, Siegel RL, Torre LA, Jemal A. Global Cancer Statistics 2018: GLOBOCAN Estimates of Incidence and Mortality Worldwide for 36 Cancers in 185 Countries. *CA Cancer J Clin* (2018) 68:394–424. doi: 10.3322/caac.21492
3. Sun Y, Li WF, Chen NY, Zhang N, Hu GQ, Xie FY, et al. Induction Chemotherapy Plus Concurrent Chemoradiotherapy Versus Concurrent Chemoradiotherapy Alone in Locoregionally Advanced Nasopharyngeal Carcinoma: A Phase 3, Multicentre, Randomised Controlled Trial. *Lancet Oncol* (2016) 17:1509–20. doi: 10.1016/S1470-2045(16)30410-7
4. Hong RL, Hsiao CF, Ting LL, Ko JY, Wang CW, Chang JTC, et al. Final Results of a Randomized Phase III Trial of Induction Chemotherapy Followed by Concurrent Chemoradiotherapy Versus Concurrent Chemoradiotherapy Alone in Patients With Stage IVA and IVB Nasopharyngeal Carcinoma-Taiwan Cooperative Oncology Group (TCOG) 1303 Study. *Ann Oncol* (2018) 29:1972–9. doi: 10.1093/annonc/mdy249
5. Ribassin-Majed L, Marguet S, Lee AWM, Ng WT, Ma J, Chan ATC, et al. What Is the Best Treatment of Locally Advanced Nasopharyngeal Carcinoma? An Individual Patient Data Network Meta-Analysis. *J Clin Oncol* (2017) 35:498–505. doi: 10.1200/jco.2016.67.4119
6. Liang ZG, Chen XQ, Niu ZJ, Chen KH, Li L, Qu S, et al. Recommendations for Updating T and N Staging Systems for Nasopharyngeal Carcinoma in the Era of Intensity-Modulated Radiotherapy. *PloS One* (2016) 11:e0168470. doi: 10.1371/journal.pone.0168470
7. Pan JJ, Ng WT, Zong JF, Chan LL, O'Sullivan B, Lin SJ, et al. Proposal for the 8th Edition of the AJCC/UICC Staging System for Nasopharyngeal Cancer in the Era of Intensity-Modulated Radiotherapy. *Cancer* (2016) 122:546–58. doi: 10.1002/cncr.29795
8. Abdel-Rahman O. Assessment of the Prognostic Value of the 8th AJCC Staging System for Patients With Clinically Staged Prostate Cancer; A Time to Sub-Classify Stage IV? *PloS One* (2017) 12:e0188450. doi: 10.1371/journal.pone.0188450
9. Nicolini A, Ferrari P, Duffy MJ. Prognostic and Predictive Biomarkers in Breast Cancer: Past, Present and Future. *Semin Cancer Biol* (2018) 52:56–73. doi: 10.1016/j.semcancer.2017.08.010
10. Thacker N, Bakhshi S, Chinnaswamy G, Vora T, Prasad M, Bansal D, et al. Management of Non-Hodgkin Lymphoma: ICMR Consensus Document. *Indian J Pediatr* (2017) 84:382–92. doi: 10.1007/s12098-017-2318-0
11. Motzer RJ, Jonasch E, Agarwal N, Beard C, Bhayani S, Bolger GB, et al. Testicular Cancer, Version 2.2015. *J Natl Compr Canc Netw* (2015) 13:772–99. doi: 10.6004/jnccn.2015.0092
12. Lieto E, Galizia G, Auricchio A, Cardella F, Mabilia A, Basile N, et al. Preoperative Neutrophil to Lymphocyte Ratio and Lymphocyte to Monocyte Ratio Are Prognostic Factors in Gastric Cancers Undergoing Surgery. *J Gastrointest Surg* (2017) 21:1764–74. doi: 10.1007/s11605-017-3515-x
13. Ethier JL, Desautels D, Templeton A, Shah PS, Amir E. Prognostic Role of Neutrophil-to-Lymphocyte Ratio in Breast Cancer: A Systematic Review and Meta-Analysis. *Breast Cancer Res* (2017) 19:2. doi: 10.1186/s13058-016-0794-1
14. Yao JJ, Zhu FT, Dong J, Liang ZB, Yang LW, Chen SY, et al. Prognostic Value of Neutrophil-to-Lymphocyte Ratio in Advanced Nasopharyngeal Carcinoma: A Large Institution-Based Cohort Study From an Endemic Area. *BMC Cancer* (2019) 19:37. doi: 10.1186/s12885-018-5236-2
15. Liao LJ, Hsu WL, Wang CT, Lo WC, Cheng PW, Shueng PW, et al. Prognostic Impact of Pre-Treatment Neutrophil-to-Lymphocyte Ratio (NLR) in Nasopharyngeal Carcinoma: A Retrospective Study of 180 Taiwanese Patients. *Clin Otolaryngol* (2018) 43:463–9. doi: 10.1111/coa.12992
16. Chen L, Hu CS, Chen XZ, Hu GQ, Cheng ZB, Sun Y, et al. Adjuvant Chemotherapy in Patients With Locoregionally Advanced Nasopharyngeal Carcinoma: Long-Term Results of a Phase 3 Multicentre Randomised Controlled Trial. *Eur J Cancer* (2017) 75:150–8. doi: 10.1016/j.ejca.2017.01.002
17. Kim YS, Ahn YC, Lee CG, Cho KH, Moon SH, Wu HG, et al. The Role of Adjuvant Chemotherapy After Definitive Chemoradiation Therapy in Locoregionally Advanced Nasopharyngeal Carcinoma in a Non-Endemic Area: Multi-Institutional Retrospective Study Using Propensity Score Matching Analysis. *Int J Radiat Oncol Biol Phys* (2018) 100:1326. doi: 10.1016/j.ijrobp.2017.12.054
18. Liang ZG, Chen XQ, Lin GX, Yu BB, Chen KH, Zhong QL, et al. Significant Survival Benefit of Adjuvant Chemotherapy After Concurrent Chemoradiotherapy in Locally Advanced High-Risk Nasopharyngeal Carcinoma. *Sci Rep* (2017) 7:41449. doi: 10.1038/srep41449
19. Harrell FEJr., Lee KL, Mark DB. Multivariable Prognostic Models: Issues in Developing Models, Evaluating Assumptions and Adequacy, and Measuring and Reducing Errors. *Stat Med* (1996) 15:361–87. doi: 10.1002/(sici)1097-0258(19960229)15:4<361::aid-sim168>3.0.co;2-4
20. Rms E F C.OMMAJ.R.X.X.X H. *Regression Modeling Strategies. R Package Version 5.1-2*. Available at: http://biostat.mc.vanderbilt.edu/wiki/Main/RmS (Accessed January 06, 2018).
21. Yang S, Zhao K, Ding X, Jiang H, Lu H. Prognostic Significance of Hematological Markers for Patients With Nasopharyngeal Carcinoma: A Meta-Analysis. *J Cancer* (2019) 10:2568–77. doi: 10.7150/jca.26770
22. Ye L, Oei RW, Kong F, Xu T, Shen C, Wang X, et al. Prognostic Values of Hematological Biomarkers in Nasopharyngeal Carcinoma Patients Treated With Intensity-Modulated Radiotherapy. *Eur Arch Otorhinolaryngol* (2018) 275:1309–17. doi: 10.1007/s00405-018-4956-x
23. Ocana A, Nieto-Jimenez C, Pandiella A, Templeton AJ. Neutrophils in Cancer: Prognostic Role and Therapeutic Strategies. *Mol Cancer* (2017) 16:137. doi: 10.1186/s12943-017-0707-7
24. Taube JM, Galon J, Sholl LM, Rodig SJ, Cottrell TR, Giraldo NA, et al. Implications of the Tumor Immune Microenvironment for Staging and Therapeutics. *Mod Pathol* (2018) 31:214–34. doi: 10.1038/modpathol.2017.156
25. Spiegel A, Brooks MW, Houshyar S, Reinhardt F, Ardolino M, Fessler E, et al. Neutrophils Suppress Intraluminal NK Cell-Mediated Tumor Cell Clearance and Enhance Extravasation of Disseminated Carcinoma Cells. *Cancer Discov* (2016) 6:630–49. doi: 10.1158/2159-8290.cd-15-1157
26. Wang TT, Zhao YL, Peng LS, Chen N, Chen W, Lv YP, et al. Tumour-Activated Neutrophils in Gastric Cancer Foster Immune Suppression and Disease Progression Through GM-CSF-PD-L1 Pathway. *Gut* (2017) 66:1900–11. doi: 10.1136/gutjnl-2016-313075
27. Kajioka H, Kagawa S, Ito A, Yoshimoto M, Sakamoto S, Kikuchi S, et al. Targeting Neutrophil Extracellular Traps With Thrombomodulin Prevents Pancreatic Cancer Metastasis. *Cancer Lett* (2021) 497:1–13. doi: 10.1016/j.canlet.2020.10.015
28. Liu LT, Chen QY, Tang LQ, Guo SS, Guo L, Mo HY, et al. Neoadjuvant or Adjuvant Chemotherapy Plus Concurrent CRT Versus Concurrent CRT Alone in the Treatment of Nasopharyngeal Carcinoma: A Study Based on EBV DNA. *J Natl Compr Canc Netw* (2019) 17:703–10. doi: 10.6004/jnccn.2018.7270
29. Huang CL, Sun ZQ, Guo R, Liu X, Mao YP, Peng H, et al. Plasma Epstein-Barr Virus DNA Load After Induction Chemotherapy Predicts Outcome in Locoregionally Advanced Nasopharyngeal Carcinoma. *Int J Radiat Oncol Biol Phys* (2019) 104:355–61. doi: 10.1016/j.ijrobp.2019.01.007
30. Lee AWM, Lee VHF, Ng WT, Strojan P, Saba NF, Rinaldo A, et al. A Systematic Review and Recommendations on the Use of Plasma EBV DNA

for Nasopharyngeal Carcinoma. *Eur J Cancer* (2021) 153:109–22. doi: 10.1016/j.ejca.2021.05.022

Conflict of Interest: The authors declare that the research was conducted in the absence of any commercial or financial relationships that could be construed as a potential conflict of interest.

Publisher's Note: All claims expressed in this article are solely those of the authors and do not necessarily represent those of their affiliated organizations, or those of the publisher, the editors and the reviewers. Any product that may be evaluated in this article, or claim that may be made by its manufacturer, is not guaranteed or endorsed by the publisher.

frontiers in Oncology

ORIGINAL RESEARCH
published: 16 November 2021
doi: 10.3389/fonc.2021.769665

Identification of Prognostic Biomarkers Originating From the Tumor Stroma of Betel Quid-Associated Oral Cancer Tissues

*Yi-Hong Liu[1,2], Yu-Lian Chen[2], Ting-Yu Lai[2,3], Ying-Chieh Ko[2], Yu-Fu Chou[4], Peir-Rong Chen[4], Jenn-Ren Hsiao[5], Jang-Yang Chang[2,6], Shine-Gwo Shiah[2], Jeng-Woei Lee[7], Jia-Ling Yang[1] and Su-Fang Lin[2]**

[1] Institute of Biotechnology, National Tsing Hua University, Hsinchu, Taiwan, [2] National Institute of Cancer Research, National Health Research Institutes, Miaoli County, Taiwan, [3] Institute of Bioinformatics and Structural Biology, National Tsing Hua University, Hsinchu, Taiwan, [4] Department of Otolaryngology, Tzu Chi University Hospital, Hsinchu, Taiwan, [5] Department of Otolaryngology, Head and Neck Collaborative Oncology Group, National Cheng Kung University Hospital, College of Medicine, National Cheng Kung University, Tainan, Taiwan, [6] Institute of Biotechnology and Pharmaceutical Research, National Health Research Institutes, Miaoli County, Taiwan, [7] Department of Life Sciences, Tzu Chi University, Hualien, Taiwan

OPEN ACCESS

Edited by:
Shiyu Song,
Virginia Commonwealth University Health System, United States

Reviewed by:
Lin Wang,
Peking University Hospital of Stomatology, China
Marco Mascitti,
Marche Polytechnic University, Italy

***Correspondence:**
Su-Fang Lin
sflin@nhri.edu.tw

Specialty section:
This article was submitted to Head and Neck Cancer, a section of the journal Frontiers in Oncology

Received: 02 September 2021
Accepted: 29 October 2021
Published: 16 November 2021

Citation:
Liu Y-H, Chen Y-L, Lai T-Y, Ko Y-C, Chou Y-F, Chen P-R, Hsiao J-R, Chang J-Y, Shiah S-G, Lee J-W, Yang J-L and Lin S-F (2021) Identification of Prognostic Biomarkers Originating From the Tumor Stroma of Betel Quid-Associated Oral Cancer Tissues. Front. Oncol. 11:769665. doi: 10.3389/fonc.2021.769665

Background: Partial epithelial-mesenchymal transition (p-EMT) is a distinct clinicopathological feature prevalent in oral cavity tumors of The Cancer Genome Atlas. Located at the invasion front, p-EMT cells require additional support from the tumor stroma for collective cell migration, including track clearing, extracellular matrix remodeling and immune evasion. The pathological roles of otherwise nonmalignant cancer-associated fibroblasts (CAFs) in cancer progression are emerging.

Methods: Gene set enrichment analysis was used to reveal differentially enriched genes and molecular pathways in OC3 and TW2.6 xenograft tissues, representing mesenchymal and p-EMT tumors, respectively. R packages of genomic data science were executed for statistical evaluations and data visualization. Immunohistochemistry and Alcian blue staining were conducted to validate the bioinformatic results. Univariate and multivariate Cox proportional hazards models were performed to identify covariates significantly associated with overall survival in clinical datasets. Kaplan–Meier curves of estimated overall survival were compared for statistical difference using the log-rank test.

Results: Compared to mesenchymal OC3 cells, tumor stroma derived from p-EMT TW2.6 cells was significantly enriched in microvessel density, tumor-excluded macrophages, inflammatory CAFs, and extracellular hyaluronan deposition. By translating these results to clinical transcriptomic datasets of oral cancer specimens, including the Puram single-cell RNA-seq cohort comprising ~6000 cells, we identified the expression of stromal *TGFBI* and *HYAL1* as independent poor and protective biomarkers, respectively, for 40 Taiwanese oral cancer tissues that were all derived from betel quid users. In The Cancer Genome Atlas, *TGFBI* was a poor marker not only for head and neck

cancer but also for additional six cancer types and *HYAL1* was a good indicator for four tumor cohorts, suggesting common stromal effects existing in different cancer types.

Conclusions: As the tumor stroma coevolves with cancer progression, the cellular origins of molecular markers identified from conventional whole tissue mRNA-based analyses should be cautiously interpreted. By incorporating disease-matched xenograft tissue and single-cell RNA-seq results, we suggested that *TGFBI* and *HYAL1*, primarily expressed by stromal CAFs and endothelial cells, respectively, could serve as robust prognostic biomarkers for oral cancer control.

Keywords: prognostic biomarkers, oral cancer, partial epithelial-mesenchymal transition (p-EMT), tumor stroma, myofibroblastic CAF (myCAF), inflammatory CAF (iCAF), hyaluronidase

INTRODUCTION

In Taiwan, the population of betel quid users significantly declined *via* a successful nationwide oral cancer screening program initiated 22 years ago. However, the 5-year survival rate (~ 56%), death ranking in all cancers (fourth for males, sixth for all), and death of middle age (60 as male median) have remained serious concerns in recent years (1). In addition, a retrospective study indicated that approximately one-third of oral cancer patients had local recurrence (34.6%, 146/422), and approximately one-fifth of 5-year survivors still experienced recurrence (18.1%, 23/127) (2). These data prompted local researchers to devote more efforts to encouraging hesitant patients for curative surgery (3), setting optimal measures for adjuvant radiotherapy (50–60 Gy) (4) and adequate surgical margins (≥ 5 mm for good overall survival) (5), among others. Regrettably, molecular biomarkers that can reliably forecast oral cancer prognosis are still unavailable.

In tumor biology, partial epithelial-mesenchymal transition (p-EMT), a.k.a. hybrid E/M status, EMT continuum or EMT spectrum, is referred to as varied intermediate stages where epithelial cells dedifferentiate to their mesenchymal counterparts (6). In contrast to fully mesenchymal cancer cells that invade alone, p-EMT cells migrate collectively and directionally in the tumor stroma, notably angiolymphatic and perineural invasions. During cluster advancement, intercellular adherent junctions and cadherins are responsible for multicellular integrity and cell-cell coordination; extracellular matrix metalloproteinases (MMPs) and basement membrane type IV collagens are essential for track clearing and secondary extracellular matrix remodeling, respectively (7).

Previously, Puram et al. revealed the ecosystems of ~6,000 cells from 18 treatment-naïve oral cancer specimens, including 5 matched lymph node metastases, by using high-resolution single-cell RNA sequencing (scRNA-seq). Their results indicated that greater than 70% of oral cavity tumors in the cancer genome atlas (TCGA) are malignant-basal type, which displays either EMT or p-EMT as hallmarks (8). Subsequent experiments using quantitative immunohistochemistry assays (PDPN, LAMB3, LAMC2) further revealed that p-EMT is statistically associated with nodal metastasis and perineural invasion in 99 primary oral cancer tissues, providing p-EMT as a useful indicator for decision-making intraoperatively (e.g., N0 neck dissection) or postoperatively (e.g., adjuvant therapy) (9).

Independently, our prior study showed that DDR1, COL4A5, COL4A6 and PDPN are statistically associated with angiolymphatic invasion in matched tumor-adjacent normal tissues from 40 Taiwanese oral cancer patients. In addition, inhibition of DDR1 kinase activity in p-EMT oral cancer cells (TW2.6) disrupted cell cohesiveness in a 2D culture, reduced spheroid invasion in a collagen gel matrix, and suppressed angiolymphatic invasion in xenograft tissues (10). It is worth noting that compared to a mesenchymal subtype (OC3) that has a similar growth rate and clonogenicity *in vitro*, p-EMT TW2.6 repeatedly grew faster (e.g., 32 *vs.* 81 days to reach 500 mm^3) in immunodeficient mice (NOG) despite their tumor-bearing rates were similar (11).

The tumor stroma is regarded as the nonmalignant part of a tumor that is interconnected by extracellular matrices (ECMs) with infiltrated immune cells, vascular or lymphatic vessels, and cancer-associated fibroblasts (CAFs). In head and neck cancer, tumor-stroma interactions, including tumor budding and tumor-stroma ratio, have emerged as powerful clinicopathological predictors for tumor aggression and patient survival (12–14). CAFs gained their name through the finding that activated fibroblasts proliferate and accelerate the growth of several epithelial tumors during malignant progression, a phenomenon reminiscent of wound repair and fibrosis (15, 16). Importantly, the Sahai Lab demonstrated that stromal fibroblasts are required for guiding collective cancer cell invasion of squamous cell carcinoma in an organotypic culture model (17). In addition, scRNA-seq methodology has explicitly revealed the presence of two functionally discrete CAF subtypes in clinical samples, designated myofibroblastic (myCAF) and inflammatory (iCAF) (18–22). Of importance, both variants coevolve with tumor progression in which iCAFs seemed to precede myCAFs (21, 23).

In conventional bulk transcriptomic analysis, tumor- and stroma-derived transcripts are admixed, which greatly limits precise molecular stratification and cell type-driven therapies (8, 24, 25). To circumvent this inherent ambiguity, various computational pipelines were developed to infer tumor-infiltrated stromal components in a given tissue, including ESTIMATE (26), CIBERSORTx (27), and TIMER (28).

Alternatively, an RNA-seq-based hypothesis-free workflow, namely, to extract the human and the mouse reads from patient-derived xenograft tissues, followed by composite transcriptomic analysis of tumor (human) and stroma (mouse) interactions, has been established recently (29–31).

Along the same vein, our prior results showed that the stroma of mesenchymal OC3 tumors harbored a statistically higher extent of mouse fibroblasts than p-EMT TW2.6 tumors. By translating the most significantly expressed gene matrix into clinical datasets of oral cancer tissues, we showed that the summed expression of *FN1*, *TGFB2*, *TGFBR2*, and *TGFBI*, dubbed the CAF index, is a poor indicator of overall survival for oral cancer (n=40) and the PANCAN (n=9,356) cohorts (11). Here, we continued to investigate the molecular interactions between tumor cells and stromal components in p-EMT TW2.6 tumors.

MATERIALS AND METHODS

Cell Culture, Animal Experiment, and mRNA-Seq Analysis of Xenograft Tissues

Please refer to prior study for details (11). Briefly, CGHNC8, C9, K2, K6 (32), OC3 (33), OEC-M1 (34), and TW2.6 (35) were kindly provided by researchers at distinct institutions in Taiwan. OC3 and TW2.6 were selected for two independent animal studies. We measured the tumor size and mouse weight twice a week. For Exp1, all tumors were collected on day 68. For Exp2, to obtain tumors with ~500 mm^3 in size, tumors of TW2.6-NOG and OC3-NOG were collected on day 32 and day 81, respectively. Total RNAs of each cell line and xenograft tissue were extracted by TRIzol® reagent (Invitrogen Life Technologies, Carlsbad, CA, USA), cleaned up by RNeasy column (Qiagen, Hilden, Germany), and subjected to an Agilent Bioanalyzer (Agilent, Santa Clara, CA, USA) for RNA Integrity Number (RIN) assessment. Only samples that had an RIN > 7 were selected for mRNA amplification and sequencing (stranded paired-end, Illumina platform, San Diego, CA, USA).

Antibodies

Anti-Pecam1 (ab28364) was purchased from Abcam (Cambridge, UK); anti-Adgre1 (#70076S) was from Cell Signaling (Danvers, MA, USA).

Immunohistochemical (IHC) Staining

Sections were dewaxed, rehydrated, and incubated with Trilogy™ (Cell Marque, Rocklin, CA, USA) (10 mM citrate buffer, pH 6.0 for Adgre1) at 121°C for 10 min to unmask antigens. At room temperature (RT), the slides were immersed in 3% hydrogen peroxide for 15 min to quench endogenous peroxidase activity followed by 1% bovine serum albumin for 60 min to block nonspecific antigenic sites. Slides were incubated with indicated primary antibodies at 4°C overnight (Pecam1, 1:100, Adgre1, 1:1500). After washing with 1X TBS containing 0.05% Tween 20, slides were incubated with horseradish peroxidase-conjugated secondary antibodies and developed by chromogen diaminobenzidine using the DakoReal™ EnVision™ kit (#K5007, DAKO, Glostrup, Denmark). All slides were counterstained with Mayer's hematoxylin and scanned by a Pannoramic MIDI scanner (3DHISTECH, Budapest, Hungary).

Alcian Blue Staining

Alcian blue staining kit (ab150662, Abcam, Cambridge, UK) was used to detect hyaluronan deposition in the xenograft tissues according to the manufacturer's instruction. Briefly, dewaxed and rehydrated FFPE tissue sections were incubated with Alcian Blue Solution for 30 min at RT, slides were counterstained with Nuclear Fast Red Solution for 5 min at RT and scanned by a Pannoramic MIDI scanner (3DHISTECH).

Quantitation of FFPE Scanned Images

To quantitate the immunostaining of Pecam1, Adgre1, and Alcian blue staining in the xenograft tissues, scanned images at 100× magnification were digitized and quantitated by using ImageJ plugged-in with the *Immunohistochemistry Image Analysis Toolbox* (v1.40p) (NIH, Bethesda, MD, USA). Quantitation results were visualized by R package *ggplot2* (v3.3.3). Statistical differences between OC3 and TW2.6 groups were evaluated by two-sample t-test of means (*compare_means*), as denoted in each plot.

Bioinformatic Analyses

Cell line dataset (GSE150469): human reference genome (hg19) aligned reads for individual genes (n=21,916) were used to compute expression values in transcripts per kilobase million (TPM) by using *Cufflinks* (v2.1.1). R *pheatmap* (v1.0.12) was used to visualize the relative expression levels of indicated genes in each cell line. Xenograft tissue dataset (GSE149496): as described previously (11), R *XenofilteR* (v1.8) processed human (hg38) and mouse (mm10) aligned reads for individual genes were used to perform gene quantification in TPM values. The resulting gene numbers for human and mouse are 17,759 and 16,374, respectively. In the exploratory analysis, R package *limma* (v3.40.6) was used to compute differentially expressed genes followed by *Volcano* plots for visualization. To identify biological pathways enriched in the OC3- and TW2.6 tumor stroma, the mouse expression matrix was subjected to gene set enrichment analysis (GSEA) (36). Enrichment was considered significant when false discovery rate (FDR) was less than 5%. R *ggcorrplot* (v0.1.3) was used to calculate and visualize the correlation matrix comprising genes of interest. The *Pearson* correlation coefficient was computed; p-value < 0.05 was considered significant. R *ggplot2* (v3.3.3) was used to visualize the relative expression levels of indicated genes in the OC3- and TW2.6 stroma. Unpaired two-sample t-test of means was applied to evaluate statistical differences; p-value < 0.05 was considered significant. R *pheatmap* (v1.0.12) was used to visualize the relative expression levels of indicated genes in each tissue. *In silico* enumeration of cell fractions was conducted by using CIBERSORTx according to its online documentation of which the 'single cell RNA-seq HNSCC' and 'LM 22' were used as signature matrices, respectively (27). Puram scRNA-seq dataset (GSE103322): the raw expression matrix was acquired from the

UCSC Cell Browser portal. Expression values (TP100K) were normalized, scaled, and log-transformed by using R *Seurat* (v4.0.3) (37). *DotPlot* was used to visualize the average expression and fraction of indicated genes across eleven cell types comprising 5,902 cells. NCKU-OrCA-40TN dataset (GSE37991): this normalized microarray dataset comprises 18,047 genes for further analysis. R *ggcorrplot* was used to calculate and visualize the correlation matrix composed of 20 selected stromal genes. The *Pearson* correlation coefficient was computed; p-value < 0.05 was considered significant. R *survival* (v3.2-7) was used to assess the univariate and multivariate Cox proportional hazards of indicated clinical features and genes. The Cancer Genome Atlas (TCGA) datasets: for each indicated cancer type, the expression matrix of 20 stromal genes and associated clinical information were acquired from the UCSC Xena platform (38), followed by univariate Cox proportional hazards assessment and dichotomized Kaplan–Meier overall survival curves prediction by using R *survival* (v3.2-7).

RESULTS

Higher Microvessel Density Was Detected in the Mouse Stroma of the p-EMT TW2.6 Tumors

A recent consensus statement of epithelial-mesenchymal transition (EMT) research reiterated the importance of associating cellular characteristics, rather than the expression of a single or a small set of molecular markers, with EMT phenotypes (6). To comply with these guidelines, we inspected the expression levels of core EMT transcription factors, p-EMT hallmarks, and canonical epithelial markers and mesenchymal regulators (6, 9, 10, 39, 40) in a set of seven Taiwanese cell lines derived from the oral cavity. Among these, while the oral cancer cell line OC3 has the highest mesenchymal propensity, TW2.6 and OEC-M1 are hypothetically p-EMT cells since they maintain both epithelial and mesenchymal genes (**Figures 1A, B**). Indeed, we demonstrated that TW2.6, but not OC3 or OEC-M1, displayed p-EMT multicellular characteristics *in vitro* and *in vivo* (10). In addition, mesenchymal OC3 repeatedly grew slower and smaller than its p-EMT TW2.6 counterpart *in vivo* [**Figure 1C** and ref (11)], a phenomenon consistent with one prior study in that head and neck cancer tissues of the inflammatory mesenchymal subtype had a better prognosis (24).

Next, exploratory analysis of differentially expressed genes (DEGs) in the OC3 and TW2.6 xenograft tissues revealed that (1) compared to the OC3 cells expressing various innate immunity responsive genes, TW2.6 cells expressed MYC and E2F targets involved in cell proliferation and cell adhesion (**Supplementary Figure 1A**); (2) compared to the OC3 stroma harboring various extracellular matrix (ECM)- and TGFβ axis-related transcripts, the TW2.6 stroma was characterized by proangiogenic factors and immune-related genes. Gene set enrichment analysis (GSEA) also confirmed that while the epithelial-mesenchymal transition hallmark is uniquely enriched in the OC3 stroma, angiogenesis and immune-related molecular processes are recurrently detected in the TW2.6 stromal compartment (**Supplementary Figure 1B**).

To validate that the p-EMT TW2.6 stroma had higher angiogenesis processes than the OC3 group, we first performed correlational analysis of stromal *Pecam1* expression, a microvessel density surrogate, with that of each well-established proangiogenic and endothelial index gene recently established in > 10,000 human tumors (41). The results indicated that the expression of tumor cell-derived *VEGFA*, *IGFBP3*,

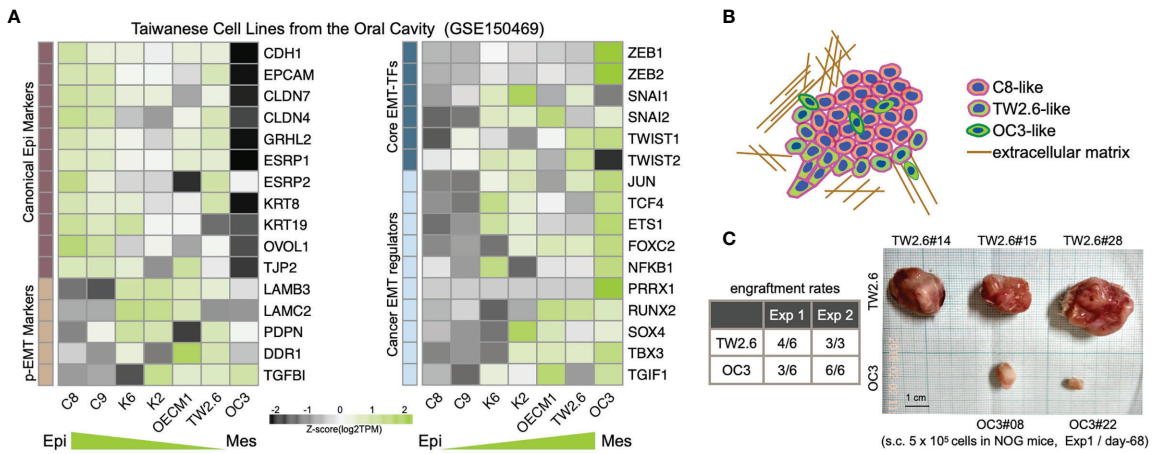

FIGURE 1 | Molecular and tumorigenic features of the mesenchymal OC3 and p-EMT TW2.6 oral cancer cell lines. **(A)** Transcriptomic heatmaps of epithelial-mesenchymal transition (EMT)-related genes in five oral cancer cell lines (C8, C9, TW2.6, OECM1, OC3) and two HPV 16-E6/E7 immortalized oral keratinocyte lines (K2, K6). Epi, epithelial; Mes, mesenchymal; p-EMT, partial EMT. **(B)** A hypothetical drawing of an *in vivo* tumor tissue admixed with C8-, TW2.6- and OC3-like cells. **(C)** Engraftment rates derived from the first experiment (Exp 1) were determined at Day 68 after cell injection. In the second experiment (Exp 2), to reach a tumor mass of similar size (~ 500 mm^3), Day 32 and Day 81 were used as sacrifice times for TW2.6 and OC3, respectively (11).

EFNA1, *EFNB1*, *IGF2*, *PDGFA* and stroma-derived *Angpt2*, *Cdh5*, *Esam*, *Esm1*, *Icam2*, and *Tie1* was statistically correlated with that of *Pecam1* (**Figure 2A**) and elevated in p-EMT TW2.6 tumors (**Figure 2B**). In parallel, immunohistochemistry using a *Pecam1* antibody not only verified significantly increased vascular densities but also prominent angiolymphatic invasions in the p-EMT TW2.6 tissues compared to their mesenchymal OC3 counterparts (**Figure 2C**). Taken together, these results strongly suggest that a higher blood supply from the tumor stroma might contribute to fostering better growth of p-EMT TW2.6 cells *in vivo*.

Tumor Cell-Excluded Macrophages Were Detected in p-EMT TW2.6 Tumors

The other prominent expression feature enriched in the TW2.6 stroma is immune-related molecular signatures, including various cytokines and chemokines (e.g., *Il6*, *Cxcl9*, *Cxcl10*, *Cxcl12*). At first, this seemed perplexing since prior results showed that stronger innate immunity was present in OC3 tumor cells (11). To resolve this confusion, we performed *in silico* enumeration of cell fractions available at the CIBERSORTx portal (27). We first employed 'scRNA-seq HNSCC' as a signature matrix, since both OC3 and TW2.6 cells are derived from the oral cavity. As expected, while no significant difference was detected in the tumor compartment (primarily consisting of 'malignant' cells), the 'fibroblast' cell fraction was significantly higher in the OC3 stroma than in the TW2.6 stroma, which is consistent with our prior results (11) (**Supplementary Figures 2A, B**). Importantly, the constituents of other immune cell populations did not differ significantly between the two groups. Alternatively, using LM22, the default signature matrix comprising cell type-specific genes derived from 22 leukocytes revealed two immune populations, i.e., 'Macrophage-M1' and 'Tγδ', were statistically elevated in the TW2.6 stroma. Further delineation of hallmark genes comprising each LM22 cell type revealed that instead of authentic immune cell markers, increased expression of stromal *Cxcl9*, *Cxcl10*, *Cxcl11* (Macrophage-M1) and *Ccl5* (Tγδ) were likely to be the leading genes contributing to the statistical enrichments (**Supplementary Figures 2C, D**).

Given that 'macrophage' represents the major (57.2 ± 6.7%) immune cell type residing in the host stroma by CIBERSORTx

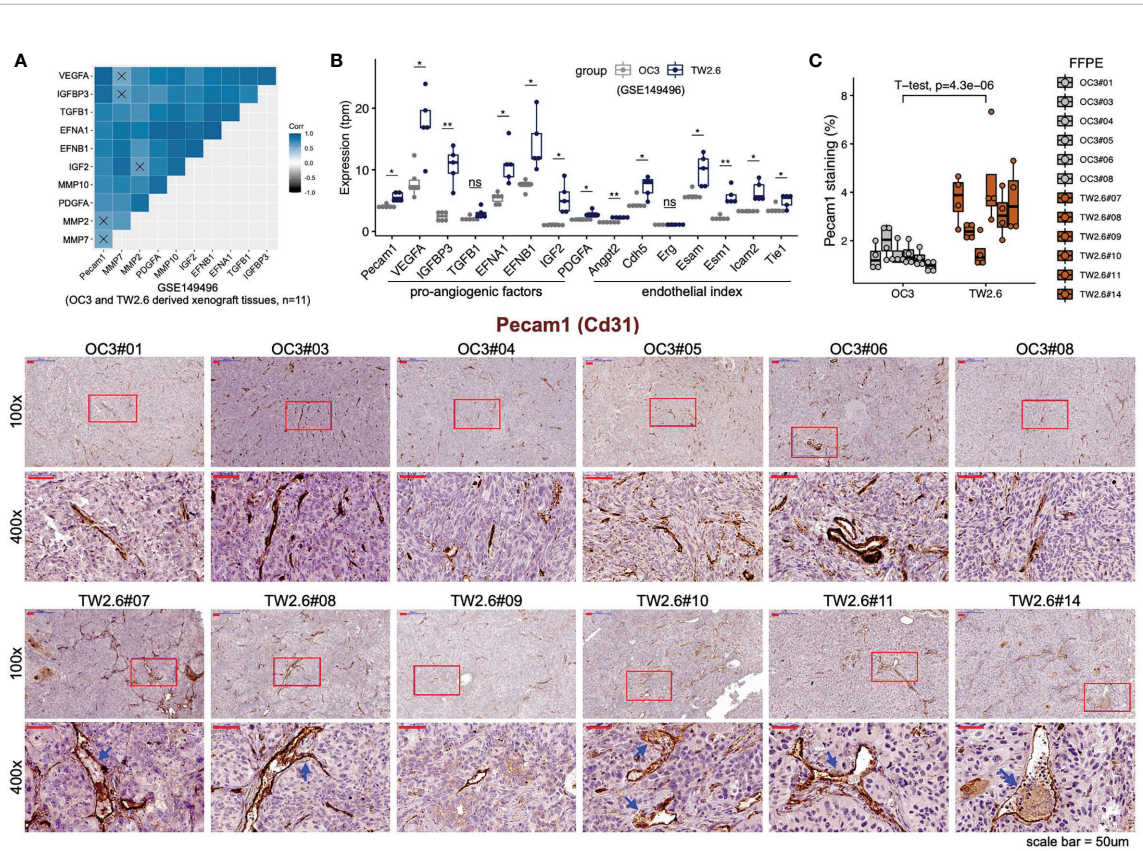

FIGURE 2 | Statistical enrichment of microvessel density in the p-EMT TW2.6 tumor stroma. **(A)** Correlational expression matrix of stromal *Pecam1* and indicated proangiogenic genes in graft tumors (OC3, n=6; TW2.6, n=5). Crosses (×) indicate $p > 0.05$. **(B)** Box plots showing the expression of *Pecam1*, proangiogenic, and endothelial index (41) genes in xenograft tissues. Two-sample t-tests of means were used to evaluate significant differences. *$p < 0.05$, **$p < 0.01$, ns, not significant. **(C)** Quantitation (mean ± SEM of four 100x magnification fields for each section) and representative images of the indicated tissue sections stained for murine Pecam1 (brown). The p value of two-sample t-test of means is denoted. Blue arrowheads denote angiolymphatic invasions (ALIs) only detected in the TW2.6 tumors, a phenomenon consistent with our prior study (10). Note that TW2.6-NOG11 was not included in RNA-seq analysis.

analysis, immunohistochemistry using an antibody against the panmacrophage marker Adgre1 (F4/80) was performed to visualize the infiltration of macrophages in each tumor section. Unexpectedly, the spatial locations of macrophages were significantly different between the OC3 and TW2.6 groups. In the majority of OC3 tissues, the tumor cells are interdigitated with irregular Adgre1-positive macrophages and are accompanied by high staining backgrounds. By contrast, in the TW2.6 group, Adgre1-positive prototypical macrophages were frequently detected in the tumor margins, a phenomenon reminiscent of 'immune privileged' sites detected in clinical head and neck cancer tissues (42). Note that no significant difference in macrophage staining was noticed between the OC3 and TW2.6 groups after background subtractions (**Figures 3A, B**), which is consistent with the CIBERSORTx results. Intriguingly, as depicted in **Figure 3C**, the simultaneous upregulation of murine signature genes of tumor-associated macrophages (43) and downregulation of major histocompatibility class II molecules required for antigen presentation in TW2.6 tissues reinforces the accumulation of anergic tumor-associated macrophages surrounding p-EMT TW2.6 tumor cells.

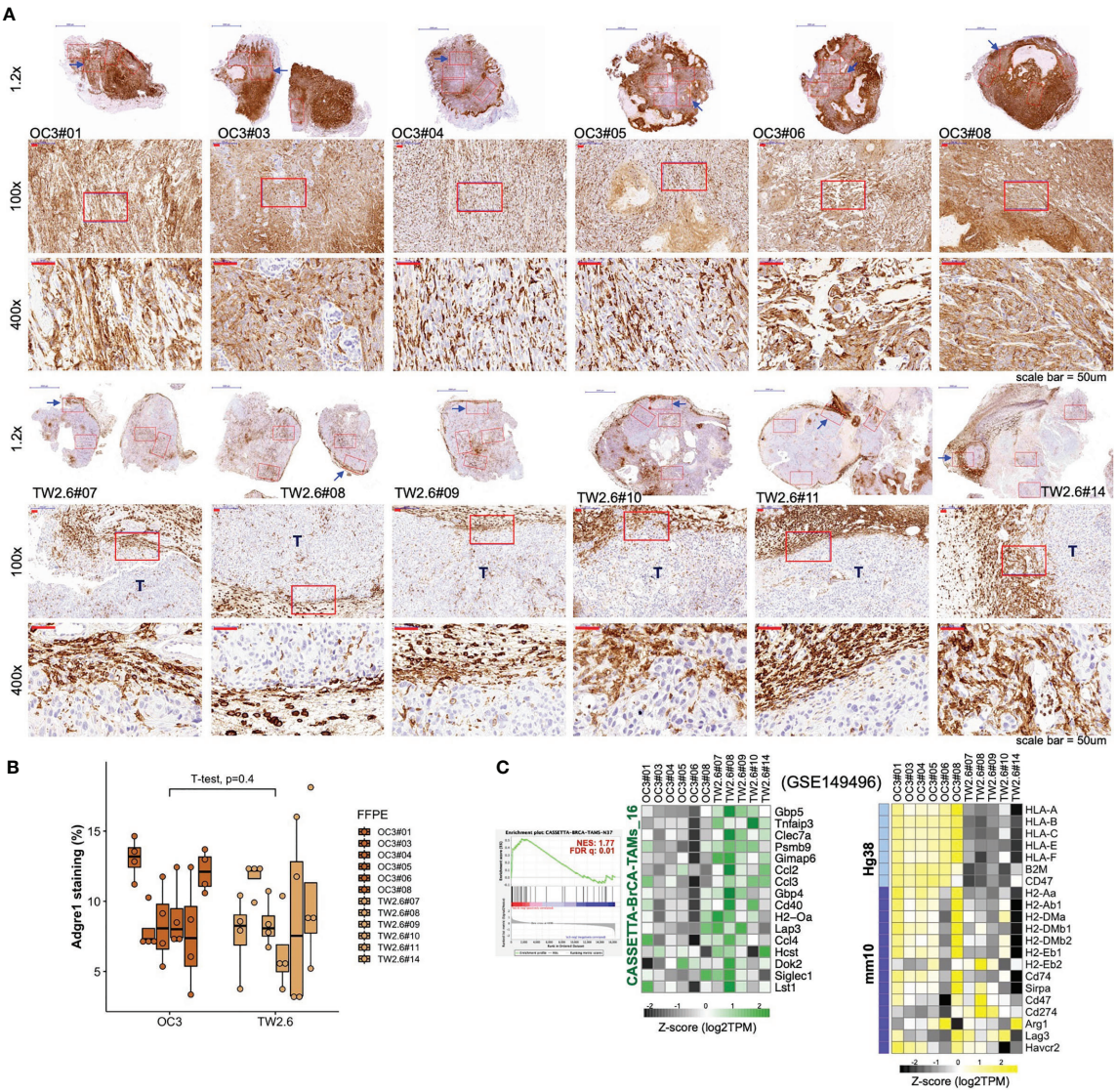

FIGURE 3 | Macrophages in the OC3 and TW2.6 stroma are geographically different. **(A)** Representative images and **(B)** quantitation (mean ± SEM of four 100x magnification fields from each section) of the indicated tissue sections stained for murine Adgre1 (brown). The p value of two-sample t-test of means is denoted. **(C)** (Left) GSEA enrichment end-plot and heatmap showing signature genes of tumor-associated macrophages (43) that are statistically enriched in the TW2.6 stroma. (Right) Heatmap showing the expression of human major histocompatibility (MHC) class-I (Hg38)- and mouse MHC class-II (mm10)-related genes in each xenograft tissue.

OC3 and TW2.6 Tumors Are Enriched With Gene Signatures of Myofibroblastic and Inflammatory CAFs, Respectively

Recent scRNA-seq studies have shown that the inflammatory subtype of CAFs (iCAFs) secretes a variety of inflammatory mediators (e.g., IL6 and CXCL12), whereas the myofibroblastic counterpart (myCAFs) primarily expresses ECM molecules (e.g., FN1 and type I collagen) (18–23). Of special interest, by microarray-based transcriptomics, Costea et al. identified two distinct subtypes of CAFs from clinical oral cancer tissues, designated CAF-N (normal-like) and CAF-D (divergent) (44). CAF-N is intrinsically motile, secretory, proangiogenic, and hyaluronan-rich. CAF-D is less migratory and secretes high levels of TGFβ but is unresponsive to it. Compared to CAF-D, the CAF-N population displayed a greater (85.33% *vs*. 50%) and faster (7 *vs*. 14 days) tumor-promoting incidence of otherwise nontumorigenic oral dysplastic cells in the immunodeficient mice (NSG) and significantly deeper invasion of malignant cells in the 3D biometrices constructed *in vitro*. The authors proposed that a switch from an earlier secretory CAF-N to a later $TGF\beta^{high}$ CAF-D occurred during oral cancer progression.

To test the hypothesis that inflammatory cytokines detected in the TW2.6 stroma might come from the iCAF cell population, in GSEA we applied customized gene matrix transposed (gmt) file of each newly identified stromal cell population as summarized in **Table 1**. Interestingly, this approach explicitly assigned enrichment of myCAF and CAF-D to the OC3 stroma and iCAF, tumor-associated macrophages, endothelial cells, and perivascular-like cells to the TW2.6 stroma (**Figure 4A**). In addition, a great number of inflammatory mediators are overlapping genes of the iCAF and immune-related pathways (e.g., IL6/JAK/STAT3 and inflammatory responses), which supports our hypothesis that CAFs of the TW2.6 stroma might be the principle source for the immune-related signatures (**Figure 4B**).

We were aware that two caveats are inherent to the current study: (1) immunodeficient NOG xenografts were used, which retained only limited innate immunity, and (2) human orthologous genes might not be entirely functional in mice. With these concerns, we performed cell type-gene expression analysis using the scRNA-seq dataset of oral cancer tissues in which the presence of CAF subtypes, including myCAFs and iCAFs, has been previously noted (8, 19, 21, 23). The results showed that except for *IL6*, which was enriched in the iCAF population of xenograft tissues but myofibroblasts in the clinical samples, hallmark genes for myCAFs, iCAFs, and myofibroblasts were fairly consistent between the xenograft and clinical oral cancer tissues, suggesting a certain extent of conservation in non-immune stromal cell populations preserved in the current study (**Figure 4C**).

Statistically Higher Hyaluronan Accumulation Was Detected in p-EMT TW2.6 Tumors

Another notable feature repeatedly linked to the secretory iCAF population is increased levels of hyaluronan synthases, including *HAS1* and *HAS2* (18, 19, 44). Interestingly, in our system, significantly increased expression of synthases (*HAS2*, *HAS3*) and hyaluronidases (*HYAL1*, *HYAL3*, *HYAL4*) was detected in the tumor cells but not in the stromal portion of TW2.6 tumors (**Supplementary Figure 3A**). Subsequent experiments using Alcian blue staining of OC3 and TW2.6 xenograft tissues confirmed that prominent hyaluronan staining was detected in five out of six TW2.6 tissues compared to sporadic Alcian blue-positive mast cells revealed in the OC3 tissues (**Supplementary Figure 3B**). Thus, our data partly support prior scRNA-seq studies in that iCAFs are frequently present in a hyaluronan-rich tumor microenvironment.

Translation of Xenograft Results Into Clinical Application

Thus far, our results provide evidence that certain stromal cell populations are preferentially associated with the most invasive yet uncommon EMT (OC3) or p-EMT (TW2.6) tumor cells, which is very different from a real clinical specimen that comprises cells at variable EMT states, e.g., only tumor cells at the invasion front display a p-EMT phenotype (6). A complementary experiment is to correlate stromal genes of interest with transcriptomic datasets from clinical bulk tissues, an approach we employed to identify the CAF index (summed expression of *TGFBI*, *TGFB2*, *TGFBR2*, *FN1*) (11). Specifically, the Puram oral cancer scRNA-seq (GSE103322) and NCKU-OrCA-40TN (GSE37991) datasets were chosen for cell type mapping and survival analysis, respectively. Of note, the latter is a microarray dataset comprising 40 matched pairs of betel quid-associated oral squamous cell carcinoma and adjacent normal tissues. Due to treatment-related death, only 38 cases were included for survival analysis. In addition, except for recurrence, none of the other clinical features were statistical

TABLE 1 | Gene matrices of stromal cell populations used in GSEA analysis.

yyyy/mm	Authors	Cancer	Stromal sub-populations
2013/07	COSTEA et al. (44)	OSCC	CAF-D, CAF-N
2019/04	CASSETTA et al. (43)	BRCA	TAM
2019/08	ELYADA et al. (18)	PDAC	myCAF, iCAF, apCAF
2020/02	DOMINGUEZ et al. (19)	PDAC	myCAF, iCAF, endothelials
2020/04	SOMERVILLE et al. (20)	PSC	myCAF, iCAF
2020/08	WU et al. (22)	TNBC	myCAF, iCAF, imPVL, dPVL
2020/09	KIEFFER et al. (21)	BRCA	myCAF, iCAF

OSCC, oral squamous cell carcinoma; BRCA, breast cancer; PDAC, pancreatic ductal adenocarcinoma; PSC, pancreatic stellate cell; TNBC, triple-negative breast cancer; CAF, cancer-associated fibroblast; TAM, tumor-associated macrophage; PVL, perivascular-like cell.

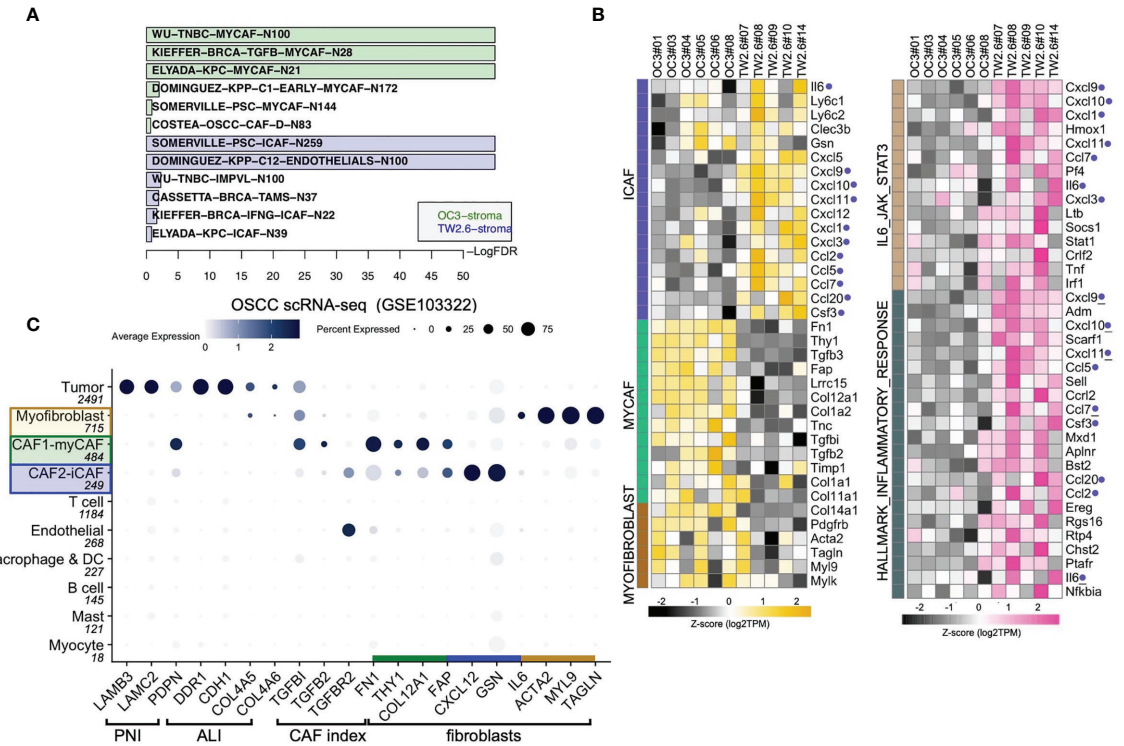

FIGURE 4 | Molecular signatures of myCAF and iCAF were enriched in OC3 and TW2.6 stroma, respectively. **(A)** Bar chart showing cell types with significant enrichments (FDR < 5%) in OC3 or TW2.6 stroma by gene set enrichment analysis (GSEA). Cell type-specific gene matrices in each study (summarized in **Table 1**) were extracted and converted to gene matrix transposed (gmt) files used in GSEA. N, gene number of indicated gene matrix. **(B)** Heatmaps showing the expression of the indicated genes classified as stromal fibroblasts (left) or immune-related (right) molecular signatures. Blue dots refer to replicates present in both heatmaps. **(C)** Dot plot denotes RNA expression of the indicated genes (*x*-axis) across eleven cell types (*y*-axis) composing the scRNA-seq dataset. Dot size indicates the proportion of cells within the indicated cell type expressing the indicated gene; color intensity represents the binned count-based expression level [log(scaled normalized count + 1)] among expressing cells. OSCC, oral squamous cell carcinoma; PNI, perineural invasion; ALI, angiolymphatic invasion. CAF index is referred to (11).

covariates for overall survival in univariate Cox proportional hazards model assessment (**Table 2**), an inherent limitation of a small cohort. Further TCGA collections with larger sample sizes will be included as validation datasets to complement this caveat.

First, genes identified in the xenograft experiments were validated for their primary origins of expression by cell typing of the scRNA-seq database, including myofibroblasts (*IL6*, *ACTA2*, *MYL9*, *TAGLN*), myCAFs (*TGFBI*, *TGFB2*, *FN1*, *THY1*, *COL12A1*, *FAP*, *HAS1*, *HAS2*), iCAFs (*FAP*, *CXCL12*, *GSN*), endothelial cells (*PECAM1*, *TGFBR2*, *HYAL1*, *HYAL2*), mast cells (*HYAL3*), T cells (*HYAL4*) and tumor cells (*HAS3*) (**Figures 4C**, **5A**). Next, in the 40 tumor tissues of NCKU-OrCA-40TN, the *Pearson* correlation coefficient of each paired gene was computed and clustered by cell type to inspect their expression consistency. As depicted in **Figure 5B**, (1) the expression of myCAF genes correlated with each other the best. (2) Myofibroblast genes share partial similarities to iCAFs and myCAFs, suggesting myofibroblasts might be progenitors of both CAF subtypes. (3) The expression of *PECAM1*, a microvessel density proxy, was inversely correlated with myCAF-*HAS2* and *TGFBI* but significantly correlated with iCAF-*CXCL12* and myofibroblast-*ACTA2*. (4) The expression of *HYAL1* is inversely related to myCAF genes but positively related to tumor cell *HAS3*.

Third, a univariate Cox proportional hazards model was performed to compute the hazard ratios (HRs) of overall survival associated with each stroma-originating gene in the NCKU-OrCA-40TN cohort. Accordingly, 6 out of 20 selected genes revealed statistical significance, including *TGFBI* (HR 11, 95% CI 2.4–50, p=0.0021), *TGFB2*, *COL12A1*, *IL6*, *HAS2*, and *HYAL1* (HR 0.15, 95% CI 0.042–0.55, *p*=0.0039) (**Table 2**). Multivariable Cox analysis revealed these 6 genes are confounding covariates (**Figure 5C** upper panel), which was not unexpected since 4 of them (*TGFBI*, *TGFB2*, *COL12A1* and *HAS2*) are derived from myCAFs. As cancer recurrence is a known prognostic factor for overall survival, we included it in multivariate Cox analysis. The results showed that *TGFBI* and *HYAL1*, respectively, remained statistically significant in multivariate Cox models (**Figure 5C** lower panel). These data suggested that both genes could serve as robust prognostic factors in betel quid-oral cancer. It is worth noting that *TGFBI* and *HYAL1* should act independently rather than combined, as

TABLE 2 | Cox proportional hazards analysis of NCKU-OrCA-40TN.

Feature/Gene	HR (95% CI) p value[#]	Notes
Age	1.5 (0.55-4.2) p=0.42	above 49 (n=20) *vs*. under 49 (n=18)
Alcohol	1.3 (0.36-4.6) p=0.7	no (n=8) *vs*. yes (n=30)
Diagnosis	1.8 (0.58-5.8) p=0.3	buccal (n=14) *vs*. tongue (n=24) Carcinoma
ALI	1.9 (0.67-5.3) p=0.23	no (n=20) *vs*. yes (n=18)
PNI	2.7 (0.76-9.6) p=0.12	no (n=14) *vs*. yes (n=24)
LNmeta	1.8 (0.65-5) p=0.26	no (n=21) *vs*. yes (n=17)
TNMstage	1.8 (0.58-5.8) p=0.3	I/II (n=14) *vs*. III/IVA (n=24)
TxModality	1 (0.36-2.8) p=0.99	Op only (15) *vs*. OpRT or OpCCRT (17 + 6)
Recurrence	7 (2.5-20) p=0.00024***	no (n=28) *vs*. yes (n=10)
EMT.Salt	4.2 (1.3-14) p=0.015*	higher score toward mesenchymal, composed of 14 genes
EMT.76GS	0.16 (0.043-0.56) p=0.0044**	higher score toward epithelial, composed of 76 genes
CAF index	13 (2.8-57) p=0.0011**	TGFBI+TGFB2+TGFBR2+FN1
TGFBI	11 (2.4-50) p=0.0021**	CAF index, myCAF
TGFB2	4.9 (1.4-17) p=0.015*	CAF index, myCAF
TGFBR2	1.3 (0.49-3.7) p=0.57	CAF index, endothelial cell
FN1	1.8 (0.63-5) p=0.28	CAF index, myCAF
THY1	1.1 (0.38-2.9) p=0.92	myCAF
COL12A1	3.2 (1.1-9.5) p=0.041*	myCAF
FAP	2.6 (0.88-7.6) p=0.085	myCAF, iCAF
CXCL12	1 (0.37-2.8) p=0.98	iCAF
GSN	0.55 (0.19-1.6) p=0.27	iCAF
IL6	3.4 (1.1-11) p=0.038*	myofibroblast, iCAF
ACTA2	0.6 (0.21-1.7) p=0.34	myofilbroblast
MYL9	1.1 (0.38-2.9) p=0.91	myofilbroblast
TAGLN	1.4 (0.49-3.8) p=0.55	myofilbroblast
HAS1	1.3 (0.45-3.5) p=0.66	hyaluronic acid synthase, myCAF
HAS2	5.8 (1.6-21) p=0.0068**	hyaluronic acid synthase, myCAF
HAS3	0.42 (0.14-1.2) p=0.11	hyaluronic acid synthase, tumor cell
HYAL1	0.15 (0.042-0.55) p=0.0039**	hyaluronidase, endothelial cell
HYAL2	1 (0.36-2.8) p=1	hyaluronidase, endothelial cell
HYAL3	0.78 (0.28-2.2) p=0.63	hyaluronidase, mast cell
HYAL4	0.85 (0.31-2.3) p=0.75	hyaluronidase, T cell
PECAM1	1.7 (0.6-4.7) p=0.32	microvessel density surrogate, endothelial cell

[#]*Significance codes: ***< 0.001, **< 0.01, *< 0.05. ALI, angiolymphatic invasion; PNI, perineural invasion; LNmeta, lymph node metastasis; Op, operation; OpRT, operation plus radiotherapy; OpCCRT, operation plus concurrent chemoradiotherapy.*

both lost partial significance in bivariate Cox assessment (*TGFBI* 8.23 95% CI 1.66–40.79, p=0.01, *HYAL* 0.23, 95% CI 0.06–0.88, p=0.032).

To validate our findings in larger TCGA cancer datasets, we first performed univariable Cox analysis and Kaplan–Meier curves stratified by low- and high-expression groups for each of the 20 stromal genes in the head and neck cancer cohort (HNSC, n=519). The results indicated that while high expression levels of *TGFBI*, *FAP* and *IL6* were statistically prognostic for poorer survival; the expression of *HYAL1* did not reach statistical significance for better survival (**Figure 6A**). It is worth noting that HNSC comprises 11 anatomic subsites including tonsil and larynx, such heterogeneity in tissue source might interfere with precisely identifying stromal biomarkers specific to each HNSC subtype. Next, same approach was used to evaluate *TGFBI* and *HYALI* in the other 32 TCGA cancer types. Interestingly, kidney renal clear cell carcinoma (KIRC, n=533) and uveal melanoma (UVM, n=80) concurrently displayed *TGFBI* and *HYAL1* as poor and good biomarkers, respectively (**Figure 6B**). In addition, the expression of *TGFBI* was also a poor indicator for bladder urothelial carcinoma (BLCA, n=406), breast invasive carcinoma (BRCA, n=841), cervical squamous cell carcinoma and endocervical adenocarcinoma (CESC, n=302), and glioblastoma multiforme (GBM, n=153); and the expression of *HYAL1* was a statistical protective marker for kidney renal papillary cell carcinoma (KIRP, n=287) and pheochromocytoma (n=148) (**Figure 6C**). Taken together, the prognostic values of *TGFBI* and *HYAL1* identified from betel quid-associated oral cancer tissues (**Figure 6D**) were recapitulated by seven (n=2834) and four (n=1048) TCGA cancer types, respectively.

DISCUSSION

Through meta-analysis of disease-matching transcriptomic xenograft tumor tissue and scRNA-seq datasets, this study extracted 20 stromal genes representative of myCAFs, iCAFs, myofibroblasts, and endothelial cells in a betel quid-oral cancer cohort comprising 40 tissues (**Table 2**). In univariate Cox proportional hazards assessment of overall survival, 6 out of these 20 genes exhibited statistical predictability. In multivariate Cox analysis interacting with cancer recurrence, *TGFBI* and *HYAL1* remained statistically significant for poor and good prognosis, respectively (**Figure 5C**). In thirty-three TCGA transcriptomic cohorts, *TGFBI* was a poor indicator of seven cancer types, including head and neck cancer; *HYAL1* was a

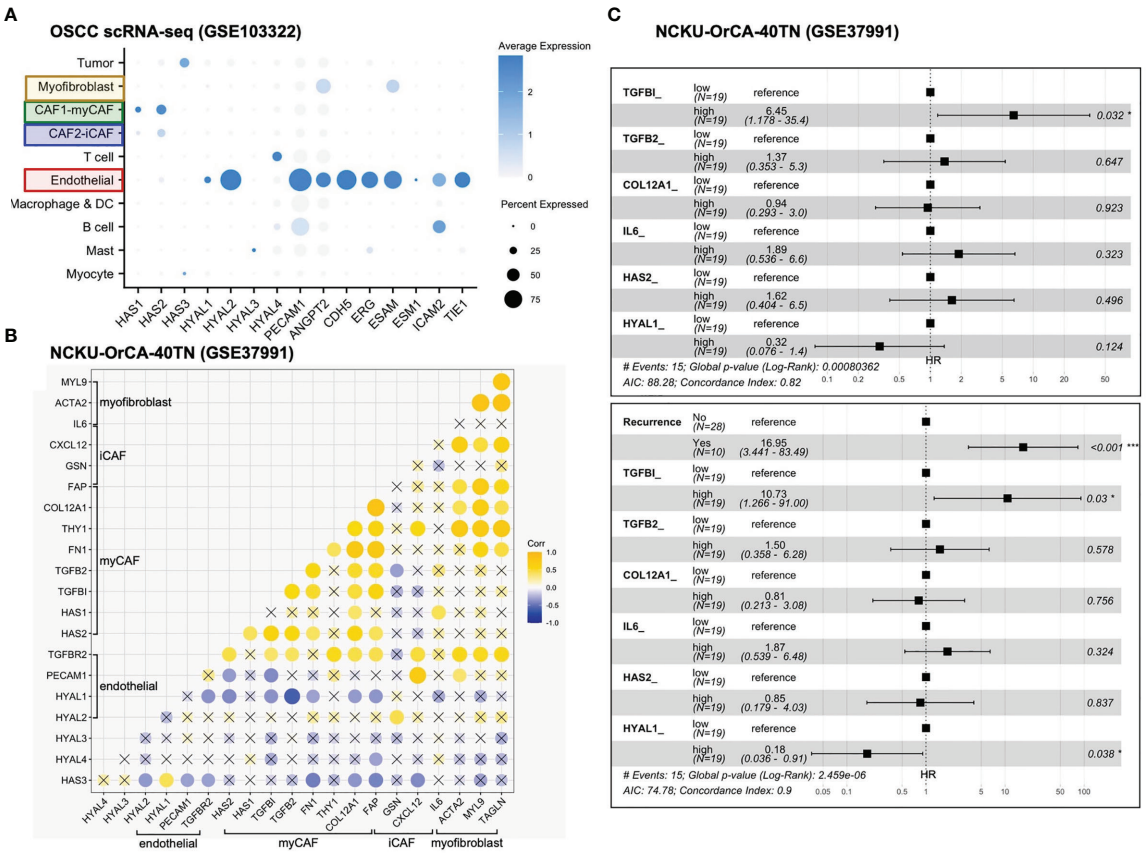

FIGURE 5 | Stromal *TGFBI* and *HYAL1* are poor and protective prognostic biomarkers, respectively, for NCKU-OrCA-40TN. **(A)** Dot plot denotes the cell origins of hyaluronan synthase (HAS1–3), hyaluronidase (HYAL1–4) and endothelial hallmark genes (PECAM1 ~ TIE1), which were included as controls. Dot size indicates the proportion of cells within the indicated cell type expressing the indicated gene; color intensity represents the binned count-based expression level [log(scaled normalized count + 1)] among expressing cells. OSCC, oral squamous cell carcinoma. **(B)** Correlational expression matrix of stroma-originating genes in the NCKU-OrCA-40TN cohort. Crosses (×) indicate $p > 0.05$ **(C)** Forest plots representing the prognostic hazard ratios (HR) of overall survival assessed by 6 stromal genes (upper plot) or stromal genes plus cancer recurrence (lower plot). *$p < 0.05$, ***$p < 0.001$.

protective marker for four cancer types, including kidney renal clear cell carcinoma and uveal melanoma.

With an unprecedented pace, scRNA-seq methodology has successfully deciphered the complexity and heterogeneity of tumor ecosystems composed of tumor cells and various stromal components. Among these, the two distinct molecular subtypes of cancer-associated fibroblasts, iCAFs and myCAFs, attracted special attention due to their relevance to cancer cell invasion and treatment resistance. In oral cancer, malignant p-EMT cells located at the invasion front are in proximity to CAFs (FAP+PDPN+) and are statistically associated with nodal metastasis and perineural invasion (8, 9). In breast cancer, while iCAFs (PDGFRB+, ACTA2-, CD34+, MCAM-) were implicated in cytotoxic T cell dysfunction of tripe-negative breast cancer (22), myCAFs (ecm) and myCAFs (TGFβ) were shown to be the primary resistance elements of immunotherapies (21). In pancreatic ductal adenocarcinoma, increased levels of the myCAF (LRRC15+) signature correlated with poor response to anti-PD-L1 therapy in an immunotherapy clinical trial (19). In a murine melanoma model, iCAFs (S1 immune), myCAFs (S2 desmoplastic), and myofibroblasts (S3 contractile, ACTA2^{high}) were temporally linked to disease progression (23).

Another stromal population, vascular endothelial cells, is also therapy relevant. In a comprehensive transcriptomic study comprising 10,767 human tumors with variable extents of vascularity, Kahn et al. revealed that both the endothelial index (**Figure 2B**) and vascular microenvironment signatures are independent predictors of disease outcome (41). In this regard, motile and secretory iCAFs (and their equivalents with different designations) were linked to angiogenesis, variably implicated by the increased expression of *CXCL12/SDF-1*, *VEGFA*, *CCL2*, *FGFs*, *PDGFs*, and hyaluronic acid synthase (*HAS1*, *HAS2*) (18, 19, 23, 44). Distinct from the other proangiogenic factors, hyaluronan is a linear, anionic polysaccharide required for normal tissue homeostasis. The degradation of high molecular weight (HMW-HA, > 500 kDa) to low molecular weight hyaluronan (LMW-HA, 7–200 kDa) is mediated by hyaluronidases (HYAL1–4). Emerging evidence indicates that

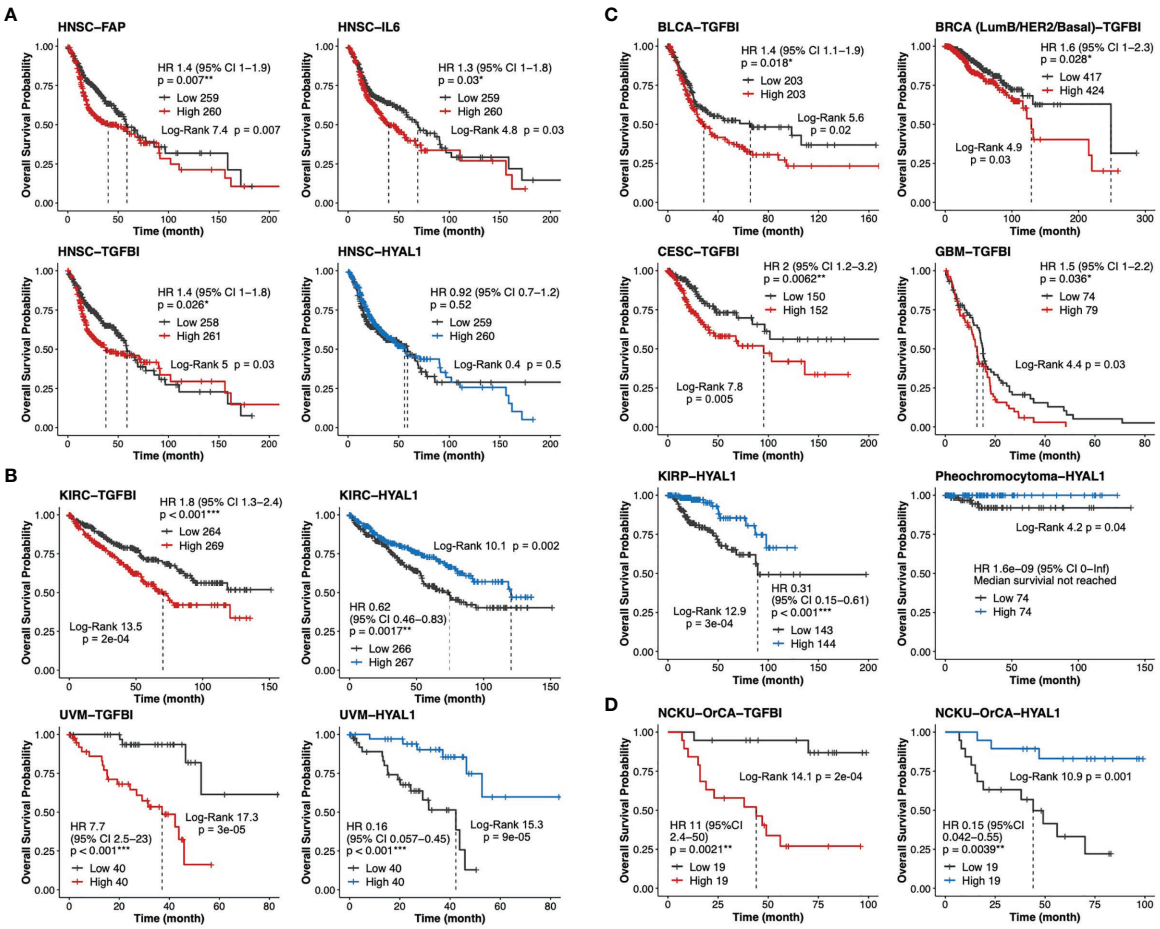

FIGURE 6 | Validation of *TGFBI* and *HYAL1* in The Cancer Genome Atlas (TCGA) datasets. **(A)** Dichotomized Kaplan-Meier curves of estimated overall survival for *FAP*, *IL6*, *TGFBI* and *HYAL1* in the head neck cancer cohort (HNSC, n=519). **(B)** Kaplan-Meier curves for *TGFBI* and *HYAL1* in kidney renal clear cell carcinoma (KIRC, n=533) and uveal melanoma (UVM, n=80). **(C)** Kaplan-Meier curves for *TGFBI* in bladder urothelial carcinoma (BLCA, n=406), invasive breast cancer (BRCA, n=841), cervical squamous cell carcinoma and endocervical adenocarcinoma (CESC, n=302), and glioblastoma multiforme (GBM, n=153); *HYAL1* in kidney renal papillary cell carcinoma (KIRP, n=287), and pheochromocytoma (n=148). **(D)** Kaplan-Meier curves for *TGFBI* and *HYAL1* in the NCKU-OrCA-40TN cohort (GSE37991, n=38). *p < 0.05, **p < 0.01, ***p < 0.001.

while LMW-HA participates in neoangiogenesis, tumor cell proliferation, migration, and invasion; in an established tumor, accumulated HMW-HA increases the intratumor interstitial fluid pressure, which blocks neoangiogenesis at the cost of reducing immune surveillance and drug delivery efficacy [reviewed in 45)].

In the oral cancer scRNA-seq study, the expression of *TGFBI* came from myCAFs, myofibroblasts and tumor cells (**Figure 4C**). TGFBI is a secretory extracellular matrix protein that mediates binding to other matrices, including fibronectin, laminin, and collagen of types I, II, IV, etc. As a direct target of TGFβ, TGFBI plays a tumor-suppressive role in early precancerous lesions but acts to promote tumor progression in later stages. Indeed, TGFBI is one of the p-EMT hallmark proteins present in oral cancer tissues (8) and is implicated in DDR1-mediated angiolymphatic invasions in the NCKU-OrCA-40TN cohort (10). Whether TGFBI produced by myCAFs and myofibroblasts is functionally different from that secreted by tumor cells awaits further investigation.

As the pathologic roles of otherwise nonmalignant stromal cell populations are beginning to emerge, prognostic biomarkers originating from the tumor stroma might illuminate a new avenue for cancer control. Indeed, while we should be more cautious about defining the tumor cell EMT spectrum in a real specimen (6), it is inspiring to learn that "the CAF-targeted therapy will take its place in the toolkit of the oncologist within the next 10 years" (46)!

CONCLUSIONS

Through integrative studies of disease-matching xenograft tumor and scRNA-seq datasets, we established nonmalignant stromal cell populations preferentially cohabitate with oral cancer cells

residing in EMT and p-EMT states, the most invasive and deleterious components within a tumor. Hallmark genes representative of myofibroblasts, myCAFs, iCAFs, and endothelial cells were assessed for Cox hazard ratios and Kaplan-Meier curves of overall survival in clinical datasets. MyCAF-*TGFBI* and endothelial-*HYAL1* were poor and good prognosis markers, respectively, for 40 betel quid-associated oral cancer tissues. In 33 TCGA datasets, *TGFBI* was recapitulated as a poor indicator for seven cancer types, including head and neck cancer comprising 519 patients. Our results not only disclose novel targets for oral cancer control, but also provide feasible applications, e.g, a single immunohistochemical assay of TGFBI from treatment naïve or recurred tumor biopsies, to assist clinical decision-making.

DATA AVAILABILITY STATEMENT

The datasets presented in this study can be found in online repositories. The names of the repository/repositories and accession number(s) can be found below: GSE149496, GSE150469.

ETHICS STATEMENT

The studies involving human participants were reviewed and approved by the Research Ethics Committee of National Health Research Institutes (Protocol No: EC1040407-E) for the use of clinical samples and patient data. Written informed consent for participation was not required for this study in accordance with the national legislation and the institutional requirements. The animal study was reviewed and approved by the Institutional Animal Care and Use Committee of National Health Research Institutes, Taiwan (Protocol No: NHRI-IACUC-106057-M1-A).

AUTHOR CONTRIBUTIONS

YHL, YFC, PRC, JWL, and SFL conceptualized this study. YCK, TYL, and YLC prepared xenograft tissues. YHL and YLC performed immunohistochemical assays and histological staining. YHL, TYL, YCK, and SFL performed bioinformatic analyses. JRH provides patient data. JRH, YFC, PRC, and JYC interpreted clinical data and survival analyses. SGS, JWL, JLY, and SFL participated in formal analysis, result validation, and are major contributors in writing the manuscript. All authors contributed to the article and approved the submitted version.

FUNDING

This study was supported by the Taiwan National Health Research Institutes (NHRI CA-110-PP-05), Ministry of Health and Welfare (MOHW 110-TDU-B-212-144013 and -144026) and the Ministry of Science and Technology (MOST 108-2320-B-400-019). The NHRI institutional library paid for the open access publication fees for this manuscript.

ACKNOWLEDGMENTS

The authors acknowledge the Clinical and Industrial Genomic Application Development Service Center of National Core Facility for Biopharmaceuticals, Taiwan (MOST108-2319-B-010-001) and Genomics Core and Bioinformatics-Biology Service Core at the Institute of Molecular Biology of Academia Sinica for RNA-seq analyses. We are indebted to the Taiwan NHRI Microarray Core, Laboratory Animal Center, and Pathology Core Laboratory for assistance with Partek Flow, animal studies, and FFPE section preparations. Yi-Hong Liu and Ting-Yu Lai carried out their thesis research under the auspices of the Graduate Program of Biotechnology in Medicine, National Tsing Hua University and National Health Research Institutes.

SUPPLEMENTARY MATERIAL

The Supplementary Material for this article can be found online at: https://www.frontiersin.org/articles/10.3389/fonc.2021.769665/full#supplementary-material

REFERENCES

1. Taiwan Cancer Registry. *Health Promotion Administration, Ministry of Health and Welfare, Taiwan*. Available at: https://www.hpa.gov.tw (Accessed 2021/07/01).
2. Chou HC, Lin HW, Yang JH, Lin PY, Cheng SJ, Wu YH, et al. Clinical Outcomes of Oral Cancer Patients Who Survive for More Than 5 Years in Taiwan. *J Formosan Med Assoc Taiwan Yi Zhi* (2019) 118(12):1616–22. doi: 10.1016/j.jfma.2019.07.022
3. Wang CP, Liao LJ, Chiang CJ, Hsu WL, Kang CJ, Wang CC, et al. Patients With Oral Cancer do Not Undergo Surgery as Primary Treatment: A Population-Based Study in Taiwan. *J Formosan Med Assoc Taiwan Yi Zhi* (2020) 119(1 Pt 3):392–8. doi: 10.1016/j.jfma.2019.06.011
4. Cheng YJ, Tsai MH, Chiang CJ, Tsai ST, Liu TW, Lou PJ, et al. Adjuvant Radiotherapy After Curative Surgery for Oral Cavity Squamous Cell Carcinoma and Treatment Effect of Timing and Duration on Outcome-A Taiwan Cancer Registry National Database Analysis. *Cancer Med* (2018) 7 (7):3073–83. doi: 10.1002/cam4.1611
5. Lin MC, Leu YS, Chiang CJ, Ko JY, Wang CP, Yang TL, et al. Adequate Surgical Margins for Oral Cancer: A Taiwan Cancer Registry National Database Analysis. *Oral Oncol* (2021) 119:105358. doi: 10.1016/j.oraloncology.2021.105358
6. Yang J, Antin P, Berx G, Blanpain C, Brabletz T, Bronner M, et al. Guidelines and Definitions for Research on Epithelial-Mesenchymal Transition. *Nat Rev Mol Cell Biol* (2020) 21(6):341–52. doi: 10.1038/s41580-020-0237-9
7. Friedl P, Gilmour D. Collective Cell Migration in Morphogenesis, Regeneration and Cancer. *Nat Rev Mol Cell Biol* (2009) 10(7):445–57. doi: 10.1038/nrm2720
8. Puram SV, Tirosh I, Parikh AS, Patel AP, Yizhak K, Gillespie S, et al. Single-Cell Transcriptomic Analysis of Primary and Metastatic Tumor Ecosystems in Head and Neck Cancer. *Cell* (2017) 171(7):1611–24. doi: 10.1016/j.cell.2017.10.044

9. Parikh AS, Puram SV, Faquin WC, Richmon JD, Emerick KS, Deschler DG, et al. Immunohistochemical Quantification of Partial-EMT in Oral Cavity Squamous Cell Carcinoma Primary Tumors is Associated With Nodal Metastasis. *Oral Oncol* (2019) 99:104458. doi: 10.1016/j.oraloncology.2019.104458
10. Chen YL, Tsai WH, Ko YC, Lai TY, Cheng AJ, Shiah SG, et al. Discoidin Domain Receptor-1 (DDR1) is Involved in Angiolymphatic Invasion in Oral Cancer. *Cancers (Basel)* (2020) 12(4):e841. doi: 10.3390/cancers12040841
11. Ko YC, Lai TY, Hsu SC, Wang FH, Su SY, Chen YL, et al. Index of Cancer-Associated Fibroblasts Is Superior to the Epithelial-Mesenchymal Transition Score in Prognosis Prediction. *Cancers (Basel)* (2020) 12(7):e1718. doi: 10.3390/cancers12071718
12. Zhang XL, Jiang C, Zhang ZX, Liu F, Zhang F, Cheng YF. The Tumor-Stroma Ratio is an Independent Predictor for Survival in Nasopharyngeal Cancer. *Oncol Res Treat* (2014) 37(9):480–4. doi: 10.1159/000365165
13. Ho YY, Wu TY, Cheng HC, Yang CC, Wu CH. The Significance of Tumor Budding in Oral Cancer Survival and its Relevance to the Eighth Edition of the American Joint Committee on Cancer Staging System. *Head Neck* (2019) 41(9):2991–3001. doi: 10.1002/hed.25780
14. Mascitti M, Zhurakivska K, Togni L, Caponio VCA, Almangush A, Balercia P, et al. Addition of the Tumour-Stroma Ratio to the 8th Edition American Joint Committee on Cancer Staging System Improves Survival Prediction for Patients With Oral Tongue Squamous Cell Carcinoma. *Histopathology* (2020) 77(5):810–22. doi: 10.1111/his.14202
15. Camps JL, Chang SM, Hsu TC, Freeman MR, Hong SJ, Zhau HE, et al. Fibroblast-Mediated Acceleration of Human Epithelial Tumor Growth *In Vivo*. *Proc Natl Acad Sci USA* (1990) 87(1):75–9. doi: 10.1073/pnas.87.1.75
16. Dvorak HF. Tumors: Wounds That do Not Heal. Similarities Between Tumor Stroma Generation and Wound Healing. *N Engl J Med* (1986) 315(26):1650–9. doi: 10.1056/NEJM198612253152606
17. Gaggioli C, Hooper S, Hidalgo-Carcedo C, Grosse R, Marshall JF, Harrington K, et al. Fibroblast-Led Collective Invasion of Carcinoma Cells With Differing Roles for RhoGTPases in Leading and Following Cells. *Nat Cell Biol* (2007) 9(12):1392–400. doi: 10.1038/ncb1658
18. Elyada E, Bolisetty M, Laise P, Flynn WF, Courtois ET, Burkhart RA, et al. Cross-Species Single-Cell Analysis of Pancreatic Ductal Adenocarcinoma Reveals Antigen-Presenting Cancer-Associated Fibroblasts. *Cancer Discovery* (2019) 9(8):1102–23. doi: 10.1158/2159-8290.CD-19-0094
19. Dominguez CX, Müller S, Keerthivasan S, Koeppen H, Hung J, Gierke S, et al. Single-Cell RNA Sequencing Reveals Stromal Evolution Into LRRC15^{+} Myofibroblasts as a Determinant of Patient Response to Cancer Immunotherapy. *Cancer Discovery* (2020) 10(2):232–53. doi: 10.1158/2159-8290.cd-19-0644
20. Somerville TD, Biffi G, Dassler-Plenker J, Hur SK, He XY, Vance KE, et al. Squamous Trans-Differentiation of Pancreatic Cancer Cells Promotes Stromal Inflammation. *Elife* (2020) 9:e53381. doi: 10.7554/eLife.53381
21. Kieffer Y, Hocine HR, Gentric G, Pelon F, Bernard C, Bourachot B, et al. Single-Cell Analysis Reveals Fibroblast Clusters Linked to Immunotherapy Resistance in Cancer. *Cancer Discovery* (2020) 10(9):1330–51. doi: 10.1158/2159-8290.cd-19-1384
22. Wu SZ, Roden DL, Wang C, Holliday H, Harvey K, Cazet AS, et al. Stromal Cell Diversity Associated With Immune Evasion in Human Triple-Negative Breast Cancer. *EMBO J* (2020) 39(19):e104063. doi: 10.15252/embj.2019104063
23. Davidson S, Efremova M, Riedel A, Mahata B, Pramanik J, Huuhtanen J, et al. Single-Cell RNA Sequencing Reveals a Dynamic Stromal Niche That Supports Tumor Growth. *Cell Rep* (2020) 31(7):107628. doi: 10.1016/j.celrep.2020.107628
24. Keck MK, Zuo Z, Khattri A, Stricker TP, Brown CD, Imanguli M, et al. Integrative Analysis of Head and Neck Cancer Identifies Two Biologically Distinct HPV and Three non-HPV Subtypes. *Clin Cancer Res* (2015) 21(4):870–81. doi: 10.1158/1078-0432.CCR-14-2481
25. Guinney J, Dienstmann R, Wang X, de Reynies A, Schlicker A, Soneson C, et al. The Consensus Molecular Subtypes of Colorectal Cancer. *Nat Med* (2015) 21(11):1350–6. doi: 10.1038/nm.3967
26. Yoshihara K, Shahmoradgoli M, Martinez E, Vegesna R, Kim H, Torres-Garcia W, et al. Inferring Tumour Purity and Stromal and Immune Cell Admixture From Expression Data. *Nat Commun* (2013) 4:2612. doi: 10.1038/ncomms3612
27. Newman AM, Steen CB, Liu CL, Gentles AJ, Chaudhuri AA, Scherer F, et al. Determining Cell Type Abundance and Expression From Bulk Tissues With Digital Cytometry. *Nat Biotechnol* (2019) 37(7):773–82. doi: 10.1038/s41587-019-0114-2
28. Li T, Fu J, Zeng Z, Cohen D, Li J, Chen Q, et al. TIMER2.0 for Analysis of Tumor-Infiltrating Immune Cells. *Nucleic Acids Res* (2020) 48(W1):W509–W14. doi: 10.1093/nar/gkaa407
29. Bradford JR, Wappett M, Beran G, Logie A, Delpuech O, Brown H, et al. Whole Transcriptome Profiling of Patient-Derived Xenograft Models as a Tool to Identify Both Tumor and Stromal Specific Biomarkers. *Oncotarget* (2016) 7(15):20773–87. doi: 10.18632/oncotarget.8014
30. Woo XY, Srivastava A, Graber JH, Yadav V, Sarsani VK, Simons A, et al. Genomic Data Analysis Workflows for Tumors From Patient-Derived Xenografts (PDXs): Challenges and Guidelines. *BMC Med Genomics* (2019) 12(1):92. doi: 10.1186/s12920-019-0551-2
31. Evrard YA, Srivastava A, Randjelovic J, Doroshow JH, Dean DA2nd, Morris JS, et al. Systematic Establishment of Robustness and Standards in Patient-Derived Xenograft Experiments and Analysis. *Cancer Res* (2020) 80(11):2286–97. doi: 10.1158/0008-5472.CAN-19-3101
32. Lu YC, Chen YJ, Wang HM, Tsai CY, Chen WH, Huang YC, et al. Oncogenic Function and Early Detection Potential of miRNA-10b in Oral Cancer as Identified by microRNA Profiling. *Cancer Prev Res (Philadelphia Pa)* (2012) 5(4):665–74. doi: 10.1158/1940-6207.CAPR-11-0358
33. Lin SC, Liu CJ, Chiu CP, Chang SM, Lu SY, Chen YJ. Establishment of OC3 Oral Carcinoma Cell Line and Identification of NF-Kappa B Activation Responses to Areca Nut Extract. *J Oral Pathol Med Off Publ Int Assoc Oral Pathologists Am Acad Oral Pathol* (2004) 33(2):79–86. doi: 10.1111/j.1600-0714.2004.00034.x
34. Chen JH, Lim JS, Shyu KW, Meng CL. Direct Cytotoxicity of Garlic on Human Oral Cancer Cells. *Zhonghua Ya Yi Xue Hui Za Zhi* (1988) 7(1):13–8.
35. Kok SH, Hong CY, Lin SK, Lee JJ, Chiang CP, Kuo MY. Establishment and Characterization of a Tumorigenic Cell Line From Areca Quid and Tobacco Smoke-Associated Buccal Carcinoma. *Oral Oncol* (2007) 43(7):639–47. doi: 10.1016/j.oraloncology.2006.07.007
36. Subramanian A, Tamayo P, Mootha VK, Mukherjee S, Ebert BL, Gillette MA, et al. Gene Set Enrichment Analysis: A Knowledge-Based Approach for Interpreting Genome-Wide Expression Profiles. *Proc Natl Acad Sci USA* (2005) 102(43):15545–50. doi: 10.1073/pnas.0506580102
37. Butler A, Hoffman P, Smibert P, Papalexi E, Satija R. Integrating Single-Cell Transcriptomic Data Across Different Conditions, Technologies, and Species. *Nat Biotechnol* (2018) 36(5):411–20. doi: 10.1038/nbt.4096
38. Goldman MJ, Craft B, Hastie M, Repecka K, McDade F, Kamath A, et al. Visualizing and Interpreting Cancer Genomics Data *via* the Xena Platform. *Nat Biotechnol* (2020) 38(6):675–8. doi: 10.1038/s41587-020-0546-8
39. Tan TZ, Miow QH, Miki Y, Noda T, Mori S, Huang RY, et al. Epithelial-Mesenchymal Transition Spectrum Quantification and its Efficacy in Deciphering Survival and Drug Responses of Cancer Patients. *EMBO Mol Med* (2014) 6(10):1279–93. doi: 10.15252/emmm.201404208
40. Nieto MA, Huang RY, Jackson RA, Thiery JP. EMT: 2016. *Cell* (2016) 166(1):21–45. doi: 10.1016/j.cell.2016.06.028
41. Kahn BM, Lucas A, Alur RG, Wengyn MD, Schwartz GW, Li J, et al. The Vascular Landscape of Human Cancer. *J Clin Invest* (2021) 131(2):e136655. doi: 10.1172/JCI136655
42. Lyford-Pike S, Peng S, Young GD, Taube JM, Westra WH, Akpeng B, et al. Evidence for a Role of the PD-1:PD-L1 Pathway in Immune Resistance of HPV-Associated Head and Neck Squamous Cell Carcinoma. *Cancer Res* (2013) 73(6):1733–41. doi: 10.1158/0008-5472.CAN-12-2384
43. Cassetta L, Fragkogianni S, Sims AH, Swierczak A, Forrester LM, Zhang H, et al. Human Tumor-Associated Macrophage and Monocyte Transcriptional Landscapes Reveal Cancer-Specific Reprogramming, Biomarkers, and Therapeutic Targets. *Cancer Cell* (2019) 35(4):588–602 e10. doi: 10.1016/j.ccell.2019.02.009
44. Costea DE, Hills A, Osman AH, Thurlow J, Kalna G, Huang X, et al. Identification of Two Distinct Carcinoma-Associated Fibroblast Subtypes With Differential Tumor-Promoting Abilities in Oral Squamous Cell

Carcinoma. *Cancer Res* (2013) 73(13):3888–901. doi: 10.1158/0008-5472.CAN-12-4150
45. Liu M, Tolg C, Turley E. Dissecting the Dual Nature of Hyaluronan in the Tumor Microenvironment. *Front Immunol* (2019) 10:947. doi: 10.3389/fimmu.2019.00947
46. Sahai E, Astsaturov I, Cukierman E, DeNardo DG, Egeblad M, Evans RM, et al. A Framework for Advancing Our Understanding of Cancer-Associated Fibroblasts. *Nat Rev Cancer* (2020) 20(3):174–86. doi: 10.1038/s41568-019-0238-1

Conflict of Interest: The authors declare that the research was conducted in the absence of any commercial or financial relationships that could be construed as a potential conflict of interest.

Publisher's Note: All claims expressed in this article are solely those of the authors and do not necessarily represent those of their affiliated organizations, or those of the publisher, the editors and the reviewers. Any product that may be evaluated in this article, or claim that may be made by its manufacturer, is not guaranteed or endorsed by the publisher.

frontiers in Oncology

ORIGINAL RESEARCH
published: 23 November 2021
doi: 10.3389/fonc.2021.709865

Identification of Hypoxia-Related Molecular Classification and Associated Gene Signature in Oral Squamous Cell Carcinoma

Chen Li[1†], Xin Chen[2†], Xiaolin Ren[2,3], Jia-lin Chen[1], Hao Chen[1], Jing-jia Yu[1], Qiu-chi Ran[1], Shuang Kang[1], Xi-meng Chen[1] and Zhen-jin Zhao[1]*

[1] Department of Orthodontics, The First Clinic of Stomatological Hospital of China Medical University, Shenyang, China, [2] Department of Neurosurgery, The First Hospital of China Medical University, Shenyang, China, [3] Department of Neurosurgery, Shenyang Red Cross Hospital, Shenyang, China

OPEN ACCESS

Edited by:
Heming Lu,
People's Hospital of Guangxi Zhuang Autonomous Region, China

Reviewed by:
Marcos Santos,
University of Brasilia, Brazil
Zaixiang Tang,
Soochow University Medical College, China
Dong Zhang,
Shandong University, China

***Correspondence:**
Zhen-jin Zhao
zjzhao@cmu.edu.cn

[†]These authors have contributed equally to this work

Specialty section:
This article was submitted to Head and Neck Cancer, a section of the journal Frontiers in Oncology

Received: 14 May 2021
Accepted: 29 October 2021
Published: 23 November 2021

Citation:
Li C, Chen X, Ren X, Chen J-l, Chen H, Yu J-j, Ran Q-c, Kang S, Chen X-m and Zhao Z-j (2021) Identification of Hypoxia-Related Molecular Classification and Associated Gene Signature in Oral Squamous Cell Carcinoma. Front. Oncol. 11:709865. doi: 10.3389/fonc.2021.709865

The high heterogeneity of oral squamous cell carcinoma (OSCC) is the main obstacle for individualized treatment. Recognizing the characteristics of different subtypes and investigating the promising strategies for each subclass are of great significance in precise treatment. In this study, we systematically evaluated hypoxia-mediated patterns together with immune characteristics of 309 OSCC patients in the TCGA training set and 97 patients in the GSE41613 testing set. We further identified two different hypoxia subtypes with distinct immune microenvironment traits and provided treatment programs for the two subclasses. In order to assess hypoxia level individually, we finally constructed a hypoxia-related risk score, which could predict the clinical outcome and immunotherapy response of OSCC patients. In summary, the recognition of different hypoxia patterns and the establishment of hypoxia-related risk score might enhance our understanding of the tumor microenvironment of OSCC and provide more personalized treatment strategies in the future.

Keywords: oral squamous cell carcinoma (OSCC), hypoxia, subtyping, immune microenvironment, immunotherapy

INTRODUCTION

Oral squamous cell carcinoma (OSCC) is one of the most common malignant tumors of head and neck squamous cell carcinoma (HNSC), accounting for 90% of neoplasms of the head and neck (1). Despite the development of surgery, radiotherapy, and chemotherapy, the prognosis of OSCC is still unsatisfactory with an average 5-year survival probability ranging from 45% to 50% due to the high incidence of recurrence and metastasis (2–4). Recently, more and more studies have concentrated on the generation of genomic signatures for risk stratification and further survival prediction in OSCC patients (5–7). However, most prognostic signatures were deficient in clinical transformation and few of them were applied to routine practice. As a heterogeneous disease, it is of great necessity to precisely understand the molecular properties of OSCC in order to achieve individualized treatment under different subtypes.

Hypoxia is one of the critical hallmarks of cancer, which is associated with tumor malignancy and angiogenesis together with therapeutic resistance (8, 9). Currently, the significant role of hypoxia in driving tumor immunosuppression and immune escape has caused widespread concern. Evidence has revealed that T cells as well as natural killer (NK) cells under a hypoxia microenvironment always behave in an exhausted state, leading to their dysfunction in killing tumor cells (10). What is more, the hypoxia status can also promote some inhibitory immune cells like regulatory T cells (Tregs) and M2 macrophage infiltration together with the secretion of suppressive molecules like VEGFA, causing the formation of an immunosuppressive microenvironment (11–13). Even though hypoxia-related subclasses have been explored in many cancer types, the features of different subtypes and their clinical benefit in OSCC are still unknown. Therefore, investigating the distinct subtypes based on hypoxia status during tumorigenesis and development might provide new insights into the treatment and prognostic detection of OSCC.

Recently, immune checkpoint blockade (ICB) therapy has been reported to improve overall survival (OS) in distinct cancer types (14–20). Nevertheless, the proportion of benefited patients still remains low. Growing evidence has revealed a tight association between hypoxia and tumor immunotherapy across multiple tumor types (21). However, the effect of hypoxia on the immune microenvironment as well as the efficacy of immunotherapy in OSCC remains less known.

In the present study, a consensus clustering based on hypoxia genes was conducted and validated in two OSCC cohorts, characterizing two different hypoxia states of OSCC samples for the first time. Moreover, the prognostic features, hypoxia traits, gene mutation alterations, immune infiltration, and the promising treatment strategy for each subtype were analyzed and investigated. For clinical practice, we further constructed a hypoxia prognostic risk score model which could further predict the OS and ICB therapy response for OSCC patients. These findings suggested an indispensable role of hypoxia states in directing therapeutic plans for OSCC.

MATERIAL AND METHODS

Data Collection and Processing

The Cancer Genome Atlas (TCGA) mRNA sequence data [htseq-FPKM in log2(x + 1) transformed] together with clinical information of OSCC were obtained from the UCSC Xena browser (GDC hub: https://gdc.xenahubs.net). For validation, microarray profiles of GSE41613 containing clinical annotations were extracted by GEOquery R package. The mentioned clinical traits are demonstrated in **Table 1**. The batch effects normalized mRNA data of pancancer with clinical information were downloaded from UCSC Xena browser. The hypoxia gene set containing 200 classical hypoxia-associated genes was obtained from gene set enrichment analysis (GSEA) (http://www.gsea-msigdb.org/). Expression data of OSCC cell lines [TPM in log2(x + 1) transformed) were downloaded from the Broad Institute Cancer Cell Line Encyclopedia (CCLE) project (https://portals.broadinstitute.org/ccle/) (22). Drug sensitivity data (area under the curve—AUC) of OSCC cells from the Cancer Therapeutics Response Portal (CTRP v.2.0) and PRISM Repurposing dataset (19Q4) were acquired from the dependency map (DepMap) portal (https://depmap.org/portal/). The ICB treatment cohort GSE91061 (23) was downloaded from the GEO database [FPKM in log2(x + 1)] transformed and used for subsequent validation. The CheckMate 009 (CM-009), CheckMate 010 (CM-010), and CheckMate 025 (CM-025) (24) were combined together to investigate the significance of our risk score [FPKM in log2(x + 1)]. We also downloaded RNA-seq (count values) data of IMvigor210 cohort (25) with clinical information by the "IMvigor210CoreBiologies" R package and transformed it into FPKM values. The log2(FPKM + 1) was calculated on expression data for further comparison.

TABLE 1 | Clinical and molecular information included in the study.

Cohort	TCGA-RNA-seq, OSCC (n = 309)	GSE41613, OSCC (n = 97)
Database	TCGA	GSE41613
Age (years)	61.82 ± 13.06	
Gender		
Male	209	66
Female	100	31
Overall survival (months)	29.72 ± 29.44	44.13 ± 26.52
Angiolymphatic invasion		
Yes	71	
No	159	
Unavailable	79	
Perineural invasion		
Yes	133	
No	109	
Unavailable	67	

Consensus Clustering Analysis

Unsupervised clustering was applied to recognize different hypoxia patterns and classify OSCC patients for further analysis. A consensus hierarchical clustering algorithm based on the expression of 34 prognostic hypoxia genes was conducted by the "ConsensusClusterPlus" R package with Euclidean distance and Ward.D2's linkage (number of bootstraps=50, item subsampling proportion = 0.8, feature subsampling proportion = 0.8).

Survival Analysis

Univariate Cox regression analysis was conducted to identify prognostic hypoxia genes and clinical events. Multivariate Cox regression analysis was performed to recognize independent prognostic factors. The Kaplan–Meier survival curve was applied to analyze the prognostic significance between distinct groups.

Single-Sample Gene Set Enrichment Analysis

The hypoxia-associated gene sets were downloaded from GSEA. The single-sample gene set enrichment analysis (ssGSEA)

algorithm in "GSVA" R package was conducted to calculate the hypoxia score of each OSCC patient.

Mutation Analysis

The MAF file of OSCC containing the detailed mutation information of the training set was downloaded from TCGA (https://portal.gdc.cancer.gov/) and further processed. The "maftool" R package was performed to analyze gene mutant features between two OSCC subclasses.

Function Enrichment Analysis

The "Limma" R package was applied to identify differential genes between two clusters with a standard of |log FC| >1.2 and adjusted *P*-value <0.05. Further gene ontology (GO) function enrichment of selected genes was performed by ClueGO in Cytoscape.

Tumor Microenvironment Analysis

The immune score and the tumor purity were calculated by the ESTIMATE algorithm (26). The CIBERSORT algorithm was applied to evaluate the *LM22* gene signatures in OSCC subtypes (27). What is more, the Epic algorithm was also used to calculate the contents of immune cell infiltration in the microenvironment (28).

Screening Potential Agents of Cluster 2

k-Nearest neighbor (k-NN) imputation was performed to impute the missing AUC values of the CTRP and PRISM datasets. Before imputation, drugs with more than 20% of missing data were excluded. Furthermore, the "pRRophetic" R package was performed to measure the AUC values of samples by ridge regression.

Development and Validation of Predictive Risk Score

Considering the difference of each platform, before developing or validating the risk score, we conducted z-scale of the mRNA data in each platform (TCGA, GSE41613, GSE91061, CM cohorts, and IMvigor210). Then, the "glmnet" R package was performed to filter the prognosis-related hypoxia genes by LASSO Cox regression analysis with a 10-fold cross-validation. After identifying the significant genes, their regression coefficients (β) were estimated by multivariate Cox regression *via* LASSO, and we calculated the risk score of each OSCC patient by the formula as follows:

$$\text{Risk score} = \Sigma_i Coefficient(mRNAi) \times Expression(mRNAi)$$

Establishment of a Nomogram

Univariate Cox and multivariate Cox regression analyses of some clinical traits were first performed and finally determined a sum of four independent prognostic factors for further establishment. Afterward, a nomogram with the four factors was developed for predicting 1- and 3-year OS of OSCC patients. The calibration plot was performed to estimate the accuracy and consistency of the prognostic models. Survival net benefits of each variable were estimated with decision curve analysis (DCA) by "stdca.R."

Other Bioinformatics Analysis

Principal components analysis (PCA) was applied to verify the hypoxia patterns of different subtypes. Potential ICB response was predicted by the tumor immune dysfunction and exclusion (TIDE) algorithm (29). The "upsetR" R package was used to visualize the intersections between promising agents in different subtypes.

Statistical Analysis

R 4.0.2 (https://www.r-project.org/) was mainly used for statistical analysis. Student's *t*-test or one-way analysis of variance was used to analyze differences between groups in variables with a normal distribution. Categorical variables between two groups were compared using chi-square test. A two sided *P*-value <0.05 was considered statistically significant.

RESULTS

Identification of Two Hypoxia-Associated Clusters in OSCC

As depicted in **Figure 1A**, a brief flowchart was demonstrated to introduce our study. Considering the critical role of hypoxia condition in the tumor microenvironment, we summarized a sum of 188 classical hypoxia-stimulated genes available from GSEA and estimated their prognostic value for further classification (**Table S1**). Univariate Cox proportional hazards model was conducted and finally filtered 34 genes with significant risks on survival of patients in the training set (**Figures S1A, B**). Hence, based on the expression similarity of the 34 hypoxia-related gene signature, the consensus clustering method was used to cluster the samples. We selected $k = 2$ as the optimal number of clusters, which could divide all samples into two groups with less correlation between groups in the training and testing cohorts (**Figures 1B, C**). Then, PCA was conducted to compare the transcriptional profile between these two clusters in the two cohorts, suggesting a significant distinction between these two subgroups (**Figures 1D, E**). In order to evaluate the clinical relevance of this clustering, the survival analysis between the two subclasses was conducted. In these two sets, cluster 2 was consistently associated with worse prognosis, highlighting the potential clinical utility of this hypoxia-associated subtyping (**Figures 1F, G**).

Distinct Hypoxia Conditions Between the Two OSCC Clusters

To better understand the hypoxia status of the two clusters, we conducted the ssGSEA algorithm to calculate the scores of some hypoxia-associated processes. As expected, patients in cluster 2 were enriched in higher hypoxia condition in the training and testing cohorts (**Figure 2A**). What is more, a total of nine hypoxia-associated key genes were also verified to be highly expressed in cluster 2, which was consistent with the aforesaid ssGSEA result (**Figure 2B**). Hence, we could define cluster 2 as a "high hypoxia subclass" compared with cluster 1.

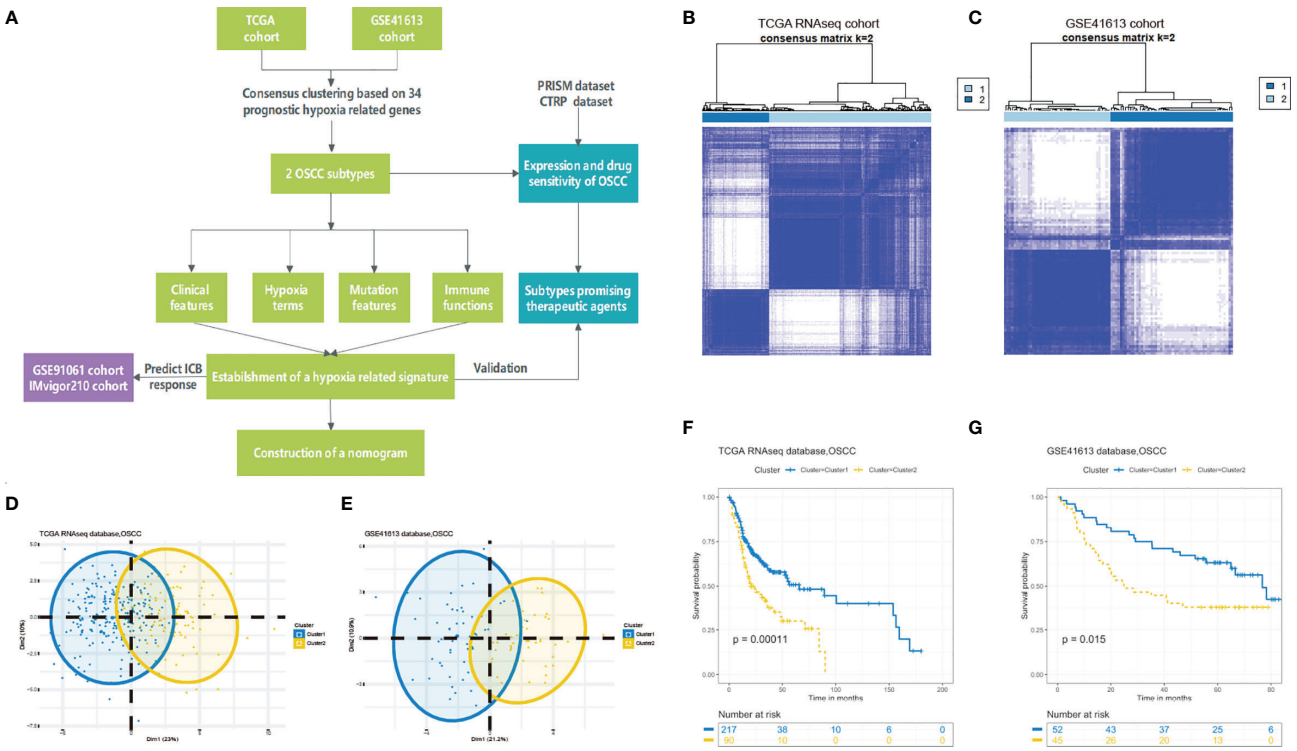

FIGURE 1 | Identification of hypoxia-related clusters in oral squamous cell carcinoma (OSCC). **(A)** Overview of the analysis procedures. **(B, C)** Unsupervised clustering of OSCC patients based on the hypoxia-associated genes generated two clusters in the TCGA and GSE41613 cohorts. **(D, E)** Principal component analysis based on hypoxia genes distinguished two identified subtypes in different cohorts. **(F, G)** Kaplan–Meier survival analysis of overall survival between the two clusters in the two cohorts.

Mutation Alterations in the Two Subclasses

Recent studies have reported the hypoxia phenotype associated with gene mutations (30). We further investigated the difference of gene mutations among these two clusters. As illustrated in the waterfall plot, differently mutated genes were detected between the two clusters and *GNPTAB* was finally identified as the most differentially highly mutated gene in cluster 2 (**Figure 3A**) ($P < 0.01$). Furthermore, based on the oncodriveCLUST algorithm, we predicted *HRAS* as the driver gene candidate in cluster 1 and *MAST4* in cluster 2 (**Figure 3B**). What is more, tumor mutational burden (TMB) was significantly increased in cluster 2 (**Figure 3C**).

High Correlation Between Hypoxia-Related Gene-Based Clusters With Immune Infiltration

To obtain deeper insights into the molecular characteristics of the two OSCC clusters, we conducted the differentially expressed genes (DEGs) analysis and their GO analysis in the training dataset. With a threshold of |log2 FC| >1.2 and adjusted *P*-value <0.05, a sum of 55 DEGs were identified for the two clusters. The expressions of DEG between these two clusters were demonstrated by a heatmap (**Figure S2A**). GO analysis based on Cytoscape showed that the cluster-specific genes were significantly enriched in immune cell infiltration, suggesting a distinct immune difference between these two clusters (**Figure S2B**).

Immune Microenvironment Features Between the Two Clusters

To reveal the difference of these two clusters on the tumor microenvironment, we first calculated the immune score and tumor purity both in the training and testing sets based on the ESTIMATE algorithm. We found that the immune score was decreased and purity score was elevated in cluster 2 compared with cluster 1 (**Figures 4A** and **S3A**). With the significant difference in immune score and purity score identified between clusters, we further compared the relative ratio of 22 kinds of immune cells by the CIBERSORT algorithm. There existed six immune cell populations significantly differently enriched between the two clusters in the training set and nine immune cells in the testing set (**Figures 4B** and **S3B**). Combined, macrophages M0, activated mast cells, were enriched in cluster 2, while CD8 T cells, resting mast cells, were deficient in both two sets. We further conducted the Epic algorithm to validate our results and found that only CD8 T cells were consistently lacking in cluster 2 in the two cohorts (**Figures 4C** and **S3C**). CD8 T cell, also known as cytotoxic T cell (CTL), exerted a critical role in

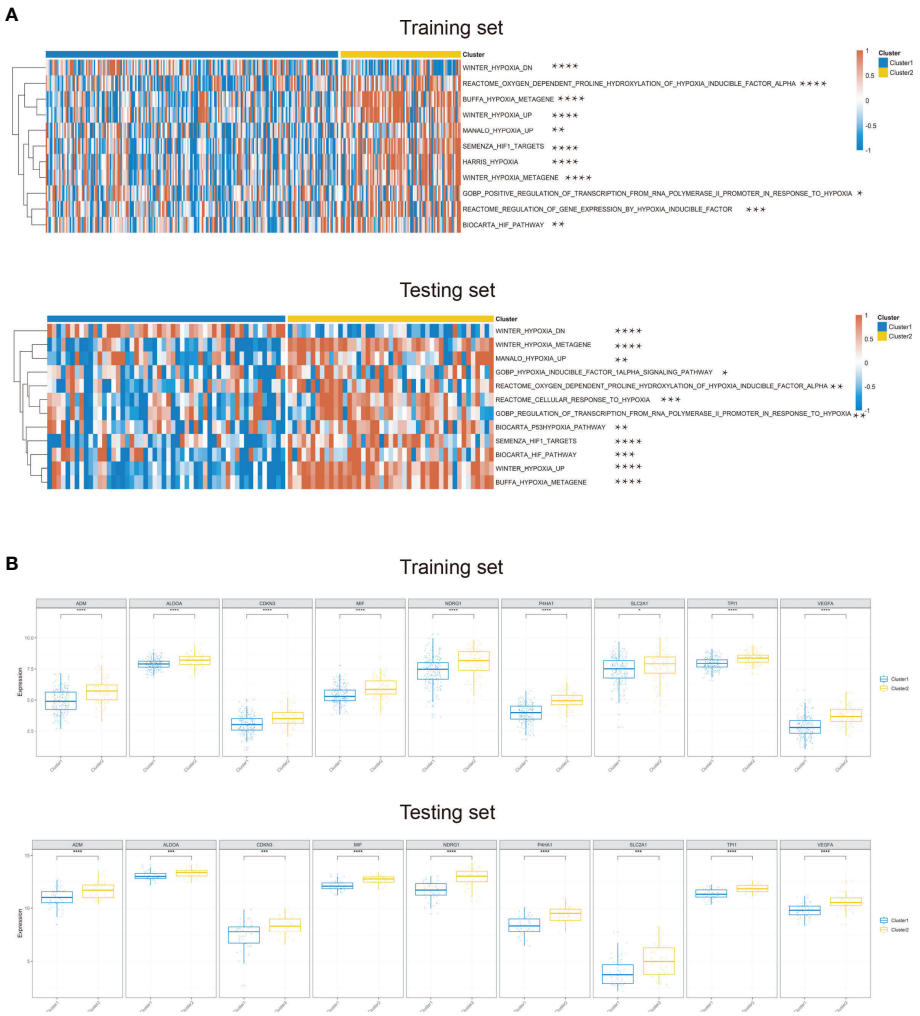

FIGURE 2 | Differential hypoxia conditions across two identified clusters. **(A)** Heatmap of the significant differential hypoxia pathways of two OSCC clusters based on ssGSEA in the training set and testing set. **(B)** The expression of nine hypoxia key genes upregulated in cluster 2 in the training and testing sets (*$P < 0.05$, **$P < 0.01$, ***$P < 0.001$, ****$P < 0.0001$).

antitumor immunity. We further examined two indicators of T-cell killing ability between the two clusters. Similarly, cluster 2 also exhibited lower CYT score and IFNG expression than cluster 1 in the training set and testing set, which was consistent with previous studies that showed an association between high CYT levels and higher patient OS (**Figures 4D** and **S3D**). Taken together, it was the lower composition of CD8 T cells and their disability of killing tumor cells that led a worse prognosis in cluster 2.

Identification of the Potential Treatment Strategy of the Two Clusters

After investigating the distinct molecular and biological characters between these two clusters, we sought to explore specific treatment options for each cluster. Considering the vital role of CD8 T cells in immunotherapy and their significant differences between the two clusters, we further assessed their immunotherapy response based on the TIDE method. In both training set and testing set, the TIDE score was significantly lower in cluster 1 compared with cluster 2, indicating patients in cluster 1 might be more sensitive to ICB therapy (**Figure 5A**). For cluster 2 patients, we hoped to seek for traditional chemotherapeutics to achieve targeted therapy. After the filtering procedure described in the *Material and Methods*, we finally obtained 16 OSCC cells with 913 drugs in the PRISM and 22 OSCC cells with 465 drugs in the CTRP dataset. The pRRophetic package with a built-in ridge regression model was then applied to predict the drug response of clinical samples in the training set based on their expression profiles, and the estimated AUC value of each compound in each sample was thus obtained. We finally identified four agents simultaneously with lower AUC values in cluster 2 both in the PRISM- and CTRP-predicted datasets (**Figures 5B, C** and **S4**). To further filter a more therapeutically significant drug in OSCC, we took

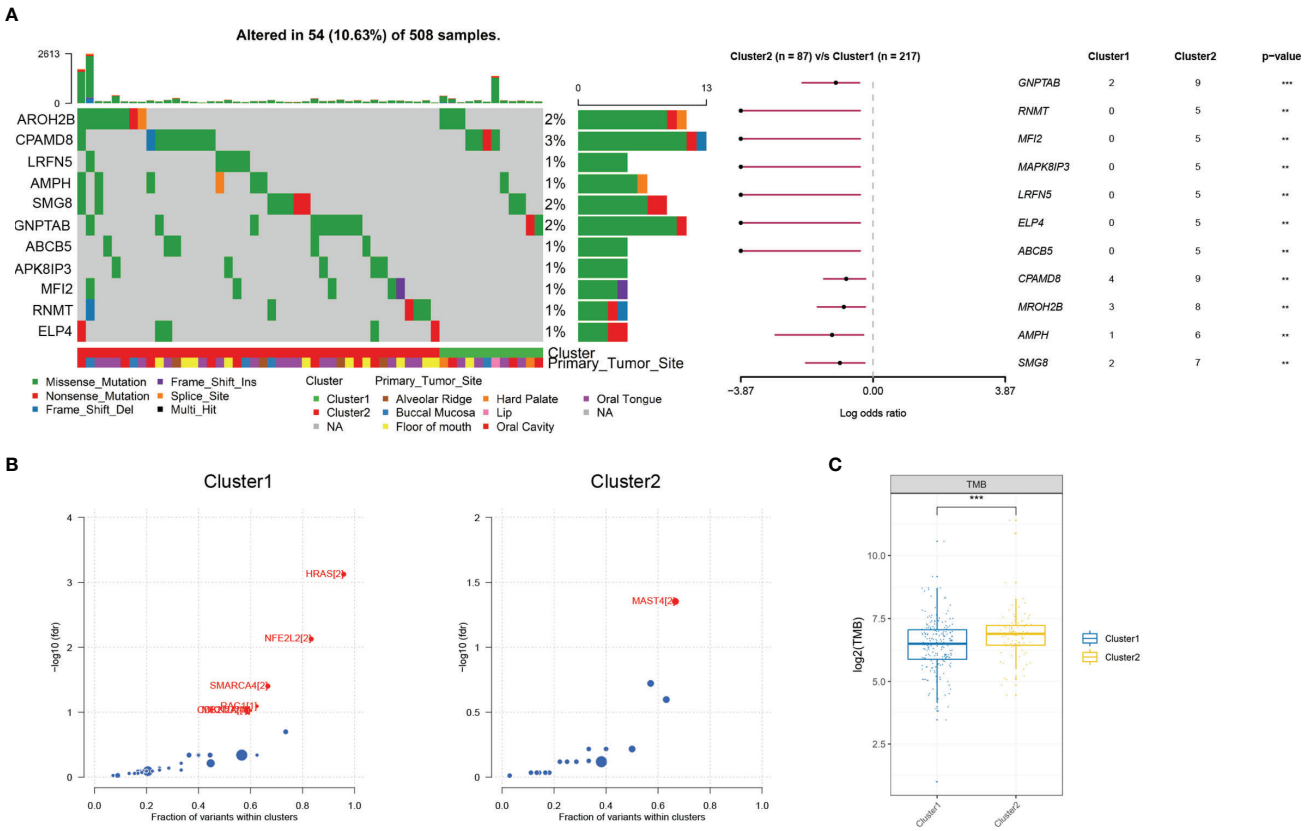

FIGURE 3 | Mutational alterations between two hypoxia clusters in the TCGA cohort. **(A)** Top 11 most differently mutated genes depicted in the two clusters. **(B)** *HRAS* or *MAST4* respectively identified as the driver gene candidate for cluster 1 or cluster 2. **(C)** Tumor mutational burden significantly increased in cluster 2 (**$P < 0.01$, ***$P < 0.001$).

their clinical phase and experimental evidence from the literature into account. Finally, we identified only bortezomib as the optimal drug that has the potential for cluster 2 treatment (**Figure 5D**).

Development and Validation of Hypoxia-Associated Prognostic Signature

To establish a signature for clinical implications, it is of great significance to filter the most representative genes of each cluster. Considering HIF1A serving as the key transcription factor in hypoxia, we intersected the DEGs between the two clusters with 4,748 potential targets of HIF1A in OSCC and found a sum of 6 candidate genes in the intersection (**Figure 6A**), identified as "Clustering-specific hypoxia-related genes." To obtain the most powerful prognostic markers, the LASSO Cox regression analysis was conducted (**Figure 6B**). A total of five gene signatures were generated and the coefficients were estimated by multivariate Cox regression *via* LASSO (**Table S2**). There existed a transcriptional difference between the two clusters (**Figure 6C**). After calculating the risk scores of the signature based on the regression coefficients, we intriguingly found that cluster 2 possessed a higher score in the two cohorts (**Figures 6D, E**). Further survival analysis revealed that patients in the high-score group exhibited significantly worse prognosis than OSCC patients or cluster 1 patients with low-score (**Figures 6F, G**). Although there was no significant survival difference between high and low scores in cluster 2 in the training set ($P = 0.1$) and testing set ($P = 0.13$), it was still obvious that a high hypoxia score was associated with the tendency toward worse prognosis (**Figures 6F, G**). The results were consistent with the above data that cluster 2 conferred the poorer prognosis. In order to determine the prognostic significance of the signature in other organ sites, we conducted the survival analysis of our hypoxia score across 33 TCGA cancer types. Similarly, the hypoxia risk score also served as an unfavorable prognostic biomarker for pancancer (**Figure 6H**). What is more, the predicted AUC values of bortezomib from CTRP and PRISM were also decreased in the high hypoxia score group, validating its promising clinical value for high-risk OSCC patients (**Figures 6I, J**).

Construction of a Nomogram for Predicting OSCC Survival

To verify whether the hypoxia-related signature was an independent prognostic factor, univariate and multivariate Cox regression analyses were conducted (**Figures 7A, B**). The results in univariate Cox regression revealed that risk score, age, and

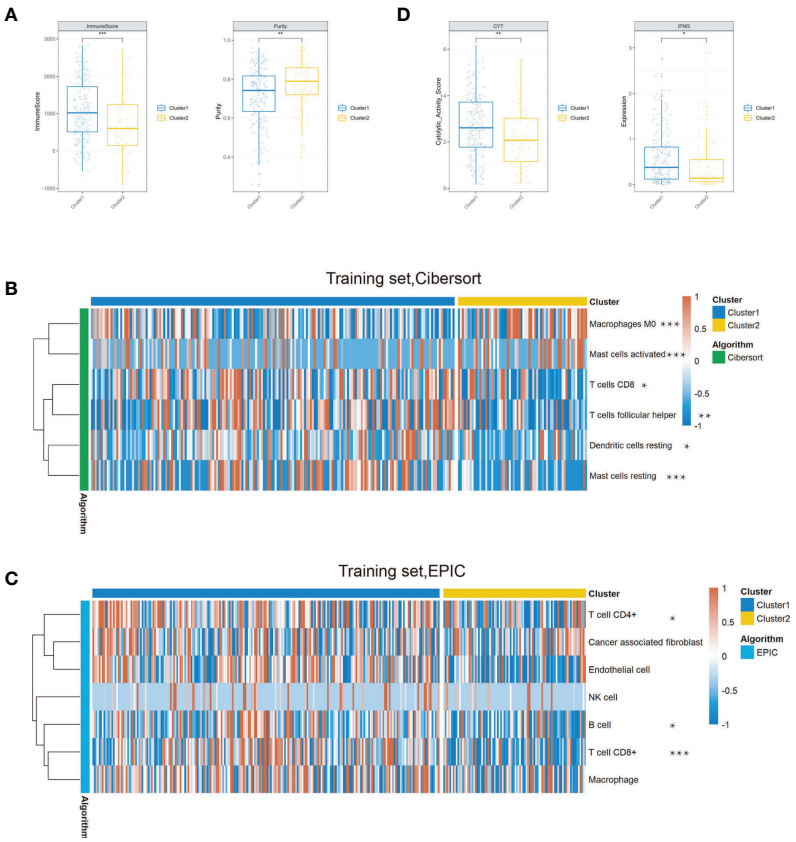

FIGURE 4 | Comparison of the immune conditions and TME between the two clusters in the training set. **(A)** Cluster 2 occupied a lower immune score and a higher purity than cluster 1. **(B)** Composition of the six significantly differential immune cells between the two clusters based on the CIBERSORT algorithm. **(C)** The Epic algorithm illustrated the immune cell difference between the two clusters. **(D)** The CYT score and IFNG expression significantly decreased in cluster 2 (*$P < 0.05$, **$P < 0.01$, ***$P < 0.001$).

angiolymphatic and perineural invasion had a significant association with the OS of OSCC patients. In multivariate Cox regression, risk score, age, and angiolymphatic and perineural invasion were identified as independent prognostic factors of OSCC. Then, we applied these four independent factors to establish a nomogram for predicting OSCC 1- and 3-year OS (**Figure 7C**). With the score increasing, the OS of patients decreased. Moreover, the calibration plots at 1 and 3 years approached 45 degrees, indicating a great performance of the established nomogram (**Figure 7D**). Meanwhile, DCA was performed to compare the clinical usability and benefits of the nomogram with that of the age and angiolymphatic and perineural invasion. As shown in **Figure 7E**, compared with age and angiolymphatic and perineural invasion, the 1-year DCA curves of the new nomogram showed larger net benefits across a range of death risk.

Predictive Value of Hypoxia-Related Risk Score in Immunotherapy

Immunotherapy has been proven relevant to improve survival in the treatment of multiple tumor types. Thus, identification of patients who will benefit most from ICB treatment is of great necessity. Our analysis revealed that the TIDE was significantly increased in the high hypoxia score group, indicating its crucial role in regulating immune response (**Figure 8A**). Based on three immunotherapy cohorts, we identified that patients with a high hypoxia score group always exhibited clinical disadvantages and markedly shortened survival ($P = 0.026$ in GSE91061, $P = 0.039$ in CM009+010+025 cohorts, and $P = 0.029$ in IMvigor210) (**Figures 8B, C, E**). In CM009+010+025 cohorts, the chi-squared test conducted between low and high hypoxia score groups demonstrated significantly better therapeutic outcomes in low score patients (**Figure 8D**). Similarly, patients with high hypoxia scores exhibited less treatment effectiveness in the IMvigor210 cohort (**Figure 8F**). We also compared the hypoxia score levels in the three immune subtypes of IMvigor210. The immune-inflamed subtype showed significantly the lowest risk score, which further confirmed our analysis above (**Figure 8G**). In addition, TMB was significantly decreased in the high-score group (**Figure 8H**). In all, our results strongly suggested that hypoxia score was associated with the response to immunotherapy and could further effectively predict the prognosis of patients.

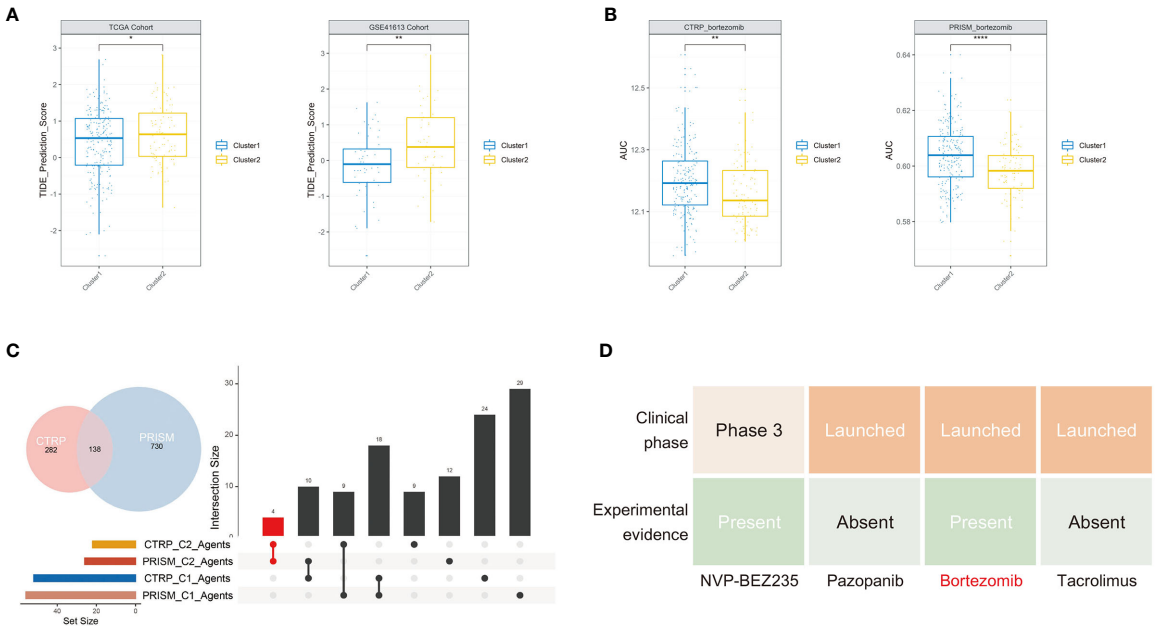

FIGURE 5 | Potential treatment strategy of the two clusters. **(A)** Cluster 2 group occupied a significantly higher TIDE score in the two cohorts. **(B)** The predicted AUC values of bortezomib from the CTRP and PRISM cohorts were decreased in cluster 2 patients. **(C)** The upsetR plot revealed only the AUC of four agents simultaneously decreased in cluster 2 patients estimated by the CTRP and PRISM cohorts. **(D)** Identification of the most promising cluster 2-specific agents according to evidence from multiple sources (*$P < 0.05$, **$P < 0.01$, ****$P < 0.0001$).

DISCUSSION

The tumor microenvironment is composed of not only the solid tumor tissue but also the surrounding vessels, fibroblasts, distinct immune cells, and extracellular matrix (31, 32). The imbalance between excessive oxygen demand and insufficient oxygen supply shaped a hypoxic microenvironment, leading to a malignant progression of tumor (33). As a hallmark of tumor, hypoxia exerts a crucial significance in different biological processes, including multiple metabolic forms, immune escape, angiogenesis, and metastasis (34). What is more, the crosstalk between tumor cells and other non-tumor cells under a hypoxic microenvironment could also induce therapeutic resistance, resulting in failure of treatment and poor clinical outcome. Considering hypoxia as an emerging biomarker and target in cancer therapy, exploring the effect of hypoxia in the tumor microenvironment is of great necessity.

Up till now, more and more studies emphasize the importance of molecular subtyping, which could direct individualized treatment (35, 36). The classification based on hypoxia genes and the generation of related signatures have been conducted in many cancer types including breast cancer, lung adenocarcinoma, and glioma to discriminate high-risk subclass and to predict survival (21, 37, 38). However, the relationships between hypoxia with clinical outcomes, genomic alterations, and therapeutic responses remain obscure in OSCC. Identifying different hypoxia patterns and generating a related signature in OSCC are beneficial to deepen our understanding of hypoxic microenvironment in OSCC progression and improve the outcome of cancer treatment.

In our study, we recognized two hypoxia-associated patterns that have different characteristics by unsupervised clustering of the gene expression of hypoxia genes. Cluster 2 patients were characterized by higher hypoxia degree, leading to a survival disadvantage over cluster 1. We also explored different mutated patterns between the two clusters. Moreover, we identified hypoxia signature genes by conducting differentially expressed analysis between the two subtypes. In agreement with the association of hypoxia status with abnormal immune response, we found that the signature genes were correlated with distinct immune cell infiltration. In the tumor microenvironment (TME), CD8 + CTLs are the immune cells of first choice for targeting cancer. During cancer progression, CTL encounters dysfunction and exhaustion due to immune-related tolerance and immunosuppression in TME, all of which contribute to adaptive immune resistance. Through multiple algorithms in the two databases, we identified CD8 T cells consistently deficient in cluster 2, which might be a major cause of its poorer prognosis and its worse immunotherapy response.

Thinking of the heterogeneity of hypoxia conditions, it was essential to quantify the hypoxia-associated character in OSCC. Hence, we further established a hypoxia-related scoring system and validated it in two cohorts. The estimated risk score was elevated in cluster 2, which was consistent with its worse prognostic significance. Multivariate Cox analysis also revealed the score as an independent prognostic factor in OSCC. Furthermore, the predictive potential of this prognostic risk

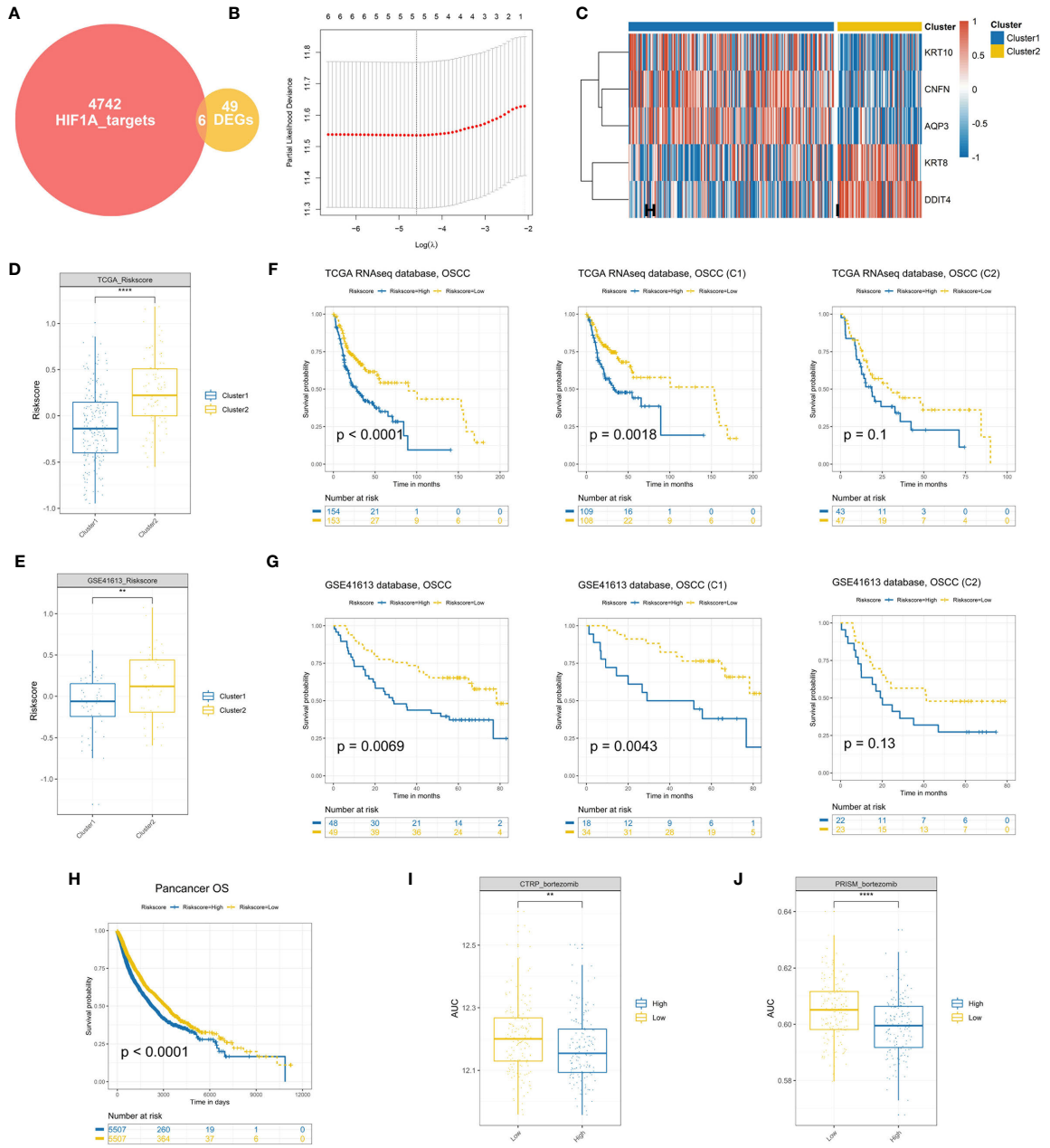

FIGURE 6 | Establishment and validation of a hypoxia prognostic signature **(A)**. A total of six candidate genes were identified in the intersection of "HIF1A targets" and "DEGs." **(B)** Cross-validation for tuning parameter selection in the proportional hazards model. **(C)** Differential expression of genes in hypoxia signature. **(D, E)** Cluster 2 patients conferred a significantly higher hypoxia risk scores in the TCGA and GSE41613 cohorts. **(F, G)** Survival analysis of the hypoxia-associated signature in OSCC or OSCC subtypes. **(H)** The prognostic significance of the established signature across 33 cancer types. **(I, J)** The predicted AUC values of bortezomib from the CTRP and PRISM datasets were decreased in the high-risk score OSCC patients (**$P < 0.01$, ****$P < 0.0001$).

score model was generated by combining it with several clinical features in a risk assessment nomogram.

In view of the clinical significance of our study, we respectively investigated different treatment strategies for distinct subclasses in line with the concept of precision treatment. For cluster 1 with a better prognosis, we recommended the recently widely used ICB treatment, while for cluster 2 patients, we screened bortezomib as the promising agent to improve the outcome of this subtype. What is more, the ideal drug was also applied to OSCC patients with high hypoxia-related risk score, indicating its clinical transforming value. In addition, the risk score we established could also predict the efficacy of immune checkpoint therapy and

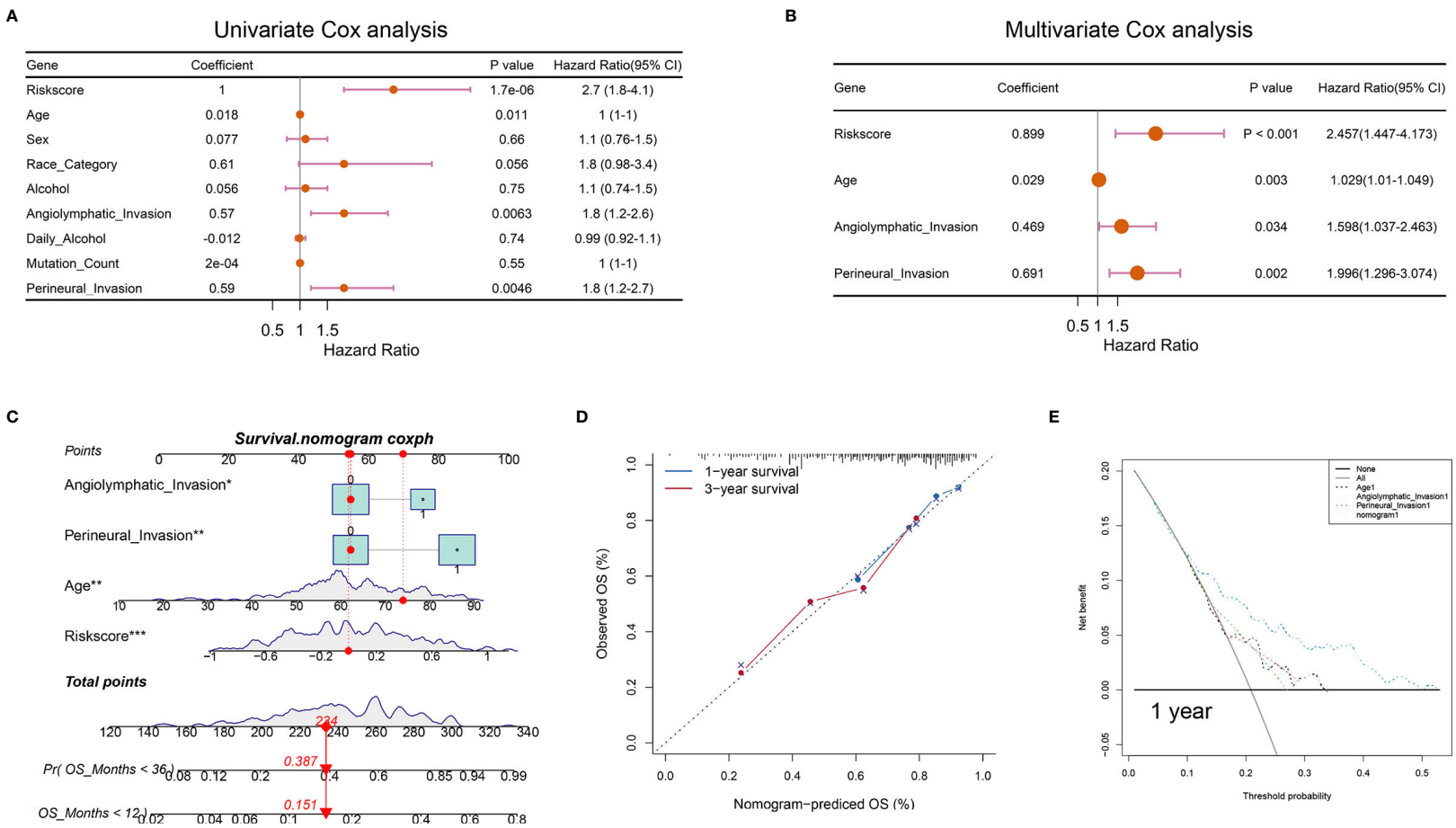

FIGURE 7 | Nomograms according to the OS-associated hypoxia scores for OSCC patients in the TCGA cohort. **(A, B)** The univariate and multivariate Cox regression analyses of OS-associated variables. **(C)** Establishment of a nomogram to predict the OS of OSCC patients. **(D)** The calibration curve revealed the high consistency between the nomogram-predicted OS with actual OS. **(E)** Decision curve analysis for the nomogram and other clinical features in the prediction of prognosis of OSCC patients at 1-year point (*$P < 0.05$, **$P < 0.01$, ***$P < 0.001$).

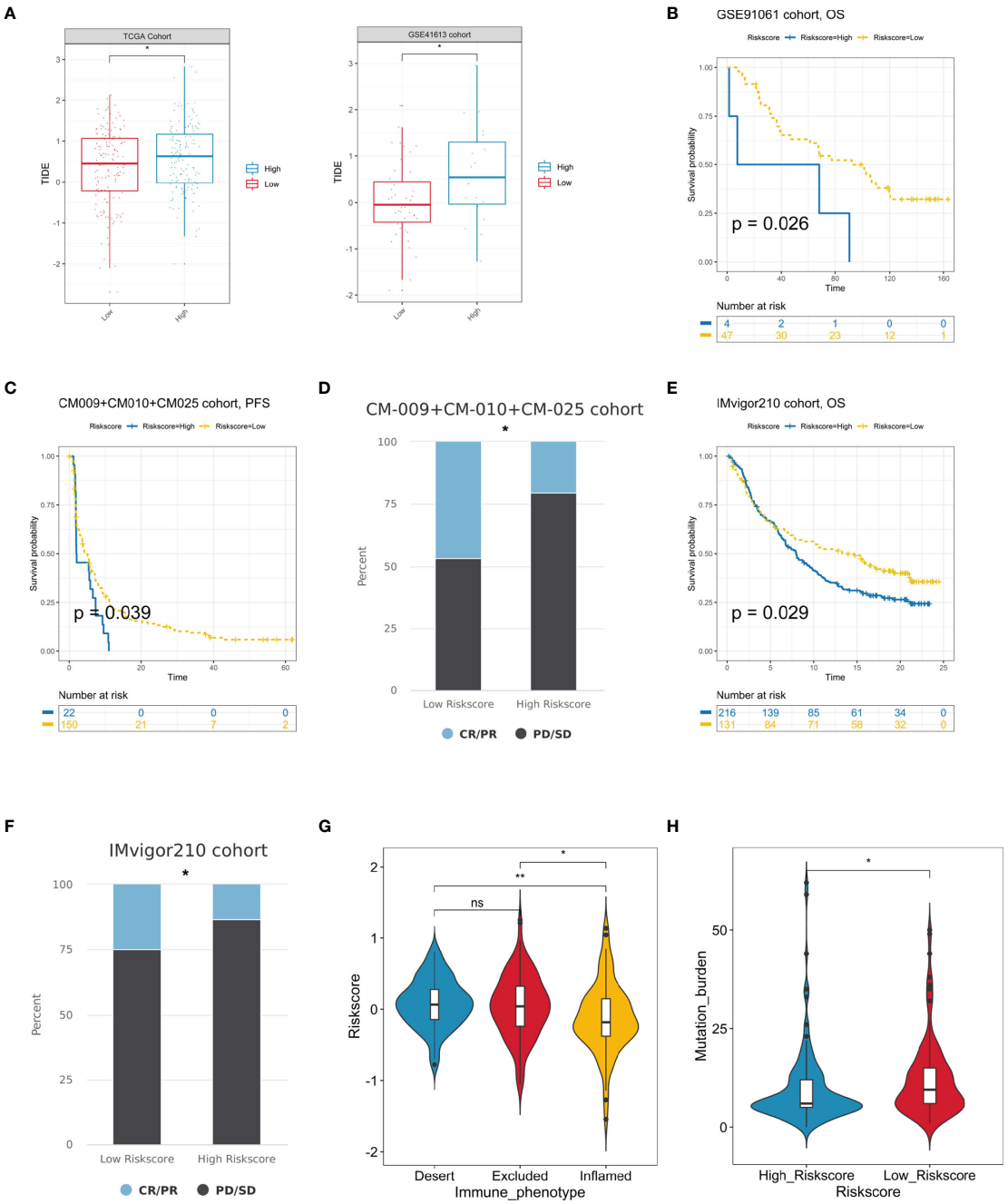

FIGURE 8 | Prediction of immunotherapeutic benefits by hypoxia score. **(A)** TIDE scores were increased in the high hypoxia risk score group in the TCGA and GSE41613 cohorts. **(B, C)** The survival analysis of the high and low hypoxia risk score groups in the GSE91061 and CM-009+CM-010+CM025 immunotherapy cohorts. **(D)** The immunotherapy response patients (CR/PR) more distributed in lower risk score patients, while non-response ones (PD/SD) enriched in higher risk score patients in the CM-009+CM-010+CM025 cohorts. **(E)** High-risk score patients occupied a significantly reduced overall survival in the Imvigor210 cohort. **(F)** Various fractions of clinical outcome patients in the high and low hypoxia risk score groups in the IMvigor210 cohort. **(G)** The difference of hypoxia risk scores in the three immune subtype groups in the IMvigor210 cohort. **(H)** Differences in TMB between high- and low-risk score groups in the IMvigor210 cohort (ns, no significance, $^{*}P < 0.05$, $^{**}P < 0.01$).

might promote personalized OSCC immunotherapy in future ICB treatment.

In summary, we recognized two different subclasses with a distinct immune microenvironment in OSCC based on hypoxia condition and explored the treatment of each subtype. We also established an individual hypoxia-associated score system which could predict the survival and the efficacy of immunotherapy. These findings provide a novel, efficient, and accurate predictive

model in the prognosis and response to immunotherapy, thus promoting personalized cancer chemotherapy and immunotherapy in the future.

DATA AVAILABILITY STATEMENT

The original contributions presented in the study are included in the article/**Supplementary Material**. Further inquiries can be directed to the corresponding author.

AUTHOR CONTRIBUTIONS

Concept and design: CL and ZZ. Data download and curation: XC, XR, JC, HC, JY, XMC, and SK. Data analyses: CL, XC, XR, and QR. Manuscript writing and revision: CL, XC, XR, and ZZ. All authors contributed to the article and approved the submitted version.

ACKNOWLEDGMENTS

We thank the members of Dr. Zhao ZJ's laboratory for help with our study.

SUPPLEMENTARY MATERIAL

The Supplementary Material for this article can be found online at: https://www.frontiersin.org/articles/10.3389/fonc.2021.709865/full#supplementary-material

Supplementary Figure 1 | Screening of the significantly prognostic hypoxia genes in TCGA cohort. **(A)** Univariate Cox regression analysis of 200 classical hypoxia stimulated genes in TCGA cohort (The forest plot only illustrated the significant genes).

Supplementary Figure 2 | Identification of the DEGs and related functions between two clusters in TCGA cohorts. **(A)** The DEGs heatmap between two clusters in OSCC. **(B)** Cluego illustrated a high correlation with immune cells infiltration.

Supplementary Figure 3 | The TME characteristics between two clusters in GSE41613 cohort. **(A)** Cluster2 patients conferred lower immune scores and higher tumor purity than Cluster1. **(B)** The significant immune cells difference between two clusters estimated by Cibersort algorithm. **(C)** EPIC algorithm revealed 7 immune cells difference in two clusters. **(D)** The CYT score but not the IFNG expression significantly decreased in Cluster2 patients. (*P < 0.05, **P < 0.01, ***P < 0.001, ****P < 0.0001, NS, not significant)

Supplementary Figure 4 | Compare of two Clusters' predicted AUC of another three drugs in TCGA cohorts. **(A)** The AUC values of another three agents predicted from CTRP and PRISM **(B)** were significantly decreased in Cluster2 patients. **P < 0.01, ***P < 0.001, ****P < 0.0001)

REFERENCES

1. Comprehensive Genomic Characterization of Head and Neck Squamous Cell Carcinomas. *Nature* (2015) 517:576–82. doi: 10.1038/nature14129
2. Zhang L, Meng X, Zhu XW, Yang DC, Chen R, Jiang Y, et al. Long Non-Coding RNAs in Oral Squamous Cell Carcinoma: Biologic Function, Mechanisms and Clinical Implications. *Mol Cancer* (2019) 18:102. doi: 10.1186/s12943-019-1021-3
3. Bray F, Ferlay J, Soerjomataram I, Siegel RL, Torre LA, Jemal A. Global Cancer Statistics 2018: GLOBOCAN Estimates of Incidence and Mortality Worldwide for 36 Cancers in 185 Countries. *CA Cancer J Clin* (2018) 68:394–424. doi: 10.3322/caac.21492
4. Quan J, Johnson NW, Zhou G, Parsons PG, Boyle GM, Gao J, et al. Potential Molecular Targets for Inhibiting Bone Invasion by Oral Squamous Cell Carcinoma: A Review of Mechanisms. *Cancer Metastasis Rev* (2012) 31:209–19. doi: 10.1007/s10555-011-9335-7
5. Huang GZ, Wu QQ, Zheng ZN, Shao TR, Chen YC, Zeng WS. M6A-Related Bioinformatics Analysis Reveals That HNRNPC Facilitates Progression of OSCC *via* EMT. *Aging (Albany NY)* (2020) 12:11667–84. doi: 10.18632/aging.103333
6. Hou C, Cai H, Zhu Y, Huang S, Song F, Hou J. Development and Validation of Autophagy-Related Gene Signature and Nomogram for Predicting Survival in Oral Squamous Cell Carcinoma. *Front Oncol* (2020) 10:558596. doi: 10.3389/fonc.2020.558596
7. Wang J, Wang Y, Kong F, Han R, Song W, Chen D, et al. Identification of a Six-Gene Prognostic Signature for Oral Squamous Cell Carcinoma. *J Cell Physiol* (2020) 235:3056–68. doi: 10.1002/jcp.29210
8. Gilkes DM, Semenza GL, Wirtz D. Hypoxia and the Extracellular Matrix: Drivers of Tumour Metastasis. *Nat Rev Cancer* (2014) 14:430–9. doi: 10.1038/nrc3726
9. Muz B, de la Puente P, Azab F, Azab AK. The Role of Hypoxia in Cancer Progression, Angiogenesis, Metastasis, and Resistance to Therapy. *Hypoxia (Auckl)* (2015) 3:83–92. doi: 10.2147/HP.S93413
10. Krzywinska E, Kantari-Mimoun C, Kerdiles Y, Sobecki M, Isagawa T, Gotthardt D, et al. Loss of HIF-1α in Natural Killer Cells Inhibits Tumour Growth by Stimulating Non-Productive Angiogenesis. *Nat Commun* (2017) 8:1597. doi: 10.1038/s41467-017-01599-w
11. Sasidharan Nair V, Saleh R, Toor SM, Cyprian FS, Elkord E. Metabolic Reprogramming of T Regulatory Cells in the Hypoxic Tumor Microenvironment. *Cancer Immunol Immunother* (2021). doi: 10.1007/s00262-020-02842-y
12. Norris PC, Libreros S, Serhan CN. Resolution Metabolomes Activated by Hypoxic Environment. *Sci Adv* (2019) 5:eaax4895. doi: 10.1126/sciadv.aax4895
13. Park MJ, Iyer S, Xue X, Bragazzi Cunha J, Gu S, Moons D, et al. HIF1-Alpha Regulates Acinar Cell Function and Response to Injury in Mouse Pancreas. *Gastroenterology* (2018) 154:1630–4.e3. doi: 10.1053/j.gastro.2018.01.037
14. Hugo W, Zaretsky JM, Sun L, Song C, Moreno BH, Hu-Lieskovan S, et al. Genomic and Transcriptomic Features of Response to Anti-PD-1 Therapy in Metastatic Melanoma. *Cell* (2016) 165:35–44. doi: 10.1016/j.cell.2016.02.065
15. Ferris RL, Blumenschein G Jr, Fayette J, Guigay J, Colevas AD, Licitra L, et al. Nivolumab for Recurrent Squamous-Cell Carcinoma of the Head and Neck. *N Engl J Med* (2016) 375:1856–67. doi: 10.1056/NEJMoa1602252
16. Rizvi NA, Hellmann MD, Snyder A, Kvistborg P, Makarov V, Havel JJ, et al. Cancer Immunology. Mutational Landscape Determines Sensitivity to PD-1 Blockade in non-Small Cell Lung Cancer. *Science* (2015) 348:124–8. doi: 10.1126/science.aaa1348
17. Brahmer J, Reckamp KL, Baas P, Crinò L, Eberhardt WE, Poddubskaya E, et al. Nivolumab Versus Docetaxel in Advanced Squamous-Cell Non-Small-Cell Lung Cancer. *N Engl J Med* (2015) 373:123–35. doi: 10.1056/NEJMoa1504627
18. Shitara K, Özgüroğlu M, Bang YJ, Di Bartolomeo M, Mandalà M, MH R, et al. Pembrolizumab Versus Paclitaxel for Previously Treated, Advanced Gastric or Gastro-Oesophageal Junction Cancer (KEYNOTE-061): A Randomised, Open-Label, Controlled, Phase 3 Trial. *Lancet* (2018) 392:123–33. doi: 10.1016/S0140-6736(18)31257-1
19. Fuchs CS, Doi T, Jang RW, Muro K, Satoh T, Machado M, et al. Safety and Efficacy of Pembrolizumab Monotherapy in Patients With Previously Treated Advanced Gastric and Gastroesophageal Junction Cancer: Phase 2 Clinical KEYNOTE-059 Trial. *JAMA Oncol* (2018) 4:e180013. doi: 10.1001/jamaoncol.2018.0013
20. Kang YK, Boku N, Satoh T, Ryu MH, Chao Y, Kato K, et al. Nivolumab in Patients With Advanced Gastric or Gastro-Oesophageal Junction Cancer Refractory to, or Intolerant of, at Least Two Previous Chemotherapy

Regimens (ONO-4538-12, ATTRACTION-2): A Randomised, Double-Blind, Placebo-Controlled, Phase 3 Trial. *Lancet* (2017) 390:2461–71. doi: 10.1016/S0140-6736(17)31827-5
21. Shi R, Bao X, Unger K, Sun J, Lu S, Manapov F, et al. Identification and Validation of Hypoxia-Derived Gene Signatures to Predict Clinical Outcomes and Therapeutic Responses in Stage I Lung Adenocarcinoma Patients. *Theranostics* (2021) 11:5061–76. doi: 10.7150/thno.56202
22. Ghandi M, Huang FW, Jané-Valbuena J, Kryukov GV, Lo CC, McDonald ER3rd, et al. Next-Generation Characterization of the Cancer Cell Line Encyclopedia. *Nature* (2019) 569:503–8. doi: 10.1038/s41586-019-1186-3
23. Riaz N, Havel JJ, Makarov V, Desrichard A, Urba WJ, Sims JS, et al. Tumor and Microenvironment Evolution During Immunotherapy With Nivolumab. *Cell* (2017) 171:934–49.e16. doi: 10.1016/j.cell.2017.09.028
24. Braun DA, Hou Y, Bakouny Z, Ficial M, Sant' Angelo M, Forman J, et al. Interplay of Somatic Alterations and Immune Infiltration Modulates Response to PD-1 Blockade in Advanced Clear Cell Renal Cell Carcinoma. *Nat Med* (2020) 26:909–18. doi: 10.1038/s41591-020-0839-y
25. Mariathasan S, Turley SJ, Nickles D, Castiglioni A, Yuen K, Wang Y, et al. Tgfβ Attenuates Tumour Response to PD-L1 Blockade by Contributing to Exclusion of T Cells. *Nature* (2018) 554:544–8. doi: 10.1038/nature25501
26. Bindea G, Mlecnik B, Tosolini M, Kirilovsky A, Waldner M, Obenauf AC, et al. Spatiotemporal Dynamics of Intratumoral Immune Cells Reveal the Immune Landscape in Human Cancer. *Immunity* (2013) 39:782–95. doi: 10.1016/j.immuni.2013.10.003
27. Newman AM, Steen CB, Liu CL, Gentles AJ, Chaudhuri AA, Scherer F, et al. Determining Cell Type Abundance and Expression From Bulk Tissues With Digital Cytometry. *Nat Biotechnol* (2019) 37:773–82. doi: 10.1038/s41587-019-0114-2
28. Racle J, de Jonge K, Baumgaertner P, Speiser DE, Gfeller D. Simultaneous Enumeration of Cancer and Immune Cell Types From Bulk Tumor Gene Expression Data. *Elife* (2017) 6. doi: 10.7554/eLife.26476
29. Jiang P, Gu S, Pan D, Fu J, Sahu A, Hu X, et al. Signatures of T Cell Dysfunction and Exclusion Predict Cancer Immunotherapy Response. *Nat Med* (2018) 24:1550–8. doi: 10.1038/s41591-018-0136-1
30. Bristow RG, Hill RP. Hypoxia and Metabolism. Hypoxia, DNA Repair and Genetic Instability. *Nat Rev Cancer* (2008) 8:180–92. doi: 10.1038/nrc2344
31. Wu T, Dai Y. Tumor Microenvironment and Therapeutic Response. *Cancer Lett* (2017) 387:61–8. doi: 10.1016/j.canlet.2016.01.043
32. Bader JE, Voss K, Rathmell JC. Targeting Metabolism to Improve the Tumor Microenvironment for Cancer Immunotherapy. *Mol Cell* (2020) 78:1019–33. doi: 10.1016/j.molcel.2020.05.034
33. Secomb TW, Hsu R, Ong ET, Gross JF, Dewhirst MW. Analysis of the Effects of Oxygen Supply and Demand on Hypoxic Fraction in Tumors. *Acta Oncol* (1995) 34:313–6. doi: 10.3109/02841869509093981
34. Schito L, Semenza GL. Hypoxia-Inducible Factors: Master Regulators of Cancer Progression. *Trends Cancer* (2016) 2:758–70. doi: 10.1016/j.trecan.2016.10.016
35. Satyal U, Sikder RK, McConkey D, Plimack ER, Abbosh PH. Clinical Implications of Molecular Subtyping in Bladder Cancer. *Curr Opin Urol* (2019) 29:350–6. doi: 10.1097/MOU.0000000000000641
36. Torres C, Grippo PJ. Pancreatic Cancer Subtypes: A Roadmap for Precision Medicine. *Ann Med* (2018) 50:277–87. doi: 10.1080/07853890.2018.1453168
37. Gong PJ, Shao YC, Huang SR, Zeng YF, Yuan XN, Xu JJ, et al. Hypoxia-Associated Prognostic Markers and Competing Endogenous RNA Co-Expression Networks in Breast Cancer. *Front Oncol* (2020) 10:579868. doi: 10.3389/fonc.2020.579868
38. Lin W, Wu S, Chen X, Ye Y, Weng Y, Pan Y, et al. Characterization of Hypoxia Signature to Evaluate the Tumor Immune Microenvironment and Predict Prognosis in Glioma Groups. *Front Oncol* (2020) 10:796. doi: 10.3389/fonc.2020.00796

Conflict of Interest: The authors declare that the research was conducted in the absence of any commercial or financial relationships that could be construed as a potential conflict of interest.

Publisher's Note: All claims expressed in this article are solely those of the authors and do not necessarily represent those of their affiliated organizations, or those of the publisher, the editors and the reviewers. Any product that may be evaluated in this article, or claim that may be made by its manufacturer, is not guaranteed or endorsed by the publisher.

frontiers in Oncology

ORIGINAL RESEARCH
published: 25 November 2021
doi: 10.3389/fonc.2021.735993

A Novel Lipid Prognostic Signature of ADCY2, LIPE, and OLR1 in Head and Neck Squamous Cell Carcinoma

Xiaolei Gao[1,2,3,4†], Na Zhao[5,6,7†], Liying Dong[2], Xuan Zheng[2], Yixin Zhang[2], Chong Ding[1,2], Shuyan Zhao[8], Zeyun Ma[9*] and Yixiang Wang[1,2*]*

[1] Central Laboratory, Peking University School and Hospital of Stomatology, Beijing, China, [2] Department of Oral and Maxillofacial Surgery, Peking University School and Hospital of Stomatology, Beijing, China, [3] National Engineering Laboratory for Digital and Material Technology of Stomatology, Peking University School and Hospital of Stomatology, Beijing, China, [4] Beijing Key Laboratory of Digital Stomatology, Peking University School and Hospital of Stomatology, Beijing, China, [5] Department of Restorative Dentistry and Biomaterials Sciences, Harvard School of Dental Medicine, Boston, MA, United States, [6] Department of Prosthodontics, Shanghai Stomatological Hospital, Fudan University, Shanghai, China, [7] Shanghai Key Laboratory of Craniomaxillofacial Development and Diseases, Shanghai Stomatological Hospital, Fudan University, Shanghai, China, [8] The Fifth Clinical Division, Peking University School and Hospital of Stomatology, Beijing, China, [9] Department of VIP Service, Peking University School and Hospital of Stomatology, Beijing, China

OPEN ACCESS

Edited by:
Yong Yin,
Shandong Cancer Hospital, China

Reviewed by:
Vito Carlo Alberto Caponio,
University of Foggia, Italy
Jinyun Li,
Ningbo University, China

***Correspondence:**
Yixiang Wang
kqwangyx@bjmu.edu.cn
Zeyun Ma
kqmzy101@sina.com
Shuyan Zhao
dbliu2012@163.com

†These authors have contributed equally to this work

Specialty section:
This article was submitted to Head and Neck Cancer, a section of the journal Frontiers in Oncology

Received: 04 July 2021
Accepted: 03 November 2021
Published: 25 November 2021

Citation:
Gao X, Zhao N, Dong L, Zheng X, Zhang Y, Ding C, Zhao S, Ma Z and Wang Y (2021) A Novel Lipid Prognostic Signature of ADCY2, LIPE, and OLR1 in Head and Neck Squamous Cell Carcinoma. Front. Oncol. 11:735993. doi: 10.3389/fonc.2021.735993

Simple Summary: Clinically, aberrant lipid metabolism is responsible for overweight and/or obesity. Overweight is considered as an independent factor of cancer risk in 2019. Therefore, lipid metabolic reprogramming is an emerging hallmark of malignancy. It is an urgent need to comprehensively understand the relationship among lipid metabolism and HNSCC and identify a valuable biomarker for predicting prognosis of HNSCC patients. Three new findings were found in this study. Firstly, we identified the lipid-related differentially expressed genes (DEGs) by using the GEO microarrays and TCGA dataset. A novel lipid-related mRNA prognostic signature (LRPS, consisting of ADCY2, LIPE and OLR1) was developed, which could predict the survival and prognosis of HNSCC patients as an independent effective prognostic factor. Secondly, we found that the LRPS could indicate the type of infiltrated immune cells in HNSCC tumor microenvironment. Thirdly, we verified that the LPPS score could interpret the TP53 status of HNSCC. Our new findings indicated that LRPS has a potential to be a promising indicator of overall survival, TP53 status, and immune characteristics in HNSCC, and perhaps can monitor and guide the treatment efficacy and prognosis of HNSCC in the future.

Background: Head and neck squamous cell carcinoma (HNSCC) is characterized by a high frequency of lymph node metastasis and a high mortality. Lipid metabolic reprogramming is an emerging carcinogen as its role in fulfilling cancer growth and spread. However, little is known about the correlation between lipid metabolism and HNSCC.

Materials and Methods: Expressions of lipid-related genes were obtained from the Cancer Genome Atlas (TCGA) and Gene expression Omnibus (GEO) databases for differential and functional analyses. A total number of 498 patients from TCGA with

complete information were included to identify a lipid-related prognostic signature (LRPS), based on ADCY2, LIPE, and OLR1, by using univariate and multivariate Cox regression analyses. LRPS-high and LRPS-low groups were accordingly divided to pathway and cell enrichment analyses.

Results: LRS-low patients had a better overall survival and relapse - free survival than LRS-high ones in HNSCC. The LRPS-high group was significantly related to perineural invasion of cancer, cancer-related pathways, high TP53 mutation rate, high proportion of natural killer T cells (NKT), dendritic cells, monocytes, Treg, and M1 and M2 macrophage infiltration in HNSCC tumor tissues. Conversely, the LRPS-low group correlated with DNA damage-related and T-cell-regulated pathways, low frequency of mutated TP53, and high infiltration of B cells and CD4+ effector cells including Th1 and Th2.

Conclusion: LRPS has a potential to be a promising indicator of overall survival, prognosis, TP53 status, and immune characteristics in HNSCC.

Keywords: head and neck squamous cell carcinoma, survival, lipid-related prognostic signature, TP53 status, immune characteristics

INTRODUCTION

Head and neck squamous cell carcinoma (HNSCC) is the most common type of the head and neck cancers, with a high risk for recurrence and poor survival under the advanced treatment approaches. The incidence of HNSCC was increased by 36.3% during the past 10 years, from ~482,000 HNSCC patients in 2008 to ~657,000 cases in 2018 (1, 2). Smoking, alcohol assumption, and virus infection are recognized as important carcinogenic factors (3). Recent studies implicate that abnormal lipid metabolism may be related with HNSCC development and progression (4, 5).

Lipid metabolic reprogramming is an emerging hallmark of malignancy (6). Overwhelming lipid anabolic and catabolic processes are essential for the uncontrolled cell proliferation and rapid cancer growth. Simultaneously, lipids constitute most of the cell membranes and serve as signaling molecules. Theoretically, fatty acids and cholesterol synthesis provide carcinogenesis and metastasis with a range of metabolic fuels and substrates, as well as pro-tumor signaling cytokines (7–11). Furthermore, the roles of lipid metabolites in protecting cancer cells from harmful conditions (like endoplasmic reticulum stress, reactive oxygen species, and drug toxicity) have been substantiated in various cancers (12, 13). Some oncolipid-activated signaling pathways, such as sterol regulatory element-binding proteins and stearoyl-CoA desaturases, have been identified to be the potential targets for cancer treatment in the future (6, 14, 15).

Clinically, aberrant lipid metabolism is responsible for overweight and obesity. Overweight is considered as an independent factor of cancer risk by the American Cancer Society, which released a report entitled Cancer Facts & Figures in 2019 (16). Nowadays, it is estimated that 5% of cancers in men and 11% in women are attributed to overweight (17). Experimental evidence indicates that high-fat diet-induced obesity not only promotes carcinogenesis, but also induces lymphangiogenesis and lymphatic metastasis *in vivo* (18–20). Conversely, diet-caused weight loss was shown to reduce cancer risk (21). Furthermore, a deliberate weight loss has been proved to reverse the effects of obesity-induced oxidative stress, inflammatory activities, and oncogenesis (22). Reduction of DNA damage responses in overweight mice was also observed after an administration of energy restriction (23).

In this study, we firstly identified the lipid-related differentially expressed genes (DEGs) by using the GEO microarrays and the TCGA dataset. A novel lipid-related mRNA prognostic signature (LRPS, consisting of ADCY2, LIPE, and OLR1) was developed for predicting survival of HNSCC patients. Accordingly, HNSCC patients were divided into high-risk and low-risk groups according to their LRPS signature, and gene-set enrichment analysis (GSEA) and cell enrichment analysis were used to elucidate the potential mechanisms.

Abbreviations: HNSCC, Head and neck squamous cell carcinoma; TCGA, The Cancer Genome Atlas; GEO, Gene expression Omnibus; LRPS, Lipid-related prognostic signature; NKT, Natural killer T cell; DEGs, Differentially expressed genes; GSEA, Gene-set enrichment analysis; GO, Gene ontology; DAVID, The Database for Annotation, Visualization, and Integration Discovery; BP, Biological processes; CC, Cellular component; MF, Molecular function; PPI, Protein–protein interaction; HSC, Hematopoietic stem cells; MSC, Mesenchymal stem cells; TMB, Total mutation burden; EMT, Epithelial–mesenchymal transition; ADCY2, Adenylate cyclase 2; LIPE, Lipase E, hormone sensitive type; CSCs, Cancer stem cells.

MATERIALS AND METHODS

Ethics Approval

The original datasets in our study were downloaded from the TCGA database and GEO dataset. We downloaded and analyzed

the study data in accordance with the relevant data policies of TCGA database and GEO datasets, and therefore, no additional ethics approval was needed.

Data Source

The original datasets comparing the mRNA expression profiles between tumors and adjacent normal tissues were obtained from the three GEO databases [GSE30784 (containing 167 oral squamous cell carcinoma, 17 dysplasia, and 45 normal oral tissues), GSE37991 (containing 40 male oral squamous cell carcinoma biopsies), and GSE65858 (containing 290 HNSCC biopsies)] and a TCGA dataset (containing 498 HNSCC biopsies). The clinical samples from the TCGA database with complete clinical information of patients were selected. The microarray data of GSE30784, GSE37991, and GSE65858 were based on GPL570 (Affymetrix Human Genome U133 Plus 2.0 Array), GPL6883 (Illumina HumanRef-8 v3.0 expression beadchip), and GPL10558 (Illumina HumanHT-12 V4.0 expression beadchip), respectively. The corresponding clinical information of patients with HNSCC was also acquired from the TCGA database (up to July 19, 2019). A total of 498 HNSCC patients with detailed follow-up time were included for the following analyses.

Data Processing and Differential Expression Analysis

The GEO data were processed and analyzed using GEO2R (https://www.ncbi.nlm.nih.gov/geo/geo2r/). TCGA mRNA counts were normalized and analyzed by R packages (DESeq2 package) ($p < 0.01$, $|\log2FC| > 2$).

Functional Enrichment Analyses

Gene ontology (GO) and KEGG pathway enrichment analyses were performed using the DAVID online database (the Database for Annotation, Visualization, and Integration Discovery) (24, 25). The enriched biological processes (BP), cellular component (CC), and molecular function (MF) were obtained to analyze the DEGs.

Protein–Protein Interaction Analysis

The STRING online database (http://string-db.org) was performed for PPI analysis. Cytoscape software was employed to construct the PPI network (26). MCODE tool of Cytoscape was performed to identify gene cluster of the PPI network. Degree cutoff ≥ 2, node score cutoff ≥ 0.2, K-core ≥ 2, and max depth = 100 was set as the threshold value.

Prognostic Signature Generation and Validation

The TCGA original dataset was performed as a training cohort. Univariate and multivariate Cox proportional hazards regression analyses were carried out to identify potential genetic predictors for HNSCC survival. Kaplan–Meier survival analysis with log-rank test was performed in R package. An internal dataset derived from the original TCGA served as a validation cohort using the bootstrap resampling method (27). Multivariate survival analysis was then performed to assess the association between the signature and clinical pathological index, namely, age, gender, lymphovascular invasion, margin status, recurrence, lymphatic metastasis, perineural invasion, cancer status, and nodal extracapsular spread.

Pathway Enrichment and Immune Enrichment Analyses

Gene-set enrichment analysis (GSEA) was performed using GSEA software with the criteria $p < 0.05$ and FDR < 0.25 (28, 29) and visualized using clusterProfiler packages of R (30). mRNA expression profiles were uploaded to xCell online software to evaluate the immunocyte heterogeneity of LRPS-high and LRPS-low groups (31).

Statistical Analysis

Statistical analyses were performed using GraphPad Prism 8.4 and R software (version 3.6.3); $p < 0.05$ was considered statistically significant. A nonparametric *t*-test was performed to compare continuous variables and χ^2 test was used to compare categorical variables between two groups. ANOVA test was utilized to compare more than two groups.

RESULTS

Lipid-Associated DEGs in HNSCC

To explore the lipid-related genes in HNSCC, 37 lipid-metabolic channels and 4 lipid-related signaling pathways (**Supplementary Files S1**) were selected based on KEGG pathway databases, and then analyzed in the TCGA database and GEO datasets using R packages. The result showed that a total of 65 genes significantly abnormally expressed in all three independent cohorts including TCGA, GSE30784, and GSE37991. The 26 upregulated and 39 downregulated lipid-related DEGs in total are listed in **Table 1**. The top 20 DEGs from the TCGA database are listed in **Figure 1**, and all lipid-related DEGs in GEO datasets are shown in **Supplementary Figure S1** ($p < 0.01$, $|\log2FC| > 2$).

Comprehensive Analysis of Molecular Characteristics in DEGs

Potential functions were then investigated in biological processes of the DEGs in HNSCC. GO analysis was performed and visualized in **Figure 2A**. The module of BP showed that the oxidation–reduction process, cholesterol homeostasis, sphingolipid biosynthetic process, and lipid metabolic and catabolic processes were commonly enriched. CC showed that the DEGs were significantly enriched in extracellular exosome, endoplasmic reticulum (membrane), and lipid particle. With regard to the module of molecular function (MF), the DEGs were mainly involved in iron ion binding and oxidoreductase activity.

Next, KEGG pathway enrichment analysis was used to figure out functions of the proteins encoded by the DEGs. As shown in **Figure 2B**, the DEGs were closely associated with arachidonic acid metabolism, PPAR signaling pathway, regulation of lipolysis in adipocytes, and metabolic pathways. $p < 10^{-5}$ was recognized as significantly enrichment categories.

TABLE 1 | The lipid-related DEGs among GSE30784, GSE37991, and TCGA.

Genes	LogFC	*p*-value	Functions
APOC2	2.17	5.02E−08	Cholesterol metabolism
ADCY3	0.71	1.08E−10	Regulation of lipolysis in adipocytes
ACOT7	1.23	3.22E−19	Fatty acid elongation
CYP27B1	2.48	4.06E−20	Steroid biosynthesis
CERS2	0.62	1.42E−10	Sphingolipid metabolism
DHCR7	1.01	3.61E−06	Steroid biosynthesis
GLA	0.76	1.09E−12	Sphingolipid metabolism; glycerolipid metabolism
GPX7	1.00	8.32E−07	Arachidonic acid metabolism
GPX8	1.28	1.69E−14	Arachidonic acid metabolism
GNAI1	0.76	7.48E−09	Regulation of lipolysis in adipocytes
HSD17B6	2.11	3.21E−37	Steroid hormone biosynthesis
HACD3	0.66	4.74E−13	Fatty acid elongation; fatty acid metabolism; biosynthesis of unsaturated fatty acids
LPCAT1	1.72	8.18E−27	Glycerophospholipid metabolism; ether lipid metabolism
MMP1	3.08	1.22E−13	PPAR signaling pathway
OLR1	2.04	7.42E−10	PPAR signaling pathway
PCSK9	2.77	1.62E−19	Cholesterol metabolism
PLPP4	4.34	3.17E−27	Glycerophospholipid metabolism; glycerolipid metabolism
PIK3CD	1.24	3.39E−16	Regulation of lipolysis in adipocytes
PPT1	0.77	1.85E−15	Fatty acid elongation; fatty acid metabolism
PLA2G7	1.98	2.09E−17	Ether lipid metabolism
SCARB1	0.73	3.19E−06	Fat digestion and absorption; cholesterol metabolism
SLC16A1	1.37	2.64E−17	Fatty acid biosynthesis
SQLE	0.82	4.82E−08	Steroid biosynthesis
SCD5	0.93	6.99E−08	Fatty acid metabolism; biosynthesis of unsaturated fatty acids; PPAR signaling pathway; AMPK signaling pathway
SPHK1	1.08	1.68E−11	Sphingosine degradation; sphingolipid metabolism
SLC2A1	1.76	1.40E−18	Adipocytokine signaling pathway
ADH1B	−5.36	9.21E−79	Fatty acid degradation
ADCY2	−2.20	1.24E−16	Regulation of lipolysis in adipocytes
AQP7	−4.11	2.31E−94	Regulation of lipolysis in adipocytes
ALOX12	−2.51	1.43E−29	Arachidonic acid metabolism
ACER1	−2.50	8.28E−17	Sphingosine biosynthesis; sphingolipid metabolism

(Continued)

TABLE 1 | Continued

Genes	LogFC	*p*-value	Functions
ADIPOQ	−5.67	7.00E−43	Adipocytokine signaling pathway; PPAR signaling pathway; AMPK signaling pathway
ASPG	−1.47	2.44E−10	Cholesterol metabolism
ACADSB	−1.68	1.66E−43	Fatty acid degradation; fatty acid metabolism
ADH7	−1.79	8.69E−09	Fatty acid degradation
CYP3A5	−3.05	3.18E−54	Steroid hormone biosynthesis
CYP11A1	−2.21	4.01E−15	Steroid hormone biosynthesis
CAB39L	−2.14	6.29E−111	AMPK signaling pathway
CHPT1	−1.64	5.19E−23	Ether lipid metabolism; glycerophospholipid metabolism; phosphatidylcholine (PC) biosynthesis
CH25H	−1.60	1.70E−16	Primary bile acid biosynthesis
CYP2E1	−1.89	9.28E−14	Steroid hormone biosynthesis; arachidonic acid metabolism; linoleic acid metabolism
CYP2J2	−1.63	1.15E−25	Arachidonic acid metabolism; linoleic acid metabolism
DEGS2	−1.69	5.96E−14	Ceramide biosynthesis; sphingosine biosynthesis; sphingolipid metabolism
EPHX2	−1.63	3.40E−26	Arachidonic acid metabolism
FABP3	−3.03	3.73E−49	PPAR signaling pathway
GDPD3	−2.25	4.37E−30	Ether lipid metabolism
GPX3	−2.45	2.91E−44	Arachidonic acid metabolism
GPD1L	−2.66	2.88E−117	Glycerophospholipid metabolism
GPD1	−5.09	6.26E−148	Glycerophospholipid metabolism
HMGCS2	−4.71	5.67E−51	Synthesis and degradation of ketone bodies; PPAR signaling pathway; MVA pathway
LIPE	−1.35	7.95E−18	Regulation of lipolysis in adipocytes
MGLL	−1.95	1.49E−44	Regulation of lipolysis in adipocytes; glycerolipid metabolism; acylglycerol degradation
PLA2G2A	−2.52	8.11E−15	Fat digestion and absorption; ether lipid metabolism; glycerophospholipid metabolism; arachidonic acid metabolism; linoleic acid metabolism; alpha-linolenic acid metabolism
PLIN1	−5.44	4.74E−149	Regulation of lipolysis in adipocytes; PPAR signaling pathway
PLIN4	−4.40	6.43E−114	PPAR signaling pathway
PLIN5	−3.28	5.54E−69	PPAR signaling pathway
PLA2G16	−1.48	2.10E−13	Regulation of lipolysis in adipocytes; ether lipid metabolism; glycerophospholipid metabolism; arachidonic acid metabolism; linoleic acid metabolism; alpha-linolenic acid metabolism
PTGDS	−1.76	2.86E−16	Arachidonic acid metabolism
PPARG	−2.21	5.74E−29	PPAR signaling pathway
SLC2A4	−4.30	6.92E−102	Adipocytokine signaling pathway
SLC27A6	−3.55	1.00E−38	PPAR signaling pathway
SORBS1	−2.76	3.87E−64	PPAR signaling pathway

(Continued)

TABLE 1 | Continued

Genes	LogFC	*p*-value	Functions
SULT2B1	−1.50	1.13E−11	Steroid hormone biosynthesis
SORT1	−1.43	3.82E−31	Cholesterol metabolism
TM7SF2	−1.82	5.62E−26	Cholesterol biosynthesis; steroid biosynthesis

LogFC, log Fold Change.

To figure out the relationship between the DEGs in HNSCC, the PPI network was constructed by STRING online database (**Figure 2C**). The central node genes (more than 10 connections or interactions) and the top 10 highly connected genes were identified, namely, PPARG, LIPE, SLC27A6, CYP2E1, ADIPOQ, PLA2G16, PLIN1, PLA2G2A, CYP2J2, and SLC2A4 (**Supplementary Files S2**). MCODE plugin from Cytoscape was used for the key module within the PPI network. The two most significant modules were identified for further pathway enrichment analysis. Module 1 consisted of 13 hub genes, namely, LIPE, PPARG, ADIPOQ, SLC2A1, SLC2A4, SLC27A6, MGLL, PLIN1, PLIN4, FABP3, CYP2E1, ALOX12, and CYP2J2 (**Figure 2D**). Module 2 included 5 hub genes, namely, SQLE, DHCR7, HMGCS2, TM7SF2, and CH25H (**Figure 2E**). Pathway enrichment analysis revealed that the hub genes in module 1 were closely correlated with PPAR signaling pathway ($p = 2.58 \times 10^{-6}$) and AMPK signaling pathway ($p = 8.29 \times 10^{-4}$). Module 2 was mainly enriched in steroid biosynthesis ($p = 4.80 \times 10^{-5}$) (**Supplementary Files S2**).

Identification of a Lipid-Related Prognostic Signature of HNSCC

To verify whether the lipid-related DEGs could be potential prognostic markers for HNSCC, the univariate and multivariate Cox analyses were performed to analyze the lipid-related DEGs as predictors for survival in TCGA patients with HNSCC (**Supplementary Files S3**, Model dataset). Univariate Cox analysis showed that ADCY2, OLR1, and LIPE significantly affected the overall survival of patients with HNSCC among the DEGs (**Figures 3A, B** and **Supplementary Files S4**). Next, a lipid-related prognostic signature (LRPS), containing LIPE, ADCY2, and OLR1, was constructed based on the coefficient

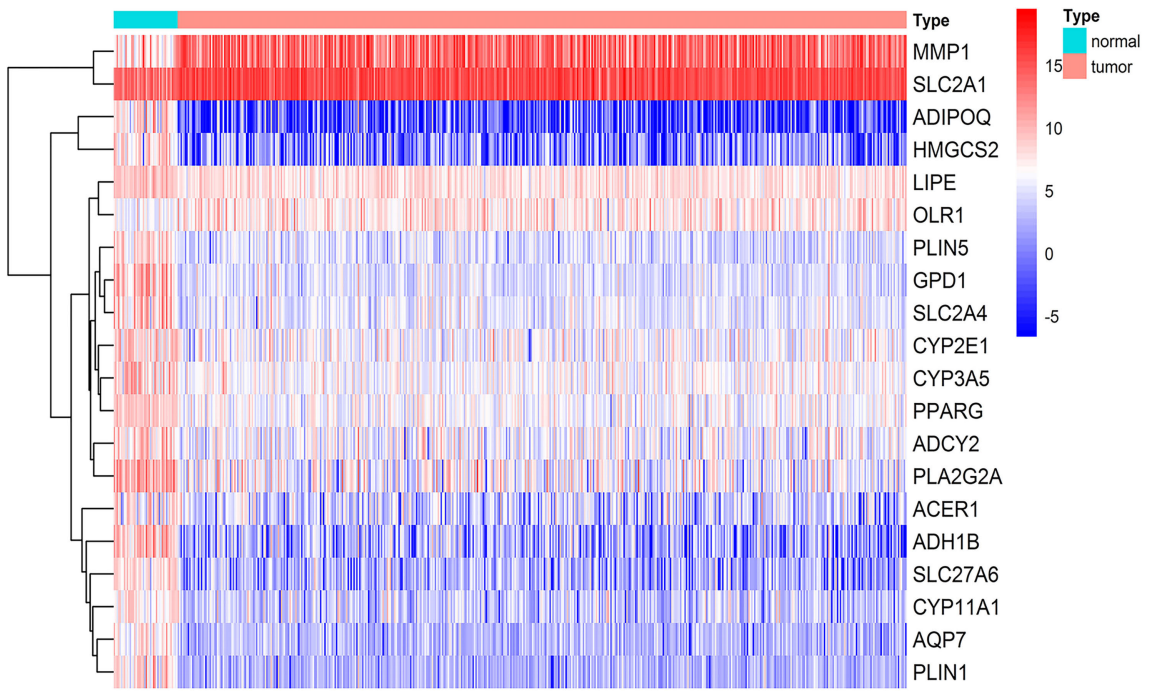

FIGURE 1 | Lipid-related differentially expressed genes (DEGs) in HNSCC. Top 20 of the 65 genes involving lipid metabolism showed abnormal expression in HNSCC from the TCGA database including 44 normal tissues and 502 tumors ($p < 0.01$, $|logFC| > 2$). The color from blue to red represents the gene expressions from high to low between tumors *vs.* normal tissues.

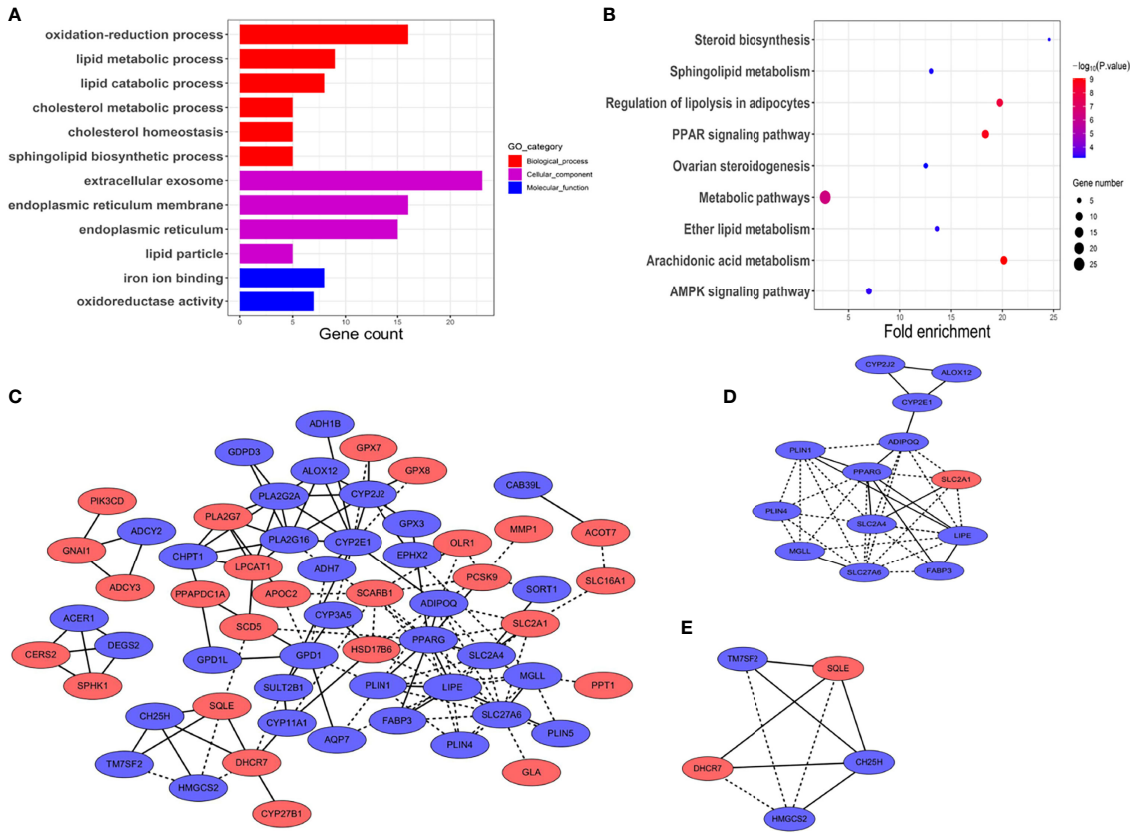

FIGURE 2 | Functional vanalyses and PPT network of the DEGs. **(A)** GO analysis including biological processes, cellular components, and molecular functions. The *x*-axis shows gene counts enriched in these processes. ($p < 0.01$, FDR < 0.05). **(B)** Pathway analysis of the DEGs showed the common pathways in the KEGG database. The size of the points represented the numbers of the enriched genes; the bigger the size, the more genes enriched. Blue to red points represented statistical significance from low significance to high significance ($p < 0.01$, FDR < 0.05). **(C)** PPI network of the DEGs. Blue represents down-expressed genes, and red denotes up-expressed genes. Solid lines represent known interactions from curated databases or experimentally determined. Dotted lines represent predicted interactions. **(D, E)** Key module genes, namely, module 1 and module 2, with scores of 6.17 and 4.5, respectively.

of multivariate Cox analysis and mRNA expression of the three genes, the risk score = (−0.15) × LIPE + (0.08) × ADCY2 + (0.09) × OLR1 (**Figure 3C**). Subsequently, the LRPS containing LIPE, ADCY2, and OLR1 was selected to predict the prognosis of HNSCC patients through the TCGA and GEO databases.

The patients were accordingly divided into the high-risk group (n = 249) and low-risk group (n = 249) based on the risk score (**Figures 4A, B**), finding that the HNSCC patients in the high-risk group had a poorer 5-year overall survival (36.9%, HR = 0.377, 95% CI = 29.8%-45.7%) than those in the low-risk group (55.9%, HR = 0.566, 95% CI = 47.07%–66.5%) ($p = 4.889 \times 10^{-6}$) (**Figure 4C** and **Supplementary Files S5**). The concordance indices (C-index) of the lipid signature showed a higher specificity and sensitivity for predicting 3-, 5-, and 10-year overall survival (C-index = 0.645, 0.592, and 0.66, respectively, **Figure 4D**).

The LRPS was validated in the GSE65858 database. A total of 290 patients with HNSCC were subdivided into LRPS-high and -low groups according to the risk score, and survival analysis showed that the LRPS-high group had poorer 5-year overall survival than the LRPS-low group with a high effectivity (**Figures S2A, B**). We also established an internal TCGA dataset by bootstrap resampling method to validate the effectiveness of the LRPS (**Supplementary Files S3**, Validation dataset). The clinical characteristics within the two datasets had no significant differences using *t*-test analysis (**Supplementary Table S1**). The validation database was calculated and divided in the same way as the original group (**Figure S3**). Five-year overall survival analysis demonstrated that the high-risk group (37.92%, 95% CI: 30.71%–46.8%) was significantly poorer than its counterpart (59%, 95% CI: 51.1%–68.2%, $p < 0.001$, **Supplementary Files S5**). Taken together, the lipid-based signature of ADCY2, LIPE, and OLR1 could effectively predict the HNSCC patients' survival.

LRPS Was an Independent Indicator of Prognosis and Closely Correlated to HNSCC Recurrence

Univariate Cox regression analysis showed that age, gender, lymphovascular invasion and metastasis, nodal extracapsular spread, perineural invasion, margin status, recurrence, cancer

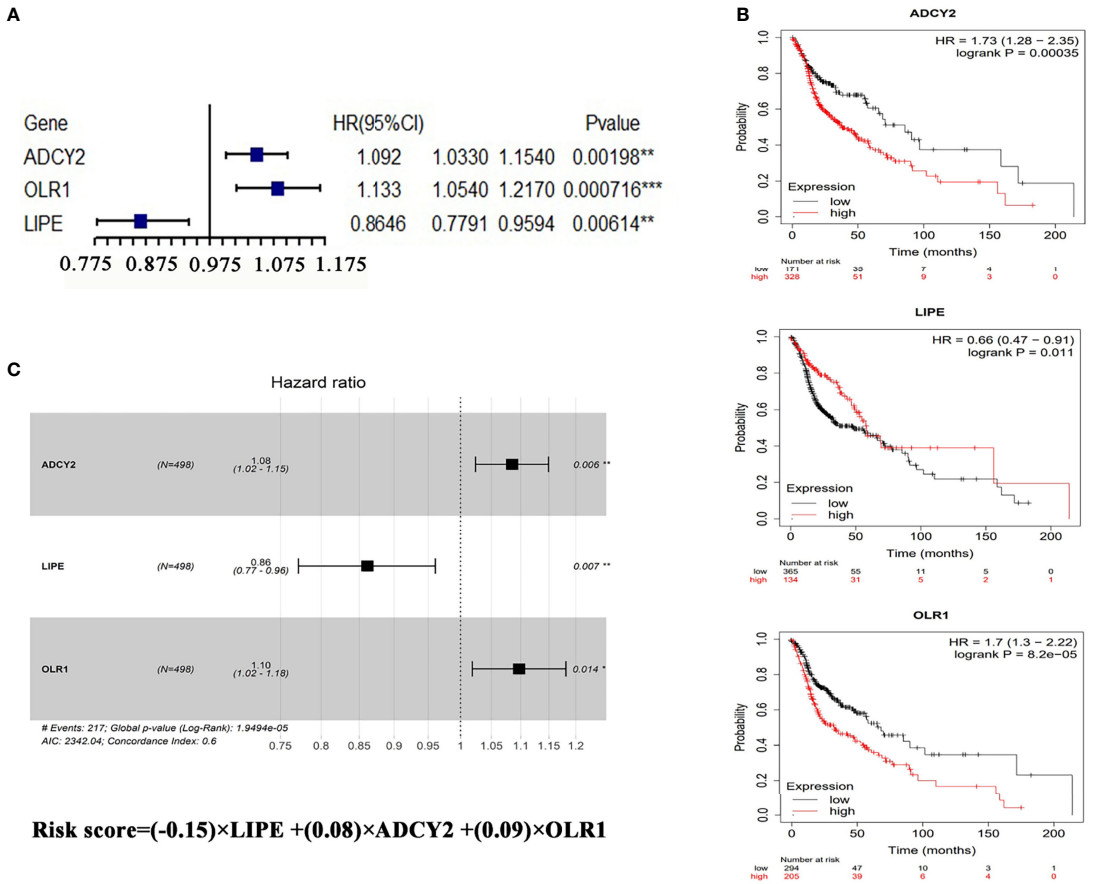

FIGURE 3 | Prognostic analysis of LRPS genes. **(A)** Univariate Cox analysis of OLR1, ADCY2, and LIPE. **(B)** Survival analysis of the three genes in HNSCC according to the Kaplan–Meier Plotter online database (http://kmplot.com/analysis/index.php?p=background). **(C)** The risk score performed using multivariate Cox analysis of the three genes. *p < 0.05, **p < 0.01, ***p < 0.001.

status, and LRPS score were significantly correlated with HNSCC prognosis (**Figure 5A**). Multivariate Cox analysis determined LRPS as an independent predictor after adjustment by other pathologic characteristics (**Figure 5B**). We evaluated the clinicopathologic factors in HNSCC among LRPS-high and LRPS-low groups (**Table 2**). Meanwhile, the LRPS could also independently predict the overall survival of HNSCC patients from the GEO database (**Figures S2C, D**). Statistically, LRPS-high patients were more prone to suffering relapse than the LRPS-low counterparts (52.73% *vs.* 22.92%, $p = 0.0024$). A high LRPS score had affinity relation with perineural invasion, compared with a low LRPS score (54.59% and 38.41% respectively, $p = 0.0027$). There were no significant differences within age, sex, alcohol and smoking history, tumor size and stage, lymphovascular invasion, and metastasis between the LRPS-high and LRPS-low groups.

Furthermore, based on the primary tumor sites, the data were classified into four subgroups: oral cavity, tongue, larynx, and pharynx. The results showed that the proportion of oral cavity and larynx samples were almost equally distributed between the high risk and low risk, but there were more cases of tongue and fewer pharynx in the high-risk than in the low-risk group ($p < 0.0001$, Fisher test; **Figure 6A**). Meanwhile, the samples with HPV test results were subdivided into positive and negative groups, and the data were performed to analyze the association between HPV status and the lipid signature. Surprisingly, we found that almost all HPV-positive samples showed a low risk for LRPS, while HPV-negative samples had a high risk for LRPS ($p < 0.0001$, Fisher test; **Figure 6B**).

Molecular and Immune Characteristics in Different LRPS Subgroups

Since the lipid signature could increase the risk for recurrence, we sought to illuminate potential mechanisms regulating cancer relapse. Different LRPS groups were performed to GSEA and xCell analyses. We observed that the LRPS-high group significantly positively correlated to focal adhesion, MAPK signaling pathway, neuroactive ligand–receptor interaction, cancer-related pathway, and TGFβ signaling pathway. The LRPS-low group was mainly enriched and negatively related to apoptosis, cell cycle, oxidative phosphorylation, p53 signaling pathway, and T-cell receptor signaling pathway (**Figure 7A**, $p < 0.05$, FDR < 0.25).

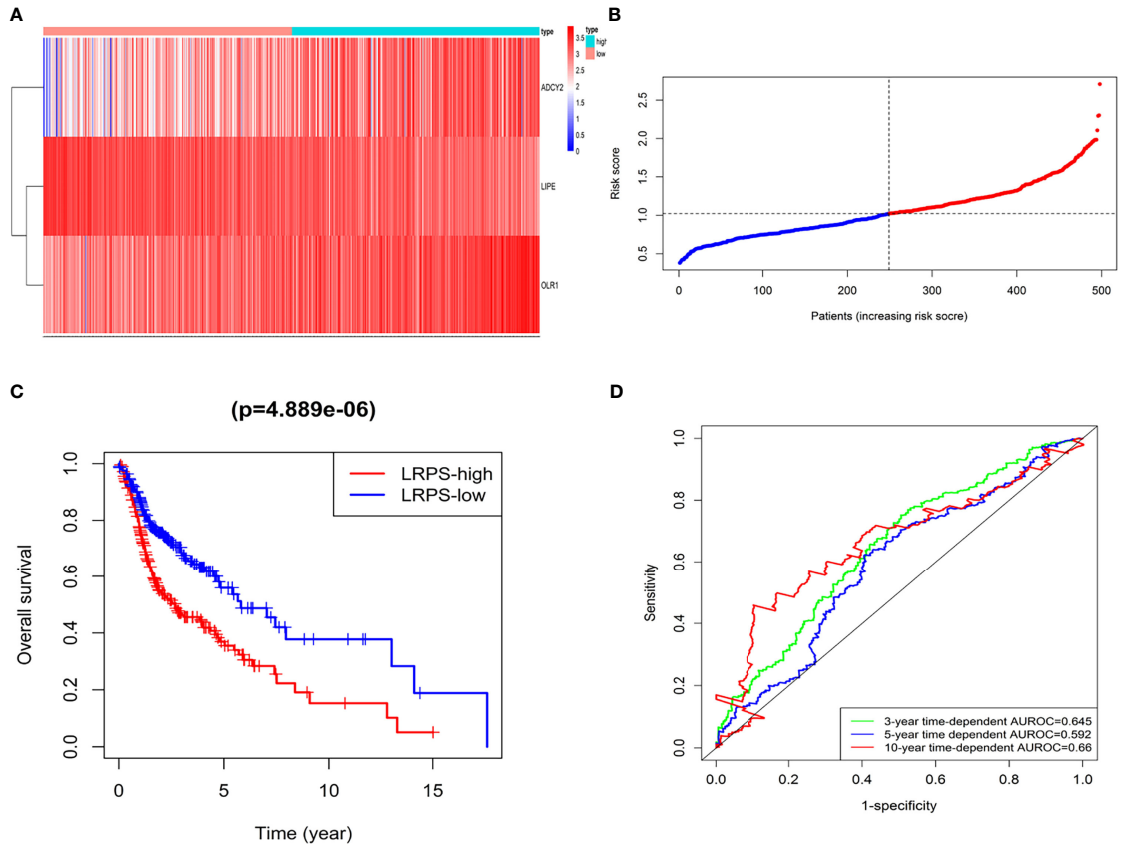

FIGURE 4 | LRPS in the TCGA model dataset. **(A)** Heatmap for the mRNA expression distribution in TCGA cohort by risk score, with red representing high expression and blue representing low expression. **(B)** The risk scores for patients with HNSCC were plotted in ascending order. **(C)** The survival rates of HNSCC patients between the LRPS-high group and LRPS-low group ($p = 4.889 \times 10^{-6}$). **(D)** C-index values of ROC analysis.

xCell analyses revealed that compared with adjacent normal tissues, the tumors that had a high LRPS score were more infiltrated in NKT, dendritic cells, monocytes, Treg, and M1 and M2 macrophages, which is in line with the inflammatory niche of the HNSCC tumor microenvironment. In addition, a proportion of B cells and $CD4^+$ T effector cells including Th1 and Th2 significantly decreased in the LRPS-high group compared with the LRPS-low group, implicating that there is a suppressive immunity in the LRPS-high group (**Figure 7B**). Notably, hematopoietic stem cells (HSCs) and mesenchymal stem cells (MSCs) were observed enriched in the LRPS-high group ($p < 0.001$). The above results indicated a possible changed immune milieu of primary tumor sites with an increased risk for HNSCC progression.

Finally, gene mutations were further analyzed to explore the molecular nature of the LRPS subgroups, and the top 10 genes with the highest mutation rates were identified (**Figure 8A**). Genomic analysis showed that HNSCC endowed a high frequency of TP53 mutations, as high as about 71%, suggesting a vital role on tumor bioactivities. Our results showed a higher mutation rate of TP53 in LRPS-high patients than those with low LRPS score (82% *vs.* 60%), underlying a potential crosstalk between altered lipid metabolism and TP53 status. Missense variations were the most popular in both LRPS-high and -low groups. Importantly, TP53 showed a significantly higher mutation rate in the LRPS-high than in the LRPS-low group (**Figure 8B**, $p < 0.0001$, Fisher's exact test). In addition, TTN, CDKN2A, FAT1, FRGB1, MUC16, CSMD3, PIK3CA, and SYNE1 were higher than 16% in both groups. The correlation between LRPS score and total mutation burden (TMB) was further explored, suggesting that the LRPS score was slightly correlated with total mutation burden ($r = -0.11$, $p = 0.015$, **Figure S4**).

DISCUSSION

The first new finding of the manuscript is that we identify the novel lipid prognostic signature of ADCY2, LIPE, and OLR1, which can predict the survival and prognosis of HNSCC patients as an independent effective prognostic factor. Meanwhile, our data may explain how lipidomics affects the prognosis and survival of patients with HNSCC through affecting tumor microenvironment *via* immunosuppression.

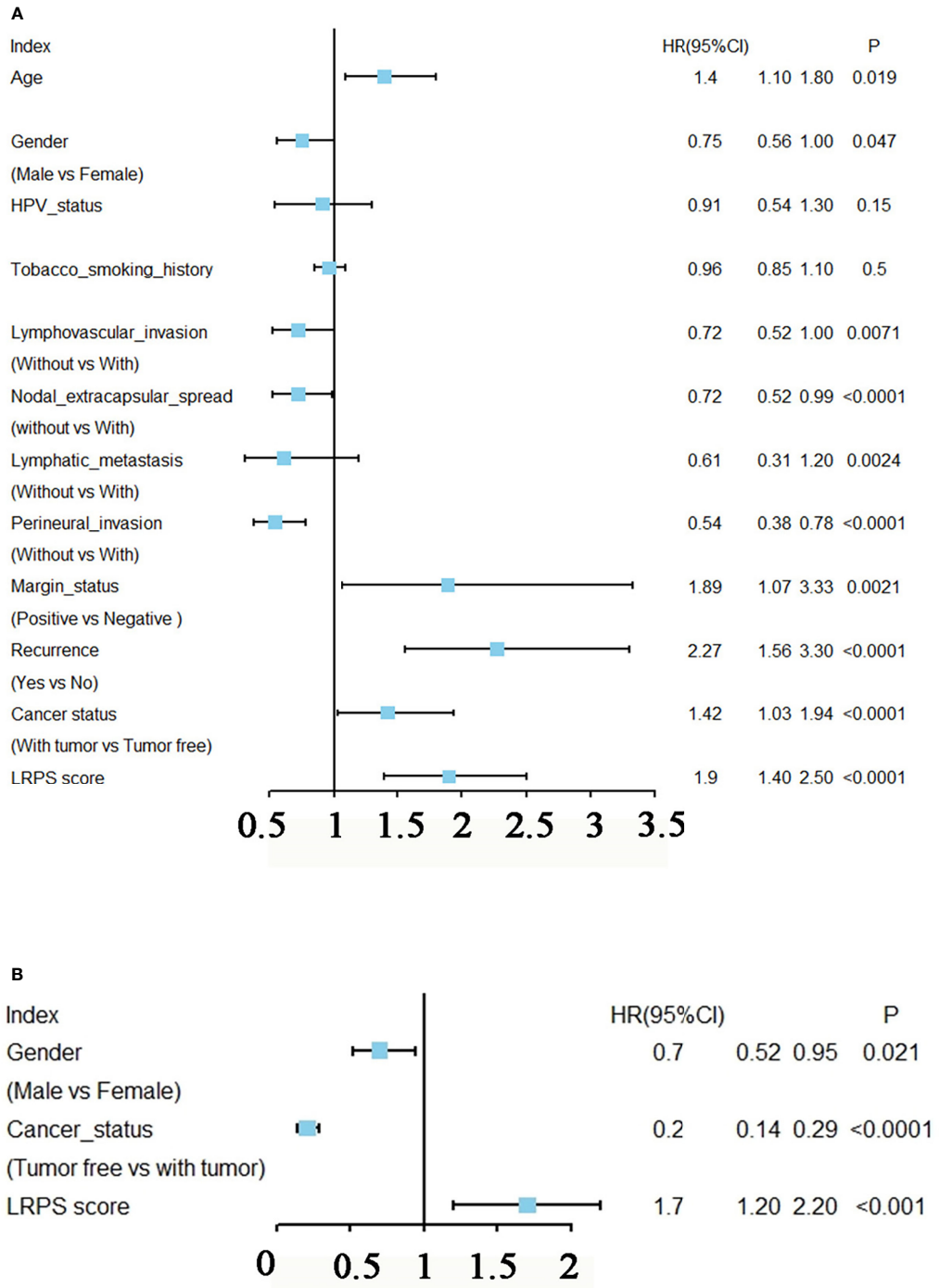

FIGURE 5 | Prognostic analysis of LRPS in HNSCC. **(A)** Univariate Cox analysis of clinicopathologic factors and the LPRS score in TCGA-HNSCC patients. **(B)** Multivariate Cox analysis of the significant factors according to results from the univariate Cox analysis ($p < 0.05$).

In recent years, lipid metabolism has come into a sharp focus on cancer initiation and progression owing to its essential role in HNSCC and striking contribution to cancer development. In this study, we, for the first time, identified a novel LRPS of HNSCC through univariate and multivariate Cox analyses, which were performed to analyze the lipid-related DEGs as predictors for survival in TCGA patients with HNSCC. ADCY2, OLR1, and LIPE significantly predicted the overall survival of HNSCC

TABLE 2 | The differences of clinical pathological characteristics between LRPS-high and LRPS-low.

Variables	Patients (*n*)	LRPS-high (*n*)	LRPS-low (*n*)	*p*-value
Age at diagnosis (years)	498	248	250	>0.9999
≤60	243	121	122	
>60	255	127	128	
Gender	498	248	250	0.6851
Male	366	180	186	
Female	132	68	64	
Alcohol history	487	241	246	0.0657
Yes	330	173	157	
No	157	68	89	
Smoking history	493	244	249	>0.9999
Yes	488	242	246	
No	5	2	3	
Clinical T stage	483	243	240	0.3943
T1–T2	175	93	82	
T3–T4	308	150	158	
Clinical stage	484	243	241	0.3907
I–II	113	61	52	
III–IV	371	182	189	
Histological stage	479	241	238	0.9163
G1–G2	358	181	177	
G3–G4	121	60	61	
Lymphatic metastasis	405	212	193	0.6143
With	235	126	109	
Without	170	86	84	
Distant metastasis	473	238	235	>0.9999
With	5	3	2	
Without	468	235	233	
Lymphovascular invasion	337	181	156	0.6492
With	119	66	53	
Without	218	115	103	
Perineural invasion	349	185	164	**0.0027****
With	164	101	63	
Without	185	84	101	
Recurrence	103	55	48	**0.0024****
With	40	29	11	
Without	63	26	37	

**, *level of significance, p < 0.01.*

among the lipid DEGs. When the three genes were combined to indicate the prognosis of HNSCC patients, it showed that the LRPS-high group was highly related to poor prognosis.

OLR1 is a stimulator of epithelial–mesenchymal transition (EMT) and involved in PPAR pathway, regulated by the secondary messenger cyclin adenosine monophosphate (cAMP). OLR1 promotes migration and metastatic spread in different pathways, such as TBC1D3/OLR1/TNFα/NF-κB, OLR1/c-Myc/HMGA2, oxLDL/OLR1/VEGF-C, and PI3K/Akt/GSK3β (32–36). Recently, LOX-1Δ4, an alternative OLR1 isoform, has been shown to directly drive non-tumorigenic breast epithelial cells into fast proliferation status (37). More importantly, OLR1 is also reported to be positively correlated with the occurrence of lymphatic metastases in pancreatic cancers (38).

Adenylate cyclase 2 (ADCY2) encodes the adenylate cyclase that catalyzes ATP to transform to the second messenger cyclic adenosine monophosphate (cAMP). The latter is a crucial signal in cell fate, inflammation, and many other bioactivities, and is also greatly involved in the growth and differentiation of MSCs. Zhao et al. have reported E2-induced ADCY2 as a positive regulator in MSCs (39). In colorectal cancer, ADCY2 could also be an important prognostic marker (40).

Lipase E, hormone-sensitive type (LIPE) increases both the levels of free cholesterol and free fatty acids, and plays an important role in adipocyte function and lipid and glucose homeostasis (41). More importantly, LIPE encodes the rate-limiting enzyme of lipolysis, and homozygous null mutation of LIPE results in marked inhibition of lipolysis, leading to multiple symmetric lipomatosis (42). Our studies showed that LIPE played a central role in the protein–protein interactions of the DEGs, significantly related to the survival rate of patients with HNSCC.

The second new finding of the study is that the LRPS can indicate the type of the infiltrated immune cells in the HNSCC tumor microenvironment. Comprehensive analyses indicated a diverse characteristic of LRPS subgroups. Lumps of the LRPS-high group showed a higher infiltration of inflammation-associated cells, including dendritic cells, M1 and M2 macrophages, and monocytes, yet a lower proportion of

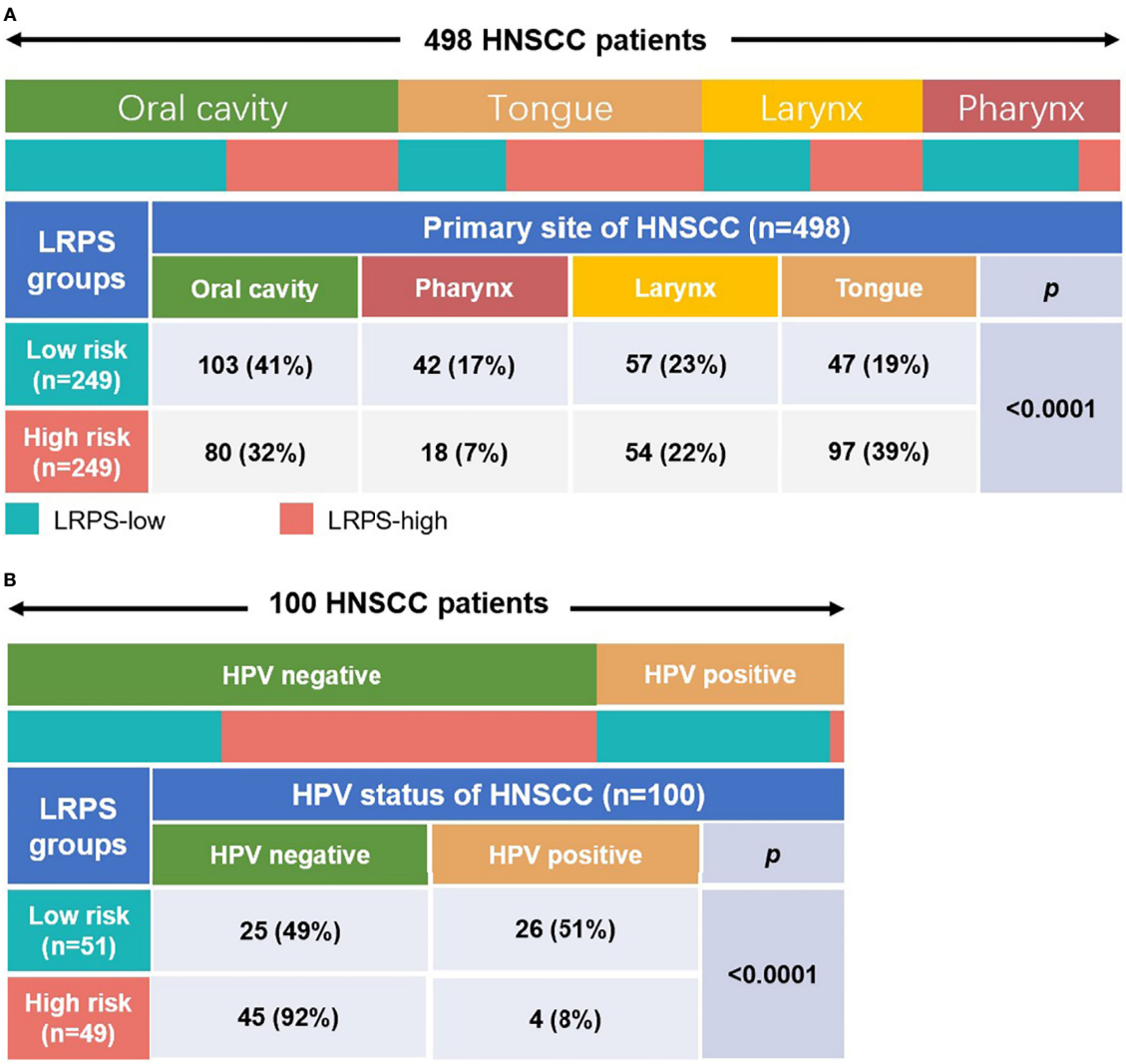

FIGURE 6 | Distribution of primary tumor sites and the HPV status in different LRPS subgroups. **(A)** Heatmap and table showing the distribution of HNSCC primary sites (oral cavity, pharynx, larynx, and tongue) between the LRPS subgroups. **(B)** Heatmap and table showing the distribution of different HPV status between the two LRPS subgroups. The distributions of the primary site subtypes and HPV status in the LRPS subgroups were compared through the Fisher test.

immunocytes (B cells and pro B cells, CD8+ Tcm) compared with the LRPS-low group. The finding is also supported by the new concept that the infectious, chronic irritated, and inflammatory infiltration induces cancer and promotes neoplastic risk.

Macrophages are the main source of tissue repairment-related growth factors and cytokines after activation, such as TGFβ1, TNFα, TGFα, and IL1 (43). These factors partly contributed to carcinogenesis *via* different signaling pathways. Numerous studies further showed a strong correlation between macrophage abundance and poor cancer prognosis, including thyroid cancer, lung cancer, and hepatocellular cancer (44–47). Compromised immunity was also observed in our results, consistent with the research that shows that high-fat diet-induced obesity accelerates tumor growth by impairing CD8+ T-cell function (48). These observations could partly elucidate that the patients with LRPS high score were more subject to a poor survival because of the inflammatory-rich and immunodeficient conditions.

Intriguingly, we found that LRPS-low harbors more Th1 and Th2 cells and fewer Treg cells in HNSCC. By contrast, LRPS-high has more Treg cells, consistent with the results from Whiteside group, which found a large number of Treg cells in the peripheral circulation of patients with HNSCC (49). Treg cells serve as one of the culprits that suppress anti-tumor immune response. Tumor within a niche of Treg cells is recognized as an unfavorable factor of cancer prognosis (50).

We further found that the patients with high LRPS score were more susceptible to recurrence because of increased infiltration of MSCs and HSCs in the tumor microenvironment. Recent data have proposed lipid metabolic rewiring as a new hallmark of

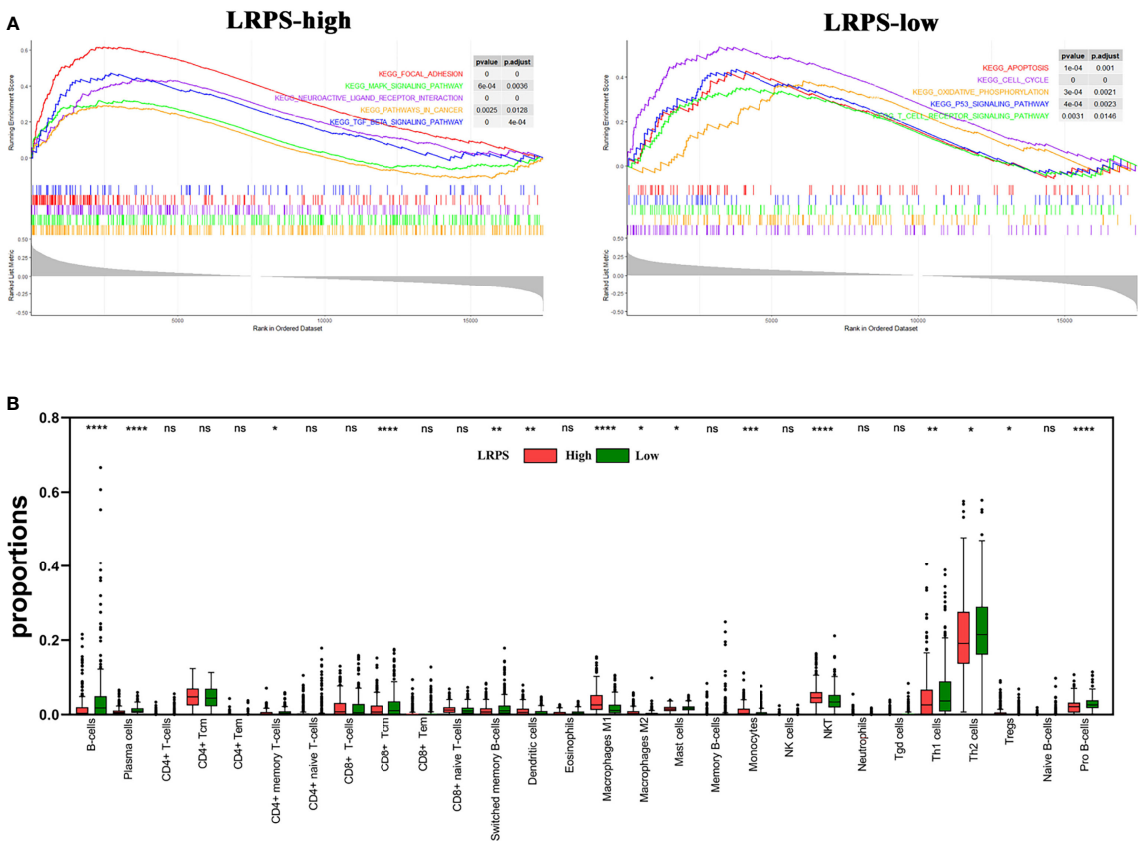

FIGURE 7 | Molecular characteristics of LPRS subgroups. **(A)** Gene sets enrichment in the LRPS-high and LRPS-low groups, respectively ($p < 0.05$, FDR < 0.25). **(B)** The proportions of immunocytes within tumor microenvironment in different LRPS subgroup (ns, no significance; *$p < 0.05$; **$p < 0.01$; ***$p < 0.001$; ****$p < 0.0001$). NK cells, natural killer cells; NKT, natural killer T cells; Tgd cells, gamma delta T cells.

cancer stem cells (CSCs) owing to its modification on stem-like cells' properties (51).

Taken together, these results affirmed that abnormal lipid metabolism exerts a great impact on immune cells' function in the tumor microenvironment, just influencing the progression and prognosis of HNSCC.

The third new finding of the study is that LPPS score can interpret the TP53 status of HNSCC. Our results showed that there were fewer LRPS-high samples in HPV-positive HNSCCs, which was in accordance with the negative relationship between HPV status and p53 mutation frequency (52). We also found a significant higher mutation rate of TP53 in LRPS-high patients than those with low LRPS score, underlying a potential crosstalk between altered lipid metabolism and TP53 status. Wild-type p53 supervises the cell damage response to various stimuli, and recent findings increasingly link p53 to lipid metabolism. P53 suppresses lipid biosynthesis *via* inhibiting lipogenesis, yet induces fatty acid oxidation as an alternative energy source to glycolysis in the condition of nutritional deficiency (53, 54), implicating p53 as a positive regulator of catabolism (increase fatty acid levels) and an inhibitor of anabolism (decrease fatty acid levels) in the process of fatty acid metabolism. Otherwise, loss of p53 can lead to cell malignant transformation. As expected, mutated p53 exert a great impact on carcinogenesis through regulating gene transcription related to cell cycle, DNA repair, immunity and energetic activities, and so on. This gain of function of mutated p53 has been validated in various human cancers including breast, prostate, colon, pancreas, and head and neck cancers (55–60). Our data further supported that p53 mutations did cooperate with abnormal lipid metabolism to promote cancer progression in HNSCC, though more laboratory investigations are needed in the future.

Though the LRPS has great potential for predicting HNSCC survival and p53 status, there are some limitations. The training and validation cohorts were retrospective, and more findings need to be validated prospectively. Moreover, the value of LRPS is not validated by *in vitro* and *in vivo* assays. Therefore, more studies are needed in the future.

CONCLUSION

Our data confirmed that the three lipid-related genes play a pivotal role in tumorigenesis and recurrence of HNSCC,

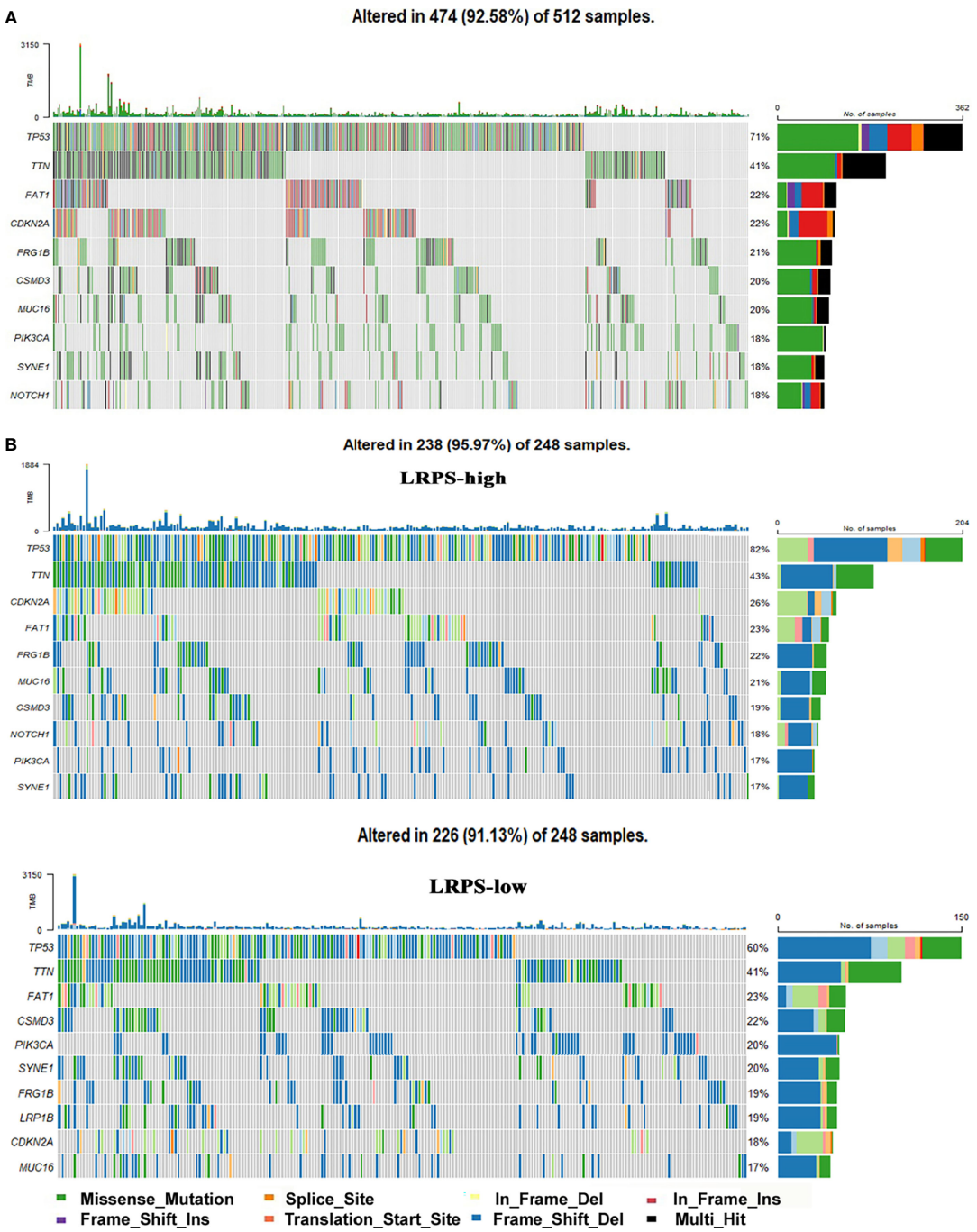

FIGURE 8 | Genomic mutations in the LRPS. **(A)** Genomic mutation signature in the patients with HNSCC from the TCGA database. **(B)** Significantly mutated genes in LRPS-high and LRPS-low subgroups. The top 10 mutated genes are listed; the right shows mutation percentage and the top shows the overall mutation rates of different cohorts.

potentially by suppressing anti-tumor immunity and reflecting TP53 mutations status. LRPS has a potential to be a promising indicator of overall survival, prognosis, TP53 status, and immune characteristics in HNSCC, and perhaps could monitor and guide the treatment efficacy and prognosis of HNSCC in the future.

DATA AVAILABILITY STATEMENT

Publicly available datasets were analyzed in this study. These data can be found here:. The original datasets comparing the mRNA expression profiles between tumors and adjacent normal tissues were obtained from the GEO databases (GSE30784, GSE37991

and GSE65858) and the TCGA dataset. The microarray data of GSE30784 and GSE37991 were based on GPL570 (Affymetrix Human Genome U133 Plus 2.0 Array) and GPL6883 (Illumina HumanRef-8 v3.0 expression beadchip) and GPL10558 (Illumina HumanHT-12 V4.0 expression beadchip), respectively. The corresponding clinical information of patients with HNSCC was also acquired from TCGA database (up to July 19, 2019). A total of 498 HNSCC patients with detailed follow-up time were included for the following analyses.

AUTHOR CONTRIBUTIONS

Conceptualization: YW, ZM, and SZ Data curation: XG. Formal analysis: XG, NZ, CD, LD, XZ, and YZ. Supervision: YW. Writing—original draft: XG. Writing—review and editing: YW, ZM, and SZ. All authors contributed to the article and approved the submitted version.

FUNDING

This research was funded by Research Grants from the Natural Science Foundation of Beijing Municipality (grant No. 7182181), the National Nature Science Foundation of China (grant Nos. 81772873, 81970920, and 81900983), and Shanghai Science and Technology Young Talents Sailing Program (19YF1442500).

SUPPLEMENTARY MATERIAL

The Supplementary Material for this article can be found online at: https://www.frontiersin.org/articles/10.3389/fonc.2021.735993/full#supplementary-material

Supplementary Figure 1 | Lipid-related differentially expressed genes (DEGs) in HNSCC of GEO datasets. **(A, B)** showed 65 lipid DEGs in GEO database, GSE30784 and GSE37991 respectively (p<0.01, |logFC|>2). The color from blue to red represented the gene expressions from high to low between tumors *vs.* normal tissues.

Supplementary Figure 2 | LRPS in the GEO dataset. **(A)** Survival analysis showed a significant difference between high-risk group and low-risk group in GSE65858 dataset (p=4.304×10-5). **(B)** The 5-year ROC value in the GEO group is 0.811.

Supplementary Figure 3 | LRPS in the TCGA validation dataset. **(A, B)** Three mRNA expression and risk score division in the TCGA validation dataset. **(C)**. Survival analysis showed a significant difference between high-risk group and low-risk group in TCGA validation dataset (p=1.337×10-5). **(D)**. The 3-year, 5-year and 10-year ROC values in the validation group are 0.625, 0.618 and 0.592, respectively.

Supplementary Figure 4 | The relationship between LRPS and tumor mutational burden. Correlation analysis between LRPS score and total tumor mutational burden (TMB) in HNSCC from TCGA database.

File S1 | List of full lipid-related pathways and the corresponding genes from KEGG database.

File S2 | List of protein–protein interaction (PPI) results from 65 lipid DEGs and two key modules within the PPI.

File S3 | The LRPS expression and the corresponding clinical information of high-risk and low-risk groups in the model dataset and the validation dataset, respectively.

File S4 | Results of all DEGs in HNSCC using univariate Cox analysis.

File S5 | Kaplan–Meier results of LRPS-high and -low subgroups in the model dataset and validation dataset, respectively.

Supplementary Table 1 | Clinical pathological characteristics comparison between the testing dataset and validation dataset.

REFERENCES

1. Ferlay J, Shin HR, Bray F, Forman D, Mathers C, Parkin DM. Estimates of Worldwide Burden of Cancer in 2008: GLOBOCAN 2008. *Int J Cancer* (2010) 127:2893–917. doi: 10.1002/ijc.25516
2. Bray F, Ferlay J, Soerjomataram I, Siegel RL, Torre LA, Jemal A. Global Cancer Statistics 2018: GLOBOCAN Estimates of Incidence and Mortality Worldwide for 36 Cancers in 185 Countries. *CA Cancer J Clin* (2018) 68:394–424. doi: 10.3322/caac.21492
3. Marur S, Forastiere AA. Head and Neck Squamous Cell Carcinoma: Update on Epidemiology, Diagnosis, and Treatment. *Mayo Clin Proc* (2016) 91:386–96. doi: 10.1016/j.mayocp.2015.12.017
4. Pascual G, Avgustinova A, Mejetta S, Martín M, Castellanos A, Attolini CS, et al. Targeting Metastasis-Initiating Cells Through the Fatty Acid Receptor CD36. *Nature* (2017) 541:41–5. doi: 10.1038/nature20791
5. Hu Q, Peng J, Chen X, Li H, Song M, Cheng B, et al. Obesity and Genes Related to Lipid Metabolism Predict Poor Survival in Oral Squamous Cell Carcinoma. *Oral Oncol* (2019) 89:14–22. doi: 10.1016/j.oraloncology.2018.12.006
6. Cheng C, Geng F, Cheng X, Guo D. Lipid Metabolism Reprogramming and Its Potential Targets in Cancer. *Cancer Commun (Lond)* (2018) 38:27. doi: 10.1186/s40880-018-0301-4
7. Boroughs LK, DeBerardinis RJ. Metabolic Pathways Promoting Cancer Cell Survival and Growth. *Nat Cell Biol* (2015) 17:351–9. doi: 10.1038/ncb3124
8. Zaidi N, Lupien L, Kuemmerle NB, Kinlaw WB, Swinnen JV, Smans K. Lipogenesis and Lipolysis: The Pathways Exploited by the Cancer Cells to Acquire Fatty Acids. *Prog Lipid Res* (2013) 52:585–9. doi: 10.1016/j.plipres.2013.08.005
9. Riscal R, Skuli N, Simon MC. Even Cancer Cells Watch Their Cholesterol! *Mol Cell* (2019) 76:220–31. doi: 10.1016/j.molcel.2019.09.008
10. Ding X, Zhang W, Li S, Yang H. The Role of Cholesterol Metabolism in Cancer. *Am J Cancer Res* (2019) 9:219–27.
11. Luo X, Cheng C, Tan Z, Li N, Tang M, Yang L, et al. Emerging Roles of Lipid Metabolism in Cancer Metastasis. *Mol Cancer* (2017) 16:76. doi: 10.1186/s12943-017-0646-3
12. Cao Y. Adipocyte and Lipid Metabolism in Cancer Drug Resistance. *J Clin Invest* (2019) 129:3006–17. doi: 10.1172/JCI127201
13. Liu Q, Luo Q, Halim A, Song G. Targeting Lipid Metabolism of Cancer Cells: A Promising Therapeutic Strategy for Cancer. *Cancer Lett* (2017) 401:39–45. doi: 10.1016/j.canlet.2017.05.002
14. Ray U, Roy SS. Aberrant Lipid Metabolism in Cancer Cells - The Role of Oncolipid-Activated Signaling. *FEBS J* (2018) 285:432–43. doi: 10.1111/febs.14281
15. Fritz V, Benfodda Z, Rodier G, Henriquet C, Iborra F, Avancès C, et al. Abrogation of *De Novo* Lipogenesis by Stearoyl-CoA Desaturase 1 Inhibition Interferes With Oncogenic Signaling and Blocks Prostate Cancer Progression in Mice. *Mol Cancer Ther* (2010) 9:1740–54. doi: 10.1158/1535-7163.MCT-09-1064
16. American Cancer Society. Cancer Facts&Figures 2(019). Available at: http://www.cancer.org/research/cancer-facts-statistics/all-cancer-factsfigures/cancer-facts-figures-2019.html.

17. Islami F, Sauer AG, Miller KD, Siegel RL, Fedewa SA, Jacobs EJ, et al. Proportion and Number of Cancer Cases and Deaths Attributable to Potentially Modifiable Risk Factors in the United States. *CA Cancer J Clin* (2018) 68:31–54. doi: 10.3322/caac.21440
18. Kim YM, Kim J, Baik SJ, Chun J, Youn YH, Park H. Sarcopenia and Sarcopenic Obesity as Novel Risk Factors for Gastric Carcinogenesis: A Health Checkup Cohort Study. *Front Oncol* (2019) 9:1249. doi: 10.3389/fonc.2019.01249
19. Zimta AA, Tigu AB, Muntean M, Cenariu D, Slaby O, Berindan-Neagoe I. Molecular Links Between Central Obesity and Breast Cancer. *Int J Mol Sci* (2019) 20:5364. doi: 10.3390/ijms20215364
20. Jung JI, Cho HJ, Jung YJ, Kwon SH, Her S, Choi SS, et al. High-Fat Diet-Induced Obesity Increases Lymphangiogenesis and Lymph Node Metastasis in the B16F10 Melanoma Allograft Model: Roles of Adipocytes and M2-Macrophages. *Int J Cancer* (2015) 136:258–70. doi: 10.1002/ijc.28983
21. Pendyala S, Neff LM, Suárez-Fariñas M, Holt PR. Diet-Induced Weight Loss Reduces Colorectal Inflammation: Implications for Colorectal Carcinogenesis. *Am J Clin Nutr* (2011) 93:234–42. doi: 10.3945/ajcn.110.002683
22. Izquierdo AG, Carreira MC, Amil M, Mosteiro CS, Garcia-Caballero T, Fernandez-Quintela A, et al. An Energy Restriction-Based Weight Loss Intervention Is Able to Reverse the Effects of Obesity on the Expression of Liver Tumor-Promoting Genes. *FASEB J* (2020) 34:2312–25. doi: 10.1096/fj.201901147RR
23. Setayesh T, Mišík M, Langie SAS, Godschalk R, Waldherr M, Bauer T, et al. Impact of Weight Loss Strategies on Obesity-Induced DNA Damage. *Mol Nutr Food Res* (2019) 63:e1900045. doi: 10.1002/mnfr.201900045
24. Huang da W, Sherman BT, Lempicki RA. Systematic and Integrative Analysis of Large Gene Lists Using DAVID Bioinformatics Resources. *Nat Protoc* (2009) 4:44–57. doi: 10.1038/nprot.2008.211
25. Huang da W, Sherman BT, Lempicki RA. Bioinformatics Enrichment Tools: Paths Toward the Comprehensive Functional Analysis of Large Gene Lists. *Nucleic Acids Res* (2009) 37:1–13. doi: 10.1093/nar/gkn923
26. Shannon P, Markiel A, Ozier O, Baliga NS, Wang JT, Ramage D, et al. Cytoscape: A Software Environment for Integrated Models of Biomolecular Interaction Networks. *Genome Res* (2003) 13:2498–504. doi: 10.1101/gr.1239303
27. Grunkemeier GL, Wu Y. Bootstrap Resampling Methods: Something for Nothing? *Ann Thorac Surg* (2004) 77:1142–4. doi: 10.1016/j.athoracsur.2004.01.005
28. Mootha VK, Lindgren CM, Eriksson K, Subramanian A, Sihag S, Lehar J, et al. PGC-1alpha-Responsive Genes Involved in Oxidative Phosphorylation Are Coordinately Downregulated in Human Diabetes. *Nat Genet* (2003) 34:267–73. doi: 10.1038/ng1180
29. Subramanian A, Tamayo P, Mootha VK, Mukherjee S, Ebert BL, Gillette MA, et al. Gene Set Enrichment Analysis: A Knowledge-Based Approach for Interpreting Genome-Wide Expression Profiles. *Proc Natl Acad Sci USA* (2005) 102:15545–50. doi: 10.1073/pnas.0506580102
30. Yu G, Wang L, Han Y, He Q. Clusterprofiler: An R Package for Comparing Biological Themes Among Gene Clusters. *OMICS* (2012) 16:284–7. doi: 10.1089/omi.2011.0118
31. Aran D, Hu Z, Butte AJ. Xcell: Digitally Portraying the Tissue Cellular Heterogeneity Landscape. *Genome Biol* (2017) 18:220. doi: 10.1186/s13059-017-1349-1
32. Wang B, Zhao H, Zhao L, Zhang Y, Wan Q, Shen Y, et al. Up-Regulation of OLR1 Expression by TBC1D3 Through Activation of Tnfα/NF-κb Pathway Promotes the Migration of Human Breast Cancer Cells. *Cancer Lett* (2017) 408:60–70. doi: 10.1016/j.canlet.2017.08.021
33. Ma C, Xie J, Luo C, Yin H, Li R, Wang X, et al. OxLDL Promotes Lymphangiogenesis and Lymphatic Metastasis in Gastric Cancer by Upregulating VEGF–C Expression and Secretion. *Int J Oncol* (2019) 54:572–84. doi: 10.3892/ijo.2018.4648
34. Yang G, Xiong G, Feng M, Zhao F, Qiu J, Liu Y, et al. OLR1 Promotes Pancreatic Cancer Metastasis *via* Increased C-Myc Expression and Transcription of HMGA2. *Mol Cancer Res* (2020) 18:685–97. doi: 10.1158/1541-7786.MCR-19-0718
35. González-Chavarría I, Fernandez E, Gutierrez N, González-Horta EE, Sandoval F, Cifuentes P, et al. LOX-1 Activation by oxLDL Triggers an Epithelial Mesenchymal Transition and Promotes Tumorigenic Potential in Prostate Cancer Cells. *Cancer Lett* (2018) 414:34–43. doi: 10.1016/j.canlet.2017.10.035
36. Li C, Zhang J, Wu H, Li L, Yang C, Song S, et al. Lectin-Like Oxidized Low-Density Lipoprotein Receptor-1 Facilitates Metastasis of Gastric Cancer Through Driving Epithelial-Mesenchymal Transition and PI3K/Akt/GSK3β Activation. *Sci Rep* (2017) 7:45275. doi: 10.1038/srep45275
37. Pucci S, Polidoro C, Greggi C, Amati F, Morini E, Murdocca M, et al. Pro-Oncogenic Action of LOX-1 and Its Splice Variant LOX-1Δ4 in Breast Cancer Phenotypes. *Cell Death Dis* (2019) 10:53. doi: 10.1038/s41419-018-1279-1
38. Zhang J, Zhang L, Li C, Yang C, Li L, Song S, et al. LOX-1 Is a Poor Prognostic Indicator and Induces Epithelial-Mesenchymal Transition and Metastasis in Pancreatic Cancer Patients. *Cell Oncol (Dordr)* (2018) 41:73–84. doi: 10.1007/s13402-017-0360-6
39. Zhao G, Li X, Miao H, Chen S, Hou Y. Estrogen Promotes cAMP Production in Mesenchymal Stem Cells by Regulating ADCY2. *Int J Stem Cells* (2020) 13:55–64. doi: 10.15283/ijsc19139
40. Yu SJ, Yu JK, Ge W, Hu H, Yuan Y, Zheng S. SPARCL1, Shp2, MSH2, E-Cadherin, P53, ADCY-2 and MAPK Are Prognosis-Related in Colorectal Cancer. *World J Gastroenterol* (2011) 17:2028–36. doi: 10.3748/wjg.v17.i15.2028
41. Albert JS, Yerges-Armstrong LM, Horenstein RB, Pollin TI, Sreenivasan UT, Chai S, et al. Null Mutation in Hormone-Sensitive Lipase Gene and Risk of Type 2 Diabetes. *N Engl J Med* (2014) 370:2307–15. doi: 10.1056/NEJMoa1315496
42. Zolotov S, Xing C, Mahamid R, Shalata A, Sheikh-Ahmad M, Garg A. Homozygous LIPE Mutation in Siblings With Multiple Symmetric Lipomatosis, Partial Lipodystrophy, and Myopathy. *Am J Med Genet A* (2017) 173:190–4. doi: 10.1002/ajmg.a.37880
43. Coussens LM, Werb Z. Inflammation and Cancer. *Nature* (2002) 420:860–7. doi: 10.1038/nature01322
44. Bingle L, Brown NJ, Lewis CE. The Role of Tumour-Associated Macrophages in Tumour Progression: Implications for New Anticancer Therapies. *J Pathol* (2002) 196:254–65. doi: 10.1002/path.1027
45. Chen JJ, Lin YC, Yao PL, Yuan A, Chen HY, Shun CT, et al. Tumor-Associated Macrophages: The Double-Edged Sword in Cancer Progression. *J Clin Oncol* (2005) 23:953–64. doi: 10.1200/JCO.2005.12.172
46. Ryder M, Ghossein RA, Ricarte-Filho JC, Knauf JA, Fagin JA. Increased Density of Tumor-Associated Macrophages Is Associated With Decreased Survival in Advanced Thyroid Cancer. *Endocr Relat Cancer* (2008) 15:1069–74. doi: 10.1677/ERC-08-0036
47. Zhu XD, Zhang JB, Zhuang PY, Zhu HG, Zhang W, Xiong YQ, et al. High Expression of Macrophage Colony-Stimulating Factor in Peritumoral Liver Tissue Is Associated With Poor Survival After Curative Resection of Hepatocellular Carcinoma. *J Clin Oncol* (2008) 26:2707–16. doi: 10.1200/JCO.2007.15.6521
48. Ringel AE, Drijvers JM, Baker GJ, Catozzi A, García-Cañaveras JC, Gassaway BM, et al. Obesity Shapes Metabolism in the Tumor Microenvironment to Suppress Anti-Tumor Immunity. *Cell* (2020) 183:1848–66.e26. doi: 10.1016/j.cell.2020.11.009
49. Schaefer C, Kim GG, Albers A, Hoermann K, Myers EN, Whiteside TL. Characteristics of CD4+CD25+ Regulatory T Cells in the Peripheral Circulation of Patients With Head and Neck Cancer. *Br J Cancer* (2005) 92:913–20. doi: 10.1038/sj.bjc.6602407
50. Tanaka A, Sakaguchi S. Regulatory T Cells in Cancer Immunotherapy. *Cell Res* (2017) 27:109–18. doi: 10.1038/cr.2016.151
51. Li H, Feng Z, He ML. Lipid Metabolism Alteration Contributes to and Maintains the Properties of Cancer Stem Cells. *Theranostics* (2020) 10:7053–69. doi: 10.7150/thno.41388
52. The Cancer Genome Atlas Network. Comprehensive Genomic Characterization of Head and Neck Squamous Cell Carcinomas. *Nature* (2015) 517:576–82. doi: 10.1038/nature14129
53. Ide T, Brown-Endres L, Chu K, Ongusaha PP, Ohtsuka T, El-Deiry WS, et al. GAMT, a P53-Inducible Modulator of Apoptosis, Is Critical for the Adaptive Response to Nutrient Stress. *Mol Cell* (2009) 36:379–92. doi: 10.1016/j.molcel.2009.09.031
54. Yahagi N, Shimano H, Matsuzaka T, Najima Y, Sekiya M, Nakagawa Y, et al. P53 Activation in Adipocytes of Obese Mice. *J Biol Chem* (2003) 278:25395–400. doi: 10.1074/jbc.M302364200

55. Stein Y, Rotter V, Aloni-Grinstein R. Gain-Of-Function Mutant P53: All the Roads Lead to Tumorigenesis. *Int J Mol Sci* (2019) 20:6197. doi: 10.3390/ijms20246197
56. Xiao G, Lundine D, Annor GK, Canar J, Ellison V, Polotskaia A, et al. Gain-Of-Function Mutant P53 R273H Interacts With Replicating DNA and PARP1 in Breast Cancer. *Cancer Res* (2020) 80:394–405. doi: 10.1158/0008-5472.CAN-19-1036
57. Zhao Y, Ding L, Wang D, Ye Z, He Y, Ma L, et al. EZH2 Cooperates With Gain-of-Function P53 Mutants to Promote Cancer Growth and Metastasis. *EMBO J* (2019) 38:e99599. doi: 10.15252/embj.201899599
58. Nakayama M, Oshima M. Mutant P53 in Colon Cancer. *J Mol Cell Biol* (2019) 11:267–76. doi: 10.1093/jmcb/mjy075
59. Fiorini C, Cordani M, Padroni C, Blandino G, Di Agostino S, Donadelli M. Mutant P53 Stimulates Chemoresistance of Pancreatic Adenocarcinoma Cells to Gemcitabine. *Biochim Biophys Acta* (2015) 1853:89–100. doi: 10.1016/j.bbamcr.2014.10.003
60. Zhou G, Wang J, Zhao M, Xie TX, Tanaka N, Sano D, et al. Gain-Of-Function Mutant P53 Promotes Cell Growth and Cancer Cell Metabolism *via* Inhibition of AMPK Activation. *Mol Cell* (2014) 54:960–74. doi: 10.1016/j.molcel.2014.04.024

Conflict of Interest: The authors declare that the research was conducted in the absence of any commercial or financial relationships that could be construed as a potential conflict of interest.

frontiers in Oncology

ORIGINAL RESEARCH
published: 29 November 2021
doi: 10.3389/fonc.2021.764258

A New Dynamic Response to Therapy Assessment in Postoperative Patients With Low-Risk Differentiated Thyroid Cancer Treated Without Radioactive Iodine

Ping Dong[1†], *Li Wang*[2†], *Liu Xiao*[1], *Liu Yang*[1], *Rui Huang*[1*] *and Lin Li*[1*]

[1] *Department of Nuclear Medicine, West China Hospital, Sichuan University, Chengdu, China,* [2] *Department of Pancreatic Surgery, West China Hospital, Sichuan University, Chengdu, China*

OPEN ACCESS

Edited by:
Heming Lu,
People's Hospital of Guangxi Zhuang Autonomous Region, China

Reviewed by:
Chentian Shen,
Shanghai Jiao Tong University, China
Shilpi Sharma,
Narayana Superspeciality Hospital, Gurugram, India

***Correspondence:**
Lin Li
lilinhuaxi@sina.com
Rui Huang
huangrui1977@163.com

[†]*These authors have contributed equally to this work*

Specialty section:
This article was submitted to Head and Neck Cancer, a section of the journal Frontiers in Oncology

Received: *25 August 2021*
Accepted: *11 November 2021*
Published: *29 November 2021*

Citation:
Dong P, Wang L, Xiao L, Yang L, Huang R and Li L (2021) A New Dynamic Response to Therapy Assessment in Postoperative Patients With Low-Risk Differentiated Thyroid Cancer Treated Without Radioactive Iodine. Front. Oncol. 11:764258. doi: 10.3389/fonc.2021.764258

Background: Total thyroidectomy (TT) or lobectomy without radioactive iodine (RAI) is becoming a common management for patients with low-risk differentiated thyroid cancer (DTC). However, the assessment of response to therapy for these patients remains controversial. The aim of this study was to propose and validate a new dynamic evaluation strategy to assess the response to therapy in patients with low-risk DTC treated with TT or lobectomy but without RAI.

Methods: We performed a retrospective analysis of 543 adult patients with low-risk DTC who underwent TT or lobectomy without RAI therapy. Follow-up consisted of trends of serum thyroglobulin (Tg), anti-thyroglobulin antibody (TgAb) levels and neck ultrasonography (US) were conducted every 6–24 months. Response to therapy assessments were defined as excellent response, biochemical incomplete response, structural incomplete response, and indeterminate response according to the follow-up findings.

Results: At a median follow-up of 51 months (range 33–66 months), 517 (95%) had excellent response, while the other 26 had either biochemical incomplete response (an increasing trend of suppressed serum Tg levels, n=9; an increasing trend of TgAb levels, n=3) or indeterminate response (a stable or decreasing trend of suppressed serum Tg levels, but a stable positive trend of TgAb levels, n=14). No patients had structural incomplete response or no deaths related to thyroid cancer. The risk of incomplete response was significantly higher in lobectomy than in TT ($p<0.001$).

Conclusion: Our study proposed and validated a new dynamic response to therapy assessment depending on trends of suppressed serum Tg, TgAb levels, and neck US findings which could be an appropriate tool for postoperative follow-up in low-risk DTC patients without RAI therapy. Our findings provided further evidence to support no routine recommendation of RAI after surgery in low-risk DTC.

Keywords: differentiated thyroid cancer, low-risk, response to therapy assessment, thyroglobulin, neck ultrasonography

INTRODUCTION

The prevalence of low-risk differentiated thyroid cancer (DTC) is increasing significantly, which mainly due to the early diagnosis of thyroid microcarcinoma (TMC) by using neck ultrasonography (US) (1–4). Optimal management of DTC usually requires interdisciplinary cooperation, including surgery, risk-adapted postoperative radioactive iodine (RAI) therapy, individualized thyroid hormone therapy, and follow-up for the detection of patients with persistent or recurrent disease (5–7). Recently, considering factors such as the excellent prognosis of low-risk DTC (5, 8), absence of significant reduction in recurrence rate or disease-free survival in low-risk patients treated with RAI (9, 10), scarce evidence concerning the usefulness of RAI in improving disease-specific mortality in low-risk DTC (5), and potential side effects on RAI [e.g., chronic sialadenitis (11, 12), secondary malignancies (13, 14)], the 2015 American Thyroid Association (ATA) guidelines recommend performing conservative strategies, namely, total thyroidectomy (TT) or lobectomy without RAI ablation, for low-risk DTC patients (5). Thus, in China, TT or lobectomy without RAI ablation is becoming a common management for patients with low-risk DTC.

Although the above-mentioned conservative strategies are gradually becoming accepted, the assessment of response to therapy for these patients remains controversial. According to the 2015 ATA guidelines, periodic measurements of serum thyroglobulin (Tg) on thyroid hormone therapy and neck US should be considered during the follow-up of patients with low-risk DTC who underwent TT or lobectomy without RAI ablation (5), but the roles played by each of these methods are not specially defined. In 2016, Momesso et al. proposed a dynamic risk stratification method (mainly based on neck US findings and different suppressed serum Tg cutoff values, namely, Tg <0.2, 0.2–5, or >5 ng/mL for TT; Tg <30 or >30 ng/mL for lobectomy, to stratify assessments as excellent response, indeterminate response, biochemical incomplete response and structural incomplete response) to evaluate the response to initial surgery in low-risk DTC patients who did not undergo RAI therapy (15). However, since this evaluation system could be affected by the size of remnant tissue, the results vary significantly [e.g., excellent response, 94.1% as reported by Momesso et al. (15) *versus* 71.7% as reported by Park et al. (16)].

The current study attempted to use a dynamic evaluation strategy based on the trends of suppressed Tg, anti-thyroglobulin antibody (TgAb) levels and neck US findings to determine the response to therapy in Chinese low-risk DTC patients treated with surgery alone (TT or lobectomy) after a median follow-up of 51 months and identify risk factors associated with incomplete response.

MATERIAL AND METHODS

Patients

This retrospective study was approved by the Institutional Research Ethics Committee of West China Hospital of Sichuan University (# 20201158). The requirement for written informed consent was waived because this study was of retrospective design and used only de-identified clinicopathologic data.

Electronic medical records at West China Hospital of Sichuan University, Chengdu, China, were retrospectively reviewed for adult patients with low-risk DTC who underwent TT or lobectomy without RAI remnant ablation therapy between July 2015 and September 2016. The inclusion criteria were as follows: patients aged >18 years at the time of surgery; patients with documented low-risk DTC who underwent lobectomy with isthmusectomy or TT, and/or central/lateral neck dissection, without RAI remnant ablation therapy, with thyroid-stimulating hormone (TSH) suppressive therapy; and those who were routinely followed up every 6–24 months with the determination of serum TSH, Tg and TgAb levels and neck US findings. The exclusion criteria were histopathological diagnosis other than DTC, history of other cancers, presence of other conditions that have clinical significance, and absence of sufficient follow-up data.

Laboratory Studies and Follow-Up Protocol

Serum Tg, TgAb, and TSH levels were measured 1.5–3 months post-operation and during routine follow-up every 6–24 months in our hospital. Between July 2015 and May 2020, serum Tg, TgAb, and TSH levels were measured using a fully automated electrochemiluminescent immunoassay analyzer (Cobas® e 601, Immunoassay Analyzer, Roche, Switzerland) with a measuring range of 0.04–500 ng/mL, 10–4000 IU/mL, and 0.005–100 mIU/L, respectively. After May 2020, serum Tg, TgAb, and TSH levels were measured using a new generation of electrochemiluminescent immunoassay analyzer (Cobas® e 801, Immunoassay Analyzer, Roche, Switzerland). Neck US examination was performed by experienced operators, using color Doppler scanners with multi-frequency probes (7.5–10 MHz), every 6 months during the first year post-operation and repeated at 12- to 24- month intervals thereafter.

The trends of suppressed serum Tg and TgAb levels were evaluated at the same TSH levels and defined as stable (the change of Tg or TgAb levels <20% when comparing the three consecutive Tg or TgAb levels), decreasing (the decrease of Tg or TgAb levels ≥20%) or increasing (the increase of Tg or TgAb levels ≥20%). Positive TgAb was defined as serum TgAb level ≥60 IU/mL, which might interfere with Tg measurement (16, 17). When the serum TgAb level was <60 IU/mL, serum TgAb status was defined as negative (16).

Neck US examination included the analysis of the thyroid bed, remnant thyroid tissue, and lymph node regions. A negative neck US result was defined as an empty thyroid bed with the jugular and carotid vessels in a medial location or no abnormalities in the remnant thyroid tissue, and as the absence of suspicious lymph nodes (LNs).

Response to Therapy Assessments

Response to therapy assessments at the last follow-up were defined as excellent response, biochemical incomplete response, structural incomplete response, and indeterminate response, which mainly depended on the trends of serum suppressed Tg, TgAb levels and neck US findings with

avoidance of the size of remnant tissue. The definitions of each response to therapy assessment at the last follow-up for patients who underwent TT or lobectomy without RAI are shown in **Table 1** (15, 16, 18, 19).

Statistical Analysis

Continuous variables were presented as means and standard deviations or median values with ranges, and categorical variables were calculated as frequencies or percentages. A comparison of continuous variables was performed with Student's t-test, and that of categorical variables was performed using Pearson's χ^2 test or Fisher's exact test. Prognostic factors associated with incomplete response at the last follow-up were analyzed using logistic regression. A p-value of <0.05 was considered statistically significant. Statistical analyses were performed using IBM SPSS statistical software (version 23.0 for Mac OS X).

RESULTS

Study Cohort

Between July 2015 and September 2016, a total of 634 patients were included (**Figure 1**). Seventeen patients were not included in the follow-up: 14 had other cancers (six with breast cancer, three with lung cancer, one with squamous cell carcinoma, one with esophageal cancer, one with colon cancer, one with renal cell carcinoma, and one with ovarian cancer), while 3 had a history of other conditions that had clinical significance (one with gastrointestinal stromal tumor, one with familial adenomatous polyposis, and one with uremia). Seventy-four patients could not be evaluated because of insufficient follow-up data. Finally, 543 patients were evaluated: 471 (87%) who underwent TT and 72 (13%) who underwent lobectomy.

Clinical Characteristics

The demographic characteristics and clinical features of the 543 patients included in the study are shown in **Table 2**. Mean patient age was 43 years; 79% were female, and all patients had low-risk papillary thyroid cancers. TMC was found in 420 (77%) of the 543 patients, wherein 19% had multifocal disease. Neck dissection was performed in 540 (99%) of the 543 patients, wherein 77% had N0. Central cervical LN metastases were found in 125 (23%) of the 543 patients, including 73 (58%) with one LN metastasis, 34 (27%) with two LN metastases, and 18 (15%) with three or four LN metastases. No patients had lateral LN cervical metastases. Based on the 8th American Joint Cancer Committee TNM staging system, 97% and 3% patients had stage I and stage II, respectively. For thyroid surgery specific complications, rates of transient hypoparathyroidism and vocal cord paralysis in TT were higher than those in lobectomy.

Patients who underwent lobectomy were younger than those who underwent TT (p=0.014). More unifocal disease and TMCs were found in patients who underwent lobectomy than in those who underwent TT (p=0.005 and p=0.013, respectively). There were no significant differences in LN metastasis or TNM staging between the TT and lobectomy cohorts (**Table 2**).

Response to Therapy Assessments

At the last follow-up (median follow-up, 51 months; range, 33–66 months), 517 (95%) of the 543 patients had excellent response (**Table 3**). Of the other 26 patients, 12 had biochemical incomplete response (an increasing trend of suppressed serum Tg levels, n=9; an increasing trend of TgAb levels, n=3), 14 had indeterminate response (a stable or decreasing trend of suppressed serum Tg levels, but a stable positive trend of TgAb levels). No patients had structural incomplete response or no deaths related to thyroid cancer.

Excellent response and fewer biochemical incomplete response were found in patients who underwent TT than in those who underwent lobectomy (p<0.001). There were no significant differences in the indeterminate incomplete response between the two groups (**Table 3**).

Prognostic Factors Associated With Incomplete Response

Details and the results of univariate analysis of prognostic factors associated with incomplete response in low-risk DTC patients treated with TT or lobectomy without RAI therapy at the last follow-up are presented in **Table 4**. The risk of incomplete response at the last follow-up was not related to the patient's age, sex, primary tumor, or nodal status (**Table 4**). The risk of incomplete response was significantly higher in patients who underwent lobectomy than their counterpart (odds ratio=6.529, p=0.001).

TABLE 1 | The definitions of a new response to therapy assessment in patients with low-risk DTC who underwent total thyroidectomy or lobectomy without RAI.

	Definitions
Excellent response	Negative neck US[a] and a stable or decreasing trend of suppressed serum Tg[b] and negative TgAb[c] levels
Biochemical incomplete response	Negative neck US and an increasing trend of suppressed serum Tg or TgAb levels
Structural incomplete response	Structural evidence of disease regardless of serum Tg or TgAb levels
Indeterminate response	A stable or decreasing trend of suppressed serum Tg levels, and nonspecific neck US findings or a stable positive trend of TgAb levels

DTC, differentiated thyroid cancer; RAI, radioactive iodine; US, ultrasonography; TgAb, anti-thyroglobulin antibody; Tg, thyroglobulin.

[a]A negative neck US result was defined as an empty thyroid bed with the jugular and carotid vessels in a medial location or no abnormalities in the remnant thyroid tissue, and as the absence of suspicious lymph nodes.

[b]Trend of suppressed serum Tg was evaluated at the similar thyrotropin levels and defined as: stable (the change of Tg levels <20% when comparing the three consecutive Tg levels), decreasing (the decrease of Tg levels ≥20%) or increasing (the increase of Tg levels ≥20%).

[c]Positive serum TgAb was defined as TgAb level ≥60 IU/mL; negative TgAb was defined as <60 IU/mL. The trends in the change of TgAb levels were defined as stable (the change of TgAb levels <20% when comparing the three consecutive TgAb levels), decreasing (the decrease of TgAb levels ≥20%), or increasing (the increase of TgAb levels ≥20%).

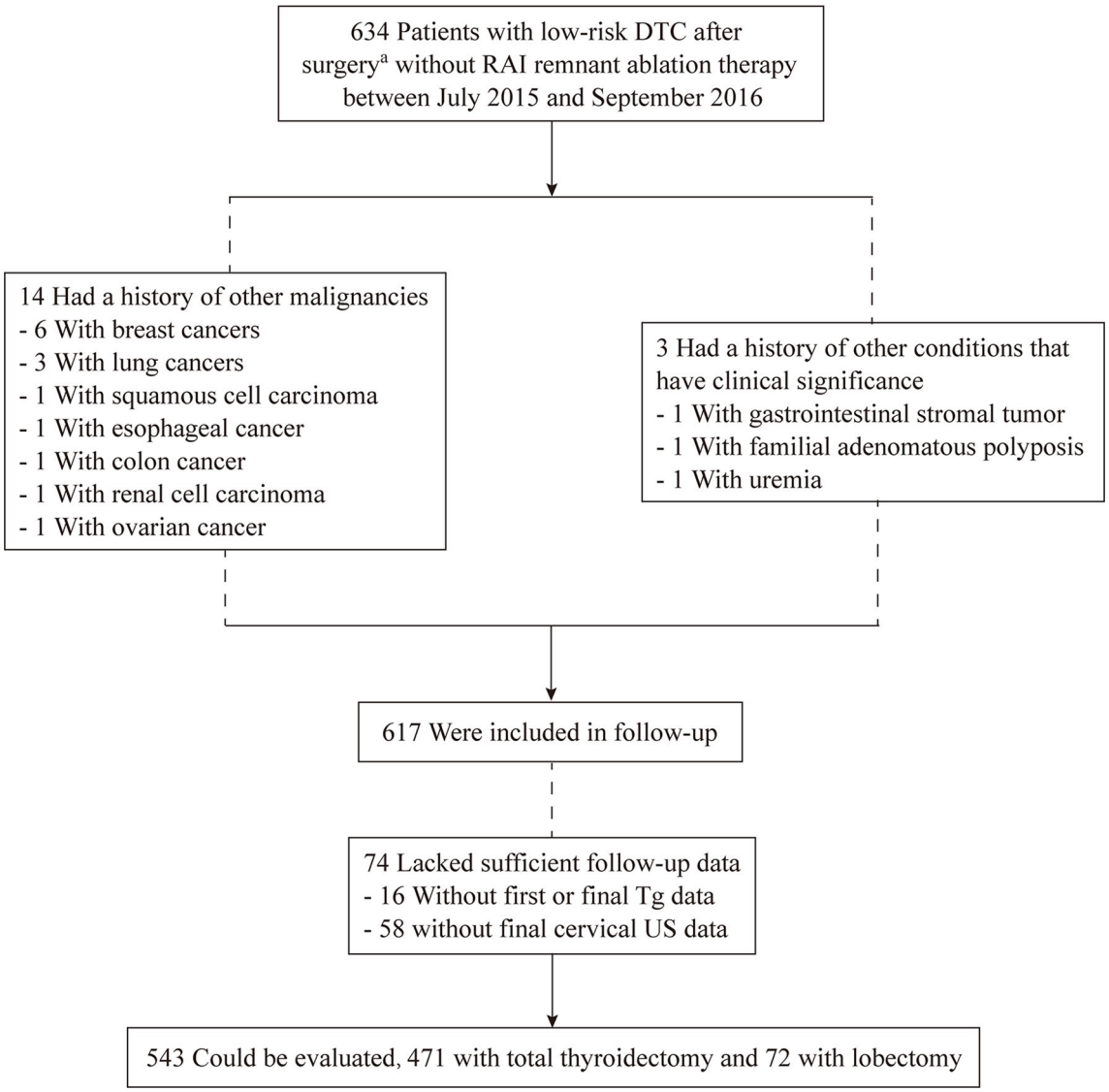

FIGURE 1 | Flow chart of inclusion-exclusion of patients with low-risk differentiated thyroid cancer without radioiodine ablation at the study. [a]Patients underwent lobectomy + isthmusectomy + ipsilateral central neck dissection or total thyroidectomy +/- central/lateral neck dissection.

DISCUSSION

In this study, we proposed and validated a new dynamic response to therapy assessment depending on trends of suppressed serum Tg, TgAb levels, and neck US findings in patients with low-risk DTC who underwent TT or lobectomy without RAI therapy. Response to therapy assessments were defined as excellent response, biochemical incomplete response, structural incomplete response, and indeterminate response, which mainly depended on the trends of suppressed serum Tg, TgAb levels and neck US findings without interference of the size of remnant tissue. Our findings show that, at the last follow-up, 95% of patients with low-risk DTC who underwent TT or lobectomy without RAI ablation therapy had excellent response. This rate in our cohort was similar to that (94.1%) reported by Momesso et al. (15), thus conforming the definition used in our study might be reasonable and reliable. Furthermore, the proportion of patients (97%) with excellent response among those who underwent TT in our study was similar to the proportion (98%) reported by Schlumberger et al. who performed a 5-year follow-up study of a randomized, phase 3, equivalence trial (ESTIMABL1, two thyrotropin-stimulation methods: thyroid hormone withdrawal *versus* the use of recombinant human TSH, and two RAI ablation doses:1.1 GBq *versus* 3.7 GBq) (20). Thus, our study provided further evidence to support no routine recommendation of RAI after surgery in low-risk DTC. The proportion of patients with biochemical incomplete response or indeterminate response in our study was in accordance with the 10-year recurrence rate of

TABLE 2 | Baseline characteristics of the patients.

	Entire Cohort (n = 543)	Surgery		p
		Total thyroidectomy[b] (n = 471)	Lobectomy[c] (n = 72)	
Age (years), median (range)	43 (19–79)	44 (19–79)	40 (19–60)	0.014
Sex, no. of patients (%)				0.046
Male	116 (21)	94 (20)	22 (31)	
Female	427 (79)	377 (80)	50 (69)	
Size of largest focus (mm), mean (range)	8.6 (1.5–29)	8.8 (1.5–29)	7.4 (4–15)	0.009
Focality, no. of patients (%)				0.005
Unifocal	440 (81)	373 (79)	67 (93)	
Multifocal	103 (19)	98 (21)	5 (7)	0.927
2 foci	84 (81)	80 (82)	4 (80)	
3–5 foci	19 (19)	18 (18)	1 (20)	
T classification[a], no. of patients (%)				0.013
T1a	420 (77)	355 (75)	65 (90)	
T1b	108 (20)	101 (21)	7 (10)	
T2	15 (3)	15 (3)	0 (0)	
N classification[a], no. of patients (%)				0.228
N0	418 (77)	367 (78)	51 (71)	
N1a	125 (23)	104 (22)	21 (29)	0.839
1 LN	73 (58)	59 (57)	14 (67)	
2 LN	34 (27)	29 (28)	5 (24)	
3–4 LN	18 (15)	16 (15)	2 (9)	
TNM Staging[a], no. of patients (%)				0.708
Stage I	527 (97)	456 (97)	71 (99)	
Stage II	16 (3)	15 (3)	1 (1)	
Follow-up duration (months), mean (range)	49 (31–64)	49 (32–64)	47 (31–62)	0.021

T, tumor; N, node; LN, lymph node; M, metastasis.

[a]TNM staging is determined by eighth American Joint Cancer Committee TNM staging system.

[b]There were 3 patients underwent total thyroidectomy, 129 patients underwent total thyroidectomy + ipsilateral central neck dissection, 334 patients underwent total thyroidectomy + bilateral central neck dissection, 5 patients underwent total thyroidectomy + bilateral central and lateral neck dissection.

[c]There were 72 patients underwent lobectomy + isthmusectomy + ipsilateral central neck dissection.

TABLE 3 | Response to therapy assessments at the last follow-up in the study subjects.

Response to therapy assessments[a]	Total (n = 543)	Total thyroidectomy (n = 471)	Lobectomy (n = 72)	p
Excellent response %	517 (95)	457 (97)	60 (83)	<0.001
Biochemical incomplete response %	12 (2)	3 (1)	9 (13)	<0.001
Indeterminate incomplete response %	14 (3)	11 (2)	3 (4)	0.413

[a]There were no patients with structural incomplete response.

1%–2%, which is expected for patients with low-risk DTC. During our follow-up, no patients had structural incomplete response, which may be explained by the aggressive prophylactic lymph node dissection and insufficient follow-up duration (21, 22).

According to the 2015 ATA guidelines, lobectomy may be sufficient for a unifocal intrathyroidal low-risk carcinoma sized <4 cm in diameter in patients with no prior head and neck radiation, familial thyroid cancer, or clinically detectable cervical LN metastases (5). In the present study, type of surgery was found to be a prognostic factor associated with incomplete response in low-risk DTC patients without RAI therapy at the last follow-up. Particularly, we found that the risk of biochemical incomplete response was significantly higher in patients who underwent lobectomy (seven and two patients due to increasing trends of suppressed serum Tg and TgAb levels, respectively), when compared to TT (two and one patients due to an increasing trend of suppressed serum Tg and TgAb levels, respectively). For low-risk DTC patients treated with lobectomy, an increase in Tg values over time suggested a growing thyroid tissue or tumor, and an increase in TgAb values suggested coexistent Hashimoto thyroiditis in residual thyroid tissues (especially in patients diagnosed with Hashimoto thyroiditis by surgical histopathology) or tumor relapse (5, 23–25).

The present study has several strengths. First, postoperative risk assessment, assessment of potential benefits and side effects of RAI therapy, and patients' preferences and values had been adequately considered during post-operative management (observation and individualized thyroid hormone therapy without RAI ablation). Second, all the included patients underwent TT or lobectomy by experienced thyroid surgeons in our hospital who had more than 10 years of thyroidectomy experience. Third, all the serum Tg, TgAb, and TSH levels of all patients were measured by electrochemiluminescent immunoassay in our laboratory to ensure the accuracy and reliability. Finally, considering that neck US is operator-

TABLE 4 | Univariate analysis of prognostic factors associated with incomplete response at the last follow-up in 543 patients.

	No. of incomplete responses/no. of patients (%)	Odds ratio	95% CI	p
Age (years)				
≤55	24/458 (5.2)	1 (ref)		
>55	2/85 (2.4)	2.295	0.532–9.897	0.265
Sex				
Male	5/116 (4.3)	1 (ref)		
Female	21/427 (4.9)	0.871	0.321–2.362	0.786
Surgery				
Lobectomy	12/72 (16.7)	1 (ref)		
Total thyroidectomy	14/471 (3.0)	6.529	2.885–14.774	<0.001
Focality				
Unifocal	22/440 (5.0)	1 (ref)		
Multifocal	4/103 (3.9)	1.303	0.439–3.865	0.634
T classification[a]				
T1a	22/420 (5.2)	1 (ref)		
T1b/T2	4/123 (3.3)	1.644	0.556–4.866	0.369
N classification[a]				
N0	19/418 (4.5)	1 (ref)		
N1a	7/125 (5.6)	0.803	0.329–1.956	0.629

T, tumor; N, node.

[a]*TNM staging is determined by eighth American Joint Cancer Committee TNM staging system.*

dependent, all high-resolution neck US scans were performed by experienced specialists to evaluate structural abnormalities to ensure the accuracy in our center. However, this study has several limitations. First, the 51-month (median) follow-up period chosen for this study might be suboptimal. Although most recurrences (80%) in low-risk DTC patients occurred during the first 3-5 years of follow-up, some recurrence or incomplete response might be missed (26, 27). Second, the single-institutional study design creates selection biases that are difficult to control. Third, this retrospective study enrolled a relatively small cohort of patients who underwent lobectomy.

In conclusion, our study validates that the newly proposed dynamic response to therapy assessment depending on trends of suppressed serum Tg, TgAb levels, and neck US findings could be an appropriate tool for postoperative follow-up in low-risk DTC patients without RAI therapy. Our findings provide further evidence to support no routine recommendation of RAI after surgery in low-risk DTC.

DATA AVAILABILITY STATEMENT

The original contributions presented in the study are included in the article/supplementary material. Further inquiries can be directed to the corresponding authors.

ETHICS STATEMENT

The studies involving human participants were reviewed and approved by the Institutional Research Ethics Committee of West China Hospital of Sichuan University. Written informed consent for participation was not required for this study in accordance with the national legislation and the institutional requirements.

AUTHOR CONTRIBUTIONS

PD, LW, RH and LL designed this research. PD, LW, LX and LY collected the data and performed the statistical analyses. PD, LW and RH reviewed the results, interpreted the data, and wrote the manuscript. PD, LW, RH and LL discussed and edited the paper. All authors contributed to the article and approved the submitted version.

FUNDING

This study was supported by the 1.3.5 Project for Disciplines of Excellence, West China Hospital, Sichuan University (No. ZYGD18016).

REFERENCES

1. Brito JP, Hay ID, Morris JC. Low Risk Papillary Thyroid Cancer. *BMJ* (2014) 348:g3045. doi: 10.1136/bmj.g3045
2. Ahn HS, Kim HJ, Welch HG. Korea's Thyroid-Cancer "Epidemic"–Screening and Overdiagnosis. *N Engl J Med* (2014) 371(19):1765–7. doi: 10.1056/NEJMp1409841
3. Veiga LH, Neta G, Aschebrook-Kilfoy B, Ron E, Devesa SS. Thyroid Cancer Incidence Patterns in Sao Paulo, Brazil, and the U.S. SEER Program, 1997-2008. *Thyroid* (2013) 23(6):748–57. doi: 10.1089/thy.2012.0532
4. Brito JP, Morris JC, Montori VM. Thyroid Cancer: Zealous Imaging has Increased Detection and Treatment of Low Risk Tumours. *BMJ* (2013) 347: f4706. doi: 10.1136/bmj.f4706
5. Haugen BR, Alexander EK, Bible KC, Doherty GM, Mandel SJ, Nikiforov YE, et al. American Thyroid Association Management Guidelines for Adult Patients With Thyroid Nodules and Differentiated Thyroid Cancer: The American Thyroid Association Guidelines Task Force on Thyroid Nodules and Differentiated Thyroid Cancer. *Thyroid* (2016) 26(1):1–133. doi: 10.1089/thy.2015.0020

6. Campenni A, Barbaro D, Guzzo M, Capoccetti F, Giovanella L. Personalized Management of Differentiated Thyroid Cancer in Real Life - Practical Guidance From a Multidisciplinary Panel of Experts. *Endocrine* (2020) 70 (2):280–91. doi: 10.1007/s12020-020-02418-x
7. Tuttle RM, Ahuja S, Avram AM, Bernet VJ, Bourguet P, Daniels GH, et al. Controversies, Consensus, and Collaboration in the Use of (131)I Therapy in Differentiated Thyroid Cancer: A Joint Statement From the American Thyroid Association, the European Association of Nuclear Medicine, the Society of Nuclear Medicine and Molecular Imaging, and the European Thyroid Association. *Thyroid* (2019) 29(4):461–70. doi: 10.1089/thy.2018.0597
8. Lamartina L, Handkiewicz-Junak D. Follow-Up of Low Risk Thyroid Cancer Patients: Can We Stop Follow-Up After 5 Years of Complete Remission? *Eur J Endocrinol* (2020) 182(5):D1–D16. doi: 10.1530/EJE-19-0960
9. Nascimento C, Borget I, Troalen F, Al Ghuzlan A, Deandreis D, Hartl D, et al. Ultrasensitive Serum Thyroglobulin Measurement Is Useful for the Follow-Up of Patients Treated With Total Thyroidectomy Without Radioactive Iodine Ablation. *Eur J Endocrinol* (2013) 169(5):689–93. doi: 10.1530/EJE-13-0386
10. Kim HJ, Kim SW. Radioactive Iodine Ablation Does Not Prevent Recurrences in Patients With Papillary Thyroid Microcarcinoma. *Clin Endocrinol (Oxf)* (2013) 79(3):445. doi: 10.1111/cen.12131
11. Jeong SY, Kim HW, Lee SW, Ahn BC, Lee J. Salivary Gland Function 5 Years After Radioactive Iodine Ablation in Patients With Differentiated Thyroid Cancer: Direct Comparison of Pre- and Postablation Scintigraphies and Their Relation to Xerostomia Symptoms. *Thyroid* (2013) 23(5):609–16. doi: 10.1089/thy.2012.0106
12. Choi JS, Hong SB, Hyun IY, Lim JY, Kim YM. Effects of Salivary Secretion Stimulation on the Treatment of Chronic Radioactive Iodine-Induced Sialadenitis. *Thyroid* (2015) 25(7):839–45. doi: 10.1089/thy.2014.0525
13. Rubino C, de Vathaire F, Dottorini ME, Hall P, Schvartz C, Couette JE, et al. Second Primary Malignancies in Thyroid Cancer Patients. *Br J Cancer* (2003) 89(9):1638–44. doi: 10.1038/sj.bjc.6601319
14. Brown AP, Chen J, Hitchcock YJ, Szabo A, Shrieve DC, Tward JD. The Risk of Second Primary Malignancies Up to Three Decades After the Treatment of Differentiated Thyroid Cancer. *J Clin Endocrinol Metab* (2008) 93(2):504–15. doi: 10.1210/jc.2007-1154
15. Momesso DP, Vaisman F, Yang SP, Bulzico DA, Corbo R, Vaisman M, et al. Dynamic Risk Stratification in Patients With Differentiated Thyroid Cancer Treated Without Radioactive Iodine. *J Clin Endocrinol Metab* (2016) 101 (7):2692–700. doi: 10.1210/jc.2015-4290
16. Park S, Kim WG, Song E, Oh HS, Kim M, Kwon H, et al. Dynamic Risk Stratification for Predicting Recurrence in Patients With Differentiated Thyroid Cancer Treated Without Radioactive Iodine Remnant Ablation Therapy. *Thyroid* (2017) 27(4):524–30. doi: 10.1089/thy.2016.0477
17. Jeon MJ, Kim WG, Jang EK, Choi YM, Lee YM, Sung TY, et al. Thyroglobulin Level in Fine-Needle Aspirates for Preoperative Diagnosis of Cervical Lymph Node Metastasis in Patients With Papillary Thyroid Carcinoma: Two Different Cutoff Values According to Serum Thyroglobulin Level. *Thyroid* (2015) 25(4):410–6. doi: 10.1089/thy.2014.0544
18. Janovsky CC, Maciel RM, Camacho CP, Padovani RP, Nakabashi CC, Yang JH, et al. A Prospective Study Showing an Excellent Response of Patients With Low-Risk Differentiated Thyroid Cancer Who Did Not Undergo Radioiodine Remnant Ablation After Total Thyroidectomy. *Eur Thyroid J* (2016) 5(1):44–9. doi: 10.1159/000442048
19. Suss SKA, Mesa CO Jr, Carvalho GA, Miasaki FY, Chaves CP, Fuser DC, et al. Clinical Outcomes of Low and Intermediate Risk Differentiated Thyroid Cancer Patients Treated With 30mci for Ablation or Without Radioactive Iodine Therapy. *Arch Endocrinol Metab* (2018) 62(2):149–56. doi: 10.20945/2359-3997000000025
20. Schlumberger M, Leboulleux S, Catargi B, Deandreis D, Zerdoud S, Bardet S, et al. Outcome After Ablation in Patients With Low-Risk Thyroid Cancer (ESTIMABL1): 5-Year Follow-Up Results of a Randomised, Phase 3, Equivalence Trial. *Lancet Diabetes Endocrinol* (2018) 6(8):618–26. doi: 10.1016/S2213-8587(18)30113-X
21. Ross DS, Litofsky D, Ain KB, Bigos T, Brierley JD, Cooper DS, et al. Recurrence After Treatment of Micropapillary Thyroid Cancer. *Thyroid* (2009) 19 (10):1043–8. doi: 10.1089/thy.2008.0407
22. Durante C, Montesano T, Attard M, Torlontano M, Monzani F, Costante G, et al. Long-Term Surveillance of Papillary Thyroid Cancer Patients Who do Not Undergo Postoperative Radioiodine Remnant Ablation: Is There a Role for Serum Thyroglobulin Measurement? *J Clin Endocrinol Metab* (2012) 97 (8):2748–53. doi: 10.1210/jc.2012-1123
23. Verburg FA, Luster M, Cupini C, Chiovato L, Duntas L, Elisei R, et al. Implications of Thyroglobulin Antibody Positivity in Patients With Differentiated Thyroid Cancer: A Clinical Position Statement. *Thyroid* (2013) 23(10):1211–25. doi: 10.1089/thy.2012.0606
24. Kim WG, Yoon JH, Kim WB, Kim TY, Kim EY, Kim JM, et al. Change of Serum Antithyroglobulin Antibody Levels Is Useful for Prediction of Clinical Recurrence in Thyroglobulin-Negative Patients With Differentiated Thyroid Carcinoma. *J Clin Endocrinol Metab* (2008) 93(12):4683–9. doi: 10.1210/jc.2008-0962
25. Chung JK, Park YJ, Kim TY, So Y, Kim SK, Park DJ, et al. Clinical Significance of Elevated Level of Serum Antithyroglobulin Antibody in Patients With Differentiated Thyroid Cancer After Thyroid Ablation. *Clin Endocrinol (Oxf)* (2002) 57(2):215–21. doi: 10.1046/j.1365-2265.2002.01592.x
26. Durante C, Montesano T, Torlontano M, Attard M, Monzani F, Tumino S, et al. Papillary Thyroid Cancer: Time Course of Recurrences During Postsurgery Surveillance. *J Clin Endocrinol Metab* (2013) 98(2):636–42. doi: 10.1210/jc.2012-3401
27. Kim H, Kim TH, Choe JH, Kim JH, Kim JS, Oh YL, et al. Patterns of Initial Recurrence in Completely Resected Papillary Thyroid Carcinoma. *Thyroid* (2017) 27(7):908–14. doi: 10.1089/thy.2016.0648

Conflict of Interest: The authors declare that the research was conducted in the absence of any commercial or financial relationships that could be construed as a potential conflict of interest.

frontiers in Oncology

ORIGINAL RESEARCH
published: 29 November 2021
doi: 10.3389/fonc.2021.766902

Worst Pattern of Perineural Invasion Redefines the Spatial Localization of Nerves in Oral Squamous Cell Carcinoma

Yong Fu[1†], Xinwen Zhang[1†], Zhuang Ding[1], Nisha Zhu[1], Yuxian Song[1], Xiaoxin Zhang[1], Yue Jing[1], Yijun Yu[1], Xiaofeng Huang[2], Lei Zhang[2], Qingang Hu[1], Yanhong Ni[1*] and Liang Ding[1*]*

[1] Central Laboratory of Stomatology, Nanjing Stomatological Hospital, Medical School of Nanjing University, Nanjing, China, [2] Department of Oral Pathology, Nanjing Stomatological Hospital, Medical School of Nanjing University, Nanjing, China

OPEN ACCESS

Edited by:
Qin Lin,
First Affiliated Hospital of Xiamen University, China

Reviewed by:
Marco Mascitti,
Marche Polytechnic University, Italy
Michaelina Macluskey,
University of Dundee, United Kingdom

***Correspondence:**
Yanhong Ni
niyanhong12@163.com
Liang Ding
879269339@qq.com
Qingang Hu
qghu@nju.edu.cn

[†]These authors have contributed equally to this work

Specialty section:
This article was submitted to Head and Neck Cancer, a section of the journal Frontiers in Oncology

Received: 30 August 2021
Accepted: 08 November 2021
Published: 29 November 2021

Citation:
Fu Y, Zhang X, Ding Z, Zhu N, Song Y, Zhang X, Jing Y, Yu Y, Huang X, Zhang L, Hu Q, Ni Y and Ding L (2021) Worst Pattern of Perineural Invasion Redefines the Spatial Localization of Nerves in Oral Squamous Cell Carcinoma. Front. Oncol. 11:766902. doi: 10.3389/fonc.2021.766902

As a key histopathological characteristic of tumor invasion, perineural invasion (PNI) assists tumor dissemination, whereas the current definition of PNI by dichotomy is not accurate and the prognostic value of PNI has not reached consensus. To define PNI status in each patient when mixed types of PNI occurred simultaneously, we here further subclassified the traditional PNI in 183 patients with oral squamous cell carcinoma (OSCC). The spatial localization of nerves in OSCC microenvironment was thoroughly evaluated and successfully concluded into four types of PNI: 0, tumor cells away from nerves; 1, tumor cells encircling nerves less than 33%; 2, tumor cells encircling nerves at least 33%; and 3, tumor cells infiltrating into nerve sheathes. Sequentially, patients were stratified by single and mixed types of PNI. Traditionally, types 0 and 1 were defined as PNI^-, while types 2 and 3 were PNI^+, which predicted shorter survival time. When multiple types of PNI existed within one tumor, patients with higher score of PNI types tended to have a relatively worse prognosis. Therefore, to define the status of PNI more precisely, the new variable worst pattern of PNI (WPNI) was proposed, which was taken as the highest score of PNI types present in each patient no matter how focal. Results showed that patients with WPNI 1 had longest survival time, and WPNI 2 correlated with better overall survival ($p = 0.02$), local-regional recurrence-free survival ($p = 0.03$), and distant metastasis-free survival ($p = 0.046$) than WPNI 3. Multivariate Cox analysis confirmed that only WPNI 3 could independently predict patients' prognosis, which could be explained by a more damaged immune response in WPNI 3 patients with less $CD3^+CD8^+$ T cells and $CD19^+$ B cells. Conclusively, WPNI by trichotomy provide more meticulous and precise pathological information for tumor-nerve interactions in OSCC patients.

Keywords: tumor-nerve interaction, worst pattern of perineural invasion (WPNI), oral squamous cell carcinoma (OSCC), prognostic biomarker, immune balance

INTRODUCTION

Oral squamous cell carcinoma (OSCC) represents the most common epithelial malignancy in the head and region, with nearly 350,000 new cases and 180,000 deaths in 2018 globally (1). Smoking, alcohol drinking, and betel quid chewing are reported as lifestyle-related pathogenic risk factors (2). At present, the primary choice for OSCC treatment is still surgical resection supplemented with/without postoperative radiotherapy, chemotherapy, or concurrent chemoradiotherapy (3). Although strategies for OSCC diagnosis and treatment are both constantly being optimized, the 5-year overall survival rate remains about 60% (3). With OSCC progression, patients eventually die of tumor recurrence and metastasis (2). Typically, lymphovascular route represents the main pathway for OSCC metastasis while nerves as the potential pathway have attracted increasing attentions in recent years (4).

In the tumor microenvironment, nerves have been neglected by researchers (5). However, in addition to interacting with immune cells, fibroblasts, and endothelial cells, tumor cells can also interact with nerves (6). Morphologically, the best example of tumor-nerve interaction is perineural invasion (PNI), which assists tumor dissemination and has been recognized as a negative prognostic factor for several cancers (7–10). Although PNI is included in clinical diagnosis including OSCC (11), there is still lack of a standardized definition consensus among pathologists (12, 13). In 1985, Batsakis et al. described PNI as tumor cells invaded in, around, and through peripheral nerves (14), nerves were surrounded by tumor cells in whole or in part, or tumor cells were observed inside the endoneurium (15). With traditional dichotomies, PNI was classified as positive (presence, PNI^+) or negative (absence, PNI^-).

However, debates on the spatial relationship between tumor cells and nerves in PNI have existed for decades due to this dichotomy. On the one hand, Liebig et al. optimized PNI to the definition that tumor cells are closely adjacent to the peripheral nerves and encircle no less than 33% of their circumferences or tumor cells within any of the three layers of nerve sheaths; however, the judgement of PNI in clinical practice was still quite subjective (13, 15, 16). Consequently, the detection rate of positive PNI in the same tumor type varied greatly across cohorts (4). Additionally, a few studies still argued that PNI failed to predict survival (17–20). However, on another hand, intratumoral heterogeneity within a single tumor microenvironment (TME) is the intrinsic driver for the simultaneous existence of several PNI types. The status of PNI in each patient as mixed types of PNI coexist and their clinical outcomes are unclear, which promoted us to identify a histopathological indicator to efficiently capture the feature of tumor-nerve interaction patterns.

In this study, in order to further classify the traditional PNI, we thoroughly evaluated the spatial localization of nerves in OSCC microenvironment. Then, the new variable, the worst pattern of PNI (WPNI) was proposed and investigated for its clinical significance. Moreover, as increasing evidence suggests that peripheral nerves profoundly alter the immune response in both inflammatory diseases and cancers (21–23), we also explored whether the imbalance of the immune system was associated with different WPNI scores in OSCC patients.

MATERIALS AND METHODS

Patients and Tissue Samples

A total of 183 patients with primary OSCC treated in the Department of Oral and Maxillofacial Surgery at Nanjing Stomatological Hospital from January 2013 to December 2014 were included in this retrospective study (**Table 1**). Patients' demographic data (age and sex), clinicopathological parameters (tumor site, pathologic T stage, pathologic N stage, pathologic TNM stage, tumor differentiation, worst pattern of invasion (WPOI), PNI, local-regional control and distant metastasis), and treatment modalities (radiotherapy and chemotherapy) were included and analyzed. Inclusion criteria included the following: (1) patients with a pathological diagnosis of OSCC; (2) patients who were primarily treated with surgery; and (3) patients with complete clinicopathological data and available tissue specimens. The exclusion criteria included preoperative

TABLE 1 | Clinicopathological features of 183 OSCC patients in this study.

Features	*n* (%)
Age (years): median (range)	61 (26–83)
Follow-up (months): median (range)	73 (2–87)
Sex	
Female	78 (42.6)
Male	105 (57.4)
Tumor site	
Buccal mucosa	33 (18.0)
Tongue	84 (45.9)
Gingiva	33 (18.0)
Others	33 (18.0)
Pathologic T stage	
T1	66 (36.1)
T2	91 (49.7)
T3	14 (7.7)
T4	12 (6.6)
Pathologic N stage	
N0	118 (64.5)
N1	38 (20.8)
N2	27 (14.8)
Tumor TNM stage	
I	46 (25.1)
II	57 (31.1)
III	45 (24.6)
IV	35 (19.1)
Tumor differentiation	
Well	163 (89.1)
Moderately/Poor	20 (10.9)
Worst pattern of invasion (WPOI)	
1–3	95 (51.9)
4–5	88 (48.1)
Radiotherapy	
Without	114 (62.3)
With	69 (37.7)
Chemotherapy	
Without	159 (86.9)
With	24 (13.1)

TNM, tumor-node-metastasis.

chemotherapy or radiotherapy, failure to undergo surgery, and the inability to obtain pathological slides. The pathological stages and the histological grade of OSCC were separately classified based on the guidelines of the 7th edition of AJCC Cancer Staging and the protocol of WHO. This study was conducted in full accordance with ethical principles and was approved by the Medical Ethics Committee of the Nanjing Stomatological Hospital, Medical School of Nanjing University [approval number: 2019NL-009(KS)].

Study Design

Based on distinct spatial localization of nerves in OSCC microenvironment, 183 OSCC patients were stratified by five types of PNI as indicated in **Figure 1I**. Through evaluation of their prognostic value, we tried to determine which type of PNI showed the highest risk of death, especially when mixed types of PNI occurred in one patient. Finally, we introduced the new variable worst pattern of PNI (WPNI) to define the PNI status of OSCC patients and further evaluated its predictive ability for the clinical outcome.

PNI Types and the WPNI

The traditional PNI were subclassified into four types: 0, tumor cells away from nerves; 1, tumor cells encircling nerves less than 33%; 2, tumor cells encircling nerves at least 33%; and 3, tumor cells infiltrating into nerve sheathes. The new variable WPNI was taken as the highest score of PNI types present in each patient no matter how focal, which was similar to WPOI (24). Two oral pathologists independently reviewed all hematoxylin-eosin (H&E)-stained slides to recognize and record the existing PNI types and where disagreement occurred, consensus would be reached through a discussion.

Immunohistochemistry

Immunohistochemical staining was performed on 4-μm-thick formalin-fixed, paraffin-embedded tissue sections. After baking all sections at 70°C for 45 min, they were incubated with xylene three times for 10 min each and then treated with gradient ethanol for 5 min in each solution. Antigen unmasking was performed by boiling the sections in sodium citrate buffer (pH 6.0), blocking with 3% hydrogen peroxide for 10 min at room temperature and washing. Cytokeratin-5/6 (kit-0018) and S-100β (kit-0007), both ready-to-use and purchased from Maixin (Maixin Biotech Co., Ltd., Fuzhou, China), were used to label tumor epithelial cells and nerves, respectively, at 4°C overnight. Then, the Super-MaxVision mouse/rabbit Universal HRP Kit (TPB-0015, Typing Biotech Co., Ltd., Nanjing, China) was used for DAB chromogen staining followed by nuclear staining using hematoxylin. Sections were covered with neutral gum and dried at room temperature.

Flow Cytometry

The T/B/NK cells data in preoperative blood of primary OSCC patients was immediately collected and analyzed using flow cytometry. To identify and determine the percentages of mature human lymphocyte subsets in erythrocyte-lysed whole blood, including T cells ($CD3^+$), B cells ($CD19^+$), helper/inducer T cells ($CD3^+CD4^+$), suppressor/cytotoxic T cells ($CD3^+CD8^+$), and natural killer (NK) lymphocytes ($CD3^-CD16^+$ and/or $CD56^+$), BD Multitest™ CD3-FITC/CD8-PE/CD45-PerCP/CD4-APC reagent and BD Multitest™ CD3-FITC/CD16-PE+CD56-PE/CD45-PerCP/CD19-APC reagent were used according to the manufacturer's instructions (Cat No. 340503, BD Biosciences, Franklin Lakes, NJ, USA), and samples were then quantified by flow cytometry on a FACS Calibur instrument. To determine the absolute counts of the lymphocyte subsets listed above, the total numbers of preoperative peripheral lymphocytes determined by the Automated Haematology Analyser XS Series (XS-1000i, Sysmex Corporation, Japan) were collected from the clinical laboratory. Since both tests came from the same batch of blood samples, we ignored the possible errors caused by the use of different detection instruments. Herein, the TBNK data of 62.3%

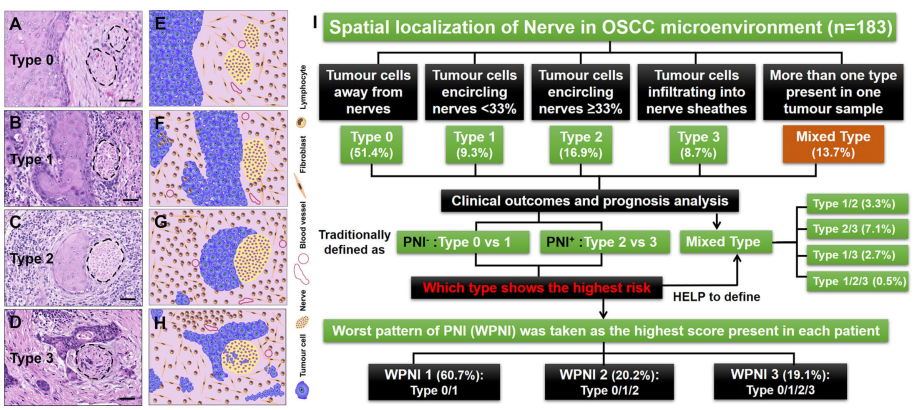

FIGURE 1 | Illustrations for patterns of tumor-nerve interaction and the study design. **(A)** PNI type 0, tumor cells away from nerves. **(B)** PNI type 1, tumor cells encircling nerves less than 33%. **(C)** PNI type 2, tumor cells encircling nerves at least 33%. **(D)** PNI type 3, tumor cells infiltrating into nerve sheathes. **(E–H)** The cartoon diagrams corresponding to **(A–D)**. **(I)** Flow diagram illustrating the management of OSCC patients stratified by different types of PNI. The dashed circles represented the peripheral nerves. Scale bars: 20 μm.

(114/183) of OSCC patients were successfully collected and the detailed characteristic data are listed in the **Supplementary Table S1**.

Statistical Analysis

Survival curves were calculated by the Kaplan-Meier method and compared by the log-rank test. The hazard ratio (HR) was calculated using the Cox proportional hazard regression model. Overall survival (OS) was defined as the time from surgery to death from any cause. Local-regional recurrence-free survival (LRFS) and distant metastasis-free survival (DMFS) were defined as the time from surgery to the occurrence of local-regional recurrence and distant metastasis or death from any cause, respectively.

For descriptive analysis, categorical variables are expressed as numbers and percentages, and continuous variables are expressed as median values and ranges. The Chi-square test was used to compare the correlations between the baseline factors and the morphological classifications of PNI. All hypothesis generation tests were two sided, and differences between groups were analyzed using Student's *t*-test, with a significance level of 0.05: $^{*}p < 0.05$; $^{**}p < 0.01$; and $^{***}p < 0.001$. Data analysis and visualization were performed on the Windows platform using IBM SPSS 24.0 and GraphPad Prism 8.0.

RESULTS

OSCC Microenvironment Has Heterogeneous Patterns of Tumor-Nerve Interaction

A total of 183 patients with primary OSCC were enrolled in this study, and 904 H&E-stained slides were thoroughly reviewed. Based on the spatial localization of nerves in the OSCC microenvironment, we observed that OSCC has heterogeneous patterns of tumor-nerve interaction. Therefore, tumor cells could be found away from nerves, which was defined here as PNI type 0 (**Figures 1A, E**). The conditions that tumor cells encircling nerves <33% and ≥33% were separately divided into PNI type 1 (**Figures 1B, F**) and type 2 (**Figures 1C, G**). Once tumor cells were observed infiltrating into nerve sheathes, this pattern was defined as PNI type 3 (**Figures 1D, H**). Importantly, if more than one type of PNI simultaneously occurred in one tumor sample, this condition was concluded into the mixed PNI type. As the PNI type 0 could be present in all OSCC samples, its coexistence with other types was not considered mixed PNI types. Thus, there were 94 (51.4%), 17 (9.3%), 31 (16.9%), and 16 (8.7%) patients with single type of PNI, types 0–3, respectively. In addition, the remaining 25 (13.7%) patients had the mixed PNI type (**Figure 1I**).

Mixed Types of PNI Are Present in One OSCC Patient

In this study, we found that PNI^{-} status contained two patterns of tumor-nerve interaction, that is PNI types 0 and 1, while PNI^{+} status consisted of PNI types 2 and 3. The traditional PNI^{-} patients did not contain any mixed types of PNI. However, in the PNI^{+} patients, the mixed types of PNI consisted of type 1/2 (6, 3.3%), type 2/3 (13, 7.1%), type 1/3 (5, 2.7%), and type 1/2/3 (1, 0.5%) (**Figure 1I**). Through immunohistochemical staining on sequential tissue sections, we showed that PNI types 0–3 simultaneously occurred in the same one OSCC sample (**Figure 2**).

The PNI Status of OSCC Patients Should Be Subdivided Into Three Types of WPNI

In order to determine the prognostic value of PNI and its subtypes in our cohort, Kaplan-Meier analyses were firstly performed between the traditional PNI^{+} and PNI^{-} OSCC patients. Patients with the traditional PNI^{+} status showed a significantly lower OS than the PNI^{-} patients ($p < 0.0001$) (**Figure 3A**). Next, we did subgroup analysis and found that in the PNI^{-} patients, PNI types 0 and 1 both indicated high 5-year OS (87.2% *vs*. 88.2%, respectively; $p = 0.89$) (**Figure 3B**). However, in the PNI^{+} patients, PNI type 3 tended to indicate a decreased 5-year OS than PNI type 2 (68.8% *vs*. 74.2%, respectively) though statistically not significant ($p = 0.52$) (**Figures 3C, D**). Most importantly, patients with the mixed PNI types had the worst 5-year OS (40.0%) (**Figure 3C**).

In order to determine the contribution of PNI subtypes to the decrease of OS, we further drew and compared the OS curves within the mixed PNI types. As a result, PNI type 1/2 showed the best OS, followed by PNI types 1/3, 2/3, and 1/2/3 (**Figure 4A**). In detail, the proportion of deaths tended to increase from 13%

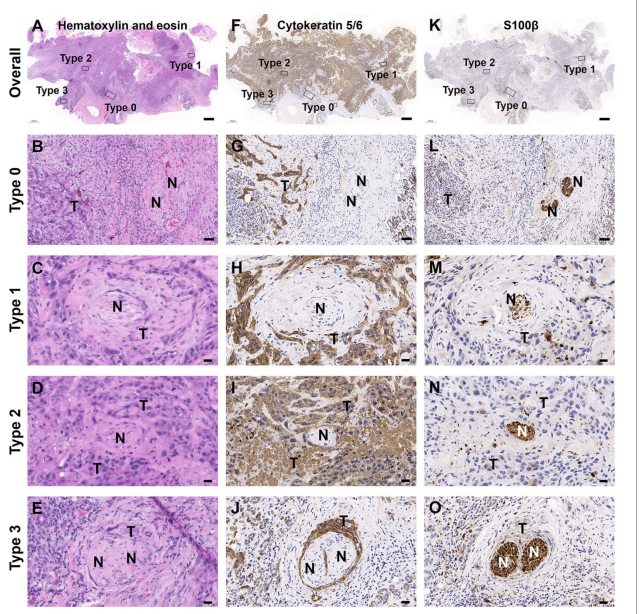

FIGURE 2 | Mixed PNI types simultaneously occurred in one OSCC sample. **(A–E)** H&E images. **(F–J)** Tumor cells labeled with cytokeratin 5/6. **(K–O)** Nerves labeled with S100β. The bold "T" and "N" represented tumor cells and nerves, respectively. Scale bars: **(A**, **F**, **K)** 1,000 μm, **(B**, **G**, **L)** 50 μm, and **(C–E**, **H–J**, **M–O)** 20 μm.

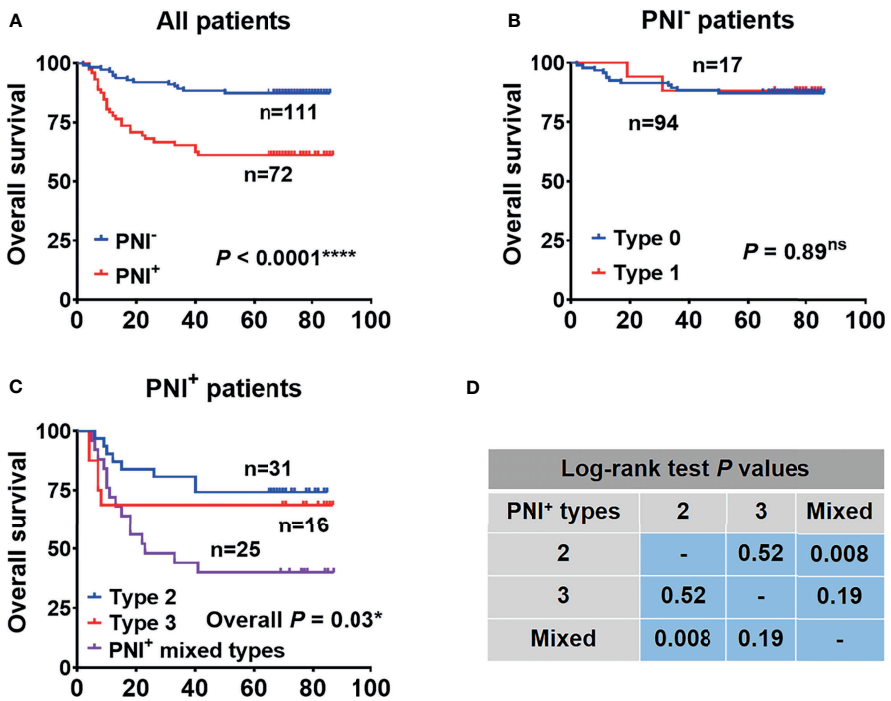

FIGURE 3 | The overall survival analysis performed between patients with the traditional PNI by dichotomy **(A)** and subgroup analysis separately in PNI⁻ **(B)** and PNI⁺ **(C)** patients. **(D)** The results of log-rank test in **(C)**. *p<0.05; ****p<0.0001; ns, not significant.

(n = 2, PNI type 1/2) to 20% (n = 3, PNI type 1/3), and then to 60% (n = 9, PNI type 2/3) (**Figure 4B**). Based on the OS analysis above, the highest PNI type perfectly indicated the patients' survival outcome. Thus, we here introduced the variable WPNI, which took the highest score present in each patient, to define the PNI status (**Figure 4C**). Thus, as PNI type 0 or 1 was redefined as WPNI 1, mixed PNI types of 1/2 were reclassified as WPNI 2. Meanwhile, we took the mixed PNI types 1/3, 2/3, and 1/2/3 as WPNI 3.

WPNI 3 OSCC Patients Showed the Worst Clinical Outcome, Prognosis, and Immune Response

To investigate the correlation between the clinicopathological features and the new WPNI scoring system, 111 (60.7%), 37 (20.2%), and 35 (19.1%) OSCC patients were reclassified into WPNI 1, WPNI 2, and WPNI 3, respectively (**Figure 1I**). Chi-square test was performed and presented that higher WPNI indicated enhanced tumor lymph node metastasis

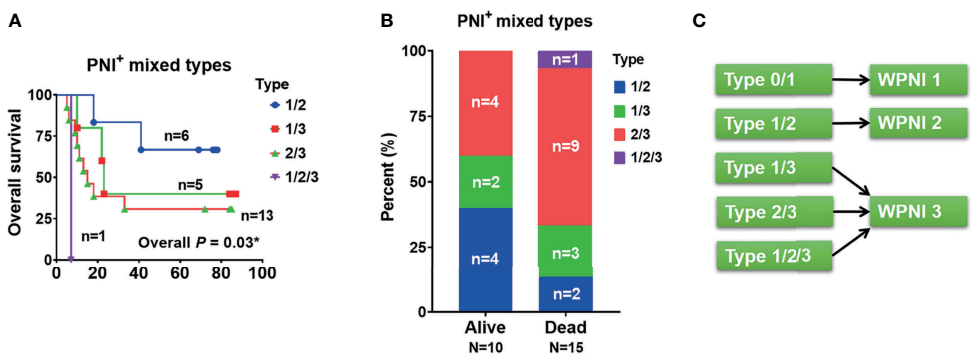

FIGURE 4 | The PNI status of OSCC patients should be subdivided into three types of WPNI. **(A)** The overall survival curves were drawn and compared within PNI⁺ patients with mixed PNI types. **(B)** The stack graph showing the frequency distribution in PNI⁺ patients with mixed PNI types. **(C)** As the highest PNI type perfectly indicated the patients' survival outcome, PNI type 0 or 1 was redefined as WPNI 1, the mixed PNI type 1/2 was reclassified as WPNI 2, and the mixed PNI types 1/3, 2/3, and 1/2/3 were combined as WPNI 3. *p<0.05.

(LN metastasis, χ^2 = 15.96, p < 0.001) and more aggressive pattern of tumor invasion (WPOI, χ^2 = 16.27, p < 0.001) (**Table 2**). Moreover, the rate of local-regional recurrence and distant metastasis after OSCC operation also significantly increased with higher WPNI score (**Table 2**).

To evaluate the prognostic value of the WPNI model on OS, LRFS, and DMFS, Kaplan-Meier analysis and log-rank test were performed. In all three survival models, WPNI 1 indicated the best prognosis while WPNI 3 predicated the worst prognosis (**Figures 5A–C**). As for WPNI 2, it had significantly better OS (p = 0.02), LRFS (p = 0.03), and DMFS (p = 0.046) than WPNI 3, which both indicated the traditionally PNI^+ status. Furthermore, univariate Cox analysis showed that pathologic N stage, TNM stage, and WPNI were significantly negative predictors for OS, LRFS, and DMFS (**Table 3**). Tumor differentiation and WPOI could successfully predict OS and LRFS, but not DMFS (**Table 3**). To exclude the effects of confounders, multivariate Cox analysis was also performed that WPNI 3 was the only variable to independently predict OS (HR = 3.80, 95% CI = 1.83–7.86, p < 0.001), LRFS (HR = 3.85, 95% CI = 1.81–8.18, p < 0.001), and DMFS (HR = 5.29, 95% CI = 1.83–15.28, p = 0.002) (**Table 3**).

As reported that tumor-infiltrating lymphocytes significantly correlated with PNI (25, 26), we further explored whether OSCC patients with different WPNI scores had changed lymphocyte subsets in the preoperative peripheral blood. The gating strategy for grouping cell populations is shown in **Figure 5D**. Although the proportion of lymphocyte subsets did not significantly change with different WPNI scores (**Figure 5E**), the absolute number of total T cells ($CD3^+$), inhibitory T cells ($CD3^+CD8^+$), and B cells ($CD19^+$) were all significantly decreased in WPNI 3 patients (p = 0.01, p = 0.01, and p = 0.008, respectively; **Figure 5F**), further suggesting a possible imbalance in immune response.

TABLE 2 | Clinicopathological features and their associations with the WPNI scoring system.

Features	WPNI			χ^2	p-value
	1 (n = 111)	2 (n = 37)	3 (n = 35)		
Sex				2.48	0.29
Female	52 (46.8%)	12 (32.4%)	14 (40.0%)		
Male	59 (53.2%)	25 (67.6%)	21 (60.0%)		
Age				1.13	0.57
≤60	53 (47.7%)	17 (45.9%)	20 (57.1%)		
>60	58 (52.3%)	20 (54.1%)	15 (42.9%)		
Tumor site				6.01	0.42
Buccal mucosa	21 (18.9%)	7 (18.9%)	5 (14.3%)		
Tongue	48 (43.2%)	17 (45.9%)	19 (54.3%)		
Gingiva	24 (21.6%)	3 (8.1%)	6 (17.1%)		
Others	18 (16.2%)	10 (27.0%)	5 (14.3%)		
Pathologic T				2.59	0.29
T1+T2	97 (87.4%)	33 (89.2%)	27 (77.1%)		
T3+T4	14 (12.6%)	4 (10.8%)	8 (22.9%)		
Pathologic N				15.96	<0.001***
N0	84 (75.7%)	16 (43.2%)	18 (51.4%)		
N1+N2	27 (24.3%)	21 (56.8%)	17 (48.6%)		
Tumor TNM stage				12.36	0.002**
I+II	74 (66.7%)	15 (40.5%)	14 (40.0%)		
III+IV	37 (33.3%)	22 (59.5%)	21 (60.0%)		
Tumor differentiation				3.73	0.15
Well	102 (91.9%)	33 (89.2%)	28 (80.0%)		
Moderately/Poor	9 (8.1%)	4 (10.8%)	7 (20.0%)		
Worst pattern of invasion				16.27	<0.001***
1–3	70 (63.1%)	16 (43.2%)	9 (25.7%)		
4–5	41 (36.9%)	21 (56.8%)	26 (74.3%)		
Radiotherapy				7.70	0.02*
Without	78 (70.3%)	18 (48.6%)	18 (51.4%)		
With	33 (29.7%)	19 (51.4%)	17 (48.6%)		
Chemotherapy				2.20	0.32
Without	97 (87.4%)	34 (91.9%)	28 (80.0%)		
With	14 (12.6%)	3 (8.1%)	7 (20%)		
Local-regional recurrence				21.81	<0.001***
No	98 (88.3%)	28 (75.7%)	18 (51.4%)		
Yes	13 (11.7%)	9 (24.3%)	17 (48.6%)		
Distant metastasis				12.78	<0.001***
No	105 (94.6%)	32 (86.5%)	25 (71.4%)		
Yes	6 (5.4%)	5 (13.5%)	10 (28.6%)		

WPNI, worst pattern of perineural invasion; TNM, tumor-node-metastasis.
**p<0.05; **p<0.01; ***p<0.001.*

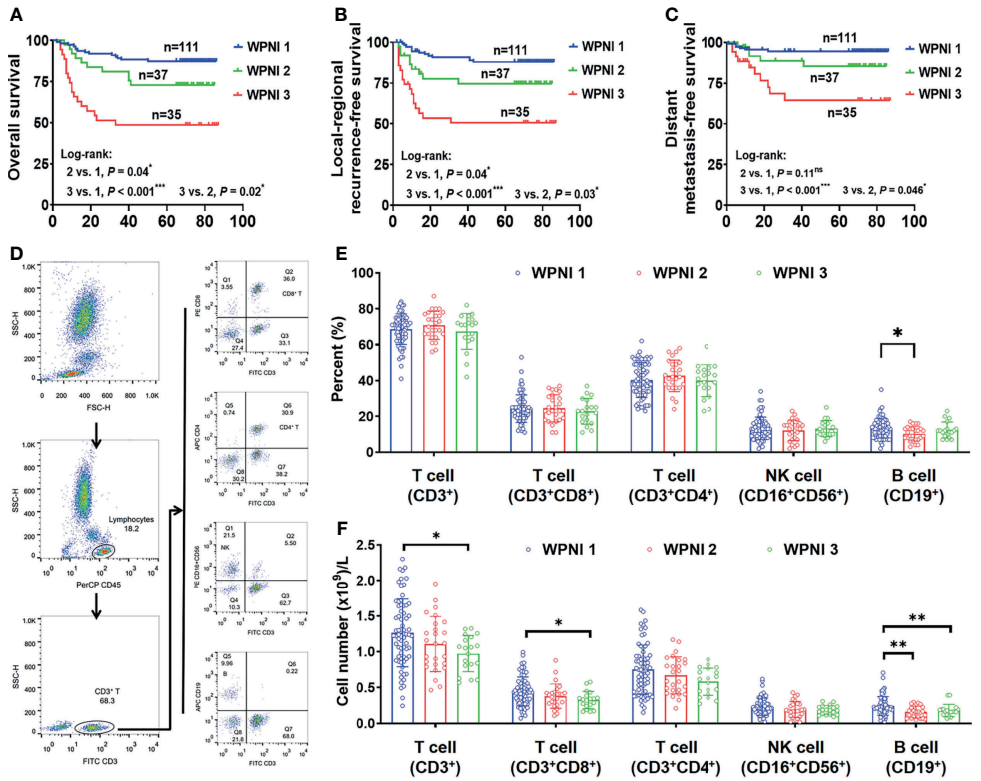

FIGURE 5 | WPNI 3 OSCC patients showed the worst prognosis and immune response. **(A–C)** Kaplan-Meier analysis for overall survival **(A)**, local-regional recurrence-free survival **(B)**, and distant metastasis-free survival **(C)** in patients stratified by the WPNI scoring system. **(D)** The gating strategy for flow cytometry analysis. **(E, F)** Comparison of the circulating lymphocytes among OSCC patients with different WPNI scores.

TABLE 3 | Univariate and multivariate analysis for OS, LRFS, and DMFS.

Features	Univariate analysis			Multivariate analysis		
	HR	95%CI	*p*-value	HR	95%CI	*p*-value
OS						
Pathologic N stage (N1+N2 *vs*. N0)	6.89	3.46–13.74	<0.001***	4.47	1.00–20.00	0.050
Tumor TNM stage (III+IV *vs*. I+II)	6.03	2.88–12.61	<0.001***	1.27	0.26–6.21	0.766
Tumor differentiation (moderately/poor *vs*. well)	3.00	1.47–6.11	0.002**	1.73	0.50–3.71	0.161
WPOI (4–5 *vs*. 1–3)	2.70	1.40–5.19	0.003**	1.42	0.70–2.89	0.337
Chemotherapy (with *vs*. without)	2.41	1.18–4.90	0.015*	1.19	0.57–2.50	0.637
WPNI (2 *vs*. 1)	2.27	1.01–5.10	0.048*	1.32	0.57–3.06	0.513
WPNI (3 *vs*. 1)	5.72	2.84–11.53	<0.001***	3.80	1.83–7.86	<0.001***
LRFS						
Pathologic N stage (N1+N2 *vs*. N0)	3.72	1.95–7.11	<0.001***	2.59	0.57–11.75	0.219
Tumor TNM stage (III+IV *vs*. I+II)	3.13	1.60–6.09	0.001**	1.10	0.23–5.17	0.907
Tumor differentiation (moderately/poor *vs*. well)	2.40	1.10–5.23	0.028*	1.29	0.56–2.93	0.550
WPOI (4–5 *vs*. 1–3)	3.54	1.72–7.27	0.001**	2.17	1.00–4.72	0.051
WPNI (2 *vs*. 1)	2.33	1.00–5.46	0.051	1.47	0.61–3.53	0.387
WPNI (3 *vs*. 1)	5.67	2.75–11.69	<0.001***	3.85	1.81–8.18	<0.001***
DMFS						
Sex (male *vs*. female)	3.12	1.05–9.29	0.040*	2.50	0.83–7.58	0.104
Pathologic N stage (N1+N2 *vs*. N0)	3.80	1.57–9.19	0.003**	3.04	0.38–24.05	0.292
Tumor TNM stage (III+IV *vs*. I+II)	3.15	1.27–7.82	0.013*	0.89	0.11–7.38	0.912
WPNI (2 *vs*. 1)	2.60	0.79–8.51	0.115	1.58	0.45–5.47	0.474
WPNI (3 *vs*. 1)	7.01	2.54–19.38	<0.001***	5.29	1.83–15.28	0.002**

OS, overall survival; LRFS, local-regional recurrence-free survival; DMFS, distant metastasis-free survival; HR, hazard ratio; 95% CI, 95% confidence interval; TNM, tumor-node-metastasis; WPOI, worst pattern of invasion; WPNI, worst pattern of perineural invasion.
**p<0.05; **p<0.01; ***p<0.001.*

DISCUSSION

Classical PNI types in different studies showed inconsistent prognostic value. Thus, alternative PNI-related characteristics were developed to test their rationality. Karina et al. retrospectively analyzed the prognostic value of PNI, number of PNIs, distance between PNI and cancer center, and diameter of invaded nerves in PNI using 318 OSCC samples and showed that classical PNI classification (PNI^- *vs.* PNI^+) could not predict the prognosis successfully (27). In contrast, an increased number of PNIs could independently predict a higher risk of local recurrence, and the prognosis worsened when the diameter of the invaded nerves exceeded 1 mm. In addition, a single PNI or PNI occurring outside the cancer center had no effect on the prognosis. Wei et al. also found that with an increased number of PNIs, the prognosis of patients worsened, but the author pointed out that how to quantify the number of PNIs needs further study (28). Miller et al. classified PNI into "PNI in tumor center," "PNI at tumor border," "PNI outside tumor center," and "no PNI" in head and neck cancer and found that this classification system could not effectively predict local recurrence (29). However, in 200 patients with oral tongue SCC, Caponio et al. presented that intratumoral PNI combined with tumor grading and WPOI could successfully predict lymph-node metastasis and advocated integrating PNI in the 8th edition of the AJCC Cancer staging system (30).

Given that PNI reflects the interaction between tumor cells and nerves (31), and it has been proven to be an active process (15), tumor cells "away from" nerves to "encircling" them and finally "infiltrating into" nerve sheathes can coexist in one tumor. Notably, tumor cells encircling nerves were empirically divided into two conditions based on the cutoff value of 33% which was empirically adopted (16). Moreover, intratumoral heterogeneity might be the intrinsic driver for the simultaneous existence of several PNI types within a single tumor microenvironment (TME). For the first time, we classified the traditional PNI^- status into WPNI 1, which represented an early stage of tumor cells invading nerves. Survival analysis confirmed that OSCC patients with WPNI 1 did have a good prognosis. However, the traditional PNI^+ indicator should be critically evaluated for its further subclassification. In this study, PNI^+ successfully predicated worse survival, but we found that WPNI 2 had significantly better survival than WPNI 3. We believed that as the late stage of tumor cells invading nerves, WPNI 3 contributed mainly to the predictive ability of the traditionally PNI^+ status. Multivariate Cox analysis confirmed that only WPNI 3 could independently predict the patients' survival. So, tumor cell-mediated destruction of nerve sheaths and their subsequent invasion significantly accelerate tumor progression. Once tumor cells entered the nerve microenvironment, they would have convenient routes and abundant nutrition for their distant metastasis (32).

Inflammatory infiltration related to PNI has been intensively investigated (33–35); we here focused on how the circulating lymphocytes changed with different stages of tumor cells invading nerves. In pancreatic ductal adenocarcinomas, infiltrating $CD8^+$ T cells significantly decreased in the PNI^+ samples accompanied with elevated levels of acetylcholine (25). In OSCCs, higher $CD8^+$ T cells at the parenchyma of the invading edge and peripheral stroma both indicated improved overall and recurrence-free survival (36). In our study, WPNI 3, but not WPNI 2, represented significantly lower circulating $CD8^+$ T cells than WPNI 1. Most importantly, WPNI 3 implies the destructed nerve sheathes, which means more possibility for neurotransmitters such as norepinephrine spilling into OSCC microenvironment (37). What is more, B cells also decreased as WPNI scores increase, indicating the damaged immune response.

In conclusion, PNI tends to be an active and continuous process in which tumor cells move far away from nerves to invade the nerve sheaths, which reflects clinically worsening survival. Therefore, the WPNI scoring system, which takes the highest score to refine the traditional PNI status, may be worth further clinical evaluation and promotion.

DATA AVAILABILITY STATEMENT

The original contributions presented in the study are included in the article/**Supplementary Material**. Further inquiries can be directed to the corresponding authors.

ETHICS STATEMENT

The studies involving human participants were reviewed and approved by The Research Ethics Committee of Nanjing Stomatological Hospital. The patients/participants provided their written informed consent to participate in this study.

AUTHOR CONTRIBUTIONS

QH, YN, and LD designed this study. YF and XWZ performed all the experiments. YF, XWZ, and ZD collected clinical data. NZ, YS, and XXZ interpreted the data. YJ, YY, XH, and LZ offered technical support. YF and XWZ wrote the manuscript. All authors contributed to the article and approved the submitted version.

FUNDING

This work was supported by the National Natural Science Foundation of China (81902754, 81702680, 82002865, 81772880), Natural Science Foundation of Jiangsu Province (BK20190304, BE2020628), and Nanjing Medical Science and Technology Development Foundation (YKK19091, YKK20153).

SUPPLEMENTARY MATERIAL

The Supplementary Material for this article can be found online at: https://www.frontiersin.org/articles/10.3389/fonc.2021.766902/full#supplementary-material

REFERENCES

1. Bray F, Ferlay J, Soerjomataram I, Siegel RL, Torre LA, Jemal A. Global Cancer Statistics 2018: GLOBOCAN Estimates of Incidence and Mortality Worldwide for 36 Cancers in 185 Countries. *CA Cancer J Clin* (2018) 68:394–424. doi: 10.3322/caac.21492
2. Chai AWY, Lim KP, Cheong SC. Translational Genomics and Recent Advances in Oral Squamous Cell Carcinoma. *Semin Cancer Biol* (2020) 61:71–83. doi: 10.1016/j.semcancer.2019.09.011
3. Zanoni DK, Montero PH, Migliacci JC, Shah JP, Wong RJ, Ganly I, et al. Survival Outcomes After Treatment of Cancer of the Oral Cavity (1985-2015). *Oral Oncol* (2019) 90:115–21. doi: 10.1016/j.oraloncology.2019.02.001
4. Chen SH, Zhang BY, Zhou B, Zhu CZ, Sun LQ, Feng YJ. Perineural Invasion of Cancer: A Complex Crosstalk Between Cells and Molecules in the Perineural Niche. *Am J Cancer Res* (2019) 9:1–21.
5. Jurcak N, Zheng L. Signaling in the Microenvironment of Pancreatic Cancer: Transmitting Along the Nerve. *Pharmacol Ther* (2019) 200:126–34. doi: 10.1016/j.pharmthera.2019.04.010
6. Tan X, Sivakumar S, Bednarsch J, Wiltberger G, Kather JN, Niehues J, et al. Nerve Fibers in the Tumor Microenvironment in Neurotropic Cancer-Pancreatic Cancer and Cholangiocarcinoma. *Oncogene* (2021) 40:899–908. doi: 10.1038/s41388-020-01578-4
7. Salcedo MP, Sood AK, Dos Reis R, Ramalingam P, Chen C, Frumovitz M, et al. Perineural Invasion (PNI) in Vulvar Carcinoma: A Review of 421 Cases. *Gynecol Oncol* (2019) 152:101–5. doi: 10.1016/j.ygyno.2018.10.035
8. Nair D, Mair M, Singhvi H, Mishra A, Nair S, Agrawal J, et al. Perineural Invasion: Independent Prognostic Factor in Oral Cancer That Warrants Adjuvant Treatment. *Head Neck* (2018) 40:1780–7. doi: 10.1002/hed.25170
9. Knijn N, Mogk SC, Teerenstra S, Simmer F, Nagtegaal ID. Perineural Invasion is a Strong Prognostic Factor in Colorectal Cancer: A Systematic Review. *Am J Surg Pathol* (2016) 40:103–12. doi: 10.1097/pas.0000000000000518
10. Bapat AA, Hostetter G, Von Hoff DD, Han H. Perineural Invasion and Associated Pain in Pancreatic Cancer. *Nat Rev Cancer* (2011) 11:695–707. doi: 10.1038/nrc3131
11. Tai SK, Li WY, Yang MH, Chu PY, Wang YF. Perineural Invasion in T1 Oral Squamous Cell Carcinoma Indicates the Need for Aggressive Elective Neck Dissection. *Am J Surg Pathol* (2013) 37:1164–72. doi: 10.1097/PAS.0b013e318285f684
12. Dunn M, Morgan MB, Beer TW. Perineural Invasion: Identification, Significance, and a Standardized Definition. *Dermatol Surg* (2009) 35:214–21. doi: 10.1111/j.1524-4725.2008.34412.x
13. Buchanan L, De'Ambrosis B, DeAmbrosis K, Warren T, Huilgol S, Soyer HP, et al. Defining Incidental Perineural Invasion: The Need for a National Registry. *Australas J Dermatol* (2014) 55:107–10. doi: 10.1111/ajd.12129
14. Batsakis JG. Nerves and Neurotropic Carcinomas. *Ann Otol Rhinol Laryngol* (1985) 94:426–7.
15. Schmitd LB, Scanlon CS, D'Silva NJ. Perineural Invasion in Head and Neck Cancer. *J Dent Res* (2018) 97:742–50. doi: 10.1177/0022034518756297
16. Liebig C, Ayala G, Wilks JA, Berger DH, Albo D. Perineural Invasion in Cancer: A Review of the Literature. *Cancer* (2009) 115:3379–91. doi: 10.1002/cncr.24396
17. Groot VP, Rezaee N, Wu W, Cameron JL, Fishman EK, Hruban RH, et al. Patterns, Timing, and Predictors of Recurrence Following Pancreatectomy for Pancreatic Ductal Adenocarcinoma. *Ann Surg* (2018) 267:936–45. doi: 10.1097/sla.0000000000002234
18. Elharram M, Margel D, Finelli A, Trachtenberg J, Evans A, van der Kwast TH, et al. Perineural Invasion on Prostate Biopsy Does Not Predict Adverse Pathological Outcome. *Can J Urol* (2012) 19:6567–72.
19. Ng JC, Koch MO, Daggy JK, Cheng L. Perineural Invasion in Radical Prostatectomy Specimens: Lack of Prognostic Significance. *J Urol* (2004) 172:2249–51. doi: 10.1097/01.ju.0000143973.22897.f8
20. Elsahwi KS, Barber E, Illuzzi J, Buza N, Ratner E, Silasi DA, et al. The Significance of Perineural Invasion in Early-Stage Cervical Cancer. *Gynecol Oncol* (2011) 123:561–4. doi: 10.1016/j.ygyno.2011.08.028
21. Pavlov VA, Chavan SS, Tracey KJ. Molecular and Functional Neuroscience in Immunity. *Annu Rev Immunol* (2018) 36:783–812. doi: 10.1146/annurev-immunol-042617-053158
22. Cervantes-Villagrana RD, Albores-García D, Cervantes-Villagrana AR, García-Acevez SJ. Tumor-Induced Neurogenesis and Immune Evasion as Targets of Innovative Anti-Cancer Therapies. *Signal Transduct Target Ther* (2020) 5:99. doi: 10.1038/s41392-020-0205-z
23. Hutchings C, Phillips JA, Djamgoz MBA. Nerve Input to Tumours: Pathophysiological Consequences of a Dynamic Relationship. *Biochim Biophys Acta Rev Cancer* (2020) 1874:188411. doi: 10.1016/j.bbcan.2020.188411
24. Brandwein-Gensler M, Teixeira MS, Lewis CM, Lee B, Rolnitzky L, Hille JJ, et al. Oral Squamous Cell Carcinoma: Histologic Risk Assessment, But Not Margin Status, is Strongly Predictive of Local Disease-Free and Overall Survival. *Am J Surg Pathol* (2005) 29:167–78. doi: 10.1097/01.pas.0000149687.90710.21
25. Yang MW, Tao LY, Jiang YS, Yang JY, Huo YM, Liu DJ, et al. Perineural Invasion Reprograms the Immune Microenvironment Through Cholinergic Signaling in Pancreatic Ductal Adenocarcinoma. *Cancer Res* (2020) 80:1991–2003. doi: 10.1158/0008-5472.Can-19-2689
26. Huang Y, Lin C, Kao HK, Hung SY, Ko HJ, Huang YC, et al. Digital Image Analysis of CD8+ and CD3+ Tumor-Infiltrating Lymphocytes in Tongue Squamous Cell Carcinoma. *Cancer Manag Res* (2020) 12:8275–85. doi: 10.2147/cmar.S255816
27. Aivazian K, Ebrahimi A, Low TH, Gao K, Clifford A, Shannon K, et al. Perineural Invasion in Oral Squamous Cell Carcinoma: Quantitative Subcategorisation of Perineural Invasion and Prognostication. *J Surg Oncol* (2015) 111:352–8. doi: 10.1002/jso.23821
28. Wei PY, Li WY, Tai SK. Discrete Perineural Invasion Focus Number in Quantification for T1-T2 Oral Squamous Cell Carcinoma. *Otolaryngol Head Neck Surg* (2019) 160:635–41. doi: 10.1177/0194599818808510
29. Miller ME, Palla B, Chen Q, Elashoff DA, Abemayor E, St John MA, et al. A Novel Classification System for Perineural Invasion in Noncutaneous Head and Neck Squamous Cell Carcinoma: Histologic Subcategories and Patient Outcomes. *Am J Otolaryngol* (2012) 33:212–5. doi: 10.1016/j.amjoto.2011.06.003
30. Caponio VCA, Troiano G, Togni L, Zhurakivska K, Santarelli A, Laino L, et al. Pattern and Localization of Perineural Invasion Predict Poor Survival in Oral Tongue Carcinoma. *Oral Dis* (2021). doi: 10.1111/odi.13900
31. Zahalka AH, Frenette PS. Nerves in Cancer. *Nat Rev Cancer* (2020) 20:143–57. doi: 10.1038/s41568-019-0237-2
32. Amit M, Na'ara S, Gil Z. Mechanisms of Cancer Dissemination Along Nerves. *Nat Rev Cancer* (2016) 16:399–408. doi: 10.1038/nrc.2016.38
33. de Matos FR, Lima E, Queiroz LM, da Silveira EJ. Analysis of Inflammatory Infiltrate, Perineural Invasion, and Risk Score can Indicate Concurrent Metastasis in Squamous Cell Carcinoma of the Tongue. *J Oral Maxillofac Surg* (2012) 70:1703–10. doi: 10.1016/j.joms.2011.08.023
34. Wang Y, Zhai J, Zhang T, Han S, Zhang Y, Yao X, et al. Tumor-Associated Neutrophils Can Predict Lymph Node Metastasis in Early Gastric Cancer. *Front Oncol* (2020) 10:570113. doi: 10.3389/fonc.2020.570113
35. Pagès F, Berger A, Camus M, Sanchez-Cabo F, Costes A, Molidor R, et al. Effector Memory T Cells, Early Metastasis, and Survival in Colorectal Cancer. *N Engl J Med* (2005) 353:2654–66. doi: 10.1056/NEJMoa051424
36. Shimizu S, Hiratsuka H, Koike K, Tsuchihashi K, Sonoda T, Ogi K, et al. Tumor-Infiltrating CD8(+) T-Cell Density Is an Independent Prognostic Marker for Oral Squamous Cell Carcinoma. *Cancer Med* (2019) 8:80–93. doi: 10.1002/cam4.1889
37. Shang ZJ, Liu K, Liang DF. Expression of Beta2-Adrenergic Receptor in Oral Squamous Cell Carcinoma. *J Oral Pathol Med* (2009) 38:371–6. doi: 10.1111/j.1600-0714.2008.00691.x

Conflict of Interest: The authors declare that the research was conducted in the absence of any commercial or financial relationships that could be construed as a potential conflict of interest.

frontiers in Oncology

ORIGINAL RESEARCH
published: 29 November 2021
doi: 10.3389/fonc.2021.764798

Comprehensive Analysis of m^{6}A Regulators Characterized by the Immune Cell Infiltration in Head and Neck Squamous Cell Carcinoma to Aid Immunotherapy and Chemotherapy

Zhiqiang Yang[1†], Xiaoping Ming[2†], Shuo Huang[2†], Minlan Yang[2], Xuhong Zhou[2*] and Jiayu Fang[2*]*

[1] Department of Spine Surgery and Musculoskeletal Tumor, Zhongnan Hospital of Wuhan University, Wuhan, China,
[2] Department of Otorhinolaryngology-Head and Neck Surgery, Zhongnan Hospital of Wuhan University, Wuhan, China

OPEN ACCESS

Edited by:
Heming Lu,
People's Hospital of Guangxi Zhuang Autonomous Region, China

Reviewed by:
Gaurisankar Sa,
Bose Institute, India
Zi-Qi Zheng,
Sun Yat-Sen University Cancer Center (SYSUCC), China

***Correspondence:**
Jiayu Fang
366619601@qq.com
Minlan Yang
yangml@whu.edu.cn
Xuhong Zhou
zhouxuhong66@126.com

[†]These authors have contributed equally to this work

Specialty section:
This article was submitted to Head and Neck Cancer, a section of the journal Frontiers in Oncology

Received: 26 August 2021
Accepted: 01 November 2021
Published: 29 November 2021

Citation:
Yang Z, Ming X, Huang S, Yang M, Zhou X and Fang J (2021) Comprehensive Analysis of m^{6}A Regulators Characterized by the Immune Cell Infiltration in Head and Neck Squamous Cell Carcinoma to Aid Immunotherapy and Chemotherapy. Front. Oncol. 11:764798. doi: 10.3389/fonc.2021.764798

Background: N6-Methyladenosine (m^{6}A), which is a prevalent regulator of mRNA expression, has gathered increasing study interests. Though the role of m^{6}A as being important in many biological processes (such as growth and proliferation of cancers) has been well documented, its potential role in tumor immune microenvironment (TIME) has rarely been analyzed.

Methods: We downloaded RNA expression, single nucleotide polymorphism (SNP), and copy number variation (CNV) data from The Cancer Genome Atlas (TCGA). We then curated 21 m^{6}A regulators and clustered patients into three m^{6}A subtypes and m^{6}A-related gene subtypes and compared them based on overall survival (OS). The combination of CIBERSORT as well as ssGSEA quantified the infiltration levels of immune cells and immune-related functions. The m^{6}A scores were determined by using principal component analysis (PCA) algorithm. Furthermore, we evaluate the correlation of m^{6}A regulators with immune and response to therapy.

Results: Three m^{6}A clusters were identified based on the TCGA-HNSCC cohort, and there were significant associations among them in overall outcomes and caner-related pathways. We found that three m^{6}A clusters were consistent with three phenotypes: immune-inflamed, immune-dessert, and immune-excluded. HNSCC patients were divided into high– and low–m^{6}A score groups based on the cutoff of m^{6}A score. Patients with lower m^{6}A score had better overall survival outcome. Further analysis indicated that patients with higher m^{6}A score presented higher tumor mutation burden (TMB). In addition, patients in low–m^{6}A score subgroup had high chemotherapeutics sensitivity. GEO cohort confirmed patients with low m^{6}A score demonstrated significant overall survival advantages and clinical benefits. Low m^{6}A score carry an increased

neoantigen load, eliciting a response to immunotherapy, and its value in predicting survival outcomes of immunotherapy was also confirmed in three anti-PD-1 cohorts.

Conclusions: Our study demonstrated that m^{6}A regulators are closely related to TIME and the m^{6}A score was an effective prognostic biomarker and predictive indicator for immunotherapy and chemotherapeutics. Comprehensive evaluation of m^{6}A regulators in tumors will extend our understanding of TIME and effectively guide increasing study investigations on immunotherapy and chemotherapy strategies for HNSCC.

Keywords: HNSCC, m^{6}A regulator, TIME, m^{6}A score, therapy

INTRODUCTION

Head and neck squamous cell carcinoma (HNSCC) remains the primary cause of cancer death worldwide, with approximately 890,000 newly diagnosed cases per year (1). More than 50% of patients will present with local recurrence or node metastasis within 5 years caused by resistance to conventional treatment (2). Conventional treatments include surgery, radiotherapy, and chemotherapy based on the stage of patients, but most HNSCC exhibit weak prognosis because of the complex mechanisms whereby the RNA modifications were associated with different immune cell infiltrations.

Immunotherapy may provide significant therapeutic effects in identifying and eliminating tumor cells by activating patients' immune defense system (3). This treatment yields new insights with unparalleled and synergistic survival benefits into multiple clinical management (4, 5). For example, inhibitors of CTLA-4 as well as anti-PD-1/L1 antibodies, which are representative immune checkpoint inhibitors, have achieved a marked clinical response in patient's treatment (6–8). Nevertheless, a major limitation of this treatment (the imbalance of the immune system) is that a minority of patients could benefit from immunotherapy. In addition, numerous cytokines (such as IL-10 and IL-17) and immunosuppressive cells (derived from marrow) are components of the tumor immune microenvironment (TIME) promoting immune escape (9). Thus, the regulatory mechanism and the novel markers of HNSCC should be urgently investigated by comprehensively parsing the components of TIME so that the ideal HNSCC subgroups for guiding and predicting therapeutic responsiveness could be identified.

The methylation modification of the N6 adenosine (m^{6}A), which is the most common type of posttranscriptional modification on RNA and mediate above 60% of RNA methylation, plays crucial roles in a series of cancer processes and progression and immunomodulatory abnormalities (10). To be specific, the aberrant methylation of m^{6}A is close to cancer stem cell differentiation, cancer immune response, and microRNA (miRNA) editing; they also play an essential role in the progression of various cancers (11–13). The m^{6}A methylation levels in tumors mainly depend on the expression of m^{6}A regulatory proteins, which is controlled by the expression of "writers"—methyltransferases, the "erasers"—demethylases, and "readers"—binding proteins in cell (14, 15). The writers, which include methyltransferase like (METTL)14, METTL3, WT1-associated protein (WTAP), Casitas B-lineage proto-oncogene like 1 (CBLL1), KIAA1429, ZC3H13, and RNA-binding motif protein 15 (RBM15), RBM15B, promote m^{6}A RNA methylation (16–18). The erasers, which include fat mass- and obesity-associated protein (FTO) and α-ketoglutarate-dependent dioxygenase alkB homolog 5 (ALKBH5), remove m^{6}A methylation (19). The readers, which include YTH domain-containing 1 (YTHDC1), YTHDC2, YTH N6-methyl-adenosine RNA-binding protein 1 (YTHDF1), YTHDF2, YTHDF3, and heterogeneous nuclear ribonucleoprotein C (HNRNPC), insulin-like growth factor 2 mRNA-binding protein 2 (IGF2BP2), IGF2BP3, ELAV-like RNA-binding protein 1 (ELAVL1), heterogeneous nuclear ribonucleoprotein A2B1 (HNRNPA2B1), and LRPPRC, can bind proteins to the m^{6}A methylation site (20).

Increasing evidence has demonstrated that the dysregulated expression of m^{6}A regulators plays a vital regulatory role in tumor progression and patient prognosis (21, 22).

Lan et al. showed that m^{6}A-modified GATA3 pre-mRNA was mediated by KIAA1429, stimulating the RNA-binding protein to undergo separation and promoting GATA3 pre-mRNA degradation (23). Among patients with hepatocellular carcinoma, overexpression of KIAA1429 was significantly associated with poor clinical prognosis. Also, shRNA silencing of KIAA1429 suppressed hepatocellular carcinoma cell proliferation and tumorigenesis both *in vitro* and *in vivo*.

In the study of Chen et al., WTAP was found to be highly expressed in osteosarcoma cancer (24), and Cox analysis showed that it was an independent prognostic factor for overall survival. Mechanistically, WTAP, as an oncogene, regulated osteosarcoma proliferation and metastasis *via* PI3K/AKT pathway *in vitro* and *in vivo*. The study of Yi et al. divided patients into two subtypes determined *via* the consensus clustering for 15 m^{6}A methylation regulators, which could stratify the prognosis of patients (25). They also established the risk score based on six m^{6}A regulators, which was an independent prognostic indicator of patients.

However, the role of risk score in immunotherapy and chemotherapy was not analyzed. In addition, whether m^{6}A methylation regulators have the interface of copy number

Abbreviations: CNV, copy number variation; DC, dendritic cell; DEGs, differentially expressed genes; EMT, epithelial-mesenchymal transition; GEO, Gene-Expression Omnibus; GSVA, Gene set variation analysis; HR, hazard ratios; ICB, immunological checkpoint blockade; m^{6}A, N6-methyladenosine; Pan-F-TBRS, Pan-fibroblast TGFb response signature; PCA, principal component analysis; ssGSEA, single-sample gene-set enrichment analysis; TCGA, The Cancer Genome Atlas; IPS, immunophenoscore; TIDE, tumor immune dysfunction and exclusion; TIME, tumor immune microenvironment.

variations (CNVs) or the correlation of tumor mutation burden (TMB) has yet to be fully explored.

Using public databases, Li et al. showed that higher expression of METTL3 was associated with poorer survival prognosis in colorectal carcinoma (CRC) metastatic tissues (26). *In vivo*, they found that METTL3 is linked to CRC development through maintaining SOX2 expression.

Recently, most studies have revealed the correlation between immune cell infiltration and m^{6}A modification, but the carcinogenic pathways of m^{6}A methylation in TIME remains unclear. Han et al. reported that lysosomal protease, marked and recognized by YTHDF1, induced the degradation of tumor neoantigens (27). Compared with WT mice, they observed higher levels of CD8+ cytotoxic T cells and NK cells in tumors from YTHDF1 knockout mice, which suggest that an enhanced antitumor response occurs in the absence of YTHDF1. In melanoma cells, Chong et al. demonstrated that interferon-gamma (IFN-γ)-induced cytotoxicity could be decreased by FTO *in vitro* by suppressing the expression of cell-intrinsic genes PD-1, CXCR4, and SOX10, at least partially through YTHDF2-mediated decay process (28). Moreover, they found that knockdown of FTO enabled an antimelanoma response *via* upregulating the expression level of IFN-γ in mice. Another study demonstrated that METTL3-mediated m^{6}A of CD40 and CD80 promoted DC activation and maturation, which contributed to increased antigen presentation and T-cell stimulation *in vivo* and *in vitro* (29). Also, the METTL3-mediated mRNA modification is essential in cancer progression. Consequently, these results indicated that m^{6}A are vital mediators of TME, emphasizing potential promising targets in enhancing therapeutic response to clinical immunotherapy. However, almost all studies focused on one or two m^{6}A regulators owing to existing technical limitations. Thus, the combined analysis of multiple m^{6}A regulators in HNSCC, including the interactions between the m^{6}A regulators and CNVs and TMB, will enhance our understanding of TIME (30).

In our study, we systematically assessed the relationship between m^{6}A methylation and prognosis, CNVs, TMB, and TIME based on the next-generation sequencing data of HNSCC samples. Three clustering subtypes were identified *via* "ConsensusClusterPlus" method, and these three subtypes were closely linked to three phenotypes: immune-inflamed, immune-excluded, and immune-desert (7). Moreover, we constructed a scoring model, m^{6}A score, to quantify HNSCC of individual cases. Also, the relationships between scoring model, ICI treatment, TIME, and cancer-related pathways were thoroughly analyzed to further explore the effect of m^{6}A regulators in HNSCC. The whole study suggested that m^{6}A regulators play an indispensable role in TIME and in assisting to make therapeutic strategies on HNSCC.

METHODS

The Collection and Pretreatment of Datasets and Samples

The genomics data and clinical information of 528 HNSCC samples and 43 adjacent normal tissues were procured from the public TCGA (https://cancergenome.nih.gov/). The selection criteria were used as follows: (1) histologically confirmed HNSCC and (2) complete clinical and OS data. Lastly, 479 patients with the corresponding clinical information, including age, gender, stage, HPV subtype, and radiation therapy were collected for further analysis. The mutation data (e.g., somatic mutation and copy number variation data) was downloaded from the UCSC Xena (https://gdc.xenahubs.net/). Twenty-one m^{6}A regulators were collected based on published literature. Next, the differential expression of the 21 m^{6}A regulators was presented in a heatmap. Nonsynonymous mutation and synonymous mutation counts were defined as tumor mutation burden. The GSE65858 (N = 267) from GEO was used as the validation cohort. The detailed information of clinical data and 21 m^{6}A regulators are shown in **Supplementary Tables S1**–**S3**.

The Consensus Clustering of 21 m6A Regulators by Consensus Cluster Plus

To elucidate the biological function of the m^{6}A regulators in HNSCC, ConsensusClusterPlus package based on Euclidean distance and Wards linkage was employed to classify the patients into different distinct m^{6}A subtypes (31). The "PCA" package was used to investigate gene-expression arrays among distinct m^{6}A subgroups.

Gene Set Variation Analysis

We utilized the gene set variation analysis ("GSVA") package to investigate the biological processes among different m^{6}A subgroups (32). The well-defined biological pathways and functions were derived from the Hallmarker gene set "c2.cp.kegg.v7.4.symbols.gmt" and "c5.go.v7.4.symbols.gmt" (download from MSigDB database v7.4) and IMvigor210CoreBiologies package (33, 34). The "ClusterProfiler" package was used to determine the Gene Ontology (GO) annotation of m^{6}A-related genes (the cutoff value were q-value <0.05 and p-value <0.05) (35).

Immune Cell Infiltration and Immune-Related Function Estimation by ssGSEA

The relative abundance and activity levels of 23 immune cell types, obtained from published signature gene lists, were quantified using the single sample gene set enrichment analysis (ssGSEA) in R package GSVA (36, 37). In this study, the innate immune cells (including natural killer (NK) cells, CD56dim NK cells, CD56bright NK cells, dendritic cells (DCs), plasmacytoid dendritic cells (pDC), immature DCs (iDC), neutrophils, mast cells, and macrophages) and the adaptive immune cells (including B cells, T cells, CD8 T cells, T follicular helper (TFH), Th1, Th2, Th17, and Treg cells) comprised these signatures. In addition, we also used ssGSEA to explore the relationship between different m^{6}A subtypes and immune-related pathways (such as cytolytic activity, T-cell co-stimulation, inflammation promoting, and parainflammation) in HNSCC expression profile of TCGA. The biosimilarity of the infiltrating immune cells and immune-related functions were estimated by the Gaussian fitting model.

To Calculate the Immunotherapy Predictors: IPS, TIDE, and ESTIMATE

Immunophenoscore (IPS) is an effective predictor of response to immune therapy *via* characterizing the determinant factors of cancer immunogenicity and antigenomes (37). The major histocompatibility complex (MHC)-related molecules, checkpoints or immunomodulators (CP), effector cells (EC), and suppressor cells (SC) developed the IPS scoring scheme. The sum of the four classes, calculated by averaging the Z-scores, was defined as the IPS. To predict immune checkpoint blockade response (ICB), we utilized the tumor immune dysfunction and exclusion (TIDE) method to model tumor immune evasion mechanisms, including the dysfunction of T-cell dysfunction in tumors with high infiltration of cytotoxic T lymphocytes (CTLs) and the prevention of T cell in tumors with exclusion of CTLs (38). For patients with higher TIDE score, cancers more likely to occur immune escape in these patients' body, thus ICB treatment might bring these patients less and short-lasting clinical benefits. The ESTIMATE algorithm was used to evaluate the tumor cellularity and tumor purity, which were composed of the TIME, based on expression matrixes. The analysis method is integrated in the "ESTIMATE " package (39). We extracted these gene expression data from RNASeqV2 data to predict different infiltration levels of immune cells and the proportion of stromal cells. Tumor purity is the summation of stromal score and immune score from individual cases. The tumor sample with higher immune scores and lower tumor purity indicated that it had an abundance of immune cell infiltration.

The Identification of Significant Mutational Genes and Signatures

The mutation annotation format (maf) file was analyzed using MutSigCV algorithm to identify significant SMGs based on the significance threshold, and the maf data were processed using the "maftools" package (40). MutSigCV measures the significance of nonsilent somatic mutations in a gene based on the background mutation rates by silent mutations (41). The false discovery rates (q-values) were then calculated, and genes with statistical significance (q-values ≤0.1) were set as SMGs (**Supplementary Table S4**). We then utilized the waterfall plot to visualize the mutation information of these significant SMGs in the TCGA cohort. Furthermore, we applied Fisher's test to detect mutually exclusive or co-occurring ratio of m^{6}A regulators. Mutational signatures were determined using the genomic data by adopting ExtractSignatures function that applies the Bayesian nonnegative matrix factorization-based framework (42). The optimal number of mutational signatures for the TCGA cohort could be detected by the SignatureEnrichment function and then it automatically assigned a given signature to each sample.

DEGs Associated With the m6A Phenotypes

Patients were grouped into the three m^{6}A clusters based on consensus clustering algorithm to identify differentially expressed genes (DEGs) associated with the m^{6}A modification. The "limma" package was implemented to determine DEGs between three m^{6}A clusters (43). The significance filtering cutoff of DEGs were set as the significance-adjusted p-value <0.001.

The Construction of the m6A Gene Signature

The overlapped DEGs identified from DEGs were used to perform the univariate Cox regression. The consensus clustering algorithm was utilized to define the number of gene clusters. The prognosis-related genes were extracted for further analysis. We then curated the final genes determined to conduct principal component analysis (PCA), and principal component 1 and 2 were extracted to construct the m^{6}A score (44, 45). This method has an advantage of mainly focusing on positively correlated (or negatively correlated) genes. We then define the m^{6}A score of each patient by adopting a similar formula based on the previous studies:

$$\text{m}^6\text{A score} = \sum(\text{PC1}_i) + \sum(\text{PC2}_i)$$

To determine the TMB of each patient, we also counted the nonsynonymous and synonymous mutation counts in the TCGA cohort (46). The association with TMB and m^{6}A score was evaluated by Spearman's method based on survival curve.

The Correlation Between m6A Score and Biological Pathways

Mariathasan et al. constructed a panel of signatures that stored genes associated with various biological pathways, including (1) immune-checkpoint; (2) CD8 T-effector signature; (3) epithelial-mesenchymal transition (EMT), including EMT1, EMT2, and EMT3; (4) pan-fibroblast TGFb response signature (Pan-F-TBRS); (5) Fanconi anemia pathway; (6) homologous recombination; (7) base excision repair; (8) WNT target; (9) DNA damage repair; (10) mismatch repair; (11) nucleotide excision repair; (12) DNA replication; (13) antigen processing; (14) cell cycle regulation; (15) FGFR3-related genes; and (16) cell cycle (34, 47). We performed the Spearman's method to explore the correlation between m^{6}A score and these biological pathways.

The Genomic and Clinical Information of Immune-Checkpoint Cohorts

We systematically performed a search for the ICB cohorts in the public databases, which could be available for detailed genomic and clinical information. Three independent anti-PD-L1 cohorts, IMvigor210 cohort (patients with metastatic urothelial cancer treated with atezolizumab) (34), Riaz et al. cohort (patients with metastatic melanoma treated with nivolumab) (48), and GSE78220 cohort (patients with metastatic melanoma treated with pembrolizumab) (49), were finally downloaded to analyze the predictive value of the m^{6}A score for immunotherapy. The raw gene expression data of all cohorts were normalized.

To Evaluate the Sensitivity of Chemotherapeutic Drugs

We used the largest public pharmacogenomics database, Genomics of Drug Sensitivity in Cancer (GDSC), to predict the

sensitivity of different drugs between high– and low–m^{6}A score subgroups (50). The prediction process used was the "pRRophetic" package where the half-maximal inhibitory concentration (IC_{50}) was estimated by ridge regression model based on gene expression profiles (51).

Statistical Analyses

The statistical analyses were generated by using R version 4.1.0. To compare more than two groups, statistical significance was estimated by the Kruskal-Wallis test. Student's *t*-test was used to compare the difference between two subgroups (52). Kaplan-Meier analysis generated the differences between m^{6}A subgroups and prognosis *via* the "survminer" package. To determine the optimal cutoff values of each cohort, we used the "surv-cutpoint" function from the "survival" package. We adopted Cox regression to calculate the hazard ratios (HR) of m^{6}A regulators and m^{6}A-related genes. The multivariate Cox regression was used to evaluate the independent prognostic factors. The "forestplot" package was employed to show the results of Cox regression analysis for m^{6}A score in the GEO cohort and TCGA cohort. We assessed the specificity and sensitivity of m^{6}A score through drawing receiver operating characteristic (ROC) curve by using "pROC" and "'timeROC" package. Also, the Spearman's method was used to compute the correlation coefficient. All comparisons were presented by the *p*-values (two-tailed), whereby <0.05 indicated statistical significance.

RESULTS

The Genetic Landscape of 21 m6A Regulators in HNSCC

We firstly identified 21 m^{6}A regulators (including eight "writers," 11 "readers," and two "erasers") in the TCGA cohort. **Figure 1A** and **Supplementary Figure S1A** summarize the significant biological processes and functions of 21 m^{6}A regulators conducted by Metascape database. Then, the waterfall plot presented the incidence of copy number variations and the ratio of somatic mutations of 21 m^{6}A regulators. A total of 72 of the 479 (15.03%) patients experienced mutations, mainly including missense mutation, splice site, and nonsense mutation. In **Figure 1B**, we found that KIAA1429 exhibited the highest mutation frequency, followed by LRPPRC and YTHDC2, while YTHDC1, YTHDF2, IGF2BP2, HNRNPC, METTL14, and RBM15B did not show any mutations. The results of mutation co-occurrence examined the significant relationship between IGF2BP3 and FTO, RBM15 and YTHDF1, LRPPRC and YTHDF2 (**Supplementary Figure S1B**). Further investigation revealed the CNV frequency of 21 m^{6}A regulators. Most m^{6}A regulators showed the prevalent deletions in copy number, while IGF2BP2, YTHDC1, and CBLL1 had a widespread frequency of CNV amplification (**Figure 1C**). **Figure 1D** shows the location of CNV of all m^{6}A regulators on chromosomes. We further demonstrated that the expressions of ALKBH5, METTL3, YTHDF2, and YTHDC2 were significantly downregulated in tumor samples, and in contrast the expression of CBLL1, METTL14, IGF2BP2, IGF2BP3, KIAA1429, YTHDF1, and YTHDC1 were significantly upregulated in tumor samples (**Figure 1E**). Compared with normal tissues, m^{6}A regulators (such as CBLL1 and YTHDF1) with amplificated CNV demonstrated markedly higher expression, and YTHDF2 and YTHDC2 with prevalent CNV deletions were markedly decreased in the tumor (**Figures 1C, E**). Spearman's method presented the correlation among these m^{6}A regulators (**Supplementary Figure S1C**). We found that IGF2BP2 showed no significant correlation with some m^{6}A regulators (RBM15B, YTHDC2, RBM15, YTHDF2, and METTL14). We then ascertain the prognostic value of 21 m^{6}A regulators using the Cox regression. The Cox regression revealed that YTHDC2 was a protective factor, significantly associated with prolonged overall survival rate, while HNRNPA2B1 was a risk factor (**Supplementary Figures S1D, E**). Based on these results, we demonstrated that m^{6}A regulators had significant heterogeneity of genomic and transcriptomic alteration landscape between normal and HNSCC samples.

The Identification of m6A Subgroups Mediated by 21 m6A Regulators

The TCGA dataset with available survival and clinical information were enrolled into the training cohort. The regulator network comprehensively depicted the whole interactions of 21 m^{6}A regulators and their prognostic significance (**Figure 2A**). We found that not only eraser genes were all risk factors, while some of the writer and reader genes were favorable factors. Moreover, we demonstrated that the connection among 21 m^{6}A regulators were positively correlated. These results indicated that cross-talk among the 21 regulators probably play critical roles in the formation of different m^{6}A modifications and pathogenesis and progression in individual tumors. Based on the hypotheses, we utilized unsupervised clustering to classify samples into different m^{6}A clusters. Moreover, we could completely distinguish one m^{6}A cluster from other clusters based on PCA (**Figure 2B**). Accordingly, three distinct m^{6}A clusters were eventually identified, including 128 cases in m^{6}A cluster A, 247 cases in m^{6}A cluster B, and 121 cases in m^{6}A cluster C (**Figure 2C**; **Supplementary Figures S2A, B**).

Among these clusters, m^{6}A cluster A, m^{6}A cluster B, and m^{6}A cluster C, patients in m^{6}A cluster A had an advantage in overall survival rate, whereas m^{6}A cluster C revealed the poorer prognosis in the TCGA cohort (p = 0.022). In the validation cohort (GEO cohort), the identical analyses obtained similar results (p = 0.049, **Figure 2D**; **Supplementary Figure S2C**).

In the TCGA cohort, multivariate Cox regression further demonstrated that patients in m^{6}A cluster C had worst overall survival rate after adjusting clinical parameters [m^{6}A cluster C *vs.* m^{6}A cluster A, HR, 1.68 (95% CI, 1 to 2.8), p = 0.049, **Supplementary Figure S4A**]. However, there was no statistical significance between m^{6}A cluster C and prognostic outcome in the GEO cohort [m^{6}A cluster C *vs.* m^{6}A cluster A, HR, 1.47 (95% CI, 0.88 to 2.47), p = 0.143, **Supplementary Figure S4B**]. We also noticed that the 21 m^{6}A regulators showed different significances between the three m^{6}A clusters. In detail, KIAA1429 and FTO were significantly elevated in m^{6}A cluster A; CBLL1, IGF2BP2,

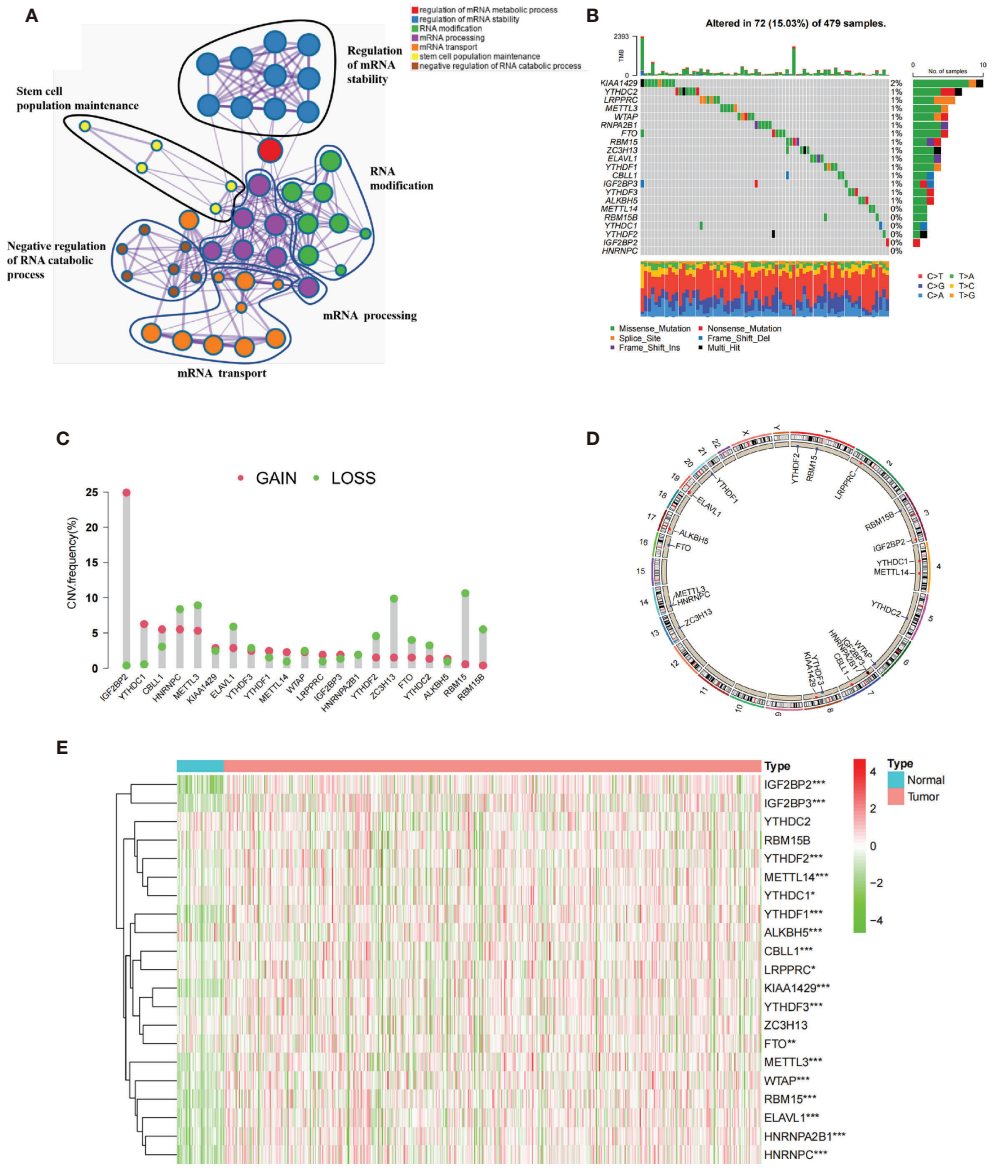

FIGURE 1 | The genetic landscape of 21 m^{6}A regulators in HNSCC. **(A)** The functional enrichment network of 21 m^{6}A regulators visualized by Metascape. Different circles represented different annotations. **(B)** Seventy-two of the 479 patients showed different genetic alterations, including missense mutation, splice site, and nonsense mutation. **(C)** The CNV of 21 m^{6}A regulators. The column represented the alteration frequency. The green dots represented deletion of CNV. The pink dots represented amplification of CNV. **(D)** The location of CNV alteration of m^{6}A regulators in cell. **(E)** The different expression level of 21 m^{6}A regulators between normal and HNSCC (*$p < 0.05$; **$p < 0.01$; ***$p < 0.001$).

and IGF2BP3 were significantly elevated in m^{6}A cluster B; and WTAP, ALKBH5, and RBM15 were significantly elevated in m^{6}A cluster C (**Supplementary Figures S2B, C**).

The Distinct Immune Landscapes of TIME in m6A Clusters

To explore the biological functions and pathways underlying these m^{6}A clusters, we performed GSVA enrichment analysis against the GO and KEGG gene sets (**Supplementary Figures S3A, B**). As shown in the GSVA analysis, m^{6}A cluster A was markedly enriched in immune activation-related pathways. Intriguingly, m^{6}A cluster C was markedly associated with carcinogenic pathways, such as DNA replication, nucleotide excision repair, and mismatch repair pathways. Whereas, m^{6}A cluster B was highly enriched in both carcinogenic and stromal-related signaling pathways.

The heatmap visualized the infiltration levels of 23 immune cells among three m^{6}A clusters (**Figure 3A**). Antitumor lymphocyte cells, such as activated CD8+ T cells, and NK cells, were mainly enriched in the m^{6}A cluster A. However,

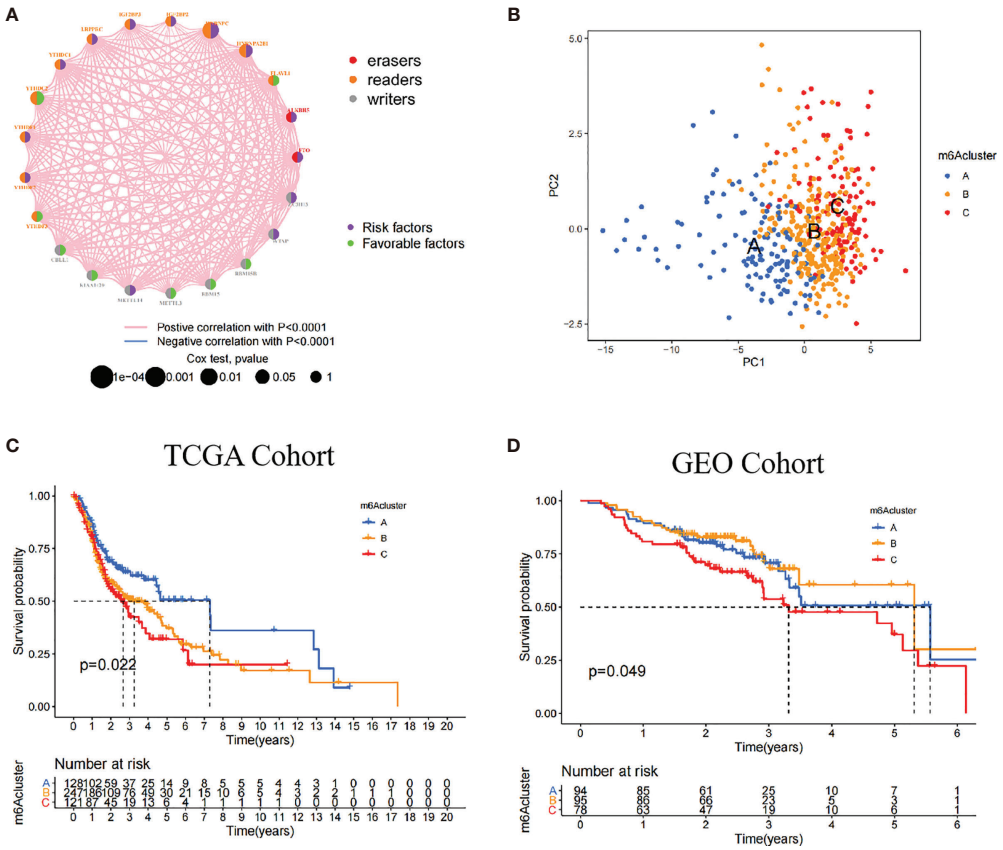

FIGURE 2 | Patterns of m^{6}A methylation modification. **(A)** The interaction of 21 m^{6}A regulators in HNSCC. The different RNA modifications were depicted by different colored circles. Readers, orange; writers, gray; erasers, red. Favorable factors were indicated by the green circle, and risk factors were indicated by the purple circle. **(B)** The remarkable difference between different three m^{6}A clusters was plotted *via* principal component analysis. **(C)** Kaplan-Meier curves of overall survival (OS) in TCGA cohort with three m^{6}A clusters (p = 0.022). **(D)** Kaplan-Meier curves of overall survival (OS) in GEO cohort with three m^{6}A clusters (p = 0.049). The patients in m^{6}A cluster C showed worse OS than in other clusters.

regulatory T cells and type 1/2/17 T helper cells were mainly enriched in the m^{6}A cluster B. To our surprise, innate immune cells including natural killer cell, macrophage, eosinophil, mast cell, and MDSC were increased in the m^{6}A cluster C. To explore the subsets of immune cell in TIME, CIBERSORT package was further used to characterize the immune cell infiltration based on the expression file. We observed the consistent result in the **Figure 3B**. Previous studies revealed a novel immune phenotype, immune-excluded phenotype, with an abundance of immune cells, retained in the tumor stroma rather than in the parenchyma. Therefore, we speculated that the m^{6}A cluster B with higher stromal score exhibited an ineffective antitumor immune response (**Figure 3E**). Cancer-related pathway analyses demonstrated that the m^{6}A cluster B was related to TGF-β and WNT-target pathways, which further corroborated with our hypothesis (**Supplementary Figures S4C, D**). In **Figure 3C**, we found that m^{6}A cluster A exhibited the highest immune scores, followed by m^{6}A cluster B and m^{6}A cluster C. Conversely, m^{6}A cluster C had a higher tumor purity than m^{6}A cluster B and m^{6}A cluster A, suggesting that tumors in m^{6}A cluster B and m^{6}A cluster A are surrounded by more immune cells and stromal cells (**Figure 3D**).

Then, we examined the association between 21 m^{6}A regulators and immune cells *via* Spearman's method. We focused on the regulator HNRNPA2B1, an independent prognostic risk factor based on the above results (**Supplementary Figures S1D, E**), which was negatively correlated with numerous immune cells (**Supplementary Figure S5A**). The ESTIMATE showed that low-expression subgroup of HNRNPA2B1 exhibited higher immune score, which confirmed the above findings (**Supplementary Figure S5B**).

We also found that low-expression subgroup of HNRNPA2B1 exhibited a significant increased among 23 immune cells (**Supplementary Figure S5C**). The low-expression subgroup of HNRNPA2B1 also exhibited elevated expression of HLA molecules (**Supplementary Figure S5D**). Subsequent function enrichment analyses found that low-expression subgroup of HNRNPA2B1 exhibited an obvious enhancement in immune activation including T-cell costimulation and type I/II IFN responses, which hinted that the expression of HNRNPA2B1 might affect the efficacy

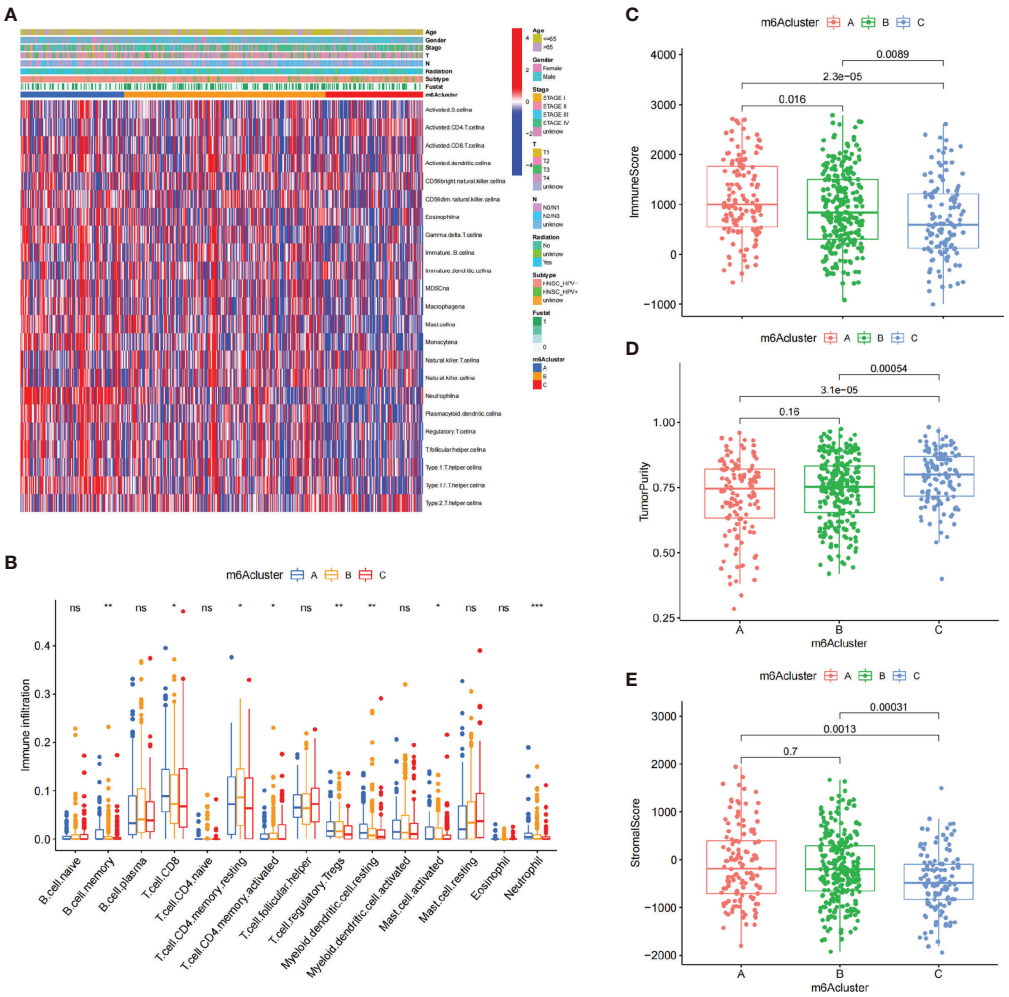

FIGURE 3 | The characteristics of TIME in three m^{6}A clusters. **(A)** The heatmap showed the result of the consensus clustering in the TCGA cohort. Clinical information included age, gender, survival status, HPV subtypes, radiation, and stage. **(B)** The infiltration of immune cells in the three m^{6}A clusters using the CIBERSORT. *$p < 0.05$; **$p < 0.01$; ***$p < 0.001$. **(C–E)** The analysis of the immune score **(C)**, tumor purity **(D)**, and stromal score **(E)** among three m^{6}A clusters. ns, no significance.

of immunotherapy (**Supplementary Figure S5D**). Thus, we investigated two anti-PD-L1 immunotherapy cohorts (IMvigor210 cohort and GSE78220 cohort). In the IMvigor210 cohort, patients with low expression of HNRNPA2B1 had prolonged overall survival rate (**Supplementary Figure S5E**). In the GSE78220 cohort, there was no significant survival trend (**Supplementary Figure S5F**). Therefore, we speculated that HNRNPA2B1-mediated m^{6}A methylation modification may enhance the antitumor response *via* promoting the activation of immune cells.

The m6A-Related DEGs in HNCSS

To identify the biological behaviors (e.g., genetic alterations and expression perturbations) of these m^{6}A clusters, we fixed attention on the m^{6}A-related transcriptional expression alterations across three m^{6}A clusters in HNSCC. The Venn diagram determined 4,269 overlapping differentially expressed genes (DEGs) (**Figure 4A**). A total of 311 DEGs related to prognosis were considered the representative m^{6}A-related genes (**Supplementary Table S5**). GO enrichment analysis revealed that the biological processes related to RNA transcription and modification were significant functions (**Figure 4B**). Similar to the above analysis, unsupervised clustering method based on the expression of these 311 DEGs separated patients into three stable gene clusters (gene clusters A–C) in the TCGA cohort (**Supplementary Figure S6A**). **Figure 4C** demonstrates that three m^{6}A gene cluster had different clinicopathological features. We found that patients in m^{6}A gene cluster C exhibited advanced clinical stage. In addition, patients receiving radiotherapy were mainly concentrated in the m^{6}A gene cluster A, while patients with negative HPV subtype were represented by the m^{6}A gene clusters B and C.

The survival analysis further indicated that the three m^{6}A gene clusters had significant prognostic differences in HNSCC samples. m^{6}A gene cluster A was proven to be related to better prognostic outcome, while patients in m^{6}A gene cluster C was associated with poorer outcome (**Figure 4D**). The Cox regression

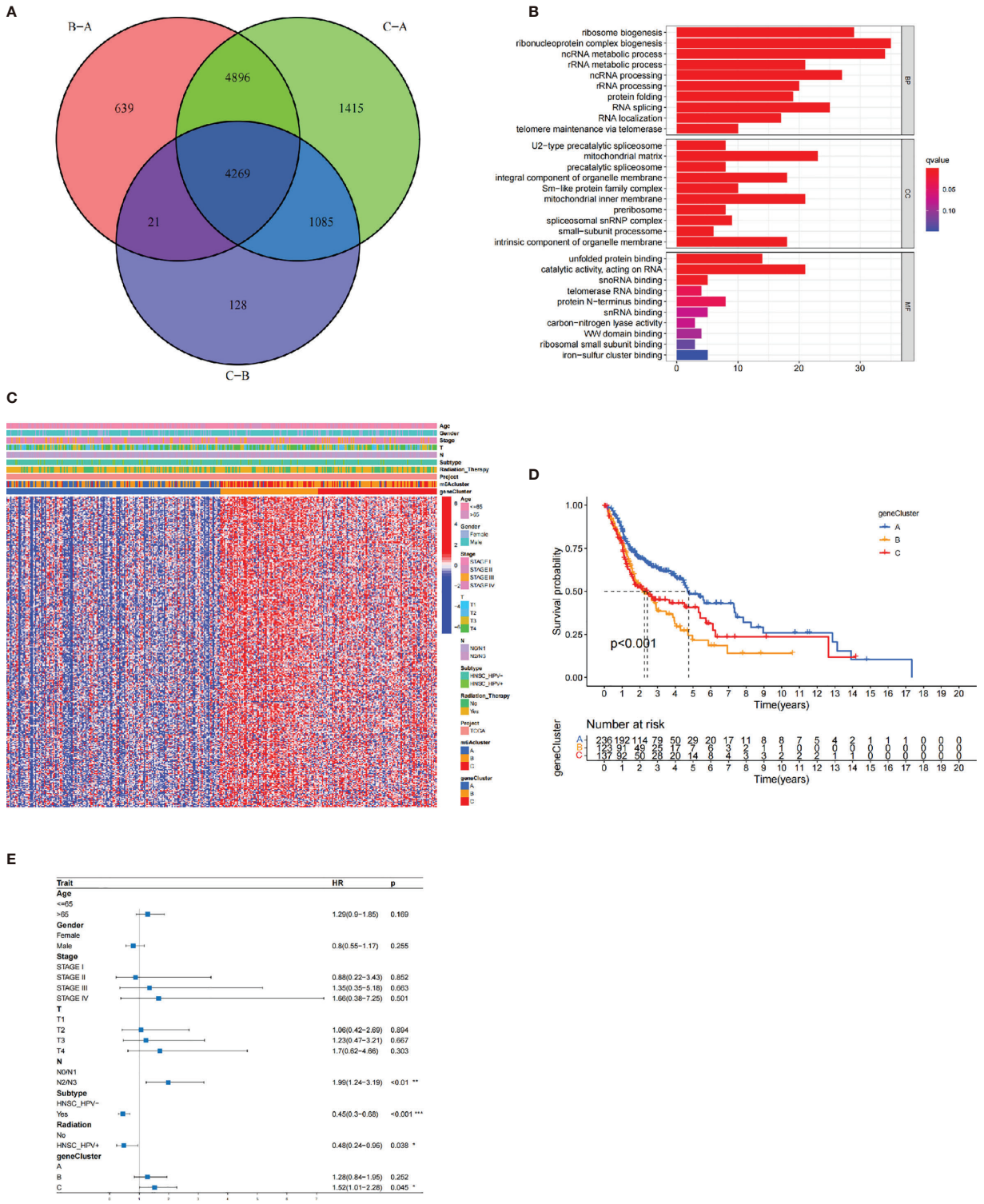

FIGURE 4 | The construction of m^{6}A gene clusters and functional annotation. The 4,269 differentially expressed genes (DEGs) among three m^{6}A clusters were shown in the Venn plot. **(B)** GO enrichment analysis of 311 prognosis-related DEGs. **(C)** The consensus clustering based on prognosis-related DEGs classified patients into three gene clusters, respectively. **(D)** The Kaplan-Meier curves of the three m^{6}A gene clusters ($p < 0.001$). **(E)** The multivariate Cox regression-estimated prognostic value of m^{6}A gene clusters in TCGA cohort.

determined m^{6}A gene cluster C (*vs.* m^{6}A gene cluster A) as an independent risk factor after considering age, gender, stage, HPV subtype, and radiotherapy [HR, 1.52 (95% CI, 1.01 to 2.28), p = 0.045; **Figure 4E**]. **Supplementary Figure S6B** observes the different expression levels of the 21 m^{6}A regulators, which were consistent with our expected results.

The Construction of Prognostic Signatures and Exploration of Its Characteristics of Clinical Traits

Accordingly, the above results showed that the m^{6}A regulators played a nonnegligible role in regulating prognosis and TIME. However, these analyses were only based on the overall population and could not interpret the heterogeneity and complexity of m^{6}A regulators individually. Based on these identified m^{6}A-related genes, we developed a scoring scheme, considered m^{6}Ascore, to quantify individual patients.

The alluvial diagram visualized the quantification changes of patients (**Figure 5A**). These results illustrated that m^{6}A gene clusters B and C were linked to higher m^{6}A score, whereas m^{6}A gene cluster A exhibited lower m^{6}A score. Notably, m^{6}A cluster C showed the highest m^{6}A score, followed by m^{6}A cluster B, while m^{6}A cluster A revealed the lowest m^{6}A score (**Supplementary Figure S7A**). Furthermore, we conducted the analysis of Spearman's correlation to illustrate the patterns of m^{6}A regulators. The heatmap indicated that m^{6}A score was

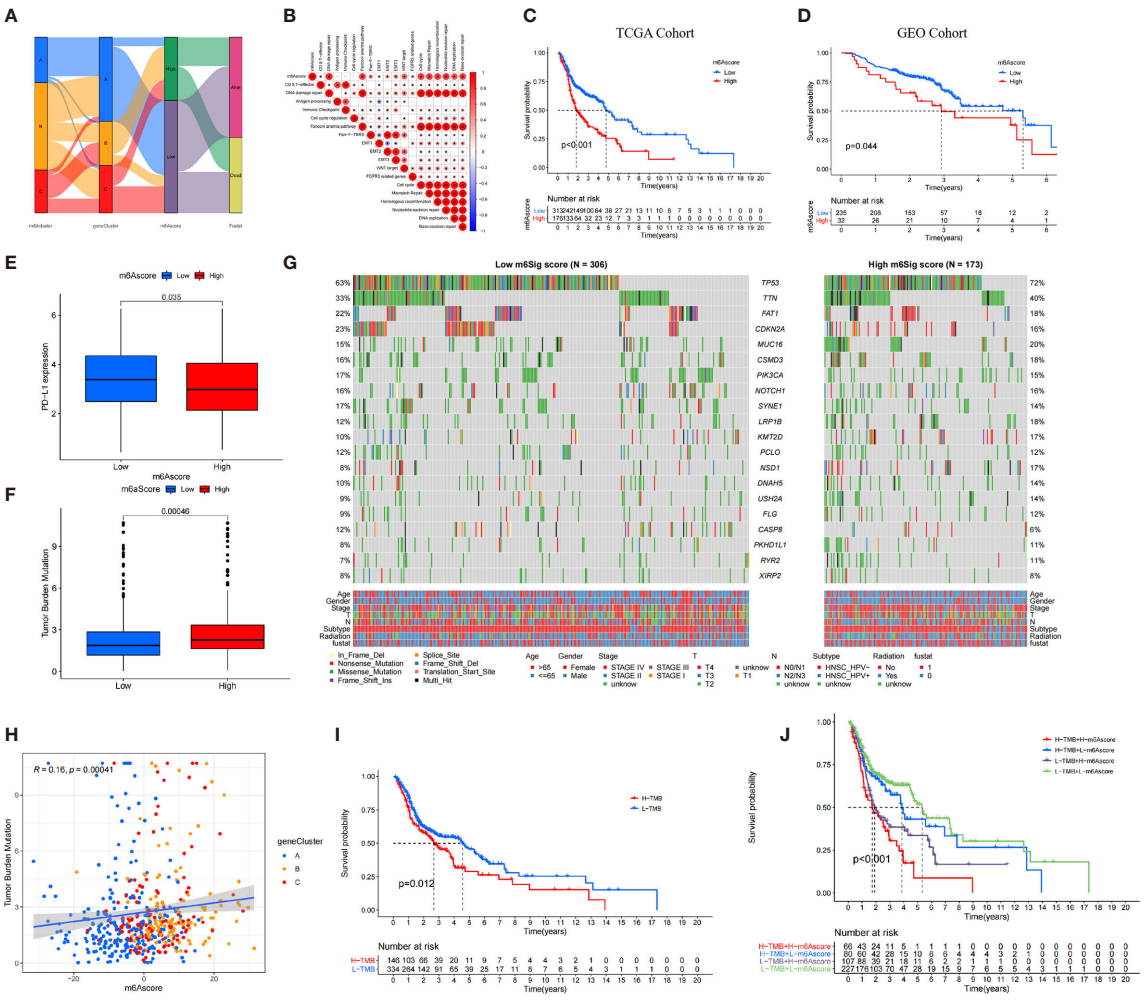

FIGURE 5 | The construction of m6A score and explore its relevant genetic features. **(A)** Alluvial diagram of m6A clusters in groups with m6A geneCluster, m6A score, and survival status. **(B)** Correlations between m6A score and the known biological gene signatures using Spearman analysis. **(C, D)** The survival analysis of patients in high and low m6A score subgroups in the TCGA cohort **(C)** and GEO cohort **(D)**. **(E)** Comparison of PD-L1 expression level in high versus low m6A score subgroups. **(F)** The distribution of tumor mutation load (TMB) in high versus low m6A score subgroups. **(G)** The waterfall of mutational landscape in TCGA stratified by low (left panel) and high m6Sig score (right panel) subgroups. Each column represented one patient. Age, Gender, Survival status, HPV subtypes, Radiation, Stage were shown as patient annotations. **(H)** There was a significant positive correlation between the m6A score and TMB (R = 0.16, p < 0.001). **(I)** Kaplan-Meier curves for patients in high and low TMB subgroups. H, high; L, Low (P=0.012). **(J)** Kaplan-Meier curves for patient in the TCGA cohort stratified by both m6A score and TMB. H, high; L, Low; TMB, tumor mutation load (P < 0.001).

positively correlated with WNT target signatures, cell cycle signatures, and EMT pathways (**Figure 5B**).

There was an inverse trend between the m^{6}A score and the immune score (R = −0.35, p = 2.3e−16) and stromal score (R = −0.08, p = 0.076), which demonstrated the crosstalk between m^{6}A score and TIME (**Supplementary Figure S7B, C**). Compared with the high m^{6}A score, patients in low–m^{6}A score subgroup had higher relative level of immune checkpoint molecules and CD8 effector cells. However, high m^{6}A scores were significantly associated with stromal pathways (**Supplementary Figure S7D**).

Furthermore, we determined the prognostic value of m^{6}A score in predicting patients' survival outcome. Based on the cutoff value of 3.3615, we divided patients into low– or high–m^{6}A score subgroups. As expected, patients with low–m^{6}A score were associated with a prominent prognosis (p < 0.001, **Figure 5C**), and the ROC validated the predictive accuracy of the m^{6}A score (AUC = 0.634, **Supplementary Figure S7E**). Integrating the clinical information (e.g., age, gender, stage, HPV subtype, and radiotherapy), multivariate Cox regression confirmed that the high m^{6}A score was an independent prognostic factor for evaluating survival outcome (high m^{6}A score *vs*. low m^{6}A score; HR, 0.61 [95% CI, 0.44 to 0.86], p < 0.01, **Supplementary Figure S7G**).

We also investigated the relationship between the m^{6}A score and level and found that the expression level of PD-L1 was elevated in the low–m^{6}A score subgroup than in the high m^{6}A score subgroup (**Figure 5E**). The constructed m^{6}A score was validated in the GEO cohort by integrating clinical genomic information. The m^{6}A score displayed the potential predictive value in GEO cohort (AUC = 0.672, **Supplementary Figure S7F**), and patients in low–m^{6}A score subgroup had a better survival outcome (p = 0.044; **Figure 5D**). Multivariate Cox regression also confirmed that the m^{6}A score was an independent prognostic biomarker in GEO cohort [HR, 0.52 (95% CI, 0.3 to 0.92), p = 0.024; **Supplementary Figure S7H**]. We then further analyzed the distribution of somatic mutated gene between low– and high–m^{6}A score subgroups. As shown in **Figure 5G**, high m^{6}A score subgroup presented more tumor somatic mutations than the low–m^{6}A score group. Increasing studies have demonstrated and there was a link between the TMB and immunotherapy responses. Consequently, we further explored the distribution of TMB in low– and high–m^{6}A score subgroups. We confirmed that the low–m^{6}A score group had lower TMB frequencies (**Figure 5F**). The m^{6}A score was markedly positively correlated with TMB (R = 0.16, p = 0.00041; **Figure 5H**). In addition, we found that patients with low TMB frequencies demonstrated a survival benefit (p = 0.012; **Figure 5I**), while patients with low m^{6}A score showed significant survival advantages among patients with low TMB frequencies (**Figure 5J**).

The prognostic value of m^{6}A score subjected to various clinical parameters was also estimated. We found that patients in low m^{6}A score had a better survival outcome than those in m^{6}A score among different subgroups (**Supplementary Figure S8**). Furthermore, the OS of patients with radiotherapy in the high– and low–m^{6}A score groups was superior, but patients with low m^{6}A score benefited significantly more than those with high m^{6}A score from radiotherapy. Accordingly, patients with low m^{6}A score were more likely to benefit for survival from radiotherapy than those with high m^{6}A score.

The Role of m^{6}A Score in Predicting Immunotherapy Benefits

TIDE and IPS served as novel imunotherapeutic predictors and are strongly suggested to evaluate the response of immunotherapy to patients. We revealed that TIDE was significantly decreased in the low–m^{6}A score subgroup, and IPS was significantly elevated in the low–m^{6}A score subgroup (IPS: p = 0.0014, **Supplementary Figure S9A**; TIDE: p = 0.0035, **Supplementary Figure S9B**). In detail, the levels of the four groups were significantly increased in the low m^{6}A score group (**Supplementary Figures S9C–F**).

We investigated whether the m^{6}A score could predict immunotherapy response to ICB treatment based on three cohorts. Among IMvigor210 cohort and Riaz et al. cohort, patients with low m^{6}A score exhibited clinical benefits markedly (IMvigor210 cohort, p < 0.001, **Figure 6A**; Riaz et al. cohort, p = 0.048, **Figure 6J**). In GSE78220 cohort, the survival curve presented an opposite result due to the small number of samples (**Figure 6H**). The immunotherapeutic advantages and anti-PD-1/L1 response to patients were confirmed in the low– and high–m^{6}A score subgroups (**Figures 6B, C, I, K**).

We investigated the difference between m^{6}A score and three immune phenotypes in the IMvigor210 cohort and found that lower m^{6}A score was remarkably associated with excluded immune phenotype, indicating that immune checkpoint inhibitors are less effective for these patients (**Figure 6D**). Furthermore, we revealed that EMT were significantly activated in tumors with low m^{6}A score (**Figure 6E**). **Figure 6F** indicates that individuals with a combination of high m^{6}A score and low neoantigen burden showed a poorer prognosis. The ROC curves implied that m^{6}A score was a robust biomarker to assess clinical prognosis of patients under immunotherapy (**Figure 6G**). In summary, our work strongly demonstrated that m^{6}A regulators was significantly correlated with TIME and mediated prognostic response to immunotherapy.

The Low–m^{6}A Score Group Showed More Sensitivity to Chemotherapies

Considering the frequent use of chemotherapy in the treatment of HNSCC, we further explored the response of patients with 138 different types of drugs. In detail, the GDSC dataset was used to predict the IC_{50} of the selected drugs based on the "pRRophetic" package. A total of 54 drugs demonstrated obviously lower IC_{50} in the low–m^{6}A score group (**Supplementary Figure S10**). Based on the guidelines of the National Comprehensive Cancer Network (53) and Chinese Society of Clinical Oncology (54), we summarized all the drugs used for the treatment of head and neck tumor (including cisplatin, methotrexate, cetuximab, afatinib, capecitabine, oxaliplatin, carboplatin, docetaxel, nivolumab, camrelizumab, gemcitabine, nimotuzumab, 5-FU, paclitaxel, pembrolizumab, toripalimab, and nedaplatin).

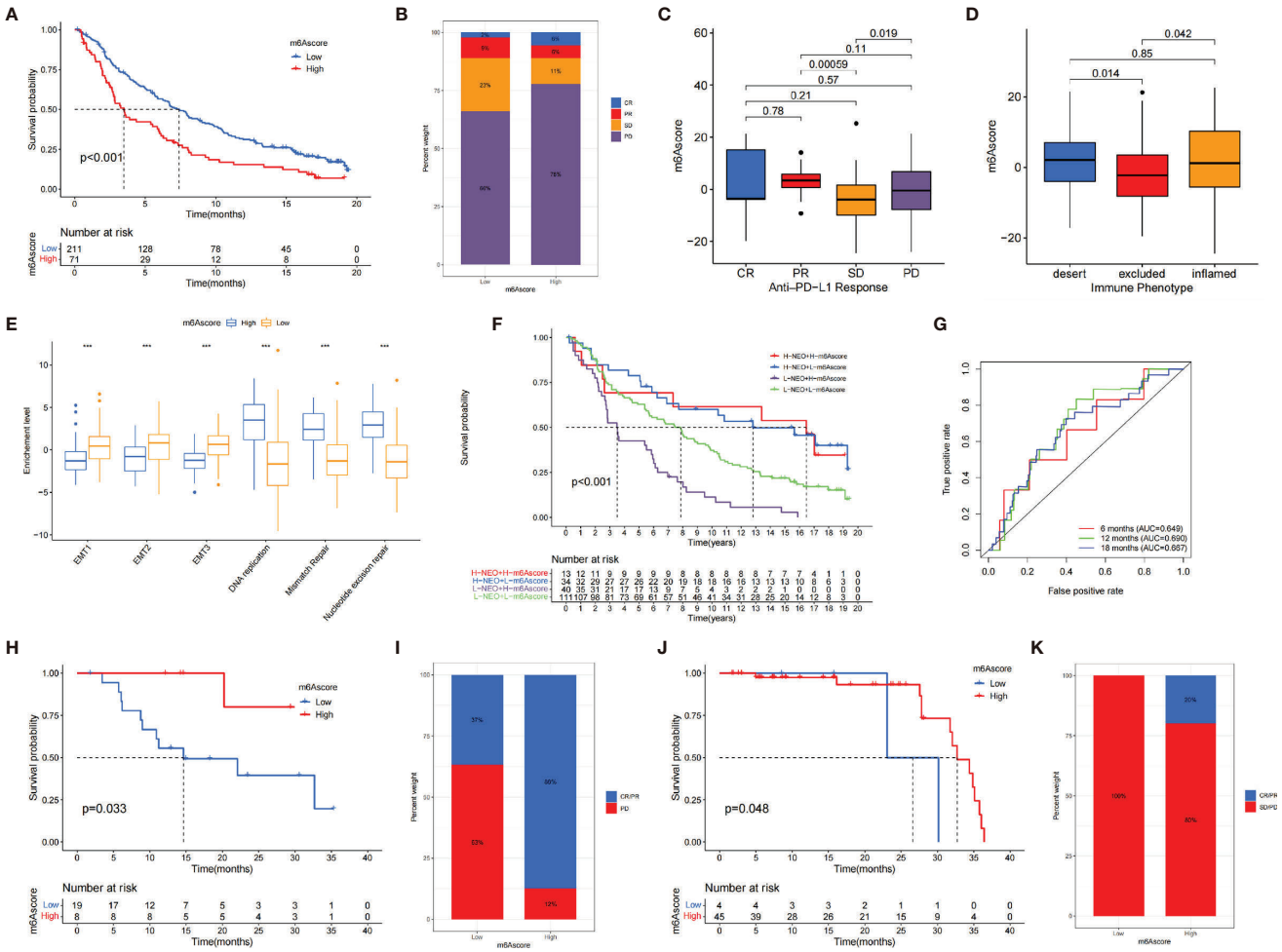

FIGURE 6 | The role of m^{6}A score in anti-PD-1/L1 cohorts. **(A)** The survival analysis of patients in low and high m^{6}A score subgroups in the IMvigor210 cohort ($p < 0.001$). **(B)** The proportion of patients with different response to immunotherapy in IMvigor210 cohort. SD, stable disease; PD, progressive disease; CR, complete response; PR, partial response. **(C)** Distribution of m^{6}A score in different response groups. **(D)** The tumor immune phenotypes were validated in IMvigor210 cohort. **(E)** Differences in EMT pathways and DNA repair-related pathways between low and high m^{6}A score groups (*$p < 0.05$; **$p < 0.01$; ***$p < 0.001$). **(F)** The survival analysis of patients who received immunotherapy stratified by both m^{6}A score and neoantigen burden. H, high; L, low; NEO, neoantigen burden ($p < 0.001$). **(G)** The AUC of the quantification of m^{6}A score in patients treated with immunotherapy (6 months, AUC = 0.649; 12 months, AUC = 0.690; 18 months, AUC = 0.667). **(H)** The survival analysis of patients in low– and high–m^{6}A score subgroups in the GSE78220 cohort ($p = 0.033$). **(I)** The proportion of patients with different responses to immunotherapy in GSE78220 cohort. **(J)** The survival analysis of patients in low– and high–m^{6}A score subgroups in the Riaz et al. cohort ($p = 0.048$). **(K)** The proportion of patients with different immunotherapy response in Riaz et al. cohort.

However, only paclitaxel presented obvious lower IC_{50} in the low–m^{6}A score group. The finding suggested that patients with low m^{6}A score were more sensitive to the treatment of paclitaxel than those with high m^{6}A score in HNSCC.

DISCUSSION

Increasing evidence shows that m^{6}A methylation, the most common posttranscriptional modification, exerts a crucial regulation on immunity, inflammation, as well as antitumor effects involving in interaction with various m^{6}A regulators. Furthermore, since most studies just revealed the modulation of one or two regulators in the contexture of TIME, the comprehensive characteristics of immune cell mediated by integrated various m^{6}A regulators is essential to elucidate the potential mechanism of m^{6}A methylation in TIME. So far, the effects of m^{6}A regulators on the TIME of HNSCC have not been explained comprehensively. Identifying the contribution of m^{6}A regulators in TIME will enhance our understanding of antitumor response mediated by m^{6}A methylation and facilitating more effective strategies on immunotherapy and chemotherapy.

In our study, we established three immune phenotypes based on 21 m^{6}A regulators, which were correlated with survival outcomes and diverse TIME characterization in HNSCC. The m^{6}A cluster A had high infiltration level of adaptive immune cells,

corresponding to the immune-inflamed phenotype. The m6A cluster B had high infiltration level of innate immune cells and stroma cells, corresponding to the immune-excluded phenotype. The m^{6}A cluster C was characterized by the inhibition of TIME, corresponding to the immune-desert phenotype. The immune-inflamed phenotype showed a large infiltration proportion of immune cell TIME (7). The immune excluded, known as nonhot tumors, means that immune cells were penetrated in the stroma rather than parenchyma. In our study, we found that the immune-desert phenotypes lacked activated and priming T cell, which were correlated with the immune escape demonstrated by previous studies (34, 55, 56). We also revealed that the m^{6}A cluster A was significantly associated with elevated infiltration of lymphocyte, supporting its predictive value on immunotherapy. Based on the above results, we found m6A cluster B exhibited a significantly high level of stroma activation, including Wnt signaling pathway and TGF-β pathway, which impeded the activation of T-lymphocyte cells (57). Therefore, we presumed that patients in m^{6}A cluster B may benefit from ICB treatment as well as TGF-β blockade treatment.

The overlapped DEGs identified from three m^{6}A phenotype were significantly associated with RNA modification and immune-related pathways, suggesting that these DEGs were "true" m^{6}A-related genes. We then further identified three transcriptomic subtypes based on m^{6}A-related genes. This result demonstrated that all m^{6}A regulators played a key role in shaping TIME. After, we established a scoring system, named m^{6}A score, to distinguish heterogeneity of each patient derived from m^{6}A modification, thus precisely guiding therapeutic strategies for HNSCC. As observed, the m^{6}A modification pattern characterized by the immune-desert phenotype exhibited a higher m^{6}A score, while the pattern characterized by the immune-inflamed phenotype showed a lower m^{6}A score.

Further analyses showed that the m^{6}A score could serve as a prognostic biomarker, which was also associated with mutation-related signatures and TMB. These results suggested that the m^{6}A score could be a preferable marker in predicting genomic aberrations.

We verified that the m^{6}A score was strongly associated with the predictors of ICB treatment, implying that the m^{6}A methylation could affect the response of immunotherapy to patients. In the IMvigor210 cohort, we validated the accuracy of the determined immune phenotype (34) and found that the m^{6}A score integrated with various biomarkers (e.g., neoantigen load, TMB, the components of TIME) could more effectively predict prognosis of patients receiving immunotherapy. Actually, we also confirmed the prediction ability of the m^{6}A score in the anti-PD-1/L1 immune response *via* two independent immunotherapy cohorts, which showed significant difference between nonresponders partial responders, and completed responders. We further found that patients with low m^{6}A score might be more sensitive to anticancer drugs than high m^{6}A score based on the GDSC. These above findings suggested that m^{6}A score was a reliable tool, which could be used to comprehensively determine the immune-related phenotypes and guide clinical treatment decision to immunotherapy and anticancer drugs.

Furthermore, we also elucidated the specific m^{6}A regulators in the regulation of TIME. Recent studies have confirmed that m^{6}A could enhance the stability of mRNA and transport the specific mRNAs to the cytoplasm mainly through the binding proteins of HNRNPA2B1 in cell (58). Also, HNRNPA2B1 was recognized as an oncogene as it promotes tumor growth and migration in various cancers (59–61). Our analyses revealed that the expression of HNRNPA2B1 was upregulated in tumor and associated with decreased survival rate. Furthermore, higher expression of HNRNPA2B1 exhibited a lower infiltration trend of various types of DC, indicating that HNRNPA2B1 may be involved in the activation of DC. We also evaluated the mutated driver genes, the critical foundation of tumor diagnosis, therapeutic selections, *via* analyzing the TCGA cohort.

Although 21 m^{6}A regulators are added into the mode, novel-identified regulators need to be curated to optimize the accuracy of the m^{6}A score. Since there is a lack of appropriate immunotherapy cohorts based on HNSCC, we hope that different regimens (e.g., anti-PD-1/L1 or anti-CTLA-4) across HNSCC cohorts will verify our conclusion. Furthermore, only retrospective datasets were used to identify the m^{6}A regulators and m^{6}A score; thus, a series of prospective cohorts receiving immunotherapy were needed. Moreover, as not all cohorts exhibited that patients in low–m^{6}A score subgroup benefits from ICB treatment, we needed a large and multicenter clinical population sample combined with more clinical features to confirm and improve the accuracy of the model.

In conclusion, our work comprehensively evaluated the TIME characteristics of m^{6}A regulators based on different cohorts. This integrated analysis indicated m^{6}A modification could not be ignored as its vital role in regulating tumor immunity. Comprehensive evaluation of m^{6}A modification in TIME will guide more effective and important immunotherapeutic strategies.

DATA AVAILABILITY STATEMENT

Publicly available datasets were analyzed in this study. The datasets generated during the current studyare available in the Cancer Genome Atlas (TCGA) public dataset (https://portal.gdc.cancer.gov/) and the Gene-Expression Omnibus (GEO) public dataset (https://www.ncbi.nlm.nih.gov/geo/).

AUTHOR CONTRIBUTIONS

JF and ZY performed all analysis as well as wrote the manuscript. XM and MY participated in data analysis. All authors participated in reviewing the manuscript and approved the final version.

SUPPLEMENTARY MATERIAL

The Supplementary Material for this article can be found online at: https://www.frontiersin.org/articles/10.3389/fonc.2021.764798/full#supplementary-material

REFERENCES

1. Bray F, Ferlay J, Soerjomataram I, Siegel RL, Torre LA, Jemal A. Global Cancer Statistics 2018: GLOBOCAN Estimates of Incidence and Mortality Worldwide for 36 Cancers in 185 Countries. *CA: Cancer J Clin* (2018) 68 (6):394–424. doi: 10.3322/caac.21492
2. Shield KD, Ferlay J, Jemal A, Sankaranarayanan R, Chaturvedi AK, Bray F, et al. The Global Incidence of Lip, Oral Cavity, and Pharyngeal Cancers by Subsite in 2012. *CA: Cancer J Clin* (2017) 67(1):51–64. doi: 10.3322/caac.21384
3. Zhang X-M, Song L-J, Shen J, Yue H, Han Y-Q, Yang C-L, et al. Prognostic and Predictive Values of Immune Infiltrate in Patients With Head and Neck Squamous Cell Carcinoma. *Hum Pathol* (2018) 82:104–12. doi: 10.1016/j.humpath.2018.07.012
4. Seiwert TY, Burtness B, Mehra R, Weiss J, Berger R, Eder JP, et al. Safety and Clinical Activity of Pembrolizumab for Treatment of Recurrent or Metastatic Squamous Cell Carcinoma of the Head and Neck (KEYNOTE-012): An Open-Label, Multicentre, Phase 1b Trial. *Lancet Oncol* (2016) 17(7):956–65. doi: 10.1016/S1470-2045(16)30066-3
5. Garassino MC, Gadgeel S, Esteban E, Felip E, Speranza G, Domine M, et al. Patient-Reported Outcomes Following Pembrolizumab or Placebo Plus Pemetrexed and Platinum in Patients With Previously Untreated, Metastatic, non-Squamous non-Small-Cell Lung Cancer (KEYNOTE-189): A Multicentre, Double-Blind, Randomised, Placebo-Controlled, Phase 3 Trial. *Lancet Oncol* (2020) 21(3):387–97. doi: 10.1016/S1470-2045(19)30801-0
6. Rosenberg JE, Hoffman-Censits J, Powles T, van der Heijden MS, Balar AV, Necchi A, et al. Atezolizumab in Patients With Locally Advanced and Metastatic Urothelial Carcinoma Who Have Progressed Following Treatment With Platinum-Based Chemotherapy: A Single-Arm, Multicentre, Phase 2 Trial. *Lancet* (2016) 387(10031):1909–20. doi: 10.1016/S0140-6736(16)00561-4
7. Chen DS, Mellman I. Elements of Cancer Immunity and the Cancer-Immune Set Point. *Nature* (2017) 541(7637):321–30. doi: 10.1038/nature21349
8. Le DT, Durham JN, Smith KN, Wang H, Bartlett BR, Aulakh LK, et al. Mismatch Repair Deficiency Predicts Response of Solid Tumors to PD-1 Blockade. *Sci (New York NY)* (2017) 357(6349):409–13. doi: 10.1126/science.aan6733
9. Ferris RL, Whiteside TL, Ferrone S. Immune Escape Associated With Functional Defects in Antigen-Processing Machinery in Head and Neck Cancer. *Clin Cancer Res* (2006) 12(13):3890–5. doi: 10.1158/1078-0432.CCR-05-2750
10. Wang T, Kong S, Tao M, Ju S. The Potential Role of RNA N6-Methyladenosine in Cancer Progression. *Mol Cancer* (2020) 19(1):88. doi: 10.1186/s12943-020-01204-7
11. Zhao BS, Roundtree IA, He C. Post-Transcriptional Gene Regulation by mRNA Modifications. *Nat Rev Mol Cell Biol* (2017) 18(1):31–42. doi: 10.1038/nrm.2016.132
12. Chen M, Wei L, Law C-T, Tsang FH-C, Shen J, Cheng CL-H, et al. RNA N6-Methyladenosine Methyltransferase-Like 3 Promotes Liver Cancer Progression Through YTHDF2-Dependent Posttranscriptional Silencing of SOCS2. *Hepatology* (2018) 67(6):2254–70. doi: 10.1002/hep.29683
13. Li H-B, Tong J, Zhu S, Batista PJ, Duffy EE, Zhao J, et al. mA mRNA Methylation Controls T Cell Homeostasis by Targeting the IL-7/STAT5/SOCS Pathways. *Nature* (2017) 548(7667):338–42. doi: 10.1038/nature23450
14. Zaccara S, Ries RJ, Jaffrey SR. Reading, Writing and Erasing mRNA Methylation. *Nat Rev Mol Cell Biol* (2019) 20(10):608–24. doi: 10.1038/s41580-019-0168-5
15. Yang Y, Hsu PJ, Chen Y-S, Yang Y-G. Dynamic Transcriptomic mA Decoration: Writers, Erasers, Readers and Functions in RNA Metabolism. *Cell Res* (2018) 28(6):616–24. doi: 10.1038/s41422-018-0040-8
16. Wang Y, Li Y, Toth JI, Petroski MD, Zhang Z, Zhao JC. N6-Methyladenosine Modification Destabilizes Developmental Regulators in Embryonic Stem Cells. *Nat Cell Biol* (2014) 16(2):191–8. doi: 10.1038/ncb2902
17. Ping X-L, Sun B-F, Wang L, Xiao W, Yang X, Wang W-J, et al. Mammalian WTAP Is a Regulatory Subunit of the RNA N6-Methyladenosine Methyltransferase. *Cell Res* (2014) 24(2):177–89. doi: 10.1038/cr.2014.3
18. Pendleton KE, Chen B, Liu K, Hunter OV, Xie Y, Tu BP, et al. The U6 snRNA mA Methyltransferase METTL16 Regulates SAM Synthetase Intron Retention. *Cell* (2017) 169(5):824–35.e14. doi: 10.1016/j.cell.2017.05.003
19. Huang Y, Yan J, Li Q, Li J, Gong S, Zhou H, et al. Meclofenamic Acid Selectively Inhibits FTO Demethylation of M6a Over ALKBH5. *Nucleic Acids Res* (2015) 43(1):373–84. doi: 10.1093/nar/gku1276
20. Meyer KD, Jaffrey SR. Rethinking mA Readers, Writers, and Erasers. *Annu Rev Cell Dev Biol* (2017) 33:319–42. doi: 10.1146/annurev-cellbio-100616-060758
21. Chen X-Y, Zhang J, Zhu J-S. The Role of mA RNA Methylation in Human Cancer. *Mol Cancer* (2019) 18(1):103. doi: 10.1186/s12943-019-1033-z
22. Shulman Z, Stern-Ginossar N. The RNA Modification N-Methyladenosine as a Novel Regulator of the Immune System. *Nat Immunol* (2020) 21(5):501–12. doi: 10.1038/s41590-020-0650-4
23. Lan T, Li H, Zhang D, Xu L, Liu H, Hao X, et al. KIAA1429 Contributes to Liver Cancer Progression Through N6-Methyladenosine-Dependent Post-Transcriptional Modification of GATA3. *Mol Cancer* (2019) 18(1):186. doi: 10.1186/s12943-019-1106-z
24. Chen S, Li Y, Zhi S, Ding Z, Wang W, Peng Y, et al. WTAP Promotes Osteosarcoma Tumorigenesis by Repressing HMBOX1 Expression in an mA-Dependent Manner. *Cell Death Dis* (2020) 11(8):659. doi: 10.1038/s41419-020-02847-6
25. Yi L, Wu G, Guo L, Zou X, Huang P. Comprehensive Analysis of the PD-L1 and Immune Infiltrates of mA RNA Methylation Regulators in Head and Neck Squamous Cell Carcinoma. *Mol Ther Nucleic Acids* (2020) 21:299–314. doi: 10.1016/j.omtn.2020.06.001
26. Li T, Hu P-S, Zuo Z, Lin J-F, Li X, Wu Q-N, et al. METTL3 Facilitates Tumor Progression *via* an mA-IGF2BP2-Dependent Mechanism in Colorectal Carcinoma. *Mol Cancer* (2019) 18(1):112. doi: 10.1186/s12943-019-1038-7
27. Han D, Liu J, Chen C, Dong L, Liu Y, Chang R, et al. Anti-Tumour Immunity Controlled Through mRNA mA Methylation and YTHDF1 in Dendritic Cells. *Nature* (2019) 566(7743):270–4. doi: 10.1038/s41586-019-0916-x
28. Yang S, Wei J, Cui Y-H, Park G, Shah P, Deng Y, et al. mA mRNA Demethylase FTO Regulates Melanoma Tumorigenicity and Response to Anti-PD-1 Blockade. *Nat Commun* (2019) 10(1):2782. doi: 10.1038/s41467-019-10669-0
29. Wang H, Hu X, Huang M, Liu J, Gu Y, Ma L, et al. Mettl3-Mediated mRNA mA Methylation Promotes Dendritic Cell Activation. *Nat Commun* (2019) 10 (1):1898. doi: 10.1038/s41467-019-09903-6
30. Chen Y-T, Shen J-Y, Chen D-P, Wu C-F, Guo R, Zhang P-P, et al. Identification of Cross-Talk Between mA and 5mc Regulators Associated With Onco-Immunogenic Features and Prognosis Across 33 Cancer Types. *J Hematol Oncol* (2020) 13(1):22. doi: 10.1186/s13045-020-00854-w
31. Wilkerson MD, Hayes DN. ConsensusClusterPlus: A Class Discovery Tool With Confidence Assessments and Item Tracking. *Bioinf (Oxford England)* (2010) 26(12):1572–3. doi: 10.1093/bioinformatics/btq170
32. Hänzelmann S, Castelo R, Guinney J. GSVA: Gene Set Variation Analysis for Microarray and RNA-Seq Data. *BMC Bioinf* (2013) 14:7. doi: 10.1186/1471-2105-14-7
33. Subramanian A, Tamayo P, Mootha VK, Mukherjee S, Ebert BL, Gillette MA, et al. Gene Set Enrichment Analysis: A Knowledge-Based Approach for Interpreting Genome-Wide Expression Profiles. In: *Proceedings of the National Academy of Sciences of the United States of America*, vol. 102. PNAS, USA (2005). p. 15545–50.
34. Mariathasan S, Turley SJ, Nickles D, Castiglioni A, Yuen K, Wang Y, et al. Tgfβ Attenuates Tumour Response to PD-L1 Blockade by Contributing to Exclusion of T Cells. *Nature* (2018) 554(7693):544–8. doi: 10.1038/nature25501
35. Yu G, Wang L-G, Han Y, He Q-Y. Clusterprofiler: An R Package for Comparing Biological Themes Among Gene Clusters. *OMICS* (2012) 16 (5):284–7. doi: 10.1089/omi.2011.0118
36. Jia Q, Wu W, Wang Y, Alexander PB, Sun C, Gong Z, et al. Local Mutational Diversity Drives Intratumoral Immune Heterogeneity in Non-Small Cell Lung Cancer. *Nat Commun* (2018) 9(1):5361. doi: 10.1038/s41467-018-07767-w
37. Charoentong P, Finotello F, Angelova M, Mayer C, Efremova M, Rieder D, et al. Pan-Cancer Immunogenomic Analyses Reveal Genotype-Immunophenotype Relationships and Predictors of Response to Checkpoint Blockade. *Cell Rep* (2017) 18(1):248–62. doi: 10.1016/j.celrep.2016.12.019
38. Jiang P, Gu S, Pan D, Fu J, Sahu A, Hu X, et al. Signatures of T Cell Dysfunction and Exclusion Predict Cancer Immunotherapy Response. *Nat Med* (2018) 24(10):1550–8. doi: 10.1038/s41591-018-0136-1

39. Yoshihara K, Shahmoradgoli M, Martínez E, Vegesna R, Kim H, Torres-Garcia W, et al. Inferring Tumour Purity and Stromal and Immune Cell Admixture From Expression Data. *Nat Commun* (2013) 4:2612. doi: 10.1038/ncomms3612
40. Mayakonda A, Lin D-C, Assenov Y, Plass C, Koeffler HP. Maftools: Efficient and Comprehensive Analysis of Somatic Variants in Cancer. *Genome Res* (2018) 28(11):1747–56. doi: 10.1101/gr.239244.118
41. Chen H, Chong W, Yang X, Zhang Y, Sang S, Li X, et al. Age-Related Mutational Signature Negatively Associated With Immune Activity and Survival Outcome in Triple-Negative Breast Cancer. *Oncoimmunology* (2020) 9(1):1788252. doi: 10.1080/2162402X.2020.1788252
42. Chen H, Chong W, Teng C, Yao Y, Wang X, Li X. The Immune Response-Related Mutational Signatures and Driver Genes in Non-Small-Cell Lung Cancer. *Cancer Sci* (2019) 110(8):2348–56. doi: 10.1111/cas.14113
43. Ritchie ME, Phipson B, Wu D, Hu Y, Law CW, Shi W, et al. Limma Powers Differential Expression Analyses for RNA-Sequencing and Microarray Studies. *Nucleic Acids Res* (2015) 43(7):e47. doi: 10.1093/nar/gkv007
44. Zeng D, Li M, Zhou R, Zhang J, Sun H, Shi M, et al. Tumor Microenvironment Characterization in Gastric Cancer Identifies Prognostic and Immunotherapeutically Relevant Gene Signatures. *Cancer Immunol Res* (2019) 7(5):737–50. doi: 10.1158/2326-6066.CIR-18-0436
45. Zhang B, Wu Q, Li B, Wang D, Wang L, Zhou YL. mA Regulator-Mediated Methylation Modification Patterns and Tumor Microenvironment Infiltration Characterization in Gastric Cancer. *Mol Cancer* (2020) 19(1):53. doi: 10.1186/s12943-020-01170-0
46. Turajlic S, Litchfield K, Xu H, Rosenthal R, McGranahan N, Reading JL, et al. Insertion-And-Deletion-Derived Tumour-Specific Neoantigens and the Immunogenic Phenotype: A Pan-Cancer Analysis. *Lancet Oncol* (2017) 18(8):1009–21. doi: 10.1016/S1470-2045(17)30516-8
47. Şenbabaoğlu Y, Gejman RS, Winer AG, Liu M, Van Allen EM, de Velasco G, et al. Tumor Immune Microenvironment Characterization in Clear Cell Renal Cell Carcinoma Identifies Prognostic and Immunotherapeutically Relevant Messenger RNA Signatures. *Genome Biol* (2016) 17(1):231. doi: 10.1186/s13059-016-1092-z
48. Riaz N, Havel JJ, Makarov V, Desrichard A, Urba WJ, Sims JS, et al. Tumor and Microenvironment Evolution During Immunotherapy With Nivolumab. *Cell* (2017) 171(4):934–49.e16. doi: 10.1016/j.cell.2017.09.028
49. Hugo W, Zaretsky JM, Sun L, Song C, Moreno BH, Hu-Lieskovan S, et al. Genomic and Transcriptomic Features of Response to Anti-PD-1 Therapy in Metastatic Melanoma. *Cell* (2016) 165(1):35–44. doi: 10.1016/j.cell.2016.02.065
50. Yang W, Soares J, Greninger P, Edelman EJ, Lightfoot H, Forbes S, et al. Genomics of Drug Sensitivity in Cancer (GDSC): A Resource for Therapeutic Biomarker Discovery in Cancer Cells. *Nucleic Acids Res* (2013) 41(Database issue):D955–61. doi: 10.1093/nar/gks1111
51. Geeleher P, Cox NJ, Huang RS. Clinical Drug Response can be Predicted Using Baseline Gene Expression Levels and *In Vitro* Drug Sensitivity in Cell Lines. *Genome Biol* (2014) 15(3):R47. doi: 10.1186/gb-2014-15-3-r47
52. Hazra A, Gogtay N. Biostatistics Series Module 3: Comparing Groups: Numerical Variables. *Indian J Dermatol* (2016) 61(3):251–60. doi: 10.4103/0019-5154.182416
53. Pfister DG, Spencer S, Adelstein D, Adkins D, Anzai Y, Brizel DM, et al. Head and Neck Cancers, Version 2.2020, NCCN Clinical Practice Guidelines in Oncology. *J Natl Compr Canc Netw* (2020) 18(7):873–98. doi: 10.6004/jnccn.2020.0031
54. Chinese Society of Clinical Oncology (CSCO) Diagnosis and Treatment Guidelines for Head and Neck Cancer 2018 (English Version). *Chin J Cancer Res* (2019) 31(1):84–98. doi: 10.21147/j.issn.1000-9604.2019.01.05
55. Kim JM, Chen DS. Immune Escape to PD-L1/PD-1 Blockade: Seven Steps to Success (or Failure). *Ann Oncol* (2016) 27(8):1492–504. doi: 10.1093/annonc/mdw217
56. Panagi M, Voutouri C, Mpekris F, Papageorgis P, Martin MR, Martin JD, et al. TGF-β Inhibition Combined With Cytotoxic Nanomedicine Normalizes Triple Negative Breast Cancer Microenvironment Towards Anti-Tumor Immunity. *Theranostics* (2020) 10(4):1910–22. doi: 10.7150/thno.36936
57. Tauriello DVF, Palomo-Ponce S, Stork D, Berenguer-Llergo A, Badia-Ramentol J, Iglesias M, et al. Tgfβ Drives Immune Evasion in Genetically Reconstituted Colon Cancer Metastasis. *Nature* (2018) 554(7693):538–43. doi: 10.1038/nature25492
58. Liu Y, Shi S-L. The Roles of hnRNP A2/B1 in RNA Biology and Disease. *Wiley Interdiscip Rev RNA* (2021) 12(2):e1612. doi: 10.1002/wrna.1612
59. Wang H, Liang L, Dong Q, Huan L, He J, Li B, et al. Long Noncoding RNA MiR503hg, a Prognostic Indicator, Inhibits Tumor Metastasis by Regulating the HNRNPA2B1/NF-κb Pathway in Hepatocellular Carcinoma. *Theranostics* (2018) 8(10):2814–29. doi: 10.7150/thno.23012
60. Zhang Y, Huang W, Yuan Y, Li J, Wu J, Yu J, et al. Long Non-Coding RNA H19 Promotes Colorectal Cancer Metastasis *via* Binding to Hnrnpa2b1. *J Exp Clin Cancer Res* (2020) 39(1):141. doi: 10.1186/s13046-020-01619-6
61. Meng L-D, Shi G-D, Ge W-L, Huang X-M, Chen Q, Yuan H, et al. Linc01232 Promotes the Metastasis of Pancreatic Cancer by Suppressing the Ubiquitin-Mediated Degradation of HNRNPA2B1 and Activating the A-Raf-Induced MAPK/ERK Signaling Pathway. *Cancer Lett* (2020) 494:107–20. doi: 10.1016/j.canlet.2020.08.001

Conflict of Interest: The authors declare that the research was conducted in the absence of any commercial or financial relationships that could be construed as a potential conflict of interest.

Publisher's Note: All claims expressed in this article are solely those of the authors and do not necessarily represent those of their affiliated organizations, or those of the publisher, the editors and the reviewers. Any product that may be evaluated in this article, or claim that may be made by its manufacturer, is not guaranteed or endorsed by the publisher.

frontiers in Oncology

ORIGINAL RESEARCH
published: 07 December 2021
doi: 10.3389/fonc.2021.774455

Predictive Value of a Combined Model Based on Pre-Treatment and Mid-Treatment MRI-Radiomics for Disease Progression or Death in Locally Advanced Nasopharyngeal Carcinoma

Le Kang[1,2,3†], Yulin Niu[4†], Rui Huang[1], Stefan (YUJIE) Lin[5], Qianlong Tang[1,3], Ailin Chen[1,3], Yixin Fan[1,3], Jinyi Lang[1], Gang Yin[1‡] and Peng Zhang[1*‡]*

[1] Department of Radiation Oncology, Sichuan Cancer Hospital & Institute, Sichuan Cancer Center, School of Medicine, University of Electronic Science and Technology of China, Radiation Oncology Key Laboratory of Sichuan Province, Chengdu, China, [2] Department of Hematology and Oncology, Anyue County People's Hospital, Ziyang, China, [3] Graduate School, Chengdu Medical College, Chengdu, China, [4] Department of Transplantation Surgery, The Affiliated Hospital of Guizhou Medical University, Guiyang, China, [5] University of Southern California, Viterbi School of Engineering Applied Data Science, Los Angeles, CA, United States

Purpose: A combined model was established based on the MRI-radiomics of pre- and mid-treatment to assess the risk of disease progression or death in locally advanced nasopharyngeal carcinoma.

Materials and Methods: A total of 243 patients were analyzed. We extracted 10,400 radiomics features from the primary nasopharyngeal tumors and largest metastatic lymph nodes on the axial contrast-enhanced T1 weighted and T2 weighted in pre- and mid-treatment MRI, respectively. We used the SMOTE algorithm, center and scale and box-cox, Pearson correlation coefficient, and LASSO regression to construct the pre- and mid-treatment MRI-radiomics prediction model, respectively, and the risk scores named P score and M score were calculated. Finally, univariate and multivariate analyses were used for P score, M score, and clinical data to build the combined model and grouped the patients into two risk levels, namely, high and low.

Result: A combined model of pre- and mid-treatment MRI-radiomics successfully categorized patients into high- and low-risk groups. The log-rank test showed that the high- and low-risk groups had good prognostic performance in PFS (P<0.0001, HR: 19.71, 95% CI: 12.77–30.41), which was better than TNM stage (P=0.004, HR:1.913, 95% CI:1.250–2.926), and also had an excellent predictive effect in LRFS, DMFS, and OS.

Conclusion: Risk grouping of LA-NPC using a combined model of pre- and mid-treatment MRI-radiomics can better predict disease progression or death.

Keywords: radiomics, nasopharyngeal carcinoma, prognosis, prediction model, magnetic resonance imaging

OPEN ACCESS

Edited by:
Heming Lu,
People's Hospital of Guangxi Zhuang Autonomous Region, China

Reviewed by:
Wenbing Lv,
Southern Medical University, China
Youping Xiao,
Fujian Provincial Cancer Hospital, China

***Correspondence:**
Peng Zhang
izhangpeng@163.com
Gang Yin
cxqyguestc@163.com

[†]These authors have contributed equally to this work and share first authorship

[‡]These authors have contributed equally to this work and share corresponding authorship

Specialty section:
This article was submitted to Head and Neck Cancer, a section of the journal Frontiers in Oncology

Received: *12 September 2021*
Accepted: *04 November 2021*
Published: *07 December 2021*

Citation:
Kang L, Niu Y, Huang R, Lin S(YUJIE), Tang Q, Chen A, Fan Y, Lang J, Yin G and Zhang P (2021) Predictive Value of a Combined Model Based on Pre-Treatment and Mid-Treatment MRI-Radiomics for Disease Progression or Death in Locally Advanced Nasopharyngeal Carcinoma. Front. Oncol. 11:774455. doi: 10.3389/fonc.2021.774455

INTRODUCTION

Nasopharyngeal carcinoma (NPC) is epithelial carcinoma originating from the inner layer of the nasopharyngeal mucosa. In 2018, there were 129,000 new cases of NPC in the world (1). The TNM stage system is widely used in risk stratification and therapeutic decision in NPC, and about 70% are diagnosed with locally advanced stage (2). Concurrent chemoradiotherapy with or without induction chemotherapy is the standard treatment with locally advanced nasopharyngeal carcinoma (LA-NPC). However, it is worth noting that there are still significant differences in clinical outcomes among the same TNM stage and similar treatment in LA-NPC; metastasis and recurrence, especially the former, are the considerable causes of treatment failure (3). The 5-year progression-free survival (PFS) for stage III and IVa in NPC were 68.7–87% and 50.4–68%, and the 5-year overall survival (OS) were 75.5–91.4% and 58.3–75%, respectively (4–6). Therefore, developing individualized methods to predict the effect in LA-NPC is necessary.

Radiomics is an algorithm that could automatically extract high-dimensional quantitative features from medical images. These features are extracted from the whole tumor in different ways. They can provide comprehensive information about tumor phenotype, tumor microenvironment, and response to treatment to characterize tumor heterogeneity (7, 8). Magnetic resonance imaging (MRI) was the preferred imaging modality for diagnosis and local stage of NPC (9). Previous studies had shown that MRI-radiomics is an independent risk factor for distant metastasis, local recurrence, and PFS in NPC (10–12). Most of these studies focus on primary tumors of the nasopharynx. A recent study showed that primary tumors and metastatic lymph nodes have different biological characteristics (13). Therefore, it is necessary to consider adding metastatic lymph node information to radiomics based on primary nasopharyngeal tumors.

Due to individualized differences, different NPCs have different responses to chemoradiotherapy, leading to differences in tumor cell populations (i.e., differences in tumor heterogeneity). Currently, there is no literature report on constructing an MRI-radiomics model during chemoradiotherapy to predict LA-NPC. This study aims to screen features associated with PFS labeling in pre- and mid-treatment MRI-radiomics, respectively, to construct a model to predict disease progression or death in LA-NPC (stage III–IVa).

MATERIAL AND METHOD

Patient

This retrospective study was approved by the institutional review board of our institution. Informed consent from patients was exempted due to the retrospective nature of this study. The experiment included newly diagnosed LA-NPC (stage III-IVa) in Sichuan Cancer Hospital from January 2015 to December 2016. The inclusion criteria were as follows: (1) histologically confirmed LA-NPC (restage according to AJCC 8th edition) and at least one metastatic lymph node. Previous studies associated with head and neck cancer have shown that the radiomics features of increasing the region of interest (ROI) of the lymph nodes provide a better predictive power than those from primary tumors alone (14, 15). According to the definition of Ho et al. (16), the diagnostic criteria of N + include central necrosis, extracapsular spread, the shortest diameter of cervical lymph nodes >10 mm, and the shortest diameter of retropharyngeal lymph nodes >5 mm. (2) pre- and mid-treatment (20 times of radiotherapy) MRI examination of nasopharynx and neck, MRI sequence included axial contrast-enhanced T1 weighted imaging (CET1WI), and axial T2 weighted imaging (T2WI); (3) radical chemoradiotherapy were completed; (4) have available clinical data. The exclusion criteria were (1) motion artifacts, blurring, and in-continuity in MRI images; (2) history of anticancer therapy before baseline MRI scans, such as radiotherapy, chemotherapy, immunotherapy, and surgery; (3) patients with distant metastasis; (4) recurrence or complicated with other malignant tumors; (5) incomplete radiotherapy planning records. Finally, a total of 243 patients were included in further analysis.

Pre-treatment clinical characteristics were collected through the Health Information System (HIS) of Sichuan Cancer Hospital. The characteristics include age, sex, cigarette smoking, alcohol consumption, family history, WHO type, platelet count (PLT), neutrophil count, lymphocyte count, monocyte count, platelet-to-lymphocyte ratio (PLR), neutrophil-to-lymphocyte ratio (NLR), lymphocyte-to-monocyte ratio (LMR), hemoglobin (HB), C-reactive protein (CRP), alanine aminotransferase (ALT), aspartate aminotransferase (AST), lactate dehydrogenase (LDH), alkaline phosphatase (ALP), serum albumin, cumulative dose of radiotherapy, image-guided radiotherapy (IGRT), TNM stage, induction chemotherapy, targeted therapy.

Treatment

The treatment regimen was concurrent chemoradiotherapy ± induction chemotherapy. The chemotherapy regimen was platinum-based single or dual drug (cisplatin ± paclitaxel), beginning on the first day of radiotherapy. Gross tumor volume (GTV), included both primary nasopharyngeal tumor (GTVnx) and metastatic lymph nodes (GTVln) as demonstrated by clinical, endoscopic, and imaging data. All ROI segmentations were firstly manually performed by a radiation oncologist who had 3 years of experience in NPC radiotherapy and then validated by a senior radiation oncologist who had 10 years of experience. GTV was planned to receive a total dose of 66–76 Gy with conventional fractionation (2.1–2.25 Gy per fraction, five fractions per week). Some patients were treated with anti-EGFR monoclonal antibodies during radiotherapy simultaneously. Nasopharynx and neck MRI were reexamined at 20 times of radiotherapy.

Follow-Up and Survival Endpoint

MRI scan showed soft tissue swelling or space-occupying and then by histopathology to determine local recurrence. Distant metastasis was diagnosed synthetically by clinical symptoms,

physical examination, imaging data, and histopathology. The main endpoint was PFS, while loco-recurrence-free survival (LRFS), distant metastasis-free survival (DMFS), and OS were secondary endpoints. PFS was defined as the time during the tumor progressing (for any aspect) or at death (for any reason) and the first MRI scan. LRFS was defined as the time between the first local recurrence and the first MRI scan. DMFS was defined as the time between the first distant metastasis and the first MRI scan. OS was defined as the time between the death of any cause and the first MRI scan.

MRI Check

The MRI equipment was Siemens Magnetom Avanto-1.5T/ Magnetom Skyra-3T. Some scanning parameters were as follows: T2WI sequence of Magnetom Avanto-1.5T scan was repetition time (TR): 4,890 ms; echo time (TE): 80 ms; field of view (FOV): 340×340 mm; matrix: 320×320 mm; thickness: 3 mm; gap: 3.6 mm. CET1WI sequence was TR: 695 ms; TE: 12 ms; FOV: 300×320; matrix: 320×280; thickness: 3 mm; gap: 3.6 mm. T2WI sequence of Magnetom Skyra-3T scan was TR: 5,290 ms; TE: 85 ms; FOV: 340×340 mm; matrix: 320×320 mm; thickness: 3 mm; gap: 3.6 mm. CET1WI sequence was TR: 769 ms; TE: 12 ms; FOV: 300×320 mm; matrix: 320×280; thickness: 3 mm; gap: 3.6 mm. CET1WI was treated with gadolinium meglumine at a dose of 0.2 mmol/kg.

Image Acquisition and Segmentation

The MRI image was exported through PACS and saved in DICOM format. The saved image was then imported into the MIM planning system for ROI drawing. To ensure the accuracy of the sketch, we used manual segmentation to outline the masses on the CET1WI and T2WI sequence of the primary nasopharyngeal tumor and metastatic lymph nodes in pre- and mid-treatment (as shown in **Figure 1**). The resulting 3D mass area was ROI. In this study, the metastatic lymph nodes with the largest short diameter were selected as the target lesions for GTVln, which is consistent with the study of Bologna (17).

Image Preprocessing

The uAI Research Portal (Version: 430 sp1) was used to image preprocessing. We processed the image by several filters, including Box Mean, Additive Gaussian Noise, Binomial Blur, Curvature Flow, Box Sigma, Laplacian of Gaussian (LoG), Wavelet, Normalize, Laplacian Sharpening, Discrete Gaussian, Mean, Speckle Noise, Recursive Gaussian, Shot Noise/Poisson Noise filter. In our study, four different LoG filtered images were obtained through different combinations. After three times of wavelet decomposition, the wavelet images of eight various frequency bands were finally obtained, and normalize filter adjusted all MRI images to 255 gray levels in order to standardize the scanning parameters and machinery differences reflected on the images.

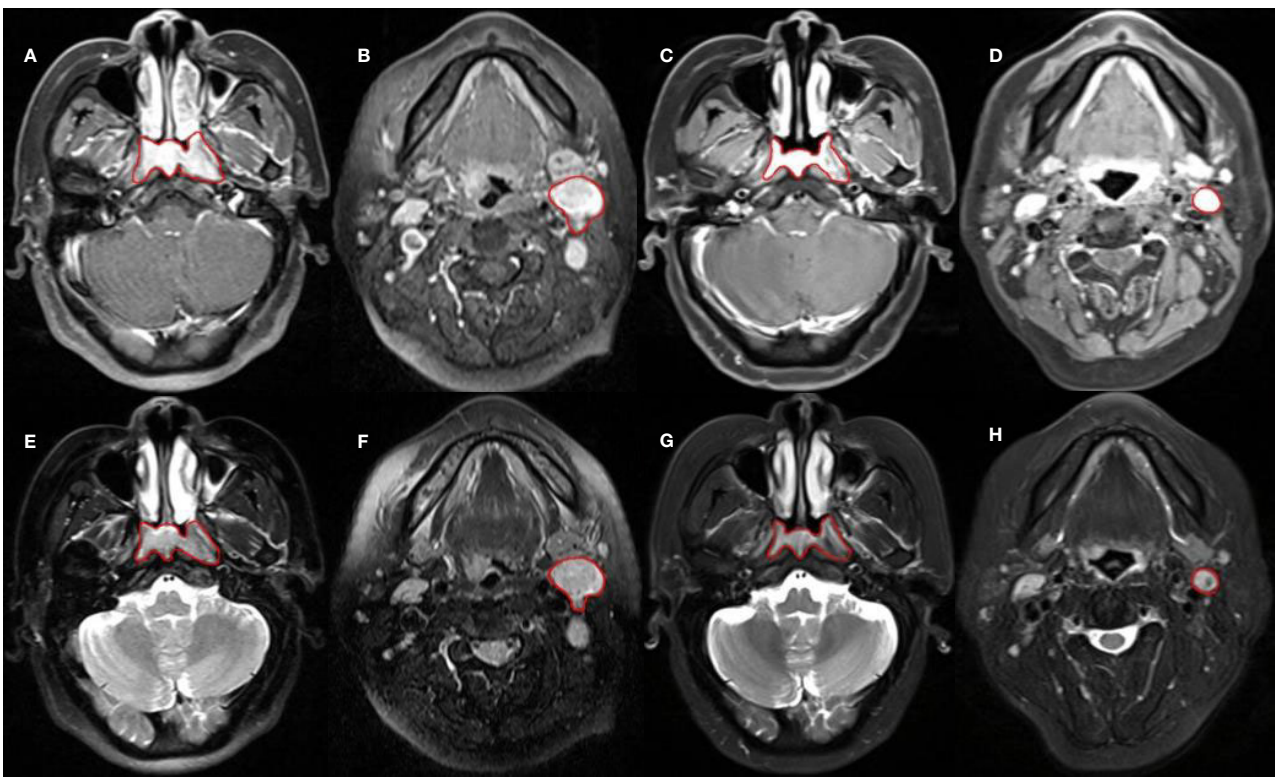

FIGURE 1 | Sketch of ROI. **(A–D)** are CET1WI sequences; from left to right, they are GTVnx and GTVln in pre-treatment, GTVnx and GTVln in mid-treatment. **(E–H)** are T2WI sequences; from left to right, they are GTVnx and GTVln in pre-treatment, GTVnx and GTVln in mid-treatment.

Radiomics Feature Extraction

The uAI Research Portal was also used for feature extraction. Features of different categories were considered: 14 shape features, 18 first-order statistics features, 21 features computed on gray level co-occurrence matrix (GLCM), 16 features computed on gray level run-length matrix (GLRLM), 16 features computed on gray level size zone matrix (GLSZM), 14 features computed on gray level dependence matrix (GLDM), and 5 features computed on gray level dependence matrix (GLDM), a total of 104 radiomics features. The original and filtered image generated 25 groups, so each ROI extracted a total of 2,600 features. Finally, from each image type (CET1WI or T2WI), 2,600 radiomics features were extracted from both the primary tumors and the largest affected lymph node on pre- and mid-treatment, for a total of 20,800 features, namely, 10,400 for pre- and mid-treatment, respectively. Excel S1 and S2 of **Supplementary Materials** shown the all radiomics feature in pre- and mid-treatment.

Radiomics Feature Selection, Model Building, and Validation

To avoid the influence of class imbalance (85 cases of progress/death *vs* 158 cases of disease-free survival) on the model building, we used a SMOTE algorithm to oversample the original dataset of pre- and mid-treatment, respectively. After amplification, the dataset was randomly divided into a training dataset (476/595) and a test dataset (119/595) according to 4:1. The model building was based on the training dataset, after being preprocessed by center and scale and Box-cox; the feature with no difference between categories was removed. The Pearson correlation coefficient was used to remove redundant features. LASSO regression was used for a further selection of the remaining features, which is consistent with most previous studies (10–12, 18, 19). Then, 20 MRI-radiomics that were most closely related to PFS tags were selected, and the importance of features in the model was sorted. Finally, we selected the top five features respectively to create a radiomics model of pre- and mid-treatment. At the same time, the prediction ability of the model was tested in the training, test, and original dataset by ROC curve and confusion matrix. Eventually, we received the radiomics risk score of pre-treatment named P score and mid-treatment named M score.

Final Model Development and Risk Stratification

The clinical information, P score, and M score were analyzed by Cox univariate analysis, and we selected the variables with $P < 0.05$ (bilateral test) to Cox multivariate analysis. According to the results of multiple factors, we chose the variables with $P < 0.05$ (bilateral test) to train a multivariate Cox proportional hazard regression model, and the predicted values of linear predictive variables of PFS were obtained. The higher the predictive value, the greater the risk of progress/death. The median of the predictive value was used as the threshold for risk stratification. Finally, we compared the Kaplan-Meier survival curves between different risk groups and TNM stages at different clinical endpoints.

Statistical Analysis

All statistical analyses were conducted using SPSS (version 26.0), GraphPad Prism (version 8), and R software (version 3.5.2). LASSO logistic regression was completed by the "glment" package. The Kaplan–Meier survival analyses were presented by GraphPad Prism. $P < 0.05$ was considered as statistically significant.

RESULT

A total of 243 patients were included for the final analysis. The median follow-up period was 52.7 months (range 10.6–72 months). The specific clinical data were shown in **Table 1**.

Establishment and Validation of Pre-Treatment MRI-Radiomics Prediction Model

In the pre-treatment prediction model, there were 243 samples in the original dataset, which were expanded to 595 samples by SMOTE algorithm. After randomly grouping according to 4:1, there were 476 samples in the training dataset and 119 samples in the test dataset. Top five of 20 radiomics features were selected, including three from primary nasopharynx tumors and two from metastatic lymph nodes. **Supplementary Figure S1** shown the 20 radiomics feature in pre-treatment. Then the pre-treatment radiomics model to predict PFS in LA-NPC was established by logistic regression. The AUC value of the pre-treatment prediction model in the training dataset was 0.8003 (95% CI:0.7613–0.8392). The average AUC value of five times 10-fold cross-validation in the training dataset was 0.7905 (95% CI: 0.7506–0.8304). The AUC value in the original dataset was 0.773 (95% CI: 0.7126–0.8334). The AUC value in the test dataset was 0.8527 (95% CI: 0.7843–0.921). The ROC curve was shown in **Figure 2**.

The results of the confusion matrix (**Figure 3**) of the three datasets (training dataset, original dataset, and test dataset) in this study were as follows: the accuracy, precision, sensitivity, specificity, and F1 values of the training dataset were 0.725, 0.704, 0.618, 0.805, and 0.658, respectively. In the original dataset, they were 0.728, 0.614, 0.600, 0.797, and 0.607, respectively. In the test dataset, they were 0.790, 0.795, 0.686, 0.868 0.737, respectively. Finally, according to the weighted coefficient of logistic regression analysis, we obtained a formula for calculating the risk value of each LA-NPC patient:

$$\begin{aligned}\text{Logit(P score)} = &-0.5747\\ &+ 0.7722 * \text{normalize\_firstorder\_Mean\_PGTVlnT1}\\ &+1.0464 * \text{boxmean\_glcm\_ClusterShade\_PGTVnxT1}\\ &+0.9113 * \text{Log\_firstorder\_Log}-\text{sigma}-2-\text{mm}-3\text{D}-\\ &\text{Maximum\_PGTVlnT1}\\ &+0.6325 * \text{normalize\_gldm\_DependenceVariance\_}\\ &\text{PGTVnxT2}\\ &+0.7434 * \text{wavelet\_glszm\_wavelet}-\text{HHH}-\\ &\text{SmallAreaEmphasis\_PGTVnxT2}\end{aligned}$$

TABLE 1 | Clinical baseline data of the subjects (N=243).

Clinical features	Percentage/mean ± SD/median (interquartile range)
Age (years)	49.28 ± 10.678
Sex (N/%)	
Male	75.3% (183/243)
Female	24.7% (60/243)
Cigarette smoking (N/%)	
No	53.1% (129/243)
Yes	46.9% (114/243)
Alcohol consumption (N/%)	
No	77.4% (188/243)
Yes	22.6% (55/243)
Family history of cancer (N/%)	
No	93.8% (228/243)
Yes	6.2% (15/243)
WHO histological type (N/%)	
Type I	0.8% (2/243)
Type II	99.2% (241/243)
Neutrophil count (10^9/L)	3.96 (3.08–4.85)
Lymphocyte count (10^9/L)	1.51 (1.22–1.93)
Monocyte count (10^9/L)	0.36 (0.27–0.45)
PLT (10^9/L)	195 (161–244)
HB (g/L)	140 (130–150)
NLR	2.48 (1.95–3.55)
PLR	131.5 (101.4–164.6)
LMR	4.39 (3.25–5.84)
CRP (mg/L)	3.55 (2.28–5.33)
ALT (U/L)	24 (16–34)
AST (U/L)	23 (19–28)
Albumin (g/L)	43.2 (41.4–45.2)
LDH (U/L)	178 (153-205)
ALP (U/L)	82 (69-99)
T stage	
T1	4.1% (10/243)
T2	34.2% (83/243)
T3	29.6% (72/243)
T4	32.1% (78/243)
N stage	
N1	11.1% (27/243)
N2	63.8% (155/243)
N3	25.1% (61/243)
TNM stage	
III	47.7% (116/243)
IVa	52.3% (127/243)
induction chemotherapy	
No	39.1% (95/243)
Yes	60.9% (148/243)
IGRT	
No	16.9% (41/243)
Yes	83.1% (202/243)
Targeted therapy	
No	92.2% (224/243)
Yes	7.8% (19/243)
Cumulative radiation dose (Gy)	44.60 ± 1.11
Clinical endpoints	
None	65.4% (159/243)
Recurrence	14.0% (34/243)
Distant metastasis	18.9% (46/243)
Recurrence and distant metastasis	3.7% (9/243)
Death	21.8% (53/243)

Establishment and Validation of Mid-Treatment MRI-Radiomics Prediction Model

In the mid-treatment prediction model, the original dataset after oversampling and grouping showed 476 samples in the training dataset and 119 samples in the test dataset. Five radiomics features were selected, including three from primary nasopharyngeal tumor and two from metastatic lymph nodes. **Supplementary Figure S2** shown the 20 radiomics feature in mid-treatment.

Then the mid-treatment radiomics model to predict PFS in LA-NPC was established by logistic regression. The AUC value of this model in the training dataset was 0.9253 (95% CI: 0.9025–0.9482). The average AUC value of five times 10-fold cross-validation in the training dataset was 0.9205 (95% CI: 0.8967–0.9442), and the AUC value in the original dataset was 0.8884 (95% CI: 0.8467–0.93). The AUC value in the test dataset was 0.8849 (95% CI: 0.8286–0.9413) (**Figure 4**).

The results of the confusion matrix (**Figure 5**) of the three datasets (training dataset, original dataset, and test dataset) in this study were as follows: the accuracy, precision, sensitivity, specificity and F1 values in the training dataset were 0.851, 0.867, 0.770, 0.912, 0.816, respectively; in the original dataset, they were 0.798, 0.714, 0.706, 0.848, 0.710, respectively; and in the test dataset were 0.773, 0.740, 0.725, 0.809, 0.733, respectively.

Finally, according to the weighted coefficient of logistic regression analysis, we obtained a formula for calculating the risk value of each LA-NPC patient:

$$\begin{aligned}\text{Logit (M score)} = {} & -0.9557 \\ & - 1.5915 * \text{shotnoise\_shape\_SurfaceVolumeRatio\_MGTVnxT1} \\ & -0.2544 * \text{wavelet\_gldm\_wavelet} - \text{HLH} - \\ & \quad \text{LargeDependenceHighGrayLevelEmphasis\_MGTVlnT1} \\ & -0.5678 * \text{wavelet\_firstorder\_wavelet} - \text{LHL} - \text{Mean\_MGTVnxT1} \\ & -0.9758 * \text{normalize\_glszm\_HighGrayLevelZoneEmphasis\_MGTVlnT1} \\ & +1.3875 * \text{normalize\_gldm\_LargeDependenceLowGrayLevelEmphasis} \\ & \text{\_MGTVnxT1}\end{aligned}$$

Final Model Development and Risk Stratification

In univariate Cox analysis, age, alkaline phosphatase, T stage, TNM stage, P score, M score were significantly correlated with PFS. Subsequent multivariate Cox analysis showed that P score (HR: 13.515, 95% CI: 5.185–35.230) and M score (HR: 17.604, 95% CI: 8.113–38.195) were independent risk factors for PFS, as shown in **Table 2**.

We put P score and M score into multivariate Cox regression model, and the predicted values of PFS linear predictive variables were obtained. The median predicted value was used as a threshold to classify high- and low-risk patients. In terms of prognostic power for PFS, the high- and low-risk groups (P<0.0001, HR: 19.17, 95% CI: 12.77–30.41) was significantly prognostic than TNM stage (P=0.004, HR: 1.913, 95% CI: 1.250–2.926). Similar results could be found by looking at the Kaplan-Meier curves for LRFS, DMFS, OS of the high-/low-risk groups and TNM stage, for as far as LRFS is concerned, the log-rank test showed P < 0.0001 (HR: 44.61, 95%

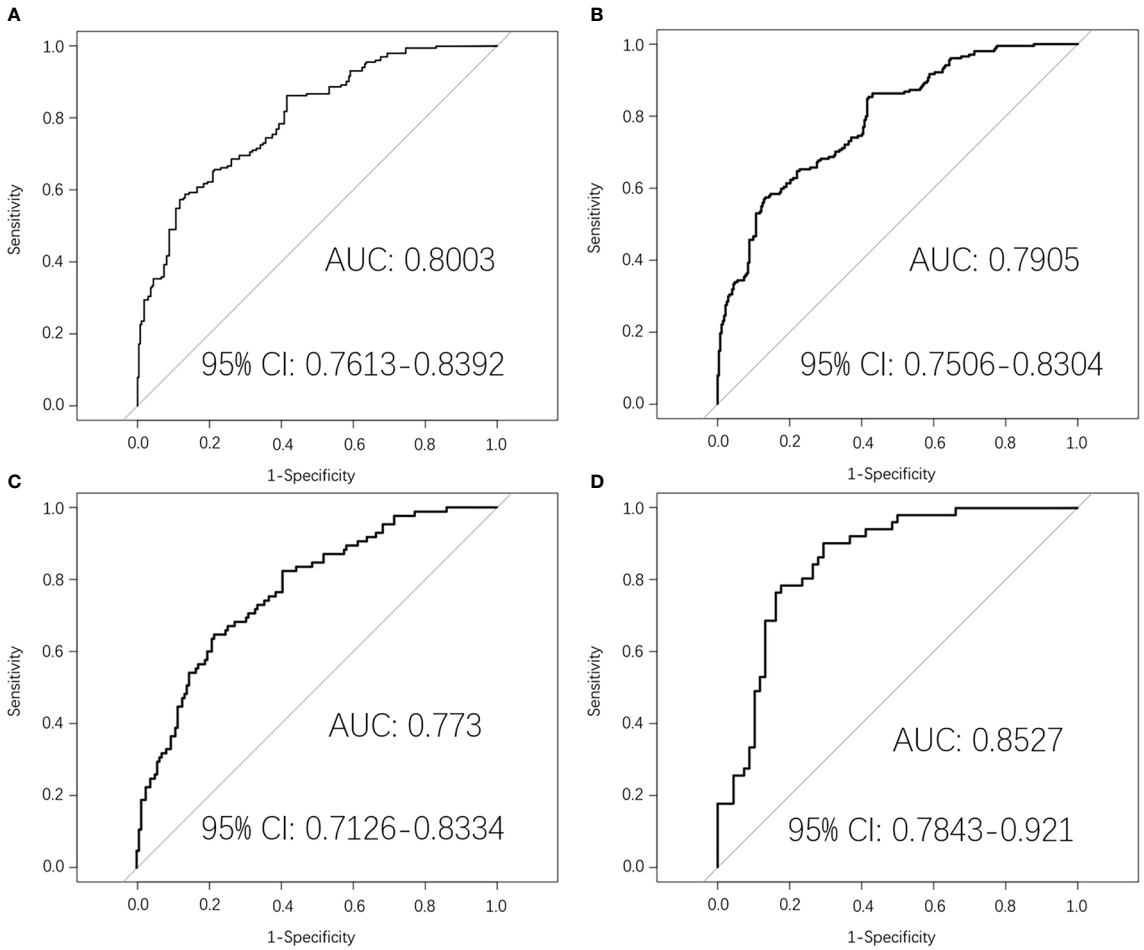

FIGURE 2 | Pre-treatment MRI-radiomics model in each dataset predicted the ROC curves of the PFS in LA-NPC. **(A)** shows the ROC curve of the MRI-radiomics model in the training dataset of pre-treatment, and **(B)** shows the average ROC curve of 10-fold cross-validation of the MRI-radiomics model in the training dataset. **(C, D)** represent the ROC curve of the MRI-radiomics model in the original dataset and test dataset, respectively.

CI: 22.60–88.05), P=0.6270 (HR: 0.8464, 95% CI: 0.4321–1.658), respectively; for DMFS concerned, P < 0.0001 (HR: 14.11, 95% CI: 7.864–25.30) and P=0.0788 (HR: 1.700, 95% CI: 0.9536–3.030), respectively; for OS concerned, P < 0.0001 (HR: 20.18, 95% CI: 11.75–34.66), P=0.0016 (HR: 2.532, 95% CI: 1.478–4.339), respectively (**Figure 6**).

DISCUSSION

In recent years, radiomics has developed rapidly in medicine, and good results have been achieved in predicting the effect of tumors. MRI is a standard imaging method in NPC, and it has unique advantages. First of all, MRI can provide superior anatomical information (such as spatial location) and has good soft tissue contrast-detection ability. Secondly, different MRI sequences may be sensitive to critical components of tumor physiology, such as blood flow and cell density, and MRI also can distinguish regions in the tumor that contain different environments that may affect local cell phenotypes and genotypes, such as blood flow changes. Finally, MRI can be the non-invasive and repeated examination of the tumor to evaluate the treatment response to be integrated into the treatment strategy. So, the MRI image was used to establish the LA-NPC prediction model through radiomics. This study explored the value of MRI-radiomics features on pre- and mid-treatment in predicting effect in LA-NPC. The results showed that the M score and P score were independent prognostic indexes of PFS. Finally, we put them into the multivariate Cox model to calculate the risk score. We successfully stratified the risk of the LA-NPC. Through the Log-rank test, we found that MRI-radiomics showed good predictive ability in PFS, LRFS, DMFS, and OS.

By screening the pre-treatment MRI-radiomics features, we got 20 radiomics features related to PFS in LA-NPC. It is better to consider that the ratio between the amount of data and the number of features that can be accommodated by logistic regression is more

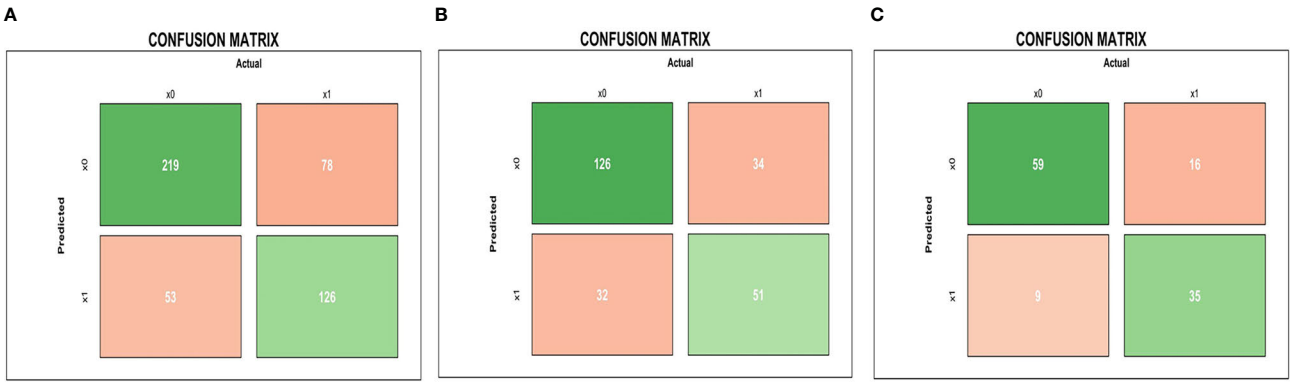

FIGURE 3 | Pre-treatment MRI-radiomics model in each dataset predicted the confusion matrix of PFS in LA-NPC. **(A–C)** represent the confusion matrix of the MRI-radiomics model of pre-treatment in the training dataset, the original dataset, and the test dataset, respectively.

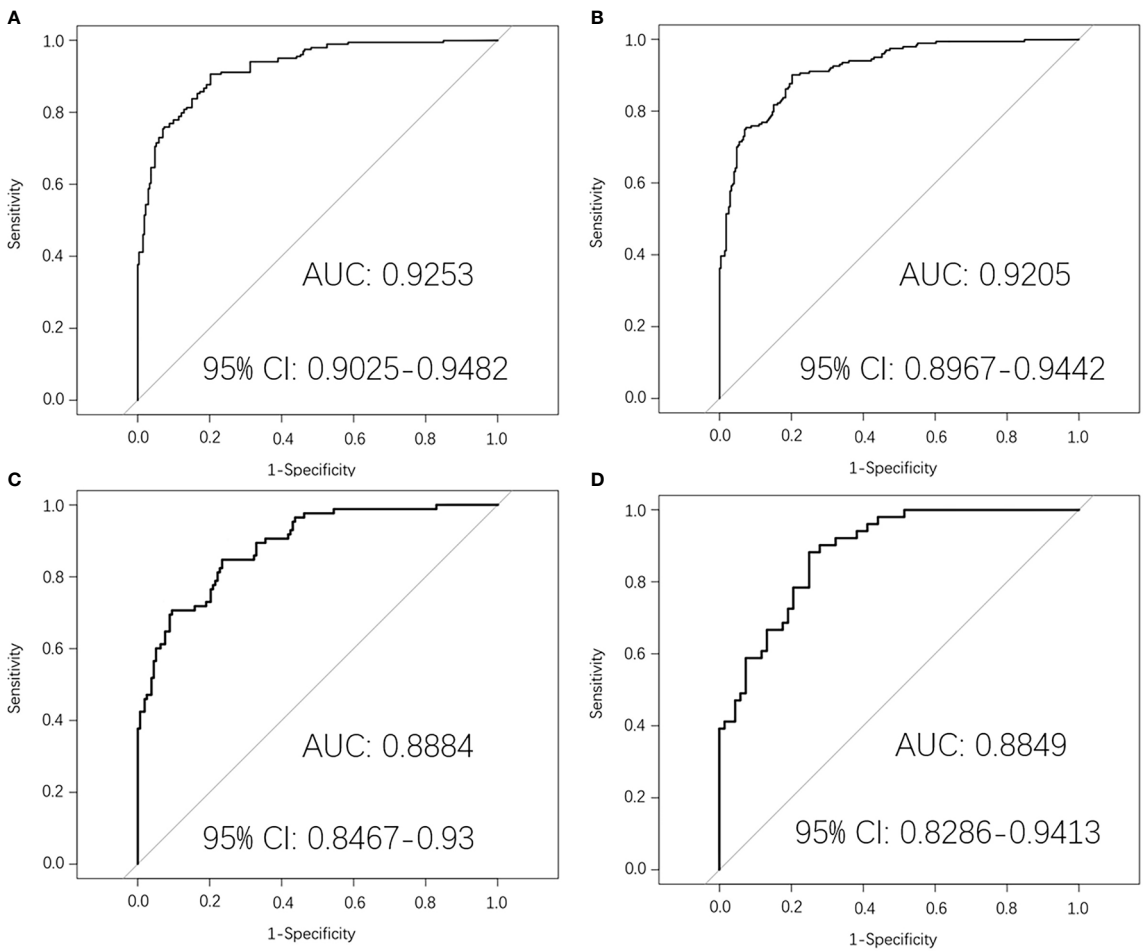

FIGURE 4 | Mid-treatment MRI-radiomics model in each dataset predicted the ROC curves of the PFS in LA-NPC. **(A)** shows the ROC curve of the MRI-radiomics model in the training dataset of mid-treatment, and **(B)** shows the average ROC curve of 10-fold cross-validation of the MRI-radiomics model in the training dataset. **(C, D)** represent the ROC curve of the MRI-radiomics model in the original dataset and test dataset, respectively.

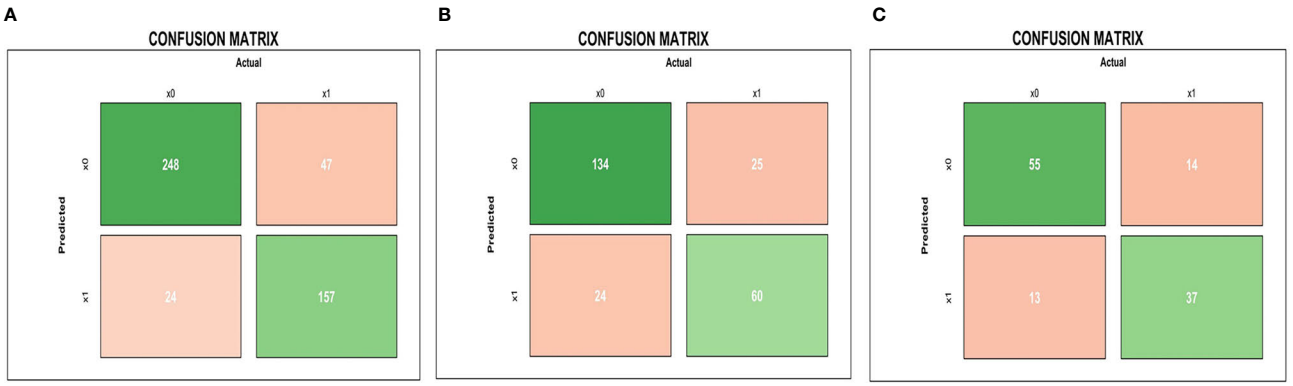

FIGURE 5 | Mid-treatment MRI-radiomics model in each dataset predicted the confusion matrix of PFS in LA-NPC. **(A–C)** represent the confusion matrix of the MRI-radiomics model of mid-treatment in the training dataset, the original dataset, and the test dataset, respectively.

than 20:1 (20). We selected the top five features to establish a pre-treatment prediction model, and the risk score named P score was calculated (21). In previous studies, an MRI-based model on primary nasopharyngeal tumors had been proved to be a significant prognostic biomarker for PFS in LA-NPC (22, 23). Furthermore, the research by Yang et al. indicated that an MRI-based model on metastatic lymph nodes is a significant risk factor for PFS in LA-NPC (24). Thus, MRI-radiomics features from both metastatic lymph nodes and primary nasopharynx tumors contribute to PFS prediction in LA-NPC, which is consistent with our research. As far as we know, there is no related research on the radiomics features of mid-treatment. Similarly, we calculated the risk score of mid-treatment named M score. The MRI-radiomics model of pre- and mid-treatment was internally validated by 10-fold cross-validation in the training dataset. The average AUC values were 0.7905 (95% CI: 0.7506–0.8304) and 0.9205 (95% CI: 0.8967–0.9442), respectively, which indicates that the model has good repeatability. In addition, the two models have high AUC values in both original and test datasets (**Figures 2**, **4**), which shows that the model has good generalization ability and portability. Furthermore, the performance of the two models in the confusion matrix in different datasets (**Figures 3**, **5**) is also outstanding.

Comparing the radiomics features included in the two models, the pre-treatment prediction model had two first-order features (average eigenvalues and maximum eigenvalues) and three texture features (GLCM, GLDM, GLSZM); the mid-treatment prediction model had one shape feature (surface area/volume ratio), one first-order feature (average eigenvalue), and three texture features (GLDM, GLSZM). The shape features reflect the volume, sphere, surface area/volume ratio of the tumor. Previous studies had found that primary tumor volume is closely related to local control, distant metastasis, and OS in NPC (25). Zhang et al. worked on the development and validation of an MRI-based model (including surface area/volume ratio) for predicting distant metastasis of NPC. The model has good evaluation ability in the validation cohort (C index: 0.74, 95% CI: 0.58–0.85) (11). First-order statistical features are the simplest statistical descriptors, including gray average, maximum, minimum, variance, percentile, etc. (24). GLCM can reveal the spatial complexity of tumors and may provide information about central necrosis or tumor metastasis-dependent factors, such as yes-related proteins (13). Several studies had shown that GLCM is closely related to the recurrence, metastasis, and OS of NPC (10–12, 17, 18, 24, 26). Zhang et al. demonstrated that GLSZM is associated with the risk of distant metastasis of NPC (10). Farhan et al. found significant differences between recurrent and non-recurrent regions in seven features (including GLSZM) in the radiomics analysis of intratumoral spatial heterogeneity in LA-NPC (19). GLDM quantifies the dependence between the gray values of adjacent pixels and the gray values of central pixels within a certain distance, and its predictive value in NPC had been confirmed by Zhang et al. (10).

We also found that three of the features in the pre-treatment prediction model came from CET1WI, and two were from T2WI, while all the features of the mid-treatment prediction model came from CET1WI. By comparing the accuracy, precision, sensitivity, specificity, F1 value, and AUC value of the two models, we noticed that the mid-treatment prediction model is better than the pre-treatment in training and original dataset, which may indicate that T2WI mainly reflects the density and boundary of the tumor. However, CET1WI reflects the heterogeneity and structure within the tumor (such as tumor angiogenesis) (27), which is crucial for judging the prognosis. Zhang et al. also found that the contribution of CET1WI to the model is more significant than that of T2WI (11), which is consistent with the results of their another study (the radiomics prediction based on CET1WI sequence is better than T2WI sequence or combined with CET1WI and T2W sequence) (28). Jiang et al. also proposed that using CET1WI to build a model produces better results than T2WI (29).

The features' inconsistency between pre- and mid-treatment prediction model is attributed to LASSO regression. In the screening radiomics features, LASSO regression will compress some relatively unimportant features, adjust the coefficients to zero for insignificant parameters, and rank the importance of

TABLE 2 | Identification of risk factors of PFS by univariate and multivariate Cox models.

	Univariate Cox regression		Multivariate Cox regression	
	HR (95% CI)	**Pvalue**	**HR (95% CI)**	**Pvalue**
Age (years)	1.028 (1.007–1.050)	0.008	1.011 (0.990–1.033)	0.295
Sex (Female *vs* Male)	1.530 (0.876–2.672)	0.135	–	–
Cigarette smoking (No *vs* Yes)	1.026 (0.671–1.571)	0.905	–	–
Alcohol consumption (No *vs* Yes)	1.282 (0.794–2.069)	0.309	–	–
Family history (No *vs* Yes)	1.747 (0.843–3.621)	0.133	–	–
WHO type (I *vs* II type)	20.421 (0.002–243908)	0.529	–	–
Neutrophil count (10^9/L)	0.957 (0.818–1.119)	0.582	–	–
Lymphocyte count (10^9/L)	1.144 (0.849–1.541)	0.377	–	–
Monocyte count (10^9/L)	0.847 (0.430–1.669)	0.631	–	–
PLT (10^9/L)	1.000 (0.996–1.003)	0.790	–	–
HB (g/L)	1.001 (0.989–1.014)	0.837	–	–
NLR	0.970 (0.856–1.099)	0.632	–	–
PLR	0.999 (0.996–1.002)	0.431	–	–
LMR	1.001 (0.984–1.019)	0.871	–	–
CRP (mg/L)	1.015 (0.988–1.042)	0.277	–	–
ALT (U/L)	0.998 (0.990–1.006)	0.638	–	–
AST (U/L)	0.994 (0.975–1.014)	0.556	–	–
Albumin (g/L)	1.004 (0.999–1.010)	0.134	–	–
LDH (U/L)	1.000 (0.996–1.003)	0.787	–	–
ALP (U/L)	1.004 (1.000–1.008)	0.034	1.005 (0.999–1.011)	0.102
T stage	1.349 (1.056–1.723)	0.016	0.946 (0.687–1.303)	0.734
N stage	1.411 (0.978–2.035)	0.066	–	–
TNM stage (III *vs* IVa)	1.915 (1.223–3.000)	0.005	0.697 (0.397–1.225)	0.210
IC (No *vs* Yes)	0.861 (0.554–1.340)	0.507	–	–
IGRT (No *vs* Yes)	1.035 (0.584–1.837)	0.905	–	–
Targeted therapy (No *vs* Yes)	1.244 (0.574–2.696)	0.580	–	–
Cumulative radiation dose (Gy)	0.966 (0.792–1.179)	0.737	–	–
P score	24.257 (10.375–56.716)	0.000	13.515 (5.185–35.230)	0.000
M score	23.046 (11.678–45.478)	0.000	17.604 (8.113–38.195)	0.000

features, for example, "wavelet_firstorder_wavelet_LHH-Mean_GTVnxT1" ranks thirteenth in the Pre-treatment prediction model and sixteenth in the mid-treatment, showing the features included in the pre-treatment model are not entirely useless, just their importance has changed. It also indicates that the tumor cell population has changed after chemoradiotherapy, leading to changes in heterogeneity within the tumor.

We compared the Kaplan-Meier survival curves between different risk groups and TNM stages at different clinical endpoints. The results showed that the high- and low-risk group had an excellent ability to predict PFS (P<0.0001 HR: 19.17, 95% CI: 12.77–30.41) was better than the TNM stage (P=0.004, HR: 1.913, 95% CI: 1.250–2.926). The MRI-radiomics model's ability to predict the LA-NPC effect is better than the TNM stage had been confirmed in some studies, consistent with our study (12, 18, 26). Interestingly, we tested the high- and low-risk group at other endpoints and found that they all performed well in LRFS, DMFS, and OS, which was similar to some of the results of Marco Bologna (26), who used OS as the label for radiomics features screening, and the final prediction model also had good predictive ability in LRFS. In the study, our radiomics features were labeled with PFS, which includes patients with recurrence, metastasis, and death according to the definition, so the features we screened have predictive values for different endpoints.

Marius suggested several considerations when conducting radiomics studies (30). Firstly, in addition to randomized clinical trials, the class imbalance is common, especially in retrospective studies using routine clinical data. There is little uniformity between interesting and non-interesting events in the cohort. For example, in our study, about 35% of patients had events of interest (progress/death). When evaluating MRI-radiomics features to predict PFS in NPC, we must take the imbalance between the percentage of patients with and without interesting events (35%) into account. The classifier that assigns all the cases in the sample to the "no event of interest" group seems to have a 65% correct rate. Still, it doesn't make clinical sense because it cannot actually distinguish whether interesting events have occurred by MRI in LA-NPC. Therefore, the overall accuracy and sensitivity, specificity, AUC value should be reported. Our study also used a SMOTE algorithm to balance the impact of class to reduce data imbalance on the research (31). Secondly, overfitting occurs when a model with many input parameters or too many degrees of freedom "memorizes" data. In addition to the features related to disease, the model also contains features reflecting image noise and random fluctuations. Generally, there are two processing methods: reducing the number of features, or performing regularization on the data. Here we compared the Pearson correlation coefficients to check and avoid collinearity between variables, and used LASSO regression for feature selection to avoid overfitting. Besides, the SMOTE algorithm balances the class distribution by synthesizing a small number of samples, which reduces the possibility of overfitting.

This study has two main advantages. Firstly, our research is the only one that demonstrates the predictive effect of the mid-

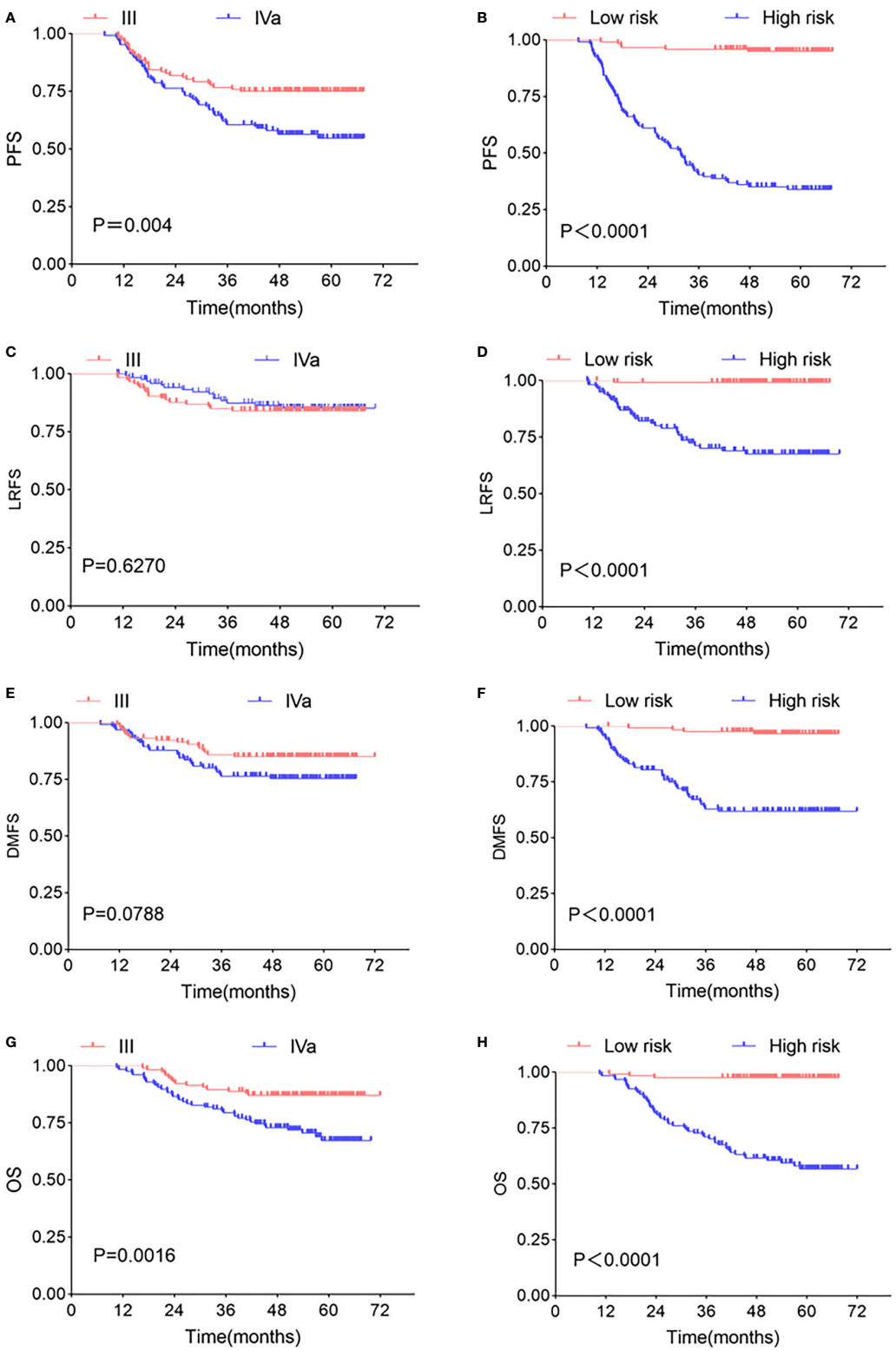

FIGURE 6 | Kaplan-Meier survival curve. Kaplan-Meier survival curves of TNM stages and two risk groups at different clinical endpoints. TNM stages in PFS **(A)**, LRFS **(C)**, DMFS **(E)**, OS **(G)** survival curve, high- and low-risk groups in PFS **(B)**, LRFS **(D)**, DMFS **(F)**, OS **(H)** survival curve. The P-value in the figure is obtained by the log-rank test.

treatment radiomics features on PFS in LA-NPC. We found that the use of radiomics information of mid-treatment can more comprehensively evaluate the response of LA-NPC to treatment and better evaluate the prognosis. On the other hand, we indirectly confirmed that the heterogeneity of tumors would change during chemoradiotherapy. The Cox model combined the pre- and mid-treatment radiomics features for risk stratification and found an excellent predictive effect across different clinical endpoints. Secondly, it had been proved that the population of different genomes is one reason for the clinical heterogeneity of radiotherapy efficacy (32). It is well known that radiomics is assumed to represent the histological heterogeneity of solid tumors (33). Although more than 90% of LA-NPC had positive lymph nodes, previous studies ignored metastatic lymph nodes (22, 23). We also collected the radiomics features of primary nasopharyngeal tumors and metastatic lymph nodes to describe tumor biological characteristics better.

This study also has some limitations. Firstly, this study is a retrospective study conducted by a single agency in non-endemic areas of NPC and lacks external validation. It is necessary to perform a large-sample multicenter prospective validation in NPC endemic and non-endemic regions to obtain strong evidence of clinical application. Secondly, the disunity of the treatment plan will also affect the prediction effect of the model. Finally, MRI-radiomics models and statistical analysis algorithms are unfamiliar and complex to the clinic. To solve this problem, we can set up a website or application, and doctors can upload images and clinical variables to obtain results.

CONCLUSION

The MRI-radiomics model (pre- and mid-treatment) is a powerful tool to predict the disease progression/death in LA-NPC. We calculate the risk score of disease progression/death in LA-NPC by combining the radiomics characteristics of pre- and mid-treatment and stratify the patients with high and low risk, which can not only predict the PFS in LA-NPC but also predict the LRFS, DMFS, and OS.

DATA AVAILABILITY STATEMENT

The original contributions presented in the study are included in the article/**Supplementary Material**. Further inquiries can be directed to the corresponding authors.

AUTHOR CONTRIBUTIONS

PZ, GY, LK, and YN designed this study. LK, YN, RH, SL, QT, AC, and YF conducted the study and analyzed the results, development of the model, and drafted the manuscript under the supervision of JL, PZ, and GY. LK took part in the drawing target outline, data extraction, development of the model, YN took part in the research general design, data extraction, development of the model,and they carried out the main part of the study, they contributed equally to this work and share first authorship. PZ and GY have contributed equally to this work and share corresponding authorship. The remaining authors are ranked by their contribution to research. All authors contributed to the article and approved the submitted version.

FUNDING

Key research and development Program of Science and Technology Department of Sichuan Province "Application of Multimodal Radiomics and Artificial Intelligence in Precise Treatment of Head and neck Tumors", item no. 2019YFG0185. Liangshan science and Technology Bureau of Sichuan provence, item no.18YYJS0094. Key R & D support Plan of Chengdu Science and Technology Bureau,item no.2021-YF05-02382-SN.

SUPPLEMENTARY MATERIAL

The Supplementary Material for this article can be found online at: https://www.frontiersin.org/articles/10.3389/fonc.2021.774455/full#supplementary-material

REFERENCES

1. Bray F, Ferlay J, Soerjomataram I, Siegel RL, Torre LA, Jemal A. Global Cancer Statistics 2018: GLOBOCAN Estimates of Incidence and Mortality Worldwide for 36 Cancers in 185 Countries. *CA Cancer J Clin* (2018) 68 (6):394–424. doi: 10.3322/caac.21492
2. Pan JJ, Ng WT, Zong JF, Lee SW, Choi HC, Chan LL, et al. Prognostic Nomogram for Refining the Prognostication of the Proposed 8th Edition of the AJCC/UICC Staging System for Nasopharyngeal Cancer in the Era of Intensity-Modulated Radiotherapy. *Cancer* (2016) 122(21):3307–15. doi: 10.1002/cncr.30198
3. Sun X, Su S, Chen C, Han F, Zhao C, Xiao W, et al. Long-Term Outcomes of Intensity-Modulated Radiotherapy for 868 Patients With Nasopharyngeal Carcinoma: An Analysis of Survival and Treatment Toxicities. *Radiother Oncol* (2014) 110(3):398–403. doi: 10.1016/j.radonc.2013.10.020
4. Guo R, Tang LL, Mao YP, Du XJ, Chen L, Zhang ZC, et al. Proposed Modifications and Incorporation of Plasma Epstein-Barr Virus DNA Improve the TNM Staging System for Epstein-Barr Virus-Related Nasopharyngeal Carcinoma. *Cancer* (2019) 125(1):79–89. doi: 10.1002/cncr.31741
5. Wu S, Quan R, Han L, Zhang H, Zhang B, Xu G, et al. Analysis of Intensity-Modulated Radiotherapy for Patients With Nasopharyngeal Carcinoma. *Med (Baltimore)* (2020) 99(30):e21325. doi: 10.1097/MD.0000000000021325
6. Tang LL, Chen YP, Mao YP, Wang ZX, Guo R, Chen L, et al. Validation of the 8th Edition of the UICC/AJCC Staging System for Nasopharyngeal Carcinoma From Endemic Areas in the Intensity-Modulated Radiotherapy Era. *J Natl Compr Canc Netw* (2017) 15(7):913–9. doi: 10.6004/jnccn.2017.0121
7. Gillies RJ, Kinahan PE, Hricak H. Radiomics: Images Are More Than Pictures, They Are Data. *Radiology* (2016) 278(2):563–77. doi: 10.1148/radiol.2015151169
8. Aerts HJ, Velazquez ER, Leijenaar RT, Parmar C, Grossmann P, Carvalho S, et al. Decoding Tumour Phenotype by Noninvasive Imaging Using a Quantitative Radiomics Approach. *Nat Commun* (2014) 5:4006. doi: 10.1038/ncomms5006
9. King AD, Bhatia KS. Magnetic Resonance Imaging Staging of Nasopharyngeal Carcinoma in the Head and Neck. *World J Radiol* (2010) 2(5):159–65. doi: 10.4329/wjr.v2.i5.159

10. Zhang L, Dong D, Li H, Tian J, Ouyang F, Mo X, et al. Development and Validation of a Magnetic Resonance Imaging-Based Model for the Prediction of Distant Metastasis Before Initial Treatment of Nasopharyngeal Carcinoma: A Retrospective Cohort Study. *EBioMedicine* (2019) 40:327–35. doi: 10.1016/j.ebiom.2019.01.013
11. Zhang L, Zhou H, Gu D, Tian J, Zhang B, Dong D, et al. Radiomic Nomogram: Pretreatment Evaluation of Local Recurrence in Nasopharyngeal Carcinoma Based on MR Imaging. *J Cancer* (2019) 10(18):4217–25. doi: 10.7150/jca.33345
12. Shen H, Wang Y, Liu D, Lv R, Huang Y, Peng C, et al. Predicting Progression-Free Survival Using MRI-Based Radiomics for Patients With Nonmetastatic Nasopharyngeal Carcinoma. *Front Oncol* (2020) 10:618. doi: 10.3389/fonc.2020.00618
13. Lee CK, Jeong SH, Jang C, Bae H, Kim YH, Park I, et al. Tumor Metastasis to Lymph Nodes Requires YAP-Dependent Metabolic Adaptation. *Sci (New York NY)* (2019) 363(6427):644–9. doi: 10.1126/science.aav0173
14. Bogowicz M, Tanadini-Lang S, Guckenberger M, Riesterer O. Combined CT Radiomics of Primary Tumor and Metastatic Lymph Nodes Improves Prediction of Loco-Regional Control in Head and Neck Cancer. *Sci Rep* (2019) 9(1):15198. doi: 10.1038/s41598-019-51599-7
15. Park SH, Hahm MH, Bae BK, Chong GO, Jeong SY, Na S, et al. Magnetic Resonance Imaging Features of Tumor and Lymph Node to Predict Clinical Outcome in Node-Positive Cervical Cancer: A Retrospective Analysis. *Radiat Oncol* (2020) 15(1):86. doi: 10.1186/s13014-020-01502-w
16. Ho FC, Tham IW, Earnest A, Lee KM, Lu JJ. Patterns of Regional Lymph Node Metastasis of Nasopharyngeal Carcinoma: A Meta-Analysis of Clinical Evidence. *BMC Cancer* (2012) 12:98. doi: 10.1186/1471-2407-12-98
17. Bologna M, Corino V, Calareso G, Tenconi C, Alfieri S, Iacovelli NA, et al. Baseline MRI-Radiomics Can Predict Overall Survival in Non-Endemic EBV-Related Nasopharyngeal Carcinoma Patients. *Cancers (Basel)* (2020) 12(10). doi: 10.3390/cancers12102958
18. Zhang LL, Huang MY, Li Y, Liang JH, Gao TS, Deng B, et al. Pretreatment MRI Radiomics Analysis Allows for Reliable Prediction of Local Recurrence in non-Metastatic T4 Nasopharyngeal Carcinoma. *EBioMedicine* (2019) 42:270–80. doi: 10.1016/j.ebiom.2019.03.050
19. Akram F, Koh PE, Wang F, Zhou S, Tan SH, Paknezhad M, et al. Exploring MRI Based Radiomics Analysis of Intratumoral Spatial Heterogeneity in Locally Advanced Nasopharyngeal Carcinoma Treated With Intensity Modulated Radiotherapy. *PloS One* (2020) 15(10):e0240043. doi: 10.1371/journal.pone.0240043
20. Liu X, Luo HN, Tian WD, Lu J, Li G, Wang L, et al. Diagnostic and Prognostic Value of Plasma microRNA Deregulation in Nasopharyngeal Carcinoma. *Cancer Biol Ther* (2013) 14(12):1133–42. doi: 10.4161/cbt.26170
21. Wang QQ, Yu SC, Qi X, Hu YH, Zheng WJ, Shi JX, et al. [Overview of Logistic Regression Model Analysis and Application]. *Zhonghua Yu Fang Yi Xue Za Zhi* (2019) 53(9):955–60. doi: 10.3760/cma.j.issn.0253-9624.2019.09.018
22. Zhang B, Tian J, Dong D, Gu D, Dong Y, Zhang L, et al. Radiomics Features of Multiparametric MRI as Novel Prognostic Factors in Advanced Nasopharyngeal Carc Inoma. *Clin Cancer Res* (2017) 23(15):4259–69. doi: 10.1158/1078-0432.CCR-16-2910
23. Mao J, Fang J, Duan X, Yang Z, Cao M, Zhang F, et al. Predictive Value of Pretreatment MRI Texture Analysis in Patients With Primary Nasopharyngeal Carcinoma. *Eur Radiol* (2019) 29(8):4105–13. doi: 10.1007/s00330-018-5961-6
24. Yang K, Tian J, Zhang B, Li M, Xie W, Zou Y, et al. A Multidimensional Nomogram Combining Overall Stage, Dose Volume Histogram Parameters and Radiomics to Predict Progression-Free Survival in Patients With Locoregionally Advanced Nasopharyngeal Carcinoma. *Oral Oncol* (2019) 98:85–91. doi: 10.1016/j.oraloncology.2019.09.022
25. Wu Z, Zeng RF, Su Y, Gu MF, Huang SM. Prognostic Significance of Tumor Volume in Patients With Nasopharyngeal Carcinoma Undergoing Intensity-Modulated Radiation Therapy. *Head Neck* (2013) 35(5):689–94. doi: 10.1002/hed.23010
26. Ouyang FS, Guo BL, Zhang B, Dong YH, Zhang L, Mo XK, et al. Exploration and Validation of Radiomics Signature as an Independent Prognostic Biomarker in Stage III -IVb Nasopharyngeal Carcinoma. *Oncotarget* (2017) 8(43):74869–79. doi: 10.18632/oncotarget.20423
27. Ibrahim MA, Dublin AB. *Magnetic Resonance Imaging (MRI), Gadolinium*. StatPearls. Treasure Island, USA: StatPearls Publishing LLC (2018).
28. Zhang L, Wu X, Liu J, Zhang B, Mo X, Chen Q, et al. MRI-Based Deep-Learning Model for Distant Metastasis-Free Survival in Locoregionally Advanced Nasopha Ryngeal Carcinoma. *J Magn Reson Imaging* (2021) 53(1):167–78. doi: 10.1002/jmri.27308
29. Jiang X, Li J, Kan Y, Yu T, Chang S, Sha X, et al. MRI Based Radiomics Approach With Deep Learning for Prediction of Vessel Invasion in Early-Stage Cervical Cancer. *IEEE/ACM Trans Comput Biol Bioinform* (2021) 18(3). doi: 10.1109/TCBB.2019.2963867
30. Mayerhoefer ME, Materka A, Langs G, Häggström I, Szczypiński P, Gibbs P, et al. Introduction to Radiomics. *J Nucl Med* (2020) 61(4):488–95. doi: 10.2967/jnumed.118.222893
31. Blagus R, Lusa L. SMOTE for High-Dimensional Class-Imbalanced Data. *BMC Bioinf* (2013) 14:106. doi: 10.1186/1471-2105-14-106
32. Scott JG, Berglund A, Schell MJ, Mihaylov I, Fulp WJ, Yue B, et al. A Genome-Based Model for Adjusting Radiotherapy Dose (GARD): A Retrospective, Cohort-Based Study. *Lancet Oncol* (2017) 18(2):202–11. doi: 10.1016/S1470-2045(16)30648-9
33. Scalco E, Rizzo G. Texture Analysis of Medical Images for Radiotherapy Applications. *Br J Radiol* (2017) 90(1070):20160642. doi: 10.1259/bjr.20160642

Conflict of Interest: The authors declare that the research was conducted in the absence of any commercial or financial relationships that could be construed as a potential conflict of interest.

frontiers in Oncology

ORIGINAL RESEARCH
published: 21 December 2021
doi: 10.3389/fonc.2021.776979

Prognostic Value of an Immune-Related Gene Signature in Oral Squamous Cell Carcinoma

Chao Zhu[1], *Liqun Gu*[2], *Mianfeng Yao*[1], *Jiang Li*[1*] and *Changyun Fang*[1*]

[1] Department of Stomatology, Xiangya Hospital, Central South University, Changsha, China, [2] Department of Pediatric Stomatology, Xiangya Stomatological Hospital, Central South University, Changsha, China

The prognosis and immunotherapy response rates are unfavorable in patients with oral squamous cell carcinoma (OSCC). The tumor microenvironment is associated with tumor prognosis and progression, and the underlying mechanisms remain unclear. We obtained differentially expressed immune-related genes from OSCC mRNA data in The Cancer Genome Atlas (TCGA) database. Overall survival-related risk signature was constructed by univariate Cox regression analysis and LASSO Cox regression analysis. The prognostic performance was validated with receiver operating characteristic (ROC) analysis and Kaplan–Meier survival curves in the TCGA and Gene Expression Omnibus (GEO) datasets. The risk score was confirmed to be an independent prognostic factor and a nomogram was built to quantify the risk of outcome for each patient. Furthermore, a negative correlation was observed between the risk score and the infiltration rate of immune cells, as well as the expression of immunostimulatory and immunosuppressive molecules. Functional enrichment analysis between different risk score subtypes detected multiple immune-related biological processes, metabolic pathways, and cancer-related pathways. Thus, the immune-related gene signature can predict overall survival and contribute to the personalized management of OSCC patients.

Keywords: immune-related genes, oral squamous cell carcinoma, prognosis, tumor microenvironment, immunotherapy

OPEN ACCESS

Edited by:
Shiyu Song,
Virginia Commonwealth University Health System, United States

Reviewed by:
Tito Poli,
University of Parma, Italy
Martin Kauke,
Brigham and Women's Hospital and Harvard Medical School, United States

***Correspondence:**
Jiang Li
lijiangsun@csu.edu.cn
Changyun Fang
fangcy@csu.edu.cn

Specialty section:
This article was submitted to Head and Neck Cancer, a section of the journal Frontiers in Oncology

Received: *14 September 2021*
Accepted: *25 November 2021*
Published: *21 December 2021*

Citation:
Zhu C, Gu L, Yao M, Li J and Fang C (2021) Prognostic Value of an Immune-Related Gene Signature in Oral Squamous Cell Carcinoma. Front. Oncol. 11:776979. doi: 10.3389/fonc.2021.776979

INTRODUCTION

Oral squamous cell carcinoma (OSCC) is one of the common malignant neoplasms in the head and neck region (1), leading to approximately 1.8% cancer-related death worldwide in 2020 (2). In the United States, there are an estimated 35,540 new cases and 6,980 deaths in 2021. In spite of the advantages of multimodal therapy including surgical resection, with or without radiotherapy or chemotherapy, the 5-year survival rate is approximately 50% (3). The challenge highlights the need to identify prognostic biomarkers to predict survival in patients with OSCC.

Over the past decade, immunotherapy has proven to be an effective treatment for various cancers. The identification of possible mechanisms of immune evasion has improved the understanding of cancer immunotherapy (4). Cancer immunotherapy, particularly immune checkpoint inhibitors (ICIs), has shown durable anti-tumor activity and improved survival in patients with head and neck squamous cell carcinoma (HNSCC) (5). Despite initial enthusiasm,

only a small number of patients have benefited from immunotherapy (6, 7). The complex interactions between cancer and the immune system have elucidated the role of the immune system in cancer development. To estimate the potential response to ICIs treatment, further exploration of predictive biomarkers is necessary.

In this study, we aimed to assess the correlation between immune-related genes and the prognosis and immune landscape of OSCC. Finally, we further performed functional enrichment analysis to explore the underlying mechanisms.

MATERIALS AND METHODS

Data Sources

RNA sequencing and clinical data of 325 OSCC and 32 normal oral cavity samples in The Cancer Genome Atlas (TCGA) database were obtained from the UCSC Xena data portal[1] and eBioPortal[2] database. The GSE41613 and GSE42743 were obtained from the Gene Expression Omnibus (GEO) database[3] (8). The gene expression data of the GEO database were normalized by rma method using affy R package (9).

Construction of Risk Score Model

To identify differentially expressed genes (DEGs) between normal and tumor samples in the TCGA dataset, RNA sequencing data were performed using the limma R package with a cutoff of $|\log_2 FC| \geq 1.5$ and a false discovery rate (FDR) < 0.05 (10). We extracted immune-related DEGs from the identified DEGs based on the ImmPort database[4] (11). Univariate Cox regression analysis was used to estimate the association between the expression of immune-related DEGs and overall survival (OS) of patients. Next, the LASSO regression model was conducted to identify key prognostic genes using the glmnet R package (12). Risk scores for each OSCC sample were derived based on the expression of prognostic genes and their corresponding regression coefficient.

Internal and External Validation of the Prognostic Signature

Patients in the TCGA dataset were randomly divided into a training set ($n = 162$) and a testing set ($n = 163$) for internal validation. The GSE41613 and GSE42743 datasets were used as the external validation cohort. Overall survival (OS), disease-specific survival (DSS), and progression-free survival (PFS) were plotted using Kaplan–Meier curves and calculated using Cox regression analysis. Patients were divided into high-risk and low-risk groups based on the median value of the risk score. Time-dependent receiver operating characteristic (ROC) curve was performed to assess the predictive efficiency of the prognostic signature using the timeROC R package (13). Independent prognostic factors were identified by multivariate Cox regression analysis using the survival R package (14). Furthermore, all independent prognostic factors obtained by multivariate Cox regression were used to construct a predictive nomogram by the rms R package to assess the 1-year, 3-year, and 5-year OS of the patients. Its predictive capacities were estimated by the corresponding calibration curve and the consistency index (C Index). Then, decision curve analysis (DCA) was performed by the dcurver R package to investigate the clinical utility of the nomogram model.

Estimation of the Immune Landscape

We estimated the expressions of 782 genes from 28 types of immune cells to quantify the infiltration ratio of immune cells (15). The ratio of immune cell infiltration was calculated by the ssGSEA method through the Gene Set Variation Analysis (GSVA) R package and visualized by heatmap R package (16, 17). The stromal, immune, and estimate scores were quantified by the estimate R package (18). Data on stromal fraction, leukocyte fraction, scores of six representative signatures, and the gene set of immune-related markers were obtained from a previously published study from the TCGA group (19).

Functional Enrichment Analysis

Functional enrichment analysis of Gene Ontology (GO) terms, Kyoto Encyclopedia of Genes and Genomes (KEGG) pathways, and Hallmark pathways was analyzed using the GSEA software v4.1.0 and visualized by ggplot2 R package (20, 21).

Statistical Analysis

Data comparison between two groups was performed by two-tailed *t*-test and multiple *t*-tests with FDR < 0.05 for continuous comparisons. Data comparison between three groups was performed by one-way ANOVA test. Correlations between ssGSEA scores of 28 immune cells and risk scores or the expression of the prognostic signature were determined by Pearson correlation test. In all analyses, $p < 0.05$ was considered statistically significant. All statistical analyses were conducted by GraphPad Prism v8.0.2 and R software v4.0.5.

RESULTS

Identification of the Candidate Immune-Related Genes

Differential expression analysis was performed between normal and tumor samples. A total of 1,313 upregulated genes and 1,615 downregulated genes were identified (**Figure S1A**). By comparing the DEGs and immunologically relevant genes, 249 genes overlapped (**Figure S1B**), and the expression of these genes was shown in the heatmap (**Figure S1C**). Univariate Cox regression analysis was performed to explore the correlation between the expression of 249 immune-related DEGs and OS in

[1] https://xenabrowser.net
[2] https://www.cbioportal.org
[3] https://www.ncbi.nlm.nih.gov/geo/
[4] https://www.immport.org

patients with OSCC. In total, 16 candidate immune-related genes were identified (**Figure S1D**).

Construction and Internal Validation of the Prognostic Signature

The LASSO Cox regression analysis was used to further identify 9 key genes, namely, Apolipoprotein D (APOD), Oxidized Low Density Lipoprotein Receptor 1(OLR1), Stanniocalcin-2 (STC2), Dickkopf-related protein 1 (DKK1), Tumor necrosis factor receptor superfamily member 19 (TNFRSF19), tumor necrosis factor receptor superfamily member 4 (TNFRSF4), Defensin Beta 1(DEFB1), Cytotoxic T-Lymphocyte Associated Protein 4 (CTLA4), and Cathepsin G (CTSG) (**Figures S1E, F**). Risk scores were calculated according to the expression of these prognostic genes weighted by the coefficients in the regression analysis for each OSCC sample. Patients from the training set, the testing test, and the entire TCGA set were divided into high-risk and low-risk groups based on the median value of the risk score, respectively. A higher proportion of deaths was observed in the high-risk group than that in the low-risk group (first and second panel of **Figures 1A–C**). The 9 genes were differentially expressed between the high-risk and low-risk groups (bottom panel of **Figures 1A–C** and **Figure S2**). To assess the predictive performance of the 9-gene prognostic signature, time-dependent ROC analyses were performed in the training, testing, and whole TCGA set to estimate the 1-year, 3-year, and 5-year OS probability (**Figures 1D–F**). Patients with low-risk scores showed longer OS, DSS, and PFS in the training, testing, and whole TCGA set (**Figures 2A–C**). We also found higher proliferation scores and wound healing scores in the high-risk group (**Figures S3A, B**). Together, these supported the predictive ability of the prognostic signature.

External Validation of the Prognostic Model in the GEO Cohort

Patients in the GEO datasets were divided into high-risk and low-risk groups by the median value of risk scores. The high-risk group had a higher proportion of deaths compared to the low-risk group (**Figures 3A, B**). The ROC analysis verified the predictive efficiency of estimating the 1-year, 3-year, and 5-year OS probability (**Figures 3C, D**). The patients in the high-risk group had a worse prognosis (**Figures 3E, F**).

The Risk Score is an Independent Prognostic Factor and Its Relationship to Clinical Characteristics

Multivariate Cox-regression analysis was performed using risk scores and clinical parameters as covariates to evaluate the independence of the risk score. The result demonstrated that the risk score can be considered as an independent predictor (TCGA: **Figure 4A**, GEO: **Figures S4A, B**). Then, we analyzed the correlation between the prognostic signature and clinical characteristics. In the TCGA cohort, the risk score was significantly different among different histologic stage and

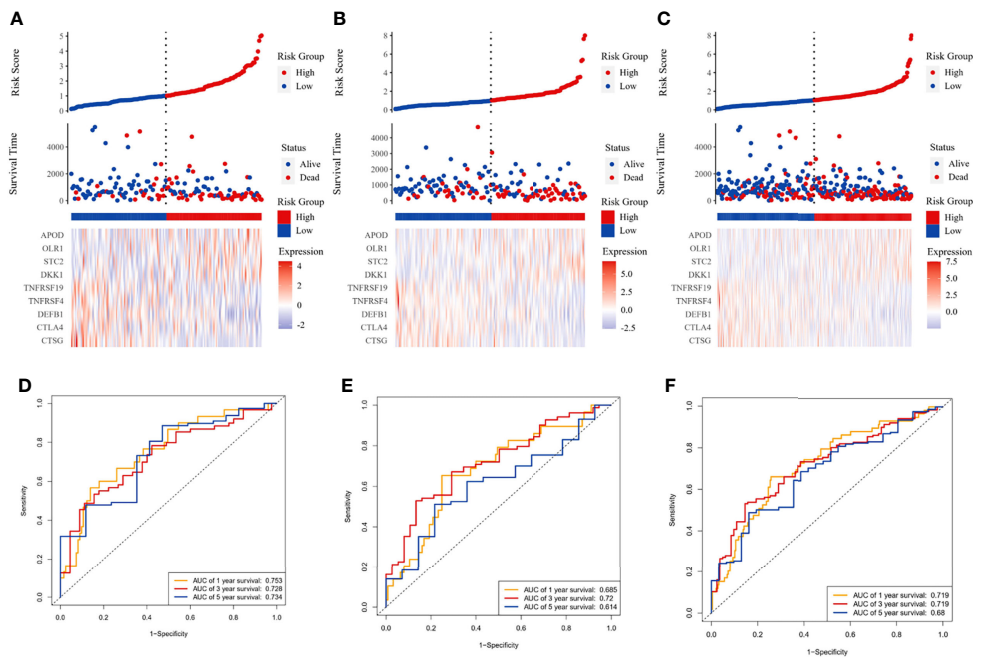

FIGURE 1 | Immune-related prognostic model construction in the TCGA cohort. The prognostic significance of risk scores was evaluated using the training set **(A, D)**, the testing set **(B, E)**, and the whole TCGA set **(C, F)**, respectively. **(A–C)** The first panel from top represents the risk score distribution of the samples. The intersecting point represents the median of risk scores. The second panel from the top was the distribution of OS status and risk scores. The bottom panel was the heatmap of the mRNA expression of the nine immune-related DEGs. **(D–F)** The ROC curve for predicting 1-, 3-, and 5-year overall survival probability.

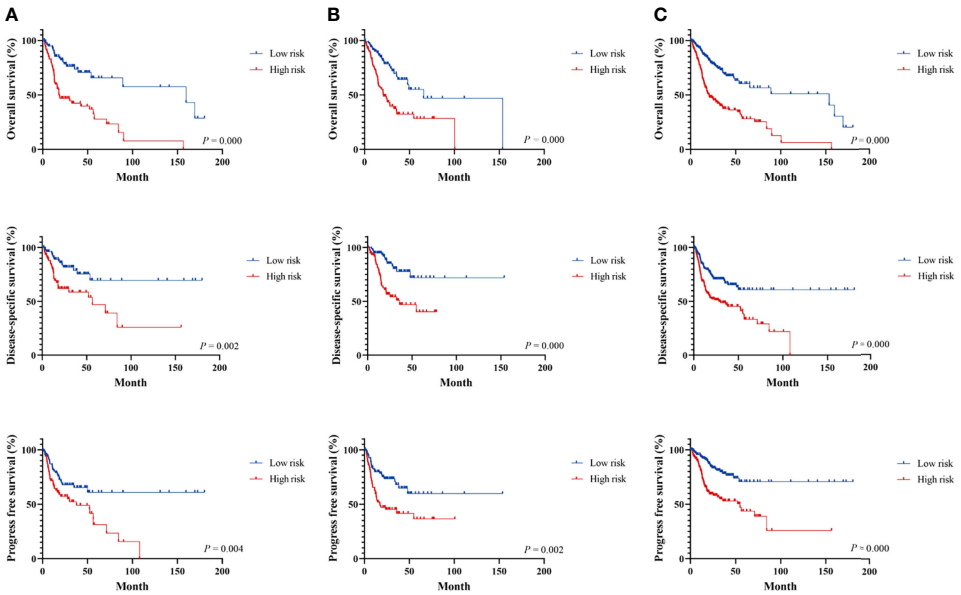

FIGURE 2 | Survival analysis of immune-related signature in the TCGA cohort. Kaplan–Meier curves for the survival rate of OSCC patients between the high-risk and low-risk groups in the training **(A)**, testing **(B)**, and whole TCGA set **(C)**, respectively. *p*-values for significance (<0.05) calculated using Cox regression analysis.

pathologic stage (**Figures 4C, D**). There were no differences between the risk score and age and gender (**Figures 4B, E**). In addition, OS was significantly shorter in high-risk patients with the same pathologic stage, and lymphovascular invasion status compared with low-risk patients (**Figures 4F, G**). In the GEO cohort, risk scores were higher in the stage III/IV group (**Figures S4C, D**), and the risk score could differentiate patients with the same pathological stage (**Figures S4E, F**).

Development and Assessment of the Predictive Nomogram

The nomogram model was constructed using the independent factors including age, risk scores, pathologic stage, and lymphovascular invasion status in the TCGA dataset (**Figure 5A**). The calibration curve was close to the standard curve showing the accuracy of the predictive nomogram in predicting the probability of OS over 1, 3, and 5 years (**Figures 5B–D**). Then, we performed a decision curve analysis (DCA) for age, risk scores, pathologic stage, lymphovascular invasion status, and combined nomogram model to evaluate the clinical utility of the nomogram (**Figures 5E–G**).

Correlation Between Tumor Immune Microenvironment and the Prognostic Signature

We compared the infiltration ratio of 28 immune cells. The high-risk group showed a relatively lower ratio of immune cell infiltration, including cells with anti-tumor activity and immunosuppressive activity (TCGA: **Figures 6A, B**; GEO: **Figure 7**). In addition, a positive correlation was observed between the ssgsea score of these two categories of immune cells in the high-risk and low-risk groups (**Figure 6C**). We compared the infiltration ratio of these two categories of immune cells in different risk groups and observed that the low-risk group was characterized by higher anti-tumor and pro-tumor immunity (**Figures 6D, E**). The risk score was negatively correlated with the enrichment score for most types of immune cells. The expression of CTSG, CTLA4, TNFRSF4, APOD, and OLR1 was positively correlated with the enrichment score of most immune cells, and the expression of STC2 was negatively correlated with it (**Figure 6F**). Using the ESTIMATE database, we observed higher stromal scores, immune scores, and estimate scores in the low-risk group (**Figures 8A–C**). We compared the stromal fraction and leukocyte fraction of these two groups in the TCGA cohort. The results showed that the stromal fraction and leukocyte fraction were higher in the low-risk group (**Figures S3C, D**). In addition, scores of macrophage regulation, lymphocyte infiltration and IFN-γ response were higher in the low-risk group in the TCGA cohort (**Figures S3E–G**). While, scores of homologous recombination defects were lower in the low-risk group and no differences were found in TGF-β response (**Figures S3H, I**). After analyzing the expression profiles of 75 immune-related genes in different risk groups, it was observed that the expression of immune-stimulatory and suppressive genes was relatively higher in the low-risk group (**Figures 8D–F**). When comparing the expression levels of several important inhibitory checkpoint molecules between the high-risk and low-risk groups, we found that the expression levels of Programmed cell death protein 1 (PD-1), Programmed death-ligand 2 (PD-L2), Cytotoxic T-Lymphocyte Associated Protein 4 (CTLA4), T-cell immunoglobulin 3 (TIM3), Lymphocyte activation gene 3 (LAG3), Indoleamine 2,3-dioxygenase 1 (IDO1), and T-cell immunoreceptor with immunoglobulin and immunoreceptor

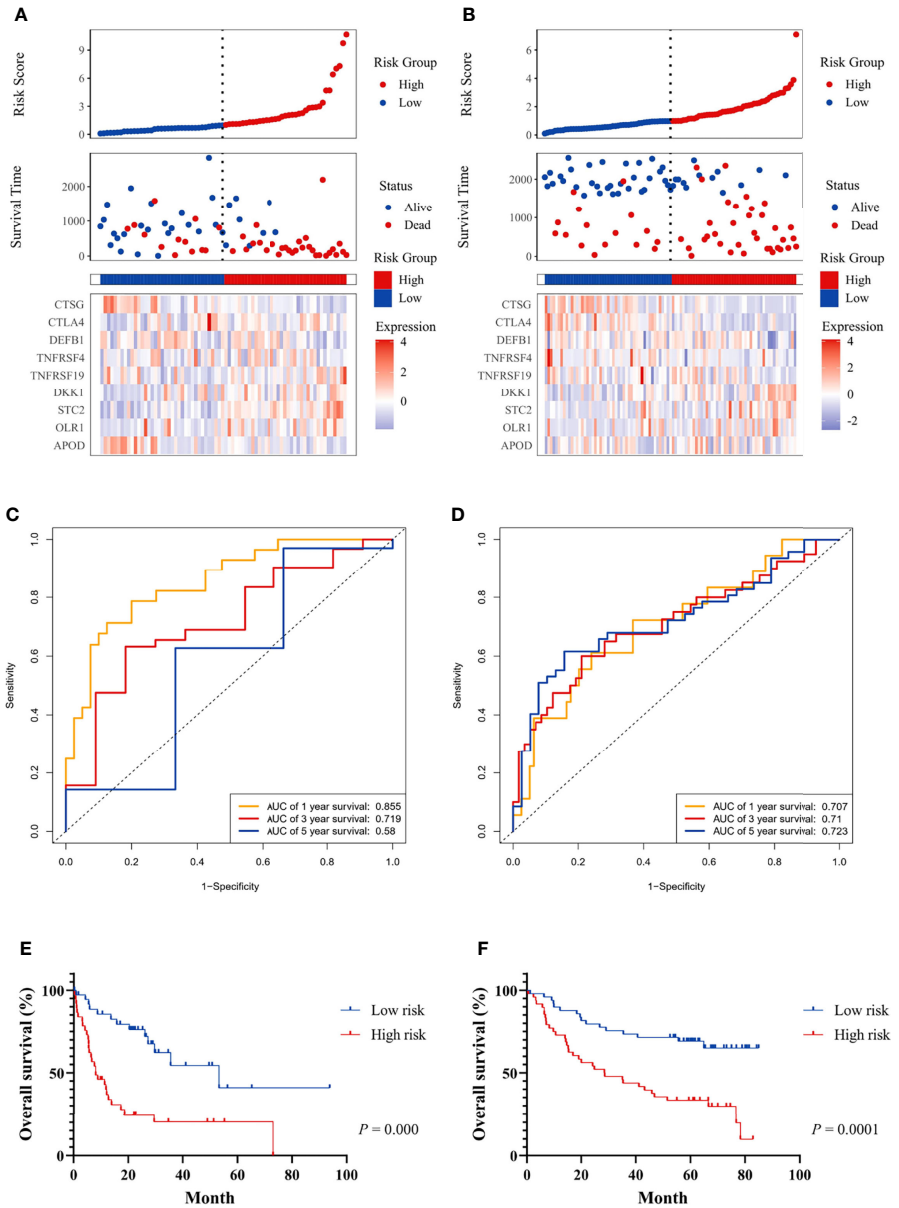

FIGURE 3 | The prognostic significance of the risk score and survival analysis were evaluated using the GEO validation cohort. The prognostic significance of risk scores was evaluated using the validation datasets GSE42743 **(A)** and GSE41613 **(B)**, respectively. The first from top represents the risk scores distribution of the samples. The intersecting point represents the median of risk scores. The second from top was the distribution of OS status and risk scores. The bottom panel was the heatmap of the mRNA expression of the nine immune-related DEGs. The ROC curve for predicting 1-, 3-, and 5-year overall survival probability in GSE42743 **(C)** and GSE41613 **(D)**. Kaplan–Meier curves for the survival rate of OSCC patients between the high-risk and low-risk groups in GSE42743 **(E)** and GSE41613 **(F)**. *P* values for significance (<0.05) calculated using Cox regression analysis.

tyrosine-based inhibitory motif domains (TIGIT) were higher in the low-risk group (**Figures 8G–I**).

Functional Enrichment Analysis

GO enrichment analysis for different risk groups revealed the following top immune-related GO terms: T-cell receptor complex, plasma membrane signaling receptor complex, and immunoglobulin complex in cellular components (**Figure 9A**); antigen binding, cytokine receptor activity, and CCR chemokine receptor binding in molecular functions (**Figure 9B**); defense response to bacterium, humoral immune response, and immune response regulation signaling pathway in biological process (**Figure 9C**). KEGG pathway analysis showed that immune-related pathways and metabolic pathways were enriched in the low-risk group, while the pentose phosphate pathway (PPP), spliceosome pathway, and homologous recombination (HR)

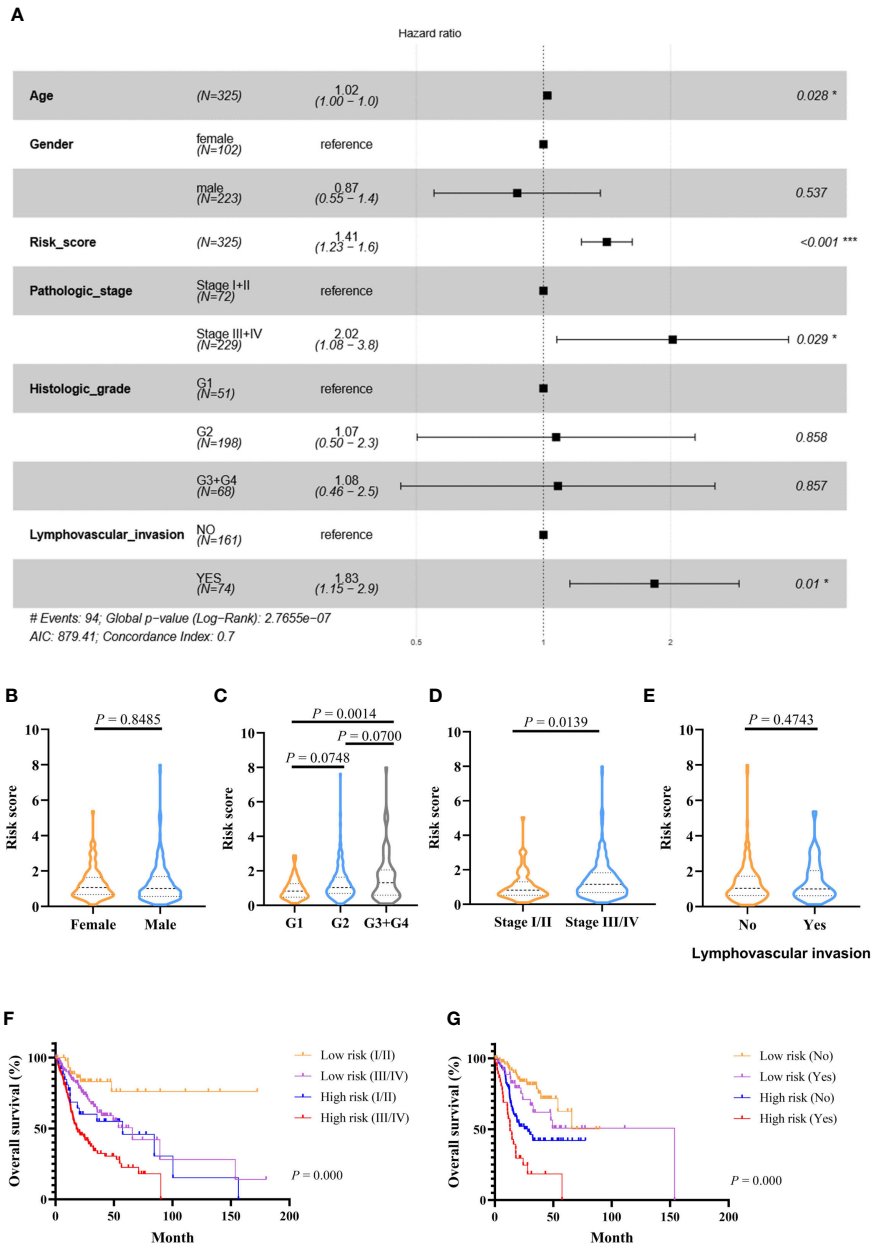

FIGURE 4 | Prognostic values of the immune-related signature model in the TCGA cohort. **(A)** Multivariate Cox regression analysis regarding OS in OSCC. **(B–E)** The distribution of risk scores in OSCC samples stratified by gender, histologic stage, pathologic stage, and lymphovascular invasion. **(F)** Kaplan–Meier curves for patients stratified by both pathologic stage and risk scores. **(G)** Kaplan–Meier curves for patients stratified by both lymphovascular invasion and risk scores. $p < 0.05$ shows significant difference. Survival significance calculated using Cox regression analysis. # just indicates the Events number. *p value < 0.05, **p value < 0.01, ***p value < .001.

pathway were enriched in the high-risk group (**Figure 9D**). Furthermore, hallmark pathway analysis revealed that glycolysis, mammalian target of rapamycin complex 1 (mTORC1) signaling, and G2M checkpoint were enriched in the high-risk group, whereas IL6/Jak/Stat3 signaling, Interferon-γ response, and allograft rejection were enriched in the low-risk group (**Figure 9E**).

DISCUSSION

ICIs are effective in the treatment of multiple cancers and have greatly improved the outcomes of patients. The limitation is that only a small number of patients benefit from ICIs treatment, including HNSCC (6, 7). Immune cells are key regulatory components of the tumor microenvironment (TME) and play

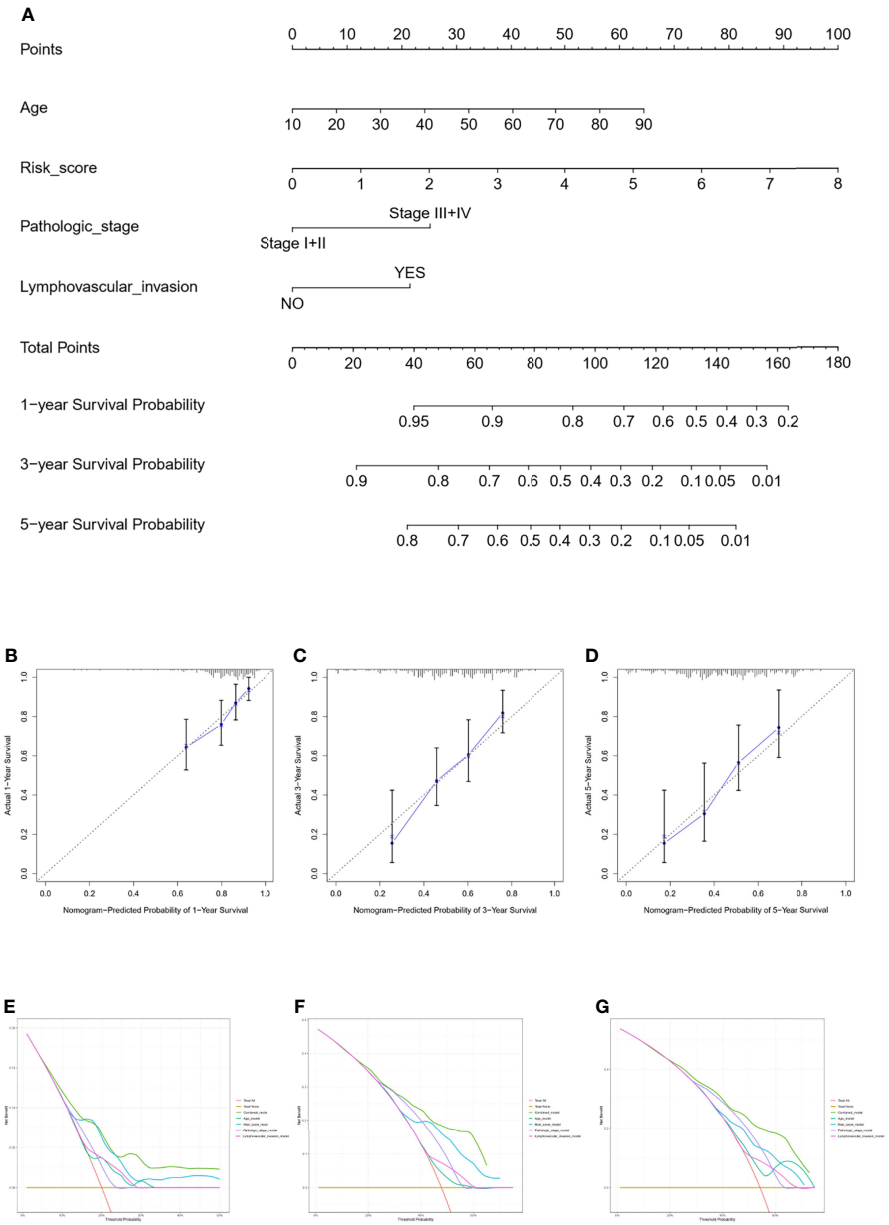

FIGURE 5 | Nomogram for predicting the survival probability of OSCC patients in the TCGA cohort. The nomogram for prediction of the 1-, 3-, and 5-year survival probability for OSCC patients **(A)**. The calibration curve for prediction of the 1-year **(B)**, 3-year **(C)**, and 5-year **(D)** survival probability for OSCC patients. The DCA curves of the age, risk score, pathologic stage, lymphovascular invasion, and combined nomogram model compared for 1-year **(E)**, 3-year **(F)**, and 5-year **(G)** OS of OSCC.

an important role in tumor growth and progression (22). Immune cell infiltration is associated with the survival rate of OSCC patients (23). However, the underlying mechanisms still need further elucidation.

In this study, we firstly identified immune-related genes that are differentially expressed between normal and tumor tissues. Then, univariate Cox regression analysis screened 16 survival-related genes. These survival-related genes have the potential to be biomarkers for prognosis. Furthermore, we established an immune-related risk signature, which is composed of 9 genes (APOD, OLR1, STC2, DKK1, TNFRSF19, TNFRSF4, DEFB1, CTLA4, and CTSG). APOD, OLR1, STC2, and DKK1 were overexpressed in high-risk patients. APOD has been reported to exhibit tumor suppressive activity in some types of tumors (24). OLR1, STC2, and DKK1 correlate with tumor evolution and immunosuppressive effects (25–29). TNFRSF19, TNFRSF4, DEFB1, CTLA4, and CTSG were identified as protective genes. High expression of TNFRSF19 is associated with poor prognosis in various types of cancer (30, 31). TNFRSF4, a T-cell co-stimulatory molecule, enhances $CD8^+$ T-cell infiltration (32). DEFB1 suppresses

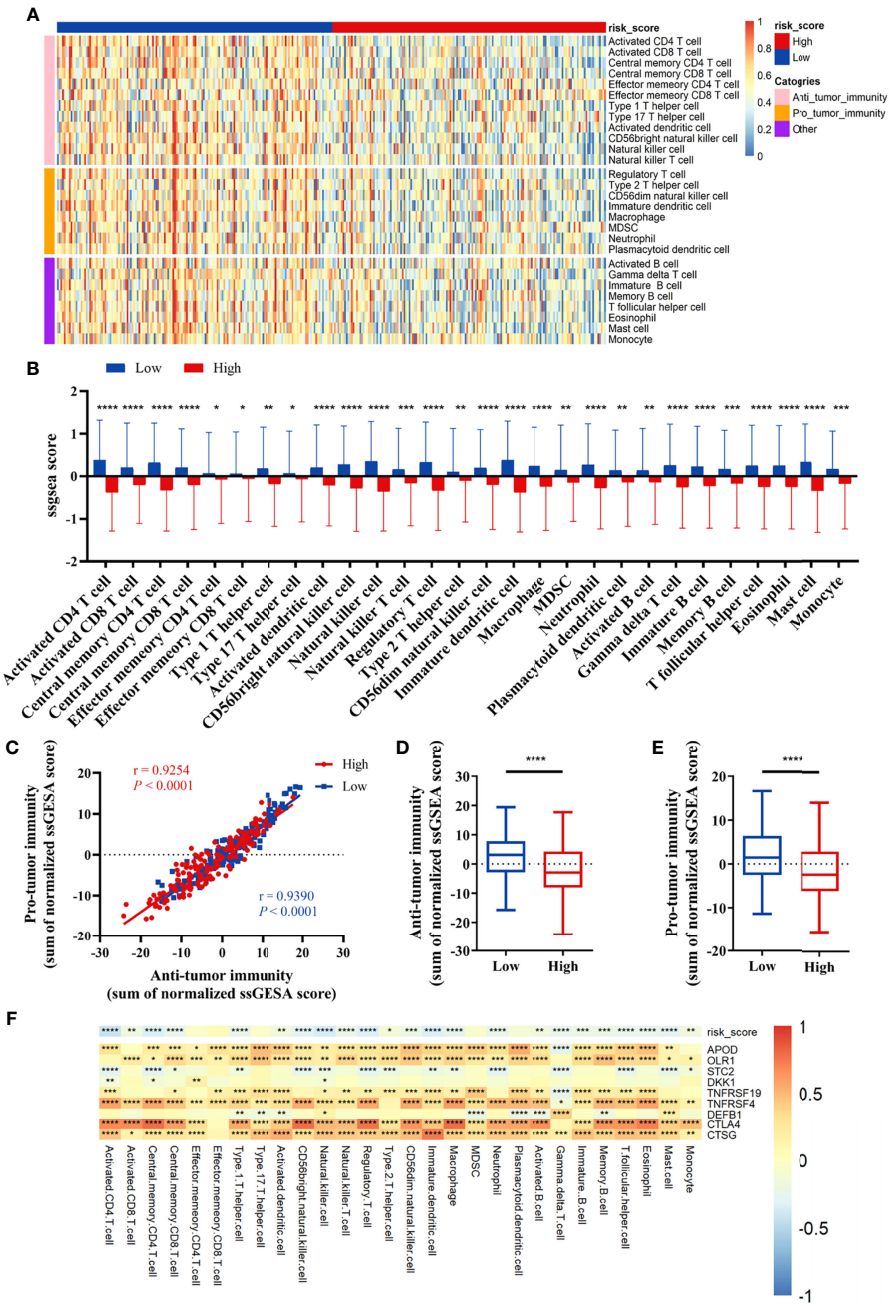

FIGURE 6 | Correlation between immune cell infiltration and the prognostic signature in the TCGA cohort. **(A, B)** The infiltration ratio of 28 immune cells. **(C)** Correlation of the cells with anti-tumor immunity and pro-tumor immunity. **(D, E)** Anti-tumor immunity and pro-tumor immunity scores of the risk score model. **(F)** The correlation between the immune-related signature and the ssGSEA scores of 28 immune cells. All *p*-values for significance (<0.05) represent comparisons *via* two-tailed *t*-test and multiple *t*-tests with FDR < 0.05. **p*-value < 0.05, ***p*-value < 0.01, ****p*-value < 0.001, and *****p*-value < 0.0001.

tumor migration and invasion in OSCC (33). CTLA-4 is a negative regulator of T-cell activation, and CTLA-4 inhibitors have been shown to promote antitumor immunity (34). CTSG is regarded as an immune-related biomarker in OSCC and inhibits OSCC cell proliferation, migration, and invasion (35). The specific role of the immune-related genes needs further investigation.

The immune-related signature could be used as an independent predictor of the prognosis in the TCGA cohort and GEO cohort. The signature could divide OSCC patients into high-risk and low-risk groups with statistically different survival outcomes. The higher proliferation score and wound healing score in the high-risk group could partially explain the worse prognosis of patients with high-risk

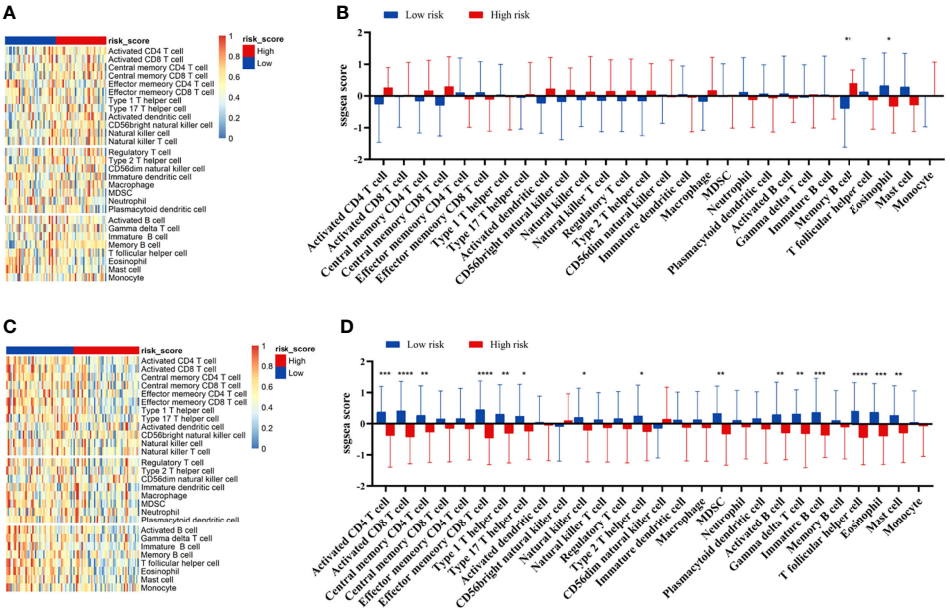

FIGURE 7 | Correlation between immune cell infiltration and the prognostic signature in the GEO cohort. The infiltration ratio of 28 immune cells in GEO42743 **(A, B)** and GEO41613 **(C, D)**. All *p*-values for significance (<0.05) represent comparisons *via* two-tailed multiple *t*-tests with FDR < 0.05. **p*-value < 0.05, ***p*-value < 0.01, ****p*-value < 0.001, and *****p*-value < 0.0001.

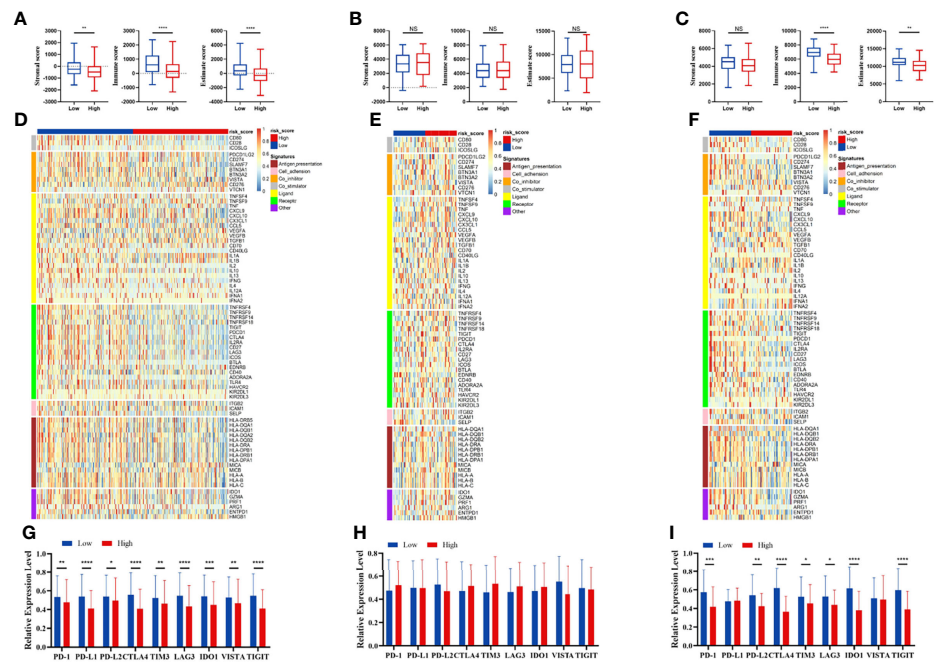

FIGURE 8 | Immune patterns of the risk score model. Comparison of stromal scores, immune scores, and estimate scores between the high-risk and low-risk patients in the TCGA **(A)**, GSE42743 **(B)**, and GSE41613 **(C)**. The expression level of immune-related signatures in the TCGA **(D)**, GSE42743 **(E)** and GSE41613 **(F)**. The expression level of immune checkpoint molecules in the TCGA **(G)**, GSE42743 **(H)** and GSE41613 **(I)**. All *p*-values for significance (<0.05) represent comparisons *via* two-tailed *t*-test and multiple *t*-tests with FDR < 0.05. **p*-value < 0.05, ***p*-value < 0.01, ****p*-value < 0.001, *****p*-value < 0.0001, and NS (not significant).

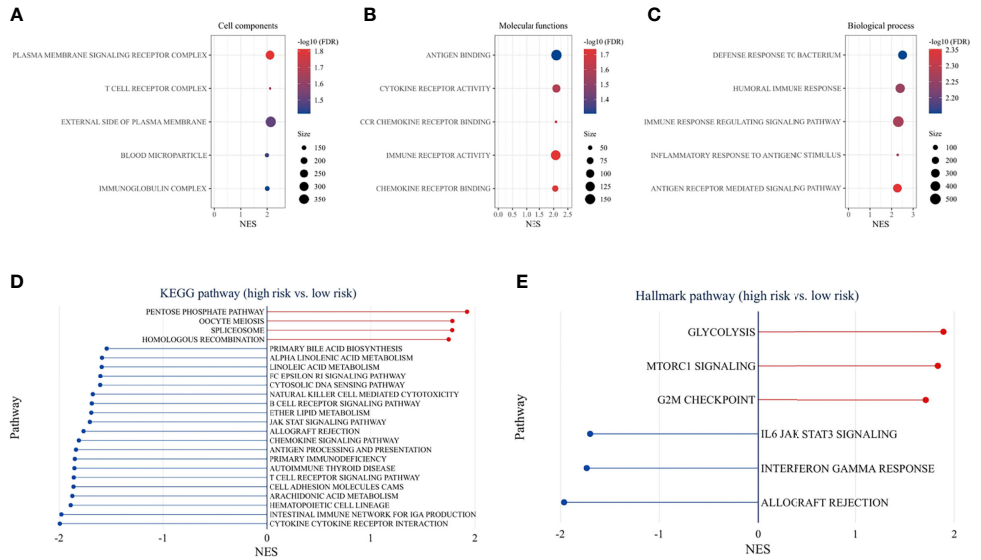

FIGURE 9 | Functional enrichment analysis. GO pathway enrichment analysis revealed top 5 GO terms in cellular components **(A)**, molecular functions **(B)**, and biological process **(C)**. KEGG pathway analysis **(D)** and hallmark pathway analysis **(E)** between the high-risk and low-risk groups ($p < 0.05$ and FDR <25% were controlled).

scores. In addition, the risk score could stratify patients with the same pathological stage, and lymphovascular invasion status. Additionally, the nomogram model further demonstrated that the risk signature can predict long-term prognosis. To assess the clinical utility of our signature, the DCA curve revealed that the nomogram joined the risk score, and clinical factors have a higher predictive efficiency than a single clinical factor. These data suggest that this immune-related risk signature can predict the prognosis of OSCC patients.

Immune cell infiltration has been reported to be an important indicator of tumor prognosis. Immune scores, as well as scores for macrophages, lymphocyte infiltration and IFN-γ response were higher in the low-risk group. These indicate a complex intratumoral immune state. Then, we analyzed the immune cell infiltration and immune-related signatures of the high-risk and low-risk groups. The risk score was negatively correlated with the infiltration ratio of immune cells, suggesting that tumor cell infiltration is indicative of better prognosis. The low-risk group had a higher proportion of anti-tumor immune cells, including activated $CD4^+$ T cells, activated $CD8^+$ T cells, and natural killer (NK) cells. In addition, we also found higher levels of immunosuppressive cells, such as Treg cells, macrophages, and myeloid-derived suppressor cells (MDSCs) in the low-risk group. $CD8^+$ T cells and NK cells, representing an activated phenotype, were higher expressed in the low-risk group, and correlated with better survival in HNSCC (36). These indicate that both anti-tumor immune cells and immunosuppressive cells are infiltrated in the TME in the low-risk group. Together, these findings suggest that the low-risk group is of the "hot tumor" phenotype, while the high-risk group is of the "cold tumor" phenotype, which could explain the difference in survival rates (37).

Consistent with immune cell infiltration phenotype, immune stimulatory factors and immune inhibitory factors were both higher expressed in the low-risk group. Co-expression of inhibitory factors had been observed following the infiltration of T cells (37, 38). The expression of negative regulatory immune checkpoints, including PD-1, PD-L2, CTLA-4, TIM3, LAG3, IDO1, and TIGIT, was relatively higher expressed in the low-risk group. The infiltration of immunosuppressive cells and elevated inhibitory pathways in the low-risk group may be negative feedback of anti-tumor immune activation. Collectively, these findings suggest that the low-risk group may be more sensitive to ICIs treatment.

To understand the mechanisms underlying the signature, functional enrichment analysis was performed between risk groups. GO analysis detected that immune-related GO terms were enriched in the low-risk group. KEGG pathway analysis showed that immune-related pathways and metabolic pathways were enriched in the low-risk group, while the PPP, spliceosome pathway, and HR pathway were enriched in the high-risk group. Further analysis of hallmark pathways revealed that glycolysis, mammalian target of rapamycin complex 1 (mTORC1) signaling, and G2/M checkpoint were enriched in the high-risk group, whereas IL6/Jak/Stat3 signaling, Interferon-γ response, and allograft rejection were enriched in the low-risk group. Recent studies have shown that IFN-γ upregulates immunosuppressive molecules such as PD-L1, PD-L2 and IDO1, in cancer and host cells (38, 39), thereby increasing the response likelihood to ICIs therapy. Cell metabolism is crucial for tumor immunity (40). On the one hand, fatty acids are required for anti-tumor effects, including the development and effector functions of $CD8^+$ T cells (41). However, it was also found that fatty acids are important for Treg survival and function (42). Fatty acid metabolism can modulate the TME, and the adaptation of immune metabolism may partly explain the immune cell infiltration and expression of immune-related genes in the TME. In the high-risk group, cancer-related pathways were activated, which promoted the malignant

transformation of the tumor and indicated a poor prognosis. Increased glycolytic activity in high-risk patients may lead to glucose competition within the TME, thereby limiting T-cell proliferation and effector functions (43). The PPP is another important metabolic pathway that helps cancer cells to meet anabolic requirements for nucleic acid synthesis, nicotinamide-adenine dinucleotide phosphate (NADPH) production, fatty acid synthesis and cell survival, as well as scavenging oxidative stress (44). Activation of mammalian target of rapamycin complex 1 (mTORC1) has been reported to stimulate PPP (45). An emerging role of spliceosome in cancer and immunity has been studied. Aberrant splicing contributes to cancer progression and immune dysregulation (46, 47). Spliceosome inhibitors have exhibited antitumor effects in cancer cells (48). The HR pathway is essential for DNA double-strand break (DSB) repair. Activation of HR in the high-risk group represented the onset of DNA damage. Higher HR deficits were found in the high-risk group, suggesting sensitivity to targeted therapy with poly ADP-ribose polymerase inhibitors (PARPi) (49) and DNA-damaging reagents (50). G2/M checkpoint was activated in the high-risk group in response to DNA damage. Small molecules targeting the G2/M checkpoint have shown promising results in preclinical studies (51). In summary, the low-risk group is the immune flamed phenotype and may potentially benefit from ICIs treatment, while targeting metabolic pathways, DNA damage or repair, and spliceosome may improve outcomes in the high-risk group.

The limitation is that the study is based on data available online. Further prospective studies with larger samples are needed to assess the clinical relevance of this signature, as well as *in vitro* and *in vivo* experimental studies to estimate its biological function in OSCC.

CONCLUSION

In summary, we have established an immune-related prognostic signature that can predict the prognosis of patients with OSCC and potentially identify patients who may benefit from immunotherapy and therapies targeting metabolic pathways, DNA damage or repair, and spliceosome. These findings may provide insights into the precise management of OSCC.

DATA AVAILABILITY STATEMENT

The datasets presented in this study can be found in online repositories. The names of the repository/repositories and accession number(s) can be found at: UCSC Xena data portal (https://xenabrowser.net), eBioPortal (https://www.cbioportal.org), GSE41613 and GSE42743 from GEO database (https://www.ncbi.nlm.nih.gov/geo/), and ImmPort database (https://www.immport.org).

ETHICS STATEMENT

Ethical review and approval was not required for the study on human participants in accordance with the local legislation and institutional requirements. Written informed consent for participation was not required for this study in accordance with the national legislation and the institutional requirements.

AUTHOR CONTRIBUTIONS

CZ designed this study and analyzed the data. CZ and LG carried out data acquisition. JL and MY helped interpret the data and prepared all figures. CZ, LG, JL, and CF wrote the manuscript. All authors contributed to the article and approved the submitted version.

FUNDING

This work was supported by the National Natural Science Foundation of China (Grant No. 82071129) and the China Scholarship Council (Grant No. 201906370170 and No. 202106375007).

SUPPLEMENTARY MATERIAL

The Supplementary Material for this article can be found online at: https://www.frontiersin.org/articles/10.3389/fonc.2021.776979/full#supplementary-material

REFERENCES

1. Chi AC, Day TA, Neville BW. Oral Cavity and Oropharyngeal Squamous Cell Carcinoma—An Update. *CA: A Cancer J Clin* (2015) 65(5):401–21. doi: 10.3322/caac.21293
2. Sung H, Ferlay J, Siegel RL, Laversanne M, Soerjomataram I, Jemal A, et al. Global Cancer Statistics 2020: GLOBOCAN Estimates of Incidence and Mortality Worldwide for 36 Cancers in 185 Countries. *CA: A Cancer J Clin* (2021) 71(3):209–49. doi: 10.3322/caac.21660
3. Siegel RL, Miller KD, Fuchs HE, Jemal A. Cancer Statistics, 2021. *CA: A Cancer J Clin* (2021) 71(1):7–33. doi: 10.3322/caac.21654
4. Schreiber RD, Old LJ, Smyth MJ. Cancer Immunoediting: Integrating Immunity's Roles in Cancer Suppression and Promotion. *Science* (2011) 331(6024):1565–70. doi: 10.1126/science.1203486
5. Waldman AD, Fritz JM. Lenardo MJ. A Guide to Cancer Immunotherapy: From T Cell Basic Science to Clinical Practice. *Nat Rev Immunol* (2020) 20 (11):651–68. doi: 10.1038/s41577-020-0306-5
6. Ferris RL, Blumenschein G Jr, Fayette J, Guigay J, Colevas AD, Licitra L, et al. Nivolumab for Recurrent Squamous-Cell Carcinoma of the Head and Neck. *N Engl J Med* (2016) 375(19):1856–67. doi: 10.1056/NEJMoa 1602252
7. Cohen EEW, Soulieres D, Le Tourneau C, Dinis J, Licitra L, Ahn MJ, et al. Pembrolizumab Versus Methotrexate, Docetaxel, or Cetuximab for Recurrent or Metastatic Head-and-Neck Squamous Cell Carcinoma (KEYNOTE-040): A Randomised, Open-Label, Phase 3 Study. *Lancet* (2019) 393(10167):156–67. doi: 10.1016/S0140-6736(18)31999-8
8. Lohavanichbutr P, Méndez E, Holsinger FC, Rue TC, Zhang Y, Houck J, et al. A 13-Gene Signature Prognostic of HPV-Negative OSCC: Discovery and

External Validation. *Clin Cancer Res* (2013) 19(5):1197–203. doi: 10.1158/1078-0432.Ccr-12-2647
9. Gautier L, Cope L, Bolstad BM, Irizarry RA. Affy—Analysis of Affymetrix GeneChip Data at the Probe Level. *Bioinformatics* (2004) 20(3):307–15. doi: 10.1093/bioinformatics/btg405
10. Ritchie ME, Phipson B, Wu D, Hu Y, Law CW, Shi W, et al. Limma Powers Differential Expression Analyses for RNA-Sequencing and Microarray Studies. *Nucleic Acids Res* (2015) 43(7):e47. doi: 10.1093/nar/gkv007
11. Bhattacharya S, Dunn P, Thomas CG, Smith B, Schaefer H, Chen J, et al. ImmPort, Toward Repurposing of Open Access Immunological Assay Data for Translational and Clinical Research. *Sci Data* (2018) 5(1):180015. doi: 10.1038/sdata.2018.15
12. Friedman JH, Hastie T, Tibshirani R. Regularization Paths for Generalized Linear Models. *Via Coordinate Descent 2010* (2010) 33(1):22. doi: 10.18637/jss.v033.i01
13. Blanche P, Dartigues J-F, Jacqmin-Gadda H. Estimating and Comparing Time-Dependent Areas Under Receiver Operating Characteristic Curves for Censored Event Times With Competing Risks. *Stat Med* (2013) 32(30):5381–97. doi: 10.1002/sim.5958
14. Therneau TM. *A Package for Survival Analysis in R*. New York: Springer (2021).
15. Charoentong P, Finotello F, Angelova M, Mayer C, Efremova M, Rieder D, et al. Pan-Cancer Immunogenomic Analyses Reveal Genotype-Immunophenotype Relationships and Predictors of Response to Checkpoint Blockade. *Cell Rep* (2017) 18(1):248–62. doi: 10.1016/j.celrep.2016.12.019
16. Hanzelmann S, Castelo R, Guinney J. GSVA: Gene Set Variation Analysis for Microarray and RNA-Seq Data. *BMC Bioinf* (2013) 14(1):7. doi: 10.1186/1471-2105-14-7
17. Core Team R. *R: A Language and Environment for Statistical Computing*. Vienna, Austria: R Foundation for Statistical Computing (2021).
18. Yoshihara K, Shahmoradgoli M, Martinez E, Vegesna R, Kim H, Torres-Garcia W, et al. Inferring Tumour Purity and Stromal and Immune Cell Admixture From Expression Data. *Nat Commun* (2013) 4(1):2612. doi: 10.1038/ncomms3612
19. Thorsson V, Gibbs DL, Brown SD, Wolf D, Bortone DS, Ou Yang TH, et al. The Immune Landscape of Cancer. *Immunity* (2018) 48(4):812–30.e14. doi: 10.1016/j.immuni.2018.03.023
20. Wickham H. *Ggplot2: Elegant Graphics for Data Analysis*. New York: Springer-Verlag (2016).
21. Subramanian A, Tamayo P, Mootha VK, Mukherjee S, Ebert BL, Gillette MA, et al. Gene Set Enrichment Analysis: A Knowledge-Based Approach for Interpreting Genome-Wide Expression Profiles. *Proc Natl Acad Sci U.S.A.* (2005) 102(43):15545–50. doi: 10.1073/pnas.0506580102
22. Grivennikov SI, Greten FR, Karin M. Immunity, Inflammation, and Cancer. *Cell* (2010) 140(6):883–99. doi: 10.1016/j.cell.2010.01.025
23. Troiano G, Rubini C, Togni L, Caponio VCA, Zhurakivska K, Santarelli A, et al. The Immune Phenotype of Tongue Squamous Cell Carcinoma Predicts Early Relapse and Poor Prognosis. *Cancer Med* (2020) 9(22):8333–44. doi: 10.1002/cam4.3440
24. Georgila K, Vyrla D, Drakos E. Apolipoprotein A-I (ApoA-I), Immunity, Inflammation and Cancer. *Cancers* (2019) 11(8):1097. doi: 10.3390/cancers11081097
25. Roche FP, Pietilä I, Kaito H, Sjöström EO, Sobotzki N, Noguer O, et al. Leukocyte Differentiation by Histidine-Rich Glycoprotein/Stanniocalcin-2 Complex Regulates Murine Glioma Growth Through Modulation of Antitumor Immunity. *Mol Cancer Ther* (2018) 17(9):1961–72. doi: 10.1158/1535-7163.Mct-18-0097
26. Murdocca M, De Masi C, Pucci S, Mango R, Novelli G, Di Natale C, et al. LOX-1 and Cancer: An Indissoluble Liaison. *Cancer Gene Ther* (2021) 28:1088–98. doi: 10.1038/s41417-020-00279-0
27. Esseghir S, Kennedy A, Seedhar P, Nerurkar A, Poulsom R, Reis-Filho JS, et al. Identification of NTN4, TRA1, and STC2 as Prognostic Markers in Breast Cancer in a Screen for Signal Sequence Encoding Proteins. *Clin Cancer Res* (2007) 13(11):3164–73. doi: 10.1158/1078-0432.Ccr-07-0224
28. Haas MS, Kagey MH, Heath H, Schuerpf F, Rottman JB, Newman W. mDKN-01, a Novel Anti-DKK1 mAb, Enhances Innate Immune Responses in the Tumor Microenvironment. *Mol Cancer Res* (2021) 19(4):717–25. doi: 10.1158/1541-7786.Mcr-20-0799
29. D'Amico L, Mahajan S, Capietto A-H, Yang Z, Zamani A, Ricci B, et al. Dickkopf-Related Protein 1 (Dkk1) Regulates the Accumulation and Function of Myeloid Derived Suppressor Cells in Cancer. *J Exp Med* (2016) 213(5):827–40. doi: 10.1084/jem.20150950
30. Deng C, Lin Y-X, Qi X-K, He G-P, Zhang Y, Zhang H-J, et al. TNFRSF19 Inhibits Tgfβ Signaling Through Interaction With Tgfβ Receptor Type I to Promote Tumorigenesis. *Cancer Res* (2018) 78(13):3469–83. doi: 10.1158/0008-5472.Can-17-3205
31. Loftus JC, Dhruv H, Tuncali S, Kloss J, Yang Z, Schumacher CA, et al. TROY (TNFRSF19) Promotes Glioblastoma Survival Signaling and Therapeutic Resistance. *Mol Cancer Res* (2013) 11(8):865–74. doi: 10.1158/1541-7786.Mcr-13-0008
32. Gough MJ, Ruby CE, Redmond WL, Dhungel B, Brown A, Weinberg AD. OX40 Agonist Therapy Enhances CD8 Infiltration and Decreases Immune Suppression in the Tumor. *Cancer Res* (2008) 68(13):5206–15. doi: 10.1158/0008-5472.Can-07-6484
33. Han Q, Wang R, Sun C, Jin X, Liu D, Zhao X, et al. Human Beta-Defensin-1 Suppresses Tumor Migration and Invasion and Is an Independent Predictor for Survival of Oral Squamous Cell Carcinoma Patients. *PloS One* (2014) 9(3):e91867. doi: 10.1371/journal.pone.0091867
34. Hodi FS, O'Day SJ, McDermott DF, Weber RW, Sosman JA, Haanen JB, et al. Improved Survival With Ipilimumab in Patients With Metastatic Melanoma. *New Engl J Med* (2010) 363(8):711–23. doi: 10.1056/NEJMoa1003466
35. Huang GZ, Wu QQ, Zheng ZN, Shao TR, Li F, Lu XY, et al. Bioinformatics Analyses Indicate That Cathepsin G (CTSG) Is a Potential Immune-Related Biomarker in Oral Squamous Cell Carcinoma (OSCC). *Onco Targets Ther* (2021) 14:1275–89. doi: 10.2147/OTT.S293148
36. Mandal R, Şenbabaoğlu Y, Desrichard A, Havel JJ, Dalin MG, Riaz N, et al. The Head and Neck Cancer Immune Landscape and Its Immunotherapeutic Implications. *JCI Insight* (2016) 1(17):e89829. doi: 10.1172/jci.insight.89829
37. Hanna GJ, Liu H, Jones RE, Bacay AF, Lizotte PH, Ivanova EV, et al. Defining an Inflamed Tumor Immunophenotype in Recurrent, Metastatic Squamous Cell Carcinoma of the Head and Neck. *Oral Oncol* (2017) 67:61–9. doi: 10.1016/j.oraloncology.2017.02.005
38. Spranger S, Spaapen RM, Zha Y, Williams J, Meng Y, Ha TT, et al. Up-Regulation of PD-L1, IDO, and T(regs) in the Melanoma Tumor Microenvironment Is Driven by CD8(+) T Cells. *Sci Transl Med* (2013) 5(200):200ra116. doi: 10.1126/scitranslmed.3006504
39. Ayers M, Lunceford J, Nebozhyn M, Murphy E, Loboda A, Kaufman DR, et al. IFN-γ–Related mRNA Profile Predicts Clinical Response to PD-1 Blockade. *J Clin Invest* (2017) 127(8):2930–40. doi: 10.1172/JCI91190
40. Bader JE, Voss K, Rathmell JC. Targeting Metabolism to Improve the Tumor Microenvironment for Cancer Immunotherapy. *Mol Cell* (2020) 78(6):1019–33. doi: 10.1016/j.molcel.2020.05.034
41. Zhang Y, Kurupati R, Liu L, Zhou XY, Zhang G, Hudaihed A, et al. Enhancing $CD8^+$ T Cell Fatty Acid Catabolism Within a Metabolically Challenging Tumor Microenvironment Increases the Efficacy of Melanoma Immunotherapy. *Cancer Cell* (2017) 32(3):377–91.e9. doi: 10.1016/j.ccell.2017.08.004
42. Wang H, Franco F, Tsui Y-C, Xie X, Trefny MP, Zappasodi R, et al. CD36-Mediated Metabolic Adaptation Supports Regulatory T Cell Survival and Function in Tumors. *Nat Immunol* (2020) 21(3):298–308. doi: 10.1038/s41590-019-0589-5
43. Chang C-H, Qiu J, O'Sullivan D, Buck Michael D, Noguchi T, Curtis Jonathan D, et al. Metabolic Competition in the Tumor Microenvironment Is a Driver of Cancer Progression. *Cell* (2015) 162(6):1229–41. doi: 10.1016/j.cell.2015.08.016
44. Patra KC, Hay N. The Pentose Phosphate Pathway and Cancer. *Trends Biochem Sci* (2014) 39(8):347–54. doi: 10.1016/j.tibs.2014.06.005
45. Düvel K, Yecies JL, Menon S, Raman P, Lipovsky AI, Souza AL, et al. Activation of a Metabolic Gene Regulatory Network Downstream of mTOR Complex 1. *Mol Cell* (2010) 39(2):171–83. doi: 10.1016/j.molcel.2010.06.022
46. Yang H, Beutler B, Zhang D. Emerging Roles of Spliceosome in Cancer and Immunity. *Protein Cell* (2021). doi: 10.1007/s13238-021-00856-5
47. El Marabti E, Younis I. The Cancer Spliceome: Reprograming of Alternative Splicing in Cancer. *Front Mol Biosci* (2018) 5:80(80). doi: 10.3389/fmolb.2018.00080
48. Zhang D, Hu Q, Liu X, Ji Y, Chao H-P, Liu Y, et al. Intron Retention is a Hallmark and Spliceosome Represents a Therapeutic Vulnerability in Aggressive Prostate Cancer. *Nat Commun* (2020) 11(1):2089. doi: 10.1038/s41467-020-15815-7

49. Mateo J, Carreira S, Sandhu S, Miranda S, Mossop H, Perez-Lopez R, et al. DNA-Repair Defects and Olaparib in Metastatic Prostate Cancer. *N Engl J Med* (2015) 373(18):1697–708. doi: 10.1056/NEJMoa1506859
50. Lord CJ, Ashworth A. BRCAness Revisited. *Nat Rev Cancer* (2016) 16(2):110–20. doi: 10.1038/nrc.2015.21
51. Visconti R, Della Monica R, Grieco D. Cell Cycle Checkpoint in Cancer: A Therapeutically Targetable Double-Edged Sword. *J Exp Clin Cancer Res* (2016) 35(1):153. doi: 10.1186/s13046-016-0433-9

Conflict of Interest: The authors declare that the research was conducted in the absence of any commercial or financial relationships that could be construed as a potential conflict of interest.

frontiers in Oncology

ORIGINAL RESEARCH
published: 03 January 2022
doi: 10.3389/fonc.2021.713815

Prediction Model of Distant Metastasis in Oral Cavity Squamous Cell Carcinoma With or Without Regional Lymphatic Metastasis

*Hsueh-Ju Lu[1,2], Yu-Wei Chiu[3,4], Wen-San Lan[5], Chih-Yu Peng[3,4], Hsien-Chun Tseng[2,6], Chung-Han Hsin[2,7], Chun-Yi Chuang[2,7], Chun-Chia Chen[2,8], Wei-Shiou Huang[1,2] and Shun-Fa Yang[5,9]**

[1] Division of Hematology and Oncology, Department of Internal Medicine, Chung Shan Medical University Hospital, Taichung, Taiwan, [2] School of Medicine, Chung Shan Medical University, Taichung, Taiwan, [3] Department of Dentistry, Chung Shan Medical University Hospital, Taichung, Taiwan, [4] School of Dentistry, Chung Shan Medical University, Taichung, Taiwan, [5] Institute of Medicine, Chung Shan Medical University, Taichung, Taiwan, [6] Department of Radiation Oncology, Chung Shan Medical University Hospital, Taichung, Taiwan, [7] Department of Otolaryngology, Chung Shan Medical University Hospital, Taichung, Taiwan, [8] Division of Plastic Surgery, Department of Surgery, Chung Shan Medical University Hospital, Taichung, Taiwan, [9] Department of Medical Research, Chung Shan Medical University Hospital, Taichung, Taiwan

OPEN ACCESS

Edited by:
Shiyu Song,
Virginia Commonwealth University Health System, United States

Reviewed by:
Shahram Ghanaati,
Goethe University Frankfurt, Germany
Li-Ang Lee,
Linkou Chang Gung Memorial Hospital, Taiwan

***Correspondence:**
Shun-Fa Yang
ysf@csmu.edu.tw

Specialty section:
This article was submitted to Head and Neck Cancer, a section of the journal Frontiers in Oncology

Received: 24 May 2021
Accepted: 08 December 2021
Published: 03 January 2022

Citation:
Lu H-J, Chiu Y-W, Lan W-S, Peng C-Y, Tseng H-C, Hsin C-H, Chuang C-Y, Chen C-C, Huang W-S and Yang S-F (2022) Prediction Model of Distant Metastasis in Oral Cavity Squamous Cell Carcinoma With or Without Regional Lymphatic Metastasis. Front. Oncol. 11:713815. doi: 10.3389/fonc.2021.713815

Patients with oral cavity squamous cell carcinoma (OCSCC) who develop distant metastasis (DM) face poor outcomes, and effective prediction models of DM are rare. A total of 595 patients with OCSCC were retrospectively enrolled in this study. Because pathological N staging significantly influences the development and mechanisms of DM, the patients were divided into nodal-negative (pN–) and -positive (pN+) groups. Clinical outcomes, prognoses, and prediction models were analyzed separately for both groups. Overall, 8.9% (53/595) of these patients developed DM. Among the DM cases, 84.9% (45/53) of them developed DM within the first 3 years. The median overall survival, locoregional recurrence-free survival, time until DM development, and postmetastatic survival were 19.8, 12.7, 14.6, and 4.1 months, respectively. Distinguishing patients who only developed locoregional recurrence from those with DM according to locoregional conditions was difficult. Age, surgical margin, and early locoregional recurrence were predictors of DM that were independent of time until DM in the pN– group; the lymphocyte-to-monocyte ratio, presence of lymphovascular invasion, and early locoregional recurrence in the pN+ group were determined. If one point was scored for each factor, then two scoring systems were used to classify the patients into low- (score = 0), intermittent- (score = 1), or high- (score = 2 or 3) risk for the pN– and pN+ groups. According to this scoring system, the 3-year DM rates for the low, intermittent, and high risk subgroups were 0.0%, 5.9%, and 17.8% for the pN– group and 7.1%, 44.9%, and 82.5% for the pN+ group, respectively. These systems also effectively predicted DM, and

the areas under the curve predicted DM occurring within the first 3 years were 0.744 and 0.820 for the pN– and pN+ groups, respectively. In conclusion, effective scoring models were established for predicting DM.

Keywords: oral cavity squamous cell carcinoma, distant metastasis, lymphatic metastasis, prediction model, oral cancer

INTRODUCTION

Oral cavity squamous cell carcinoma (OCSCC) is one of the most common types of head and neck squamous cell carcinoma (HNSCC), which is the sixth most common cancer globally and the fourth most common cancer in the Taiwanese male population (1, 2). In addition, 5% to 15% of patients with curative OCSCC develop distant metastasis (DM) during follow-up, for which the prognosis is poor (3–5). The median survival rate is 12.5 mo for those with metastatic HNSCC (6) and 3 mo for those with metastatic OCSCC (4). Thus, metastatic OCSCC research and management is critical.

Unlike locoregional recurrence, for which salvage surgery is a curative option, metastatic OCSCC can generally only be treated with palliative therapies (7–9). Although approved novel agents could prolong survival, most provide no long-term clinical benefit (7–9). The outcomes of DM are also influenced by its clinical presentation; several studies have reported that the number of metastatic lesions significantly influences the survival rates of patients with DM (4, 6). Patients who develop single metastasis or oligometastasis have higher survival rates than do those who develop multiple metastases (4, 6). Unfortunately, most lesions form multiple metastases, with 15% to 30% of cases of DM detected during follow-up for a single metastasis or oligometastasis. Metastatic-direct therapy, such as surgical resection, radiotherapy, and radiofrequency ablation, also influences survival rates, but only cases of single metastasis or oligometastasis are suitable for these aggressive therapy treatments (6). Therefore, the early detection of single and oligometastatic lesions is crucial and influences the outcomes and choice of metastatic-direct therapy.

These single and oligometastatic lesions can be detected through regular screening, but because of the relatively low rate of DM among patients with OCSCC, the cost-effectiveness of regular screening for these patients must be considered. Effective biomarkers that predict DM may provide a suitable method for selecting eligible patients for screening. Several studies have discussed predicting DM (4, 5, 10–14), and pathological neck lymph node involvement was considered to significantly influence the development of DM (15, 16). The primary tumor was long thought to passively permeate the lymphatic system and spread to the regional lymph nodes; the permeated tumor cells would then enter the lymph node vasculature and disseminate to distant organs through the lymphatic system or blood vessel system (17). However, some patients can develop DM without initial pathological neck lymph node involvement (5). The DM model now considers the additional effects of components of primary tumor biology, such as tumor microenvironment, the vascular endothelial growth factor family, and epithelial-mesenchymal transition (17). Primary tumors actively enter the primary tumor lymphatics and primary tumor vasculature simultaneously. The tumor cells then directly metastasize to distant organs through both of these systems. Because the mechanisms of DM can differ between patients with and without neck lymph metastasis, prediction models should be formulated independent of this factor. In addition, though these models should ideally be applied to all patients with OCSCC, only clinicopathological variables are analyzed because these factors can be widely available in clinical settings.

In this study, we enrolled all patients newly diagnosed with OCSCC at Chung Shan Medical University Hospital between 2010 and 2016. Data regarding clinicopathological variables were retrospectively extracted and analyzed. Because pathological N status is highly influential to the DM development (4, 5), the predictors for the patients were analyzed with or without the presence of regional lymph node metastasis. Enrollees were divided into nodal-negative and -positive groups, and the clinical outcomes, prognoses, and the prediction models of these groups were analyzed separately. We hope that these models can be applied in clinical practice, especially in the early detection of DM.

METHODS AND MATERIALS

Study Design, Research Setting, and Patient Selection

This was a single-institute cohort study. Patients newly diagnosed with OCSCC at Chung Shan Medical University Hospital between January 2010 and December 2016 were retrospectively enrolled. The patients were staged according to the American Joint Committee on Cancer staging system (seventh edition) (18) and underwent curative resection at initial diagnosis. At the timing of screening, the patients with locoregional recurrence but who were not newly diagnosed or who experienced secondary primary malignancies were excluded because the factors, such as tumor recurrence and metastatic lesions from secondary primary malignancies, might influence the calculation of time-dependent prognostic and predictive factors. The other exclusion criteria were as follows: patients who did not undergo curative surgery, who received a previous diagnosis and treatment for other HNSCCs, and/or those classified as stage IVC at initial diagnosis. This study was approved by the institutional review board of Chung Shan Medical University Hospital (IRB No. CS2-20050).

Clinical Characteristics

The clinical data we recorded were the same as those in our previous study and were accessed from the patients' medical charts (19). We took note of the basic clinicopathological variables included age, sex, primary tumor features (location, staging, and pathological features), and nodal conditions. Adjuvant therapy, included adjuvant chemoradiotherapy, adjuvant radiotherapy, and adjuvant chemotherapy, were also documented. Biochemistry laboratory data documented within 7 d before curative surgery were also compiled. DM-associated information was recorded, such as the numbers and sites of metastatic lesions and their subsequent treatments.

Classification of Patients With and Without Pathological Neck Lymph Node Involvement

Lymphatic and blood vessels are the two primary systems that allow tumor cells to develop into regional metastasis or DM. Because the mechanisms of DM development through the lymphatic or blood vessel systems may differ (17), the phenotypes and predictors are discussed separately herein. Our patients were divided into nodal-negative and -positive groups according to their initial pathological N stage, which was determined in order to identify the influence of regional lymph node metastasis. The patients of both groups were then classified into disease-free status (without disease progression), locoregional recurrence only, and DM with any locoregional status groups to discuss the impact of distant metastasis in clinical outcomes. Prognostic factors and prediction models for DM were separately established for both nodal-negative and -positive groups (**Figure 1**).

Definition of DM

At the time of writing, monitoring of patients with OCSCC includes imaging studies, such as computed tomography (CT), magnetic resonance imaging (MRI), positron emission tomography-computed tomography, and whole-body bone scanning. Patients should undergo CT and MRI every 3 to 6 mo for the first 2 y and then every 6 to 12 mo in the next 3 to 5 y after curative treatment. PET-CT is conducted when the status of the primary lesion cannot be ascertained *via* CT or MRI. Whole body bone scan (WBBS) should be performed every 6 mo in the

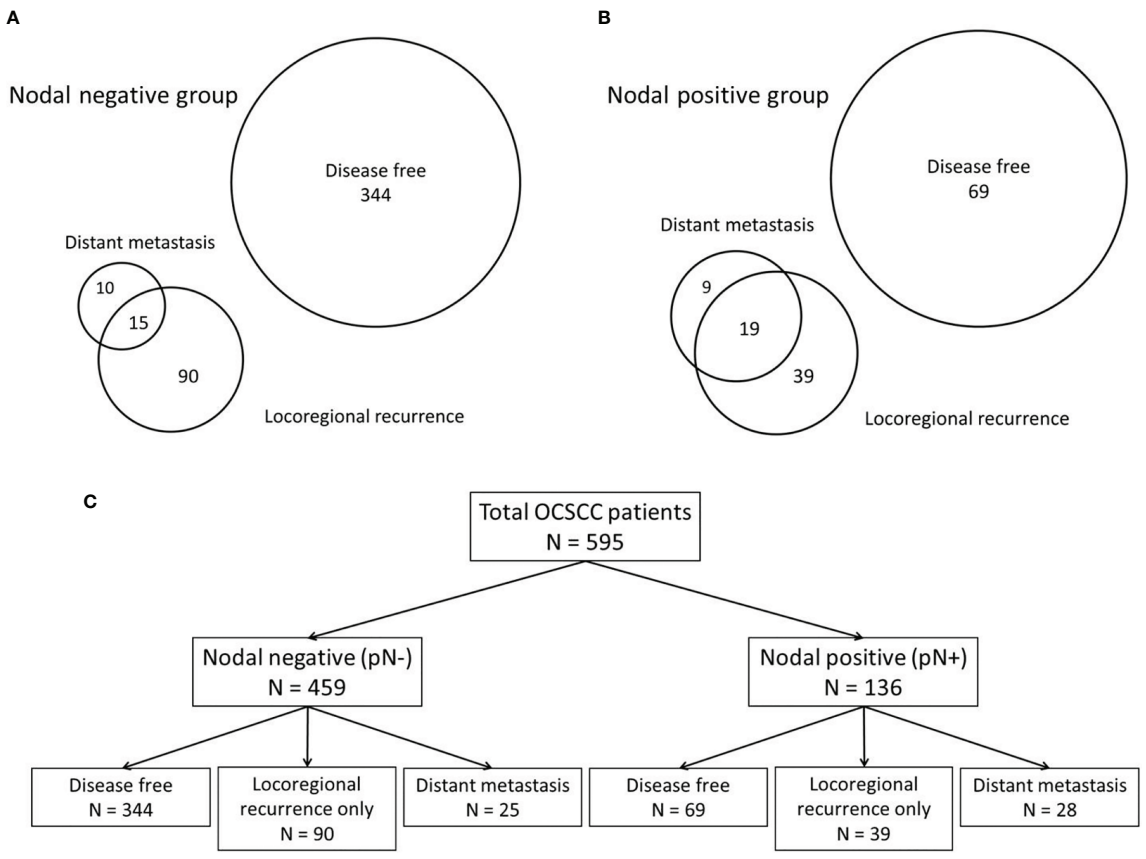

FIGURE 1 | The patients were classified according to their patterns of disease progression. According to the patterns of disease progression, the patients were classified into those with disease-free development (without disease progression), locoregional recurrence only, and distant metastasis with any locoregional status. **(A)** Venn diagram of the nodal-negative group. **(B)** Venn diagram of the nodal-positive group. **(C)** The classifications of both the nodal-negative and -positive groups according to the patterns of disease progression.

first year and then performed again if patients report local bone pain. Here, the imaging studies were evaluated by two independent radiologists; if they could not reach a consensus, then the equivocal patterns were discussed at tumor board conferences.

Statistical Analysis

Overall survival (OS) was calculated from the date of diagnosis to the date of death or last follow-up. The locoregional recurrence-free survival (LRFS) rate was calculated from the date of disease diagnosis to the date of local or regional recurrence. Time until DM was defined as the date of disease diagnosis until the date of detection of DM. Postmetastatic survival (PMS) was calculated from the date of DM detection to the date of death or the last follow-up.

Correlations between the clinicopathological parameters were analyzed using a χ^2 or Fisher's exact test. Cox forward stepwise regression analyses were used to identify the independent factors for PMS and for the time until DM. Only the variables with P values of <.05 in univariate analyses were enrolled in the forward multivariate analysis. A two-sided P value of <.05 was statistically significant. We utilized the time-dependent receiver operating characteristic (ROC) curve in our prediction models (20). Survival analyses were estimated using the Kaplan-Meier method, and the log-rank test was used to compare the survival curves. SPSS (version 21.0, IBM Corp., Armonk, NY, USA) was used for all statistical analyses.

RESULTS

Baseline Characteristics

A total of 595 patients newly diagnosed with OCSCC were retrospectively enrolled in this study. These patients received curative surgical resection. The patients at recurrent stages or with secondary primary malignancies were excluded. In accordance with the initial pathological N staging, the patients were divided into nodal-negative (77.1% [459/595]) and -positive groups (22.9% [136/595]). Mean age of all was 53.9 (28.3-90.3) (nodal-negative group, 53.9 [28.3-90.3]; nodal-positive group, 54.2 [29.2-88.2]) (**Figure S1**). Overall, 8.9% (53/595) of the included patients developed DM during the follow-up period (5.4% [25/459] and 20.6% [28/136] for the nodal-negative and -positive groups, respectively). The basic patient characteristics are presented in **Table 1**.

Clinical Outcomes

In accordance with disease progression patterns, the patients were classified as disease-free (without disease progression), having locoregional recurrence only, and having DM with any locoregional status. The distributions of the progression patterns were significantly different between the nodal-negative and -positive groups (P <.001). The percentage of these three patterns were 72.8% (334/459), 19.6% (90/459), and 5.4% (25/459) in the nodal-negative group, and 50.7% (69/136), 28.7% (39/136), and 20.6% (28/136) in the nodal-positive group (**Figure 1**).

For all included OCSCC patients, the OSs of the patients who were disease-free (without disease progression), had locoregional recurrence only, and had DM with any locoregional status were significantly different. 3-y OS of these three patterns were 93.1%, 56.8%, and 22.1%, respectively (P <.001), and 5-y OS were 88.5%, 47.5%, and 12.3%, respectively (P <.001) (**Figure 2A**). In both the nodal-negative and -positive groups, the patients who developed DM had also significantly poorer OS than those of the patients without DM (**Figures 2B, C**).

However, the patients who developed locoregional recurrence only and DM with any locoregional status had similar 6-mo LRFS rates (77.5% and 74.0%, respectively, P = .344) (**Figure 2D**). For the nodal-negative group, the 6-mo LRFS rates of these two progression patterns were 80.0% and 87.5%, respectively (P = .338) (**Figure 2E**). And for the nodal-positive group, the 6-mo LRFS rates were 71.8% and 61.5%, respectively (P = .275) (**Figure 2F**). Although the patients who developed DM had poor outcomes, it was difficult to distinguish the patients who developed DM or locoregional recurrence only according to the phenotypes of early locoregional recurrence. Effective predictive models are required to ensure that patients at risk of DM undergo regular screening for the early detection of DM.

Patients Who Developed DM

For the patients who developed DM, the most common metastatic sites were the lung (67.9%), bone (43.4%), and mediastinal lymph node (28.3%). Most metastases (64.2% [34/53]) were multiple metastatic lesions (metastatic lesions ≥ 3). The basic characteristics of the patients who developed DM are listed in **Table 2**.

The median OS of the patients who developed DM was 19.8 mo (28.0 and 17.3 mo for the nodal-negative and -positive groups, respectively, P = .009). The median LRFS period was 12.7 mo (16.1 and 8.3 mo, respectively, P = .105). The median time until DM was 14.6 mo (19.2 and 10.8 mo, respectively, P = .013). And PMS was only 4.1 mo (5.4 and 3.3 mo, respectively, P = .349). Almost 85% (84.9% [45/53]) of the DM events occurred within the first 3 y (nodal-negative group: 76% [19/25]; nodal positive group: 92.9% [26/28]) (**Figure 3**).

Histologically poor differentiation (hazard ratio [HR] 95% confidence interval [CI]: 2.39 [1.13–5.06], P = .023) and pleural metastasis (HR [95% CI]: 3.88 [1.67–9.00], P = .002) were independent factors for PMS. The number of metastatic lesions (HR [95% CI]: 2.01 [1.04–3.90], P = .037) was also a significant factor in the univariate analysis (**Table S1**).

The Role of Adjuvant Therapy in DM

The distributions of patients receiving adjuvant therapy or not were the same in both the nodal-negative and -positive groups (P = .231, and.335, respectively) (**Table 1**). Among the patients with DM, 47.2% (25/53) of them had received adjuvant therapy. The advanced staging (nodal-positive) group had a greater administration of adjuvant therapy than did the lower staging (nodal-negative) group (nodal-positive vs. -negative, 57.1% vs. 36.0%, P = .017) (**Table 2**). Although adjuvant therapy did not impact time until DM in statistics, it seemed to be a trend that adjuvant therapy decreased DM occurrence in the nodal-positive group (HR: 0.869, P = .694) (**Table S2**).

TABLE 1 | Basic characteristics of OCSCC patients with or without distant metastasis.

	pN negative			pN positive		
	Non-distant metastasis N = 434	**Distant metastasis N = 25**	***P* value**	**Non-distant metastasis N = 108**	**Distant metastasis N = 28**	***P* value**
Age ≥ 65 y	61 (14.1)	8 (32.0)	**0.022**	15 (13.9)	3 (10.7)	0.467
Male	400 (92.2)	22 (88.0)	0.327	95 (88.0)	22 (78.6)	0.164
Personal history						
Smoking	302/431 (70.1)	13/25 (52.0)	**0.050**	72/107 (67.3)	16/28 (57.1)	0.216
Alcohol	252/428 (58.9)	12/25 (48.0)	0.193	74/107 (69.2)	16/28 (57.1)	0.164
Betel nut	294/431 (68.2)	17/25 (68.0)	0.569	74/108 (68.5)	20/28 (71.4)	0.483
Primary tumor site			0.173			0.437
Check mucosa	162 (37.3)	12 (48.0)		41 (38.0)	8 (28.6)	
Oral tongue	136 (31.3)	5 (20.0)		33 (30.6)	8 (28.6)	
Gum	73 (16.8)	4 (16.0)		19 (17.6)	7 (25.0)	
Lip	40 (9.2)	2 (8.0)		8 (7.4)	1 (3.6)	
Mouth floor	13 (3.0)	0 (0.0)		4 (3.8)	1 (3.6)	
Retromolar trigone	5 (1.2)	0 (0.0)		1 (0.9)	1 (3.6)	
Hard palate	2 (0.5)	1 (4.0)		0 (0.0)	1 (3.6)	
Others	3 (0.7)	1 (4.0)		2 (1.9)	1 (3.6)	
Pathologic T staging						
T1-T2	363 (83.6)	16 (64.0)	**0.018**	68 (63.6)	12 (46.2)	0.081
T3-T4	71 (16.4)	9 (36.0)		39 (36.4)	14 (53.8)	
Pathologic N staging			NA			0.203
N0	434 (100.0)	25 (100.0)		0 (0.0)	0 (0.0)	
N1	0 (0.0)	0 (0.0)		47 (43.5)	7 (25.0)	
N2A	0 (0.0)	0 (0.0)		0 (0.0)	0 (0.0)	
N2B	0 (0.0)	0 (0.0)		58 (53.7)	20 (71.4)	
N2C	0 (0.0)	0 (0.0)		3 (2.8)	1 (3.6)	
N3	0 (0.0)	0 (0.0)		0 (0.0)	0 (0.0)	
Pathologic TNM staging			**0.019**			NA
Stage I-II	362 (83.4)	16 (16.6)		0 (0.0)	0 (0.0)	
Stage III-IV	72 (16.6)	9 (36.0)		107 (100)	26 (100)	
Histological grade			0.465			0.550
Well	153 (35.3)	6 (20.0)		9 (8.3)	2 (7.1)	
Moderately	237 (54.6)	18 (72.0)		78 (72.2)	17 (60.7)	
Poorly	32 (7.4)	2 (8.0)		19 (17.6)	8 (28.6)	
Undifferentiated	1 (0.2)	0 (0.0)		0 (0.0)	0 (0.0)	
Unknown	11 (2.5)	0 (0.0)		2 (1.9)	1 (3.6)	
Pathologic feature						
Primary tumor size ≥ 2 cm	198/432 (45.8)	13/25 (52.0)	0.345	78/107 (72.9)	26/28 (92.9)	**0.018**
Extracapsular spread	NA	NA	NA	46/108 (42.6)	11/28 (39.3)	0.463
Depth of invasion ≥ 1 cm	92/394 (23.4)	10/24 (41.7)	**0.042**	43/91 (47.3)	15/21 (71.4)	**0.038**
Lymphovascular invasion	12/405 (3.0)	0/25 (0.0)	0.483	19/103 (18.4)	10/25 (40.0)	**0.024**
Perineural invasion	97/405 (24.0)	7/25 (28.0)	0.400	66/104 (63.5)	19/24 (79.2)	0.108
Surgical margin	264/412 (64.1)	20/25 (80.0)	0.076	74/101 (73.3)	19/26 (73.1)	0.582
Pathologic nodal status						
Lymph node dissection	330/434 (76.0)	18/25 (72.0)	0.400	108/108 (100.0)	28/28 (100.0)	NA
Number of LN dissection ≥15	288/434 (66.4)	17/25 (68.0)	0.528	97/107 (90.4)	23/27 (85.2)	0.301
Positive lymph node ≥ 3	NA	NA	NA	38/107 (35.5)	15/27 (55.6)	**0.047**
Lymph node ratio ≥ 6%	NA	NA	NA	64/107 (59.8)	20/27 (74.1)	0.125
Adjuvant therapy			0.231			0.335
Adjuvant chemoradiotherapy	47 (10.8)	5 (20.0)		50 (46.3)	16 (57.1)	
Adjuvant radiotherapy	51 (11.8)	3 (12.0)		9 (8.3)	0 (0.0)	
Adjuvant chemotherapy	4 (0.9)	1 (4.0)		2 (1.9)	0 (0.0)	
None	332 (76.5)	16 (64.0)		47 (43.5)	12 (42.9)	
Locoregional recurrence < 6 m	17/412 (4.1)	3/24 (12.5)	0.090	11/102 (10.8)	10/26 (38.5)	**0.002**
Preoperative biochemistry data						
White blood count > 10,000/μL	42/400 (10.5)	3/24 (12.5)	0.479	20/102 (19.6)	3/24 (12.5)	0.314
Hemoglobin < 10g/dL	7/400 (1.8)	0/24 (0.0)	0.663	9/102 (8.8)	4/24 (16.7)	0.215
Platelet count > 450,000/μ)	3/400 (0.8)	0/24 (0.0)	0.839	3/102 (2.9)	0/24 (0.0)	0.527
N/L ratio > 2.5	158/370 (42.7)	14/24 (58.3)	0.100	39/98 (39.8)	14/24 (58.3)	0.079
Lymph/Mono < 2.5	25/370 (6.8)	2/24 (8.3)	0.503	9/98 (9.2)	5/24 (20.8)	0.110
Lymph/PLT ratio <0.01	247/369 (66.9)	20/24 (83.3)	0.070	77/98 (78.6)	22/24 (91.7)	0.115

NA, not applicable.

Bold values mean that P value of <.05 was statistically significant.

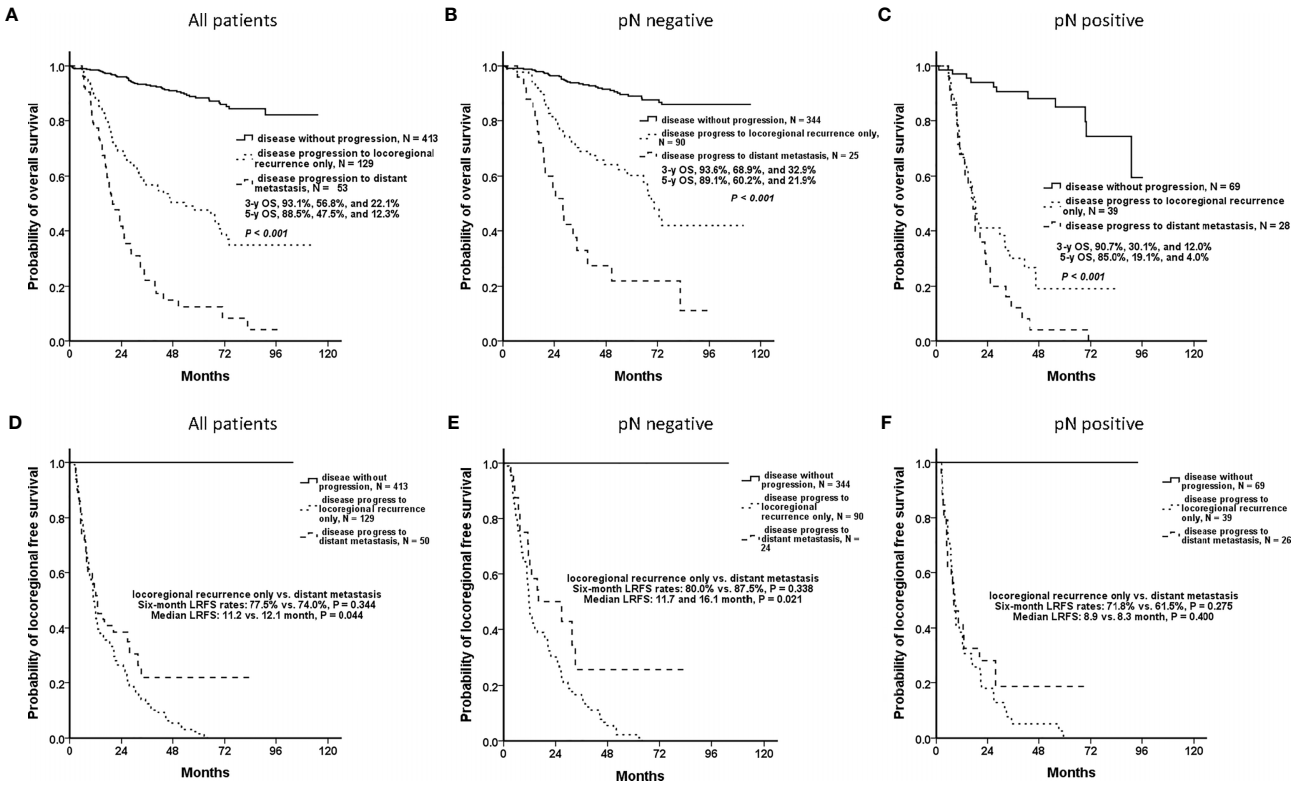

FIGURE 2 | Clinical outcomes of patients who were disease-free, had locoregional recurrence only, and had distant metastasis (DM) with any locoregional status. In accordance with disease progression patterns, the patients were classified as those who were disease-free (without disease progression), who had locoregional recurrence only, and had DM with any locoregional status. **(A)** Overall, the patients who had DM had significantly worsened overall survival (OS) than did the others (P <.001). **(B, C)** In both the nodal-negative and -positive groups, the patients who developed DM had significantly poorer OS than those of the patients without DM. **(D)** The patients who developed locoregional recurrence only and DM with any locoregional status had similar 6-mo locoregional recurrence-free survival (LRFS) rates (77.5% and 74.0%, respectively, P = .344). It was difficult to differentiate both disease patterns at the early phase. **(E)** For the nodal-negative group, the 6-mo LRFS rates of the patients who developed locoregional recurrence only and who had DM were 80.0% and 87.5%, respectively (P = .338), and the median LRFS periods were 11.7 and 16.1 mo, respectively (P = .021). **(F)** For the nodal-positive group, the 6-mo LRFS rates were 71.8% and 61.5%, respectively (P = .275), and the median LRFS periods were 8.9 and 8.3 mo, respectively (P = .400).

DM Prediction Model for Patients With OCSCC

Prediction models for DM were established separately for the nodal-negative and -positive groups because their DM development processes may have differed. In the nodal-negative group, ages greater than 65 y (HR [95% CI]: 3.78 [1.51–9.44], P = .004), surgical margin of less than 5 mm (HR [95% CI]: 3.15 [1.06–9.35], P = .038), and a locoregional recurrence of less than 6 mo (HR [95% CI]: 7.03 [2.02–24.50], P = 0.002) were independent factors for the time until DM. Lymphovascular invasion (HR [95% CI]: 2.81 [1.01–7.86], P = .048), a locoregional recurrence of less than 6 mo (HR [95% CI]: 24.35 [8.00–74.11], P <.001), and a lymphocyte-to-monocyte ratio of less than 2.5 (HR [95% CI]: 5.38 [1.33–21.72], P = .018) were independent factors for the nodal-positive group (**Table S2**). The calculation for the Akaike information criterion of the independent factors is in **Table S3**.

Each independent factor was scored 1 point, and two predictive models were established separately for the nodal-negative and -positive groups. Both models could classify patients into low- (score 0), intermittent- (score 1), and high- (score 2 or 3) risk groups. And 3-y DM rate of these three risk groups were 0.0%, 5.9%, and 17.8% in the nodal-negative group, and 7.1%, 44.9%, and 82.5% in the nodal-positive group, respectively (**Figures 4A, B**). In addition, these models were found to be effective predictors of DM events. The areas under the curve (AUCs) that predicted DM occurring within the first 1 y were 0.858 and 0.848 for the nodal-negative and -positive models, respectively. In addition, up to 85% of the DM events occurred within the first 3 y, and the AUCs predicted this event were 0.744 and 0.820 for both two groups, respectively (**Figures 4C, D**). The AUC, sensitivity, and specificity of each score are presented in **Table 3**.

DISCUSSION

A total of 595 patients with OCSCC were retrospectively enrolled in this study. Overall, 8.9% of the included patients developed

TABLE 2 | The presentations of metastatic lesions.

	Patients with distant metastasis (N = 53)			
		pN negative N = 25	pN positive N = 28	P value
Age ≥ 65 y	11(20.8)	8 (32.0)	3 (10.7)	0.058
Male	44(83.0)	22 (88.0)	22(78.6)	0.295
Personal history				
Smoking	29(54.7)	13(52.0)	16(57.1)	0.460
Alcohol	37(69.8)	12(48.0)	16(57.1)	0.348
Betel nut	28(52.8)	17(68.0)	20(71.4)	0.510
Initial pathologic staging				
pT>2	23/51(43.4)	9/25(36.0)	14/26(53.8)	0.159
pN+	28/53(52.8)	NA	NA	NA
Initial pathologic staging				**<0.001**
Stage I-II	16(31.4)	16(64.0)	0(0.0)	
Stage III-IV	35(68.6)	9(36.0)	26(100)	
Initial histologic type				
Poorly differentiated	10/52 (19.2)	2/25(8.0)	8/27(29.6)	0.050
Initial pathologic feature				
Primary tumor size ≥ 2cm	39/53(73.6)	13/25(52.0)	26/28(92.9)	0.001
Extracapsular spread	11/53(20.8)	0/25(0.0)	11/28(39.3)	<0.001
Depth of invasion >1 cm	25/45(55.6)	10/24(41.7)	15/21(71.4)	0.044
Lymphovascular invasion	10/50(20.0)	0/25(0.0)	10/25(40.0)	<0.001
Perineural invasion	26/49(53.1)	7/25(28.0)	19/24(79.2)	<0.001
Surgical margin	39/51(76.5)	20/25(80.0)	19/26(73.1)	0.401
Adjuvant therapy				**0.017**
Adjuvant chemoradiotherapy	21(39.6)	5(20.0)	16(57.1)	
Adjuvant radiotherapy	3(5.7)	3(12.0)	0(0.0)	
Adjuvant chemotherapy	1(1.9)	1(4.0)	0(0.0)	
None	28(52.8)	16(64.0)	12(42.9)	
Metastatic site				
Lung	36(67.9)	15(60.0)	21(75.0)	0.191
Bone	23(43.4)	14(56.0)	9(32.1)	**0.070**
Mediastinal lymph node	15(28.3)	7(28.0)	8(28.6)	0.603
Pleura	9(17.0)	3(12.0)	6(21.4)	0.295
Liver	6(11.3)	2(8.0)	4(14.3)	0.391
Intra-abdominal organ	3(5.7)	1(4.0)	2(7.1)	0.543
Skin	2(3.8)	2(8.0)	0(0.0)	0.218
Pericardium	1(1.9)	0(0.0)	1(3.6)	0.528
Number of metastatic lesions				0.452
1	13(24.5)	8(32.0)	5(17.9)	
2	6(11.3)	3(12.0)	3(10.7)	
≥3	34(64.2)	14(56.0)	20(71.4)	
Treatment for metastatic lesions				0.285
Palliative chemotherapy	28(52.8)	12(48.0)	16(57.1)	
Local radiotherapy	8(15.1)	6(24.0)	2(7.1)	
Palliative chemotherapy and local radiotherapy	1(1.9)	0(0.0)	1(3.6)	
Best supportive care	15(28.3)	6(24.0)	9(32.1)	
Loss follow up	1(1.9)	1(4.0)	8(15.1)	

Bold values mean that P value of <.05 was statistically significant.

DM during the follow-up period, with 85% of DM events occurring within the first 3 y following the date of initial diagnosis. Among the patients who developed DM, the median OS, LRFS, time until DM, and PMS were 19.8, 12.7, 14.6, and 4.1 mo, respectively. The lung, bone, and mediastinal lymph nodes were the most common metastatic sites. Histologically poor differentiation and pleural metastasis were independent factors of PMS. Because the phenotypes of locoregional recurrence between the patients who developed DM or locoregional recurrence only were similar, DM was difficult to detect early. Two scoring models predicting DM development were established to distinguish the influence of regional lymph node metastasis. These models could predict DM events occurring within the first 3 y after diagnosis for each patient in the nodal-negative and positive groups. The AUCs of these two models were 0.744 and 0.820, respectively.

In addition, although the mechanism between aging and cancer metastasis in OCSCC was unknown, the results showed that aging influenced the occurrence of DM for both the nodal-negative and -positive groups. In our study, age ≥ 80 y was an independent factor for time until DM in univariant Cox regression for all patients (HR [95% CI]: 8.880 [2.579–30.581], $P = .001$). For the nodal-negative group, ages between 70–80 and ≥ 80 y were significant (ages between 70–80 y, HR [95% CI]: 5.0668 [1.811–14.182], $P = .002$; ages ≥ 80 y, HR [95% CI]: 8.890 [1.056–74.856], $P = .044$). An age ≥ 80 y was also independent (HR [95% CI]: 8.656 [1.731–43.292],

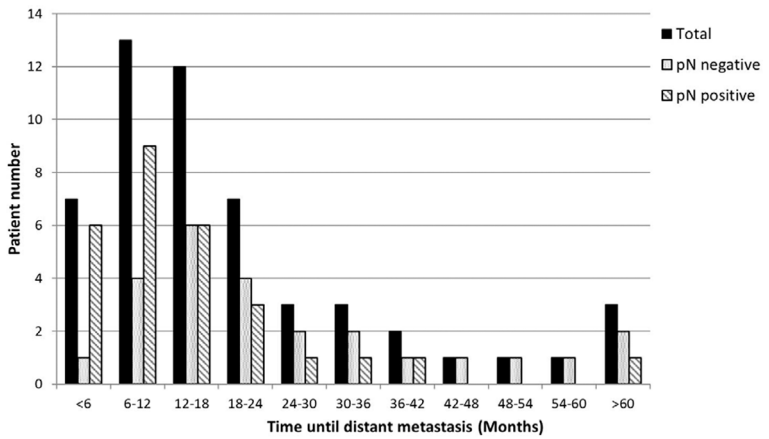

FIGURE 3 | The distribution of time until distant metastasis. Most (84.9%, 45/53) of the DM events occurred within the first 3 y (nodal-negative group, 76% [19/25]; nodal-positive group, 92.9% [26/28]).

P = .009) for the nodal-positive group (**Table S3**). Several studies have reported that extracellular matrix degradation may be the reason why cancer metastasis occurred more in elderly patients than in younger patients (21, 22). Future studies are warranted for OCSCC in this issue.

In Taiwan, up to 70% of HNSCC cases are OCSCC (2), and the PMS of patients with OCSCC was significantly poorer than that of non-OCSCC patients. One study has reported that the proportions of patients with cancer of the oral cavity, oropharynx, hypopharynx, and larynx who achieve 2-y PMS are 8.9%, 33.3%, 12.1%, and 21.1%, respectively (P <.001) (23). Thus, although the DM rate is lower among patients with OCSCC than among those without OCSCC (14, 24), predicting and managing DM in patients with OCSCC is a major challenge in clinical practice.

Although the shortened period of locoregional control (locoregional recurrence < 6 mo) was found to be independent of time until DM, it was initially difficult to identify the patients who would develop DM; the phenotypes and 6-mo LRFS rate were not significantly different between the patients who developed DM and those with locoregional recurrence only. According to Allen et al. (17), primary tumors actively enter both primary tumor lymphatics and primary tumor vasculature simultaneously and disseminate to distant organs through the lymphatic and blood vessel systems. For locoregional conditions, the mechanisms of tumor-induced lymphangiogenesis and lymph node metastasis have been widely discussed. These mechanisms include the expression of VEGFs, angiopoietins, insulin-like growth factors, and fibroblast growth factors (25), some of which have salient roles in the development of DM (26, 27). Detailed molecular analyses on this topic are warranted in the future.

In addition to locoregional recurrence, DM may develop directly from the primary tumor. In our study, almost 85% of DM events occurred within the first 3 y for the nodal-negative and -positive groups, as reported in other studies (4, 5). The time until DM development was unrelated to nodal status, and the DM process did not depend solely on lymphatic drainage. Metastatic tumor cells enter the primary tumor vasculature directly from the primary tumor lesions (17). These metastatic tumor cells are aggressive and invasive; compared with the genetic profiles of the primary tumor lesions, those of the matched lesions indicated enrichment in hypoxia, angiogenesis, EMT, and glycolysis (12). Other metastatic-related functions, such as cell differentiation, extracellular matrix organization, tissue development, adhesion, immune response, and cancer metabolism, have also been reported (28, 29). The molecular signals of DM differ from those of locoregional recurrence in that the process of DM development does not depend on lymph node metastasis.

Several studies investigated DM predictors on the basis of clinicopathological parameters (10, 11). Hosni et al. found that 14.1% (63/447) of patients with OCSCC in their study were diagnosed with DM during follow-up. Pathological N2 or N3 (pN2 or pN3) and histological grade 2 or 3 (G2–3) were independent factors for DM. However, only patients who received curative surgery followed by adjuvant chemotherapy or chemoradiotherapy were enrolled in this study (10). In addition, Huang et al. classified 312 patients with OCSCC into high-, intermittent-, and low-risk groups according to their human papillomavirus (HPV) viral loads, pN2 status, and tumor depth. The 5-y DM rates for these three groups were 74%, 17%, and 1% (P <.001), respectively, and the concordance index was 0.78 (11). Although the model effectively predicted DM in patients with OCSCC, only 5.4% (17/312) of these patients were classified as high-risk with subsequent intensive treatments and follow-up strategies. In our study, patients were divided into nodal-negative and -positive groups, with predictive models established separately for each group. In addition to the shortened interval of locoregional control, other independent factors were related to cancer metastasis, such as age, surgical margin, and lymphovascular invasion status (30–32). In the nodal-negative group, although only 5.4% (25/459) of the patients developed DM during the follow-up period, most

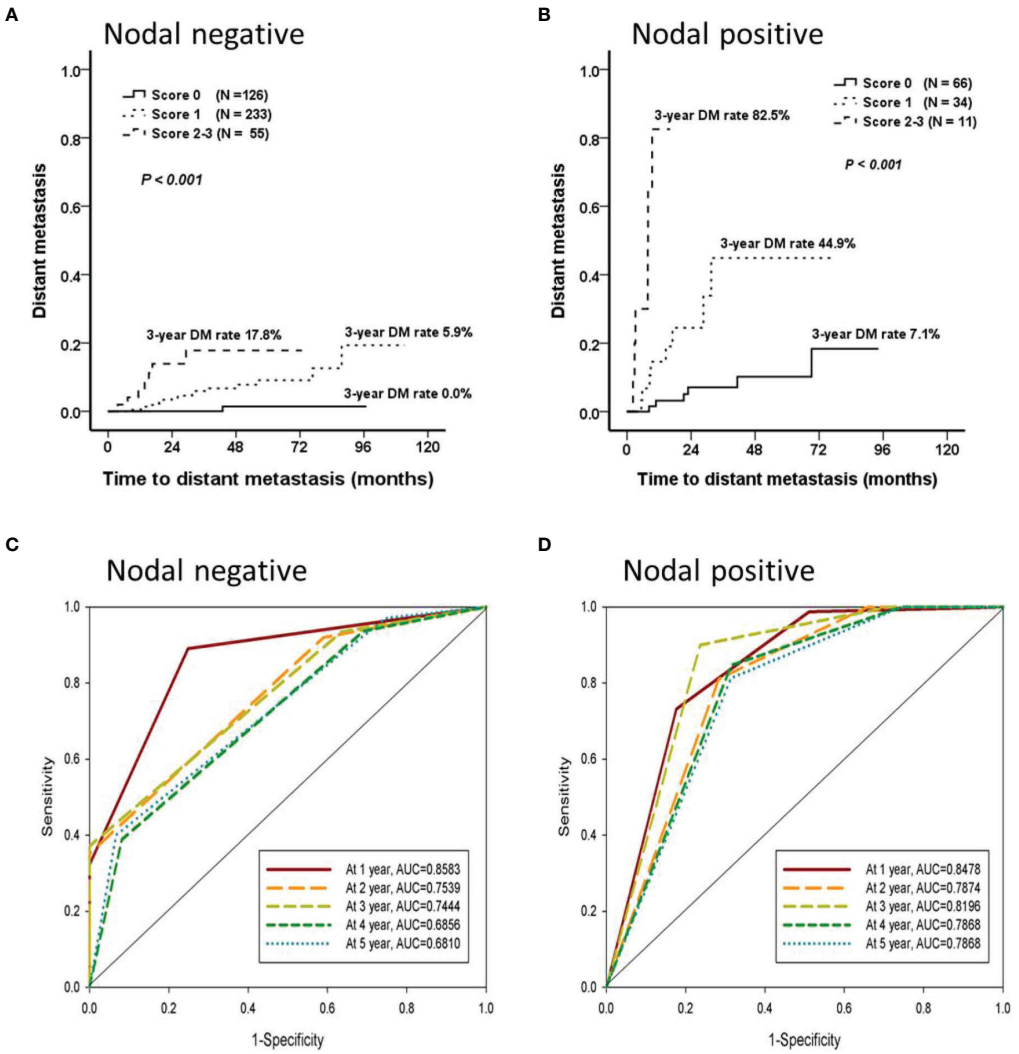

FIGURE 4 | The prediction model for distant metastasis. Cox forward stepwise regression analyzes were used to identify the independent factors for the time until DM. Age, surgical margin, and early locoregional recurrence were predictors of DM that were independent of time until DM in the nodal-negative group; the lymphocyte-to-monocyte ratio, presence of lymphovascular invasion, and early locoregional recurrence in the nodal-positive group were determined. Each independent factor was scored 1 point, and two predictive models could classify patients from both the nodal-negative and -positive groups into low- (score 0), intermittent- (score 1), or high- (score 2 or 3) risk groups separately. **(A, B)** The nodal-negative and -positive 3-y DM rates were 0.0%, 5.9%, and 17.8% and 7.1%, 44.9%, and 82.5%, respectively. **(C, D)** These models were effective predictors of DM events occurring within the first 3 y. The areas under the curve (AUCs) of the nodal-negative and -positive models were 0.744 and 0.820, respectively.

(77.1% [459/595]) of the patients with OCSCC were in this group, and this first predictive model was established for them. By contrast, for the nodal-positive group, almost 40.5% (45/111) of the patients were classified as intermittent- to high-risk, and the 3-y DM rates were 44.9% to 82.5%. Both models effectively predicted the development of DM (AUCs predicted DM occurring within the first 3 y, with 0.744 and 0.820 for the nodal-negative and -positive groups, respectively).

In this study, we hoped to provide flexible models to predict DM in clinical practice. Only the parameters which were available in the clinical setting were enrolled for analysis. The patients who missed the score factors would be eliminated in prediction models. The weight of each score factor was different, which might affect the power of the prediction models. In the future, we hoped that artificial intelligence, such as machine learning and deep learning, could be involved in the development of these prediction models.

This study had some limitations. First, although we established a predictive model for DM development, only a single-institute analysis was undertaken; the validation of our results with a large population is required. Second, DM was detected on the basis of image diagnosis and not from autopsy results. Micrometastatic lesions may therefore not have been detected and could constitute missed diagnoses. Third, although molecular information, such as HPV infection status, is vital for

TABLE 3 | Areas under the curve (AUCs), sensitivity, and specificity of the score models to predict distant metastasis.

	pN negative group			pN positive group		
	AUC	**Sensitivity**	**Specificity**	**AUC**	**Sensitivity**	**Specificity**
DM within the first 1 year	0.858			0.848		
Score ≥1		100.0%	32.3%		82.3%	73.1%
Score ≥2		75.1%	89.0%		48.8%	98.7%
Score ≥3		0.0%	100.0%		0.0%	100.0%
DM within the first 2 years	0.754			0.787		
Score ≥1		100.0%	35.1%		71.6%	81.0%
Score ≥2		41.0%	92.0%		34.1%	100.0%
Score ≥3		0.0%	100.0%		0.0%	100.0%
DM within the first 3 years	0.744			0.820		
Score ≥1		100.0%	37.1%		76.3%	90.0%
Score ≥2		36.4%	93.5%		28.5%	100.0%
Score ≥3		0.0%	100.0%		0.0%	100.0%
DM within the first 4 years	0.686			0.787		
Score ≥1		91.8%	38.9%		68.5%	84.6%
Score ≥2		30.9%	93.6%		25.6%	100.0%
Score ≥3		0.0%	100.0%		0.0%	100.0%
DM within the first 5 years	0.681			0.787		
Score ≥1		93.3%	40.0%		68.5%	81.3%
Score ≥2		25.4%	97.0%		25.6%	100.0%
Score ≥3		0.0%	100.0%		0.0%	100.0%

predicting DM development in patients with OCSCC (11), only the information available in the patients' medical charts were analyzed.

CONCLUSION

DM development may occur directly through both the lymphatic and blood vessel systems, though the DM development mechanisms of these two systems may differ. In this study, we established two scoring models that could effectively predict DM events within the first 3 y following diagnosis of each patient in both nodal-negative and -positive groups. A validation study is required to verify our findings.

DATA AVAILABILITY STATEMENT

The raw data supporting the conclusions of this article will be made available by the authors, without undue reservation.

ETHICS STATEMENT

The studies involving human participants were reviewed and approved by Institutional Review Board of Chung Shan Medical University Hospital. The patients/participants provided their written informed consent to participate in this study.

AUTHOR CONTRIBUTIONS

H-JL and S-FY proposed the study concept and study design. H-JL edited the manuscript, and S-FY approved the final version to be published. H-JL and W-SL participated in the data collection, statistical analysis, and manuscript preparation. H-JL, Y-WC, C-YP, H-CT, C-HH, C-YC, and W-SH contributed to the collection of clinical information and data processing. All of the authors agree to be accountable for all aspects of the work.

FUNDING

This study was supported by research grants to H-JL from the Chung Shan Medical University Hospital, Taiwan (CSH-2020-A-016 and CSH-2020-D-009).

ACKNOWLEDGMENTS

This is a short text to acknowledge the contributions of specific colleagues, institutions, or agencies that aided the efforts of the authors.

SUPPLEMENTARY MATERIAL

The Supplementary Material for this article can be found online at: https://www.frontiersin.org/articles/10.3389/fonc.2021.713815/full#supplementary-material

REFERENCES

1. Siegel RL, Miller KD, Jemal A. Cancer Statistics, 2020. *CA Cancer J Clin* (2020) 70:7–30. doi: 10.3322/caac.21590
2. *Cancer Registry Annual Report*. Taiwan: Health Promotion Administration (2017).
3. Colevas AD, Yom SS, Pfister DG, Spencer S, Adelstein D, Adkins D, et al. NCCN Guidelines Insights: Head and Neck Cancers, Version 1.2018. *J Natl Compr Canc Netw* (2018) 16:479–90. doi: 10.6004/jnccn.2018.0026
4. Hosni A, Huang SH, Xu W, Su J, Bayley A, Bratman SV, et al. Distant Metastases Following Postoperative Intensity-Modulated Radiotherapy for

Oral Cavity Squamous Cell Carcinoma. *JAMA Otolaryngol Head Neck Surg* (2017) 143:368–75. doi: 10.1001/jamaoto.2016.3668
5. Duprez F, Berwouts D, De Neve W, Bonte K, Boterberg T, Deron P, et al. Distant Metastases in Head and Neck Cancer. *Head Neck* (2017) 39:1733–43. doi: 10.1002/hed.24687
6. Beckham TH, Leeman JE, Xie P, Li X, Goldman DA, Zhang Z, et al. Long-Term Survival in Patients With Metastatic Head and Neck Squamous Cell Carcinoma Treated With Metastasis-Directed Therapy. *Br J Cancer* (2019) 121:897–903. doi: 10.1038/s41416-019-0601-8
7. Ferris RL, Blumenschein GJr., Fayette J, Guigay J, Colevas AD, Licitra L, et al. Nivolumab for Recurrent Squamous-Cell Carcinoma of the Head and Neck. *N Engl J Med* (2016) 375:1856–67. doi: 10.1056/NEJMoa1602252
8. Burtness B, Harrington KJ, Greil R, Soulieres D, Tahara M, de Castro GJr., et al. Pembrolizumab Alone or With Chemotherapy Versus Cetuximab With Chemotherapy for Recurrent or Metastatic Squamous Cell Carcinoma of the Head and Neck (KEYNOTE-048): A Randomised, Open-Label, Phase 3 Study. *Lancet* (2019) 394:1915–28. doi: 10.1016/S0140-6736(19)32591-7
9. Vermorken JB, Mesia R, Rivera F, Remenar E, Kawecki A, Rottey S, et al. Platinum-Based Chemotherapy Plus Cetuximab in Head and Neck Cancer. *N Engl J Med* (2008) 359:1116–27. doi: 10.1056/NEJMoa0802656
10. Hosni A, Huang SH, Chiu K, Xu W, Su J, Lu L, et al. Validation of Distant Metastases Risk-Groups in Oral Cavity Squamous Cell Carcinoma Patients Treated With Postoperative Intensity-Modulated Radiotherapy. *Radiother Oncol* (2019) 134:10–6. doi: 10.1016/j.radonc.2019.01.014
11. Huang CG, Lee LA, Tsao KC, Liao CT, Yang LY, Kang CJ, et al. Human Papillomavirus 16/18 E7 Viral Loads Predict Distant Metastasis in Oral Cavity Squamous Cell Carcinoma. *J Clin Virol* (2014) 61:230–6. doi: 10.1016/j.jcv.2014.07.007
12. Alfieri S, Carenzo A, Platini F, Serafini MS, Perrone F, Galbiati D, et al. Tumor Biomarkers for the Prediction of Distant Metastasis in Head and Neck Squamous Cell Carcinoma. *Cancers (Basel)* (2020) 12(4):922. doi: 10.3390/cancers12040922
13. Arellano-Garcia ME, Li R, Liu X, Xie Y, Yan X, Loo JA, et al. Identification of Tetranectin as a Potential Biomarker for Metastatic Oral Cancer. *Int J Mol Sci* (2010) 11:3106–21. doi: 10.3390/ijms11093106
14. Lim JY, Lim YC, Kim SH, Kim JW, Jeong HM, Choi EC. Predictive Factors of Isolated Distant Metastasis After Primary Definitive Surgery Without Systemic Treatment for Head and Neck Squamous Cell Carcinoma. *Oral Oncol* (2010) 46:504–8. doi: 10.1016/j.oraloncology.2010.02.005
15. Merino OR, Lindberg RD, Fletcher GH. An Analysis of Distant Metastases From Squamous Cell Carcinoma of the Upper Respiratory and Digestive Tracts. *Cancer* (1977) 40:145–51. doi: 10.1002/1097-0142(197707)40:1<145::aid-cncr2820400124>3.0.co;2-9
16. Leemans CR, Tiwari R, Nauta JJ, van der Waal I, Snow GB. Regional Lymph Node Involvement and its Significance in the Development of Distant Metastases in Head and Neck Carcinoma. *Cancer* (1993) 71:452–6. doi: 10.1002/1097-0142(19930115)71:2<452::aid-cncr2820710228>3.0.co;2-b
17. Allen CT, Law JH, Dunn GP, Uppaluri R. Emerging Insights Into Head and Neck Cancer Metastasis. *Head Neck* (2013) 35:1669–78. doi: 10.1002/hed.23202
18. Edge SB, Compton CC. The American Joint Committee on Cancer: The 7th Edition of the AJCC Cancer Staging Manual and the Future of TNM. *Ann Surg Oncol* (2010) 17:1471–4. doi: 10.1245/s10434-010-0985-4
19. Lu HJ, Tseng SW, Peng CY, Tseng HC, Hsin CH, Chen HL, et al. Predictors of Early Progression After Curative Resection Followed by Platinum-Based Adjuvant Chemoradiotherapy in Oral Cavity Squamous Cell Carcinoma. *Postgrad Med* (2021) 133:377–84. doi: 10.1080/00325481.2020.1809869
20. Kamarudin AN, Cox T, Kolamunnage-Dona R. Time-Dependent ROC Curve Analysis in Medical Research: Current Methods and Applications. *BMC Med Res Methodol* (2017) 17:53. doi: 10.1186/s12874-017-0332-6
21. Ecker BL, Kaur A, Douglass SM, Webster MR, Almeida FV, Marino GE, et al. Age-Related Changes in HAPLN1 Increase Lymphatic Permeability and Affect Routes of Melanoma Metastasis. *Cancer Discov* (2019) 9:82–95. doi: 10.1158/2159-8290.CD-18-0168
22. Zou J, Guo S, Xiong MT, Xu Y, Shao J, Tong Z, et al. Ageing as Key Factor for Distant Metastasis Patterns and Prognosis in Patients With Extensive-Stage Small Cell Lung Cancer. *J Cancer* (2021) 12:1575–82. doi: 10.7150/jca.49681
23. Kang HS, Roh JL, Kim MJ, Cho KJ, Lee SW, Kim SB, et al. Predictive Factors for Long-Term Survival in Head and Neck Squamous Cell Carcinoma Patients With Distant Metastasis After Initial Definitive Treatment. *J Cancer Res Clin Oncol* (2016) 142:295–304. doi: 10.1007/s00432-015-2043-x
24. Leon X, Quer M, Orus C, del Prado Venegas M, Lopez M. Distant Metastases in Head and Neck Cancer Patients Who Achieved Loco-Regional Control. *Head Neck* (2000) 22:680–6. doi: 10.1002/1097-0347(200010)22:7<680::aid-hed7>3.0.co;2-j
25. Karatzanis AD, Koudounarakis E, Papadakis I, Velegrakis G. Molecular Pathways of Lymphangiogenesis and Lymph Node Metastasis in Head and Neck Cancer. *Eur Arch Otorhinolaryngol* (2012) 269:731–7. doi: 10.1007/s00405-011-1809-2
26. Siriwardena BS, Kudo Y, Ogawa I, Udagama MN, Tilakaratne WM, Takata T. VEGF-C is Associated With Lymphatic Status and Invasion in Oral Cancer. *J Clin Pathol* (2008) 61:103–8. doi: 10.1136/jcp.2007.047662
27. Sopo M, Anttila M, Hamalainen K, Kivela A, Yla-Herttuala S, Kosma VM, et al. Expression Profiles of VEGF-A, VEGF-D and VEGFR1 are Higher in Distant Metastases Than in Matched Primary High Grade Epithelial Ovarian Cancer. *BMC Cancer* (2019) 19:584. doi: 10.1186/s12885-019-5757-3
28. Rickman DS, Millon R, De Reynies A, Thomas E, Wasylyk C, Muller D, et al. Prediction of Future Metastasis and Molecular Characterization of Head and Neck Squamous-Cell Carcinoma Based on Transcriptome and Genome Analysis by Microarrays. *Oncogene* (2008) 27:6607–22. doi: 10.1038/onc.2008.251
29. Lu HJ, Hsieh CC, Yeh CC, Yeh YC, Wu CC, Wang FS, et al. Clinical, Pathophysiologic, and Genomic Analysis of the Outcomes of Primary Head and Neck Malignancy After Pulmonary Metastasectomy. *Sci Rep* (2019) 9:12913. doi: 10.1038/s41598-019-49212-y
30. Kuperman DI, Auethavekiat V, Adkins DR, Nussenbaum B, Collins S, Boonchalermvichian C, et al. Squamous Cell Cancer of the Head and Neck With Distant Metastasis at Presentation. *Head Neck* (2011) 33:714–8. doi: 10.1002/hed.21529
31. Eldeeb H, Macmillan C, Elwell C, Hammod A. The Effect of the Surgical Margins on the Outcome of Patients With Head and Neck Squamous Cell Carcinoma: Single Institution Experience. *Cancer Biol Med* (2012) 9:29–33. doi: 10.3969/j.issn.2095-3941.2012.01.005
32. Huang S, Zhu Y, Cai H, Zhang Y, Hou J. Impact of Lymphovascular Invasion in Oral Squamous Cell Carcinoma: A Meta-Analysis. *Oral Surg Oral Med Oral Pathol Oral Radiol* (2021) 131:319–28 e1. doi: 10.1016/j.oooo.2020.10.026

Conflict of Interest: The authors declare that the research was conducted in the absence of any commercial or financial relationships that could be construed as a potential conflict of interest.

frontiers in Oncology

REVIEW
published: 05 January 2022
doi: 10.3389/fonc.2021.767134

Radiomics for Diagnosis and Radiotherapy of Nasopharyngeal Carcinoma

Yu-mei Zhang[1], Guan-zhong Gong[2], Qing-tao Qiu[2], Yun-wei Han[1], He-ming Lu[3] and Yong Yin[1,2]**

[1] Department of Oncology, The Affiliated Hospital of Southwest Medical University, Luzhou, China, [2] Department of Radiotherapy, Shandong Cancer Hospital and Institute, Shandong First Medical University and Shandong Academy of Medical Sciences, Jinan, China, [3] Department of Radiotherapy, People's Hospital of Guangxi Zhuang Autonomous Region, Nanning, China

Nasopharyngeal carcinoma (NPC) is a malignant tumor of the head and neck. The primary clinical manifestations are nasal congestion, blood-stained nasal discharge, headache, and hearing loss. It occurs frequently in Southeast Asia, North Africa, and especially in southern China. Radiotherapy is the main treatment, and currently, imaging examinations used for the diagnosis, treatment, and prognosis of NPC include computed tomography (CT), magnetic resonance imaging (MRI), positron emission tomography (PET)-CT, and PET-MRI. These methods play an important role in target delineation, radiotherapy planning design, dose evaluation, and outcome prediction. However, the anatomical and metabolic information obtained at the macro level of images may not meet the increasing accuracy required for radiotherapy. As a technology used for mining deep image information, radiomics can provide further information for the diagnosis and treatment of NPC and promote individualized precision radiotherapy in the future. This paper reviews the application of radiomics in the diagnosis and treatment of nasopharyngeal carcinoma.

Keywords: nasopharyngeal carcinoma, computerized tomography, magnetic resonance imaging, positron emission computed tomography, radiomics

OPEN ACCESS

Edited by:
Xiance Jin,
Wenzhou Medical University, China

Reviewed by:
Wenbing Lv,
Southern Medical University, China
Zhiyong Xu,
Shanghai Jiaotong University, China

****Correspondence:***
Yong Yin
yinyongsd@126.com
He-ming Lu
luhming3632@163.com

Specialty section:
This article was submitted to Head and Neck Cancer, a section of the journal Frontiers in Oncology

Received: *30 August 2021*
Accepted: *13 December 2021*
Published: *05 January 2022*

Citation:
Zhang Y-m, Gong G-z, Qiu Q-t, Han Y-w, Lu H-m and Yin Y (2022) Radiomics for Diagnosis and Radiotherapy of Nasopharyngeal Carcinoma. Front. Oncol. 11:767134. doi: 10.3389/fonc.2021.767134

1 INTRODUCTION

Compared with other head and neck tumors, NPC has unique epidemiological, etiological, clinical, and genetic characteristics (1). According to the data of the International Agency for Research on Cancer, there are approximately 133,354 new cases of NPC, which accounts for only 0.7% of all cancers diagnosed in 2020. More than 70% of new cases occur in East and Southeast Asia, and South China is also an area with a high incidence. The age-standardized mortality rate in China is 1.6/100000, which is approximately twice that of NPC worldwide (2). Therefore, accurate treatment of NPC is imperative.

Because of the specific anatomical position and important adjacent structures of NPCs and the high sensitivity of NPC to radiotherapy, the main treatment for NPC is a comprehensive treatment based on radiotherapy. During radiotherapy, the medical images applied to NPC include magnetic resonance imaging (MRI), computed tomography (CT), positron emission tomography (PET)-CT, and PET-MRI

(3). These various medical imaging methods have distinct characteristics. MRI has high contrast for different tissues, which provides high-resolution images of soft tissue; however, it requires a long acquisition time (4). CT has advantages in imaging bone and vascular invasion, and image acquisition is rapid; thus, it is well tolerated by patients (5, 6). In contrast to anatomical imaging, PET-CT combines biological metabolic information, and PET-MRI combines metabolic information with high-resolution soft-tissue images, and therefore, they are expected to become new methods for the diagnosis and treatment of NPC (5–7). These imaging methods have played a crucial role in target delineation, planning, quantitative evaluation, radiotherapy response tracking, and outcome and toxicity prediction of NPCs (8–11). However, the application of traditional images is aimed at diagnosing and treating diseases from a macro perspective. Patients with similar stages and grades of tumor experience different therapeutic effects with the same treatment due to the internal heterogeneity of the tumor (12). Only analyzing the disease from an anatomical level cannot meet the needs of treatment. With the increase in standards for radiotherapy, hidden information in images is valuable for improving NPC treatments. Radiomics is a technology that involves mining deep information in images, which has been used widely in the diagnosis, treatment, and prognosis of lung, esophageal, breast, rectal, and prostate cancers (13–16). There is an increasing number of studies investigating the diagnosis and treatment of NPC using radiomics. For example, one study applied metabolic information obtained from PET-CT to the treatment of head and neck squamous cell carcinoma with the aim of performing dose painting (17).

2 RADIOMICS

As an emergent field of transformational research, radiomics extracts quantitative features from medical images to decode the heterogeneity derived from tumor regions, metastatic lesions, and normal tissues, and explore microscopic changes in morphological and functional images (18). There are four steps in radiomics studies, which comprise image acquisition, tumor segmentation, feature extraction, and model development and validation (19) (**Figure 1**). Radiomics is distinct from traditional radiology, where images are not only interpreted visually; moreover, quantitative analyses are possible because the images are the data.

Radiomics statistical features can be divided into first-order, second-order, and high-order features. A first-order statistical feature describes the distribution of individual voxel values without considering the spatial relationship (20). Second-order features are usually described as 'texture' features; they describe the statistical correlation between voxels with similar (or dissimilar) contrast values and provide a measurement of intratumor heterogeneity. The high-order statistical method applies a filter grid to the image to extract repeated or non-repeated patterns (19). These data are combined with clinical data to develop models to improve the accuracy of diagnostic, treatment, and prognostic predictions. Mining image information and combining clinical medicine with engineering may become routine practice in the diagnosis and treatment of NPC in the future. Furthermore, radiomics will allow oncologists to establish relevant tumor databases and use this data to provide decision support for the diagnosis and treatment of tumors (21).

3 RADIOMICS SIGNATURE

When researchers make predictions about diagnosis or treatment based on radiomics, they need to first clarify the diseases and problems to be studied, and then collect relevant clinical data, such as hemoglobin, lymphocytes, etc. The features which are extracted from the volume of interest and related

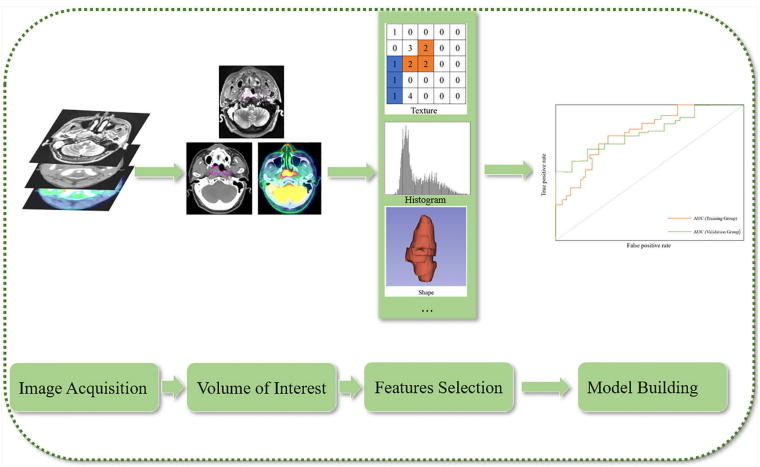

FIGURE 1 | Flow chart of radiomics.

clinical parameters are filtered through various ways, such as Cox proportional hazards model and classifier, and then the final required model is established (22).

4 APPLICATION OF RADIOMICS FOR THE DIAGNOSIS AND TREATMENT OF NPC

Most imaging studies on NPC have focused on MRI data, and few have reported on the use of CT, PET-CT, and PET-MRI images. Moreover, studies have focused predominantly on prognosis, and there is currently a lack of exploratory and prospective studies, even though retrospective studies can provide valuable clinical guidance for diagnosis, differential diagnosis, treatment, recurrence, and prognosis of the disease.

4.1 Diagnosis

4.1.1 Diagnosis

The resolution of soft tissue on MRI is significantly superior to that of CT and PET-CT and can effectively show the range of parapharyngeal space, skull base, and intracranial tumors. It is the gold standard for the evaluation of NPC (5–7). NPC is prone to distant metastasis; therefore, PET-CT is now used to evaluate distant metastasis by providing systemic anatomical and metabolic information. The National Comprehensive Cancer Network guidelines (23) recommend MRI and PET-CT for the diagnosis of NPC. The TNM staging system (based on tumor size, regional lymph node involvement, and distant metastases) that is currently used to guide the diagnosis and treatment of NPC is regarded as the gold standard. However, during diagnosis and treatment, patients at similar stages have exhibited different treatment responses, which may be due to the internal heterogeneity of the tumor. Thus, Zhu et al. (24) developed a radiomics model that combined the features extracted from MRI data with clinical information to analyze the survival subgroups of early NPC (validation group C-index: 0.814), compared it with the T (C-index: 0.803) and TNM staging systems (C-index: 0.765), and concluded that performance of the radiomics model was superior to the TNM staging system. This may have a significant impact on individualized diagnoses, treatments, and prognoses of NPC in the future.

Compared with CT, MRI has a higher resolution of soft tissue, which is advantageous for imaging NPCs. Research on the application of CT combined with radiomics to the diagnosis and staging of disease remains limited. PET-MRI combines the metabolic characteristics of PET and the high-resolution characteristics of MRI (6). Compared with MRI, the increased [^{18}F]-fluorodeoxyglucose (FDG) uptake of PET-MRI can better show the subtle changes in local lesions, and it can also provide a more suitable anatomical reference than can PET-CT (5). Chan et al. (25) found that the sensitivity, specificity, and accuracy for the diagnosis of primary tumors of head and neck MRI were 94.2%, 90.9%, and 99.5% (p = 0.75), respectively, 99.6%, 98.3%, and 99.2% (p = 0.92) for head and neck [^{18}F]-FDG PET-CT, respectively, and 98.2%, 96.3%, and 99.3% (p = 0.87) for [^{18}F]-FDG PET-MRI, respectively. The positive predictive value of PET-MRI in the diagnosis of distant metastasis (93.1%) is higher than that of MRI and PET-CT (78.8% and 83.3%, respectively). This was a prospective study that suggested that this imaging method has better diagnostic capabilities for nasopharyngeal cancer and may play an important role in the diagnosis and treatment of NPC in the future.

In a study of PET-MRI combined with radiomics, Feng et al. (26) developed a radiomics model of FDG PET-MRI and reported areas under the curve (AUC) of the training group based on T2-weighted imaging and PET models of 0.85 and 0.84, respectively, and those of the validation group of 0.83 and 0.82, respectively, which offers great promise for the clinical staging of NPCs. In terms of internal heterogeneity of tumors, Akram et al. (27) showed that the imaging features Neighboring Gray Tone Difference Matrix-busyness extracted from MRI data before and after treatment may reflect differences between recurrent and non-recurrent areas in tumors; moreover, they demonstrated the potential of radiomics in the identification of radiation resistance in tumors before treatment to select dose increments.

4.1.2 Differential Diagnosis

Radiomics is advantageous not only for the diagnosis of diseases but also for differential diagnoses. The clinical manifestations and medical images of radiation-induced osteonecrosis and bone metastasis of the cervical spine are similar (28). Furthermore, the two conditions require different treatment methods and thus, require differentiation before treatment. The AUCs of MRI-based radiomics nomogram training and validation groups have been reported to be 0.725 and 0.720, respectively (28). Although CT and MRI are not applicable for differentiating between tumor recurrence and inflammation (29), PET-CT can distinguish between these two conditions; however, the high uptake of inflammation can affect the diagnosis of recurrence. The diagnostic performance of NPC images based on PET-CT imaging was evaluated using 42 cross combinations of six feature selection methods and seven classifiers. The optimal combination of feature selection and machine learning methods (the cross-combination fisher score [FSCR] + random forest [RF], FSCR + k-nearest neighborhood [KNN], FSCR + support vector machines [SVM] with radial basis function kernel [RBF-SVM], and minimum redundancy maximum relevance [MRMR] + RBF-SVM) to identify the two diseases were obtained (AUCs of 0.883, 0.867, 0.892, and 0.883, respectively; sensitivity: 0.833, 0.864, 0.831, and 0.750, respectively; specificity 1, 1, 0.873, and 1, respectively). Compared with the standard uptake value (SUV), total lesion glycolysis, and other indices, radiomics showed a higher AUCs (0.867–0.892 vs. 0.817), although the difference was not statistically significant (p = 0.462–0.560) (**Table 1**).

4.2 Treatment

4.2.1 Treatment Response Prediction

Radiotherapy is the main treatment for NPC during the early stage and radiotherapy and chemotherapy are the primary treatments during in late stage (6). For patients with intensity-modulated radiotherapy, weight loss, tumor regression, and other factors can result in large dose errors when applying the

originally planned irradiation (30). In such cases, adaptive radiotherapy may be a better treatment option. Adaptive radiotherapy is usually administered to patients during radiation therapy, and the processes of imaging, sketching, and planning are repeated. The current radiotherapy system presents a significant economic burden for patients, and treatment is time-consuming and labor-intensive. Patients who need adaptive radiotherapy should be identified before treatment to improve treatment response. Yu et al. (30) used tumor marker features in MRI images acquired before treatment, and feature modeling (using enhanced T1 and T2 images provided AUCs of the enhanced T1, T2, and combined model verification groups of 0.852, 0.750, and 0.930, respectively), which may offer a basis for determining patient eligibility for adaptive radiotherapy and developing personalized treatments to reduce dose error. For the treatment response of NPC patients with advanced local progression to induction chemotherapy, Zhao et al. (31) developed a nomogram that combined multi-sequence MRI features before treatment with clinical parameters to predict the treatment effect in non-epidemic NPC areas. The model (training and validation group C-index: 0.952 vs. 0.863) had better predictive ability than the model developed using clinical parameters alone (training and validation group C-index: 0.708 vs. 0.549). In addition, in a study by Piao et al. (32), the AUC of the combined model was highest (AUC: 0.905) with the separate modeling of ClusterShade_angle135_offset 4 and Correlation_AllDirection_offshel_SD features based on enhanced magnetic resonance sequence imaging (AUC: 0.804 and 0.762, respectively). The combined model of the two features can help to determine the sensitivity and drug resistance in patients undergoing neoadjuvant chemotherapy, which is crucial for treatment scheme selection and treatment plan modification in patients with NPC.

4.2.2 Prognosis Prediction

Most imaging studies have focused on the prognosis of NPC. These studies (33–36) demonstrate the effectiveness of conventional MRI in evaluating progression-free survival (PFS), disease-free survival, and overall survival in patients with NPC, in combination with clinical information, such as lymph nodes, Epstein-Barr virus, and tumor stage, which can guide personalized treatment selection and improve the quality of care. Ouyang et al. (33) calculated and analyzed the Radscore and found it can predict PFS as a biomarker. Shen et al. (34) developed five models based on different combinations of data: model 1: clinical data; model 2: overall staging; model 3: radiomics; model 4: radiomics + overall staging; and model 5: radiomics + overall staging + EB virus). Model 5 had a high C-index for predicting PFS (training group 0.805, validation group 0.874). Yang et al. (36) suggested a nomogram integrating lymph node, Dose Volume Histogram signature, reflecting planning score and TNM stage, that had a C-index of 0.811 for the prediction of PFS, which showed better performance than using TNM alone (C-index: 0.613). Furthermore, another study (37) used different combinations of PET, CT, and relevant clinical data to develop models and found that the model combining all three factors had the highest prediction performance (C-indices of the training and validation cohorts were 0.71–0.76 and 0.67–0.73, respectively). Another found that subregional radiomics analysis of NPC outperformed the whole tumor (C-index, 0.69 vs. 0.58) and the traditional AJCC (American Joint Committee on Cancer) staging system for PFS prediction (38).

Radiomics can predict not only treatment effects but also recurrence before treatment, which can improve treatment decision-making. For the prediction of recurrence, most studies use MRI images. Zhang et al. (39) developed models based on MRI radiomics to predict distant metastasis (AUCs of the training and validation groups: 0.827 and 0.792, respectively) and divided patients into low- and high-risk groups based on a risk cutoff score of 0.37 to indicate the risk of metastasis and determine the treatment strategy. A subsequent study (40) introduced a nomogram to radiomics to study local recurrence and found that the nomogram (C-index: 0.74) predicted recurrence more accurately than did radiomics and clinical variables (C-index: 0.59). The study by Raghavan et al. (41) preferred the prediction model, which not only predicted recurrence but also emphasized whether recurrence would occur in the form of local or distant metastasis. The AUC, sensitivity, and specificity of the local recurrence model were 0.82, 0.73, and 0.74, respectively, whereas those of the model for predicting distant metastasis were 0.92, 0.79, and 0.84, respectively. In addition, another study (42) combined machine learning with features extracted from MRI and applied different feature selection and classifier methods to determine the optimal combination (random forest + random forest), which laid a foundation for future studies of local recurrence and distant metastasis prediction combining MRI features with relevant clinical information. Li et al. (43) used radiomics with machine learning to analyze the radiation resistance of local recurrence (artificial neural network: 0.812; KNN:0.775; SVM: 0.732) using existing MRI data, which provided quantitative and objective evaluations of patients with NPC without requiring additional radiation exposure. Furthermore, NPCs with in-field recurrences could be differentiated from NPCs (AUCs: 0.727–0.835).

4.2.3 Prediction of Side Effects

Radiomics can also be applied to the prediction of radiotherapy reactions the following radiotherapy for NPC. In a study of patients with acute xerostomia after radiotherapy (44), parotid CT images and saliva volume were acquired before, during, and after treatment to develop a model to predict changes in saliva volume after early radiotherapy (accuracy: 0.9220, sensitivity: 100%). The difference between the statistical and real values can then be used to predict the degree of dry mouth by predicting the amount of saliva. The diagnosis of radiation-induced brain injury in NPC mainly depends on MRI; however, MRI has limited use for early diagnoses and can only be used to evaluate morphological changes in late radiation-induced brain injury in the temporal lobe. Radiomics can examine microscopic characteristics, which can be used as markers as a basis for the treatment of early brain injury. Zhang et al. (45) developed three models combining machine learning and MRI radiomics; the

TABLE 1 | Data of relevant models in references.

Purpose		Authors	Imaging	Application	Method/model	Results
Diagnosis	Diagnosis	Zhu et al. (24)	MRI	staging	support vector machine classifier	C-index : training&validation group : 0.827&0.814 (based on model), 0.815&0.803(based on T), 0.842&0.756(based on TNM)
		Feng et al. (26)	PET-MRI	staging	logistic regression models	AUC: training group:0.84(PET),0.85(T2-weighted); validation group:0.82(PET),0.83(T2-weighted)
	Differential diagnosis	Zhong et al. (28)	MRI	cervical spine osteoradionecrosis and bone metastasis	nomogram model	AUC: training group : 0.725 ; validation group:0.720
		Du et al. (29)	PET-CT	recurrence and inflammation	7 types of machine learning classifiers	optimal combination of feature selection and machine learning methods
Treatment						
	Treatment response prediction	Yu et al. (30)	MRI	pretreatment prediction of adaptive radiation	logistic regression model	AUC: training group: 0.962(CET1-w), 0.895(T2-weighted),0.984(joint T1-T2); validation group:0.852 (CET1-w), 0.750(T2-weighted),0.930(joint T1-T2)
		Zhao et al. (31)	MRI	predict the response to induction chemotherapy and survival	support vector machine, radiomics nomogram	C-index : training&validation group:0.952&0.863 (radiomics signature with clinical data),0.708&0.549 (clinical nomogram alone)
		Piao et al. (32)	MRI	early response of neoadjuvant chemotherapy	Cox regression model	AUC: 0.905(combined), 0.804 (ClusterShade_angle135_offset 4)、0.762 (Correlation_AllDirection_offshel_SD)
	Prognosis prediction					
		Ouyang et al. (33)	MRI	radiomics signature as a prognostic biomarker	multivariate Cox proportional hazards model	Hazard ratio (HR): 5.14(discovery set), 7.28(validation set)
		Shen et al. (34)	MRI	predicting progression-free survival (PFS)	Cox model	Model 5 incorporating radiomics, overall stage, and EBV DNA yielded the highest C-index for predicting PFS (training cohorts: 0.805, validation cohorts: 0.874)
		Ming et al. (35)	MRI	disease free-survival (DFS), overall survival (OS), distant metastasis-free survival (DMFS)	Cox regression model	C-index : validation group: 0.751(DFS)、0.845(OS)、0、643(DMFS)
		Yang et al. (36)	MRI	PFS	Nomogram	C-index: validation group: 0.811(including three factors),0.613(just TNM)
		Lv et al. (37)	PET-CT	PFS	Cox regression model	C-index: validation group: 0.67–0.73
		Xu et al. (38)	PET-CT	PFS	Cox's proportional hazard model	C-index: 0.69(S3), 0.58(whole tumor)
		Zhang et al. (39)	MRI	distant metastasis	logistic regression model	AUC: training&validation groups: 0.827&0.792
		Zhang et al. (40)	MRI	local recurrence	Cox proportional hazard model, nomogram	C-index: validation groups: 0.74(radiomic features and multiple clinical variables)
		Raghavan et al. (41)	MRI	recurrence	multivariate logistic regression model, Cox proportional model	local recurrence model: 0.82(AUC), 0.73(sensitivity), and 0.74(specificity);distant metastasis model: 0.92 (AUC), 0.79(sensitivity), and 0.84(specificity)
		Zhang et al. (42)	MRI	optimal machine-learning methods for the radiomics-based prediction of local failure and distant failure	machine-learning methods	optimal combination random forest + random forest AUC:0.8464 ± 0.0069
		Li et al. (43)	MRI	recurrence patterns	machine-learning methods,support vector machine (SVM) models	NPCs with in-field recurrences (NPC-IFR) and NPCs with non-progression disease (NPC-NPD) could be differentiated (AUCs: 0.727–0.835).
	Prediction of side effects	Liu et al. (44)	CT	prediction of Acute Xerostomia	support vector regression	accuracy: 0.9220, sensitivity: 100%
		Zhang et al. (45)	MRI	radiation-Induced Brain Injury	Random forest method	AUC: validation groups: 0.830 (model1), 0.773 (model2), and 0.716(model3)
	Stability characteristic study	Liang et al. (46)	MRI	Moddicom (v. 0.51),Pyradiomics (v. 2.1.2)	Spearman's rank correlation	Selection of stable features of the disease is key.
		Lu et al. (47)	PET-CT	different contrast agents	ICC	features extracted from [11C] choline are more stable than those extracted from the [18F]-FDG contrast agent.
		Yang et al. (48)	PET-MRI	robust radiomic features	intraclass correlation coefficient (ICC) and	voxel size: 0.5 × 0.5 × 1.0 mm3; normalized grey level:64 and 128

(Continued)

TABLE 1 | Continued

Purpose	Authors	Imaging	Application	Method/model	Results
	Lv et al. (49)	PET-CT	robustness	spearman correlation coefficient ICC	poor absolute-scale robustness still has good diagnostic performance.

AUCs of the validation group were 0.830 (95% confidence interval [CI]: 0.823–0.837), 0.773 (95% CI: 0.763–0.782), and 0.716 (95% CI: 0.699–0.733), respectively, which offers promise for applying radiomics to the study of related complications.

4.2.4 Stability Characteristic Study

Because there are numerous methods to extract radiomics features, obtaining robust features is vital for the generalizability of radiomics models. Liang et al. (46) used two different feature extraction tools to extract features from different NPC MRI sequences. Different extraction methods had varying effects on the features, which may impact model development. Thus, the selection of stable features of the disease is key. In a study on PET-CT radiomics characteristics under different contrast agents, Lu et al. (47) selected [^{18}F]-FDG and [^{11}C] choline to examine segmentation and discretization and revealed that discretization has a greater impact on features than does segmentation, and features extracted from [^{11}C] choline are more stable than those extracted from the [^{18}F]-FDG contrast agent. Yang et al. (48) evaluated the reproducibility of features extracted from PET-MRI and found that a voxel size of $0.5 \times 0.5 \times 1.0$ mm^3 in PET, T2, and diffusion-weighted imaging data and a larger bin size allow the acquisition of stable characteristics. Although these studies focused on the definition and mode of feature generation, Lv et al. (49) analyzed the robustness of feature matrix parameters and found that poor absolute-scale robustness retained good diagnostic performance (**Table 1**).

5 FUTURE

Artificial intelligence technologies and radiomics will be applied in the diagnosis and treatment of NPC in the field of target delineation, dose evaluation, plan design, outcome prediction, to realize the individualized clinical adaptive precision radiotherapy. However, there is still a significant gap between research and clinical application, which requires relevant modeling to not only meet or even exceed the industry gold standard but also solve some medical ethical problems (20). At present, many studies on radiomics are focused on NPC. However, radiomics may be extended to diseases other than tumors in the future and provide a reference for the majority of patients by establishing databases and other measures. In addition, radiomics can reduce medical costs and makes full use of medical image data to reduce injuries caused by invasive punctures; relevant models can solve problems of treatment and prognosis to save on medical costs and realize individualized treatment.

6 CONCLUSION

Multimodal imaging combined with radiomics offers new opportunities and methods for studying the diagnosis, treatment, and prognosis of NPC. The combination of radiomics and machine learning assists in the diagnosis and treatment of NPC. However, machine learning in radiomics is primarily applied to model selection. Although radiomics has numerous unique advantages, it also carries significant challenges, such as the need for big datasets for tumor model development, data sharing between different medical institutions, and various imaging protocols. Considerable progress is still needed to apply radiomics models to clinical practice. Future developments of radiomics require further forward-looking research and applications to promote individualized and intelligent treatment.

AUTHOR CONTRIBUTIONS

Y-MZ designed the study and wrote this paper. G-ZG, H-ML, Q-TQ, Y-WH, and YY conceived the study and revised the paper. All authors contributed to the article and approved the submitted version.

FUNDING

This work was supported by the National Science Foundation of Shandong Province (ZR2020MH227) and the Guangxi Key Research and Development Plan (AB17195005).

ACKNOWLEDGMENTS

We would like to thank journal experts for editing the language of the manuscript.

REFERENCES

1. Llorente JL, López F, Suárez C, Hermsen MA. Sinonasal Carcinoma: Clinical, Pathological, Genetic and Therapeutic Advances. *Nat Rev Clin Oncol* (2014) 11(8):460–72. doi: 10.1038/nrclinonc.2014.97
2. Sung H, Ferlay J, Siegel RL, Laversanne M, Soerjomataram I, Jemal A, et al. Global Cancer Statistics 2020: GLOBOCAN Estimates of Incidence and Mortality Worldwide for 36 Cancers in 185 Countries. *CA Cancer J Clin* (2021) 71:209–49. doi: 10.3322/caac.21660
3. Chen YP, Chan ATC, Le QT, Blanchard P, Sun Y, Ma J. Nasopharyngeal Carcinoma. *Lancet* (2019) 394(10192):64–80. doi: 10.1016/S0140-6736(19)30956-0

4. Chung NN, Ting LL, Hsu WC, Lui LT, Wang PM. Impact of Magnetic Resonance Imaging Versus CT on Nasopharyngeal Carcinoma: Primary Tumor Target Delineation for Radiotherapy. *Head Neck* (2004) 26(3):241–6. doi: 10.1002/hed.10378
5. Rumboldt Z, Gordon L, Gordon L, Bonsall R, Ackermann S. Imaging in Head and Neck Cancer. *Curr Treat Options Oncol* (2006) 7(1):23–34. doi: 10.1007/s11864-006-0029-2
6. Nayak U, Prasad RS, Sekhar S. *Clinical Radiology of Head and Neck Tumors*. Singapore: Springer Press (2018).
7. Huang SH, Chien CY, Lin WC, Fang FM, Wang PW, Lui CC, et al. A Comparative Study of Fused FDG PET/MRI, PET/CT, MRI, and CT Imaging for Assessing Surrounding Tissue Invasion of Advanced Buccal Squamous Cell Carcinoma. *Clin Nucl Med* (2011) 36(7):518–25. doi: 10.1097/RLU.0b013e318217566f
8. Abdel Khalek Abdel Razek A, King A. MRI and CT of Nasopharyngeal Carcinoma. *AJR Am J Roentgenol* (2012) 198(1):11–8. doi: 10.2214/AJR.11.6954
9. Li CH, Wu VW, Chiu G. A Dosimetric Evaluation on Applying RTOG-Based and CT/MRI-Based Delineation Methods to Brachial Plexus in Radiotherapy of Nasopharyngeal Carcinoma Treated With Helical Tomotherapy. *Br J Radiol* (2019) 92(1102):20170881. doi: 10.1259/bjr.20170881
10. Manavis J, Sivridis L, Koukourakis MI. Nasopharyngeal Carcinoma: The Impact of CT-Scan and of MRI on Staging, Radiotherapy Treatment Planning, and Outcome of the Disease. *Clin Imaging* (2005) 29(2):128–33. doi: 10.1016/j.clinimag.2004.04.004
11. Bogowicz M, Vuong D, Huellner MW, Pavic M, Andratschke N, Gabrys HS, et al. CT Radiomics and PET Radiomics: Ready for Clinical Implementation? *Q J Nucl Med Mol Imaging* (2019) 63(4):355–70. doi: 10.23736/S1824-4785.19.03192-3
12. Xu Y, Zheng ZS, Gao Y, Duan SY, Chen C, Rong J, et al. High Expression of IMPDH2 Is Associated With Aggressive Features and Poor Prognosis of Primary Nasopharyngeal Carcinoma. *Sci Rep* (2017) 7(1):745. doi: 10.1038/s41598-017-00887-1
13. Avanzo M, Stancanello J, Pirrone G, Sartor G. Radiomics and Deep Learning in Lung Cancer. *Strahlenther Onkol* (2020) 196(10):879–87. doi: 10.1007/s00066-020-01625-9
14. Sah BR, Owczarczyk K, Siddique M, Cook GJR, Goh V. Radiomics in Esophageal and Gastric Cancer. *Abdom Radiol* (2019) 44(6):2048–58. doi: 10.1007/s00261-018-1724-8
15. Valdora F, Houssami N, Rossi F, Calabrese M, Tagliafico AS. Rapid Review: Radiomics and Breast Cancer. *Breast Cancer Res Treat* (2018) 169(2):217–29. doi: 10.1007/s10549-018-4675-4
16. Sun Y, Reynolds HM, Parameswaran B, Wraith D, Finnegan ME, Williams S, et al. Multiparametric MRI and Radiomics in Prostate Cancer: A Review. *Australas Phys Eng Sci Med* (2019) 42(1):3–25. doi: 10.1007/s13246-019-00730-z
17. Yan D, Chen S, Krauss DJ, Chen PY, Chinnaiyan P, Wilson GD. Tumor Voxel Dose-Response Matrix and Dose Prescription Function Derived Using 18f-FDG PET/CT Images for Adaptive Dose Painting by Number. *Int J Radiat Oncol Biol Phys* (2019) 104(1):207–18. doi: 10.1016/j.ijrobp.2019.01.077
18. Gillies RJ, Kinahan PE, Hricak H. Radiomics: Images Are More Than Pictures, They Are Data. *Radiology* (2016) 278(2):563–77. doi: 10.1148/radiol.2015151169
19. Lambin P, Rios-Velazquez E, Leijenaar R, Carvalho S, van Stiphout RG, Granton P, et al. Radiomics: Extracting More Information From Medical Images Using Advanced Feature Analysis. *Eur J Cancer* (2012) 48(4):441–6. doi: 10.1016/j.ejca.2011.11.036
20. Avanzo M, Stancanello J, El Naqa I. Beyond Imaging: The Promise of Radiomics. *Phys Med* (2017) 38:122–39. doi: 10.1016/j.ejmp.2017.05.071
21. Mayerhoefer ME, Materka A, Langs G, Häggström I, Szczypiński P, Gibbs P, et al. Introduction to Radiomics. *J Nucl Med* (2020) 61(4):488–95. doi: 10.2967/jnumed.118.222893
22. Parmar C, Barry JD, Hosny A, Quackenbush J, Aerts HJWL. Data Analysis Strategies in Medical Imaging. *Clin Cancer Res* (2018) 1:24(15):3492–9. doi: 10.1158/1078-0432.CCR-18-0385
23. Pfister DG, Spencer S, Adelstein D, Adkins D, Anzai Y, Brizel DM, et al. Head and Neck Cancers, NCCN Clinical Practice Guidelines in Oncology. *J Natl Compr Canc Netw* (2020) 18(7):873–98. doi: 10.6004/jnccn.2020.0031
24. Zhuo EH, Zhang WJ, Li HJ, Zhang GY, Jing BZ, Zhou J, et al. Radiomics on Multi-Modalities MR Sequences Can Subtype Patients With Non-Metastatic Nasopharyngeal Carcinoma (NPC) Into Distinct Survival Subgroups. *Eur Radiol* (2019) 29(10):5590–9. doi: 10.1007/s00330-019-06075-1
25. Chan SC, Yeh CH, Yen TC, Ng SH, Chang JT, Lin CY, et al. Clinical Utility of Simultaneous Whole-Body 18F-FDG PET/MRI as a Single-Step Imaging Modality in the Staging of Primary Nasopharyngeal Carcinoma. *Eur J Nucl Med Mol Imaging* (2018) 45(8):1297–308. doi: 10.1007/s00259-018-3986-3
26. Feng Q, Liang JT, Wang LY, Niu JL, Ge XH, Pang PP, et al. Radiomics Analysis and Correlation With Metabolic Parameters in Nasopharyngeal Carcinoma Based on PET/MR Imaging. *Front Oncol* (2020) 10:1619. doi: 10.3389/fonc.2020.01619
27. Akram F, Koh PE, Wang F, Zhou S, Tan SH, Paknezhad M, et al. Exploring MRI Based Radiomics Analysis of Intratumoral Spatial Heterogeneity in Locally Advanced Nasopharyngeal Carcinoma Treated With Intensity Modulated Radiotherapy. *PloS One* (2020) 15(10):e0240043. doi: 10.1371/journal.pone.0240043
28. Zhong X, Li L, Jiang HL, Yin JX, Lu BG, Han W, et al. Cervical Spine Osteoradionecrosis or Bone Metastasis After Radiotherapy for Nasopharyngeal Carcinoma? The MRI-Based Radiomics for Characterization. *BMC Med Imaging* (2020) 20(1):104. doi: 10.1186/s12880-020-00502-2
29. Du DY, Feng H, Lv WB, Ashrafinia S, Yuan QY, Wang QS, et al. Machine Learning Methods for Optimal Radiomics-Based Differentiation Between Recurrence and Inflammation: Application to Nasopharyngeal Carcinoma Post-Therapy PET/CT Images. *Mol Imaging Biol* (2020) 22(3):730–8. doi: 10.1007/s11307-019-01411-9
30. Yu TT, Lam SK, To LH, Tse KY, Cheng NY, Fan YN, et al. Pretreatment Prediction of Adaptive Radiation Therapy Eligibility Using MRI-Based Radiomics for Advanced Nasopharyngeal Carcinoma Patients. *Front Oncol* (2019) 9:1050. doi: 10.3389/fonc.2019.01050
31. Zhao L, Gong J, Xi YB, Xu M, Li C, Kang XW, et al. MRI-Based Radiomics Nomogram May Predict the Response to Induction Chemotherapy and Survival in Locally Advanced Nasopharyngeal Carcinoma. *Eur Radiol* (2020) 30(1):537–46. doi: 10.1007/s00330-019-06211-x
32. Piao YF, Jiang C, Wang L, Yan FQ, Ye ZM, Fu ZF, et al. The Usefulness of Pretreatment MR-Based Radiomics on Early Response of Neoadjuvant Chemotherapy in Patients With Locally Advanced Nasopharyngeal Carcinoma. *Oncol Res* (2021) 28(6):605–13. doi: 10.3727/096504020X16022401878096
33. Ouyang FS, Guo BL, Zhang B, Dong YH, Zhang L, Mo XK, et al. Exploration and Validation of Radiomics Signature as an Independent Prognostic Biomarker in Stage III-IVb Nasopharyngeal Carcinoma. *Oncotarget* (2017) 8(43):74869–79. doi: 10.18632/oncotarget.20423
34. Shen HS, Wang Y, Liu DH, Lv RF, Huang YY, Peng C, et al. Predicting Progression-Free Survival Using MRI-Based Radiomics for Patients With Nonmetastatic Nasopharyngeal Carcinoma. *Front Oncol* (2020) 10:618. doi: 10.3389/fonc.2020.00618
35. Ming X, Oei RW, Zhai RP, Kong FF, Du CR, Hu CS, et al. MRI-Based Radiomics Signature Is a Quantitative Prognostic Biomarker for Nasopharyngeal Carcinoma. *Sci Rep* (2019) 9(1):10412. doi: 10.1038/s41598-019-46985-0
36. Yang KX, Tian JF, Zhang B, Li M, Xie WJ, Zou YT, et al. A Multidimensional Nomogram Combining Overall Stage, Dose Volume Histogram Parameters and Radiomics to Predict Progression-Free Survival in Patients With Locoregionally Advanced Nasopharyngeal Carcinoma. *Oral Oncol* (2019) 98:85–91. doi: 10.1016/j.oraloncology
37. Lv WB, Yuan QY, Wang QS, Ma JH, Feng QJ, Chen WF, et al. Radiomics Analysis of PET and CT Components of PET/CT Imaging Integrated With Clinical Parameters: Application to Prognosis for Nasopharyngeal Carcinoma. *Mol Imaging Biol* (2019) 21(5):954–64. doi: 10.1007/s11307-018-01304-3
38. Xu H, Lv WB, Feng H, Du DY, Yuan QY, Wang QS, et al. Subregional Radiomics Analysis of PET/CT Imaging With Intratumor Partitioning: Application to Prognosis for Nasopharyngeal Carcinoma. *Mol Imaging Biol* (2020) 22(5):1414–26. doi: 10.1007/s11307-019-01439-x
39. Zhang L, Dong D, Li HL, Tian J, Ouyang F, Mo XK, et al. Development and Validation of a Magnetic Resonance Imaging-Based Model for the Prediction

of Distant Metastasis Before Initial Treatment of Nasopharyngeal Carcinoma: A Retrospective Cohort Study. *EBioMedicine* (2019) 40:327–35. doi: 10.1016/j.ebiom.2019.01.013
40. Zhang L, Zhou HY, Gu DS, Tian J, Zhang B, Dong D, et al. Radiomic Nomogram: Pretreatment Evaluation of Local Recurrence in Nasopharyngeal Carcinoma Based on MR Imaging. *J Cancer* (2019) 10(18):4217–25. doi: 10.7150/jca.33345
41. Raghavan Nair JK, Vallières M, Mascarella MA, El Sabbagh N, Duchatellier CF, Zeitouni A, et al. Magnetic Resonance Imaging Texture Analysis Predicts Recurrence in Patients With Nasopharyngeal Carcinoma. *Can Assoc Radiol J* (2019) 70(4):394–402. doi: 10.1016/j.carj.2019.06.009
42. Zhang B, He X, Ouyang F, Gu D, Dong YH, Zhang L, et al. Radiomic Machine-Learning Classifiers for Prognostic Biomarkers of Advanced Nasopharyngeal Carcinoma. *Cancer Lett* (2017) 403:21–7. doi: 10.1016/j.canlet.2017.06.004
43. Li SS, Wang KC, Hou Z, Yang J, Ren W, Gao SB, et al. Use of Radiomics Combined With Machine Learning Method in the Recurrence Patterns After Intensity-Modulated Radiotherapy for Nasopharyngeal Carcinoma: A Preliminary Study. *Front Oncol* (2018) 8:648. doi: 10.3389/fonc.2018.00648
44. Liu YX, Shi HY, Huang SJ, Chen XC, Zhou HM, Chang H, et al. Early Prediction of Acute Xerostomia During Radiation Therapy for Nasopharyngeal Cancer Based on Delta Radiomics From CT Images. *Quant Imaging Med Surg* (2019) 9(7):1288–302. doi: 10.21037/qims.2019.07.08
45. Zhang B, Lian ZY, Zhong LM, Zhang X, Dong YH, Chen QY, et al. Machine-Learning Based MRI Radiomics Models for Early Detection of Radiation-Induced Brain Injury in Nasopharyngeal Carcinoma. *BMC Cancer* (2020) 20 (1):502. doi: 10.1186/s12885-020-06957-4
46. Liang ZG, Tan HQ, Zhang F, Rui Tan LK, Lin L, Lenkowicz J, et al. Comparison of Radiomics Tools for Image Analyses and Clinical Prediction in Nasopharyngeal Carcinoma. *Br J Radiol* (2019) 92(1102):20190271. doi: 10.1259/bjr.20190271
47. Lu LJ, Lv WB, Jiang J, Ma JH, Feng QJ, Rahmim A, et al. Robustness of Radiomic Features in [11C]Choline and [18F]FDG PET/CT Imaging of Nasopharyngeal Carcinoma: Impact of Segmentation and Discretization. *Mol Imaging Biol* (2016) 18(6):935–45. doi: 10.1007/s11307-016-0973-6
48. Yang PF, Xu L, Cao ZZ, Wan YD, Xue Y, Jiang YK, et al. Extracting and Selecting Robust Radiomic Features From PET/MR Images in Nasopharyngeal Carcinoma. *Mol Imaging Biol* (2020) 22(6):1581–91. doi: 10.1007/s11307-020-01507-7
49. Lv WB, Yuan QY, Wang QS, Ma JH, Jiang J, Yang W, et al. Robustness Versus Disease Differentiation When Varying Parameter Settings in Radiomics Features: Application to Nasopharyngeal PET/Ct. *Eur Radiol* (2018) 28 (8):3245–54. doi: 10.1007/s00330-018-5343-0

Conflict of Interest: The authors declare that the research was conducted in the absence of any commercial or financial relationships that could be construed as a potential conflict of interest.

Publisher's Note: All claims expressed in this article are solely those of the authors and do not necessarily represent those of their affiliated organizations, or those of the publisher, the editors and the reviewers. Any product that may be evaluated in this article, or claim that may be made by its manufacturer, is not guaranteed or endorsed by the publisher.

frontiers in Oncology

ORIGINAL RESEARCH
published: 11 January 2022
doi: 10.3389/fonc.2021.739182

An Immune Feature-Based, Three-Gene Scoring System for Prognostic Prediction of Head-and-Neck Squamous Cell Carcinoma

Yamin Zhang[1,2†], *Xiayan Luo*[1†], *Jing Yu*[1], *Kejia Qian*[1] *and Huiyong Zhu*[1*]

[1] *Department of Oral and Maxillofacial Surgery, The First Affiliated Hospital of Zhejiang University School of Medicine, Hangzhou, China,* [2] *School of Stomatology, Key Laboratory of Oral Biomedical Research of Zhejiang Province, Hangzhou, China*

OPEN ACCESS

Edited by:
Min Yao,
University Hospitals Cleveland Medical Center, United States

Reviewed by:
Kee Howe Wong,
Royal Marsden NHS Foundation Trust, United Kingdom
Xuan Zhou,
Tianjin Medical University Cancer Institute and Hospital, China

***Correspondence:**
Huiyong Zhu
zhuhuiyong@zju.edu.cn

[†]These authors have contributed equally to this work and share first authorship

Specialty section:
This article was submitted to Head and Neck Cancer, a section of the journal Frontiers in Oncology

Received: *10 July 2021*
Accepted: *14 December 2021*
Published: *11 January 2022*

Citation:
Zhang Y, Luo X, Yu J, Qian K and Zhu H (2022) An Immune Feature-Based, Three-Gene Scoring System for Prognostic Prediction of Head-and-Neck Squamous Cell Carcinoma. Front. Oncol. 11:739182. doi: 10.3389/fonc.2021.739182

Head-and-neck squamous cell carcinoma (HNSCC) is characterized by a high frequency of neck lymph node metastasis (LNM), a key prognostic factor. Therefore, identifying the biological processes during LNM of HNSCC has significant clinical implications for risk stratification. This study performed Gene Ontology enrichment analysis of differentially expressed genes between tumors with LNM and those without LNM and identified the involvement of immune response in the lymphatic metastasis of HNSCC. We further identified greater infiltrations of $CD8^+$ T cells in tumors than in adjacent normal tissues through immunochemistry in the patient cohort (n = 62), indicating the involvement of $CD8^+$ T cells in the antitumor immunity. Hierarchical clustering analysis was conducted to initially identify the candidate genes relevant to lymphocyte-mediated antitumor response. The candidate genes were applied to construct a LASSO Cox regression analysis model. Three genes were eventually screened out as progression-related differentially expressed candidates in HNSCC and a risk scoring system was established based on LASSO Cox regression model to predict the outcome in patients with HNSCC. The score was calculated using the formula: 0.0636 × CXCL11 − 0.4619 × CXCR3 + 0.2398 × CCR5. Patients with high scores had significantly worse overall survival than those with low scores ($p < 0.001$). The risk score showed good performance in characterizing tumor-infiltrating lymphocytes and provided a theoretical basis for stratifying patients receiving immune therapies. Additionally, a nomogram including the risk score, age, and TNM stage was constructed. The prediction model displayed marginally better discrimination ability and higher agreement in predicting the survival of patients with HNSCC compared with the TNM stage.

Keywords: HNSCC, lymph node metastasis, tumor-infiltrating lymphocyte, CD8+ T cell, LASSO, risk-scoring system

1 INTRODUCTION

Head-and-neck squamous cell carcinoma (HNSCC) is the most common malignant tumor arising from the head-and-neck cancers (1); it typically arises in the oral cavity, oropharynx, larynx, and hypopharynx (2, 3). HNSCC is characterized by frequent local invasiveness and neck lymph node metastasis (LNM), which have been identified as key prognostic factors. Despite advancements in diagnostic and therapeutic modalities, the prognosis of patients with HNSCC remains poor (4). Accurate prediction of prognosis assists in decision-making regarding adjuvant treatment after tumor resection. Currently, prognostic prediction and treatment decisions regarding HNSCC are based on the American Joint Committee on Cancer TNM staging system (5). However, the sensitivity and accuracy of this system for prognostic prediction are reduced by the individual heterogeneity (6). Accurate predictors are thus needed.

Innate and adaptive immunity can exert antitumor effect through recognition and elimination of malignant cells (7, 8). Increasing evidence suggests that densities of tumor-infiltrating lymphocytes (TILs) reflect the antitumor immunity process in the tumor environment and can predict overall survival (OS) of patients with cancer, including those with HNSCC (9–11). TILs comprise at least 28 different types (12), among which T lymphocytes are considered the central players (13). Besides T lymphocytes, various myeloid cells, such as dendritic cells (DCs), natural killer (NK) cells, and macrophages, also infiltrate the tumor microenvironment (TME) to exert their antitumor effects (14). Some studies have focused on the correlations between the infiltration of one or several immune cells in HNSCC tumors and prognosis (15–17). However, immunity in the tumor environment is mutually regulated by multiple TILs, which demands a comprehensive analysis of the TIL profiles.

Generally, TILs can effectively eliminate cancer cells at their early stages (8). However, cancer cells can evade the immune surveillance and resist the cytotoxic effect of cytotoxic T lymphocytes by hijacking immune-checkpoint pathways (18, 19), allowing the occurrence of advanced tumors. Multiple immune checkpoints, especially those expressed on the T-lymphocyte markers have been reported. Numerous clinical trials in various tumors have proven the efficiency of immune-checkpoint blockade (ICB) therapies, especially those that target cytotoxic T-lymphocyte-associated protein 4 (CTLA) and programmed cell death protein 1 (PD-1)/programmed cell death 1 ligand 1 (PD-L1) (20, 21). However, the clinical responses of ICB antibodies strongly depend on the composition of the TME (22, 23). As a result, the clinical benefit of patients with cancer from ICB therapies has great heterogeneity. A key challenge is the identification of patients potentially suitable for ICB therapies. Currently, the advancement of next-generation sequencing technologies and computational techniques allows analysis of the infiltration of immune cells (24–26). Based on the comprehensive insight of TIL profiles, we can better investigate the antitumor response and predict outcomes in patients with cancer. Some efficient risk scoring systems based on immune features have been reported in prediction of HNSCC outcome (27, 28). However, their clinical applications were somewhat limited by complex variables incorporated in prediction models.

In this study, we performed RNA sequencing in patients with HNSCC with different LNM statuses and found that the differentially expressed genes (DEGs) between HNSCC tumors with LNM and those without LNM were enriched in immune-response pathways. After estimating the abundance of TILs, we found that $CD8^+$ T cells had greater estimated abundance in tumors with LNM, which was also verified in our HNSCC cohort by immunohistochemistry (IHC). Therefore, we focused on T-lymphocyte-related genes in the follow-up study. We developed a prognostic risk-scoring system based on the TIL-related genes, and the ability of the system in reflecting tumor immune environment was also evaluated.

2 MATERIALS AND METHODS

2.1 RNA-Sequencing Profiles

2.1.1 Sample Preparations and Procedures

Samples from LNM^- primary tumors ($n = 4$) and LNM^+ primary tumors ($n = 5$) were cut into small specimens. The total RNA was extracted using Trizol reagent (Invitrogen, Carlsbad, CA, USA) following the manufacturer's procedure. The purity and quantity of total RNA were analyzed using NanoDrop ND 1000 (NanoDrop, Wilmington, DE, USA), and the integrity of the RNA was assessed using Agilent 2100 with RIN number >7.0. Poly(A) RNA was purified from total RNA (5 μg) using poly T oligo attached magnetic beads using two rounds of purification (Invitrogen). The mRNA was then fragmented into small pieces using divalent cations under elevated temperature. Subsequently, the cleaved RNA fragments were reverse-transcribed to create the final cDNA library in accordance with the protocol for the mRNA-sequencing sample preparation kit (Illumina, San Diego, CA, USA). Lastly, we performed the 150-bp paired-end sequencing on an Illumina X Ten (LC Bio, Hangzhou, China) following the recommended protocols.

2.1.2 Data Processing

The HISAT package (version 2.0.4) (29) was used to align the raw RNA sequences to the hg19 human reference genome (http://genome.ucsc.edu/). The mapped reads were assembled using StringTie (version 1.3.4) (30), and transcriptomes were merged using Perl scripts. The expression level for mRNAs was calculated by exon per million mapped reads (FRKM) using StringTie. The DEGs with |log2 (fold change)| >1 and p-value <0.05 were selected using "edgeR" (version 3.20.9) (31).

2.1.3 Data Analyses

Gene Oncology (GO) enrichment was performed for DEGs using the GO database (http://geneontology.org/). The DEGs with significant differential expression ($p < 0.01$, log2|FC|>2) in top 20 enriched GO terms were selected and applied to GO enrichment analysis of ImmunoSystem Process using Cytoscape 3.1.0 (32). KEGG pathway analysis of the DEGs was

also performed using the KEGG pathway database (https://www.genome.jp/kegg/pathway.html). Cell-type Identification by Estimating Relative Subsets of RNA Transcripts (CIBERSORT) (http://cibersort.stanford.edu) was used for TIL profiles. The algorithm was run using the leukocyte matrix (LM22) signature and 1,000 permutations for the estimation of relative fractions of multiple TILs in gene expression profiles of admixtures (26, 33, 34). Samples with statistically significant deconvolution result across all cell subsets (p-value <0.05) were included in the consequent analysis. The relative fractions of 22 TILs were summarized by means ± standard errors of the means (SEM).

2.2 IHC

2.2.1 Sample Preparations and Procedures

A patient cohort (n = 62) with a histopathological diagnosis of primary HNSCC was enrolled in this study. All patients underwent surgical tumor resection and neck lymph node dissection (elective or therapeutic neck dissection) under general anesthesia at the First Affiliated Hospital of Zhejiang University from January 2018 to June 2021. The exclusion criteria were as follows: (i) chemotherapy, radiotherapy, or biological treatment before surgery; (ii) immune deficiency or immune system disease; (iii) inadequate clinicopathological medical records; (iv) previous history of other malignant tumors; and (v) previous history of primary tumors arising from the head and neck.

Demographical and clinicopathological data—sex, age, primary region of tumorigenesis, tumor size, and N status—were collected by a retrospective review of medical records and postoperative pathological reports. T and N staging was performed using the TNM staging system of the American Joint Committee on Cancer, 7th Edition. Because of the retrospective study design, power calculation was not performed. The sample size was equal to the number of patients treated in our institution during the recruitment period. The collection and the preservation of the samples were approved by the Ethics Committee of the First Affiliated Hospital, College of Medicine, Zhejiang University, and written informed consent was obtained from all participants.

Segments of tumor tissues (n = 62) and adjacent normal tissues (n = 24) (mucosa 5 cm beyond the edge of the carcinoma) were collected and repeatedly washed in phosphate-buffered saline (pH 7.4) to remove mucus and blood and then fixed in formalin, dehydrated, embedded in paraffin, and sectioned. Moreover, 4-μm-thick paraffin sections of samples were deparaffinized in xylene, rehydrated through graded alcohols, repaired with antigen retrieval through hot citric acid buffer (pH 6), and blocked with 3% bovine serum albumin. These sections were then incubated with antibody-CD4 (NCL-L-CD4-1F6, Leica Biosystems, Milton Keynes, UK), antibody-CD8 (NCL-L-CD8-4B11, Leica Biosystems, UK), antibody-Foxp3 (ab20034, Abcam, Cambridge, MA, USA), and secondary antibodies (Servicebio, Wuhan, China) successively at an appropriate dilution. Finally, sections were treated with 3,3′-diaminobenzidine, counterstained with hematoxylin, dehydrated through graded ethanol, cleared in xylene, and mounted with resin mounting medium.

2.2.2 Quantitative Evaluation of Immunostaining Density

Immunostaining reactions were separately assessed by two independent pathologists who were blinded to the clinical data of the patients. A positive reaction was defined as clear brown staining. The interface of the tumor/normal tissues were screened at a low-power field (×100). Subsequently, areas containing the highest number of positively stained cells (hot spots) were selected. In the selected field, 3–8 separate areas of intense cells were captured in a ×200 field. These images were captured using an inverted microscope (Leica, Wetzlar, Germany).

We used the IHC Profile plugged in ImageJ software (USA) to semiautomatically calculate the intensity of positive cytoplasmic membrane staining and percentage of positive staining area. Antigen-expressed cells in each IHC image were divided into four levels (high positive, positive, low-positive, and negative) according to their density and assigned values of 3, 2, 1, and 0, respectively. We multiplied the value of positive cells and percentage of positive areas to obtain the IHC score of each marker based on the Barnes' score method.

2.2.3 Associations of TILs With Clinicopathological Features

Patients were divided into high- and low-infiltration groups based on their IHC scores of immune markers (CD8, CD4, and Foxp3). The Chi-squared test was performed to determine the associations of the immune markers with the clinicopathological features of patients with HNSCC.

2.3 Database Mining

2.3.1 Data Acquisition

We mined The Cancer Genome Atlas (TCGA) database (https://portal.gdc.cancer.gov/) to extract the transcriptome data, pathological stage, and survival status of patients with HNSCC diagnosed between 1993 and 2013 (n = 501).

2.3.2 Data Analyses

2.3.2.1 Correlations of TIL-Related Genes by Pearson's Analysis and Hierarchical Clustering Analysis

Pearson's analysis was performed to screen DEGs closely related to CD8, CD4, and Foxp3, which were involved in the pathway of activation, differentiation, and migration of T cells. The correlation values were clustered and visualized through hierarchical clustering analysis (HCA) in the R software.

2.3.2.2 Survival-Related Hub Gene Screening Using the LASSO Cox Regression Analysis

To identify the hub gene signatures relevant to survival of patients, we used a linear regression technique based on the LASSO algorithm in "glmnet" R (version 4.1-1). The most suitable signatures were selected by the LASSO Cox regression model when the minimum penalization coefficient (lambda) was obtained after running crossvalidation likelihood 1,000 times. The selected gene signatures were then applied to establish a risk-

scoring system, by weighting the expression levels of gene signatures and corresponding regression coefficients. To validate its efficiency in predicting patients' prognosis, patients with HNSCC were divided into the low- and high-risk groups based on their risk scores (median risk score as cutoff point). Survival rates of the two groups were calculated using the Kaplan–Meier (KM) method and compared using log-rank test. The time-dependent receiver operating characteristic curve (ROC) analysis was performed to assess the area under curve (AUC) for the 1-, 3-, and 5-year OS, thus checking the survival prediction accuracy of the prognostic model.

2.3.2.3 Survival Analysis

The correlations between the survival-related genes and OS of patients with HNSCC were analyzed using KM plotter database (http://kmplot.com/analysis/) (35). Cox proportional hazards regression analysis was performed to calculate the log-rank *p*-values, hazard ratios (HRs), and 95% confidence intervals (CIs). KM survival plots were generated to visualize the survival differences in patients with different mRNA expression levels of target genes (median as cutoff point).

2.3.2.4 Associations Between the Risk Scores and Tumor Immune Microenvironment

The abundance of TILs in HNSCC tumors was estimated using the CIBERSORT algorithm. Tumors were divided into the high-risk and low-risk group (median as cutoff point). The estimated infiltration fractions of TILs between the two groups were compared using the Mann–Whitney *U* test. We also investigated the associations of the risk scores with the infiltrations of lymphoid and myeloid cells, respectively, using Pearson's correlation test. Comparison of the overall infiltrations of lymphoid and myeloid cells between the two groups was also performed using the Mann–Whitney *U* test. Additionally, the associations of the risk scores with a set of immune checkpoints were analyzed using Pearson's correlation test.

2.4 Quantitative Real-Time Polymerase Chain Reaction

The relative expression levels of the survival-related hub genes were further identified in LNM^- (n = 18) and LNM^+ primary tumors (n = 18). Total RNA was isolated from collected tumor tissues using RnaExTM Total RNA Isolation Solution (GK3006, GENEray, Shanghai, China). Moreover, 1 μg of total RNA was used to synthesize cDNA. The quantitative real-time polymerase chain reaction (qRT-PCR) was performed using 500 ng cDNA per 10 μl reaction. Each reaction was conducted with iQTM SYBR® Green Supermix (Bio-Rad, Hercules, CA, USA). Gene amplification was conducted on thermal cycler programmed as follows: initial denaturation at 95°C for 5 min followed by 35 cycles at 95°C for 10 s, annealing at 60°C for 20 s, 72°C for 1 min, extending at 72°C for 5 min. Each sample was analyzed in triplicate. Relative expression levels were normalized to glyceraldehyde-3-phosphate dehydrogenase (GAPDH). The relative expression of targets in LNM^+ tumors compared with LNM^- tumors was calculated using $2^{-\triangle\triangle ct}$. The primer sequences are presented in **Table 1**.

TABLE 1 | Primers used in qRT-PCR.

Primer	Sequence
CXCL10_F	TATTTCCCTCACCTTTCCC
CXCL10_R	GCAGATTTGATTGCATACCTT
CXCL11_F	GAAAGGTGGGTGAAAGGAC
CXCL11_R	TGCAACAAGTAAGAACGTGAA
CCR5_F	TGTTTGCGTCTCTCCCA
CCR5_R	CCAGCCCCAAGATGACTA
GAPDH_F	CCTTCCGTGTCCCCACT
GAPDH_R	GCCTGCTTCACCACCTTC

2.5 Univariate and Multivariate Cox Regression Analyses

A total of 439 patients with complete clinical data from the TCGA dataset were evaluated, and univariate and multivariate Cox regression analyses were employed to investigate whether the risk score was an independent risk factor for the OS of patients with HNSCC. The OS rates were calculated using the KM method and log-rank test. We included age, grade, T stage, N stage, and TNM stage into the univariate Cox model, considering their potential prognostic roles. The risk score was classified into four levels by quartiles (low, low-medium, medium-high, and high); age of patients was classified into four age bands (<50, 50–60, 60–70, ≥70 years). Variables showing statistically significant effect (p-value <0.05) in the univariate analysis were included in the multivariate Cox regression model. Variables with p-values <0.05 in the multivariate Cox model were considered independent prognostic factors. The forest was used to display the HR, p-value, and 95% CI of each variable using the "forestplot" R package.

2.6 Construction and Assessment of the Nomogram Model

For convenient application of the established risk-scoring system in clinical work, we established a nomogram prediction model based on the risk scores and clinical parameters to predict outcomes of patients with HNSCC. Variables identified as independent risk factors were included to construct a nomogram prediction model to predict OS of patients with HNSCC. The discrimination of the constructed nomogram model was measured and compared using Harrell's concordance index (c-index). The predicted accuracy of the nomogram for prediction of 1-, 3-, and 5-year survival of patients with HNSCC was shown in the calibration curves and compared with that of the TNM stage (36).

2.7 Statistical Analysis

All statistical analyses and plots were conducted using GraphPad Prism (version 8.0) and R software (version 4.0.5). Student's t-test was used for groupwise comparisons of normally distributed continuous variables; the Mann–Whitney *U* test was used for groupwise comparisons of variables with abnormal distributions. The Chi-squared test was used to analyze the associations between the TILs and clinicopathological features. Pearson's correlation test was used to analyze correlations between groups. Correlation values were used to conduct HCA. The KM method was used to calculate survival rates. LASSO regression analysis was performed to filter key genes and

establish the risk-scoring system. The accuracies of the diagnostic and prognostic prediction models were generated using ROC curves and calculated using the AUC. Univariate and multivariate Cox hazard regression analyses were performed for screening independent risk factors for the OS of patients with HNSCC. A nomogram was constructed based on parameters selected by multivariate Cox regression analysis. The discrimination abilities of the prognostic models were measured using the c-index. All statistical tests were two sided, and p-value <0.05 was considered statistically significant.

3 RESULTS

3.1 Identification of Biological Processes in Tumors During LNM of HNSCC Tumors

A total of 258 upregulated genes and 265 downregulated genes were identified in tumors with LNM compared with tumors without LNM (|log2 fold-change| >1 and p-value <0.05). DEGs were significantly enriched in extracellular matrix and immune-related GO terms ($p < 0.01$) (**Figure 1A**). Similarly, KEGG pathway analysis yielded DEGs enriched mostly in the cytokine-cytokine receptor interaction pathway (**Figure 1B**). We found the 198 DEGs enriched in the top 20 GO terms were mainly enriched in the immune system process pathways of complement activation (classical pathway) (53.85%), positive regulation of cytokines involved in immunity (34.63%), NK-mediated immunity (7.69%), and T-cell chemotaxis (3.85%) (**Figure 1C**). Among them, CCL26, MYB, CDH26, GATA3, CXCL10, CXCL11, IL6, and CCL20 were involved in the pathway of activation, differentiation, and migration of T cells.

3.2 Identification of Infiltrated TILs in HNSCC Tumors

We compared the average infiltration levels of TILs and found that $CD8^+$ T cells were greater in LNM^+ tumors than in LNM^- tumors (0.173 ± 0.044 versus 0.103 ± 0.022, respectively) (**Figure 2A**). IHC confirmed the expression of CD8 in tumor tissues and adjacent normal tissues. $CD8^+$ T cells infiltrated the tumor stroma, invasive margin, and center, whereas $CD4^+$ and $Foxp3^+$ T cells mainly infiltrated the tumor stroma and invasive margin (**Figure 2B**). The IHC scores of CD8 and CD4 were significantly higher in tumor tissues ($p < 0.05$) while those of Foxp3 showed no significant difference ($p > 0.05$) (**Figure 2C**).

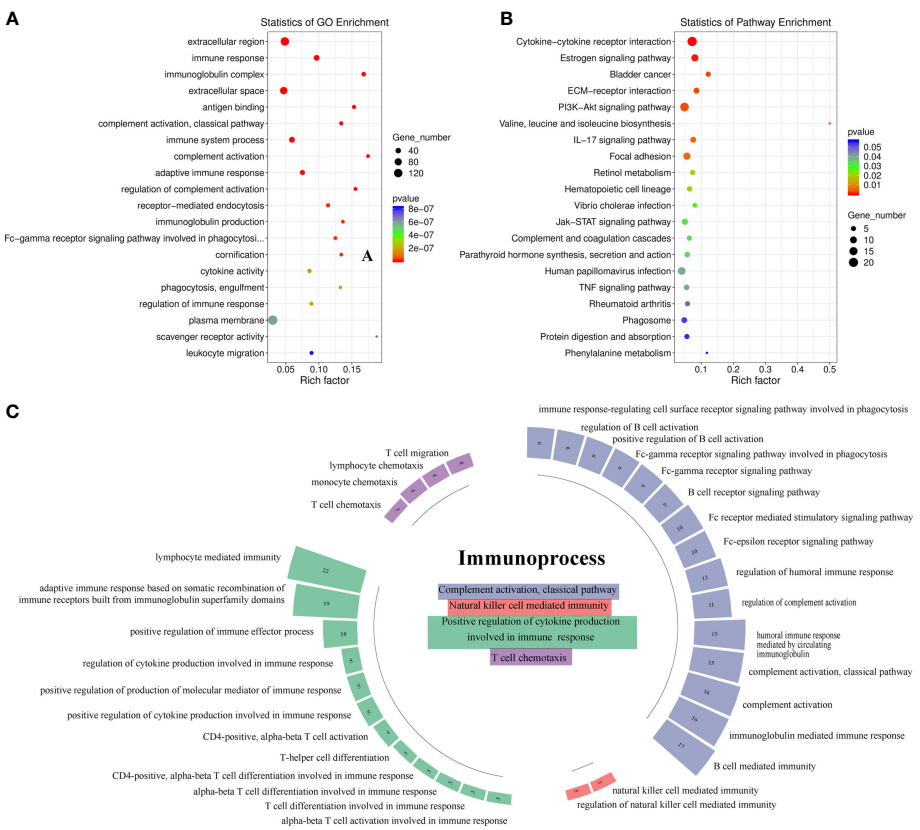

FIGURE 1 | Identification of the immune process involved in antitumor lymphatic metastasis response in head-and-neck squamous cell carcinoma patients (n = 9). **(A)** Gene Ontology (GO) enrichment analysis of 523 differentially expressed gene (DEGs). The top 20 GO terms with the smallest p-value in the enrichment analysis results are presented. **(B)** KEGG pathway analysis of 523 DEGs. The top 20 pathways with the highest enrichment factor are shown. **(C)** Immunosystem process pathway enrichment analysis of 198 DEGs involved in the top 20 GO terms. Numbers in boxes indicate numbers of genes involved in corresponding immune pathways.

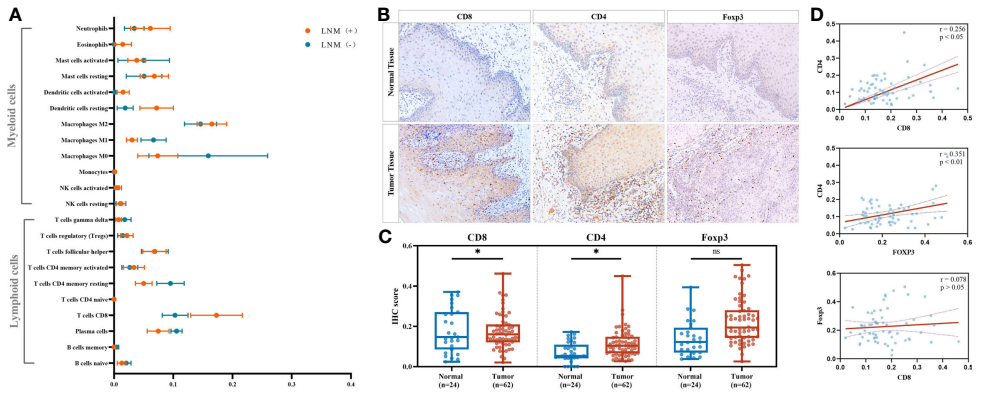

FIGURE 2 | Identifying significant tumor-infiltrating lymphocyte (TIL) subtypes engaging in antitumor lymphatic metastasis response. **(A)** Comparison of the estimated fractions of 22 TILs in tumors with LNM (n = 5) and those without LNM (n = 4). All values were represented by mean ± SEM. **(B)** Representative immunohistochemistry (IHC) images of CD8, CD4, and FOXP3 in adjacent normal tissues and tumor tissues. Images were obtained under a light microscope at magnifications of ×200. **(C)** Comparison of the IHC scores between normal tissues (n = 24) and tumor tissues (n = 62) by Mann–Whitney U test. *p < 0.05; ns, p > 0.05. **(D)** Correlations of the IHC scores of CD8, CD4, and FOXP3 in tumor tissues (n = 62) by Pearson's correlation test. TIL, tumor-infiltrating lymphocytes; LNM, lymph-node metastasis; SEM, standard error of mean.

The protein expression levels of CD8 and CD4 were significantly correlated (r = 0.256, p < 0.05), whereas CD8 and Foxp3 showed no statistically significant correlation (r = 0.078, p > 0.05) (**Figure 2D**). Additionally, the protein expression level of Foxp3 was highly relevant to that of CD4 (r = 0.351, p < 0.01). As shown in **Table 2**, the CD8 expression level was significantly associated with LNM status (p = 0.001) but not with sex, age, tumor site, tumor burden, or degree of differentiation. CD4 and Foxp3 showed no significant correlations with clinicopathological characteristics (p > 0.05).

3.3 Identification of TIL-Related Genes

Among the DEGs involved in T-cell regulation, CXCL10 and CXCL11 were identified to be highly correlated with TIL-characterizing gene sets (CD8A, CD4, and Foxp3) (p < 0.00001) (**Figure 3A**). Additionally, CXCR3 and CCR5 were highly correlated with both CXCL10 and CXCL11 (r > 0.613, p < 0.0001) (**Figure 3B**). Consistently, the chemokines were positively associated with a series of effector immune cells, including M2 macrophages, resting NK cells, resting mast cells, $CD8^+$ T cells, and activated memory $CD4^+$ T cells (TAM CD4) (r > 0.04, p < 0.001) (**Figure 3C**). Additionally, they were negatively associated with M1 macrophages, activated mast cells, plasma cells, and naïve $CD4^+$ T cells (**Figure 3C**). Comprehensively, CXCL10, CXCL11, CXCR3, and CCR5 were TIL-related chemokines, involved in the accumulation of TILs in HNSCC.

3.4 Establishment and Validation of the Risk-Scoring System

CXCL11, CXCR3, and CCR5 were screened to be candidate genes related to prognosis of patients with HNSCC through LASSO Cox regression analysis (**Figures 4A, B**). A risk-scoring system was then established based on the formula generated according to the expression of the three genes, which could calculate the risk scores of patients with HNSCC. The risk-scoring system was established as follows: risk score = (0.0636) * CXCL11 + (−0.4619) ;* CXCR3 + (0.2398) * ;CCR5. Patients with high-risk scores had significantly worse OS than low-risk patients (log-rank p < 0.001) (**Figures 4C–F**). The risk score was identified to be an independent risk factor for patients with HNSCC (HR, 1.586; 95% CI, 1.21~2.077). The prediction accuracy of the system had a good performance in predicting 1-year OS (AUC, 0.606; 95% CI, 0.551–0.66) and 3-year OS (AUC, 0.642; 95% CI, 0.59–0.695). In contrast, the system showed relatively poor performance in predicting 5-year OS (AUC, 0.599; 95% CI, 0.519–0.679) (**Figure 4G**).

3.5 Validation of Prognosis-Related Candidate Genes

Of the three genes, CXCR3 had significant associations with OS of patients with HNSCC (HR, 0.64; 95% CI, 0.49–0.84; log-rank p = 0.001), so did CCR5 (HR, 0.76; 95% CI, 0.58–1; log-rank p = 0.048). Interestingly, patients with high expression of CXCL11 also had the tendency to live longer than those with low expression of CXCL11 (HR, 0.82; 95% CI, 0.62–1.07), but not statistically significant (log-rank p = 0.15) (**Figure 5A**). Also, the relative expression level of CXCL11 was significantly lower in LNM^+ tumors compared with that in LNM^- tumors (p < 0.05), whereas CCR5 showed significant higher expression in LNM^+ tumors compared with that in LNM^- tumors (p < 0.05). The relative expression level of CXCR3 in LNM^+ tumors was mildly higher but not statistically significant (p = 0.436) (**Figure 5B**).

3.6 Ability of the Risk-Scoring System to Reflect the TIL Landscape

Among the 22 TILs, M0, M1, and M2 macrophages had the highest infiltration rates (24.7%, 12.6%, and 10.8%, respectively), followed by resting memory $CD4^+$ T cells (TRM CD4), follicular helper T cells (Tfh), $CD8^+$ T cells, and resting NK cells. Ten

TABLE 2 | The Chi-square test of the associations between IHC scores and clinicopathological characteristics.

Variables	Cases	CD8			CD4			FOXP3		
		Low (%)	High (%)	*p*-value	Low (%)	High (%)	*p*-value	Low (%)	High (%)	*p*-value
Gender										
Male	34	15 (44.1%)	19 (55.9%)	0.307	15 (44.1%)	19 (55.9%)	0.307	16 (47.1%)	18 (52.9%)	0.61
Female	28	16 (57.1%)	12 (42.9%)		16 (57.1%)	12 (42.9%)		15 (53.6%)	13 (46.4%)	
Age										
≤Median	32	17 (53.1%)	15 (46.9%)	0.611	17 (53.1%)	15 (46.9%)	0.611	16 (50.0%)	16 (50.0%)	1
>Median	30	14 (46.7%)	16 (53.3%)		14 (46.7%)	16 (53.3%)		14 (46.7%)	16 (53.3%)	
Region										
Gingiva	16	9 (56.3%)	7 (43.8%)	0.501	7 (43.8%)	9 (56.3%)	0.779	6 (37.5%)	10 (62.5%)	0.368
Tongue	30	16 (53.3%)	14 (46.7%)		15 (50.0%)	15 (50%)		15 (50.0%)	15 (50%)	
Others	16	6 (37.5%)	10 (62.5%)		9 (56.3%)	7 (43.8%)		10 (62.5%)	6 (37.5%)	
Tumor size										
≤2 cm	23	13 (56.5%)	10 (43.5%)	0.43	13 (56.5%)	10 (43.5%)	0.43	11 (47.8%)	12 (52.2%)	0.793
>2 cm	39	18 (46.2%)	21 (53.8%)		18 (46.2%)	21 (53.8%)		20 (51.3%)	19 (48.7%)	
Differentiation degree										
Well	28	17 (60.7%)	11 (39.3%)	0.126	13 (46.4%)	15 (53.6%)	0.61	14 (50 %)	14 (50 %)	1
Moderately/Poorly	34	14 (41.2%)	20 (58.8%)		18 (52.9%)	16 (47.1%)		17 (50 %)	17 (50 %)	
LNM										
LNM (–)	35	24 (68.6%)	11 (31.4%)	**0.001**	18 (51.4%)	17 (48.6%)	0.798	17 (48.6%)	18 (51.4%)	0.798
LNM (+)	27	7 (25.9%)	20 (74.1%)		13 (48.1%)	14 (51.9%)		14 (51.9%)	13 (48.1%)	

LNM, lymph node metastasis; LNM(–), absence of lymph node metastasis; LNM(+), presence of lymph node metastasis.
The numbers in bold indicate statistical significance.

subtypes of TILs (naïve B cells, memory B cells, naïve $CD4^+$ T cells, TAM CD4, γδT cells, activated NK cells, monocytes, resting dendritic cells, eosinophils, and neutrophils) showed low abundance in both high- and low-risk patients (<5%) (**Figure 6A**). As for the remaining 12 types of TILs, we compared their abundance in high- and low-risk groups and found that 11 of them showed significant differences. Among these TIL subtypes, seven types of TILs (resting mast cells, $CD8^+$ T cells, Tregs, resting NK cells, TRM CD4, M2 macrophages, and M1 macrophages) had significantly higher abundance in low-risk groups. In contrast, four types of TILs (activated mast cells, plasma cells, activated DCs, and M0 macrophages) had significantly higher abundance in high-risk groups. Tfhs showed no difference in the infiltration between the two groups ($p > 0.05$) (**Figure 6B**).

Intriguingly, with the increase in the risk scores, the overall abundance of lymphoid cells continuously decreased ($r = -0.454$, $p < 0.0001$) and that of myeloid cells increased ($r = 0.487$, $p < 0.0001$) (**Figure 7A**). Consistently, the lymphoid cells had greater infiltration in the low-risk groups ($p < 0.0001$) and the myeloid cells had greater infiltration in high-risk groups ($p < 0.0001$) (**Figures 7B, C**).

3.7 Validating the Associations of the Risk Scores and Immune Checkpoints

The risk scores were significantly correlated with CD27 ($r = -0.7948$, $p < 0.0001$), ICOS ($r = -0.6251$, $p < 0.0001$), PDCD1 ($r = -0.5958$, $p < 0.0001$), LAG3 ($r = -0.5662$, $p < 0.0001$), TIGIT ($r = -0.5302$, $p < 0.0001$), CTLA4 ($r = -0.486$, $p < 0.0001$), IDO1 ($r = -0.4519$, $p < 0.0001$), HAVCR2 ($r = -0.3021$, $p < 0.0001$), and CD274 ($r = -0.251$, $p < 0.0001$) (**Figure 8**).

3.8 Identifying the Prognostic Role of the Risk Scores

Risk score, TNM stage, and age were independent risk factors for OS of patients with HNSCC through univariate and multivariate Cox regression analyses (**Figures 9A, B**). Patients with low–medium-, median–high-, and high-risk scores had significantly higher mortality risks than those with low-risk scores (HR = 1.653, 1.666, and 2.554, respectively, $p < 0.05$). Patients at stage III and stage IV had significantly higher mortality risk than those at stage I ($p < 0.05$). The risk of death for patients aged >70 years was significantly higher than that of those aged <50 years (HR = 1.689; 95% CI, 1.032–2.764; $p < 0.05$) (**Figure 9C**).

3.9 Construction and Validation of a Nomogram Prediction Model

A nomogram was constructed to predict the OS of patients with HNSCC based on identified independent risk factors (risk score, TNM stage, and age) (**Figure 10A**). The prediction model displayed better discrimination ability than the TNM stage for predicting OS (c-index = 0.64 vs. 0.57, respectively). The calibration curves for probability of 1-, 3-, and 5-year OS showed good agreement between nomogram prediction and actual observation, which also performed better than the TNM stage (**Figures 10B, C**).

4 DISCUSSION

Although the associations between TILs and cancer outcomes vary according to cell specificity and tumor heterogeneity, pan-cancer analysis had revealed that higher estimated T-cell fractions are generally correlated with superior survival (37). Massive evidence supports the antitumor role of $CD3^+$ T and

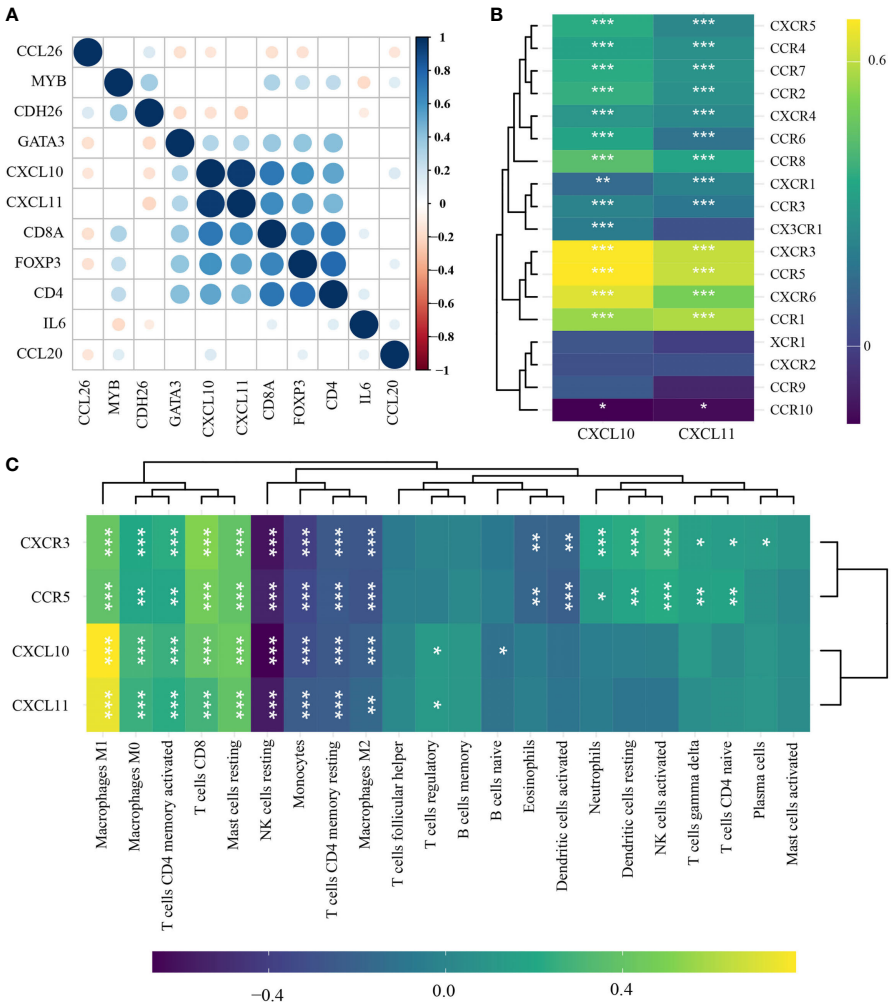

FIGURE 3 | Identification of TIL-related genes in head-and-neck squamous cell carcinoma (n = 501) by Pearson's correlation test and hierarchical cluster analysis. **(A)** Correlations among immune-related differentially expressed gene (DEGs), CD8A, CD4, and Foxp3. **(B)** Correlations of CXCL10 and CXCL11 with chemokine ligands. **(C)** Correlations of CXCL10, CXCL11, CXCR3, and CCR5 with the abundance of TILs. *p < 0.05; **p < 0.01; ***p < 0.001. TILs, tumor-infiltrating lymphocytes.

CD8$^+$ T cells in colorectal cancer (38), breast cancer (39), and nonsmall cell lung cancer (40). Strong infiltration of CD8$^+$ T cells has been generally associated with a favorable prognosis of patients with cancer (41–43). Moreover, immunotherapies are mainly aimed to reinvigorate antitumor immunity mediated by CD8$^+$ cytotoxic T lymphocytes (CTLs) (23). CD4$^+$ T cells can eliminate tumor cells by promoting the functions of CTLs or modulating the TME (44, 45). Greater infiltrations of CD4$^+$ and CD8$^+$ T lymphocytes have been identified to be associated with improved OS for HNSCC (46, 47). Consistently, we found higher CD8$^+$ and CD4$^+$ T-cell infiltration in HNSCC tumor tissues than adjacent normal tissues (p < 0.05) in our cohort. The density of CD8 and CD4 was highly correlated (r = 0.256, p < 0.05), indicating their synergy in the TME. The prognostic role of tumor-infiltrating FoxP3$^+$ T lymphocytes in patients with HNSCC is controversial. Boxberg et al. reported that patients with HNSCC with lower density of Foxp3$^+$ T lymphocytes tended to have worse OS and disease-free survival (48). In contrast, Mehtap et al. reported that FoxP3 was correlated with advanced tumor stages and poor prognosis (49). A pan-cancer meta-analysis revealed the heterogeneity of the prognostic roles of FoxP3s among tumor sites and the antitumor role of FoxP3 in HNSCC (OR, 0.69; 95% CI, 0.50~0.95; p < 0.05). It is hypothesized that the positive effect of FoxP3$^+$ Tregs may be partially attributed to its ability to suppress inflammatory response, which may promote tumor progression (50, 51).

In this study, we found that both innate and adaptive immune responses engaged in the lymphatic metastatic process of HNSCC tumors, which reminded us the importance of investigating TILs. Among tumor-infiltrating T lymphocytes, CD8$^+$ T cells seemed to actively participate in the antitumor LNM response in patients with HNSCC, which was also identified through the Chi-squared analysis of the IHC scores of CD8 (p = 0.001). Considering the cytotoxic effect of CD8$^+$ T cells and regulation function of CD4$^+$ T

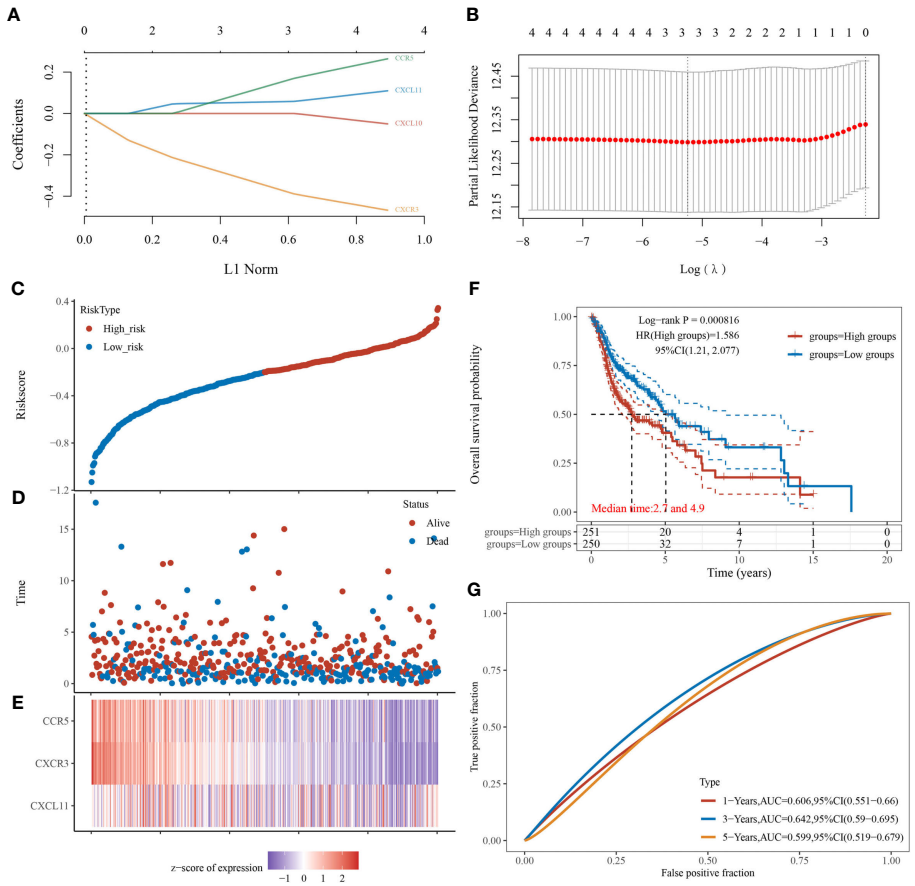

FIGURE 4 | Establishment and verification of the risk-scoring system in patients with head-and-neck squamous cell carcinoma (n = 501). **(A)** LASSO coefficient profiles of CXCL10, CXCL11, CXCR3, and CCR5. **(B)** Partial likelihood deviance of variables revealed by LASSO-based Cox regression model. **(C)** Patients with HNSCC were divided into high- and low-risk groups (median as the cutoff) based on the risk scores. **(D)** Scatterplot of the survival status of patients with different risk scores. Abscissa represents risk score, and ordinate represents survival status. **(E)** Heatmap of expression levels of CXCL11, CXCR3, and CCR5 in tumors with different risk scores. **(F)** Kaplan–Meier analysis and log-rank test of patients with high- and low-risk scores. **(G)** Predictive accuracy of the risk-scoring system by time-dependent receiver operating characteristic curve (ROC) analysis.

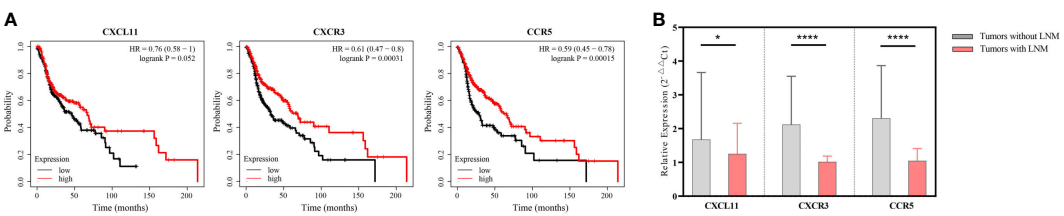

FIGURE 5 | Identifying the prognostic role of CXCL11, CXCR3, and CCR5 in patients with head-and-neck squamous cell carcinoma (HNSCC). **(A)** Survival curves of HNSCC patients stratified by mRNA expression levels (median as the cutoff) (n = 501). **(B)** Comparing the relative expression levels of CXCL11, CXCR3, and CCR5 in tumors without lymphatic metastases (n = 18) and those with lymphatic metastases (n = 18) by unpaired Student's t-test. Error bars represent the mean ± SEM. *p < 0.05; ns, $p \geq 0.05$.

cells and Tregs in tumor immunity, chemokines closely related to the three TIL subtypes can reflect tumor immune environment to some degree. The role of CXCL11 in tumor immunity is controversial. Notably, CXCL11 can promote antitumor immunity to benefit survival, as in patients with colon adenocarcinoma (52). However, CXCL11 is a potential antagonist of CXCL10 and CXCL11 because of its higher affinity for CXCR3 (53). CXCL11 also binds to CXCR7,

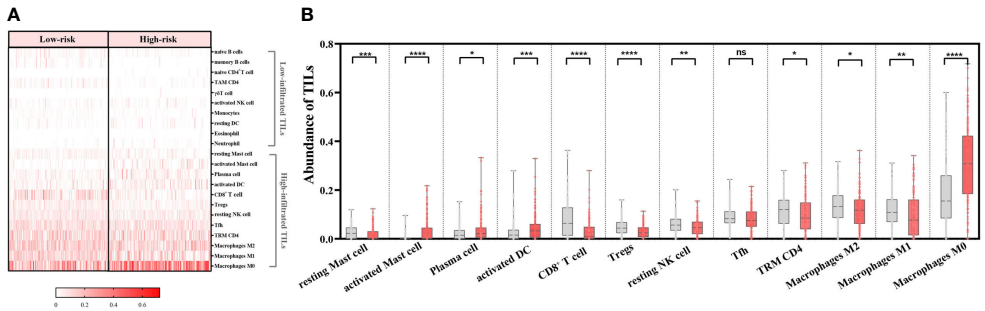

FIGURE 6 | Ability of the risk-scoring system to characterize the tumor-infiltrating lymphocyte (TIL) landscapes in patients with head-and-neck squamous cell carcinoma (n = 439). **(A)** Heatmap of abundance of 22 TILs in the low- and high-risk groups. **(B)** Comparing the abundance of 12 TILs between the low- and high-risk groups by Mann–Whitney U test. ****$p < 0.0001$; ***$p < 0.001$; **$p < 0.01$; *$p < 0.05$; ns, $p \geq 0.05$. Grey columns represent the low-risk group, and red columns represent the high-risk group.

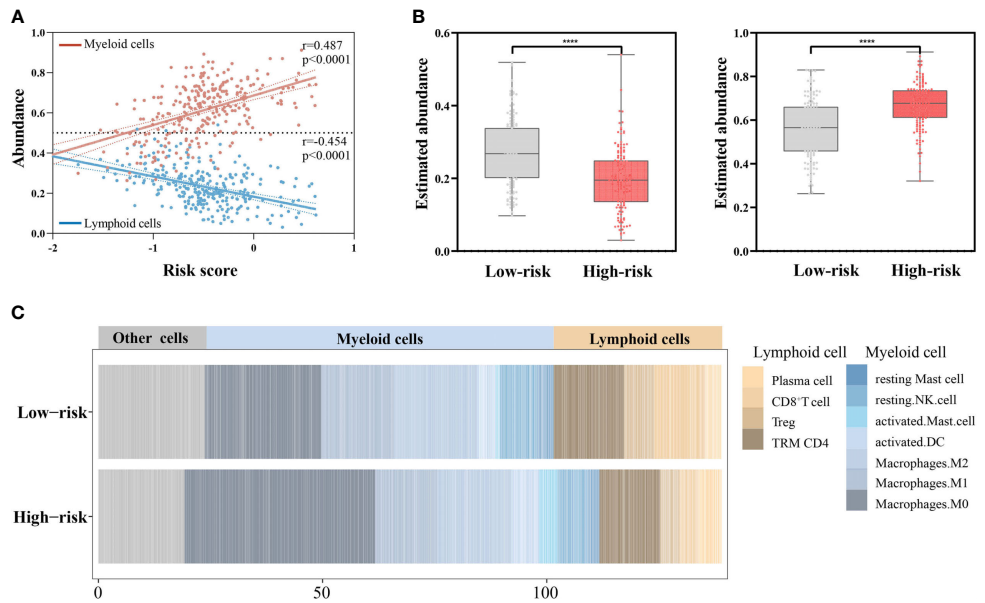

FIGURE 7 | Associations of the risk scores with abundance of lymphoid cells and myeloid cells (n = 439). **(A)** Correlations of the risk scores with abundance of lymphoid cells and myeloid cells by Pearson's correlation test. **(B)** Comparing the abundance of lymphoid cells (left) and myeloid cells (right) between the low- and high-risk groups by Mann–Whitney U test. ****$p < 0.0001$. **(C)** Stacked column plots of abundance of TILs in low- and high-risk groups.

implicating it in tumor invasiveness (54). The mechanism underlying the function of CXCL11 in the tumor environment may explain its negative association with prognosis. Additionally, the role of CCR5 in HNSCC tumor immunity is also intriguing. In our study, we found that patients with HNSCC with higher CCR5 expression had significantly better OS (HR, 0.59; 95% CI, 0.45–0.78). However, CCR5 contributes to negative effect (coefficient, 0.2398) on survival rates in LASSO regression model. Also, CCR5 had significantly higher expression in tumors with LNM than in those without LNM ($p < 0.05$) in our cohort. Some studies reported that greater cytoplasmic CCR5 expression is correlated with a poor prognosis of patients with cancer because it induces cancer hallmarks (55), cancer homing to metastatic sites (56), and tumor invasion (57). A few studies also focused on the tumor-promoting role of CCR5 in HNSCC (58–60), which are consistent with our partial findings. Thus, CCR5 may not be an independent prognostic factor for outcome of patients with HNSCC, and further investigation is warranted.

In contrast to the immune surveillance role of lymphocytes in the TME, myeloid cells may promote tumor growth and metastasis through by favoring the TME (61–63). Zhang et al. implicated the role of $CD8^+$ T cells in attenuating the protumor activity of myeloid cells in the premetastatic TME by compromising Stat3, which indicated its therapeutic potential (64). Consistently, the competition for between lymphoid cells and myeloid cells in TME of HNSCC were also presented in our study. Tumors with higher

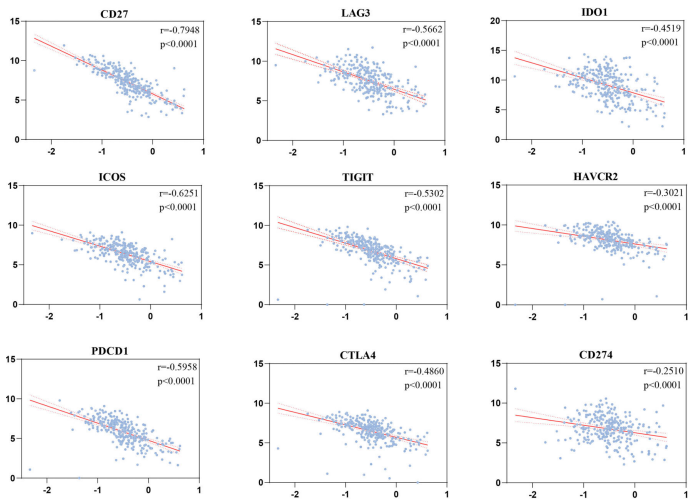

FIGURE 8 | Correlations of the risk scores with immune checkpoints by Pearson's correlation test (n = 501).

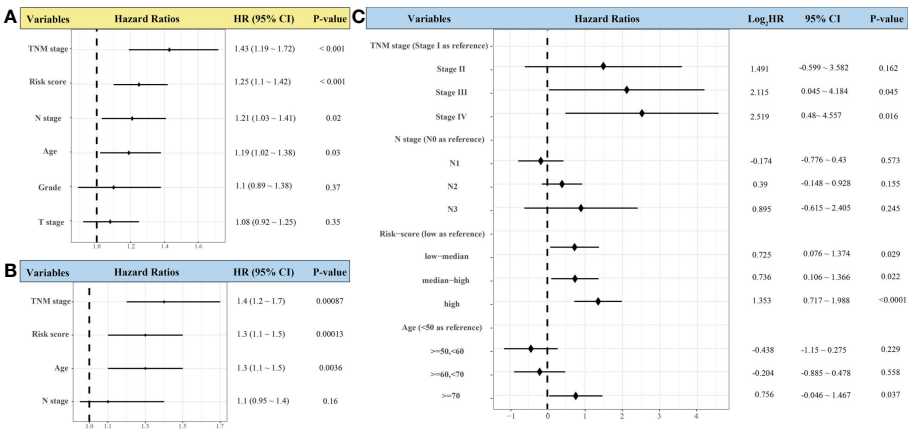

FIGURE 9 | Forest plots showing univariate **(A)** and multivariate Cox regression analyses **(B, C)** of the effect of variables on overall survival of patients with head-and-neck squamous cell carcinoma (n = 439).

risk scores tended to be infiltrated by greater abundance of myeloid cells and less abundance of lymphoid cells, and had worse prognosis, compared with those with lower risk scores. Although, many studies have assessed the abundance of individual lymphocytes or myeloid cells in tumor tissues to predict the prognosis of patients and potential sensitivity to adjuvant chemotherapy and immunotherapy (12). However, the tumor immune microenvironment is an intricated assembly of varieties of TILs. They interact to shape the TME that may be antitumor or tumor promoting. Based on this, the risk-scoring system we established in the study comprehensively evaluates the infiltrations of various significant TILs and provides a more reliable theoretical basis for stratifying patients receiving immune therapies.

This study had some limitations. First, the method used to quantify the density of IHC markers may not fully reflect *in vivo* expression patterns. Second, the performance of the risk scores in predicting OS of patients with HNSCC was unsatisfactory. We speculate that it may be because the risk-scoring system only includes genes closely relevant to the tumor immune microenvironment. However, the TME not only consists of immune cells but also fibroblasts, endothelial cells, normal epithelial cells, nutrients, etc. These admixtures have been extensively researched and thought to involve in the tumor growth (65). Additionally, the prognosis or tumor progression is mainly regulated by tumor cells. Therefore, more genes associated with tumor progression should be incorporated into the system to improve the prediction accuracy of prognosis of patients with HNSCC. Third, the discrimination of constructed nomogram was limited (c-index, 0.64; 95% CI, 0.55–0.73), despite its better performance than TNM stage. We speculate that it may be because the risk score only evaluates the patient's prognosis from the perspective of tumor LNM. However, tumor progression is a

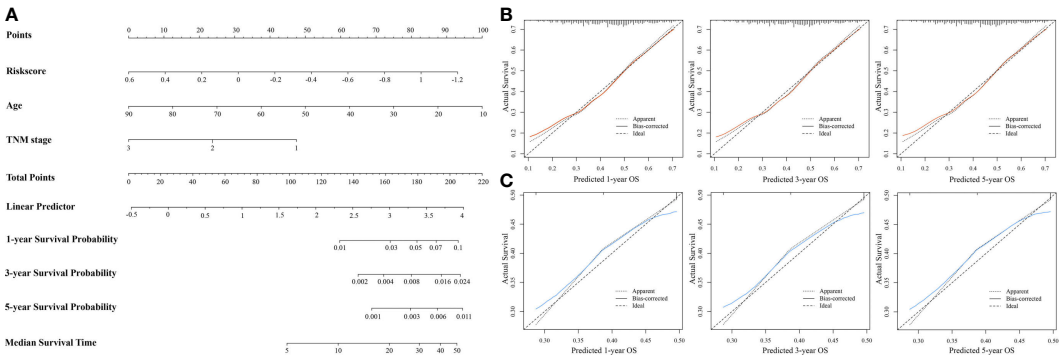

FIGURE 10 | Establishment and evaluation of nomogram prediction model for overall survival (OS) of patients with head-and-neck squamous cell carcinoma (n = 439). **(A)** Nomogram based on independent risk factors for OS in patients with HNSCC. **(B)** Calibration curves of the nomogram model for 1-, 3-, and 5-year OS. **(C)** Calibration curves of TNM stage for 1-, 3-, and 5-year OS.

complicated process in which tumor cells interact with TME for mutual promotion. Therefore, some indicators related to the invasive ability of tumor cells and identified to be independent risk factors (e.g., HPV status, depth of invasion, extranodal extension) should also be included in the prediction model to improve the reliability, which were not assessed in this study due to the retrospective nature of the data (66–68). There is still room for improvement of the nomogram in the prognosis prediction of HNSCC. Prospective cohort studies involving a large number of patients are needed to improve it in the future.

5 CONCLUSION

We identified the involvement of $CD8^+$ T cells in antitumor immunity during the process of tumor lymphatic metastasis and established an immune-feature-based three-gene-signature risk-scoring system to predict HNSCC prognosis. The risk-scoring system had good performance in characterizing the immune landscape in HNSCC and might benefit clinical patient risk stratification. The constructed nomogram could be a robust supplement to the TNM stage in the prediction of clinical prognoses. Further demonstrations of their prediction values in the clinical level are needed in the future.

DATA AVAILABILITY STATEMENT

The sequencing data from this study are publicly available under GEO series number GSE176221 through the NCBI Gene Expression Omnibus (GEO) (http://www.ncbi.nlm.nih.gov/geo) (69).

ETHICS STATEMENT

The studies involving human participants were reviewed and approved by the Ethics Committee of the First Affiliated Hospital, College of Medicine, Zhejiang University. The patients/participants provided their written informed consent to participate in this study. Written informed consent was obtained from the individual(s) for the publication of any potentially identifiable images or data included in this article.

AUTHOR CONTRIBUTIONS

HZ and YZ initiated, designed, and coordinated the study. YZ performed data acquisition, analysis, and interpretation. XL performed prediction model establishment. JY provided clinical information and performed the prognostic validation of the candidate genes. KQ collected tissues. All authors contributed to the article and approved the submitted version.

ACKNOWLEDGMENTS

We acknowledge TCGA and GEO databases for providing their platforms and contributors for uploading their meaningful datasets. We thank the patients for their participation in this study. We thank Dr. Chen Yin for the revision of the manuscript.

REFERENCES

1. Gupta B, Johnson NW, Kumar N. Global Epidemiology of Head and Neck Cancers: A Continuing Challenge. *Oncology* (2016) 91(1):13–23. doi: 10.1159/000446117
2. Johnson DE, Burtness B, Leemans CR, Lui VWY, Bauman JE, Grandis JR. Head and Neck Squamous Cell Carcinoma. *Nat Rev Dis Primers* (2020) 6 (1):92. doi: 10.1038/s41572-020-00224-3
3. Pfister DG, Spencer S, Brizel DM, Burtness B, Busse PM, Caudell JJ, et al. Head and Neck Cancers, Version 1.2015. *J Natl Compr Canc Netw* (2015) 13 (7):847–55; quiz 856. doi: 10.6004/jnccn.2015.0102
4. Pulte D, Brenner H. Changes in Survival in Head and Neck Cancers in the Late 20th and Early 21st Century: A Period Analysis. *Oncologist* (2010) 15 (9):994–1001. doi: 10.1634/theoncologist.2009-0289
5. Edge SB, Compton CC. The American Joint Committee on Cancer: The 7th Edition of the AJCC Cancer Staging Manual and the Future of

TNM. *Ann Surg Oncol* (2010) 17(6):1471–4. doi: 10.1245/s10434-010-0985-4
6. Muzaffar J, Bari S, Kirtane K, Chung CH. Recent Advances and Future Directions in Clinical Management of Head and Neck Squamous Cell Carcinoma. *Cancers (Basel)* (2021) 13(2):338. doi: 10.3390/cancers13020338
7. Kather JN, Halama N. Harnessing the Innate Immune System and Local Immunological Microenvironment to Treat Colorectal Cancer. *Br J Cancer* (2019) 120(9):871–82. doi: 10.1038/s41416-019-0441-6
8. T GS. Innate and Adaptive Immune Cells in Tumor Microenvironment. *Gulf J Oncolog* (2021) 1(35):77–81.
9. Pretscher D, Distel LV, Grabenbauer GG, Wittlinger M, Buettner M, Niedobitek G. Distribution of Immune Cells in Head and Neck Cancer: CD8+ T-Cells and CD20+ B-Cells in Metastatic Lymph Nodes are Associated With Favourable Outcome in Patients With Oro- and Hypopharyngeal Carcinoma. *BMC Cancer* (2009) 9:292. doi: 10.1186/1471-2407-9-292
10. Balermpas P, Rodel F, Weiss C, Rodel C, Fokas E. Tumor-Infiltrating Lymphocytes Favor the Response to Chemoradiotherapy of Head and Neck Cancer. *Oncoimmunology* (2014) 3(1):e27403. doi: 10.4161/onci.27403
11. Balermpas P, Michel Y, Wagenblast J, Seitz O, Weiss C, Rodel F, et al. Tumour-Infiltrating Lymphocytes Predict Response to Definitive Chemoradiotherapy in Head and Neck Cancer. *Br J Cancer* (2014) 110 (2):501–9. doi: 10.1038/bjc.2013.640
12. Bindea G, Mlecnik B, Tosolini M, Kirilovsky A, Waldner M, Obenauf AC, et al. Spatiotemporal Dynamics of Intratumoral Immune Cells Reveal the Immune Landscape in Human Cancer. *Immunity* (2013) 39(4):782–95. doi: 10.1016/j.immuni.2013.10.003
13. Rivoltini L, Carrabba M, Huber V, Castelli C, Novellino L, Dalerba P, et al. Immunity to Cancer: Attack and Escape in T Lymphocyte-Tumor Cell Interaction. *Immunol Rev* (2002) 188:97–113. doi: 10.1034/j.1600-065x.2002.18809.x
14. Demaria O, Cornen S, Daeron M, Morel Y, Medzhitov R, Vivier E. Harnessing Innate Immunity in Cancer Therapy. *Nature* (2019) 574(7776):45–56. doi: 10.1038/s41586-019-1593-5
15. Chen YP, Wang YQ, Lv JW, Li YQ, Chua MLK, Le QT, et al. Identification and Validation of Novel Microenvironment-Based Immune Molecular Subgroups of Head and Neck Squamous Cell Carcinoma: Implications for Immunotherapy. *Ann Oncol* (2019) 30(1):68–75. doi: 10.1093/annonc/mdy470
16. Chakraborty P, Karmakar T, Arora N, Mukherjee G. Immune and Genomic Signatures in Oral (Head and Neck) Cancer. *Heliyon* (2018) 4(10):e00880. doi: 10.1016/j.heliyon.2018.e00880
17. Chen J, Yang J, Li H, Yang Z, Zhang X, Li X, et al. Single-Cell Transcriptomics Reveal the Intratumoral Landscape of Infiltrated T-Cell Subpopulations in Oral Squamous Cell Carcinoma. *Mol Oncol* (2021) 15(4):866–86. doi: 10.1002/1878-0261.12910
18. Kakimi K, Karasaki T, Matsushita H, Sugie T. Advances in Personalized Cancer Immunotherapy. *Breast Cancer* (2017) 24(1):16–24. doi: 10.1007/s12282-016-0688-1
19. Li B, Chan HL, Chen P. Immune Checkpoint Inhibitors: Basics and Challenges. *Curr Med Chem* (2019) 26(17):3009–25. doi: 10.2174/0929867324666170804143706
20. Ouyang T, Cao Y, Kan X, Chen L, Ren Y, Sun T, et al. Treatment-Related Serious Adverse Events of Immune Checkpoint Inhibitors in Clinical Trials: A Systematic Review. *Front Oncol* (2021) 11:621639. doi: 10.3389/fonc.2021.621639
21. Sharon E, Streicher H, Goncalves P, Chen HX. Immune Checkpoint Inhibitors in Clinical Trials. *Chin J Cancer* (2014) 33(9):434–44. doi: 10.5732/cjc.014.10122
22. Spitzer MH, Carmi Y, Reticker-Flynn NE, Kwek SS, Madhireddy D, Martins MM, et al. Systemic Immunity Is Required for Effective Cancer Immunotherapy. *Cell* (2017) 168(3):487–502.e15. doi: 10.1016/j.cell.2016.12.022
23. Petitprez F, Meylan M, de Reynies A, Sautes-Fridman C, Fridman WH. The Tumor Microenvironment in the Response to Immune Checkpoint Blockade Therapies. *Front Immunol* (2020) 11:784. doi: 10.3389/fimmu.2020.00784
24. Newman AM, Steen CB, Liu CL, Gentles AJ, Chaudhuri AA, Scherer F, et al. Determining Cell Type Abundance and Expression From Bulk Tissues With Digital Cytometry. *Nat Biotechnol* (2019) 37(7):773–82. doi: 10.1038/s41587-019-0114-2
25. Li T, Fan J, Wang B, Traugh N, Chen Q, Liu JS, et al. TIMER: A Web Server for Comprehensive Analysis of Tumor-Infiltrating Immune Cells. *Cancer Res* (2017) 77(21):e108–10. doi: 10.1158/0008-5472.CAN-17-0307
26. Charoentong P, Finotello F, Angelova M, Mayer C, Efremova M, Rieder D, et al. Pan-Cancer Immunogenomic Analyses Reveal Genotype-Immunophenotype Relationships and Predictors of Response to Checkpoint Blockade. *Cell Rep* (2017) 18(1):248–62. doi: 10.1016/j.celrep.2016.12.019
27. Yang J, Xie K, Li C. Immune-Related Genes Have Prognostic Significance in Head and Neck Squamous Cell Carcinoma. *Life Sci* (2020) 256:117906. doi: 10.1016/j.lfs.2020.117906
28. Chen Y, Li ZY, Zhou GQ, Sun Y. An Immune-Related Gene Prognostic Index for Head and Neck Squamous Cell Carcinoma. *Clin Cancer Res* (2021) 27 (1):330–41. doi: 10.1158/1078-0432.CCR-20-2166
29. Kim D, Langmead B, Salzberg SL. HISAT: A Fast Spliced Aligner With Low Memory Requirements. *Nat Methods* (2015) 12(4):357–60. doi: 10.1038/nmeth.3317
30. Pertea M, Pertea GM, Antonescu CM, Chang TC, Mendell JT, Salzberg SL. StringTie Enables Improved Reconstruction of a Transcriptome From RNA-Seq Reads. *Nat Biotechnol* (2015) 33(3):290–5. doi: 10.1038/nbt.3122
31. Robinson MD, McCarthy DJ, Smyth GK. Edger: A Bioconductor Package for Differential Expression Analysis of Digital Gene Expression Data. *Bioinformatics* (2010) 26(1):139–40. doi: 10.1093/bioinformatics/btp616
32. Shannon P, Markiel A, Ozier O, Baliga NS, Wang JT, Ramage D, et al. Cytoscape: A Software Environment for Integrated Models of Biomolecular Interaction Networks. *Genome Res* (2003) 13(11):2498–504. doi: 10.1101/gr.1239303
33. Chen B, Khodadoust MS, Liu CL, Newman AM, Alizadeh AA. Profiling Tumor Infiltrating Immune Cells With CIBERSORT. *Methods Mol Biol* (2018) 1711:243–59. doi: 10.1007/978-1-4939-7493-1_12
34. Newman AM, Liu CL, Green MR, Gentles AJ, Feng W, Xu Y, et al. Robust Enumeration of Cell Subsets From Tissue Expression Profiles. *Nat Methods* (2015) 12(5):453–7. doi: 10.1038/nmeth.3337
35. Nagy A, Munkacsy G, Gyorffy B. Pancancer Survival Analysis of Cancer Hallmark Genes. *Sci Rep* (2021) 11(1):6047. doi: 10.1038/s41598-021-84787-5
36. Iasonos A, Schrag D, Raj GV, Panageas KS. How to Build and Interpret a Nomogram for Cancer Prognosis. *J Clin Oncol* (2008) 26(8):1364–70. doi: 10.1200/JCO.2007.12.9791
37. Gentles AJ, Newman AM, Liu CL, Bratman SV, Feng W, Kim D, et al. The Prognostic Landscape of Genes and Infiltrating Immune Cells Across Human Cancers. *Nat Med* (2015) 21(8):938–45. doi: 10.1038/nm.3909
38. Galon J, Mlecnik B, Bindea G, Angell HK, Berger A, Lagorce C, et al. Towards the Introduction of the 'Immunoscore' in the Classification of Malignant Tumours. *J Pathol* (2014) 232(2):199–209. doi: 10.1002/path.4287
39. Salgado R, Denkert C, Demaria S, Sirtaine N, Klauschen F, Pruneri G, et al. The Evaluation of Tumor-Infiltrating Lymphocytes (TILs) in Breast Cancer: Recommendations by an International TILs Working Group 2014. *Ann Oncol* (2015) 26(2):259–71. doi: 10.1093/annonc/mdu450
40. Donnem T, Kilvaer TK, Andersen S, Richardsen E, Paulsen EE, Hald SM, et al. Strategies for Clinical Implementation of TNM-Immunoscore in Resected Nonsmall-Cell Lung Cancer. *Ann Oncol* (2016) 27(2):225–32. doi: 10.1093/annonc/mdv560
41. Galon J, Costes A, Sanchez-Cabo F, Kirilovsky A, Mlecnik B, Lagorce-Pages C, et al. Type, Density, and Location of Immune Cells Within Human Colorectal Tumors Predict Clinical Outcome. *Science* (2006) 313(5795):1960–4. doi: 10.1126/science.1129139
42. Mahmoud SM, Paish EC, Powe DG, Macmillan RD, Grainge MJ, Lee AH, et al. Tumor-Infiltrating CD8+ Lymphocytes Predict Clinical Outcome in Breast Cancer. *J Clin Oncol* (2011) 29(15):1949–55. doi: 10.1200/JCO.2010.30.5037
43. Gao Q, Qiu SJ, Fan J, Zhou J, Wang XY, Xiao YS, et al. Intratumoral Balance of Regulatory and Cytotoxic T Cells Is Associated With Prognosis of Hepatocellular Carcinoma After Resection. *J Clin Oncol* (2007) 25 (18):2586–93. doi: 10.1200/JCO.2006.09.4565
44. Kennedy R, Celis E. Multiple Roles for CD4+ T Cells in Anti-Tumor Immune Responses. *Immunol Rev* (2008) 222:129–44. doi: 10.1111/j.1600-065X.2008.00616.x

45. Borst J, Ahrends T, Babala N, Melief CJM, Kastenmuller W. CD4(+) T Cell Help in Cancer Immunology and Immunotherapy. *Nat Rev Immunol* (2018) 18(10):635–47. doi: 10.1038/s41577-018-0044-0
46. Nguyen N, Bellile E, Thomas D, McHugh J, Rozek L, Virani S, et al. Tumor Infiltrating Lymphocytes and Survival in Patients With Head and Neck Squamous Cell Carcinoma. *Head Neck* (2016) 38(7):1074–84. doi: 10.1002/hed.24406
47. Fridman WH, Pages F, Sautes-Fridman C, Galon J. The Immune Contexture in Human Tumours: Impact on Clinical Outcome. *Nat Rev Cancer* (2012) 12 (4):298–306. doi: 10.1038/nrc3245
48. Boxberg M, Leising L, Steiger K, Jesinghaus M, Alkhamas A, Mielke M, et al. Composition and Clinical Impact of the Immunologic Tumor Microenvironment in Oral Squamous Cell Carcinoma. *J Immunol* (2019) 202(1):278–91. doi: 10.4049/jimmunol.1800242
49. Boduc M, Roessler M, Mandic R, Netzer C, Guldner C, Walliczek-Dworschak U, et al. Foxp3 Expression in Lymph Node Metastases in Patients With Head and Neck Cancer. *Acta Otolaryngol* (2017) 137(11):1215–9. doi: 10.1080/00016489.2017.1353705
50. Shang B, Liu Y, Jiang SJ, Liu Y. Prognostic Value of Tumor-Infiltrating FoxP3+ Regulatory T Cells in Cancers: A Systematic Review and Meta-Analysis. *Sci Rep* (2015) 5:15179. doi: 10.1038/srep15179
51. Echarti A, Hecht M, Buttner-Herold M, Haderlein M, Hartmann A, Fietkau R, et al. CD8+ and Regulatory T Cells Differentiate Tumor Immune Phenotypes and Predict Survival in Locally Advanced Head and Neck Cancer. *Cancers (Basel)* (2019) 11(9):1398. doi: 10.3390/cancers11091398
52. Cao Y, Jiao N, Sun T, Ma Y, Zhang X, Chen H, et al. CXCL11 Correlates With Antitumor Immunity and an Improved Prognosis in Colon Cancer. *Front Cell Dev Biol* (2021) 9:646252. doi: 10.3389/fcell.2021.646252
53. Colvin RA, Campanella GS, Manice LA, Luster AD. CXCR3 Requires Tyrosine Sulfation for Ligand Binding and a Second Extracellular Loop Arginine Residue for Ligand-Induced Chemotaxis. *Mol Cell Biol* (2006) 26 (15):5838–49. doi: 10.1128/MCB.00556-06
54. Puchert M, Obst J, Koch C, Zieger K, Engele J. CXCL11 Promotes Tumor Progression by the Biased Use of the Chemokine Receptors CXCR3 and CXCR7. *Cytokine* (2020) 125:154809. doi: 10.1016/j.cyto.2019.154809
55. Gao D, Fish EN. Chemokines in Breast Cancer: Regulating Metabolism. *Cytokine* (2018) 109:57–64. doi: 10.1016/j.cyto.2018.02.010
56. Zi J, Yuan S, Qiao J, Zhao K, Xu L, Qi K, et al. Treatment With the C-C Chemokine Receptor Type 5 (CCR5)-Inhibitor Maraviroc Suppresses Growth and Induces Apoptosis of Acute Lymphoblastic Leukemia Cells. *Am J Cancer Res* (2017) 7(4):869–80.
57. Velasco-Velazquez M, Jiao X, de la Fuente M, Pestell TG, Ertel A, Lisanti MP, et al. CCR5 Antagonist Blocks Metastasis of Basal Breast Cancer Cells. *Cancer Res* (2012) 72(15):3839–50. doi: 10.1158/0008-5472.CAN-11-3917
58. Khademi B, Razmkhah M, Erfani N, Gharagozloo M, Ghaderi A. SDF-1 and CCR5 Genes Polymorphism in Patients With Head and Neck Cancer. *Pathol Oncol Res* (2008) 14(1):45–50. doi: 10.1007/s12253-008-9007-2
59. Gonzalez-Arriagada WA, Lozano-Burgos C, Zuniga-Moreta R, Gonzalez-Diaz P, Coletta RD. Clinicopathological Significance of Chemokine Receptor (CCR1, CCR3, CCR4, CCR5, CCR7 and CXCR4) Expression in Head and Neck Squamous Cell Carcinomas. *J Oral Pathol Med* (2018) 47(8):755–63. doi: 10.1111/jop.12736
60. Aggarwal S, Sharma SC, S ND. Dynamics of Regulatory T Cells (Tregs) in Patients With Oral Squamous Cell Carcinoma. *J Surg Oncol* (2017) 116 (8):1103–13. doi: 10.1002/jso.24782
61. Hiratsuka S, Watanabe A, Aburatani H, Maru Y. Tumour-Mediated Upregulation of Chemoattractants and Recruitment of Myeloid Cells Predetermines Lung Metastasis. *Nat Cell Biol* (2006) 8(12):1369–75. doi: 10.1038/ncb1507
62. Kim S, Takahashi H, Lin WW, Descargues P, Grivennikov S, Kim Y, et al. Carcinoma-Produced Factors Activate Myeloid Cells Through TLR2 to Stimulate Metastasis. *Nature* (2009) 457(7225):102–6. doi: 10.1038/nature07623
63. Deng J, Liu Y, Lee H, Herrmann A, Zhang W, Zhang C, et al. S1PR1-STAT3 Signaling is Crucial for Myeloid Cell Colonization at Future Metastatic Sites. *Cancer Cell* (2012) 21(5):642–54. doi: 10.1016/j.ccr.2012.03.039
64. Zhang W, Zhang C, Li W, Deng J, Herrmann A, Priceman SJ, et al. CD8+ T-Cell Immunosurveillance Constrains Lymphoid Premetastatic Myeloid Cell Accumulation. *Eur J Immunol* (2015) 45(1):71–81. doi: 10.1002/eji.201444467
65. Aran D, Sirota M, Butte AJ. Systematic Pan-Cancer Analysis of Tumour Purity. *Nat Commun* (2015) 6:8971. doi: 10.1038/ncomms9971
66. Kann BH, Hicks DF, Payabvash S, Mahajan A, Du J, Gupta V, et al. Multi-Institutional Validation of Deep Learning for Pretreatment Identification of Extranodal Extension in Head and Neck Squamous Cell Carcinoma. *J Clin Oncol* (2020) 38(12):1304–11. doi: 10.1200/JCO.19.02031
67. Amin MB, Greene FL, Edge SB, Compton CC, Gershenwald JE, Brookland RK, et al. The Eighth Edition AJCC Cancer Staging Manual: Continuing to Build a Bridge From a Population-Based to a More "Personalized" Approach to Cancer Staging. *CA Cancer J Clin* (2017) 67(2):93–9. doi: 10.3322/caac.21388
68. Matos LL, Dedivitis RA, Kulcsar MAV, de Mello ES, Alves VAF, Cernea CR. External Validation of the AJCC Cancer Staging Manual, 8th Edition, in an Independent Cohort of Oral Cancer Patients. *Oral Oncol* (2017) 71:47–53. doi: 10.1016/j.oraloncology.2017.05.020
69. Barrett T, Wilhite SE, Ledoux P, Evangelista C, Kim IF, Tomashevsky M, et al. NCBI GEO: Archive for Functional Genomics Data Sets–Update. *Nucleic Acids Res* (2013) 41(Database issue):D991–5. doi: 10.1093/nar/gks1193

Conflict of Interest: The authors declare that the research was conducted in the absence of any commercial or financial relationships that could be construed as a potential conflict of interest.

frontiers in Oncology

ORIGINAL RESEARCH
published: 19 January 2022
doi: 10.3389/fonc.2021.766650

Establishing a Predictive Nomogram for Cervical Lymph Node Metastasis in Patients With Papillary Thyroid Carcinoma

Qiao Hu[1], Wang-Jian Zhang[2†], Li Liang[1†], Ling-Ling Li[1†], Wu Yin[3], Quan-Li Su[1] and Fei-Fei Lin[1]*

[1] Department of Ultrasound, The People's Hospital of Guangxi Zhuang Autonomous Region & Guangxi Academy of Medical Sciences, Nanning, China, [2] School of Public Health, Sun Yet-Sen University, Guangzhou, China, [3] Department of Pathology, The People's Hospital of Guangxi Zhuang Autonomous Region & Guangxi Academy of Medical Sciences, Nanning, China

Objectives: The purpose of this study was to establish a nomogram for predicting cervical lymph node metastasis (CLNM) in patients with papillary thyroid carcinoma (PTC).

Materials and Methods: A total of 418 patients with papillary thyroid carcinoma undergoing total thyroidectomy with cervical lymph node dissection were enrolled in the retrospective study from January 2016 to September 2019. Univariate and multivariate Logistic regression analysis were performed to screen the clinicopathologic, laboratory and ultrasound (US) parameters influencing cervical lymph nodes metastasis and develop the predicting model.

Results: CLNM was proved in 34.4% (144/418) of patients. In the multivariate regression analysis, Male, Age < 45 years, Tumor size > 20mm, multifocality, ambiguous boundary, extracapsular invasion and US-suggested lymph nodes metastasis were independent risk factors of CLNM ($p < 0.05$). Prediction nomogram showed an excellent discriminative ability, with a C-index of 0.940 (95% confidence interval [CI], 0.888-0.991), and a good calibration.

Conclusion: The established nomogram showed a good prediction of CLNM in patients with PTC. It is conveniently used and should be considered in the determination of surgical procedures.

Keywords: nomogram, papillary thyroid carcinoma, cervical lymph node, metastasis, predictor

OPEN ACCESS

Edited by:
Yong Yin,
Shandong Cancer Hospital, China

Reviewed by:
Franz Rödel,
University Hospital Frankfurt, Germany
Shilpi Sharma,
Narayana Superspeciality Hospital, India

****Correspondence:***
Qiao Hu
xyyxyhq@163.com

[†]These authors have contributed equally to this work

Specialty section:
This article was submitted to Head and Neck Cancer, a section of the journal Frontiers in Oncology

Received: *29 August 2021*
Accepted: *27 December 2021*
Published: *19 January 2022*

Citation:
Hu Q, Zhang W-J, Liang L, Li L-L, Yin W, Su Q-L and Lin F-F (2022) Establishing a Predictive Nomogram for Cervical Lymph Node Metastasis in Patients With Papillary Thyroid Carcinoma. Front. Oncol. 11:766650. doi: 10.3389/fonc.2021.766650

INTRODUCTION

Papillary thyroid carcinoma (PTC) originates from the thyroid follicular epithelium and is the major pathological type among thyroid malignancies, accounting for approximately 80% of all thyroid cancers (1). PTC is more common in female patients, and the incidence rate in women is three times that in men. Although PTC is considered to be an indolent tumor with low malignancy, slow disease progression, and good prognosis (2), 20–50% of patients still have early cervical lymph node metastasis (CLNM), leading to a high risk of local recurrence (3).

CLNM of PTC usually manifests as sequential lymph node metastasis from the central area to the lateral cervical area (4). However, some PTCs may undergo direct lateral lymph node metastasis (LLNM) without central lymph node metastasis, which is called "skip metastasis" (5). CLNM is the strongest risk factor for local recurrence and the prognosis of PTC patients and is an important indicator for determining the surgical approach before surgery (6).

Prophylactic cervical lymph node dissection (CLND) has always been controversial (7, 8). Some scholars believe that CLND can change the tumor–node–metastasis (TNM) staging of some patients, and reduce their risk of postoperative recurrence (9). Other studies suggest that there is still not enough evidence to show that prophylactic CLND is beneficial in reducing the recurrence rate and improving the prognosis, and it increases the risk of potential surgical complications such as recurrent laryngeal nerve injury and reduced parathyroid function (10). Therefore, it is necessary to efficiently and accurately assess the presence or absence of CLNM before surgery.

Ultrasound has the advantages of real-time, noninvasive, dynamic, and simple operation and has become the preferred tool for cervical lymph nodes examination. However, due to the complex anatomical location of cervical lymph nodes and interference by air echoes in the trachea, the detection rate of central lymph node metastasis by ultrasound is very limited, and the sensitivity of conventional ultrasound in the diagnosis of central lymph node metastasis is low, at only 20–33% (11). In addition, ultrasound cannot detect some occult lymph nodes metastasis. In recent years, some scholars have attempted to use clinical data and imaging data to assess the risk faced by PTC patients before surgery and screen out the patients most likely to develop CLNM to compensate for the low sensitivity of conventional ultrasound at directly diagnosing CLNM. Hu et al. (5) used clinicopathological data to analyze the risk factors for skip metastasis in PTC patients. Their results suggest that age > 55 years, tumor located in the upper portion, and unilaterality were independent risk factors of skip metastasis. In another study, a radiomic model established based on anatomical and functional magnetic resonance images was used to screen independent risk factors for CLNM in PTC patients (12). Tong et al. (13) established a nomogram model based on the central lymph node status suggested by conventional ultrasound and computed tomography (CT) images, which could be used to predict LLNM in PTC patients before surgery. No previous reports have established a quantitative risk assessment model for the screened risk factors, and there is no unified method for the preoperative prediction of CLNM in PTC patients. Thus, the purpose of our study was to establish a nomogram model for the preoperative prediction of CLNM of PTC based on clinical, pathological, and ultrasound imaging characteristics and to test its predictive efficacy.

MATERIALS AND METHODS

Patients

This study was performed with the approval of the Ethics Committee of the People's Hospital of Guangxi Zhuang Autonomous Region, China (IRB No. KY-KJT-2019-04). The informed consent requirement was obtained from all participants. A total of 418 PTC patients (109 males and 309 females, aged 9-75 y with a median age of 43 y) were enrolled between January 2016 and September 2019. Inclusion criteria: ① preoperative thyroid fine-needle aspiration biopsy or postoperative pathology diagnosed PTC; ② complete clinical, pathological, and conventional ultrasound image data; ③ first thyroid surgery (thyroid lobectomy or any type of thyroidectomy) and undergoing CLND (at least central lymph nodes dissection); and ③ pathology confirming the presence or absence of lymph node metastasis. The exclusion criteria were as follows: ① non-PTC pathology; ② other treatments before surgery (such as iodine-131 or surgical history); ③ incomplete ultrasound, clinical, or pathological data; ④ distant metastasis; and ⑤ malignant tumors at other sites. The clinical, serological, and pathological data of the included cases were retrospectively analyzed, including age (<45 years, 45-55 years, or >55 years), sex, bilaterality (unilateral or bilateral), tumor size (maximum diameter <10 mm, 10-20 mm, or >20 mm), Hashimoto's thyroiditis (absent or present), serum thyroid-stimulating hormone (TSH), thyroid peroxidase antibodies (TPOAb), triiodothyronine (T3), thyroxine (T4), free triiodothyronine (FT3), free thyroxine (FT4), and the expression of galectin-3, cytokeratin (CK)-19, and CK-34 in tumor specimens.

The surgical range of cervical lymph node dissection of the enrolled patients were determined based on the preoperative fine-needle aspiration cytological examination and/or the intraoperative rapid frozen pathological results: ① unilateral PTC: excision of the affected lobe plus isthmus and lymph nodes dissection of the ipsilateral central region (level VI); x2461; bilateral lymph nodes dissection in the central region for patients with isthmus or bilateral PTC; ③ lymph nodes dissection of the affected lateral cervical region if preoperative ultrasound reported lymph node metastasis in the lateral cervical region (levels II, III, and IV) and fine-needle aspiration cytology indicated suspicious positivity; ④ additional lymph node dissection in level V if lymph node metastasis in level V was suspected.

Ultrasonography Imaging

Preoperative conventional ultrasound examination was performed using a GE Logiq E9 ultrasound system (GE Healthcare Life Sciences, Chicago, IL, USA) with a 6-15 MHz linear transducer. The patients were placed in the supine position with the neck extended. The thyroid and cervical lymph nodes were scanned on multiple sections, and their characteristics were recorded, including tumor position (left, right, others), internal component (solid, not solid), echogenicity (hypoecho, not hypoecho), taller than wide (absent or present), multifocality (single or multiple), margin (regular or irregular), boundary (legible or ambiguous). The presence or absence of microcalcification (defined as a maximum diameter of calcification ≤1 mm) and the presence or absence of extracapsular invasion (defined as contact between the nodule and the anterior and/or posterior capsule of the thyroid, such that the continuity of the capsule line was interrupted or obscured by nodules that could not be explored), and the sonographic assessment of the cervical lymph nodes (**Figures 1**, **2**). Blinded to the clinical and pathological information, two ultrasound physicians with more than 2 years of experience were responsible for the

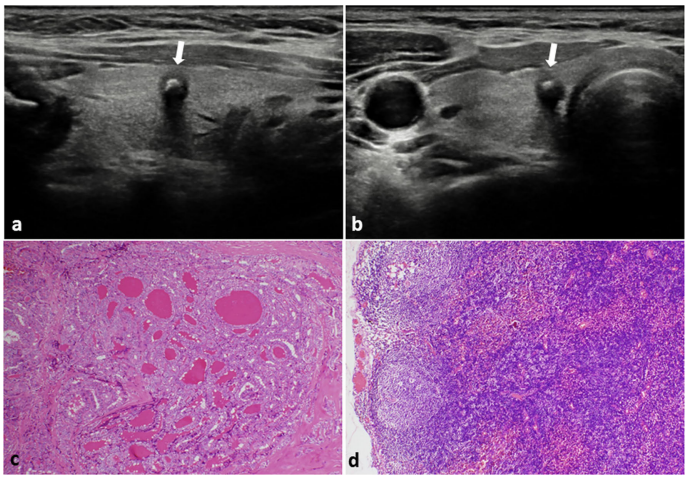

FIGURE 1 | PTC with negative CLNM in a 48-year-old female. **(A)** Longitudinal sonogram and **(B)** Transverse sonogram showing a 5×5×6 mm hypoechoic nodule in the right lobe of thyroid (arrow). The nodule was regular, legible, with a taller than wide shape and absence of extracapsular invasion. A bulky calcification (> 1 mm) was observed inside the nodule. Histological examination of the tumor **(C)** and lymph nodes **(D)** indicated no lymph nodes metastasis in the central area of the neck. H-E × 100.

interpretation of sonographic images. In cases of discrepancies, the two physicians reanalyzed and discussed together to reach a consensus.

Statistical Analysis

R language 3.5.3 statistical software was used for data analysis. Continuous variables were presented as mean ± standard deviation (SD), and comparisons between groups were performed with Student's *t*- test or analysis of variance. Categorical data were expressed as the number of cases or percentages (%), and comparisons between the groups were performed with the Chi-square test. The risk factors with $P < 0.1$ were screened by univariate analysis and were included in the multivariate logistic regression analysis. The stepwise regression was used to identify the independent predicting factors for CLNM in PTC patients, from which a nomogram model was plotted and established (14). The concordance index (C-index) and 95% confidence interval (CI) were used to evaluate the discriminability of the nomogram model. The range of the C-index is 0–1. The closer the C-index is to 1, the better the model differentiates patients and the more accurate the predictive performance. The calibration curve was used to evaluate the agreement between the predicted probability of CLNM in the nomogram of PTC and the actual probability value. The X-axis represents the predicted probability calculated by the nomogram, and the Y-axis represents the actual pathological assessment of lymph node metastasis. Falling on the 45° diagonal reference line indicated that the prediction was in good agreement with pathology. $P<0.05$ indicated that a difference was statistically significant.

RESULTS

The demographic data of patients are shown in **Table 1**. Out of 418 patients, postoperative pathological results showed that 144 patients (144/418, 34.4%) had positive CLNM, of whom 99 cases had central lymph node metastasis, 28 cases had central and lateral lymph node metastasis, and 17 cases had skip metastasis of LLNM; 274 cases (274/418, 65.6%) were negative for CLNM.

Univariate Analysis of Risk Factors for CLNM

Univariate analysis showed that when comparing the CLNM-positive and -negative groups, there were statistically significant differences in factors such as gender, age, expression of galectin-3, tumor size, boundary, margin, bilaterality, taller than wide, multifocality, tumor position, echogenicity, presence of microcalcification, extracapsular invasion, and US suggested CLNM ($P < 0.1$). There was no significant difference in the expression level of TSH, TPOAb, T3, T4, FT3, FT4, CK-19, and CK-34, tumor internal components, and the presence or absence of thyroiditis between the CLNM-positive group and the CLNM-negative group ($P > 0.1$) (**Table 2**).

Multivariate Analysis of Risk Factors for CLNM

The risk factors with statistically significant differences in the univariate analysis were included in the multivariate logistic regression analysis. Seven variables (including male sex, age <45 years, tumor maximum diameter > 20mm, multifocality, ambiguous boundary, extracapsular invasion, and US suggested CLNM) were proved to be independent predicting factors associated with CLNM (**Table 3**). The ranking of the odds ratio (OR) value was as follows: US suggested CLNM > tumor size > extracapsular invasion > gender > multifocality > boundary > age.

Establishment of Nomogram Model

The nomogram model was established using the seven independent risk predictors: gender, age, multifocality, tumor

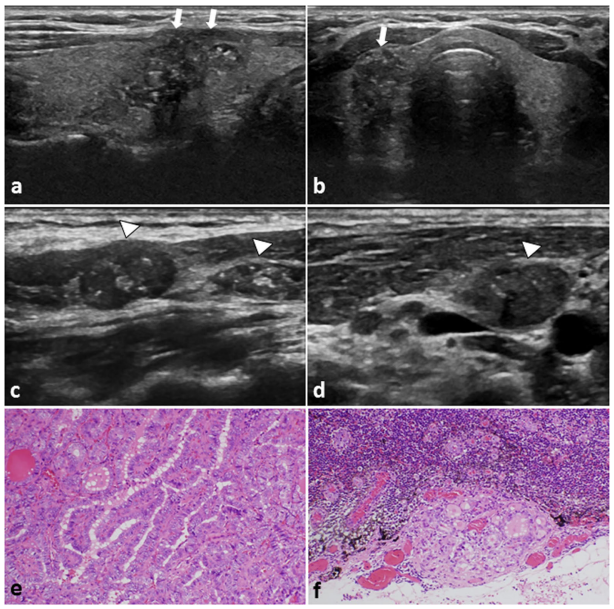

FIGURE 2 | A 29-year-old female PTC patient with positive CLNM. **(A)** Longitudinal sonogram and **(B)** Transverse sonogram showing a hypoechoic lesion in the right lobe of thyroid (arrows). The tumor size is 26×17×16mm, irregular, ambiguous, had multiple microcalcification (≤ 1 mm) inside, and hard to be distinguish from the anterior thyroid capsule. Conventional US of the lymph nodes on **(C)** Level III and **(D)** level IV area of the neck. The lymph nodes were approximately rounded, lymphatic hilus structure disappeared, and with scattered calcification inside (arrowheads). These features on US suggest the cervical lymph nodes metastasis. Histological examination confirmed the **(E)** thyroid papillary carcinoma in the right lobe, and **(F)** revealed lateral cervical lymph nodes metastasis. H-E × 200.

size, extracapsular invasion, boundary, and US suggested CLNM (**Figure 3**). The model score axis (2-9) corresponded to the score of each predictor from bottom to top, and then the total score was calculated to find the risk of CLNM corresponding to the last risk axis. The C-index of the nomogram was 0.940 (95% CI, 0.888-0.991), suggesting that the nomogram model has a favorable prediction performance of CLNM. The calibration curve displayed good fitting with the 45° reference line suggesting that the predictive model was in good consistency with the actual condition of lymph node metastasis (**Figure 4**).

DISCUSSION

Nomogram model is a predictive tool, which uses a visually graphical representation of a statistical predictive model that to generate a numerical probability of a clinical event (15). Nomograms are widely used to predict clinical disease onset and patient prognosis, especially in the field of cancer (16). Tong et al. (13) proposed a radiomics nomogram, which incorporated the radiomics signature and the ultrasound and contrast enhanced CT-reported cervical lymph node status, for the prediction lateral lymph node metastasis in patients with PTC. The radiomic nomogram demonstrated a best predictive performance than either the radiomic signature or the US- or CT- reported lateral cervical lymph node status with an area under the ROC curve and a C-index of 0.914 (95% CI, 0.842-0.987) and 0.927 (95% CI, 0.856-0.980), respectively. However, CT has the limits of radiation and costly, and has a risk of contrast agent allergy. It has been reported that the incidence of hypersensitivity reactions related to iodinated contrast media ranges from 0.004–3.0% (17). Several scholars recommended CT as a complementary modality for detecting the extent of tumor involvement in the airway or esophagus as well as detecting extra nodal tumor extension (18). In our present study, a quantitative nomogram model for the preoperative prediction of CLNM of PTC was established based on laboratory serum indicators, pathology, and non-invasive ultrasound imaging characteristics. This nomogram model exhibited a promising value with an excellent discriminative ability of a C-index of 0.940 (95% CI, 0.888-0.991), and a good calibration.

The results of the present study showed that male sex, age <45 years, multifocality, tumor maximum diameter >20 mm, extracapsular invasion, ambiguous boundary, and lymph node metastasis suggested by ultrasound were independent risk predictors for CLNM of PTC. The risk of CLMN in male patients was 2.82 times that of female patients. Some scholars believe that men (especially young men) have a high basal metabolism, which accelerates the spread of tumors and puts them at greater risk for CLNM (19). This finding is consistent with the results of Gui et al. (20). PTC can occur in various age groups, with a high incidence in 30–60 years old. This study analyzed the relationship between age and CLNM and found that the risk of CLNM in PTC patients <45 years old was significantly higher than that in other age groups (P=0.021). This is consistent with the conclusion of Zheng et al. (21) that age is an independent risk factor for the development of CLNM of PTC. However, Xue et al. (22) reported no difference in lymph nodes metastasis between patients <45 years old and patients ≥45 years old. The explanation for the inconsistent results may be related to the relatively small sample size and the bias of case selection in the study of Xue et al.

Multiple lesions are a clinicopathological feature of PTC, having an incidence of approximately 23–40% in PTC patients. Compared with single lesions, multifocal PTC is more invasive, and the more cancer lesions a person has, the higher their degree of malignancy, the more prone they are to lymph node metastasis, and the poorer the prognosis will be (23). Cyclooxygenase-2 (COX-2) and vascular endothelial growth factor (VEGF) are highly expressed in multifocal PTC (24). High expression of COX-2 and VEGF is closely related to the extent of PTC invasion and lymph node metastasis. COX-2 can catalyze the synthesis of a large amount of prostaglandin E2 (PGE2), which not only promotes cell proliferation and inhibits apoptosis but also promotes tumor angiogenesis. VEGF promotes neovascularization, increases vascular permeability, and plays an important role in tumor nutrient transport before angiogenesis. The results of present study also showed that the risk of CLNM of multifocal PTC was 2.67 times that of a single lesion. A study on multifocal PTC found that multiple

TABLE 1 | Patients characteristics.

	Case number	Central lymph node metastasis		Positive rate	*P*-Value
		Negative	Positive		
Gender					
Female	309	215	94	30.42%	0.006
Male	109	59	50	45.87%	
Age					
< 45 years	230	139 (50.73%)	91	39.57%	0.051
45-55 years	109	80 (29.20%)	29	26.61%	
> 55 years	79	55 (20.07%)	24	30.38%	
TPOAb	418	46.11 ± 137.83*	54.54 ± 169.68*		0.376
TSH	418	1.96 ± 1.98*	1.98 ± 1.59*		0.323
T3	418	1.47 ± 0.39*	1.48 ± 0.32*		0.303
T4	418	101.12 ± 19.40*	101.40 ± 20.98*		0.426
FT3	418	5.35 ± 0.97*	5.36 ± 0.91*		0.895
FT4	418	11.72 ± 2.73*	11.33 ± 2.28 *		0.725
Multifocality					
Multiple	115	55	60	52.17%	<0.001
Single	303	219	84	27.72%	
Galectin-3					
–	21	18	3	14.29%	0.047
+	397	257	140	35.26%	
CK19					
–	11	8	3	27.27%	0.729
+	407	265	142	34.89%	
CK34					
–	22	16	6	27.27%	0.493
+	396	258	138	34.85%	
Position					
Others	74	37	37	50.00%	0.008
Left lobe	153	112	41	26.80%	
Right lobe	191	125	66	34.55%	
Hashimoto's thyroiditis					
Absent	327	216	111	33.94%	0.724
Present	91	58	33	36.26%	
US suggested CLNM					
Absent	290	253	37	12.76%	<0.001
Present	128	21	107	83.59%	
Tumor size					
<10mm	185	156	29	15.68%	<0.001
10-20mm	135	89	46	34.07%	
>20mm	98	29	69	70.41%	
Component					
Solid	378	245	133	35.19%	0.400
Solid cystic	40	29	11	27.50%	
Echogenicity					
Hypoecho	401	259	142	35.41%	0.072
Isoecho	17	15	2	11.76%	
Taller than wide					
Absent	302	185	117	38.74%	0.005
Present	116	89	27	23.28%	
Margin					
Irregular	177	93	84	47.46%	<0.001
Regular	241	181	60	24.90%	
Boundary					
Ambiguous	223	116	107	47.98%	<0.001
Legible	195	158	37	18.97%	
Microcalcification					
Absent	92	75	17	18.48%	<0.001
Present	326	199	127	38.96%	
Extracapsular invasion					
Absent	292	239	53	18.15%	<0.001
Present	126	35	91	72.22%	

(Continued)

TABLE 1 | Continued

	Case number	Central lymph node metastasis		Positive rate	*P*-Value
		Negative	Positive		
bilaterality					
Absent	353	246	107	30.31%	<0.001
Present	65	28	37	56.92%	

**Mean ± standard deviation.*

TPOAb, Thyroid Peroxidase antibody; TSH, thyroid stimulating hormone; T3, triiodothyronine; T4, thyroxine; FT3, free triiodothyronine; FT4, free thyroxine; US, ultrasound; CLNM, cervical lymph node metastasis.

TABLE 2 | Univariate analysis of risk factors associated with CLNM in PTC patients.

Factors		OR	95% CI		*P*-Value
Gender	(male vs. female)	1.938	1.238	3.034	0.004
Age					
	<45 years	1			
	45-55 years	0.554	0.336	0.9136	0.021
	>55 years	0.667	0.386	1.153	0.146
TPOAb(U/mL)		0.782	0.508	1.206	0.266
TSH(uIU/mL)		1.005	0.898	1.125	0.926
T3 (nmol/L)		1.075	0.605	1.909	0.805
T4 (nmol/L)		1.000	0.990	1.011	0.896
FT3 (pmol/L)		1.0111	0.8121	1.257	0.925
FT4 (pmol/L)		0.938	0.860	1.024	0.155
Multifocality	(single vs. multiple)	2.844	1.824	4.434	<0.001
Galectin	(negative vs. positive)	4.354	0.985	19.247	0.052
CK19	(negative vs. positive)	1.619	0.322	8.146	0.559
CK34	(negative vs. positive)	1.492	0.529	4.239	0.453
bilaterality	(unilateral vs. bilateral)	3.0381	1.7689	5.218	<0.001
Position					
	left lobe	0.466	0.196	1.1087	0.084
	right lobe	0.672	0.289	1.563	0.356
	others	1.439	0.546	3.790	0.462
Hashimoto's thyroiditis	(absent vs. present)	1.107	0.682	1.798	0.681
US suggested CLNM	(absent vs. present)	34.840	19.483	62.304	<0.001
Tumor size					
	<10mm	1			
	10-20mm	2.780	1.632	4.736	<0.001
	>20mm	13.256	7.337	23.952	<0.001
Component	(solid vs. solid cystic)	0.6987	0.338	1.443	0.333
Echogenicity	(hypoechoic vs. others)	0.243	0.0548	1.079	0.063
Taller than wide	(absent vs. present)	0.4797	0.2947	0.7827	0.003
Margin	(regular vs. irregular)	0.3677	0.2427	0.556	<0.001
Boundary	(ambiguous vs. legible)	3.939	2.527	6.141	<0.001
Microcalcification	(absent vs. present)	2.816	1.589	4.986	<0.001
Extracapsularinvasion	(absent vs. present)	11.724	7.179	19.146	<0.001

OR, odds ratio; PTC, papillary thyroid carcinoma; US, ultrasound; CLNM, cervical lymph node metastasis.

TABLE 3 | Multivariate analysis of predictive factors associated with CLNM in PTC patients.

Variables	OR	95% CI	*P*-Value
Gender (Male)	2.823	1.269-6.279	0.011
Age (<45 years)	1.806	1.095-2.979	0.021
Multifocality	2.666	1.225-5.802	0.013
US suggested CLNM	33.192	14.867-74.101	<0.001
Tumor size (10-20mm)	1.833	0.795-4.223	0.155
Tumor size (>20mm)	6.635	2.541-17.324	<0.001
Boundary (ambiguous)	2.046	1.002-4.414	0.042
Extracapsular invasion	5.532	2.556-11.971	<0.001

OR, odds ratio; PTC, papillary thyroid carcinoma; US, ultrasound; CLNM, cervical lymph node metastasis.

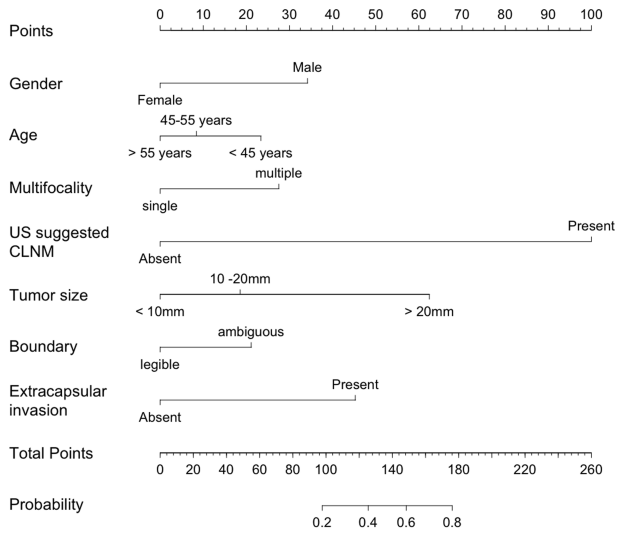

FIGURE 3 | Nomogram for predicting CLNM in patients with papillary thyroid carcinoma. CLNM, cervical lymph node metastasis; US, ultrasound.

lesions could be accurately identified in 75.9% of cases by ultrasonography (25). There was no significant difference between their multifocal findings determined by ultrasound and their histopathological findings. Therefore, the prediction model based on ultrasound features is reliable and feasible.

Tumor size has always been considered an important predictor of CLNM in patients with PTC. The larger the tumor volume, the higher the risk of CLMN. The mechanism may be related to the overexpression of VEGF. With the enlargement of nodules, the intra-tumor vessels are induced by various angiogenic factors to proliferate rapidly, forming many disorganized vascular networks. The active angiogenesis of the tumor increased the risk of CLNM (26, 27). However, the prediction thresholds reported by previous studies are different. Ahn et al. (28) reported that a tumor diameter ≥ 1 cm was a risk factor for CLNM, while Yan et al. (29) believed that tumor diameter had predictive value when it was ≥ 0.25 cm. The results of this present study found that the risk of developing CLNM of tumors with a maximum diameter of 10–20 mm and >20 mm was 1.83 and 6.63 times that of tumors with a maximum diameter of < 10 mm.

Extracapsular invasion of the thyroid is another independent predictor for CLNM (30). Kamaya et al. (31) reported that the criteria for ultrasound assessment of capsule invasion in PTC were that the nodule was adjacent to the capsule (i.e., there was no normal thyroid tissue between the nodule and the capsule), regardless of whether the capsule was interrupted. Jin et al. (32) suggested that the risk of CLNM was higher when the contact area between the nodule and the capsule was greater than 25%. Wang et al. (33) showed that tumor invasion and breakthrough of the thyroid capsule increased the likelihood of invading the lymphatic ducts and increased the risk of CLNM, and the distance between the tumor and the capsule was negatively correlated with the rate of lymph node metastasis. In our present study, the risk of CLNM in PTC patients with extracapsular invasion was significantly higher than that of patients without extracapsular invasion, which is consistent with the results of previous studies

The results of this study also indicated that an ambiguous boundary is an important factor for predicting lymph node metastasis, which is in line with the report of Xue et al. (22). Tumor metastasis required cancer cells invasion into the stroma, migration into the vessels, and proliferation in the lymph nodes (34).The invasive growth characteristics of the tumor cause the loss of a clear boundary between the tumor and the surrounding normal tissues.

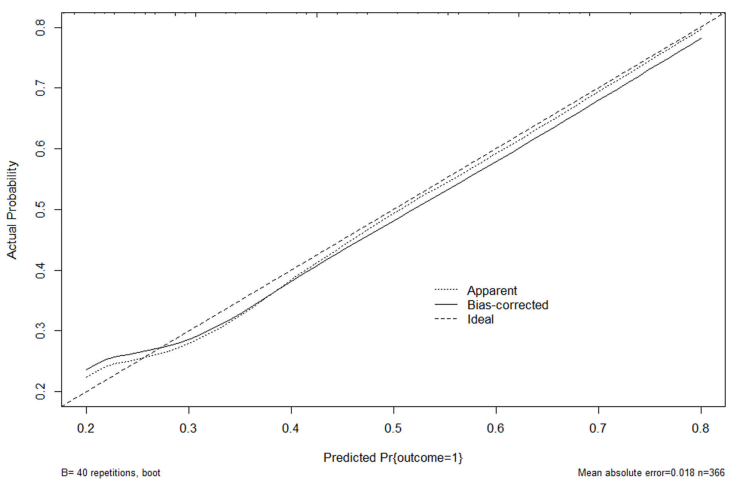

FIGURE 4 | Calibration curve for internal validation of the CLNM nomograms. Nomogram predicted CLNM probabilities are plotted on the x-axis; actual CLNM probabilities are plotted on the y-axis. The dashed line along the 45-degree line passing through the point of origin represents a perfect calibration model in which the predicted probabilities are consistent with the actual probabilities. US, ultrasound; CLNM, cervical lymph node metastasis.

On ultrasound, metastatic lymph nodes of PTC is recognized as round-like, calcified, cystic, and disordered or absent lymphatic hilus structure. In this study, any of the above changes detected by ultrasound examination was suspected lymph node metastasis. Ultrasound suggested lymph node metastasis accounted for the highest score in the nomogram model established in the present study, which may become one of the most important indicators for the prediction of CLNM.

Microcalcification is the deposition of calcium salts caused by vascular and fibrous hyperplasia, which reflects the rapid growth of cancer cells and is a typical ultrasound manifestation of PTC. However, the effect of microcalcification on CLNM of PTC is controversial. The presence of microcalcifications, especially the presence of diffuse microcalcifications, has been highly correlated with CLNM, and 91.8% of the thyroid lesions with diffuse microcalcifications developed central lymph node metastasis (27). Bai et al. (35) found that the presence of microcalcifications in PTC was significantly correlated with lymph node metastasis and clinical stage. Some cytokines, such as bone morphogenetic protein-1 and osteopontin, are highly expressed in tumors with microcalcifications (36), which are associated with the invasiveness of PTC. However, the results of this study showed that microcalcification was only statistically significant in univariate analysis, as multivariate analysis did not indicate that microcalcification was an independent risk factor for CLMN. The relationship between microcalcifications and CLNM needs to be further studied.

Hashimoto's thyroiditis is a risk factor for the development of PTC (37). However, there is no consensus on the relationship between Hashimoto's thyroiditis and CLNM in PTC patients. Hashimoto's thyroiditis is a protective factor against CLNM, as the probability of developing CLNM is lower in PTC patients with Hashimoto's thyroiditis (38). Zhou et al. (39) reported that TPO Ab <1 kU/L was an independent risk factor for central lymph node metastasis, but this was not confirmed in the study of Qu et al. (40). In our present study, there was no significant difference in the incidence of CLNM between PTC patients with Hashimoto's thyroiditis and PTC patients without a Hashimoto's thyroiditis background. TPOAb was not an independent risk factor for CLNM. The differences in the results of these studies may be related to the differences in the samples of different studies. The study of Zhou et al. only included unifocal PTC, and only central lymph node metastasis was analyzed. In this study, we included both unifocal PTC and multifocal PTC, and included both central lymph node metastasis and LLNM in the statistical analysis.

The present study has some limitations. First, the establishment of the nomogram model was based on a retrospective study of single-center samples, which may have a selection bias. Second, relatively few study subjects were included in this study, so the established nomogram model still requires prospective and big data studies to further verify its accuracy. Third, this study only included patients with PTC in China, and the applicability of the results to other pathological types of thyroid cancer (such as follicular thyroid carcinoma and medullary carcinoma) or populations of other races or countries needs to be further explored.

In summary, male sex, age <45 years, multifocality, maximum tumor diameter > 20 mm, extracapsular invasion, ambiguous boundary, and US suggested CLNM were independent risk factors for CLNM in patients with PTC. This study successfully established a nomogram model for predicting CLNM of PTC, which can help in the preoperative quantitative prediction of CLNM and should be considered in the determination of surgical procedures.

DATA AVAILABILITY STATEMENT

The original contributions presented in the study are included in the article/supplementary material. Further inquiries can be directed to the corresponding author.

ETHICS STATEMENT

The studies involving human participants were reviewed and approved by the Ethics Committee of the People's Hospital of Guangxi Zhuang Autonomous Region. Written informed consent to participate in this study was provided by the participants' legal guardian/next of kin.

AUTHOR CONTRIBUTIONS

All authors listed have made a substantial, direct, and intellectual contribution to the work, and approved it for publication.

FUNDING

This study was supported by the National Natural Science Foundation of China (No. 81660292, 81260223), Guangxi Natural Science Foundation project (2020GXNSFAA259014), and Guangxi medical high-level personnel training "139" project. The funders had no role in study design, data collection and analysis, decision to publish, or preparation of the manuscript.

REFERENCES

1. National Cancer Institute. *Cancer Stat Facts: Thyroid Cancer* (2020). Available at: https://seer.cancer.gov/statfacts/html/thyro.html (Accessed June 8, 2020).
2. Liu T, Zhou S, Yu J, Guo Y, Wang Y, Zhou J, et al. Prediction of Lymph Node Metastasis in Patients With Papillary Thyroid Carcinoma: A Radiomics Method Based on Preoperative Ultrasound Images. *Technol Cancer Res Treat* (2019) 18:1533033819831713. doi: 10.1177/1533033819831713
3. Wang Y, Nie F, Wang G, Liu T, Dong T, Sun Y. Value of Combining Clinical Factors, Conventional Ultrasound, and Contrast-Enhanced Ultrasound Features in Preoperative Prediction of Central Lymph Node Metastases of Different Sized Papillary Thyroid Carcinomas. *Cancer Manag Res* (2021) 13:3403–15. doi: 10.2147/CMAR.S299157

4. Kwon HK, Cheon YI, Shin SC, Sung ES, Lee JC, Kim IJ, et al. Risk Factors of Suprasternal Lymph Node Metastasis in Papillary Thyroid Carcinoma With Clinical Lateral Cervical Lymph Node Metastasis. *Gland Surg* (2021) 2:512–20. doi: 10.21037/gs-20-368
5. Hu D, Lin H, Zeng X, Wang T, Deng J, Su X. Risk Factors for and Prediction Model of Skip Metastasis to Lateral Lymph Nodes in Papillary Thyroid Carcinoma. *World J Surg* (2020) 5:1498–505. doi: 10.1007/s00268-019-05332-0
6. Zheng CM, Ji YB, Song CM, Ge MH, Tae K. Number of Metastatic Lymph Nodes and Ratio of Metastatic Lymph Nodes to Total Number of Retrieved Lymph Nodes Are Risk Factors for Recurrence in Patients With Clinically Node Negative Papillary Thyroid Carcinoma. *Clin Exp Otorhinolaryngol* (2018) 11:58–64. doi: 10.21053/ceo.2017.00472
7. Aydin OU, Soylu L, Ozbas S, Ilgan S, Bilezikci B, Gursoy A, et al. The Risk of Hypoparathyroidism After Central Compartment Lymph Node Dissection in the Surgical Treatment of Pt1, N0 Thyroid Papillary Carcinoma. *Eur Rev Med Pharmacol Sci* (2016) 9:1781–7.
8. Soydal Ç, Özkan E, Küçük NÖ, Kir KM. Effect of the Application of Prophylactic Central Compartment Lymph Node Dissectionon Radioiodine Ablation Doses in Patients With Papillary Thyroid Carcinoma. *Turk J Med Sci* (2016) 4:1078–82. doi: 10.3906/sag-1505-40
9. Liu H, Li Y, Mao Y. Local Lymph Node Recurrence After Central Neck Dissection in Papillary Thyroid Cancers: A Meta Analysis. *Eur Ann Otorhinolaryngol Head Neck Dis* (2019) 6:481–7. doi: 10.1016/j.anorl.2018.07.010
10. Deng L, Cao Y, Lin J. Regional Recurrence Rate of Lymph-Node-Positive Thyroid Carcinoma After Selective or Comprehensive Neck Dissection. *Oral Oncol* (2019) 90:147–9. doi: 10.1016/j.oraloncology.2018.11.034
11. Zhao H, Li H. Meta-Analysis of Ultrasound for Cervical Lymph Nodes in Papillary Thyroid Cancer: Diagnosis of Central and Lateral Compartment Nodal Metastases. *Eur J Radiol* (2019) 112:14–21. doi: 10.1016/j.ejrad.2019.01.006
12. Hu W, Wang H, Wei R, Wang L, Dai Z, Duan S, et al. MRI-Based Radiomics Analysis to Predict Preoperative Lymph Node Metastasis in Papillary Thyroid Carcinoma. *Gland Surg* (2020) 5:1214–26. doi: 10.21037/gs-20-479
13. Tong Y, Li J, Huang Y, Zhou J, Liu T, Guo Y, et al. Ultrasound-Based Radiomic Nomogram for Predicting Lateral Cervical Lymph Node Metastasis in Papillary Thyroid Carcinoma. *Acad Radiol* (2020) 8:S1076–6332(20)30440-2. doi: 10.1016/j.acra.2020.07.017
14. Tang LQ, Li CF, Li J, Chen WH, Chen QY, Yuan LX, et al. Establishment and Validation of Prognostic Nomograms for Endemic Nasopharyngeal Carcinoma. *J Natl Cancer Inst* (2015) 1:djv291. doi: 10.1093/jnci/djv291
15. Iasonos A, Schrag D, Raj GV, Panageas KS. How to Build and Interpret a Nomogram for Cancer Prognosis. *J Clin Oncol* (2008) 8:1364–70. doi: 10.1200/JCO.2007.12.9791
16. Liang W, Zhang L, Jiang G, Wang Q, Liu L, Liu D, et al. Development and Validation of a Nomogram for Predicting Survival in Patients With Resected Non-Small-Cell Lung Cancer. *J Clin Oncol* (2015) 8:861–9. doi: 10.1200/JCO.2014.56.6661
17. Sohn KH, Kim GW, Lee SY, Kim HS, Cho SH, Han JK, et al. Immediate and Delayed Hypersensitivity After Intra-Arterial Injection of Iodinated Contrast Media: A Prospective Study in Patients With Coronary Angiography. *Eur Radiol* (2019) 29:5314–21. doi: 10.1007/s00330-019-06138-3
18. Suh CH, Baek JH, Choi YJ, Lee JH. Performance of CT in the Preoperative Diagnosis of Cervical Lymph Node Metastasis in Patients With Papillary Thyroid Cancer: A Systematic Review and Meta-Analysis. *AJNR Am J Neuroradiol* (2017) 38:154–61. doi: 10.3174/ajnr.A4967
19. Zhang L, Wei WJ, Ji QH, Zhu YX, Wang ZY, Wang Y, et al. Risk Factors for Neck Nodal Metastasis in Papillary Thyroid Microcarcinoma: A Study of 1066 Patients. *J Clin Endocrinol Metab* (2012) 4:1250–7. doi: 10.1210/jc.2011-1546
20. Gui CY, Qiu SL, Peng ZH, Wang M. Clinical and Pathologic Predictors of Central Lymph Node Metastasis in Papillary Thyroid Microcarcinoma: A Retrospective Cohort Study. *J Endocrinol Invest* (2018) 4:403–9. doi: 10.1007/s40618-017-0759-y
21. Zheng X, Peng C, Gao M, Zhi J, Hou X, Zhao J, et al. Risk Factors for Cervical Lymph Node Metastasis in Papillary Thyroid Microcarcinoma: A Study of 1,587 Patients. *Cancer Biol Med* (2019) 1:121–30. doi: 10.20892/j.issn.2095-3941.2018.0125
22. Xue K, Qi Z, Shi W, Jia S. Relevant Factors Between Ultrasound Imaging Features of Papillary Thyroid Micropapillary Carcinoma and Cervical Lymph Node Metastases. *Chin J Ultrasound Med* (2020) 4:306–9.
23. Kim HJ, Park HK, Byun DW, Suh K, Yoo MH, Min YK, et al. Number of Tumor Foci as Predictor of Lateral Lymph Node Metastasis in Papillary Thyroid Carcinoma. *Head Neck* (2015) 5:650–4. doi: 10.1002/hed.23650
24. Fu X, Zhang H, Chen Z, Yang Z, Shi D, Liu T, et al. TFAP2B Overexpression Contributes to Tumor Growth and Progression of Thyroid Cancer Through the COX-2 Signaling Pathway. *Cell Death Dis* (2019) 6:397. doi: 10.1038/s41419-019-1600-7
25. Al Afif A, Williams BA, Rigby MH, Bullock MJ, Taylor SM, Trites J, et al. Multifocal Papillary Thyroid Cancer Increases the Risk of Central Lymph Node Metastasis. *Thyroid* (2015) 9:1008–12. doi: 10.1089/thy.2015.0130
26. Zhao L, Yan H, Pang P, Fan X, Jia X, Zang L, et al. Thyroid Nodule Size Calculated Using Ultrasound and Gross Pathology as Predictors of Cancer: A 23-Year Retrospective Study. *Diagn Cytopathol* (2019) 3:187–93. doi: 10.1002/dc.24068
27. Tian X, Song Q, Xie F, Ren L, Zhang Y, Tang J, et al. Papillary Thyroid Carcinoma: An Ultrasound-Based Nomogram Improves the Prediction of Lymph Node Metastases in the Central Compartment. *Eur Radiol* (2020) 11:5881–93. doi: 10.1007/s00330-020-06906-6
28. Ahn JE, Lee JH, Yi JS, Shong YK, Hong SJ, Lee DH, et al. Diagnostic Accuracy of CT and Ultrasonography for Evaluating Metastatic Cervical Lymph Nodes in Patients With Thyroid Cancer. *World J Surg* (2008) 7:1552–8. doi: 10.1007/s00268-008-9588-7
29. Yan H, Zhou X, Jin H, Li X, Zheng M, Ming X, et al. A Study on Central Lymph Node Metastasis in 543 Cn0 Papillary Thyroid Carcinoma Patients. *Int J Endocrinol* (2016) 2016:1878194. doi: 10.1155/2016/1878194
30. Yang Y, Chen C, Chen Z, Jiang J, Chen Y, Jin L, et al. Prediction of Central Compartment Lymph Node Metastasis in Papillary Thyroid Microcarcinoma. *Clin Endocrinol (Oxf)* (2014) 2:282–8. doi: 10.1111/cen.12417
31. Kamaya A, Tahvildari AM, Patel BN, Willmann JK, Jeffrey RB, Desser TS. Sonographic Detection of Extracapsular Extension in Papillary Thyroid Cancer. *J Ultrasound Med* (2015) 12:2225–30. doi: 10.7863/ultra.15.02006
32. Jin WX, Ye DR, Sun YH, Zhou XF, Wang OC, Zhang XH, et al. Prediction of Central Lymph Node Metastasis in Papillary Thyroid Microcarcinoma According to Clinicopathologic Factors and Thyroid Nodule Sonographic Features: A Case-Control Study. *Cancer Manag Res* (2018) 10:3237–43. doi: 10.2147/CMAR.S169741
33. Wang QC, Cheng W, Wen X, Li JB, Jing H, Nie CL. Shorter Distance Between the Nodule and Capsule has Greater Risk of Cervical Lymph Node Metastasis in Papillary Thyroid Carcinoma. *Asian Pac J Cancer Prev* (2014) 2:855–60. doi: 10.7314/apjcp.2014.15.2.855
34. Xie N, Wang C, Liu X, Li R, Hou J, Chen X, et al. Tumor Budding Correlates With Occult Cervical Lymph Node Metastasis and Poor Prognosis in Clinical Early-Stage Tongue Squamous Cell Carcinoma. *J Oral Pathol Med* (2015) 4:266–72. doi: 10.1111/jop.12242
35. Bai Y, Zhou G, Nakamura M, Ozaki T, Mori I, Taniguchi E, et al. Survival Impact of Psammona Body, Stromal Calcification, and Bone Formation in Papillary Thyroid Carcinoma. *Mod Pathol* (2009) 7:887–94. doi: 10.1038/modpathol.2009.38
36. Ferreira LB, Lima RT, Bastos ACSDF, Silva AM, Tavares C, Pestana A, et al. OPNa Overexpression Is Associated With Matrix Calcification in Thyroid Cancer Cell Lines. *Int J Mol Sci* (2018) 10:2990. doi: 10.3390/ijms19102990
37. Uhliarova B, Hajtman A. Hashimoto's Thyroiditis - an Independent Risk Factor for Papillary Carcinoma. *Braz J Otorhinolaryngol* (2018) 6:729–35. doi: 10.1016/j.bjorl.2017.08.012
38. Zhu F, Shen YB, Li FQ, Fang Y, Hu L, Wu YJ. The Effects of Hashimoto Thyroiditis on Lymph Node Metastases in Unifocal and Multifocal Papillary Thyroid Carcinoma: A Retrospective Chinese Cohort Study. *Med (Baltimore)* (2016) 6:e2674. doi: 10.1097/MD.0000000000002674
39. Zhou J, Zhou SC, Li JW, Wang Y, Chen YL, Wang F, et al. Risk Factors of Central Neck Lymph Node Metastasis Following Solitary Papillary Thyroid Carcinoma. *Chin J Ultrasonogr* (2019) 3:235–40. doi: 10.3760/cma.j.issn.1004-4477.2019.03.009
40. Qu N, Zhang L, Lin DZ, Ji QH, Zhu YX, Wang Y. The Impact of Coexistent Hashimoto's Thyroiditis on Lymph Node Metastasis and Prognosis in Papillary Thyroid Microcarcinoma. *Tumour Biol* (2016) 6:7685–92. doi: 10.1007/s13277-015-4534-4

Conflict of Interest: The authors declare that the research was conducted in the absence of any commercial or financial relationships that could be construed as a potential conflict of interest.

this article, or claim that may be made by its manufacturer, is not guaranteed or endorsed by the publisher.

frontiers in Oncology

ORIGINAL RESEARCH
published: 20 January 2022
doi: 10.3389/fonc.2021.770241

A Robust Metabolic Enzyme-Based Prognostic Signature for Head and Neck Squamous Cell Carcinoma

Zizhao Mai[1], *Huan Chen*[1], *Mingshu Huang*[1], *Xinyuan Zhao*[1*] *and Li Cui*[1,2*]

[1] *Stomatological Hospital, Southern Medical University, Guangzhou, China,* [2] *Division of Oral Biology and Medicine, School of Dentistry, University of California, Los Angeles, CA, United States*

Background: Head and neck squamous cell carcinoma (HNSCC) is still a menace to public wellbeing globally. However, the underlying molecular events influencing the carcinogenesis and prognosis of HNSCC are poorly known.

Methods: Gene expression profiles of The Cancer Genome Atlas (TCGA) HNSCC dataset and GSE37991 were downloaded from the TCGA database and gene expression omnibus, respectively. The common differentially expressed metabolic enzymes (DEMEs) between HNSCC tissues and normal controls were screened out. Then a DEME-based molecular signature and a clinically practical nomogram model were constructed and validated.

Results: A total of 23 commonly upregulated and 9 commonly downregulated DEMEs were identified in TCGA HNSCC and GSE37991. Gene ontology analyses of the common DEMEs revealed that alpha-amino acid metabolic process, glycosyl compound metabolic process, and cellular amino acid metabolic process were enriched. Based on the TCGA HNSCC cohort, we have built up a robust DEME-based prognostic signature including *HPRT1*, *PLOD2*, *ASNS*, *TXNRD1*, *CYP27B1*, and *FUT6* for predicting the clinical outcome of HNSCC. Furthermore, this prognosis signature was successfully validated in another independent cohort GSE65858. Moreover, a potent prognostic signature-based nomogram model was constructed to provide personalized therapeutic guidance for treating HNSCC. *In vitro* experiment revealed that the knockdown of TXNRD1 suppressed malignant activities of HNSCC cells.

Conclusion: Our study has successfully developed a robust DEME-based signature for predicting the prognosis of HNSCC. Moreover, the nomogram model might provide useful guidance for the precision treatment of HNSCC.

Keywords: head and neck squamous cell carcinoma (HNSCC), metabolic enzyme, prognostic signature, survival analysis, The Cancer Genome Atlas

OPEN ACCESS

Edited by:
Heming Lu,
People's Hospital of Guangxi Zhuang Autonomous Region, China

Reviewed by:
Jinhui Liu,
Nanjing Medical University, China
Vito Carlo Alberto Caponio,
University of Foggia, Italy
Baochang He,
Fujian Medical University, China

****Correspondence:***
Xinyuan Zhao
zhaoxinyuan1989@smu.edu.cn
Li Cui
zsucllj@ucla.edu

Specialty section:
This article was submitted to Head and Neck Cancer, a section of the journal Frontiers in Oncology

Received: *03 September 2021*
Accepted: *16 December 2021*
Published: *20 January 2022*

Citation:
Mai Z, Chen H, Huang M, Zhao X and Cui L (2022) A Robust Metabolic Enzyme-Based Prognostic Signature for Head and Neck Squamous Cell Carcinoma. Front. Oncol. 11:770241. doi: 10.3389/fonc.2021.770241

Abbreviations: HNSCC, Head and neck squamous cell carcinoma; TCGA, The Cancer Genome Atlas; DEME, differentially expressed metabolic enzyme; HPV, human papillomavirus; OS, overall survival; GEO, Gene Expression Omnibus; DEG, differentially expressed gene; GO, Gene Ontology; LASSO, least absolute shrinkage and selection operator; RSN, Robust Spline Normalization; PVDF, polyvinylidene difluoride; MTT, 3-(4, 5-dimethylthiazol-2-yl)-2, 5-diphenyltetrazolium bromide; DMSO, Dimethyl sulfoxide; EdU, 5-Ethynyl-2′-deoxyuridine; AUC, area under the curve; OD, optical density.

INTRODUCTION

Head and neck squamous cell carcinoma (HNSCC) is cancer that arises from squamous cells in the area of the head and neck. HNSCC represents up to 90% of tumors in the head and neck region, which includes malignancy of the oral cavity, pharynx, and larynx (1, 2). The initiation and development of HNSCC are mainly caused by genetic alterations, human papillomavirus (HPV) infection, and consumption of tobacco, alcohol, and areca-nut, etc (3). Although surgery, radiochemotherapy, targeted therapy, and immunotherapy have been significantly advanced, patients with HNSCC have a median five-year overall survival (OS) rate of approximately 66% (4). HNSCC is usually treatable if detected at the earliest stage. Unfortunately, patients often present with advanced clinical stages at the time of diagnosis that is incurable or requires aggressive treatment, leading to an unfavorable prognosis (5). This highlights the significance of developing novel and robust molecular signatures for precisely evaluating the clinical outcome of HNSCC, which contributes to therapeutic guidance for HNSCC (6, 7).

Metabolic alterations of tumors were first found nearly a century ago, but only recently has reprogrammed metabolism been deemed as a cancer hallmark (8, 9). For example, nutrient uptake and biosynthesis are required in the early stages of cancer progression, while oxidative phosphorylation and oxidative stress resistance occur in the later stages of tumor growth (10). Therefore, reprogrammed metabolism has become a topic of renewed interest, and reversing abnormal metabolic processes might be a novel approach for the treatment of HNSCC (11). However, it is still uncertain which key metabolic enzymes affect the dismal prognosis of HNSCC.

The Cancer Genome Atlas (TCGA, http://cancergenome.nih.gov/) and NCBI-Gene Expression Omnibus (GEO, http://www.ncbi.nlm.nih.gov/geo/) are international public databases that archive and freely distribute next-generation sequencing, microarray, and other formats of high-throughput datasets, which are valuable resources for improving our understanding of cancer development (12, 13). In this study, we first identified the common differentially expressed metabolic enzymes (DEMEs) in TCGA HNSCC and GSE37991 cohort. Afterward a robust DEME-based signature was successfully built up and validated for predicting the clinical outcome of HNSCC. Moreover, a clinically practical nomogram model was constructed to accurately estimate HNSCC prognosis.

MATERIALS AND METHODS

Data Source

The original GEO datasets GSE37991 and GSE65858 were downloaded from NCBI GEO databases. The data of GSE37991 and GSE65858 were based on GPL6883 (Illumina HumanRef-8 v3.0 expression beadchip) and GPL10558 (Illumina HumanHT-12 V4.0 expression beadchip), respectively. For the TCGA HNSCC cohort, the raw data and corresponding clinical information were downloaded from the TCGA data portal. The tumor located in lips, tongue, oral cavity, oropharynx, larynx, and hypopharynx were selected. The format of the TCGA HNSCC downloaded data was HTseq-FPKM, and the formats of GSE37991 and GSE65858 were normalized microarray data.

The RNA-seq data of the TGCA HNSCC cohort included 521 HNSCC samples and 44 normal control samples. Forty-three out of 44 normal samples were matched to the HNSCC tumor samples. Only one normal sample from the salivary gland was not matched to the tumor samples. Two hundred and seventy HNSCC tumor samples were included in the microarray data of GSE65858, which did not include normal control samples. The microarray data of the GSE37991 cohort included 40 HNSCC samples and 40 paired normal samples. Regarding the inclusion/exclusion criteria for the enrolled patients, both tumor and normal control samples in TCGA HNSCC and GSE37991 cohorts were included for the differential expression analysis. For the construction of risk signature, only the tumor samples in TCGA HNSCC, GSE37991 and GSE65858 cohorts were considered, and all normal control samples were excluded. The patients without clinical characteristics such as follow-up time, follow-up status, age, gender, clinical stage, T stage or N stage were excluded. Besides, the patients with the TX stage and NX stage were also excluded due to the disturbance to grouping. The clinical characteristics including age, gender, stage of the HNSCC tumor samples in the TCGA HNSCC discovery cohort and GSE65858 validation cohort were summarized in **Tables S1** and **S2**, respectively.

Data Pre-Processing and Differential Expression Analysis

Briefly, the probes that have no expression in most of the samples were excluded. The FPKM data of the TCGA HNSCC cohort was converted to TPM format for further analysis. For GSE37991, data normalization was achieved with GeneSpring GX software (Agilent Technologies). For GSE65858, the data was first processed within the R/Bioconductor. Then the expression values were subjected to $\log_2$-transformation and the normalization was performed using Robust Spline Normalization (RSN). Batch effects of expression BeadChips were corrected using ComBat.

The DEMEs in GSE37991 and TCGA HNSCC cohort were identified by the edgeR package. Absolute $\log_2$FC>1 and p<0.05 were selected as the demarcation criteria based on Benjamini & Hochberg (BH) procedure. The common differentially expressed genes (DEGs) between GSE37991 and TCGA HNSCC cohort were identified by the intersect function in R.

Gene Ontology Enrichment Analysis

Gene Ontology (GO) enrichment analysis was performed using the DAVID (the Database for Annotation, Visualization and Integration Discovery).

Prognostic Signature Generation and Validation

TCGA HNSCC cohort and GSE65858 were used as discovery and validation cohorts, respectively. DEMEs were demonstrated to be correlative with the OS of HNSCC by univariate Cox

proportional hazards regression analysis, which adopted the statistics from the TCGA HNSCC cohort. Subsequently, the most optimum DEMEs were chosen by the approach of the least absolute shrinkage and selection operator (LASSO) regression. The independent DEME-based prognostic signature was determined by the multivariate Cox proportional hazards regression analysis. Afterward a risk score model was constructed with this independent DEME-based prognostic signature. The summation of each DEME's score was computed as a risk score for each HNSCC patient: risk score = $\Sigma_{i=1}^{n}\ \beta i \times Ei$ (14). On basis of the median value of the risk scores, the TCGA HNSCC cohort was divided into a low-risk group and a high-risk group. We compared the OS between low- and high-risk groups and assessed the differential survival distinguished by clinicopathological parameters between low- and high-risk groups. Similarly, the GSE65858 validation cohort was classified into low- and high-risk groups according to the above risk score model built up by the TCGA HNSCC cohort. Besides, the OS and the survival distinction were likewise differentiated by clinicopathological parameters between low- and high-risk groups.

Nomogram Model Construction

A nomogram model including the risk score and other clinicopathological indices was constructed. The calibration curves were used to assess the accuracy for predicting 1-year OS and 3-year OS of HNSCC.

Cell Culture and Transfection

Both SCC1 and SCC23 were cultured in Dulbecco's modified Eagle's medium (DMEM) (Gibco, USA) supplemented with 10% fetal bovine serum and 1% penicillin/streptomycin. Cells were grown in a 37°C, 5% CO_2 cell incubator in a humidified atmosphere. The cells were transfected with siTXNRD1 and siCTRL using Lipofectamine® RNA iMAX Transfection Reagent (Invitrogen, Carlsbad, CA, USA).

Western Blot

The protein samples were separated on 4-20% SDS-PAGE gels and then transferred to polyvinylidene difluoride (PVDF) membranes. Following by blocking in 5% skimmed milk for 1 hr at room temperature, the blots were then probed with primary antibody against TXNRD1 (1:1000, Proteintech, Chicago, IL, USA) at 4°C overnight. The corresponding HRP-conjugated secondary antibody was used to incubate the membranes for 1 hr at room temperature. The signal was detected with ECL kits.

MTT Assay

The cells were seeded into the 96-wells of the plate at a density of 3,000 cells per well in 200 µl cell culture media. MTT solution (20 µl,5 mg/ml) was added to each well at the indicated time points and incubated for 4 hrs at 37°C. Dimethyl sulfoxide (DMSO) was added to dissolve the precipitate after removing the supernatant. A microculture plate reader (Tecan, Mannedorf, Switzerland) was used to measure the absorbance at 570 nm.

5-Ethynyl-2′-Deoxyuridine Assay

According to the manufacturer's instructions, the Click-iT™ 5-Ethynyl-2′-deoxyuridine (EdU) Cell Proliferation Kit for Imaging (Invitrogen) was used to perform the EdU assay. Briefly, EdU was added to the cells and incubated at 37°C for 2 hrs. Subsequently, 3.7% formaldehyde was used to fix the cells at room temperature for 20 min. After washing three changes of PBS, 0.5% Triton X-100 was added to increase the permeability of the cellular membrane. 1× Click-iT reaction cocktail was used to stain the cells in the dark at room temperature for 30 min. Then, the cell nucleus was stained by Hoechst 33342 dye. A confocal laser scanning microscope (Olympus, Center Valley, PA) was used to capture at least four random images per well.

Statistical Analysis

The volcano plot and heatmaps were drawn by the "ggplot2" package of R software. The univariate and multivariate Cox regression analyses incorporated the clinical characteristics including age, gender, clinical stage, and risk score. The independent prognostic factors for HNSCC were identified by the univariate and multivariate Cox regression analyses. The Kaplan-Meier method and log-rank test were performed to calculate the OS distinguish between different groups. A *p*-value less than 0.05 is considered statistically significant.

RESULTS

The Common DEMEs Between GSE37991 and TCGA HNSCC

The volcano plot was used to visualize the distribution of metabolic enzymes between cancer and normal tissues from the GSE37991 and TCGA HNSCC cohort. The significantly downregulated or upregulated metabolic enzymes were represented as green or red dots, respectively (**Figure 1A**). In total, 478 (402 upregulated and 76 downregulated) and 223 (102 upregulated and 121 downregulated) significantly changed metabolic enzymes were identified in GSE37991 and TCGA HNSCC cohort, respectively. The detailed information of the significantly changed metabolic enzymes was summarized in **Tables S3** and **S4**. The common DEMEs (23 upregulated and 9 downregulated) between GSE37991 and TCGA HNSCC cohort were shown in **Figure 1B**.

Gene Ontology

Gene ontology (GO) analysis of the DEMEs showed that small molecule catabolic process, alpha-amino acid metabolic process, glycosyl compound metabolic process, cellular amino acid metabolic process, organophosphate catabolic process, protein tetramerization, nucleoside metabolic process, nucleobase-containing small molecule catabolic process, aspartate family amino acid metabolic process, purine-containing compound catabolic process were the enriched (**Figure 2A**).

Identification of the Prognostic Signature

The survival-related DEMEs in the TCGA HNSCC cohort were identified by the univariate Cox regression, and *ASNS*, *CYP27B1*, *TXNRD1*, *GATM*, *PLOD2*, *FUT6*, and *HPRT1* were harvested. Based on the HRs, *GATM* and *FUT6* were protective genes, while *ASNS*, *CYP27B1*, *TXNRD1*, *PLOD2*, and *HPRT1* were risky genes

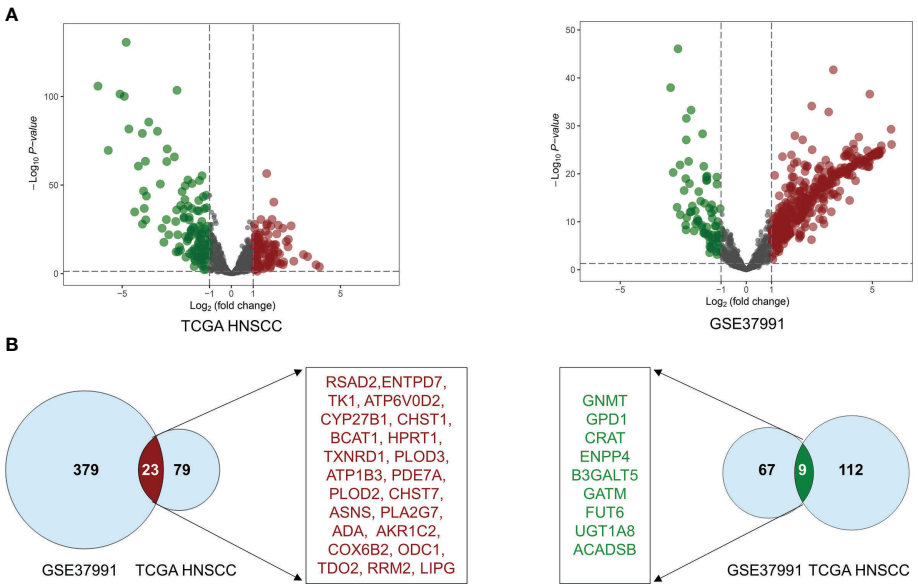

FIGURE 1 | The significant alteration of DEMEs between TCGA HNSCC cohort and GSE37991. **(A)** The volcano plot showed significant alteration of DEMEs between normal controls and tumor tissues from HNSCC. The fold changes (log_2-scaled) were shown in the X-axis, and the *p* values (log_{10}-scaled) were shown in the Y-axis. Each gene was represented by a dot, and the significantly downregulated or upregulated DEMEs were represented by the green or red color. **(B)** The common DEMEs between the TCGA HNSCC cohort and GSE37991 were shown in Venn diagrams.

(**Figure 2B**). The LASSO regression analysis identified six optimal DEMEs including *ASNS*, *CYP27B1*, *TXNRD1*, *PLOD2*, *FUT6*, and *HPRT1*. The risk score for each patient was computed as follows: risk score = (0.308) **ASNS* + (0.228) * *CYP27B1* + (0.284) * *TXNRD1* + (0.174) * *PLOD2* + (-0.092) * *FUT6* + (0.362) * *HPRT1*. Subsequently, the HNSCC patients were divided into high- and low-risk groups based on the median value of risk scores (**Figure 3A**). The survival time and survival status of each HNSCC patient in TCGA HNSCC were presented in a scatter plot (**Figure 3B**). The expression levels of *ASNS*, *CYP27B1*, *TXNRD1*, *PLOD2*, *FUT6*, and *HPRT1* in each HNSCC patient were shown with a heatmap (**Figure 3C**). Besides, survival analysis demonstrated that the OS of the high-risk group was significantly lower compared to the low-risk group (**Figure 3D**). We then stratified the HNSCC patients with different clinical indices including age, gender, clinical stage, T stage, and N stage. As shown in **Figures 4A–E**, the low-risk group got remarkably better OS than the high-risk group for the HNSCC patients with age>60 (p=0.003), or with female gender (p=0.023) or with male gender (p=0.022), or at the clinical stage III-IV (p<0.001), or at the stage T3-4 (p=0.003), or with node metastasis (p=0.005).

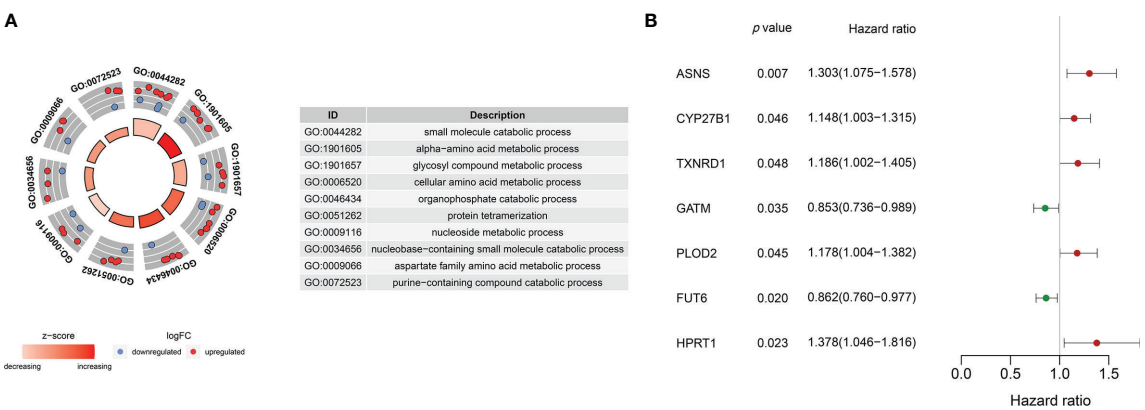

FIGURE 2 | **(A)** Gene ontology analyses of the common DEMEs. **(B)** *ASNS*, *CYP27B1 TXNRD1*, *GATM*, *PLOD2*, *FUT6*, and *HPRT1* were significantly correlative with survival in the TCGA HNSCC cohort.

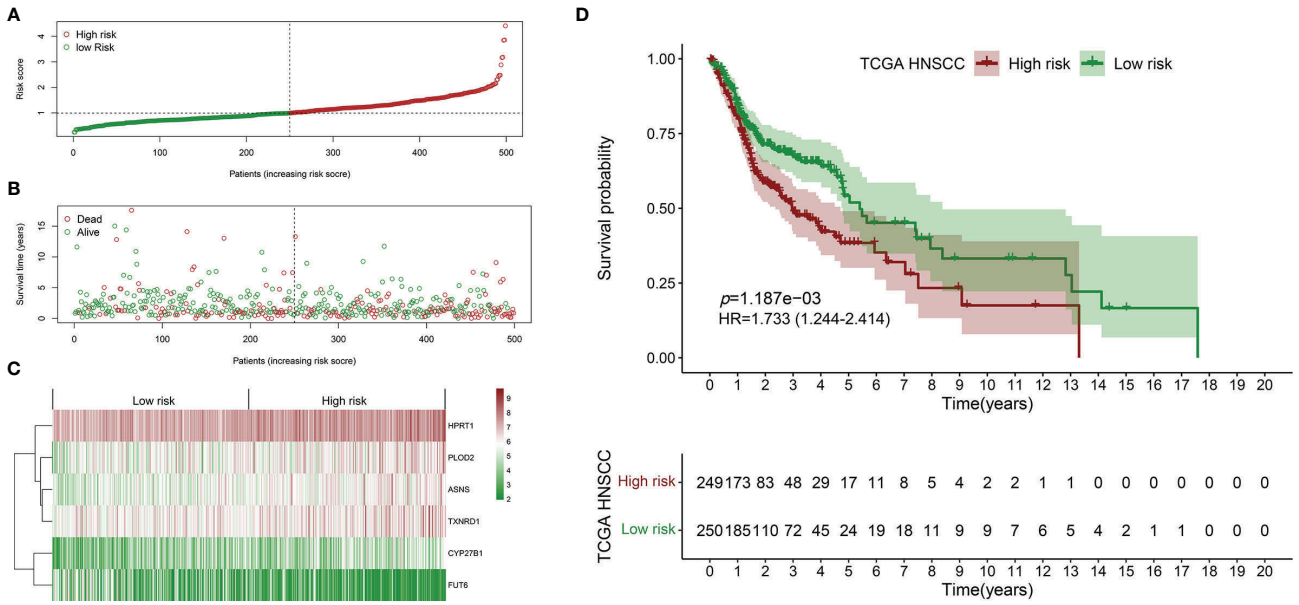

FIGURE 3 | Establishment of the prognostic signature using the TCGA HNSCC cohort. **(A)** Scatter plot of the risk scores distribution. **(B)** Scatter plot of the OS and OS status distribution in the low-and high-risk groups. **(C)** The six prognostic DEMEs expression pattern between low- and high-risk groups was shown in the heatmap. **(D)** The low-risk group got remarkably better OS than the high-risk group for the HNSCC patients.

Validation of the Prognostic Signature in an Independent Cohort GSE65858

Similarly, the HNSCC patients in GSE65858 were divided into high- and low-risk groups using the same median risk score in the TCGA HNSCC cohort (**Figure 5A**). The survival status, survival time, and expression level of prognosis-related DEMEs in each HNSCC patient were shown in **Figures 5B, C**. More importantly, the HNSCC patients in the high-risk group suffered a significantly poorer OS than those in the low-risk group (**Figure 5D**). As displayed in **Figures 6A–E**, the low-risk group got remarkably better OS than the high-risk group for the HNSCC patients with age ≤ 60 (p=0.026), or with male gender (p=0.009), or at the clinical stage III-IV (p=0.027), or the stage T3-4 (p=0.030).

The Risk Score Is an Independent Prognostic Factor for HNSCC

In the TCGA HNSCC cohort, the univariate Cox regression analysis showed that age (p =0.014, HR=1.020), gender (p =0.045, HR=0.695) and risk score (p<0.001, HR=2.116) were significantly associated with survival (**Figure 7A**). The multivariate Cox regression analysis revealed that only risk score (p<0.001, HR=2.047) was the independent prognostic factor for HNSCC (**Figure 7B**). Similarly, in GSE65858, the univariate Cox regression analysis showed that age (p =0.013, HR=1.027), clinical stage (p=0.001, HR=1.615) and risk score (p=0.024, HR=1.715) were significantly correlated with survival (**Figure 7C**). The multivariate Cox regression analysis showed that age (p =0.015, HR=1.027), clinical stage (p=0.001, HR=1.637) and risk score (p=0.023, HR=1.710) were independent prognostic factors for HNSCC (**Figure 7D**).

Nomogram Model Prediction

The risk score, age, gender and clinical stage were incorporated into the nomogram model to forecast the clinical outcome of HNSCC (**Figure 8**). A total nomogram-based score was obtained for each HNSCC patient derived from the clinicopathological parameters and their corresponding points. The 1-year OS or 3-year OS of HNSCC patients was forecasted with the nomogram model. The calibration curves showed that the nomogram model we built up exhibited excellent conformance for predicting the 1-year OS or 3-year OS of HNSCC (**Figures 9A, B**). The C indices of the nomogram model are 0.658 or 0.616 for predicting the 1-year OS or 3-year OS of HNSCC, respectively.

Knockdown of TXNRD1 Suppressed Malignant Activities of HNSCC Cells *In Vitro*

The expression level of TXNRD1 was significantly reduced in HNSCC cells following siTXNRD1 treatment (**Figure 10A**). Compared to the siCTRL treated cells, the MTT assay showed that the optical density (OD) values were markedly lower in TXNRD1-knockdown cells at indicated time points (**Figure 10B**). Similarly, the EdU assay showed the percentage of EdU-positive cells was dramatically lower in HNSCC cells treated with siTXNRD1 (**Figure 10C**).

DISCUSSION

Metabolic reprogramming has been demonstrated to be essential for regulating the carcinogenesis of HNSCC. The energy

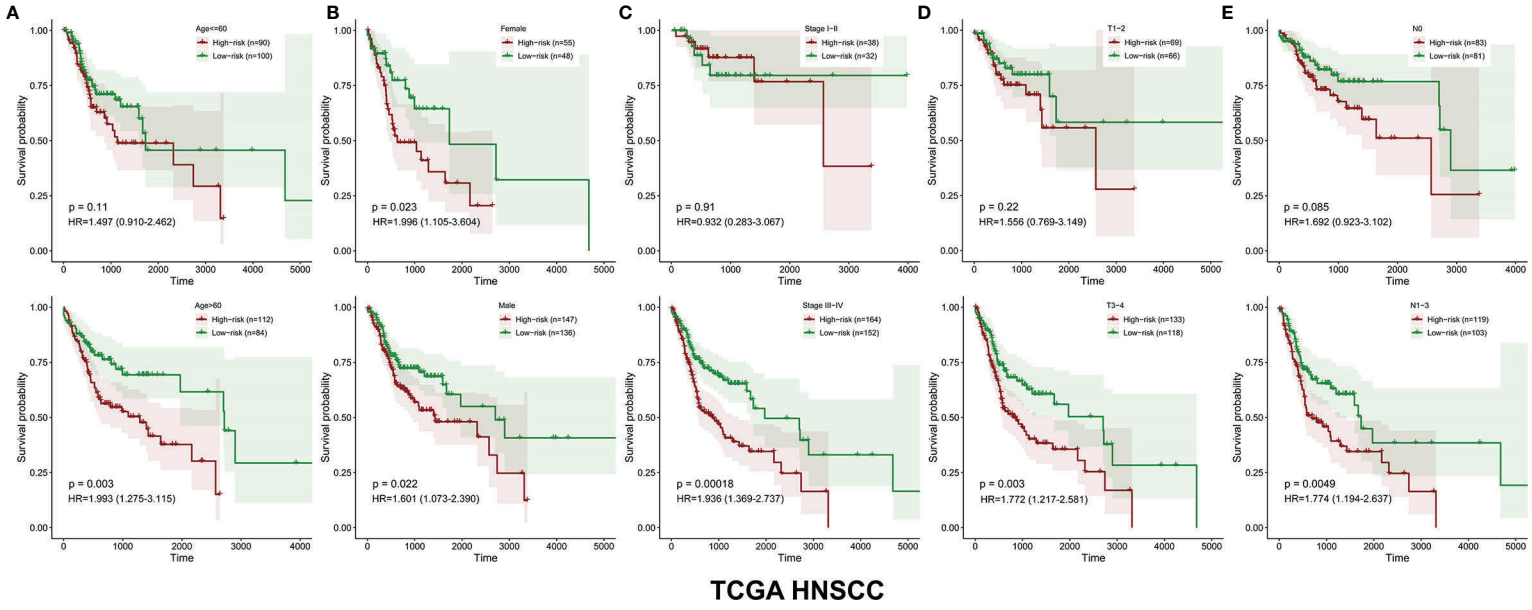

FIGURE 4 | The OS distinction between the low- and high-risk groups was classified by age, gender, clinical stage, T stage, and N stage in the TCGA HNSCC cohort **(A–E)**.

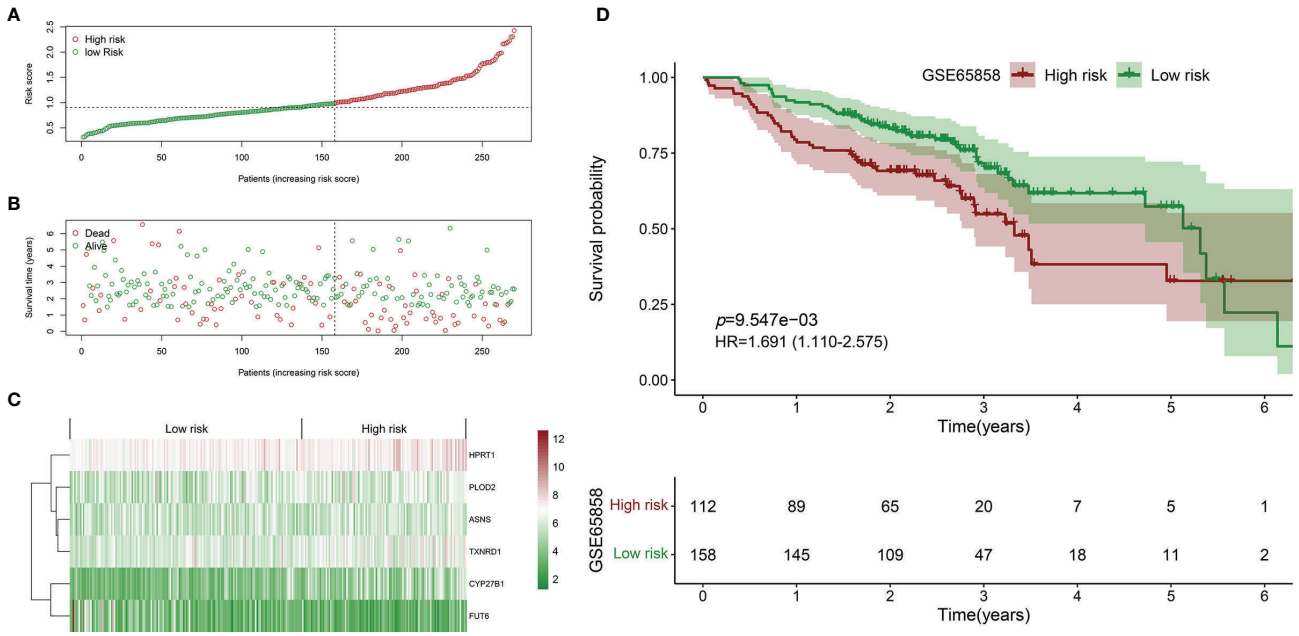

FIGURE 5 | Validation of the prognostic biomarker using the GSE65858 validation cohort. **(A)** Scatter plot of the risk scores distribution. **(B)** Scatter plot of the OS and OS status distribution in the low-and high-risk groups. **(C)** The six prognostic DEMEs expression pattern between low- and high-risk groups was shown in the heatmap. **(D)** The low-risk group got remarkably better OS than the high-risk group for the HNSCC patients.

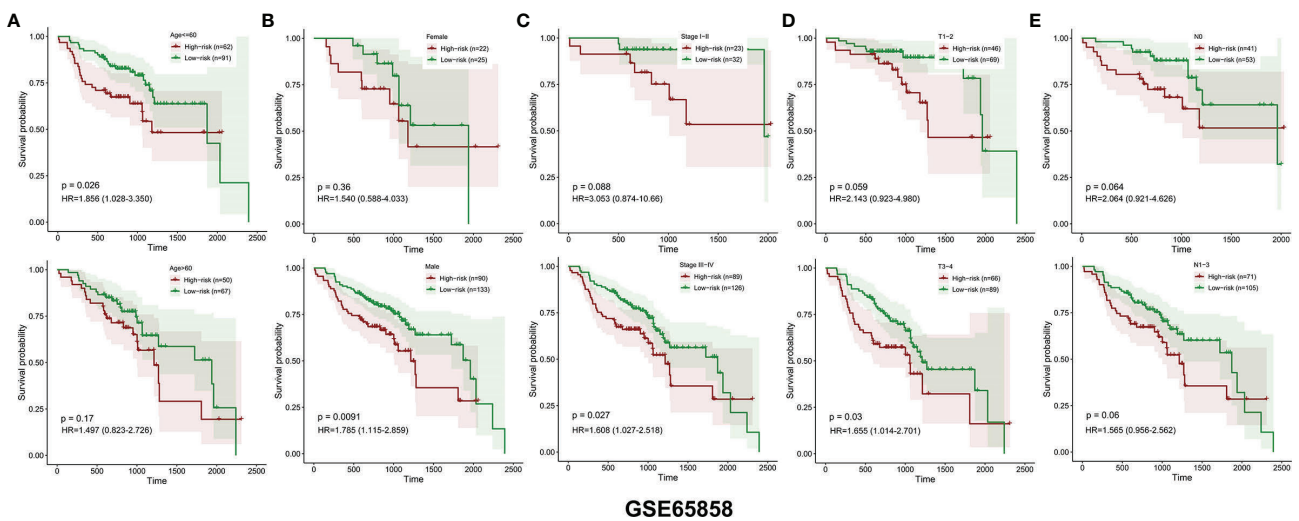

FIGURE 6 | The OS distinction between the low- and high-risk groups was classified by age, gender, clinical stage, T stage, and N stage in the GSE65858 validation cohort **(A–E)**.

consumption of neoplastic cells is increased to maintain their continuous growth and rapid proliferation (15). Nonetheless, the underlying molecular mechanisms for metabolic reprogramming in HNSCC are still unclear. Therefore, it's urgently needed to figure out the potential metabolic enzymes that are correlative with the carcinogenesis of HNSCC. In this study, the common DEMEs between the TCGA HNSCC cohort and GSE37991 were identified. GO analyses of the common DEMEs revealed that the small molecule catabolic process, alpha-amino acid metabolic process, glycosyl compound metabolic process, etc., were

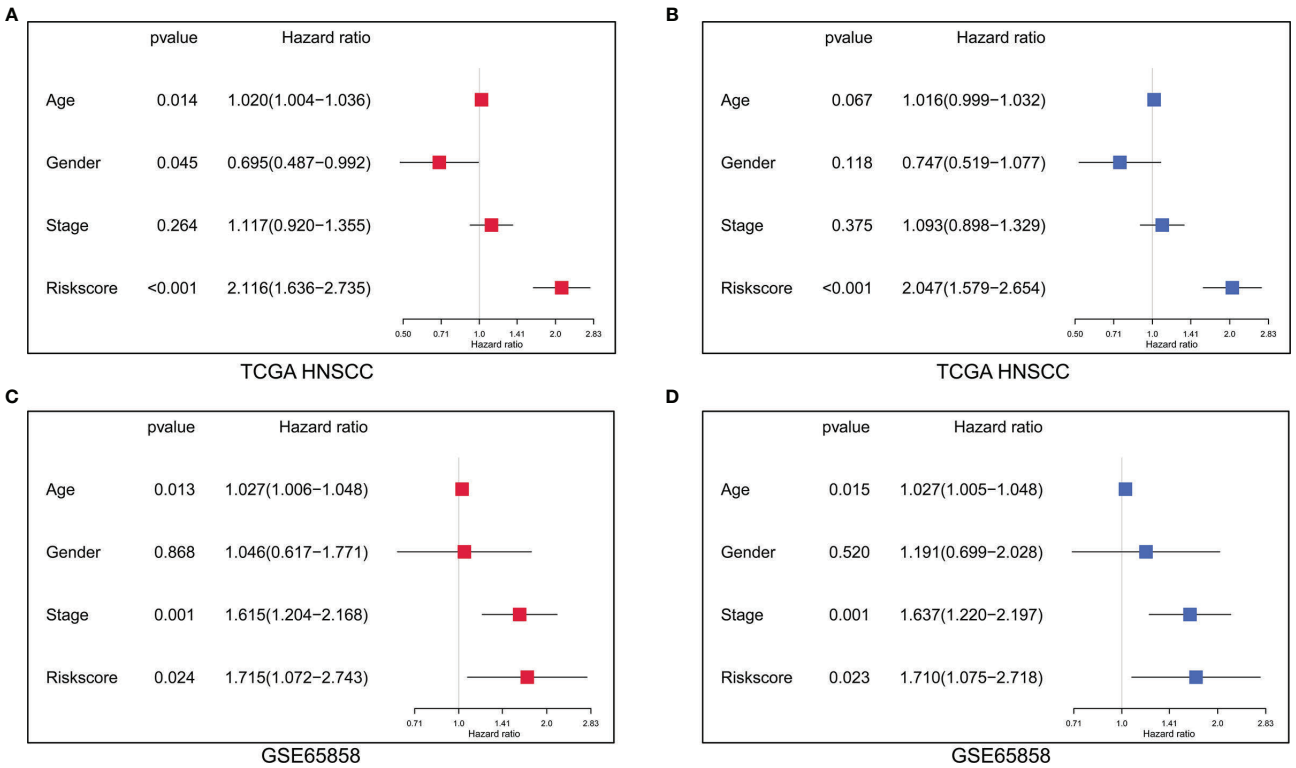

FIGURE 7 | The independent prognostic factors were revealed by univariate and multivariate Cox regression analysis. **(A)** Age, gender and risk score were significantly correlated with survival in the TCGA HNSCC cohort by univariate Cox regression analysis. **(B)** The risk score was the independent prognostic indicator in the TCGA HNSCC cohort by multivariate Cox regression analysis. **(C)** Age, clinical stage and risk score were significantly associated with survival in the GSE65858 cohort by univariate Cox regression analysis. **(D)** Age, clinical stage and risk score were the independent prognostic indices in the GSE65858 cohort by multivariate Cox regression analysis.

enriched. In addition, a robust DEME-based prognostic signature including *HPRT1, PLOD2, ASNS, TXNRD1, CYP27B1*, and *FUT6* was constructed based on the TCGA HNSCC cohort. More importantly, this six-gene prognosis signature was successfully validated in another independent cohort GSE65858. Moreover, we have built up a robust risk score-based nomogram model which might provide personalized therapeutic guidance for treating HNSCC. *In vitro* experiment revealed that the knockdown of TXNRD1 suppressed malignant activities of HNSCC cells.

Based on our study, *ASNS*, *CYP27B1*, *TXNRD1*, *PLOD2*, *HPRT1* are identified as risky genes, and *FUT6* is deemed as the protective gene. ASNS catalyzed the ATP-dependent conversion of aspartate to asparagine, which promoted the proliferation of tumor cells through acting as an amino acid exchange factor (16). Downregulation of ASNS led to the suppression of asparagine synthesis by p53 and the unbalance between asparagine and aspartate, which subsequently inhibited the proliferation of neoplasm cells (17). Overexpression of ASNS facilitated the growth, metastasis, and chemoresistance of neoplasm cells, and a metabolic vulnerability was shown in specified cancer models with low-ASNS expression (18). CYP27B1, the vitamin D metabolizing enzyme, was upregulated at the beginning of the cancer carcinogenesis process with an increased expression of the vitamin D receptor (19). Besides, CYP27B1 may weaken the anticancer functions by locally altering the catabolic and anabolic progress of active vitamin D in cancer (20). On the contrary, CYP27B1 inhibited the proliferation, invasion, and migration of ovarian cancer cells *in vitro* (21). TXNRD1 is increased in head and neck cancer, breast cancer, and lung cancer, and its overexpression is correlative with poor prognosis (22, 23). Suppression of TXNRD1 inhibited the proliferation and induced apoptosis of hepatocellular carcinoma cells by modulating redox balance *in vitro* (24). In addition, TXNRD1 may promote DNA replication, tumorigenicity, and drug resistance by inducing the generation of reactive oxygen species (25). Increased expression of PLOD2 has been found in many types of cancer including breast cancer, colorectal cancer, hepatocellular carcinoma, esophageal squamous cell carcinoma, etc. (26) In HNSCC, PLOD2 is essential for the invasion and metastasis by activating the function of integrin β1 (27). In terms of mechanism, PLOD2 induced collagen cross-linking and maturation, and thus affected the biogenesis of the extracellular matrix of cancer-associated fibroblasts and stellate cells in the tumor microenvironment (26, 28). HPRT1 is located on

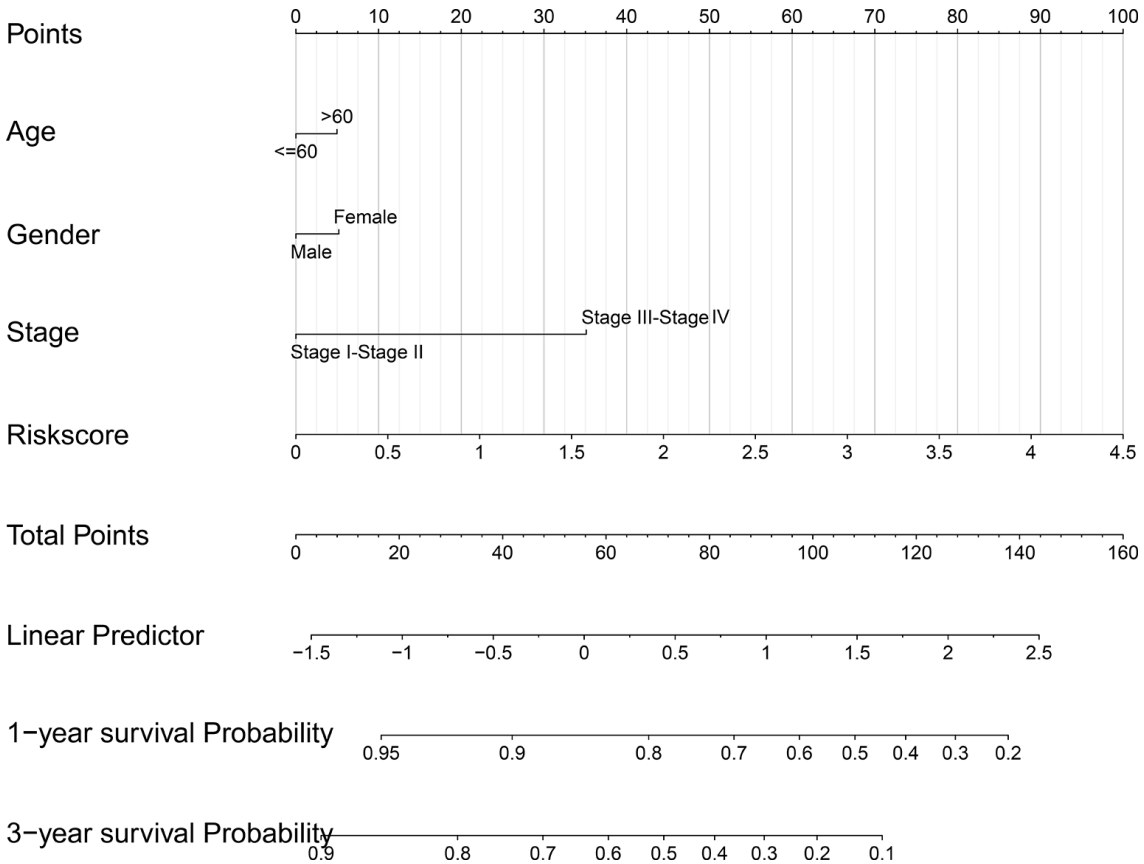

FIGURE 8 | The nomogram prediction model was constructed with the risk score and other clinicopathological indices.

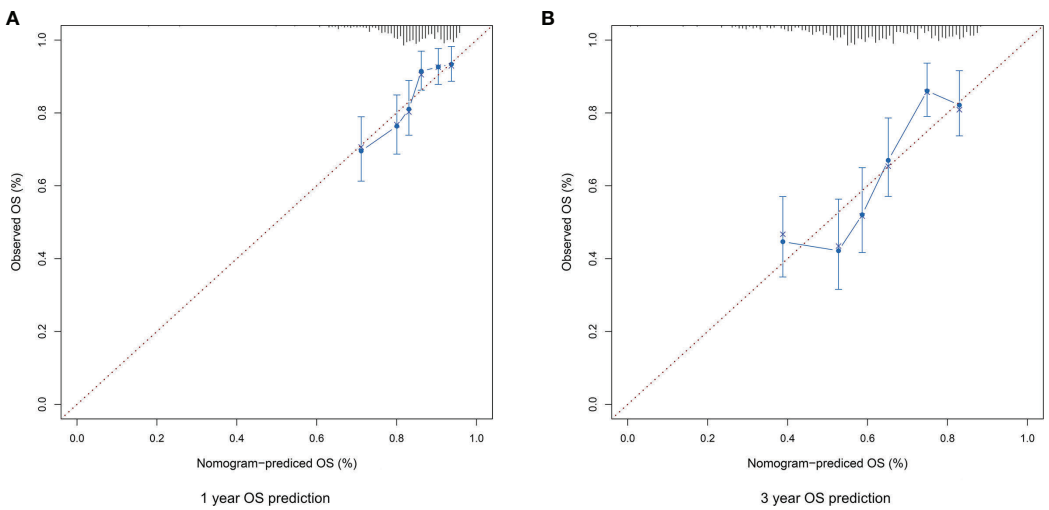

FIGURE 9 | **(A)** The calibration plot for internal validation of the nomogram for 1-year OS prediction. **(B)** The calibration plot for internal validation of the nomogram for 3-year OS prediction.

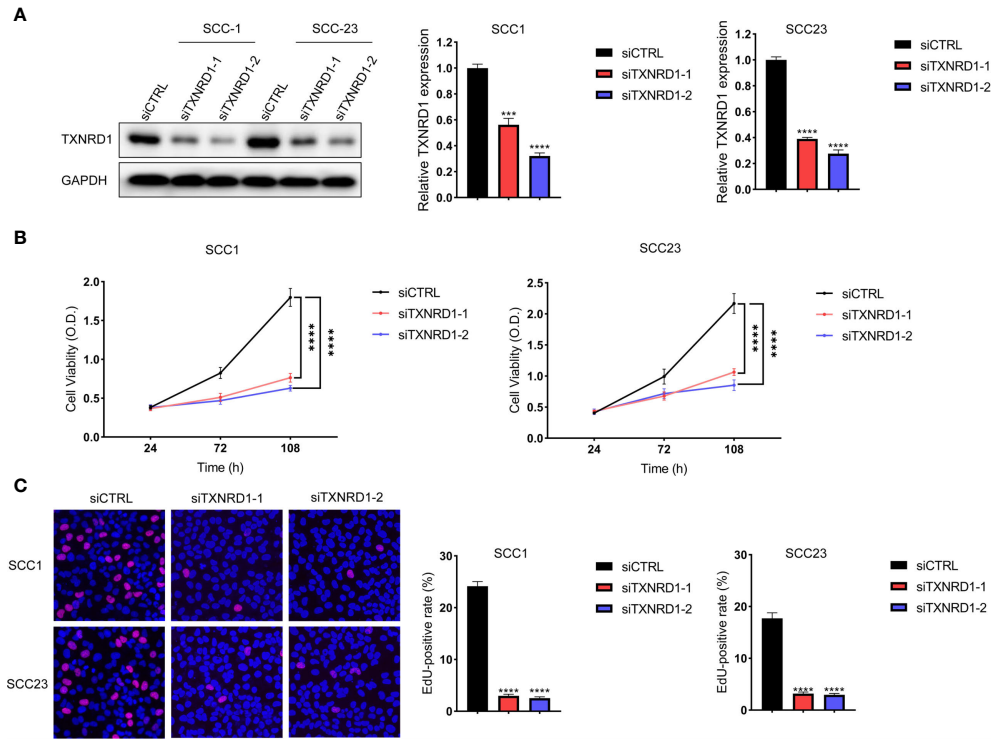

FIGURE 10 | Knockdown of TXNRD1 suppressed malignant activities of HNSCC cells in vitro. **(A)** The expression level of TXNRD1 was significantly reduced in HNSCC cells following siTXNRD1 treatment. **(B)** Compared to the siCTRL treated cells, the OD values were markedly lower in TXNRD1-knockdown cells at indicated time points. **(C)** The EdU assay showed the percentage of EdU-positive cells was dramatically lower in HNSCC cells treated with siTXNRD1. ***P < 0.001. ****P < 0.0001.

chromosome X and supplies recycled nucleotides to the cell cycle for DNA and RNA synthesis (29). Increased expression of HPRT1 was observed in many cancer types, indicating that HPRT1 may be a potential diagnostic and prognostic marker (30). FUT6 produced glycans for tumor cells *via* the PI3K/Akt signaling pathway, which was regulated by miR-125a-3p in colorectal cancer (31). Overexpression of FUT6 inhibited the malignant activities of neoplasm cells by suppressing the dimerization and phosphorylation of epidermal growth factor receptors (32).

Our robust metabolic enzyme-based risk signature has several advantages compared to the gene model with existing signatures. Firstly, to the best of our knowledge, currently few metabolic enzyme-based prognostic signatures are available for predicting the prognosis of HNSCC. Secondly, most prognostic signatures included up to 10 genes, which might be not facilitated for clinical application. Our model has simplified the number of genes in the risk signature to six. Thirdly, compared to many existing prognostic signatures, we have successfully constructed a metabolic enzyme-based nomogram model which showed great promise for therapeutic guidance for HNSCC. Fourthly, the multivariate analysis showed that metabolic enzyme-based prognostic signature was more robust for predicting the prognosis of HNSCC compared to the TNM stage.

Although our study might provide clinical guidance for treating HNSCC, several limitations are needed to be considered. Firstly, the detailed clinicopathological information such as M stage and HPV infection status is missing in most HNSCC patients. Therefore, the importance of these clinicopathological parameters couldn't be included in the nomogram model. Secondly, most patients in the TCGA HNSCC cohort are whites. The effectiveness of the prognostic signature in other races is warranted for further validation. Thirdly, the AUC value of our metabolic-enzyme based risk signature was not high (data not shown), and needs further improvement. However, it is very difficult to use a risk model or a panel of biomarkers to accurately predict the prognosis of HNSCC. In the clinical setting, many clinicopathological parameters such as clinical symptoms, psychological condition and systemic diseases should be combined to comprehensively evaluate the clinical outcome of HNSCC. Finally, large-scale cohorts are needed to verify our DEME-based prognostic signature.

CONCLUSIONS

In summary, our study has identified the common DEMEs between HNSCC and normal controls, which may be correlative with the initiation and development of HNSCC. In addition, we have successfully built up and validated a robust DEME-based

prognostic signature. Moreover, the nomogram model might provide useful guidance for the precision treatment of HNSCC.

DATA AVAILABILITY STATEMENT

The datasets presented in this study can be found in online repositories. The names of the repository/repositories and accession number(s) can be found in the article/**Supplementary Material**.

AUTHOR CONTRIBUTIONS

Conceptualization and funding acquisition, XZ and LC. ZM, XZ, and LC designed and coordinated the study. ZM and HC performed the statistical analysis. HC and MH participated in the collection of database and analysis tools. ZM, XZ, and LC drafted the paper. All authors have read and agreed to the submitted version of the manuscript.

FUNDING

This work was supported by the National Natural Science Foundation of China (81901006). Guangdong Basic and Applied Basic Research Foundation (2020A1515110051).

SUPPLEMENTARY MATERIAL

The Supplementary Material for this article can be found online at: https://www.frontiersin.org/articles/10.3389/fonc.2021.770241/full#supplementary-material

REFERENCES

1. Economopoulou P, de Bree R, Kotsantis I, Psyrri A. Diagnostic Tumor Markers in Head and Neck Squamous Cell Carcinoma (HNSCC) in the Clinical Setting. *Front Oncol* (2019) 9:827. doi: 10.3389/fonc.2019.00827
2. Vigneswaran N, Williams MD. Epidemiologic Trends in Head and Neck Cancer and Aids in Diagnosis. *Oral Maxillofac Surg Clin North Am* (2014) 26 (2):123–41. doi: 10.1016/j.coms.2014.01.001
3. Hashibe M, Brennan P, Chuang SC, Boccia S, Castellsague X, Chen C, et al. Interaction Between Tobacco and Alcohol Use and the Risk of Head and Neck Cancer: Pooled Analysis in the International Head and Neck Cancer Epidemiology Consortium. *Cancer Epidemiol Biomarkers Prev* (2009) 18 (2):541–50. doi: 10.1158/1055-9965.EPI-08-0347
4. Johnson DE, Burtness B, Leemans CR, Lui VWY, Bauman JE, Grandis JR. Head and Neck Squamous Cell Carcinoma. *Nat Rev Dis Primers* (2020) 6 (1):92. doi: 10.1038/s41572-020-00224-3
5. Sanderson RJ, Ironside JA. Squamous Cell Carcinomas of the Head and Neck. *BMJ* (2002) 325(7368):822–7. doi: 10.1136/bmj.325.7368.822
6. Shin YY, Seo Y, Oh SJ, Ahn JS, Song MH, Kang MJ, et al. Melatonin and Verteporfin Synergistically Suppress the Growth and Stemness of Head and Neck Squamous Cell Carcinoma Through the Regulation of Mitochondrial Dynamics. *J Pineal Res* (2021) 72(1):e12779. doi: 10.1111/jpi.12779
7. Su SC, Yeh CM, Lin CW, Hsieh YH, Chuang CY, Tang CH, et al. A Novel Melatonin-Regulated lncRNA Suppresses TPA-Induced Oral Cancer Cell Motility Through Replenishing PRUNE2 Expression. *J Pineal Res* (2021) 71 (3):e12760. doi: 10.1111/jpi.12760
8. Weyandt JD, Thompson CB, Giaccia AJ, Rathmell WK. Metabolic Alterations in Cancer and Their Potential as Therapeutic Targets. *Am Soc Clin Oncol Educ Book* (2017) 37:825–32. doi: 10.14694/EDBK_175561. 10.1200/EDBK_175561.
9. Cui L, Zhao X, Jin Z, Wang H, Yang SF, Hu S. Melatonin Modulates Metabolic Remodeling in HNSCC by Suppressing MTHFD1L-Formate Axis. *J Pineal Res* (2021) 71(4):e12767. doi: 10.1111/jpi.12767
10. Faubert B, Solmonson A, DeBerardinis RJ. Metabolic Reprogramming and Cancer Progression. *Science* (2020) 368(6487):eaaw5473. doi: 10.1126/science.aaw5473
11. Pavlova NN, Thompson CB. The Emerging Hallmarks of Cancer Metabolism. *Cell Metab* (2016) 23(1):27–47. doi: 10.1016/j.cmet.2015.12.006
12. Barrett T, Edgar R. Mining Microarray Data at NCBI's Gene Expression Omnibus (GEO)*. *Methods Mol Biol* (2006) 338:175–90. doi: 10.1385/1-59745-097-9:175
13. Clough E, Barrett T. The Gene Expression Omnibus Database. *Methods Mol Biol* (2016) 1418:93–110. doi: 10.1007/978-1-4939-3578-9_5
14. Cao M, Cai J, Yuan Y, Shi Y, Wu H, Liu Q, et al. A Four-Gene Signature-Derived Risk Score for Glioblastoma: Prospects for Prognostic and Response Predictive Analyses. *Cancer Biol Med* (2019) 16(3):595–605. doi: 10.20892/j.issn.2095-3941.2018.0277
15. Cazzaniga M, Bonanni B. Relationship Between Metabolic Reprogramming and Mitochondrial Activity in Cancer Cells. Understanding The Anticancer Effect of Metformin and Its Clinical Implications. *Anticancer Res* (2015) 35 (11):5789–96.
16. Krall AS, Xu S, Graeber TG, Braas D, Christofk HR. Asparagine Promotes Cancer Cell Proliferation Through Use as an Amino Acid Exchange Factor. *Nat Commun* (2016) 7:11457. doi: 10.1038/ncomms11457
17. Deng L, Yao P, Li L, Ji F, Zhao S, Xu C, et al. P53-Mediated Control of Aspartate-Asparagine Homeostasis Dictates LKB1 Activity and Modulates Cell Survival. *Nat Commun* (2020) 11(1):1755. doi: 10.1038/s41467-020-15573-6
18. Chiu M, Taurino G, Bianchi MG, Kilberg MS, Bussolati O. Asparagine Synthetase in Cancer: Beyond Acute Lymphoblastic Leukemia. *Front Oncol* (2019) 9:1480. doi: 10.3389/fonc.2019.01480
19. Bises G, Kallay E, Weiland T, Wrba F, Wenzl E, Bonner E, et al. 25-Hydroxyvitamin D3-1alpha-Hydroxylase Expression in Normal and Malignant Human Colon. *J Histochem Cytochem* (2004) 52(7):985–9. doi: 10.1369/jhc.4B6271.2004
20. Zhalehjoo N, Shakiba Y, Panjehpour M. Gene Expression Profiles of CYP24A1 and CYP27B1 in Malignant and Normal Breast Tissues. *Mol Med Rep* (2017) 15(1):467–73. doi: 10.3892/mmr.2016.5992
21. Huo X, Sun H, Qian Q, Ma X, Peng P, Yu M, et al. CYP27B1 Downregulation: A New Molecular Mechanism Regulating EZH2 in Ovarian Cancer Tumorigenicity. *Front Cell Dev Biol* (2020) 8:561804. doi: 10.3389/fcell.2020.561804
22. Bhatia M, McGrath KL, Di Trapani G, Charoentong P, Shah F, King MM, et al. The Thioredoxin System in Breast Cancer Cell Invasion and Migration. *Redox Biol* (2016) 8:68–78. doi: 10.1016/j.redox.2015.12.004
23. Leone A, Roca MS, Ciardiello C, Costantini S, Budillon A. Oxidative Stress Gene Expression Profile Correlates With Cancer Patient Poor Prognosis: Identification of Crucial Pathways Might Select Novel Therapeutic Approaches. *Oxid Med Cell Longev* (2017) 2017:2597581. doi: 10.1155/2017/2597581
24. Lee D, Xu IM, Chiu DK, Leibold J, Tse AP, Bao MH, et al. Induction of Oxidative Stress Through Inhibition of Thioredoxin Reductase 1 Is an Effective Therapeutic Approach for Hepatocellular Carcinoma. *Hepatology* (2019) 69(4):1768–86. doi: 10.1002/hep.30467
25. Fu B, Meng W, Zeng X, Zhao H, Liu W, Zhang T. TXNRD1 Is an Unfavorable Prognostic Factor for Patients With Hepatocellular Carcinoma. *BioMed Res Int* (2017) 2017:4698167. doi: 10.1155/2017/4698167
26. Du H, Pang M, Hou X, Yuan S, Sun L. PLOD2 in Cancer Research. *BioMed Pharmacother* (2017) 90:670–6. doi: 10.1016/j.biopha.2017.04.023

27. Ueki Y, Saito K, Iioka H, Sakamoto I, Kanda Y, Sakaguchi M, et al. PLOD2 Is Essential to Functional Activation of Integrin Beta1 for Invasion/Metastasis in Head and Neck Squamous Cell Carcinomas. *iScience* (2020) 23(2):100850. doi: 10.1016/j.isci.2020.100850
28. Qi Y, Xu R. Roles of PLODs in Collagen Synthesis and Cancer Progression. *Front Cell Dev Biol* (2018) 6:66. doi: 10.3389/fcell.2018.00066
29. Stout JT, Caskey CT. HPRT: Gene Structure, Expression, and Mutation. *Annu Rev Genet* (1985) 19:127–48. doi: 10.1146/annurev.ge.19.120185.001015
30. Sedano M,J, Ramos I, Choudhari E,R, Harrison L, Subramani A,R, Lakshmanaswamy R, et al. Hypoxanthine Phosphoribosyl Transferase 1 Is Upregulated, Predicts Clinical Outcome and Controls Gene Expression in Breast Cancer. *Cancers (Basel)* (2020) 12(6):1522. doi: 10.3390/cancers12061522
31. Liang L, Gao C, Li Y, Sun M, Xu J, Li H, et al. miR-125a-3p/FUT5-FUT6 Axis Mediates Colorectal Cancer Cell Proliferation, Migration, Invasion and Pathological Angiogenesis via PI3K-Akt Pathway. *Cell Death Dis* (2017) 8 (8):e2968. doi: 10.1038/cddis.2017.352
32. Liu YC, Yen HY, Chen CY, Chen CH, Cheng PF, Juan YH, et al. Sialylation and Fucosylation of Epidermal Growth Factor Receptor Suppress Its Dimerization and Activation in Lung Cancer Cells. *Proc Natl Acad Sci USA* (2011) 108(28):11332–7. doi: 10.1073/pnas.1107385108

Conflict of Interest: The authors declare that the research was conducted in the absence of any commercial or financial relationships that could be construed as a potential conflict of interest.

Publisher's Note: All claims expressed in this article are solely those of the authors and do not necessarily represent those of their affiliated organizations, or those of the publisher, the editors and the reviewers. Any product that may be evaluated in this article, or claim that may be made by its manufacturer, is not guaranteed or endorsed by the publisher.

frontiers in Oncology

ORIGINAL RESEARCH
published: 27 January 2022
doi: 10.3389/fonc.2022.730785

Treatment Stratification in First-Line Recurrent or Metastatic Head and Neck Cancer, on Behalf of the EORTC Young Investigator Head and Neck Cancer Group

Konrad Klinghammer[1,2*†], *Luigi Lorini*[3], *Daan Nevens*[4], *Christian Simon*[5], *Jean-Pascal Machiels*[6] *and Paolo Bossi*[3]

[1] Department of Hematology, Oncology and Cancer Immunology, Charité—Universitätsmedizin, Berlin, Germany, [2] Charité Comprehensive Cancer Center, Berlin, Germany, [3] Medical Oncology Unit, Department of Medical and Surgical Specialties, Radiological Sciences and Public Health, ASST Spedali Civili of Brescia, University of Brescia, Brescia, Italy, [4] Iridium Netwerk, Radiation Oncology Department, University of Antwerp, Antwerp, Belgium, [5] Department of Otolaryngology, Head and Neck Surgery, University of Lausanne, CHUV, Lausanne, Switzerland, [6] Institut Roi Albert II, Department of Medical Oncology, Cliniques Universitaires Saint-Luc and Institut de Recherche Clinique et Expérimentale (Pole MIRO), UC Louvain, Brussels, Belgium

OPEN ACCESS

Edited by:
Shiyu Song,
Virginia Commonwealth University Health System, United States

Reviewed by:
Jason Fleming,
Aintree University Hospital, United Kingdom
Stefan Kasper-Virchow,
Essen University Hospital, Germany

***Correspondence:**
Konrad Klinghammer
konrad.klinghammer@charite.de

†Corporate member of Freie Universität Berlin and Humboldt-Universität zu Berlin

Specialty section:
This article was submitted to Head and Neck Cancer, a section of the journal Frontiers in Oncology

Received: *25 June 2021*
Accepted: *05 January 2022*
Published: *27 January 2022*

Citation:
Klinghammer K, Lorini L, Nevens D, Simon C, Machiels J-P and Bossi P (2022) Treatment Stratification in First-Line Recurrent or Metastatic Head and Neck Cancer, on Behalf of the EORTC Young Investigator Head and Neck Cancer Group. Front. Oncol. 12:730785. doi: 10.3389/fonc.2022.730785

Multiple factors differentially influence treatment decisions in the first line treatment of recurrent/metastatic HNSCC. The EORTC Young investigator group launched a survey among treating physicians to explore the main influencing factors for treatment stratification. The questionnaire was posted as a web-survey link from May to August 2020. Next to defining the factors that mostly influence therapeutic decision the survey was complemented by a clinical case discussion of five patient cases. A total of 118 responses from 19 countries were collected. The key factors identified to guide treatment decision were performance status, PD-L1 Expression, time from last systemic treatment above or below 6 months, and disease burden.

Prospective evaluation of patient characteristics and additional potential predictive biomarkers for novel treatment options remains an important question to stratify personalized treatment for RM HNSCC.

Keywords: head and neck squamous cell carcinoma, PD-L1 CPS, treatment stratification, survey, HNSCC

INTRODUCTION

Head and neck squamous cell carcinoma (HNSCC) represents the sixth most common type of cancer with 0.65 million new cases and 0.33 million deaths annually worldwide (1). Despite recent advances in the diagnosis and treatment of HNSCC, the median survival for patients with incurable, recurrent, or metastatic disease remains poor at around 10–15 months (2). Treatment intensification failed to improve outcome (3). To date, the epidermal growth factor receptor (EGFR)-targeted antibody cetuximab and programmed death receptor-1 (PD-1) antibodies nivolumab and pembrolizumab are approved as targeted agents for the treatment of HNSCC. With the introduction of immunotherapies both in first and second line treatments of HNSCC, the

therapeutic options for patients have increased (4). Toxicities and QoL were favorable with immunotherapeutic treatment in comparison to chemotherapy (5). However, not all patients respond to PD-1 inhibition and for some patients with autoimmune diseases the risk of deterioration with such treatment modalities is essential. Multiple factors have been discussed, which differentially influence treatment decisions in the first line treatment of recurrent/metastatic HNSCC. However there is a lack of scientific evidence to provide adequate patient selection for tailored treatment (6, 7).

The EORTC young investigator group launched a survey among physicians treating head and neck cancer patients, to ask what are the main influencing factors used to stratify treatment for chemotherapy and cetuximab versus immunotherapy alone versus immunotherapy in combination with chemotherapy. Furthermore, we asked the participants to make treatment decisions for particular case presentation taking PD-L1 expression into consideration.

METHODS

The questionnaire was posted as a web-survey link in the EORTC (European Organization for Research and Treatment of Cancer) head and neck cancer (HNC) mailing list reaching 419 EORTC members from May to August 2020. The questionnaire can be found in the **Appendix**. Data were collected *via* Survey Monkey (www.surveymonkey.com) and descriptive analyses were performed.

The survey consisted of 17 items divided in two parts: 12 items in part one and five clinical cases in part two. The participants were medical oncologists, radiation oncologists, and surgeons (otolaryngologist and maxillofacial).

In the first part of the survey we evaluated the experience in treating HNSCC and the environment where each respondent worked (presence or not of a multidisciplinary team). This was followed by the key questions regarding the factors that mostly influence therapeutic decision in the recurrent/metastatic (R/M) setting to choose chemotherapy plus anti-EGFR agent or chemotherapy in combination with immunotherapy (IO) or IO alone. Items to choose were burden of disease, time from last systemic treatment, presence of locoregional or metastatic disease, performance status (PS), tumor pain, hypercalcemia, treatment schedule, risk of bleeding, patient age, PD-L1 combined positivity score (CPS), and the presence of caregiver.

In the second part we proposed five clinical cases with different characteristics and asked the preferred treatment based on three different PD-L1 CPS value (PD-L1 CPS <1; PD-L1 CPS 1–19; PD-L1 CPS ≥20).

RESULTS

Collection of Questionnaires

There were 118 responses to the questionnaire. The participants were predominantly male (61%), 53.9% of responders had an age between 40 and 55 years. The majority of participants (43.6%) treated 6–15 HNC patients per month. Countries that mainly contributed to the survey included Italy (40%), Germany (19%), France (6%), Netherlands (6%) Switzerland (6%), and Belgium (6%). Participants were medical oncologists (58.6%), radiation oncologists (20.7%), and head and neck surgeons (20.7%). Of these participants, 43.6% had more than 15 years of experience in head and neck cancer treatment and more than 95% of responders reported to work as part of an HNC multidisciplinary team in their hospital that discusses patients with both curative and palliative intent. Regarding the reimbursement policy for drugs used in R/M HNSCC, in the majority of the countries of the participants, cetuximab in first line only with cisplatin in combination with 5-fluorouracil (67.5%) and nivolumab in platinum resistant patients (92.1%) are reimbursed. Descriptive data of the responders are provided in **Table 1**.

Factors Mostly Influencing Treatment Decisions

Within the questionnaire, physicians were asked to rate 5 factors to stratify the treatment for platinum in combination with cetuximab (e.g., EXTREME or TPEX protocol) in first-line treatment of R/M HNSCC (8, 9). The main factors identified were performance status, time from last systemic treatment >6 months, and a high burden of disease, respectively 82.8, 64.6, and 61.2% of responders. Moreover, we asked the main factors leading to choosing immunotherapy as monotherapy in the same setting, which were performance status (72.2%), PD-L1 CPS ≥20 (72.2%), and time from last systemic treatment <6 months (53.9%).

In the setting of combined treatment with chemotherapy and immunotherapy, physicians guided their decision on performance status and burden of disease (both 69.8%) and PD-L1 CPS 1–19 (62.2%). In **Table 2** factors that mainly influenced treatment decision are summarized.

Clinical Case Discussion

In our survey we proposed 5 different clinical cases in different settings of R/M HNSCC according to pain, extension of disease, comorbidity, presence of caregiver, performance status, and time from last systemic treatment. We asked the participants to choose the preferred therapy (between chemotherapy + cetuximab, IO alone or IO + chemotherapy) regarding three alternative PD-L1 CPS (<1; 1–19; ≥20).

The first clinical case illustrated a male patient of 58 years old with an ECOG of 0 and with history of hypertension and previous hepatitis B (30 years ago). He was a previous smoker (20 packs/years). He consulted an Otorhinolaryngology specialist for having moderate dysphagia. He was diagnosed with an ulcerated lesion at the base of the tongue and right tonsil, and 4–5 cm nodes on the right neck (level IIa). The subsequent magnetic resonance imaging (MRI) and fluorodeoxyglucose–positron emission tomography (FDG-PET) confirmed the presence of an ulcerated right oropharyngeal lesion, pathologic nodes and showed bilateral lung nodules. Final clinical staging was cT4aN2bM1. In **Table 3**, we report the decisions based on different PD-L1 CPS values from the responders.

TABLE 1 | Participants characteristics.

Participants number (118)	Characteristics	Number (%)
Gender	Female	46 (38.9)
	Male	77 (61)
Age (years)	<40	39 (33.3)
	40–55	65 (53.8)
	>55	15 (12.8)
	No response	1
Specialty	Medical Oncology	68 (58.6)
	Radiation Oncology	24 (20.7)
	Otolaryngologist (ENT)/Maxillo Facial Surgeon	24 (20.7)
	No respone	2
Years of experience in treatment of HN Cancer (years)	<5	21 (17.9)
	5–15	45 (38.4)
	>15	51 (43.5)
	No response	2
New RM/HNSCC seen per month in each center	1–5	34 (29.1)
	6-15	51 (43.6)
	>15	32 (27.4)
	No response	1
Presence of HN multidisciplinary team in each center	Yes	114 (97.4)
	No	3 (2.6)
	No response	1
Type of RM/HNSCC cases discussed in HN multidisciplinary team	All cases with curative intent	6 (5.2)
	All cases with curative and palliative intent	103 (88.8)
	Not all cases discussed	7 (6)
	No response	2
Reimbursed policy in each country for specific drug	Cetuximab in first line	
	Yes	82 (75.2)
	No	27 (24.8)
	No response	9
	Cetuximab in second line	
	Yes	60 (57.1)
	No	45 (42.9)
	No response	13
	Cetuximab only with Cisplatin + 5-Fluorouracil chemotherapy	
	Yes	75 (67.6)
	No	36 (32.4)
	No response	7
	Pembrolizumab in first line	
	Yes	52 (47.3)
	No	58 (52.7)
	No response	8

HN, head and neck; RM HNSCC, recurrent metastatic head and neck squamous cell carcinoma.

The second clinical case described a male patient of 62 years old diagnosed with HNSCC. He was a current smoker (120 packs/year) without relevant comorbidities, ECOG 0, who underwent a total laryngectomy + right (IIa–IIb–III,V) and left (II–III–IV) selective neck dissection (SND), right hemithyroidectomy and voice prosthesis placement. Based on TNM VIII edition the tumor was classified as pT3 pN2c cM0, R0, squamous cell carcinoma (SCC) with extracapsular extension (ENE+). The patient received adjuvant radiochemotherapy with cisplatin at a cumulative dose of platinum of 240 mg/m^2. Two years later a computer tomography (CT) scan showed two lung nodules (10 and 8 mm) in the left upper lobe and another peribronchial nodule (8 mm) in the right lower lobe, with unsuccessful biopsy attempt. FDG-PET revealed next to the known lesion a large mass localized to left side of L5-S1 and left hemisacrum with bone erosion. The patient complained of left lower back pain with impaired ambulation, weight loss (5%) due to anorexia and asthenia. PS ECOG 1. Palliative radiotherapy (20 Gy) on L5-S1 was delivered. In **Table 4**, we report the decisions for systemic treatment of the responders regarding this case based on different PD-L1 CPS value.

The third clinical case described a male patient, 71 years old, PS ECOG 0, never smoker. He had a history of ulcerative colitis that was diagnosed at the age of 54 and treated with mesalazine in the clinical phase of remission. He had a left tonsillectomy with partial excision of the base of tongue plus modified left neck dissection (levels I–IV), with final diagnosis of SCC, p16+ and HPV 16 + pT2 pN2b cM0, R0, ENE+, stage III. This treatment was followed by 3 months of adjuvant concomitant chemoradiotherapy on the neck nodes (66/54 Gy) and cisplatin cumulative dose 260 mg/m^2. Three months later FDG-PET showed mediastinal and right hilar nodes (dimension 17 × 7 and 22 × 12 mm) and a small nodule at the right lower lung with maximum diameter of 8 mm. Bronchoscopy and sampling of the node confirmed the diagnosis of SCC, p16 positive. The patient had no signs or symptoms and maintained a social life and working activities. **Table 5** summarizes the answers of the responders of the questionnaire.

The fourth clinical case described a female patient of 47 years old, with a PS ECOG 2 due to comorbidities with mild mental impairment, anxiety and depression. A caregiver was present to help her with her everyday needs. Medical history revealed arterial hypertension and polyarticular juvenile idiopathic arthritis since her childhood in treatment with methylprednisolone 4 mg. She underwent a mandibulectomy + maxillectomy + right selective neck dissection. The pathology report revealed a grade 2 SCC of the oral cavity, pT4b pN2b (2/55 ENE-) cM0. She underwent adjuvant concomitant chemoradiotherapy, with RT up to 60/54 Gy, and with a cumulative cisplatin dose of 200 mg/m^2. After three months, due to the appearance of mild dyspnea, a chest CT scan was performed with evidence of left pleural effusion and progression of disease at the lung and a bone lesion art the sternum. In **Table 6**, we report the treatment decision of our responders, based on different PD-L1 CPS values.

The fifth clinical case was about a male patient, 74 years old, ECOG 1. In October 2014 he underwent concomitant chemoradiotherapy for a supraglottic laryngeal SCC, cT2 cN2 cM0 (up to 70 Gy) with cumulative cisplatin dose of 300 mg/m^2. Eleven months later he underwent neck dissection due to nodal relapse. Furthermore, 3 years after initial diagnosis, level V on the left was re-irradiated due to unresectable relapse. Another 2 years later a CT showed vascularized tissue with irregular margins of 32 × 32 mm at the left laterocervical site adjacent to the surgical clips. The patient complained about pain localized to the tumor recurrence. Here we report decisions based on different PD-L1 CPS values from responders (**Table 7**).

DISCUSSION

Treatment decision in R/M HNSCC remains challenging. No internationally accepted treatment guideline exists to guide the

TABLE 2 | Factors that mostly influence treatment decision.

Immunotherapy alone		Immunotherapy + Chemotherapy		Combination of Platinum + Cetuximab	
Characteristics	**% of participants**	**Characteristics**	**% of participants**	**Characteristics**	**% of participants**
Perfomance status ECOG	72.7%	Perfomance status ECOG	69.8%	Perfomance status ECOG	82.8%
PD-L1 CPS ≥20	72.2%	High burden of disease	69.8%	Time from last systemic treatment > or ≤6 months	64.7%
Time from last systemic treatment <6 months	53.9%	PD-L1 CPS 1-19	62.3%	High burden of disease	61.2%
Low burden of disease	48.7%	Time from last systemic treatment <6 months	44.3%	Age	44%
Presence of metastatic disease	40.9%	Presence of metastatic disease	41.5%	PD-L1 CPS <1	40.5%
Age	33.9%	Presence of locoregional relapse	34%	Presence of metastatic disease	36.2%
PD-L1 CPS 1-19	27.8%	PD-L1 CPS ≥20	33%	Presence of locoregional relapse	33.6%
Patients wish	26.1%	Tumor pain	33%	Tumor pain	32.8%
Presence of locoregional relapse	25.2%	Age	28.3%	Patients wish	22.4%
Treatment schedule	14%	Presence of caregiver	17%	Risk of bleeding	13.8%
Tumor pain	10.4%	Risk of bleeding	15.1%	Presence of caregiver	13.8%
Presence of caregiver	7.8%	Patient's wish	8.5%	Treatment schedule	10.3%
Risk of bleeding	5.2%	Treatment schedule	6.6%	Hypercalcemia	3.5%
Hypercalcemia	0.9%	Hypercalcemia	1.9%		

TABLE 3 | Clinical Case 1—Preferred therapy according to CPS value.

	IO alone (%)	IO+ chemotherapy (%)	Chemotherapy + cetuximab (%)
CPS <1	2 (1.9)	12 (11.9)	**87 (86.1)**
CPS 1–19	7 (7)	**79** (79)	14 (14)
CPS ≥20	**46 (46)**	43 (43)	11 (11)

Most frequent answers in the different PD-L1 CPS groups are depicted in bold.

TABLE 4 | Clinical Case 2—Preferred therapy according to CPS value.

	IO alone (%)	IO+ chemotherapy (%)	Chemotherapy + cetuximab (%)
CPS <1	6 (6.5)	8 (8.7)	**78 (84.8)**
CPS 1–19	25 (26.8)	**52 (55.9)**	16 (17.2)
CPS ≥20	**54 (58.1)**	31 (33.3)	11 (8.6)

Most frequent answers in the different PD-L1 CPS groups are depicted in bold.

TABLE 5 | Clinical Case 3—Preferred therapy according to CPS value.

	IO alone (%)	IO+ chemotherapy (%)	chemotherapy + cetuximab (%)
CPS <1	20 (21.5)	8 (8.6)	**65 (69.9)**
CPS 1–19	**47 (50)**	22 (23.4)	25 (26.6)
CPS ≥20	**70 (74.5)**	9 (9.6)	15 (15.9)

Most frequent answers in the different PD-L1 CPS groups are depicted in bold.

TABLE 6 | Clinical Case 4—Preferred therapy according to CPS value.

	IO alone (%)	IO+ chemotherapy (%)	Chemotherapy + cetuximab (%)
CPS <1	19 (22.6)	7 (8.3)	**58 (69.1)**
CPS 1–19	**39 (43.8)**	20 (22.5)	30 (33.7)
CPS ≥20	**51 (56)**	12 (13.2)	28 (30.7)

Most frequent answers in the different PD-L1 CPS groups are depicted in bold.

TABLE 7 | Clinical Case 5—Preferred therapy according to CPS value.

	IO alone (%)	IO+ chemotherapy (%)	Chemotherapy + cetuximab (%)
CPS <1	14 (16.3)	8 (9.3)	**64 (74.4)**
CPS 1–19	28 (32.2)	**48 (55.2)**	11 (12.6)
CPS ≥20	**49 (55.7)**	32 (36.4)	7 (7.9)

Most frequent answers in the different PD-L1 CPS groups are depicted in bold.

decision-making process. Medical treatment is considered the standard approach in the palliative setting, however for a minority of patients salvage surgery or (re-)irradiation might be an option. The survey was answered by the EORTC members of the Head and Neck cancer group, which represents a community of experts of the field and therefore is not representative for all physicians. CheckMate-141, Keynote-040, and Keynote-48 trials (2, 10, 11) led to the introduction of immune checkpoint inhibitors (ICIs) into the palliative treatment of HNSCC in platinum sensitive or resistant patients, thus providing an alternative to chemotherapy, which is beneficial in regard to tumor control for a subset of patients. However, toxicities which impair quality of life do occur more often with chemotherapy combinations, which has led to the widespread use of immunotherapies. Currently, PD-L1 expression is the only established biomarker to stratify treatment decisions (12). However, a multitude of other factors play a minor or major role in deciding for or against a chemotherapeutic regimen with or without the combination with ICIs. Stzurz and Vermorken in their editorial commentary to Keynote-048 showed the complexity of therapeutic choices in R/M HNSCC, other than PD-L1 CPS values (12). Physicians have to consider multiple variables, namely, biological age (from fitness to frailty), tumor dynamics, and burden of disease. In our survey, the most important decision factor in the palliative setting was the performance status of the patient for the three treatment options given. We interpreted this in the way that good performance status is a fundamental

prerequisite for receiving chemotherapy, otherwise this treatment being detrimental for the patient. On the opposite, immunotherapy could be perceived as a treatment with less toxicity, therefore suitable also for patients with lower PS. However, it should be acknowledged that PS is also the strongest predictor of PFS and OS in patients treated with immunotherapy (13). Next to performance status, treatment decision for immunotherapy alone or in combination with chemotherapy is mainly guided by the time from last platinum-based treatment and PD-L1 expression. This is in line with the published data of platinum refractory disease (10, 14) and the inclusion criteria of the Keynote-48 trial (2). Currently, limited data from prospective clinical trials exist regarding the dynamics of response under checkpoint inhibition. Due to the limited overall response rate achieved with immunotherapy alone (less than 20% in the unselected population) (2, 10), the majority of physicians participating in this survey voted for the combination with chemotherapy when a situation of high tumor burden exists. It should be underlined that obtaining response to treatment is crucial in particular when facing disease with high tumor burden and corresponding symptoms (15). The survey was complemented by a clinical case discussion, which took most factors guiding treatment decisions into account. Responses appeared to be guided by PD-L1 CPS as one of the most important factors; however, also in case of high PD-L1 CPS, there was a relatively high quote of respondents choosing combination of chemotherapy plus IO, mainly in cases where the high tumor burden (case #1) or the symptoms (mainly pain) complained by the patients justified the need to achieve tumor response (case #2 and #5). It is interesting to observe that also in the third case responses were guided by PD-L1 CPS expression, even in presence of an autoimmune comorbidity. The anamnesis of ulcerative colitis did not lead the majority of participants of the survey to avoid IO, possibly due to the fact that the autoimmune disease was reported as being under control and without high steroid use. Until recently, no large cases series of patients with inflammatory bowel disease and immune checkpoint inhibition have been published, and patients with active autoimmune diseases have been excluded from most of clinical trials leading to registration of IO in the different cancer sites. Also, the fourth case presented with the comorbidity of a polyarticular juvenile idiopathic arthritis, in active treatment with low steroid dose; the disease-free interval since last platinum dose was 3 months, therefore prompting many respondents to propose the use of IO alone. About one-third of the physicians would have chosen a combination of chemotherapy and cetuximab, considered to be less at risk of toxicities than IO.

Given the obvious limitations of such a survey in general, the collected responses were in line with current treatment recommendations by the European Society of Medical Oncology (ESMO) (6). There is broad consent of treatment with ICI in platinum refractory or nonsymptomatic PD-L1 positive tumor patients. For patients with low or negative PD-L1 expression the choice of the appropriate chemotherapy combination with or without IO has not been defined and especially elderly and frail patients, who do represent a large proportion of patients, remain not adequately represented in trials. This makes general treatment recommendations impossible. The aim of systemic treatment should always be evaluated, if being primarily directed to achieve treatment response or to prolong overall survival. Discussion with the patient and caregivers should also be a central point in treatment choice, evaluating preferences and expectations of the patient. Geriatric assessments or evaluation of the frailty of the patient should be prospectively evaluated to improve patient outcome in this vulnerable population (16). These points highlight a field of missing data in the decision process for the right treatment. Considering all these factors, we support treatment personalization as being crucial in clinical decision making, in a time where different treatments are available for R/M HNSCC patients.

Conclusion

Immunotherapy has changed the therapeutic landscape in RM HNSCC. Our survey showed how clinical decisions in a real world setting are based mostly on performance status, PD-L1 CPS expression, burden of disease, and time from last systemic treatment. Prospective evaluation of patient characteristics and additional potential predictive biomarkers for novel treatment options remain an important quest to stratify personalized treatment for RM HNSCC.

DATA AVAILABILITY STATEMENT

The original contributions presented in the study are included in the article/**Supplementary Material**. Further inquiries can be directed to the corresponding author.

ETHICS STATEMENT

Ethical review and approval was not required for the study on human participants in accordance with the local legislation and institutional requirements. The patients/participants provided their written informed consent to participate in this study.

AUTHOR CONTRIBUTIONS

KK: Conceptualization, Data curation, Formal analysis, Funding acquisition, Investigation, Methodology, Project administration, Resources, Writing—Original draft, and review & editing. LL: Conceptualization, Data curation, Formal analysis, Investigation, Methodology, Project administration, Resources, Writing—Original draft, and review & editing. DN: Conceptualization, Data curation, Formal analysis, Investigation, Methodology, Project administration, Resources, Writing—Original draft, and review & editing. CS: Supervision, and Writing—Review & editing. J-PM: Supervision, and Writing—Review & editing. PB: Conceptualization, Data curation, Formal analysis, Investigation, Methodology, Project administration, Resources, Writing—Original draft, and review & editing. All authors contributed to the article and approved the submitted version.

ACKNOWLEDGMENTS

We thank Sofia Gomes and Catherine Fortpied at the EORTC Headquarters for their support in distributing the survey and reviewing the manuscript.

SUPPLEMENTARY MATERIAL

The Supplementary Material for this article can be found online at: https://www.frontiersin.org/articles/10.3389/fonc.2022.730785/full#supplementary-material

REFERENCES

1. Cramer JD, Burtness B, Le QT, Ferris RL. The Changing Therapeutic Landscape of Head and Neck Cancer. *Nat Rev Clin Oncol* (2019) 16 (11):669–83. doi: 10.1038/s41571-019-0227-z
2. Burtness B, Harrington KJ, Greil R, Soulieres D, Tahara M, de Castro G Jr, et al. Pembrolizumab Alone or With Chemotherapy Versus Cetuximab With Chemotherapy for Recurrent or Metastatic Squamous Cell Carcinoma of the Head and Neck (KEYNOTE-048): A Randomised, Open-Label, Phase 3 Study. *Lancet* (2019) 394(10212):1915–28. doi: 10.1016/S0140-6736(19) 32591-7
3. Klinghammer K, Gauler T, Dietz A, Grunwald V, Stohlmacher J, Knipping S, et al. Cetuximab, Fluorouracil and Cisplatin With or Without Docetaxel for Patients With Recurrent and/or Metastatic Squamous Cell Carcinoma of the Head and Neck (CeFCiD): An Open-Label Phase II Randomised Trial (AIO/ IAG-KHT Trial 1108). *Eur J Cancer* (2019) 122:53–60. doi: 10.1016/ j.ejca.2019.08.018
4. Borel C, Jung AC, Burgy M. Immunotherapy Breakthroughs in the Treatment of Recurrent or Metastatic Head and Neck Squamous Cell Carcinoma. *Cancers (Basel)* (2020) 12(9):2691. doi: 10.3390/cancers12092691
5. Harrington KJ, Ferris RL, Blumenschein GJr., Colevas AD, Fayette J, Licitra L, et al. Nivolumab Versus Standard, Single-Agent Therapy of Investigator's Choice in Recurrent or Metastatic Squamous Cell Carcinoma of the Head and Neck (CheckMate 141): Health-Related Quality-of-Life Results From a Randomised, Phase 3 Trial. *Lancet Oncol* (2017) 18(8):1104–15. doi: 10.1016/S1470-2045(17)30421-7
6. Machiels JP, Rene Leemans C, Golusinski W, Grau C, Licitra L, Gregoire V, et al. Squamous Cell Carcinoma of the Oral Cavity, Larynx, Oropharynx and Hypopharynx: EHNS-ESMO-ESTRO Clinical Practice Guidelines for Diagnosis, Treatment and Follow-Up. *Ann Oncol* (2020) 31(11):1462–75. doi: 10.1016/j.annonc.2020.07.011
7. Oliveira TB, Mesia R, Falco A, Hsieh JC, Yokota T, Saada-Bouzid E, et al. Defining the Needs of Patients With Recurrent and/or Metastatic Head and Neck Cancer: An Expert Opinion. *Crit Rev Oncol Hematol* (2021) 157:103200. doi: 10.1016/j.critrevonc.2020.103200
8. Vermorken JB, Mesia R, Rivera F, Remenar E, Kawecki A, Rottey S, et al. Platinum-Based Chemotherapy Plus Cetuximab in Head and Neck Cancer. *N Engl J Med* (2008) 359(11):1116–27. doi: 10.1056/NEJMoa0802656
9. Guigay J, Auperin A, Fayette J, Saada-Bouzid E, Lafond C, Taberna M, et al. Cetuximab, Docetaxel, and Cisplatin Versus Platinum, Fluorouracil, and Cetuximab as First-Line Treatment in Patients With Recurrent or Metastatic Head and Neck Squamous-Cell Carcinoma (GORTEC 2014-01 TPExtreme): A Multicentre, Open-Label, Randomised, Phase 2 Trial. *Lancet Oncol* (2021) 22(4):463–75. doi: 10.1016/S1470-2045(20)30755-5
10. Ferris RL, Blumenschein GJr., Fayette J, Guigay J, Colevas AD, Licitra L, et al. Nivolumab for Recurrent Squamous-Cell Carcinoma of the Head and Neck. *N Engl J Med* (2016) 375(19):1856–67. doi: 10.1056/ NEJMoa1602252
11. Cohen EEW, Soulieres D, Le Tourneau C, Dinis J, Licitra L, Ahn MJ, et al. Pembrolizumab Versus Methotrexate, Docetaxel, or Cetuximab for Recurrent or Metastatic Head-and-Neck Squamous Cell Carcinoma (KEYNOTE-040): A Randomised, Open-Label, Phase 3 Study. *Lancet* (2019) 393(10167):156–67. doi: 10.1016/S0140-6736(18)31999-8
12. Szturz P, Vermorken JB. Translating KEYNOTE-048 Into Practice Recommendations for Head and Neck Cancer. *Ann Transl Med* (2020) 8 (15):975. doi: 10.21037/atm.2020.03.164
13. Matsuki T, Okamoto I, Fushimi C, Takahashi H, Okada T, Kondo T, et al. Real-World, Long-Term Outcomes of Nivolumab Therapy for Recurrent or Metastatic Squamous Cell Carcinoma of the Head and Neck and Impact of the Magnitude of Best Overall Response: A Retrospective Multicenter Study of 88 Patients. *Cancers (Basel)* (2020) 12(11):3427. doi: 10.3390/cancers12113427
14. Argiris A, Harrington KJ, Tahara M, Schulten J, Chomette P, Ferreira Castro A, et al. Evidence-Based Treatment Options in Recurrent and/or Metastatic Squamous Cell Carcinoma of the Head and Neck. *Front Oncol* (2017) 7:72. doi: 10.3389/fonc.2017.00072
15. Hecht M, Hahn D, Wolber P, Hautmann MG, Reichert D, Weniger S, et al. Treatment Response Lowers Tumor Symptom Burden in Recurrent and/or Metastatic Head and Neck Cancer. *BMC Cancer* (2020) 20(1):933. doi: 10.1186/s12885-020-07440-w
16. Szturz P, Bossi P, Vermorken JB. Systemic Treatment in Elderly Head and Neck Cancer Patients: Recommendations for Clinical Practice. *Curr Opin Otolaryngol Head Neck Surg* (2019) 27(2):142–50. doi: 10.1097/MOO.0000000000000526

Conflict of Interest: KK: Advisory board participation, invited speaker or conference honoraria from: Merck, Sanofi, Merck Sharp & Dohme, Bristol-Myers Squibb. CS: grants from Roche, grants from Intuitive, personal fees from Pfizer, personal fees from Merck, personal fees from MSD, personal fees from Seattle Genetics, outside the submitted work. J-PM: Advisory board member or speaker with honoraria (managed by my Institution): Pfizer, Roche, Astra/Zeneca, Bayer, Innate, Merck Serono, Boerhinger, BMS, Novartis, Janssen, Incyte, Cue Biopharma, ALX Oncology, iTEOS, eTheRNA. Travel expenses: Amgen, BMS, Pfizer, MSD. Data safety monitoring board with honoraria: Debio, Nanobiotix, Psioxus; Uncompensated advisory role: MSD; EORTC: investigator and study coordinator, H & N group Chair. PB: Advisory board participation or conference honoraria from: Merck, Sanofi, Merck Sharp & Dohme, Sun Pharma, Angelini, Molteni, Bristol-Myers Squibb, GSK. The remaining authors declare that the research was conducted in the absence of any commercial or financial relationships that could be construed as a potential conflict of interest.

Publisher's Note: All claims expressed in this article are solely those of the authors and do not necessarily represent those of their affiliated organizations, or those of the publisher, the editors and the reviewers. Any product that may be evaluated in this article, or claim that may be made by its manufacturer, is not guaranteed or endorsed by the publisher.

frontiers in Oncology

ORIGINAL RESEARCH
published: 31 January 2022
doi: 10.3389/fonc.2021.792024

Multi-Organ Omics-Based Prediction for Adaptive Radiation Therapy Eligibility in Nasopharyngeal Carcinoma Patients Undergoing Concurrent Chemoradiotherapy

*Sai-Kit Lam[1], Yuanpeng Zhang[1], Jiang Zhang[1], Bing Li[1], Jia-Chen Sun[1], Carol Yee-Tung Liu[1], Pak-Hei Chou[1], Xinzhi Teng[1], Zong-Rui Ma[1], Rui-Yan Ni[1], Ta Zhou[1], Tao Peng[1], Hao-Nan Xiao[1], Tian Li[1], Ge Ren[1], Andy Lai-Yin Cheung[1,2], Francis Kar-Ho Lee[3], Celia Wai-Yi Yip[3], Kwok-Hung Au[3], Victor Ho-Fun Lee[4], Amy Tien-Yee Chang[5], Lawrence Wing-Chi Chan[1] and Jing Cai[1]**

[1] Department of Health Technology and Informatics, The Hong Kong Polytechnic University, Hong Kong, Hong Kong SAR, China, [2] Department of Clinical Oncology, Queen Mary Hospital, Hong Kong, Hong Kong SAR, China, [3] Department of Clinical Oncology, Queen Elizabeth Hospital, Hong Kong, Hong Kong SAR, China, [4] Department of Clinical Oncology, The University of Hong Kong5Comprehensive Oncology Centre, Hong Kong Sanatorium & Hospital, Hong Kong, Hong Kong SAR, China, [5] Comprehensive Oncology Centre, Hong Kong Sanatorium & Hospital, Hong Kong, Hong Kong SAR, China*

OPEN ACCESS

Edited by:
Shiyu Song, Virginia Commonwealth University Health System, United States

Reviewed by:
Weiwei Zong, Henry Ford Health System, United States
Chenbin Liu, Peking Union Medical College (CAS), China

***Correspondence:**
Jing Cai
jing.cai@polyu.edu.hk

Specialty section:
This article was submitted to Head and Neck Cancer, a section of the journal Frontiers in Oncology

Received: *09 October 2021*
Accepted: *01 December 2021*
Published: *31 January 2022*

Citation:
Lam S-K, Zhang Y, Zhang J, Li B, Sun J-C, Liu CY-T, Chou P-H, Teng X, Ma Z-R, Ni R-Y, Zhou T, Peng T, Xiao H-N, Li T, Ren G, Cheung AL-Y, Lee FK-H, Yip CW-Y, Au K-H, Lee VH-F, Chang AT-Y, Chan LW-C and Cai J (2022) Multi-Organ Omics-Based Prediction for Adaptive Radiation Therapy Eligibility in Nasopharyngeal Carcinoma Patients Undergoing Concurrent Chemoradiotherapy. Front. Oncol. 11:792024. doi: 10.3389/fonc.2021.792024

Purpose: To investigate the role of different multi-organ omics-based prediction models for pre-treatment prediction of Adaptive Radiotherapy (ART) eligibility in patients with nasopharyngeal carcinoma (NPC).

Methods and Materials: Pre-treatment contrast-enhanced computed tomographic and magnetic resonance images, radiotherapy dose and contour data of 135 NPC patients treated at Hong Kong Queen Elizabeth Hospital were retrospectively analyzed for extraction of multi-omics features, namely Radiomics (R), Morphology (M), Dosiomics (D), and Contouromics (C), from a total of eight organ structures. During model development, patient cohort was divided into a training set and a hold-out test set in a ratio of 7 to 3 *via* 20 iterations. Four single-omics models (R, M, D, C) and four multi-omics models (RD, RC, RM, RMDC) were developed on the training data using Ridge and Multi-Kernel Learning (MKL) algorithm, respectively, under 10-fold cross validation, and evaluated on hold-out test data using average area under the receiver-operator-characteristics curve (AUC). The best-performing single-omics model was first determined by comparing the AUC distribution across the 20 iterations among the four single-omics models using two-sided student *t*-test, which was then retrained using MKL algorithm for a fair comparison with the four multi-omics models.

Results: The R model significantly outperformed all other three single-omics models (all p-value<0.0001), achieving an average AUC of 0.942 (95%CI: 0.938-0.946) and 0.918 (95%CI: 0.903-0.933) in training and hold-out test set, respectively. When trained with MKL, the R model (R_MKL) yielded an increased AUC of 0.984 (95%CI: 0.981-0.988) and 0.927 (95%CI: 0.905-0.948) in training and hold-out test set respectively, while

demonstrating no significant difference as compared to all studied multi-omics models in the hold-out test sets. Intriguingly, Radiomic features accounted for the majority of the final selected features, ranging from 64% to 94%, in all the studied multi-omics models.

Conclusions: Among all the studied models, the Radiomic model was found to play a dominant role for ART eligibility in NPC patients, and Radiomic features accounted for the largest proportion of features in all the multi-omics models.

Keywords: nasopharyngeal carcinoma, adaptive radiotherapy, radiomics, dosiomics, multiomics approach

INTRODUCTION

Nasopharyngeal carcinoma (NPC) presents immediate proximity to a variety of surrounding critical healthy organs such as spinal cord and brainstem within an intricated nose-pharynx ministry, dysfunction of which can incur catastrophic complications. At present, concurrent chemo-radiotherapy (CCRT) is a standard-of-care remedy for advanced NPC patients; adoption of Intensity-modulated Radiotherapy (IMRT) allows for highly conformal and precise dose delivery to the treatment targets, meanwhile protecting the adjacent healthy tissues. Notably, the success of treatment relies on an assumption that the patient anatomy remains throughout the 6-7 weeks of IMRT course. In response to treatment perturbations, however, tumors and surrounding healthy organs may exhibit significant morphometric volume and/or geometric alterations, which may jointly alter patient anatomy and jeopardize the efficacy of the original treatment plan (1–3). The issue of these variabilities can be more detrimental in the IMRT era, where slight anatomic deviations may deleteriously lead to significant dosimetric consequences due to the sharp dose falloff beyond the target lesions. Confronted with this, Adaptive Radiotherapy (ART), a modification of the original treatment plan, has been introduced to compensate for these patient-specific variations. The dosimetric and clinical benefits of ART for NPC patients have been well-documented in the literature (1–7).

Notwithstanding, ART generally involves re-imaging, re-segmentations of tumor and organs-at-risk (OARs), and re-planning, requiring a highly specialized multidisciplinary team. This labor-intensive and time-consuming nature of ART procedures preclude the feasibility of routine ART practice on a patient basis in clinic. In light of this, tremendous effort has been constantly made to evaluate the underlying morphometric and geometric variations of patient anatomy amid the radiotherapy course, in the hope of streamlining clinical implementation of ART (8–20).

Radiation dose has long been regarded as a prime attribute for morphometric volume change of tumors, neck lesions and bilateral parotid glands throughout the treatment course. Bahl et al. (8) prospectively analyzed volumetric alterations in 20 NPC patients between pre-treatment computed tomography (CT) and mid-treatment CT at the 17^{th} fraction. They reported approximately 30% shrinkage of high-risk gross-tumor-volume (GTV), which was accompanied with a significantly increased median dose of 7.2-7.7 Gy to and reduced volume of bilateral parotid glands. Another prospective study by Cheng et al. (9) demonstrated that the anatomic tissue shrinkage was dependent on radiation dose received. They analyzed repeated planning CT and magnetic resonance images (MRI) at 30-Gy and 50-Gy intervals and reported that the shrinkage of both primary NPC tumor and nodal lesions against pre-treatment baselines were higher when 50-Gy was delivered (13% and 29%, respectively) than that when 30-Gy was given (9% and 16%, respectively) and a similar trend was also observed for bilateral parotid glands. Further evidence was also observed by Hu et al. (10) who analyzed 40 re-planned NPC patients and confirmed the significant shrinkage of 35% in clinical-target-volume, and by Murat et al. (11) who reported a median reduction of 27% and 43% in primary and nodal GTV, respectively, in 48 re-planned head-and-neck cancer patients.

Notably, volumetric shrinkages of these organ structures are often accompanied with geometric shifts of internal structures (12, 13) and/or body contour modification (14, 15), which may in concert contribute to an elevated risk of ill-fitted immobilization cast during daily setup (14, 15) and/or detrimental consequences following treatment [e.g., overdosing to OARs (7, 16, 17), underdosing to targets (7, 12)], triggering the demand for ART. In view of this, research community has introduced numerous criteria as ART triggers (11, 12, 18–20), mainly on dosimetric aspects. Nevertheless, most of these factors require close monitoring throughout the radiotherapy course for each patient, pre-treatment prediction of ART eligibility is greatly demanding. Further, these factors are deficient in capturing inter-patient disparity in intrinsic biologic response of tissue upon receiving treatment perturbation.

Until more recently, emerging Radiomics has opened up opportunities for divulging concealed biologic traits and genetic association of tumor and organ structures (21–23). There is mounting evidence in the literature showing the power of Radiomics in predicting treatment response on the ground of volume shrinkage in various cancer diseases (24–29), which has laid great foundation for Radiomics prediction of ART demand in cancer patients. Ramella et al. performed radiomic analysis on pre-treatment CT images of replanned non-small cell lung cancer patients and generated a radiomic signature for prediction of tumor shrinkage during chemo-radiotherapy, yielding an Area Under the Receiver Characteristics Curves (AUC) of 0.82 (27). For the first time, Yu et al. generated several radiomic models for ART eligibility in NPC patients using tumoral radiomic features from multi-parametric pre-

treatment MRI, achieving AUCs ranging from 0.75 to 0.93 (15). It is worth noting that ART eligibility is multifactorial in nature. Joint response of multiple organ structures upon treatment perturbations, treatment aggressiveness, and pre-treatment geometric and morphologic condition of patient anatomy, may all come into play for triggering ART.

Therefore, it is pertinent to investigate the role of these attributes, in the form of -omics features, from multiple relevant organ structures within head-and-neck regions using pre-treatment CT, MRI, contours, and three-dimensional dose map for prediction of ART eligibility in NPC patients, which constituted the main objective of this present study. The success of this study may provide the community with valuable insights into developing ART screening strategies in future, particularly in view of the soaring demand of ART in this vulnerable subgroup of cancer sufferers in the IMRT era.

METHODS AND MATERIALS

Patient Data

This study is a retrospective analysis of 261 NPC patients who received radiotherapy at Hong Kong Queen Elizabeth Hospital between 2012 and 2015. Patient informed consent was waived due to the retrospective nature of this study. Patients were included if they (1) were diagnosed with biopsy-proven primary NPC without presence of distant metastasis and co-existing tumors of other types at presentation (2), underwent curative concurrent chemo-RT (CCRT) or CCRT plus adjuvant chemotherapy (AC), and (3) were treated with Helical Tomotherapy. Patients were excluded if they (1) received induction chemotherapy before CCRT treatment, or (2) received RT-alone without concurrent chemotherapy, or (3) did not receive injection of contrast agent for obtaining planning contrast-enhanced CT (CECT) images or planning contrast-enhanced T1-w (CET1-w) MR images, or (4) did not have complete set of clinical/image data. The binary status of whether or not an individual patient has undergone ART treatment during their main course of RT at the discretion of radiation oncologist was chosen as the clinical endpoint for this study. Patients were labelled as 1 if he/she has received ART treatment, otherwise were labelled as 0.

Image Acquisition

All the enrolled patients underwent pre-treatment planning CECT and MRI scans, which were retrospectively retrieved in Digital Imaging and Communications in Medicine (DICOM) format, archived using Picture Archiving and Communication System (PACs). Details of imaging parameters can be found in **Supplementary A1**.

Volume-of-Interest (VOI) Definition

There were a total of 8 different VOIs of organ structures involved in this study, including gross-tumor-volume of primary NPC tumor (GTVnp) and metastatic lymph nodes (GTVn), ipsi-lateral parotid gland (IpsiPG), contra-lateral parotid gland (ContraPG), brainstem (BS), spinal cord (SC), high-dose and low-dose regions of nodal planning target volume (PTVn_high_dose for the PTVn with the prescribed dose level of 70-Gy, PTVn_low_dose for the PTVn with the prescribed dose level of 60-Gy, respectively). **Figure 1** illustrates location of each VOI involved in this study.

GTVnp was manually delineated on axial CT slices after registration with planning MR images, and GTVn was delineated on CECT images by an experienced radiation oncologist specializing in head-and-neck cancers with accreditations, in accordance with International Consensus Guidelines for the CT-based delineation of neck levels (30). To determine whether each

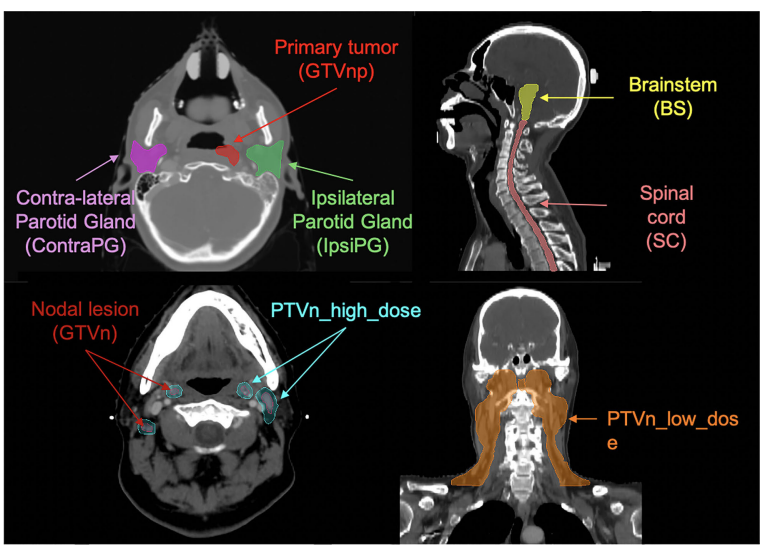

FIGURE 1 | Illustration of the eight VOIs involved in this study.

of the segmented parotid glands (PG) belongs to IpsiPG or ContraPG for each patient, the minimum geometric distance between a particular voxel point on the PG volume and all voxel points on the GTVnp surface was first determined. This procedure was repeated for another voxel point on the PG volume until the minimum distances between each of all the voxel points on the PG volume and the GTVnp surface were determined. Lastly, a median value of these calculated minimum distances was obtained to determine the overall proximity of that PG to the GTVnp for each patient. The PG with smaller median value of the minimum distances was denoted as IpsiPG, otherwise it was denoted as ContraPG. All segmentations were carried out using Varian ARIA and Eclipse treatment planning system v13 (Varian Medical Systems Inc, Palo Alto, CA).

Multi-Omics Feature Extraction

Radiomics (R) and Morphology (M)

Prior to radiomic feature extraction, a series of image preprocessing steps were performed on CECT and MR images according to well-recognized recommendations from the Image Biomarker Standardisation Initiative (IBSI) guidelines (31), using our in-house developed Python-based (v3.7.3) platform. Details of the image preprocessing procedures can be found in **Supplementary A2**.

In this study, 4 different VOIs of organ structures (GTVnp, GTVn, IpsiPG and ContraPG) were involved in radiomic feature calculations. Extraction of radiomic features was performed using the publicly available SimpleITK (v1.2.4) and PyRadiomics (v2.2.0) packages embedded in our platform in accordance with the IBSI guidelines (31). Radiomic features can be generally divided into three major families: morphologic features, first-order statistics, and texture features which can be further categorized into Gray Level Difference Matrix (GLDM), Gray Level Cooccurrence Matrix (GLCM), Gray Level Run Length Matrix (GLRLM), Gray Level Size Zone Matrix (GLSZM), Neighboring Gray Tone Difference Matrix (NGTDM) classes. Radiomic feature calculations were performed on CECT, CET1-w and T2-w MR images, with and without being filtered by Laplacian of Gaussian (LoG) filter (kernel size: 1-mm, 3-mm, 6-mm) and wavelet filters (HHH, HLL, LHL, LLH, LHH, HLH, HHL, LLL). In this study, morphologic features of all the 4 VOIs were separated from the radiomic feature set, resulting in a total of 6,348 radiomic features for each studied VOI. A total of 14 morphologic features, including elongation, flatness, least axis length, major axis length, minor axis length, maximum 2D diameter column, maximum 2D diameter row, maximum 2D diameter slice, maximum 3D diameter, mesh volume, sphericity, surface area, surface volume ratio, voxel volume, for each of the 4 VOIs (i.e., GTVnp, GTVn, IpsiPG, and ContraPG) were combined to form a set of 56 features. Detailed definitions of the radiomic and morphologic features can be found on the Pyradiomics documentation (https://pyradiomics.readthedocs.io/en/latest/features.html).

Dosiomics (D)

All the 8 different VOIs of organ structures were employed for dosiomic feature calculation using RT dose data. Conventional dose-volume histogram (DVH) does not contain information on spatial dose distribution within irradiated organs. By contrast, dosiomics is capable of characterizing spatial pattern of local radiation dose distributions within the 8 studied VOIs. It has been extensively studied in various predictive modelling for cancer prognosis and treatment responses (32, 33). In this study, dosiomic features of DVH curve points for the 8 VOIs were calculated based on the method adopted by Gabryś et al. (34), examples include but not limited to maximum dose, minimum dose, mean dose, volume of the VOI receiving at least certain dose levels, and minimum dose received by certain volume of the VOI. Besides, spatial dose distribution within each studied VOI was extracted to comprehensively depict the heterogeneity of deposited dose, such as dose gradients along the three imaging axes (x-, y- and z-directions). The definitions of these features were described in a previous publication by Buettner et al. (35). Further, the three-dimensional (3D) dose distribution within each studied VOI was transformed into a 3D image, such that radiomics-alike dosiomics features were subsequently calculated using the PyRadiomics package; examples include first-order dose statistics, GLDM, GLCM, GLRLM, GLSZM and NGTDM. A total of 1608 dosiomic features were extracted from the 8 VOIs in this study.

Contouromics (C)

In this work, we extracted features that depict complex geometric relationships between 4 pairs of VOIs of organ structures (GTVnp and IpsiPG, GTVnp and ContraPG, GTVnp and SC, and PTVn_low_dose and SC), on the ground that the implementation of ART is triggered by change of geometric relationship of different internal organs within head and neck regions. These features were extracted from the RT contour data. For the first time, they were termed as "Contouromics" in this study. For each of the VOI pairs, a series of contouromic features were calculated from a distance descriptor overlap-volume histogram (OVH), as adopted in a previous publication (36); for instance, the maximum and minimum distances between SC and PTVn_low_dose during the treatment planning stage were calculated as the distances on the OVH at zero and full volume, respectively. In this study, the calculation of OVH was implemented using the algorithm employed in a previous publication (37). Besides, an angle descriptor projection-overlap-volume (POV), defined as one VOI that overlaps with the parallel projection of another VOI at specific projection angle, was used for further divulging potential contouromic features from the VOI pairs. A total of 132 contouromic features were extracted from the 4 pairs of VOIs in this study. **Table 1** summarizes the sources of VOIs involved in calculation of the four types of -omics features studied.

Determination of Optimal Feature Selection (FS) Algorithms for Each -Omics Dataset

Feature dimensionality reduction is considered essential in machine learning when it comes to minimizing the risk of model overfitting. Although there are a multitude of unsupervised and supervised FS algorithms currently available for assessing redundancy and outcome relevance of the studied features, an optimal combination of both kinds of FS algorithms

TABLE 1 | Summarizes the sources of VOIs involved in calculation of the four types of -omics features studied.

Radiomics (R)	Morphology (M)	Dosiomics (D)	Contouromics (C)
CECT-GTVnp	GTVnp	GTVnp	PTVn_low_dose-SC
CECT-GTVn	GTVn	GTVn	GTVnp-IpsiPG
CECT-IpsiPG	IpsiPG	IpsiPG	GTVnp-ContraPG
CECT-ContraPG	ContraPG	ContraPG	GTVnp-SC
CET1w-GTVnp		BS	
CET1w-IpsiPG		SC	
CET1w-ContraPG		PTVn_high_dose	
T2w-GTVnp		PTVn_low_dose	
T2w-IpsiPG			
T2w-ContraPG			

remains unclear. In this study, a total of 6 unsupervised and 4 supervised FS algorithms that have been commonly adopted in machine learning were studied (38) and are publicly available (https://jundongl.github.io/scikit-feature/algorithms.html), giving rise to a resultant amount of 24 FS combinations **(Supplementary Figure S1).**

A proper selection of FS combination for a particular feature set is crucial to ensure that the final selected features of a prediction model are of high discriminability (i.e., high score of Area Under the Receiver Operating Characteristics Curve, AUC score) and high reproducibility under multiple train/test splits of the dataset (i.e., high feature output stability score). To this end, we adopted a strategic workflow **(Supplementary Figure S2)** to calculate both scores and determined the optimal FS combination using a decision graph **(Supplementary Figure S3)** for a particular -omics dataset. More details can be found in **Supplementary A3**.

Development and Evaluation of ART Prediction Models

In this study, a total of 4 single-omics models (R, M, D, C) and 4 multi-omics models (RM from R+M, RD from R+D, RC from R+C, RMDC from R+M+D+C) were developed using the corresponding -omics features from multiple VOIs of organ structures.

Figure 2 shows a schematic diagram for model development. The patient cohort was divided into a training dataset and a hold-out test dataset in a ratio of 7 to 3 *via* 20 iterations. The optimal supervised FS algorithm was applied only to the training dataset of each iteration to maintain clinical relevance of the remnant features. The optimal unsupervised FS algorithm was subsequently applied to remove highly redundant features, leading to a reduced feature set of K features. Development of prediction models was conducted with the initial K features using the Ridge algorithm (for single-omics model) or Multi-Kernel Learning (MKL) algorithm (for multi-omics model) *via* a 10-fold cross-validation (CV) within the training set to mitigate the risk of model overfitting. Evaluation of model discriminability, in aspects of AUC, was performed on the hold-out test set of each iteration. The model development process was repeated on (K-1) features after removing the feature of the lowest ranking of frequency of occurrence across the 20 iterations until one feature remained in the feature set. An optimal prediction model was finally determined when the average AUC on the hold-out test datasets reached its maximum.

With regard to the model training algorithm, Ridge classifier was adopted for generation of the 4 single-omics models. It is a typical statistical approach for resolving bias-variance trade-off with the use of a linear function; the principles and advantages of Ridge algorithm have been well-documented (39). On the other hand, MKL algorithm was applied for development of multi-omics models in this study. Unlike single-omics features, different types of multi-omics data may contain distinctly different data representations. Ridge algorithm is deficient in capturing the difference in representations of multi-omics data and non-linear relationship between predictors and prediction outcome. Therefore, MKL was adopted in this study with an attempt to divulging complementary (non-linear) relationship between different types of -omics features and prediction outcomes. Specifically, two types of kernels (Gaussian and Polynomial) with a range of kernel parameters were applied. Each kernel was embedded into the feature space of a given multi-omics feature set for subsequent multi-omics fusion. **Supplementary Figure S4** illuminates the multi-omics fusion framework in our study. More details of the MKL algorithms can be found in **Supplementary A4** and a previous publication (40).

Model Comparison and Statistical Analysis

For single-omics models, discriminability of the final radiomic model (R), in terms of distribution of the AUC scores across the 20 iterations, was compared against the other 3 single-omics models (M, D, and C) in both training and hold-out test datasets. For multi-omics models, discriminability of the final RMDC model was compared against the other 3 multi-omics models (RM, RD, and RC) in both training and hold-out test datasets. Further, we also compared the best-performing single-omics model against all the 4 studied multi-omics models (RM, RD, RC, and RMDC). With this regard, the selected single-omics model was firstly re-trained using MKL algorithm for achieving a fair comparison with multi-omics models.

Statistical estimates of model discriminability in terms of average AUC, its standard deviation (STD) and 95% confident interval (95%CI) across the 20 iterations for all the studied prediction models were reported in this study. Two-sided paired student *t*-test was employed for the abovementioned comparisons. On the other hand, Chi-square test was employed to assess statistical difference of categorical patient clinical factors between patients who received ART and those who did not, while two-sided student *t*-test was applied for continuous clinical factors. A p-value of ≤ 0.05 was considered statistically significant.

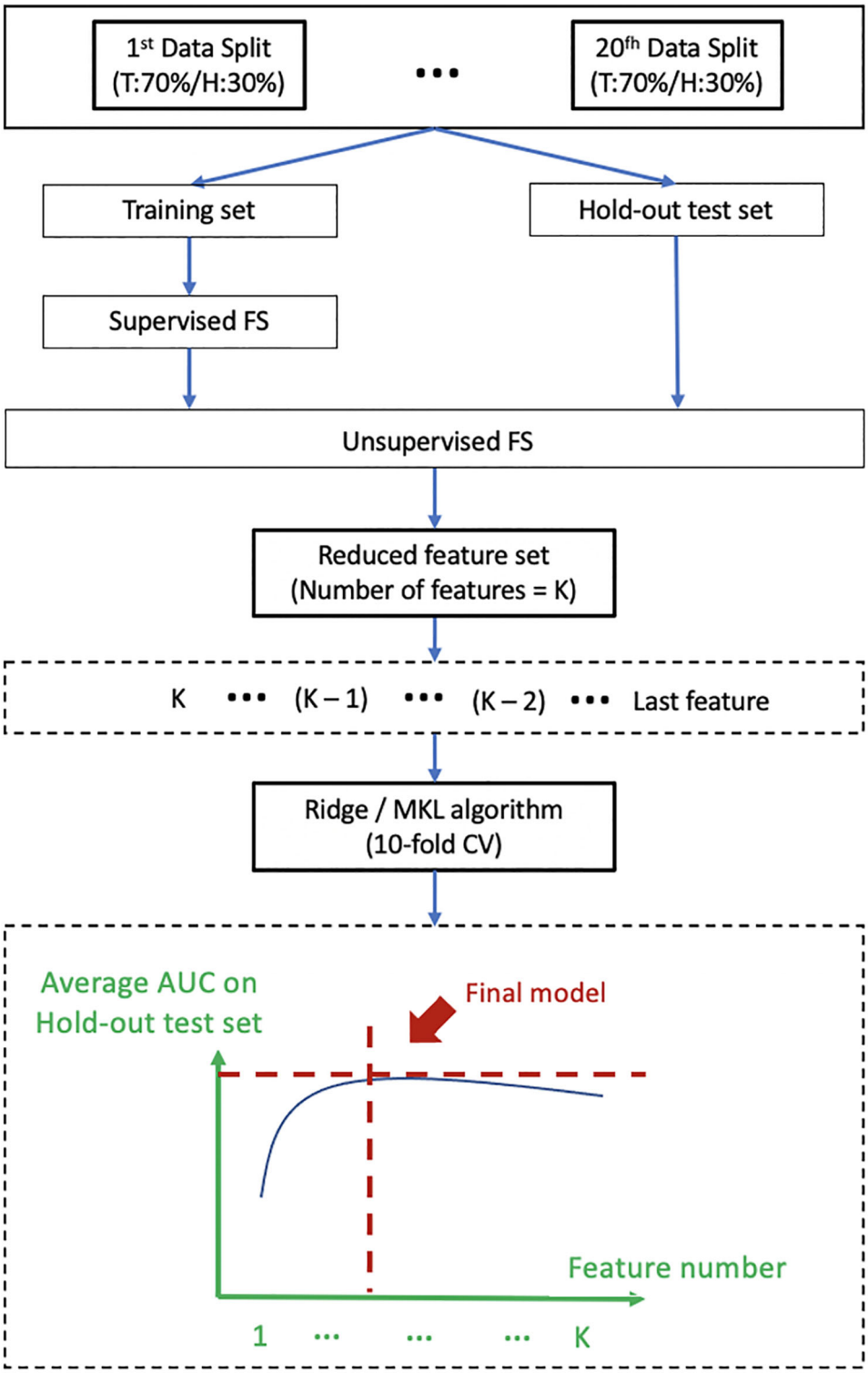

FIGURE 2 | Shows a schematic diagram for model development. T, Training set; H, Hold-out test set; FS, feature selection; MKL, Multi-Kernel Learning; CV, Cross-Validation; AUC, Area Under the Receiver Operating Characteristics Curves.

RESULTS

Patient Characteristics

A total of 135 NPC patients (35 experienced ART, approximately 26%) were finally considered eligible for this study. **Table 2** summarizes major characteristics of the patients. There were no statistically significant differences in the studied clinical factors between patients who experienced ART and those who did not.

Optimal FS Combination Determination and Model Development

Optimal combinations of FS algorithms for the 4 single-omics datasets (R, M, D, C) and the 4 multi-omics datasets (RM, RD, RC, RMDC) were determined using the decision graphs (**Supplementary Figures S5A–H**) and were summarized in **Supplementary Table S1**.

Supplementary Figures S6A–D and **S7A–D** illustrate the change of average AUC scores (and its STD shown in shadow) in both training and hold-out test sets against varying number of features for the 4 single-omics models and the 4 multi-omics models, respectively. Final models were determined when the average AUC scores on the hold-out test sets reached its maximum.

Table 3 summarizes the total number and distribution of the selected features in the final models. Interestingly, it can be observed that radiomic features are dominant in all the four multi-omics models, compared to M, C, and D features.

Model Comparison

Figures 3A, B indicates box-whisker plots of the average AUC distributions for the final single-omics models, and **Figures 3C, D** for the multi-omics models and the Radiomic models trained by using MKL algorithms, in training and hold-out test sets. A summary of the statistical estimates of model performance is provided in **Tables 4A, B**.

From **Figures 3A, B** and **Table 4A**, it can be seen that the Radiomic model (R) significantly outperformed all other studied single-omics models (p-value < 0.0001), achieving an average AUC of 0.942 (STD: 0.009, 95%CI: 0.938-0.946) in the training set and 0.918 (STD: 0.034, 95%CI: 0.903-0.933) in the hold-out set.

The Dosiomic model (D) was the second best single-omics model with an average AUC of 0.895 (STD: 0.018, 95%CI: 0.887-0.903) in the training set and 0.811 (STD: 0.029, 95%CI: 0.798-0.824) in the hold-out set. This was followed by the Morphologic model (M) which yielded an average AUC of 0.740 (STD: 0.032,

TABLE 2 | Patient clinical characteristics.

Clinical factor		Data/p-value	
Age		p-value = 0.142	
Average, Range	54		27 - 81
Gender		p-value = 0.348	
Male (no.,%)	101		75
Female (no.,%)	34		25
WHO Histologic subtype*		p-value = 0.544	
Type-1 (no., %)	4		3
Type-2 (no., %)	3		2
Type-3 (no., %)	128		95
T-Stage		p-value = 0.133	
T1 (no., %)	9		7
T2 (no., %)	9		7
T3 (no., %)	94		70
T4 (no., %)	23		17
N-Stage		p-value = 0.146	
N0 (no., %)	1		1
N1 (no., %)	22		16
N2 (no., %)	98		73
N3 (no., %)	14		10
Overall stage (7^{th} AJCC)		p-value = 0.077	
Stage-I (no., %)	1		1
Stage-II (no., %)	7		5
Stage-III (no., %)	92		68
Stage-IVA (no., %)	23		17
Stage-IVB (no., %)	12		9
Initial size of primary tumor (mm^3)		p-value = 0.341	
Average, range	43,482		4,537 - 184,333
Initial size of nodal lesion (mm^3)		p-value = 0.202	
Average, range	31,078		501 - 330,143
Initial total tumor burden (primary + nodal lesion) (mm^3)		p-value = 0.153	
Average, range	74,560		7,886 - 438,998
Pre-treatment body weight (kg)		p-value = 0.265	
Average, range	63		37-102

**WHO histologic subtype of NPC: Type 1: Keratinizing squamous cell carcinoma; Type 2: Non-keratinizing differentiated carcinoma; Type 3: Non-keratinizing undifferentiated carcinoma. AJCC, American Joint Committee on Cancer.*

TABLE 3 | A summary of total number and distribution of selected features in the final models.

	Number of Final Selected Features				
	Total	**R**	**M**	**C**	**D**
Radiomics (R)	11	11	*	*	*
Morphology (M)	9	*	9	*	*
Contouromics (C)	10	*	*	10	*
Dosiomics (D)	18	*	*	*	18
Radiomics (R_MKL)	23	23	*	*	*
RM	33	31	2	*	*
RC	28	27	*	1	*
RD	38	30	*	*	8
RDCM	55	36	3	9	7

Not applicable.

95%CI: 0.726-0.754) in the training set and 0.643 (STD: 0.078, 95%CI: 0.608-0.677) in the hold-out set, while the Contouromic model (C) was the most underperforming model, producing an average AUC of 0.664 (STD: 0.052, 95%CI: 0.641-0.687) in the training set and 0.550 (STD: 0.082, 95%CI: 0.514-0.586) in the hold-out test set.

From **Figures 3C, D** and **Table 4B**, it can be observed that the RMDC model had the highest AUC of 0.997 (STD: 0.003, 95%CI: 0.995-0.998) in the training set and 0.943 (STD: 0.029, 95%CI: 0.931-0.956) in the hold-out set, compared to other types of multi-omics models. While it statistically outperformed the other three studied multi-omics models (RM, RD, and RC) in the training set, it did not reach the statistical significant level in the hold-out test set.

Notably, when the R model was re-trained using MKL algorithm (referred to as R_MKL model), the average AUC boosted to 0.984 (STD: 0.008, 95%CI: 0.981-0.988) in the training set and 0.927 (STD: 0.050, 95%CI: 0.905-0.948) in the hold-out set. The development and performance of the R_MKL model can be seen in **Supplementary Figure S7E**, **Figures 3C, D** and **Table 4B**. Surprisingly, further comparisons between the R_MKL model and all the 4 studied multi-omics models

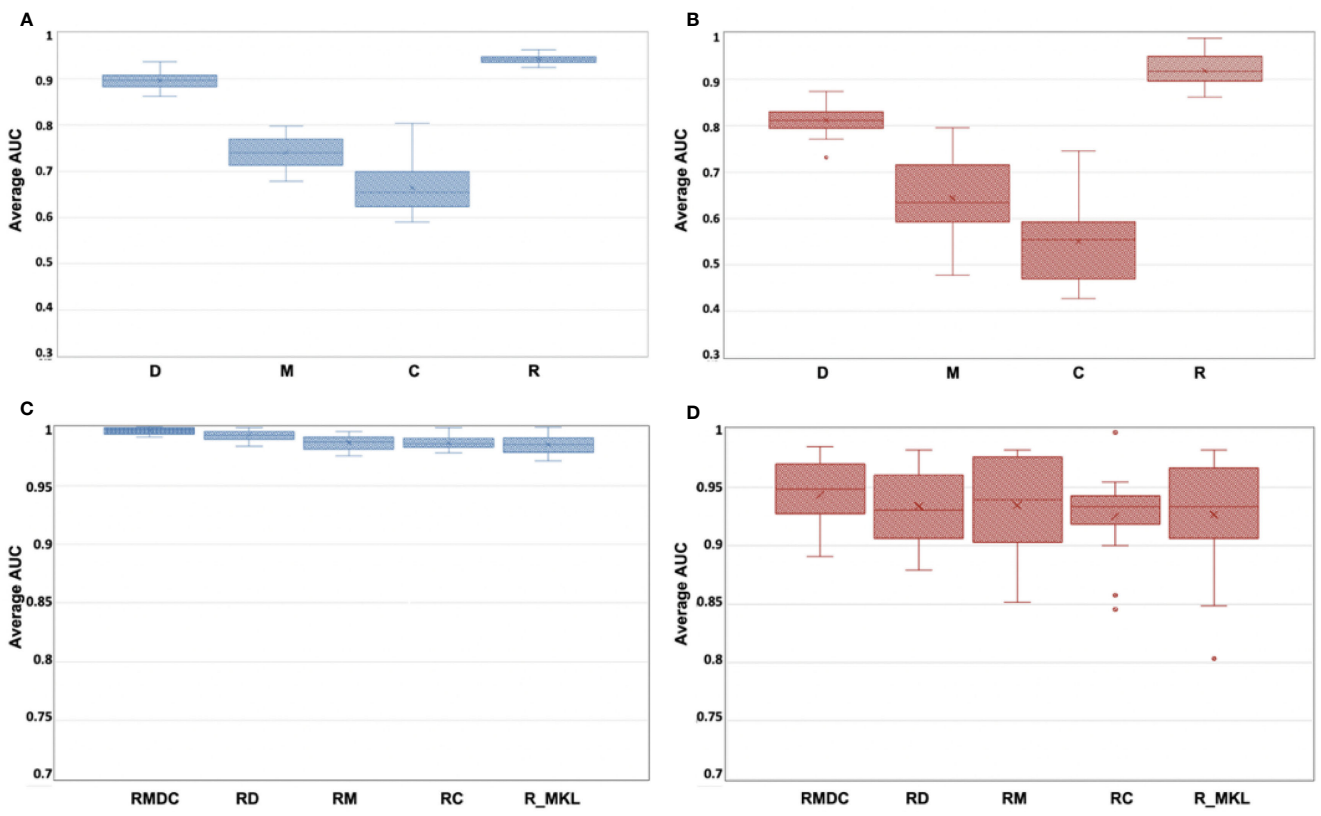

FIGURE 3 | **(A–D)** Box-whisker plots of the average AUC distribution for the final single-omics models in training set **(A)** and hold-out test set **(B)**, and for the multi-omics models and the Radiomic models trained by using MKL algorithms in training **(C)** and hold-out test set **(D)**.

TABLE 4(A-B) | A summary of statistical estimates on performance of single-omics models (4A), multi-omics models and the Radiomic model trained by using MKL algorithm (4B).

Table 4A	Training Set				Hold-out test set			
	Avg. AUC	STD	95% CI	p-value	Avg. AUC	STD	95% CI	p-value
Single-omics Model								
Radiomics (R)	0.94	0.01	(0.938,0.946)	Ref	0.92	0.03	(0.903,0.933)	Ref
Morphology (M)	0.74	0.03	(0.726,0.754)	<0.0001*	0.64	0.08	(0.608,0.677)	<0.0001*
Contouromics (C)	0.664	0.052	(0.641,0.687)	<0.0001*	0.55	0.082	(0.514,0.586)	<0.0001*
Dosiomics (D)	0.9	0.02	(0.887,0.903)	<0.0001*	0.81	0.03	(0.798,0.824)	<0.0001*

Table 4B	Training Set					Hold-out test set				
	Avg. AUC	STD	95% CI	p-value		Avg. AUC	STD	95% CI	p-value	
Multi-omics Model										
RM	0.99	0.01	(0.983,0.989)	<0.0001*	0.47	0.93	0.04	(0.916,0.952)	0.36	0.62
RD	0.99	0	(0.990,0.994)	<0.01*	<0.001*	0.93	0.03	(0.920,0.947)	0.37	0.64
RC	0.99	0.01	(0.984,0.989)	<0.0001*	0.42	0.93	0.04	(0.909,0.941)	0.14	0.92
RMDC	1	0	(0.995,0.998)	Ref	<0.0001*	0.94	0.03	(0.931,0.956)	Ref	0.21
Radiomic Model (trained by MKL)										
R_MKL	0.98	0.01	(0.981,0.988)	<0.0001*	Ref	0.93	0.05	(0.905,0.948)	0.21	Ref

The symbol (*) represents meeting the level of statistical significance (p < 0.05).

indicated that there were no significant differences in model discriminability between R_MKL and all other multi-omics models in the hold-out test set **(Figure 3D** and **Table 4B)**.

DISCUSSION

ART aims to compensate for patient-specific anatomic variations in NPC patients between fractions, while routine ART implementation on patient basis would undoubtedly pose immense burden to clinic. Previously, we were the first to demonstrate the capability of tumoral Radiomics from pre-treatment MRI for prediction of ART eligibility in NPC patients (15). In this study, we investigated a variety of single-omics and multi-omics models from multi-modal images, with an eye towards identifying their roles in predicting ART eligibility in NPC and providing insights into development of ART eligibility screening strategy in NPC in the long run. In this discussion, we attempted to highlight key findings of our study, scrutinize possible underlying reasons, and provide research community with potential directions in the future.

Results of our study showed that the R model significantly outperformed all other studied single-omics models (i.e., M, C and D models, all p-value < 0.0001), achieving an average AUC of 0.942 (STD: 0.009, 95%CI: 0.938-0.946) in the training set and 0.918 (STD: 0.034, 95%CI: 0.903-0.933) in the hold-out test set **(Figures 3A, B** and **Table 4A)**. Among the studied multi-omics models, the RMDC had the highest average AUC in both cohorts **(Figures 3C, D** and **Table 4B)**, however, its difference to the other three models (RM, RD and RC) did not reach the level of statistical significance in the hold-out test sets **(Table 4B)**. Surprisingly, there was no statistical difference between the R_MKL and all the studied multi-omics models in the hold-out set **(Table 4B)**. In other words, addition of other types of -omics features into a radiomic model did not demonstrate statistically significant improvement in model performance, suggesting the dominant role of Radiomic features in prediction of multifactorial ART eligibility in NPC. Besides, Radiomic features accounted for majority of the final selected features, ranging from 64% to 94%, in all the studied multi-omics models **(Table 3)**. We speculated that the dominant role of Radiomics found in this study could partially be explained by both the unique nature of Radiomics and the multi-factorial nature of the ART eligibility.

First, the outstanding predictability of Radiomics in this study may largely lie in its unique capability in unraveling intrinsic tissue property regarding response to treatment perturbations, which can be tissue-type dependent and patient-specific. There is mounting evidence in the literature showing the power of Radiomics in predicting treatment response in various cancer diseases (24–29). For instance, Hou et al. investigated CECT-based biomarkers for prediction of therapeutic response to chemo-radiotherapy in esophageal carcinoma and reported the discriminability of their model in AUC ranging from 0.686 to 0.727 (24). Wang et al. developed a radiomic signature combining features from multi-modal MR imaging sequences for prediction of early treatment response to induction chemotherapy in NPC patients, achieving an AUC of 0.822 (25). Piao et al. devised a MR-based radiomic model to distinguish sensitive and resistant tumors in NPC patients following induction chemotherapy, yielding an AUC of 0.905 (26). In these studies, the tumor response was defined in accordance with the Response Evaluation Criteria in Solid Tumors (RECIST) *via* quantitative assessment of tumor shrinkage, which follows the same line of thought as in this present study. Apart from this, Ramella et al. performed radiomic analysis of pre-treatment CT images of replanned non-small-cell lung cancer patients and generated a radiomic signature for prediction of tumor shrinkage during chemo-radiotherapy, yielding an AUC of 0.82 (27). Yu et al. analyzed tumoral radiomic features from multi-parametric pre-treatment MRI of NPC patients and developed several prediction models for ART eligibility, achieving AUC ranging from 0.750 to 0.930 (15). All the above evidence indicates the outstanding capability of Radiomics in

divulging patient-specific intrinsic tissue biologic characteristics for discerning respondent and non-respondent cancer patients upon treatment perturbations, laying great foundation for predicting patient-specific anatomic variations for ART eligibility for NPC in this study.

By contrast, Dosimoics mainly characterizes aggressiveness of a specific treatment plan by capturing dose statistics from the entire three-dimensional dose distribution map within each of the studied organ structures, while it appears to convey little information on tissue responsiveness upon treatment perturbations. To a degree, this may shed some light on the well-recognized phenomenon where the same-staged patients experienced a diverse range of treatment outcome/response following identical treatment (same degree of treatment aggressiveness). Herein, we emphasize that results of our study do not deny the potential of Dosiomics in predicting treatment response. Indeed, it is worth noting that the D model was the second best-performing model in this study, giving rise to an average AUC of 0.895 (STD: 0.018, 95%CI: 0.887-0.903) in the training set and 0.811 (STD: 0.029, 95%CI: 0.798-0.824) in the hold-out test set **(Figures 3A, B** and **Table 4A)**. This result appears in agreement with most of the previous studies investigating triggering factors for ART in NPC (8–20), where radiation dose deposited was regarded as a prime factor for morphologic volume shrinkage of targets and OARs during the RT course, which may in turn incur intolerable dosimetric deviations from initial treatment plan and hence trigger ART implementation. For instance, Cheng et al. (9) analyzed repeated planning CT and MR scans at 30 and 50-Gy intervals. They reported that the shrinkage of both primary tumor and nodal lesions were higher when 50-Gy was delivered (13% and 29%, respectively) than that when 30-Gy was given (9% and 16%, respectively) and similar trend was also observed for bilateral parotid glands, which jointly led to significant increase in doses to numerous critical OARs, triggering implementation of ART. In this regard, several research groups have also suggested to incorporate dosimetric deviations in targets and/or OARs (such as parotid glands) as part of the ART regimen (12, 18–20). Of note, although Dosiomics has recently been studied for prediction of toxicity (32, 34, 41–43) and prognosis (33, 44) in cancer patients, its potential in treatment response prediction, in particular on the basis of the RECIST criteria, has not been reported. Future studies in this aspect are recommended to confirm its capability in this regard.

On the other hand, Morphologic and Contouromic features merely depict initial morphometric characteristics and geometric relationship between organs, respectively. They share commonality in their distinct disparity against Radiomics in that they both carry little or no underlying biologic information of the studied organ structures. This may in part explain the fair-to-poor predictive performance of the M and C models in our study, yielding an AUC of 0.643 (STD: 0.078, 95%CI: 0.608-0.677) and 0.550 (STD: 0.082, 95%CI: 0.514-0.582) in the hold-out test set, respectively **(Figures 3A, B** and **Table 4A)**.

In addition, the multifactorial nature of ART eligibility in the context of NPC disease may further elucidate why Radiomics plays a dominant role in this study, irrespective of additional types of -omics features. ART eligibility in NPC depends on multiple organs located in a confined space of head-and-neck regions. GTVnp, GTVn and bilateral parotid glands are all bulky organ structures within the nose-pharynx ministry, responsiveness of these structures upon treatment perturbations jointly determines the degree of patient-specific alternations in anatomy, hence affecting the demand for ART. Given the unique superiority of Radiomics in unravelling intrinsic tissue biologic response, we inferred that the role of Radiomics could become increasingly important when more organ structures come into play in contributing to the studied outcome (i.e., the ART eligibility), compared with other types of -omics features. This may, to some extent, provide an insight into our findings that Radiomic features accounted for the largest proportion of the final selected features in all the studied multi-omics models **(Table 3)**; and that the multi-organ-based R model performed far better than other single-omics models (all p-value < 0.0001) **(Table 4A)**; and that incorporating Morphologic and/or Dosiomic and/or Contouromic features into the radiomic model did not demonstrate statistically significant improvement in the hold-out test set **(Table 4B)** (all p-value > 0.05). Herein, we highlight that findings of this study may provide research community with valuable insights into development of pre-treatment stratification strategies for ART eligibility in NPC patients, potentially facilitating clinical implementation of ART in the future.

Although there exists a lack of studies on revealing multi-omics in prediction of multi-organ triggering outcome, results from a few studies in the literature may worth our attention. Sheikh et al. investigated radiomics and dosimetric features from bilateral parotid and submandibular glands (i.e., four separated organ structures) for predicting xerostomia, and reported that addition of dosimetric and clinical factors into a joint-CT-MR radiomic model did not lead to statistically significant improvement in model performance (45), which appears to be in line with our current findings. By contrast, Jiang et al. reported superior model performance when using both radiomic and dosimetric features from five lung sub-regions for predicting radiation pneumonitis than when using radiomic features alone (46), which may appear contradictive to our findings. However, it should be noted that the features in their studies were essentially derived from a single organ – the same lung tissue, rather than individual separated organ structures as in this current work. Further, unlike the present work, only CT-based radiomics was adopted in their study, which may lead to a relatively weaker predictive power than as if it were developed from multi-modal images that capture complementary tissue characteristics. Notwithstanding, this presents an interesting area to be explored and a close scrutinization of different types of features in prediction of a multi-organ contributing outcome is highly warranted in the future to further affirm the role of radiomics in context.

This study has several limitations. First, our models were developed and validated in a small-sized single cohort of NPC patients who received CCRT under Tomotherapy machine. While we believe such a homogeneous dataset is advantageous for model building, findings of our study require further validation in a large multi-cohort study. However, it is worth noting that the goal of this study was to assess the role of different omics-based prediction models for ART eligibility in NPC, instead of developing a

generalizable model for clinical adoption. Thus, results of this study still deserve great attention in the community. Second, this study employed a large number of features for model building, which may lead to model overfitting in a small-sized cohort. In this regard, we deployed a strategic approach of determining optimal FS combinations that were used for feature dimensionality reduction prior to model development. The remnant feature sets were of high outcome relevance and low feature redundancy, and only 10 to 33 and 37 to 55 features were input to the modelling algorithms for developing single-omics and multi-omics models, respectively.

CONCLUSION

Comparisons among all the studied models indicated that the Radiomic model was found to play a dominant role for ART eligibility in NPC patients; and Radiomic features accounted for the largest proportion of features in all the four multi-omics models, suggesting its governing power in ART eligibility prediction.

DATA AVAILABILITY STATEMENT

The patients' clinical and DICOM data are not publicly available for patient privacy protection purposes. Requests to access these datasets should be directed to the corresponding author.

AUTHOR CONTRIBUTIONS

SL, YZ, JZ, BL, XT, ZM, TZ, TP, HX, TL, GR, AnC, FL, KA, VL, AmC, and LC contributed to study design, methodology development, results interpretation, and manuscript review. SL, JS, CL, BC, RN, FL, CY, and KA offered administrative and material support for clinical data and imaging data collection. SL and YZ constructed and validated the models. SL wrote the manuscript. JC supervised the study. All authors contributed to the article and approved the submitted version.

FUNDING

This research was partly supported by research grants of Innovation and Technology Fund (ITS/080/19), the Innovation and Technology Commission, and Project of Strategic Importance Fund (P0035421), The Hong Kong Polytechnic University, The Government of the Hong Kong Special Administrative Region.

SUPPLEMENTARY MATERIAL

The Supplementary Material for this article can be found online at: https://www.frontiersin.org/articles/10.3389/fonc.2021.792024/full#supplementary-material

REFERENCES

1. Wang R, Zhang S, Zhou L, Zhang G, Yu H, Lin X, et al. Volume and Dosimetric Variations During Two-Phase Adaptive Intensity-Modulated Radiotherapy for Locally Advanced Nasopharyngeal Carcinoma. *BioMed Mater Eng* (2014) 24(1):1217–25. doi: 10.3233/BME-130923
2. Lu J, Ma Y, Chen J, Wang L, Zhang G, Zhao M, et al. Assessment of Anatomical and Dosimetric Changes by a Deformable Registration Method During the Course of Intensity-Modulated Radiotherapy for Nasopharyngeal Carcinoma. *J Radiat Res* (2014) 55(1):97–104. doi: 10.1093/jrr/rrt076
3. Zhao L, Wan Q, Zhou Y, Deng X, Xie C, Wu S. The Role of Replanning in Fractionated Intensity Modulated Radiotherapy for Nasopharyngeal Carcinoma. *Radiother Oncol* (2011) 98(1):23–7. doi: 10.1016/j.radonc.2010.10.009
4. Deng S, Liu X, Lu H, Huang H, Shu L, Jiang H, et al. Three-Phase Adaptive Radiation Therapy for Patients With Nasopharyngeal Carcinoma Undergoing Intensity-Modulated Radiation Therapy: Dosimetric Analysis. *Technol Cancer Res Treat* (2017) 16(6):910–6. doi: 10.1177/1533034617709396
5. Wang W, Yang H, Hu W, Shan G, Ding W, Yu C, et al. Clinical Study of the Necessity of Replanning Before the 25th Fraction During the Course of Intensity-Modulated Radiotherapy for Patients With Nasopharyngeal Carcinoma. *Int J Radiat Oncol Biol Phys* (2010) 77(2):617–21. doi: 10.1016/j.ijrobp.2009.08.036
6. Chitapanarux I, Chomprasert K, Nobnaop W, Wanwilairat S, Tharavichitkul E, Jakrabhandu S, et al. A Dosimetric Comparison of Two-Phase Adaptive Intensity-Modulated Radiotherapy for Locally Advanced Nasopharyngeal Cancer. *J Radiat Res* (2015) 56(3):529–38. doi: 10.1093/jrr/rru119
7. Mnejja W, Daoud H, Fourati N, Sahnoun T, Siala W, Farhat L, et al. Dosimetric Impact on Changes in Target Volumes During Intensity-Modulated Radiotherapy for Nasopharyngeal Carcinoma. *Rep Pract Oncol Radiother* (2020) 25(1):41–5. doi: 10.1016/j.rpor.2019.12.012
8. Bahl A, Elangovan A, Dracham CB, Kaur S, Oinam AS, Trivedi G, et al. Analysis of Volumetric and Dosimetric Changes in Mid Treatment CT Scan in Carcinoma Nasopharynx: Implications for Adaptive Radiotherapy. *J Exp Ther Oncol* (2019) 13(1):33–9.
9. Cheng HCY, Wu VWC, Ngan RKC, Tang KW, Chan CCL, Wong KH, et al. A Prospective Study on Volumetric and Dosimetric Changes During Intensity-Modulated Radiotherapy for Nasopharyngeal Carcinoma Patients. *Radiother Oncol* (2012) 104(3):317–23. doi: 10.1016/j.radonc.2012.03.013
10. Hu YC, Tsai KW, Lee CC, Peng NJ, Chien JC, Tseng HH, et al. Which Nasopharyngeal Cancer Patients Need Adaptive Radiotherapy? *BMC Cancer* (2018) 18(1):1234. doi: 10.1186/s12885-018-5159-y
11. Surucu M, Shah KK, Mescioglu I, Roeske JC, Small W, Choi M, et al. Decision Trees Predicting Tumor Shrinkage for Head and Neck Cancer: Implications for Adaptive Radiotherapy. *Technol Cancer Res Treat* (2016) 15(1):139–45. doi: 10.1177/1533034615572638
12. Bhide SA, Davies M, Burke K, Mcnair HA, Hansen V, Barbachano Y, et al. Weekly Volume and Dosimetric Changes During Chemoradiotherapy With Intensity-Modulated Radiation Therapy for Head and Neck Cancer: A Prospective Observational Study. *Int J Radiat Oncol Biol Phys* (2010) 76 (5):1360–8. doi: 10.1016/j.ijrobp.2009.04.005
13. Barker JL, Garden AS, Ang KK, O'Daniel JC, Wang H, Court LE, et al. Quantification of Volumetric and Geometric Changes Occurring During Fractionated Radiotherapy for Head-And-Neck Cancer Using an Integrated CT/Linear Accelerator System. *Int J Radiat Oncol Biol Phys* (2004) 59(4):960–70. doi: 10.1016/j.ijrobp.2003.12.024
14. Noble DJ, Yeap PL, Seah SYK, Harrison K, Shelley LEA, Romanchikova M, et al. Anatomical Change During Radiotherapy for Head and Neck Cancer, and Its Effect on Delivered Dose to the Spinal Cord. *Radiother Oncol* (2019) 130:32–8. doi: 10.1016/j.radonc.2018.07.009
15. Yu TT, Lam SK, To LH, Tse KY, Cheng NY, Fan YN, et al. Pretreatment Prediction of Adaptive Radiation Therapy Eligibility Using MRI-Based Radiomics for Advanced Nasopharyngeal Carcinoma Patients. *Front Oncol* (2019) 9:1050. doi: 10.3389/fonc.2019.01050
16. Jin X, Han C, Zhou Y, Yi J, Yan H, Xie C. A Modified VMAT Adaptive Radiotherapy for Nasopharyngeal Cancer Patients Based on CT-CT Image Fusion. *Radiat Oncol* (2013) 8(1):277. doi: 10.1186/1748-717x-8-277
17. Hansen EK, Bucci MK, Quivey JM, Weinberg V, Xia P. Repeat CT Imaging and Replanning During the Course of IMRT for Head-And-Neck Cancer. *Int*

J Radiat Oncol Biol Phys (2006) 64(2):355–62. doi: 10.1016/j.ijrobp.2005.07.957
18. Brown E, Owen R, Harden F, Mengersen K, Oestreich K, Houghton W, et al. Head and Neck Adaptive Radiotherapy: Predicting the Time to Replan. *Asia Pac J Clin Oncol* (2016) 12(4):460–7. doi: 10.1111/ajco.12516
19. Gai X, Wei Y, Tao H, Zhu J, Li B. Clinical Study of the Time of Repeated Computed Tomography and Replanning for Patients With Nasopharyngeal Carcinoma. *Oncotarget* (2017) 8(16):27529–40. doi: 10.18632/oncotarget.16770
20. Yao WR, Xu SP, Liu B, Cao XT, Ren G, Du L, et al. Replanning Criteria and Timing Definition for Parotid Protection-Based Adaptive Radiation Therapy in Nasopharyngeal Carcinoma. *BioMed Res Int* (2015) 2015:1–8. doi: 10.1155/2015/476383
21. Gillies RJ, Kinahan PE, Hricak H. Radiomics: Images Are More Than Pictures, They Are Data. *Radiology* (2016) 278(2):563–77. doi: 10.1148/radiol.2015151169
22. Sun R, Limkin EJ, Vakalopoulou M, Dercle L, Champiat S, Han SR, et al. A Radiomics Approach to Assess Tumour-Infiltrating CD8 Cells and Response to Anti-PD-1 or Anti-PD-L1 Immunotherapy: An Imaging Biomarker, Retrospective Multicohort Study. *Lancet Oncol* (2018) 19(9):1180–91. doi: 10.1016/s1470-2045(18)30413-3
23. Xing L, Krupinski EA, Cai J. Artificial Intelligence Will Soon Change the Landscape of Medical Physics Research and Practice. *Med Physics* (2018) 45(5):1791–3. doi: 10.1002/mp.12831
24. Hou Z, Ren W, Li S, Liu J, Sun Y, Yan J, et al. Radiomic Analysis in Contrast-Enhanced CT: Predict Treatment Response to Chemoradiotherapy in Esophageal Carcinoma. *Oncotarget* (2017) 8(61):104444–54. doi: 10.18632/oncotarget.22304info:doi/10.18632/oncotarget.22304
25. Wang G, He L, Yuan C, Huang Y, Liu Z, Liang C, et al. Imaging Radiomics Signatures for Response Prediction to Induction Chemotherapy in Patients With Nasopharyngeal Carcinoma. *Eur J Radiol* (2018) 98:100–6. doi: 10.1016/j.ejrad.2017.11.007
26. Piao Y, Jiang C, Wang L, Yan F, Ye Z, Fu Z, et al. The Usefulness of Pretreatment MR-Based Radiomics on Early Response of Neoadjuvant Chemotherapy in Patients With Locally Advanced Nasopharyngeal Carcinoma. *Oncol Res* (2021) 28(6):605–13. doi: 10.3727/096504020x16022401878096
27. Ramella S, Fiore M, Greco C, Cordelli E, Sicilia R, Merone M, et al. A Radiomic Approach for Adaptive Radiotherapy in Non-Small Cell Lung Cancer Patients. *PloS One* (2018) 13(11):e0207455. doi: 10.1371/journal.pone.0207455
28. Colen RR, Rolfo C, Ak M, Ayoub M, Ahmed S, Elshafeey N, et al. Radiomics Analysis for Predicting Pembrolizumab Response in Patients With Advanced Rare Cancers. *J Immunother Cancer* (2021) 9(4):e001752. doi: 10.1136/jitc-2020-001752
29. Klaassen R, Larue RTHM, Mearadji B, van der Woude SO, Stoker J, Lambin P, et al. Feasibility of CT Radiomics to Predict Treatment Response of Individual Liver Metastases in Esophagogastric Cancer Patients. *PloS One* (2018) 13(11):e0207362. doi: 10.1371/journal.pone.0207362
30. Grégoire V, Levendag P, Ang KK, Bernier J, Braaksma M, Budach V, et al. CT-Based Delineation of Lymph Node Levels and Related CTVs in the Node-Negative Neck: DAHANCA, EORTC, GORTEC, NCIC, RTOG Consensus Guidelines. *Radiother Oncol* (2003) 69(3):227–36. doi: 10.1016/j.radonc.2003.09.011
31. Zwanenburg A, Vallières M, Abdalah MA, Aerts HJWL, Andrearczyk V, Apte A, et al. The Image Biomarker Standardization Initiative: Standardized Quantitative Radiomics for High-Throughput Image-Based Phenotyping. *Radiology* (2020) 295(2):328–38. doi: 10.1148/radiol.2020191145
32. Lee SH, Han P, Hales RK, Voong KR, Noro K, Sugiyama S, et al. Multi-View Radiomics and Dosiomics Analysis With Machine Learning for Predicting Acute-Phase Weight Loss in Lung Cancer Patients Treated With Radiotherapy. *Phys Med Biol* (2020) 65(19):195015. doi: 10.1088/1361-6560/ab8531
33. Wu A, Li Y, Qi M, Lu X, Jia Q, Guo F, et al. Dosiomics Improves Prediction of Locoregional Recurrence for Intensity Modulated Radiotherapy Treated Head and Neck Cancer Cases. *Oral Oncol* (2020) 104:104625. doi: 10.1016/j.oraloncology.2020.104625
34. Gabryś HS, Buettner F, Sterzing F, Hauswald H, Bangert M. Design and Selection of Machine Learning Methods Using Radiomics and Dosiomics for Normal Tissue Complication Probability Modeling of Xerostomia. *Front Oncol* (2018) 8:35. doi: 10.3389/fonc.2018.00035
35. Buettner F, Miah AB, Gulliford SL, Hall E, Harrington KJ, Webb S, et al. Novel Approaches to Improve the Therapeutic Index of Head and Neck Radiotherapy: An Analysis of Data From the PARSPORT Randomised Phase III Trial. *Radiother Oncol* (2012) 103(1):82–7. doi: 10.1016/j.radonc.2012.02.006
36. Wu B, Ricchetti F, Sanguineti G, Kazhdan M, Simari P, Chuang M, et al. Patient Geometry-Driven Information Retrieval for IMRT Treatment Plan Quality Control. *Med Phys* (2009) 36(12):5497–505. doi: 10.1118/1.3253464
37. Zhang J, Wu QJ, Ge Y, Wang C, Sheng Y, Palta J, et al. Knowledge-Based Statistical Inference Method for Plan Quality Quantification. *Technol Cancer Res Treat* (2019) 18:1533033819857758. doi: 10.1177/1533033819857758
38. Li J, Cheng K, Wang S, Morstatter F, Trevino RP, Tang J, et al. Feature Selection: A Data Perspective. *ACM Comput Surv* (2017) 50(6):1–45. doi: 10.1145/3136625
39. Hoerl AE, Kennard RW. Ridge Regression — 1980: Advances, Algorithms, and Applications. *Am J Math Manag Sci* (1981) 1(1):5–83. doi: 10.1080/01966324.1981.10737061
40. Rakotomamonjy A, Bach F, Canu S, Grandvalet Y. SimpleMKL. *J Mach Learn Res* (2008) 9:2491–521.
41. Rossi L, Bijman R, Schillemans W, Aluwini S, Cavedon C, Witte M, et al. Texture Analysis of 3D Dose Distributions for Predictive Modelling of Toxicity Rates in Radiotherapy. *Radiother Oncol* (2018) 129(3):548–53. doi: 10.1016/j.radonc.2018.07.027
42. Liang B, Tian Y, Chen X, Yan H, Yan L, Zhang T, et al. Prediction of Radiation Pneumonitis With Dose Distribution: A Convolutional Neural Network (CNN) Based Model. *Front Oncol* (2019) 9:1500. doi: 10.3389/fonc.2019.01500
43. Adachi T, Nakamura M, Shintani T, Mitsuyoshi T, Kakino R, Ogata T, et al. Multi-Institutional Dose-Segmented Dosiomic Analysis for Predicting Radiation Pneumonitis After Lung Stereotactic Body Radiation Therapy. *Med Phys* (2021) 48(4):1781–91. doi: 10.1002/mp.14769
44. Buizza G, Paganelli C, D'Ippolito E, Fontana G, Molinelli S, Preda L, et al. Radiomics and Dosiomics for Predicting Local Control After Carbon-Ion Radiotherapy in Skull-Base Chordoma. *Cancers* (2021) 13(2):339. doi: 10.3390/cancers13020339
45. Sheikh K, Lee SH, Cheng Z, Lakshminarayanan P, Peng L, Han P, et al. Predicting Acute Radiation Induced Xerostomia in Head and Neck Cancer Using MR and CT Radiomics of Parotid and Submandibular Glands. *Radiat Oncol* (2019) 14(1):131. doi: 10.1186/s13014-019-1339-4
46. Jiang W, Song Y, Sun Z, Qiu J, Shi L. Dosimetric Factors and Radiomics Features Within Different Regions of Interest in Planning CT Images for Improving the Prediction of Radiation Pneumonitis. *Int J Radiat Oncol Biol Phys* (2021) 110(4):1161–70. doi: 10.1016/j.ijrobp.2021.01.049

Conflict of Interest: The authors declare that the research was conducted in the absence of any commercial or financial relationships that could be construed as a potential conflict of interest.

frontiers in Oncology

ORIGINAL RESEARCH
published: 03 February 2022
doi: 10.3389/fonc.2021.779882

The Role of the EZH2 and H3K27me3 Expression as a Predictor of Clinical Outcomes in Salivary Duct Carcinoma Patients: A Large-Series Study With Emphasis on the Relevance to the Combined Androgen Blockade and HER2-Targeted Therapy

Natsuki Saigusa[1†], Hideaki Hirai[1†], Yuichiro Tada[2], Daisuke Kawakita[3], Masato Nakaguro[4], Kiyoaki Tsukahara[5], Satoshi Kano[6], Hiroyuki Ozawa[7], Takahito Kondo[8], Kenji Okami[9], Takafumi Togashi[10], Yukiko Sato[11], Makoto Urano[12], Manami Kajiwara[1], Tomotaka Shimura[13], Chihiro Fushimi[2], Akira Shimizu[5], Isaku Okamoto[5], Takuro Okada[5], Takayoshi Suzuki[6], Yorihisa Imanishi[7], Yoshihiro Watanabe[7], Akihiro Sakai[9], Koji Ebisumoto[9], Yuichiro Sato[10], Yoshitaka Honma[14], Keisuke Yamazaki[15], Yushi Ueki[15], Toyoyuki Hanazawa[16], Yuki Saito[17], Hideaki Takahashi[18], Mizuo Ando[19], Shinji Kohsaka[20], Takashi Matsuki[21] and Toshitaka Nagao[1]*

[1] Department of Anatomic Pathology, Tokyo Medical University, Tokyo, Japan, [2] Department of Head and Neck Oncology and Surgery, International University of Health and Welfare, Mita Hospital, Tokyo, Japan, [3] Department of Otorhinolaryngology, Head and Neck Surgery, Nagoya City University Graduate School of Medical Sciences, Nagoya, Japan, [4] Department of Pathology and Laboratory Medicine, Nagoya University Hospital, Nagoya, Japan, [5] Department of Otorhinolaryngology, Head and Neck Surgery, Tokyo Medical University, Tokyo, Japan, [6] Department of Otolaryngology Head and Neck Surgery, Faculty of Medicine and Graduate School of Medicine, Hokkaido University, Sapporo, Japan, [7] Department of Otorhinolaryngology Head and Neck Surgery, Keio University School of Medicine, Tokyo, Japan, [8] Department of Otorhinolaryngology, Head and Neck Surgery, Tokyo Medical University Hachioji Medical Center, Tokyo, Japan, [9] Department of Otolaryngology Head and Neck Surgery, Tokai University School of Medicine, Isehara, Japan, [10] Department of Head and Neck Surgery, Niigata Cancer Center Hospital, Niigata, Japan, [11] Department of Pathology, Cancer Institute Hospital, Japanese Foundation for Cancer Research, Tokyo, Japan, [12] Department of Diagnostic Pathology Bantane Hospital Fujita Health University, School of Medicine, Nagoya, Japan, [13] Department of Otolaryngology, Showa University Fujigaoka Hospital, Yokohama, Japan, [14] Department of Head and Neck, Esophageal Medical Oncology, National Cancer Center Hospital, Tokyo, Japan, [15] Department of Otolaryngology Head and Neck Surgery, Niigata University Graduate School of Medical and Dental Sciences, Niigata, Japan, [16] Department of Otolaryngology, Head and Neck Surgery, Chiba University Graduate School of Medicine, Chiba, Japan, [17] Department of Otolaryngology - Head and Neck Surgery, Faculty of Medicine, The University of Tokyo, Tokyo, Japan, [18] Department of Otorhinolaryngology, Head and Neck Surgery, Yokohama City University, School of Medicine, Yokohama, Japan, [19] Department of Otolaryngology-Head & Neck Surgery, Okayama University Graduate School of Medicine, Dentistry and Pharmaceutical Sciences, Okayama, Japan, [20] Division of Cellular Signaling, National Cancer Center Research Institute, Tokyo, Japan, [21] Department of Otorhinolaryngology, Head and Neck Surgery, Kitasato University School of Medicine, Kanagawa, Japan

Objective: Salivary duct carcinoma (SDC) is a highly aggressive and uncommon tumor arising not only *de novo* but also in pleomorphic adenoma. Androgen receptor (AR)- and HER2-targeted therapy have recently been introduced for SDC as promising treatment options; however, no predictive biomarkers have yet been established. EZH2 and

OPEN ACCESS

Edited by:
Min Yao,
University Hospitals Cleveland Medical Center, United States

Reviewed by:
Mario Airoldi,
Oncology Department, Italy
Ashish V. Chintakuntlawar,
Mayo Clinic, United States
Vincent Vander Poorten,
KU Leuven, Belgium

***Correspondence:**
Toshitaka Nagao
nagao-t@tokyo-med.ac.jp

[†]These authors have contributed equally to this work and share first authorship

Specialty section:
This article was submitted to Head and Neck Cancer, a section of the journal Frontiers in Oncology

Received: *20 September 2021*
Accepted: *27 December 2021*
Published: *03 February 2022*

Citation:
Saigusa N, Hirai H, Tada Y, Kawakita D, Nakaguro M, Tsukahara K, Kano S, Ozawa H, Kondo T, Okami K, Togashi T, Sato Y, Urano M, Kajiwara M, Shimura T, Fushimi C, Shimizu A, Okamoto I, Okada T, Suzuki T, Imanishi Y, Watanabe Y, Sakai A, Ebisumoto K, Sato Y, Honma Y, Yamazaki K, Ueki Y, Hanazawa T, Saito Y, Takahashi H, Ando M, Kohsaka S, Matsuki T and Nagao T (2022) The Role of the EZH2 and H3K27me3 Expression as a Predictor of Clinical Outcomes in Salivary Duct Carcinoma Patients: A Large-Series Study With Emphasis on the Relevance to the Combined Androgen Blockade and HER2-Targeted Therapy. Front. Oncol. 11:779882. doi: 10.3389/fonc.2021.779882

H3K27me3 are closely linked to the development and progression of various cancers, and EZH2 is also expected to be a desirable therapeutic target. We therefore explored the clinicopathological and prognostic implications of EZH2 and H3K27me3 in a large cohort of SDC patients, focusing on their impact on the therapeutic efficacy of AR- or HER2-targeted therapy.

Materials and Methods: The EZH2 and H3K27me3 immunohistochemical expression and *EZH2* Y646 gain-of-function mutation status were examined in 226 SDCs, and the relationship with the clinicopathological factors as well as clinical outcomes were evaluated within the three groups depending on the treatment: AR-targeted (combined androgen blockade with leuprorelin acetate and bicalutamide; 89 cases), HER2-targeted (trastuzumab and docetaxel; 42 cases), and conventional therapy (112 cases).

Results: EZH2 and H3K27me3 were variably immunoreactive in most SDCs. A positive correlation was found between the expression of EZH2 and H3K27me3. The EZH2 expression in the SDC component was significantly higher than that in the pre-existing pleomorphic adenoma component. *EZH2* Y646 was not identified in any cases. EZH2-high cases more frequently had an advanced clinical stage and aggressive histological features than EZH2-low cases. An EZH2-high status in patients treated with AR-targeted therapy was associated with a significantly shorter progression-free and overall survival as well as a lower objective response rate and clinical benefit rate. In addition, a H3K27me3-high status in patients treated with AR-targeted therapy was related to a shorter overall survival. Conversely, there was no association between the EZH2 and H3K27me3 expression and the clinical outcomes in the conventional or HER2-targeted therapy groups.

Conclusions: A high expression of EZH2 and H3K27me3 in SDC might be a predictor of a poor efficacy of AR-targeted therapy. Our data provide new insights into the role of EZH2 and H3K27me3 in therapeutic strategies for SDC.

Keywords: salivary duct carcinoma, EZH2, H3K27me3, androgen receptor, HER2, combined androgen blockade (CAB), prognosis, therapeutic effect

INTRODUCTION

Salivary duct carcinoma (SDC) is a highly aggressive and uncommon tumor that accounts for as many as 10% of all salivary gland malignancies (1, 2). It can occur not only as *de novo* carcinoma but also as a malignant component of carcinoma ex pleomorphic adenoma (PA) (1, 3). SDC is histologically comparable to high-grade mammary ductal carcinoma. SDC shows a high rate of metastasis, and systemic chemotherapy is required for patients with metastatic disease.

Most SDCs characteristically express androgen receptor (AR), and approximately 40% are positive for HER2 (4–6). Recently, based on these biomarker profiles, treatments targeting AR and HER2 have been developed as a promising optional therapy in recurrent/metastatic or unresectable locally advanced SDCs (7–14). AR-targeted therapy demonstrated equivalent efficacy and less toxicity for patients with AR-positive SDC than conventional chemotherapy (9, 10, 14, 15). Furthermore, HER2-targeted therapy showed more encouraging efficacy with a higher response rate in HER2-positive SDC patients than conventional or AR-targeted therapy (8–11). However, since SDCs often express both AR and HER2, selecting the most appropriate treatment remains difficult.

In the past decade, there have been remarkable advances in research on therapy-relevant biomarkers linked to biological behavior in various cancers. At present, little is known concerning the mechanisms and factors related to resistance to targeted therapy in patients with SDC, although a few possible adverse biomarkers of SDC patients treated with AR-targeted therapy, such as AR-related molecules, have been reported (3, 16–19). However, how to apply such strategies in clinical practice remains challenging (19). For this reason, precise immunohistochemical biomarkers that reflect the clinicopathological status or predict the prognosis and therapeutic effect are awaited (3–6, 19).

Enhancer of zeste homolog 2 (EZH2), a specific histone methyltransferase of histone H3 at Lys 27 (H3K27), has been garnering attention as a prognostic factor as well as an attractive target for cancer therapy. EZH2 plays an important role in the

epigenetic maintenance of the repressive chromatin mark. It forms the polycomb repressive complex 2 (PRC2) and demonstrates histone methyltransferase activity (20). PRC2 recruitment to chromatin causes H3K27 trimethylation (H3K27me3), which is normally related to gene repression and plays a crucial role in tumor development (21). Furthermore, the *EZH2* Y646 gain-of-function mutation is involved in tumorigenesis (22–24). In fact, the overexpression of EZH2 has been shown to be associated with invasive growth and poor clinical outcomes in many malignant tumors, including breast, prostate, gastric, endometrial and hematologic cancers, even though the prognostic impact of H3K27me3 expression is variable (25–29). Furthermore, the overexpression of EZH2 is related to resistance to AR- and HER2-targeted therapy in prostate and breast cancers, respectively (30, 31).

An EZH2 inhibitor was approved by the U.S. Food and Drug Administration for use against epithelioid sarcoma and follicular lymphoma in 2020 (32). In addition, several clinical trials concerning EZH2 inhibitor therapy for different types of malignant tumors are ongoing (ClinicalTrials.gov: NCT02601950, NCT01897571 and NCT04407741) (33, 34). To our knowledge, however, the roles of EZH2 and H3K27me3 in SDC have not yet been described.

We therefore examined the EZH2 and H3K27me3 protein expression and *EZH2* Y646 activating mutations and evaluated their relationship with the clinicopathological factors and prognosis of SDC in a large cohort of patients. Furthermore, we sought to analyze the association of EZH2/H3K27me3 expression with survival outcomes and therapeutic effect within differently (AR- or HER2-targeted) treated groups of patients with SDC.

MATERIALS AND METHODS

This study was approved by the Institutional Ethics Review Board of each participating institution.

Patients

All patients underwent a central pathological review by an expert pathologist (T.N.) according to the rigorous histomorphological criteria for SDC (**Figure 1**). We recruited 226 patients who were diagnosed with and received treatment for SDC at 7 institutions between 1994 and 2019, and AR- and HER2-tageted therapy started in 2012 and 2011, respectively. As shown in the study flow diagram (**Figure 2**), we classified total 226 patients into 3 independent cohort groups: the conventional therapy group (Cohort A; 112 cases, 49.6%), the AR-targeted therapy group (Cohort B; 89 cases, 39.4%), and the HER2-targeted therapy group (Cohort C; 42 cases, 18.6%). The conventional therapy group (Cohort A) was defined as SDC patients who did not receive either AR-targeted therapy (combined androgen blockade therapy [CAB]: leuprorelin acetate and bicalutamide) (9) or HER2-targeted therapy (trastuzumab and docetaxel) (11–13). Patients who had been treated before the introduction of targeted therapy were also assigned to the conventional therapy group (Cohort A), even if they were positive for AR and/or HER2. Almost all patients in the conventional therapy group (Cohort A) (109 of 112 cases, 97%) received radical surgical resection with or without radiotherapy/systemic therapy, which is considered a typical treatment in general clinical practice. In addition, Cohorts B and C included 17 patients who received both AR- and HER2-targeted therapy. The details of AR- and HER2-targeted therapy were previously reported (9, 11).

We retrospectively reviewed the patient records to obtain information about the age, sex, tumor size, lymph node metastasis, distant metastasis, and survival. The TNM classification was determined in accordance with the 8th edition of the International Union Against Cancer (35).

Histopathology

The histopathological analysis regarding tumor grading was performed using a previously reported histological risk stratification model, which was determined by 4 histological features (prominent nuclear pleomorphism, mitosis ≥30/10 high-power fields, vascular invasion and high poorly differentiated cluster) (36). The total number of positive factors was considered to indicate low risk to high risk, as follows: low risk, 0 to 1 point; intermediate risk, 2 to 3 points; high risk, 4 points.

Immunohistochemistry (IHC) and Fluorescence *In Situ* Hybridization (FISH)

For IHC, formalin-fixed, paraffin-embedded tumor tissue was cut into 4-μm-thick sections. A polymer-based detection system with heat-mediated antigen retrieval was conducted using the primary antibodies shown in **Supplementary Table 1**. Diaminobenzidine was applied to detect antigen-antibody reactions. The EZH2 and H3K27me3 labelling index (LI) (0–100%) was determined by counting the number of immunoreactive nuclei in at least 1,000 cells (**Figure 1**). We also compared the EZH2/H3K27me3 expression among normal salivary glands, the PA component and carcinoma.

HER2 was considered to be positive based on an HER2 IHC score of 3+ and/or *HER2* amplification, as determined by a FISH analysis, in accordance with the ASCO/CAP guideline for evaluating breast cancer (5, 37). The analysis methods of immunohistochemical staining for Ki-67, AR, p53, p-Akt, mTOR, PTEN, EGFR and CK5/6 were reported previously by our group (5, 37–40)

Gene Mutation Analyses

We extracted DNA from paraffin-embedded sections using a QIAamp DNA FFPE Tissue Kit (Qiagen, Hilden, DE, USA) and DNA was purified using a QIAquick Spin Kit (Qiagen). DNA purity was tested using a NanoDrop (Thermo Scientific, Waltham, MA, USA). For the detection of mutations, DNA was amplified with primers flanking regions in exon 16 of the *EZH2* gene encompassing codon 646. We amplified the region with the following primers: forward primer 5'-TGG GGG ATT TTT ATC AAA G-3'/reverse primer 5'-TCA AAC CCA CAG ACT TAC CT-3'. Polymerase chain reaction products were sequenced in both sense and antisense directions using a BigDye Terminator v3.1 cycle sequencing kit on an ABI 3730

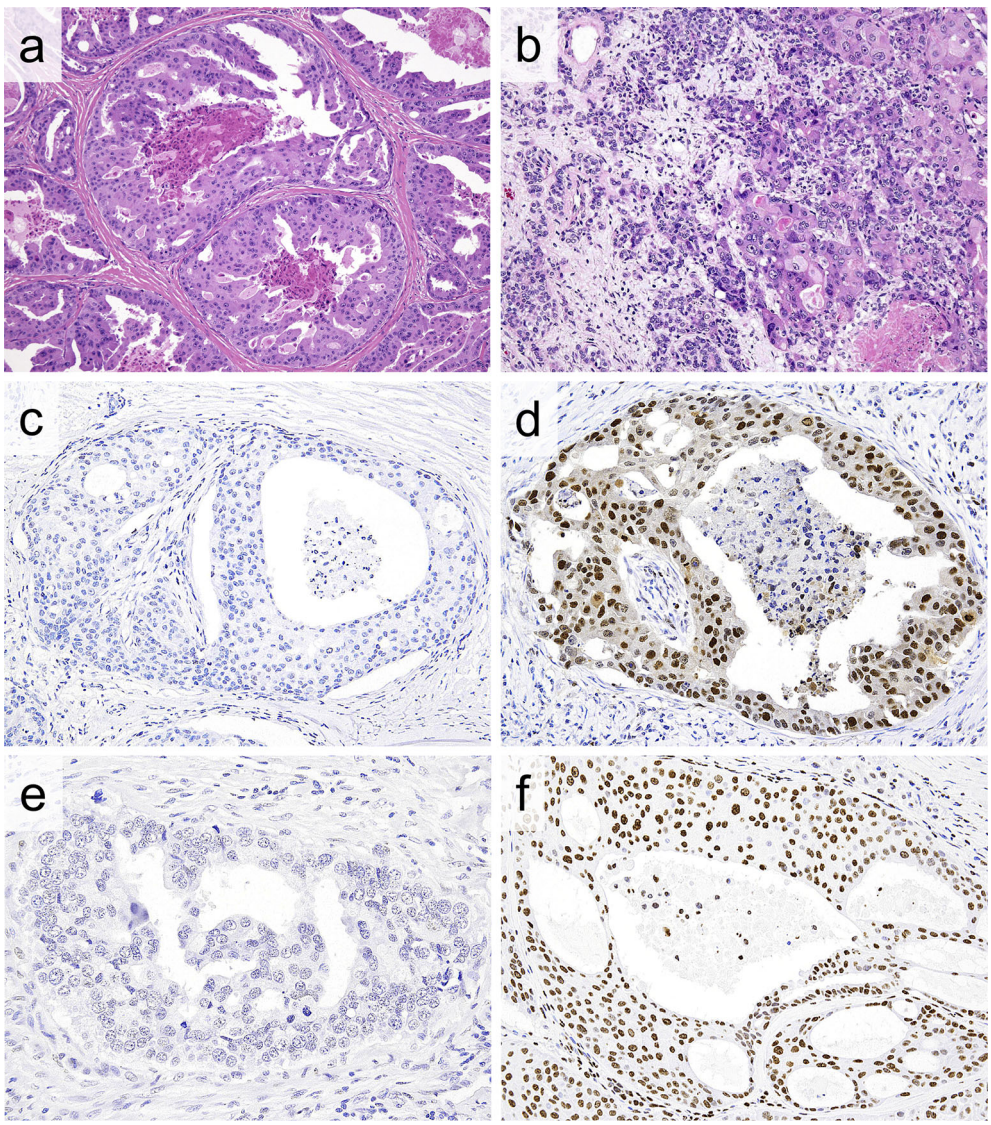

FIGURE 1 | **(A, B)** Representative histologic features of salivary duct carcinoma (SDC). **(A)** Dilated ductal structures with a papillary, "Roman-bridge," or cribriform growth accompanied by comedo necrosis. **(B)** SDC ex pleomorphic adenoma composed of SDC (right portion) and a preexisting pleomorphic adenoma component (left portion). Note carcinoma cells exhibiting large pleomorphic nuclei and abundant eosinophilic cytoplasm. **(C, D)** Immunohistochemically, the EZH2 labelling index (LI) is low (0%) **(C)** and high (90%) **(D)** in SDC. **(D)** Diffuse and strong nuclear and weak cytoplasmic EZH2 immunoreactivity. **(E, F)** Likewise, the H3K27me3 LI is low (0%) **(E)** and high (90%) **(F)** in SDC. **(F)** Diffuse and strong nuclear H3K27me3 immunoreactivity.

instrument (Applied Biosystems, Inc., Foster City, CA, USA). Sanger sequencing was performed for *TP53* (exons 4–10), *PIK3CA* (exons 9 and 20) *and HRAS* (exons 1-2) (38).

Statistical Analyses

Non-continuous variables were compared using the chi-squared test. Continuous variables were compared using the Mann-Whitney U test or Wilcoxon's signed-rank test. Spearman's rank correlation test was used to evaluate the correlation between the expression of proteins. The association between the EZH2/H3K27me3 expression and the overall survival (OS) or progression-free survival (PFS) was evaluated using the Kaplan-Meier product-limit method and univariate and multivariate Cox proportional hazards models. Furthermore, in the AR- and HER2-targeted therapy groups (Cohorts B and C), the relationship between the EZH2/H3K27me3 expression and clinical benefit rate (CBR) or objective response rate (ORR) was also analyzed using univariate and multivariate Cox proportional hazards models. The potential confounders in the multivariate analysis included the age, sex, primary tumor site, separate T, N, and M classification, first-line treatment, histological origin and AR- and HER2-targeted therapy. Conventional therapy group (Cohort A), AR-targeted therapy group (Cohort B), and HER2-targeted therapy group (Cohort C) were independent cohorts classified based on a difference of therapy,

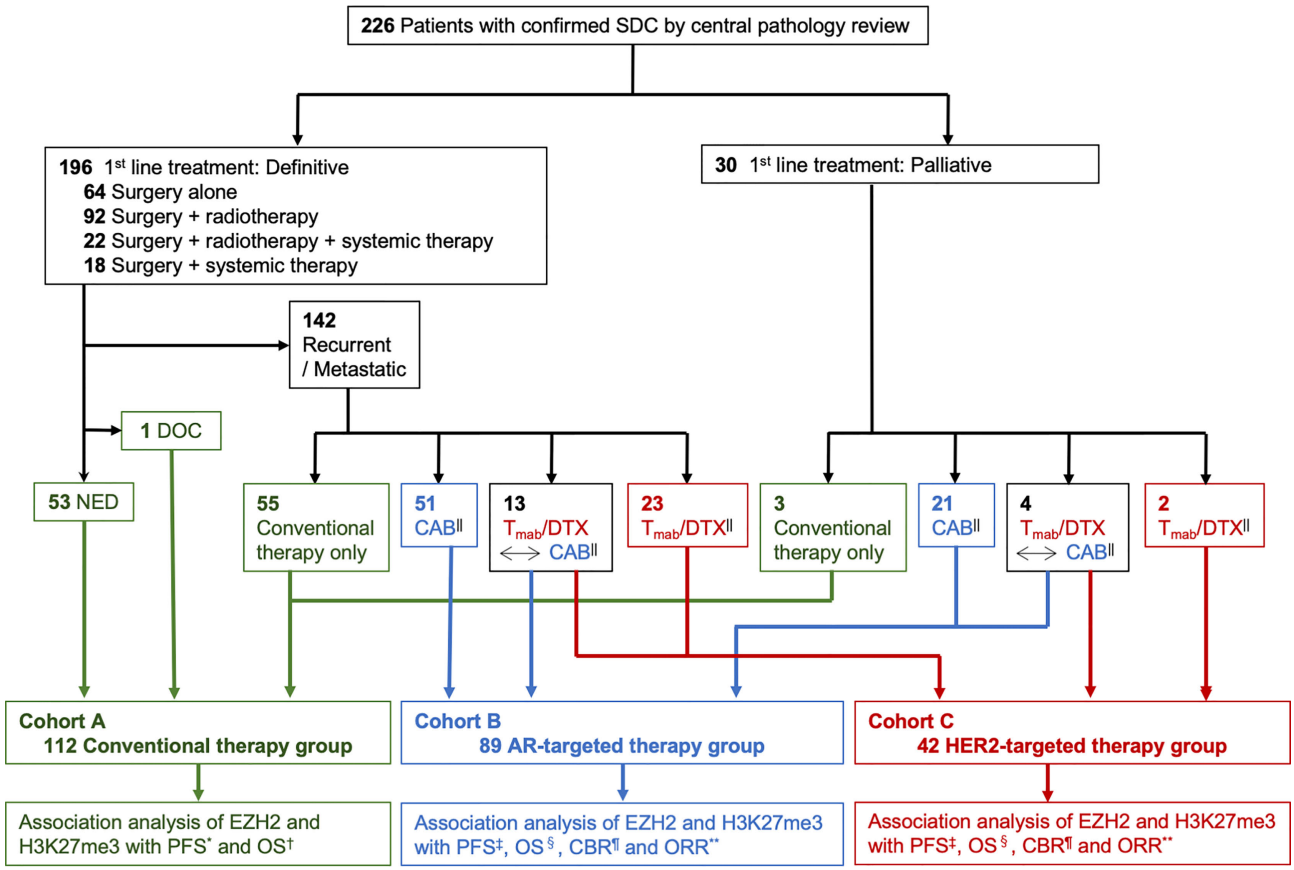

FIGURE 2 | Study flow diagram. SDC, salivary duct carcinoma; DOC, dead of other cause; NED, no evidence of disease; Tmab/DTX, trastuzumab and docetaxel; CAB, combined androgen blockade; AR, androgen receptor; HER2, human epidermal growth factor receptor type 2; PFS, progression free survival; OS, overall survival; CBR, clinical benefit rate; ORR, objective response rate. * Time from the start of any treatment to the diagnosis of progressive disease. † Time from the start of any treatment to death from any cause or the last follow-up. ‡ Time from the start of AR- or HER2-targeted therapy to the diagnosis of progressive disease or death from any cause. § Time from the start of AR- or HER2-targeted therapy to death from any cause or the last follow-up. ‖ ± conventional therapy. ¶ The percentage of patients who achieved a complete response (CR), partial response (PR) or stable disease for at least 24 weeks. ** The percentage of patients who achieved CR or PR.

but not clinical outcomes. Therefore, we estimated the optimal cut-off values for the EZH2 and H3K27me3 expression according to survival in each cohort. The PFS in the conventional therapy group (Cohort A) was defined as the length of time from the start of any treatment to the diagnosis of progressive disease, while the OS in the conventional therapy was defined as the length of time from the start of any treatment to death from any cause. The PFS in the AR- and HER2-targeted therapy groups (Cohorts B and C) was defined as the length of time from the start of AR- and HER2-targeted therapy to the diagnosis of progressive disease or death from any cause, respectively, while the OS in the AR- and HER2-targeted therapy groups (Cohorts B and C) was defined as the length of time from the start of AR- and HER2-targeted therapy to death from any cause or the last follow-up, respectively.

The therapeutic effect of AR- and HER2-targeted therapy was evaluated according to the ORR, defined as the percentage of patients who achieved a complete response (CR) or partial response (PR) and CBR, which was defined as the percentage of patients who achieved CR, PR or stable disease (SD) for at least 24 weeks. Tumor assessments were performed within 4 weeks before the initiation of AR- and HER2-targeted therapy using computed tomography and/or magnetic resonance imaging and were repeated every 6–8 weeks until disease progression, death, or up to 2 years after the initiation of treatment. Thereafter, assessment was continued every 3 months in surviving patients. Patient response was determined based on the Response Evaluation Criteria in Solid Tumors (version 1.1) (41). All statistical analyses were performed using the STATA software program (version 16; StataCorp, College Station, TX, USA). All tests were two-sided, and *P* values of < 0.05 were considered to indicate statistical significance.

RESULTS

Patients' Characteristics

The distribution of the patient characteristics is shown in **Table 1**. The case series included 194 males and 32 females with a median age of 63 (range, 26-94) years old. Eighty-three SDC cases (43%) and

TABLE 1 | Patients' characteristics.

	Total cohort n = 226		Cohort A		Cohort B*		Cohort C*	
			Conventional therapy group n = 112		AR-targeted therapy group n = 89		HER2-targeted therapy group n = 42	
	n	%	n	%	n	%	n	%
Age (years)								
≤65	125	55	59	53	41	46	29	69
>65	101	45	53	47	48	54	13	31
Sex								
Male	194	86	95	85	81	91	32	76
Female	32	14	17	15	8	9	10	24
Primary site								
Parotid gland	172	76	92	82	61	69	28	67
Others	53	23	20	18	27	30	14	33
Unknown	1	1	0	0	1	1	0	0
Histological origin								
CXPA	115	51	42	37	37	42	5	12
de novo	83	37	67	60	29	33	32	76
undefined	28	12	3	3	23	25	5	12
AR expression								
<20%	32	14	27	24	0	0	5	12
≥20%	194	86	85	76	89	100	37	88
HER2 status								
Negative	131	58	62	55	67	75	2	5
Positive	95	42	50	45	22	25	40	95
T classification								
1	21	9	8	7	–	–	–	–
2	59	26	31	28	–	–	–	–
3	46	21	21	19	–	–	–	–
4a	91	40	49	44	–	–	–	–
4b	7	3	3	3	–	–	–	–
Unknown	2	1	0	0				
N classification								
0	94	42	60	54	–	–	–	–
1	15	7	9	8	–	–	–	–
2	114	50	43	38	–	–	–	–
3	3	1	0	0	–	–	–	–
M classification								
0	194	86	106	95	–	–	–	–
1	32	14	6	5	–	–	–	–
First-line treatment								
Surgery	196	87	109	97	–	–	–	–
Radiation	123	54	57	51	–	–	–	–
Systemic therapy	65	29	23	21	–	–	–	–

*CXPA, carcinoma ex pleomorphic adenoma; AR, androgen receptor; HER2, human epidermal growth factor receptor type 2. *Cohorts B and C included 17 patients who received both AR- and HER2-targeted therapy.*

115 cases (57%) were classified as *de novo* and carcinoma ex PA, respectively (**Figure 1**). Bone-only metastasis was found in 4 cases in the AR- group (Cohort B) and 1 case in the HER2-targeted therapy group (Cohort C). In the conventional therapy group (Cohort A), 42 of 112 cases (37.5%) were treated with systemic therapy, either at the time of the initial treatment or at the time of recurrence/metastasis.

The median follow-up period of all patients was 3.7 (range 0.04-19.0) years. The 5-year OS rate in all patients was 46.9% (95% confidence interval [CI] 39.8%-53.7%), and the 5-year PFS rate was 23.5% (95% CI 18.0%-29.4%). The median OS of all patients was 4.4 (95% CI 3.7-5.9) years, and the median PFS was 1.0 (95% CI 0.9-1.3) years. In addition, the median follow-up period of conventional therapy group (Cohort A) was 4.0 (range 0.04-19.0) years. The median OS of conventional therapy group (Cohort A) was 5.8 (95% CI 3.4-8.7) years, and the median PFS was 2.6 years (95% CI not significant).

Efficacy of AR-Targeted Therapy

The median follow-up period in the AR-targeted therapy group (Cohort B) was 1.9 (range 0.1-6.6) years. The responses in patients treated with CAB are shown by waterfall plots in **Supplementary Figure 1**. Four (4.5%), 20 (22.5%), 42 (47.2%), and 23 (25.8%) patients showed CR, PR, SD, and PD, respectively. The ORR was 27.0% (95% CI 18.7%–37.2%). Forty-two patients with SD maintained their status for more than 24 weeks and CBR was 74.2% (95% CI 63.9–82.3%). The median PFS was 0.46 (95% CI 0.36–0.58) years, and the median OS was 2.33 (95% CI 1.86-3.17) years.

Efficacy of HER2-Targeted Therapy

The median follow-up period in the HER2-targeted therapy group (Cohort C) was 2.3 (range 0.3-8.4) years. The responses in patients treated with HER2-targeted therapy are shown by waterfall plots in **Supplementary Figure 1**. Five (12.2%), 22 (53.7%), 11 (26.8%) and 3 (7.3%) patients showed CR, PR, SD and PD, respectively. The ORR was 65.9% (95% CI 49.8%–79.0%). Eleven patients with SD maintained the status for more than 24 weeks and CBR was 92.7% (95% CI 79.0%–97.7%). The median PFS was 0.80 (95% CI 0.56–0.93) years, and the median OS was 2.91 (95% CI 2.27-3.27) years.

The Expression of EZH2 and H3K27me3 With Clinicopathological Correlation

In virtually all cases, both EZH2 and H3K27me3 were expressed in at least a limited part of the SDC (97.8% and 99.1%, respectively). The cut-off values for a low/high LI of EZH2 and H3K27me3 were 60% and 65%, respectively, based on the median value. A total of 124 cases (54.9%) and 102 cases (45.1%) were thus classified into the EZH2-low and EZH2-high groups, respectively (mean EZH2 expression LI: 48.8%). Likewise, 112 cases (52.6%) and 101 cases (47.4%) were categorized into the H3K27me3-low and H3K27me3-high groups, respectively (mean H3K27me3 expression LI: 52.8%) (**Figure 1**). A weak positive correlation was found between the expression of EZH2 and H3K27me3 (r = 0.357, P < 0.001) (**Supplementary Figure 2**).

The EZH2 expression of the surrounding non-neoplastic salivary gland tissues and pre-existing PA components was very low (mean EZH2 expression LI: 1.8% and 4.2%, respectively), and the value in the SDC was significantly higher than that in the PA component (P < 0.001), while that in the PA component was higher than that in normal salivary gland tissue (P = 0.002) (**Supplementary Figure 3**). In contrast, H3K27me3 expression was also observed in the surrounding non-neoplastic salivary gland tissues and pre-existing PA components to varying degrees in almost all cases (mean H3K27me3 expression LI: 39.1% and 52.0%, respectively). The expression of H3K27me3 in the PA component and SDC was higher than that in the normal salivary gland tissue (P = 0.038 and < 0.001, respectively); however, the H3K27me3 expression in the PA component and SDC was not significantly associated (P = 0.885) (**Supplementary Figure 3**).

The correlations between the EZH2/H3K27me3 expression and the clinicopathological factors and various biomarkers are summarized in **Table 2** and **Supplementary Table 2**. High-EZH2-LI cases more frequently had an advanced N and M classification compared with low-EZH2-LI cases (P = 0.005 and < 0.001, respectively), while there was no notable relationship between the EZH2 expression and T classification. In addition, an EZH2-high tumor was associated with the presence of prominent nuclear pleomorphism, intermediate or high histological risk group, carcinoma ex PA, higher Ki-67 LI and the aberrant expression of p53 in comparison to an EZH2-low tumor (P < 0.001, = 0.015, = 0.014, < 0.001 and = 0.005, respectively). In contrast, an H3K27me3-high status was associated with a low p-Akt and high EGFR expression (P = 0.036 and 0.034, respectively). A weak positive correlation was found between the expression of H3K27me3 and AR (r = 0.350, P < 0.001) (**Supplementary Figure 4**).

Association Between the EZH2/H3K27me3 Expression and Clinical Outcomes

We estimated the optimal cut-off values based on survival in each cohort (Cohorts A-C). Consequently, cut-off values between the low and high LI of EZH2 and H3K27me3 in conventional therapy group (Cohort A) were determined to be 35% and 50%, respectively. These in AR-targeted therapy group (Cohort B) were 60% and 80%, respectively. Furthermore, these in HER2-targeted therapy group (Cohort C) were determined to be 65% and 70%, respectively.

In the conventional therapy group (Cohort A), although the high expression of H3K27me3 was associated with a significantly longer PFS only in the univariate analysis (P = 0.011), there were no other significant prognostic associations (**Table 3** and **Figure 3**).

In the AR-targeted therapy group (Cohort B), univariate and multivariate analyses revealed that an EZH2-high status was associated with a significantly shorter PFS (P < 0.001) (**Table 4** and **Figure 4**). A significant relationship between an EZH2-high status and a shorter OS was identified in the univariate analysis (P = 0.042), but not in the multivariate analysis. Furthermore, an EZH2-high status was associated with reduced ORR and CBR values in the univariate (P = 0.003 and 0.002, respectively) and multivariate analyses (P = 0.039 and 0.007, respectively). Furthermore, an H3K27me3-high status was associated with a shorter OS in the univariate and multivariate analyses (P = 0.027 and 0.047, respectively). There was no significant association between the H3K27me3 expression and the PFS, ORR or CBR. Waterfall plots of the maximum tumor size change from baseline according to EZH2 and H3K27me3 status are shown in **Figure 5**.

In contrast, no significant association was identified between the EZH2/H3K27me3 expression and therapeutic effect in the HER2-targeted therapy group (Cohort C) (**Table 4** and **Figures 6**, **7**).

EZH2 Y646 Activating Mutations

Two hundred and twenty-two of the 226 cases were available for gene sequencing. There were no patients with *EZH2* Y646 gain-of-function mutations.

DISCUSSION

The present findings suggested that the EZH2 and H3K27me3 expression was a predictive factor of AR-targeted therapy in SDC (42). Conversely, there was no significant association between the EZH2/H3K27me3 expression and clinical outcomes in the conventional or HER2-targeted therapy group.

In prostate cancer, the activated EHZ2 pathway is associated with resistance to AR-targeted therapy. First, this is because the overexpression of EZH2 promotes neuroendocrine differentiation

TABLE 2 | Patient characteristics and the correlation between the EZH2/H3K27me3 expression and clinicopathological factors.

Clinicopathological factors		EZH2 expression			H3K27me3 expression		
	n (%)	<60% n = 124	≥60% n = 102	*P*	<65% n = 112	≥65% n = 101	*P*
H3K27me3 expression, mean ± SD (%)		46.2 ± 25.2	61.5 ± 22.4	<0.001*	NA	NA	NA
Age, mean ± SD, years		62.7 ± 12.7	63.4 ± 12.0	0.886	62.0 ± 13.3	63.4 ± 10.9	0.588
Sex							
Male	194 (86)	106	88	0.865	96	86	0.907
Female	32 (14)	18	14		16	15	
Histologic origin							
De novo	83 (43)	57	26	0.014*	41	38	0.391
CXPA	115 (57)	59	56		64	46	
T classification							
1-2	80 (36)	46	34	0.562	34	41	0.116
3-4	144 (64)	77	67		77	59	
N classification							
0	94 (42)	62	32	0.005*	45	46	0.429
1-2	132 (58)	62	70		67	55	
M classification							
0	194 (86)	117	77	<0.001*	101	84	0.131
1	32 (14)	7	25		11	17	
Prominent nuclear pleomorphism							
Absent	68 (35)	52	16	<0.001*	36	30	0.744
Present	128 (65)	67	61		69	52	
Mitosis (/10 HPF)							
<30	98 (50)	65	33	0.108	49	45	0.265
≥30	98 (50)	54	44		56	37	
Lymphatic invasion							
Absent	119 (58)	71	48	0.827	57	55	0.056
Present	86 (42)	50	36		53	29	
Vascular invasion							
Absent	88 (43)	52	36	0.987	47	36	0.986
Present	117 (57)	69	48		63	48	
Perineural invasion							
Absent	104 (51)	62	42	0.861	55	41	0.869
Present	101 (49)	59	42		55	43	
Histologic risk stratification model†							
Low risk	43 (22)	33	10	0.015*	22	20	0.576
Intermediate or high risk	153 (78)	86	67		83	62	
AR expression, mean ± SD (%)		63.3 ± 32.0	62.3 ± 31.8	0.925	55.4 ± 34.2	70.5 ± 27.7	0.001*
HER2 status							
Negative	131 (58)	76	55	0.264	62	62	0.373
Positive	95 (42)	48	47		50	39	
Ki-67 LI, mean ± SD (%)		36.9 ± 23.3	50.5 ± 20.7	<0.001*	42.8 ± 24.4	42.9 ± 21.3	0.883
p53							
NE	127 (56)	80	47	0.005*	60	60	0.391
EN/EP	99 (44)	44	55		52	41	
TP53							
Wild-type	64 (35)	42	22	0.111	25	34	0.106
Mutation	118 (65)	63	55		62	50	

*EZH2, enhancer of zeste homologue 2; H3K27me3, histone H3 trimethylation at lysine 27; SD, standard deviation; NA, not available; CXPA, carcinoma ex pleomorphic adenoma; HPF, high-power fields; AR, androgen receptor; HER2, human epidermal growth factor receptor type 2; LI, labeling index; NE, not extreme; EN/EP, extreme negative/positive. †The histologic risk stratification model was determined by 4 histologic features (prominent nuclear pleomorphism, mitosis ≥30/10 HPF, vascular invasion, and high PDC). The total number of positive factors among these 4 was defined as indicating low to high risk as follows: low risk, 0 to 1 point; intermediate risk, 2 to 3 points; high risk, 4 points. *Statistically significant association (P < 0.05).*

and resistance to AR-targeted therapy through ataxia telangiectasia-mutated (ATM) upregulation (43, 44). Although this relationship was not investigated in this study, we are greatly interested in investigating this issue by reviewing recurrent/metastatic SDC cases with resistance to AR-targeted therapy as a future challenge. Targeting EZH2 represents a way of restoring AR signaling in neuroendocrine-differentiated tumor cells (44, 45). Second, EZH2 directly binds to the promoter of prostate-specific antigen, an AR-targeted gene, and inhibits its expression in CAB-resistant prostatic cancer cells (46). Third, EZH2 activates *AR* gene transcription through direct occupancy at its promoter (47). Therefore, there is the possibility that combination treatment targeting EZH2 and AR is an effective novel therapeutic regimen for the treatment

TABLE 3 | The association between EZH2 or H3K27me3 expression and clinical outcomes in patients with salivary duct carcinoma treated with conventional therapy.

		Progression-free survival						Overall survival					
		Univariate analysis			Multivariate analysis			Univariate analysis			Multivariate analysis		
	n	HR	95% CI	*P*	HR	95% CI	*P*	HR	95% CI	*P*	HR	95% CI	*P*
EZH2 expression													
≥35%	60	1.00	–	–	1.00	–	–	1.00	–	–	1.00	–	–
<35%	52	0.73	0.43-1.23	0.235	0.69	0.38-1.24	0.210	0.78	0.47-1.30	0.347	0.70	0.39-1.28	0.247
H3K27me3 expression													
≥50%	56	1.00	–	–	1.00	–	–	1.00	–	–	1.00	–	–
<50%	55	1.99	1.17-3.39	0.011*	1.51	0.77-2.96	0.227	1.56	0.94-2.59	0.086	0.97	0.52-1.80	0.924

Adjusted by age, sex, primary tumor site, TNM classification, first-line treatment, and histologic origin.
HR, hazard ratio; CI, confidence interval; EZH2, enhancer of zeste homologue 2; H3K27me3, histone H3 trimethylation at lysine 27.
**Statistically significant association (P<0.05).*

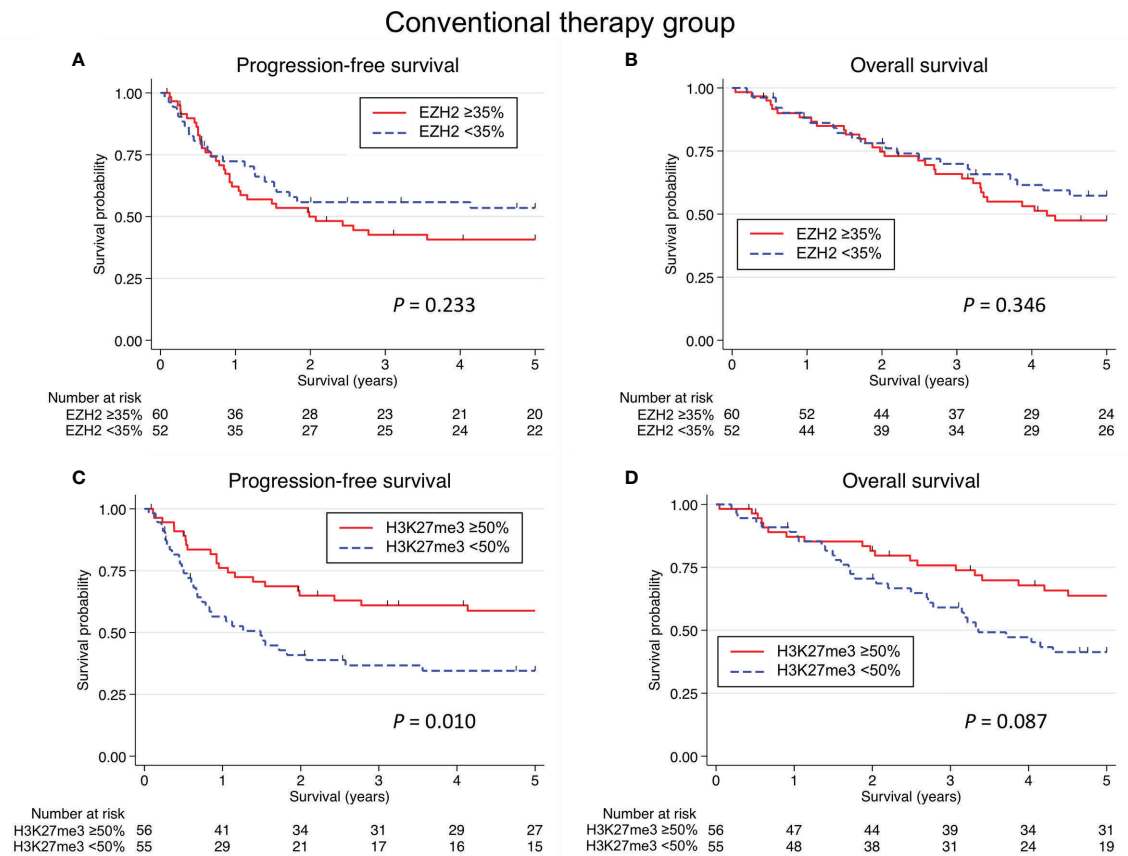

FIGURE 3 | Kaplan-Meier survival curves according to the EZH2/H3K27me3 expression in salivary duct carcinoma with conventional therapy. No significant association was identified between the EZH2 expression and the progression-free survival (PFS) **(A)** or overall survival (OS) **(B)**. **(C)** A low expression of H3K27me3 was associated with a significantly shorter PFS (*P* = 0.010), but there was no significant association between the H3K27me3 expression and the PFS in multivariate analysis. **(D)** Although a low expression of H3K27me3 tented to be associated with a shorter OS (*P* = 0.087), no significant relation between the H3K27me3 expression and the OS was detected in univariate and multivariate analyses.

of castration-resistant prostate cancer (CRPC) (46). The use of the EZH2 inhibitor tazemetostat in combination with AR-targeted therapy is currently being evaluated for its safety in CRPC (NCT04179864) (44).

In this study, the high-EZH2 expression was associated with a significantly shorter PFS and indicated a predictive factor of a poor efficacy of AR-targeted therapy assessed by ORR and CBR. The present findings suggest that SDC patients with EZH2-high status may be unsuitable for AR-targeted therapy. Combination treatment targeting EZH2 and AR might overcome resistance of AR-targeted therapy in SDC patients. Validation *via* prospective clinical trials is warranted in order to improve

TABLE 4 | The association between EZH2 or H3K27me3 expression and clinical outcomes in patients with salivary duct carcinoma treated with AR- or HER2-targeted therapy.

Variable			AR-targeted therapy									
			PFS					OS				
	n	%	median (months; 95% CI)	Univariate analysis HR (95% CI)	*P*	Multivariate analysis HR (95% CI)	*P*	median (months; 95% CI)	Univariate analysis HR (95% CI)	*P*	Multivariate analysis HR (95% CI)	*P*
EZH2 expression												
*≥60%	53	60	4.4 (2.9-5.5)	1.00	–	1.00	–	24.9 (19.3-36.0)	1.00	–	1.00	–
<60%	36	40	8.7 (7.0-11.2)	0.42 (0.26-0.68)	<0.001*	0.18 (0.09-0.36)	<0.001*	39.2 (22.2-52.2)	0.57 (0.33-0.98)	0.042*	0.53 (0.27-1.03)	0.060
H3K27me3 expression												
≥80%	32	40	5.5 (3.9-6.7)	1.00	–	1.00	–	22.4 (14.4-40.8)	1.00	–	1.00	–
<80%	48	60	5.6 (2.9-9.0)	0.63 (0.38-1.04)	0.070	0.56 (0.29-1.08)	0.081	36.0 (24.5-52.2)	0.53 (0.30-0.93)	0.027*	0.46 (0.21-0.99)	0.047*

			ORR					CBR				
				Univariate analysis		Multivariate analysis			Univariate analysis		Multivariate analysis	
			ORR % (95% CI)	OR (95% CI)	*P*	OR (95% CI)	*P*	CBR % (95% CI)	OR (95% CI)	*P*	OR (95% CI)	*P*
EZH2 expression												
≥60%	53	60	15.1 (7.6-27.7)	1.00	–	1.00	–	66.0 (52.1-77.7)	1.00	–	1.00	–
<60%	36	40	44.4 (28.8-61.2)	4.50 (1.66-12.22)	0.003*	15.56 (2.82-85.79)	0.002*	86.1 (70.0-94.3)	3.19 (1.06-9.60)	0.039*	7.81 (1.75-34.88)	0.007*
H3K27me3 expression												
≥80%	32	40	25.0 (12.7-43.4)	1.00	–	1.00	–	84.4 (66.7-93.6)	1.00	–	1.00	–
<80%	48	60	31.3 (19.5-46.0)	1.36 (0.50-3.73)	0.546	2.05 (0.49-8.56)	0.327	66.7 (51.9-78.7)	0.37 (0.12-1.14)	0.084	0.32 (0.08-1.31)	0.113

Variable			HER2-Targeted Therapy									
			PFS					OS				
				Univariate analysis		Multivariate analysis			Univariate analysis		Multivariate analysis	
	n	%	median (months; 95% CI)	HR (95% CI)	*P*	HR (95% CI)	*P*	median (months; 95% CI)	HR (95% CI)	*P*	HR (95% CI)	*P*
EZH2 expression												
≥65%	21	50	9.8 (5.9-13.8)	1.00	–	1.00	–	30.3 (13.8-39.7)	1.00	–	1.00	–
<65%	21	50	9.7 (6.3-11.3)	1.13 (0.56-2.27)	0.730	1.30 (0.57-2.94)	0.534	35.7 (16.3-61.3)	0.74 (0.34-1.60)	0.450	0.51 (0.18-1.46)	0.211
H3K27me3 expression												
≥70%	18	47	9.8 (6.6-11.9)	1.00	–	1.00	–	35.7 (NS)	1.00	–	1.00	–
<70%	20	63	9.7 (5.3-13.1)	1.13 (0.55-2.34)	0.743	1.38 (0.45-4.30)	0.573	35.4 (12.2-49.4)	1.47 (0.64-3.36)	0.367	1.31 (0.38-4.49)	0.662

(Continued)

TABLE 4 | Continued

			ORR					CBR				
				Univariate analysis		Multivariate analysis			Univariate analysis		Multivariate analysis	
			ORR % (95% CI)	OR (95% CI)	*P*	OR (95% CI)	*P*	CBR % (95% CI)	OR (95% CI)	*P*	OR (95% CI)	*P*
EZH2 expression												
≥65%	21	50	66.7 (43.2-84.0)	1.00	–	1.00	–	95.2 (70.2-99.4)	1.00	–	1.00	–
<65%	21	50	65.0 (41.0-83.2)	0.93 (0.26-3.38)	0.910	0.49 (0.08-3.00)	0.442	90.0 (65.4-97.7)	0.45 (0.04-5.39)	0.529	NS	–
H3K27me3 expression												
≥70%	18	47	77.8 (51.4-92.0)	1.00	–	1.00	–	94.4 (66.0-99.3)	1.00	–	1.00	–
<70%	20	63	57.9 (34.1-78.5)	0.39 (0.09-1.65)	0.202	0.66 (0.09-4.74)	0.676	94.7 (67.5-99.4)	1.06 (0.06-18.30)	0.969	NS	–

Adjustment by age, sex, primary tumor site, TNM classification, first-line treatment, histological origin, AR-targeted therapy (in HER2-targeted therapy group), HER2-targeted therapy (in AR-targeted therapy group).

AR, androgen receptor; HER2, human epidermal growth factor receptor type 2; PFS, progression-free survival; OS, overall survival; CBR, clinical benefit rate (complete response + partial response + stable disease ≥24 weeks); ORR, objective response rate (complete response + partial response); HR, hazard ratio; CI, confidence interval; EZH2, enhancer of zeste homologue 2; H3K27me3, histone H3 trimethylation at lysine 27.

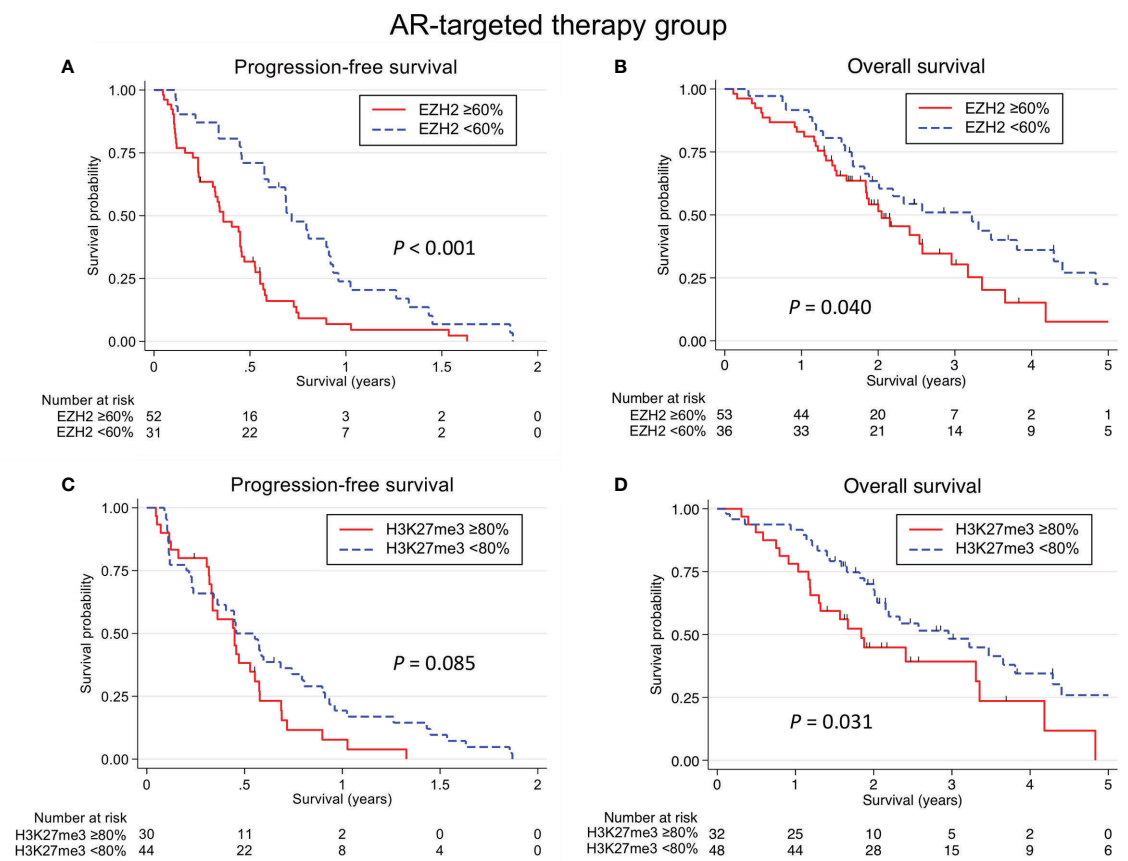

FIGURE 4 | Kaplan-Meier survival curves according to the EZH2/H3K27me3 expression in salivary duct carcinoma treated with AR-targeted therapy. An EZH2-high status was associated with a significantly shorter progression-free survival (PFS) **(A)** and overall survival (OS) **(B)** (*P* <0.001 and *P* = 0.040, respectively). **(C)** There was no significant association between the H3K27me3 expression and the PFS. **(D)** An H3K27me3-high status was associated with a shorter OS (*P* = 0.031).

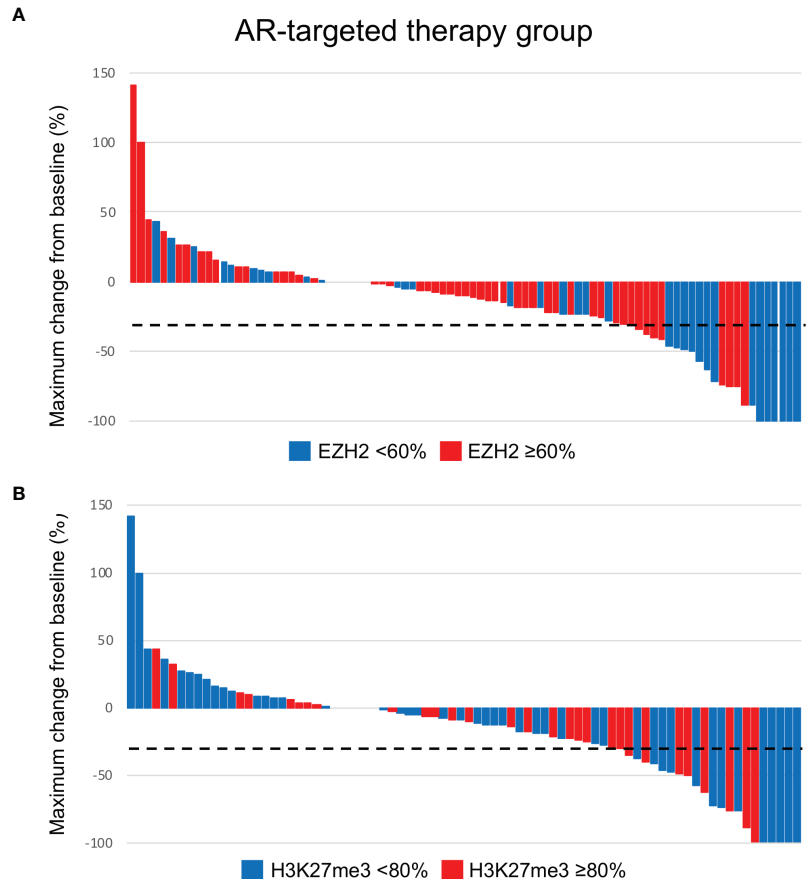

FIGURE 5 | Waterfall plots of maximum changes from baseline according to the EZH2 **(A)** and H3K27me3 **(B)** status in patients who received AR-targeted therapy. The dotted line indicates -30% of maximum change from baseline.

therapy selection and develop treatment strategies tailored for SDC patients.

In SDC patients with AR-targeted therapy, the H3K27me3 expression was not a predictive factor, but it was significantly associated with the OS. EZH2 is supposed to promote tumor progression in both an H3K27me3-dependent and H3K27me3-independent manner in cases of malignant tumor (22). Regarding the H3K27me3-dependent function, EZH2 catalyzes H3K27me3, which mediates chromatin compaction and results in the transcriptional repression of downstream genes, including tumor suppressor genes (22, 48). In contrast, as H3K27me3-independent functions, EZH2 not only promotes the methylation of non-histone proteins but also acts as a co-activator for transcription factors. These activities contribute to transcriptional suppression and co-activation (49, 50). Because the expression of EZH2 and H3K27me3 showed a weakly positive correlation in this study, the aggressiveness of SDC may be—at least partially—related to the H3K27me3-dependent function of EZH2.

In breast cancer, EZH2 activity is reported to be correlated with resistance to HER2-targeted therapy (31). However, for the present cohort of SDC patients treated with HER2-targeted therapy, as with conventional therapy, there was no association between the EZH2/H3K27me3 expression and therapeutic effect. On the other hand, we are also interested in the efficacy of certain drugs (*e.g.* trastuzumab deruxtecan) in the low-HER2 expression tumors, even in SDC (51).

An EZH2-high status was associated with aggressive clinicopathological features, including advanced N and M classification, the presence of prominent nuclear pleomorphism, intermediate or high histological risk group, a high Ki-67 LI and the aberrant expression of p53. Similar to the current findings on SDC, in various cancers, the association between the expression of EZH2 and tumor progression has been indicated (25–29). In salivary gland tumors, although the amount of data is very limited, adenoid cystic carcinoma with a high EZH2 expression showed a high Ki-67 LI (52). SDC cases with the high expression of EZH2 exhibited various aggressive clinicopathological features, but there was no significant association with the survival of patients in the conventional therapy group. One of the reasons that caused the discrepancy may be a difference in the patient population that was analyzed: all patients in **Table 2** and the conventional therapy group in **Table 3**. However, further studies are warranted to clarify the role of EZH2 in the regulation of

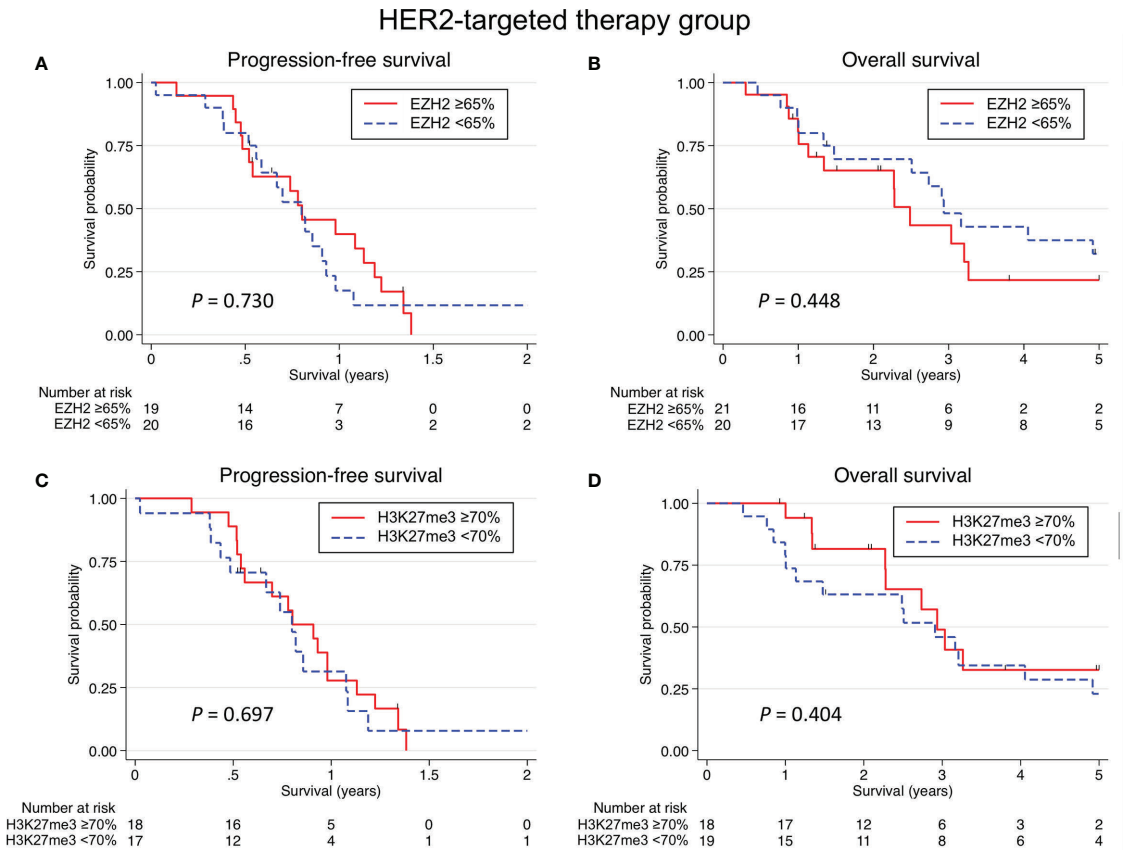

FIGURE 6 | Kaplan-Meier survival curves according to the EZH2/H3K27me3 expression in salivary duct carcinoma treated with HER2-targeted therapy. No significant association was identified between the EZH2 expression and the progression-free survival (PFS) **(A)** or overall survival (OS) **(B)**. There was also no significant association between the H3K27me3 expression and the PFS **(C)** or OS **(D)**.

biological behavior of the tumor. The *EZH2* Y646 gain-of-function mutation was not identified in SDC, in contrast to reports of its presence in lymphoma (22–24).

In colon cancer, EZH2 but not H3K27me3 expression is associated with progression from adenoma to carcinoma (53, 54). One previous report found that the majority of malignant salivary gland tumors, such as mucoepidermoid carcinoma and adenoid cystic carcinoma, showed positive EZH2 immunoreactivity, but all the investigated benign tumors, including PA, were negative (55), although no SDC cases were included in that study. In our cohort, nearly all cases with an SDC component of carcinoma ex PA expressed EZH2, whereas the PA component showed almost no expression of EZH2. In line with these findings for colon cancer, EZH2 may contribute to the malignant transformation from PA to SDC.

In our study, the ORR, median PFS, and median OS were 27.0%, 0.46 years, and 2.33 years, respectively, in the anti-androgen therapy group (n=89). On the other hand, according to the two European cohorts reported (n=34 and n=17) in the relevant literature, the outcomes varied: the ORR, median PFS, and median OS were 17.7-64.7%, 0.33-0.91 years, 1.41-3.66 years, respectively (10, 14). Thus, the outcomes of patients who received anti-androgen therapy do not necessarily seem considerably poor in comparison to the European cohorts. However, the discrepancy may be due differences in the cohort size, patient characteristics, regimens, and method of survival assessment.

In this study, we thought that it was not appropriate to apply common pre-set cut-offs when analyzing independent cohort groups. Because this is the first investigation to examine the EZH2 and H3K27me3 expression in SDC, there are no known optimal cut-off values for the EZH2 and H3K27me3 expression for any subject (e.g., clinicopathological factors in total cases or clinical outcomes in different therapeutic cohorts). Also, the biological behavior of each cohort (Cohorts A to C) varies in the present study. Therefore, in this study, to investigate the clinicopathological correlation of the EZH2 and H3K27me3 expression in the total cases we used the median values as the cutoff values. Alternatively, in Cohorts A to C, we individually estimated cut-off values according to survival. Due to the relatively small sample size in each group, internal validation was not conducted in this study. The most suitable cut-off values for the EZH2 and H3K27me3 expression should be reevaluated in a much larger series in future studies.

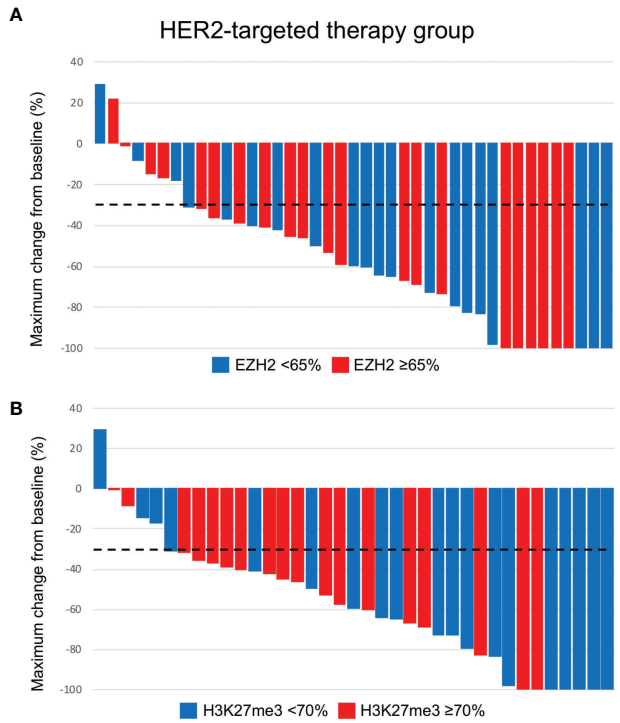

FIGURE 7 | Waterfall plots of maximum changes from baseline according to the EZH2 **(A)** and H3K27me3 **(B)** status in patients who received HER2-targeted therapy. The dotted line indicates -30% of maximum change from baseline.

Several limitations associated with the present study warrant mention. First, the nonrandomized and retrospective design may have introduced bias into the data collection. Second, in this study, functional analyses of EZH2 and H3K27me3 were not performed, and could not find out details of subcellular molecular mechanisms. Further comprehensive studies, including a clinical trial, *in vitro* cell culture and patient-derived xenograft experiments, are needed to clarify the biological role of EZH2 and H3K27me3 in the development and progression of SDC.

In conclusion, the present study showed that EZH2 and H3K27me3 are frequently but unevenly expressed in SDC. In SDC patients treated with AR-targeted therapy, the high expression of EZH2 and H3K27me3 was a potential predictor of a poor efficacy of the treatment. In addition, there is a possibility that an EZH2-high status was associated with resistance to AR-targeted therapy.

DATA AVAILABILITY STATEMENT

The original contributions presented in the study are included in the article/**Supplementary Material**. Further inquiries can be directed to the corresponding author.

ETHICS STATEMENT

The studies involving human participants were reviewed and approved by The Institutional Review Board of the International University of Health and Welfare Mita Hospital (No. 5-19-58). The patients/participants provided their written informed consent to participate in this study.

AUTHOR CONTRIBUTIONS

All authors contributed to the study conception, study design, material preparation, and data collection. Data analysis was performed by NS, HH, YT, DK, and TN. The first draft of the manuscript was written by NS and HH, and all authors commented on previous versions of the manuscript. All authors read and approved the final manuscript.

FUNDING

This work was supported by a JSPS Grant-in-Aid for Scientific Research (C) to YT (no.21K09616), TN (no. 20K07417), TM (no. 20K07597) and DK (no. 20K10508) and a Grant-in-Aid for Young Scientists to HH (no. 19K16568) and CF (no. 21K16835).

ACKNOWLEDGMENTS

The authors thank M. Yokotsuka for performing the gene mutation analysis and Y. Yamamoto for performing the immunohistochemical analysis.

SUPPLEMENTARY MATERIAL

The Supplementary Material for this article can be found online at: https://www.frontiersin.org/articles/10.3389/fonc.2021.779882/full#supplementary-material

REFERENCES

1. Nagao T, Licitra L, Loening T, Vielh P, Williams M. Salivary Duct Carcinoma. In: A El-Naggar, J Chan, J Grandis, T Takata, P Slootweg, editors. *World Health Organization Classification of Tumours, 4th*. Lyon: IARC (2017). p. 173–4.
2. D'heygere E, Meulemans J, Vander Poorten V. Salivary Duct Carcinoma. *Curr Opin Otolaryngol Head Neck Surg* (2018) 26:142–51. doi: 10.1097/MOO.0000000000000436
3. Nakaguro M, Tada Y, Faquin WC, Sadow PM, Wirth LJ, Nagao T. Salivary Duct Carcinoma: Updates in Histology, Cytology, Molecular Biology, and Treatment. *Cancer Cytopathol* (2020) 128:693–703. doi: 10.1002/cncy.22288
4. Masubuchi T, Tada Y, Maruya S, Osamura Y, Kamata SE, Miura K, et al. Clinicopathological Significance of Androgen Receptor, HER2, Ki-67 and EGFR Expressions in Salivary Duct Carcinoma. *Int J Clin Oncol* (2015) 20:35–44. doi: 10.1007/s10147-014-0674-6
5. Takase S, Kano S, Tada Y, Kawakita D, Shimura T, Hirai H, et al. Biomarker Immunoprofile in Salivary Duct Carcinomas: Clinicopathological and Prognostic Implications With Evaluation of the Revised Classification. *Oncotarget* (2017) 8:59023–35. doi: 10.18632/oncotarget.19812

6. Boon E, Bel M, van Boxtel W, van der Graaf WTA, van Es RJJ, Eerenstein SEJ, et al. A Clinicopathological Study and Prognostic Factor Analysis of 177 Salivary Duct Carcinoma Patients From The Netherlands. *Int J Cancer* (2018) 143:758–66. doi: 10.1002/ijc.31353
7. Alfieri S, Granata R, Bergamini C, Resteghini C, Bossi P, Licitra LF, et al. Systemic Therapy in Metastatic Salivary Gland Carcinomas: A Pathology-Driven Paradigm? *Oral Oncol* (2017) 66:58–63. doi: 10.1016/j.oraloncology.2016.12.016
8. van Boxtel W, Boon E, Weijs WLJ, van den Hoogen FJA, Flucke UE, van Herpen CML. Combination of Docetaxel, Trastuzumab and Pertuzumab or Treatment With Trastuzumab-Emtansine for Metastatic Salivary Duct Carcinoma. *Oral Oncol* (2017) 72:198–200. doi: 10.1016/j.oraloncology.2017.06.023
9. Fushimi C, Tada Y, Takahashi H, Nagao T, Ojiri H, Masubuchi T, et al. A Prospective Phase II Study of Combined Androgen Blockade in Patients With Androgen Receptor-Positive Metastatic or Locally Advanced Unresectable Salivary Gland Carcinoma. *Ann Oncol* (2018) 29:979–84. doi: 10.1093/annonc/mdx771
10. Boon E, van Boxtel W, Buter J, Baatenburg de Jong RJ, van Es RJJ, Bel M, et al. Androgen Deprivation Therapy for Androgen Receptor-Positive Advanced Salivary Duct Carcinoma: A Nationwide Case Series of 35 Patients in The Netherlands. *Head Neck* (2018) 40:605–13. doi: 10.1002/hed.25035
11. Takahashi H, Tada Y, Saotome T, Akazawa K, Ojiri H, Fushimi C, et al. Phase II Trial of Trastuzumab and Docetaxel in Patients With Human Epidermal Growth Factor Receptor 2-Positive Salivary Duct Carcinoma. *J Clin Oncol* (2019) 37:125–34. doi: 10.1200/JCO.18.00545
12. Geiger JL, Ismaila N, Beadle B, Caudell JJ, Chau N, Deschler D, et al. Management of Salivary Gland Malignancy: ASCO Guideline. *J Clin Oncol* (2021) 39:1909–41. doi: 10.1200/JCO.21.00449
13. National Comprehensive Caner Network. *Head and Neck Cancers* (2021). Available at: https://www.nccn.org/professionals/physician_gls/pdf/head-and-neck.pdf (Accessed july 25, 2021).
14. Locati LD, Perrone F, Cortelazzi B, Lo Vullo S, Bossi P, Dagrada G, et al. Clinical Activity of Androgen Deprivation Therapy in Patients With Metastatic/Relapsed Androgen Receptor-Positive Salivary Gland Cancers. *Head Neck* (2016) 38:724–31. doi: 10.1002/hed.23940
15. Viscuse PV, Price KA, Garcia JJ, Schembri-Wismayer DJ, Chintakuntlawar AV. First Line Androgen Deprivation Therapy vs. Chemotherapy for Patients With Androgen Receptor Positive Recurrent or Metastatic Salivary Gland Carcinoma-A Retrospective Study. *Front Oncol* (2019) 9:701. doi: 10.3389/fonc.2019.00701
16. van Boxtel W, Verhaegh GW, van Engen-van Grunsven IA, van Strijp D, Kroeze LI, Ligtenberg MJ, et al. Prediction of Clinical Benefit From Androgen Deprivation Therapy in Salivary Duct Carcinoma Patients. *Int J Cancer* (2020) 146:3196–206. doi: 10.1002/ijc.32795
17. Cappelletti V, Miodini P, Reduzzi C, Alfieri S, Daidone MG, Licitra L, et al. Tailoring Treatment of Salivary Duct Carcinoma (SDC) by Liquid Biopsy: ARv7 Expression in Circulating Tumor Cells. *Ann Oncol* (2018) 29:1599–601. doi: 10.1093/annonc/mdy141
18. Dalin MG, Desrichard A, Katabi N, Makarov V, Walsh LA, Lee KW, et al. Comprehensive Molecular Characterization of Salivary Duct Carcinoma Reveals Actionable Targets and Similarity to Apocrine Breast Cancer. *Clin Cancer Res* (2016) 22:4623–33. doi: 10.1158/1078-0432.CCR-16-0637
19. Lassche G, Tada Y, van Herpen C, Jonker MA, Nagao T, Saotome T, et al. Predictive and Prognostic Biomarker Identification in a Large Cohort of Androgen Receptor-Positive Salivary Duct Carcinoma Patients Scheduled for Combined Androgen Blockade. *Cancers* (2021) 13:3527. doi: 10.3390/cancers13143527
20. Ketel CS, Andersen EF, Vargas ML, Suh J, Strome S, Simon JA. Subunit Contributions to Histone Methyltransferase Activities of Fly and Worm Polycomb Group Complexes. *Mol Cell Biol* (2005) 25:6857–68. doi: 10.1128/MCB.25.16.6857-6868.2005
21. Han Li C, Chen Y. Targeting EZH2 for Cancer Therapy: Progress and Perspective. *Curr Protein Pept Sci* (2015) 16:559–70. doi: 10.2174/1389203716666150409100233
22. Gan L, Yang Y, Li Q, Feng Y, Liu T, Guo W. Epigenetic Regulation of Cancer Progression by EZH2: From Biological Insights to Therapeutic Potential. *biomark Res* (2018) 6:10. doi: 10.1186/s40364-018-0122-2
23. Bödör C, Grossmann V, Popov N, Okosun J, O'Riain C, Tan K, et al. EZH2 Mutations are Frequent and Represent an Early Event in Follicular Lymphoma. *Blood* (2013) 122:3165–8. doi: 10.1182/blood-2013-04-496893
24. Huet S, Xerri L, Tesson B, Mareschal S, Taix S, Mescam-Mancini L, et al. EZH2 Alterations in Follicular Lymphoma: Biological and Clinical Correlations. *Blood Cancer J* (2017) 7:e555. doi: 10.1038/bcj.2017.32
25. Bachmann IM, Halvorsen OJ, Collett K, Stefansson IM, Straume O, Haukaas SA, et al. EZH2 Expression is Associated With High Proliferation Rate and Aggressive Tumor Subgroups in Cutaneous Melanoma and Cancers of the Endometrium, Prostate, and Breast. *J Clin Oncol* (2006) 24:268–73. doi: 10.1200/JCO.2005.01.5180
26. Cai GH, Wang K, Miao Q, Peng YS, Chen XY. Expression of Polycomb Protein EZH2 in Multi-Stage Tissues of Gastric Carcinogenesis. *J Dig Dis* (2010) 11:88–93. doi: 10.1111/j.1751-2980.2010.00420.x
27. Fiskus W, Wang Y, Sreekumar A, Buckley KM, Shi H, Jillella A, et al. Combined Epigenetic Therapy With the Histone Methyltransferase EZH2 Inhibitor 3-Deazaneplanocin A and the Histone Deacetylase Inhibitor Panobinostat Against Human AML Cells. *Blood* (2009) 114:2733–43. doi: 10.1182/blood-2009-03-213496
28. Liu J, Liang L, Huang S, Nong L, Li D, Zhang B, et al. Aberrant Differential Expression of EZH2 and H3K27me3 in Extranodal NK/T-Cell Lymphoma, Nasal Type, Is Associated With Disease Progression and Prognosis. *Hum Pathol* (2019) 83:166–76. doi: 10.1016/j.humpath.2018.08.025
29. Oh EJ, Yang WI, Cheong JW, Choi SE, Yoon SO. Diffuse Large B-Cell Lymphoma With Histone H3 Trimethylation at Lysine 27: Another Poor Prognostic Phenotype Independent of C-Myc/Bcl2 Coexpression. *Hum Pathol* (2014) 45:2043–50. doi: 10.1016/j.humpath.2014.07.002
30. Bai Y, Zhang Z, Cheng L, Wang R, Chen X, Kong Y, et al. Inhibition of Enhancer of Zeste Homolog 2 (EZH2) Overcomes Enzalutamide Resistance in Castration-Resistant Prostate Cancer. *J Biol Chem* (2019) 294:9911–23. doi: 10.1074/jbc.RA119.008152
31. Hirukawa A, Singh S, Wang J, Rennhack JP, Swiatnicki M, Sanguin-Gendreau V, et al. Reduction of Global H3K27me(3) Enhances HER2/ErbB2 Targeted Therapy. *Cell Rep* (2019) 29:249–57. doi: 10.1016/j.celrep.2019.08.105
32. Marsh S, Jimeno A. Tazemetostat for the Treatment of Multiple Types of Hematological Malignancies and Solid Tumors. *Drugs Today (Barc)* (2020) 56:377–87. doi: 10.1358/dot.2020.56.6.3147937
33. Gounder M, Schöffski P, Jones RL, Agulnik M, Cote GM, Villalobos VM, et al. Tazemetostat in Advanced Epithelioid Sarcoma With Loss of INI1/SMARCB1: An International, Open-Label, Phase 2 Basket Study. *Lancet Oncol* (2020) 21:1423–32. doi: 10.1016/S1470-2045(20)30451-4
34. Morschhauser F, Tilly H, Chaidos A, McKay P, Phillips T, Assouline S, et al. Tazemetostat for Patients With Relapsed or Refractory Follicular Lymphoma: An Open-Label, Single-Arm, Multicentre, Phase 2 Trial. *Lancet Oncol* (2020) 21:1433–42. doi: 10.1016/S1470-2045(20)30441-1
35. Brierley JD, Gospodarowicz MK, Wittekind C. *TNM Classfication of Malignant Tumours. 8th*. Hoboken: Wiley-Blackwell (2017) p. 47–9. doi: 10.1002/9780471420194.tnmc07.pub3
36. Nakaguro M, Sato Y, Tada Y, Kawakita D, Hirai H, Urano M, et al. Prognostic Implication of Histopathologic Indicators in Salivary Duct Carcinoma: Proposal of a Novel Histologic Risk Stratification Model. *Am J Surg Pathol* (2020) 44:526–35. doi: 10.1097/PAS.0000000000001413
37. Wolff AC, Hammond MEH, Allison KH, Harvey BE, Mangu PB, Bartlett JMS, et al. Human Epidermal Growth Factor Receptor 2 Testing in Breast Cancer: American Society of Clinical Oncology/College of American Pathologists Clinical Practice Guideline Focused Update. *J Clin Oncol* (2018) 36:2105–22. doi: 10.1200/JCO.2018.77.8738
38. Shimura T, Tada Y, Hirai H, Kawakita D, Kano S, Tsukahara K, et al. Prognostic and Histogenetic Roles of Gene Alteration and the Expression of Key Potentially Actionable Targets in Salivary Duct Carcinomas. *Oncotarget* (2018) 9:1852–67. doi: 10.18632/oncotarget.22927
39. Boyle DP, McArt DG, Irwin G, Wilhelm-Benartzi CS, Lioe TF, Sebastian E, et al. The Prognostic Significance of the Aberrant Extremes of P53 Immunophenotypes in Breast Cancer. *Histopathology* (2014) 65:340–52. doi: 10.1111/his.12398
40. Sakr RA, Barbashina V, Morrogh M, Chandarlapaty S, Andrade VP, Arroyo CD, et al. Protocol for PTEN Expression by Immunohistochemistry in Formalin-Fixed Paraffin-Embedded Human Breast Carcinoma. *Appl*

Immunohistochem Mol Morphol (2010) 18:371–4. doi: 10.1097/PAI.0b013e3181d50bd5
41. Eisenhauer EA, Therasse P, Bogaerts J, Schwartz LH, Sargent D, Ford R, et al. New Response Evaluation Criteria in Solid Tumours: Revised RECIST Guideline (Version 1.1). *Eur J Cancer* (2009) 45:228–47. doi: 10.1016/j.ejca.2008.10.026
42. Adolfsson J, Steineck G. Prognostic and Treatment-Predictive Factors-is There a Difference? *Prostate Cancer Prostatic Dis* (2000) 3:265–8. doi: 10.1038/sj.pcan.4500490
43. Yin Y, Xu L, Chang Y, Zeng T, Chen X, Wang A, et al. N-Myc Promotes Therapeutic Resistance Development of Neuroendocrine Prostate Cancer by Differentially Regulating miR-421/ATM Pathway. *Mol Cancer* (2019) 18:11. doi: 10.1186/s12943-019-0941-2
44. Schmidt KT, Huitema ADR, Chau CH, Figg WD. Resistance to Second-Generation Androgen Receptor Antagonists in Prostate Cancer. *Nat Rev Urol* (2021) 18:209–26. doi: 10.1038/s41585-021-00438-4
45. Zhang Y, Zheng D, Zhou T, Song H, Hulsurkar M, Su N, et al. Androgen Deprivation Promotes Neuroendocrine Differentiation and Angiogenesis Through CREB-EZH2-TSP1 Pathway in Prostate Cancers. *Nat Commun* (2018) 9:4080. doi: 10.1038/s41467-018-06177-2
46. Shankar E, Franco D, Iqbal O, El-Hayek V, Gupta S. Novel Approach to Therapeutic Targeting of Castration-Resistant Prostate Cancer. *Med Hypotheses* (2020) 140:109639. doi: 10.1016/j.mehy.2020.109639
47. Kim J, Lee Y, Lu X, Song B, Fong KW, Cao Q, et al. Polycomb- and Methylation-Independent Roles of EZH2 as a Transcription Activator. *Cell Rep* (2018) 25:2808–20. doi: 10.1016/j.celrep.2018.11.035
48. He A, Shen X, Ma Q, Cao J, von Gise A, Zhou P, et al. PRC2 Directly Methylates GATA4 and Represses its Transcriptional Activity. *Genes Dev* (2012) 26:37–42. doi: 10.1101/gad.173930.111
49. Kim E, Kim M, Woo DH, Shin Y, Shin J, Chang N, et al. Phosphorylation of EZH2 Activates STAT3 Signaling *via* STAT3 Methylation and Promotes Tumorigenicity of Glioblastoma Stem-Like Cells. *Cancer Cell* (2013) 23:839–52. doi: 10.1016/j.ccr.2013.04.008
50. Xu K, Wu ZJ, Groner AC, He HH, Cai C, Lis RT, et al. EZH2 Oncogenic Activity in Castration-Resistant Prostate Cancer Cells is Polycomb-Independent. *Science* (2012) 338:1465–9. doi: 10.1126/science.1227604
51. Tsurutani J, Iwata H, Krop I, Jänne PA, Doi T, Takahashi S, et al. Targeting HER2 With Trastuzumab Deruxtecan: A Dose-Expansion, Phase I Study in Multiple Advanced Solid Tumors. *Cancer Discovery* (2020) 10:688–701. doi: 10.1158/2159-8290
52. Vékony H, Raaphorst FM, Otte AP, van Lohuizen M, Leemans CR, van der Waal I, et al. High Expression of Polycomb Group Protein EZH2 Predicts Poor Survival in Salivary Gland Adenoid Cystic Carcinoma. *J Clin Pathol* (2008) 61:744–9. doi: 10.1136/jcp.2007.054262
53. Nakazawa T, Kondo T, Ma D, Niu D, Mochizuki K, Kawasaki T, et al. Global Histone Modification of Histone H3 in Colorectal Cancer and its Precursor Lesions. *Hum Pathol* (2012) 43:834–42. doi: 10.1016/j.humpath.2011.07.009
54. Ohuchi M, Sakamoto Y, Tokunaga R, Kiyozumi Y, Nakamura K, Izumi D, et al. Increased EZH2 Expression During the Adenoma-Carcinoma Sequence in Colorectal Cancer. *Oncol Lett* (2018) 16:5275–81. doi: 10.3892/ol.2018.9240
55. Hajósi-Kalcakosz S, Vincze E, Dezső K, Paku S, Rókusz A, Sápi Z, et al. EZH2 is a Sensitive Marker of Malignancy in Salivary Gland Tumors. *Diagn Pathol* (2015) 10:163. doi: 10.1186/s13000-015-0392-z

Conflict of Interest: The authors declare that the research was conducted in the absence of any commercial or financial relationships that could be construed as a potential conflict of interest.

Publisher's Note: All claims expressed in this article are solely those of the authors and do not necessarily represent those of their affiliated organizations, or those of the publisher, the editors and the reviewers. Any product that may be evaluated in this article, or claim that may be made by its manufacturer, is not guaranteed or endorsed by the publisher.

frontiers in Oncology

ORIGINAL RESEARCH
published: 24 February 2022
doi: 10.3389/fonc.2021.771556

A Comprehensive Risk Assessment and Stratification Model of Papillary Thyroid Carcinoma Based on the Autophagy-Related LncRNAs

Yongrun Mu[1], Fuling Song[2], Kai Yuan[3], Zili Zhang[4], Yan Lu[3,5], Rongzhan Fu[3] and Dongsheng Zhou[3]**

[1] Department of Head and Neck Surgery Department, Shandong Cancer Hospital Affiliated to Shandong First Medical University, Jinan, China, [2] Department of Cardiology, The First Affiliated Hospital of Shandong First Medical University & Shandong Provincial Qianfoshan Hospital, Jinan, China, [3] Department of Thyroid Surgery Department, The First Affiliated Hospital of Shandong First Medical University & Shandong Provincial Qianfoshan Hospital, Jinan, China, [4] The Fourth People's Hospital of Jinan, The Third Affiliated Hospital of Shandong First Medical University, Jinan, China, [5] Shandong First Medical University, Jinan, China

OPEN ACCESS

Edited by:
Heming Lu,
People's Hospital of Guangxi Zhuang Autonomous Region, China

Reviewed by:
Yong-Fa Zhang,
Fudan University, China
Yaojun Zhang,
Sun Yat-sen University Cancer Center (SYSUCC), China

***Correspondence:**
Rongzhan Fu
furongzhan2014@163.com
Dongsheng Zhou
sysucczds@163.com

Specialty section:
This article was submitted to Head and Neck Cancer, a section of the journal Frontiers in Oncology

Received: *06 September 2021*
Accepted: *16 November 2021*
Published: *24 February 2022*

Citation:
Mu Y, Song F, Yuan K, Zhang Z, Lu Y, Fu R and Zhou D (2022) A Comprehensive Risk Assessment and Stratification Model of Papillary Thyroid Carcinoma Based on the Autophagy-Related LncRNAs. Front. Oncol. 11:771556. doi: 10.3389/fonc.2021.771556

Background: Papillary thyroid carcinoma (PTC) is one of the most common malignant carcinomas in the endocrine system, and it has a growing incidence worldwide. Despite the development of diagnosis and treatment modalities for thyroid carcinoma, the outcome remains uncertain. Autophagy participates in the process of cancer invasion, malignancy, metastasis, and drug resistance. Emerging research has shown that long noncoding RNAs (lncRNAs) play an important role in the process of different types of cancers. However, the interaction between the process of autophagy and lncRNA and the value of autophagy-related lncRNA for risk assessment, prediction of drug sensitivity, and prognosis prediction in PTC patients remains unknown.

Materials and Methods: We screened 1,283 autophagy-related lncRNAs and identified 144 lncRNAs with prognostic value in The Cancer Genome Atlas (TCGA) cohorts. Univariate and multivariate Cox regression analyses were used to establish the prognosis-related autophagy-related lncRNA risk classification consisting of 10 lncRNAs to indicate the level of risk, according to which the patients were grouped into high-risk group and low risk-group.

Results: The high-risk group had dramatically worse overall survival compared with the low-risk group. Cox regression analysis was performed to confirm the independent prognostic value of the autophagy-related lncRNA risk stratification, and the time-dependent receiver operating characteristic curves of the risk stratification were 0.981 (1 year), 0.906 (3 years), and 0.963 (5 years). LncRNA CRNDE (LINC00180) is overexpressed in the tumor, and its high expression matched with poorer survival state.

So, we chose it for further experiment. Finally, knockdown of the CRNDE in PTC increased the sensitivity to sorafenib.

Conclusion: Collectively, we successfully established a novel risk stratification for PTC based on the expression profiles of autophagy-related lncRNAs.

Keywords: Autophagy, LncRNA, Papillary thyroid carcinoma, Prognosis, Sorafenib

INTRODUCTION

Thyroid carcinoma is the most common endocrine malignant tumor, and 90% of this tumor type is made up of papillary carcinoma histologically (1). The improvement of thyroid-based diagnostic procedures, such as radiographic imaging and fine-needle aspiration, has contributed directly to the rapid increase of new discovered cases (2). Similarly, papillary carcinoma accounts for most of the increase (3). However, the other histological subtypes (anaplastic, medullary, and follicular) do not change markedly (4, 5). The sharp increase in mortality due to PTC has garnered increased concern from the public (3, 6, 7).

With the research on papillary carcinoma mainly focused on genetics, transcriptomics proteomics, and epigenetics, mechanistic knowledge is growing rapidly. Therefore, determining the correlation of the clinicopathological information with the genomic alternations and transcriptome has become a new area of research for many researchers (8).

The increasing risk of small thyroid nodes due to overdiagnosis alone remains controversial among clinical decision makers. Although the eighth edition of the American Joint Committee on Cancer–Union for International Cancer Control (AJCC–UICC) staging system describes that most patients at low risk have a lower mortality for differentiated thyroid cancer, there is a crucial discussion about initial therapeutic decision-making and the clinical management of those newly diagnosed (9), especially regarding the requirement for active surveillance or thyroid surgery (1).

Autophagy is a type II programmed cell death process, which directly controls physiological mechanisms by degradation of proteins and organelles to achieve homeostasis (10). It is an important pathway necessary to adjust to various stresses (11). Nevertheless, dysregulation of autophagy involved in multiple diseases, including cancer (12–14), results in both tumor suppression and oncogenesis at different stages of cancer development.

Long noncoding RNAs (lncRNAs) are a type of noncoding RNA whose length is more than 200 base pairs (15, 16). These play a role in diverse biological processes of cancer, such as tumor prognosis, immune system, and cell proliferation (17, 18).

There is still no proper risk stratification for guiding the decision maker to make the choice to perform surgery and for predicting the outcome following thyroidectomy. Here, we established a risk stratification based on the expression profiles of autophagy-related lncRNAs to predict the risk level of patients with PTC.

MATERIALS AND METHODS

Thyroid Carcinoma Data Sets

We extracted the expression data and the matched clinical information of patients with papillary thyroid carcinoma (PTC) from The Cancer Genome Atlas (TCGA, https://cancergenome.nih.gov/). Then, we classified the RNAs into either protein-coding function or lncRNA using the Ensemble human genome browser (19). The expression data for all the messenger RNAs (mRNAs) and lncRNAs in the cohort were log2 transformed [log2(FPKM+1)] for downstream analyses. A total of 508 patients whose pathological subtype is PTC were included in the study, and those whose survival time was less than 30 days were excluded because their death is likely to be classified under surgery-related death.

Cell Culture

PTC cell lines BCPAP, TPC-1, and K1 were used in the following experiment. TPC-1 and K1 were cultured in Roswell Park Memorial Institute-1640 medium (Gibco, USA) containing 10% fetal bovine serum (FBS) (Gibco, USA) and 1% antibiotics (P/S) (Gibco, NY, USA), and BCPAP was cultured in Dulbecco's modified Eagle's medium (DMEM) (Gibco, USA) containing 10% FBS (Gibco, USA) and 1% antibiotics. All samples were placed in an incubator (Thermo, USA) with 5% CO_2 at 37°C. Cells were dissociated with 0.25% trypsin at a ratio of 1:3 when their density reached 80%.

Cell Transfection

The small interfering RNAs (siRNA) were utilized for knocking down CRNDE, and scrambled siRNA (si-NC) was used as the negative control. The sequences were shown in **Supplementary Table S1**. All of them were synthesized by RiboBio (Shanghai, China). Cell transfection was performed with Lipofectamine 2000 (Invitrogen, USA) according to the product instructions. After harvesting for 48 h, the efficiency of knocking down was identified using qRT-PCR.

Cell Treatment and Proliferation Assay

Cell proliferation was measured using the Cell Counting Kit-8 (CCK-8) Assay (MedChemExpress, China) according to the manufacturer's instructions. Briefly, PTC cells with and without transfection (4×10^3 cells/well) were cultured in a 96-well plate in the presence or absence of sorafenib (MedChemExpress, China) (2 μM), and the cell viability was observed by measuring absorbance at 450 nm (24, 48, and 72 h) in a microplate reader after incubation with CCK-8 solution (10 μl) for 2 h.

RNA Extraction and Quantitative Real-Time Polymerase Chain Reaction

TRIzol (Invitrogen, CA) was used to extract total RNA from PTC cells. Here, 1 ml of TRIzol reagent was added to a 3.5-cm dish and incubated for 10 min. Following this step, 0.2 ml of chloroform was added to the dish. All the contents of the dish were transferred into tubes and shaken vigorously for 16 s. After standing in ice for 10 min, the tubes were centrifuged at 12,000 rpm for 25 min at 4°C. Finally, the RNA was washed with 75% ethyl alcohol and dissolved in diethylpyrocarbonate (DEPC) water. Then, 1 μg extracted RNA retrieved in the above step was reverse-transcribed into cDNA in a 20-μl reaction volume by using the First Strand cDNA Synthesis Kit (Takara, Japan) according to the manufacturers' instructions. The cDNA was used as a template for real-time PCR by using matched primers. The sequences used in quantitative PCR were shown in **Supplementary Table S1**. The length of amplified products was within 300 bp. The real-time PCR was performed with a 20-μl reaction system containing 2 μl cDNA, 2 μl of mix of primer, 4 μl dd H_2O, and 10 μl SYBR Green Real-Time PCR Master Mix (Takara, Japan). The detailed reaction conditions were set by referring to the manufacturers' instructions. Data were analyzed by using the ΔΔCt method, where the endogenous housekeeping gene *β-actin* was used as a quantity and quality control.

Obtaining Autophagy-Associated Gene Sets and Identification of Autophagy-Related LncRNAs by Coexpression Analysis

A total of 232 autophagy genes were obtained from the Human Autophagy Database (HADb; http://www.autophagy.Lu), which provides a comprehensive and up-to-date list of human genes involved in autophagy and is shown in **Supplementary Table S2**. The Pearson correlation coefficient was calculated between the expression of autophagy genes and autophagy-related lncRNAs. Autophagy-related lncRNAs were selected based on the absolute value of the coefficient being >0.3 ($|R|>0.3$), and a P value <0.001 was considered significant. Detailed information on the correlation between lncRNAs and autophagy-related genes is shown in **Supplementary Table S3**.

Construction of a Protein–LncRNA Interaction Network

To further explore the interaction between lncRNAs and autophagy genes, we established an lncRNA and mRNA network using the Search Tool for the Retrieval of Interacting Genes/Proteins (STRING). The software Cytoscape 3.8.1 was used to visualize the relationship between lncRNAs and mRNAs.

Construction of the Prognostic Risk Stratification

Univariate and multivariate Cox regression analyses were performed to identify potential autophagy-related lncRNAs with prognostic value. The autophagy lncRNAs with a P value <0.01 were submitted to the next step to perform the multivariate Cox regression analysis. The risk stratification based on the expression of autophagy-related lncRNAs was established by using the candidate lncRNAs obtained from the multivariate Cox regression. The linear risk formula was RiskScore = (Coef1 × Expression Gene1) + (Coef2 × Expression Gene2) + (Coef3 × Expression Gene 3) + (Coef4 × Expression Gene4) + (Coef5 × Expression Gene5) +……+ (Coef Gene N × Expression Gene N).

Based on the expression profiles of autophagy-related lncRNAs, we conducted a principal component analysis (PCA) to investigate the difference between the high-risk group and low-risk group.

Gene Set Enrichment Analysis

Gene set enrichment analysis (GSEA) was performed using GSEA software (Version 4.1.0). All operations were performed as previously described (19–22). The results of GSEA were visualized using an enrichment map. Each analysis of gene set permutation was calculated 1,000 times, and pathways enriched in specific phenotypes were sorted by normalized enrichment score (NES) and P value. Relevant gene sets were obtained from the gene set database of Kyoto Encyclopedia of Genes and Genomes (KEGG) pathways detailed in **Supplementary Figure S2**.

Statistical Analysis

A Cox regression model was employed to construct the risk stratification. The hazard ratio (HR) and associated 95% confidence interval (CI) were calculated. From the analysis of two subgroups based on the median value of risk score, the overall survival (OS) times of the high-risk and low-risk subgroups were calculated and analyzed *via* Kaplan–Meier test and compared using the log-rank test. The time-dependent receiver operating characteristic (ROC) curve was used to evaluate the predictive accuracy of the autophagy-related lncRNAs.

RESULTS

Identification of Prognostic Autophagy-Related LncRNAs in Papillary Thyroid Carcinoma

By constructing the coexpression network of the 232 autophagy genes, a total of 1,283 autophagy-related lncRNAs were obtained (**Figures 1A–D**). Then, we performed Cox proportional hazards analysis to obtain 144 autophagy lncRNAs with significant prognostic value by analyzing the expression profile (**Figure 1**). There were 32 lncRNAs with low risk (HR <1) and 112 lncRNAs with high risk (HR >1) (**Supplementary Table S4**). Following this, multivariate Cox analysis was performed to further screen 10 lncRNAs from 144 autophagy lncRNAs with prognostic value, and they were AC008063.1, AC011297.1, FAM201A, AC092279.1, LINC00900, AL162231.2, CRNDE, TONSL-AS1, LINC02454, and AC004918.3 (**Figures 4A–J**) (**Supplementary Table S5**).

Construction of a Prognostic Model

Then, these optional lncRNAs were submitted to the next step to construct the prognostic risk stratification of autophagy-related

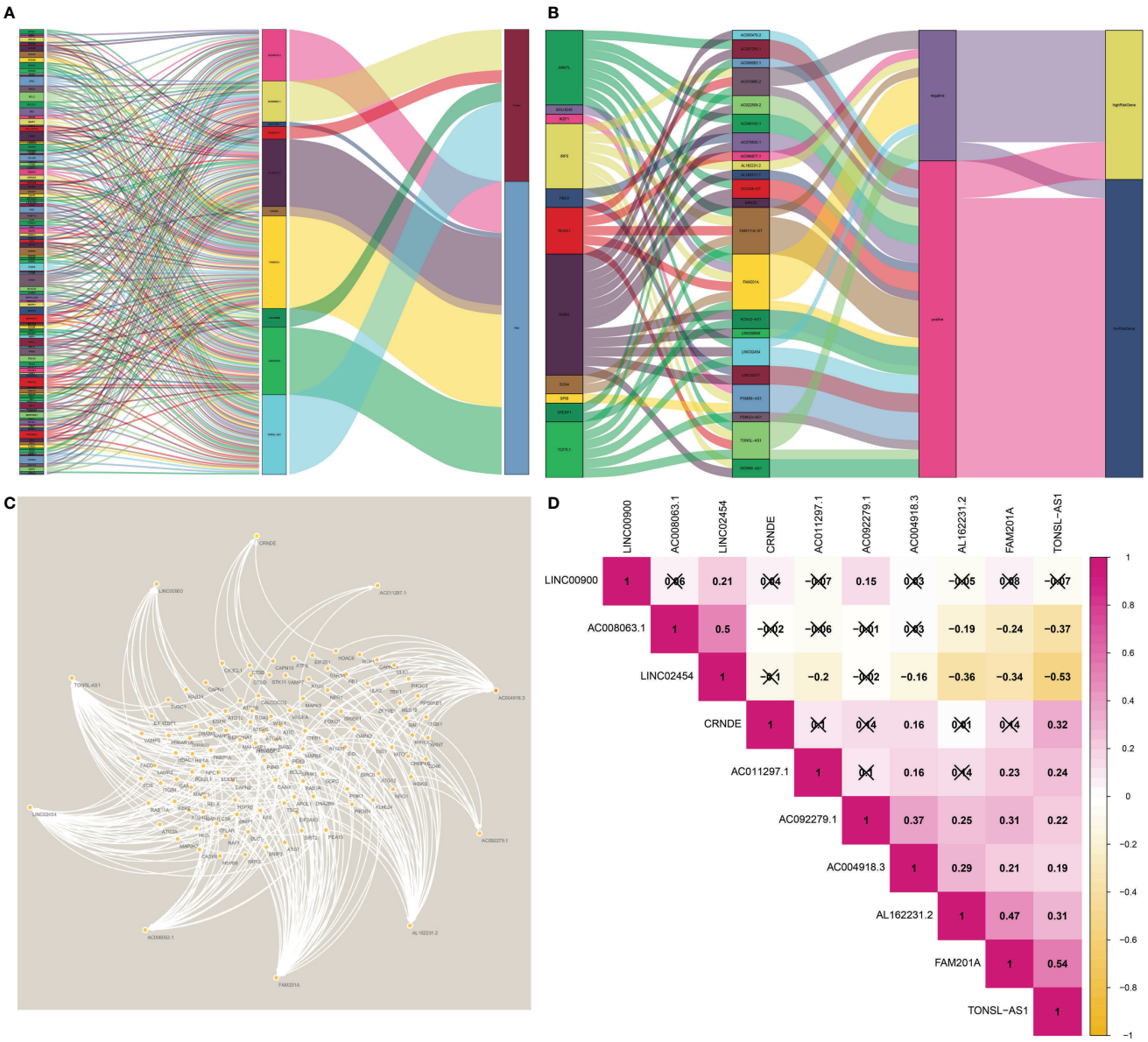

FIGURE 1 | Construction of the regulation network of the long noncoding RNAs (lncRNAs) with prognostic value and autophagy genes in papillary thyroid carcinoma (PTC). **(A)** The coexpression network of the 10 autophagy-related lncRNAs–messenger RNAs (mRNAs) with prognostic value was constructed and visualized using Sankey diagram between prognostic risk-related lncRNAs, mRNAs, and risk types (risk or protective). **(B)** The coexpression network of autophagy-related lncRNAs and matched transcriptional factors was constructed and visualized using Sankey diagram. **(C)** The network of autophagy gene and autophagy-related lncRNA. **(D)** The correlation of expression levels of lncRNAs involved in the risk stratification.

lncRNAs. We established a coexpression network of autophagy-related lncRNAs with prognostic value and mRNAs, as shown in (**Figures 1A, C**). And the formula is as follows:

Risk score = (AC008063.1*-1.740157523) + (AC011297.1*0.171231624) + (FAM201A*0.895715416) + (AC092279.1*-3.730086976) + (LINC00900*-2.38496601) + (AL162231.2*0.671649156) + (CRNDE*0.450612252) + (TONSL-AS1*-0.79310585) + (LINC02454*0.588168097) + (AC004918.3*2.412626944).

Based on the risk formula and median risk score, the PTC patients were divided into a high-risk group and a low-risk group (**Figure 2A**). Kaplan–Meier survival analysis showed that patients in the high-risk group had shorter OS than that in the low-risk group (**Figure 2B**), which suggested that the risk stratification had good prognostic prediction ability.

A scatter plot of survival status and risk curve were made in order to display the risk score and the corresponding survival

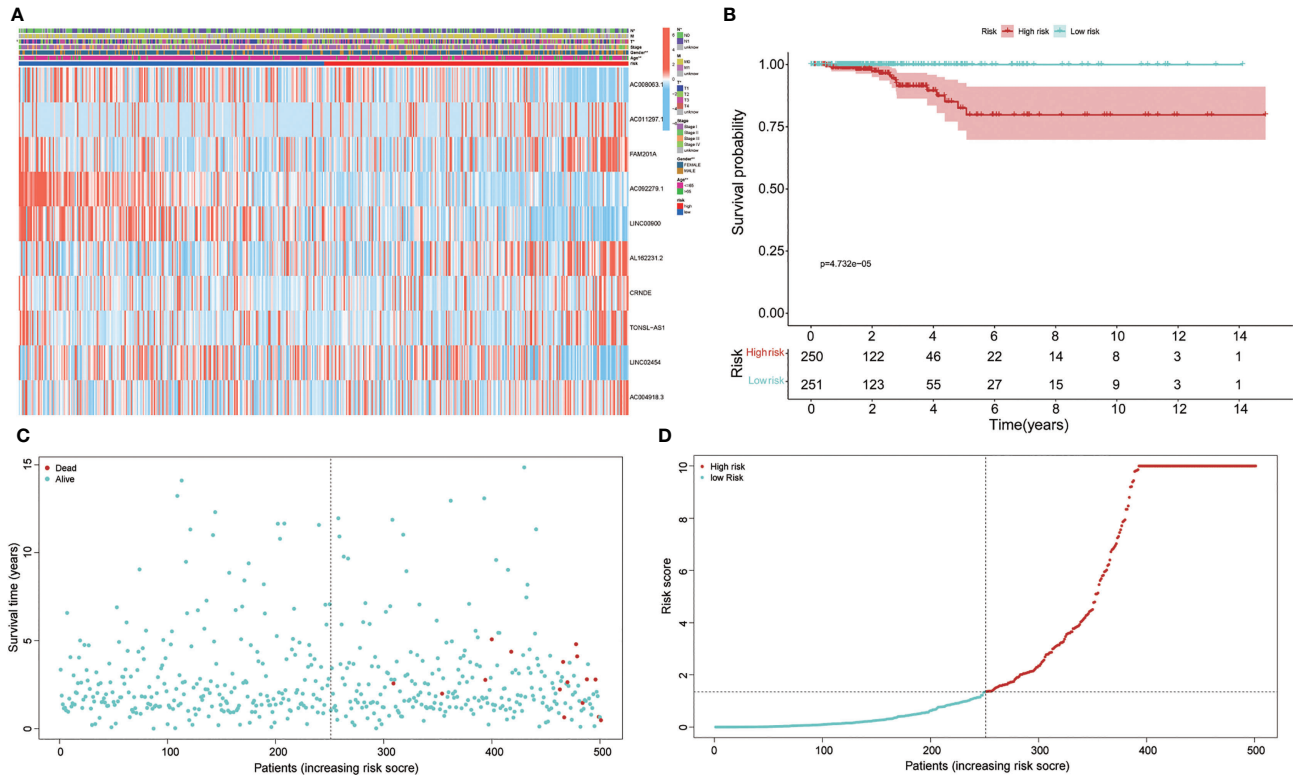

FIGURE 2 | Prognosis and expression of risk genes in the two groups of papillary thyroid carcinoma (PTC) patients. **(A)** The heatmap displayed the expression levels of autophagy-related long noncoding RNAs (lncRNAs) in the high-risk and low-risk groups. **(B)** Kaplan–Meier survival analysis of the high-risk and low-risk groups based on the risk stratification. **(C)** The scatter plot based on the survival status of each patient. The different colors matched the status of survival and death. **(D)** The risk curve was drawn based on the risk score of each sample. The different colors matched the status of risk.

status of PTC patients, the results of which showed that the higher risk score corresponded to higher mortality. At the same time, the heatmap was drawn based on these 10 autophagy-related lncRNAs in the PTC samples (**Figure 2A**). The survival curve (**Figures 2B–D**). The heatmaps displayed the expression of these elements in the high-risk group and low-risk group. Hence, these results indicate that all 10 autophagy lncRNAs have good prognostic value for PTC (**Figures 2**, **3**).

Evaluation of the Risk Stratification Based on the 10 Autophagy-Related LncRNAs as an Independent Prognostic Factor for Papillary Cancer Patients

Univariate and multivariate Cox regression analyses were employed to determine whether the risk stratification based on autophagy-related lncRNAs was an independent prognostic factor of PTC. The HR and 95% CI of the risk score based on the risk stratification were 1.003014104–1.00616136988199 ($P < 0.05$) in the univariate Cox regression analysis and 1.004196324–1.00559955694039 ($P < 0.05$) in the multivariate Cox regression analysis (**Figures 3D, E**). The results showed that the risk stratification based on autophagy-related lncRNAs was a powerful significant prognostic factor of PTC, independent of clinicopathological characteristics such as tumor size, metastasis of lymph node and distant metastasis, sex, and TNM stage. The ROC curve was plotted to evaluate and estimate the predictive specificity and sensitivity of the risk stratification based on the autophagy-related lncRNAs (**Figure 8**). The time-dependent area under the curve (AUC) for 1, 3, and 5 years was 0.981, 0.901, and 0.963, respectively (**Figure 3B**). At the same time, the AUC of the other clinical characteristic including T, N, M, age, and TNM (stage) was calculated, and the AUC value of the risk score exceeded most of the others (**Figure 3C**). These results indicate that the risk stratification based on autophagy-related lncRNAs was an effective independent prognostic factor for PTC patients. Subgroup analysis was performed based on the risk stratification (**Figures 5C–N**). Besides, those patients both with high tumor mutation burden (TMB) levels and high risk exhibited a poorer survival state (**Figures 5A, B**). PCA results show that the model has an excellent ability to distinguish high-risk and low-risk patients (**Figures 6A–D**). DNA stemness score (DNAss) and RNA stemness score (RNAss) presented significant differences among the two subgroups (**Figures 6E, F**). Different risk types possessed different TIME statuses, Immunogenomics features (**Figure 7**).

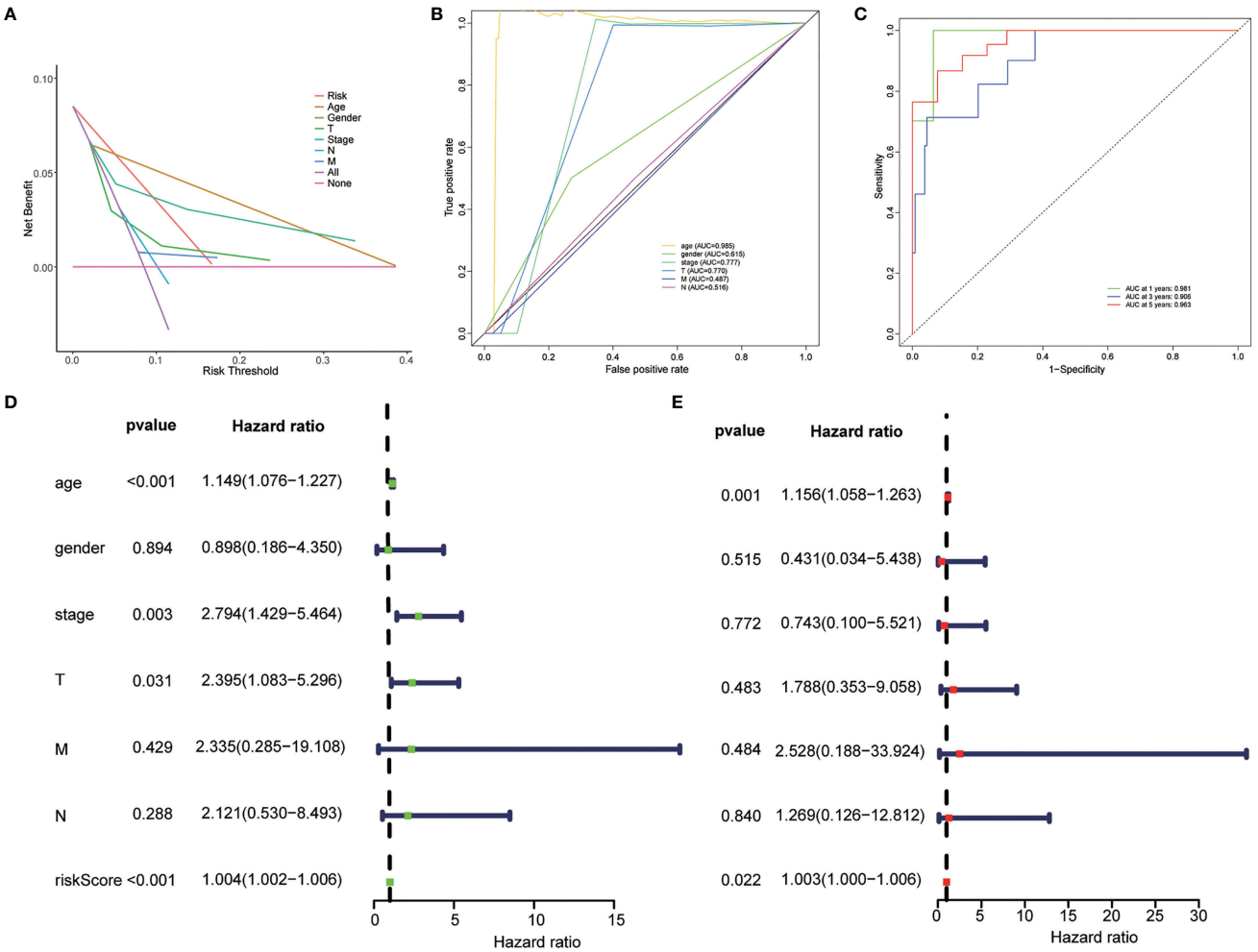

FIGURE 3 | Evaluation of the clinical utility of the risk stratification. **(A)** DCA curve was drawn based on the risk stratification. **(B)** The area under the curve (AUC) value of clinical features according to the receiver operating characteristic (ROC) curves. Clinical features: Age, TNM stage, gender, T (tumor size), N (lymph node metastasis), and M (distant metastasis). **(C)** ROC curve of the risk stratification showing the prognostic performance of the autophagy-related long noncoding RNA (lncRNA) risk stratification. **(D)** The univariate Cox regression analysis of the risk model score and clinical features regarding prognostic value. **(E)** The multivariate Cox regression analysis of the risk model score and clinical features regarding prognostic value.

Knocking Down CRNDE Significantly Improves the Sensitivity of Papillary Thyroid Carcinoma Cell Line for Sorafenib

Interestingly, most of the risk genes involved in the stratification system with higher expression in PTC samples matched better prognosis (**Figures 4F**, **8R**). After further validation, we found that those patients with higher CRNDE expression matched worse survival state.

We tried to evaluate the association between the risk stratification and the efficacy of chemotherapeutics based on the THCA cohort of TCGA project. Interestingly, the results showed that higher risk score based on the risk stratification was associated with higher half inhibitory concentration (IC50) of sorafenib ($P < 0.01$) (**Figure 8K**).

Next, we chose lncRNA CRNDE from the 10 autophagy lncRNAs and investigated if it could mediate cancer cell survival under sorafenib challenge. By directly knocking down CRNDE in the PTC cell line (Bacap-1, TPC-1, and K1), CCK-8 assay showed that knocking down CRNDE partially increased the effects of sorafenib-induced cell death in PTC cells with si-CRNDE transfection (**Figures 8I–III**). All those results suggested that CRNDE plays a positive role in tumorigenesis and may regulate the sorafenib sensitivity of PTC cells (**Figures 8IV–VI**).

DISCUSSION

Over the past year, the diagnostic rate of thyroid cancer has increased rapidly because of the popularization and widespread application of various imaging techniques. PTC lists on top of head and neck cancers. Currently, the comprehensive treatment strategy of combining surgery, thyroid hormone

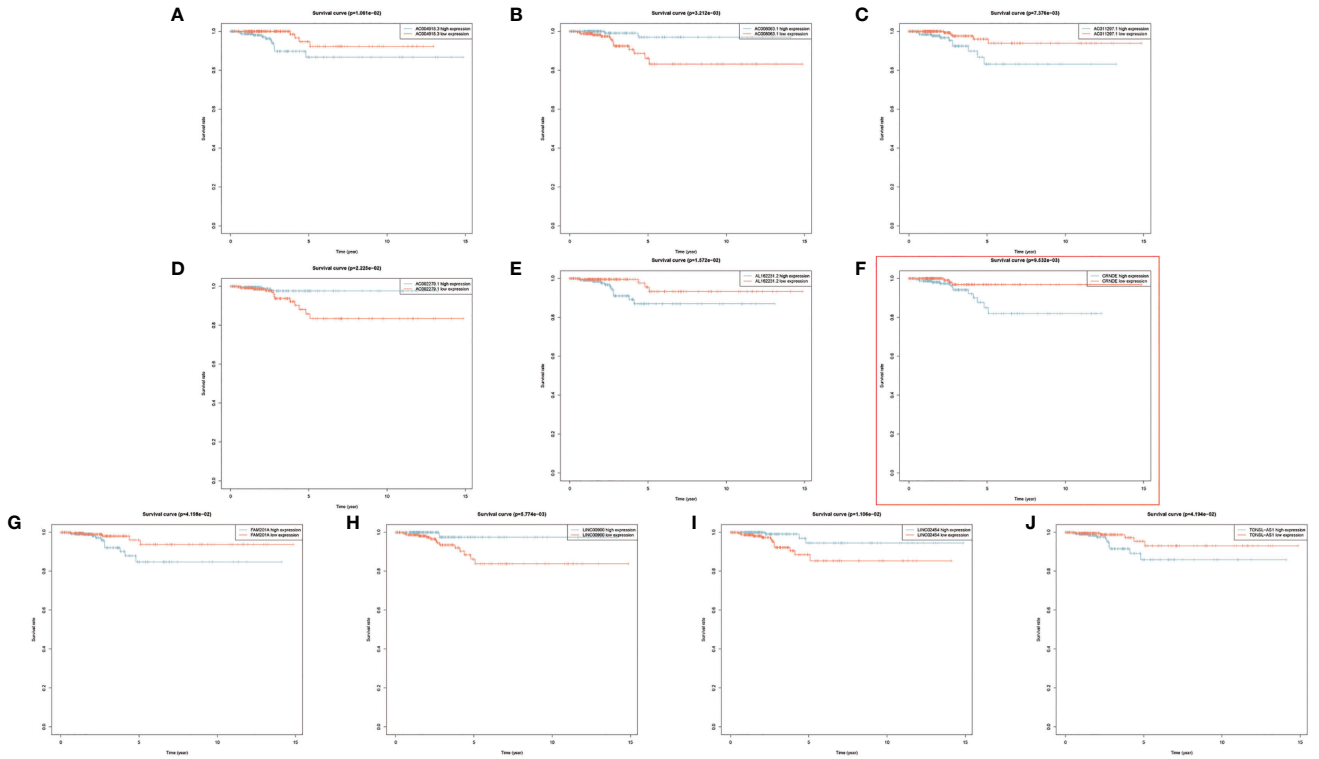

FIGURE 4 | **(A–J)** Kaplan–Meier survival analyses of 10 prognostic risk-related autophagy-related long noncoding RNA (lncRNA).

therapy, and internal radiotherapy is widely accepted. However, the definitive molecular mechanisms contributing to the malignant phenotype of PTC remain poorly explored. The high occurrence of thyroid cancer has been shown to have a close relationship with daily iodine intake and disorders of thyroid-stimulating hormone (TSH) levels, and a strong association was also proven that some PTC patients exposited to ionizing radiation (23).

Abnormal expression state of specific genes including tumor suppressor genes and oncogenes and epigenetics process such as methylation of promoters and acetylation of histone are involved in the heterogeneity of PTC. The common classical oncogenic alterations are found in the tumorigenesis of PTC, among which activating mutation in BRAF lists as first among common genetic alterations. BRAF V600E mutation has been verified as a powerful prognostic marker to evaluate the risk of PTC (24). The mutation of BRAF gene has a strong correlation with aggressive clinical characteristics such as metastasis of lymph node, extra thyroid diffusion, high recurrence rate, and resistance to radioactive iodine. Mutation of BRAF reduces the ability of cancer cells to take up iodine. The status of telomerase reverse transcriptase (TERT) mutation has been discovered to serve as an independent prognostic factor for PTC (25). NTRK, HRAS, KRAS, NRAS, RET, RET/PTC, and PAX8/PPARγ gene mutations were proven as oncogenic driver mutations in tumorigenesis of PTC (26–28). The unique oncogene duet of coexisting BRAF V600E and TERT promoter mutations is widely proven to be a robust genetic background promoting thyroid cancer aggressiveness (29–31). Systematic identification and analysis of these oncogenic alterations will help clinical decision makers better diagnose, predict the prognosis, and make the appropriate treatment decision.

Currently, the exploration of molecular biomarkers and development of relative risk stratification are of great interest in cancer research, including screening for new effective diagnostic biomarkers of early-stage cancer, establishing new risk stratifications to predict the OS of cancer patients and new drug research and development.

The discovery of thousands of noncoding RNAs has changed the conventional concept that biological processes are mostly regulated by genes with protein-coding ability (32). There is much research indicating that lncRNAs participate in the process of tumorigenesis. More recently, lncRNAs are associated with various biological behaviors of PTC, including autophagy (33–35), invasion (36, 37), and metastasis (38) by acting as cancer oncogenes or suppressor genes. Although accumulating evidence has shown that the mRNA expression profile could be regarded as a powerful predictive tool for patients suffering from cancer, the risk stratification based on the lncRNA profile has been shown to have an excellent prognostic value because lncRNAs act in a functional mode that is different from that of mRNA with coding ability (39–42). The abnormal expression of particular lncRNAs in cancer is a response to cancer progression, and they

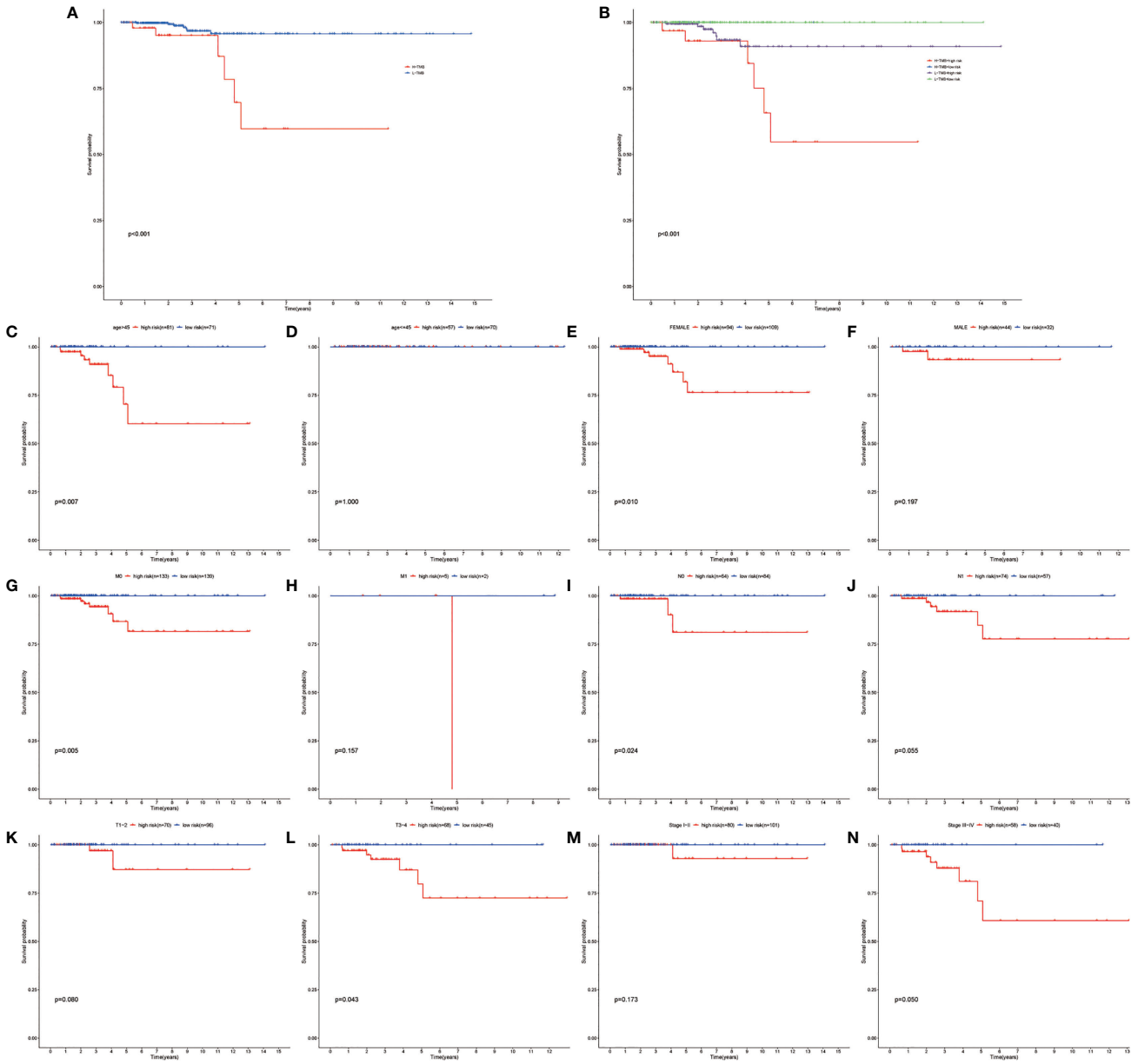

FIGURE 5 | Performing the survival analysis combining TMB with risk stratification. **(A)** Kaplan–Meier survival analyses of high-TMB and low-TMB papillary thyroid carcinoma (PTC) group. **(B)** Kaplan–Meier survival analyses of high TMB combined with high risk, high TMB combined with low risk, low TMB combined with high-risk group, and low TMB combined with low-risk group. **(C–N)** Kaplan–Meier survival analyses of the autophagy-related long noncoding RNA (lncRNA) risk stratification in different subgroups.

could serve as powerful independent biomarkers for diagnosis and prognosis. However, the prognostic value of lncRNAs in PTC has not been systematically explored. Meanwhile, it is often difficult to accurately risk stratify and make an optimal benefit–harm balance of management of PTC, particularly for the risk stratification of small nodules and prediction of OS.

In this study, we established a risk stratification based on the expression profile of autophagy lncRNAs. In order to identify target lncRNAs, we performed coexpression analysis and obtained 1,283 autophagy-related lncRNAs ($|R|>0.3$ and P value <0.001). After performing univariate and multivariate analyses, autophagy-related lncRNAs with independent prognostic values were selected to construct a risk score model by using matched expression levels. According to the median risk score, the patients were assigned to the high-risk group and low-risk group. Consistent with our assumptions, patients in the high-risk group tended to have worse OS than that in those in the low-risk group. We draw the ROC curve and

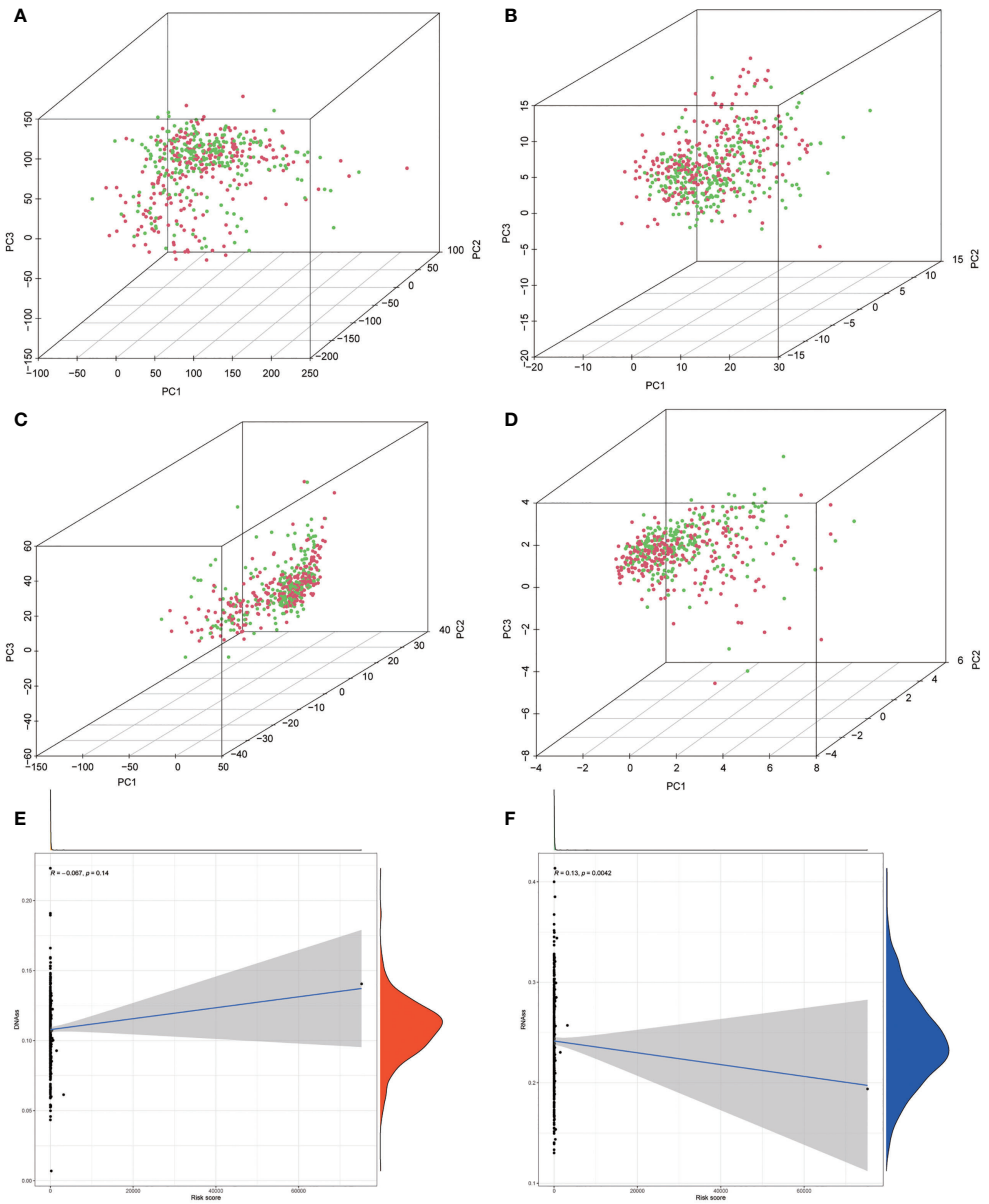

FIGURE 6 | **(A–D)** Principal component analysis (PCA) between the low-risk and high-risk groups based on risk stratification. **(A)** The whole genome. **(B)** Autophagy-related encoding genes. **(C)** Autophagy-related long noncoding RNA (lncRNA). **(D)** The risk model of the 10 autophagy-related lncRNA expression profiles. **(E, F)** The correlation among risk stratification and tumor stem cell score (based on RNA expression and DNA methylation). **(E)** The correlation between the risk stratification and DNA stemness index. **(F)** The correlation between the risk stratification and RNA stemness index.

calculated its AUC value. All the results showed that the risk stratification could easily classify the risk state of PTC. Among the lncRNAs composing the risk stratification, AC008063.1, AC092279.1, LINC00900, and LINC02454 were protective factors. AC004918.3, AC011297.1, AL162231.2, CRNDE, FAM201A, and TONSL-AS1 were risk-related factors. Besides, we employed the Cox regression analysis and certified that the risk stratification is an independent factor of PTC. At the same time, we evaluated the clinical value of the risk stratification in clinical characteristics including age, gender, tumor, node, metastasis, and TNM staging classification. We also made comprehensive and systematic estimation of tumor-infiltrating cells through different databases and immunosuppressed molecules based on the risk stratification.

The initial intervention of PTC always starts with surgical resection of the gland with primary tumor and the metastatic lymph nodes (43, 44). However, the management of advanced

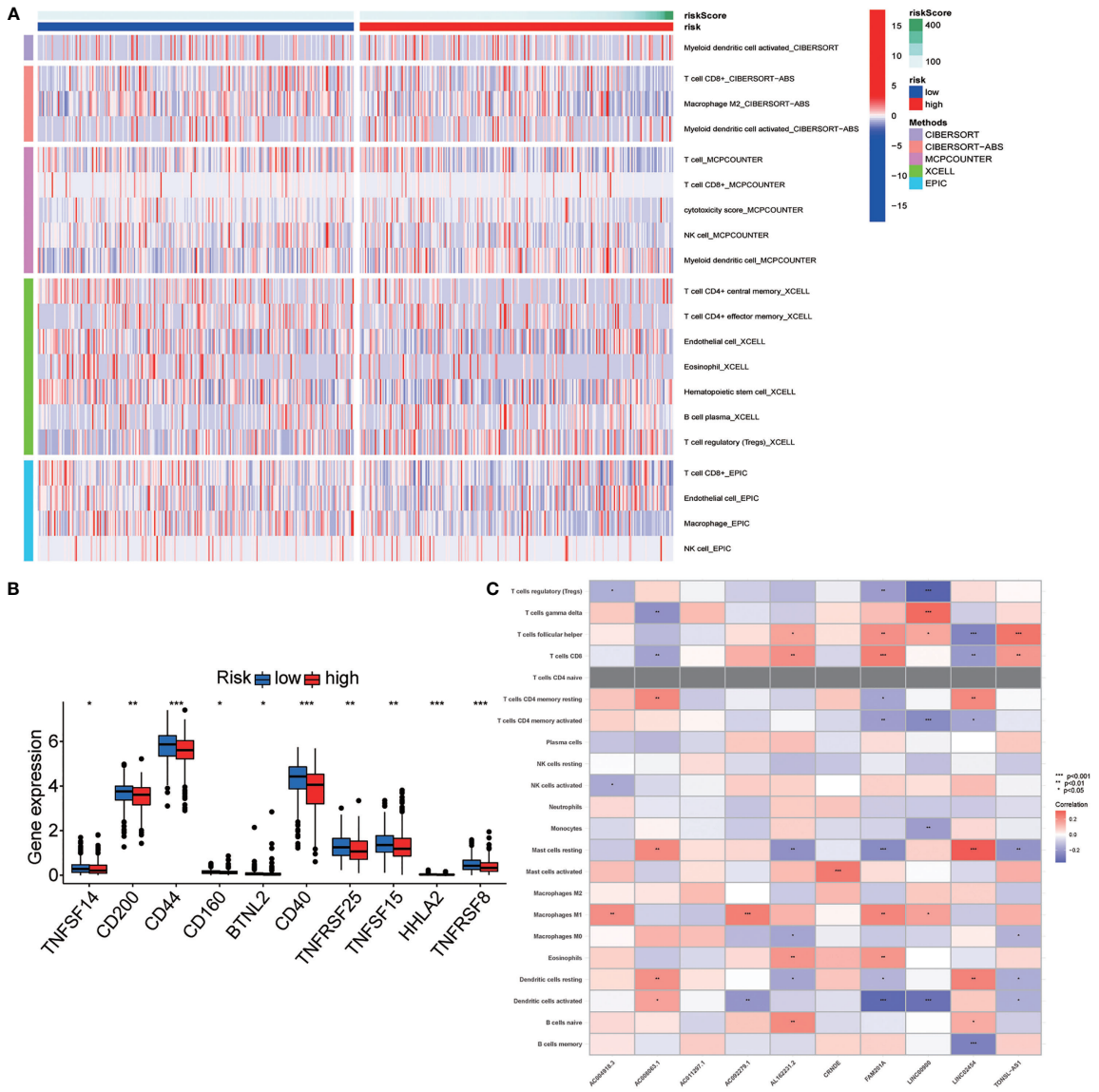

FIGURE 7 | Exploration of the association of the risk stratification with tumor immunity. **(A)** Immune infiltration statuses among high-risk group and low-risk group through TIMER, CIBERSORT, XCELL, QUANTISEQ, MCPcounter, EPIC, and CIBERSORT database. **(B)** Differential expression checkpoint gene in papillary thyroid carcinoma (PTC) sample of high-risk and low-risk patients. **(C)** Correlation between the long noncoding RNA (lncRNA) involved in the risk stratification and immune cell infiltration. Symbols *, **, *** means that p-value <0.05, <0.01 and <0.001, respectively.

PTC patients with a high risk of recurrent disease and exhibiting radioactive iodine refractoriness is still full of intractability after undergoing total thyroidectomy (45, 46). The patients mentioned above may be candidates to benefit from drug therapy. Therefore, we explored the association between the risk stratification and the efficacy of common chemotherapeutics based on the THCA cohort of TCGA project. The IC50 of sorafenib in the high-risk group is higher than that of the low-risk group. A risk lncRNA CRNDE was chosen for further study, and the experimental evidence showed that knocking down CRNDE might enhance sensitivity to sorafenib in *in vitro* experiments.

We hope the risk stratification based on the autophagy-related lncRNAs helps the clinical worker identify patients with conventionally high risk of PTC and could contribute to the management of patients with PTC.

Our research focused on autophagy-related lncRNAs, and there are certain limitations in our research. First, our studies were based on TCGA cohort and need to be further validated using another additional cohort with a long follow-up time. While low mortality is a characteristic of PTC, there is an absence of cohorts with sufficiently long follow-up. Furthermore, further experiments need to be carried out to

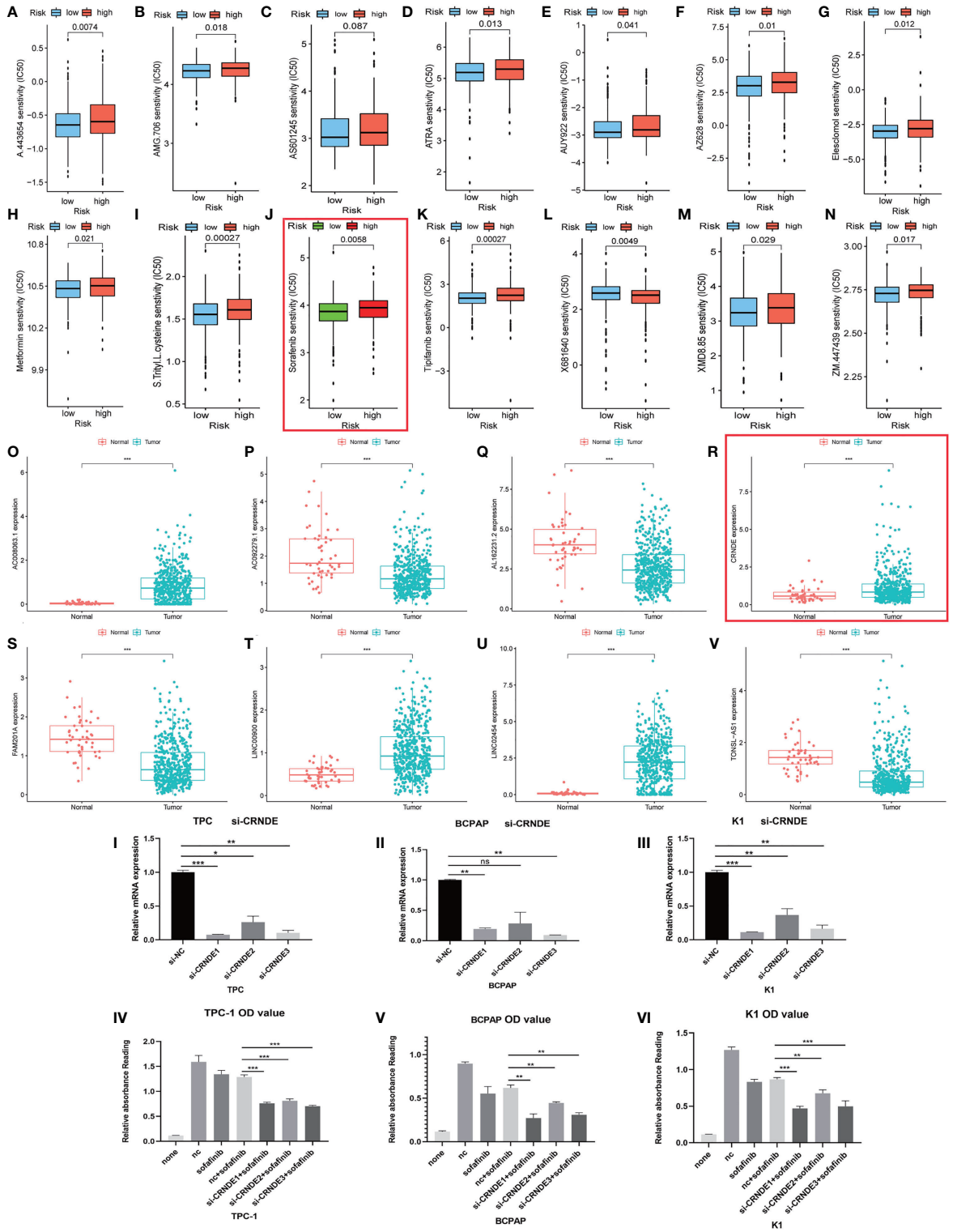

FIGURE 8 | Evaluation and valuation of the prediction ability of sensitivity of risk stratification for common clinical chemotherapies and targeted therapies. **(A–N)** The risk stratification also can act as a powerful predictor of chemosensitivity for clinical chemotherapeutics. **(O–V)** The expression of 10 long noncoding RNAs (lncRNAs) in papillary thyroid carcinoma (PTC) and normal tissue. (IV–VI) Here, 2 μM sorafenib was added after knocking down CRNDE in three PTC cell lines. I-III: Efficiency of knocking down were confirmed with qRT-PCR. Symbols *, **, *** means that p-value <0.05, <0.01 and <0.001, respectively. The expanded form of ns means that no significance.

determine the mechanisms and functions of these autophagy-related lncRNAs in the tumorigenesis of PTC.

DATA AVAILABILITY STATEMENT

The original contributions presented in the study are included in the article/**Supplementary Material**. Further inquiries can be directed to the corresponding authors.

AUTHOR CONTRIBUTIONS

Conception and design: DZ and RF. Administrative support: KY and YL. Provision of data: YM. Collection and assembly of data: YM. Data analysis and interpretation: YM, FS, and YL. Article writing: YM and ZZ. All authors contributed to the article and approved the submitted version.

FUNDING

This study was funded by the National Natural Science Foundation (81702752), Shandong Province Natural Science Foundation (ZR2017BH076), and Shandong Province Science and Technology Key Project (2017GSF18145).

ACKNOWLEDGMENTS

We thank the researchers who gave their data for this analysis from TCGA.

SUPPLEMENTARY MATERIAL

The Supplementary Material for this article can be found online at: https://www.frontiersin.org/articles/10.3389/fonc.2021.771556/full#supplementary-material

REFERENCES

1. Wang TS, Sosa JA. Thyroid Surgery for Differentiated Thyroid Cancer - Recent Advances and Future Directions. *Nat Rev Endocrinol* (2018) 14 (11):670–83. doi: 10.1038/s41574-018-0080-7
2. Sosa JA, Hanna JW, Robinson KA, Lanman RB. Increases in Thyroid Nodule Fine-Needle Aspirations, Operations, and Diagnoses of Thyroid Cancer in the United States. *Surgery* (2013) 154(6):1420–6. doi: 10.1016/j.surg.2013.07.006
3. Kitahara CM, Sosa JA. The Changing Incidence of Thyroid Cancer. *Nat Rev Endocrinol* (2016) 12(11):646–53. doi: 10.1038/nrendo.2016.110
4. Davies L, Welch HG. Increasing Incidence of Thyroid Cancer in the United States, 1973-2002. *JAMA* (2006) 295(18):2164–7. doi: 10.1001/jama.295.18.2164
5. Chen AY, Jemal A, Ward EM. Increasing Incidence of Differentiated Thyroid Cancer in the United States, 1988-2005. *Cancer* (2009) 115(16):3801–7. doi: 10.1002/cncr.24416
6. Cramer JD, Fu P, Harth KC, Margevicius S, Wilhelm SM. Analysis of the Rising Incidence of Thyroid Cancer Using the Surveillance, Epidemiology and End Results National Cancer Data Registry. *Surgery* (2010) 148(6):1142–52. doi: 10.1016/j.surg.2010.10.016
7. Kent WDT, Hall SF, Isotalo PA, Houlden RL, George RL, Groome PA. Increased Incidence of Differentiated Thyroid Carcinoma and Detection of Subclinical Disease. *CMAJ Can Med Assoc J = J l'Association medicale Can* (2007) 177(11):1357–61. doi: 10.1503/cmaj.061730
8. Grimm D. Current Knowledge in Thyroid Cancer-From Bench to Bedside. *Int J Mol Sci* (2017) 18(7):1549. doi: 10.3390/ijms18071529
9. Tuttle RM, Haugen B, Perrier ND. Updated American Joint Committee on Cancer/Tumor-Node-Metastasis Staging System for Differentiated and Anaplastic Thyroid Cancer (Eighth Edition): What Changed and Why? *Thyroid Off J Am Thyroid Assoc* (2017) 27(6):751–6. doi: 10.1089/thy.2017.0102
10. Mathew R, Karantza-Wadsworth V, White E. Role of Autophagy in Cancer. *Nat Rev Cancer* (2007) 7(12):961–7. doi: 10.1038/nrc2254
11. Levine B, Kroemer G. Biological Functions of Autophagy Genes: A Disease Perspective. *Cell* (2019) 176(1-2):11–42. doi: 10.1016/j.cell.2018.09.048
12. Katheder NS, Khezri R, O'Farrell F, Schultz SW, Jain A, Rahman MM. Microenvironmental Autophagy Promotes Tumour Growth. *Nature* (2017) 541(7637):417–20. doi: 10.1038/nature20815
13. Kimmelman AC, White E. Autophagy and Tumor Metabolism. *Cell Metab* (2017) 25(5):1037–43. doi: 10.1016/j.cmet.2017.04.004
14. Levy JMM, Towers CG, Thorburn A. Targeting Autophagy in Cancer. *Nat Rev Cancer* (2017) 17(9):528–42. doi: 10.1038/nrc.2017.53
15. Beermann J, Piccoli MT, Viereck J, Thum T. Non-Coding RNAs in Development and Disease: Background, Mechanisms, and Therapeutic Approaches. *Physiol Rev* (2016) 96(4):1297–325. doi: 10.1152/physrev.00041.2015
16. Consortium, E.P. An Integrated Encyclopedia of DNA Elements in the Human Genome. *Nature* (2012) 489(7414):57–74. doi: 10.1038/nature11247
17. Huarte M. The Emerging Role of lncRNAs in Cancer. *Nat Med* (2015) 21 (11):1253–61. doi: 10.1038/nm.3981
18. Atianand MK, Caffrey DR, Fitzgerald KA. Immunobiology of Long Noncoding RNAs. *Annu Rev Immunol* (2017) 35:177–98. doi: 10.1146/annurev-immunol-041015-055459
19. Subramanian A, Tamayo P, Mootha VK, Mukherjee S, Ebert BL, Gillette MA. Gene Set Enrichment Analysis: A Knowledge-Based Approach for Interpreting Genome-Wide Expression Profiles. *Proc Natl Acad Sci United States America* (2005) 102(43):15545–50. doi: 10.1073/pnas.0506580102
20. Liberzon A, Subramanian A, Pinchback R, Thorvaldsdottir H, Tamayo P, Mesirov JP. Molecular Signatures Database (MSigDB) 3.0. *Bioinformatics* (2011) 27(12):1739–40. doi: 10.1093/bioinformatics/btr260
21. Liberzon A, Birger C, Thorvaldsdóttir H, Ghandi M, Mesirov JP, Tamayo P, et al. The Molecular Signatures Database (MSigDB) Hallmark Gene Set Collection. *Cell Syst* (2015) 1(6):417–25. doi: 10.1016/j.cels.2015.12.004
22. Targonski CA, Shearer CA, Shealy BT, Smith MC, Feltus FA. Uncovering Biomarker Genes With Enriched Classification Potential From Hallmark Gene Sets. *Sci Rep* (2019) 9(1):9747. doi: 10.1038/s41598-019-46059-1
23. Inskip PD. Thyroid Cancer After Radiotherapy for Childhood Cancer. *Med Pediatr Oncol* (2001) 36(5):568–73. doi: 10.1002/mpo.1132
24. Xing M, Haugen BR, Schlumberger M. Progress in Molecular-Based Management of Differentiated Thyroid Cancer. *Lancet (London England)* (2013) 381(9871):1058–69. doi: 10.1016/S0140-6736(13)60109-9
25. Park J, Lee S, Kim K, Park H, Ki C-S, Oh YL, et al. Promoter Mutations and the 8th Edition TNM Classification in Predicting the Survival of Thyroid Cancer Patients. *Cancers* (2021) 13(4):648. doi: 10.3390/cancers13040648
26. Pekova B, Sykorova V, Mastnikova K, Vaclavikova E, Moravcova J, Vlcek P, et al. Fusion Genes in Thyroid Carcinomas: Clinicopathological Characteristics and Their Impacts on Prognosis. *Cancers* (2021) 13(8):1932. doi: 10.3390/cancers13081932
27. Pekova B, Sykorova V, Dvorakova S, Vaclavikova E, Moravcova J, Katra R, et al. RET, NTRK, ALK, BRAF, and MET Fusions in a Large Cohort of Pediatric Papillary Thyroid Carcinomas. *Thyroid Off J Am Thyroid Assoc* (2020) 30(12):1771–80. doi: 10.1089/thy.2019.0802
28. Prasad ML, Vyas M, Horne MJ, Virk RK, Morotti R, Liu Z. NTRK Fusion Oncogenes in Pediatric Papillary Thyroid Carcinoma in Northeast United States. *Cancer* (2016) 122(7):1097–107. doi: 10.1002/cncr.29887
29. Liu R, Zhang T, Zhu G, Xing M. Regulation of Mutant TERT by BRAF V600E/MAP Kinase Pathway Through FOS/GABP in Human Cancer. *Nat Commun* (2018) 9(1):579. doi: 10.1038/s41467-018-03033-1
30. Kim KJ, Kim SG, Tan J, Shen X, Viola D, Elisei R, et al. BRAF V600E Status may Facilitate Decision-Making on Active Surveillance of Low-Risk Papillary

Thyroid Microcarcinoma. *Eur J Cancer (Oxford Engl 1990)* (2020) 124:161–9. doi: 10.1016/j.ejca.2019.10.017
31. Tan J, Liu R, Zhu G, Umbricht CB, Xing M. Promoter Mutation Determines Apoptotic and Therapeutic Responses of -Mutant Cancers to BRAF and MEK Inhibitors: Achilles Heel. *Proc Natl Acad Sci United States America* (2020) 117 (27):15846–51. doi: 10.1073/pnas.2004707117
32. Schmitt AM, Chang HY. Long Noncoding RNAs in Cancer Pathways. *Cancer Cell* (2016) 29(4):452–63. doi: 10.1016/j.ccell.2016.03.010
33. Yang L-X, Wu J, Guo M-L, Zhang Y, Ma S-G. Suppression of Long Non-Coding RNA TNRC6C-AS1 Protects Against Thyroid Carcinoma Through DNA Demethylation of STK4 via the Hippo Signalling Pathway. *Cell proliferation* (2019) 52(3):e12564. doi: 10.1111/cpr.12564
34. Zhao Y, Zhao L, Li J, Zhong L. Silencing of Long Noncoding RNA RP11-476D10.1 Enhances Apoptosis and Autophagy While Inhibiting Proliferation of Papillary Thyroid Carcinoma Cells via microRNA-138-5p-Dependent Inhibition of LRRK2. *J Cell Physiol* (2019) 234(11):20980–91. doi: 10.1002/jcp.28702
35. Qin Y, Sun W, Zhang H, Zhang P, Wang Z, Dong W, et al. LncRNA GAS8-AS1 Inhibits Cell Proliferation Through ATG5-Mediated Autophagy in Papillary Thyroid Cancer. *Endocrine* (2018) 59(3):555–64. doi: 10.1007/s12020-017-1520-1
36. Dai W, Jin X, Han L, Huang H, Ji Z, Xu X, et al. Exosomal lncRNA DOCK9-AS2 Derived From Cancer Stem Cell-Like Cells Activated Wnt/β-Catenin Pathway to Aggravate Stemness, Proliferation, Migration, and Invasion in Papillary Thyroid Carcinoma. *Cell Death Dis* (2020) 11(9):743. doi: 10.1038/s41419-020-02827-w
37. Sun W, Qin Y, Wang Z, Dong W, He L, Zhang T, et al. The /miR-491 Axis Modulates Papillary Thyroid Cancer Invasion and Metastasis Through Tgm2/Nfkb/FN1 Signaling. *Front Oncol* (2021) 11:610547. doi: 10.3389/fonc.2021.610547
38. Feng J, Zhou Q, Yi H, Ma S, Li D, Xu Y, et al. A Novel lncRNA N384546 Promotes Thyroid Papillary Cancer Progression and Metastasis by Acting as a Competing Endogenous RNA of miR-145-5p to Regulate AKT3. *Cell Death Dis* (2019) 10(6):433. doi: 10.1038/s41419-019-1637-7
39. Peng F, Wang R, Zhang Y, Zhao Z, Zhou W, Chang Z, et al. Differential Expression Analysis at the Individual Level Reveals a lncRNA Prognostic Signature for Lung Adenocarcinoma. *Mol Cancer* (2017) 16(1):98. doi: 10.1186/s12943-017-0666-z
40. Zhou C, Wang S, Zhou Q, Zhao J, Xia X, Chen W, et al. A Long Non-Coding RNA Signature to Improve Prognostic Prediction of Pancreatic Ductal Adenocarcinoma. *Front Oncol* (2019) 9:1160. doi: 10.3389/fonc.2019.01160
41. Shukla S, Evans JR, Malik R, Feng FY, Dhanasekaran SM, Cao X, et al. Development of a RNA-Seq Based Prognostic Signature in Lung Adenocarcinoma. *J Natl Cancer Institute* (2017) 109(1):djw200. doi: 10.1093/jnci/djw200
42. Zhu X, Tian X, Yu C, Shen C, Yan T, Hong J, et al. A Long Non-Coding RNA Signature to Improve Prognosis Prediction of Gastric Cancer. *Mol Cancer* (2016) 15(1):60. doi: 10.1186/s12943-016-0544-0
43. Schlumberger M, Tahara M, Wirth LJ, Robinson B, Brose MS, Elisei R, et al. Lenvatinib Versus Placebo in Radioiodine-Refractory Thyroid Cancer. *New Engl J Med* (2015) 372(7):621–30. doi: 10.1056/NEJMoa1406470
44. Ancker OV, Krüger M, Wehland M, Infanger M, Grimm D. Multikinase Inhibitor Treatment in Thyroid Cancer. *Int J Mol Sci* (2019) 21(1). doi: 10.3390/ijms21010010
45. Brose MS, Nutting CM, Jarzab B, Elisei R, Siena S, Bastholt L, et al. Sorafenib in Radioactive Iodine-Refractory, Locally Advanced or Metastatic Differentiated Thyroid Cancer: A Randomised, Double-Blind, Phase 3 Trial. *Lancet (London England)* (2014) 384(9940):319–28. doi: 10.1016/S0140-6736(14)60421-9
46. Cabanillas ME, Ryder M, Jimenez C. Targeted Therapy for Advanced Thyroid Cancer: Kinase Inhibitors and Beyond. *Endocrine Rev* (2019) 40(6):1573–604. doi: 10.1210/er.2019-00007

Conflict of Interest: The authors declare that the research was conducted in the absence of any commercial or financial relationships that could be construed as a potential conflict of interest.

Publisher's Note: All claims expressed in this article are solely those of the authors and do not necessarily represent those of their affiliated organizations, or those of the publisher, the editors and the reviewers. Any product that may be evaluated in this article, or claim that may be made by its manufacturer, is not guaranteed or endorsed by the publisher.

frontiers in Oncology

ORIGINAL RESEARCH
published: 03 March 2022
doi: 10.3389/fonc.2021.752018

Prognostic Impact of Pattern of Mandibular Involvement in Gingivo-Buccal Complex Squamous Cell Carcinomas: Marrow and Mandibular Canal Staging System

Abhishek Mahajan[1†], Navnath Dhone[2†], Richa Vaish[3], Ankita Singhania[1], Akshat Malik[3], Kumar Prabhash[4], Ankita Ahuja[1], Nilesh Sable[1], Pankaj Chaturvedi[3], Vanita Noronha[4], Sarbani Gosh Laskar[5], Ujjwal Agarwal[1], Shreya Shukla[1], Gouri Pantvaidya[3], Prathamesh Pai[3], Atanu Bhattacharjee[6], Vijay Patil[4], Asawari Patil[7], Munita Bal[7], Swapnil Rane[7], Shivakumar Thiagarajan[3] and Anil D' Cruz[3]*

[1] Department of Radiodiagnosis and Imaging, Tata Memorial Hospital, Homi Bhabha National Institute, Mumbai, India, [2] Senior Resident Department of Radiodiagnosis, Tata Memorial Hospital, Homi Bhabha National Institute, Mumbai, India, [3] Department of Head and Neck Surgery, Tata Memorial Hospital, Homi Bhabha National Institute, Mumbai, India, [4] Department of Medical Oncology, Tata Memorial Hospital, Homi Bhabha National Institute, Mumbai, India, [5] Department of Radiation Oncology, Tata Memorial Hospital, Homi Bhabha National Institute, Mumbai, India, [6] Section of Biostatistics Centre for Cancer Epidemiology, Tata Memorial Centre Homi Bhabha National Institute, Mumbai, India, [7] Department of Pathology, Tata Memorial Hospital, Homi Bhabha National Institute, Mumbai, India

Purpose: To study the pattern of mandibular involvement and its impact on oncologic outcomes in patients with gingivo-buccal complex squamous cell carcinoma (GBC-SCC) and propose a staging system based on the pattern of bone involvement (MMC: Marrow and mandibular canal staging system) and compare its performance with the 8th edition of the American Joint Committee on Cancer (AJCC8).

Methods: This retrospective observational study included treatment-naïve GBC-SCC patients who underwent preoperative computed tomography (CT) imaging between January 1, 2012, and March 31, 2016, at a tertiary care cancer center. Patients with T4b disease with high infratemporal fossa involvement, maxillary erosion, and follow-up of less than a year were excluded. The chi-square or Fisher's exact test was used for descriptive analysis. Kaplan–Meier estimate and log-rank test were performed for survival analysis. Multivariate analysis was done using Cox regression analysis after making adjustments for other prognostic factors. p-Value <0.05 was considered as significant. Based upon the survival analysis with different patterns of bone invasion, a new staging system was proposed "MMC: Marrow and mandibular canal staging system". "Akaike information criterion" (AIC) was used to study the relative fitted model of the various staging (TNM staging—AJCC8) with respect to survival parameters.

Results: A total of 1,200 patients were screened; 303 patients were included in the study. On radiology review, mandibular bone was involved in 62% of patients. The pattern of bone involvement was as follows: deep cortical bone erosion (DCBE) in 23%, marrow in 34%, and marrow with the mandibular canal in 43% of patients. Patients with DCBE and

OPEN ACCESS

Edited by:
Hui Wang,
Hunan Cancer Hospital, China

Reviewed by:
Derfel Ap Dafydd,
Royal Marsden Hospital, United Kingdom
John Adeoye,
The University of Hong Kong, Hong Kong SAR, China
Wen-Wei Sung,
Chung Shan Medical University Hospital, Taiwan

***Correspondence:**
Abhishek Mahajan
drabhishek.mahajan@yahoo.in

[†]*These authors share first authorship*

Specialty section:
This article was submitted to Head and Neck Cancer, a section of the journal Frontiers in Oncology

Received: *02 August 2021*
Accepted: *31 December 2021*
Published: *03 March 2022*

Citation:
Mahajan A, Dhone N, Vaish R, Singhania A, Malik A, Prabhash K, Ahuja A, Sable N, Chaturvedi P, Noronha V, Gosh Laskar S, Agarwal U, Shukla S, Pantvaidya G, Pai P, Bhattacharjee A, Patil V, Patil A, Bal M, Rane S, Thiagarajan S and D' Cruz A (2022) Prognostic Impact of Pattern of Mandibular Involvement in Gingivo-Buccal Complex Squamous Cell Carcinomas: Marrow and Mandibular Canal Staging System. Front. Oncol. 11:752018. doi: 10.3389/fonc.2021.752018

no bone involvement (including superficial cortical) had similar survival [disease-free survival (DFS) and locoregional recurrence-free survival (LRRFS)], and this was significantly better than those with marrow with or without mandibular canal involvement (for both DFS and LRRFS). Patients with DCBE were staged using the MMC, and when compared with the AJCC8, the MMC system was better for the prediction of survival outcomes, as AIC values were lower compared with those of the AJCC8. There was a significant association ($p = 0.013$) between the type of bone involvement and the pattern of recurrence.

Conclusions: For GBC-SCC, only marrow with or without mandibular canal involvement is associated with poorer survival outcomes. As compared with the AJCC8, the proposed Mahajan et al. MMC staging system downstages DCBE correlates better with survival outcomes.

Keywords: head and neck squamous cell carcinoma, oral cancer (OC), AJCC 8th edition, gingivo-buccal squamous cell carcinoma, imaging—computed tomography, imaging, prognostic model, outcome assessment

INTRODUCTION

Squamous cell carcinoma is the most common histology of the oral cavity cancers. There are a multitude of factors that impact the prognosis of patients with these tumors. Amongst these, mandibular bone erosion (through the cortical bone of the mandible: deep cortical and/or marrow) is found to be an important factor (1–5). According to widely accepted staging systems, its presence is considered to be stage T4a (6). The probability of mandibular bone erosion is higher with buccal mucosa lesions in close proximity to the mandible and gingival cancers, which occur due to invasion of the mandible through the occlusal surface (7–9).

Over recent years, it has often been argued that mandibular bone erosion needs to be characterized further. The Japan Society for Oral Tumors (JSOT) has defined T4 cancer as the invasion of the mandibular canal (10–12). Ebrahimi et al. based the T stage on size and depth of invasion for tumor categories T1–T3 and T4 in the presence of marrow invasion (13). In contrast, a few reports have suggested that tumor size correlates with adverse prognosis and that bone invasion is not an independent predictor of survival (14–16). On the contrary, some studies have reported that tumor size and marrow invasion are independent predictors of reduced survival (13, 17–19). In view of such varied evidence and lack of clarity, this study aims to evaluate the association of various patterns of mandibular bone involvement and their impact on survival. Based upon the findings, we also endeavored to develop a staging system that would reflect the implications of various types of bone invasion-superficial cortical erosion (erosive bony involvement), deep cortical erosion (infiltrative bony involvement), marrow involvement (infiltrative bony involvement), and mandibular canal involvement (infiltrative bony involvement), as assessed on imaging in a better way.

MATERIAL AND METHODS

This is a retrospective study on treatment-naïve gingivo-buccal complex squamous cell carcinoma (GBC-SCC) patients who underwent preoperative CT imaging between January 1, 2012, and March 31, 2016, at a tertiary care cancer center. The patients who underwent treatment with curative intent were included. Since surgery is the mainstay of treatment for these cancers, only those patients who underwent definitive surgical management at our center were included in the study.

Patients

Overall, 1,200 patients were screened. We excluded patients with stage T4b with high infratemporal fossa involvement, maxillary erosion, those with follow-up of less than 1 year, and cases where digital imaging and communications in medicine (DICOM) images were not available for review. Analysis was performed on 303 patients in our study (**Figure 1**). The Institutional Ethics Committee approval was obtained. Since it is a retrospective study, the waiver of consent was granted. The demographic, treatment, histopathological, and follow-up details were obtained from the electronic medical records.

Image Evaluation

Two senior head and neck radiologists with experience of over 10 and 6 years and one junior radiologist with experience of over 3 years reviewed the CT images independently (AbM, NS, and ND, respectively). The imaging review was performed on reconstructed DICOM data. The soft-tissue algorithm and bone window or bone algorithm reformations and axial images were analyzed on a volume viewer integrated within the picture archiving and communication system (PACS) using triangulation.

The various patterns of bone involvement reported on imaging were as follows: erosive infiltration, i.e., superficial cortical erosion with subtle outer cortical erosion without complete breach. Infiltrative invasion included deep cortical erosion with outer cortical breach and disease reaching up to the inner cortical layer, marrow involvement with disease eroding both the cortices and reaching up to the mandibular marrow, and mandibular canal involvement with disease eroding the inferior alveolar canal, obliteration of fat, or excessive

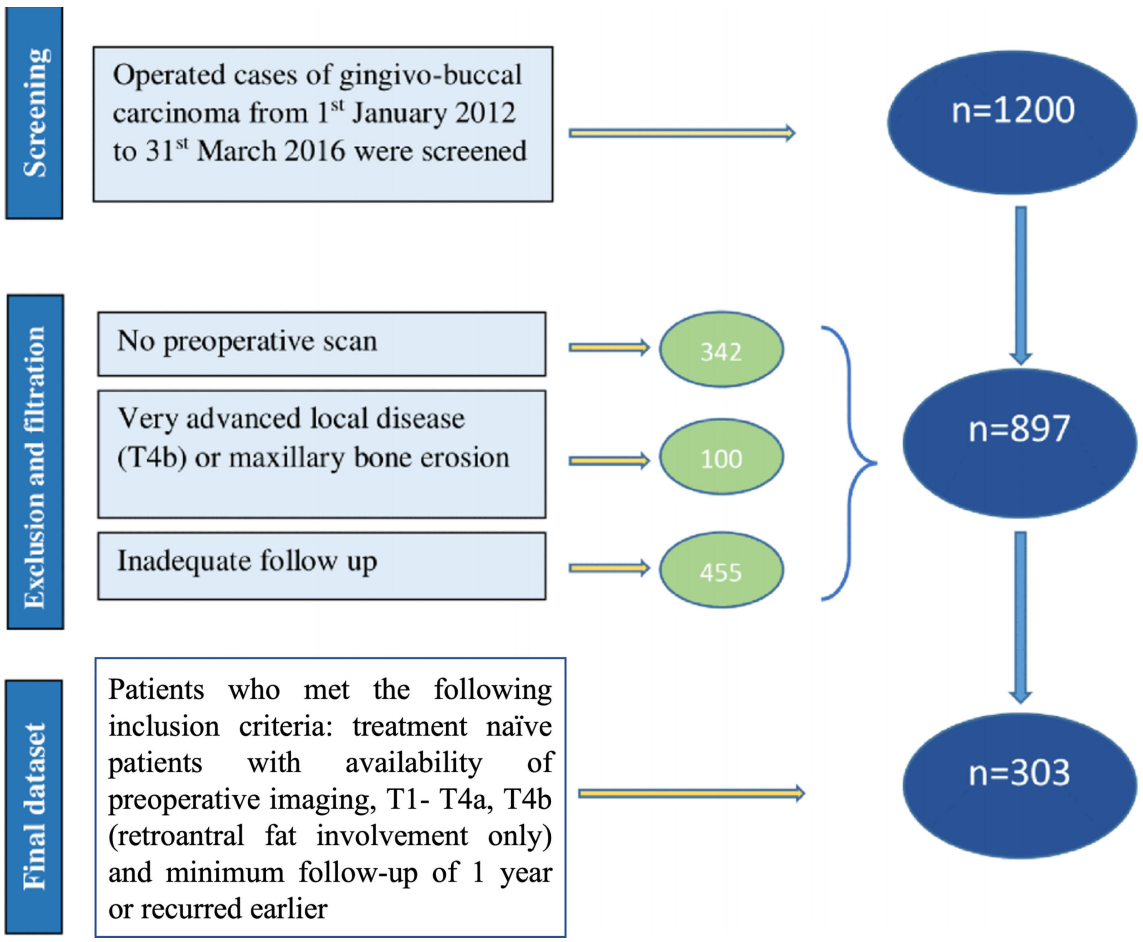

FIGURE 1 | Consort diagram; 1,200 patients were screened, and 303 were included who met the inclusion criteria.

enhancement within the mandibular foramen, with or without widening or erosion of the foramen, which was regarded as the perineural spread. **Figure 2** shows a line diagram of the described patterns of mandibular involvement. As the 8th edition of the American Joint Committee on Cancer (AJCC8) does not consider superficial cortical erosion for upstaging the disease, patients with superficial cortical erosion were included with patients having no bone erosion.

Pathology Evaluation

The pathology reports of all tumors exhibiting bone invasion on imaging were reviewed. The bone invasion was categorized as present or absent in the final report. In cases where there was inadequate information regarding the extent of bone invasion, the second review of the pathology slides was performed by a senior head and neck pathologist (SR, AP, and MB).

Statistical Considerations

The analysis was performed using SPSS version 21 and R software (IBM Corp). The chi-square or Fisher's exact test was used for descriptive analysis. The overall survival (OS) was calculated from the date of surgery to death due to any cause. Disease-free survival (DFS) was defined from the date of surgery to any disease recurrence. Locoregional recurrence-free survival (LRRFS) was calculated from the date of surgery to the locoregional recurrence. The patients were censored if they were lost to follow-up or on the last follow-up date in case the event did not occur. Kaplan–Meier estimate and log-rank test were performed for survival analysis. Multivariate analysis was done using Cox regression analysis after making adjustments for other prognostic factors. p-Value <0.05 was considered significant.

MMC: Marrow and Mandibular Canal Staging System

Based upon the survival analysis with different patterns of bone invasion, a new staging system was proposed, "*MMC: Marrow and mandibular canal staging system*" (**Table 1**). The patients with no bone erosion/superficial cortical erosion and deep cortical bone erosion were staged based on the size and depth of invasion. Only marrow invasion with or without mandibular canal involvement was considered to be T4a. The patients were restaged according to this system, and this staging system was compared with the AJCC8 staging system.

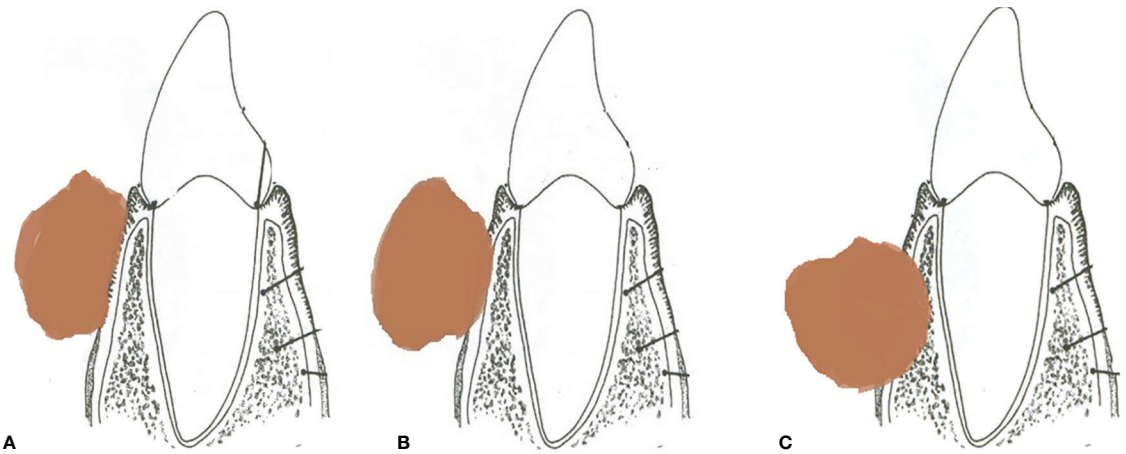

FIGURE 2 | **(A)** Line diagram of tumor eroding the superficial cortex. **(B)** Tumor with deep cortical erosion. **(C)** Tumor with marrow involvement.

"Akaike information criterion" (AIC) was used to study the relative fitted model of the various staging (TNM staging—AJCC8) with respect to OS, DFS, and LRRFS. AIC estimates the best-fitted model, relative to other models, thus providing the means for each model selection. R software and survival package were used to calculate the AIC values.

RESULTS

Patient Characteristics

We screened 1,200 patients, out of whom 303 patients met the inclusion criteria and were included in the final analysis. The mean age of the cohort was 52.86 years (30 to 84 years). Of these, 258 (85%) were males and 45(15%) were females. The personal habits revealed that most of the patients 263 (86.8%) were tobacco chewers/smokers; 27 (8.9%) had multiple habits. Out of 303 patients, 261 (86%) underwent segmental mandibulectomy, and 42 (14%) underwent marginal mandibulectomy. A total of 206 (68%) patients received adjuvant chemoradiation, 71 (23%) received adjuvant radiotherapy, and 26 (9%) did not warrant any adjuvant therapy. Relevant patient demographic and clinicopathological data are summarized in **Table 2**. The pathological nodal staging was done using the AJCC8 staging system. All the patients underwent neck dissection. The majority of them were N0, 154 (51%); N1, 16 (5%); N2, 53 (18%); and N3, 80 (26%). Positive bony and mucosal margins were seen in 8 (3%) and 7 (2%) of cases, respectively.

Patterns of Bone Involvement

According to the radiology review, mandibular bone was involved in 187 (62%) patients. Out of these, deep cortical erosion was seen in 43 (23%), marrow was involved in 64 (34%), and mandibular canal involvement was seen in 80 (43%) patients.

Survival Analysis

In our study, the mean OS was 26 months, the mean DFS was 24.6 months, and the mean LRRFS was 24.7 months. The cohorts were stratified based on the type of bone erosion. **Figures 3–5** depict the Kaplan–Meier survival curves for the various patterns of bone involvement. No bone erosion or deep cortical bone

TABLE 1 | Marrow mandibular canal staging system.

T stage	Definition
T1	Tumor ≤ 2 cm in greatest dimensions with DOI ≤ 5 mm
T2	Tumor ≤ 2 cm in greatest dimensions with DOI >5 mm and ≤10 mm
	Tumor >2 to ≤4 cm in greatest dimensions with DOI ≤ 10 mm
T3	Tumor >2 to ≤ 4 cm in greatest dimensions with DOI > 10 mm
	Tumor > 4 cm in greatest dimensions with DOI ≤ 10 mm
T4a	Tumor > 4 cm in greatest dimensions with DOI >10 mm
	Tumor invades into mandibular marrow* with or without mandibular canal, maxillary sinus, retroantral fat or skin of face.
T4b	Tumor invades masticator space, pterygoid plates, or skull base or encases internal carotid artery

DOI, depth of invasion.

**Deep cortical erosion is not considered to be T4a in the marrow mandibular canal (MMC) staging system.*

TABLE 2 | Demographic, histopathological, and clinical details of the whole cohort (n = 303).

Variable	Bone erosion		p value
	No Bone Erosion/Deep Cortical Erosion	Marrow with or without Mandibular Canal Involvement	
Gender			
Male	137	121	0.63
Female	22	23	
Preoperative treatment			
None	101	107	
Neoadjuvant chemotherapy (NACT)	56	36	0.19
Radiotherapy (RT)	1	0	
Concurrent chemoradiotherapy (CTRT)	1	1	
Type of surgery			
Marginal mandibulectomy	40	2	<0.001
Segmental mandibulectomy	119	142	
Adjuvant therapy			
None	23	3	0.001
RT	37	34	
CTRT	99	107	
Pathological skin involvement			
Absent	117	119	0.07
Present	42	25	
Pathological node involvement			
Absent	86	68	0.25
Present	73	76	
Extracapsular spread			
Absent	102	83	0.29
Present	57	61	
Lymphovascular invasion			
Absent	156	137	0.2
Present	3	7	
Perineural Invasion			
Absent	129	106	0.13
Present	30	38	
Histopathological grade of tumour			
Well differentiated	25	13	0.17
Moderate differentiated	106	99	
Poorly differentiated	28	32	
Mucosal margins			
Free	157	139	0.26
Positive	2	5	
Bone margins			
Free	158	137	0.03
Involved	1	7	
Pathological T stage AJCC 8			
T1	17	0	<0.001
T2	34	0	
T3	24	0	
T4a	84	144	
MMC T staging system			
T1	23	0	<0.001
T2	50	0	
T3	32	0	
T4a	54	144	
Pathological Nodal staging			
N0	86	68	0.07
N1	10	6	
N2	31	22	
N3	32	48	

AJCC8, 8th edition of the American Joint Committee on Cancer; MMC, Marrow and mandibular canal staging system.

involvement had a significantly better outcome compared with marrow or mandibular canal involvement (DFS, p = 0.023; LRRFS p = 0.013). However, the difference in OS between the 2 groups was not significant (p = 0.82). Marrow involvement had a similar survival (DFS and LRRFS) to mandibular canal invasion (for DFS, p = 0.59; for LRRFS p = 0.77). There was a significant survival difference (DFS and LRRFS) between the deep cortex and marrow (for DFS, p = 0.005; for LRRFS, p = 0.017) and the

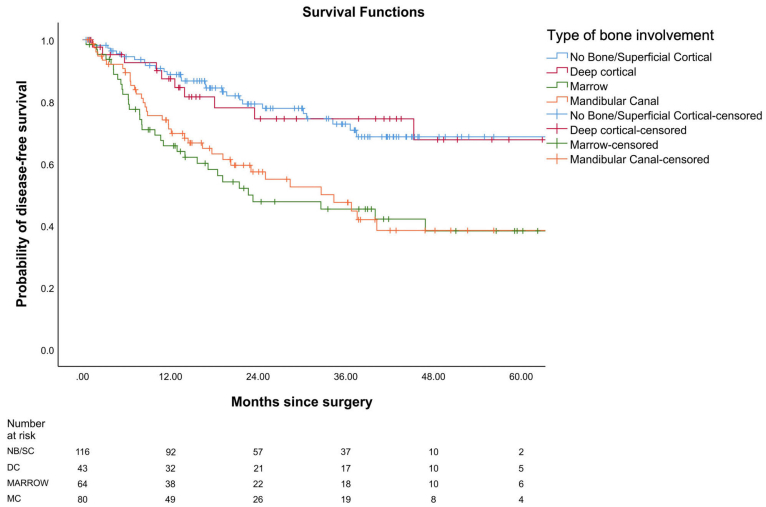

FIGURE 3 | Comparison of Kaplan–Meier survival curves of disease-free survival (DFS) for different patterns of bone involvement.

deep cortex and mandibular canal involvement (for DFS, p = 0.01; for LRRFS p = 0.006).

When the patients were stratified based on extracapsular spread (ECS), there was statistically worse DFS and LRRFS in patients with marrow/canal involvement as compared with no bone erosion/deep cortical erosion in the ECS-negative subgroup (p = 0.023 and p = 0.013, respectively). However, the difference in the 2 groups was not statistically significant (p = 0.389 for DFS; p = 0.641 for LRRFS) in the ECS-positive subgroup. The type of bone was an independent prognostic factor for DFS on multivariate analysis after making adjustments for known histopathological prognostic factors and retroantral fat involvement involvement p < 0.001 (**Table 3**). Other independent prognostic factors were retroantral fat involvement, skin involvement, and tumor grade. The type of bone involvement was the only independent prognostic factor for LRRFS on multivariate analysis, p < 0.001 (**Table 4**).

Marrow and Mandibular Canal Classification—Stage Migration and Comparison With 8th Edition of the American Joint Committee on Cancer

As per the final histopathology report, patients were staged according to the AJCC8 and MMC classifications (**Table 2**). In the MMC classification, patients with deep cortex involvement

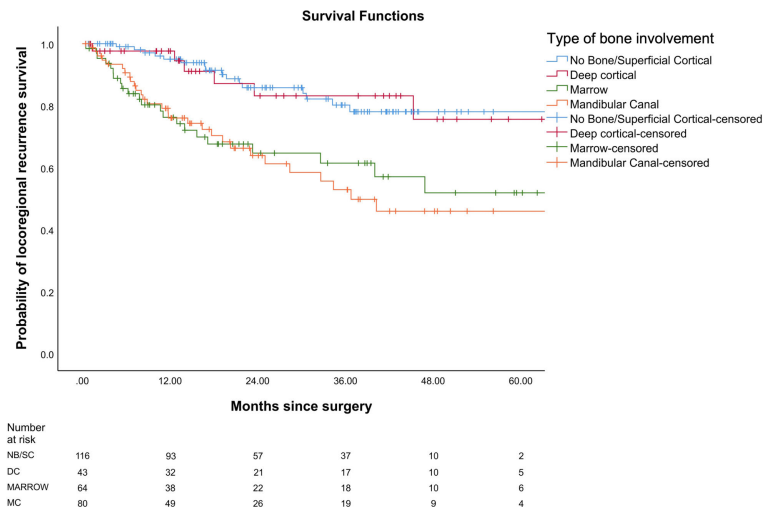

FIGURE 4 | Comparison of Kaplan–Meier survival curves of locoregional recurrence-free survival (LRRFS) for different patterns of bone involvement.

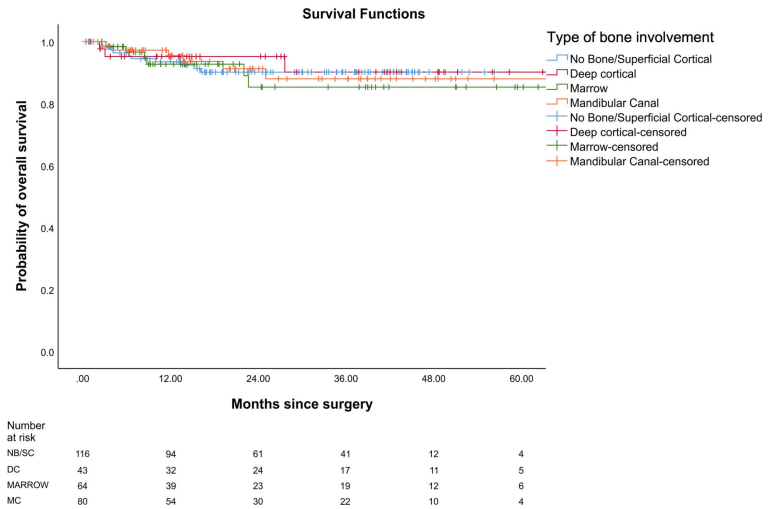

FIGURE 5 | Comparison of Kaplan–Meier survival curves of overall survival (OS) for different patterns of bone involvement.

were downstaged from T4 to the stage according to the size of the tumor and depth of invasion. Out of 228 T4 patients (according to the AJCC8), 30 patients were downstaged to T1–T3. Out of these 30 patients, 6 were restaged to T1, 16 were restaged to T2, and 8 were restaged as T3. When the two staging systems were compared using AIC, the MMC system turned out to be a better staging system for the prediction of survival, as the AIC values of the MMC staging system for LRRFS, DFS, and OS were lower compared with those of the AJCC8 (**Table 5**).

Patterns of Recurrence

Table 6 shows the pattern of recurrence with respect to the types of bone involvement. Further, we evaluated if the type of bone erosion had any impact on the pattern of recurrence. The recurrence occurred in 23.3% of patients with deep cortical and no bone involvement versus 48.6% of patients with marrow and mandibular canal involvement, which was statistically significant ($p = 0.023$). There was a statistically significant association between the type of bone erosion and the type of recurrence ($p = 0.013$).

DISCUSSION

The prognosis of oral squamous cell carcinoma depends upon a multitude of factors. Several of these are included in the staging system. Bone invasion has been considered as an adverse prognostic factor for a long time, thus meriting adjuvant therapy (2). Over the last few decades, it has been shown that superficial cortical erosion for alveolar primaries does not portend a poorer prognosis; such tumors are, therefore, staged according to their size (13).

There have been several studies that have further tried to understand and characterize the type of bone erosion and its effect on prognosis (20, 21). They have differentiated bone erosion as erosive (superficial cortical erosion) and infiltrative (deep cortical, marrow involvement, and mandibular canal involvement) and looked at their impact on the prognosis and survival. It has been observed that cortical bone erosion may not impact survival and only marrow invasion impacts prognosis. A recent meta-analysis found that only marrow invasion impacted overall and disease-free survival (22). On the contrary, few other studies did not show such an association between any type of bone erosion and survival (14–16). Probably this is the reason why staging systems, rather than characterizing the type of bone erosion, continue to mention merely mandibular bone erosion as present or absent.

Studies on this aspect have looked at all subsites of the oral cavity combined. It is prudent to understand that a buccal mucosa or a lower alveolus cancer is more likely to erode mandibular bone as compared with a tongue cancer (8, 9). They cannot be kept on the same pedestal while making any meaningful conclusions regarding upstaging the disease in presence of bone erosion. Another important aspect that these studies have not considered is the pathological depth of invasion, which plays an important role in assessing the prognosis and has recently been incorporated in the AJCC staging system (23, 24). In our study, we utilized the AJCC8 to stage the patients; thus, the depth of invasion was included in the staging process. As mentioned earlier, we only included buccal mucosa and lower alveolus cancer patients in the study, which is the most relevant cohort. We also excluded patients with high infratemporal fossa and maxillary erosion. This was done to exclusively analyze the prognostic impact of the type of mandibular bone erosion on survival.

On multivariate analysis, type of bone erosion had an independent prognostic impact on DFS and LRRFS ($p < 0.001$ and $p < 0.001$, respectively) after making adjustments for other prognostic factors (**Tables 3** and **4**, respectively). Deep cortical

TABLE 3 | Multivariate analysis of disease-free survival in patients with gingivo-buccal squamous cell carcinoma.

Variable	Events (n)	Hazard Ratio	95% CI	p-Value
Bone involvement				
No bone involvement/deep bone involvement	37	0.42	028–0.65	**<0.001**
Marrow with or without mandibular canal involvement	70	1.0	Reference	
Retroantral fat involvement				
Present	8	5.3	2.29–12.26	**<0.001**
Absent	99	1.0	Reference	
Pathological skin Involvement				
Present	28	1.68	1.06–2.65	**0.026**
Absent	79	1.0	Reference	
Pathological node Involvement				
Present	60	1.56	0.81–3.0	0.18
Absent	47	1.0	Reference	
Pathological extracapsular spread				
Present	48	0.81	0.42–1.59	0.56
Absent	59	1.0	Reference	
Lymphovascular invasion				
Present	6	1.31	0.54–3.14	0.54
Absent	101	1.0	Reference	
Perineural invasion				
Present	32	1.04	0.65–1.66	0.86
Absent	75	1.0	Reference	
Histopathological grade of tumor				
Poor	33	2.13	1.36–3.34	**<0.001**
Moderate	67	1.0	Reference	
Histopathological grade of tumour				
Well	7	0.70	0.31-1.57	0.40
Moderate	67	1.0	Reference	
Mucosal Margin				
Positive	2	0.82	0.18-3.62	0.80
Free	105	1.0	Reference	
Bony Margin				
Positive	3	0.52	0.14-1.88	0.32
Free	104	1.0	Reference	

Bold means p value significant.

erosion had survival similar to cases with no bone erosion. In contrast, marrow and mandibular canal involvement had similar survival (DFS and LRRFS), which was statistically worse than that seen with deep cortical erosion and no bone erosion for DFS and LRRFS (**Figures 3**, **4**).

Based on the results of univariate analysis, patients with deep cortical or no bone involvement were included together, and patients with marrow and mandibular canal were included together for further analysis. We found marrow and mandibular canal involvement to be statistically significantly poorer than no bone or deep cortical erosion for DFS and LRRFS (p =0.023 and p =0.013, respectively). It has also been hypothesized by a few studies that mandibular canal involvement may be associated with higher chances of distant metastasis (25–27). In our study, we found a statistically significant association between type of recurrence and the type of bone erosion (p = 0.013).

There have been few studies that have tried to restage the disease based upon the type of bone erosion. As per Ebrahimi et al., cortex involvement had a similar outcome as no bone involvement (13). They proposed a staging system where the disease was upstaged by 1 T category in the presence of marrow invasion. Another study proposed the JSOT classification, where the tumor was classified as T4a only when there was the involvement of the mandibular canal (10, 11). Involvement of the mandibular marrow without canal involvement was classified according to size; however, these patients performed equally badly as those with canal involvement. Bone erosion was completely ignored in another staging system, where the classification was based upon the soft tissue involvement alone (28). They did not consider bone involvement important for staging the tumor. In all these studies, cases without bone erosion were staged as per the size of the tumor. For staging, they had used the 7th edition of the AJCC, where the impact of depth of invasion was not considered. In the present study, we have staged the patients as per the AJCC8 and have considered the depth of invasion for all the patients.

As per the AJCC8 classification system, the tumor is classified as T4a even on mandibular cortical involvement. But the results of our study show that the cortical involvement did not affect the survival of the patient. Hence, we proposed an MMC classification system in which we downstaged tumors with superficial or deep cortical erosion based solely upon their size and depth of invasion (**Table 1**). Only those having marrow involvement with or without mandibular canal involvement were staged as T4a. This staging was labeled as MMC. The results of our study also show that T classification based upon the MMC staging was a better predictor of OS, DFS, and LRRFS as compared with the AJCC8 (**Table 5**).

TABLE 4 | Multivariate analysis of locoregional recurrence-free survival in patients with gingivo-buccal squamous cell carcinoma.

Variable	Events (n)	Hazard Ratio	95% CI	p-Value
Bone involvement				
No bone involvement/deep bone involvement	23	0.33	0.19–0.55	**<0.001**
Marrow with or without mandibular canal involvement	51	1	Reference	
Retroantral fat involvement				
Present	4	1.5	0.50–4.49	0.47
Absent	70	1	Reference	
Pathological skin Involvement				
Present	19	1.64	0.94–2.84	0.08
Absent	55	1	Reference	
Pathological node Involvement				
Present	38	0.77	0.31–1.87	0.57
Absent	36	1	Reference	
Pathological extracapsular spread				
Present	32	1.5	0.61–3.71	0.37
Absent	42	1	Reference	
Lymphovascular invasion				
Present	1	0.21	0.02–1.63	0.14
Absent	73	1	Reference	
Perineural invasion				
Present	18	0.89	0.49–1.60	0.71
Absent	56	1	Reference	
Histopathological grade of tumor				
Poor	20	1.55	0.89–2.70	0.12
Moderate	48	1	Reference	
Histopathological grade of tumour				
Well	6	0.7	0.29–1.69	0.44
Moderate	48	1	Reference	
Mucosal Margin				
Positive	2	0.85	0.17.4.21	0.85
Free	72	1	Reference	
Bony Margin				
Positive	3	1.37	0.35–5.26	0.64
Free	71	1	Reference	

Bold means p value significant.

TABLE 5 | AIC values of AJCC8 and MMC staging system with respect to survival.

Survival	AIC Values	
	AJCC8 Staging	MMC Staging
LRRFS	266.61	8.92
DFS	1,165.56	82.46
OS	818.98	74.26

LRRFS, locoregional recurrence-free survival; DFS, disease-free survival; OS, overall survival; AIC, Akaike information criterion; AJCC8, 8th edition of the American Joint Committee on Cancer; MMC, Marrow and mandibular canal staging system.

TABLE 6 | Pattern of bone involvement with pattern of recurrence.

Type of Bone Involvement	Number of Recurrences	Site of Recurrence			
		Local	Regional	Distant	Combination
No bone involved and deep cortical bone erosion (159 cases)	37 (23.3%)	17 (46%)	5 (13.5%)	11 (29.7%)	4 (10.8%)
Marrow with or without mandibular canal (144 cases)	70 (48.6%)	43 (61.4%)	8 (11.4%)	14 (20%)	5 (7.1%)

The limitation of our study is that it is retrospective. We also did not study the impact of superficial bone erosion on the prognosis. Moreover, information about the pattern of invasion on histopathology for these patients was not available. In spite of these limitations, this study provided a large sample size focusing on the relevant subsite of the oral cancers, the buccal mucosa.

CONCLUSION

In this study, we found that for GBC-SCC, bone erosion with marrow as well as mandibular canal involvement, and not cortical erosion, is associated with poorer survival outcomes. The marrow with or without mandibular canal involvement has a higher incidence of recurrence, and there was a statistically significant association between the type of bone involvement and pattern of recurrence. T classification based upon the proposed Mahajan et al. MMC staging system, which downstages deep cortical bone involvement, is a better predictor for survival as compared with the AJCC8.

DATA AVAILABILITY STATEMENT

The original contributions presented in the study are included in the article/supplementary material. Further inquiries can be directed to the corresponding author.

ETHICS STATEMENT

The studies involving human participants were reviewed and approved by IEC TMC. The ethics committee waived the requirement of written informed consent for participation.

AUTHOR CONTRIBUTIONS

Study concept: ND, AbM, and AkM. Study design: ND, AbM, and AkM. Data acquisition: ND, AbM, and AS. Quality control of data algorithms: ND, AbM, AkM, and AB. Statistical analysis: ND, AbM, AkM, and AB. Manuscript preparation: all authors. Manuscript editing: ND, AbM, and AkM. Manuscript reviewing: all authors.

REFERENCES

1. Choi S, Myers JN. Molecular Pathogenesis of Oral Squamous Cell Carcinoma: Implications for Therapy. *J Dental Res* (2008) 87(1):14–32. doi: 10.1177/154405910808700104
2. Mahajan A, Ahuja A, Sable N, Stambuk HE. Imaging in Oral Cancers: A Comprehensive Overview of Imaging Findings for Staging and Treatment Planning. *Oral Oncol* (2020) 104:104658. doi: 10.1016/j.oraloncology.2020.104658
3. Jadhav KB, Gupta N. Clinicopathological Prognostic Implicators of Oral Squamous Cell Carcinoma: Need to Understand and Revise. *North Am J Med Sci* (2013) 5(12):671. doi: 10.4103/1947-2714.123239
4. Ash CS, Nason RW, Abdoh AA, Cohen MA. Prognostic Implications of Mandibular Invasion in Oral Cancer. *Head Neck: J Sci Specialties Head Neck* (2000) 22(8):794–8. doi: 10.1002/1097-0347(200012)22:8<794::AID-HED8>3.0.CO;2-W
5. Majumdar B, Patil S, Sarode SC, Sarode GS, Rao RS. Clinico-Pathological Prognosticators in Oral Squamous Cell Carcinoma: An Update. *Trans Res Oral Oncol* (2017) 2:2057178X17738912. doi: 10.1177/2057178X17738912
6. Lydiatt WM, Patel SG, O'Sullivan B, Brandwein MS, Ridge JA, Migliacci JC, et al. Head and Neck Cancers—Major Changes in the American Joint Committee on Cancer Eighth Edition Cancer Staging Manual. *CA: Cancer J Clin* (2017) 67(2):122–37. doi: 10.3322/caac.21389
7. Chaukar DA, Dandekar M, Kane S, Arya S, Purandare N, Rangarajan V, et al. Invasion of the Mandible in Gingivobuccal Complex Cancers: Histopathological Analysis of Routes of Tumour Entry and Correlation With Preoperative Assessment. *Oral Oncol* (2018) 86:181–7. doi: 10.1016/j.oraloncology.2018.09.022
8. Pandey M, Rao LP, Das SR, Mathews A, Chacko EM, Naik BR. Patterns of Mandibular Invasion in Oral Squamous Cell Carcinoma of the Mandibular Region. *World J Surg Oncol* (2007) 5(1):12. doi: 10.1186/1477-7819-5-12
9. Wang W, Adeoye J, Thomson P, Choi SW. Statistical Profiling of Oral Cancer and the Prediction of Outcome. *J Oral Pathol Med* (2021) 50(1):39–46. doi: 10.1111/jop.13110
10. Omura K. Current Status of Oral Cancer Treatment Strategies: Surgical Treatments for Oral Squamous Cell Carcinoma. *Int J Clin Oncol* (2014) 19 (3):423–30. doi: 10.1007/s10147-014-0689-z
11. Izumo T, Kirita T, Ariji E, Ozeki S, Okada N, Okabe S, et al. General Rules for Clinical and Pathological Studies on Oral Cancer: A Synopsis. *Jpn J Clin Oncol* (2012) 42(11):1099–109. doi: 10.1093/jjco/hys141
12. Sasaki T, Imai Y, Fujibayashi T. New Proposal for T Classification of Gingival Carcinomas Arising in the Maxilla. *Int J Oral Maxillofac Surg* (2004) 33:349–52. doi: 10.1016/j.ijom.2003.09.004
13. Ebrahimi A, Murali R, Gao K, Elliott MS, Clark JR. The Prognostic and Staging Implications of Bone Invasion in Oral Squamous Cell Carcinoma. *Cancer* (2011) 117(19):4460–7. doi: 10.1002/cncr.26032
14. Platz H, Fries R, Hudec M, Tjoa AM, Wagner RR. The Prognostic Relevance of Various Factors at the Time of the First Admission of the Patient: Retrospective DÖSAK Study on Carcinoma of the Oral Cavity. *J Maxillofac Surg* (1983) 11:3–12. doi: 10.1016/S0301-0503(83)80005-8
15. Overholt SM, Eicher SA, Wolf P, Weber RS. Prognostic Factors Affecting Outcome in Lower Gingival Carcinoma. *Laryngoscope* (1996) 106(11):1335–9. doi: 10.1097/00005537-199611000-00006
16. Soo KC, Spiro RH, King W, Harvey W, Strong EW. Squamous Carcinoma of the Gums. *Am J Surg* (1988) 156(4):281–5. doi: 10.1016/S0002-9610(88)80292-7
17. Bobdey S, Sathwara J, Jain A, Saoba S, Balasubramaniam G. Squamous Cell Carcinoma of Buccal Mucosa: An Analysis of Prognostic Factors. *South Asian J Cancer* (2018) 7(1):49. doi: 10.4103/sajc.sajc_317_16
18. Yoshida S, Shimo T, Murase Y, Takabatake K, Kishimoto K, Ibaragi S, et al. The Prognostic Implications of Bone Invasion in Gingival Squamous Cell Carcinoma. *Anticancer Res* (2018) 38(2):955–62. doi: 10.21873/anticanres.12309
19. Fried D, Mullins B, Weissler M, Shores C, Zanation A, Hackman T, et al. Prognostic Significance of Bone Invasion for Oral Cavity Squamous Cell Carcinoma Considered T1/T2 by American Joint Committee on Cancer Size Criteria. *Head Neck* (2014) 36(6):776–81. doi: 10.1002/hed.23367
20. Mücke T, Hölzle F, Wagenpfeil S, Wolff KD, Kesting M. The Role of Tumor Invasion Into the Mandible of Oral Squamous Cell Carcinoma. *J Cancer Res Clin Oncol* (2011) 137:165–71. doi: 10.1007/s00432-010-0870-3
21. Momin MA, Okochi K, Watanabe H, Imaizumi A, Omura K, Amagasa T, et al. Diagnostic Accuracy of Cone-Beam CT in the Assessment of Mandibular Invasion of Lower Gingival Carcinoma: Comparison With Conventional Panoramic Radiography. *Eur J Radiol* (2009) 72:75–81. doi: 10.1016/j.ejrad.2008.06.018
22. Li C, Lin J, Men Y, Yang W, Mi F, Li L. Does Medullary Versus Cortical Invasion of the Mandible Affect Prognosis in Patients With Oral Squamous Cell Carcinoma? *J Oral Maxillofac Surg* (2017) 75(2):403–15. doi: 10.1016/j.joms.2016.08.005
23. Omar EA. The Outline of Prognosis and New Advances in Diagnosis of Oral Squamous Cell Carcinoma (OSCC): Review of the Literature. *J Oral Oncol* (2013) 2013. doi: 10.1155/2013/519312

24. Urist MM, O'Brien CJ, Soong SJ, Visscher DW, Maddox WA. Squamous Cell Carcinoma of the Buccal Mucosa: Analysis of Prognostic Factors. *Am J Surg* (1987) 154(4):411–4. doi: 10.1016/0002-9610(89)90014-7
25. Okura M, Yanamoto S, Umeda M, Otsuru M, Ota Y, Kurita H, et al. Prognostic and Staging Implications of Mandibular Canal Invasion in Lower Gingival Squamous Cell Carcinoma. *Cancer Med* (2016) 5(12):3378–85. doi: 10.1002/cam4.899
26. Patel RS, Dirven R, Clark JR, Swinson BD, Gao K, O'Brien CJ. The Prognostic Impact of Extent of Bone Invasion and Extent of Bone Resection in Oral Carcinoma. *Laryngoscope* (2008) 118:780–5. doi: 10.1097/MLG.0b013e31816422bb
27. Wong RJ, Keel SB, Glynn RJ, Varvares MA. Histological Pattern of Mandibular Invasion by Oral Squamous Cell Carcinoma. *Laryngoscope* (2000) 110:65–72. doi: 10.1097/00005537-200001000-00013
28. Matsushita Y, Yanamoto S, Yamada SI, Mori H, Adachi M, Takahashi H, et al. Correlation Between Degree of Bone Invasion and Prognosis in Carcinoma of the Mandibular Gingiva: Soft Tissue Classification Based on UICC Classification. *J Oral Maxillofac Surg Med Pathol* (2015) 27(5):631–6. doi: 10.1016/j.ajoms.2014.12.002

Conflict of Interest: The authors declare that the research was conducted in the absence of any commercial or financial relationships that could be construed as a potential conflict of interest.

frontiers in Oncology

ORIGINAL RESEARCH
published: 11 March 2022
doi: 10.3389/fonc.2022.772816

Integrative Pan-Cancer Analysis of KIF15 Reveals Its Diagnosis and Prognosis Value in Nasopharyngeal Carcinoma

Jinglin Mi[1†], Shanshan Ma[1†], Wei Chen[1,2†], Min Kang[1,3], Meng Xu[1], Chang Liu[1], Bo Li[1], Fang Wu[1,3], Fengju Liu[4], Yong Zhang[1], Rensheng Wang[1,3] and Li Jiang[1*]*

[1] Department of Radiation Oncology, The First Affiliated Hospital of Guangxi Medical University, Nanning, China, [2] Department of Oncology, Yunfu People's Hospital, Yunfu, China, [3] Key Laboratory of High-Incidence-Tumor Prevention & Treatment (Guangxi Medical University), Ministry of Education, Nanning, China, [4] Department of Pathology, The First Affiliated Hospital of Guangxi Medical University, Nanning, China

OPEN ACCESS

Edited by:
Heming Lu,
People's Hospital of Guangxi Zhuang Autonomous Region, China

Reviewed by:
Zheng Chen,
Fudan University, China
Liangfang Shen,
Central South University, China
Li Rongqing,
The First Affiliated Hospital of Kunming Medical University, China

***Correspondence:**
Li Jiang
jiangligxmu@163.com
Rensheng Wang
13807806008@163.com

[†]These authors share first authorship

Specialty section:
This article was submitted to Head and Neck Cancer, a section of the journal Frontiers in Oncology

Received: 08 September 2021
Accepted: 18 February 2022
Published: 11 March 2022

Citation:
Mi J, Ma S, Chen W, Kang M, Xu M, Liu C, Li B, Wu F, Liu F, Zhang Y, Wang R and Jiang L (2022) Integrative Pan-Cancer Analysis of KIF15 Reveals Its Diagnosis and Prognosis Value in Nasopharyngeal Carcinoma. Front. Oncol. 12:772816. doi: 10.3389/fonc.2022.772816

Background: KIF15 plays a vital role in many biological processes and has been reported to influence the occurrence and development of certain human cancers. However, there are few systematic evaluations on the role of KIF15 in human cancers, and the role of KIF15 in the diagnosis and prognosis of nasopharyngeal carcinoma (NPC) also remains unexplored. Therefore, this study aimed to conduct a pan-cancer analysis of KIF15 and evaluate its diagnostic and prognostic potential in NPC.

Methods: The expression pattern, prognostic value, molecular function, tumor mutation burden, microsatellite instability, and immune cell infiltration of KIF15 were examined based on public databases. Next, the diagnostic value of KIF15 in NPC was analyzed using the Gene Expression Omnibus (GEO) database and immunohistochemistry (IHC). Kaplan–Meier curves, Cox regression analyses, and nomograms were used to evaluate the effects of KIF15 expression on NPC prognosis. Finally, the effect of KIF15 on NPC was explored by *in vitro* experiments.

Results: The expression of KIF15 was significantly upregulated in 20 out of 33 cancer types compared to adjacent normal tissue. Kyoto Encyclopedia of Genes and Genomes enrichment (KEGG) analysis showed that KIF15 could participate in several cancer-related pathways. The increased expression level of KIF15 was correlated with worse clinical outcomes in many types of human cancers. Additionally, KIF15 expression was related to cancer infiltration of immune cells, tumor mutation burden, and microsatellite instability. In the analysis of NPC, KIF15 was significantly upregulated based on the GEO database and immunohistochemistry. A high expression of KIF15 was negatively associated with the prognosis of patients with NPC. A nomogram model integrating clinical characteristics and KIF15 expression was established, and it showed good predictive ability with an area under the curve value of 0.73. KIF15 knockdown significantly inhibited NPC cell proliferation and migration.

Conclusions: Our findings revealed the important and functional role of KIF15 as an oncogene in pan-cancer. Moreover, high expression of KIF15 was found in NPC tissues, and was correlated with poor prognosis in NPC. KIF15 may serve as a potential therapeutic target in NPC treatment.

Keywords: KIF15, pan-cancer analysis, nasopharyngeal carcinoma, diagnosis, prognosis

INTRODUCTION

Cancer has become the leading cause of morbidity and mortality in low- and high-income countries around the world (1). Due to population aging and growth, the global number of patients with cancer is predicted to increase (2). Despite great advances in diagnostic and therapeutic methods of treating cancer in recent years, the survival outcome and quality of life of patients remains unsatisfactory (3). Among all types of cancers, nasopharyngeal carcinoma (NPC) is endemic to southeast Asia, north Africa, and southern China. According to GLOBOCAN estimates, the age-standardized rate of NPC is 4–25 cases per 100,000 individuals in these regions (4, 5). The tumorigenesis and progression of NPC are closely related to genetic factors, environmental effects, and Epstein–Barr virus (EBV) infection (6). Advanced NPC had worse clinical outcomes due to delayed diagnosis and distant metastasis are the critical factors for treatment failure (7). Consequently, it is necessary to identify novel biomarkers and investigate the molecular mechanisms for improving early diagnosis and prognosis of NPC.

The kinesin superfamily (KIF) is an important microtubule-dependent motor protein that participates in the transport of various cargos including vesicles, membranous organelles, and mRNAs (8). To date, more than 45 KIF members have been found in mammalian cells and they are classified into 14 families base on their structural features (9). KIF15, a member of kinesin-12 family, is a plus end-directed motor with an N-terminal motor domain that plays a key role in bipolar spindle assembly (10). During cell division, dysregulation of KIF15 can result in aberrant cell proliferation, tumorigenesis, and tumor aggressiveness (11). Recently, KIF15 has been proven to be over-expressed in various cancers including gastric cancer, hepatocellular carcinoma, and lung adenocarcinoma (12–14). However, the functions of KIF15 in pan-cancer are not fully understood. Moreover, there is a lack of evidence on the effects of KIF15 expression on the diagnosis and prognosis of NPC.

In the present study, we comprehensively analyzed the expression signature, prognostic value, and associated pathways of KIF15 across 33 types of human cancers using multiple databases. Subsequently, the correlations between KIF15 and tumor mutation burden (TMB), microsatellite instability (MSI), and immune infiltration degree were investigated. We further analyzed the mRNA expression of KIF15 in NPC tissues and normal tissues using the Gene Expression Omnibus (GEO) database. Immunohistochemical analysis (IHC) was utilized to verify the protein expression level of KIF15 and its diagnostic and prognostic value in NPC. RNA interference was conducted to silence the KIF15 expression to investigate its molecular function in the NPC cell lines. The results of our study could contribute to a better understanding of the effects of KIF15 on cancer (specifically NPC) occurrence, development, and prognosis.

MATERIALS AND METHODS

Analysis of KIF15 Differential Expression in Pan-Cancer

The Cancer Genome Atlas (TCGA) is a web-based, publicly available database, which contains more than 2.5 petabytes of genomic, transcriptomic, and proteomic data of over 20,000 cancer patients across 33 different cancer types (http://cancergenome.nih.gov/). Gene expression data and clinical data of TCGA were downloaded using the University of California, Santa Cruz Xena (UCSC Xena) online tool. Wilcoxon test was used to assess the expression levels of KIF15 in various cancers based on TCGA database. The Oncomine database is a useful platform that provides a powerful series of analyses, including comparison gene expression signatures, clusters, and gene-set modules (www.oncomine.org). The Kaplan-Meier plotter is capable of evaluating the potential role of mRNA, miRNA, and proteins in 21 cancer types (http://kmplot.com/analysis/). The expression pattern of KIF15 in pan-cancer was further verified by Oncomine database and Kaplan-Meier plotter database. The clinical relationship between KIF15 expression level and patients' cancer stage was evaluated using limma package and RColorBrewer package was used to visualized the results, we used 'avereps' function from limma package to condense the microarray data object so that values for within-array replicate probes are replaced with their average, for each cancer type, we compared gene expression differences of KIF15 between each of the two cancer stages using the Wilcox test. *P* values were set as statistically significant according to the following: $^{*}P<0.05$; $^{**}P<0.01$ and $^{***}P<0.001$.

Analysis of KIF15 Expression and Prognosis in Pan-Cancer

To evaluate the KIF15 potential prognostic value in pan-cancer, univariate Cox regression and Kaplan-Meier (KM) method were used to analyze overall survival (OS), disease-free interval (DFI), disease-specific survival (DSS) and progression-free interval (PFI) based on TCGA database. The GEPIA web-based platform was applied to analyze the KIF15 expression level in pan-cancer (http://gepia2.cancer-pku.cn). A *P* value <0.05 was set as significantly different.

Meta-analysis was carried out using Review Manager (RevMan) version 5.3. The eligible studies were searched for on public databases, including PubMed, PrognoScan and Chinese National Knowledge Infrastructure (CNKI) up to December 31, 2021. The search strategy was as follows: ("KIF15" or "kinesin family member 15") AND ("tumor" or "cancer" or "carcinoma" or "malignancy") AND ("survival" or "outcome" or "prognostic"). The inclusion criteria were: (1) the expression level of KIF15 was detected in human cancer; (2) the correlation of KIF15 expression and OS or Disease-free survival (DFS) or Relapse-Free Survival (RFS) or Local relapse-free survival (LRFS) or Distant metastasis-free survival (DMFS) was evaluated; and (3) the hazard ratios (HRs) with 95% confidence intervals (CIs) could be acquired directly or estimated. The exclusion criteria were: (1) articles that were reviews, case reports, letters, meeting abstracts, or expert opinions; (2) duplicate literature; and (3) data that were insufficiently detailed or the needed descriptive or inferential statistics could not be calculated.

We evaluated the correlation between KIF15 and the survival results (OS, RFS, and DMFS) by the pooled HR and 95% CIs. A $P<0.05$ was regarded to be statistically significant. Higgins I^2 statistics and the chi-square Q test were applied to analyze the heterogeneity of different studies. When the heterogeneity was statistically significant ($P>0.1$ or $I^2<50\%$), the fixed-effect model (FEM) was built; otherwise, the random-effect model (REM) was built. A funnel plot and the Egger test were used to evaluate publication bias.

Functional Analysis of KIF15 Related Genes

The GEPIA database was utilized to identify the significantly related genes of KIF15 in human cancers. The correlation coefficient was calculated using the Pearson method and the top 100 genes most relevant to KIF15 were selected. GO and Kyoto Encyclopedia of Genes and Genomes (KEGG) enrichment analyses was performed to investigate the biological functions of these genes by Database for Annotation, Visualization, and Integrated Discovery (DAVID) (https://david.ncifcrf.gov/). Next, a protein–protein interaction (PPI) network was constructed and visualized by Cytoscape (version 8.2). The functional state of KIF15 in different cancer types was explored using CancerSEA database (http://biocc.hrbmu.edu.cn/CancerSEA/). CancerSEA is the first comprehensive database that offers a cancer single-cell functional state atlas; it contains 14 functional states of 41,900 cancer single cells across 25 cancer types. Association between KIF15 and functional state in various single-cell datasets was determined by a correlation strength >0.3 and a false discovery rate (FDR) (Benjamini & Hochberg) <0.05.

Correlation Between KIF15 Expression and Tumor Immunity

The Tumor Immune Estimation Resource (TIMER) web server is an interactive database that helps comprehensively analyze immune cell infiltration (B cells, CD4+ T cells, CD8+ T cells, neutrophils, macrophages, and dendritic cells) in difference cancer types (https://cistrome.shinyapps.io/timer/). We applied "Gene" module of TIMER to evaluate the correlation between KIF15 expression and the six immune cell subtypes from the expression file.

TMB is defined as the total count of somatic insertions, base substitutions, and deletions in each coding area of the tumor genome. The Perl language and R software (version 4.1.1) were used to calculate the total TMB score of each TCGA cancer case and analyze its relationship with KIF15 expression level in pan-cancer (15). MSI is defined as the number of insertion or deletion events in short tandem repeat DNA tracts. Analysis of the correlation between KIF15 expression and MSI was performed by R software (16). Relationship between KIF15 expression and immune signatures was investigated. These immune signatures contained BTLA, CD200, TNFRSF14, NRP1, LAIR1, TNFSF4, CD244, LAG3, ICOS, CD40LG, CTLA4, CD48, CD28, CD200R1, HAVCR2, ADORA2A, CD276, KIR3DL1, CD80, PDCD1, LGALS9, CD160, TNFSF14, IDO2, ICOSLG, TMIGD2, VTCN1, IDO1, PDCD1LG2, HHLA2, TNFSF18, BTNL2, CD70, TNFSF9, TNFRSF8, CD27, TNFRSF25, VSIR, TNFRSF4, CD40, TNFRSF18, TNFSF15, TIGIT, CD274, CD86, CD44 and TNFRSF9, according to previous reports (15–17).The limma package and RColorBrewer package of R software were used to evaluate the correlation between KIF15 expression and the selected immunologic genes in pan-cancer.

Genetic Alteration Analysis of KIF15

cBioPortal for Cancer Genomics database (http://cbioportal.org) were utilized to analysis the KIF15 alteration frequency, copy number alteration and mutation type in various cancer types from TCGA.

GEO Database Analysis of NPC

Three gene expression profiling datasets GSE12452, GSE53819, and GSE61218 were obtained from the GEO database. The GSE12452 microarray contained 31 NPC samples and 10 normal samples, the GSE53819 microarray included 18 NPC samples and 18 non-cancerous samples, the GSE61218 microarray included 10 NPC tissue samples and six normal samples. The expression level of KIF15 was evaluated by wilcoxon, and P-values <0.05 were set as statistically significant.

Immunohistochemistry and Evaluation

From April 2011 to December 2015, 158 formalin-fixed, paraffin-embedded NPC and 33 normal nasopharyngeal epithelium (NNE) tissues were collected in The First Affiliated Hospital of Guangxi Medical University. The patient tumors were newly diagnosed, non-metastatic, measurable, and pathologically confirmed to be NPC. The study was approved by the ethics committee of The First Affiliated Hospital of Guangxi Medical University.

First, the paraffin-embedded tissue sections were dewavered and rehydrated, then the antigen retrieval was carried out, and the endogenous peroxidase activity was blocked by 3% hydrogen peroxide for 25 min at 25°C. After being incubated with KIF15 primary antibody (Abcam, 1:200) at 4°C overnight, the sections were incubated by the secondary antibody for 90 min at room temperature. The immunoreactive score was calculated by

multiplying the proportion of positive cells and the staining intensity. The cell positivity scores were determined as follows: <5% for zero; 5%–25% for one; 26%–50% for two; 51%–75% for three; and 76%–100% for four. The staining intensity scores were determined according to the following: 0 for no staining; 1 for light yellow; 2 for yellow; and 3 for brown. The final immunoreactive score were determined according to the following: 0 for negative, 1-3 for weak staining, 4-7 for moderate staining and, 8-12 for intense staining. All the NPC patients were divided into KIF15 high expression group and low expression group base on median immunoreactive score.

Gene Set Enrichment Analysis (GSEA) of KIF15

GSEA was conducted using GSEA (version 4.0.1) with the Molecular Signatures Database (MSigDB). Samples were separated into high or low KIF15 expression groups based on the median KIF15 expression. The gene set "c2.cp.kegg.v7.1.symbols.gmt" of MSigDB gene set was chose as a reference gene set. A pathway with adj P-value<0.05, false discovery rate (FDR) <0.25 and normalized enrichment score (NES) >1.5 was considered as significantly enriched.

Cell Lines and Transfection

The normal human nasopharyngeal epithelial cell line (NP69) and NPC cell line (CNE1, CNE2, HONE1, C666-1) were obtained from Guangxi Medical University Nasopharyngeal Cancer Research Laboratory. The NP69 cells were cultured in keratinocyte-SFM medium (Invitrogen, Carlsbad, USA) containing bovine pituitary extract (BD Biosciences, San Diego, CA, USA). Human NPC cells were cultured in RPMI-1640 medium supplemented with 10% fetal bovine serum (Gibco), 1% streptomycin/penicillin was added to the medium. All the cells were incubated in a humidified atmosphere with 5% CO_2 at 37°C. NPC cell was transfected with siRNAs targeting KIF15 or control siRNA (RuiSai, Shanghai, China) using Lipofectamine 3000 (Invitrogen, Carlsbad, USA). The target sequences were GCGGTTATAATGGTACCAT (siKIF15-1), and GCTGGAAAGAGTTTCCTTT (siKIF15-2).

Quantitative Real Time Polymerase Chain Reaction (qRT-PCR)

Total RNA from NPC cell was extracted using TRIzol reagent (Life Technologies Corporation, Carlsbad, USA), cDNA was generated using the PrimeScript RT reagent kit according to the manufacturer's protocol (Takara Bio, Kusatsu, Japan). Then, the TB Green Premix Ex Taq II kit (Takara Bio) was applied for qRT-PCR. The relative RNA expression was determined by $2^{-\triangle\triangle ct}$ method, with GAPDH being the internal control. The primers sequences were as follows: KIF15: Forward: 5'-TGGAG GATGGAGGAATAG-3'; Reverse: 3'-CCACCAGGTTG AGTAGGG-5'. GAPDH: Forward: 5'-GGATTGTCTGGCA GTAGCC-3'; Reverse: 3'-ATTGTGAAAGGCAGGGAG-5'.

Cell Viability and Colony Formation Assays

Cells were planted into 96 well plates (1500 cells/well) after 24 hours of transfection. CCK-8 reaction reagent (Dojindo, Japan) was used to measure cell viability at 0h, 24h, 48h, 72h. 10 μl of CCK-8 solution was added into each well and incubated for 2 h. The OD value was measured with the microplate reader at 450 nm. In order to explore proliferation, colony formation assay was performed. After incubation in 6-well plates at 1500/well, the formation of cell colonies was detected after 14 days. In brief, cells were subjected to methanol fixation and stained by crystal violet solution. clones contained at least 50 cells were counted for analysis.

Scratch Assay

5×10^5 cells/well were seeded into 6-well plates. Subsequently, 10μl pipette tip was used to create a wound on the confluent cell monolayer. Then, we used inverted microscope to take photos of wound closure at 0 and 24 h and the wound healing distance was analyzed.

Transwell Assay

After resuspending by serum-free medium, 5×10^4 cells containing RPMI 1640 medium without FBS were plated in the upper chamber, and 500 ul of 10% FBS RPMI 1640 medium was added to the lower chamber. The number of cells that had migrated after 24 h was measured under three random fields.

Statistical Analysis

Differences in clinical characteristics (Gender, Age, Histological type, T stage, N stage and TNM stage) between the groups were evaluated using the chi square test, while 5 year-OS between the groups were evaluated using KM analysis with the log-rank test. OS, RFS, and DMFS were defined as the period from the day of first treatment to day of death, relapse and distant metastasis due to any reason. Statistical analysis and visualization were conducted with SPSS (version 24.0; IBM, New York, USA), GraphPad Prism (version 8.0), and R software. Results with $P<0.05$ was regarded as statistically significant. We conducted univariate and multivariate cox regression analyses for the selection of features. The selection of candidate features depended on comprehensive consideration of their clinical value and statistical significance. The nomogram model was generated with 5-year OS endpoint by the rms package of R software. Concordance index (C-index), receiver operating characteristic (ROC) curve, and the calibration curve were used to evaluate the predictive accuracy for the nomogram. After calculating the total scores by nomogram, patients were divided into low- or high-risk subgroups by using the X-tile software (version 3.6.1; Yale University, New Haven, CT, USA) (18).

RESULTS

KIF15 mRNA Expression and Clinical Association in Pan-Cancer

The abbreviations of the 33 TCGA cancer types are shown in **Table 1**. In TCGA database, KIF15 was upregulated in 20 cancer types, including BLCA, BRCA, CESC, CHOL, COAD, ESCA, GBM, HNSC, KICH, KIRC, LIHC, LUAD, LUSC, PCPG, PRAD, READ, SARC, STAD, THCA and UCEC (**Figure 1A**). Likewise,

in the Oncomine database, the expression level of KIF15 was significantly increased in bladder, brain and CNS, breast, cervical, colorectal, esophageal, gastric, head and neck, lung, and ovarian cancers, as well as lymphoma and sarcoma; while significantly decreased in leukemia. (**Figure 1B**). Detailed data of KIF15 expression levels in Oncomine database are shown in **Supplementary Table 1**. In the Kaplan-Meier plotter database, KIF15 was differentially highly expressed in 18 cancer types, including adrenal, bladder, breast, colorectal, esophageal, liver, lung, ovarian, pancreatic, prostate, rectal, renal, skin cancer, stomach, thyroid, and uterine cancers and acute myeloid leukemia, while less expressed in testicular cancer (**Figure 1C**). In short, KIF15 could serve as an oncogene in pan-cancer. In addition, the expression level of KIF15 significantly related to patients' cancer stage in ACC, BRCA, COAD, ESCA, KICH, KIRC, KIRP, LIHC, LUSC, SKCM, TGCT, and THCA based on TCGA database (**Figure 2**).

Correlation Analysis Between the Expression of KIF15 and Prognostic Value

Univariate cox regression analyses are shown as forest charts in **Figure 3**. High KIF15 expression positively correlated with poorer OS in ACC, KICH, KIRC, KIRP, LGG, LIHC, MESO, PAAD, PCPG, PRAD, READ, while it correlated with better OS in READ and THYM (**Figure 3A**). For DFI, high KIF15 expression remarkably correlated with worse survival in KIRP, LIHC, LUAD, PAAD, PRAD, SARC, and THCA (**Figure 3B**). For DSS, it was found that high KIF15 expression significantly correlated with worse prognosis in ACC, KICH, KIRC, KIRP, LGG, LIHC, LUAD, MESO, PAAD, PRAD, SARC, and UCEC, while it correlated with better prognosis in COAD (**Figure 3C**). For PFI, high KIF15 expression positively correlated with worse survival in ACC, KICH, KIRC, KIRP, LGG, LIHC, LUAD, MESO, PAAD, PCPG, PRAD, SARC but correlated with better survival in COAD and GBM (**Figure 3D**).

A K-M survival curve was used to demonstrate the effect of KIF15 on prognosis, as shown in **Figure 4**. For OS, increased KIF15 expression showed worse prognosis in ACC, KICH, KIRC, KIRP, LGG, LIHC, MESO, PAAD, and SARC but better prognosis in COAD, STAD, and THYM (**Figure 4A**). For DFI, increased KIF15 expression showed worse prognosis in KIRP, LIHC, LUAD, PAAD, SARC, and THCA (**Figure 4B**). For DSS, increased KIF15 expression showed worse prognosis in ACC, KICH, KIRC, KIRP, LGG, LIHC, LUAD, MESO, PAAD, PRAD and SARC, but better prognosis in COAD (**Figure 4C**). For PFI, increased KIF15 expression showed worse prognosis in ACC, KIRC, KIRP, LGG, LIHC, LUAD, MESO, PAAD, PRAD, SARC, and UVM but better prognosis in COAD and GBM (**Figure 4D**). Together, higher expression levels of KIF15 represented an unfavorable prognostic indicator in pan-cancer. Additionally, based on the GEPIA platform, higher mRNA expression levels of KIF15 also indicated a worse prognostic outcome in pan-cancer (**Figures 4E, F**).

A meta-analysis was performed to further clarify the prognostic value of KIF15 in cancers. The flowchart of literature retrieval process is shown in **Supplementary Figure 1**. The basic characteristics of all included studies (12, 14, 19–29) or datasets are shown in **Supplementary Table 2** and **Supplementary Table 3**. Results of the forest plots demonstrated that high KIF15 expression significantly correlated to a worse OS (HR 1.25, 95% CI 1.14–1.37, P<0.0001); RFS (HR 1.31, 95% CI 1.13–1.53, P = 0.0003); and DMFS (HR 1.51, 95% CI 1.32–1.73, P<0.00001) (**Supplementary Figure 2**). Significant heterogeneity in meta-analysis was observed (OS, P<0.00001, I^2 = 60%; RFS, P = 0.01, I^2 = 53%), and thus a REM was adopted. For the sensitivity analysis of OS, after exclusion of Liu et al., Song et al., and Duke OC, the heterogeneity was reduced (P=0.0003, I^2 = 48%), while no significant change occurred with the HR of 1.30 (95% CI 1.19–1.43, P<0.00001). For the sensitivity analysis of RFS, after exclusion of GSE31210, the heterogeneity decreased (P=0.23, I^2 = 22%), while the HR slightly decreased to 1.23 (95% CI 1.09–1.38, P=0.0006) (**Supplementary Figure 3**). Thus, the summarized results in the meta-analysis were relatively reliable and stable. In summary, these integrated analyses suggest that high expression of KIF15 may serve as a poor prognostic biomarker in most cancers.

TABLE 1 | Abbreviations of the 33 cancer types in the The Cancer Genome Atlas database.

ACC	Adrenocortical carcinoma
BLCA	Bladder urothelial carcinoma
BRCA	Breast invasive carcinoma
CESC	Cervical squamous cell carcinoma and Endocervical adenocarcinoma
CHOL	Cholangiocarcinoma
COAD	Colon adenocarcinoma
DLBC	Lymphoid neoplasm diffuse large B-cell lymphoma
ESCA	Esophageal carcinoma
GBM	Glioblastoma multiforme
HNSC	Head and Neck squamous cell carcinoma
KICH	Kidney chromophobe
KIRC	Kidney renal clear cell carcinoma
KIRP	Kidney renal papillary cell carcinoma
LAML	Acute myeloid leukemia
LGG	Brain lower grade glioma
LIHC	Liver hepatocellular carcinoma
LUAD	Lung adenocarcinoma
LUSC	Lung squamous cell carcinoma
MESO	Mesothelioma
OV	Ovarian serous cystadenocarcinoma
PAAD	Pancreatic adenocarcinoma
PCPG	Pheochromocytoma and Paraganglioma
PRAD	Prostate adenocarcinoma
READ	Rectum adenocarcinoma
SARC	Sarcoma
SKCM	Skin cutaneous melanoma
STAD	Stomach adenocarcinoma
TGCT	Testicular germ cell tumors
THCA	Thyroid carcinoma
THYM	Thymoma
UCEC	Uterine corpus endometrial carcinoma
UCS	Uterine carcinosarcoma
UVM	Uveal melanoma

Molecular Mechanism of KIF15 in Pan-Cancer

The interaction between KIF15 and its related genes are displayed in **Figure 5A**. KEGG and GO enrichment analysis were carried out to explore the potential functions of KIF15 in cancer. The results indicated that KIF15 and its related genes were significantly

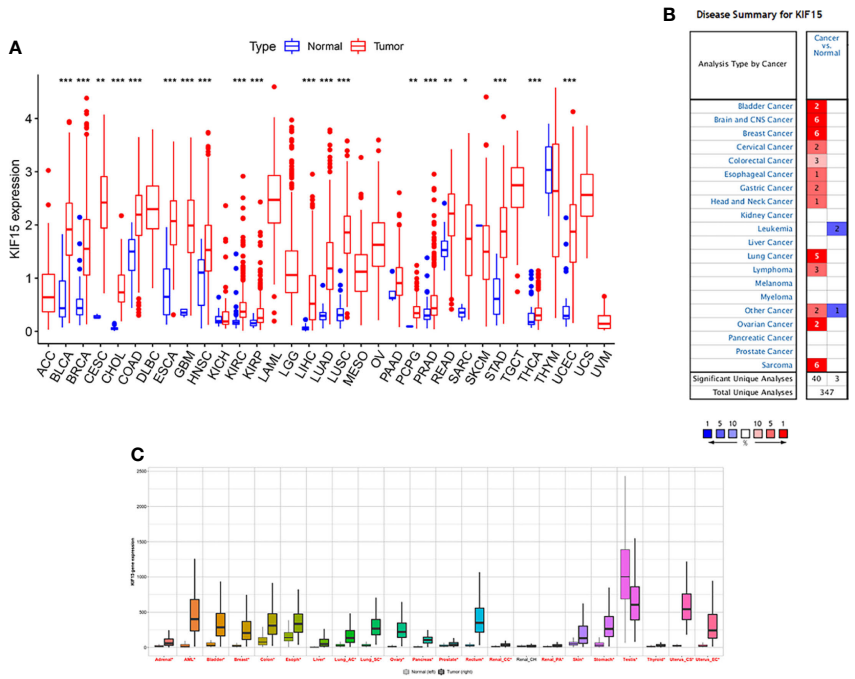

FIGURE 1 | The expression level of KIF15 in pan-cancer. **(A)** Differential expression of KIF15 between tumor and normal tissues of KIF15 in TCGA. **(B)** Differential expression of KIF15 between tumor and normal tissues of KIF15 in Oncomine. **(C)** Differential expression of KIF15 between tumor and normal tissues of KIF15 in Kaplan–Meier plotter. *$P < 0.05$; **$P < 0.01$ and ***$P < 0.001$.

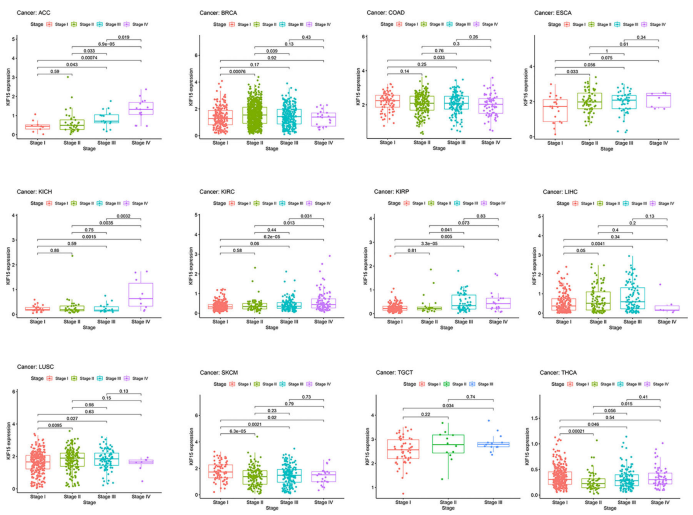

FIGURE 2 | Correlation of KIF15 mRNA expression and different pathological stages of certain cancers in TCGA.

associated with cell division, mitotic nuclear division, and sister chromatid cohesion; they may also have association with the p53 signaling pathway, the cell cycle, and DNA replication (**Figures 5B, C**). In the analysis of CancerSEA database, the functional state of KIF15 was explored at the single-cell level in 14 types of cancer. KIF15 was found to be positively associated with cell cycle, DNA damage, DNA repair, and proliferation in multiple cancer types (**Supplementary Figure 4**).

Genetic Alteration of KIF15 in Pancancer

As is shown in **Figure 6**. Mutation status of KIF15 was evaluated, the highest alteration rate of KIF15 (8.13%) appears in patients

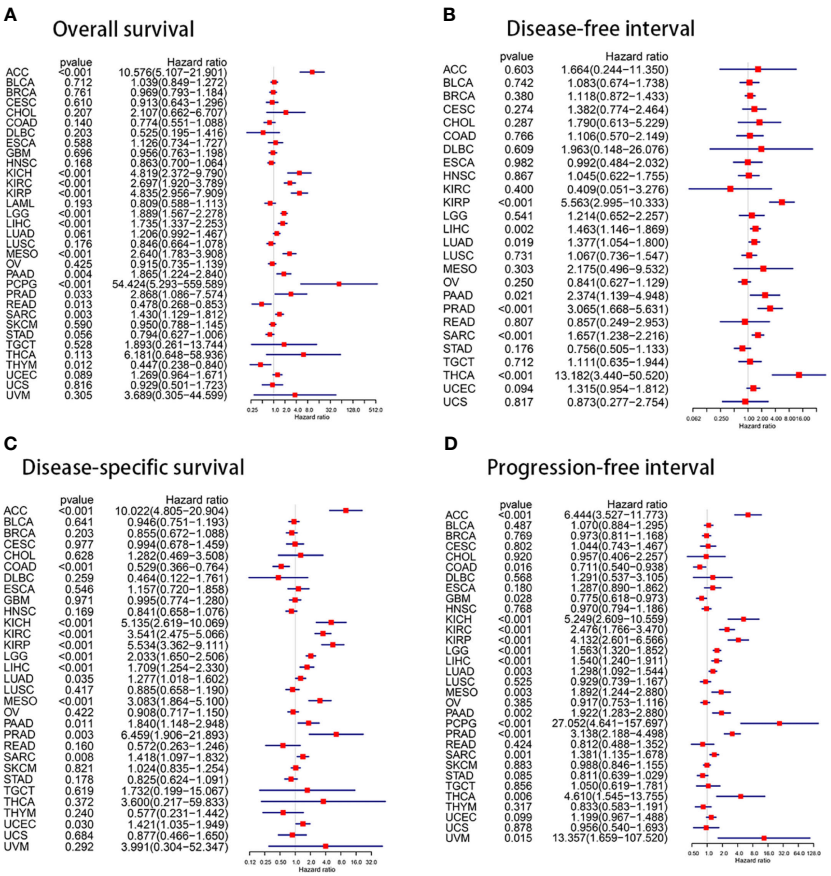

FIGURE 3 | The prognosis value of KIF15 of differ cancers using Univariate Cox proportional hazards models. **(A)** Overall survival (OS). **(B)** Disease-free survival (DFI). **(C)** Disease-specific survival (DSS). **(D)** Progression-free interval (PFI).

with uterine corpus endometrial carcinoma with "mutation" as the primary type. The "deep deletion" type (4.17%) of copy number alteration was the primary type in the diffuse large B-Cell lymphoma cases.

Relationship Between KIF15 and Immune-Related Factors

Studies have proven that immune cell infiltration is significantly correlated with survival in cancers. Tumor purity is a vital factor that affects the evaluation of immune infiltration. Therefore, the relationship between KIF15 expression and immune cell infiltration in pan-cancer was explored. Notably, the results indicated that HNSC, KIRC, LGG, LIHC, PRAD, and THYM were six cancer types most strongly associated with KIF15 expression in immune cell infiltrating level, including B cells, CD8+ T cells, CD4+ T cells, macrophages, neutrophils, and dendritic cells (**Supplementary Figure 5**). TMB and MSI were also analyzed. For TMB, it was found that KIF15 gene expression was positively related to ACC, BLCA, BRCA, COAD, HNSC, KICH, LGG, LUAD, LUSC, MESO, PAAD, PRAD, READ, SARC, SKCM, STAD, and UCEC but negatively related to THYM. For MSI, we found that KIF15 gene expression was positively related to BLCA, ESCA, LUSC, MESO, READ, SARC, STAD, and UCEC but was negatively related to DLBC. Moreover, correlation between KIF15 and immune gene set was analyzed, and the expression of several important immune-related genes was significantly related to KIF15 expression level in pan-cancer, such as CTLA4, IDO1, and LAG3 (**Figure 7**). In summary, our findings showed that high expression of KIF15 played an important role in immune-related factors.

KIF15 Expression in NPC Tissue

Regarding the key functional role of KIF15 in cancers, we detected the expression level of KIF15 in NPC tissue through the GEO datasets and IHC. Based on the analyses of three microarrays (GSE12452, GSE53819, and GSE61218), KIF15 expression was found to be upregulated in NPC tissues compared to the normal controls (P<0.05) (**Figures 8A–C**). A diagnostic ROC curve was performed between the two groups, and KIF15 exhibited high diagnostic value in the three microarrays (area under the curve, AUC= 0.9584, 0.7191, and 0.9833, respectively) (**Figures 8D–F**). For IHC, Compared with the NNE tissue, KIF15 expression was significantly upregulated

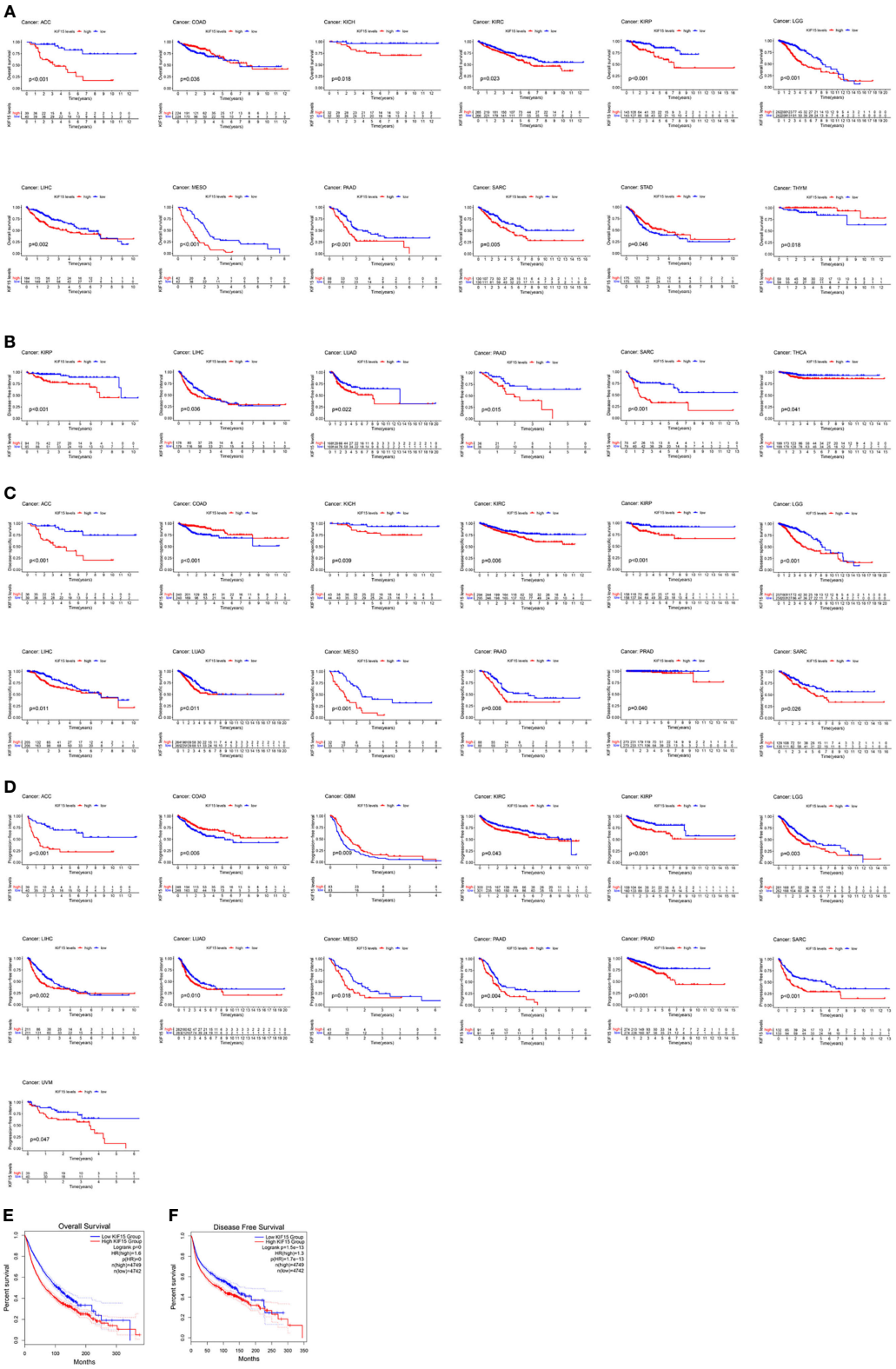

FIGURE 4 | The prognostic value of KIF15 in different cancers using Kaplan–Meier method. **(A)** Overall survival (OS). **(B)** Disease-free survival (DFI). **(C)** Disease-specific survival (DSS). **(D)** Progression-free interval (PFI). **(E)** OS curve of KIF15 in all cancer based on GEPIA. **(F)** Disease-free survival (DFS) curve of KIF15 in all cancer based on GEPIA.

TABLE 2 | Correlation between the expression level of KIF15 and clinicopathological characteristics of patients with nasopharyngeal carcinoma.

Variables	Case	KIF15 expression		
		low	high	*P-value*
Gender				
Female	39	17	22	
Male	119	62	57	0.356†
Age (y)				
< 45	73	35	38	
≥ 45	85	44	41	0.632†
Histological type				
WHO II	14	6	8	
WHO III	144	73	71	0.576†
T stage				
T1-2	65	40	25	
T3-4	93	39	54	0.015†
N stage				
N0-1	56	37	19	
N2-3	102	42	60	0.003†
TNM stage				
I-II	32	23	9	
III-IV	126	56	70	0.006†
5 year-OS		78.5%	58.2%	0.0044‡

OS, overall survival. †chi square test, ‡log-rank test.

in NPC tissues (**Figure 9A**). As shown in **Table 2**, high KIF15 expression level positively correlated with T stage (*P*=0.015), N stage (*P*=0.003), and clinical stage (*P*=0.006). the median follow-up period was 76 months (range, 4-80 months). After 5-year follow-up, 62 (78.5%) patients in low KIF expression group were alive, 46 (58.2%) patients in low KIF expression group were alive. The result indicated that increased KIF15 expression correlated with worse OS for NPC (P=0.0044). (**Figure 9B**). To identify the independent prognostic factor in NPC, univariate analysis was used to assess the prognostic value of clinical features and KIF expression level. These results indicated that age (*P*=0.078), T stage (*P*=0.023), N stage (*P*=0.007), and KIF15 expression level (*P*=0.006) were significantly correlated with the OS (**Table 3**). According to the multivariate cox analysis, age, T stage, N stage, and KIF15 expression level were incorporated to build a nomogram model (**Figure 10A**). The C-index of the model was 0.695 (95% CI 0.62–0.765) and was verified by 1000-replication bootstrapping analysis. The calibration curves for predicting 3- and 5-year OS also indicated a satisfactory predictive accuracy (**Figures 10B, C**). ROC curve analysis revealed that the model had an effective predictive ability, with an AUC value of 0.730 (**Figure 10D**). Subsequently, based on the total score of each case, all the patients were divided into either a low-risk (score<136) or high-risk group by X-tile software. KM survival curves showed that the OS in the high-risk group was significantly reduced below that of the low-risk group (**Figure 10E**).

KIF15 Related Pathways

As is shown in **Figure 11**, GSEA analysis of GSE12450 indicated that high expression of KIF15 significantly related to DNA repair (NES = 2.424, p.adj = 0.013, FDR = 0.008), DNA replication (NES = 2.737, p.adj = 0.013, FDR = 0.008) and PLK1 pathway (NES = 2.301, p.adj = 0.013, FDR = 0.008).

Primary Validation of the Effect of KIF15 in NPC Cells

Using RT-PCR, we found that the mRNA expression level of KIF15 was increased in NPC cell lines, especially in CNE1, compared to the NP69 ($p < 0.001$) (**Figure 12A**). Therefore, CNE1 cell line was selected for further study. Besides, We verified that KIF15 expression level was significantly repressed upon si-KIF15 transfection (**Figure 12B**). CCK8 and colony formation assays indicated that downregulation of KIF15 remarkably reduced the proliferation of CNE1 (**Figures 12C, D**). Wound healing was remarkedly suppressed by KIF15 silencing in CNE1 (**Figure 12E**). The Transwell assay indicated that the migration of CNE1 cells were significantly suppressed by KIF15 silencing (**Figure 12F**).

DISCUSSION

NPC, one of the major types of head and neck cancer, is a malignant tumor arising from the nasopharyngeal mucosal lining (30). Because of its challenging anatomical location, radiochemotherapy is regarded as the mainstay of treatment (31). However, an anatomy-based staging system is not enough to predict prognosis and treatment efficiency of NPC. Thus, it is necessary to investigate the incorporation of clinical features and novel biomarkers for the improvement of the efficacy of prediction.

Kinesins are a type of conserved protein that modulate the movement of certain important functional molecules, including chromosomes, protein complexes, mRNAs, and organelles in cells during mitosis (32). Thus, they are critical for protein sorting and appropriate positioning of different biological

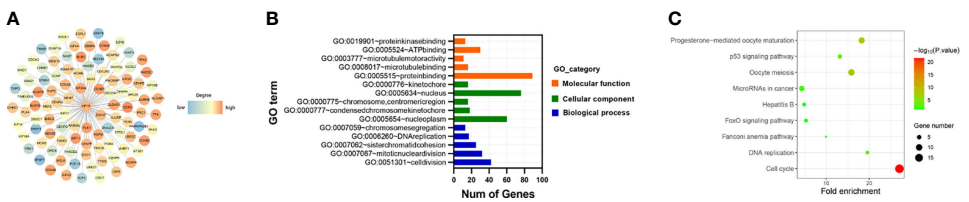

FIGURE 5 | Functional analysis of KIF15 and relevant genes. **(A)** Protein–protein interaction (PPI) network display the top 100 relevant genes of KIF15. **(B)** Gene Oncology (GO) analysis of KIF15 and relevant genes. **(C)** Kyoto Encyclopedia of Genes and Genomes (KEGG) analysis of KIF15 and relevant genes.

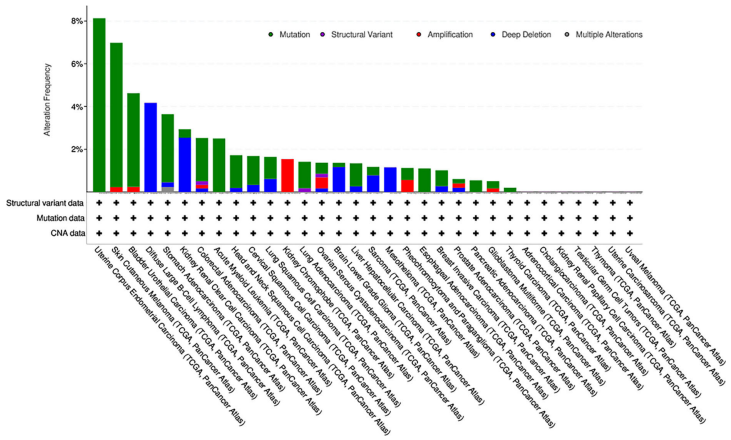

FIGURE 6 | The alteration frequency with mutation type of KIF15 in different cancer types from TCGA database.

molecules. Reportedly, the kinesin family features are prominent in facilitating a variety of biological processes such as cell morphology, cytoskeletal dynamics, cell division, and cell migration (8). These findings have demonstrated a very promising role of the kinesin family in cancer. For instance, KIF23 is highly expressed in gastric cancer and is correlated with a worse prognosis of patients (33). KIF21B has been identified as an oncogene in the development and migration of NSCLC (34). Additionally, KIF20B could promote cancer growth by promoting cell proliferation in tongue cancer (35). However, the effect of most kinesin families in tumorigenesis are not completely understood.

KIF15 is a member of the kinesin family that directs kinesin-like motor enzymes involved in mitotic spindle assembly (36). The aberrant expression of KIF15 could lead to abnormal cell replication, differentiation, and thus cause tumorigenesis. The expression pattern and functional roles of KIF15 in tumor pathogenesis, especially in NPC, have not been comprehensively investigated. The results of our pan-cancer analysis revealed that KIF15 expression was significantly upregulated in most type of cancers, suggesting that KIF15 might act as an oncogene in pan-cancers. Based on KM and univariate analyses, it was found that high expression of KIF15 indicated poor survival in several cancers, including OS, DFI, DSS, and PFI. Our results from the clinical correlation test showed that KIF15 expression level was increased in advanced pathological stages in ACC, KICH, KIRC, KIRP, LIHC, LUAD, and TGCT. Moreover, the results of IHC revealed that KIF15 had a higher expression level in NPC tissues, and it was significantly correlated with the poor prognosis of patients with NPC. Previous studies have indicated that KIF15 plays a vital role in the disease progression of most cancers. Gao et al. have found that the upregulation of KIF15 in breast cancer tissues was positively related to TNM stage, tumor size, and lymph node metastasis; while downregulation of KIF15 inhibited cell proliferation and tumor proliferation *in vitro* and *in vivo* (37). Research by Li et al. has shown that over-expression of KIF15 promoted the cancer stem cell (CSC) phenotype and malignancy through phosphoglycerate dehydrogenase (PHGDH)-regulated intracellular reactive oxygen species disorders in HCC (38). Wang et al. have also shown that KIF15 promoted pancreatic cancer growth by enhancing G1/S phase transition by affecting the MEK–ERK signalling pathway (25). These findings are consistent with that of ours, which indicated that KIF15 is a promising diagnostic and prognostic biomarker in pan-cancer, as well as NPC.

Functional enrichment analysis showed that KIF15 may be involved in the p53 signaling pathway, the cell cycle, DNA replication and FOXO pathway. The well-known cancer suppressor gene, p53, closely controls various cellular signals involved in the cell-cycle, apoptosis, and senescence (39). A study based on machine learning showed that KIF20A and KIF23 were regulated by p53 and correlated with malignant transformation and tumor stage (40). Further, KIF15 knockdown strongly enhanced the expression of p53 and p21 protein in breast cancer cells (37). KIF15 is involved in Burkitt lymphoma cell activity *via* mediating the expression of p53 (41). Loss or mutation of p53 in tumor might have an impact on the recruitment and activity of myeloid and T cells, which contribute to immune evasion and tumor development, in addition, p53 can also affect the immune cells, causing different outcomes that can impede or promoting cancer progression (42, 43). The cell cycle is one of the most important topics studied in cancer biology. Over-expression of KIF15 increases the cyclin-D1, CDK2, p-RB expression, and accelerated G1/S transition in pancreatic cancer cells (25). KIF15 suppression has been shown to cause cell cycle arrest at the G0/G1 phase in breast cancer cells, indicating that knockdown of KIF15 inhibited the malignant behavior of breast cancer cells (27). Abnormal DNA replication is a hallmark of the cancer process, and previous studies have indicated that KIF15 and other kinesin genes were significantly enriched in DNA replication in bladder and endometrial cancers (29, 44). Accumulating evidence revealed that the FOXO family of transcription factors plays an important role in regulating the progression and function of tumor microenvironment (TME). FOXOs promote antitumor activity by negatively inducing the

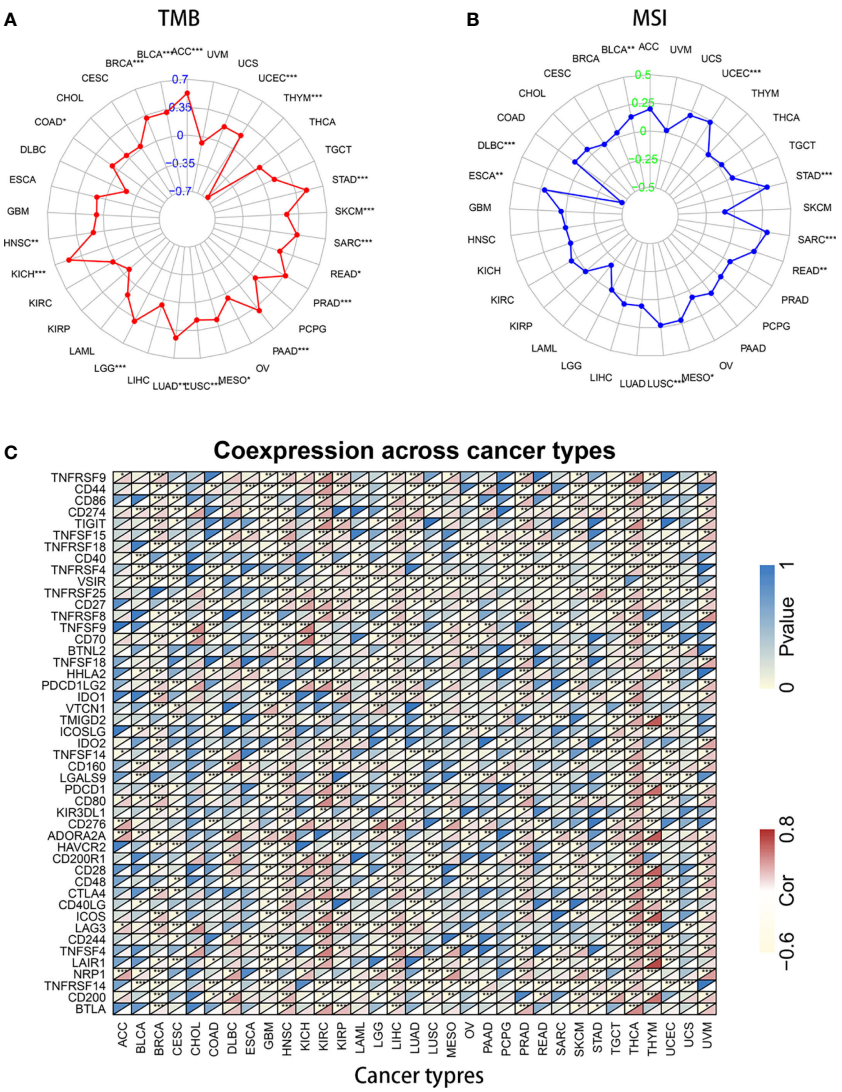

FIGURE 7 | Association of KIF15 mRNA expression with tumor mutational burden (TMB), microsatellite instability (MSI) and immune genes. **(A)** A radar map shows the relationship of KIF15 and TMB. **(B)** A radar map shows the relationship of KIF15 and MSI. **(C)** Heatmap shows the relationship of KIF15 and immune genes. *$P < 0.05$; **$P < 0.01$ and ***$P < 0.001$.

expression of immunosuppressive proteins, including PD-L1 and VEGF in stromal cells or tumor cell, and thus promote immunotolerant state in the TME (45).

TMB is an emerging characteristic of cancer and is tightly associated with MSI (46). Both TMB and MSI are considered to be biomarkers for the favorable immune checkpoint blockade treatment response in cancer (47, 48). For TMB, we found that KIF15 gene expression was positively associated with ACC, BLCA, BRCA, COAD, HNSC, KICH, LGG, LUAD, LUSC, MESO, PAAD, PRAD, READ, SARC, SKCM, STAD, and UCEC but was negatively associated with THYM. We suspect that a high neoantigens load led to the dysregulation of KIF15, and thus affected the development of cancer. For MSI, we found that KIF15 gene expression was positively associated with BLCA, ESCA, LUSC, MESO, READ, SARC, STAD, UCEC but was negatively associated with DLBC, suggesting that MSI may change the expression of KIF15 (15). Several kinesin superfamily have been found to link with tumor immune cells infiltration. For example, Ren et al. found that KIF20A expression was strong positive association with Th2 cells, Treg cells and Macrophages, while a negative association with Th17 cells, Mast cells and NK cells (49). Kim et al. indicated that KIF18A act as a key dendritic cells differentiation and activation regulator (50). Qiu et al. shown that KIF18B expression was associated closely with tumor immunity and interacted with various immune cells and genes markers (15). However, researches investigating the possible role of KIF15 in the regulation of tumor immunity are seldom. A study constructed a decision tree using mutations in PIK3CA, MEF2C, SLC11A1, and KIF15 to divided patient sub-cohorts

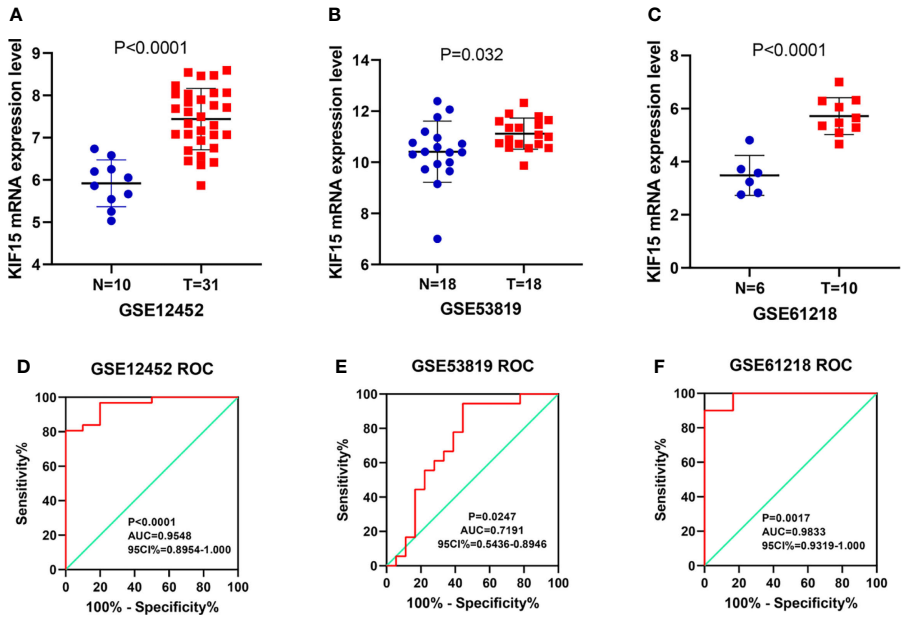

FIGURE 8 | The expression of KIF15 in nasopharyngeal carcinoma (NPC) and normal tissues were investigated by GEO database. **(A–C)** KIF15 was significantly upregulated in NPC tissue in three datasets. **(D–F)** The diagnostic operating characteristic (ROC) curves of KIF15 in NPC and normal tissues in three datasets.

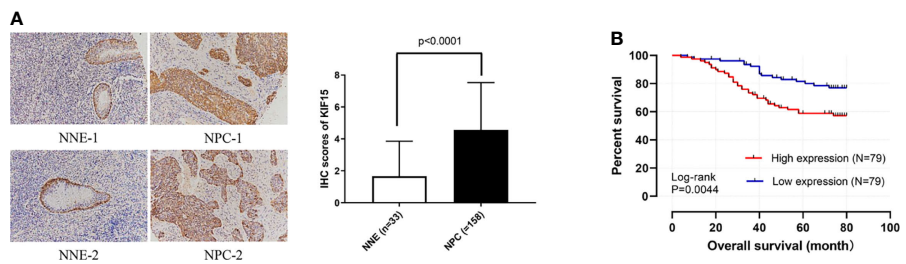

FIGURE 9 | Preliminary experimental verification of KIF15 in patients with nasopharyngeal carcinoma (NPC). **(A)** Immunohistochemical analysis of KIF15 protein expression between nasopharyngeal carcinoma (NPC) and normal tissues (200×). **(B)** Kaplan–Meier survival curves for KIF15 in NPC.

with elevated PD-L1 expression, which contribute to identify the novel prognostic biomarkers of Gastric Cancer (51). Result of our study indicates new antigen generation was related to KIF15, further experiments are needed to investigate the regulator role of KIF15 in TME.

Tumor cells as well as the tumor microenvironment (TME) could secrete or express different signaling molecules, which act on immune checkpoints expressed in immune cells to inhibit immune responses (52). Several kinesin family genes have been linked to immune infiltration. For example, KIF18B expression significantly correlated negatively with the purity of stromal cells and immune cells in seven types of cancer (15). Likewise, KIF1A expression negatively correlated with infiltration levels of 16 types of immune cells in ovarian carcinoma (53). KIF20A had a strong positive association with Th2 cells, Treg cells, and macrophages but a negative association with Th17 cells, mast cells, and NK cells in renal clear cell carcinoma (49). However, the effects of KIF15 in cancer immunity and cancer microenvironment have been seldomly reported, and further investigation is urgently needed to clarify its role in cancer. In our study, expression of KIF15 significantly related to B cell, CD8+ T cell, CD4+ T cell, macrophage, neutrophil, and dendritic cell infiltration in HNSC, KIRC, LGG, LIHC, PRAD, and THYM. Macrophages have high plasticity in response to different external signals and directly influence various steps in tumor development, such as tumor cell proliferation, stemness, and immunosuppression (54). Neutrophils participate in almost every step of oncogenesis, and in recent years, the neutrophil-to-lymphocyte ratio has been regarded as a prognostic indicator of worse OS in cancer (55). Dendritic cells are a critical factor in antitumor immunity due to their potent

TABLE 3 | Evaluation of the prognostic factors of nasopharyngeal carcinoma based on univariate and multivariate COX regression.

	Univariate Cox regression			Multivariate Cox regression		
	HR	**95% CI**	***P*-value**	**HR**	**95% CI**	***P*-value**
Gender (Female vs. Male)	0.683	0.341-1.365	0.280	–	-	-
Age (≥45 vs. <45)	1.681	0.943-2.99	0.078	1.957	1.092-3.506	0.024
T stage (T3–4 vs. T1–2)	2.019	1.102-3.699	0.023	1.637	0.885-3.028	0.116
N stage (N2–3 vs. N0–1)	2.590	1.294-5.180	0.007	2.355	1.155-4.801	0.018
TNM stage (III–IV vs. I–II)	1.815	0.816-4.036	0.144	–	–	–
Histological type (WHO III vs. WHO II)	1.626	0.506-5.224	0.415	–	–	–
KIF15 expression (High vs. Low)	2.284	1.272-4.104	0.006	1.902	1.047-3.454	0.035

HR, hazard ratio; CI, confidence interval.

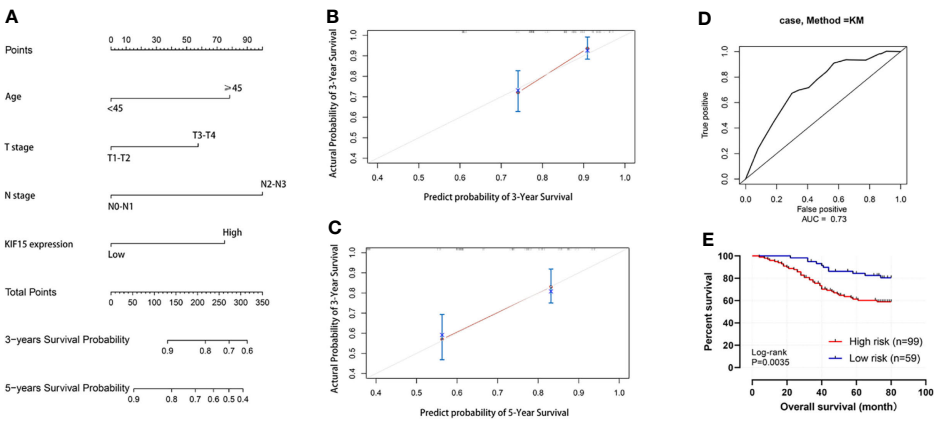

FIGURE 10 | Nomogram for predicting the prognosis of NPC patient. **(A)** Nomogram. **(B, C)** 3-year and 5-year calibration curves. **(D)** Operating characteristic (ROC) curves for the mode. **(E)** Survival curve of high-risk and low-risk groups.

antigen-presenting ability, therefore, dendritic cells are a critical target in any effort to generate immunotherapy against cancer (56). In short, our results suggest a likely regulatory role of KIF15 in tumor immunology.

Moreover, we selected several common immune genes and examined their correlation with KIF15 expression levels in various cancer types. Among these genes, CTLA4 has presently garnered much attention. CTL-associated antigen 4 (CTLA4) is the first immune checkpoint receptor to be clinically targeted. It regulates T-cell activation by competing with the co-stimulatory molecule CD28, CTLA4 and CD28 shared ligands, CD80 (also known as B7.1), and CD86 (also known as B7.2) (57). Once antigen recognition has started, CD28 signalling intensely amplifies TCR signalling to activate T cells (58). In this study, KIF15 significantly related to CTLA4 expression in 17 out of 33 cancer types. Indoleamine 2, 3-dioxygenase 1 (IDO1) is a novel immune checkpoint target, which is a type of a rate-limiting metabolic enzyme that transforms tryptophan (Trp) into downstream kynurenines (Kyn). Some studies have demonstrated that IDO1 was associated with potently regulating immunosuppressive effects in cancer (59). According to our findings, KIF15 was highly related to IDO1 expression in 11 out of 33 cancer types. Inhibitory receptors (IRs) have a potential role in regulating the immune response and are regulators of T cell dysfunction in autoimmune diseases. Lymphocyte Activation Gene 3 (LAG3), also known as CD223, is currently one of the most promising new IR targets in the clinic. It is expressed by both activated and exhausted CD4+ and CD8+ T cells as well as by regulatory T cells (60). In the present study, it was found that KIF15 was closely related to the expression of LAG3 in 16 out of 33 cancer types. Thus, KIF15 might serve as novel cancer therapeutic targets.

To the best of our knowledge, this is the first study that focused on the value of KIF15 from a pan-cancer perspective. We successfully explored the role of KIF15 in NPC; however, further functional experiments are still needed to clarify its effect on tumor biological process *in vivo* and *in vitro*. Despite the limitation of our

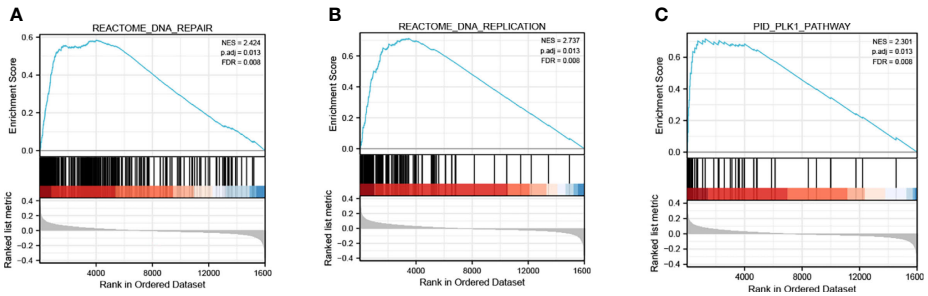

FIGURE 11 | Enrichment plots of GSEA from GSE12452 dataset. **(A–C)** KIF15 related signaling pathways in c2.cp.kegg.v7.1.symbols.gmt.

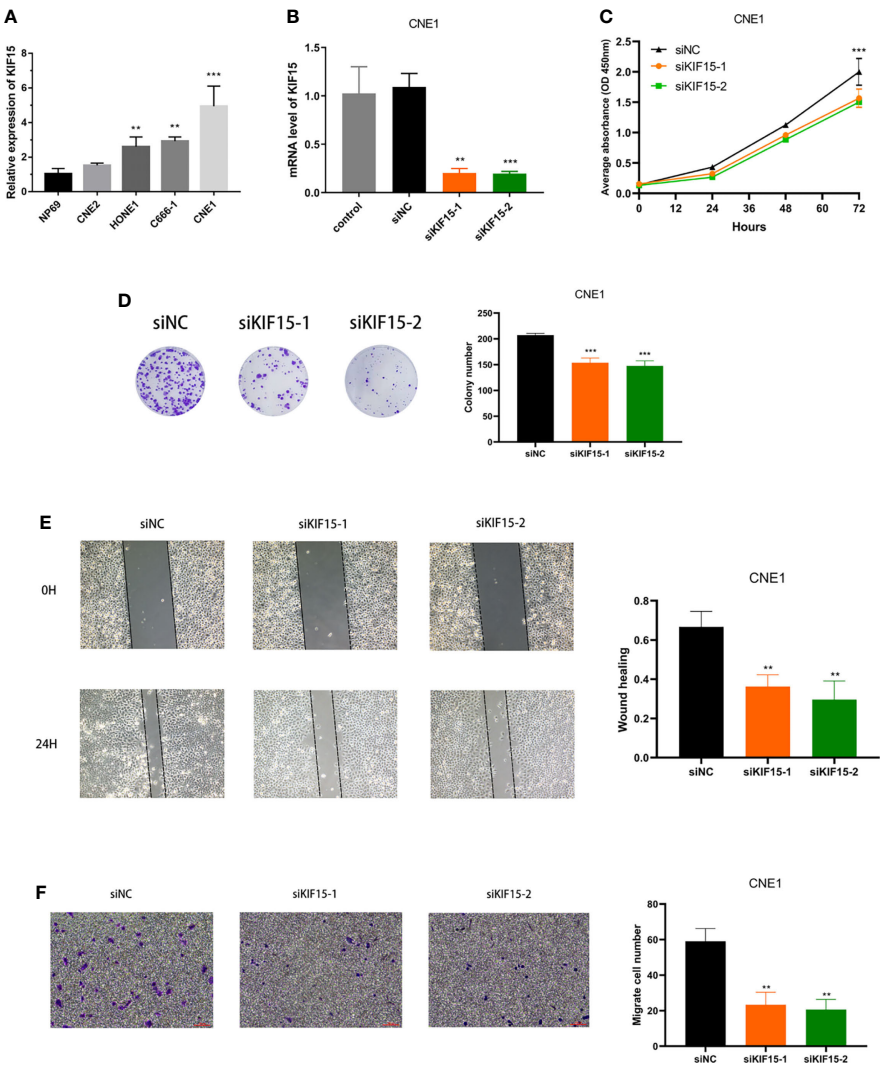

FIGURE 12 | Effect of KIF15 in NPC cell proliferation and migration. **(A)** qRT-PCR analysis of KIF15 expression level in normal and NPC cell lines. **(B)** qRT-PCR analysis confirmed the knockdown efficacy of KIF15 in NPC cell line CNE1. **(C, D)** CCK-8 and colony formation assay were applied to examine the proliferation ability of KIF15 knockdown cells. **(E, F)** Wound-healing and transwell assay employed to detect the migration ability of KIF15 knockdown cells. $^{**}P < 0.01$ and $^{***}P < 0.001$.

study, we conclude that KIF15 could be a promising prognostic biomarker in pan-cancer as well as in NPC.

CONCLUSION

In the present study, a pan-cancer investigation was performed revealing that KIF15 played a vital role in prognosis, molecular function, signaling pathways, and tumor immunity in differ cancer types based on public databases. Furthermore, we demonstrated that KIF15 was highly expressed in NPC tissue and could be considered as a novel diagnostic and prognostic biomarker of NPC.

DATA AVAILABILITY STATEMENT

The original contributions presented in the study are included in the article/**Supplementary Material**. Further inquiries can be directed to the corresponding authors.

ETHICS STATEMENT

Written informed consent was obtained from the individual(s) for the publication of any potentially identifiable images or data included in this article.

AUTHOR CONTRIBUTIONS

LJ and RW conceived and designed the study. JM, SM, and WC organize and carried out the research. MK, MX, CL, BL, and FW helped to analyze the data of the study. FL and YZ performed the experiments. JM wrote the paper. All authors contributed to the article and approved the submitted version.

FUNDING

This work was supported by the Guangxi Medical and Health Appropriate Technology Development and Promotion Application Project (No. S2017020), the Key Research and Development Program of Guangxi (No. Guike AB18281003), the "139" Program for high-level medical talents in Guangxi, Innovation Team of The First Affiliated Hospital of Guangxi Medical University, Guangxi Science and Technology Program Project (GK AD17129013), and the National Natural Science Foundation of China (No. 82060019, 82060494).

SUPPLEMENTARY MATERIAL

The Supplementary Material for this article can be found online at: https://www.frontiersin.org/articles/10.3389/fonc.2022.772816/full#supplementary-material

REFERENCES

1. Soerjomataram I, Bray F. Planning for Tomorrow: Global Cancer Incidence and the Role of Prevention 2020-2070. *Nat Rev Clin Oncol* (2021) 28 (15):2529–37. doi: 10.1038/s41571-021-00514-z
2. Bray F, Jemal A, Grey N, Ferlay J, Forman D. Global Cancer Transitions According to the Human Development Index (2008-2030): A Population-Based Study. *Lancet Oncol* (2012) 13(8):790–801. doi: 10.1016/s1470-2045(12)70211-5
3. Ferlay J, Colombet M, Soerjomataram I, Dyba T, Randi G, Bettio M, et al. Cancer Incidence and Mortality Patterns in Europe: Estimates for 40 Countries and 25 Major Cancers in 2018. *Eur J Cancer* (2018) 103:356–87. doi: 10.1016/j.ejca.2018.07.005
4. Wong KCW, Hui EP, Lo KW. Nasopharyngeal Carcinoma: An Evolving Paradigm. *Nat Rev Clin Oncol* (2021) 18(11):679–95. doi: 10.1038/s41571-021-00524-x
5. Sung H, Ferlay J, Siegel RL. Global Cancer Statistics 2020: GLOBOCAN Estimates of Incidence and Mortality Worldwide for 36 Cancers in 185 Countries. *CA Cancer J Clin* (2021) 71(3):209–49. doi: 10.3322/caac.21660
6. Chen YP, Chan ATC, Le QT, Blanchard P, Sun Y, Ma J. Nasopharyngeal Carcinoma. *Lancet* (2019) 394(10192):64–80. doi: 10.1016/s0140-6736(19)30956-0
7. Liu L, Wang H, Yan C. An Integrated Analysis of mRNAs and miRNAs Microarray Profiles to Screen miRNA Signatures Involved in Nasopharyngeal Carcinoma. *Technol Cancer Res Treat* (2020) 19:1533033820956998. doi: 10.1177/1533033820956998
8. Hirokawa N, Noda Y, Tanaka Y, Niwa S. Kinesin Superfamily Motor Proteins and Intracellular Transport. *Nat Rev Mol Cell Biol* (2009) 10(10):682–96. doi: 10.1038/nrm2774
9. Miki H, Setou M, Kaneshiro K, Hirokawa N. All Kinesin Superfamily Protein, KIF, Genes in Mouse and Human. *Proc Natl Acad Sci USA* (2001) 98 (13):7004–11. doi: 10.1073/pnas.111145398
10. Eskova A, Knapp B, Matelska D, Reusing S, Arjonen A, Lisauskas T, et al. An RNAi Screen Identifies KIF15 as a Novel Regulator of the Endocytic Trafficking of Integrin. *J Cell Sci* (2014) 127(Pt 11):2433–47. doi: 10.1242/jcs.137281
11. Yu X, He X, Heindl LM, Song X, Fan J, Jia R. KIF15 Plays a Role in Promoting the Tumorigenicity of Melanoma. *Exp Eye Res* (2019) 185:107598. doi: 10.1016/j.exer.2019.02.014
12. Ding L, Li B, Yu X, Li Z, Li X, Dang S, et al. KIF15 Facilitates Gastric Cancer *via* Enhancing Proliferation, Inhibiting Apoptosis, and Predict Poor Prognosis. *Cancer Cell Int* (2020) 20:125. doi: 10.1186/s12935-020-01199-7
13. Sun YF, Wu HL, Shi RF, Chen L, Meng C. KIF15 Promotes Proliferation and Growth of Hepatocellular Carcinoma. *Anal Cell Pathol (Amst)* (2020) 2020:6403012. doi: 10.1155/2020/6403012
14. Qiao Y, Chen J, Ma C, Liu Y, Li P, Wang Y, et al. Increased KIF15 Expression Predicts a Poor Prognosis in Patients With Lung Adenocarcinoma. *Cell Physiol Biochem* (2018) 51(1):1–10. doi: 10.1159/000495155
15. w_ss_sfst_s.ddsQiu MJ, Wang QS, Li QT, Zhu LS, Li YN, Yang SL, et al. KIF18B is a Prognostic Biomarker and Correlates With Immune Infiltrates in Pan-Cancer. *Front Mol Biosci* (2021) 8:559800. doi: 10.3389/fmolb.2021.559800
16. Wang B, Zhong JL, Li HZ, Wu B, Sun DF, Jiang N, et al. Diagnostic and Therapeutic Values of PMEPA1 and its Correlation With Tumor Immunity in Pan-Cancer. *Life Sci* (2021) 277:119452. doi: 10.1016/j.lfs.2021.119452
17. Xu WX, Zhang J, Hua YT, Yang SJ, Wang DD, Tang JH. An Integrative Pan-Cancer Analysis Revealing LCN2 as an Oncogenic Immune Protein in Tumor Microenvironment. *Front Oncol* (2020) 10:605097. doi: 10.3389/fonc.2020.605097
18. Camp RL, Dolled-Filhart M, Rimm DL. X-Tile: A New Bio-Informatics Tool for Biomarker Assessment and Outcome-Based Cut-Point Optimization. *Clin Cancer Res* (2004) 10(21):7252–9. doi: 10.1158/1078-0432.ccr-04-0713

19. Chen J, Li S, Zhou S, Cao S, Lou Y, Shen H, et al. Kinesin Superfamily Protein Expression and its Association With Progression and Prognosis in Hepatocellular Carcinoma. *J Cancer Res Ther* (2017) 13(4):651–9. doi: 10.4103/jcrt.JCRT_491_17
20. Kitagawa A, Masuda T, Takahashi J, Tobo T, Noda M, Kuroda Y, et al. KIF15 Expression in Tumor-Associated Monocytes Is a Prognostic Biomarker in Hepatocellular Carcinoma. *Cancer Genomics Proteomics* (2020) 17(2):141–9. doi: 10.21873/cgp.20174
21. Liu J, Meng H, Li S, Shen Y, Wang H, Shan W, et al. Identification of Potential Biomarkers in Association With Progression and Prognosis in Epithelial Ovarian Cancer by Integrated Bioinformatics Analysis. *Front Genet* (2019) 10:1031. doi: 10.3389/fgene.2019.01031
22. Shen J, Yu S, Sun X, Yin M, Fei J, Zhou J. Identification of Key Biomarkers Associated With Development and Prognosis in Patients With Ovarian Carcinoma: Evidence From Bioinformatic Analysis. *J Ovarian Res* (2019) 12 (1):110. doi: 10.1186/s13048-019-0578-1
23. Sheng J, Xue X, Jiang K. Knockdown of Kinase Family 15 Inhibits Cancer Cell Proliferation *In Vitro* and its Clinical Relevance in Triple-Negative Breast Cancer. *Curr Mol Med* (2019) 19(2):147–55. doi: 10.2174/1566524019666190308122108
24. Song X, Zhang T, Wang X, Liao X, Han C, Yang C, et al. Distinct Diagnostic and Prognostic Values of Kinesin Family Member Genes Expression in Patients With Breast Cancer. *Med Sci Monit* (2018) 24:9442–64. doi: 10.12659/msm.913401
25. Wang J, Guo X, Xie C, Jiang J. KIF15 Promotes Pancreatic Cancer Proliferation *via* the MEK-ERK Signalling Pathway. *Br J Cancer* (2017) 117 (2):245–55. doi: 10.1038/bjc.2017.165
26. Yan X, Liu XP, Guo ZX, Liu TZ, Li S. Identification of Hub Genes Associated With Progression and Prognosis in Patients With Bladder Cancer. *Front Genet* (2019) 10:408. doi: 10.3389/fgene.2019.00408
27. Zeng H, Li T, Zhai D, Bi J, Kuang X, Lu S, et al. ZNF367-Induced Transcriptional Activation of KIF15 Accelerates the Progression of Breast Cancer. *Int J Biol Sci* (2020) 16(12):2084–93. doi: 10.7150/ijbs.44204
28. Zhang L, He M, Zhu W. Identification of a Panel of Mitotic Spindle-Related Genes as a Signature Predicting Survival in Lung Adenocarcinoma. *J Cell Physiol* (2020) 235(5):4361–75. doi: 10.1002/jcp.29312
29. Zhao H, Bo Q, Wu Z, Liu Q, Li Y, Zhang N, et al. KIF15 Promotes Bladder Cancer Proliferation *via* the MEK-ERK Signaling Pathway. *Cancer Manag Res* (2019) 11:1857–68. doi: 10.2147/cmar.s191681
30. Mai HQ, Chen QY, Chen D, Hu C, Yang K, Wen J, et al. Toripalimab or Placebo Plus Chemotherapy as First-Line Treatment in Advanced Nasopharyngeal Carcinoma: A Multicenter Randomized Phase 3 Trial. *Nat Med* (2021) 27(9):1536–43. doi: 10.1038/s41591-021-01444-0
31. Chen YP, Liu X, Zhou Q, Yang KY, Jin F, Zhu XD, et al. Metronomic Capecitabine as Adjuvant Therapy in Locoregionally Advanced Nasopharyngeal Carcinoma: A Multicentre, Open-Label, Parallel-Group, Randomised, Controlled, Phase 3 Trial. *Lancet* (2021) 398(10297):303–13. doi: 10.1016/s0140-6736(21)01123-5
32. Miki H, Okada Y, Hirokawa N. Analysis of the Kinesin Superfamily: Insights Into Structure and Function. *Trends Cell Biol* (2005) 15(9):467–76. doi: 10.1016/j.tcb.2005.07.006
33. Liang WT, Liu XF, Huang HB, Gao ZM, Li K. Prognostic Significance of KIF23 Expression in Gastric Cancer. *World J Gastrointest Oncol* (2020) 12 (10):1104–18. doi: 10.4251/wjgo.v12.i10.1104
34. Sun ZG, Pan F, Shao JB, Yan QQ, Lu L, Zhang N. Kinesin Superfamily Protein 21B Acts as an Oncogene in non-Small Cell Lung Cancer. *Cancer Cell Int* (2020) 20:233. doi: 10.1186/s12935-020-01323-7
35. Li ZY, Wang ZX, Li CC. Kinesin Family Member 20B Regulates Tongue Cancer Progression by Promoting Cell Proliferation. *Mol Med Rep* (2019) 19 (3):2202–10. doi: 10.3892/mmr.2019.9851
36. Drechsler H, McAinsh AD. Kinesin-12 Motors Cooperate to Suppress Microtubule Catastrophes and Drive the Formation of Parallel Microtubule Bundles. *Proc Natl Acad Sci U.S.A.* (2016) 113(12):E1635–1644. doi: 10.1073/pnas.1516370113
37. Gao X, Zhu L, Lu X, Wang Y, Li R, Jiang G. KIF15 Contributes to Cell Proliferation and Migration in Breast Cancer. *Hum Cell* (2020) 33(4):1218–28. doi: 10.1007/s13577-020-00392-0
38. Li Q, Qiu J, Yang H, Sun G, Hu Y, Zhu D, et al. Kinesin Family Member 15 Promotes Cancer Stem Cell Phenotype and Malignancy *via* Reactive Oxygen Species Imbalance in Hepatocellular Carcinoma. *Cancer Lett* (2020) 482:112–25. doi: 10.1016/j.canlet.2019.11.008
39. Levine AJ, Oren M. The First 30 Years of P53: Growing Ever More Complex. *Nat Rev Cancer* (2009) 9(10):749–58. doi: 10.1038/nrc2723
40. Saghaleyni R, Sheikh M. A Machine Learning-Based Investigation of the Cancer Protein Secretory Pathway. *PLoS Comput Biol* (2021) 17(4):e1008898. doi: 10.1371/journal.pcbi.1008898
41. Wang Z, Chen M, Fang X, Hong H, Yao Y, Huang H. KIF15 is Involved in Development and Progression of Burkitt Lymphoma. *Cancer Cell Int* (2021) 21(1):261. doi: 10.1186/s12935-021-01967-z
42. Agupitan AD, Neeson P, Williams S, Howitt J, Haupt S, Haupt Y. P53: A Guardian of Immunity Becomes Its Saboteur Through Mutation. *Int J Mol Sci* (2020) 21(10):3452. doi: 10.3390/ijms21103452
43. Blagih J, Buck MD, Vousden KH. P53, Cancer and the Immune Response. *J Cell Sci* (2020) 133(5):jcs237453. doi: 10.1242/jcs.237453
44. Liu Y, Chen P. Comprehensive Analysis of the Control of Cancer Stem Cell Characteristics in Endometrial Cancer by Network Analysis. *Comput Math Methods Med* (2021) 2021:6653295. doi: 10.1155/2021/6653295
45. Deng Y, Wang F, Hughes T, Yu J. FOXOs in Cancer Immunity: Knowns and Unknowns. *Semin Cancer Biol* (2018) 50:53–64. doi: 10.1016/j.semcancer.2018.01.005
46. Steuer CE, Ramalingam SS. Tumor Mutation Burden: Leading Immunotherapy to the Era of Precision Medicine? *J Clin Oncol* (2018) 36 (7):631–2. doi: 10.1200/jco.2017.76.8770
47. Chan TA, Yarchoan M, Jaffee E, Swanton C, Quezada SA, Stenzinger A, et al. Development of Tumor Mutation Burden as an Immunotherapy Biomarker: Utility for the Oncology Clinic. *Ann Oncol* (2019) 30(1):44–56. doi: 10.1093/annonc/mdy495
48. Le DT, Uram JN, Wang H, Bartlett BR, Kemberling H, Eyring AD, et al. PD-1 Blockade in Tumors With Mismatch-Repair Deficiency. *N Engl J Med* (2015) 372(26):2509–20. doi: 10.1056/NEJMoa1500596
49. Ren X, Chen X, Ji Y, Li L, Li Y, Qin C, et al. Upregulation of KIF20A Promotes Tumor Proliferation and Invasion in Renal Clear Cell Carcinoma and is Associated With Adverse Clinical Outcome. *Aging (Albany NY)* (2020) 12 (24):25878–94. doi: 10.18632/aging.202153
50. Kim S, Cho YB, Song CU, Eyun SI. Kinesin Family Member KIF18A is a Critical Cellular Factor That Regulates the Differentiation and Activation of Dendritic Cells. *Genes Genomics* (2020) 42(1):41–6. doi: 10.1007/s13258-019-00875-x
51. Menyhárt O, Pongor LS, Győrffy B. Mutations Defining Patient Cohorts With Elevated PD-L1 Expression in Gastric Cancer. *Front Pharmacol* (2018) 9:1522. doi: 10.3389/fphar.2018.01522
52. Sharma P, Hu-Lieskovan S, Wargo JA, Ribas A. Primary, Adaptive, and Acquired Resistance to Cancer Immunotherapy. *Cell* (2017) 168(4):707–23. doi: 10.1016/j.cell.2017.01.017
53. Lu X, Li G, Liu S, Wang H, Zhang Z, Chen B. Bioinformatics Analysis of KIF1A Expression and Gene Regulation Network in Ovarian Carcinoma. *Int J Gen Med* (2021) 14:3707–17. doi: 10.2147/ijgm.s323591
54. Najafi M, Hashemi Goradel N, Farhood B, Salehi E, Nashtaei MS, Khanlarkhani N, et al. Macrophage Polarity in Cancer: A Review. *J Cell Biochem* (2019) 120(3):2756–65. doi: 10.1002/jcb.27646
55. Mollinedo F. Neutrophil Degranulation, Plasticity, and Cancer Metastasis. *Trends Immunol* (2019) 40(3):228–42. doi: 10.1016/j.it.2019.01.006
56. Veglia F, Gabrilovich DI. Dendritic Cells in Cancer: The Role Revisited. *Curr Opin Immunol* (2017) 45:43–51. doi: 10.1016/j.coi.2017.01.002
57. Chen DS, Mellman I. Elements of Cancer Immunity and the Cancer-Immune Set Point. *Nature* (2017) 541(7637):321–30. doi: 10.1038/nature21349
58. Pardoll DM. The Blockade of Immune Checkpoints in Cancer Immunotherapy. *Nat Rev Cancer* (2012) 12(4):252–64. doi: 10.1038/nrc3239
59. Zhai L, Ladomersky E, Lenzen A, Nguyen B, Patel R, Lauing KL, et al. IDO1 in Cancer: A Gemini of Immune Checkpoints. *Cell Mol Immunol* (2018) 15 (5):447–57. doi: 10.1038/cmi.2017.143
60. Ruffo E, Wu RC, Bruno TC, Workman CJ, Vignali DAA. Lymphocyte-Activation Gene 3 (LAG3): The Next Immune Checkpoint Receptor. *Semin Immunol* (2019) 42:101305. doi: 10.1016/j.smim.2019.101305

Conflict of Interest: The authors declare that the research was conducted in the absence of any commercial or financial relationships that could be construed as a potential conflict of interest.

this article, or claim that may be made by its manufacturer, is not guaranteed or endorsed by the publisher.

frontiers in Oncology

ORIGINAL RESEARCH
published: 24 March 2022
doi: 10.3389/fonc.2022.817692

Neoadjuvant Chemoradiotherapy for Oral Cavity Cancer: Predictive Factors for Response and Interim Analysis of the Prospective INVERT-Trial

Jens von der Grün[1,2,3,4], Ria Winkelmann[5], Iris Burck[6], Daniel Martin[1,2,3,4], Franz Rödel[1,2,3,4], Peter Johannes Wild[5], Katrin Bankov[5], Andreas Weigert[7], Ivan-Maximiliano Kur[7], Christian Brandts[2,3,4,8], Natalie Filmann[9], Christian Issing[4,10], Philipp Thönissen[11], Anna Maria Tanneberger[11], Claus Rödel[1,2,3,4], Shahram Ghanaati[11†] and Panagiotis Balermpas[1,12†]*

[1] Department of Radiotherapy and Oncology, Goethe-University Frankfurt, Frankfurt, Germany, [2] German Cancer Research Center (DKFZ), Heidelberg, Germany, [3] German Cancer Consortium (DKTK), Partner Site Frankfurt a. M., Goethe-University Frankfurt, Frankfurt, Germany, [4] Frankfurt Cancer Institute (FCI), Goethe-University Frankfurt, Frankfurt, Germany, [5] Dr. Senckenberg Institute of Pathology, Goethe-University Frankfurt, Frankfurt, Germany, [6] Department of Diagnostic and Interventional Radiology, Goethe-University Frankfurt, Frankfurt, Germany, [7] Institute of Biochemistry I, Faculty of Medicine, Goethe-University Frankfurt, Frankfurt, Germany, [8] Department of Medicine, Hematology/Oncology, Goethe-University Frankfurt, Frankfurt, Germany, [9] Institute of Biostatistics and Mathematical Modelling, Goethe-University Frankfurt, Frankfurt, Germany, [10] Department of Otorhinolaryngology, Goethe-University Frankfurt, Frankfurt, Germany, [11] Department of Oral, Maxillofacial and Facial Plastic Surgery, Goethe-University Frankfurt, Frankfurt, Germany, [12] Department of Radiation Oncology, University Hospital Zurich, Zurich, Switzerland

OPEN ACCESS

Edited by:
Yong Yin,
Shandong Cancer Hospital, China

Reviewed by:
Chia-Jung Busch,
University of Greifswald, Germany
Ali-Farid Safi,
Harvard University, United States

***Correspondence:**
Jens von der Grün
jens.vondergruen@kgu.de

[†]These authors have contributed equally to this work and share last authorship

Specialty section:
This article was submitted to Head and Neck Cancer, a section of the journal Frontiers in Oncology

Received: 18 November 2021
Accepted: 02 March 2022
Published: 24 March 2022

Citation:
von der Grün J, Winkelmann R, Burck I, Martin D, Rödel F, Wild PJ, Bankov K, Weigert A, Kur I-M, Brandts C, Filmann N, Issing C, Thönissen P, Tanneberger AM, Rödel C, Ghanaati S and Balermpas P (2022) Neoadjuvant Chemoradiotherapy for Oral Cavity Cancer: Predictive Factors for Response and Interim Analysis of the Prospective INVERT-Trial. Front. Oncol. 12:817692. doi: 10.3389/fonc.2022.817692

Background: To study neoadjuvant chemoradiotherapy (nCRT) and potential predictive factors for response in locally advanced oral cavity cancer (LA-OCC).

Methods: The INVERT trial is an ongoing single-center, prospective phase 2, proof-of-principle trial. Operable patients with stage III-IVA squamous cell carcinomas of the oral cavity were eligible and received nCRT consisting of 60 Gy with concomitant cisplatin and 5-fluorouracil. Surgery was scheduled 6-8 weeks after completion of nCRT. Explorative, multiplex immunohistochemistry (IHC) was performed on pretreatment tumor specimen, and diffusion-weighted magnetic resonance imaging (DW-MRI) was conducted prior to, during nCRT (day 15), and before surgery to identify potential predictive biomarkers and imaging features. Primary endpoint was the pathological complete response (pCR) rate.

Results: Seventeen patients with stage IVA OCC were included in this interim analysis. All patients completed nCRT. One patient died from pneumonia 10 weeks after nCRT before surgery. Complete tumor resection (R0) was achieved in 16/17 patients, of whom 7 (41%, 95% CI: 18-67%) showed pCR. According to the Clavien-Dindo classification, grade 3a and 3b complications were found in 4 (25%) and 5 (31%) patients, respectively; grade 4-5 complications did not occur. Increased changes in the apparent diffusion coefficient signal intensities between MRI at day 15 of nCRT and before surgery were associated with better response (p=0.022). Higher abundances of programmed cell death protein 1 (PD1)

positive cytotoxic T-cells (p=0.012), PD1+ macrophages (p=0.046), and cancer-associated fibroblasts (CAFs, p=0.036) were associated with incomplete response to nCRT.

Conclusion: nCRT for LA-OCC followed by radical surgery is feasible and shows high response rates. Larger patient cohorts from randomized trials are needed to further investigate nCRT and predictive biomarkers such as changes in DW-MRI signal intensities, tumor infiltrating immune cells, and CAFs.

Keywords: neoadjuvant chemoradiotherapy, oral cavity cancer, multiplexed immunofluorescence, diffusion-weighted magnetic resonance imaging, predictive biomarker

1 INTRODUCTION

The standard treatment for locally advanced oral cavity cancer (LA-OCC) is primary surgery followed by risk-adapted adjuvant radiotherapy/chemoradiotherapy (RT/CRT) or definitive CRT for functionally inoperable tumors (1–5). Following combined modality treatment, local recurrences and distant metastases occur in about 25% of patients with locally advanced head and neck squamous cell carcinoma (LA-HNSCC) (1, 2). However, local control rates for the subgroup of LA-OCC remain inferior to those of LA-HNSCC with most locoregional failures emerging in field of prior RT (6–8). Furthermore, high-dose, postoperative RT/CRT to the oral cavity is challenging following extensive reconstructive surgery and can be delayed due to prolonged postoperative recovery or possible complications associated with surgery (6, 9, 10). Also, better vascularization and oxygenation in the unoperated tissue is associated with increased radiosensitivity and early systemic therapy could potentially reduce metastatic spread of these tumors (11). Some rare complications, such as fibula transplant- or flap-necrosis related to RT could be avoided in case of preoperative treatment, and in case of occurrence, the necrotic jaw could be resected during surgery (9). To improve local tumor control and overcome some of the limitations of primary or postoperative radiotherapy (PORT), a limited number of retrospective and prospective studies investigated neoadjuvant RT/CRT in LA-OCC. These studies mostly showed encouraging local control rates despite utilizing partly outdated RT-techniques, doses, and time intervals between treatment modalities (12). To study neoadjuvant CRT (nCRT) we launched a prospective, single-arm trial investigating nCRT followed by surgery in LA-OCC. We here report on first results regarding feasibility and early efficacy with a particular focus on potential predictive biomarkers for pathologic complete response (pCR) based on pretreatment immune contextures and diffusion-weighted magnetic resonance imaging (DW-MRI) signal changes during treatment.

2 PATIENTS AND METHODS

2.1 Patient Selection

The INVERT trial is an ongoing, single-center, prospective phase II trial. Eligible patients were 18 years or older with histologically confirmed, primary diagnosis of locally advanced HNSCC of the oral cavity stage III-IVA defined by UICC TNM version 8. Mandatory staging included MRI of the neck, and computed tomography (CT) of the chest and abdomen. Additional key inclusion criteria were Eastern Cooperative Oncology Group (ECOG) status of ≤2 and adequate organ function. The study received approval by the ethics committee of the Goethe-University Frankfurt, Frankfurt, Germany (approval number 208/12). A written informed consent was provided by each patient. The INVERT treatment schedule is shown in **Supplementary Figure 1**. The study protocol synopsis in English language is provided as **Supplementary Table 1**, the complete protocol in German language as supplementary document 1.

2.2 Chemoradiotherapy

Neoadjuvant RT consisted of 60.0/54.9/50.1 Gy in 30 fractions, applied to the primary tumor region, involved/high risk neck levels, and the elective neck levels according to current guidelines, respectively (13, 14). Intensity-modulated radiotherapy (IMRT) with a simultaneously integrated boost (SIB) concept was used. Therapy was delivered by 6 MeV photon energy using a linear accelerator (Versa HD^{TM}, Elekta). Two cycles of chemotherapy (CTX) were applied on days 1–5, and 29–33 of the RT consisting of 5-fluorouracil (5-FU) (600 mg/m² per day) as a continuous 120-h intravenous infusion, and cisplatin (20 mg/m² per day) as short intravenous infusion (15). For patients who were ineligible for cisplatin, carboplatin area und curve (AUC) 1 was applied alternatively on days 1–5, and 29–33. For patients with contraindications for 5-FU, cisplatin monotherapy was applied.

2.3 Surgery

Radical surgery following nCRT was performed according to the initial extension of the primary tumor as marked by pretreatment tattooing. Elective neck dissection was performed according to pretreatment staging information. Elective, ipsilateral supraomohyoid neck dissection (SOHND) was conducted for clinically negative neck nodes (cN0), and was extended to the neck levels I-V for pathologically positive nodes. In these cases, and for tumors crossing midline, contra-lateral SOHND was performed and also extended to the neck levels I-V for positive, contra-lateral nodes. Surgical reconstruction

consisted of locoregional flaps, myocutaneous flaps, free flaps, or bone grafts as one- or two-stage surgical procedures.

2.4 Objectives

The primary endpoint, pCR, was defined as ypT0N0 after surgery. Acute and late adverse events from CRT and surgery were graded according to the National Cancer Institute Common Terminology Criteria for Adverse Events (NCI-CTCAE) version 4.0. Furthermore, surgical complications were graded on the basis of the Clavien-Dindo classification (16, 17). Explorative immune cell counts and DWI-MRI signal intensities were assessed to identify potential predictive bio- and imaging markers for pCR.

2.5 Pathological Assessment of Tumor Response

For pathological assessment, the tissue was extensively worked up. The tumor bed was formaldehyde-fixed and paraffin-embedded (FFPE) in total; ypTNM staging was applied according to the UICC TNM classification of malignant tumors (Union internationale contre le cancer, Version 8, 2017). Furthermore, tumor regression grading of the primary tumor was performed as described by Braun et al. (18): Grade 1: No or devitalized tumor cells; grade 2: small nests of vital tumor cells which do not exceed 5% of the whole lesion; grade 3: 5%-50% vital tumor cells; grade 4: more than 50% vital tumor cells. Also, for residual primary tumors, patterns of response to neoadjuvant CRT were evaluated as introduced by Nagtegaal et al. (19) and reported as tumor fragmentation versus shrinkage.

2.6 Radiological Assessment of Tumor Response

Diffusion-weighted, gadolinium enhanced MRI was performed prior to RT (day -14 to day 0; MRI 1), during RT (day 15, MRI 2), and prior to surgery (day 72 to 86, MRI 3).

2.6.1 Magnetic Resonance Imaging Protocol

All MRI scans were performed using a 1.5-T system (MAGNETOM Avantofit, Siemens Healthineers) with a dedicated head and neck coil. Standard axial turbo inversion recovery magnitude (TIRM) (repetition time ms/echo time ms 3270/36; matrix size, 320 × 252; slice thickness, 6 mm), axial DW (diffusion-weighted) (repetition time ms/echo time ms, 3980/55; matrix size, 160 × 160; section thickness, 5 mm); axial unenhanced T1-weighted turbo spin-echo sequences (repetition time ms/echo time ms, 659/12; matrix size, 384 × 324; section thickness, 4 mm); axial T2-weighted turbo spin-echo sequences (repetition time ms/echo time ms, 7010/83; matrix size, 384 × 365; section thickness, 4 mm) were acquired. Axial contrast-enhanced T1-weighted multipoint Dixon sequences with fat suppression (repetition time ms/echo time ms, 604/12; matrix size, 320 × 277; section thickness, 4 mm) were also performed. Contrast administration was performed by injection of 0.1 ml gadobutrol per kilogram body weight (flow rate of 2 ml/s) with a power injector (Accutron MR; Medtron, Saarbrücken, Germany), followed by application of 20 ml saline (flow rate of 2 ml/s).

2.6.2 Image Analysis

All MRI scans were analyzed on a commercially available PACS workstation (Centricity 4.2, GE Healthcare, Dornstadt, Germany). Two different observers (one radiology department resident, one senior staff member) quantitatively analyzed the MR series in consensus. Tumor signal intensities were assessed on diffusion-weighted, T2-weighted, and contrast-enhanced images using dedicated regions of interest (ROI) with a standardized radius of 5mm, placed on solid portions of the tumors. The signal intensity of the upper cervical spinal cord was also measured. The tumor signal intensities were expressed as a tumor to spine signal intensity ratio. Furthermore, ADC (apparent diffusion coefficient) were calculated with two b factors (0, 1,000 s/mm2) by placing ROIs over the solid tumor regions. Subsequently, the signal intensities of the tumors were independently assessed qualitatively by the two raters. The higher value was taken into account for the analysis in the event of unequal assessment by the two raters. Tumor signal intensities were evaluated on diffusion-weighted and T2-weighted images using a 5-point scale compared with the spinal cord (1 = hypointense, 2 = slightly hypointense, 3 = isointense, 4 = slightly hyperintense and 5 = markedly hyperintense). The images of the gadolinium-enhanced T1-weighted images were assessed using a 4-point scale compared to the submandibular gland (1 = no enhancement, 2 = weak enhancement, 3 = moderate enhancement, and 4 marked enhancement) (20).

2.7 Multiplexed Immunofluorescence

Pretreatment FFPE tissue sections were assessed before staining by an experienced head and neck pathologist. Each section contained the following three tumor compartments: tumor, invasive front, and tumor microenvironment (TME, stroma). Next, the pretreatment tissue sections (2 µm thick) were deparaffinized by 1 hour incubation at 60°C and stained with Opal 7-Color Automation immunohistochemistry (IHC) Kits (Akoya Bioscience) in the BOND-RX Multiplex IHC Stainer (Leica). Each section was put through 6 sequential rounds of staining, which included blocking in 5% BSA followed by incubation with primary antibodies of two panels (T-cell panel: CD3, Ventana, 790-4341; CD4, Abcam, ab133616; PD-1, Sigma, HPA035981-100UL; CD163, Abcam, ab182422; CD8, DAKO, M710301-2; FoxP3, Abcam, ab20034; TME panel: PD-L1, Spring, M4422; Pan-Cytokeratin (Pan-CK), Abcam, ab7753; alpha-smooth muscle actin (aSMA), Sigma, F377; Vimentin, Abcam, ab92547; CD45, Abcam, ab10558; Ki67, Abcam, ab16667), corresponding secondary HRP-conjugated antibodies (Akoya Biosciences, ARH1001A) and Opal fluorophores as described before (21). Nuclei were counterstained with 4′,6-diamidino-2-phenylindole (DAPI) contained in the Opal 7-Color Automation IHC Kits, and slides were mounted with Fluoromount-G (SouthernBiotech). Imaging was performed with the VectraPolaris imaging system (Akoya Bioscience), and

images were analyzed by using the Phenotyping application of the inForm software V2.5 (Akoya Bioscience). The following markers were used to identify specific cell types for input into the training algorithm: T-Helper Cells: CD3+ CD4+; Exhausted T-Helper Cells CD3+ CD4+ PD1+; Cytotoxic T-cells: CD3+ CD8+; Exhausted Cytotoxic T-Cells: CD3+ CD8+ PD1+; Macrophages: CD163+; PD1+ macrophages: CD163+ PD1+; Regulatory T-cells (Tregs): CD3+ CD4+ FoxP3+; Cancer-associated fibroblasts (CAFs): aSMA+ Vimentin+; PD-L1+ CAFs: aSMA+ Vimentin+ PD-L1+; Immune cells: CD45+; PD-L1+ immune cells: CD45+ PD-L1+. Proliferating immune cells: CD45+ Ki67+.

2.8 Statistics and Analysis

The primary clinical objective of this pilot study is to estimate the pCR rate and to calculate the corresponding 95% confidence interval. The assumed probability for pCR on which the case number calculation was based was 50%. In order for the overall statistical length to be less than 40% (+/- 20%), data from a total of n=26 patients must be available for analysis (exact Clopper-Pearson calculation using PASS 2008 software). Since the primary endpoint of pCR is achieved after surgery, we expect only a small drop out of at most 5%, resulting in a total number of 28 patients to be recruited.

Statistical analyses were performed using SPSS (IBM SPSS Statistics, v25.0, Armonk, NY, USA) and R [R Core Team (2020). R Foundation for Statistical Computing, Vienna, Austria]. Confidence intervals for binomial variables were calculated using the Clopper–Pearson method. Associations between categorical variables were evaluated by the Pearson chi-squared test. Regarding qualitative and quantitative MRI analysis, the Wilcoxon signed-rank test was used for nonparametric, related samples. Further, the Mann-Whitney U test was nonparametric, nonrelated samples for quantitative MRI analysis. Cohen's Kappa test was used to assess the overall inter-rater variability in the qualitative MRI evaluation (22). For multiplexed immunofluorescence analysis, overall average marker percentages were dichotomized between "high" and "low" abundance by median value. All tests were two-sided and a p-value of $p \leq 0.05$ was considered as significant during all statistical procedures.

3 RESULTS

3.1 Patient Characteristics

Until the data cutoff for this interim analysis in July 2021, 17 of 26 planned patients were enrolled in this trial. All patients had stage IVA tumors of the oral cavity, mostly with osseus tumor infiltration (15/17, 88%); 59% (10/17) of the patients were men, and median age was 63 years by the time of first diagnosis. **Table 1** summarizes the patient characteristics. The consort diagram is shown in **Supplementary Figure 2**.

3.2 Toxicity, Treatment Compliance and Efficacy

RT-related grade 3 toxic effects occurred as pain and dysphagia in 4 (24%, 95% CI: 7-50%), as mucositis in 7 (41%, 95% CI: 18-67%), and as radiation dermatitis in 2 (12%, 95% CI: 1-36%) of the patients. Chemotherapy-related grade 3 adverse effects were leukopenia in 5 (29%, 95% CI: 10-56%), and hypertension in 6 (35%, 95% CI: 14-62%) patients. One patient with comorbidities died from pneumonia ten weeks after completion of nCRT (**Supplementary Table 2**).

Full dose of RT was applied in all 17 patients. Thirteen (76%, 95% CI: 50-93%) received cisplatin and 5-FU. Three patients (18%, 95% CI: 38-43%) with contraindications against 5-FU received cisplatin monotherapy, and one patient with contraindications for cisplatin received carboplatin and 5-FU. Regarding compliance with CTX, 13 (76%, 95% CI: 50-93%) patients completed CTX as prescribed and 4 (24%, 95% CI: 7-50%) received >50%. All patients received prophylactic gastric tubes (PEG tube) to ensure adequate nutrition (**Supplementary Table 3**).

After nCRT, 16 patients underwent surgery. All patients received bilateral neck dissections and flap plastics. Complete local tumor resection (R0) was achieved in all cases (100%, 95% CI: 79-100%). NCI-CTCAE grade 3 complications were reported in 9 (56%, 95% CI: 30-80%) cases. Oral hemorrhages (4/16, 25%, 95% CI: 7-52%) and wound complications (3/16, 19%, 95% CI: 4-46%) were most common. According to the Clavien-Dindo classification, grade 3a complications were found in 4 (25%, 95% CI: 7-52%) patients, and grade 3b complications were reported in 5 (31%, 95% CI: 11-59%) patients. Grade 4-5 surgical complications did not occur (**Table 2**).

Overall, a pCR (ypT0N0) in the intention-to-treat population was achieved in 7 (41%%, 95% CI: 18-67%) of the patients and in 44% (95% CI: 20-70%) of the patients who underwent surgery: ypT0 occurred in 8 (50%, 95% CI: 25-75%) and ypN0 in 13 (81%, 95% CI: 54-96%). In the majority of the patients with residual tumor, tumor fragmentation was found rather than tumor shrinkage. Exemplary images of tumor regression patterns are shown in **Figure 1**. Downsizing of the primary tumor of > 95% was evident in 88% (14/16, 95% CI: 68-98%) of the cases (**Table 2**).

3.3 Association of Diffusion-Weighted Magnetic-Resonance Imaging and Response to Chemoradiotherapy

The test for inter-rater variability regarding the qualitative MRI evaluation showed high correlation between the two raters (kappa 0,809; p<0.001). Qualitative signal intensities changed significantly between MRI 1, MRI 2, and MRI 3 in diffusion-weighted and T1 + gadolinium series (p-values < 0.05). Exemplary, fused axial diffusion-weighted gadolineum-enhanced T1-weighted images are shown in **Figure 2**. Regarding quantitative analysis, signal intensities changed significantly when MRI 2 and MRI 3 were compared to MRI 1 in the ADC and diffusion-weighted series (p-values < 0.05), and between MRI 2 and MRI 3 in the T2 series (p=0.034) (**Supplementary Table 4**). Quantitative and qualitative changes in signal intensities were correlated with the pathological response of the primary tumor following CRT. Increased changes in the ADC signal intensity between MRI 2 and 3 were associated with < 5% residual tumor tissue (p=0.022) (**Figure 3**, **Supplementary Table 5**).

TABLE 1 | Baseline characteristics. Clinical disease stage according to UICC TNM classification (8th edition); ECOG, Eastern Cooperative Oncology Group.

Characteristic	n (%)
Total	17 (100)
Sex	
Male	10 (59)
Female	7 (41)
Age	
Median, years (range)	63 (42-76)
ECOG performance status	
0	14 (82)
1	3 (18)
History of smoking	
Yes	13 (76)
No	2 (12)
Missing	2 (12)
History of alcohol abuse	
Yes	7 (41)
No	8 (47)
Missing	2 (12)
Tumor site	
Oral cavity	17 (100)
Clinical T category	
cT1	0 (0)
cT2	2 (12)
cT3	0 (0)
cT4	15 (88)
Clinical N category	
cN0	2 (12)
cN1	1 (6)
cN2a	1 (6)
cN2b	11 (65)
cN2b	2 (12)
cN3	0 (0)
Pathological tumor differentiation	
Well differentiated (G1)	1 (6)
Moderately differentiated (G2)	16 (94)
Poorly differentiated (G3)	0 (0)
Clinical disease stage	
III	0 (0)
IVA	17 (100)

3.4 Association of Immunohistochemical Biomarkers in Pre-Treatment Tissue Specimens Imaging and Response to Chemoradiotherapy

To identify possible predictive markers for response to nCRT, the abundance of different cell populations was tested for their association with either pCR or ypT0 (**Table 3** and **Figure 4**). A higher abundance of PD1+ cytotoxic T-cells (p=0.012) and PD1+ macrophages (p=0.046) was associated with incomplete response of the primary tumor to nCRT (no ypT0). Further, an increased occurrence of PD1+ cytotoxic T-cells (p=0.036) and CAFs (p=0.036) was associated with incomplete tumor and or nodal response (no pCR).

4 DISCUSSION

Only a limited number of studies have investigated nCRT for HNSCC to date. We present preliminary clinical and

TABLE 2 | Surgical and pathological characteristics of patients who underwent surgery.

Characteristic	n (%)
Total	16 (100)
Time interval to surgery, days, median (range)	
From start of CRT to surgery	97 (69-121)
From end of CRT to surgery	56 (42-80)
Surgery	
Duration of surgery, minutes, median (range)	485 (369-802)
Neck dissection	
Ipsilateral	16 (100)
Contralateral	16 (100)
Number of dissected nodes, ipsilateral, median (range)	24 (11-60)
Number of dissected nodes, contralateral, median (range)	18 (5-39)
Flap plastic	
Regional	5 (31)
Vastus lateralis	4 (25)
Vastus lateralis and anterolateral thigh	2 (13)
Deltopectoral	2 (13)
Rectus abdominis	1 (6)
Radial forearm	1 (6)
Fibula	1 (6)
Residual tumor	
R0	16 (100)
R1/2	0 (0)
Pathologic T category	
ypT0	8 (50)
ypT1	4 (25)
ypT2	0 (0)
ypT3	0 (0)
ypT4	4 (25)
Pathologic N category	
ypN0	13 (81)
ypN1	2 (13)
ypN2a	0 (0)
ypN2b	1 (6)
ypN2c	0 (0)
ypN3	0 (0)
Tumor regression grading#	
1	8 (51)
2	6 (37)
3	1 (6)
4	1 (6)
Primary tumor regression pattern	
Tumor shrinkage	3 (19)
Tumor fragmentation	5 (31)
Pathologic complete response	8 (59)
Postoperative morbidity	
Clavien-Dindo classification	
None	5 (31)
Grade 1	1 (6)
Grade 2	1 (6)
Grade 3a	4 (25)
Grade 3b	5 (31)
Grade 4	0 (0)
Grade 5	0 (0)
NCI-CTCAE* complications	
None	5 (31)
Grade 1	1 (6)
Grade 2	1 (6)
Grade 3	9 (56)
Grade 4	0 (0)
Grade 5	0 (0)
NCI-CTCAE* complications grade ≥3	
Wound complication (including 1 loss of flap)	3 (19)
Oral hemorrhage	4 (25)
Hematoma	1 (6)
Laryngeal edema	1 (6)

**National Cancer Institute Common Terminology Criteria for Adverse Events version 5.0.*
#Tumor regression of the primary tumor following neoadjuvant chemoradiotherapy according to Braun et al., 1989. CRT, Chemoradiotherapy.

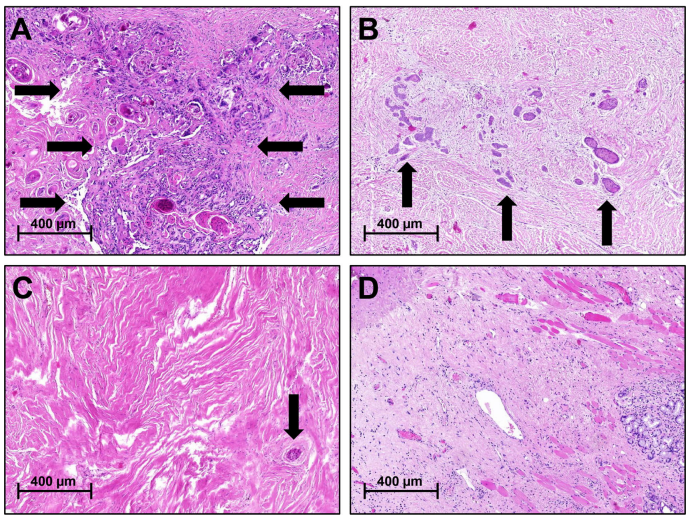

FIGURE 1 | Pathological Response Patterns Following Neoadjuvant Chemoradiotherapy. **(A)** No/minimal tumor regression, vital tumor cells, and prominent keratin pearls; **(B)** Tumor fragmentation with increased amount of fibrous connective tissue with scattered groups of vital tumor cells; **(C)** Tumor shrinkage with a solitary group of vital tumor cells embedded in fibrous connective tissue; **(D)** Complete response with no vital tumor cells within fibrous connective tissue; salivary glands, and skeletal muscles located on the right.

translational results of a single-arm, prospective trial utilizing neoadjuvant, concomitant IMRT-based CRT followed by radical surgery, and provide novel predictive biomarkers, such as immune cell infiltrates and diffusion weighted MRI imaging.

The use of nCRT is standard in different tumor entities, such as lung, esophageal and rectal cancer, with encouraging pCR rates and long-term oncologic outcomes (23–26). In HNSCC, primary surgery with risk-adapted adjuvant RT/CRT has been the standard of care for decades, but has never been tested against nCRT in a prospective, randomized trial (1, 2). A number of retrospective studies have investigated nCRT for HNSCC of different subsites with RT doses ranging from 20-50 Gy. Concomitant systemic therapy was mostly platinum-based with cumulative doses between 63–100 mg/m². The time interval from the end of CRT to surgery ranged between 1-6 weeks, resulting in pCR rates form 0-50%, and 5 years overall survival (OS) rates of 45-81% (**Supplementary Table 6**) (27–35). In 7 prospective, non-randomized trials, neoadjuvant RT doses of 40-50 Gy were applied with (n=6) or without (n=1) concomitant CTX. Again, CTX was mostly platinum-based with cumulative doses of 160-200 mg/m². Intervals from completion of RT/CRT to surgery ranged from 3-8 weeks with pCR rates from 13 to 75% (**Supplementary Table 7**) (36–44). A randomized study by Mohr et al. assigned 268 patients to surgery alone or nCRT with 36 Gy and concomitant cisplatin (12.5 mg, days 1-5), followed by radical surgery 10-14 days after CRT completion. In this study, nCRT resulted in pCR of the primary tumors in 37% of the patients, and less locoregional relapses occurred after 3 years (31% vs. 16%) (38). Yi et al. randomized patients to receive neoadjuvant RT (50 Gy) with or without concomitant cisplatin (cumulative 150 mg/m²). Following local restaging with CT/MRI and endoscopy, patients received completion CRT (total 70 Gy + cisplatin) for >80% clinical remission, followed by planned neck dissections for cN2-3 patients, or radical surgery after 6-8 weeks. Surprisingly, clinical response rates (64 vs. 70%) and pCR rates (27 vs. 43%) were lower following nCRT compared to neoadjuvant RT alone. However, local progression-free survival and OS were improved following nCRT versus neoadjuvant RT and surgery (44). Most of the patients included in the studies above would have received standard, adjuvant RT doses of 60-66 Gy resulting in disease-free survival rates of less than 50% at 5 years (1, 2). However, most of the above neoadjuvant data originate from the pre-IMRT era, where dose escalation was clearly associated with higher toxicity. Accordingly, a higher dose of 60 Gy was selected for this IMRT-based trial. Further, the cumulative doses of cisplatin in the older studies were mostly far less than the currently recommended ≥ 200mg/m² utilized in combination with 5-FU in this study (45). CTX consisting of cisplatin plus 5-FU is not the current international standard for HNSCC. However, in our department as in other German-speaking centers cisplatin (200mg/m² total) and 5-FU was the standard concomitant CTX regimen at the time the trial was designed. Furthermore, a parallel German multicentric phase III trial in the definitive CRT-setting, failed to demonstrate any benefit regarding survival or toxicity for a taxane/cisplatin combination compared to the cisplatin/5-FU regimen used in this trial, with the latter showing good 3 years OS rates of 65% (15).

The time interval between CRT and surgery was scheduled to be 6 to 8 weeks in this trial and therefore longer than in the majority of the prior trials. There is little experience regarding re-growth of HNSCC after neoadjuvant regimens in cases of delayed surgery. However, in other tumor entities treated with neoadjuvant CRT, such as rectal cancer or esophageal cancer,

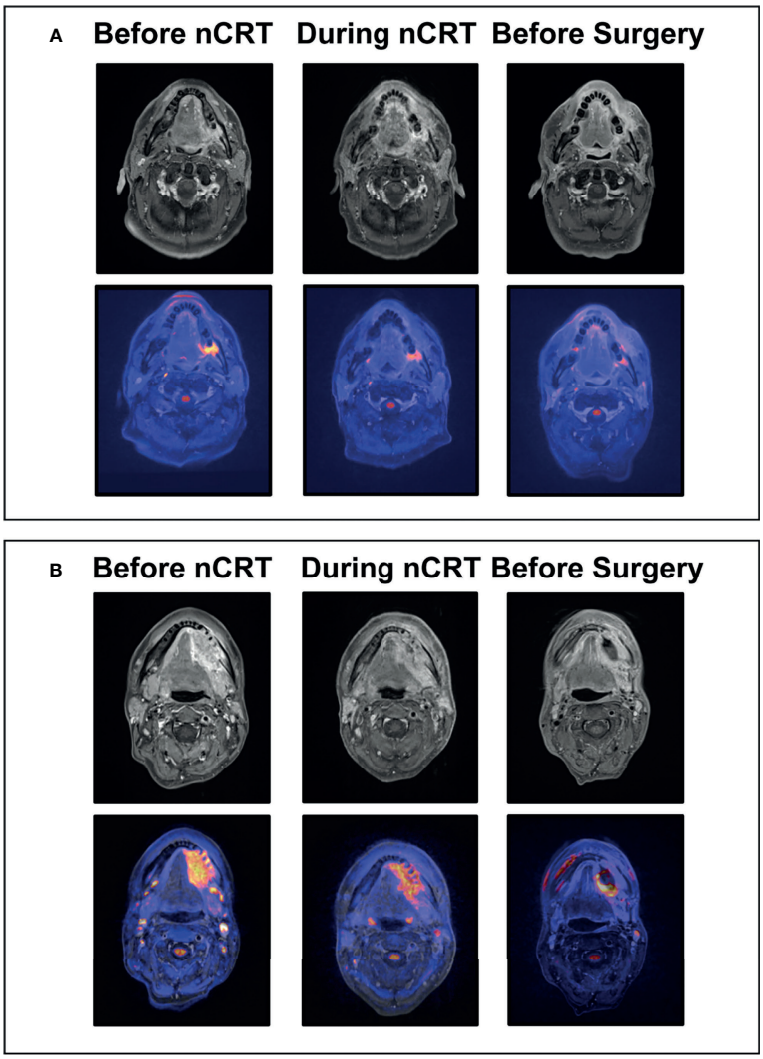

FIGURE 2 | Exemplary MRI Images of Clinical Responses to Neoadjuvant Chemoradiotherapy. **(A)** Exemplary images of a 55-year old patient with left-sided squamous cell carcinoma of the oral cavity before and during chemoradiotherapy (day 15), and prior to surgery; The top row shows representative axial gadolineum-enhanced T1-weighted images with continuous decrease in size and contrast enhancement resulting in complete clinical response prior to surgery of the primary tumor at the left retromolar region; The bottom row shows corresponding fused diffusion-weighted - gadolineum-enhanced T1-weighted images with decreasing diffusion restriction of the tumor region resulting in complete clinical response prior to surgery. **(B)** Exemplary images of a 49-year old patient with left-sided squamous cell carcinoma of the oral cavity before and during chemoradiotherapy (day 15), and prior to surgery; The top row shows representative axial gadolineum-enhanced T1-weighted images with continuous decrease in size and contrast enhancement. Markable residual tumor with contrast enhancement at the left mandibular region prior to surgery; The bottom row shows corresponding fused diffusion-weighted - gadolineum-enhanced T1-weighted images with decreasing but residual diffusion restriction of the tumor region; nCRT, Neoadjuvant chemoradiotherapy.

surgery is commonly performed 6-8 weeks after CRT completion in order to allow for prolonged tumor regression (23–26). Furthermore, in anal squamous cell carcinoma, a tumor entity with several biological parallels to HNSCC, it has been demonstrated that a final response evaluation should be performed 6 months after CRT (50-60 Gy) completion (46). Moreover, for primary CRT of HNSCC, tumor response also is only evaluated at 3 months following treatment and any residual tumor after 6 to 8 weeks after treatment is not necessarily considered as clonogenic (47). The feasibility of surgery and the frequency of postoperative complications were of special interest in this study. In all patients, complete tumor resections and adequate ND were possible. Surgical complications are frequently classified using a system introduced by Clavien and Dindo (16) which has been adapted for head and neck cancer as well (17, 48). McMahon et al. prospectively studied postoperative complications according to the CD system in 192 patients who underwent major head and neck surgeries with free flap repair. A total of 64% had any-grade complications with grade 3 or above occurring in 32% of the patients. Loss of flaps occurred in 3

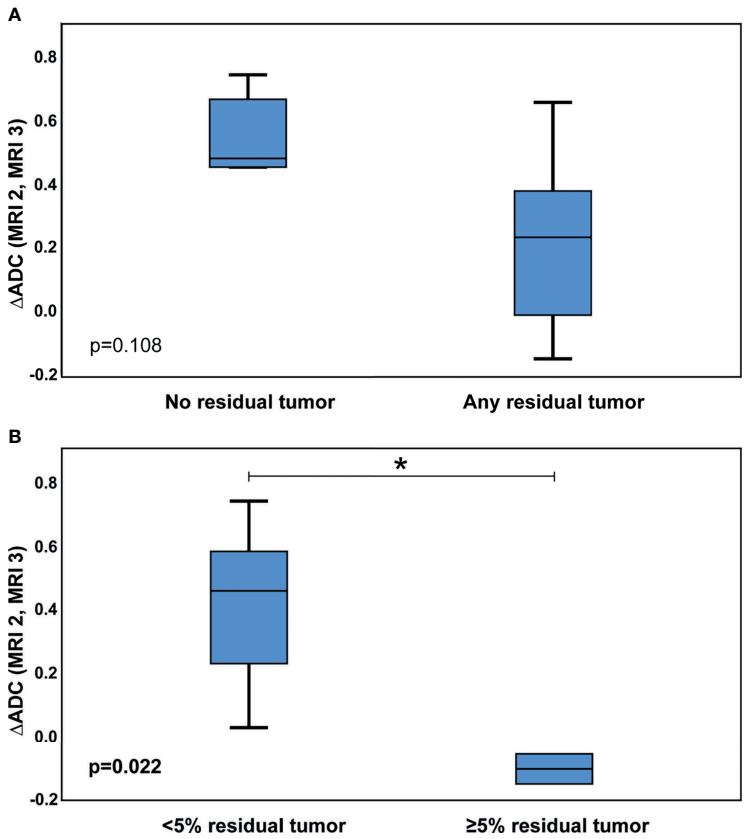

FIGURE 3 | Association of Changes in ADC Signal Intensities with Pathological Tumor Response. Delta (Δ) in ADC signal intensities of MRI 2 and MRI 3 correlated with pathological response of the primary tumor: **(A)** ΔADC, complete response of the primary tumor vs. any residual primary tumor; **(B)** ΔADC, <5% residual primary tumor vs. ≥5% residual primary tumor; ADC, Apparent diffusion coefficient; MRI, Magnetic resonance imaging; p-values according to Mann-Whitney U test; *p-value < 0,05.

patients (49). Peters et al. reported 60% overall complications from a cohort of 121 patients with more than half of them being major (grade 3-5) (50), and Grammatica et al. reported on 84 patients with 62% complication rate with 31% of grade 3 and higher (51). In the present trial, a total of 68% of the patients suffered from post-operative complications and 56% had grade 3 complications. One loss of flap and no grade 4-5 toxicities occurred in the context of surgery. Overall complications did not occur more frequently here in comparison with the rare literature on this topic.

Within our study, extended tumor regression analysis besides the general TNM classification was utilized to more precisely assess response patterns. Braun et al. developed a tumor regression grading (TRG) for HNSCC on the basis of the percentage of vital residual tumor cells (18). Analogous to a recent system introduced by Nagtegaal et al. for rectal cancer, regression patterns in this study were also distinguished between tumor fragmentation and shrinkage (19). Tumors without complete response to nCRT more likely showed fragmentation (n=5) instead of shrinkage (n=3). Prediction of tumor shrinkage following nCRT rather than tumor fragmentation would be of great value for clinicians to possibly reduce the extent of surgery, but higher patient numbers are needed to address this topic. To date, surgery for HNSCC should be performed within the initial tumor margins due to potential tumor fragmentation. Tumor fragmentation following nCRT in HNSCC possibly reflects radio-resistant, hypoxic or immune-privileged tumor subareas, and has been associated with tumor recurrence by Kiong et al. (52). This hypothesis is further supported by the following immunological findings: Multiplex IHC in this study showed that higher abundances of PD1+ cytotoxic T-cells, PD1+ macrophages, and CAFs were associated with incomplete response to nCRT. The prognostic value of immune cell infiltrates and the TME composition have been extensively studied in HNSCC within the last years (53, 54). CD8+ tumor-infiltrating lymphocytes (TILs) were shown to be prognostic factors associated with improved outcome following primary or adjuvant CRT in single- and multicenter cohorts (55, 56). On the other hand, PD1 is a prominent marker of T-cell exhaustion and inhibits anti-tumor T-cell response (57). M2-polarized (CD163+), tumor-associated macrophages (TAMs) promote tumor growth and spread (58). PD1+ expression in TAMs negatively correlates with their phagocytic effects against tumor cells (59) and high abundances of PD1+ TAMs were associated with poor outcome in gastric and muscle-invasive bladder cancer, yet (60, 61). CAFs were reported to

TABLE 3 | Association of pre-treatment immune cell infiltration and cells of the tumor microenvironment with response to neoadjuvant chemoradiotherapy.

Cell types	ypT0N0, n (%)			ypT0, n (%)		
Total n=16	**ypT0N0**	**Rest**	**p**	**ypT0**	**Rest**	**p**
T-Helper Cells						
Low	3 (37)	5 (63)		3 (37)	5 (63)	
High	4 (50)	4 (50)	0.614	5 (63)	3 (37)	0.317
Exhausted T-Helper Cells						
Low	4 (50)	4 (50)		5 (63)	3 (37)	
High	3 (37)	5 (63)	0.614	3 (37)	5 (63)	0.317
Regulatory T-Cells						
Low	4 (50)	4 (50)		5 (63)	3 (37)	
High	3 (37)	5 (63)	0.614	3 (37)	5 (63)	0.317
Cytotoxic T-Cells						
Low	3 (37)	5 (63)		4 (50)	4 (50)	
High	4 (50)	4 (50)	0.614	4 (50)	4 (50)	1.000
PD1+ cytotoxic T-Cells						
Low	6 (67)	3 (33)		7 (78)	2 (22)	
High	1 (14)	6 (86)	**0.036**	1 (14)	6 (86)	**0.012**
Macrophages						
Low	2 (25)	6 (75)		3 (37)	5 (63)	
High	5 (63)	3 (37)	0.131	5 (63)	3 (37)	0.317
PD1+ macrophages						
Low	5 (63)	3 (37)		6 (75)	2 (25)	
High	2 (25)	6 (75)	0.131	2 (25)	6 (75)	**0.046**
Cancer-associated fibroblasts						
Low	6 (67)	3 (33)		6 (67)	3 (33)	
High	1 (14)	6 (86)	**0.036**	2 (29)	5 (71)	0.131
PD-L1+ Cancer-associated fibroblasts						
Low	3 (37)	5 (63)		4 (50)	4 (50)	
High	4 (50)	4 (50)	0.614	4 (50)	4 (50)	1.000
Immune Cells						
Low	4 (44)	5 (56)		4 (44)	5 (56)	
High	3 (43)	4 (57)	0.949	4 (57)	3 (43)	0.614
PD-L1+ Immune Cells						
Low	3 (33)	6 (67)		4 (44)	5 (56)	
High	5 (57)	3 (43)	0.341	4 (57)	3 (43)	0.614
Proliferating Immune Cells						
Low	4 (40)	6 (60)		4 (50)	4 (50)	
High	3 (50)	3 (50)	0.696	3 (50)	3 (50)	1.000

P-values according to Pearson chi-squared test.
Bold values indicate p-values <0.05.

play a key role in tumor progression by secretion of growth factors and cytokines, and high αSMA levels in OCC were associated with impaired prognosis (62–65). Taken together, in patients with incomplete response to nCRT, the tumor and its microenvironment were defined by immunosuppressive stimuli and exhausted immune effector cells.

Finally, we identified an association of changes in ADC signal intensities with response to nCRT. Previously, Kato et al. identified correlations of tumor regression according to RECIST (Response evaluation criteria in solid tumors) with ADC and diffusion-weighted signal intensities in 28 HNSCC patients treated with neoadjuvant CRT, RT, or CTX (20). Median RT dose applied was 30 Gy. Imaging was performed before and after neoadjuvant treatment. To the best of our knowledge, no other study has analyzed early and late responses to nCRT *via* DW-MRI in HNSCC to predict pathological tumor response. So far, DW-MRI studies for HNSCC have mostly focused on early response prediction either during or after definitive CRT (66, 67). Kim et al. performed DW-MRI on 40 patients undergoing primary CRT for HNSCC before, during, and after therapy. Complete therapy responders showed an early increase in ADC intensity ($p<0.01$) (68). Further studies found high pretreatment ADC intensities to be associated with poor outcome in HNSCC (69, 70). Besides these encouraging results, the DW-MRI evaluation procedures to assess response to therapy have differed greatly between the previous studies and standardized evaluation protocols to improve comparability were not yet established.

We acknowledge several limitations of this study: First, the sample size is limited and allows only preliminary and exploratory hypotheses regarding the predictive biomarkers assessed. Second, the unicentric character of the study warrants caution regarding generalization of the results. Third, this interim analysis was not planned according to the study protocol. Finally, some surgical techniques and DW-MRI quantification are not completely standardized yet, which might affect interpretability. Nevertheless, immunological and radiological biomarkers were correlated with pathological responses to neoadjuvant CRT for this tumor entity for the first time.

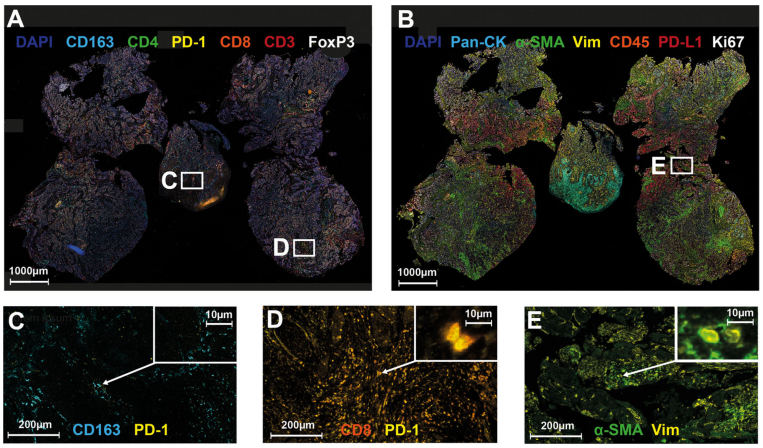

FIGURE 4 | Multiplex Immunohistochemistry and Cell Types Associated with Poor Response to Neoadjuvant Chemoradiotherapy. Representative overview of the T-cell antibody panel **(A)** and the TME panel **(B)**, and exemplary images of cell types with association to tumor response to neoadjuvant chemoradiotherapy **(C–E)**. Nuclei were counterstained with DAPI (blue). **(A)** T-cell panel: CD163 (cyan), CD4 (green), PD-1 (yellow), CD8 (orange), CD3 (red), FoxP3 (white); **(B)** TME panel: Pan-CK (cyan), aSMA (green), Vimentin (yellow), CD45 (orange), PD-L1 (red), Ki67 (white); **(C)** PD-1 positive macrophage; **(D)** PD-1 positive cytotoxic T-cell; **(E)** Cancer-associated fibroblast.

5 CONCLUSION

Neoadjuvant chemoradiotherapy for locally advanced oral cavity cancer followed by radical surgery is feasible and shows high response rates. Emerging biomarkers such as diffusion-weighted magnetic resonance imaging signal intensities, tumor immune cell infiltrates, and the tumor microenvironment are of great interest with potential predictive value regarding response following neoadjuvant treatment. Ultimately, future patient selection for organ preservation could be based on these factors following randomized, controlled trials.

DATA AVAILABILITY STATEMENT

The data presented in this study are available on request from the corresponding author. Requests to access the datasets should be directed to Jens von der Grün, jens.vondergruen@kgu.de.

ETHICS STATEMENT

The studies involving human participants were reviewed and approved by Ethics committee of the Goethe-University Frankfurt, Frankfurt, Germany; Approval No.: 208/12. The patients/participants provided their written informed consent to participate in this study.

AUTHOR CONTRIBUTIONS

Conceptualization, JG, CR, SG, and PB. Methodology, JG, NF, CR, SG, and PB. Data acquisition, JG, RW, IB, PW, KB, AW, I-MK, CB, CI, PT, AT, SG, and PB. Analysis, JG, RW, IB, DM, FR, KB, AW, I-MK, CB, NF, CI, PT, CR, AT, SG, and PB. Investigation, JG, IB, CB, PT, CR, SG, and PB. Writing—original draft preparation, JG, NF, RW, AW, I-MK, FR, IB, CR, SG, and PB. Writing—review and editing, JG, RW, IB, DM, FR, PW, KB, AW, I-MK, CB, AT, NF, CI, PT, CR, SG, and PB. Visualization, JG, IB, and DM. Project administration, JG, CR, SG, and PB. Funding acquisition, PB. All authors have read and agreed to the final version of the manuscript.

FUNDING

The study was partially funded by a research grant received by Panagiotis Balermpas for the INVERT trial by the Clinical Trial Center Network of the University Cancer Center Frankfurt, 2012.

ACKNOWLEDGMENTS

This work was supported by grants from the Mildred-Scheel-Nachwuchszentrum (MSNZ) of the German Cancer Aid to JG.

SUPPLEMENTARY MATERIAL

The Supplementary Material for this article can be found online at: https://www.frontiersin.org/articles/10.3389/fonc.2022.817692/full#supplementary-material

REFERENCES

1. Cooper JS, Pajak TF, Forastiere AA, Jacobs J, Campbell BH, Saxman SB, et al. Postoperative Concurrent Radiotherapy and Chemotherapy for High-Risk Squamous-Cell Carcinoma of the Head and Neck. *N Engl J Med* (2004) 350 (19):1937–44. doi: 10.1056/NEJMoa032646
2. Bernier J, Domenge C, Ozsahin M, Matuszewska K, Lefebvre JL, Greiner RH, et al. Postoperative Irradiation With or Without Concomitant Chemotherapy for Locally Advanced Head and Neck Cancer. *N Engl J Med* (2004) 350 (19):1945–52. doi: 10.1056/NEJMoa032641
3. National Comprehensive Cancer Network. *Head and Neck Cancers (Version 2.2020, June 09, 2020)* (2020). Available at: https://www.nccn.org/professionals/physician_gls/pdf/head-and-neck.pdf.
4. Robertson AG, Soutar DS, Paul J, Webster M, Leonard AG, Moore KP, et al. Early Closure of a Randomized Trial: Surgery and Postoperative Radiotherapy Versus Radiotherapy in the Management of Intra-Oral Tumours. *Clin Oncol (R Coll Radiol)* (1998) 10(3):155–60. doi: 10.1016/s0936-6555(98)80055-1
5. Iyer NG, Tan DS, Tan VK, Wang W, Hwang J, Tan NC, et al. Randomized Trial Comparing Surgery and Adjuvant Radiotherapy Versus Concurrent Chemoradiotherapy in Patients With Advanced, Nonmetastatic Squamous Cell Carcinoma of the Head and Neck: 10-Year Update and Subset Analysis. *Cancer* (2015) 121(10):1599–607. doi: 10.1002/cncr.29251
6. Daly ME, Le QT, Kozak MM, Maxim PG, Murphy JD, Hsu A, et al. Intensity-Modulated Radiotherapy for Oral Cavity Squamous Cell Carcinoma: Patterns of Failure and Predictors of Local Control. *Int J Radiat Oncol Biol Phys* (2011) 80(5):1412–22. doi: 10.1016/j.ijrobp.2010.04.031
7. Chan AK, Huang SH, Le LW, Yu E, Dawson LA, Kim JJ, et al. Postoperative Intensity-Modulated Radiotherapy Following Surgery for Oral Cavity Squamous Cell Carcinoma: Patterns of Failure. *Oral Oncol* (2013) 49 (3):255–60. doi: 10.1016/j.oraloncology.2012.09.006
8. Yao M, Chang K, Funk GF, Lu H, Tan H, Wacha J, et al. The Failure Patterns of Oral Cavity Squamous Cell Carcinoma After Intensity-Modulated Radiotherapy-The University of Iowa Experience. *Int J Radiat Oncol Biol Phys* (2007) 67(5):1332–41. doi: 10.1016/j.ijrobp.2006.11.030
9. Carsuzaa F, Lapeyre M, Gregoire V, Maingon P, Beddok A, Marcy PY, et al. Recommendations for Postoperative Radiotherapy in Head & Neck Squamous Cell Carcinoma in the Presence of Flaps: A GORTEC Internationally-Reviewed HNCIG-Endorsed Consensus. *Radiother Oncol* (2021) 160:140–7. doi: 10.1016/j.radonc.2021.04.026
10. Chang DT, Sandow PR, Morris CG, Hollander R, Scarborough L, Amdur RJ, et al. Do Pre-Irradiation Dental Extractions Reduce the Risk of Osteoradionecrosis of the Mandible? *Head Neck* (2007) 29(6):528–36. doi: 10.1002/hed.20538
11. Wegge M, Dok R, Nuyts S. Hypoxia and Its Influence on Radiotherapy Response of HPV-Positive and HPV-Negative Head and Neck Cancer. *Cancers (Basel)* (2021) 13(23):5959. doi: 10.3390/cancers13235959
12. Alzahrani R, Obaid A, Al-Hakami H, Alshehri A, Al-Assaf H, Adas R, et al. Locally Advanced Oral Cavity Cancers: What Is The Optimal Care? *Cancer Control* (2020) 27(1):1073274820920727. doi: 10.1177/1073274820920727
13. Gregoire V, Coche E, Cosnard G, Hamoir M, Reychler H. Selection and Delineation of Lymph Node Target Volumes in Head and Neck Conformal Radiotherapy. Proposal for Standardizing Terminology and Procedure Based on the Surgical Experience. *Radiother Oncol* (2000) 56(2):135–50. doi: 10.1016/s0167-8140(00)00202-4
14. Biau J, Lapeyre M, Troussier I, Budach W, Giralt J, Grau C, et al. Selection of Lymph Node Target Volumes for Definitive Head and Neck Radiation Therapy: A 2019 Update. *Radiother Oncol* (2019) 134:1–9. doi: 10.1016/j.radonc.2019.01.018
15. Fietkau R, Hecht M, Hofner B, Lubgan D, Iro H, Gefeller O, et al. Randomized Phase-III-Trial of Concurrent Chemoradiation for Locally Advanced Head and Neck Cancer Comparing Dose Reduced Radiotherapy With Paclitaxel/Cisplatin to Standard Radiotherapy With Fluorouracil/Cisplatin: The PacCis-Trial. *Radiother Oncol* (2020) 144:209–17. doi: 10.1016/j.radonc.2020.01.016
16. Dindo D, Demartines N, Clavien PA. Classification of Surgical Complications: A New Proposal With Evaluation in a Cohort of 6336 Patients and Results of a Survey. *Ann Surg* (2004) 240(2):205–13. doi: 10.1097/01.sla.0000133083.54934.ae
17. Vallur S, Dutta A, Arjun AP. Use of Clavien-Dindo Classification System in Assessing Head and Neck Surgery Complications. *Indian J Otolaryngol Head Neck Surg* (2020) 72(1):24–9. doi: 10.1007/s12070-019-01718-7
18. Braun OM, Neumeister B, Popp W, Scherrer R, Dobrowsky E, Dobrowsky W, et al. Histologic Tumor Regression Grades in Squamous Cell Carcinoma of the Head and Neck After Preoperative Radiochemotherapy. *Cancer* (1989) 63 (6):1097–100. doi: 10.1002/1097-0142(19890315)63:6<1097::aid-cncr2820630610>3.0.co;2-6
19. Nagtegaal ID, Glynne-Jones R. How to Measure Tumour Response in Rectal Cancer? An Explanation of Discrepancies and Suggestions for Improvement. *Cancer Treat Rev* (2020) 84:101964. doi: 10.1016/j.ctrv.2020.101964
20. Kato H, Kanematsu M, Tanaka O, Mizuta K, Aoki M, Shibata T, et al. Head and Neck Squamous Cell Carcinoma: Usefulness of Diffusion-Weighted MR Imaging in the Prediction of a Neoadjuvant Therapeutic Effect. *Eur Radiol* (2009) 19(1):103–9. doi: 10.1007/s00330-008-1108-5
21. Strack E, Rolfe PA, Fink AF, Bankov K, Schmid T, Solbach C, et al. Identification of Tumor-Associated Macrophage Subsets That are Associated With Breast Cancer Prognosis. *Clin Transl Med* (2020) 10(8): e239. doi: 10.1002/ctm2.239
22. Landis JR, Koch GG. The Measurement of Observer Agreement for Categorical Data. *Biometrics* (1977) 33(1):159–74. doi: 10.2307/2529310
23. van Hagen P, Hulshof MCCM, van Lanschot JJB, Steyerberg EW, Henegouwen M, Wijnhoven BPL, et al. Preoperative Chemoradiotherapy for Esophageal or Junctional Cancer. *N Engl J Med* (2012) 366(22):2074–84. doi: 10.1056/NEJMoa1112088
24. Sauer R, Becker H, Hohenberger W, Rödel C, Wittekind C, Fietkau R, et al. Preoperative Versus Postoperative Chemoradiotherapy for Rectal Cancer. *N Engl J Med* (2004) 351(17):1731–40. doi: 10.1056/NEJMoa040694
25. Fokas E, Allgauer M, Polat B, Klautke G, Grabenbauer GG, Fietkau R, et al. Randomized Phase II Trial of Chemoradiotherapy Plus Induction or Consolidation Chemotherapy as Total Neoadjuvant Therapy for Locally Advanced Rectal Cancer: CAO/ARO/AIO-12. *J Clin Oncol* (2019) 37 (34):3212–22. doi: 10.1200/JCO.19.00308
26. Rusch VW, Giroux DJ, Kraut MJ, Crowley J, Hazuka M, Johnson D, et al. Induction Chemoradiation and Surgical Resection for Non-Small Cell Lung Carcinomas of the Superior Sulcus: Initial Results of Southwest Oncology Group Trial 9416 (Intergroup Trial 0160). *J Thorac Cardiovasc Surg* (2001) 121(3):472–83. doi: 10.1067/mtc.2001.112465
27. Dobrowsky W, Dobrowsky E, Strassl H, Braun O, Gritzmann N, Scheiber V. Combined Modality Treatment of Advanced Cancers of the Oral Cavity and Oropharynx. *Int J Radiat Oncol Biol Phys* (1991) 20(2):239–42. doi: 10.1016/0360-3016(91)90097-n
28. Kirita T, Ohgi K, Shimooka H, Yamanaka Y, Tatebayashi S, Yamamoto K, et al. Preoperative Concurrent Chemoradiotherapy Plus Radical Surgery for Advanced Squamous Cell Carcinoma of the Oral Cavity: An Analysis of Long-Term Results. *Oral Oncol* (1999) 35(6):597–606. doi: 10.1016/s1368-8375(99)00044-5
29. Koelbl O, Rosenwald A, Haberl M, Muller J, Reuther J, Flentje M. P53 and Ki-67 as Predictive Markers for Radiosensitivity in Squamous Cell Carcinoma of the Oral Cavity? An Immunohistochemical and Clinicopathologic Study. *Int J Radiat Oncol Biol Phys* (2001) 49(1):147–54. doi: 10.1016/s0360-3016(00)01356-0
30. Freier K, Engel M, Lindel K, Flechtenmacher C, Muhling J, Hassfeld S, et al. Neoadjuvant Concurrent Radiochemotherapy Followed by Surgery in Advanced Oral Squamous Cell Carcinoma (OSCC): A Retrospective Analysis of 207 Patients. *Oral Oncol* (2008) 44(2):116–23. doi: 10.1016/j.oraloncology.2007.01.006
31. Eich HT, Loschcke M, Scheer M, Kocher M, Bongartz R, Wacker S, et al. Neoadjuvant Radiochemotherapy and Radical Resection for Advanced Squamous Cell Carcinoma of the Oral Cavity. Outcome of 134 Patients. *Strahlenther Onkol* (2008) 184(1):23–9. doi: 10.1007/s00066-008-1725-6
32. Driemel O, Ettl T, Kolbl O, Reichert TE, Dresp BV, Reuther J, et al. Outcome and Histopathologic Regression in Oral Squamous Cell Carcinoma After Preoperative Radiochemotherapy. *Strahlenther Onkol* (2009) 185(5):296–302. doi: 10.1007/s00066-009-1914-y
33. Klug C, Berzaczy D, Voracek M, Nell C, Ploder O, Millesi W, et al. Preoperative Radiochemotherapy in the Treatment of Advanced Oral

Cancer: Outcome of 276 Patients. *J Craniomaxillofac Surg* (2009) 37(6):344–7. doi: 10.1016/j.jcms.2008.11.012
34. Mucke T, Konen M, Wagenpfeil S, Kesting MR, Wolff KD, Holzle F. Low-Dose Preoperative Chemoradiation Therapy Compared With Surgery Alone With or Without Postoperative Radiotherapy in Patients With Head and Neck Carcinoma. *Ann Surg Oncol* (2011) 18(10):2739–47. doi: 10.1245/s10434-011-1643-1
35. Kreppel M, Dreiseidler T, Rothamel D, Eich HT, Drebber U, Zoller JE, et al. The Role of Clinical Versus Histopathological Staging in Patients With Advanced Oral Squamous Cell Carcinoma Treated With Neoadjuvant Radiochemotherapy Followed by Radical Surgery. *J Craniomaxillofac Surg* (2013) 41(1):22–7. doi: 10.1016/j.jcms.2012.05.005
36. Tupchong L, Scott CB, Blitzer PH, Marcial VA, Lowry LD, Jacobs JR, et al. Randomized Study of Preoperative Versus Postoperative Radiation Therapy in Advanced Head and Neck Carcinoma: Long-Term Follow-Up of RTOG Study 73-03. *Int J Radiat Oncol Biol Phys* (1991) 20(1):21–8. doi: 10.1016/0360-3016(91)90133-o
37. Slotman GJ, Doolittle CH, Glicksman AS. Preoperative Combined Chemotherapy and Radiation Therapy Plus Radical Surgery in Advanced Head and Neck Cancer. Five-Year Results With Impressive Complete Response Rates and High Survival. *Cancer* (1992) 69(11):2736–43. doi: 10.1002/1097-0142(19920601)69:11<2736::aid-cncr2820691118>3.0.co;2-s
38. Mohr C, Bohndorf W, Gremmel H, Harle F, Hausamen JE, Hirche H, et al. Preoperative Radiochemotherapy and Radical Surgery of Advanced Head and Neck Cancers–Results of a Prospective, Multicenter DOSAK Study. *Recent Results Cancer Res* (1994) 134:155–63. doi: 10.1007/978-3-642-84971-8_17
39. Glicksman AS, Slotman G, Doolittle C3rd, Clark J, Koness J, Coachman N, et al. Concurrent Cis-Platinum and Radiation With or Without Surgery for Advanced Head and Neck Cancer. *Int J Radiat Oncol Biol Phys* (1994) 30(5):1043–50. doi: 10.1016/0360-3016(94)90308-5
40. Wanebo H, Chougule P, Ready N, Safran H, Ackerley W, Koness RJ, et al. Surgical Resection is Necessary to Maximize Tumor Control in Function-Preserving, Aggressive Chemoradiation Protocols for Advanced Squamous Cancer of the Head and Neck (Stage III and IV). *Ann Surg Oncol* (2001) 8(8):644–50. doi: 10.1007/s10434-001-0644-x
41. Kessler P, Grabenbauer G, Leher A, Bloch-Birkholz A, Vairaktaris E, Neukam FW, et al. Five Year Survival of Patients With Primary Oral Squamous Cell Carcinoma. Comparison of Two Treatment Protocols in a Prospective Study. *Strahlenther Onkol* (2007) 183(4):184–9. doi: 10.1007/s00066-007-1469-8
42. Eckardt A, Sinikovic B, Hofele C, Bremer M, Reuter C. Preoperative Paclitaxel/Carboplatin Radiochemotherapy for Stage III/IV Resectable Oral and Oropharyngeal Cancer: Seven-Year Follow-Up of a Phase II Trial. *Oncol* (2007) 73(3-4):198–203. doi: 10.1159/000127420
43. Harada H, Omura K, Tomioka H, Nakayama H, Hiraki A, Shinohara M, et al. Multicenter Phase II Trial of Preoperative Chemoradiotherapy With S-1 for Locally Advanced Oral Squamous Cell Carcinoma. *Cancer Chemother Pharmacol* (2013) 71(4):1059–64. doi: 10.1007/s00280-013-2101-5
44. Yi J, Huang X, Xu Z, Liu S, Wang X, He X, et al. Phase III Randomized Trial of Preoperative Concurrent Chemoradiotherapy Versus Preoperative Radiotherapy for Patients With Locally Advanced Head and Neck Squamous Cell Carcinoma. *Oncotarget* (2017) 8(27):44842–50. doi: 10.18632/oncotarget.15107
45. Strojan P, Vermorken JB, Beitler JJ, Saba NF, Haigentz MJr., Bossi P, et al. Cumulative Cisplatin Dose in Concurrent Chemoradiotherapy for Head and Neck Cancer: A Systematic Review. *Head Neck* (2016) 38(Suppl 1):E2151–8. doi: 10.1002/hed.24026
46. Martin D, Balermpas P, Winkelmann R, Rodel F, Rodel C, Fokas E. Anal Squamous Cell Carcinoma - State of the Art Management and Future Perspectives. *Cancer Treat Rev* (2018) 65:11–21. doi: 10.1016/j.ctrv.2018.02.001
47. Mehanna H, Wong WL, McConkey CC, Rahman JK, Robinson M, Hartley AG, et al. PET-CT Surveillance Versus Neck Dissection in Advanced Head and Neck Cancer. *N Engl J Med* (2016) 374(15):1444–54. doi: 10.1056/NEJMoa1514493
48. Monteiro E, Sklar MC, Eskander A, de Almeida JR, Shrime M, Gullane P, et al. Assessment of the Clavien-Dindo Classification System for Complications in Head and Neck Surgery. *Laryngoscope* (2014) 124(12):2726–31. doi: 10.1002/lary.24817
49. McMahon JD, MacIver C, Smith M, Stathopoulos P, Wales C, McNulty R, et al. Postoperative Complications After Major Head and Neck Surgery With Free Flap Repair–Prevalence, Patterns, and Determinants: A Prospective Cohort Study. *Br J Oral Maxillofac Surg* (2013) 51(8):689–95. doi: 10.1016/j.bjoms.2013.04.015
50. Peters TTA, Post SF, van Dijk BAC, Roodenburg JLN, van der Laan BFAM, Werker PMN, et al. Free Flap Reconstruction for Head and Neck Cancer can be Safely Performed in Both Young and Elderly Patients After Careful Patient Selection. *Eur Arch Oto-Rhino-Laryngol* (2015) 272(10):2999–3005. doi: 10.1007/s00405-014-3268-z
51. Grammatica A, Piazza C, Pellini R, Montalto N, Lancini D, Vural A, et al. Free Flaps for Advanced Oral Cancer in the "Older Old" and "Oldest Old": A Retrospective Multi-Institutional Study. *Front Oncol* (2019) 9:604. doi: 10.3389/fonc.2019.00604
52. Kiong KL, Bell D, Yao CMKL, Ferrarotto R, Lewis CM. Multifocal Regression and Pathologic Response Predicts Recurrence After Neoadjuvant Chemotherapy in Head and Neck Squamous Cell Carcinoma. *Oral Oncol* (2021) 122:105520. doi: 10.1016/j.oraloncology.2021.105520
53. Budach V, Tinhofer I. Novel Prognostic Clinical Factors and Biomarkers for Outcome Prediction in Head and Neck Cancer: A Systematic Review. *Lancet Oncol* (2019) 20(6):e313-26. doi: 10.1016/S1470-2045(19)30177-9
54. Johnson DE, Burtness B, Leemans CR, Lui VWY, Bauman JE, Grandis JR. Head and Neck Squamous Cell Carcinoma. *Nat Rev Dis Primers* (2020) 6(1):92. doi: 10.1038/s41572-020-00224-3
55. Balermpas P, Michel Y, Wagenblast J, Seitz O, Weiss C, Rodel F, et al. Tumour-Infiltrating Lymphocytes Predict Response to Definitive Chemoradiotherapy in Head and Neck Cancer. *Br J Cancer* (2014) 110(2):501–9. doi: 10.1038/bjc.2013.640
56. Balermpas P, Rodel F, Rodel C, Krause M, Linge A, Lohaus F, et al. CD8+ Tumour-Infiltrating Lymphocytes in Relation to HPV Status and Clinical Outcome in Patients With Head and Neck Cancer After Postoperative Chemoradiotherapy: A Multicentre Study of the German Cancer Consortium Radiation Oncology Group (DKTK-ROG). *Int J Cancer* (2016) 138(1):171–81. doi: 10.1002/ijc.29683
57. Ribas A, Wolchok JD. Cancer Immunotherapy Using Checkpoint Blockade. *Sci* (2018) 359(6382):1350–5. doi: 10.1126/science.aar4060
58. De Palma M, Lewis CE. Macrophage Regulation of Tumor Responses to Anticancer Therapies. *Cancer Cell* (2013) 23(3):277–86. doi: 10.1016/j.ccr.2013.02.013
59. Gordon SR, Maute RL, Dulken BW, Hutter G, George BM, McCracken MN, et al. PD-1 Expression by Tumour-Associated Macrophages Inhibits Phagocytosis and Tumour Immunity. *Nat* (2017) 545(7655):495–9. doi: 10.1038/nature22396
60. Kono Y, Saito H, Miyauchi W, Shimizu S, Murakami Y, Shishido Y, et al. Increased PD-1-Positive Macrophages in the Tissue of Gastric Cancer are Closely Associated With Poor Prognosis in Gastric Cancer Patients. *BMC Cancer* (2020) 20(1):175. doi: 10.1186/s12885-020-6629-6
61. Jiang L-R, Zhang N, Chen S-T, He J, Liu Y-H, Han Y-Q, et al. PD-1-Positive Tumor-Associated Macrophages Define Poor Clinical Outcomes in Patients With Muscle Invasive Bladder Cancer Through Potential CD68/PD-1 Complex Interactions. *Front Oncol* (2021) 11:1810. doi: 10.3389/fonc.2021.679928
62. Augsten M. Cancer-Associated Fibroblasts as Another Polarized Cell Type of the Tumor Microenvironment. *Front Oncol* (2014) 4:62. doi: 10.3389/fonc.2014.00062
63. Canning M, Guo G, Yu M, Myint C, Groves MW, Byrd JK, et al. Heterogeneity of the Head and Neck Squamous Cell Carcinoma Immune Landscape and Its Impact on Immunotherapy. *Front Cell Dev Biol* (2019) 7:52. doi: 10.3389/fcell.2019.00052
64. Peltanova B, Raudenska M, Masarik M. Effect of Tumor Microenvironment on Pathogenesis of the Head and Neck Squamous Cell Carcinoma: A Systematic Review. *Mol Cancer* (2019) 18(1):63. doi: 10.1186/s12943-019-0983-5
65. Marsh D, Suchak K, Moutasim KA, Vallath S, Hopper C, Jerjes W, et al. Stromal Features are Predictive of Disease Mortality in Oral Cancer Patients. *J Pathol* (2011) 223(4):470–81. doi: 10.1002/path.2830
66. Martens RM, Noij DP, Ali M, Koopman T, Marcus JT, Vergeer MR, et al. Functional Imaging Early During (Chemo)Radiotherapy for Response Prediction in Head and Neck Squamous Cell Carcinoma; A Systematic Review. *Oral Oncol* (2019) 88:75–83. doi: 10.1016/j.oraloncology.2018.11.005

67. Chung SR, Choi YJ, Suh CH, Lee JH, Baek JH. Diffusion-Weighted Magnetic Resonance Imaging for Predicting Response to Chemoradiation Therapy for Head and Neck Squamous Cell Carcinoma: A Systematic Review. *Korean J Radiol* (2019) 20(4):649–61. doi: 10.3348/kjr.2018.0446
68. Kim S, Loevner L, Quon H, Sherman E, Weinstein G, Kilger A, et al. Diffusion-Weighted Magnetic Resonance Imaging for Predicting and Detecting Early Response to Chemoradiation Therapy of Squamous Cell Carcinomas of the Head and Neck. *Clin Cancer Res* (2009) 15(3):986–94. doi: 10.1158/1078-0432.CCR-08-1287
69. Noij DP, Pouwels PJW, Ljumanovic R, Knol DL, Doornaert P, de Bree R, et al. Predictive Value of Diffusion-Weighted Imaging Without and With Including Contrast-Enhanced Magnetic Resonance Imaging in Image Analysis of Head and Neck Squamous Cell Carcinoma. *Eur J Radiol* (2015) 84(1):108–16. doi: 10.1016/j.ejrad.2014.10.015
70. Hauser T, Essig M, Jensen A, Gerigk L, Laun FB, Munter M, et al. Characterization and Therapy Monitoring of Head and Neck Carcinomas Using Diffusion-Imaging-Based Intravoxel Incoherent Motion Parameters-Preliminary Results. *Neuroradiol* (2013) 55(5):527–36. doi: 10.1007/s00234-013-1154-9

Conflict of Interest: PW has received consulting fees and honoraria (private/institutional) for lectures by Bayer, Janssen-Cilag, Novartis, Roche, MSD, Astellas Pharma, Bristol-Myers Squibb, Thermo Fisher Scientific, Molecular Health, Sophia Genetics, Qiagen, Eli Lilly, Myriad, Hedera Dx, and Astra Zeneca.

The remaining authors declare that the research was conducted in the absence of any commercial or financial relationships that could be construed as a potential conflict of interest.

frontiers | Frontiers in Oncology

ORIGINAL RESEARCH
published: 05 April 2022
doi: 10.3389/fonc.2022.795781

The Prognostic Signature of Head and Neck Squamous Cell Carcinoma Constructed by Immune-Related RNA-Binding Proteins

Ruijie Ming[†], *Xiangrui Li*[†], *Enhao Wang*[†], *Jiahui Wei*, *Bo Liu*, *Peng Zhou*, *Wenting Yu*, *Shimin Zong*[*] *and Hongjun Xiao*[*]

Department of Otorhinolaryngology, Union Hospital, Tongji Medical College, Huazhong University of Science and Technology, Wuhan, China

OPEN ACCESS

Edited by:
Heming Lu,
People's Hospital of Guangxi Zhuang Autonomous Region, China

Reviewed by:
Jessica Dal Col,
University of Salerno, Italy
John Morton,
University of Colorado, United States

***Correspondence:**
Hongjun Xiao
xhjent_whxh@hust.edu.cn
Shimin Zong
2018XH0090@hust.edu.cn

[†]*These authors share first authorship*

Specialty section:
This article was submitted to Head and Neck Cancer, a section of the journal Frontiers in Oncology

Received: *15 October 2021*
Accepted: *04 March 2022*
Published: *05 April 2022*

Citation:
Ming R, Li X, Wang E, Wei J, Liu B, Zhou P, Yu W, Zong S and Xiao H (2022) The Prognostic Signature of Head and Neck Squamous Cell Carcinoma Constructed by Immune-Related RNA-Binding Proteins. Front. Oncol. 12:795781. doi: 10.3389/fonc.2022.795781

Purpose: This study aimed to construct a prognostic signature consisting of immune-related RNA-binding proteins (RBPs) to predict the prognosis of patients with head and neck squamous cell carcinoma (HNSCC) effectively.

Methods: The transcriptome and clinical data of HNSCC were downloaded from The Cancer Genome Atlas (TCGA) and Gene Expression Omnibus (GEO) databases. First, we ascertained the immunological differences in HNSCC, through single-sample gene set enrichment analysis, stromal and immune cells in malignant tumor tissues using expression data (ESTIMATE), and cell-type identification by estimating relative subsets of RNA transcripts (CIBERSORT) deconvolution algorithm. Then we used univariate proportional hazards (Cox) regression analysis and least absolute shrinkage and selection operator (LASSO) Cox regression analysis to screen immune-related RBPs and acquire the risk score of each sample. Subsequently, we further investigated the difference in prognosis, immune status, and tumor mutation burden in high- and low-risk groups. Finally, the efficacy of immunotherapy was measured by the tumor immune dysfunction and exclusion (TIDE) score.

Results: We derived 15 immune-related RBPs, including FRMD4A, ASNS, RAB11FIP1, FAM120C, CFLAR, CTTN, PLEKHO1, SELENBP1, CHCHD2, NPM3, ATP2A3, CFDP1, IGF2BP2, NQO1, and DENND2D. There were significant differences in the prognoses of patients in the high- and low-risk groups in the training set ($p < 0.001$) and the validation set ($p < 0.01$). Furthermore, there were statistical differences between the high-risk group and low-risk group in immune cell infiltration and pathway and tumor mutation load ($p < 0.001$). In the end, we found that patients in the low-risk group were more sensitive to immunotherapy ($p < 0.001$), and then we screened 14 small-molecule chemotherapeutics with higher sensitivity to the high-risk group ($p < 0.001$).

Conclusion: The study constructed a prognostic signature of HNSCC, which might guide clinical immunotherapy in the future.

Keywords: head and neck squamous cell carcinoma, RNA binding protein, prognostic, immune microenvironment, tumor mutation burden, copy number variations, immunotherapy, chemotherapeutic

INTRODUCTION

Head and neck squamous carcinoma (HNSCC), which has a mortality rate of 50.5%, is one of the most common tumors, accounting for 3.6% of malignant tumors (1). HNSCC is a histologically and genetically heterogeneous disease that originates from a variety of anatomical parts, including the oral cavity, tongue, salivary glands, nasopharynx, and larynx (2). Smoking, drinking, and human papillomavirus infection are the main causes of HNSCC (3). Patients with HNSCC often experience cervical lymph node metastasis, local recurrence, and resistance to radiotherapy and chemotherapy (4).

At present, the treatment strategy for HNSCC patients is still based on tumor location and disease stage, not tumor biology. Many biomolecular markers, such as proteins, DNA, RNA, and microRNA, have been proposed to detect primary and secondary malignancies in the initial stages of the disease, but the above indicators are still very limited in terms of prognostic assessment and optimization of treatment options. In order to improve the treatment outcome of HNSCC, a clinically useful method is urgently needed to identify the risk of HNSCC and judge the effectiveness of adjuvant therapy.

The tumor microenvironment (TME) plays a vital role in the occurrence, progression, and treatment response of tumors. TME includes proliferating tumor cells, tumor stroma, blood vessels, cancer-related fibroblasts, infiltrating inflammatory cells, and various related signal molecules (5, 6). In the microenvironment of HNSCC, immune cells and mesenchymal cells, as the two main non-tumor components, have caused a large number of inflammatory reactions (7). Since HNSCC is an immunosuppressive disease, immune checkpoint inhibitors have emerged as a new treatment option (8). The basic principle of immunotherapy is to block the immunosuppressive effect of immune checkpoints while activating the endogenous immune system, thus increasing the number and cytotoxicity of T cells, which is beneficial to attack tumor cells (9). Consequently, it would be valuable to investigate the role of immune cells and their regulators in the TME of HNSCC.

From the nucleus to the peripheral cytoplasm, RNA-binding proteins (RBPs) play a vital role in the post-transcriptional regulation of genes (10). RBPs are able to affect pre-mRNA processing, transport and localization, mRNA stability/degradation, and translation (11). In a variety of tumors, some RBPs were found to be dysfunctional and aberrantly regulated (12, 13). Meanwhile, RBPs are important components of the immune system, which respond quickly to inflammatory mediators and in modulating inflammatory responses (14). Considering the important role of RBPs in immunity, it is necessary to explore the relationship between RBPs and HNSCC.

This study aimed to develop a prognostic prediction model for HNSCC based on immune-related RBPs. First, we classified HNSCC patients into two immune phenotypes based on the enrichment fraction of immune cells, then screened for differentially expressed RBPs in two immune phenotypes, and defined them as immune-related RBPs. Through univariate proportional hazards (Cox) regression analysis and least absolute shrinkage and selection operator (LASSO) Cox regression analysis, we identified immune-related RBPs related to prognosis and then constructed a risk model for patients with HNSCC. Based on the validation of the prognostic relevance and predictive capacity of the risk model, we further analyzed the infiltrating immune cells and immune-related pathways, somatic mutations, copy number variations (CNVs), the efficacy of immunotherapy, and sensitivity of chemotherapeutic agents in patients with HNSCC. The results showed that the risk model consisting of immune-related RBPs can effectively differentiate the clinical outcomes and show superiority in predicting the prognosis of patients with HNSCC.

METHODS

Data Access

The transcriptome data in the fragment per kilobase million (FPKM) format and clinical data of 499 patients with HNSCC were downloaded from The Cancer Genome Atlas (TCGA) as the training set (https://portal.gdc.cancer.gov) (15) and downloaded the transcriptome data and clinical data of 97 HNSCC samples from the GSE41613 dataset of the Gene Expression Omnibus (GEO) database for validation (https://www.ncbi.nlm.nih.gov/geo/) (16). The data of somatic mutation and CNVs of patients with HNSCC were downloaded from UCSC (http://xena.ucsc.edu/) (17). The gene list of RBPs was collected from Gerstberger (10), SONAR (18), GO: RNA binding (19), poly(A) RBPs (20–24), CARIC (25), and XRNAX (26).

Immunophenotyping Based on Single-Sample Gene Set Enrichment Analysis

Single-sample gene set enrichment analysis (ssGSEA) is an algorithm based on rank ordering, which can calculate the degree of enrichment of a single sample in a given gene set (27). On this basis, the enrichment scores of immune cells and some related immune processes were calculated through the GSEA program (28, 29) and then quantified through the default parameters of the "Gene Set Variation Analysis (GSVA)" R package (30). Subsequently, the "ConsensusClusterPlus" R package was used to co-cluster the infiltration levels of 23 types of immune cells in HNSCC samples from TCGA to

identify and distinguish immune subtypes (31). In the cumulative distribution function (CDF), the K value with the largest area under the curve was selected as 2, and so the HNSCC samples were divided into two types (31). The Estimation of STromal and Immune cells in MAlignant Tumor tissues using Expression data (ESTIMATE) algorithm was utilized to calculate the immune score, stromal score, ESTIMATE score, and tumor purity (32). The immune cell infiltration calculated by the Cell-type Identification By Estimating Relative Subsets Of RNA Transcripts (CIBERSORT) deconvolution algorithm was used to verify the immune difference between the two types (33). Finally, the GSEA program was used to compare the differences in pathway enrichment between the above immunotypes from the Kyoto Encyclopedia of Genes and Genomes (KEGG) (34).

Construction and Validation of Risk Model

The "limma" R package was used to distinguish RBPs with different expressions between immunotypes. With a 1.4-fold difference and corrected p less than 0.05 as the screening conditions, 238 immune-related RBPs were obtained. Subsequently, 47 immune-related RBPs associated with prognosis were obtained through univariate proportional hazards regression ($p < 0.05$). The "glmnet" package was then utilized to perform LASSO Cox regression analysis (35). After 1,000 times of cross-validation, 15 immune-related RBPs and the correlation coefficients of the corresponding risk genes were obtained to construct a risk model at the same time. Risk score = $\Sigma_i^n Expi \times Coefi$, in which *Expi* is the expression of each risk gene and *Coefi* is its correlation coefficient. All patients were divided into a high-risk group and a low-risk group characterized by the median risk score of patients with HNSCC in the training set. The Kaplan–Meier curves were used to compare the overall survival (OS) difference of patients in the high- and low-risk groups. Receiver operating characteristic (ROC) curves were generated to evaluate the effectiveness and accuracy of the risk score in predicting the prognosis of patients with HNSCC. Next, the "ggExtra" R package was used to calculate the correlation between the risk score and the OS of patients with HNSCC. The independent correlation between the risk score and the prognosis of patients with HNSCC was then evaluated by univariate and multivariate proportional hazards regression analyses. Subsequently, a nomogram that could predict the prognosis of individual patients with HNSCC was constructed based on the stage, T stage, N stage, and risk group of patients with HNSCC through the "rms" R package (36). The C index was then used to assess the ability of the nomogram to distinguish prognosis, and a calibration chart was drawn to evaluate the accuracy of the nomogram. In addition, GSEA and gene set variation analysis (GSVA) were used to compare the differences in KEGG pathway enrichment between risk groups.

Analysis of Somatic Mutation and Copy Number Variations

The tumor mutation burden (TMB) of HNSCC samples from TCGA was analyzed through the "maftools" R package (37). The differences in TMB between the high- and low-risk groups were compared and showed the top 20 genes with the highest mutation rate and their mutation types in the high- and low-risk groups. Then the impact of TMB on the OS of patients with HNSCC was evaluated through the Kaplan–Meier survival curves. After that, gistic 2.0 was used to detect significant copy number amplification or deletion (38). In the end, the CNVs of 22 pairs of autosomes between the high- and low-risk groups were compared and showed the top 20 genes with most CNVs and their variation types.

Prediction of the Curative Effect of Immunotherapy and Chemotherapy

Tumor immune dysfunction and exclusion (TIDE) (http://tide.dfci.harvard.edu/) was used to calculate the TIDE score, which was reported to be able to predict the response of patients with a malignant tumor to immunotherapy (39). On the other hand, the "pRRophetic" R package was used to compare the half-maximal inhibitory concentration (IC50) differences of some common small-molecule chemotherapeutics between the high- and low-risk groups and screened out chemotherapeutics that may have better efficacy for patients in the high-risk group (40).

Statistical Analysis

All statistical analyses were based on R 4.0.4 software (https://www.r-project.org/). Categorical variables were tested by the chi-square test or Fisher's exact test. The t-test or Wilcoxon test was performed on continuous variables. $p < 0.05$ was deemed statistically significant.

RESULTS

Development and Validation of the Prognostic Model Based on Immunophenotyping of Head and Neck Squamous Cell Carcinoma

The flowchart of this research is shown in **Figure 1**. First, we obtained patient data from TCGA database and divided the patients into two groups according to differences in immune cells. The CIBERSORT deconvolution and ESTIMATE algorithm confirmed the difference in the immune microenvironment between the Sub1 and Sub2 groups (**Figure 1A**). After differential expression analysis, 238 immune-related RBPs were identified. Through univariate and LASSO Cox regression analysis, 15 immune-related RBPs related to prognosis were selected, and then the Kaplan–Meier curves showed the difference between the high- and low-expression immune-related RBPs groups (**Figure 1B**). Subsequently, we found that the risk score was significantly related to the OS of patients with HNSCC in training and validation sets, respectively (**Figure 1C**). In addition, the differences in immune cells and pathways between the high- and low-risk groups are further elaborated (**Figure 1D**). In terms of genes, we showed the differences in somatic mutation and CNVs (**Figure 1E**). In addition, we have also produced a nomogram combining the stage, T stage, N stage, and risk group to predict the prognosis (**Figure 1F**). In the end, the efficacy of immunotherapy was analyzed through the TIDE

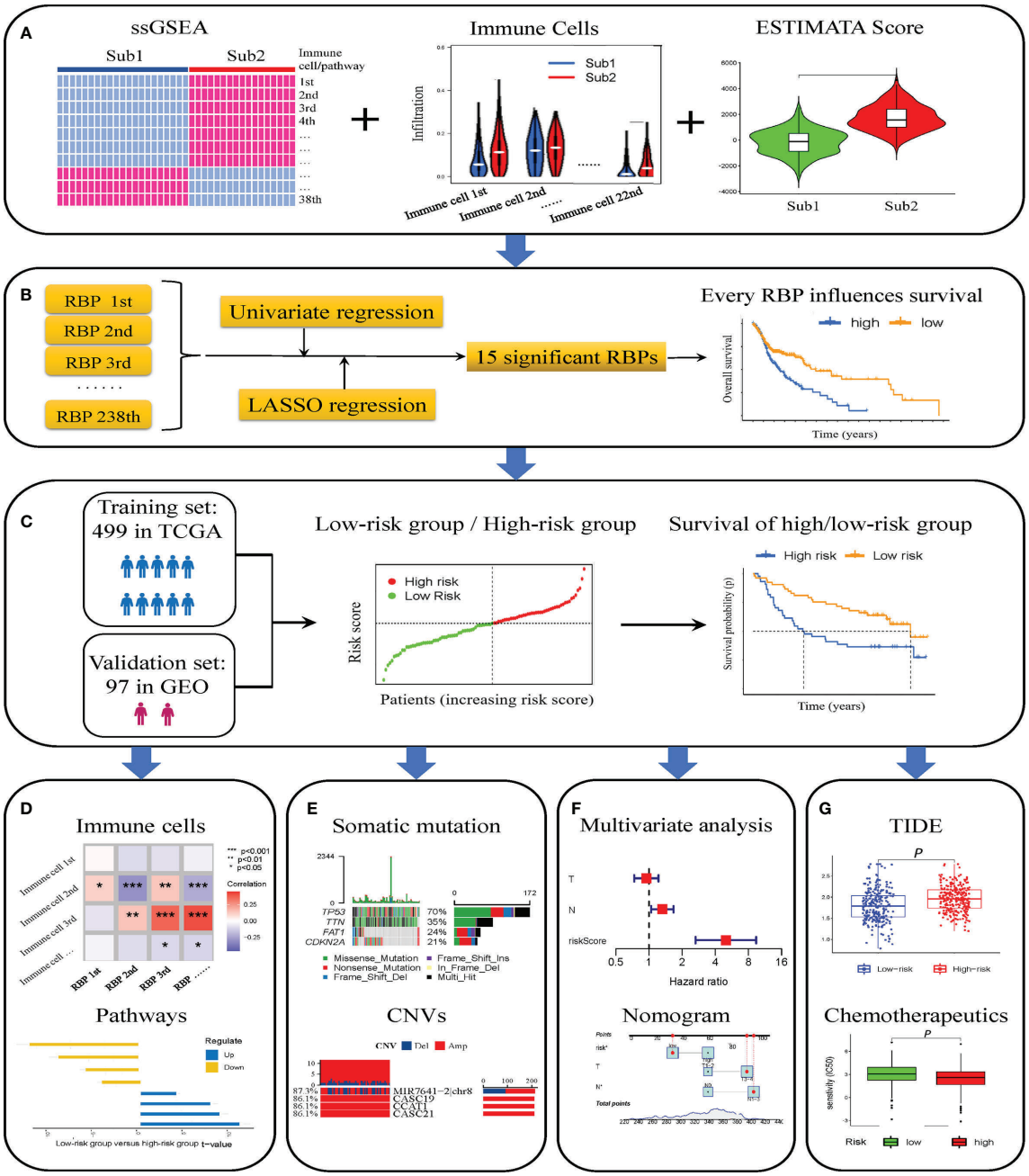

FIGURE 1 | Flowchart of this study. Two immune subtypes identified by single-sample gene set enrichment analysis (ssGSEA) and co-clustering analysis, and difference of infiltrating immune cells assessed by CIBERSORT deconvolution algorithm and ESTIMATE algorithm **(A)**. Fifteen immune-related RNA-binding proteins (RBPs) screened out through "limma" package, univariate and least absolute shrinkage and selection operator (LASSO) Cox analysis, and the Kaplan–Meier curves for high- and low-expression immune-related RBP groups **(B)**. Validation of the risk model composed of immune-related RBPs for prognosis in The Cancer Genome Atlas (TCGA) and Gene Expression Omnibus (GEO) database **(C)**. Immune cell infiltration and pathways in high- and low-risk groups **(D)**. Somatic mutation and copy number variations (CNVs) in high- and low-risk groups **(E)**. Construction and calibration of prognosis nomogram **(F)**. The differences of tumor immune dysfunction and exclusion (TIDE) score and sensitivity to chemotherapeutics of patients with head and neck squamous cell carcinoma (HNSCC) in high- and low-risk groups **(G)**. $^{*}p < 0.05$; $^{**}p < 0.01$; $^{***}p < 0.001$.

score, and the sensitivity of different risk groups to small-molecule chemotherapeutics was also revealed (**Figure 1G**).

Based on the transcriptome data of TCGA HNSCC, we evaluated and quantify 23 kinds of immune cells and 15 kinds of immune processes by ssGSEA. After that, co-clustering analysis was used to distinguish the infiltration of 23 immune cells in the HNSCC samples in TCGA. When K = 2, the CDF curve had the largest area under the curve, so all samples were divided into two types

(Sub1 and Sub2) (**Figure S1A**). Among them, there were 271 cases in the Sub1 group and 228 cases in the Sub2 group. It was worth mentioning that the immune cells and pathways were more enriched in the Sub2 group than the Sub1 group (**Figure 2A**). Compared with the Sub2 group, the Sub2 group had lower immune score (**Figure 2B**, $p < 0.001$), lower stromal score (**Figure 2C**, $p < 0.001$), lower ESTIMATE score (**Figure 2D**, $p < 0.001$), and higher tumor purity (**Figure 2E**, $p < 0.001$). For the purpose of authenticating the difference between the two types, we used the CIBERSORT deconvolution algorithm and the ESTIMATE algorithm to calculate the infiltration of immune cells. Among the Sub1 group, M0 macrophages, activated dendritic cells, and mast cells infiltrated more, while in the Sub2 group, primitive B cells, plasma cells, CD8 T cells, activated CD4 memory T cells, follicular helper T cells, Treg cells, M1 macrophages, resting mast cells, and eosinophils infiltrated more (**Figure 2F**, $p < 0.05$). As far as the human leukocyte antigen (HLA) family is concerned, the expression of the Sub1 group is lower (**Figure 2G**, $p < 0.001$). Considering the rise of immune checkpoint inhibitor therapy, we also analyzed the differences between immune checkpoints. The expressions of checkpoint LAG3, PDCD1, HAVCR2, CTLA4, and CD274 in the Sub2 group are extremely higher than that in the Sub1 group (**Figure 2H**, $p < 0.001$). In addition, as the result of pathway enrichment shows, there was more immune-related pathway enrichment in the Sub2 group, such as cytokine receptor interaction, chemokine signaling pathway, JAK-STAT signaling pathway, cell adhesion molecules cams, toll-like receptor signaling pathway, and natural killer cell-mediated cytotoxicity (**Figure 2I**, $p < 0.001$). It was worth noting that the Kaplan–Meier curves showed a better prognosis of the Sub2 group than that of the Sub1 group (**Figure 2J**, $p = 0.007$).

Construction and Validation of Risk Model

We screened 238 immune-related RBPs through the "limma" R package (**Figure 3A**). Among these 238 immune-related RBPs, most of them were highly expressed in the Sub2 group, and the others were highly expressed in the Sub1 group (**Figure 3B**). Subsequently, 47 prognostic-related immune-related RBPs were obtained through univariate proportional hazards regression (**Figure 3C**, $p < 0.05$). In order to avoid overfitting, we then used LASSO Cox regression analysis and cross-validated 1,000 times to obtain 15 immune-related RBPs and the correlation coefficients of their corresponding risk genes (**Figures 3D, E**, **Table S1**). The risk model was thus constructed:

$$\begin{aligned}\text{RiskScore} &= \textit{Exp}\text{FRMD4A}*(-0.0573) + \text{ExpASNS}*(0.1068)\\ &+\textit{Exp}\text{RAB11FIP1}*(0.1068) + \textit{Exp}\text{FAM120C} * (-0.1220)\\ &+ \text{ExpCFLAR} * (-0.0026) + \text{ExpCTTN} * (0.0341)\\ &+ \text{ExpPLEKHO1} * (-0.0663) + \text{ExpSELENBP1} * (0.0181)\\ &+ \text{ExpCHCHD2} * (0.0547) + \text{ExpNPM3} * (0.0507)\\ &+ \text{ExpATP2A3} * (0.0787) + \text{ExpCFDP1} * (0.0787)\\ &+ \text{ExpIGF2BP2} * (0.0149) + \text{ExpNQO1} * (0.0459)\\ &+ \text{ExpDENND2D} * (-0.0207).\end{aligned}$$

The negative correlation coefficient indicated that the expression of the gene was beneficial to the prognosis, and the positive value indicated no benefit or even hindrance.

We assigned TCGA data as the training set and GEO data as the validation set. According to the median risk score of patients with HNSCC in TCGA, all patients were divided into the high-risk group and low-risk group (**Figures 4A, H**). In the training and validation sets, the mortality of patients in the high-risk group was higher than that in the low-risk group (**Figures 4B, I**). In the high-risk group, ASNS, CTTN, CHCHD2, NPM3, CFDP1, IGF2BP2, and NQO1 were expressed higher, while in the low-risk group, there were higher expressions of FRMD4A, RAB11FIP1, FAM120C, CFLAR, PLEKHO1, SELENBP1, ATP2A3, and DENND2D (**Figures 4C, J**). The OS was negatively correlated with the risk score, which meant the OS of patients with HNSCC gradually decreases as the risk score increased (**Figures 4D, K**). The area under the ROC (AUC) of the risk score of the training set was 0.60 (1 year), 0.70 (3 years), and 0.64 (5 years) (**Figure 4E**). In contrast, the AUC of the validation set was 0.63 (1 year), 0.63 (3 years), and 0.64 (5 years) (**Figure 4L**). The Kaplan–Meier curves also indicated that the high-risk group had a poor prognosis (**Figures 4F, G**, $p < 0.01$).

In order to verify the validity and independence of the risk score, we combined the clinical characteristics and pathological staging data from TCGA database to perform univariate and multivariate Cox regression analyses. Univariate Cox analysis showed that age ($p < 0.05$), stage ($p < 0.001$), T ($p < 0.01$), N ($p < 0.001$), and risk score ($p < 0.001$) were significantly related to the prognosis (**Figure 5A**, **Table S2**). Multivariate analysis indicated that age ($p < 0.01$), N ($p < 0.05$), and risk score ($p < 0.001$) were significantly correlated with the prognosis (**Figure 5B**, **Table S3**). This implied that our risk model based on immune-related RBPs could be used as independent and effective indicators for the prognosis of patients with HNSCC.

In addition, we combined the stage (I–II and III–IV), T stage (T1–2 and T3–4), N stage (N0 and N1–3), and risk group (low and high) to construct 1-, 3-, and 5-year prognostic nomogram models (**Figure 5C**), which could guide clinical judgment more conveniently and effectively. For example, when an 80-year-old patient in a low-risk group is stage III–IV, T3–4, and N1–3, he would get a score of 375, which means that the probability of his survival time at less than 1 year, less than 3 years, and less than 5 years is 0.268, 0.574, and 0.698, respectively. The following calibration chart showed the difference between the OS predicted by this nomogram and the actual OS from TCGA database and suggested that the nomogram had certain accuracy (**Figure 5D**).

Finally, we evaluated the relationship between each of the 15 immune-related RBP genes in the model and the OS of patients with HNSCC. Patients with high expressions of ASNS, IGF2BP2, CFDP1, CHCHD2, CTTN, NPM3, and NQO1 have poor OS, while patients with high expressions of FRMD4A, FAM120C, ATP2A3, PLEKHO1, RAB11FIP1, DENND2D, CFLAR, and SELENBP1 have a better OS (**Figures 6A–O**, $p < 0.05$).

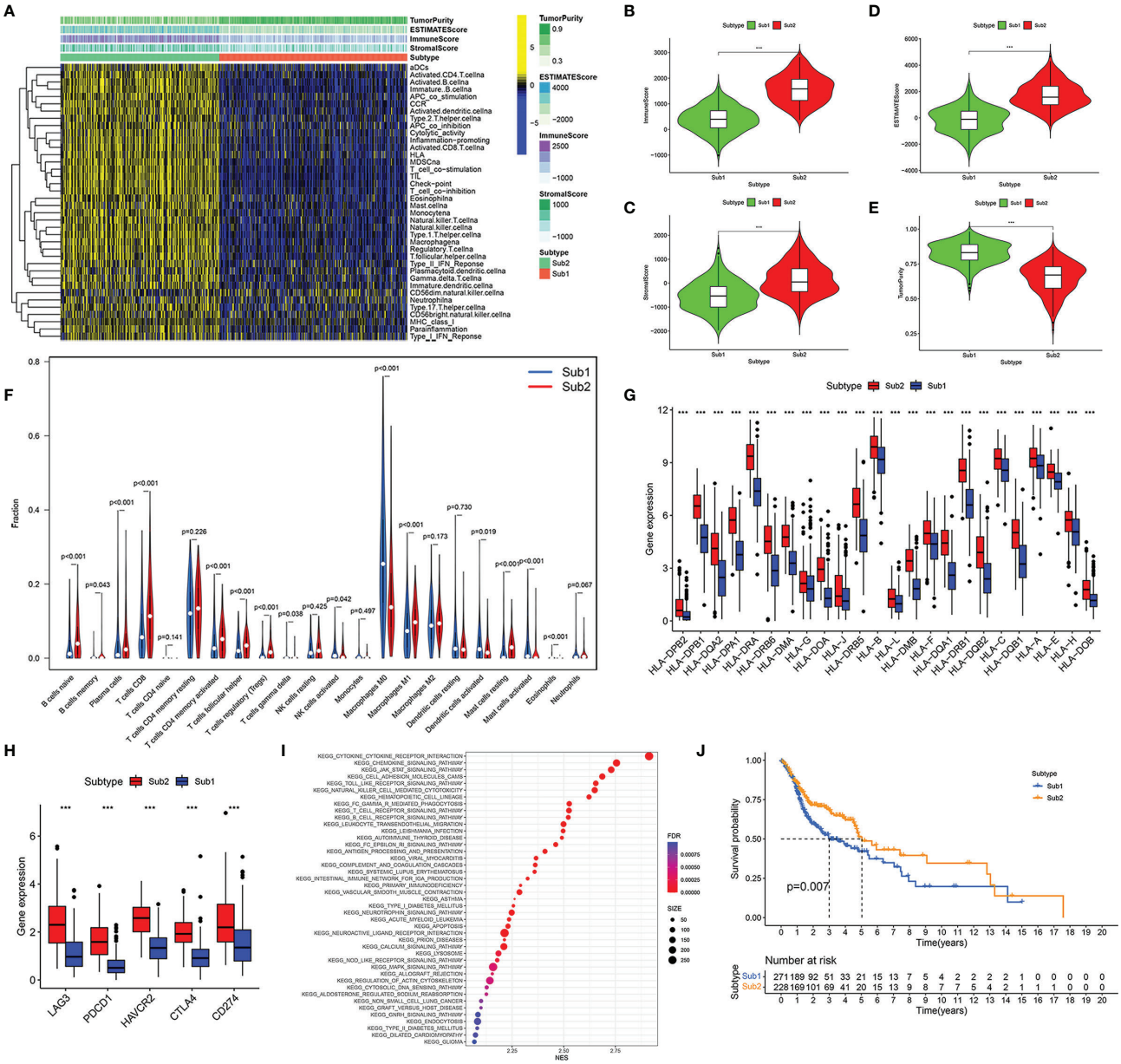

FIGURE 2 | Immune subtypes of head and neck squamous cell carcinoma (HNSCC) were identified based on the tumor-infiltrating immune cells. Heatmap of single-sample gene set enrichment analysis (ssGSEA) scores for Sub1 group (n = 271) and Sub2 group (n = 228) **(A)**. Comparison of immune score **(B)**, stromal score **(C)**, ESTIMATE score **(D)**, and tumor purity **(E)** between Sub1 and Sub2 groups. Difference of immune cell infiltration between Sub1 and Sub2 groups **(F)**. The expressions of HLA family genes in Sub1 and Sub2 groups **(G)**. The discrepancy of immune checkpoint genes between Sub1 and Sub2 groups, including LAG3, PDCD1, HAVCR2, CTLA4, and CD274 **(H)**. The divergence of enrichment pathways between Sub1 and Sub2 groups **(I)**. Kaplan–Meier curves of Sub1 and Sub2 groups **(J)**. ***p < 0.001.

Exploration of the Immune Microenvironment

The established risk model was based on immune-related RBPs, so it was necessary to confirm whether the model was related to the immune microenvironment of HNSCC. CIRBERSORT results showed that the 15 immune-related RBPs in the model all had associated immune cells (**Figure 7A**). Through the ESTIMATE algorithm, we found that the immune score, stromal score, and ESTIMATE score were lower and that the tumor purity was higher in the high-risk group (**Figures 7B–E**, $p < 0.001$). Then, we compared the expressions of the HLA family, and most of them were lower in the high-risk group

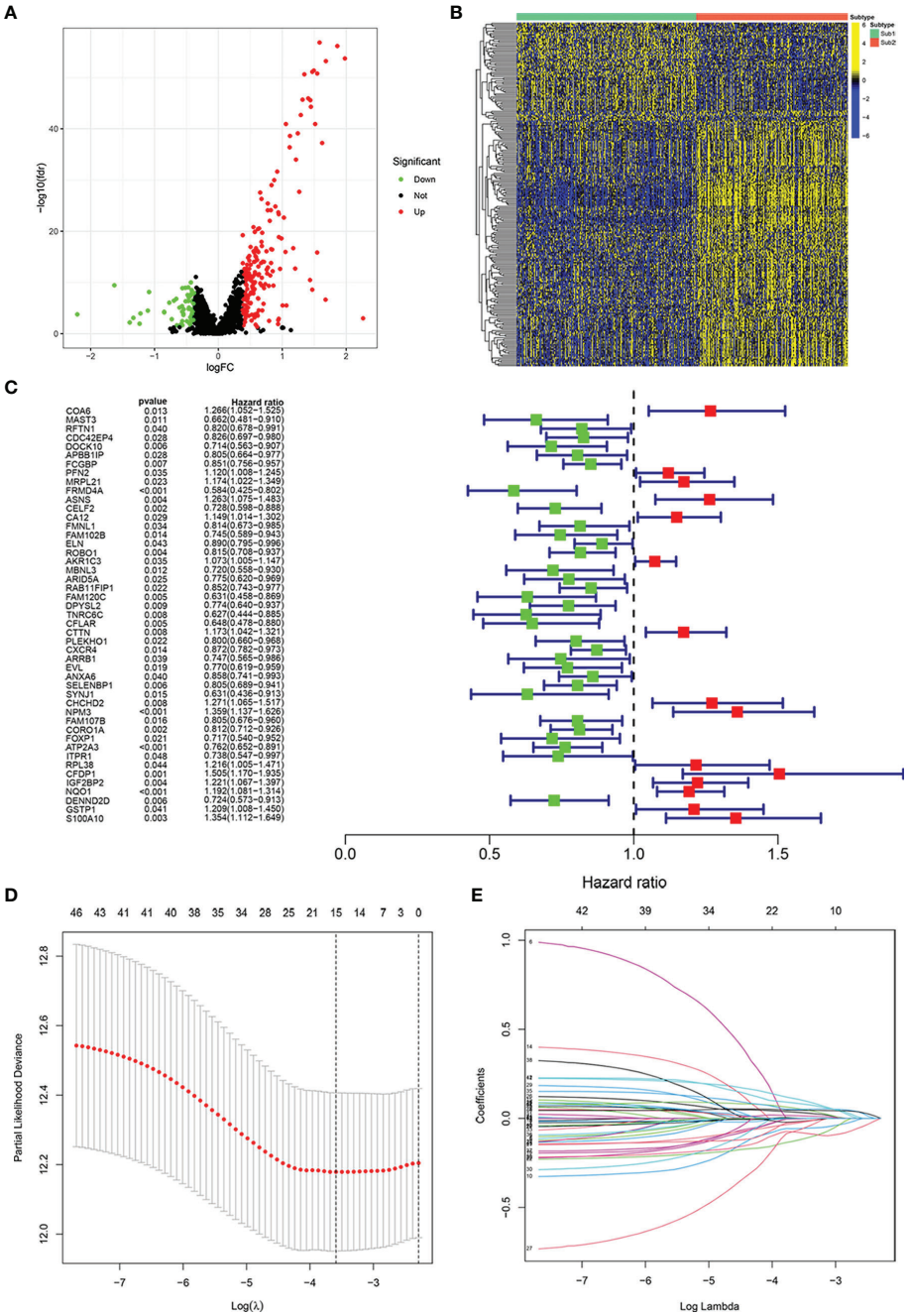

FIGURE 3 | Construction of risk model for prognosis in patients with head and neck squamous cell carcinoma (HNSCC). Volcano plot exhibiting the differentially expressed immune-related RNA-binding proteins (RBPs) between Sub1 group (n = 271) and Sub2 group (n = 228) in HNSCC **(A)**. Heatmap of differentially expressed immune-related RBPs in Sub1 and Sub2 groups **(B)**. The result of univariate Cox analysis **(C)** and least absolute shrinkage and selection operator (LASSO) Cox analysis **(D, E)**.

(**Figure 7F**, $p < 0.05$). Subsequently, the checkpoint expressions of PDCD1, CD274, CTLA4, HAVCR2, and LAG3 in the low-risk group were relatively high (**Figures 7G–K**, $p < 0.001$). Every immune checkpoint is negatively correlated with the risk score (**Figures 7L–P**, $p < 0.001$).

Analysis of Somatic Mutation and Copy Number Variations

In the high-risk group and the low-risk group, the genes with the highest mutations are TP53, TTN, FAT1, and CDKN2A. Moreover, there are more mutations of TP53, FAT1,

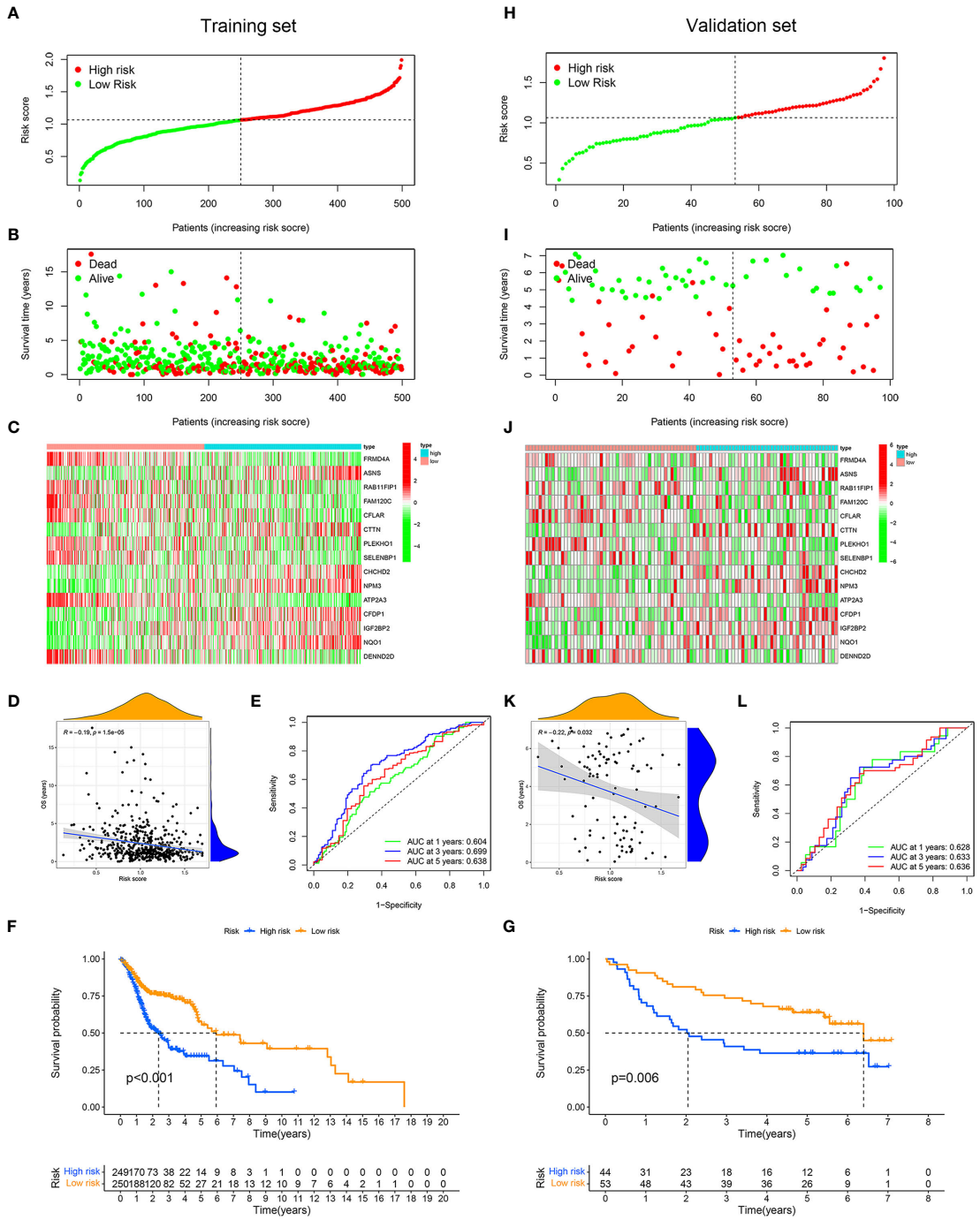

FIGURE 4 | Application and validation of the risk model for prognosis. Samples in The Cancer Genome Atlas (TCGA) dataset were designated as training set, and samples in Gene Expression Omnibus (GEO) dataset were designated as validation set. On basis of the mean risk score of samples in training set, patients were divided into high-risk (red dot) and low-risk (green dot) groups. Distribution of the risk scores of the patients in training set **(A)**. Distribution of survival time of patients in training set **(B)**. The heatmap depicting the expression difference of 15 immune-related RNA-binding proteins (RBPs) between the high-risk group and the low-risk group in training set **(C)**. Correlation between overall survival and risk score in training set **(D)**. ROC curves of risk score for predicting 1, 3, and 5 years of overall survival in training set **(E)**. Kaplan–Meier curves of high- and low-risk groups in training set **(F)**. Distribution of the risk scores of the samples in validation set **(H)**. Distribution of survival time of samples in validation set **(I)**. The heatmap showing the expression patterns of 15 immune-related RBPs between the high- and low-risk groups in validation set **(J)**. Correlation between overall survival and risk score in validation set **(K)**. Receiver operating characteristic (ROC) curves of risk score for predicting 1, 3, and 5 years of overall survival in validation set **(L)**. Kaplan–Meier curves of high- and low-risk groups in validation set **(G)**.

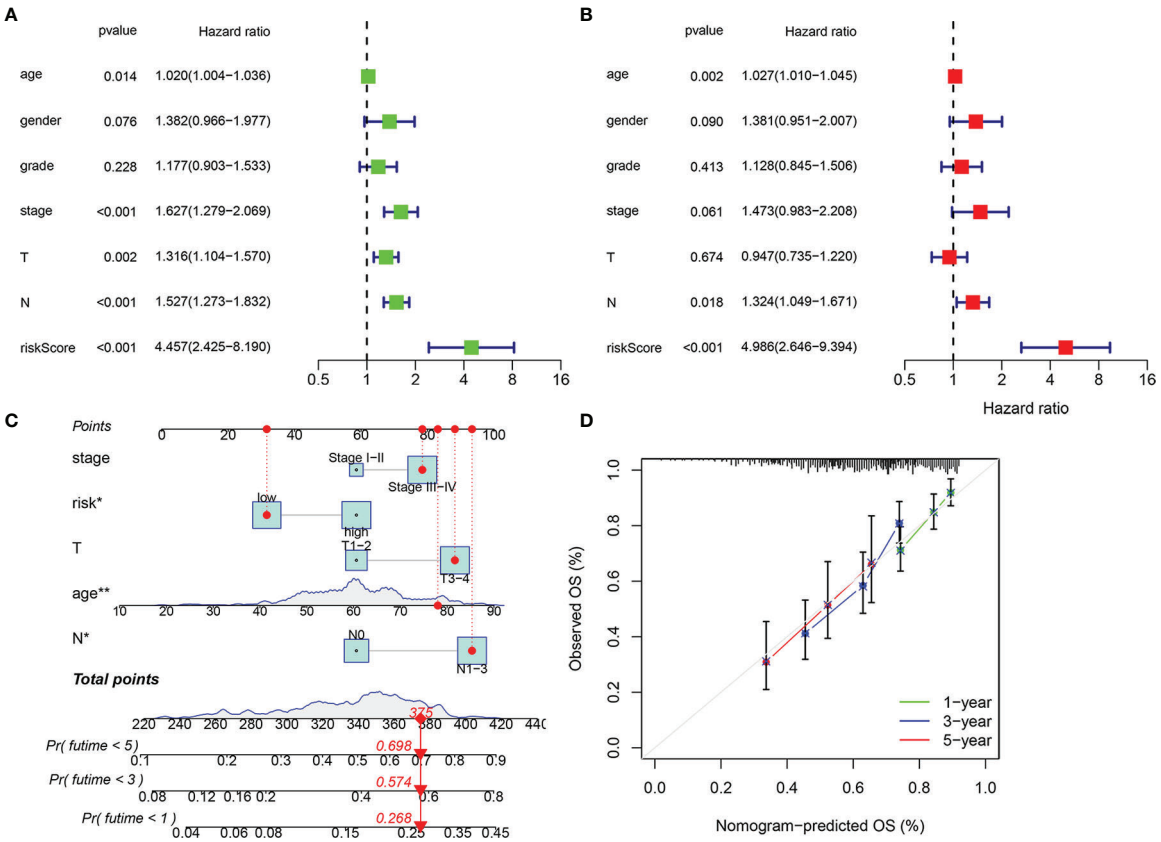

FIGURE 5 | Independence of risk score and construction of nomogram consisting of risk score and clinicopathological characteristics. Univariate Cox regression analysis was used to validate whether age, gender, grade, stage, T, N, and risk score had an independent influence on prognosis **(A)**. Multivariate Cox regression analysis was used to validate whether age, gender, grade, stage, T, N, and risk score had independent influence on prognosis **(B)**. Construction of integrated nomogram to predict survival in head and neck squamous cell carcinoma (HNSCC) **(C)**. Calibration curve for predicting 1, 3, and 5 years of overall survival **(D)**. *$p < 0.05$, **$p < 0.01$.

CDKN2A, NOTCH1, SYNE1, and NSD1 in the high-risk group, and the mutation rate of PIK3CA is higher in the low-risk group (**Figures 8A, B**). TMB is higher in the high-risk group (**Figure 8C**, $p < 0.001$). The prognosis of patients with high TMB was significantly worse than that of patients with low TMB (**Figure 8D**). Considering that the risk score was an independent prognostic factor, we evaluated the superimposed influence of TMB and risk score. The prognosis in descending order is the low-mutation and low-risk group, the high-mutation and low-risk group, the low-mutation and high-risk group, and the high-mutation and high-risk group (**Figure 8E**, $p < 0.001$).

Extensive copy number amplification was detected in 22 pairs of autosomes in all two groups. In the low-risk group, high-frequency deletion regions were found on chromosomes 3 and 13, and high-frequency amplification regions were found on chromosome 8 (**Figure 8F**). In the high-risk group, CNVs analysis indicated the following most relevant genes: MIR7641-2|chr8, CASC19, CCAT1, CASC21, CASC8, CCAT2, POU5FIB, and CSMD1 (**Figure 8G**). Among them, gene CSMD1 had a significant copy number deletion (**Figure 8G**). On the other hand, the five most correlative genes in the low-risk group included NAALADL2, TP63, LINC01206, TPRG1, and TPRG1-AS2 (**Figure 8H**).

GSEA (**Figure 9A**) and GSVA (**Figure 9B**) revealed the differences in pathway enrichment between the high- and low-risk groups. Most of the pathways enriched in the low-risk group were associated with immune responses, which may be involved in immune-related RBPs, including Fc gamma R-mediated phagocytosis, B-cell receptor signaling pathway, T-cell receptor signaling pathway, autoimmune thyroid disease, cell adhesion molecules cams, cytokine–cytokine receptor interaction, leukocyte transendothelial migration, and natural killer cell-mediated cytotoxicity.

Prediction of the Efficacy of Immunotherapy and Chemotherapy

We used the TIDE score to predict the immunotherapy response of patients with HNSCC to immunotherapy. It could be briefly described that the higher the TIDE score, the higher the likelihood of immune dysfunction or evasion, and the less likely the patient will benefit from immune checkpoint inhibitors. As a result, the TIDE score of the high-risk group

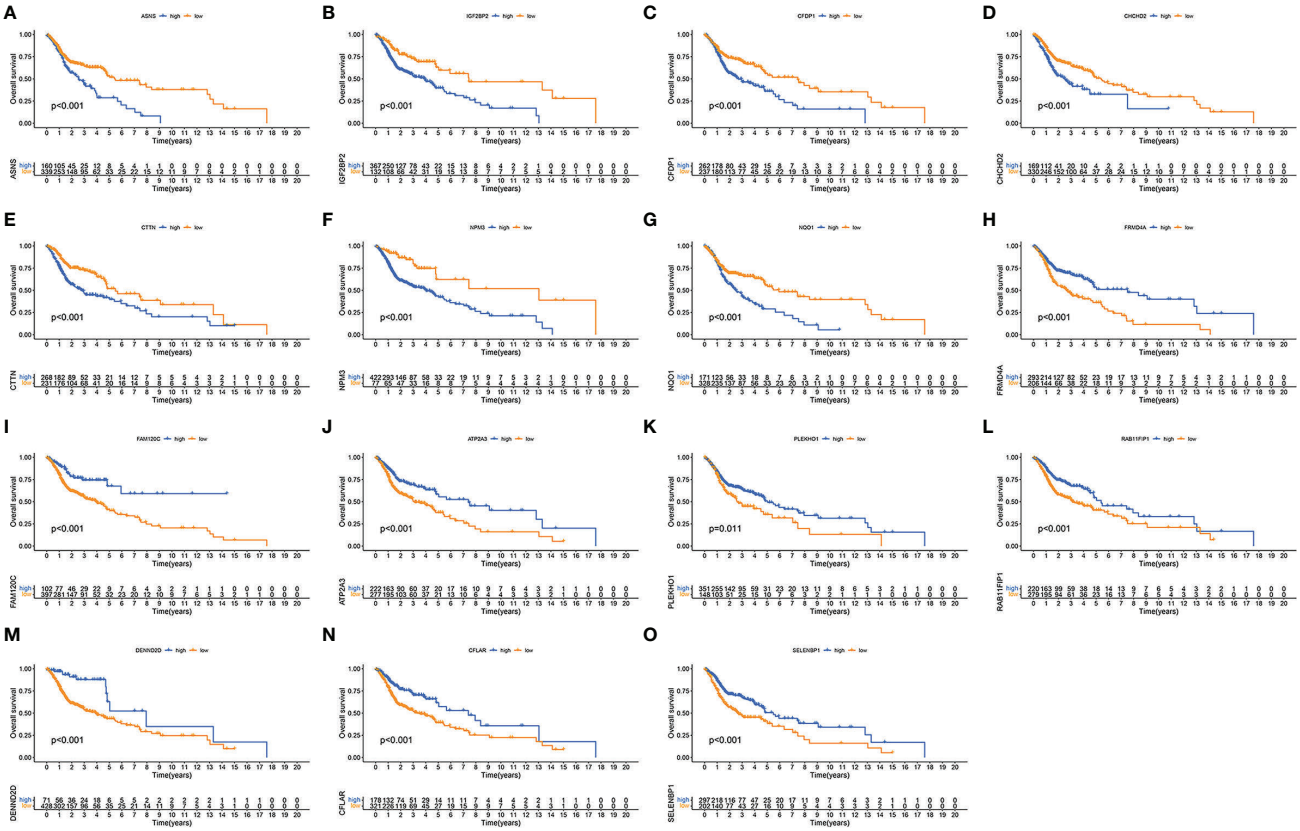

FIGURE 6 | Validation of each immune-related RNA-binding protein (RBP) in the risk model. Kaplan–Meier curves showing the differences of overall survival in high- and low-expression immune-related RBPs ASNS **(A)**, IGF2BP2 **(B)**, CFDP1 **(C)**, CHCHD2 **(D)**, CTTN **(E)**, NPM3 **(F)**, NQO1 **(G)**, FRMD4A **(H)**, FAM120C **(I)**, ATP2A3 **(J)**, PLEKHO1 **(K)**, RAB11FIP1 **(L)**, DENND2D **(M)**, CFLAR **(N)**, and SELENBP1 **(O)** between high-expression (blue) group and low-expression (yellow) group.

was significantly higher than that of the low-risk group, which means that immunotherapy is less effective in the high-risk group (**Figure 10A**, $p < 0.001$).

In addition, we screened out 14 small-molecule chemotherapeutics that may be more effective for patients with HNSCC in the high-risk group. The IC50 represents the concentration of an inhibitor that is required for 50% inhibition of carcinoma cells. A lower IC50 value means better drug sensitivity. Patients in the high-risk group were more sensitive to bosutinib, bryostatin.1, camptothecin, cytarabine, docetaxel, doxorubicin, erlotinib, gefitinib, gemcitabine, lapatinib, paclitaxel, parthenolide, sorafenib, and thapsigargin (**Figures 10B–O**, $p < 0.001$).

DISCUSSION

Immunotherapy has become an effective method for treating malignant tumors (41). Furthermore, immunosuppressant therapy has made important progress in the treatment of patients with HNSCC (42). Nevertheless, it cannot be ignored that only a limited one-third of patients respond to immunotherapy in most types of tumors (43). Further studies of immune-related RBPs in HNSCC may provide new ways to improve the clinical prognosis of patients. At present, there is an urgent need for an accurate and operational prognostic evaluation model for HNSCC in clinical practice. Based on TCGA and GEO databases and a variety of algorithms starting with ssGSEA, our study established a new model for predicting immune response, efficacy of conventional chemotherapy and immunotherapy, and individual outcome.

There are many kinds of myeloid immune cells in the HNSCC microenvironment that have a unique immune profile prior to treatment (44). In this study, we retrospectively analyzed the transcriptomic data of 499 HNSCC patients in TCGA database and further classified them into Sub1 and Sub2 on the basis of differences in immune cell infiltration. Regarding the infiltrating immune cells in the Sub1 group, M0 macrophages infiltrated more, while in the Sub2 group, there was more infiltration of naive B cells, plasma cells, T cells, and M1 macrophages. Compared with the Sub1 group, the Sub2 group had higher immune, stromal, and ESTIMATE scores but lower tumor purity, and its prognosis was significantly better than that of the Sub1 group. In addition, the expressions of the HLA family

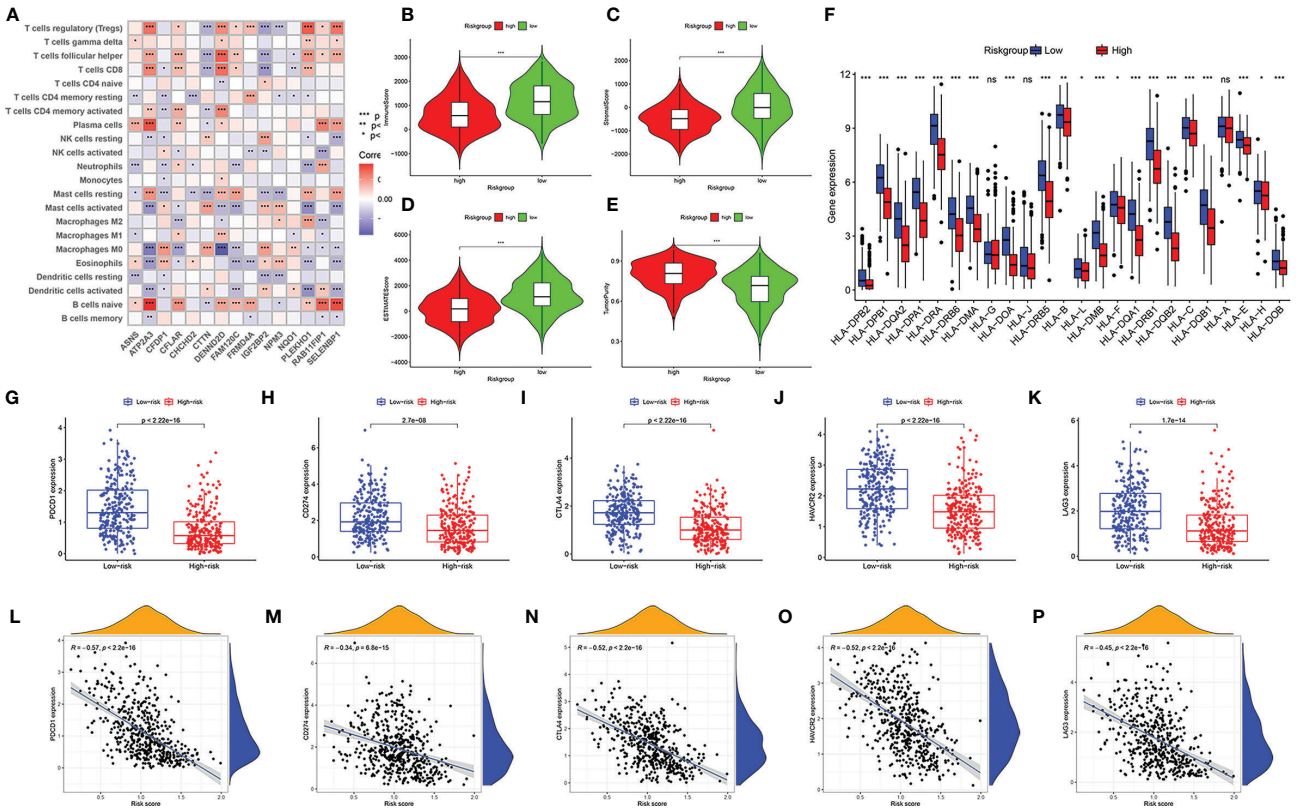

FIGURE 7 | Immune landscape of patients with head and neck squamous cell carcinoma (HNSCC) in high- and low-risk groups. Correlation matrix of 15 immune-related RNA-binding proteins (RBPs) and infiltrating immune cells **(A)**. Comparison of immune score **(B)**, stromal score **(C)**, ESTIMATE score **(D)**, and tumor purity **(E)**. The differential expressions of HLA family genes in patients with HNSCC in high- and low-risk groups **(F)**. The expression level of immune checkpoint genes PDCD1 **(G)**, CD274 **(H)**, CTLA4 **(I)**, HAVCR2 **(J)**, and LAG3 **(K)** in low-risk group and high-risk group. The correlation between risk score and immune checkpoints PDCD1 **(L)**, CD274 **(M)**, CTLA4 **(N)**, HAVCR2 **(O)**, and LAG3 **(P)**. "ns" means p ≥ 0.05, *$p < 0.05$, **$p < 0.01$, ***$p < 0.001$.

were significantly lower in the Sub1 group, which assisted tumor cells to escape the immune system (45). The immune-related pathways in the Sub2 group were more abundant.

Some RBPs are able to rapidly react to inflammatory mediators and regulate the reprogramming of immune cells to tumor-associated phenotypes (12). After recognizing the difference in RBP expressions between the Sub1 and Sub2 groups, we constructed a risk model containing 15 immune-related RBPs through univariate and LASSO Cox regression analysis. Then, according to the risk score calculated by the above model, patients with HNSCC were divided into low- and high-risk groups. Patients in the high-risk group had poorer clinical outcomes. The model even had good validity and stability in determining the prognosis at 1, 3, and 5 years, which was further confirmed in the GEO database. After confirming the risk score as an independent prognostic factor, we constructed a prognostic nomogram model according to the staging, T, N, and age of patients, which was also accurate in predicting OS at 1, 3, and 5 years.

The relationship between the prognostic characteristics of 15 immune-related RBPs and the immune microenvironment has also been investigated. In contrast with the high-risk group, the low-risk group had lower tumor purity and higher immune score, stromal score, and ESTIMATE score. In the high-risk group, M0 macrophages, activated dendritic cells, and mast cells infiltrated more, but the expression of the HLA family decreased. In the low-risk group, there were more M1 macrophages, naive B cells, CD4 memory and CD8 T cells, plasma cells, and eosinophils. This is similar to previous reports suggesting that exhausted immunity with lower survival is characterized by enrichment of stromal activation and anti-inflammatory M2 macrophage, whereas enhanced immunity associated with better prognosis is characterized by M1 macrophages providing stronger pro-inflammatory signaling, enhanced cytolytic activity, and massive lymphocyte infiltration (7). The activation of M1 macrophages is beneficial to patients because it can induce acute inflammation secreting tumor-killing molecules such as tumor necrosis factor α (TNFα) (46). On the other hand, if acute inflammation is not controlled, differentiation of M2 macrophages facilitates chronic inflammation, promoting tumor cell growth, angiogenesis, fibrosis, and immunosuppression (47), which is certainly harmful to patients. Both B cells and partial T cells also contribute to the prognosis of patients with HNSCC. As reported by Norouzian et al., the composition of B-cell

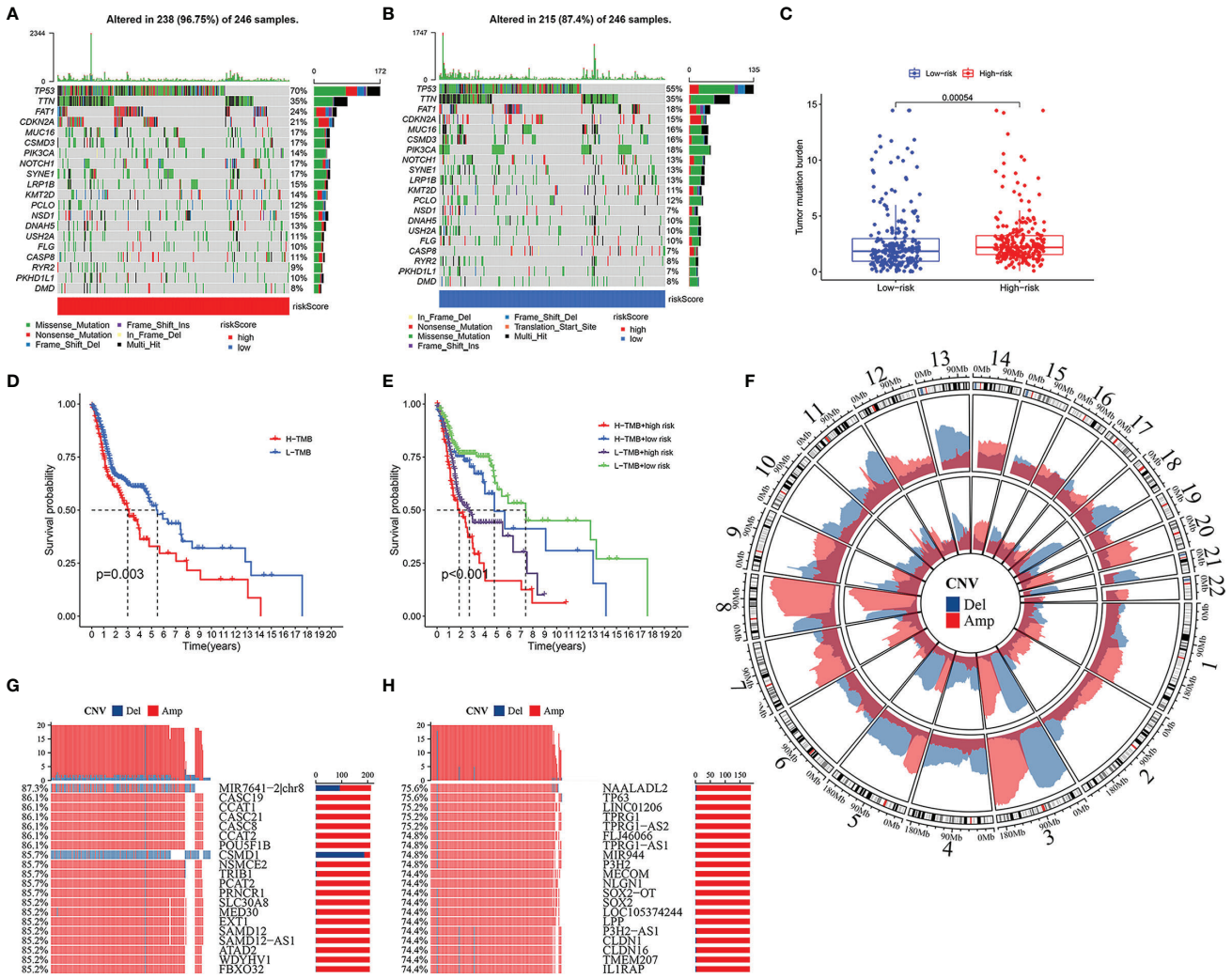

FIGURE 8 | Somatic mutation and copy number variations (CNVs) in high- and low-risk groups. Heatmap of somatic mutations in high-risk group **(A)** and low-risk group **(B)**. The difference of tumor mutation burden between high- and low-risk groups **(C)**. Kaplan–Meier curves showing the differences in high- and low-tumor mutation burden (TMB) groups **(D)**. Kaplan–Meier curves revealing the differences in high-TMB and high-risk group, high-TMB and low-risk group, low-TMB and high-risk group, and low-TMB and low-risk group **(E)**. Amplification and deletion of copy number in the high-risk group (inner) and low-risk group (outer) **(F)**. The 20 genes with maximum CNVs in high-risk group, and the percentage meaning the proportion of patients with head and neck squamous cell carcinoma (HNSCC) who suffered gene deletion (blue) or amplification (red) in high-risk group **(G)**. Top 20 genes with maximum CNVs in low-risk group, and the percentage representing the ratio of patients with HNSCC who suffered gene deletion (blue) or amplification (red) in low-risk group **(H)**.

subpopulations changes in TME of HNSCC, and the B cells with atypical memory and regulatory phenotype are significantly related to favorable prognostic (48). Notably, the high abundance of tumor-infiltrating lymphocyte B and high density of direct B-cell/CD8+ T-cell interactions predict a better outcome (49). Dense T-cell infiltration, especially cytotoxic CD8 T cells, represents superior antitumor ability (50, 51).

Based on the risk score, we further elaborated on TMB, somatic mutations, and CNVs. The high-risk group had a higher TMB, which implied a higher mortality rate. Mutations in TP53 were overwhelmingly predominant in both groups and were more frequent in the high-risk group than in the low-risk group (70% vs. 55%). As previously reported by Lawrence, TP53 mutations and CDKN2 inactivation are intimately involved in HNSCC (52). Remarkably, TP53 mutations are common and associated with a poor prognosis in patients with HNSCC (53). MIR7641 is highly expressed in the exosomes of metastatic tumor cells and can enhance the proliferation, migration, and invasion of recipient tumor cells (54, 55). Cub and Sushi Multiple Domains-1 (CSMD1) acts as a tumor suppressor, whose low expression promotes the invasion of HNSCC and gastric tumor (56, 57) and is also correlated with a poorer prognosis of HNSCC (58).

The efficacy of immunotherapy has been reported to be generally superior to that of conventional chemotherapy (42).

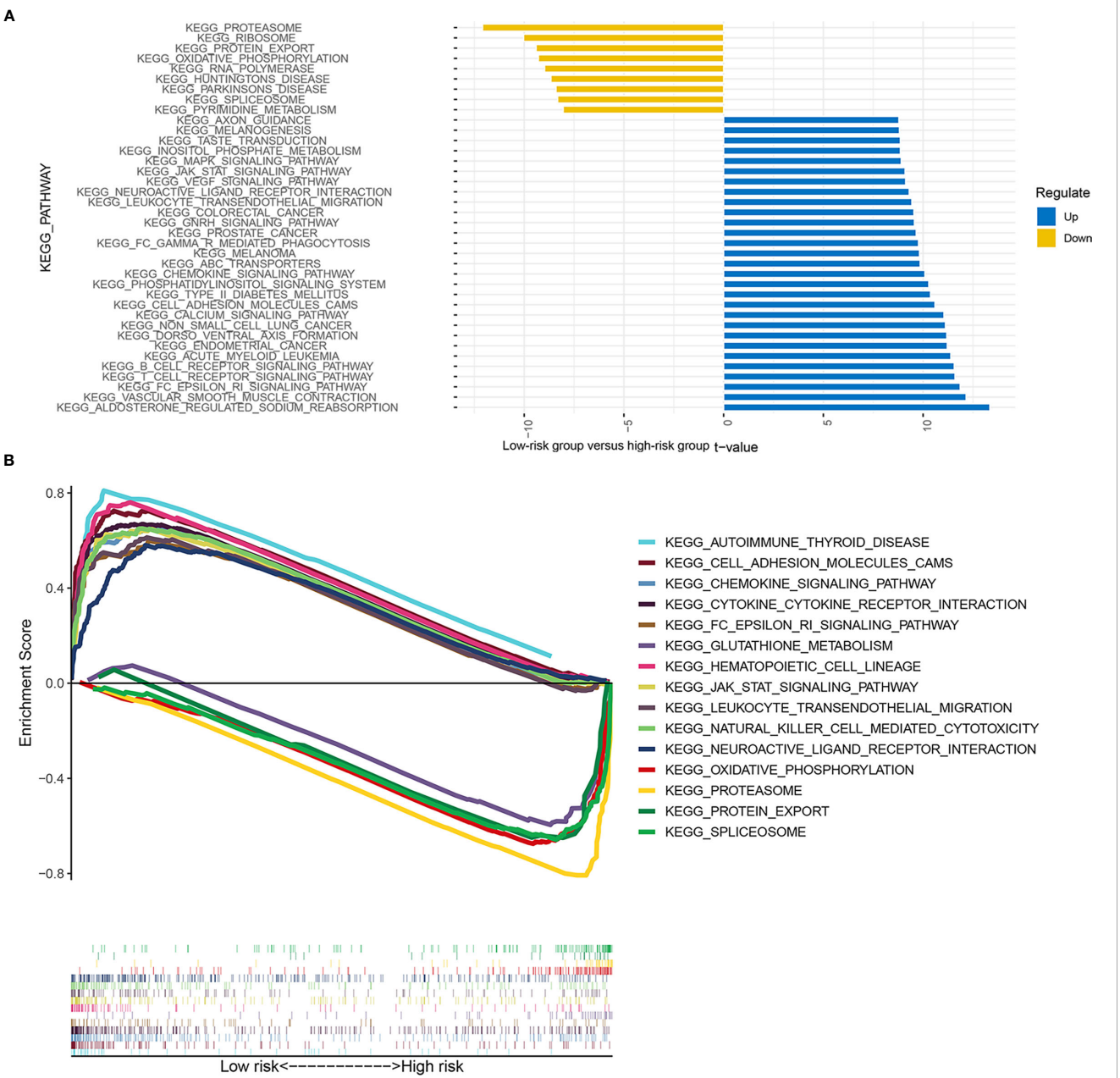

FIGURE 9 | Enrichment signaling pathways of different risk groups. The pathway enrichment of gene set variation analysis (GSVA) between the low- and high-risk groups **(A)**. The pathway enrichment of gene set enrichment analysis (GSEA) between the low- and high-risk groups **(B)**.

Besides, the combined application of PD-1/PD-L1 inhibitors and platinum drugs also shows positive therapeutic potential (59). This implies that the exploration of medication regimens is potentially valuable. On the one hand, the immune checkpoint expressions of LAG3, PDCD1, HAVCR2, CTLA4, and CD274 increased in the low-risk group. The efficacy of corresponding immune checkpoint inhibitors is better for the low-risk group but the opposite for the high-risk group. On the other hand, the low-risk group has a lower TIDE score, which means that the lower TIDE score is related to a better curative effect. TIDE can be used to identify two mechanisms of tumor immune escape: inducing T-cell immunotherapeutic dysfunction in tumors with high infiltration of cytotoxic T lymphocytes (CTLs) and blocking T-cell infiltration in tumors with low CTL in TME (39). In our study, the low-risk group had more infiltration of CTLs, so they would respond better to immunotherapy, due to better recovery from T-cell dysfunction. The high-risk group had less CTL infiltration, so they would benefit less from immunotherapy, which may be due to T-cell repulsion. In short, the low-risk group will benefit more from immunotherapy. Furthermore, we

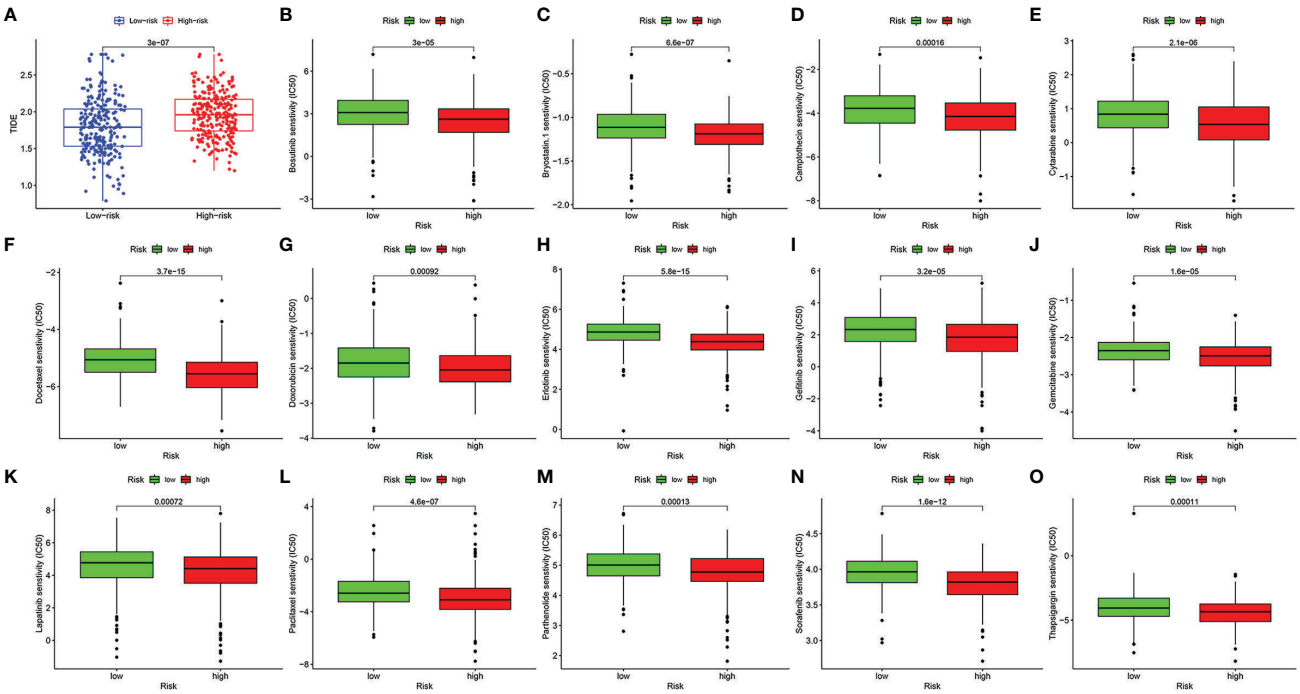

FIGURE 10 | The value of the risk model in predicting the efficacy of immunotherapy and chemotherapy. The score of tumor immune dysfunction and exclusion of patients with head and neck squamous cell carcinoma (HNSCC) in high- and low-risk groups **(A)**. The box plots of the estimated IC50 for bosutinib **(B)**, bryostatin.1 **(C)**, camptothecin **(D)**, cytarabine **(E)**, docetaxel **(F)**, doxorubicin **(G)**, erlotinib **(H)**, gefitinib **(I)**, gemcitabine **(J)**, lapatinib **(K)**, paclitaxel **(L)**, parthenolide **(M)**, sorafenib **(N),** and thapsigargin **(O)**.

screened out 15 chemotherapy drugs that are more suitable for the high-risk group. The new model constructed by immune-related RBPs could serve as a new marker to help guide the selection of chemotherapeutic drugs and distinguish who would benefit more from antitumor immunotherapy.

Some of the RBPs in this article have been reported to have a practical relationship with tumorigenesis and progression. Asparagine synthetase (ASNS) catalyzes the synthesis of the nonessential amino acid asparagine, while ASNS knockdown significantly hinders cell proliferation (60). In other words, stable ASNS gene expression guarantees the growth of tumor cells. Cortactin (CTTN) gene encodes a protein, cortacn, which plays an essential role in the migration of oral carcinoma cells by regulating filamentous actin and prominent structures on cell membranes (61). The high expression of CTTN was related to a poorer OS rate (62). Coiled-coil-helix-coiled-coil-helix domain-containing protein 2 (CHCHD2) as a small mitochondrial protein can regulate mitochondrial outer membrane permeabilization and is one of the negative regulators that mediate apoptosis (63). CHCHD2 indicates a poor prognosis and is overexpressed in hepatocellular carcinoma, breast tumor, non-small cell lung carcinoma, and renal cell carcinoma (64, 65). The loss of the human Cranio Facial Development Protein 1 (CFDP1) affects the dynamic changes of chromosomes and cell cycle progression (66). Moreover, some studies have confirmed that CFDP1 is a risk gene for pancreatic carcinoma (67, 68). High expression of insulin growth factor 2 mRNA binding protein 1 (IGF2BP1) is associated with a poor prognosis such as advanced clinical stage, increased tumor size, lymph node metastasis, and low survival rate of patients with HNSCC (69, 70). NAD(P)H quinone oxidoreductase (NQO1), a cytoplasmic enzyme that mediates the reduction of quinone substrates, is highly expressed in a multitude of tumors and can catalyze quinone drugs to poison tumor cells (71). NQO1 is considered a promising direct tumor target. For example, the drug β-lapachone, catalyzed by NQO1, triggers the innate perception of T cells in the TME, thereby enhancing antitumor capacity and even overcoming checkpoint blockade (72). Casein kinase 2-interacting protein-1 (CKIP-1, also known as PLEKHO1) inhibits tumor growth by causing inactivation of serine/threonine kinases and self-degradation of Smurf1, which is a potential oncogenic target in various tumor cells (73). Selenium binding protein 1(SELENBP1) is significantly downregulated in esophageal adenocarcinoma, ovarian tumor, and oral squamous cell carcinoma, but its overexpression can lead to incremental cellular senescence and apoptosis, as well as enhanced cytotoxicity of cisplatin (74–76). Three different genes (ATP2A1-3) encode the Ca^{2+}-ATPases from the Sarco/endoplasmic reticulum (SERCA) to maintain calcium homeostasis between the cell cytoplasm and the endoplasmic reticulum, and they have been reported to downregulate transcription in gastric and colon tumors (77). In particular, ATP2A2 gene inactivation is closely related to oral squamous

cell carcinoma (78). DENN/MADD domain-containing protein 2D (DENND2D) is less expressed in malignant tumors and is thought to contribute to the worsening prognosis and high recurrence rate (79–81). However, other RBPs may have a prospective regulatory impact on HNSCC. Some articles reported the relationship between genes FRMD4A and HNSCC. High expression of FRMD4A is associated with an increased risk of HNSCC recurrence, and the silencing of FRMD4A inhibits the growth and metastasis of human squamous cell carcinoma in skin and tongue metastases and reduces the proliferation and cell adhesion of squamous cell carcinoma (82, 83). Interestingly, in our study, patients with high expression of FRMD4A experienced a better prognosis (**Figure 6H**), which is worthy of further study. RAB proteins play the role of small GTPases in the regulation of vesicle and protein transport, membrane targeting, and fusion, and a group of them can actively or inversely regulate tumor cell generation, migration, and invasion (84). RAB11 affects the invasiveness of breast cancer cells (85). RAB11FIP1 is positively related to dendritic cells and CD4 T cells, and the low expression of RAB11FIP1 revealed a poor prognosis for lung adenocarcinoma (86). CASP8 and FADD-like apoptosis regulator (CFLAR), also known as c-FLICE-like inhibitory protein (c-FLIP), is a vital anti-apoptotic protein (87). Some studies have identified FLIP as an independent poor prognostic indicator for colorectal carcinoma, cervical carcinoma, and acute myeloid leukemia (88).

Although some studies have explored the association of RBPs with HNSCC (89, 90), our research has made further progress. On the basis of differentiated immunophenotyping, we take the lead in the screening of differentially expressed RBPs, which represents a more effective prognostic biomarker and a more accurate predictor of response to immunotherapy in different groups of patients. In general, the prognosis model system constructed based on the immune-related RBPs and clinical information of patients with HNSCC drew the landscape in the immune microenvironment of HNSCC and could effectively predict the prognosis of patients with HNSCC in the high- and low-risk groups. The nomogram based on this model is more helpful for predicting the clinical outcome of patients with HNSCC. Last but not least, the differences in immune checkpoints and TIDE scores between the high- and low-risk groups provide new ideas for the immunotherapy of patients with HNSCC.

Our study still has some limitations. First, we only used public databases to construct and verify the prognostic risk model, and we need to validate this model in subsequent clinical trials. Second, how the immune-related RBPs regulate immunity still needs to be verified by experiments *in vitro* and *in vivo*. Eventually, human papillomavirus is an independent prognostic factor for HNSCC, which is worth further stratified analysis.

CONCLUSION

In summary, the signature constructed by 15 immune-related RBPs could effectively predict the clinical outcome of patients with HNSCC. Subsequently, we demonstrated the immune landscape, TMB, CNVs, and efficacy of immunotherapy in different risk groups, which might guide clinical therapy.

DATA AVAILABILITY STATEMENT

The original contributions presented in the study are included in the article/**Supplementary Material**. Further inquiries can be directed to the corresponding authors.

AUTHOR CONTRIBUTIONS

RM and XL designed the study, performed the experiments, and plotted the data. EW collected original data. JW, BL, WY, and PZ drafted and edited the manuscript. HX and SZ reviewed the manuscript. HX and SZ supervised the project. HX and SZ funded the experiments for the study. All authors contributed to the article and approved the submitted version.

FUNDING

This study was supported by grants from the National Natural Science Foundation of China (grant numbers 81771002, 82071057).

ACKNOWLEDGMENTS

The authors gratefully acknowledge the data generated by all public datasets utilized in this research. The authors very much appreciate the efforts of all researchers in developing R package tools. The authors are very grateful to these authors for their selfless dedication to TCGA database and standardizing these data work from TCGA. The authors cherish these precious public database resources very much.

SUPPLEMENTARY MATERIAL

The Supplementary Material for this article can be found online at: https://www.frontiersin.org/articles/10.3389/fonc.2022.795781/full#supplementary-material

REFERENCES

1. Bray F, Ferlay J, Soerjomataram I, Siegel RL, Torre LA, Jemal A. Global Cancer Statistics 2018: GLOBOCAN Estimates of Incidence and Mortality Worldwide for 36 Cancers in 185 Countries. *CA Cancer J Clin* (2018) 68 (6):394–424. doi: 10.3322/caac.21492
2. Takeuchi T, Kawasaki H, Luce A, Cossu AM, Misso G, Scrima M, et al. Insight Toward the Microrna Profiling of Laryngeal Cancers: Biological Role and Clinical Impact. *Int J Mol Sci* (2020) 21(10):3693. doi: 10.3390/ijms21103693
3. Galot R, Le Tourneau C, Guigay J, Licitra L, Tinhofer I, Kong A, et al. Personalized Biomarker-Based Treatment Strategy for Patients With

Squamous Cell Carcinoma of the Head and Neck: EORTC Position and Approach. *Ann Oncol* (2018) 29(12):2313–27. doi: 10.1093/annonc/mdy452
4. Li Q, Xu L, Li Y, Yang R, Qiao Q, Wang Y, et al. P2RY14 Is a Potential Biomarker of Tumor Microenvironment Immunomodulation and Favorable Prognosis in Patients With Head and Neck Cancer. *Front Genet* (2021) 12:670746. doi: 10.3389/fgene.2021.670746
5. Quail DF, Joyce JA. Microenvironmental Regulation of Tumor Progression and Metastasis. *Nat Med* (2013) 19(11):1423–37. doi: 10.1038/nm.3394
6. New J, Arnold L, Ananth M, Alvi S, Thornton M, Werner L, et al. Secretory Autophagy in Cancer-Associated Fibroblasts Promotes Head and Neck Cancer Progression and Offers a Novel Therapeutic Target. *Cancer Res* (2017) 77(23):6679–91. doi: 10.1158/0008-5472.CAN-17-1077
7. Chen YP, Wang YQ, Lv JW, Li YQ, Chua MLK, Le QT, et al. Identification and Validation of Novel Microenvironment-Based Immune Molecular Subgroups of Head and Neck Squamous Cell Carcinoma: Implications for Immunotherapy. *Ann Oncol* (2019) 30(1):68–75. doi: 10.1093/annonc/mdy470
8. Thorsson V, Gibbs DL, Brown SD, Wolf D, Bortone DS, Ou Yang TH, et al. The Immune Landscape of Cancer. *Immunity* (2018) 48(4):812–830 e14. doi: 10.1016/j.immuni.2018.03.023
9. Ghanizada M, Jakobsen KK, Gronhoj C, von Buchwald C. The Effects of Checkpoint Inhibition on Head and Neck Squamous Cell Carcinoma: A Systematic Review. *Oral Oncol* (2019) 90:67–73. doi: 10.1016/j.oraloncology.2019.01.018
10. Gerstberger S, Hafner M, Tuschl T. A Census of Human RNA-Binding Proteins. *Nat Rev Genet* (2014) 15(12):829–45. doi: 10.1038/nrg3813
11. Dreyfuss G, Kim VN, Kataoka N. Messenger-RNA-Binding Proteins and the Messages They Carry. *Nat Rev Mol Cell Biol* (2002) 3(3):195–205. doi: 10.1038/nrm760
12. Kechavarzi B, Janga SC. Dissecting the Expression Landscape of RNA-Binding Proteins in Human Cancers. *Genome Biol* (2014) 15(1):R14. doi: 10.1186/gb-2014-15-1-r14
13. Sebestyen E, Singh B, Minana B, Pages A, Mateo F, Pujana MA, et al. Large-Scale Analysis of Genome and Transcriptome Alterations in Multiple Tumors Unveils Novel Cancer-Relevant Splicing Networks. *Genome Res* (2016) 26 (6):732–44. doi: 10.1101/gr.199935.115
14. Turner M, Diaz-Munoz MD. RNA-Binding Proteins Control Gene Expression and Cell Fate in the Immune System. *Nat Immunol* (2018) 19 (2):120–9. doi: 10.1038/s41590-017-0028-4
15. Mounir M, Lucchetta M, Silva TC, Olsen C, Bontempi G, Chen X, et al. New Functionalities in the Tcgabiolinks Package for the Study and Integration of Cancer Data From GDC and Gtex. *PloS Comput Biol* (2019) 15(3):e1006701. doi: 10.1371/journal.pcbi.1006701
16. Lohavanichbutr P, Mendez E, Holsinger FC, Rue TC, Zhang Y, Houck J, et al. A 13-Gene Signature Prognostic of HPV-Negative OSCC: Discovery and External Validation. *Clin Cancer Res* (2013) 19(5):1197–203. doi: 10.1158/1078-0432.CCR-12-2647
17. Goldman MJ, Craft B, Hastie M, Repecka K, McDade F, Kamath A, et al. Visualizing and Interpreting Cancer Genomics Data *via* the Xena Platform. *Nat Biotechnol* (2020) 38(6):675–8. doi: 10.1038/s41587-020-0546-8
18. Brannan KW, Jin W, Huelga SC, Banks CA, Gilmore JM, Florens L, et al. SONAR Discovers RNA-Binding Proteins From Analysis of Large-Scale Protein-Protein Interactomes. *Mol Cell* (2016) 64(2):282–93. doi: 10.1016/j.molcel.2016.09.003
19. Gene Ontology C, Blake JA, Dolan M, Drabkin H, Hill DP, Li N, et al. Gene Ontology Annotations and Resources. *Nucleic Acids Res* (2013) 41(Database issue):D530–5. doi: 10.1093/nar/gks1050
20. Conrad T, Albrecht AS, de Melo Costa VR, Sauer S, Meierhofer D, Orom UA. Serial Interactome Capture of the Human Cell Nucleus. *Nat Commun* (2016) 7:11212. doi: 10.1038/ncomms11212
21. Castello A, Fischer B, Frese CK, Horos R, Alleaume AM, Foehr S, et al. Comprehensive Identification of RNA-Binding Domains in Human Cells. *Mol Cell* (2016) 63(4):696–710. doi: 10.1016/j.molcel.2016.06.029
22. Castello A, Fischer B, Eichelbaum K, Horos R, Beckmann BM, Strein C, et al. Insights Into RNA Biology From an Atlas of Mammalian Mrna-Binding Proteins. *Cell* (2012) 149(6):1393–406. doi: 10.1016/j.cell.2012.04.031
23. Beckmann BM, Horos R, Fischer B, Castello A, Eichelbaum K, Alleaume AM, et al. The RNA-Binding Proteomes From Yeast to Man Harbour Conserved Enigmrbps. *Nat Commun* (2015) 6:10127. doi: 10.1038/ncomms10127
24. Baltz AG, Munschauer M, Schwanhausser B, Vasile A, Murakawa Y, Schueler M, et al. The Mrna-Bound Proteome and Its Global Occupancy Profile on Protein-Coding Transcripts. *Mol Cell* (2012) 46(5):674–90. doi: 10.1016/j.molcel.2012.05.021
25. Huang R, Han M, Meng L, Chen X. Transcriptome-Wide Discovery of Coding and Noncoding RNA-Binding Proteins. *Proc Natl Acad Sci USA* (2018) 115 (17):E3879–87. doi: 10.1073/pnas.1718406115
26. Trendel J, Schwarzl T, Horos R, Prakash A, Bateman A, Hentze MW, et al. The Human RNA-Binding Proteome and Its Dynamics During Translational Arrest. *Cell* (2019) 176(1-2):391–403 e19. doi: 10.1016/j.cell.2018.11.004
27. Zuo S, Wei M, Wang S, Dong J, Wei J. Pan-Cancer Analysis of Immune Cell Infiltration Identifies a Prognostic Immune-Cell Characteristic Score (ICCS) in Lung Adenocarcinoma. *Front Immunol* (2020) 11:1218. doi: 10.3389/fimmu.2020.01218
28. Zhang L, Zhao Y, Dai Y, Cheng JN, Gong Z, Feng Y, et al. Immune Landscape of Colorectal Cancer Tumor Microenvironment From Different Primary Tumor Location. *Front Immunol* (2018) 9:1578. doi: 10.3389/fimmu.2018.01578
29. Finotello F, Trajanoski Z. Quantifying Tumor-Infiltrating Immune Cells From Transcriptomics Data. *Cancer Immunol Immunother* (2018) 67 (7):1031–40. doi: 10.1007/s00262-018-2150-z
30. Hanzelmann S, Castelo R, Guinney J. GSVA: Gene Set Variation Analysis for Microarray and RNA-Seq Data. *BMC Bioinf* (2013) 14:7. doi: 10.1186/1471-2105-14-7
31. Wilkerson MD, Hayes DN. Consensusclusterplus: A Class Discovery Tool With Confidence Assessments and Item Tracking. *Bioinformatics* (2010) 26 (12):1572–3. doi: 10.1093/bioinformatics/btq170
32. Yoshihara K, Shahmoradgoli M, Martinez E, Vegesna R, Kim H, Torres-Garcia W, et al. Inferring Tumour Purity and Stromal and Immune Cell Admixture From Expression Data. *Nat Commun* (2013) 4:2612. doi: 10.1038/ncomms3612
33. Newman AM, Liu CL, Green MR, Gentles AJ, Feng W, Xu Y, et al. Robust Enumeration of Cell Subsets From Tissue Expression Profiles. *Nat Methods* (2015) 12(5):453–7. doi: 10.1038/nmeth.3337
34. Subramanian A, Tamayo P, Mootha VK, Mukherjee S, Ebert BL, Gillette MA, et al. Gene Set Enrichment Analysis: A Knowledge-Based Approach for Interpreting Genome-Wide Expression Profiles. *Proc Natl Acad Sci USA* (2005) 102(43):15545–50. doi: 10.1073/pnas.0506580102
35. Friedman J, Hastie T, Tibshirani R. Regularization Paths for Generalized Linear Models *via* Coordinate Descent. *J Stat Software* (2010) 33(1):1–22. doi: 10.18637/jss.v033.i01
36. Mao R, Chen Y, Xiong L, Liu Y, Zhang T. Identification of a Nomogram Based on an 8-Lncrna Signature as a Novel Diagnostic Biomarker for Head and Neck Squamous Cell Carcinoma. *Aging (Albany NY)* (2020) 12(20):20778–800. doi: 10.18632/aging.104014
37. Mayakonda A, Lin DC, Assenov Y, Plass C, Koeffler HP. Maftools: Efficient and Comprehensive Analysis of Somatic Variants in Cancer. *Genome Res* (2018) 28(11):1747–56. doi: 10.1101/gr.239244.118
38. Mermel CH, Schumacher SE, Hill B, Meyerson ML, Beroukhim R, Getz G. GISTIC2.0 Facilitates Sensitive and Confident Localization of the Targets of Focal Somatic Copy-Number Alteration in Human Cancers. *Genome Biol* (2011) 12(4):R41. doi: 10.1186/gb-2011-12-4-r41
39. Jiang P, Gu S, Pan D, Fu J, Sahu A, Hu X, et al. Signatures of T Cell Dysfunction and Exclusion Predict Cancer Immunotherapy Response. *Nat Med* (2018) 24(10):1550–8. doi: 10.1038/s41591-018-0136-1
40. Geeleher P, Cox N, Huang RS. Prrophetic: An R Package for Prediction of Clinical Chemotherapeutic Response From Tumor Gene Expression Levels. *PloS One* (2014) 9(9):e107468. doi: 10.1371/journal.pone.0107468
41. Emens LA, Ascierto PA, Darcy PK, Demaria S, Eggermont AMM, Redmond WL, et al. Cancer Immunotherapy: Opportunities and Challenges in the Rapidly Evolving Clinical Landscape. *Eur J Cancer* (2017) 81:116–29. doi: 10.1016/j.ejca.2017.01.035
42. Cohen EEW, Soulières D, Le Tourneau C, Dinis J, Licitra L, Ahn M-J, et al. Pembrolizumab Versus Methotrexate, Docetaxel, or Cetuximab for Recurrent or Metastatic Head-and-Neck Squamous Cell Carcinoma (KEYNOTE-040): A Randomised, Open-Label, Phase 3 Study. *Lancet* (2019) 393(10167):156–67. doi: 10.1016/s0140-6736(18)31999-8

43. Sharma P, Hu-Lieskovan S, Wargo JA, Ribas A. Primary, Adaptive, and Acquired Resistance to Cancer Immunotherapy. *Cell* (2017) 168(4):707–23. doi: 10.1016/j.cell.2017.01.017
44. Cillo AR, Kurten CHL, Tabib T, Qi Z, Onkar S, Wang T, et al. Immune Landscape of Viral- and Carcinogen-Driven Head and Neck Cancer. *Immunity* (2020) 52(1):183–199 e9. doi: 10.1016/j.immuni.2019.11.014
45. Jhunjhunwala S, Hammer C, Delamarre L. Antigen Presentation in Cancer: Insights Into Tumour Immunogenicity and Immune Evasion. *Nat Rev Cancer* (2021) 21(5):298–312. doi: 10.1038/s41568-021-00339-z
46. Josephs DH, Bax HJ, Karagiannis SN. Tumour-Associated Macrophage Polarisation and Re-Education With Immunotherapy. *Front Biosci (Elite Ed)* (2015) 7:293–308. doi: 10.2741/E735
47. Ruffell B, Coussens LM. Macrophages and Therapeutic Resistance in Cancer. *Cancer Cell* (2015) 27(4):462–72. doi: 10.1016/j.ccell.2015.02.015
48. Norouzian M, Mehdipour F, Balouchi Anaraki S, Ashraf MJ, Khademi B, Ghaderi A. Atypical Memory and Regulatory B Cell Subsets in Tumor Draining Lymph Nodes of Head and Neck Squamous Cell Carcinoma Correlate With Good Prognostic Factors. *Head Neck Pathol* (2020) 14 (3):645–56. doi: 10.1007/s12105-019-01095-1
49. Hladikova K, Koucky V, Boucek J, Laco J, Grega M, Hodek M, et al. Tumor-Infiltrating B Cells Affect the Progression of Oropharyngeal Squamous Cell Carcinoma *via* Cell-to-Cell Interactions With CD8(+) T Cells. *J Immunother Cancer* (2019) 7(1):261. doi: 10.1186/s40425-019-0726-6
50. Fridman WH, Zitvogel L, Sautes-Fridman C, Kroemer G. The Immune Contexture in Cancer Prognosis and Treatment. *Nat Rev Clin Oncol* (2017) 14(12):717–34. doi: 10.1038/nrclinonc.2017.101
51. Gentles AJ, Newman AM, Liu CL, Bratman SV, Feng W, Kim D, et al. The Prognostic Landscape of Genes and Infiltrating Immune Cells Across Human Cancers. *Nat Med* (2015) 21(8):938–45. doi: 10.1038/nm.3909
52. Cancer Genome Atlas N. Comprehensive Genomic Characterization of Head and Neck Squamous Cell Carcinomas. *Nature* (2015) 517(7536):576–82. doi: 10.1038/nature14129
53. Zhou G, Liu Z, Myers JN. TP53 Mutations in Head and Neck Squamous Cell Carcinoma and Their Impact on Disease Progression and Treatment Response. *J Cell Biochem* (2016) 117(12):2682–92. doi: 10.1002/jcb.25592
54. Liu Y, Hua F, Zhan Y, Yang Y, Xie J, Cheng Y, et al. Carcinoma Associated Fibroblasts Small Extracellular Vesicles With Low Mir-7641 Promotes Breast Cancer Stemness and Glycolysis by HIF-1alpha. *Cell Death Discov* (2021) 7 (1):176. doi: 10.1038/s41420-021-00524-x
55. Shen S, Song Y, Zhao B, Xu Y, Ren X, Zhou Y, et al. Cancer-Derived Exosomal Mir-7641 Promotes Breast Cancer Progression and Metastasis. *Cell Commun Signal* (2021) 19(1):20. doi: 10.1186/s12964-020-00700-z
56. Chen XL, Hong LL, Wang KL, Liu X, Wang JL, Lei L, et al. Deregulation of CSMD1 Targeted by Microrna-10b Drives Gastric Cancer Progression Through the NF-Kappab Pathway. *Int J Biol Sci* (2019) 15(10):2075–86. doi: 10.7150/ijbs.23802
57. Veeramachaneni R, Walker T, Revil T, Weck A, Badescu D, O'Sullivan J, et al. Analysis of Head and Neck Carcinoma Progression Reveals Novel and Relevant Stage-Specific Changes Associated With Immortalisation and Malignancy. *Sci Rep* (2019) 9(1):11992. doi: 10.1038/s41598-019-48229-7
58. Jung AR, Eun YG, Lee YC, Noh JK, Kwon KH. Clinical Significance of CUB and Sushi Multiple Domains 1 Inactivation in Head and Neck Squamous Cell Carcinoma. *Int J Mol Sci* (2018) 19(12):3996. doi: 10.3390/ijms19123996
59. Xue Y, Gao S, Gou J, Yin T, He H, Wang Y, et al. Platinum-Based Chemotherapy in Combination With PD-1/PD-L1 Inhibitors: Preclinical and Clinical Studies and Mechanism of Action. *Expert Opin Drug Deliv* (2021) 18(2):187–203. doi: 10.1080/17425247.2021.1825376
60. Li H, Ning S, Ghandi M, Kryukov GV, Gopal S, Deik A, et al. The Landscape of Cancer Cell Line Metabolism. *Nat Med* (2019) 25(5):850–60. doi: 10.1038/s41591-019-0404-8
61. Ramos-Garcia P, Gonzalez-Moles MA, Gonzalez-Ruiz L, Ayen A, Ruiz-Avila I, Navarro-Trivino FJ, et al. An Update of Knowledge on Cortactin as a Metastatic Driver and Potential Therapeutic Target in Oral Squamous Cell Carcinoma. *Oral Dis* (2019) 25(4):949–71. doi: 10.1111/odi.12913
62. Horn D, Gross M, Dyckhoff G, Fuchs J, Grabe N, Weichert W, et al. Cortactin Expression: Association With Disease Progression and Survival in Oral Squamous Cell Carcinoma. *Head Neck* (2018) 40(12):2685–94. doi: 10.1002/hed.25515
63. Liu Y, Clegg HV, Leslie PL, Di J, Tollini LA, He Y, et al. CHCHD2 Inhibits Apoptosis by Interacting With Bcl-X L to Regulate Bax Activation. *Cell Death Differ* (2015) 22(6):1035–46. doi: 10.1038/cdd.2014.194
64. Yao Y, Su J, Zhao L, Li R, Liu K, Wang S. CHCHD2 Promotes Hepatocellular Carcinoma and Indicates Poor Prognosis of Hepatocellular Carcinoma Patients. *J Cancer* (2019) 10(27):6822–8. doi: 10.7150/jca.31158
65. Gundamaraju R, Lu W, Manikam R. Chchd2: The Power House's Potential Prognostic Factor for Cancer? *Front Cell Dev Biol* (2020) 8:620816. doi: 10.3389/fcell.2020.620816
66. Messina G, Atterrato MT, Prozzillo Y, Piacentini L, Losada A, Dimitri P. The Human Cranio Facial Development Protein 1 (Cfdp1) Gene Encodes a Protein Required for the Maintenance of Higher-Order Chromatin Organization. *Sci Rep* (2017) 7:45022. doi: 10.1038/srep45022
67. Liu D, Zhou D, Sun Y, Zhu J, Ghoneim D, Wu C, et al. A Transcriptome-Wide Association Study Identifies Candidate Susceptibility Genes for Pancreatic Cancer Risk. *Cancer Res* (2020) 80(20):4346–54. doi: 10.1158/0008-5472.Can-20-1353
68. Zhong J, Jermusyk A, Wu L, Hoskins JW, Collins I, Mocci E, et al. A Transcriptome-Wide Association Study Identifies Novel Candidate Susceptibility Genes for Pancreatic Cancer. *J Natl Cancer Inst* (2020) 112 (10):1003–12. doi: 10.1093/jnci/djz246
69. Chou CH, Chang CY, Lu HJ, Hsin MC, Chen MK, Huang HC, et al. IGF2BP2 Polymorphisms Are Associated With Clinical Characteristics and Development of Oral Cancer. *Int J Mol Sci* (2020) 21(16). doi: 10.3390/ijms21165662
70. Paramasivam A, George R, Priyadharsini JV. Genomic and Transcriptomic Alterations in M6a Regulatory Genes are Associated With Tumorigenesis and Poor Prognosis in Head and Neck Squamous Cell Carcinoma. *Am J Cancer Res* (2021) 11(7):3688–97.
71. Oh ET, Park HJ. Implications of NQO1 in Cancer Therapy. *BMB Rep* (2015) 48(11):609–17. doi: 10.5483/bmbrep.2015.48.11.190
72. Li X, Liu Z, Zhang A, Han C, Shen A, Jiang L, et al. NQO1 Targeting Prodrug Triggers Innate Sensing to Overcome Checkpoint Blockade Resistance. *Nat Commun* (2019) 10(1):3251. doi: 10.1038/s41467-019-11238-1
73. Fu L, Zhang L. Physiological Functions of CKIP-1: From Molecular Mechanisms to Therapy Implications. *Ageing Res Rev* (2019) 53:100908. doi: 10.1016/j.arr.2019.05.002
74. Silvers AL, Lin L, Bass AJ, Chen G, Wang Z, Thomas DG, et al. Decreased Selenium-Binding Protein 1 in Esophageal Adenocarcinoma Results From Posttranscriptional and Epigenetic Regulation and Affects Chemosensitivity. *Clin Cancer Res* (2010) 16(7):2009–21. doi: 10.1158/1078-0432.CCR-09-2801
75. Huang KC, Park DC, Ng SK, Lee JY, Ni X, Ng WC, et al. Selenium Binding Protein 1 in Ovarian Cancer. *Int J Cancer* (2006) 118(10):2433–40. doi: 10.1002/ijc.21671
76. Zeng H, Zhao X, Tang C. Downregulation of SELENBP1 Enhances Oral Squamous Cell Carcinoma Chemoresistance Through KEAP1-NRF2 Signaling. *Cancer Chemother Pharmacol* (2021) 88(2):223–33. doi: 10.1007/s00280-021-04284-4
77. Meneses-Morales I, Izquierdo-Torres E, Flores-Peredo L, Rodriguez G, Hernandez-Oliveras A, Zarain-Herzberg A. Epigenetic Regulation of the Human ATP2A3 Gene Promoter in Gastric and Colon Cancer Cell Lines. *Mol Carcinog* (2019) 58(6):887–97. doi: 10.1002/mc.22978
78. Endo Y, Uzawa K, Mochida Y, Shiiba M, Bukawa H, Yokoe H, et al. Sarcoendoplasmic Reticulum Ca(2+) Atpase Type 2 Downregulated in Human Oral Squamous Cell Carcinoma. *Int J Cancer* (2004) 110(2):225–31. doi: 10.1002/ijc.20118
79. Kanda M, Nomoto S, Oya H, Takami H, Hibino S, Hishida M, et al. Downregulation of DENND2D by Promoter Hypermethylation Is Associated With Early Recurrence of Hepatocellular Carcinoma. *Int J Oncol* (2014) 44(1):44–52. doi: 10.3892/ijo.2013.2165
80. Kanda M, Shimizu D, Nomoto S, Takami H, Hibino S, Oya H, et al. Prognostic Impact of Expression and Methylation Status of DENN/MADD Domain-Containing Protein 2D in Gastric Cancer. *Gastric Cancer* (2015) 18(2):288–96. doi: 10.1007/s10120-014-0372-0
81. Ling B, Zheng H, Fu G, Yuan J, Shi T, Chen S, et al. Suppression of Non-Small Cell Lung Cancer Proliferation and Tumorigenicity by DENND2D. *Lung Cancer* (2013) 79(2):104–10. doi: 10.1016/j.lungcan.2012.10.012

82. Zheng X, Jia B, Lin X, Han J, Qiu X, Chu H, et al. FRMD4A: A Potential Therapeutic Target for the Treatment of Tongue Squamous Cell Carcinoma. *Int J Mol Med* (2016) 38(5):1443–9. doi: 10.3892/ijmm.2016.2745
83. Goldie SJ, Mulder KW, Tan DW, Lyons SK, Sims AH, Watt FM. FRMD4A Upregulation in Human Squamous Cell Carcinoma Promotes Tumor Growth and Metastasis and Is Associated With Poor Prognosis. *Cancer Res* (2012) 72 (13):3424–36. doi: 10.1158/0008-5472.CAN-12-0423
84. Tzeng HT, Wang YC. Rab-Mediated Vesicle Trafficking in Cancer. *J BioMed Sci* (2016) 23(1):70. doi: 10.1186/s12929-016-0287-7
85. Yoon SO, Shin S, Mercurio AM. Hypoxia Stimulates Carcinoma Invasion by Stabilizing Microtubules and Promoting the Rab11 Trafficking of the Alpha6beta4 Integrin. *Cancer Res* (2005) 65(7):2761–9. doi: 10.1158/0008-5472.CAN-04-4122
86. Zhang W, Chen T, Liu J, Yu S, Liu L, Zheng M, et al. RAB11FIP1: An Indicator for Tumor Immune Microenvironment and Prognosis of Lung Adenocarcinoma From a Comprehensive Analysis of Bioinformatics. *Front Genet* (2021) 12:757169. doi: 10.3389/fgene.2021.757169
87. Giogha C, Lung TW, Pearson JS, Hartland EL. Inhibition of Death Receptor Signaling by Bacterial Gut Pathogens. *Cytokine Growth Factor Rev* (2014) 25 (2):235–43. doi: 10.1016/j.cytogfr.2013.12.012
88. Humphreys L, Espona-Fiedler M, Longley DB. FLIP as a Therapeutic Target in Cancer. *FEBS J* (2018) 285(22):4104–23. doi: 10.1111/febs.14523
89. Duan X, Cheng X, Yin X, Ke Z, Song J. Systematic Analysis of the Function and Prognostic Value of RNA Binding Protein in Head and Neck Squamous Cell Carcinoma. *Eur Arch Otorhinolaryngol* (2021) 279(3):1535–47. doi: 10.1007/s00405-021-06929-9
90. Yang X, Han B, Zhang R, Su Y, Hosseini DK, Wu H, et al. Development and Validation of a RNA Binding Protein-Associated Prognostic Model for Head and Neck Squamous Cell Carcinoma. *Aging (Albany NY)* (2021) 13(6):7975–97. doi: 10.18632/aging.202848

Conflict of Interest: The authors declare that the research was conducted in the absence of any commercial or financial relationships that could be construed as a potential conflict of interest.

Publisher's Note: All claims expressed in this article are solely those of the authors and do not necessarily represent those of their affiliated organizations, or those of the publisher, the editors and the reviewers. Any product that may be evaluated in this article, or claim that may be made by its manufacturer, is not guaranteed or endorsed by the publisher.

frontiers | Frontiers in Oncology

ORIGINAL RESEARCH
published: 28 April 2022
doi: 10.3389/fonc.2022.778380

Prognostic Factors for the Therapeutic Performance of Cisplatin in Head and Neck Malignancies

Frederic Jungbauer, Lena Huber, Sonja Ludwig, Nicole Rotter, Beatrice Walter, Lena Zaubitzer and Anne Lammert*

Department for Otorhinolaryngology, Head- and Neck-Surgery, University Medical Centre Mannheim, Mannheim, Germany

Introduction: For squamous cell carcinoma of the head and neck (HNSCC), cisplatin is used as primary or adjuvant (radio)chemotherapy. In terms of dosage, two main regimens are used, weekly 40mg/m^2 or 3-weekly 100mg/m^2. For an optimal outcome, the highest possible cumulative total dose of cisplatin is aimed for. The selection of the scheme is patient-specific, but the factors for the selection of the optimal scheme have not yet been conclusively researched. The aim of this study was to find correlations between initial laboratory values and the cumulative total dose of cisplatin, as well as any correlations between early laboratory values or their dynamics and later laboratory values or their dynamics to provide support in the selection of the chemo regimen.

Material and Methods: In this retrospective study, the clinical data and laboratory values, namely glomerular filtration rate (GFR), hemoglobin, albumin, leucocyte, erythrocyte and platelet count, over the course of time of 79 patients with HNSCC who had received chemotherapy with cisplatin in our clinic between 2018 and 2021 were evaluated.

Results: Patients on 3-weekly regimens achieved a higher mean cumulative total dose of cisplatin than patients on weekly regimens (214.18 ± 65.95 vs 183.33 ± 65.2 mg/m^2). Significant positive correlations were seen for total cumulative dose of cisplatin with initial GFR (p=0.001, Pearson's r=0.364), initial hemoglobin (p=0.035, r=0.237), initial erythrocyte (p=0.002, r=0.337), and initial albumin (p=0.002, r=0.337). There were no significant correlations for initial leucocyte or platelets. Regarding the dynamics of the laboratory values under the first chemo administration, no correlation was found with later laboratory values or dynamics.

Discussion and Conclusion: As in other prospective studies, our retrospective analysis found a higher cumulative total dose in the 3-weekly regimen. As this seems to correlate positively with patient outcome, superiority of the 3-weekly regimen over the weekly regimen can be assumed. Functioning organ systems, especially of the bone marrow and kidneys, are associated with an increased cumulative total dose and can therefore be regarded as predictive factors. Regular monitoring of laboratory values is nevertheless essential throughout the entire course of chemotherapy.

Keywords: HNSCC, cisplatin, prognosis, laboratory tests, carcinoma, chemotherapy, predictive, blood values

OPEN ACCESS

Edited by:
Yong Yin,
Shandong Cancer Hospital, China

Reviewed by:
Franz Rödel,
University Hospital Frankfurt, Germany
Loredana G. Marcu,
University of Oradea, Romania

****Correspondence:***
Frederic Jungbauer
frederic.jungbauer@umm.de

Specialty section:
This article was submitted to Head and Neck Cancer, a section of the journal Frontiers in Oncology

Received: *16 September 2021*
Accepted: *04 April 2022*
Published: *28 April 2022*

Citation:
Jungbauer F, Huber L, Ludwig S, Rotter N, Walter B, Zaubitzer L and Lammert A (2022) Prognostic Factors for the Therapeutic Performance of Cisplatin in Head and Neck Malignancies. Front. Oncol. 12:778380. doi: 10.3389/fonc.2022.778380

INTRODUCTION

Cisplatin is an inorganic heavy metal complex with the molecular formula Cl2H6N2Pt. It was the first platinum-containing agent approved by the United States Food and Drug Administration for the treatment of cancer in 1978 (1). Intracellularly, cisplatin loses its chloride ions, creating a reactive species that generates linkage with the purine bases of DNA (2). Cross-linking sets DNA damage, which subsequently leads to apoptosis of the affected cell through various signal transduction pathways (3). Due to increasing resistance mechanisms to cisplatin, the underlying molecular mechanisms continue to be the focus of oncology research (4).

In the treatment of squamous cell carcinoma of the head and neck region (HNSCC), cisplatin is used both as part of primary (without previous surgery) and adjuvant (after previous surgery) radiochemotherapy (pRCT/aRCT). Possible applications have also been established in combination with other antineoplastic agents such as cetuximab or 5-fluorouracil (5-FU), as in the EXTREME regimen (5). Other platinum derivatives such as carboplatin can also be used, but because of the superiority of cisplatin, they are usually chosen only when, because of individual risk factors, therapy with cisplatin appears too risky. This may be the case, for example, if kidney function is too weak at the beginning or during the course of chemotherapy (6, 7).

The main known side effects of cisplatin are a high emetogenic potential and various organotoxic effects. Cisplatin can be nephrotoxic (8), ototoxic (9) and neurotoxic (especially with peripheral neuropathies) (10) as well as myelosuppressive (11). Appropriate premedication with e.g. cortisone, histamine antagonists and 5-hydroxytryptamine antagonists should keep nausea within tolerable limits. Because of the possible organ damage mentioned, laboratory-chemical blood checks must be carried out before and after each administration in order to be able to recognize and treat possible complications. If there are signs of incipient organ damage, an individual decision must be made as to whether chemotherapy can be continued with supportive measures, whether it must be paused, whether a switch to another agent must be made, or whether chemotherapy must be discontinued completely. Most common reasons for discontinuation or switching from cisplatin to another agent appear to be nephrotoxic and myelosuppressive effects (12). However, other factors can also result in the discontinuation of therapy, such as serious infections or even the patient's refusal to continue therapy.

Studies have shown that the outcome of patients after pRCT and aRCT depends mainly on the cumulative total dose, i.e. the added dose of all administrations of cisplatin in the course of therapy. The higher the total cumulative dose achieved, the better the outcome of patients (13). Thus, the goal of RCT is to administer as high a dose of cisplatin as possible during ongoing radiotherapy, while preserving organ function and reducing toxicity and side effects as much as possible. Various regimens are used for this purpose. The two most common are weekly administration à 40mg cisplatin/m^2 body surface area and 3-weekly administration à 100mg cisplatin/m^2 body surface area intravenously during radiotherapy (14). Currently, there are no uniform recommendations as to which therapy regimen should be selected. On the one hand, patients seem to achieve better locoregional control with the 3-weekly regimen, but on the other hand, the higher tumor toxicity also leads to more pronounced side effects than with the weekly regimen (15, 16).

The aim of this study was to demonstrate possible correlations of early laboratory chemical changes with the cumulative total dose achieved later and to be able to provide support for the selection of the cisplatin regimen based on subgroup analyses.

MATERIAL AND METHODS

All patients who had a presentation to the Interdisciplinary Head and Neck Tumor Board of the University Medical Centre Mannheim (Mannheim, Germany) from 01/2018 to 05/2021 were screened. Screening was performed only through 2018 because prior to that, cisplatin was administered mostly in combination with 5-FU, not as monotherapy. Radiation fractionation of 2Gy per day was performed in both adjuvant and primary RCT. Thus, a total cumulative dose of 60Gy was achieved at the completion of therapy. In the primary RCT, if therapy could be completed, a subsequent boost of 10Gy was applied to the tumor region.

Patients who received curative therapy and started either primary radiochemotherapy with cisplatin without another chemotherapy agent or adjuvant radiochemotherapy with cisplatin without another chemotherapy agent were included. Patients on other platinum-based chemotherapies (e.g., carboplatin), combined chemotherapeutics (e.g., cisplatin/5-FU), or palliative regimens (e.g., the EXTREME regimen with platinum/cetuximab) were not included. Clinical data such as patient age, cisplatin regimen used, and any port or percutaneous endoscopic gastrostomy (PEG) implantation were extracted from medical records. Blood sampling was done on the day of chemo administration or the day before. The control of blood values after chemotherapy administration was performed 3-7 days after chemotherapy administration. Blood values were extracted from the in-house laboratory system before and after the respective chemo administrations, namely leukocyte count, glomerular filtration rate (GFR, calculated from serum creatinine), platelet count, hemoglobin, erythrocyte count, and serum albumin. In addition to the enumerated values, their differences between before and after chemo administration, both in absolute and relative values, were also calculated.

Statistical analysis was then performed using the statistical software SPSS Statistics for Windows, version 27.0 (SPSS Inc., Chicago, Ill., USA). Descriptive analyses, t-tests, and bivariate correlations were performed. A p-value <0.05 was considered statistically significant. The results are given in absolute numbers ± standard deviation. A professional consultation took place by the local ethics committee of the University of Heidelberg and did not result in any concerns (approval number 2021-865).

RESULTS

Of the patients screened, 79 patients (n=79) were included. All patients had squamous cell carcinoma on histopathology, and the location, tumor extent, lymph node status, and distant metastasis status (according to the respective Union for International Cancer Control TNM classification) are listed in **Table 1**. The mean age was 63 years (± 9 years, range 33-80 years). 64 patients (81%) were male, 15 (19%) were female. Radiochemotherapy was started adjuvantly (after a previous resectioning surgery) in 31 patients (39.2%) and as primary/definitive therapy (without previous surgery) in 48 patients (60.8%). Chemotherapy with weekly regimen was started in 30 patients, 3-weekly regimen in 49 patients (38%/62%). A PEG was placed in 46 patients (58.2%). A port was implanted in 28 patients (35.4%). The first dose of cisplatin 3-weekly was given in 49 patients (62%), a second dose of cisplatin 3-weekly in 37 patients (47%), and a third dose of cisplatin 3-weekly in 12 patients (15%). Due to adverse events, the regimen was changed from 3-weekly to weekly in 4 patients (5%) after the first administration. The first dose of cisplatin weekly was given in 30 patients (38%), a second dose of cisplatin weekly in 32 patients (41%), a third dose of cisplatin weekly in 29 patients (37%), a fourth dose of cisplatin weekly in 25 patients (32%), a fifth dose of cisplatin weekly in 19 patients (24%), a sixth dose of cisplatin weekly in 12 patients (15%), and seven doses of cisplatin weekly in 2 patients (2.5%).

The total cumulative dose achieved was a mean of 202.47mg cisplatin/m^2 body surface area (± 66.96; range 40-300). A dose of ≥200mg/m^2 body surface area was achieved in 57 patients (72.51%). Here, a cumulative dose of >200mg/m^2 body surface area was achieved within the weekly regimen group in 56.6% of patients, and within the 3-weekly regimen group in 81.6% of patients. The agent was switched from cisplatin to carboplatin in 8 patients (10.12%) during the course of therapy, and 2 patients (2.53%) were switched to primary radioimmunotherapy with cetuximab.

12 patients (15.2%) died during the observation period, 54 patients (68.3%) were alive at the end of the observation period. In 13 patients (16.5%), death within or survival of the observation period could not be traced on the basis of the available data. Of the 12 patients who died, 8 patients had started radiochemotherapy with the weekly regimen and 4 patients with the 3-weekly regimen. On average, the deceased patients initially had significantly higher platelet levels (p=0.039), significantly lower albumin levels (p<0.001), significantly lower erythrocyte levels (p=0.019), and significantly lower hemoglobin levels (p=0.008) than the survivors. There were no significant differences in leukocyte or GFR levels compared with patients who were alive at the end of the observation period.

Significant positive correlations were seen for total cumulative dose with initial GFR (p=0.001, Pearson's r=0.364) (**Figure 1**), initial hemoglobin (p=0.035, r=0.237) (**Figure 2**), initial erythrocyte count (p=0.002, r=0.337) (**Figure 3**), and initial albumin (p=0.002, r=0.337) (**Figure 4**). There were no significant correlations for total cumulative dose with initial leukocyte (**Figure 5**) or platelet (**Figure 6**) count. There were no significant correlations of the total cumulative dose with the differences of the laboratory values pre/post-chemo administration.

When separated by gender, there was a significant difference in the change in GFR after the first chemo administration, both in absolute (p=0.007) and relative differences (p=0.012), with a greater decrease in GFR in females (-7.27ml/min; -4.13ml/min). Otherwise, there were no significant differences, not even in the total cumulative dose achieved.

In the male subgroup, there was a significant negative correlation of total cumulative dose with an increase in leukocytes after the first chemo administration (absolute value: p=0.016, r=-0.301; relative value: p=0.032, r=-0.269).

In the subgroup of women, there was a significant negative correlation of differences in erythrocytes (absolute value: p=0.03, r=-0.708; relative value: p=0.04, r=-0.695) and hemoglobin (absolute value: p=0.028, r=-0.567; relative value: p=0.023, r=-0.581) values over the first chemo administration with the total cumulative dose.

Between patients with and without PEG, as well as between patients with and without port, there were no significant differences in the values collected.

In the weekly group, the mean age (69.53 ± 7.1 years) was significantly (p<0.001) higher than that in the 3-weekly group (58.94 ± 7.75 years). The achieved total cumulative dose of cisplatin was significantly (p=0.046) higher in the 3-weekly group than in the weekly group (214.18 ± 65.95 vs. 183.33 ± 65.2 mg/m^2 body surface area) (**Figure 7**). Mean initial GFR was significantly (p<0.001) lower in the weekly group (79.9 ± 17.22ml/min) than in the 3-weekly group (94.45 ± 14.23). There were no significant differences in the remaining initial laboratory values between the two groups.

Considering only patients with a GFR ≥ 70ml/min, there is no significant difference in the total cumulative dose of cisplatin achieved between the weekly regimen (190 ± 57.82mg/m^2 body surface area) and the 3-weekly regimen (217.28 ± 62.34mg/m^2 body surface area). Patients with GFR between 60-69ml/min showed a significant difference (p=0.046) with 183.33 ± 65.2mg/m^2 body surface area in the weekly regimen and 214.18 ± 65.95mg/m^2 body surface area in the 3-weekly regimen. Patients with a GFR<60ml/min did not receive chemotherapy on the 3-weekly regimen during the screened period, so a comparison of the two regimens was not possible here.

Initial leukocyte values showed a significant positive correlation with leukocyte values after the first (p=0.009, r=0.292) and before the fifth (p=0.019, r=0.518) chemo administration. Initial GFR values showed a significant positive correlation with GFR values before the second (p<0.001, r=0.701), third (p<0.001, r=0.668), fourth (p<0.001, r=0.749), fifth (p=0.004, r=0.164) and sixth (p<0.001, r=0.886) chemo administration. Initial platelet values showed a significant positive correlation with platelet values before the second (p<0.001, r=0.537), third (p=0.001, r= 0.473), fourth (p<0.001, r=0.656), fifth (p=0.002, r=0.646) and sixth (p=0.01, r=0.709) chemo administration. Initial hemoglobin values showed a

TABLE 1 | Characteristics and initial laboratory values of the examined patients (T, tumor extent; N, lymph node status; M, distant metastasis status).

ID	Sex [male; female]	Age at start of chemotherapy [years]	T	N	M	Localization	Adj./prim. RCT	Initial regimen cisplatin [mg/m^2]	Accumulated dose cisplatin [mg/m^2]	Death during the study period	Initial leucocyte count [10E9/L]	Initial GFR [ml/min/ 1,73m^2]	Initial platelet count [10E9/L]	Initial hemoglobin [g/dL]	Initial erythrocyte count [10E12/L]	Initial albumin [g/L]
1	m	64	2	1	0	oropharynx	adj.	100	300	no	5.98	94	216	13.7	4.73	38
2	m	59	4	1	0	oral cavity / oropharynx	prim.	100	200	no	7.58	101	347	15.7	5.15	44
3	m	61	4	0	0	oral cavity	prim.	40	40	no	4.04	76	138	9.2	2.79	30.8
4	m	49	2	1	0	oropharynx	adj.	100	200	no	7.24	99	436	11.5	4	34
5	m	79	2	2	0	larynx	prim.	40	40	no	8.21	52	195	15	4.75	36.5
6	m	73	3	0	0	hypopharynx	prim.	40	160	no	6.41	73	191	14	4.25	34.8
7	m	60	3	0	0	oropharynx / hypopharynx	adj.	100	200	no	5.91	104	463	9.5	3.25	38
8	f	74	4	2	0	oropharynx / hypopharynx / larynx	prim.	40	200	no	5.5	92	240	12.9	3.9	37
9	m	50	4	3	1	larynx	adj.	100	260	no	8.35	106	631	9.8	3.4	36
10	m	53	3	2	0	oropharynx	adj.	100	300	no	8.58	111	407	12.5	4.31	37
11	m	64	3	1	0	hypopharynx / larynx	prim.	100	100	no	4.97	73	293	12.6	4.29	39
12	m	51	1	2	0	oropharynx	adj.	100	180	no	10.24	115	461	11.7	3.67	32
13	m	63	3	2	0	hypopharynx	prim.	100	300	no	8.22	85	169	14.1	5.24	35.7
14	f	59	4	1	0	nasopharynx	prim.	100	200	?	16.95	92	474	11.5	4.03	32.3
15	m	74	2	1	0	oropharynx / hypopharynx	adj.	100	200	no	6.38	82	506	11.9	3.83	28.8
16	m	58	3	3	0	hypopharynx	adj.	100	220	no	9.57	98	427	10.9	3.91	34
17	m	39	4	0	0	oropharynx	prim.	100	250	no	9.77	118	189	14.2	4.68	37
18	f	53	4	0	0	nasopharynx / oropharynx	prim.	100	200	no	7.1	109	323	13.3	4.05	31
19	f	64	4	2	0	nasopharynx / oropharynx / hypopharynx	prim.	40	160	yes	14.46	95	599	7.3	3.17	23
20	m	55	1	1	0	nasopharynx	prim.	100	300	no	5.43	94	268	14.5	4.85	36.8
21	f	59	1	1	0	oropharynx	adj.	100	100	no	9.92	96	254	12.8	4.01	35
22	f	74	3	2	0	oropharynx / larynx	prim.	40	120	yes	9.66	68	276	13.2	4.38	34
23	m	71	3	2	0	oral cavity	adj.	40	200	no	4.84	90	416	12.6	3.88	29.3
24	m	46	4	2	0	oral cavity	prim.	40	160	no	7.97	100	367	12.3	4.55	35.7
25	m	54	4	2	0	oropharynx	adj.	100	260	yes	8.89	84	389	13.7	4.79	36.3
26	m	69	3	2	0	oropharynx	adj.	40	160	no	8.79	85	286	12.5	4.07	29.8
27	m	71	4	1	0	oropharynx	prim.	40	80	yes	9.78	62	252	8.1	2.54	25.6
28	m	71	4	0	0	hypopharynx	prim.	40	240	no	9.11	70	391	13.6	3.85	33.1
29	m	65	1	0	0	larynx	prim.	40	240	no	6.07	90	213	16.4	5.28	36
30	m	72	3	0	0	larynx	prim.	40	240	no	6.54	67	278	14.6	4.66	37.2
31	m	64	2	3	0	hypopharynx	adj.	100	250	no	8.84	79	169	13.1	4.45	38.3
32	f	78	1	2	0	oropharynx	prim.	40	240	no	6.97	65	359	13.5	4.52	36
33	m	54	3	0	0	oropharynx	prim.	100	300	yes	8.06	102	309	12.7	3.94	33.8
34	m	33	2	1	0	oral cavity	adj.	100	200	no	7.91	125	364	11.4	3.69	32.3
35	f	77	3	2	0	oropharynx	prim.	40	240	no	5.98	75	284	14.2	4.66	28.4
36	m	57	4	0	0	nasopharynx	prim.	100	300	no	8.5	65	522	8.7	4.36	28.1
37	m	59	1	2	0	oropharynx	prim.	100	200	no	6.11	87	150	11.6	4	38
38	f	53	1	1	0	oropharynx	adj.	100	200	no	7.09	77	426	14	4.95	38.2
39	m	66	3	2	0	oropharynx	prim.	100	100	no	9.87	73	299	15.9	5.33	36.6
40	m	72	3	0	0	hypopharynx	prim.	100	100	no	8.28	61	236	14.3	4.27	37.5
41	m	75	3	2	0	larynx	prim.	40	240	?	6.66	68	360	11.7	4.03	39.3
42	m	72	1	2	0	oral cavity	adj.	40	240	no	5.75	56	299	15.7	5.43	36.9
43	m	57	2	1	0	oropharynx	adj.	100	100	no	5.85	104	286	9.6	3.16	24.6
44	m	65	3	2	0	hypopharynx	prim.	40	200	no	7.97	74	236	13.9	4.58	37.2
45	m	61	4	2	0	nasopharynx / oropharynx	prim.	100	200	no	10.27	96	273	13.7	4.16	34.1
46	m	63	2	2	1	oral cavity	prim.	100	200	?	9	86	337	14	4.03	37.5
47	m	66	4	0	0	oropharynx	adj.	40	120	yes	7.15	86	679	11.6	4.07	28.7
48	f	68	1	1	0	nasopharynx	prim.	100	200	?	9.56	85	327	14.3	4.68	35.9
49	f	64	2	2	0	oral cavity	adj.	100	200	no	7.24	99	242	11.5	3.86	32.4
50	f	59	2	3	0	oropharynx	adj.	40	160	yes	9.26	95	455	11.1	3.36	25.8
51	m	64	4	2	0	oropharynx	prim.	40	200	no	9.59	73	349	12.6	4.17	35.1
52	m	55	2	1	0	oropharynx	adj.	100	200	no	6.12	96	273	12.1	7	37
53	f	74	4	0	0	larynx	prim.	40	260	yes	6.83	84	256	12.5	4.95	34.5
54	m	61	3	3	0	larynx	adj.	100	300	no	11.25	107	386	13.7	4.45	37.1
55	m	64	4	2	0	oropharynx	prim.	100	300	no	14.68	93	276	13.3	4.26	35.8
56	m	57	3	2	0	larynx	prim.	100	200	no	6.73	98	248	14.7	5.22	34.6
57	m	63	1	3	0	hypopharynx	adj.	100	200	no	6.02	101	427	10	3.46	28.2
58	m	72	3	0	0	larynx	prim.	40	240	?	11.6	91	360	12.8	4.12	35.5
59	m	64	2	1	0	oropharynx	adj.	100	100	?	7.54	96	417	10.8	3.46	30.1
60	m	57	3	1	0	hypopharynx	adj.	100	300	no	12.83	104	428	10.7	3.6	31.8
61	m	63	2	0	0	oral cavity	prim.	100	200	no	7.43	91	235	14.5	4.73	34.3

(Continued)

TABLE 1 | Continued

ID	Sex [male; female]	Age at start of chemotherapy [years]	T	N	M	Localization	Adj./prim. RCT	Initial regimen cisplatin [mg/m^2]	Accumulated dose cisplatin [mg/m^2]	Death during the study period	Initial leucocyte count [10E9/L]	Initial GFR [ml/min/ 1,73m^2]	Initial platelet count [10E9/L]	Initial hemoglobin [g/dL]	Initial erythrocyte count [10E12/L]	Initial albumin [g/L]
62	m	76	4	0	0	oropharynx	prim.	40	80	yes	9.22	78	539	9.5	3.07	18.4
63	m	57	3	2	0	larynx	prim.	100	200	?	10.11	110	575	12.4	3.97	28
64	m	59	4	2	0	oropharynx	prim.	40	240	?	7.65	117	420	12.2	3.83	32.5
65	m	70	1	2	0	oral cavity	adj.	100	100	no	5.72	68	378	11.8	3.82	31.4
66	m	71	4	3	0	oropharynx / hypopharynx	prim.	40	240	?	9.36	71	192	12.5	4.04	34.4
67	m	65	4	2	1	oropharynx / hypopharynx / larynx	prim.	100	200	yes	4.39	111	275	9.4	3.21	27.5
68	m	61	4	1	0	hypopharynx	prim.	100	300	?	8.93	95	375	15.4	5.03	37.6
69	m	50	4	0	0	oral cavity	prim.	100	300	?	9.25	121	344	11.7	4.41	33.5
70	m	70	2	2	0	oropharynx	prim.	40	160	no	5.45	70	166	11.5	3.63	34.7
71	m	47	3	0	0	larynx	adj.	100	200	?	5.06	102	116	13.2	4.65	35.2
72	f	72	3	1	0	oral cavity	adj.	100	200	yes	6.93	85	287	13.8	4.46	34.5
73	m	62	2	2	0	larynx	adj.	100	100	?	8.17	82	356	12.4	3.91	31.3
74	f	70	2	0	0	neopharynx	prim.	40	240	no	7.76	125	318	11	3.63	34.7
75	m	59	1	2	0	hypopharynx	adj.	100	300	no	7.37	99	442	13.3	4.5	33.4
76	m	80	2	1	0	oropharynx	prim.	40	120	no	5.05	53	200	12.3	3.97	31.8
77	m	61	2	0	0	oropharynx	prim.	100	275	no	7.23	90	250	15.3	5.26	37.8
78	m	68	3	2	0	oropharynx	prim.	40	240	yes	9.29	96	370	11.4	3.24	29.8
79	m	65	3	2	0	larynx	adj.	100	200	no	7.59	79	313	13.1	4.39	33.3

significant positive correlation with hemoglobin values before the second ($p<0.001$, $r=0.751$), third ($p<0.001$, $r=0.512$), fourth ($p<0.001$, $r=0.786$), fifth ($p<0.001$, $r=0.758$) and sixth ($p=0.002$, $r=0.79$) chemo administration. Initial erythrocyte values showed significant positive correlation with erythrocyte values before second ($p<0.001$, $r=0.605$), third ($p<0.001$, $r=0.507$), fourth ($p<0.001$, $r=0.768$), fifth ($p<0.001$, $r=0.788$) and sixth ($p=0.002$, $r=0.795$) chemo administration. Initial albumin values showed significant positive correlation with albumin values before second ($p<0.001$, $r=0.667$), third ($p=0.012$, $r=0.372$) and fourth ($p=0.002$, $r=0.586$) chemo administration.

With respect to the individual initial laboratory values among themselves, significant positive correlations were found between leukocytes and platelets ($p=0.003$; $r=0.335$), GFR and platelets ($p=0.025$; $r=0.252$), hemoglobin level and erythrocytes ($p<0.001$; $r=0.759$), hemoglobin level and albumin ($p<0.001$; $r=0.651$), and erythrocytes and albumin ($p<0.001$; $r=0.607$).

There was a significant negative correlation between platelets and hemoglobin level ($p<0.001$; $r=-0.415$), as well as between platelets and albumin ($p<0.001$; $r=-0.409$) and platelets and erythrocytes ($p=0.006$; $r=-0.304$).

DISCUSSION

There are currently only a few randomized controlled trials comparing the two aforementioned chemo regimens. Tsan et al. described a higher average cumulative total dose of cisplatin achieved with the 3-weekly regimen and better tolerability than with the weekly regimen (17). Noronha et al. compared the 3-weekly regimen with weekly administration of 30mg cisplatin/m^2 body surface area, again finding significantly better locoregional control in the 3-weekly group and recommending it should be preferred (15). In a meta-analysis, no superiority of the weekly regimen was found in terms of patient outcome, nor were there differences in prior therapy side effects, so the authors recommend the 3-weekly regimen (18). Another meta-analysis also found no difference in overall survival, but found the weekly regimen to be less myelotoxic and nephrotoxic, but associated with increased dysphagia and body weight loss (19). Retrospective evaluations also found a higher total cumulative dose of cisplatin with the 3-weekly regimen (16), but other authors described better tolerability in terms of less toxicity with the weekly regimen (20). In addition to the two regimens listed, other regimens (such as low-dose daily cisplatin (21, 22) also exist internationally, but these are not currently established nationwide in Germany. It is to be expected that the results of this study are not directly transferable to other cisplatin regimens and that own evaluations have to be made in this respect.

An important retrospective study, in light of whose results our study is also interpreted, showed a correlation of overall survival with the total cumulative dose of cisplatin administered (13). This study was important in that it was able to correlate a targeted but more distant end point (overall survival) with a more proximate end point (total cumulative dose) and therefore allowed earlier interpretation of data.

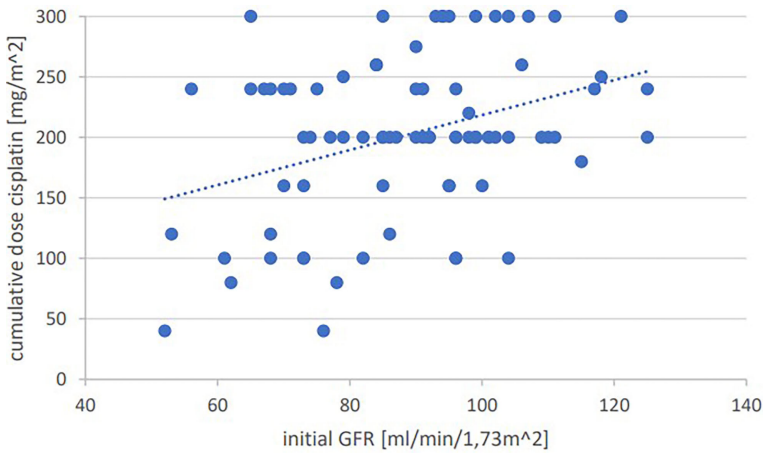

FIGURE 1 | Bivariate correlation analysis of initial GFR values [ml/min/1,73m^2] with final cumulative total dose of cisplatin achieved [mg/m^2]: p=0.001, Pearson's r=0.364; individual values as points, dashed linear trend line.

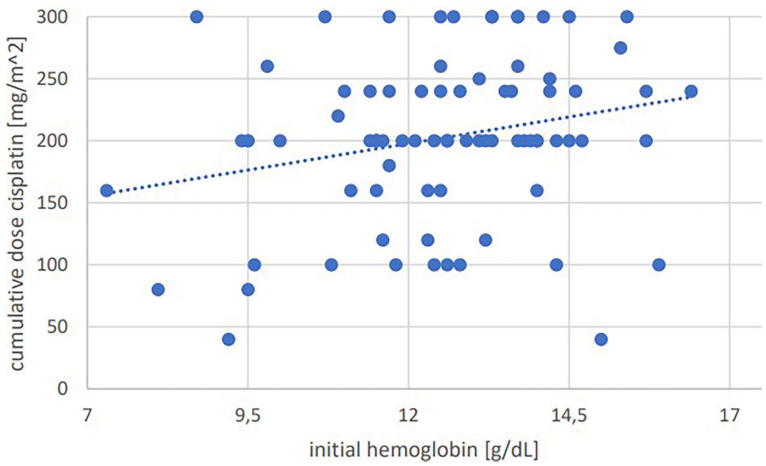

FIGURE 2 | Bivariate correlation analysis of initial hemoglobin values [g/dL] with final cumulative total dose of cisplatin achieved [mg/m^2]: p=0.035, Pearson's r=0.237; individual values as points, dashed linear trend line.

Due to the highly distressing and also potentially dangerous side effects of (radio)chemotherapy, it seems reasonable to consider not only tumor free-survival but also the overall survival of patients with regard to the evaluation of a therapy. However, due to the partly limited compliance of patients during regular tumor follow-up, the survival of all patients could not be evaluated. Of those who could be followed up, 26.6% of patients after RCT with the weekly regimen died within the observation period; in the 3-weekly regimen group, 8.1% of patients died within the observation period. The significance of the survival rates of our patients is therefore limited, also due to the relatively short observation period in relation to the 5-year survival rate of patients with HNSCC (23). Comparison of laboratory values at baseline showed significantly higher erythrocyte, hemoglobin, and albumin levels and lower platelet levels in survivors. Overall, however, it is difficult to compare patient survival between the two regimens in a retrospective study because the indication of the regimens was also based on the treating physician's assessment of which form of chemotherapy the patient could tolerate. Based on the significant differences in erythrocyte/hemoglobin and albumin levels, it can be assumed that the patients who died during the observation period were already in poorer physical condition before the start of therapy, so that their poorer survival rate cannot necessarily be attributed to the chemo regimen. Thus, a high-quality assessment of overall survival comparing cisplatin regimens remains reserved for large, prospective studies designed over an even longer time period.

Based on the study by Strojan et al. the cumulative total dose was therefore set as the primary endpoint in this study.

There were no significant differences in the total cumulative dose achieved between patients with and without PEG, and

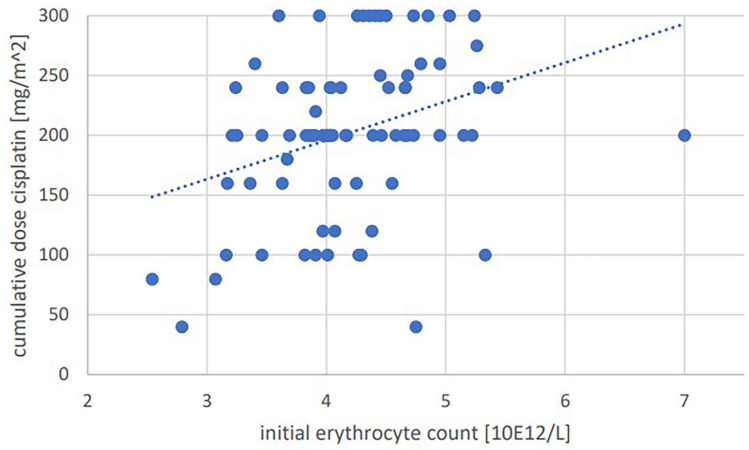

FIGURE 3 | Bivariate correlation analysis of initial erythrocyte count [10E12/L] with final cumulative total dose of cisplatin achieved [mg/m^2]: p=0.002, Pearson's r=0.337; individual values as points, dashed linear trend line.

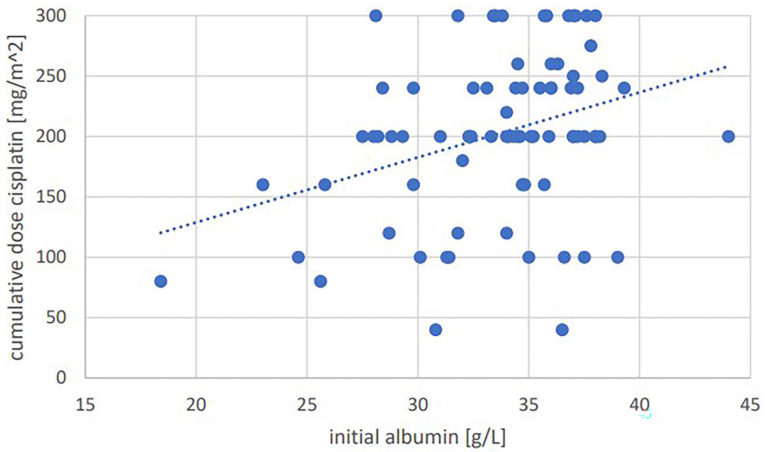

FIGURE 4 | Bivariate correlation analysis of initial albumin value [g/L] with final cumulative total dose of cisplatin achieved [mg/m^2]: p=0.002, Pearson's r=0.337; individual values as points, dashed linear trend line.

patients with and without port. Dysphagia in patients with advanced HNSCC can develop both promptly postoperatively due to extensive tumor resection and persist in aRCT (24), or develop directly in a pRCT or aRCT due to radiogenic stomatitis and xerostomia (25). If oral food intake is significantly restricted as a result, the placement of a PEG may be necessary in the medium term after temporary parenteral nutrition. The patient must be informed about the possible risks and complications (26). If extravasation occurs during intravenous administration of cisplatin, severe irritation of the affected tissue, including necrosis, may occur, necessitating immediate conservative or even surgical intervention (27). Because of the higher concentration, the risk of tissue damage is higher in the 3-weekly dosage than in the weekly dosage (28). Therefore, pretherapeutic port implantation should be evaluated, especially in patients with poor peripheral venous status. However, due to the potential peri- and postoperative complications from a port, the expected benefits must always be weighed against the potential risks (29). Thus, the indication for the mentioned devices has to be made individually for the patients, a basic superiority in the achieved cumulative total dose could not be proven in our data by PEG placement and/or port implantation, a blanket recommendation on this can therefore not be made.

Our data show that high erythrocyte, hemoglobin, GFR, and albumin values in the initial blood values, i.e., measured before the first chemotherapy dose, correlate with a high total cumulative dose achieved.

High or normal hemoglobin values, like high or normal erythrocytes, indicate adequate hematopoietic function. A high

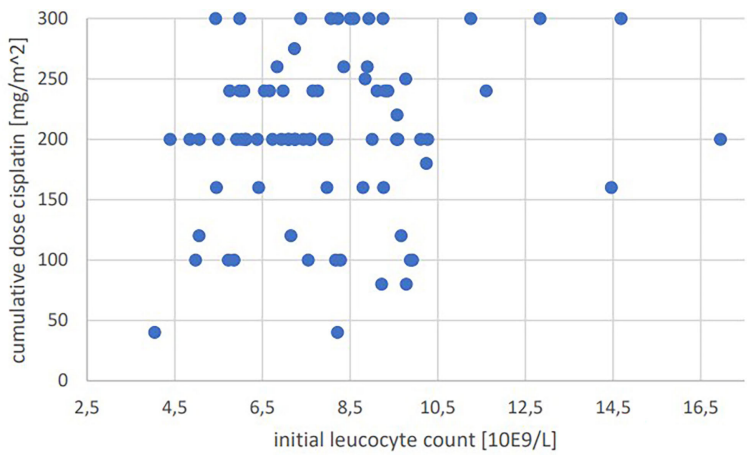

FIGURE 5 | Bivariate correlation analysis of initial leucocyte count [10E9/L] with final cumulative total dose of cisplatin achieved [mg/m^2]: p=0.177, no significant correlation; individual values as points.

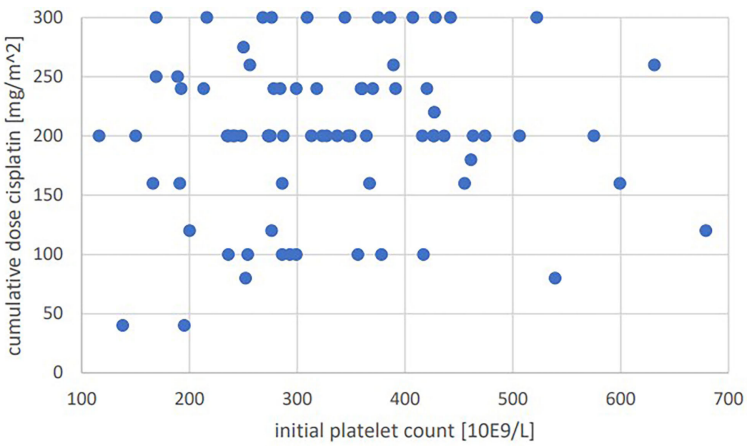

FIGURE 6 | Bivariate correlation analysis of initial platelet count [10E9/L] with final cumulative total dose of cisplatin achieved [mg/m^2]: p=0.56, no significant correlation; individual values as points.

or normal GFR indicates adequate renal function. Albumin, as the main blood transport protein, is an indirect representation of nutritional status and, in combination with other values, is known to be a predictive factor about patient outcome in long-term therapies (30).

It seems logical that high/normal values of leucocytes and platelets also indicate normal bone marrow function. The lack of correlations of leukocytes and platelets with the cumulative total dose of cisplatin in our data allows hypothesizing different explanations. On the one hand, these values in the context of reactive leukocytosis and reactive thrombocytosis are subject to higher dynamics with higher fluctuations within a few days than, for example, erythrocyte values. This makes them unsuitable for predictive estimation for the future based on a single blood draw. On the other hand, it could be suggested that the bone marrow function, which is represented by the leukocyte and platelet values, actually has no predictive/prognostic function for the patient. This is in contrast to the demonstrated correlations of hemoglobin and erythrocytes. In this regard, it could be argued that erythrocyte and hemoglobin levels do not primarily represent bone marrow function, but rather renal function. An adequate renal function plays an important role in erythrocyte formation by stimulating hematopoiesis *via* erythropoietin (31). Although this relationship is biologically beyond question, we were unable to demonstrate a significant correlation between GFR and erythrocyte/hemoglobin levels in our data. This suggests that erythrocytes are still influenced by too many other factors to assume a pure linear relationship with, and thus representation of, renal function. A final conclusion of this cannot be made in a retrospective view due to the close biological interconnectedness of the laboratory values.

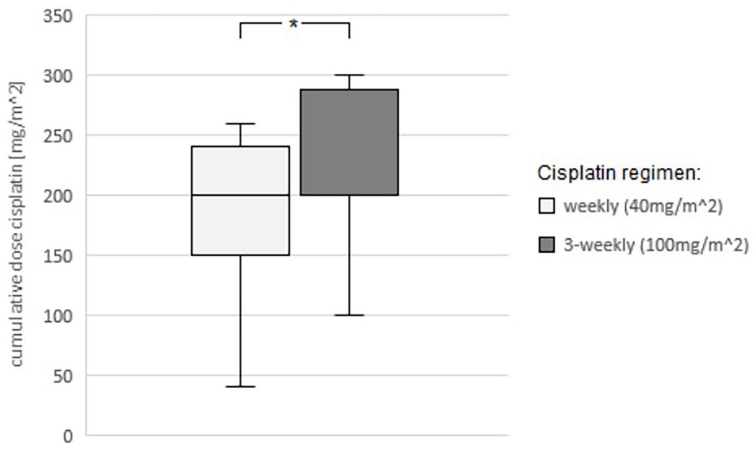

FIGURE 7 | Comparison of the average cumulative total dose of cisplatin achieved between the two regimens (weekly administration 40mg/m^2 body surface area and 3-weekly administration 100mg/m^2 body surface area). Student's t-test: p=0.046, statistically significant (*) mean CDC(weekly)= 183.33mg/m^2; mean CDC(3-weekly)=214.18mg/m^2.

In summary, patients with adequately functioning organ systems, particularly the kidney and bone marrow, have a better chance of achieving a high total cumulative dose of cisplatin than patients who already have laboratory limitations in these systems at the start of therapy. However, it must be kept in mind that although the positive correlations were statistically significant, they were with a rather moderate correlation coefficient, so the associations between good renal/bone marrow function and achieving a high total cumulative dose of cisplatin were not strictly related. Rather, the organ functions reflected in the blood values must be viewed and evaluated in conjunction with, for example, the patient's clinical presentation and other comorbidities as well, not as sole decision factors.

High/normal initial values of hemoglobin, GFR, erythrocyte count and albumin can therefore be considered predictive factors for chemotherapy with cisplatin. Yet, there are also clear positive correlations within the laboratory values, especially strong between the hemoglobin values, the erythrocytes and the albumin values. Due to their biological nature, these values are closely related and also typically move in conformity with each other, as they represent the general condition as well as, among other things, the nutritional status of the patient. Malnutrition, for example, can manifest itself both in a decreased albumin level and, in the case of pronounced substrate deficiency, in anemia. It must therefore be assumed that the individual laboratory values are not completely independent values, each of which is individually predictive of the subsequent cumulative total dose, but must be considered in their entirety.

The importance of GFR as a prognostic factor is also highlighted by the fact that in the subgroup analysis of patients with a GFR of more than 70ml/min/1.73m^2, no significant difference in the cumulative dose of cisplatin was discernible between the 3-weekly and the weekly group. This highlights the importance of good renal function for the patient's therapeutic prognosis and might even call into question the fundamental superiority of the 3-weekly regimen. Nonetheless, the superiority of this regimen in terms of higher cumulative dose of cisplatin has also been demonstrated in large randomized trials (15, 17), also in our study significantly higher cumulative doses were achieved with the 3-weekly regimen in the range between 60 and 69ml/min/1.73m^2.

However, it should be noted that in routine clinical practice the measurement is made indirectly by calculation from serum creatinine. Creatinine, in turn, is a breakdown product of muscle. Especially in (tumor) cachectic patients, creatinine may be decreased due to the lack of muscle mass, so that a false-high/good GFR value is calculated. In these cases, the renal function must be critically questioned.

In our data, there was a significant difference in the dynamics of GFR after the first chemo administration between men and women, with women showing a greater decrease in GFR. It is known from the analysis of long-term data that women show a significantly greater permanent decrease in GFR during the course after therapy with cisplatin compared to men (32). This is mainly explained by the lower average muscle percentage in women (33). Over the later chemo administrations, this sex difference in GFR dynamics was no longer detectable in our data, probably because the patients who had shown a greater GFR decline during the first administration had received targeted protective volume therapy during later chemo administrations to prevent renal failure.

The male subgroup showed a negative correlation of the dynamics of leukocyte levels over the first chemo administration with the later cumulative dose of cisplatin. Thus, the higher the leukocytes increased between before and after the first administration, the lower the cumulative dose of cisplatin at the end. It can be assumed that this correlation is due to constellations in which patients have suffered an infection, which on the one hand manifests itself in leukocytosis and on the other hand negatively influences the cumulative dose achieved

later, since the infection meant that chemotherapy had to be suspended or discontinued. A possible correlation of leukopenia after cisplatin administration with the later cumulative dose may thus be statistically masked.

A similar negative correlation was found in the subgroup of women, but here between the dynamics of erythroycyte and hemoglobin levels above the first chemo administration with the cumulative dose of cisplatin. Thus, the greater the increase in erythrocyte and hemoglobin levels between the first two blood draws, the lower the subsequent cumulative dose of cisplatin. Since high erythrocyte and hemoglobin levels tend to be prognostically favorable factors, this counterintuitive correlation is most likely explained by an exciccosis phenomenon. Renal damage and limited fluid intake may result in intravascular fluid deficiency, which is reflected in increased erythrocyte and hemoglobin levels. Since this correlation in our data is only seen in the first chemo administration, it can be assumed that in these patients exsiccosis was counteracted by supportive measures during later chemo administrations.

The correlation analyses show that GFR, platelet count, erythrocyte count, and hemoglobin levels are stable overall, and the initial values correlate with the later ones over almost the entire course of chemotherapy. In the case of leukocyte values, a consistent correlation of initial with later values is not found, which fits with the fact that leukocytosis may occur together with an increase in acute-phase proteins (34) in the context of stressful situations such as those represented by chemotherapy. At the same time, however, leukopenia may also develop due to the myelosuppressive effects of cisplatin (12). Through this, the dynamics of leukocyte values in the course of chemotherapy is much more pronounced than that of the other laboratory values, resulting in the lack of correlation evidence with the initial values. However, there was no relevant correlation of the initial laboratory values with the later dynamics of the laboratory values, nor of the dynamics of the laboratory values over the first chemo administration with the later values. It must also be considered that falsification may occur due to iatrogenic influence on laboratory parameters during the course of radiochemotherapy. While cisplatin can primarily trigger a reduction in blood count values, the treating physician can raise blood count values again by administering transfusions and bone marrow stimulation with e.g. granulocyte colony-stimulating factor (G-CSF). Substitution therapy of iron and erythropoietin in the context of anemia of chronic disease also changes the course of blood values compared to a patient in whom this substitution does not take place.

It must further be considered that radiotherapy alone at different doses also has an impact on blood counts and blood values and thus represents a potential bias on the evaluation of blood values under radiochemotherapy (35). However, in our study, significant correlations and differences were found mainly with respect to initial laboratory values, which were not yet influenced by radiotherapy, and after the first dose of chemotherapy, which was administered in parallel with the start of radiotherapy. Thus, the influence of radiation on the significant correlations and differences found can be considered absent or negligible. The later laboratory values in the course of radiochemotherapy were certainly influenced by the radiation in addition to the chemotherapy; an etiological assignment would not be possible with certainty here in the retrospective design.

In summary, our data show that neither the initial laboratory values nor their dynamics over the first chemo administration provide sufficient information about the later behavior of the laboratory values in the course of chemotherapy. Thus, subsequent leukopenia or renal failure cannot be confidently assessed after primary chemo administration and need to be monitored regularly during chemotherapy. Nevertheless, it must be critically noted that the sampling times of the blood controls after chemo administration were not standardized. Due to the fluctuations in the sampling times, in some cases of several days, a falsification of the dynamics cannot be ruled out here. In clinical routine, the partly specific temporal course of the laboratory parameters, in particular of the nadir, should be observed during the blood checks after chemo administration in order not to obtain false-good values.

However, the negative correlation of the initial platelet values with the initial erythrocyte, hemoglobin, and albumin values, i.e., the laboratory values favorable in relation to the cumulative total dose, is striking. A direct negative correlation between the initial or later platelet values and the total cumulative dose of cisplatin was not detectable in our data. However, advanced cancers are well known causes of secondary thrombocytosis (36), and the negative prognostic value of thrombocytosis and an elevated platelet/lymphocyte ratio in HNSCC patients has already been demonstrated in other retrospective studies (37). Although the value in terms of patient outcome of antiplatelet therapy (38) is not yet clear, pretherapeutic thrombocytosis before cisplatin therapy seems to have some prognostic value.

The limitations of this study are mainly due to its retrospective design. As the initial regimens were also chosen on the basis of the initial laboratory values, an asymmetry in the weekly and 3-weekly groups results, especially with regard to age and GFR. A younger patient with statistically less preexisting disease and good renal function was likely to be preferentially assigned to the 3-weekly regimen by the treating physician, whereas an older patient with statistically more preexisting internal disease and a low GFR was more likely to be placed in the weekly group. However, our results are in line with those of the literature, in which a higher cumulative total dose was achieved in the study arm with the 3-weekly regimen, even in randomized controlled trials (15, 17). Furthermore, the changes in laboratory values over the period of the RCT cannot necessarily be attributed to the chemotherapy, as iatrogenic interventions such as red blood cell transfusions or the administration of G-CSF could also have taken place. However, since these are legitimate supportive measures that are available to every patient under RCT and would not have been omitted in a prospective study, the use of the data is nevertheless justifiable. In particular, initial blood levels, for which we demonstrated a correlation with the cumulative total dose of cisplatin, are still unaffected by such supportive measures.

Our data show a higher average cumulative total dose of cisplatin in the 3-weekly group (**Figure 7**). Also, a cumulative

dose ≥200mg/m^2 body surface area was more frequently achieved with the 3-weekly regimen. If the previous findings from retrospective studies confirm that the cumulative total dose correlates positively with the outcome of the patients, the 3-weekly would in principle be preferable to the weekly regimen as far as medically justifiable.

The initial hemoglobin and erythrocyte values, the initial GFR and the initial albumin value allow a prospect of the total dose to be achieved later and should be taken into account when selecting the chemo regimen. Also, elevated platelet values are seen mainly in patients with otherwise rather low favorable prognostic parameters (erythrocytes/hemoglobin/albumin), so that at least indirectly an increased disease burden and a lower resistance might be suspected here.

The initial laboratory values as well as their changes after the first chemo administration do not allow any conclusion to be drawn about later changes in the laboratory values (especially leukopenia or kidney failure), therefore the laboratory values must be checked regularly during the entire chemotherapy in order to be able to recognize and treat any complications at an early stage.

However, rising leukocytes (mainly in men in our evaluation) and rising erythrocytes/hemoglobin (mainly in women in our evaluation) after the first chemo administration may be indications of poor outcome, as they were statistically associated with a lower cumulative dose of cisplatin in our study.

For the correct selection of the chemo regimen, especially against the background of cisplatin-resistant tumors, further factors must be investigated in the future in order to be able to make the optimal weighing of benefits and risks for the individual patient. In this regard, tumor biology and pharmacogenetic research are the main focus for patient stratification (39). This will allow the identification of patient groups with an increased risk of complications and side effects, as well as those with a possible development of resistance to cisplatin.

DATA AVAILABILITY STATEMENT

The raw data supporting the conclusions of this article will be made available by the authors, without undue reservation.

ETHICS STATEMENT

The studies involving human participants were reviewed and approved by Ethik-Kommission II of the University Heidelberg. Written informed consent for participation was not required for this study in accordance with the national legislation and the institutional requirements.

AUTHOR CONTRIBUTIONS

FJ formulated the hypothesis, conducted the data analysis and literature review, and wrote the manuscript. AL supervised the writing of the manuscript and revised it. LH, SL, NR, BW, and LZ revised and corrected the manuscript and made essential suggestions for adaptation and modification. Each author made an essential contribution to the form and content of the current manuscript.

REFERENCES

1. Kelland L. The Resurgence of Platinum-Based Cancer Chemotherapy. *Nat Rev Cancer* (2007) 7:573–84. doi: 10.1038/nrc2167
2. Goodsell DS. The Molecular Perspective: Cisplatin. *Oncologist* (2006) 11:316–7. doi: 10.1634/theoncologist.11-3-316
3. Ghosh S. Cisplatin: The First Metal Based Anticancer Drug. *Bioorg Chem* (2019) 88:102925. doi: 10.1016/j.bioorg.2019.102925
4. Galluzzi L, Vitale I, Michels J, Brenner C, Szabadkai G, Harel-Bellan A, et al. Systems Biology of Cisplatin Resistance: Past, Present and Future. *Cell Death Dis* (2014) 5:e1257. doi: 10.1038/cddis.2013.428
5. Rivera F, Garcia-Castano A, Vega N, Vega-Villegas ME, Gutierrez-Sanz L. Cetuximab in Metastatic or Recurrent Head and Neck Cancer: The EXTREME Trial. *Expert Rev Anticancer Ther* (2009) 9:1421–8. doi: 10.1586/era.09.113
6. Go RS, Adjei AA. Review of the Comparative Pharmacology and Clinical Activity of Cisplatin and Carboplatin. *J Clin Oncol* (1999) 17:409–22. doi: 10.1200/JCO.1999.17.1.409
7. Ho GY, Woodward N, Coward JI. Cisplatin Versus Carboplatin: Comparative Review of Therapeutic Management in Solid Malignancies. *Crit Rev Oncol Hematol* (2016) 102:37–46. doi: 10.1016/j.critrevonc.2016.03.014
8. Dierckes SJ, Ragsdale ME, Macik MR, Weddle KJ. Retrospective Analysis of the Incidence and Severity of Acute Kidney Injury (AKI) in Patients With Head and Neck Cancer Receiving Weekly Cisplatin With Radiotherapy (RAISe-AKI). *J Oncol Pharm Pract* (2020) 27(8):1925–7. doi: 10.1177/1078155220978454
9. Brock P, Bellman S. Ototoxicity of Cisplatinum. *Br J Cancer* (1991) 63:159–60. doi: 10.1038/bjc.1991.35
10. Meier C, Goldhirsch A, Hess C, Bazarian J, Greiner R, Beer M. Polyneuropathy After Cisplatin Treatment. *Dtsch Med Wochenschr* (1985) 110:721–5. doi: 10.1055/s-2008-1068894
11. Barabas K, Milner R, Lurie D, Adin C. Cisplatin: A Review of Toxicities and Therapeutic Applications. *Vet Comp Oncol* (2008) 6:1–18. doi: 10.1111/j.1476-5829.2007.00142.x
12. Weykamp F, Seidensaal K, Rieken S, Green K, Mende S, Zaoui K, et al. Age-Dependent Hemato- and Nephrotoxicity in Patients With Head and Neck Cancer Receiving Chemoradiotherapy With Weekly Cisplatin. *Strahlenther Onkol* (2020) 196:515–21. doi: 10.1007/s00066-019-01550-6
13. Strojan P, Vermorken JB, Beitler JJ, Saba NF, Haigentz MJr., Bossi P, et al. Cumulative Cisplatin Dose in Concurrent Chemoradiotherapy for Head and Neck Cancer: A Systematic Review. *Head Neck* (2016) 38(Suppl 1):E2151–2158. doi: 10.1002/hed.24026
14. Adelstein DJ, Li Y, Adams GL, Wagner HJr., Kish JA, Ensley JF, et al. An Intergroup Phase III Comparison of Standard Radiation Therapy and Two Schedules of Concurrent Chemoradiotherapy in Patients With Unresectable Squamous Cell Head and Neck Cancer. *J Clin Oncol* (2003) 21:92–8. doi: 10.1200/JCO.2003.01.008
15. Noronha V, Joshi A, Patil VM, Agarwal J, Ghosh-Laskar S, Budrukkar A, et al. Once-A-Week Versus Once-Every-3-Weeks Cisplatin Chemoradiation for Locally Advanced Head and Neck Cancer: A Phase III Randomized

Noninferiority Trial. *J Clin Oncol* (2018) 36:1064–72. doi: 10.1200/JCO.2017.74.9457
16. Helfenstein S, Riesterer O, Meier UR, Papachristofilou A, Kasenda B, Pless M, et al. 3-Weekly or Weekly Cisplatin Concurrently With Radiotherapy for Patients With Squamous Cell Carcinoma of the Head and Neck - A Multicentre, Retrospective Analysis. *Radiat Oncol* (2019) 14:32. doi: 10.1186/s13014-019-1235-y
17. Tsan DL, Lin CY, Kang CJ, Huang SF, Fan KH, Liao CT, et al. The Comparison Between Weekly and Three-Weekly Cisplatin Delivered Concurrently With Radiotherapy for Patients With Postoperative High-Risk Squamous Cell Carcinoma of the Oral Cavity. *Radiat Oncol* (2012) 7:215. doi: 10.1186/1748-717X-7-215
18. Jacinto JK, Co J, Mejia MB, Regala EE. The Evidence on Effectiveness of Weekly vs Triweekly Cisplatin Concurrent With Radiotherapy in Locally Advanced Head and Neck Squamous Cell Carcinoma (HNSCC): A Systematic Review and Meta-Analysis. *Br J Radiol* (2017) 90:20170442. doi: 10.1259/bjr.20170442
19. Szturz P, Wouters K, Kiyota N, Tahara M, Prabhash K, Noronha V, et al. Weekly Low-Dose Versus Three-Weekly High-Dose Cisplatin for Concurrent Chemoradiation in Locoregionally Advanced Non-Nasopharyngeal Head and Neck Cancer: A Systematic Review and Meta-Analysis of Aggregate Data. *Oncologist* (2017) 22:1056–66. doi: 10.1634/theoncologist.2017-0015
20. Bauml JM, Vinnakota R, Anna Park YH, Bates SE, Fojo T, Aggarwal C, et al. Cisplatin Every 3 Weeks Versus Weekly With Definitive Concurrent Radiotherapy for Squamous Cell Carcinoma of the Head and Neck. *J Natl Cancer Inst* (2019) 111:490–7. doi: 10.1093/jnci/djy133
21. Jeremic B, Milicic B. Influence of Low-Dose Daily Cisplatin on the Distant Metastasis-Free Survival of Patients With Locally Advanced Nonmetastatic Head and Neck Cancer Treated With Radiation Therapy. *Radiother Oncol* (2008) 87:201–3. doi: 10.1016/j.radonc.2007.12.023
22. Jeremic B, Milicic B. Pretreatment Prognostic Factors of Survival in Patients With Locally Advanced Nonmetastatic Squamous Cell Carcinoma of the Head and Neck Treated With Radiation Therapy With or Without Concurrent Chemotherapy. *Am J Clin Oncol* (2009) 32:163–8. doi: 10.1097/COC.0b013e31818254cc
23. Du E, Mazul AL, Farquhar D, Brennan P, Anantharaman D, Abedi-Ardekani B, et al. Long-Term Survival in Head and Neck Cancer: Impact of Site, Stage, Smoking, and Human Papillomavirus Status. *Laryngoscope* (2019) 129:2506–13. doi: 10.1002/lary.27807
24. Carmignani I, Locatello LG, Desideri I, Bonomo P, Olmetto E, Livi L, et al. Analysis of Dysphagia in Advanced-Stage Head-and-Neck Cancer Patients: Impact on Quality of Life and Development of a Preventive Swallowing Treatment. *Eur Arch Otorhinolaryngol* (2018) 275:2159–67. doi: 10.1007/s00405-018-5054-9
25. Nguyen NP, Moltz CC, Frank C, Vos P, Smith HJ, Karlsson U, et al. Dysphagia Following Chemoradiation for Locally Advanced Head and Neck Cancer. *Ann Oncol* (2004) 15:383–8. doi: 10.1093/annonc/mdh101
26. Schrag SP, Sharma R, Jaik NP, Seamon MJ, Lukaszczyk JJ, Martin ND, et al. Complications Related to Percutaneous Endoscopic Gastrostomy (PEG) Tubes. A Comprehensive Clinical Review. *J Gastrointestin Liver Dis* (2007) 16:407–18.
27. Bertelli G, Gozza A, Forno GB, Vidili MG, Silvestro S, Venturini M, et al. Topical Dimethylsulfoxide for the Prevention of Soft Tissue Injury After Extravasation of Vesicant Cytotoxic Drugs: A Prospective Clinical Study. *J Clin Oncol* (1995) 13:2851–5. doi: 10.1200/JCO.1995.13.11.2851
28. Jordan K, Grothe W, Schmoll HJ. Extravasation of Chemotherapeutic Agents: Prevention and Therapy. *Dtsch Med Wochenschr* (2005) 130:33–7. doi: 10.1055/s-2005-837372
29. Machat S, Eisenhuber E, Pfarl G, Stubler J, Koelblinger C, Zacherl J, et al. Complications of Central Venous Port Systems: A Pictorial Review. *Insights Imaging* (2019) 10:86. doi: 10.1186/s13244-019-0770-2
30. Whicher J, Spence C. When Is Serum Albumin Worth Measuring? *Ann Clin Biochem* (1987) 24(Pt 6):572–80. doi: 10.1177/000456328702400604
31. Batchelor EK, Kapitsinou P, Pergola PE, Kovesdy CP, Jalal DI. Iron Deficiency in Chronic Kidney Disease: Updates on Pathophysiology, Diagnosis, and Treatment. *J Am Soc Nephrol* (2020) 31:456–68. doi: 10.1681/ASN.2019020213
32. Latcha S, Jaimes EA, Patil S, Glezerman IG, Mehta S, Flombaum CD. Long-Term Renal Outcomes After Cisplatin Treatment. *Clin J Am Soc Nephrol* (2016) 11:1173–9. doi: 10.2215/CJN.08070715
33. Bredella MA. Sex Differences in Body Composition. *Adv Exp Med Biol* (2017) 1043:9–27. doi: 10.1007/978-3-319-70178-3_2
34. Koj A. Initiation of Acute Phase Response and Synthesis of Cytokines. *Biochim Biophys Acta* (1996) 1317:84–94. doi: 10.1016/S0925-4439(96)00048-8
35. Lin AJ, Rao YJ, Chin RI, Campian J, Mullen D, Thotala D, et al. Post-Operative Radiation Effects on Lymphopenia, Neutrophil to Lymphocyte Ratio, and Clinical Outcomes in Palatine Tonsil Cancers. *Oral Oncol* (2018) 86:1–7. doi: 10.1016/j.oraloncology.2018.08.008
36. Rokkam VR, Kotagiri R. "Secondary Thrombocytosis,". In: *StatPearls*. Treasure Island (FL): StatPearls Publishing (2021).
37. Rachidi S, Wallace K, Day TA, Alberg AJ, Li Z. Lower Circulating Platelet Counts and Antiplatelet Therapy Independently Predict Better Outcomes in Patients With Head and Neck Squamous Cell Carcinoma. *J Hematol Oncol* (2014) 7:65. doi: 10.1186/s13045-014-0065-5
38. Takenaka Y, Oya R, Kitamiura T, Ashida N, Shimizu K, Takemura K, et al. Platelet Count and Platelet-Lymphocyte Ratio as Prognostic Markers for Head and Neck Squamous Cell Carcinoma: Meta-Analysis. *Head Neck* (2018) 40:2714–23. doi: 10.1002/hed.25366
39. Marcu LG, Marcu DC. Current Omics Trends in Personalised Head and Neck Cancer Chemoradiotherapy. *J Pers Med* (2021) 11. doi: 10.3390/jpm11111094

Conflict of Interest: The authors declare that the research was conducted in the absence of any commercial or financial relationships that could be construed as a potential conflict of interest.

Publisher's Note: All claims expressed in this article are solely those of the authors and do not necessarily represent those of their affiliated organizations, or those of the publisher, the editors and the reviewers. Any product that may be evaluated in this article, or claim that may be made by its manufacturer, is not guaranteed or endorsed by the publisher.

frontiers | Frontiers in Oncology

ORIGINAL RESEARCH
published: 02 May 2022
doi: 10.3389/fonc.2022.762180

Asporin Interacts With HER2 to Promote Thyroid Cancer Metastasis *via* the MAPK/EMT Signaling Pathway

Shaohua Zhan[1,2,3†], *Tianxiao Wang*[4†], *Jingying Li*[2†], *Hanyang Zhu*[2], *Wei Ge*[2*] and *Jinming Li*[1*]

[1] National Center for Clinical Laboratories, Institute of Geriatric Medicine, Chinese Academy of Medical Sciences, Beijing Hospital/National Center of Gerontology, Beijing, China, [2] Institute of Basic Medical Sciences, State Key Laboratory of Medical Molecular Biology & Department of Immunology, Chinese Academy of Medical Sciences, Beijing, China, [3] Department of Laboratory Medicine, Peking University Third Hospital, Beijing, China, [4] Key Laboratory of Carcinogenesis and Translational Research, Department of Head and Neck Surgery, Peking University Cancer Hospital & Institute, Beijing, China

OPEN ACCESS

Edited by:
Qin Lin,
First Affiliated Hospital of Xiamen University, China

Reviewed by:
Gaurisankar Sa,
Bose Institute, India
Weibo Xu,
Fudan University, China

***Correspondence:**
Wei Ge
wei.ge@chem.ox.ac.uk
Jinming Li
jmli@nccl.org.cn

[†]These authors have contributed equally to this work

Specialty section:
This article was submitted to Head and Neck Cancer, a section of the journal Frontiers in Oncology

Received: 21 August 2021
Accepted: 07 April 2022
Published: 02 May 2022

Citation:
Zhan S, Wang T, Li J, Zhu H, Ge W and Li J (2022) Asporin Interacts With HER2 to Promote Thyroid Cancer Metastasis via the MAPK/EMT Signaling Pathway. Front. Oncol. 12:762180. doi: 10.3389/fonc.2022.762180

Approximately 85% of histological subtypes of thyroid cancer are papillary thyroid cancer (PTC), and the morbidity and mortality of PTC patients rapidly increased due to lymph node metastases or distant metastasis. Therefore, it needs to distill an enhanced understanding of the pathogenesis of PTC patients with lymph node metastases or distant metastasis. We employed the TMT-based quantitative proteomics approach to identify and analyze differentially expressed proteins in PTC with different degrees of lymph node metastases. Compared with paired normal tissues, asporin is overexpressed in PTC-N0, PTC-N1a, and PTC-N1b tumorous tissues *via* proteomics, western blotting, and immunohistochemistry assays. Functionally, asporin is mainly expressed in the extracellular matrix, cell membrane, and cytoplasm of PTC tumorous tissues, and promotes thyroid cancer cell proliferation, migration, and invasion. Mechanistically, asporin, interacting with HER2, co-localizes HER2 on the cell membrane and cytoplasm, and the asporin/HER2/SRC/EGFR axis upregulate the expression of EMT-activating transcription factors through the MAPK signaling pathway. Clinically, asporin can be regarded as a serological biomarker to identify PTC patients with or without lymph node metastasis, and high expression of asporin in PTC tumorous tissues is a risk factor for poor prognosis.

Keywords: papillary thyroid cancer, asporin, HER2, quantitative proteomics, tumor migration and invasiveness

INTRODUCTION

Cancer has rapidly grown in global incidence and mortality in recent years and is expected to become the leading cause of death from the non-communicable disease according to GLOBOCAN (1). Thyroid cancer is the most common endocrine malignancy, and its incidence was the highest among all cancers in the United States between 2000 and 2009 (2). Approximately 85% of

histological subtypes of thyroid cancer are papillary thyroid cancer (PTC). Although the death rate of PTC is relatively low following surgery with or without concomitant radioiodine treatment, the morbidity and mortality of PTC patients are increased greatly due to lymph node metastases (LNMs) or distant metastasis (3).

PTC is MAPK-driven cancer characterized by mutually exclusive drivers including $BRAF^{V600E}$ and mutated *RAS* (4). Importantly, the BRAF V600E oncoprotein (encoded by the $BRAF^{V600E}$ mutation) is a typical member of MAPK signaling pathway, occurring in 40%–60% of PTC patients (3). Furthermore, Xing M demonstrated that activation of MAPK signaling pathway resulted in upregulation of tumor-promoting genes (e.g. *VEGFA*, *MET*, *HIF1A, UPA*, *UPAR*, *TGFB1*, and *TSP1*) as well as downregulation of tumor suppression and thyroid genes (e.g. *TIMP3*, *SLC5A8*, *DAPK1*, *NIS, TSHR*, and *TPO*) (2). Recently, the framework of $BRAF^{V600E}$-*RAS* gene expression scores in The Cancer Genome Atlas (TCGA) indicated that PTCs differentiate into $BRAF^{V600E}$-like and *RAS*-like PTCs (5). All these studies indicated that the MAPK signaling pathway (upregulated in tumors with the $BRAF^{V600E}$ mutation) is associated with PTC aggressiveness. However, the phase 2 trial of vemurafenib targeting BRAF-mutated PTC patients showed only a 38.5% response rate, which is considerably lower than that in patients with BRAF-mutated melanoma (6). Therefore, it needs to distill an enhanced understanding of the pathogenesis of PTC patients.

Asporin belongs to the class I small leucine-rich proteoglycan (SLRP) family, which also includes biglycan and decorin (7). The name "asporin" refers to its unique aspartate resides (D-repeat) in its N-terminal domain and its 54% identity with the sequence of decorin (8). Asporin contains 380 amino acids and its D-repeat polymorphisms (residues 8–19) in the N-terminus are correlated with osteoarthritis and metastatic recurrence of prostate cancer (7, 9). Although decorin acts as a tumor suppressor and biglycan is regarded as an oncogene, asporin exerts tumor-suppressor function in triple-negative breast cancer but exerts tumor-promotor function in some types of cancer, including breast, pancreatic, colorectal, gastric, and prostate cancer (10). For example, asporin binds directly to extracellular TGF-β1 in triple-negative breast cancer and its downstream cytoplasmatic component Smad 2/3 in colorectal cancer, resulting in inhibition or activation of the TGF-β1 signaling pathway, respectively (11, 12). Therefore, it is unsurprising that asporin plays different roles depending on binding different proteins. A growing body of evidence now demonstrates that asporin acts as an extracellular matrix component or intracellular protein that positively or negatively controls proliferation, invasion, and metastasis of cancer cells by regulating the TGF-β, EGFR, and CD44 signaling pathways (10). A previous study indicated that asporin is expressed at moderate levels in thyroid normal tissues (8); however, the biological roles of asporin in thyroid cancer progression have never been investigated. The present study contributes to this field by demonstrating that asporin interacts with HER2 to promote thyroid cancer metastasis by regulating the MAPK-epithelial-to-mesenchymal transition (EMT) axis.

MATERIALS AND METHODS

Patients and Specimens

In total, 106 PTC patients were recruited from the department of head and neck surgery, Peking University Cancer Hospital & Institute, People's Republic of China. The use of human materials in this study was approved by the Ethics Committee of Peking University Cancer Hospital & Institute and informed consent was obtained from all patients. Tumorous and paired normal tissues from 53 PTC patients were used in Western blotting, immunohistochemistry (IHC), and tandem mass tag (TMT)-based mass spectrometry (MS)/MS assays. Serum samples from another 53 PTC patients were analyzed by ELISA. Tissues collected from surgical procedures and serum samples were immediately snap-frozen in dry ice and then stored at –80°C. The clinicopathological parameters of all these PTC patients are summarized in **Supplementary Table 1**.

Co-Immunoprecipitation

Immunoprecipitation was performed as previously described (13, 14). Briefly, whole-cell extracts were obtained with RIPA buffer (ab156034; Abcam) containing 1 mM PMSF and a protease inhibitor cocktail (04693132001; Roche). After centrifugation at 12,000 ×*g* for 20 min at 4°C, soluble proteins were quantified by BCA. Samples (1 mg) of proteins precleared with 30 μl protein A/G Plus-Agarose (sc-2003; Santa Cruz) were used for each immunoprecipitation experiment. Proteins were incubated with 2 μg antibodies and 30 μl protein A/G Plus-Agarose. Immunoprecipitated materials were washed four times with ice-cold wash buffer (0.1% Triton X-100, 50 mM Tris-HCl, pH 7.4, 300 mM NaCl, 5 mM EDTA, 0.02% sodium azide) and once more using 1 ml ice-cold PBS. Bound proteins were separated by SDS-PAGE, transferred onto PVDF membranes, and immunoblotted with the appropriate antibodies. Signals were detected with Enhanced Chemiluminescence kits (Millipore) according to the manufacturer's instructions. Band intensity was measured using FluorChem Q 3.4.0 software.

IHC and Evaluation of Staining

Tissue sections (5 μm thick) were de-waxed at 60°C for 30 min followed by two 5-min washes with xylene. The sections were then rehydrated by sequential 5-min washes in 100%, 95%, and 80% ethanol and distilled water. Antigen retrieval was performed by heating the tissues at 95°C for 10 min in 0.01 M citrate buffer (pH 6.0). The endogenous peroxidase activity of the tissues was blocked by 3% hydrogen peroxide for 30 min, followed by incubation with primary detection antibodies overnight at 4°C. The sections were then incubated with the Polink-2 Plus® HRP Polymer Detection System (PV-9001 and PV-9002; ZSGB-BIO) according to the manufacturer's instructions. The samples were developed using the 3, 3′-diaminobenzidine (DAB) substrate (Dako), and counterstained with hematoxylin.

The immunohistochemical staining was evaluated according to percentage and intensity. The percentage of positive cells was scored as 0–4 (0 = <10% cells; 1 = 10%–30% cells, 2 = 30%–50% cells, 3 = 50%–70% cells, and 4 = >70% cells), and the staining intensity of the positive cells was scored as 0–3 (0 =

no staining, 1 = weak staining, 2 = intermediate staining, and 3 = strong staining). The percentage and intensity scores were summed to obtain the final immunohistochemical staining scores ranging from 0–7. Based on these scores, the protein expression level was classified into three groups: 0–2 = negative staining; 3–5 = moderate staining; and 6–7 = high staining.

Immunofluorescence Staining

Immunofluorescence staining was performed as previously described (15). Briefly, BCPAP and KTC-1 cells were washed three times with PBS, fixed in 4% paraformaldehyde for 20 min, permeabilized with 0.2% Triton-X 100 for 15 min, and then blocked with 5% BSA for 60 min. Cells were incubated with primary detection antibodies (anti-asporin and anti-HER2 (sc-7301); Santa Cruz) at 4°C overnight. Cells were then incubated with appropriate secondary detection antibodies [Alexa Fluor Plus 555-conjugated anti-mouse (A32727; Thermo Fisher) or anti-rabbit (A32727) antibody and Alexa Fluor 488-conjugated anti-rabbit (A11034; Thermo Fisher)]. Cell nuclei were stained with DAPI (Sigma) at a final concentration of 0.1 mg/mL. Fluorescent images were captured on a laser confocal microscope (LSM780; ZEISS).

Transfection of Thyroid Cancer Cell Lines

Poorly differentiated thyroid cancer cell lines [B-CPAP (RRID: CVCL_0153) and KTC-1 (RRID: CVCL_6300)] and anaplastic thyroid cancer (ATC) cell lines [BHT-101 (RRID: CVCL_1085)] were kindly provided by the Stem Cell Bank of the Chinese Academy of Sciences. BCPAP and KTC-1 cells were cultured in RPMI 1640 supplemented with 10% FBS and 1% non-essential amino acids (Invitrogen, USA). BHT101 cells were cultured in DMEM supplemented with 20% FBS. All human cell lines have been authenticated using short tandem repeat profiling within this year, and all experiments were performed with mycoplasma-free cells. Small interfering RNAs (siRNAs) were obtained from Guangzhou RiboBio (China). Three siRNAs targeting the *Asporin* gene were designed and synthesized (siRNA2: 5'-GTGACGG TGTTCCATATCA-3'; siRNA4: 5'-GGAGTATGTGCTCCTAT TA-3'; siRNA5: 5'-GTGCTATTCACGAGTTGTA-3'). At the time of transfection, cells were plated onto a 6-well plate at 60%–80% confluence. Transfection was performed with RNAiMAX (13778-150; Thermo Fisher) according to the manufacturer's protocol. RNAiMAX reagent (7.5 μL) and siRNAs were diluted in Opti-MEM and incubated at room temperature for 15 min. The mixtures were then added to cells, giving a final concentration of siRNAs of 30 pmol. BCPAP, KTC-1, and BHT101 cells were cultured for 72 h after transfection and were subsequently lysed in RIPA buffer (ab156034; Abcam).

Drug Treatment

For the Afatinib assay, BCPAP and KTC-1 Cells (4×10^5) were incubated with 100 ng/ml EGF (236-EG-200; R&D Systems) for 20 min, and then incubated with or without 1 μmol/L Afatinib (S1011; Selleckchem) for 2 h. For the PLX4032 assay, BCPAP and KTC-1 Cells (4×10^5) were also incubated with 100 ng/ml EGF for 20 min and then incubated with or without 2 μmol/L PLX4032 (S1267; Selleckchem) for 4 h. After Afatinib and PLX4032 treatment, BCPAP and KTC-1 Cells were washed with ice-cold PBS three times, and whole-cell lysates were subjected to SDS–PAGE and incubated with p-EGFR^{Y845}, p-ERK1/2, t-ERK1/2, SLUG, ZEB1, ZEB2, and β-actin antibodies, respectively.

In Vitro Assays of Cell Migration and Invasion

The migratory and invasive potentials of the BCPAP, KTC-1 and BHT101 cell lines were evaluated as described previously (16). Briefly, 3×10^4 cells suspended in RPMI 1640 or DMEM media were seeded in the upper chamber of the Transwell (3422; Corning) coated with 100 μl 2% Matrigel (356234; Corning). RPMI 1640 or DMEM supplemented with 10% FBS was placed in the lower chamber as the source of chemoattractant. After 24 h of 37°C incubation, the cells remaining on the upper surface of the insert were removed using a cotton swab, and the cells on the lower surface were fixed with anhydrous methanol for 30 min and then stained with 0.2% crystal violet solution (V5265-250ML; Sigma). For each insert, cells in the center and five randomly selected peripheral fields were assessed under an inverted microscope. Migration assays were performed using the invasion assay method, except that 5×10^4 cells were seeded into the upper chamber that was not coated with Matrigel.

Cell Proliferation And Colony Formation Assays

Cell proliferation assays were performed using the Cell Counting Kit-8 (96992; Sigma) according to the manufacturer's protocol. Briefly, 5×10^3 BCPAP and KTC-1 cells in suspension were seeded into a 96-well plate (100 μl/well). After incubating the plate in a humidified incubator (37°C, 5% CO_2) for 24, 48, 72, and 96 h, 10 μL CCK-8 solution was added to each well. After incubating the plate for 2 h, the absorbance values at 450 nm and 600 nm were measured using a microplate reader (Multiskan FC; Thermo Scientific). For the colony formation assay, 3×10^3 BCPAP and KTC-1 cells suspended in RPMI 1640 containing 10% FBS were added to each well of a 6-well plate. Cells were cultured for 14 days at 37°C, and colonies were counted in three independent experiments.

TMT-Based MS/MS Analysis and Protein Identification

TMT-based MS/MS analysis was performed as previously described (17, 18). Briefly, according to the lymph node status, 48 thyroid tissues from 24 PTC patients were pooled as follows: tumorous tissues from PTC patients with N0 (N0_T), tumorous tissues from PTC patients with N1a (N1a_T), tumorous tissues from PTC patients with N1b (N1b_T), and paired normal tissues from all PTC patients (N0_N, N1a_N, and N1b_N). The four groups of proteins were reduced by incubation with 10 mM DTT for 30 min at 55°C, alkylated with 25 mm IAA for 30 min at room temperature in the dark, and then incubated with trypsin/Lys-C mix at a protein/protease ratio of 25:1 for 12 h at 37°C. Subsequently, TMT isobaric label reagents (0.8 mg TMT dissolved in 40 μL 99.9% acetonitrile) were used separately according to the manufacturer's instructions to label each

group of peptides as follows: TMT-126 for N1b_T; TMT-127 for N0_T; TMT-128 for N1a_T; TMT-131 for N0+N1a+N1b_N. All the labeled peptides in the four groups were then combined for subsequent high-performance liquid chromatography (HPLC) and LC-MS/MS analysis (18).

The MS/MS raw data were analyzed against the human reviewed Swiss-Prot FASTA database (released on 2018.03.02) using Proteome Discoverer software (Version 2.1, Thermo Scientific). The following search criteria were applied: carbamidomethylation (C, +57.021 Da) and TMT-6plex (K and peptide N-terminus) as fixed modifications and oxidation (methionine, M) as a variable modification. A maximum of two missed trypsin/Lys-C cleavages was allowed. The false discovery rate (FDR) was determined based on searches of the peptide spectrum matched against the reversed decoy database. The FDRs for peptide and protein identification were both set to 0.01. The MS/MS raw data were deposited in the ProteomeXchange Consortium *via* the PRIDE partner repository with the dataset identifier PXD007971.

Bioinformatic Analysis

The two-sided 95% prediction interval of the combined ratio distribution was used to identify the cutoffs for differentially expressed proteins (DEPs) (set as ≥1.7-fold or ≤0.4-fold) using JMP Pro 13.2.1 software (**Supplementary Figure 1A**). Gene ontology (GO) and pathway enrichment analyses were performed using the Funrich tool (Version 3.1.3). The protein-protein interaction (PPI) analysis was performed and visualized using the stringAPP plugin in Cytoscape (Version 3.7.0), with a confidence cutoff set at 0.4. TCGA-Assembler 2 software was used to download the normalized RNA-seq by expectation-maximization (RSEM) data and clinicopathological parameters of thyroid cancer (THCA) from TCGA (19). Upregulated mRNA expression was defined as a Z-score ≥1, whereas downregulated mRNA expression was defined as a Z-score ≤−1 according to the previous study (20).

Statistical Analysis

All statistical analyses were performed using SPSS 19.0 (IBM Corp., Armonk, NY, USA) and JMP Pro 13.2.1 software. Each experiment was repeated at least 3 times. ANOVA was used to evaluate differences among different groups and Tukey's HSD was further applied for pairwise comparisons. Mann–Whitney or Kruskal–Wallis tests were used to analyze the relationship between *asporin* mRNA expression and clinicopathological characteristics. The Kaplan–Meier method was used to evaluate progression-free survival (PFS) and overall survival (OS). Receiver operating characteristic (ROC) curves were generated to evaluate the diagnostic value of serum asporin in thyroid cancer. Two-tailed $P < 0.05$ was considered to indicate statistical significance.

RESULTS

Overview of Proteomic Profiles and Corresponding Bioinformatic Analysis

To comprehensively investigate the underlying mechanisms of PTC tumorigenicity with different degrees of LNMs, we obtained the global protein profiles of PTC tissues by performing TMT-based MS/MS. A total of 7,657 proteins were identified, of which 5,965 high confidence proteins without keratin were extracted with stringent criteria (q-value <0.01, unique peptide ≥2). The abundance of these 5,965 proteins was analyzed by non-supervised principal component analysis (PCA). Tumorous tissues in PTC-N0, PTC-N1a, and PTC-N1b were separated from pooled paired normal tissue (Npool_N) in Component 1, indicating that proteomic profiles in PTC tumorous tissues were distinct from paired normal tissues. Furthermore, tumorous tissues in PTC with different degrees of LNM also exhibited different profiles in terms of protein expression, resulting in a separate cluster in Component 2 (**Supplementary Figure 1B**). In further exploration of the patterns of variation among tumorous tissues in PTC-N0, PTC-N1a, and PTC-N1b, we obtained a total of 609 DEPs (q-value < 0.01, unique peptide ≥ 2, and fold change ≥ 1.7-fold or ≤ 0.4-fold) for hierarchical clustering analysis. The ratios of these 609 DEPs were grouped hierarchically into five clusters, of which 430 DEPs in cluster 5 were upregulated in N0_T, N1a_T, and N1b_T (**Figure 1A**). To further explore the biological significance of these DEPs, we performed GO and pathway enrichment analyses of these 430 DEPs. The majority of these DEPs were mainly involved in metabolism, energy pathways, cell growth, and extracellular matrix structural constituents (**Figure 1B**), which are the pathological hallmarks of cancer (21). Therefore, 70 DEPs enriched in these categories were extracted and average ratios were used to construct the PPI network. Of particular note, these DEPs were closely linked and upregulated in PTC tumorous tissues compared to the levels expressed in pooled normal tissues (**Figure 1C**).

Verification of DEPs by Western Blotting and IHC Analyses

To further validate our proteomics data, five core DEPs (VCAN, PLS3, SERP1NA1, CD55, and asporin) enriched in three different categories of PPI were analyzed by Western blotting (**Figure 2A**). VCAN, PLS3, SERP1NA1, CD55, and asporin were confirmed to be upregulated in in PTC-N0, PTC-N1a, and PTC-N1b tumorous tissues (**Figures 2A, B**); β-actin was used as an internal control. Thus, the Western blotting results were consistent with our proteomics data, and the average ratios of these five DEPs [e.g., Ratio_ave (asporin) = (N0_T/Npool_N + N1a_T/Npool_N + N1b_T/Npool_N)/3)] were 3.60, 1.84, 2.91, 2.02, and 2.31, respectively (**Figure 2C**). Asporin was selected for further investigation based on the following criteria: (a) Asporin acts as an oncogene in pancreatic, colorectal, gastric, and prostate cancer (10); (b) The roles of asporin in thyroid cancer have not been reported based in searchers of PubMed or Google. IHC performed in an independent set of PTC patients confirmed that the IHC scores of asporin were also increased in PTC tumorous tissues (**Figures 2D, E**). Furthermore, IHC staining indicated that asporin is expressed mainly in the extracellular matrix, cell membrane, and cytoplasm. Typical images of IHC staining of asporin expression are shown in **Figure 2E**. To further investigate the roles of asporin in PTC tumorigenesis, asporin RSEM data and corresponding clinicopathological parameters were successfully retrieved from the TCGA-THCA cohort.

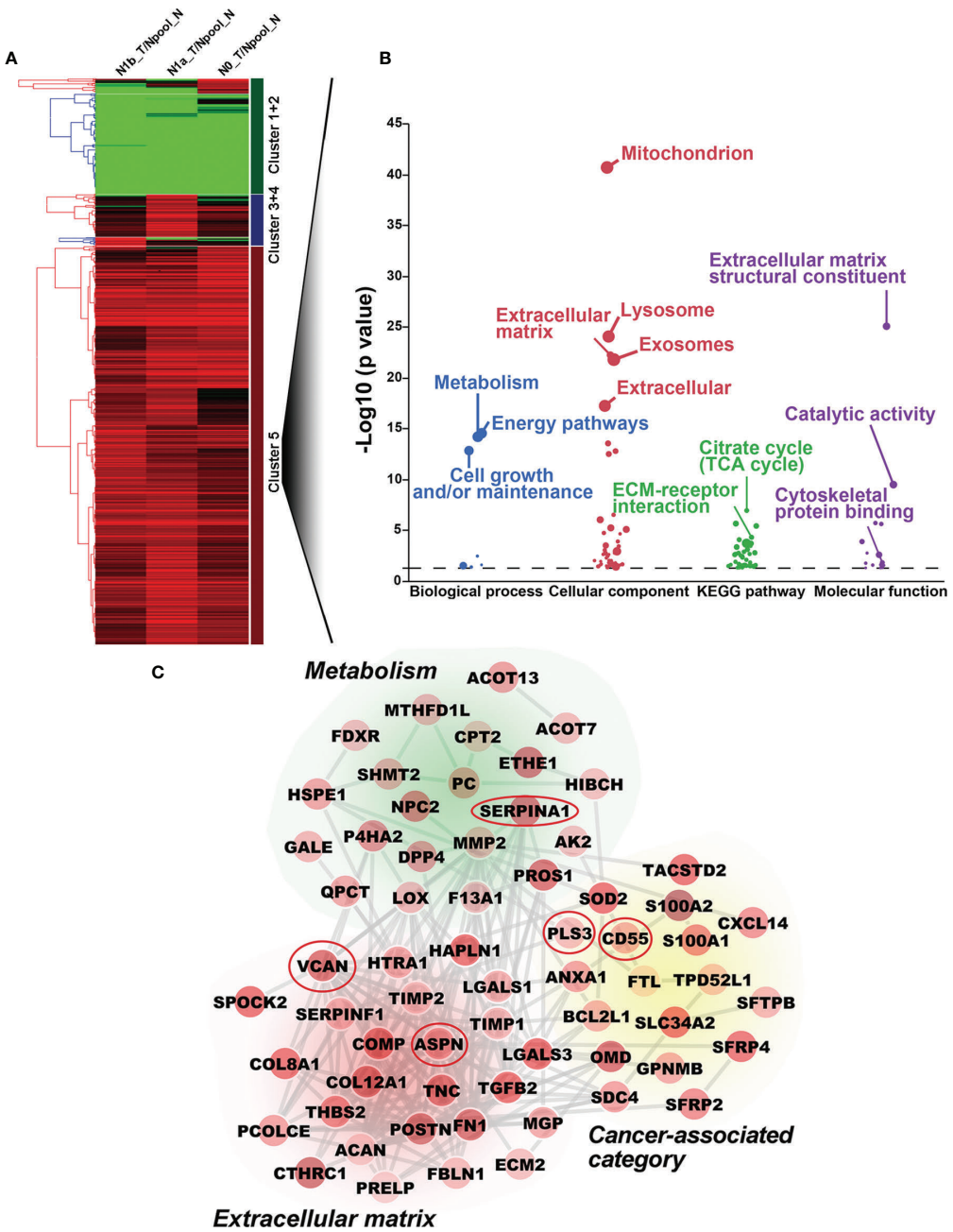

FIGURE 1 | Bioinformatic analysis of differentially expressed proteins (DEPs) by TMT-based MS/MS. **(A)** Hierarchical cluster analysis of DEPs. Upregulated and downregulated DEPs are shown in red and green, respectively. Five clusters are shown on the left of the heatmap. **(B)** Gene ontology and pathway enrichment analysis of DEPs in Cluster 5. The biological process, cellular component, biological pathway, and molecular function are shown in blue, red, green, and purple, respectively. **(C)** Protein-protein interaction network was constructed with DEPs; no connective DEPs were excluded. The average ratios of DEPs are reflected by color intensity. Upregulated and downregulated DEPs are shown in red and green, respectively. Five DEPs included in the red ovals were further investigated by Western blotting analysis.

This dataset showed that the high-level Z-scores of asporin were positively correlated with PTC patients with larger tumor classification ($P < 0.001$), LNM ($P < 0.001$), high AJCC staging ($P < 0.001$), and $BRAF^{V600E}$ mutation ($P < 0.001$) (**Table 1**). Furthermore, we found that *asporin* mRNA expression showed a significant positive association with EMT-activating transcription factors (EMT-TFs), including *β-catenin* (r = 0.207, $P < 0.001$), *SLUG* (r = 0.706, $P < 0.001$), *ZEB1* (r = 0.428, $P < 0.001$), and *ZEB2* (r = 0.522, $P < 0.001$) (**Figure 4C**). These results suggested that asporin may exert a vital

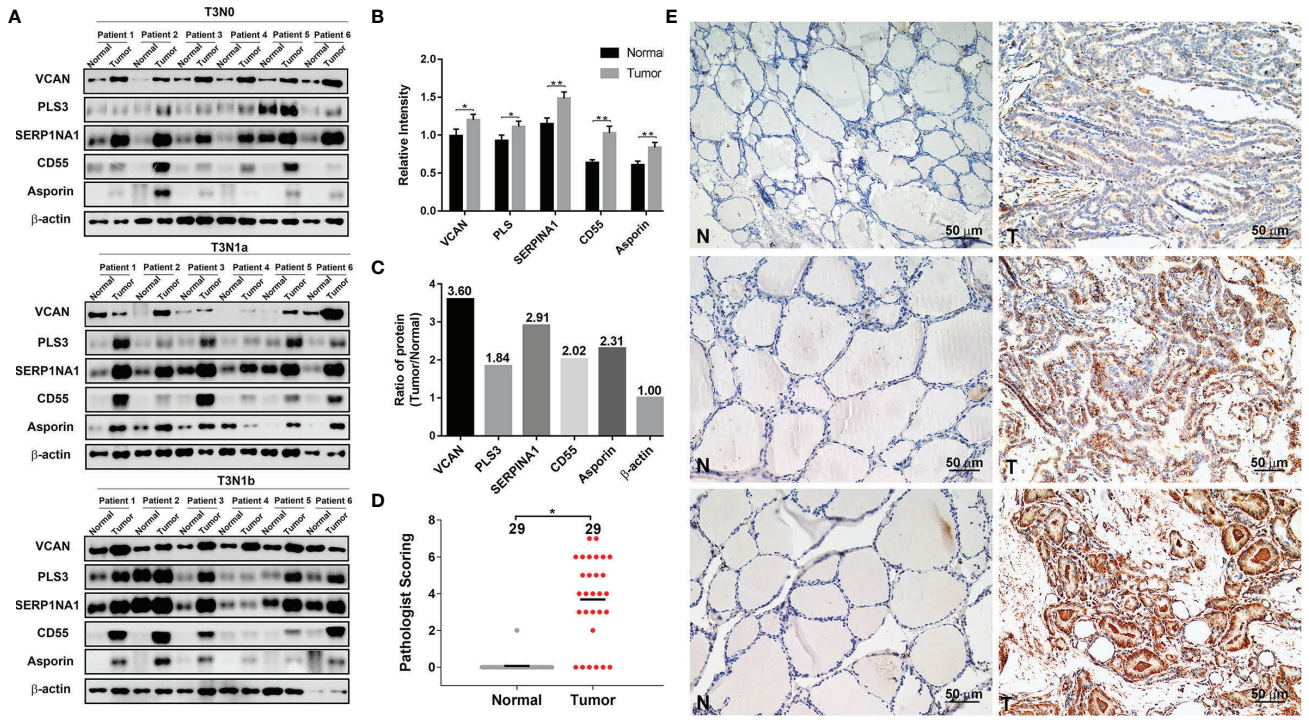

FIGURE 2 | Validation of five differentially expressed proteins (DEPs) by Western blotting and IHC analyses. **(A)** VCAN, PLS3, SERP1NA1, CD55, and asporin protein levels were validated by Western blotting analysis; β-actin was used as the loading control. **(B)** Quantification of the indicated five DEPs relative to β-actin. **(C)** The average ratios of the indicated five DEPs were identified in the TMT-based proteomics data relative to β-actin. **(D)** Histopathological scoring of asporin in 29 paraffin-embedded PTC tumorous tissues and paired normal tissues. $^{*}P < 0.05$, $^{**}P < 0.01$. **(E)** Representative images of immunohistochemical labeling of asporin in PTC tumorous tissues and paired normal tissues. Asporin was expressed mainly in the extracellular matrix, cell membrane, and cytoplasm of PTC tumorous tissues, while a very low or no signal was detectable in paired normal tissues. Paired normal (N) or tumorous (T) tissues are marked with dotted lines. Scale bars, 50 μm.

tumor-promoting function in PTC by regulating the MAPK/EMT axis.

Knockdown of Asporin Inhibits Cell Growth, Migration, and Invasion of Thyroid Cancer Cells

To further examine the ability of asporin to enhance tumor progression in thyroid cancer, we knocked down endogenous *asporin* expression in thyroid cancer cell lines by transfection with three siRNAs (**Figures 4A, B**). Compared to the cells transfected with the scramble control, CCK-8 assays showed that *asporin* knockdown inhibited the viability of BCPAP and KTC-1 cells (**Figures 3A, B**). Furthermore, siASPN also decreased the number of colonies in the colony formation assays (**Figures 3C, D**), further indicating that *asporin* knockdown inhibits the growth of thyroid cancer cells. Next, we performed Transwell assays to examine the effects of *asporin* knockdown on the invasive and metastatic potential of these cells. We found that transfection with siASPN decreased the migratory and invasive ability of BCPAP and KTC-1 cells (**Figures 3E, F**). Interestingly, migration and invasion assays showed that siASPN also significantly decreased the ability of BHT101 cells (ATC cell line) to penetrate the Transwell membrane with or without Matrigel-coating (**Supplementary Figure 2**). These results suggested that *asporin* knockdown significantly inhibits the metastatic potential of thyroid cancer cells.

Asporin Knockdown Impairs the Malignant Phenotype of Thyroid Cancer Cells by Inhibiting the MAPK/EMT Axis

Next, we investigated the molecular mechanism by which asporin promotes the malignant phenotype in thyroid cancer. TCGA-THCA cohort analysis indicated that *asporin* mRNA expression was positively associated with MAPK pathway activation and EMT-related mRNA expression. Western blotting analysis showed that asporin knockdown reduced p-ERK1/2 protein levels, but not t-ERK1/2 protein levels in BCPAP and KTC-1 cells (**Figures 4A, B**). Furthermore, siRNA-mediated silencing of asporin also resulted in the downregulation of EMT-TFs, including SLUG, ZEB1, and ZEB2, which is the downstream of the MAPK signaling pathway (**Figures 4A, B**). Of particular note, we also found that siRNA-mediated silencing of asporin resulted in the downregulation of p-ERK1/2, TWIST1, SLUG, ZEB1, and ZEB2 protein levels, and upregulation of E-cadherin in BTH101 cells (**Supplementary Figure 3**). These results indicated that asporin knockdown inhibited the tumorigenicity of thyroid cancer cells by hindering activation of the MAPK

TABLE 1 | Correlations of *Asporin* mRNA expression in tumorous tissues with clinicopathological characteristics.

Characteristics	*Asporin* mRNA expression (Z scores)				
	No.	Low (≤-1)	Moderate (-1 to 1)	High (≥1)	*P*-value
Age					
<45 years	221	30	165	26	0.29
≥45 years	269	35	181	53	
Sex					
Male	130	18	91	21	0.263
Female	360	47	255	58	
Multifocality					
Solitary	262	41	174	47	0.056
Multiple	218	22	164	32	
Tumor classification					
T1+T2	303	41	235	27	**<0.001**
T3+T4	185	24	109	52	
Lymph node classification					
N0	225	33	169	23	**<0.001**
N1	215	27	136	52	
AJCC Staging					
Stage I+II	324	44	250	30	**<0.001**
Stage III+IV	164	21	94	49	
$BRAF^{V600E}$mutation					
Yes	231	24	156	51	**<0.001**
No	245	39	181	25	

P-value indicates the probability from the nonparametric Mann–Whitney test. Bold text indicates P < 0.05.

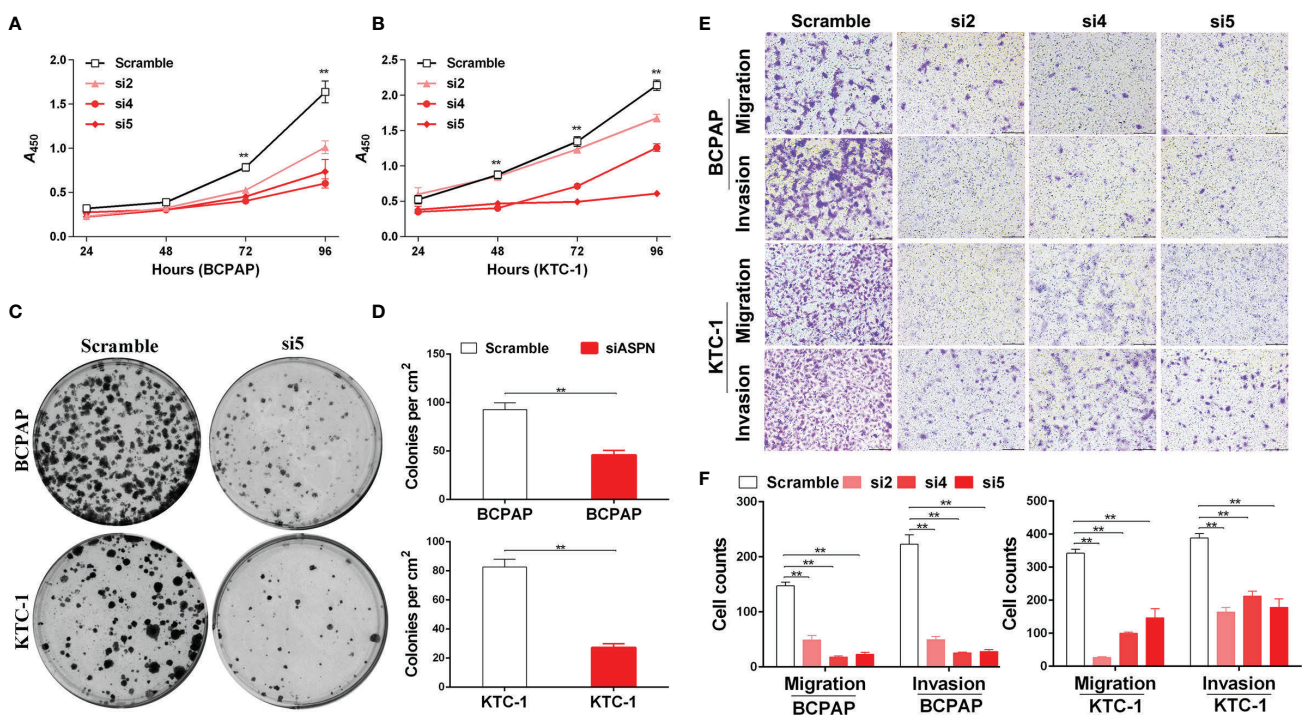

FIGURE 3 | The knockdown of asporin inhibits thyroid cancer cell growth, migration, and invasion. **(A)** CCK-8 assay of the growth rates of control or siASPN BCPAP cells. Data represents the mean ± SD of three independent experiments. $^{**}P < 0.01$(si4-si5 cultured for 72-96 h) **(B)** Growth rates of control or siASPN KTC-1 cells. $^{**}P < 0.01$(si4-si5 cultured for 48-96 h,and si2 cultured for 96 h). **(C)** Representative images of colony formation in BCPAP and KTC-1 cells. **(D)** The number of clones counted in three independent experiments. Data are expressed as mean ± SD. $^{**}P < 0.01$. **(E)** Representative images of Transwell assays of BCPAP and KTC-1 cell migration and invasion. **(F)** Cells that migrated across the chamber membrane were stained with 0.2% crystal violet solution and counted. Data represents the mean ± SD. $^{**}P < 0.01$.

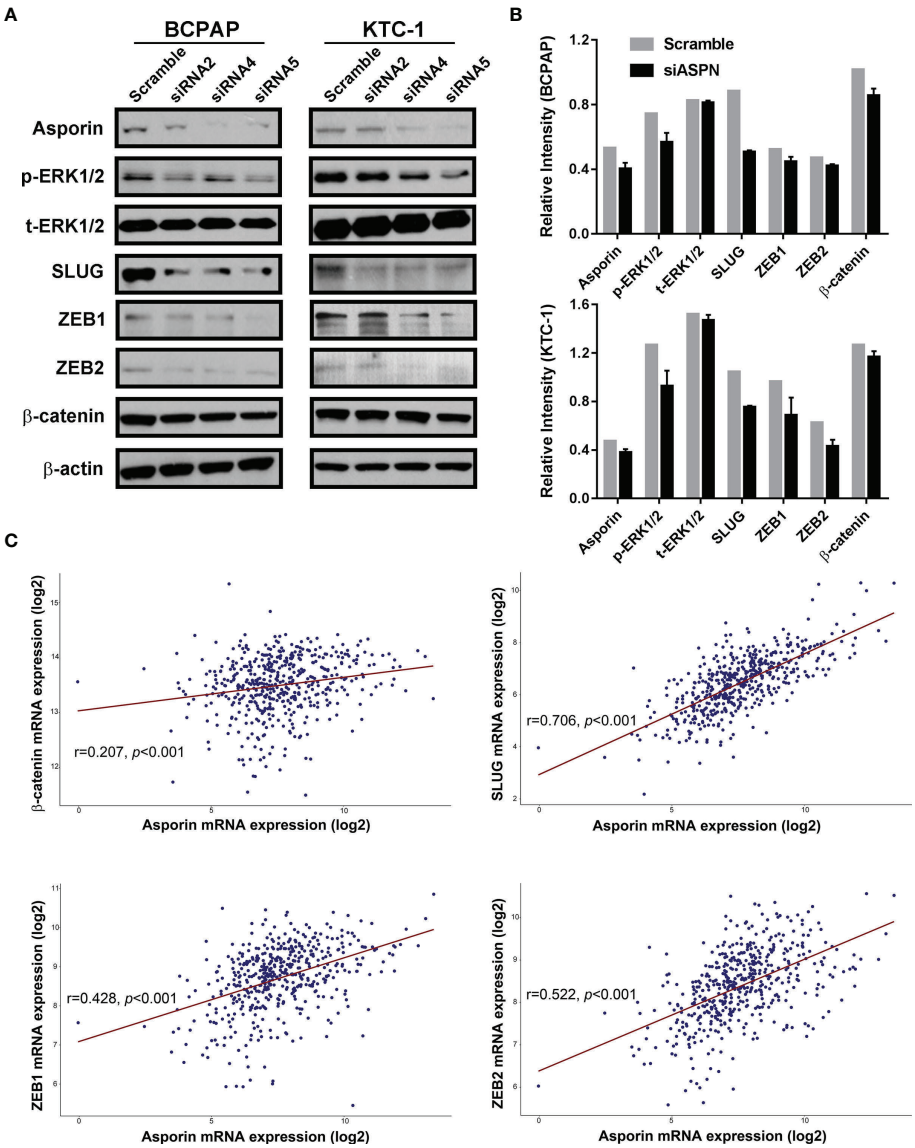

FIGURE 4 | Asporin knockdown impairs the malignant phenotype of thyroid cancer cells by inhibiting the MAPK/EMT axis. **(A)** Knockdown of asporin using three siRNAs (siASPN). Levels of proteins in the MAPK signaling pathway and its downstream EMT-TFs were downregulated in the siASPN cells, including p-ERK1/2, SLUG, ZEB1, and ZEB2. The results presented are representative of at least 3 independent experiments. **(B)** Quantification of protein levels in control and siASPN cells relative to β-actin. **(C)** TCGA-THCA cohort data analysis indicated that asporin mRNA expression was positively correlated with the expression of some EMT-TFs mRNAs, including β-catenin, SLUG, ZEB1, and ZEB2.

signaling pathway and downregulating its downstream EMT-TFs to impair the migration and invasiveness of thyroid cancer cells.

Asporin Interacts With HER2 and Activates the HER2 Signaling Pathway

Numerous studies have shown that the MAPK signaling pathway is activated by members of the EGF family, including EGFR and HER2 (22). We investigated the ability of asporin to interact with members of the EGF family in PTC using endogenous co-IP assays. Asporin was coprecipitated with HER2 but not with EGFR and SRC (**Figure 5A**), and conversely, HER2 was coprecipitated with asporin (**Figure 5B**). Furthermore, immunofluorescence assays revealed the co-localization of asporin and HER2 on the cell membrane and in the cytoplasm of BCPAP and KTC-1 cells (**Figure 5C**). These results indicated that asporin and HER2 form a complex. Knockdown of asporin expression in BCPAP and KTC-1 cell lines reduced HER2, p-HER2^{Y1248}, p-SRC^{Y418}, p-EGFR^{Y845}, and p-EGFR^{Y1173} expression, but not SRC and EGFR levels (**Figures 5D, E**). These results suggested that asporin could bind HER2 to maintain its expression level, and asporin knockdown could

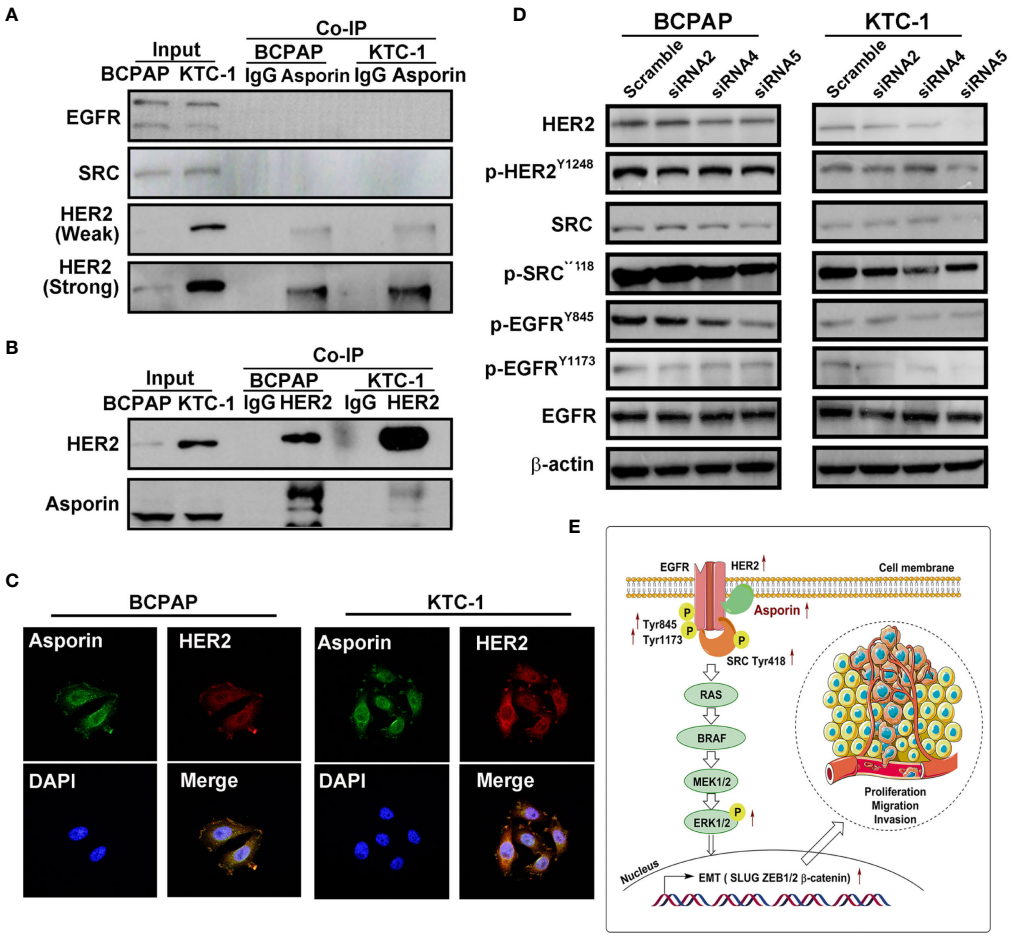

FIGURE 5 | Asporin interacts with HER2 and activates the HER2 signaling pathway. **(A, B)** Endogenous co-immunoprecipitation (co-IP) assay revealed co-IP of asporin with HER2, but not with EGFR and SRC, and conversely, HER2 was coprecipitated with asprorin; IgG was used as the isotype control. The results presented are representative of at least 3 independent experiments. **(C)** Immunofluorescence staining of asporin (green) and HER2 (red) in BCPAP and KTC-1 cells. Merged images with DAPI staining. Asporin colocalizes with HER2 in the cell membrane and cytoplasm. One representative result of at least 3 independent experiments was shown. **(D)** Equal amounts of proteins in siASPN or control cells were analyzed by immunoblotting with the indicated antibodies. **(E)** Proposed working model for asporin promoting thyroid cancer metastasis by regulating the HER2/SRC/EGFR/MAPK/EMT axis.

subsequently downregulate the expression of p-EGFR and p-SRC in BCPAP and KTC-1 cell lines.

Afatinib and PLX4032 Mimic the Effects of Asporin

Our results suggest that reduced MAPK pathway activity is due to lower EGFR/HER2 signaling which mediates the decrease in EMT regulating genes by Asporin knockdown. To confirm these results, pharmacological inhibitor assays were performed to confirm whether Afatinib (EGFR inhibitor) or PLX4032 (MAPK inhibitor) can mimic the effects of Asporin knockdown on SLUG, ZEB1, and ZEB2 expression. We found that BCPAP and KTC-1 cells treated with Afatinib can downregulate p-EGFR^{Y845}, p-ERK1/2, SLUG, ZEB1, and ZEB2 expression, but not t-ERK1/2 (**Figure 6A**). Furthermore, PLX4032 treatment results in the downregulation of p-ERK1/2, SLUG, ZEB1, and ZEB2 protein levels in BCPAP and KTC-1 cells, but not t-ERK1/2 (**Figure 6B**).

Clinical Applications of Asporin in PTC

Our *in vitro* results raised the possibility that the upregulation of asporin in serum represents a candidate biomarker in PTC. Accordingly, we examined the serological asporin levels in 54 PTC patients and 11 healthy volunteers by ELISA. The serum levels of asporin in PTC were higher than those in healthy volunteers ($P < 0.05$) (**Figure 7A**). We then used ROC curve analysis to determine the sensitivity and specificity of asporin as a biomarker in PTC. The area under the ROC curve (AUC) of asporin for discriminating PTC patients from healthy controls was 0.73, and the optimal Youden's index was 0.407 (sensitivity = 0.679, specificity = 0.727) (**Figure 7B**). More importantly, serum levels of asporin in PTC-N1a and PTC-N1b patients were higher than those of healthy volunteers and PTC-N0 patients ($P < 0.01$) (**Figure 7C**). The AUC of asporin for discriminating PTC-N1a and PTC-N1b patients with PTC-N0 patients was 0.84, and the optimal Youden's index was 0.59 (sensitivity = 0.667,

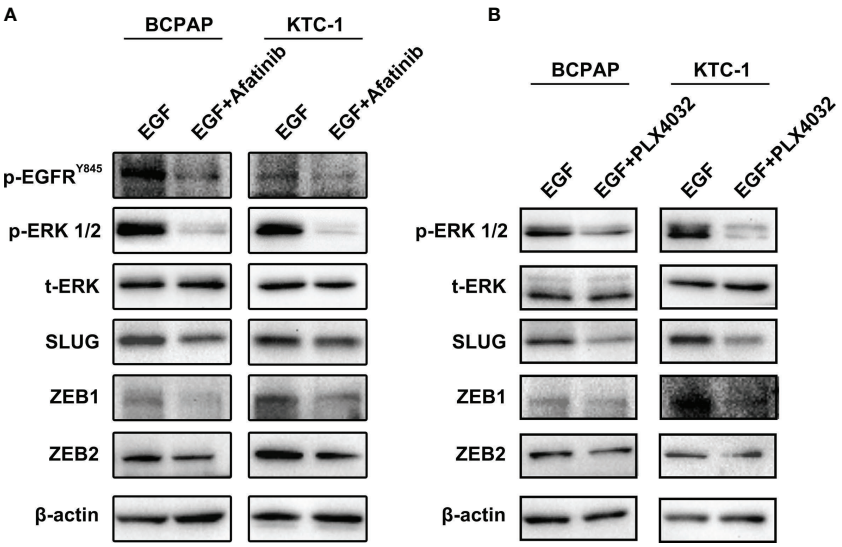

FIGURE 6 | Afatinib and PLX4032 mimic the effects of Asporin knockdown on SLUG, ZEB1, and ZEB2, expression. **(A)** Afatinib treatment can downregulate p-EGFRY845, p-ERK1/2, SLUG, ZEB1, and ZEB2 expression, but not t-ERK1/2. **(B)** PLX4032 treatment results in the downregulation of p-ERK1/2, SLUG, ZEB1, and ZEB2 protein levels, but not t-ERK1/2.

specificity = 0.923) (**Figure 7D**). These results implicated asporin as a serological biomarker that can be used to identify PTC patients with or without lymph node metastasis. Furthermore, we referred to the TCGA-THCA cohort to investigate the potential correlation of asporin expression with OS or PFS. Kaplan–Meier analysis indicated that high Z-scores for asporin in tumorous tissues were associated with significantly worse PFS (P = 0.027) and OS (P = 0.002) than those of patients with normal/low Z-scores (**Figures 7E, F**). Therefore, elevated asporin expression in tumorous tissue was found to correlate positively with a poorer prognosis, thus, also implicating asporin as a novel candidate prognostic biomarker.

DISCUSSION

Our study revealed distinct tumorous protein profiles among PTC with different degrees of LNMs and showed that DEPs in tumorous tissues are mostly enriched in the extracellular matrix, metabolism, and cell growth. The proteomics data were validated by Western blotting analysis of VCAN, PLS3, SERP1NA1, CD55, and asporin, which were confirmed to be upregulated in PTC tumorous tissues with different degrees of LNMs. Asporin was found to be expressed mainly in the extracellular matrix, cell membrane, and cytoplasm of PTC tumorous tissues, and promoted thyroid cancer cell proliferation, migration, and invasion. Asporin was also shown to co-localize with HER2 on the cell membrane and in the cytoplasm of PTC cells. Furthermore, we showed that the asporin/HER2/SRC/EGFR axis upregulated the expression of EMT-TFs *via* the MAPK signaling pathway (**Figure 5E**). Finally, ELISA assay implicates asporin as a serological biomarker to identify PTC patients with or without lymph node metastasis, and high expression of asporin in PTC tumorous tissues is a risk factor for poor prognosis.

In colorectal cancer, Wu et al. demonstrated that asporin promoted cancer cell proliferation and metastasis *via* the EGFR/SRC/cortactin signaling pathway (23). Furthermore, Ding et al. suggested that asporin also promoted tumor growth and metastasis in gastric cancer *via* the EGFR/ERK/MMP2 axis (24). However, it is far from clear how asporin activates the EGFR signaling pathway to upregulate the p-EGFR protein level. Two previous studies suggested that HER2 and EGFR are overexpressed in PTC tumorous tissues (25, 26) and that HER2 and EGFR overexpression are positively associated with extrathyroidal extension, LNM, and high TNM stage in PTC (26). In the current study, we found that asporin interacted with HER2 and asporin knockdown downregulated protein levels of HER2, p-HER2^{Y1248}, and p-EGFR^{Y1171}. Mounting evidence shows that HER2 overexpression promotes EGFR expression and activity (27–29). Furthermore, HER2/HER2, HER2/EGFR, and HER2/HER3 levels were increased by HER2 overexpression, resulting in activation of the MAPK and PI3K signaling pathways, as well as stimulation of SRC kinases (30). In breast cancer, Jeong and colleagues found that PMCA2 knockdown disrupted the interaction between HER2 and HSP90 and promoted the internalization and degradation of HER2, resulting in a reduction in the protein levels of p-EGFR, HER3, and p-HER3, but not EGFR (31). Furthermore, Yoon et al. indicated that α6β4 integrin interacted with, and increased the translation of HER2 through eIF4E, which resulted in p-EGFR overexpression and activation of Ras to promote invasion in breast cancer cells (32). However, the mechanism by which asporin regulates HER2 expression in thyroid cancer remains to be fully elucidated. However, these previous studies provide

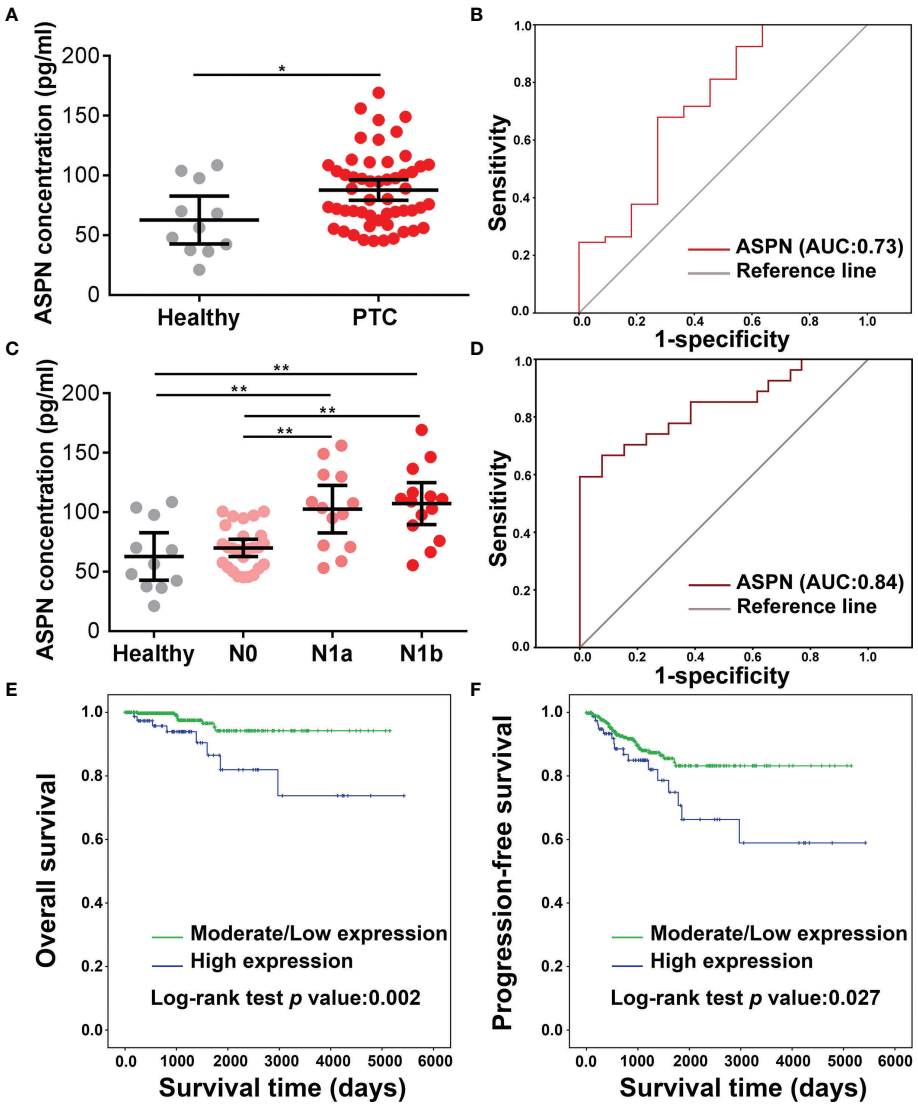

FIGURE 7 | Clinical analysis of asporin expression in serum and tumorous tissues. **(A)** The serum levels of asporin in 54 PTC patients and 11 healthy volunteers were determined by sandwich ELISA. Data are expressed as mean ± SD. *$P < 0.05$, **$P < 0.01$. **(B)** Receiver-operator characteristic (ROC) curve analysis was used to examine the diagnostic efficacy of serum asporin levels. ROC curve analysis of data for discriminating PTC patients and healthy volunteers. **(C)** Serum asporin levels in patients with PTC-N0, PTC-N1a, and PTC-N1b. **(D)** ROC curve analysis of data for differentiating PTC-N0 from PTC-N1a and PTC-N1b.**(E, F)** Kaplan–Meier curves and log-rank tests showing high expression of asporin is positively correlated with worse progression-free survival and overall survival of patients with PTC.

good evidence that asporin may regulate HER2 expression at the translational or post-translational level.

A growing body of evidence indicates that SCR activity is necessary for HER2-mediated proliferation, survival, metastasis, and angiogenesis (33), suggesting that SRC is the vital second messenger of HER2. Furthermore, HER2 interacts with SRC to increase its expression and activity (34, 35). SRC also increases HER2/HER3 dimerization and HER2 activity (36), which indicates that HER2 and SRC may create a regulatory feedback loop. Interestingly, Biscardi et al. indicated that SRC also enhanced EGFR activity by inducing phosphorylation of Tyr845 and Tyr1101 (37). In accordance with previous studies, we also found that asporin knockdown in PTC cells downregulate protein levels of HER2, p-SRC^{Y418}, and p-EGFR^{Y845}, but not the total levels of SRC protein. Collectively, the asporin/HER2/MAPK/EMT axis promoted the migration and invasion of thyroid cancer cells.

Nearly 36% of PTC patients are diagnosed with LNMs, which are correlated with local tumor recurrence and cancer-specific mortality (38). Therefore, it is important to accurately diagnose the presence and level of LNMs. Although high-resolution ultrasound imaging can be used to evaluate the extent of primary tumors and LNMs of PTC (39), the overall sensitivity is only 51%, and this imaging has limitations for the evaluation of the deeply situated retropharyngeal and mediastinal lymph

nodes (38, 39). In the present study, we found that serum asporin could not only be used to distinguish PTC patients from healthy volunteers but also to discriminate PTC-N1a and PTC-N1b patients from PTC-N0 patients. These results indicated that the combination of serum asporin levels and ultrasound imaging may be used to assess the probability that LNMs has occurred and the extent.

DATA AVAILABILITY STATEMENT

The datasets presented in this study can be found in online repositories. The names of the repository/repositories and accession number(s) can be found below:

https://www.ebi.ac.uk/pride/archive/, PXD007971.

ETHICS STATEMENT

The studies involving human participants were reviewed and approved by Ethics Committee of Peking University Cancer Hospital & Institute. The patients/participants provided their written informed consent to participate in this study.

AUTHOR CONTRIBUTIONS

JML and WG conceived and designed the study. SZ, JL, HZ and TW performed all experiments. TW collected thyroid tissues and analyzed the primary data. SZ, JL and HZ drafted the manuscript. TW, JML. and WG proofread and revised the manuscript. All authors read and approved the final manuscript.

FUNDING

This work was supported by the CAMS Innovation Fund for Medical Sciences (CIFMS #2017-I2M-3-001), the National Natural Science Foundation of China (No. 82103111 and 81971023), and Key Clinical Projects of Peking University Third Hospital (BYSYZD2021035).

SUPPLEMENTARY MATERIAL

The Supplementary Material for this article can be found online at: https://www.frontiersin.org/articles/10.3389/fonc.2022.762180/full#supplementary-material

REFERENCES

1. Bray F, Ferlay J, Soerjomataram I, Siegel RL, Torre LA, Jemal A. Global Cancer Statistics 2018: GLOBOCAN Estimates of Incidence and Mortality Worldwide for 36 Cancers in 185 Countries. *CA: Cancer J Clin* (2018) 68 (6):394–424. doi: 10.3322/caac.21492
2. Xing M. Molecular Pathogenesis and Mechanisms of Thyroid Cancer. *Nat Rev Cancer* (2013) 13(3):184–99. doi: 10.1038/nrc3431
3. Fagin JA, Wells SA Jr. Biologic and Clinical Perspectives on Thyroid Cancer. *N Engl J Med* (2016) 375(11):1054–67. doi: 10.1056/NEJMra1501993
4. Giordano TJ. Genomic Hallmarks of Thyroid Neoplasia. *Annu Rev Pathol* (2018) 13:141–62. doi: 10.1146/annurev-pathol-121808-102139
5. Cancer Genome Atlas Research N. Integrated Genomic Characterization of Papillary Thyroid Carcinoma. *Cell* (2014) 159(3):676–90. doi: 10.1016/j.cell.2014.09.050
6. Brose MS, Cabanillas ME, Cohen EE, Wirth LJ, Riehl T, Yue H, et al. Vemurafenib in Patients With BRAF(V600E)-Positive Metastatic or Unresectable Papillary Thyroid Cancer Refractory to Radioactive Iodine: A non-Randomised, Multicentre, Open-Label, Phase 2 Trial. *Lancet Oncol* (2016) 17(9):1272–82. doi: 10.1016/S1470-2045(16)30166-8
7. Kizawa H, Kou I, Iida A, Sudo A, Miyamoto Y, Fukuda A, et al. An Aspartic Acid Repeat Polymorphism in Asporin Inhibits Chondrogenesis and Increases Susceptibility to Osteoarthritis. *Nat Genet* (2005) 37(2):138–44. doi: 10.1038/ng1496
8. Lorenzo P, Aspberg A, Onnerfjord P, Bayliss MT, Neame PJ, Heinegard D. Identification and Characterization of Asporin. A Novel Member of the Leucine-Rich Repeat Protein Family Closely Related to Decorin and Biglycan. *J Biol Chem* (2001) 276(15):12201–11. doi: 10.1074/jbc.M010932200
9. Hurley PJ, Sundi D, Shinder B, Simons BW, Hughes RM, Miller RM, et al. Germline Variants in Asporin Vary by Race, Modulate the Tumor Microenvironment, and Are Differentially Associated With Metastatic Prostate Cancer. *Clin Cancer Res an Off J Am Assoc Cancer Res* (2016) 22 (2):448–58. doi: 10.1158/1078-0432.CCR-15-0256
10. Zhan S, Li J, Ge W. Multifaceted Roles of Asporin in Cancer: Current Understanding. *Front Oncol* (2019) 9:948. doi: 10.3389/fonc.2019.00948
11. Maris P, Blomme A, Palacios AP, Costanza B, Bellahcène A, Bianchi E, et al. Asporin Is a Fibroblast-Derived TGF-β1 Inhibitor and a Tumor Suppressor Associated With Good Prognosis in Breast Cancer. *PloS Med* (2015) 12(9): e1001871. doi: 10.1371/journal.pmed.1001871
12. Li H, Zhang Z, Chen L, Sun X, Zhao Y, Guo Q, et al. Cytoplasmic Asporin Promotes Cell Migration by Regulating TGF-Beta/Smad2/3 Pathway and Indicates a Poor Prognosis in Colorectal Cancer. *Cell Death Dis* (2019) 10 (2):109. doi: 10.1038/s41419-019-1376-9
13. Li H, Lai P, Jia J, Song Y, Xia Q, Huang K, et al. RNA Helicase DDX5 Inhibits Reprogramming to Pluripotency by miRNA-Based Repression of RYBP and Its PRC1-Dependent and -Independent Functions. *Cell Stem Cell* (2017) 20 (4):462–477.e466. doi: 10.1016/j.stem.2017.03.014
14. Bonifacino JS, Gershlick DC, Dell'Angelica EC. Immunoprecipitation. *Curr Protoc Cell Biol* (2016) 71. doi: 10.1002/cpcb.3
15. Donaldson JG. Immunofluorescence Staining. *Curr Protoc Cell Biol* (2015) 69:4.3.1–7. doi: 10.1002/0471143030.cb0403s69
16. Kajiro M, Hirota R, Nakajima Y, Kawanowa K, So-ma K, Ito I, et al. The Ubiquitin Ligase CHIP Acts as an Upstream Regulator of Oncogenic Pathways. *Nat Cell Biol* (2009) 11(3):312–9. doi: 10.1038/ncb1839
17. Zhan S, Li J, Wang T, Ge W. Quantitative Proteomics Analysis of Sporadic Medullary Thyroid Cancer Reveals FN1 as a Potential Novel Candidate Prognostic Biomarker. *Oncologist* (2018) 23(12):1415–25. doi: 10.1634/theoncologist.2017-0399
18. Zhan S, Wang T, Wang M, Li J, Ge W. In-Depth Proteomics Analysis to Identify Biomarkers of Papillary Thyroid Cancer Patients Older Than 45 Years With Different Degrees of Lymph Node Metastases. *Proteomics Clin Appl* (2019) 13(5):e1900030. doi: 10.1002/prca.201900030
19. Wei L, Jin Z, Yang S, Xu Y, Zhu Y, Ji Y. TCGA-Assembler 2: Software Pipeline for Retrieval and Processing of TCGA/CPTAC Data. *Bioinf (Oxf Eng)* (2018) 34(9):1615–7. doi: 10.1093/bioinformatics/btx812
20. Hindupur SK, Colombi M, Fuhs SR, Matter MS, Guri Y, Adam K, et al. The Protein Histidine Phosphatase LHPP Is a Tumour Suppressor. *Nature* (2018) 555(7698):678–82. doi: 10.1038/nature26140
21. Hanahan D, Weinberg RA. Hallmarks of Cancer: The Next Generation. *Cell* (2011) 144(5):646–74. doi: 10.1016/j.cell.2011.02.013
22. Dhillon AS, Hagan S, Rath O, Kolch W. MAP Kinase Signalling Pathways in Cancer. *Oncogene* (2007) 26(22):3279–90. doi: 10.1038/sj.onc.1210421
23. Wu H, Jing X, Cheng X, He Y, Hu L, Wu H, et al. Asporin Enhances Colorectal Cancer Metastasis Through Activating the EGFR/src/cortactin Signaling Pathway. *Oncotarget* (2016) 7(45):73402. doi: 10.18632/oncotarget.12336

24. Ding Q, Zhang M, Liu C. Asporin Participates in Gastric Cancer Cell Growth and Migration by Influencing EGF Receptor Signaling. *Oncol Rep* (2015) 33 (4):1783–90. doi: 10.3892/or.2015.3791
25. Siraj AK, Beg S, Jehan Z, Prabhakaran S, Al-Sobhi SS, Al-Dawish M, et al. The Role of HER2 Overexpression in Middle Eastern Papillary Thyroid Cancer. *Trans Cancer Res* (2017) 6(2):366–73. doi: 10.21037/tcr.2017.03.37
26. Dai YJ, Qiu YB, Jiang R, Xu M, Zhao L, Chen GG, et al. Concomitant High Expression of ERalpha36, EGFR and HER2 Is Associated With Aggressive Behaviors of Papillary Thyroid Carcinomas. *Sci Rep* (2017) 7(1):12279. doi: 10.1038/s41598-017-12478-1
27. Huang G, Chantry A, Epstein RJ. Overexpression of ErbB2 Impairs Ligand-Dependent Downregulation of Epidermal Growth Factor Receptors via a Post-Transcriptional Mechanism. *J Cell Biochem* (1999) 74(1):23–30. doi: 10.1002/(SICI)1097-4644(19990701)74:1<23::AID-JCB3>3.0.CO;2-L
28. Wang Z, Zhang L, Yeung TK, Chen X. Endocytosis Deficiency of Epidermal Growth Factor (EGF) Receptor-ErbB2 Heterodimers in Response to EGF Stimulation. *Mol Biol Cell* (1999) 10(5):1621–36. doi: 10.1091/mbc.10.5.1621
29. Hendriks BS, Wiley HS, Lauffenburger D. HER2-Mediated Effects on EGFR Endosomal Sorting: Analysis of Biophysical Mechanisms. *Biophys J* (2003) 85 (4):2732–45. doi: 10.1016/S0006-3495(03)74696-7
30. Yarden Y, Pines G. The ERBB Network: At Last, Cancer Therapy Meets Systems Biology. *Nat Rev Cancer* (2012) 12(8):553–63. doi: 10.1038/nrc3309
31. Jeong J, VanHouten JN, Dann P, Kim W, Sullivan C, Yu H, et al. PMCA2 Regulates HER2 Protein Kinase Localization and Signaling and Promotes HER2-Mediated Breast Cancer. *Proc Natl Acad Sci USA* (2016) 113(3):E282–290. doi: 10.1073/pnas.1516138113
32. Yoon SO, Shin S, Lipscomb EA. A Novel Mechanism for Integrin-Mediated Ras Activation in Breast Carcinoma Cells: The Alpha6beta4 Integrin Regulates ErbB2 Translation and Transactivates Epidermal Growth Factor Receptor/ErbB2 Signaling. *Cancer Res* (2006) 66(5):2732–9. doi: 10.1158/0008-5472.CAN-05-2941
33. Ishizawar R, Parsons SJ. C-Src and Cooperating Partners in Human Cancer. *Cancer Cell* (2004) 6(3):209–14. doi: 10.1016/j.ccr.2004.09.001
34. Vadlamudi RK, Sahin AA, Adam L, Wang RA, Kumar R. Heregulin and HER2 Signaling Selectively Activates C-Src Phosphorylation at Tyrosine 215. *FEBS Lett* (2003) 543(1-3):76–80. doi: 10.1016/S0014-5793(03)00404-6
35. Tan M, Li P, Klos KS, Lu J, Lan KH, Nagata Y, et al. ErbB2 Promotes Src Synthesis and Stability: Novel Mechanisms of Src Activation That Confer Breast Cancer Metastasis. *Cancer Res* (2005) 65(5):1858–67. doi: 10.1158/0008-5472.CAN-04-2353
36. Ishizawar RC, Miyake T, Parsons SJ. C-Src Modulates ErbB2 and ErbB3 Heterocomplex Formation and Function. *Oncogene* (2007) 26(24):3503–10. doi: 10.1038/sj.onc.1210138
37. Biscardi JS, Maa MC, Tice DA, Cox ME, Leu TH, Parsons SJ. C-Src-Mediated Phosphorylation of the Epidermal Growth Factor Receptor on Tyr845 and Tyr1101 Is Associated With Modulation of Receptor Function. *J Biol Chem* (1999) 274(12):8335–43. doi: 10.1074/jbc.274.12.8335
38. Kim E, Park JS, Son KR, Kim JH, Jeon SJ, Na DG. Preoperative Diagnosis of Cervical Metastatic Lymph Nodes in Papillary Thyroid Carcinoma: Comparison of Ultrasound, Computed Tomography, and Combined Ultrasound With Computed Tomography. *Thyroid* (2008) 18(4):411–8. doi: 10.1089/thy.2007.0269
39. Choi JS, Kim J, Kwak JY, Kim MJ, Chang HS, Kim EK. Preoperative Staging of Papillary Thyroid Carcinoma: Comparison of Ultrasound Imaging and CT. *AJR Am J Roentgenol* (2009) 193(3):871–8. doi: 10.2214/AJR.09.2386

Conflict of Interest: The authors declare that the research was conducted in the absence of any commercial or financial relationships that could be construed as a potential conflict of interest.

Publisher's Note: All claims expressed in this article are solely those of the authors and do not necessarily represent those of their affiliated organizations, or those of the publisher, the editors and the reviewers. Any product that may be evaluated in this article, or claim that may be made by its manufacturer, is not guaranteed or endorsed by the publisher.

frontiers | Frontiers in Oncology

ORIGINAL RESEARCH
published: 03 June 2022
doi: 10.3389/fonc.2022.799680

Does Reorganization of Clinicopathological Information Improve Prognostic Stratification and Prediction of Chemoradiosensitivity in Sinonasal Carcinomas? A Retrospective Study on 145 Patients

Marco Ferrari[1,2,3], Davide Mattavelli[4], Alberto Schreiber[4], Tommaso Gualtieri[4], Vittorio Rampinelli[2,4], Michele Tomasoni[4], Stefano Taboni[1,3,5], Laura Ardighieri[6], Simonetta Battocchio[6], Anna Bozzola[6], Marco Ravanelli[7], Roberto Maroldi[7], Cesare Piazza[4], Paolo Bossi[8], Alberto Deganello[4] and Piero Nicolai[1]*

[1] Section of Otorhinolaryngology—Head and Neck Surgery, Department of Neurosciences, University of Padua—"Azienda Ospedale Università di Padova", Padua, Italy, [2] Technology for Health (PhD program), Department of Information Engineering, University of Brescia, Brescia, Italy, [3] Guided Therapeutics Program International Scholar, University Health Network, Toronto, Canada, [4] Unit of Otorhinolaryngology—Head and Neck Surgery, Department of Medical and Surgical Specialties, Radiologic Sciences, and Public Health, University of Brescia—"ASST Spedali Civili di Brescia", Brescia, Italy, [5] Artificial Intelligence in Medicine and Innovation in Clinical Research and Methodology (PhD program), Department of Clinical and Experimental Sciences, University of Brescia, Brescia, Italy, [6] Unit of Pathology, "ASST Spedali Civili di Brescia", Brescia, Italy, [7] Unit of Radiology, Department of Medical and Surgical Specialties, Radiologic Sciences, and Public Health, University of Brescia—"ASST Spedali Civili di Brescia", Brescia, Italy, [8] Unit of Medical Oncology, Department of Medical and Surgical Specialties, Radiologic Sciences, and Public Health, University of Brescia—"ASST Spedali Civili di Brescia", Brescia, Italy

OPEN ACCESS

Edited by:
Heming Lu,
People's Hospital of Guangxi Zhuang Autonomous Region, China

Reviewed by:
Barbara Pichi,
Hospital Physiotherapy Institutes (IRCCS), Italy
Majid mohammed Mahmood,
Mustansiriyah University, Iraq

***Correspondence:**
Marco Ferrari
marco.ferrari@unipd.it

Specialty section:
This article was submitted to Head and Neck Cancer, a section of the journal Frontiers in Oncology

Received: *21 October 2021*
Accepted: *05 May 2022*
Published: *03 June 2022*

Citation:
Ferrari M, Mattavelli D, Schreiber A, Gualtieri T, Rampinelli V, Tomasoni M, Taboni S, Ardighieri L, Battocchio S, Bozzola A, Ravanelli M, Maroldi R, Piazza C, Bossi P, Deganello A and Nicolai P (2022) Does Reorganization of Clinicopathological Information Improve Prognostic Stratification and Prediction of Chemoradiosensitivity in Sinonasal Carcinomas? A Retrospective Study on 145 Patients. Front. Oncol. 12:799680. doi: 10.3389/fonc.2022.799680

Background: The classification of sinonasal carcinomas (SNCs) is a conundrum. Consequently, prognosis and prediction of response to non-surgical treatment are often unreliable. The availability of prognostic and predictive measures is an unmet need, and the first logical source of information to be investigated is represented by the clinicopathological features of the disease. The hypothesis of the study was that clinicopathological information on SNC could be exploited to better predict prognosis and chemoradiosensitivity.

Methods: All patients affected by SNC who received curative treatment, including surgery, at the Unit of Otorhinolaryngology—Head and Neck Surgery of the University of Brescia between October 1998 and February 2019 were included in the analysis. The institutional series was reviewed and a survival analysis was performed. Machine learning and multivariable statistical methods were employed to develop, analyze, and test 3 experimental classifications (classification #1, based on cytomorphological, histomorphological, and differentiation information; classification #2, based on differentiation information; and classification #3, based on locoregional extension) of SNC, based on the inherent clinicopathological information. The association of experimental classifications with prognosis and chemoradiosensitivity was tested.

Results: The study included 145 patients. From a prognostic standpoint, the machine learning-generated classification of SNC provided better prediction than the current World Health Organization classification. However, the prediction of the chemoradiosensitivity of SNC was not achievable.

Conclusions: Reorganization of clinicopathological information, with special reference to those related to tumor differentiation, can improve the reliability of prognosis of SNC. Prediction of chemoradiosensitivity remains an unmet need and further research is required.

Keywords: sinonasal, carcinoma, skull base (head and neck), classification, machine learning, prognosis, chemotherapy, radiotherapy

INTRODUCTION

Sinonasal carcinomas (SNC) are a heterogeneous group of cancers that include keratinizing and non-keratinizing squamous cell carcinoma (SCC), spindle cell carcinoma, lymphoepithelial carcinoma, sinonasal undifferentiated carcinoma (SNUC), NUT carcinoma, neuroendocrine carcinomas (NEC), intestinal-type (ITAC), and non-intestinal-type adenocarcinoma (NITAC) (1). SNC represent most of the malignancies diagnosed in the sinonasal tract and their treatment is histology-driven (2–4). Thus, the reliable classification of SNC is paramount to guiding the treatment that the multi-disciplinary team will offer.

The current classification of SNC is mostly based on histomorphological features, in combination, when needed, with immunohistochemical and genetic studies. However, diagnosis of SNC is universally acknowledged as a challenge since several tumor types display overlapping features, and differential diagnosis includes a variety of entities. The fact that SNC exhibit some overlapping features from a morphological standpoint is not surprising, as several authors have demonstrated that the molecular features of these cancers are partially coinciding, and signatures of several genes are necessary to correctly classify diverse SNC (5, 6). The practical implications of this challenge are remarkable: not only is the sinonasal tract the site with the highest rate of major diagnostic discrepancy in the head and neck (19.0% vs. 0.0–8.3% in sinonasal and non-sinonasal sites, respectively) (7), but Choi et al. also demonstrated that initially misdiagnosed sinonasal cancers are associated with worse prognosis compared to those correctly identified prior to treatment (8). Moreover, even SCC diagnosis, which could be considered as relatively "simple" in most areas of the head and neck, has been associated with the highest rate of diagnostic discrepancy in the nasoethmoidal compartment (9). Correct classification of SNC is of paramount importance, particularly in the era of "histology-driven" management, as the best type and sequence of treatment modalities can significantly change with histology (2–4). As an example of that, neoadjuvant chemotherapy (ChT) has been adopted for several sinonasal cancers in an attempt to achieve a number of goals such as treatment intensification, chemoselection, orbit sparing, and reduction of distant failure. However, neoadjuvant ChT can display non-negligible toxicity, and no reliable means of response prediction are available. Thus, there exists a substantial uncertainty about the opportunity to start treatment with neoadjuvant ChT in some SNC.

These data dispel any doubt that the current method of classifying SNCs can be improved. Thus, research in the field of sinonasal oncology should be oriented toward the identification of novel clustering approaches to be implemented with the current classification. The main hypothesis of this study was that the reorganization of clinicopathological information on SNC could improve the prediction of prognosis and chemoradiosensitivity. The institutional series of SNC patients at the University of Brescia was reviewed and used to test the utility of machine learning techniques in exploiting commonly available information. The resulting experimental classifications were tested as prognostic and predictive factors and compared with the current means of classifying SNC.

MATERIALS AND METHODS

Patients' Selection and Data Acquisition

All patients affected by SNC who received curative treatment, including surgery, at the Unit of Otorhinolaryngology—Head and Neck Surgery of the University of Brescia between October 1998 and February 2019 were included in the analysis. ITAC and low-grade NITAC were excluded, as they were considered remarkably different clinical entities with respect to other SNCs (10).

The following information were retrospectively gathered for each case (full details are reported in **Table S1**): demographics, oncological history, treatment characteristics, response to neoadjuvant therapy (classified according to the Response Evaluation Criteria In Solid Tumors [RECIST], version 1.1), general pathologic features, cytomorphological information, histomorphological and local invasion-related information, (immuno)histochemical and nucleic acid-based test information, locoregional extension, follow-up events, and status at last evaluation. Differentiation of tumors was described through non-mutually exclusive classes (i.e., each tumor could be attributed to more than one differentiation class), based on the criteria summarized in **Table 1**. Margin status (11), perineural invasion (PNI) (11), lymphovascular invasion (LVI) (11), and infiltrative pattern-bone invasion (IPBI) (12) were considered as previously described. The 8th TNM Edition was employed (13).

TABLE 1 | Summary of criteria to attribute squamous, glandular, neuroendocrine, mesenchymal, embryonal, and neural differentiation.

Differentiation	Attribution criteria*
Squamous	• Squamous cytomorphology • Keratinization • Expression of p63 and/or p40
Glandular	• Glandular cytomorphology • Positive staining for periodic acid-Schiff stain, Alcian blue and/or mucicarmine • Expression of cytokeratin 7, cytokeratin 20 and/or epithelial membrane antigen (MUC1/EMA)
Neuroendocrine	• Expression of CD56, synaptophysin, chromogranin A and/or neuron-specific enolase (NSE)*
Mesenchymal	• Presence of spindle cells, rhabdoid cells and/or osteoblastoid cells • Expression of vimentin, muscle-specific actin, smooth muscle alfa-actin, calponin, myogenin, desmin and/or CD117
Embryonal	• Expression of the carcinoembryonic antigen (CEA)
Neural	• Expression of SOX10, NSE*, and/or glial fibrillary acid protein (GFAP)

NSE was considered as a neural marker only when neuroendocrine markers were not expressed.

The pathologic evaluation of cases was led by the senior pathologist co-authoring this study (SB), who has 25 years of physician-level experience in the field, acquired in centers with a high volume of sinonasal cancers. A large majority of pathological reports (126/145, 86.9%) were either led or co-authored by SB. All non-SCC, non-conventional SCC, and nasoethmoidal SCC cases were analyzed in consensus by at least 2 dedicated head and neck pathologists and reviewed by SB.

Unsupervised Re-Classification of Tumors

The softwares XLSTAT and RStudio were employed to perform the following analyses. The following experimental classifications were generated to test the main hypothesis of the study.

Unsupervised Re-Classification of Tumors Based on Pathological Features

Three groups of information (1—cytomorphological; 2—histomorphological and invasion-related; and 3—differentiation) underwent adjusted-inertia Multiple Correspondence Analysis (MCA). A minimum of 2 factors were extrapolated from each MCA, whereas the third or further factors were considered only if determining >10% of inertia. Agglomerative Hierarchical Clustering (AHC), which clusters observations through Euclidean dissimilarity as per Ward's method, was applied to the factors extrapolated from MCAs. Three- to 6-cluster classifications were generated, and their association with disease-specific survival (DSS) was tested through the Cox proportional-hazards model. The classification providing the best prediction with minimum complexity was identified through analysis of the concordance index (C-index), Akaike Information Criterion (AIC), Bayesian Information Criterion (BIC), and Nagelkerke pseudo-R^2 (NPR). This classification is hereby referred to as "classification #1." The C-index expresses the goodness of fit of prognostic models. AIC and BIC estimate the prediction error of a model, whereas NPR determines how much of the variance observed in a series is explained by the variables (i.e., covariates). Thus, the higher the C-index and NPR, and the lower AIC and BIC, the better is one predictive model compared to another.

Each class of the selected classification was described in terms of cytomorphological, histomorphological- and invasion-related, and differentiation information through chi-square or Fisher's exact test, as appropriate.

Unsupervised Re-Classification of Tumors Based on Differentiation Features

Differentiation information underwent AHC. Identification of the best classification in terms of the number of clusters was selected as described for classification #1. This classification is referred to as "classification #2."

Unsupervised Re-Classification of Tumors Based on Locoregional Extension

Local and regional extension information was summarized through an adjusted-inertia MCA approach, as previously described, and underwent AHC. Identification of the best classification in terms of the number of clusters was selected with the same method described for classifications #1 and #2 but using local recurrence-free survival (LRFS) instead of DSS. This classification is referred to as "classification #3".

Prognostic Efficacy of Classifications #1 to #3 and Comparison With Available Classifications

The following time-to-event outcomes were considered to evaluate the prognostic efficacy of classifications: overall survival (OS), DSS, recurrence-free survival (RFS), LRFS, regional recurrence-free survival (RRFS), and distant recurrence-free survival (DRFS). The effect on prognosis was first tested through univariable analysis with a log-rank test (level of significance = 0.10). To measure a more reliable effect on outcomes, multivariable prognostic models were created through the Cox proportional-hazards method with an *a priori* selection of covariates for those outcomes which were impacted by classifications #1 to #3 at univariable analysis (level of significance = 0.05). The proportional hazards assumption was tested with Schoenfeld's global test (level of significance = 0.05). Factors resulting in significant multivariable analysis for DSS, LRFS, and DRFS were also tested through a competing risk analysis with Gray's test (level of significance = 0.05). Events were defined as appropriate to analyze competing risk for DSS (death of disease, death of other cause), LRFS (local recurrence, death without local recurrence), and DRFS (distant recurrence, death without distant recurrence). Causes of censorship were analyzed for DSS, RFS, LRFS, RRFS, and DRFS. Competing risk multivariable analysis was performed through a subdistribution hazard model for DSS, LRFS, and DRFS.

The following parameters were evaluated for classifications #1 to #3: independent prognostic effect (defined as the statistical significance of the classification when considered as a covariate in a multivariable model); prognostic segregation (defined as the ratio of observations clustered in a category significantly different from the reference category in a multivariable model out of the total number of patients in the series); and *a priori* applicability (evaluated as the confusion rate calculated through classification tree analysis run with the classification as the dependent variable and pathological or locoregional extension-related information as an explanatory variable, as appropriate).

Based on these parameters, classifications #1 and #2 were compared to the latest WHO classification of tumors, whereas classification #3 was compared to the pT category and stage of the latest TNM classification. Since the analysis was based on planned comparisons, multiple comparisons correction was not performed.

Sub-Analysis of Patients Receiving Neoadjuvant Chemotherapy and Assessment of Chemoradiosensitivity

Descriptive statistics of the sub-cohort of patients receiving neoadjuvant ChT were performed. Multivariable models were applied to this sub-cohort of patients, including response to ChT as a covariate.

Chemoradiosensitivity (i.e., the tendency of the tumor to respond to ChT and/or radiotherapy (RT)) was estimated based on the criteria summarized in **Table 2**. The univariable association of response to neoadjuvant ChT and chemoradiosensitivity with demographics, oncological history, treatment characteristics, pathological information, and classifications #1 to #3 was tested with chi-square or Fisher's exact test, as appropriate (level of significance = 0.10). A multivariable analysis of the same outcomes was performed using logistic regression applied to factors resulting significantly from the univariable analysis (level of significance = 0.05). The Classification Random Forest (CRF) method with "random with replacement" sampling, a subsample size of 50 observations, and the building of 100 classification trees was run to detect predictors of response to neoadjuvant ChT and chemoradiosensitivity.

RESULTS

Cohort Description

The study included 145 patients, of whom 49 (33.8%) were women and 96 (66.2%) were men. Nine (6.2%) patients were treated between 1998 and 2000, 22 (15.2%) between 2001 and 2005, 30 (20.7%) between 2006 and 2010, 42 (29.0%) between 2011 and 2015, and 42 (29.0%) between 2016 and 2019 (**Figure S1**). The mean age at surgery was 63.8 years (median: 66.3; range: 28.8–89.0; interquartile range: 54.6–74.5).

Ninety-nine (68.3%) and 46 (31.7%) patients were referred for a primary or recurrent tumor, respectively. In the latter group, 15 (32.6%) patients had received surgery; 10 (21.7%) surgery and adjuvant RT; 7 (15.2%) surgery and adjuvant ChT-RT; 6 (13.0%) definitive ChT-RT, 3 (6.5%) RT; and 1 (2.2%) surgery and adjuvant ChT. In 4 (8.7%) of the patients, previous treatments could not be traced back. In patients referred after adjuvant or definitive (ChT-)RT (26/46, 56.5%), the disease-free interval was less than 1 year in 8 (30.8%) cases, between 12 and 24 months in 4 (15.4%), between 24 and 48 months in 4 (15.4%), between 5 and 10 years in 4 (15.4%), and beyond 10 years in 2 (7.7%).

Surgery consisted of endoscopic resection without transnasal craniectomy (ER), endoscopic resection with transnasal craniectomy (ERTC), cranioendoscopic resection (CER), open maxillectomy (OM), and endoscopic-assisted craniofacial resection (EA)CFR in 30 (20.7%), 21 (14.5%), 11 (7.6%), 48 (33.1%), and 35 (24.1%) patients, respectively. Neck dissection was performed in 30 (20.7%) patients, of whom 18 (60.0%) received a unilateral therapeutic comprehensive neck dissection and 12 (40.0%) unilateral superselective (I–IIA) or selective (I–III) neck dissection (when harvest of recipient vessels before microvascular reconstruction was indicated).

Fifty-six (38.6%) patients did not receive adjuvant treatments; 70 (48.3%) underwent adjuvant RT; 15 (10.3%) adjuvant RT-ChT; and 4 (2.8%) adjuvant ChT alone. Neoadjuvant ChT was administered to 35 (24.1%) patients, of whom 31 (88.6%) received docetaxel, cisplatin/carboplatin, 5-fluorouracile (TPF) regimen and 4 (11.4%) a cisplatin and etoposide alternated to adriamycin and ifosfamide (PE-AI) protocol.

TABLE 2 | Summary of criteria to estimate chemoradiosensitivity of tumors.

Chemoradiosensitivity class	Criteria
A,"Highly chemoradiosensitive tumor"*	Complete response** following neoadjuvant ChT and/or curative-intended (ChT-)RT
B,"Moderately chemoradiosensitive tumor"*	Partial response** following neoadjuvant ChT
	At referral: local and/or regional relapse after a 2-year or longer disease-free interval since the date of completion of (ChT-)RT-including treatment
	During follow-up: local and/or regional relapse 2 or more years after completion of treatment including R1 surgery*** followed by adjuvant (ChT)-RT
C,"Chemoradioresistant tumor"*	Stable or progressing disease** after neoadjuvant ChT
	At referral: local and/or regional relapse within 2 years since the date of completion of (ChT-)RT-including treatment
	During follow-up: local and/or regional relapse within 2 years after completion of treatment including R1 surgery*** followed by adjuvant (ChT)-RT

**When a tumor had criteria designating multiple classes, the worst one was assigned. **Response was evaluated according to the Response Evaluation Criteria in Solid Tumors, version 1.1 (14). ***Patients receiving R0 surgery were excluded as chemoradiosensitivity could have been overestimated by completeness of resection.*

Pathological Features

The tumor epicenter was in the maxillary sinus and in the nasoethmoidal complex in 79 (54.5%) and 66 (45.5%) patients, respectively. Histology was distributed as follows: SCC in 91 (62.8%) patients (well/moderately differentiated in 31 [21.4%] cases, poorly differentiated in 60 [41.4%]), SNC not otherwise specified (SNCNOS) in 30 (20.7%), NEC in 10 (6.9%), high-grade NITAC (HG-NITAC) in 6 (4.1%), SNUC without molecular identifier in 5 (3.4%), and SMARCB1/INI1-deficient carcinoma (ID-SNUC) in 3 (2.1%) (**Figure 1**).

Of note, SNCNOS were poorly-to-non-differentiated SNCs that could not be classified as WHO-recognized entities. ID-SNUC was distinguished from SNUC owing to their substantially different clinical behavior (4). When considering SCCs, 64 (70.3%) were described as classical variants, 16 (17.6%) as non-keratinizing, 5 (5.5%) as adenosquamous, 3 (3.3%) as basaloid, 2 (2.2%) as spindle-cell, and 1 (1.1%) as adenomatoid. When considering NEC, 6 (60.0%) were described as small cells, 1 (10.0%) as large cells, and 3 (30.0%) were not otherwise specified. The preeminent grade of differentiation was

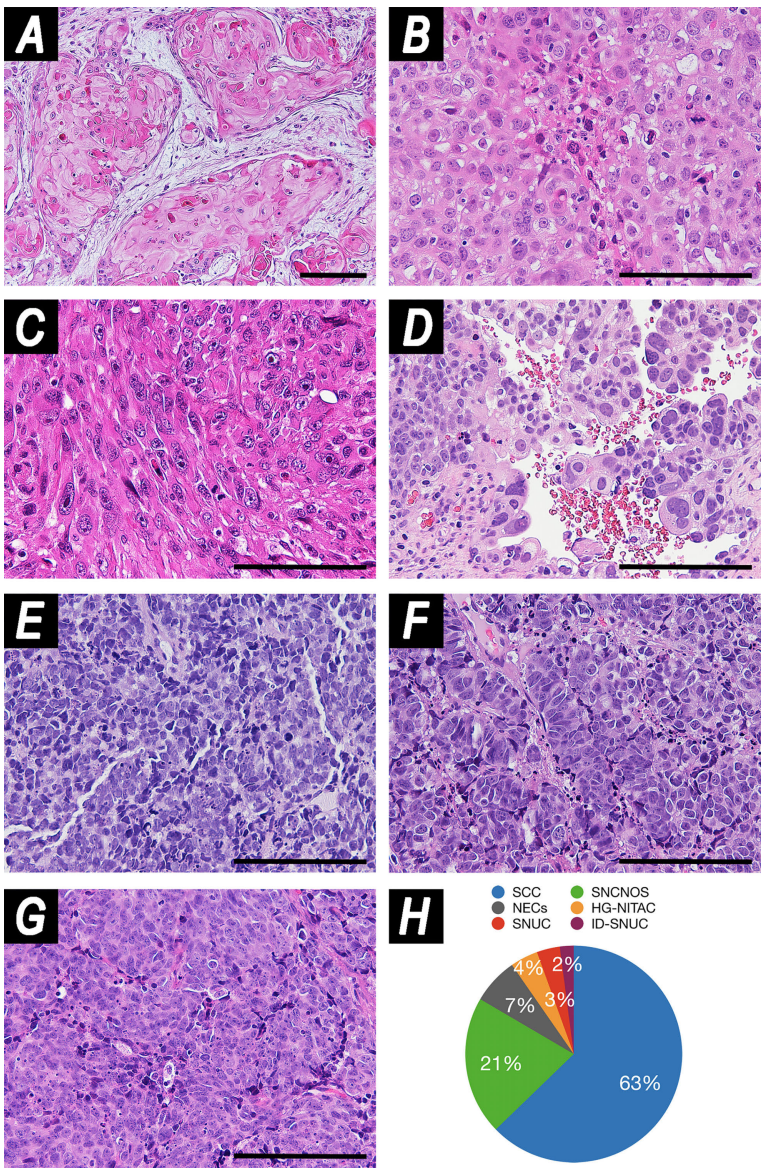

FIGURE 1 | Panel illustrating examples of histologies included in the study. **(A)** Well-differentiated squamous cell carcinoma (SCC) (hematoxylin–eosin (HE), magnification: ×100). **(B)** Poorly differentiated SCC (HE, magnification: ×200). **(C)** Spindle cell carcinoma (HE, magnification: ×200). **(D)** High-grade non-intestinal-type adenocarcinoma (HG-NITAC) (HE, magnification: ×200). **(E)** Small cell neuroendocrine carcinoma (NEC) (HE, magnification: ×200). **(F)** Large cell NEC (HE, magnification: ×200). **(G)** Sinonasal undifferentiated carcinoma (SNUC) (HE, magnification: ×200). **(H)** Pie chart displaying distribution of histologies in the series. Scale bar: 100 μm. ID-SNUC, INI1/SMARCB1-deficient sinonasal undifferentiated carcinoma; SNCNOS, sinonasal carcinoma not otherwise specified.

described as low in 33 (22.8%) tumors, high in 93 (64.1%), and unspecified in 19 (13.1%). The worst grade of differentiation was low in 21 (14.5%) tumors, high in 105 (72.4%), and unpecified in 19 (13.1%). Inverted papilloma (IP) was found in 21 (14.5%) tumors, of which 19 (13.1%) were SCC and 2 (1.4%) SNCNOS. Margins were clear (R0) in 86 (59.3%) patients and involved (R+) in 59 (40.7%).

Squamous morphology of tumor cells was observed in 107 (73.8%) cases, basaloid in 12 (8.3%), glandular in 18 (12.4%), and mesenchymal in 18 (12.4%), out of which 14 (9.7%) were spindle, 3 (2.1%) rhabdoid, and 1 (0.7%) osteoblastoid (**Figure 2**).

Keratinization was found in 38 (26.2%) cases, cellular pleomorphism in 53 (36.6%), nuclear pleomorphism in 50 (34.5%), nucleolar prominence in 30 (20.7%), abnormal mitoses in 20 (13.8%), neoplastic necrosis in 66 (45.5%), and verrucous hyperplasia in 3 (2.1%). The nucleus-to-cytoplasm ratio was classified as high in 22 (15.2%) tumors, low in 9 (6.2%), and intermediate or unspecified in 114 (78.6%).

Pattern of growth was described as solid in 125 (86.2%) tumors, papillary in 27 (18.6%), transitional-like in 8 (5.5%), lobular in 7 (4.8%), cribriform in 7 (4.8%), pagetoid in 7 (4.8%), and tubular in 2 (1.4%). Overall, PNI was observed in 44 (30.3%) cancers, and LVI in 49 (33.8%). Infiltrative-type bone invasion was observed in 85 (58.6%) patients (**Figure 3**).

According to the criteria reported in **Table 1**, squamous differentiation was observed in 114 (78.6%) tumors, glandular

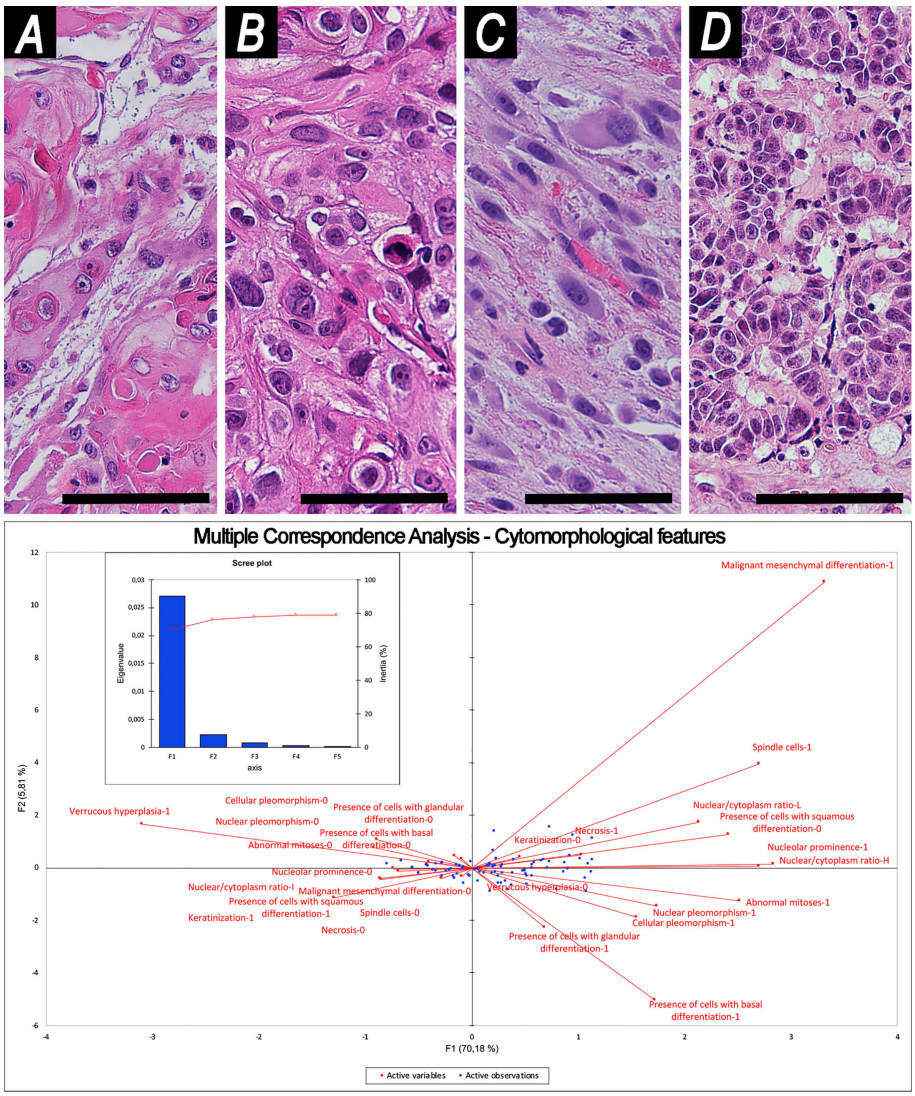

FIGURE 2 | Examples of cytomorphology and related Multiple Correspondence Analysis. **(A, B)** Squamous cell morphology [**(A)** well-differentiated; **(B)** poorly-differentiated]. **(C)** Spindle cell morphology. **(D)** Glandular cell morphology. Magnification of histological images is ×200; all are stained through hematoxylin–eosin. The bottom image shows organization of variables into cartesian axes depending on their mutual relationships. This results in 2 factors (F1, F2), represented in the y- and x-axes of the graph, which reliably summarize sample variability, as shown in the scree plot. Scale bar: 50 μm.

in 35 (24.1%), mesenchymal in 32 (22.1%), neuroendocrine in 25 (17.2%), neural in 3 (2.1%), and embryonic in 1 (0.7%). Given their rarity in the series, neural and embryonic differentiations were not considered further.

Histochemical, (immuno)histochemical, and nucleic acid-based staining employed over the study period are reported in **Table S2**. Epstein–Barr virus (EBV), human papilloma virus (HPV), and polyomavirus were searched in 16 (11.0%), 3 (2.1%), and 3 (2.1%) cases, respectively. Only one tumor was found to be EBV+. No cases associated with HPV or polyomavirus were observed. A positive stain for p16 was found in 5 of 9 (55.6%) cases in which it was tested.

The tumor involved the orbital content in 41 (28.3%) cases, the bony skull base in 41 (28.3%), the dura mater in 26 (17.9%), masticator and/or parapharyngeal space in 46 (31.7%), the facial soft tissues in 46 (31.7%), the sphenoid sinus in 37 (25.5%), the frontal sinus in 19 (13.1%), and the nasopharynx in 24 (16.6%). The pathological T category was distributed as follows: pT1 in 12 (8.3%) patients, pT2 in 16 (11.0%), pT3 in 22 (15.2%), pT4a in 43 (29.7%), and pT4b in 52 (35.9%). Eighteen (12.4%) patients had pathologically proven nodal metastases. The tumor stage was classified as I in 12 (8.3%) patients, II in 15 (10.3%), III in 21 (14.5%), IVA in 42 (29.0%), and IVB in 55 (37.9%).

Oncologic Outcomes

The mean follow-up duration was 48.2 months (median: 29.7; range: 0.8–215.6; inter-quartile range: 9.4–73.2). The status of patients at last contact was distributed as follows: died of disease in 61 (42.1%) patients; alive with no evidence of disease in 60 (41.4%); died of other causes in 7 (4.8%); and alive with evidence of disease in 4 (2.8%). Thirteen (9.0%) patients were lost at follow-up. The following data refer to the subgroup of patients for whom follow-up information is available (n = 132).

One-, 2-, 5-, and 10-year OS were 74.0, 62.5, 51.3, and 46.3%, respectively (**Figure 4**); 90% of deaths from any cause occurred within 55 months after diagnosis. One-, 2-, 5-, and 10-year DSS were 76.0, 65.0, 54.6, and 53.1%, respectively (**Figure 4**); 90% of cancer-specific deaths occurred within 50 months after diagnosis.

Sixty-nine (52.3%) patients had at least 1 recurrence. In particular, there were 31 (23.5%) local recurrences, 7 (5.3%) locoregional, 9 (6.8%) local and distant, 3 (2.3%) regional, 3 (2.3%) regional and distant, 10 (7.6%) distant, and 6 (4.5%) locoregional and distant (**Figure 4**). Cumulatively, recurrence was observed at the local, regional, and distant sites in 53 (40.2%), 19 (14.4%), and 28 (21.2%) patients, respectively.

One-, 2-, 5-, and 10-year RFS were 64.6, 54.9, 46.1, and 43.0%, respectively (**Figure 4**). One-, 2-, 5-, and 10-year LRFS were 74.3, 65.5, 57.0, and 53.3%, respectively (**Figure 4**). One-, 2-, 5-, and 10-year RRFS were 89.3, 85.1, 85.1, and 80.2%, respectively (**Figure 4**). One-, 2-, 5-, and 10-year DRFS were 87.4, 81.4, 73.1, and 70.1%, respectively (**Figure 4**). The time to observe 90% of any recurrence, local recurrence, regional recurrence, and distant recurrence was 33, 35, 32, and 43 months, respectively. The causes of censorship in the RFS (n = 63) analysis were distributed as follows: 6 (9.5%) patients died of other causes with no recurrence of disease, and 57 (90.5%) patients were alive with no recurrence of disease. The causes of censorship in the LRFS (n = 79) analysis were distributed as follows: 6 (7.6%) patients died of other causes with no local recurrence of disease, 15 (19.0%) patients died of non-locally recurrent disease, and 58 (73.4%) patients were alive with no local recurrence of disease. The causes of censorship in the RRFS (n = 113) analysis were distributed as follows: 6 (5.3%) patients died of other causes with no regional

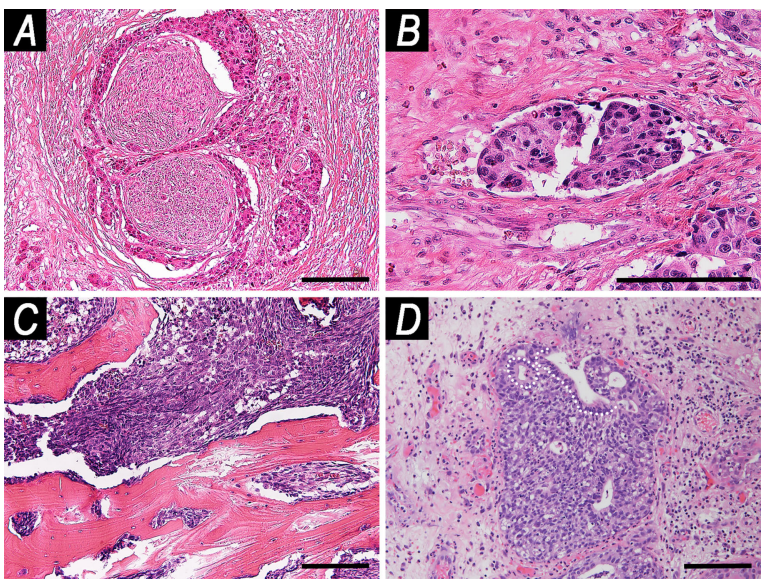

FIGURE 3 | Examples of microscopic local spread patterns. **(A)** Perineural invasion (hematoxylin–eosin (HE), magnification: ×100). **(B)** Endovascular tumor embolization (HE, magnification: ×200). **(C)** Infiltrative pattern-bone invasion (HE, magnification: ×100). **(D)** Pagetoid growth (HE, magnification: ×100). White dashed line indicates the basal lamina of glandular epithelium of a submucosal gland. The tumor grew along the glandular axis underneath the epithelium. Scale bar: 100 μm.

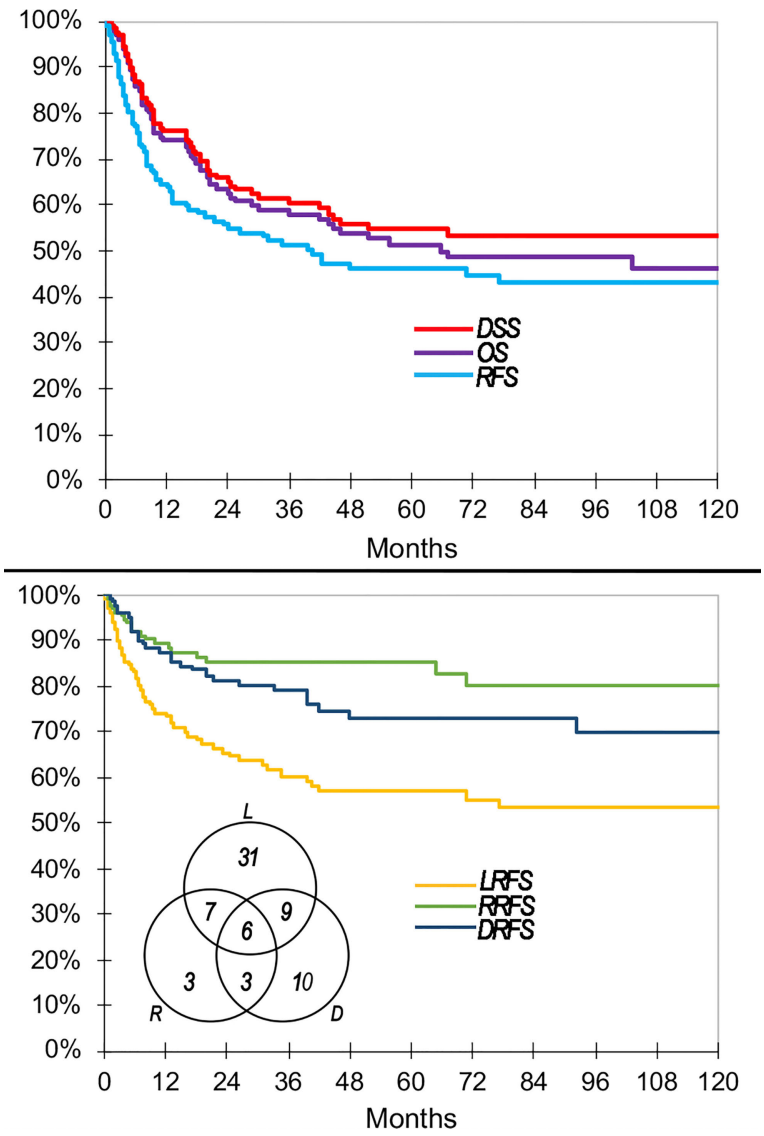

FIGURE 4 | Main oncologic outcomes of the series summarized through Kaplan–Meier curves. Venn diagram shows raw count of recurrences. DRFS, distant recurrence-free survival; DSS, disease-specific survival; LRFS, local recurrence-free survival; OS, overall survival; RFS, recurrence-free survival; RRFS, regional recurrence-free survival.

recurrence of disease, 43 (38.1%) patients died of non-regionally recurrent disease, 64 (56.6%) patients were alive with no regional recurrence of disease. The causes of censorship in the DRFS (n = 104) analysis were distributed as follows: 7 (6.7%) patients died of other causes with no distant recurrence of disease, 32 (30.8%) patients died of recurrent disease without distant metastasis, and 65 (62.5%) patients were alive with no distant recurrence of disease.

A multivariable analysis of prognostic factors is reported in **Tables S3**–**S6**. Schoenfeld's global p-value was >0.05 for all models. The results of the competing risk analysis of DSS and LRFS are summarized in **Tables S4**, **S6**, respectively. Gray's test competing risk analysis of DRFS showed that both covariates showing significance at multivariable analysis (i.e., histology according to WHO classification and locoregional extension according to classification #3) are potentially associated with informative censoring bias. The probability of informative censorship is significantly affected by the category of covariates ($p = 0.027$ and $p < 0.0001$, respectively). While the locoregional extension maintained significance in terms of distant recurrence-specific events ($p = 0.008$), histology lost significance ($p = 0.408$). The multi-variable subdistribution hazard models of DSS and LRFS did not show relevant difference compared with the respective Cox proportional hazards models, thus excluding the presence of a relevant informative censoring bias (**Table S7**). Multivariable subdistribution hazard models of DRFS showed a relevant difference compared with the respective Cox proportional

hazards models (i.e., the covariate histology lost significance) (**Table S7**). Thus, the DRFS Cox proportional hazard model was considered flawed by informative censoring and was not used to compare classifications. Given the paucity of regional failure events (n = 19) and the remarkable number of competing events, RRFS was also excluded from terms of comparison of classifications.

Classifications #1 and #2 and Comparison With WHO Classification

Cytomorphological-MCA, histomorphological and invasion-related-MCA, and differentiation-MCA generated 2 factors each, representing 76.0, 70.7, and 82.4% of variability in observations, respectively.

For classification #1, 5- and 6-cluster classifications were the best combinations of AIC/BIC and NPR (**Table S8**); since the 6-cluster classification had a 1-case class, the 5-cluster classification was selected due to better sorting of cases. Classification #1 is reported in **Table 3**. An independent prognostic effect was observed on LRFS and prognostic segregation was 15.9% ("NEC with mesenchymal features" vs. others). *A priori* applicability was suboptimal, with a confusion rate of 4.1%.

For classification #2, the 5-cluster classification generated through AHC (**Figure 5**) was associated with the best combination of AIC/BIC and NPR (**Table S9**). Classification #2 is reported in **Table 4**. An independent prognostic effect was observed on RFS and LRFS. Prognostic segregation was 37.2% for RFS ("SCC with mesenchymal features", "NEC without glandular features", and "other carcinomas" vs. others) and 26.2% for LRFS ("SCC with mesenchymal features" and "other carcinomas" vs. others) (**Figure 6**). The *a priori* applicability was optimal, with a confusion rate of 0.0% (**Figure 7**). The WHO classification (i.e., classification in SCC, SNCNOS, NEC, HG-

TABLE 3 | Classification #1 and class-specific outcomes.

Classification #1	Class 1 (n = 65)	Class 2 (n = 23)	Class 3 (n = 18)	Class 4 (n = 16)	Class 5 (n = 23)
Brief description	"Squamous cell carcinoma"	"Spindle cell and adenosquamous carcinoma"	"Papillary squamous cell carcinoma, possibly ex-inverted papilloma"	"Neuroendocrine carcinomas with glandular features"	"Neuroendocrine carcinomas with mesenchymal features"
Cytomorphological features	Squamous morphology (98.5%) Keratinization (43.1%) Rare cellular (16.9%) and nuclear (20.0%) pleomorphism Intermediate nucleus/ cytoplasm ratio (95.4%) Variable preeminent grade (G1/2: 40.0%; G3/4/X: 60.0%)	Squamous morphology (87.0%) Keratinization (26.1%) Glandular morphology (39.1%) Spindle cell (34.8%) or other mesenchymal morphology (4.3%) Frequent cellular (60.9%) and nuclear (47.8%) pleomorphism Nucleolar prominence (26.1%) Intermediate nucleus/ cytoplasm ratio (95.4%) High-grade (100.0%)	Squamous morphology (100.0%) Keratinization (22.2%) Possible cellular (38.9%) and nuclear (38.9%) pleomorphism Intermediate nucleus/ cytoplasm ratio (88.9%) Variable preeminent grade (G1/2: 27.8%; G3/4/X: 72.2%)	Rare squamous morphology (18.8%) Frequent cellular (62.5%) and nuclear (50.0%) pleomorphism Nucleolar prominence (43.8%) High nucleus/cytoplasm ratio (56.3%) High-grade (100.0%)	Rare squamous morphology (8.7%) Glandular morphology (39.1%) Spindle cell (26.1%) or other mesenchymal morphology (13.0%) Frequent cellular (47.8%) and nuclear (47.8%) pleomorphism Nucleolar prominence (52.2%) High (34.8%) or low (21.7%) nucleus/ cytoplasm ratio High-grade (91.3%)
Histomorphological features	Solid architecture (98.5%) Association with inverted papilloma (17.2%)	Solid architecture (91.3%) Cribriform architecture (17.4%) Association with inverted papilloma (13.0%)	Solid architecture (22.2%) Papillary architecture (83.3%) Association with inverted papilloma (38.9%)	Solid architecture (93.8%)	Solid architecture (91.3%) Cribriform architecture (13.0%)
Invasion-related features	PNI (38.5%) LVI (46.2%) IPBI (69.2%)	PNI (47.8%) LVI (30.4%) IPBI (56.5%)	PNI (0.0%) LVI (0.0%) IPBI (16.7%)	PNI (6.3%) LVI (31.3%) IPBI (75.0%)	PNI (30.4%) LVI (30.4%) IPBI (52.2%)
Differentiation features	Squamous (100.0%)	Squamous (100,0%) Glandular (73.9%) Mesenchymal (65.2%)	Squamous (100.0%)	Glandular (78.3%) Neuroendocrine (75.0%) Squamous (25.0%)	Mesenchymal (73.9%) Neuroendocrine (50.0%) Squamous (17.4%)
Multivariable model-adjusted* impact on LRFS (HR (95%-CI), p-value)	REF	1.83 (0.84–3.99), p = 0.130	0.21 (0.03–1.72), p = 0.144	1.18 (0.26–5.22), p = 0.833	3.47 (1.32–9.13), **p = 0.012**
Multivariable model-adjusted impact on RRFS (HR (95%-CI), p-value)**	REF	0.69 (0.14–3.52), p = 0.658	N.A., p = 0.998	2.66 (0.41–17.24), p = 0.305	8.66 (2.49–30.06), **p = 0.001**

*95% CI, 95% confidence interval; G1, well differentiated; G2, moderately differentiated; G3, poorly differentiated; G4, undifferentiated; GX, grade of differentiation not specified or not assessable (lesions defined as "high-grade" regardless of pathological features); HR, hazard ratio; IPBI, infiltrative pattern-bone invasion; LVI, lymphovascular invasion; N.A., not assessable; PNI, perineural invasion; REF, reference. *Multivariable model included: classification #1, type of surgery, classification # 3, margin status, adjuvant treatment, previous chemotherapy. **Multivariable model included: classification #1, neck dissection, orbital involvement, involvement of the masticator and/or parapharyngeal space, facial tissues involvement, sphenoid sinus involvement, margin status, adjuvant treatment. P-values less than 0.05 are highlighted in bold.*

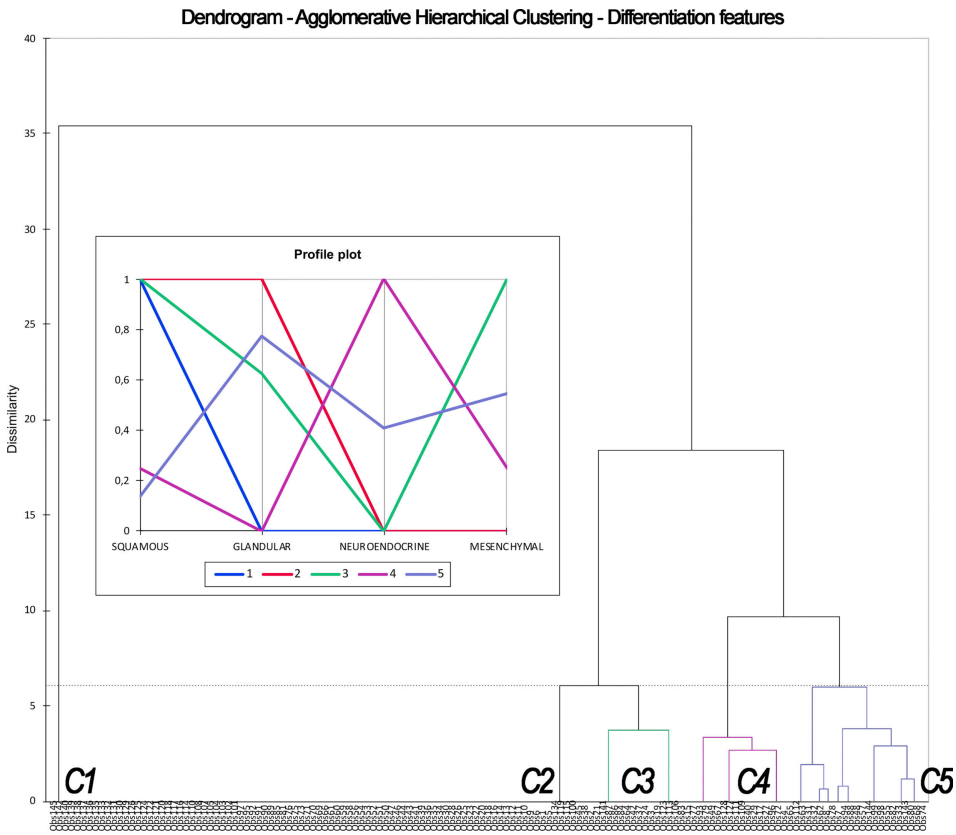

FIGURE 5 | Dendrogram and profile plot summarizing the process of Agglomerative Hierarchical Clustering based on differentiation features (i.e., leading to classification #2). This unsupervised machine learning methodology clusters observations (listed along the x-axis) based on their dissimilarity (expressed in the y-axis). Dissimilarity, which is defined according to differentiation, is maximal between clusters and minimal within each cluster. The process resulted in 5 clusters (C1–5), each one displaying a determinate frequency of squamous, glandular, neuroendocrine, and mesenchymal differentiation, as expressed by the profile plot. C1, C2, C3, C4, and C5 corresponds to cluster labeled as "squamous cell carcinoma," "squamous cell carcinoma with glandular features," "squamous cell carcinoma with mesenchymal features," "neuroendocrine carcinomas without glandular features," and "other carcinomas" in **Table 4**.

NITAC, SNUC, and ID-SNUC) had an independent prognostic effect on OS, DSS, RFS, and DRFS. Prognostic segregation was 9.0% (NEC and ID-SNUC vs. others).

When comparing RFS multivariable models including the type of surgery, locoregional extensions summarized as classification #3, margin status, type of adjuvant treatment, and either classification #2 or WHO classification, C-index, AIC, BIC, and NPR were 0.484, 577, 613, and 0.774 vs. 0.431, 579, 617, and 0.781, respectively (**Table 5**).

Classification #3 and Comparison With TNM Classification

Locoregional extension-related MCA generated 2 factors, representing 74.1% of the variability in observations. Five-cluster classification was associated with the best combination of AIC/BIC and NPR (**Table S10**). Classification #3 is reported in **Table 6**. An independent prognostic effect was observed on OS, DSS, RFS, and LRFS. Prognostic segregation was 33.8% for OS, DSS, RFS, and LRFS ("transcranial," "spheno-infracranial," and "fronto-orbito-basal" vs. others). *A priori* applicability was suboptimal, with a confusion rate of 3.4%.

Pathological T category (i.e., classification in pT1, pT2, pT3, pT4a, and pT4b) had an independent prognostic effect on OS, DSS, RFS, and LRFS. Prognostic segregation was 35.9% (pT4b vs. others) for OS, DSS, and RFS, and 65.5% for LRFS (pT4a and pT4b vs. others). The tumor stage (i.e., classification into stage I, II, III, IVA, and IVB) had an independent prognostic effect on OS, RFS, and LRFS. Prognostic segregation was 37.9% (IVB vs. others) for OS and RFS, and 66.9% for LRFS (IVA and IVB vs. others).

Response to Neoadjuvant Chemotherapy and Chemoradiosensitivity

Response to neoadjuvant ChT was distributed as follows: partial response (PR) in 15/35 (42.9%) patients; stable disease (SD) in 15/35 (42.9%); and progression of disease (PD) in 5/35 (14.3%). Histology was SCC in 14/35 (40.0%) patients, SNCNOS in 11/35 (31.4%), SNEC in 4/35 (11.4%), and SNUC, HG-NITAC, and ID-SNUC in 2/35 (5.7%) each. Fourteen/35 (40.0%) tumors were classified as pT4b, 12/35 (34.3%) as pT4a, 7/35 (20.0%) as pT3, and 2/35 (5.7%) as pT2. Chemoradiosensitivity could be estimated in 76/145 (52.4%) patients and was distributed as follows: class A in 2 (2.6%) cases, class B in 33 (43.4%), and class C in 41 (53.9%).

TABLE 4 | Classification #2 and class-specific outcomes.

Classification #2	Class 1 (n = 83)	Class 2 (n = 8)	Class 3 (n = 16)	Class 4 (n = 16)	Class 5 (n = 22)
Brief description	"Squamous cell carcinoma"	"Squamous cell carcinoma with glandular features"	"Squamous cell carcinoma with mesenchymal features"	"Neuroendocrine carcinomas without glandular features"	"Other carcinomas"
Label in Figure 5	"C1"	"C2"	"C3"	"C4"	"C5"
Label in Figures 6 and 7	"SCC"	"Glandular SCC"	"Mesenchymal SCC"	"Non-glandular NEC"	"Other SNC"
Differentiation	Squamous (100.0%) Glandular (0.0%) Mesenchymal (0.0%) Neuroendocrine (0.0%)	Squamous (100.0%) Glandular (100.0%) Mesenchymal (0.0%) Neuroendocrine (0.0%)	Squamous (100.0%) Glandular (62.5%) Mesenchymal (100.0%) Neuroendocrine (0.0%)	Squamous (25.0%) Glandular (0.0%) Mesenchymal (25.0%) Neuroendocrine (100.0%)	Squamous (13.6%) Glandular (77.3%) Mesenchymal (54.5%) Neuroendocrine (40.9%)
Multivariable model-adjusted* impact on RFS (HR (95%-CI), p-value)	REF	2.07 (0.84–5.09), p = 0.112	2.42 (1.10–5.34), **p = 0.028**	8.50 (2.60–27.74), **p = 0.0004**	2.32 (1.03–5.23), **p = 0.043**
Multivariable model-adjusted impact on LRFS (HR (95%-CI), p-value)**	REF	1.67 (0.57–4.88), p = 0.352	2.96 (1.25–7.03), **p = 0.014**	4.00 (0.86–18.59), p = 0.078	3.59 (1.42–9.08), **p = 0.007**

*95% CI, 95% confidence interval; HR, hazard ratio, *Multivariable model included: classification #2, type of surgery, classification # 3, margin status, adjuvant treatment. **Multivariable model included: classification #2, type of surgery, classification # 3, margin status, adjuvant treatment, previous chemotherapy. P-values less than 0.05 are highlighted in bold.*

Among all the tested information, only PNI and pagetoid growth were significantly associated with the response to ChT (p = 0.043 and p = 0.070, respectively, with PNI being associated with lower rate of PR and higher rate of PD, and pagetoid growth with higher rate of PR), neither of which maintained significance at multivariable analysis. The estimate of chemoradiosensitivity was associated with cellular pleomorphism (p = 0.030), solid pattern of growth (p = 0.056), pagetoid growth (p = 0.032), PNI (p = 0.001), and classification #1 (p = 0.050). However, only pagetoid growth and PNI-maintained significance at logistic regression (p = 0.030 and p = 0.007, respectively), with pagetoid growth being significantly associated with class A or B and PNI with class C. CRF was associated with a steady out-of-the-basket error between 40 and 60% when applied to both the response to neoadjuvant ChT and chemoradiosensitivity.

When the prognosis of patients receiving neoadjuvant ChT was analyzed in the multivariable model, the response to ChT affected OS, DSS, and RFS, with PD being associated with a significantly worse outcome. While margin status played a substantial prognostic role in multivariable models for all outcomes but RRFS and DRFS, its prognostic effect was lost when the analysis was limited to the subset of patients treated with neoadjuvant ChT.

DISCUSSION

Heterogeneity of Sinonasal Carcinomas

The first significant confirmatory finding of this study is that cancers grouped under the term "SNC" are extremely heterogeneous. While some dominant features, such as squamous cell morphology and a solid pattern of growth, could be demonstrated, numerous tumors displayed diverse pathological features from cytomorphological, histomorphological, and immunohistochemical standpoints. As already highlighted by other authors (15–17), this emphasizes that carcinomas of the sinonasal tract definitely have overlapping features, which probably explains difficulties in diagnosis, the high rate of diagnostic discrepancies, and suboptimal prediction of treatment response. As a glaring example of this phenomenon, according to classification #2, 62/145 (42.8%) of cases were classified as non-purely squamous SNC, of which, however, 31 (50.0%) displayed at least one of the features required to be labeled as "squamous."

Steadily Poor Prognosis of Sinonasal Carcinomas

Another relevant result of our analysis is that a substantial proportion of SNCs were associated with poor prognosis even if treatment was performed over the last 2 decades within a modern, multidisciplinary frame. As reported by Dulguerov et al., the OS of SNC progressively increased in the second half of the last century, from 28% ± 13% in the 1960s, to 36% ± 13% in the 1970s, 43% ± 15% in the 1980s, and 51% ± 14% in the 1990s (18). According to our results and consistent with a Danish population-based phase-4 cohort study performed in 2008–2015 (19), the positive trend observed by Dulguerov et al. has plateaued, with 5-year OS settled roughly around 50%. Of note, around one-third of patients included in the present series died within one year from the end of treatment, mostly owing to an early local recurrence, highlighting that a remarkable proportion of SNC is highly aggressive and poorly controlled, even if they were initially considered eligible for curative treatment. On one hand, this might be related to the large number of patients with locally advanced SNC in our study (T3/4: 117/145, 80.7%; vs. 61.4% in the recently published Danish Head and Neck Cancer (DAHANCA) group study) (19). On the other hand, this finding suggests that a relevant subgroup of SNC is not managed effectively even with contemporary treatment strategies. Interestingly, SNCNOS, namely SNC lacking a precise diagnosis according to the

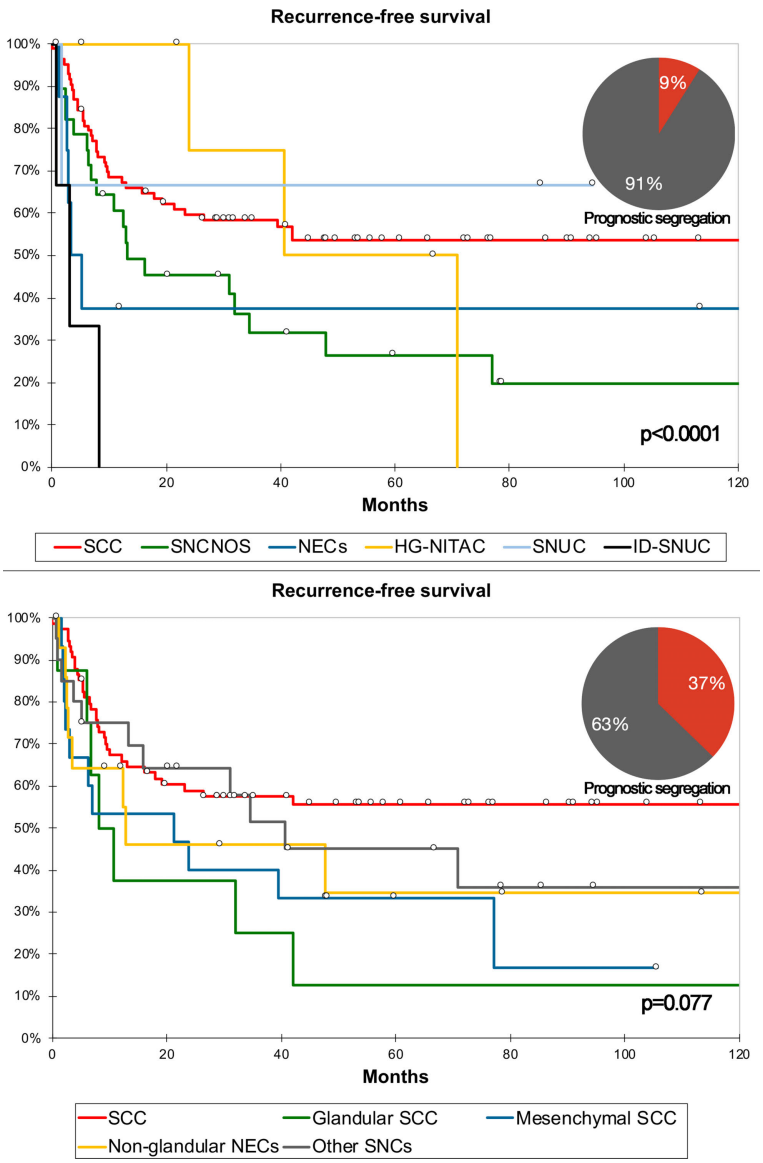

FIGURE 6 | Kaplan–Meier curves depicting recurrence-free survival of different sinonasal carcinomas (SNC) classified according to the WHO criteria and classification #2. Prognostic segregation is expressed through pie charts. P-value refers to log-rank test (see **Tables S5** and **4** for multivariable-adjusted significance). See **Table 4** for detailed definition of each group of carcinomas as per classification #2. HG-NITAC, high-grade non-intestinal-type adenocarcinoma; ID-SNUC, INI1-SMARCB1-deficient sinonasal undifferentiated carcinoma; NEC, neuroendocrine carcinoma; SCC, squamous cell carcinoma; SNCNOS, sinonasal carcinoma not otherwise specified; SNUC, sinonasal undifferentiated carcinoma.

WHO criteria, were associated with dismal OS and DSS similarly to NEC and ID-SNUC (5-year estimates: 36.6 and 41.7%, 33.3 and 37.5%, and 0.0 and 0.0%, respectively). SNUCs with normal or non-tested expression of SMARCB1/INI1, were associated with 5-year OS and DSS of 66.7%, which aligns with the 59% rate recently reported by Amit et al. in a cohort of 95 SNUCs (20). While SNUC is still considered as a wastebasket entity, the progressive exclusion from this category of aggressive SNC with specific molecular identifiers such as ID-SNUC (21), SMARCA4-deficient carcinoma (22) and NUT carcinoma (23), together with the increasing use of neoadjuvant ChT-based regimens, has led to considerable improvement in SNUC-specific outcomes, particularly when treatment is based on chemoselection (20). Our data suggest that poorly understood SNC currently bears a worse prognosis than SNUC, which in the past was unanimously considered to be associated with a dismal outcome (24–26). Among SNC with the worst prognosis, NEC and ID-SNUC represented only a small proportion (13/145, 9.0%), while SNCNOS was the second most frequent diagnosis after SCC, with 30 (20.7%) cases. This further emphasizes

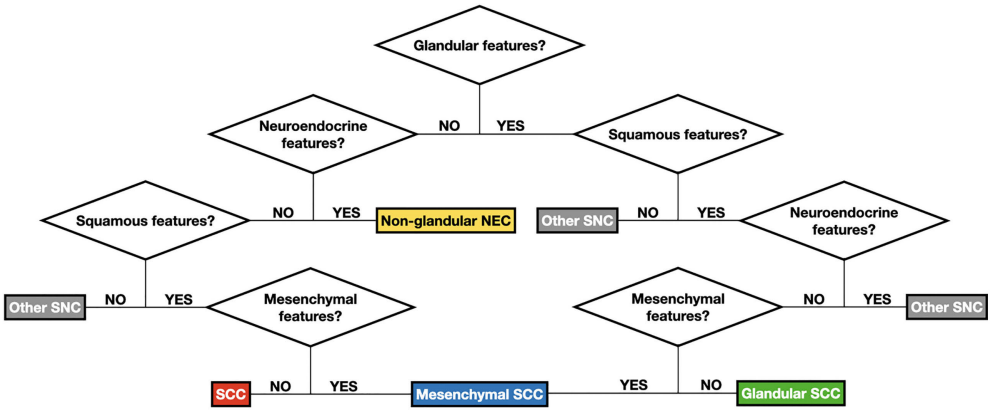

FIGURE 7 | Flow chart summarizing the logical steps to classify sinonasal carcinomas (SNC) according to classification #2. See **Table 1** for detailed description of features designating the differentiation(s) of carcinomas. See **Table 4** for de-tailed definition of each group of carcinomas as per classification #2. NEC, neuroendocrine carcinoma; SCC, squamous cell carcinoma.

the difficulty of reaching a WHO-recognized SNC diagnosis in SNC and the need for better classification of SNC to improve treatment outcomes.

The Impact of Multimodal Treatment

Adjuvant and neoadjuvant therapies have been confirmed to be of utmost importance in determining and predicting outcomes. Response to neoadjuvant ChT was associated with OS, DSS, and RFS independently of histology, locoregional extension, type of surgery, margin status, and type of adjuvant treatment (**Tables S3–S5**). In particular, patients with PD had a significantly worse prognosis than those with SD or PR following neoadjuvant ChT (**Figure 8**). Several studies from the University of Texas MD Anderson Cancer Center demonstrated the prognostic effect of response to neoadjuvant ChT in single-histology SNC series (20, 27, 28). Of note, in our series, adjuvant ChT-RT showed a remarkable positive effect on RFS and LRFS (**Figure 8**), which was, however, minimized in multivariable analysis, where adjuvant RT and ChT-RT had a similar positive impact on RFS and LRFS irrespective of histology, locoregional extension, type of surgery, margin status, and previous ChT (**Tables S5–S6**). This finding reinforces the belief that treatment of most SNC should be multimodal. Being independently associated with OS, DSS, RFS, and LRFS, margin status was confirmed as a relevant prognostic factor. The finding that margin status lost its prognostic effect on patients treated with neoadjuvant ChT is of particular interest (**Tables S3–S6**). A possible explanation might be related to a non-concentric response of SNC to ChT, as observed in other cancers (29). This would imply that the assessment of margins at definitive pathology is not a reliable estimate of microscopic residual disease. Such a hypothesis, while based on a small number of

TABLE 5 | Comparison of multivariable models in terms of concordance index (C-index), Akaike Information Criterion (AIC), Bayesian Information Criterion (BIC), and Nagelkerke pseudo-R^2 (NPR).

Model	C-index	AIC	BIC	NPR
Classification #2—RFS*	0.484	577	613	0.774
WHO—RFS*	0.431	579	617	0.781
Classification #3—OS**	0.598	529	566	0.773
Pathological T category (8th ed.)—OS**	0.318	540	577	0.717
Tumor stage (8th ed.)—OS**	0.312	545	582	0.725
Classification #3—DSS**	0.608	467	502	0.794
Pathological T category (8th ed.)—DSS**	0.322	478	513	0.748
Classification #3—RFS**	0.431	579	617	0.781
Pathological T category (8th ed.)—RFS**	0.306	591	629	0.757
Tumor stage (8th ed.)—RFS**	0.321	595	633	0.719
Classification #3—LRFS**	0.576	452	460	0.422
Pathological T category (8th ed.)—LRFS**	0.353	460	470	0.387
Tumor stage (8th ed.)—LRFS**	0.348	460	468	0.362

*DSS, disease-specific survival; LRFS, local recurrence-free survival; OS, overall survival; RFS, recurrence-free survival; WHO, World Health Organization. *Model included type of surgery, locoregional extensions summarized as classification #3, margin status, type of adjuvant treatment, and either classification #2 or WHO classification of histology. **Model included WHO classification of histology, type of surgery, margin status, type of adjuvant treatment, and locoregional extensions summarized as either classification #3, pathological T category or tumor stage.*

TABLE 6 | Classification #3 and class-specific outcomes.

Classification #3	Class 1 (n = 64)	Class 2 (n = 32)	Class 3 (n = 18)	Class 4 (n = 14)	Class 5 (n = 17)	P-value
Brief description	"Sinonasal"	"Facial"	"Transcranial"	"Spheno-infracranial"	"Fronto-orbito-basal"	–
Orbital infiltration	3.1%	46.9%	7.1%	44.4%	88.2%	<0.0001
Infiltration of the bony skull base	10.9%	9.4%	100.0%	22.2%	76.5%	<0.0001
Dural infiltration	0.0%	0.0%	100.0%	0.0%	70.6%	<0.0001
Infiltration of the masticator/parapharyngeal space	17.2%	50.0%	0.0%	83.3%	23.5%	<0.0001
Infiltration of facial tissues	0.0%	96.9%	0.0%	38.9%	47.1%	<0.0001
Infiltration of sphenoid sinus	6.3%	12.5%	35.7%	77.8%	58.8%	<0.0001
Infiltration of frontal sinus	6.3%	0.0%	0.0%	0.0%	88.2%	<0.0001
Nasopharyngeal infiltration	6.3%	0.0%	0.0%	88.9%	23.5%	<0.0001
Nodal metastasis	9.4%	15.6%	0.0%	16.7%	23.5%	0.256
5-year LRFS (95% CI)	80.2% (71.4–89.0%)	57.1% (36.0–78.1%)	33.3% (3.4–63.3%)	22.0% (0.0–46.1%)	13.3% (0.00–34.9%)	<0.0001

95% CI, 95% confidence interval; LRFS, local recurrence-free survival. Multivariable model included: classification #3, type of surgery, classification #2, margin status, adjuvant treatment. Multivariable model included: classification #3, type of surgery, classification#2, margin status, adjuvant treatment, previous chemotherapy.

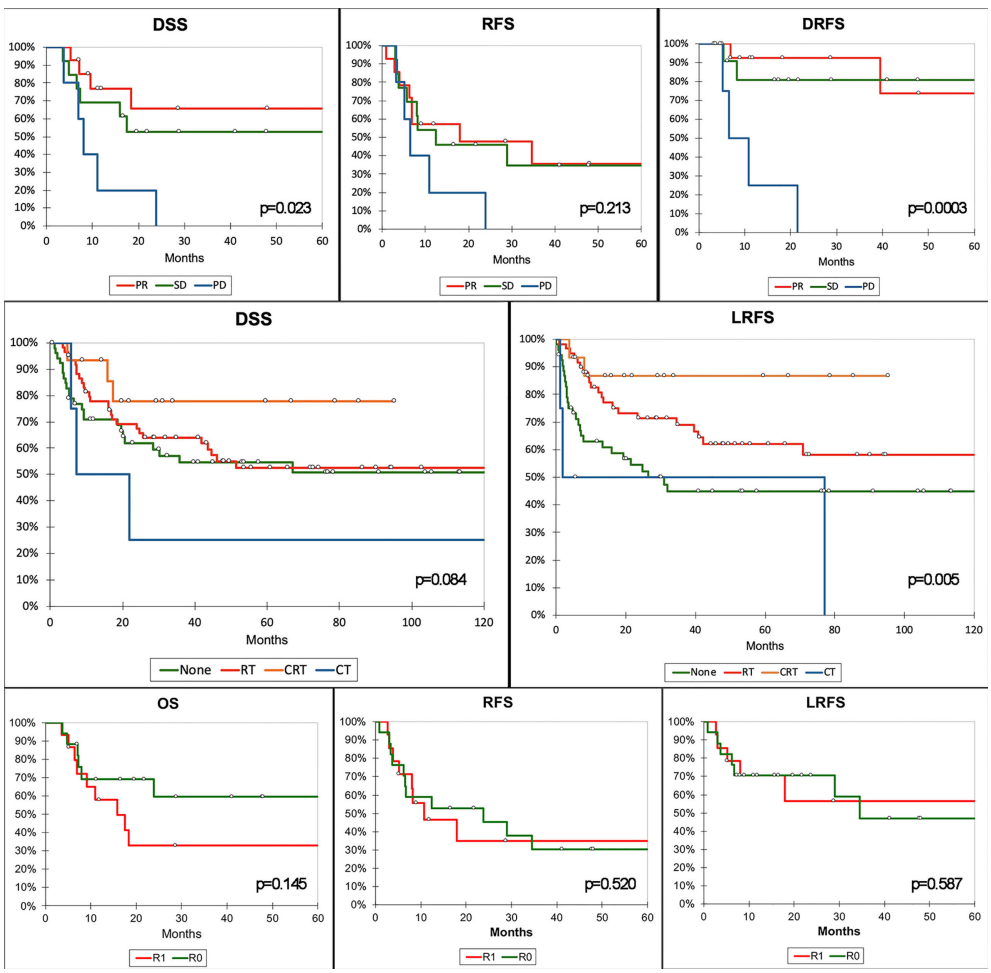

FIGURE 8 | Kaplan–Meier curves summarizing the most relevant results of the survival analysis. Top row of graphs demonstrates the poorer prognosis in terms of disease-specific (DSS), recurrence-free (RFS), and distant recurrence-free survival (DRFS) of patients with progression of disease (PD) after neoadjuvant chemotherapy compared to those with stable disease (SD) or partial response (PR). Middle row shows the protective effect of adjuvant radiotherapy (RT) and chemoradiotherapy (CRT) on local recurrence-free survival (LRFS). Of note, only CRT showed an effect on DSS at univariate analysis. Bottom row shows the absence of a relevant effect of margin status on prognosis in patients receiving neoadjuvant CT. P-value refers to log-rank test (see **Tables S3**–**S6** for multivariable-adjusted significance). CT, adjuvant chemotherapy; R0, clear margins; R1, involved margins.

patients, might suggest that the value of classical prognosticators of SNC is undermined in subjects receiving neoadjuvant therapies and warrants a systematic reappraisal of prognostic factors in these patients. However, before generalizing this finding, one should consider that it was based on patients sent for surgery after neoadjuvant ChT, which includes a majority of cases with poor response to neoadjuvant therapy and might thereby be not representative of all SNC.

Machine-Learning-Based Classification of Sinonasal Carcinomas

Three machine-learning-generated experimental classifications of SNC based on pathological features and locoregional extension were generated to test the main hypothesis of the study, which was that reorganization of clinicopathological information could improve the prediction of prognosis and chemoradiosensitivity. Each classification was compared to the respective gold standard method to describe sinonasal cancers, namely the WHO (1) and TNM classifications (13) for pathological diagnosis and description of locoregional extension, respectively. A comparison was first performed on a prognostic basis and showed that classification #2 better predicted OS than the WHO classification, whereas classification #1 could not be included in the comparison as there were no prognostic outcomes affected by both the WHO classification and classification #1 at multivariable analyses. Prognostic segregation was also better for classification #2 compared to the WHO classification, with 37.2 and 9.0% of patients being classified in the poor-prognosis category(ies), respectively. As opposed to classification #1, classification #2 was applicable *a priori*, which means that criteria to apply this classification to an external series could be found, as reported in **Figure 6**. However, two main drawbacks of this classification should be highlighted: First, criteria to designate a cancer with one or another differentiation were established arbitrarily, based on the common interpretation of some morphological and (immuno) histochemical findings (**Table 1**); second, immunohistochemistry, which is supposed to substantially aid in unveiling nuances of differentiation in a given cancer, was not systematically applied, as immunostaining was dictated by case-specific needs to achieve a diagnosis. Thus, not all cancers underwent the same set of immunostaining. Based on these findings, reorganization of pathological information, with special reference to those related to tumor differentiation, may help in improving the ability to predict outcomes of SNC-patients. However, classification #2 has been used only as a research means to test a scientific hypothesis and requires optimization and external validation prior to being proposed as an alternative prognostic tool.

Classification #3 assessed the locoregional extension of SNC and performed better than TNM classification in terms of OS, DSS, RFS, and LRFS prediction. However, the absence of *a priori* applicability prevents it from being proposed as an alternative to TNM classification. Moreover, TNM-based clustering of tumors provided better prognostic segregation. The main difference between classification #3 and TNM lies in the fact that in the former, the category is assigned by simultaneously considering the status of involvement of several sinonasal and skull base structures, whereas the latter classifies a tumor based on the infiltrated structure pertaining to the highest T category. The fact that the first method provided better prediction of several survival outcomes should prompt investigation of tumor extension in a more multidimensional fashion when T category assignment criteria are revised for the next TNM Edition. For instance, a score-based assignment based on the evaluation of tumor extension along the 6 vectors of possible growth (i.e., anterior, posterior, inferior, superior, medial, and lateral) could be considered.

Of note, the prognostic value of the experimental classification used herein should be considered in view of the unsupervised methodology of machine learning. Each classifications has been developed based on non-prognostic information, and prognostic outcomes (i.e., DSS and LRFS) were employed only to select the best among alternative clustering strategies developed blindly with respect to prognosis. This method minimizes the risk of overfitting.

Unpredictability of Response to Chemotherapy and Radiotherapy

Reliable prediction of sensitivity to ChT and/or RT is an unmet need in the field of sinonasal oncology. Amit et al. recently demonstrated that sensitivity to ChT-RT can be based on response to neoadjuvant ChT in SNUC, at the cost of a 60% rate of ChT-related grade 3–4 adverse events (20). The same group also found that a 34-gene signature predicted the response to neoadjuvant ChT in SNUC, thus paving the way towards molecular biology-based selection of locoregional treatment, which would have the potential benefit of avoiding neoadjuvant ChT-related toxicity (30). Different from SNUC, chemoselection is not effective in other SNC such as SCC (28). Since SNUC represents a minority of SNC, there is an evident need for predictive tools to identify responders to non-surgical treatment. This would, in fact, save potential responders the morbidity of invasive surgeries such as open maxillectomy and endoscopic-assisted craniofacial resection, which were performed in more than half of the patients in the present series (83/145, 57.2%). Our analysis showed that PNI and pagetoid growth affected chemoradiosensitivity independently of other factors. PNI was associated with resistance to non-surgical therapies, whereas pagetoid growth was associated with increased chemoradiosensitivity. However, this observation has limited value from a predictive perspective: first, PNI and pagetoid growth were found at definitive histological examination after surgery, and one could argue that they might have been undetectable at pre-treatment biopsy; second, even if pagetoid growth was unprecedently reported in SNC in the present study (**Figure 3D**), this pattern of local extension is rather rare (7/145 cases, 4.8%). Pagetoid growth refers to the tendency of cancer cells to spread through the epithelium, thus representing a distinct escape route along the superficial aspect of

the sinonasal tract compared to invasion of subepithelial tissues. This pattern was observed in 3 SNCNOS, 2 SCC, and 2 SNUC. Two cases were recurrent, and 3 had been treated with neoadjuvant ChT (of which 1 was a recurrent SNCNOS), thus excluding that this pattern represents an artifact induced by previous treatments (as 3 patients were treatment-naïve). PNI was observed in 44 (30.3%) patients, consistent with the findings of Gil et al. (22% in SCC, 60% in SNUC, 20% in SNCNOS) (31). The fact that PNI increased chemoradioresistance is consistent with its negative effect on prognosis, as observed in other studies (11, 32). Thus, it is reasonable to surmise that PNI represents a preeminent mechanism of resistance to therapy in SNC. Overall, it can be concluded that pathological features cannot be exploited, not even through machine learning, to infer chemoradiosensitivity of SNC, as also witnessed by the fact that CRF was unable to segregate cancers based on their estimated chemoradiosensitivity. Thus, since genomics- (30) and radiomics-based (33) signatures are efficient in segregating responders from non-responders while avoiding chemoselection, omic analysis of SNC represents the next logical step forward in sinonasal oncology research.

Limitations of the Study

Besides those already highlighted, the 1) retrospective design of this study, which included only patients treated with surgery as locoregional treatment, is the major limitation. This was imposed by the need for accurate pathological analysis of each case (that is not available in patients receiving a primary RT-based treatment), but, at the same time, it creates a considerable selection bias. In fact, some chemoradiosensitive cancers that initially responded to neoadjuvant ChT were treated with definitive ChT-RT, thus preventing inclusion in this study. 2) Given the rarity of SNC, both primary and recurrent cases were included. Removing recurrent cases would have meant decreasing the size of the series to a point of non-usability for this study. Since presentation did not significantly impact on survival, with prognosis being the first term of comparison between classifications, then the tradeoff between dramatically reducing the series size and accepting the non-/poorly-impacting approximation of including non-primary cases was considered in favor of this scientific policy. Of note, the same strategy has been adopted by several other research groups with a high reputation in the field of sinonasal cancer (34–41). However, despite there exists no sound and univocal evidence on the fact that recurrent SNC bear worse prognosis compared to primary SNC, a sufficiently large series of non-recurrent SNC would imply reducing the risk for confounders and bias. 3) Selection of staining methods to make diagnosis was dictated by case-specific needs and constraints, thus being non-systematic as an unavoidable consequence of the long inclusion period. 4) Lacking a blind re-evaluation by multiple raters, this study does not provide information on inter-rater agreement. 5) The sample size of this single-center series of rare cancers is inherently limited. 6) Even if unsupervised machine learning reduces the risk of overfitting, external validation will be essential to corroborate our findings.

CONCLUSIONS

This study confirmed that SNCs are exceedingly heterogeneous from a histological standpoint. Oncologic outcomes have plateaued since the early 2000s despite the adoption of multi-modal treatment regimens. SNCNOS, namely cancers that cannot be precisely classified as per WHO criteria, represent a non-negligible part of SNC and their prognosis is similar to that of aggressive histologies such as NEC and ID-SNUC. Re-classification of cancers through a machine learning method based on pathological information improved prediction and segregation, thus suggesting that a reappraisal of pathological and biological features of these cancers could be beneficial in terms of prognostic accuracy. However, the response to ChT and/or RT could not be predicted in this series, thus suggesting that other fields of research, such as radiomics and genomics/transcriptomics, should be exploited to identify predictive models. Of note, the classifications presented here were aimed at verifying the hypothesis of the study and are not intended to substitute the standardized method for classifying SNC.

DATA AVAILABILITY STATEMENT

The raw data supporting the conclusions of this article will be made available by the authors, without undue reservation.

ETHICS STATEMENT

The studies involving human participants were reviewed and approved by the Comitato Etico degli Spedali Civili di Brescia. Written informed consent for participation was not required for this study in accordance with the national legislation and the institutional requirements.

AUTHOR CONTRIBUTIONS

Authors contributed to the manuscript as follows: conceptualization: MF, DM, AS, VR, RM, PB, AD, and PN. Methodology: MF. Software: MF. Formal analysis: DM and MR. Data curation: MF, VR, TG, MT, ST, LA, SB, and AB. Writing of original draft: MF. Manuscript review and editing: DM, CP, PB, AD, and PN. Supervision: RM, PB, CP, AD, and PN. All authors listed have made a substantial, direct, and intellectual contribution to the work and approved it for publication.

SUPPLEMENTARY MATERIAL

The Supplementary Material for this article can be found online at: https://www.frontiersin.org/articles/10.3389/fonc.2022.799680/full#supplementary-material

REFERENCES

1. El-Naggar AK, Chan JKC, Rubin Grandis J, Takata T, Slootweg PJ. International Agency for Research on Cancer. WHO Classification of Head and Neck Tumours. Lyon, France: WHO. (2017).
2. Castelnuovo P, Turri-Zanoni M, Battaglia P, Antognoni P, Bossi P, Locatelli D. Sinonasal Malignancies of Anterior Skull Base: Histology-Driven Treatment Strategies. *Otolaryngol Clin North Am* (2016) 49:183–200. doi: 10.1016/j.otc.2015.09.012
3. López F, Lund VJ, Suárez C, Snyderman CH, Saba NF, Robbins KT, et al. The Impact of Histologic Phenotype in the Treatment of Sinonasal Cancer. *Adv Ther* (2017) 34:2181–98. doi: 10.1007/s12325-017-0605-9
4. Ferrari M, Orlandi E, Bossi P. Sinonasal Cancers Treatments: State of the Art. *Curr Opin Oncol* (2021) 33:196–205. doi: 10.1097/CCO.0000000000000726
5. De Cecco L, Serafini MS, Facco C, Granata R, Orlandi E, Fallai C, et al. A Functional Gene Expression Analysis in Epithelial Sinonasal Cancer: Biology and Clinical Relevance Behind Three Histological Subtypes. *Oral Oncol* (2019) 90:94–101. doi: 10.1016/j.oraloncology.2019.02.003
6. Takahashi Y, Gleber-Netto FO, Bell D, Roberts D, Xie TX, Abdelmeguid AS, et al. Identification of Novel Diagnostic Markers for Sinonasal Undifferentiated Carcinoma. *Head Neck* (2019) 41:2688–95. doi: 10.1002/hed.25748
7. Mehrad M, Chernock RD, El-Mofty SK, Lewis JS. Diagnostic Discrepancies in Mandatory Slide Review of Extra-Departmental Head and Neck Cases: Experience at a Large Academic Center. *Proc Arch Pathol Lab Med* (2015) 139:1539–45. doi: 10.5858/arpa.2014-0628-OA
8. Choi KY, Amit M, Tam S, Bell D, Phan J, Garden AS, et al. Clinical Implication of Diagnostic and Histopathologic Discrepancies in Sinonasal Malignancies. *Laryngoscope* (2021) 131:E1468–75. doi: 10.1002/lary.29102
9. Schreiber A, Rampinelli V, Ferrari M, Mattavelli D, Farina D, Battocchio S, et al. Diagnostic Reliability of Pretreatment Biopsy in Malignant Nasoethmoidal Tumors: A Retrospective Study of 77 Cases. *Laryngoscope* (2018) 128:1772–7. doi: 10.1002/lary.27077
10. Ferrari M, Bossi P, Mattavelli D, Ardighieri L, Nicolai P. Management of Sinonasal Adenocarcinomas With Anterior Skull Base Extension. *J Neurooncol* (2020) 150:405–17. doi: 10.1007/s11060-019-03385-8
11. Ferrari M, Ioppi A, Schreiber A, Gualtieri T, Mattavelli D, Rampinelli V, et al. Malignant Tumors of the Maxillary Sinus: Prognostic Impact of Neurovascular Invasion in a Series of 138 Patients. *Oral Oncol* (2020) 106:104672. doi: 10.1016/j.oraloncology.2020.104672
12. Brown JS, Browne RM. Factors Influencing the Patterns of Invasion of the Mandible by Oral Squamous Cell Carcinoma. *Int J Oral Maxillofac Surg* (1995) 24:417–26. doi: 10.1016/S0901-5027(05)80471-0
13. Union for International Cancer Control (UICC). *Tumor Node Metastasis (TNM) Classification of Malignant Tumours*. JD Brierley, MK Gospodarowicz, C Wittekind, editors. Hoboken, NJ, USA: Wiley-Blackwell (2016).
14. Eisenhauer EA, Therasse P, Bogaerts J, Schwartz LH, Sargent D, Ford R, et al. New Response Evaluation Criteria in Solid Tumours: Revised RECIST Guideline (Version 1.1). *Eur J Cancer* (2009) 45:228–47. doi: 10.1016/j.ejca.2008.10.026
15. Weindorf SC, Brown NA, McHugh JB, Udager AM. Sinonasal Papillomas and Carcinomas a Contemporary Update With Review of an Emerging Molecular Classification. *Arch Pathol Lab Med* (2019) 143:1304–16. doi: 10.5858/arpa.2019-0372-RA
16. Stelow EB, Jo VY, Mills SE, Carlson DL. A Histologic and Immunohistochemical Study Describing the Diversity of Tumors Classified as Sinonasal High-Grade Nonintestinal Adenocarcinomas. *Am J Surg Pathol* (2011) 35:971–80. doi: 10.1097/PAS.0b013e31821cbd72
17. Bell D, Hanna EY. Sinonasal Undifferentiated Carcinoma: Morphological Heterogeneity, Diagnosis, Management and Biological Markers. *Expert Rev Anticancer Ther* (2013) 13:285–96. doi: 10.1586/era.13.1
18. Dulguerov P, Jacobsen MS, Allal AS, Lehmann W, Calcaterra T. Nasal and Paranasal Sinus Carcinoma: Are We Making Progress? A Series of 220 Patients and a Systematic Review. *Cancer* (2001) 92:3012–29. doi: 10.1002/1097-0142(20011215)92:12<3012::aid-cncr10131>3.0.co;2-e
19. Filtenborg MV, Lilja-Fischer JK, Sharma MB, Primdahl H, Kjems J, Plaschke CC, et al. Sinonasal Cancer in Denmark 2008–2015: A Population-Based Phase-4 Cohort Study From DAHANCA. *Acta Oncol (Madr)* (2021) 60:333–42. doi: 10.1080/0284186X.2021.1874618
20. Amit M, Abdelmeguid AS, Watcherporn T, Takahashi H, Tam S, Bell D, et al. Induction Chemotherapy Response as a Guide for Treatment Optimization in Sinonasal Undifferentiated Carcinoma. *J Clin Oncol* (2019) 37:504–12. doi: 10.1200/JCO.18.00353
21. Kakkar A, Antony VM, Pramanik R, Sakthivel P, Singh CA, Jain D. SMARCB1 (INI1)–deficient Sinonasal Carcinoma: A Series of 13 Cases With Assessment of Histologic Patterns. *Hum Pathol* (2019) 83:59–67. doi: 10.1016/j.humpath.2018.08.008
22. Agaimy A, Weichert W. SMARCA4-Deficient Sinonasal Carcinoma. *Head Neck Pathol* (2017) 11:541–5. doi: 10.1007/s12105-017-0783-4
23. Stelow EB, Bellizzi AM, Taneja K, Mills SE, Legallo RD, Kutok JL, et al. NUT Rearrangement in Undifferentiated Carcinomas of the Upper Aerodigestive Tract. *Am J Surg Pathol* (2008) 32:828–34. doi: 10.1097/PAS.0b013e31815a3900
24. Gorelick J, Ross D, Marentette L, Blaivas M. Sinonasal Undifferentiated Carcinoma: Case Series and Review of the Literature. *Neurosurgery* (2000) 47:750–5. doi: 10.1097/00006123-200009000-00045
25. Houston GD. Sinonasal Undifferentiated Carcinoma: Report of Two Cases and Review of the Literature. *Oral Surg Oral Med Oral Pathol Oral Radiol Endod* (1998) 85:185–8. doi: 10.1016/S1079-2104(98)90424-3
26. Kim BS, Vongtama R, Juillard G. Sinonasal Undifferentiated Carcinoma: Case Series and Literature Review. *Am J Otolaryngol* (2004) 25:162–6. doi: 10.1016/j.amjoto.2003.12.002
27. Hanna EY, Cardenas AD, DeMonte F, Roberts D, Kupferman M, Weber R, et al. Induction Chemotherapy for Advanced Squamous Cell Carcinoma of the Paranasal Sinuses. *Arch Otolaryngol - Head Neck Surg* (2011) 137:78–81. doi: 10.1001/archoto.2010.231
28. Abdelmeguid AS, Teeramatwanich W, Roberts DB, Amit M, Ferraroto R, Glisson BS, et al. Neoadjuvant Chemotherapy for Locoregionally Advanced Squamous Cell Carcinoma of the Paranasal Sinuses. *Cancer* (2021) 127:1788–95. doi: 10.1002/cncr.33452
29. Kim TH, Kang DK, Yim H, Jung YS, Kim KS, Kang SY. Magnetic Resonance Imaging Patterns of Tumor Regression After Neoadjuvant Chemotherapy in Breast Cancer Patients: Correlation With Pathological Response Grading System Based on Tumor Cellularity. *J Comput Assist Tomogr* (2012) 36:200–6. doi: 10.1097/RCT.0b013e318246abf3
30. Takahashi Y, Gleber-Netto FO, Bell D, Roberts D, Xie TX, Abdelmeguid AS, et al. Identification of Markers Predictive for Response to Induction Chemotherapy in Patients With Sinonasal Undifferentiated Carcinoma. *Oral Oncol* (2019) 97:56–61. doi: 10.1016/j.oraloncology.2019.07.028
31. Gil Z, Carlson DL, Gupta A, Lee N, Hoppe B, Shah JP, et al. Patterns and Incidence of Neural Invasion in Patients With Cancers of the Paranasal Sinuses. *Arch Otolaryngol - Head Neck Surg* (2009) 135:173–9. doi: 10.1001/archoto.2008.525
32. Ferrari M, Migliorati S, Tomasoni M, Crisafulli V, Nocivelli G, Paderno A, et al. Sinonasal Cancer Encroaching the Orbit: Ablation or Preservation? *Oral Oncol* (2021) 114:105185. doi: 10.1016/j.oraloncology.2021.105185
33. Bologna M, Montin E, Corino VDA, Bossi P, Calareso G, Licitra L, et al. Use of Apparent Diffusion Coefficient Images to Predict Response to Induction Chemotherapy in Sinonasal Cancer. *Proc Annu Int Conf IEEE Eng Med Biol Soc* (2018) 2018:782–5. doi: 10.1109/EMBC.2018.8512306
34. Hanna E, DeMonte F, Ibrahim S, Roberts D, Levine N, Kupferman M. Endoscopic Resection of Sinonasal Cancers With and Without Craniotomy: Oncologic Results. *Arch Otolaryngol - Head Neck Surg* (2009) 135:1219–24. doi: 10.1001/archoto.2009.173
35. Nicolai P, Battaglia P, Bignami M, Villaret AB, Delù G, Khrais T, et al. Endoscopic Surgery for Malignant Tumors of the Sinonasal Tract and Adjacent Skull Base: A 10-Year Experience. *Am J Rhinol* (2008) 22:308–16. doi: 10.2500/ajr.2008.22.3170
36. Lund VJ, Wei WI. Endoscopic Surgery for Malignant Sinonasal Tumours: An Eighteen Year Experience. *Rhinology* (2015) 53:204–11. doi: 10.4193/Rhino14.318
37. Ganly I, Patel SG, Singh B, Kraus DH, Bridger PG, Cantu G, et al. Craniofacial Resection for Malignant Paranasal Sinus Tumors: Report of an International Collaborative Study. *Head Neck* (2005) 27:575–84. doi: 10.1002/hed.20165
38. Howard DJ, Lund VJ, Wei WI. Craniofacial Resection for Tumors of the Nasal Cavity and Paranasal Sinuses: A 25-Year Experience. *Head Neck* (2006) 28:867–73. doi: 10.1002/hed.20432

39. Suarez C, Llorente JL, De Leon RF, Maseda E, Lopez A. Prognostic Factors in Sinonasal Tumors Involving the Anterior Skull Base. *Head Neck* (2004) 26:136–44. doi: 10.1002/hed.10358
40. Cantu G, Solero CL, Mariani L, Lo Vullo S, Riccio S, Colombo S, et al. Intestinal Type Adenocarcinoma of the Ethmoid Sinus in Wood and Leather Workers: A Retrospective Study of 153 Cas-Es. *Head Neck* (2011) 33:535–42. doi: 10.1002/hed.21485
41. Cantu G, Solero CL, Miceli R, Mattana F, Riccio S, Colombo S, et al. Anterior Craniofacial Resection for Malignant Paranasal Tumors: A Monoinstitutional Experience of 366 Cases. *Head Neck* (2012) 34:78–87. doi: 10.1002/hed.21685

Conflict of Interest: The authors declare that the research was conducted in the absence of any commercial or financial relationships that could be construed as a potential conflict of interest.

frontiers | Frontiers in Oncology

ORIGINAL RESEARCH
published: 17 June 2022
doi: 10.3389/fonc.2022.783919

NTF2 Upregulation in HNSCC: a Predictive Marker and Potential Therapeutic Target Associated With Immune Infiltration

Guangxu Xuan[1,2†], Xin Zhang[3†], Min Zhang[3†], Minghang Yu[4,5], Yujie Zhou[5], Xiaosong He[2], Xiaopeng Hu[3], Xi Wang[4,5,6*] and Liangfa Liu[1*]*

[1] Department of Otolaryngology Head and Neck Surgery, Beijing Friendship Hospital, Capital Medical University, Beijing, China, [2] Department of Otolaryngology Head and Neck Surgery, Affiliated Hospital of Guilin Medical University, Guilin, China, [3] Department of Urology, Beijing Chao-Yang Hospital, Capital Medical University, Beijing, China, [4] Beijing Key Laboratory of Emerging Infectious Diseases, Institute of Infectious Diseases, Beijing Ditan Hospital, Capital Medical University, Beijing, China, [5] Department of Immunology, School of Basic Medical Sciences, Advanced Innovation Center for Human Brain Protection, Beijing Key Laboratory for Cancer Invasion and Metastasis, Department of Oncology, Capital Medical University, Beijing, China, [6] Beijing Institute of Infectious Diseases, Beijing, China

OPEN ACCESS

Edited by:
Hui Wang,
Hunan Cancer Hospital, China

Reviewed by:
Yuxian Song,
Nanjing Stomatological Hospital (NSH), China
Yi Bai,
Tianjin First Central Hospital, China

***Correspondence:**
Liangfa Liu
liuliangfa301@163.com
Xi Wang
xiwang@ccmu.edu.cn
Xiaopeng Hu
xiaopeng_hu@sina.com

[†]These authors have contributed equally to this work and share first authorship

Specialty section:
This article was submitted to Head and Neck Cancer, a section of the journal Frontiers in Oncology

Received: *27 September 2021*
Accepted: *13 May 2022*
Published: *17 June 2022*

Citation:
Xuan G, Zhang X, Zhang M, Yu M, Zhou Y, He X, Hu X, Wang X and Liu L (2022) NTF2 Upregulation in HNSCC: A Predictive Marker and Potential Therapeutic Target Associated With Immune Infiltration. Front. Oncol. 12:783919. doi: 10.3389/fonc.2022.783919

Background: Head and neck squamous cell carcinoma (HNSCC) is a type of malignant tumor with an increasing incidence worldwide and a meager 5-year survival rate. It is known that nuclear transporter factor 2 (NTF2) transports related proteins into the nucleus physiologically. However, the role of NTF2 in HNSCC remains unclear.

Methods: In this study, RNA-Seq data of HNSCC samples with corresponding clinical information were obtained from The Cancer Genome Atlas (TCGA) database. In addition, other expression profiling data were downloaded from the Gene Expression Omnibus (GEO) database. The differential expressions of NTF2, along with the overall survival (OS) rates were identified and analyzed. Then, the clinical features and expression levels of NTF2 were utilized to develop a prognostic model. The study also utilized the Gene Ontology (GO) and Kyoto Encyclopedia of Genes and Genomes (KEGG) methods to determine the related pathways of NTF2. Furthermore, the Tumor Immune Estimation Resource (TIMER) database was referenced to discover the immune correlation of NTF2. In this research investigation, RT-qPCR, western blotting, Cell Counting Kit-8 (CCK-8) assay, wound-healing assay, and immunohistochemical (IHC) staining methods were adopted to perform experimental verifications.

Results: This study's results confirmed that the NTF2 expressions were significantly increased in HNSCC tissue when compared with normal tissue. In addition, the high expression levels of NTF2 were found to be associated with poor prognoses, which was confirmed *via* the IHC validations of HNSCC samples with survival data. The results of functional enrichment analysis showed that the NTF2 was associated with epithelial cell growth, skin differentiation, keratosis, and estrogen metabolism. Furthermore, the expressions of NTF2 were determined to be negatively involved with immune infiltrations and correlated with immune checkpoint blockade (ICB) responses following

various ICB therapy strategies. The results of the CCK-8 assay and wound-healing assay confirmed the NTF2's promoting effects on the proliferation and migration of tumor cells.

Conclusions: This study defined a novel prognostic model associated with the expressions of NTF2, which was shown to be independently related to the OS of HNSCC. It was concluded in this study that NTF2 might be a potential diagnostic and prognostic biomarker for HNSCC.

Keywords: NTF2, HNSCC, prognostic biomarker, immune infiltration, immune checkpoint

INTRODUCTION

Head and neck squamous cell carcinoma (HNSCC) originates from the mucosal epithelium of the mouth, nasopharynx, oropharynx, hypopharynx, and larynx (1). It is currently the most common malignancy of the head and neck, and the sixth most common cancer globally (2). There are more than 650,000 new cases and 350,000 deaths from HNSCC each year worldwide (3, 4). At present, the incidence of HNSCC is increasing year by year and is expected to increase by 30% by 2030 (5, 6). Tobacco, alcohol, human papillomavirus (HPV), and Epstein-Barr virus (EBV) infections are considered to be risk factors for the high incidence of HNSCC (7–10). It has been determined that due to the asymptomatic nature of the early disease stages, along with the lack of effective screening methods, the majority of patients tend to be diagnosed with advanced squamous cell carcinoma of the head and neck, resulting in a meager 5-year survival rate (11, 12). Therefore, there is an urgent need for effective biomarkers to be identified to assist clinicians in accurately predicting clinical outcomes and provide references for personalized medical treatments to combat HNSCC.

It has long been noted that the size of the nucleus tends to correlate with the size of the cell (13–17). Nuclear transport factor 2 (NTF2, also known as NUTF2) is bound up with nuclear size regulation and was initially identified based on its ability to stimulate nuclear input in permeable cells (18, 19). It has subsequently been shown to be responsible for importing Ran-GDP into the nucleus (20, 21). It has been found that altered nuclear scaling is associated with many types of cancer, and pathologists monitor the increased grading of nuclear sizes in cancer diagnosis and prognosis processes (22, 23). It has been reported that increased nuclear size during melanoma progression is related to decreased NTF2 expressions. In addition, increased NTF2 levels in melanoma cells are known to be sufficient for reducing the nuclear size (24). While Du et al. reported that NTF2 overexpression promoted the proliferation, migration, and invasion of glioma cells, which suggests that NTF2 is an oncogene in glioma (25). However, at present, the function of NTF2 in HNSCC remains unclear.

In this study, RNA sequencing data and the corresponding clinical information of HSNCC patients from the Cancer Genome Atlas (TCGA) database were comprehensively analyzed. The differential expressions of NTF2 were examined, and its diagnostic and prognostic values were evaluated. The results were further validated with clinical patients. The relationships between the expression levels of NTF2 and immune infiltration were then analyzed, and the function of NTF2 in HNSCC cell lines was verified. Finally, NTF2 was successfully identified as a potential diagnostic and prognostic biomarker for HNSCC.

MATERIALS AND METHODS

Downloaded Data and Differential Expression Analysis

In this research investigation, the original counts and corresponding clinical information of RNA sequencing data (Level 3) for 528 HNSCC samples and 44 normal samples were obtained on July 1st, 2021 from TCGA dataset (https://portal.gdc.cancer.gov/). Also, the expression profiling data of 22 pairs of HNSCC were obtained from the Gene Expression Omnibus (GEO) database (https://www.ncbi.nlm.nih.gov/geo/). The data were analyzed in SPSS (Version 25, IBM Corp., USA), and the results were processed using Graphpad Prism (Version 8, GraphPad Software, USA). In addition, the UALCAN database (http://ualcan.path.uab.edu/) was referenced to investigate the relationships between the expression levels of NTF2 and various clinical features.

Survival Analysis

In this study, the prognostic values were determined by the Kaplan-Meier curves, and univariate and multivariate Cox regression analysis was performed. The R packages "RMS" and "RMDA" packages were utilized to perform the nomogram, calibration, and decision curve analysis (DCA) based on the results of the multivariate Cox proportional risk analysis. Nomogram and DCA were used to evaluate and compare the predictive models containing the clinical outcomes. All of the above-mentioned analysis methods and R packages were performed using R software version 4.0.3, and $P < 0.05$ was considered to be statistically significant.

Functional Enrichment Analysis

Differentially expressed genes were identified and analyzed using the "limma" R package and wilcoxon tests based on the expression levels of the NTF2 (26, 27). A false discovery rate (FDR) < 0.05 and a |log2(fold change)| >1 were set as the thresholds. Then, Gene Ontology (GO) and the Kyoto Encyclopedia of Genes and Genomes (KEGG) were utilized when using the "cluster profiler" R package. Finally, the "ggplot2" R package was adopted to visualize the experimental results.

Correlation Analysis of the NTF2 *via* Immune Infiltration, Immune Checkpoints, and ICB Responses

The Tumor Immune Estimation Resource (TIMER) database (https://cistrome.shinyapps.io/timer/) was referenced in this study to analyze six subsets of tumor-infiltrating immune cells (28). The immune checkpoint-related genes (SIGLEC15, TIGIT, CD274, HAVCR2, PDCD1, CTLA4, LAG3, and PDCD1LG2) were extracted from TCGA database to explore the tumor immunology. Then, Tumor Immune Dysfunction and Exclusion (TIDE) was used to predict the potential immune checkpoint blocking (ICB) responses (29). The R software packages "ggplot2", "pheatmap", and "ggpubr" were used in this research for graph visualization. In the aforementioned analysis processes, a P value of less than 0.05 was considered to be statistically significant.

Cell Cultures

During this study's experimental processes, human nasopharyngeal carcinoma cell line 5-8F cells and human pharyngeal squamous carcinoma cell line Fadu cells were cultured in RPMI1640 (iCell, China) and MEM medium (Gibco, USA), respectively. All of the media contained 10% heat-inactivated fetal bovine serum (FBS) and 1% penicillin/streptomycin. Also, all of the cells were incubated at 37°C under the condition of 5% CO_2.

siRNA Transfection, RNA Isolation, and Real-Time qPCR Methods

The NTF2 was knocked down in 5-8F and Fadu cell lines via siRNA transfection (Hanbio, China). Then, the 5-8F and Fadu cells were collected for subsequent studies after transfection for 48 hours.

The total RNA was extracted according to the instructions of the Trizol Reagent (Invitrogen, USA), and real-time quantitative PCR (RT-qPCR) was performed using SYBR Green (Vazyme, China). The relative expression levels of the genes were analyzed using the ΔΔCT method and normalized to GAPDH.

The specific primers and siRNA sequences were listed in **Table 1**.

Western Blotting

In order to assess the protein expression levels of the NTF2, a RIPA buffer and protease inhibitors (Gene-Protein Link, China) were used to disrupt the cells. Then, 20 μg of total protein was separated on 15% SDS-PAGE gel. The antibodies specific for NTF2 (66063-1, Proteintech, China) (1:1000) and GAPDH (T004, Affinity, China) (1:2000) were utilized for probing the proteins. Then, specific proteins were visualized using the method provided by the AI600 Imaging System (GE, USA).

Wound-Healing Assay

In the present study, 5-8F cells were inoculated in 6-well plates containing MEM with 10% FBS at a density of 4×10^5 cells/well. Subsequently, when 90% of the cells had become fused after 16 to 24 hours of culture, the confluence cells were lined with a 200 μL pipette. Then, the injured monolayer cells were washed with phosphate-buffered saline (PBS) for the purpose of removing the cell debris. In the next experimental step, the MEM with 10% FBS was replaced with a serum-free medium. Images were obtained at 0, 6, and 24 hours, and each experiment was independently performed at least three times. The scratch areas were evaluated using Image J, and the cell migration rates were calculated using the following formula:

$$\text{Migration rate}\ (\%) = (\text{original area} - \text{measured area})/\text{original area} \times 100\,\%$$

TABLE 1 | Primer and siRNA sequences of related genes.

Gene		Sequence (5'-3')
Primer-NTF2	F*	AACCCAACTAGGCGCAATTTA
	R	ACGGAAGGCTAGACAACTTCT
Primer-GAPDH	F	AAGAAGGTGGTGAAGCAGGC
	R	GAGTGGGTGTCGCTGTTGAA
siRNA-NTF2		
si1	F	CCACCAGAUGUUCCUAUUAAATT
	R	UUUAAUAGGAACAUCUGGUGGTT
si2	F	GAUGCUUGGGUUUGCACCAAUTT
	R	AUUGGUGCAAACCCAAGCAUCTT
siRNA-GAPDH	F	UAAAGUACCCUGUGCUCAATT
	R	UUGAGCACAGGGUACUUUATT

*F, forward; R, reverse.

Immunohistochemical Staining

Paraffin-embedded tissue was selected from 66 HNSCC patients who had undergone surgery in the Affiliated Hospital of Guilin Medical University between April 2012 and October 2019. The patients enrolled in this study were diagnosed with primary squamous cell carcinoma of the larynx, with no other malignancies in the mouth, oropharynx, or pharynx, and no previous history of radiotherapy or chemotherapy. In addition, both clinical and pathological data were collected, including the patients' ages, differentiation grades, lymph node metastasis, and survival periods. The follow-up and postoperative management data of the patients were collected by telephone or from outpatient medical records. The tumor stages were classified according to the tumor node metastasis (TNM) staging system (2017) of the Union for International Cancer Control (UICC). The samples obtained from the 66 HNSCC patients and ten adjacent normal tissue were each divided into 4 μm thick sections for this study's immunohistochemical (IHC) analysis process. A primary monoclonal antibody (66063-1, Proteintech, China) was used to detect the expression levels of the NTF2. Secondary antibodies to mouse IgG were obtained from the IHC kit (#CW2069, Beijing Cowin Bioscience Co., Ltd., China). Mouse IgG was used as a negative control to exclude false positive results. The staining intensity was assessed by histology score (H-score) and semi-quantitative analysis was performed by two independent pathologists who had not been informed of the sources of the clinical samples (30, 31). The following formula was applied:

$$H-score = (\text{percentage of weak intensity cells} \times 1) + (\text{percentage of moderate intensity cells} \times 2) + (\text{percentage of strong intensity cells} \times 3)$$

The studies involving human participants were reviewed and approved by the Ethics Committee of the Affiliated Hospital of Guilin Medical University. All of the patients/participants provided their written informed consent to participate in this study.

Statistical Analysis

Two-tailed student t-tests were performed in SPSS to evaluate the statistical significance in this study. The significance differences of $P < 0.05$, 0.01, and 0.001 were symbolized as *, **, and ***, respectively.

RESULTS

NTF2 Was Highly Expressed in HNSCC

The mRNA expressions of NTF2 in human cancer cells were analyzed using the UALCAN database. It was found that when compared with the corresponding normal tissue, higher expressions of NTF2 were observed in the majority of the cancer types, including HNSCC ($P < 0.001$); bladder urothelial carcinoma (BLCA); breast invasive carcinoma (BRCA); cholangiocarcinoma (CHOL); colon adenocarcinoma (COAD); esophageal carcinoma (ESCA), and so on (**Figures 1A, B**). In addition, significant increases in the NTF2 expressions in HNSCC cases were observed in 44 cases of tumor tissue with paired adjacent normal tissue ($P < 0.001$) (**Figure 1C**). Furthermore, similar results were observed in 22 pairs of HNSCC samples from the GSE6631 cohort in the GEO database ($P < 0.001$) (**Figure 1D**). Therefore, the findings suggested that NTF2 may play a vital regulatory role in the development and progression of HNSCC.

NTF2 Expression Levels and the Clinical Features of the HNSCC Patients

This study investigated the NTF2 expression levels in various HNSCC subgroups using the UALCAN database. It was observed that the NTF2 expression levels were higher in the HPV negative group than in the positive group ($P < 0.001$; **Figure 2D**). In addition, the NTF2 expression levels were significantly up-regulated in both the men and women tumor groups, respectively ($P < 0.001$) (**Figure 2A**). The same results were observed for the different age groups ($P < 0.001$; **Figure 2B**); pathological grade groups ($P < 0.001$; **Figure 2C**); HPV infection groups ($P < 0.001$; **Figure 2D**); tumor stage groups ($P < 0.001$; **Figure 2E**); and lymph node metastasis groups ($P < 0.001$; **Figure 2F**) among the HNSCC cases. However, there were no significant differences observed among the clinical subgroups.

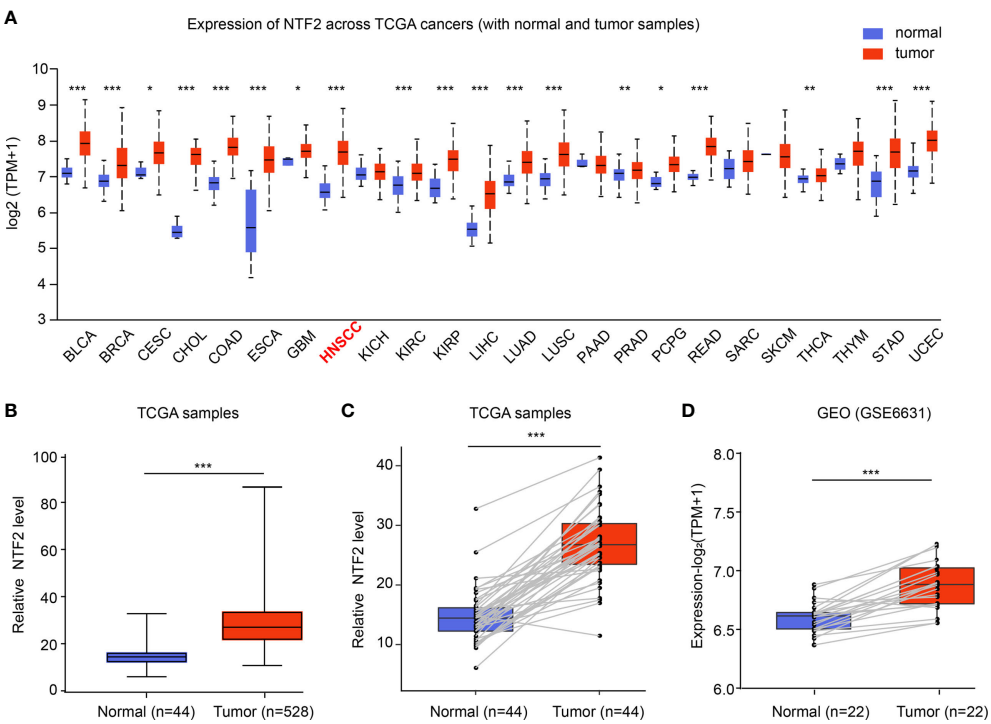

FIGURE 1 | Expression of NTF2 in HNSCC. **(A)** NTF2 expressions in different types of cancers were examined using the UALCAN database. **(B)** Analysis of NTF2 expression in HNSCC using TCGA database. Comparison of NTF2 mRNA levels in paired adjacent normal tissue and tumor tissue of HNSCC from TCGA **(C)** and GEO database **(D)**. *P < 0.05, **P < 0.01, ***P < 0.001.

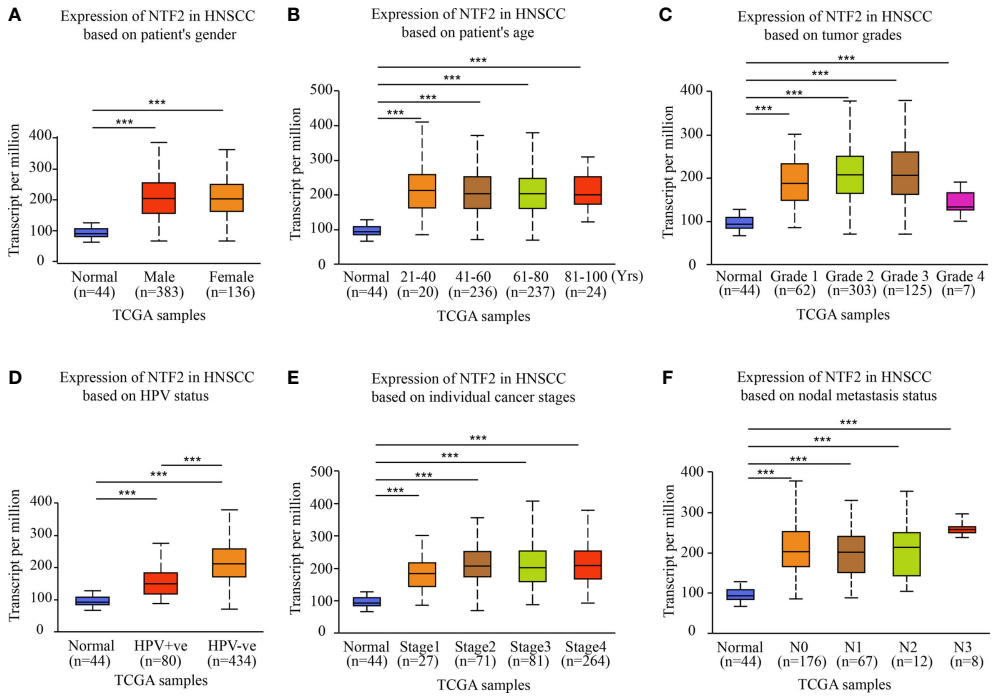

FIGURE 2 | NTF2 expressions in different groups were evaluated according to clinical features based on UALCAN database. Analysis was shown for sex **(A)**, age **(B)**, pathological grade **(C)**, HPV infection **(D)**, clinical-stage **(E)**, and lymph node metastasis status **(F)**. N0: no regional lymph node metastasis; N1: 1 to 3 cervical lymph nodes metastasis; N2: 4 to 9 cervical lymph nodes metastasis; N3: 10 or more cervical lymph nodes metastasis. ***P < 0.001.

High Expressions of NTF2 Were Observed to be Correlated With the Poor Prognoses of the HNSCC Patients

Then, the prognostic values of the NTF2 were determined. Following a median expression level, the patients were divided into the following two groups: High expression group (n = 264) and low-expression group (n = 264), as detailed in **Figure 3A**. The patients in the high expression group were observed to have remarkably higher mortality rates than those in the low-expression group (**Figure 3B**). In addition, the Kaplan-Meier survival curves also showed that the survival rates of the high expression patients were significantly lower than those of the low-expression patients (P = 0.000714; **Figure 3C**).

In the present investigation, both univariate and multivariate Cox proportional risk analyses were performed. The results revealed that the NTF2 expression levels, patient ages, and TNM stages were independent prognostic factors (**Figures 3D, E**), which were included to establish an accurate prediction model. This study's nomogram provided a graphical representation of the aforementioned factors, and the prognostic risks for an individual patient could be calculated by the points associated with each risk factor, as detailed in **Figure 3F**. In addition, as shown in **Figure 3G**, the calibration plots showed excellent agreement between the actual probabilities and the estimated probabilities at 1, 3, and 5 years.

Experimental Verifications of the Clinical Samples

An immunohistochemical staining method was used to detect the expression levels of NTF2 in the tumor samples from 66 HNSCC patients and 10 normal tissue samples. The results revealed that the NTF2 was highly expressed in the HNSCC tissue when compared with the normal tissue (**Figures 4A, B**). Meanwhile, there was no significant correlation observed between the NTF2 expression levels and the patient ages, genders, pathological grades, tumor stages, lymph node metastasis, or smoking habits (**Table 2**). The median follow-up timeframe for all of the examined patient cases was 36.2 months (ranging from 1.0 to 99.9 months). At the final follow-up times, it was determined that in 49 cases (74.2%), the patients had survived, and in 17 cases (25.8%) the patients had died. The Kaplan-Meier analysis results showed that the high expression levels of NTF2 were closely related to significant reductions in overall survival (P = 0.0066) in the HNSCC case samples (**Figure 4C**).

Functional Enrichment Analysis

In the present study, the co-expressed genes related to NTF2 were identified by mining data from TCGA database. This study's volcano map and heat map with positive and negative correlations with NTF2 in HNSCC were shown in **Figures 5A, B**, respectively. A total of 119 genes associated with NTF2 (P < 0.05) were used in the GO and KEGG enrichment analyses in order to

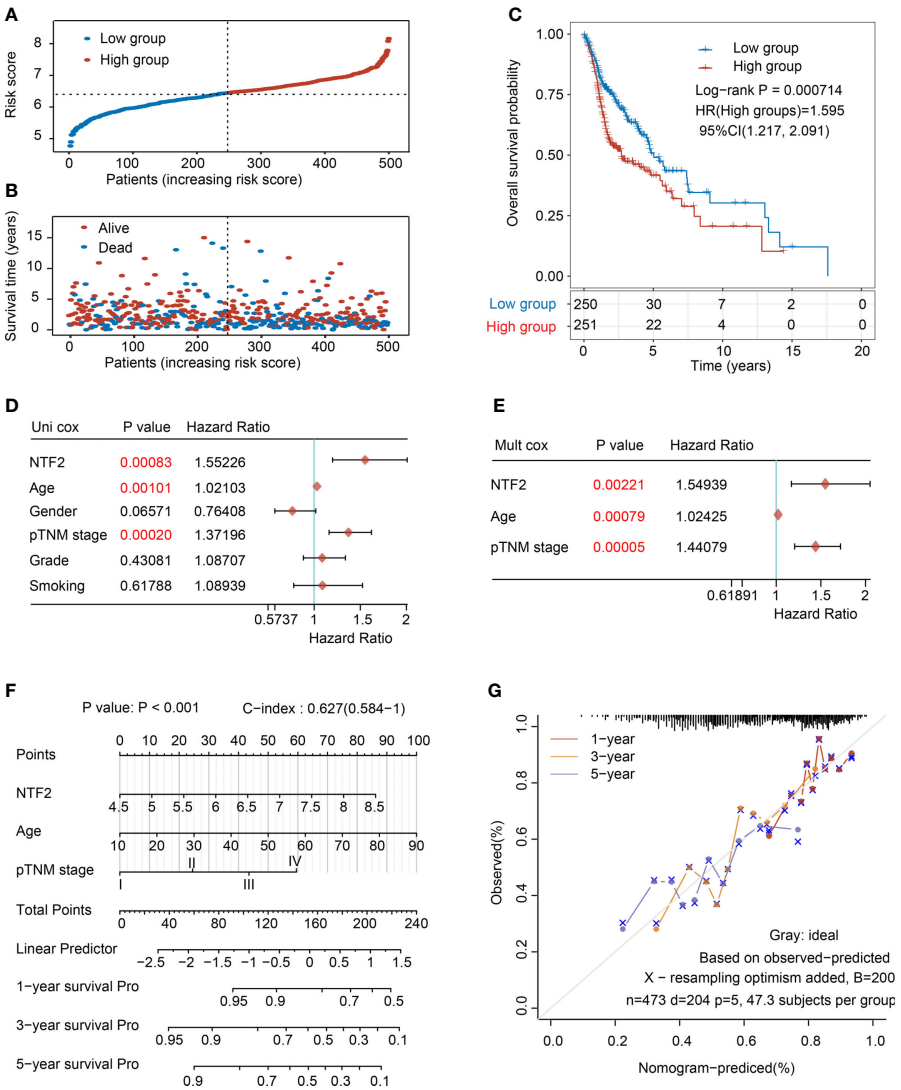

FIGURE 3 | Analysis of the prognostic risk signature based on NTF2 expression in TCGA database. **(A)** The risk score distribution of HNSCC patients. **(B)** Survival status and duration of patients. **(C)** Survival curve of NTF2 with high and low expression. The univariate **(D)** and multivariate **(E)** independent prognostic analysis of independent risk factors for overall survival (OS) in HNSCC patients. **(F)** Nomogram to predict the 1-, 3-, and 5-year overall survival of HNSCC patients. **(G)** Calibration curve for the OS nomogram model. The grey dotted line represents the ideal prediction curve.

explore relevant biological functions and pathways. The top 30 critical terms for the enrichment analysis of the biological processes (BP), cellular components (CC), and molecular functions (MF) were detailed in **Figures 5C–E**. The first 10 KEGG pathways of the related genes were shown in **Figure 5F**.

Correlation Analysis of NTF2 Expression Level With Immune Infiltration, Immune Checkpoint, and ICB Response

The associations between the NTF2 expression levels and the infiltrating immune cells were analyzed. The results showed that NTF2 expression levels were negatively correlated with the B cells (PSpearman = -0.35; $P < 0.001$); $CD4^+$ T cells (PSpearman = -0.25; $P < 0.001$); $CD8^+$ T cells (PSpearman = -0.17; $P < 0.001$); neutrophils (PSpearman = -0.17; $P < 0.001$); macrophages (PSpearman = -0.11; $P = 0.0017$); and dendritic cells (PSpearman = -0.16; $P < 0.001$) (**Figure 6A**). The immune checkpoint-related genes (SIGLEC15, TIGIT, CD274, HAVCR2, PDCD1, CTLA4, LAG3, and PDCD1LG2) were extracted and analyzed. It was found that the CD274, CTLA4, LAG3, PDCD1, and TIGIT genes displayed negative correlations with the NTF2 expressions (**Figure 6B**). The potential ICB responses indicated that the NTF2 high expression group had a poor efficacy for immune checkpoint blockade treatments (**Figure 6C**).

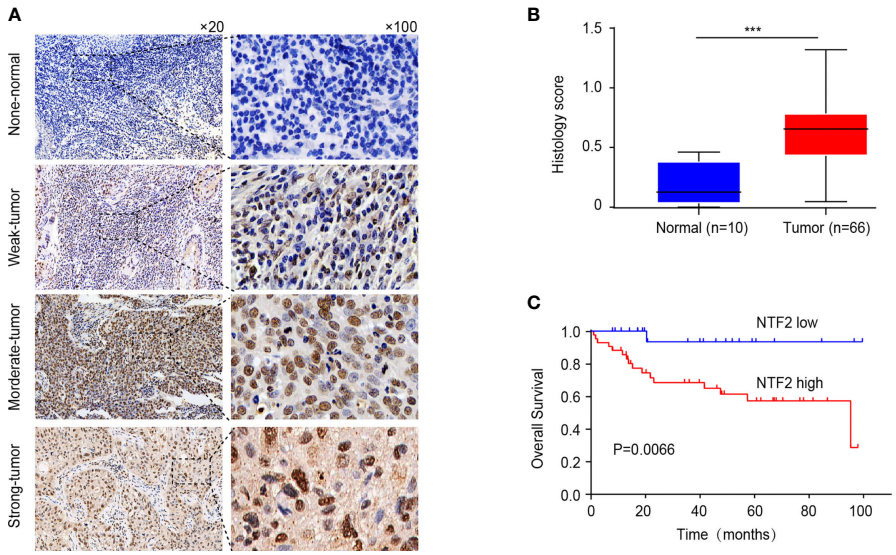

FIGURE 4 | Immunohistochemical evaluation of NTF2 as a prognostic marker. **(A)** Negative, weak, moderate, strong immunohistochemical staining of NTF2 was shown respectively in HNSCC and normal samples. **(B)** The H-scores of 66 HNSCC tissue were compared with those of 10 normal tissue. **(C)** Overall survival rate was compared between low and high expression group of NTF2 based on H-score. ***P < 0.001.

TABLE 2 | Correlation between NTF2 expression and the clinicopathological features in 66 HNSCC samples.

Characteristics	NTF2 expression		P value
	High (n = 42)	Low (n = 24)	
Age (years, mean ± SD)	62.36 ± 9.414	61.46 ± 5.956	0.675
Sex (M/F)	42/0	24/1	0.1825
Pathological differentiation			
Well	30	14	
Moderate/poor	12	10	0.2776
TNM Stage			
T1,T2	17	15	
T3,T4	25	9	0.085
Lymph node metastasis			
Yes	12	5	
No	30	19	0.4892
Smoking			
Yes	32	18	
No	10	6	0.9135

NTF2 Regulation of the Proliferation and Migration of HNSCC Cells

In order to investigate the role of NTF2 in HNSCC cells, two siRNAs targeting NTF2 (si1, si2) were transfected into 5-8F and Fadu cells respectively. It was found that when compared with the control cells treated with empty vector, the NTF2 was significantly silenced at the mRNA (**Figure 7A**) and protein levels in the knockdown group (**Figure 7B**). This study then tested the effects of cell proliferation *in-vitro*. Using the CCK-8 assay, it was found that the knockdown of the NTF2 could inhibit HNSCC cell proliferation after 48 hours (P < 0.001) and 72 hours (P < 0.001) of culturing (**Figures 7C, D**). In addition, the wound-healing assay was used to assess the capacity of cancer cell migration. The results revealed that the cells treated with NTF2 siRNAs showed lower migration rates than the control cells after 6 hours (P < 0.001) and 24 hours (P < 0.001) of culturing (**Figures 7E, F**).

DISCUSSION

Following the Global Burden of Disease study, the incidence of lip and oral cancers has increased by 36.5%, throat cancers by 23.1%, and other pharyngeal cancers by 29.9% over the past decade (32, 33). It has been found that with the increased stages of the tumor, the survival rates of HNSCC patients decreased, and the postoperative recurrence rate increased (34–36), which could not be improved by adjustments in treatment regimens (37, 38). Therefore, the development of new therapeutic targets and prognostic markers is urgently required. In previous investigations, NTF2 had been reported to reduce the nuclear sizes of melanoma cells and was found to be highly expressed in glioma tissue (24, 25). However, NTF2 had not yet been reported in HNSCC cases. This study found increased expression levels of NTF2 in TCGA and GEO databases, which was confirmed by the results obtained in this study's tissue samples. In addition, knockdown verifications of this molecule were conducted for the first time in the current investigation. The results confirmed that the downregulation of NTF2 could inhibit HNSCC cells proliferation and migration.

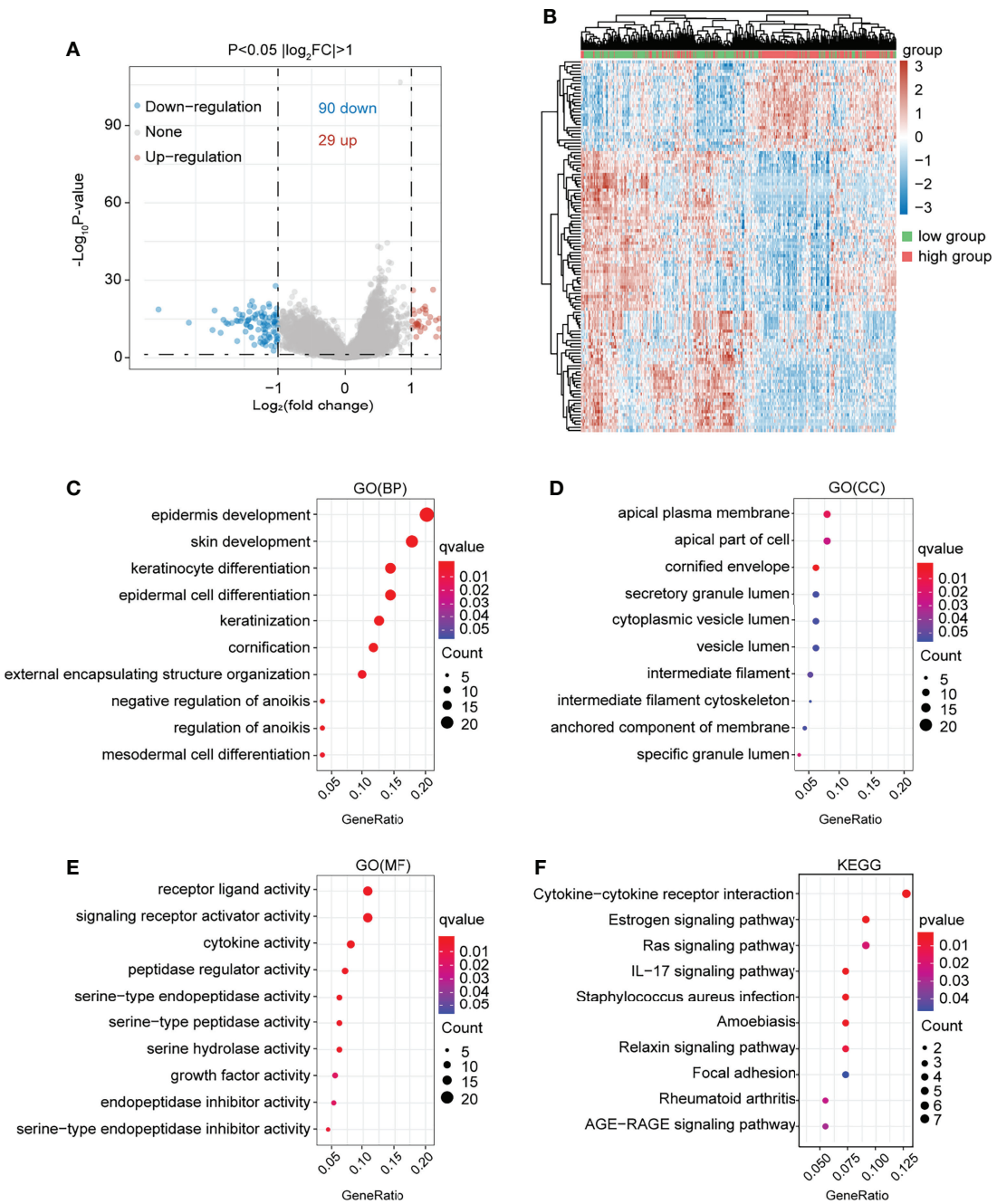

FIGURE 5 | Functional enrichment analysis of NTF2 related genes. **(A)** In the volcano map of HNSCC in TCGA database, red dots were up-regulated genes and blue dots were down-regulated genes. **(B)** Heatmap of differential genes between NTF2 high and low groups in TCGA database. **(C–E)** GO analyses. **(F)** KEGG analyses.

HPV infections are known to be associated with the majority of oropharyngeal cancers (> 70%) and are considered to be increasingly common risk factors for HNSCC (39, 40). HPV-associated tumors are modulated by helical domain mutations of the oncogene PIK3CA, loss of TRAF3, and the amplification of the cell cycle gene E2F1 (41). In this study, there was observed to be significant statistical differences in the expression levels of NTF2 between the HPV infection group and the non-HPV infection group. Therefore, the results suggested that the NTF2 may be involved in the integration of the HPV's genetic information into the host genome.

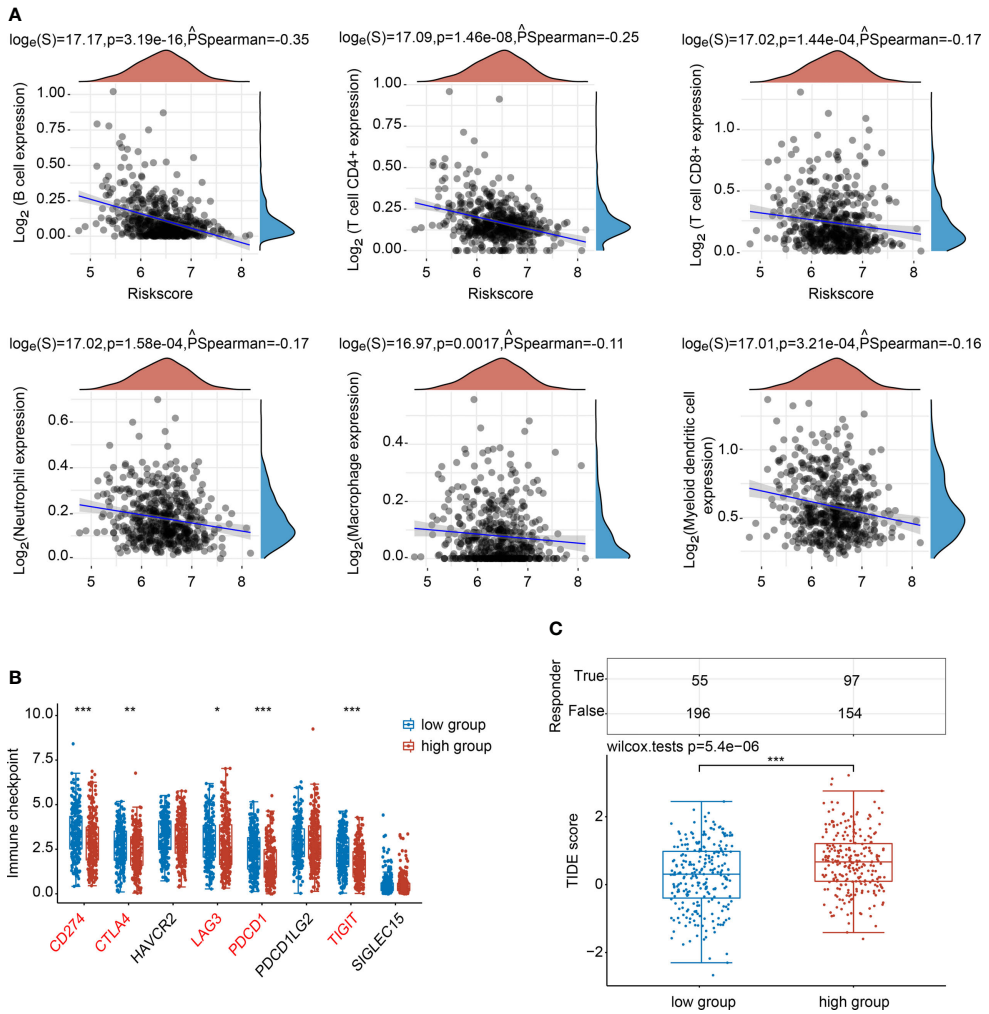

FIGURE 6 | Correlations between NTF2 and immune status in HNSCC patients. **(A)** Spearman analysis between NTF2 and immune score. **(B)** Correlation analysis between NTF2 and immune checkpoint-related gene expression using Wilcox on test. **(C)** Potential immunotherapeutic responses were predicted through the TIDE algorithm. *P < 0.05, **P < 0.01, ***P < 0.001.

Although such clinical indicators as TNM can be used to judge the prognoses of patients, they still have certain limitations (42). At present, the accumulation of public genome databases and the recent advances in bioinformatics have made it possible to acquire a comprehensive cancer genome map in large cohorts (43). However, the effects of NTF2 on tumor survival in HNSCC remain under-reported. The results obtained in this study showed that the high expressions of NUFT2 were related to the poor prognostic outcomes of the HNSCC patients in the bioinformatics database. Therefore, a nomogram was constructed in this study for the comprehensive predictions of patient survival rates in clinical settings. In addition, the prognostic effects were reconfirmed by the collected tissue samples.

TIMER web server is a comprehensive resource for the systematic analysis of immune infiltrates across diverse cancer types (28, 44). The relationships between the NTF2 expression levels and the tumor-infiltrating immune cells were analyzed in this study using the TIMER database. It was found that the NTF2 expression levels were negatively correlated with six immune cells. Therefore, it was indicated that NTF2 might indirectly alter tumor immune microenvironments. Furthermore, this study considered that immune checkpoint therapy may be less effective in patients with high expressions of NTF2, suggesting that it was a predictor of malignant prognosis.

However, it should be noted that there were still some limitations in this study. For example, the HPV infection data were not available in the clinical data. In addition, although the functions of NTF2 in cells were initially explored, the mechanisms of those functions were not investigated. Therefore, further studies should be conducted *in-vivo* and *in-vitro* to investigate the functions and mechanisms of NTF2 in HNSCC.

In conclusion, the results obtained in this study elucidated the differential expressions and clinical prognosis values of NTF2. The NTF2 immune-related functions were also discussed, which

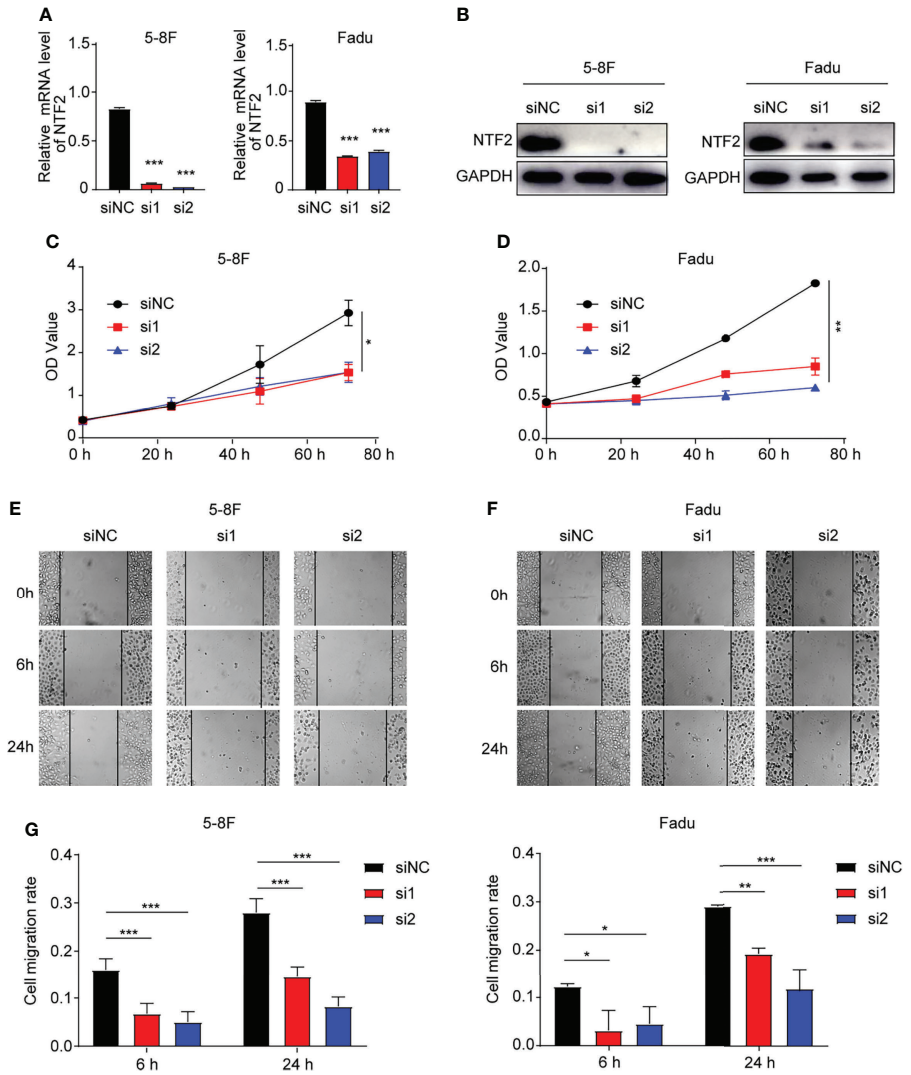

FIGURE 7 | Experimental validation. **(A, B)** Knockdown validation by qRT-qPCR and western blotting. CCK-8 assay **(C, D)** and wound-healing assay **(E, F)** were used to detect the growth and migration of NTF2-knockdown HNSCC cell lines. *P < 0.05, **P < 0.01, ***P < 0.001.

reflected the clinical and biological significance of NTF2 in HNSCC. The obtained results suggested that the NTF2 might be a potential novel tumor prognostic marker and therapeutic target in the future.

DATA AVAILABILITY STATEMENT

The datasets presented in this study can be found in online repositories. The names of the repository/repositories and accession number(s) can be found in the article/supplementary material.

ETHICS STATEMENT

The studies involving human participants were reviewed and approved by The Ethics Committee of Affiliated Hospital of Guilin Medical University. The patients/participants provided their written informed consent to participate in this study.

AUTHOR CONTRIBUTIONS

LL, XW, and XHu reviewed the manuscript and supervised the study. GX carried out the experiments, exported the figures, and wrote the first draft of the manuscript. GX, XZ, and MZ designed the research processes and finalized the manuscript. GX, MY, YZ, and XHe collected the clinical samples used in this investigation. All authors contributed to the article and approved the final manuscript.

FUNDING

This study was supported by the Research and Development Project of Scientific Research Instruments and Equipment of the Chinese Academy of Sciences - major instruments project (YJKYYQ20180039) and the Digestive Medical Coordinated Development Center of Beijing Municipal Administration of

Hospitals (No. XXZ0604), the Support Project of High-level Teachers in Beijing Municipal Universities in the Period of 13th Five-year Plan (IDHT20190510 to XW), and the National Natural Science Foundation of China (grant# 81972652 & 81171899 to XW).

ACKNOWLEDGMENTS

The authors thank TCGA and GEO for providing the open-access databases utilized in this study.

REFERENCES

1. Marur S, Forastiere AA. Head and Neck Squamous Cell Carcinoma: Update on Epidemiology, Diagnosis, and Treatment. *Mayo Clin Proc* (2016) 91 (3):386–96. doi: 10.1016/j.mayocp.2015.12.017
2. Jemal A, Bray F, Center MM, Ferlay J, Ward E, Forman D. Global Cancer Statistics. *CA Cancer J Clin* (2011) 61(2):69–90. doi: 10.3322/caac.20107
3. Ferlay J, Soerjomataram I, Dikshit R, Eser S, Mathers C, Rebelo M, et al. Cancer Incidence and Mortality Worldwide: Sources, Methods and Major Patterns in GLOBOCAN 2012. *Int J Cancer* (2015) 136(5):E359–86. doi: 10.1002/ijc.29210
4. Torre LA, Bray F, Siegel RL, Ferlay J, Lortet-Tieulent J, Jemal A. Global Cancer Statistics, 2012. *CA Cancer J Clin* (2015) 65(2):87–108. doi: 10.3322/caac.21262
5. Ferlay J, Colombet M, Soerjomataram I, Mathers C, Parkin DM, Pineros M, et al. Estimating the Global Cancer Incidence and Mortality in 2018: GLOBOCAN Sources and Methods. *Int J Cancer* (2019) 144(8):1941–53. doi: 10.1002/ijc.31937
6. Bray F, Ferlay J, Soerjomataram I, Siegel RL, Torre LA, Jemal A. Global Cancer Statistics 2018: GLOBOCAN Estimates of Incidence and Mortality Worldwide for 36 Cancers in 185 Countries. *CA Cancer J Clin* (2018) 68 (6):394–424. doi: 10.3322/caac.21492
7. Mehanna H, Beech T, Nicholson T, El-Hariry I, McConkey C, Paleri V, et al. Prevalence of Human Papillomavirus in Oropharyngeal and Nonoropharyngeal Head and Neck Cancer–Systematic Review and Meta-Analysis of Trends by Time and Region. *Head Neck* (2013) 35(5):747–55. doi: 10.1002/hed.22015
8. Jiang H, Livingston M, Room R, Gan Y, English D, Chenhall R. Can Public Health Policies on Alcohol and Tobacco Reduce a Cancer Epidemic? Australia's Experience. *BMC Med* (2019) 17(1):213. doi: 10.1186/s12916-019-1453-z
9. Blot WJ, McLaughlin JK, Winn DM, Austin DF, Greenberg RS, Preston-Martin S, et al. Smoking and Drinking in Relation to Oral and Pharyngeal Cancer. *Cancer Res* (1988) 48(11):3282–7.
10. Tsang CM, Lui V, Bruce JP, Pugh TJ, Lo KW. Translational Genomics of Nasopharyngeal Cancer. *Semin Cancer Biol* (2020) 61:84–100. doi: 10.1016/j.semcancer.2019.09.006
11. Cmelak AJ, Arneson K, Chau NG, Gilbert RW, Haddad RI. Locally Advanced Head and Neck Cancer. *Am Soc Clin Oncol Educ Book* (2013), 33:237–44. doi: 10.14694/EdBook_AM.2013.33.237
12. Matar N, Haddad A. New Trends in the Management of Head and Neck Cancers. *J Med Liban* (2011) 59(4):220–6.
13. Chan YH, Marshall WF. Scaling Properties of Cell and Organelle Size. *Organogenesis* (2010) 6(2):88–96. doi: 10.4161/org.6.2.11464
14. Levy DL, Heald R. Nuclear Size is Regulated by Importin Alpha and Ntf2 in Xenopus. *Cell* (2010) 143(2):288–98. doi: 10.1016/j.cell.2010.09.012
15. Walters AD, Bommakanti A, Cohen-Fix O. Shaping the Nucleus: Factors and Forces. *J Cell Biochem* (2012) 113(9):2813–21. doi: 10.1002/jcb.24178
16. Hara Y, Iwabuchi M, Ohsumi K, Kimura A. Intranuclear DNA Density Affects Chromosome Condensation in Metazoans. *Mol Biol Cell* (2013) 24(15):2442–53. doi: 10.1091/mbc.E13-01-0043
17. Jevtic P, Levy DL. Nuclear Size Scaling During Xenopus Early Development Contributes to Midblastula Transition Timing. *Curr Biol* (2015) 25(1):45–52. doi: 10.1016/j.cub.2014.10.051
18. Moore MS, Blobel G. Purification of a Ran-Interacting Protein That is Required for Protein Import Into the Nucleus. *Proc Natl Acad Sci USA* (1994) 91(21):10212–6. doi: 10.1073/pnas.91.21.10212
19. Paschal BM, Gerace L. Identification of NTF2, a Cytosolic Factor for Nuclear Import That Interacts With Nuclear Pore Complex Protein P62. *J Cell Biol* (1995) 129(4):925–37. doi: 10.1083/jcb.129.4.925
20. Ribbeck K, Lipowsky G, Kent HM, Stewart M, Gorlich D. NTF2 Mediates Nuclear Import of Ran. *EMBO J* (1998) 17(22):6587–98. doi: 10.1093/emboj/17.22.6587
21. Smith A, Brownawell A, Macara IG. Nuclear Import of Ran Is Mediated by the Transport Factor NTF2. *Curr Biol* (1998) 8(25):1403–6. doi: 10.1016/s0960-9822(98)00023-2
22. Chow KH, Factor RE, Ullman KS. The Nuclear Envelope Environment and Its Cancer Connections. *Nat Rev Cancer* (2012) 12(3):196–209. doi: 10.1038/nrc3219
23. Jevtic P, Levy DL. Mechanisms of Nuclear Size Regulation in Model Systems and Cancer. *Adv Exp Med Biol* (2014) 773:537–69. doi: 10.1007/978-1-4899-8032-8_25
24. Vukovic LD, Jevtic P, Zhang Z, Stohr BA, Levy DL. Nuclear Size is Sensitive to NTF2 Protein Levels in a Manner Dependent on Ran Binding. *J Cell Sci* (2016) 129(6):1115–27. doi: 10.1242/jcs.181263
25. Du Q, Liu J, Tian D, Zhang X, Zhu J, Qiu W, et al. Long Noncoding RNA LINC00173 Promotes NUTF2 Expression Through Sponging miR-765 and Facilitates Tumorigenesis in Glioma. *Cancer Manag Res* (2020) 12:7211–7. doi: 10.2147/CMAR.S262279
26. Ritchie ME, Phipson B, Wu D, Hu Y, Law CW, Shi W, et al. Limma Powers Differential Expression Analyses for RNA-Sequencing and Microarray Studies. *Nucleic Acids Res* (2015) 43(7):e47. doi: 10.1093/nar/gkv007
27. Yue C, Ma H, Zhou Y. Identification of Prognostic Gene Signature Associated With Microenvironment of Lung Adenocarcinoma. *Peerj* (2019) 7:e8128. doi: 10.7717/peerj.8128
28. Li T, Fan J, Wang B, Traugh N, Chen Q, Liu JS, et al. TIMER: A Web Server for Comprehensive Analysis of Tumor-Infiltrating Immune Cells. *Cancer Res* (2017) 77(21):e108–10. doi: 10.1158/0008-5472.CAN-17-0307
29. Jiang P, Gu S, Pan D, Fu J, Sahu A, Hu X, et al. Signatures of T Cell Dysfunction and Exclusion Predict Cancer Immunotherapy Response. *Nat Med* (2018) 24(10):1550–8. doi: 10.1038/s41591-018-0136-1
30. Maclean A, Bunni E, Makrydima S, Withington A, Kamal AM, Valentijn AJ, et al. Fallopian Tube Epithelial Cells Express Androgen Receptor and Have a Distinct Hormonal Responsiveness When Compared With Endometrial Epithelium. *Hum Reprod* (2020) 35(9):2097–106. doi: 10.1093/humrep/deaa177
31. Dogan S, Vasudevaraja V, Xu B, Serrano J, Ptashkin RN, Jung HJ, et al. DNA Methylation-Based Classification of Sinonasal Undifferentiated Carcinoma. *Mod Pathol* (2019) 32(10):1447–59. doi: 10.1038/s41379-019-0285-x
32. James SL, Abate D, Abate KH, Abay SM, Abbafati C, Abbasi N, et al. Global, Regional, and National Incidence, Prevalence, and Years Lived With Disability for 354 Diseases and Injuries for 195 Countries and Territories, 1990-2017: A Systematic Analysis for the Global Burden of Disease Study 2017. *Lancet* (2018) 392(10159):1789–858. doi: 10.1016/S0140-6736(18)32279-7
33. Simard EP, Torre LA, Jemal A. International Trends in Head and Neck Cancer Incidence Rates: Differences by Country, Sex and Anatomic Site. *Oral Oncol* (2014) 50(5):387–403. doi: 10.1016/j.oraloncology.2014.01.016
34. Ervin TJ, Clark JR, Weichselbaum RR, Fallon BG, Miller D, Fabian RL, et al. An Analysis of Induction and Adjuvant Chemotherapy in the Multidisciplinary Treatment of Squamous-Cell Carcinoma of the Head and Neck. *J Clin Oncol* (1987) 5(1):10–20. doi: 10.1200/JCO.1987.5.1.10
35. Chin D, Boyle GM, Porceddu S, Theile DR, Parsons PG, Coman WB. Head and Neck Cancer: Past, Present and Future. *Expert Rev Anticancer Ther* (2006) 6(7):1111–8. doi: 10.1586/14737140.6.7.1111
36. Bernier J. A Multidisciplinary Approach to Squamous Cell Carcinomas of the Head and Neck: An Update. *Curr Opin Oncol* (2008) 20(3):249–55. doi: 10.1097/CCO.0b013e3282faa0b1
37. Murdoch D. Standard, and Novel Cytotoxic and Molecular-Targeted, Therapies for HNSCC: An Evidence-Based Review. *Curr Opin Oncol* (2007) 19(3):216–21. doi: 10.1097/01.cco.0000264952.98166.99
38. Sher DJ, Yan J, Day A, Sumer BD, Pham NL, Khan S, et al. Comparative Effectiveness of Primary Radiotherapy Versus Surgery in Elderly Patients With Locally Advanced Oropharyngeal Squamous Cell Carcinoma. *Oral Oncol* (2019) 88:18–26. doi: 10.1016/j.oraloncology.2018.11.004

39. Stein AP, Saha S, Kraninger JL, Swick AD, Yu M, Lambert PF, et al. Prevalence of Human Papillomavirus in Oropharyngeal Cancer: A Systematic Review. *Cancer J* (2015) 21(3):138–46. doi: 10.1097/PPO.0000000000000115
40. Isayeva T, Li Y, Maswahu D, Brandwein-Gensler M. Human Papillomavirus in Non-Oropharyngeal Head and Neck Cancers: A Systematic Literature Review. *Head Neck Pathol* (2012) 6 Suppl 1:S104–20. doi: 10.1007/s12105-012-0368-1
41. Lawrence MS, Sougnez C, Lichtenstein L, Cibulskis K, Lander E, Gabriel SB, et al. Comprehensive Genomic Characterization of Head and Neck Squamous Cell Carcinomas. *Nature* (2015) 517(7536):576–82. doi: 10.1038/nature14129
42. Turri-Zanoni M, Salzano G, Lambertoni A, Giovannardi M, Karligkiotis A, Battaglia P, et al. Prognostic Value of Pretreatment Peripheral Blood Markers in Paranasal Sinus Cancer: Neutrophil-To-Lymphocyte and Platelet-to-Lymphocyte Ratio. *Head Neck* (2017) 39(4):730–6. doi: 10.1002/hed.24681
43. Leemans CR, Snijders P, Brakenhoff RH. The Molecular Landscape of Head and Neck Cancer. *Nat Rev Cancer* (2018) 18(5):269–82. doi: 10.1038/nrc.2018.11
44. Li B, Severson E, Pignon JC, Zhao H, Li T, Novak J, et al. Comprehensive Analyses of Tumor Immunity: Implications for Cancer Immunotherapy. *Genome Biol* (2016) 17(1):174. doi: 10.1186/s13059-016-1028-7

Conflict of Interest: The authors declare that the research was conducted in the absence of any commercial or financial relationships that could be construed as a potential conflict of interest.

frontiers | Frontiers in Oncology

ORIGINAL RESEARCH
published: 30 June 2022
doi: 10.3389/fonc.2022.754967

Malignant Myoepithelioma of the Head and Neck: Demographics, Clinicopathological Characteristics, Treatment, and Prognosis

Jia-Qi Wang[1,2†], *Rong-Xin Deng*[1,2†], *Hui Liu*[1,2], *Yuan Luo*[1,2], *Meng-Meng Lu*[1,2] *and Zhi-Cheng Yang*[1,2*]

[1]Department of Oral and Maxillofacial Surgery, Shanghai Stomatological Hospital & School of Stomatology, Fudan University, Shanghai, China, [2] Shanghai Key Laboratory of Craniomaxillofacial Development and Diseases, Fudan University, Shanghai, China

OPEN ACCESS

Edited by:
Heming Lu,
People's Hospital of Guangxi Zhuang Autonomous Region, China

Reviewed by:
Brandon Mullins,
Ravenel Oncology, United States
Remo Accorona,
Fondazione IRCCS Ca' Granda, Ospedale Maggiore Policlinico, Italy

***Correspondence:**
Zhi-Cheng Yang
zhichengyang1998@sina.com

[†]*These authors have contributed equally to this work*

Specialty section:
This article was submitted to Head and Neck Cancer, a section of the journal Frontiers in Oncology

Received: *07 August 2021*
Accepted: *20 May 2022*
Published: *30 June 2022*

Citation:
Wang J-Q, Deng R-X, Liu H, Luo Y, Lu M-M and Yang Z-C (2022) Malignant Myoepithelioma of the Head and Neck: Demographics, Clinicopathological Characteristics, Treatment, and Prognosis. Front. Oncol. 12:754967. doi: 10.3389/fonc.2022.754967

Malignant myoepithelioma of the head and neck (HNMM) is a rare malignancy, and its characteristics and survival rates have not been well-defined. This study aimed to define the epidemiology of HNMM and identify the prognostic factors associated with the disease. Data on all patients diagnosed with HNMM between 1991 and 2016 were gathered from the Surveillance Epidemiology and End Results (SEER) database. The demographics, clinicopathological characteristics, treatment, and prognoses of the patients were described. Cox regression analysis was used to identify the prognostic factors, and the prognostic nomograms for overall survival (OS) and disease-specific survival (DSS) were constructed. A total of 333 cases of HNMM were identified. The average age at diagnosis was 60.6 years, and 50.1% of the patients were men. After diagnosis, 46.2% of patients underwent surgery alone, 43.5% of patients underwent surgery and radiotherapy, and 3.6% of patients received only radiotherapy. Survival analysis showed that the 5-year OS and DSS for all HNMM patients were 69.7 and 82.1%, respectively. In the multivariate analysis model, the undifferentiated pathological grade ($P < 0.05$) and M1 in the M category ($P < 0.01$) were independent prognostic factors for poor OS and DSS, whereas the use of surgical resection was an independent favorable prognostic factor for both OS and DSS ($P < 0.05$). The prognostic nomograms for OS and DSS prediction were constructed; the C-index values for OS and DSS prediction were 0.78 (95% CI 0.70–0.86) and 0.79 (95% CI 0.67–0.90), respectively. In conclusion, this SEER data-based study demonstrated that HNMM patients often had a favorable prognosis, and distant metastasis, pathological grade, and the use of surgery contributed to their survival. Furthermore, we developed a prognostic nomogram to predict OS and DSS for HNMM patients to aid physicians in the clinical management of this rare disease.

Keywords: malignant myoepithelioma, head and neck cancer, SEER database, nomogram, overall survival

INTRODUCTION

A myoepithelial tumor is a rare malignancy that is composed almost exclusively of cells with myoepithelial differentiation. Myoepithelial tumors were classified among salivary gland tumors as separate entities by the World Health Organization in 1991 (1) . These can be can categorized as benign and malignant myoepitheliomas. Malignant myoepithelioma (MM) is a neoplasm that exhibits a wide morphological and cytological diversity similar to its benign counterpart, myoepithelioma, with evidence of malignant change. Due to a lack of specific symptoms or imaging characteristics, it is impossible to differentiate benign from malignant myoepitheliomas based on clinical information. Therefore, a biopsy is required for the diagnosis of this disease. Malignant myoepitheliomas often present with an infiltrative growth pattern, angiolymphatic or perineural invasion, and a propensity for metastasis and recurrence (2–4). Nagao et al. (5) reported that myoepithelial tumors with high cell proliferative activity suggest malignancy, irrespective of their histological appearance.

Malignant myoepitheliomas are often located in the salivary glands (6–8). In addition to the salivary gland, previous studies have reported that this disease may arise in other head and neck locations such as the nasal cavity, nasopharynx, and the maxillary sinus (9–14). Owing to its rarity, much of the current knowledge and clinical approaches to malignant myoepithelioma of the head and neck (HNMM) are limited to generalizations from malignant myoepitheliomas located in other anatomical regions (7). Furthermore, there is a lack of population data, and no studies so far have defined the clinicopathological characteristics and determined the factors influencing survival in a large cohort; these factors limit the understanding of this rare disease. Thus, we conducted the present study to describe the demographics, clinicopathologic characteristics, treatment regimen, and prognosis of HNMM patients using data from the Surveillance Epidemiology and End Results (SEER) database.

MATERIALS AND METHODS

Participants

A population-based search for patients diagnosed with HNMM between 1991 and 2016 was carried out in the SEER database of "SEER 18 Regs Custom Data with additional treatment fields, Nov 2018 Sub (1975–2016)" using SEER*STAT 8.3.9 software. Given that SEER is a publicly available database, institutional review board approval was not required (Ethics committee of Shanghai Stomatological Hospital). The International Classification of Diseases for Oncology (ICD-O) topography code 8982/3 was used to identify all HNMM patients. The study variables included demographic information, clinicopathological factors, treatment, and prognosis. Specific information retrieved included data on age at diagnosis, sex, race, tumor grade, anatomical site, TNM stage (AJCC 7th edition), surgery, radiotherapy, survival status, and survival time (overall survival, OS; disease-specific survival, DSS). OS was defined as the interval from initial diagnosis to death from any cause or last follow-up, and DSS was defined as the interval from initial diagnosis to death caused by this disease.

Statistical Analysis

Descriptive statistics were calculated for all demographic and clinicopathological characteristics. Survival analyses for OS and DSS were performed using the Kaplan–Meier curve and log-rank tests. Univariate and multivariate Cox regression analyses were used to assess the predictive performance of each covariate for OS and DSS. All survival analyses were performed using MedCalc software (version 15.2.2, Mariakerke, Belgium), and the prognostic nomograms for OS and DSS predictions were constructed using R version 3.6.0 (R Foundation for Statistical Computing, Vienna, Austria). $P < 0.05$ was considered statistically significant.

RESULTS

A total of 333 patients diagnosed with HNMM between 1991 and 2016 were found in the SEER database. Patient characteristics are shown in **Table 1**. Of these patients, 50.1% were women, and 72.7% were white. The average and median age at diagnosis were 60.6 and 63 years, respectively (range: 1–94 years). The salivary gland was the most affected site, followed by the oral cavity. Definitive staging was available in 67.3% of cases, with almost equal distributions at each stage (stage I, 21.9%; stage II, 25.8%; stage III, 25.0%; stage IV, 27.3%). Among 243 (OS) and 245 (DSS) patients with definitive information on metastases, lymph node and distant metastases were observed in 37/243 patients and 16/245 patients, respectively. As for the treatment regimen, 46.2% of patients underwent surgery alone, 43.6% of patients received surgery and radiotherapy, 3.6% of patients received radiotherapy alone, and 6.3% received neither. Compared with those receiving surgery plus radiotherapy, HNMM patients receiving surgery alone tended to exhibit well differentiated, early-stage tumors (TNM-I/II, T1/T2, lymph node-negative tumors) (**Supplementary Table 1**). Moreover, patients who could not receive surgery were more likely to have exhibited distant metastases (6/33 vs. 10/299).

The Kaplan–Meier curves for OS and DSS showed that the 5-year OS and DSS in the entire cohort were 69.7 and 82.1%, respectively (**Figures 1A, B**). The median OS was 118 months (95% CI, 93–177). Survival analysis revealed a statistically significant difference in OS and DSS stratified according to the stage at presentation ($P < 0.01$) (**Figures 1C, D**). Similarly, pathological grade and T/N/M categories were significantly associated with both OS and DSS (**Figure 2**). Male sex and the use of radiotherapy were associated with worse DSS ($P = 0.04$ for both). Younger age was associated with significantly better OS ($P < 0.01$). However, race and primary site were not significantly associated with OS and DSS.

As for treatment modality, surgical resection was associated with better DSS and OS (**Figures 3A, B**). A Kaplan–Meier

TABLE 1 | Patients' characteristics.

Characteristics	Total (N = 333)
Age (Year)	
Mean	60.6
Median	63
Min	1
Max	94
Sex	
Female	167 (50.1%)
Male	166 (49.9%)
Race	
White	242 (72.7%)
Black	54 (15.2%)
Other (American Indian/AK Native, Asian/Pacific Islander)	35 (10.5%)
Unknown	2 (0.6%)
Tumor Grade	
Well	42 (23.5%)
Moderately	77 (42.0%)
Poorly	34 (17.6%)
Undifferentiated	34 (16.9%)
Unknown	146
Primary Site	
Salivary Gland	245 (76.0%)
Oral Cavity	52 (13.5%)
Nasal cavity & accessory sinuses	21 (1.1%)
Pharynx & Larynx	10 (9.4%)
Other	5
TNM	
I	50
II	59
III	57
IV	58
Unknown	109
T category	
T1	52 (16.2%)
T2	66 (33.5%)
T3	67 (32.9%)
T4	45 (23.3%)
Unknown	103
N category	
N0	206 (85.6%)
N1	17 (12.8%)
N2	20 (6.6%)
Unknown	90
M category	
M0	229 (92.3%)
M1	16 (7.7%)
Unknown	88
Surgery	
Yes	299 (89.8%)
No	33
Unknown	1
Radiotherapy	
Yes	157
No	176
Treatment modality	
Surgery + radiotherapy	145 (43.6%)
Surgery Alone	154 (46.2%)
Radiotherapy Alone	12 (3.6%)
None	21 (6.3%)
Unknown	1(0.3%)

analysis was used to compare the relative survival curves for HNMM patients receiving surgical resection, radiotherapy, both, or neither (**Figures 3C, D**). Differences in OS were observed between the patients treated with surgery alone and radiotherapy alone (P = 0.01), whereas differences in DSS were observed between those treated with bimodal therapy and surgical resection (P = 0.01) (**Supplementary Table 2**).

We then further compared the efficacy of treatment modalities stratified by tumor stage and the presence of lymph node metastases. Surgery plus radiotherapy could not significantly improve OS or DSS, compared with surgery alone, among patients with late-stage (III/IV) or lymph node metastasis (P >0.05). Similarly, no significant differences were observed between treatment modalities (surgery alone vs. surgery plus radiation) among early-stage patients (I/II) (P >0.05) (**Supplementary Figure 1**).

Tables 2, **3** show the results of the univariate and multivariate Cox regression analyses for OS and DSS, respectively. In the multivariate analysis model, an absence of differentiation in terms of pathological grade (OS: HR = 5.46, 95% CI 1.62–18.4, P <0.01; DSS: HR = 8.20, 95% CI 1.31–51.4, P = 0.03) and M1 in the M category (OS: HR = 9.98, 95% CI 3.57–27, P <0.01; DSS: HR = 18.6, 95% CI 4.67–74.3, P <0.01) were independent prognostic factors for worse OS and DSS, while the use of surgical resection was an independent favorable prognostic indicator for both OS and DSS (OS: HR = 0.15, 95% CI 0.05–0.47 P <0.01; DSS: HR = 0.14, 95% CI 0.02–0.83, P = 0.03). Additionally, N2 in the N category was an independent, unfavorable, prognostic factor for OS (HR = 3.20, 95% CI 1.31–7.80, P = 0.01).

Furthermore, we constructed the prognostic nomograms for OS and DSS among HNMM patients using independent prognostic factors from multivariate Cox regression analysis. As shown in **Figure 4**, distant metastasis contributed the most to both OS and DSS, followed by pathological grade and the use of surgery. The C-index values for OS and DSS predictions were 0.78 (95% CI 0.70–0.86) and 0.79 (95% CI 0.67–0.90), respectively. The 3-, 5-, and 10-year calibration curves showed excellent agreement between the predicted and observed values (**Figure 5**).

DISCUSSION

Data on HNMM are relatively limited. In addition, there is a demand for large-scale cohort studies to determine the clinicopathological determinants of survival and treatment modalities for this rare malignancy. This study, using data from the SEER database, permitted the analysis of treatment and outcomes using population-based data relating to this rare malignancy. This study is, to our knowledge, based on the largest cohort of HNMM patients in its description of demographics and clinicopathological characteristics as well as its definition of prognostic factors.

Demographically, our results concerning age agreed with data previously reported in the literature related to HNMM, with the peak incidence recorded in the sixth decade of life (range: 14–96 years) (11, 15–17). Although age was significantly associated with OS rather than DSS, this significant association disappeared after adjusting for other variables in the multivariate Cox

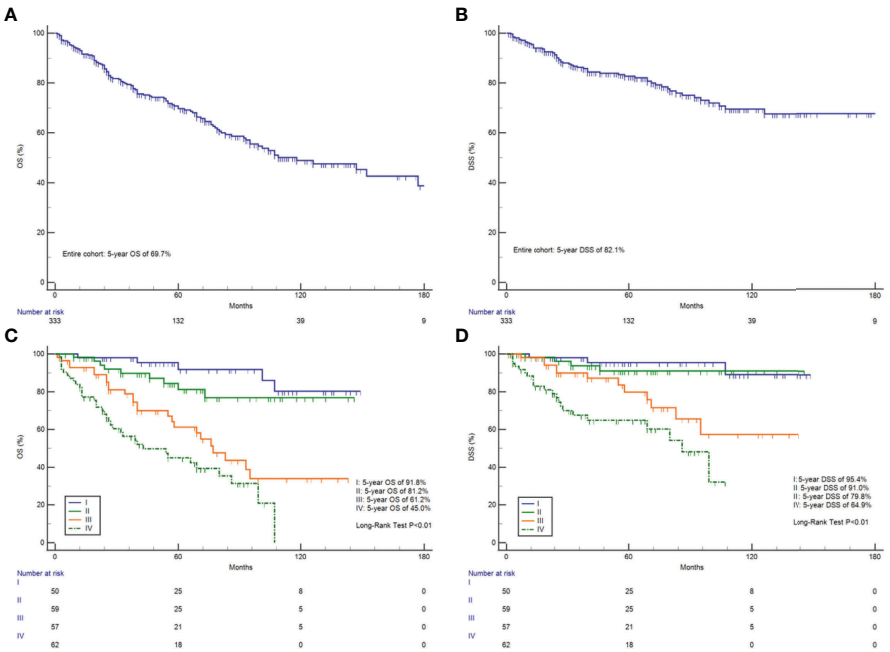

FIGURE 1 | Survival analysis. OS **(A)** and DSS **(B)** in all 333 HNMM patients; OS **(C)** and DSS **(D)** analysis stratified by AJCC-TNM staging.

regression analysis. The sex distribution results contradicted those of the previously reported studies. Nagao et al. reported a predominance of women over men (2:1) among 10 patients with MM of the salivary gland, whereas Yu et al. observed a predominance of men (1.7:1) (5, 18). However, our cohort found an equal sex distribution, with 167 women and 166 men. One possible explanation for this discrepancy is that several previous studies only focused on patients with MM of the salivary gland. In our study, we included patients with MM in other head and neck regions, not only in the salivary gland. Notably, this study is the first to suggest that male patients with HNMM have a worse prognosis than their female counterparts. Race appeared to have no statistically significant effect on the survival of HNMM patients. This finding is inconsistent with previous reports that indicate that race is an independent prognostic factor in other head and neck malignancies (19, 20).

In terms of clinicopathology, most tumors (76%) occurred in the salivary glands in this cohort; this result is consistent with the results of previous studies (17). A survival analysis stratified in terms of the primary sites showed no significant differences in DSS and OS. Patients with MM of the salivary gland had a survival rate similar to those with MM of other parts of the head and neck. This result suggests that these patients may belong to one entity. Previous studies have revealed that pathological grade is an important prognostic reference for tumors in the head and neck region (21–24). This study also indicated a significant association between pathological differentiation and survival, and multivariate analysis demonstrated that pathological differentiation was independently associated with OS and DSS. In the constructed nomograms, pathological differentiation had the second highest contribution to OS and DSS predictions. This finding demonstrates the importance of the pathological differentiation of MM located in the head and neck region on prognosis; thus, physicians should evaluate the prognosis in terms of pathological differentiation. AJCC-TNM staging plays an essential role in treatment planning and prognosis evaluation. Based on the available information, in this cohort, an equal distribution of the AJCC-TNM stage was observed among the 234 patients. Meanwhile, 19.4 and 7.7% of patients had lymph node and distant metastases, respectively, signifying the aggressive nature of this rare malignancy *via* hematogenous and lymphatic spread. Both the N and M categories were independently associated with OS and DSS. For example, patients with distant metastases have a dismal prognosis (OS, 26 months; DSS, 28 months). Therefore, an early examination and diagnosis is vital to improve survival and decrease the possibility of metastases.

Overall, the prognosis of HNMM patients is better than that of patients with other malignancies in the head and neck region (25, 26). According to the largest case series reported to date, the 5-year cumulative survival rate of 59 Chinese patients with HNMM was 62% (27). In this cohort, our data showed a 5-year OS rate of 69.7%. One possible explanation for this difference is the higher proportion of stage III (23/59 cases) and stage IV (19/59) patients in the cohort in the study by Zhao etal. (27) than in this study. Furthermore, our data revealed that a significant majority of cases (90.1%) were treated with surgical resection, and the use of surgery was an independent favorable prognostic factor. Surgery may decrease the risk of death from all causes and HNMM by 85 and 86%, respectively. Surgery

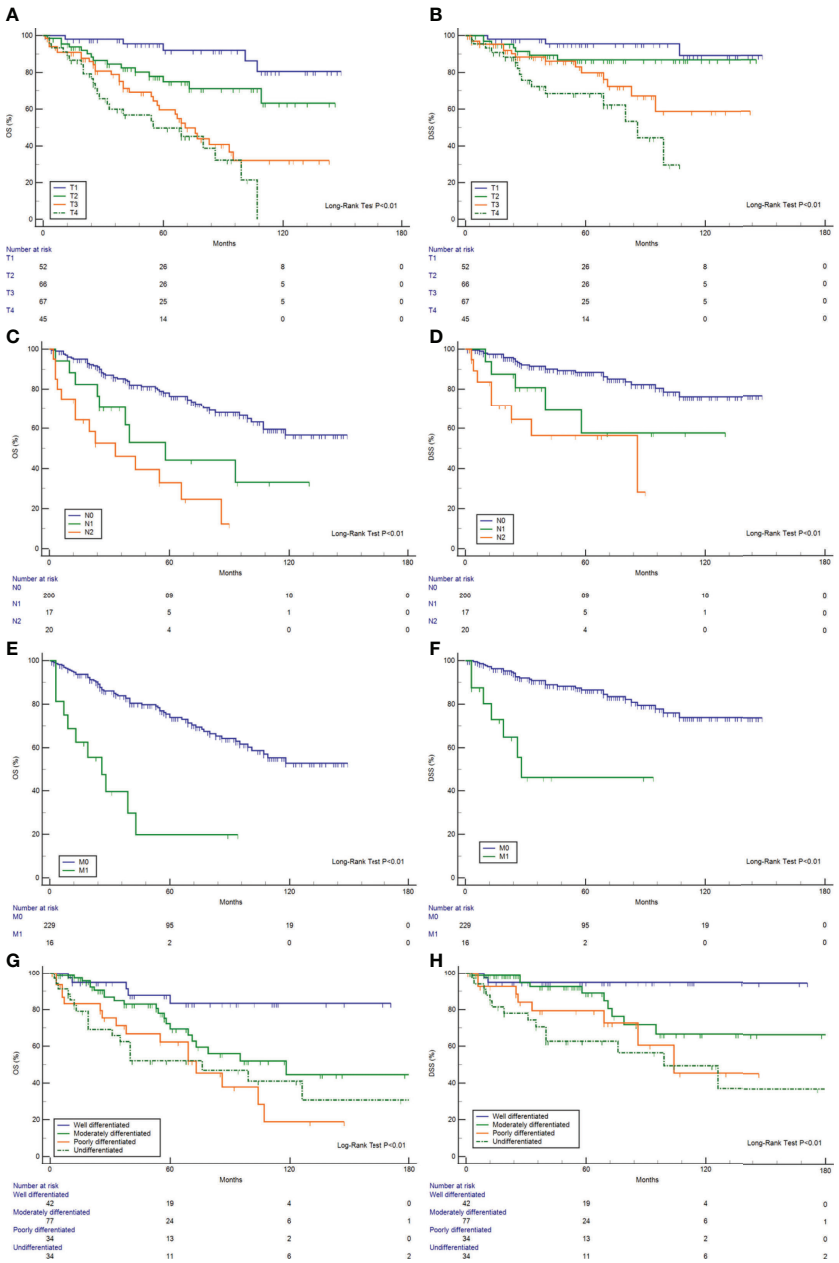

FIGURE 2 | OS and DSS analysis. **(A)** OS and T category; **(B)** OS and N category; **(C)** OS and M category; **(D)** OS and pathological grade; **(E)** DSS and T category; **(F)** DSS and N category; **(G)** DSS and M category; and **(H)** DSS and pathological grade.

significantly prolonged OS by approximately 109 months (147 months vs. 38 months). Therefore, surgery is the optimal treatment strategy for patients with HNMM. A previous study has also demonstrated that surgical resection is the preferred treatment for HNMM. However, the requirements for a first surgery are high. Furthermore, if the resection is not complete, it is easy for relapse to occur, and the operation and adjuvant treatment often do not deliver satisfactory results (27). Radiotherapy is an alternative regimen for patients who cannot tolerate surgery; it can also serve as an adjuvant treatment for patients undergoing surgery. In this cohort, approximately half of all patients (47.1%) received radiotherapy. The addition of radiotherapy to surgery did not significantly prolong the OS or DSS. Moreover, patients receiving a combination of surgery and radiotherapy had a considerably shorter duration of DSS than those who underwent surgery alone. This result may be attributed to the fact that patients receiving radiotherapy plus surgery mostly had advanced-stage tumors and that patients

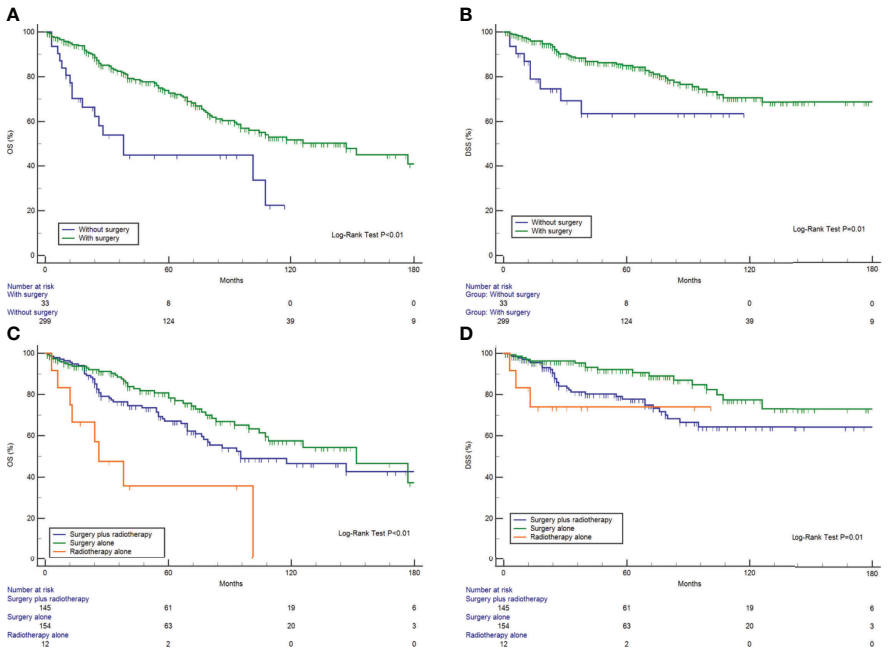

FIGURE 3 | Survival analysis stratified by surgery **(A, B)** and treatment modalities **(C, D)**.

TABLE 2 | Univariate COX regression analysis for OS and DSS.

Characteristic	OS		DSS	
	HR with 95% CI	P-value	HR with 95% CI	P-value
Age (≥61 vs <61)	2.11 (1.42–3.15)	<0.01	1.03 (0.62–1.71)	0.92
Sex (Male vs Female)	1.41 (0.97–2.06)	0.07	1.69 (1.01–2.84)	0.04
Race				
White	Reference		Reference	
Black	0.77 (0.46–1.29)	0.31	0.75 (0.37–1.54)	0.44
Other	0.54 (0.27–1.13)	0.10	0.51 (0.18–1.42)	0.20
Grade				
Well	Reference		Reference	
Moderately	2.72 (1.02–7.21)	0.04	3.17 (0.69–14.5)	0.14
Poorly	5.27 (1.93–14.4)	<0.01	6.46 (1.37–30.4)	0.02
Undifferentiated	4.98 (1.85–13.4)	<0.01	9.77 (2.22–43.1)	<0.01
Primary site				
Salivary Gland	Reference		Reference	
Oral Cavity	1.01 (0.59–1.73)	0.98	1.60 (0.84–3.07)	0.16
Nasal cavity & accessory sinuses	1.11 (0.56–2.21)	0.77	1.89 (0.84–4.25)	0.12
Pharynx & Larynx	2.84 (0.99–7.81)	0.06	2.80 (0.67–11.7)	0.16
Other	1.45 (0.46–4.61)	0.53	2.29 (0.55–9.52)	0.26
T category				
T1	Reference		Reference	
T2	3.02 (1.10–8.31)	0.03	2.29 (0.59–8.87)	0.23
T3	6.62 (2.57–17.1)	<0.01	4.85 (1.39–16.9)	0.0132
T4	9.29 (3.53–24.4)	<0.01	9.17 (2.64–31.9)	<0.01
N category				
N0	Reference		Reference	
N1	2.45 (1.21–4.97)	0.01	2.60 (1.01–6.75)	0.04
N2	5.13 (2.83–9.31)	<0.01	5.56 (2.51–12.3)	<0.01
M category (M0 vs M1)	4.82 (2.53–9.20)	<0.01	5.65 (2.48–12.9)	<0.01
Surgery (Yes vs No)	0.39 (0.23–0.66)	<0.01	0.42 (0.21–0.85)	0.016
Radiation (Yes vs No)	1.34 (0.92–1.94)	0.13	1.69 (1.01–2.83)	0.046

TABLE 3 | Multivariate COX regression analysis for OS and DSS.

Characteristic	OS		DSS	
	HR with 95% CI	P-value	HR with 95% CI	P-value
Age (≥61 vs <61)	1.35 (0.67–2.70)	0.40	N/A	N/A
Sex (Male vs Female)	N/A	N/A	1.63 (0.53–5.02)	0.40
Grade				
Well	Reference		Reference	
Moderately	3.22 (0.99–10.5)	0.06	4.31 (0.66–28.4)	0.13
Poorly	3.12 (0.88–11.0)	0.08	3.05 (0.42–22.0)	0.27
Undifferentiated	5.46 (1.62–18.4)	<0.01	8.20 (1.31–51.4)	0.03
T category				
T1	Reference		Reference	
T2	2.97 (0.80–11.0)	0.10	1.30 (0.21–8.06)	0.77
T3	2.43 (0.62–9.50)	0.20	1.79 (0.31–10.5)	0.52
T4	3.22 (0.82–12.7)	0.09	2.84 (0.47–17.3)	0.26
N category				
N0	Reference		Reference	
N1	1.02 (0.30–3.44)	0.97	1.01 (0.18–5.65)	0.99
N2	3.20 (1.31–7.80)	0.01	3.36 (0.99–11.4)	0.06
M category (M0 vs M1)	9.98 (3.57–27.9)	<0.01	18.6 (4.67–74.3)	<0.01
Surgery (Yes vs No)	0.15 (0.05–0.47)	<0.01	0.14 (0.02–0.83)	0.03
Radiation (Yes vs No)	N/A	N/A	1.11 (0.40–3.03)	0.84

Only significant factors from univariate Cox analysis were included in multivariate Cox analysis. N/A, not available.

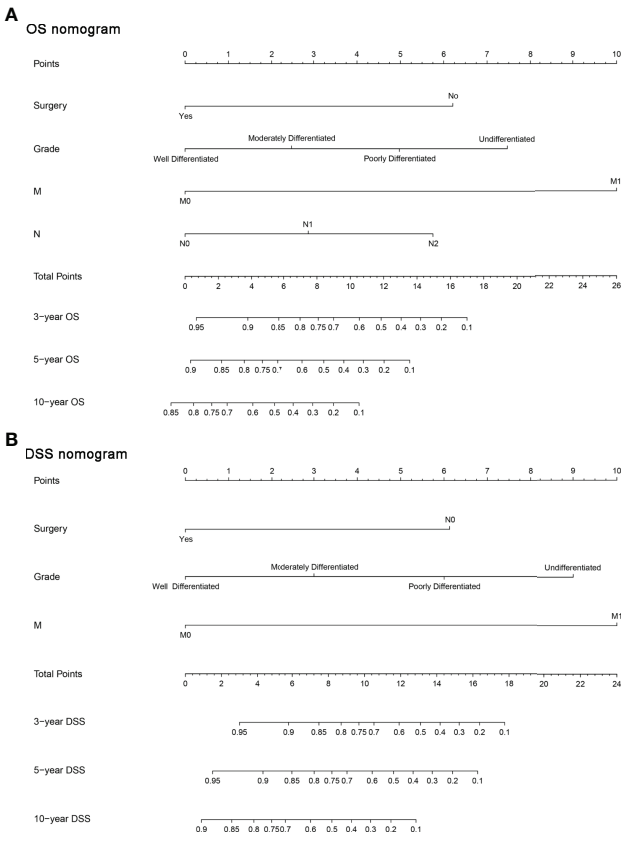

FIGURE 4 | The constructed prognostic nomogram for OS **(A)** and DSS **(B)** prediction. Each variable was assigned a score on the point scale. By summing the total score and locating it on the total point scale, a straight line was drawn down to determine the estimated probability of OS and DSS.

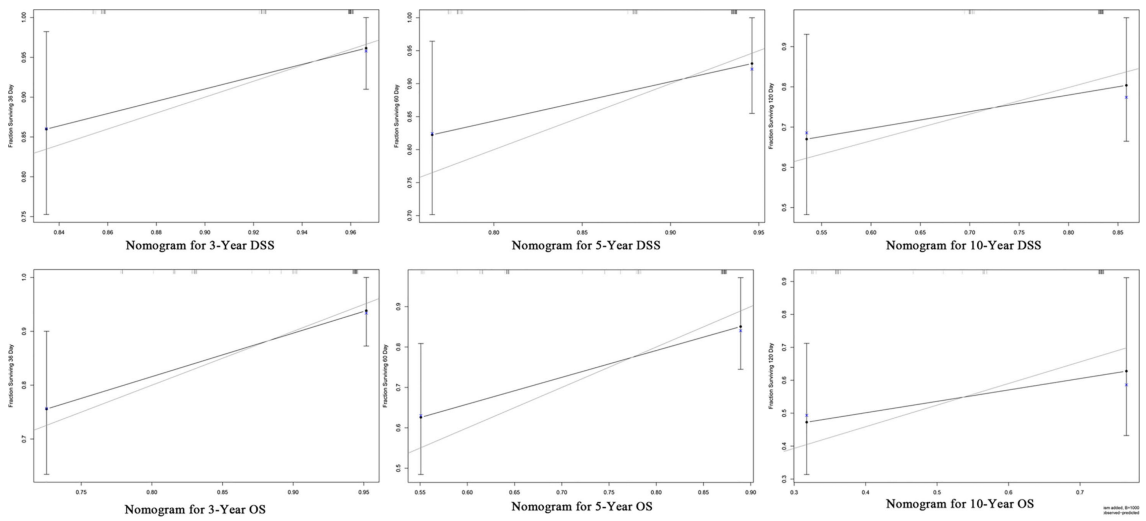

FIGURE 5 | Calibration curves for the 3-, 5-, and 10-year DSS/OS.

with radiotherapy were more likely to have late-stage tumors (76/115 vs. 43/113). Radiotherapy alone is sometimes used palliatively, as was the case in 3.6% of patients in our cohort who received radiotherapy alone. Moreover, our data showed that patients who underwent surgery alone had a substantially longer OS than those who underwent radiotherapy alone, suggesting that radiotherapy could not replace surgery among patients with HNMM. However, only 12 out of 333 patients received radiotherapy alone. Hence, it is difficult to arrive at a solid conclusion on the role of radiotherapy in HNMM owing to the small sample size. Moreover, the efficacy of chemotherapy for HNMM could not be evaluated because of insufficient information. Therefore, the optimal treatment regime for HNMM patients still needs to be confirmed in future research.

Despite a large sample size for this rare malignancy, this study has several limitations. First, certain variables could not be precisely analyzed retrospectively, including tumor recurrence and comorbidities. Second, no information on chemotherapy was available in the SEER database; thus, the analysis was limited in terms of exploring the optimal regimen for this malignancy. The lack of data on cancer control and tumor recurrence in the SEER database restricted the potential knowledge we could have gained concerning this rare disease. Third, concerns emerged regarding the misclassification and lack of clinicopathologic variables, particularly tumor grade and histological differentiation, in the database. For example, there was no information on the TNM stage for 109 patients and on the pathological grade for 146 patients.

In conclusion, HNMM is a rare malignancy that often occurs in the sixth decade of life with an equal sex distribution. It has a relatively good survival rate with a 5-year OS and DSS of 69.7 and 82.1%, respectively. Pathological grade and distant metastasis are independently associated with its prognosis. Surgical resection confers OS and DSS benefits in patients with HNMM. Furthermore, distant metastasis, pathological grade, and the use of surgery contribute to the establishment of prognostic predictions of OS and DSS among HNMM patients.

DATA AVAILABILITY STATEMENT

The original contributions presented in the study are included in the article/**Supplementary Material**. Further inquiries can be directed to the corresponding author.

AUTHOR CONTRIBUTIONS

J-QW: Study design, data collection, data analysis, and writing—original draft preparation. R-XD: Date collection, data analysis, and writing—original draft preparation. HL: Data analysis, software, and writing—reviewing. YL: Data collection and data analysis. M-ML: Writing—reviewing and editing. Z-CY: Study design, supervision, writing—reviewing and editing. All authors listed have made a substantial, direct, and intellectual contribution to the work and approved it for publication.

SUPPLEMENTARY MATERIAL

The Supplementary Material for this article can be found online at: https://www.frontiersin.org/articles/10.3389/fonc.2022.754967/full#supplementary-material

Supplementary Figure 1 | Survival analysis stratified by treatment modalities (surgery plus radiation vs surgery alone) **(A**: TNM-I/II, OS; **(B**: TNM-I/II, DSS; **(C**: TNM-III/IV, OS; **(D**: TNM-III/IV, DSS; **(E**: N1+N2, OS; **(F**: N1+N2, DSS; **(G**: N0, OS; **(H**: N0, DSS).

REFERENCES

1. Seifert G, Sobin LH. Myoepithelioma. World Health Organization International Histological Classification of Tumours. In: *Histological Typing of Salivary Gland Tumours, 2nd ed*. Berlin, Germany: Springer-Verlag (1991). p. 20–1.
2. Ogawa I, Nishida T, Miyauchi M, Sato S, Takata T. Dedifferentiated Malignant Myoepithelioma of the Parotid Gland. *Pathol Int* (2003) 53:704–9. doi: 10.1046/j.1440-1827.2003.01536.x
3. Kong M, Drill EN, Morris L, West L, Klimstra D, Gonen M, et al. Prognostic Factors in Myoepithelial Carcinoma of Salivary Glands: A Clinicopathologic Study of 48 Cases. *Am J Surg Pathol* (2015) 39:931–8. doi: 10.1097/PAS.0000000000000452
4. Vilar-Gonzalez S, Bradley K, Rico-Perez J, Vogiatzis P, Golka D, Nigam A, et al. Salivary Gland Myoepithelial Carcinoma. *Clin Transl Oncol* (2015) 17:847–55. doi: 10.1007/s12094-015-1329-4
5. Nagao T, Sugano I, Ishida Y, Tajima Y, Matsuzaki O, Konno A, et al. Salivary Gland Malignant Myoepithelioma: A Clinicopathologic and Immunohistochemical Study of Ten Cases. *Cancer* (1998) 83:1292–9. doi: 10.1002/(SICI)1097-0142(19981001)83:7<1292::AID-CNCR4>3.0.CO;2-L
6. Vazquez A, Patel TD, D'aguillo CM, Abdou RY, Farver W, Baredes S, et al. Epithelial-Myoepithelial Carcinoma of the Salivary Glands: An Analysis of 246 Cases. *Otolaryngol. Head Neck Surg* (2015) 153:569–74. doi: 10.1177/0194599815594788
7. Rastrelli M, Del Fiore P, Damiani GB, Mocellin S, Tropea S, Spina R, et al. Myoepithelioma of the Soft Tissue: A Systematic Review of Clinical Reports. *Eur J Surg Oncol* (2019) 45:1520–6. doi: 10.1016/j.ejso.2019.05.003
8. Trevino M, Moorthy C, Kafchinski L, Bustamante D. Foot Plantar Soft Tissue Malignant Myoepithelioma Tumor: Case Report and Review of the Literature. *Clin Imaging* (2020) 61:90–4. doi: 10.1016/j.clinimag.2019.11.014
9. Graadt Van Roggen JF, Baatenberg-De Jong RJ, Verschuur HP, Balhuizen JC, Slootweg PJ, Van Krieken JH. Myoepithelial Carcinoma (Malignant Myoepithelioma): First Report of an Occurrence in the Maxillary Sinus. *Histopathology* (1998) 32:239–41. doi: 10.1046/j.1365-2559.1998.00382.x
10. Zhou SH, Ruan LX, Gong L, Gong SQ. Primary Malignant Myoepithelioma of the Left Maxillary Sinus: A Case Report. *J Int Med Res* (2008) 36:362–5.
11. Hata M, Tokuuye K, Shioyama Y, Nomoto S, Inadome Y, Fukumitsu N, et al. Malignant Myoepithelioma in the Maxillary Sinus: Case Report and Review of the Literature. *Anticancer Res* (2009) 29:497–501.
12. Petersson F, Chao SS, Ng SB. Anaplastic Myoepithelial Carcinoma of the Sinonasal Tract: An Underrecognized Salivary-Type Tumor Among the Sinonasal Small Round Blue Cell Malignancies? Report of One Case and a Review of the Literature. *Head Neck Pathol* (2011) 5:144–53. doi: 10.1007/s12105-010-0226-y
13. Chen L, Fu Y, Wang H, Yang F, Liu J, Xia F, et al. Myoepithelial Carcinoma of the Nasopharynx: Rare Case Report With Clinicopathologic and Immunohistochemical Features Review of Literature. *Head Neck* (2018) 40:E62–7. doi: 10.1002/hed.25150
14. Silveira HA, Almeida LY, Nonaka CFW, Alves PM, Ribeiro-Silva A, Leon JE. Myoepithelial Carcinoma With Rhabdoid Features in the Maxillary Sinus: Immunohistochemical and *in Situ* Hybridization Analysis of a Rare Case. *Oral Oncol* (2019) 93:116–9. doi: 10.1016/j.oraloncology.2019.04.015
15. Wang J, Wu Q, Sun K, Beng C. Quantitative Multivariate Analysis of Myoepithelioma and Myoepithelial Carcinoma. *Int J Oral Maxillofac Surg* (1995) 24:153–7. doi: 10.1016/S0901-5027(06)80091-3
16. Neto AG, Pineda-Daboin K, Luna MA. Myoepithelioma of the Soft Tissue of the Head and Neck: A Case Report and Review of the Literature. *Head Neck* (2004) 26:470–3. doi: 10.1002/hed.20044
17. Li CQ, Guo ZM, Liu WW, Zhang Q, Yang AK, Yang L. [Clinical Analysis of Myoepithelial Carcinoma of Head and Neck]. *Zhonghua Er Bi Yan Hou Tou Jing Wai Ke Za Zhi* (2010) 45:124–7.
18. Yu G, Ma D, Sun K, Li T, Zhang Y. Myoepithelial Carcinoma of the Salivary Glands: Behavior and Management. *Chin Med J (Engl)* (2003) 116:163–5.
19. Mahal BA, Inverso G, Aizer AA, Bruce Donoff R, Chuang SK. Impact of African-American Race on Presentation, Treatment, and Survival of Head and Neck Cancer. *Oral Oncol* (2014) 50:1177–81. doi: 10.1016/j.oraloncology.2014.09.004
20. Zandberg DP, Liu S, Goloubeva O, Ord R, Strome SE, Suntharalingam M, et al. Oropharyngeal Cancer as a Driver of Racial Outcome Disparities in Squamous Cell Carcinoma of the Head and Neck: 10-Year Experience at the University of Maryland Greenebaum Cancer Center. *Head Neck* (2016) 38:564–72. doi: 10.1002/hed.23933
21. Bjorndal K, Krogdahl A, Therkildsen MH, Overgaard J, Johansen J, Kristensen CA, et al. Salivary Gland Carcinoma in Denmark 1990-2005: A National Study of Incidence, Site and Histology. Results of the Danish Head and Neck Cancer Group (DAHANCA). *Oral Oncol* (2011) 47:677–82. doi: 10.1016/j.oraloncology.2011.04.020
22. Schwarz S, Zenk J, Muller M, Ettl T, Wunsch PH, Hartmann A, et al. The Many Faces of Acinic Cell Carcinomas of the Salivary Glands: A Study of 40 Cases Relating Histological and Immunohistological Subtypes to Clinical Parameters and Prognosis. *Histopathology* (2012) 61:395–408. doi: 10.1111/j.1365-2559.2012.04233.x
23. Wang YL, Zhu YX, Chen TZ, Wang Y, Sun GH, Zhang L, et al. Clinicopathologic Study of 1176 Salivary Gland Tumors in a Chinese Population: Experience of One Cancer Center 1997-2007. *Acta Otolaryngol* (2012) 132:879–86. doi: 10.3109/00016489.2012.662715
24. Yibulayin F, Feng L, Wang M, Lu MM, Luo Y, Liu H, et al. Head & Neck Acinar Cell Carcinoma: A Population-Based Study Using the Seer Registry. *BMC Cancer* (2020) 20:631. doi: 10.1186/s12885-020-07066-y
25. Yu CX, Yibulayin F, Feng L, Wang M, Lu MM, Luo Y, et al. Clinicopathological Characteristics, Treatment and Prognosis of Head & Neck Small Cell Carcinoma: A SEER Population-Based Study. *BMC Cancer* (2020) 20:1208. doi: 10.1186/s12885-020-07522-9
26. Yan O, Xie W, Teng H, Fu S, Chen Y, Liu F. Nomograms Forecasting Long-Term Overall and Cancer Specific Survival of Patients With Head and Neck Neuroendocrine Carcinoma. *Front Oncol* (2021) 11:619599. doi: 10.3389/fonc.2021.619599
27. Zhao DL, Wang LZ, Cao H, Sang JZ, Gao L, Cao XD, et al. [Clinical Characteristics and Treatment of Myoepithelial Carcinoma of Head and Neck]. *Lin Chung Er Bi Yan Hou Tou Jing Wai Ke Za Zhi* (2019) 33:1085–8.

Conflict of Interest: The authors declare that the research was conducted in the absence of any commercial or financial relationships that could be construed as a potential conflict of interest.

Frontiers in Oncology

Advances knowledge of carcinogenesis and tumor progression for better treatment and management

The third most-cited oncology journal, which highlights research in carcinogenesis and tumor progression, bridging the gap between basic research and applications to imrpove diagnosis, therapeutics and management strategies.

Discover the latest Research Topics

See more →

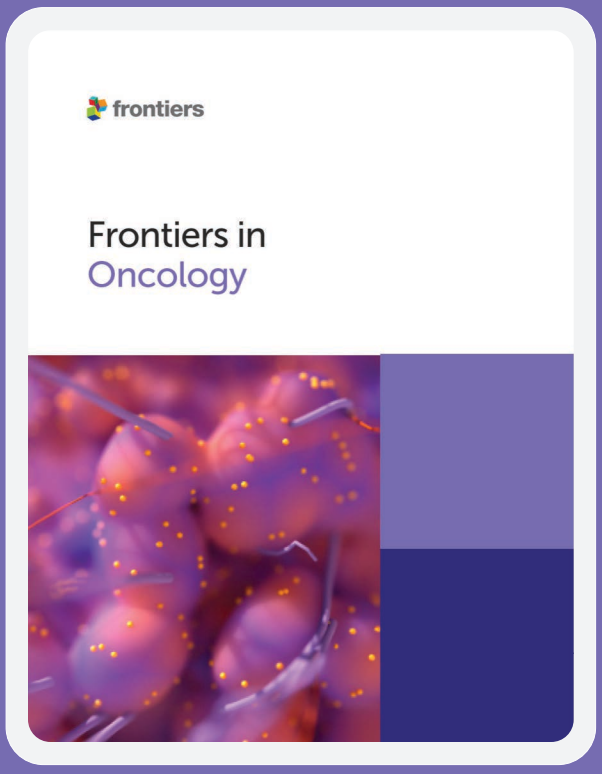

Frontiers

Avenue du Tribunal-Fédéral 34
1005 Lausanne, Switzerland
frontiersin.org

Contact us

+41 (0)21 510 17 00
frontiersin.org/about/contact